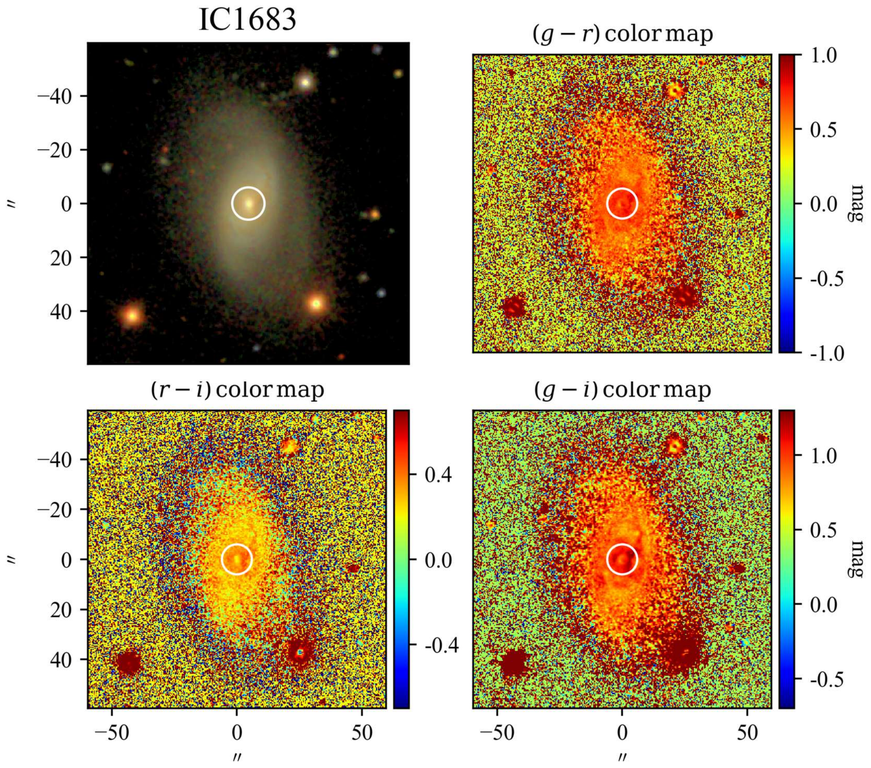

SBP decomposition of SDSS r band

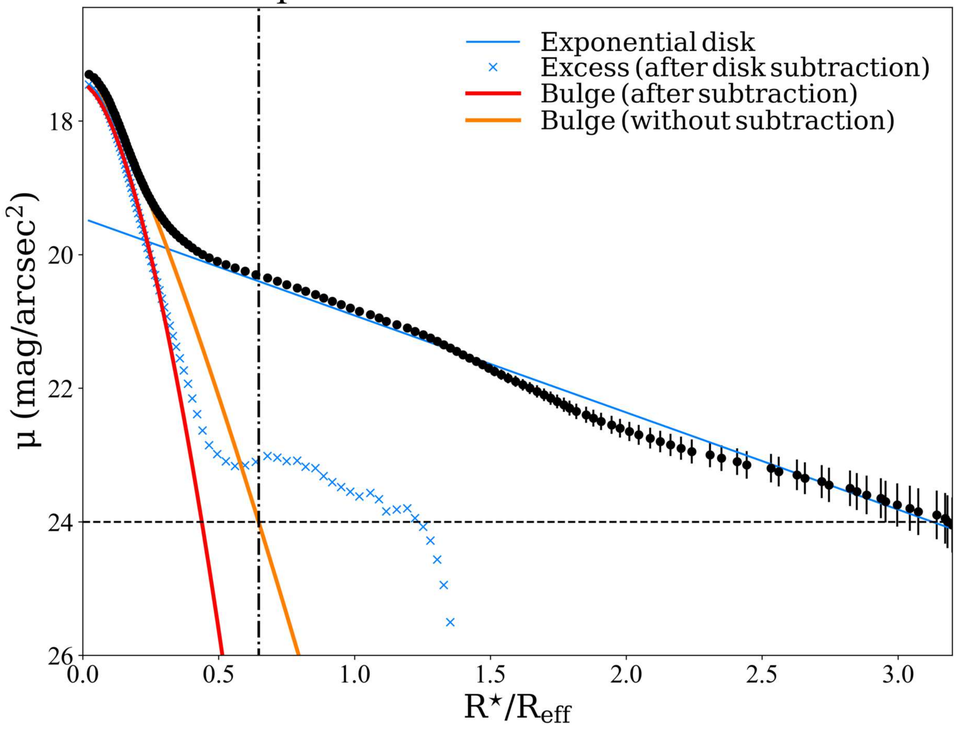

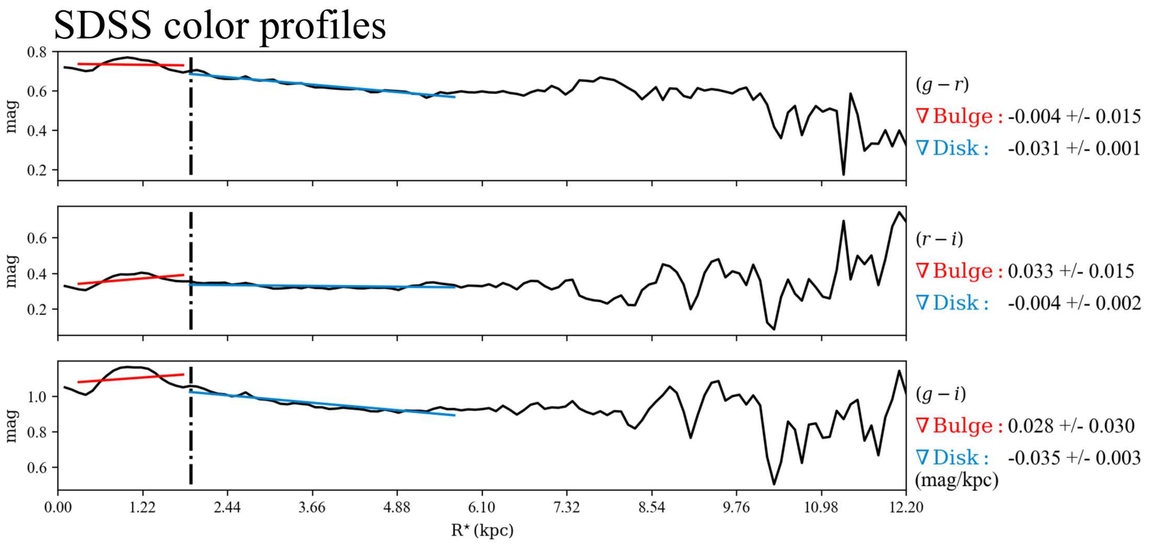

$\mathcal{RY}$ SBPs

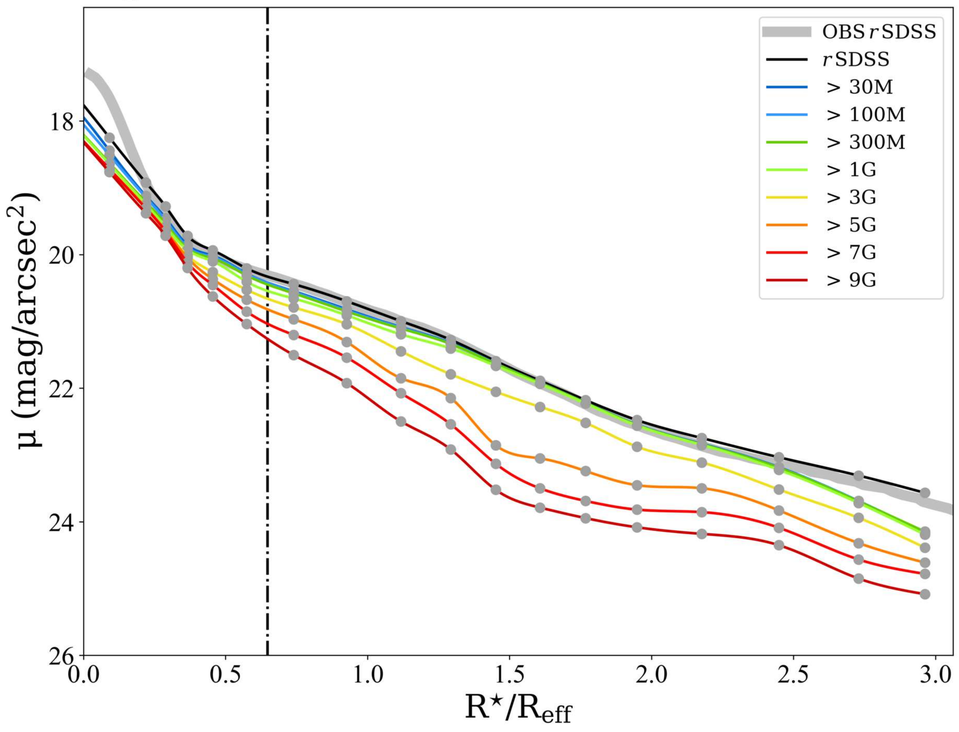

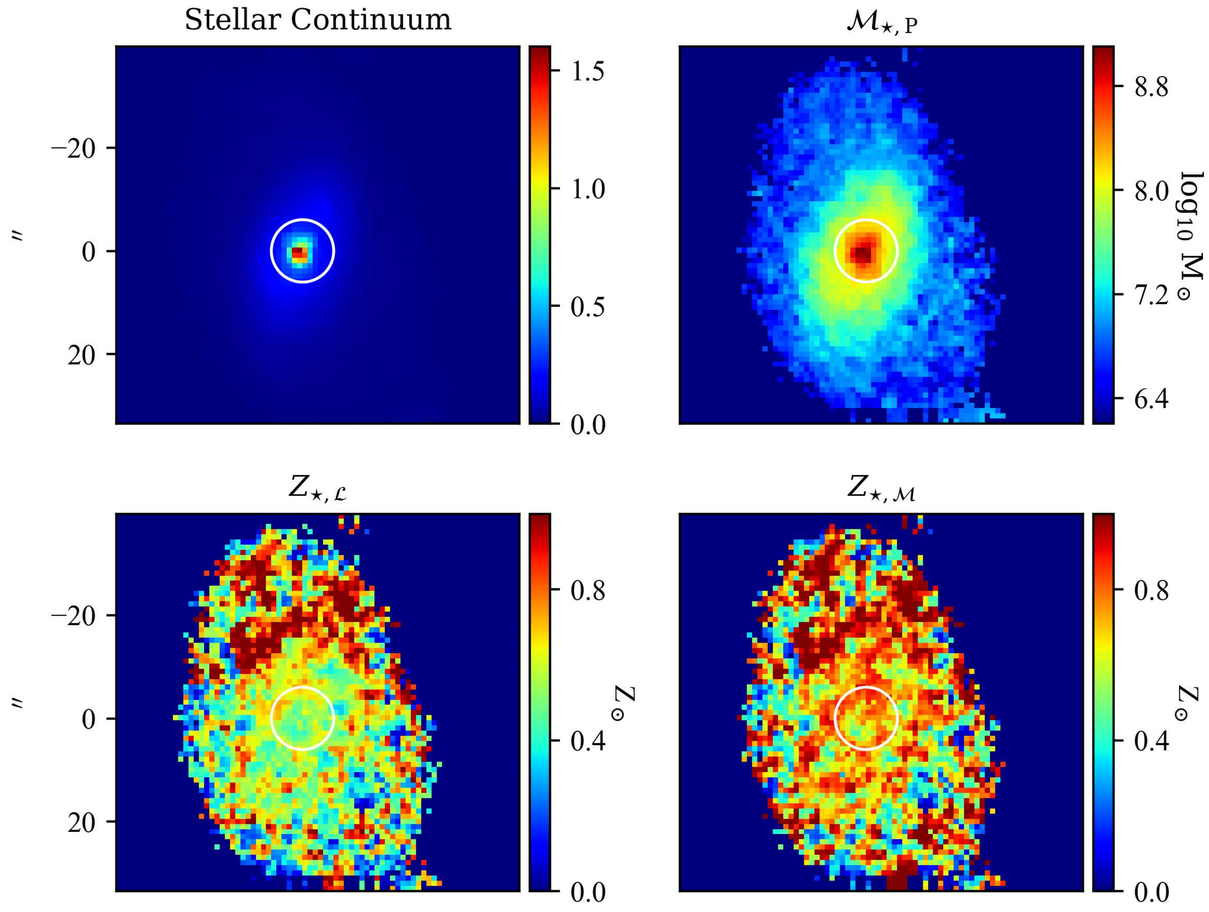

Log. of cumulative present stellar mass profiles

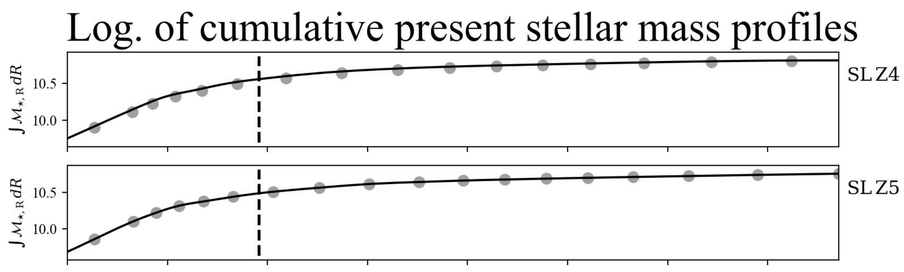

Stellar metallicity/Age & Hα flux/EW profiles

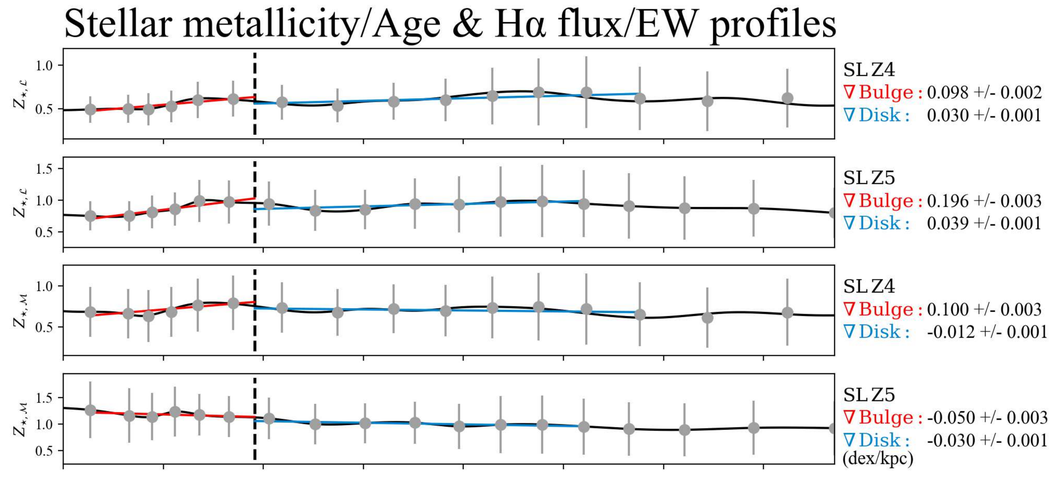

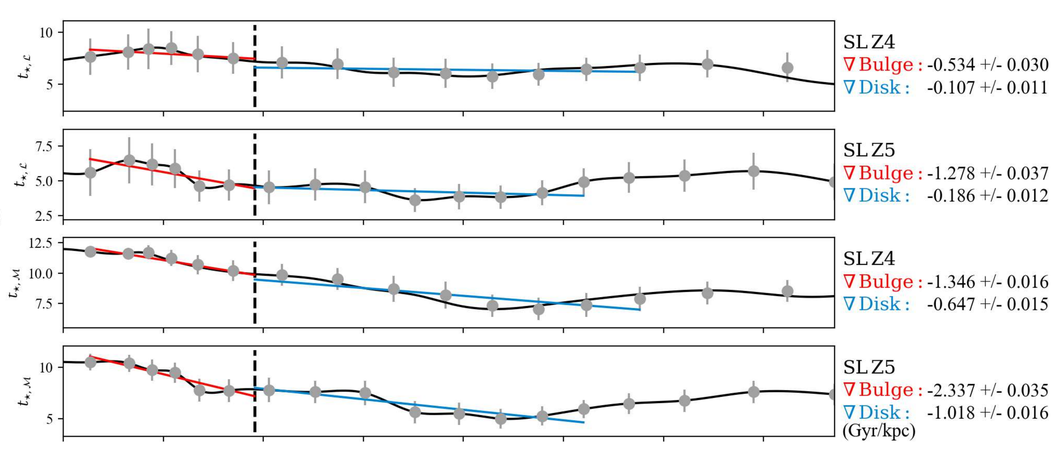

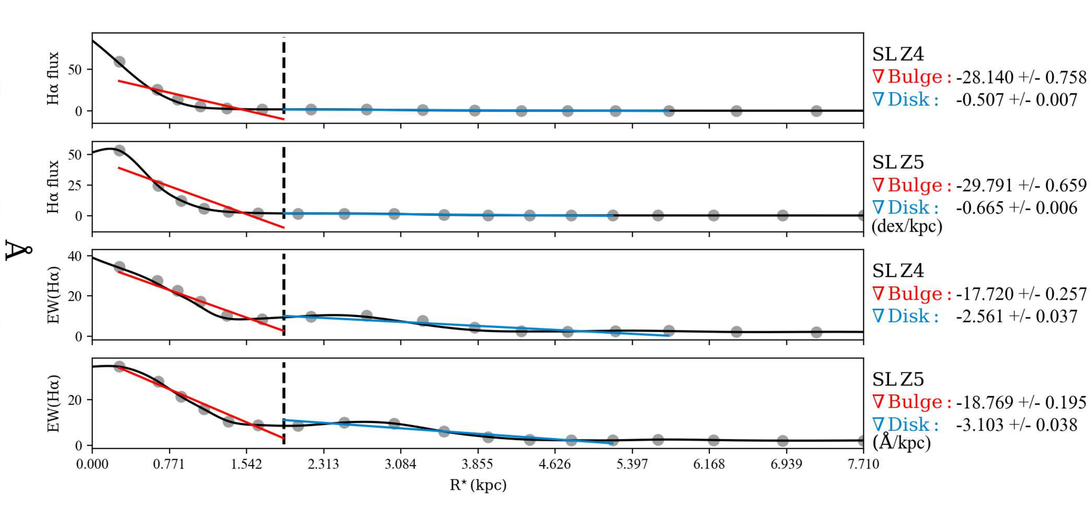

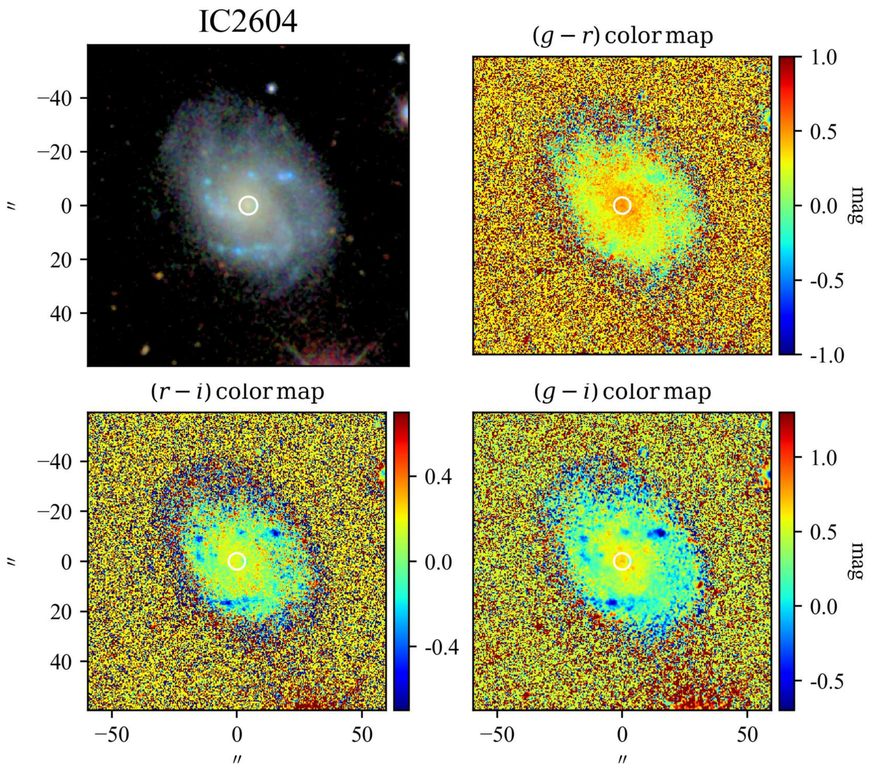

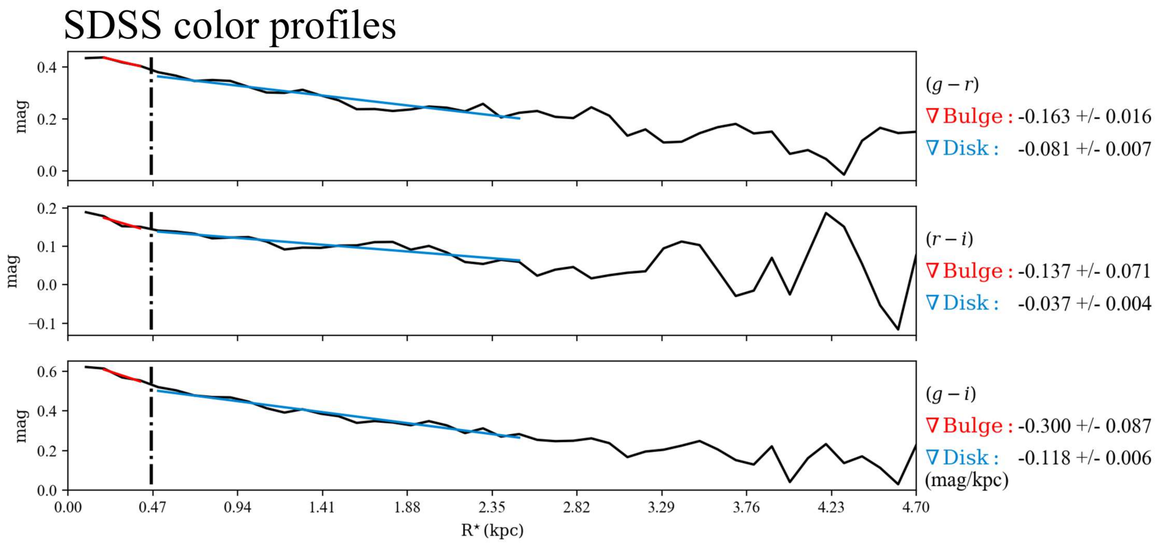

SBP decomposition of SDSS r band

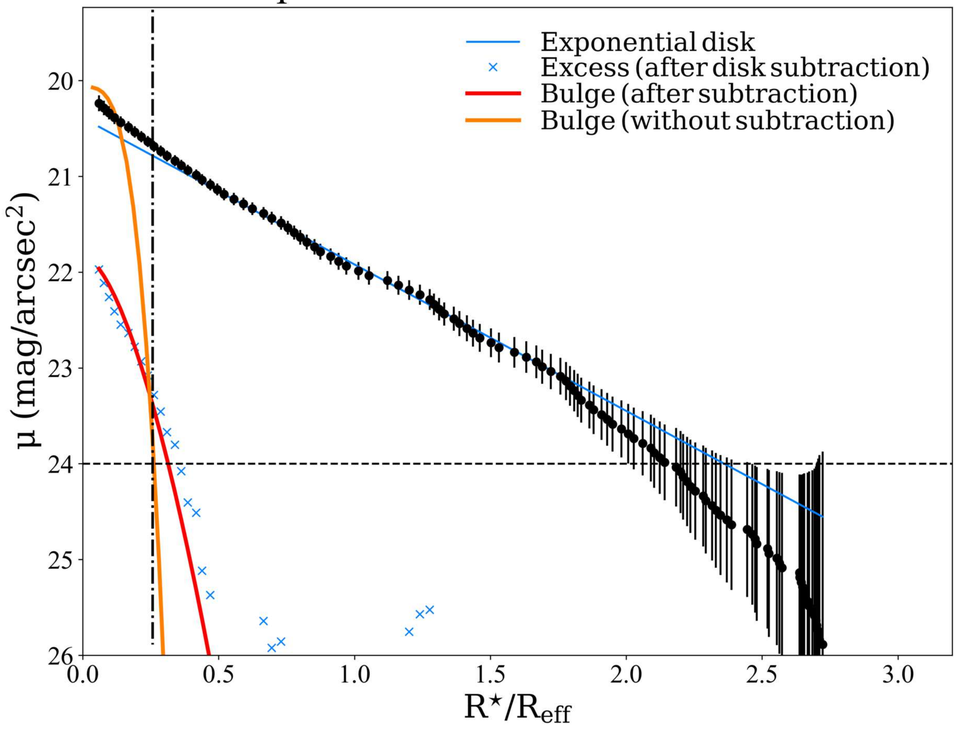

$\mathcal{RY}$ SBPs

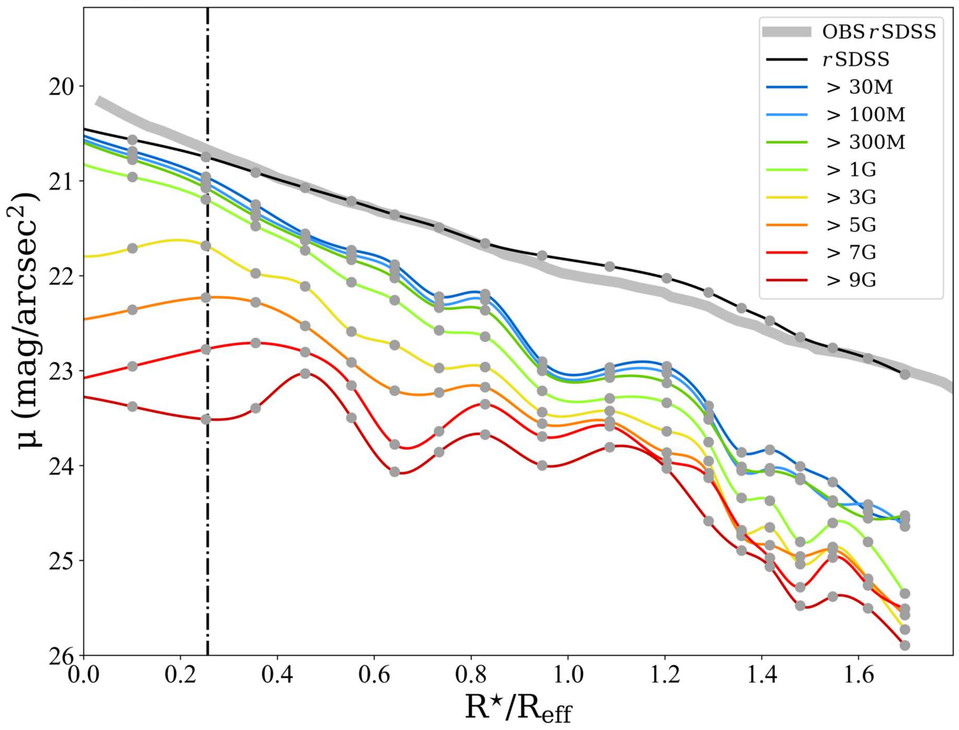

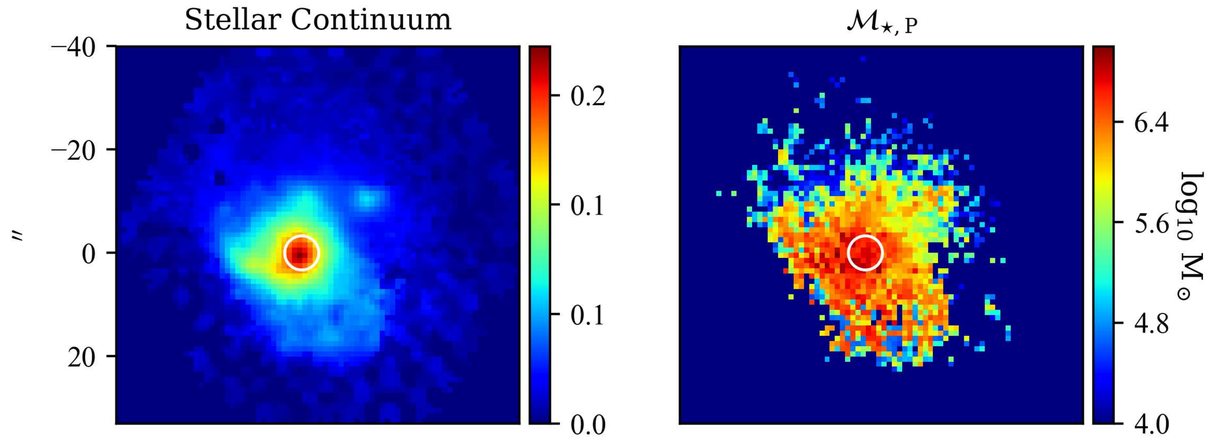

Log. of cumulative present stellar mass profiles

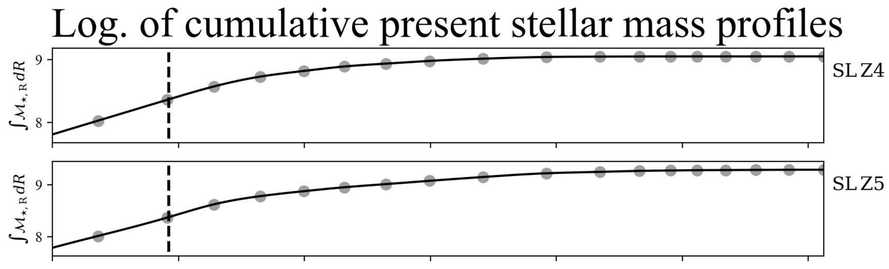

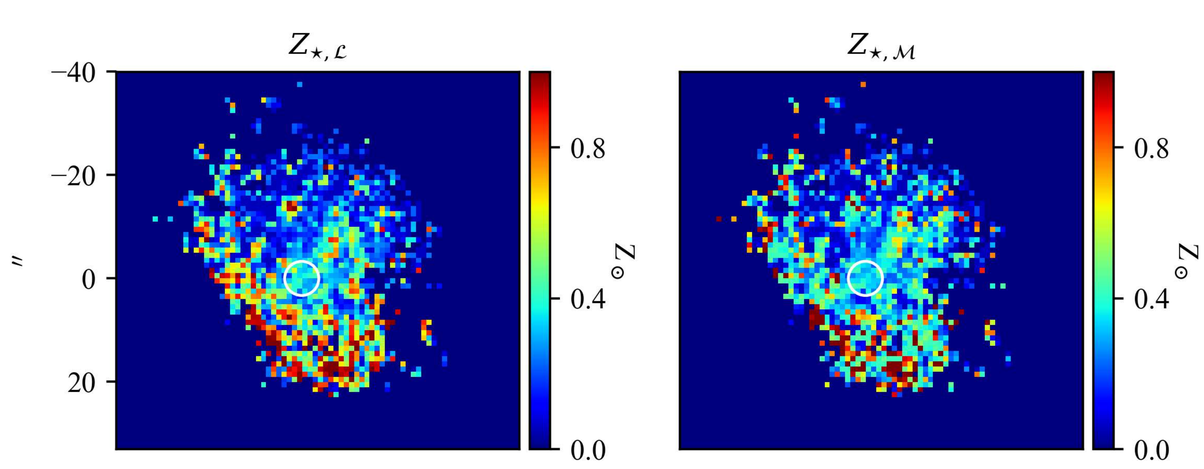

Stellar metallicity/Age & Hα flux/EW profiles

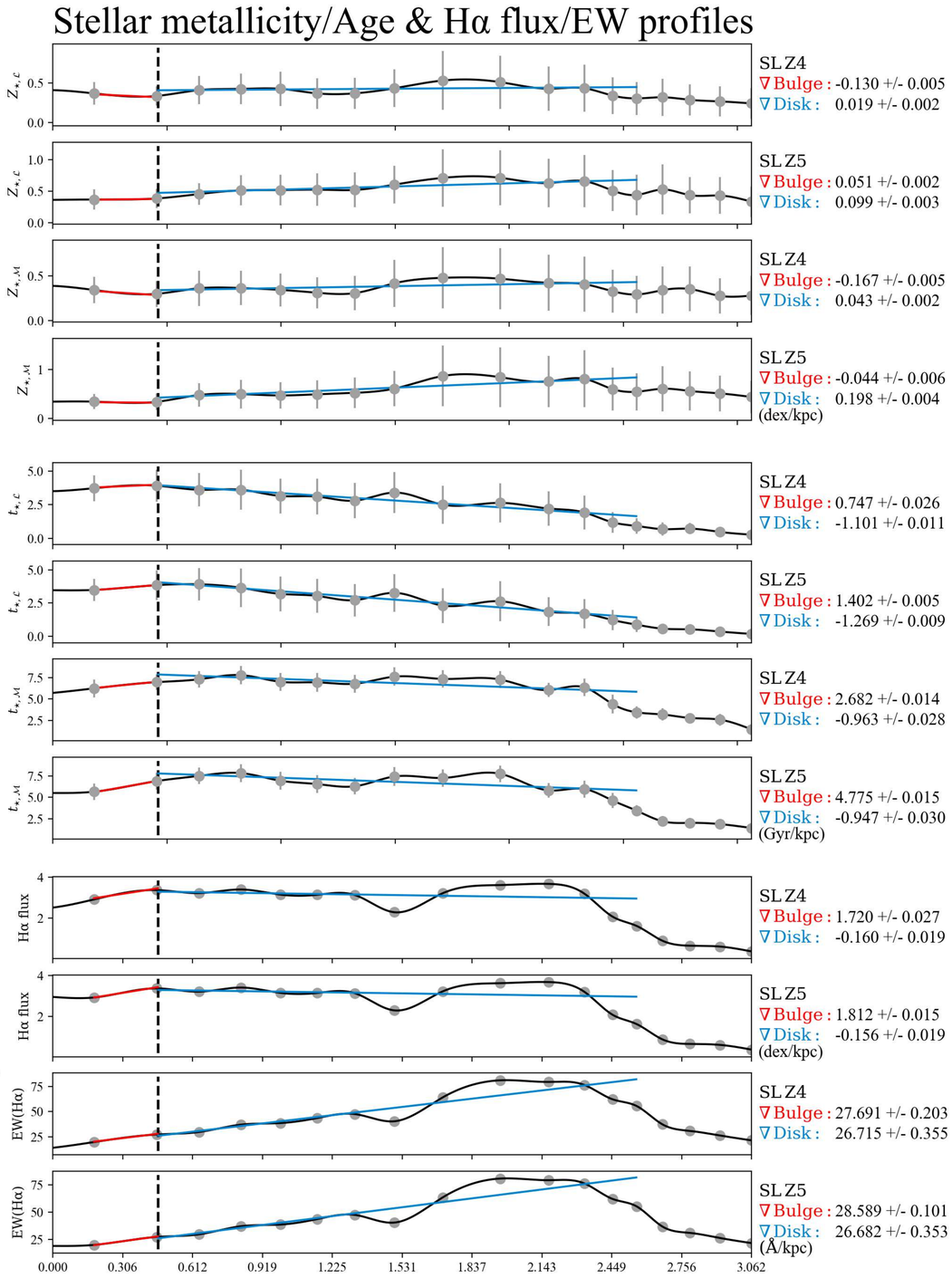

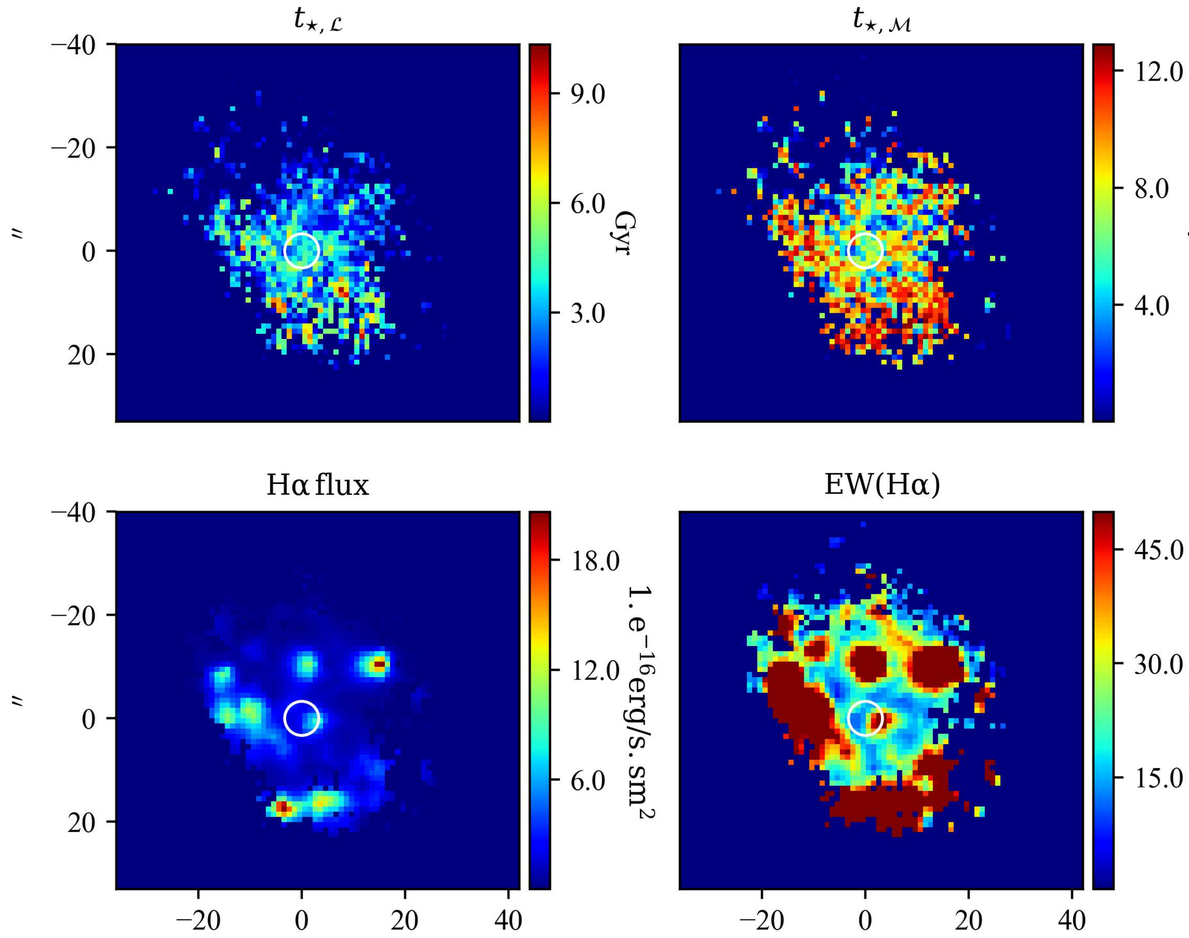

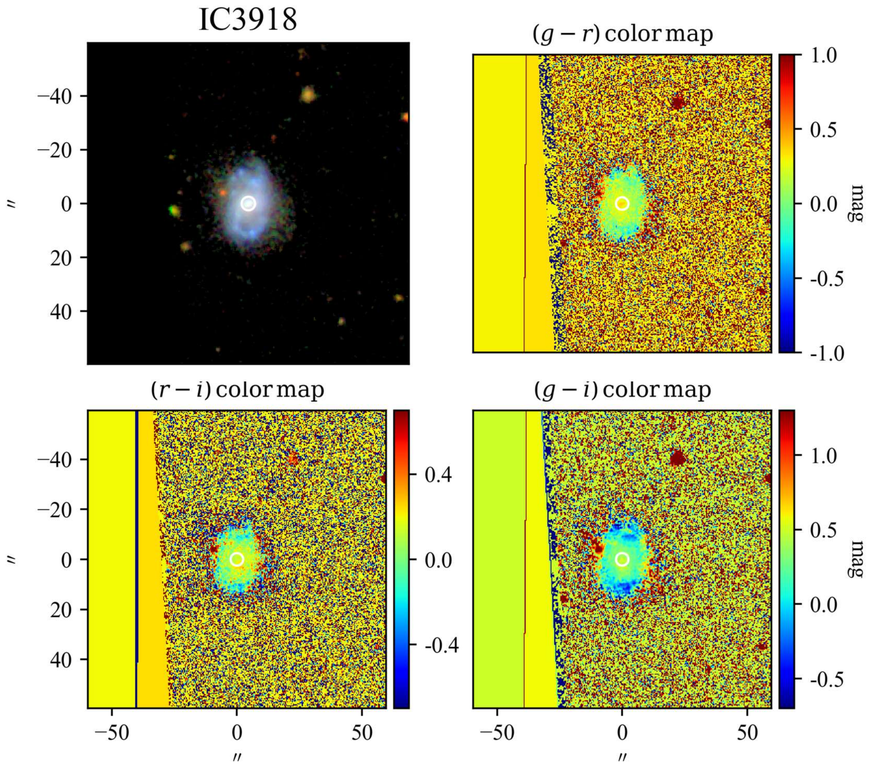

SBP decomposition of SDSS r band

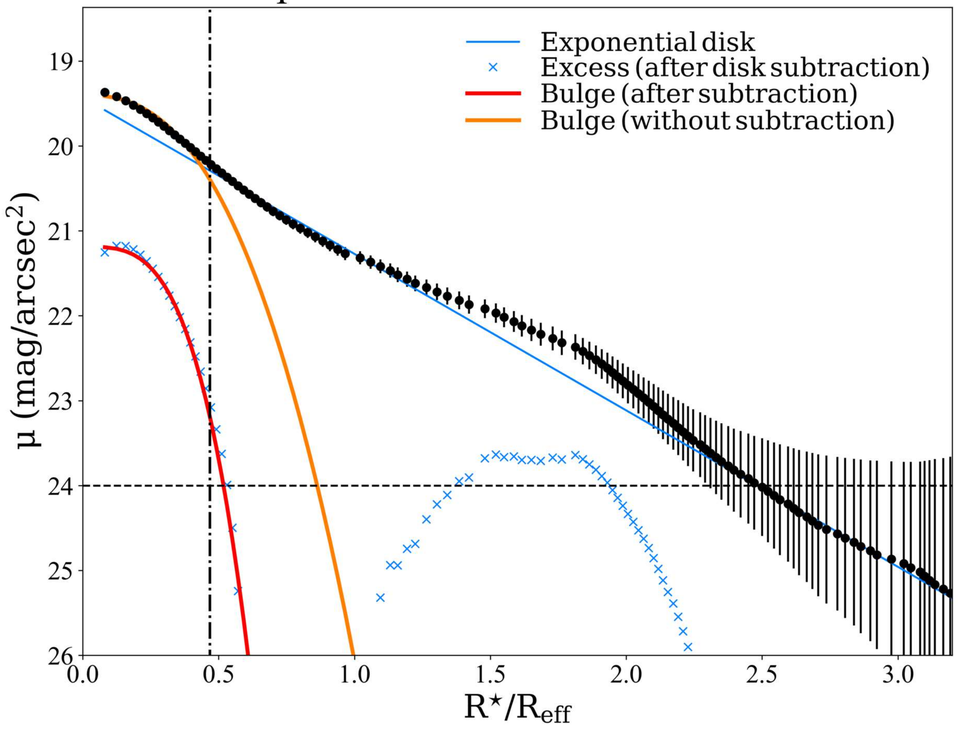

SDSS color profiles

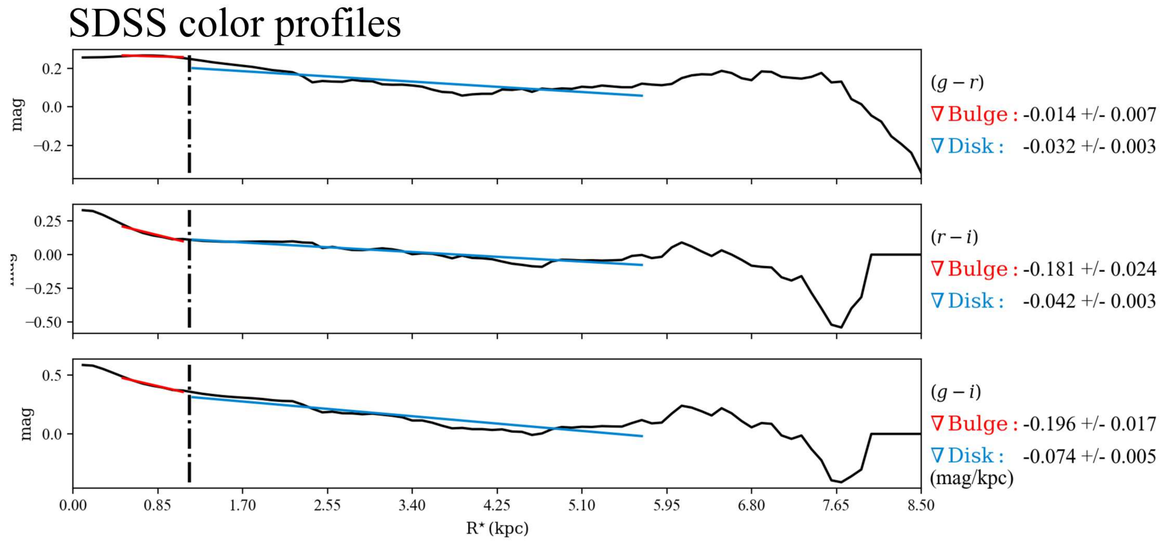

$\mathcal{RY}$ SBPs

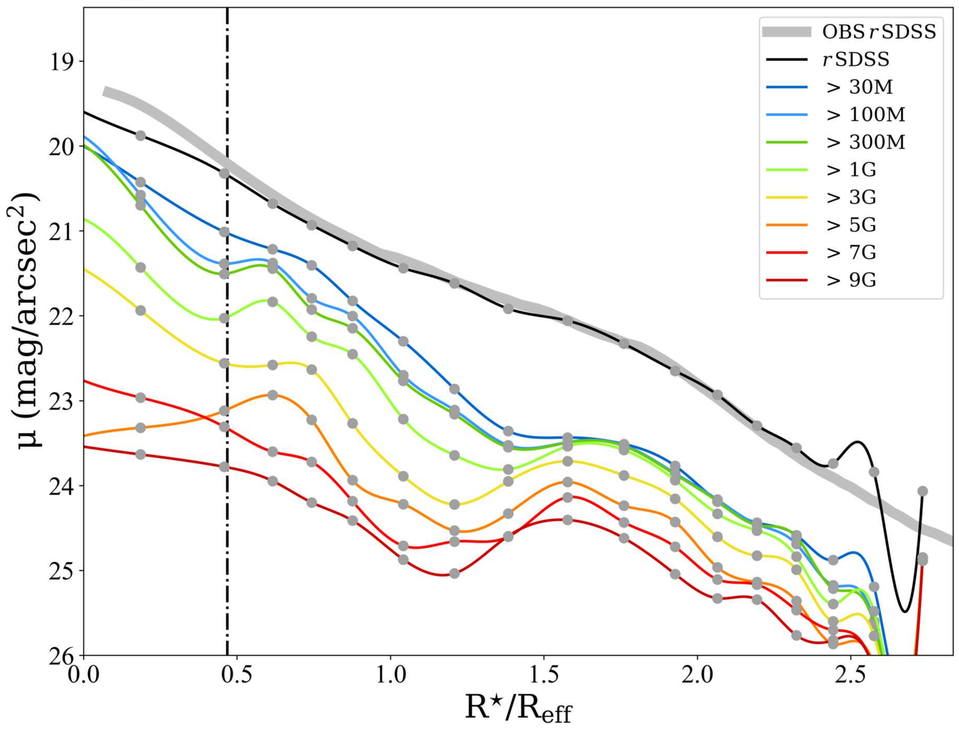

Stellar Continuum

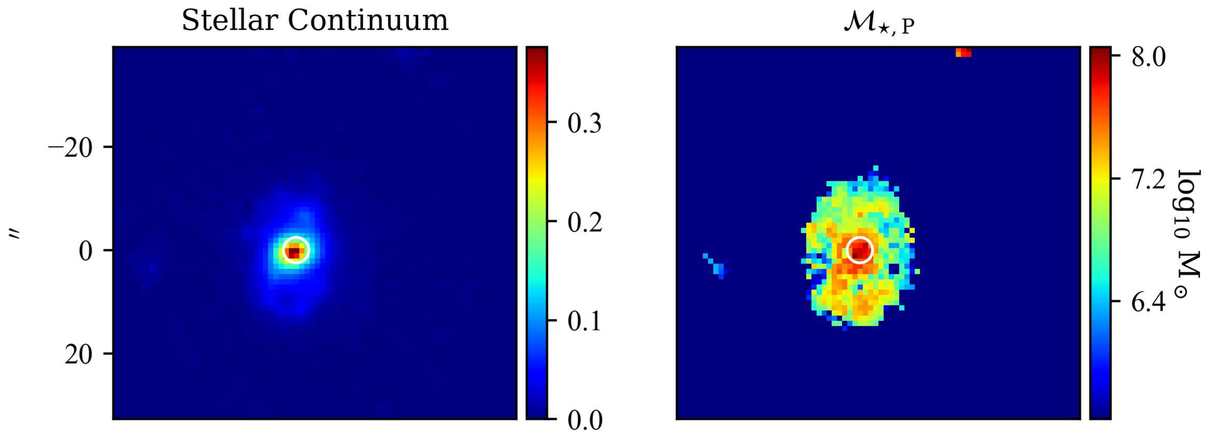

Log. of cumulative present stellar mass profiles

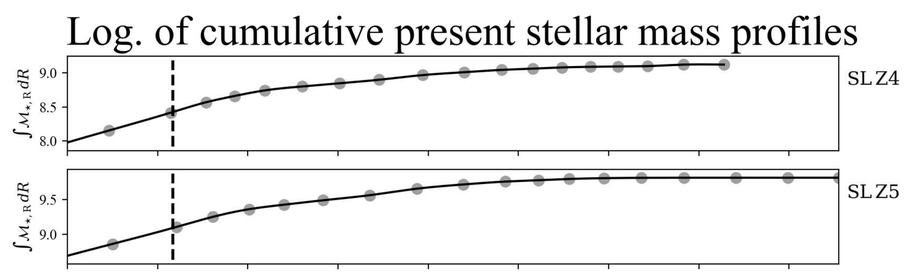

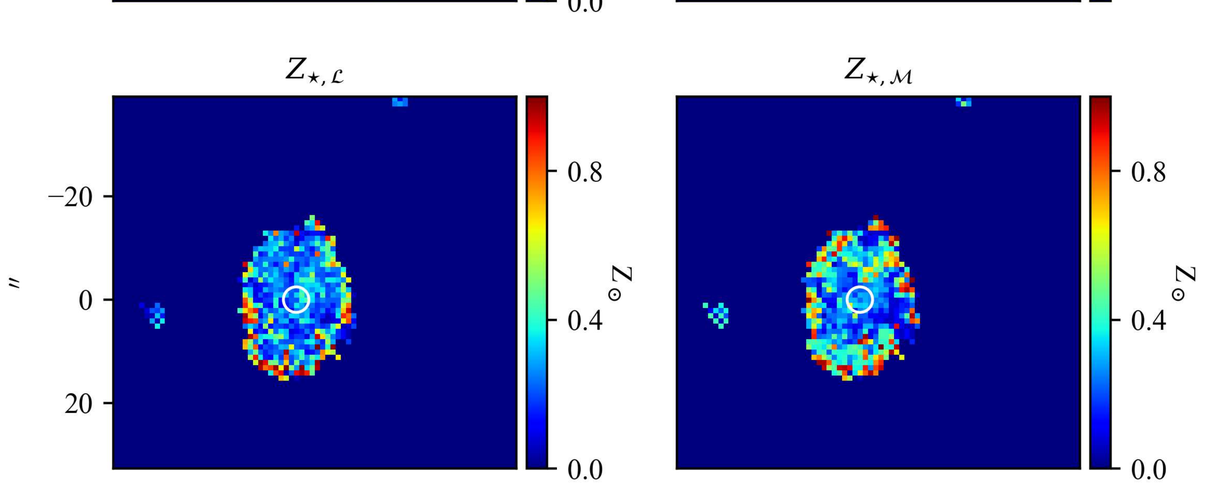

Stellar metallicity/Age & Hα flux/EW profiles

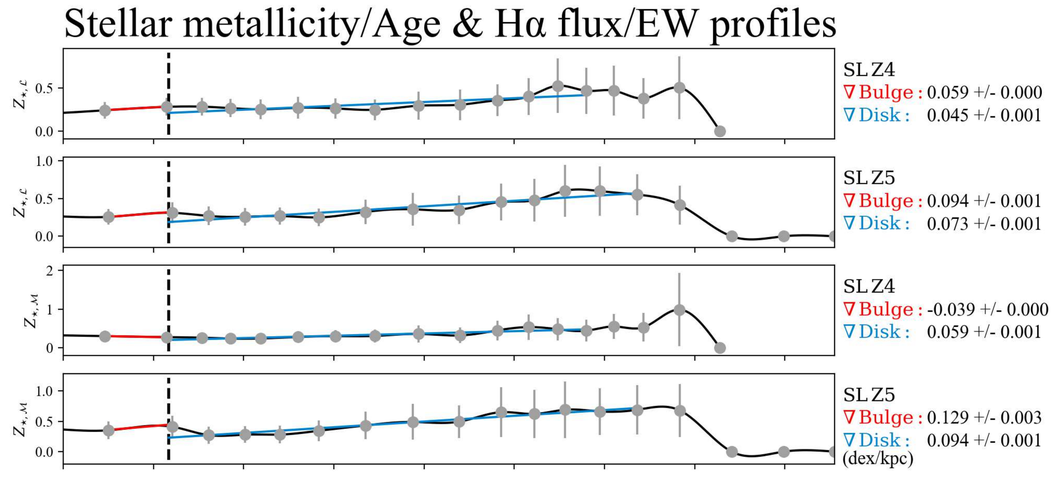

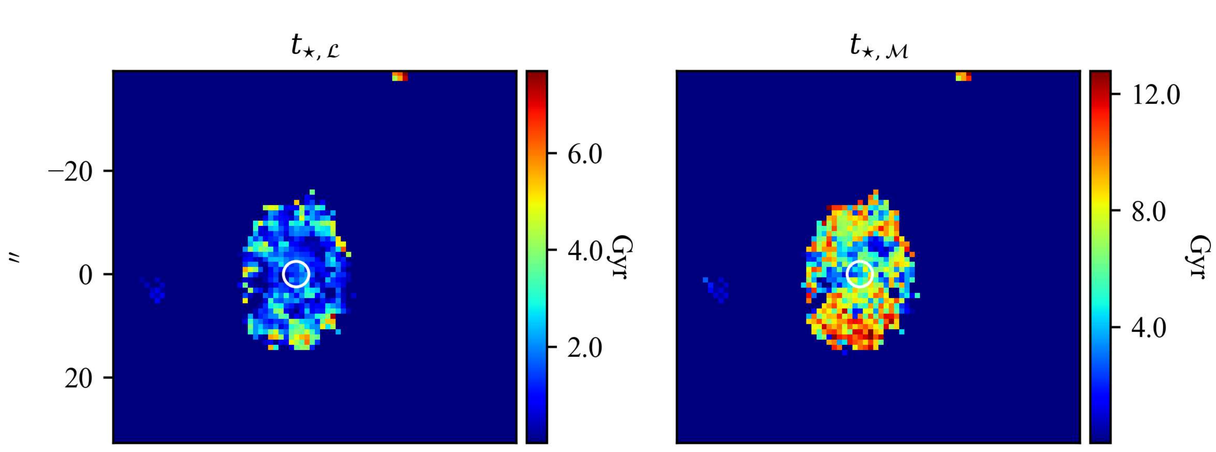

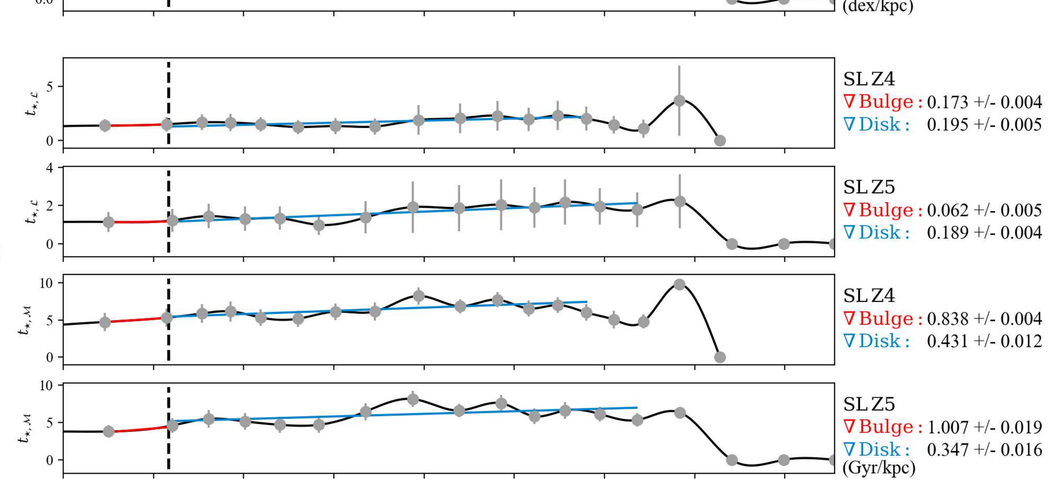

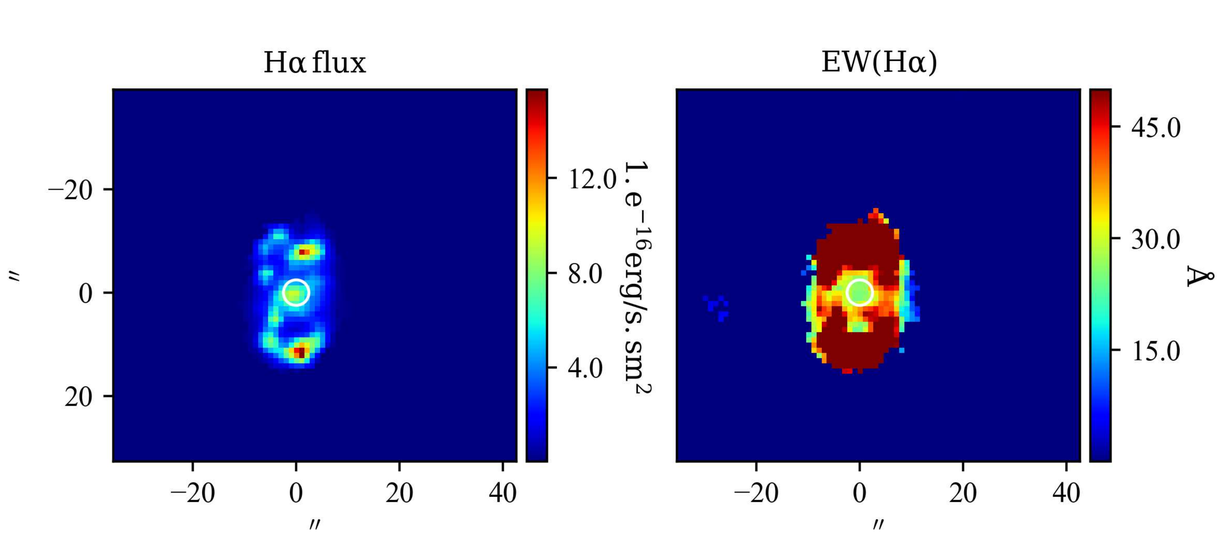

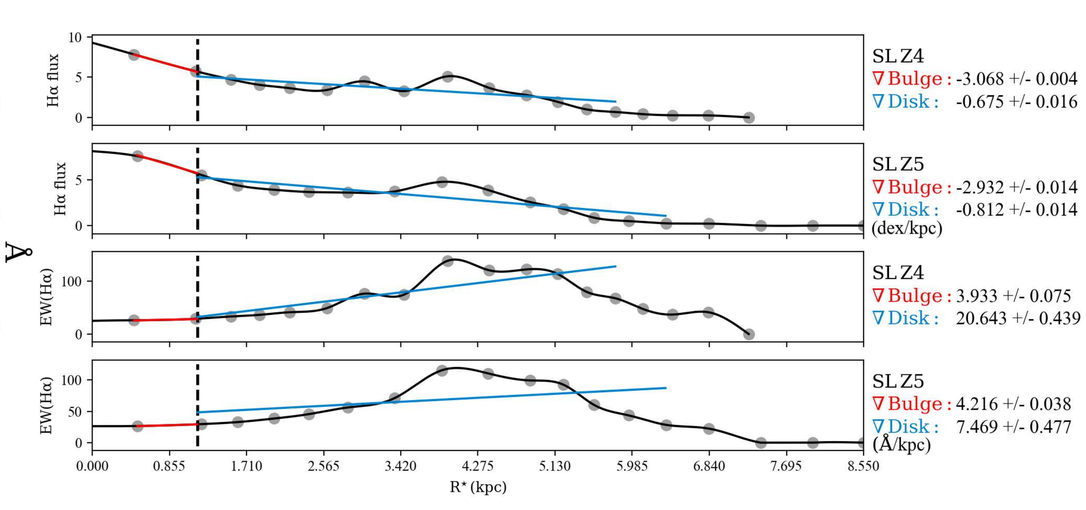

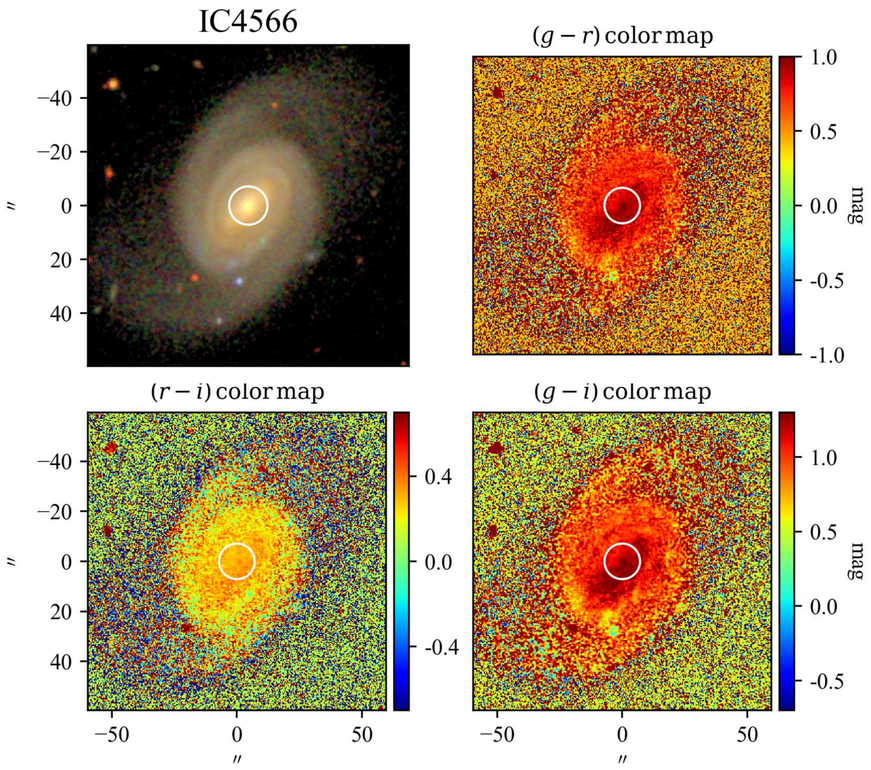

SBP decomposition of SDSS r band

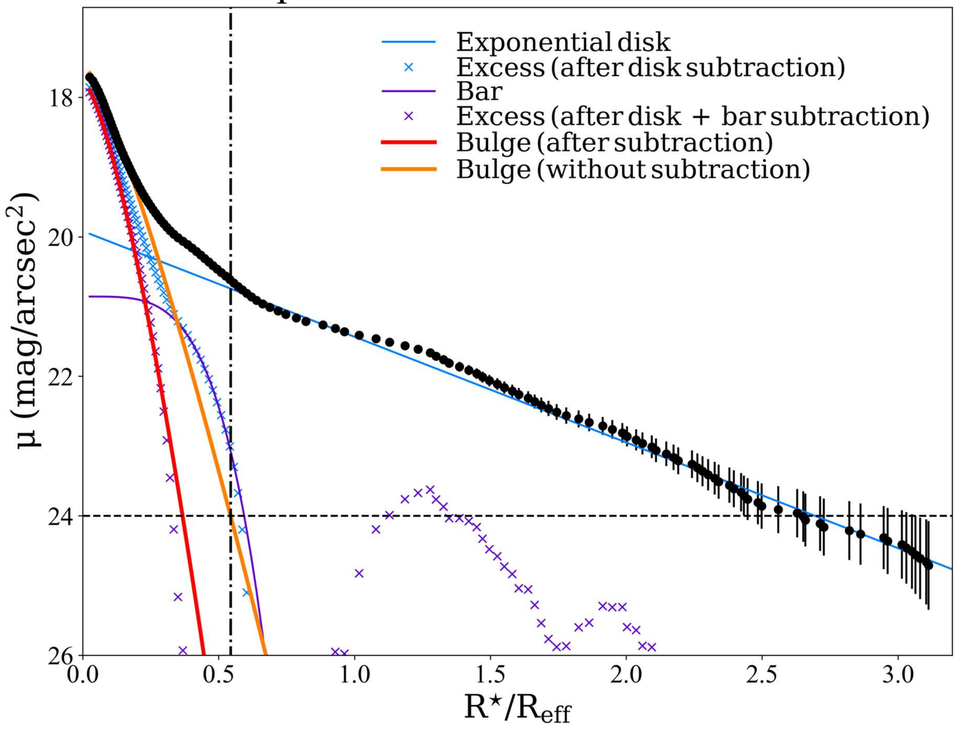

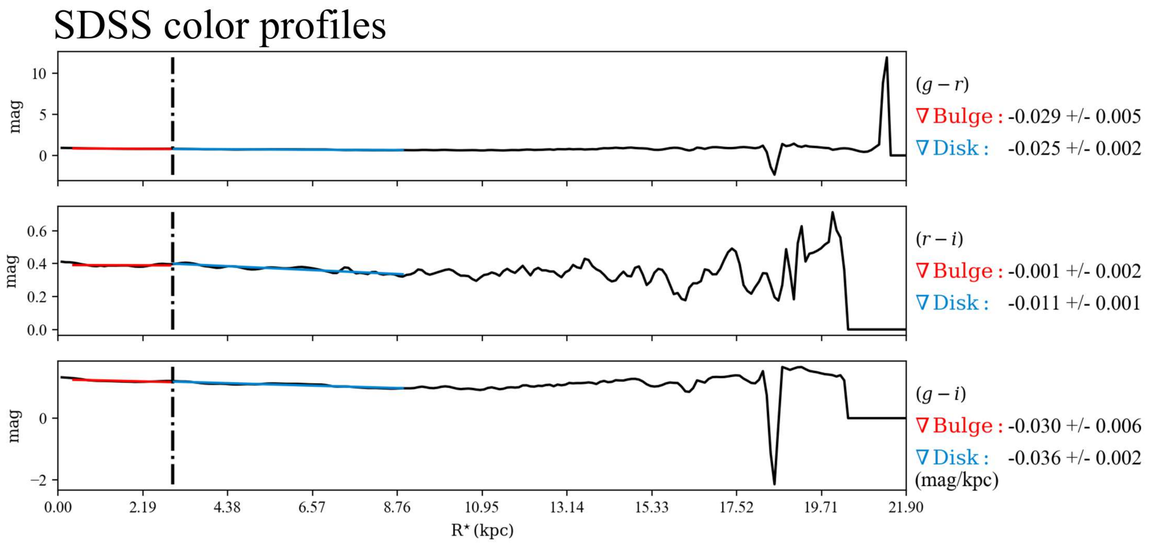

$\mathcal{RY}$ SBPs

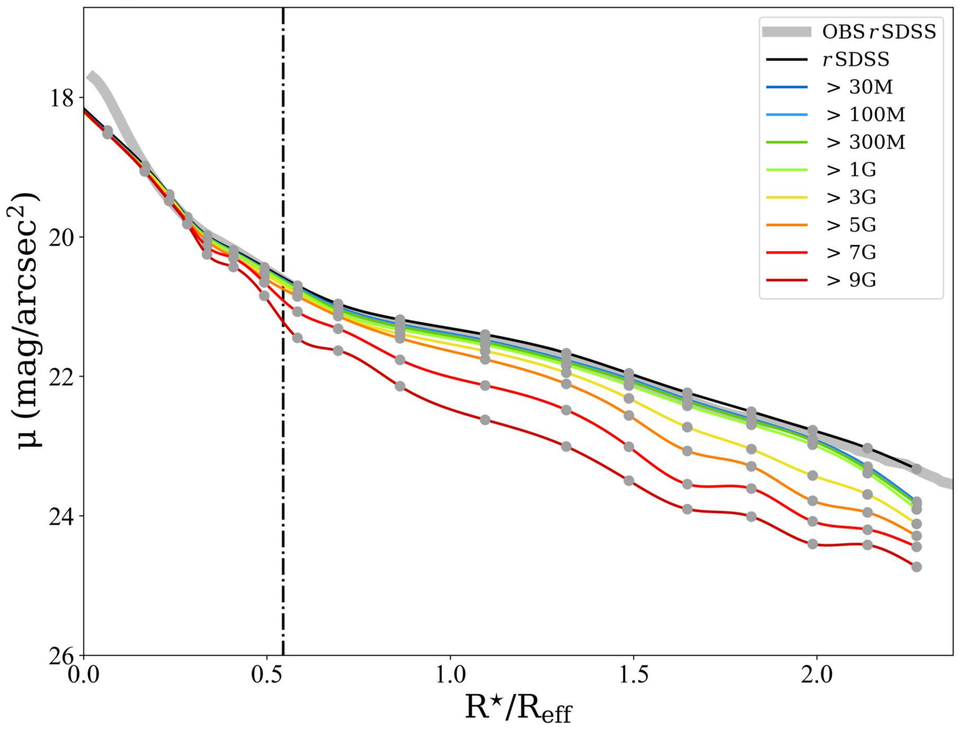

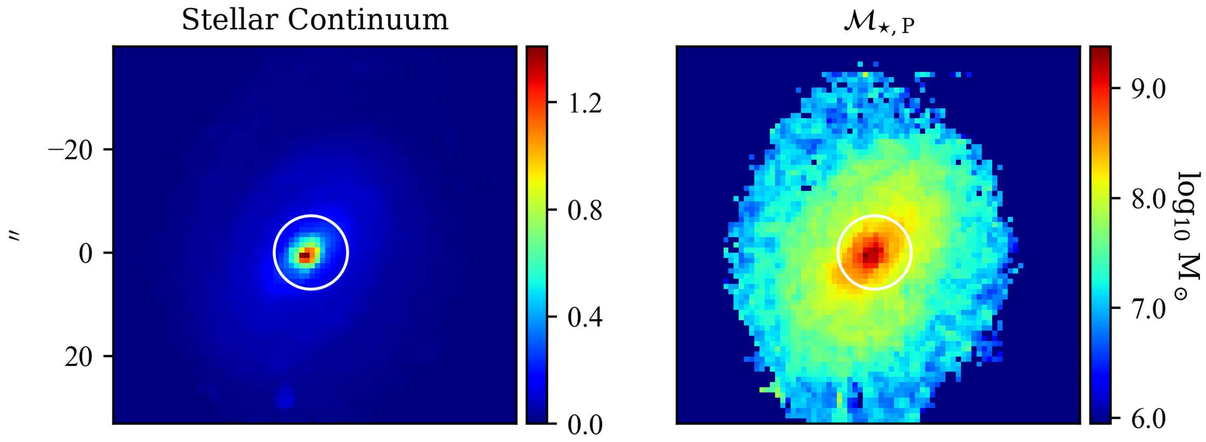

Log. of cumulative present stellar mass profiles

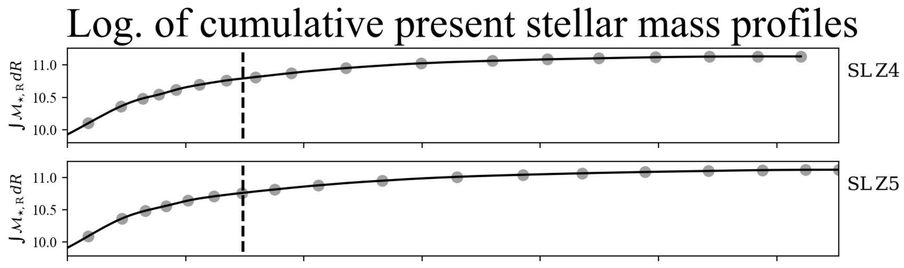

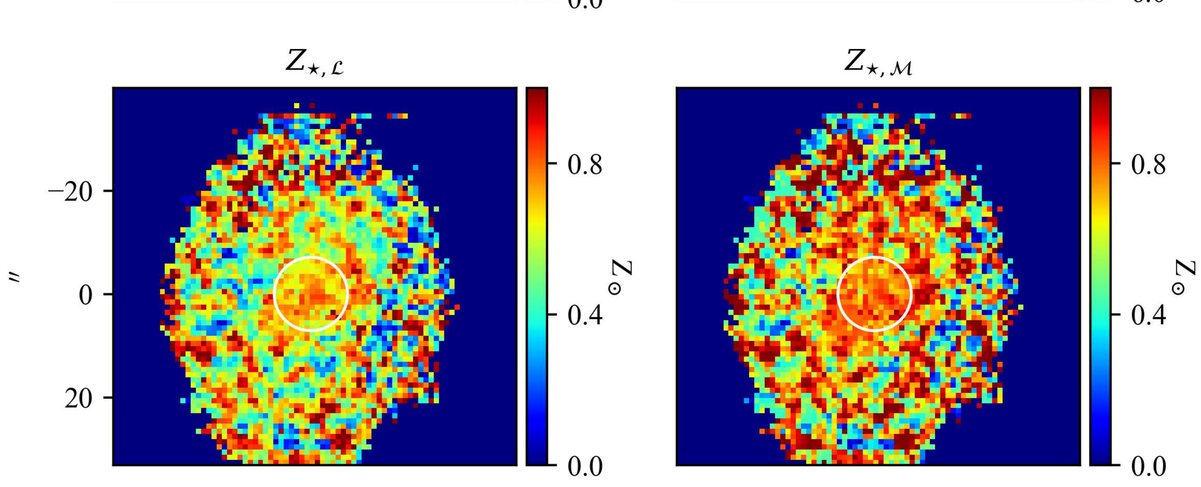

Stellar metallicity/Age & Hα flux/EW profiles

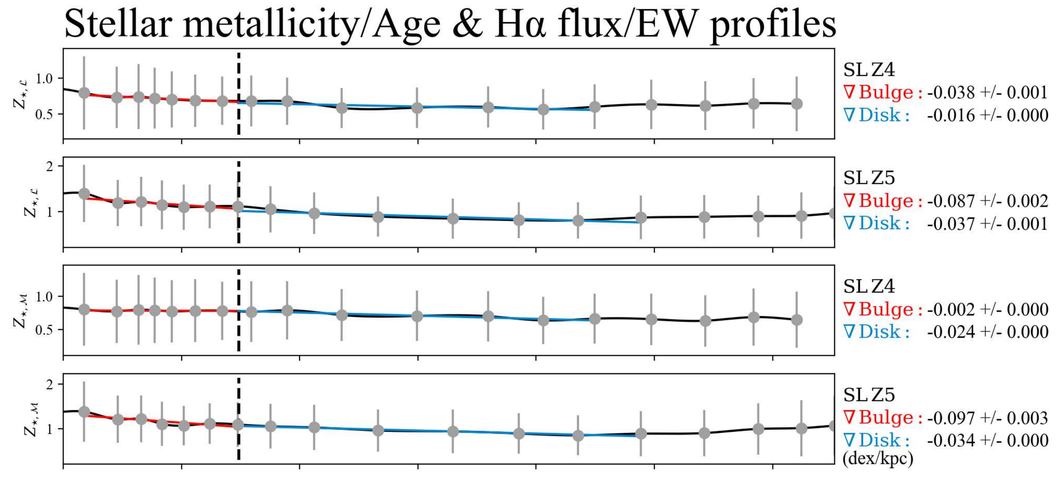

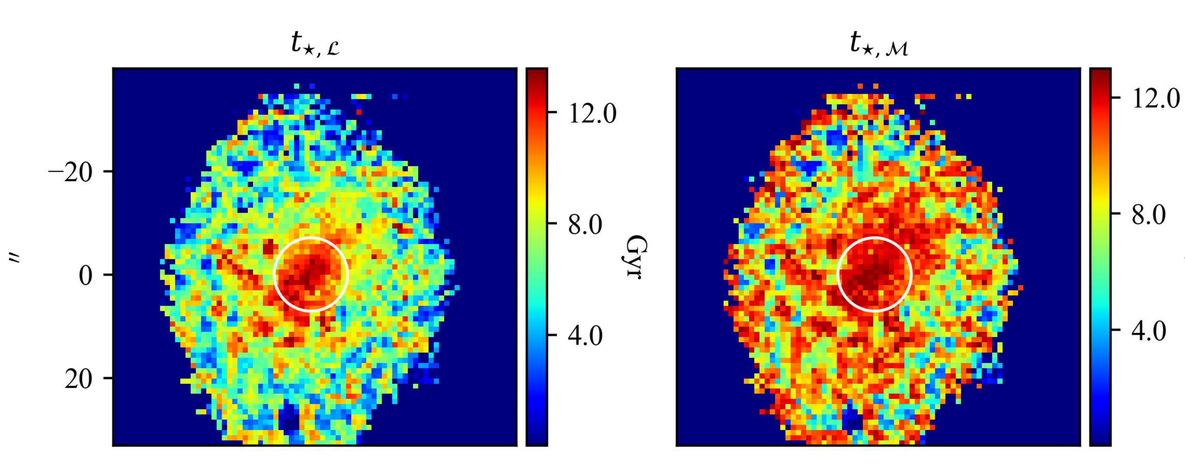

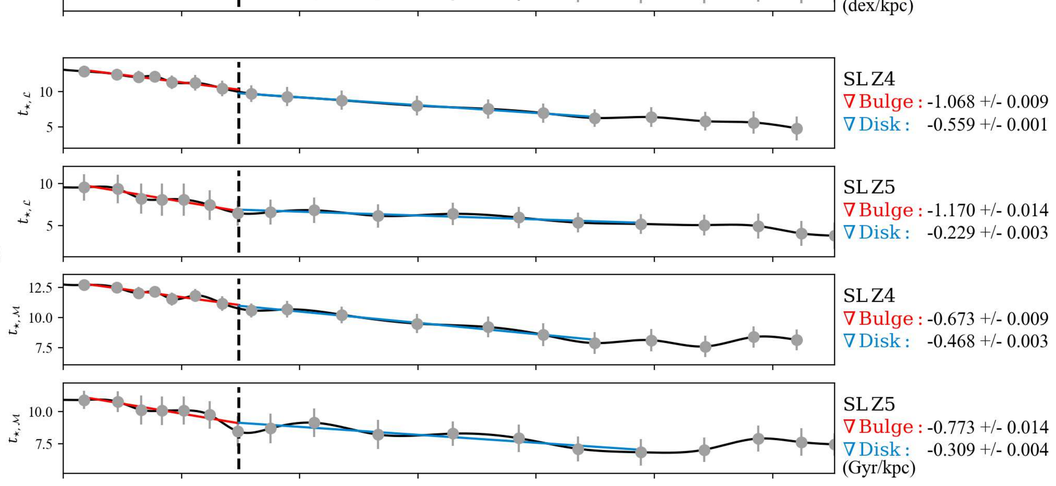

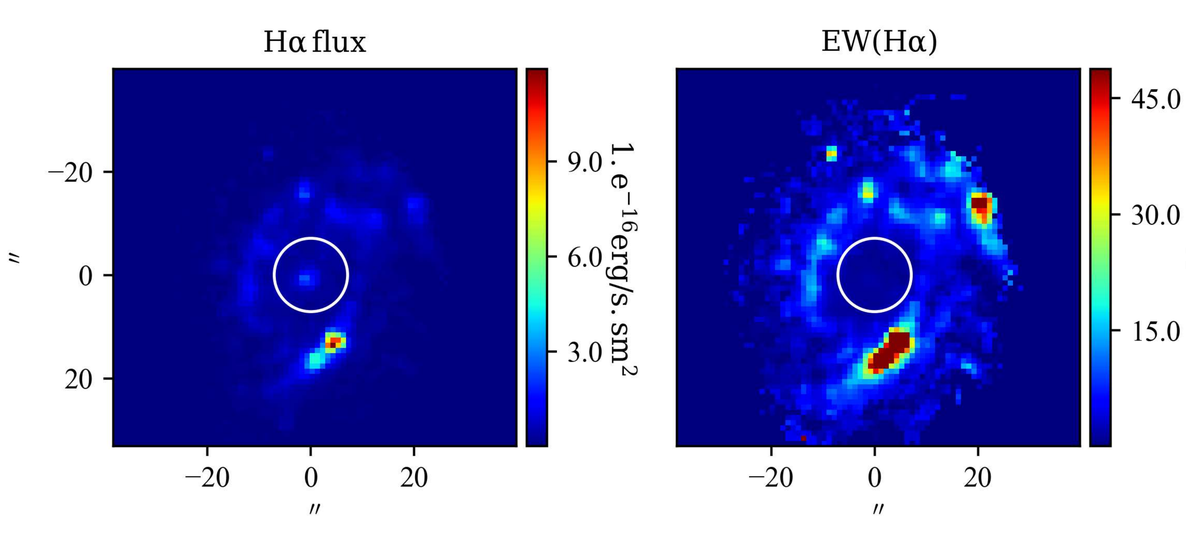

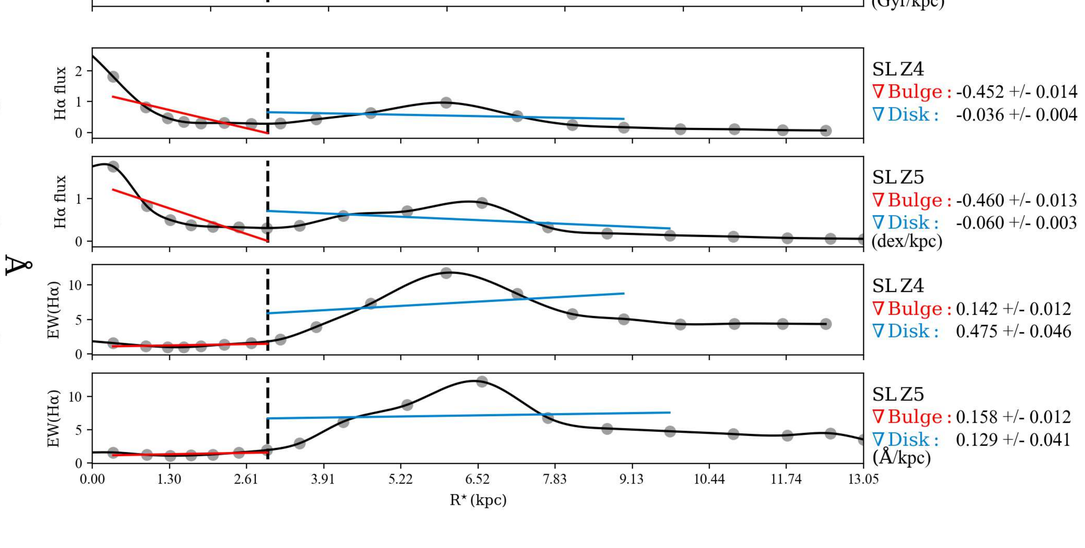

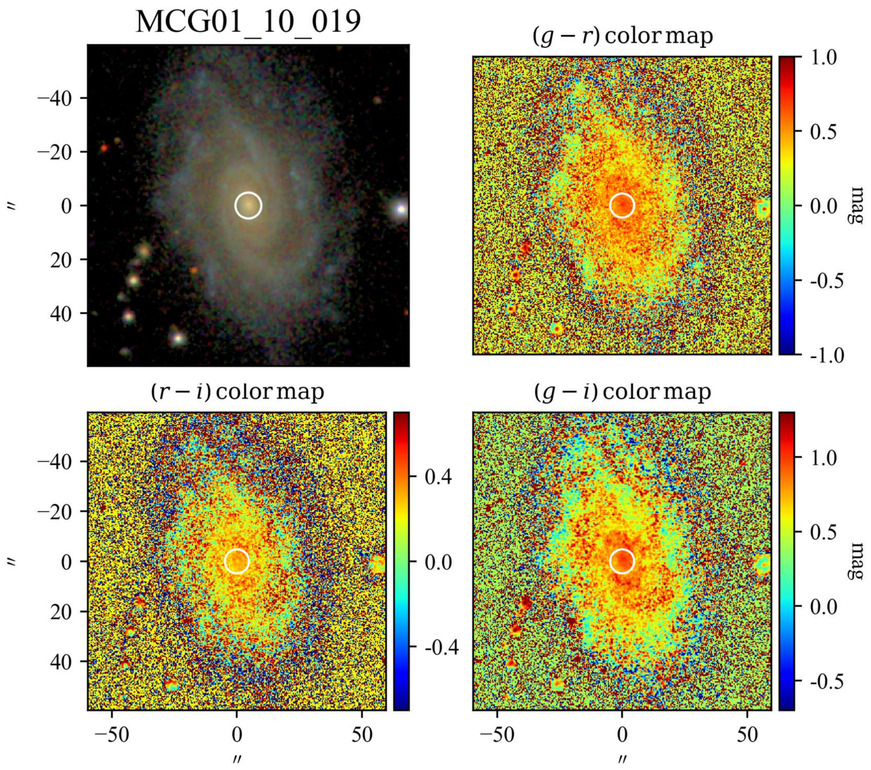

SBP decomposition of SDSS r band

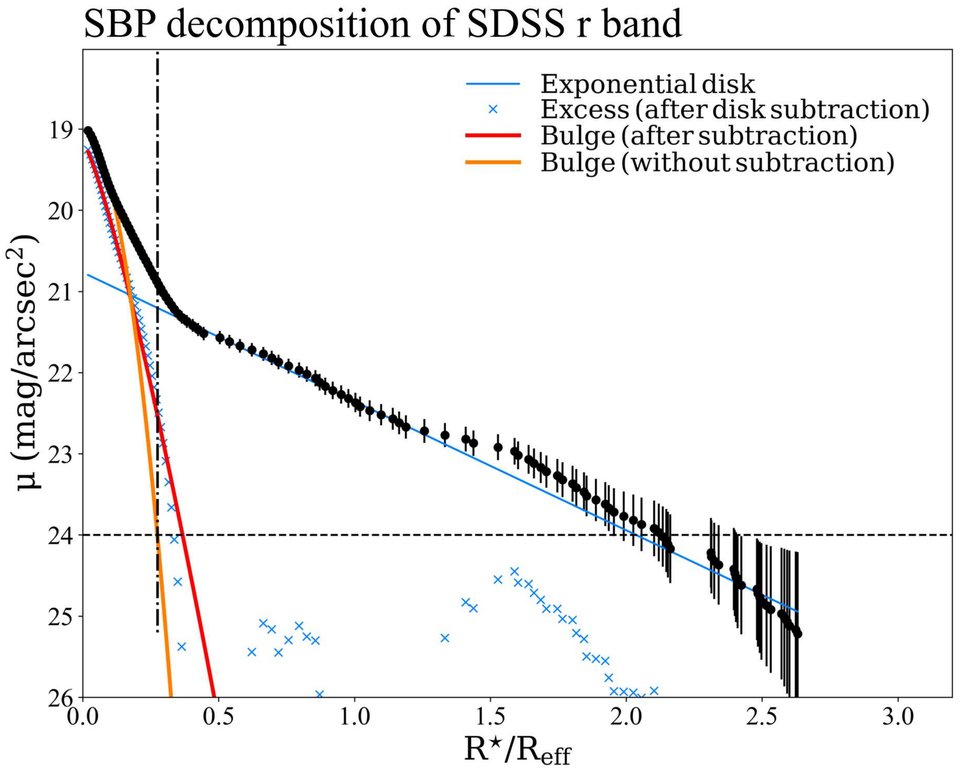

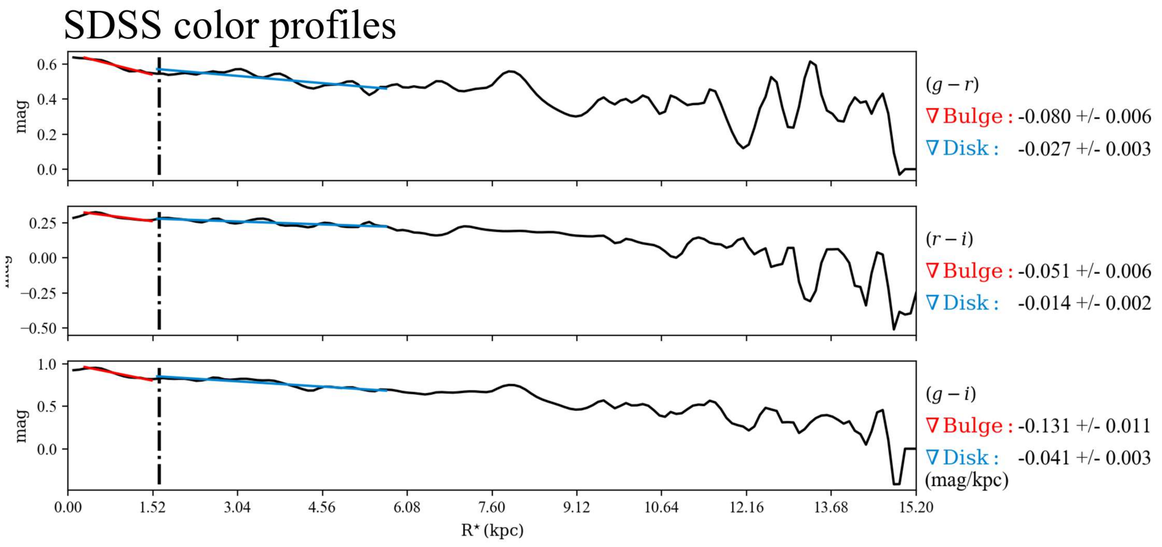

$\mathcal{RY}$ SBPs

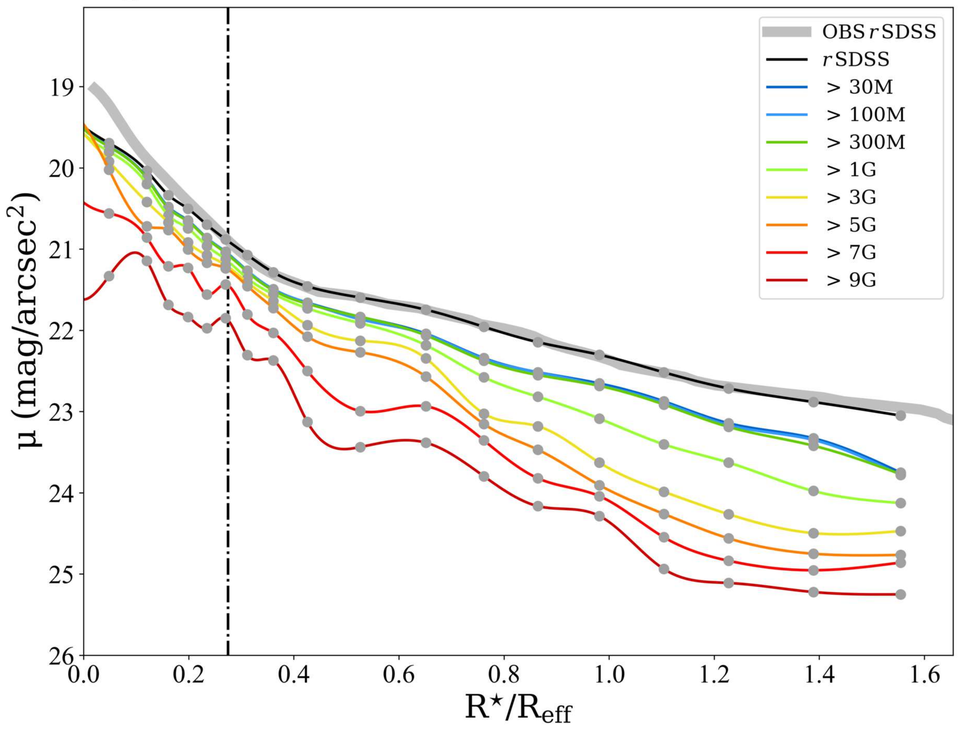

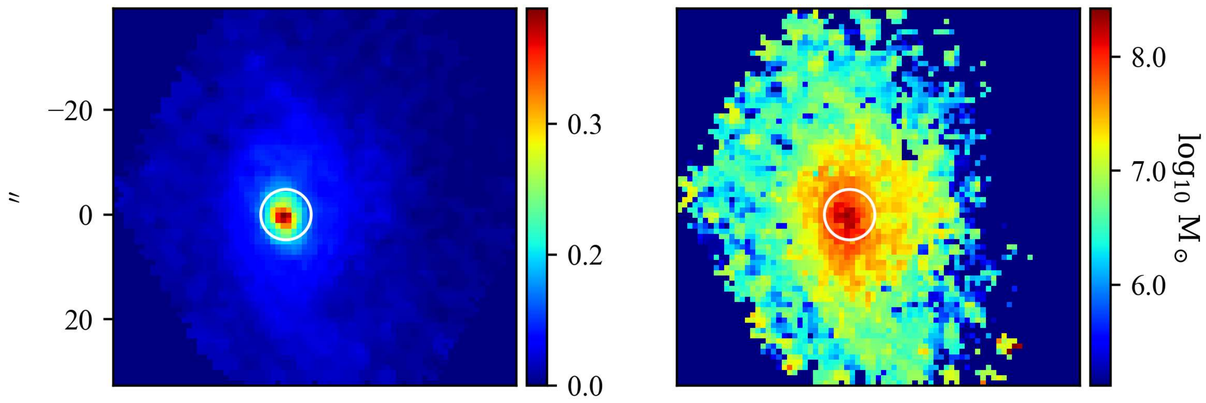

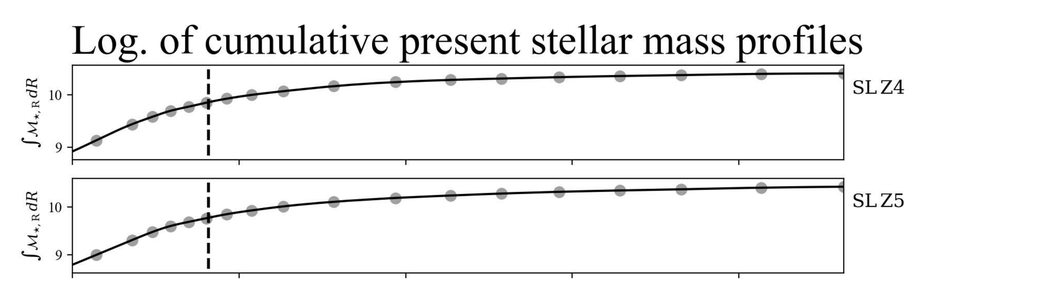

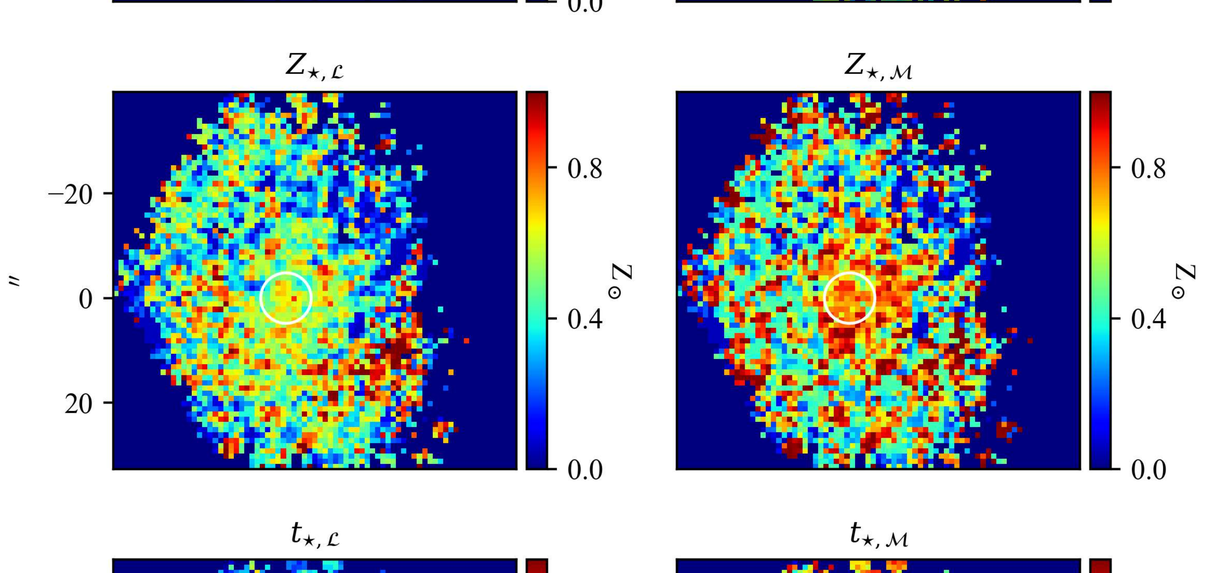

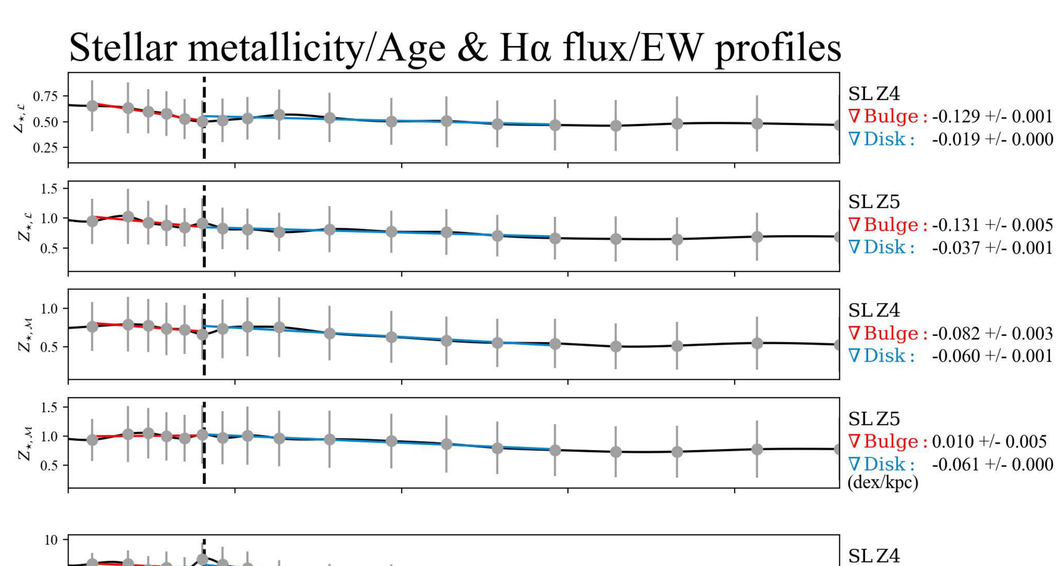

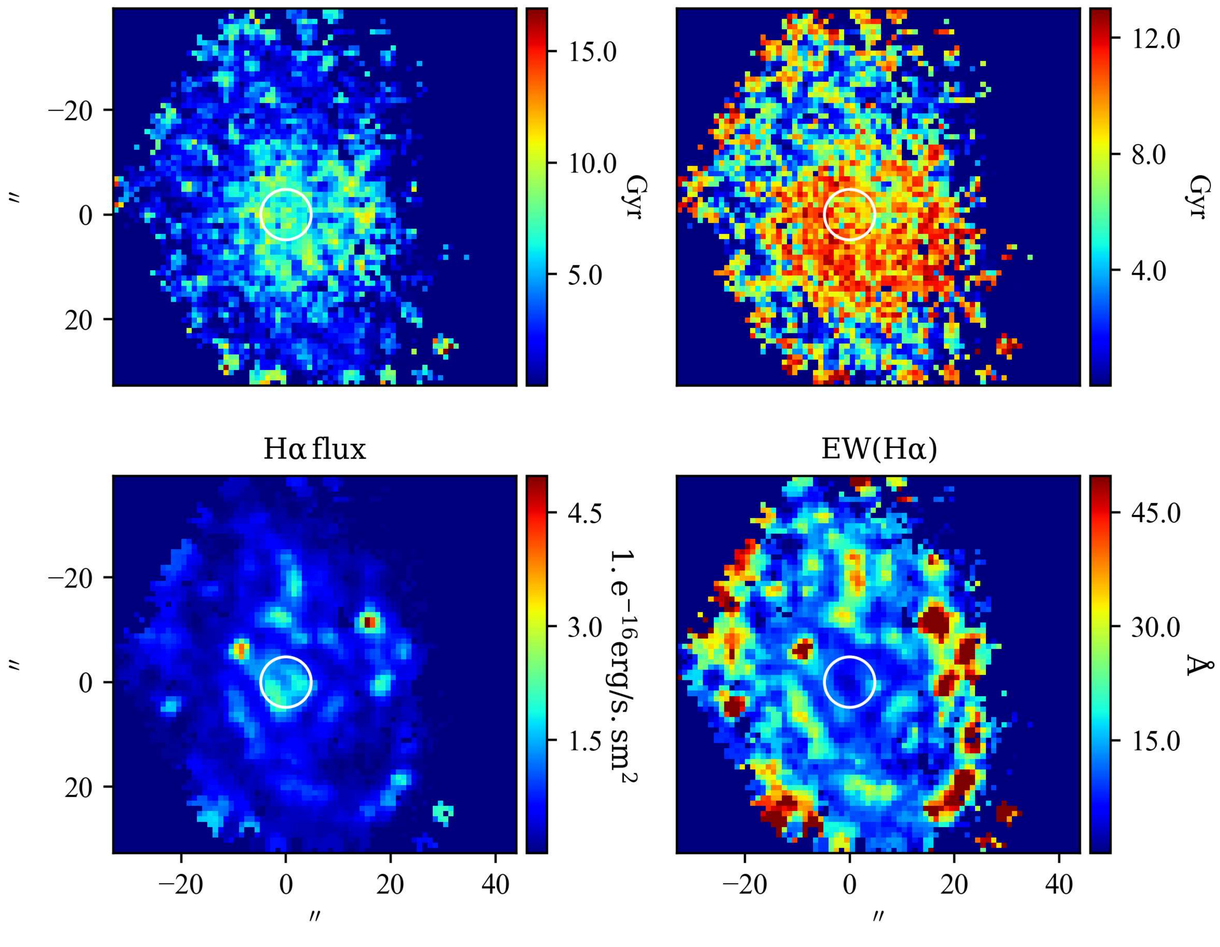

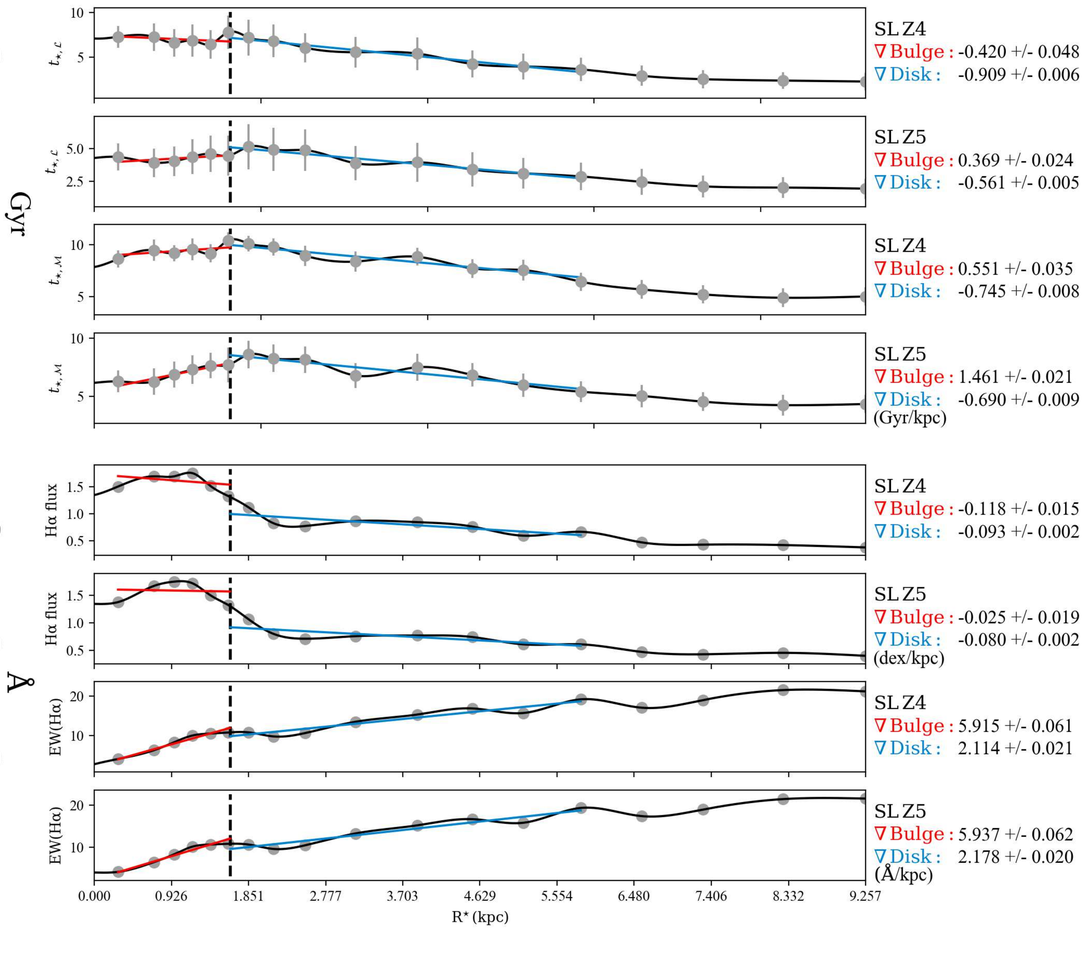

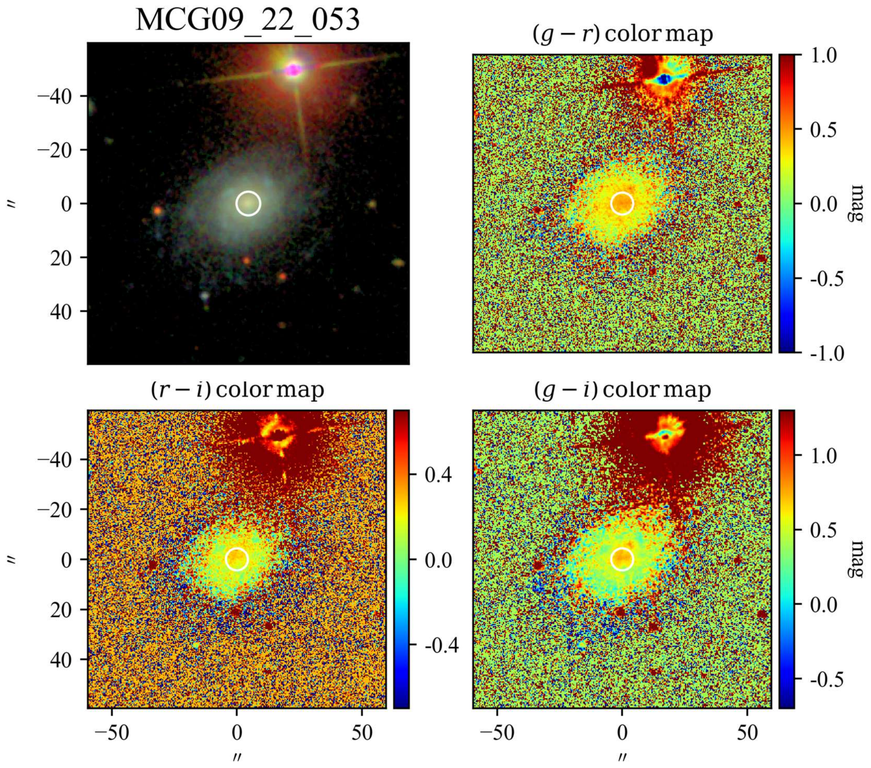

SBP decomposition of SDSS r band

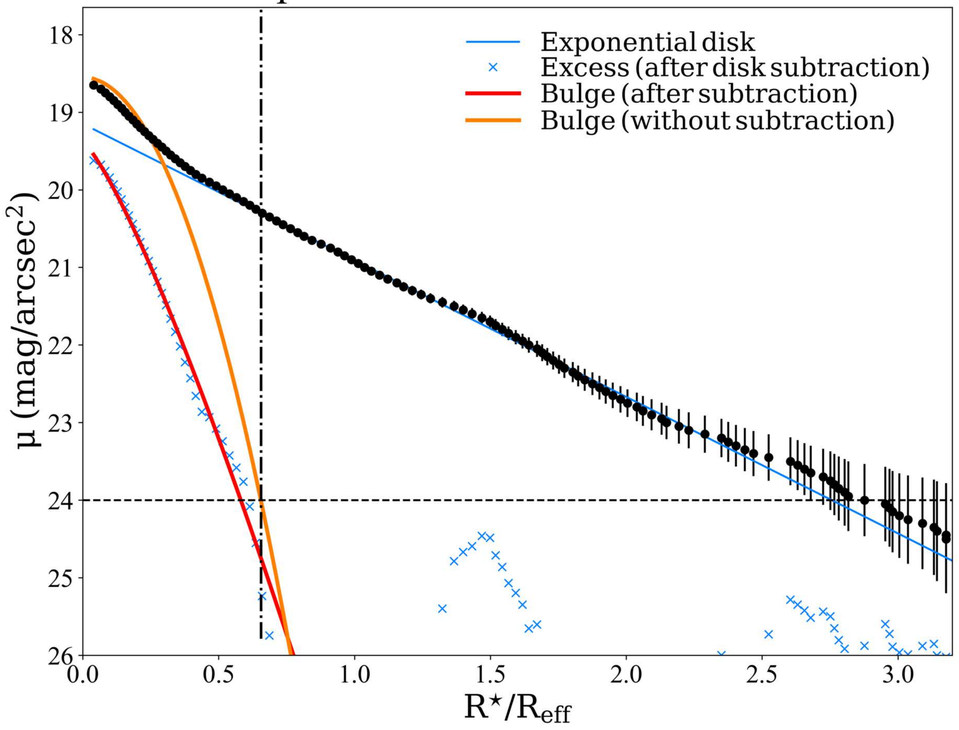

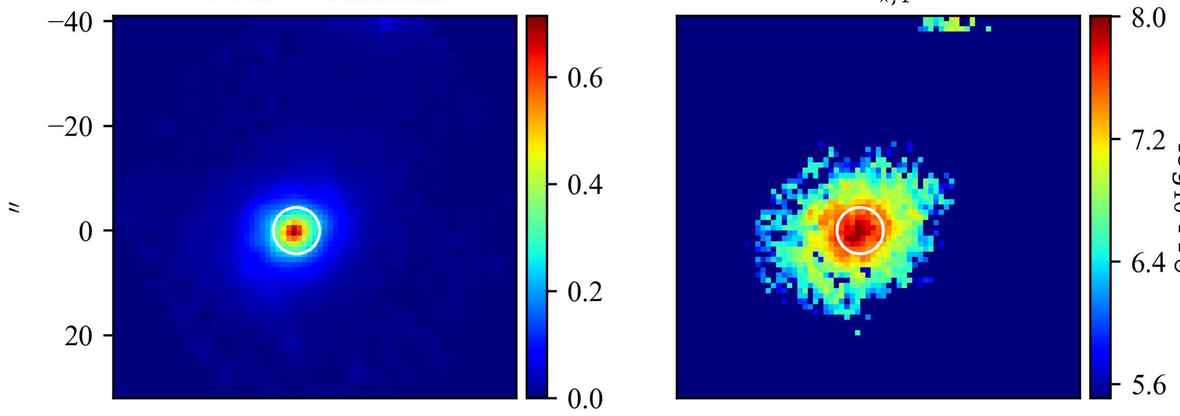

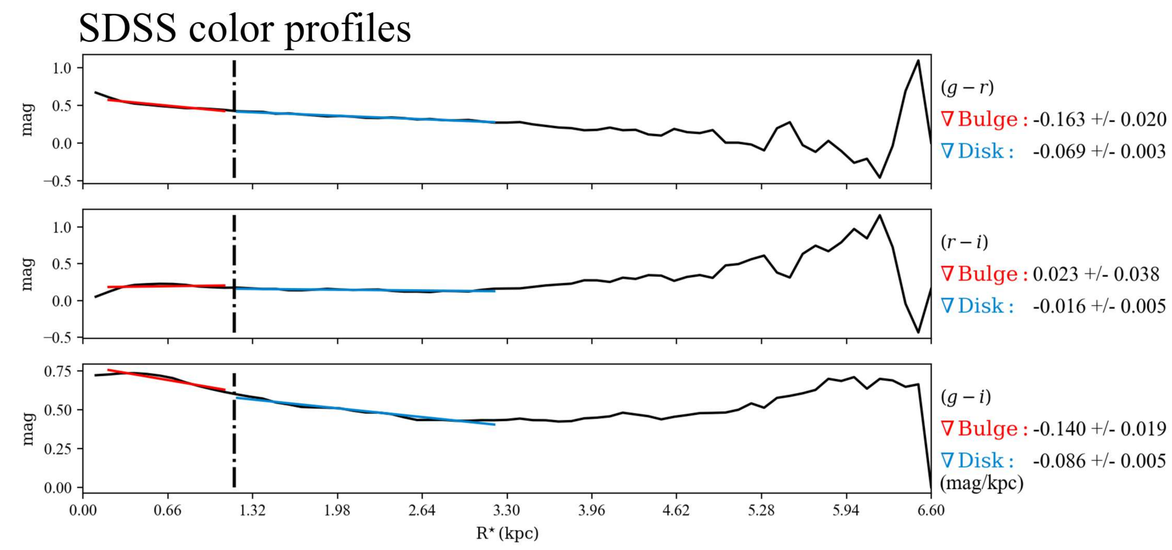

$\mathcal{RY}$ SBPs

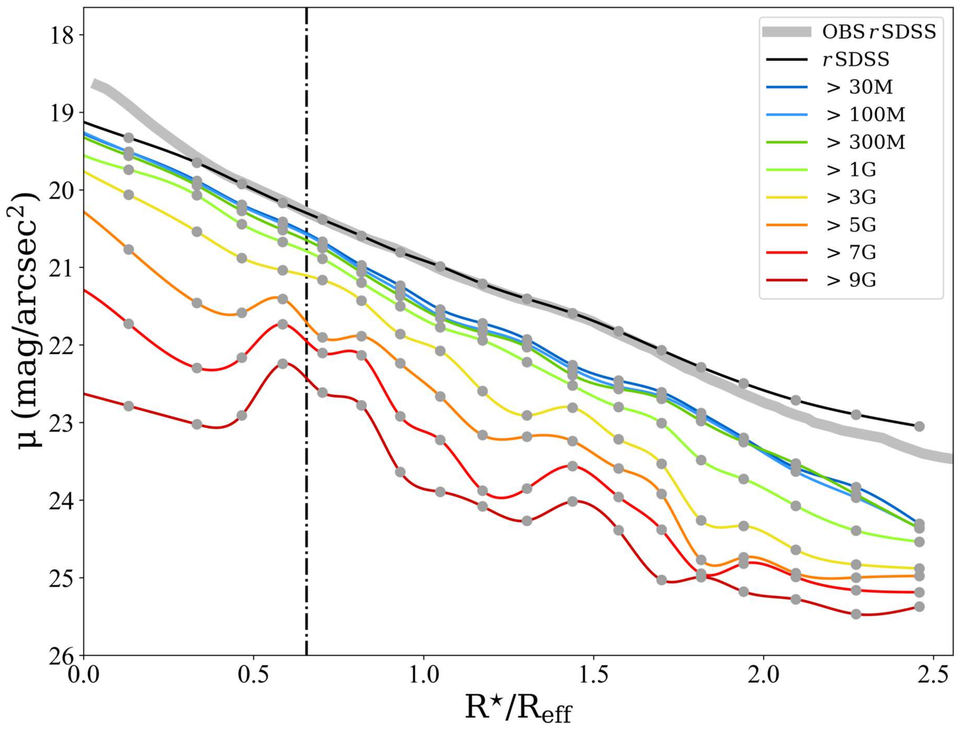

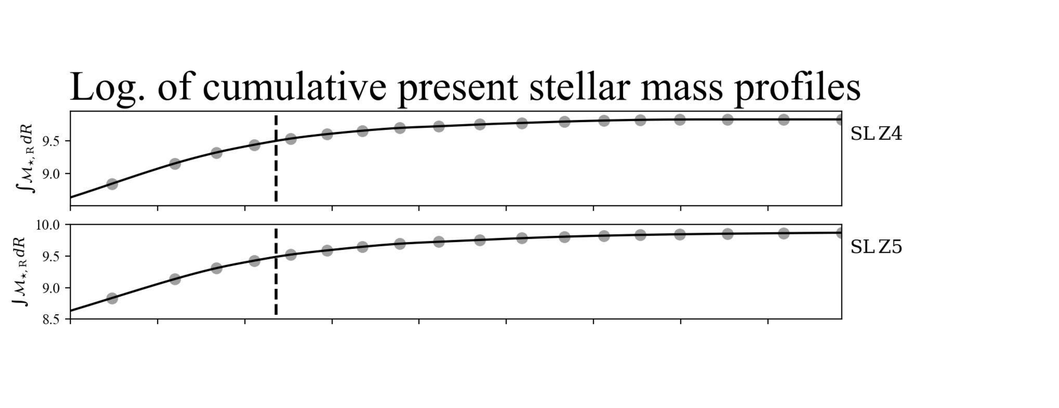

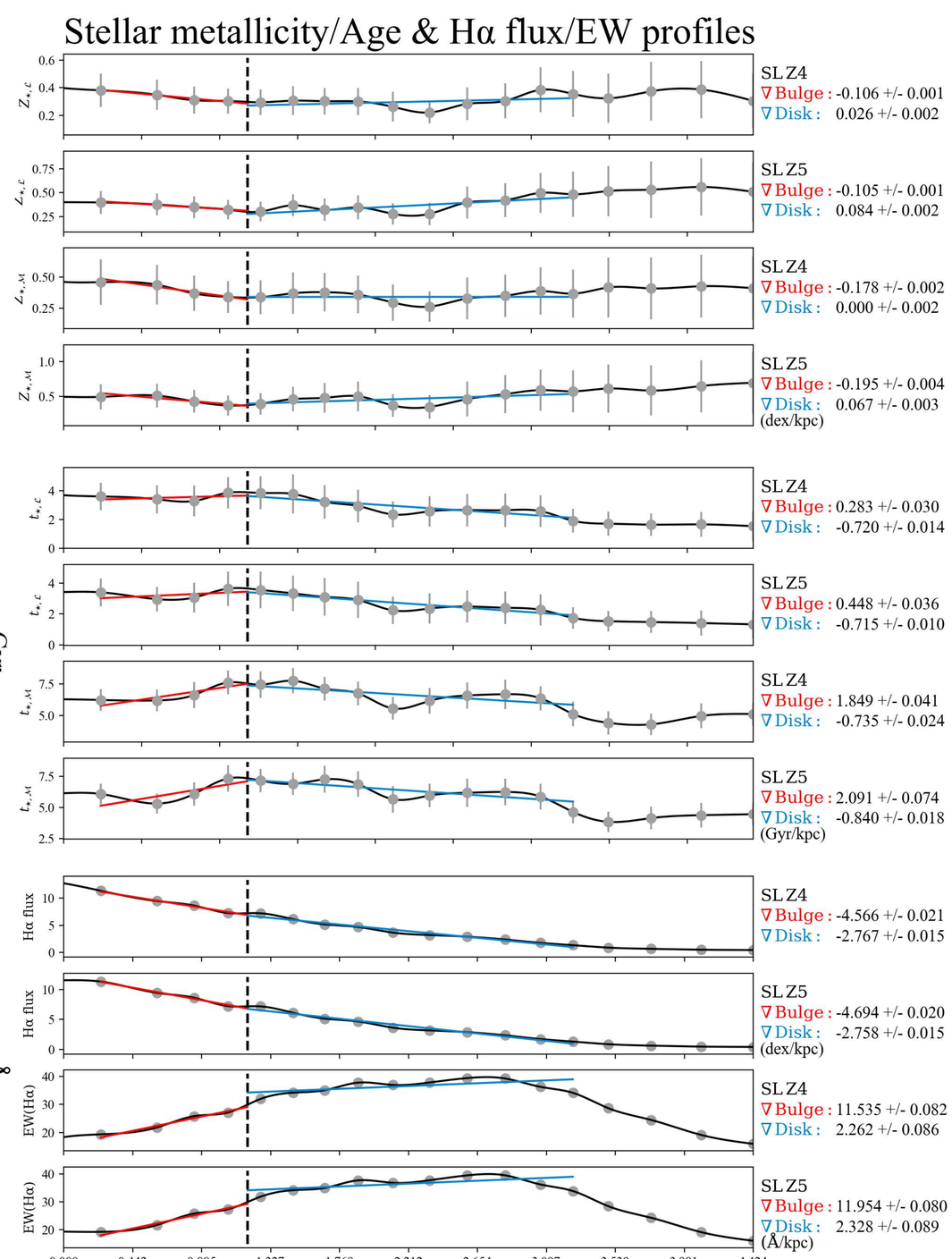

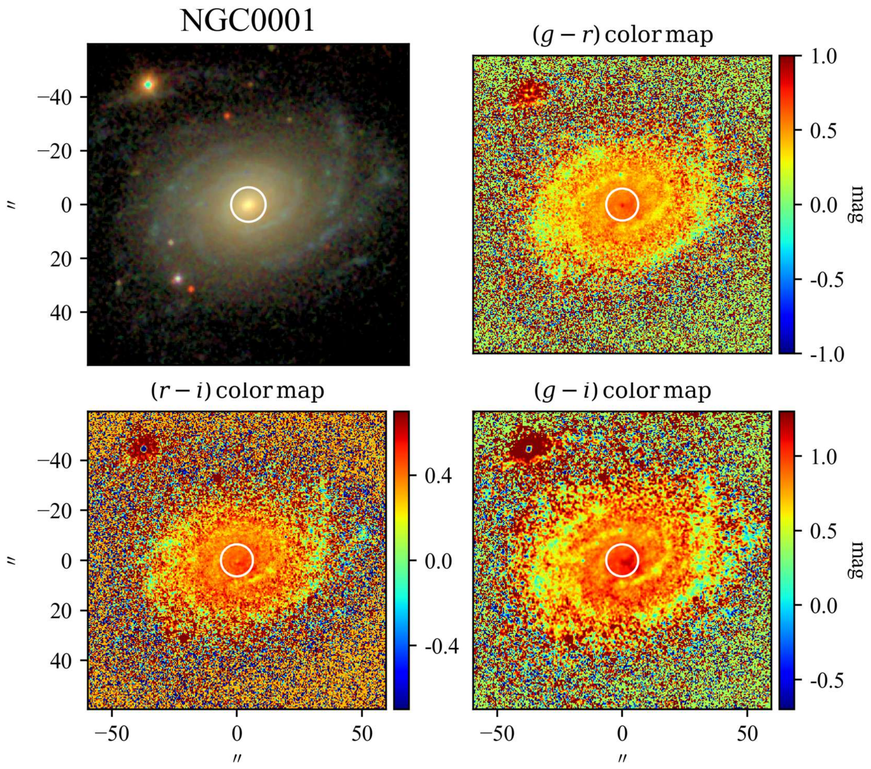
NGC0001
$(g-r)$ color map
$(r-i)$ color map
$(g-i)$ color map
mag
″

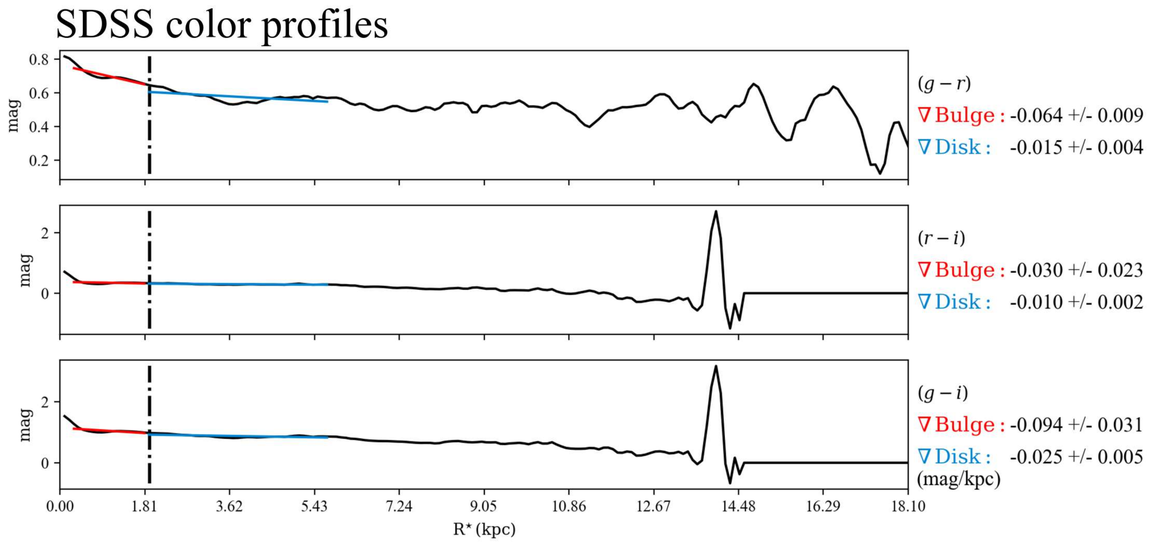
SDSS color profiles
mag
$(g-r)$
∇ Bulge : -0.064 +/- 0.009
∇ Disk : -0.015 +/- 0.004
$(r-i)$
∇ Bulge : -0.030 +/- 0.023
∇ Disk : -0.010 +/- 0.002
$(g-i)$
∇ Bulge : -0.094 +/- 0.031
∇ Disk : -0.025 +/- 0.005
(mag/kpc)
R* (kpc)

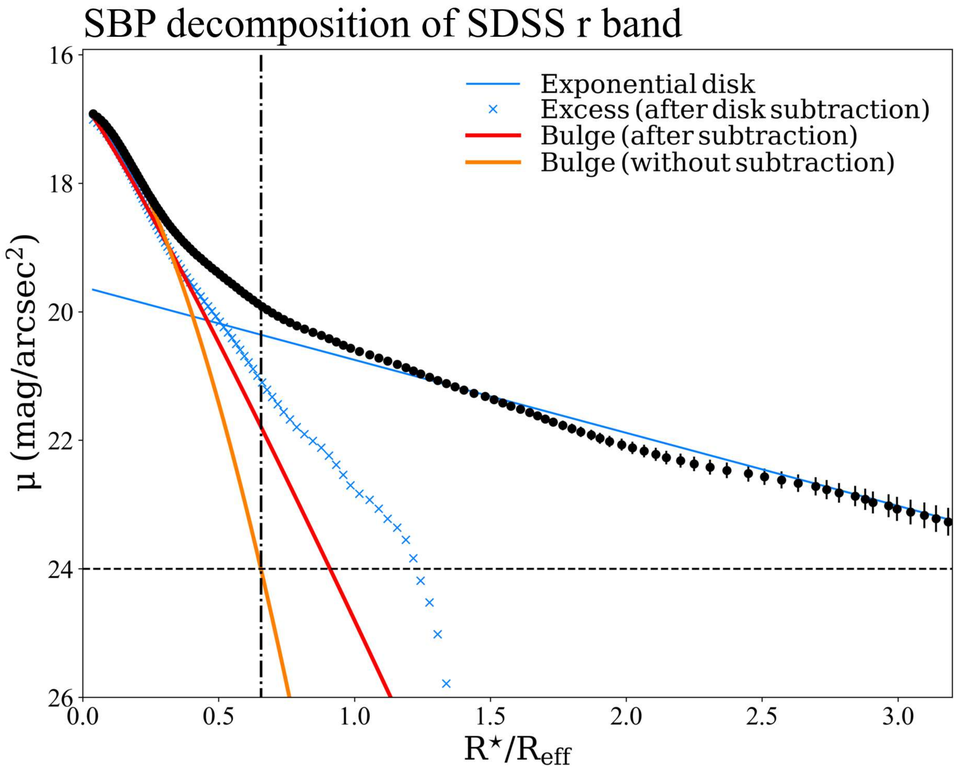
SBP decomposition of SDSS r band
Exponential disk
Excess (after disk subtraction)
Bulge (after subtraction)
Bulge (without subtraction)
μ (mag/arcsec^2)
R*/R$_{eff}$

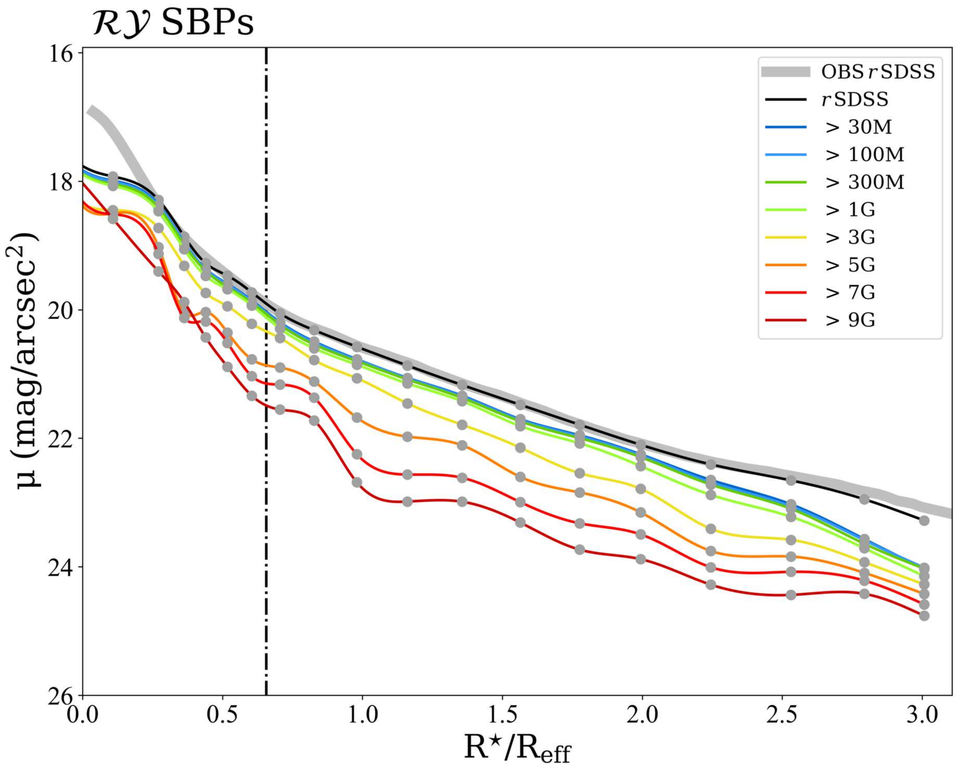
$\mathcal{RY}$ SBPs
OBS rSDSS
rSDSS
> 30M
> 100M
> 300M
> 1G
> 3G
> 5G
> 7G
> 9G
μ (mag/arcsec^2)
R*/R$_{eff}$

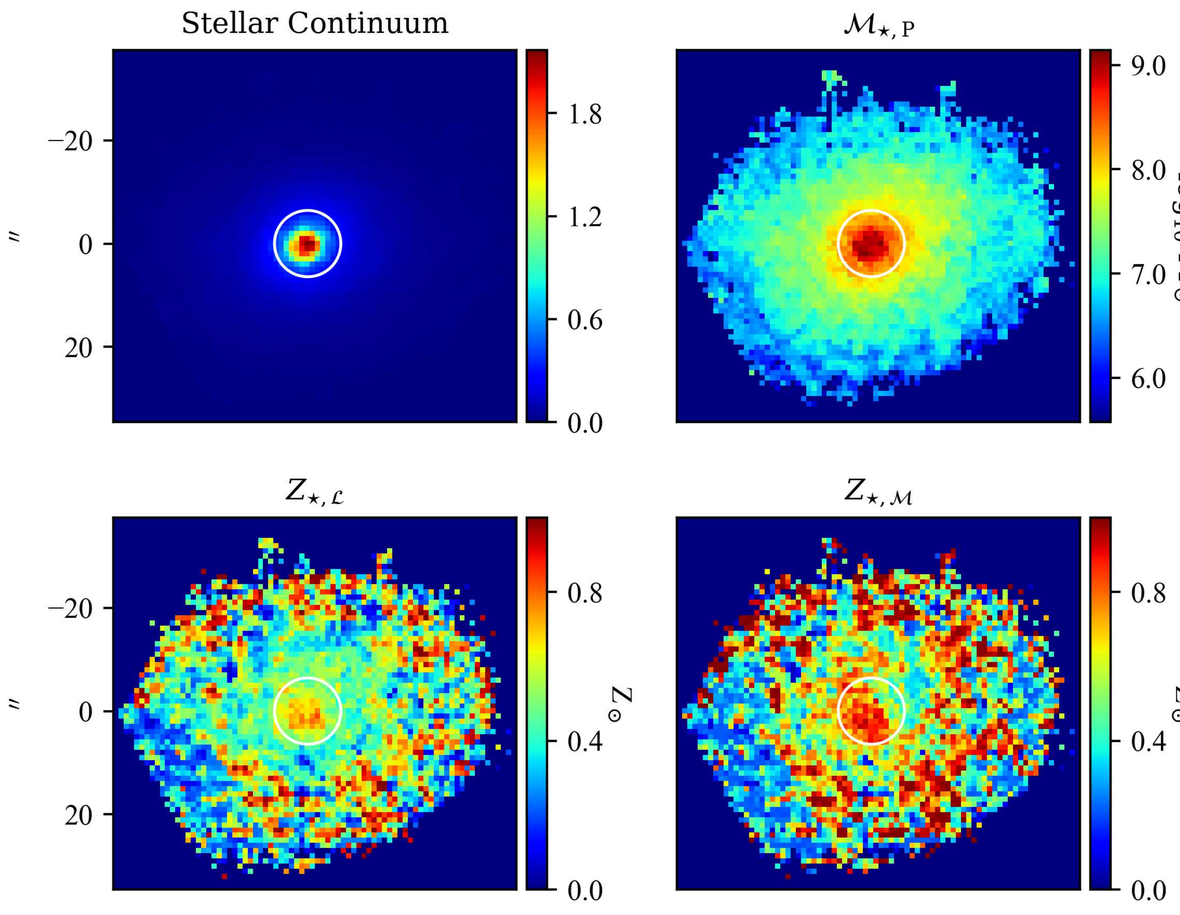
Stellar Continuum
$\mathcal{M}_{\star,\mathrm{P}}$
log$_{10}$ M$_\odot$
″

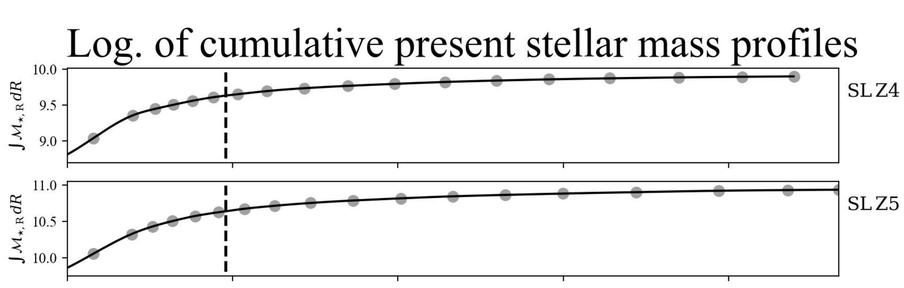
Log. of cumulative present stellar mass profiles
SL Z4
SL Z5

$Z_{\star,\mathcal{L}}$
$Z_{\star,\mathcal{M}}$
Z$_\odot$
″

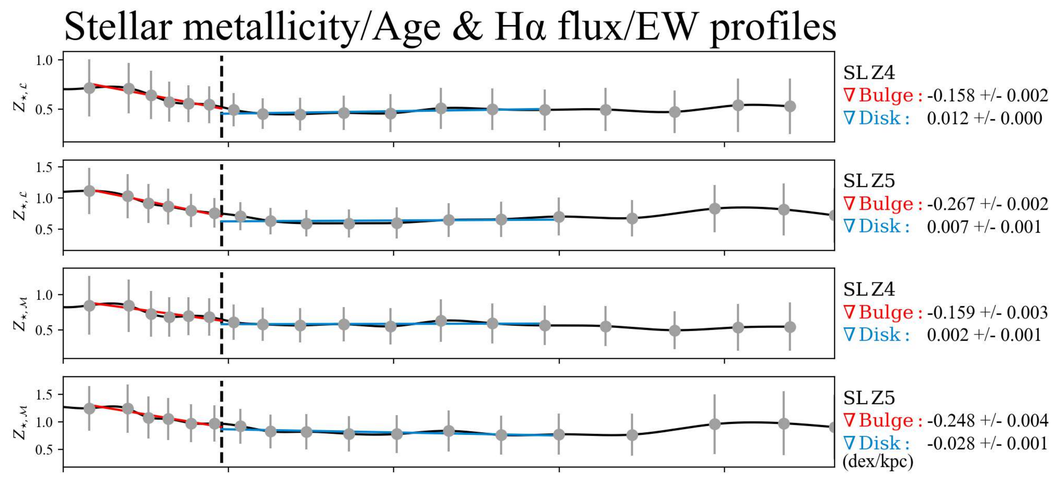
Stellar metallicity/Age & Hα flux/EW profiles
SL Z4
∇ Bulge : -0.158 +/- 0.002
∇ Disk : 0.012 +/- 0.000
SL Z5
∇ Bulge : -0.267 +/- 0.002
∇ Disk : 0.007 +/- 0.001
SL Z4
∇ Bulge : -0.159 +/- 0.003
∇ Disk : 0.002 +/- 0.001
SL Z5
∇ Bulge : -0.248 +/- 0.004
∇ Disk : -0.028 +/- 0.001
(dex/kpc)

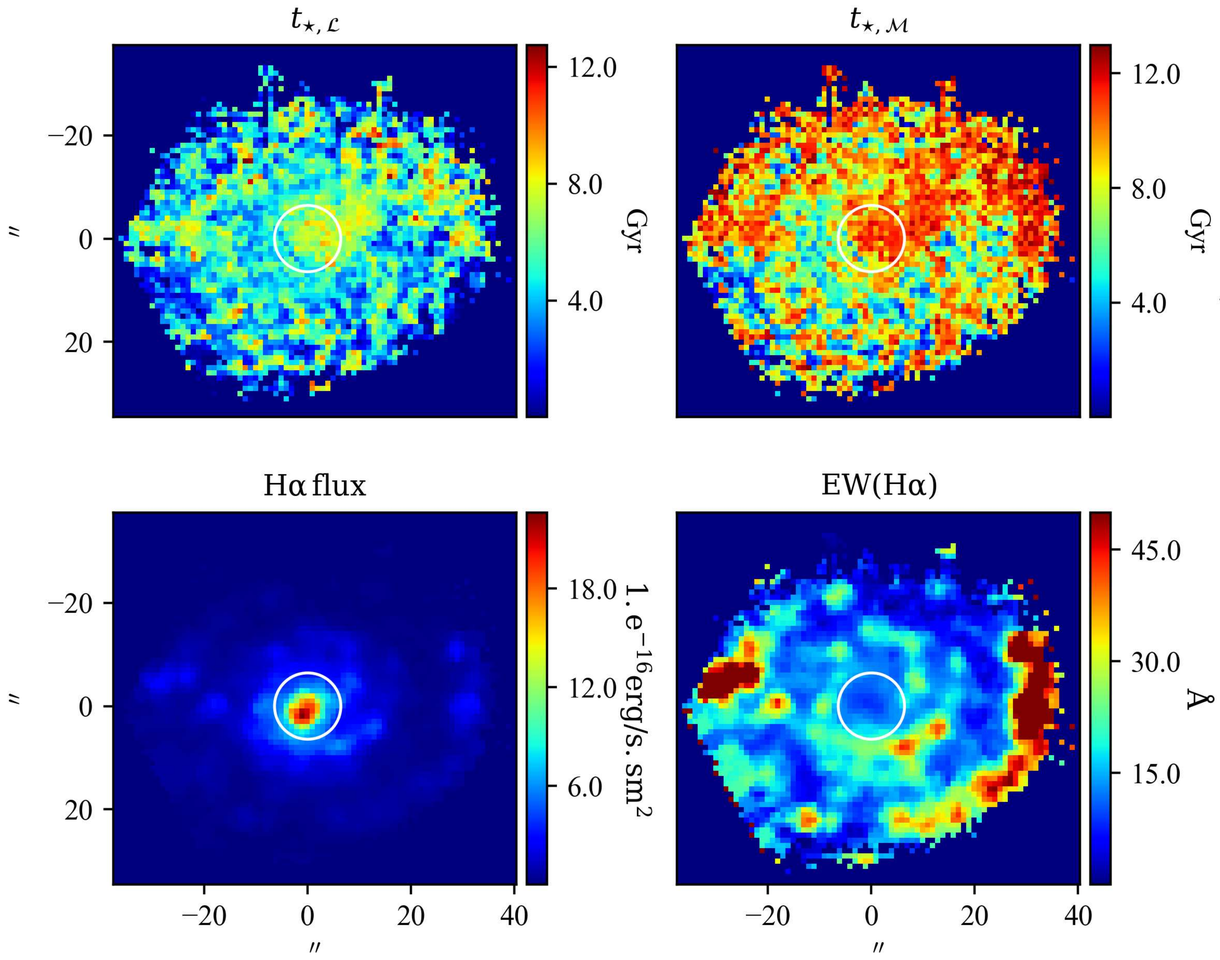
$t_{\star,\mathcal{L}}$
$t_{\star,\mathcal{M}}$
Gyr
″

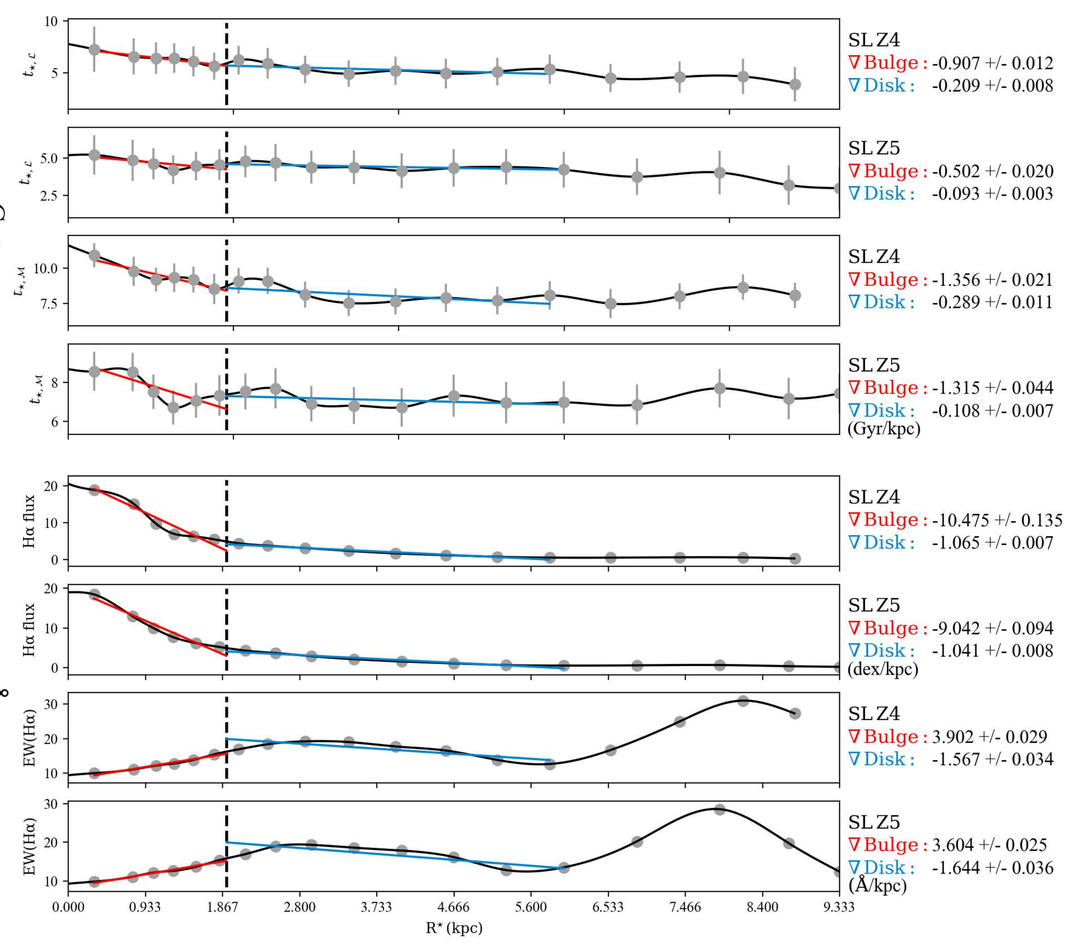
SL Z4
∇ Bulge : -0.907 +/- 0.012
∇ Disk : -0.209 +/- 0.008
SL Z5
∇ Bulge : -0.502 +/- 0.020
∇ Disk : -0.093 +/- 0.003
SL Z4
∇ Bulge : -1.356 +/- 0.021
∇ Disk : -0.289 +/- 0.011
SL Z5
∇ Bulge : -1.315 +/- 0.044
∇ Disk : -0.108 +/- 0.007
(Gyr/kpc)

Hα flux
EW(Hα)
1. e^{-16}erg/s. sm^2
Å
″

SL Z4
∇ Bulge : -10.475 +/- 0.135
∇ Disk : -1.065 +/- 0.007
SL Z5
∇ Bulge : -9.042 +/- 0.094
∇ Disk : -1.041 +/- 0.008
(dex/kpc)
SL Z4
∇ Bulge : 3.902 +/- 0.029
∇ Disk : -1.567 +/- 0.034
SL Z5
∇ Bulge : 3.604 +/- 0.025
∇ Disk : -1.644 +/- 0.036
(Å/kpc)
R* (kpc)

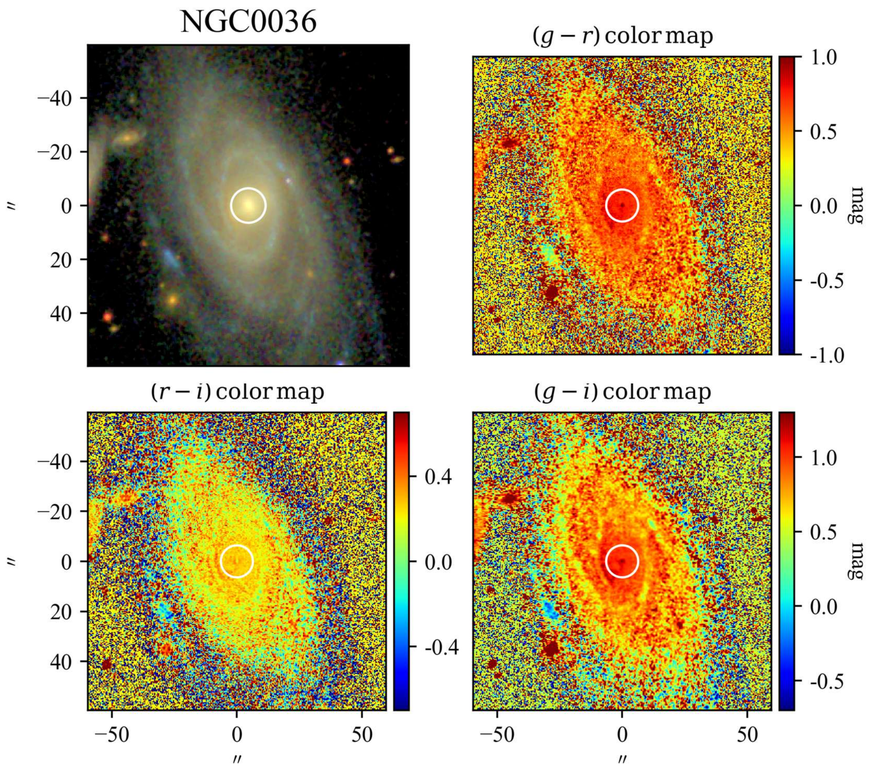

SBP decomposition of SDSS r band

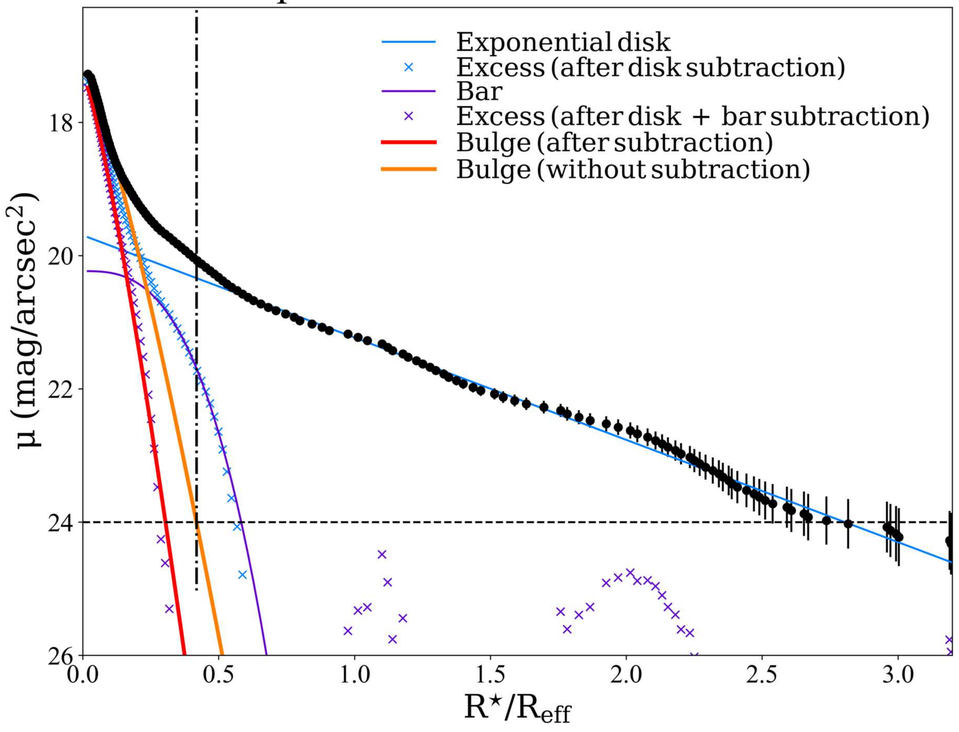

SDSS color profiles

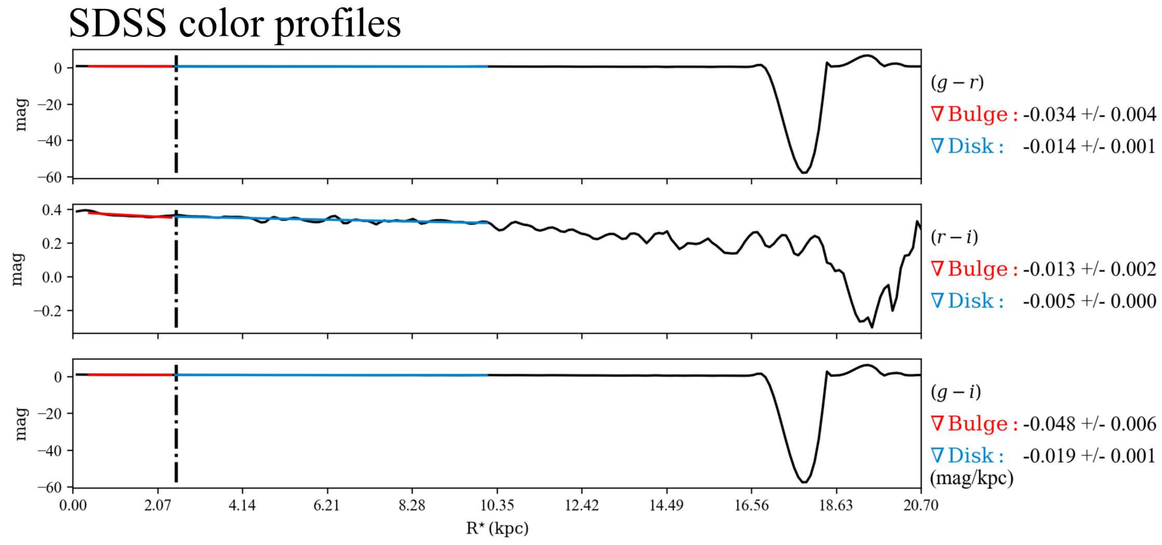

$\mathcal{RY}$ SBPs

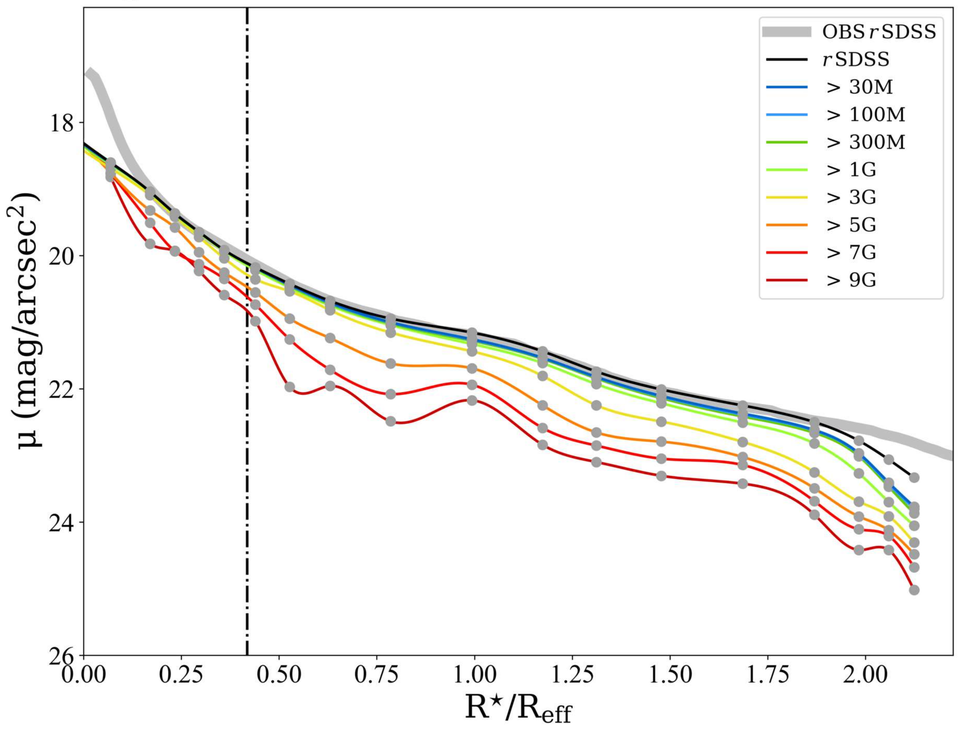

Stellar Continuum

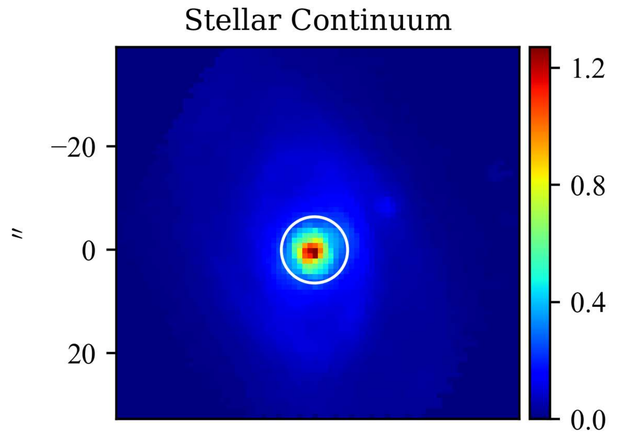

$\mathcal{M}_{\star,\,\rm P}$

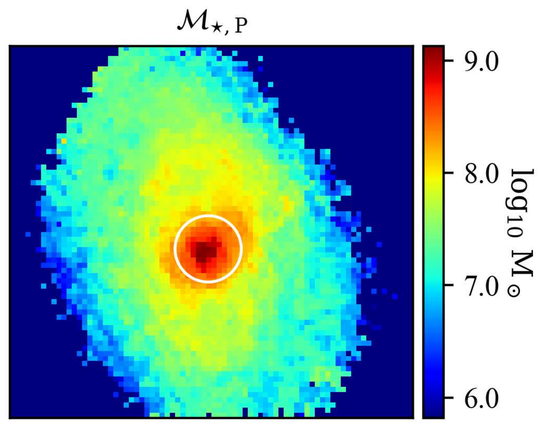

Log. of cumulative present stellar mass profiles

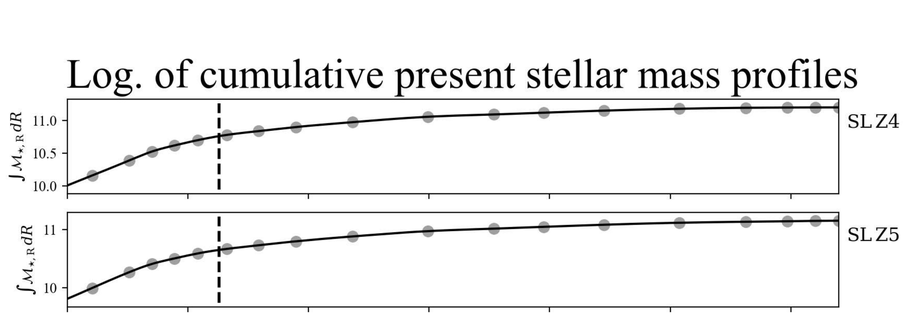

$Z_{\star,\,\mathcal{L}}$

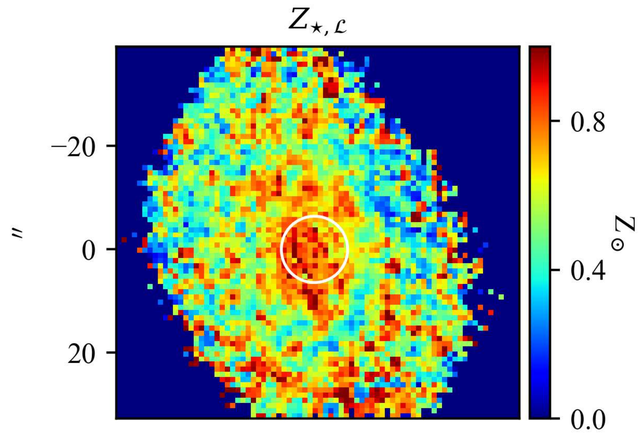

$Z_{\star,\,\mathcal{M}}$

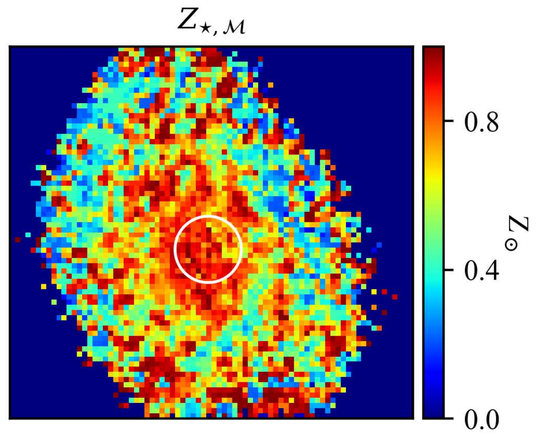

Stellar metallicity/Age & Hα flux/EW profiles

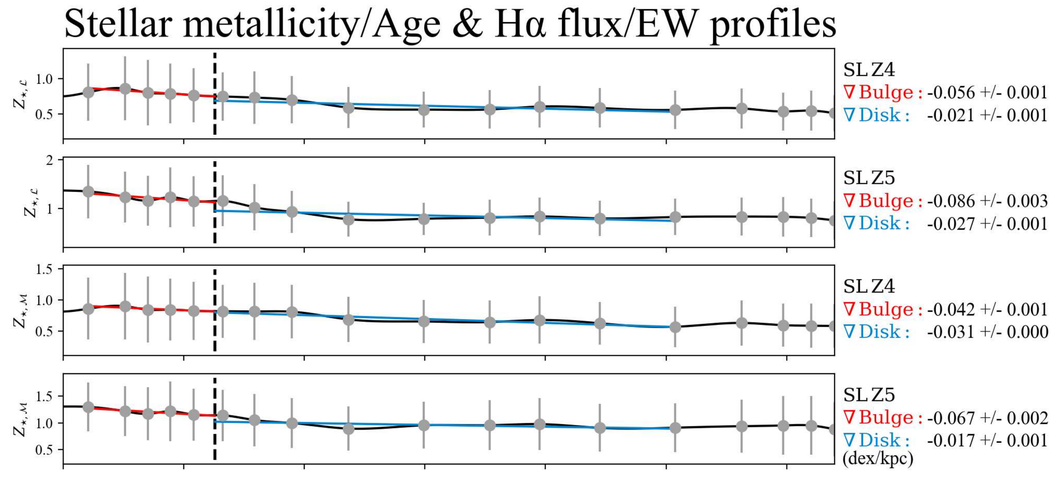

$t_{\star,\,\mathcal{L}}$

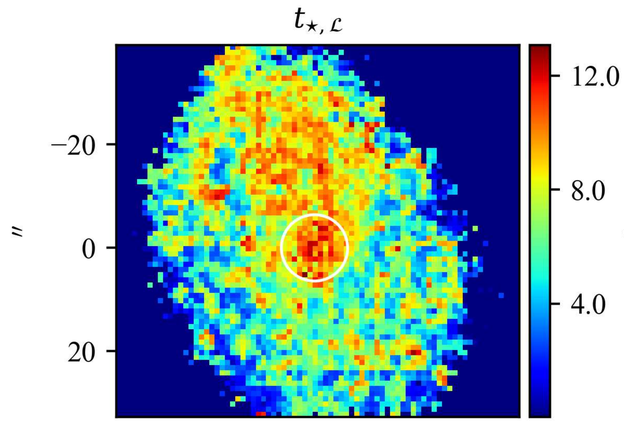

$t_{\star,\,\mathcal{M}}$

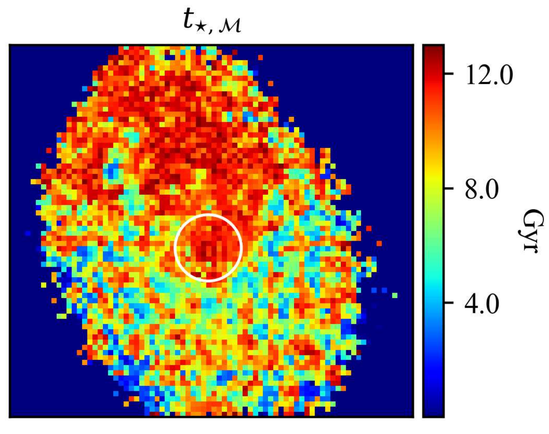

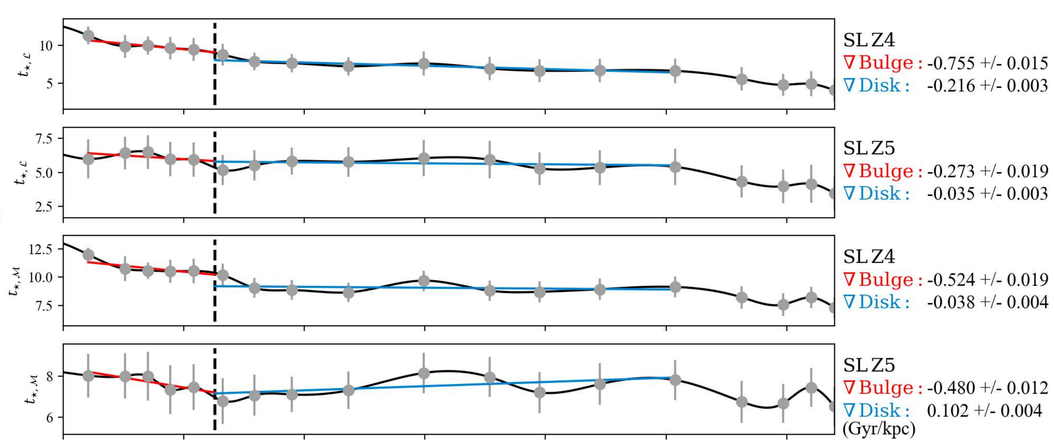

Hα flux

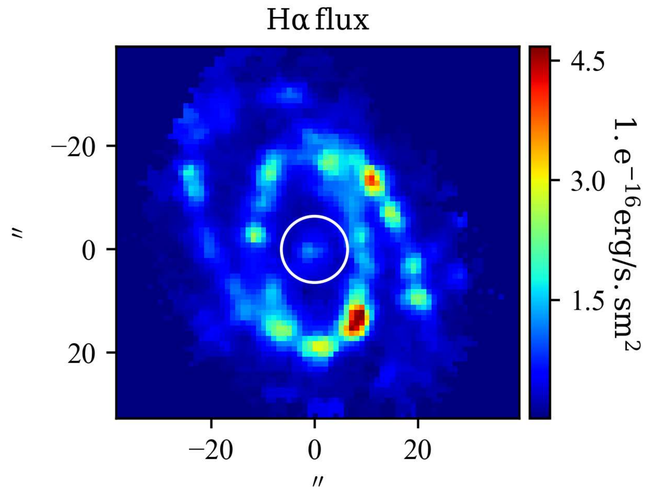

EW(Hα)

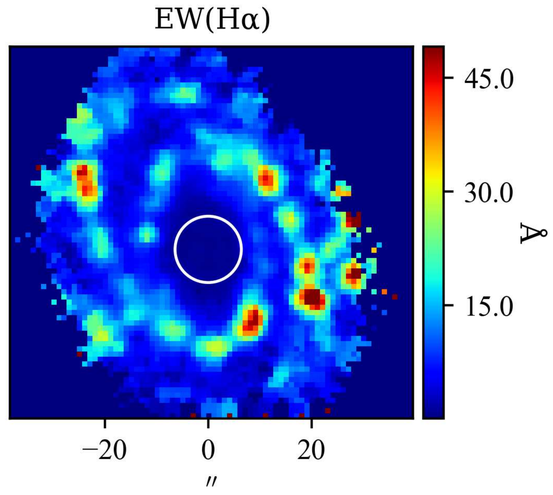

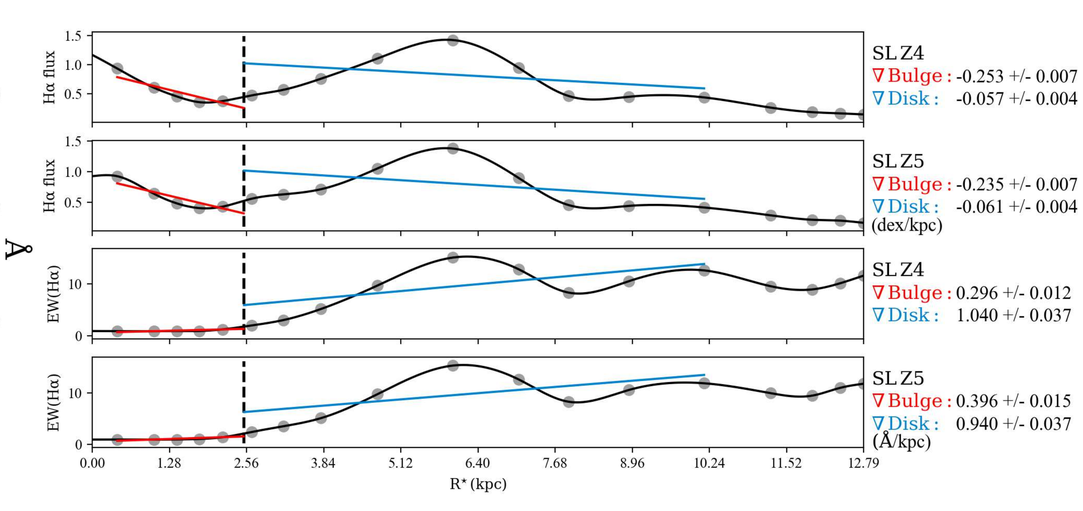

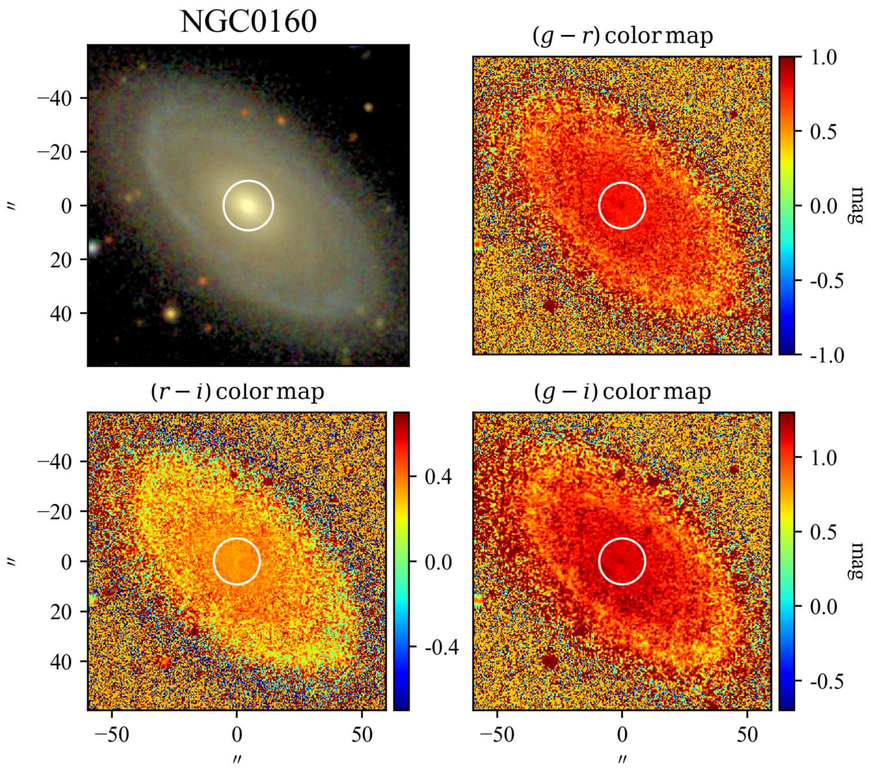

SBP decomposition of SDSS r band

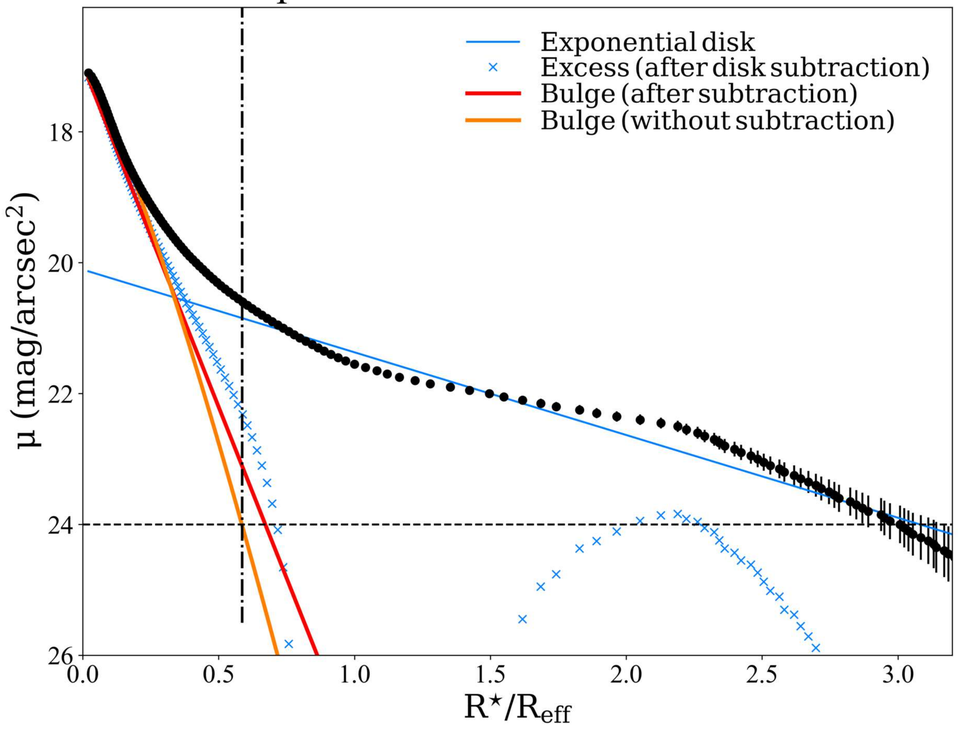

SDSS color profiles

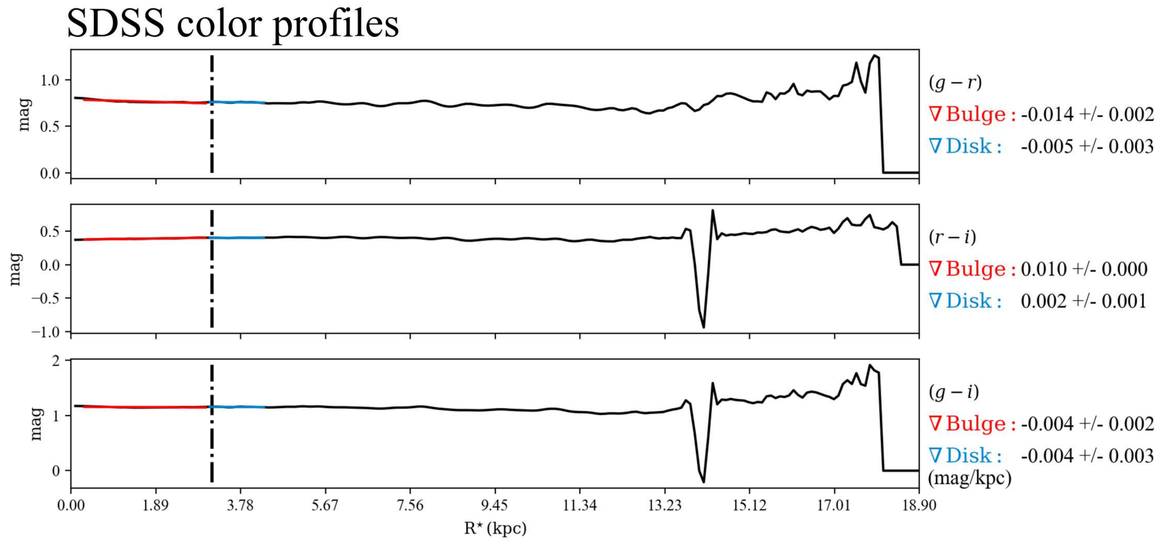

$\mathcal{RY}$ SBPs

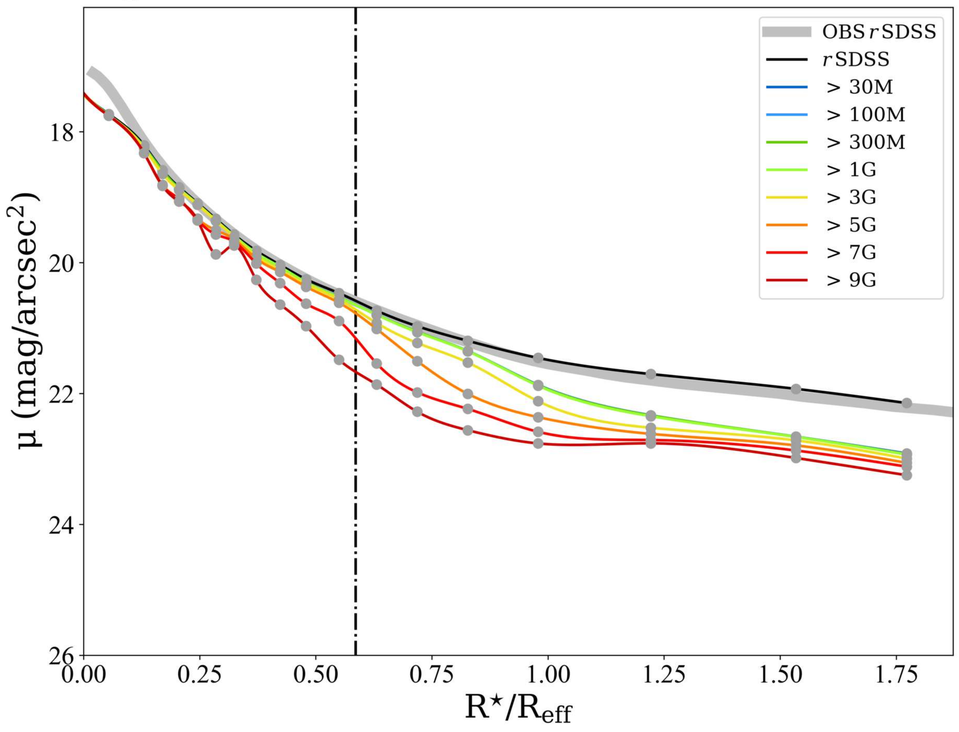

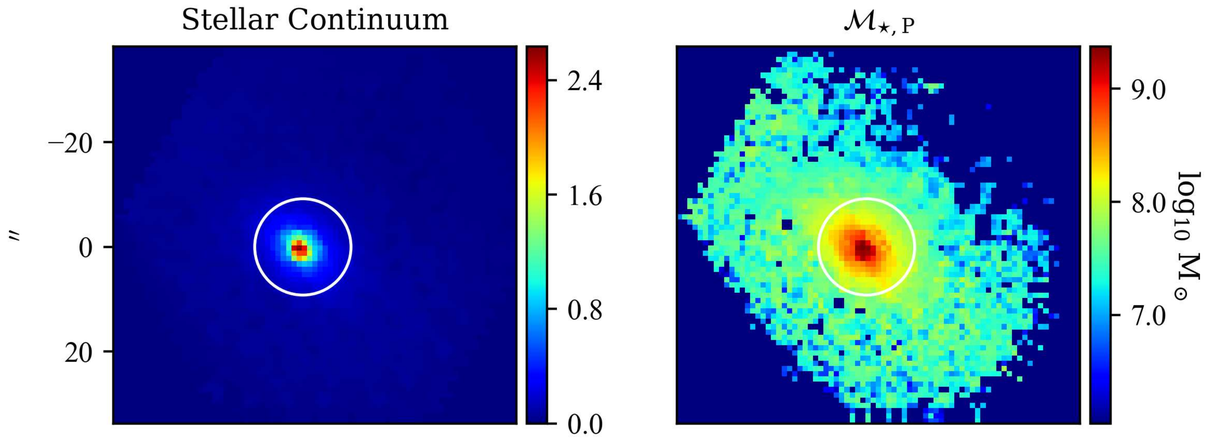

Log. of cumulative present stellar mass profiles

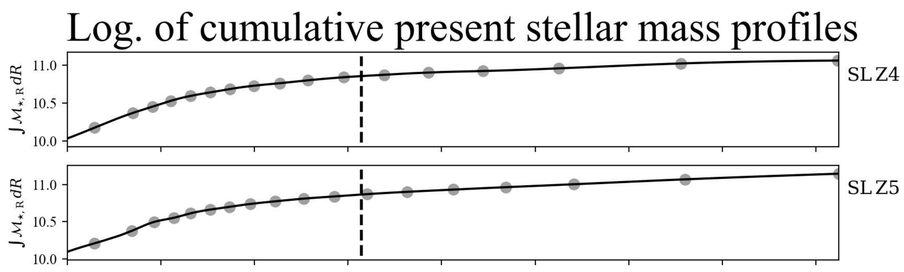

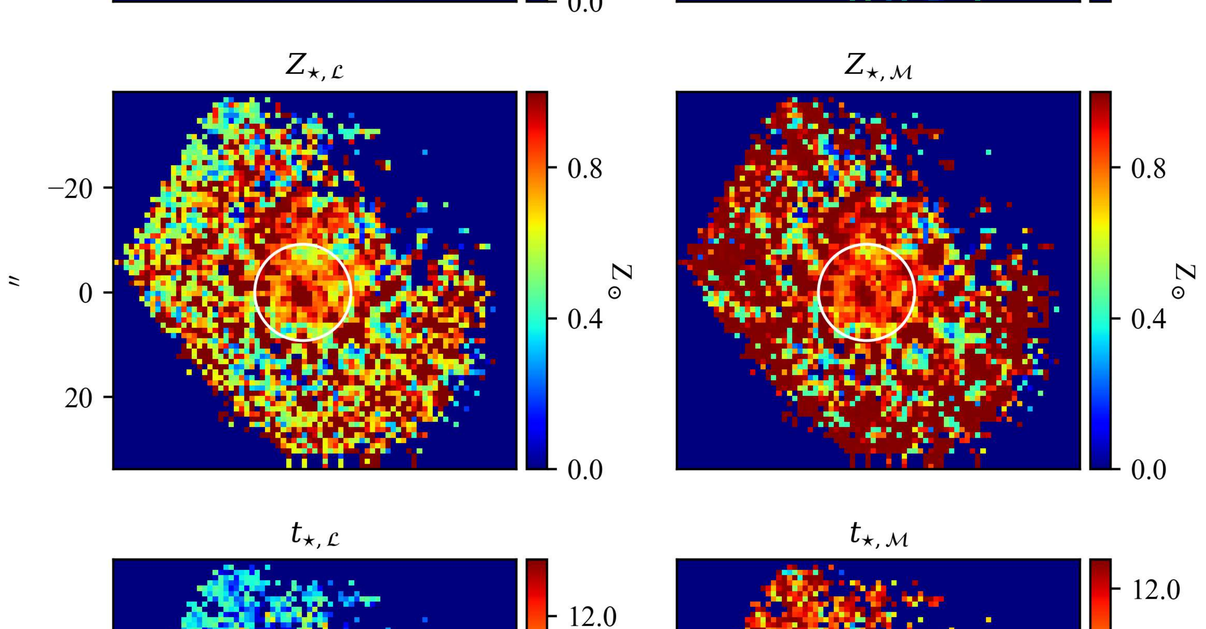

Stellar metallicity/Age & Hα flux/EW profiles

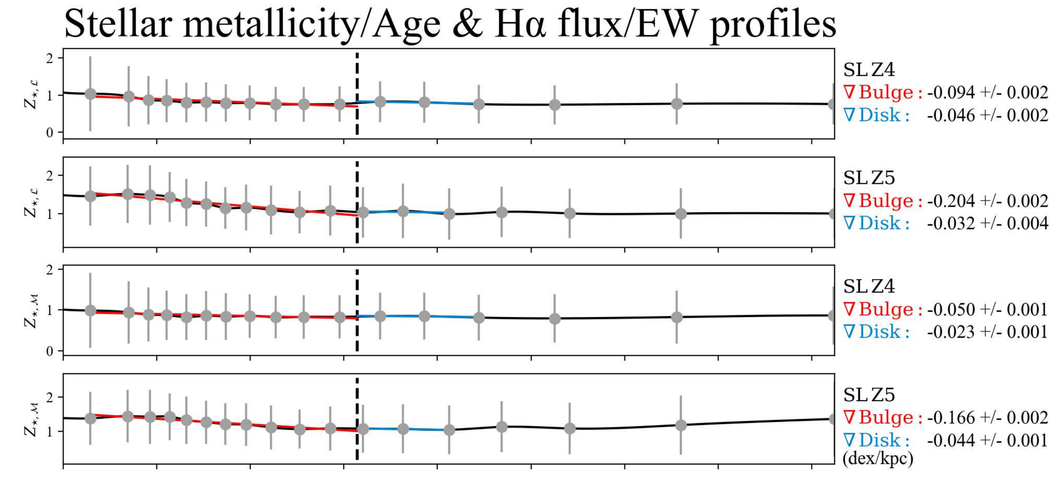

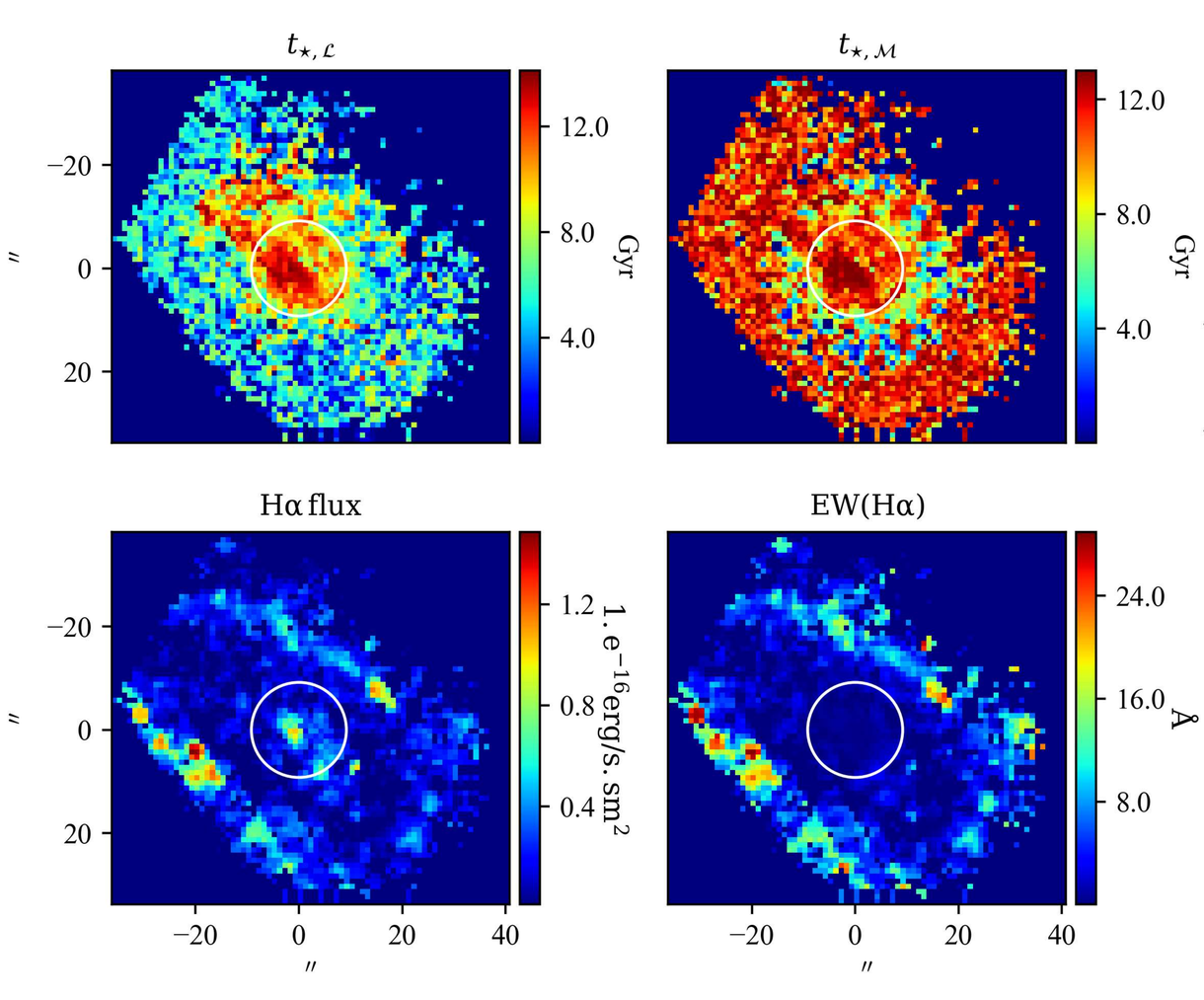

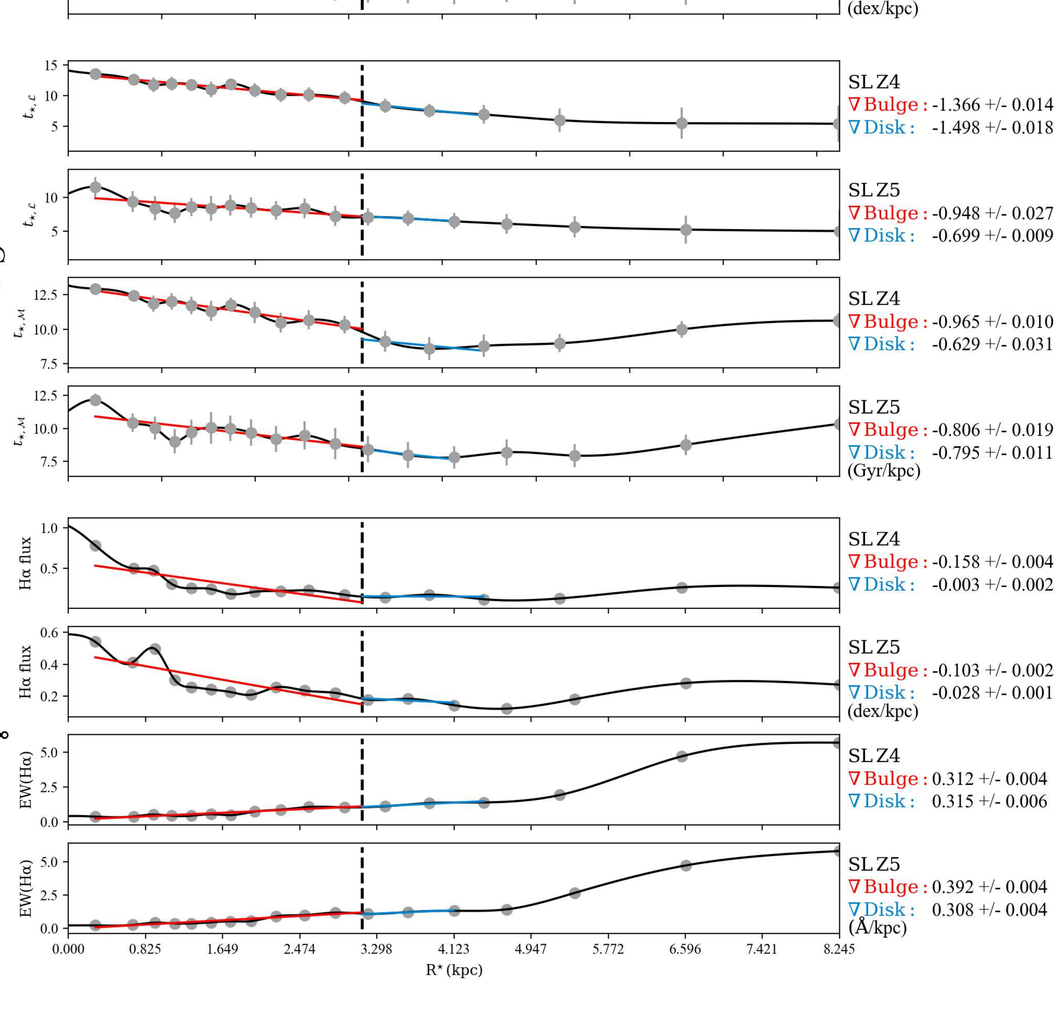

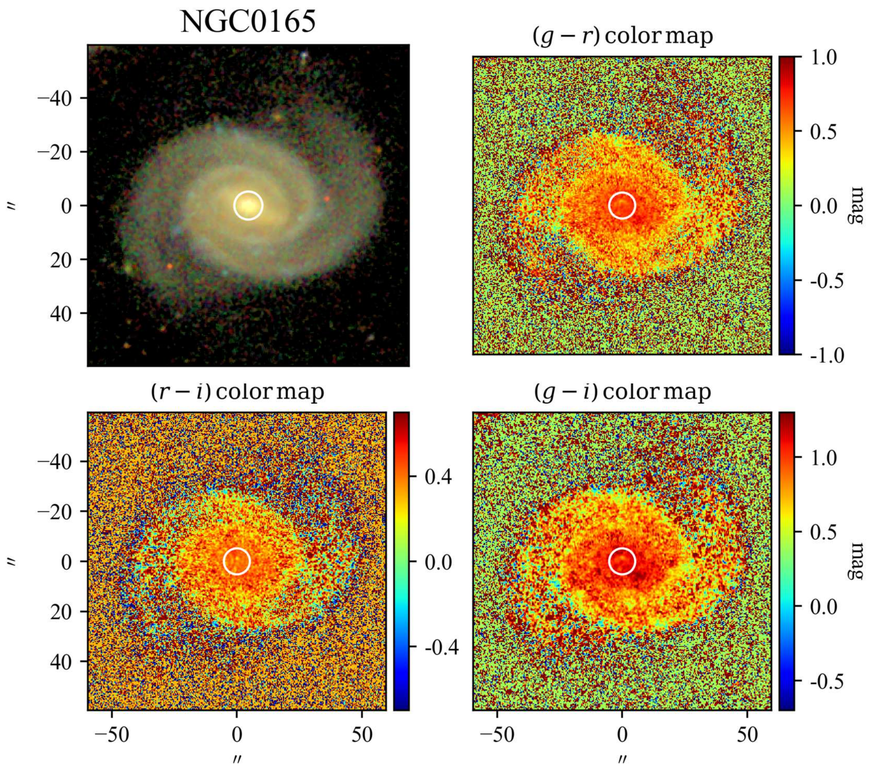

SBP decomposition of SDSS r band

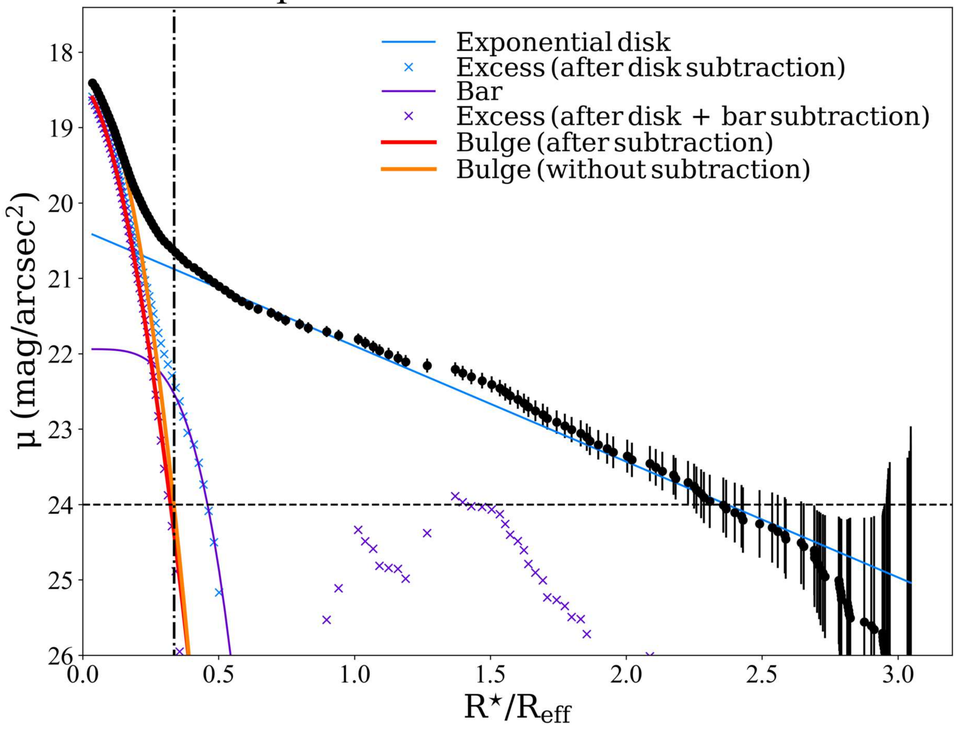

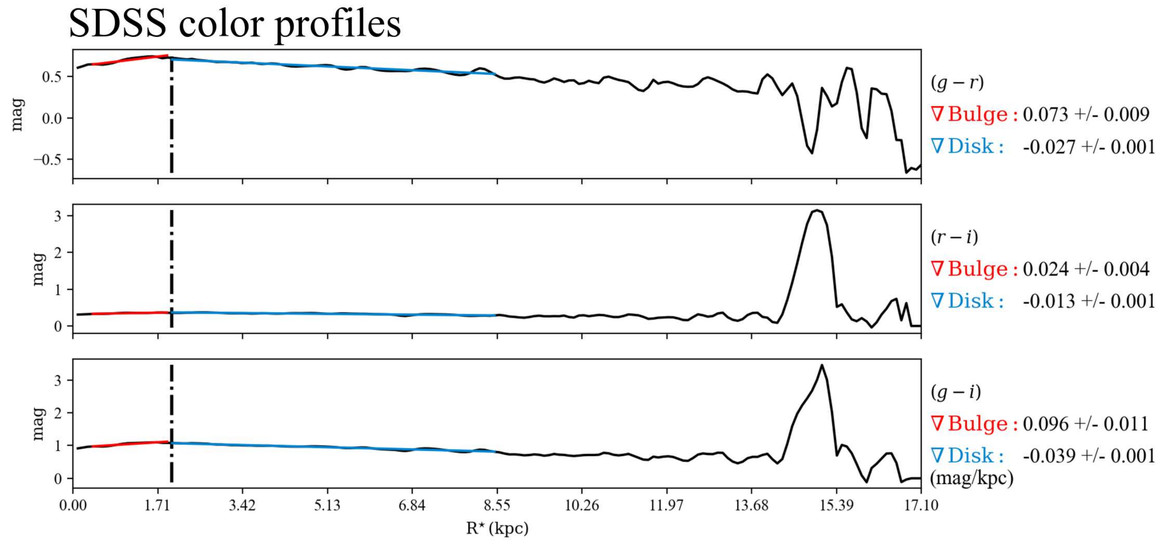

$\mathcal{RY}$ SBPs

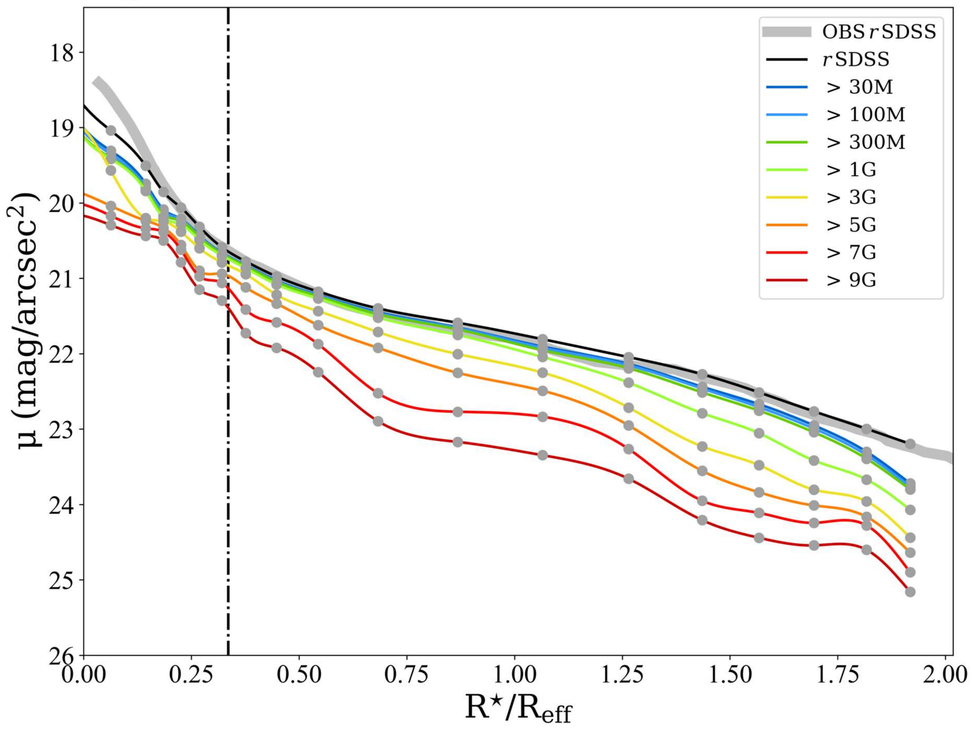

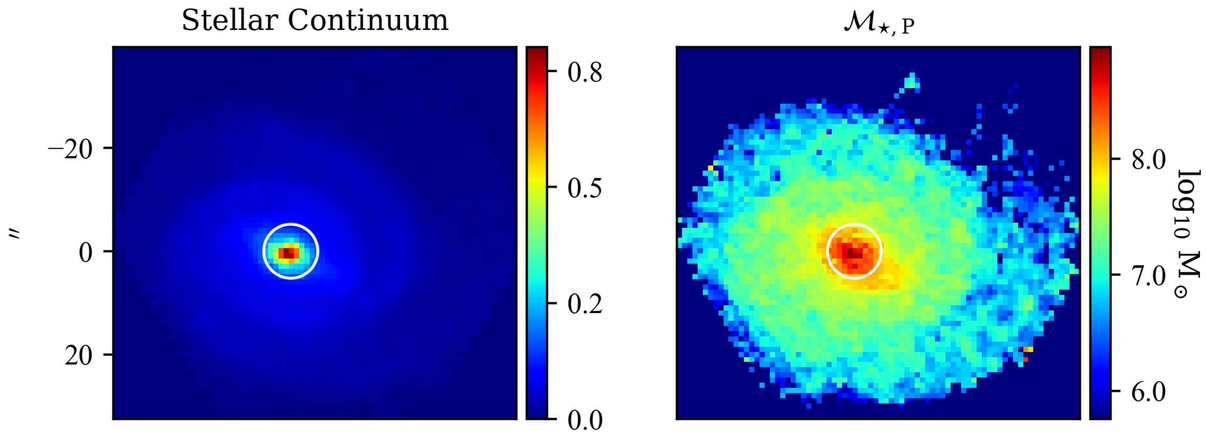

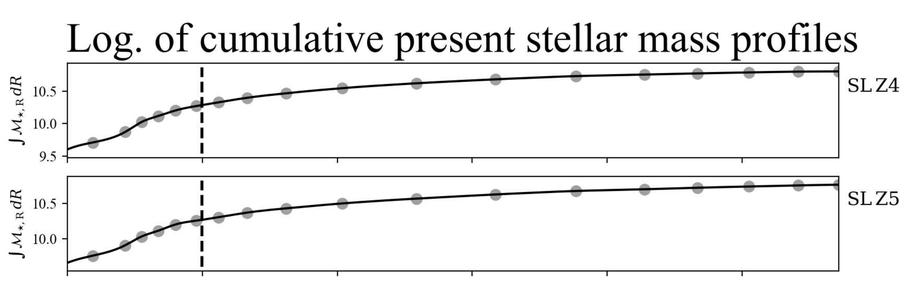

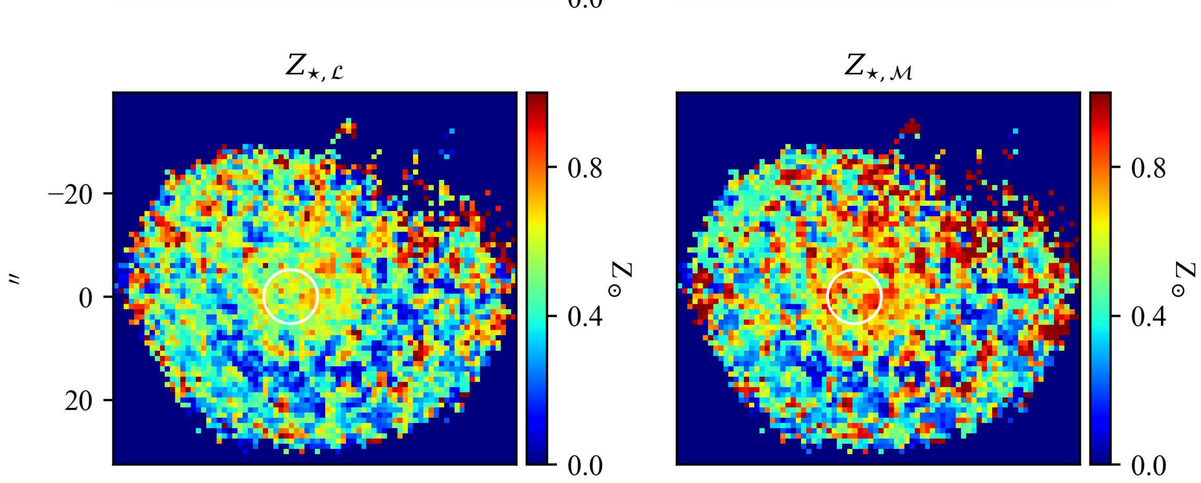

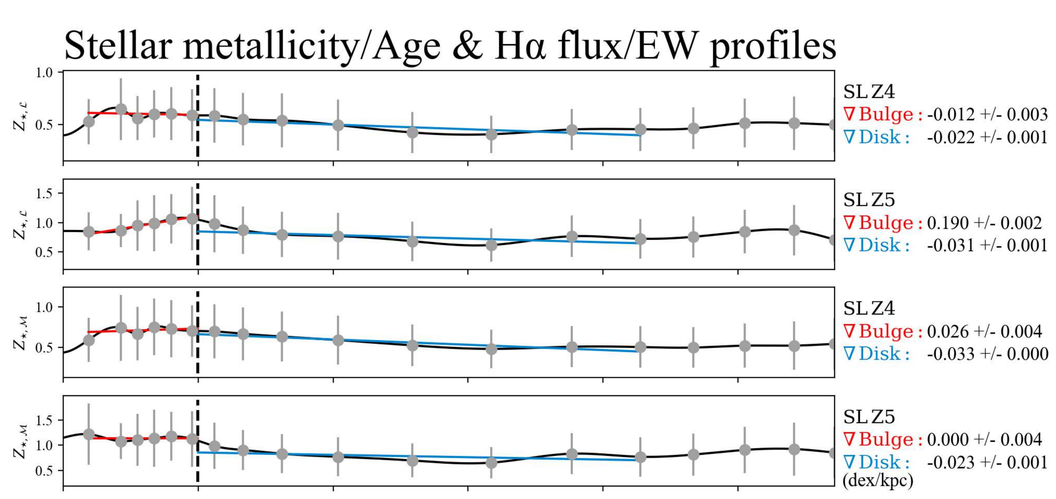

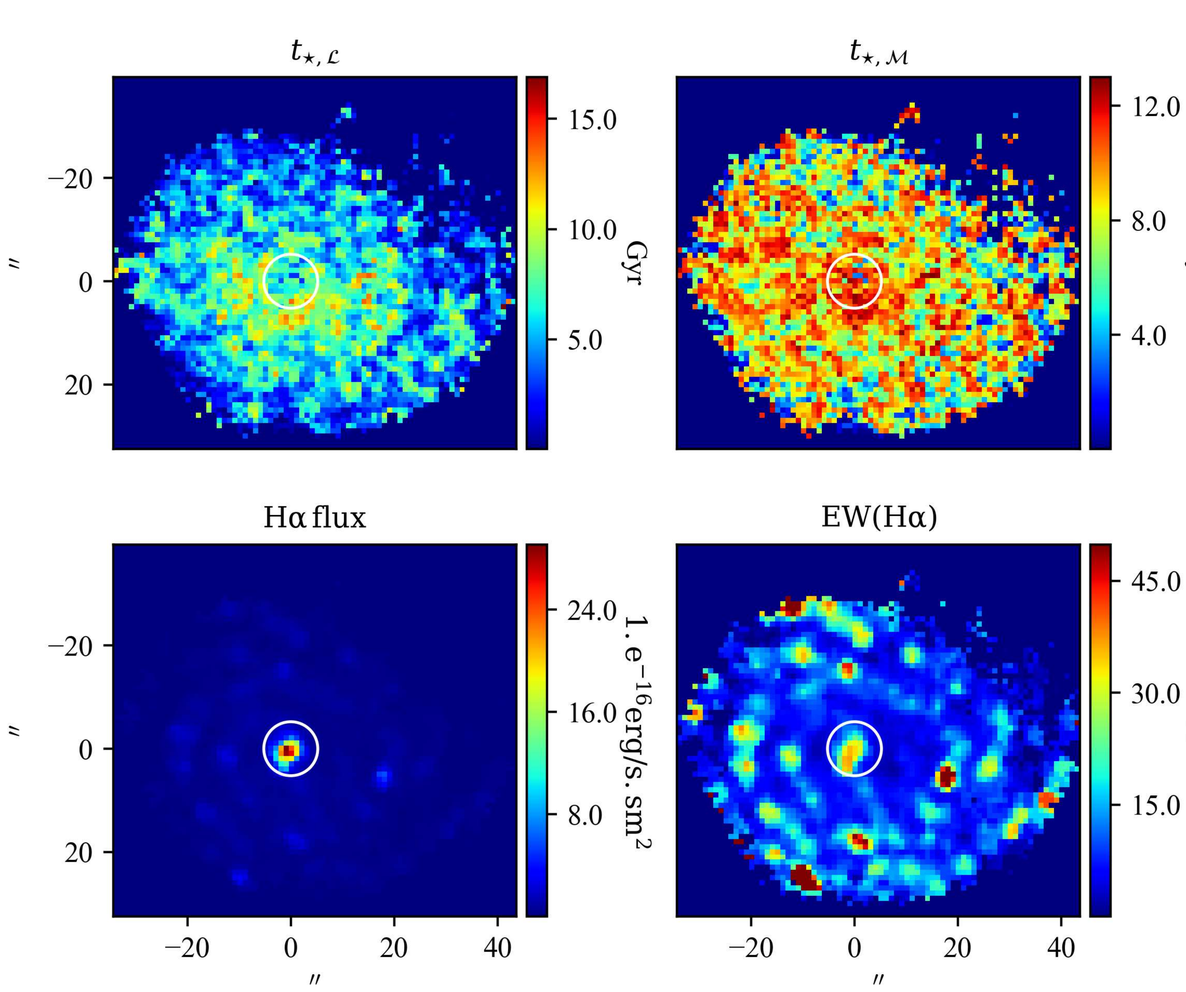

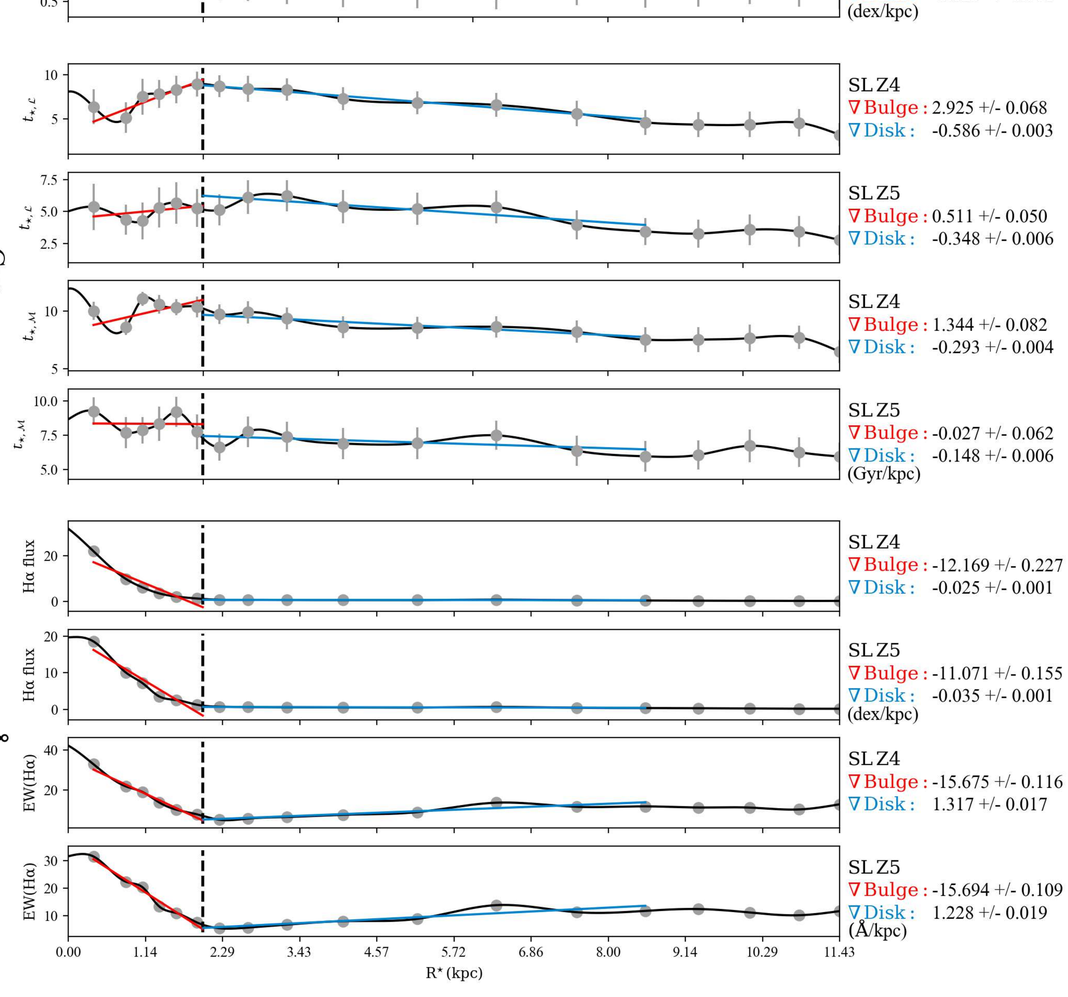

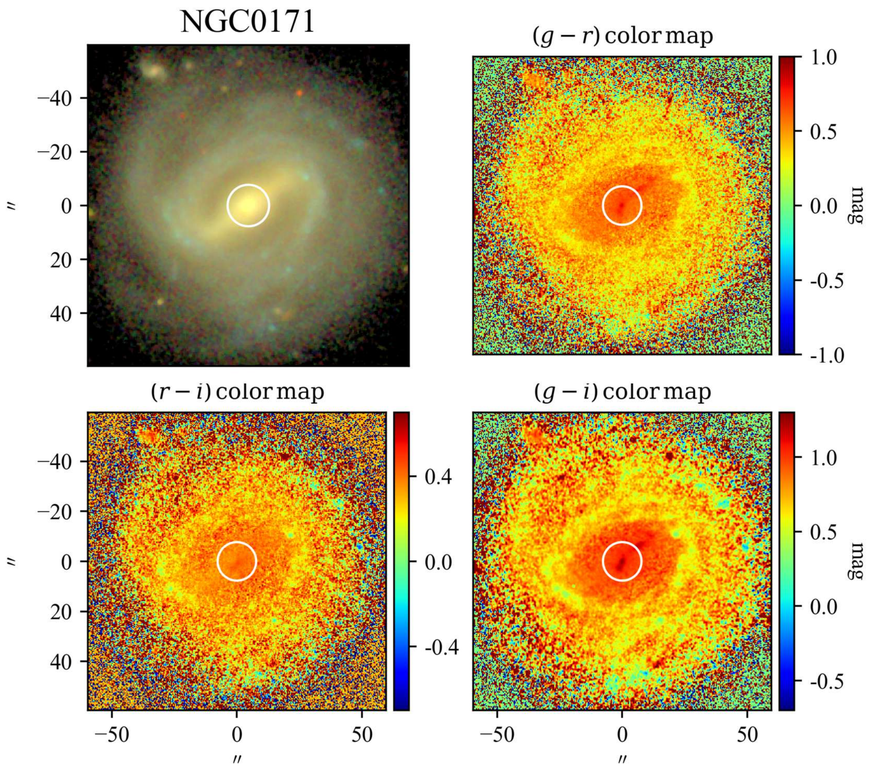

SBP decomposition of SDSS r band

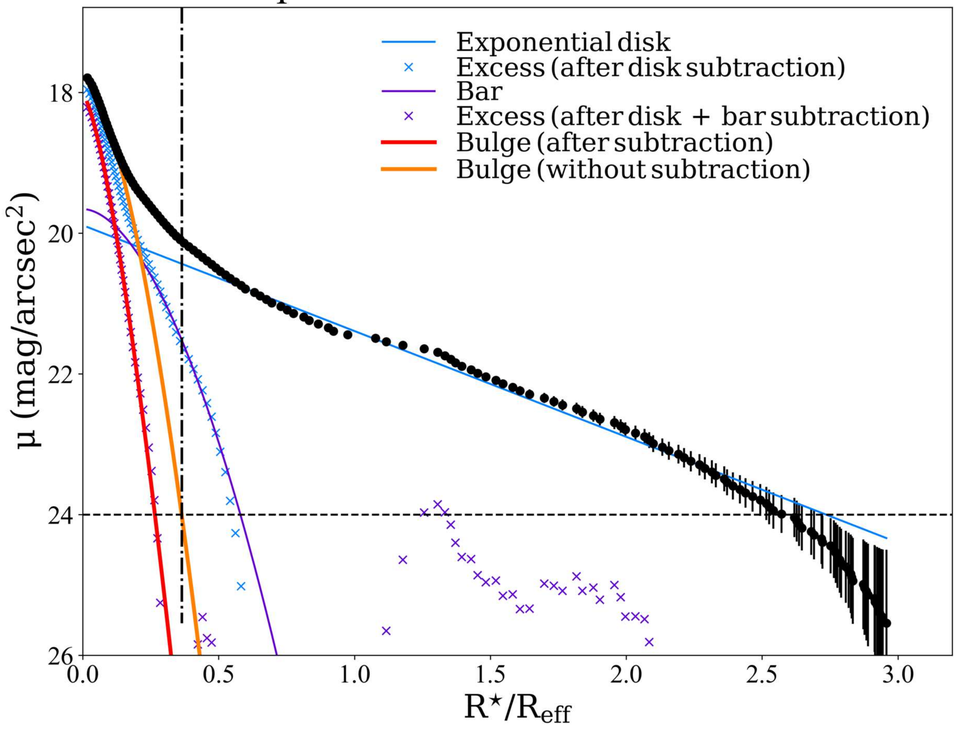

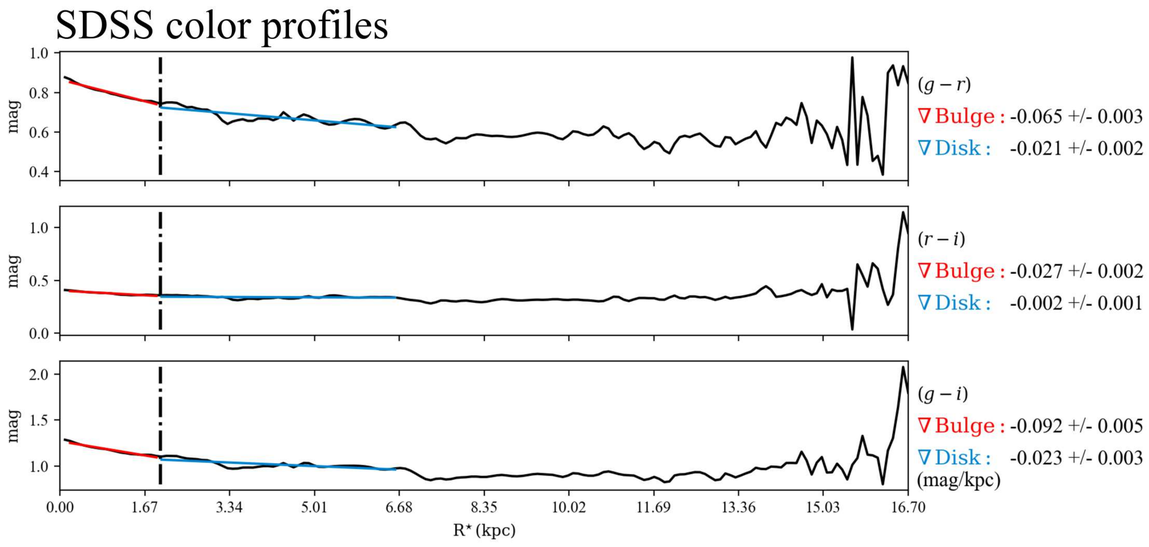

$\mathcal{RY}$ SBPs

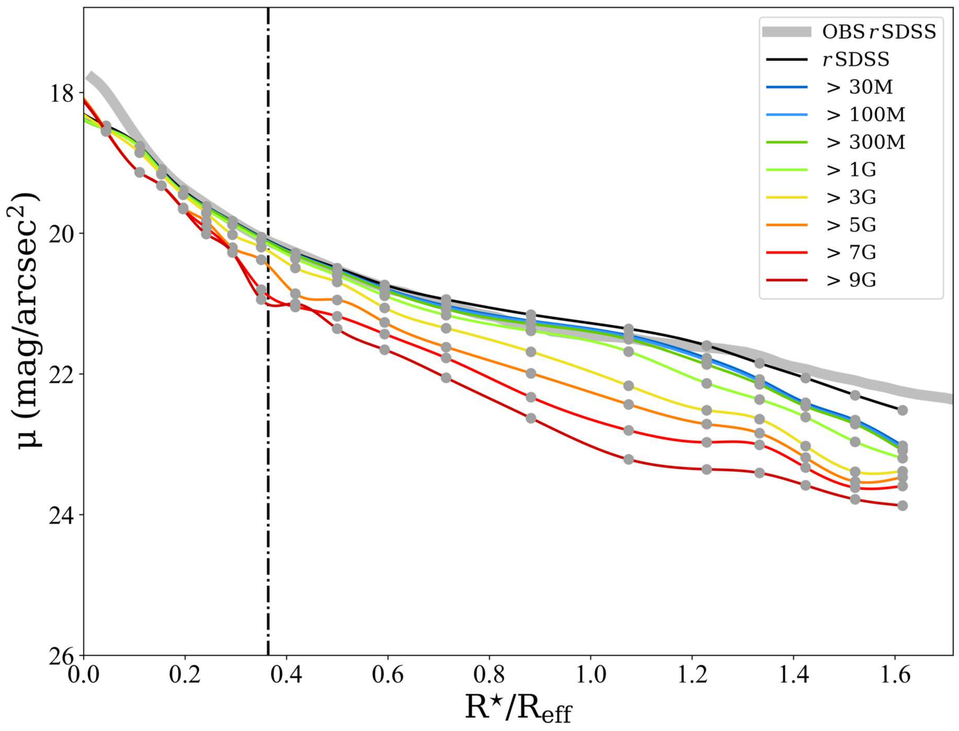

Stellar Continuum

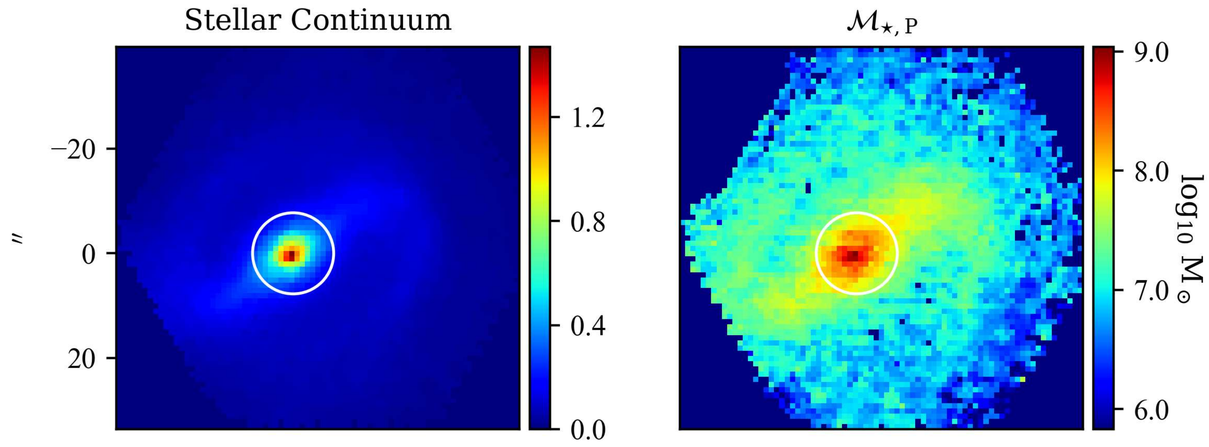

Log. of cumulative present stellar mass profiles

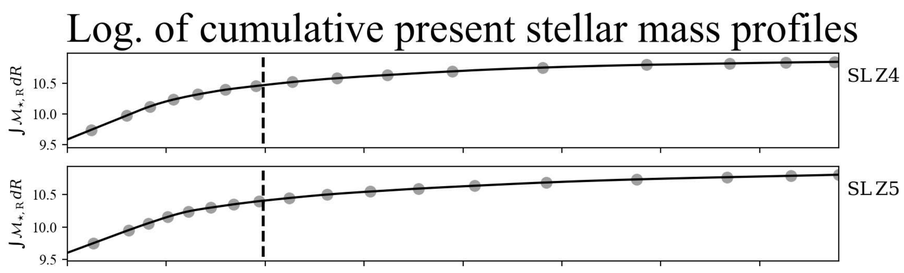

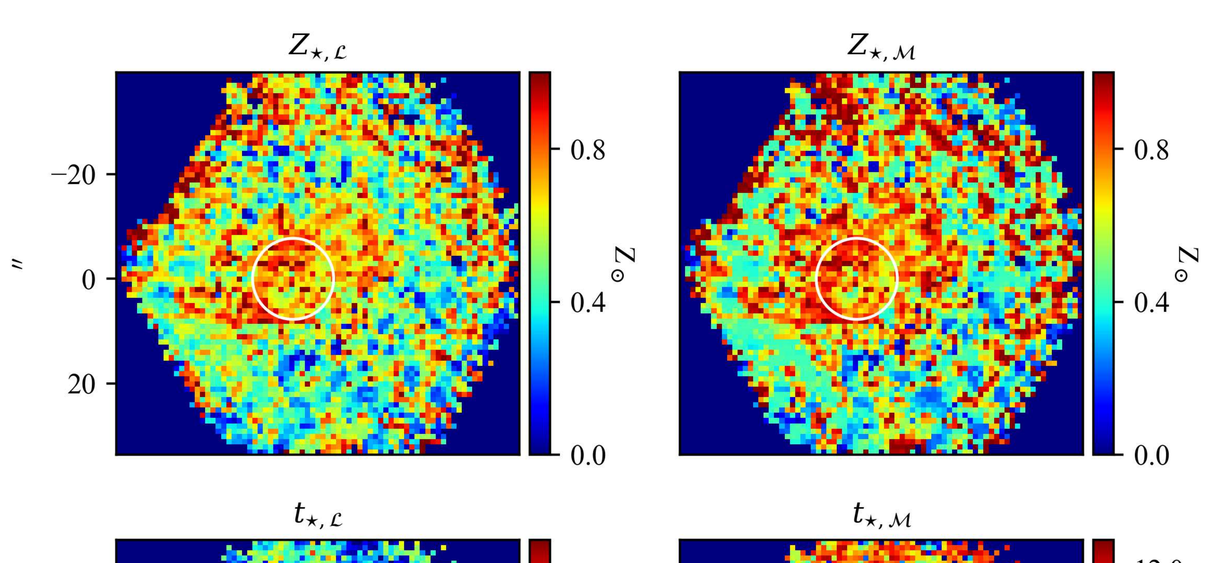

Stellar metallicity/Age & Hα flux/EW profiles

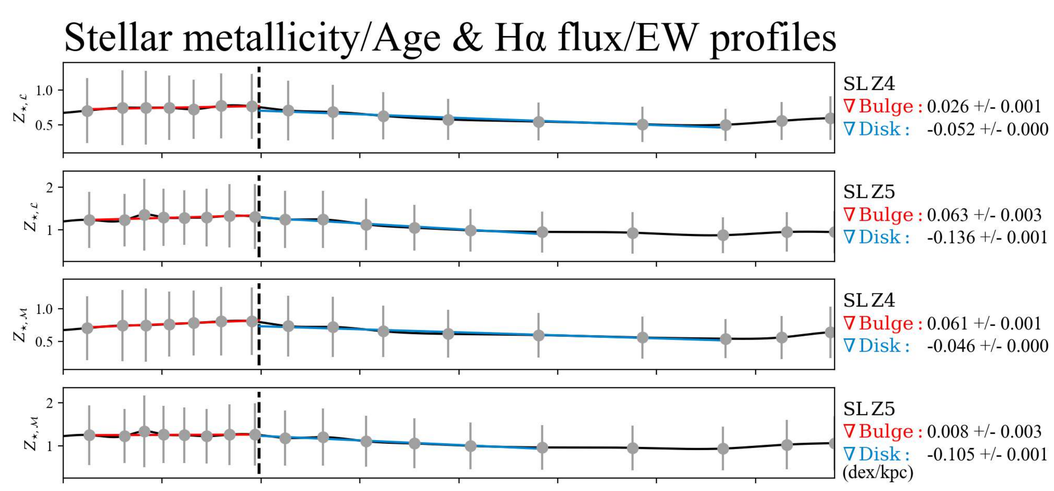

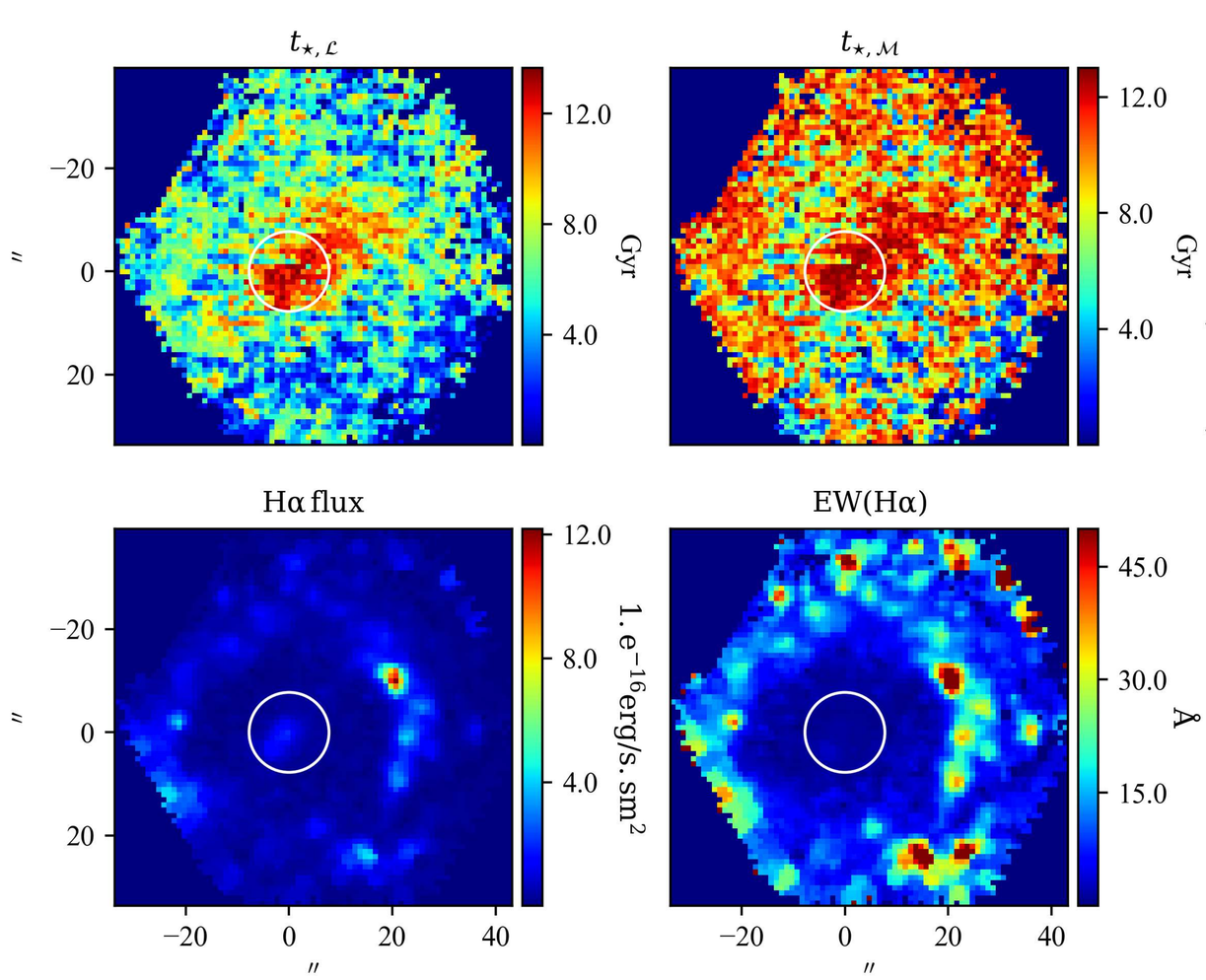

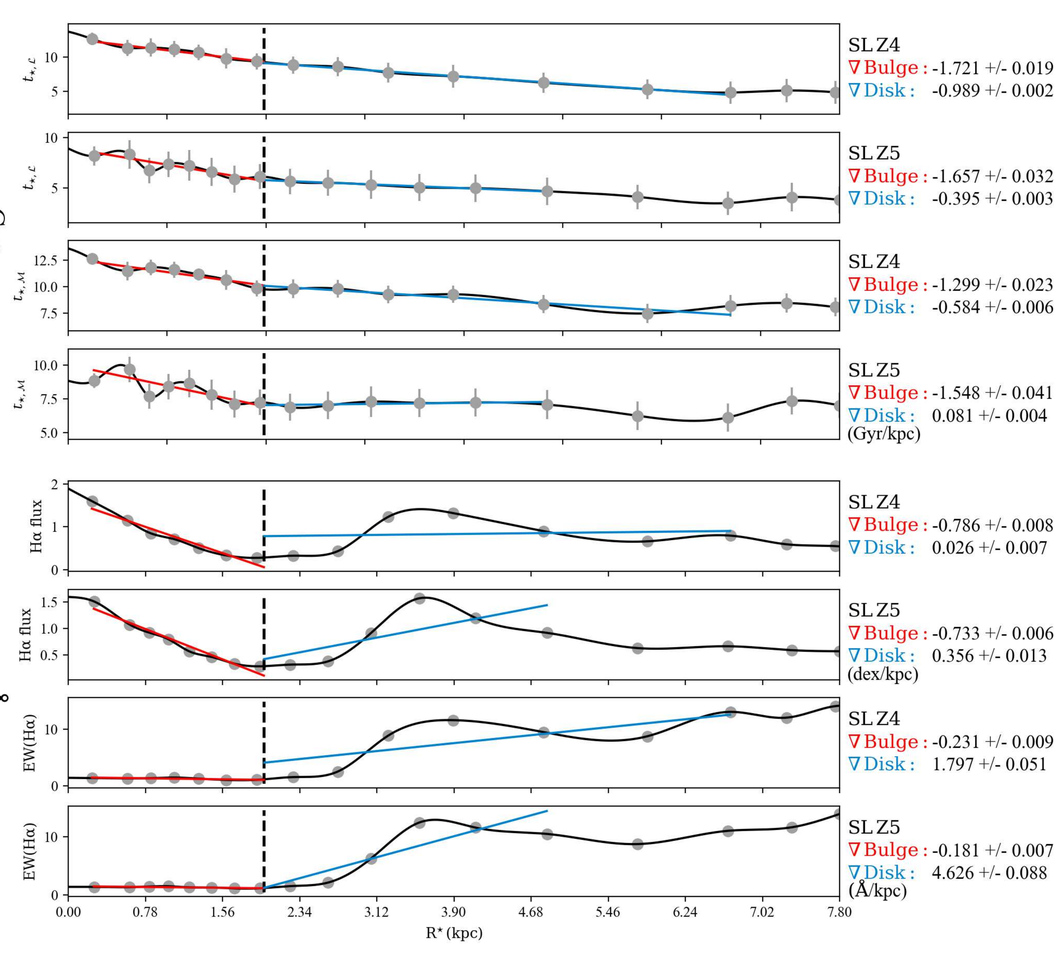

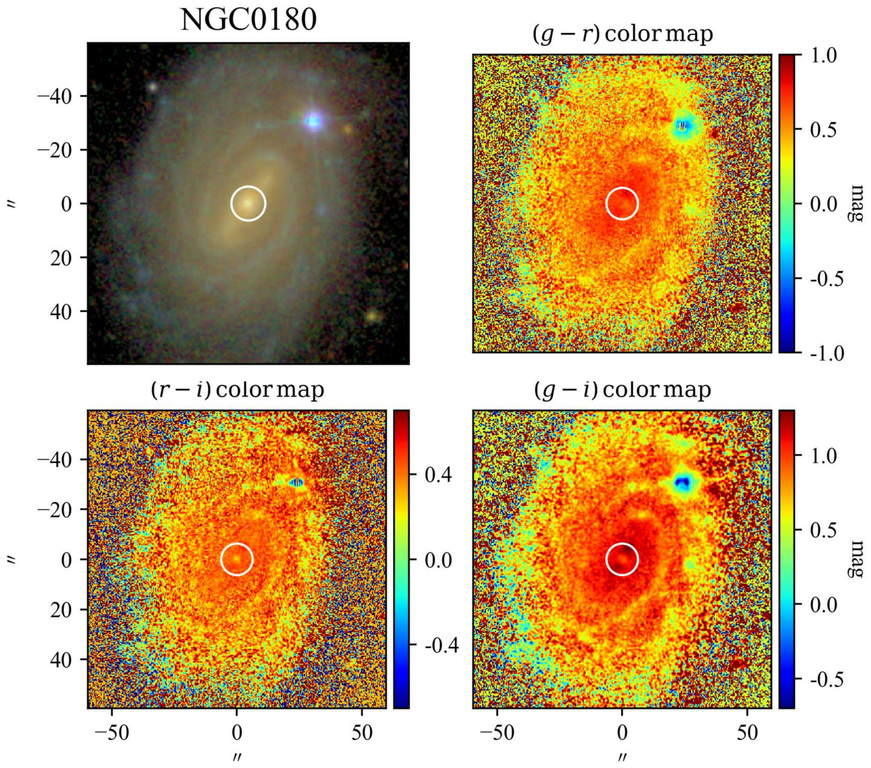

SBP decomposition of SDSS r band

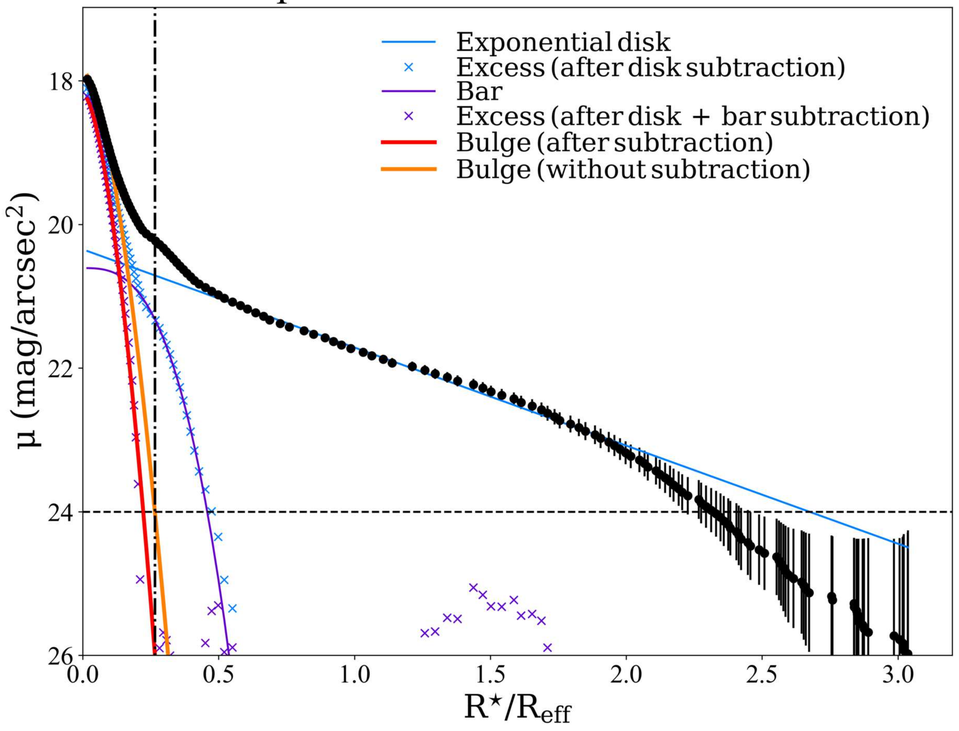

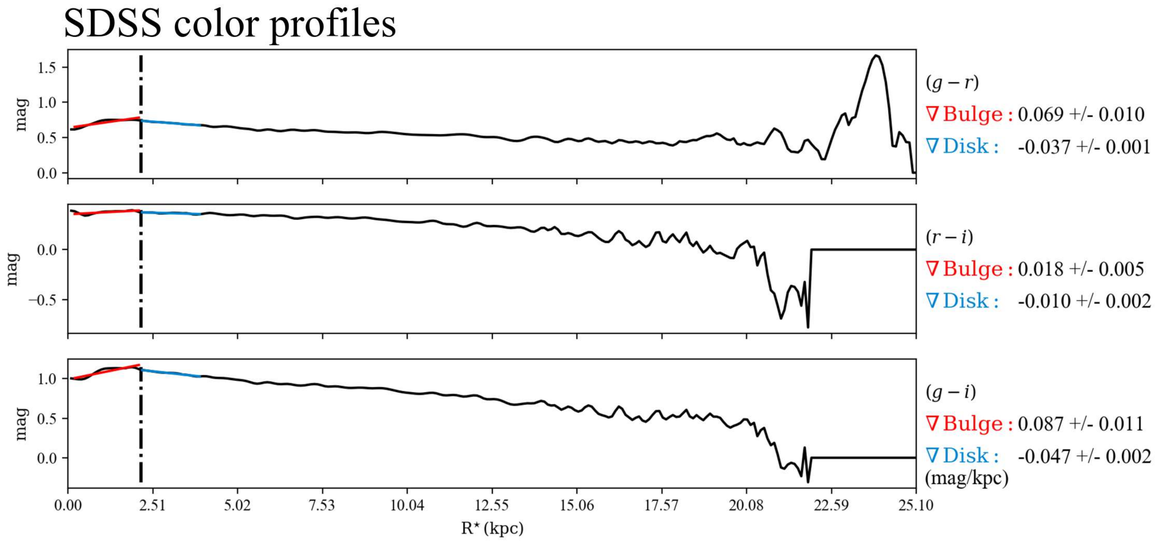

$\mathcal{RV}$ SBPs

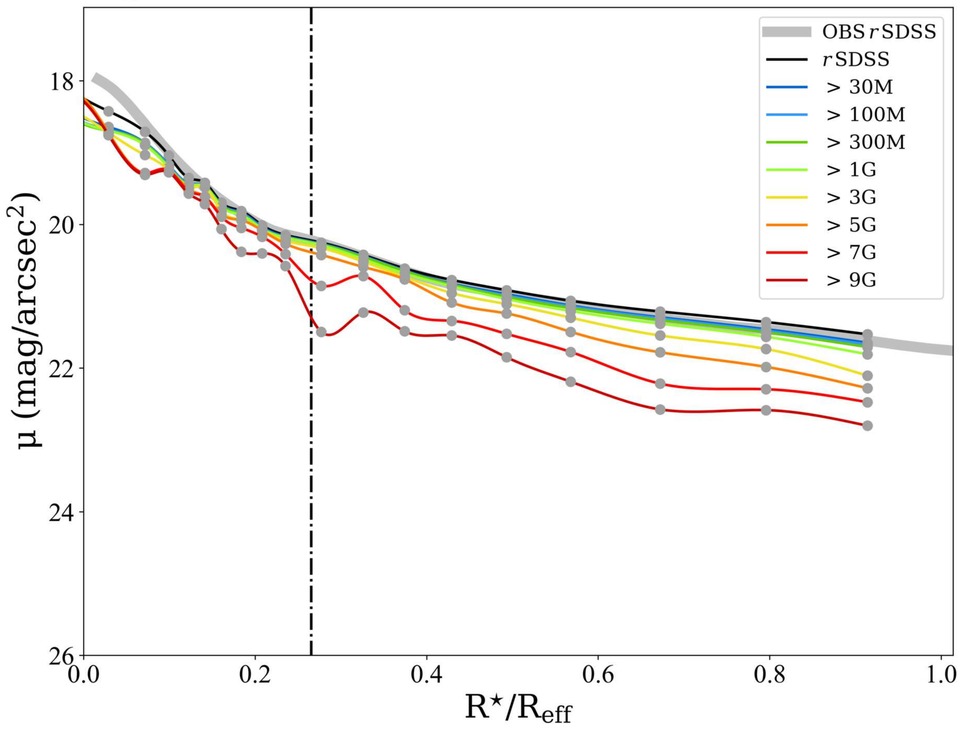

Stellar Continuum

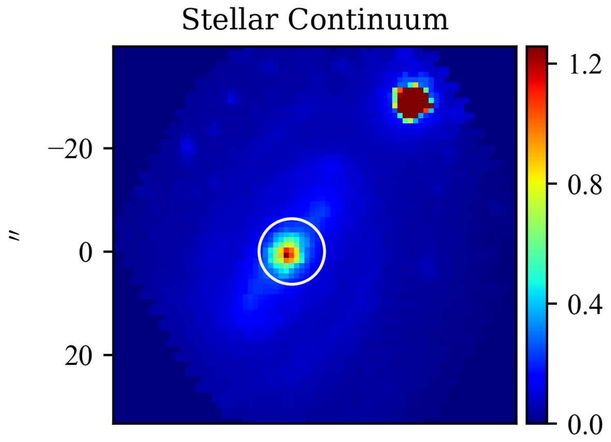

$\mathcal{M}_{\star,\mathrm{P}}$

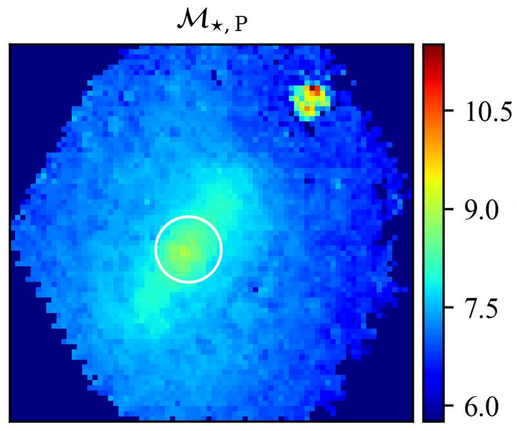

Log. of cumulative present stellar mass profiles

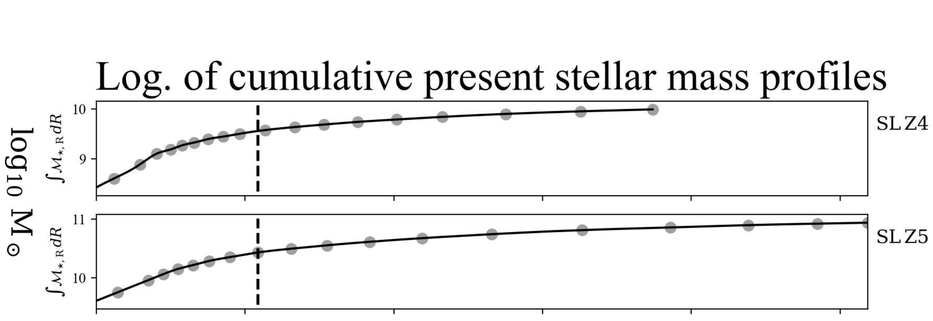

$Z_{\star,\mathcal{L}}$

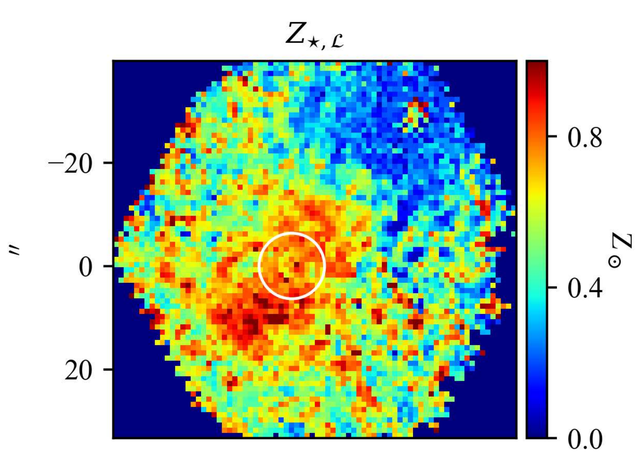

$Z_{\star,\mathcal{M}}$

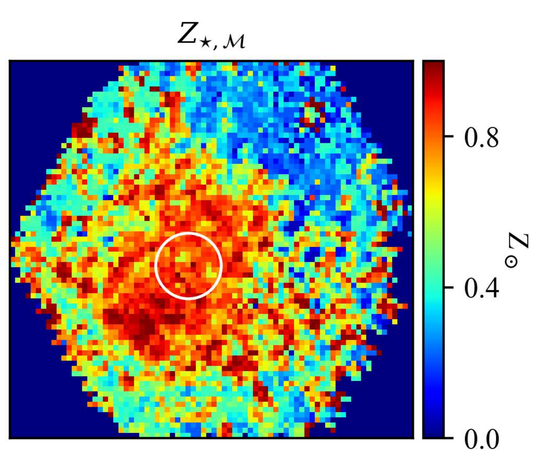

Stellar metallicity/Age & Hα flux/EW profiles

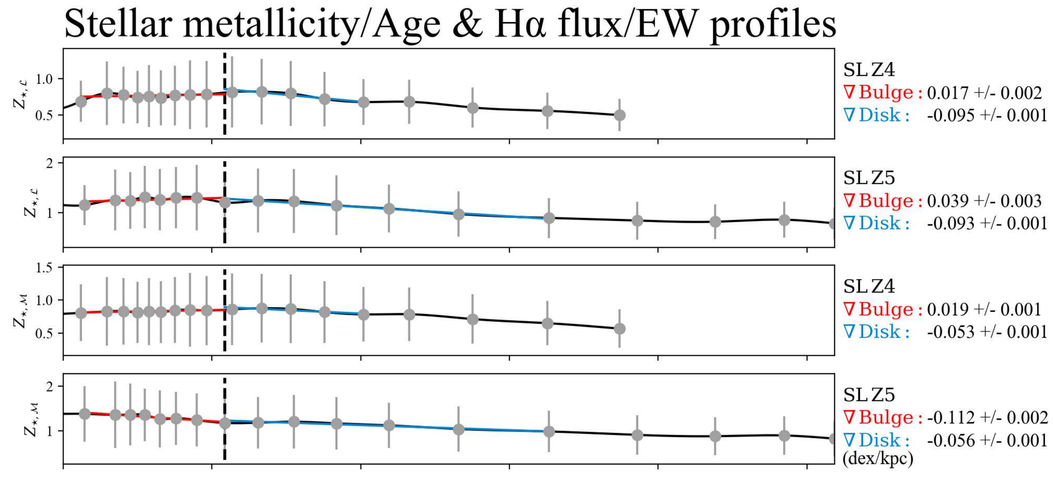

$t_{\star,\mathcal{L}}$

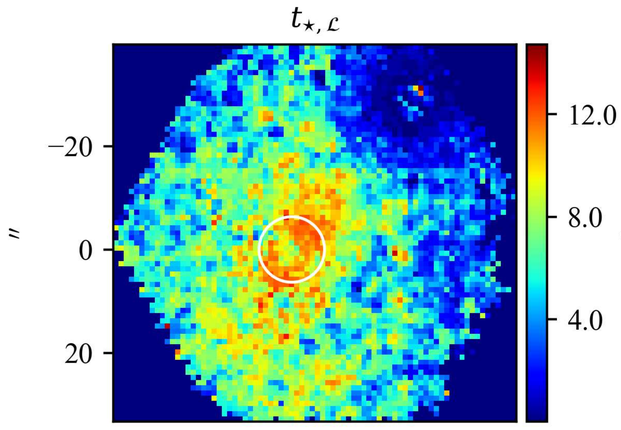

$t_{\star,\mathcal{M}}$

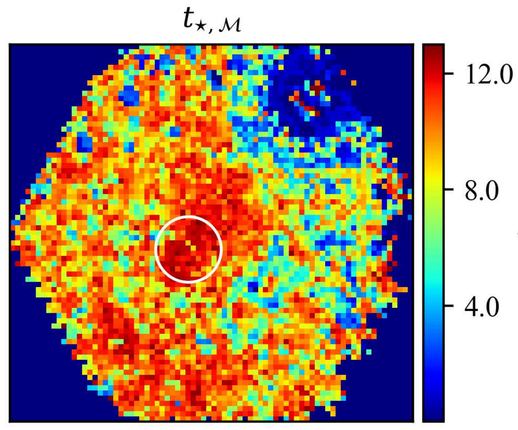

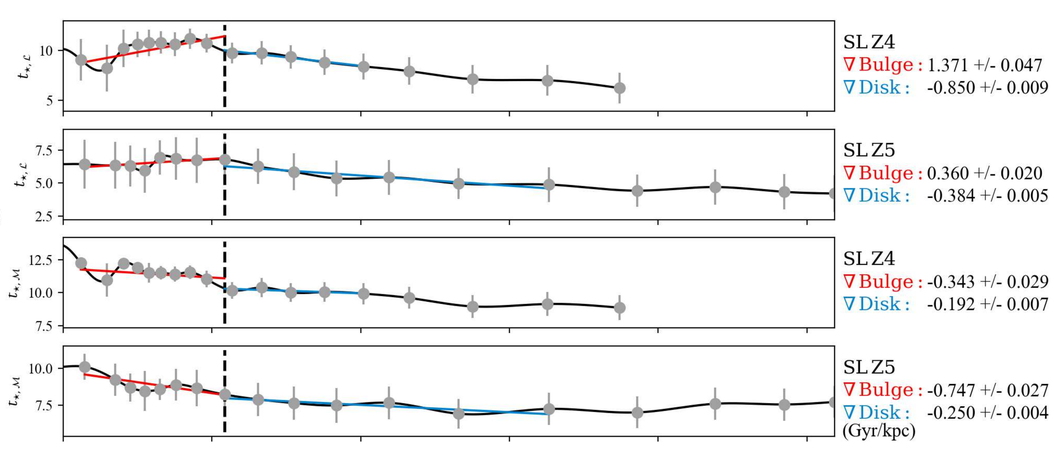

Hα flux

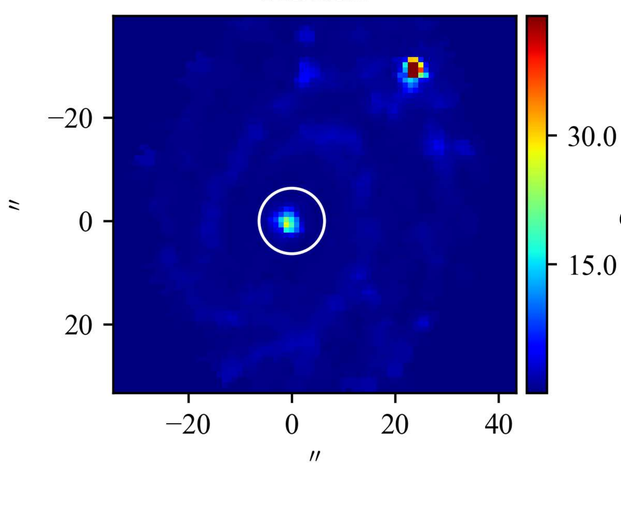

EW(Hα)

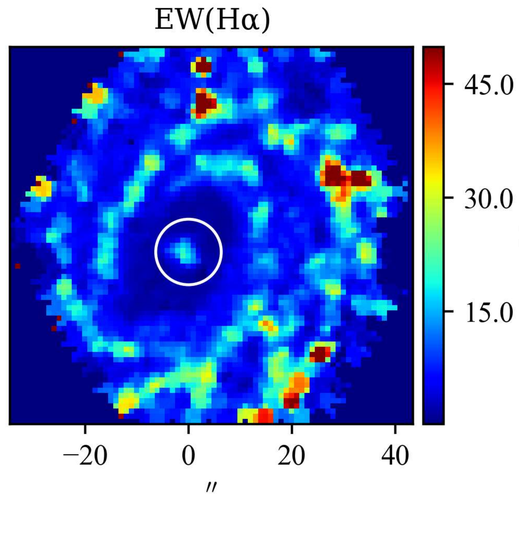

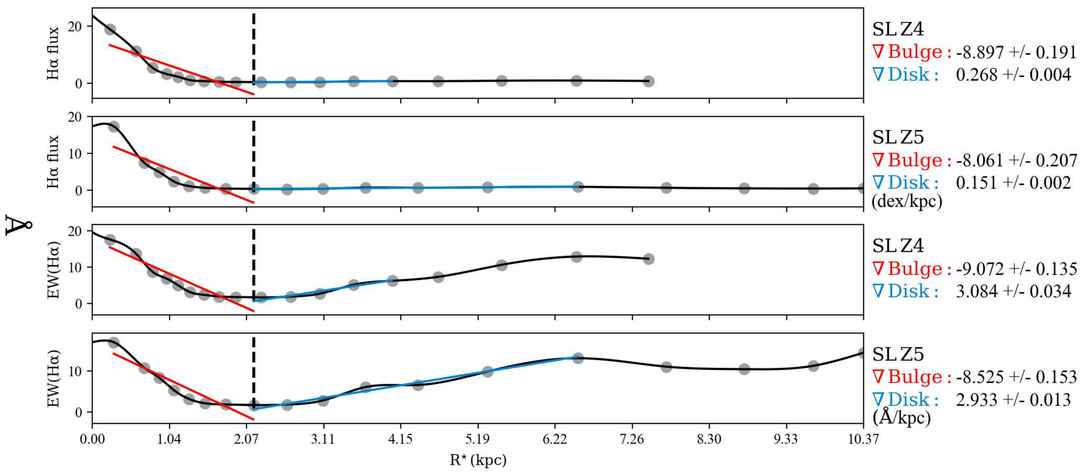

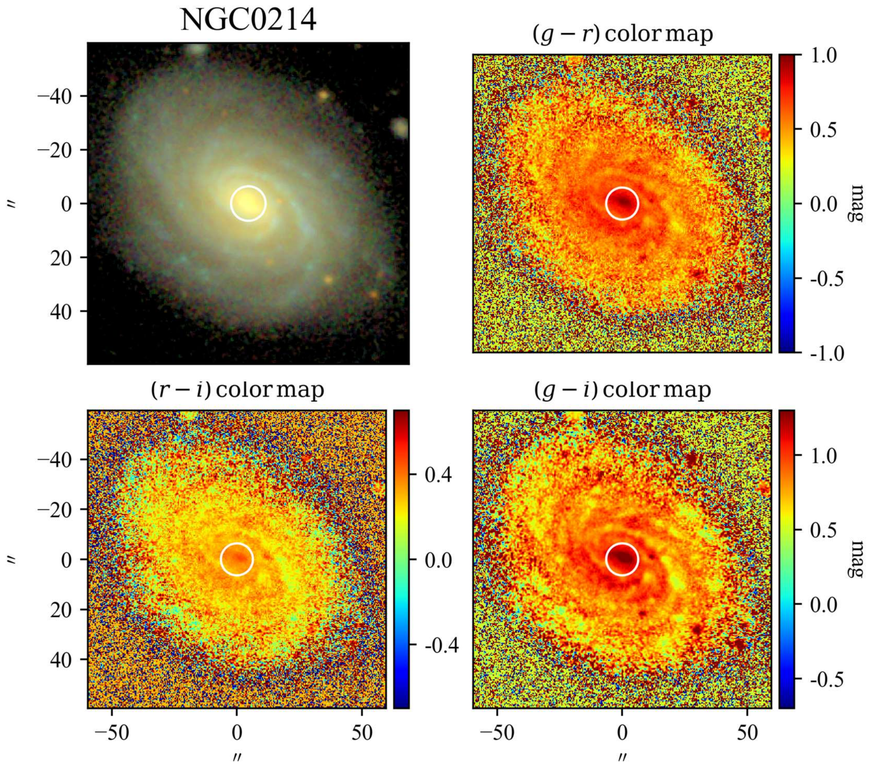

SBP decomposition of SDSS r band

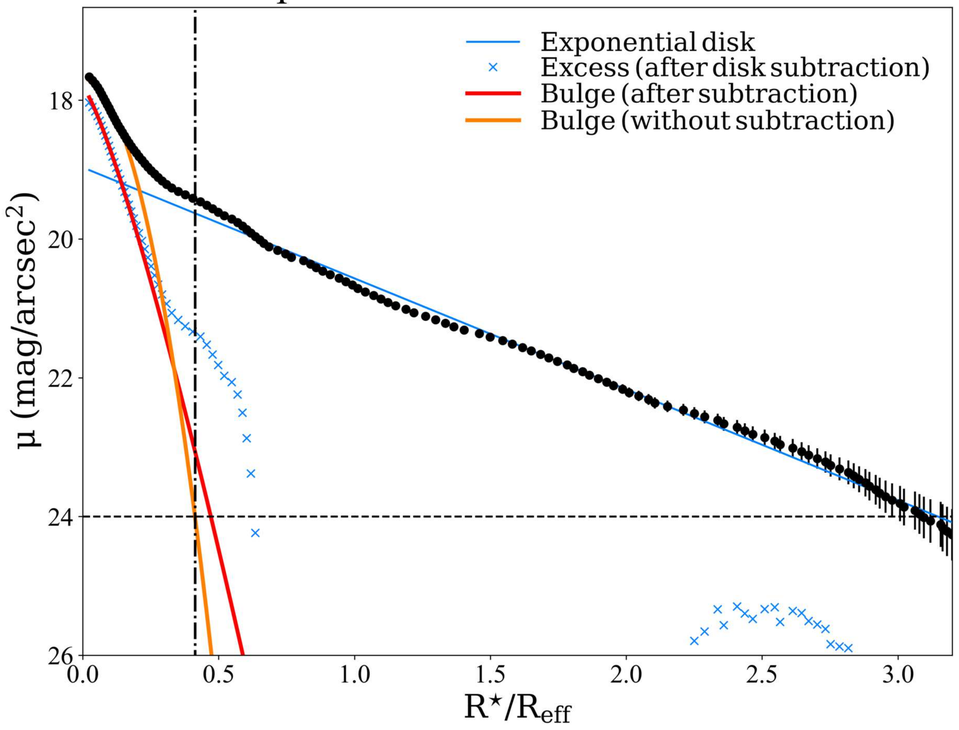

SDSS color profiles

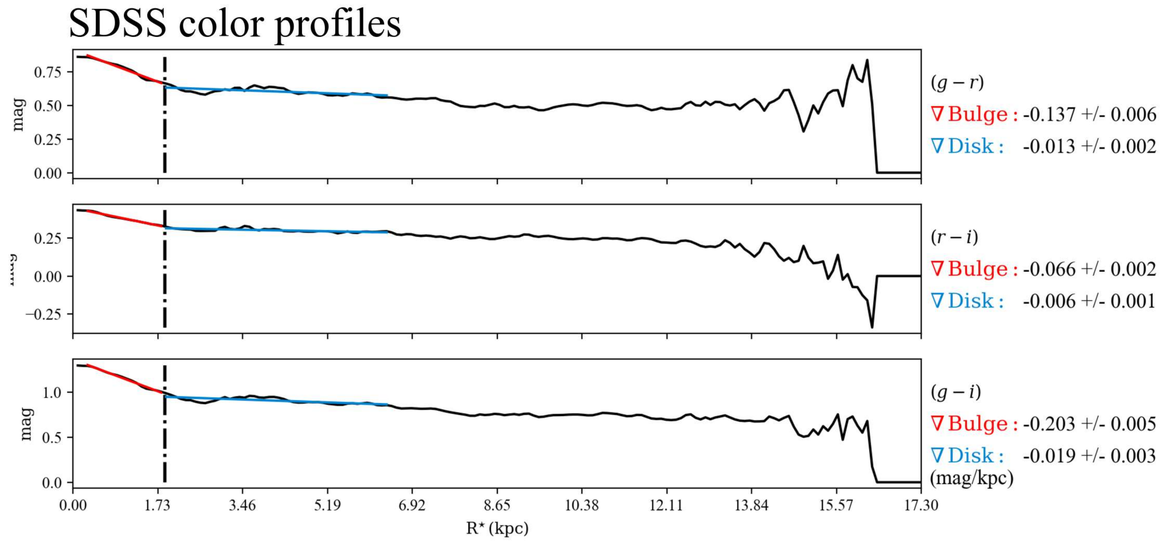

$\mathcal{RV}$ SBPs

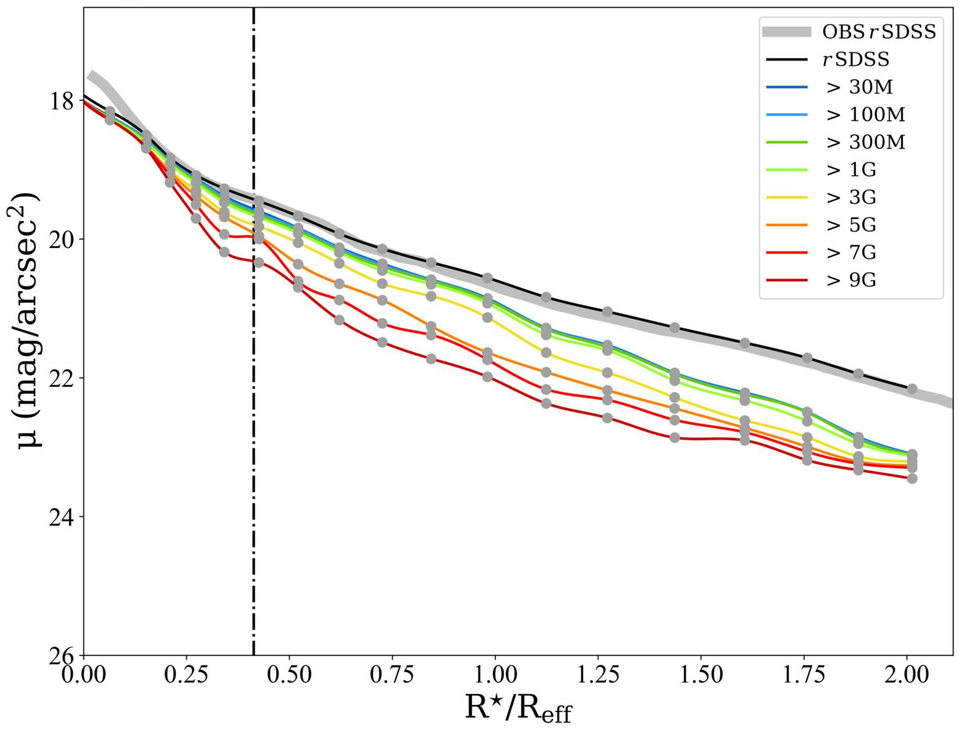

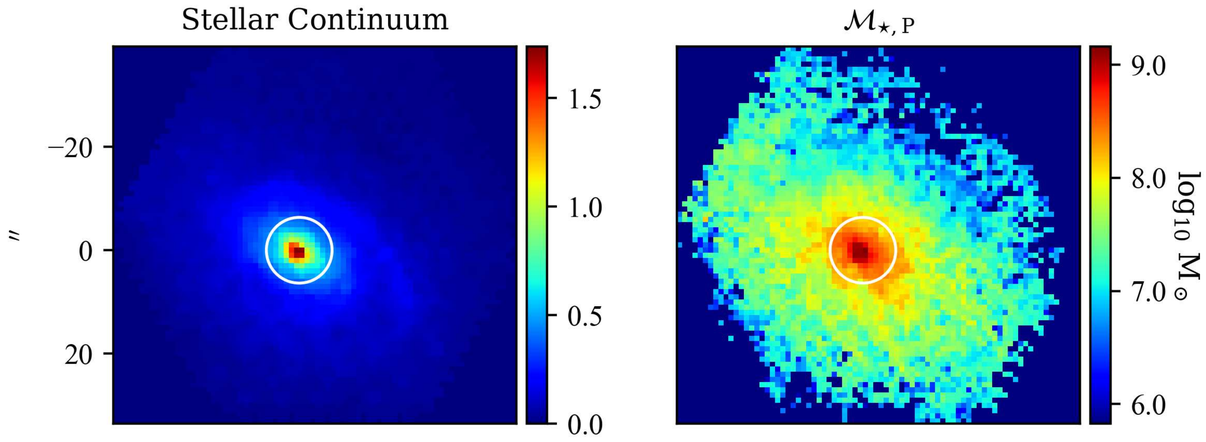

Log. of cumulative present stellar mass profiles

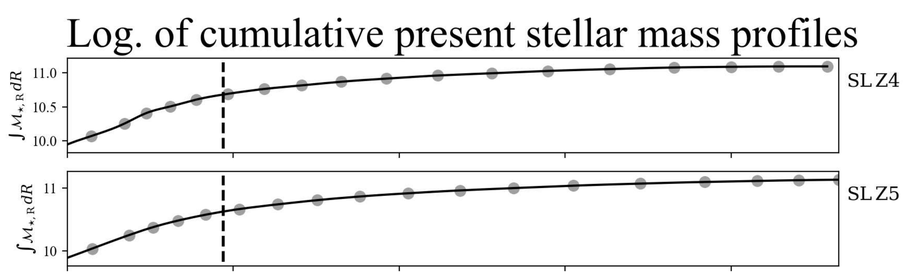

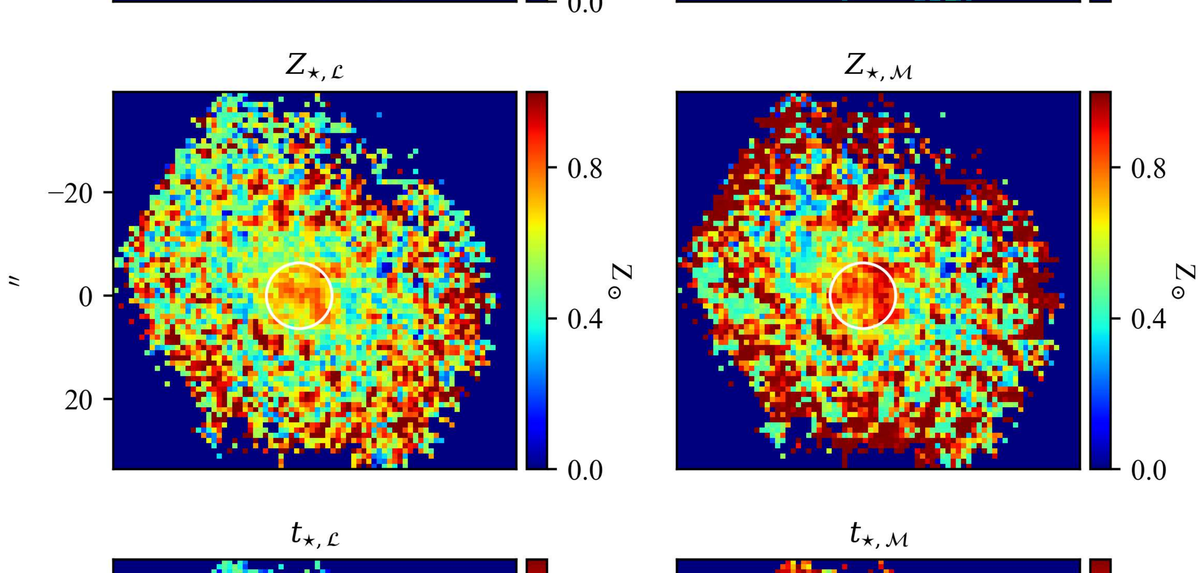

Stellar metallicity/Age & Hα flux/EW profiles

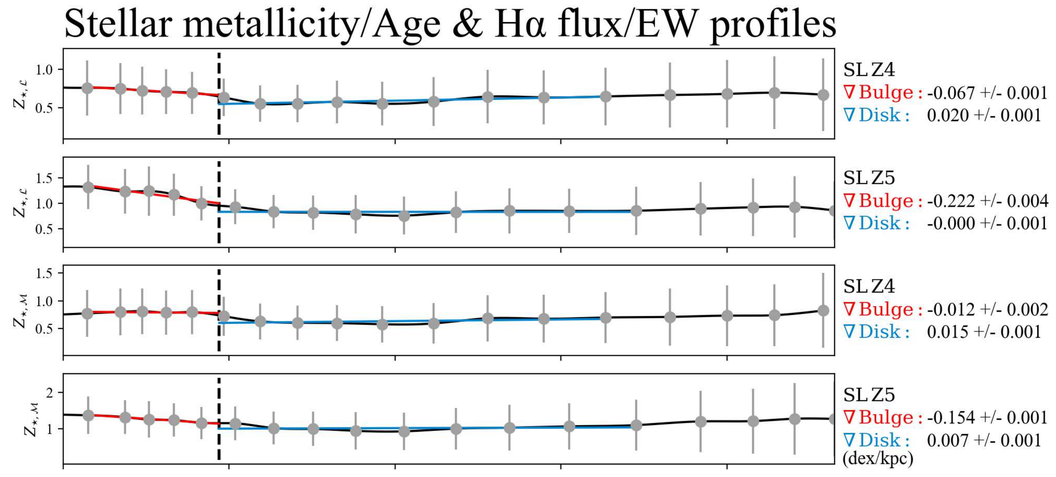

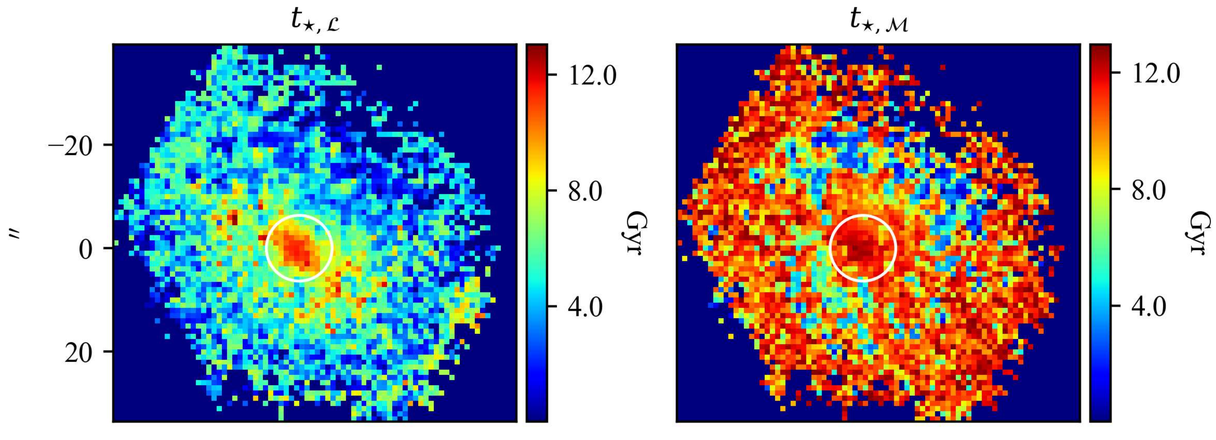

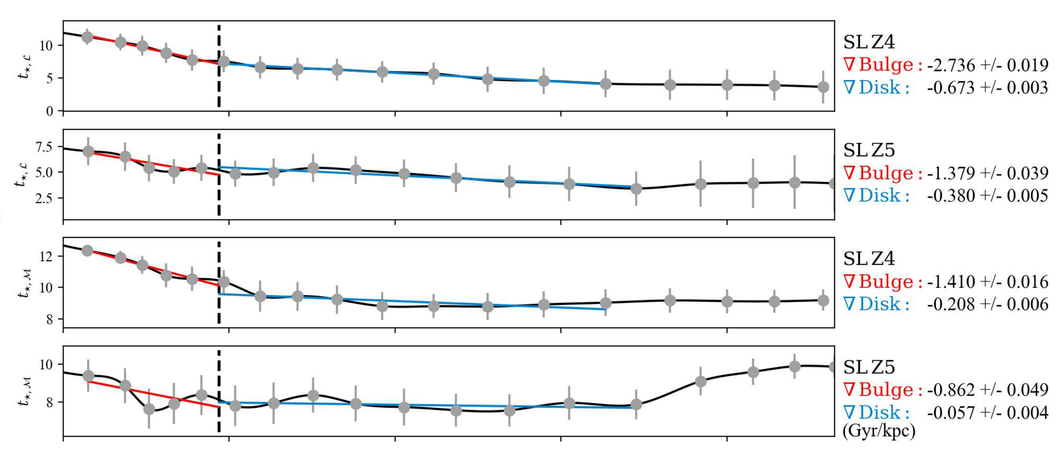

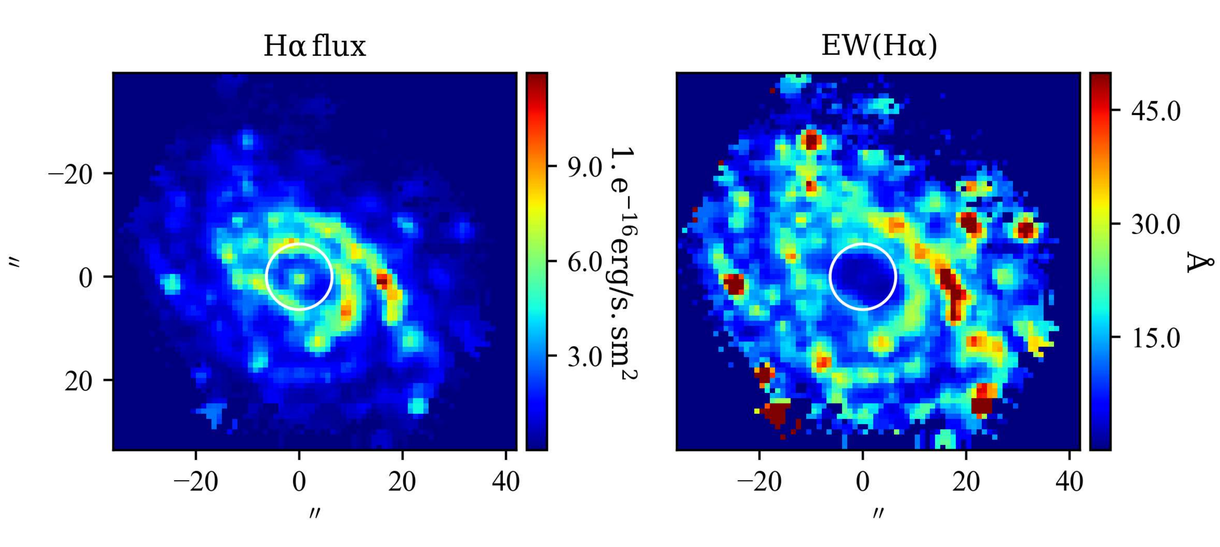

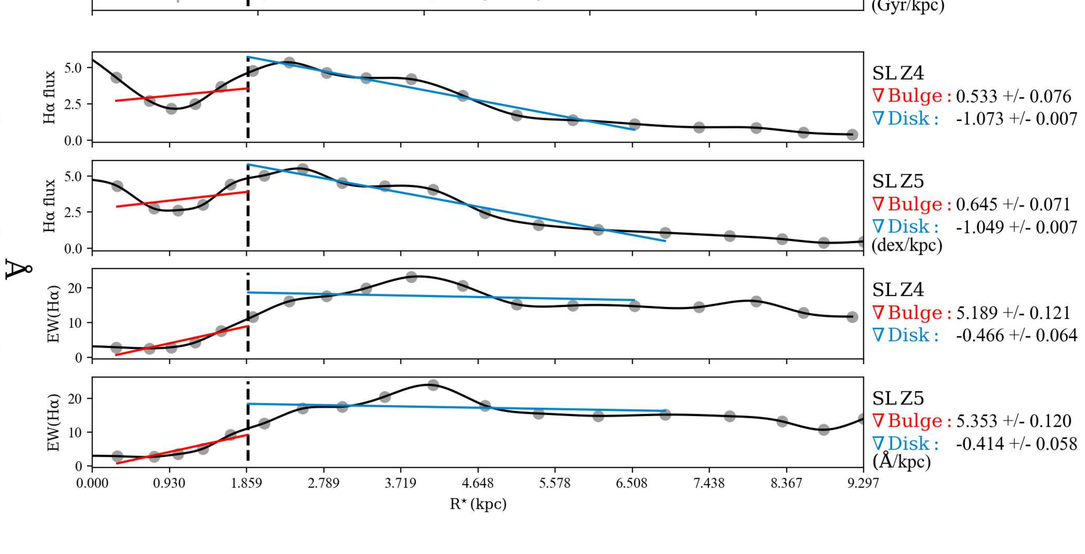

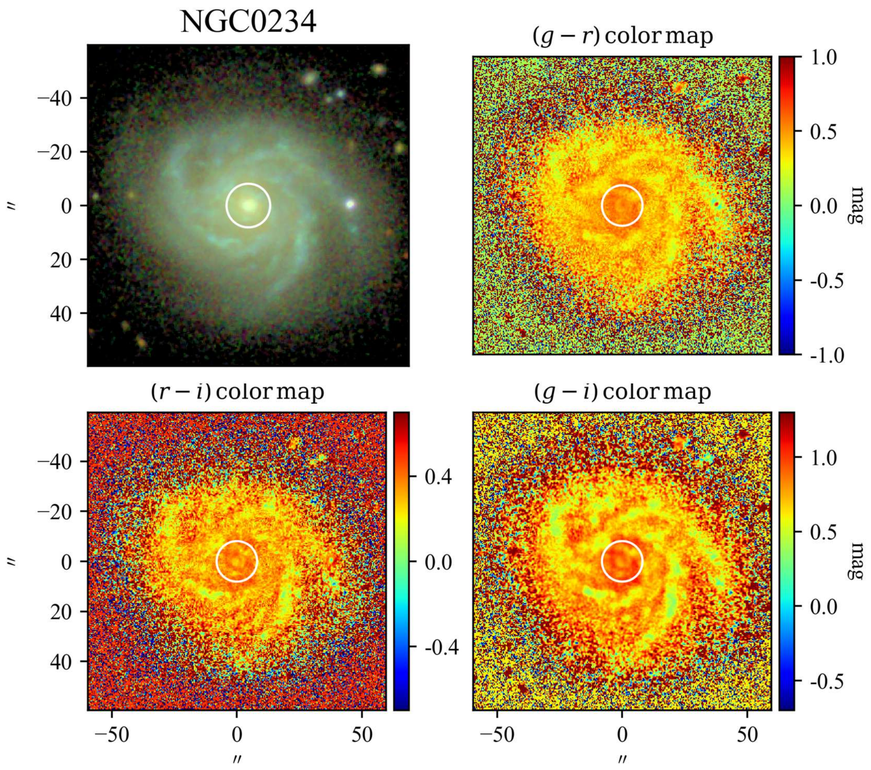

SBP decomposition of SDSS r band

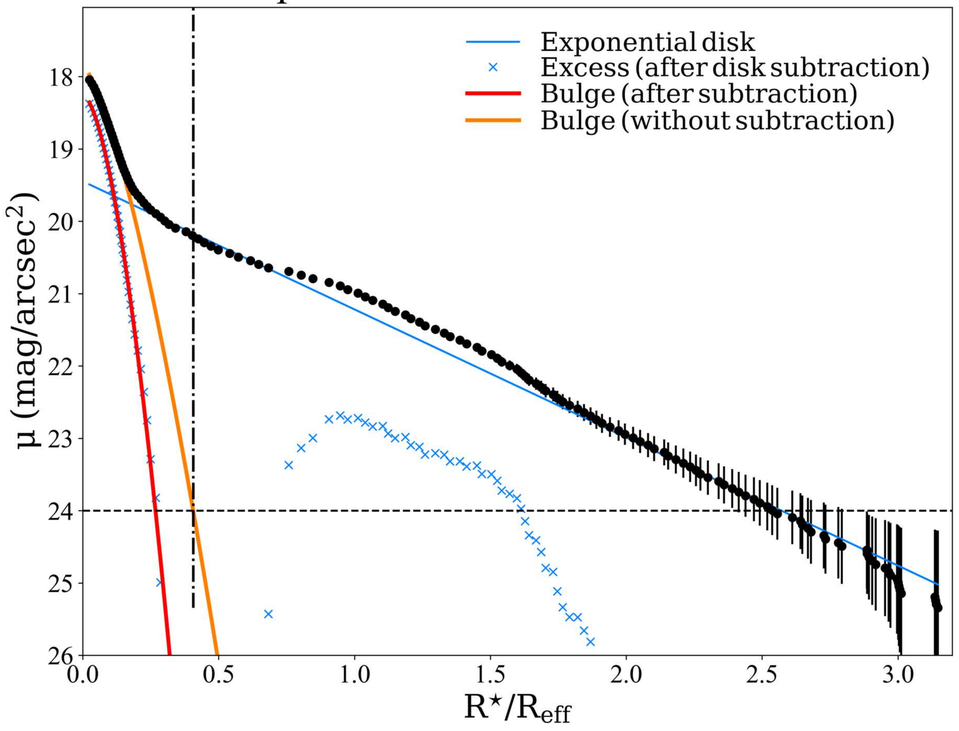

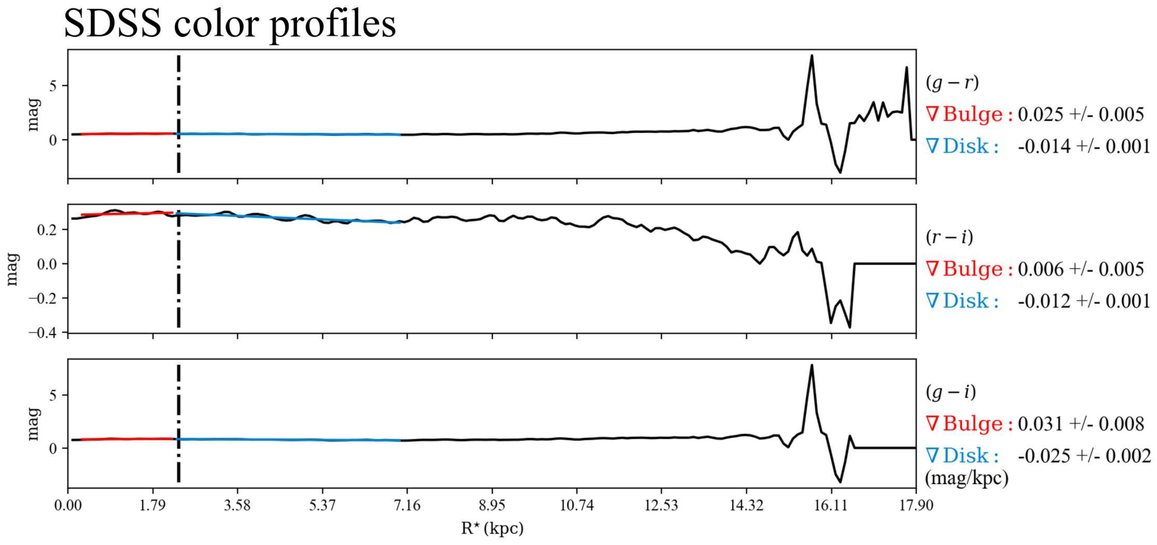

$\mathcal{RY}$ SBPs

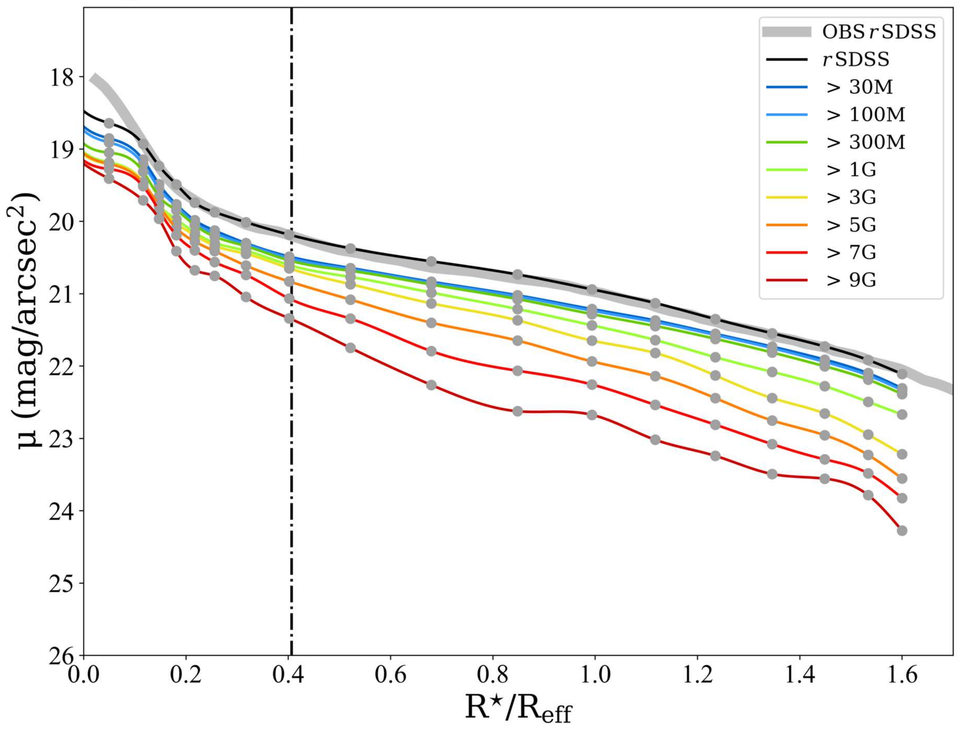

Stellar Continuum $\mathcal{M}_{\star,\mathrm{P}}$

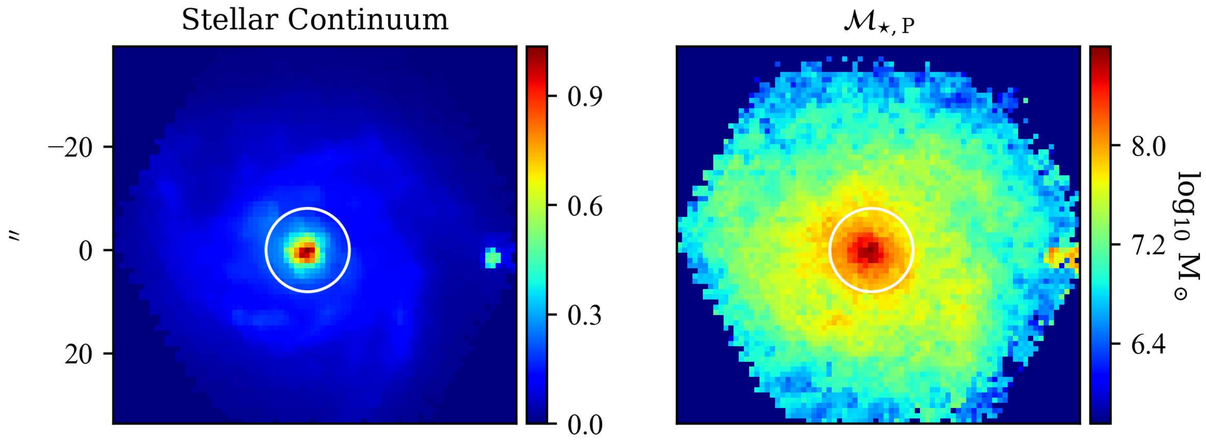

Log. of cumulative present stellar mass profiles

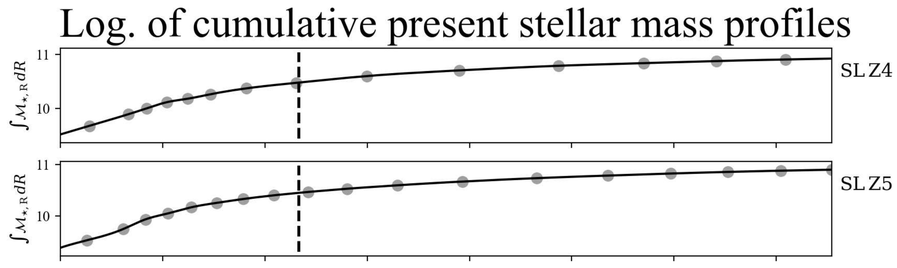

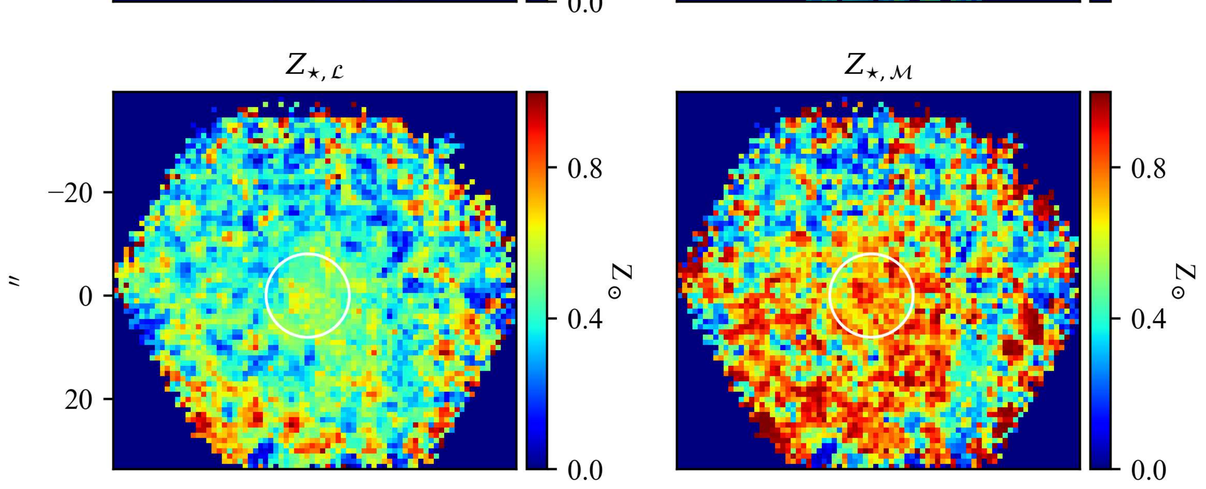

Stellar metallicity/Age & Hα flux/EW profiles

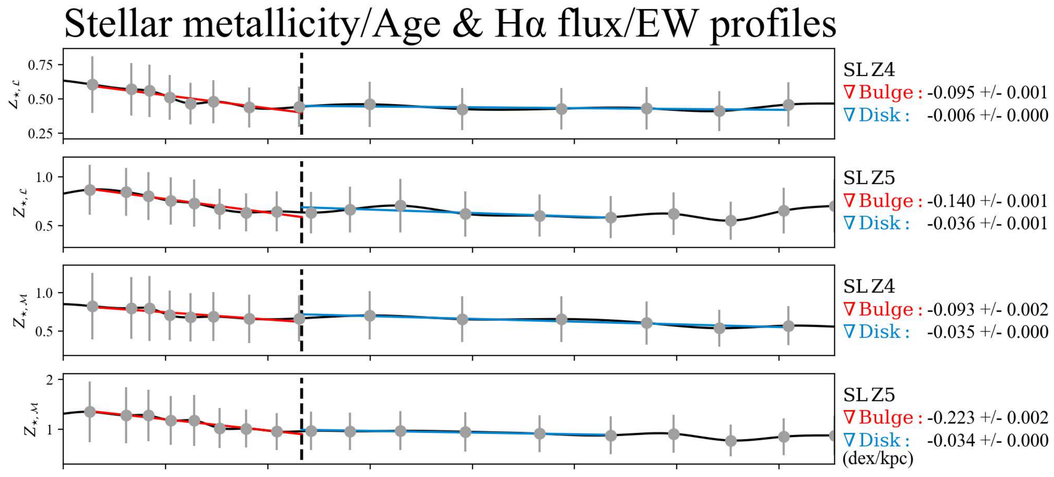

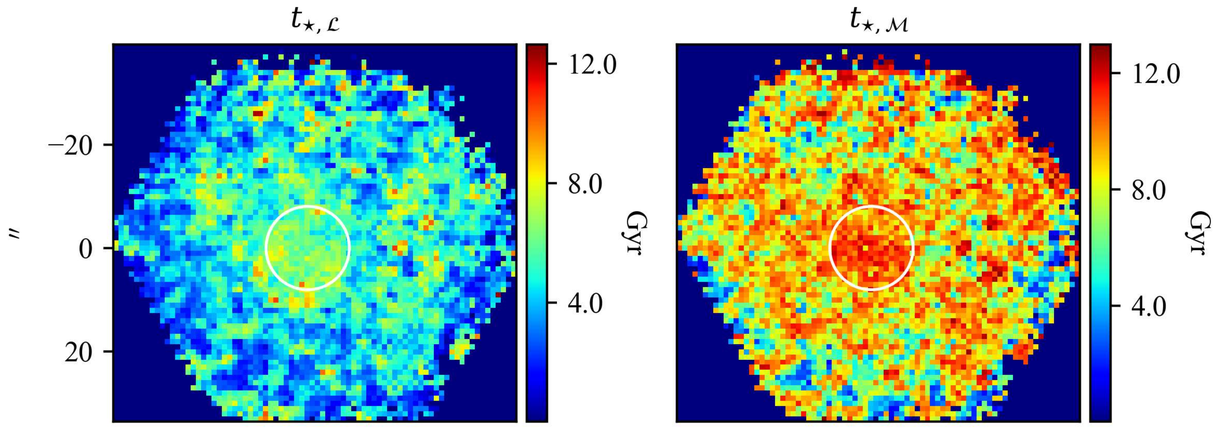

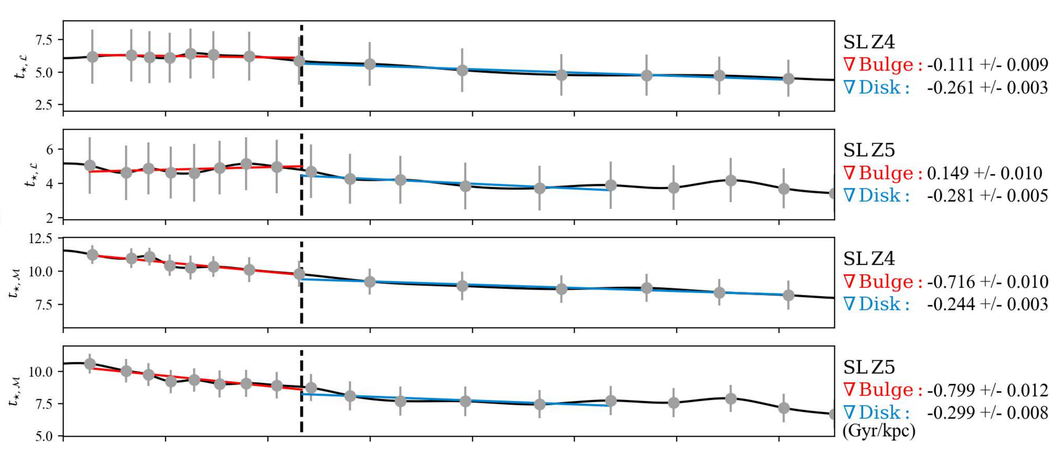

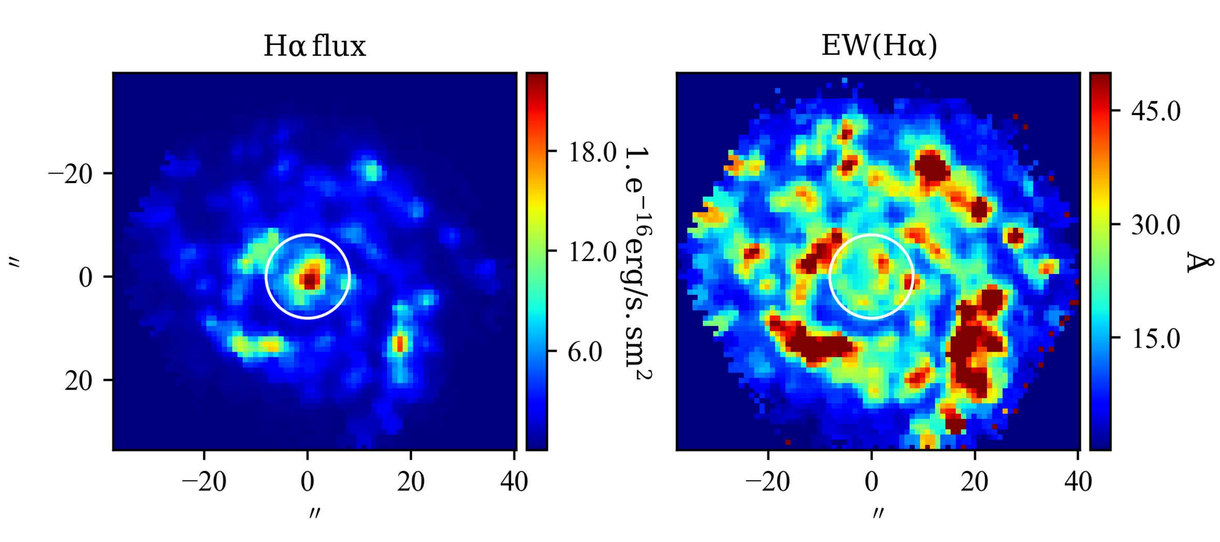

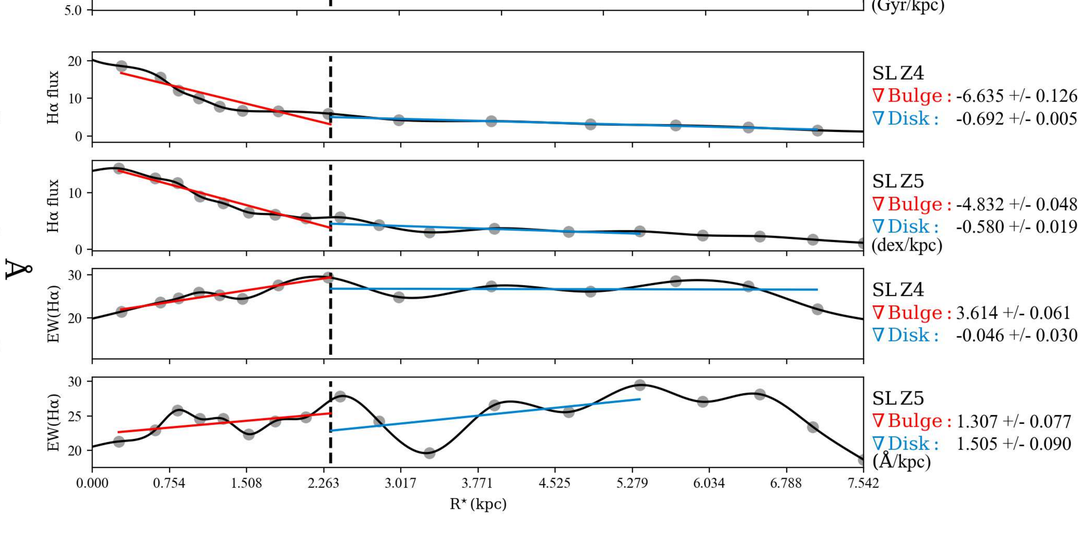

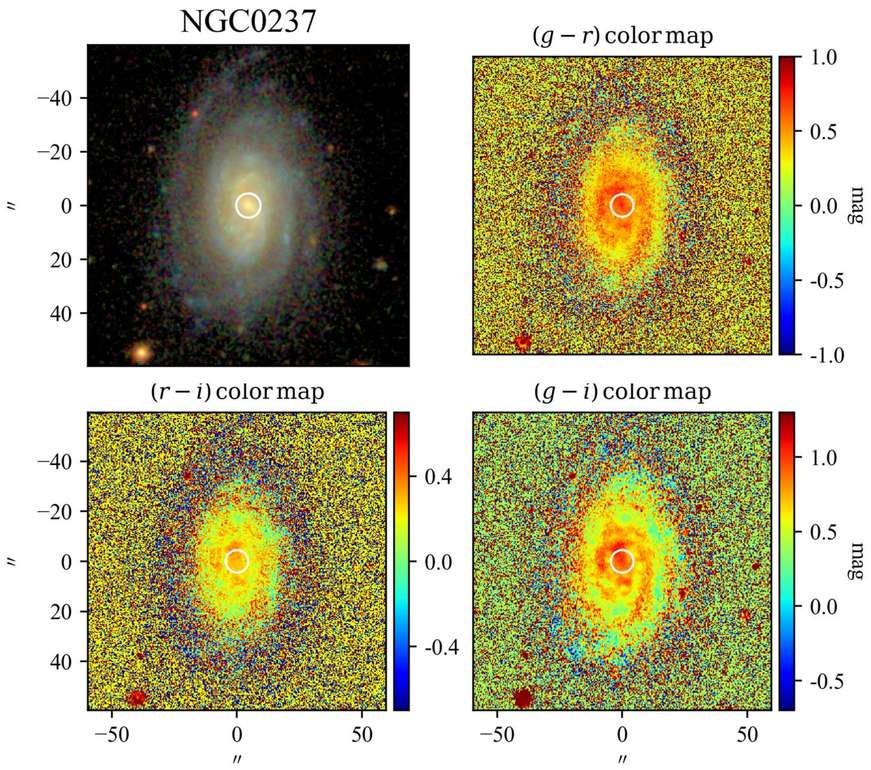

SBP decomposition of SDSS r band

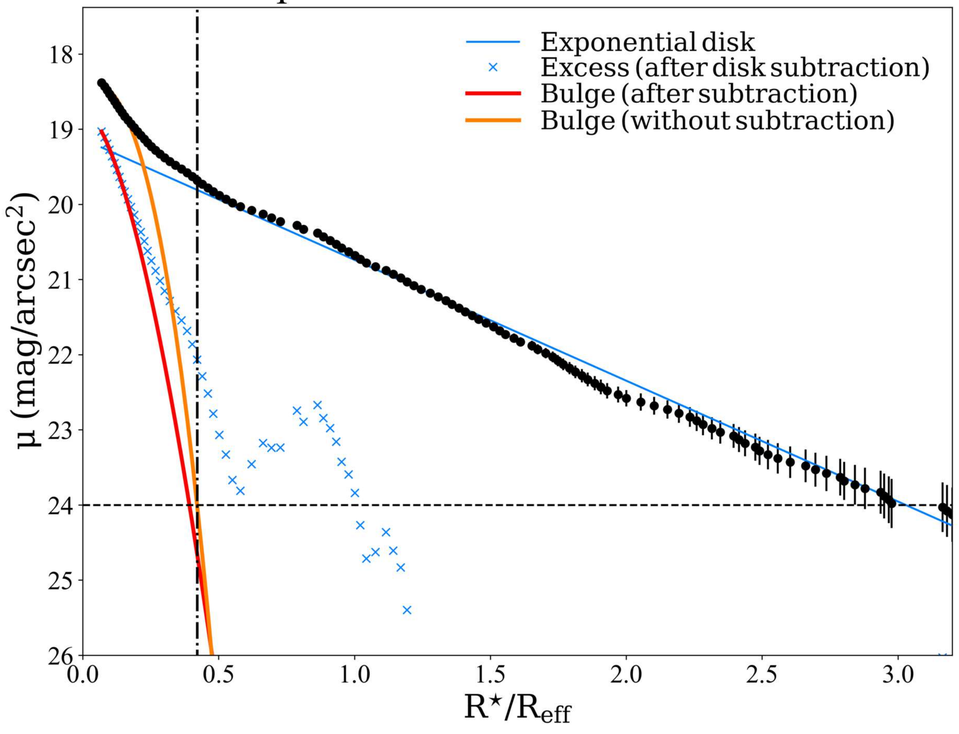

SDSS color profiles

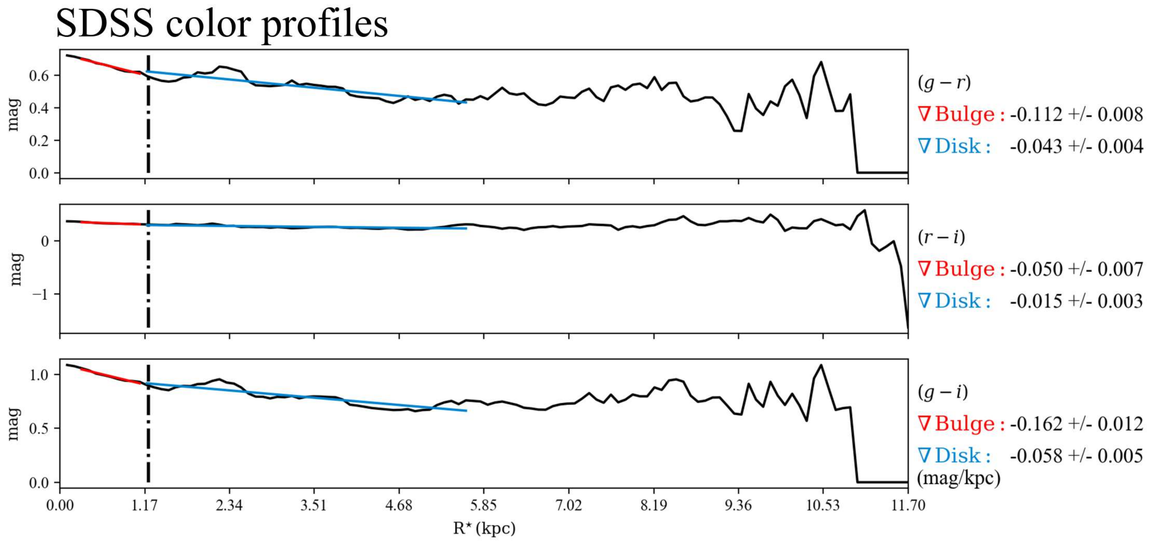

$\mathcal{RY}$ SBPs

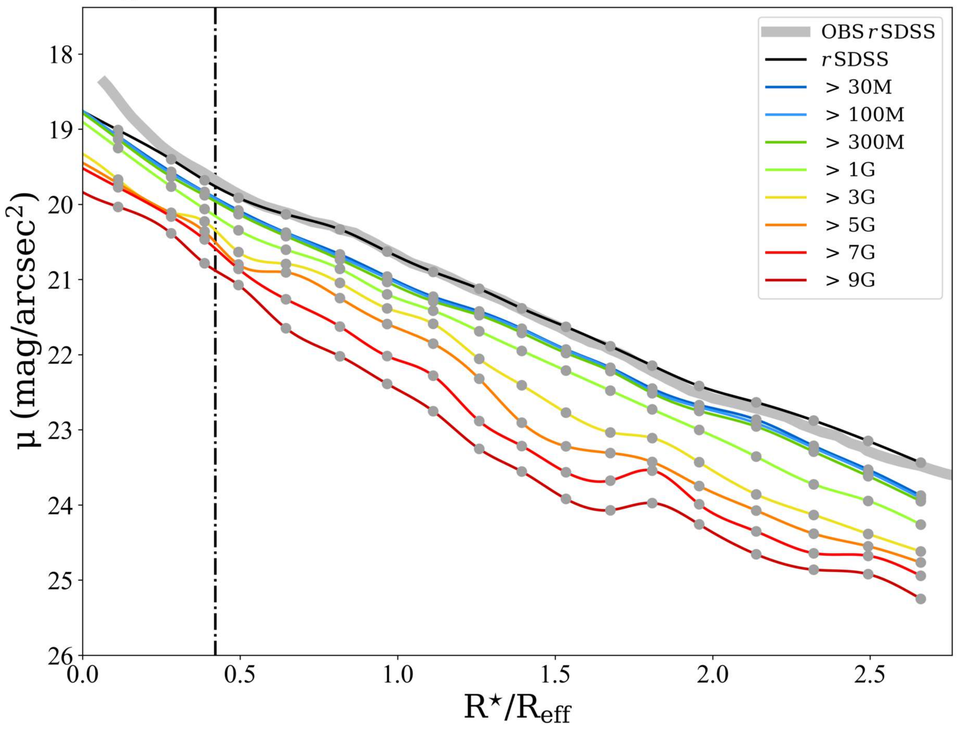

Stellar Continuum

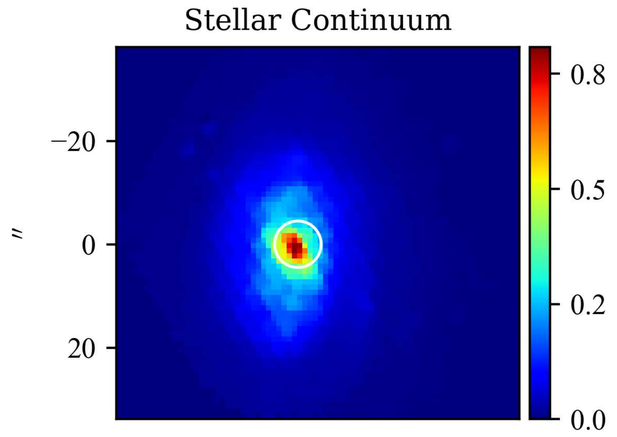

$\mathcal{M}_{\star,\mathrm{P}}$

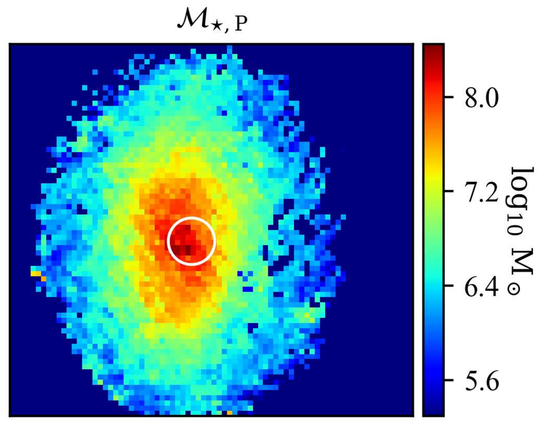

Log. of cumulative present stellar mass profiles

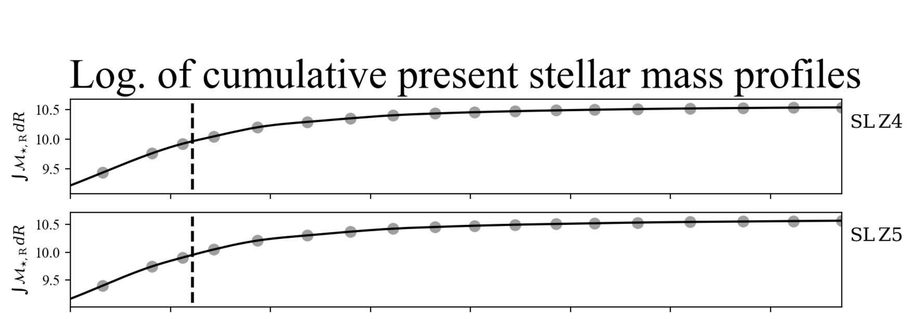

$Z_{\star,\mathcal{L}}$

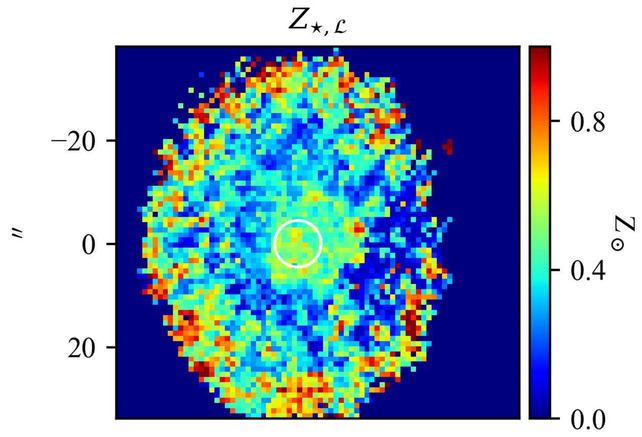

$Z_{\star,\mathcal{M}}$

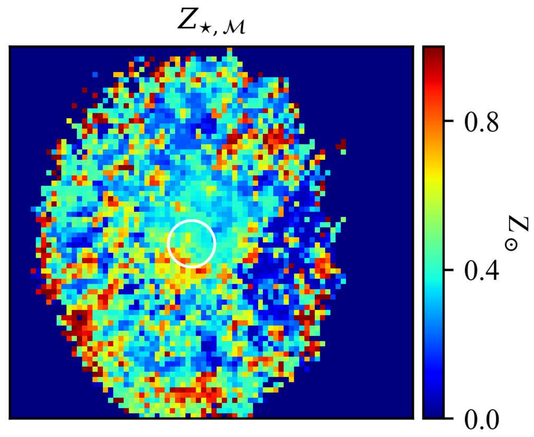

Stellar metallicity/Age & Hα flux/EW profiles

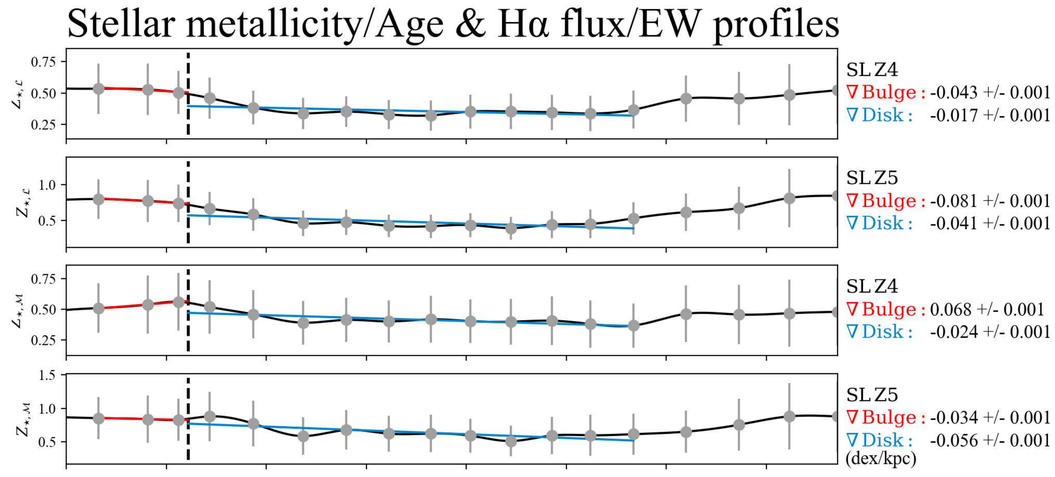

$t_{\star,\mathcal{L}}$

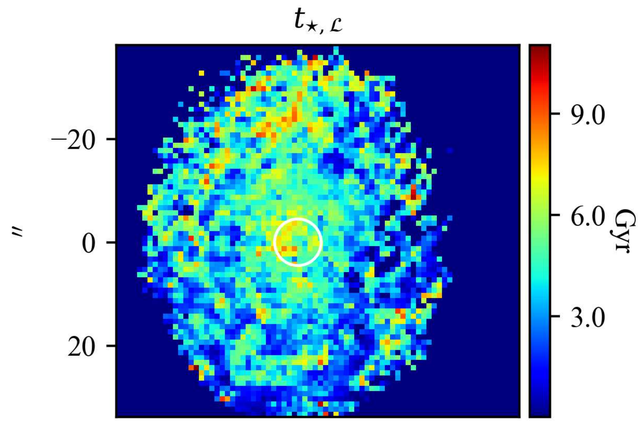

$t_{\star,\mathcal{M}}$

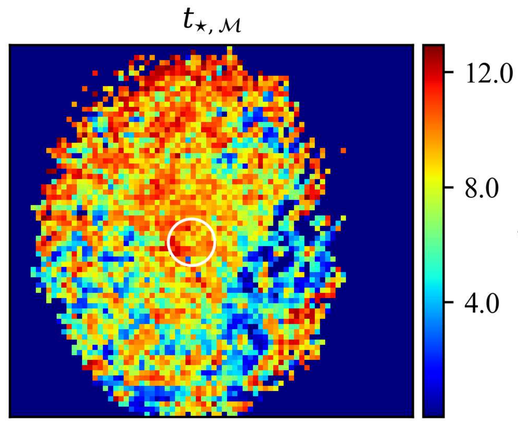

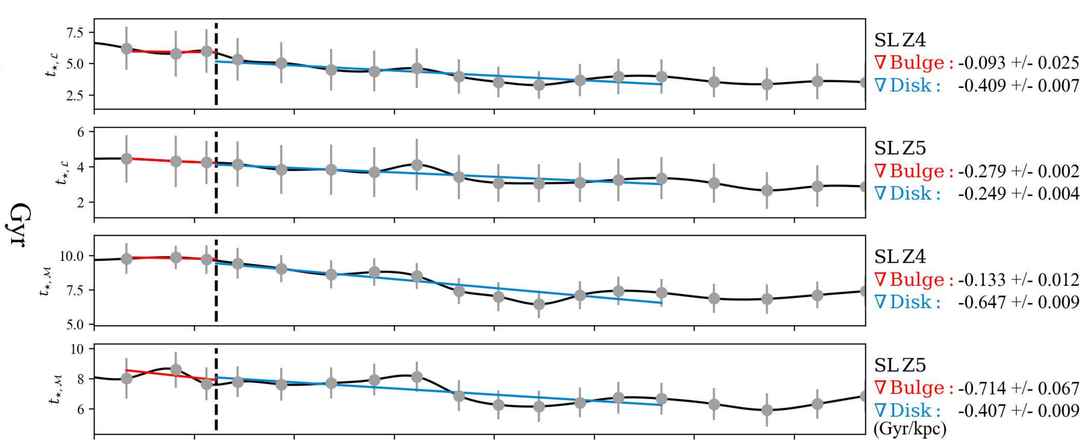

Hα flux

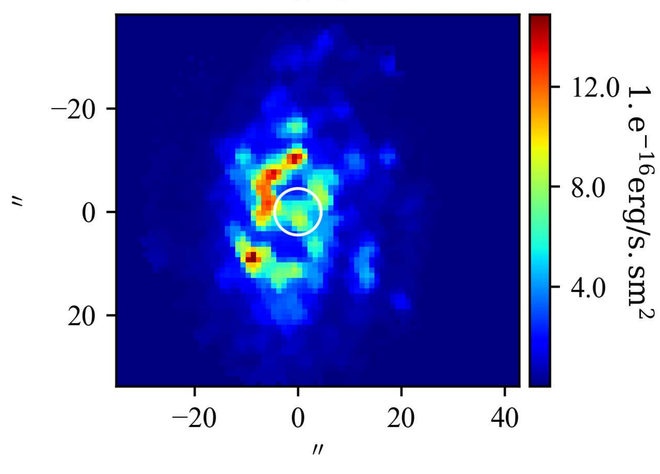

EW(Hα)

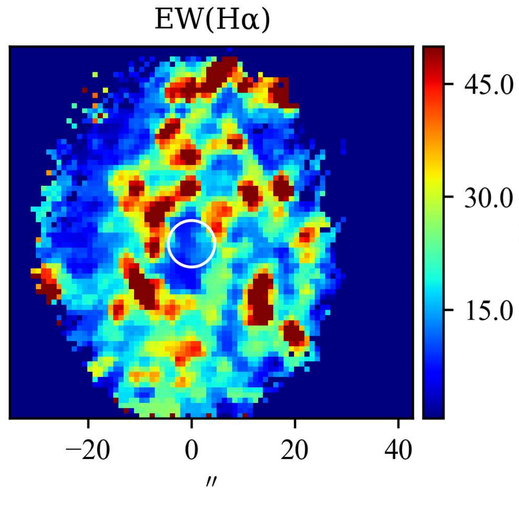

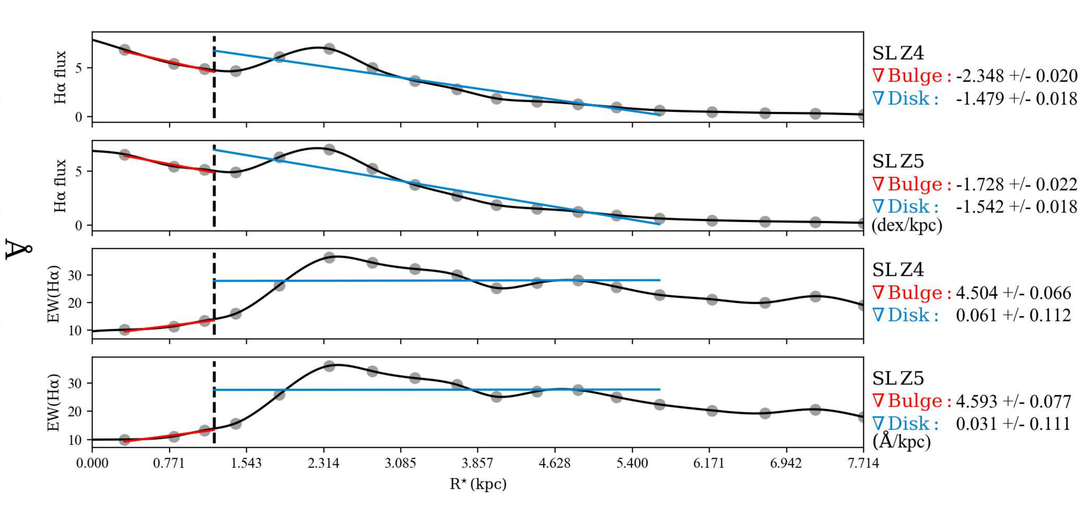

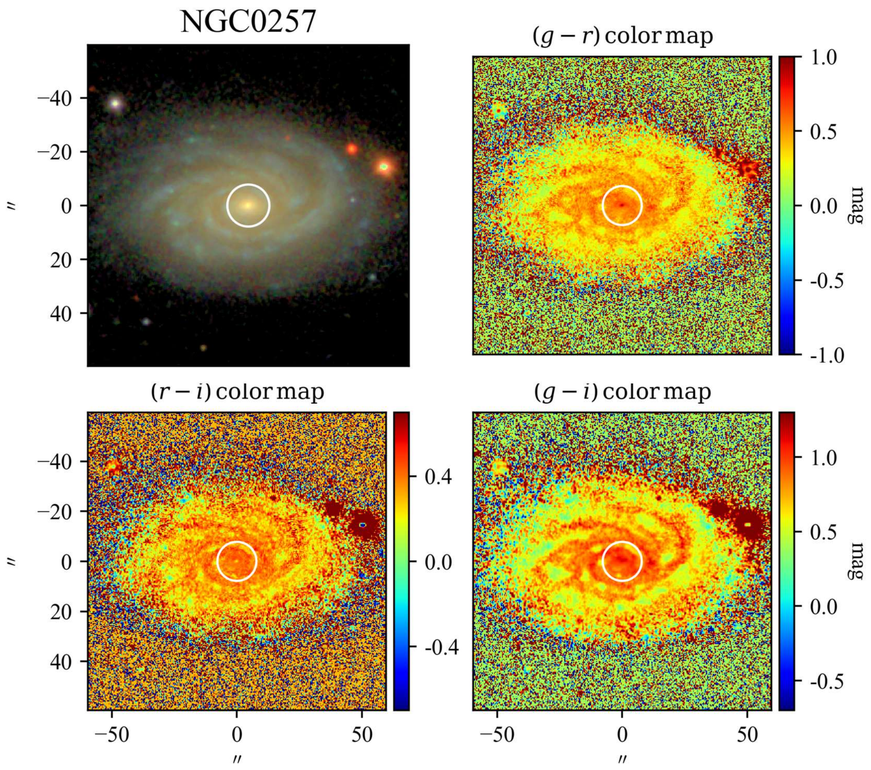

SBP decomposition of SDSS r band

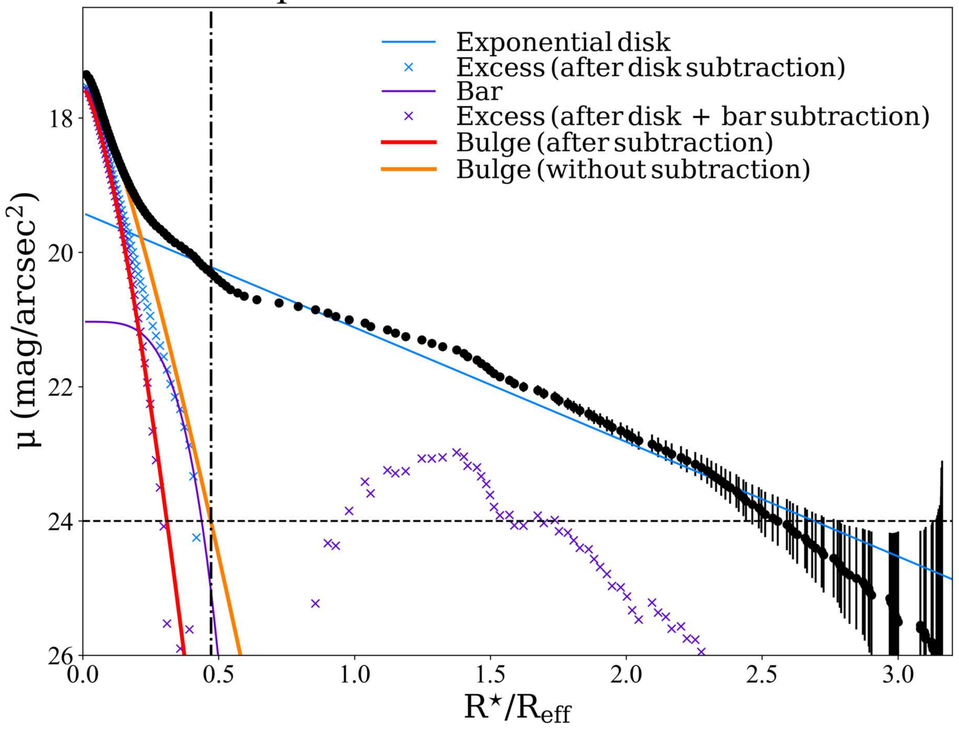

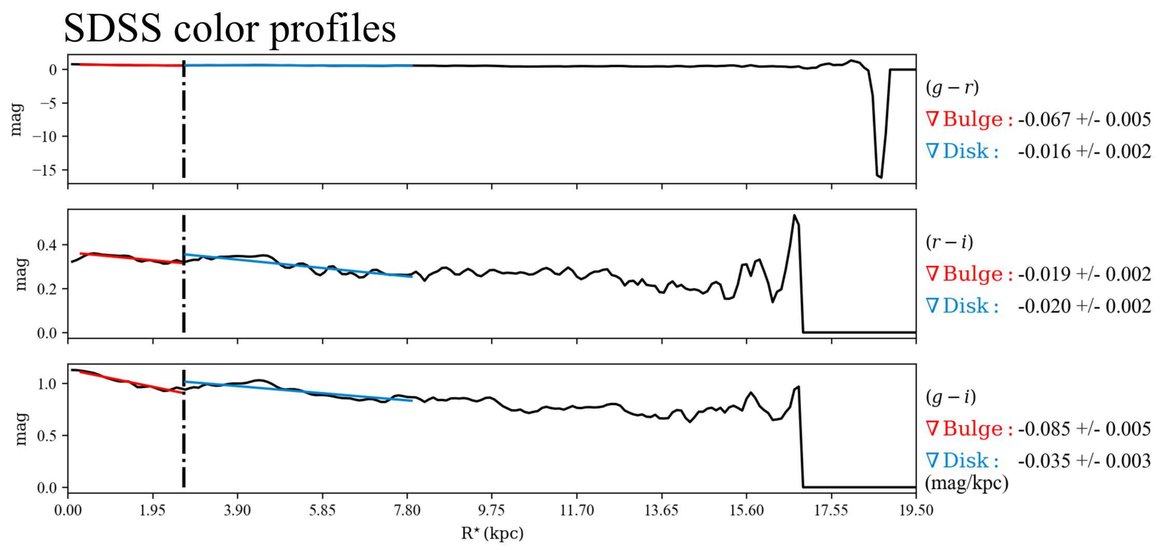

$\mathcal{RV}$ SBPs

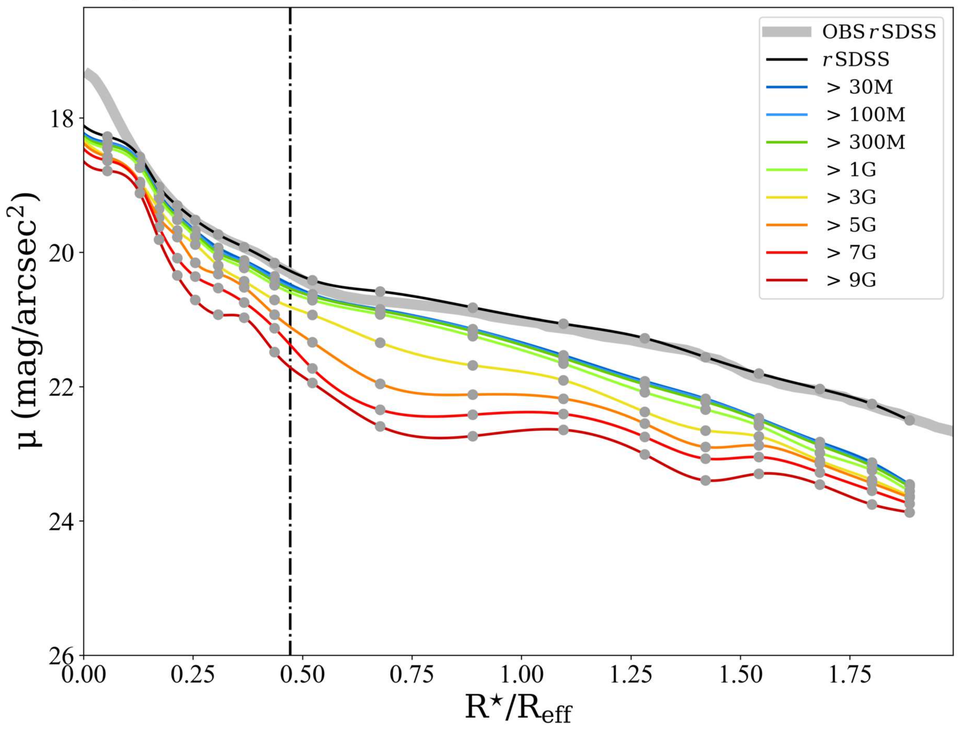

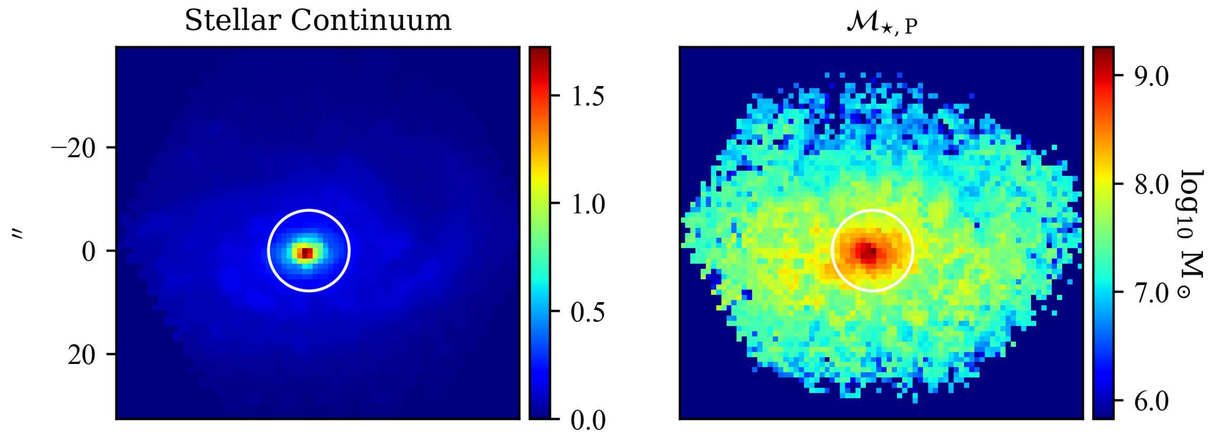

Log. of cumulative present stellar mass profiles

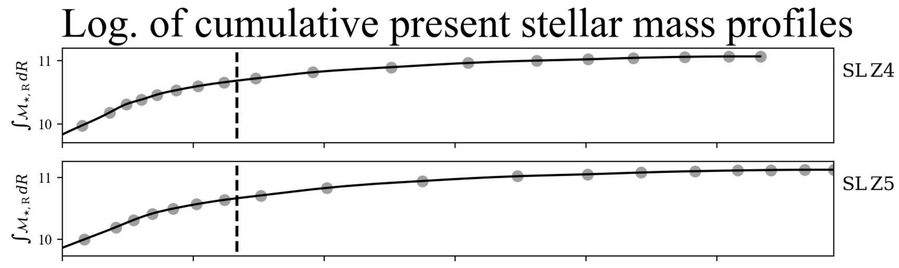

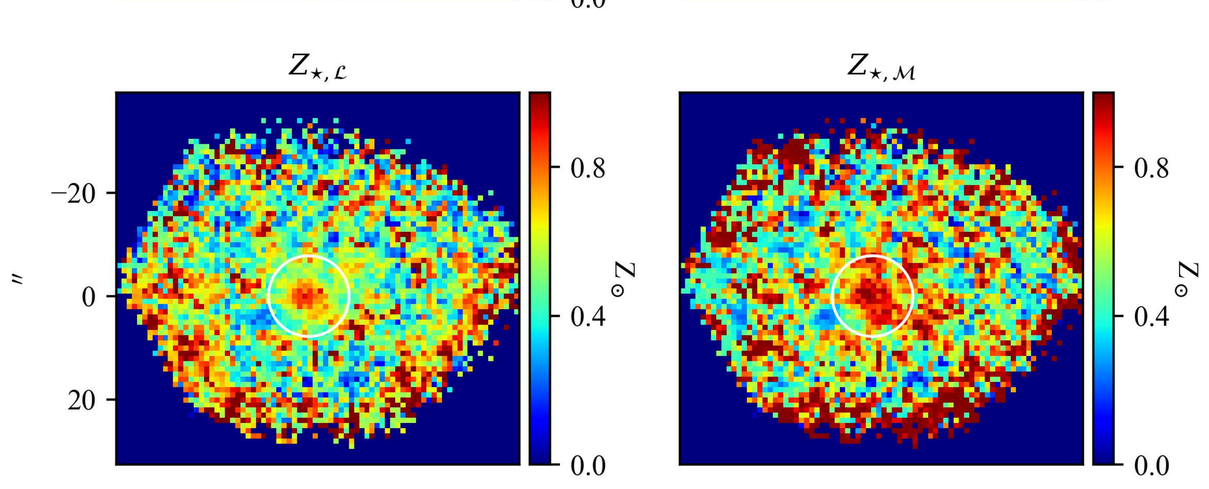

Stellar metallicity/Age & Hα flux/EW profiles

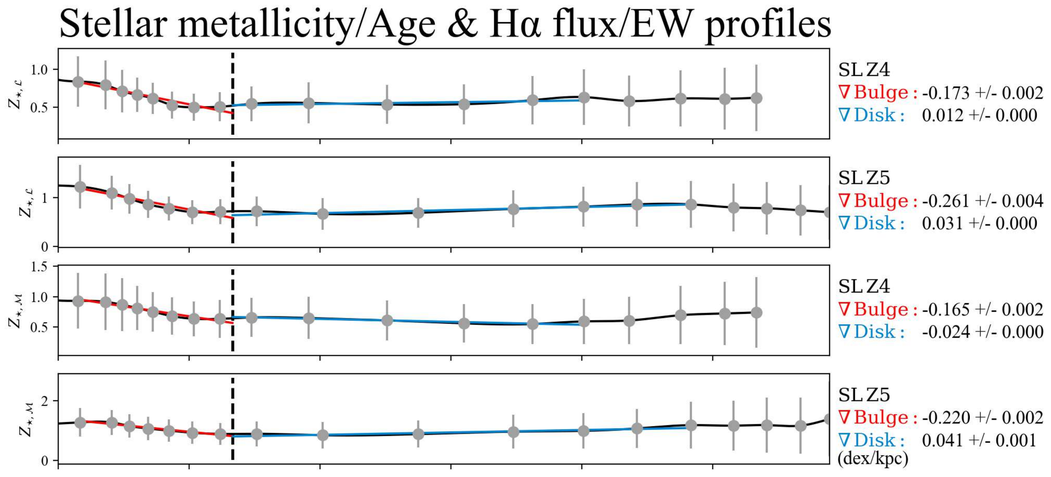

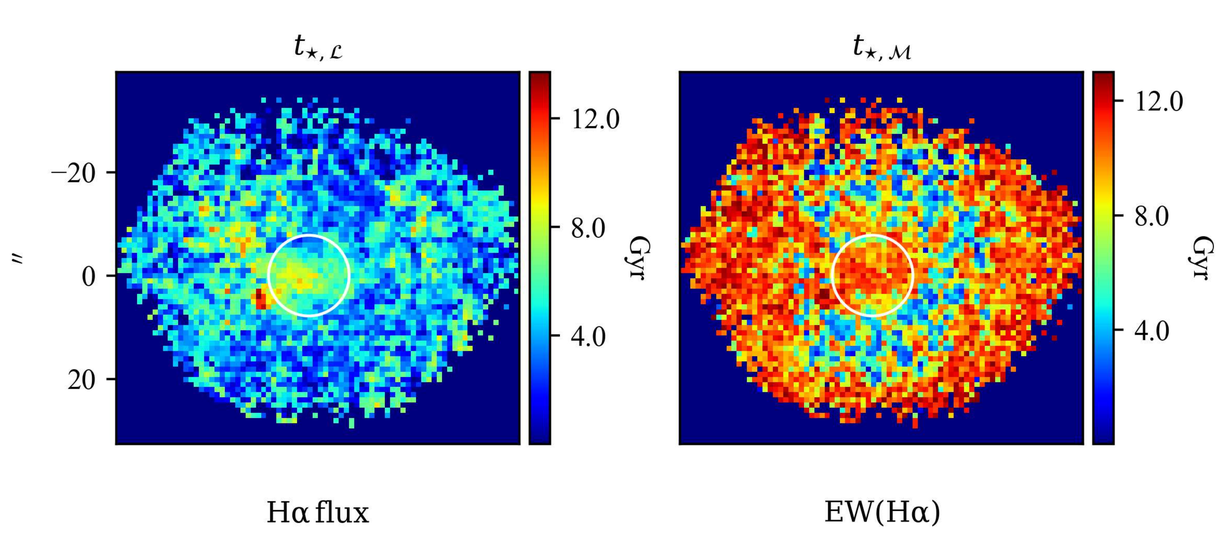

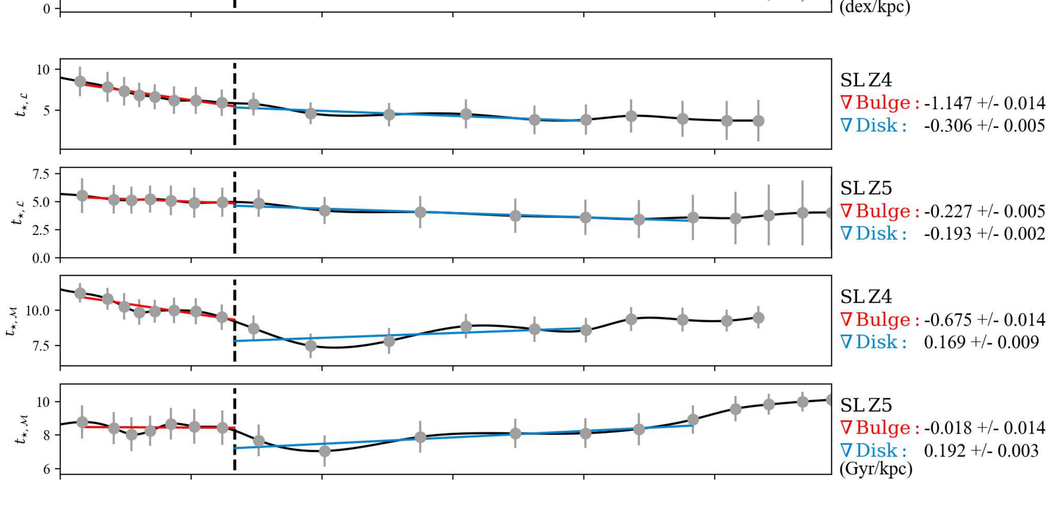

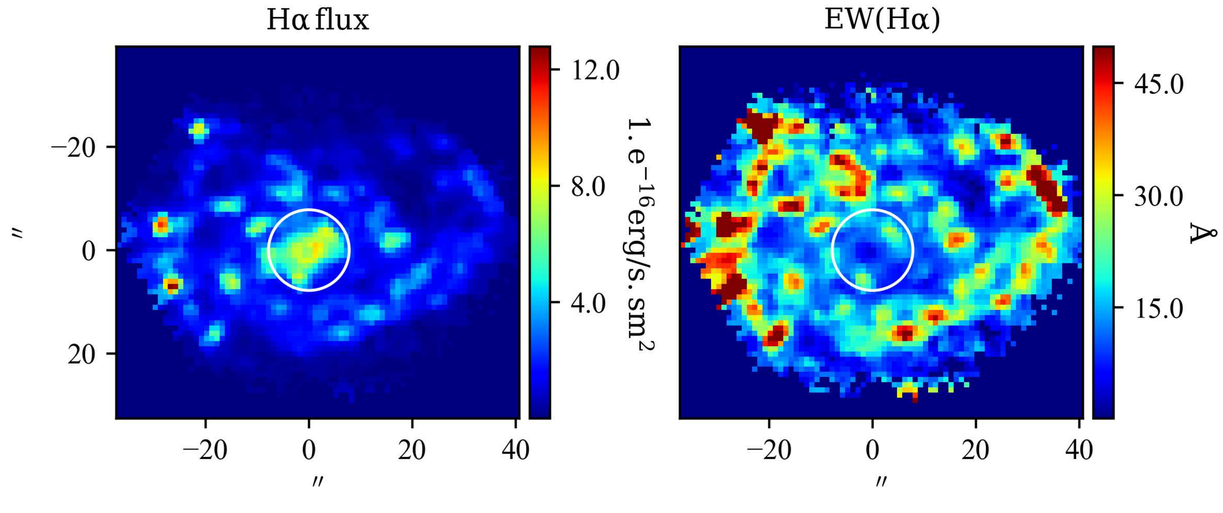

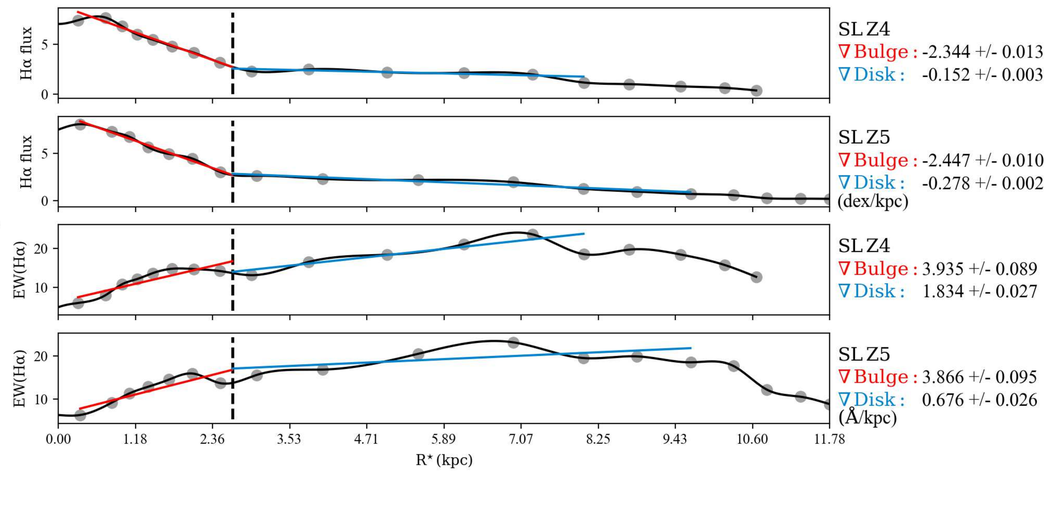

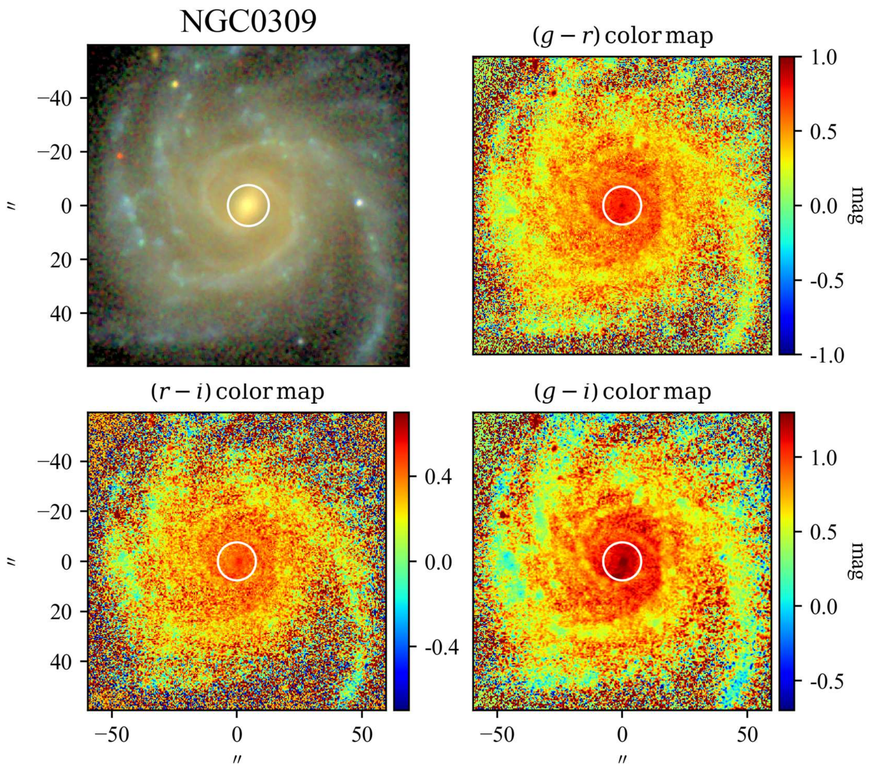

SBP decomposition of SDSS r band

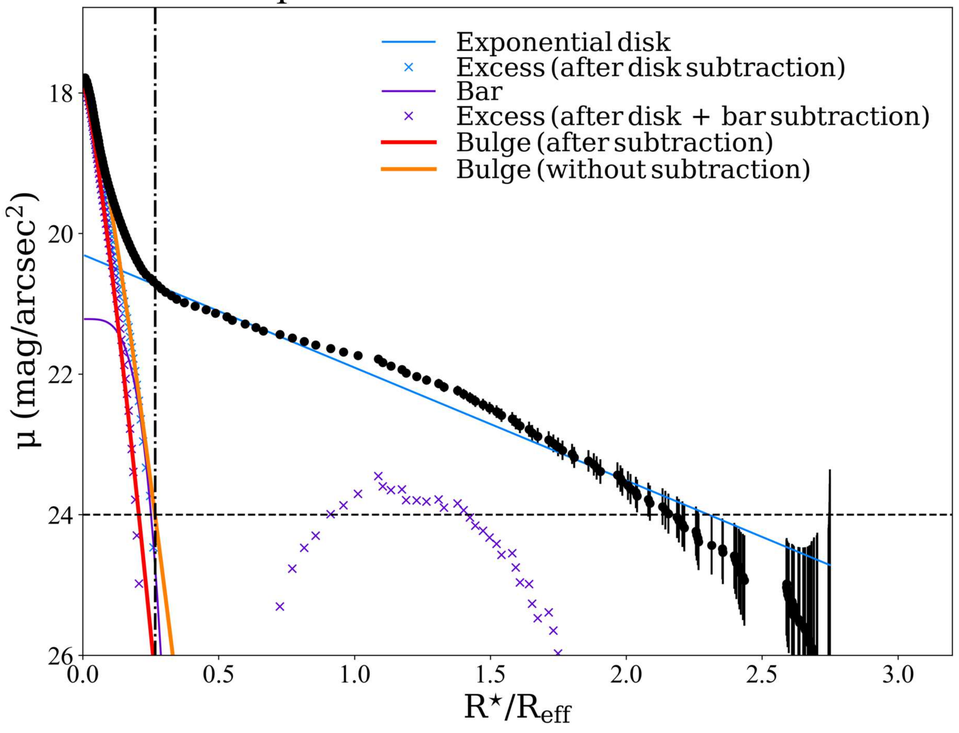

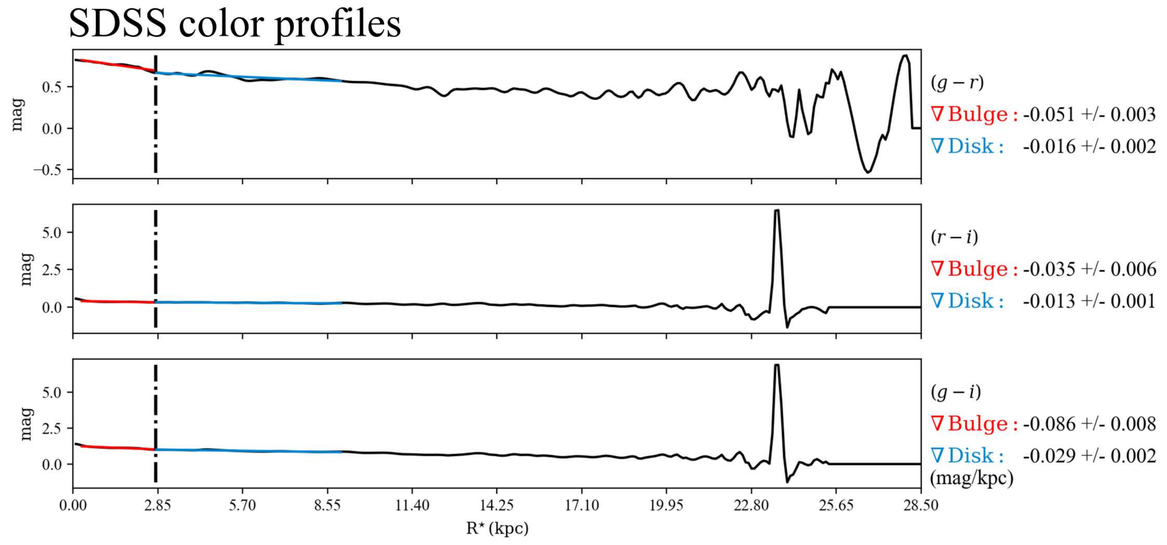

$\mathcal{RV}$ SBPs

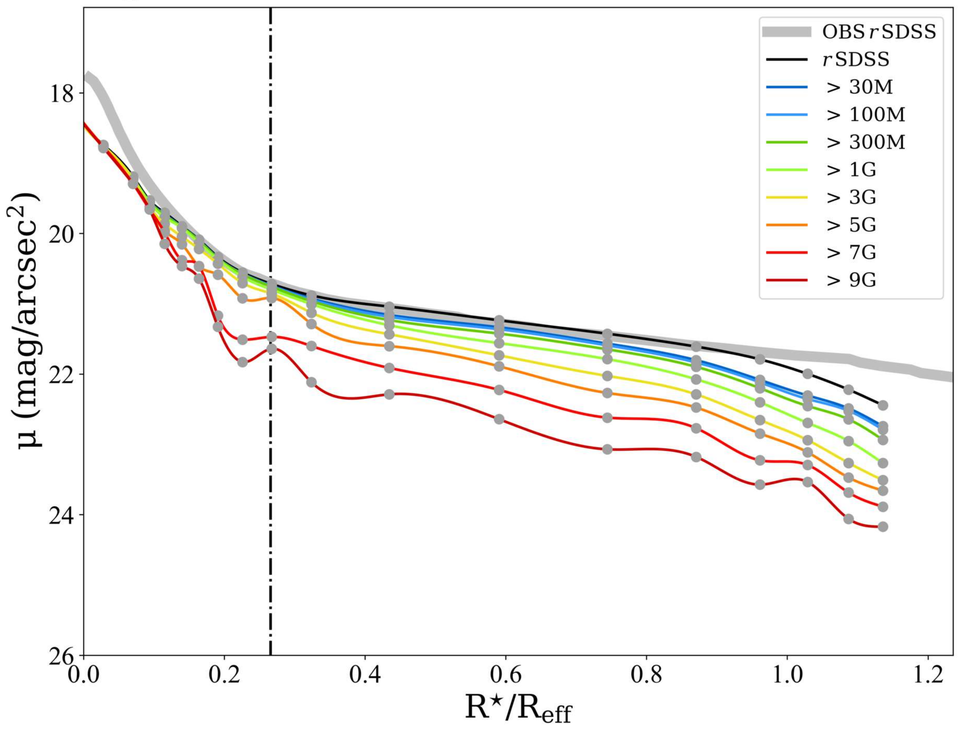

Stellar Continuum

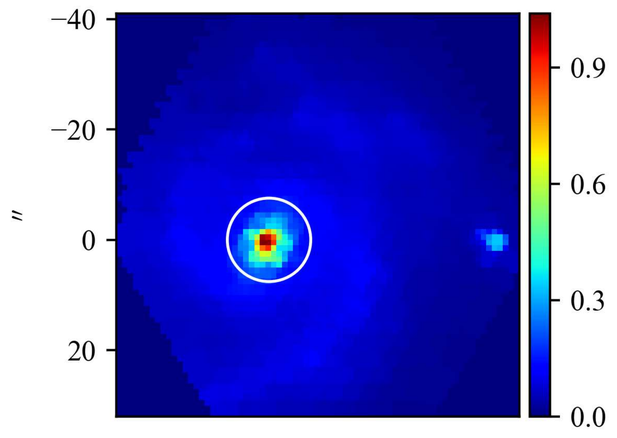

$\mathcal{M}_{\star,\mathrm{P}}$

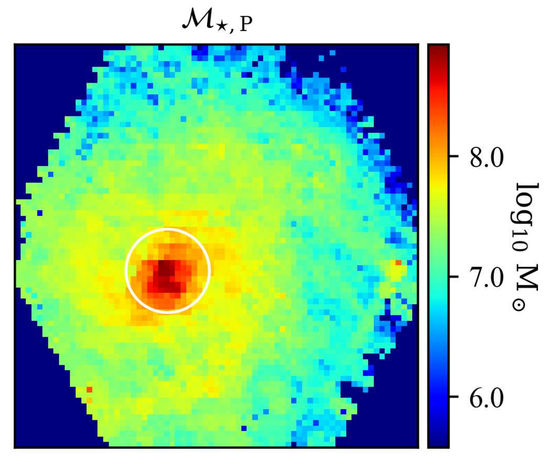

Log. of cumulative present stellar mass profiles

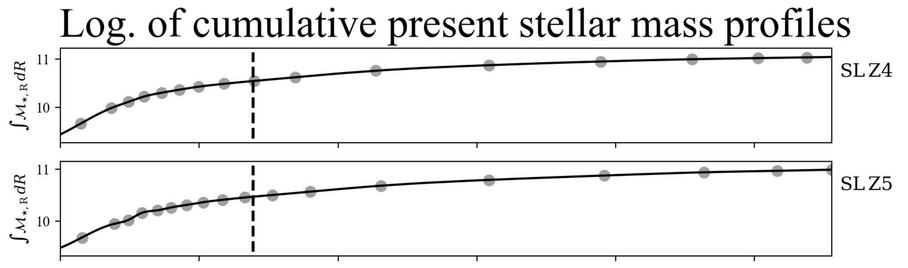

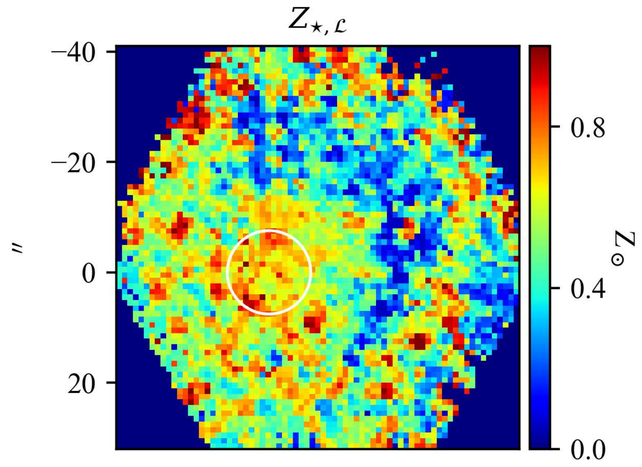

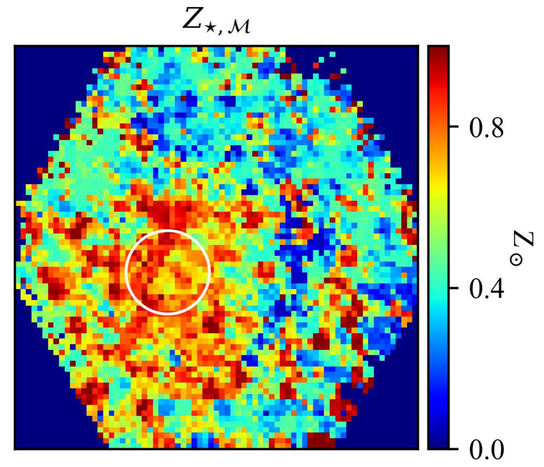

Stellar metallicity/Age & Hα flux/EW profiles

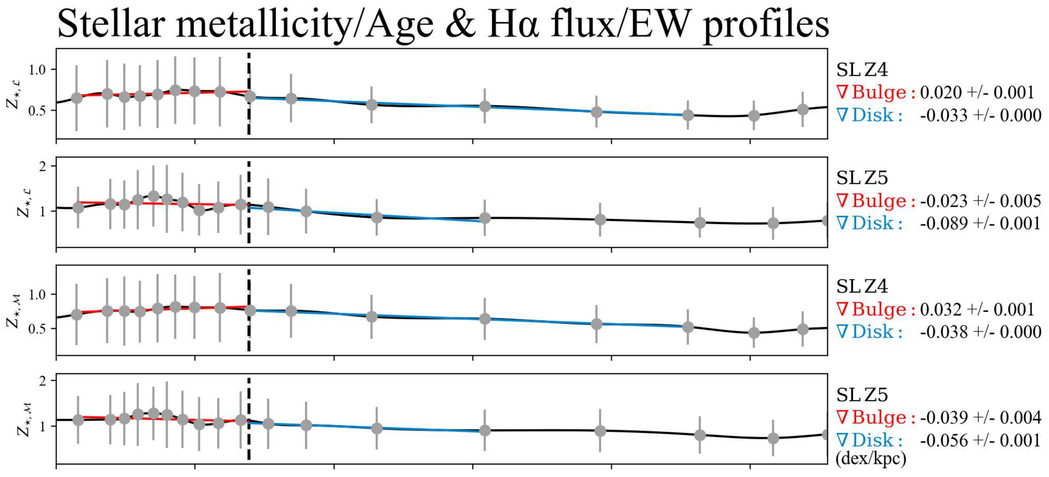

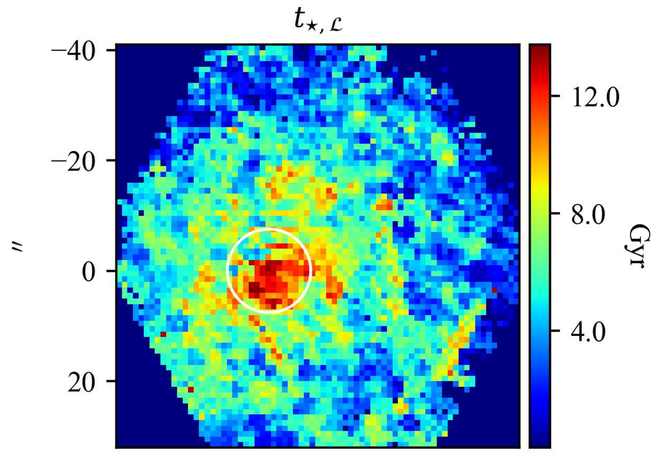

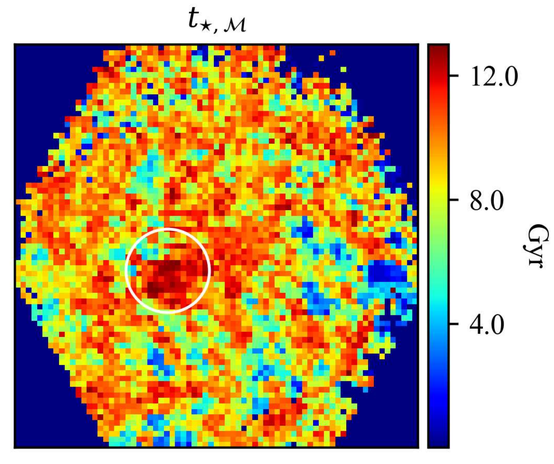

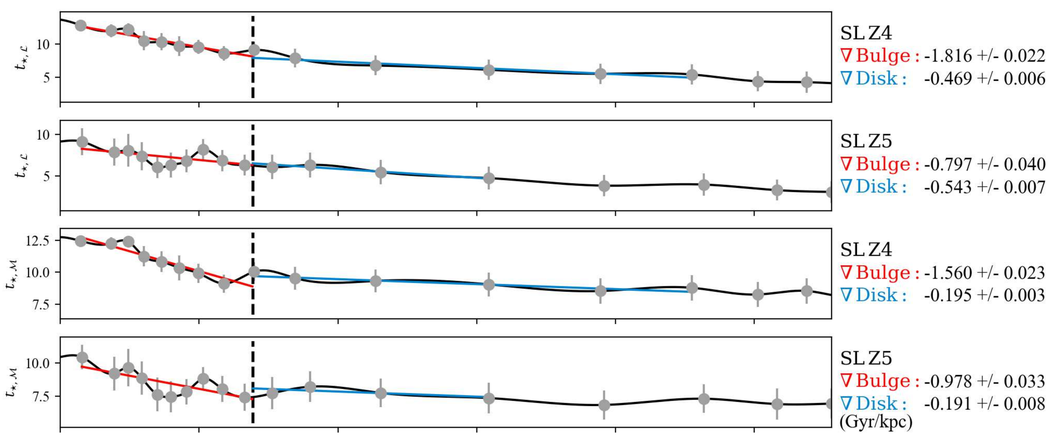

Hα flux

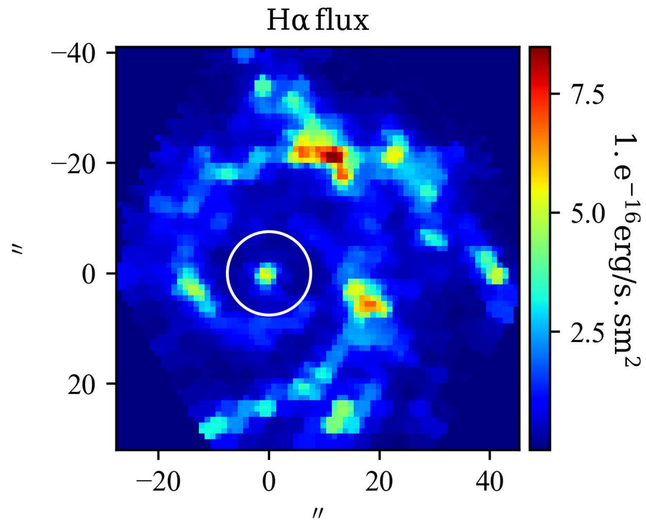

EW(Hα)

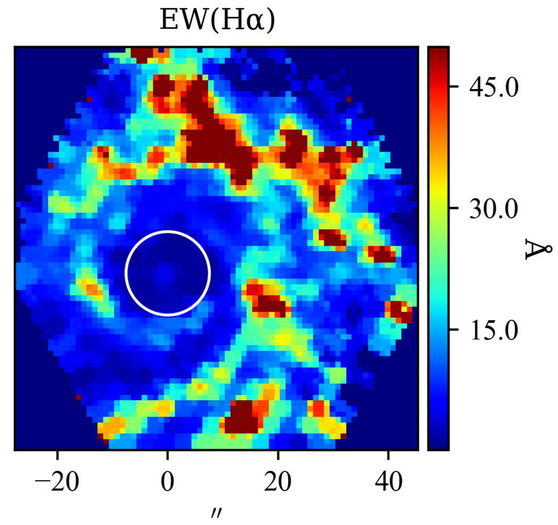

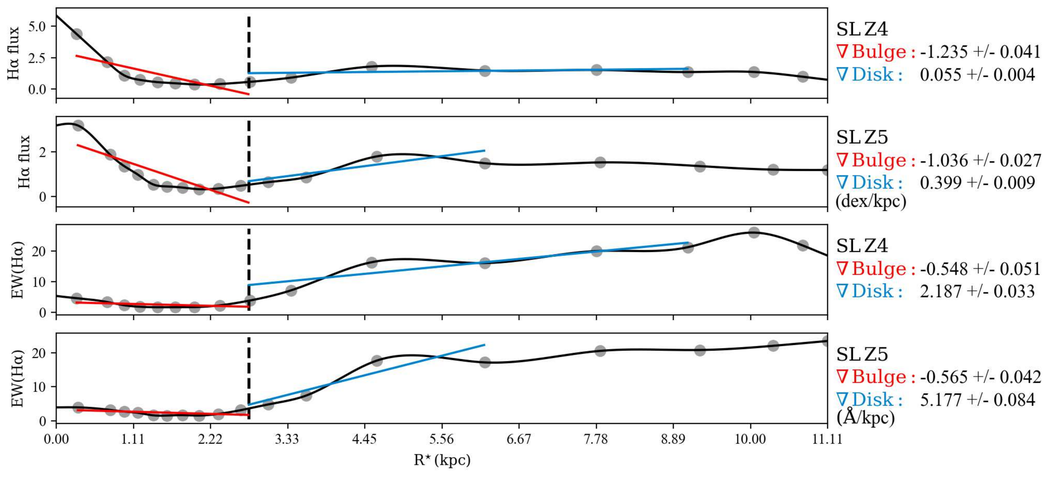

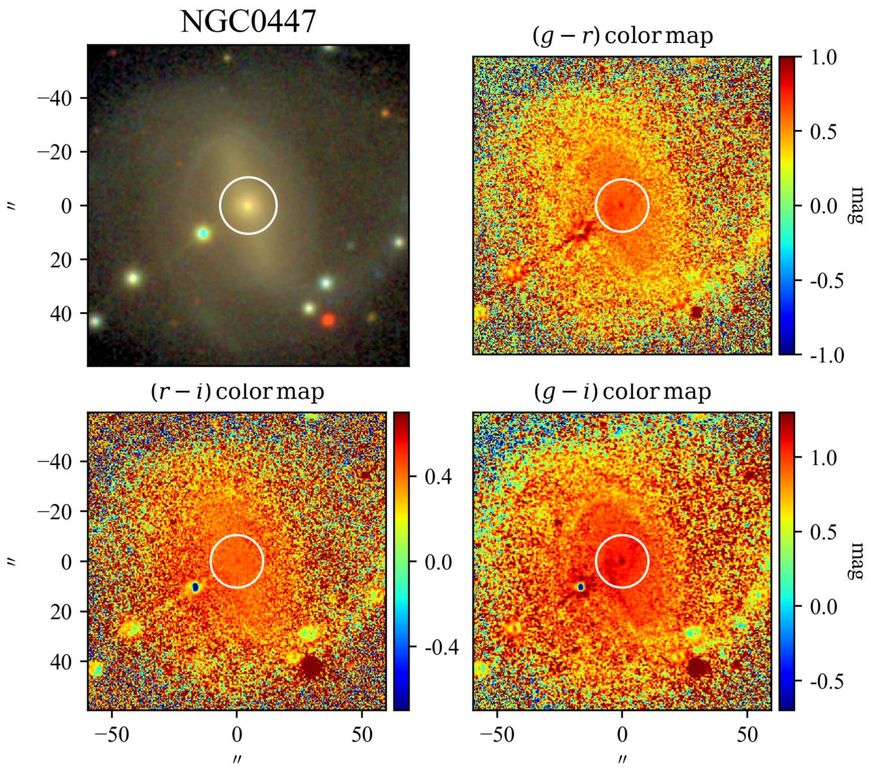

SBP decomposition of SDSS r band

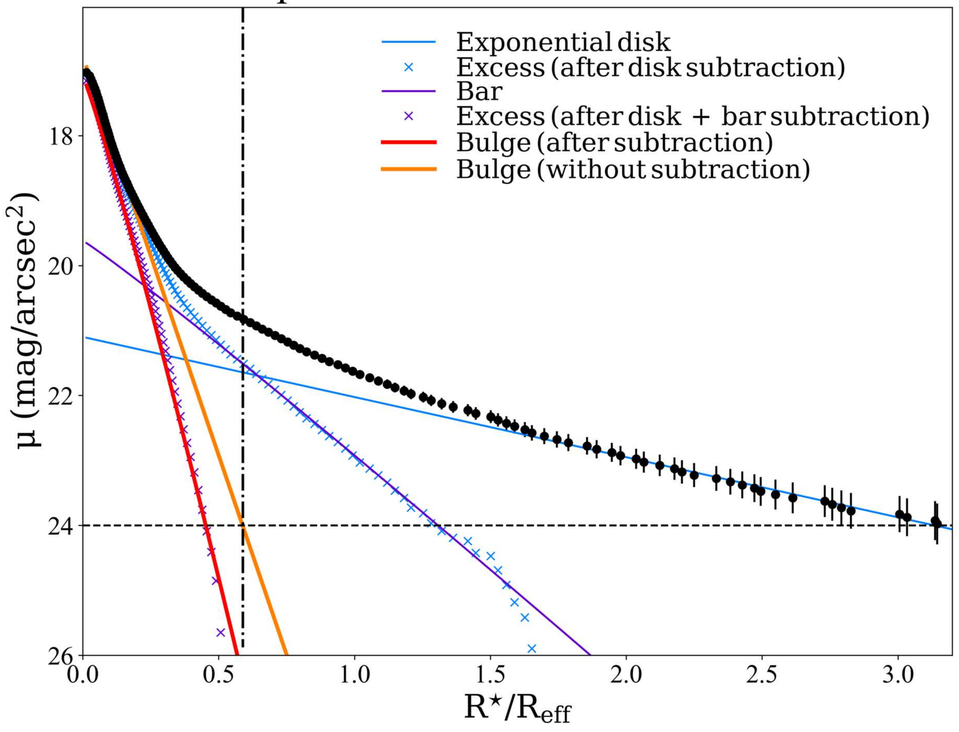

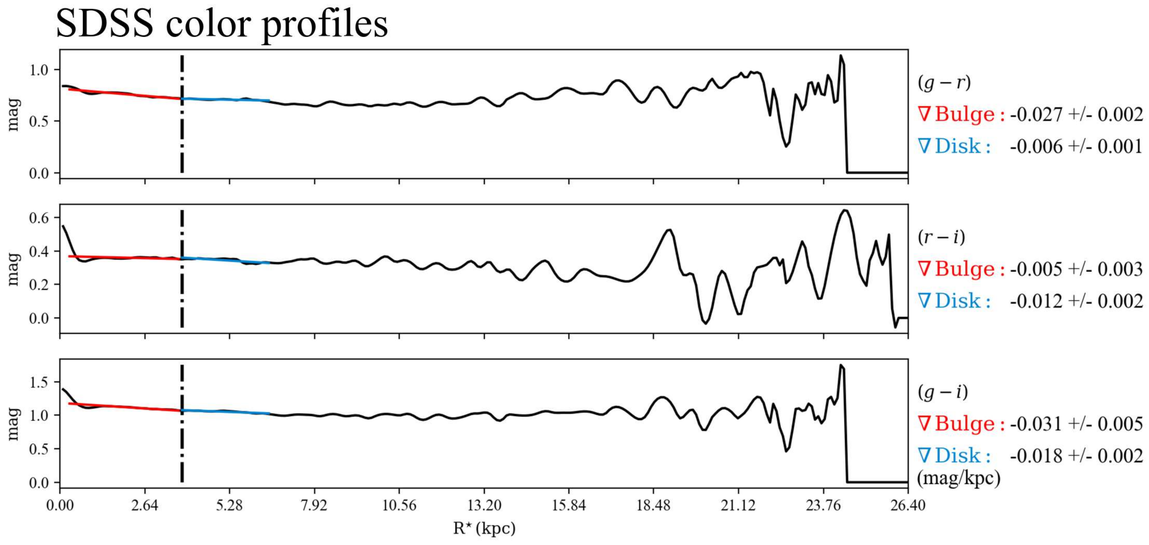

$\mathcal{RY}$ SBPs

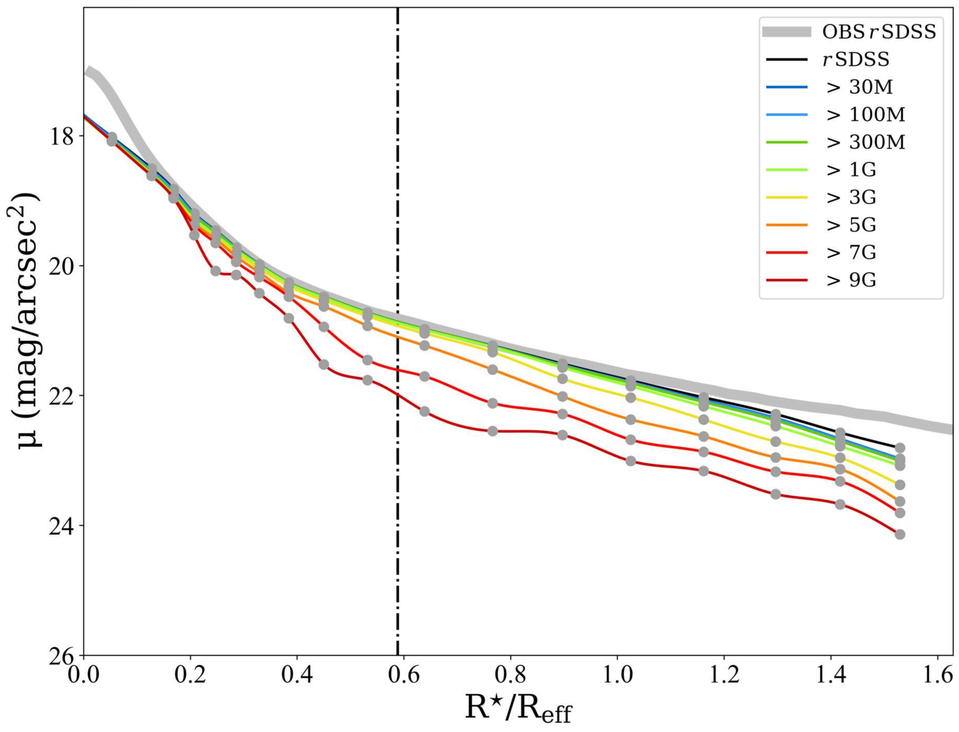

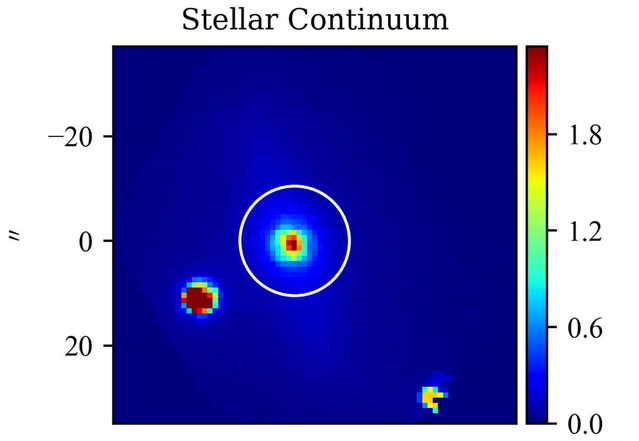

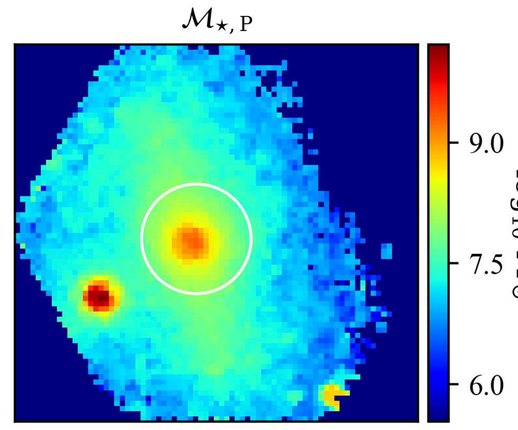

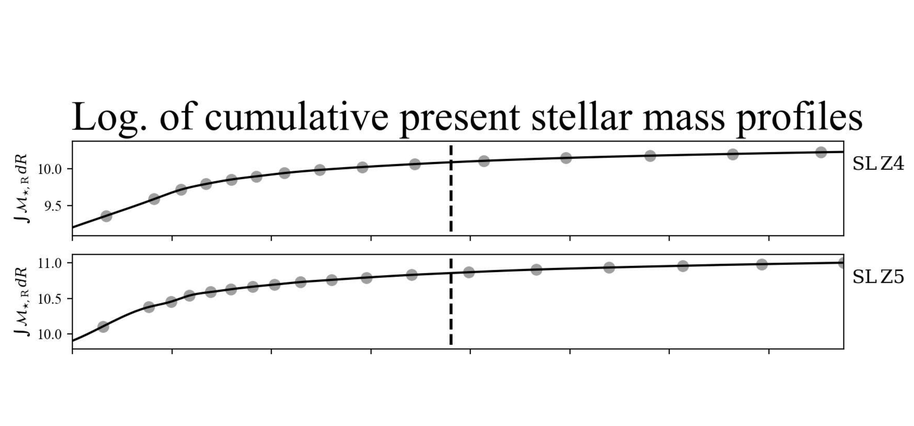

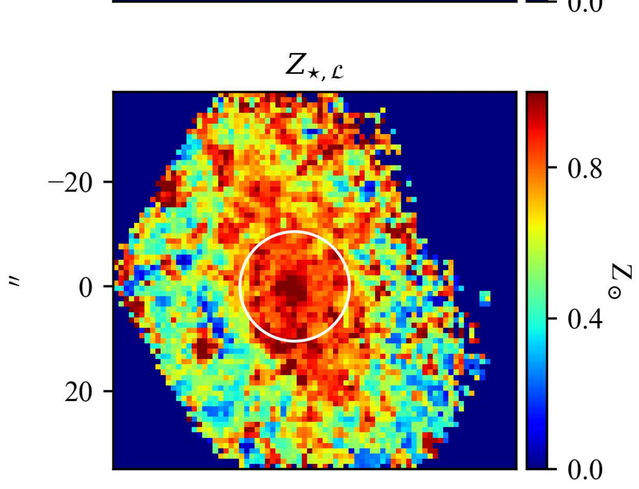

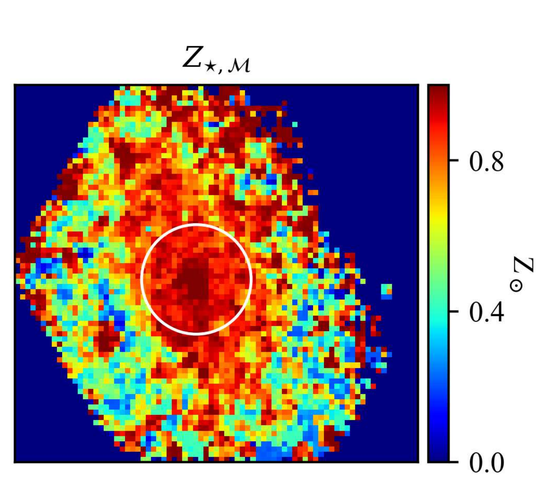

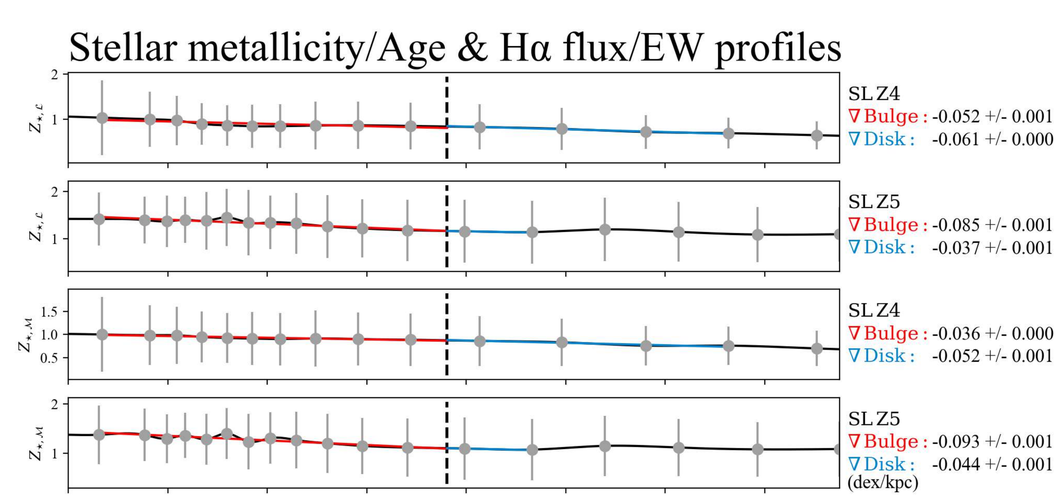

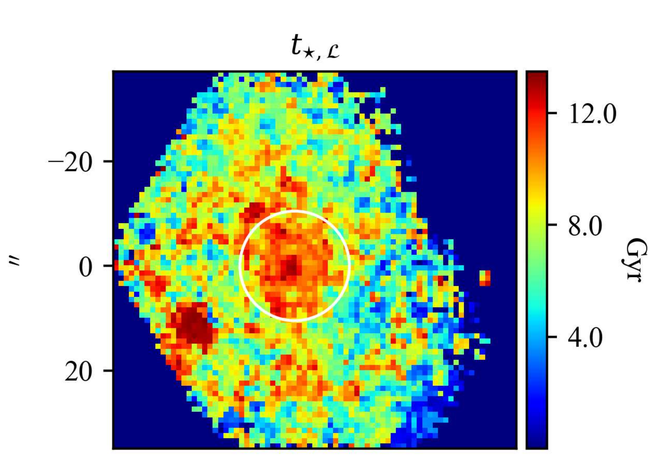

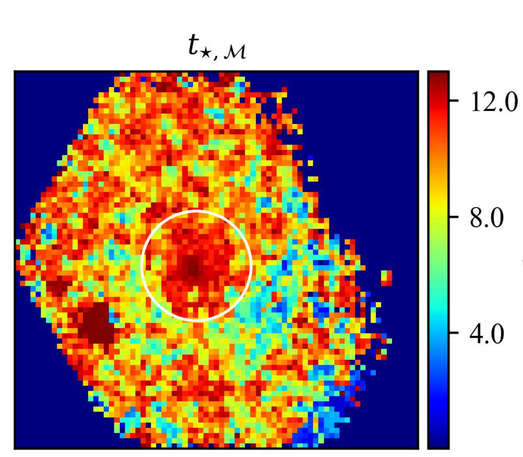

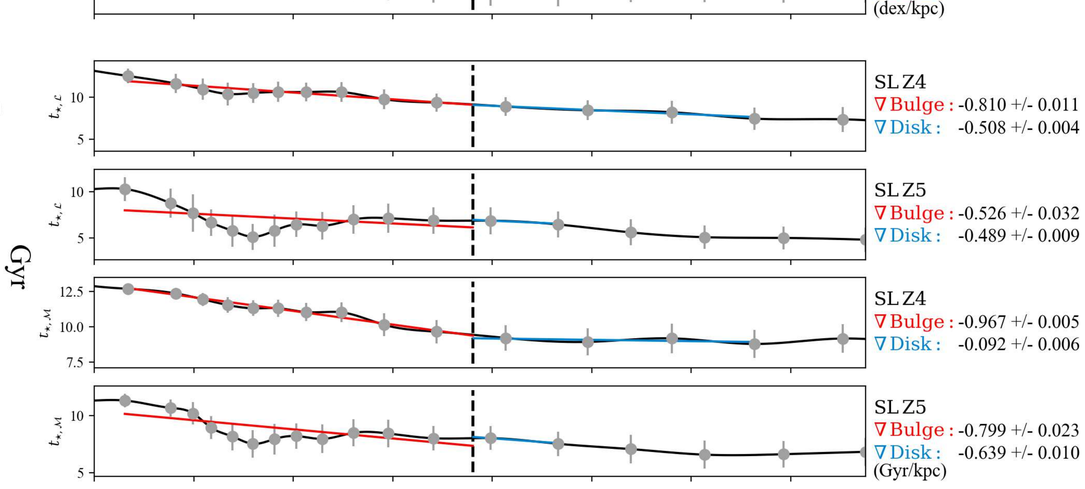

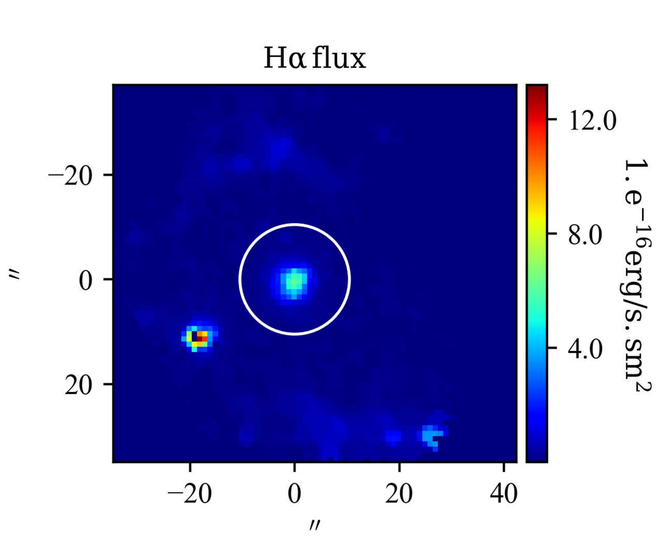

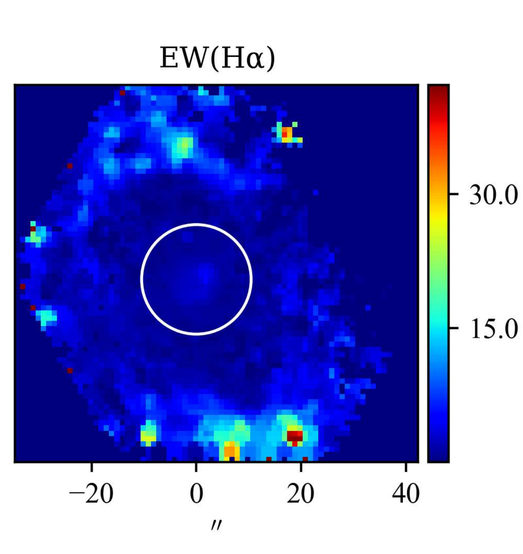

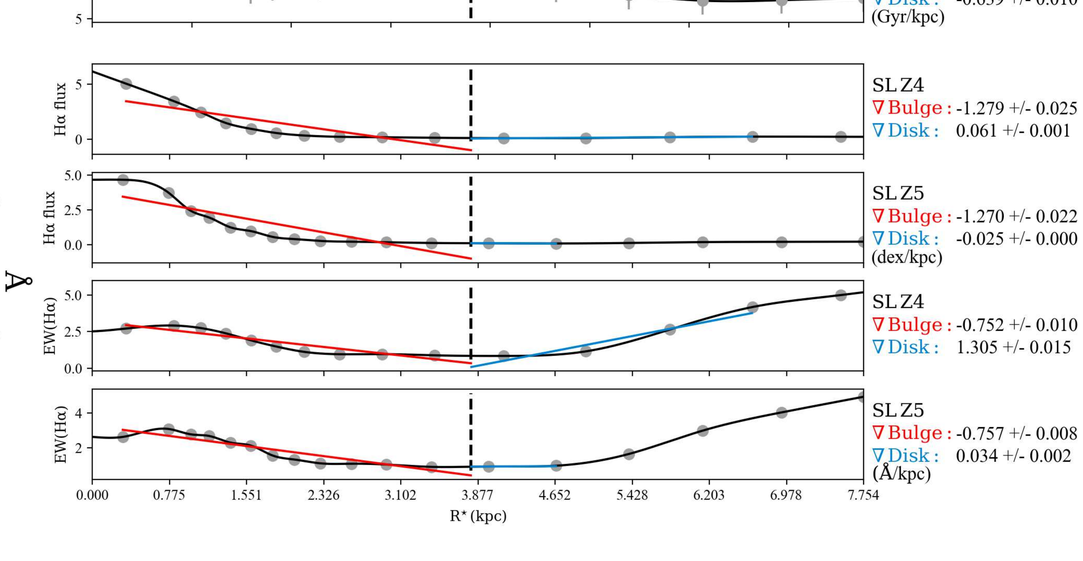

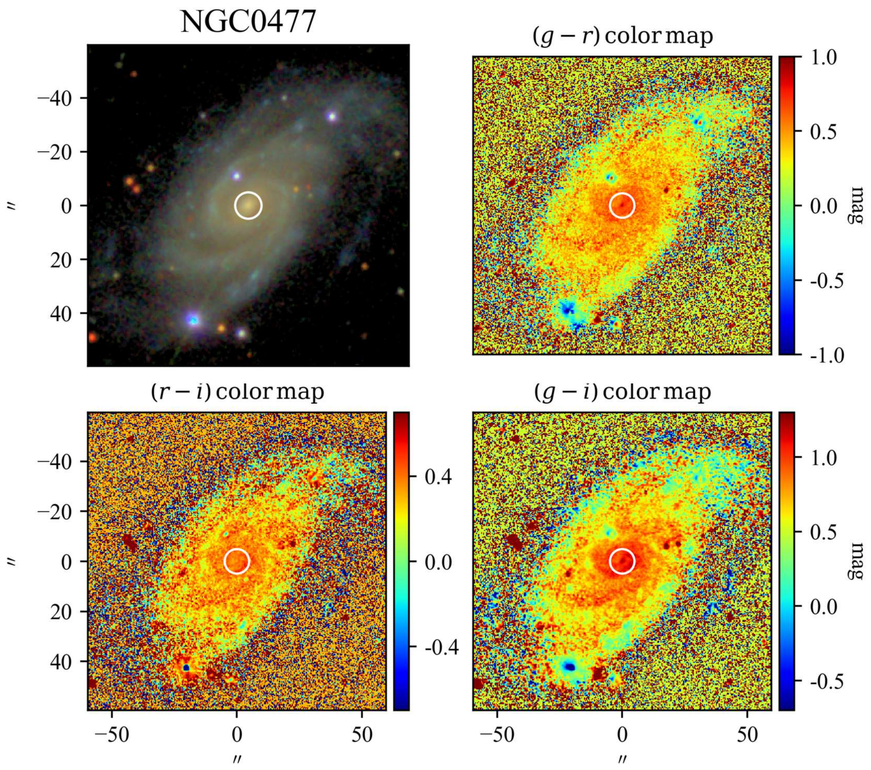

SBP decomposition of SDSS r band

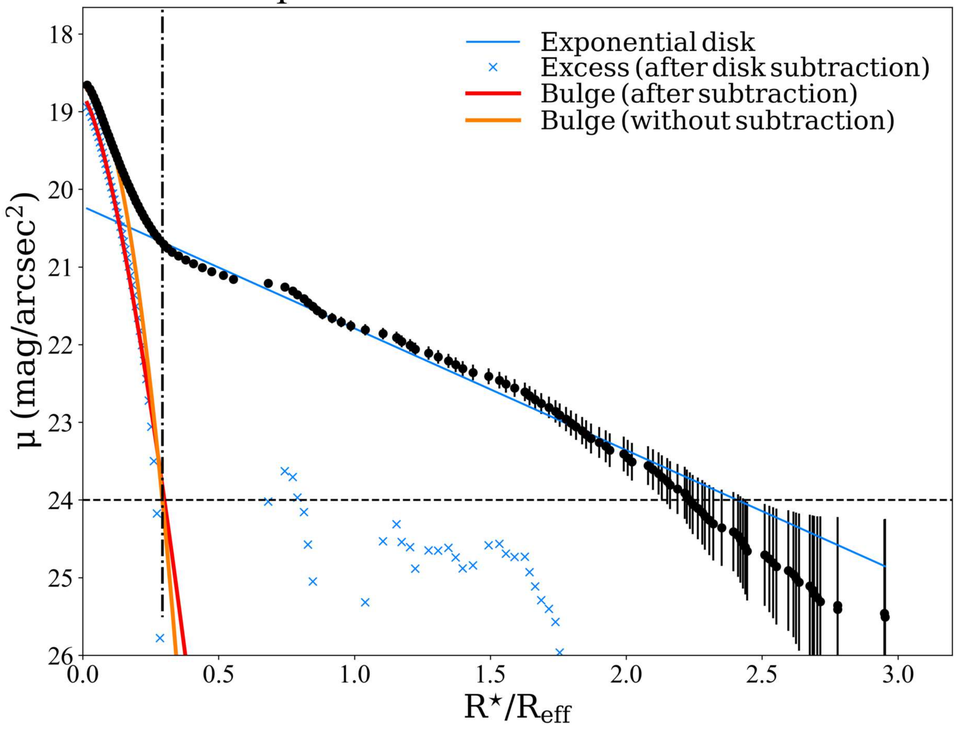

SDSS color profiles

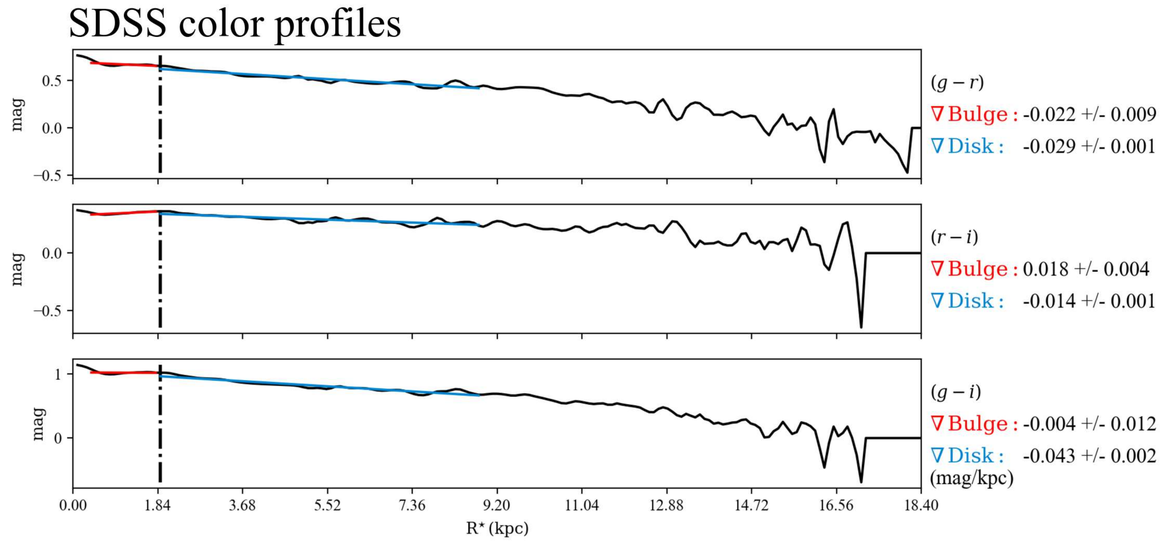

$\mathcal{RY}$ SBPs

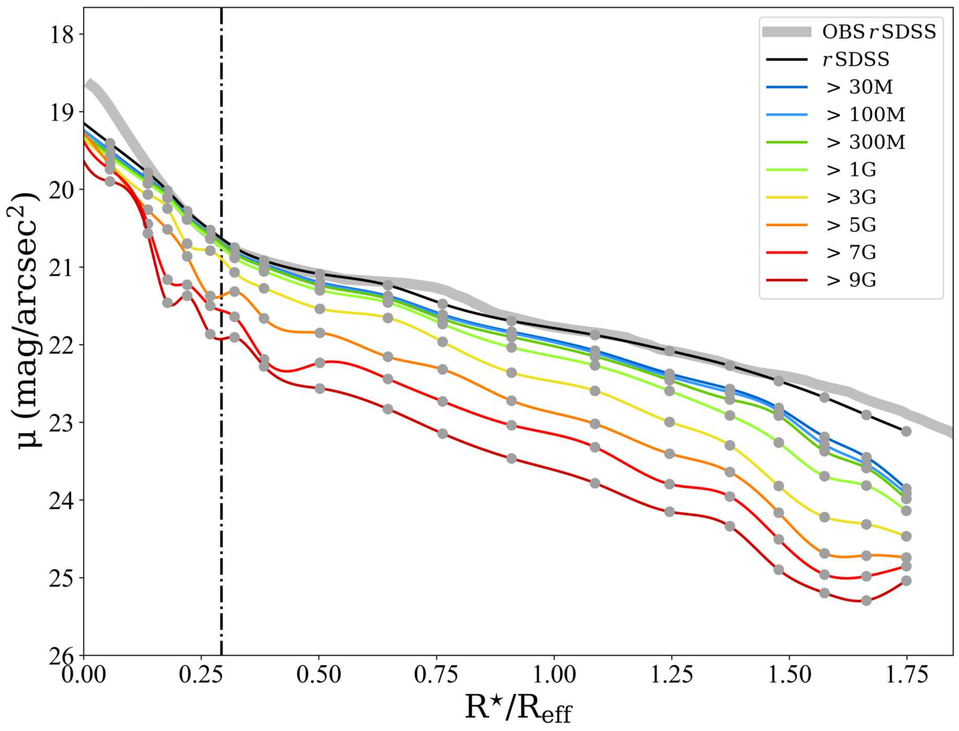

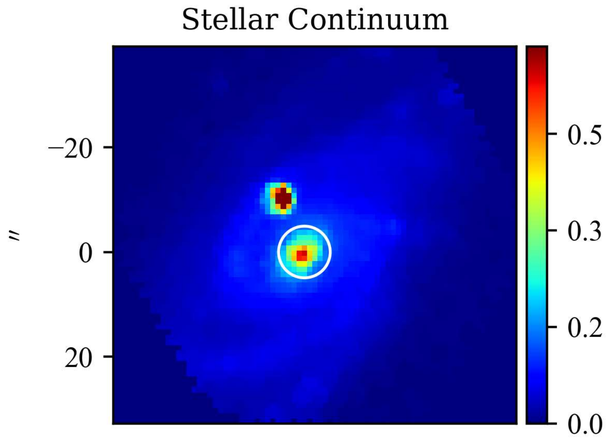

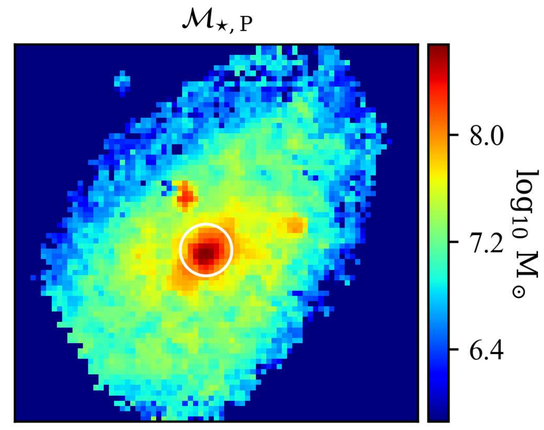

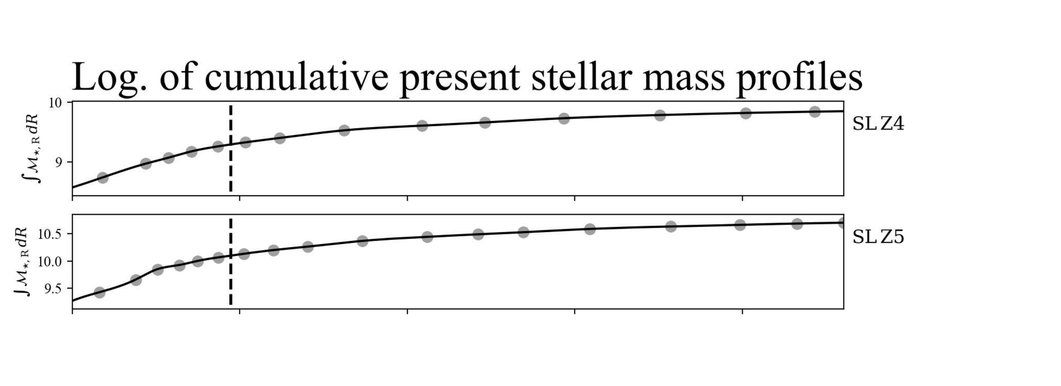

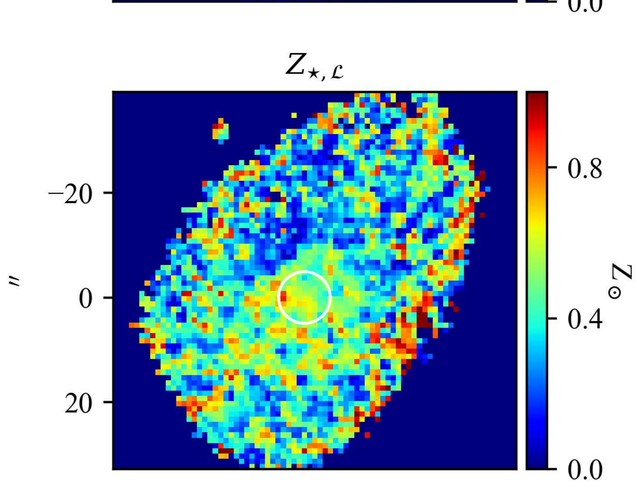

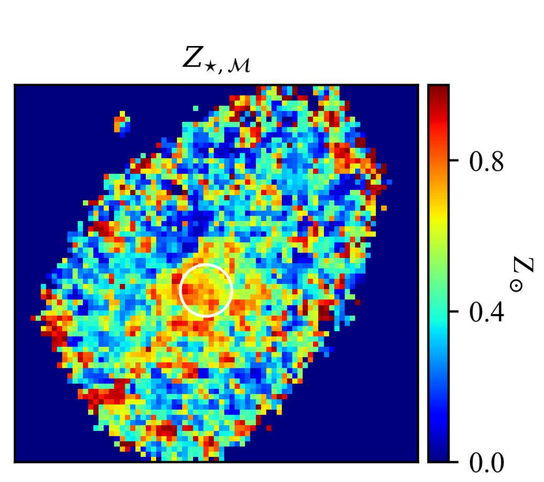

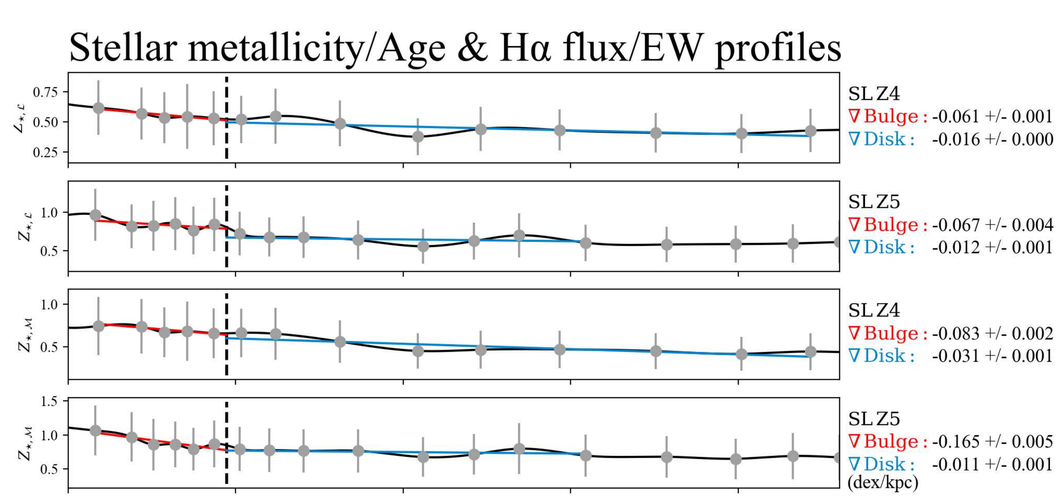

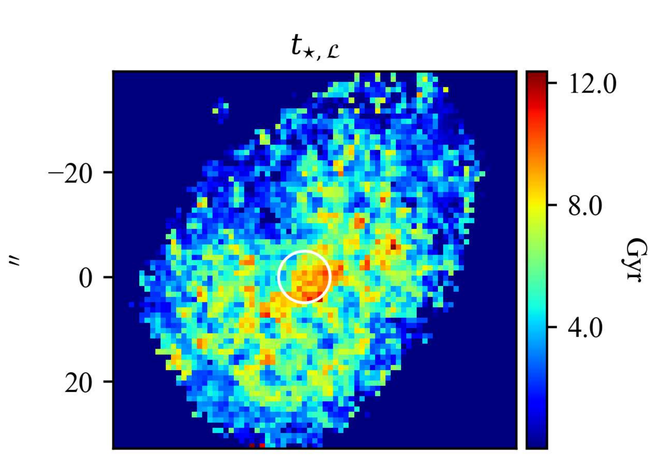

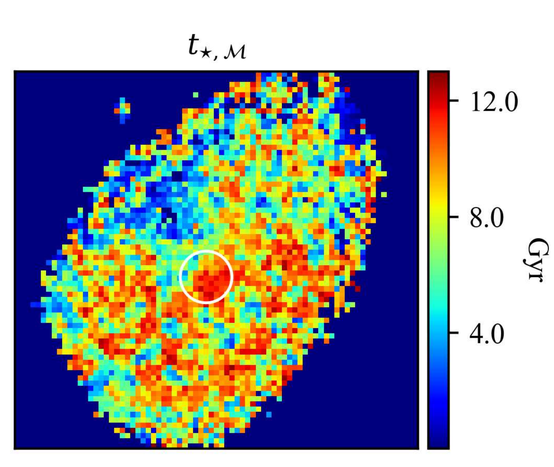

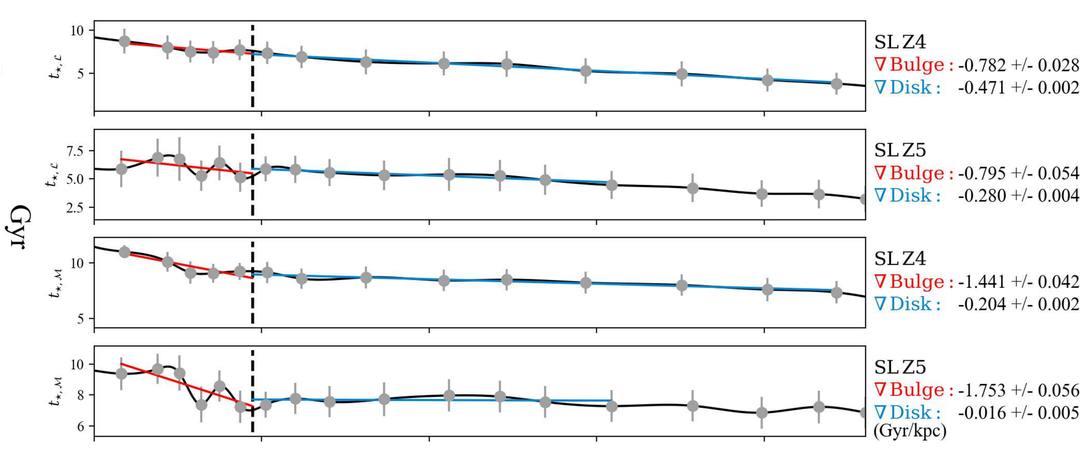

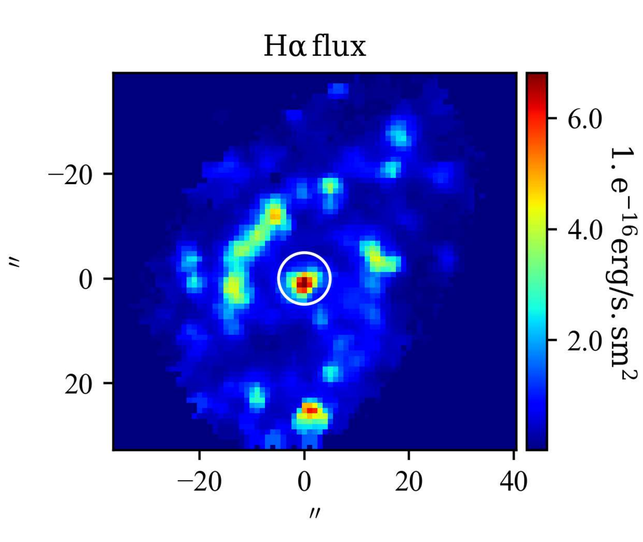

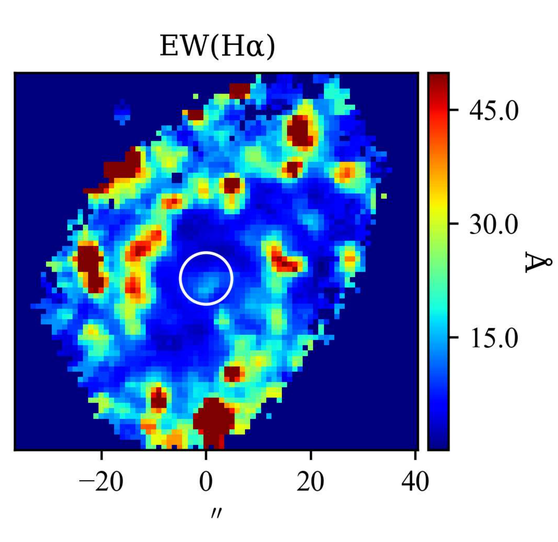

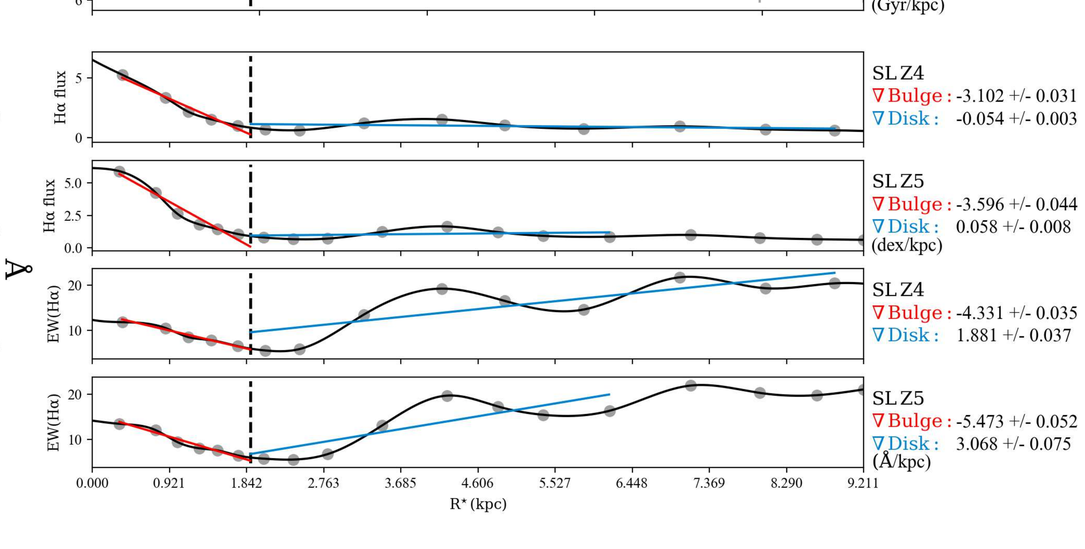

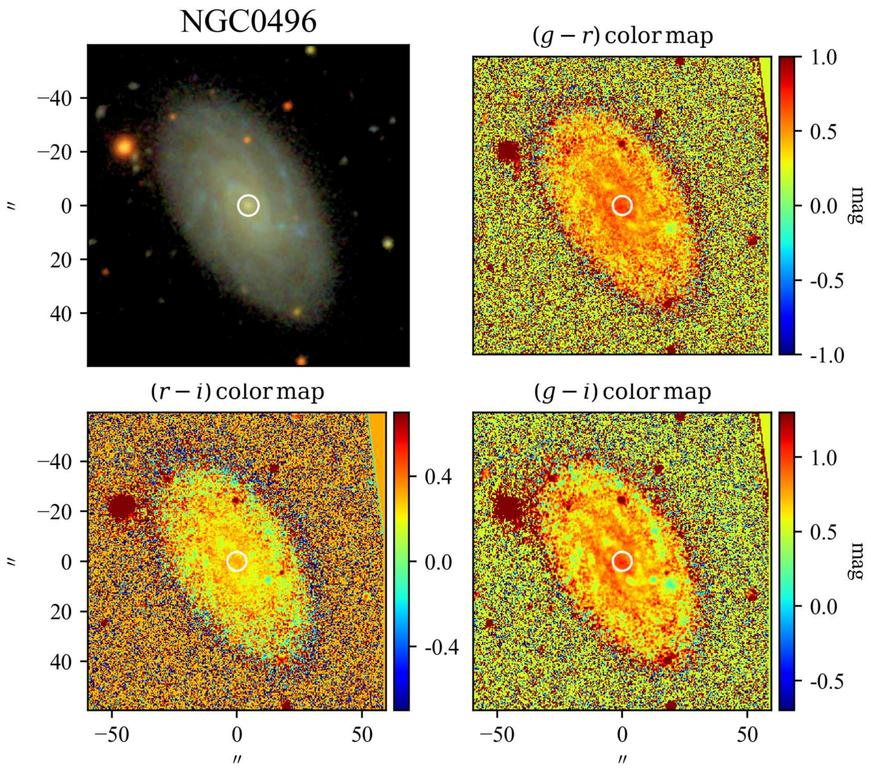

SBP decomposition of SDSS r band

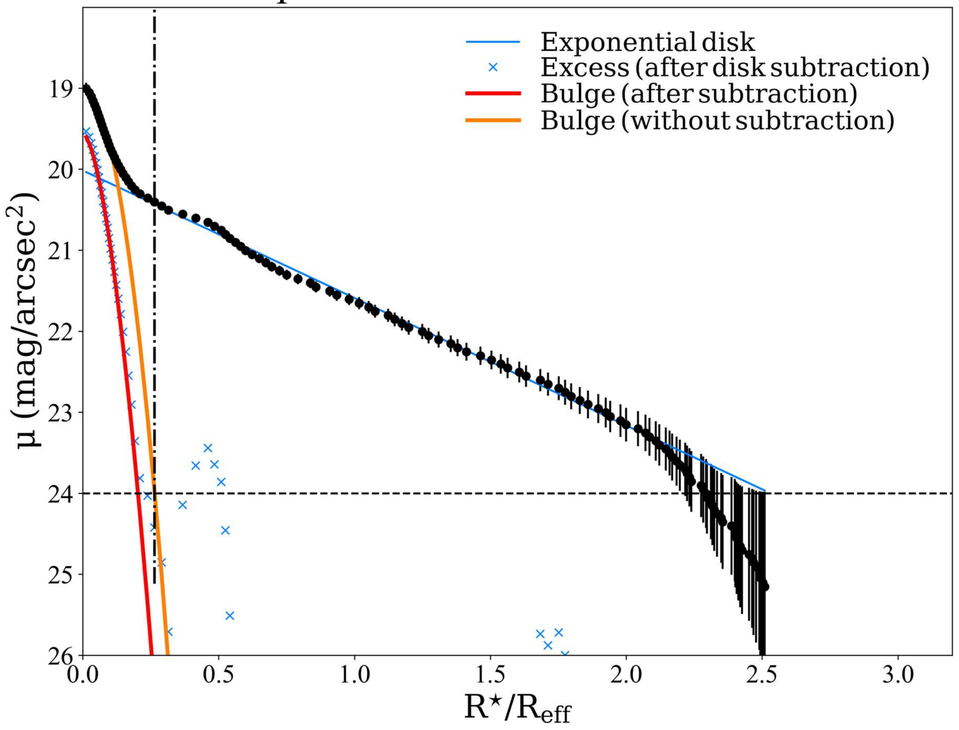

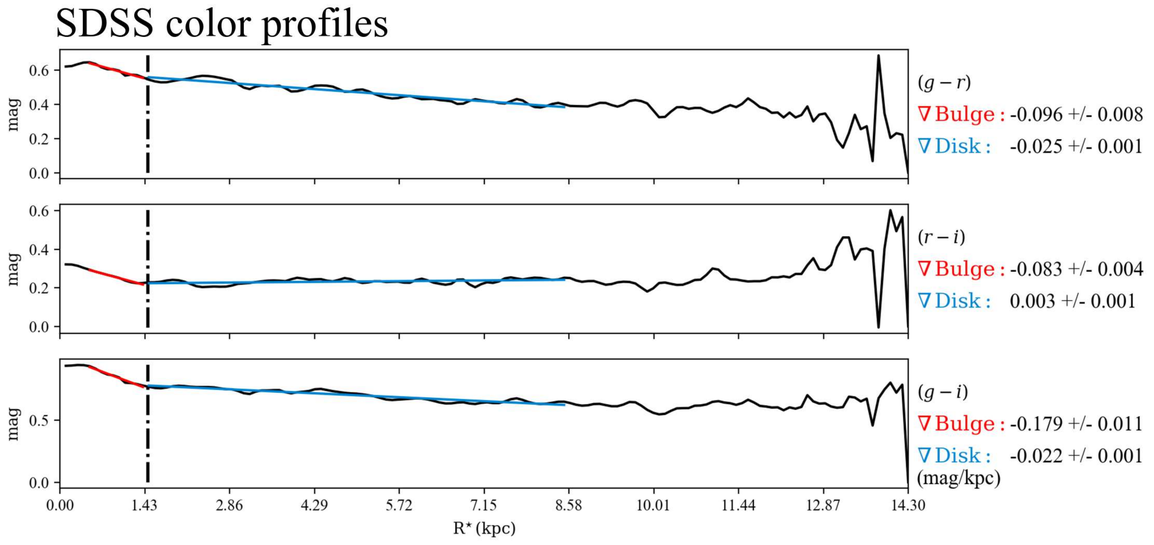

$\mathcal{RY}$ SBPs

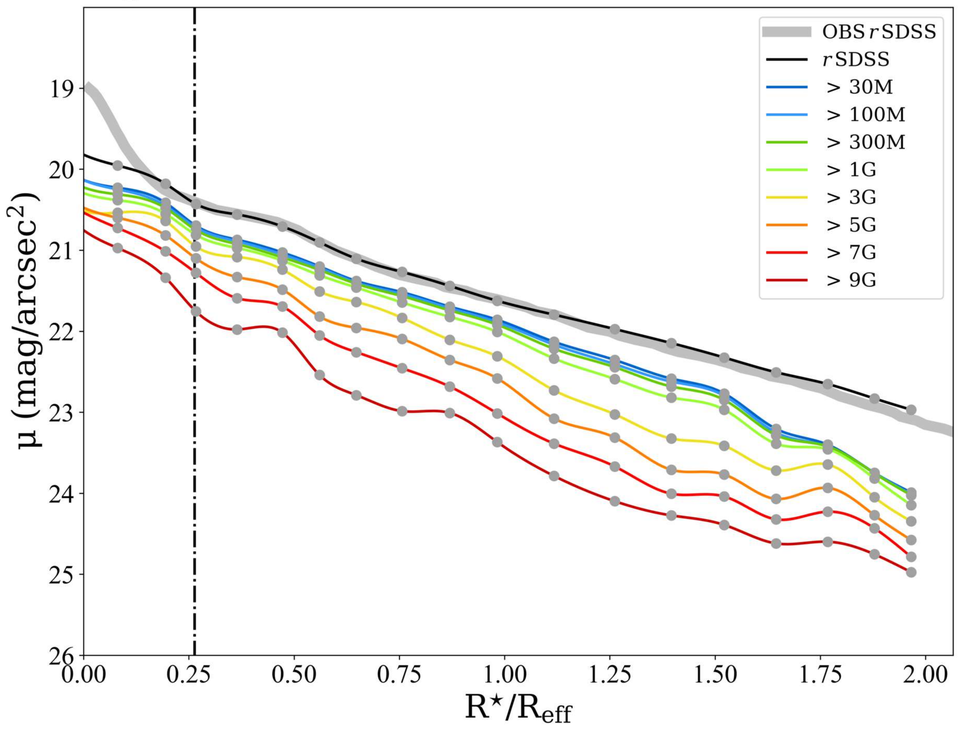

Stellar Continuum

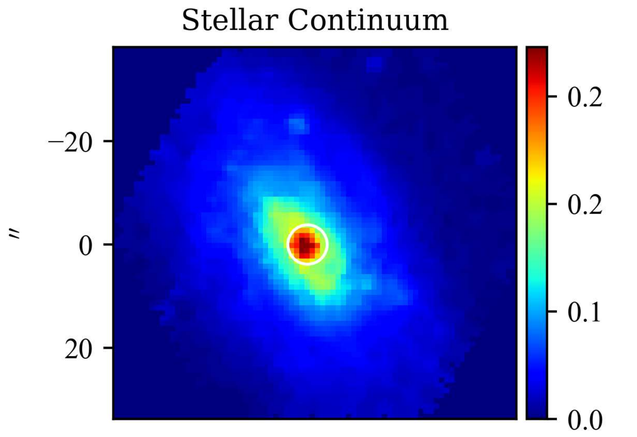

$\mathcal{M}_{\star,\mathrm{P}}$

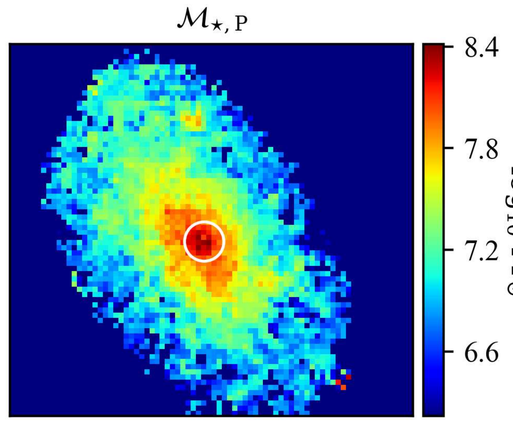

Log. of cumulative present stellar mass profiles

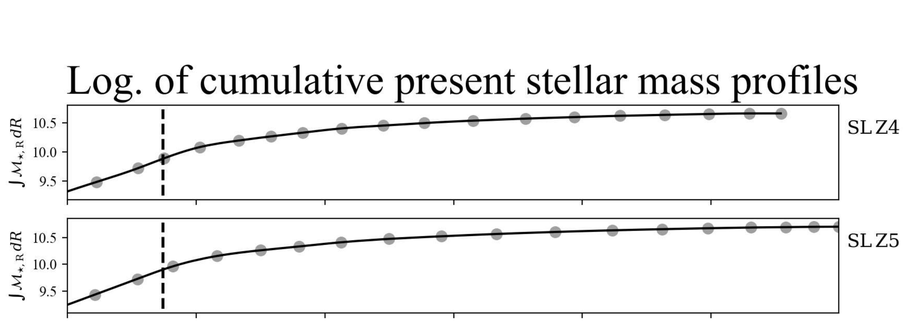

$Z_{\star,\mathcal{L}}$

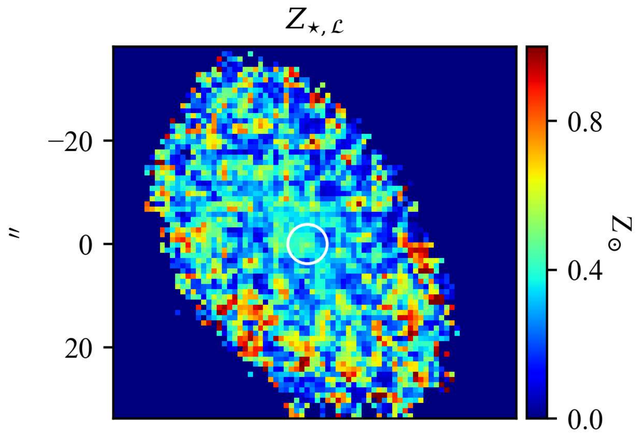

$Z_{\star,\mathcal{M}}$

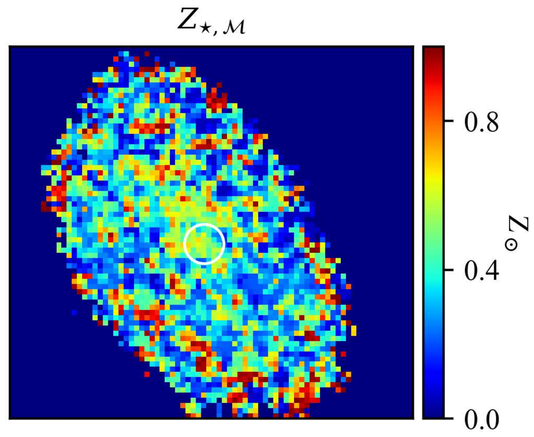

Stellar metallicity/Age & Hα flux/EW profiles

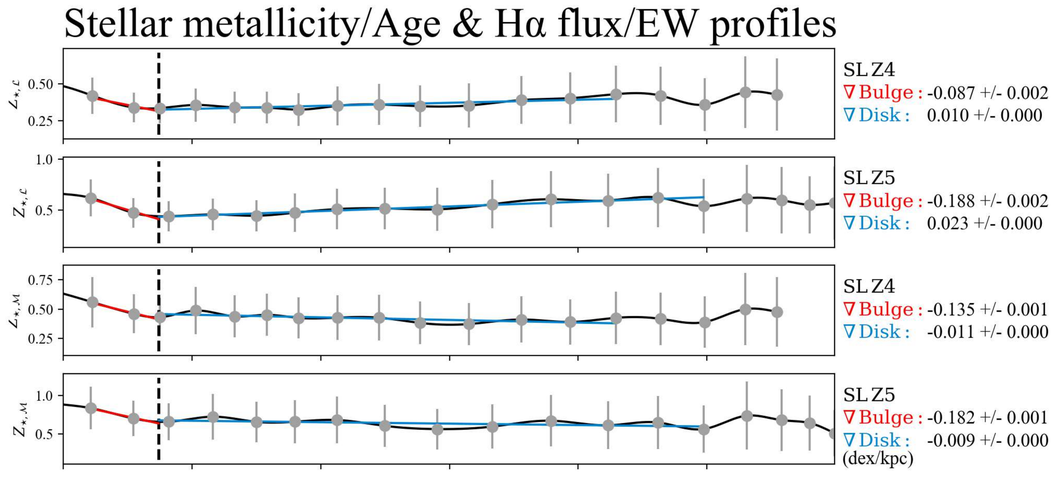

$t_{\star,\mathcal{L}}$

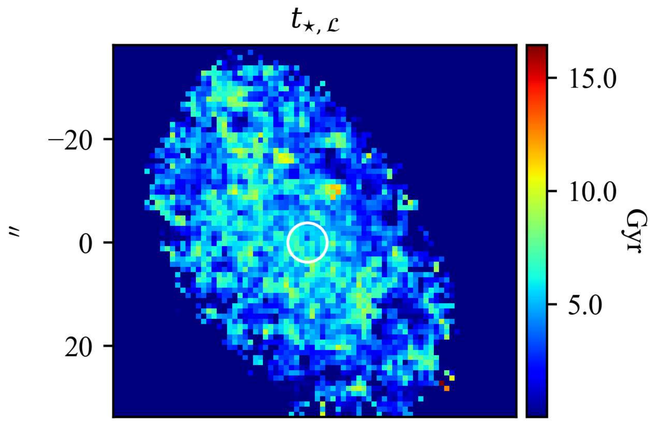

$t_{\star,\mathcal{M}}$

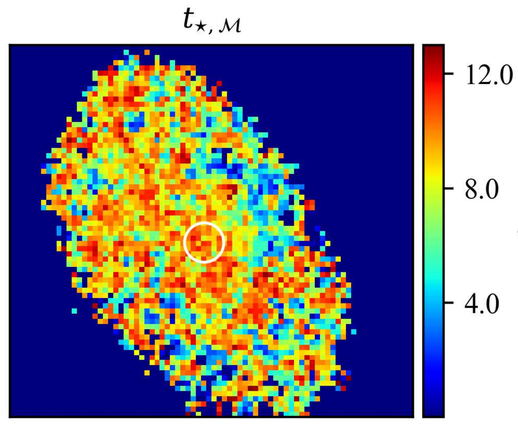

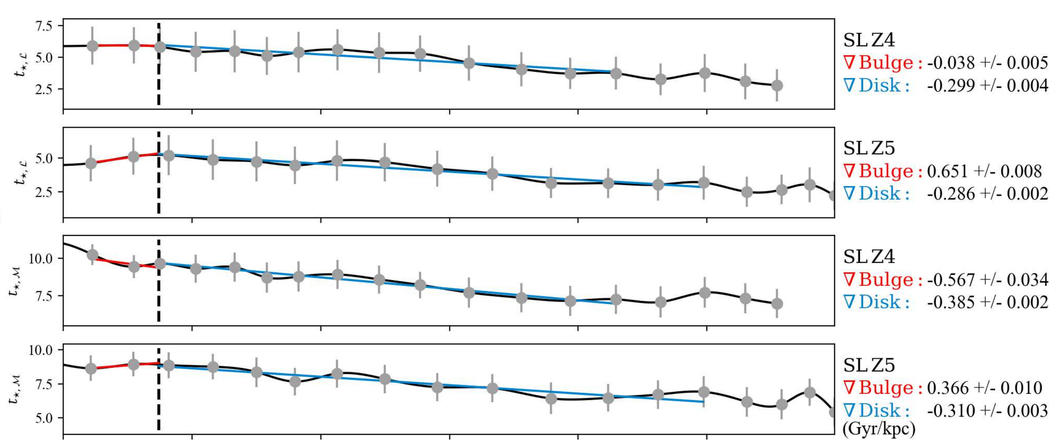

Hα flux

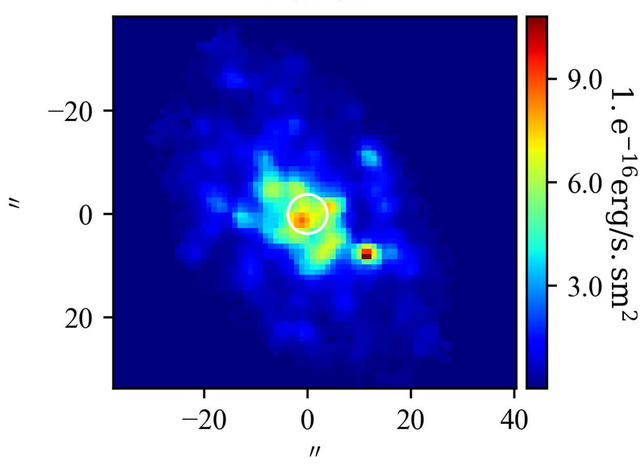

EW(Hα)

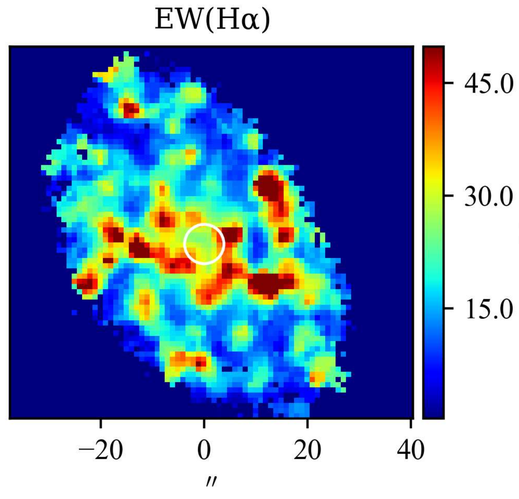

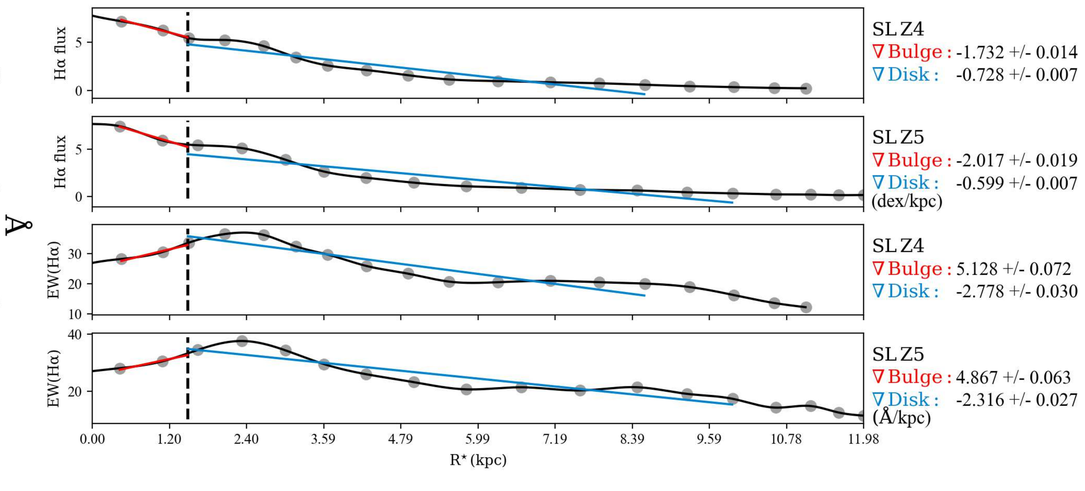

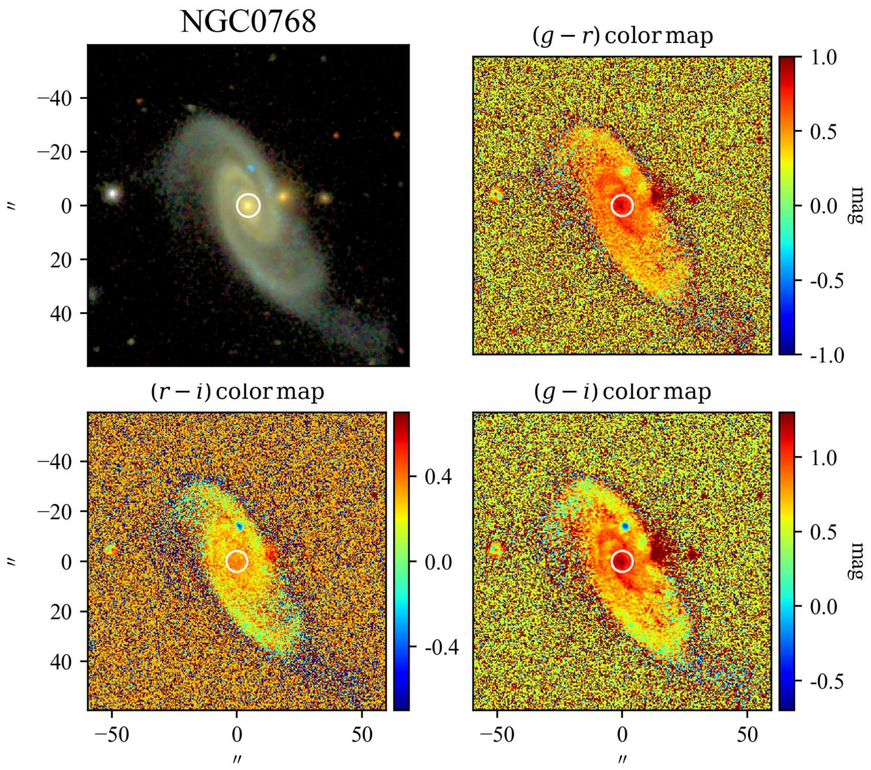

SBP decomposition of SDSS r band

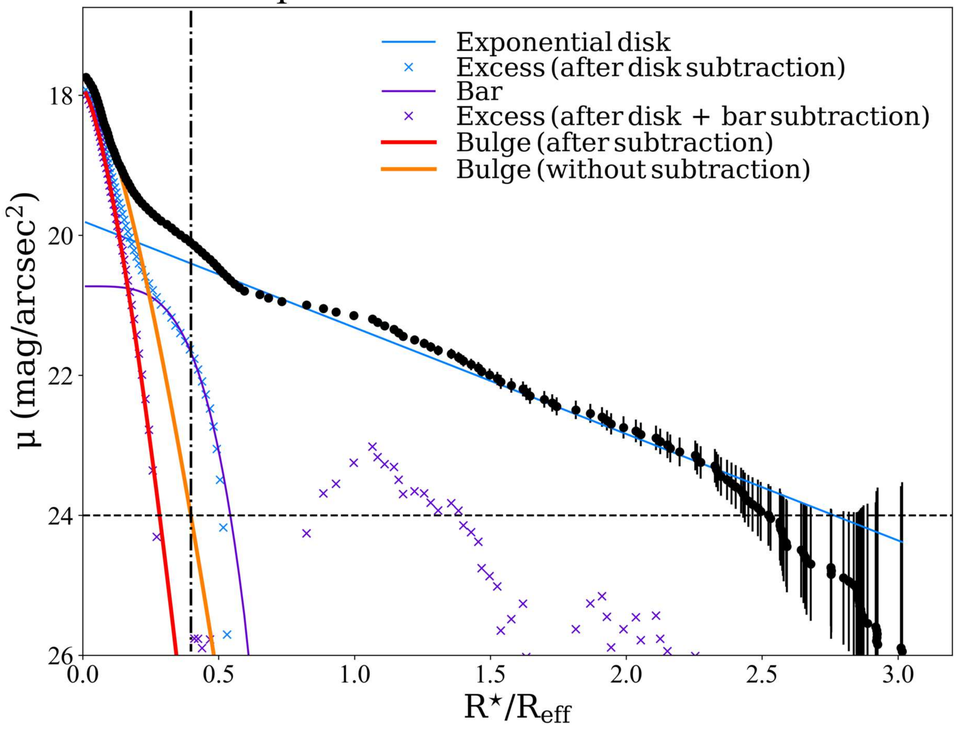

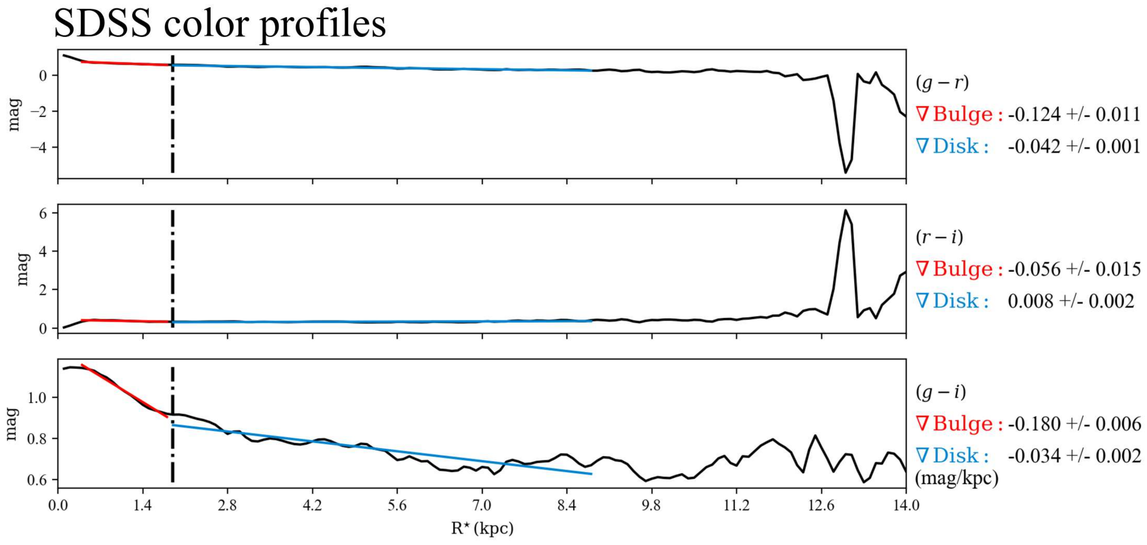

$\mathcal{RY}$ SBPs

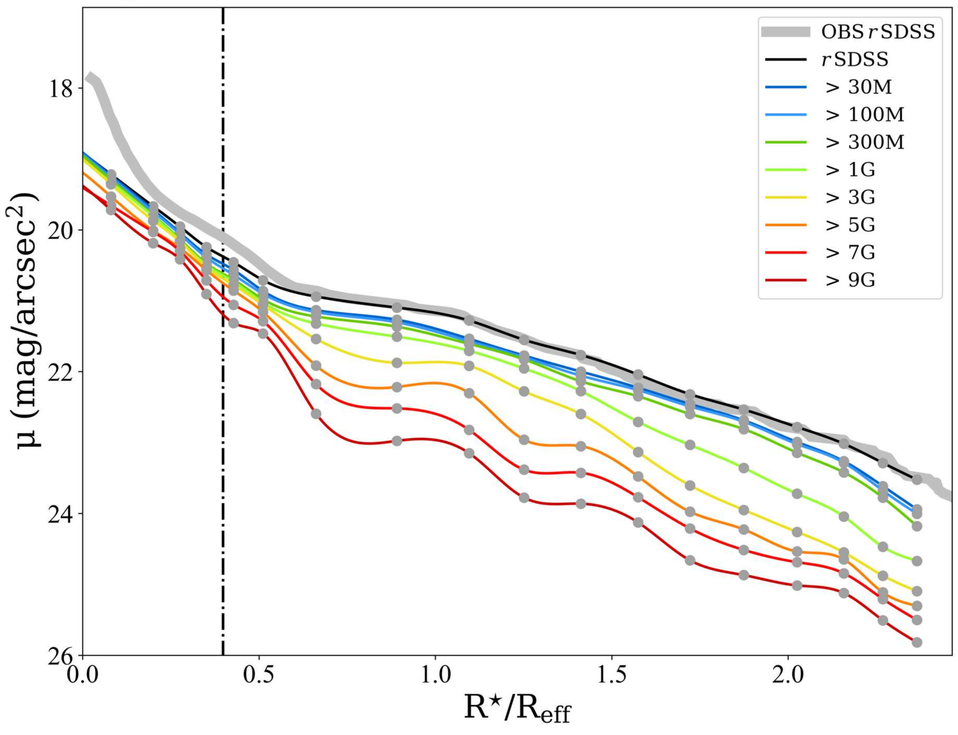

Stellar Continuum

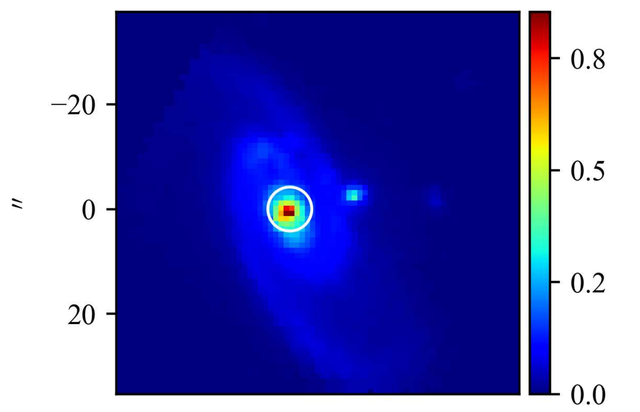

$\mathcal{M}_{\star,\mathrm{P}}$

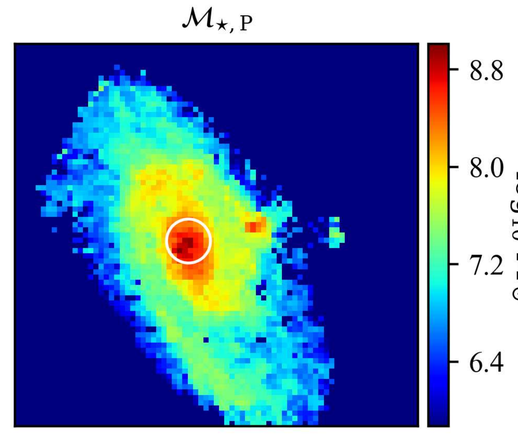

Log. of cumulative present stellar mass profiles

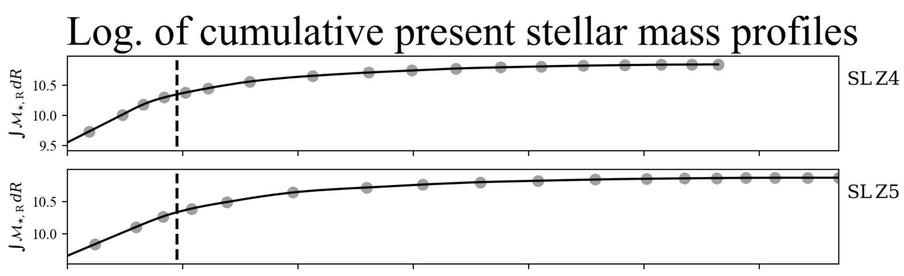

$Z_{\star,\mathcal{L}}$

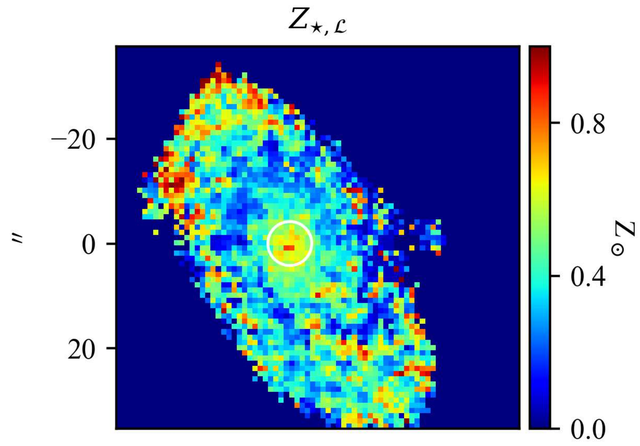

$Z_{\star,\mathcal{M}}$

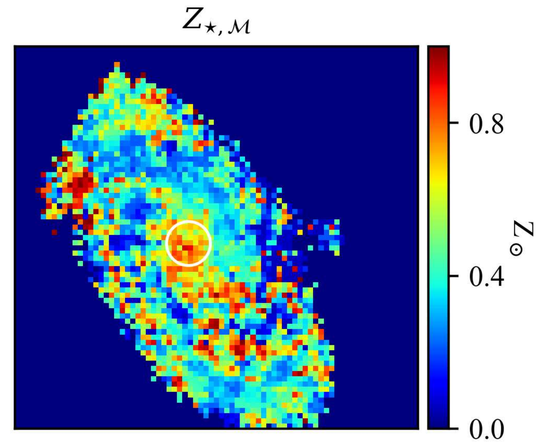

Stellar metallicity/Age & Hα flux/EW profiles

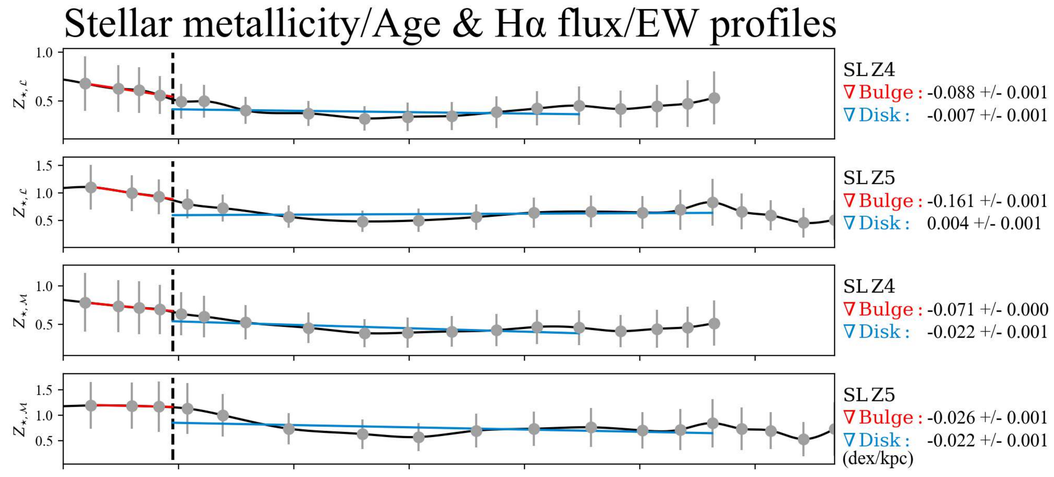

$t_{\star,\mathcal{L}}$

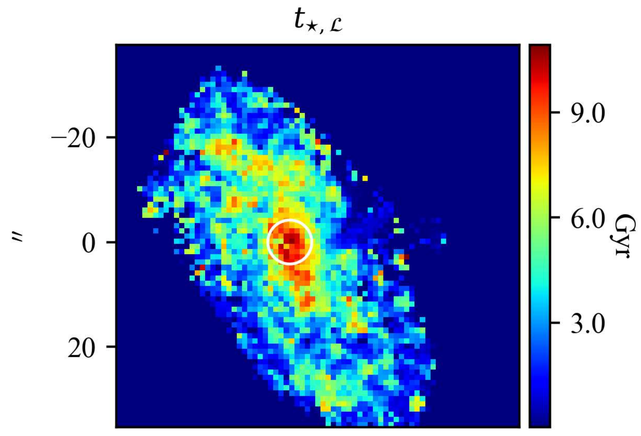

$t_{\star,\mathcal{M}}$

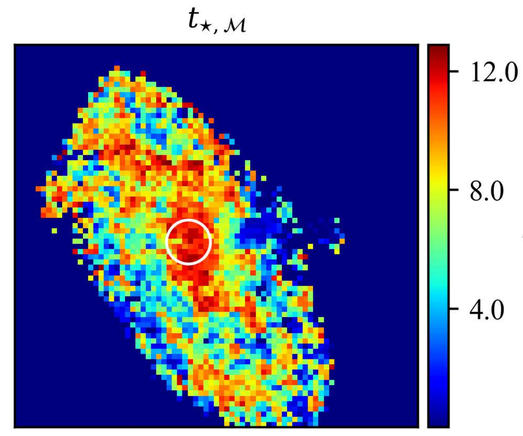

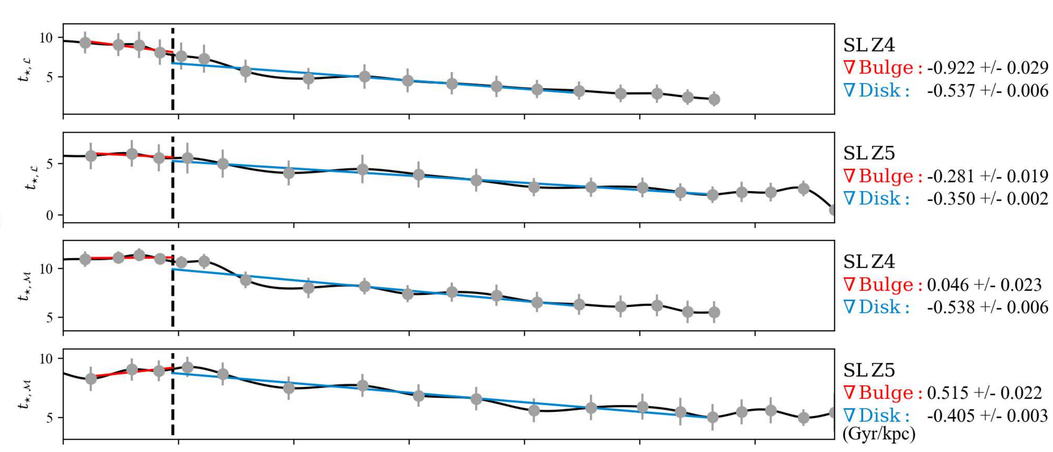

Hα flux

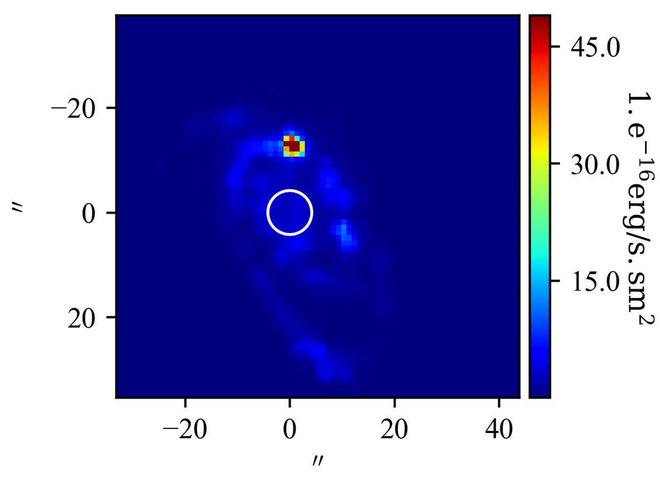

EW(Hα)

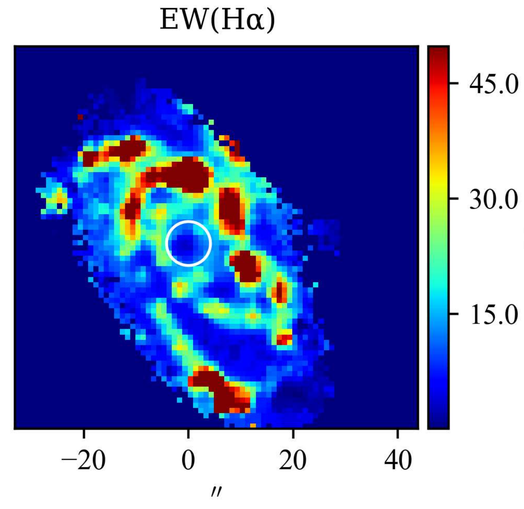

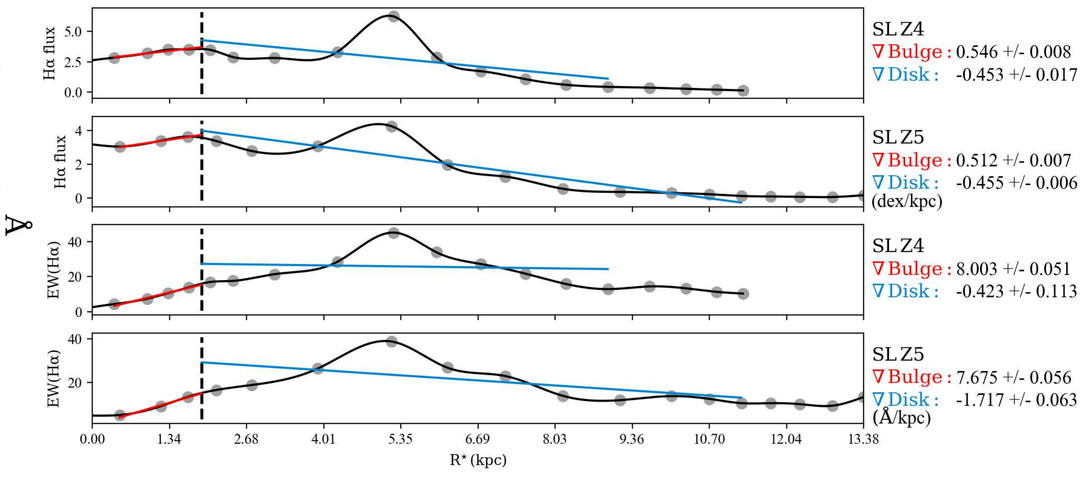

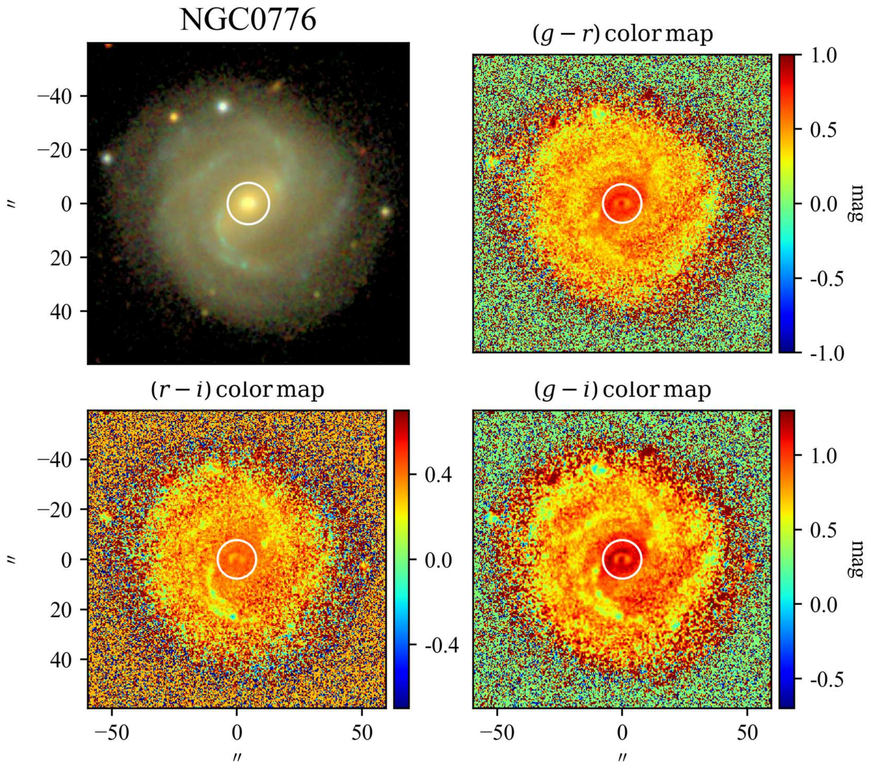

SBP decomposition of SDSS r band

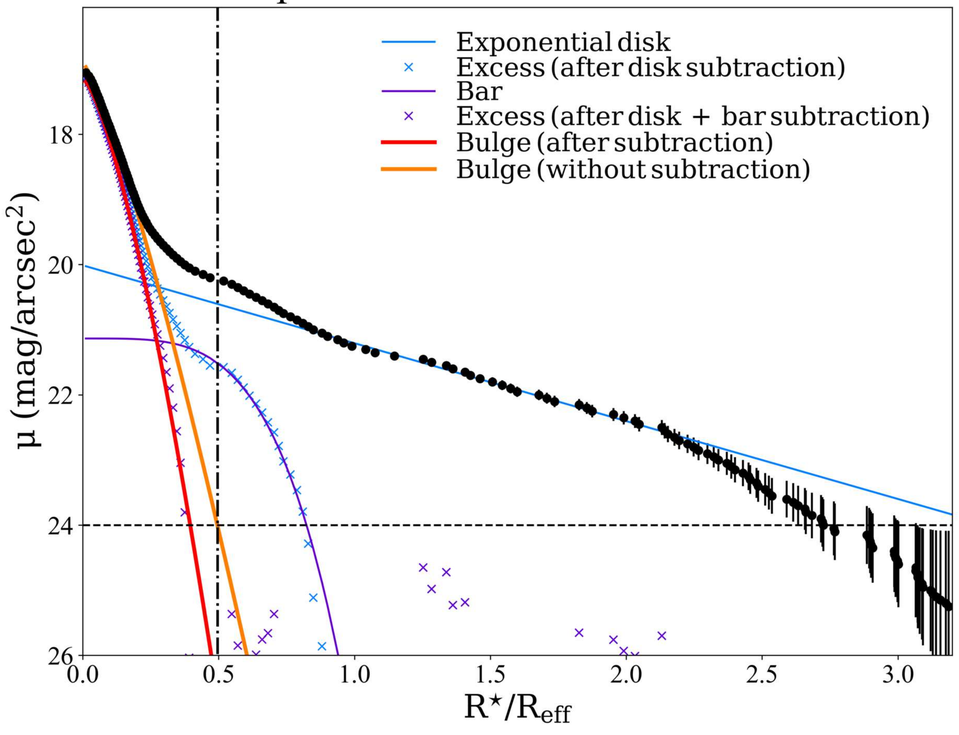

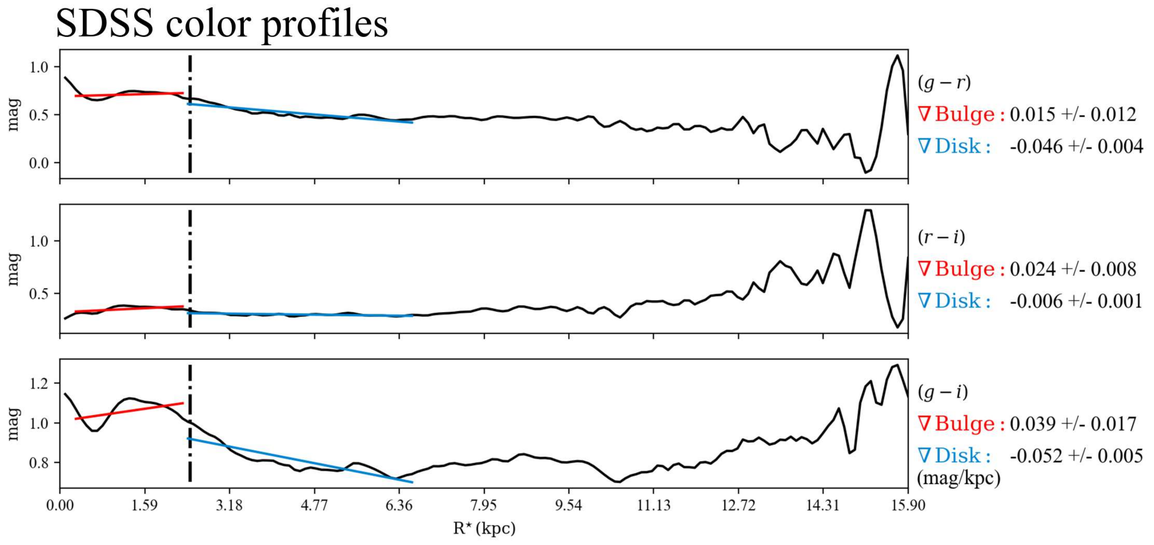

$\mathcal{RY}$ SBPs

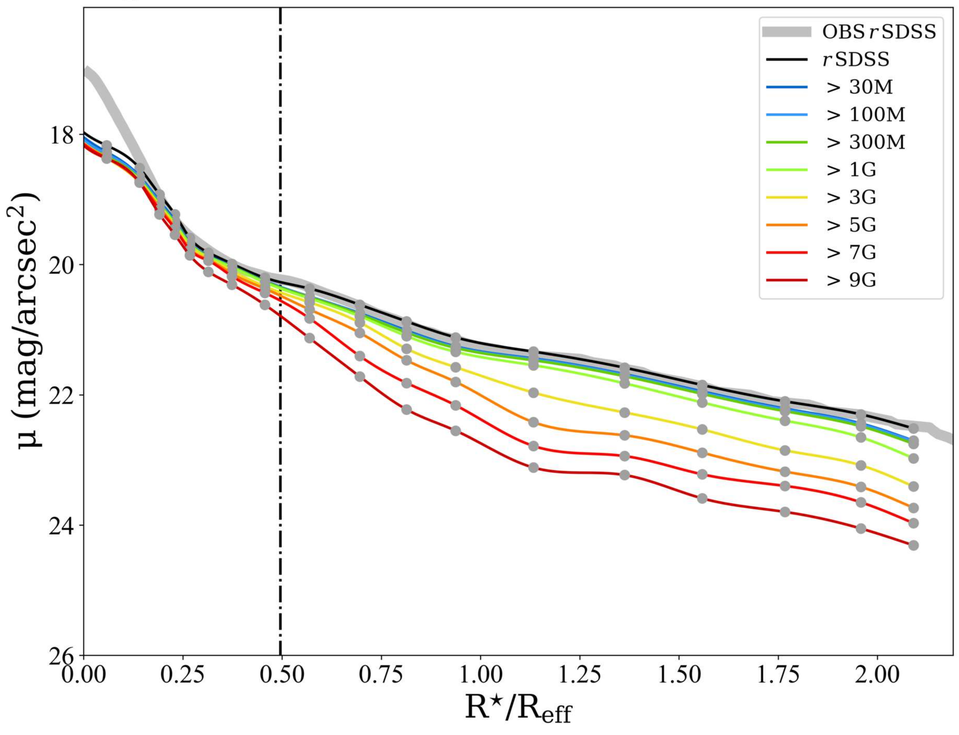

Stellar Continuum

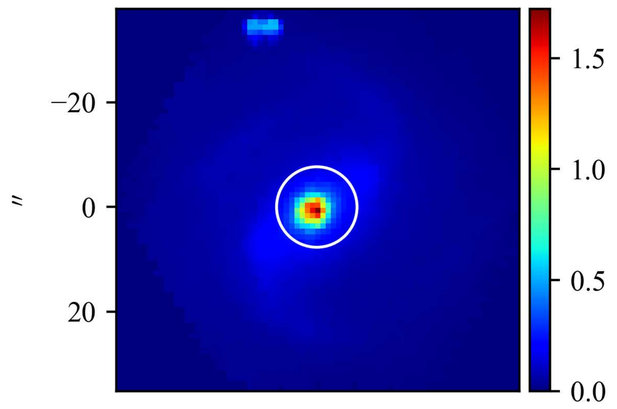

$\mathcal{M}_{\star,\mathrm{P}}$

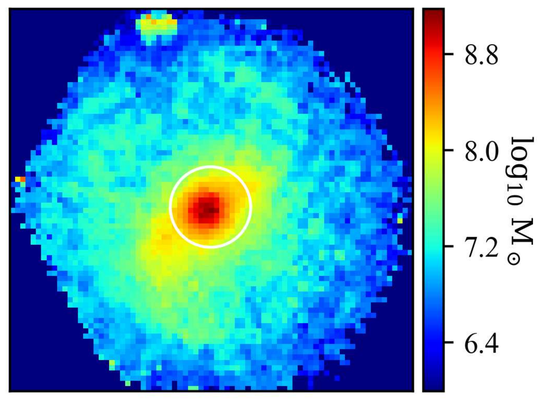

Log. of cumulative present stellar mass profiles

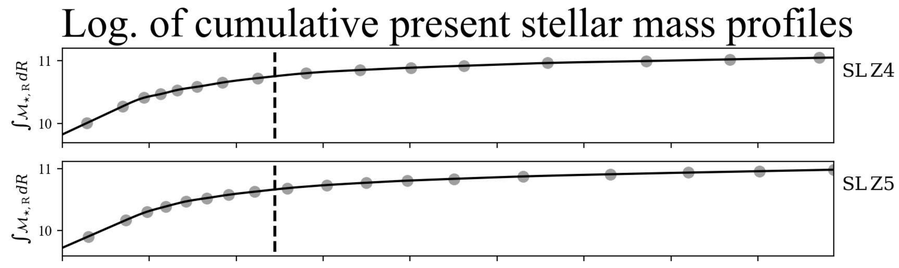

$Z_{\star,\mathcal{L}}$

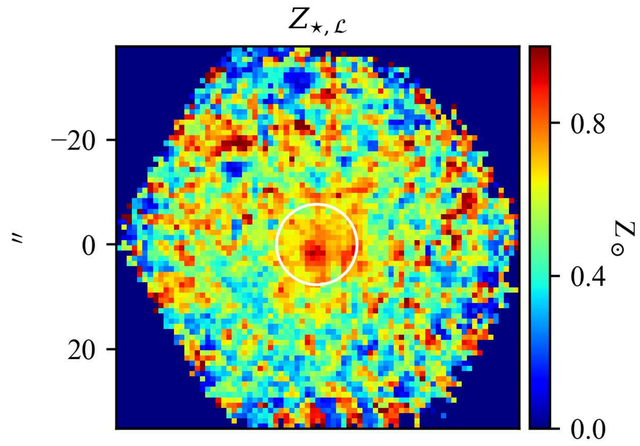

$Z_{\star,\mathcal{M}}$

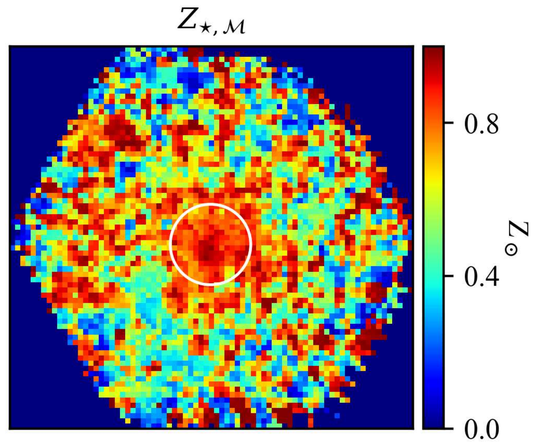

Stellar metallicity/Age & Hα flux/EW profiles

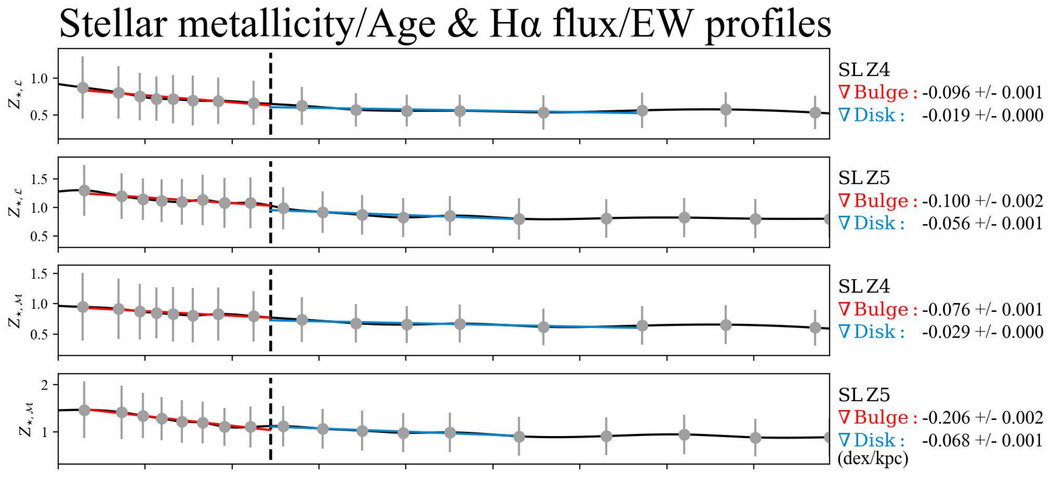

$t_{\star,\mathcal{L}}$

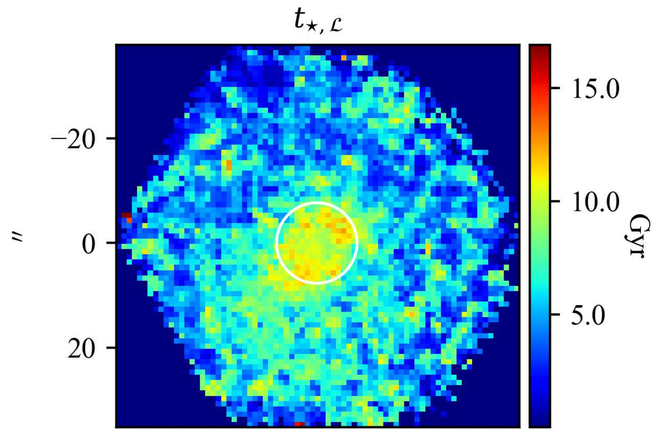

$t_{\star,\mathcal{M}}$

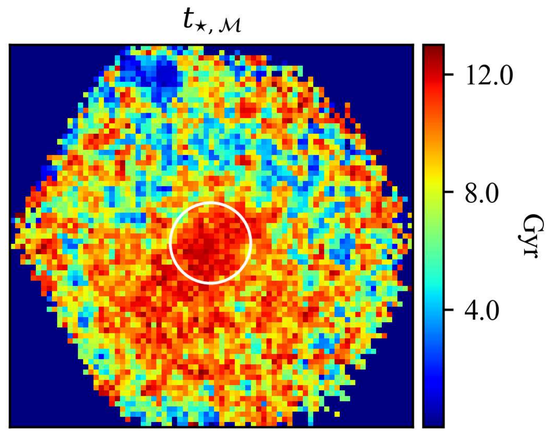

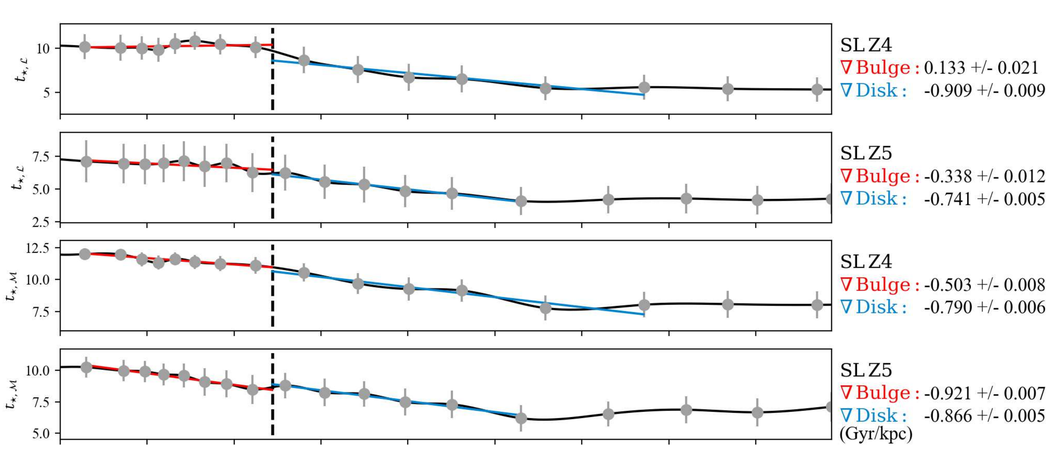

Hα flux

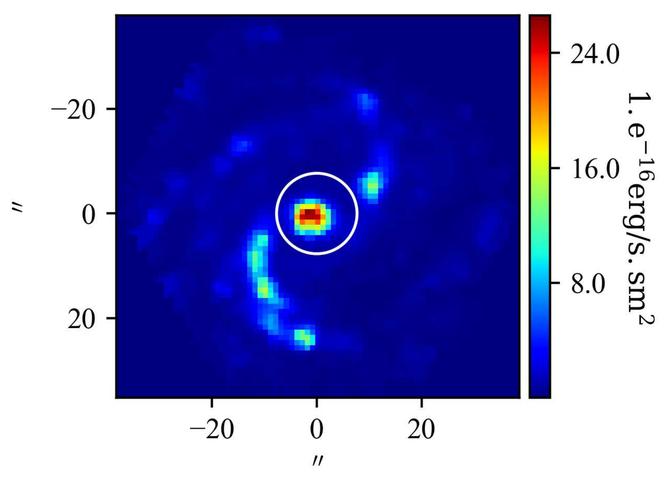

EW(Hα)

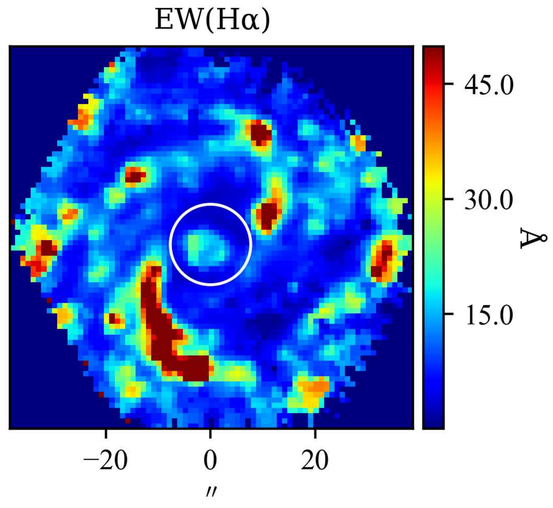

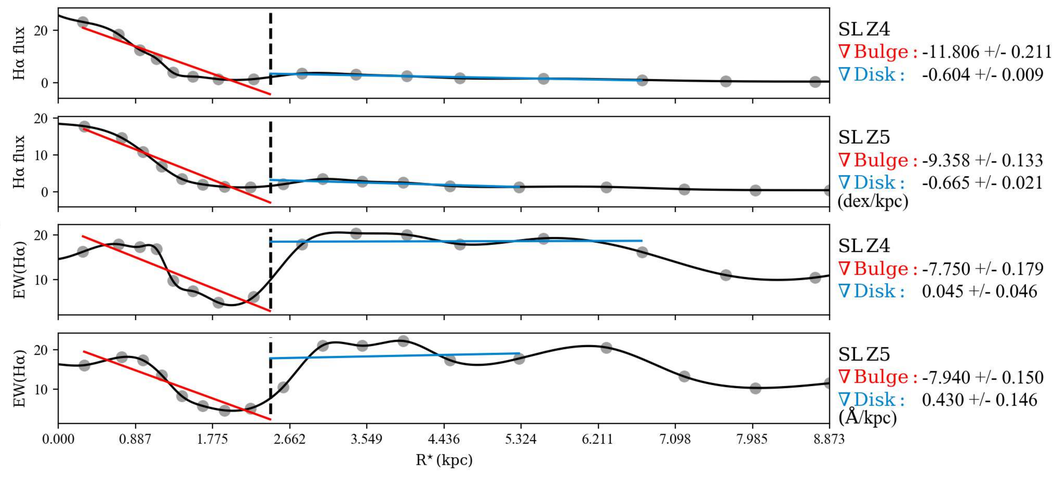

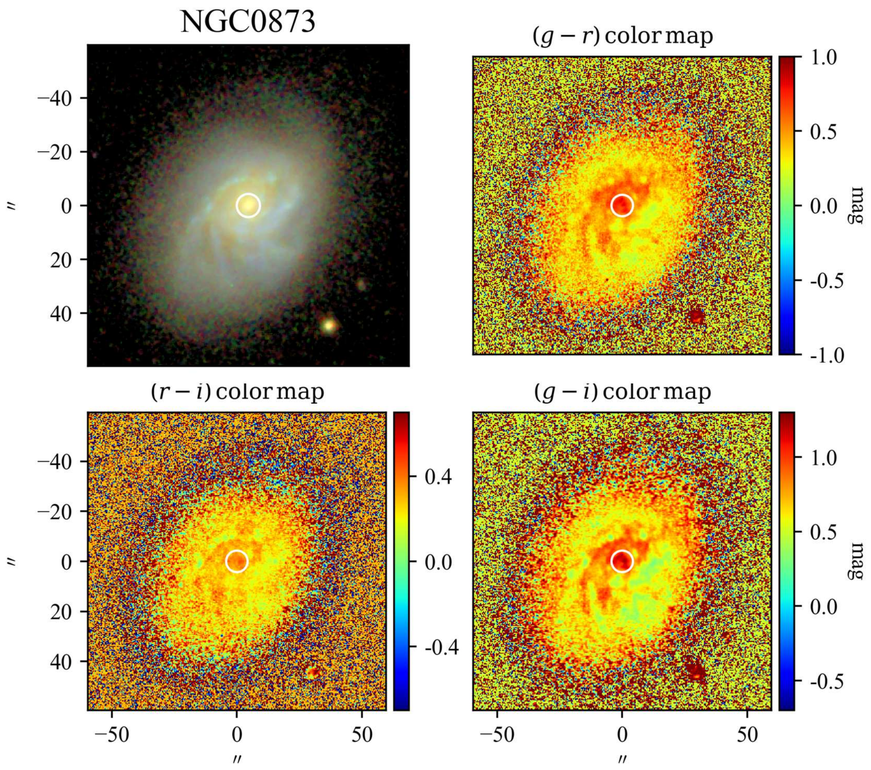

SBP decomposition of SDSS r band

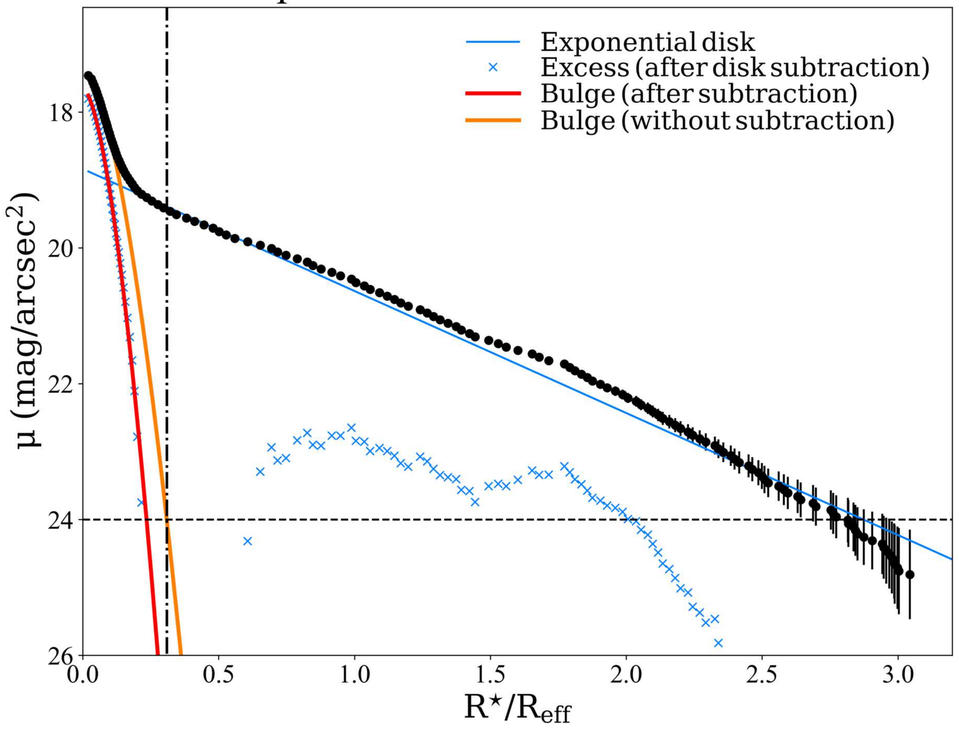

SDSS color profiles

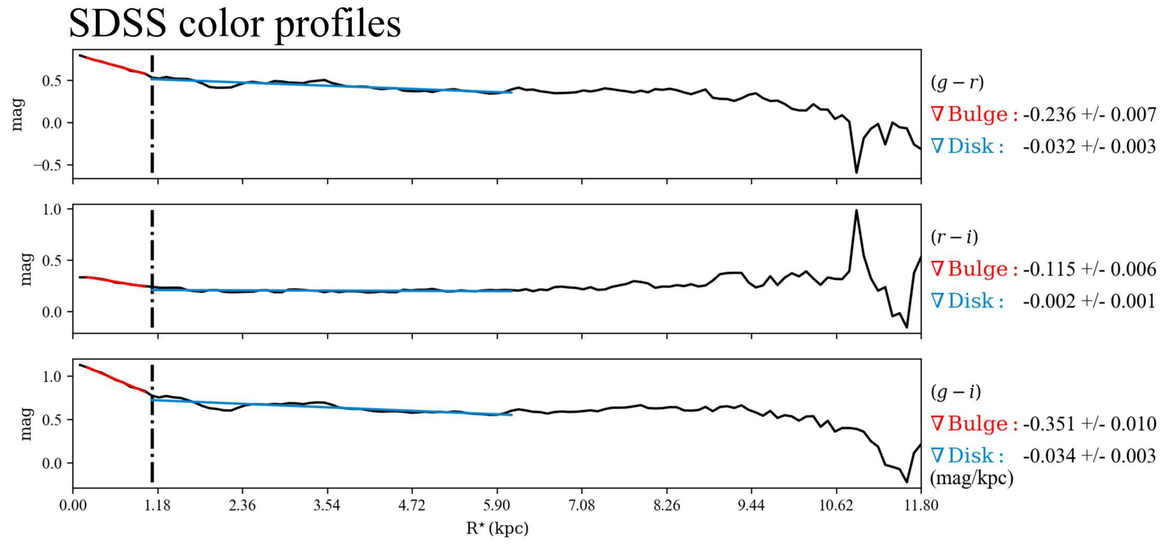

$\mathcal{RY}$ SBPs

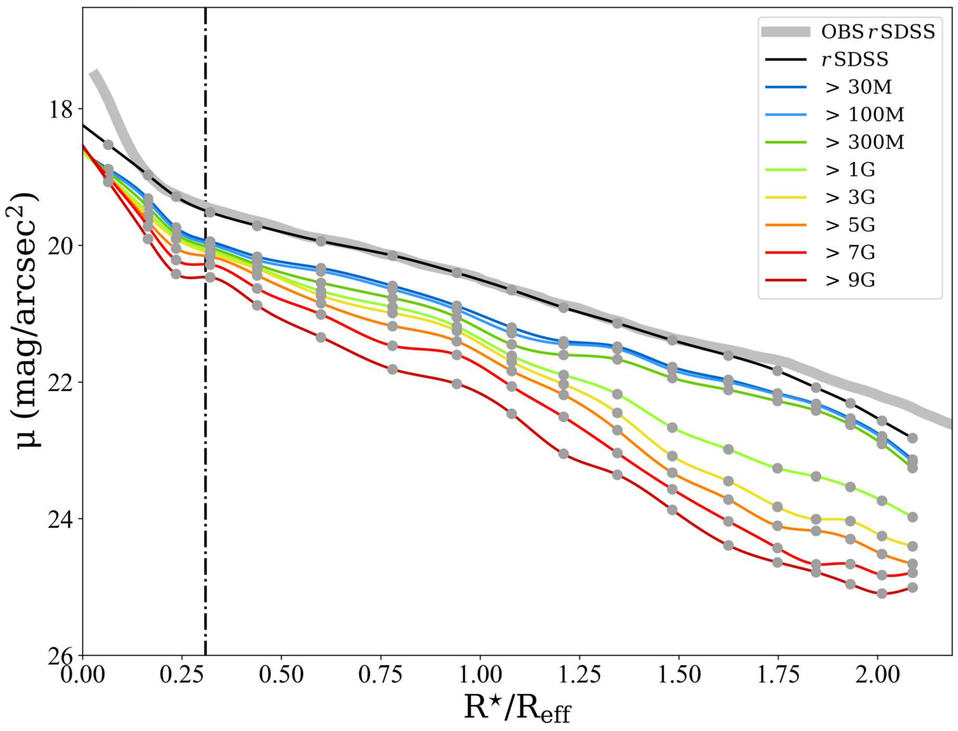

Stellar Continuum

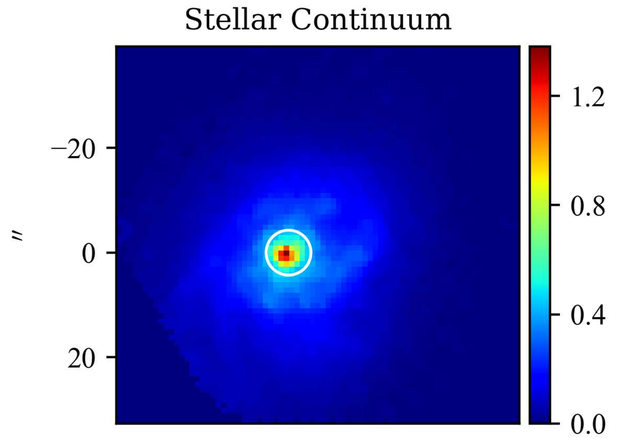

$\mathcal{M}_{\star,\mathrm{P}}$

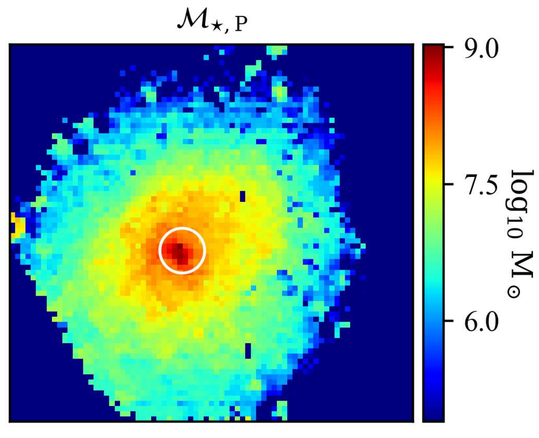

Log. of cumulative present stellar mass profiles

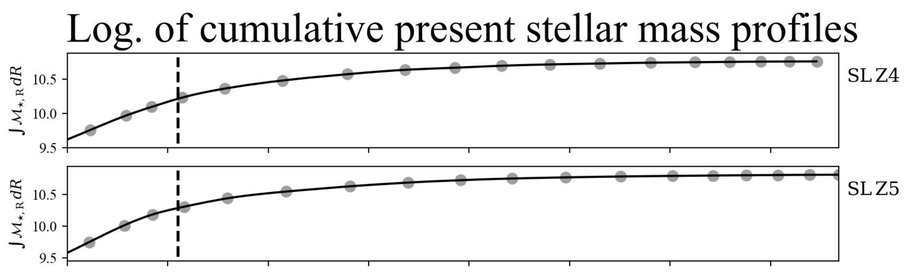

$Z_{\star,\mathcal{L}}$

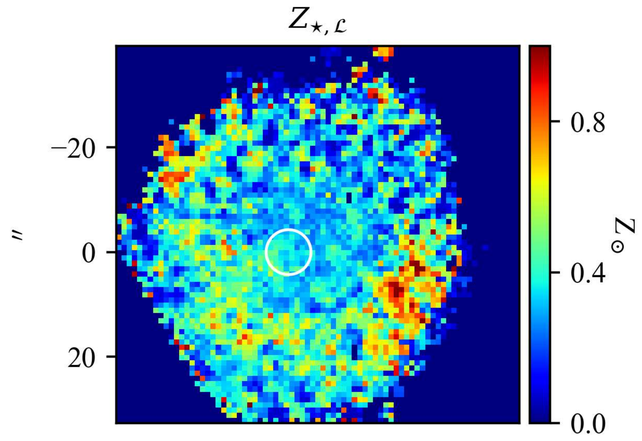

$Z_{\star,\mathcal{M}}$

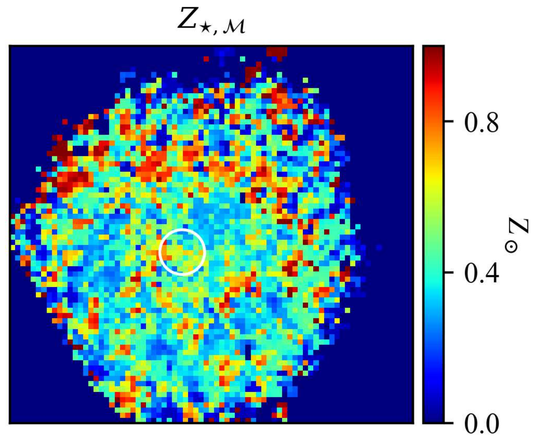

Stellar metallicity/Age & Hα flux/EW profiles

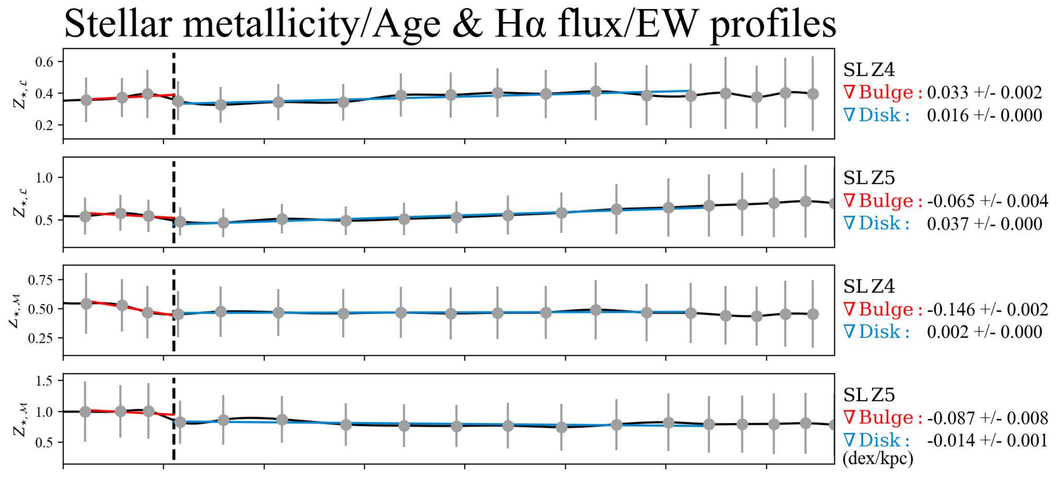

$t_{\star,\mathcal{L}}$

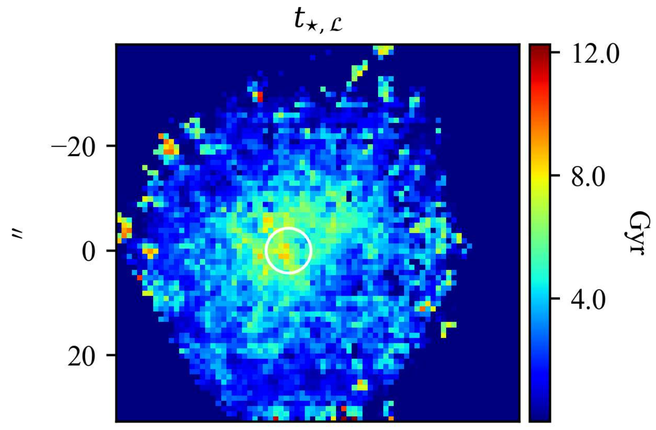

$t_{\star,\mathcal{M}}$

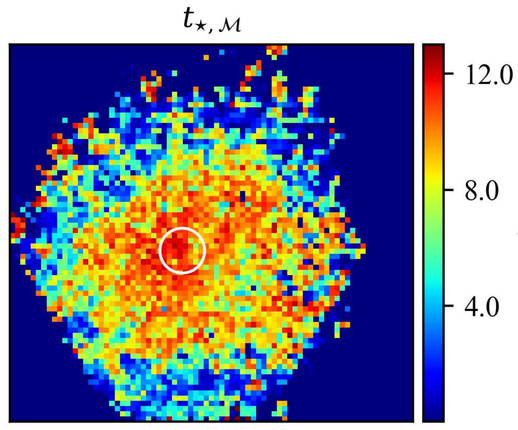

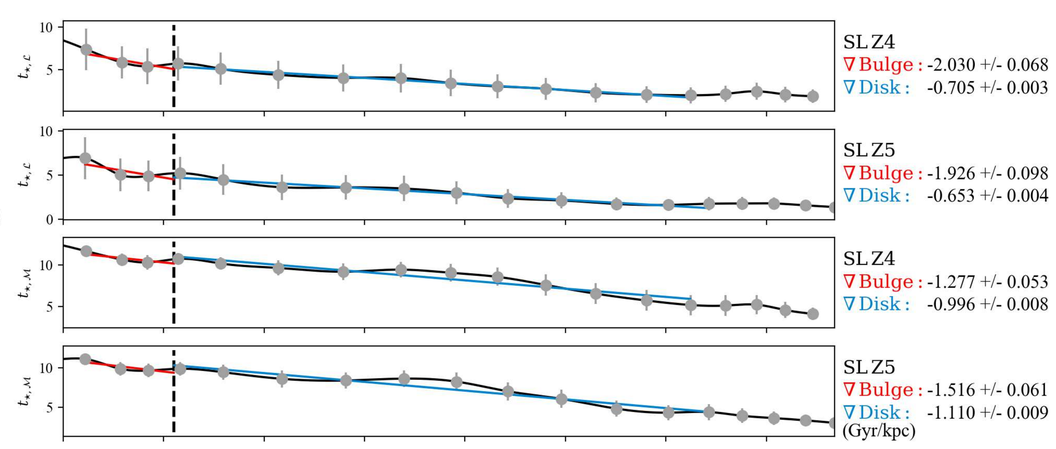

Hα flux

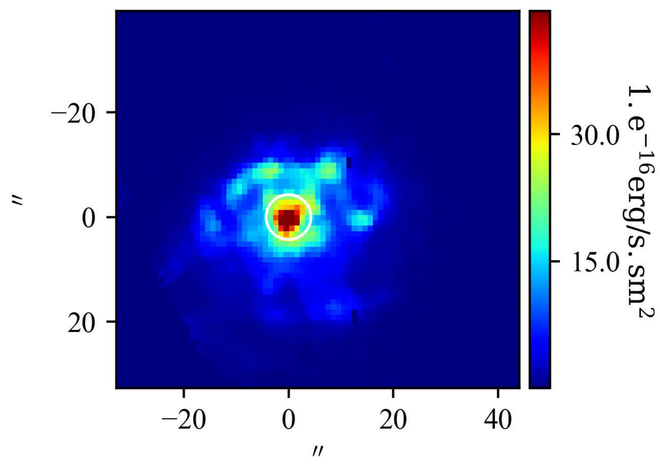

EW(Hα)

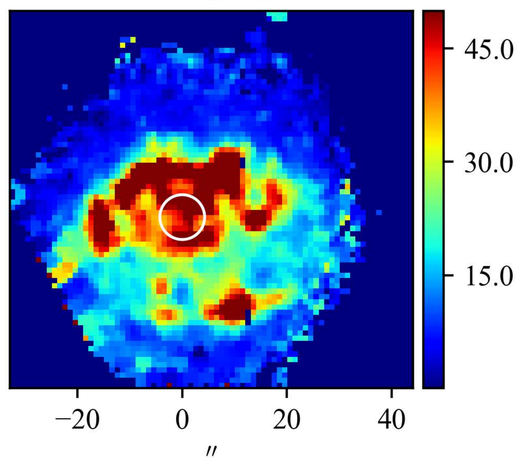

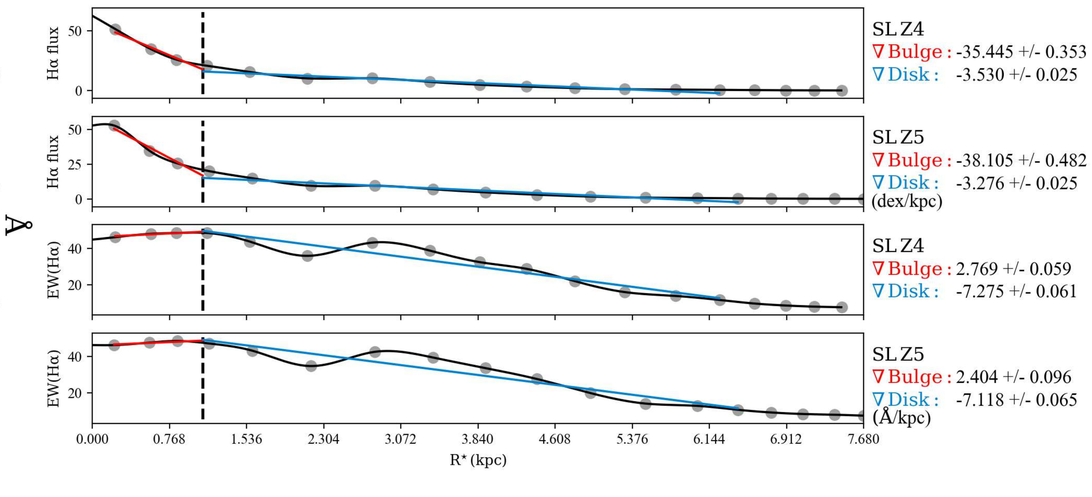

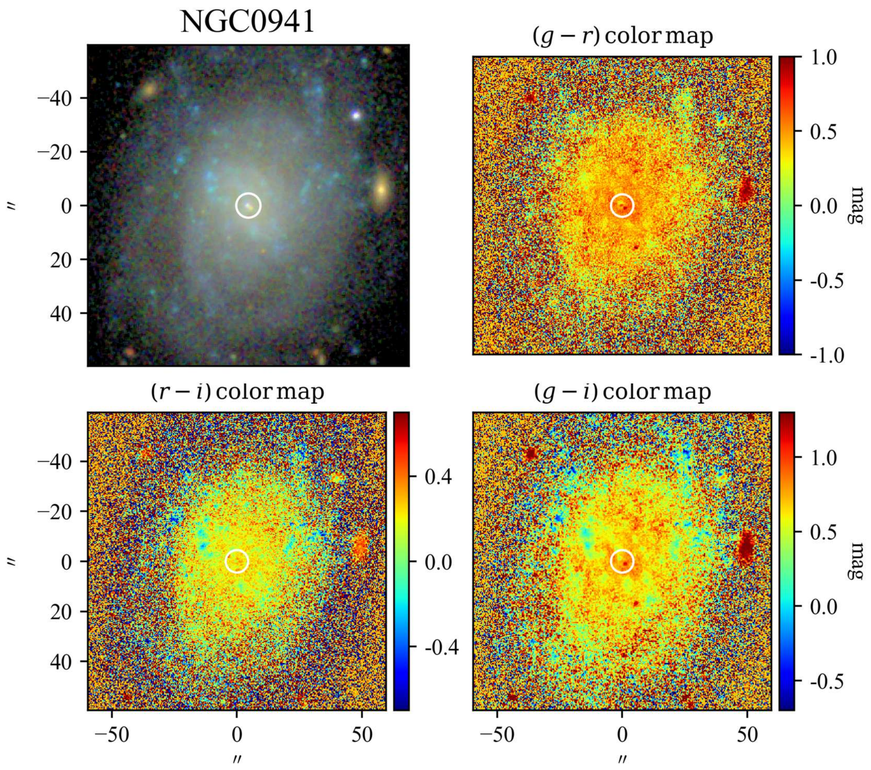

SBP decomposition of SDSS r band

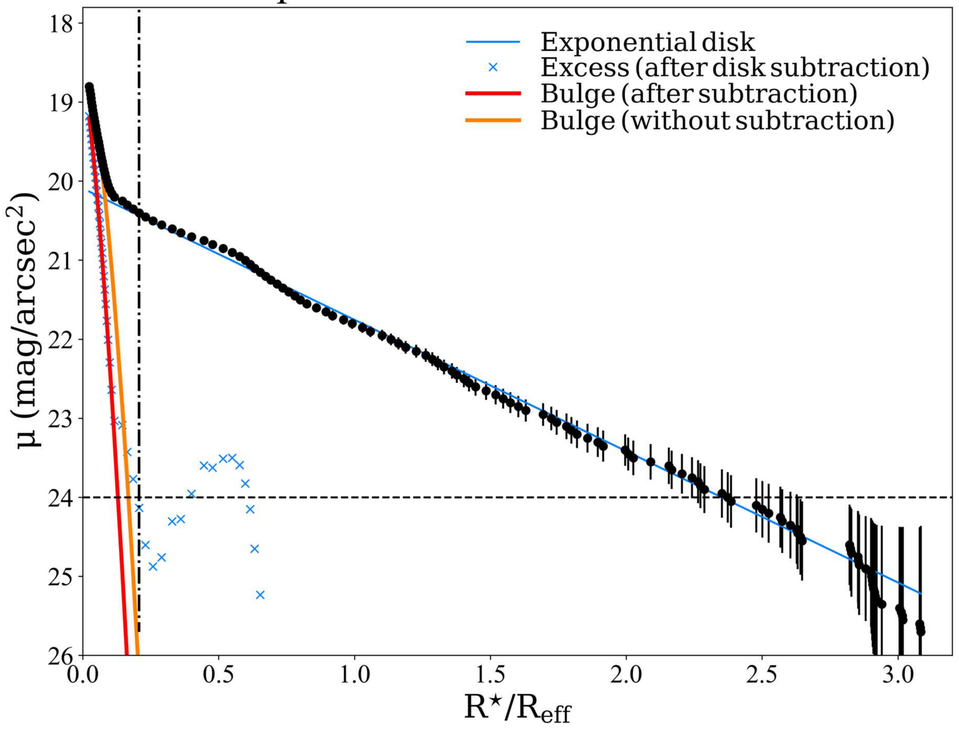

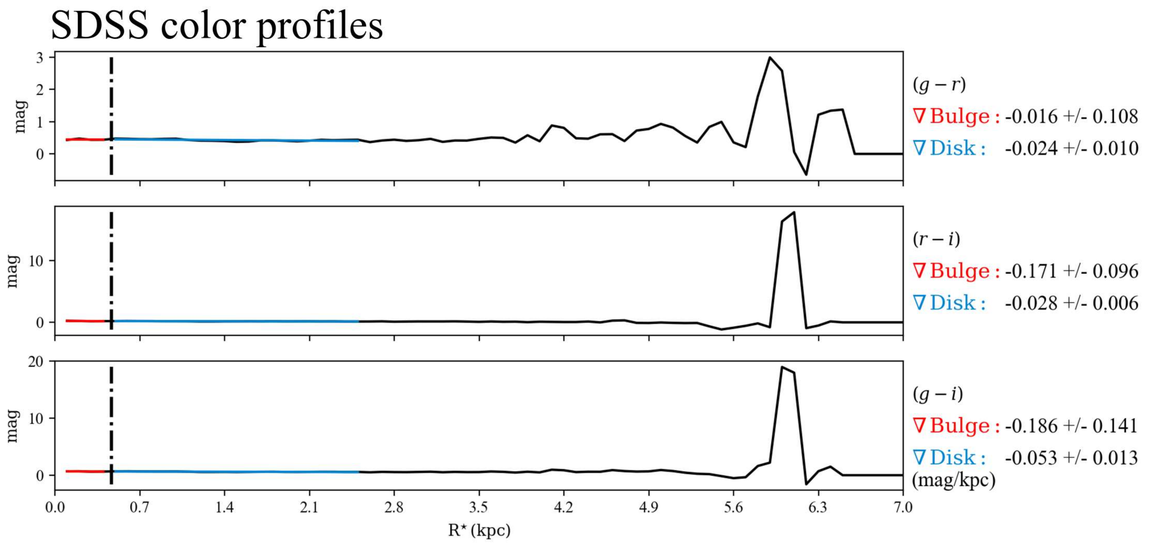

$\mathcal{RV}$ SBPs

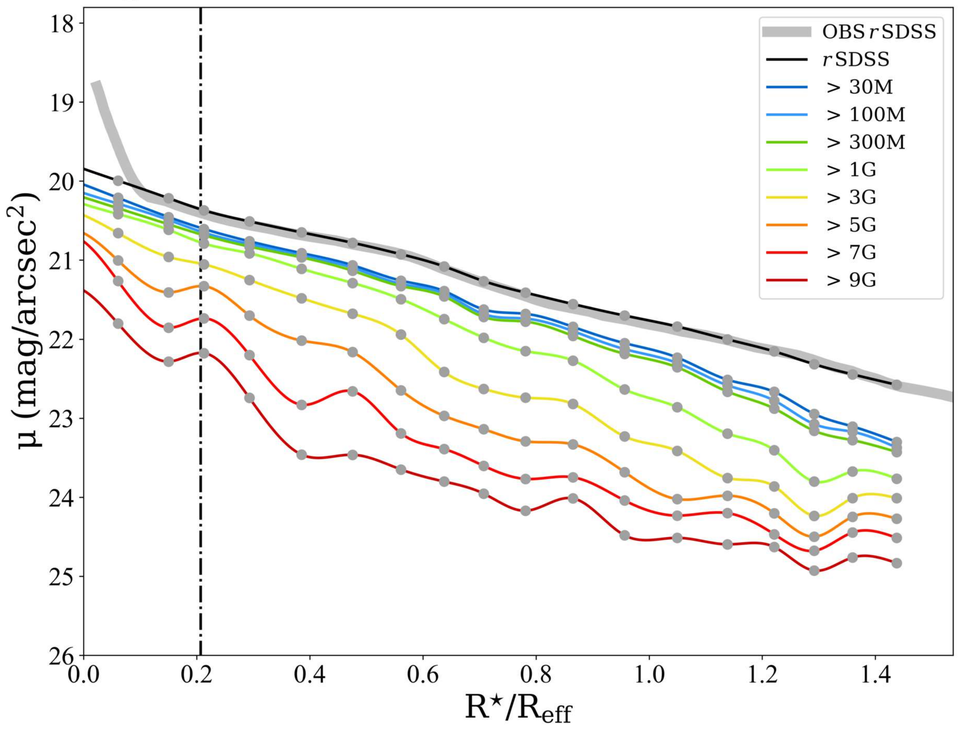

Stellar Continuum $\mathcal{M}_{\star,\rm P}$

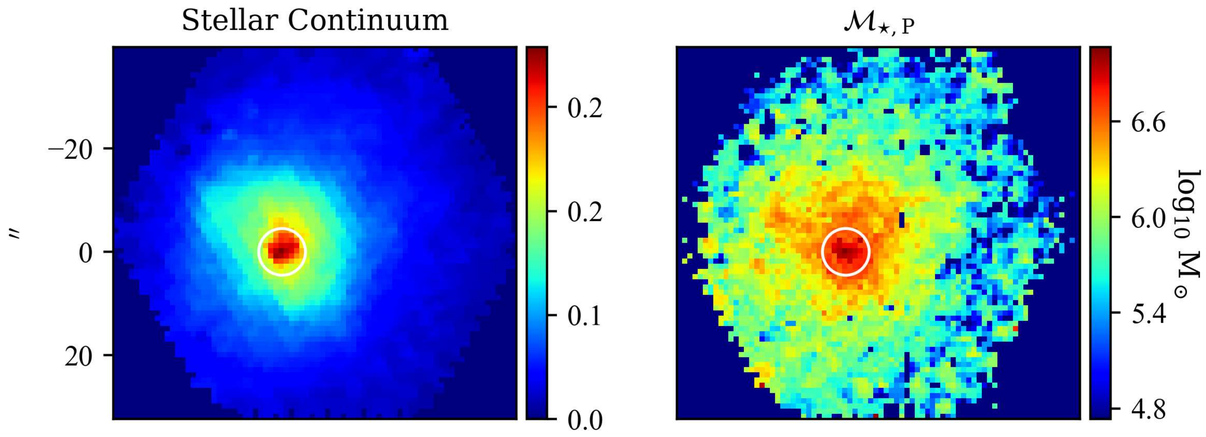

Log. of cumulative present stellar mass profiles

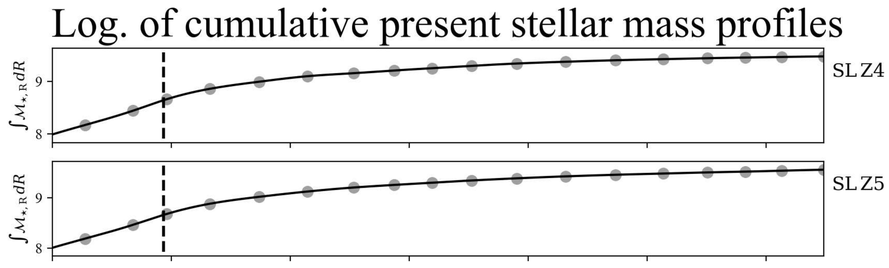

$Z_{\star,\mathcal{L}}$ $Z_{\star,\mathcal{M}}$

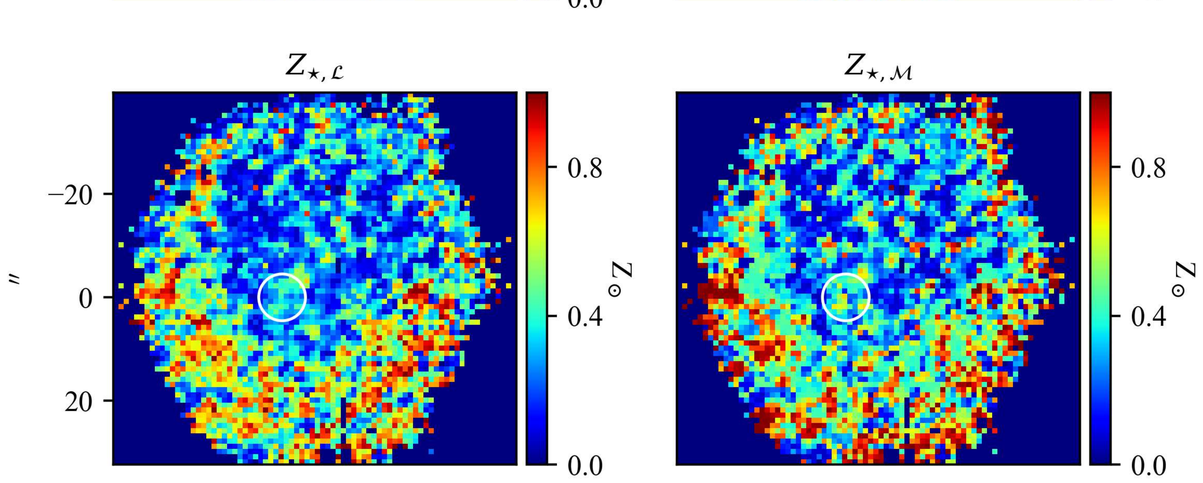

Stellar metallicity/Age & Hα flux/EW profiles

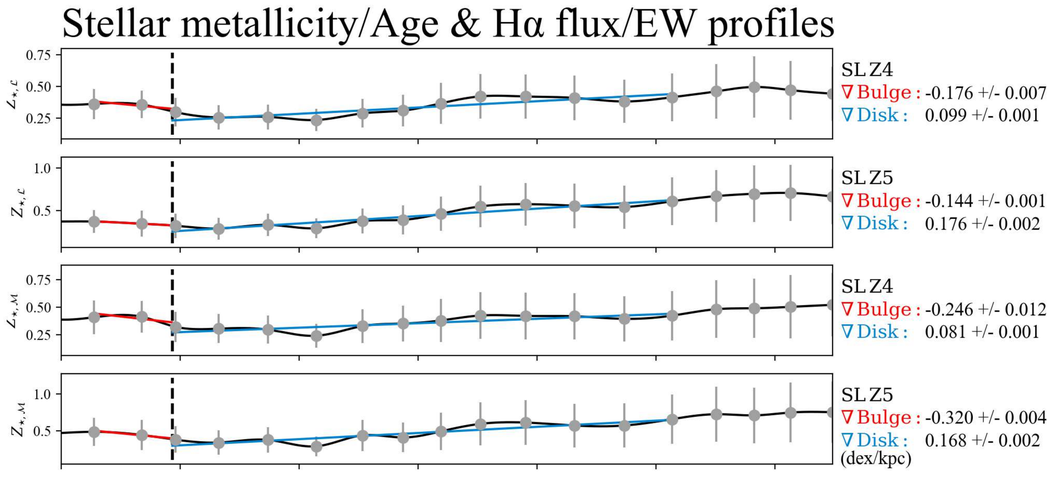

$t_{\star,\mathcal{L}}$ $t_{\star,\mathcal{M}}$

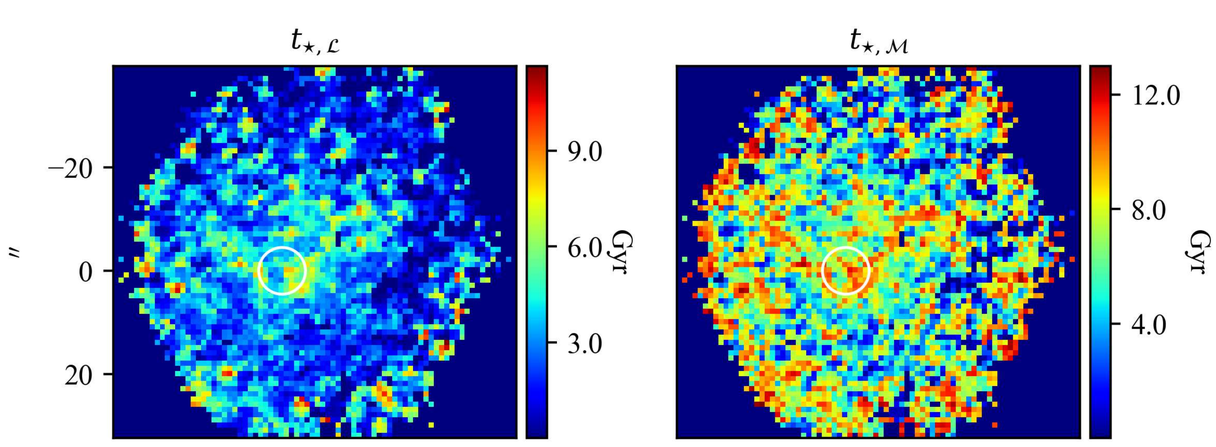

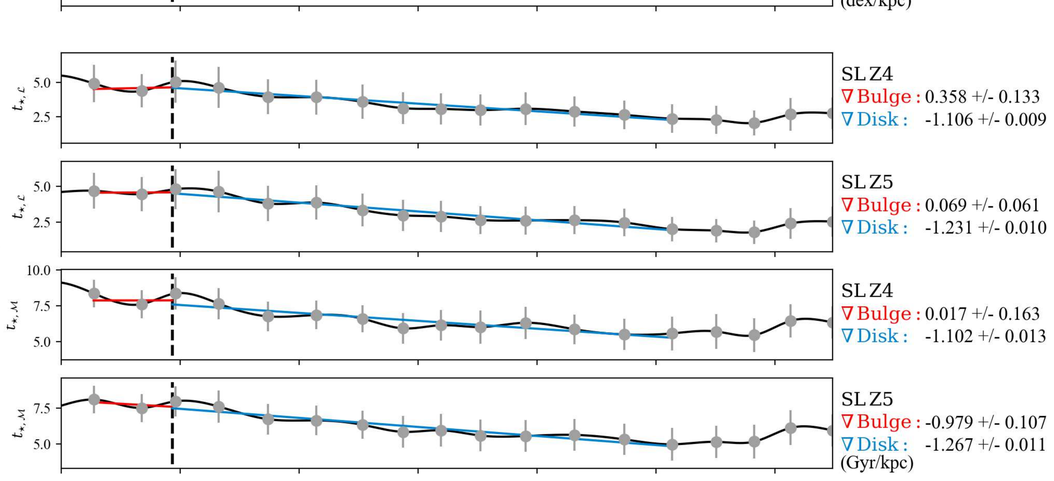

Hα flux EW(Hα)

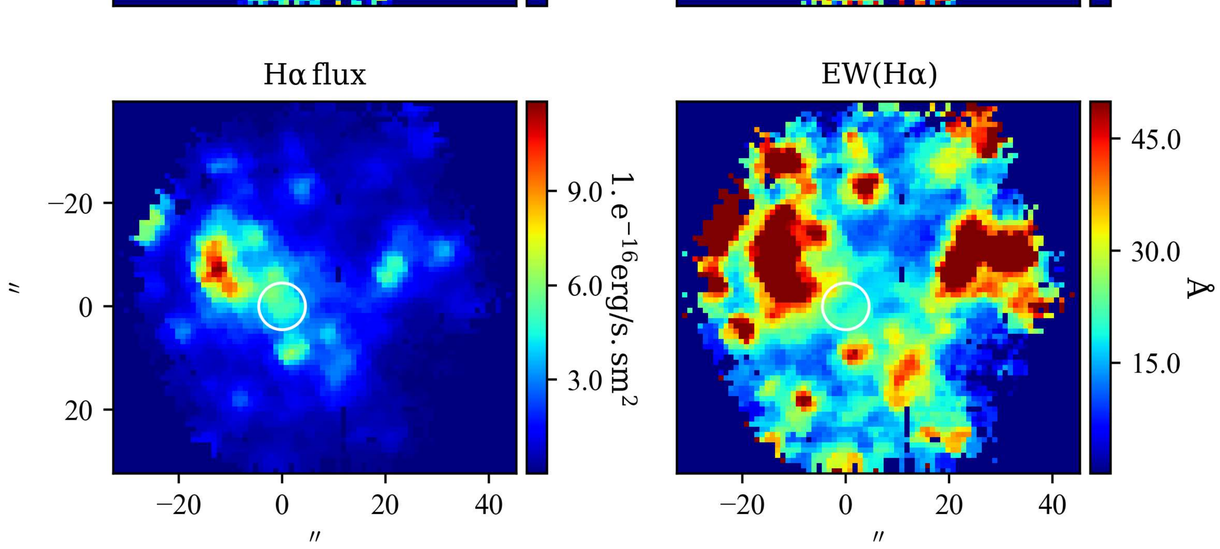

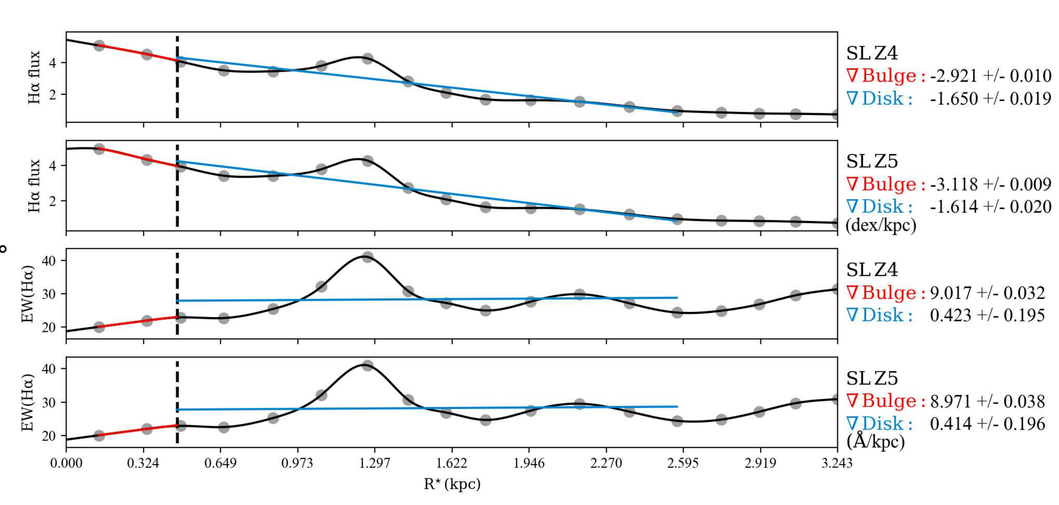

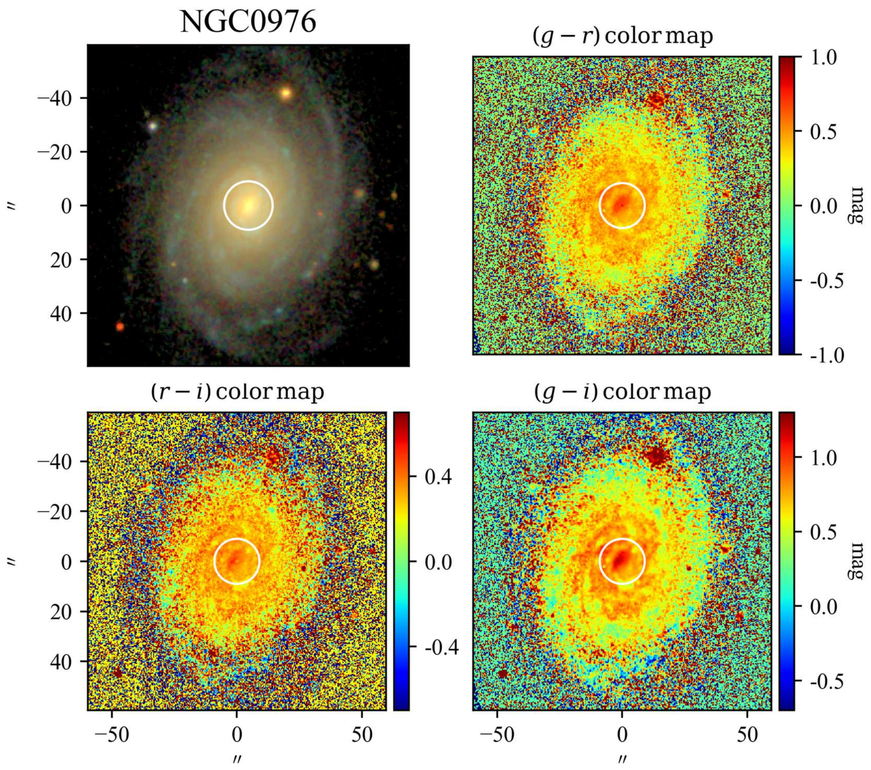

SBP decomposition of SDSS r band

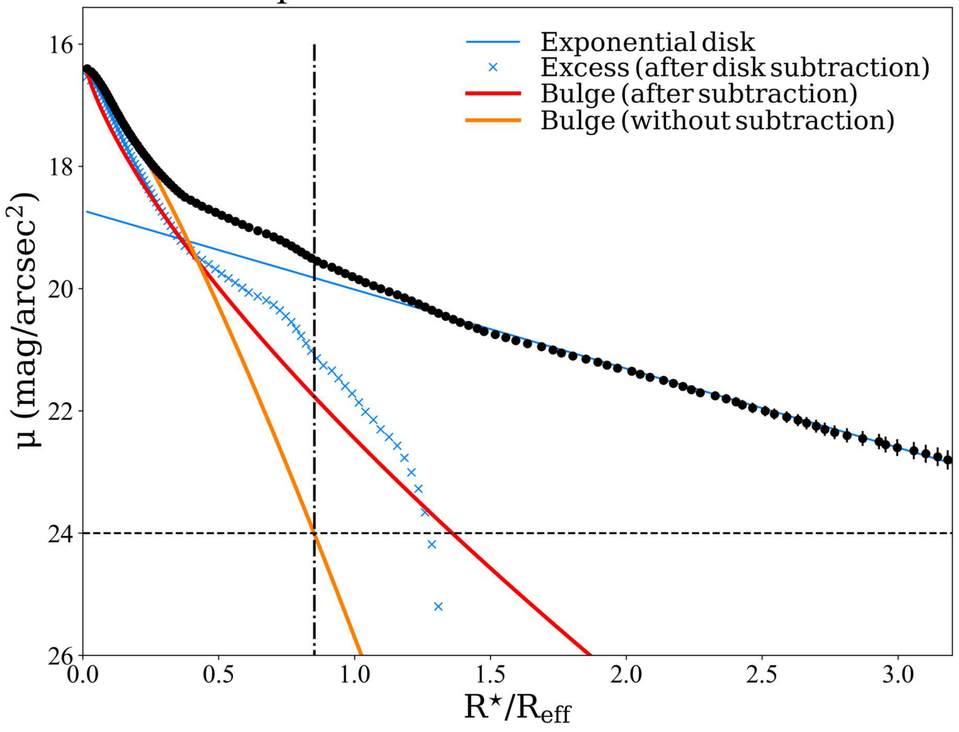

SDSS color profiles

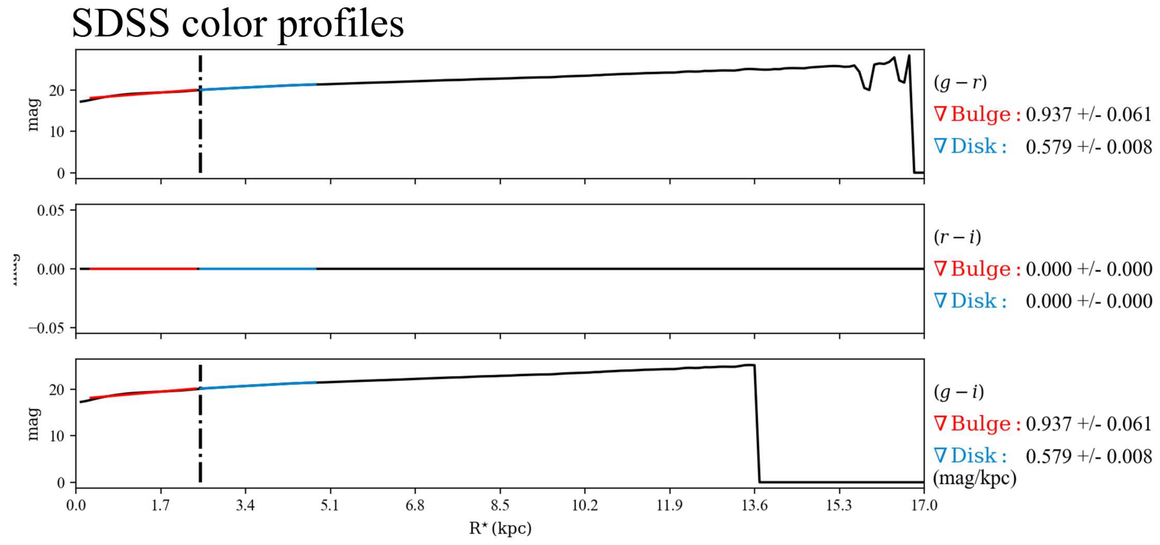

$\mathcal{RY}$ SBPs

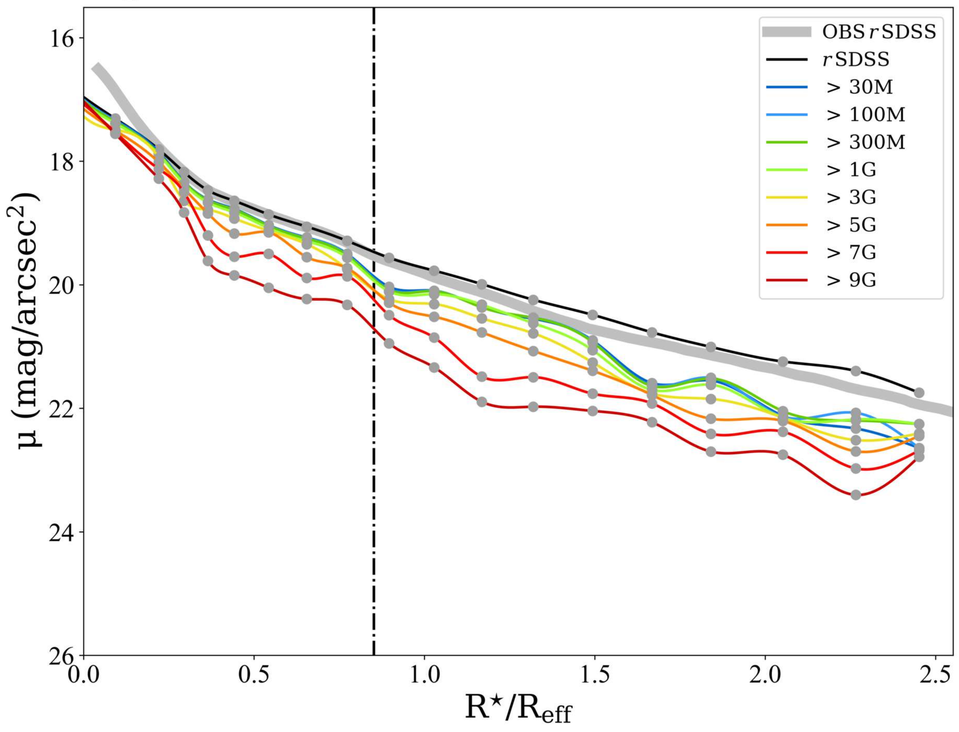

Stellar Continuum

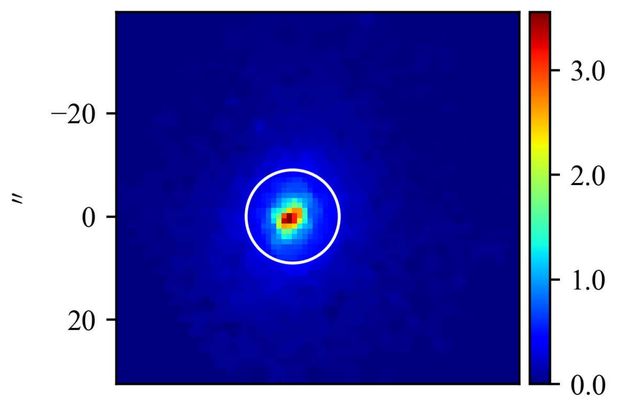

$\mathcal{M}_{\star,\,\rm P}$

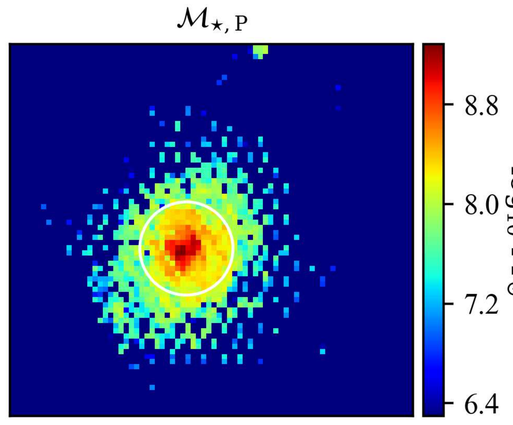

Log. of cumulative present stellar mass profiles

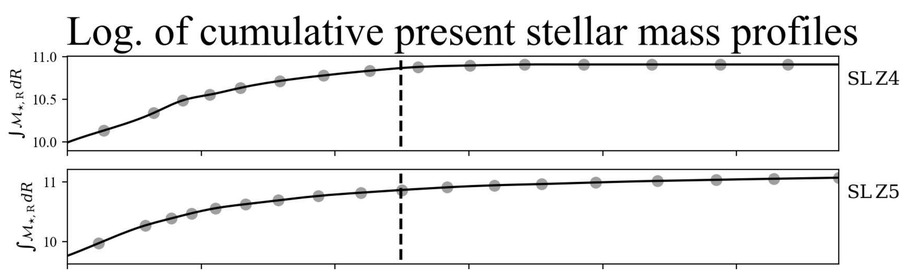

$Z_{\star,\,\mathcal{L}}$

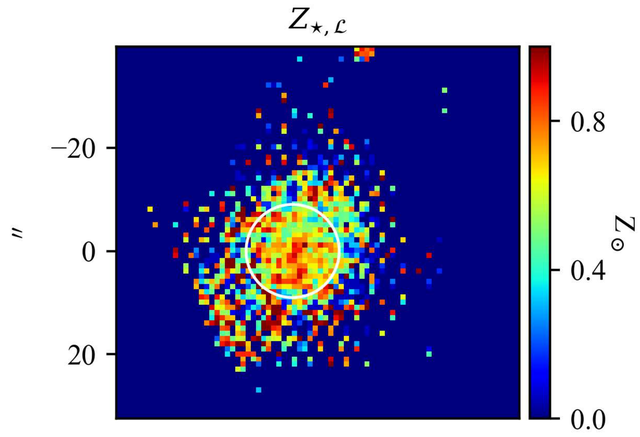

$Z_{\star,\,\mathcal{M}}$

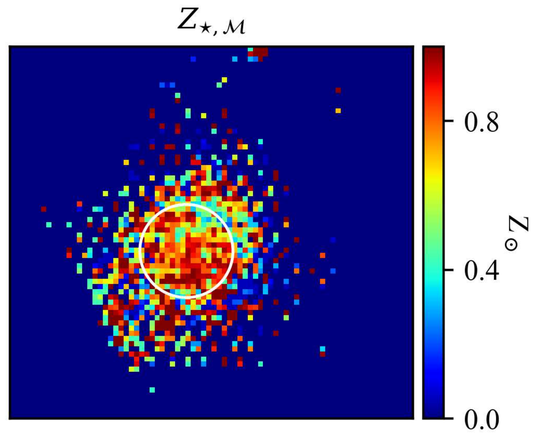

Stellar metallicity/Age & Hα flux/EW profiles

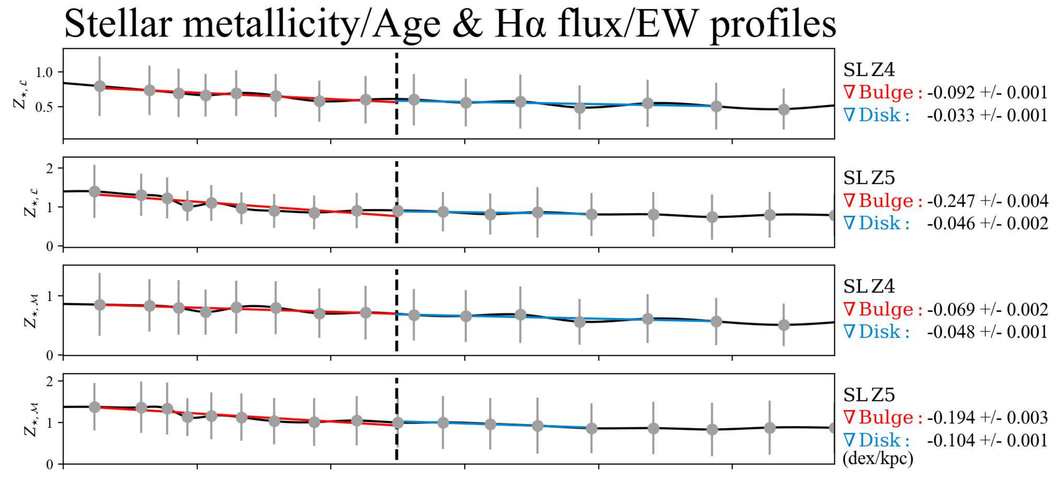

$t_{\star,\,\mathcal{L}}$

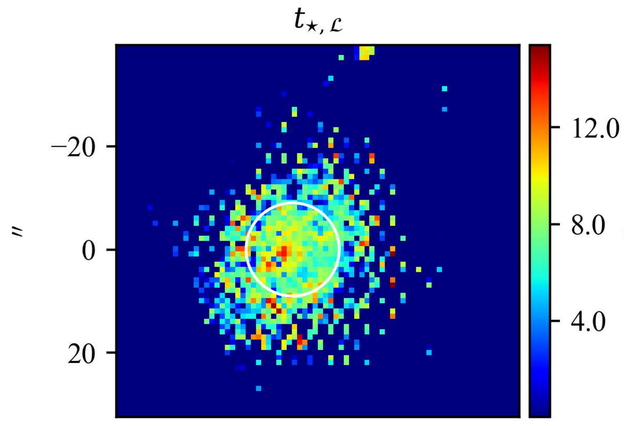

$t_{\star,\,\mathcal{M}}$

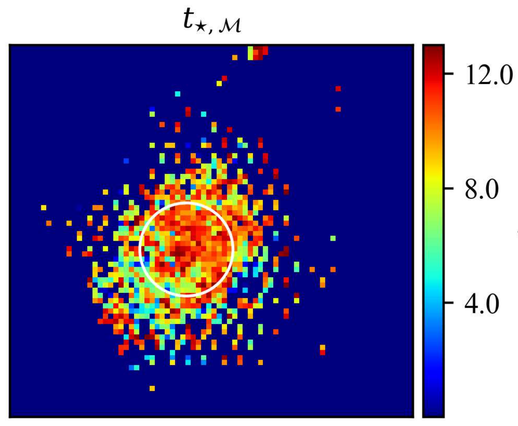

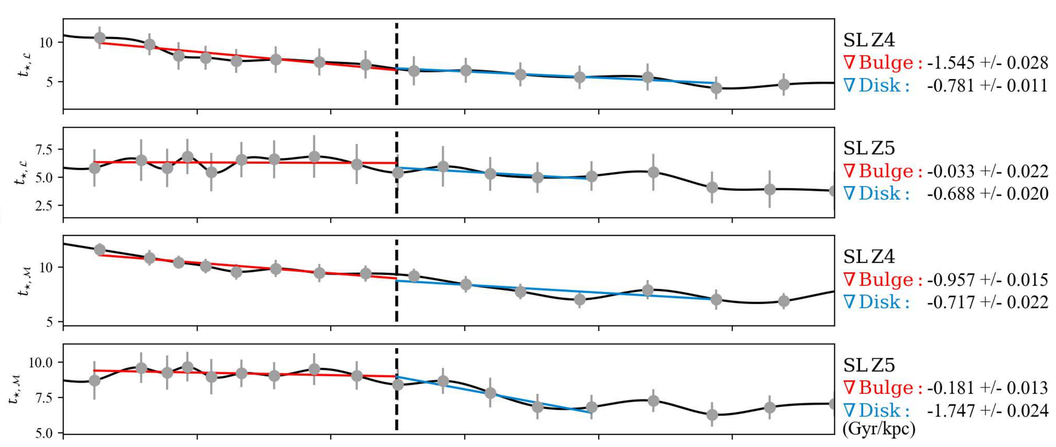

Hα flux

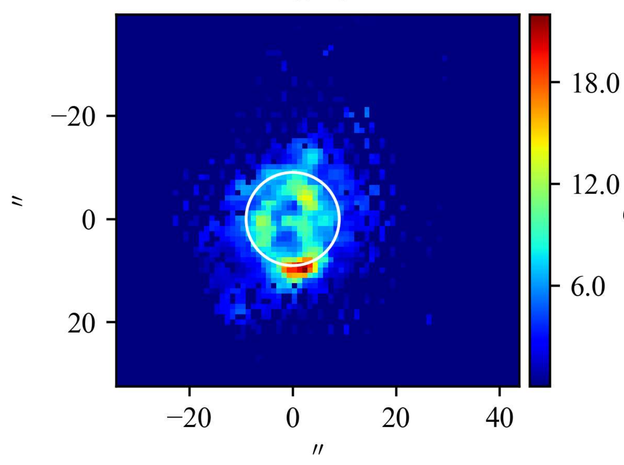

EW(Hα)

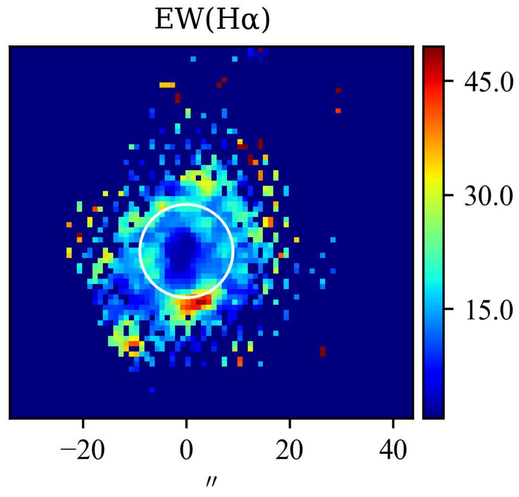

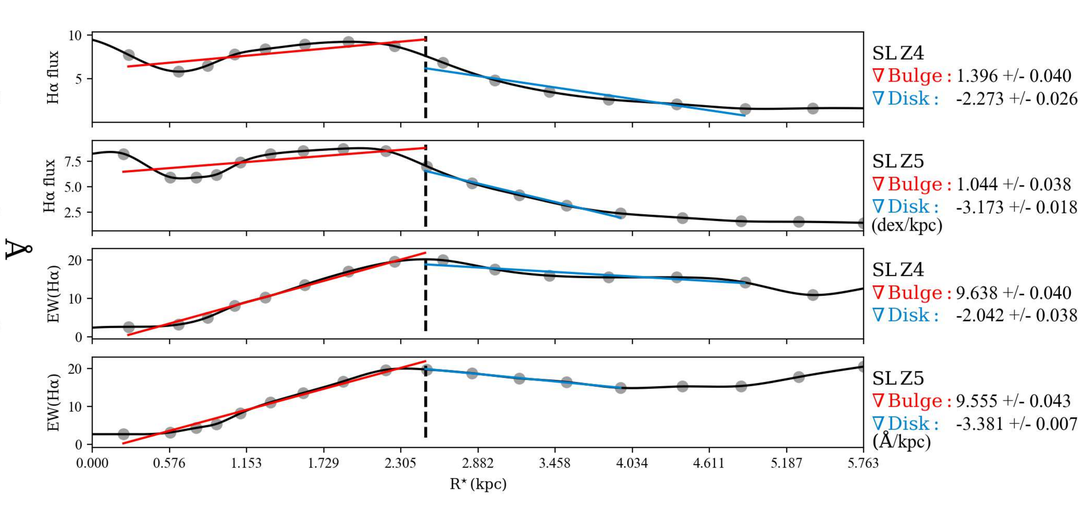

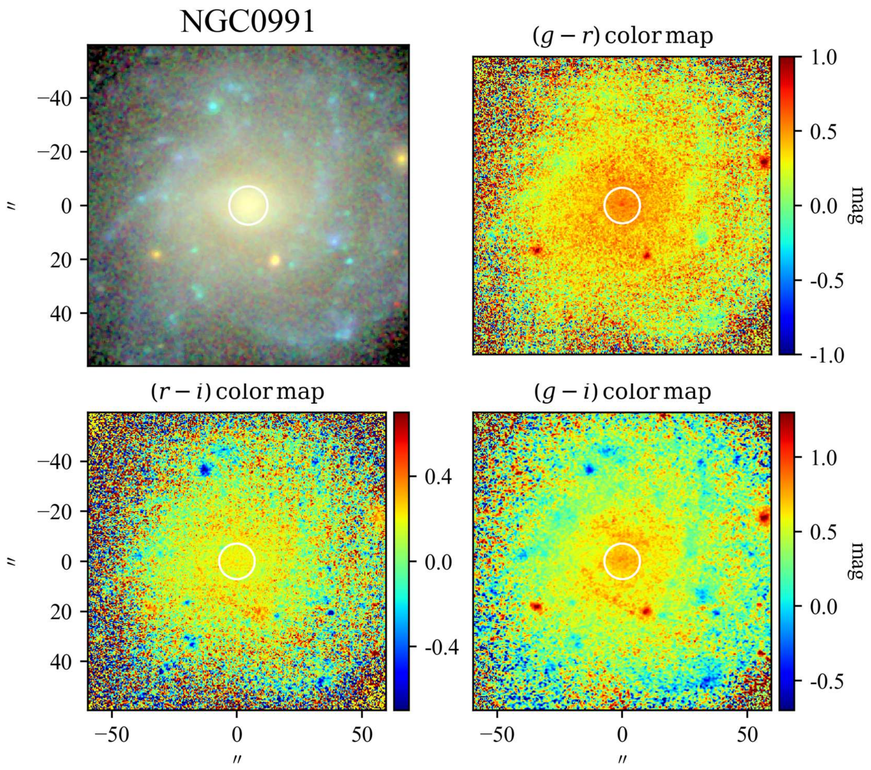

SBP decomposition of SDSS r band

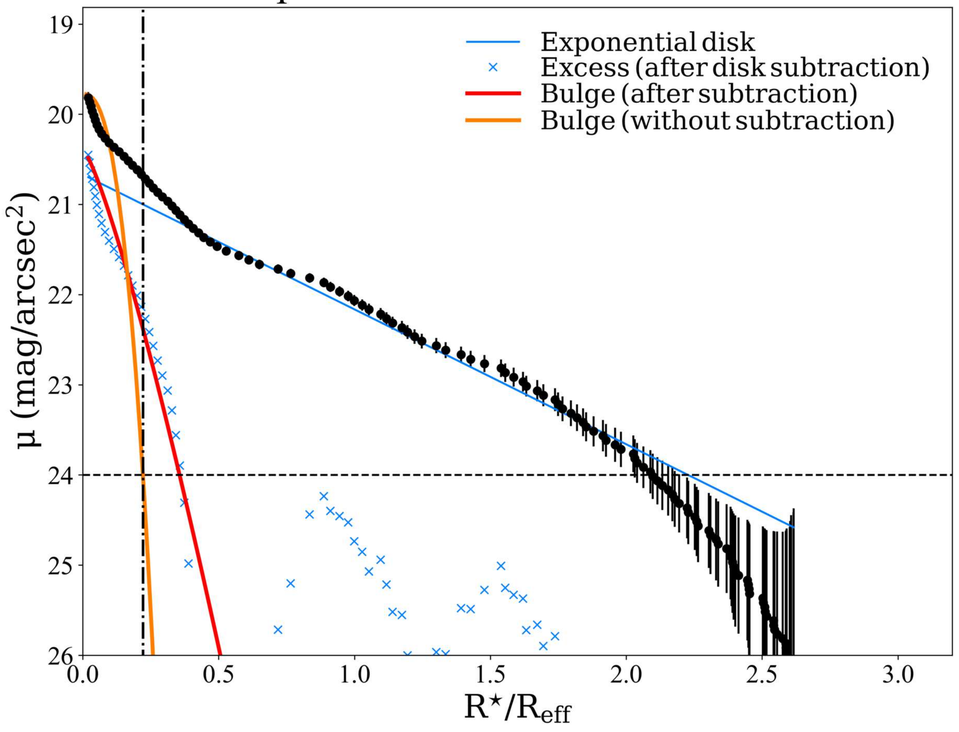

SDSS color profiles

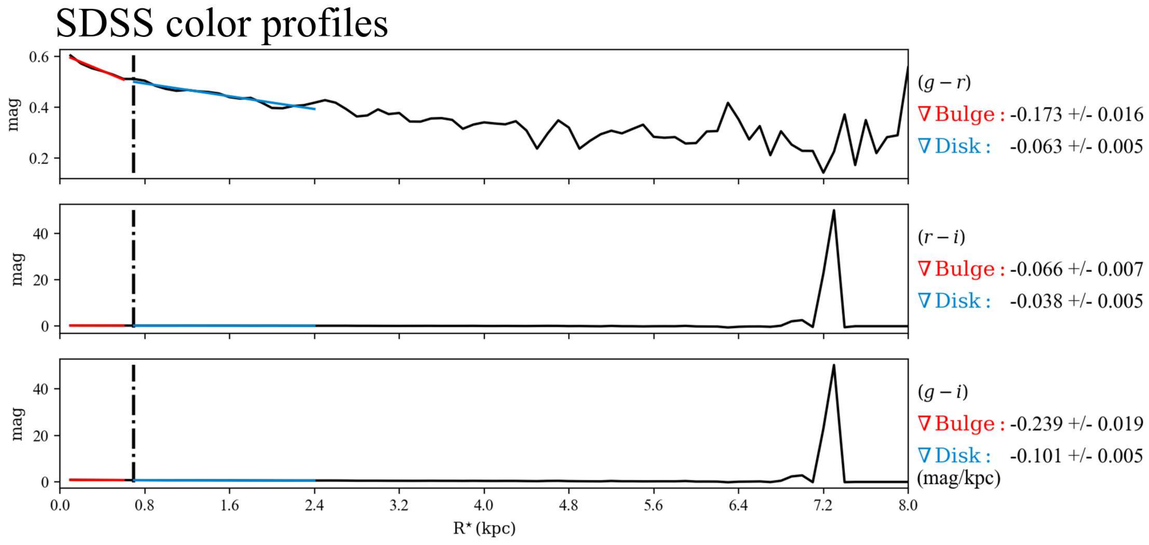

$\mathcal{RY}$ SBPs

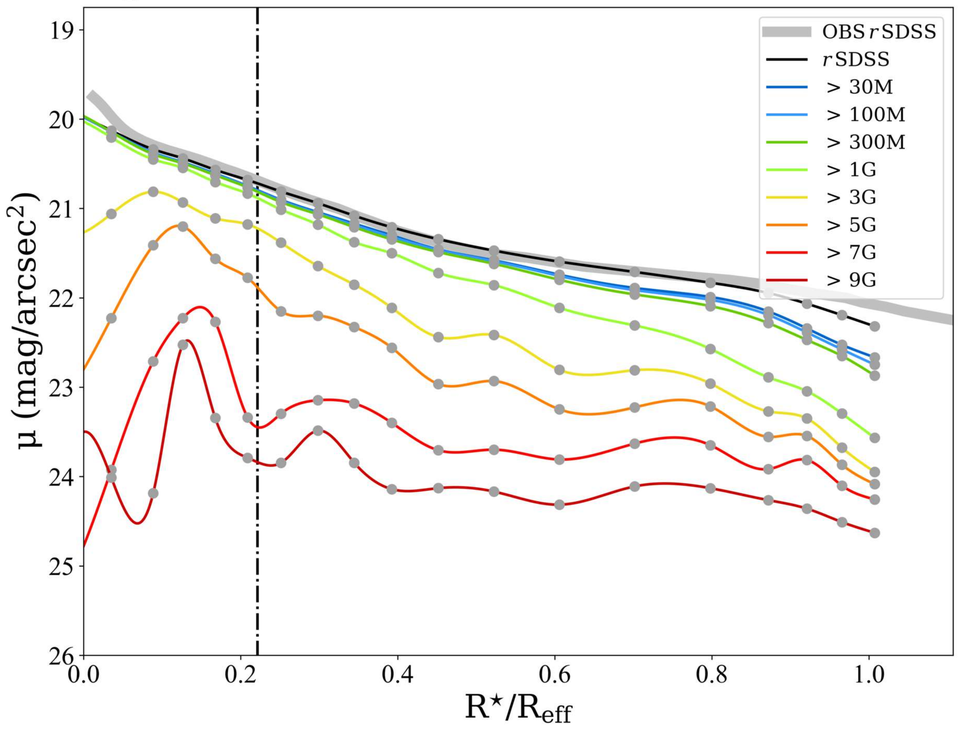

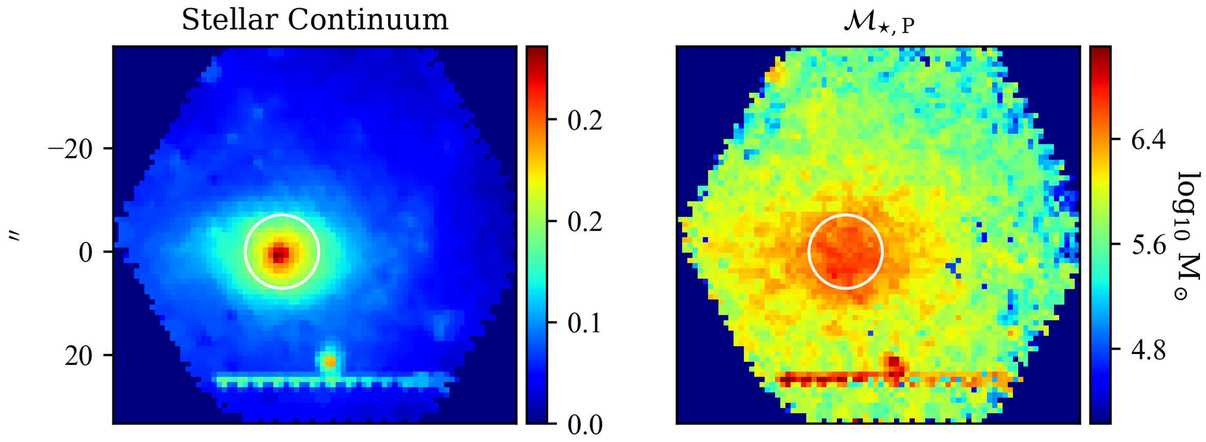

Log. of cumulative present stellar mass profiles

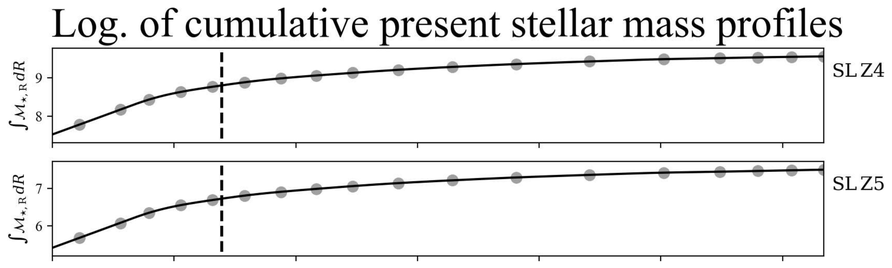

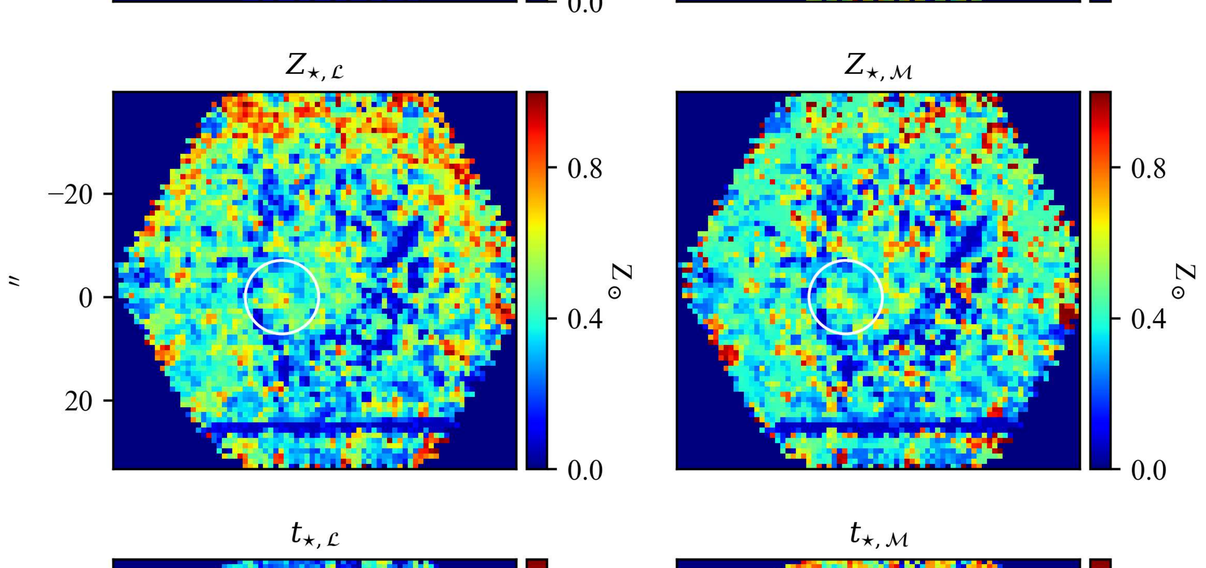

Stellar metallicity/Age & Hα flux/EW profiles

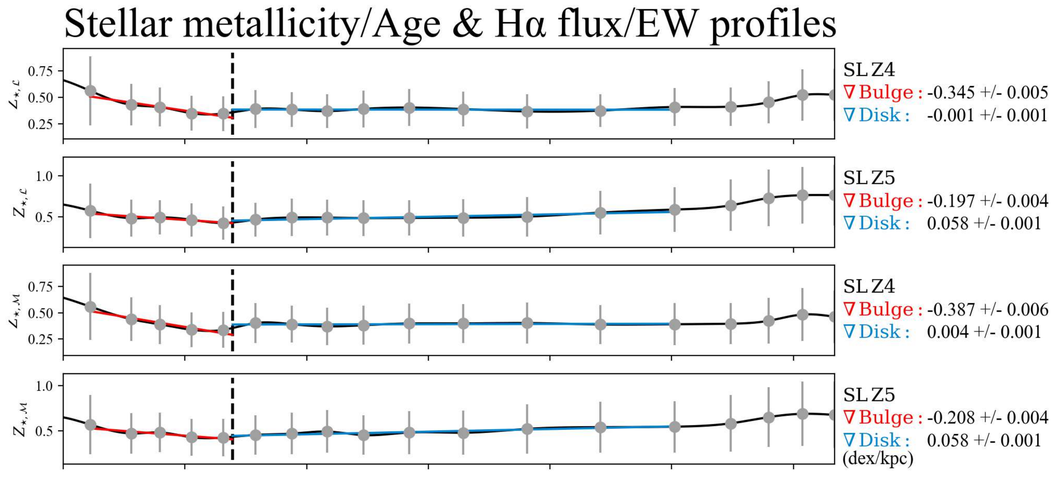

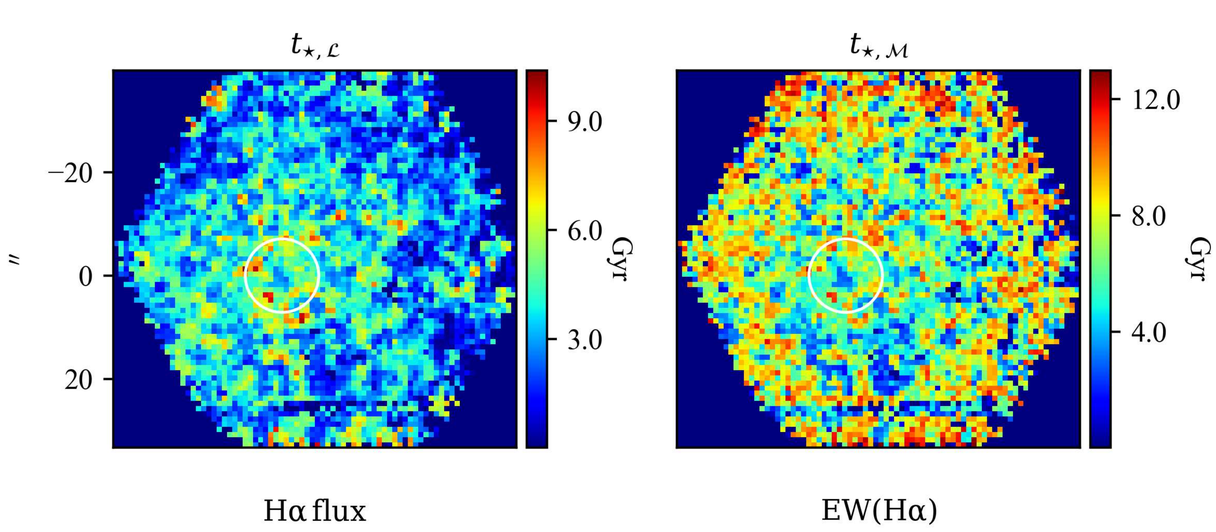

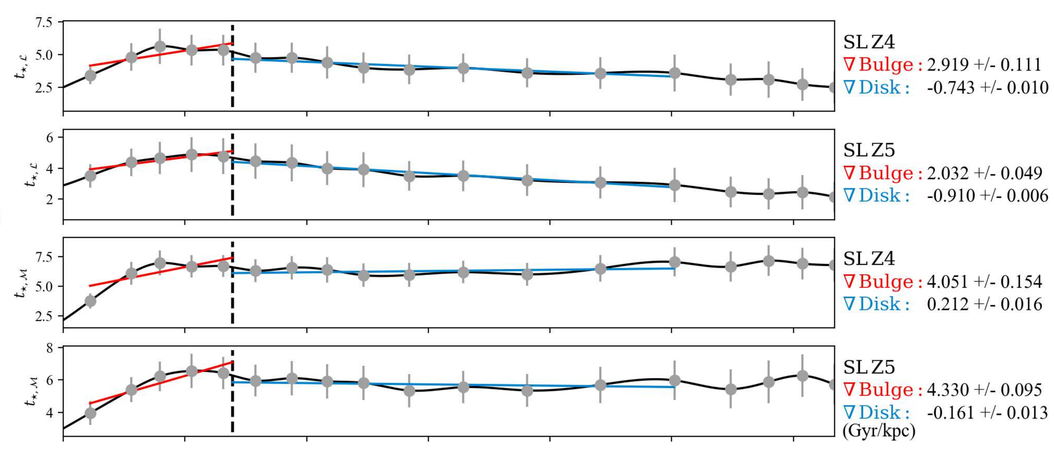

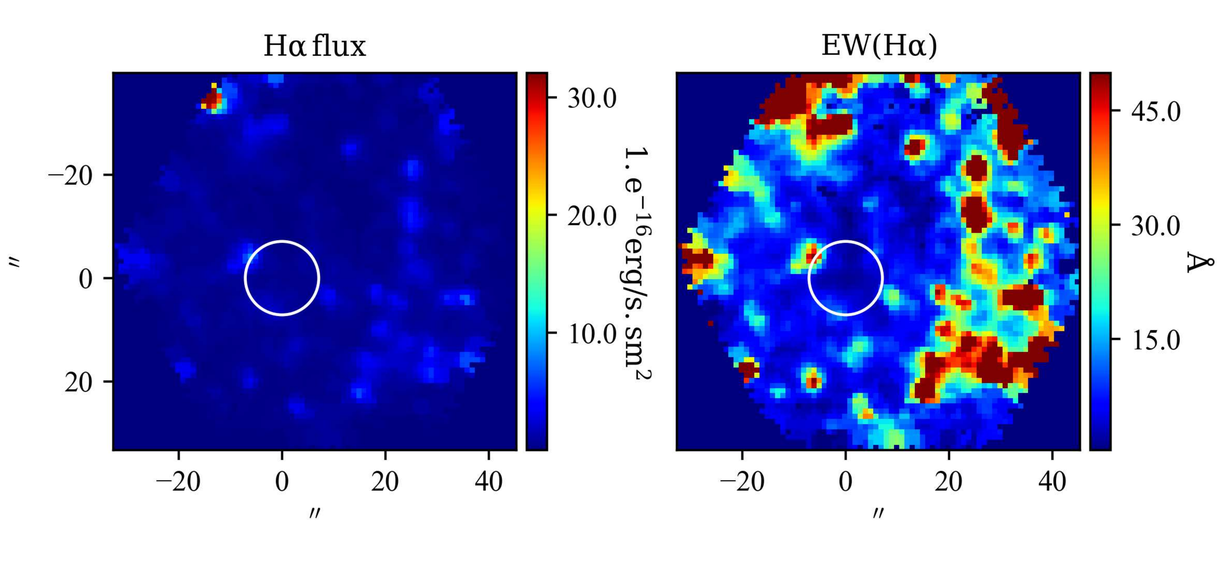

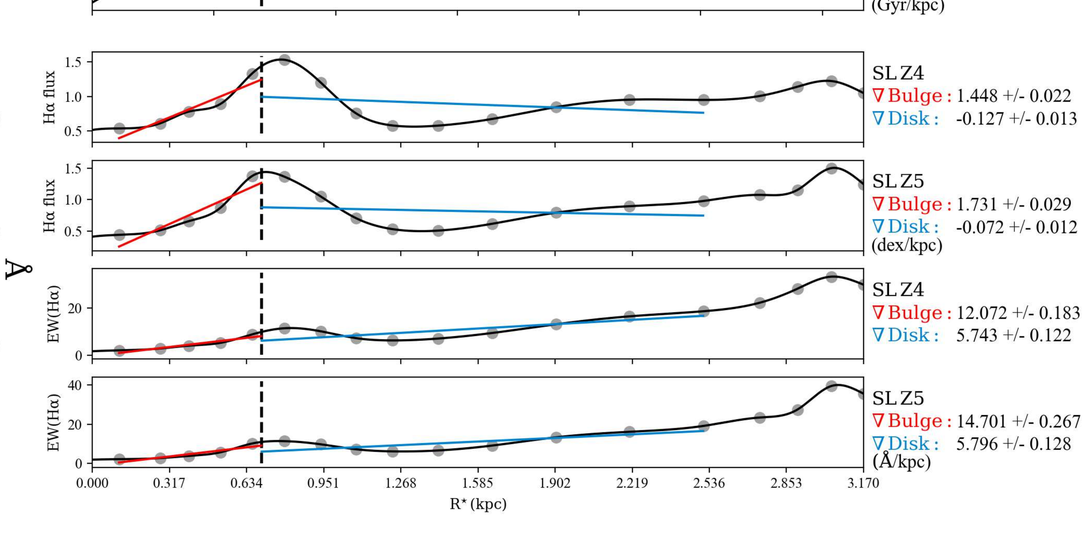

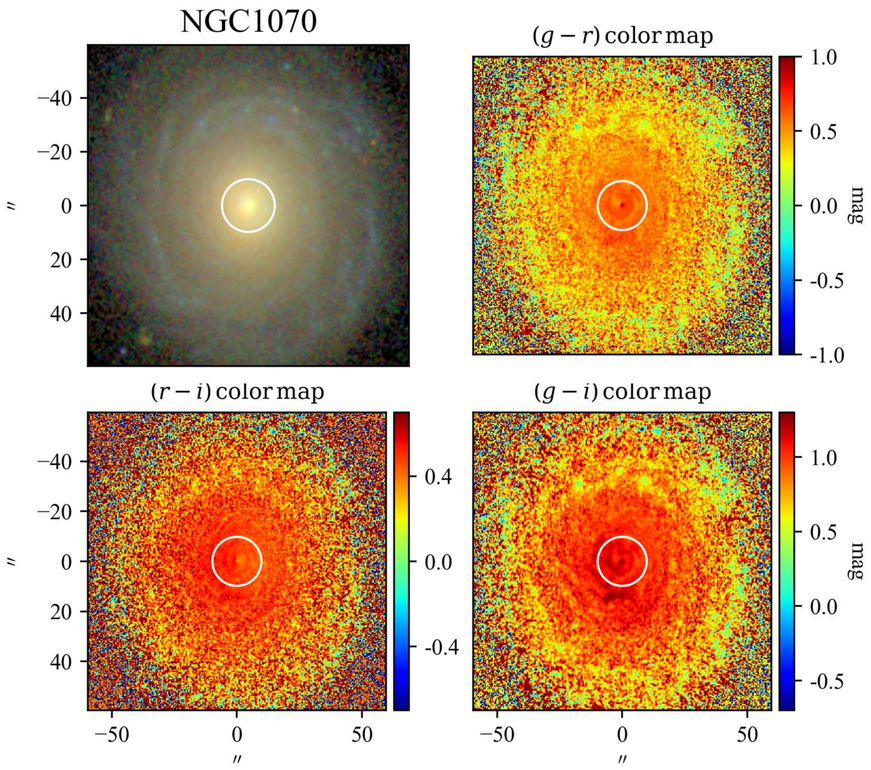

SBP decomposition of SDSS r band

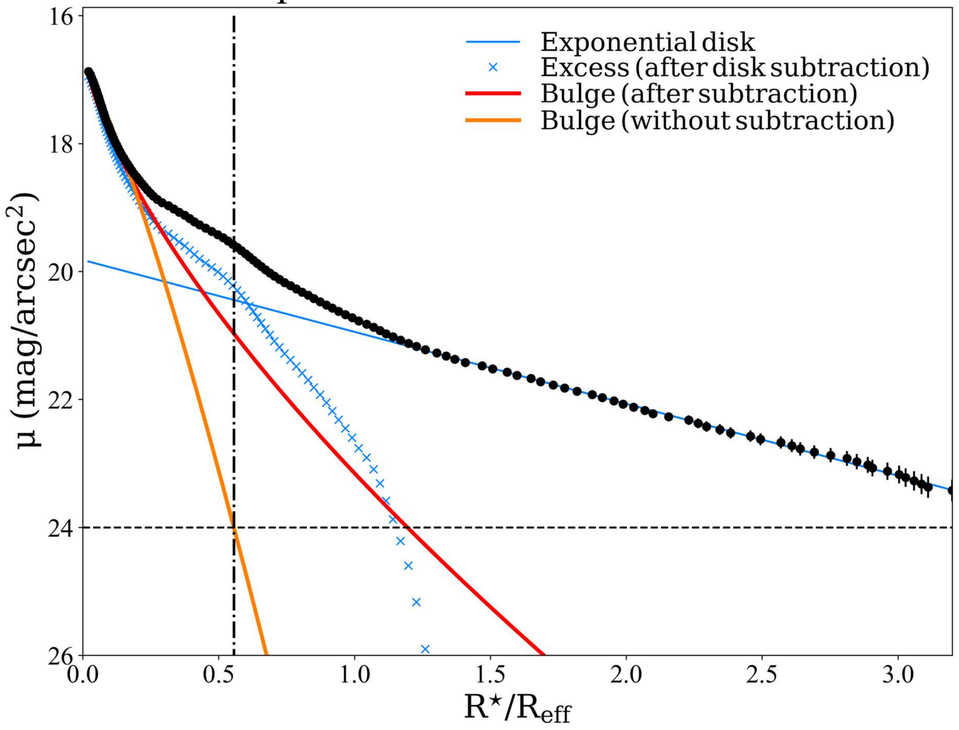

SDSS color profiles

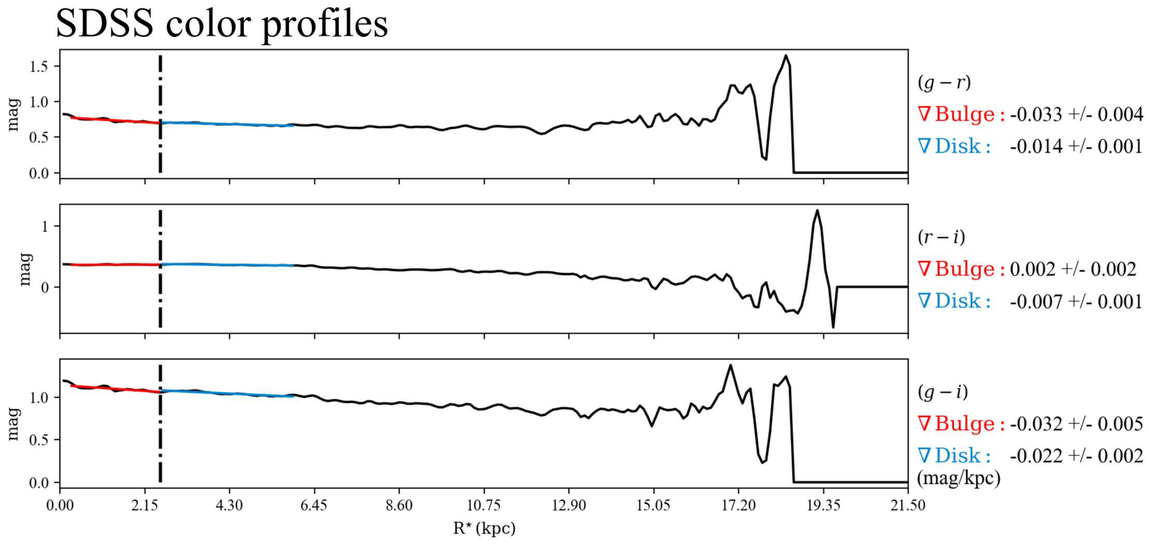

$\mathcal{RY}$ SBPs

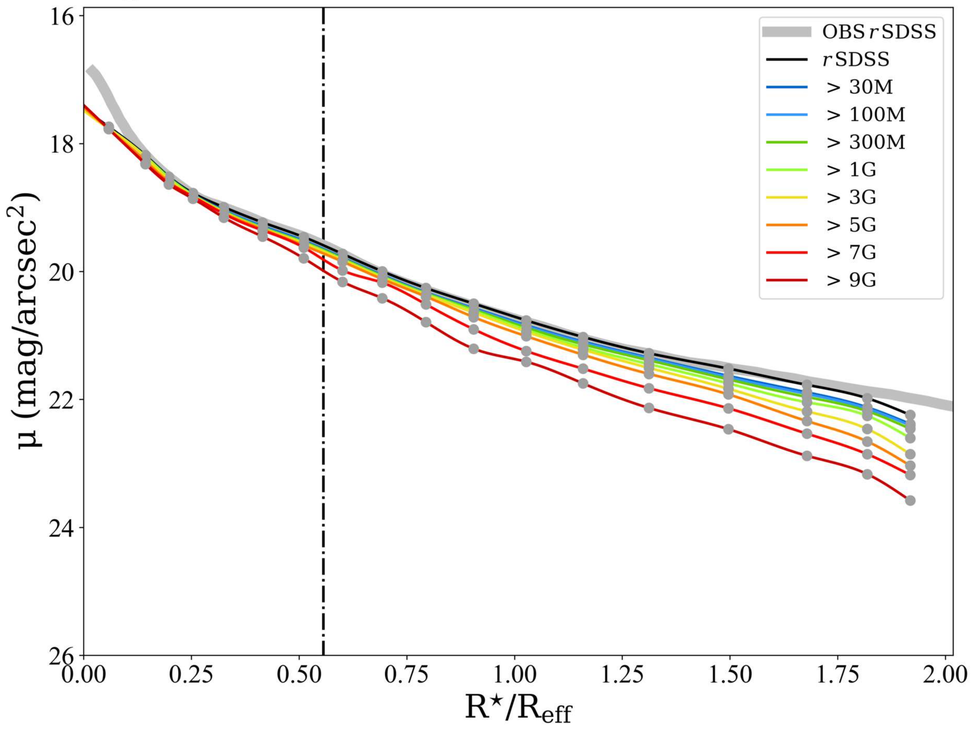

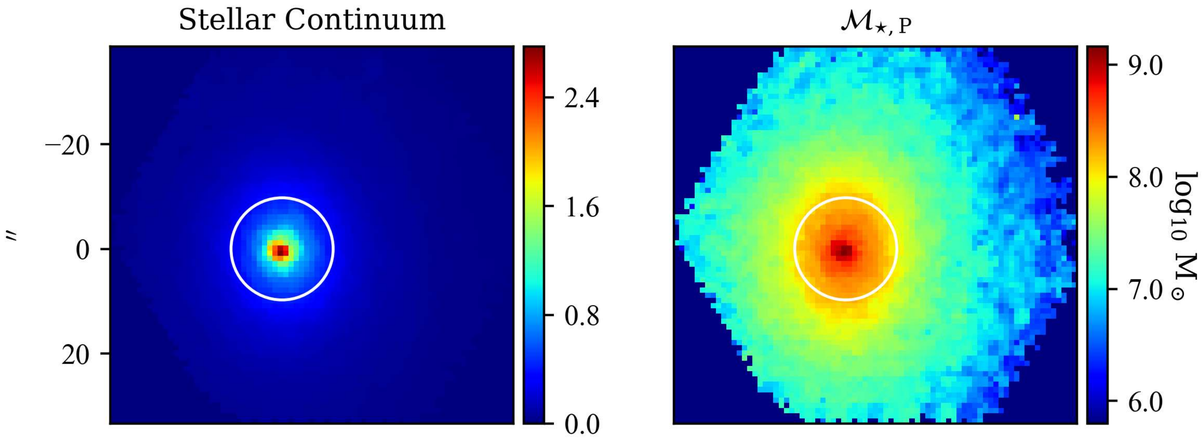

Log. of cumulative present stellar mass profiles

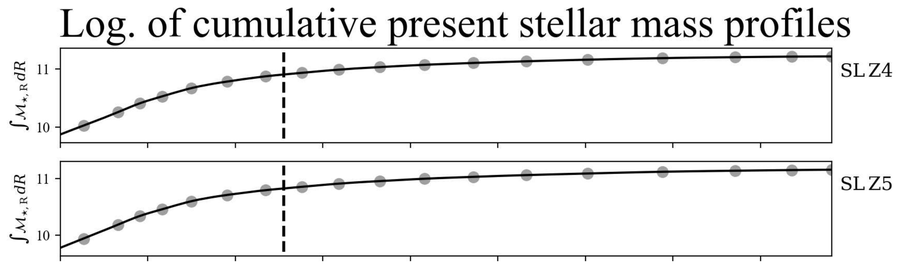

Stellar metallicity/Age & Hα flux/EW profiles

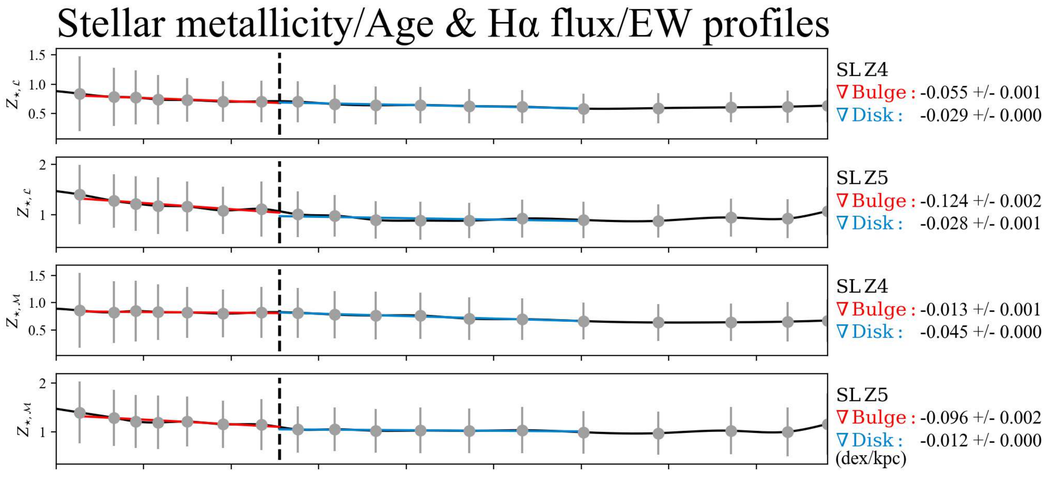

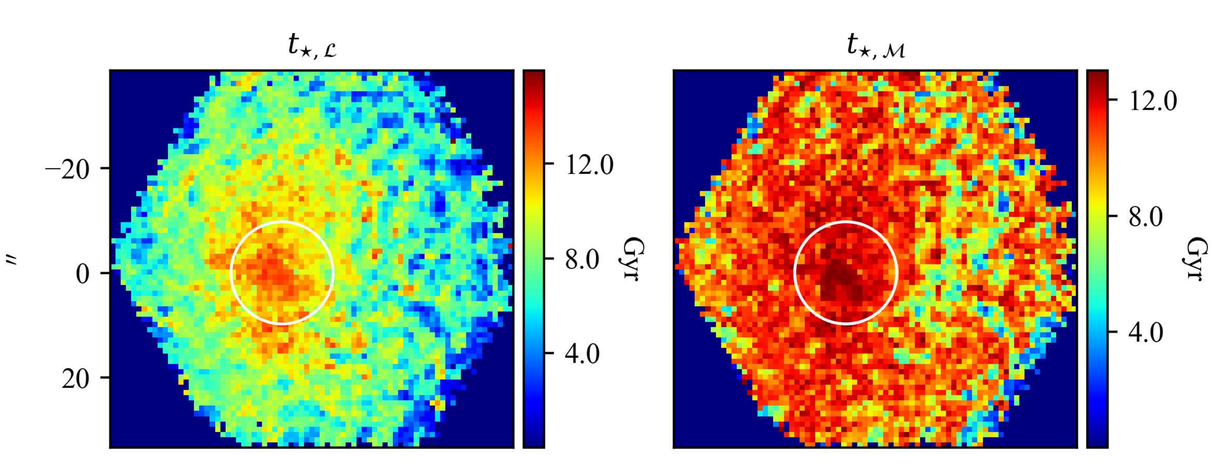

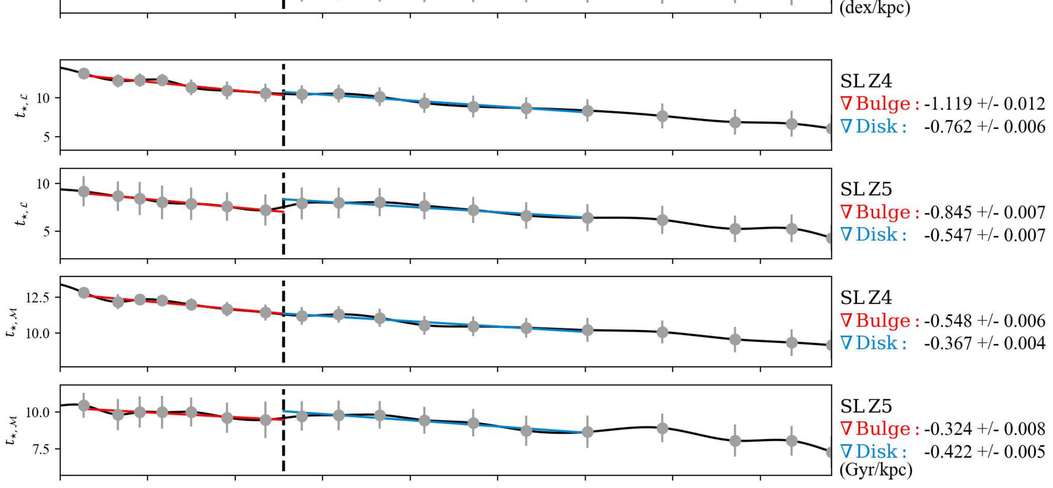

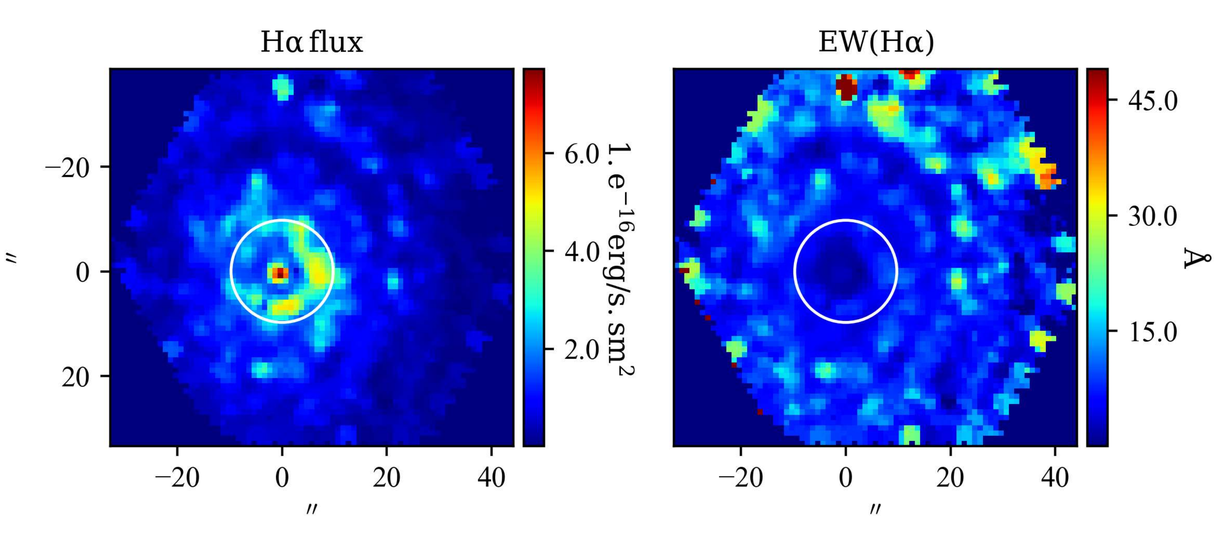

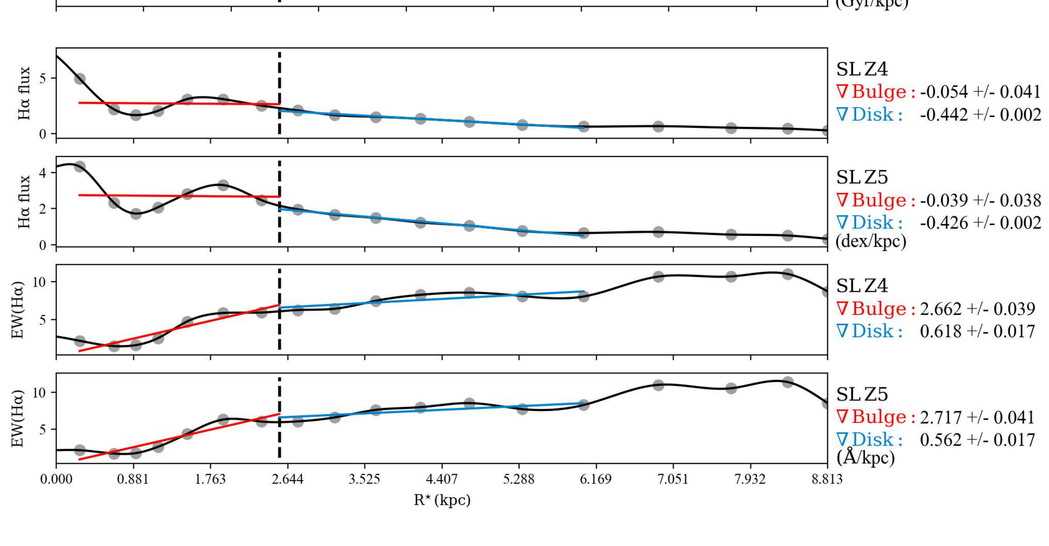

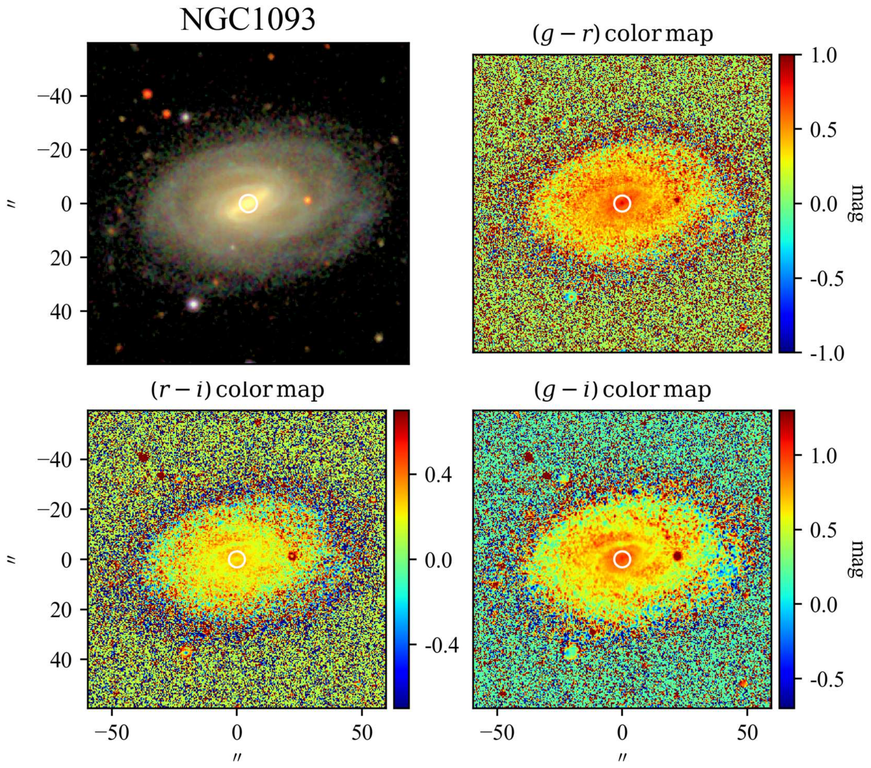

SBP decomposition of SDSS r band

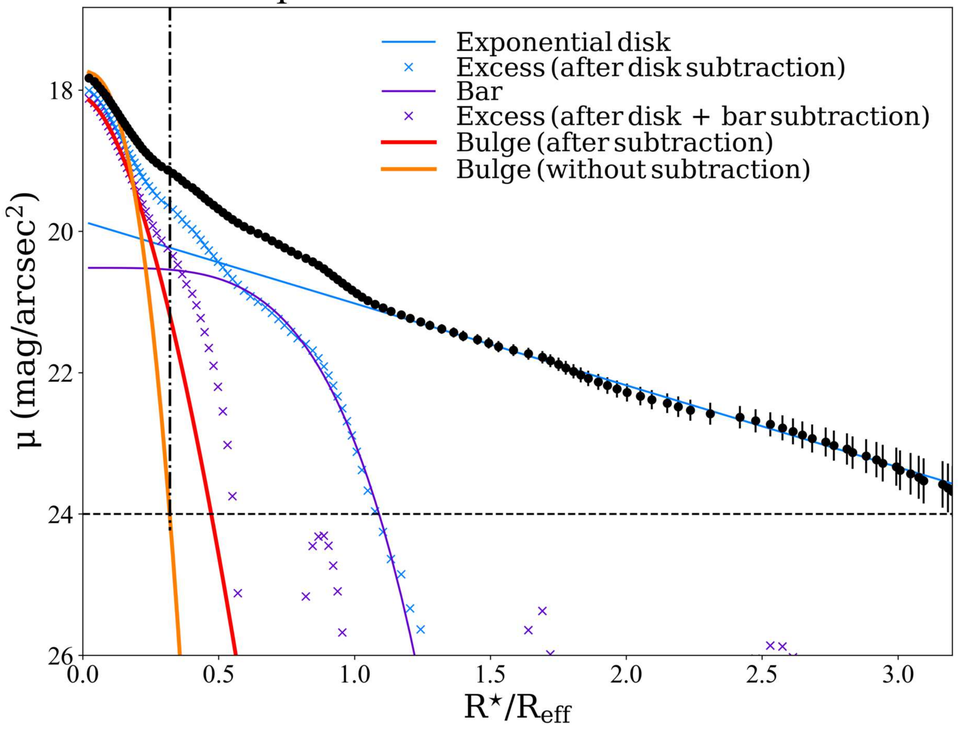

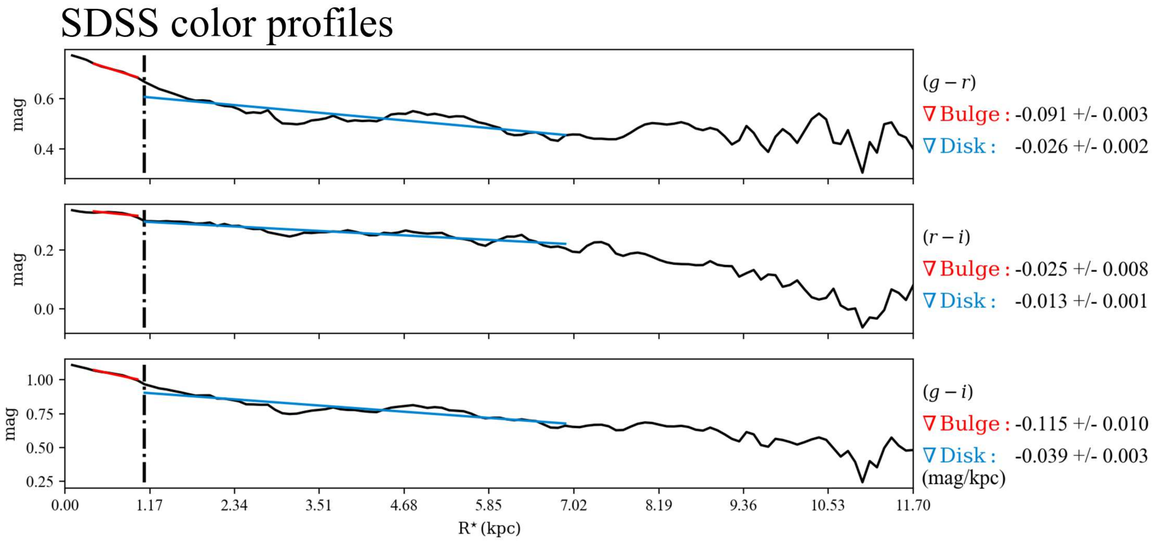

$\mathcal{RV}$ SBPs

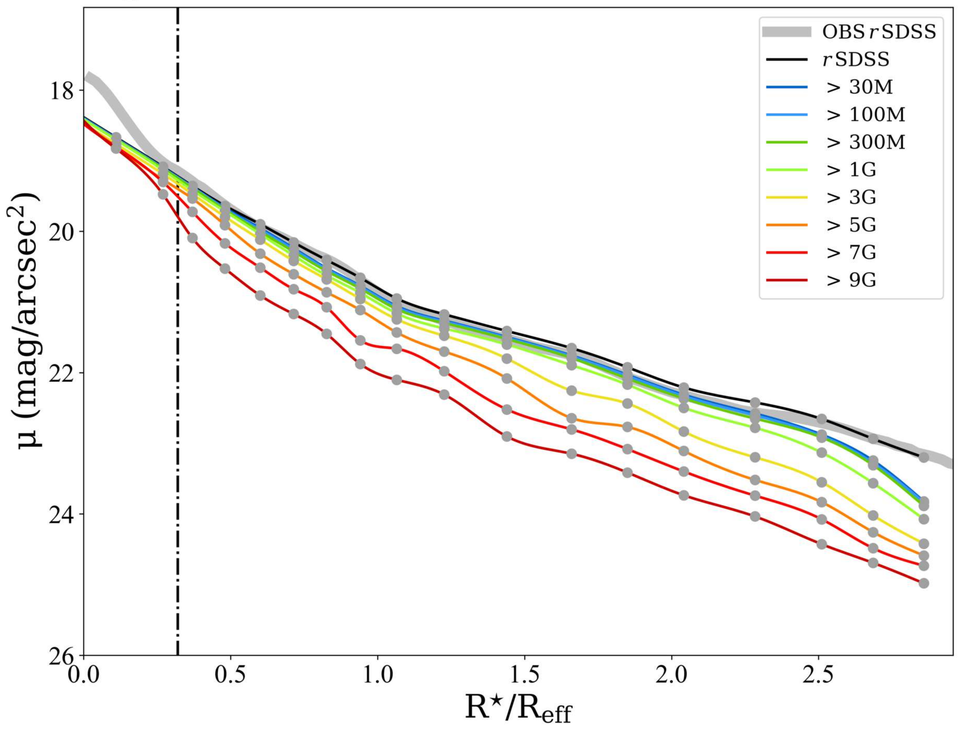

Stellar Continuum

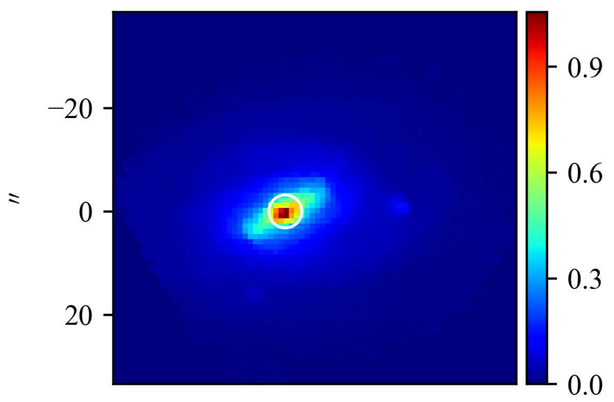

$\mathcal{M}_{\star,\mathrm{P}}$

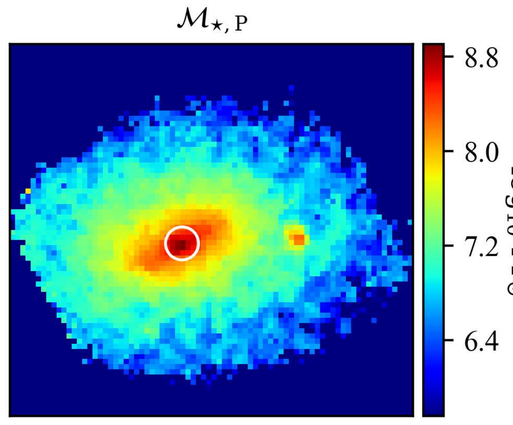

Log. of cumulative present stellar mass profiles

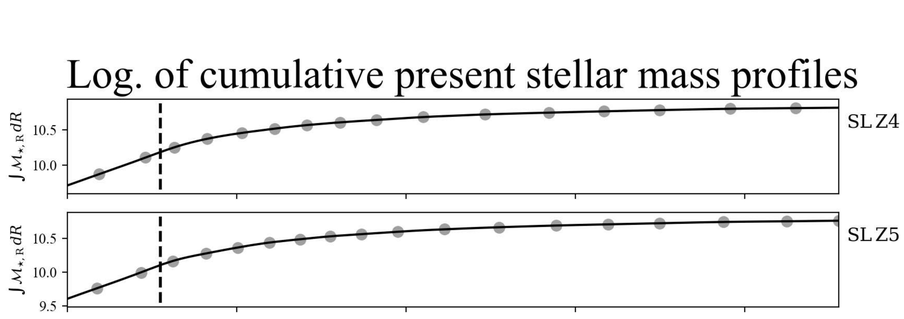

$Z_{\star,\mathcal{L}}$

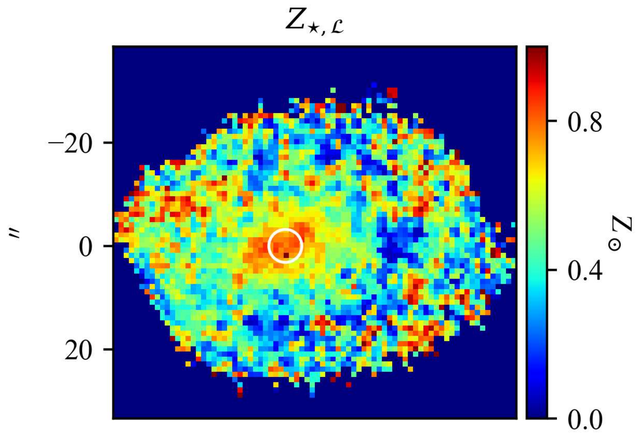

$Z_{\star,\mathcal{M}}$

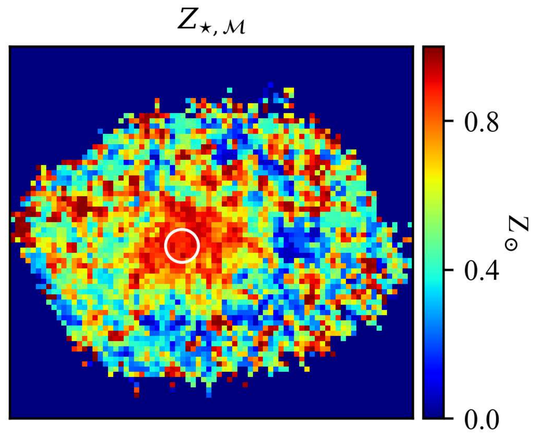

Stellar metallicity/Age & Hα flux/EW profiles

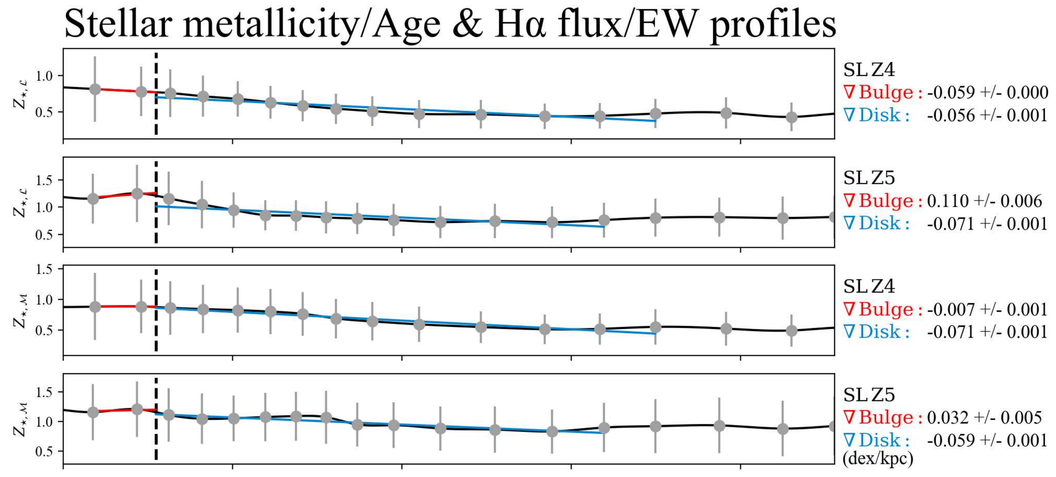

$t_{\star,\mathcal{L}}$

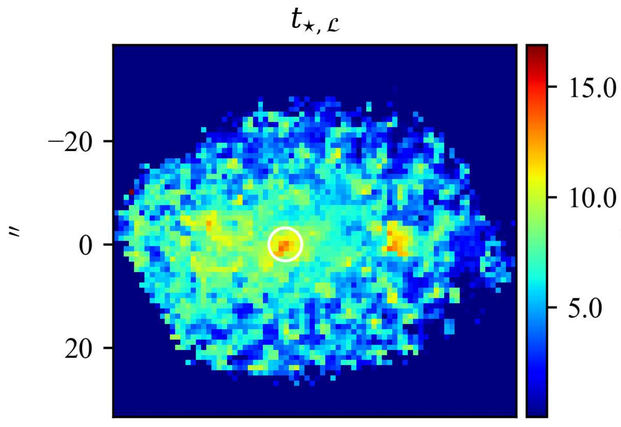

$t_{\star,\mathcal{M}}$

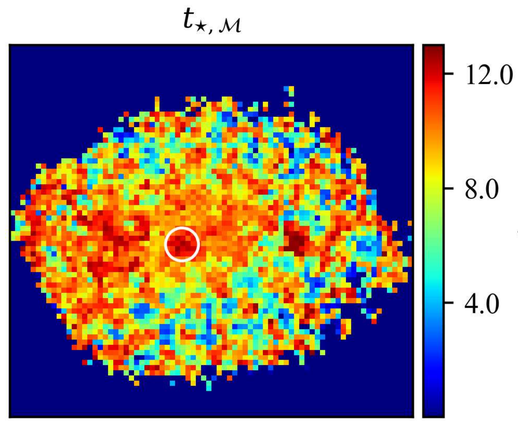

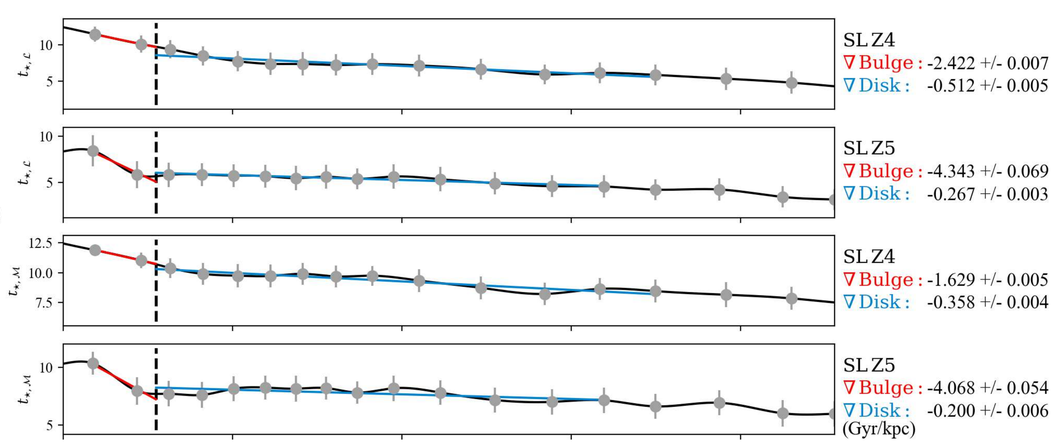

Hα flux

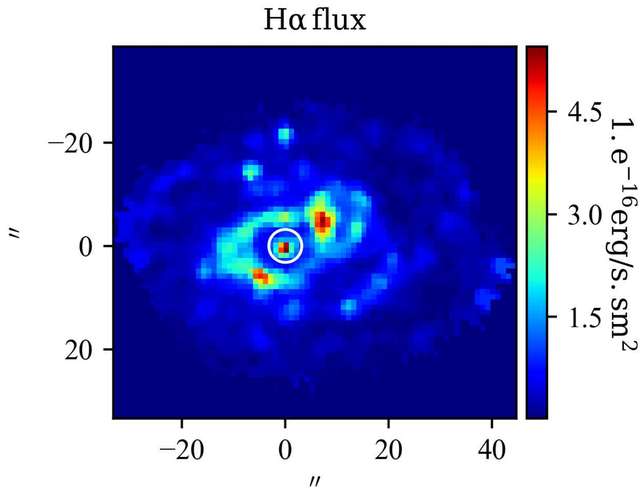

EW(Hα)

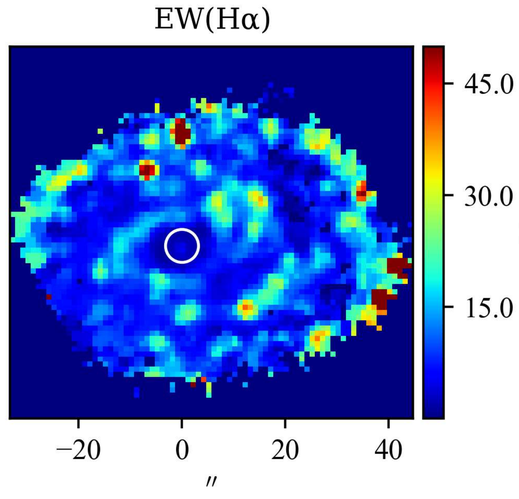

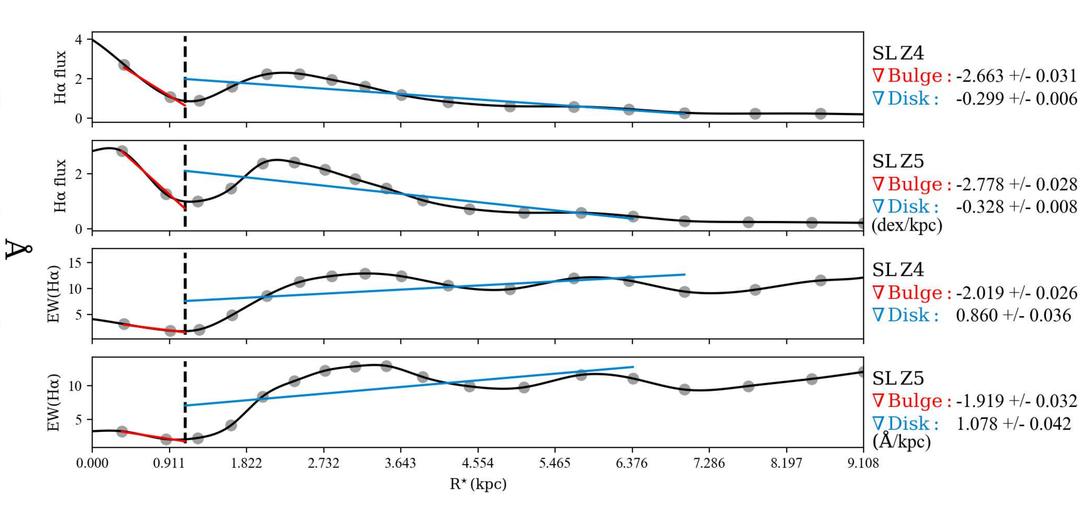

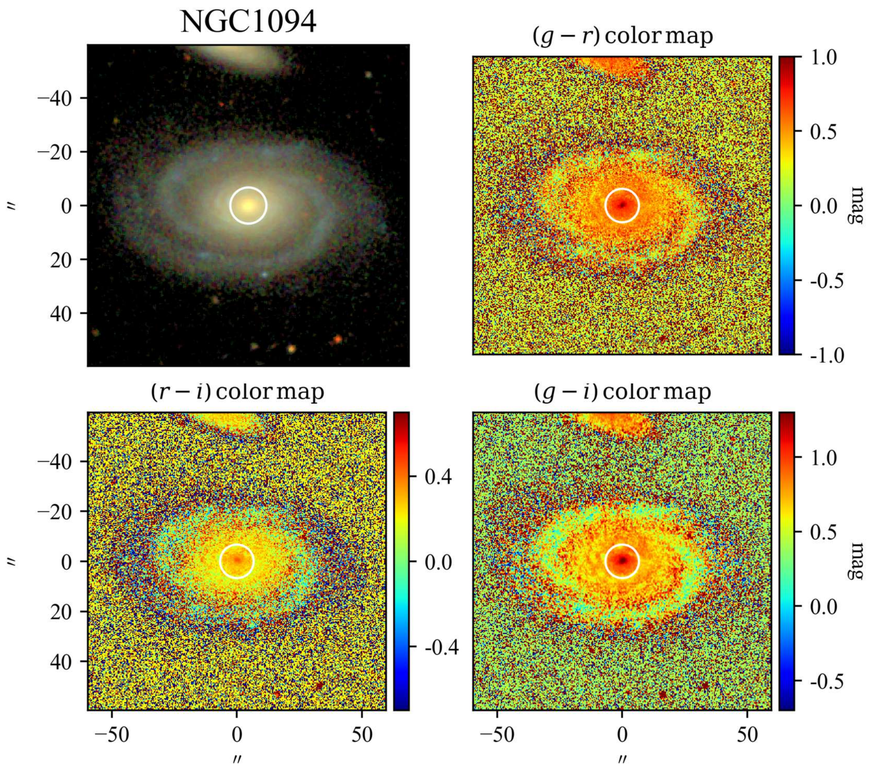

SBP decomposition of SDSS r band

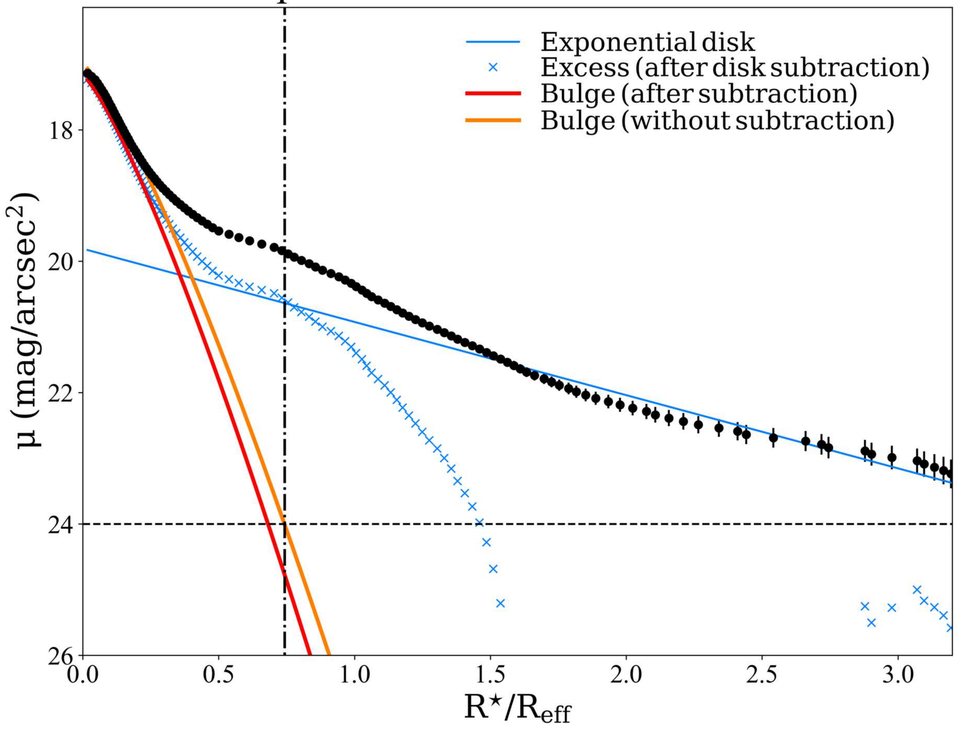

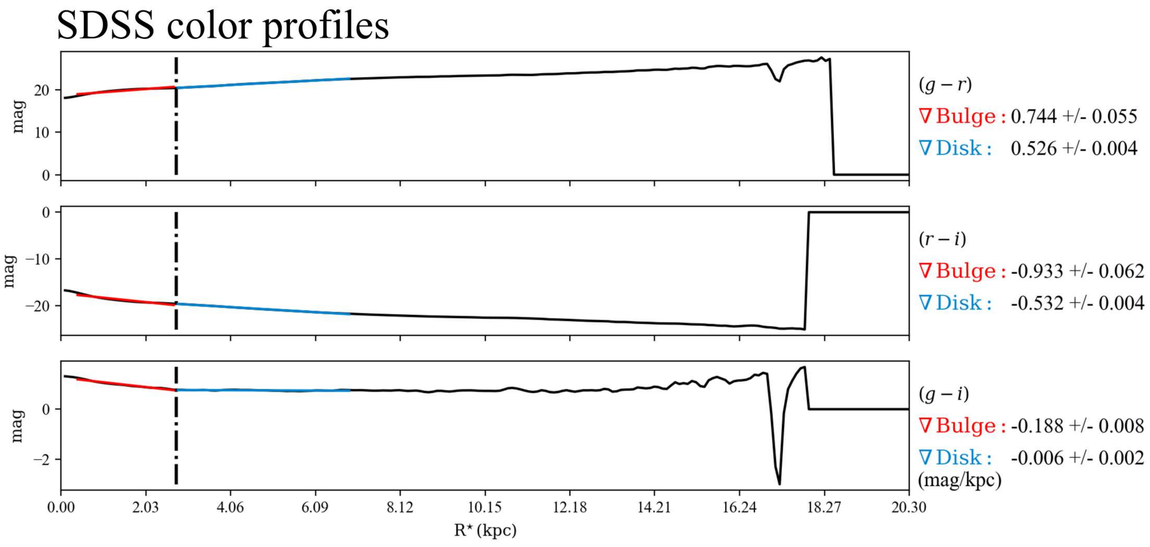

$\mathcal{RY}$ SBPs

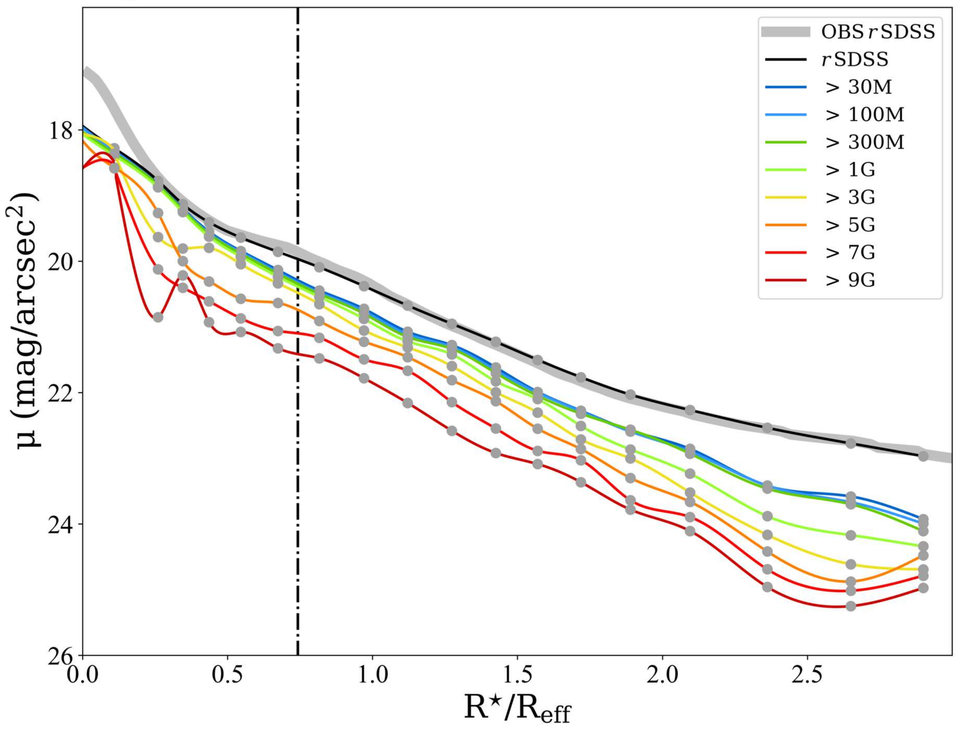

Stellar Continuum

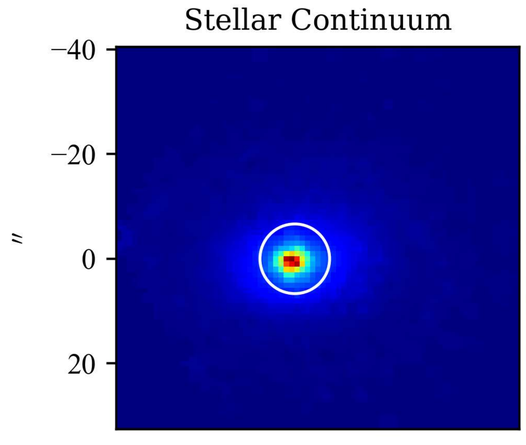

$\mathcal{M}_{\star,\mathrm{P}}$

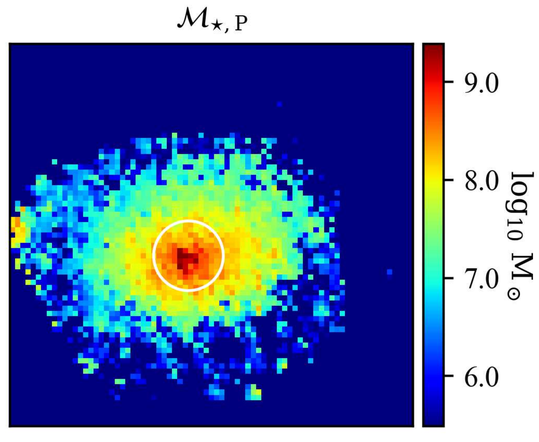

Log. of cumulative present stellar mass profiles

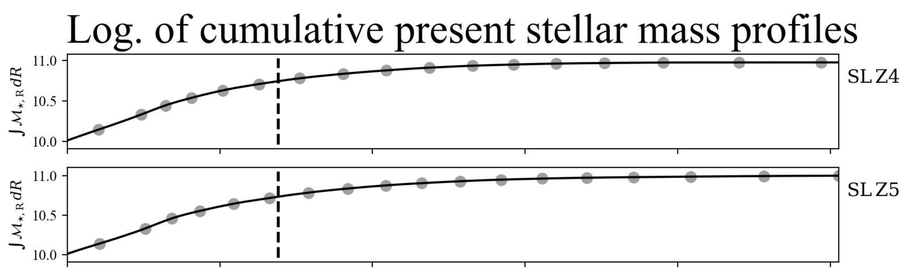

$Z_{\star,\mathcal{L}}$

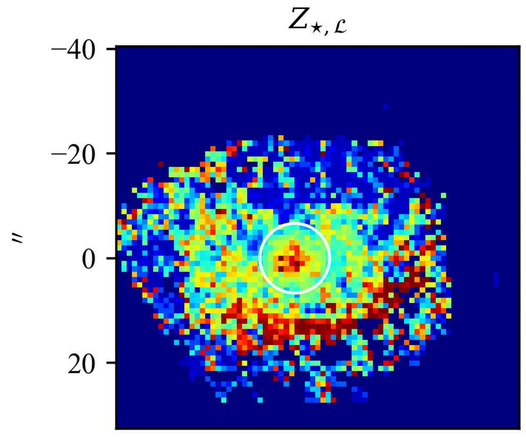

$Z_{\star,\mathcal{M}}$

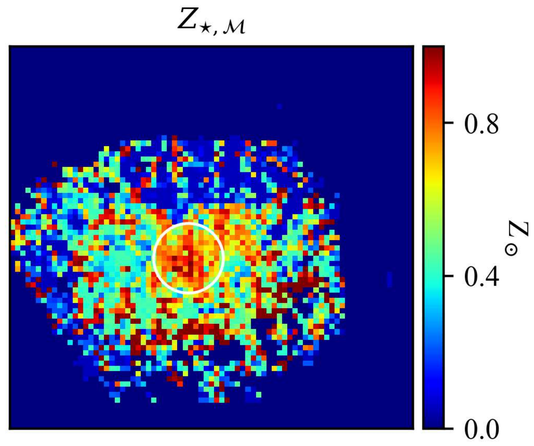

Stellar metallicity/Age & Hα flux/EW profiles

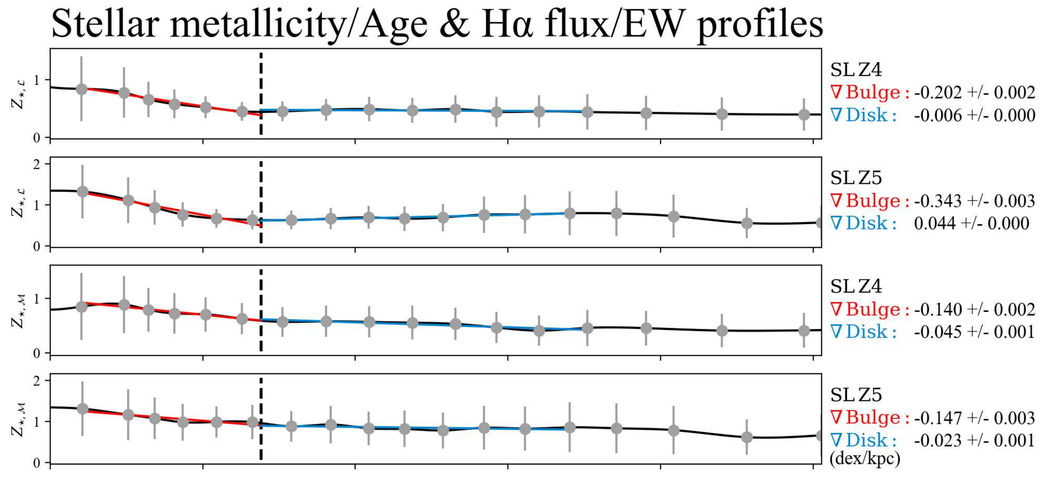

$t_{\star,\mathcal{L}}$

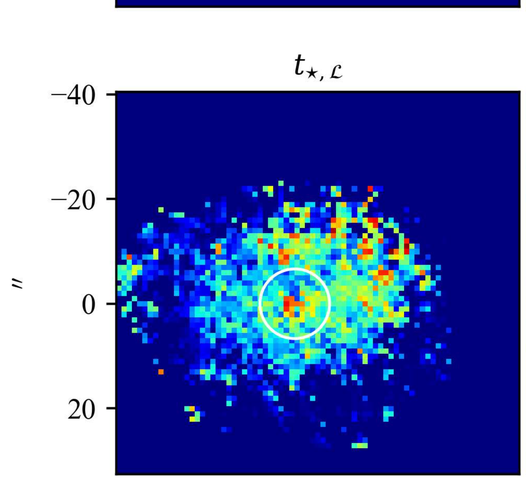

$t_{\star,\mathcal{M}}$

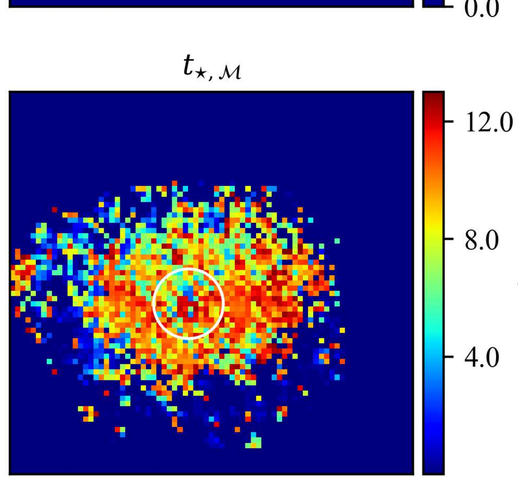

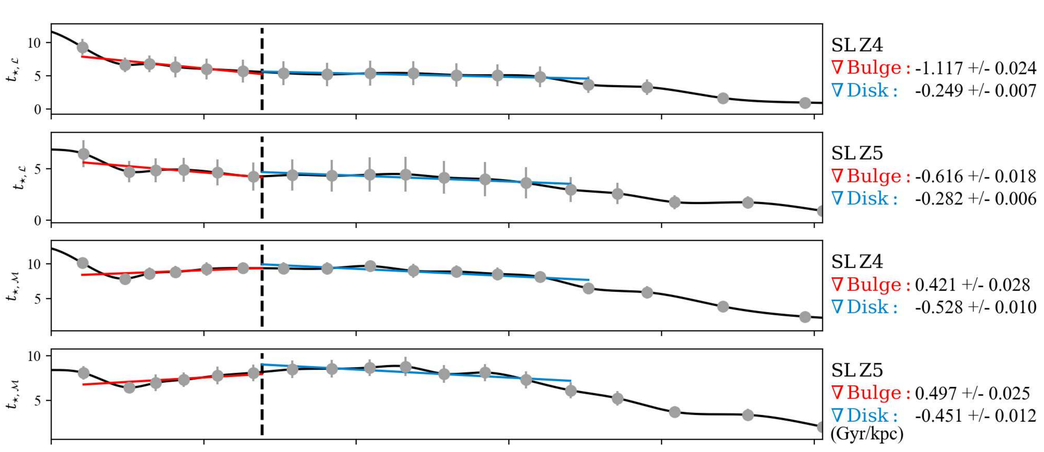

Hα flux

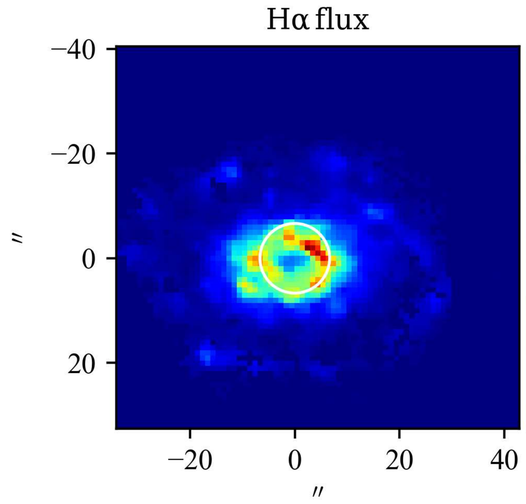

EW(Hα)

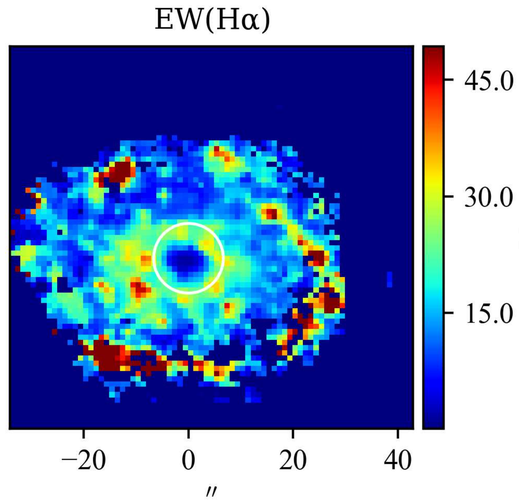

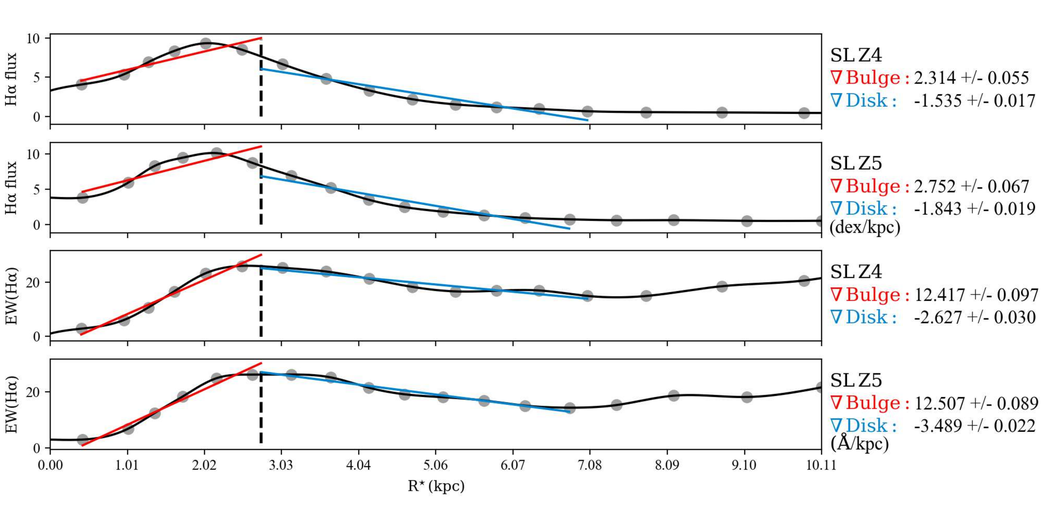

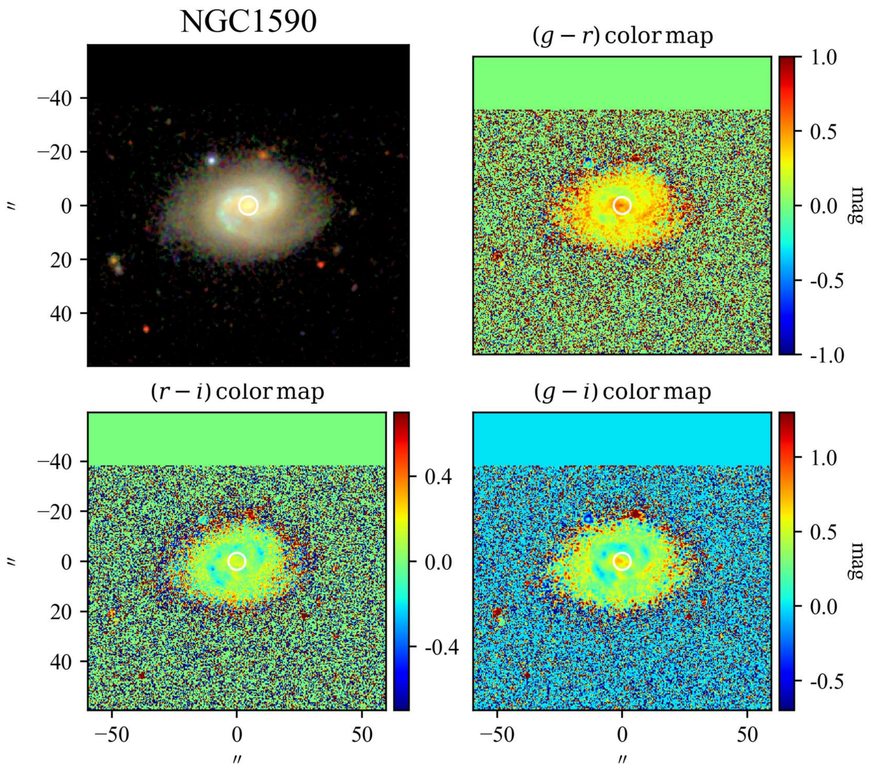

SBP decomposition of SDSS r band

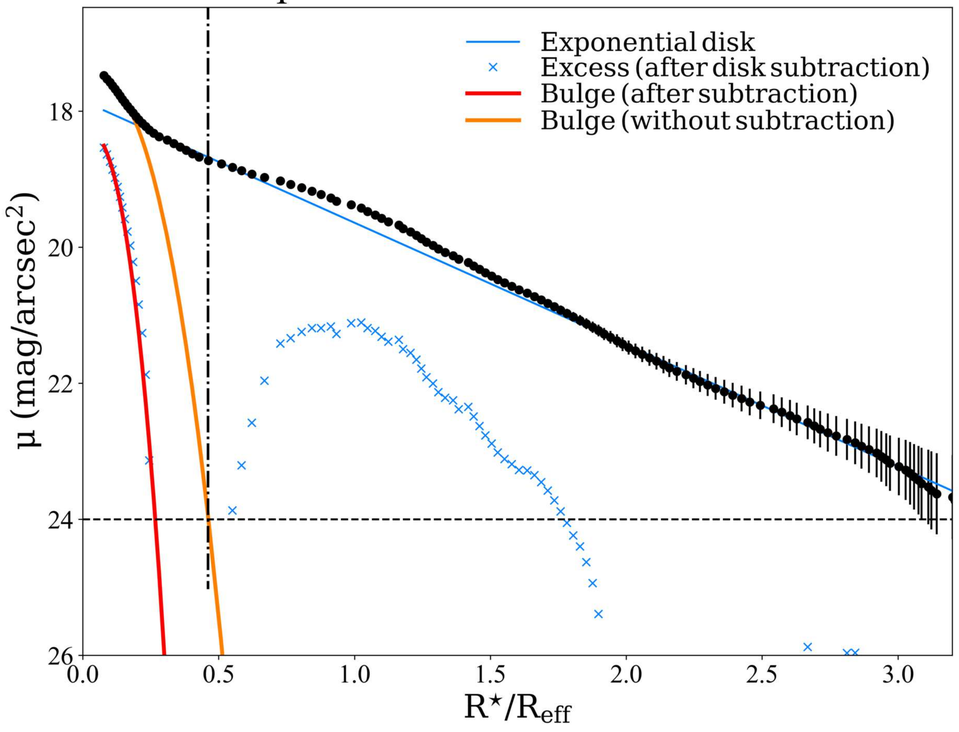

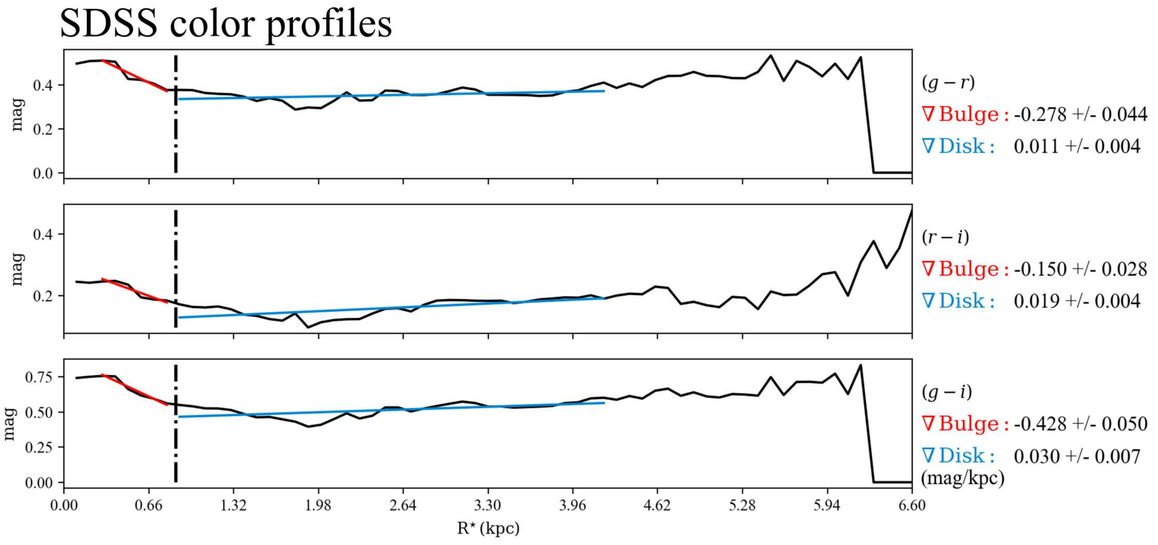

$\mathcal{RV}$ SBPs

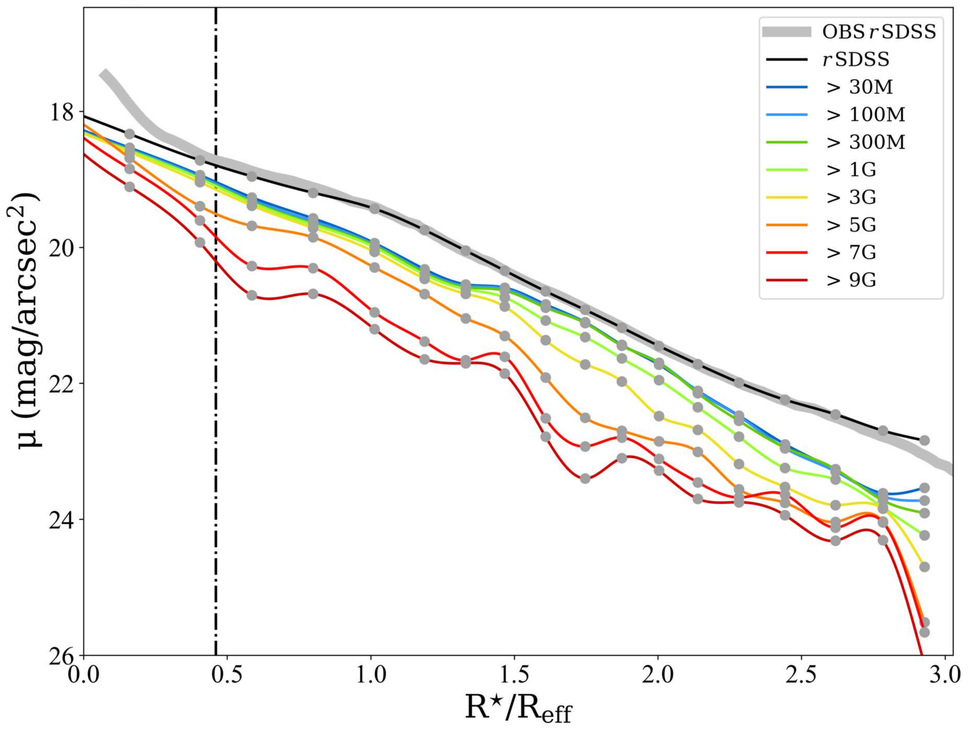

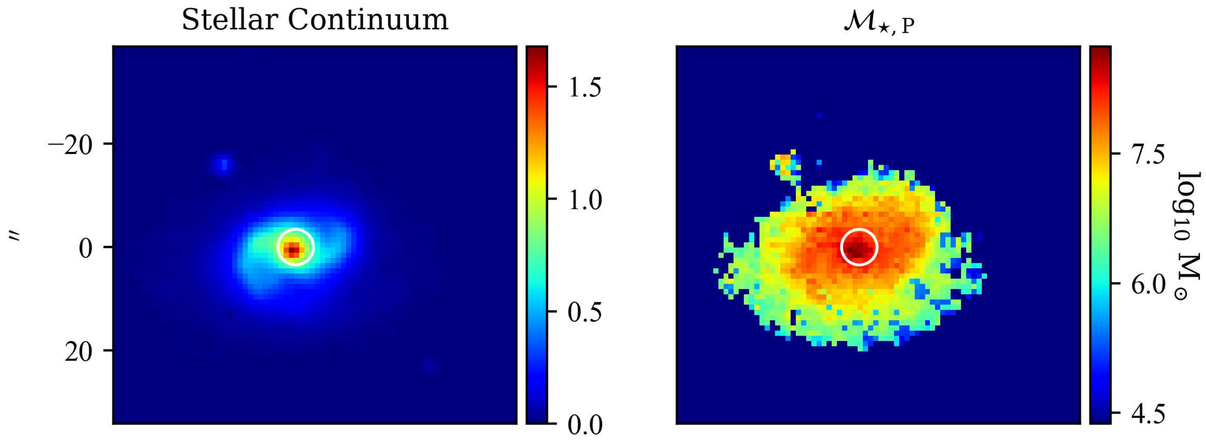

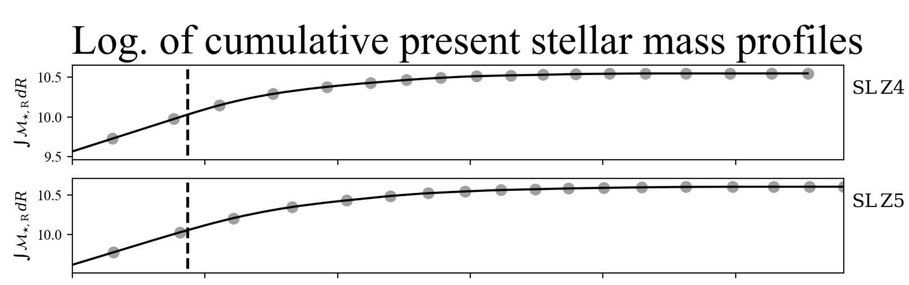

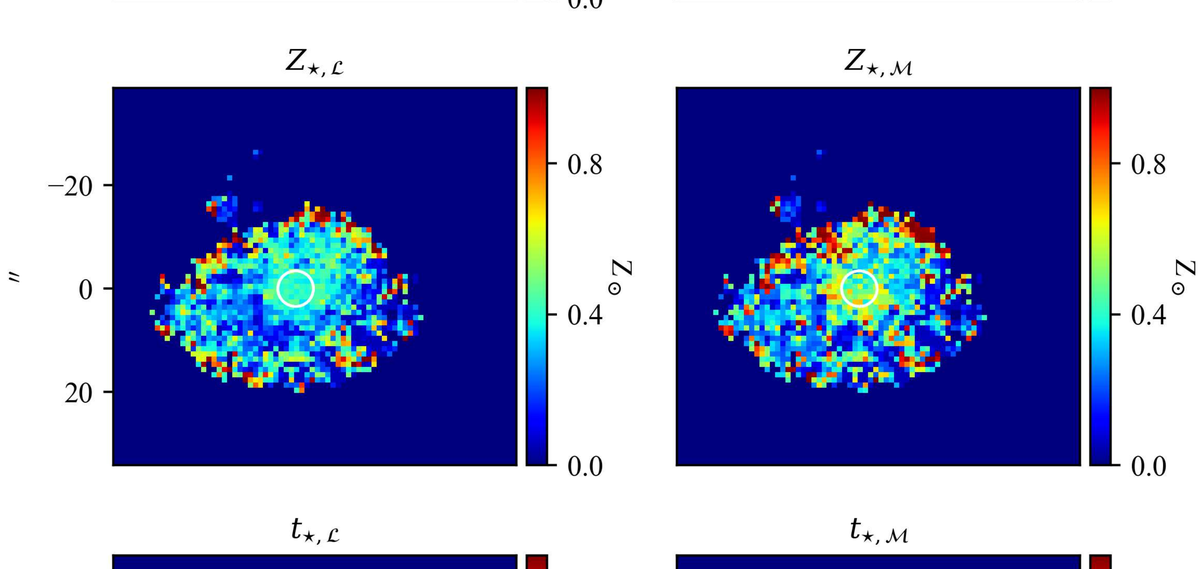

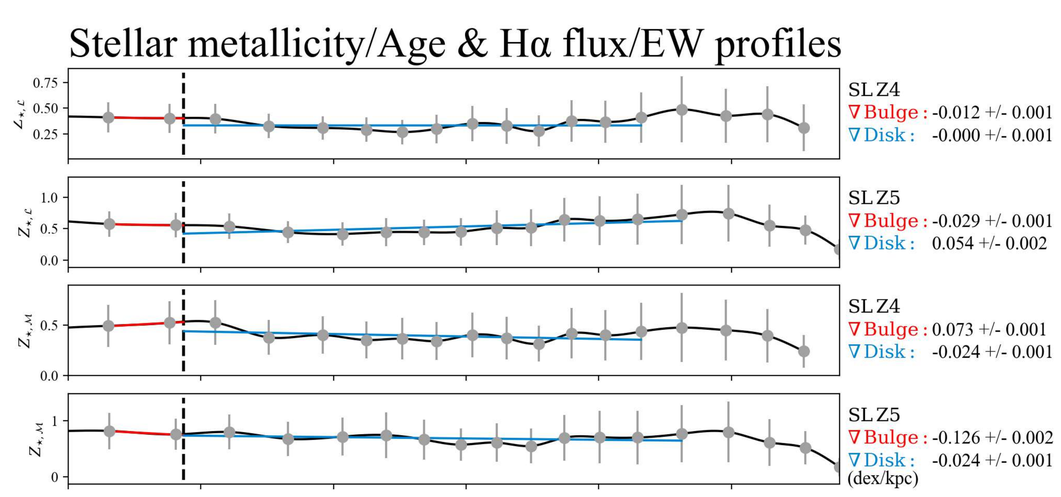

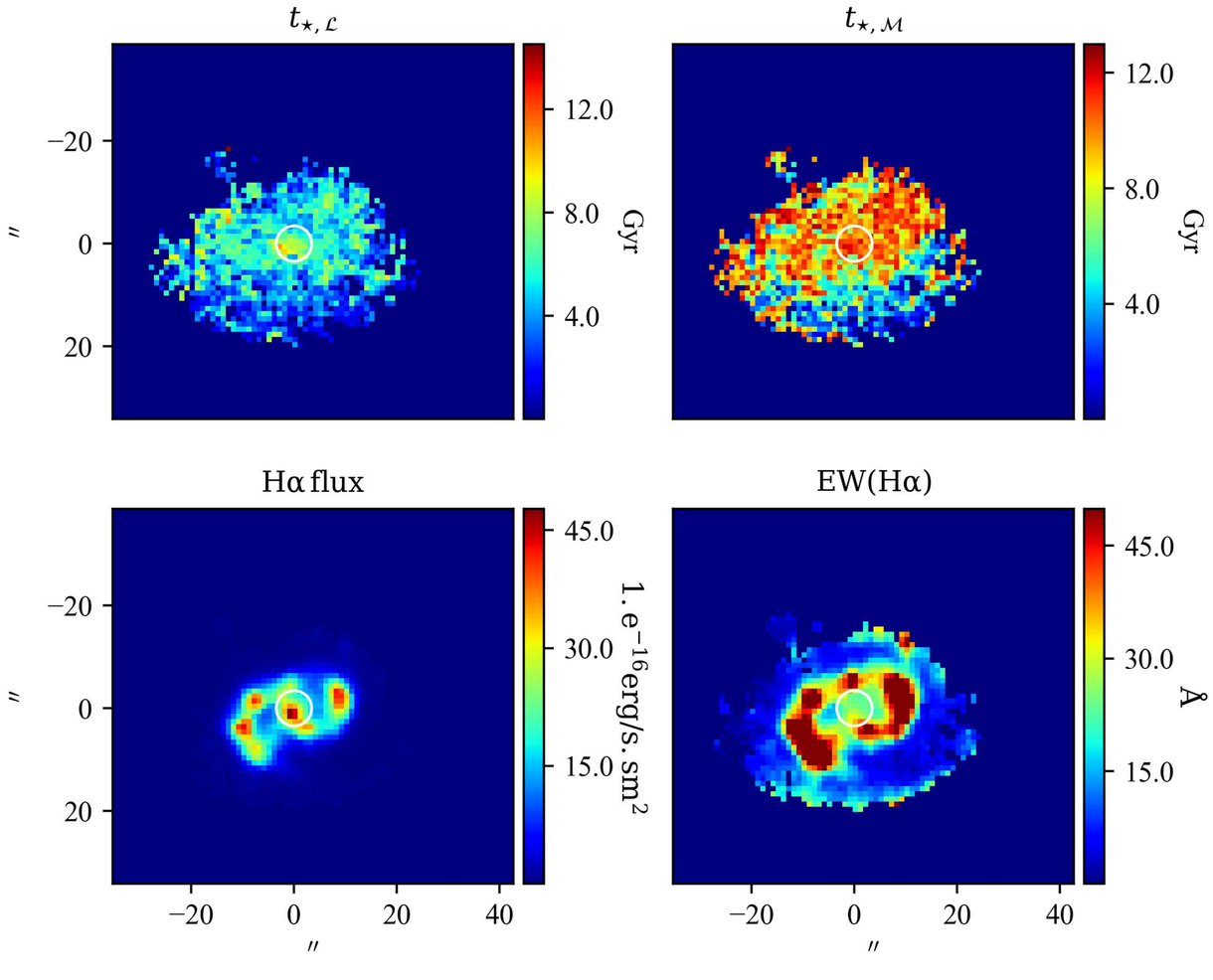

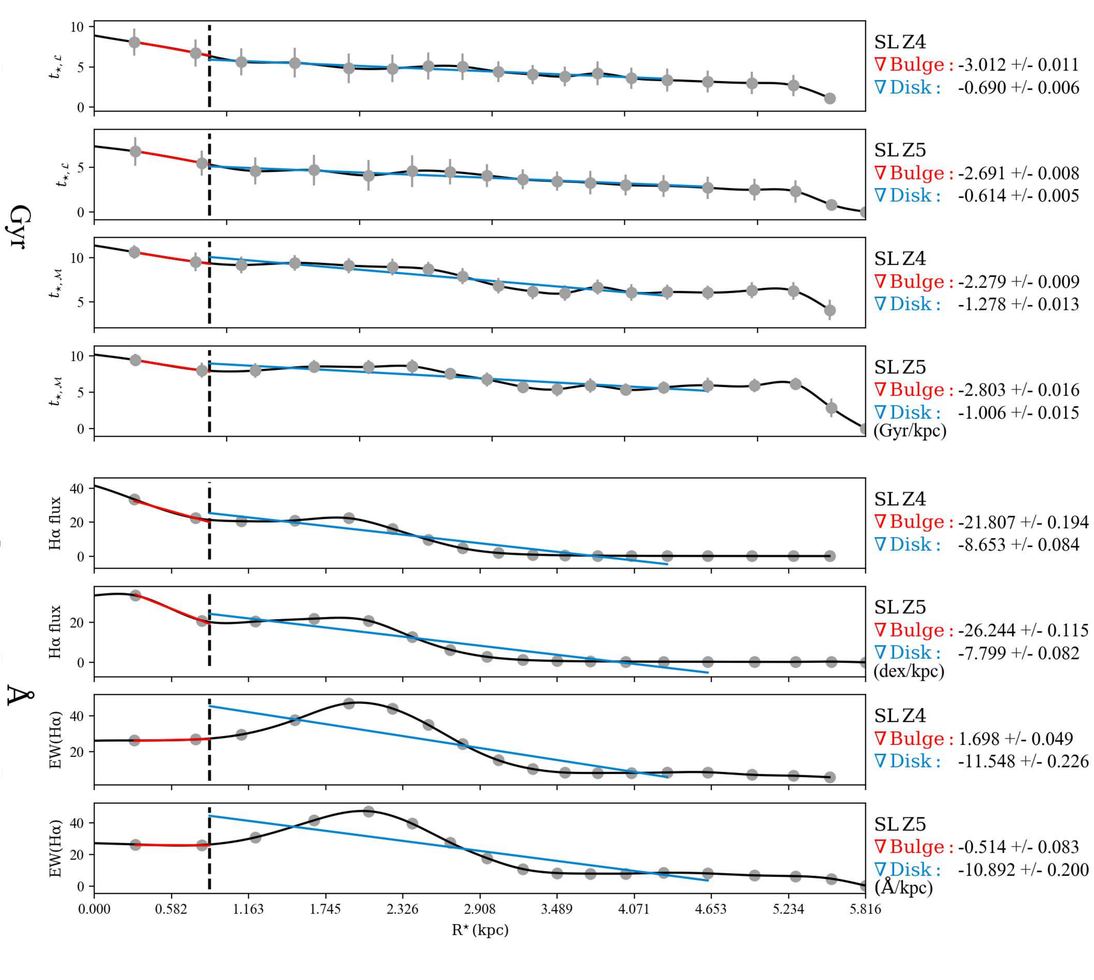

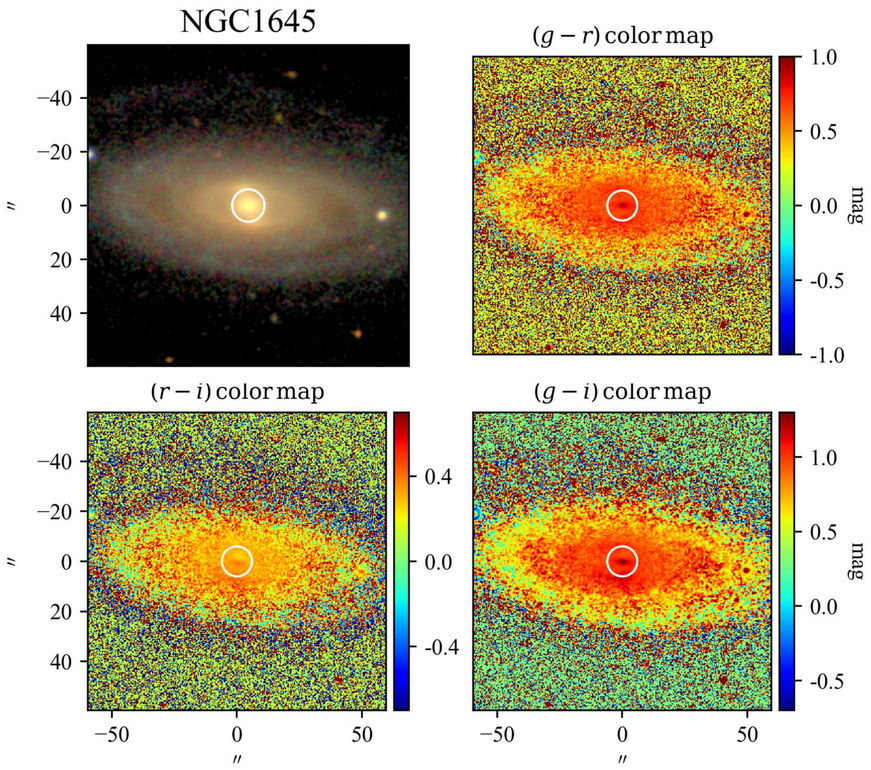

SBP decomposition of SDSS r band

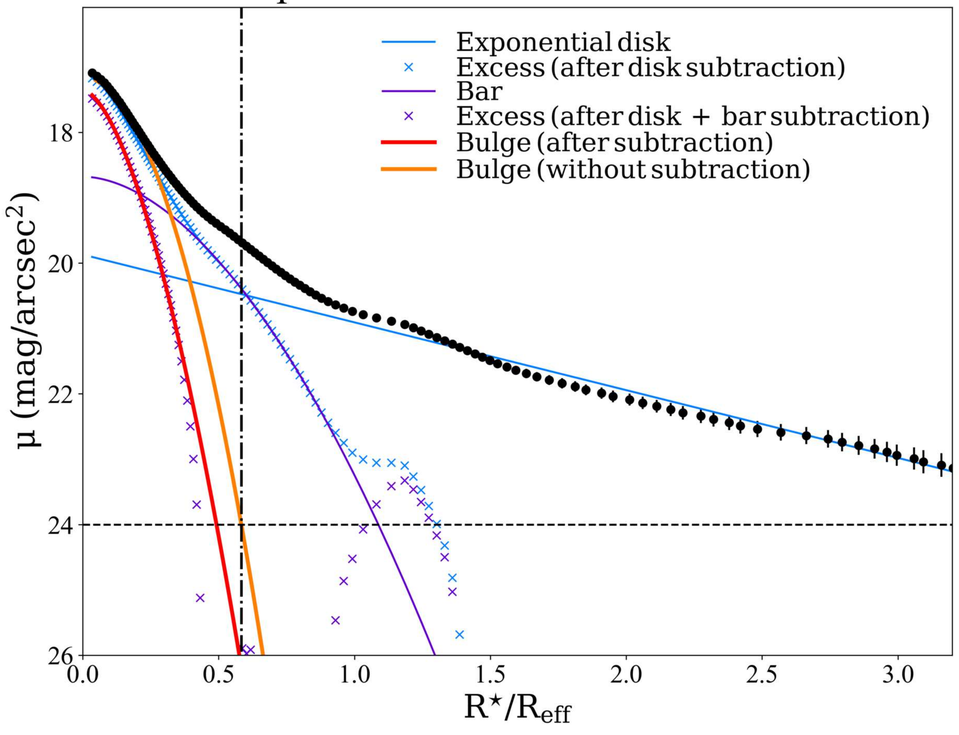

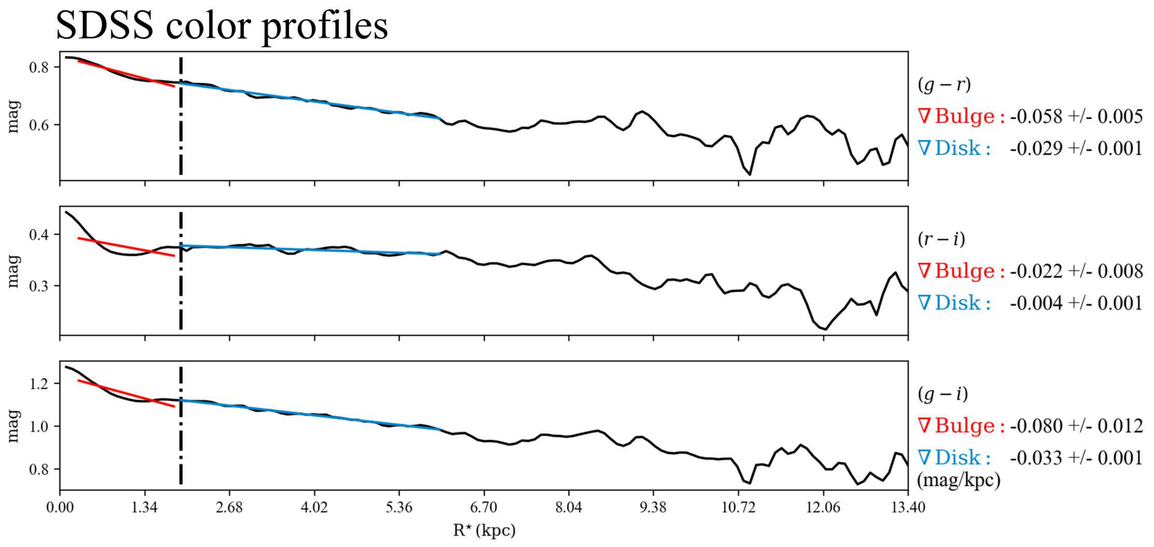

$\mathcal{RV}$ SBPs

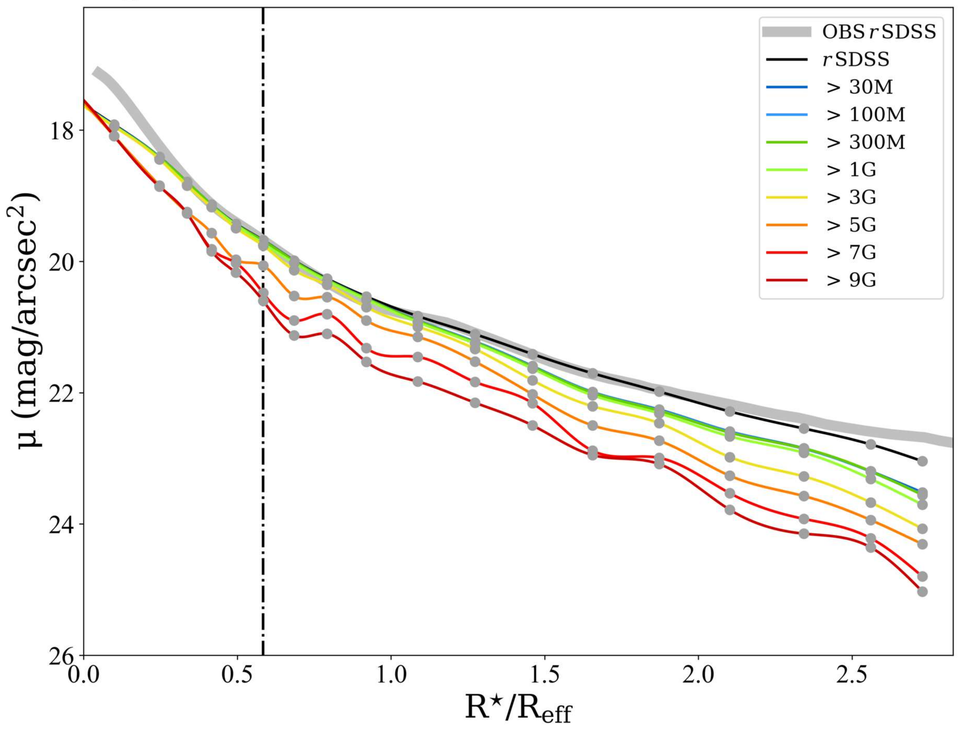

Stellar Continuum $\mathcal{M}_{\star,\mathrm{P}}$

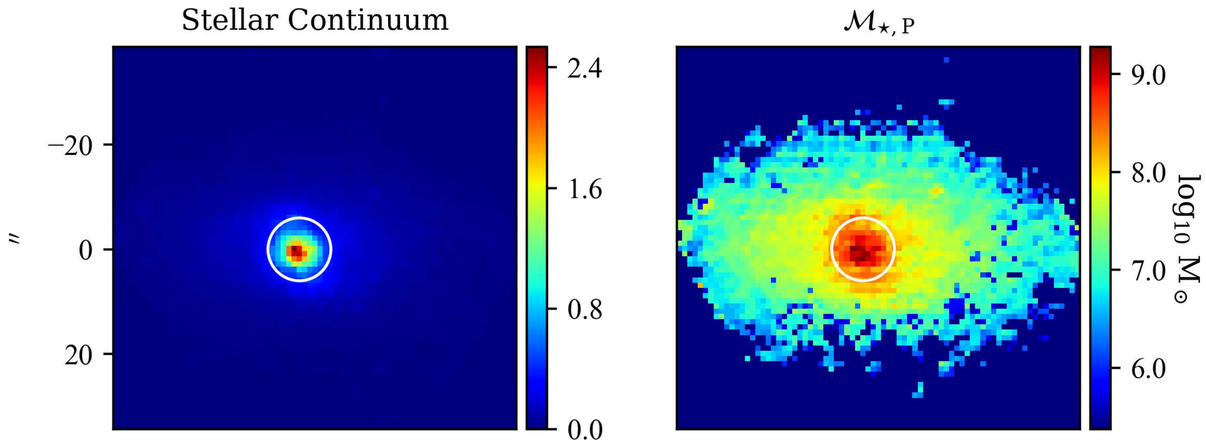

Log. of cumulative present stellar mass profiles

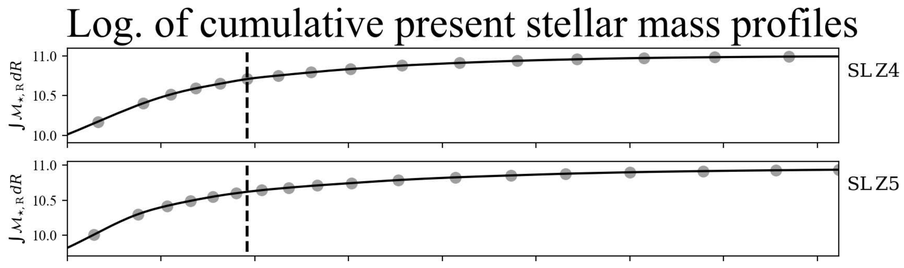

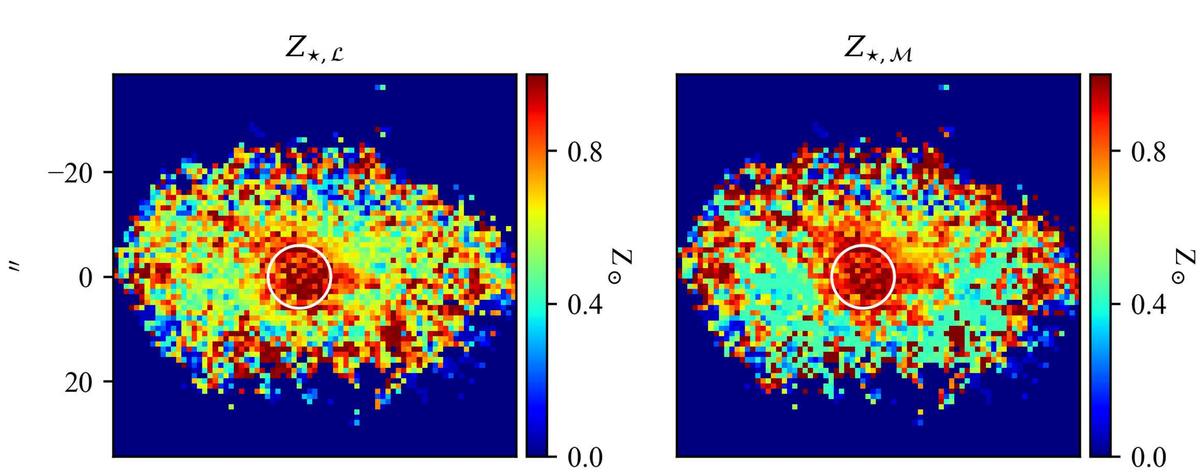

Stellar metallicity/Age & Hα flux/EW profiles

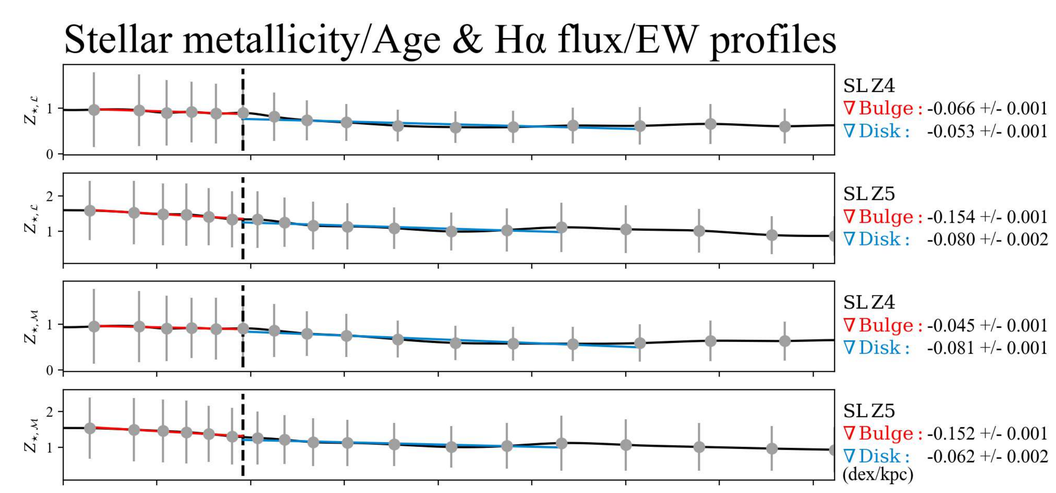

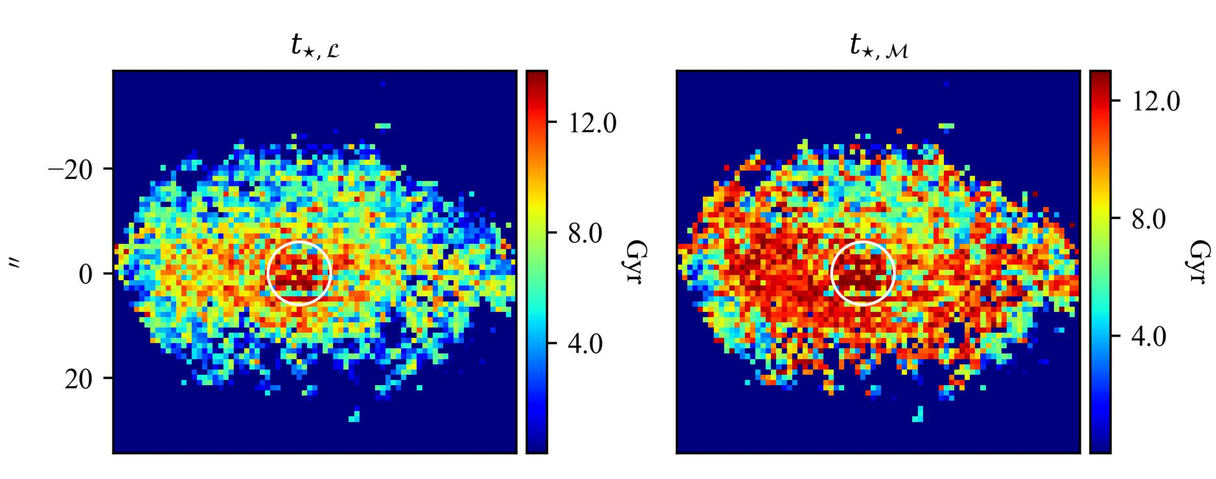

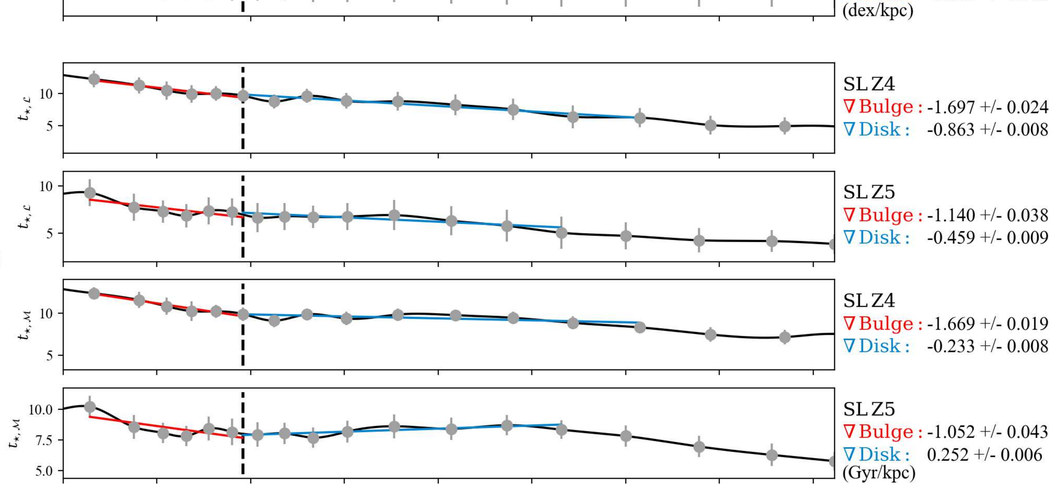

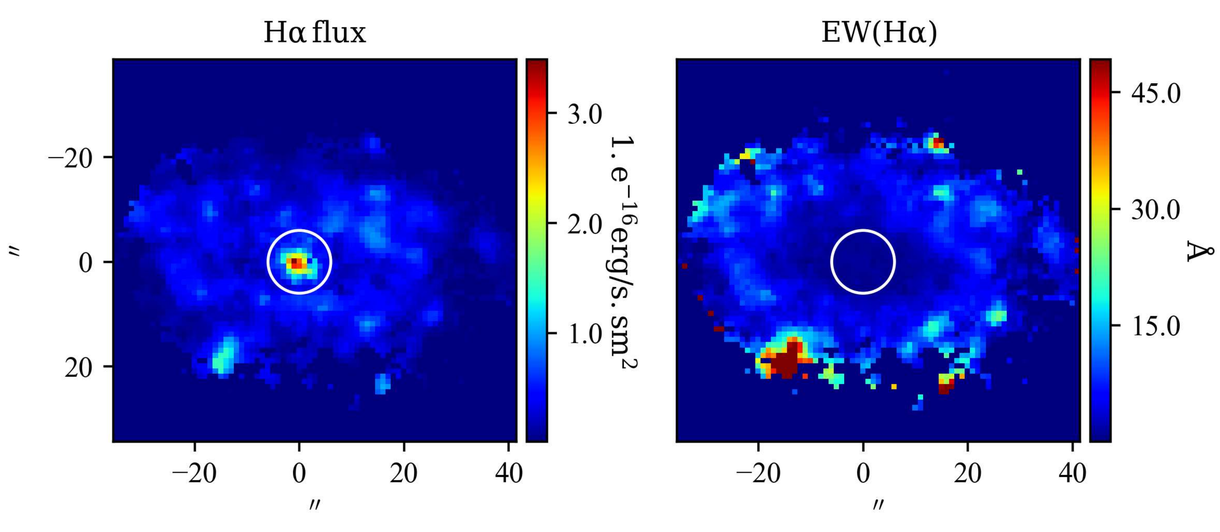

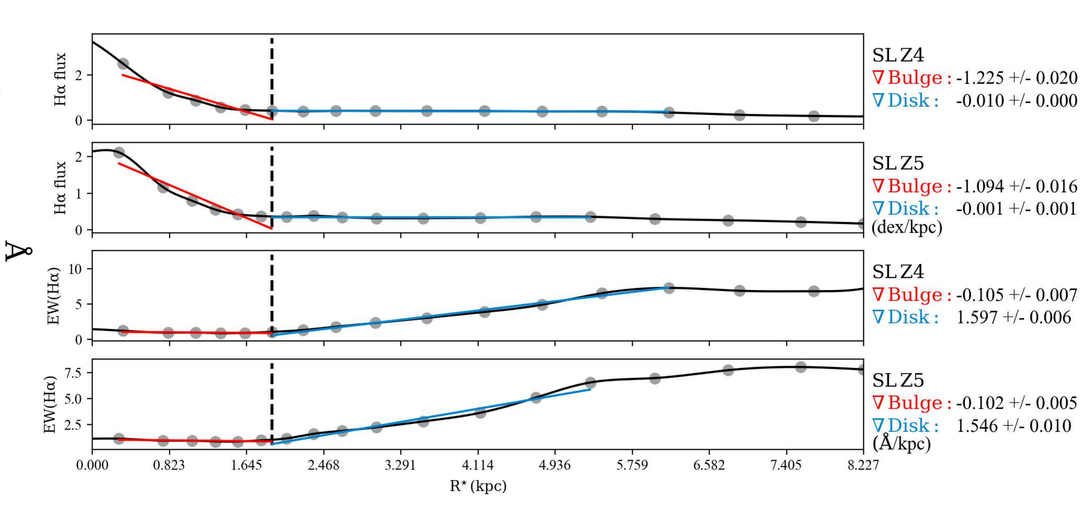

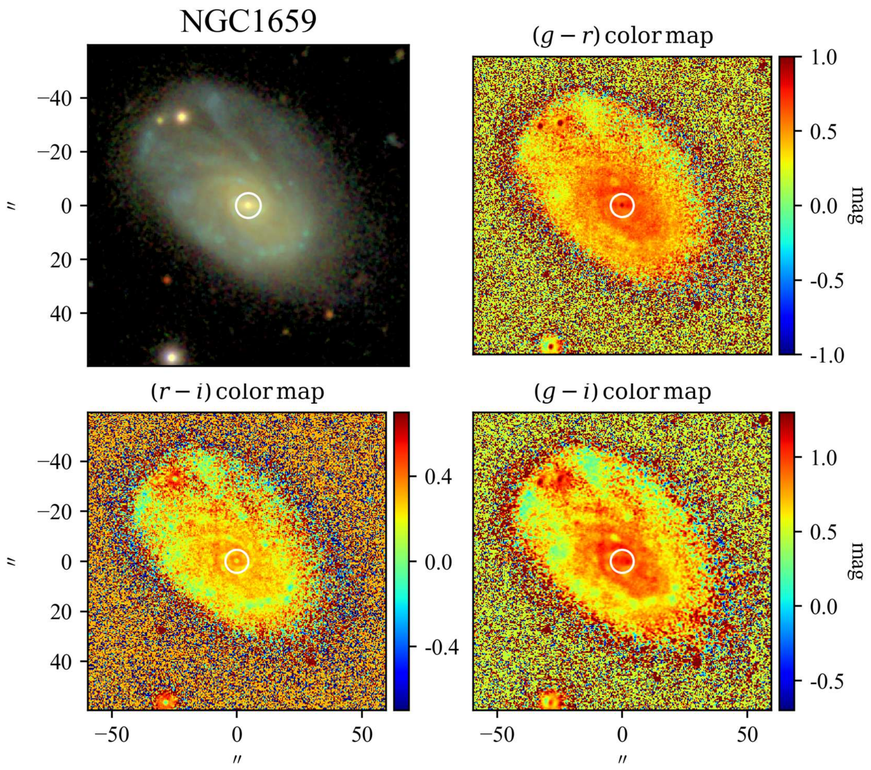

SBP decomposition of SDSS r band

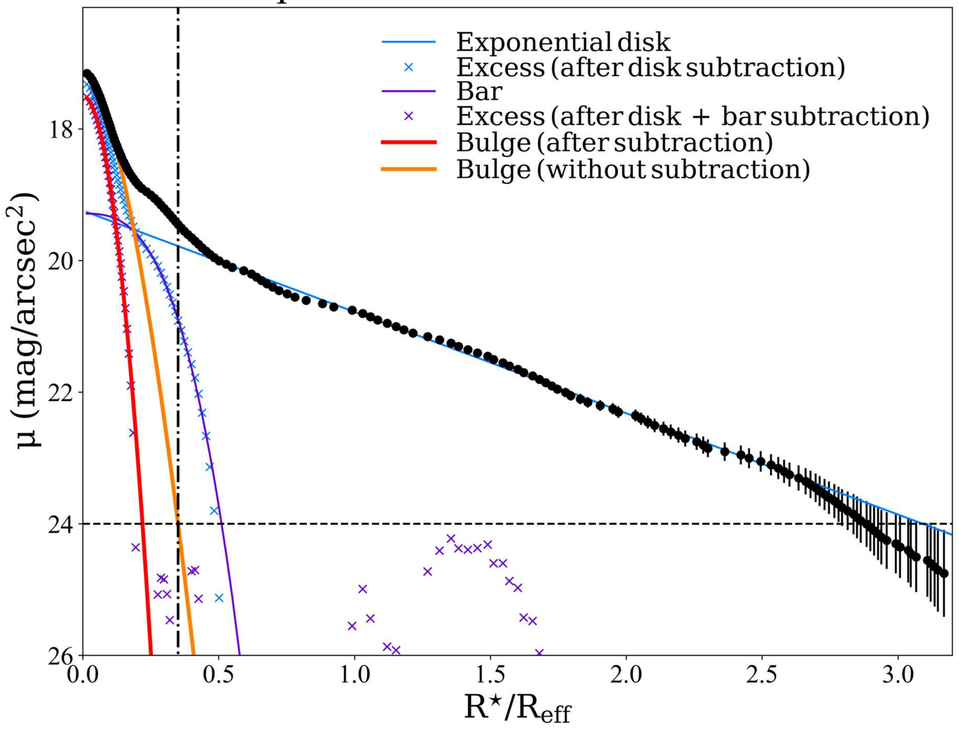

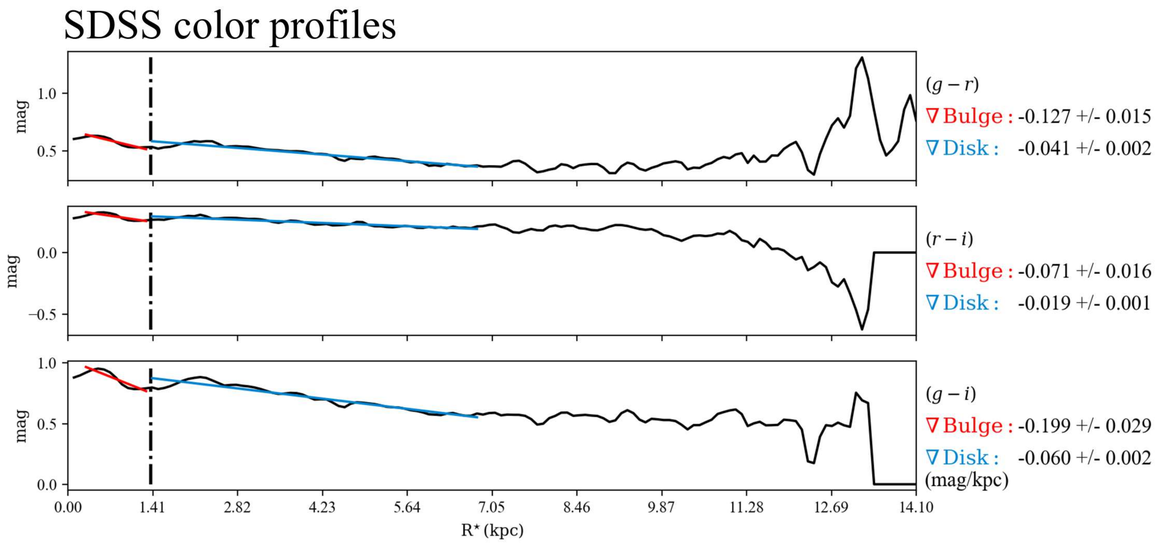

$\mathcal{RY}$ SBPs

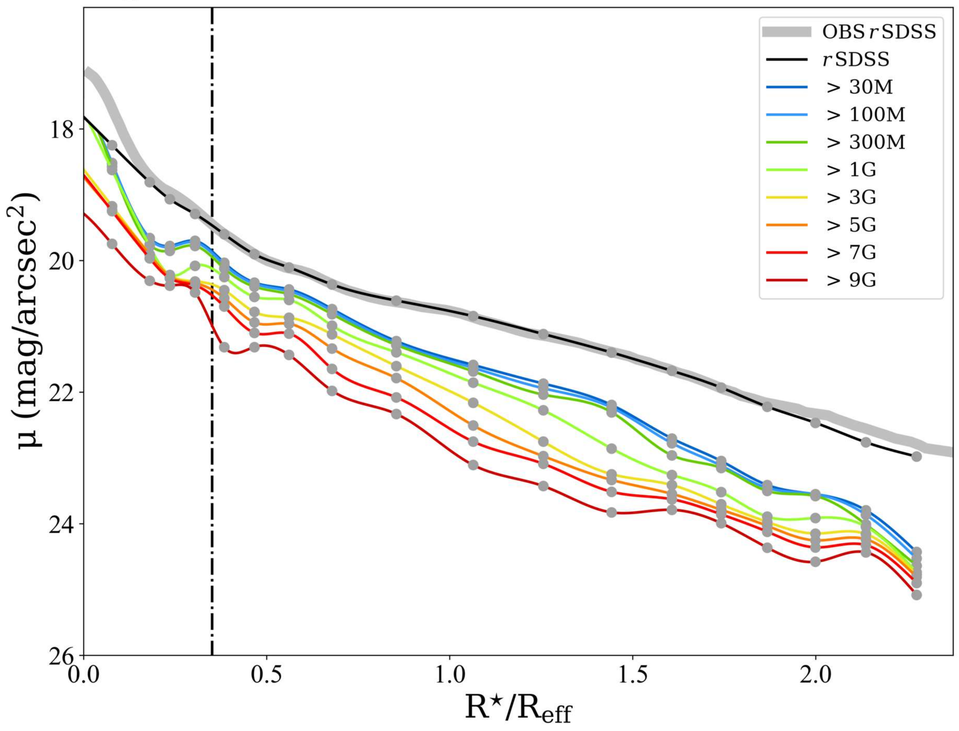

Stellar Continuum

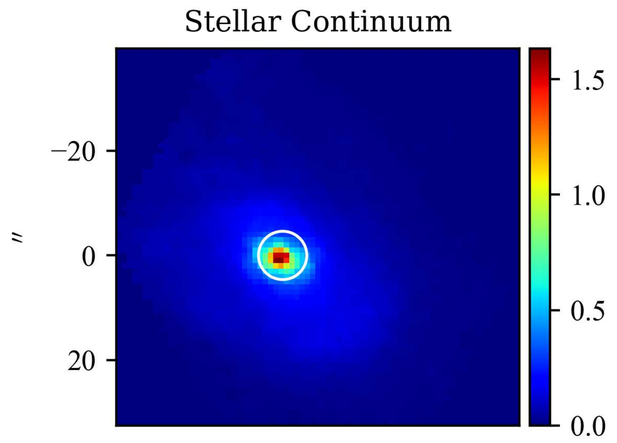

$\mathcal{M}_{\star,\mathrm{P}}$

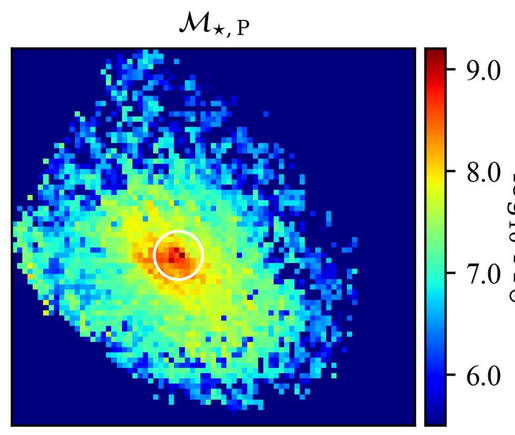

Log. of cumulative present stellar mass profiles

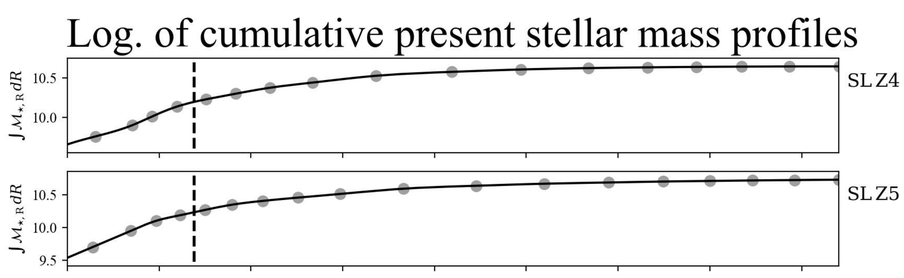

$Z_{\star,\mathcal{L}}$

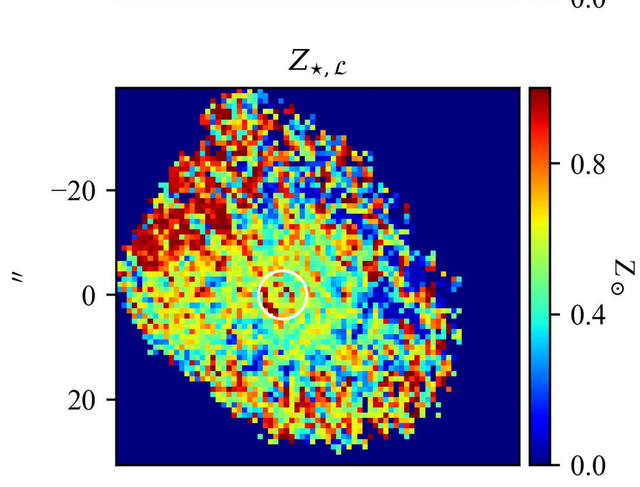

$Z_{\star,\mathcal{M}}$

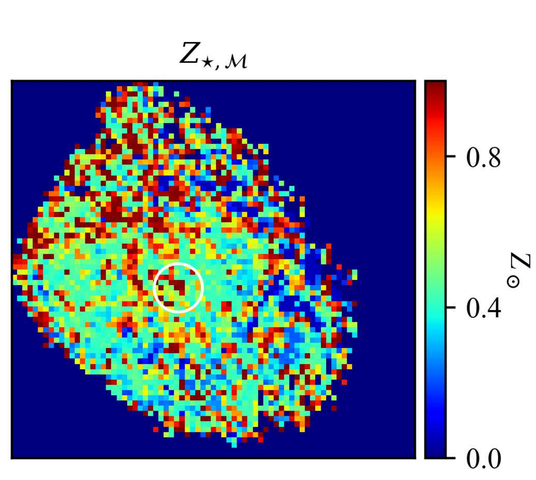

Stellar metallicity/Age & Hα flux/EW profiles

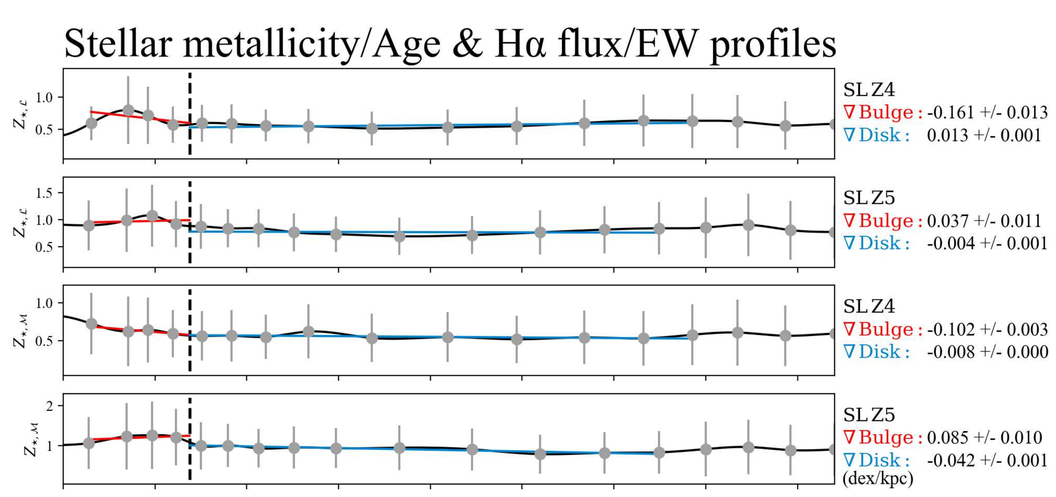

$t_{\star,\mathcal{L}}$

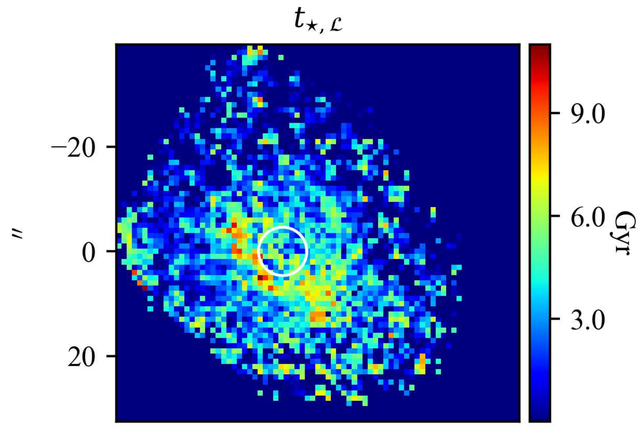

$t_{\star,\mathcal{M}}$

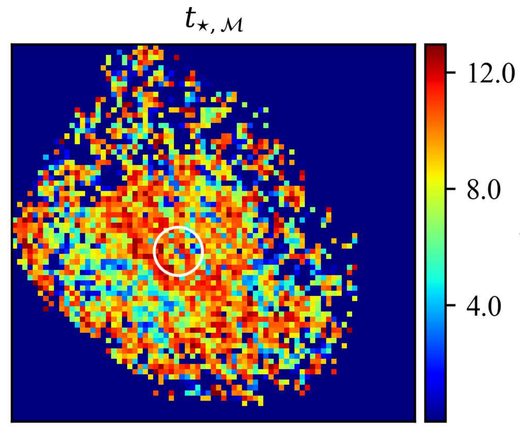

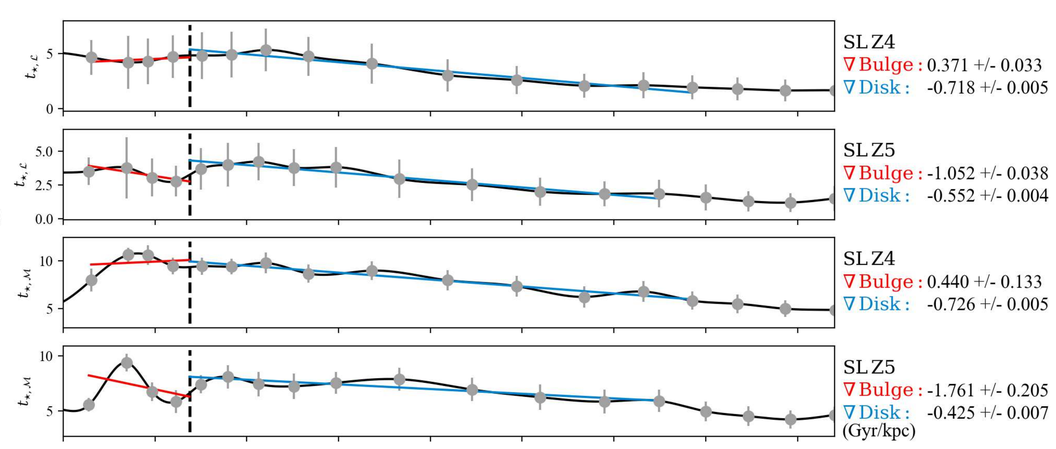

Hα flux

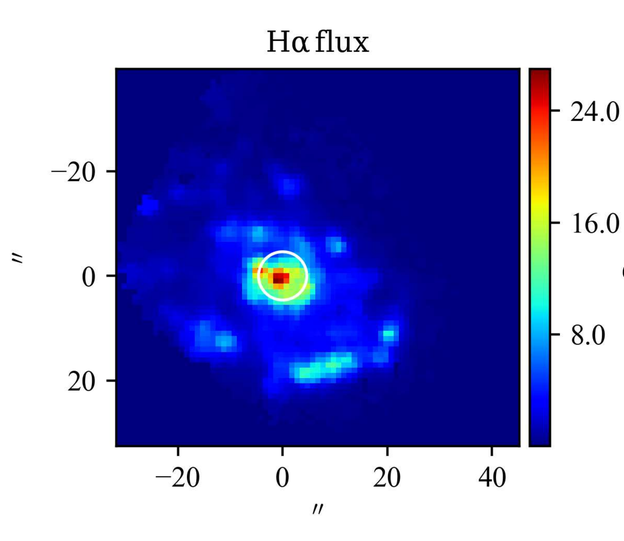

EW(Hα)

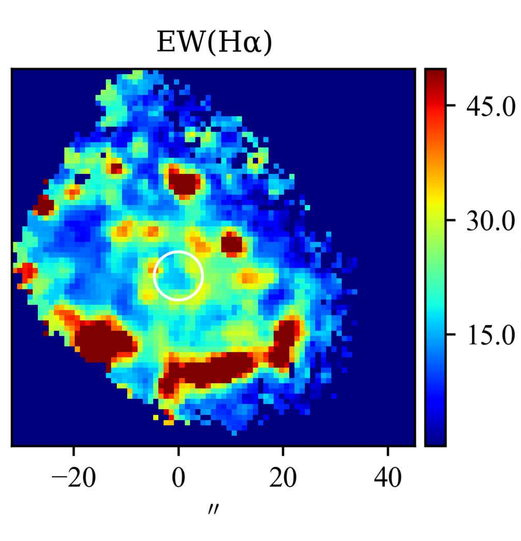

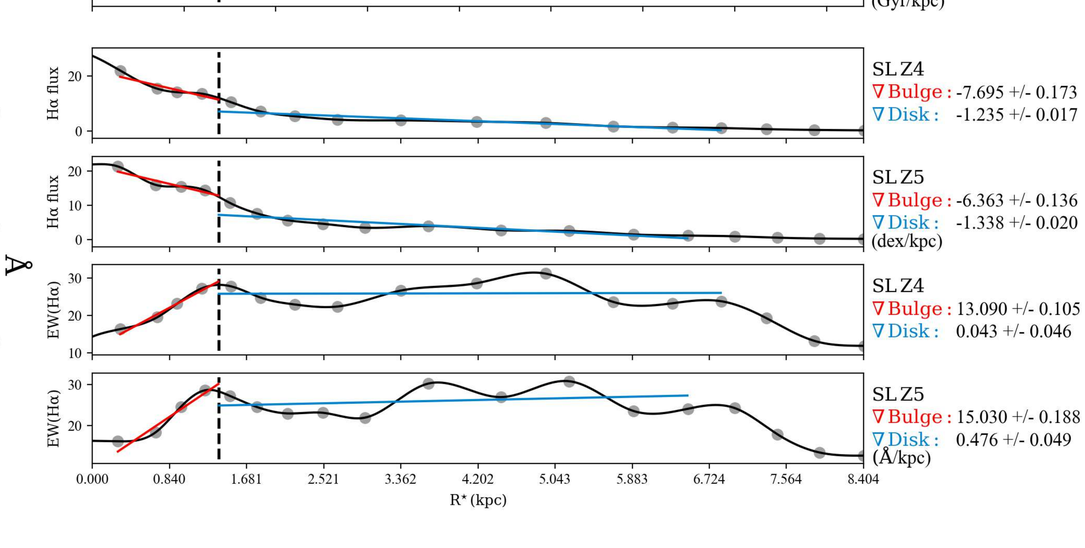

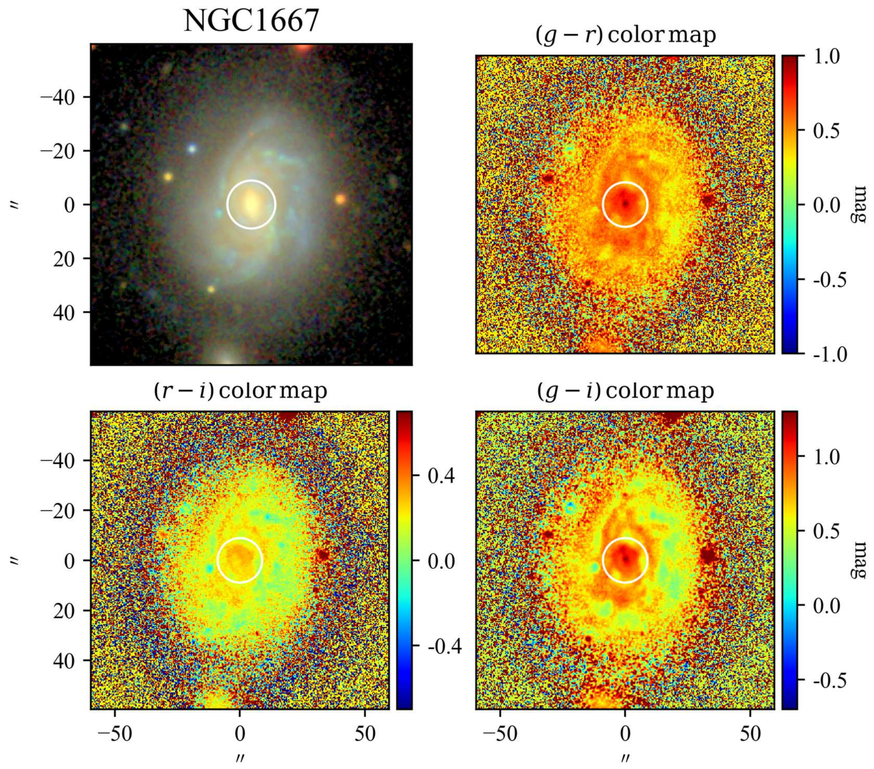
NGC1667
$(g-r)$ color map
$(r-i)$ color map
$(g-i)$ color map
mag
″

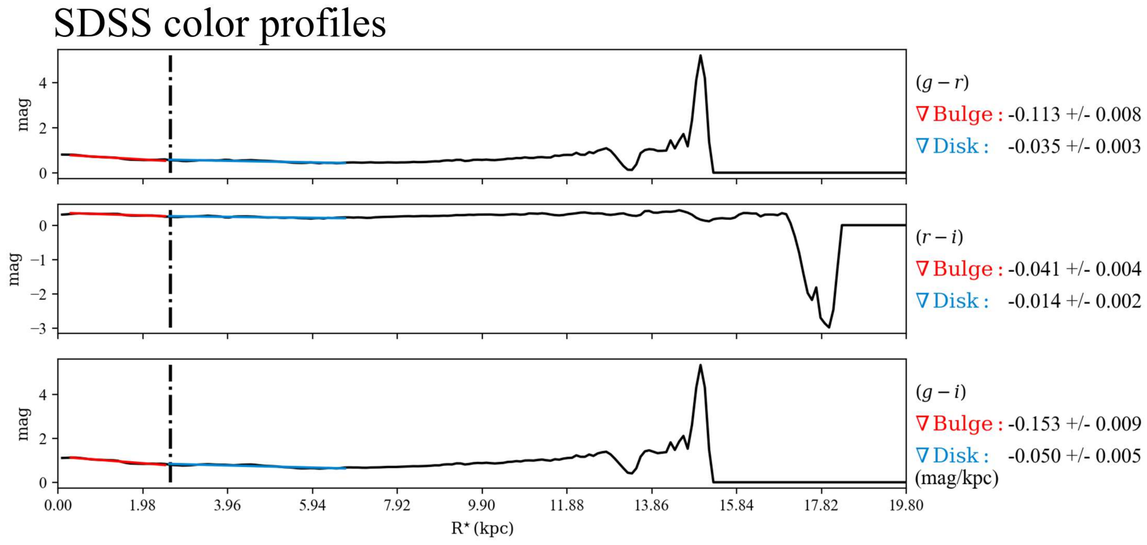
SDSS color profiles
mag
$(g-r)$
∇ Bulge : -0.113 +/- 0.008
∇ Disk : -0.035 +/- 0.003
$(r-i)$
∇ Bulge : -0.041 +/- 0.004
∇ Disk : -0.014 +/- 0.002
$(g-i)$
∇ Bulge : -0.153 +/- 0.009
∇ Disk : -0.050 +/- 0.005
(mag/kpc)
R* (kpc)

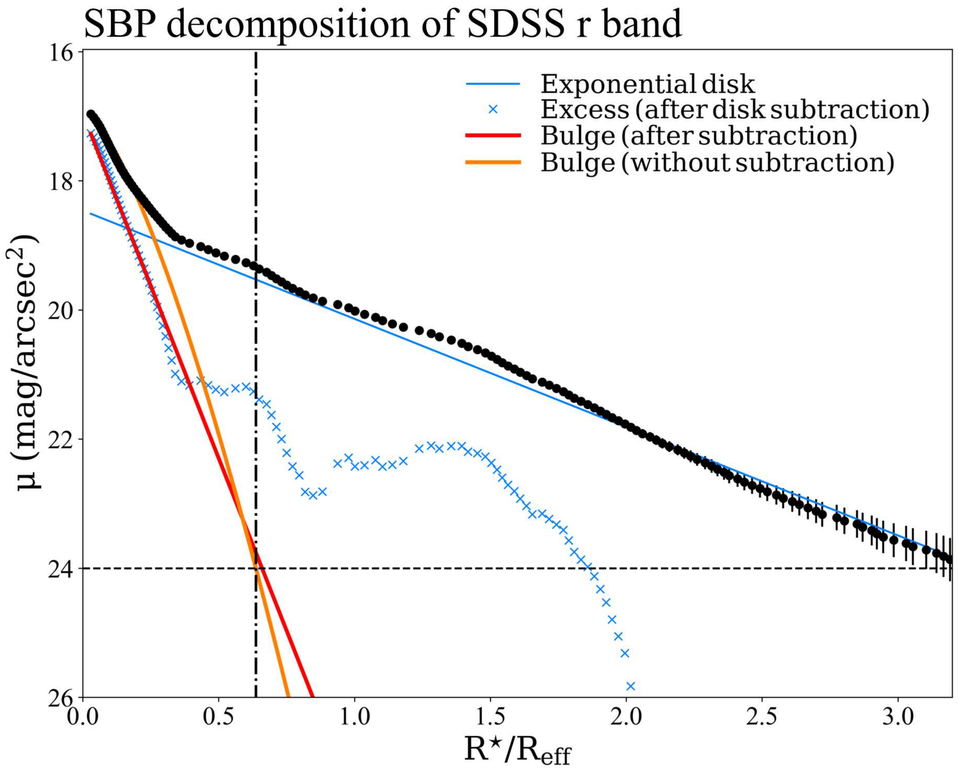
SBP decomposition of SDSS r band
Exponential disk
Excess (after disk subtraction)
Bulge (after subtraction)
Bulge (without subtraction)
μ (mag/arcsec²)
R*/Reff

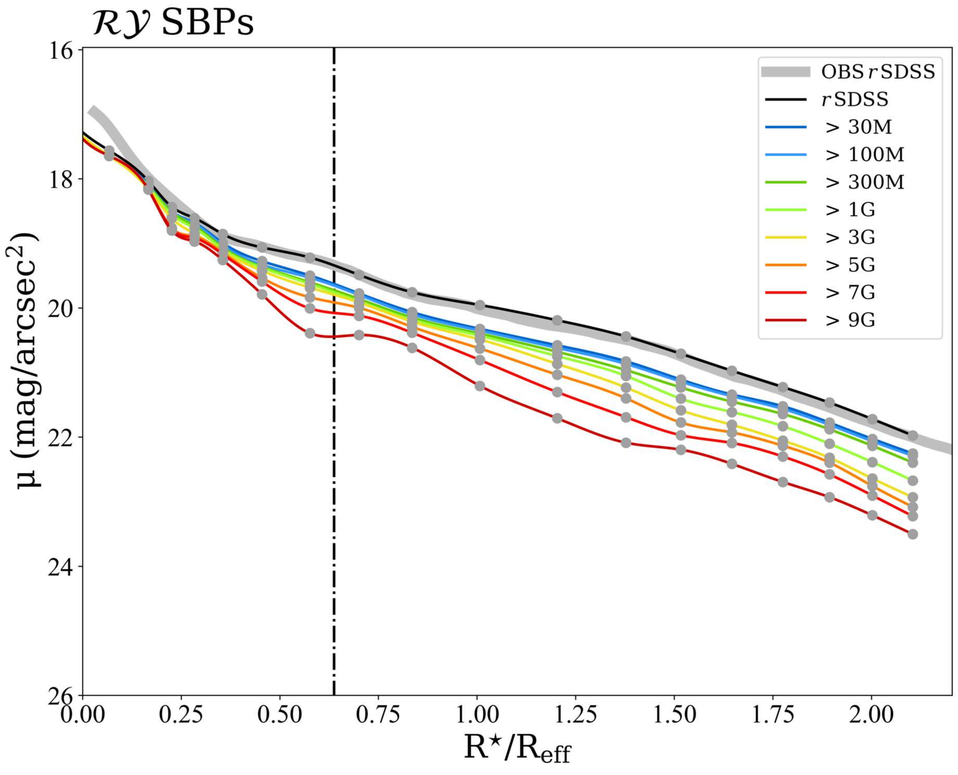
$\mathcal{RV}$ SBPs
OBS rSDSS
rSDSS
> 30M
> 100M
> 300M
> 1G
> 3G
> 5G
> 7G
> 9G
μ (mag/arcsec²)
R*/Reff

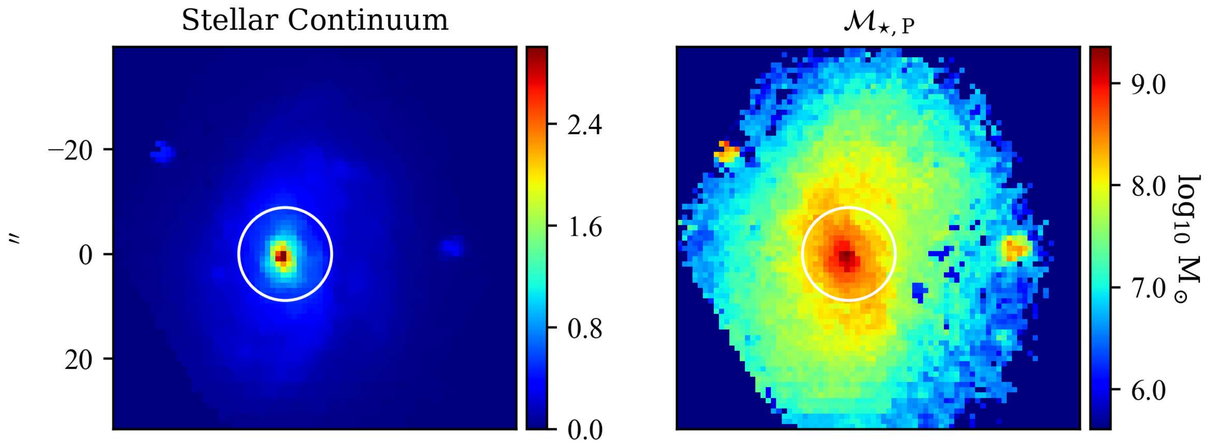
Stellar Continuum
$\mathcal{M}_{\star,\mathrm{P}}$
$Z_{\star,\mathcal{L}}$
$Z_{\star,\mathcal{M}}$
log10 M⊙
Z⊙
″

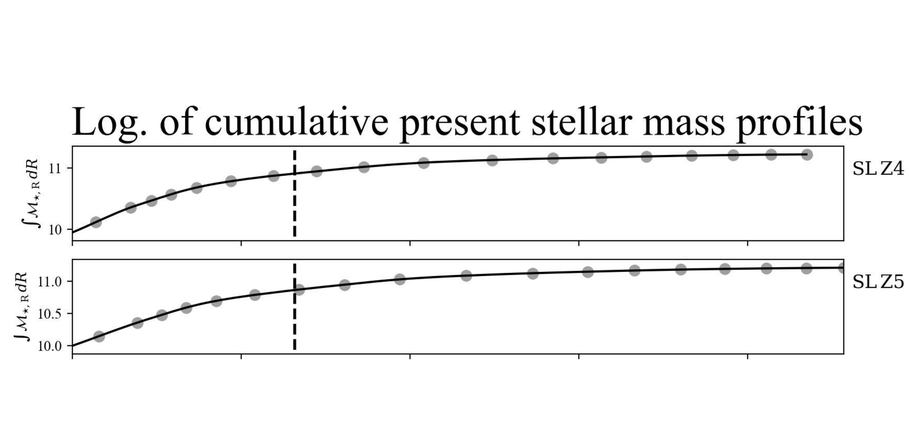
Log. of cumulative present stellar mass profiles
$\int \mathcal{M}_{\star,\mathrm{R}}\, dR$
SL Z4
SL Z5
Stellar metallicity/Age & Hα flux/EW profiles
$Z_{\star,\mathcal{L}}$
$Z_{\star,\mathcal{M}}$
SL Z4
∇ Bulge : -0.146 +/- 0.002
∇ Disk : -0.004 +/- 0.001
SL Z5
∇ Bulge : -0.327 +/- 0.003
∇ Disk : -0.015 +/- 0.001
SL Z4
∇ Bulge : -0.038 +/- 0.002
∇ Disk : -0.041 +/- 0.001
SL Z5
∇ Bulge : -0.158 +/- 0.001
∇ Disk : -0.077 +/- 0.002
(dex/kpc)

$t_{\star,\mathcal{L}}$
$t_{\star,\mathcal{M}}$
Gyr
Hα flux
EW(Hα)
1. e⁻¹⁶erg/s.sm²
Å
″

SL Z4
∇ Bulge : -3.107 +/- 0.024
∇ Disk : -0.714 +/- 0.007
SL Z5
∇ Bulge : -2.023 +/- 0.043
∇ Disk : -0.329 +/- 0.006
SL Z4
∇ Bulge : -1.226 +/- 0.013
∇ Disk : -0.543 +/- 0.007
SL Z5
∇ Bulge : -0.607 +/- 0.044
∇ Disk : -0.308 +/- 0.006
(Gyr/kpc)
SL Z4
∇ Bulge : 1.341 +/- 0.251
∇ Disk : -2.426 +/- 0.022
SL Z5
∇ Bulge : 2.066 +/- 0.209
∇ Disk : -2.347 +/- 0.015
(dex/kpc)
SL Z4
∇ Bulge : 13.007 +/- 0.217
∇ Disk : -1.454 +/- 0.114
SL Z5
∇ Bulge : 13.861 +/- 0.219
∇ Disk : -2.248 +/- 0.109
(Å/kpc)
R* (kpc)

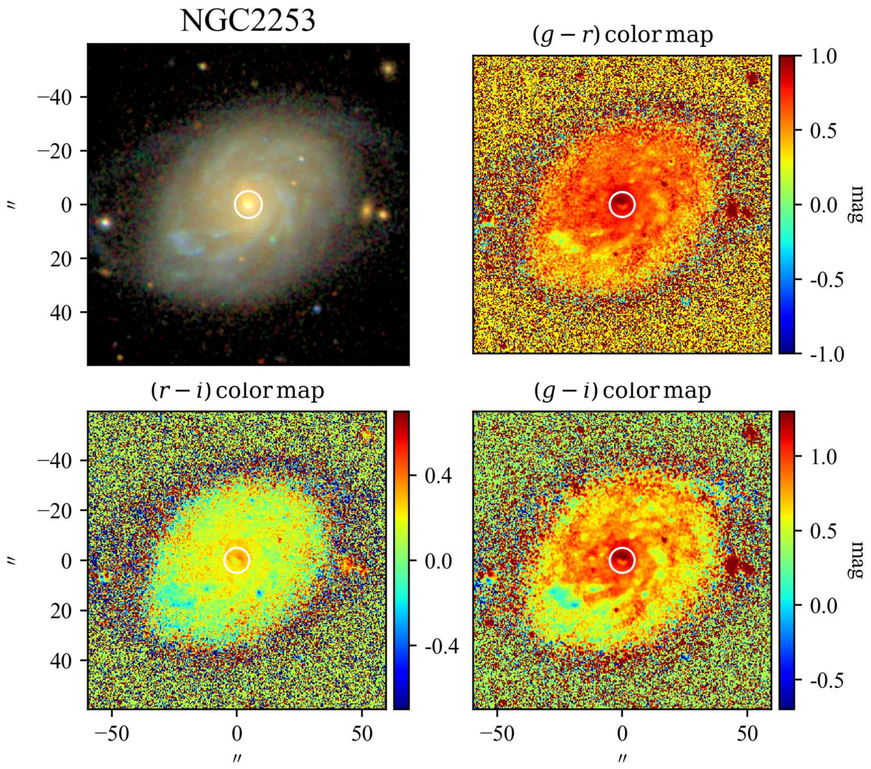
NGC2253
$(g-r)$ color map
$(r-i)$ color map
$(g-i)$ color map
mag
″

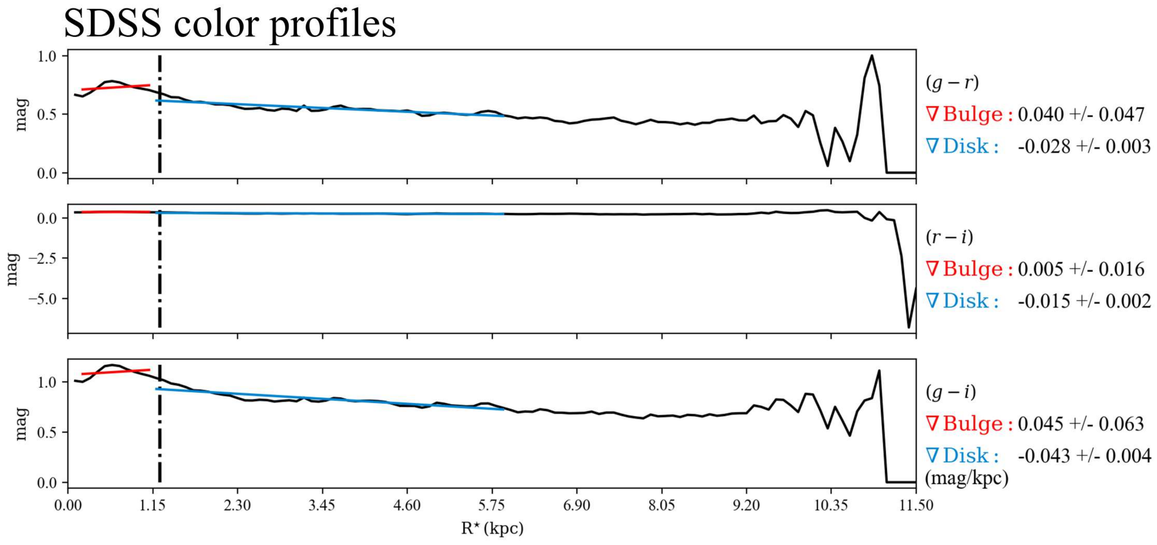
SDSS color profiles
$(g-r)$
∇ Bulge : 0.040 +/- 0.047
∇ Disk : -0.028 +/- 0.003
$(r-i)$
∇ Bulge : 0.005 +/- 0.016
∇ Disk : -0.015 +/- 0.002
$(g-i)$
∇ Bulge : 0.045 +/- 0.063
∇ Disk : -0.043 +/- 0.004
(mag/kpc)
mag
R* (kpc)

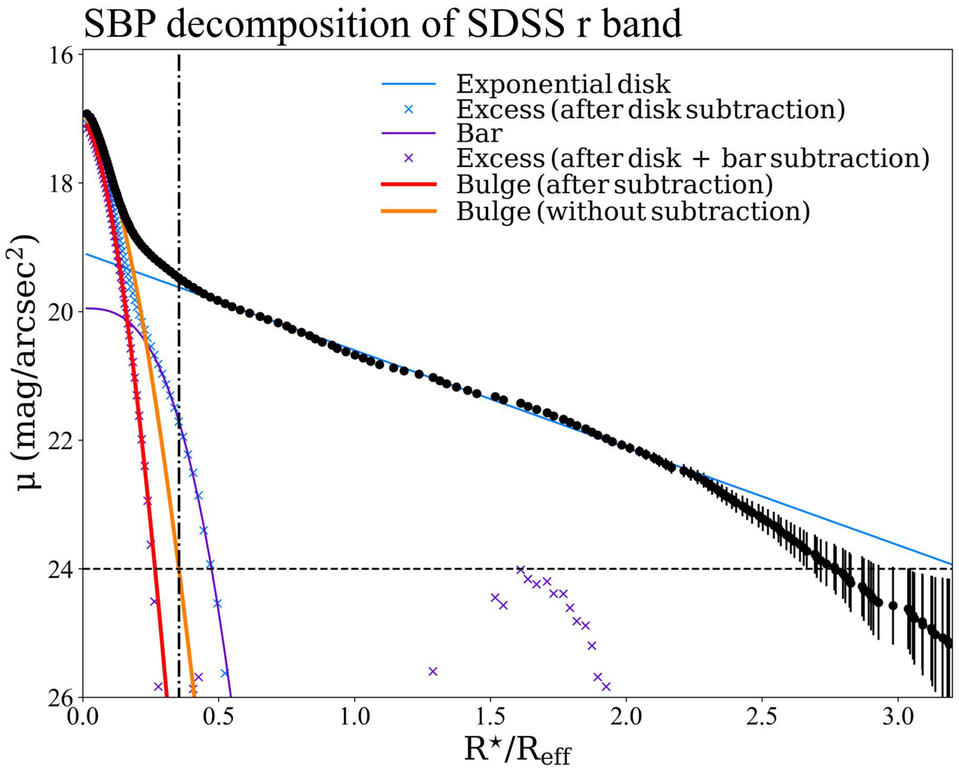
SBP decomposition of SDSS r band
Exponential disk
Excess (after disk subtraction)
Bar
Excess (after disk + bar subtraction)
Bulge (after subtraction)
Bulge (without subtraction)
μ (mag/arcsec²)
R*/Reff

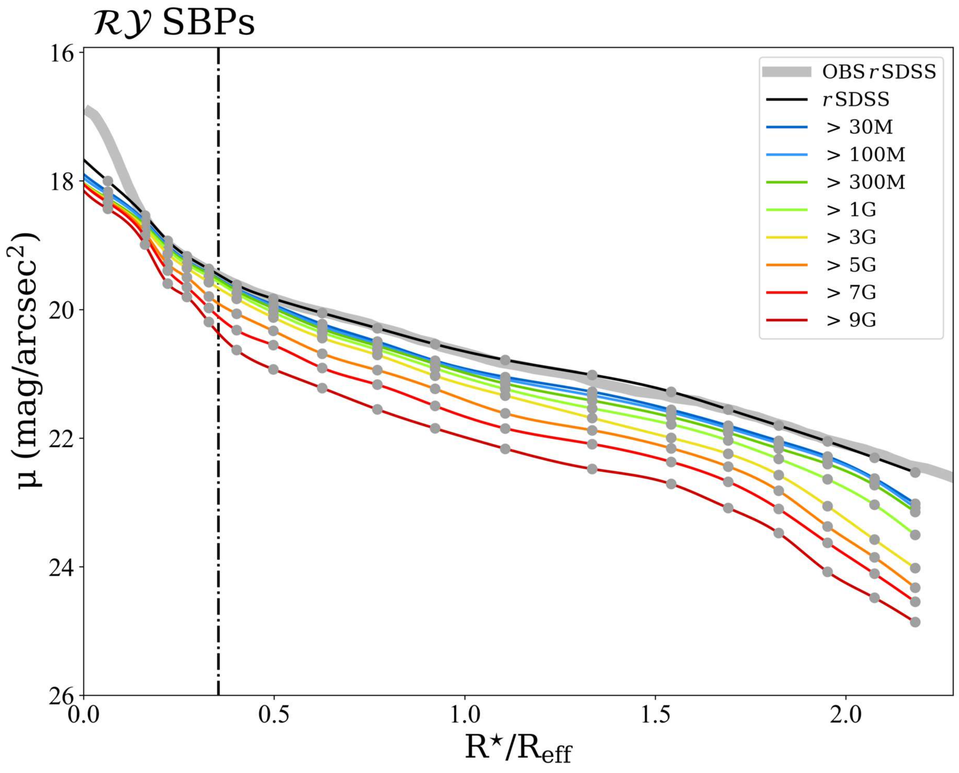
$\mathcal{RY}$ SBPs
OBS rSDSS
rSDSS
> 30M
> 100M
> 300M
> 1G
> 3G
> 5G
> 7G
> 9G
μ (mag/arcsec²)
R*/Reff

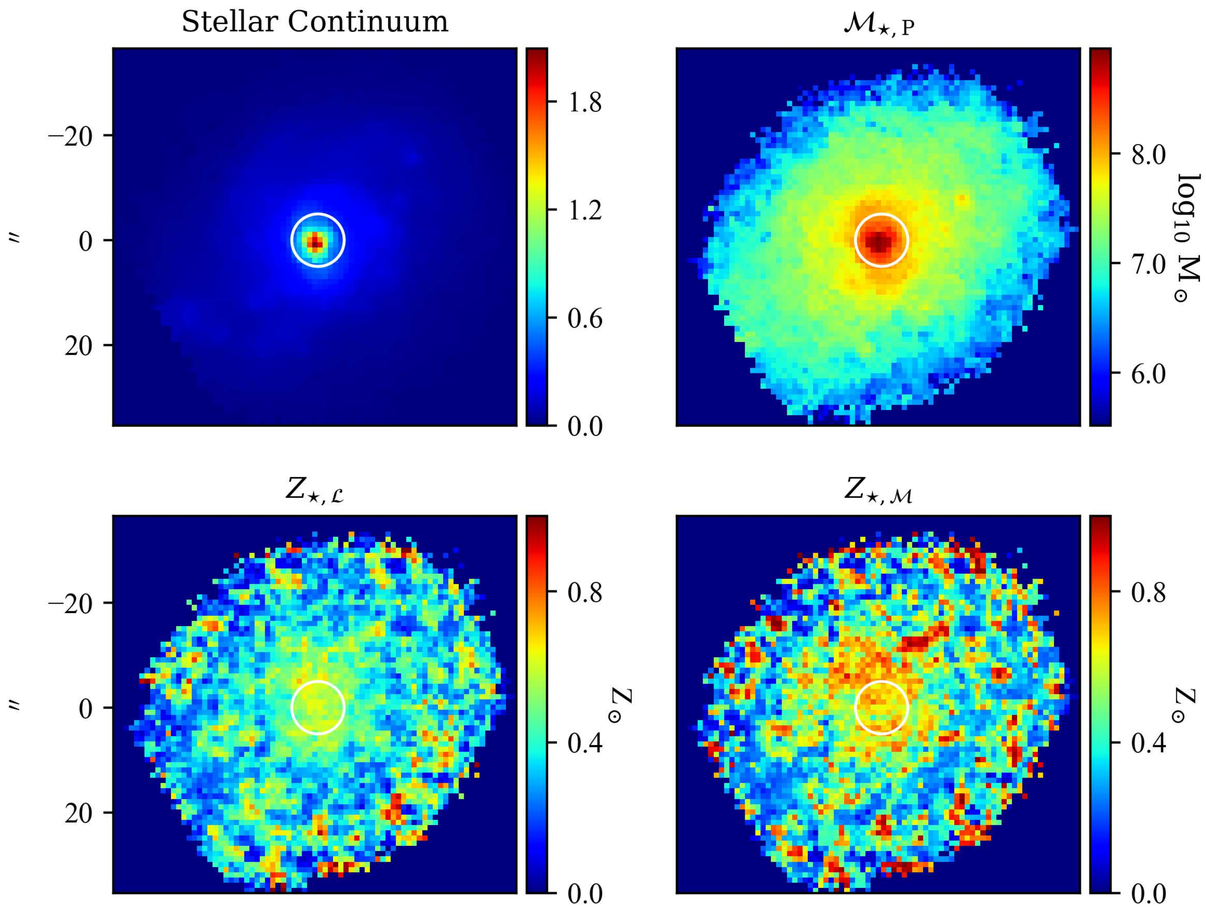
Stellar Continuum
$\mathcal{M}_{\star,\mathrm{P}}$
$\log_{10} M_\odot$
$Z_{\star,\mathcal{L}}$
$Z_{\star,\mathcal{M}}$
$Z_\odot$
″

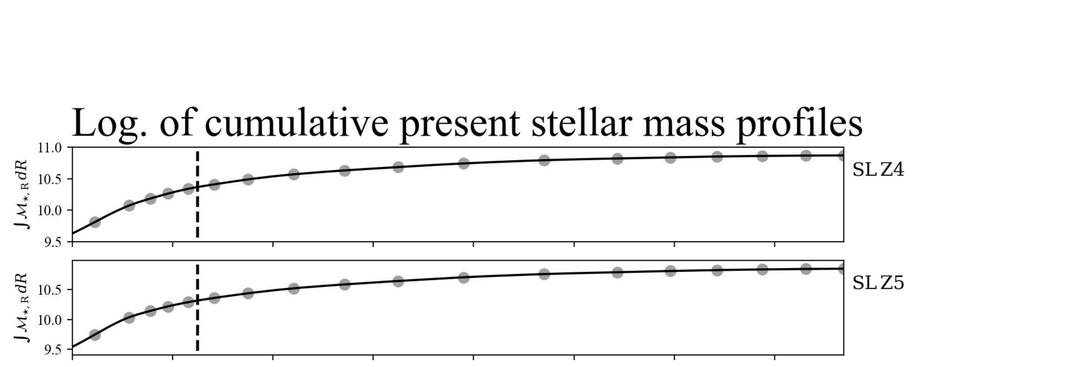
Log. of cumulative present stellar mass profiles
$\int \mathcal{M}_{\star,\mathrm{R}} dR$
SL Z4
SL Z5

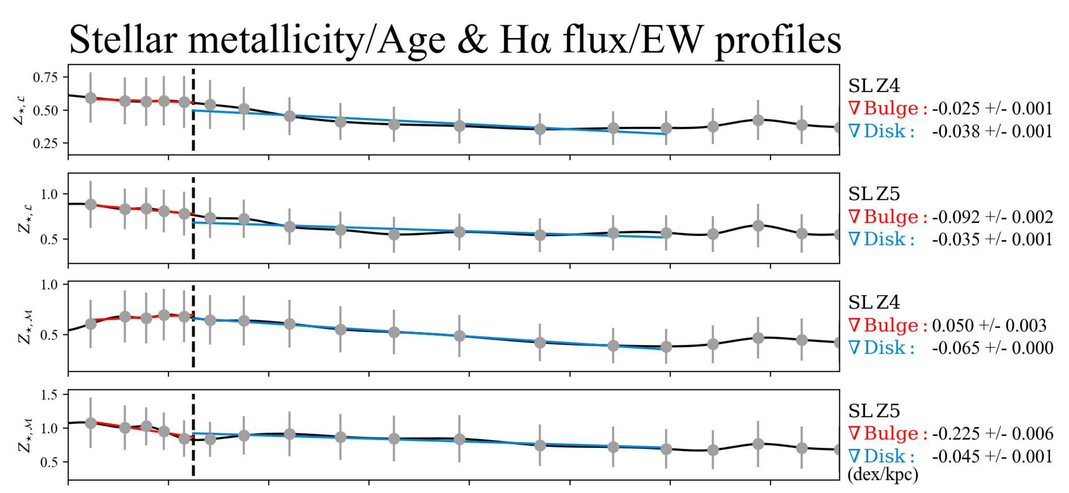
Stellar metallicity/Age & Hα flux/EW profiles
$Z_{\star,\mathcal{L}}$
SL Z4
∇ Bulge : -0.025 +/- 0.001
∇ Disk : -0.038 +/- 0.001
$Z_{\star,\mathcal{L}}$
SL Z5
∇ Bulge : -0.092 +/- 0.002
∇ Disk : -0.035 +/- 0.001
$Z_{\star,\mathcal{M}}$
SL Z4
∇ Bulge : 0.050 +/- 0.003
∇ Disk : -0.065 +/- 0.000
$Z_{\star,\mathcal{M}}$
SL Z5
∇ Bulge : -0.225 +/- 0.006
∇ Disk : -0.045 +/- 0.001
(dex/kpc)

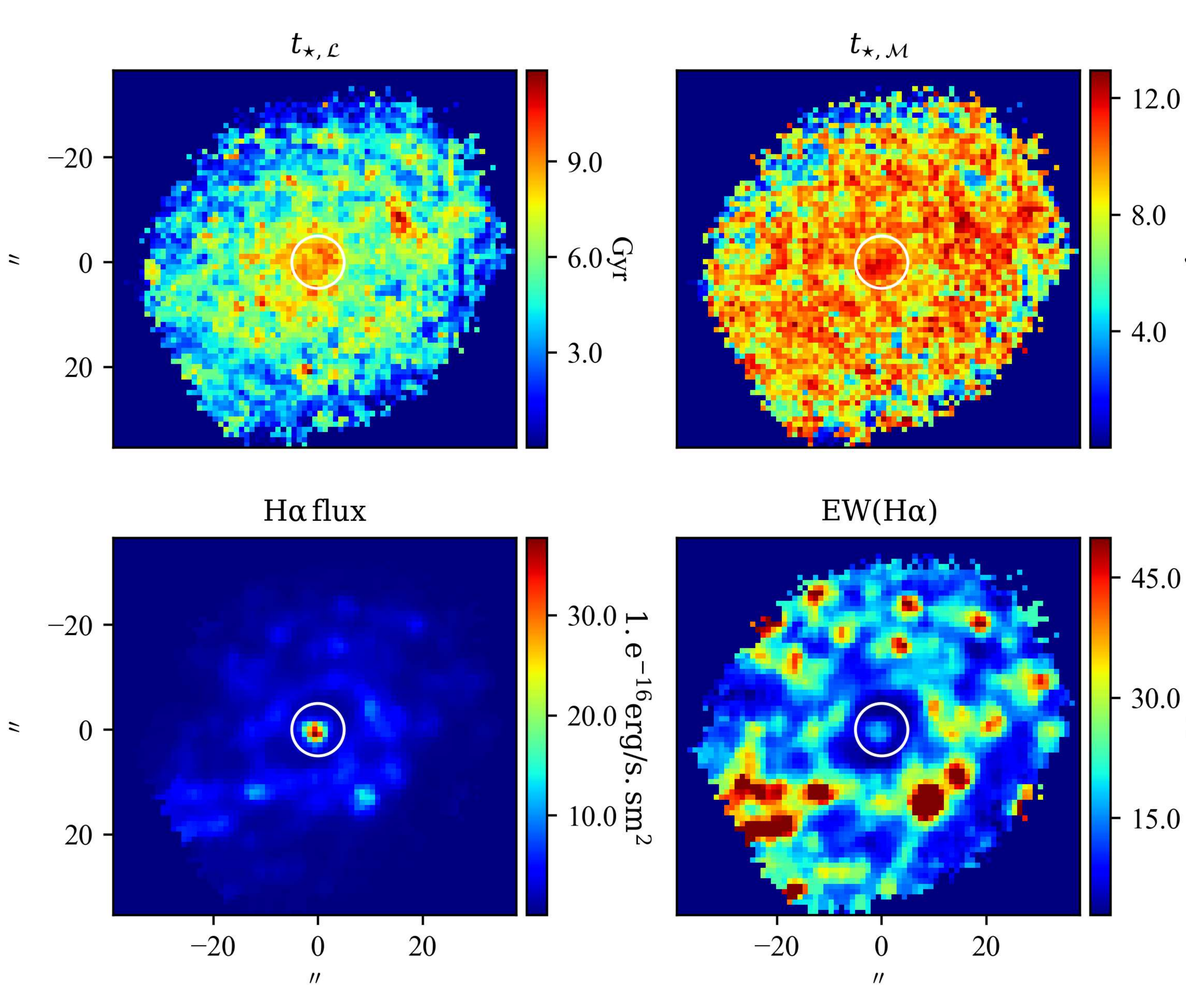
$t_{\star,\mathcal{L}}$
$t_{\star,\mathcal{M}}$
Gyr
Hα flux
EW(Hα)
$1.e^{-16}$erg/s.sm²
Å
″

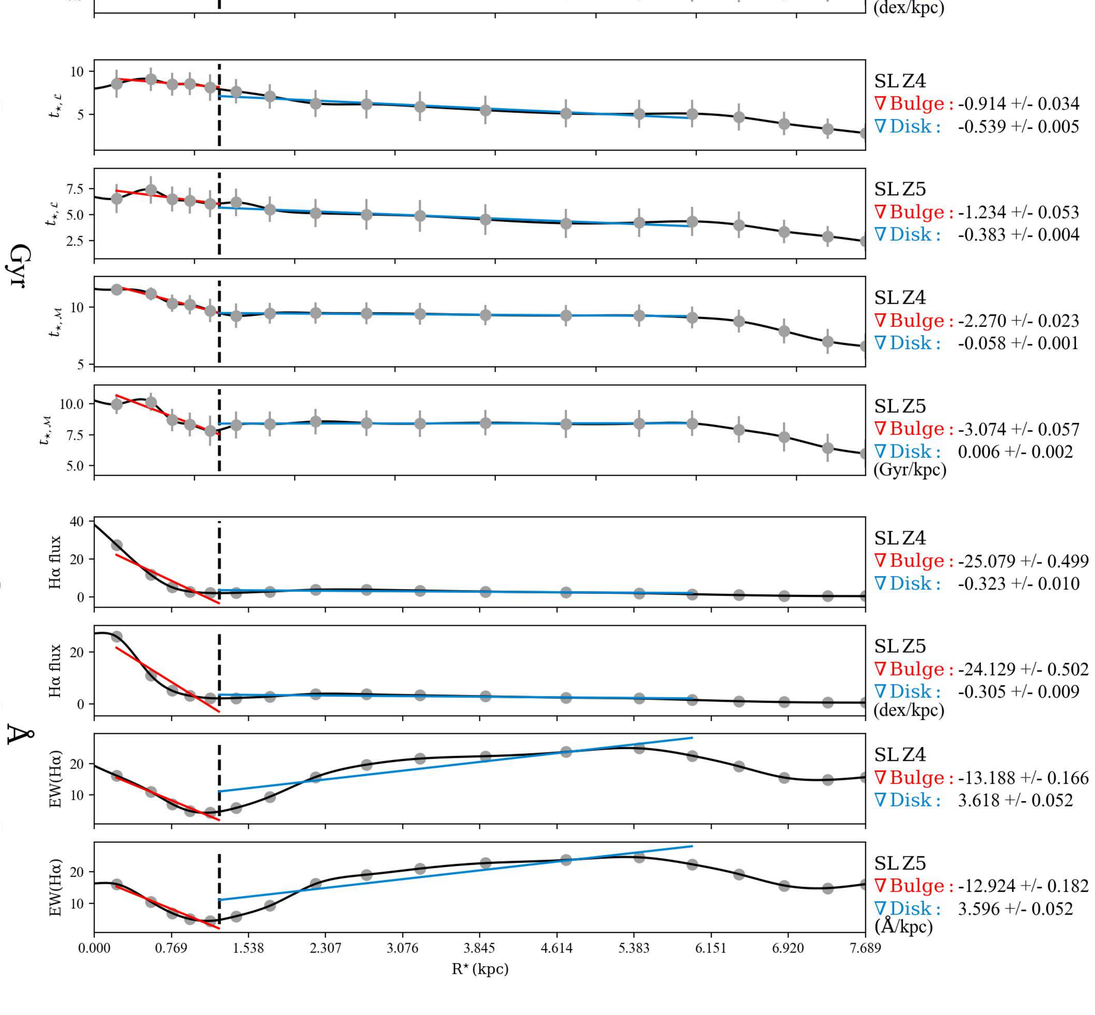
$t_{\star,\mathcal{L}}$
SL Z4
∇ Bulge : -0.914 +/- 0.034
∇ Disk : -0.539 +/- 0.005
$t_{\star,\mathcal{L}}$
SL Z5
∇ Bulge : -1.234 +/- 0.053
∇ Disk : -0.383 +/- 0.004
$t_{\star,\mathcal{M}}$
SL Z4
∇ Bulge : -2.270 +/- 0.023
∇ Disk : -0.058 +/- 0.001
$t_{\star,\mathcal{M}}$
SL Z5
∇ Bulge : -3.074 +/- 0.057
∇ Disk : 0.006 +/- 0.002
(Gyr/kpc)
Hα flux
SL Z4
∇ Bulge : -25.079 +/- 0.499
∇ Disk : -0.323 +/- 0.010
Hα flux
SL Z5
∇ Bulge : -24.129 +/- 0.502
∇ Disk : -0.305 +/- 0.009
(dex/kpc)
EW(Hα)
SL Z4
∇ Bulge : -13.188 +/- 0.166
∇ Disk : 3.618 +/- 0.052
EW(Hα)
SL Z5
∇ Bulge : -12.924 +/- 0.182
∇ Disk : 3.596 +/- 0.052
(Å/kpc)
R* (kpc)

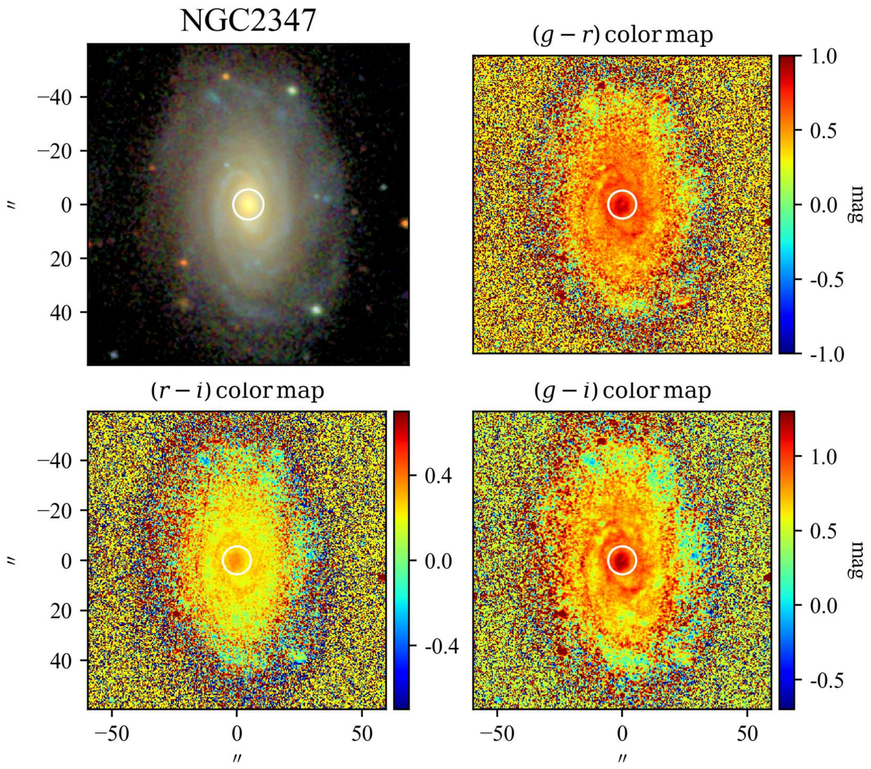
NGC2347
$(g-r)$ color map
$(r-i)$ color map
$(g-i)$ color map
mag
″

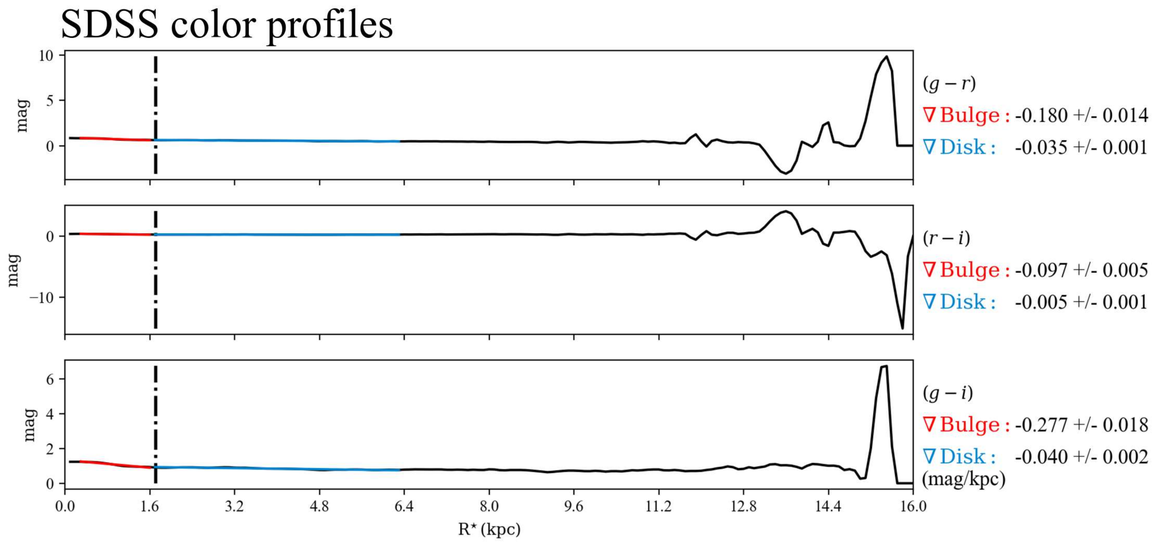
SDSS color profiles
$(g-r)$
∇ Bulge : -0.180 +/- 0.014
∇ Disk : -0.035 +/- 0.001
$(r-i)$
∇ Bulge : -0.097 +/- 0.005
∇ Disk : -0.005 +/- 0.001
$(g-i)$
∇ Bulge : -0.277 +/- 0.018
∇ Disk : -0.040 +/- 0.002
(mag/kpc)
mag
R* (kpc)

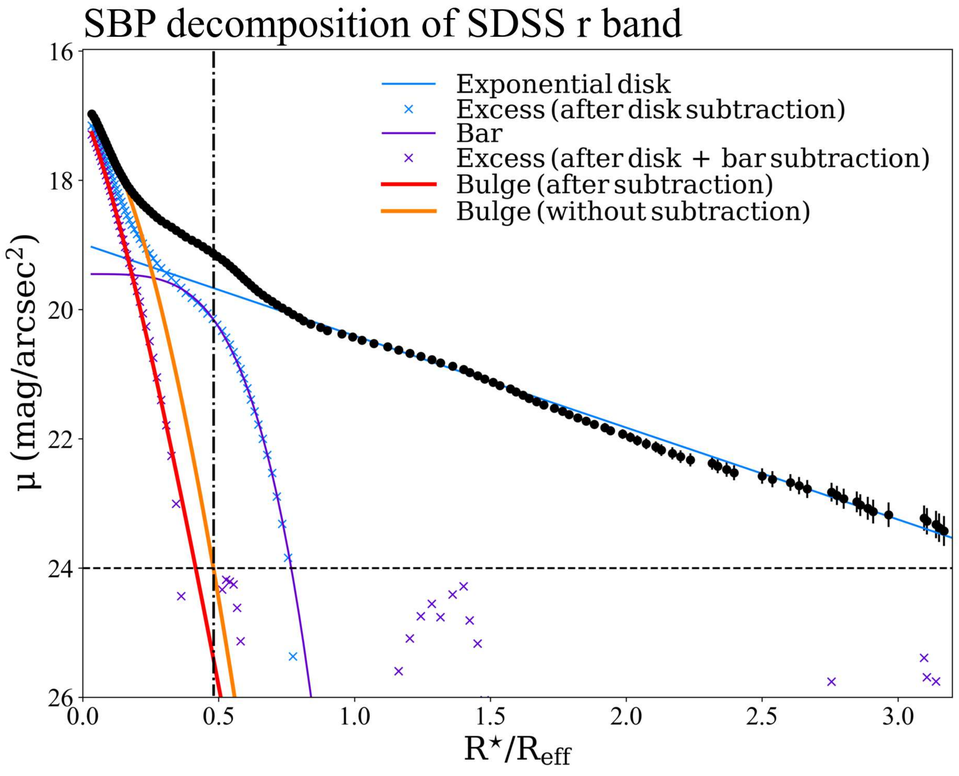
SBP decomposition of SDSS r band
Exponential disk
Excess (after disk subtraction)
Bar
Excess (after disk + bar subtraction)
Bulge (after subtraction)
Bulge (without subtraction)
μ (mag/arcsec^2)
R*/R$_{eff}$

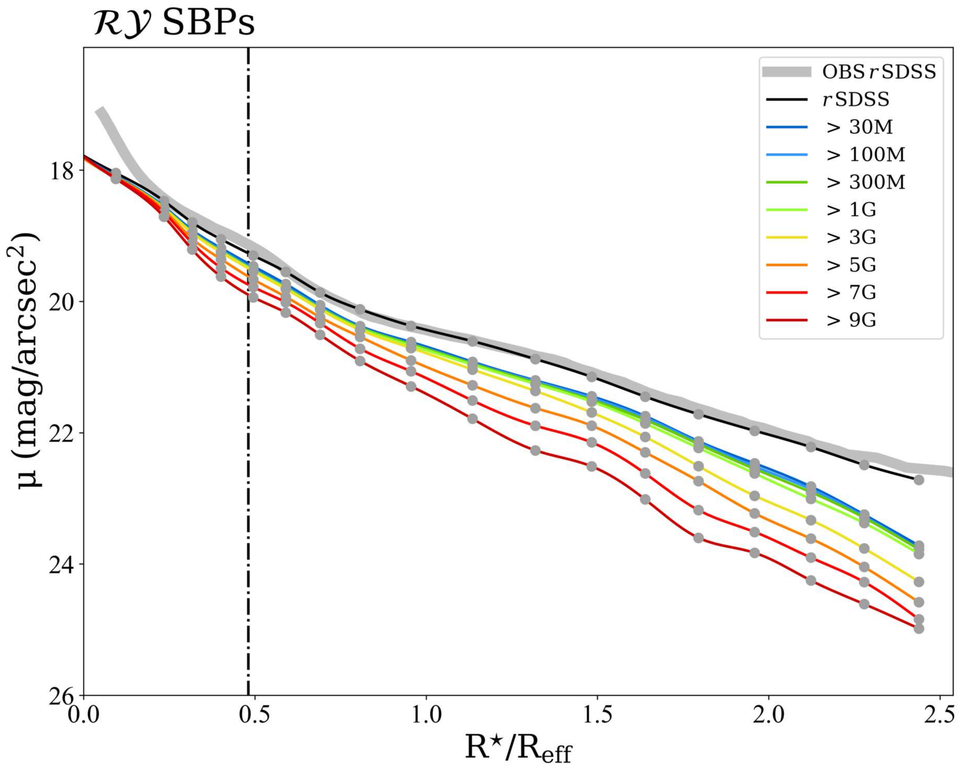
$\mathcal{RY}$ SBPs
OBS rSDSS
rSDSS
> 30M
> 100M
> 300M
> 1G
> 3G
> 5G
> 7G
> 9G
μ (mag/arcsec^2)
R*/R$_{eff}$

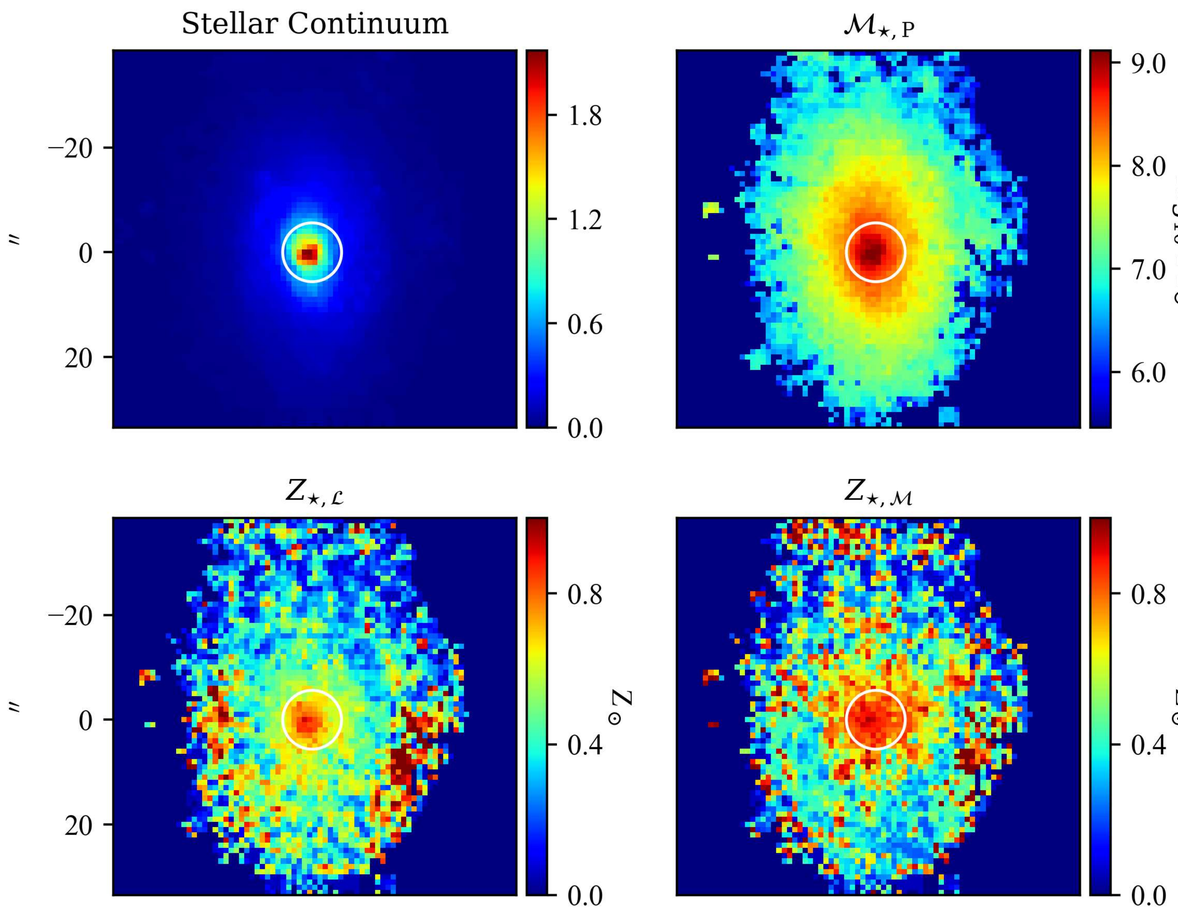
Stellar Continuum
$\mathcal{M}_{\star,\mathrm{P}}$
log$_{10}$ M$_\odot$
″

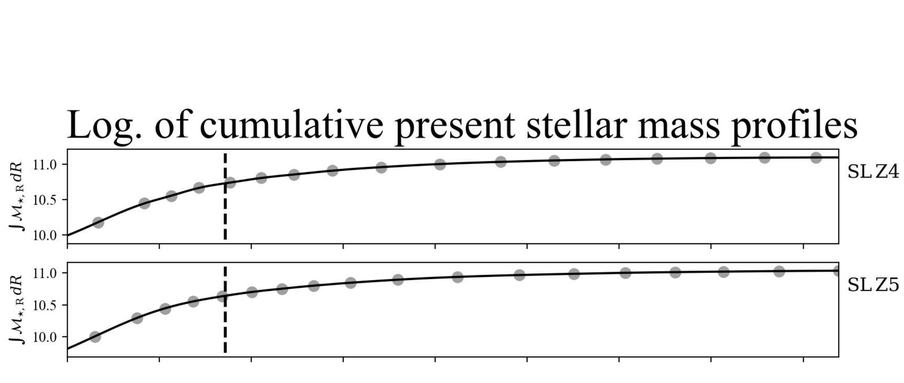
Log. of cumulative present stellar mass profiles
SL Z4
SL Z5
$\int \mathcal{M}_{\star,\mathrm{R}}\, dR$

$Z_{\star,\mathcal{L}}$
$Z_{\star,\mathcal{M}}$
Z$_\odot$
″

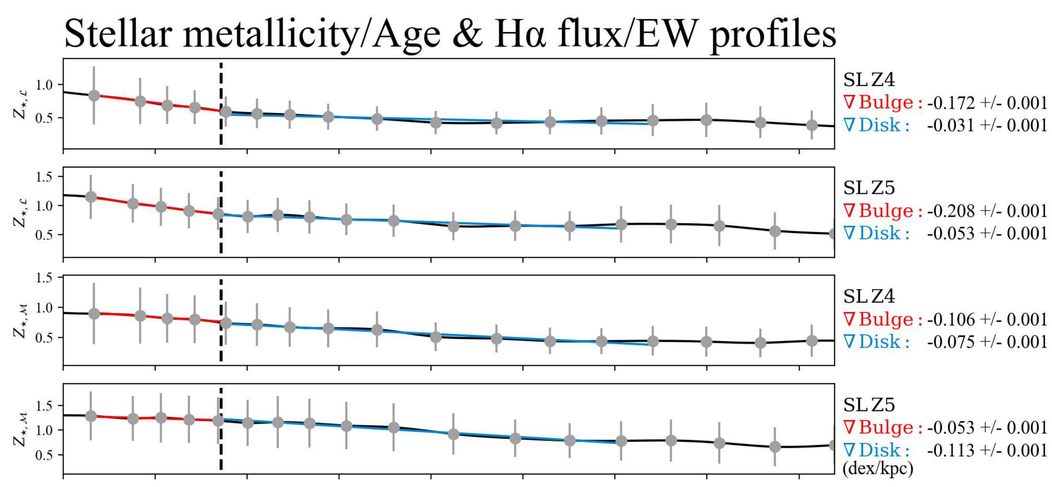
Stellar metallicity/Age & Hα flux/EW profiles
SL Z4
∇ Bulge : -0.172 +/- 0.001
∇ Disk : -0.031 +/- 0.001
SL Z5
∇ Bulge : -0.208 +/- 0.001
∇ Disk : -0.053 +/- 0.001
SL Z4
∇ Bulge : -0.106 +/- 0.001
∇ Disk : -0.075 +/- 0.001
SL Z5
∇ Bulge : -0.053 +/- 0.001
∇ Disk : -0.113 +/- 0.001
(dex/kpc)

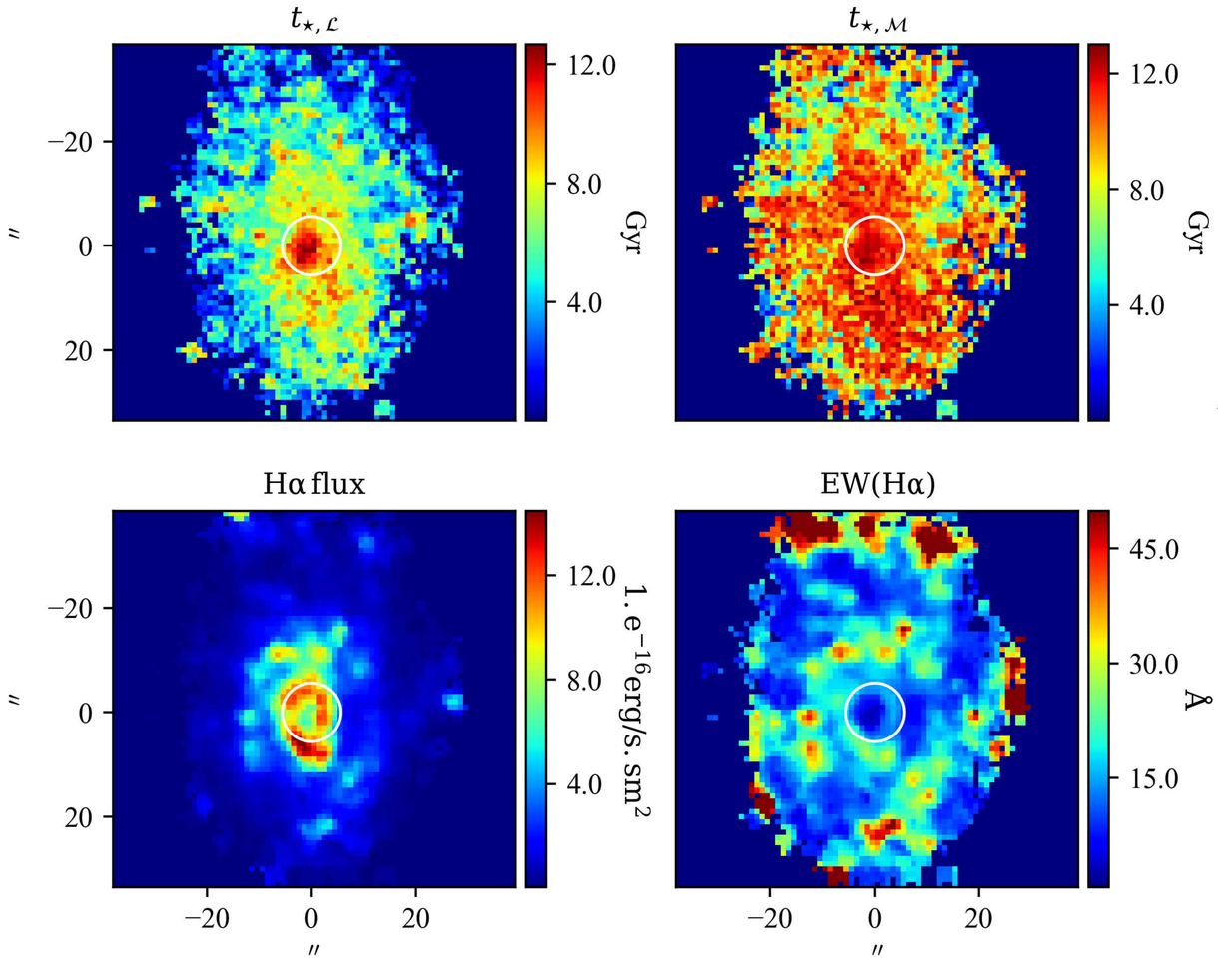
$t_{\star,\mathcal{L}}$
$t_{\star,\mathcal{M}}$
Gyr
″

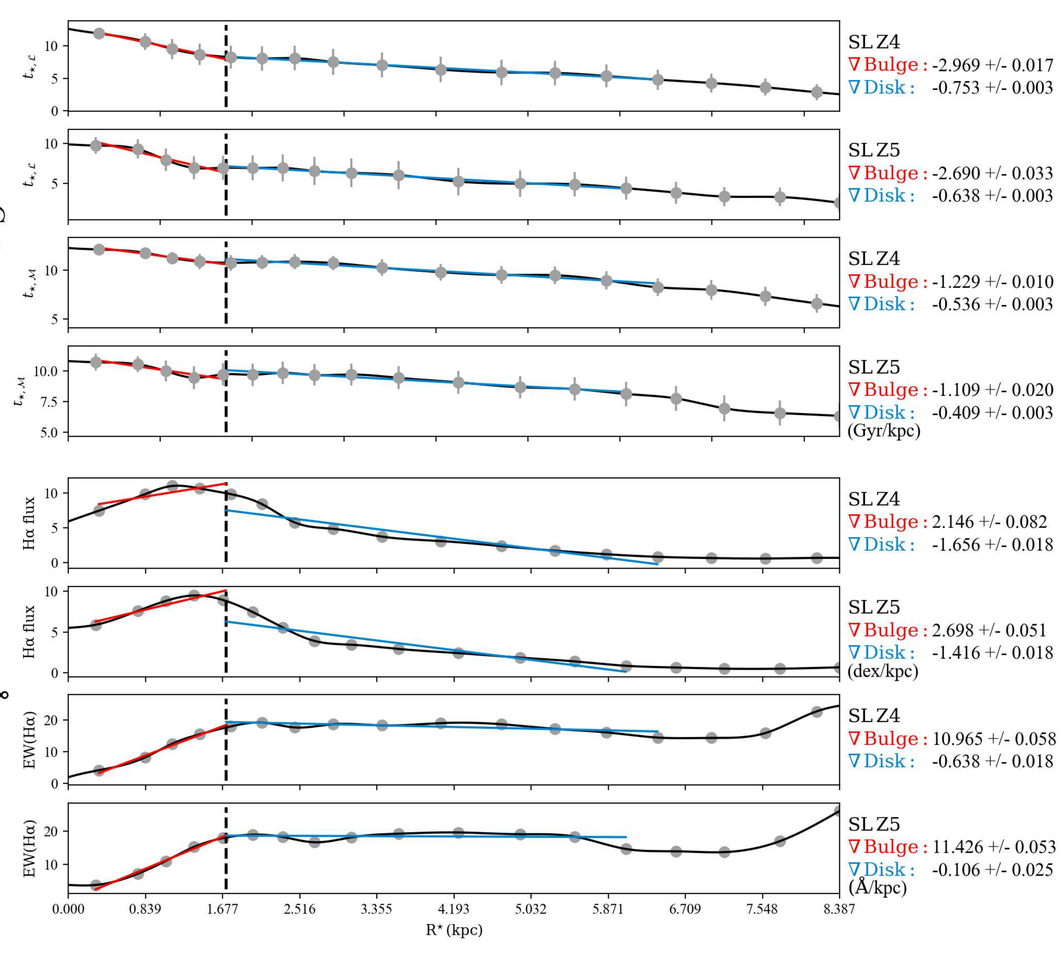
SL Z4
∇ Bulge : -2.969 +/- 0.017
∇ Disk : -0.753 +/- 0.003
SL Z5
∇ Bulge : -2.690 +/- 0.033
∇ Disk : -0.638 +/- 0.003
SL Z4
∇ Bulge : -1.229 +/- 0.010
∇ Disk : -0.536 +/- 0.003
SL Z5
∇ Bulge : -1.109 +/- 0.020
∇ Disk : -0.409 +/- 0.003
(Gyr/kpc)

Hα flux
EW(Hα)
1. e^{-16}erg/s. sm^2
Å
″

SL Z4
∇ Bulge : 2.146 +/- 0.082
∇ Disk : -1.656 +/- 0.018
SL Z5
∇ Bulge : 2.698 +/- 0.051
∇ Disk : -1.416 +/- 0.018
(dex/kpc)
SL Z4
∇ Bulge : 10.965 +/- 0.058
∇ Disk : -0.638 +/- 0.018
SL Z5
∇ Bulge : 11.426 +/- 0.053
∇ Disk : -0.106 +/- 0.025
(Å/kpc)
R* (kpc)

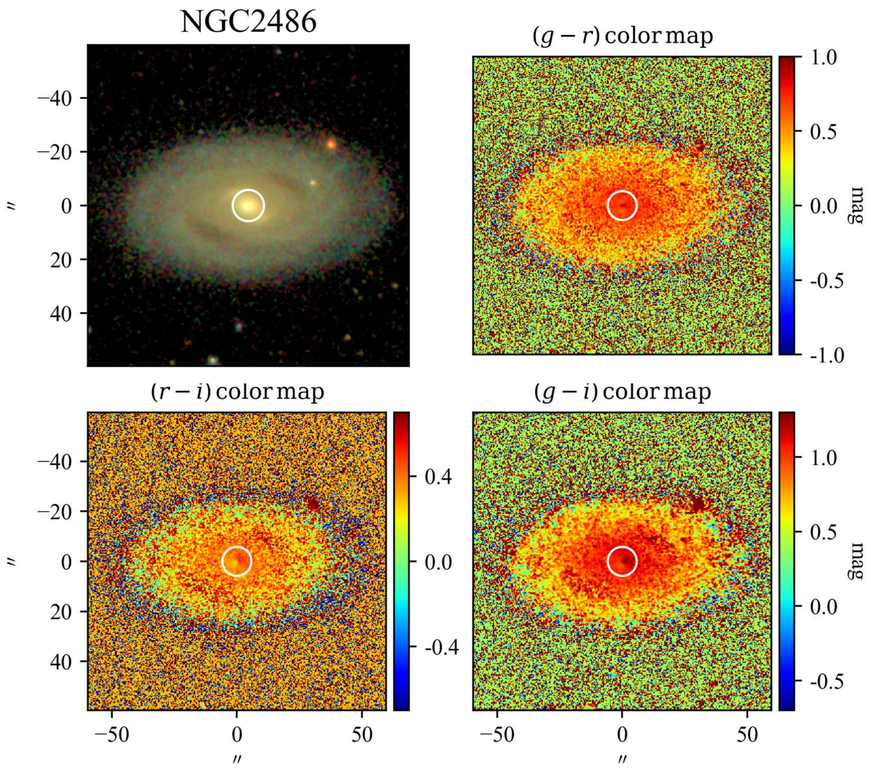

SBP decomposition of SDSS r band

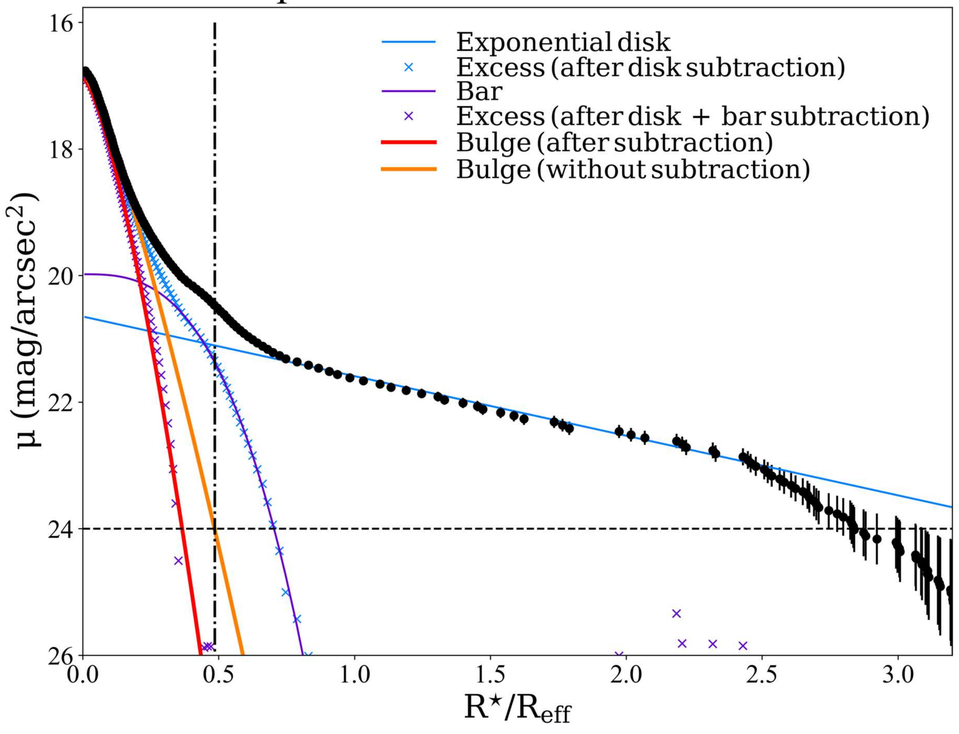

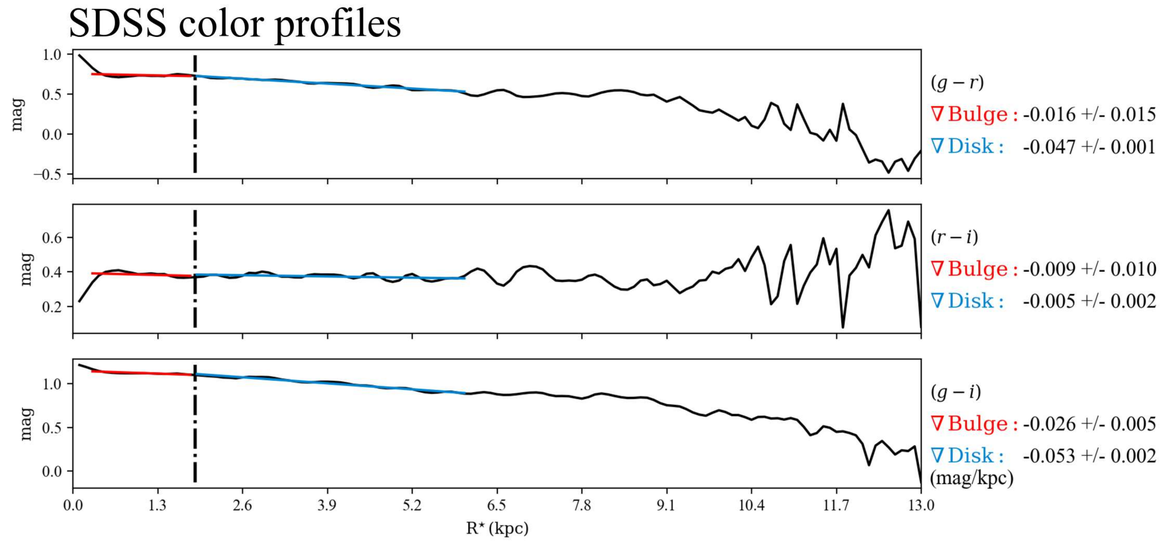

$\mathcal{RV}$ SBPs

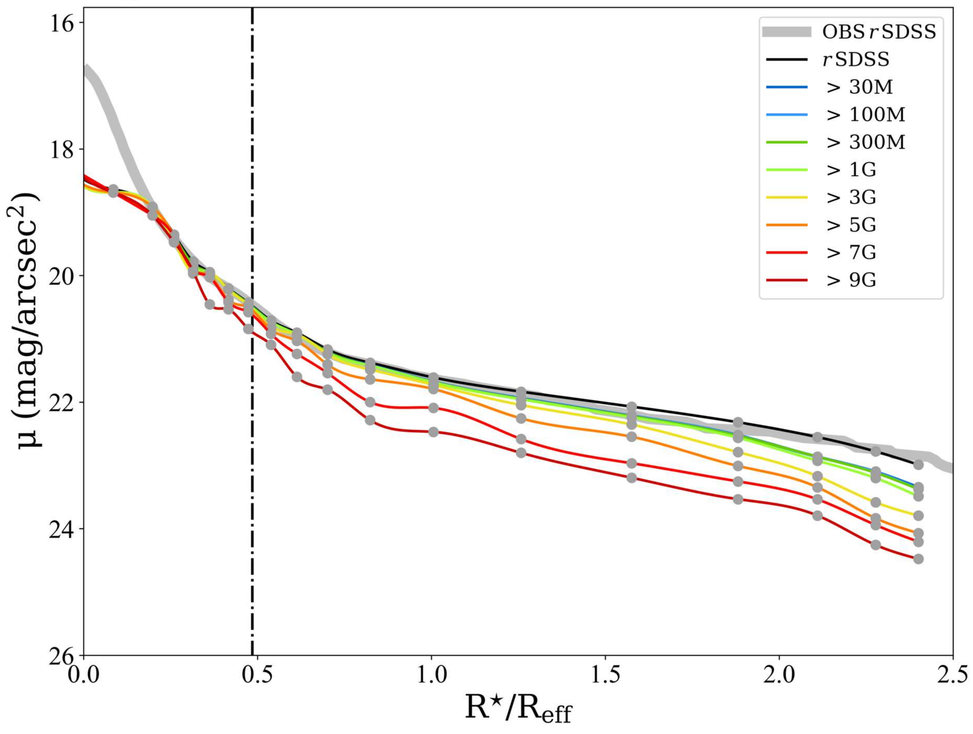

Stellar Continuum

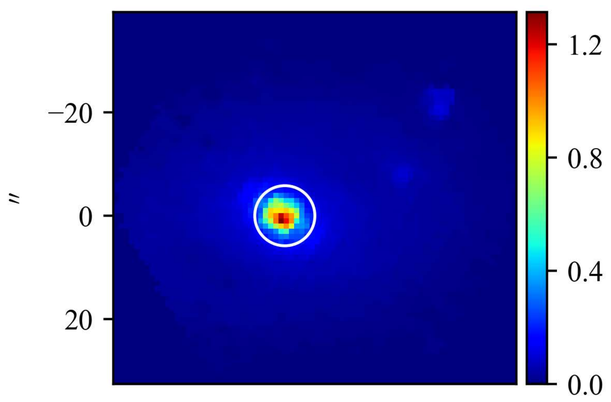

$\mathcal{M}_{\star,\mathrm{P}}$

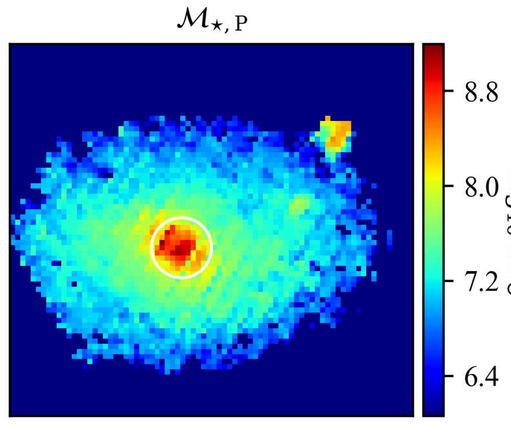

Log. of cumulative present stellar mass profiles

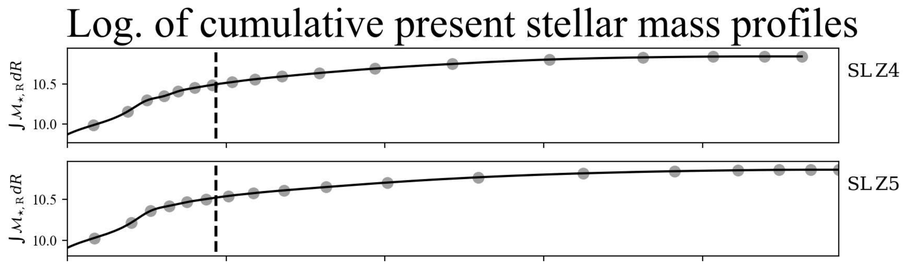

$Z_{\star,\mathcal{L}}$

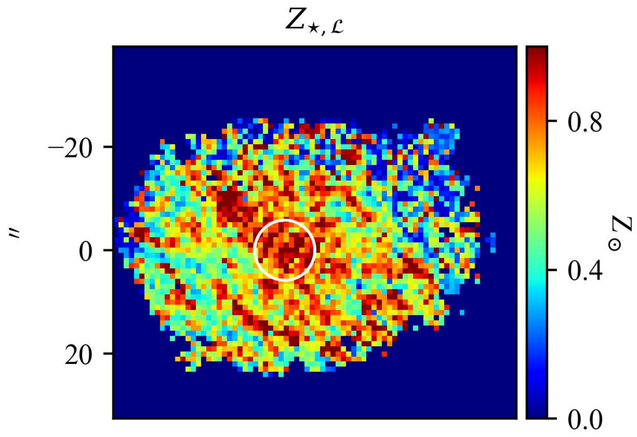

$Z_{\star,\mathcal{M}}$

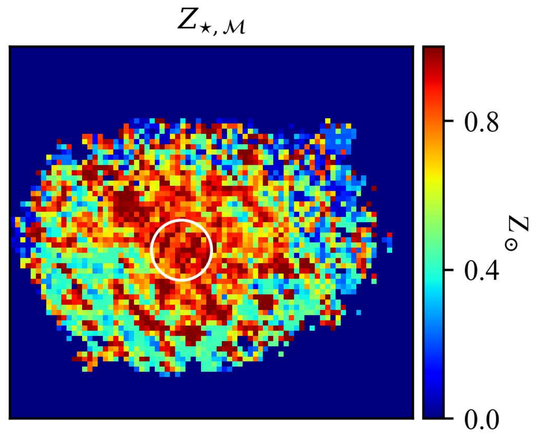

Stellar metallicity/Age & Hα flux/EW profiles

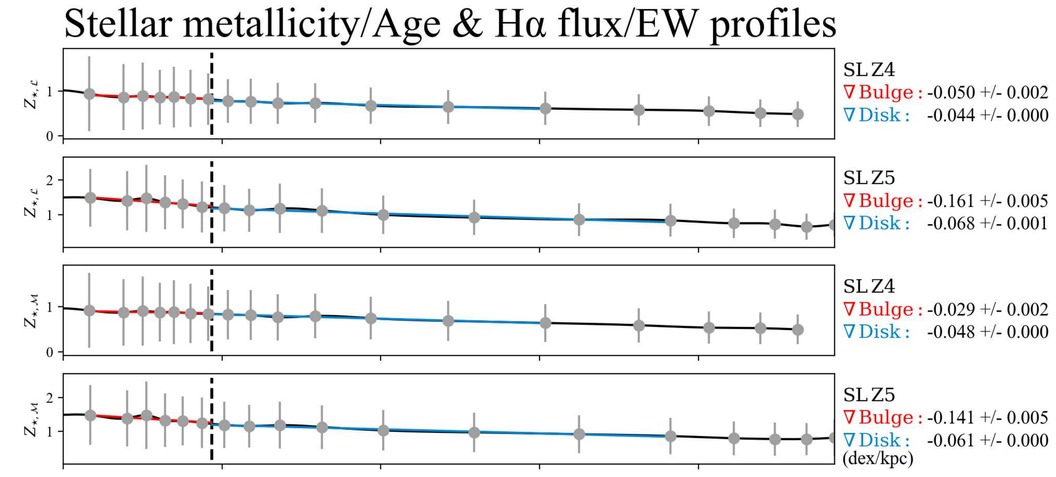

$t_{\star,\mathcal{L}}$

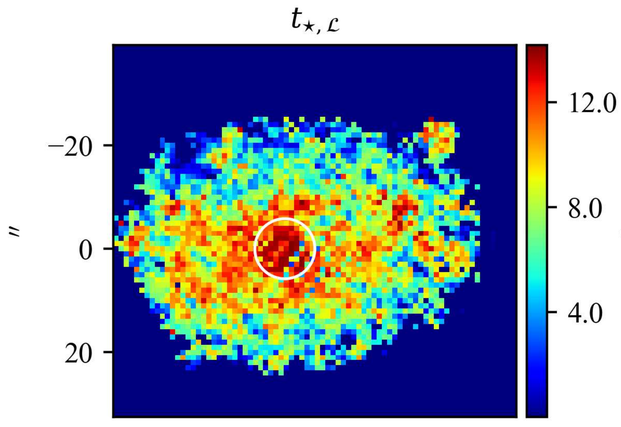

$t_{\star,\mathcal{M}}$

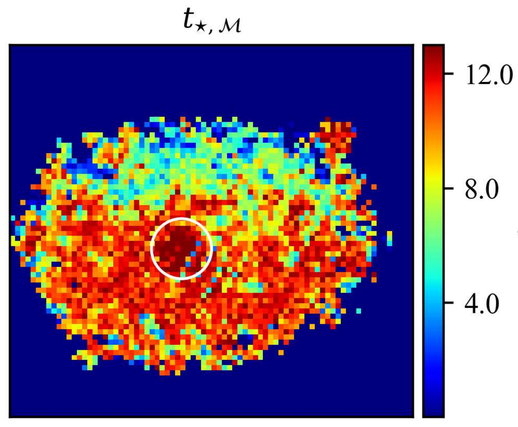

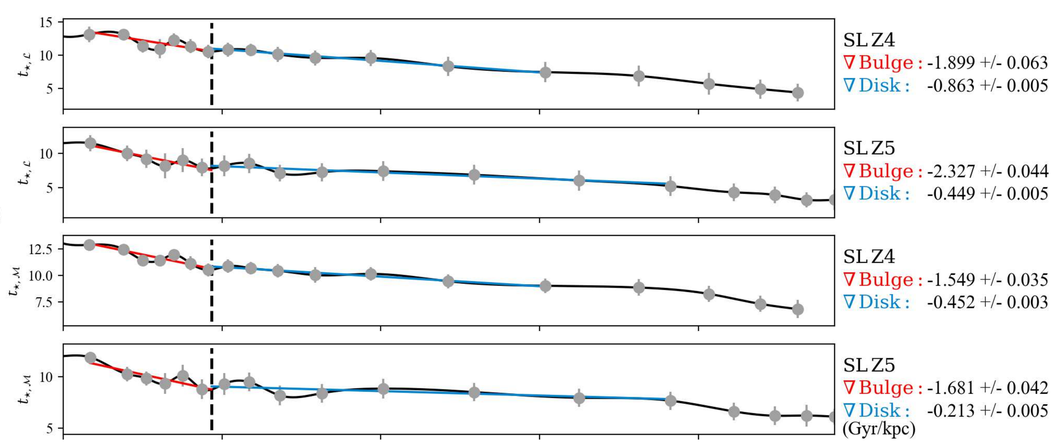

Hα flux

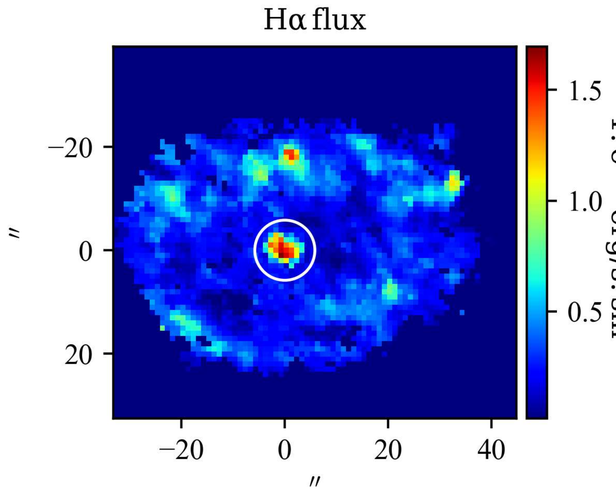

EW(Hα)

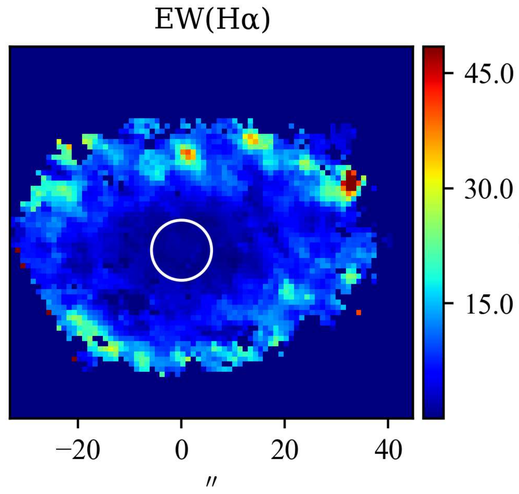

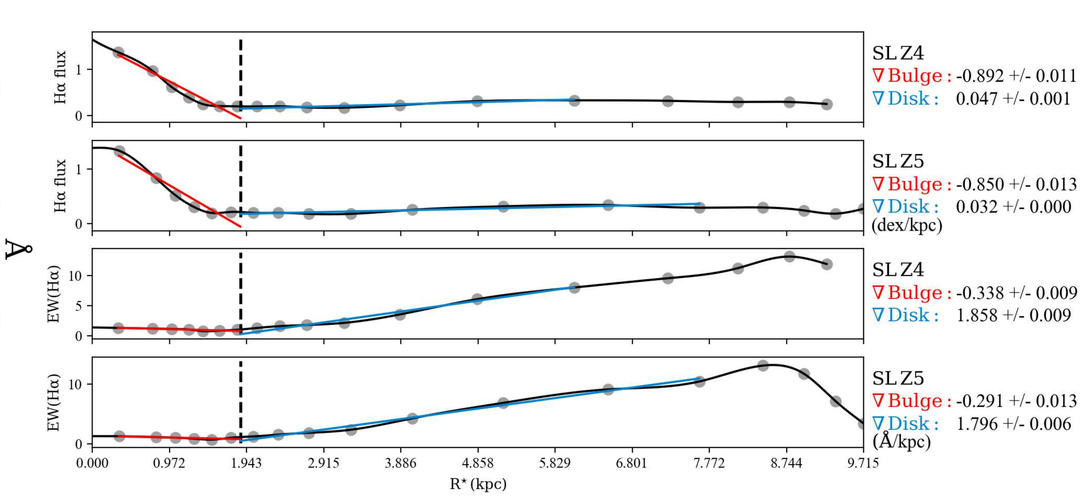

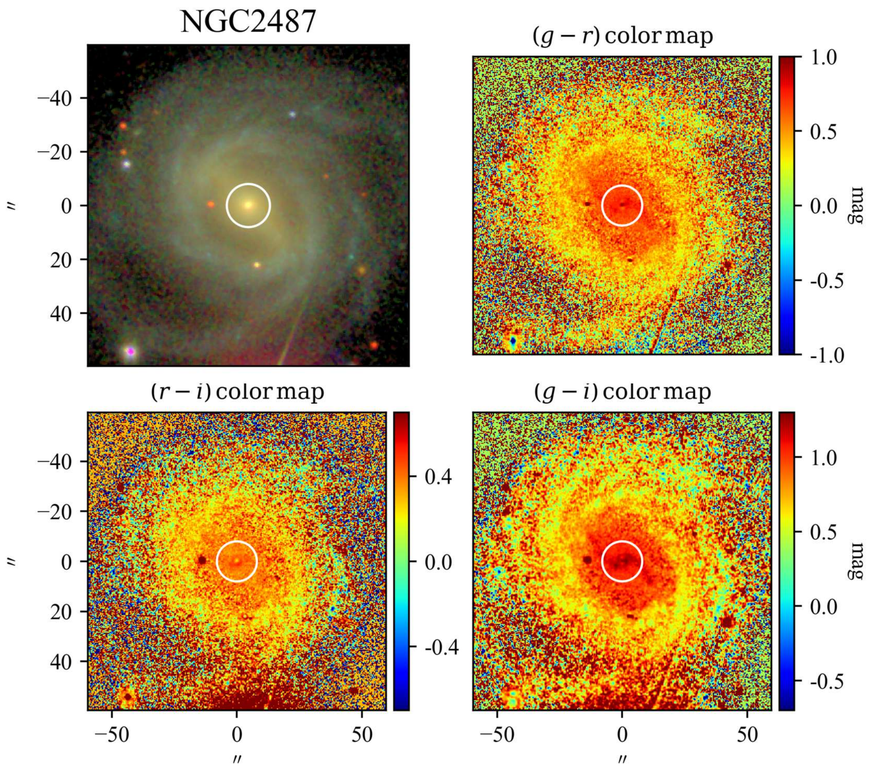

SBP decomposition of SDSS r band

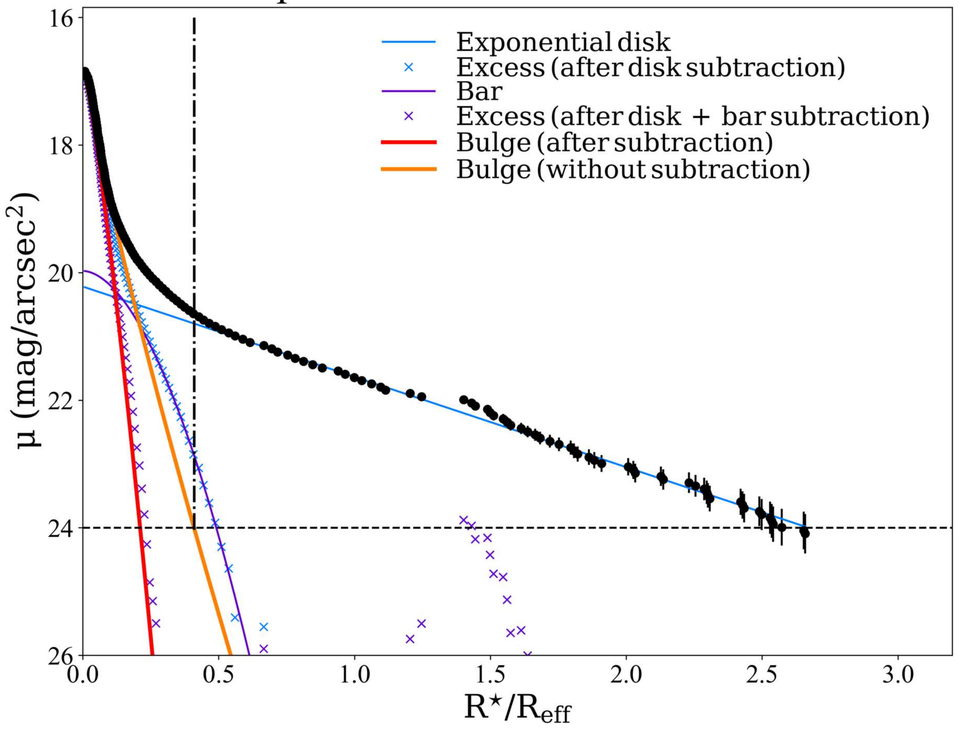

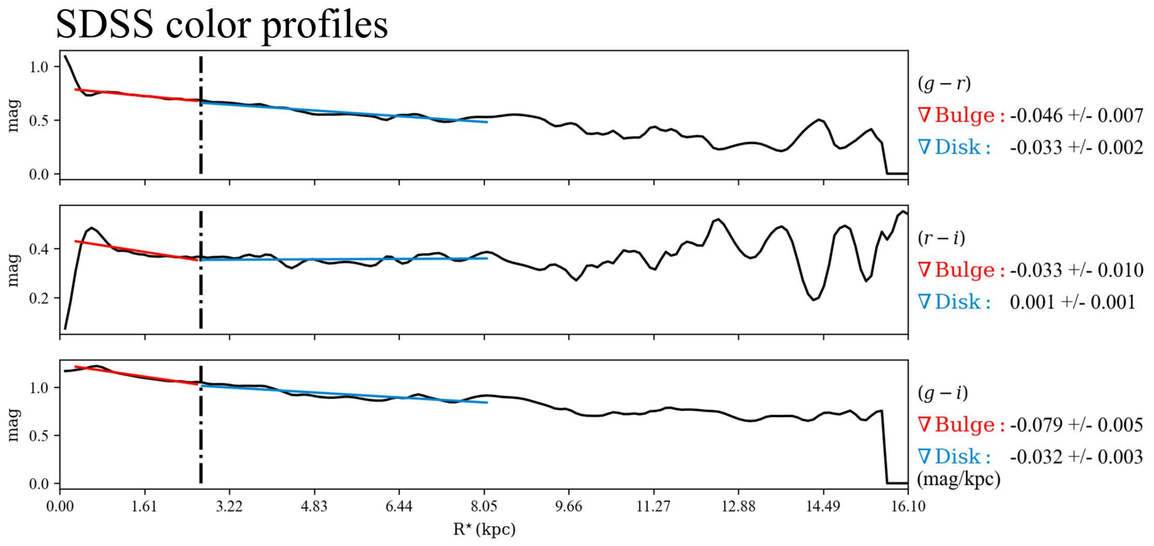

$\mathcal{RY}$ SBPs

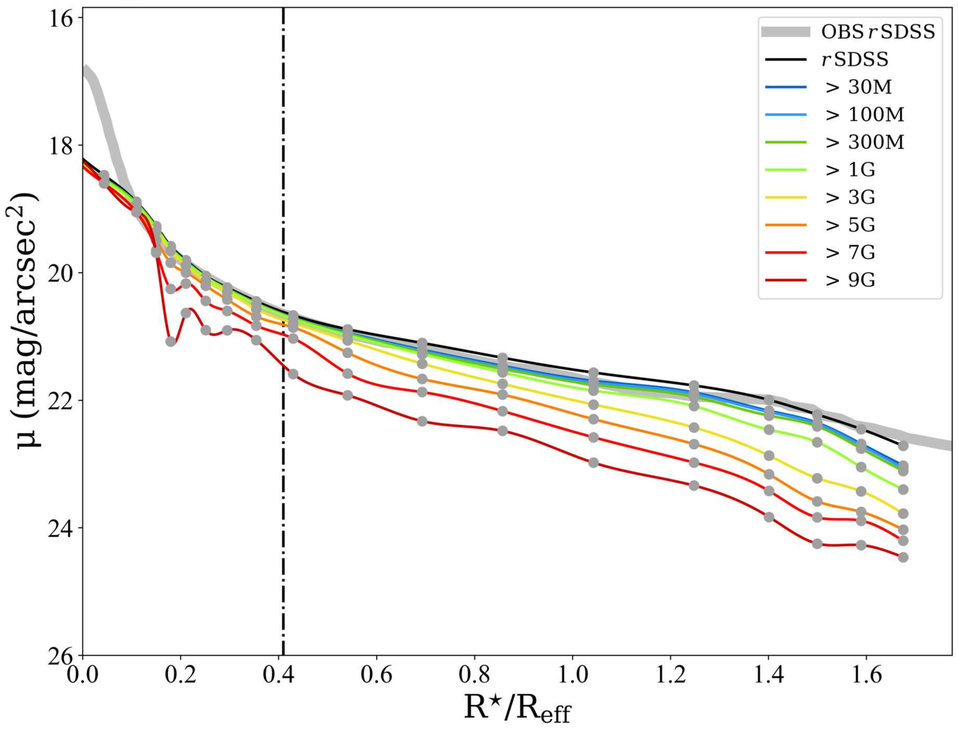

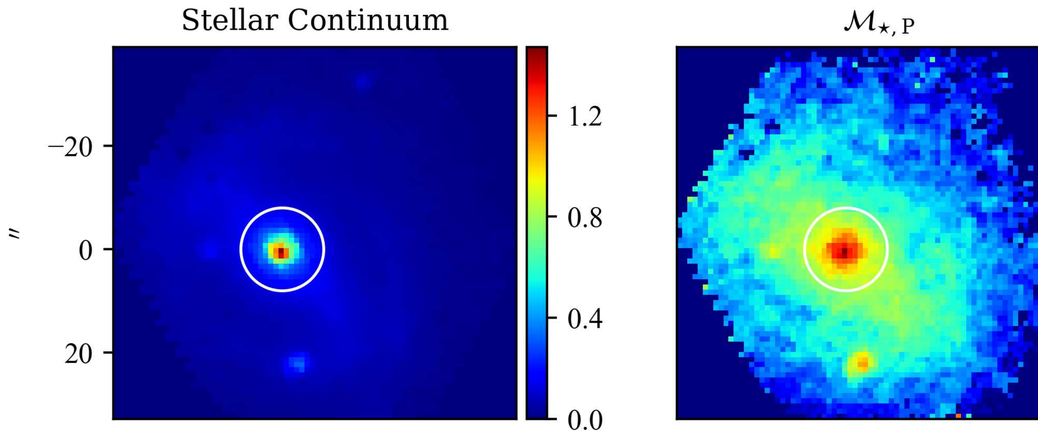

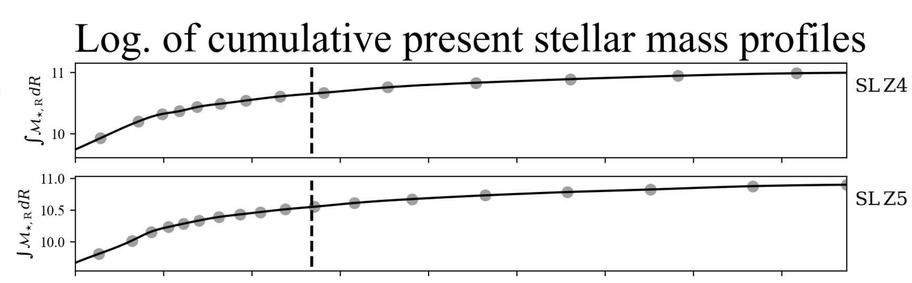

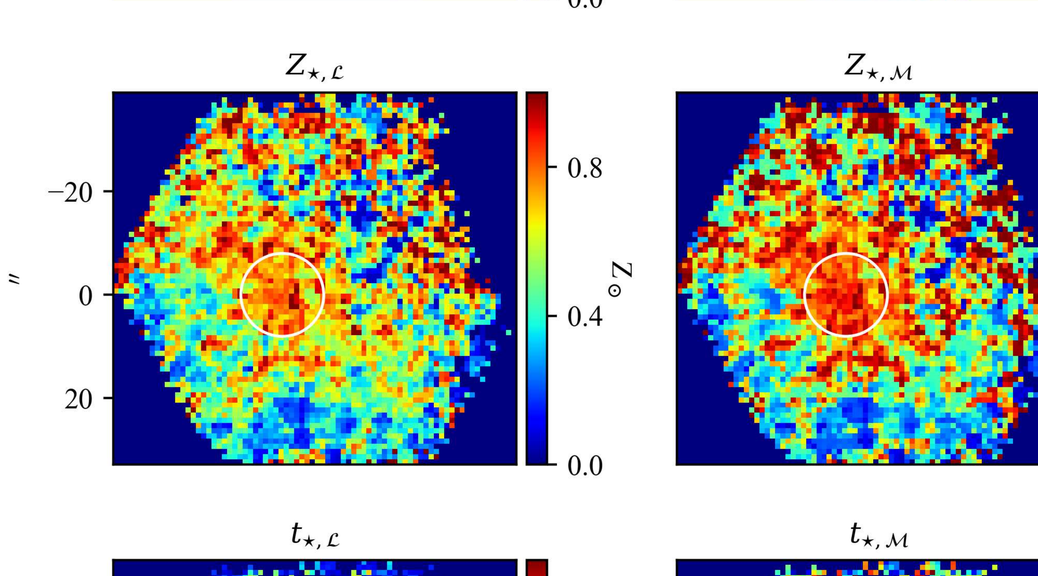

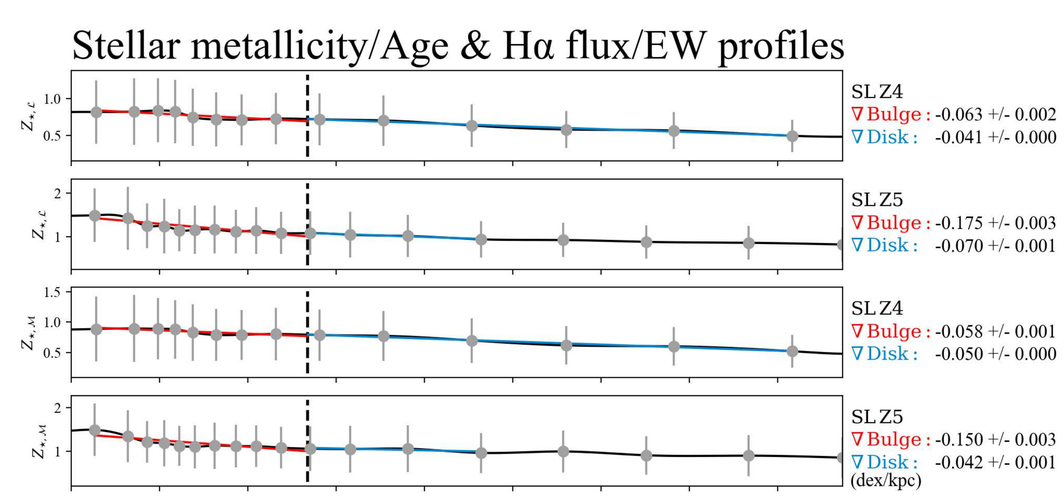

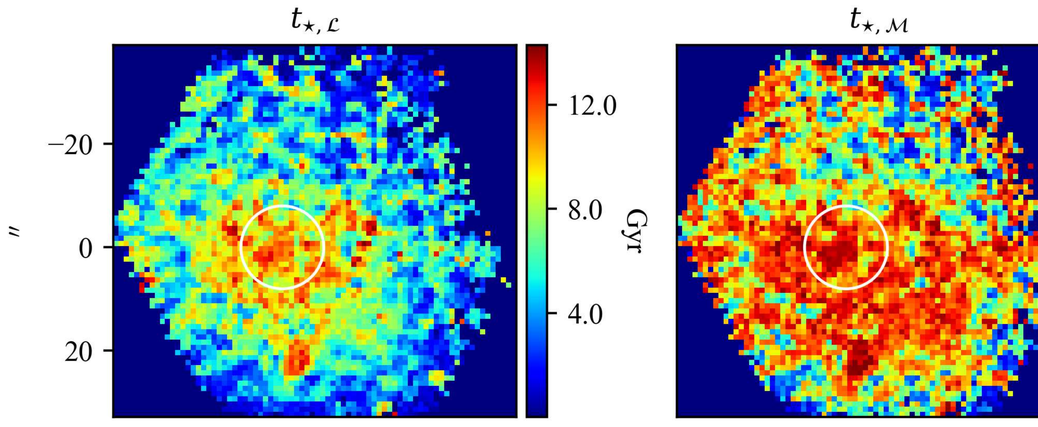

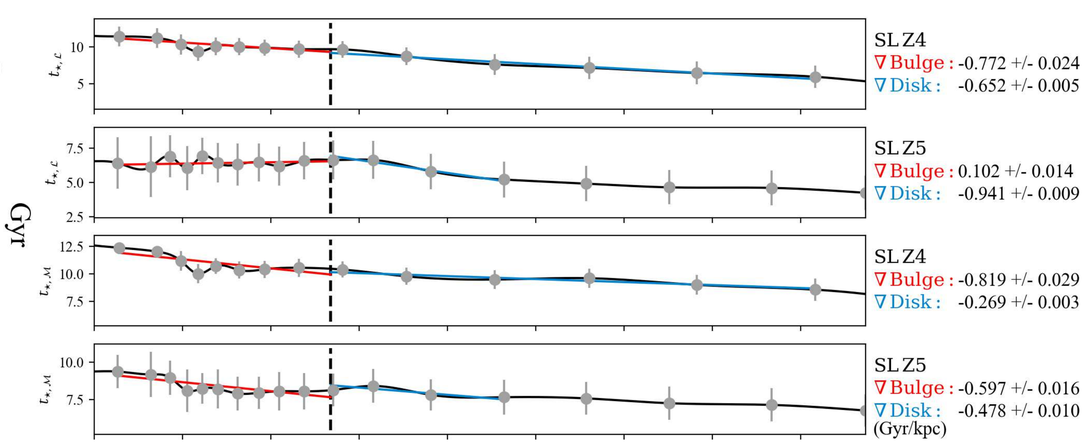

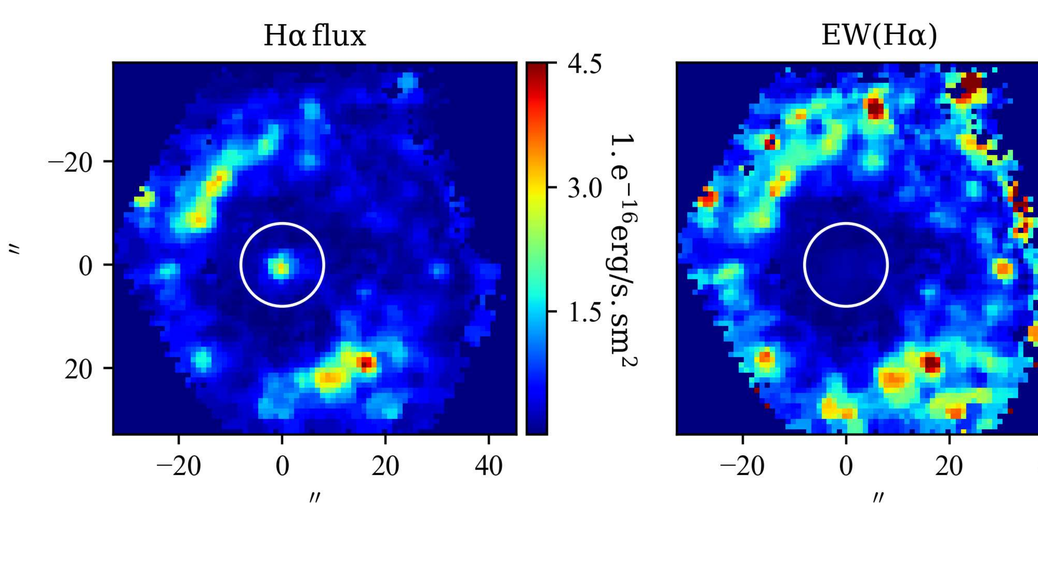

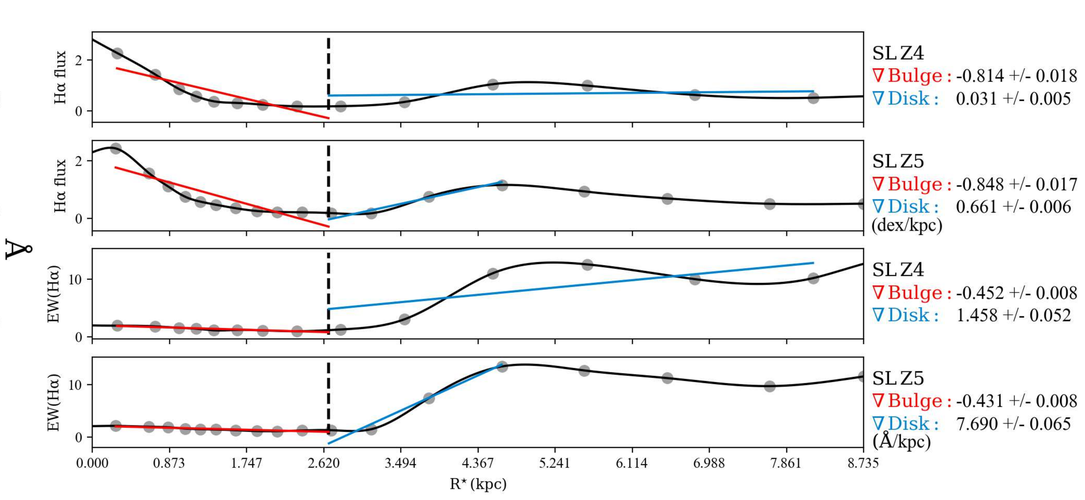

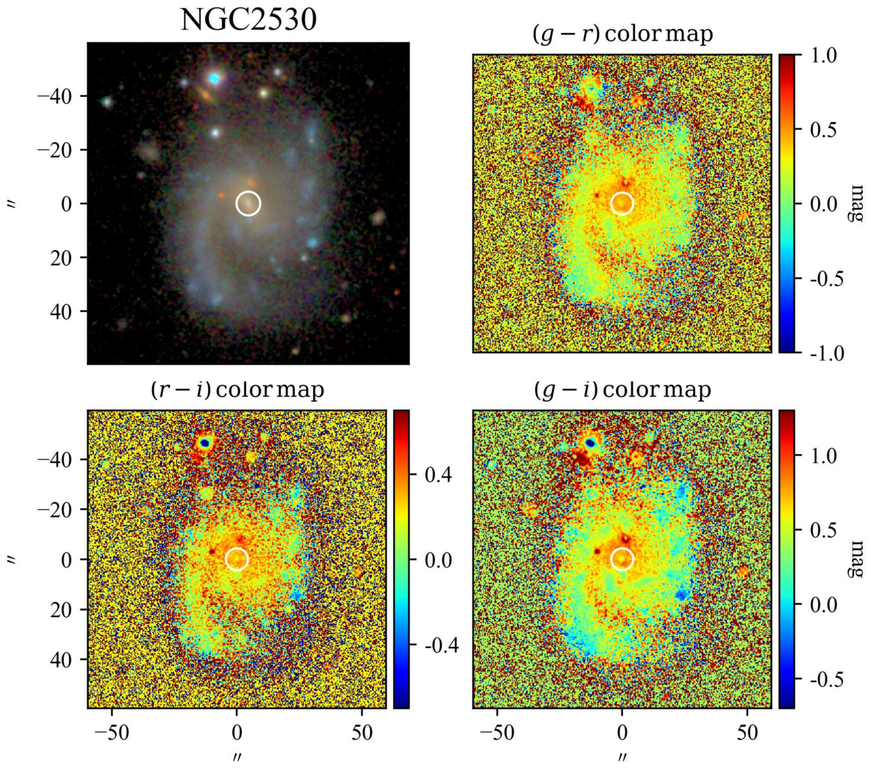

SBP decomposition of SDSS r band

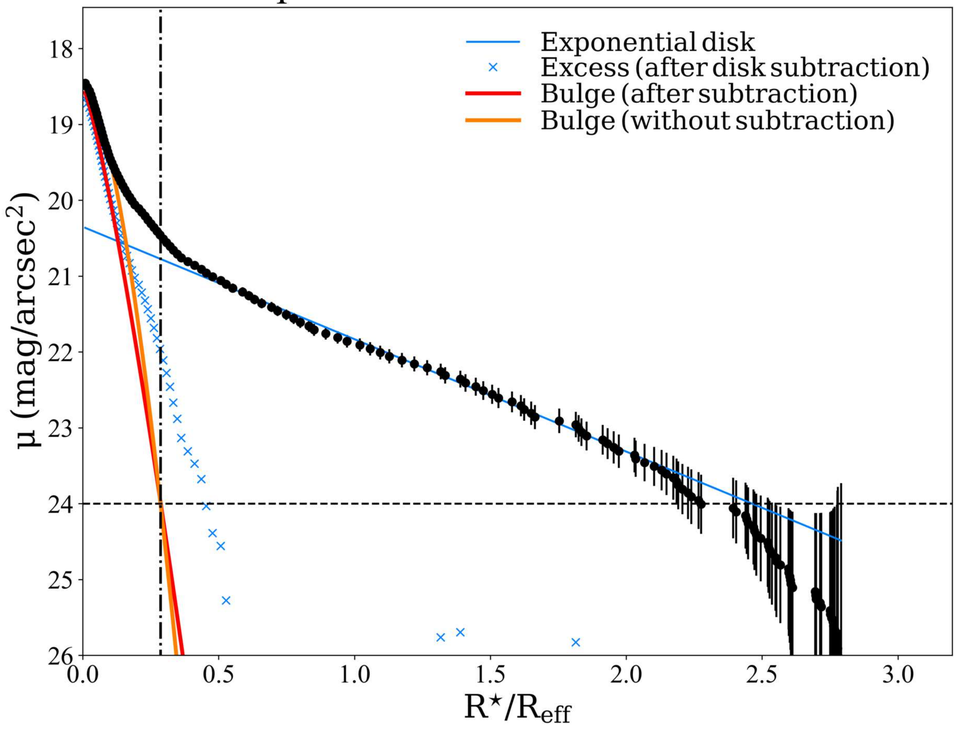

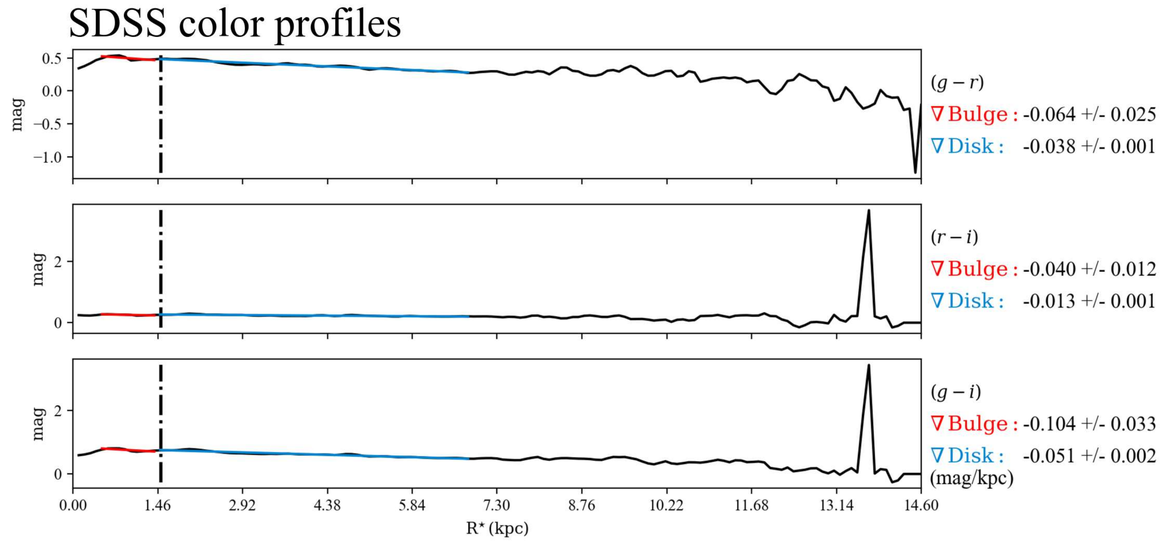

$\mathcal{RY}$ SBPs

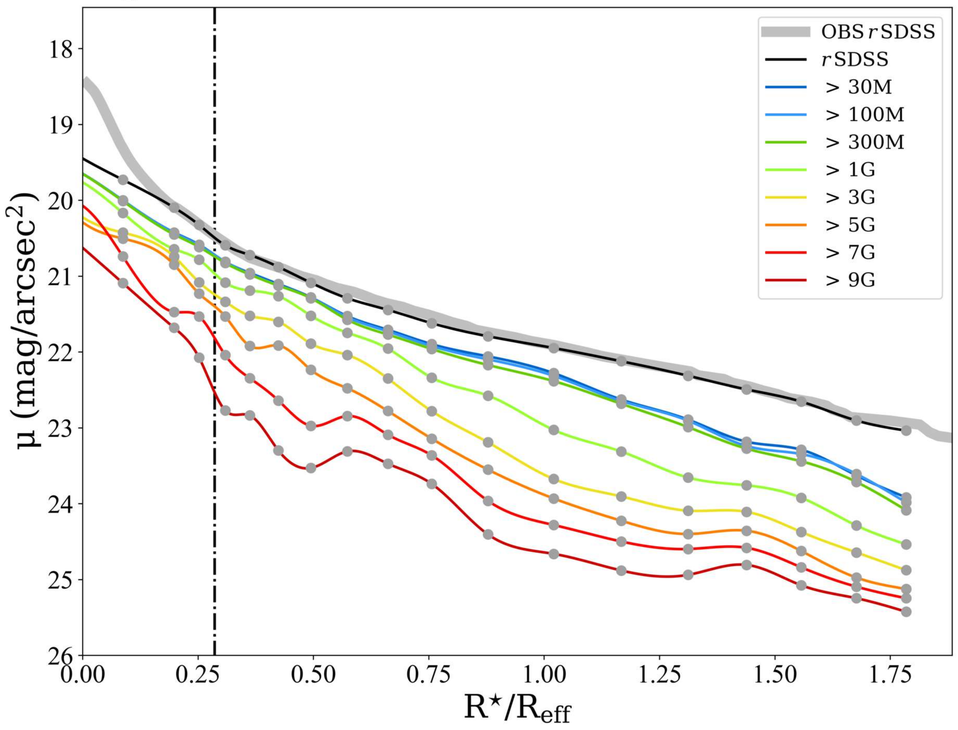

Stellar Continuum $\mathcal{M}_{\star,\mathrm{P}}$

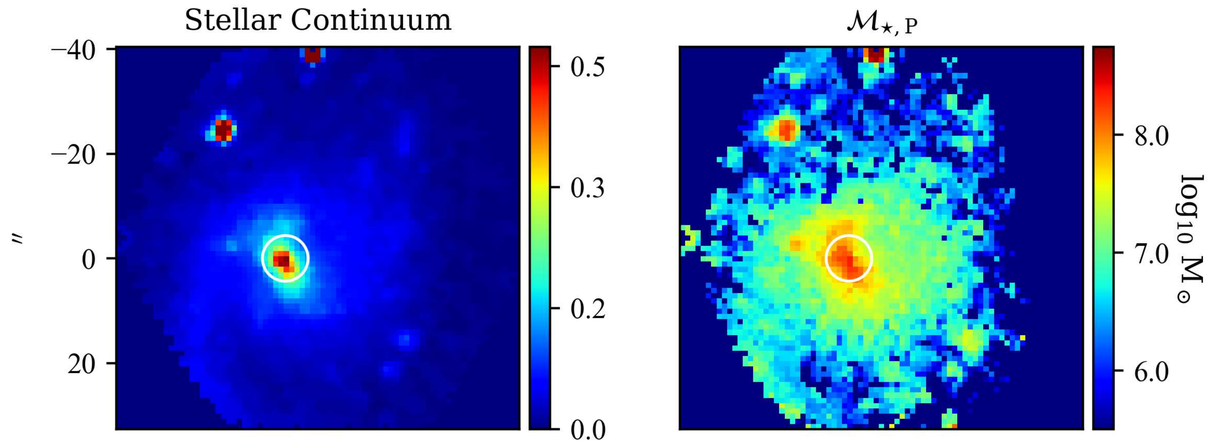

Log. of cumulative present stellar mass profiles

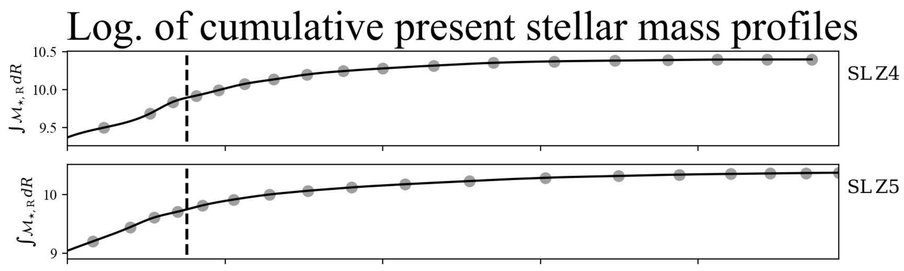

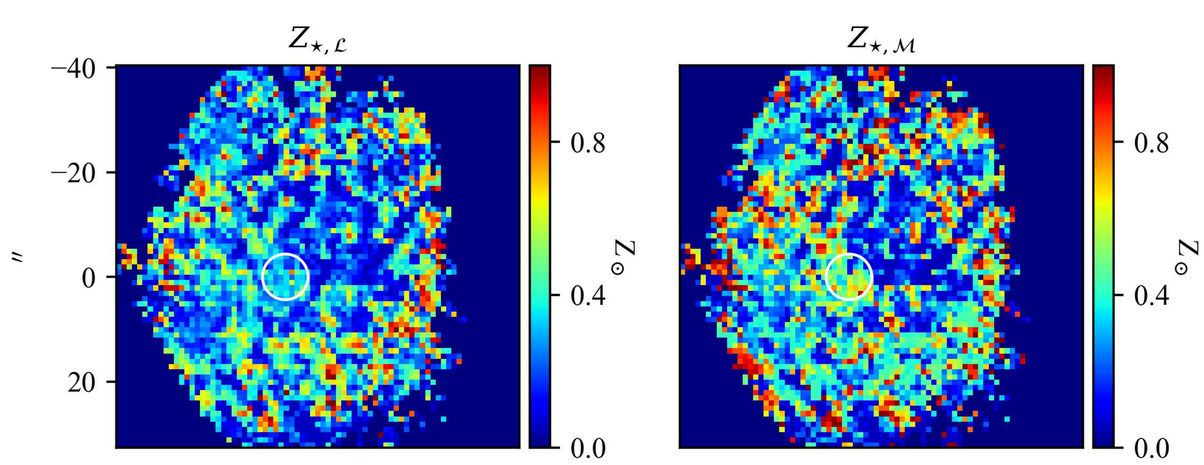

Stellar metallicity/Age & Hα flux/EW profiles

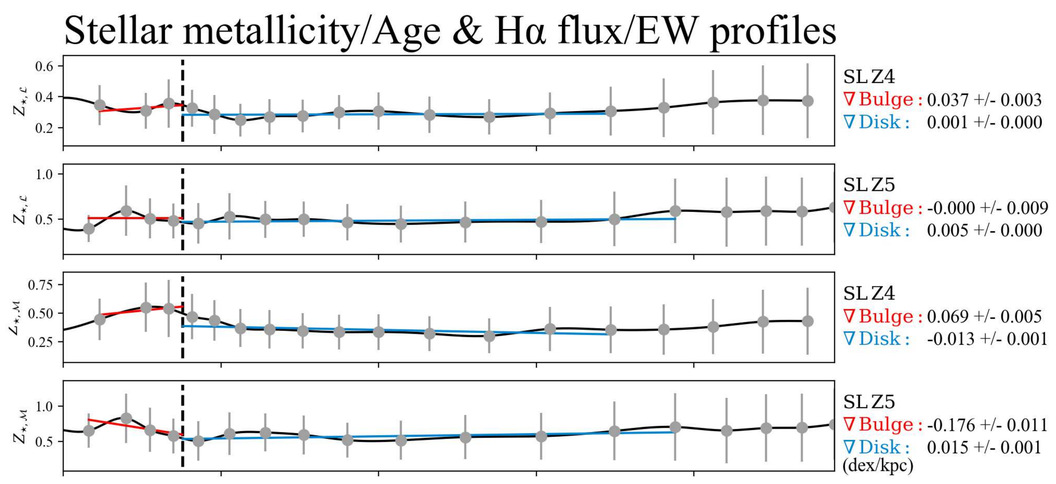

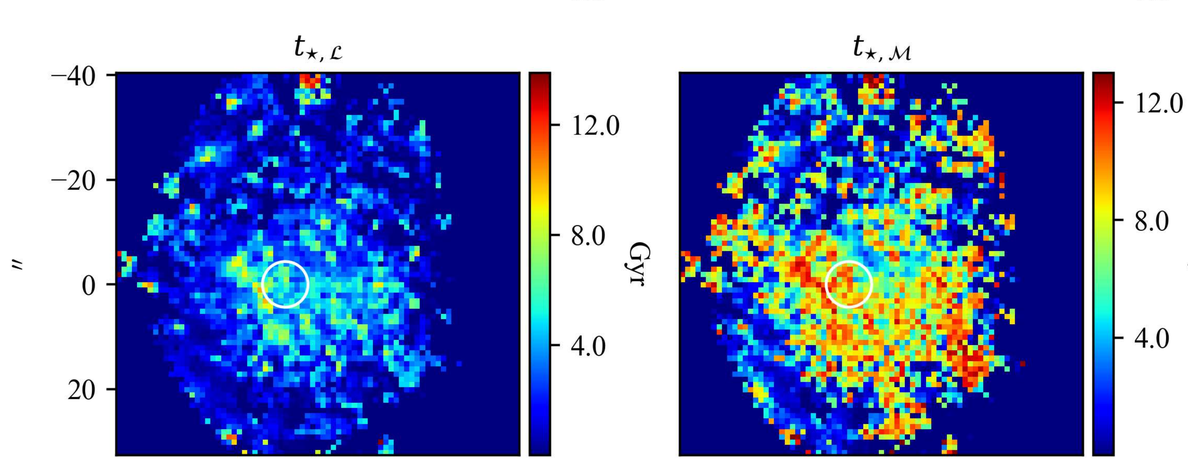

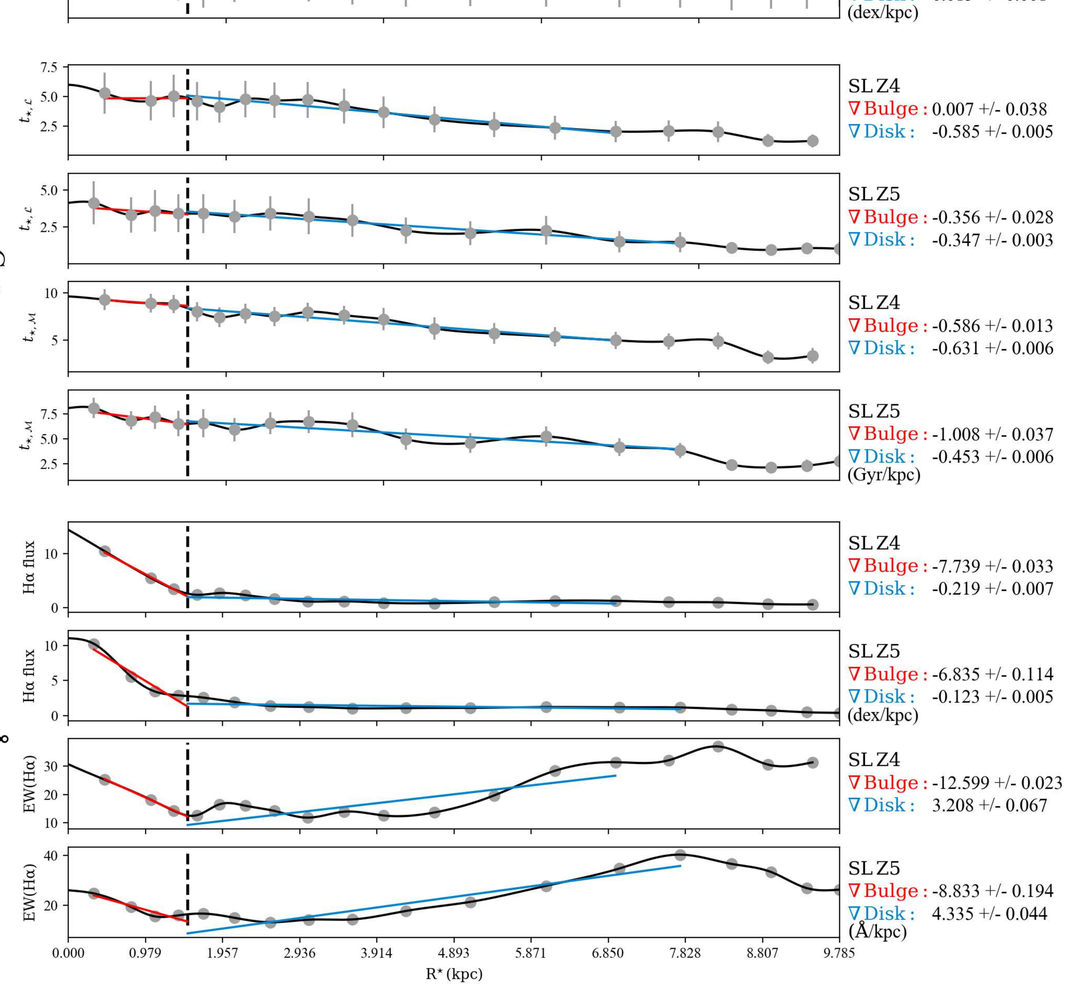

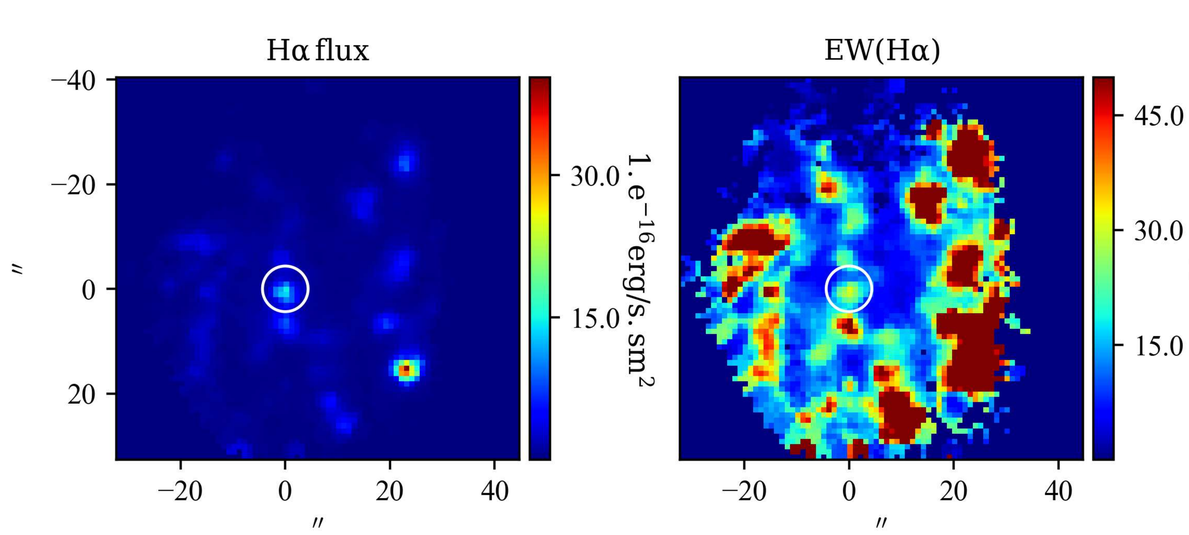

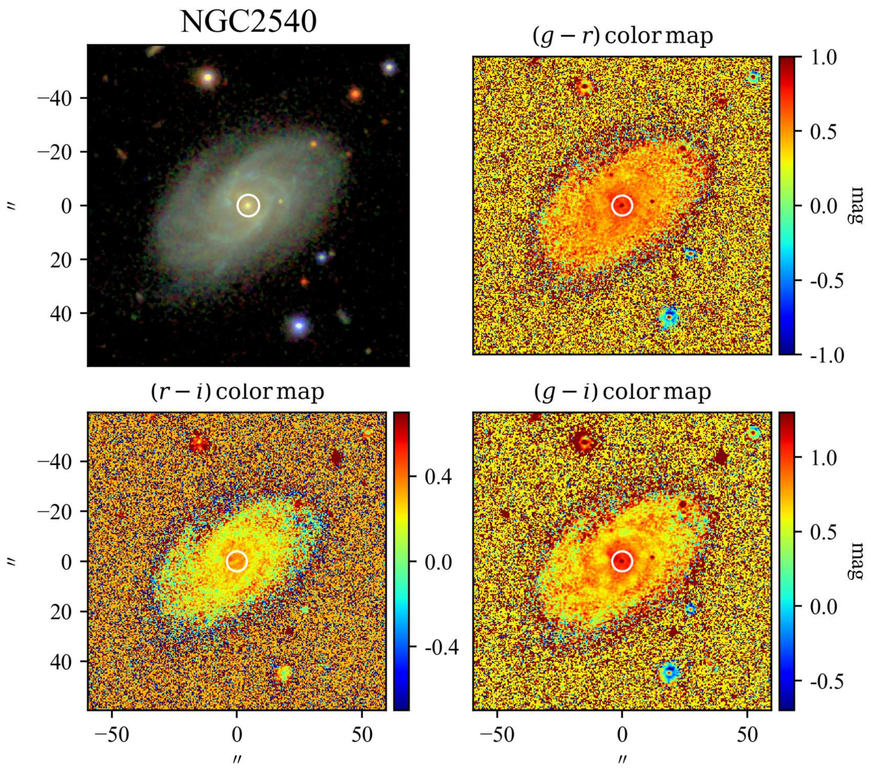

SBP decomposition of SDSS r band

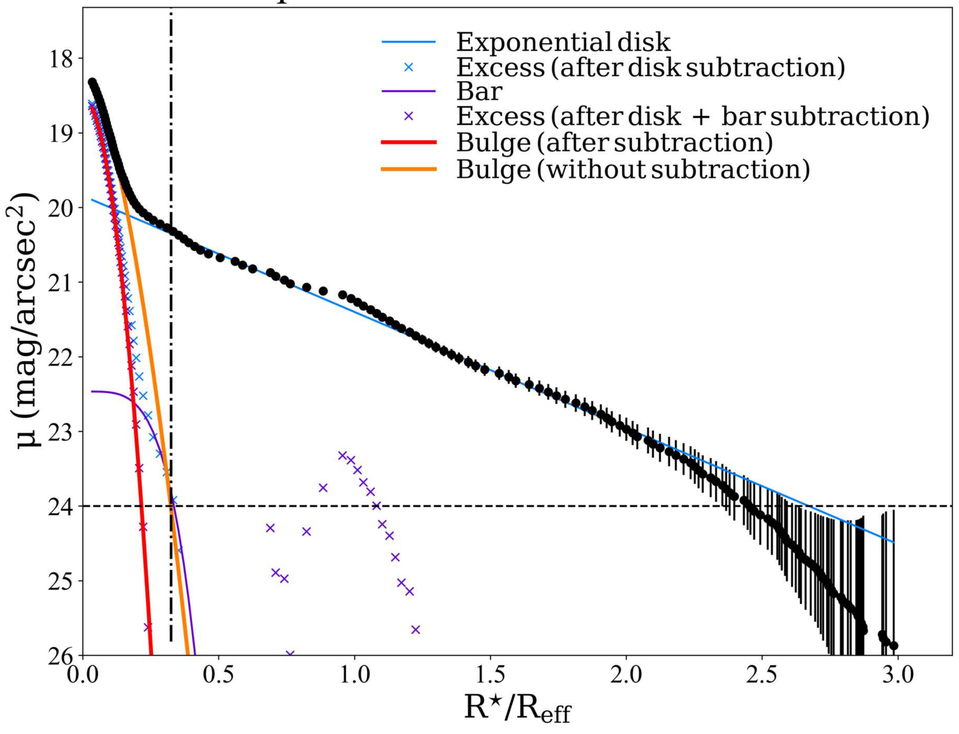

SDSS color profiles

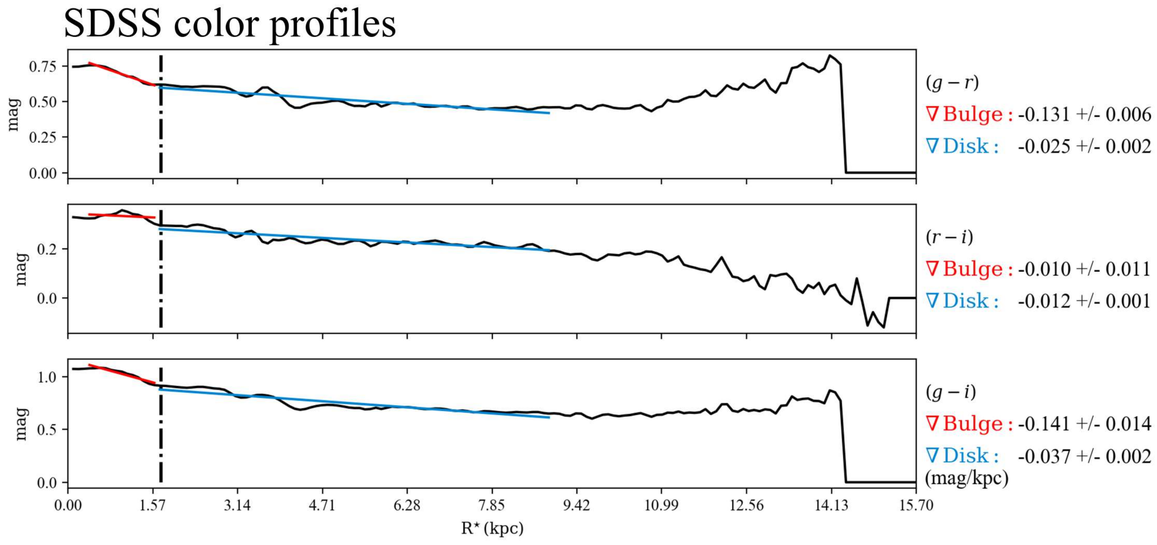

$\mathcal{RV}$ SBPs

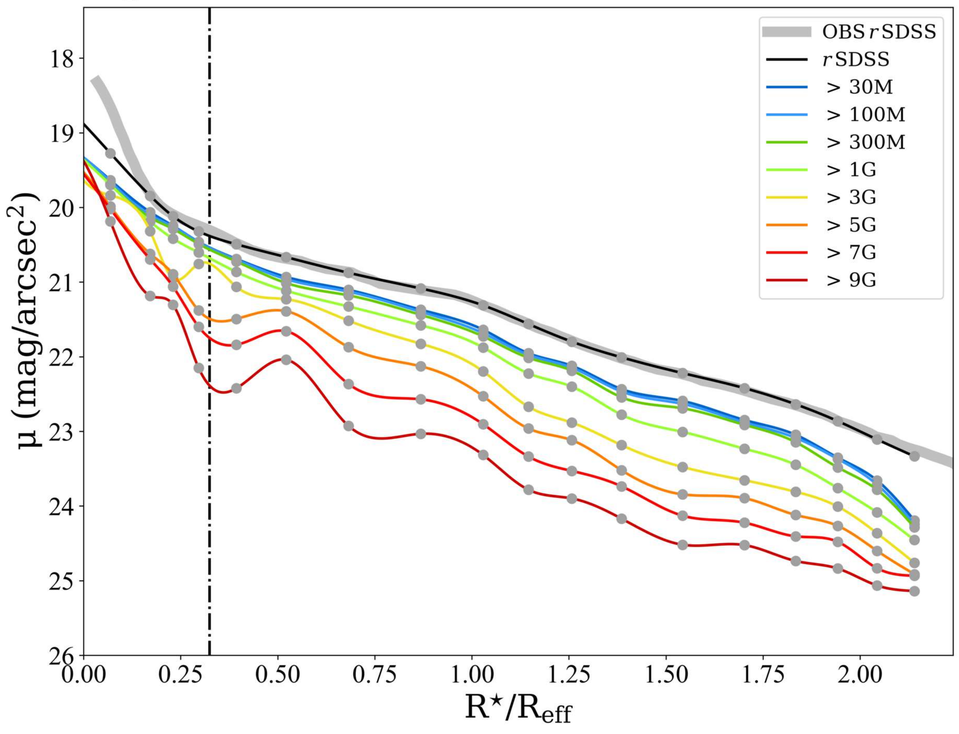

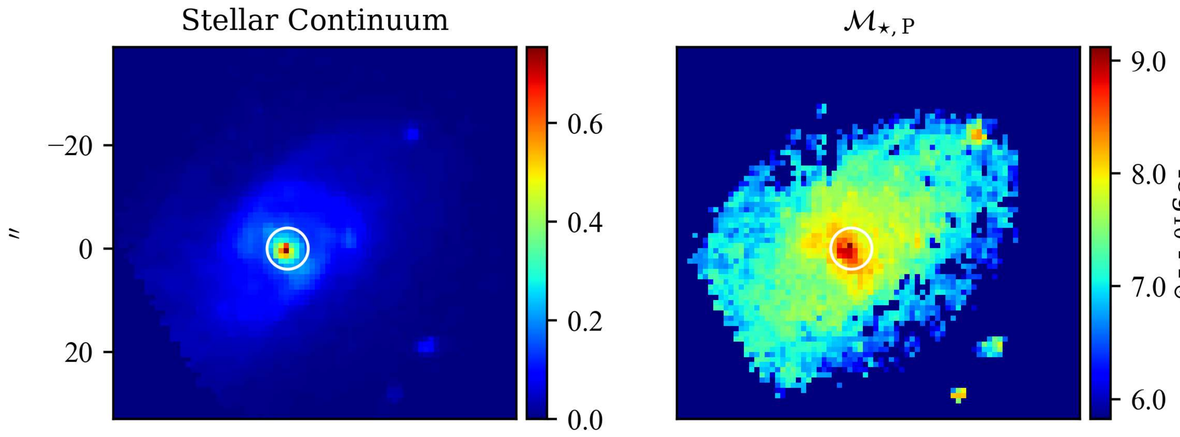

Log. of cumulative present stellar mass profiles

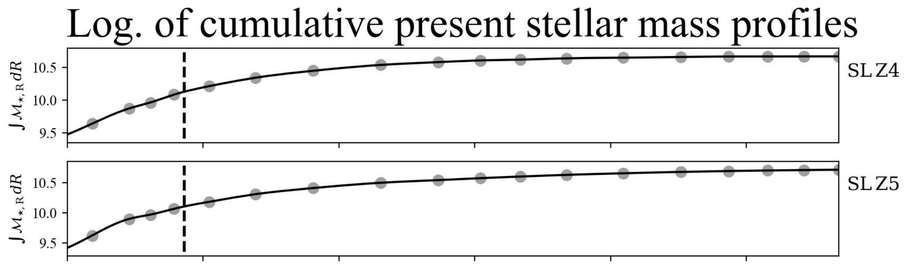

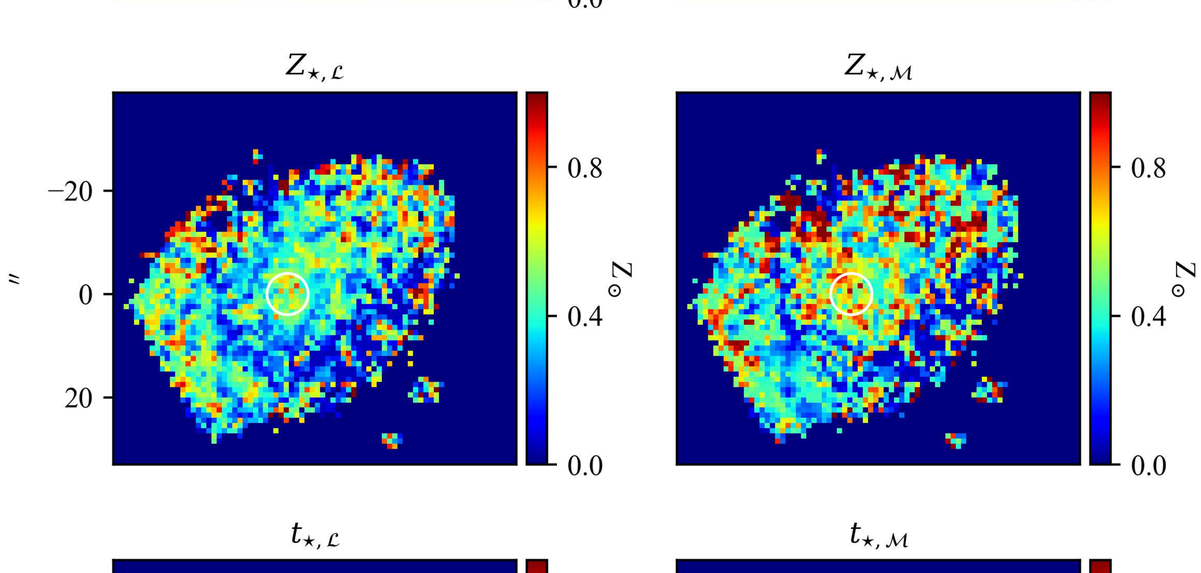

Stellar metallicity/Age & Hα flux/EW profiles

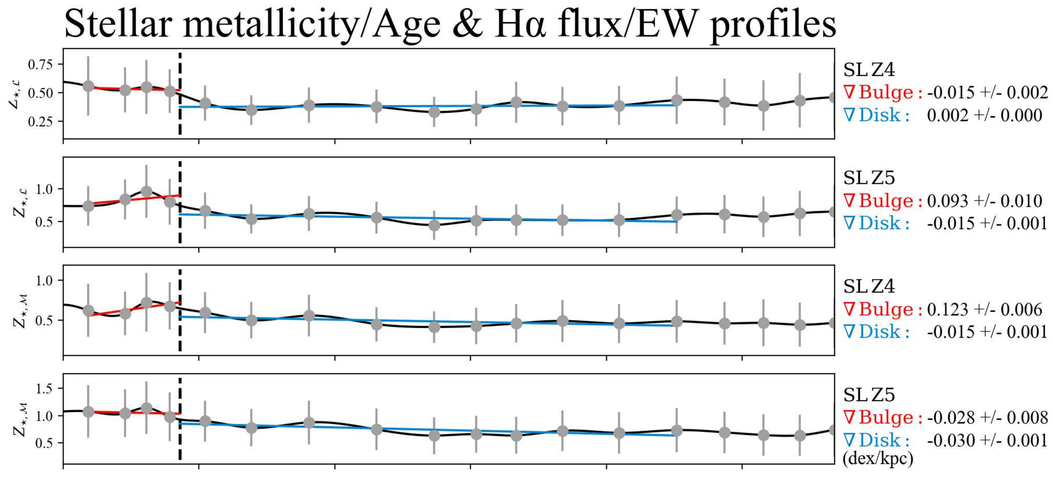

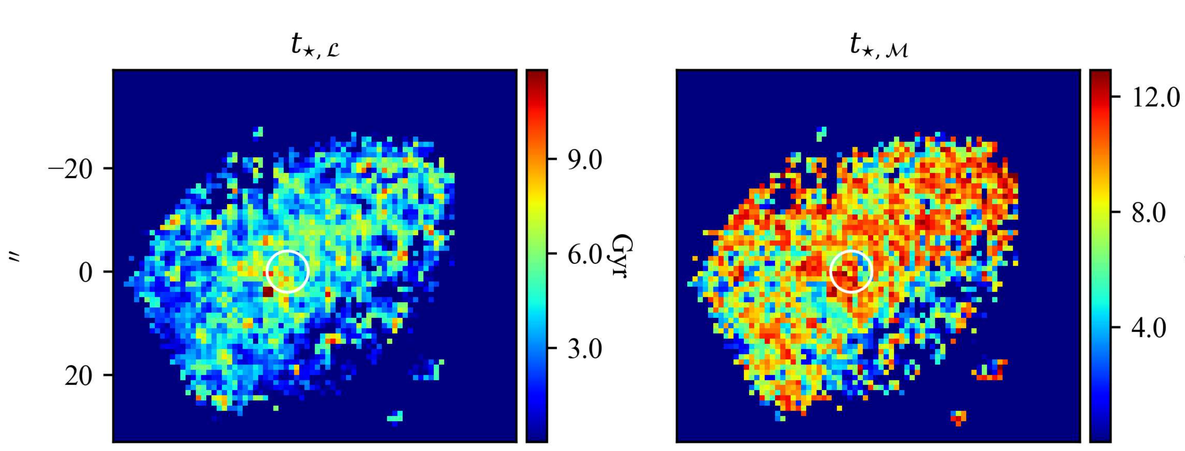

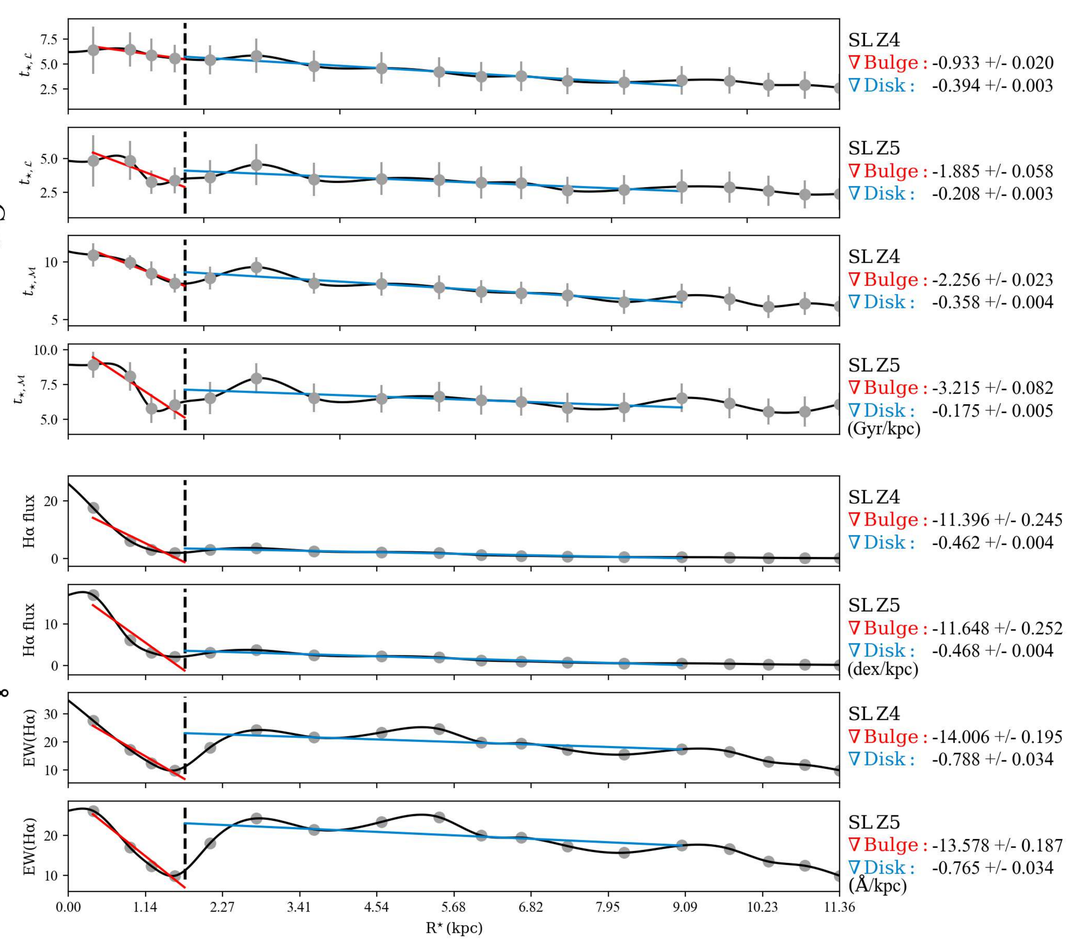

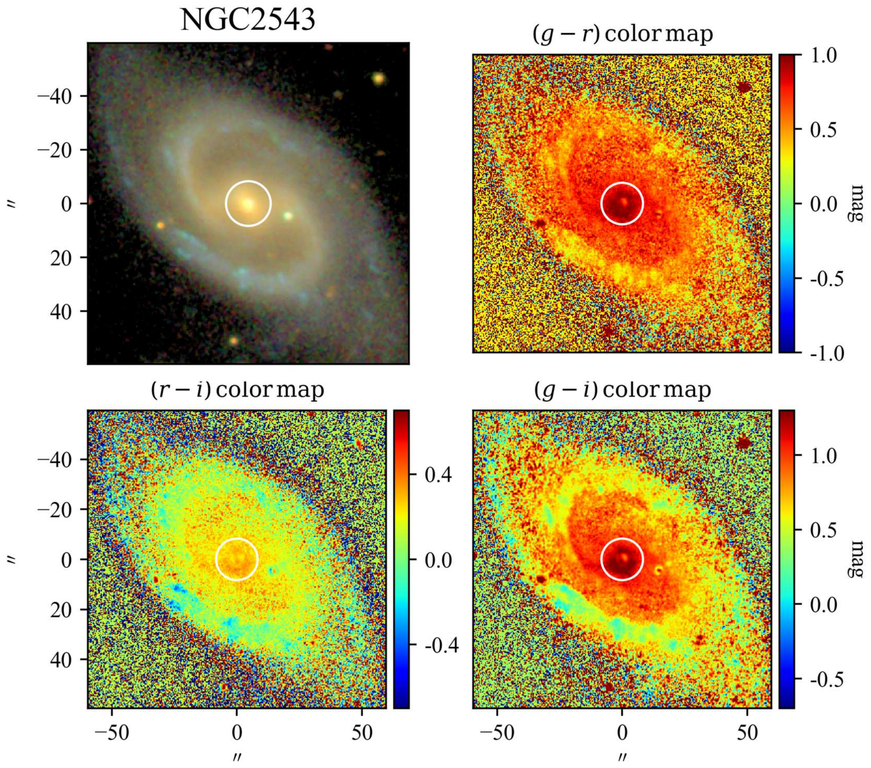

SBP decomposition of SDSS r band

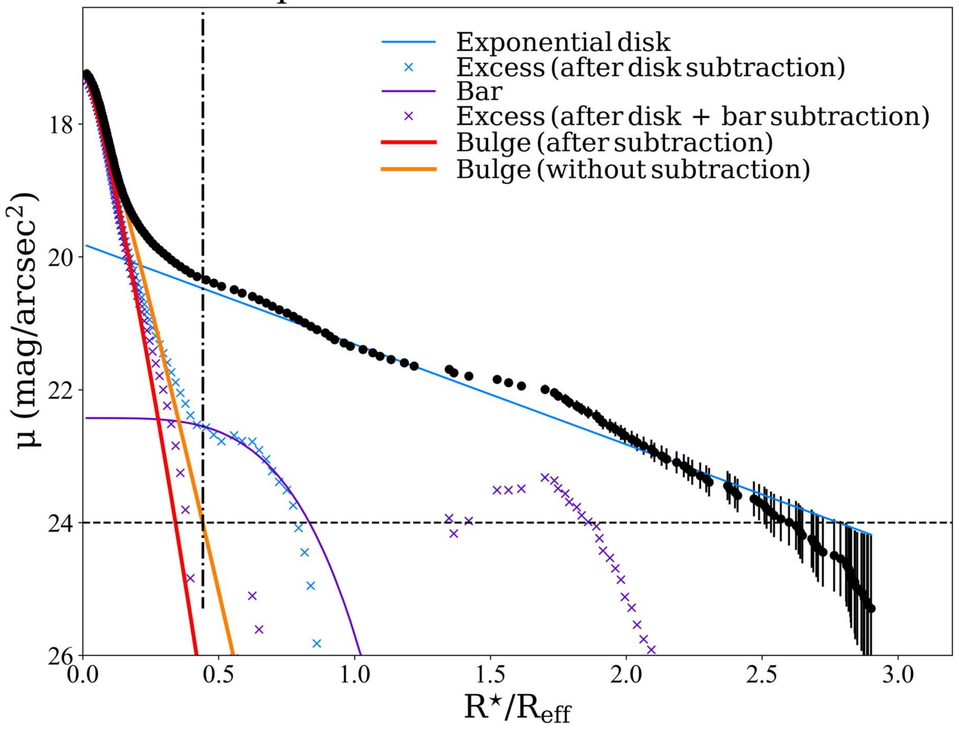

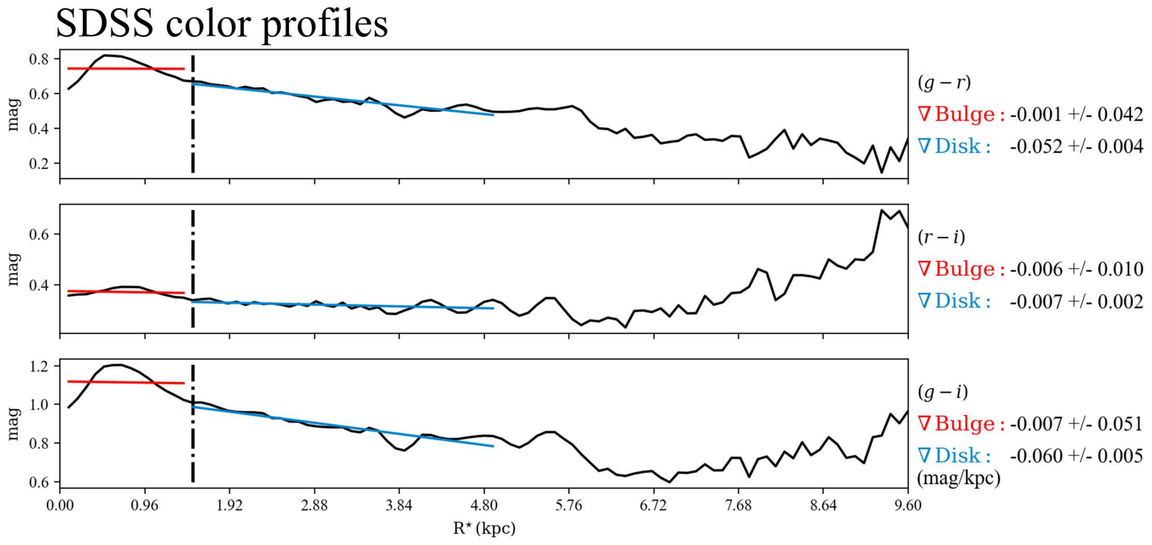

$\mathcal{RY}$ SBPs

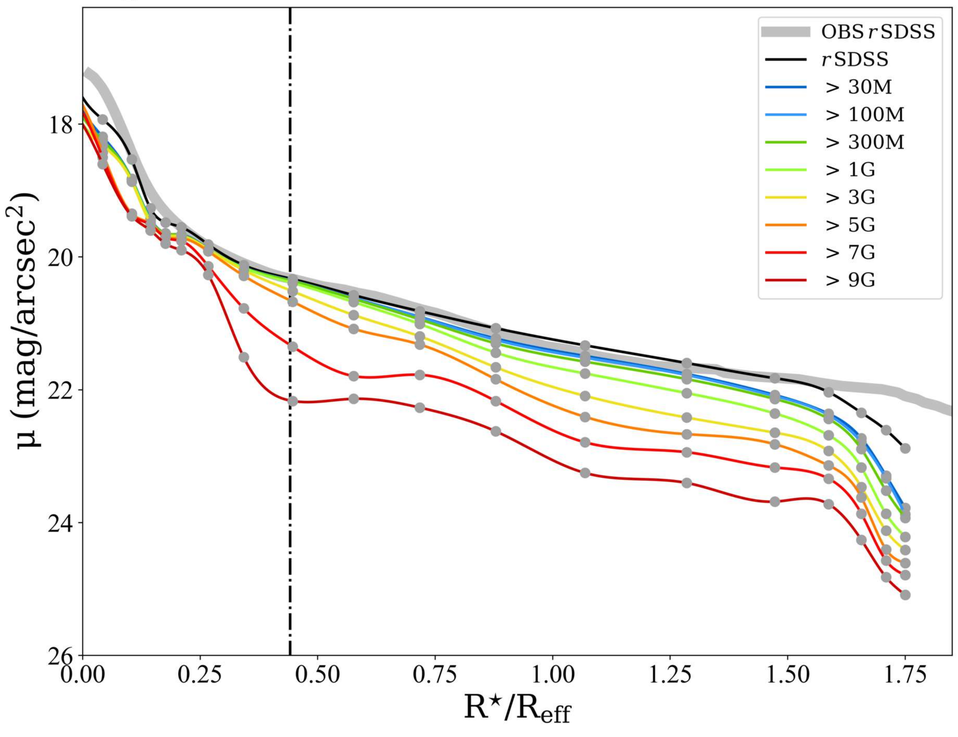

Stellar Continuum

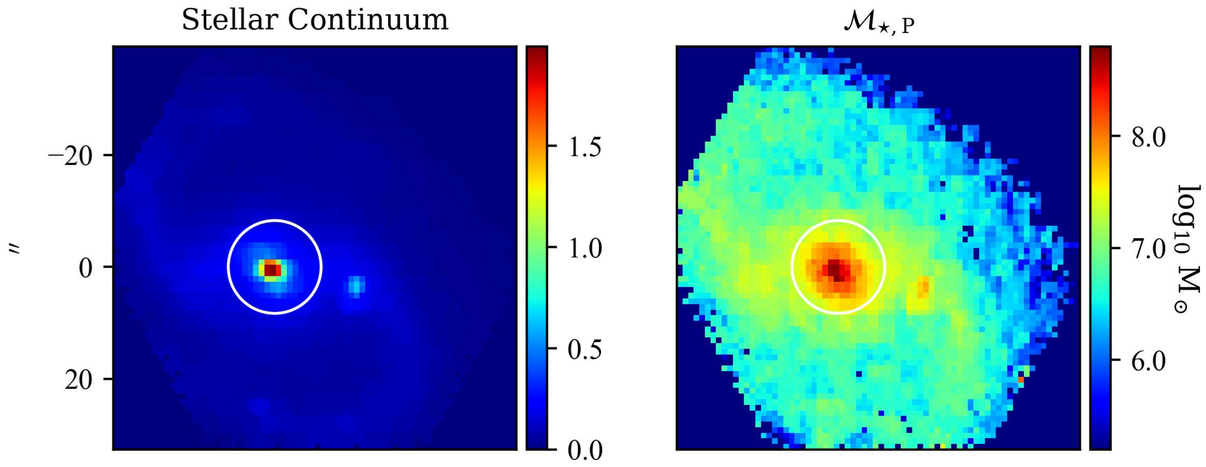

$\mathcal{M}_{\star,\mathrm{P}}$

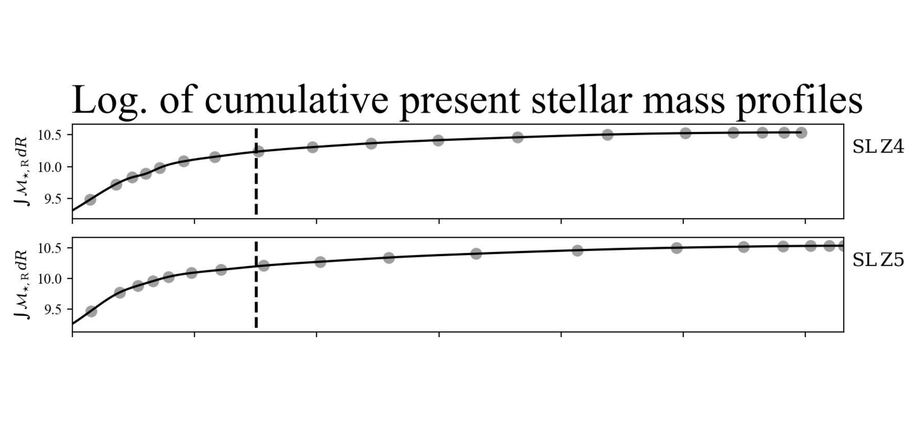

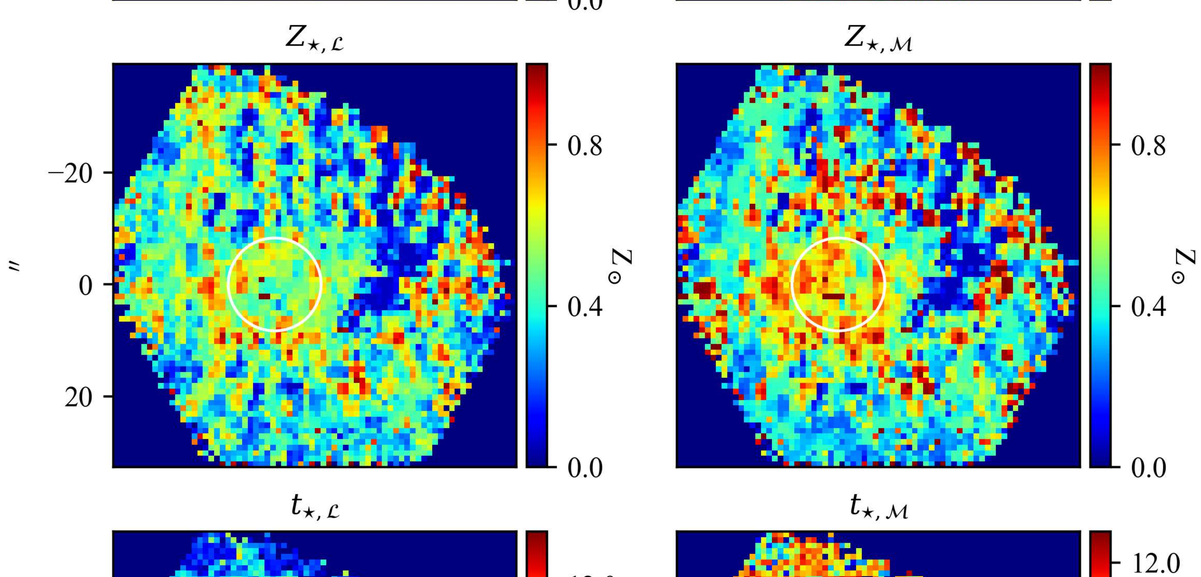

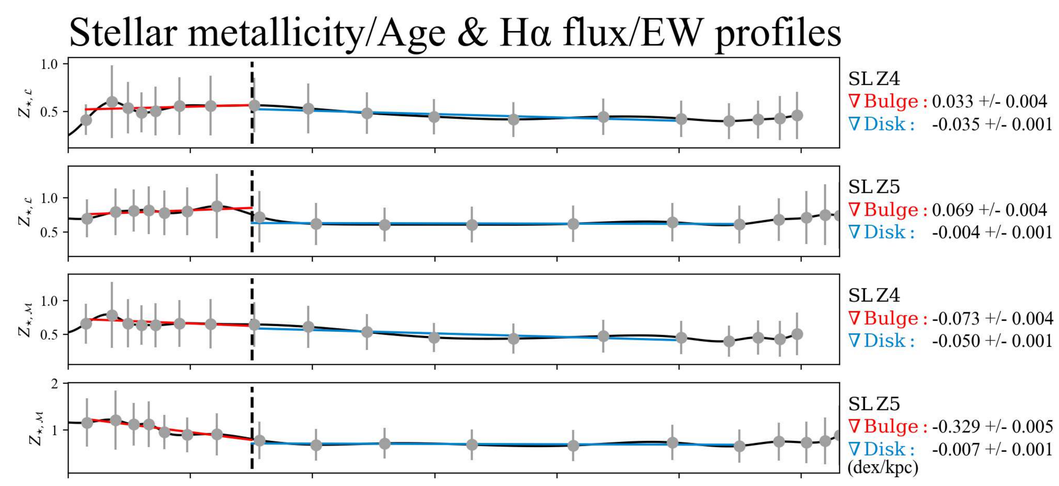

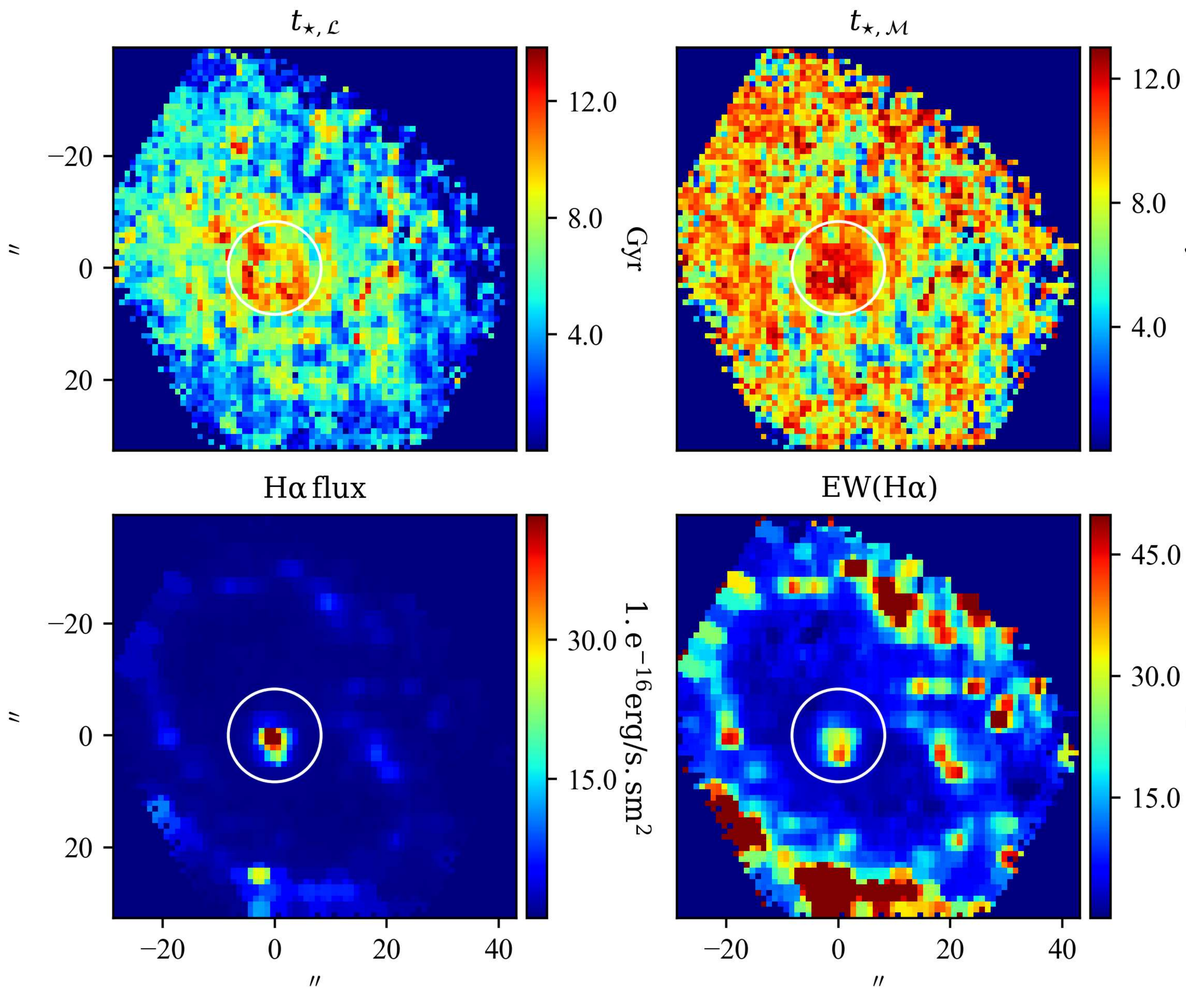

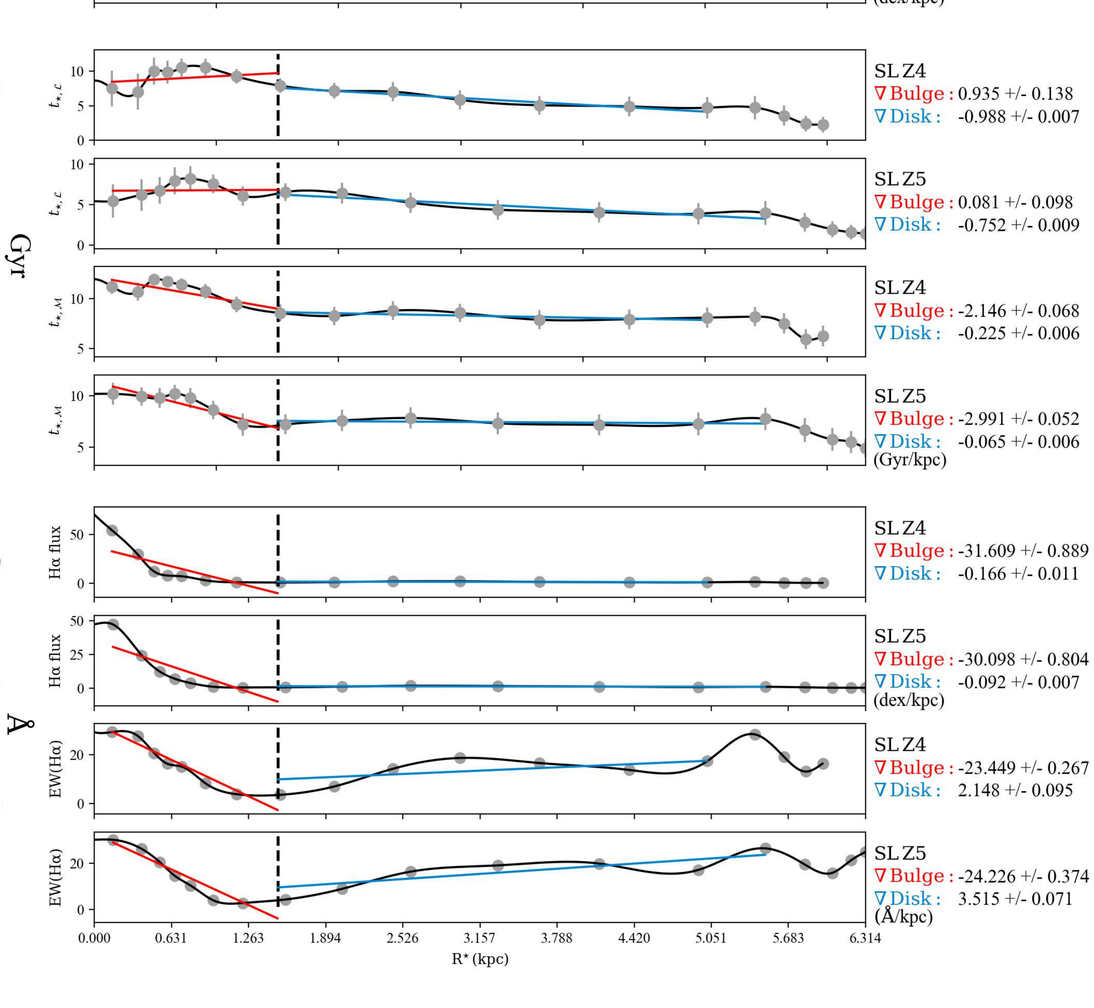

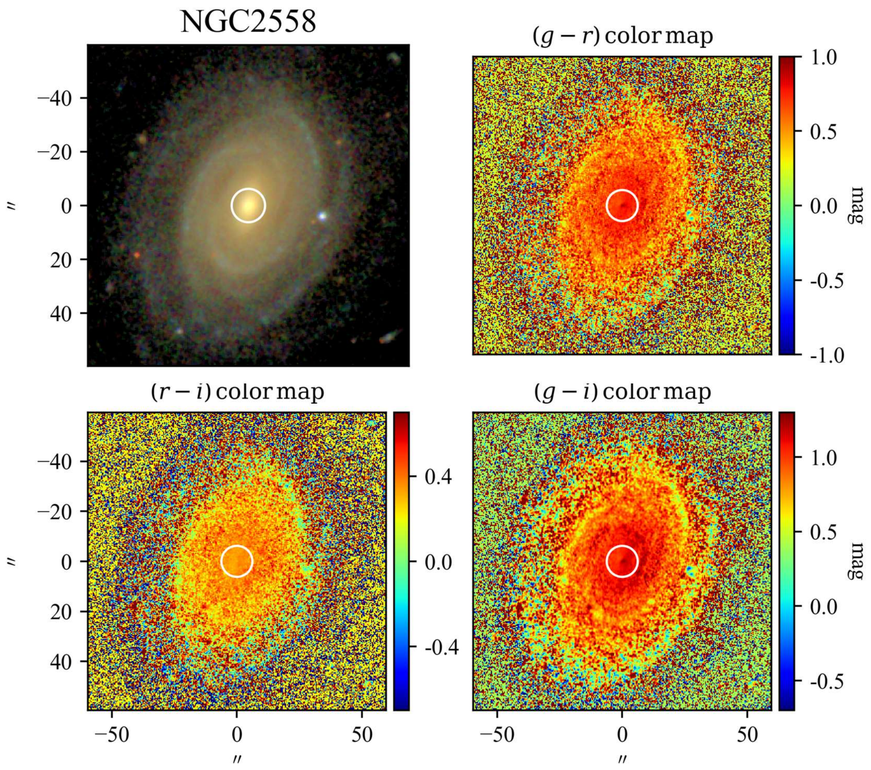

SBP decomposition of SDSS r band

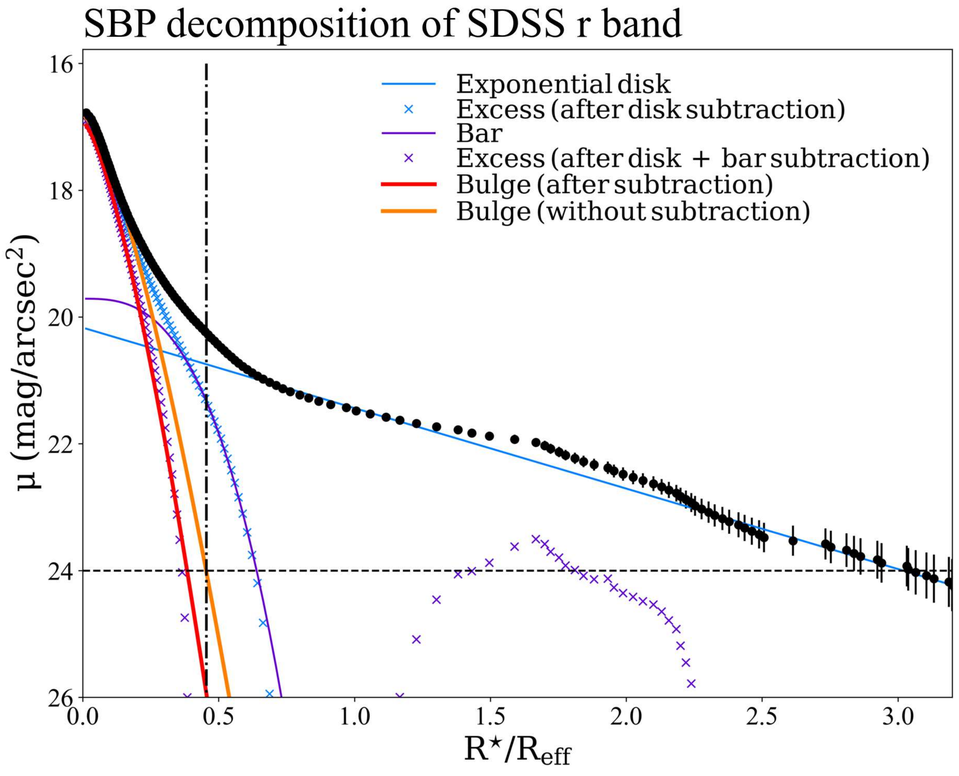

SDSS color profiles

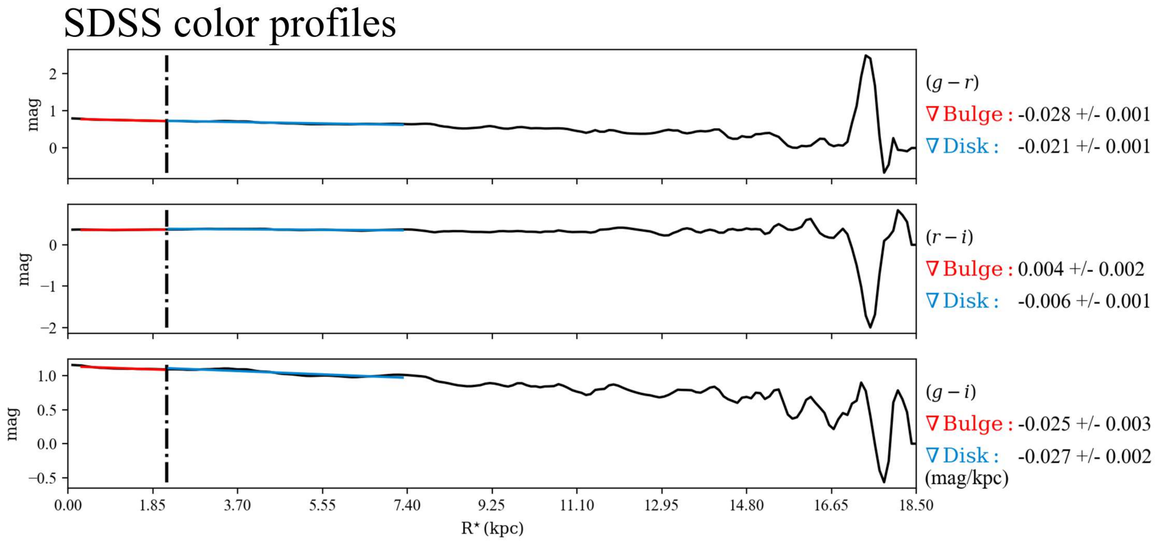

$\mathcal{RY}$ SBPs

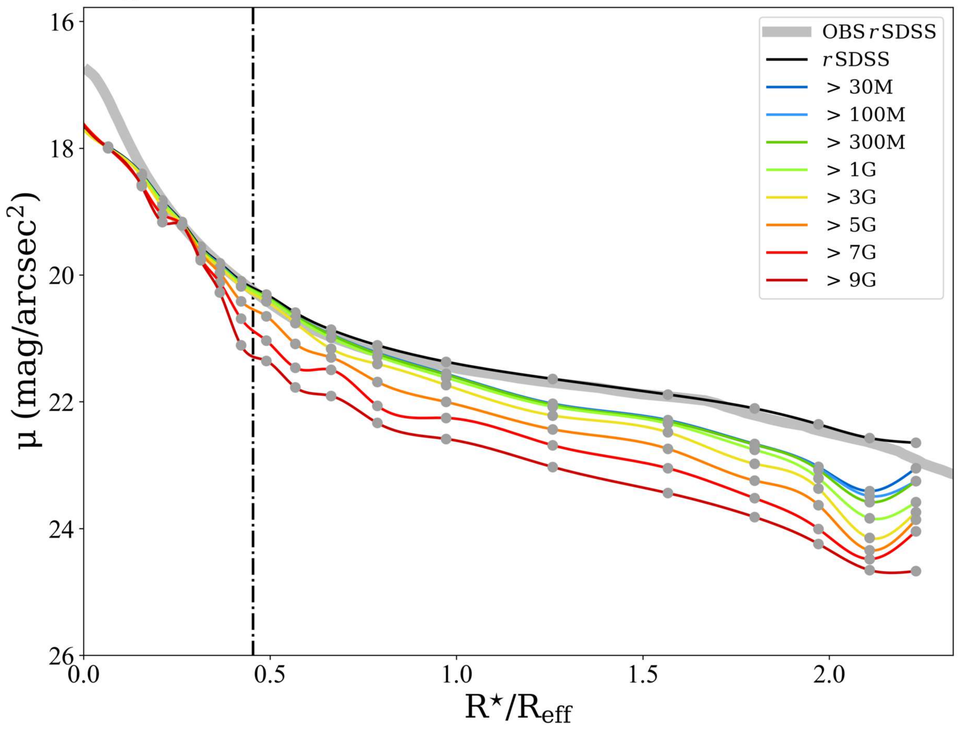

Stellar Continuum

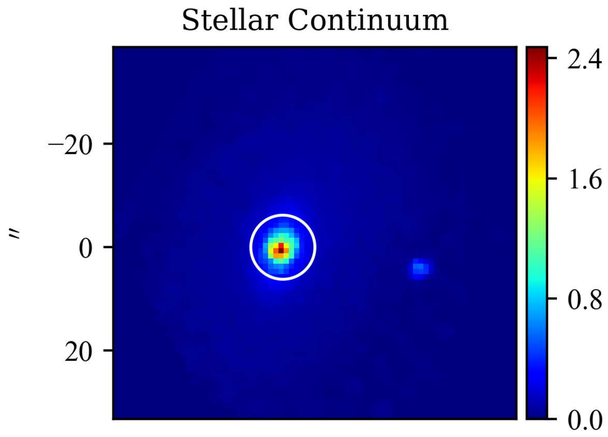

$\mathcal{M}_{\star,\mathrm{P}}$

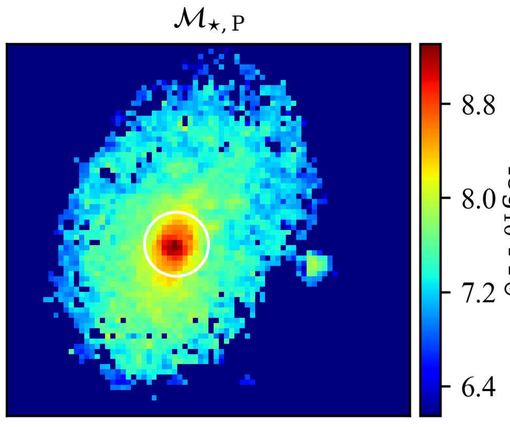

Log. of cumulative present stellar mass profiles

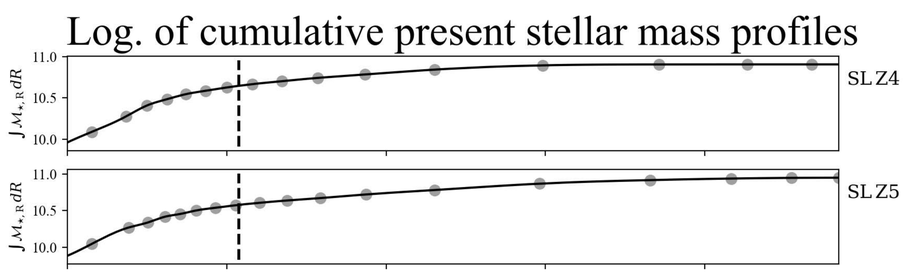

$Z_{\star,\mathcal{L}}$

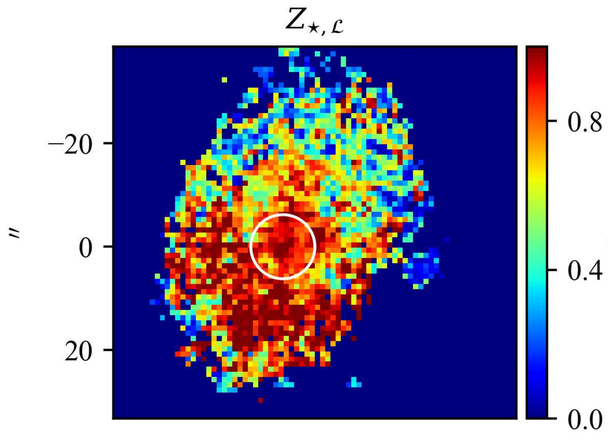

$Z_{\star,\mathcal{M}}$

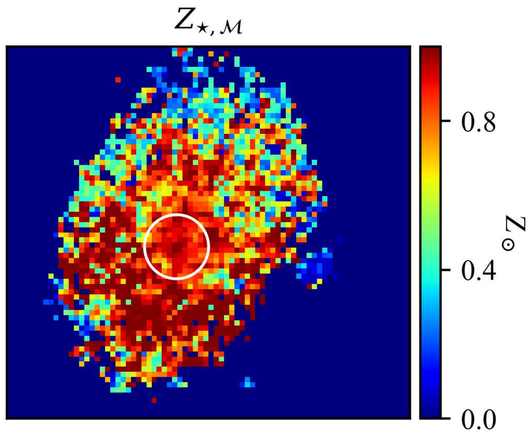

Stellar metallicity/Age & Hα flux/EW profiles

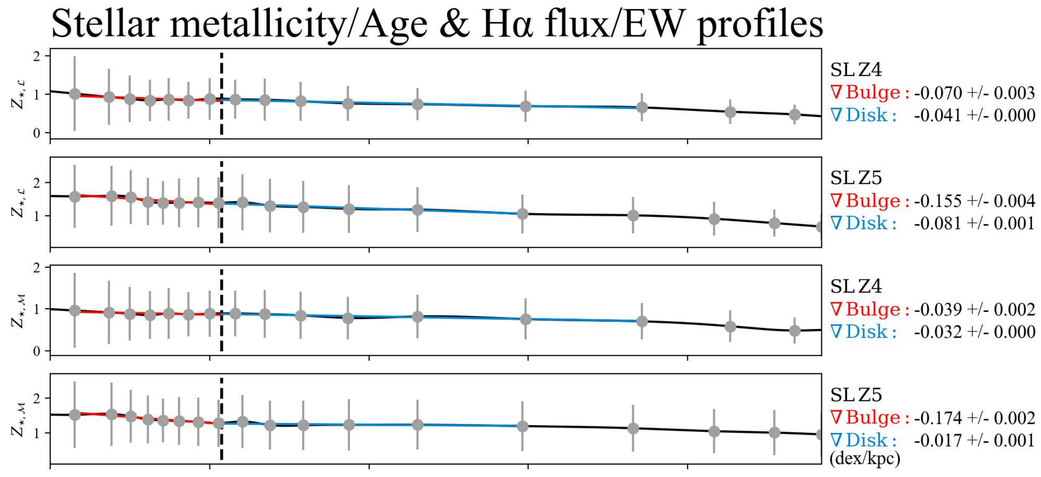

$t_{\star,\mathcal{L}}$

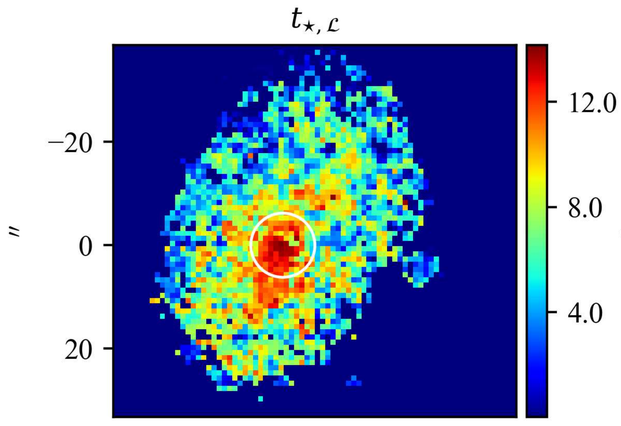

$t_{\star,\mathcal{M}}$

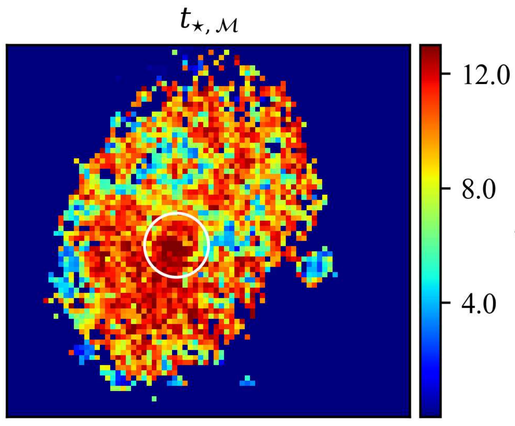

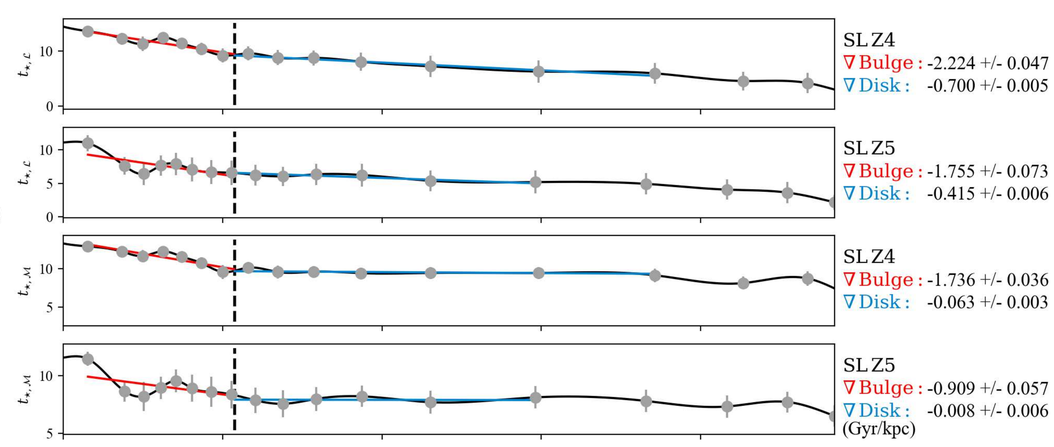

Hα flux

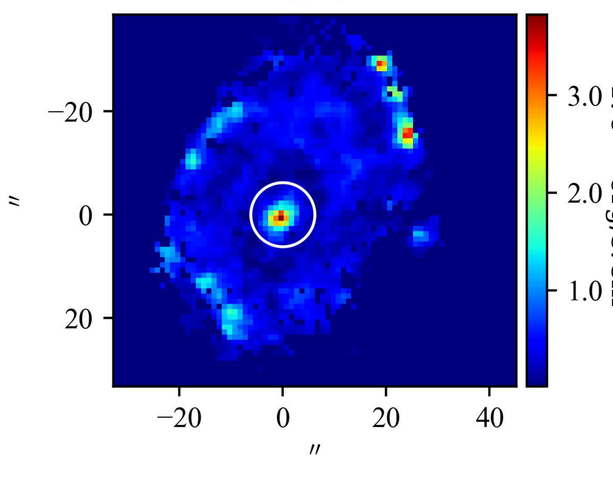

EW(Hα)

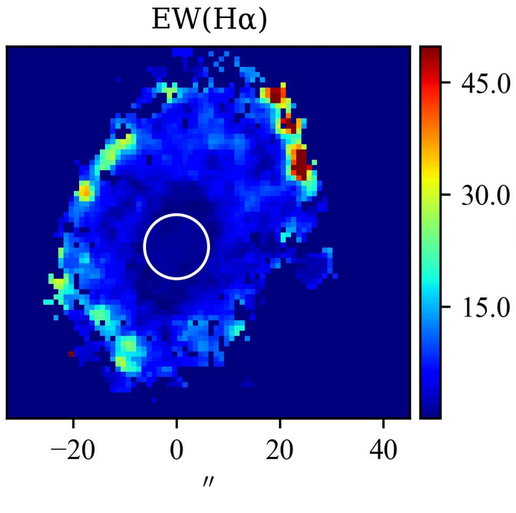

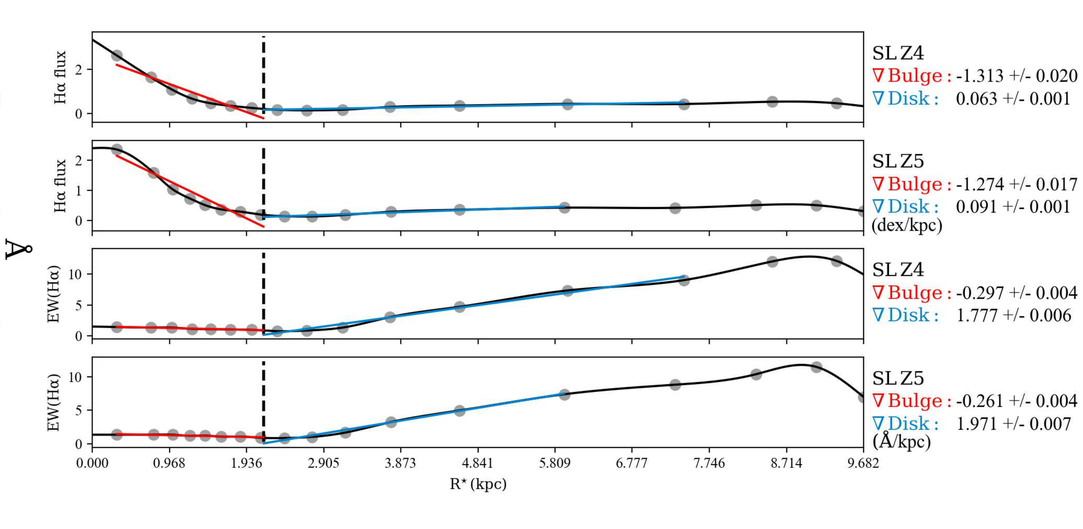

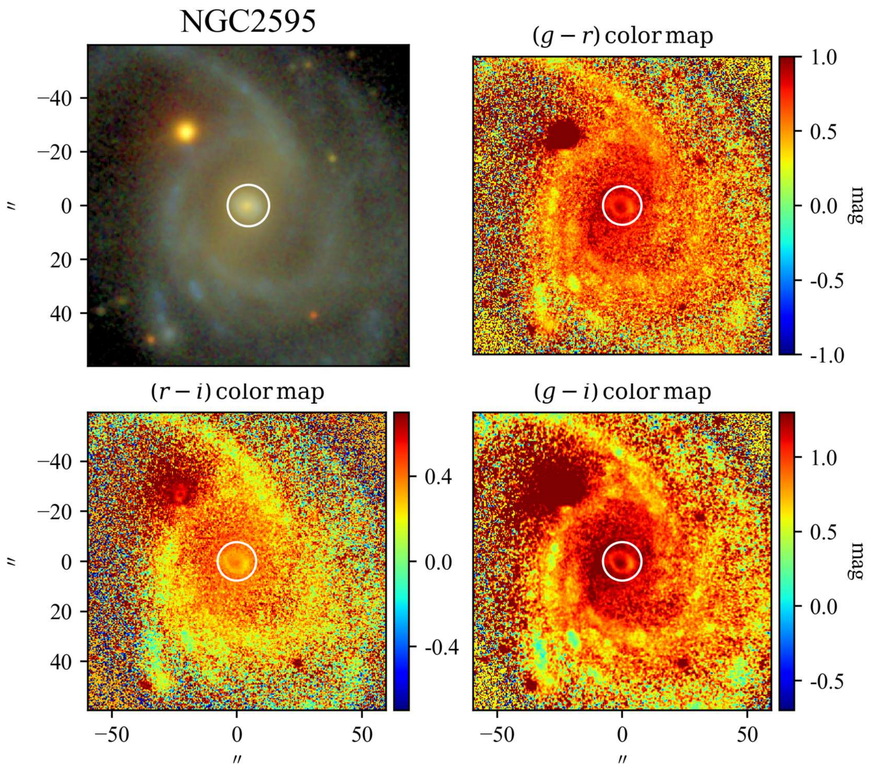

SBP decomposition of SDSS r band

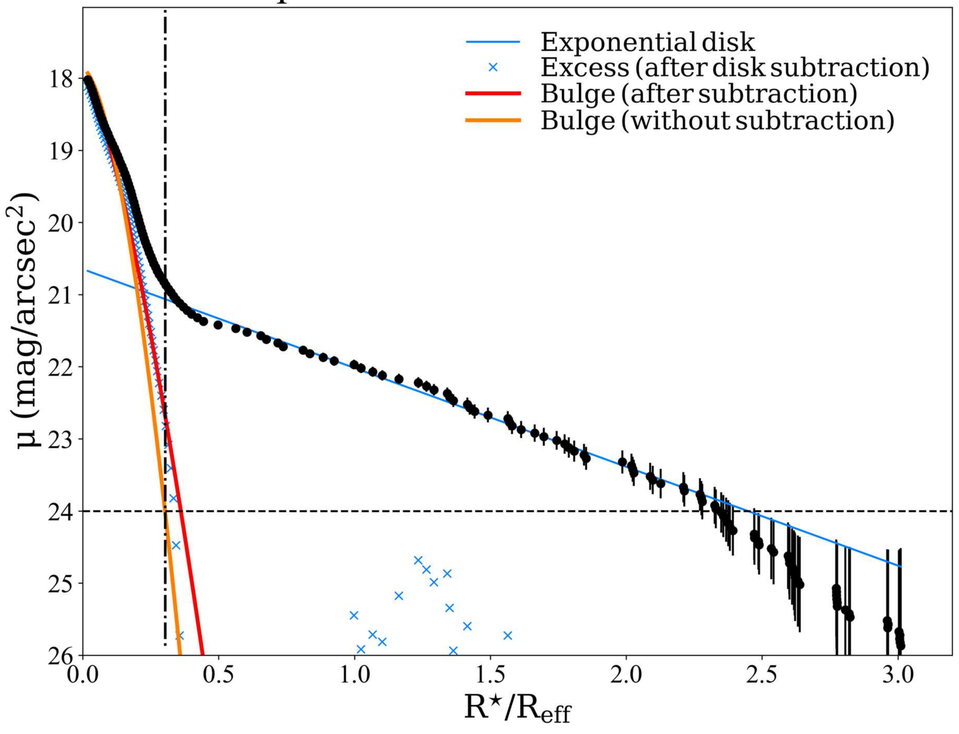

SDSS color profiles

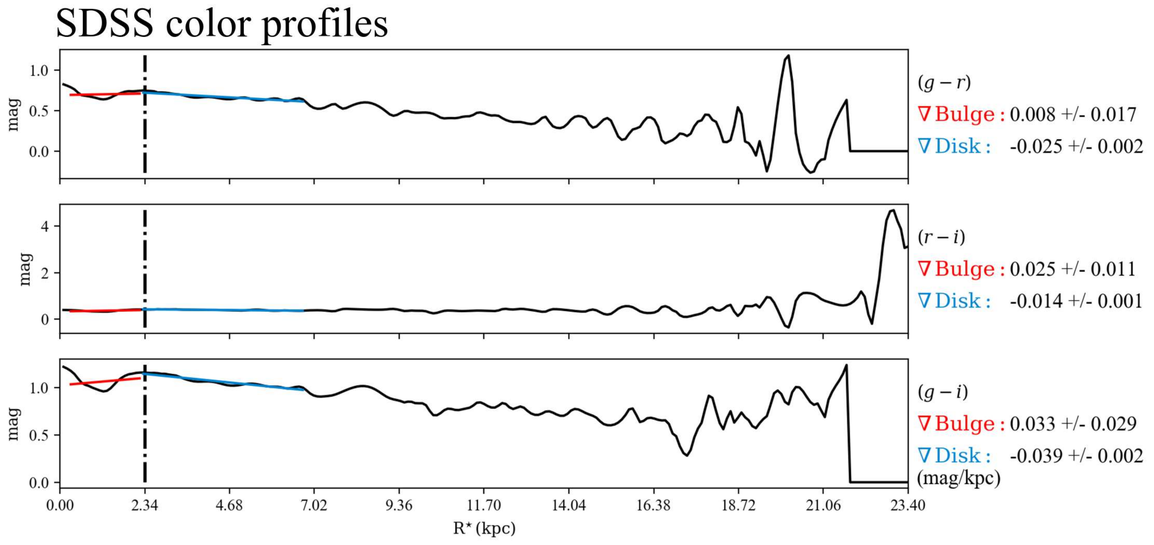

$\mathcal{RY}$ SBPs

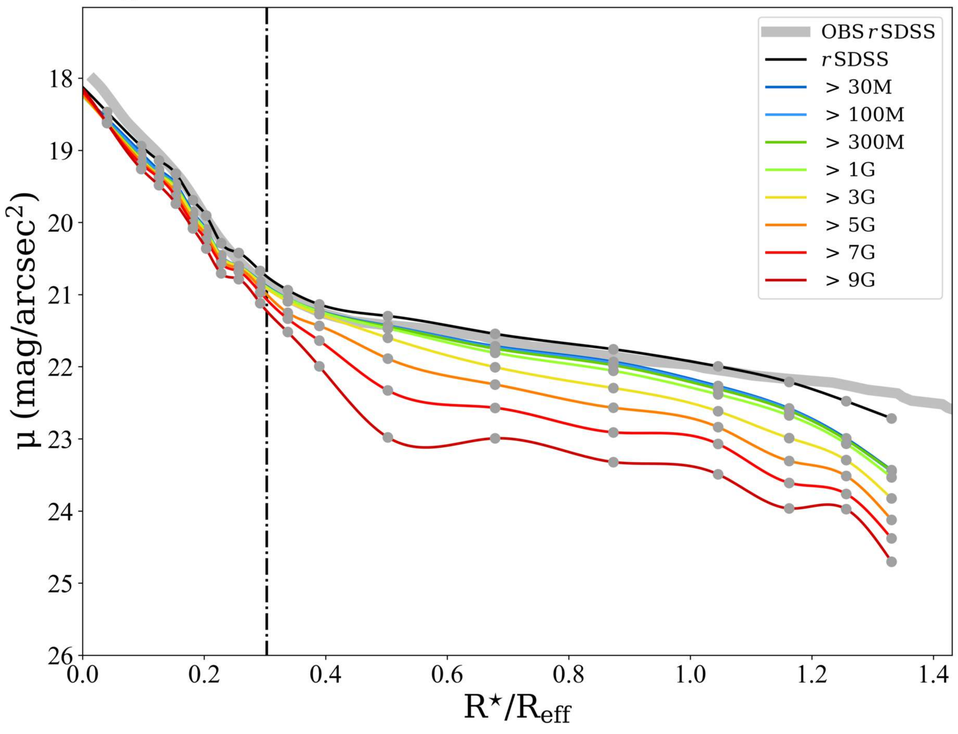

Stellar Continuum

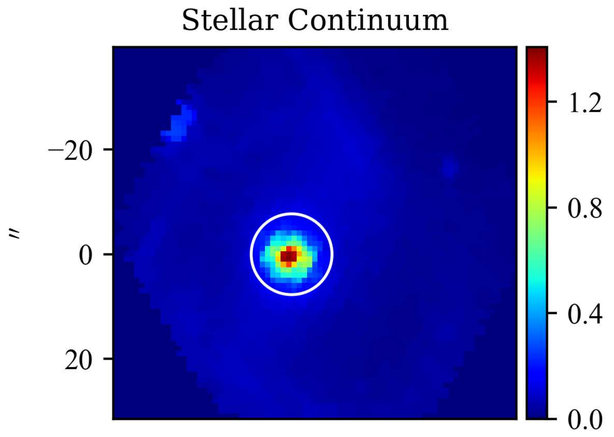

$\mathcal{M}_{\star,\mathrm{P}}$

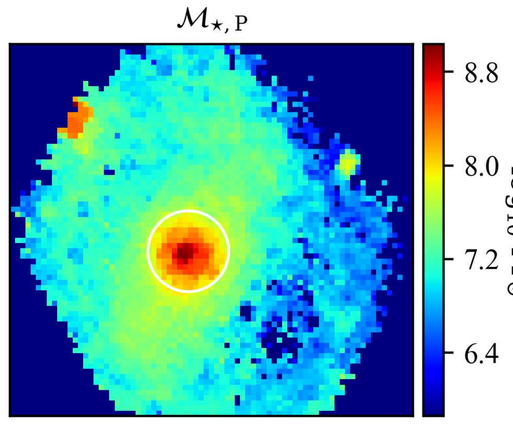

Log. of cumulative present stellar mass profiles

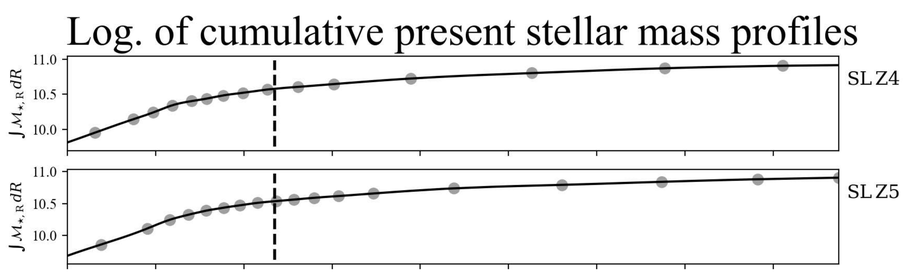

$Z_{\star,\mathcal{L}}$

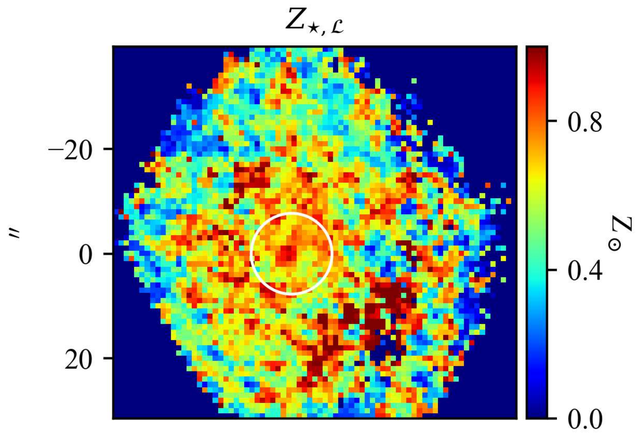

$Z_{\star,\mathcal{M}}$

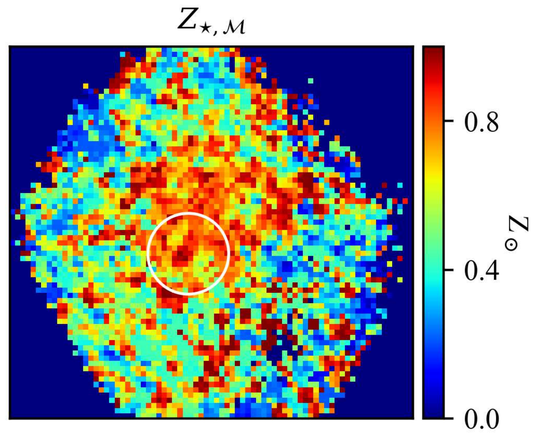

Stellar metallicity/Age & Hα flux/EW profiles

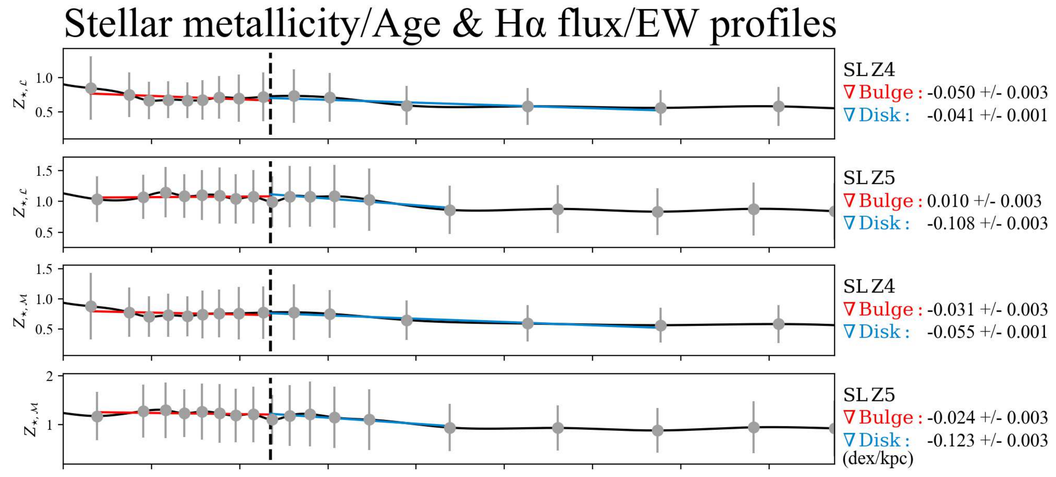

$t_{\star,\mathcal{L}}$

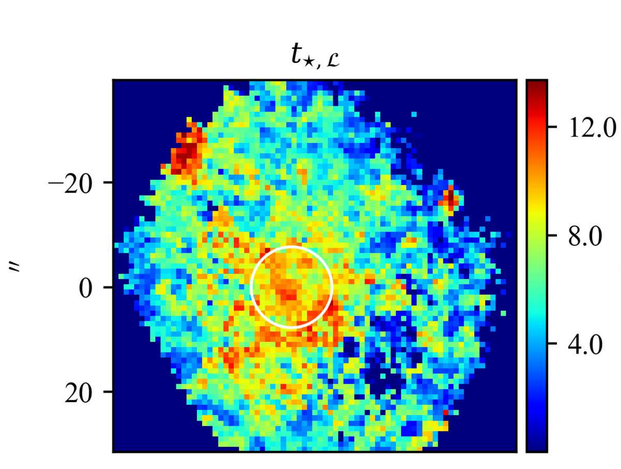

$t_{\star,\mathcal{M}}$

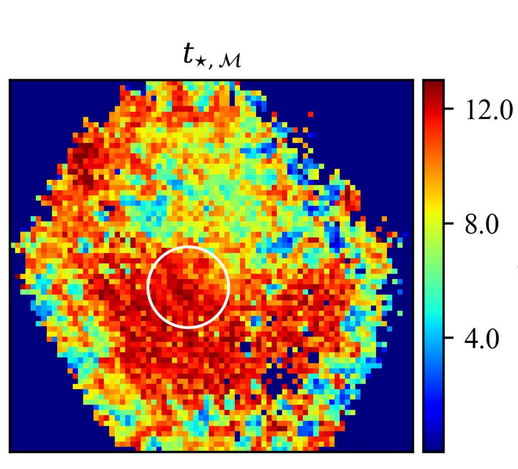

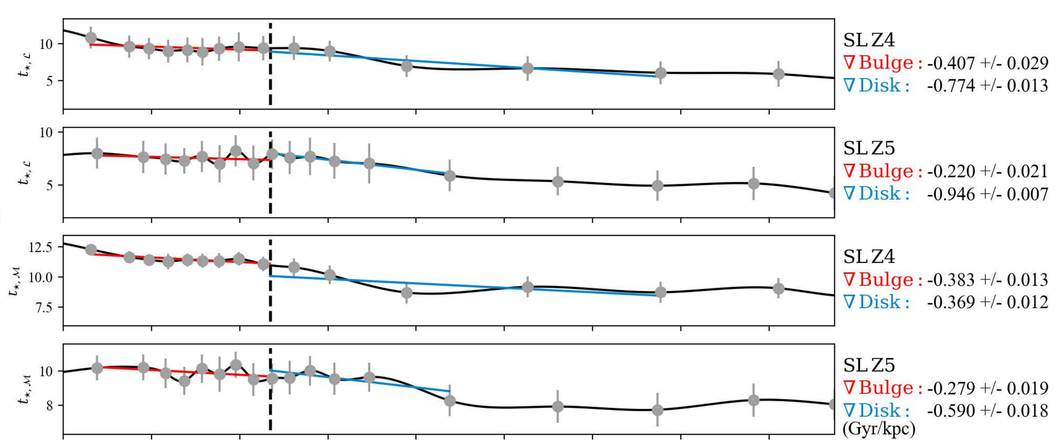

Hα flux

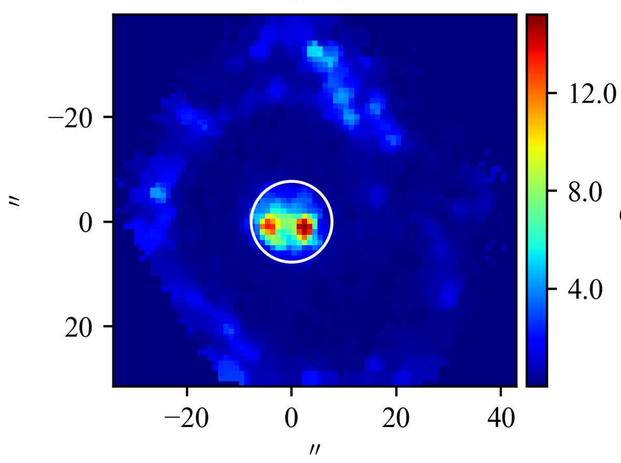

EW(Hα)

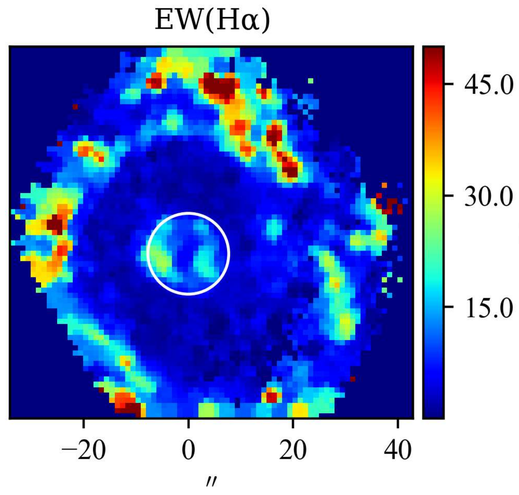

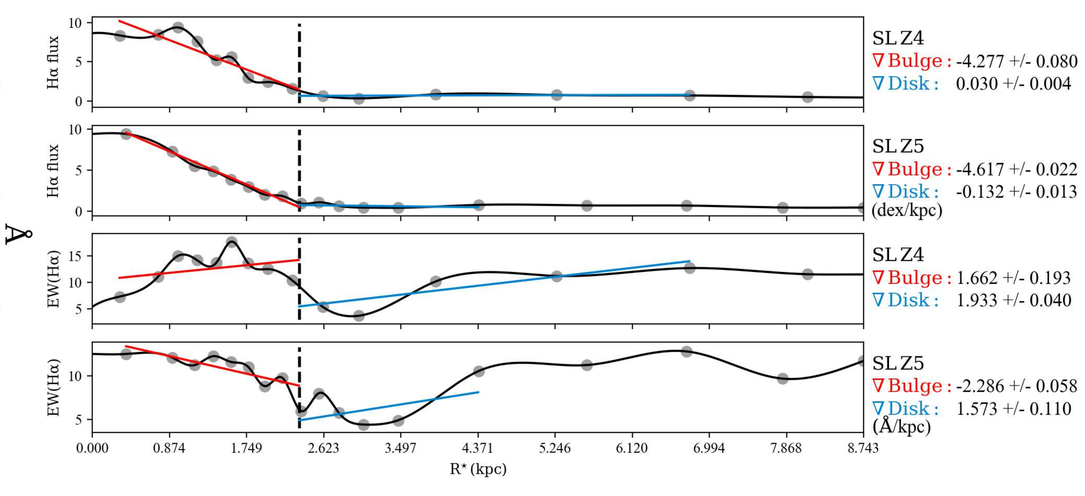

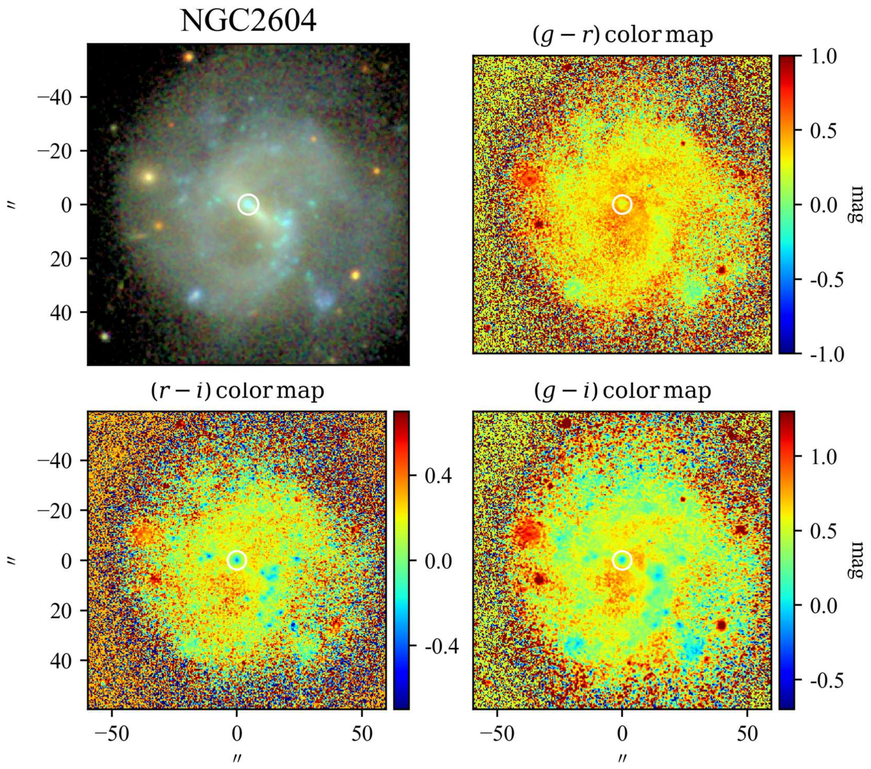
NGC2604
$(g-r)$ color map
$(r-i)$ color map
$(g-i)$ color map
mag
″

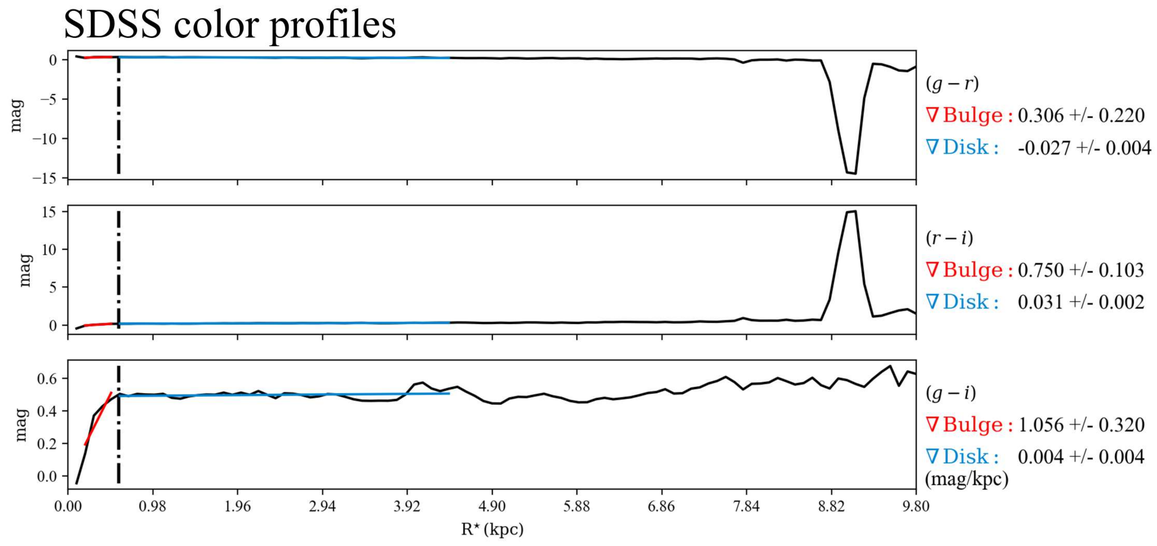
SDSS color profiles
$(g-r)$
∇ Bulge : 0.306 +/- 0.220
∇ Disk : -0.027 +/- 0.004
$(r-i)$
∇ Bulge : 0.750 +/- 0.103
∇ Disk : 0.031 +/- 0.002
$(g-i)$
∇ Bulge : 1.056 +/- 0.320
∇ Disk : 0.004 +/- 0.004
(mag/kpc)
mag
R* (kpc)

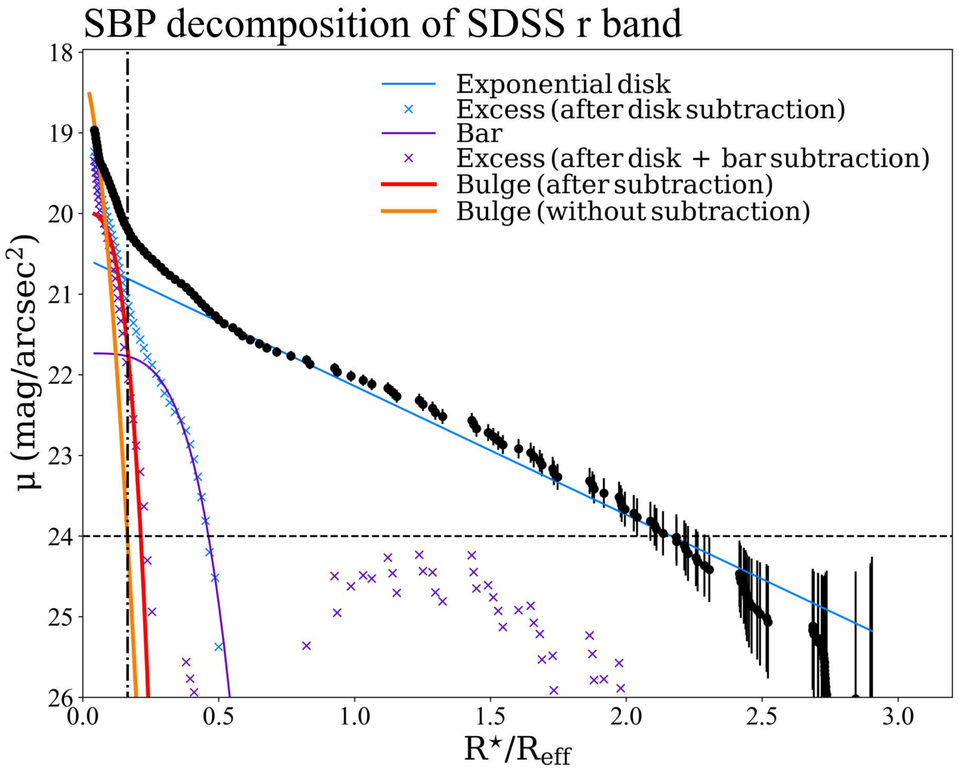
SBP decomposition of SDSS r band
Exponential disk
Excess (after disk subtraction)
Bar
Excess (after disk + bar subtraction)
Bulge (after subtraction)
Bulge (without subtraction)
μ (mag/arcsec^2)
R*/R$_{eff}$

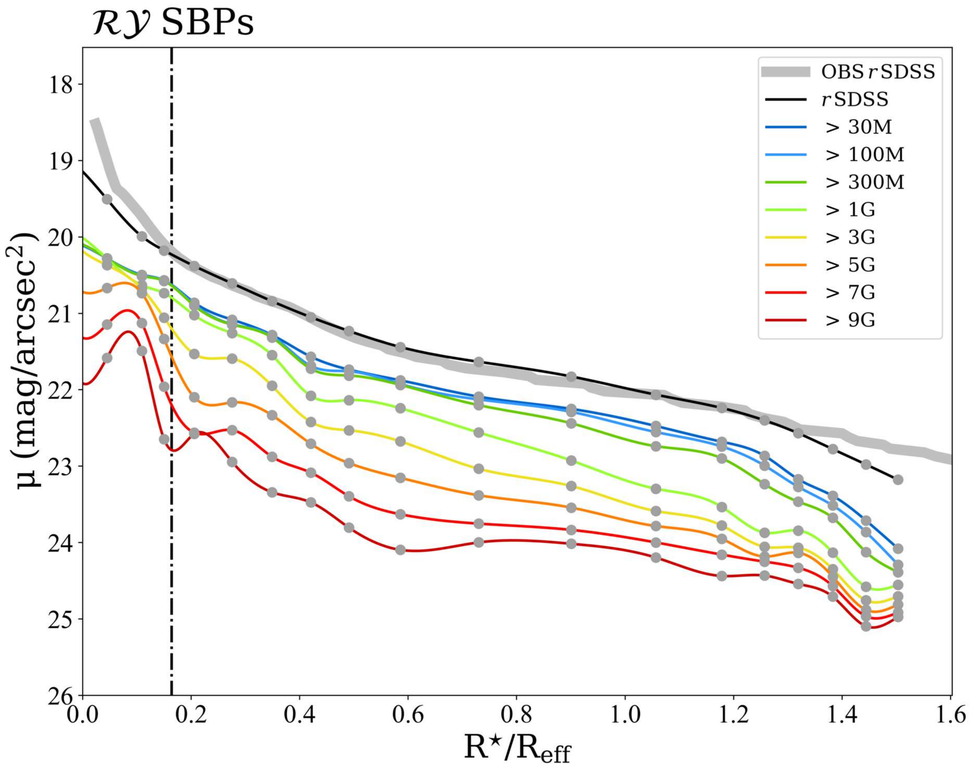
$\mathcal{RY}$ SBPs
OBS rSDSS
rSDSS
> 30M
> 100M
> 300M
> 1G
> 3G
> 5G
> 7G
> 9G
μ (mag/arcsec^2)
R*/R$_{eff}$

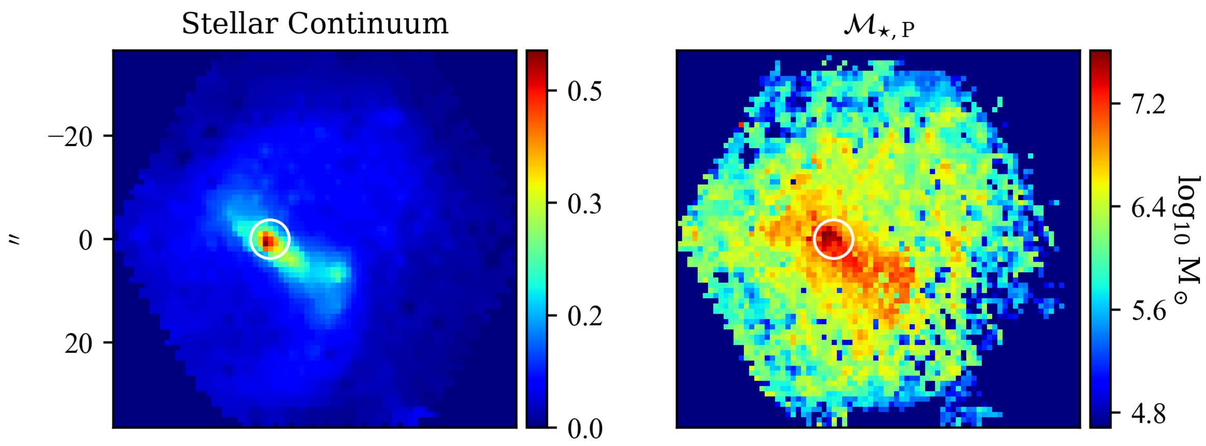
Stellar Continuum
$\mathcal{M}_{\star,\mathrm{P}}$
log$_{10}$ M$_\odot$
″

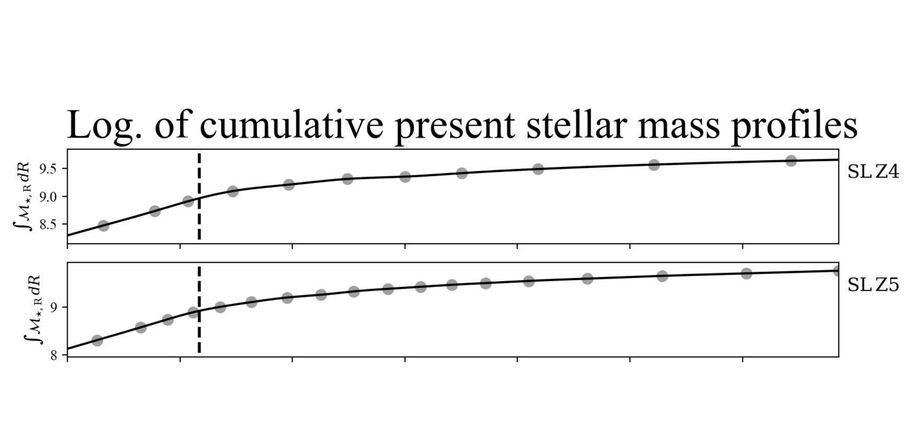
Log. of cumulative present stellar mass profiles
SL Z4
SL Z5
$\int \mathcal{M}_{\star,\mathrm{R}} dR$

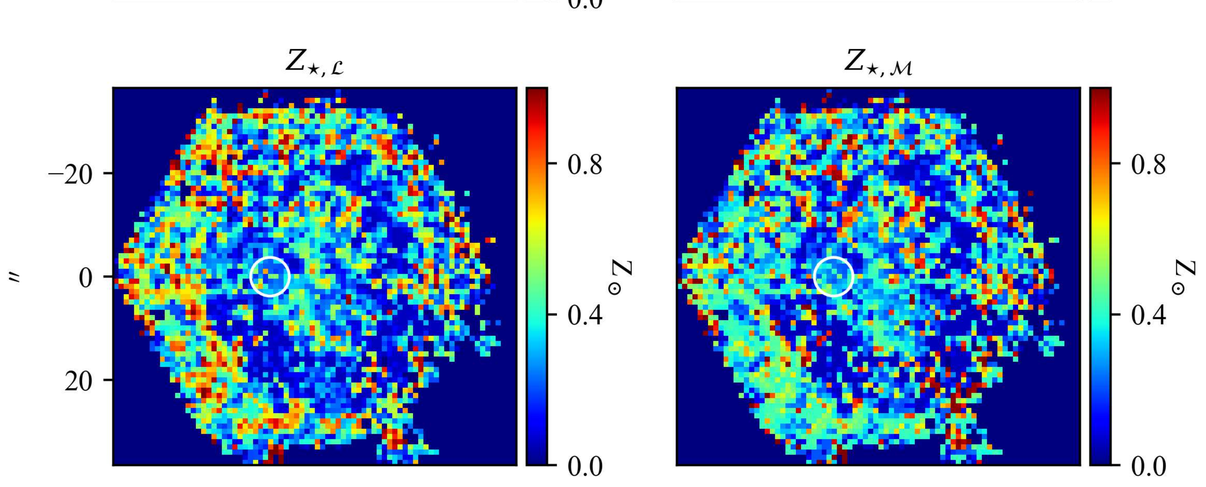
$Z_{\star,\mathcal{L}}$
$Z_{\star,\mathcal{M}}$
Z$_\odot$
″

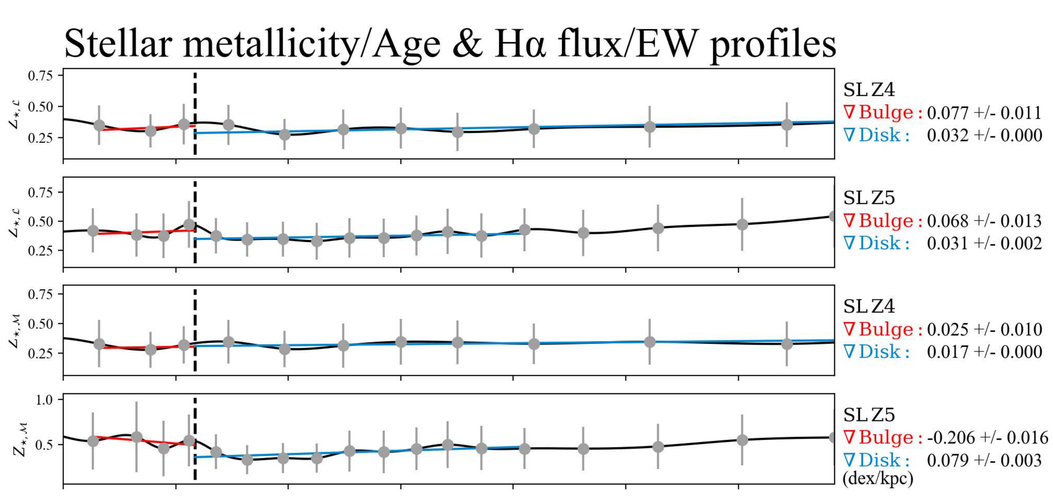
Stellar metallicity/Age & Hα flux/EW profiles
SL Z4
∇ Bulge : 0.077 +/- 0.011
∇ Disk : 0.032 +/- 0.000
SL Z5
∇ Bulge : 0.068 +/- 0.013
∇ Disk : 0.031 +/- 0.002
SL Z4
∇ Bulge : 0.025 +/- 0.010
∇ Disk : 0.017 +/- 0.000
SL Z5
∇ Bulge : -0.206 +/- 0.016
∇ Disk : 0.079 +/- 0.003
(dex/kpc)

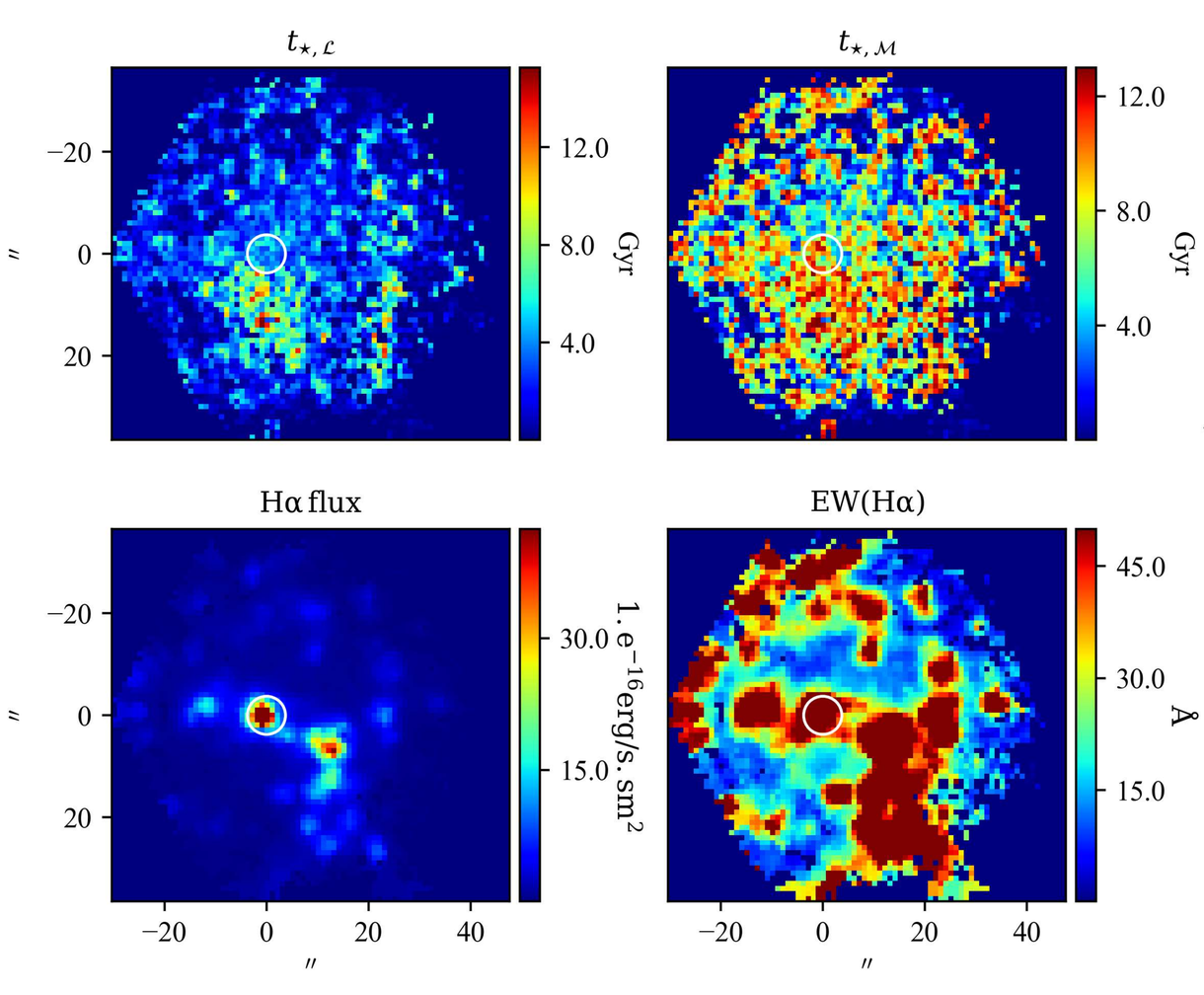
$t_{\star,\mathcal{L}}$
$t_{\star,\mathcal{M}}$
Gyr
″

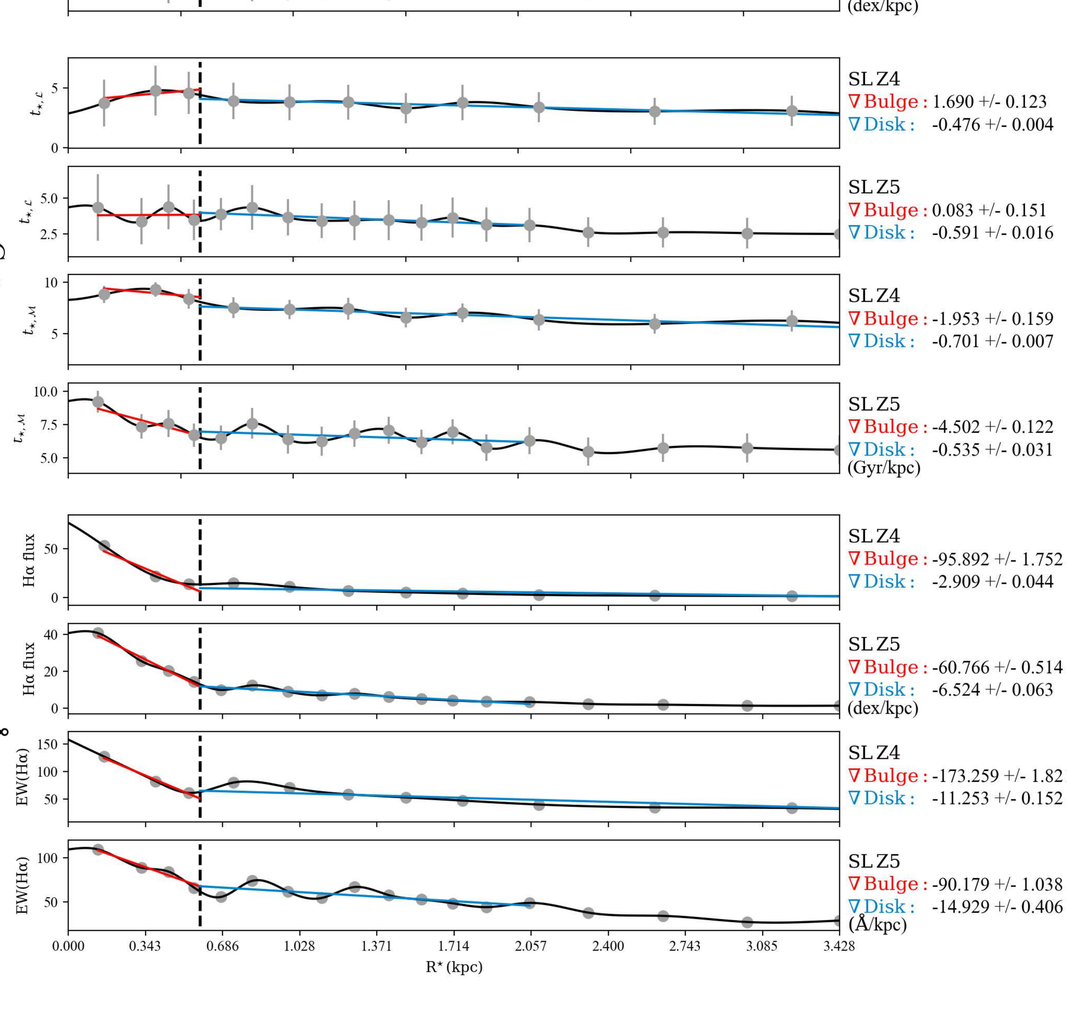
SL Z4
∇ Bulge : 1.690 +/- 0.123
∇ Disk : -0.476 +/- 0.004
SL Z5
∇ Bulge : 0.083 +/- 0.151
∇ Disk : -0.591 +/- 0.016
SL Z4
∇ Bulge : -1.953 +/- 0.159
∇ Disk : -0.701 +/- 0.007
SL Z5
∇ Bulge : -4.502 +/- 0.122
∇ Disk : -0.535 +/- 0.031
(Gyr/kpc)

Hα flux
EW(Hα)
1.e^{-16}erg/s.sm^2
Å
″

SL Z4
∇ Bulge : -95.892 +/- 1.752
∇ Disk : -2.909 +/- 0.044
SL Z5
∇ Bulge : -60.766 +/- 0.514
∇ Disk : -6.524 +/- 0.063
(dex/kpc)
SL Z4
∇ Bulge : -173.259 +/- 1.82
∇ Disk : -11.253 +/- 0.152
SL Z5
∇ Bulge : -90.179 +/- 1.038
∇ Disk : -14.929 +/- 0.406
(Å/kpc)
R* (kpc)

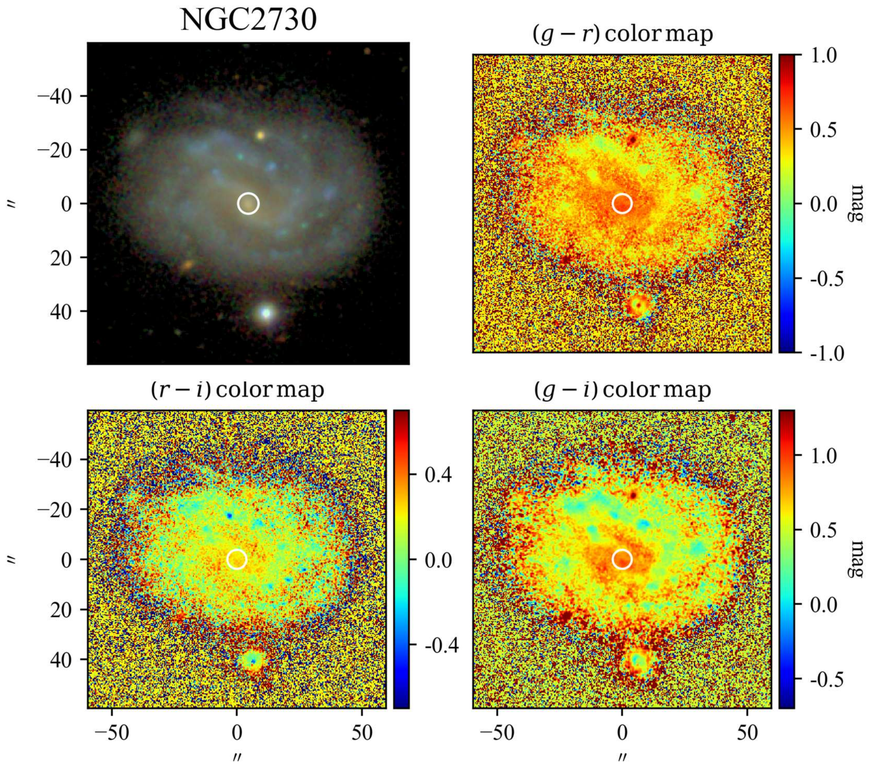

SBP decomposition of SDSS r band

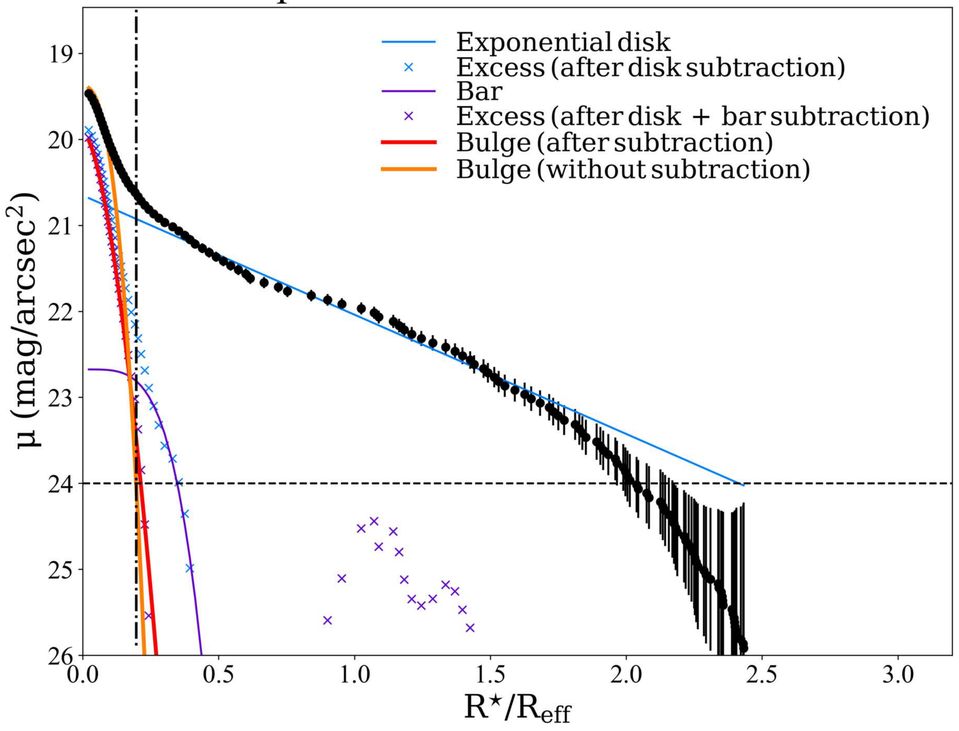

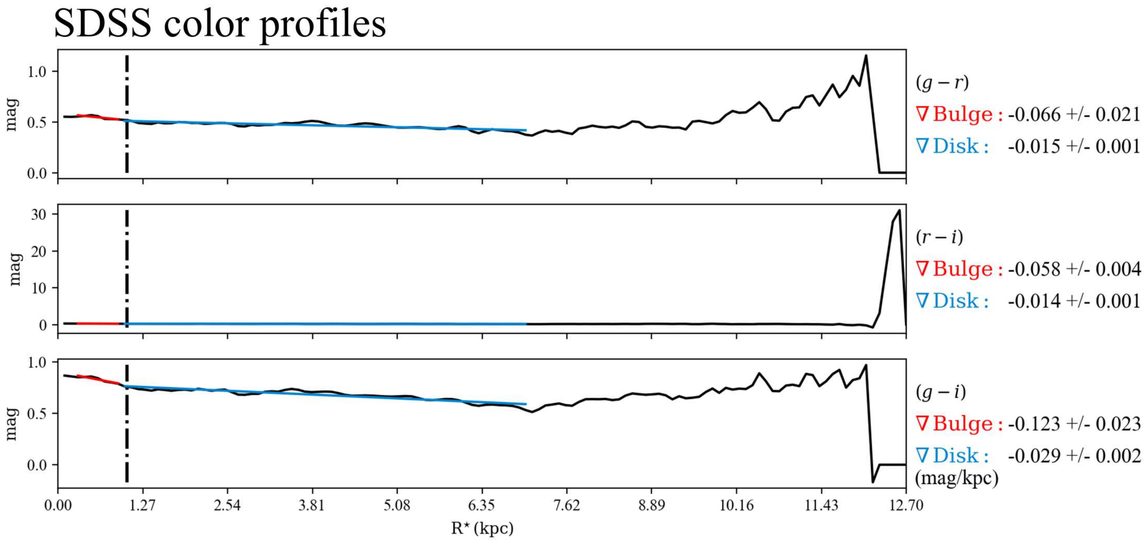

$\mathcal{RV}$ SBPs

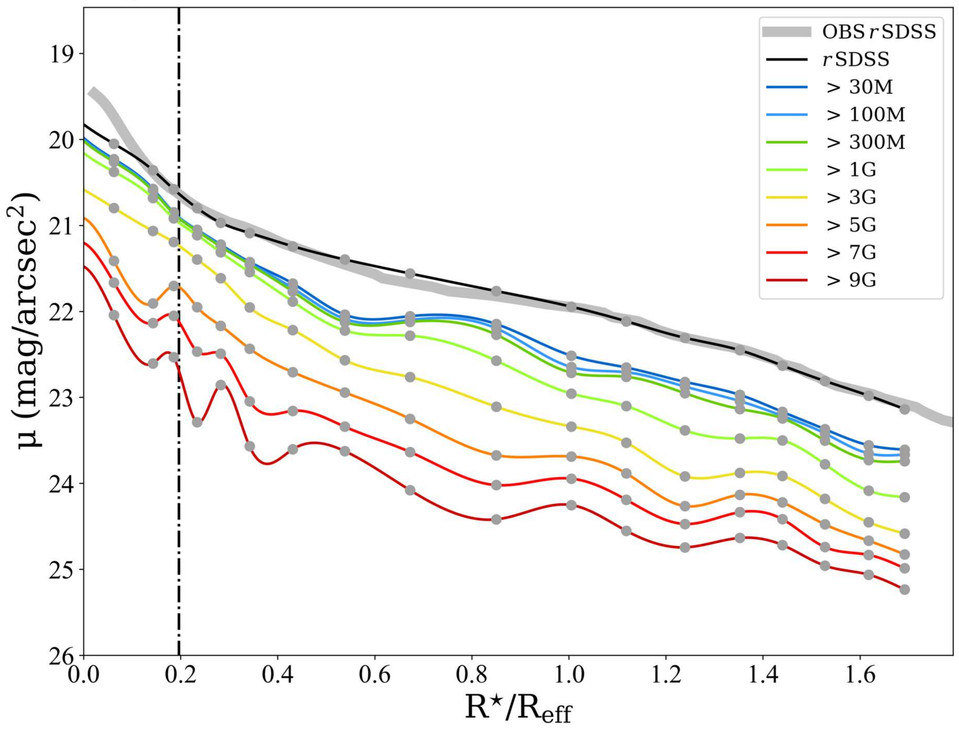

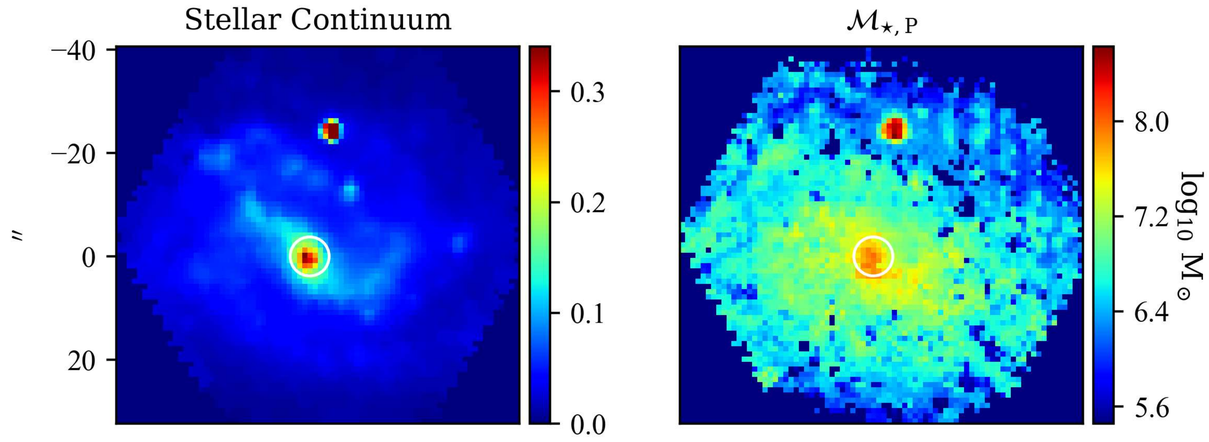

Log. of cumulative present stellar mass profiles

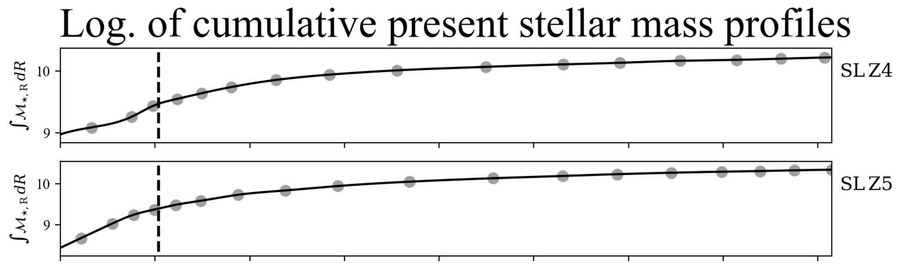

Stellar metallicity/Age & Hα flux/EW profiles

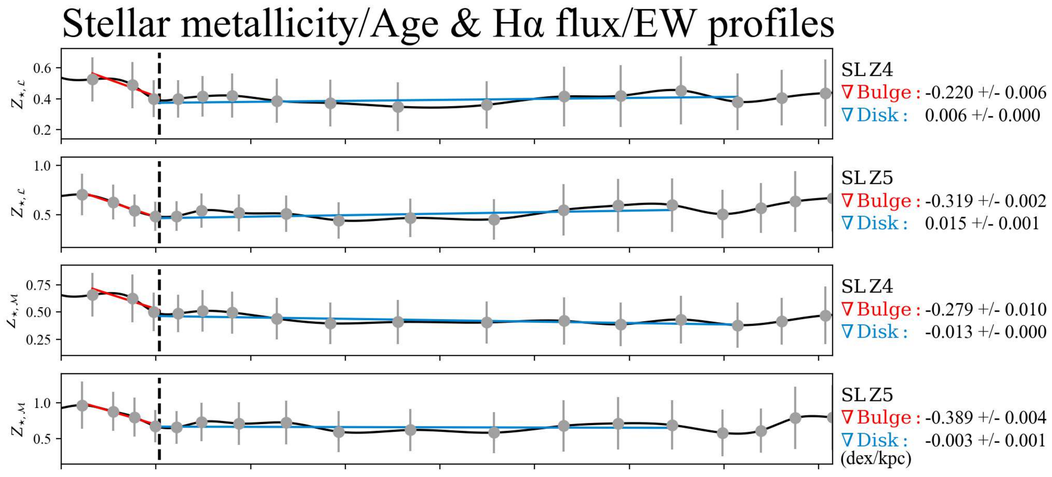

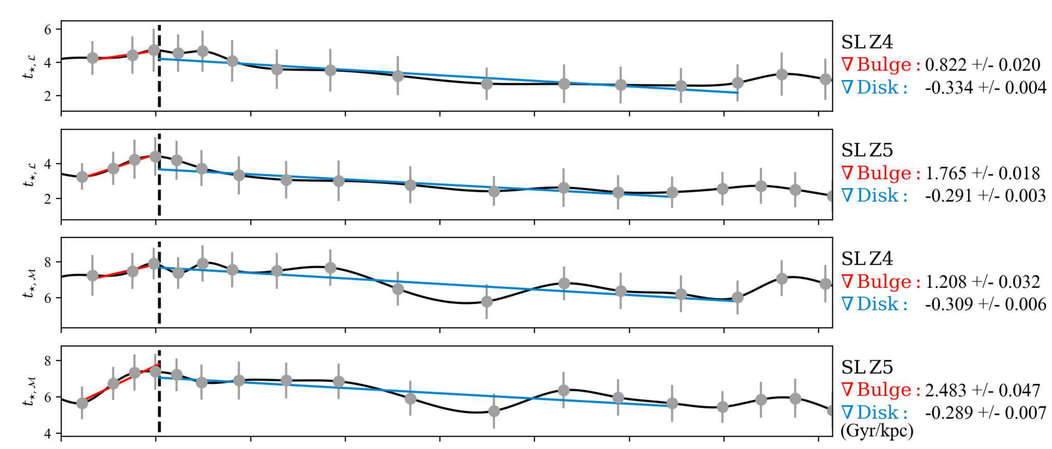

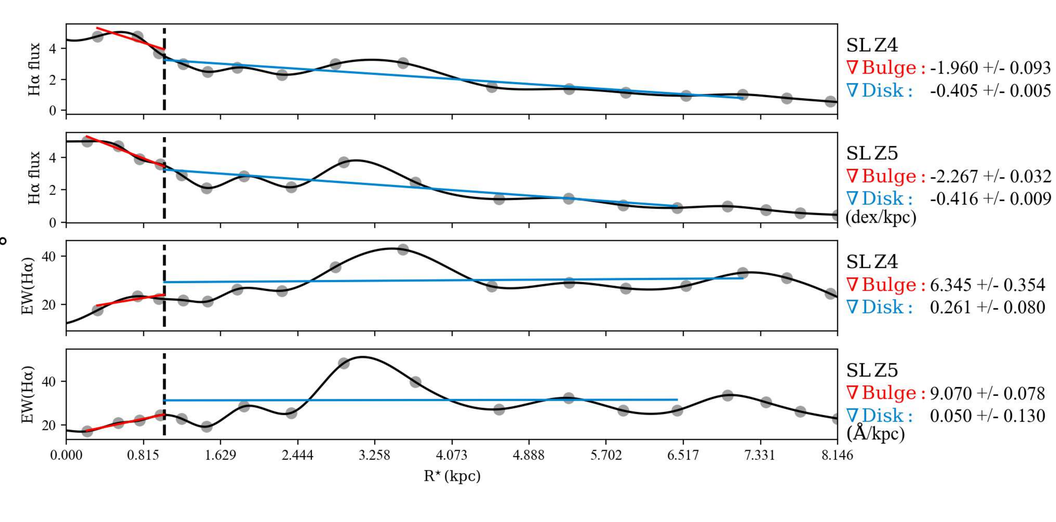

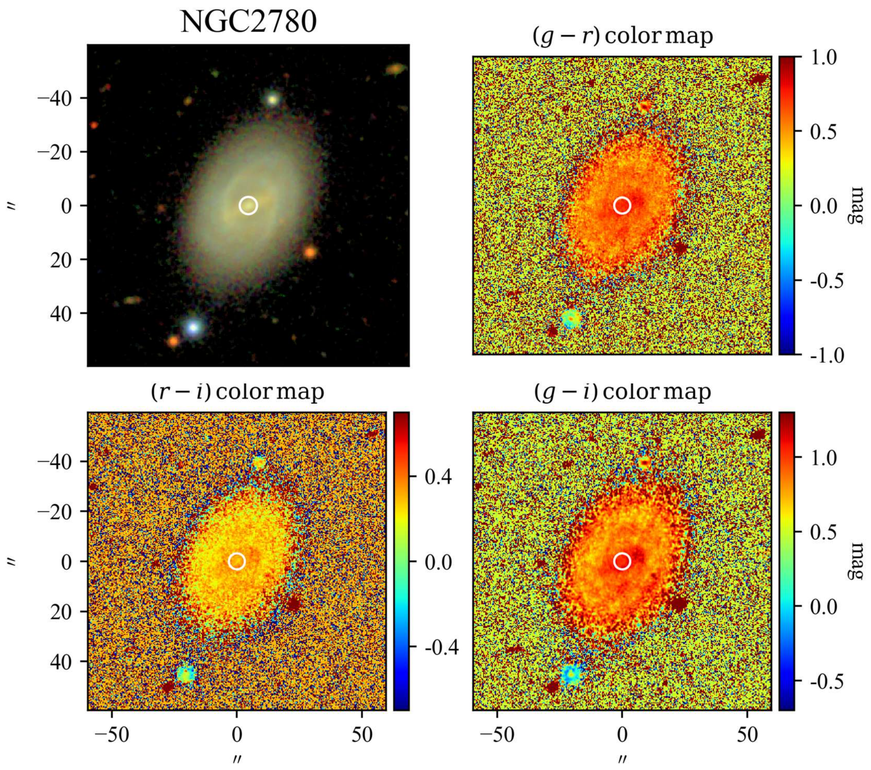

SBP decomposition of SDSS r band

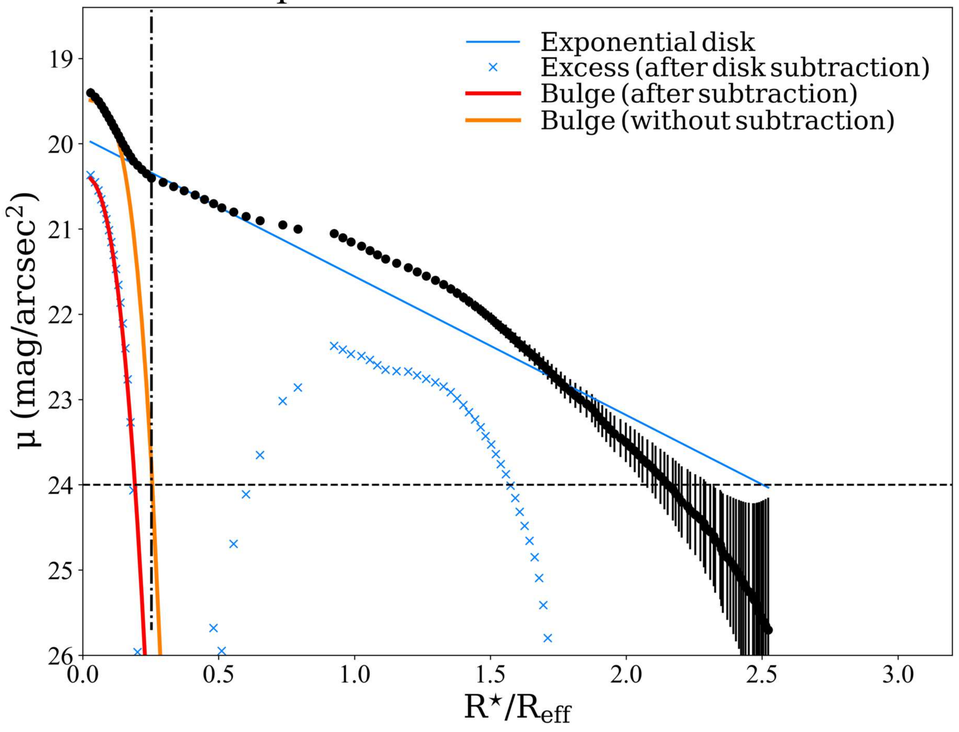

SDSS color profiles

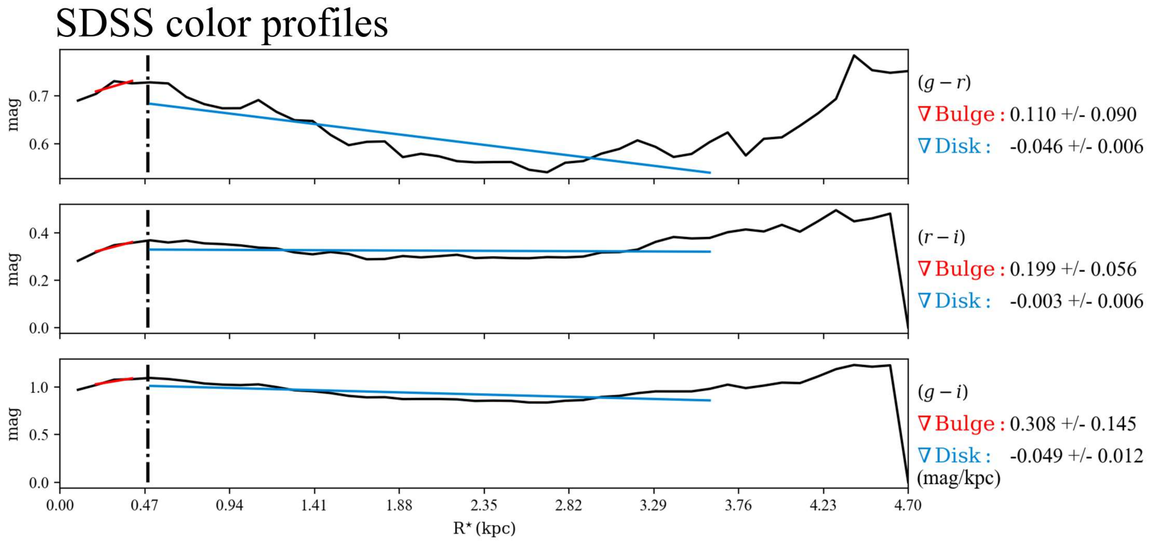

$\mathcal{RV}$ SBPs

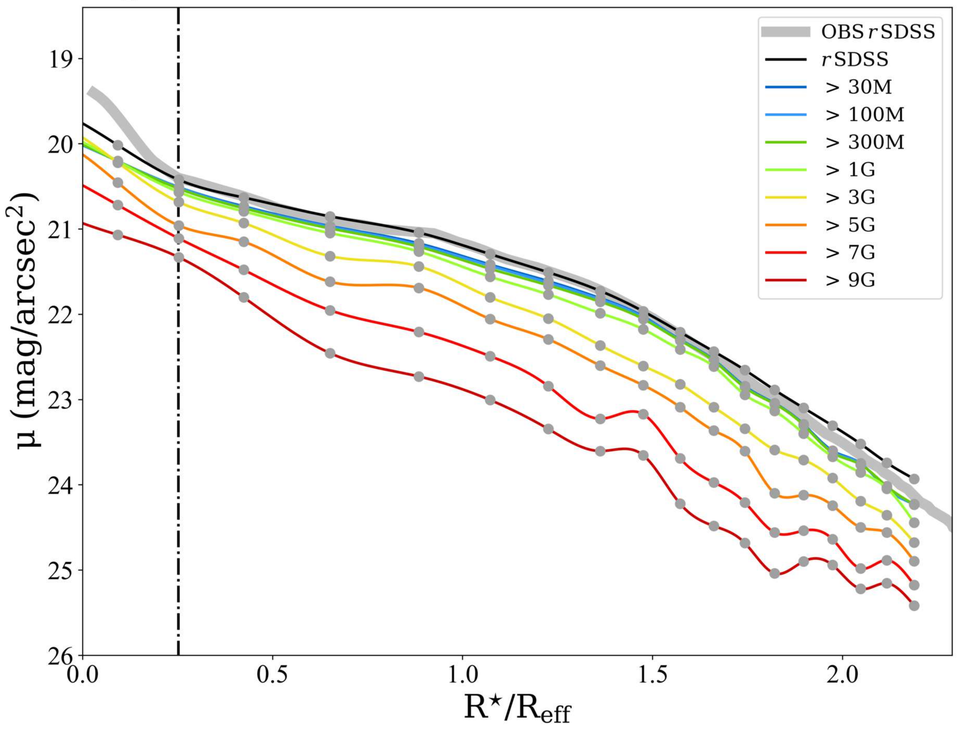

Stellar Continuum

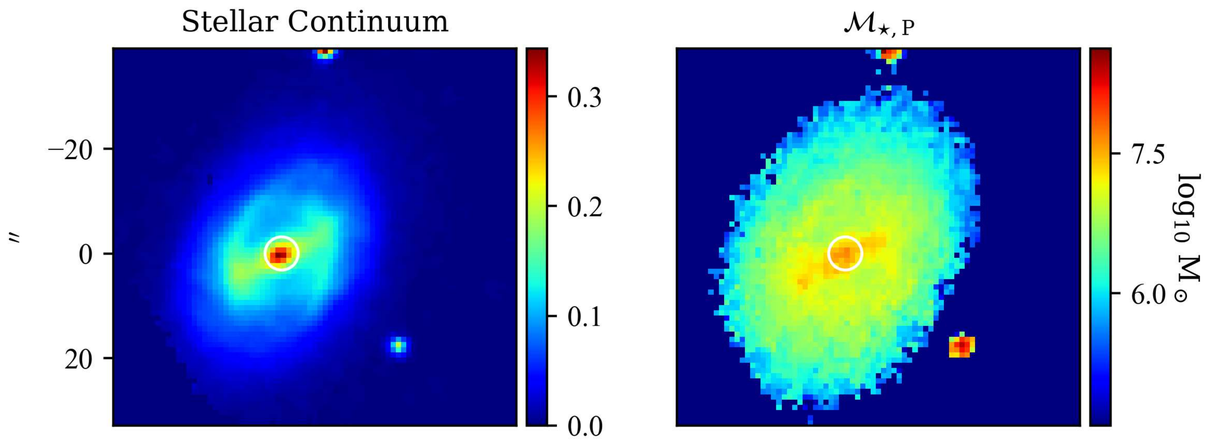

Log. of cumulative present stellar mass profiles

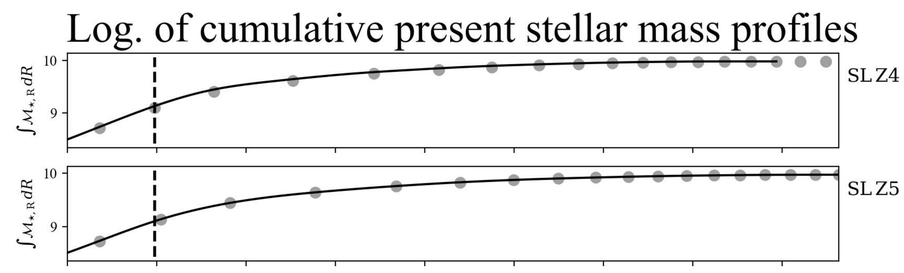

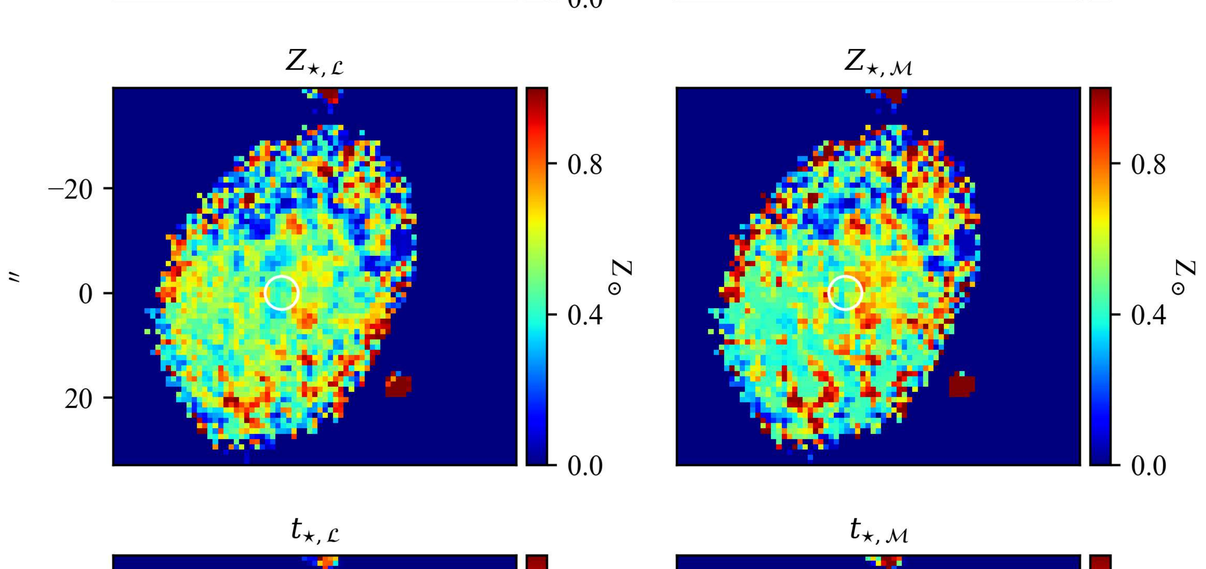

Stellar metallicity/Age & Hα flux/EW profiles

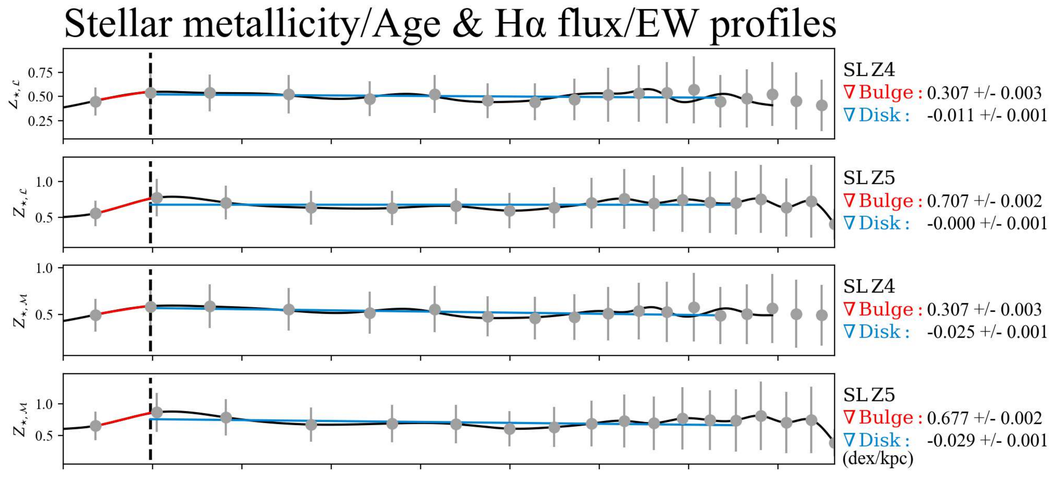

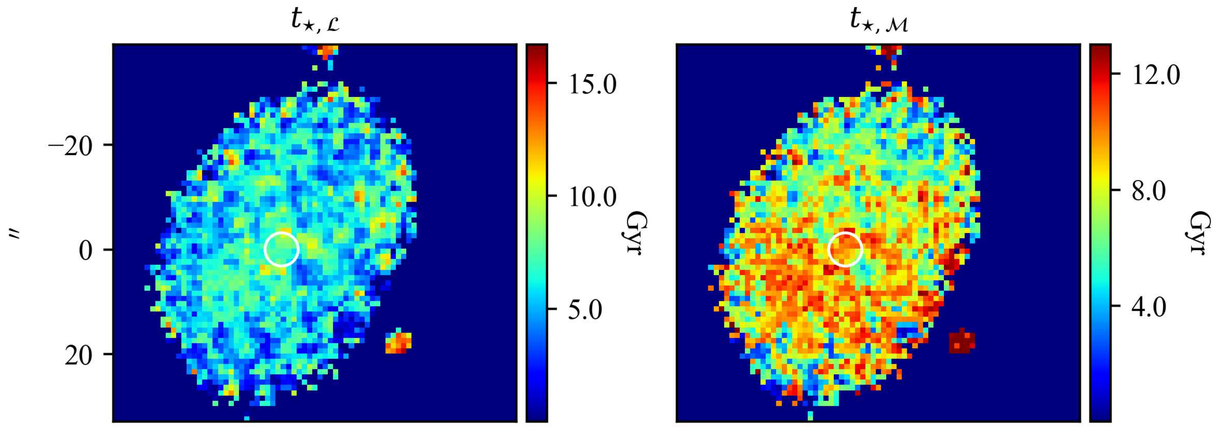

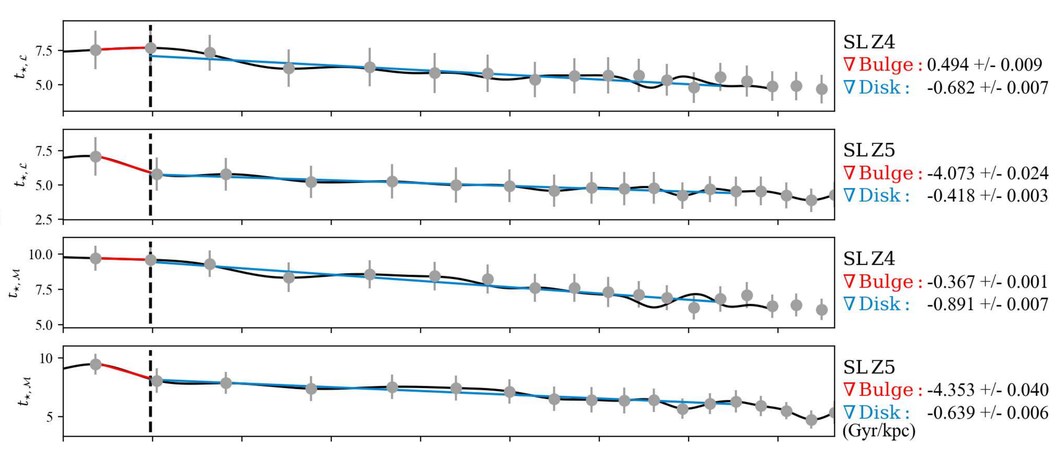

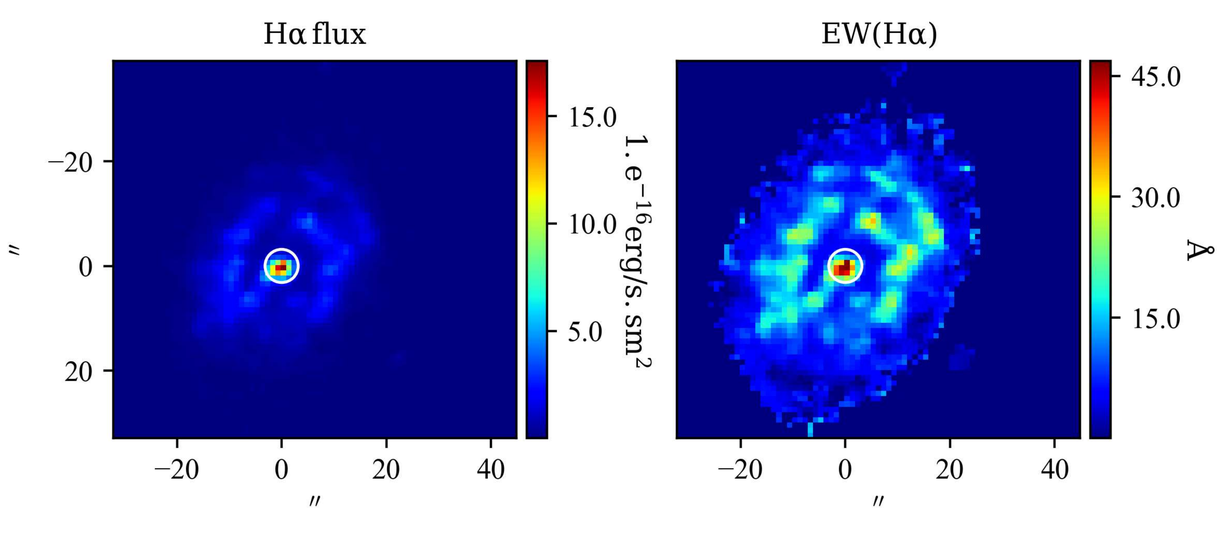

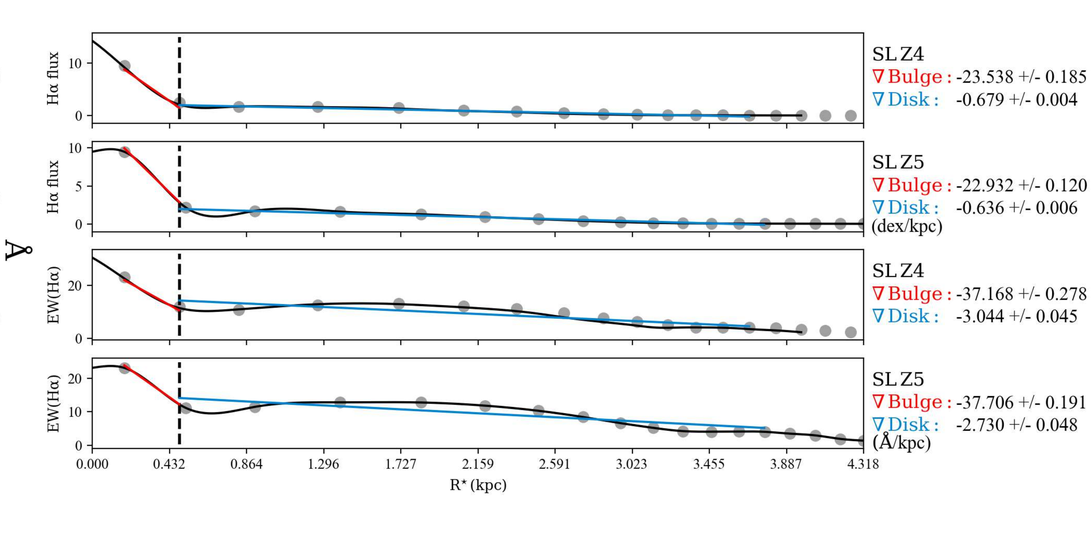

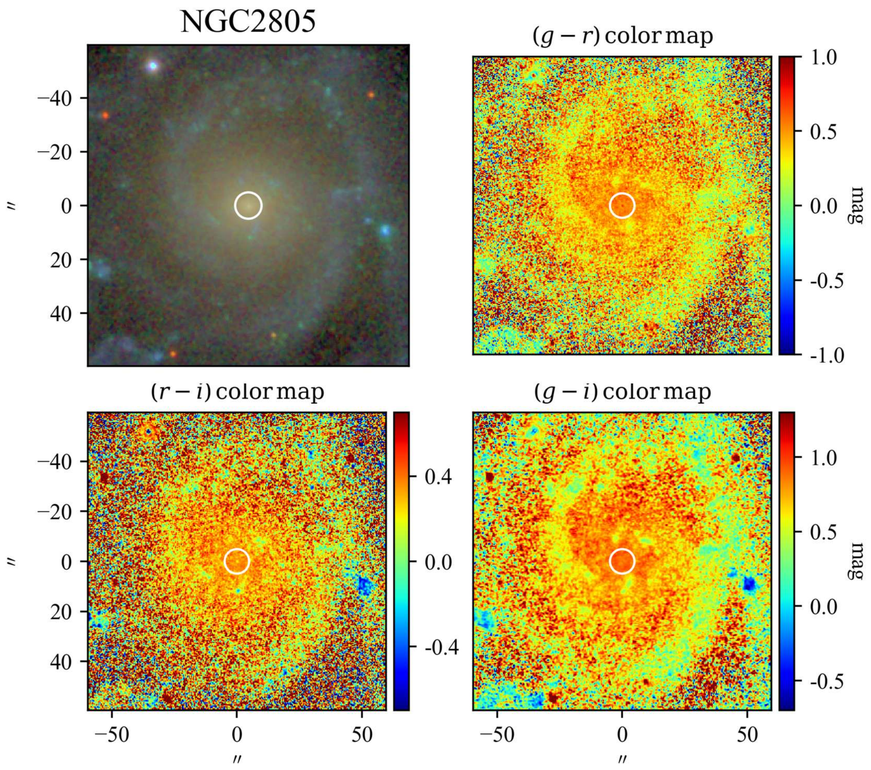

SBP decomposition of SDSS r band

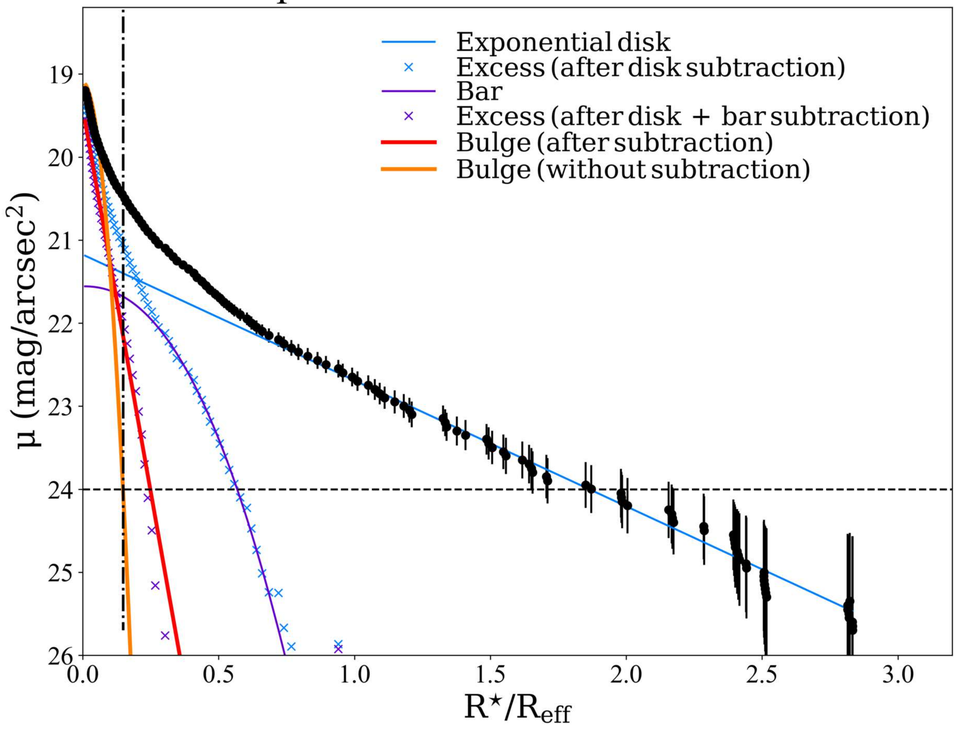

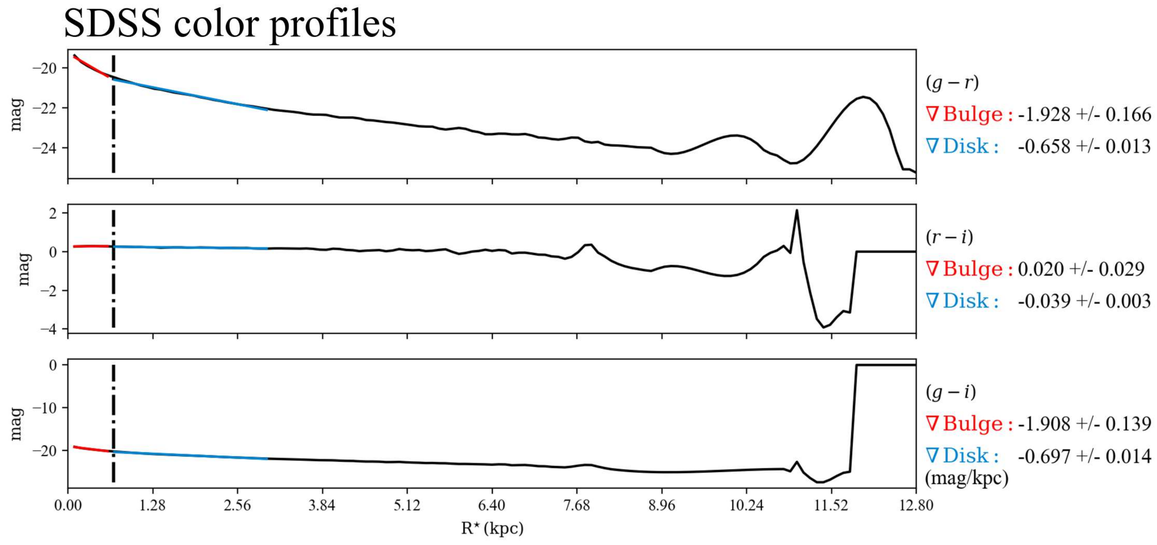

$\mathcal{RY}$ SBPs

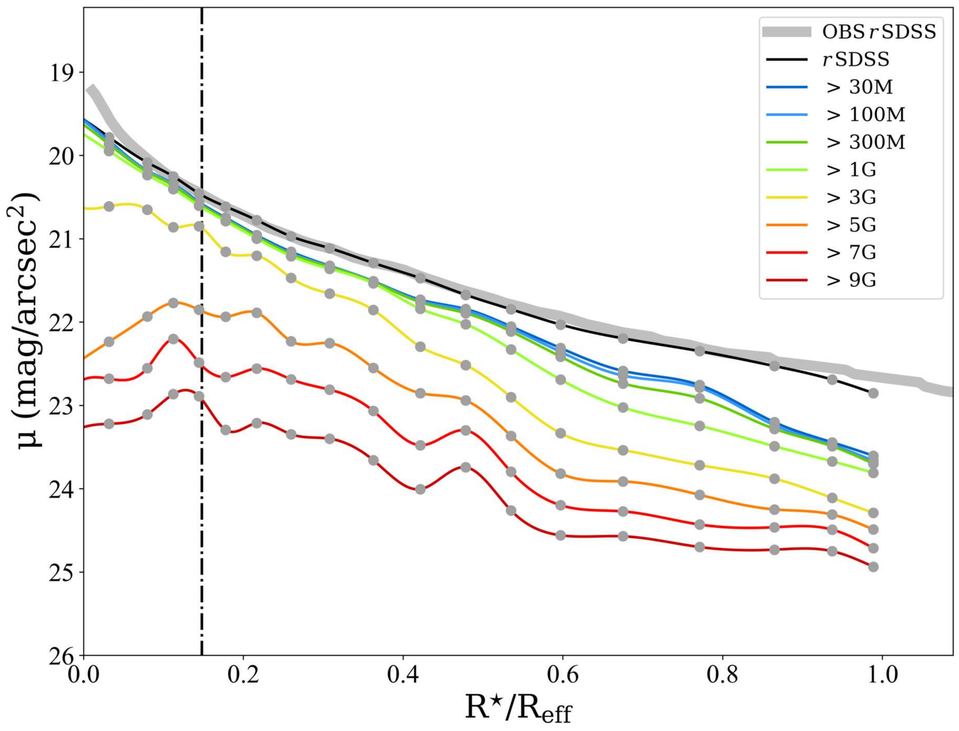

Stellar Continuum

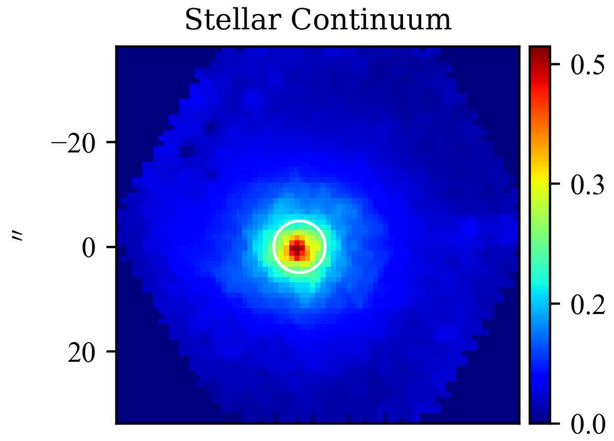

$\mathcal{M}_{\star,\mathrm{P}}$

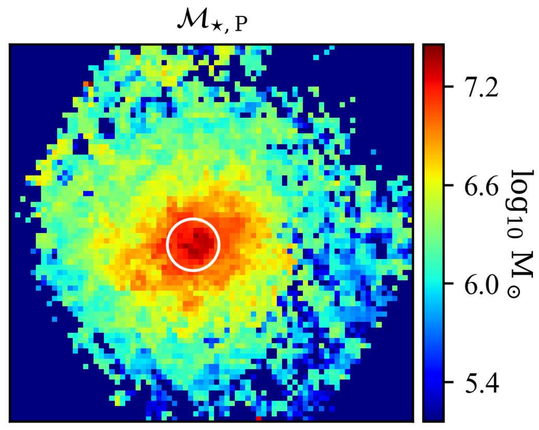

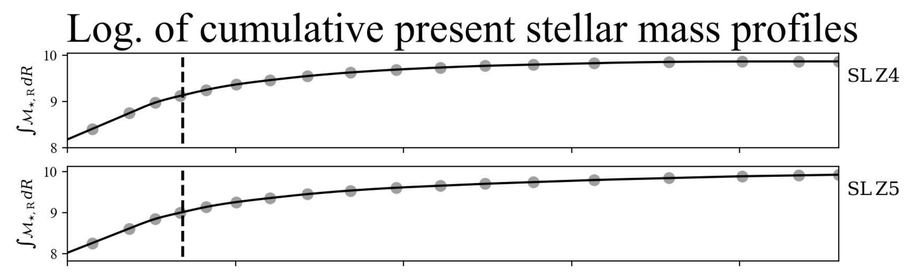

$Z_{\star,\mathcal{L}}$

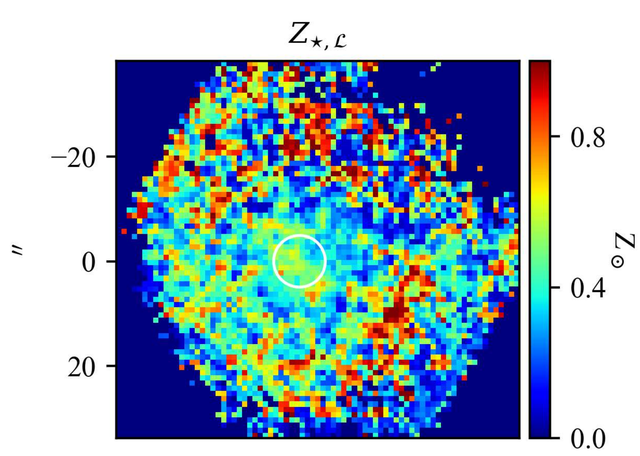

$Z_{\star,\mathcal{M}}$

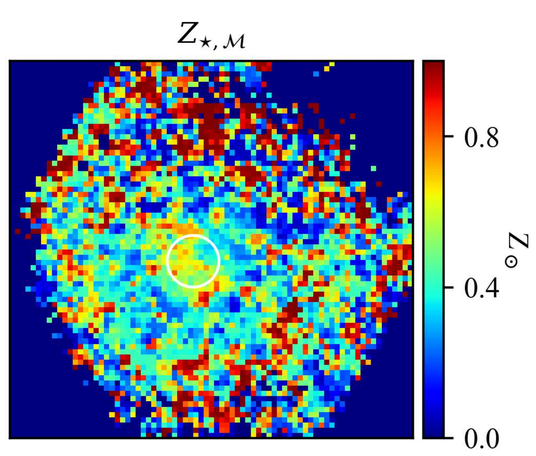

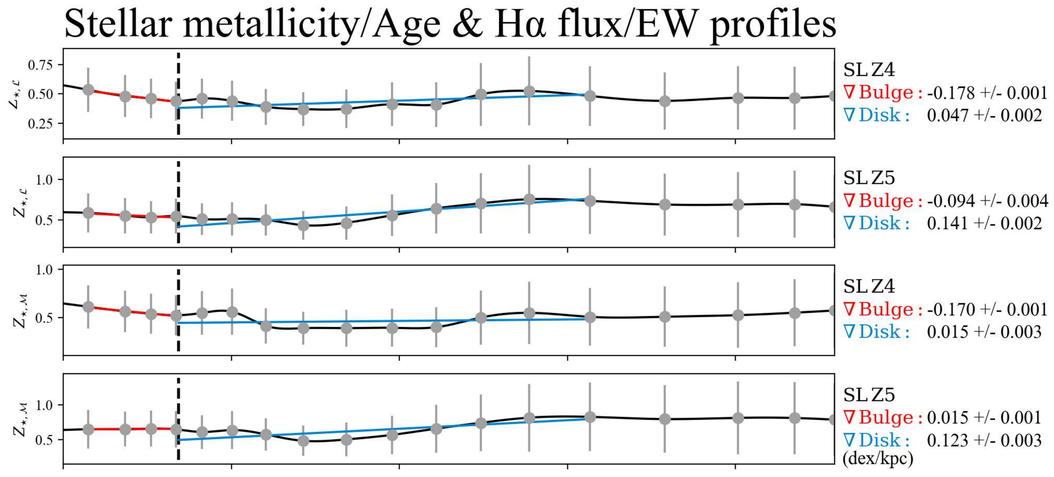

$t_{\star,\mathcal{L}}$

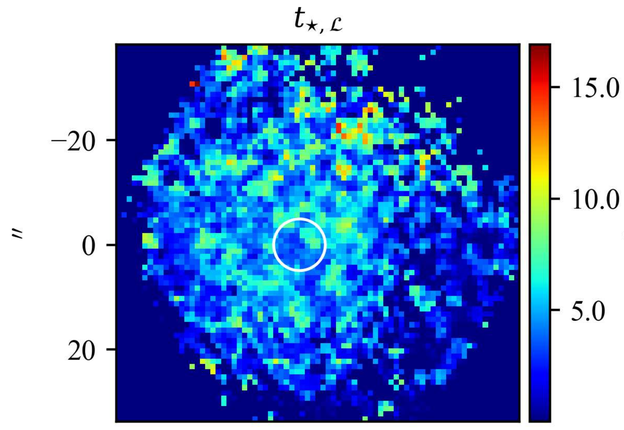

$t_{\star,\mathcal{M}}$

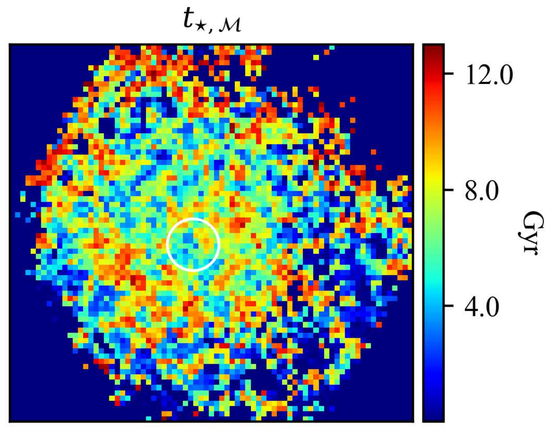

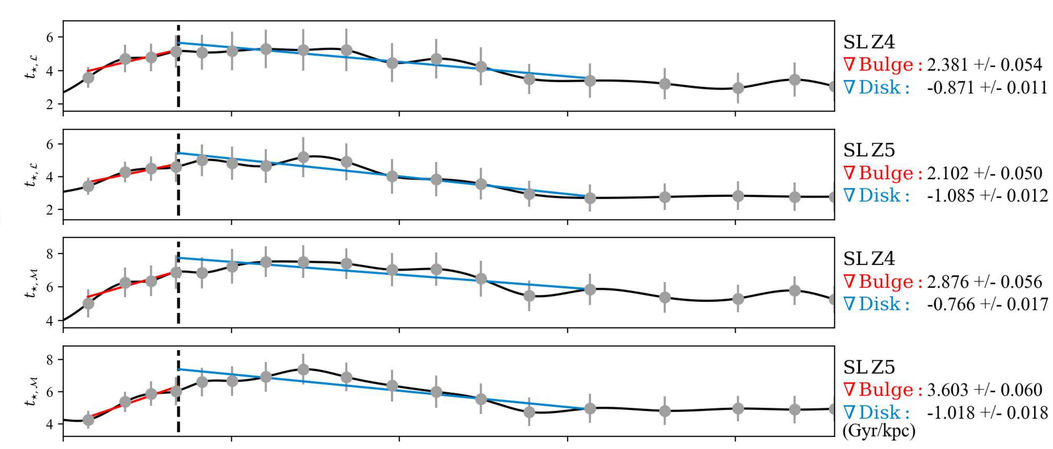

Hα flux

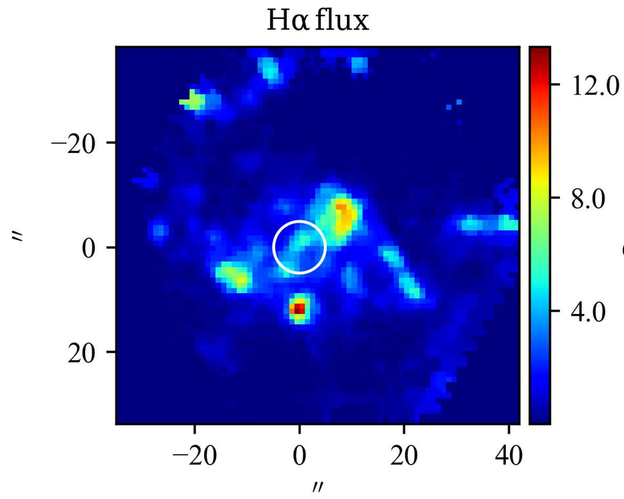

EW(Hα)

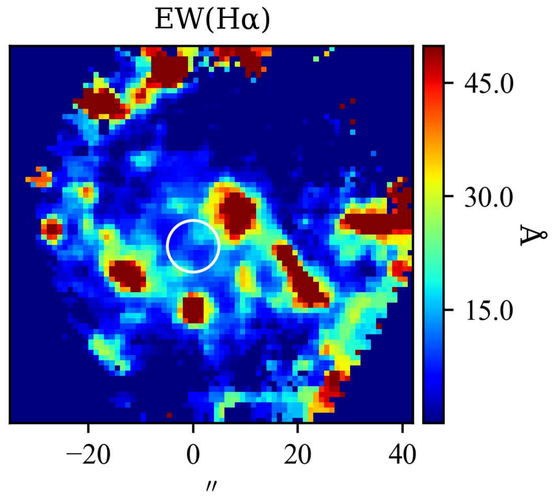

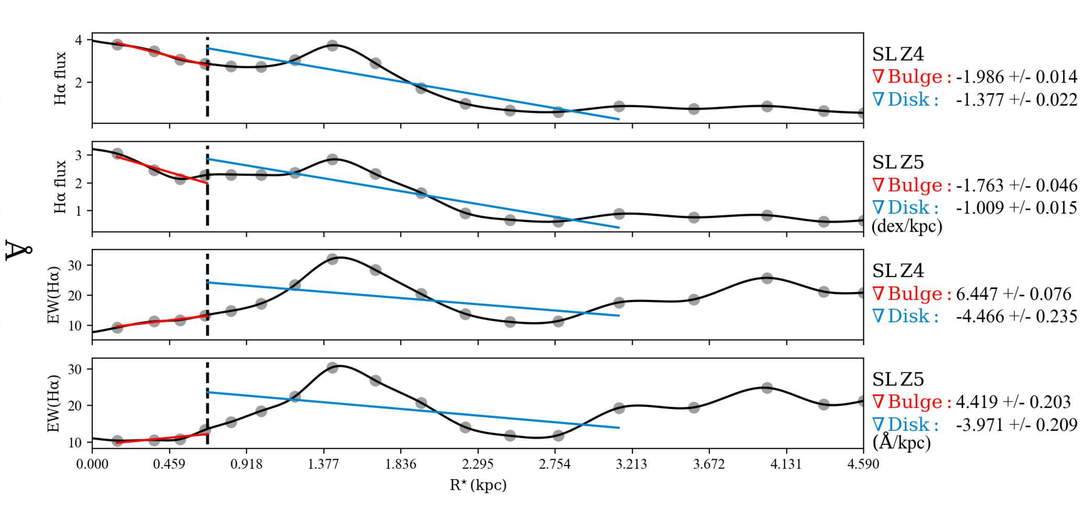

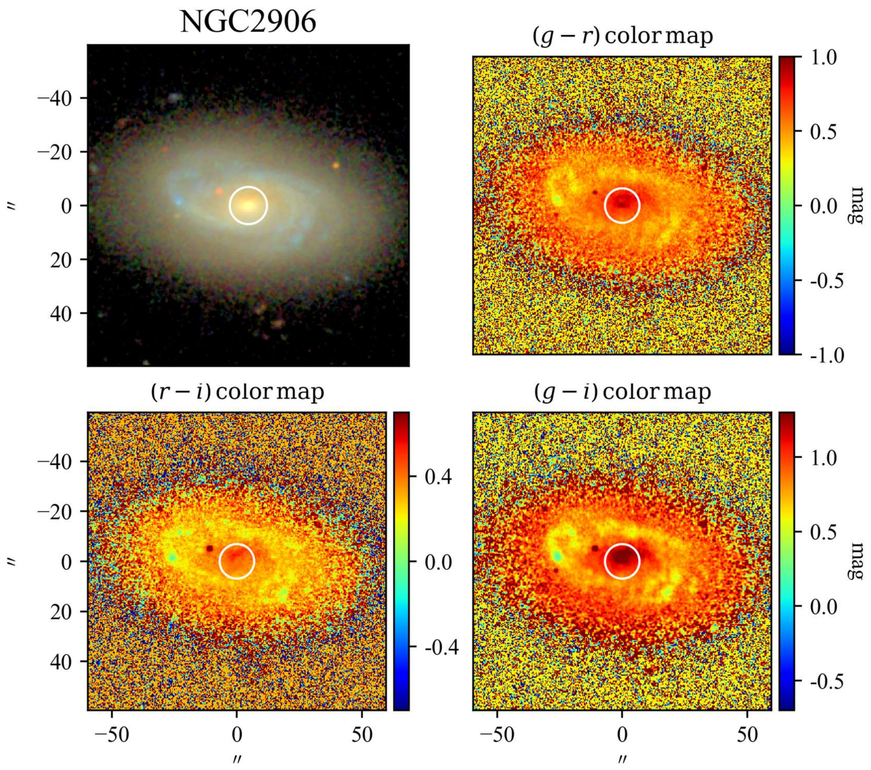

SBP decomposition of SDSS r band

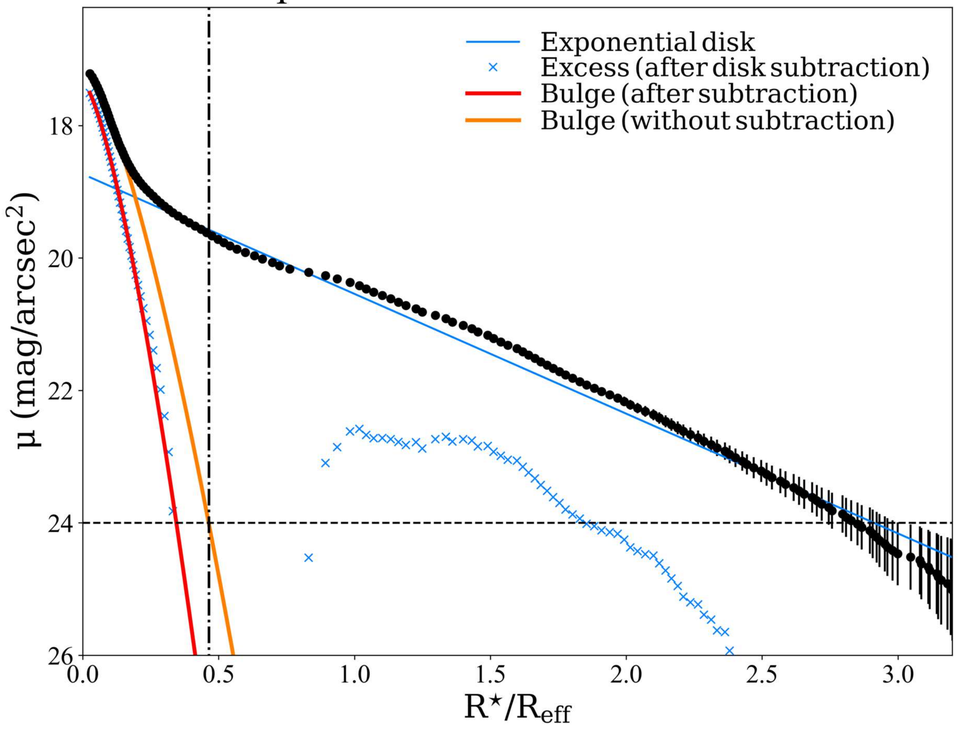

SDSS color profiles

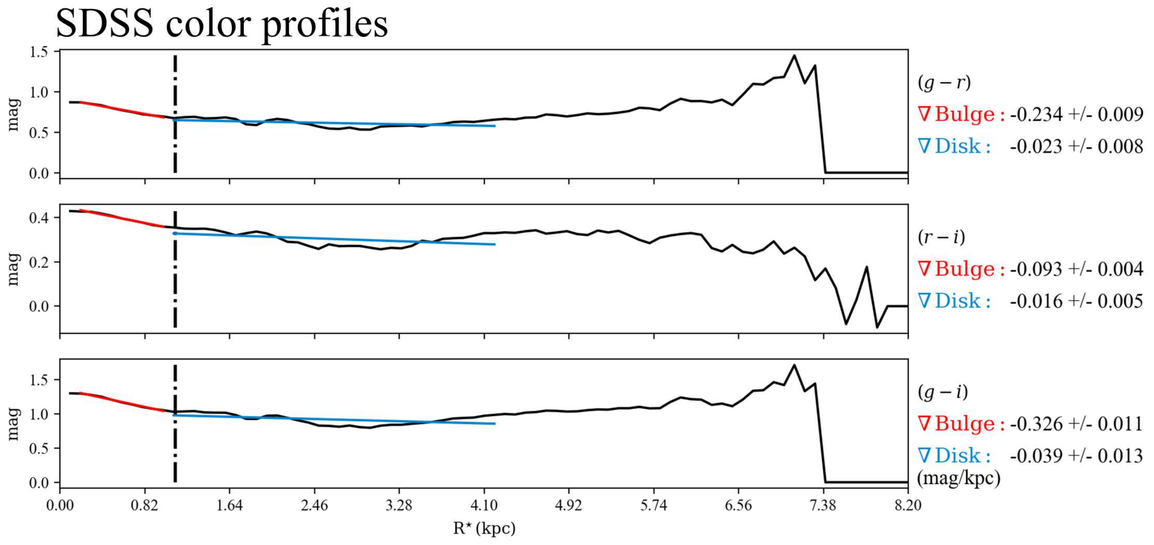

$\mathcal{RY}$ SBPs

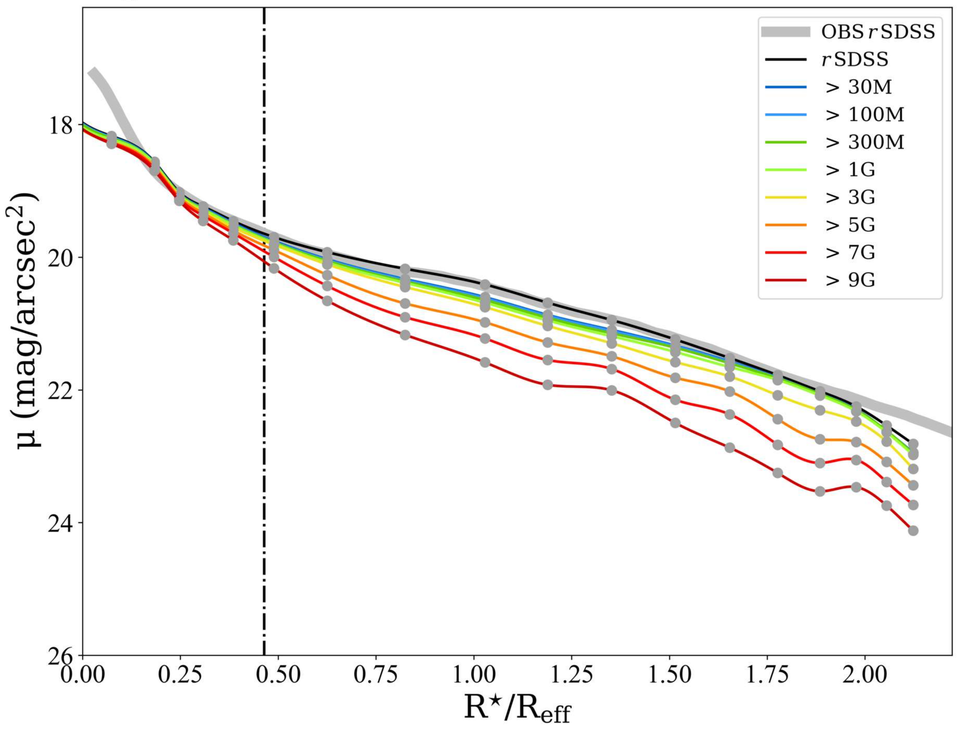

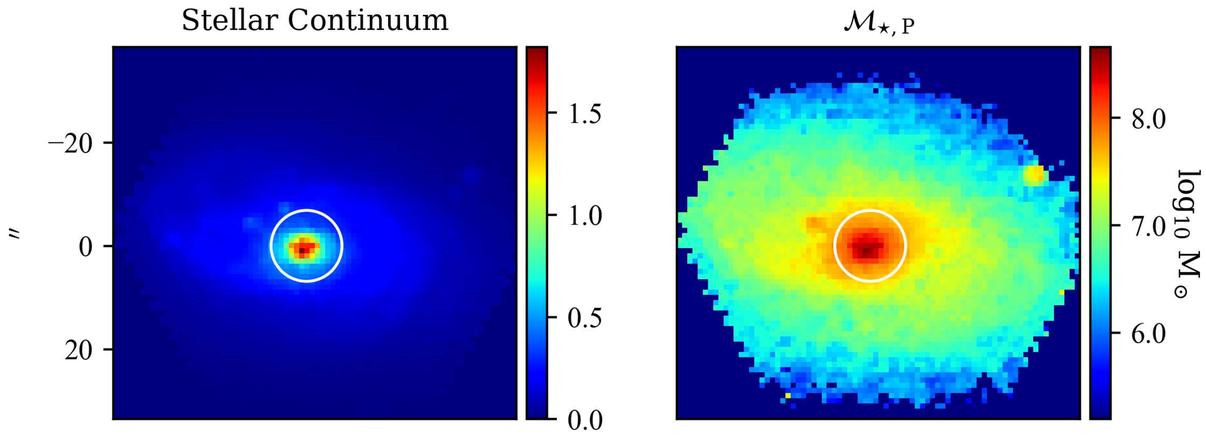

Log. of cumulative present stellar mass profiles

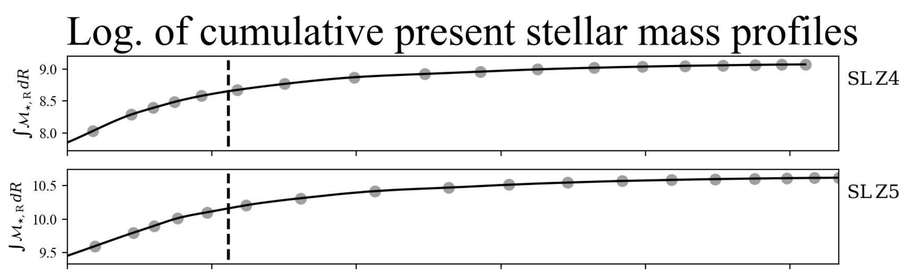

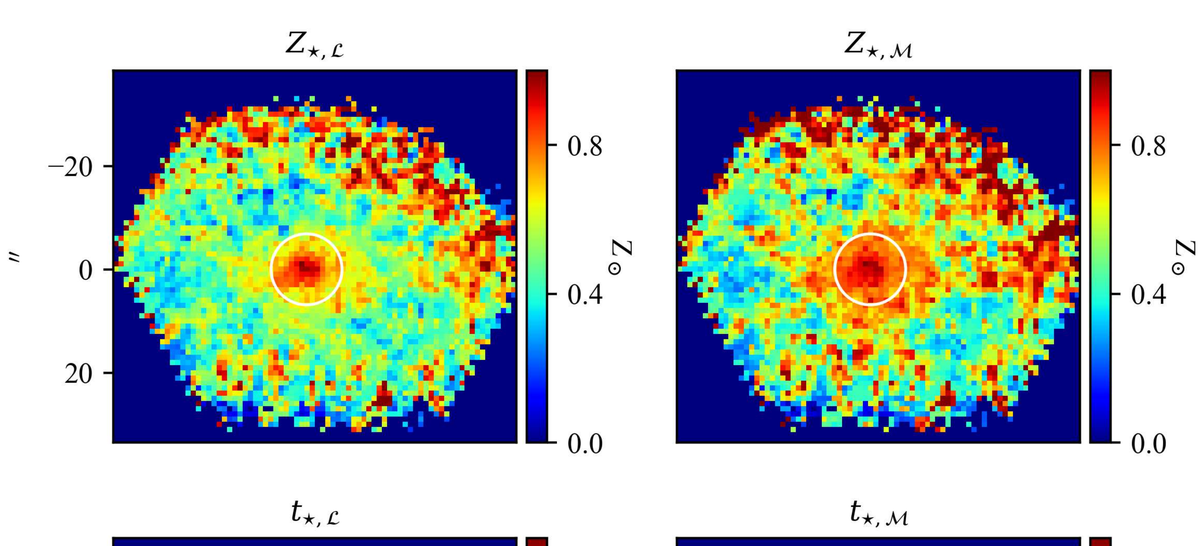

Stellar metallicity/Age & Hα flux/EW profiles

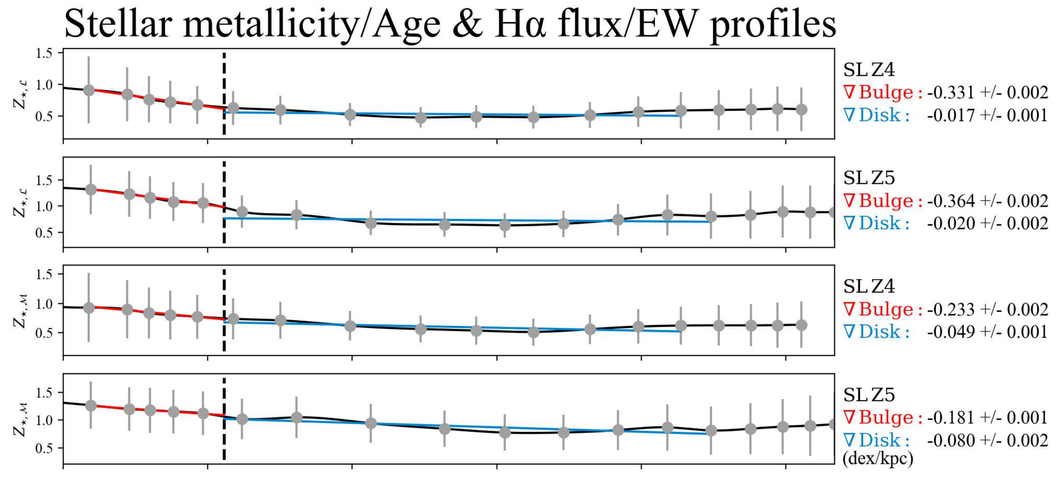

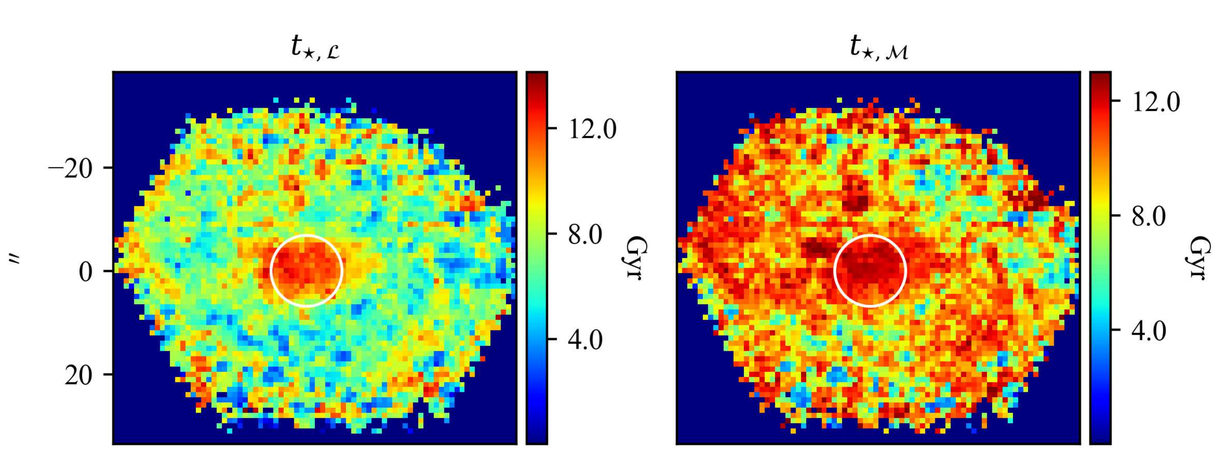

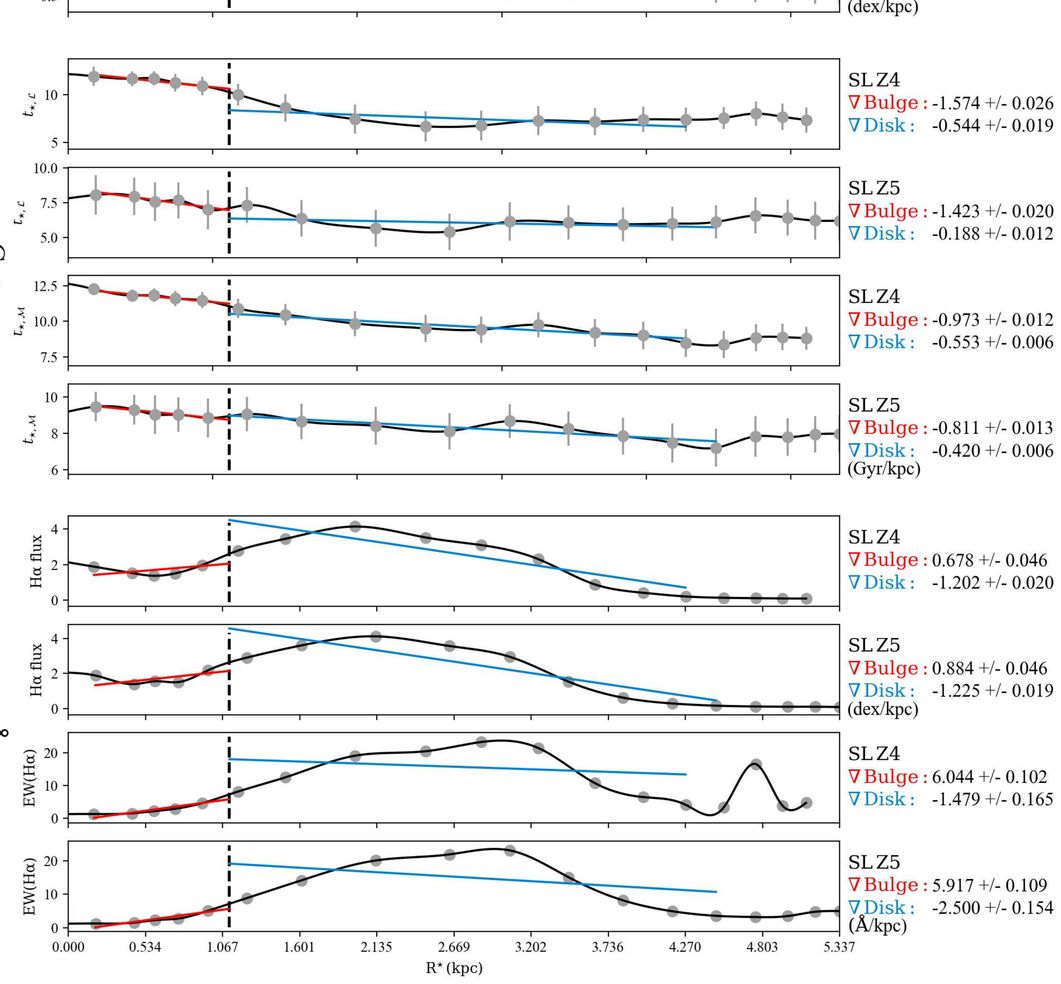

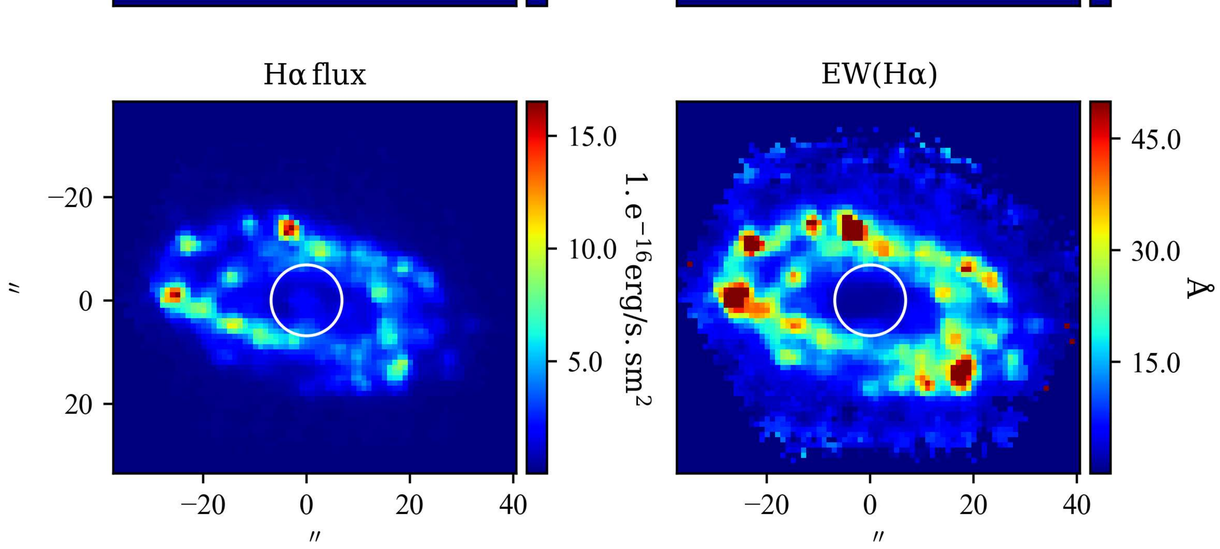

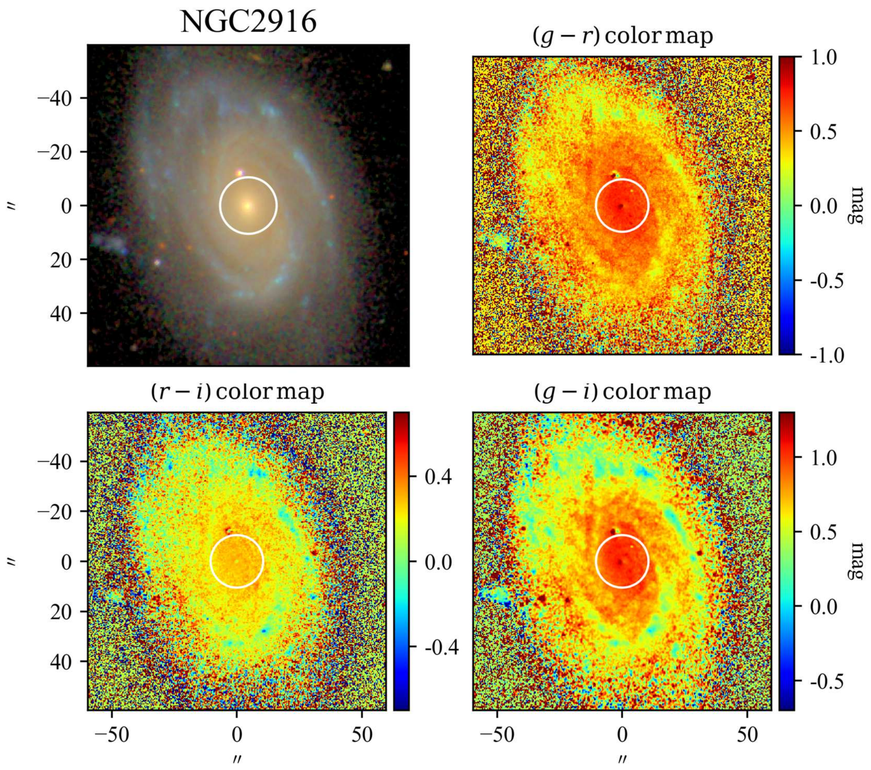

SBP decomposition of SDSS r band

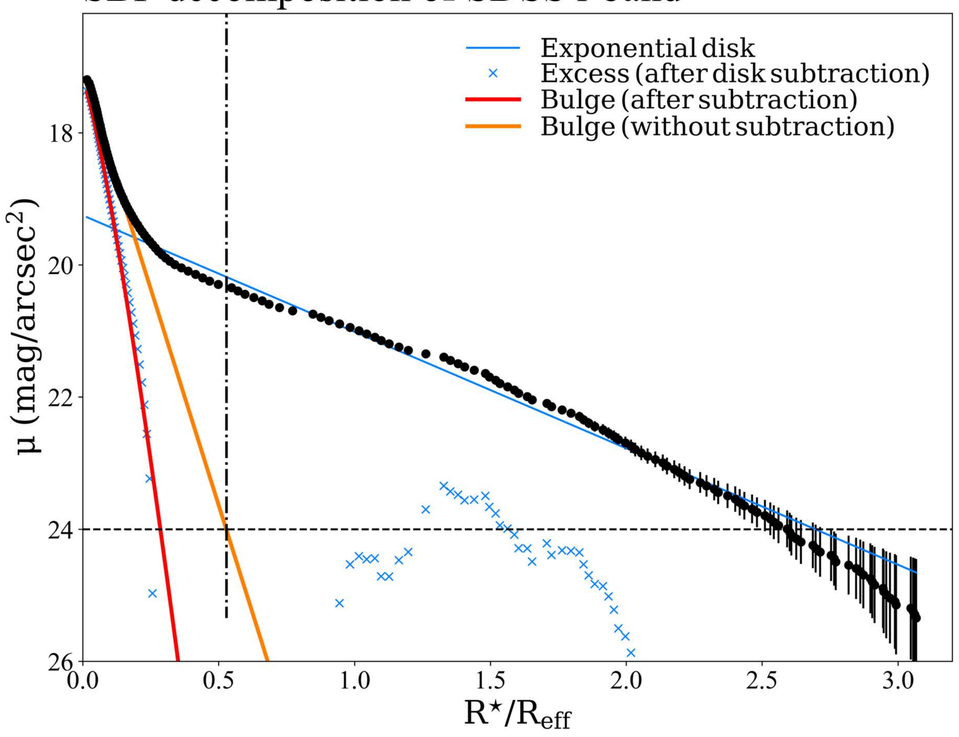

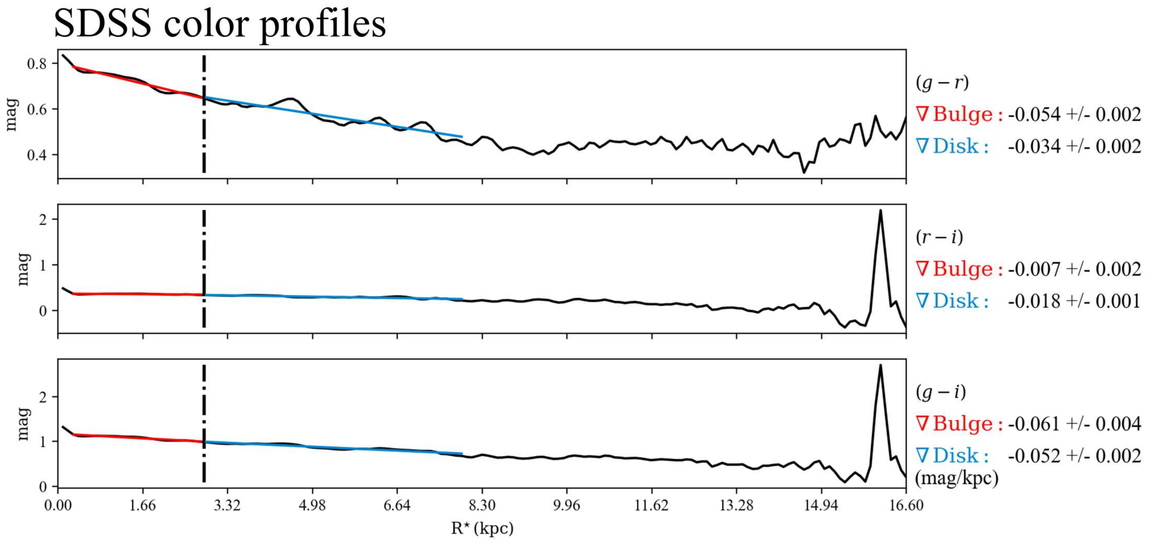

$\mathcal{RY}$ SBPs

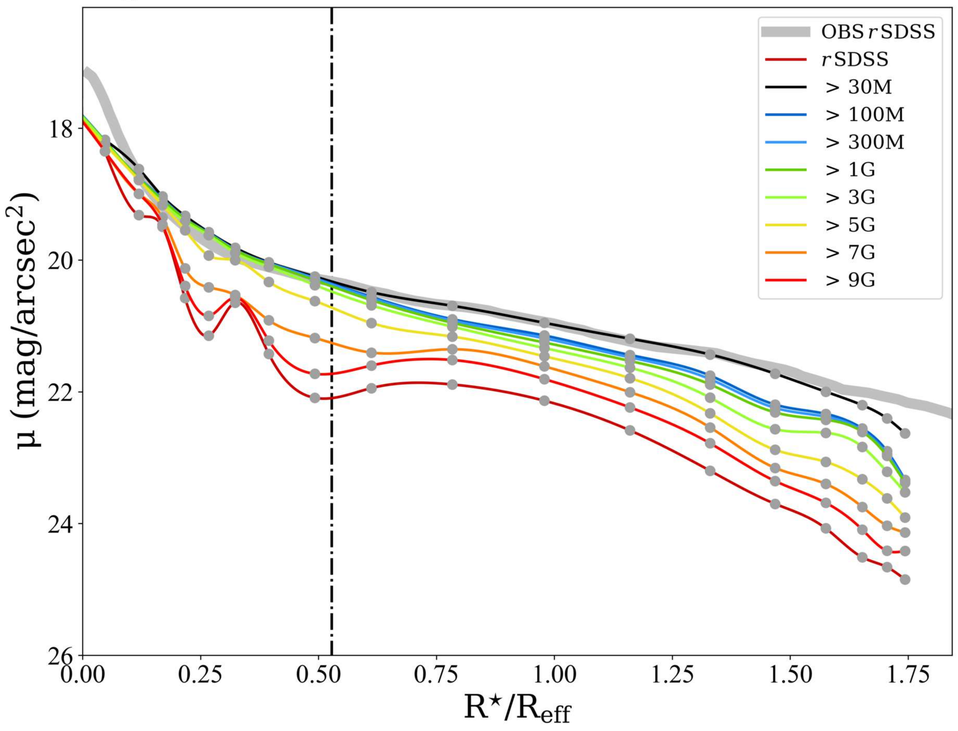

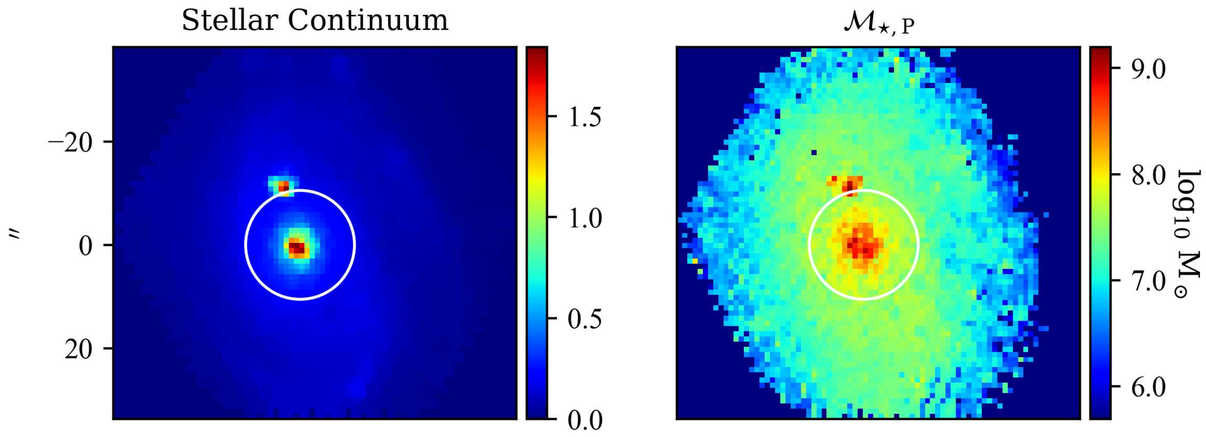

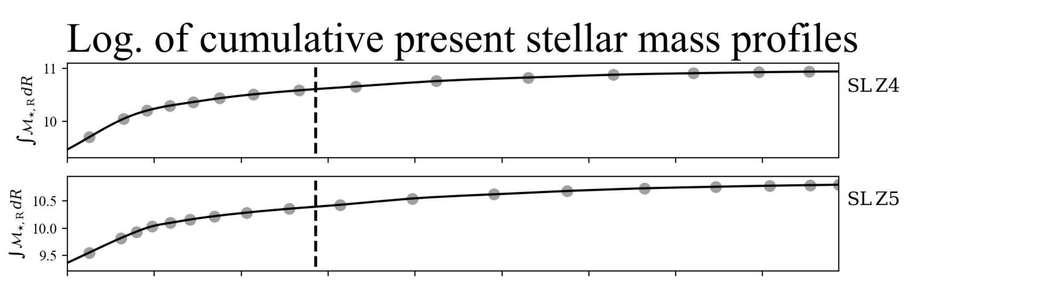

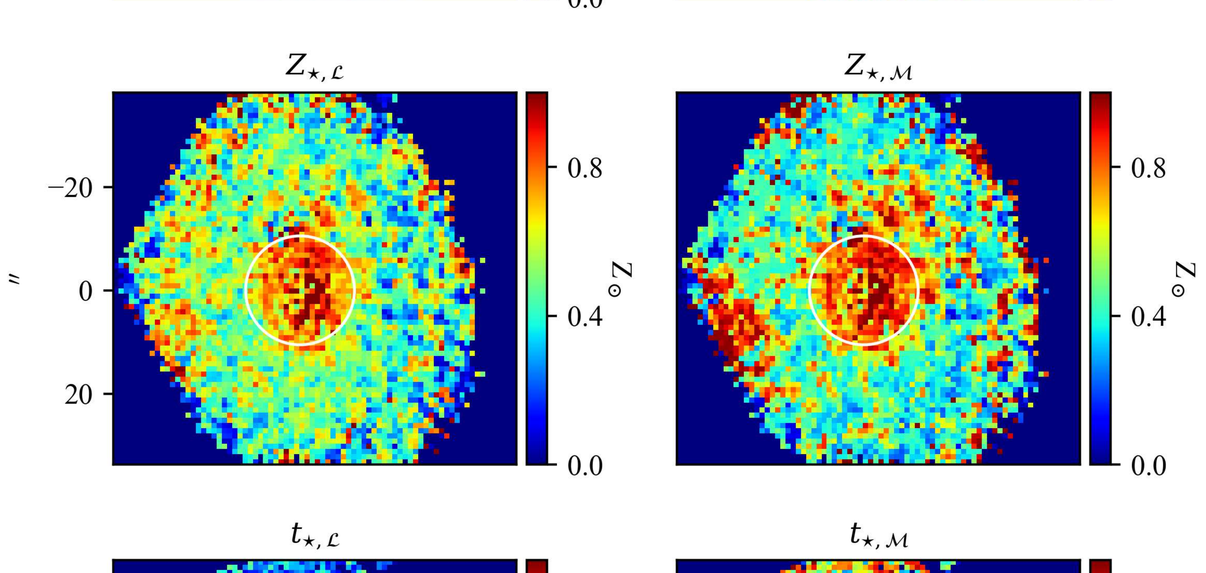

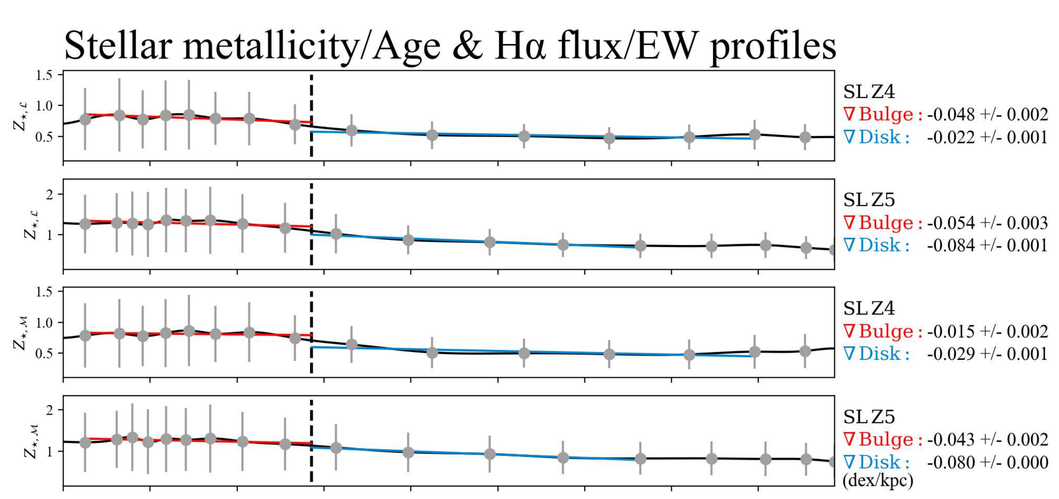

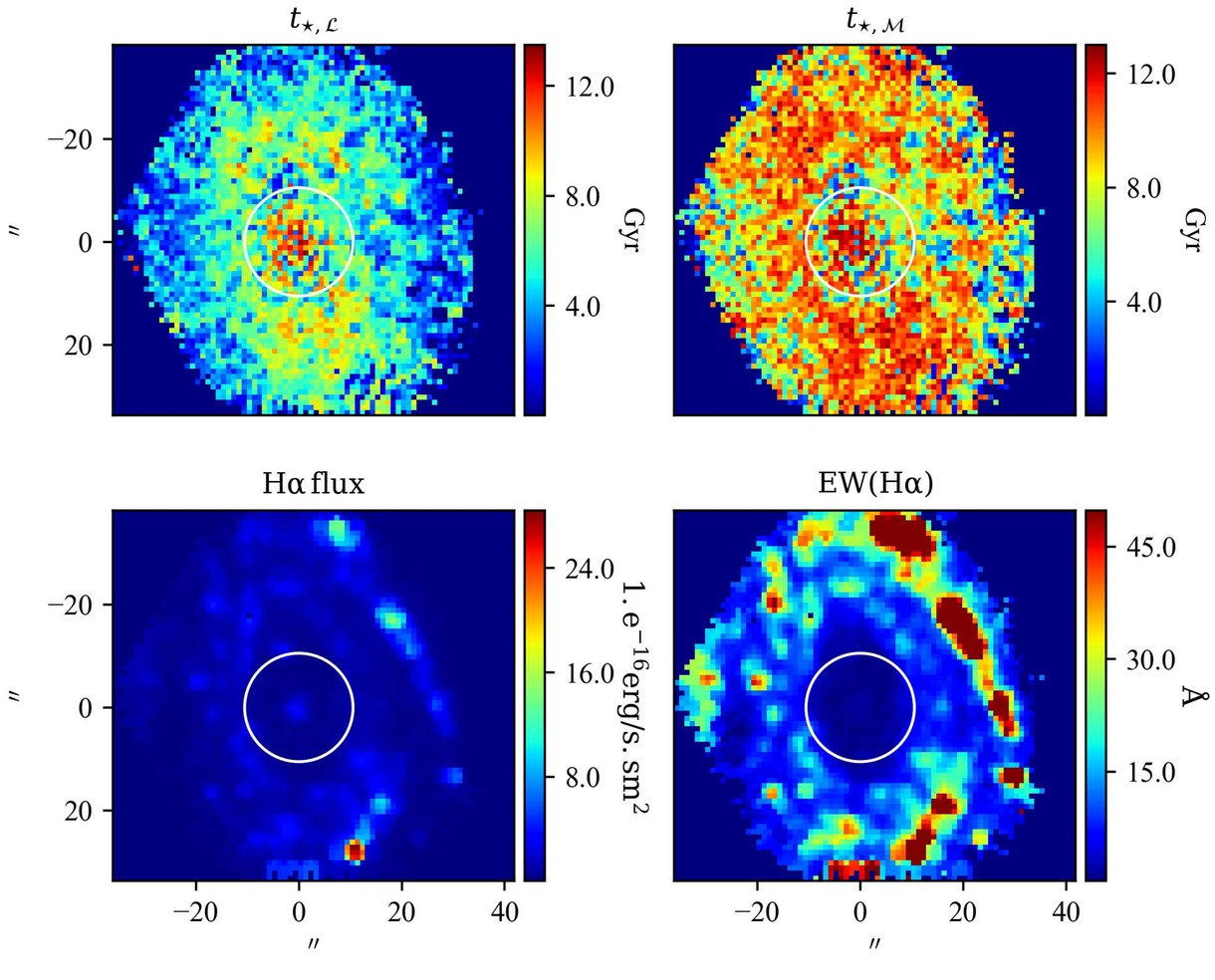

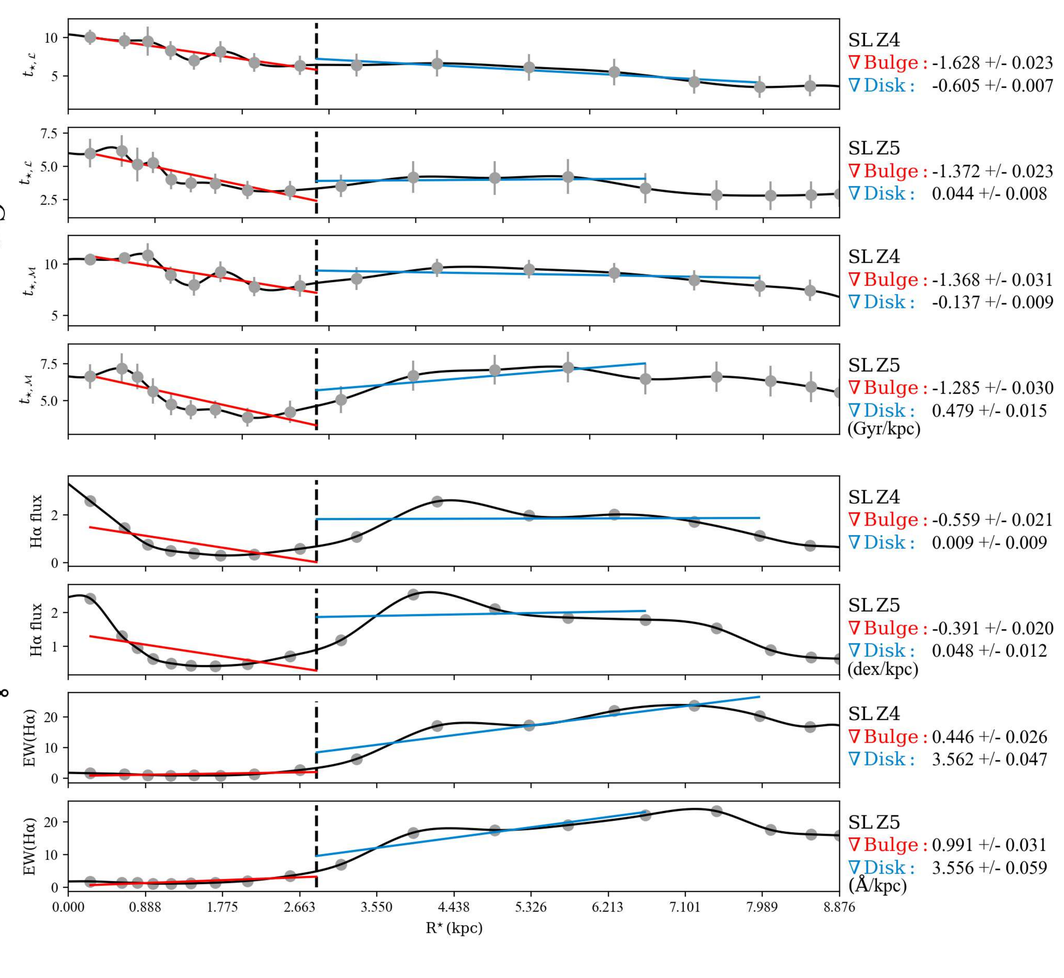

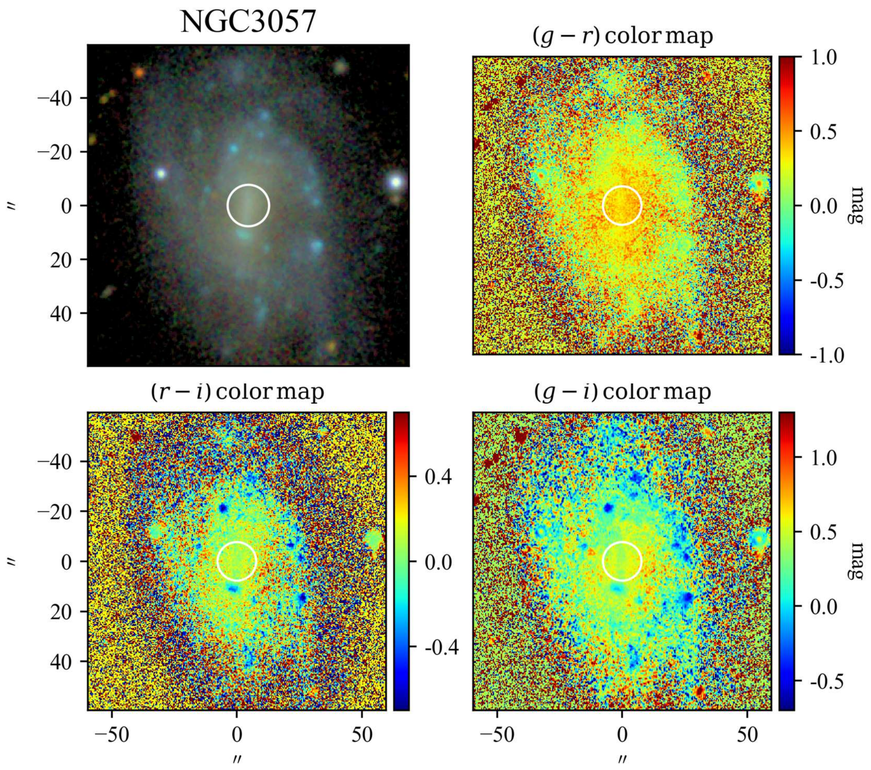

SBP decomposition of SDSS r band

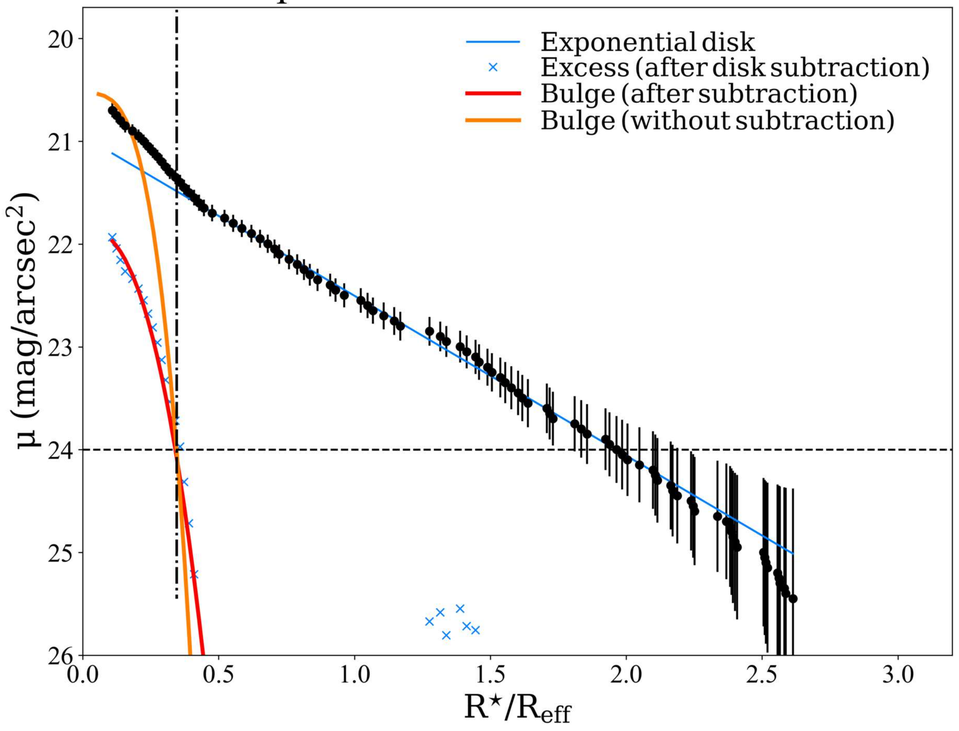

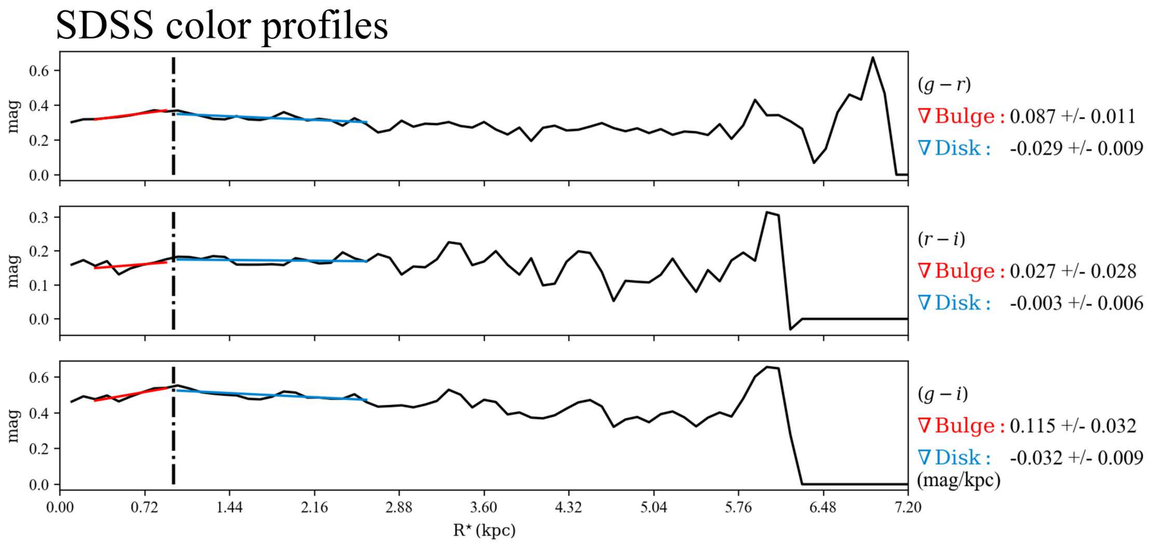

$\mathcal{RY}$ SBPs

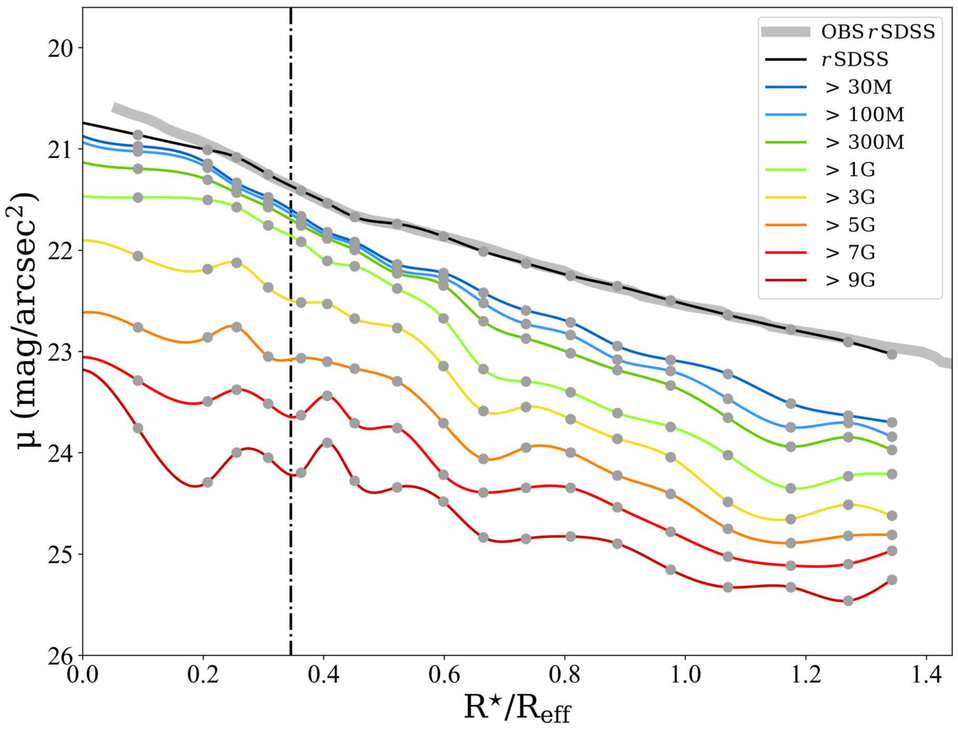

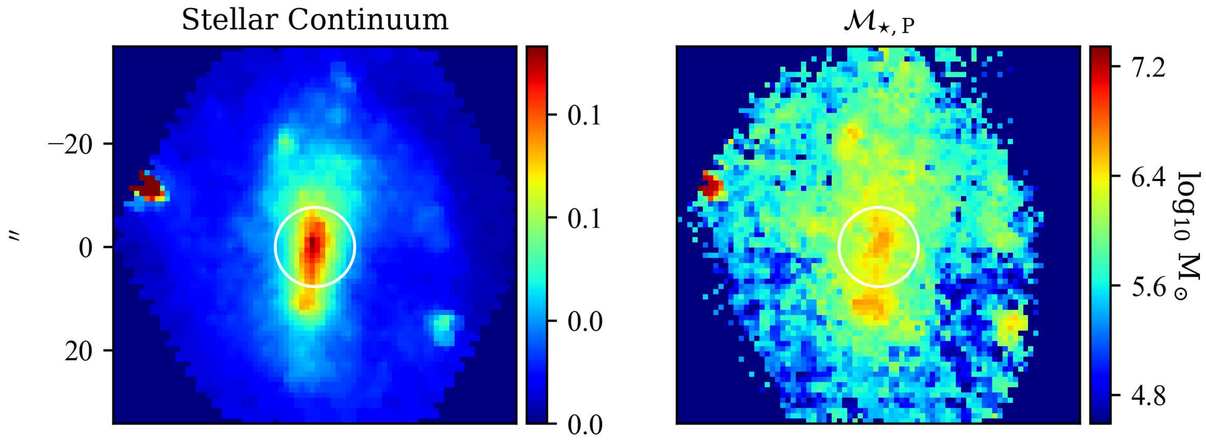

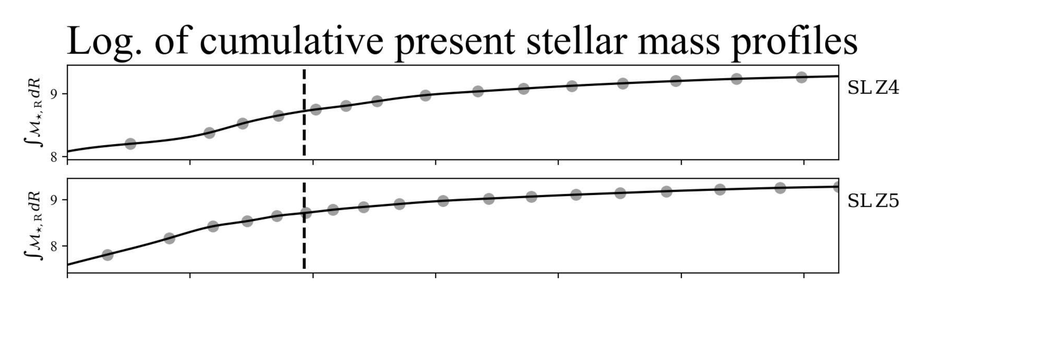

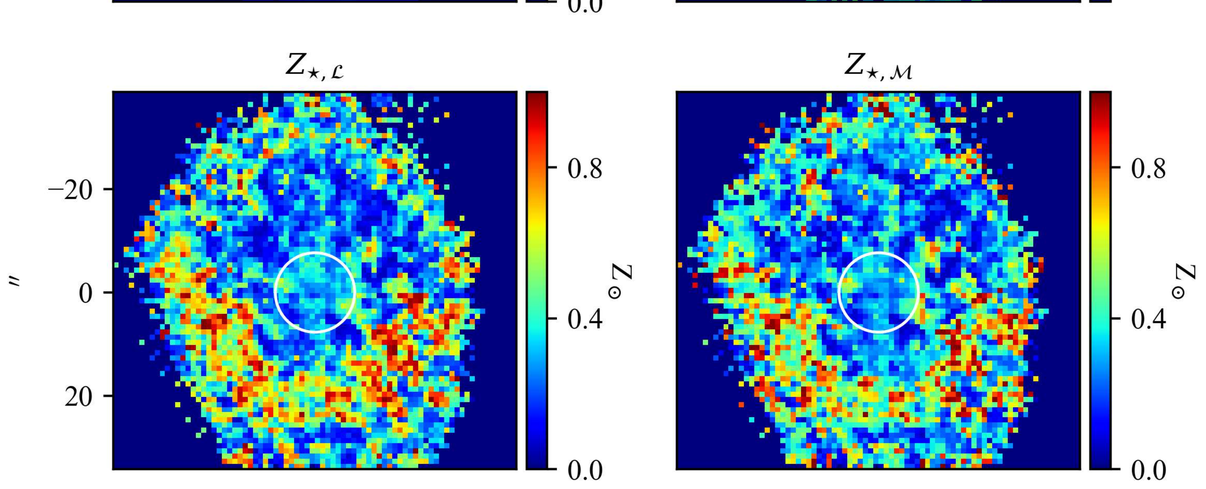

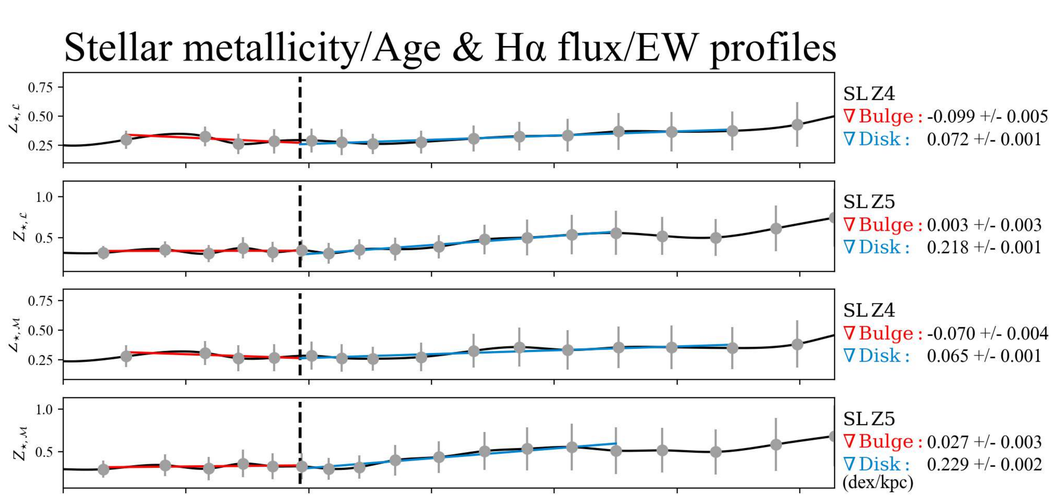

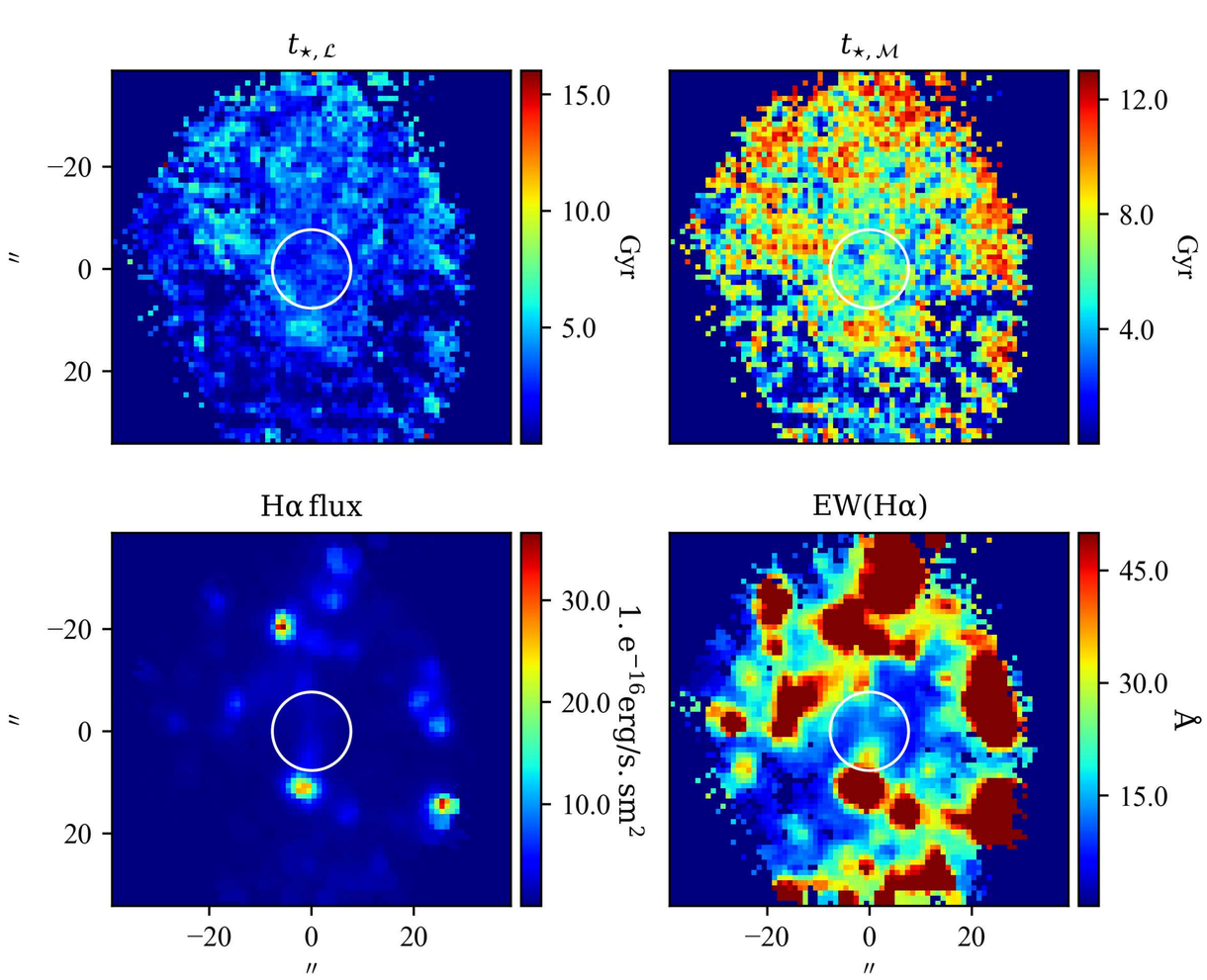

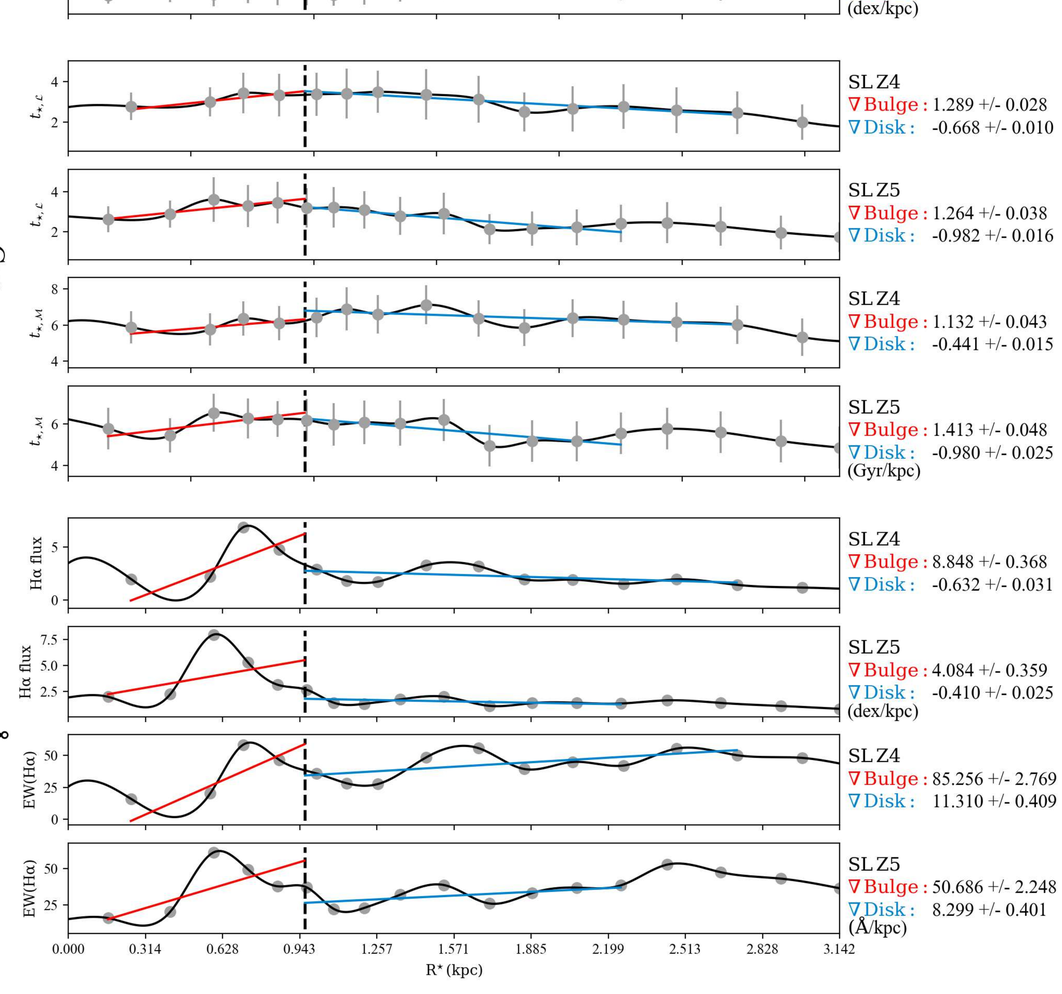

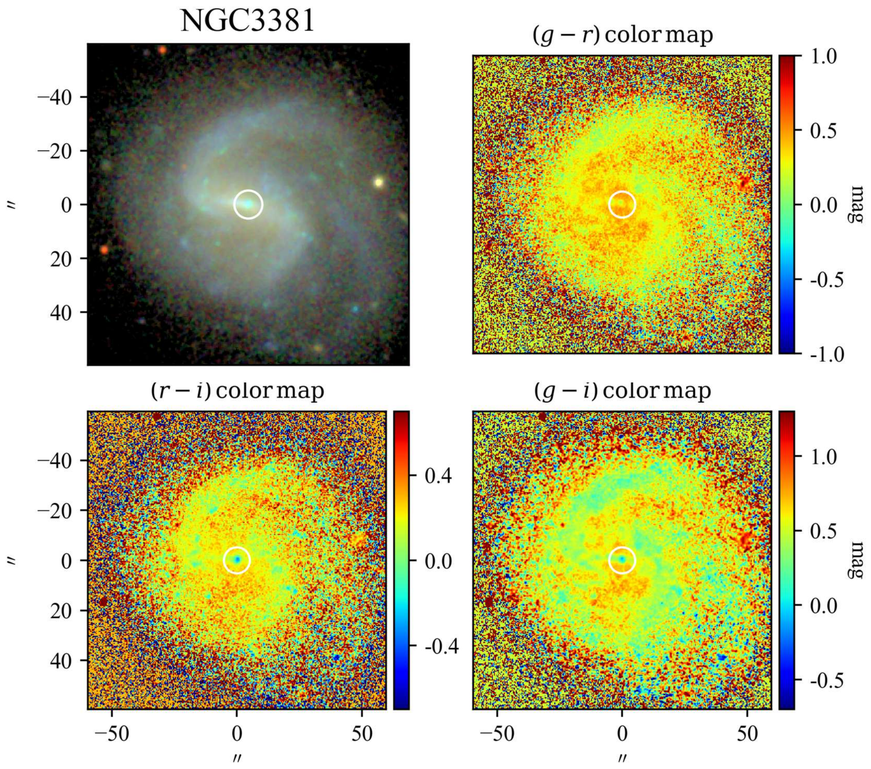
NGC3381
$(g-r)$ color map
$(r-i)$ color map
$(g-i)$ color map
mag
″

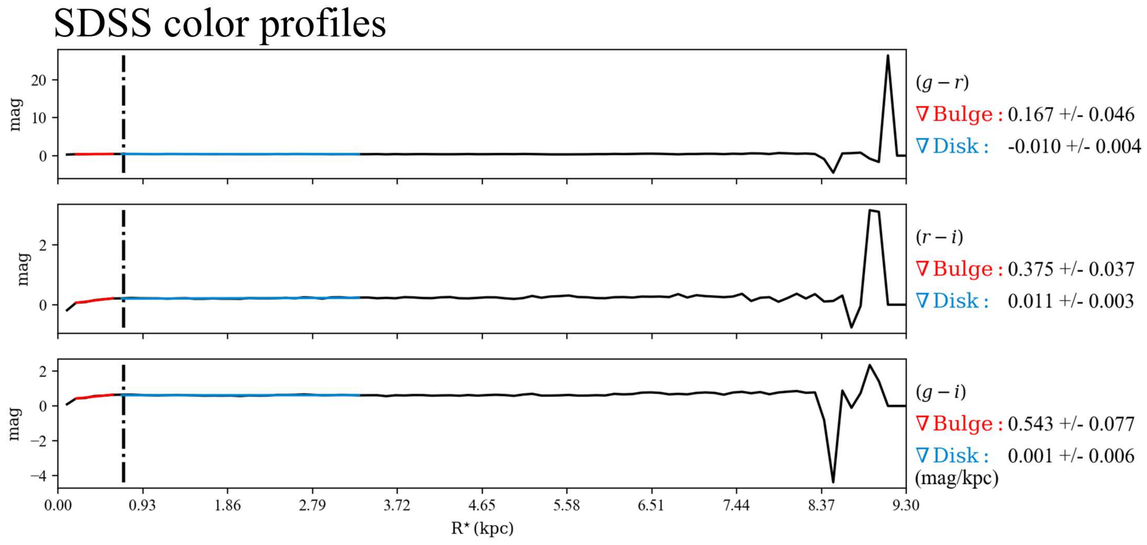
SDSS color profiles
$(g-r)$
∇ Bulge : 0.167 +/- 0.046
∇ Disk : -0.010 +/- 0.004
$(r-i)$
∇ Bulge : 0.375 +/- 0.037
∇ Disk : 0.011 +/- 0.003
$(g-i)$
∇ Bulge : 0.543 +/- 0.077
∇ Disk : 0.001 +/- 0.006
(mag/kpc)
mag
R* (kpc)

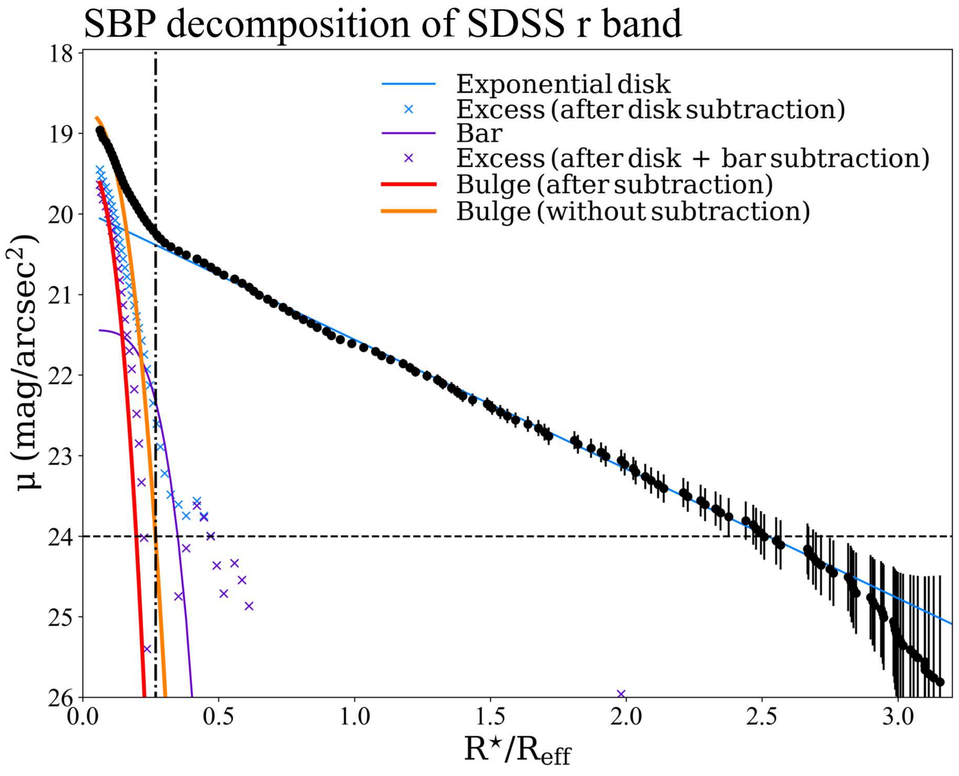
SBP decomposition of SDSS r band
Exponential disk
Excess (after disk subtraction)
Bar
Excess (after disk + bar subtraction)
Bulge (after subtraction)
Bulge (without subtraction)
μ (mag/arcsec^2)
R*/R$_{eff}$

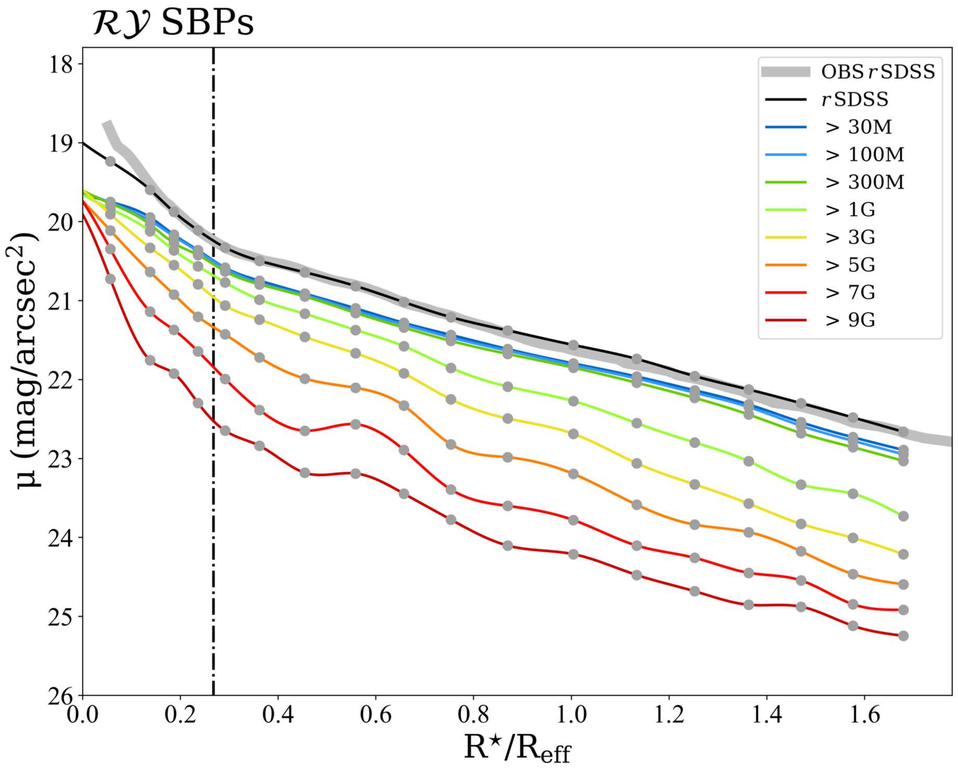
$\mathcal{RY}$ SBPs
OBS rSDSS
rSDSS
> 30M
> 100M
> 300M
> 1G
> 3G
> 5G
> 7G
> 9G
μ (mag/arcsec^2)
R*/R$_{eff}$

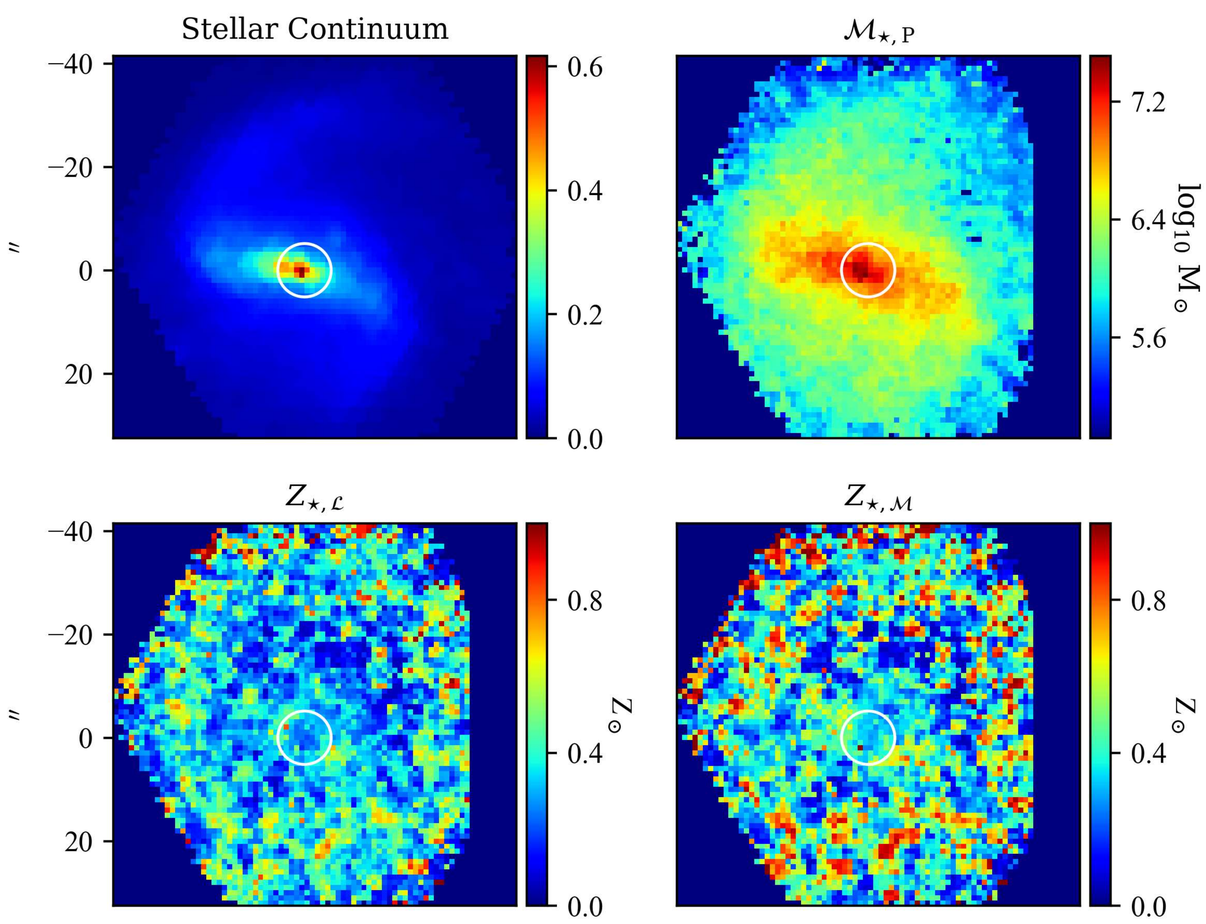
Stellar Continuum
$\mathcal{M}_{\star,\,P}$
$Z_{\star,\,\mathcal{L}}$
$Z_{\star,\,\mathcal{M}}$
log$_{10}$ M$_\odot$
Z$_\odot$
″

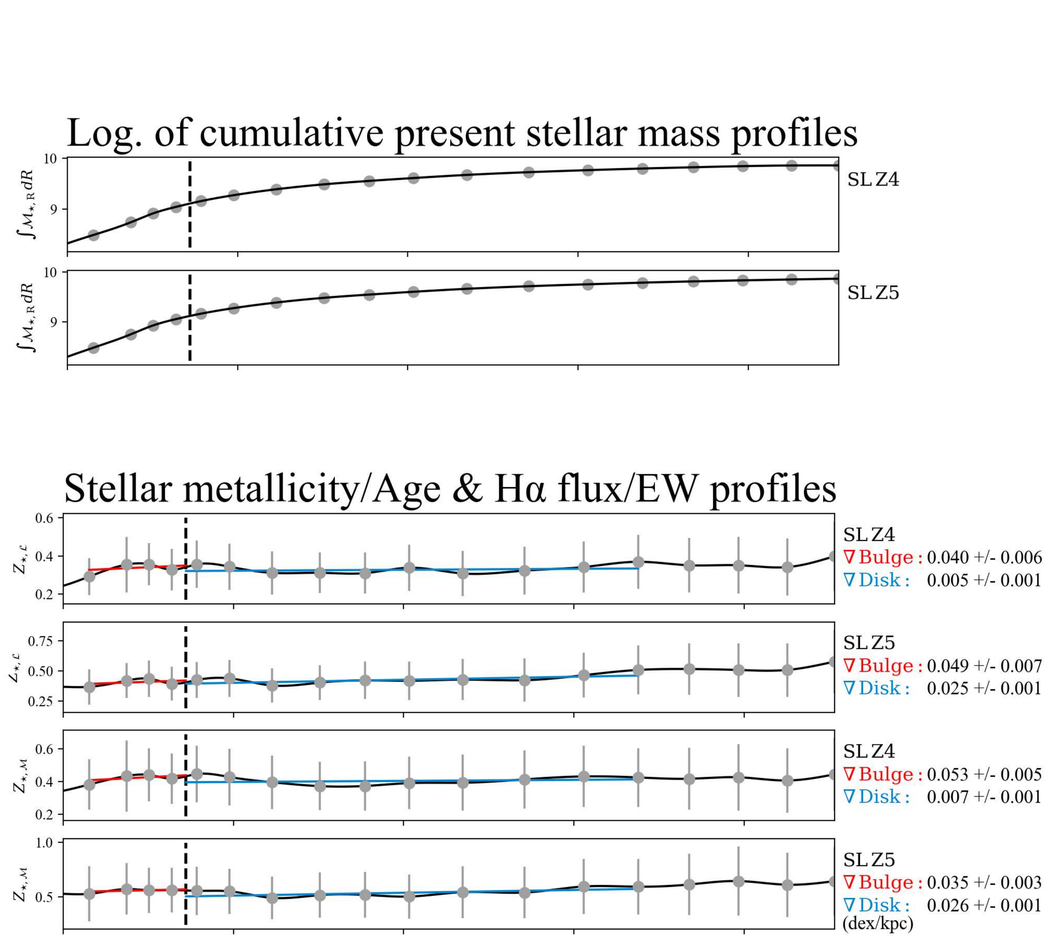
Log. of cumulative present stellar mass profiles
$\int \mathcal{M}_{\star,\,R}\,dR$
SL Z4
SL Z5
Stellar metallicity/Age & Hα flux/EW profiles
$Z_{\star,\,\mathcal{L}}$
$Z_{\star,\,\mathcal{M}}$
SL Z4
∇ Bulge : 0.040 +/- 0.006
∇ Disk : 0.005 +/- 0.001
SL Z5
∇ Bulge : 0.049 +/- 0.007
∇ Disk : 0.025 +/- 0.001
SL Z4
∇ Bulge : 0.053 +/- 0.005
∇ Disk : 0.007 +/- 0.001
SL Z5
∇ Bulge : 0.035 +/- 0.003
∇ Disk : 0.026 +/- 0.001
(dex/kpc)

$t_{\star,\,\mathcal{L}}$
$t_{\star,\,\mathcal{M}}$
Gyr
″

$t_{\star,\,\mathcal{L}}$
$t_{\star,\,\mathcal{M}}$
SL Z4
∇ Bulge : -0.975 +/- 0.038
∇ Disk : -0.490 +/- 0.003
SL Z5
∇ Bulge : -2.021 +/- 0.021
∇ Disk : -0.493 +/- 0.002
SL Z4
∇ Bulge : -2.964 +/- 0.057
∇ Disk : -0.603 +/- 0.006
SL Z5
∇ Bulge : -3.147 +/- 0.024
∇ Disk : -0.731 +/- 0.004
(Gyr/kpc)

Hα flux
EW(Hα)
1. e^{-16}erg/s. sm^2
Å
″

Hα flux
EW(Hα)
SL Z4
∇ Bulge : -93.330 +/- 1.390
∇ Disk : -1.611 +/- 0.014
SL Z5
∇ Bulge : -91.765 +/- 1.529
∇ Disk : -1.625 +/- 0.014
(dex/kpc)
SL Z4
∇ Bulge : -122.111 +/- 0.98
∇ Disk : -2.027 +/- 0.082
SL Z5
∇ Bulge : -133.318 +/- 1.55
∇ Disk : -2.171 +/- 0.084
(Å/kpc)
R* (kpc)

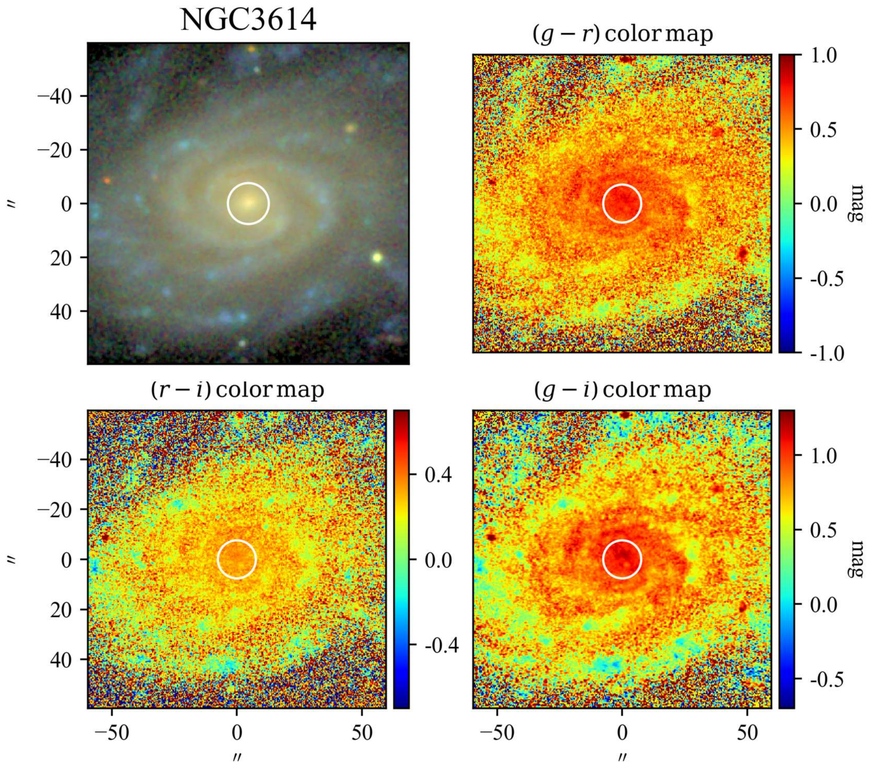

SBP decomposition of SDSS r band

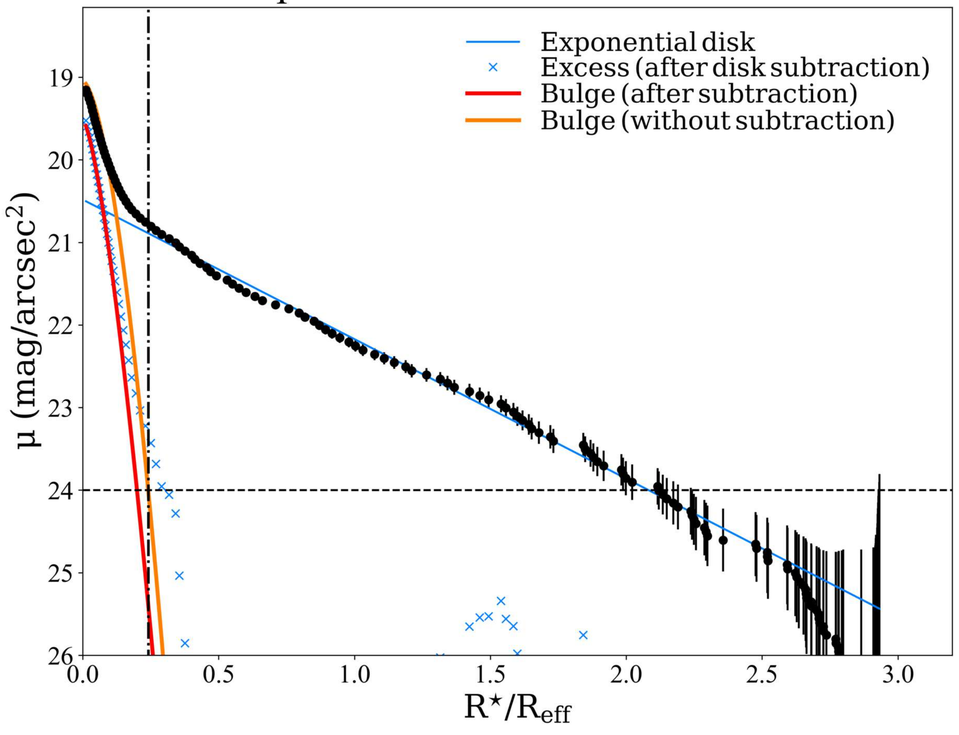

SDSS color profiles

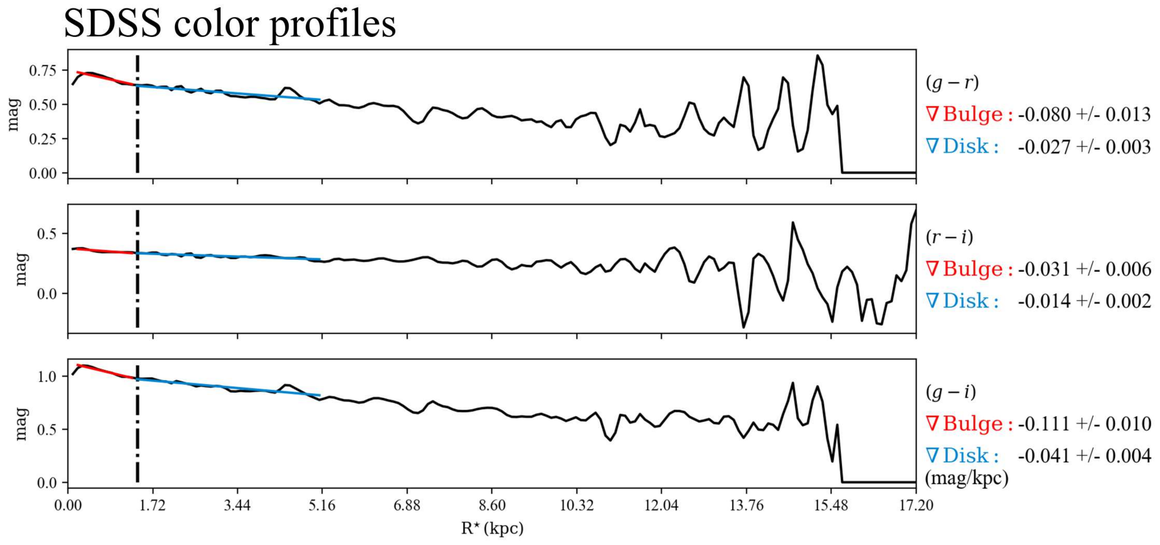

$\mathcal{RV}$ SBPs

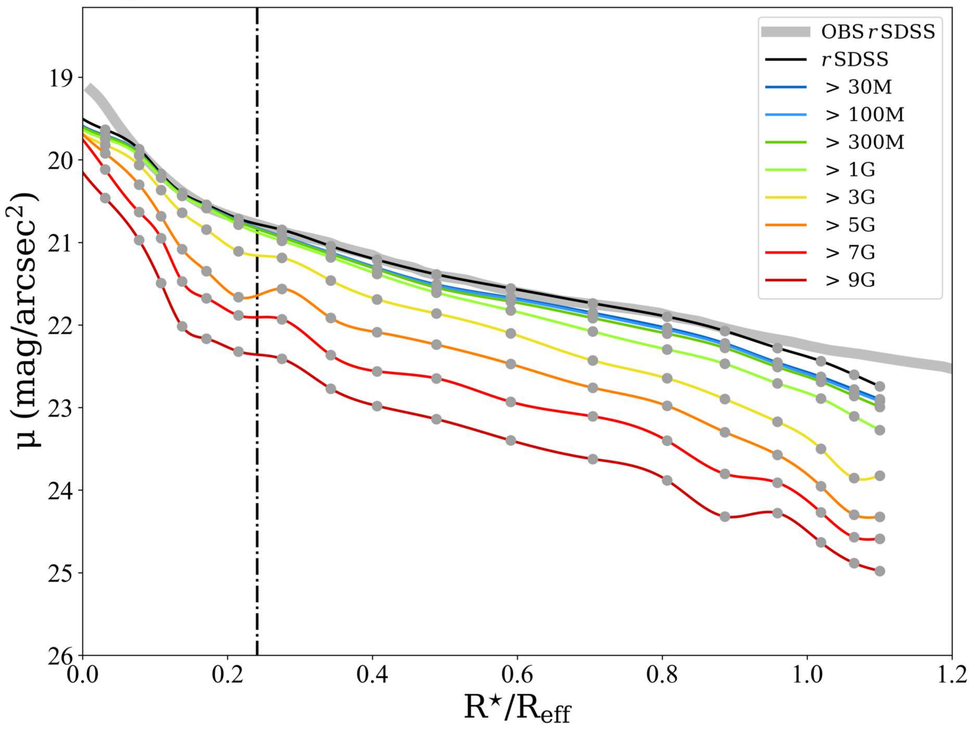

Stellar Continuum

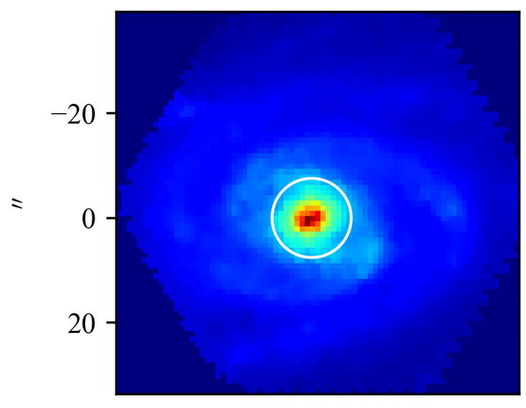

$\mathcal{M}_{\star,\,\rm P}$

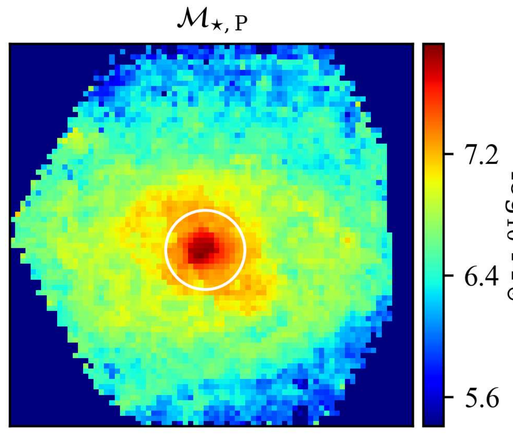

Log. of cumulative present stellar mass profiles

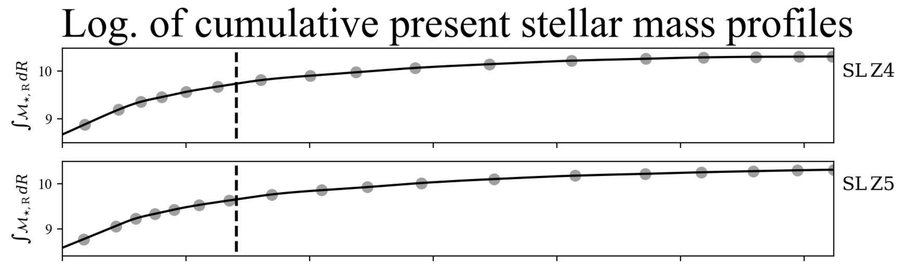

$Z_{\star,\,\mathcal{L}}$

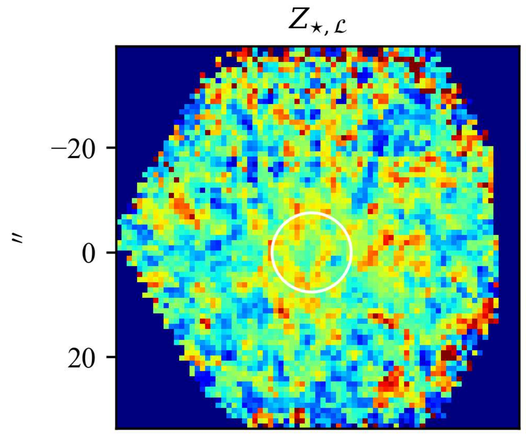

$Z_{\star,\,\mathcal{M}}$

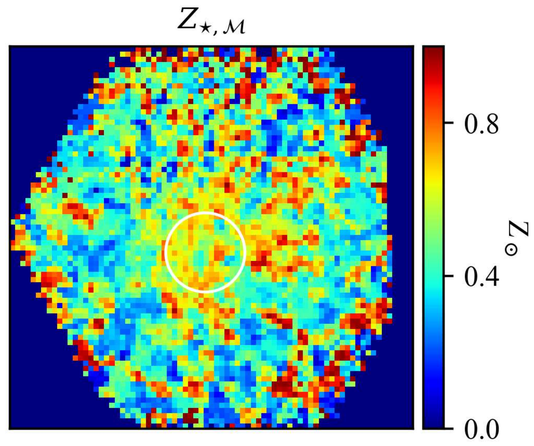

Stellar metallicity/Age & Hα flux/EW profiles

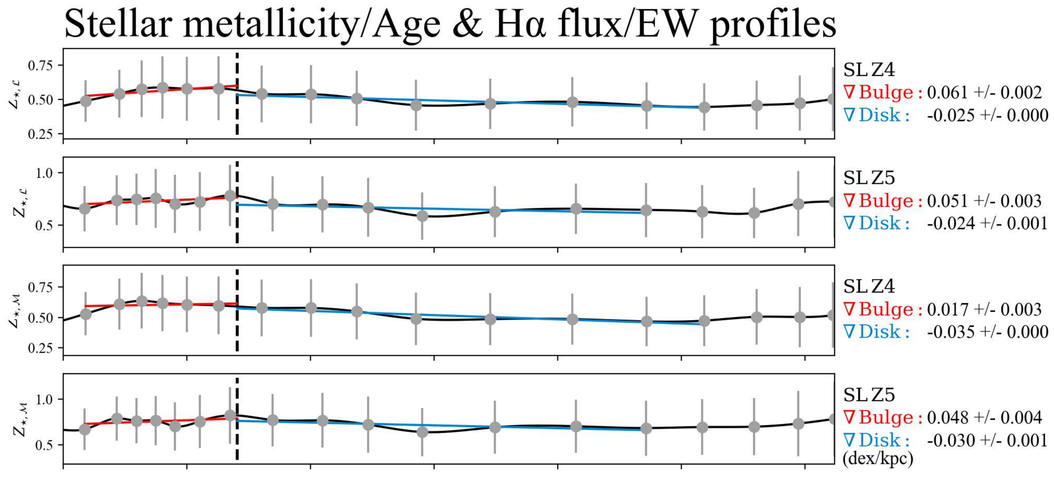

$t_{\star,\,\mathcal{L}}$

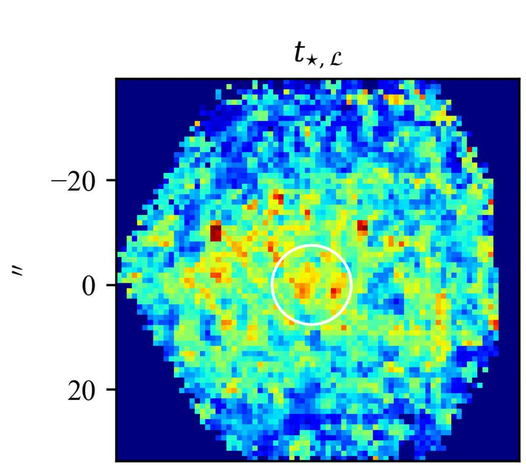

$t_{\star,\,\mathcal{M}}$

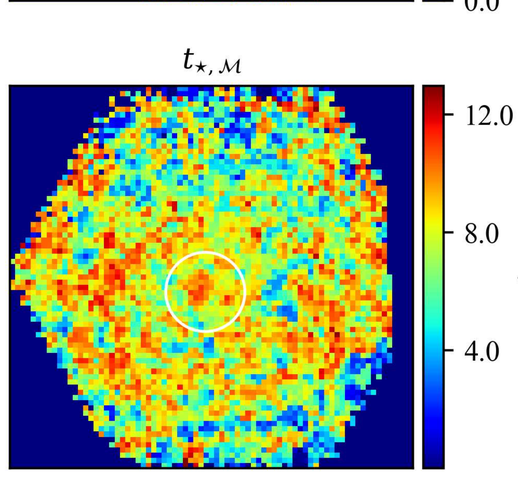

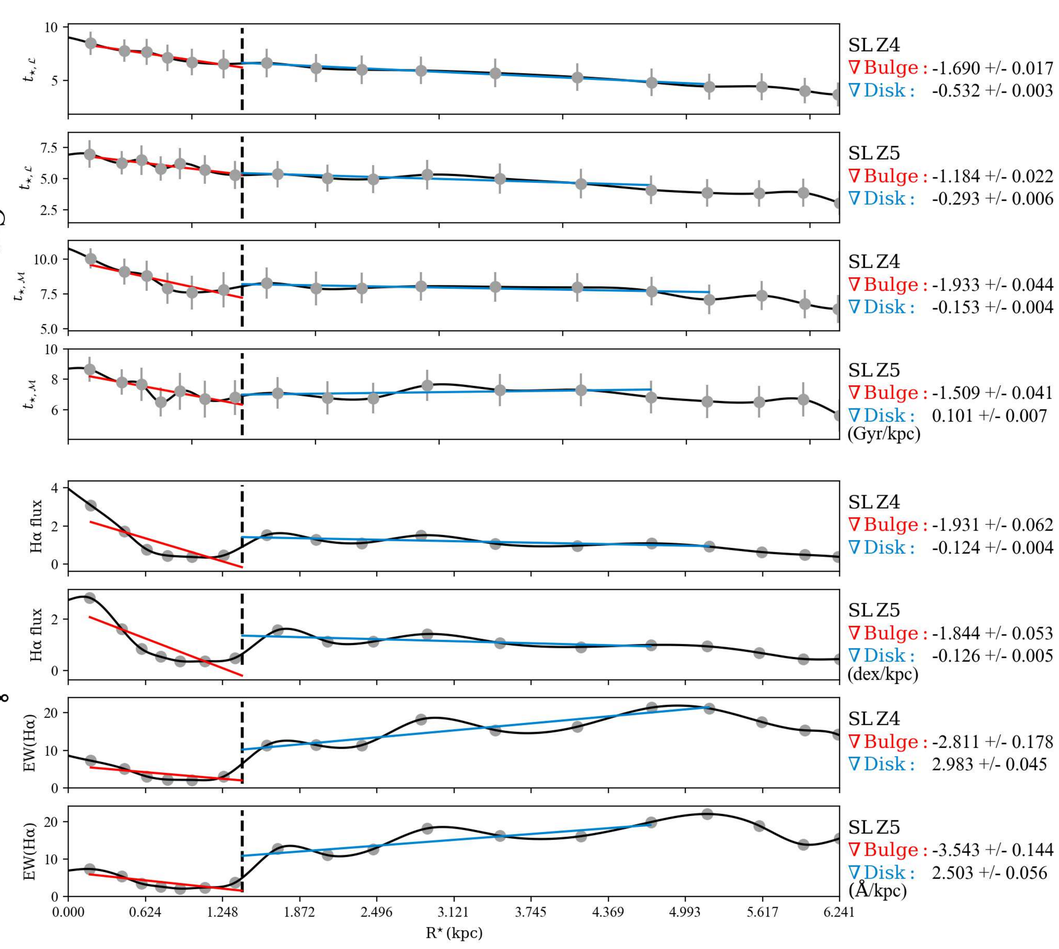

Hα flux

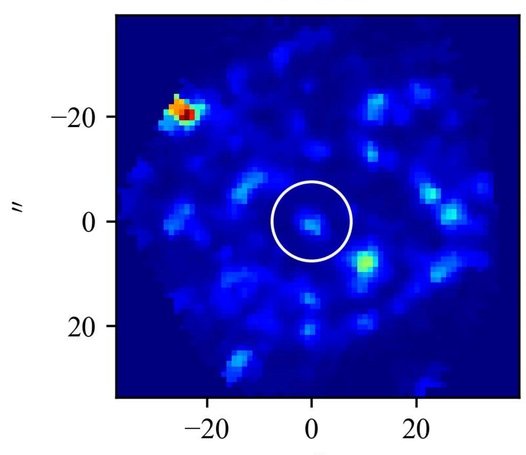

EW(Hα)

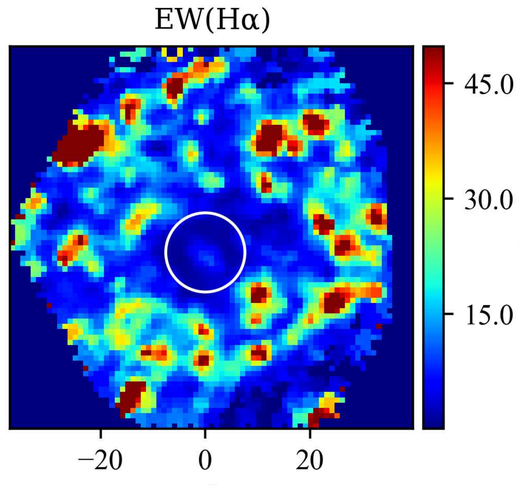

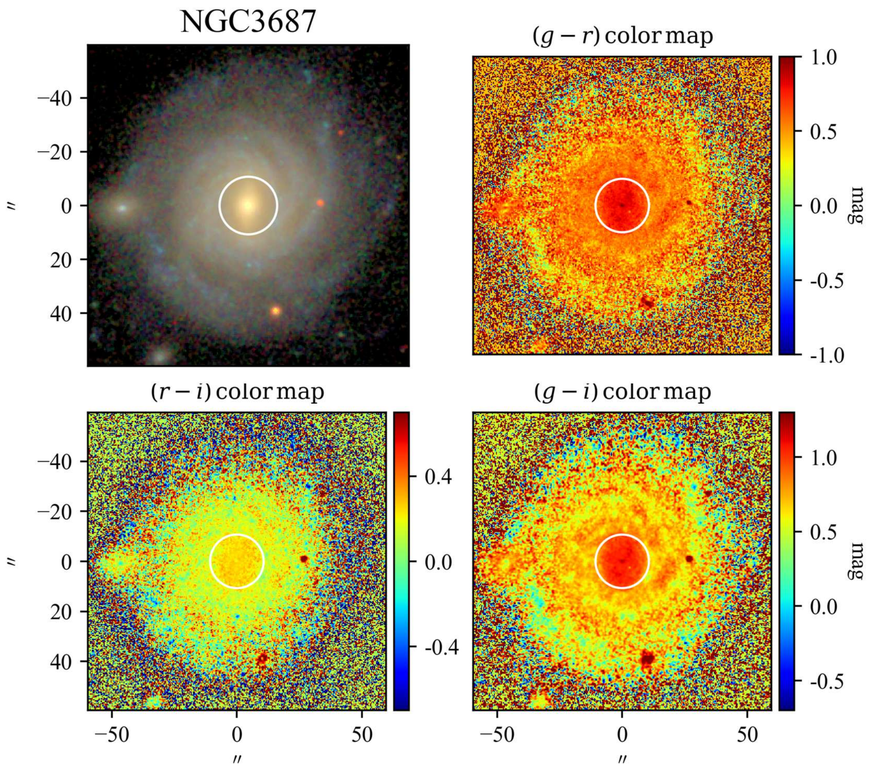

SBP decomposition of SDSS r band

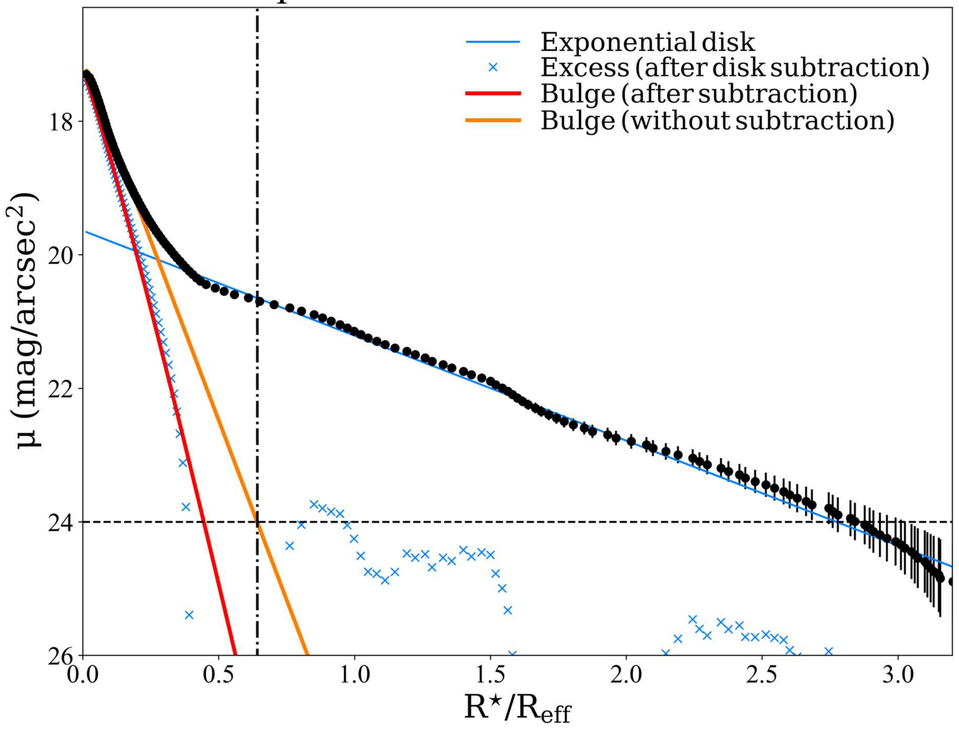

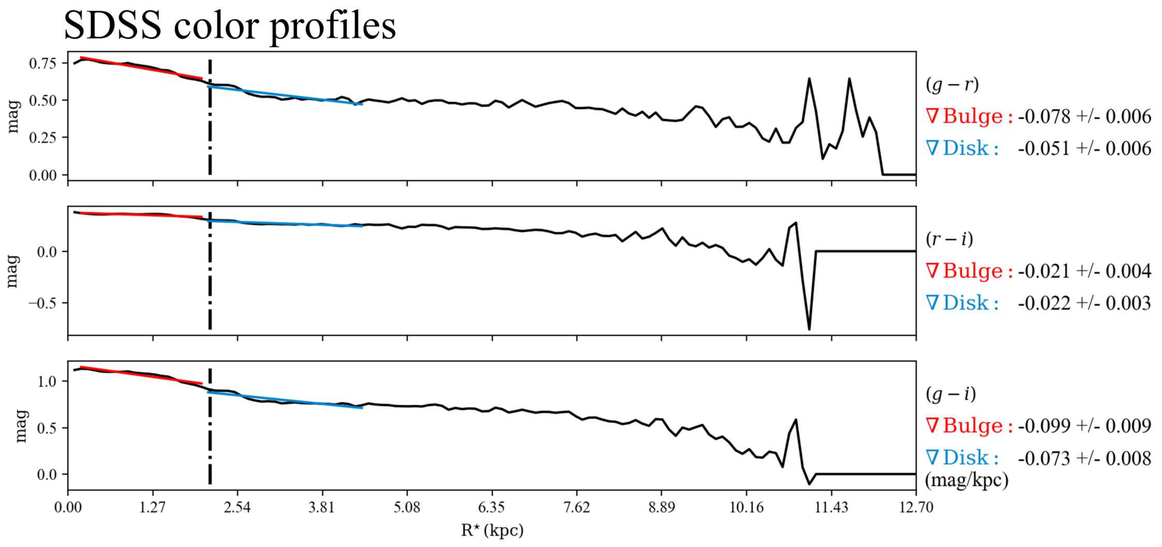

$\mathcal{RV}$ SBPs

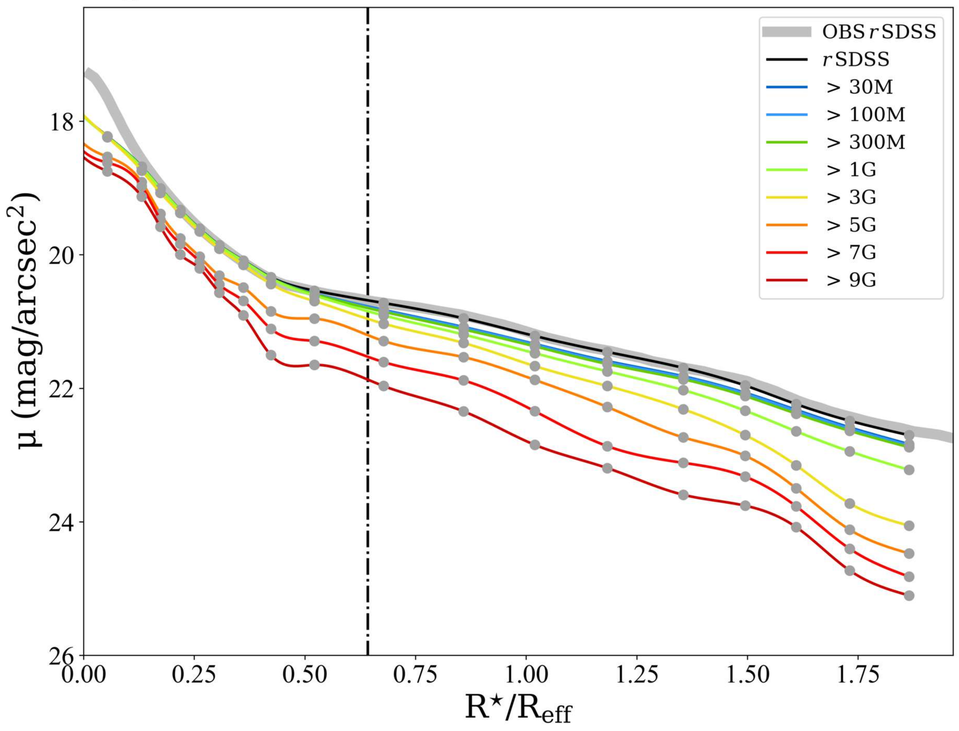

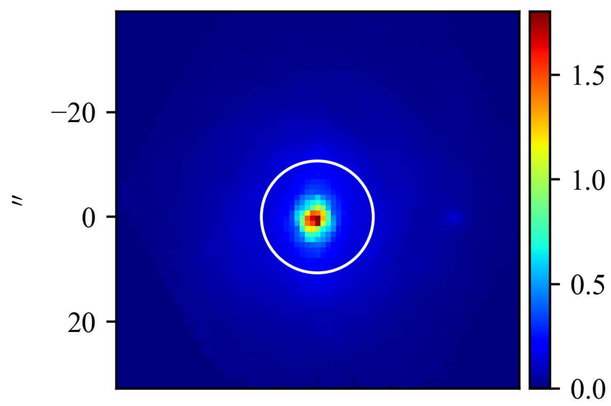

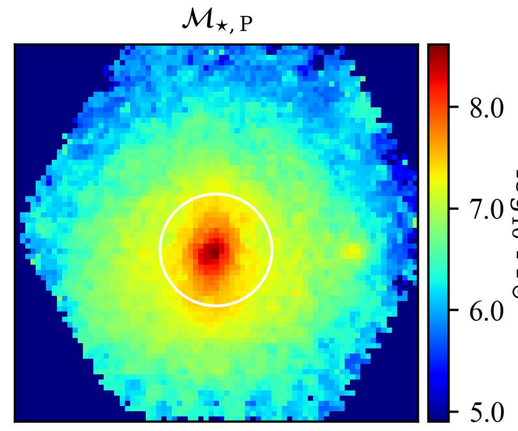

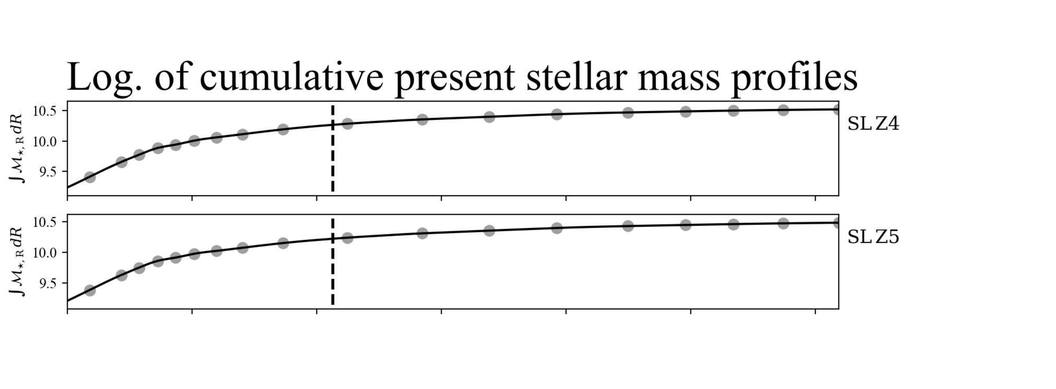

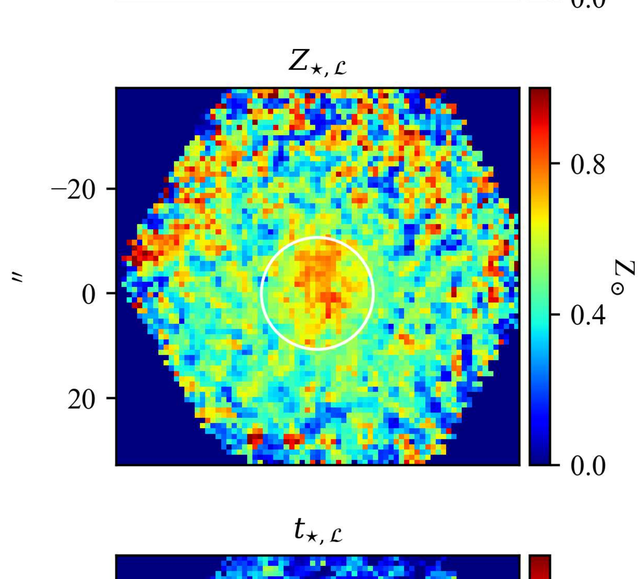

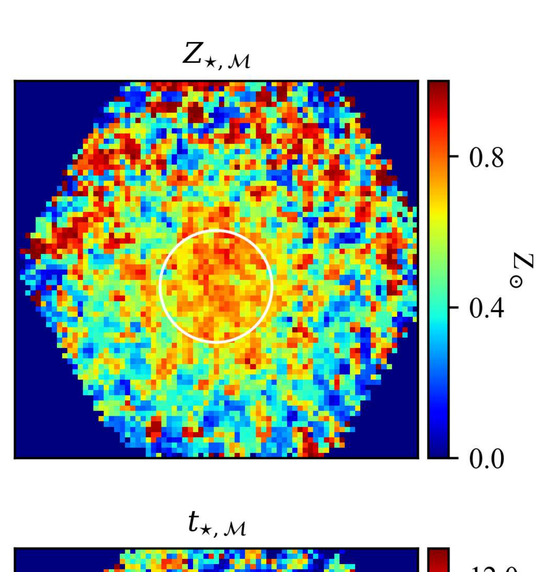

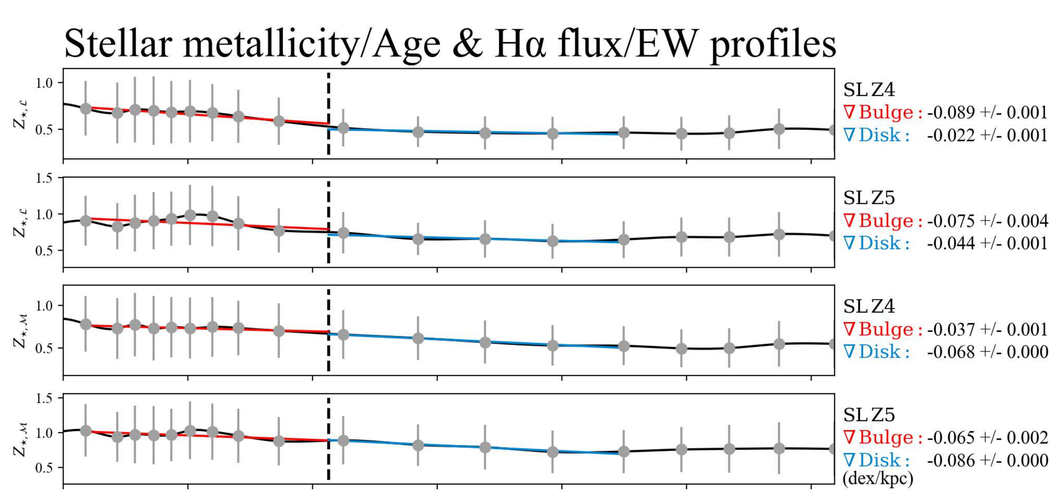

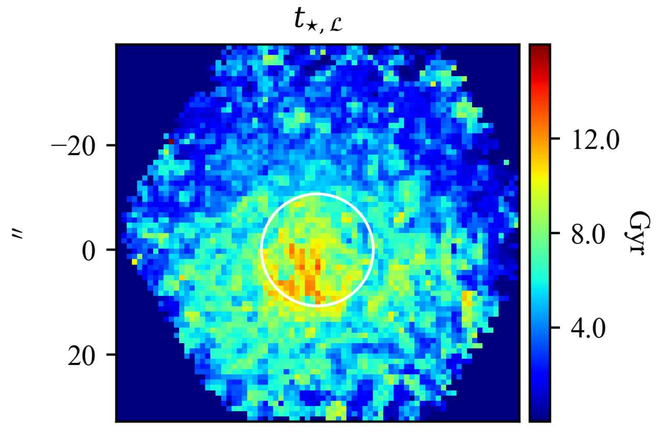

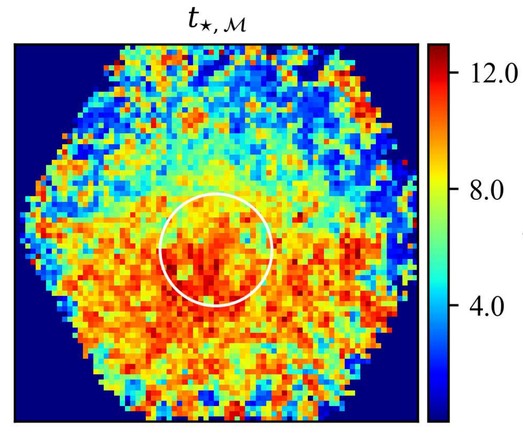

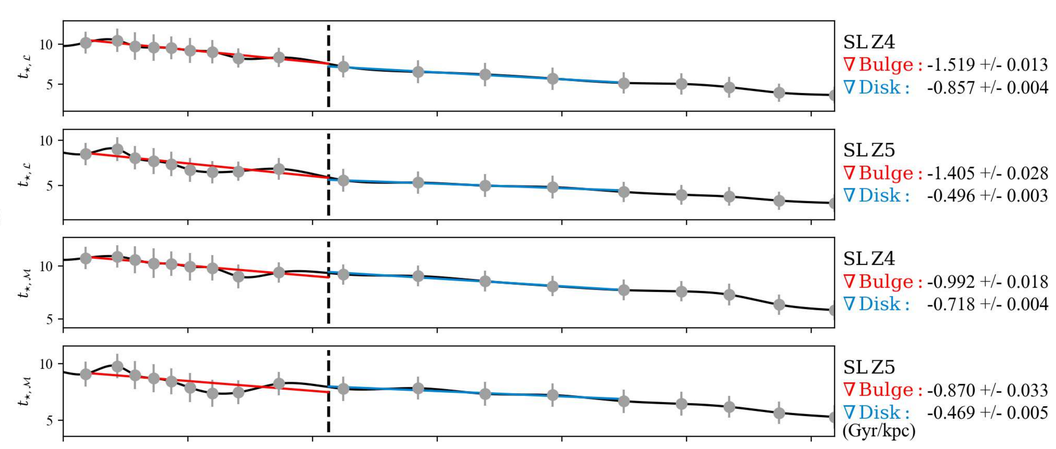

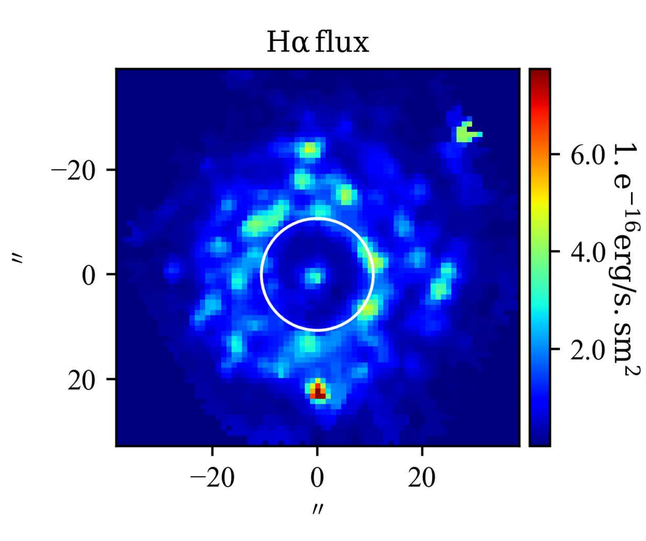

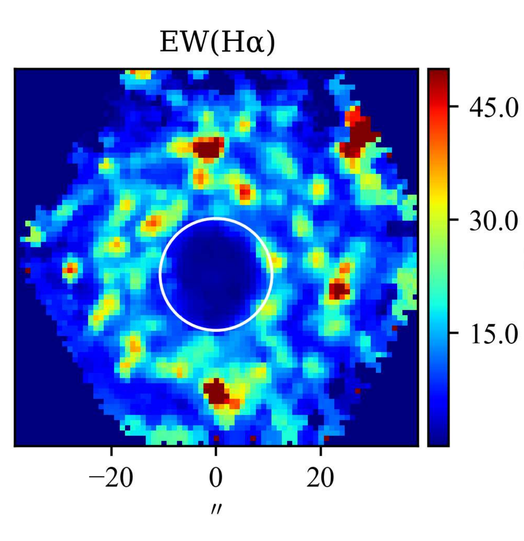

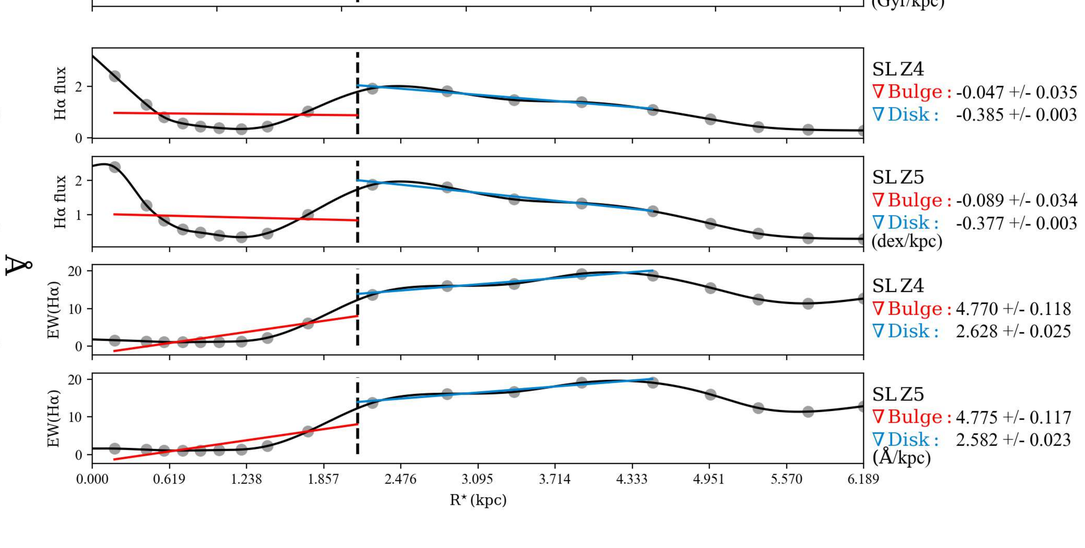

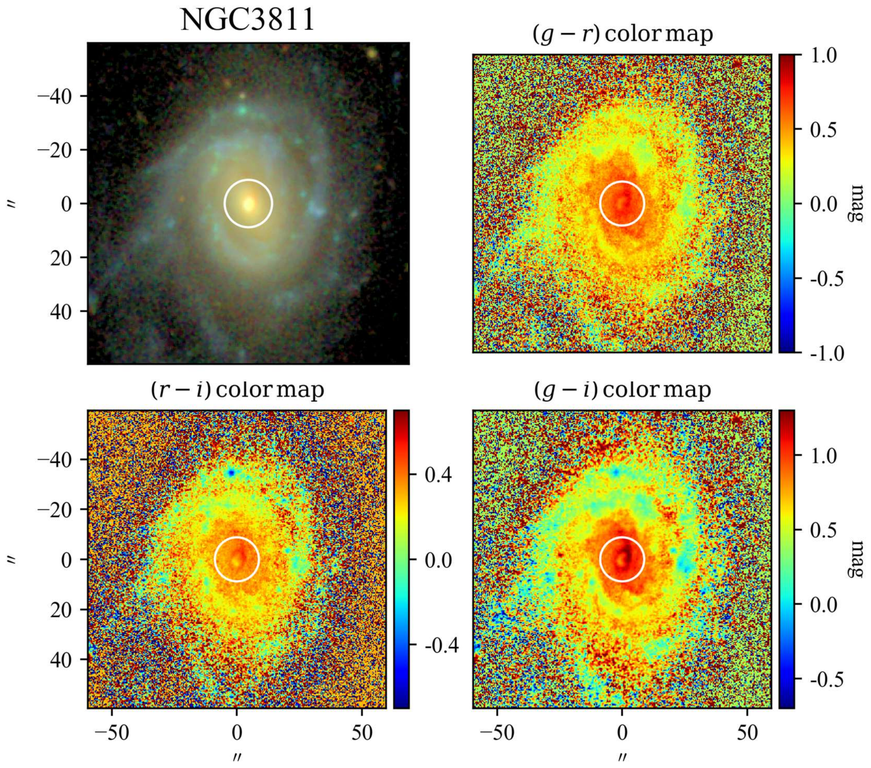

SBP decomposition of SDSS r band

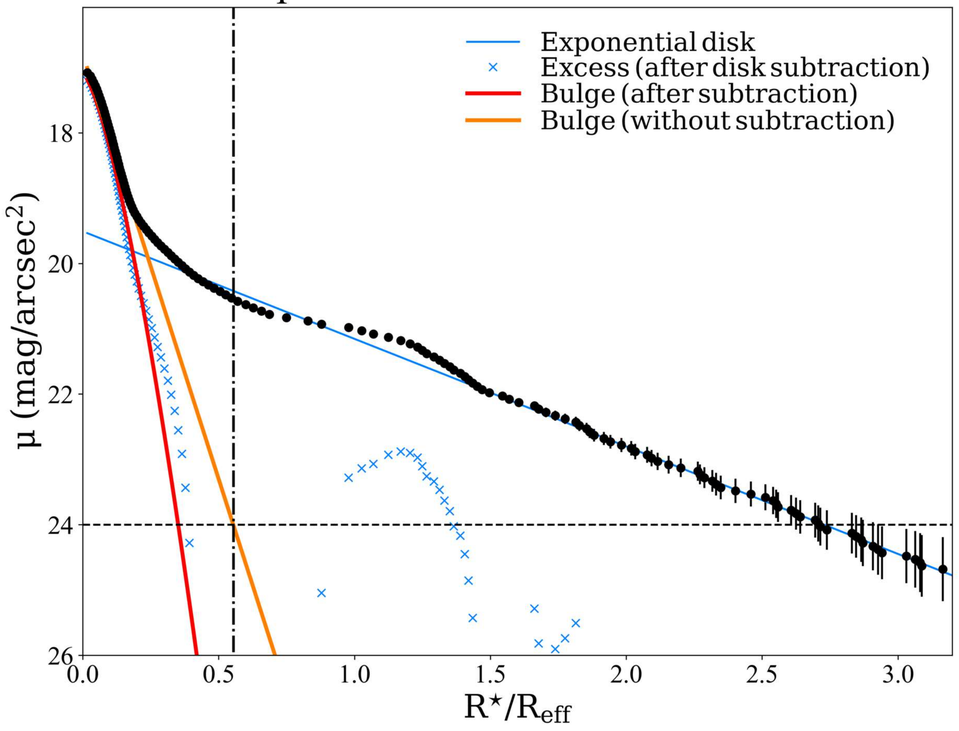

SDSS color profiles

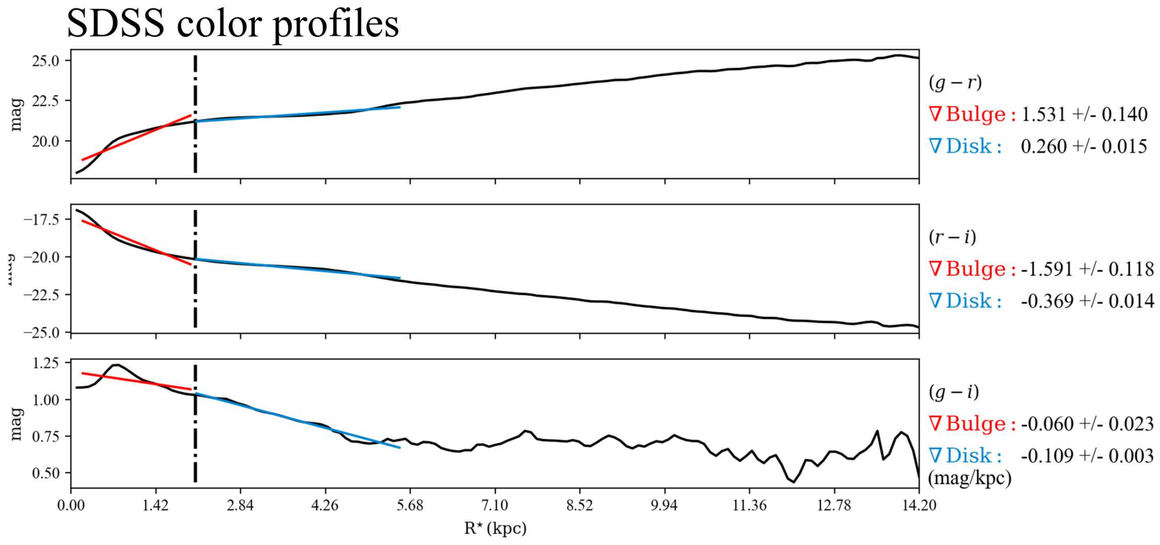

$\mathcal{RY}$ SBPs

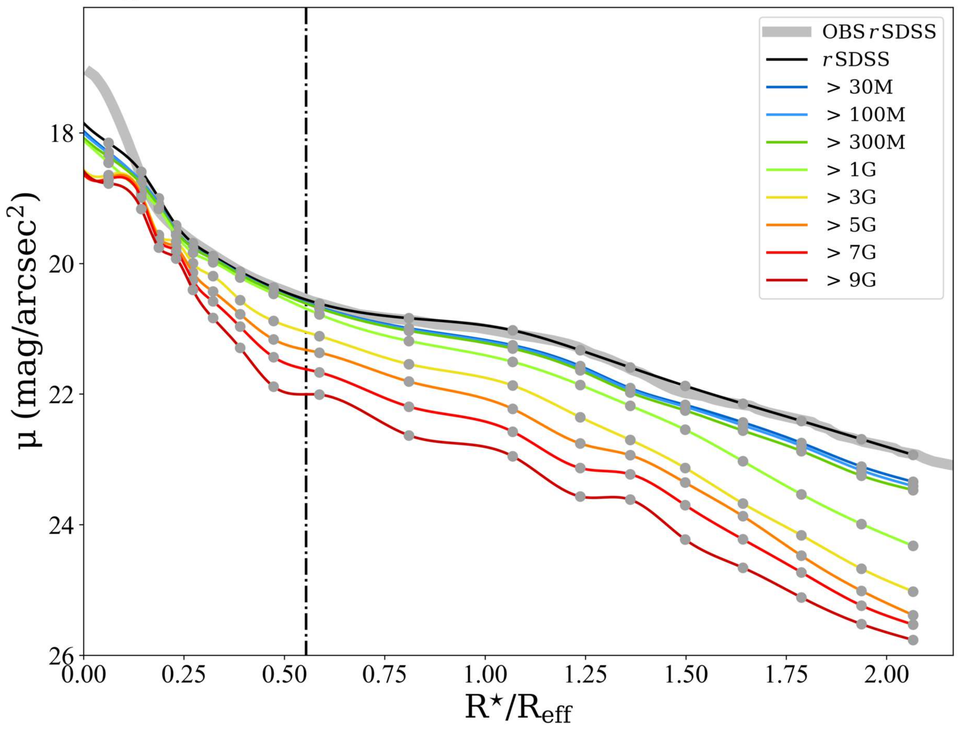

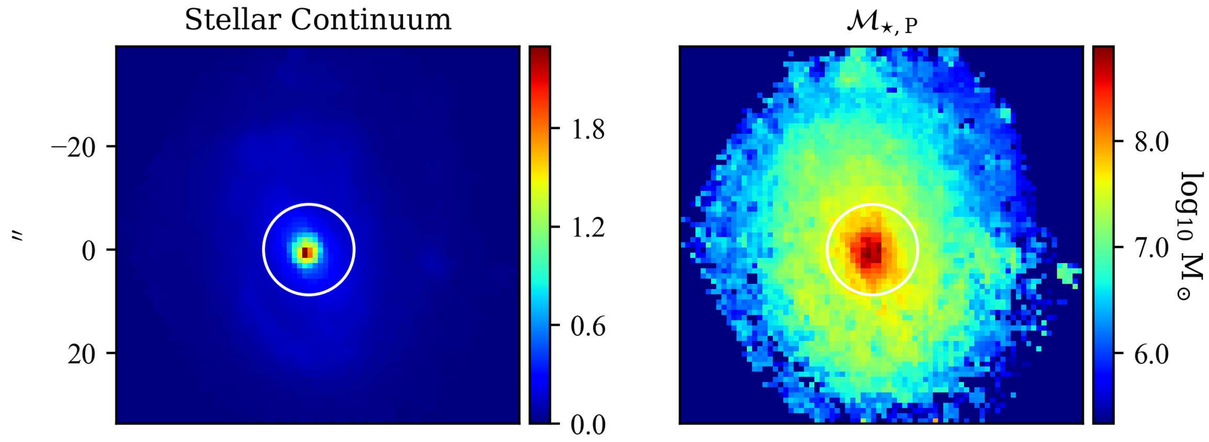

Log. of cumulative present stellar mass profiles

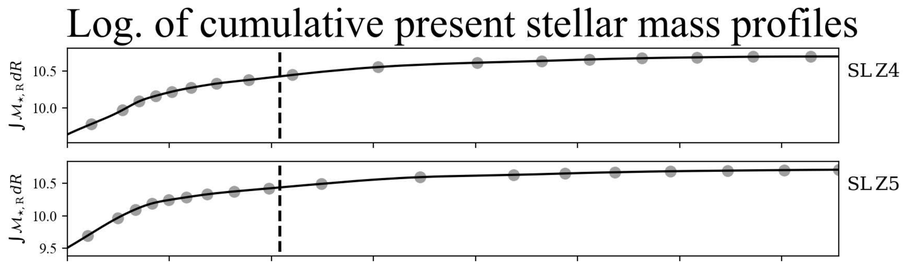

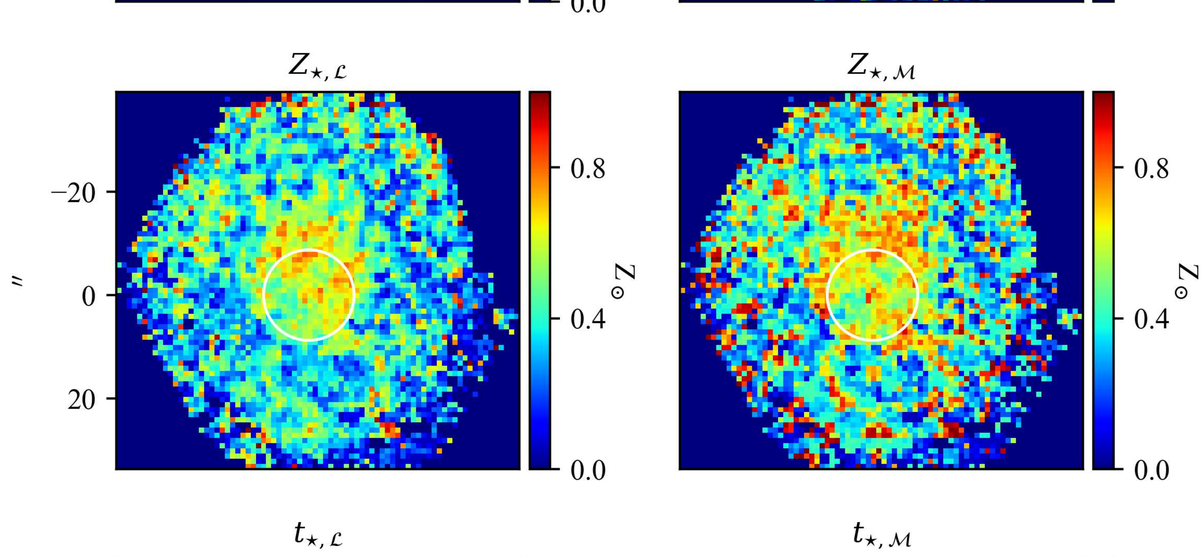

Stellar metallicity/Age & Hα flux/EW profiles

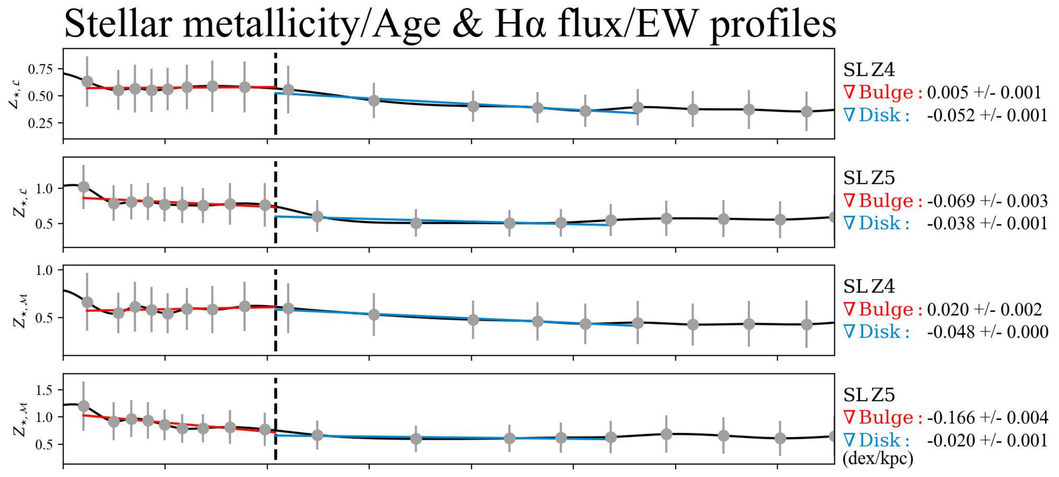

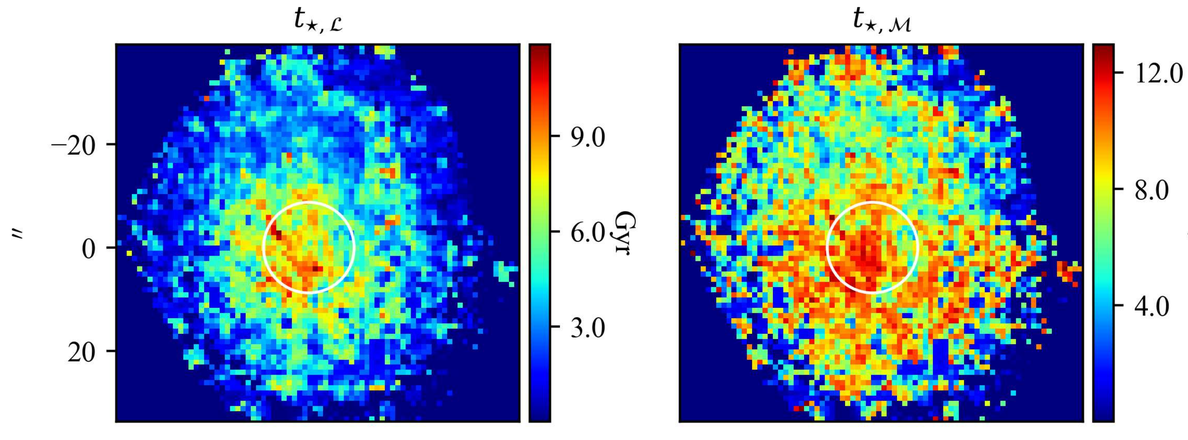

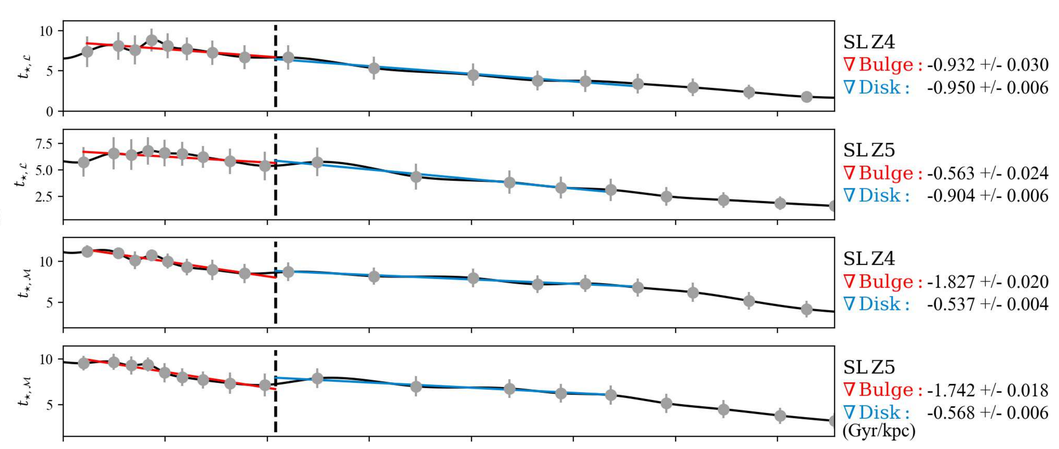

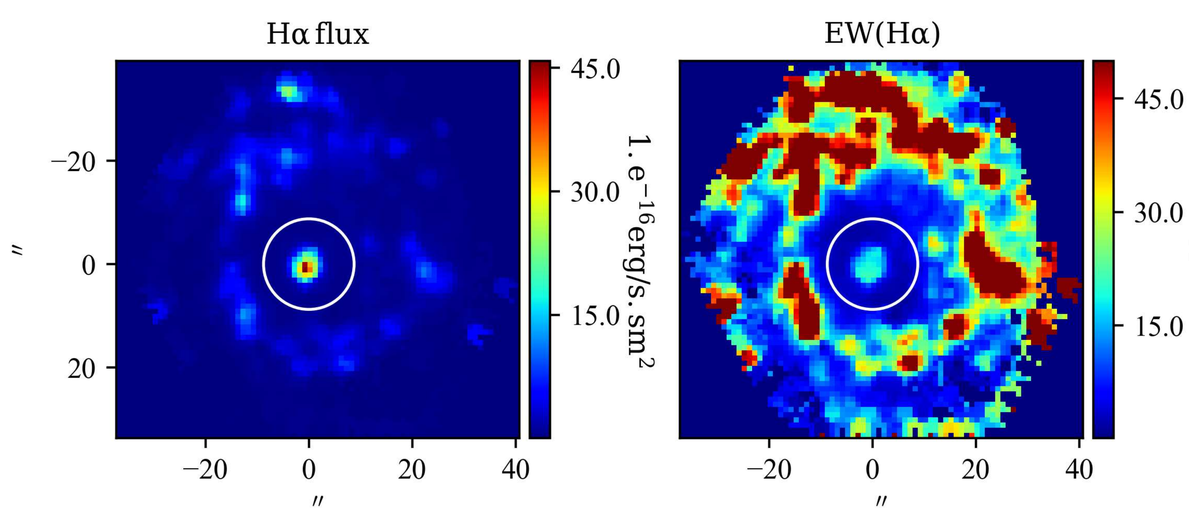

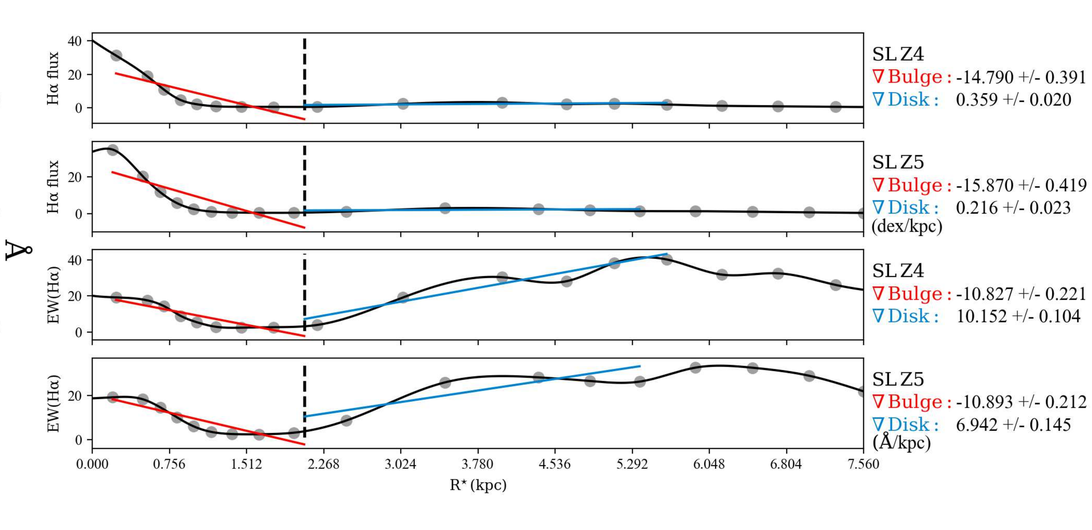

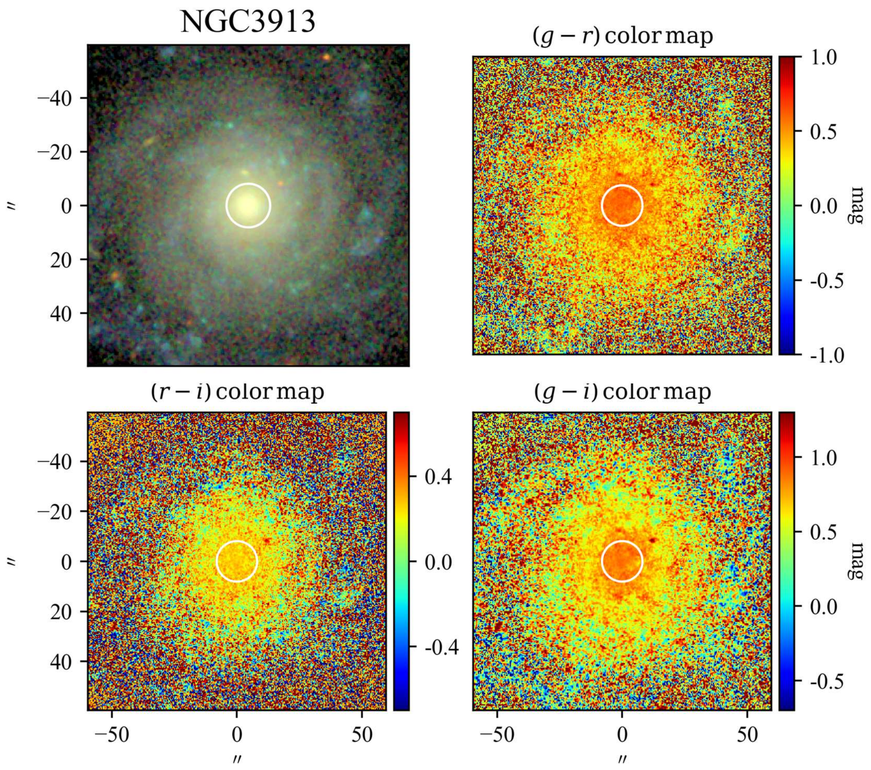

SBP decomposition of SDSS r band

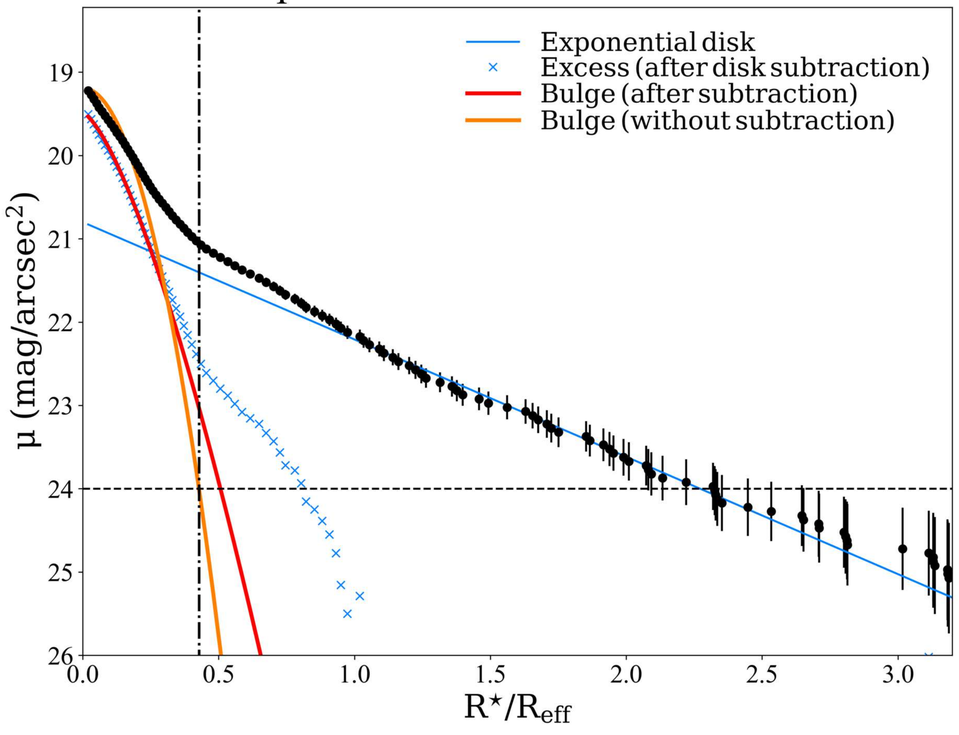

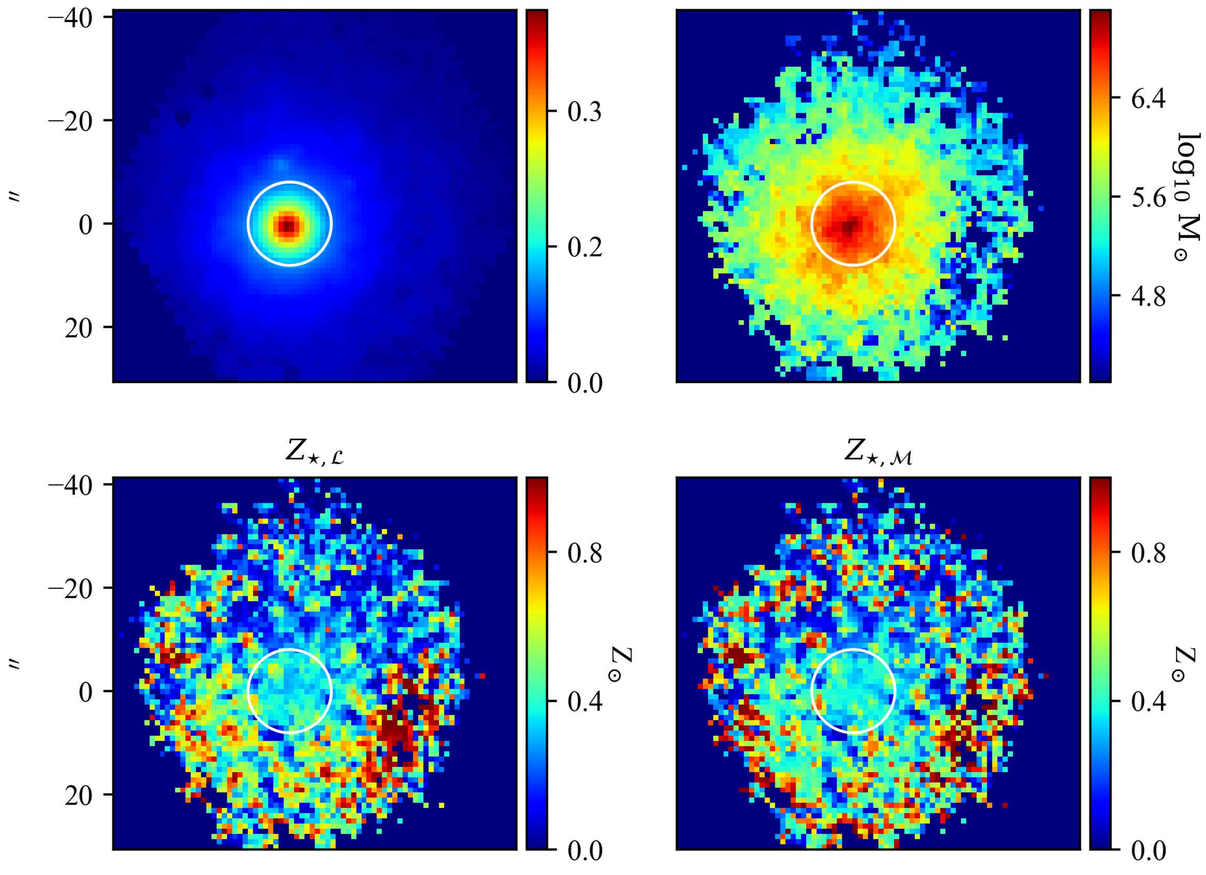

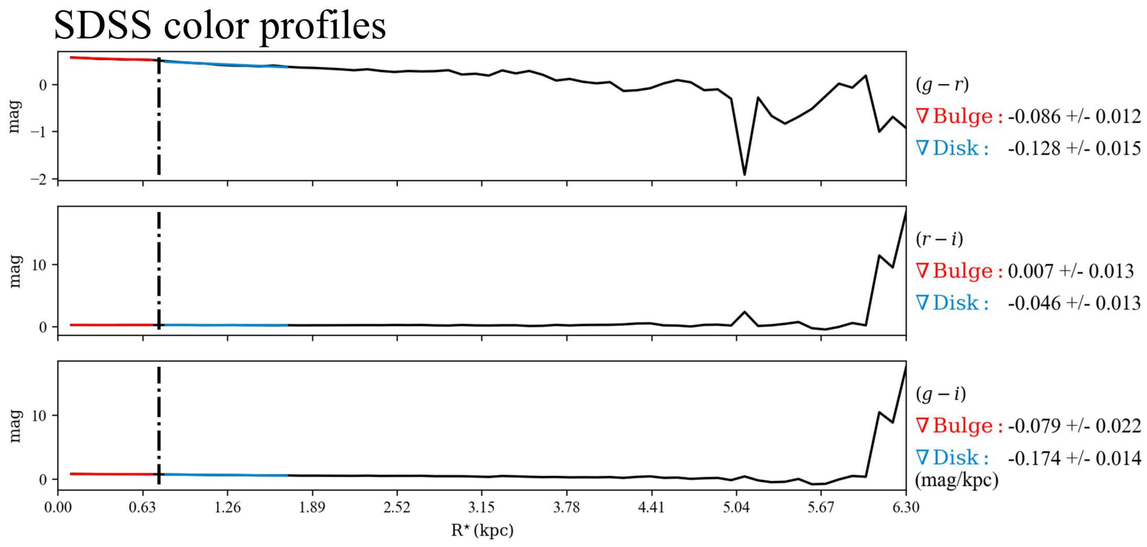

$\mathcal{RY}$ SBPs

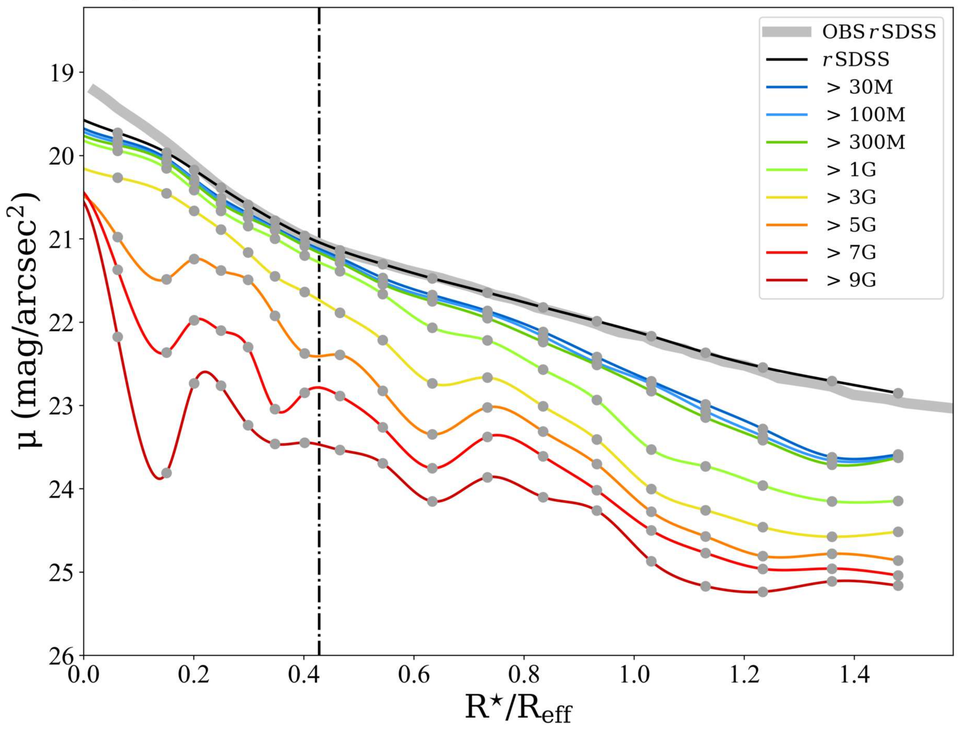

Log. of cumulative present stellar mass profiles

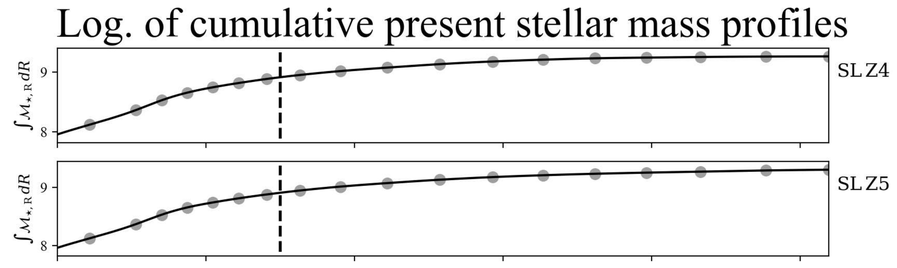

Stellar metallicity/Age & Hα flux/EW profiles

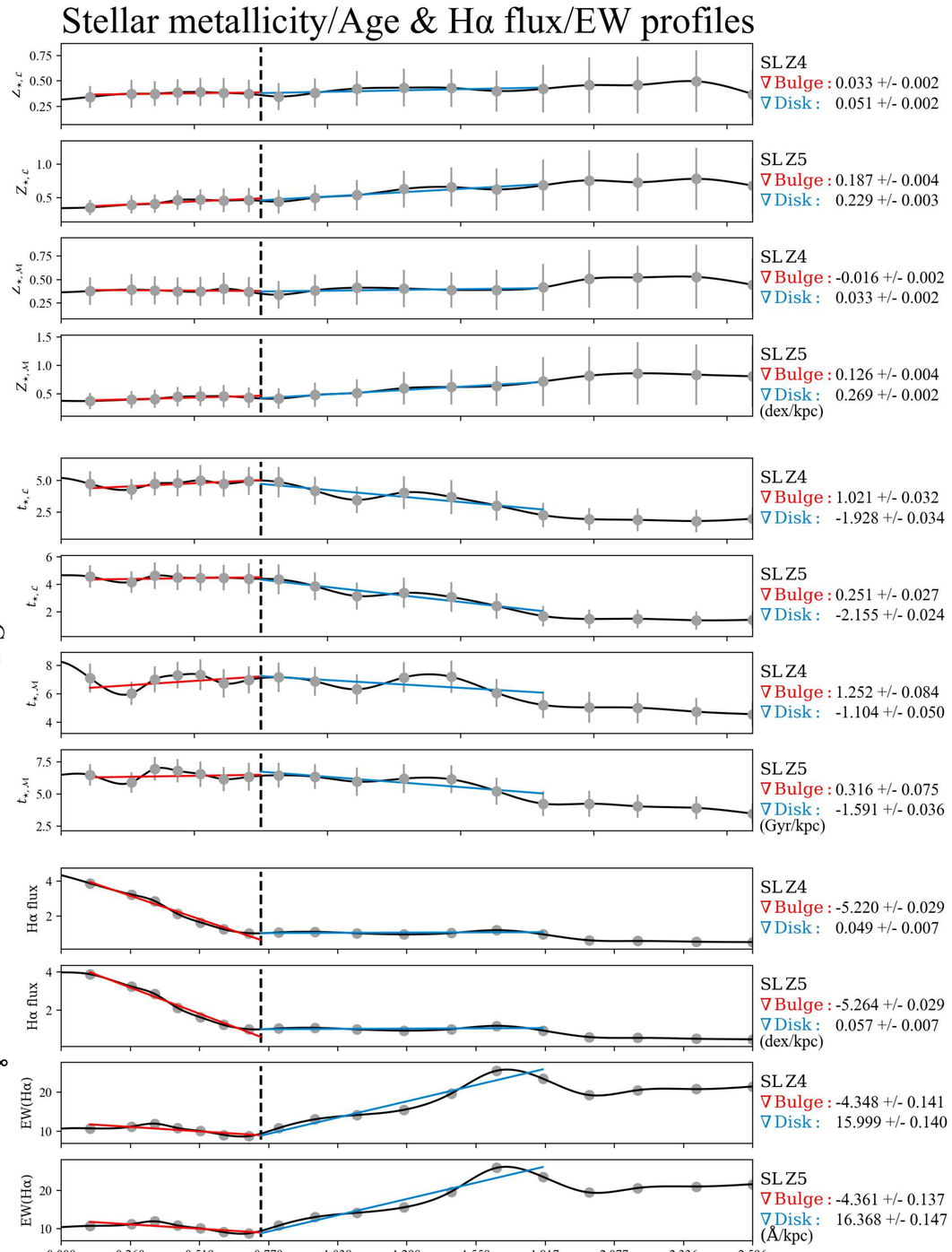

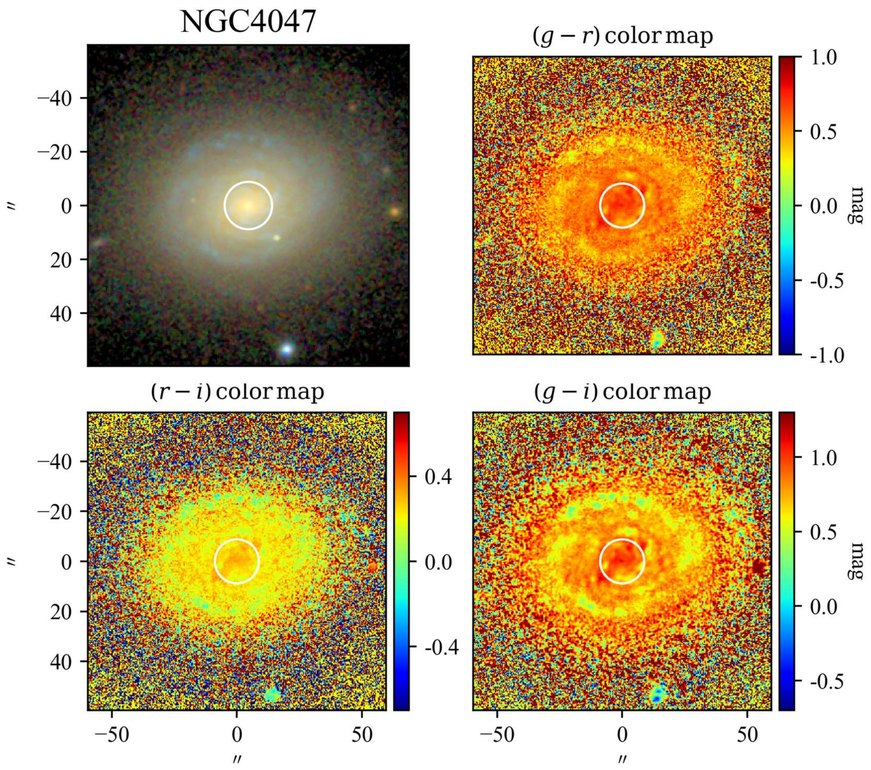

SBP decomposition of SDSS r band

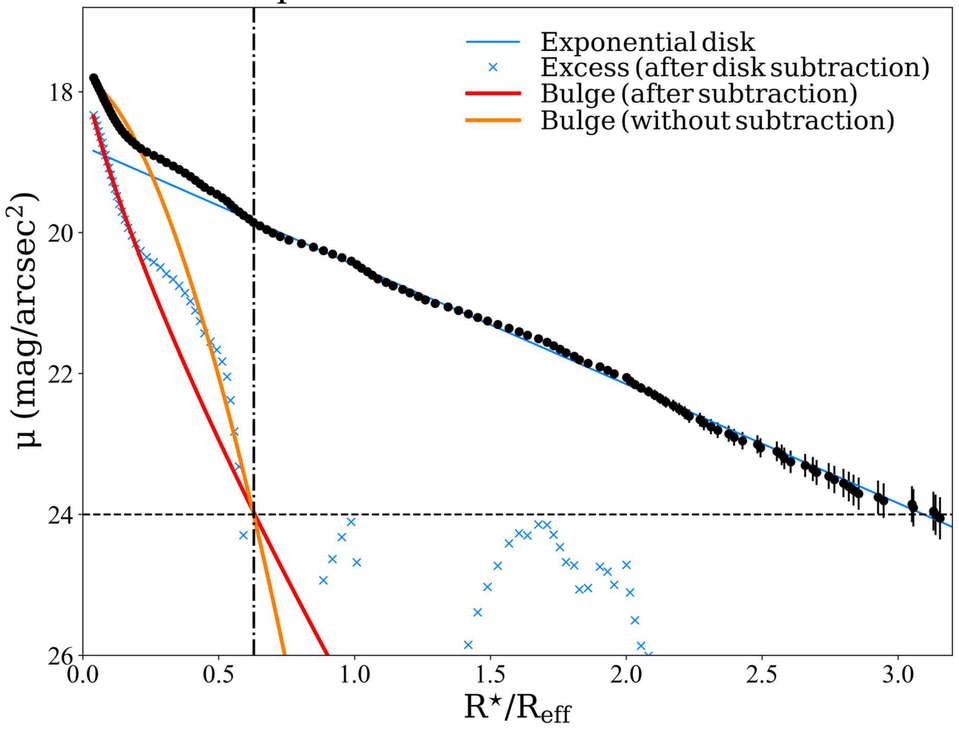

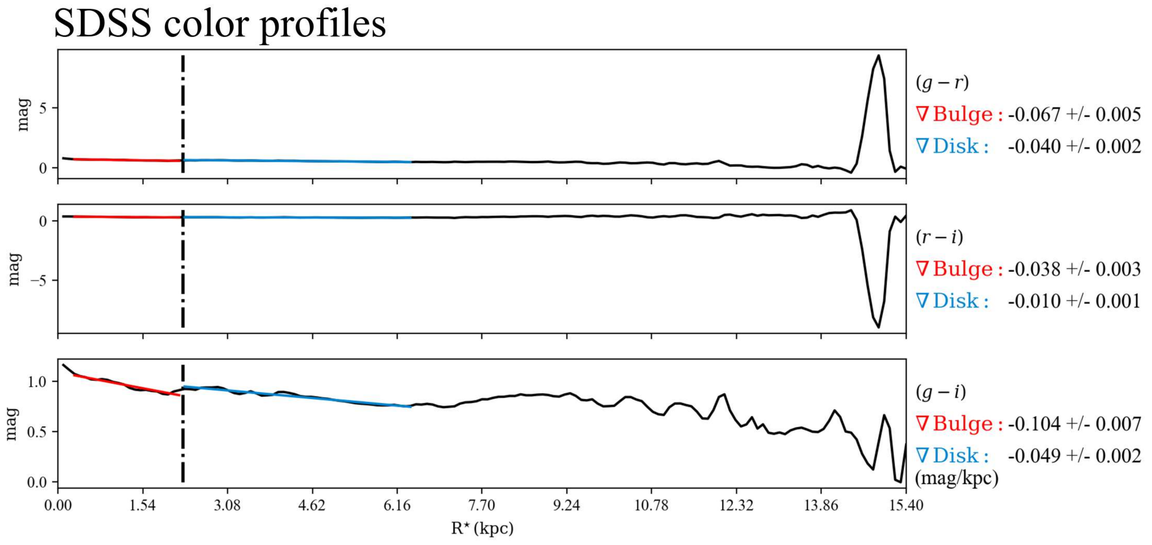

$\mathcal{RV}$ SBPs

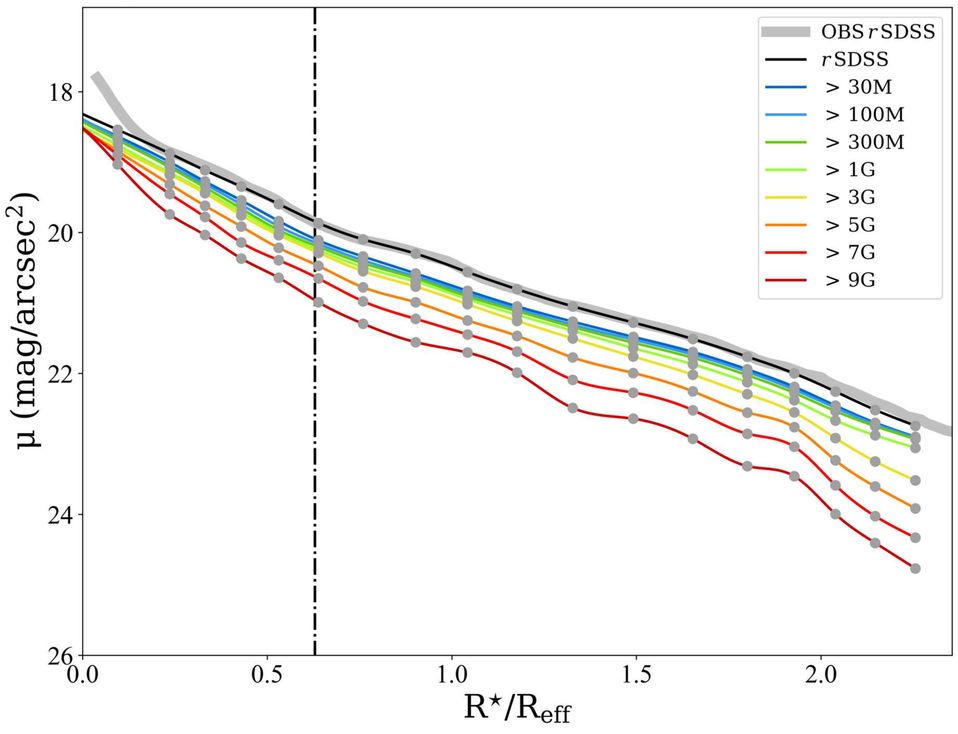

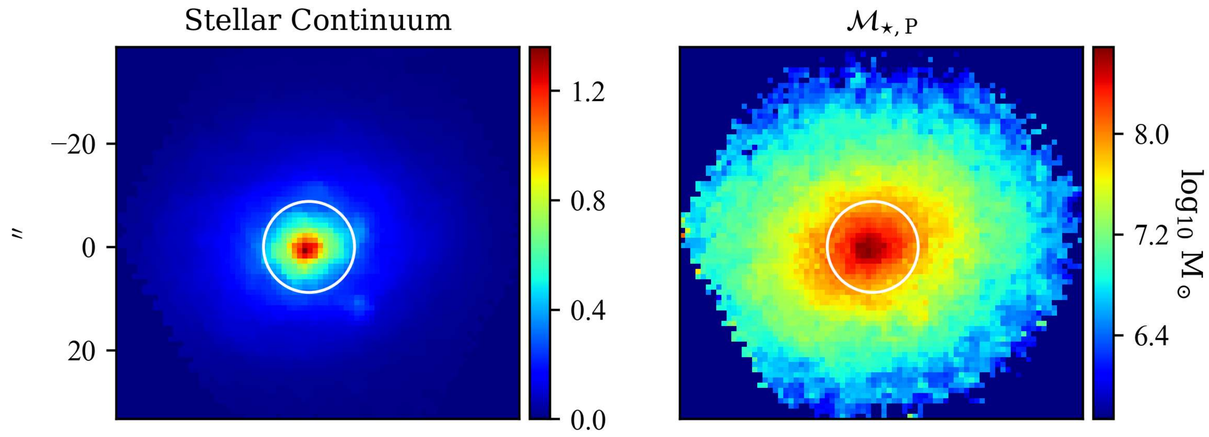

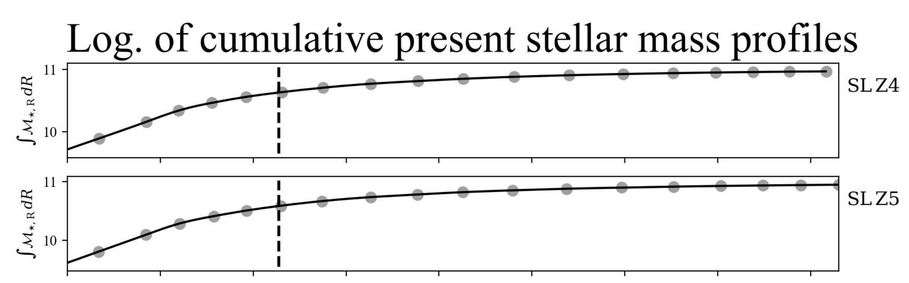

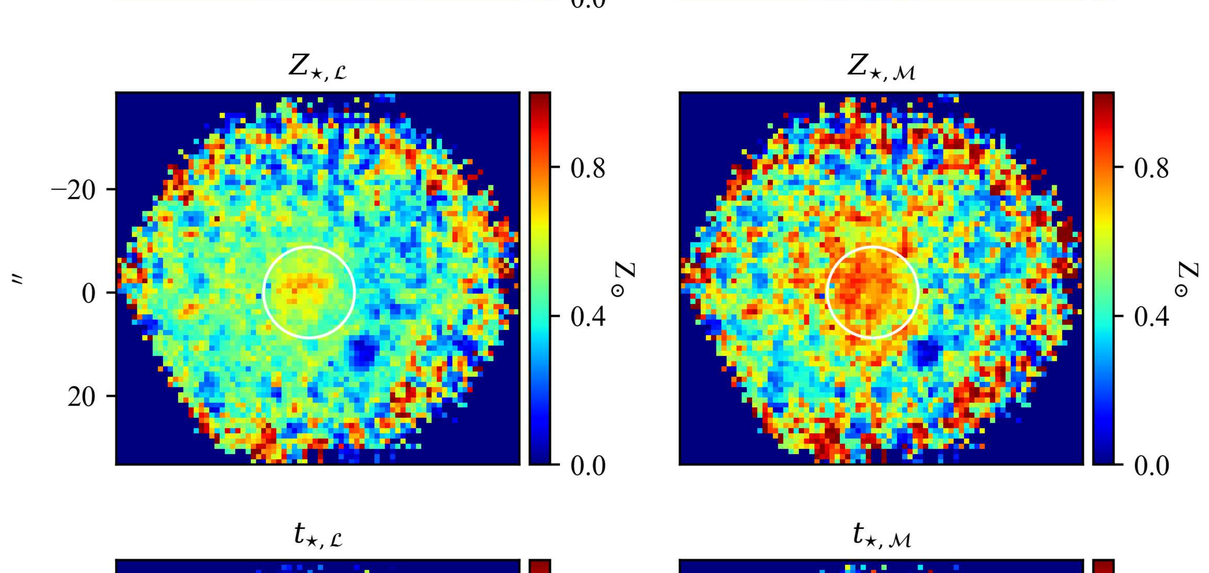

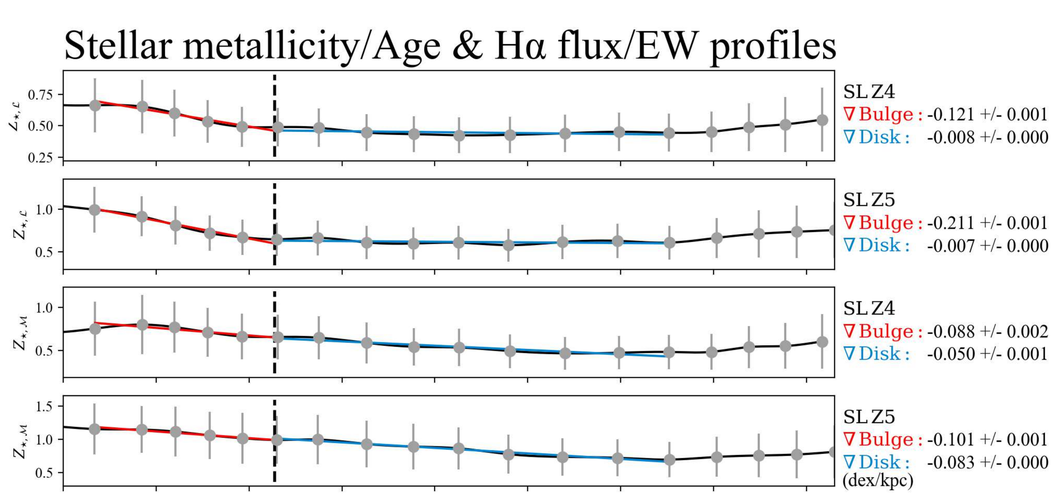

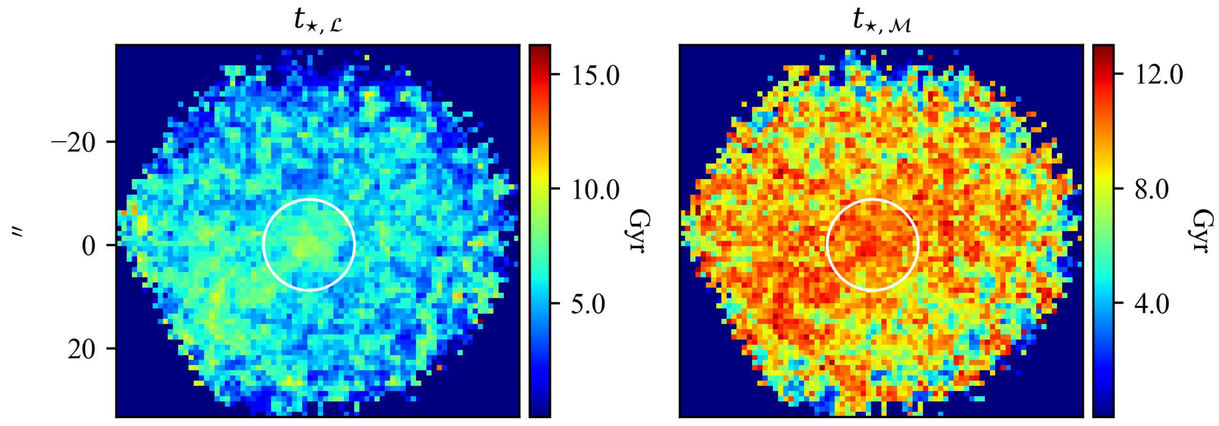

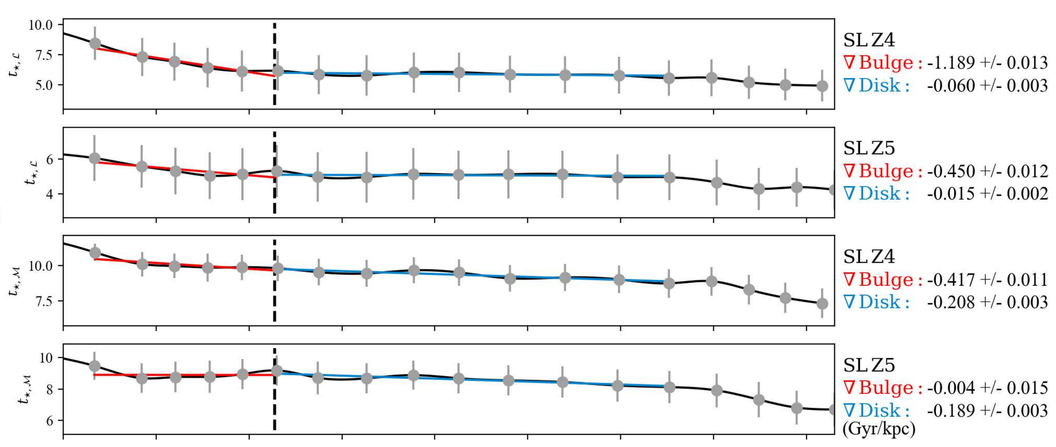

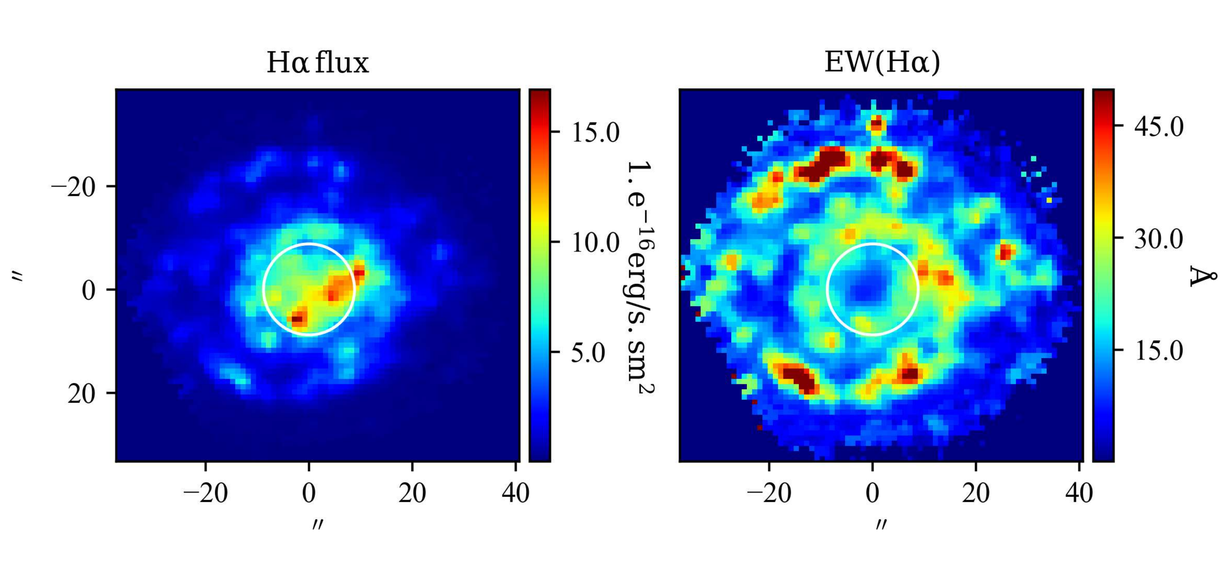

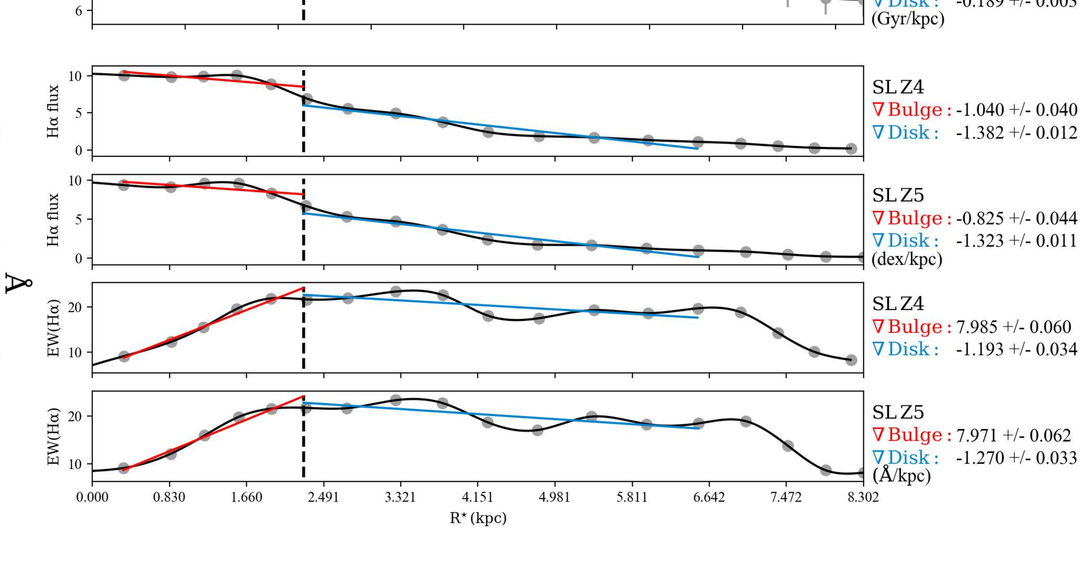

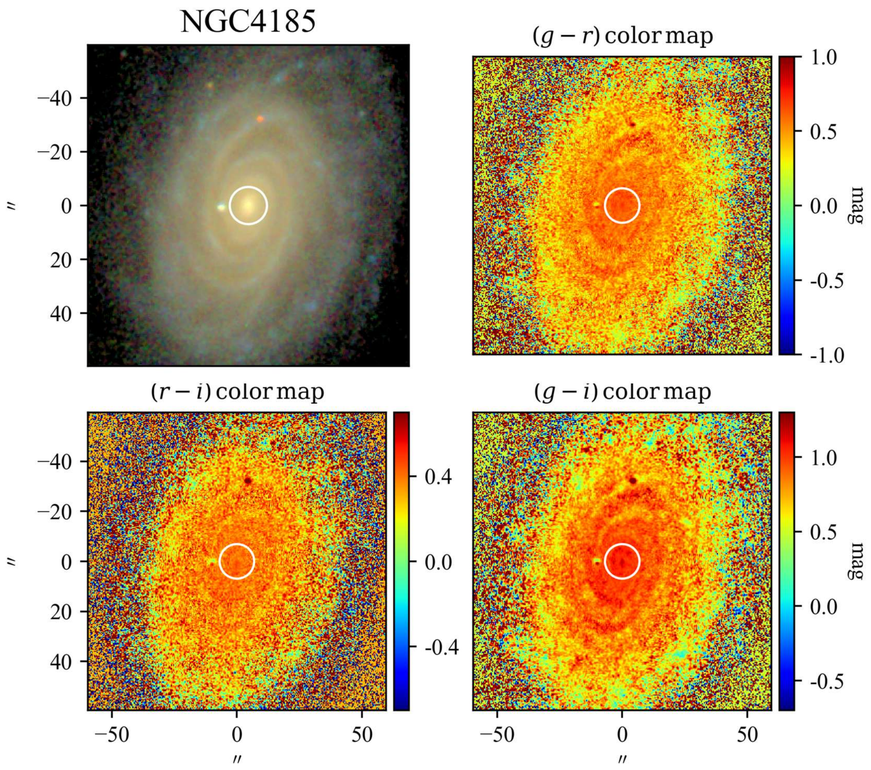

SBP decomposition of SDSS r band

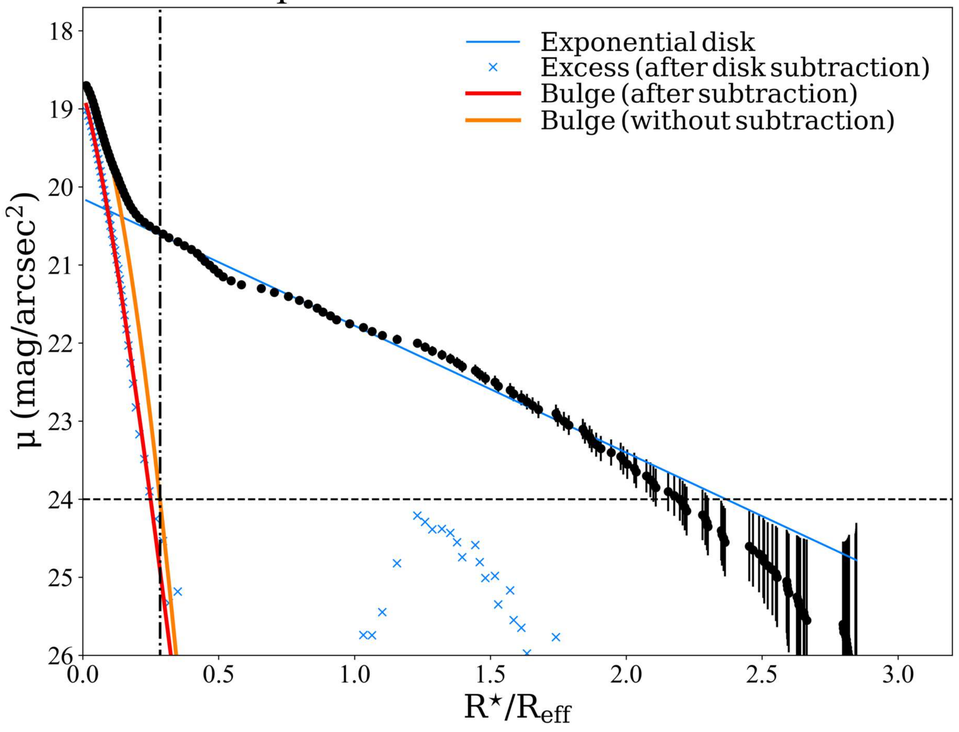

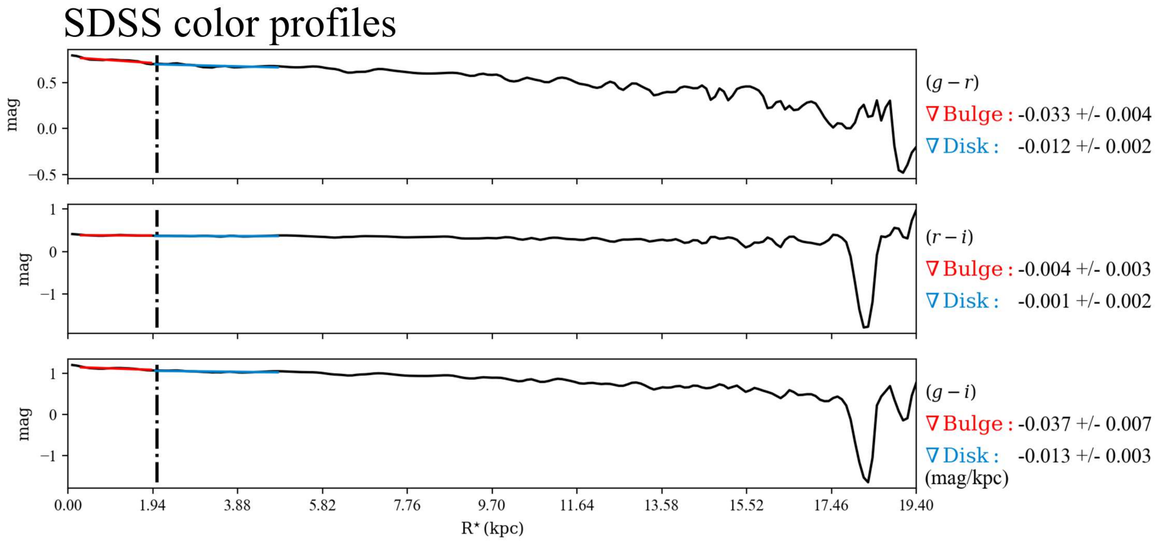

$\mathcal{RY}$ SBPs

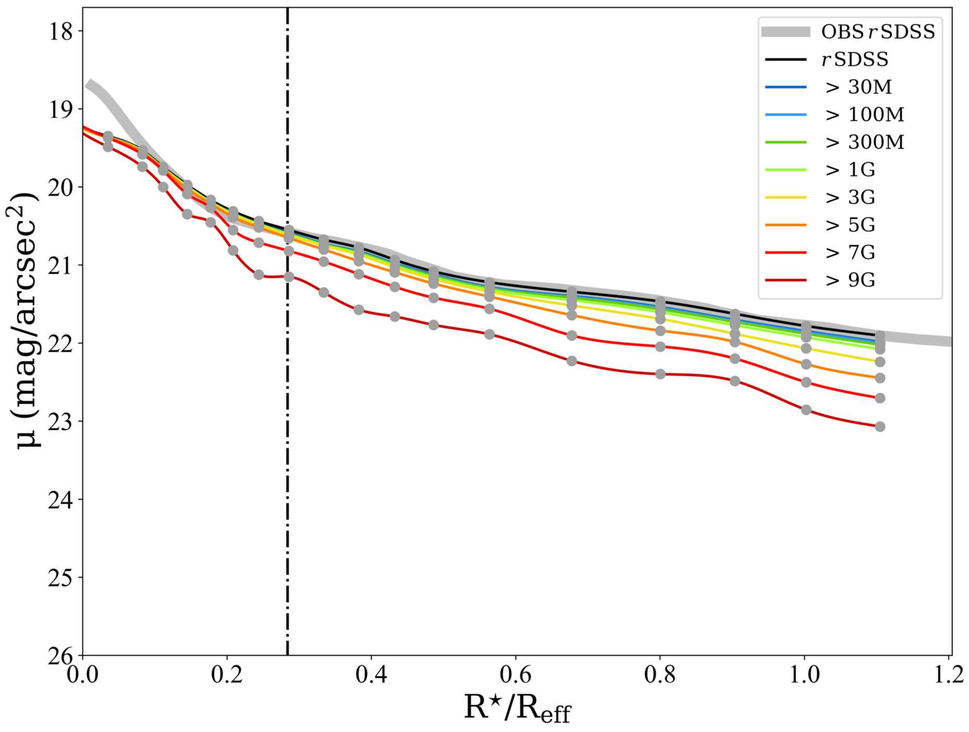

Stellar Continuum

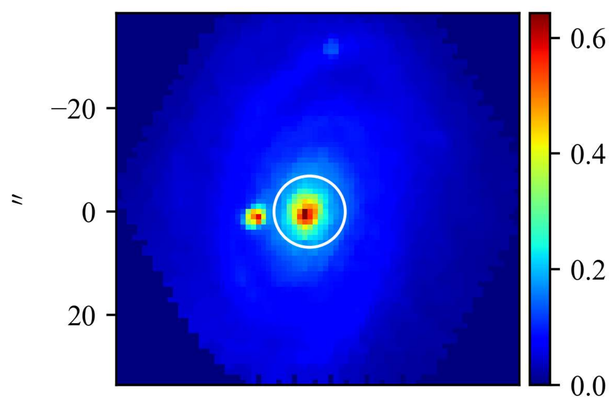

$\mathcal{M}_{\star,\mathrm{P}}$

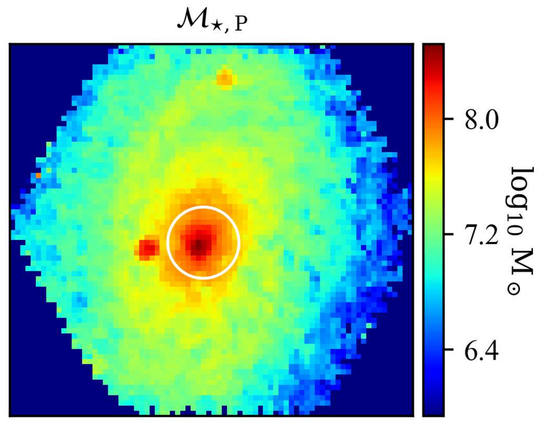

Log. of cumulative present stellar mass profiles

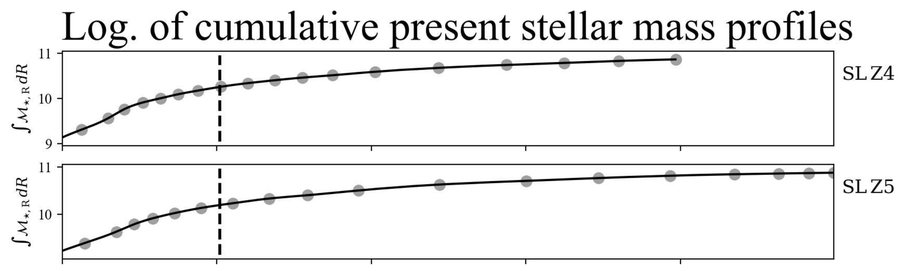

$Z_{\star,\mathcal{L}}$

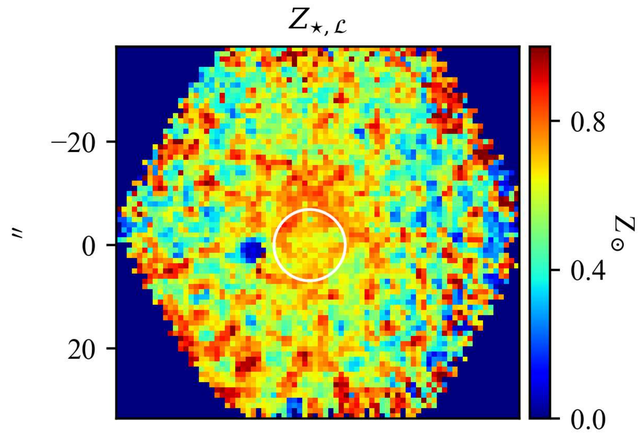

$Z_{\star,\mathcal{M}}$

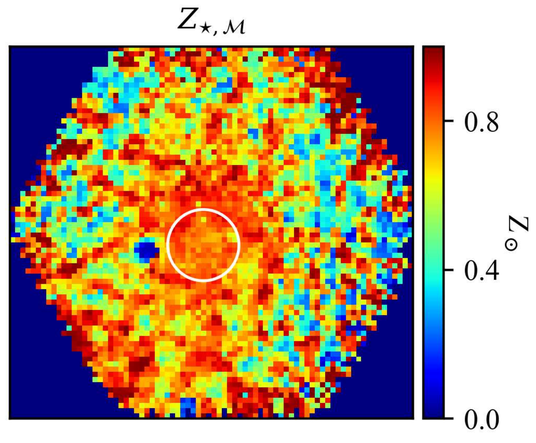

Stellar metallicity/Age & Hα flux/EW profiles

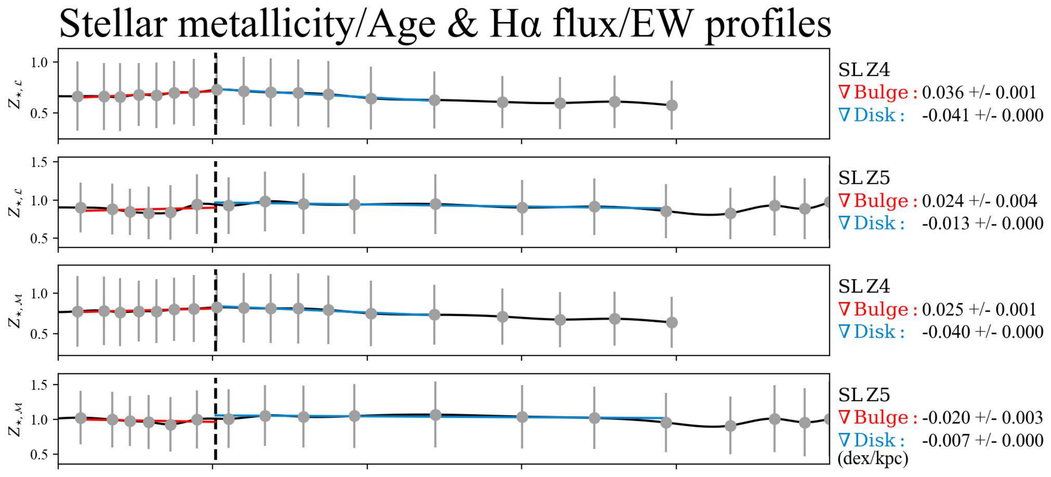

$t_{\star,\mathcal{L}}$

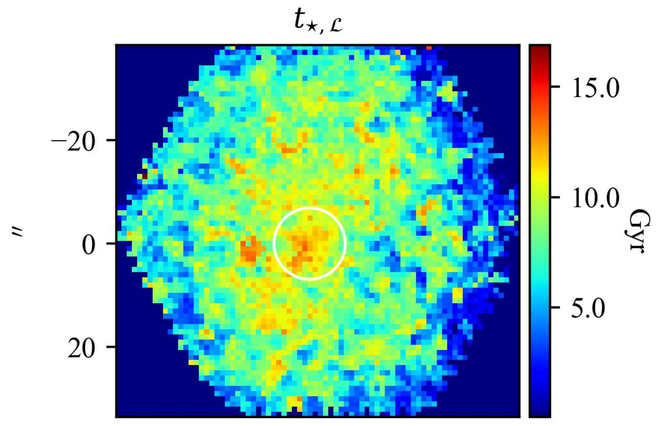

$t_{\star,\mathcal{M}}$

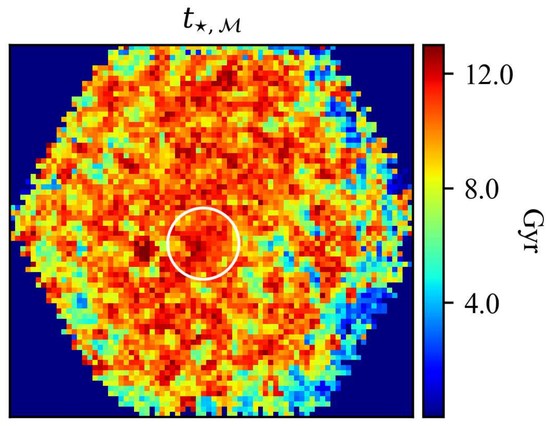

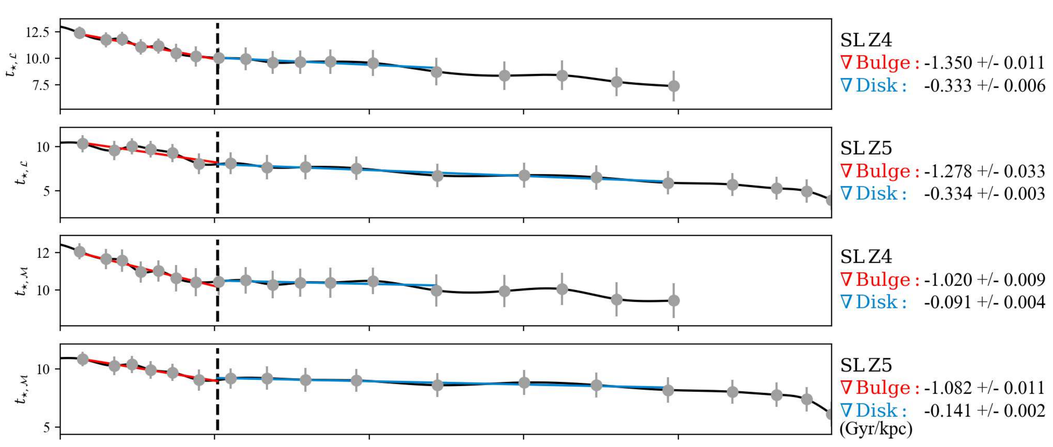

Hα flux

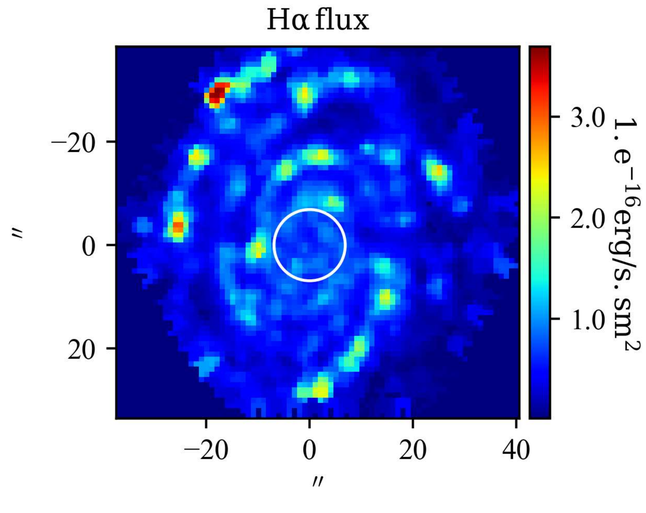

EW(Hα)

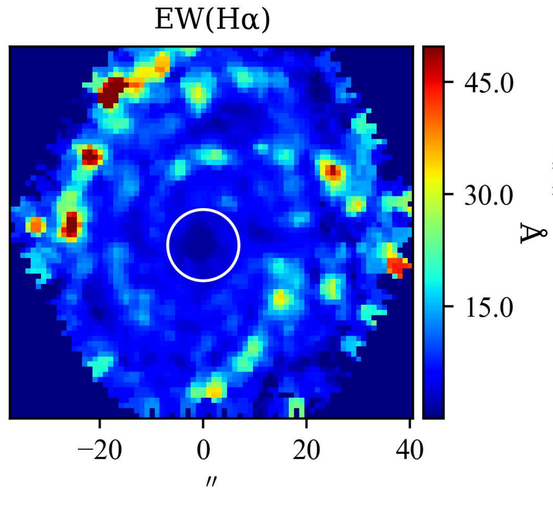

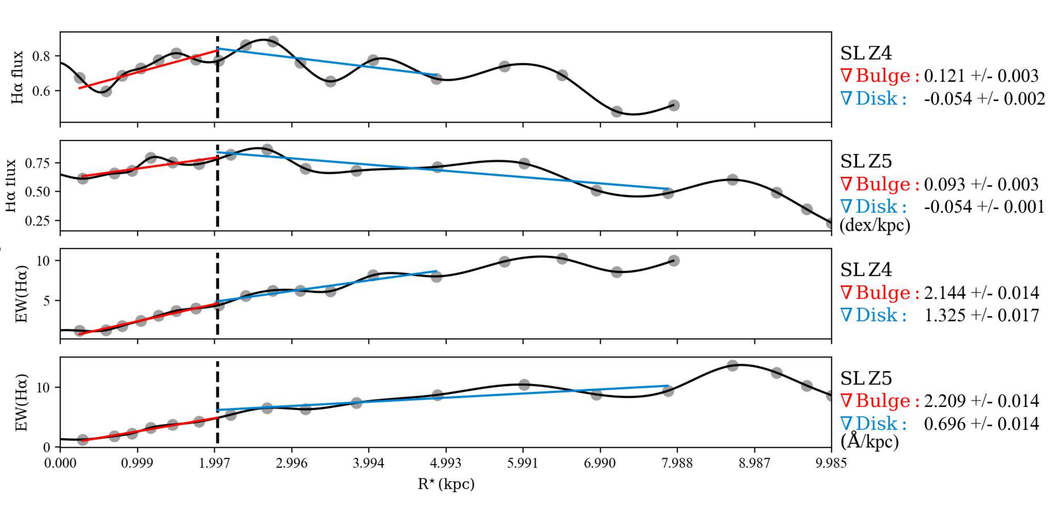

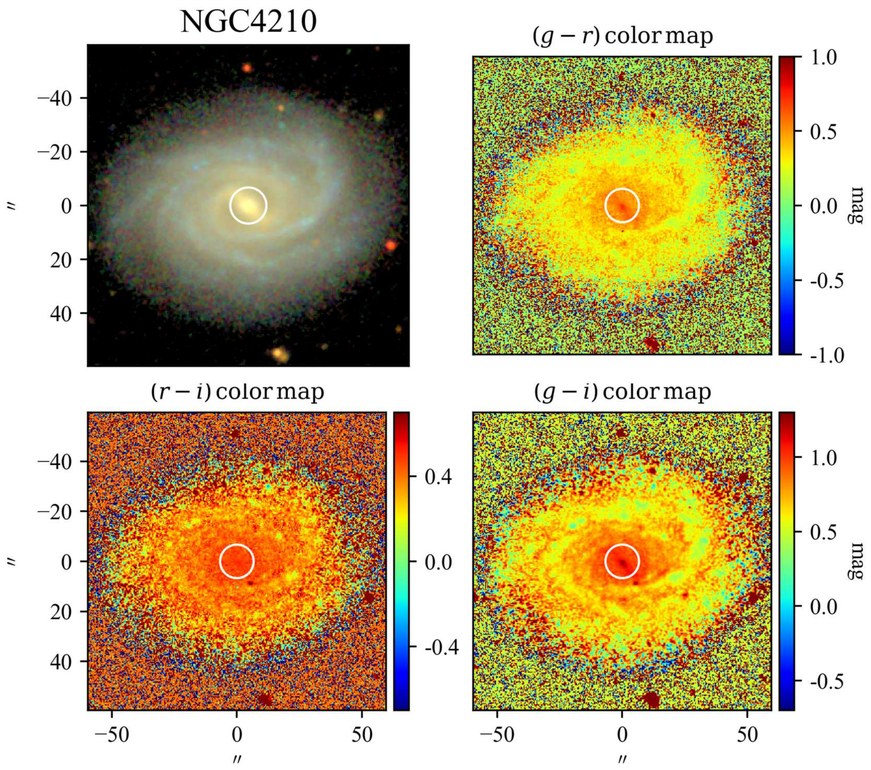

SBP decomposition of SDSS r band

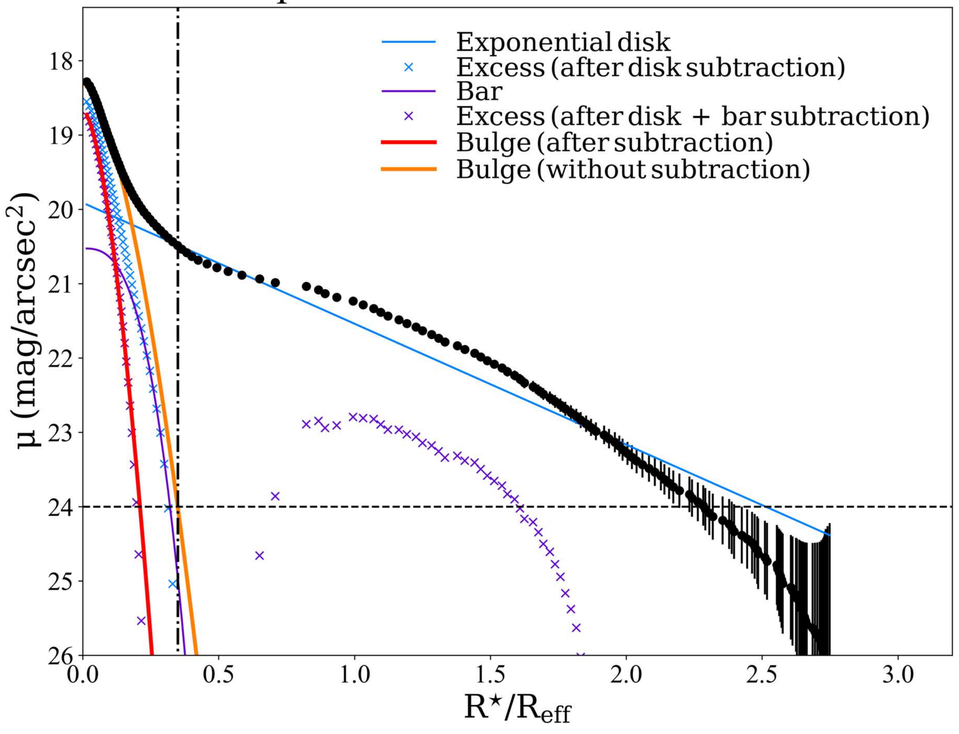

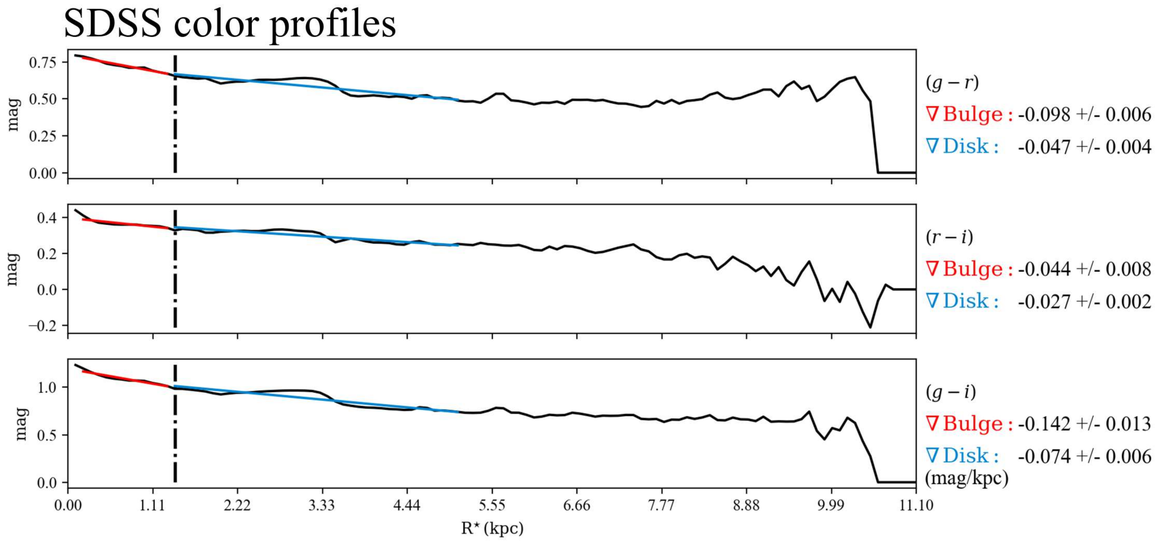

$\mathcal{RV}$ SBPs

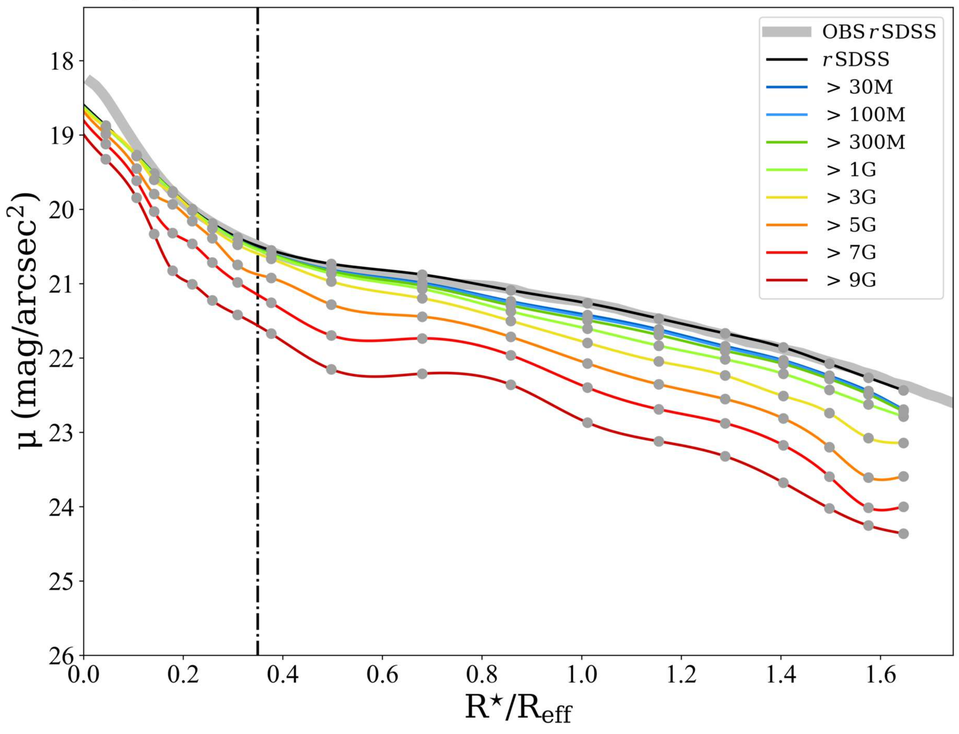

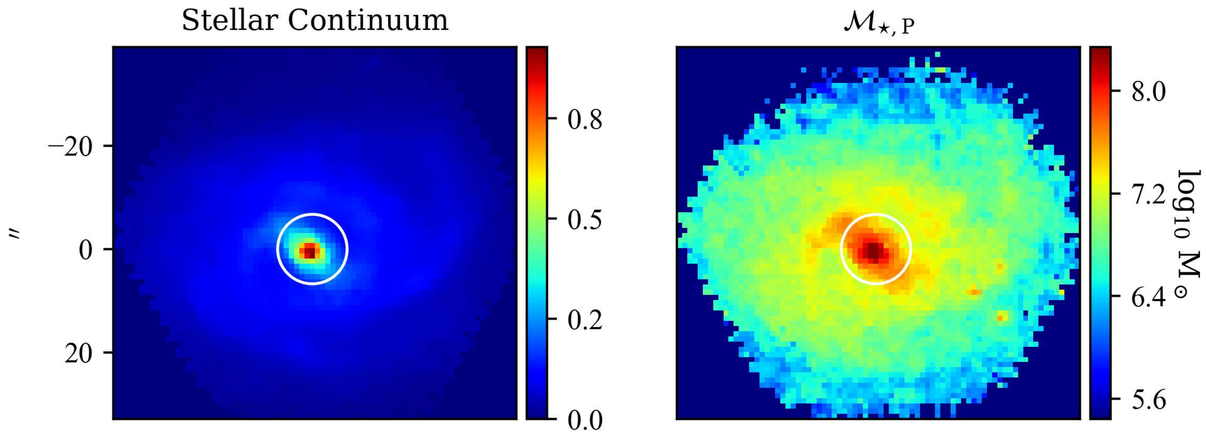

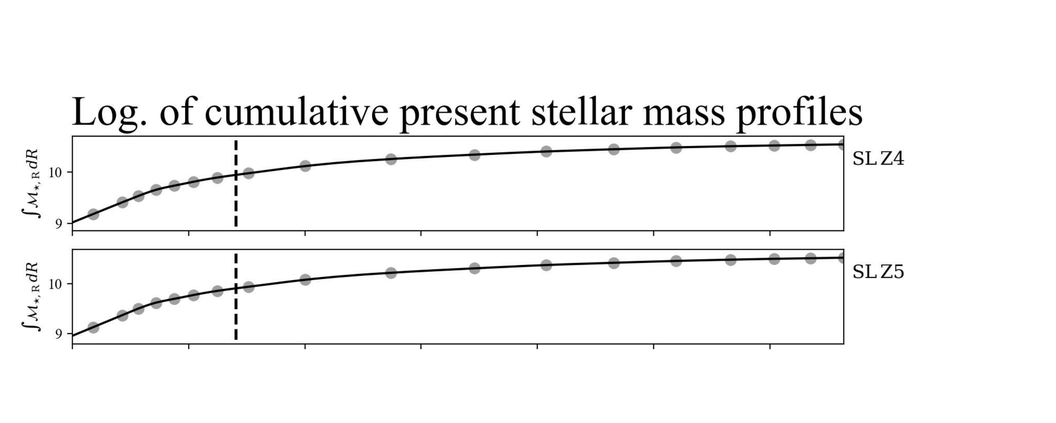

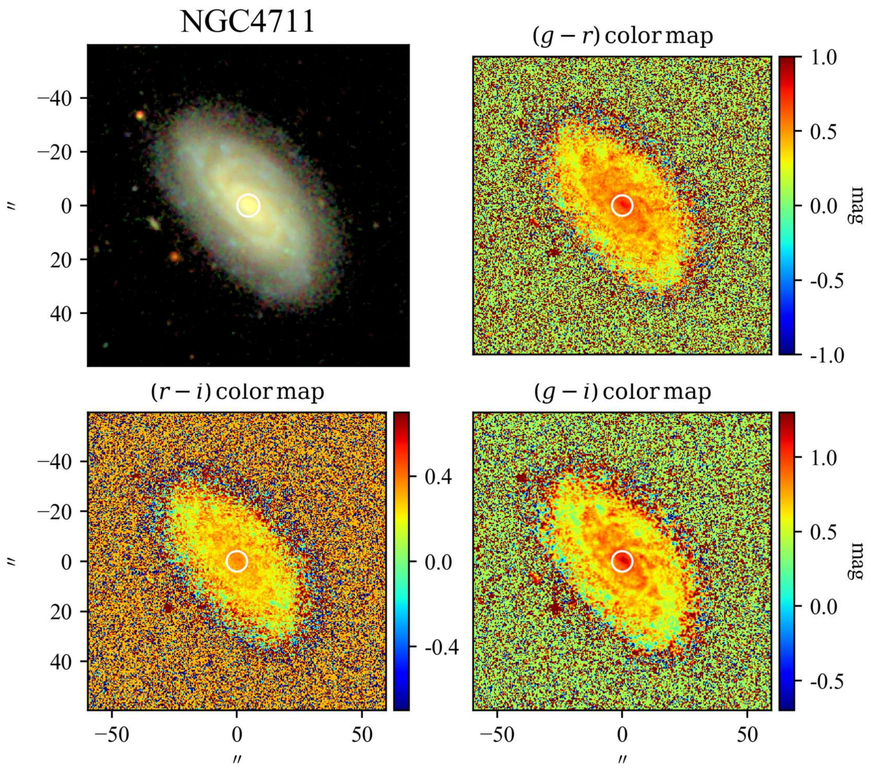

SBP decomposition of SDSS r band

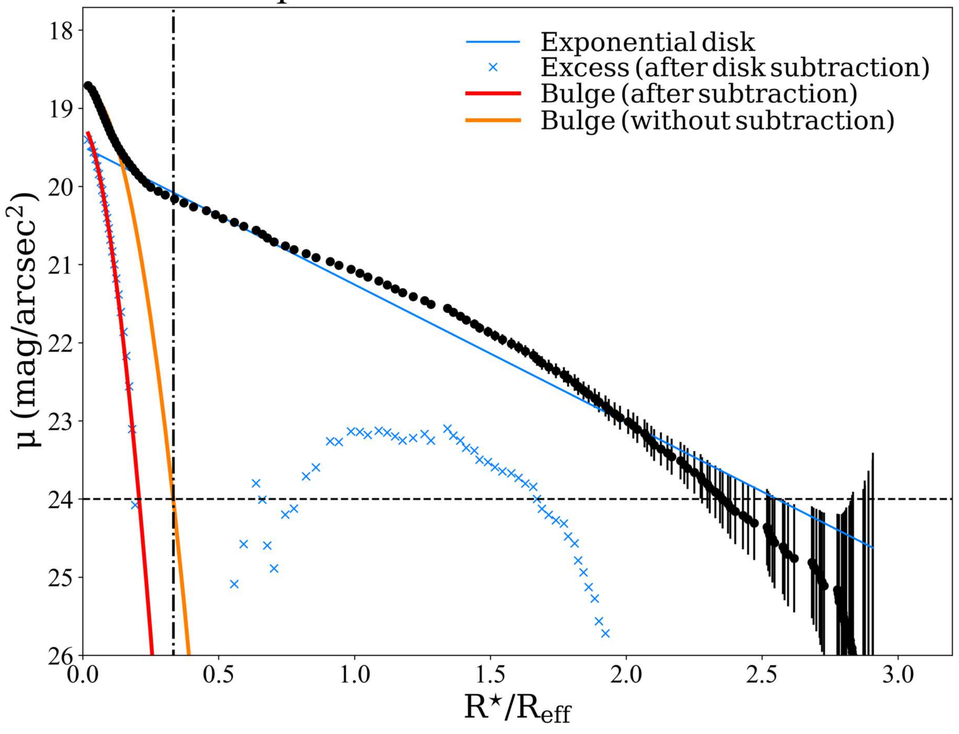

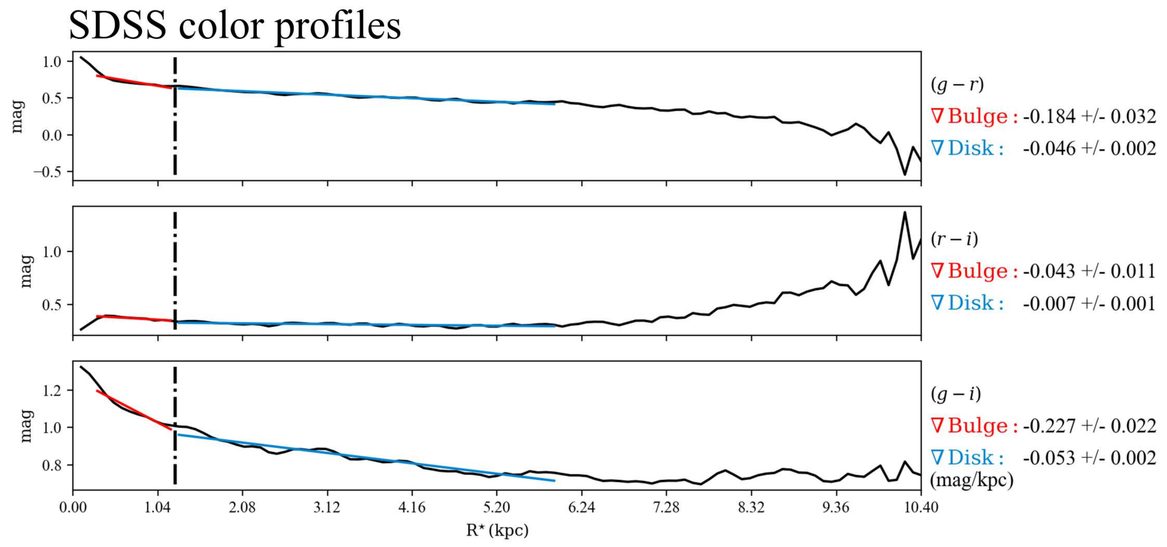

$\mathcal{RV}$ SBPs

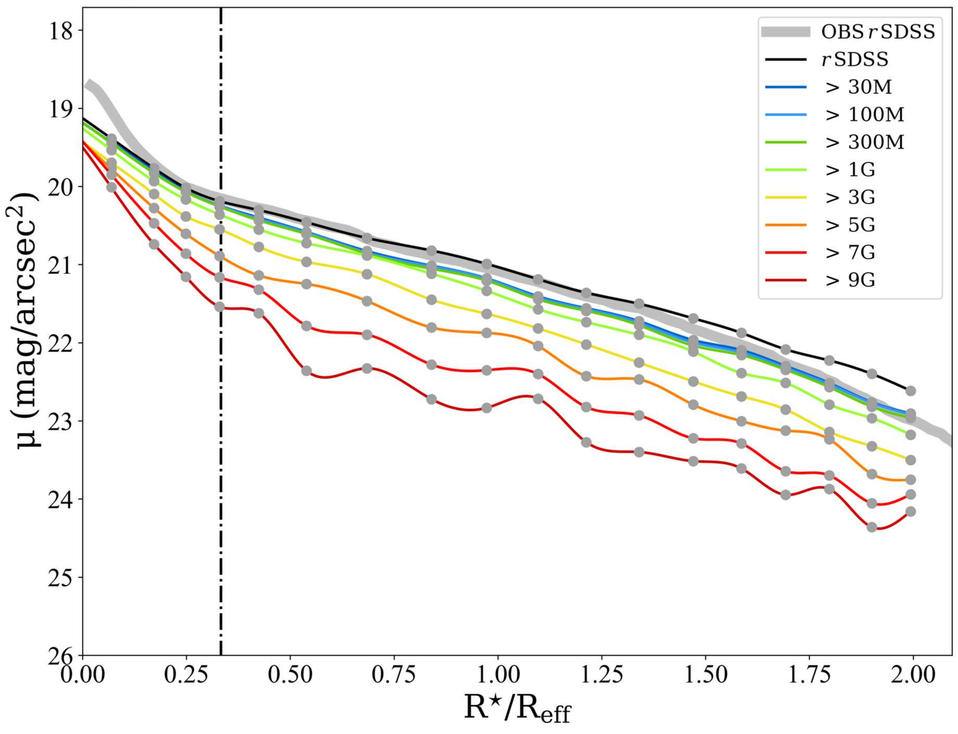

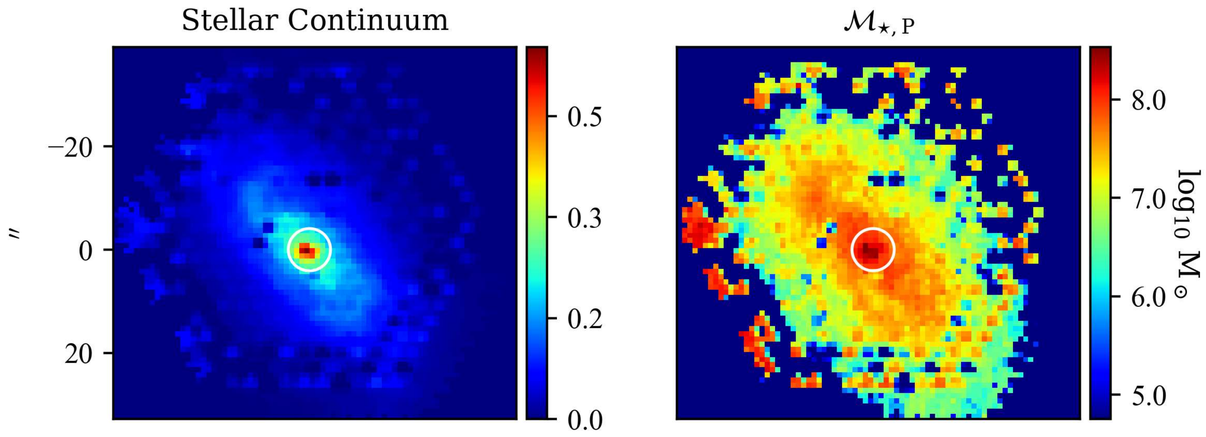

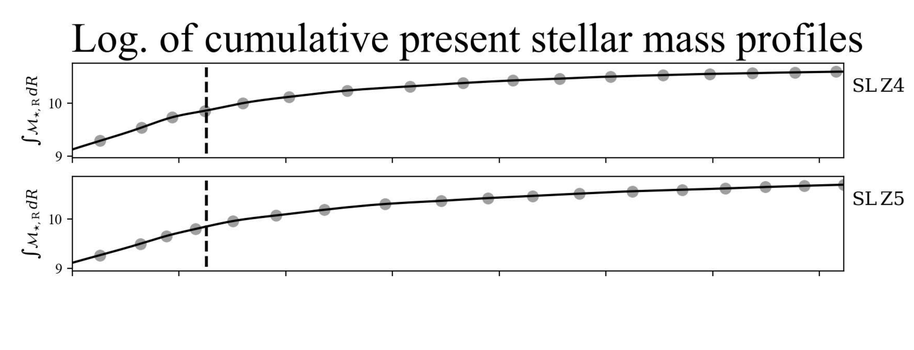

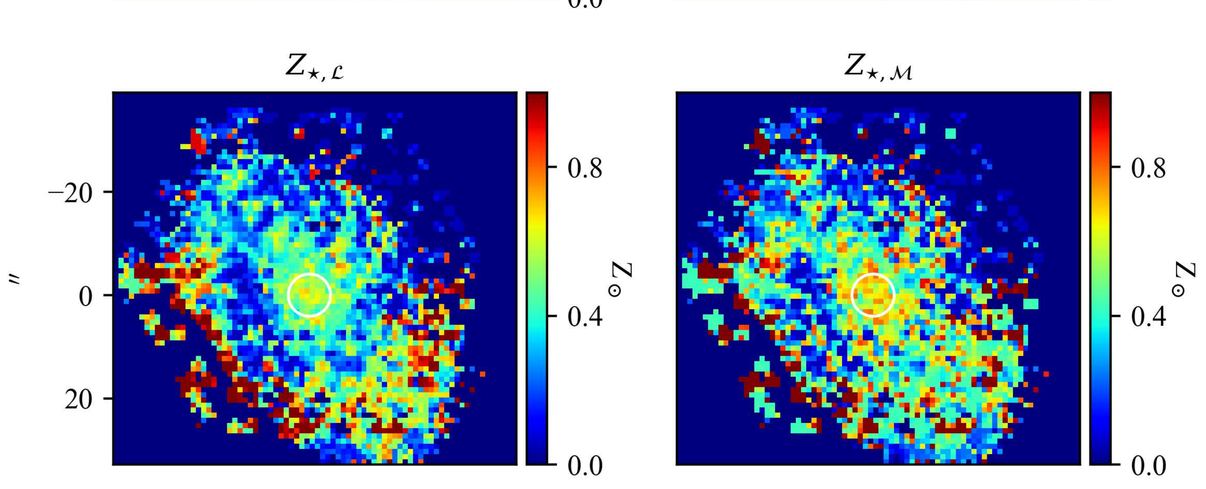

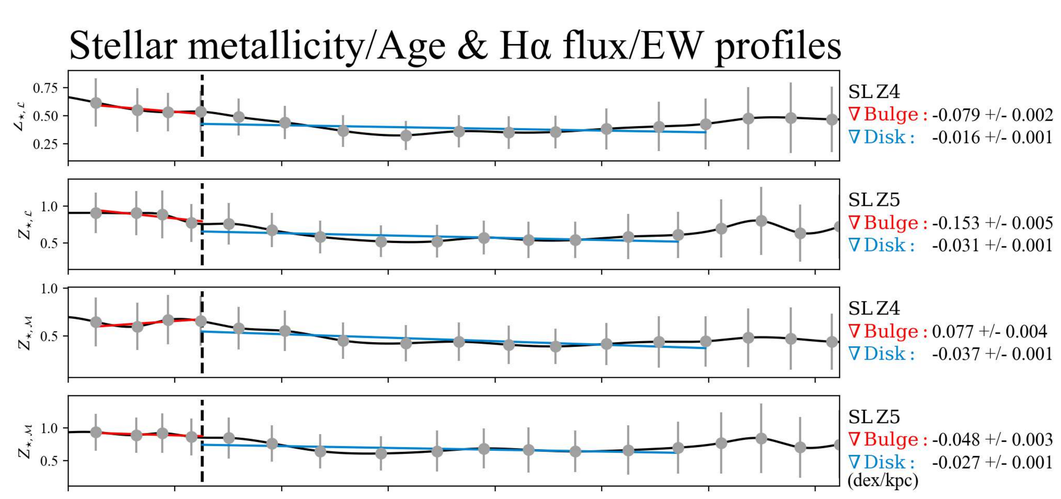

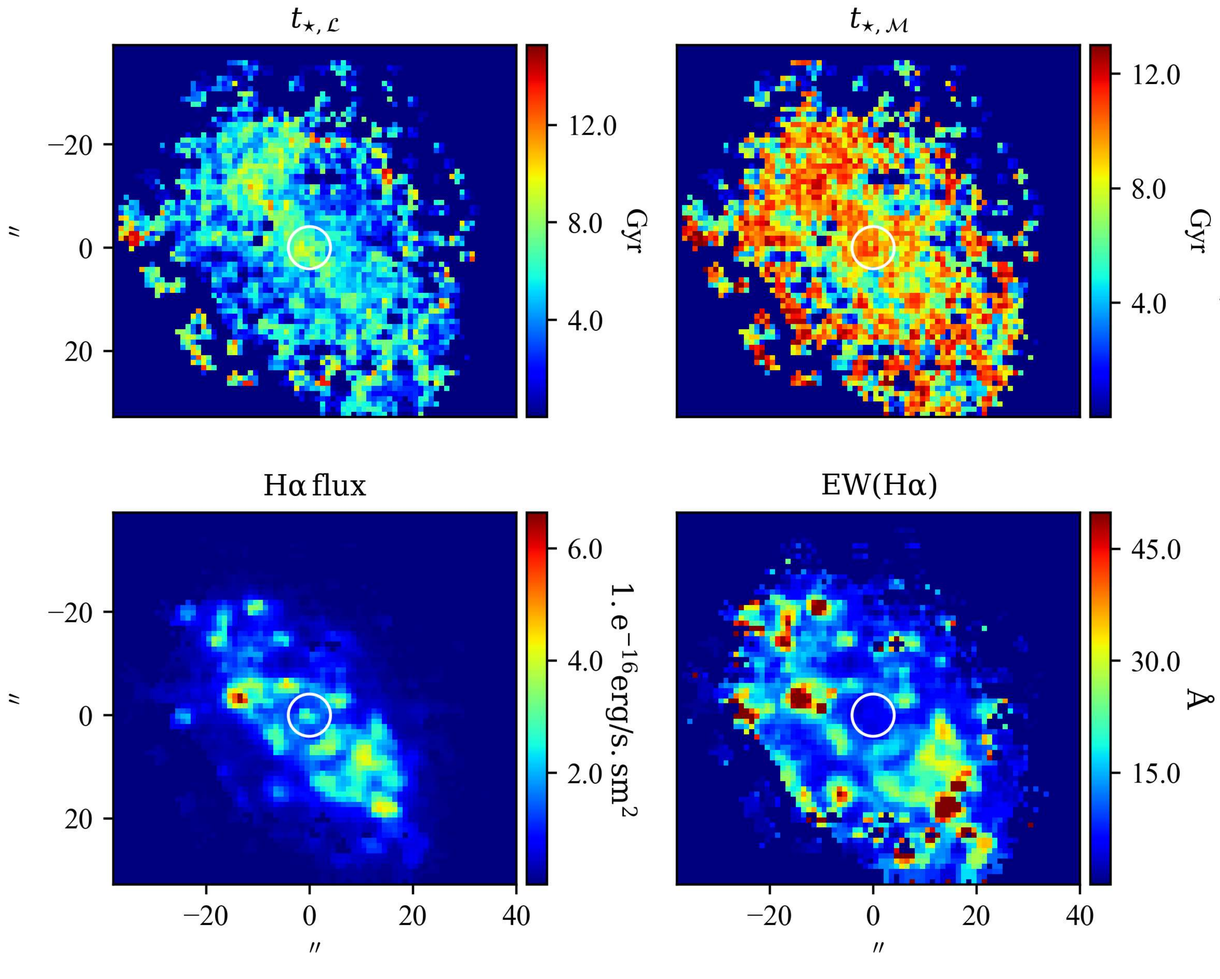

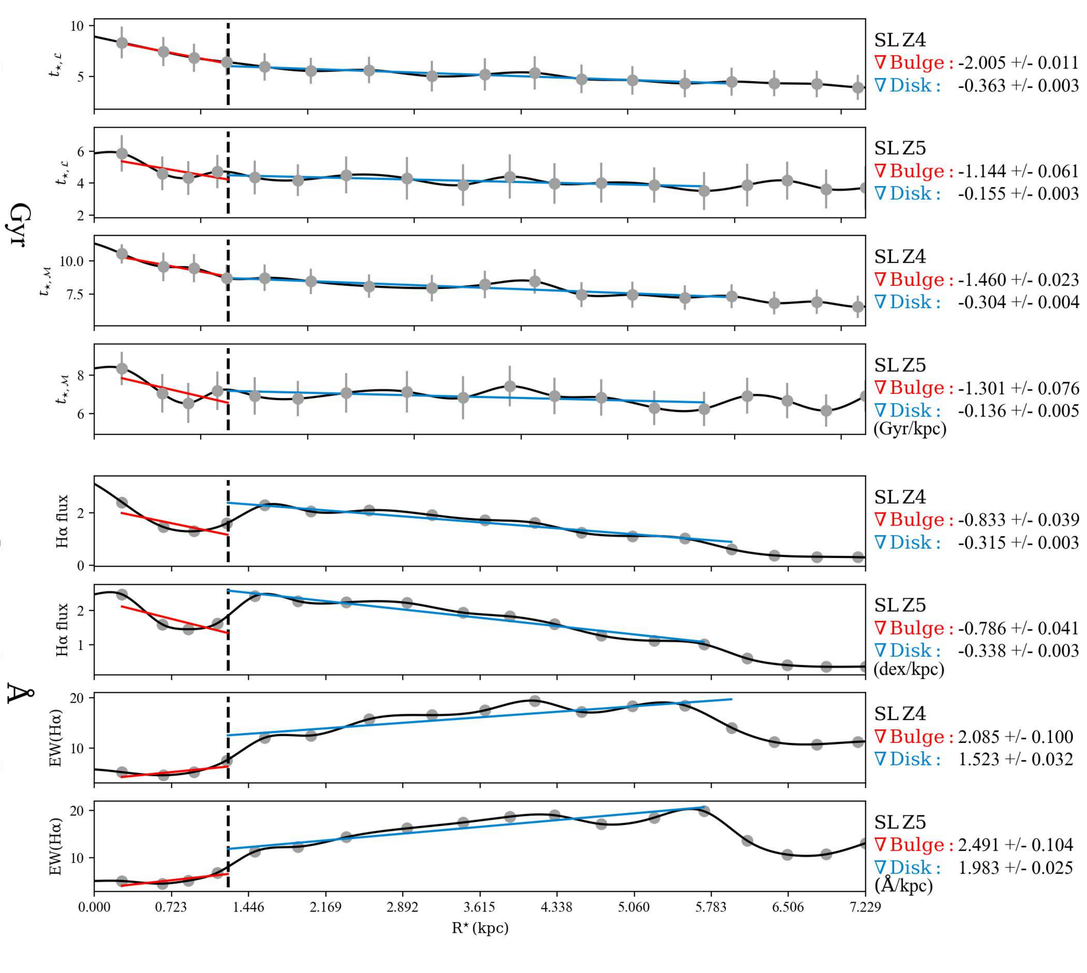

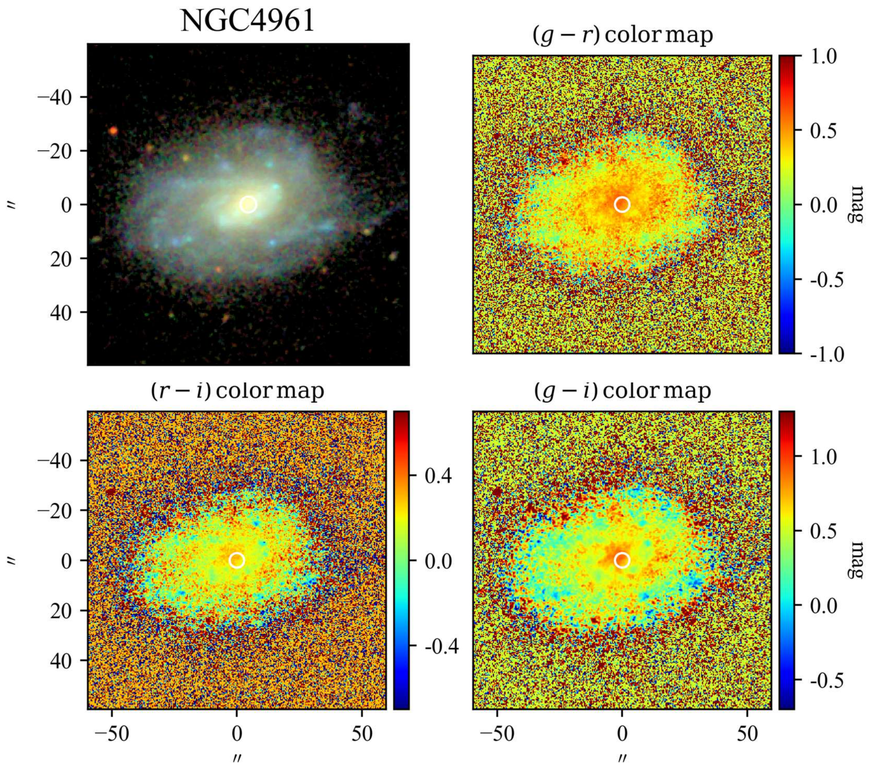
NGC4961
$(g-r)$ color map
$(r-i)$ color map
$(g-i)$ color map
mag
″

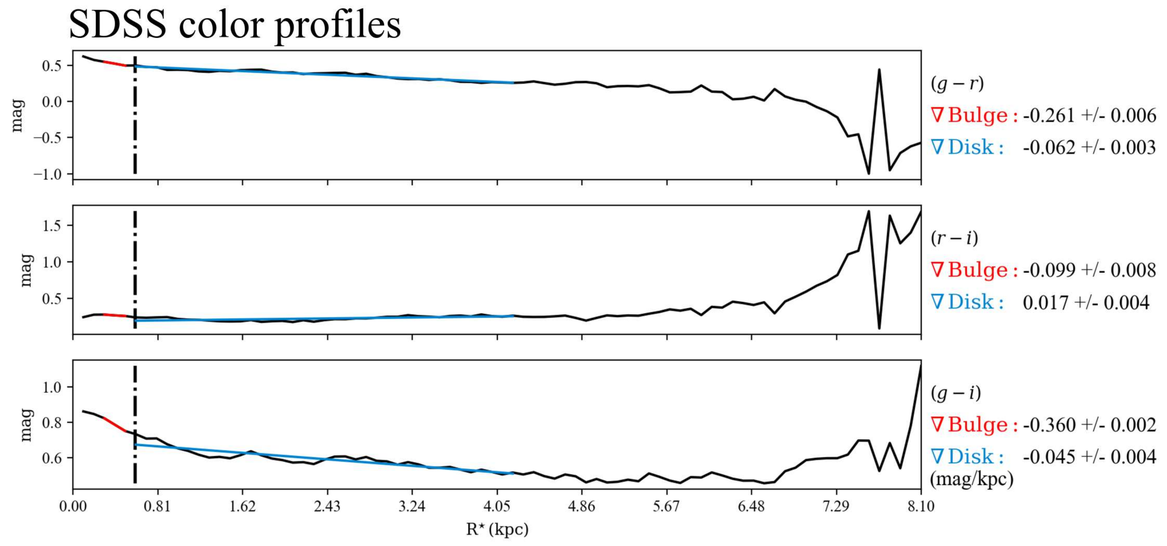
SDSS color profiles
$(g-r)$
∇ Bulge : -0.261 +/- 0.006
∇ Disk : -0.062 +/- 0.003
$(r-i)$
∇ Bulge : -0.099 +/- 0.008
∇ Disk : 0.017 +/- 0.004
$(g-i)$
∇ Bulge : -0.360 +/- 0.002
∇ Disk : -0.045 +/- 0.004
(mag/kpc)
mag
R* (kpc)

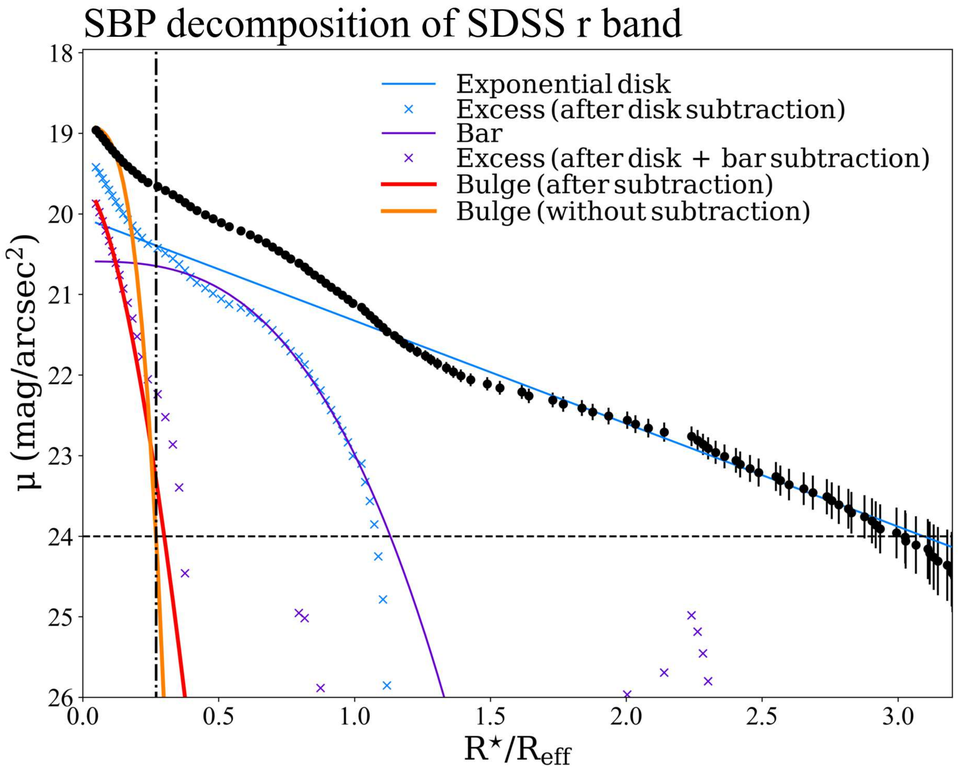
SBP decomposition of SDSS r band
Exponential disk
Excess (after disk subtraction)
Bar
Excess (after disk + bar subtraction)
Bulge (after subtraction)
Bulge (without subtraction)
μ (mag/arcsec²)
R*/Reff

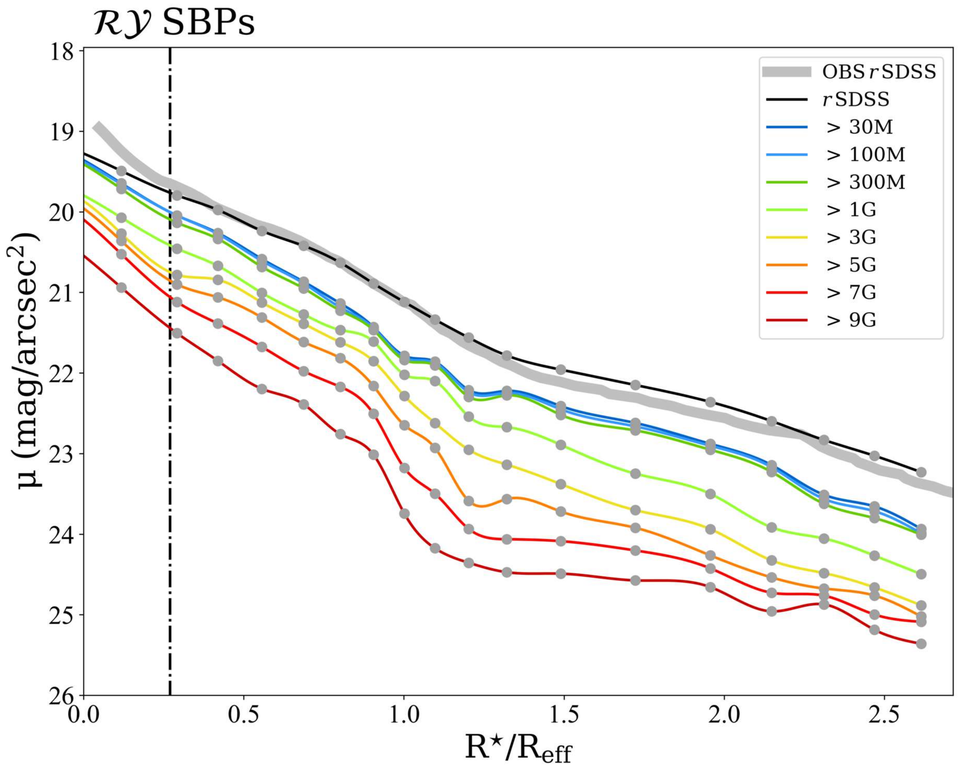
$\mathcal{RY}$ SBPs
OBS rSDSS
rSDSS
> 30M
> 100M
> 300M
> 1G
> 3G
> 5G
> 7G
> 9G
μ (mag/arcsec²)
R*/Reff

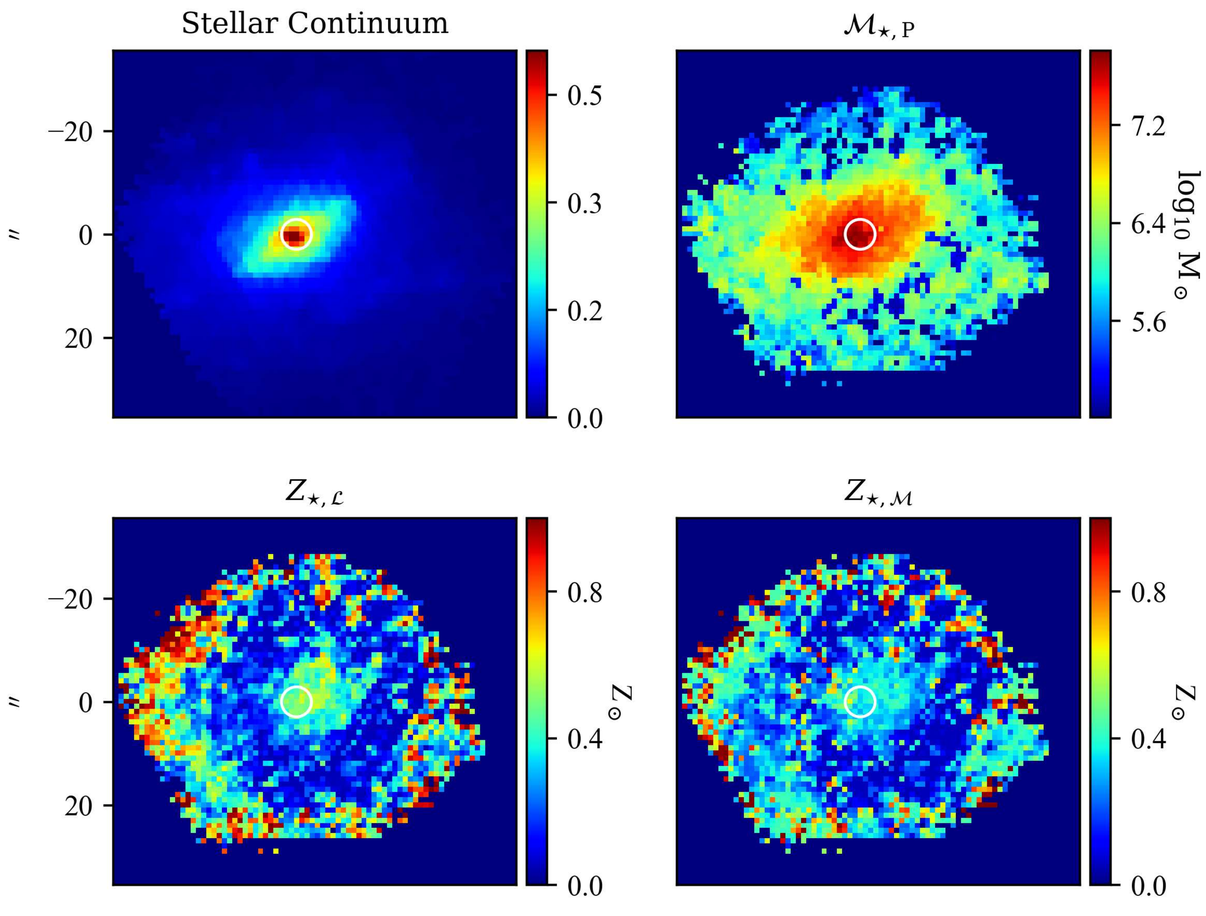
Stellar Continuum
$\mathcal{M}_{\star,\mathrm{P}}$
$Z_{\star,\mathcal{L}}$
$Z_{\star,\mathcal{M}}$
log10 M⊙
Z⊙
″

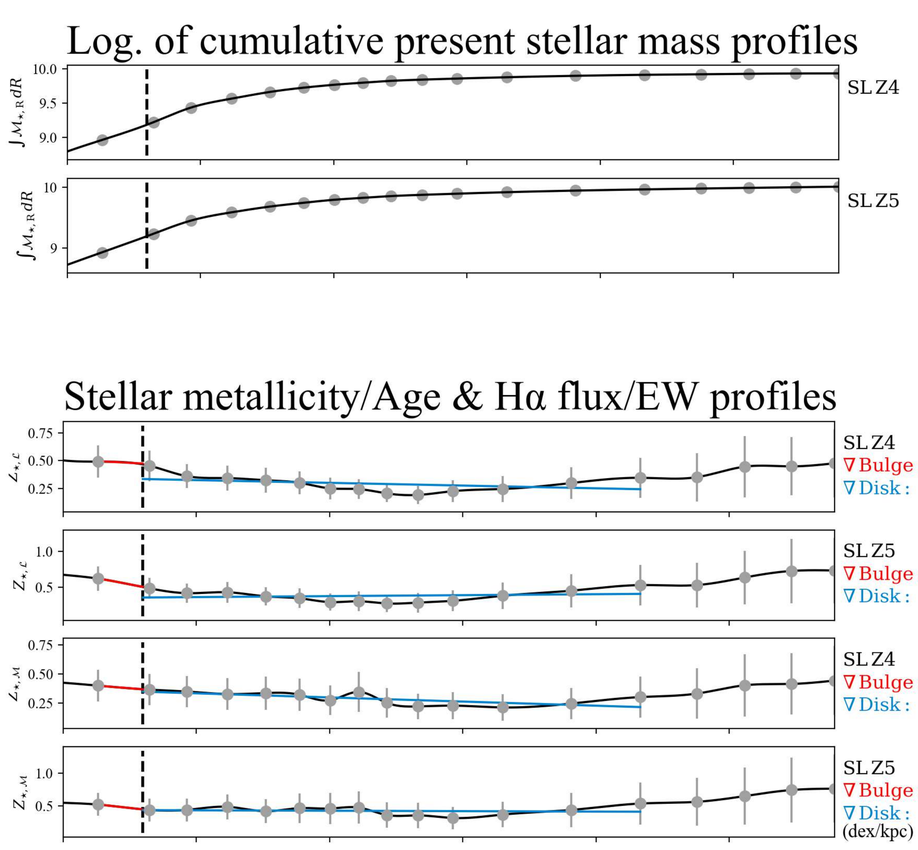
Log. of cumulative present stellar mass profiles
SL Z4
SL Z5
Stellar metallicity/Age & Hα flux/EW profiles
SL Z4
∇ Bulge : -0.065 +/- 0.002
∇ Disk : -0.025 +/- 0.001
SL Z5
∇ Bulge : -0.354 +/- 0.001
∇ Disk : 0.014 +/- 0.002
SL Z4
∇ Bulge : -0.093 +/- 0.000
∇ Disk : -0.035 +/- 0.001
SL Z5
∇ Bulge : -0.224 +/- 0.000
∇ Disk : -0.006 +/- 0.001
(dex/kpc)

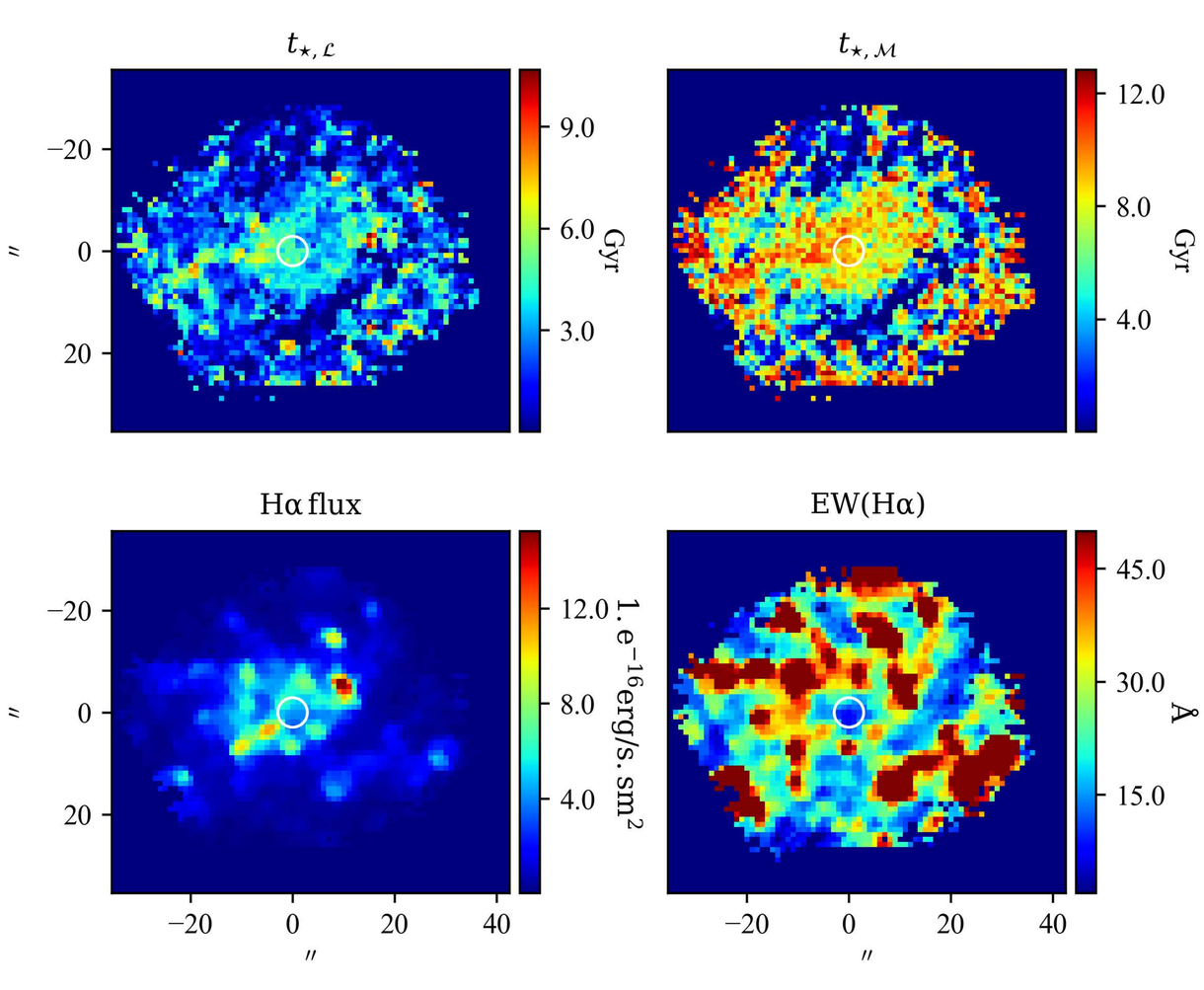
$t_{\star,\mathcal{L}}$
$t_{\star,\mathcal{M}}$
Gyr
Hα flux
EW(Hα)
1. e⁻¹⁶erg/s. sm²
Å
″

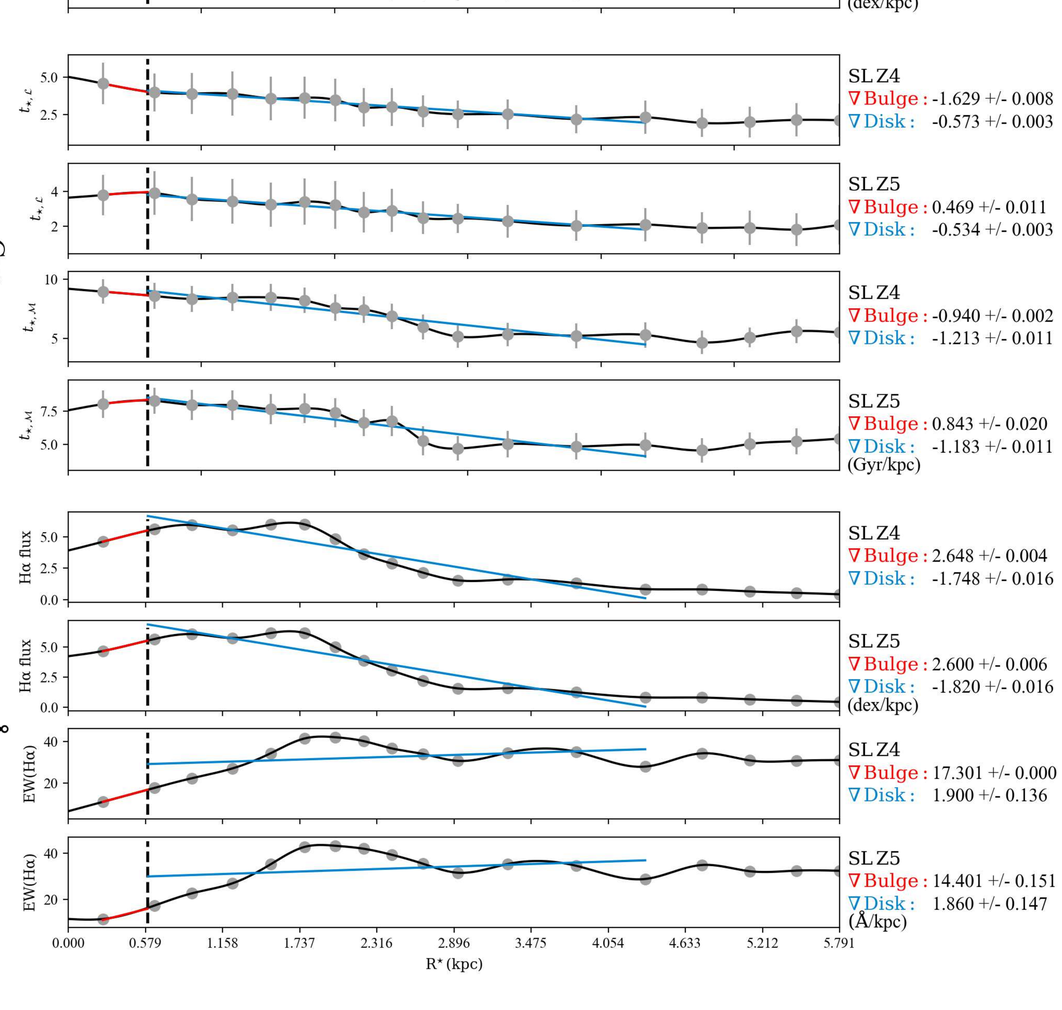
SL Z4
∇ Bulge : -1.629 +/- 0.008
∇ Disk : -0.573 +/- 0.003
SL Z5
∇ Bulge : 0.469 +/- 0.011
∇ Disk : -0.534 +/- 0.003
SL Z4
∇ Bulge : -0.940 +/- 0.002
∇ Disk : -1.213 +/- 0.011
SL Z5
∇ Bulge : 0.843 +/- 0.020
∇ Disk : -1.183 +/- 0.011
(Gyr/kpc)
Hα flux
∇ Bulge : 2.648 +/- 0.004
∇ Disk : -1.748 +/- 0.016
SL Z5
∇ Bulge : 2.600 +/- 0.006
∇ Disk : -1.820 +/- 0.016
(dex/kpc)
EW(Hα)
∇ Bulge : 17.301 +/- 0.000
∇ Disk : 1.900 +/- 0.136
SL Z5
∇ Bulge : 14.401 +/- 0.151
∇ Disk : 1.860 +/- 0.147
(Å/kpc)
R* (kpc)

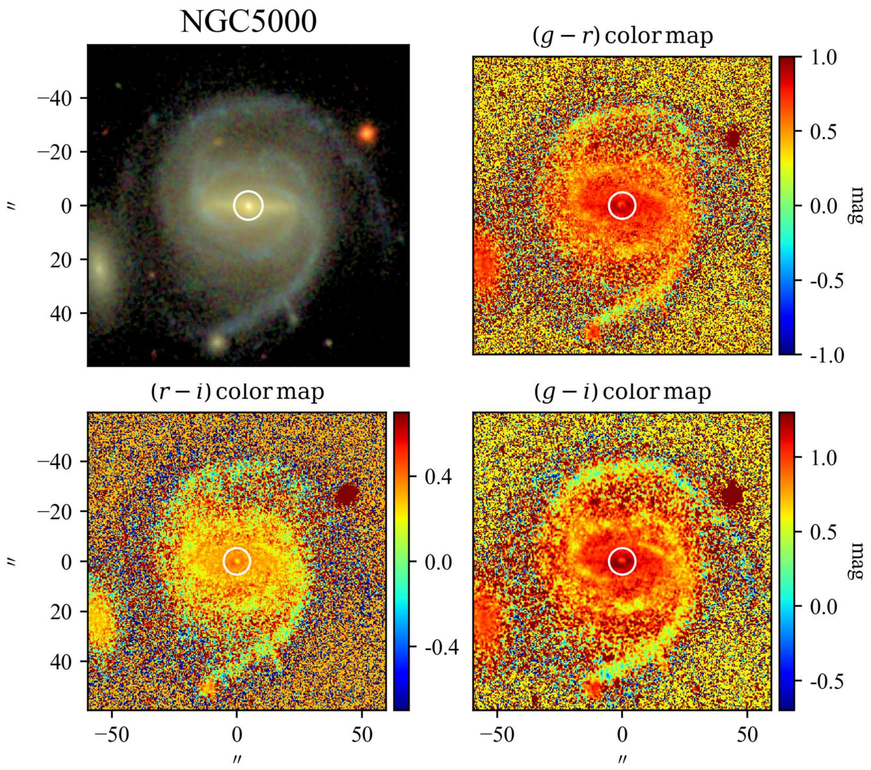

SBP decomposition of SDSS r band

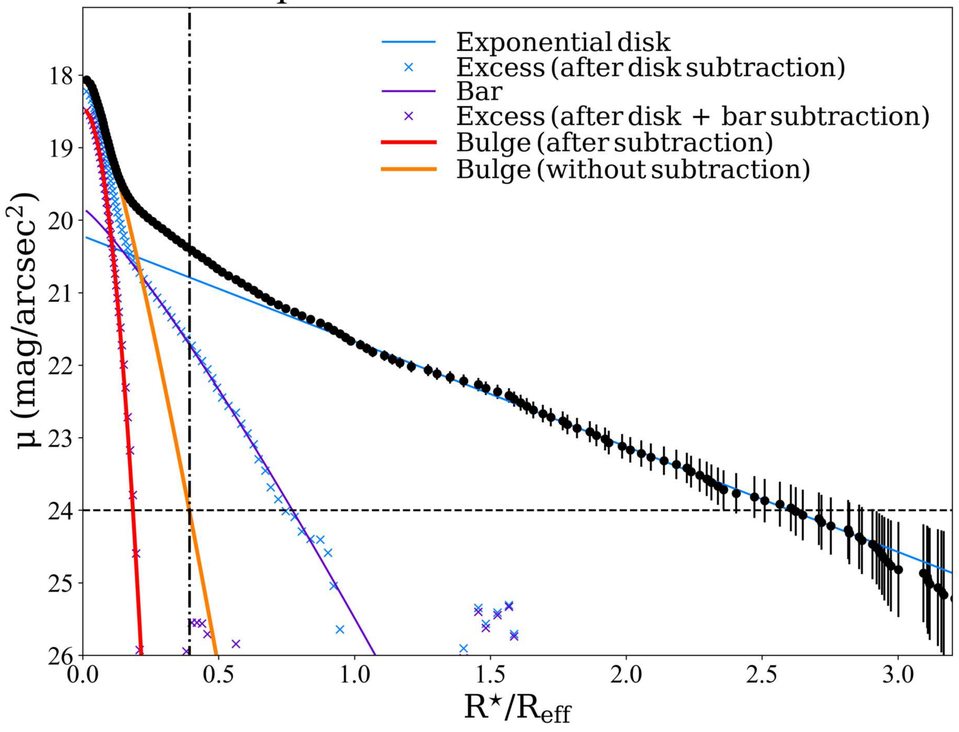

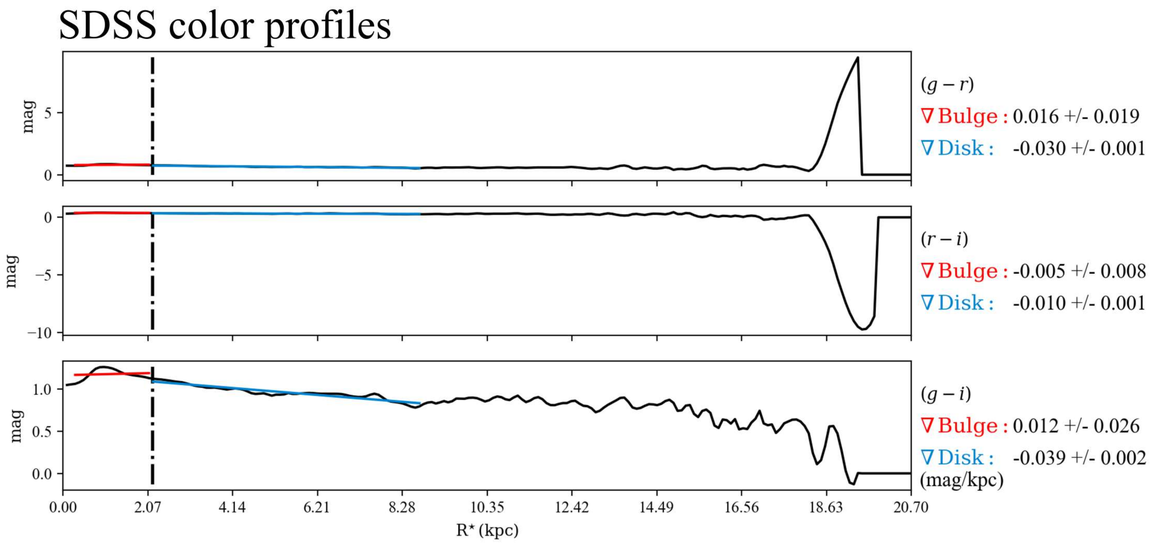

$\mathcal{RV}$ SBPs

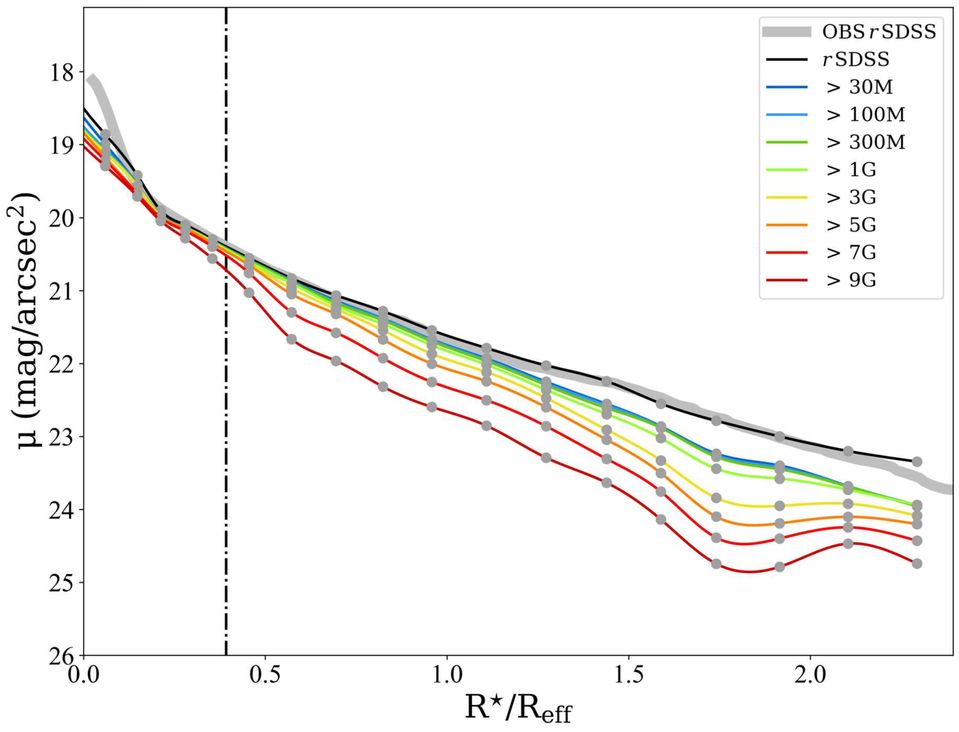

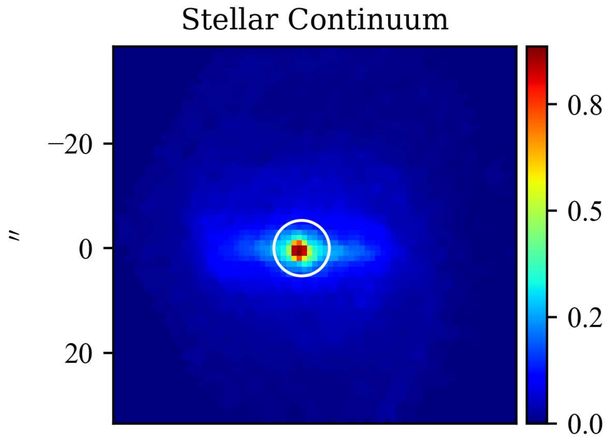

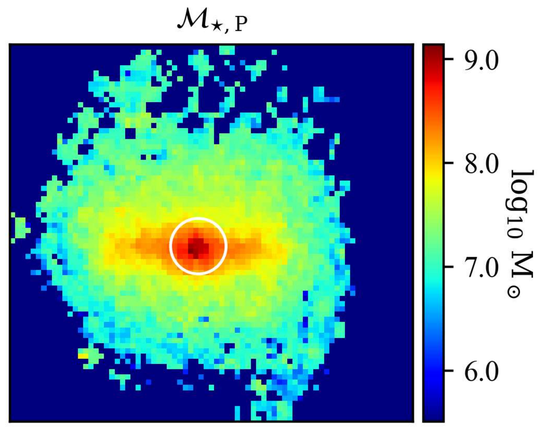

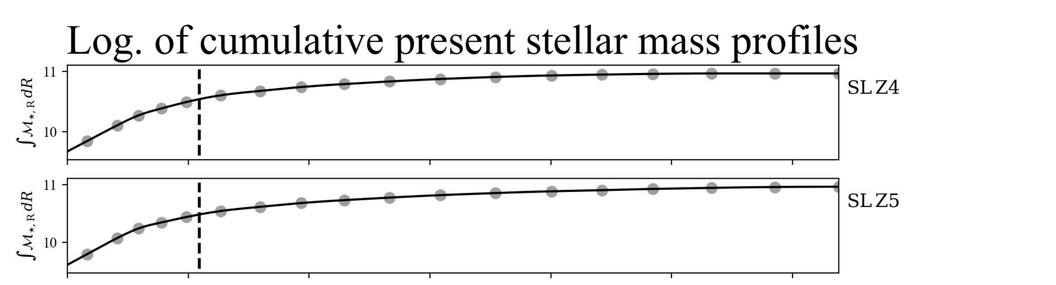

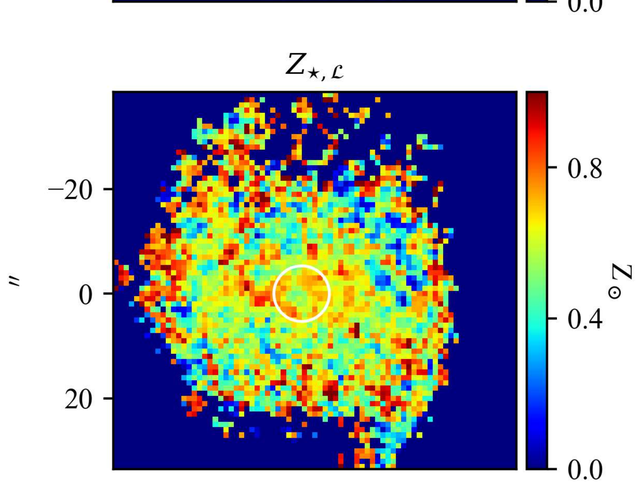

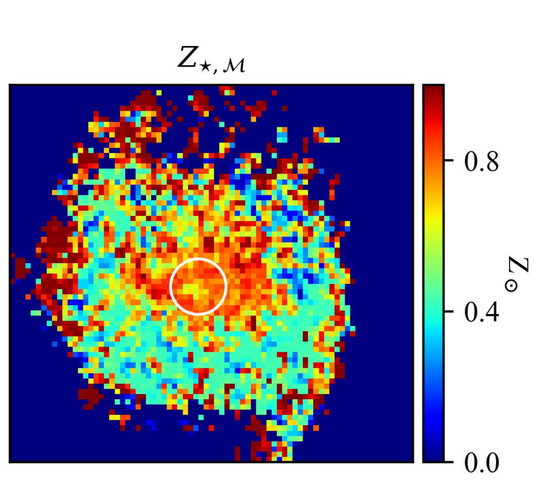

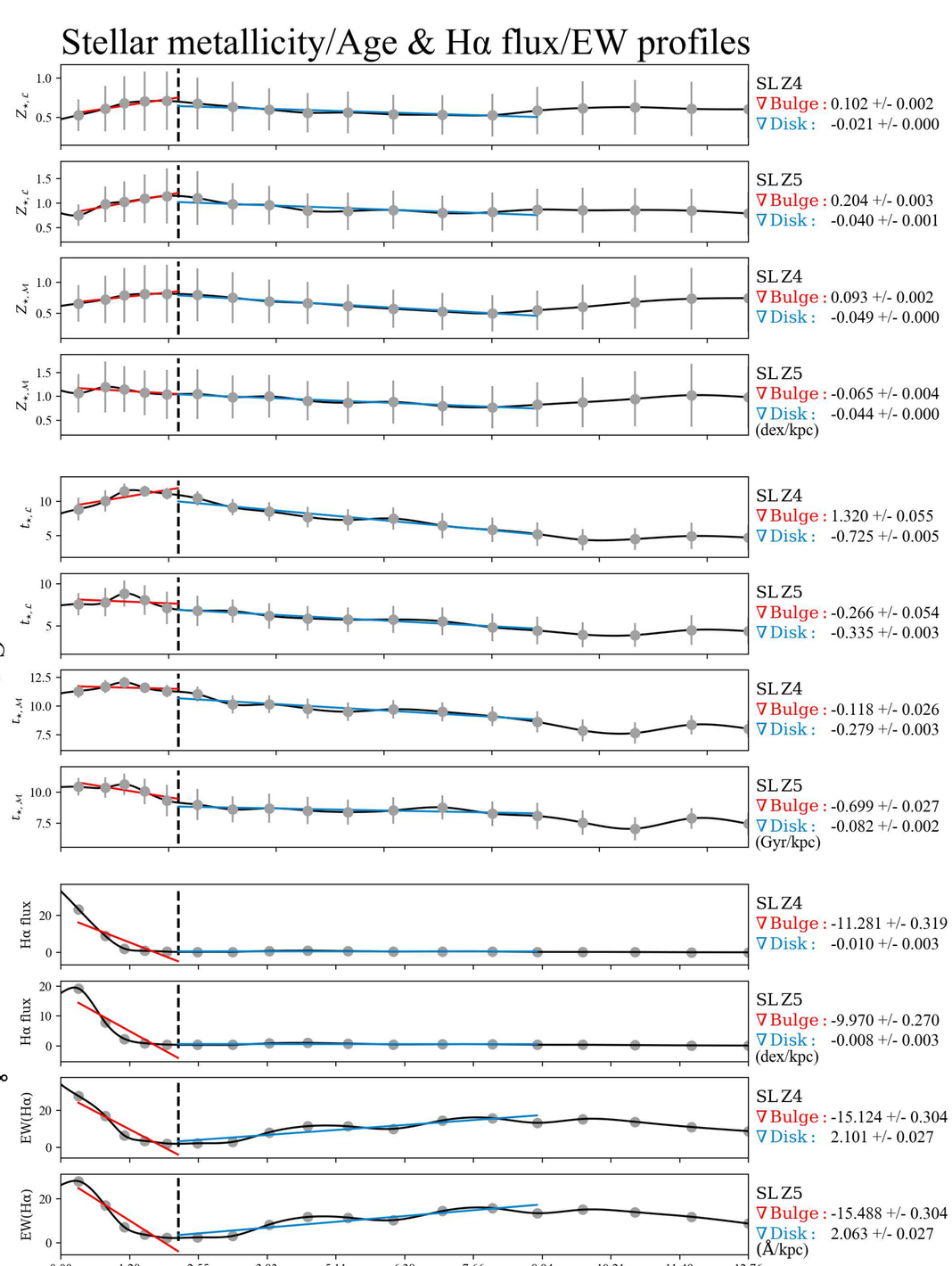

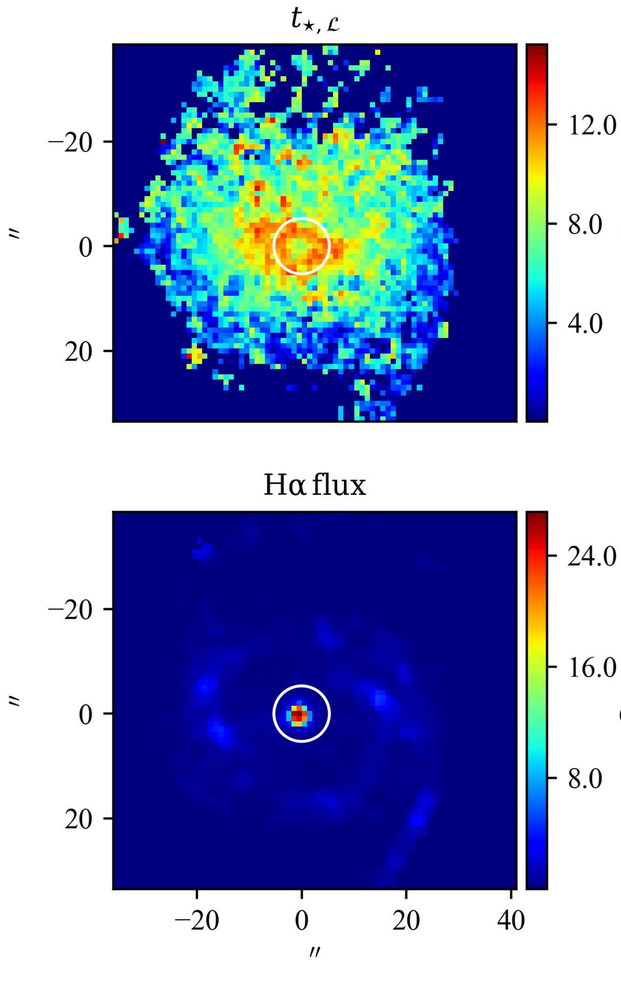

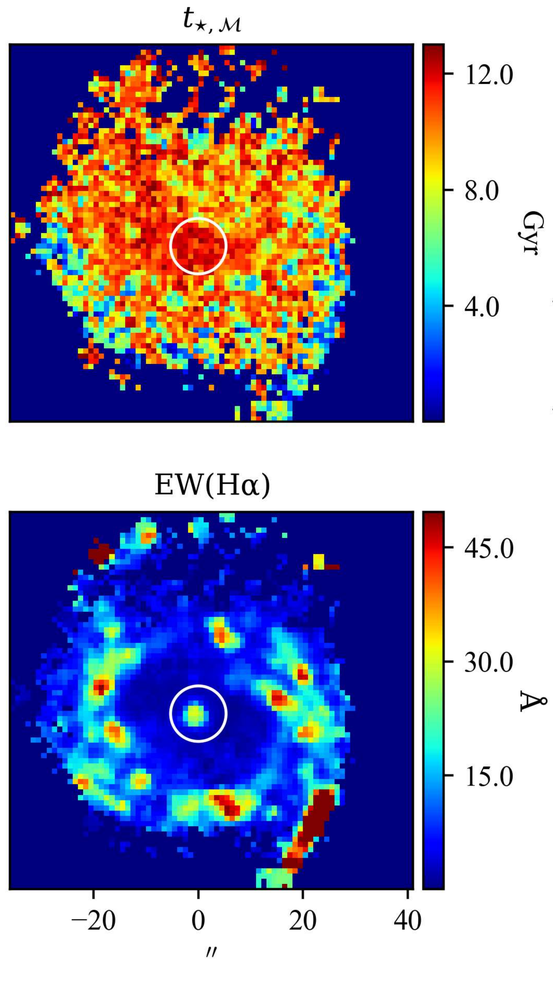

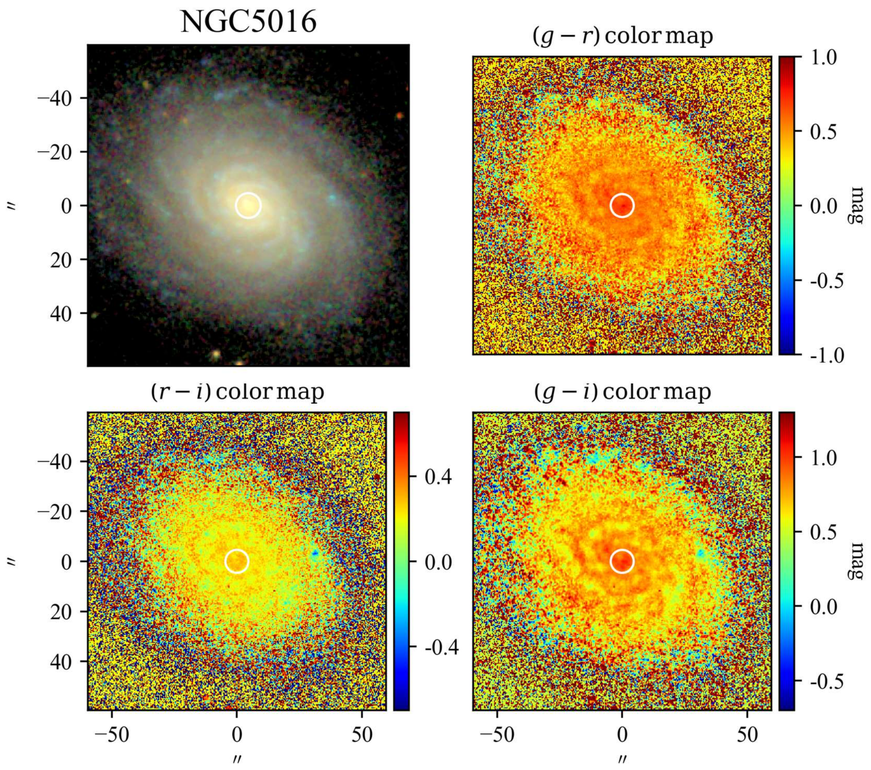

SBP decomposition of SDSS r band

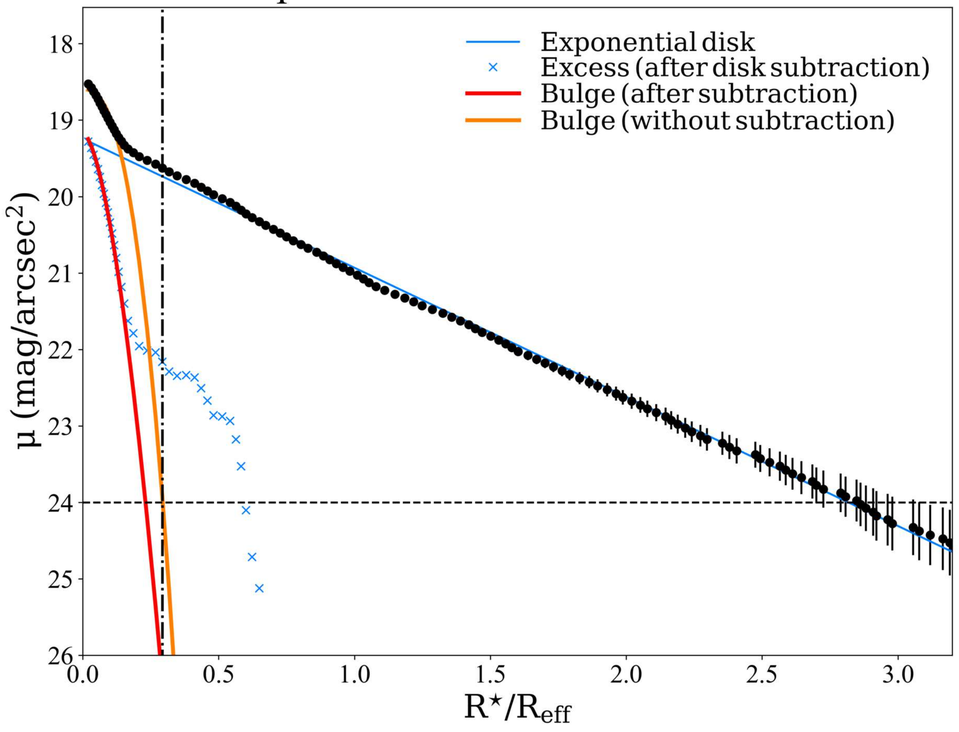

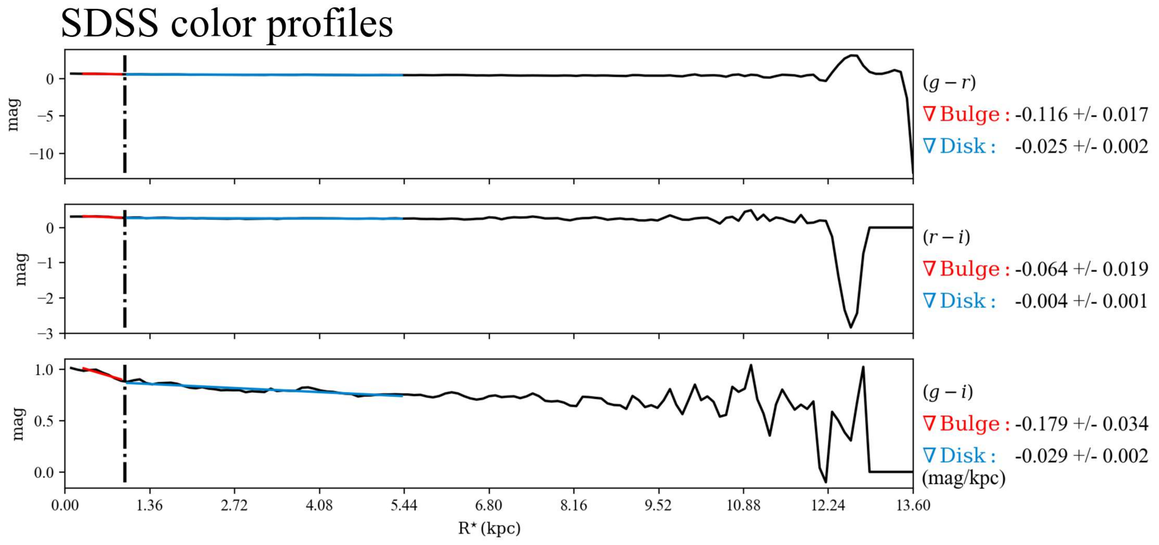

$\mathcal{RY}$ SBPs

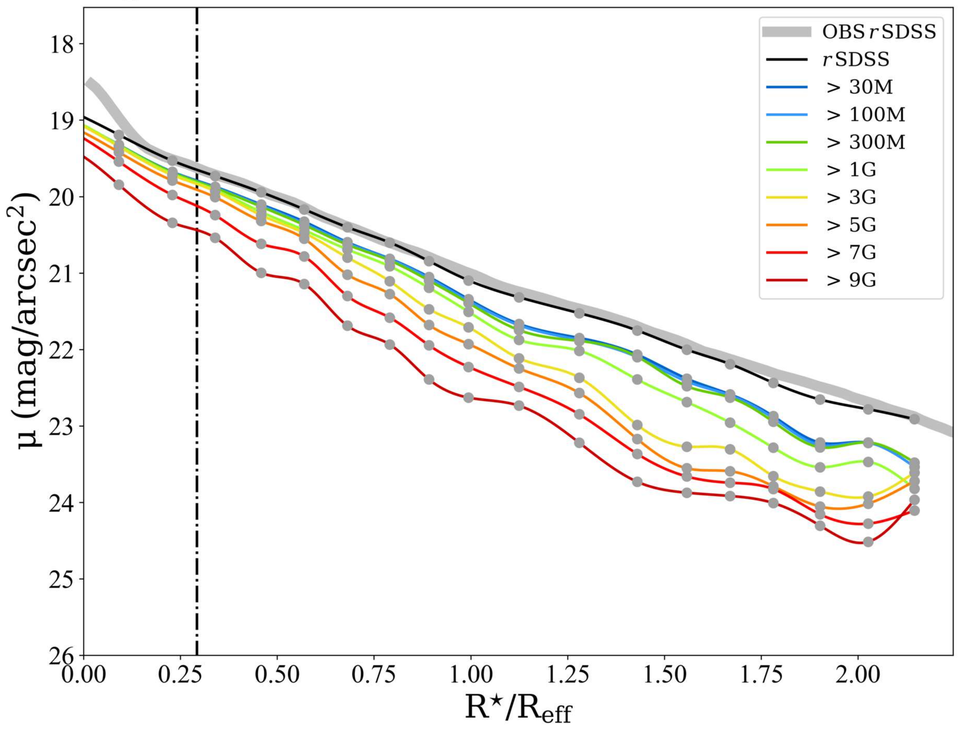

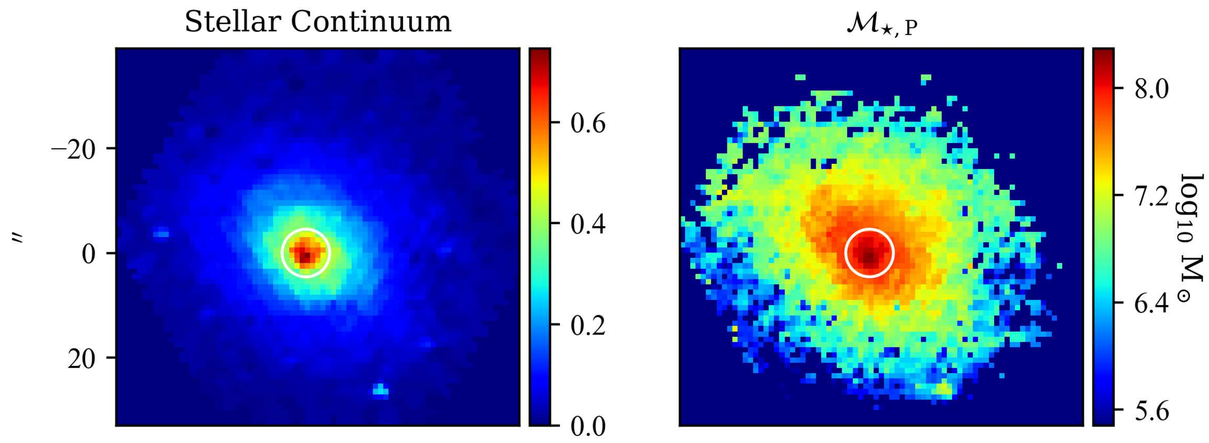

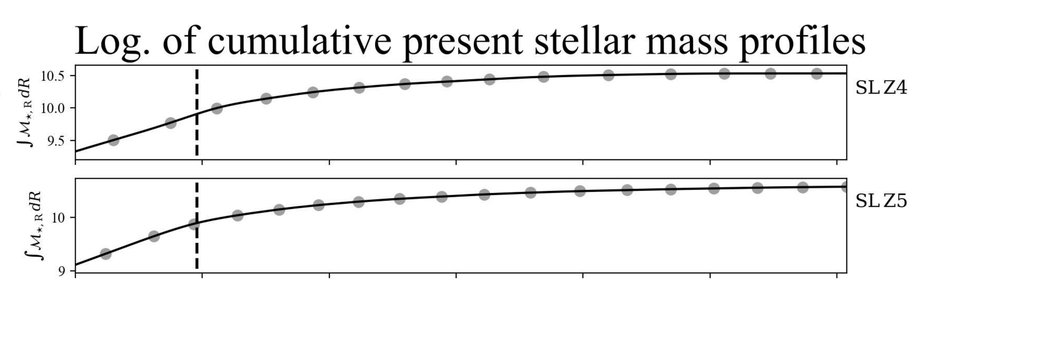

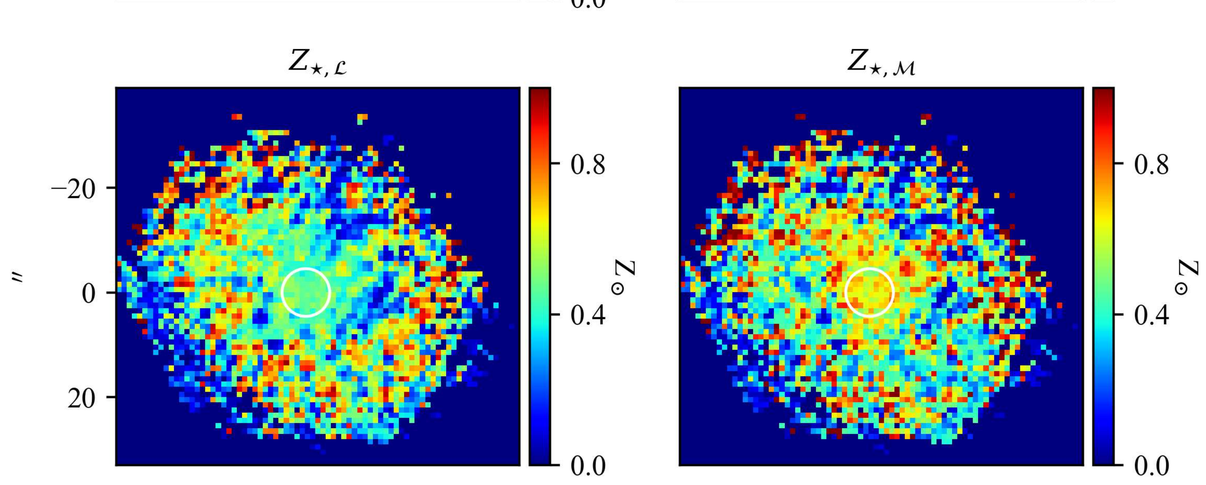

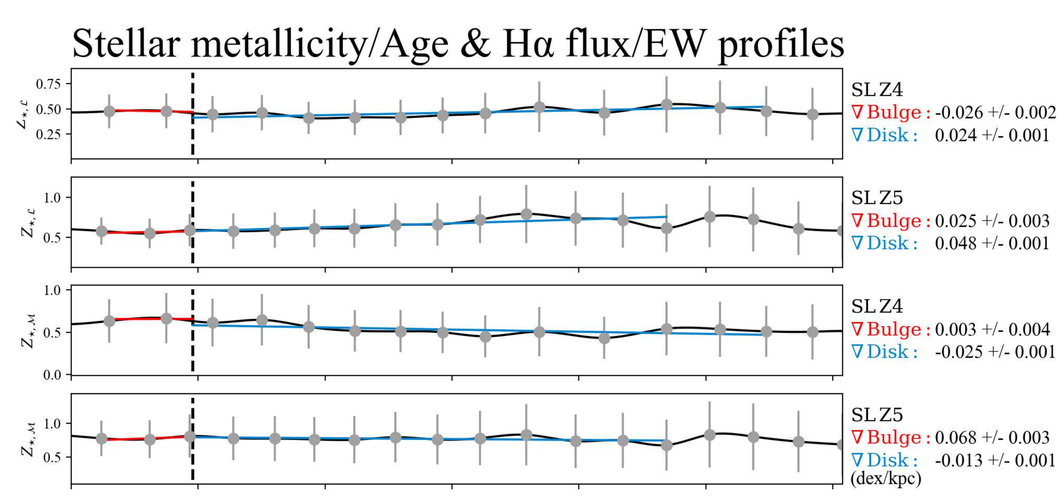

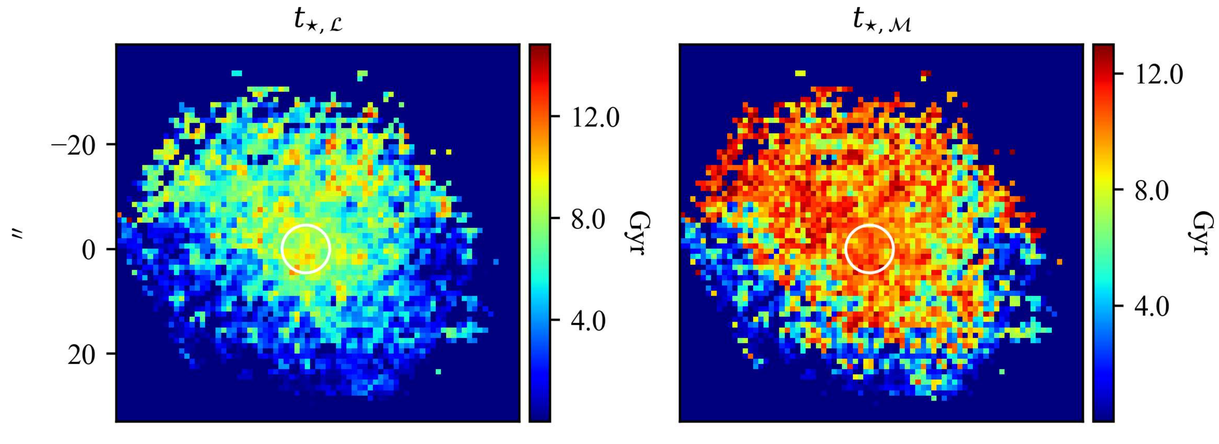

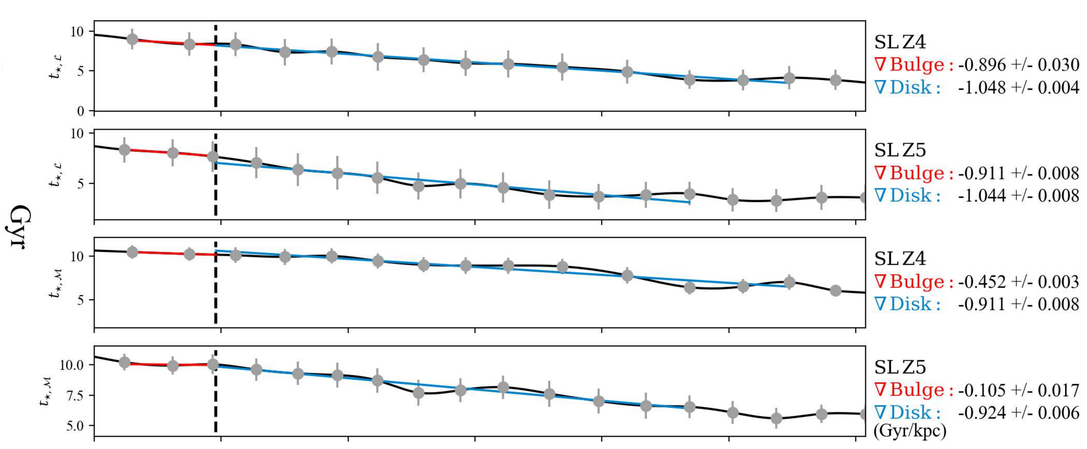

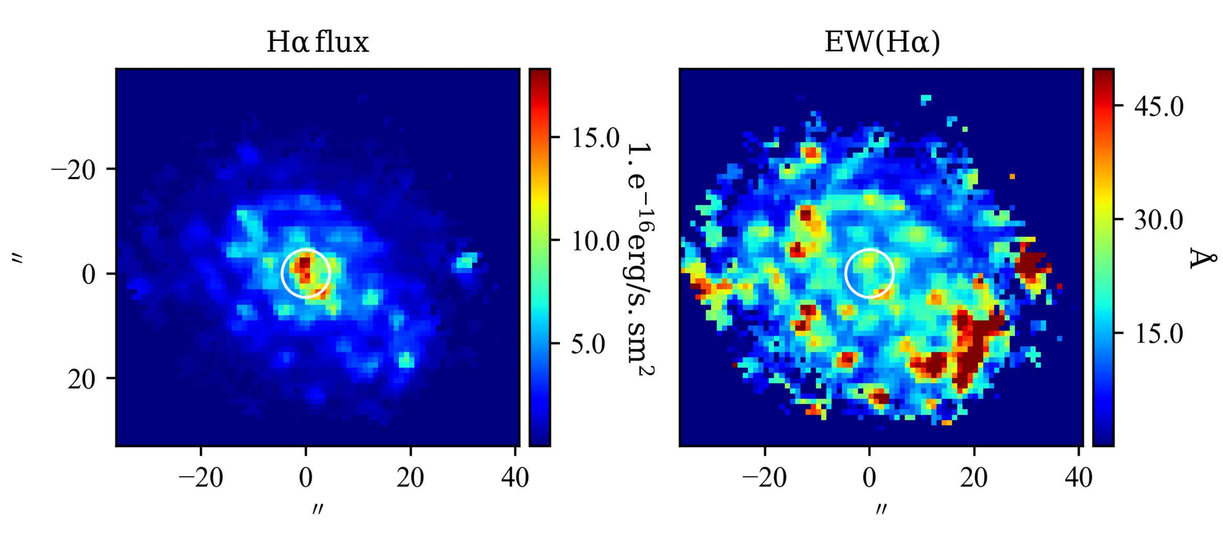

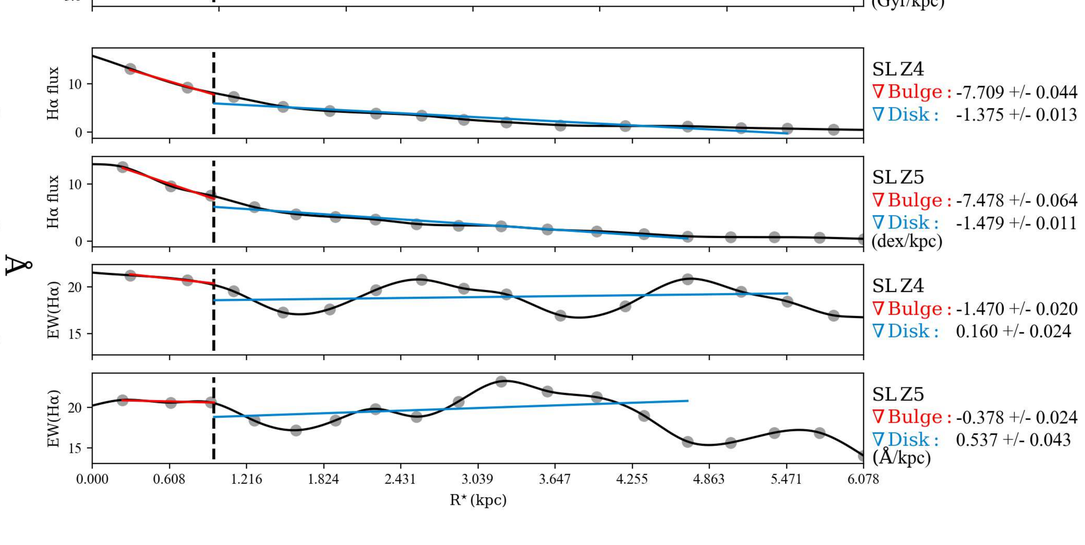

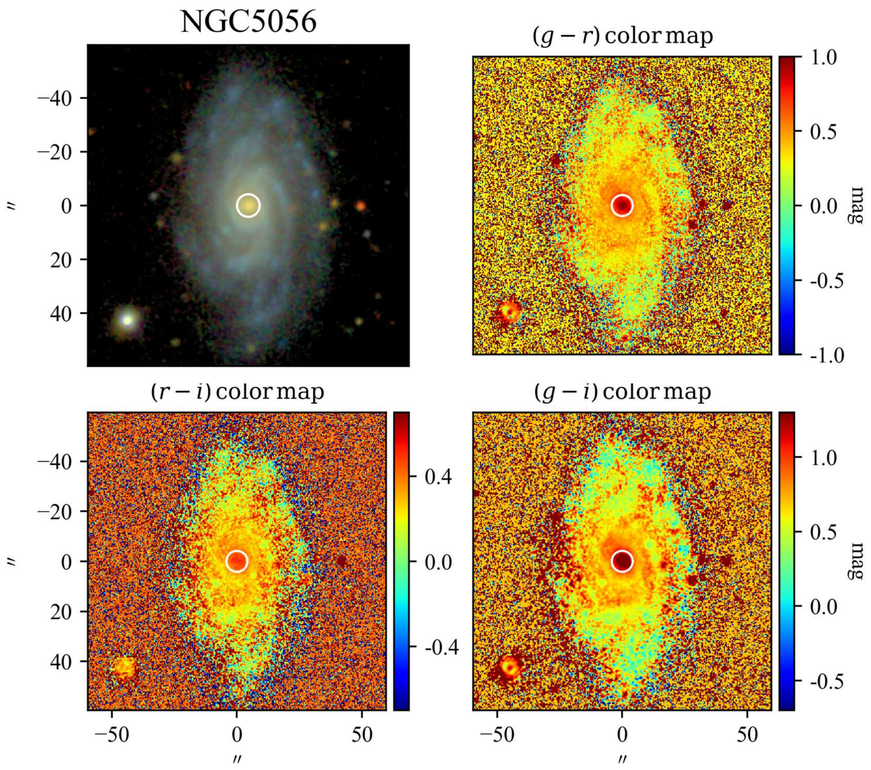

SBP decomposition of SDSS r band

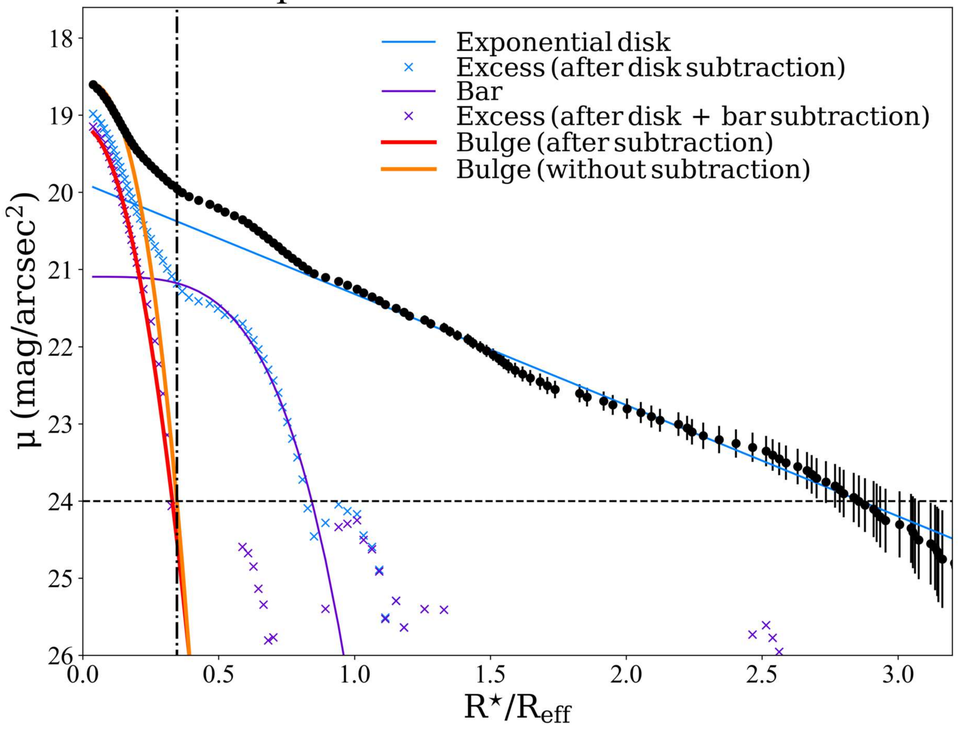

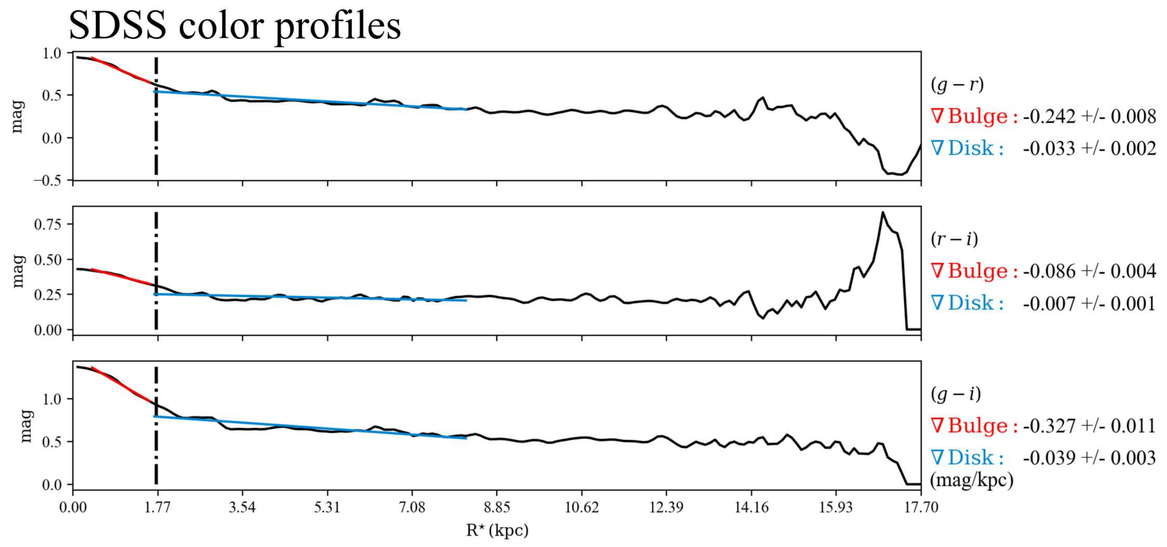

$\mathcal{RV}$ SBPs

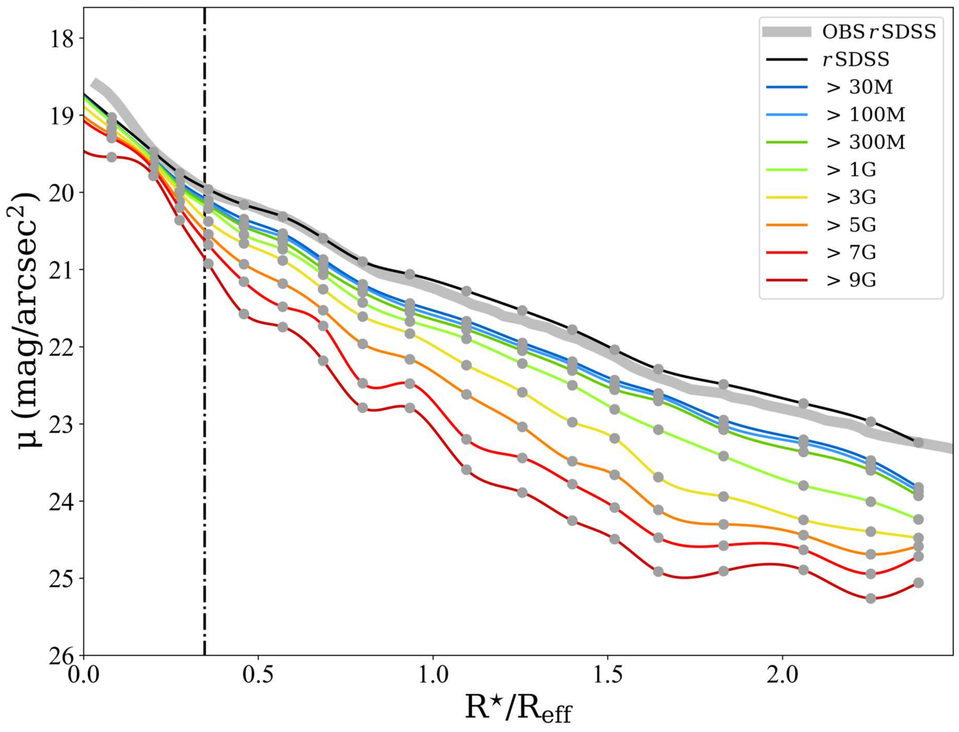

Stellar Continuum

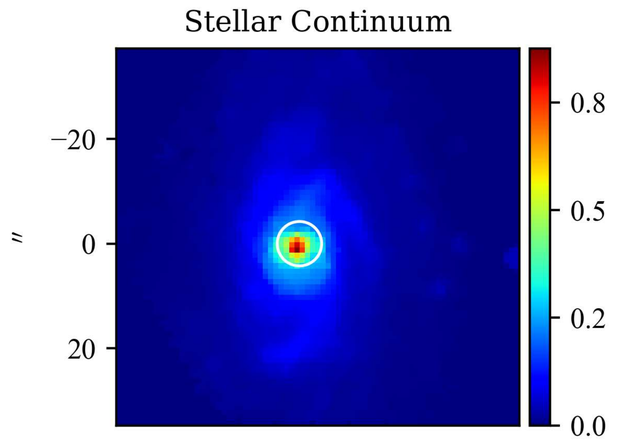

$\mathcal{M}_{\star,\mathrm{P}}$

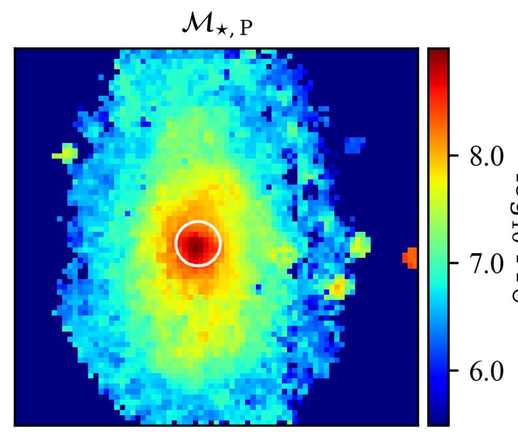

Log. of cumulative present stellar mass profiles

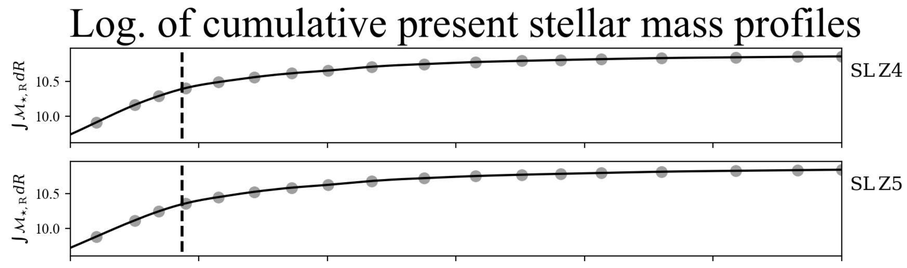

$Z_{\star,\mathcal{L}}$

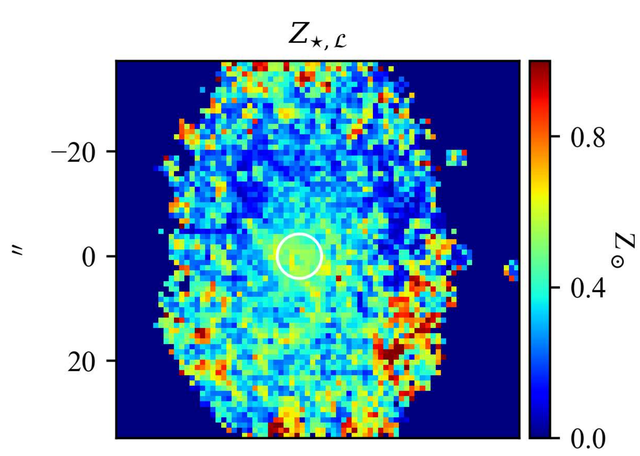

$Z_{\star,\mathcal{M}}$

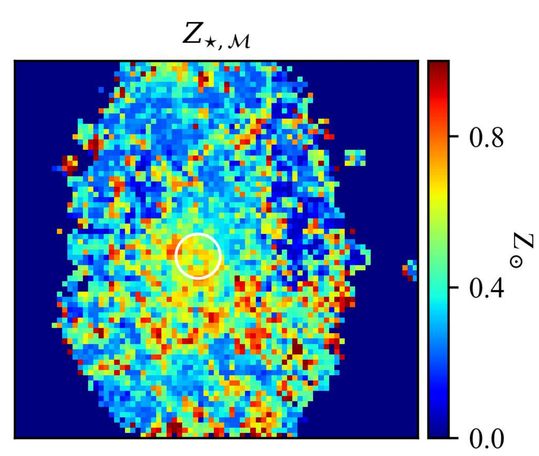

Stellar metallicity/Age & Hα flux/EW profiles

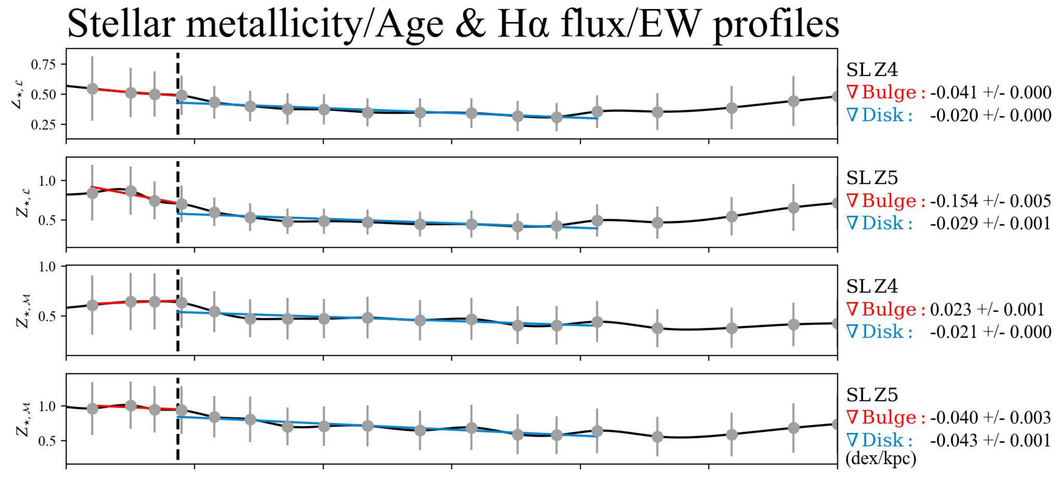

$t_{\star,\mathcal{L}}$

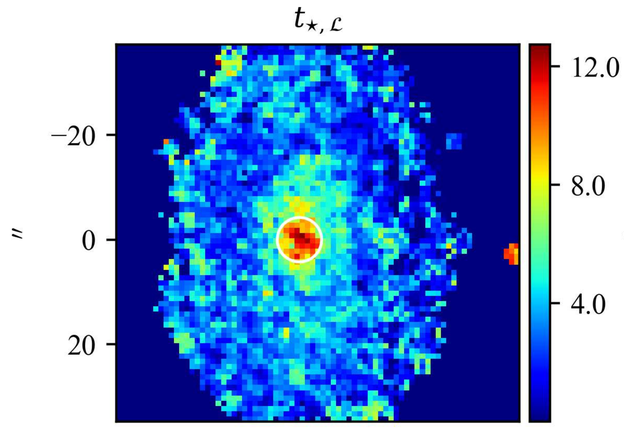

$t_{\star,\mathcal{M}}$

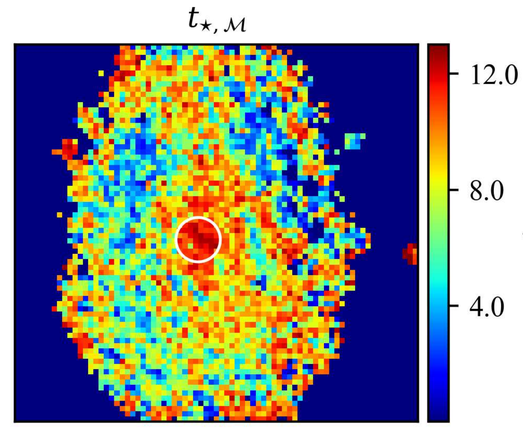

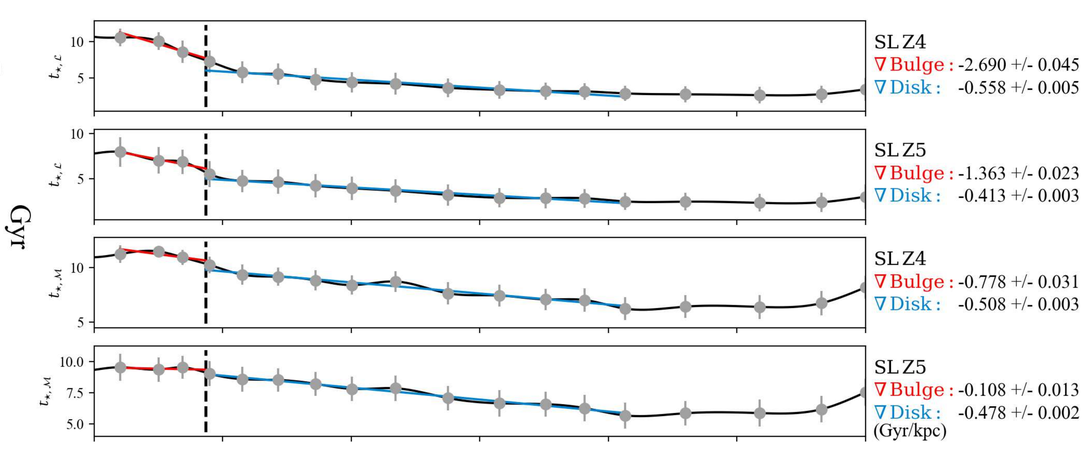

Hα flux

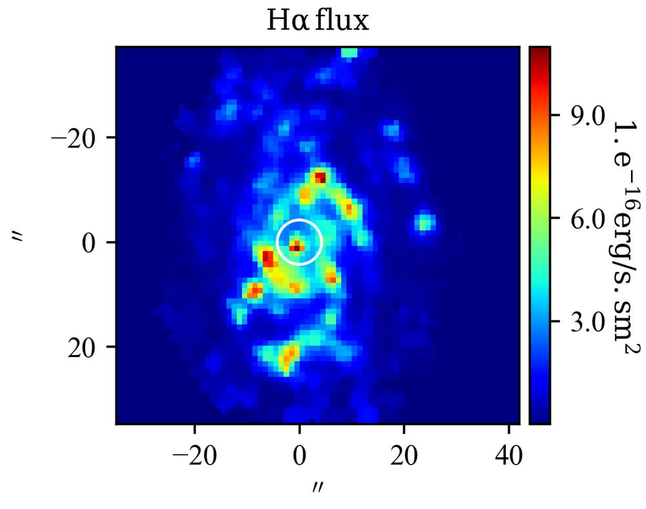

EW(Hα)

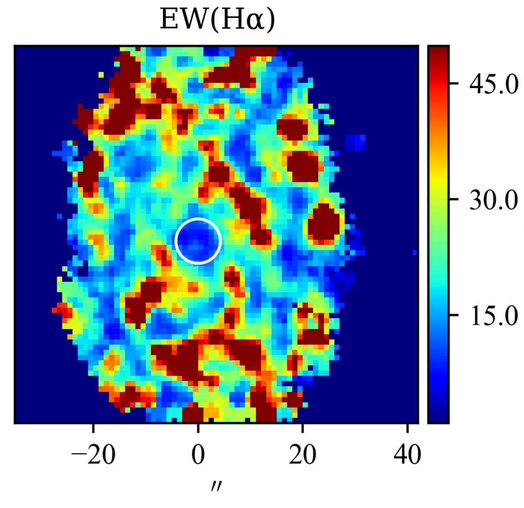

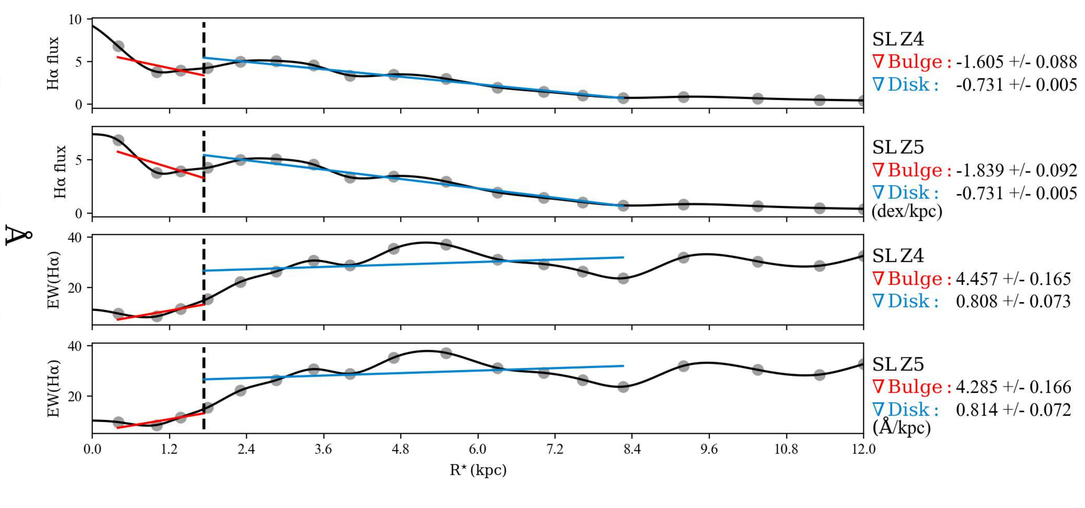

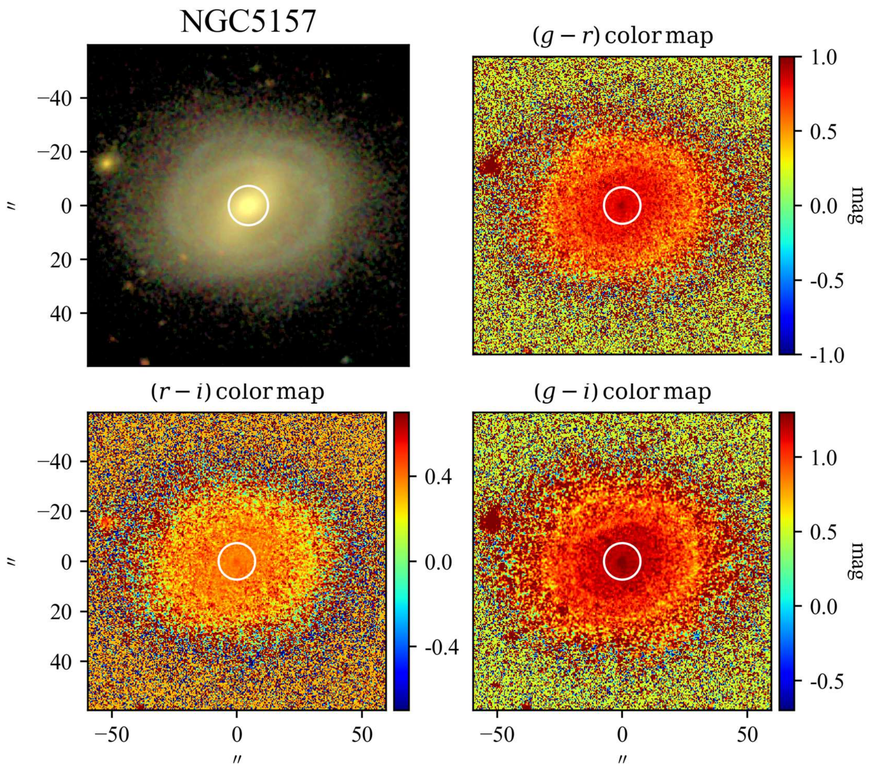

SBP decomposition of SDSS r band

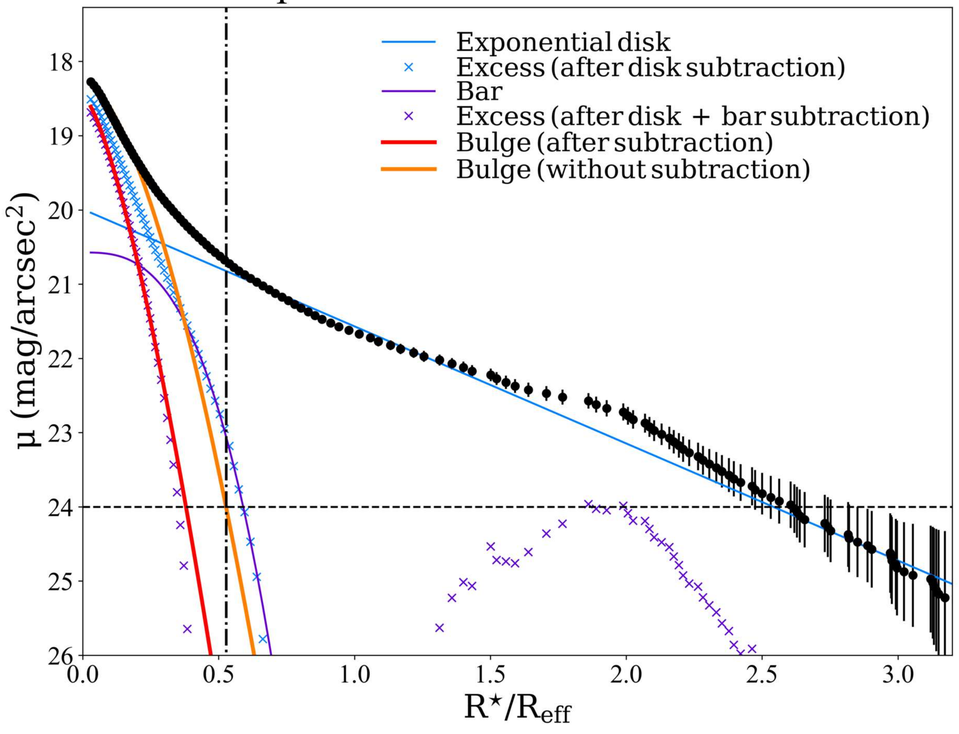

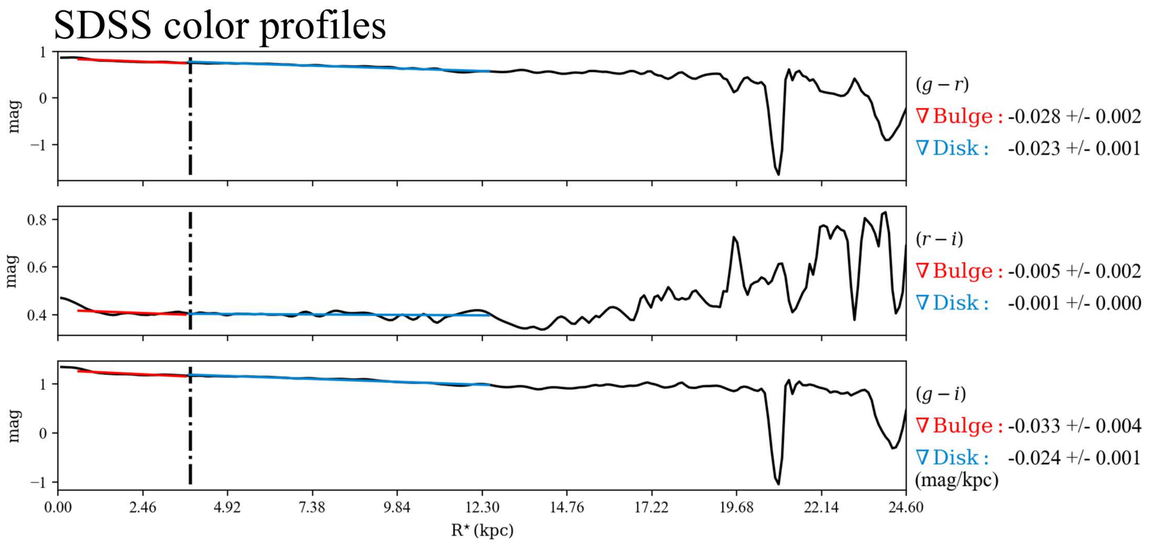

$\mathcal{RV}$ SBPs

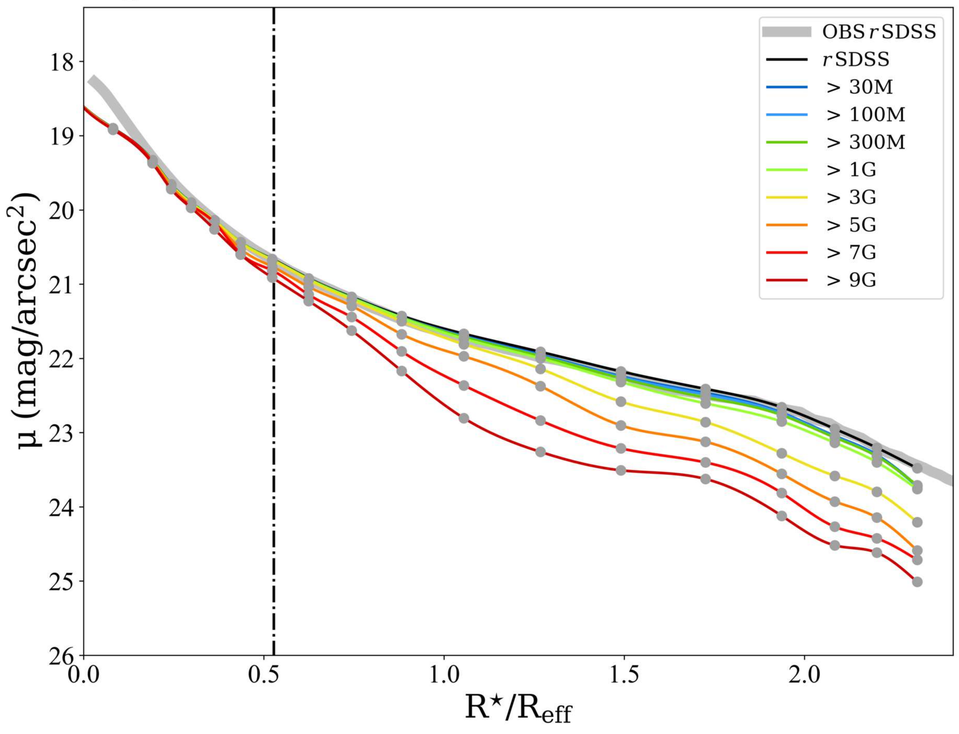

Stellar Continuum

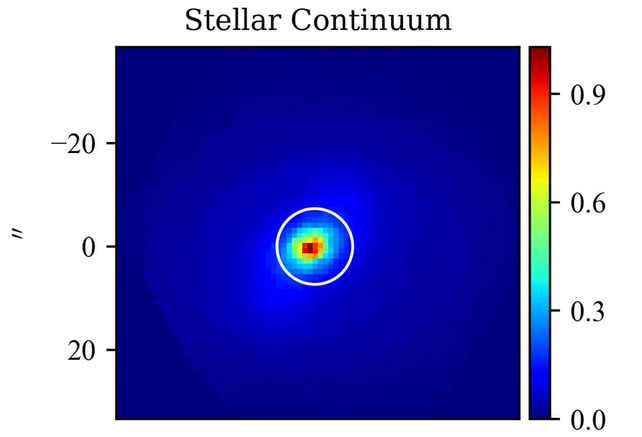

$\mathcal{M}_{\star,\mathrm{P}}$

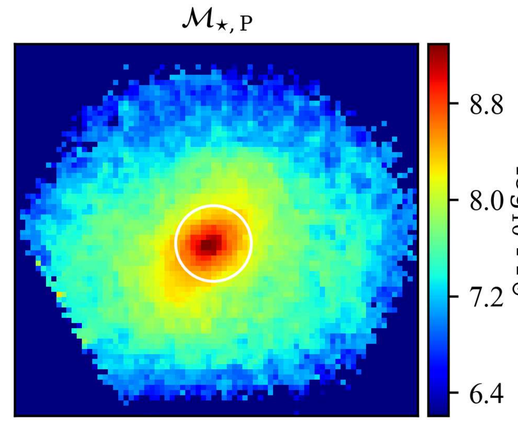

Log. of cumulative present stellar mass profiles

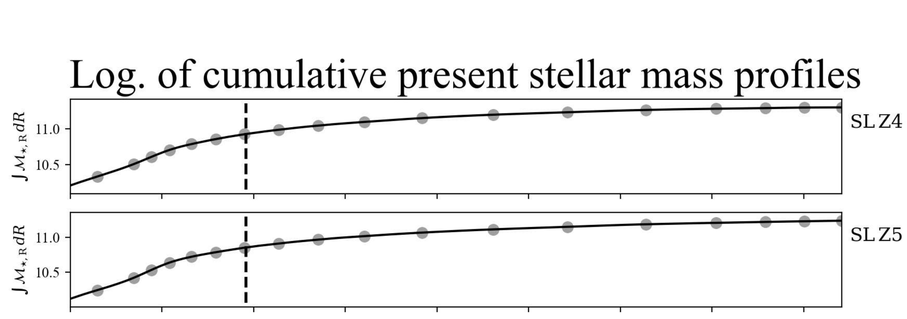

$Z_{\star,\mathcal{L}}$

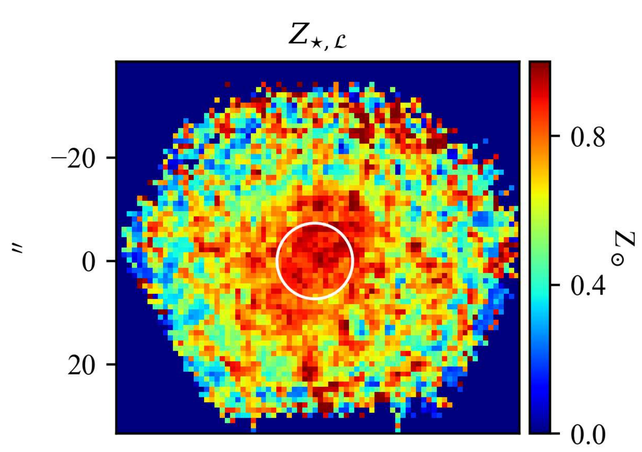

$Z_{\star,\mathcal{M}}$

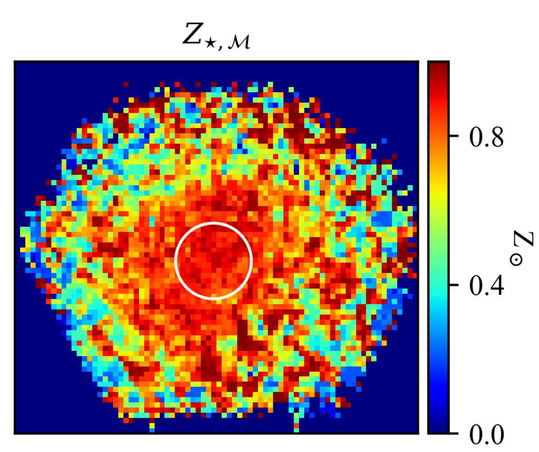

Stellar metallicity/Age & Hα flux/EW profiles

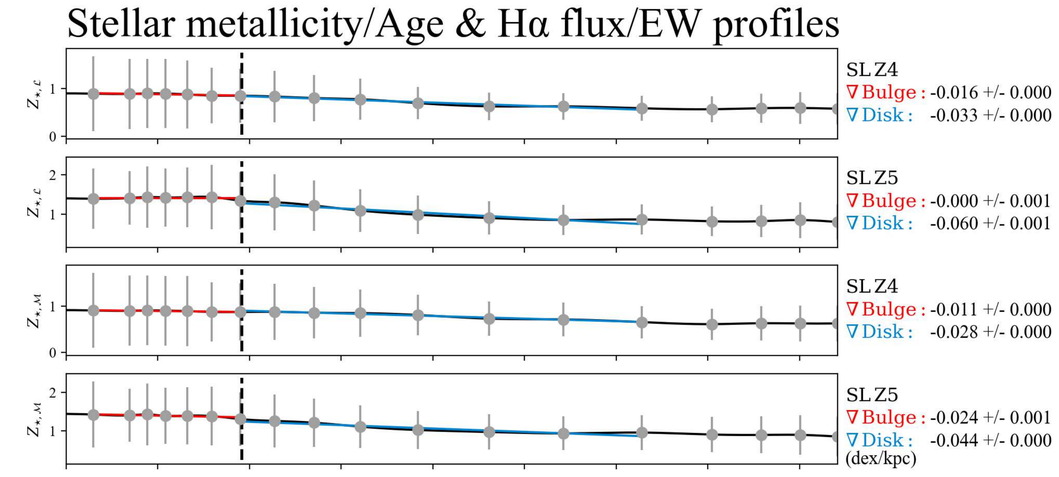

$t_{\star,\mathcal{L}}$

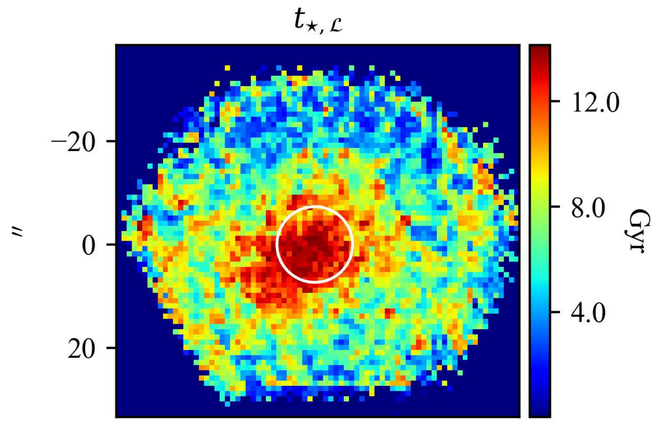

$t_{\star,\mathcal{M}}$

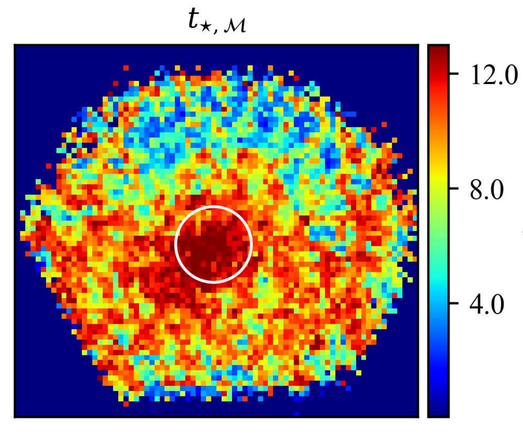

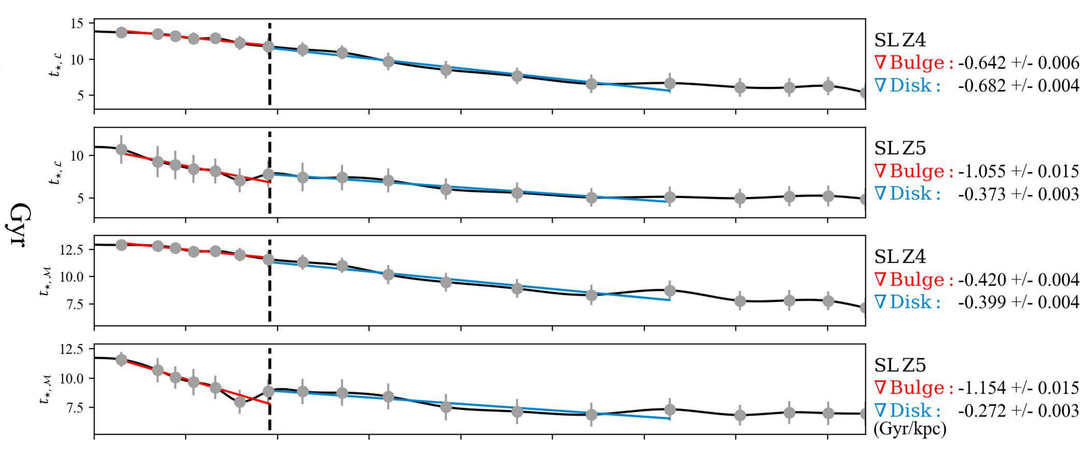

Hα flux

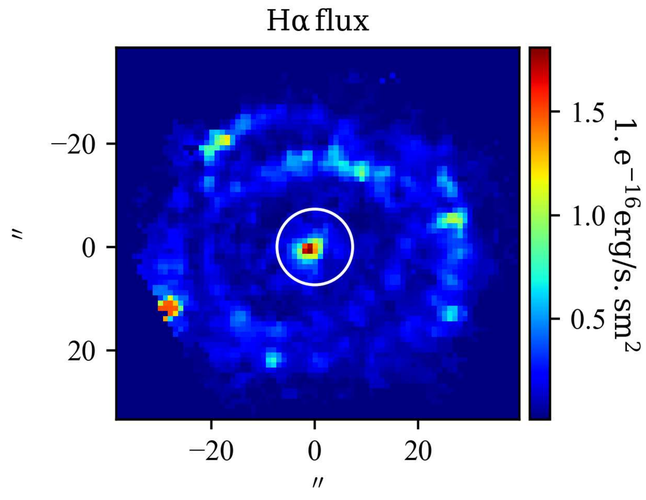

EW(Hα)

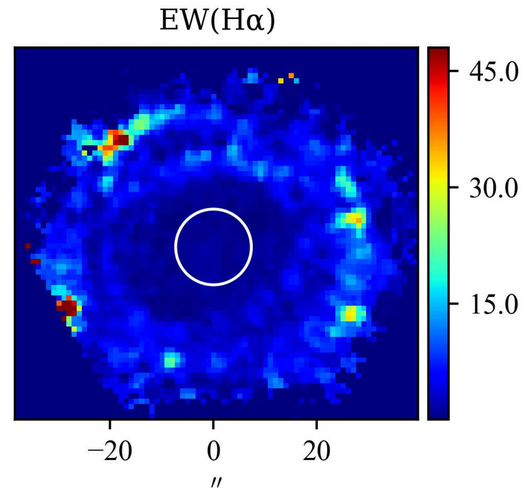

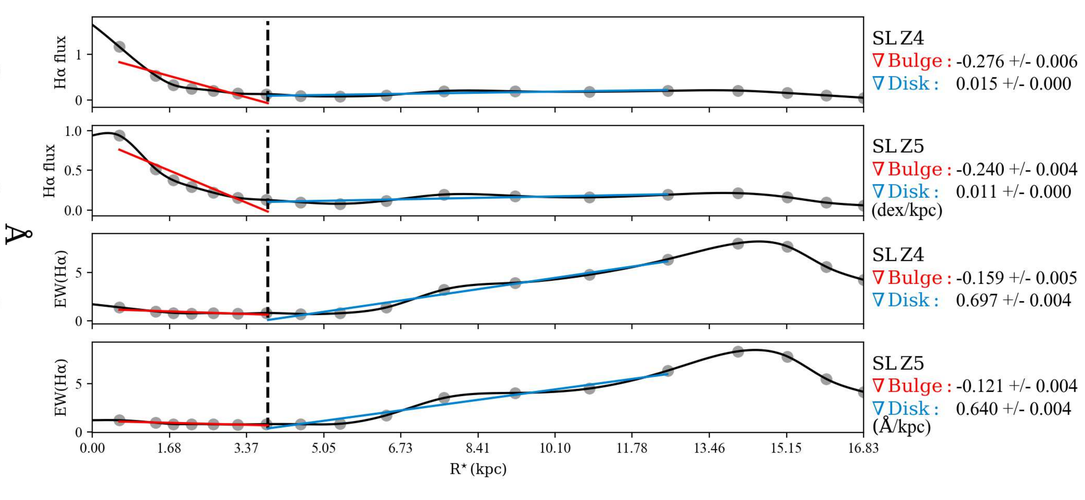

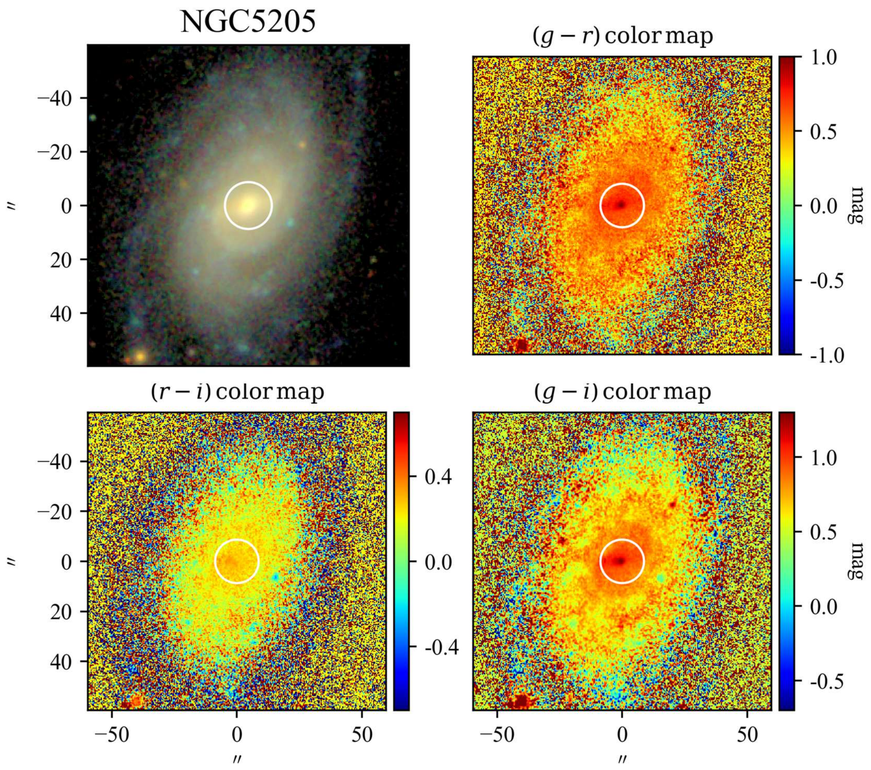

SBP decomposition of SDSS r band

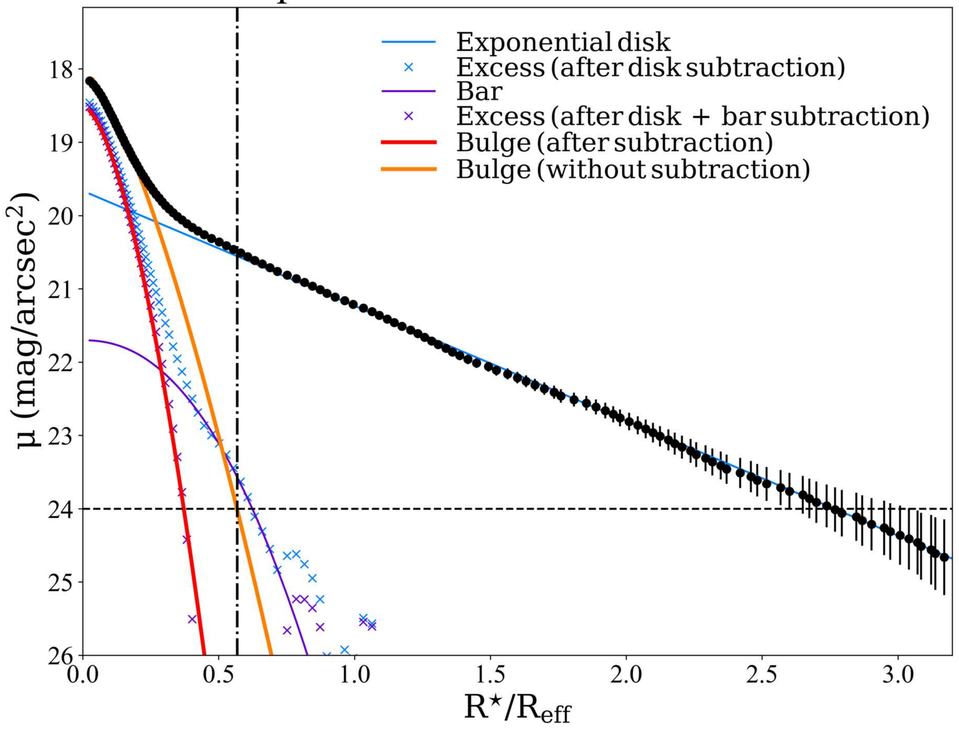

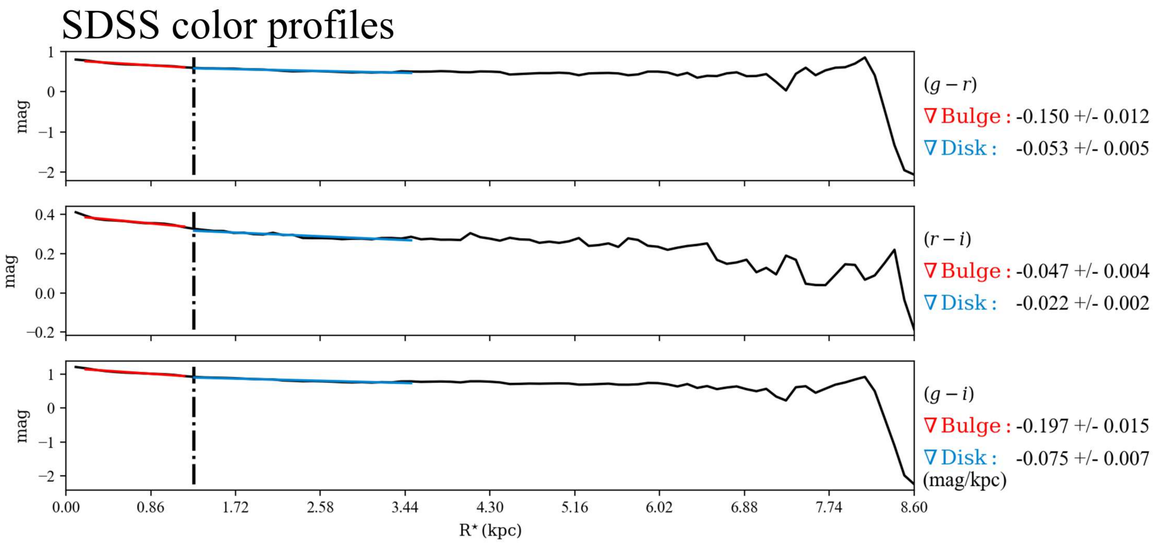

$\mathcal{RV}$ SBPs

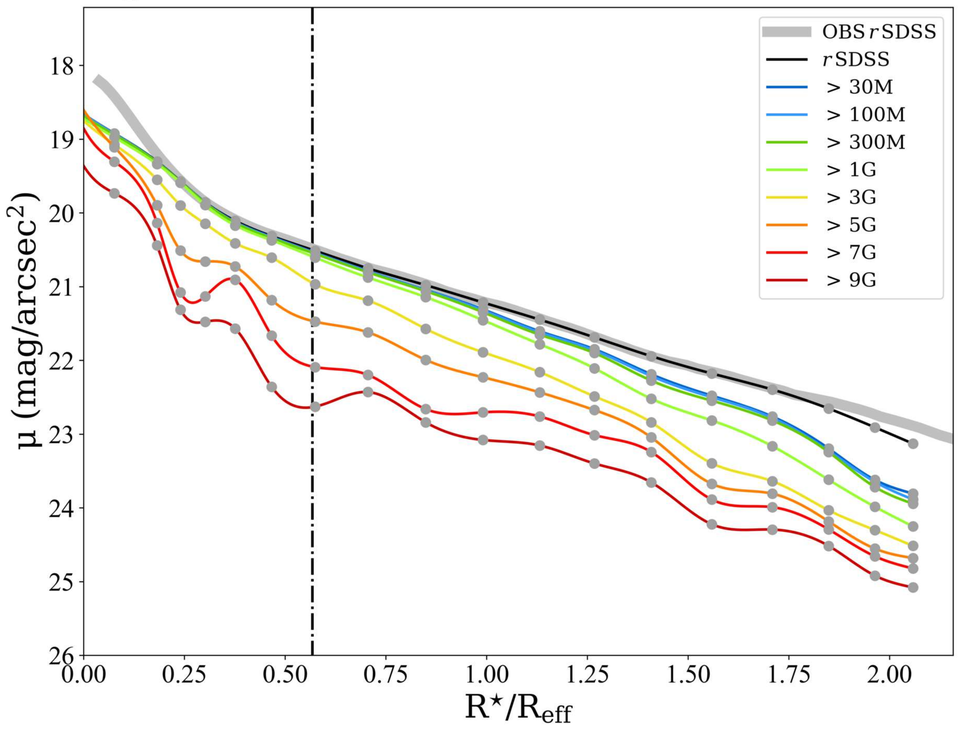

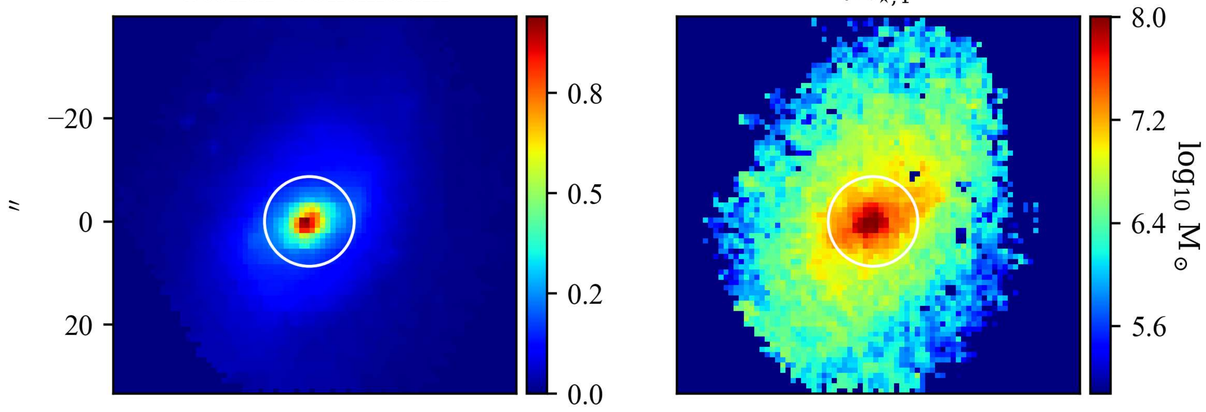

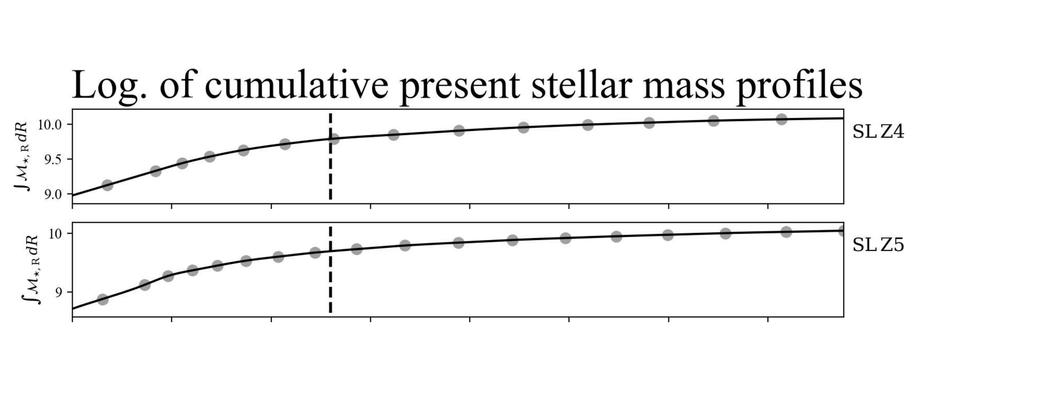

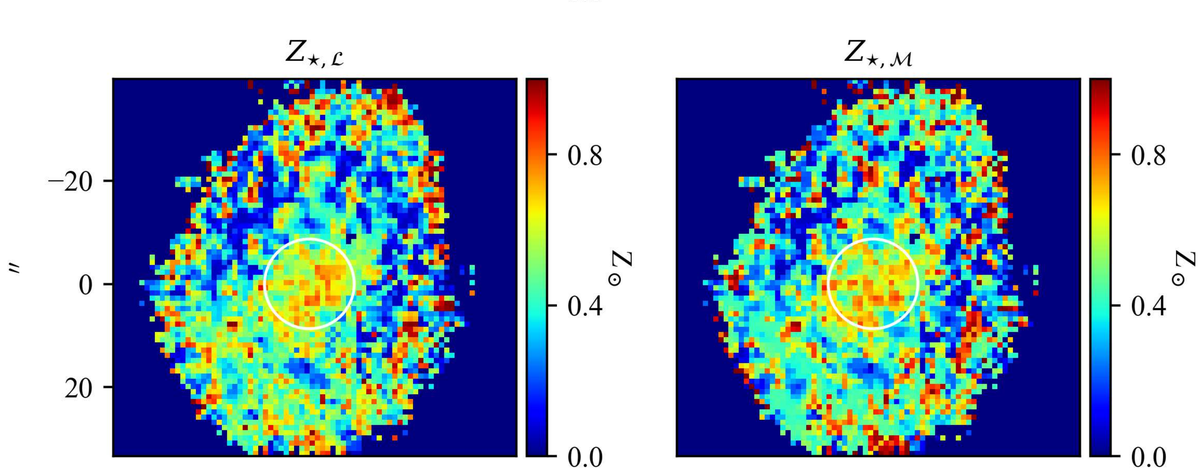

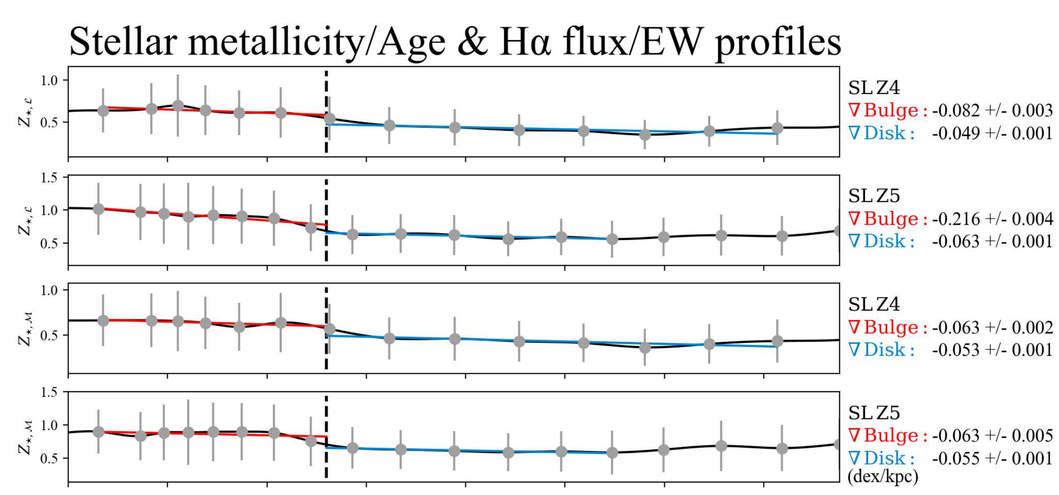

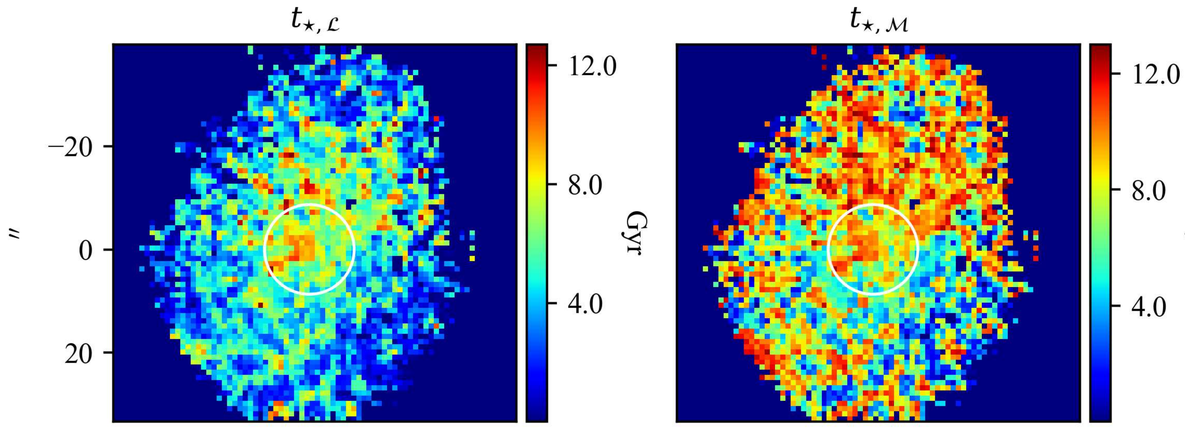

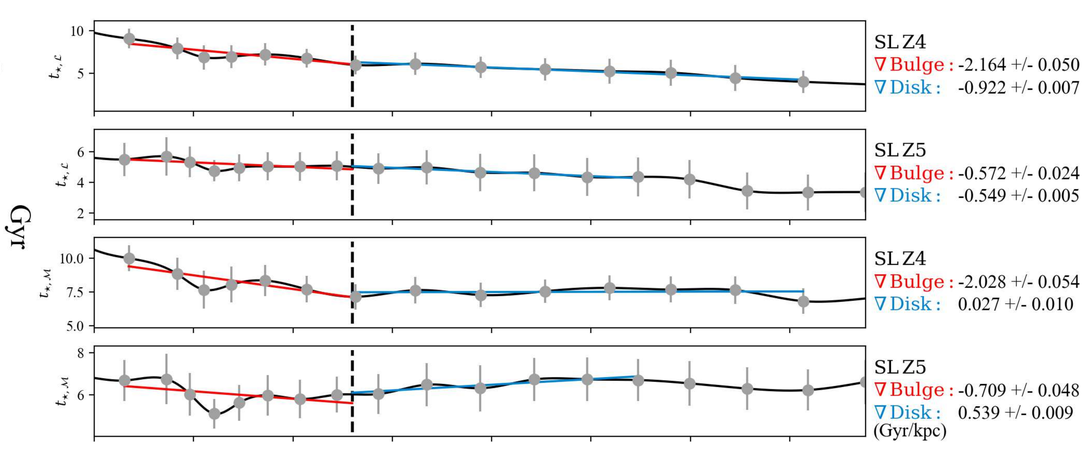

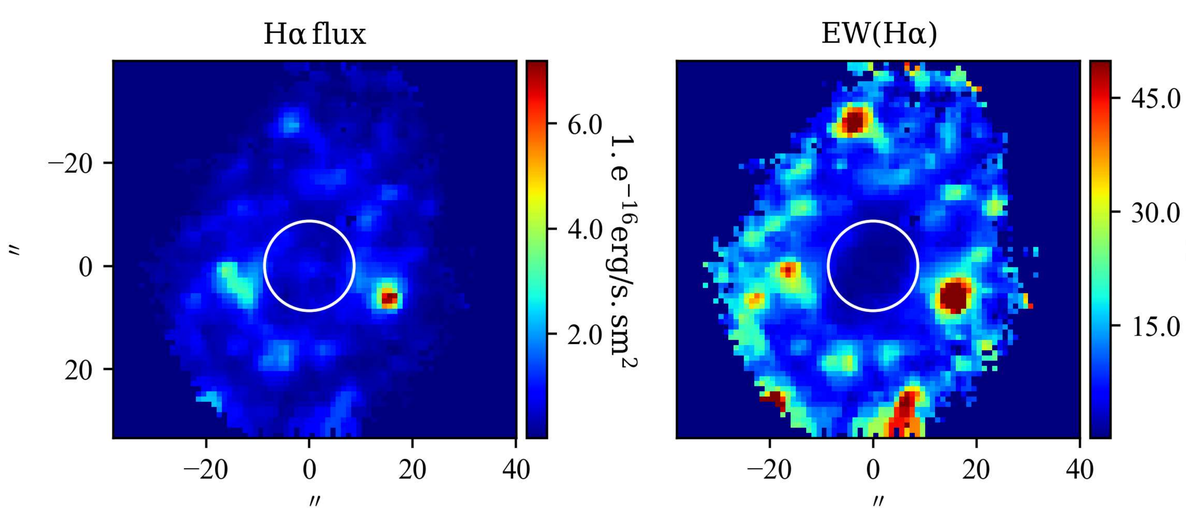

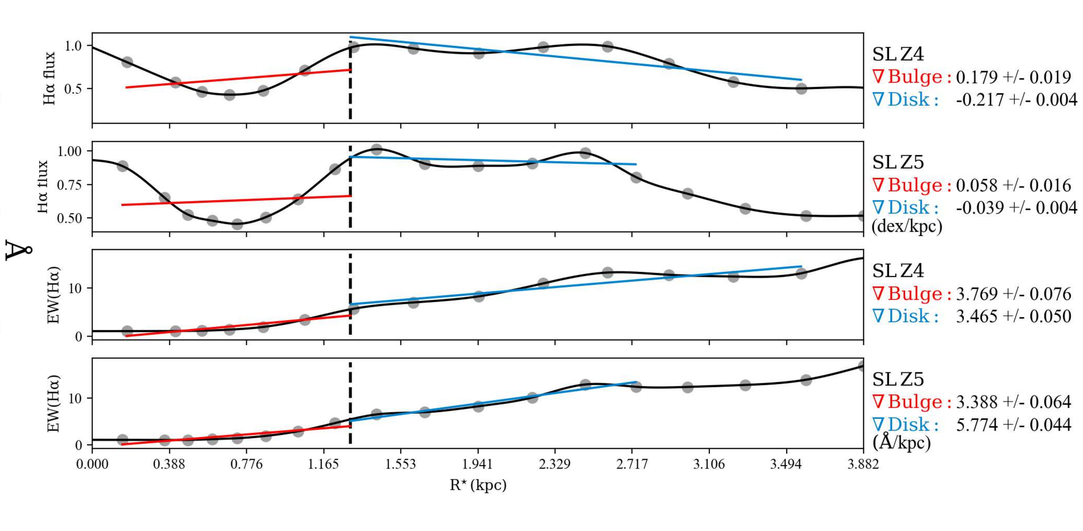

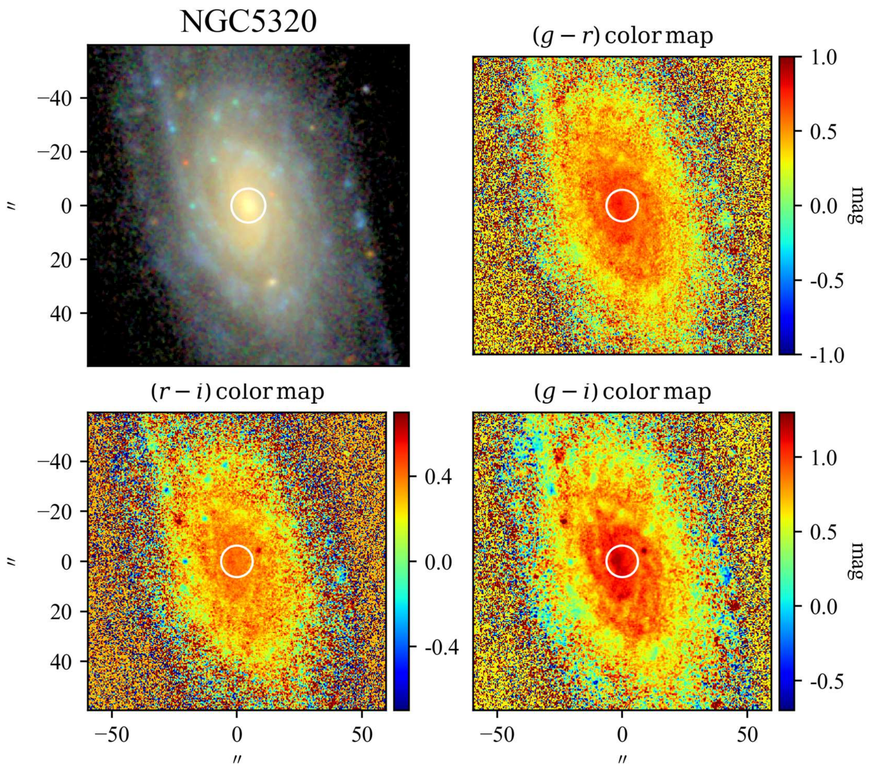

SBP decomposition of SDSS r band

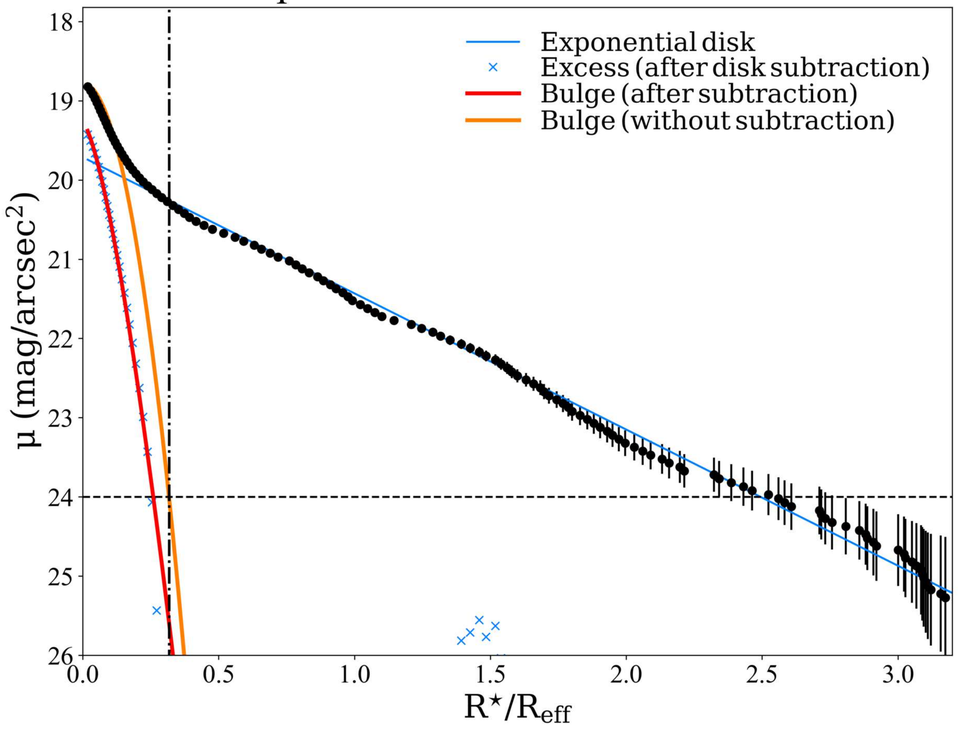

SDSS color profiles

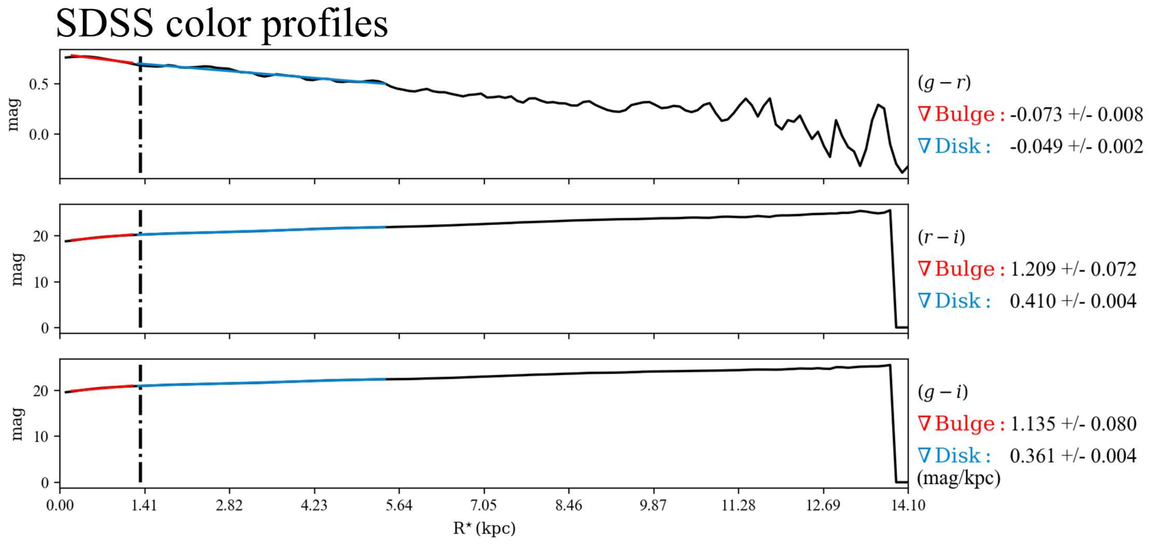

$\mathcal{RY}$ SBPs

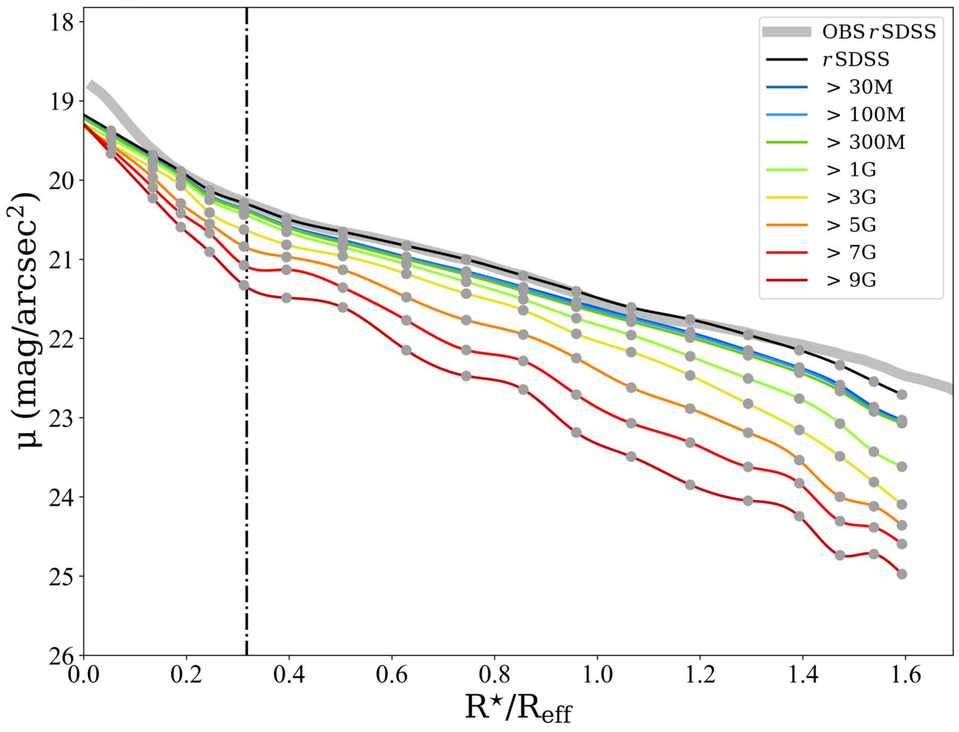

Stellar Continuum

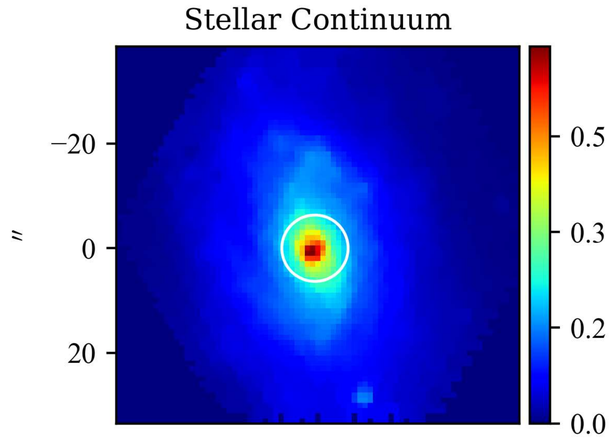

$\mathcal{M}_{\star,\rm P}$

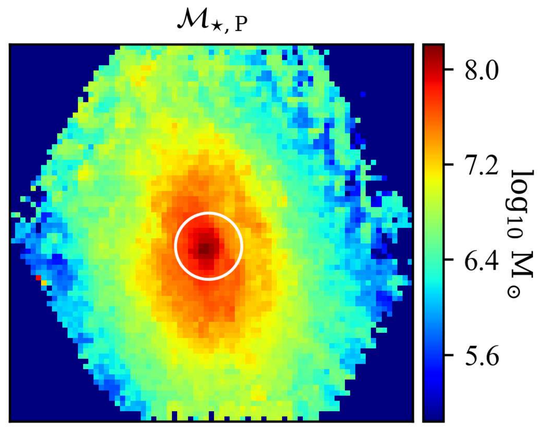

Log. of cumulative present stellar mass profiles

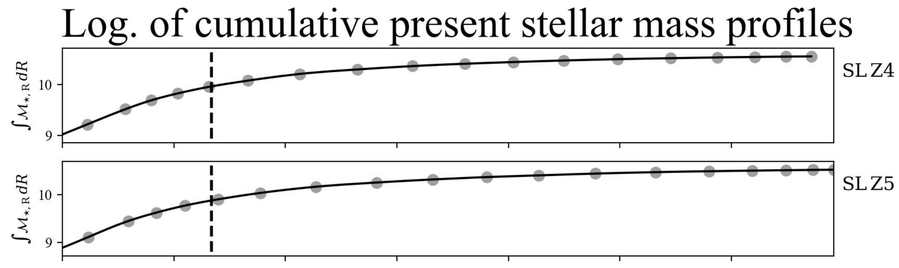

$Z_{\star,\mathcal{L}}$

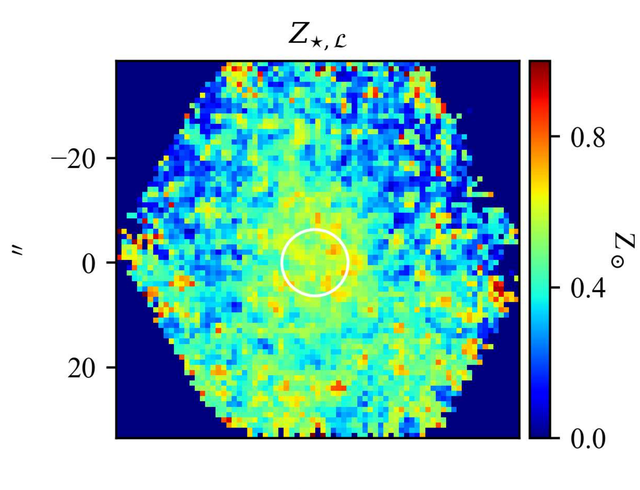

$Z_{\star,\mathcal{M}}$

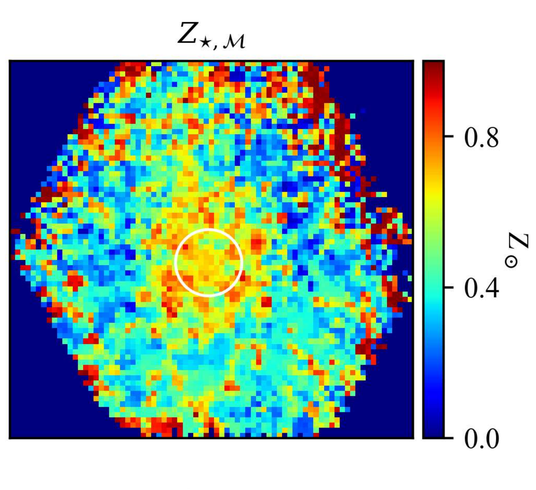

Stellar metallicity/Age & Hα flux/EW profiles

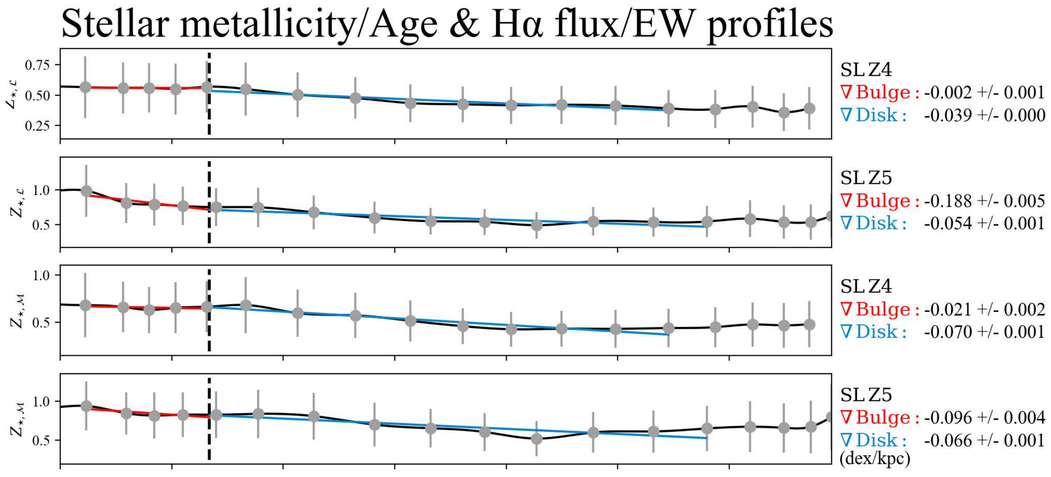

$t_{\star,\mathcal{L}}$

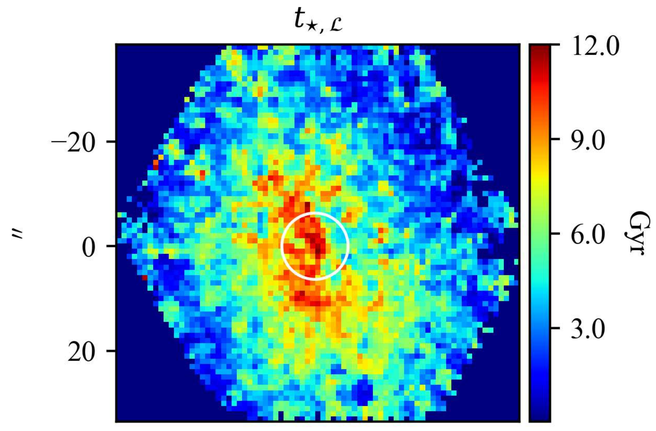

$t_{\star,\mathcal{M}}$

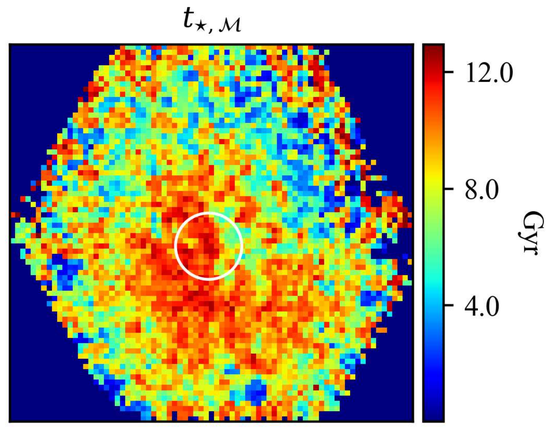

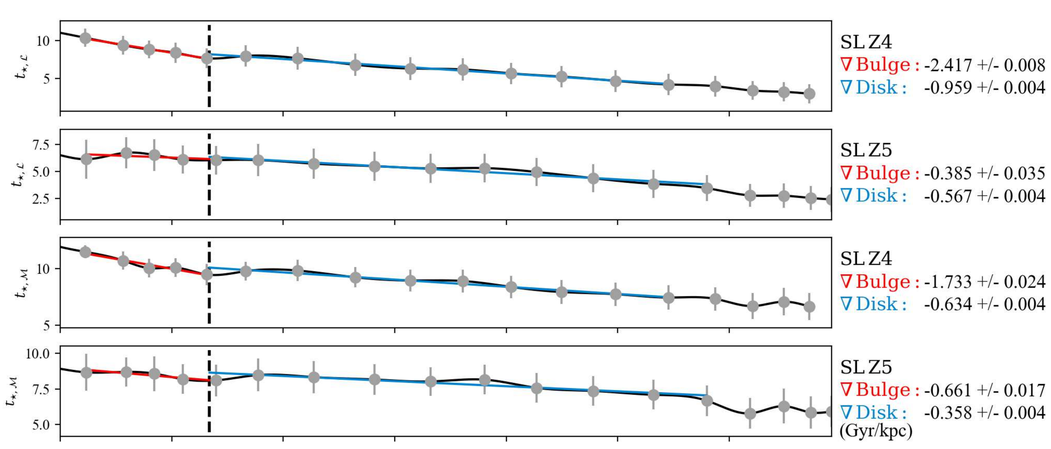

Hα flux

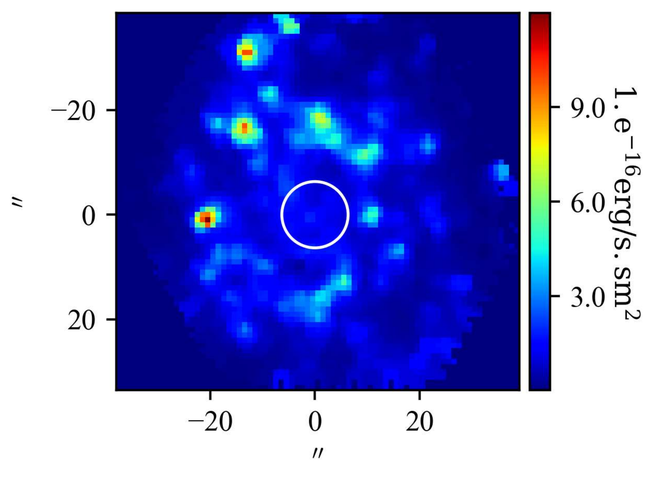

EW(Hα)

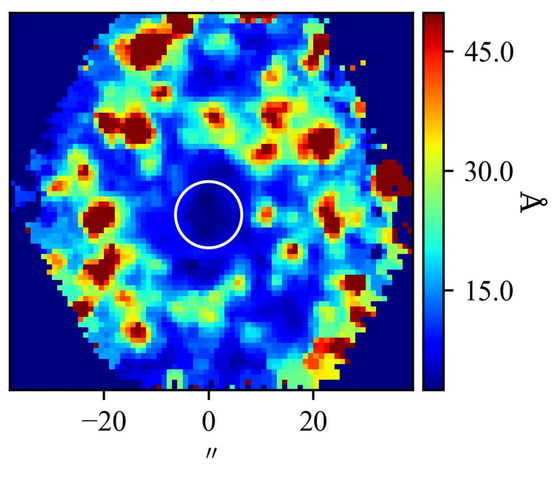

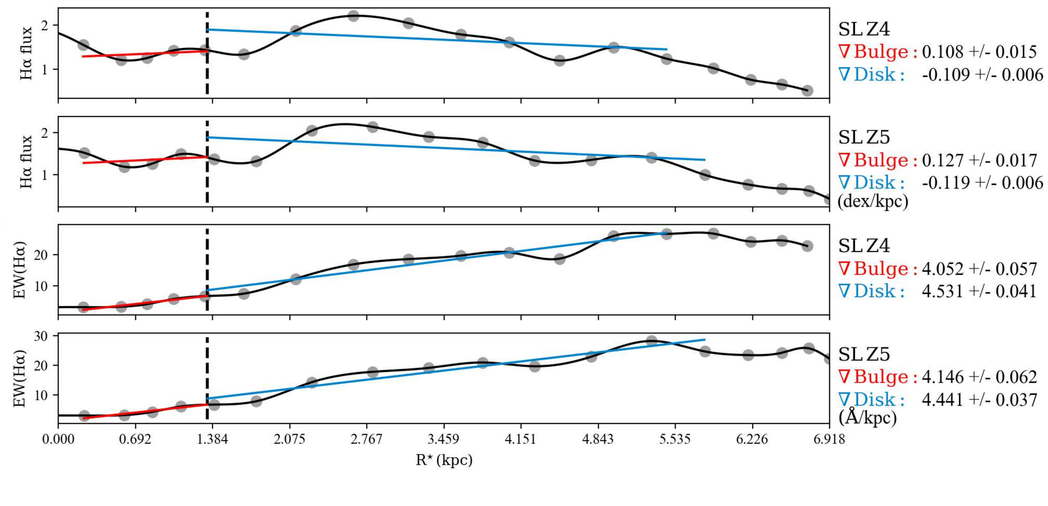

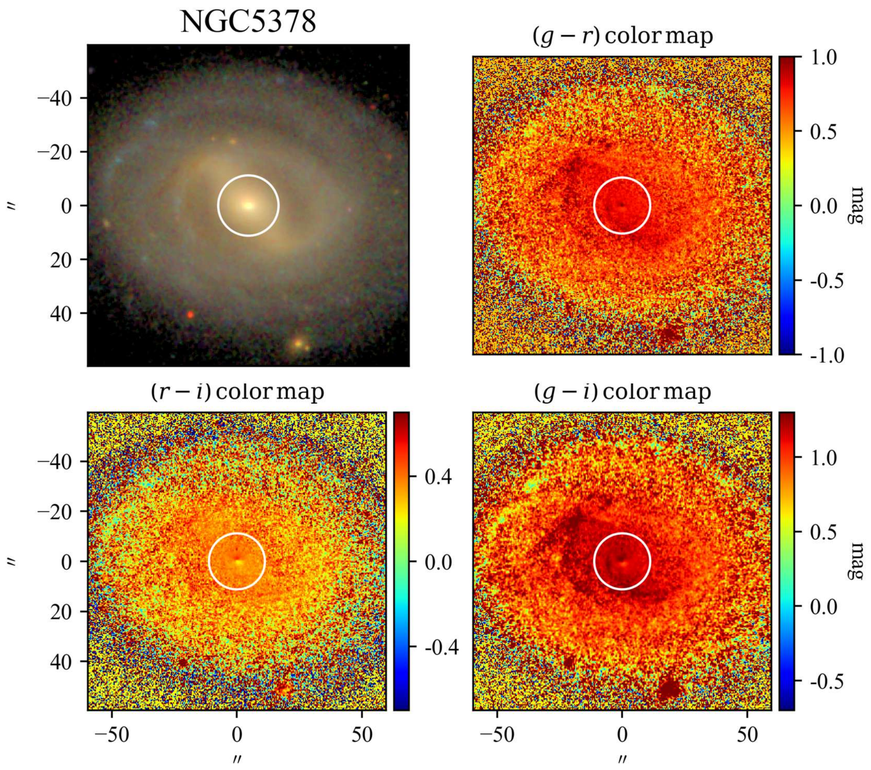

SBP decomposition of SDSS r band

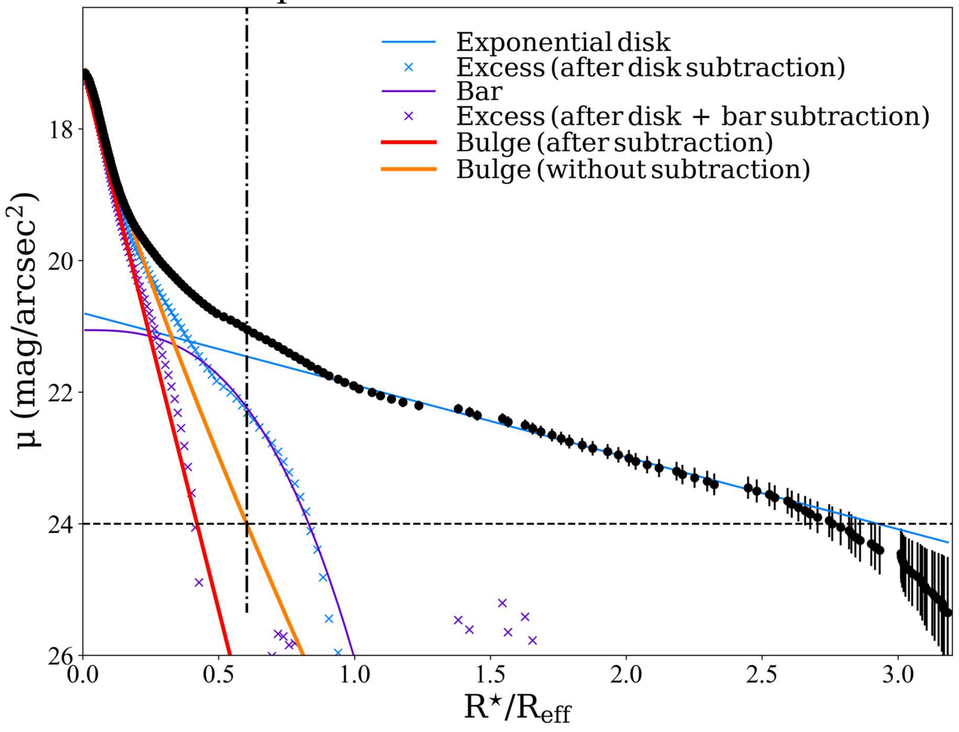

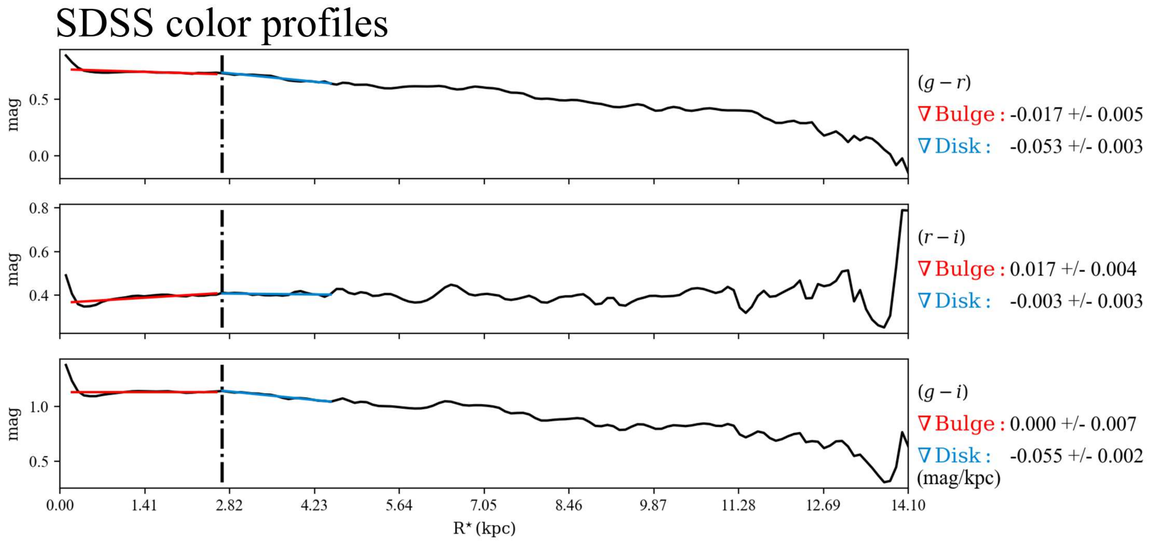

$\mathcal{RY}$ SBPs

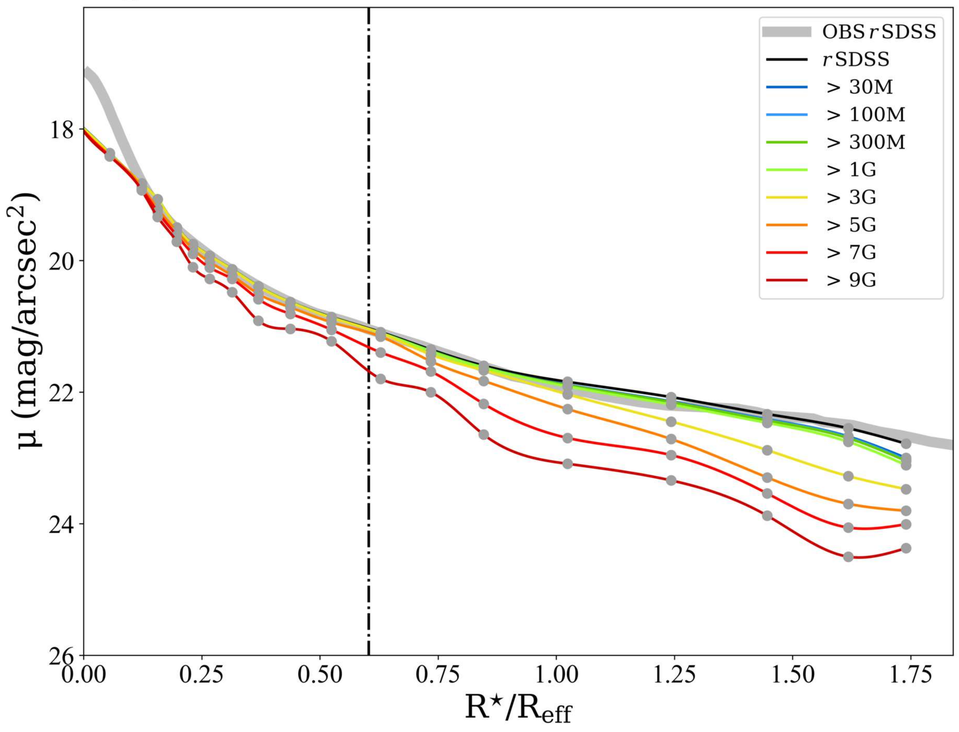

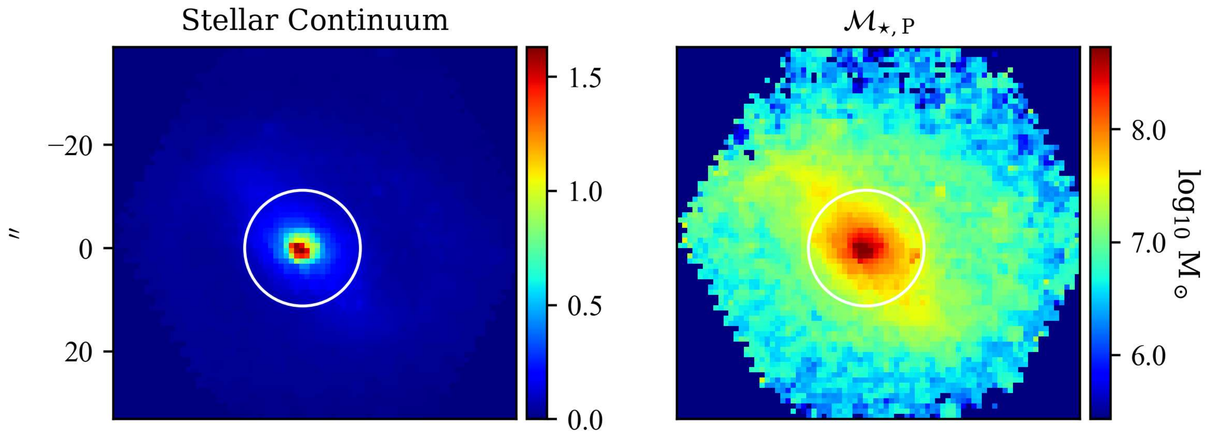

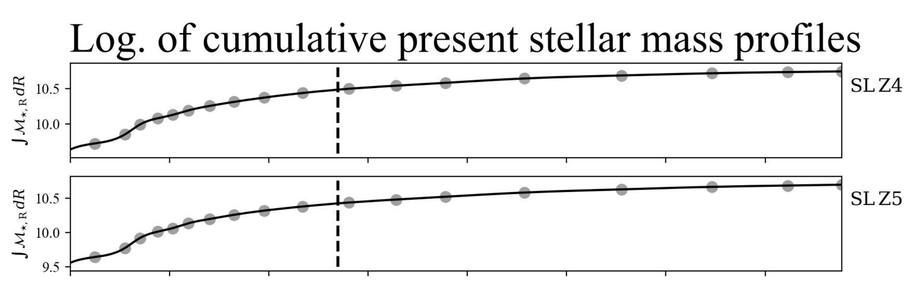

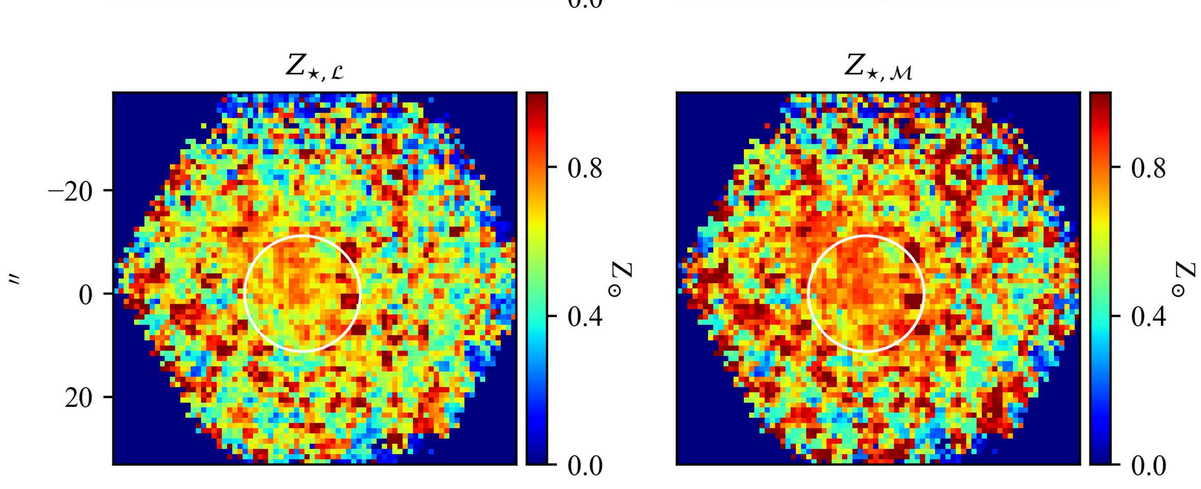

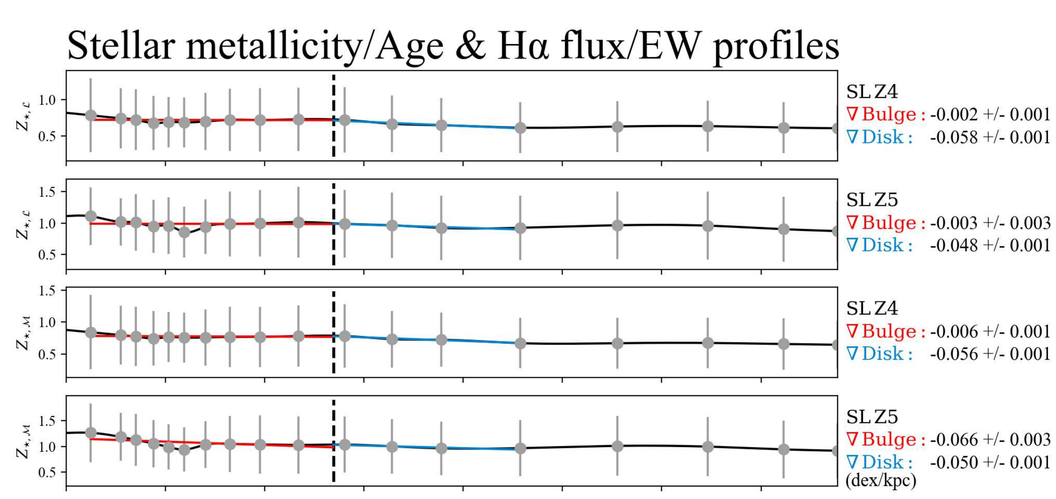

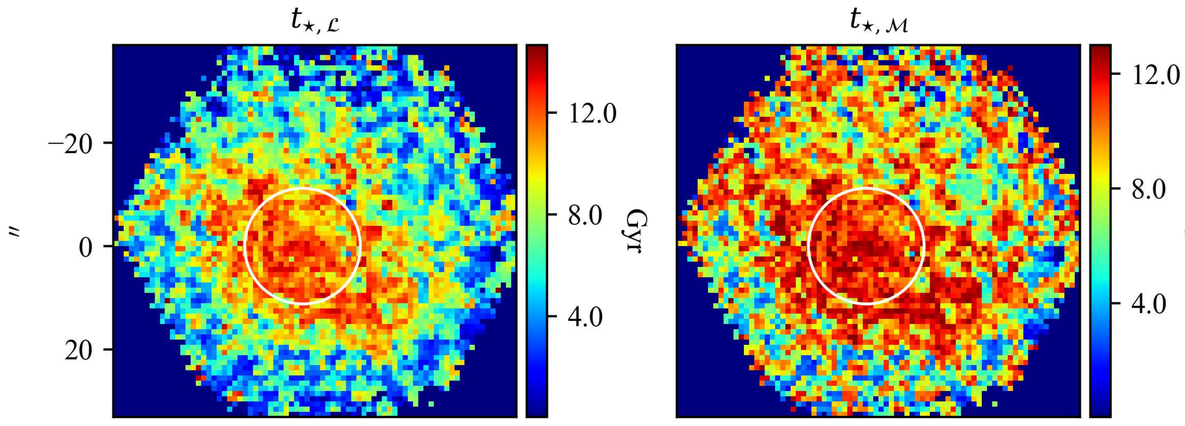

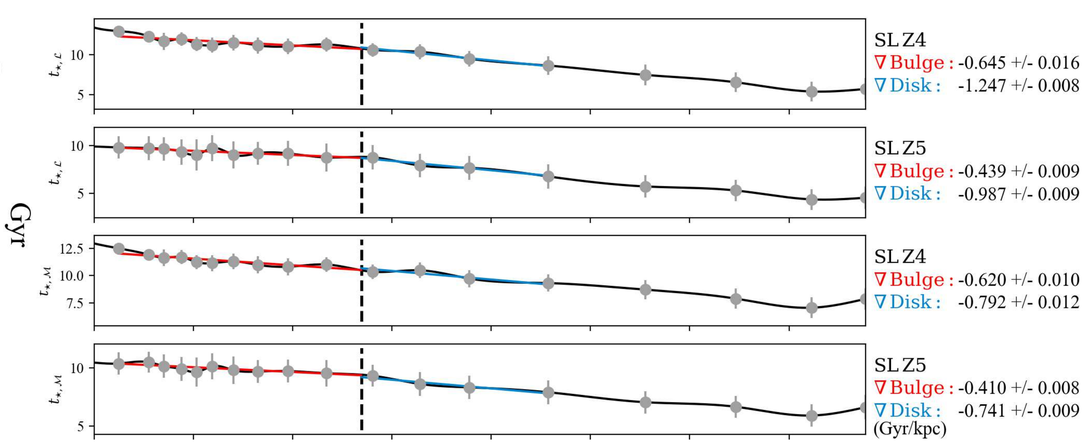

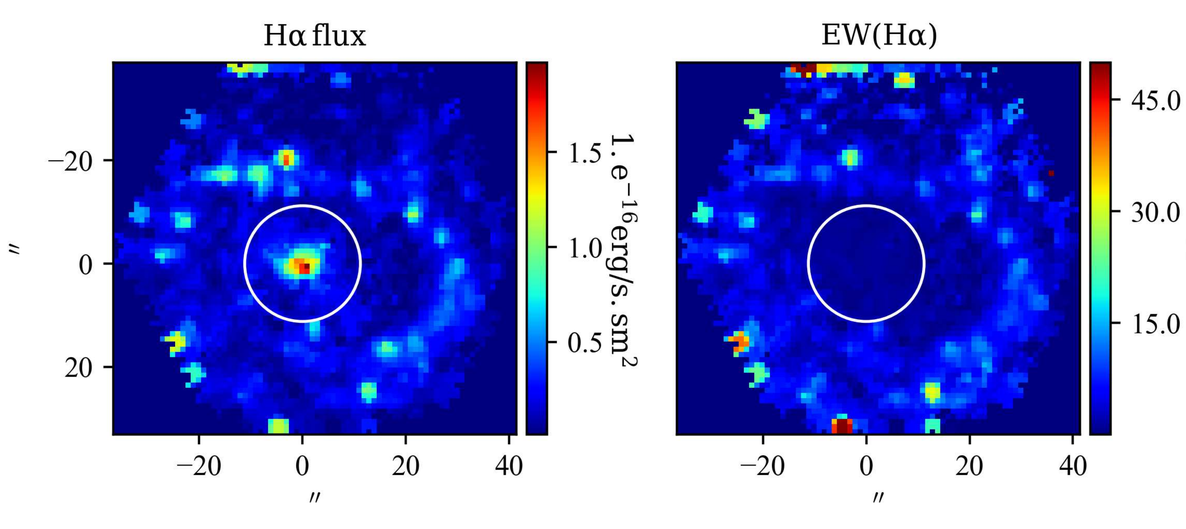

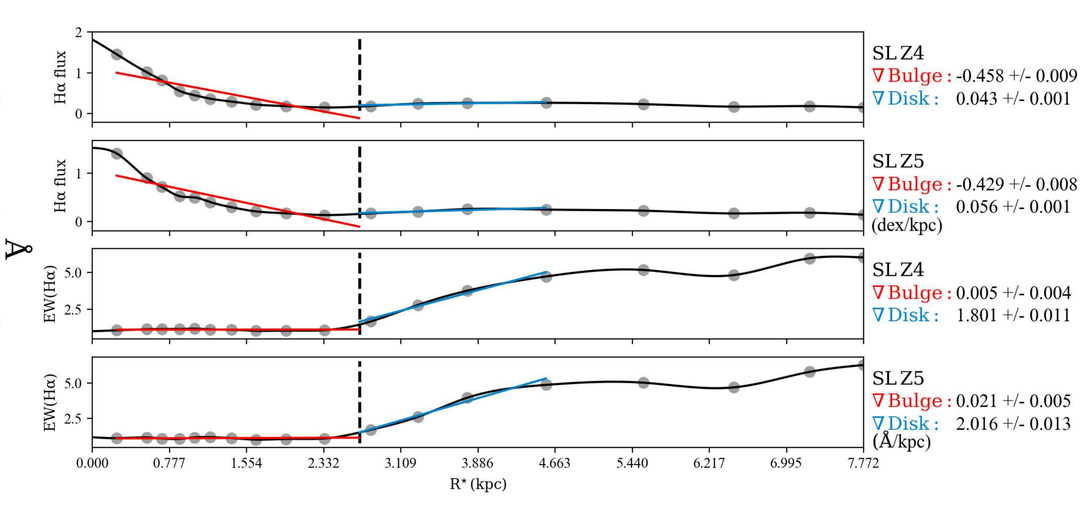

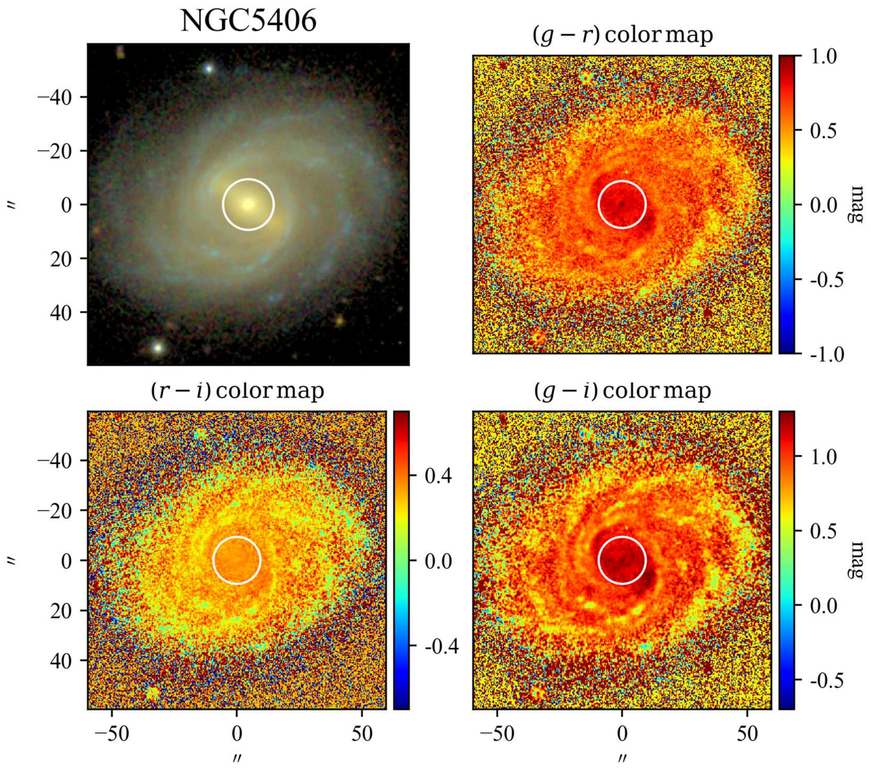
NGC5406
$(g-r)$ color map
$(r-i)$ color map
$(g-i)$ color map
mag
″

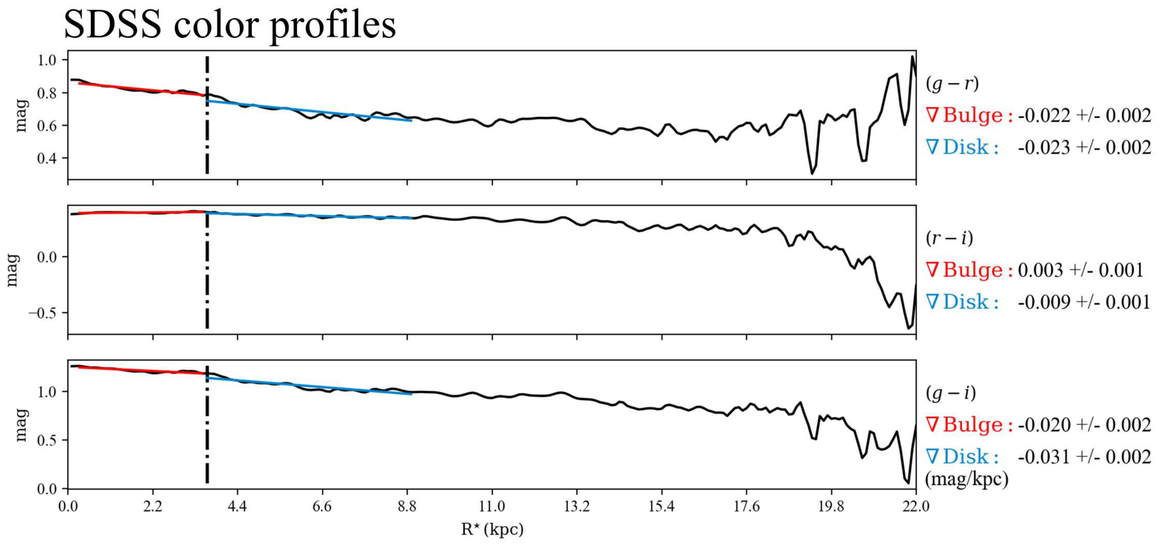
SDSS color profiles
$(g-r)$
∇ Bulge : -0.022 +/- 0.002
∇ Disk : -0.023 +/- 0.002
$(r-i)$
∇ Bulge : 0.003 +/- 0.001
∇ Disk : -0.009 +/- 0.001
$(g-i)$
∇ Bulge : -0.020 +/- 0.002
∇ Disk : -0.031 +/- 0.002
(mag/kpc)
mag
R* (kpc)

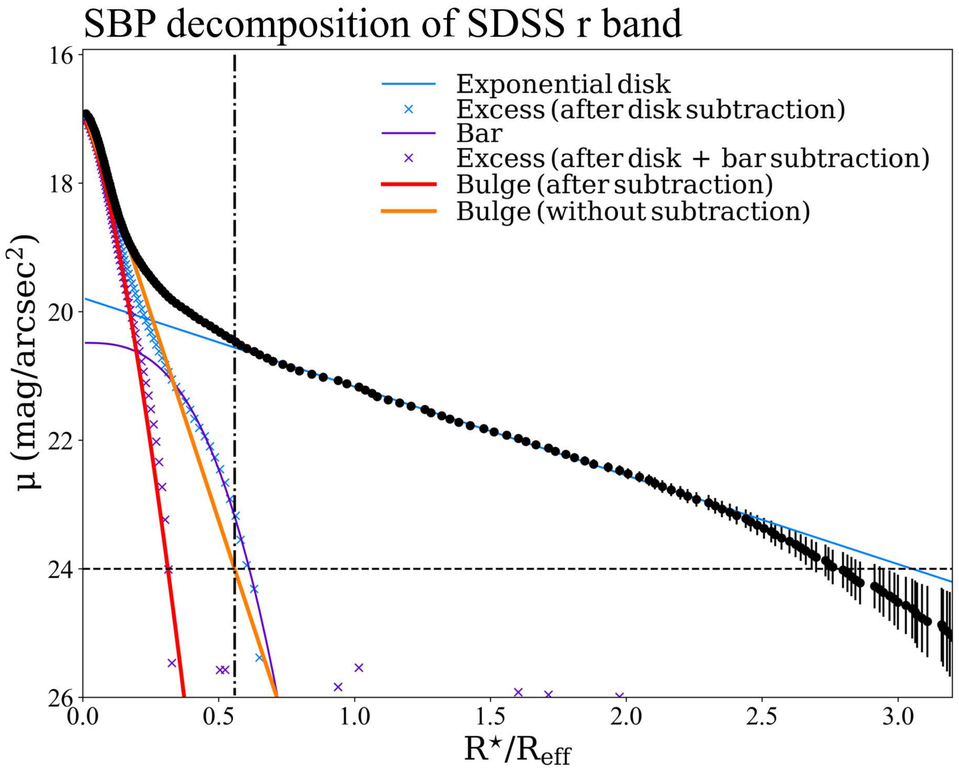
SBP decomposition of SDSS r band
Exponential disk
Excess (after disk subtraction)
Bar
Excess (after disk + bar subtraction)
Bulge (after subtraction)
Bulge (without subtraction)
μ (mag/arcsec^2)
R*/R$_{eff}$

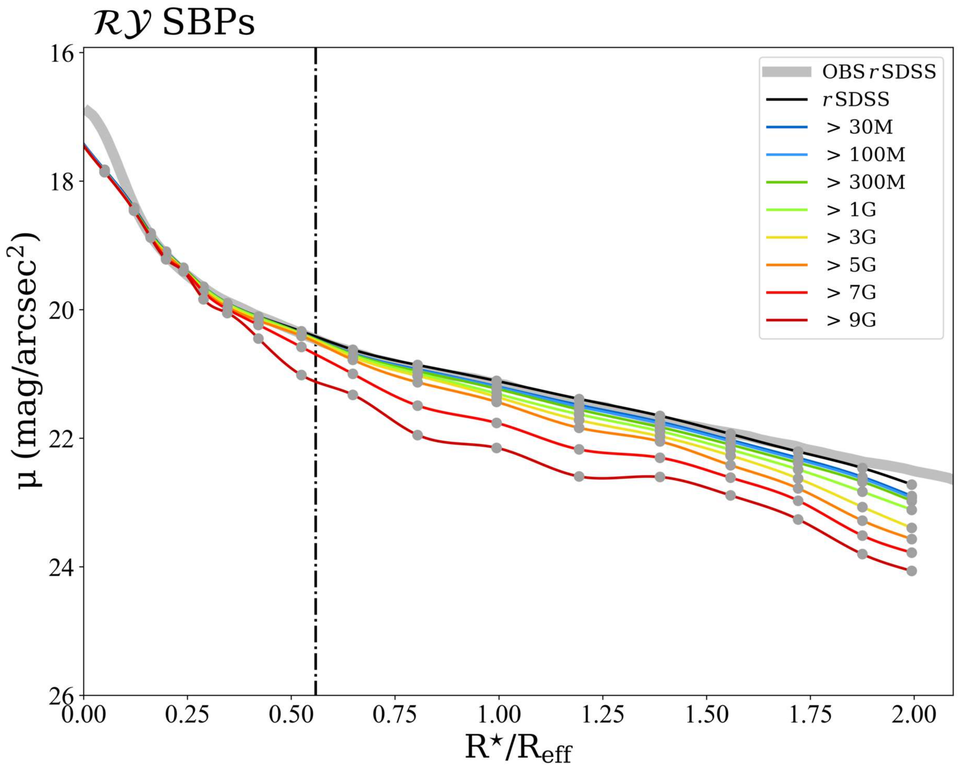
$\mathcal{RY}$ SBPs
OBS rSDSS
rSDSS
> 30M
> 100M
> 300M
> 1G
> 3G
> 5G
> 7G
> 9G
μ (mag/arcsec^2)
R*/R$_{eff}$

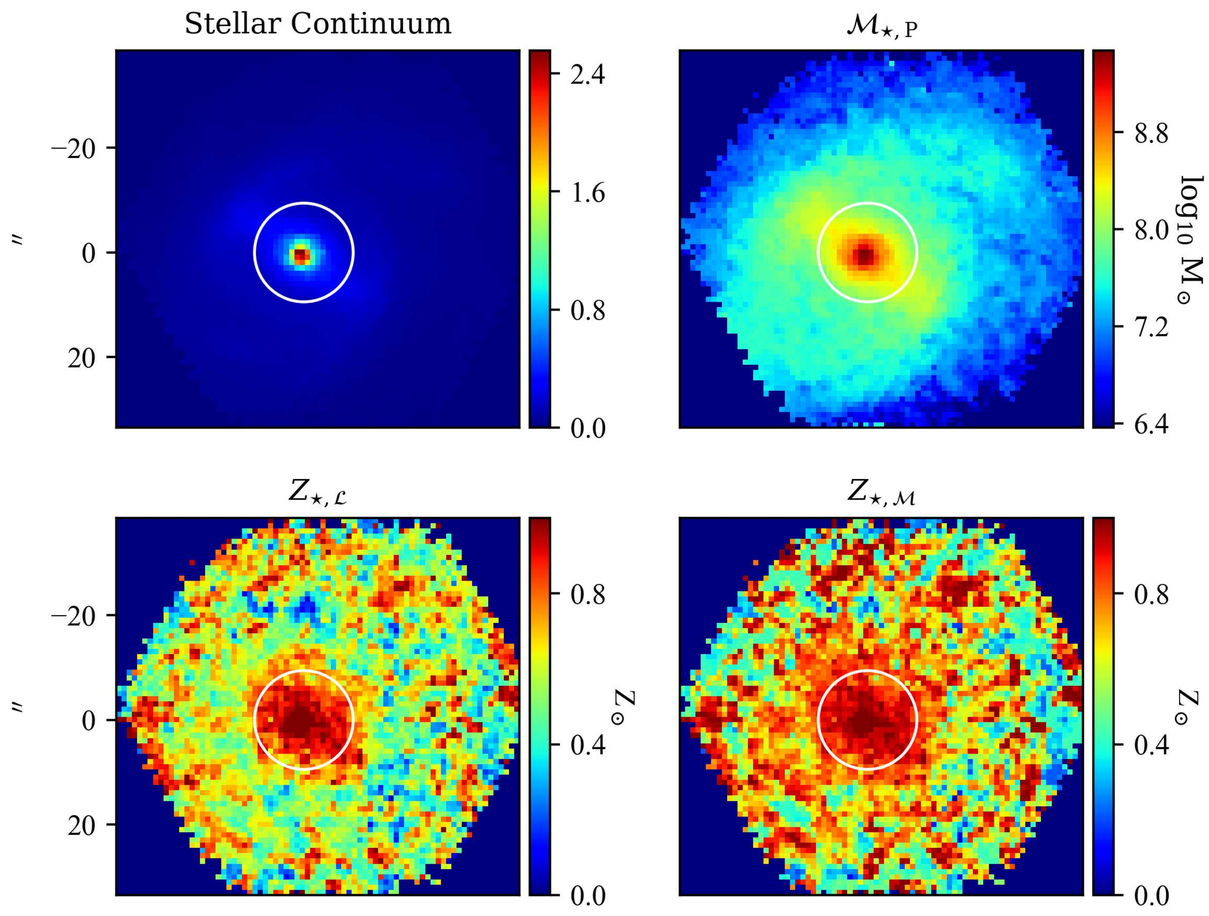
Stellar Continuum
$\mathcal{M}_{\star,\mathrm{P}}$
$Z_{\star,\mathcal{L}}$
$Z_{\star,\mathcal{M}}$
log$_{10}$ M$_\odot$
Z$_\odot$
″

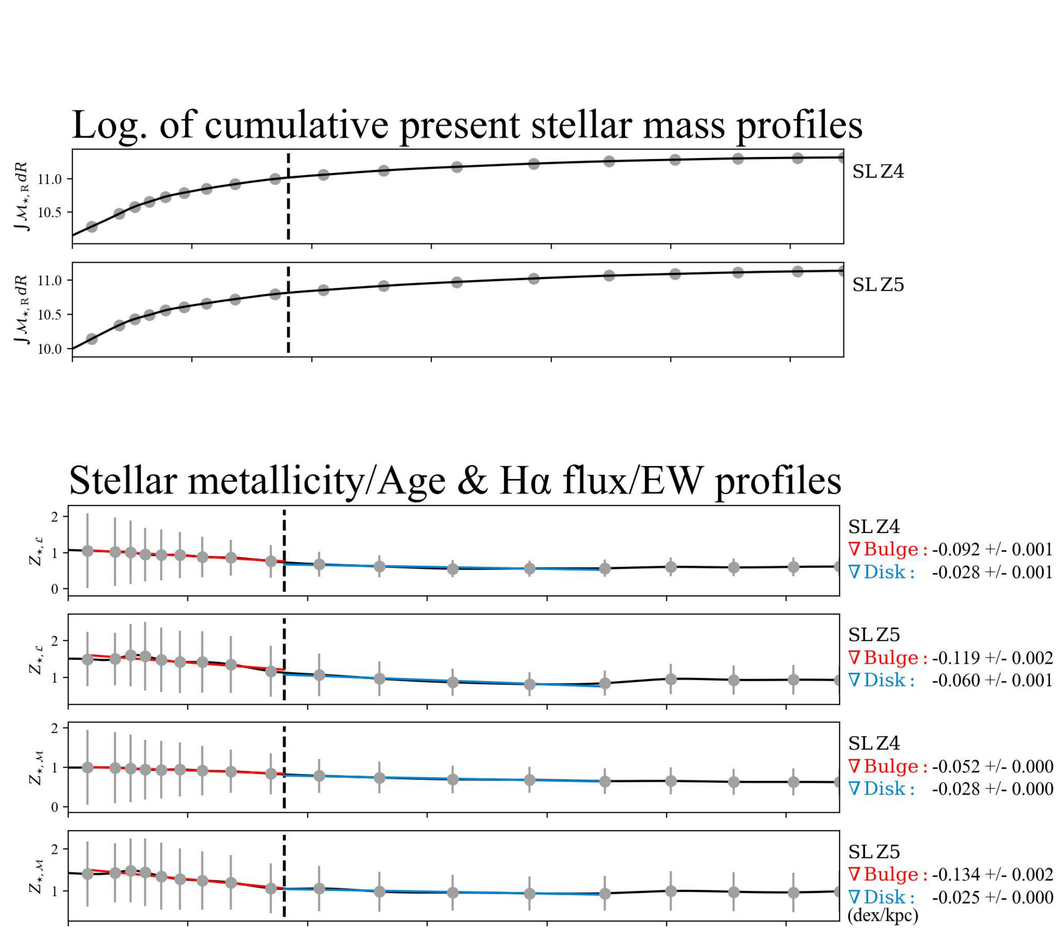
Log. of cumulative present stellar mass profiles
$\int \mathcal{M}_{\star,\mathrm{R}} dR$
SL Z4
SL Z5
Stellar metallicity/Age & Hα flux/EW profiles
$Z_{\star,\mathcal{L}}$
$Z_{\star,\mathcal{M}}$
SL Z4
∇ Bulge : -0.092 +/- 0.001
∇ Disk : -0.028 +/- 0.001
SL Z5
∇ Bulge : -0.119 +/- 0.002
∇ Disk : -0.060 +/- 0.001
SL Z4
∇ Bulge : -0.052 +/- 0.000
∇ Disk : -0.028 +/- 0.000
SL Z5
∇ Bulge : -0.134 +/- 0.002
∇ Disk : -0.025 +/- 0.000
(dex/kpc)

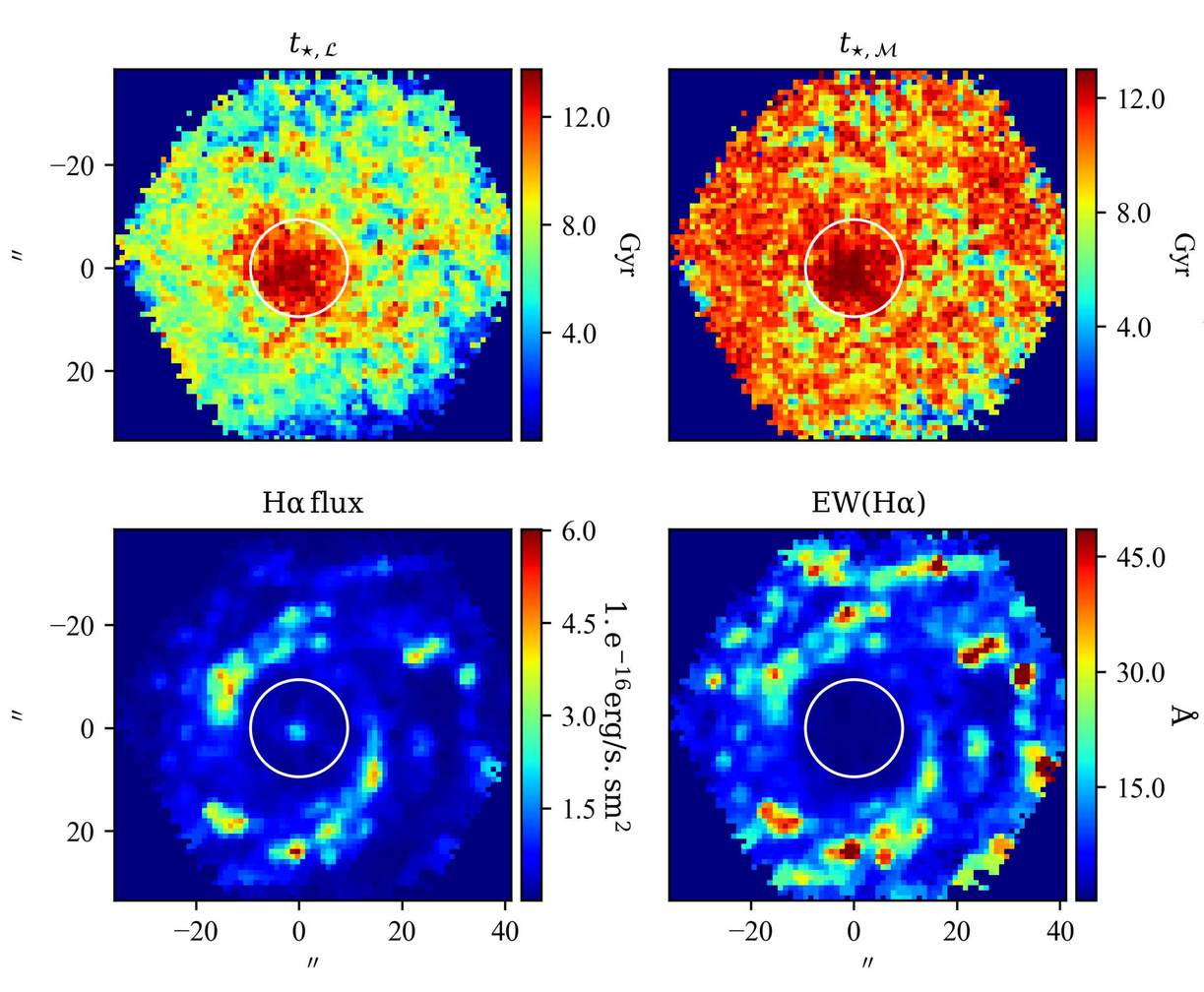
$t_{\star,\mathcal{L}}$
$t_{\star,\mathcal{M}}$
Gyr
Hα flux
EW(Hα)
1. e^{-16}erg/s. sm^2
Å
″

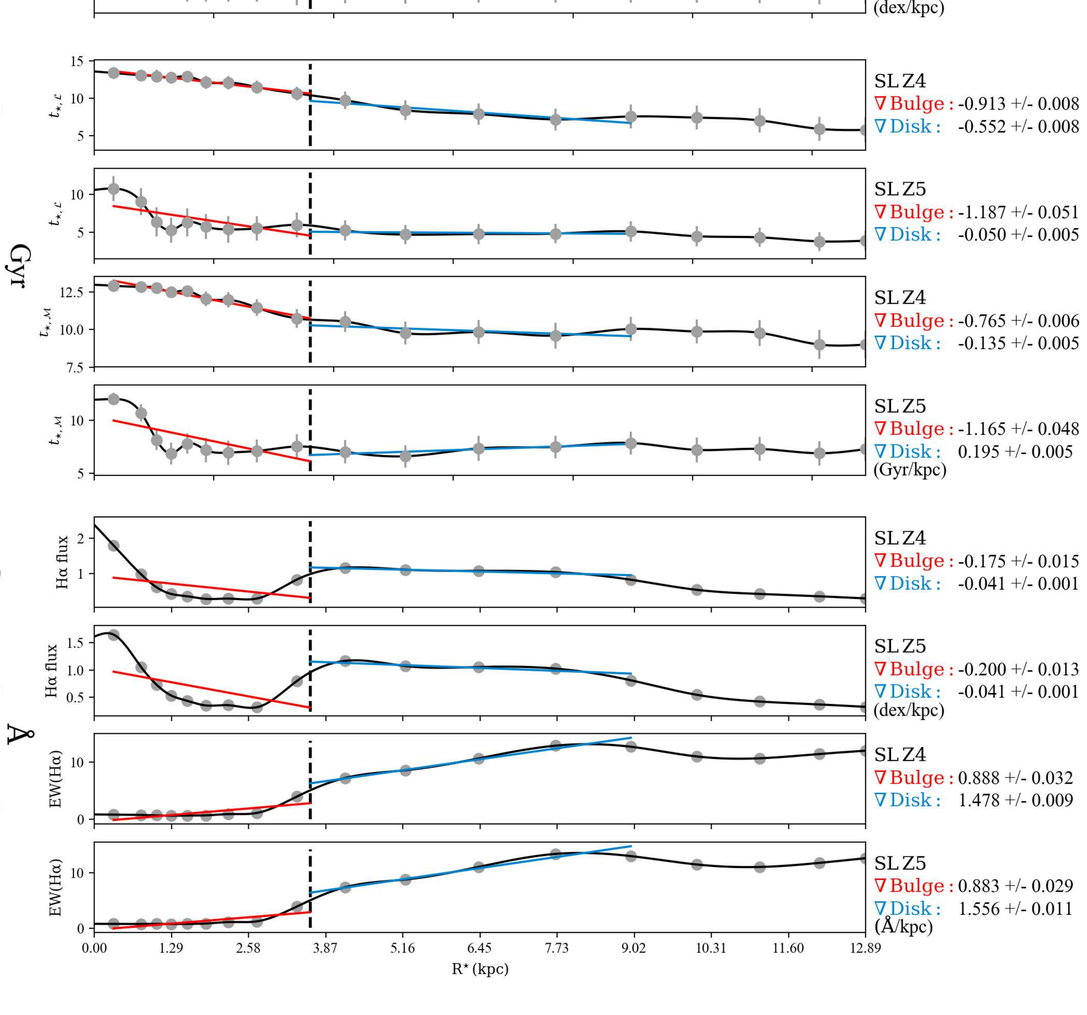
SL Z4
∇ Bulge : -0.913 +/- 0.008
∇ Disk : -0.552 +/- 0.008
SL Z5
∇ Bulge : -1.187 +/- 0.051
∇ Disk : -0.050 +/- 0.005
SL Z4
∇ Bulge : -0.765 +/- 0.006
∇ Disk : -0.135 +/- 0.005
SL Z5
∇ Bulge : -1.165 +/- 0.048
∇ Disk : 0.195 +/- 0.005
(Gyr/kpc)
SL Z4
∇ Bulge : -0.175 +/- 0.015
∇ Disk : -0.041 +/- 0.001
SL Z5
∇ Bulge : -0.200 +/- 0.013
∇ Disk : -0.041 +/- 0.001
(dex/kpc)
SL Z4
∇ Bulge : 0.888 +/- 0.032
∇ Disk : 1.478 +/- 0.009
SL Z5
∇ Bulge : 0.883 +/- 0.029
∇ Disk : 1.556 +/- 0.011
(Å/kpc)
R* (kpc)

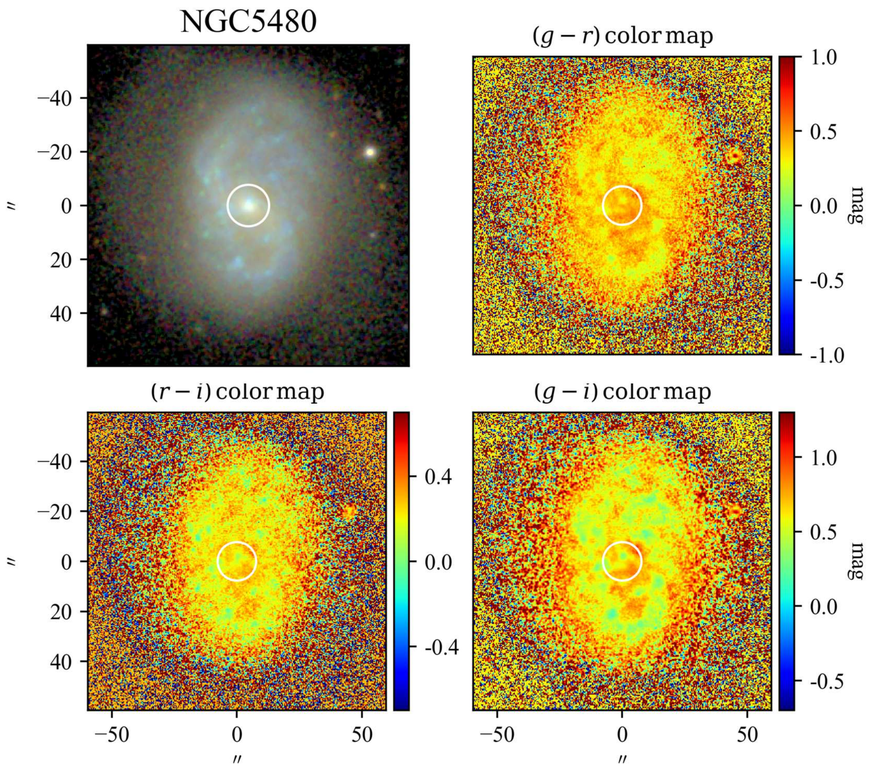

SBP decomposition of SDSS r band

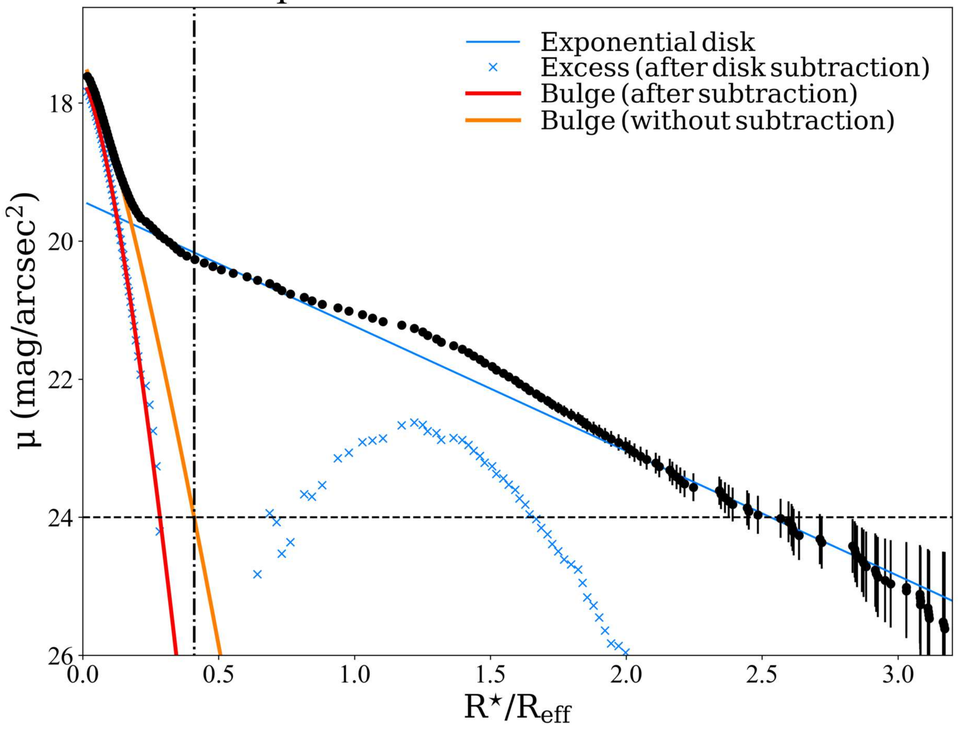

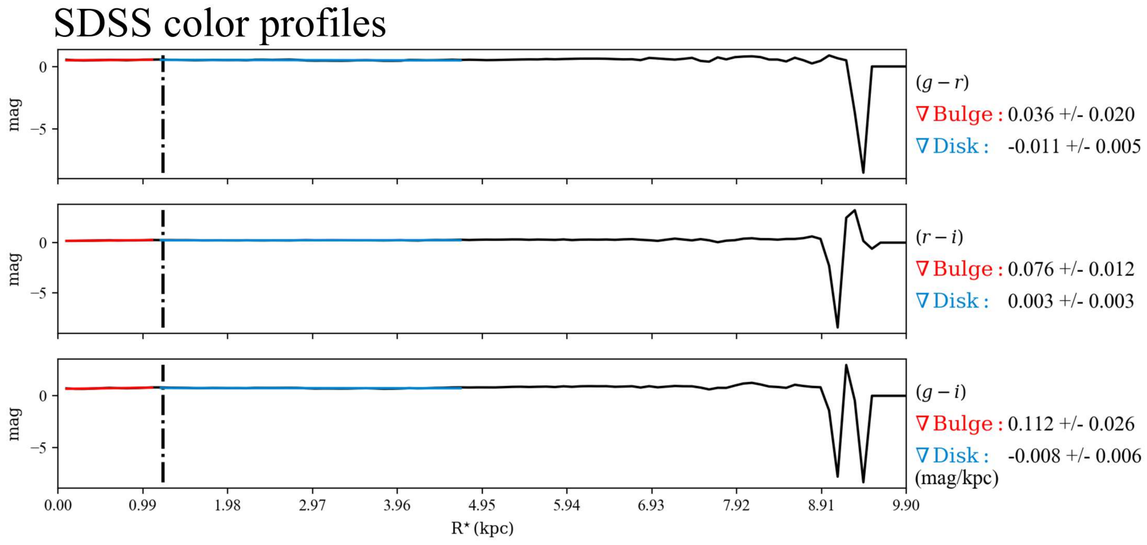

$\mathcal{RY}$ SBPs

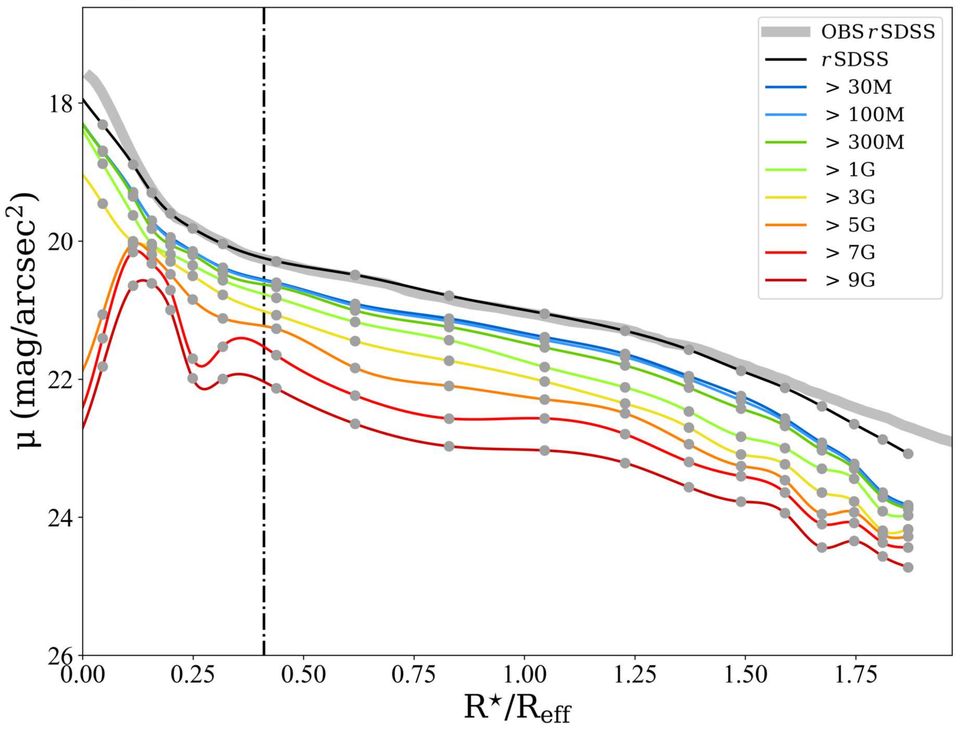

Stellar Continuum $\mathcal{M}_{\star,\mathrm{P}}$

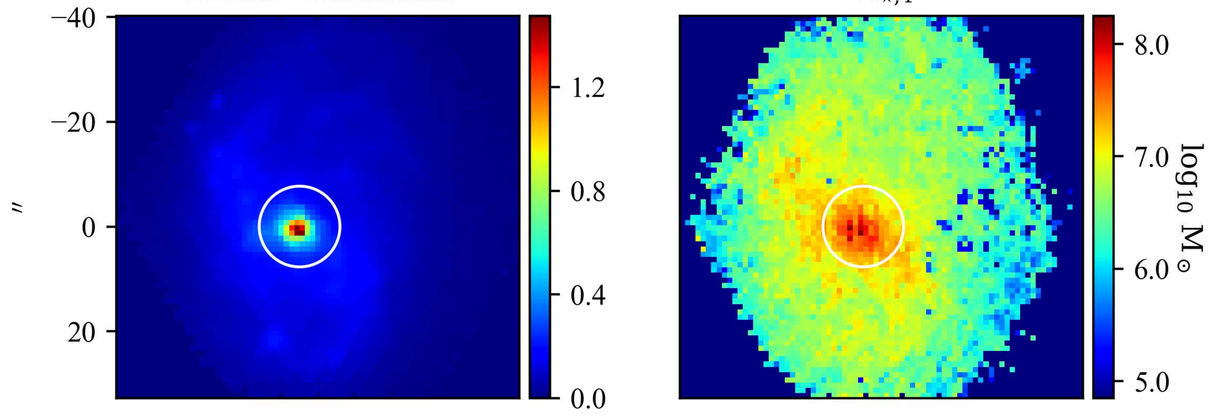

Log. of cumulative present stellar mass profiles

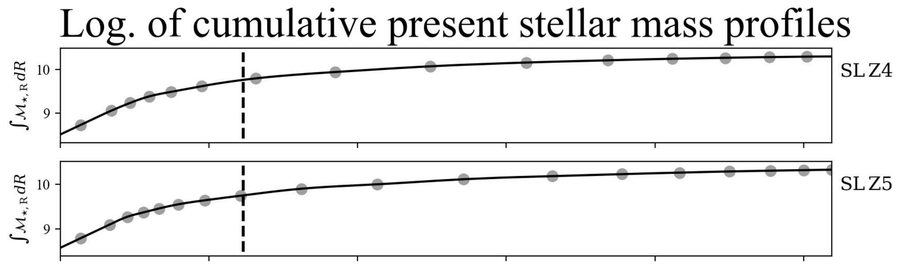

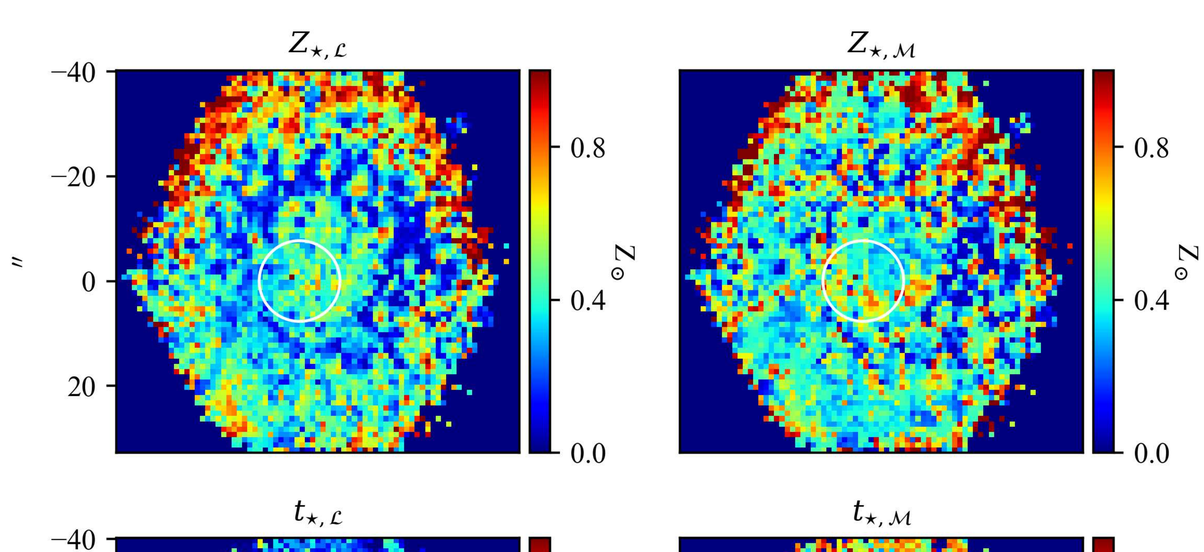

Stellar metallicity/Age & Hα flux/EW profiles

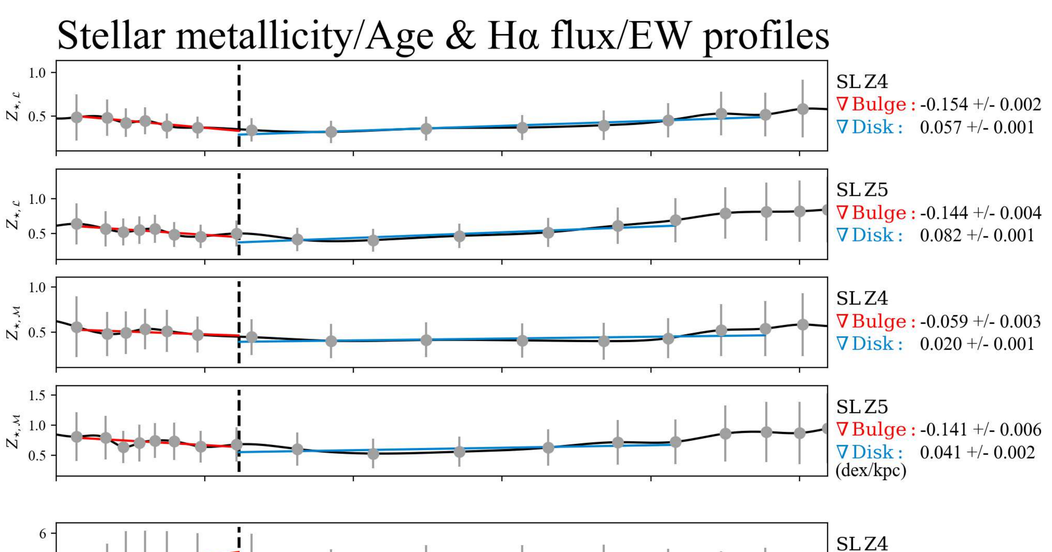

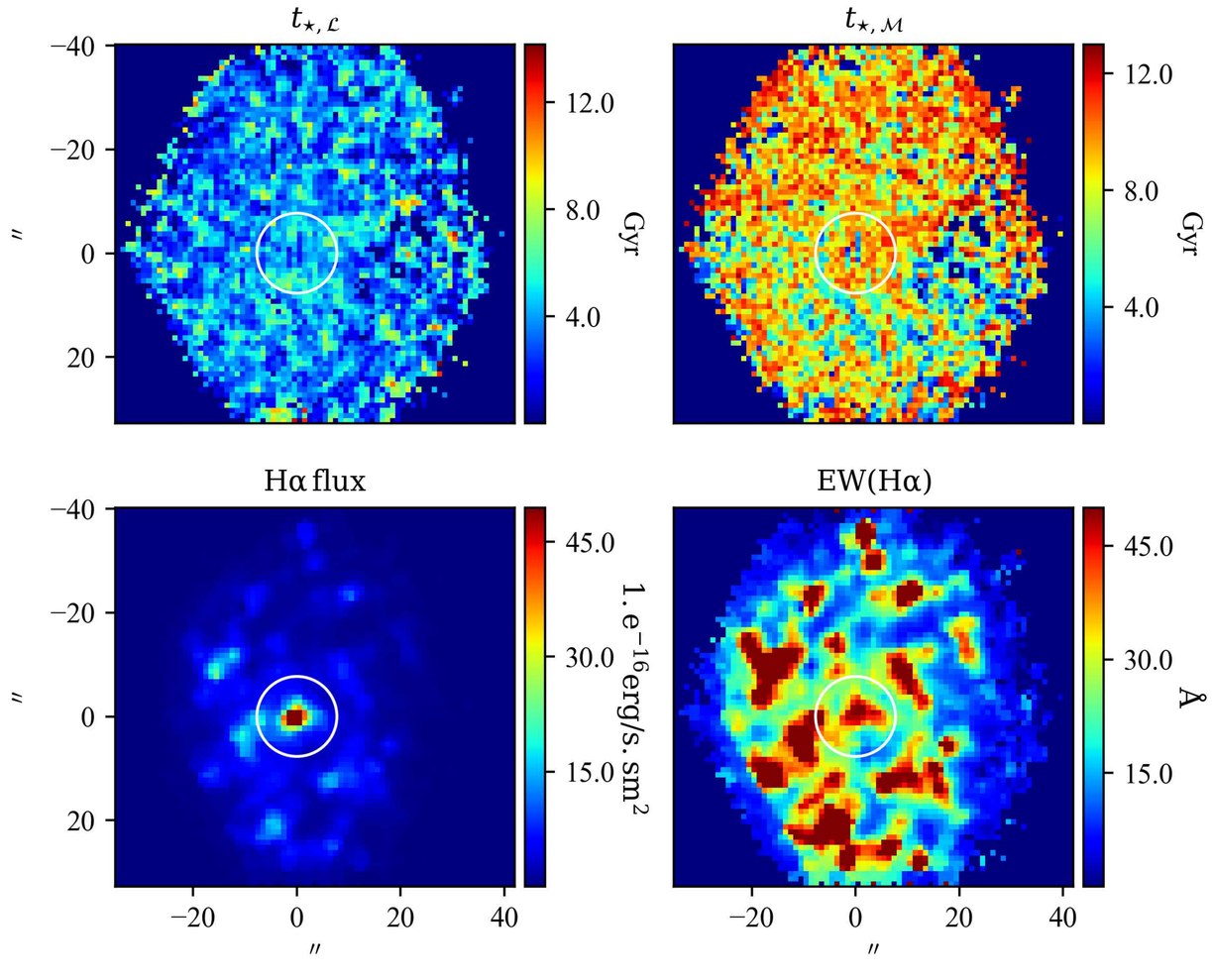

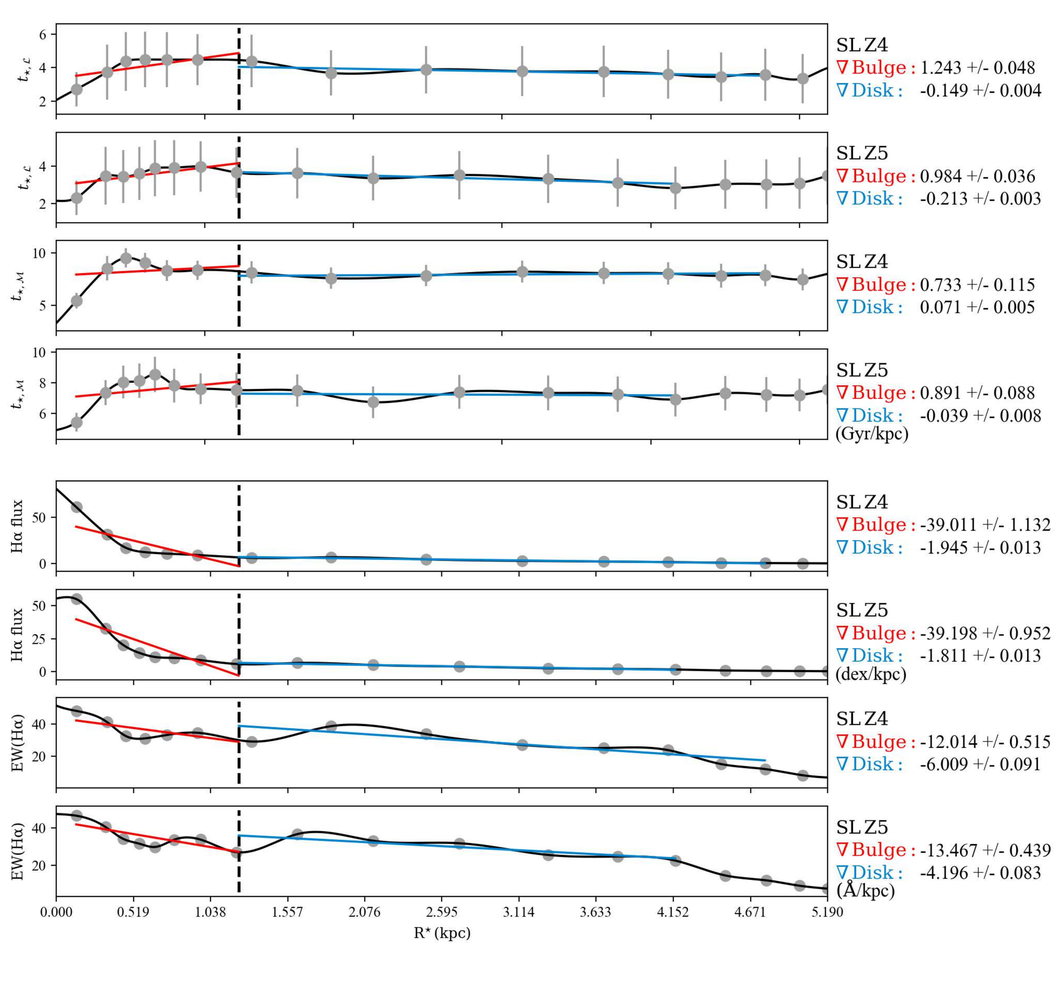

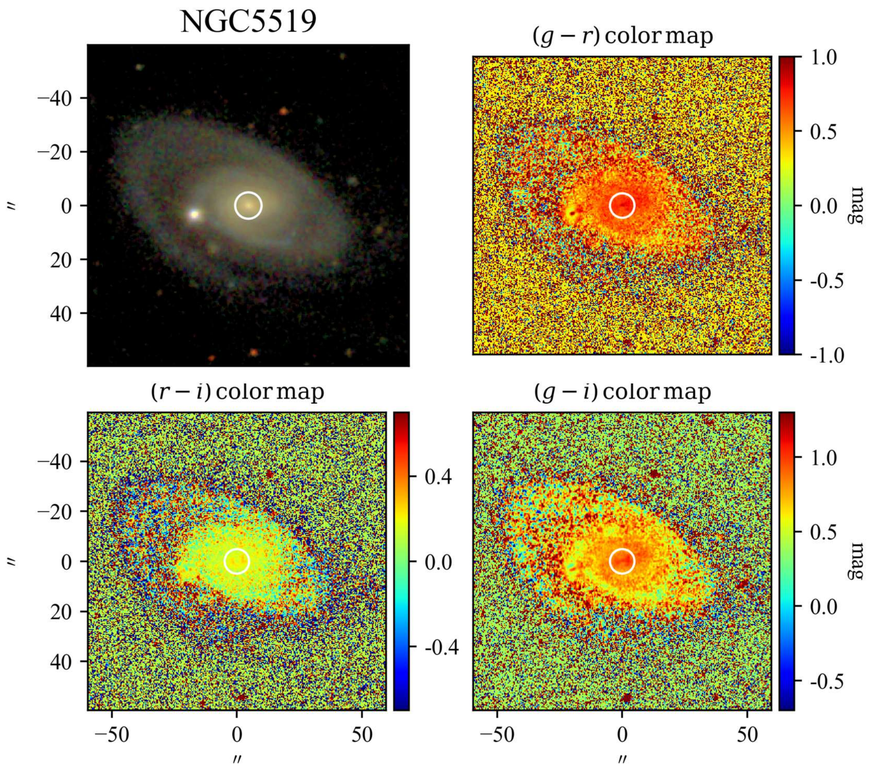

SBP decomposition of SDSS r band

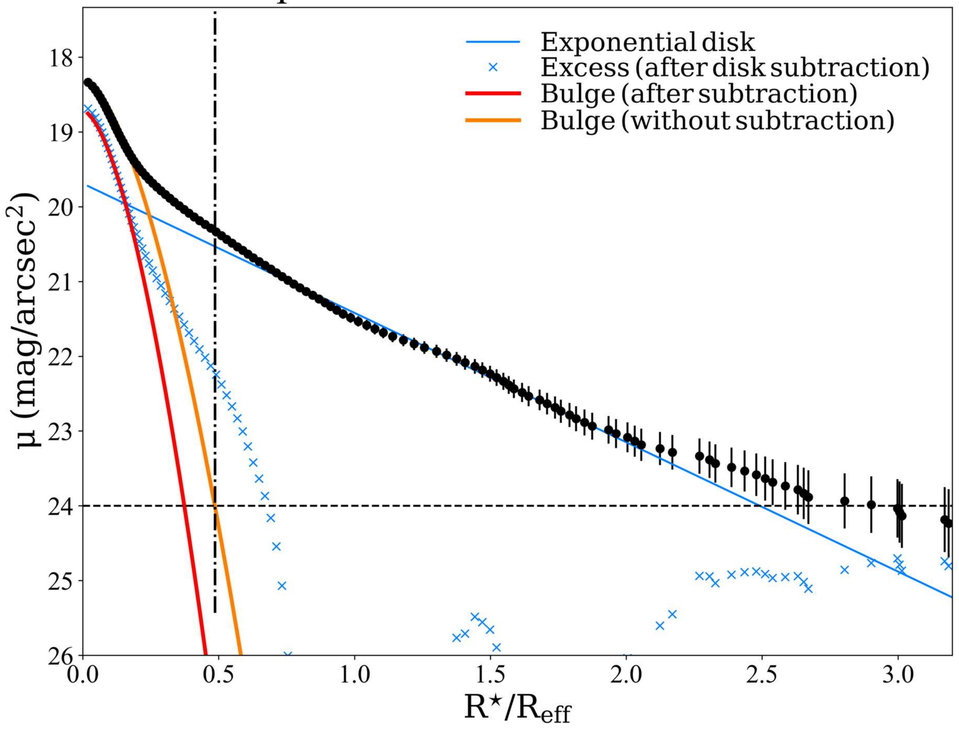

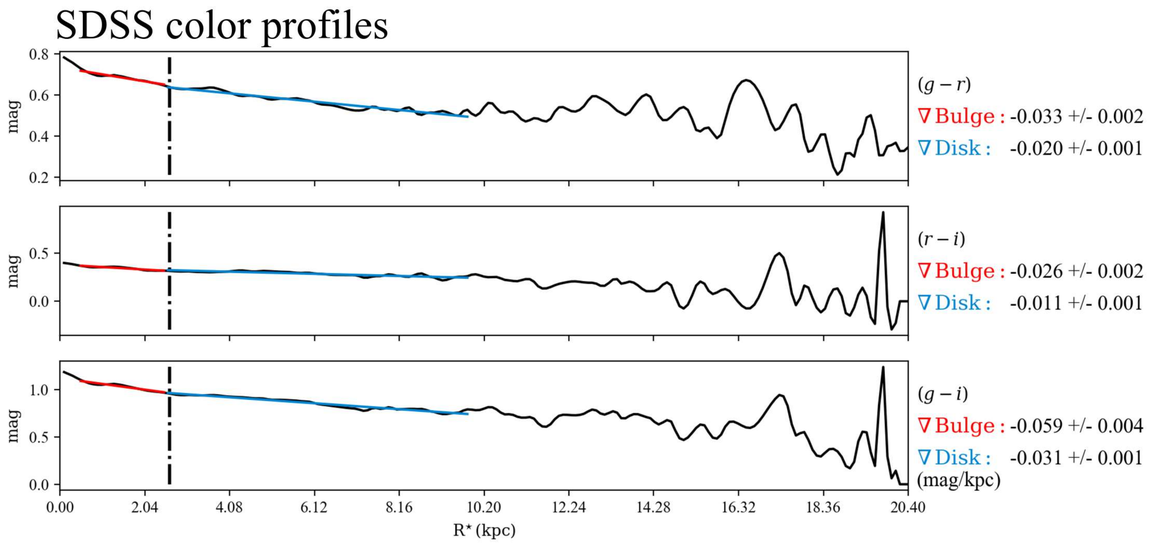

$\mathcal{RY}$ SBPs

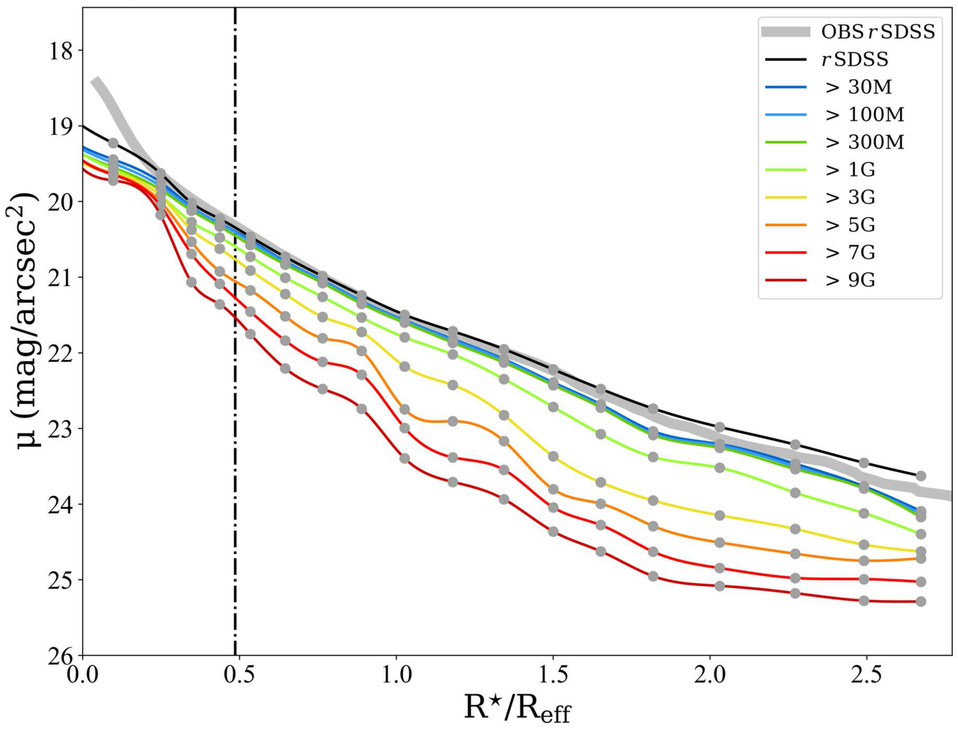

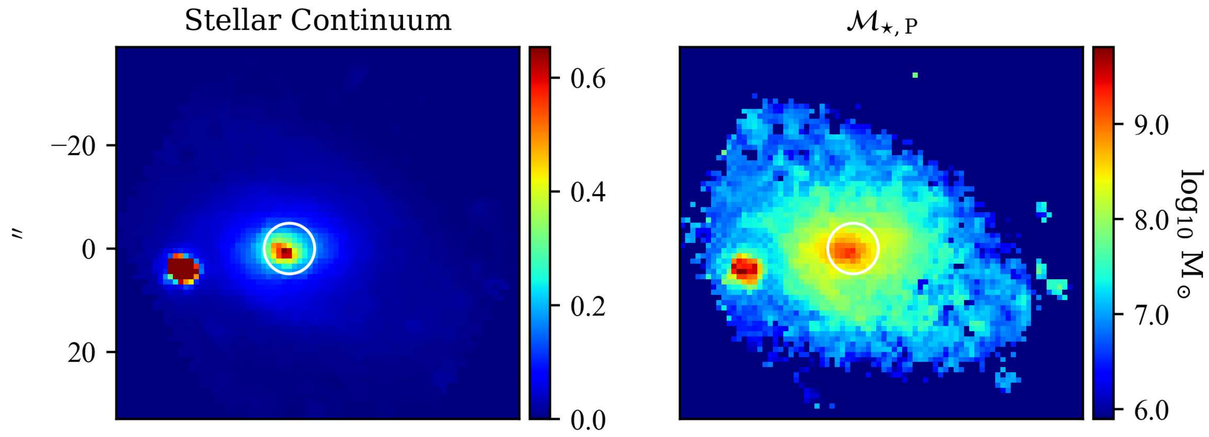

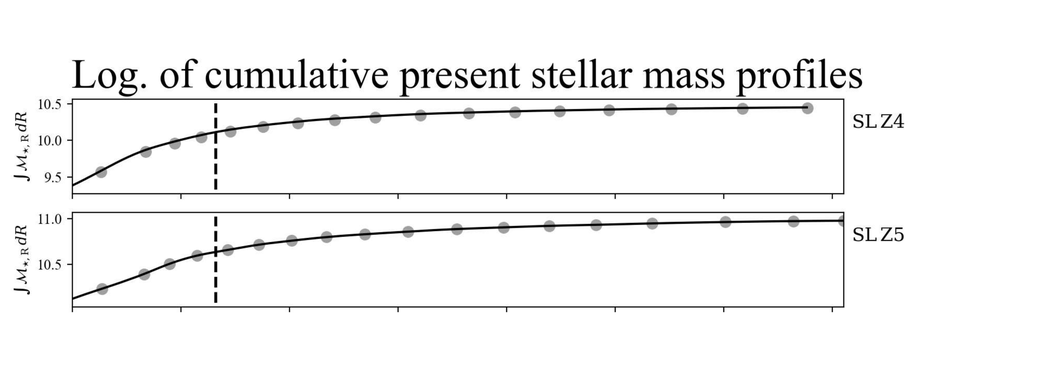

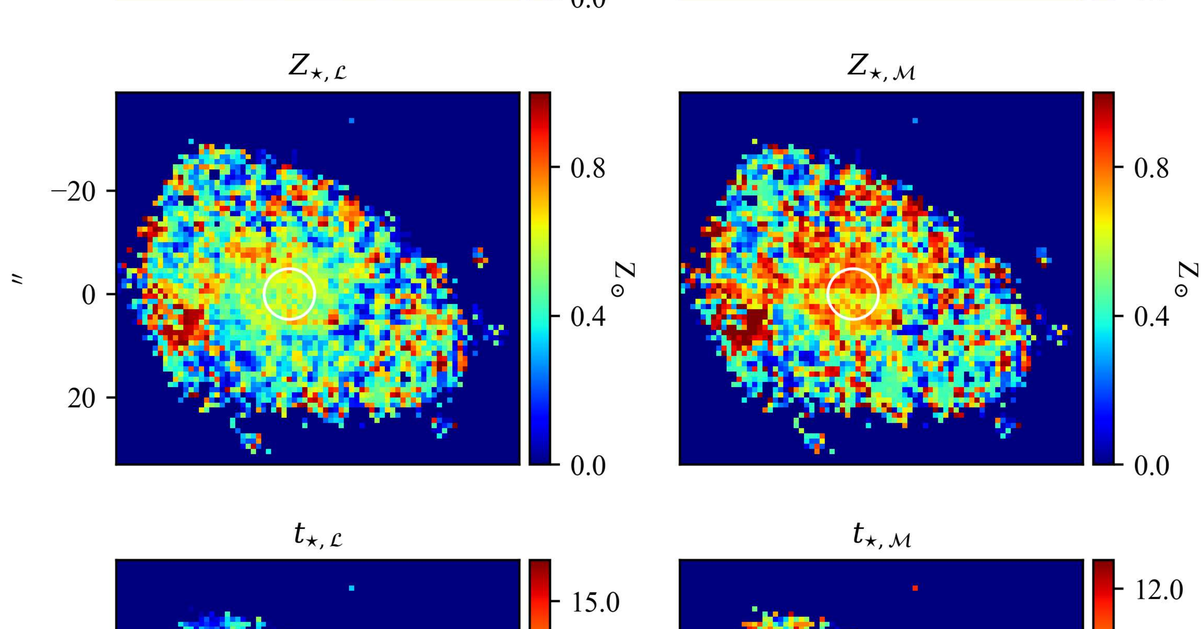

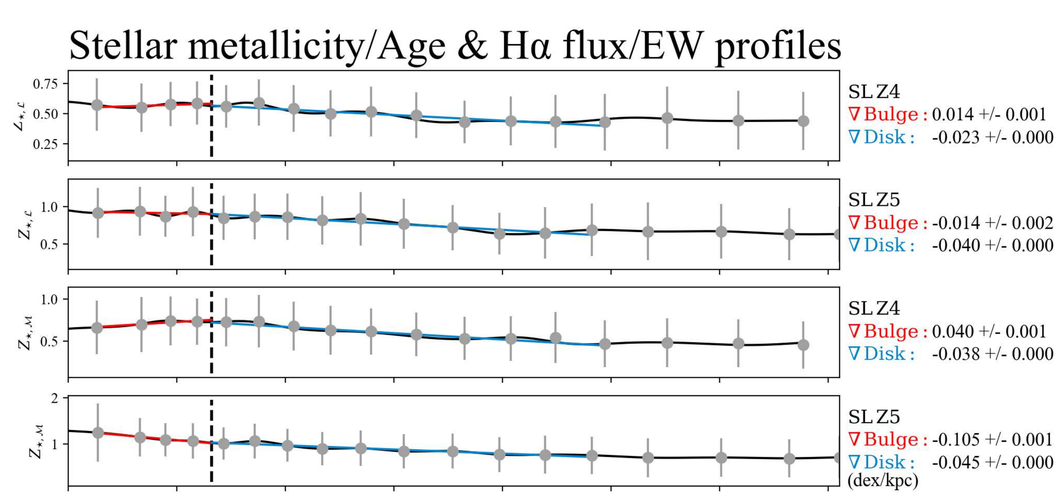

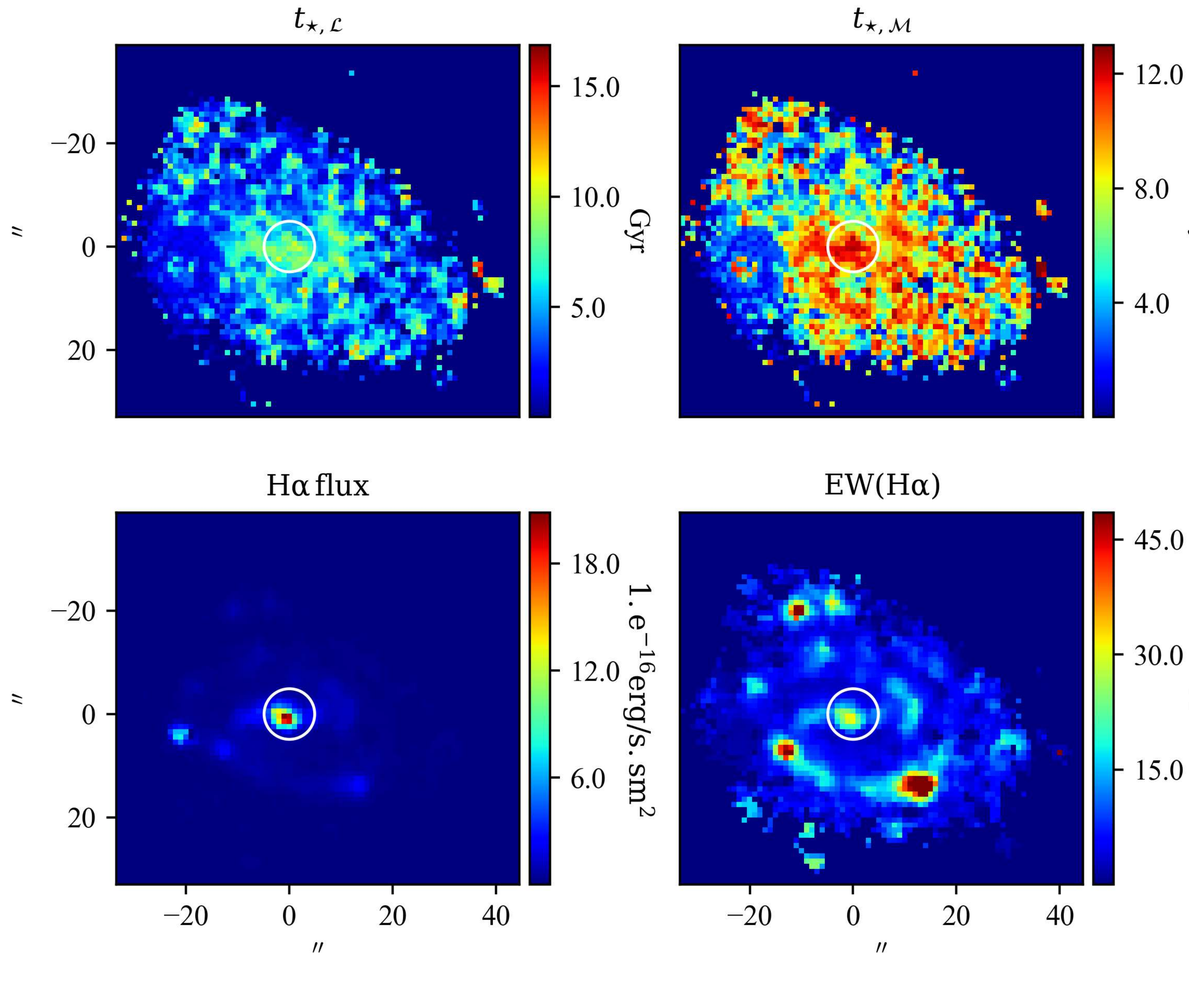

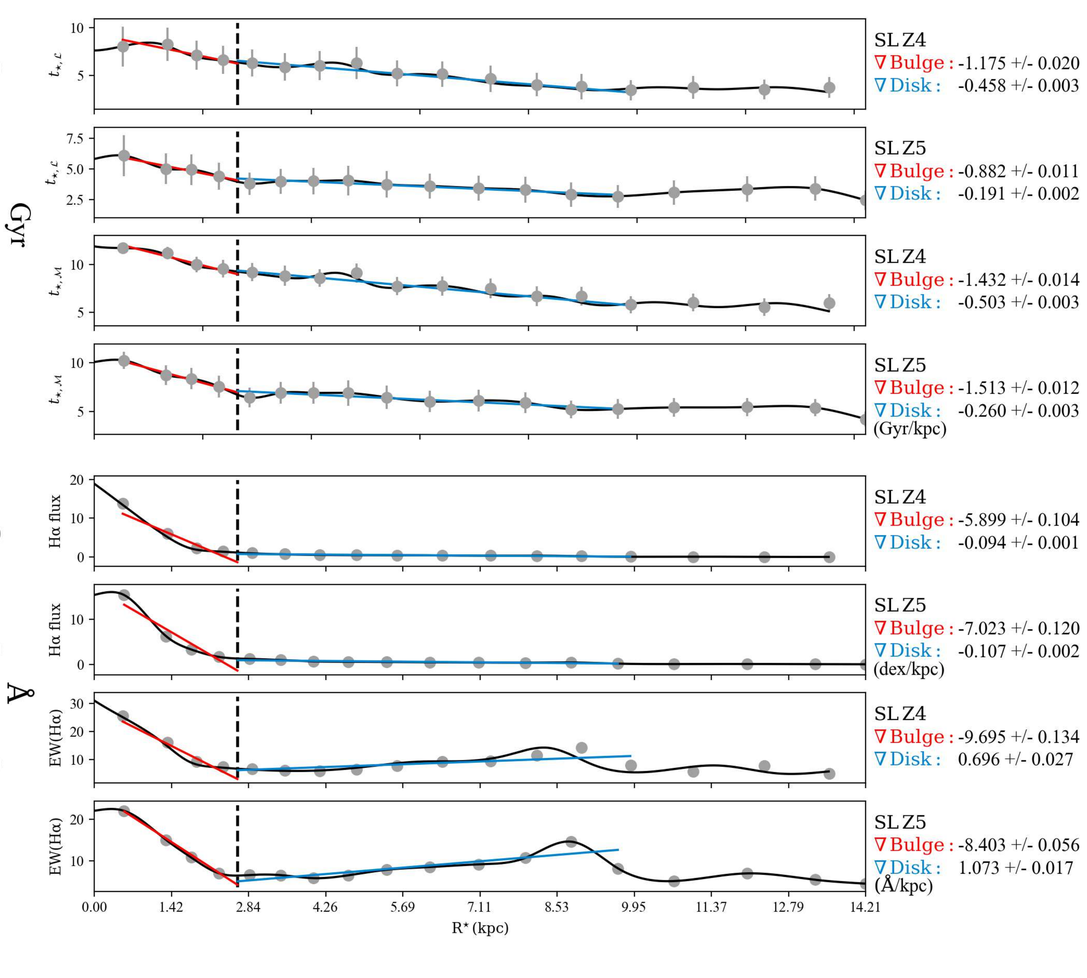

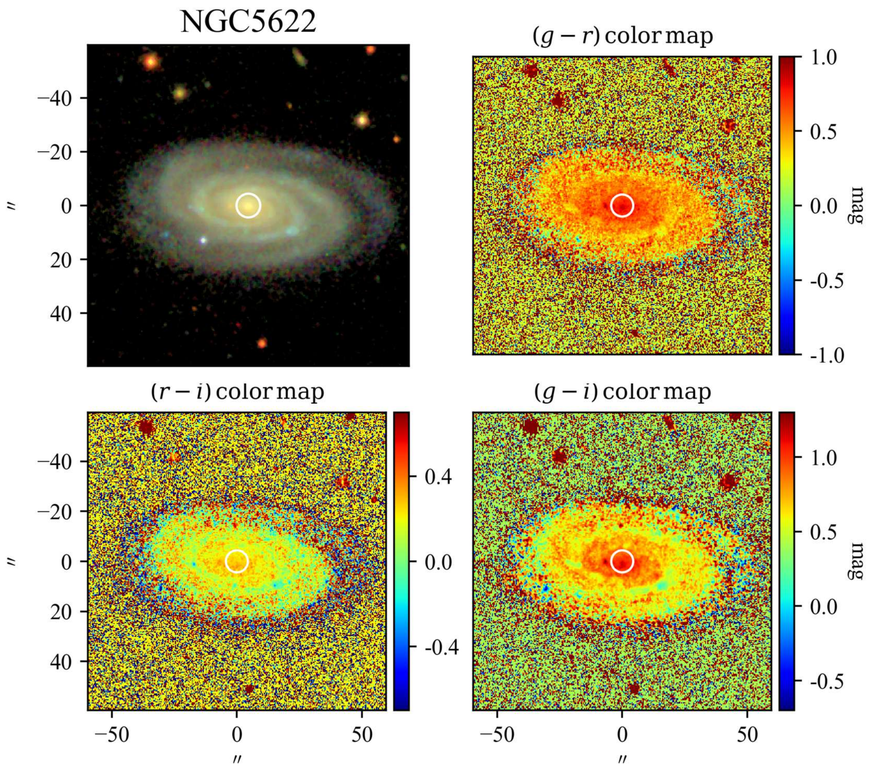

SBP decomposition of SDSS r band

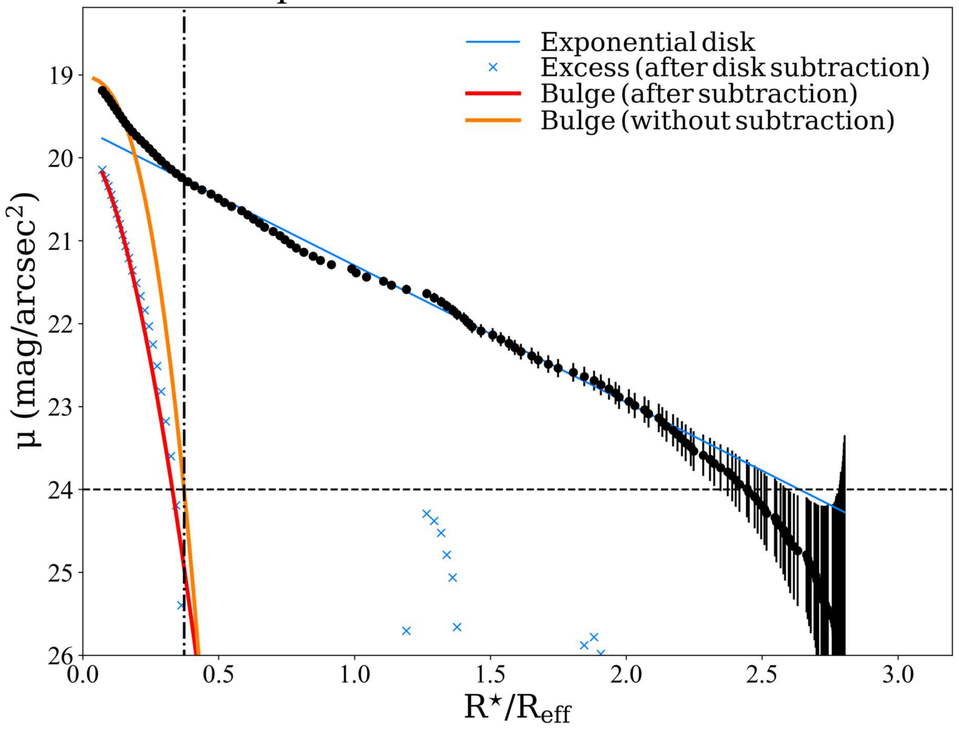

SDSS color profiles

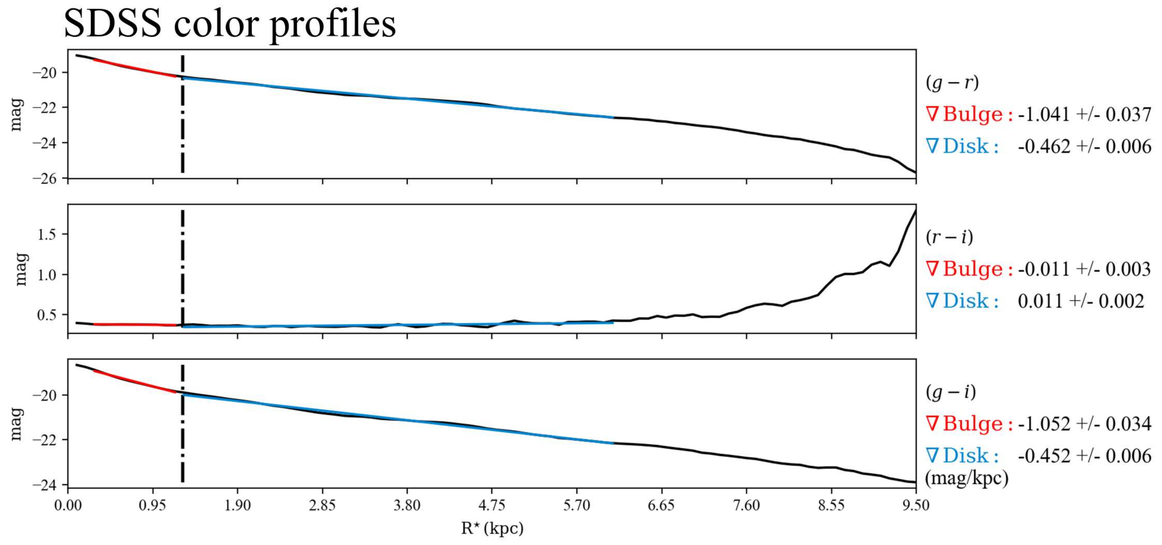

$\mathcal{RY}$ SBPs

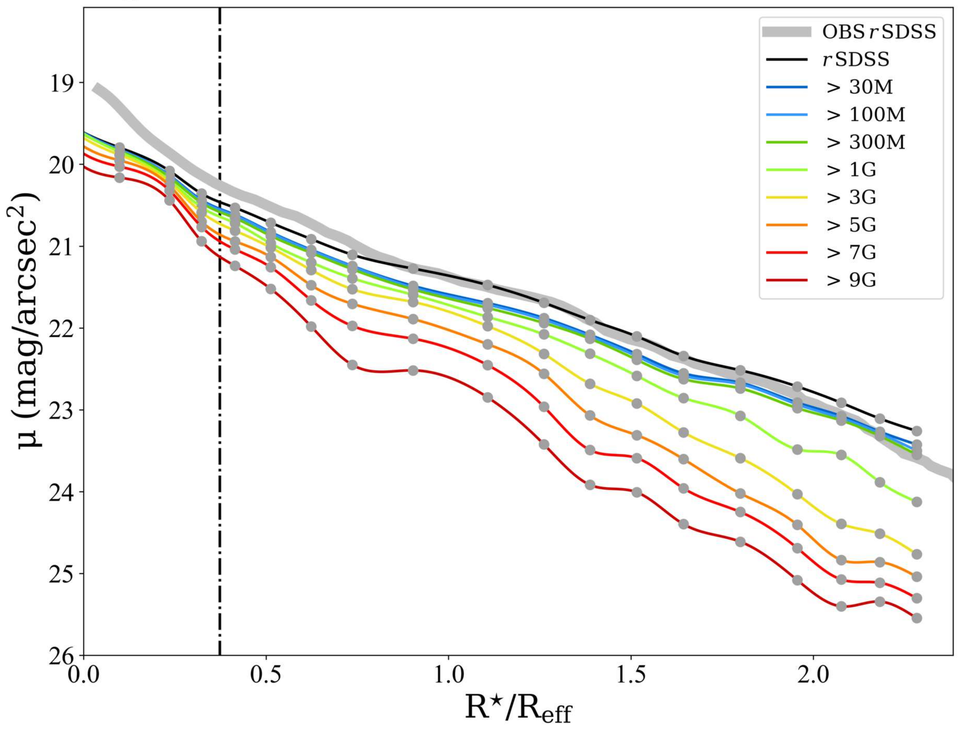

Stellar Continuum

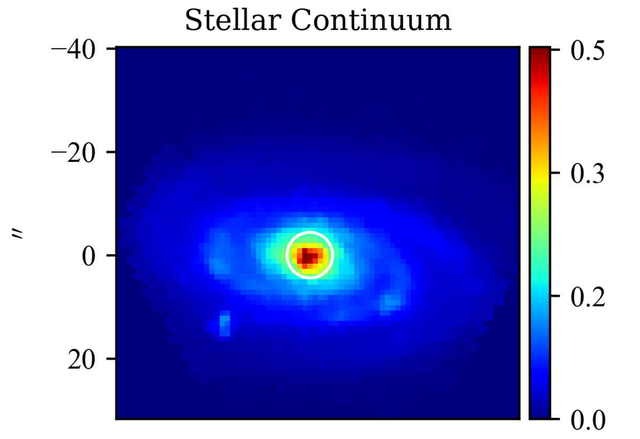

$\mathcal{M}_{\star,\,\rm P}$

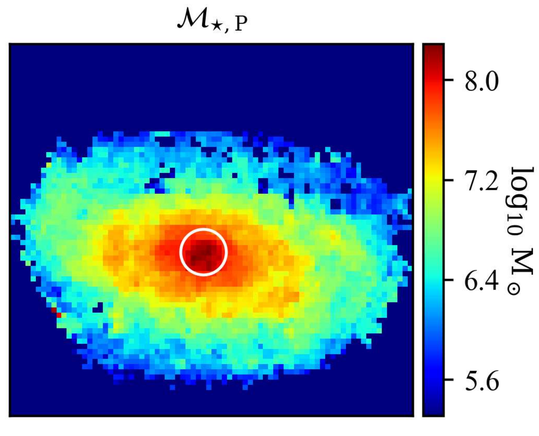

Log. of cumulative present stellar mass profiles

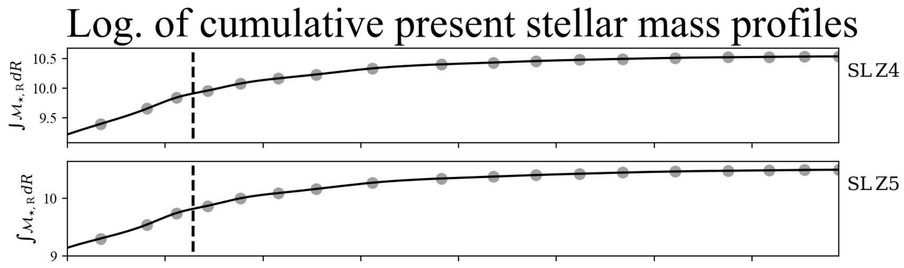

$Z_{\star,\,\mathcal{L}}$

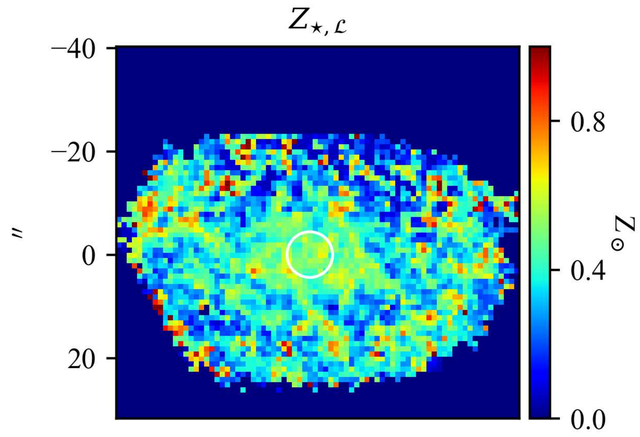

$Z_{\star,\,\mathcal{M}}$

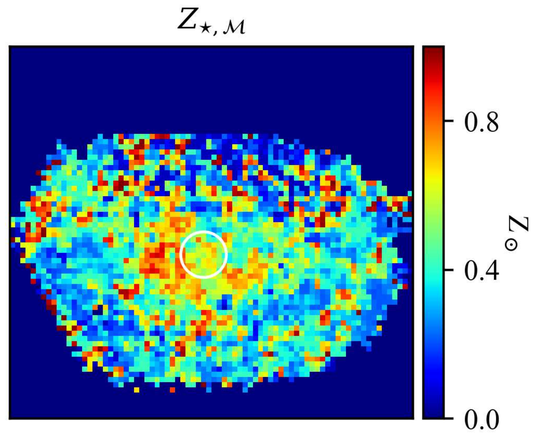

Stellar metallicity/Age & Hα flux/EW profiles

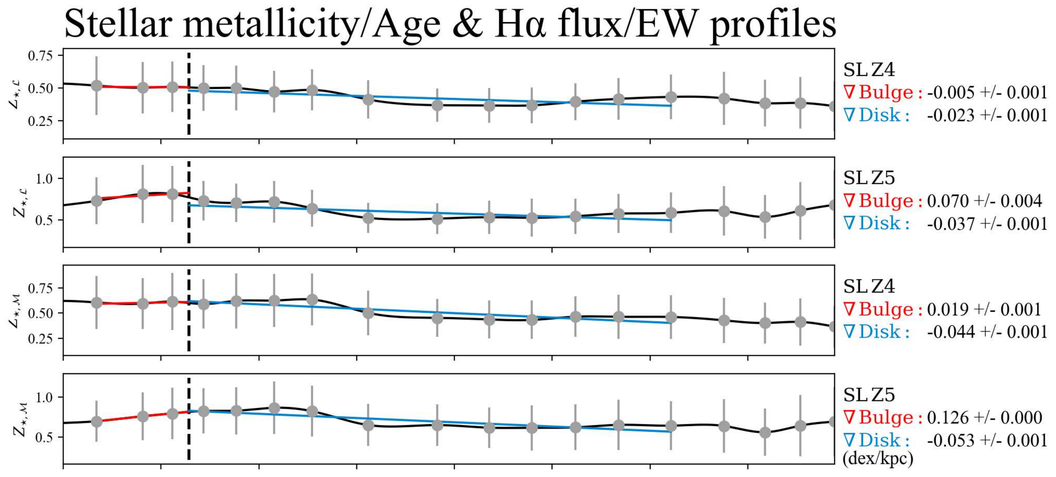

$t_{\star,\,\mathcal{L}}$

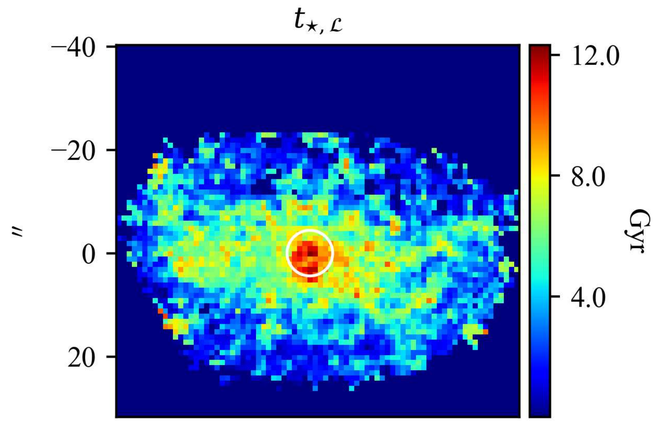

$t_{\star,\,\mathcal{M}}$

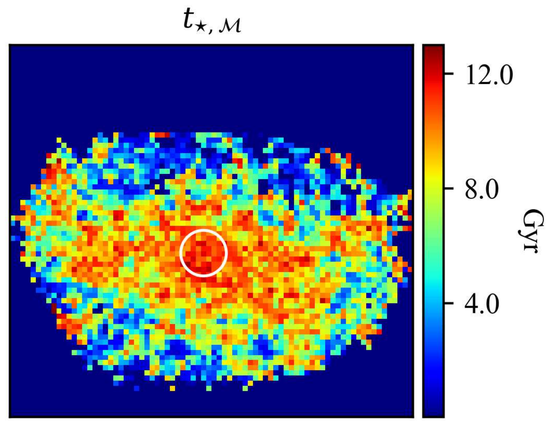

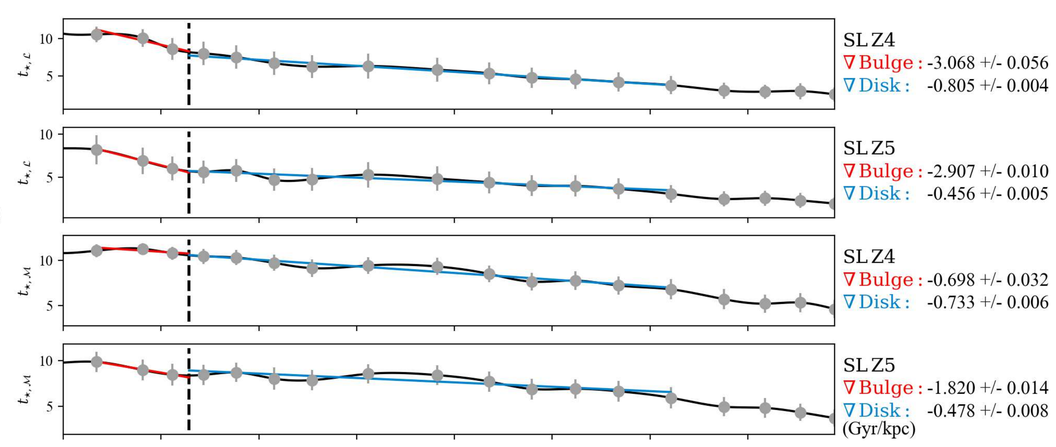

Hα flux

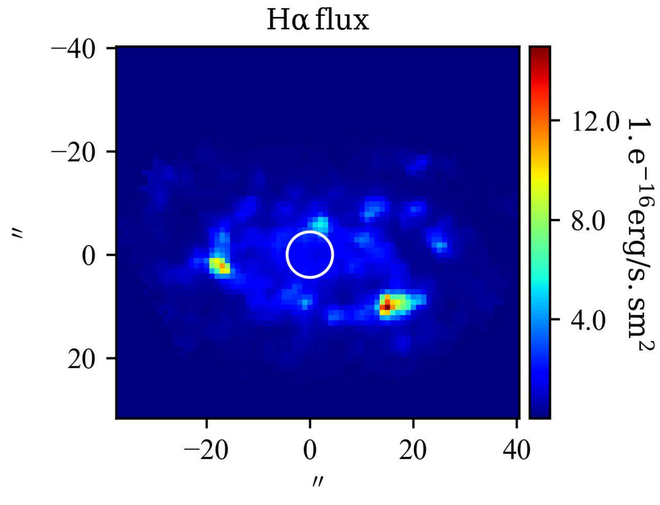

EW(Hα)

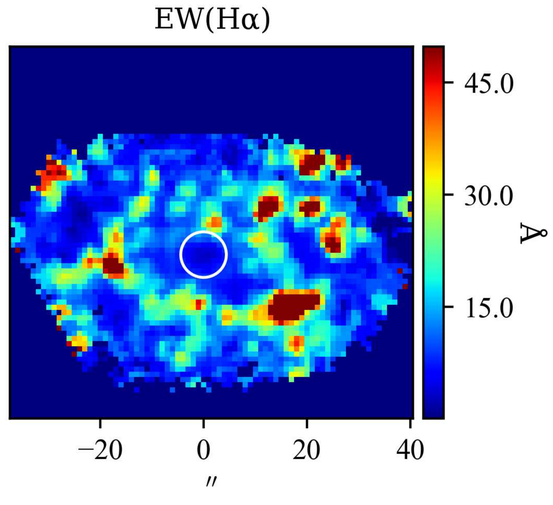

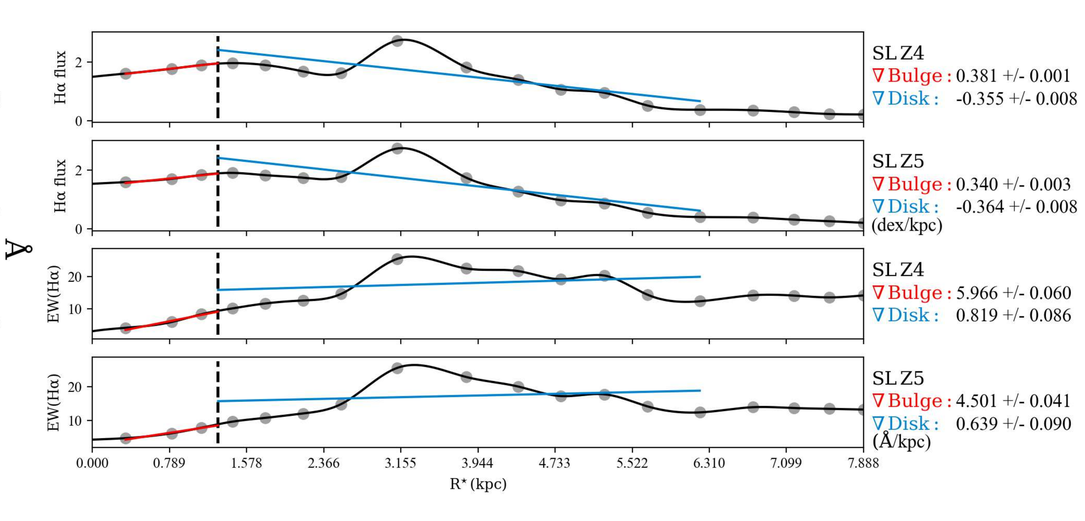

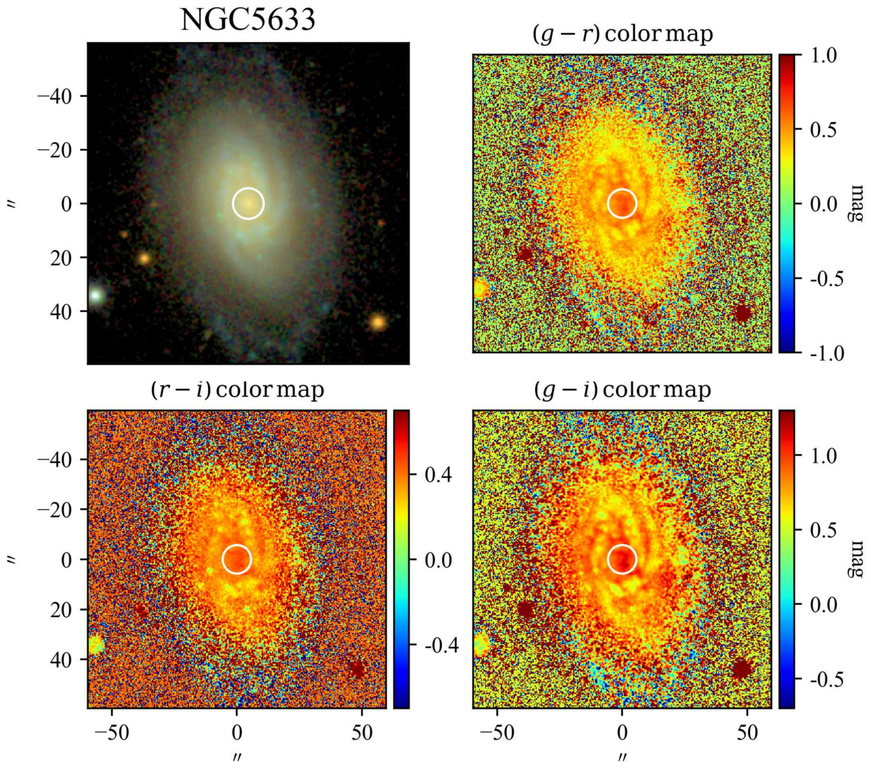

SBP decomposition of SDSS r band

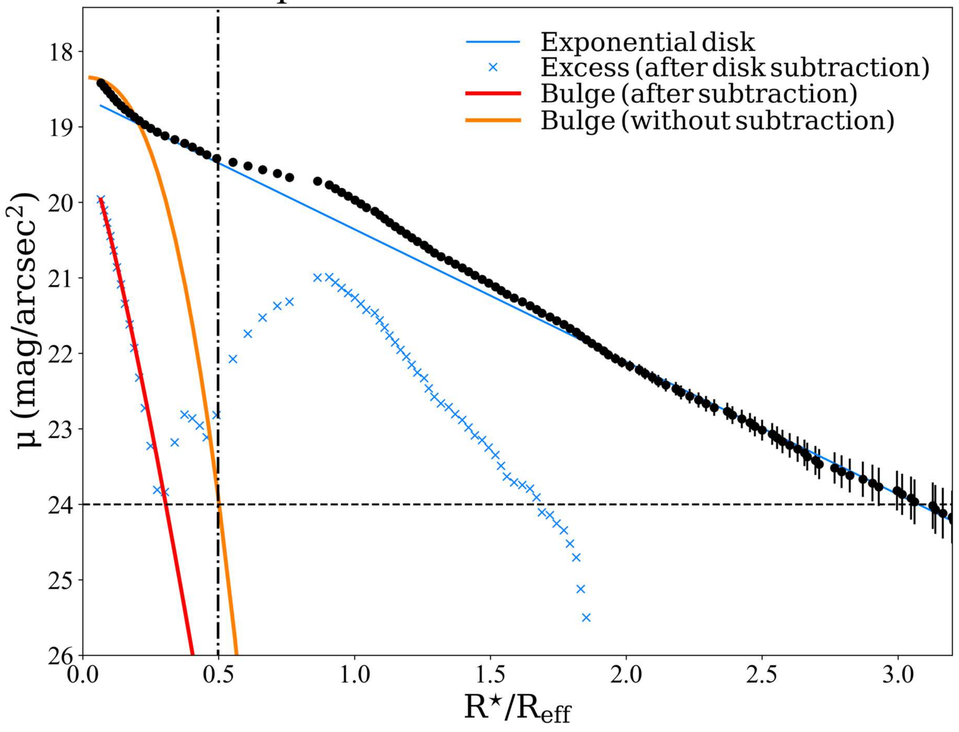

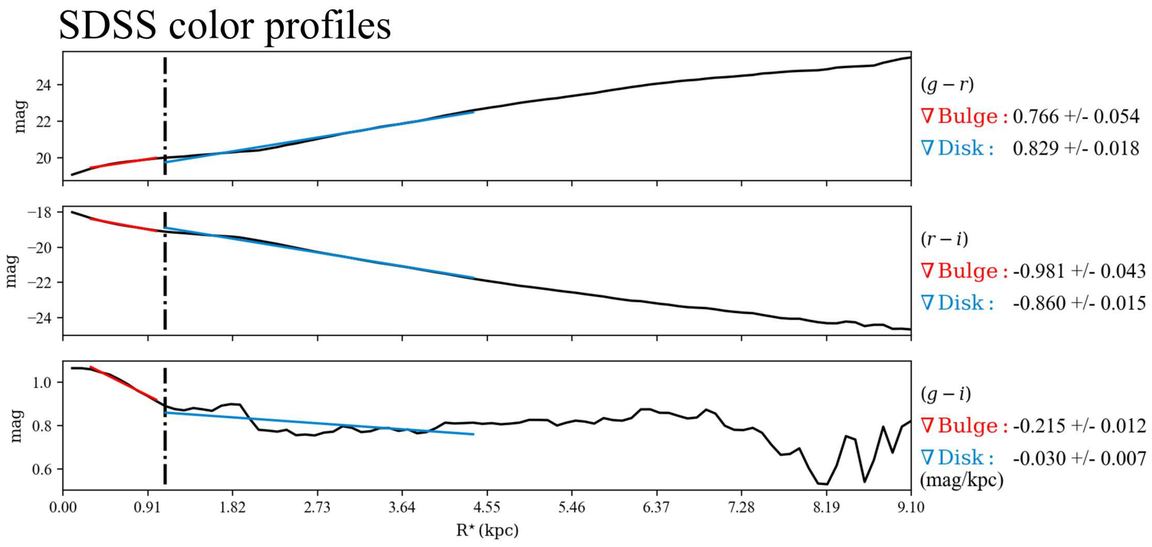

$\mathcal{RV}$ SBPs

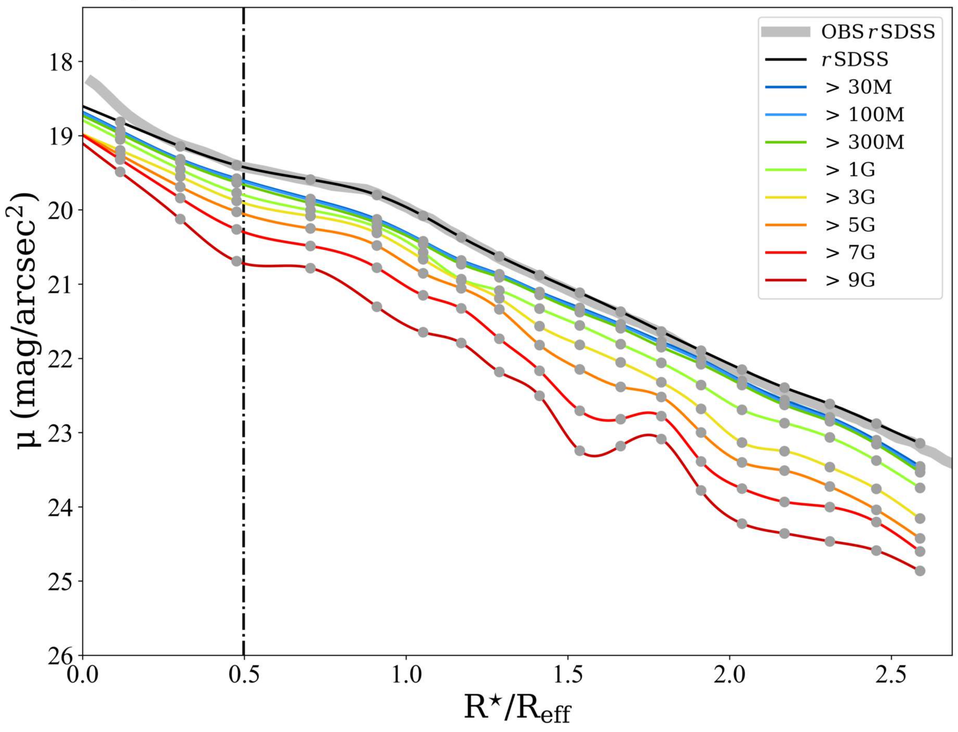

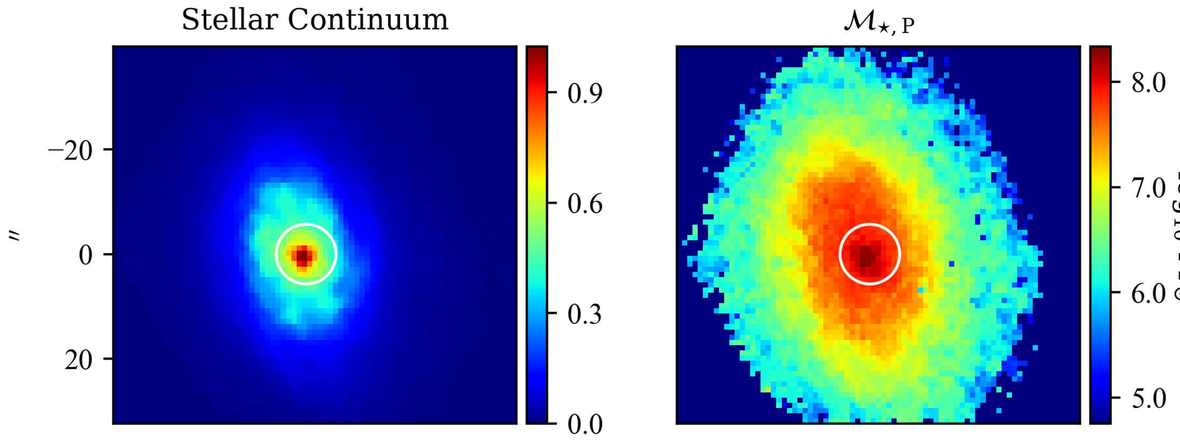

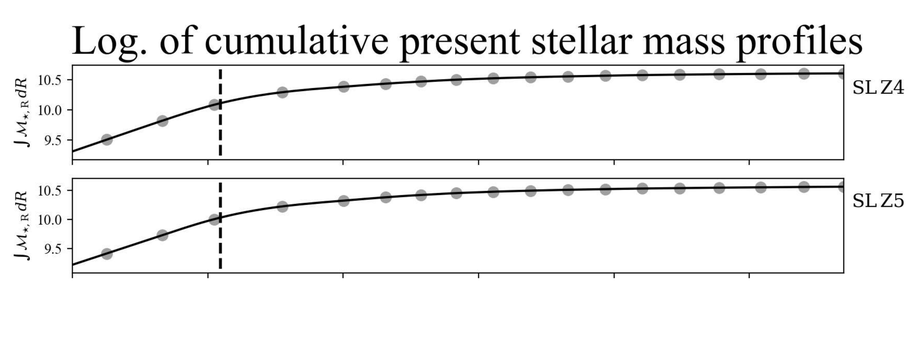

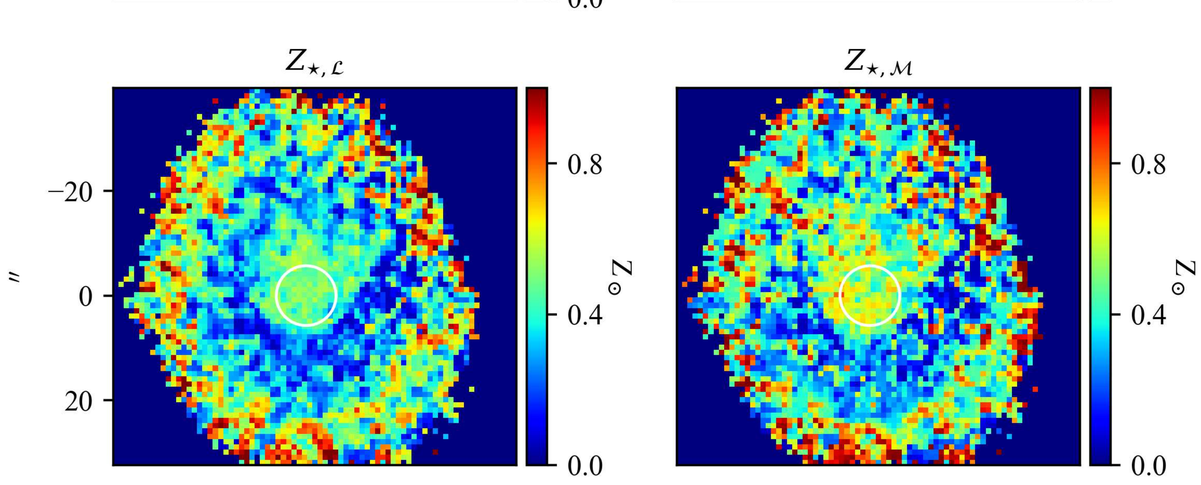

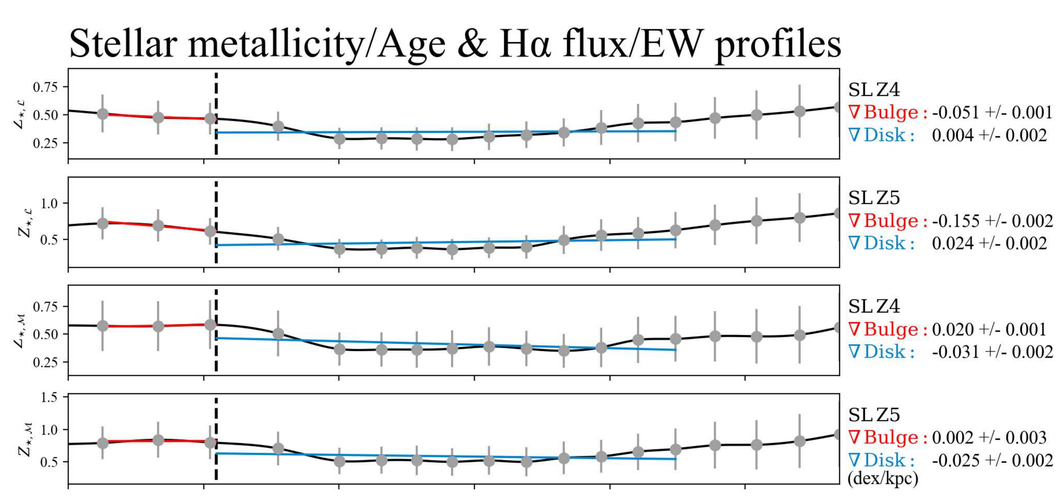

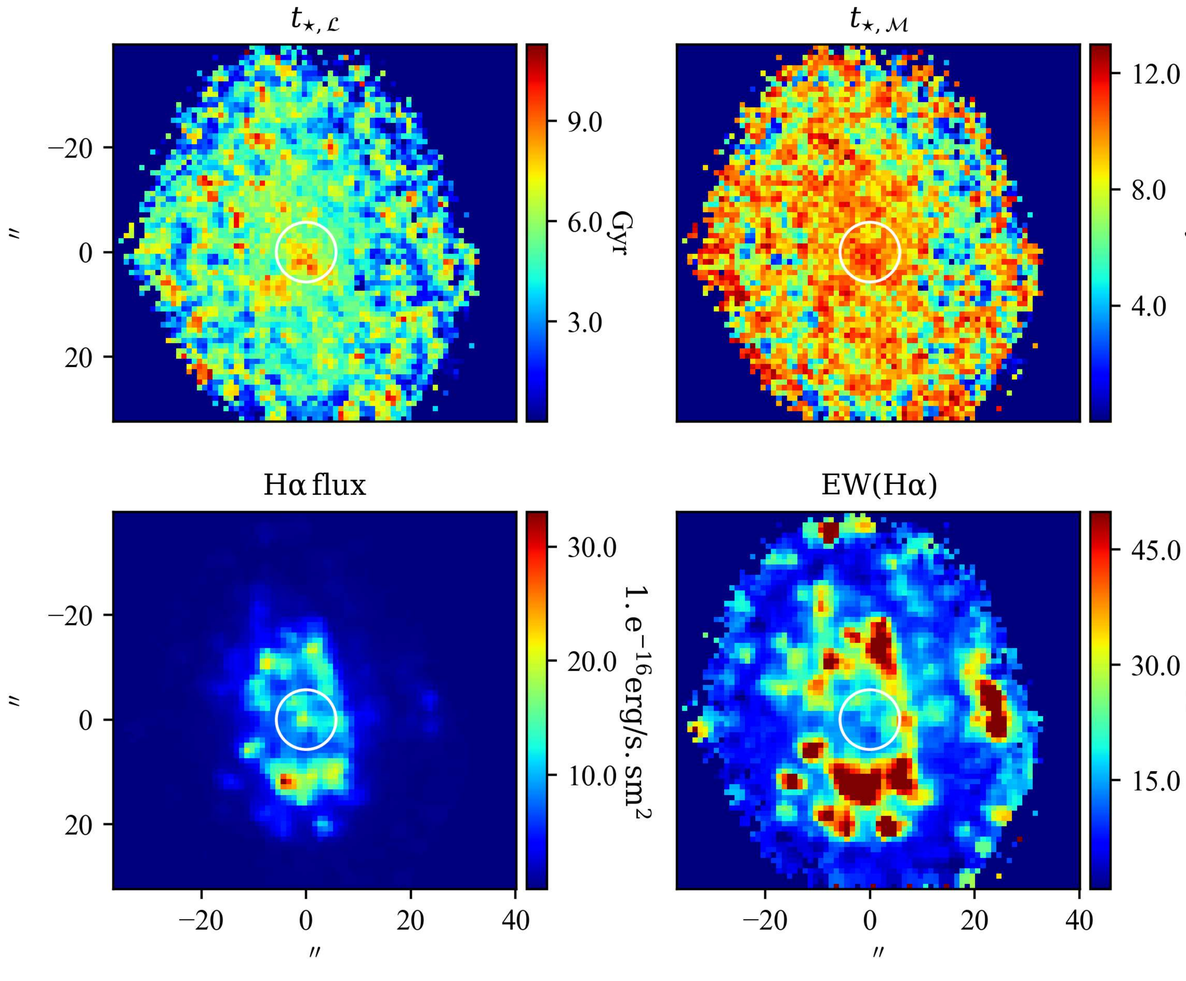

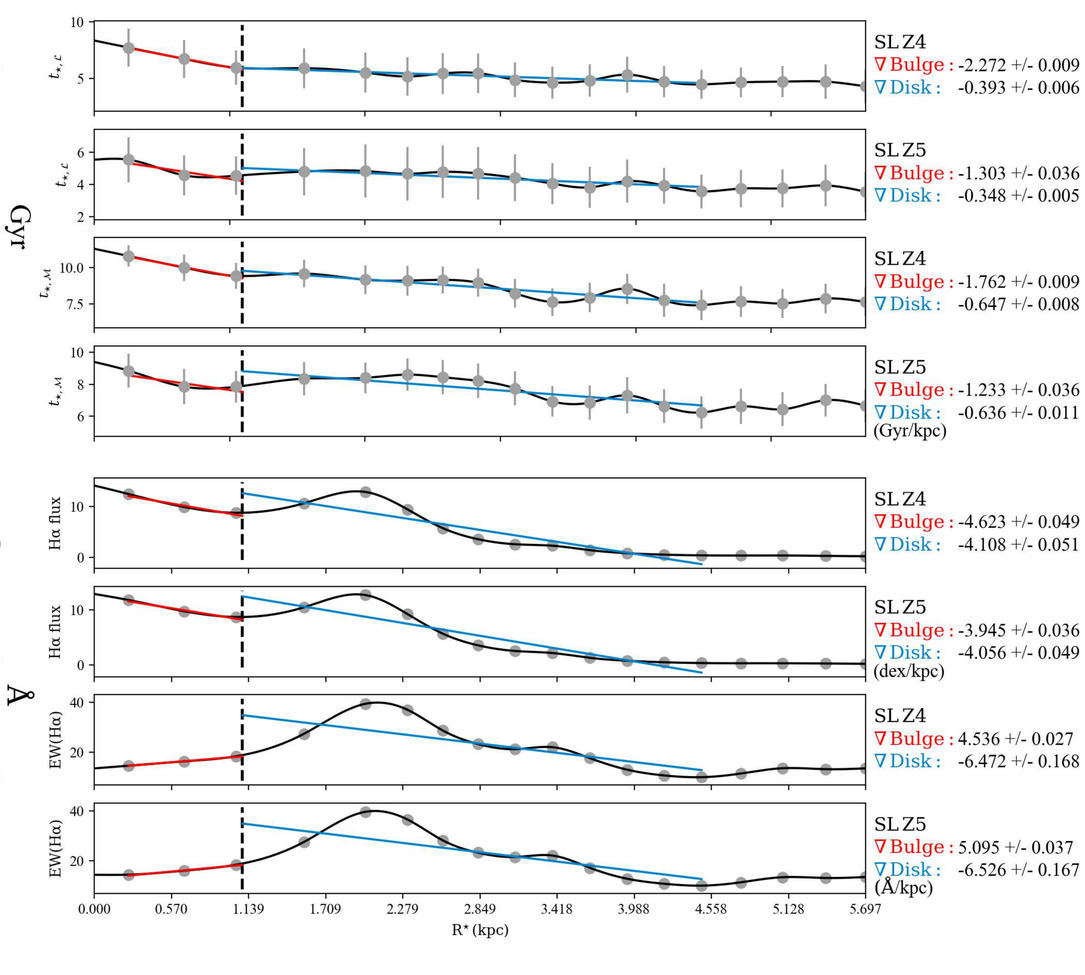

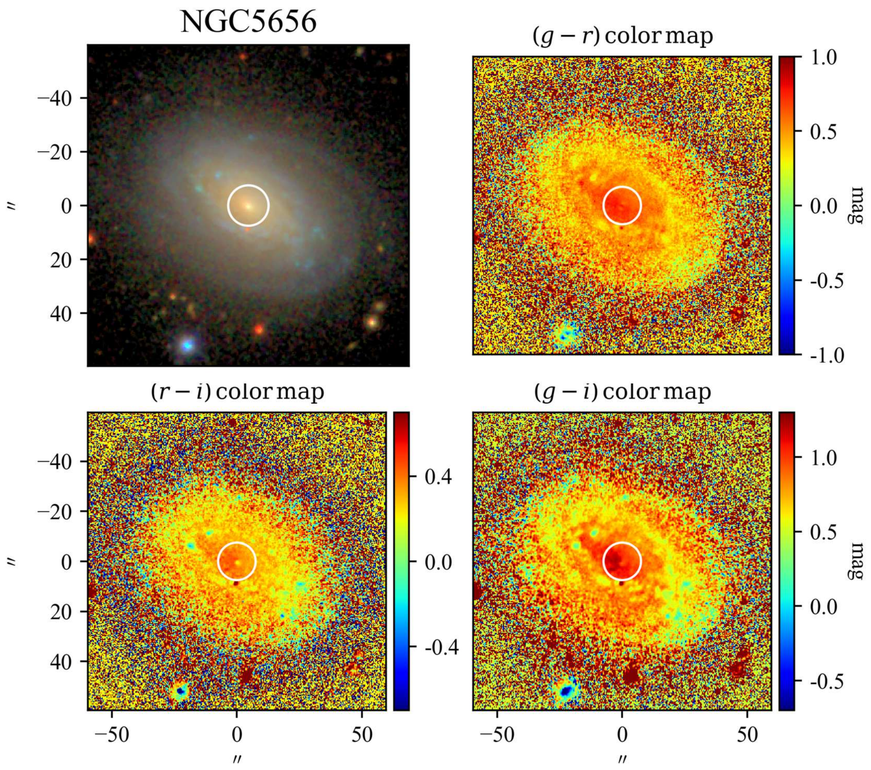

SBP decomposition of SDSS r band

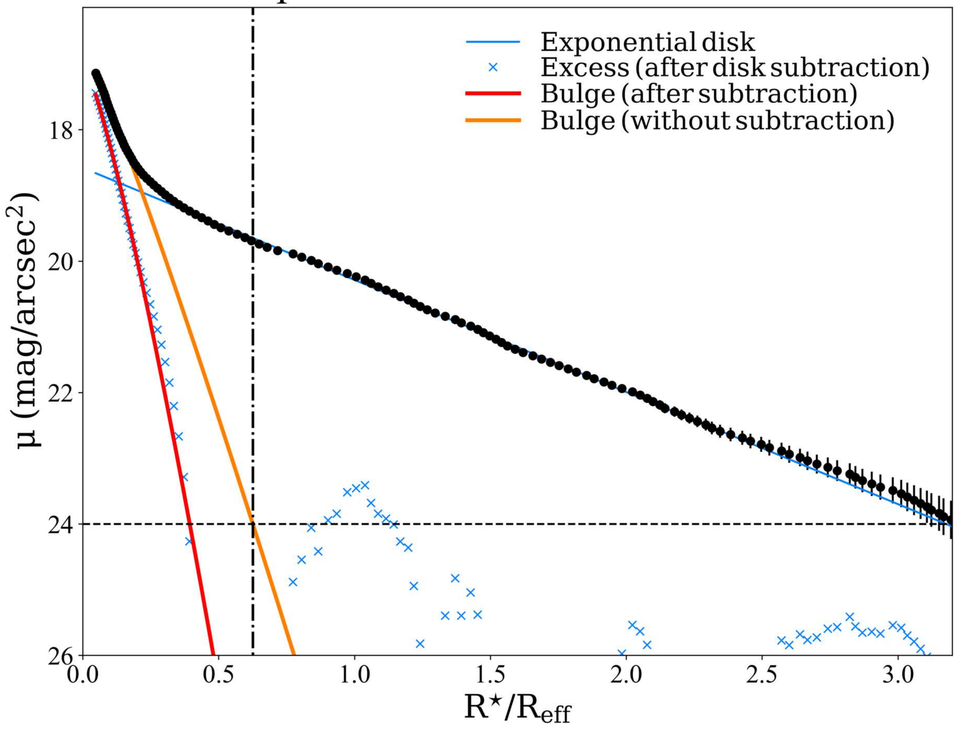

SDSS color profiles

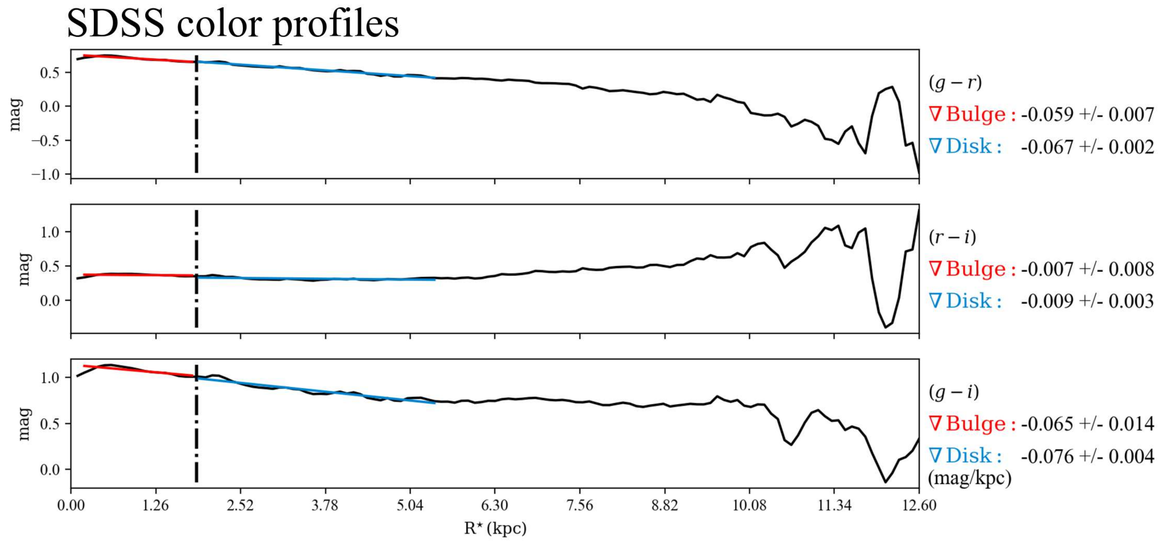

$\mathcal{RY}$ SBPs

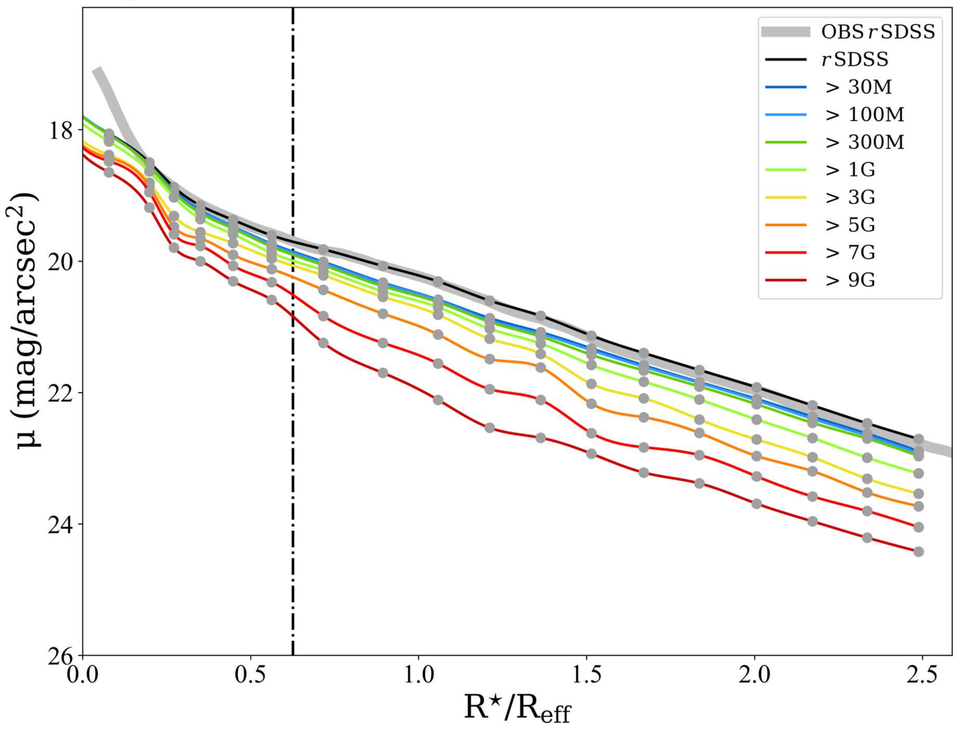

Stellar Continuum $\mathcal{M}_{\star,\mathrm{P}}$

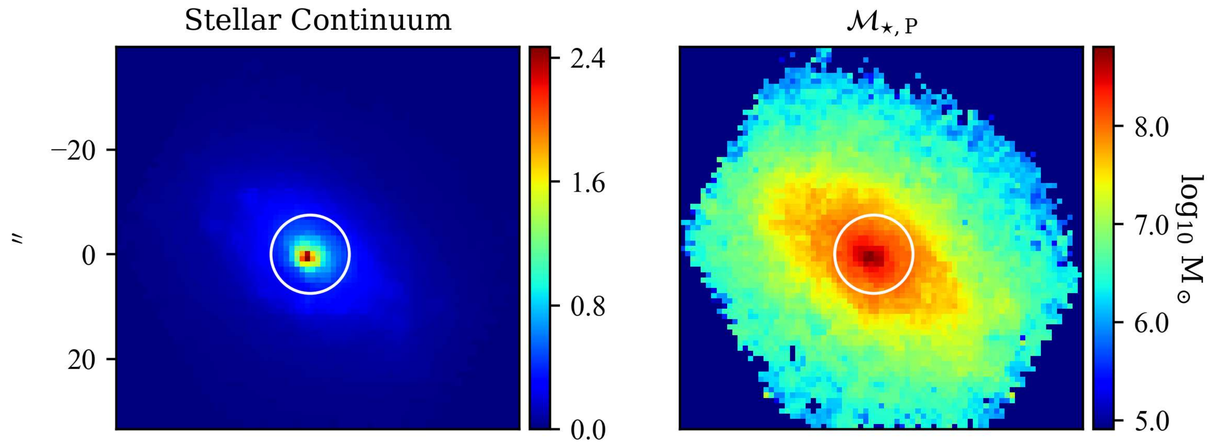

Log. of cumulative present stellar mass profiles

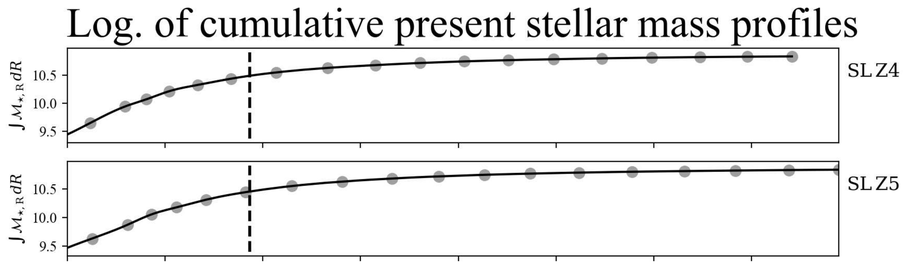

$Z_{\star,\mathcal{L}}$ $Z_{\star,\mathcal{M}}$

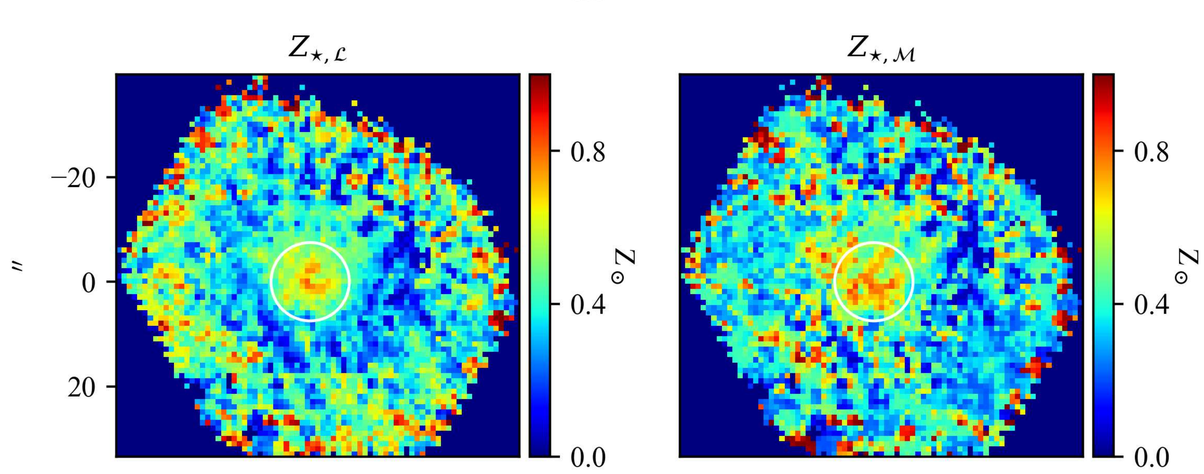

Stellar metallicity/Age & Hα flux/EW profiles

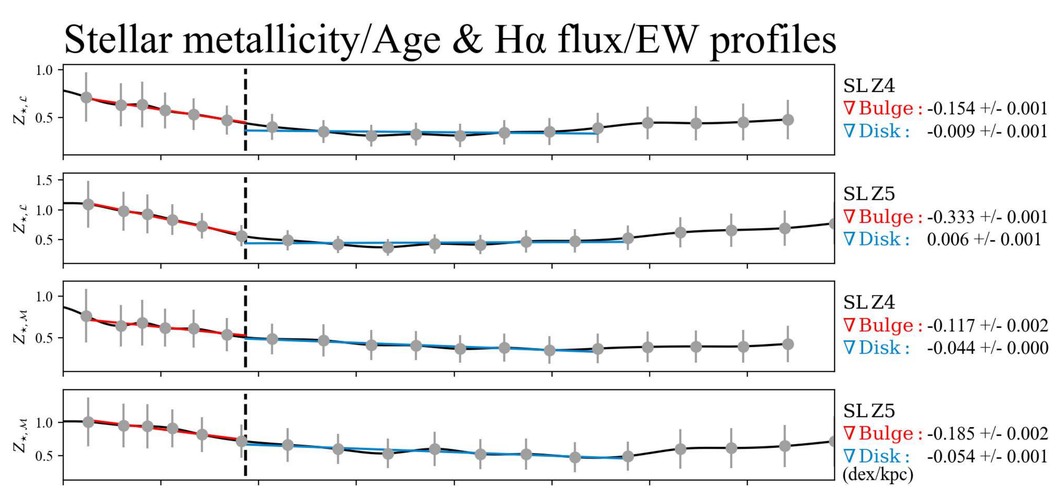

$t_{\star,\mathcal{L}}$ $t_{\star,\mathcal{M}}$

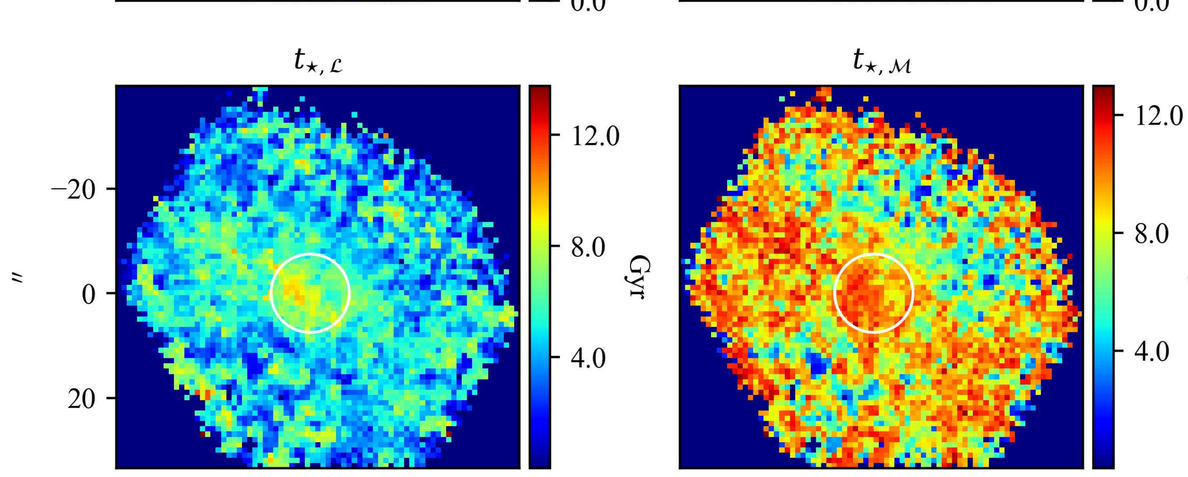

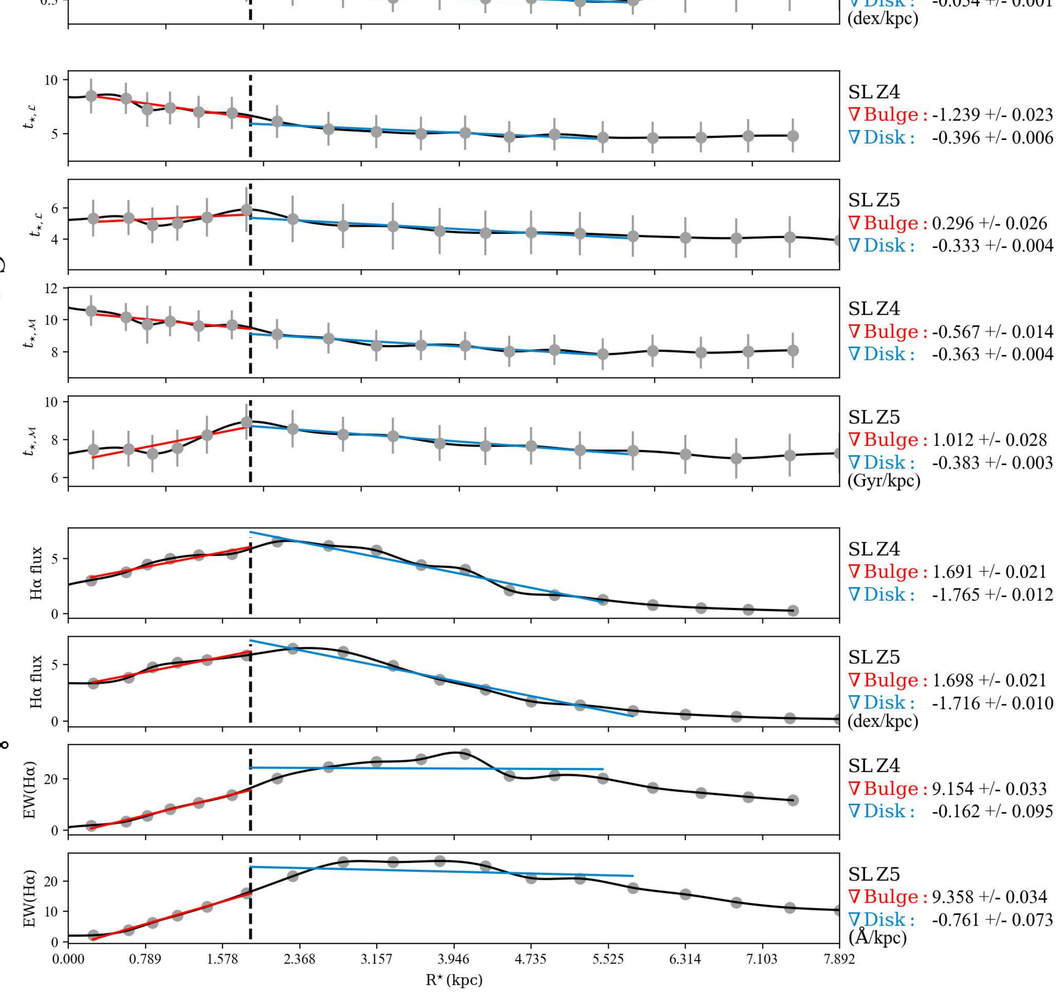

Hα flux EW(Hα)

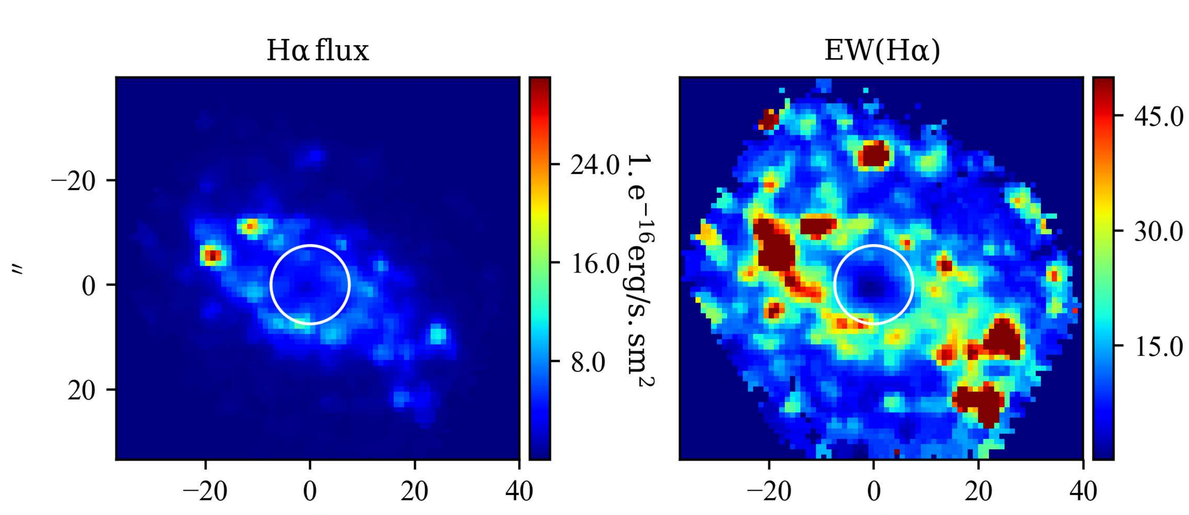

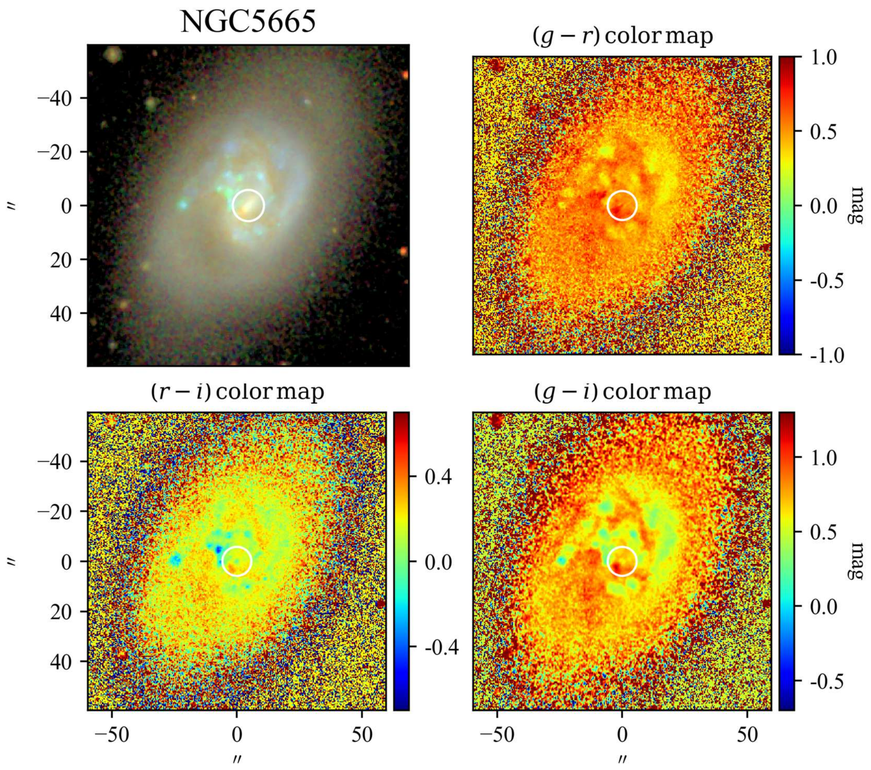

SBP decomposition of SDSS r band

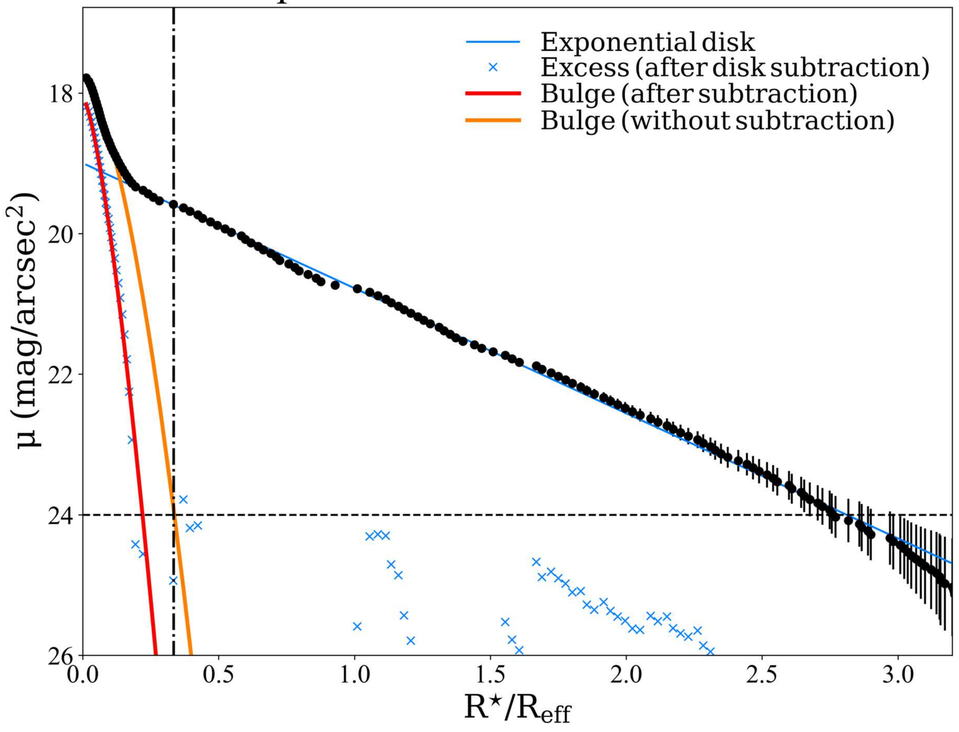

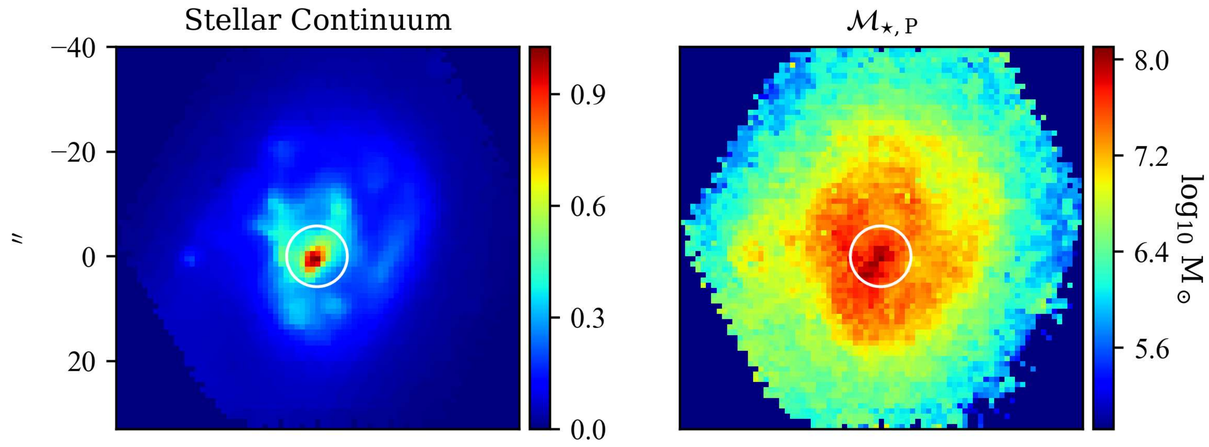

SDSS color profiles

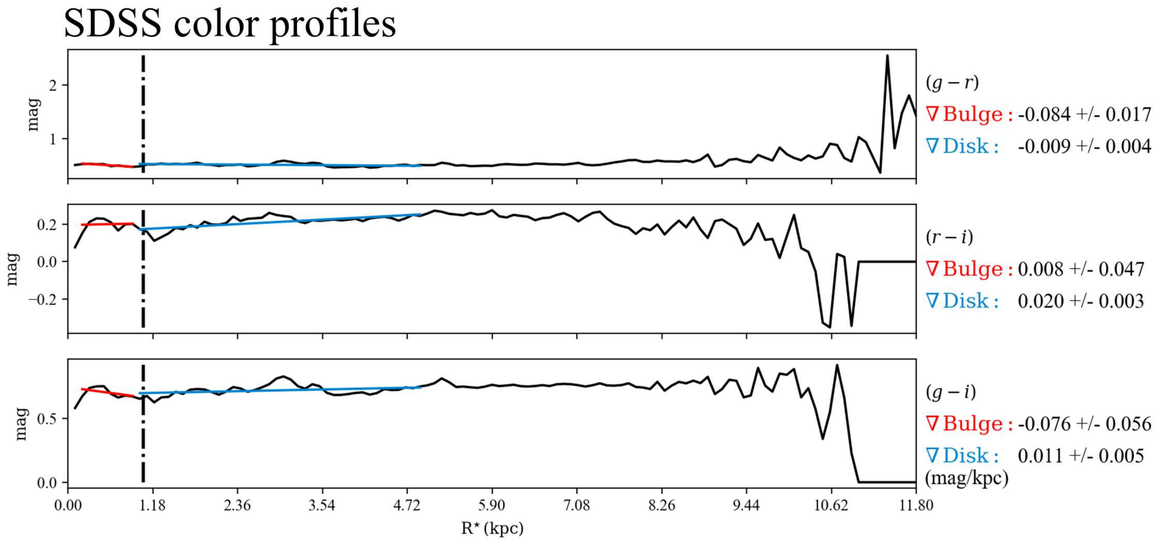

$\mathcal{RY}$ SBPs

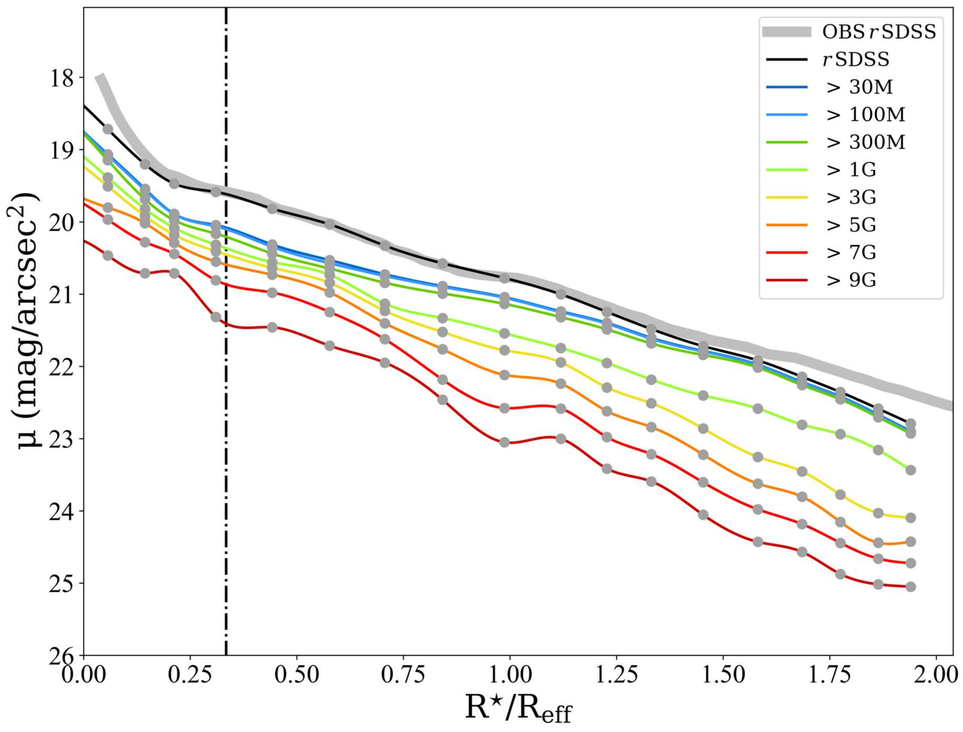

Log. of cumulative present stellar mass profiles

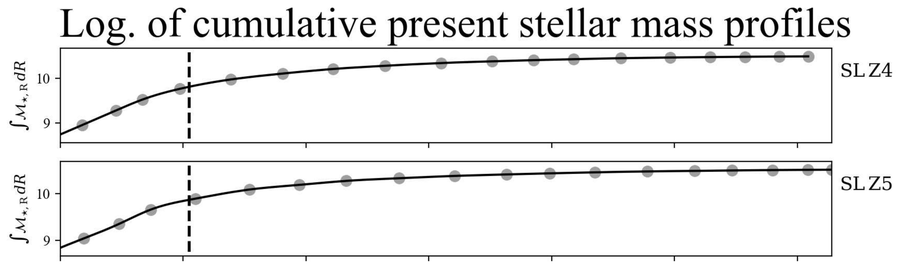

Stellar metallicity/Age & Hα flux/EW profiles

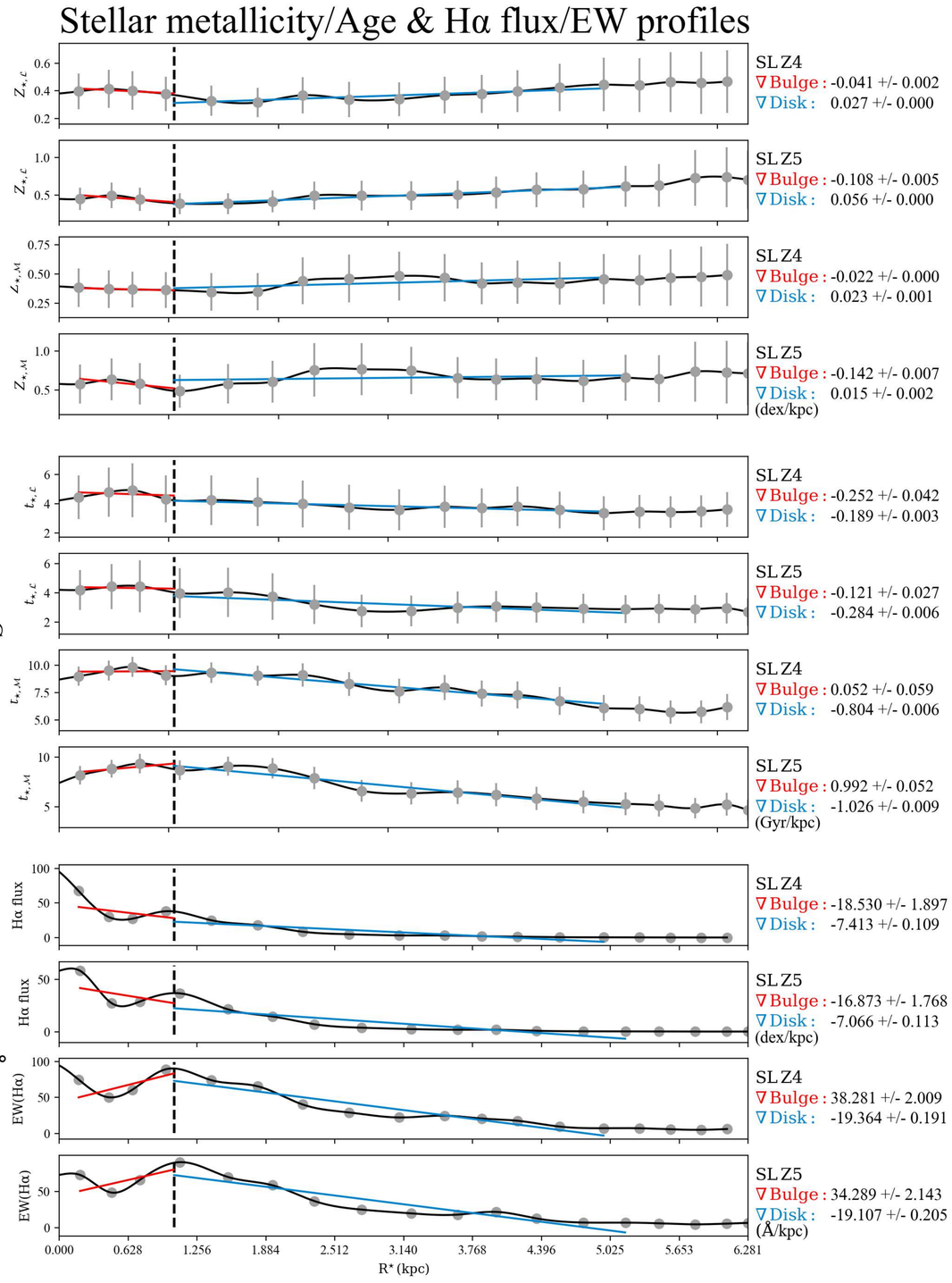

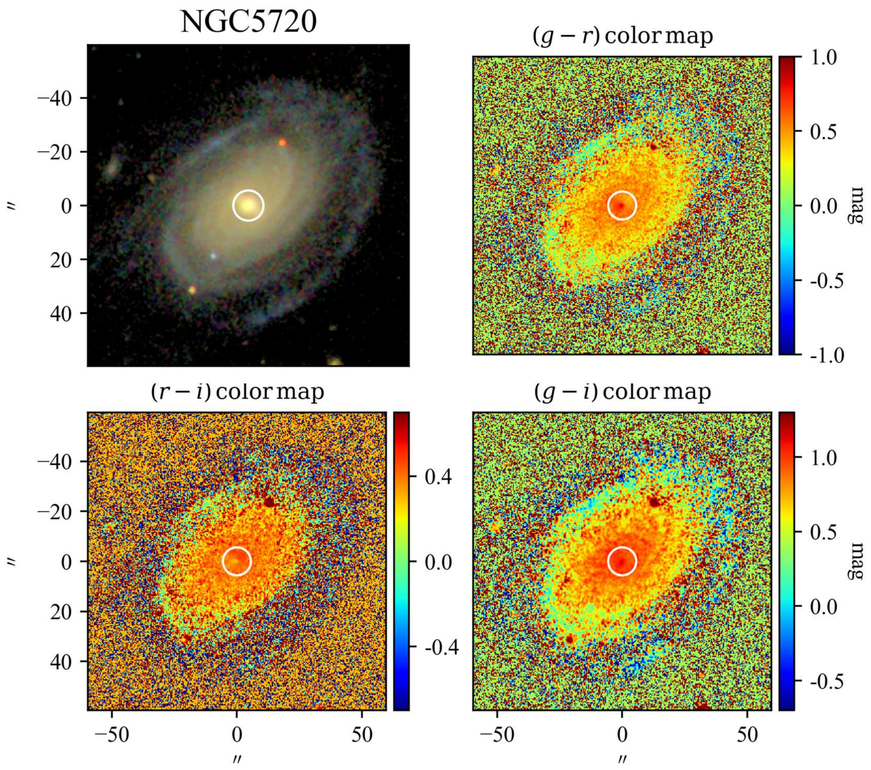

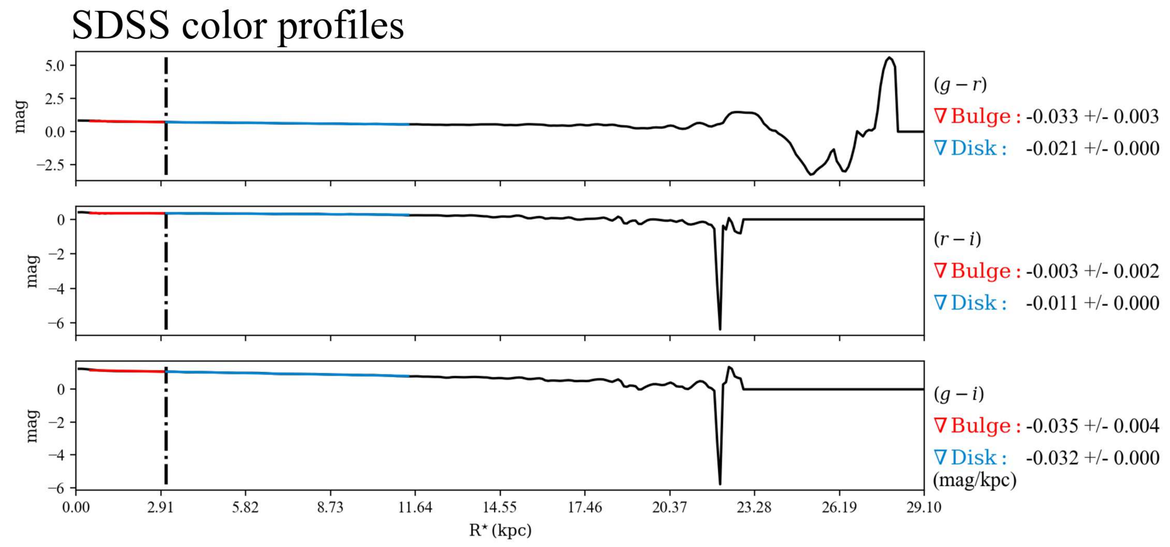

SBP decomposition of SDSS r band

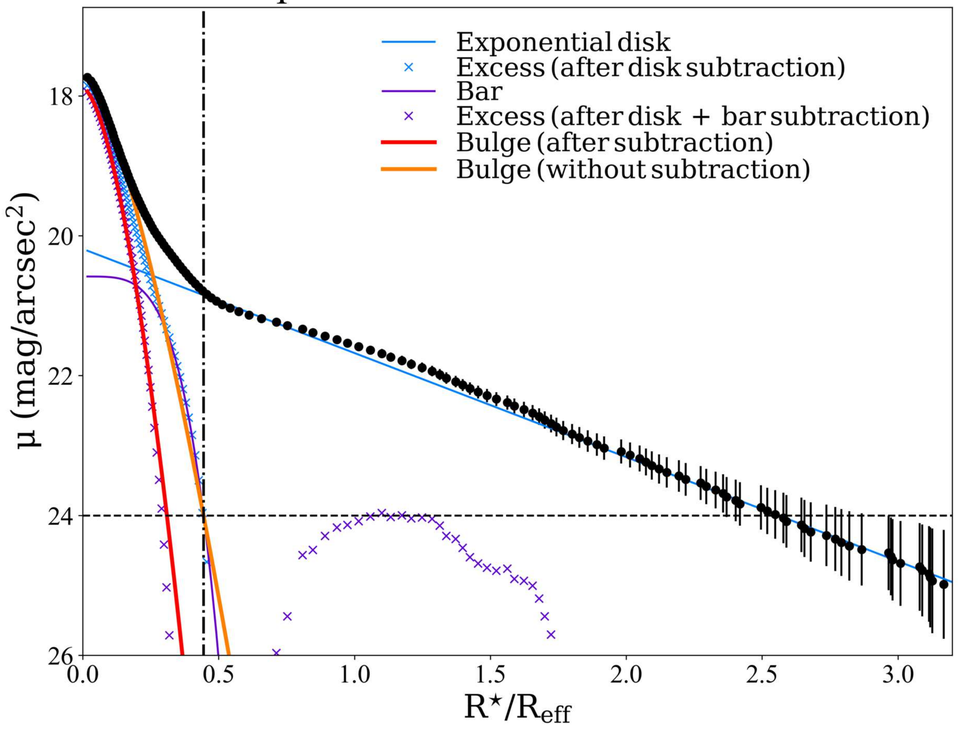

$\mathcal{RY}$ SBPs

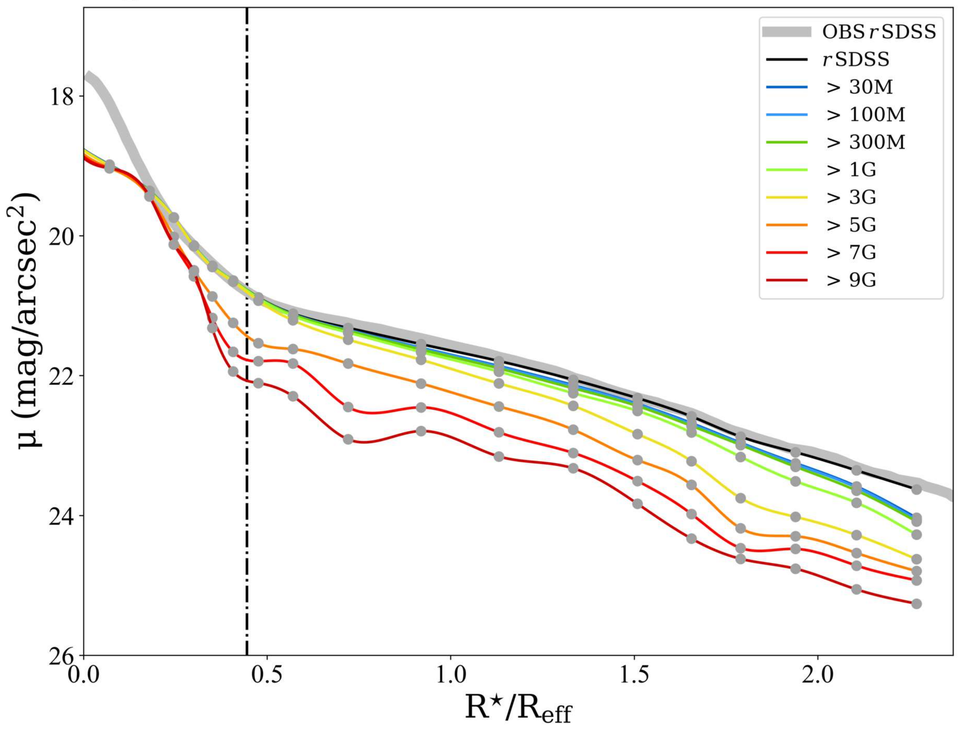

Stellar Continuum

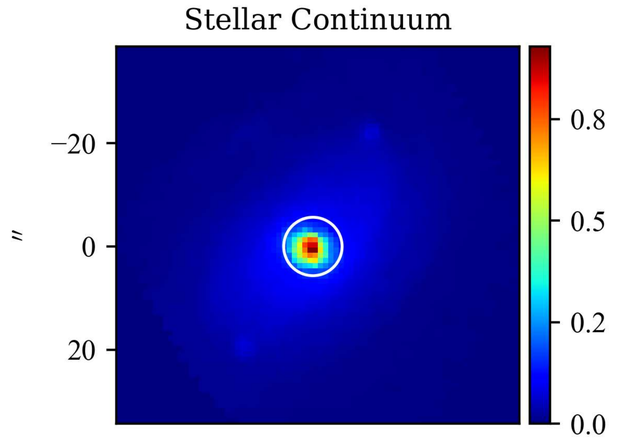

$\mathcal{M}_{\star,\mathrm{P}}$

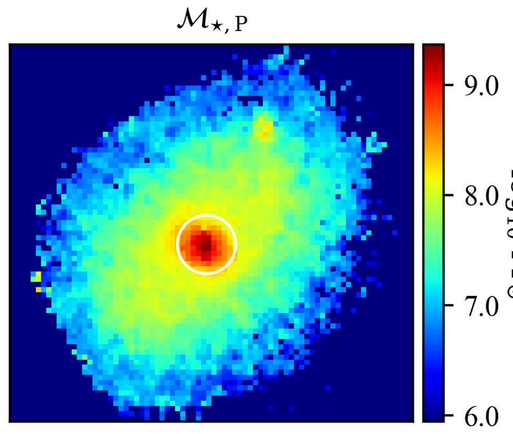

Log. of cumulative present stellar mass profiles

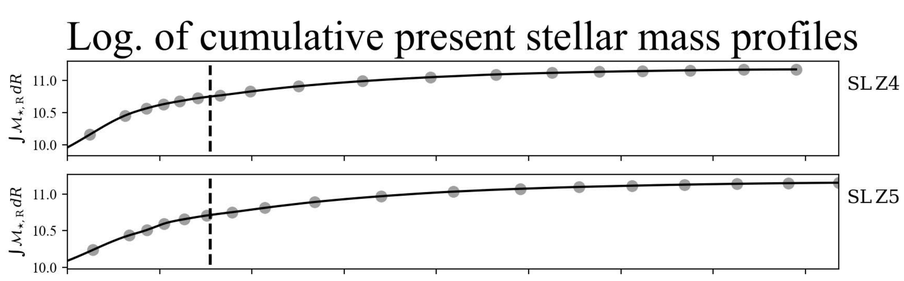

$Z_{\star,\mathcal{L}}$

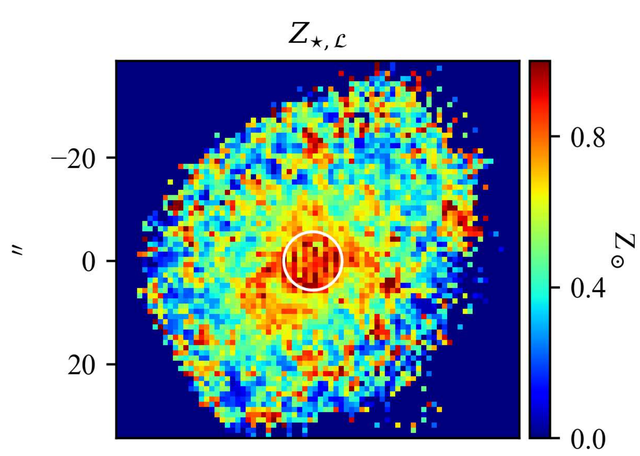

$Z_{\star,\mathcal{M}}$

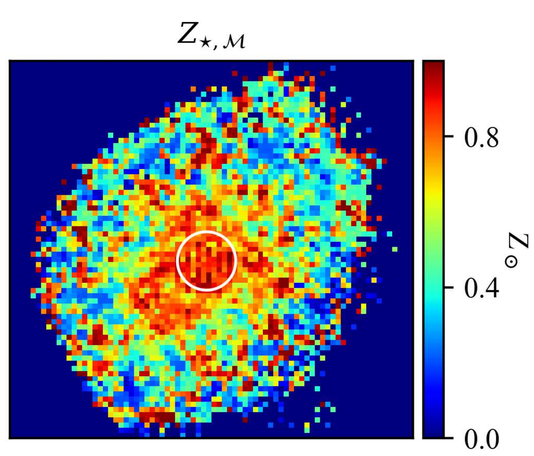

Stellar metallicity/Age & Hα flux/EW profiles

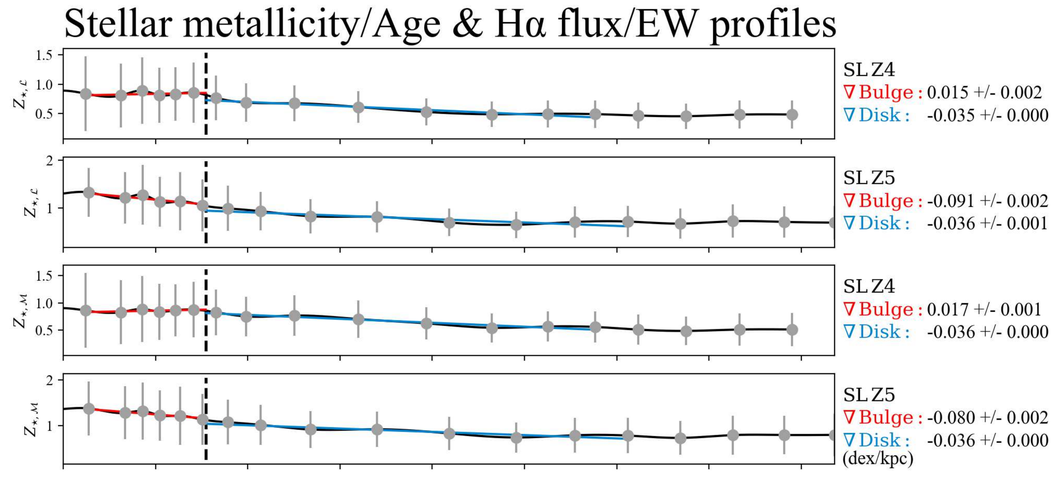

$t_{\star,\mathcal{L}}$

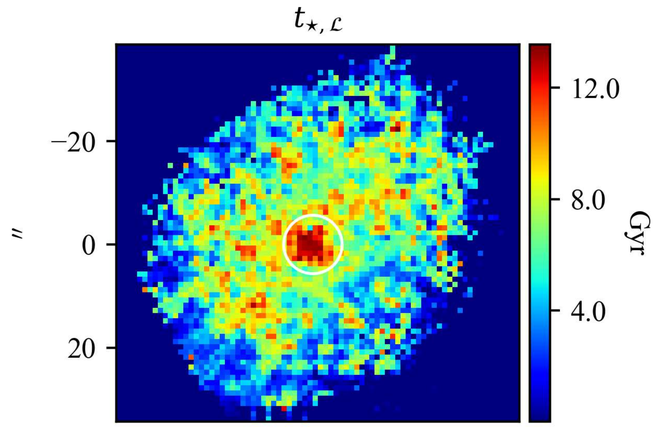

$t_{\star,\mathcal{M}}$

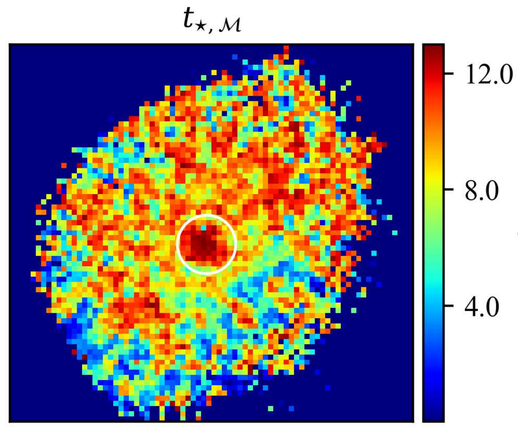

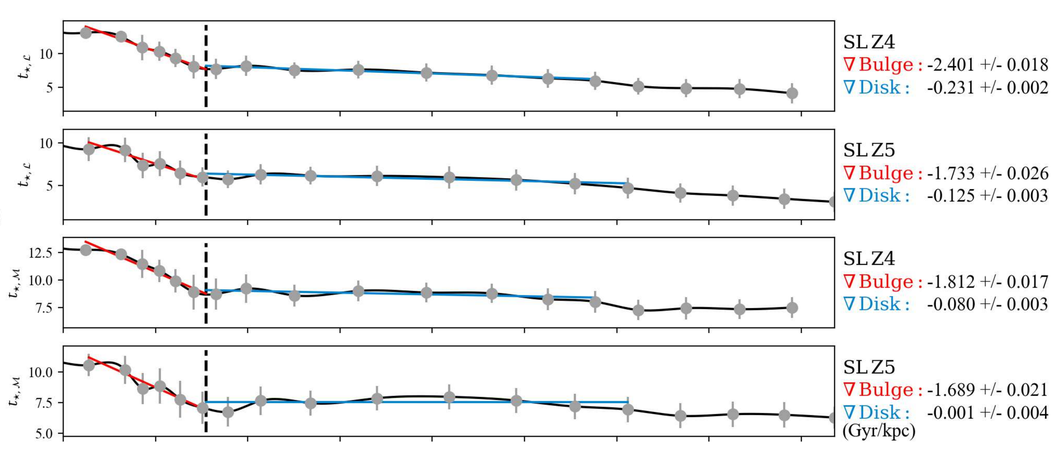

Hα flux

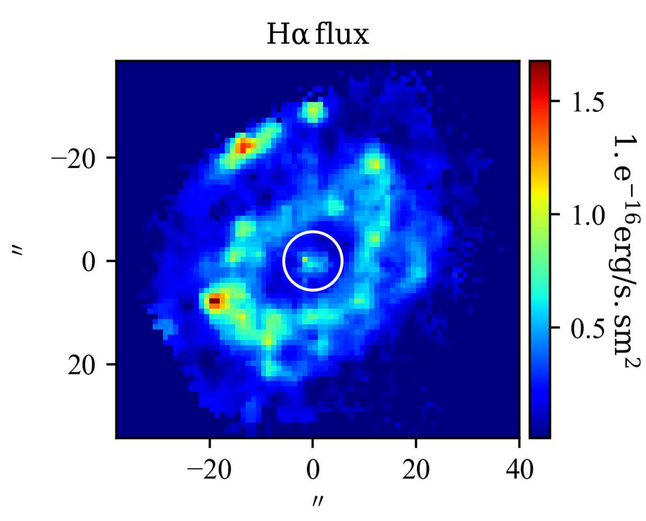

EW(Hα)

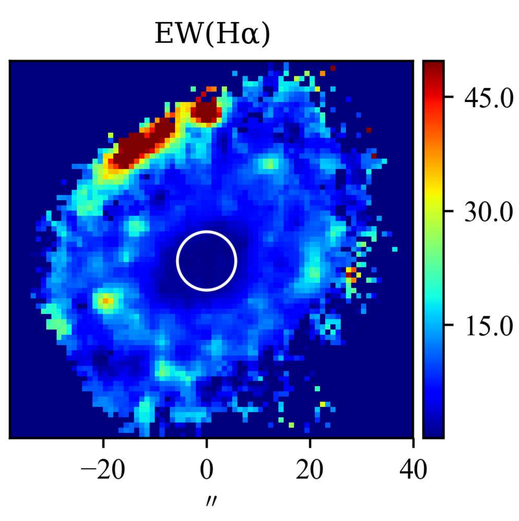

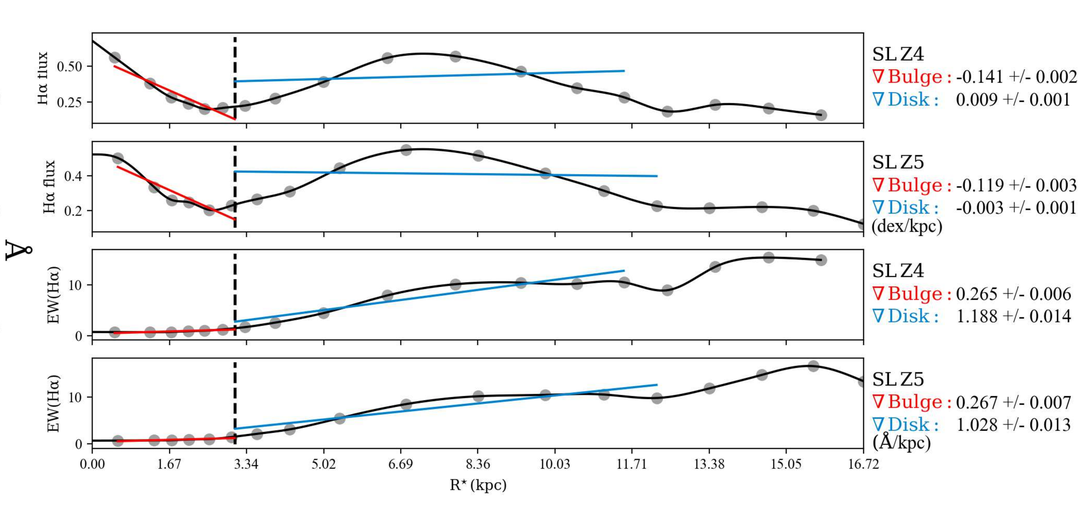

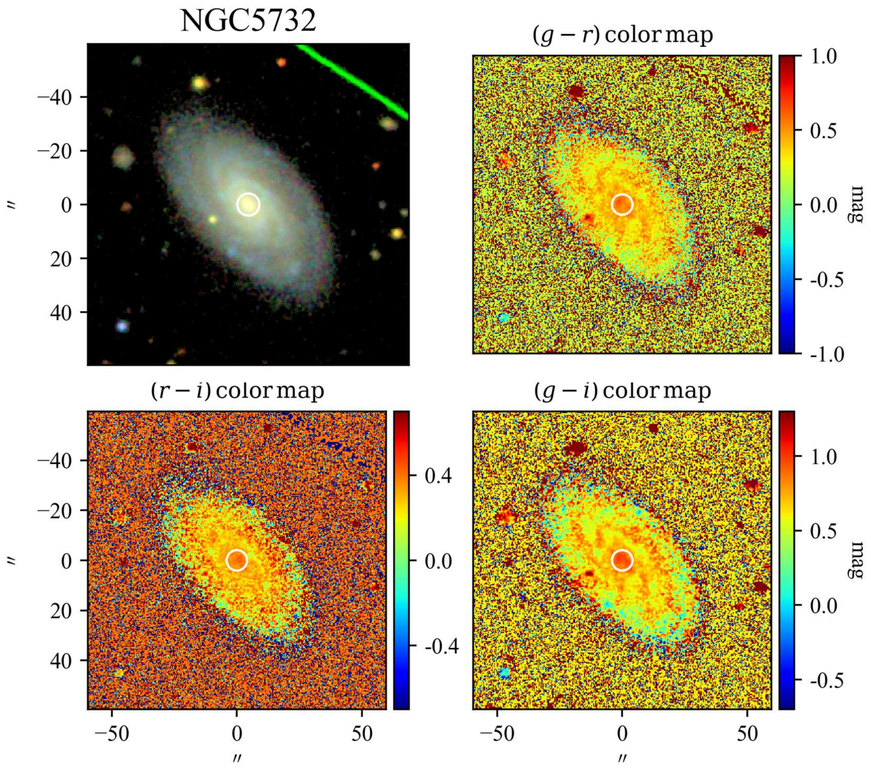
NGC5732
(g − r) color map
(r − i) color map
(g − i) color map
mag
″

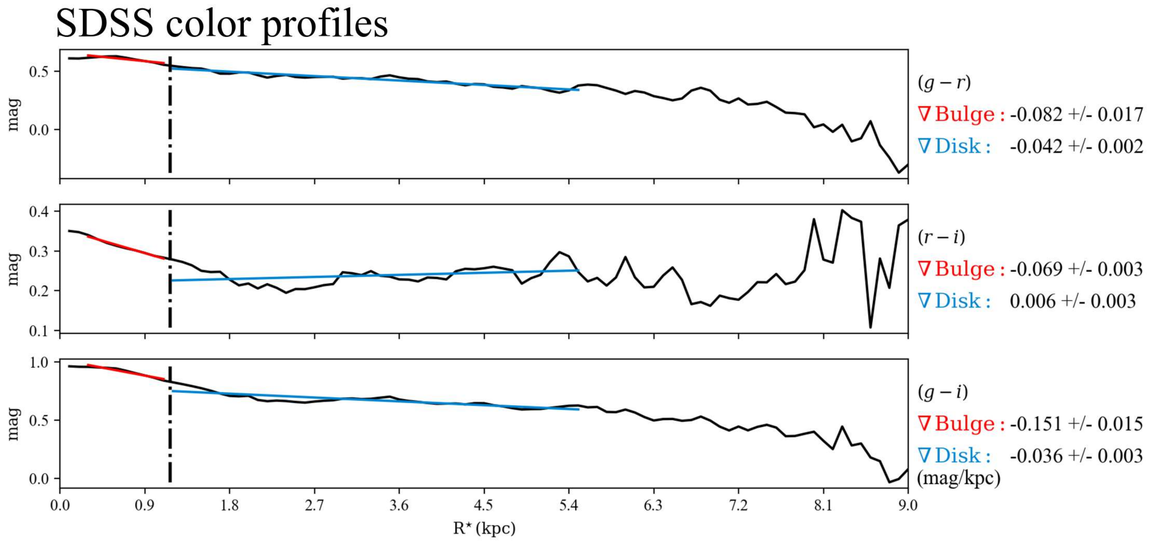
SDSS color profiles
(g − r)
∇ Bulge : -0.082 +/- 0.017
∇ Disk : -0.042 +/- 0.002
(r − i)
∇ Bulge : -0.069 +/- 0.003
∇ Disk : 0.006 +/- 0.003
(g − i)
∇ Bulge : -0.151 +/- 0.015
∇ Disk : -0.036 +/- 0.003
(mag/kpc)
mag
R* (kpc)

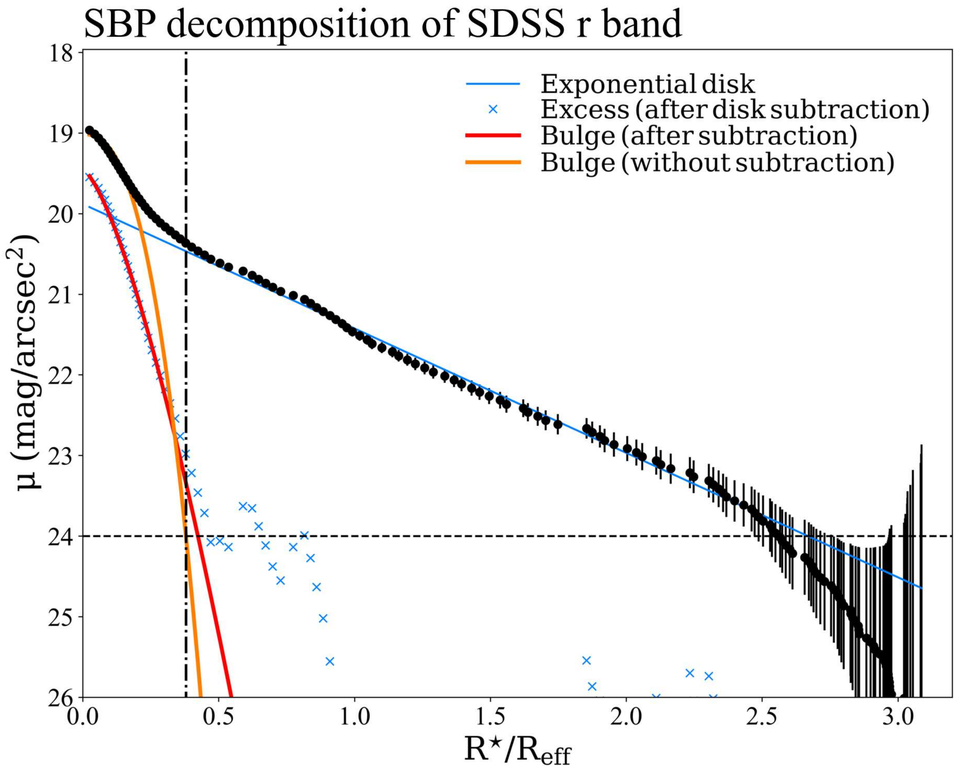
SBP decomposition of SDSS r band
Exponential disk
Excess (after disk subtraction)
Bulge (after subtraction)
Bulge (without subtraction)
μ (mag/arcsec²)
R*/Reff

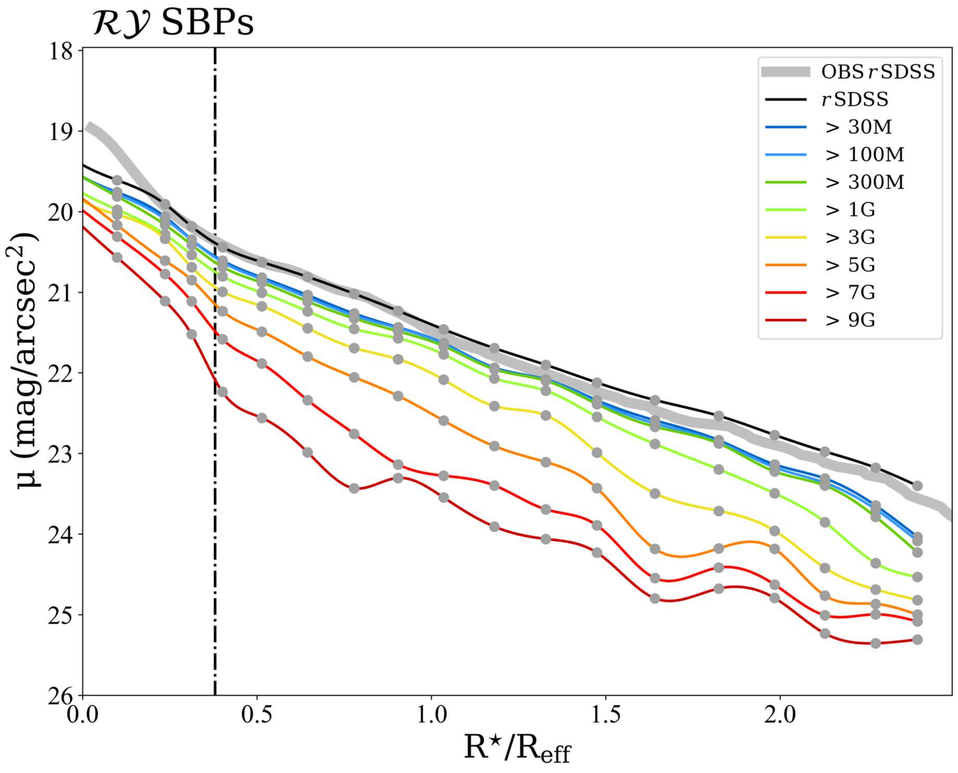
$\mathcal{RV}$ SBPs
OBS r SDSS
r SDSS
> 30M
> 100M
> 300M
> 1G
> 3G
> 5G
> 7G
> 9G
μ (mag/arcsec²)
R*/Reff

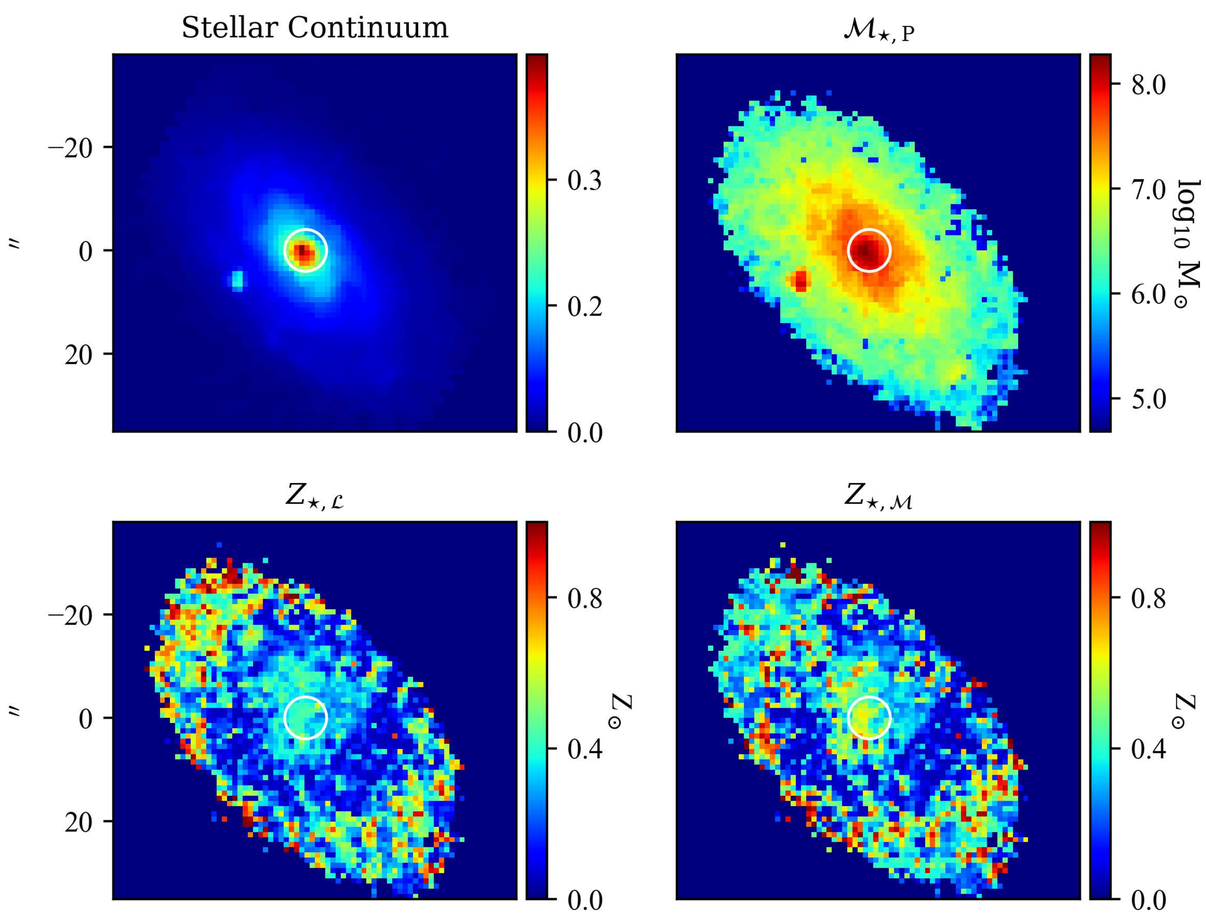
Stellar Continuum
$\mathcal{M}_{\star,\mathrm{P}}$
$Z_{\star,\mathcal{L}}$
$Z_{\star,\mathcal{M}}$
$t_{\star,\mathcal{L}}$
$t_{\star,\mathcal{M}}$
Hα flux
EW(Hα)
″

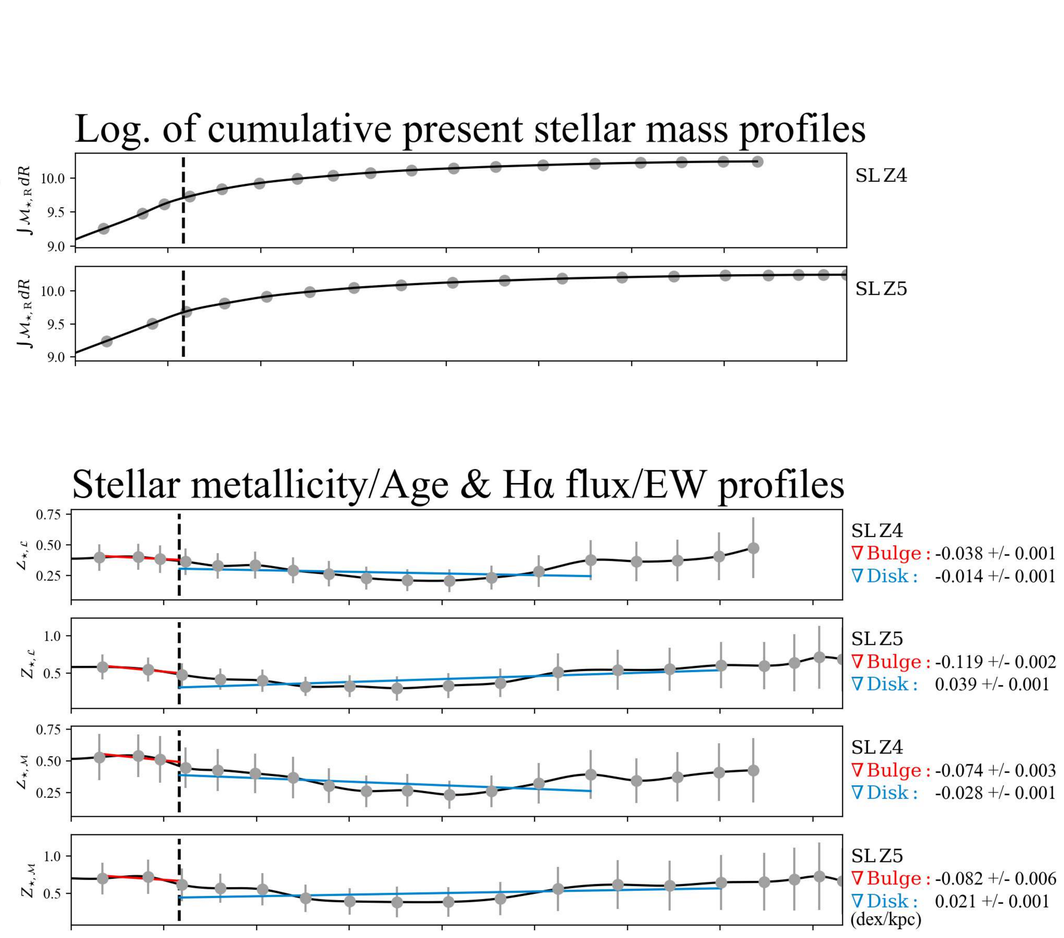
Log. of cumulative present stellar mass profiles
SL Z4
SL Z5
Stellar metallicity/Age & Hα flux/EW profiles
SL Z4
∇ Bulge : -0.038 +/- 0.001
∇ Disk : -0.014 +/- 0.001
SL Z5
∇ Bulge : -0.119 +/- 0.002
∇ Disk : 0.039 +/- 0.001
SL Z4
∇ Bulge : -0.074 +/- 0.003
∇ Disk : -0.028 +/- 0.001
SL Z5
∇ Bulge : -0.082 +/- 0.006
∇ Disk : 0.021 +/- 0.001
(dex/kpc)
SL Z4
∇ Bulge : -0.994 +/- 0.016
∇ Disk : -0.324 +/- 0.005
SL Z5
∇ Bulge : 0.078 +/- 0.005
∇ Disk : -0.370 +/- 0.003
SL Z4
∇ Bulge : -0.833 +/- 0.029
∇ Disk : -0.574 +/- 0.004
SL Z5
∇ Bulge : -0.183 +/- 0.014
∇ Disk : -0.457 +/- 0.003
(Gyr/kpc)
SL Z4
∇ Bulge : -3.912 +/- 0.017
∇ Disk : -0.922 +/- 0.008
SL Z5
∇ Bulge : -3.232 +/- 0.022
∇ Disk : -0.708 +/- 0.007
(dex/kpc)
SL Z4
∇ Bulge : 1.389 +/- 0.039
∇ Disk : -2.848 +/- 0.087
SL Z5
∇ Bulge : 2.911 +/- 0.059
∇ Disk : -1.631 +/- 0.052
(Å/kpc)
R* (kpc)

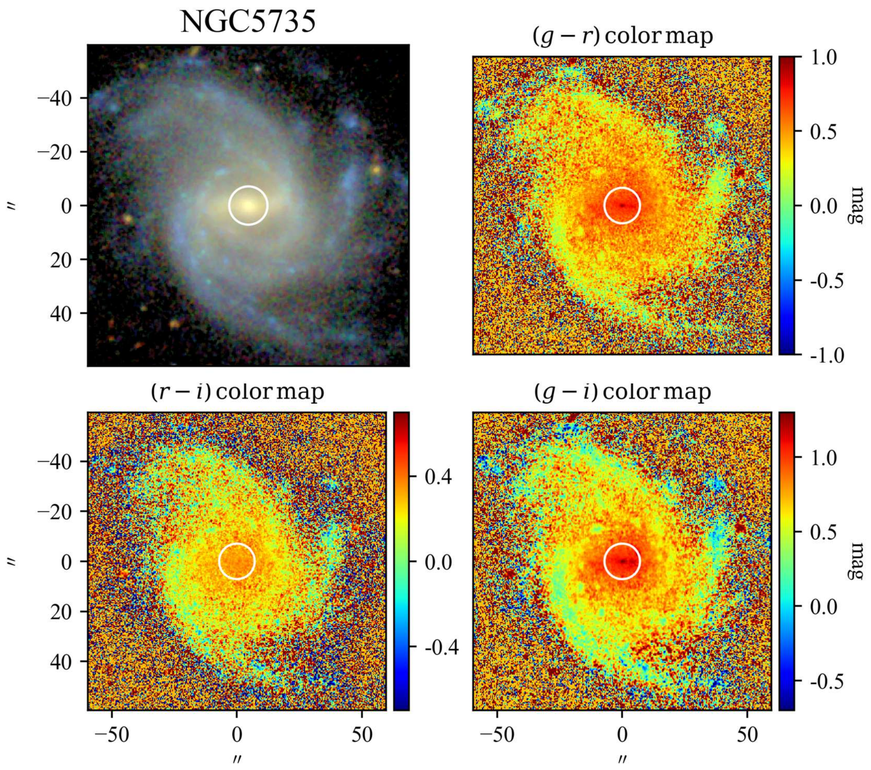

SBP decomposition of SDSS r band

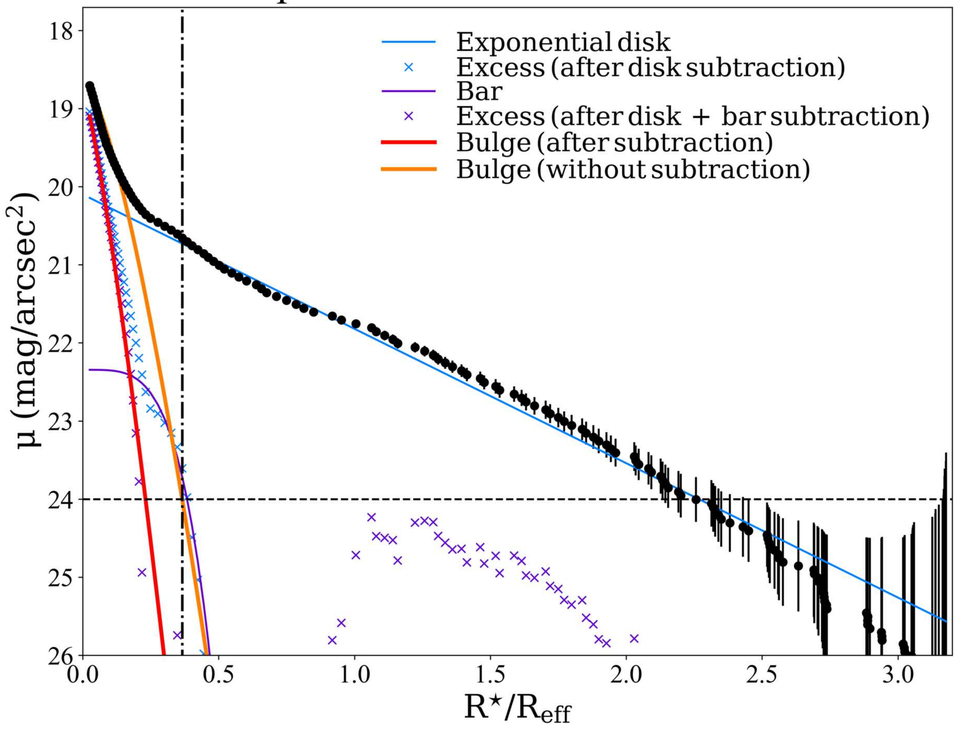

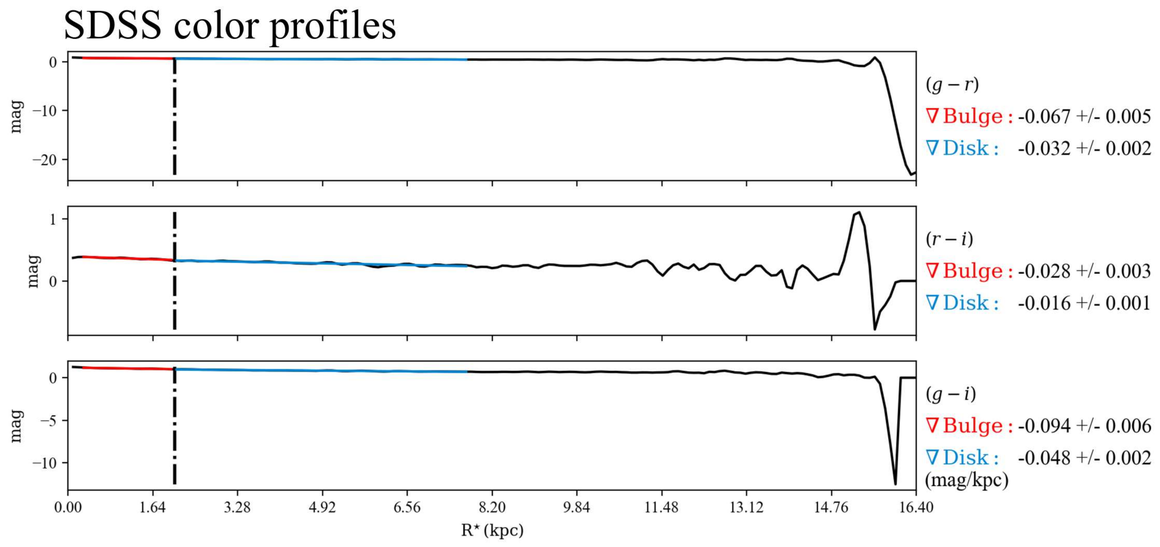

$\mathcal{RV}$ SBPs

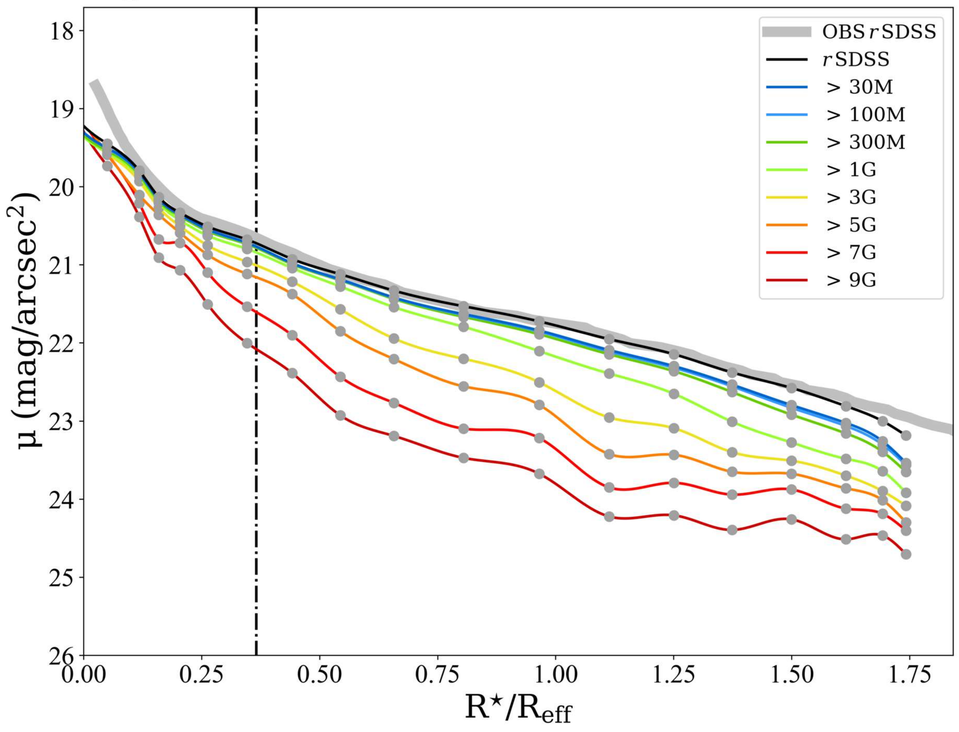

Stellar Continuum

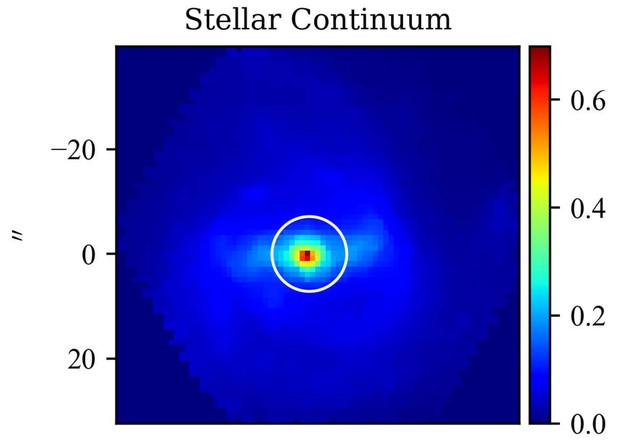

$\mathcal{M}_{\star,\mathrm{P}}$

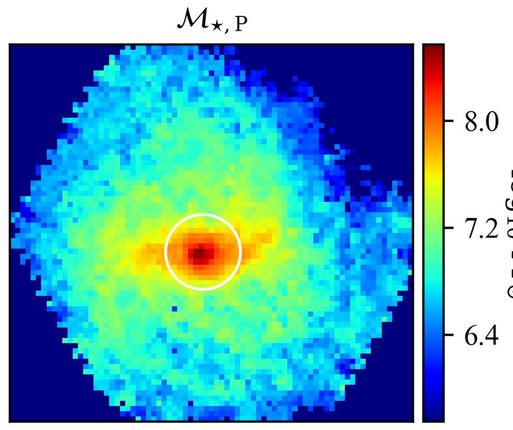

Log. of cumulative present stellar mass profiles

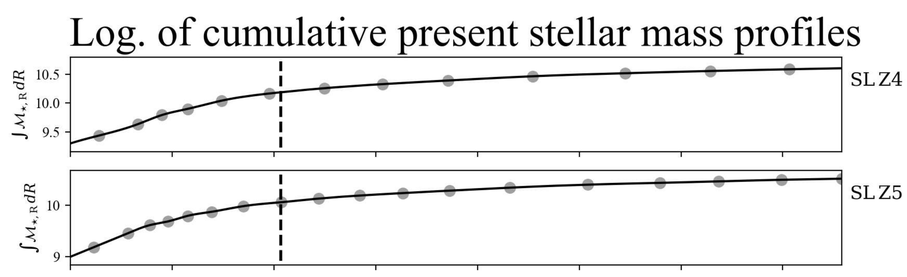

$Z_{\star,\mathcal{L}}$

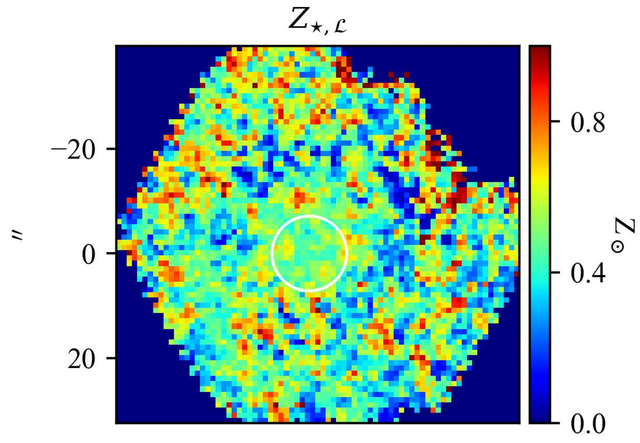

$Z_{\star,\mathcal{M}}$

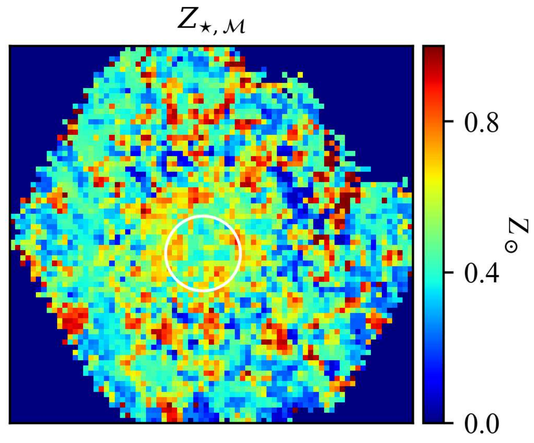

Stellar metallicity/Age & Hα flux/EW profiles

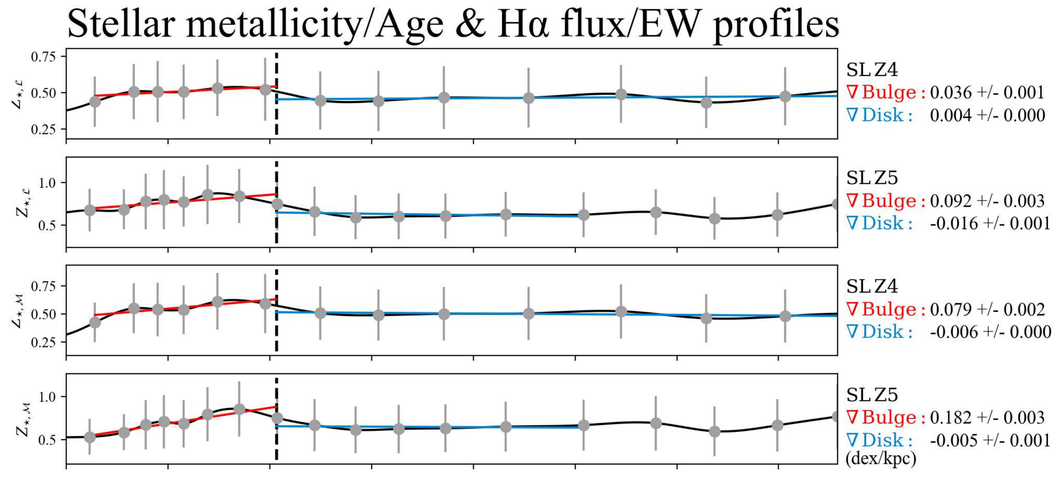

$t_{\star,\mathcal{L}}$

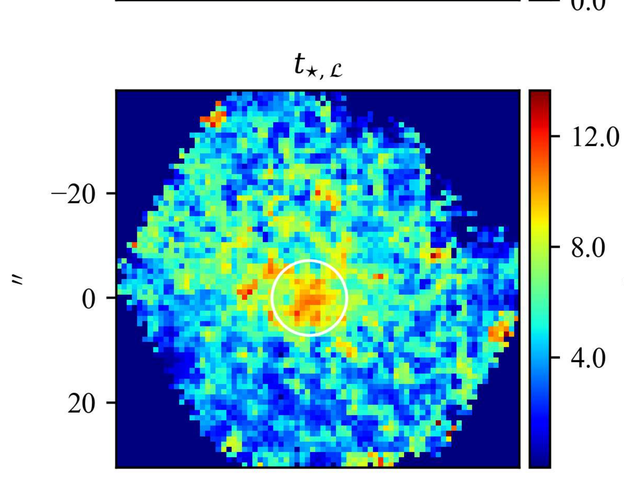

$t_{\star,\mathcal{M}}$

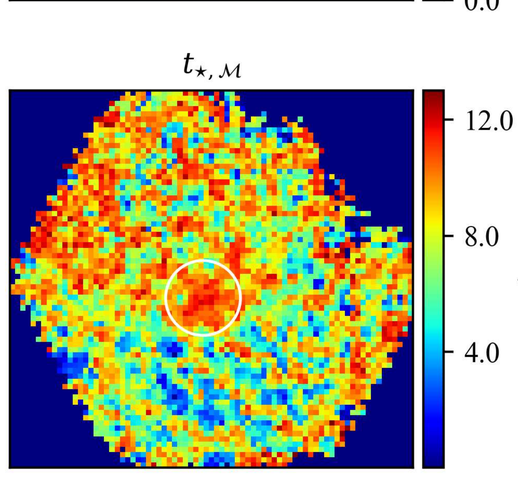

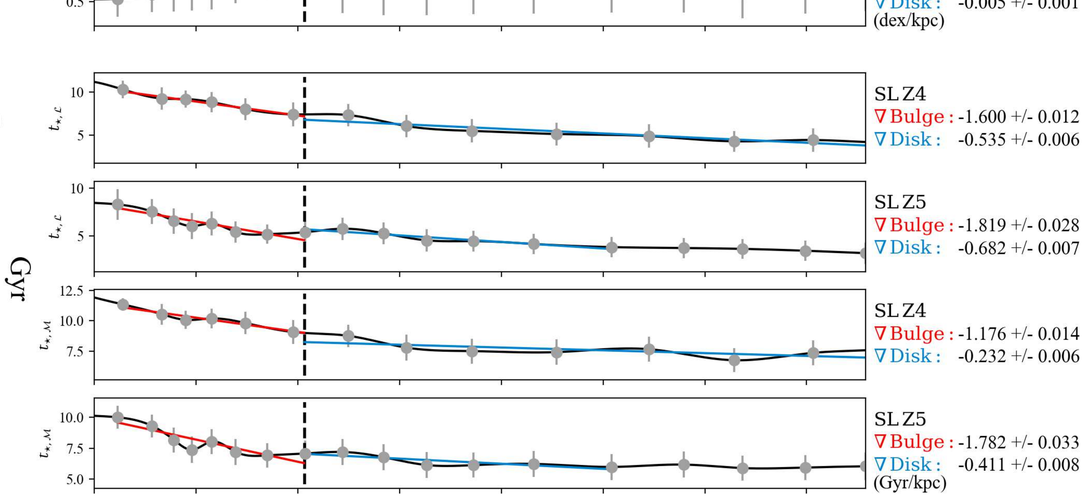

Hα flux

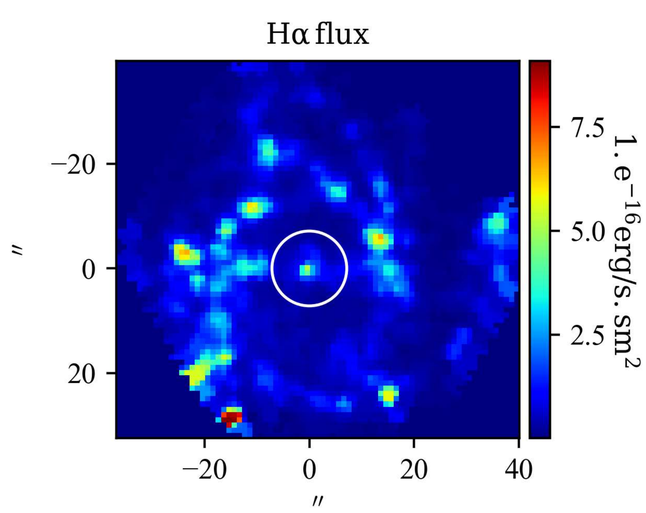

EW(Hα)

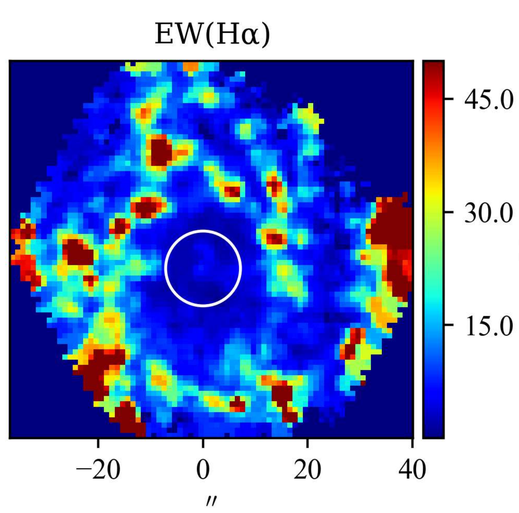

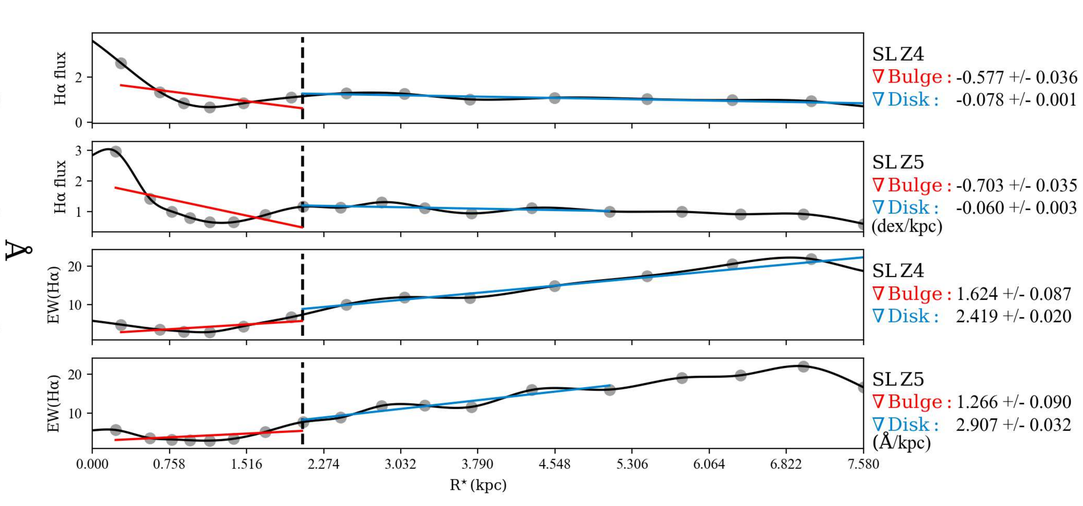

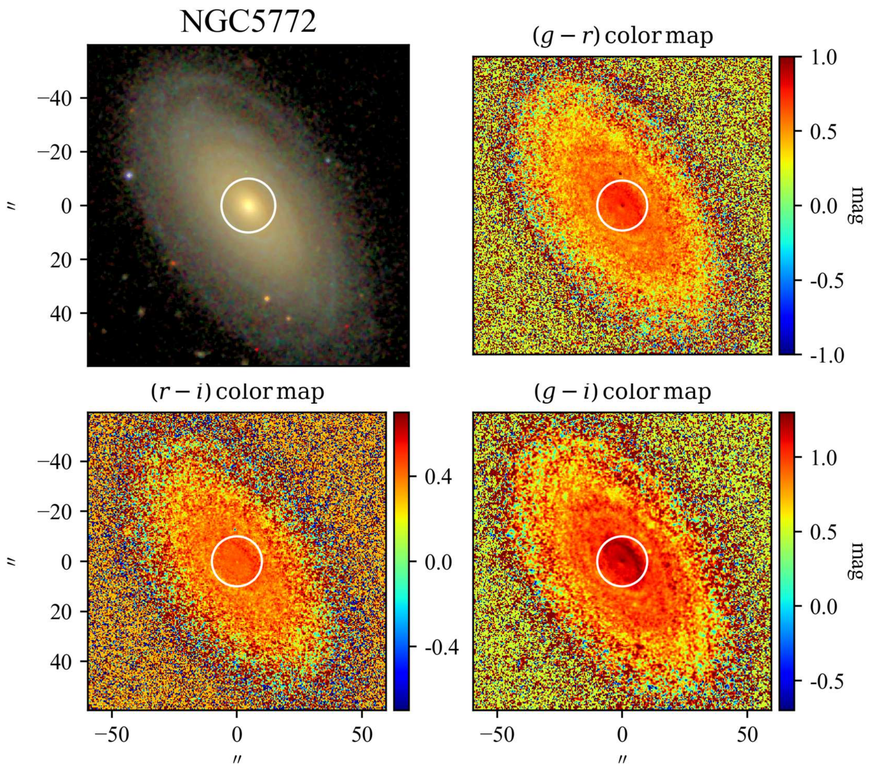

SBP decomposition of SDSS r band

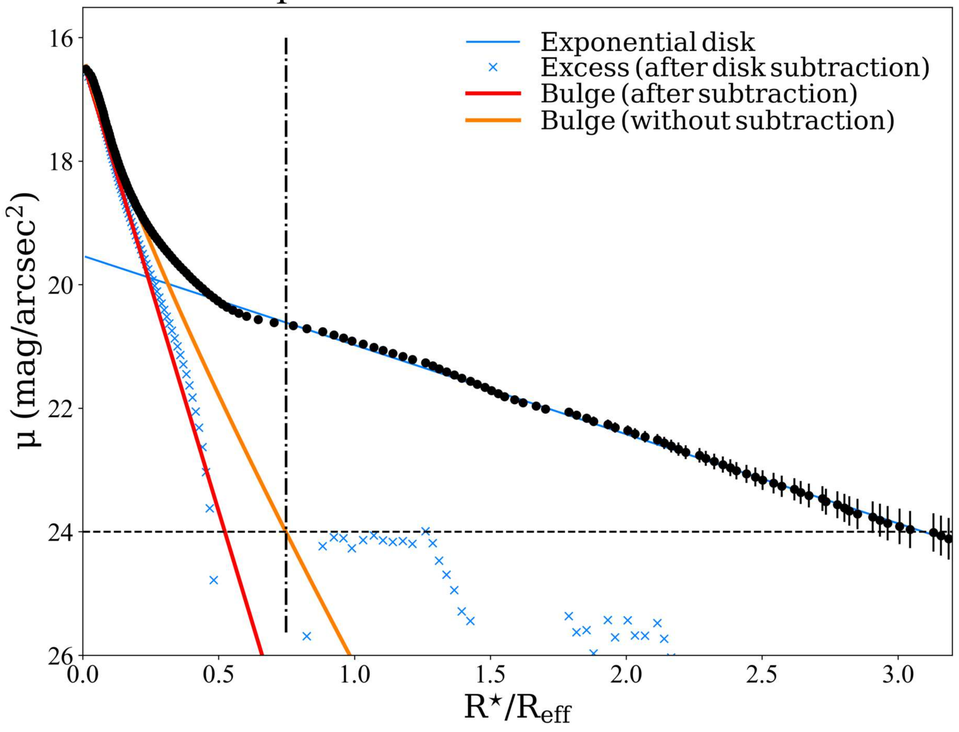

SDSS color profiles

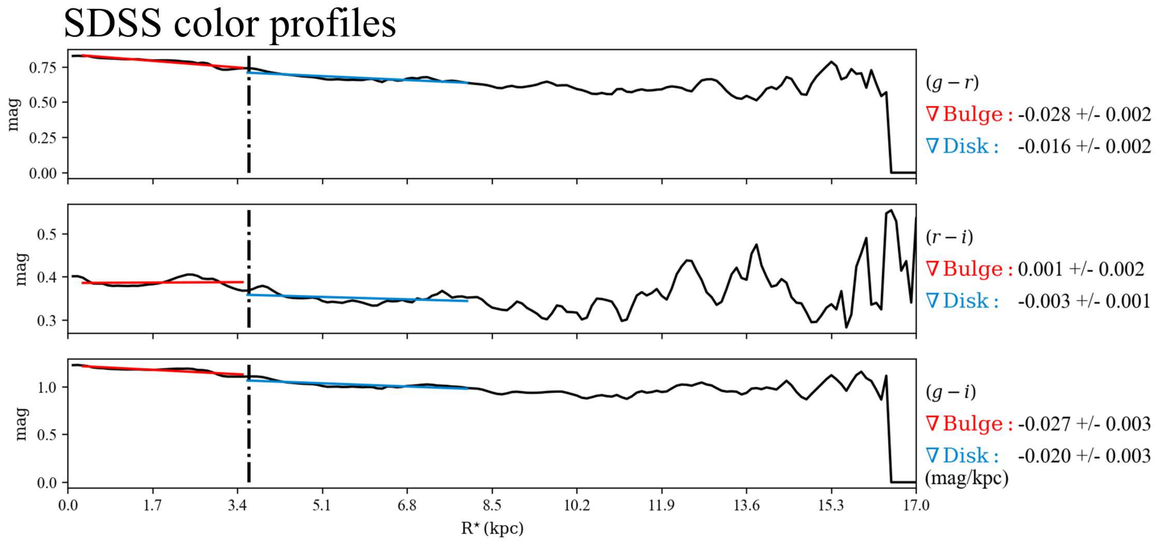

$\mathcal{RY}$ SBPs

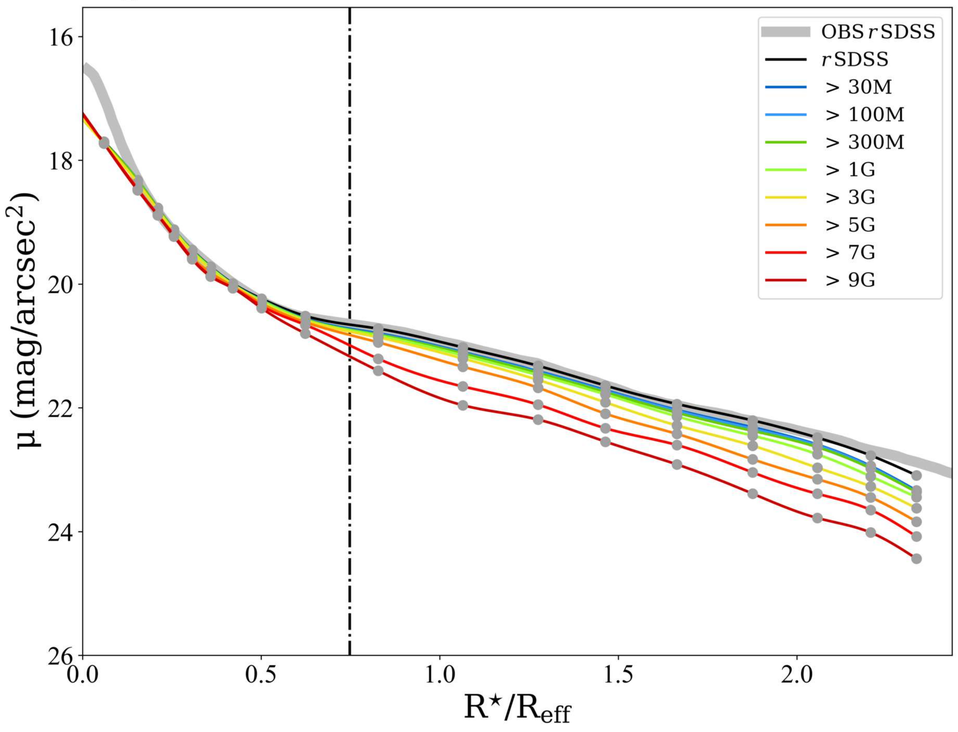

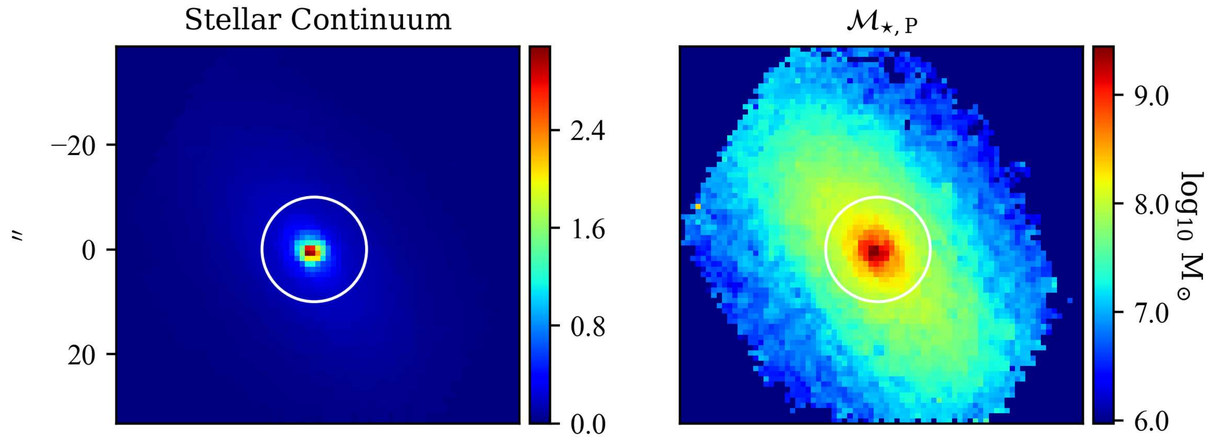

Log. of cumulative present stellar mass profiles

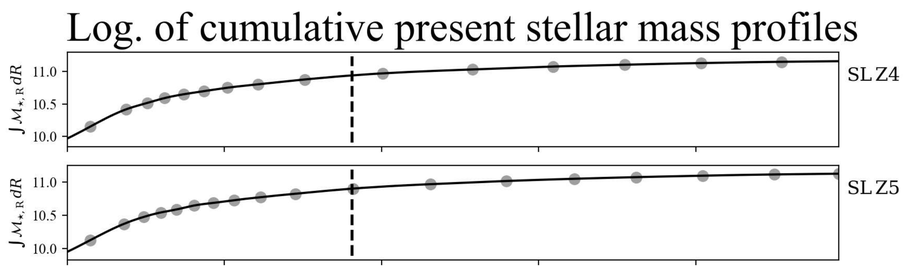

Stellar metallicity/Age & Hα flux/EW profiles

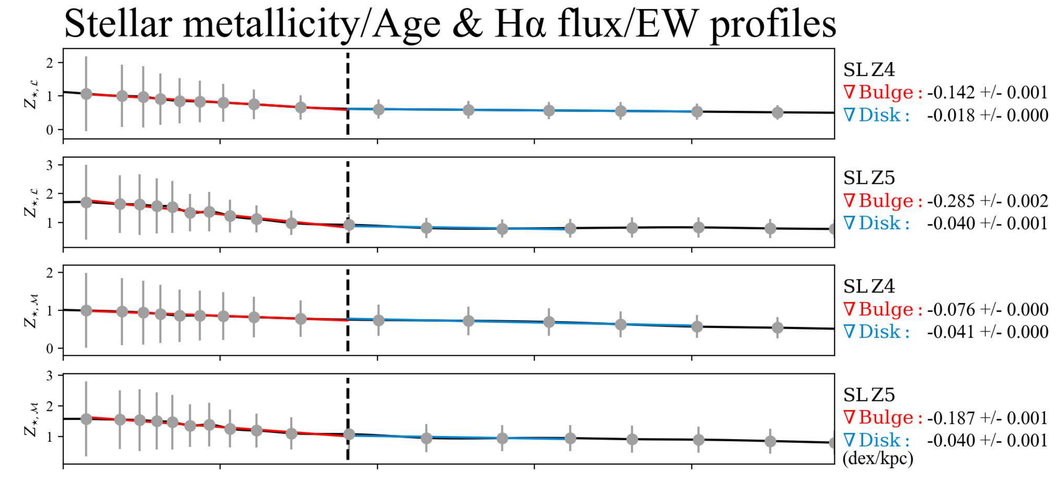

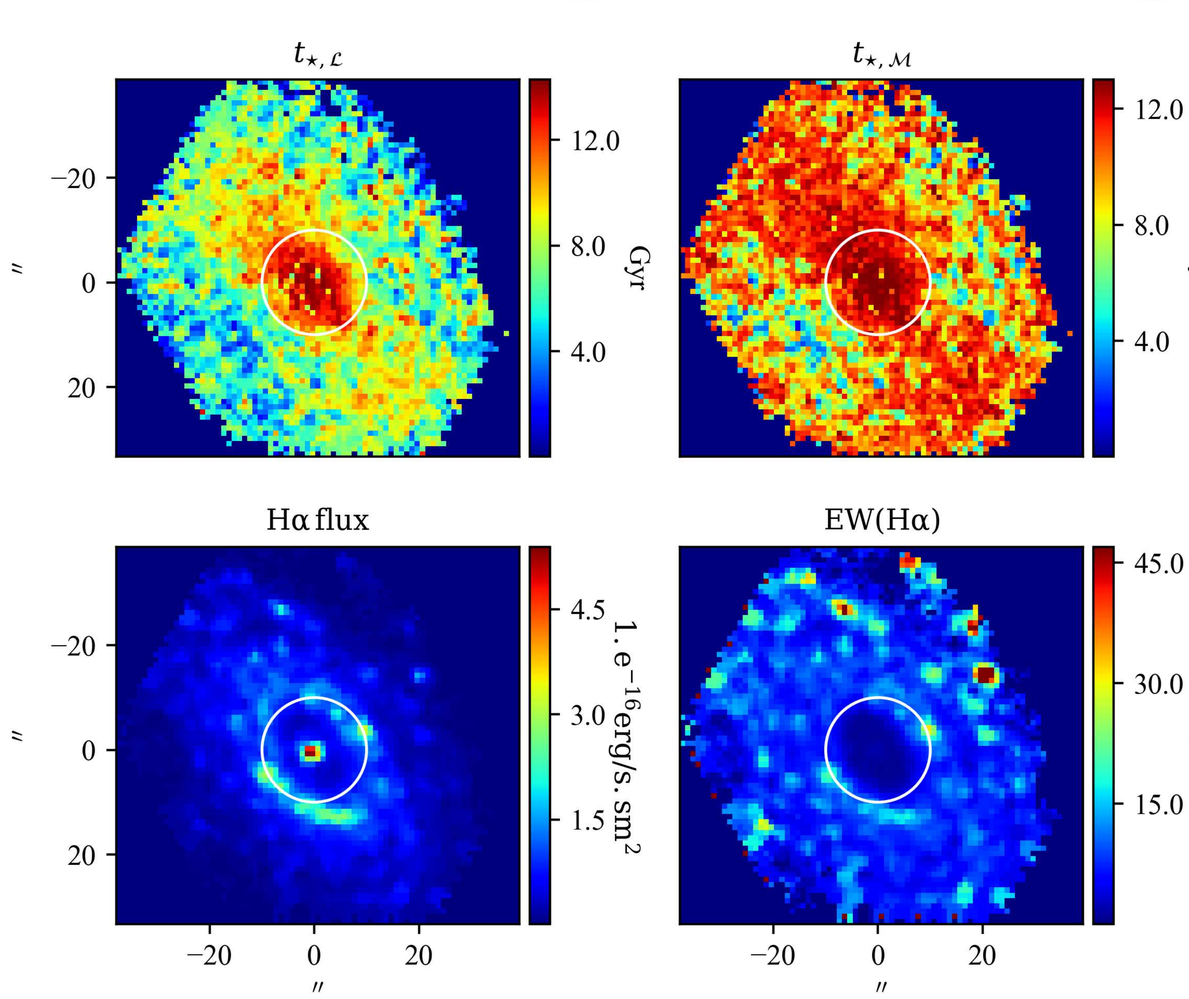

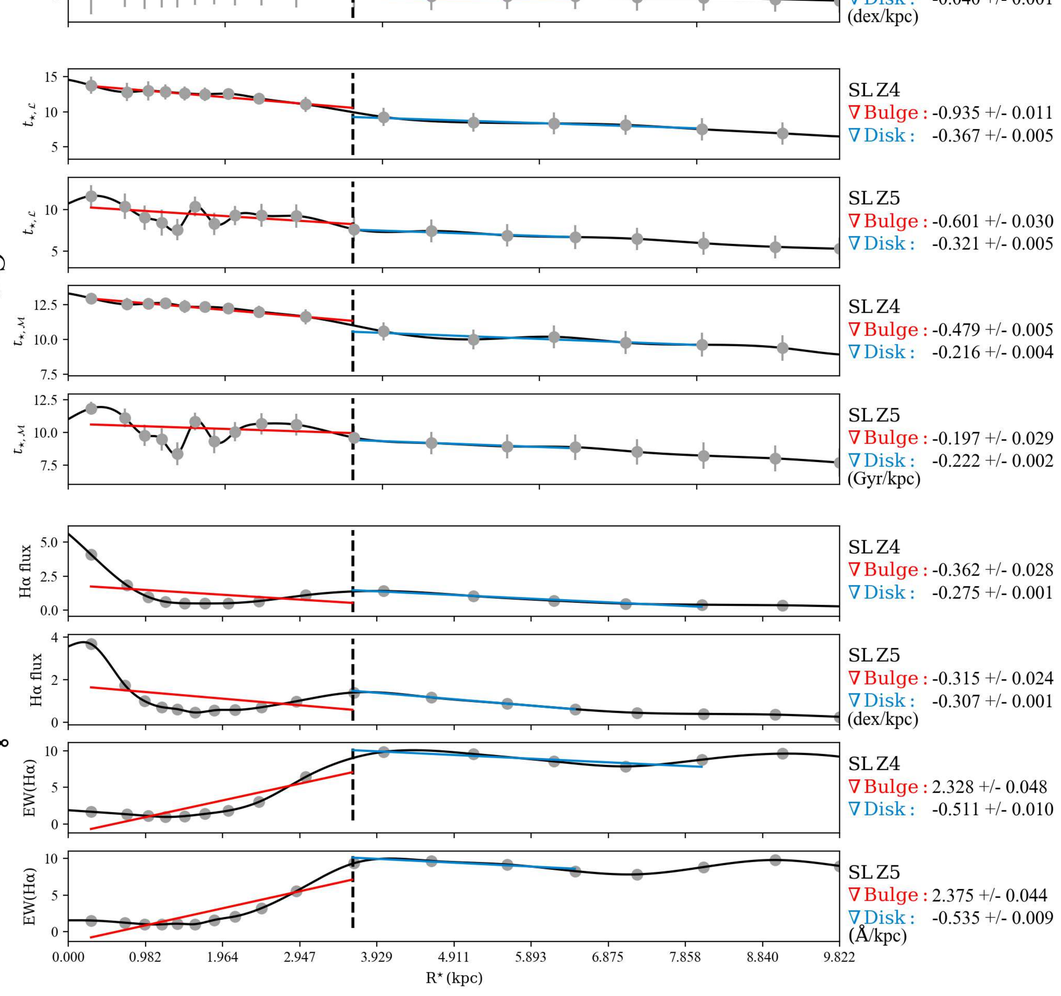

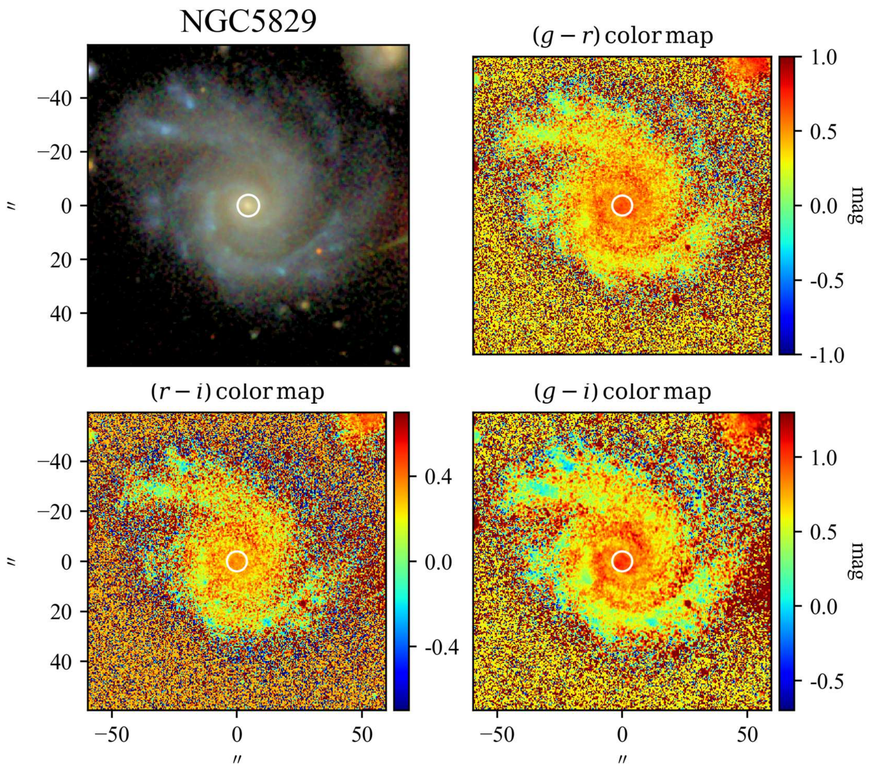

SBP decomposition of SDSS r band

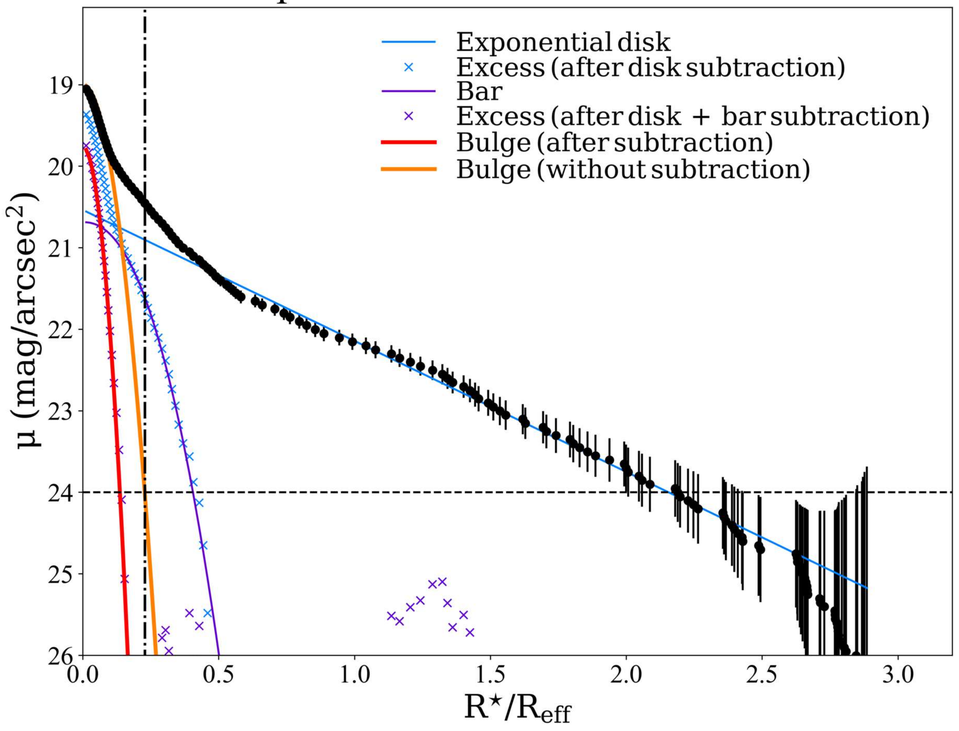

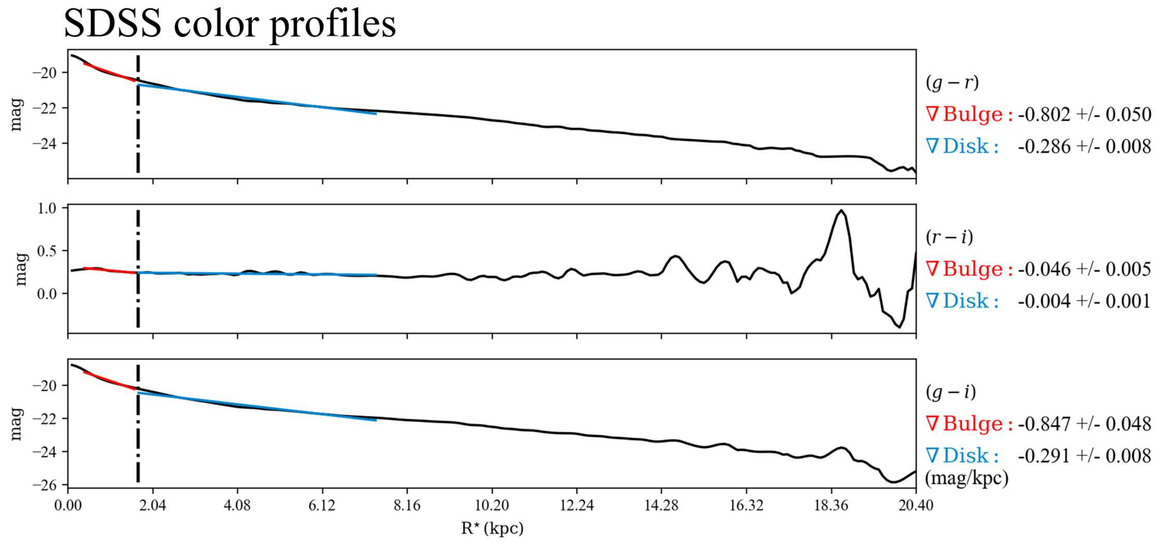

$\mathcal{RV}$ SBPs

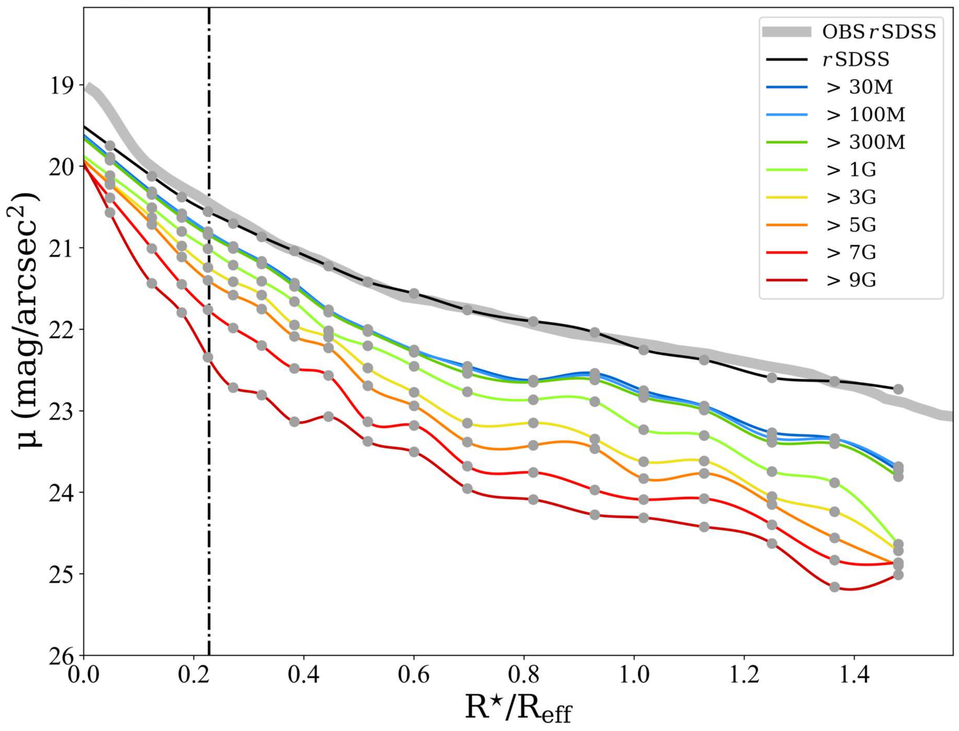

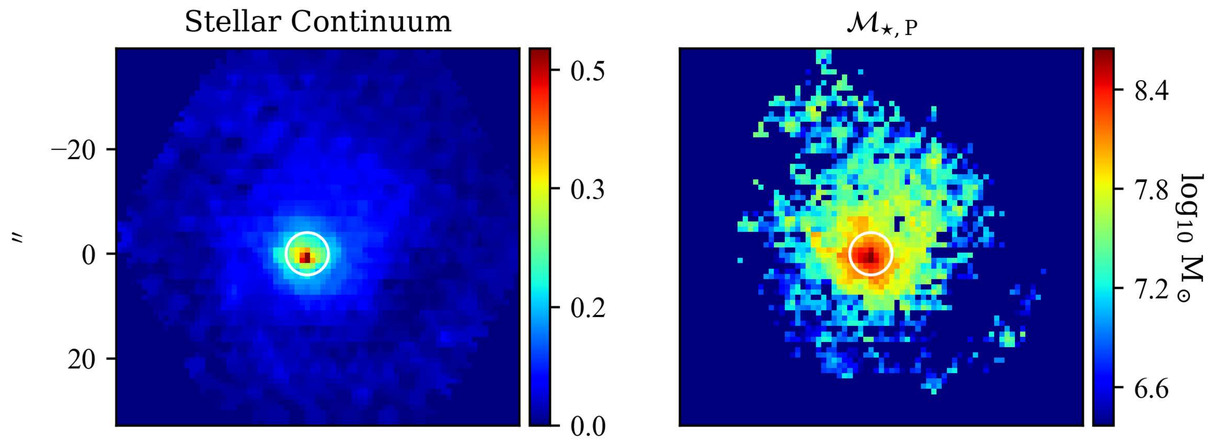

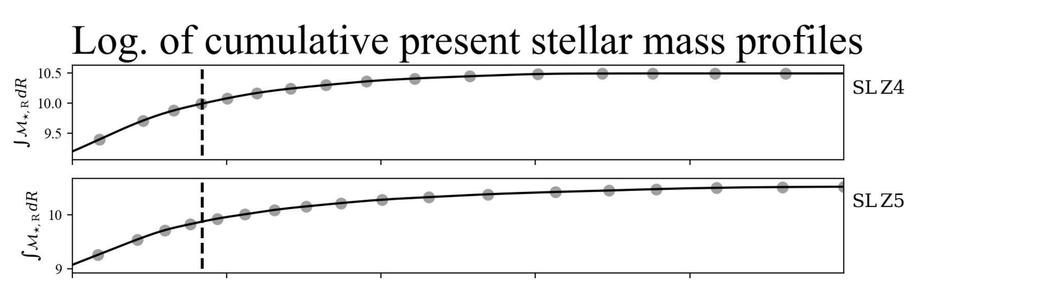

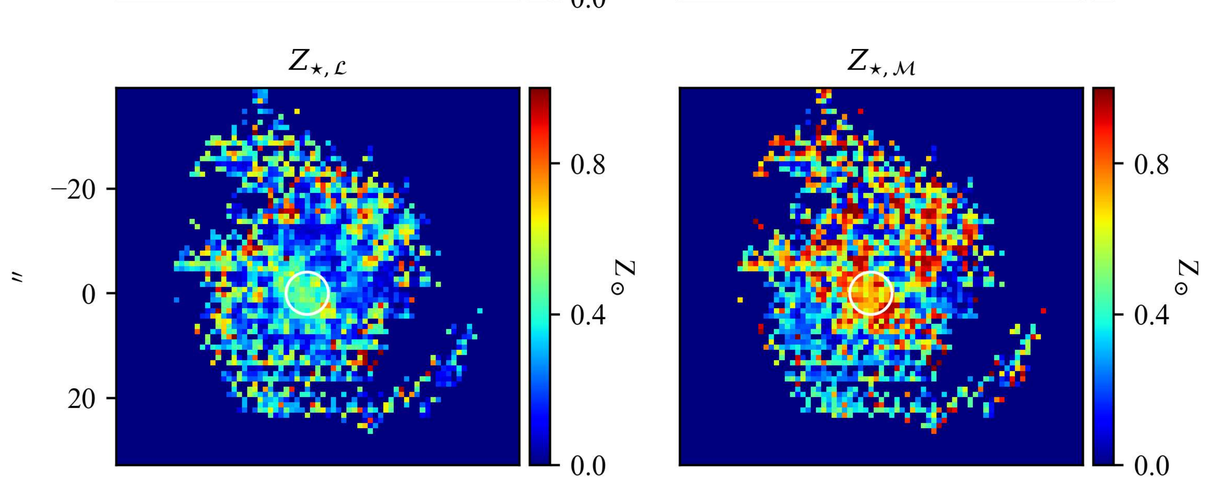

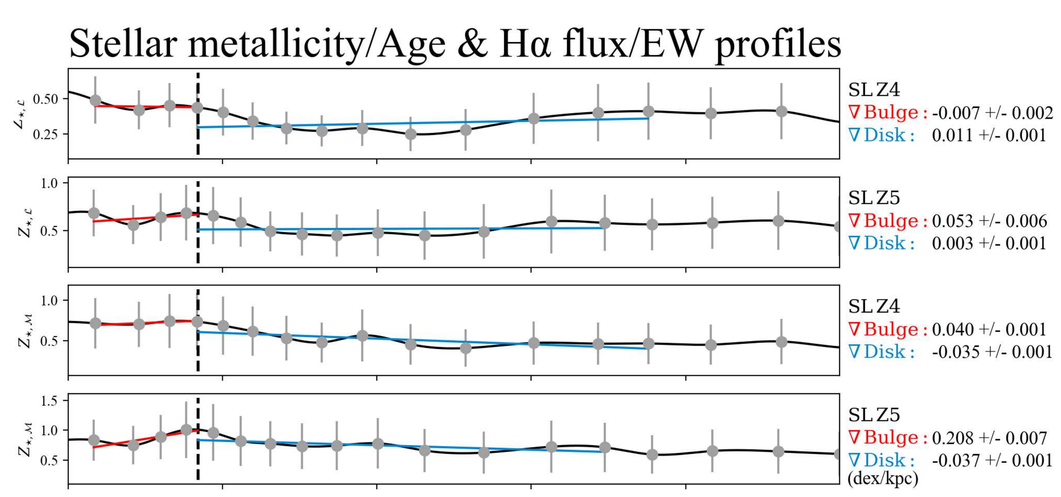

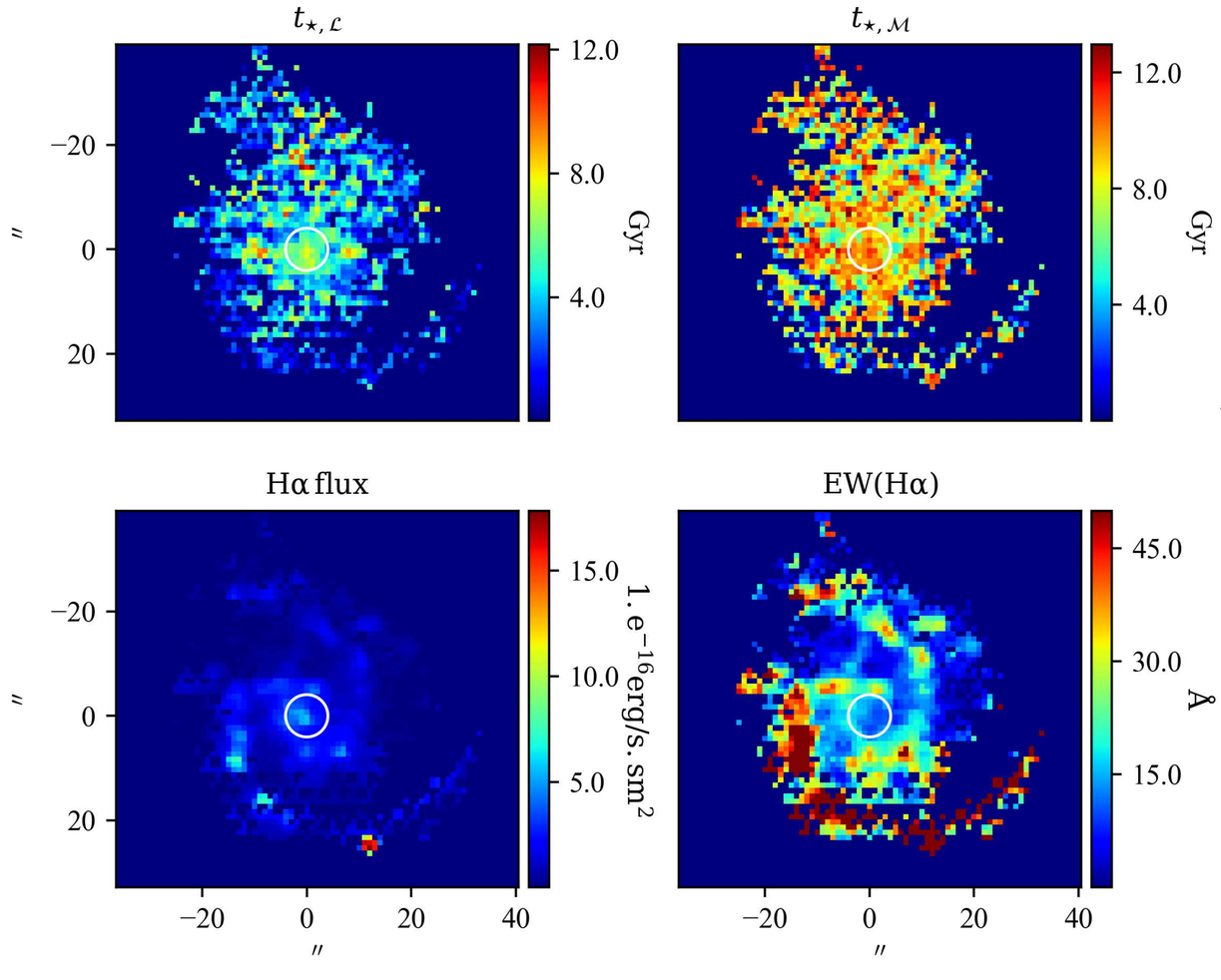

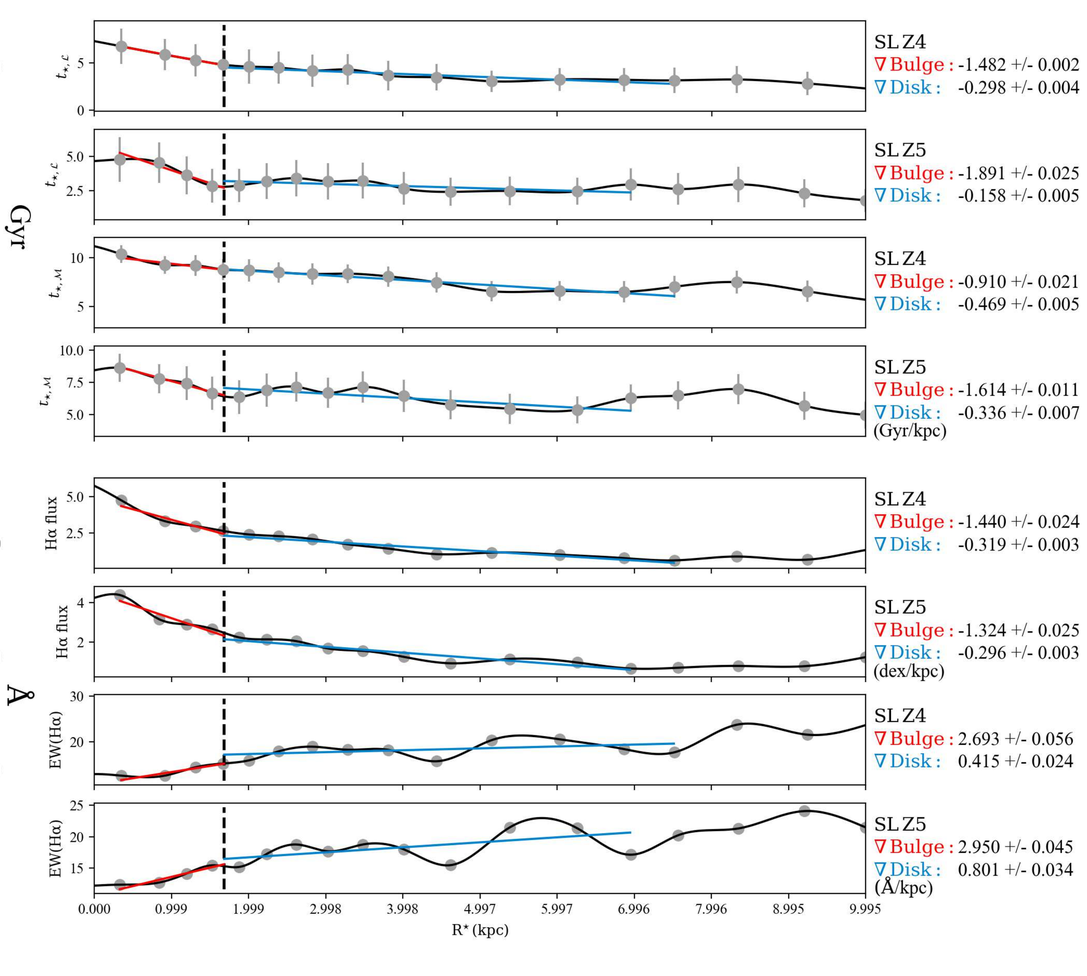

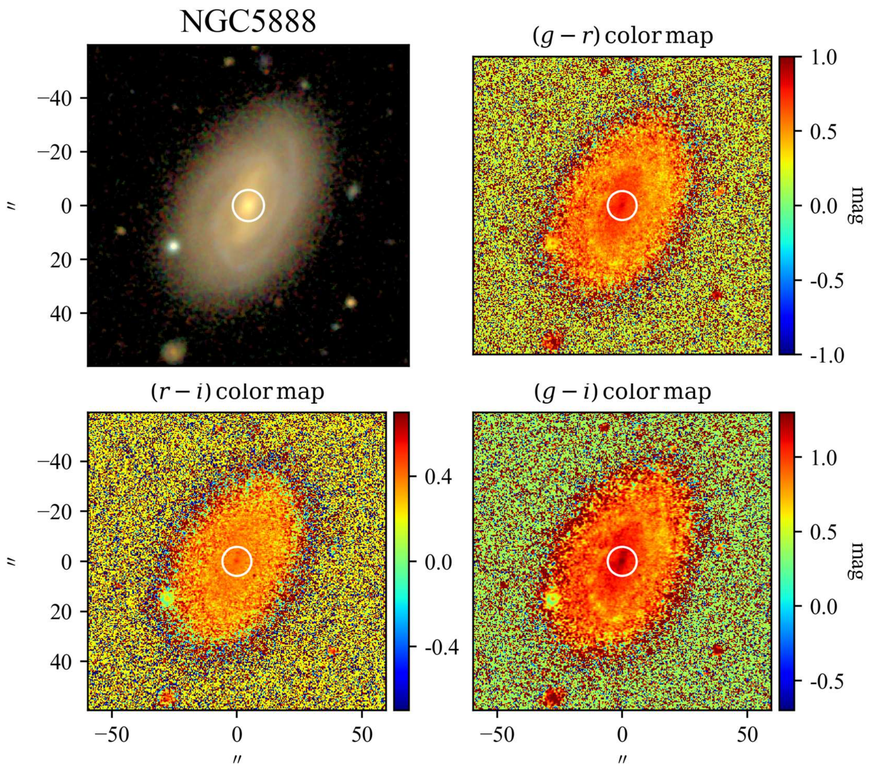

SBP decomposition of SDSS r band

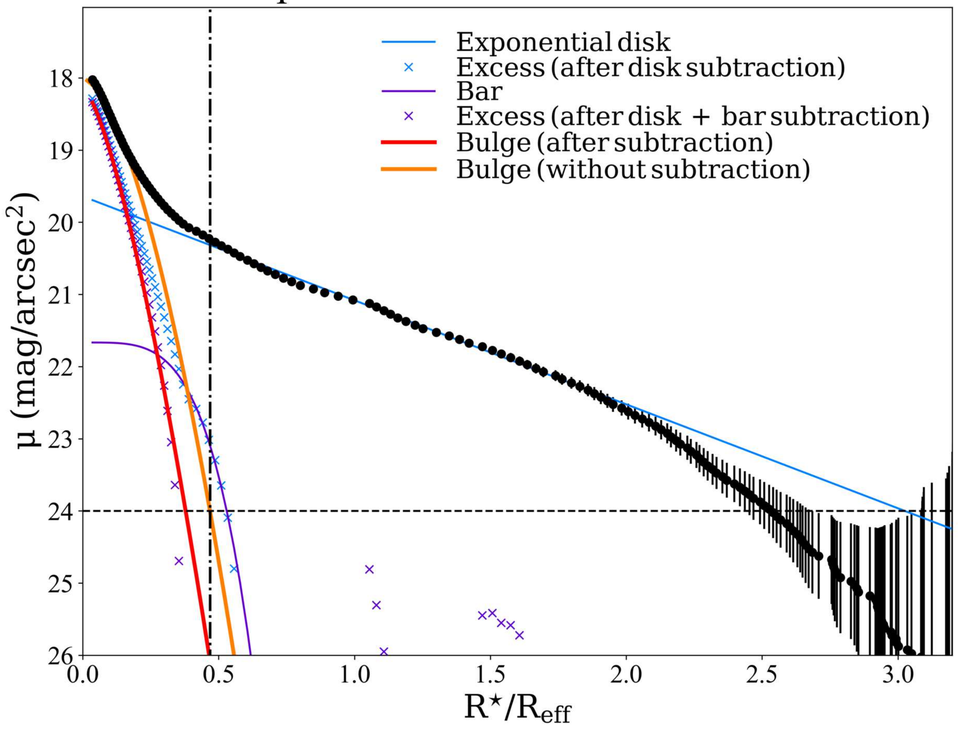

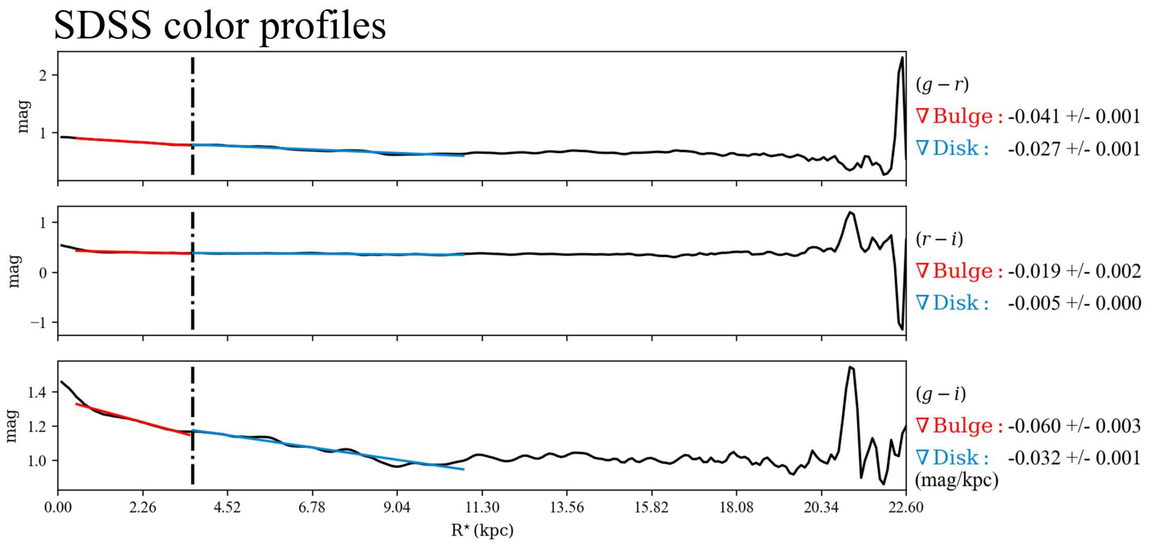

$\mathcal{RY}$ SBPs

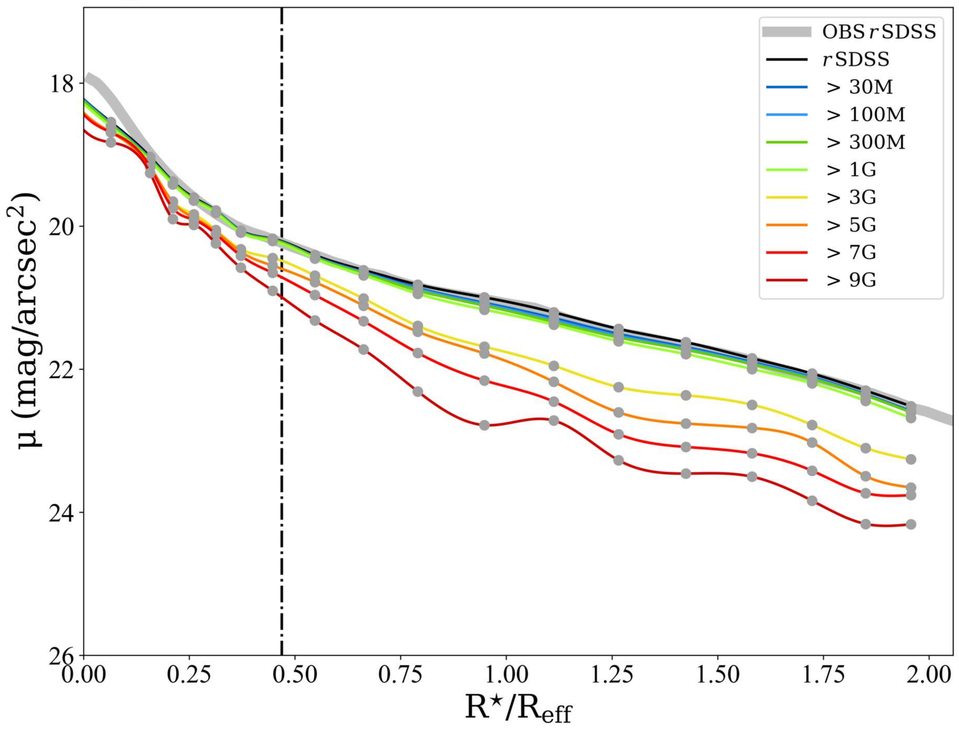

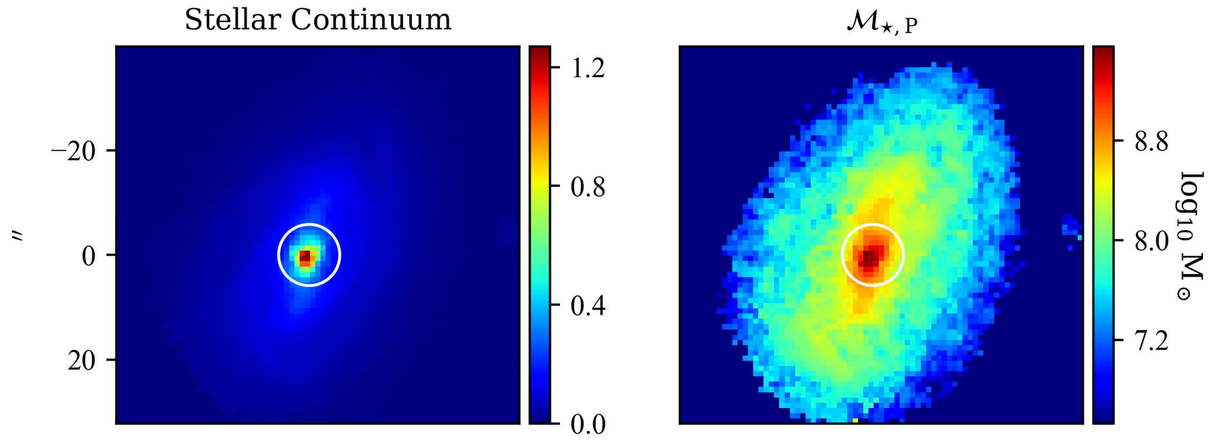

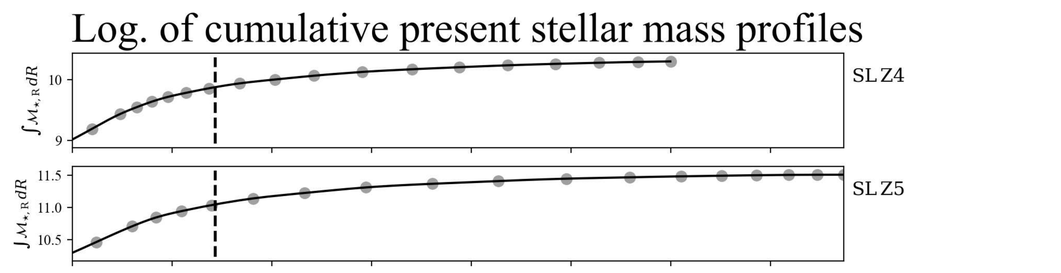

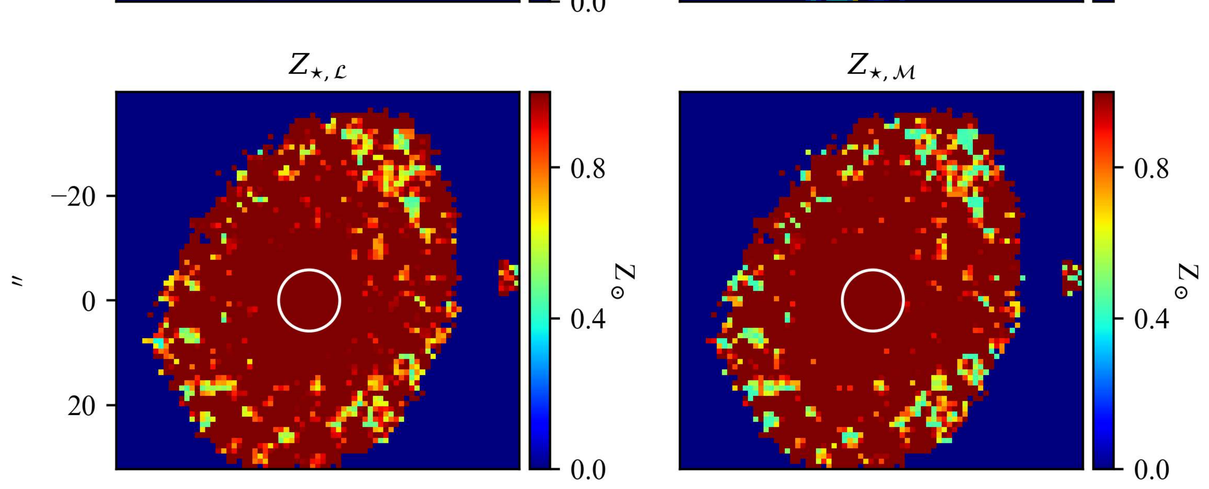

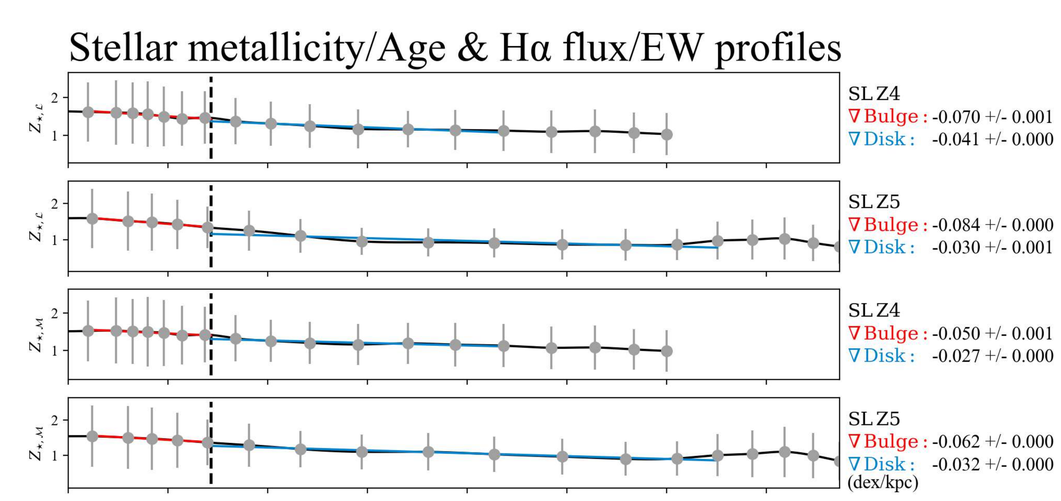

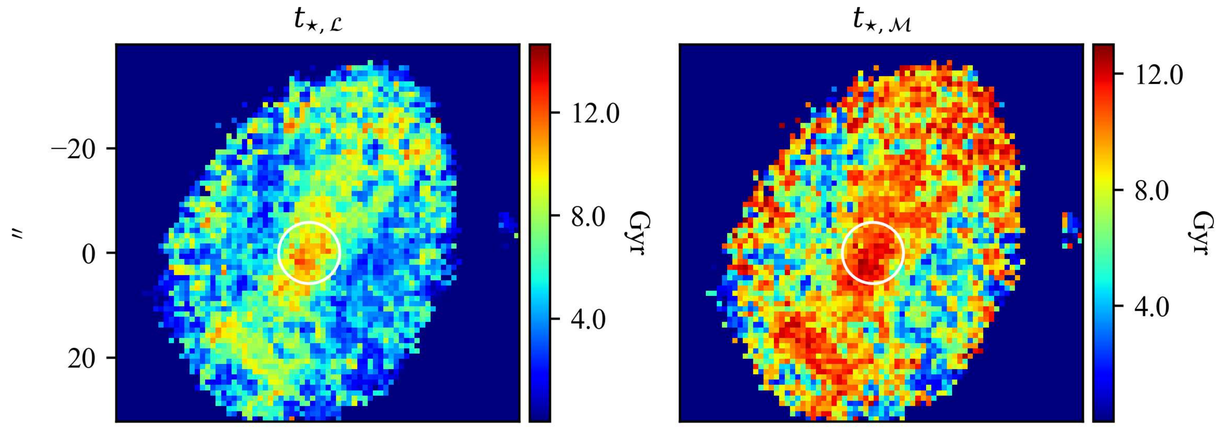

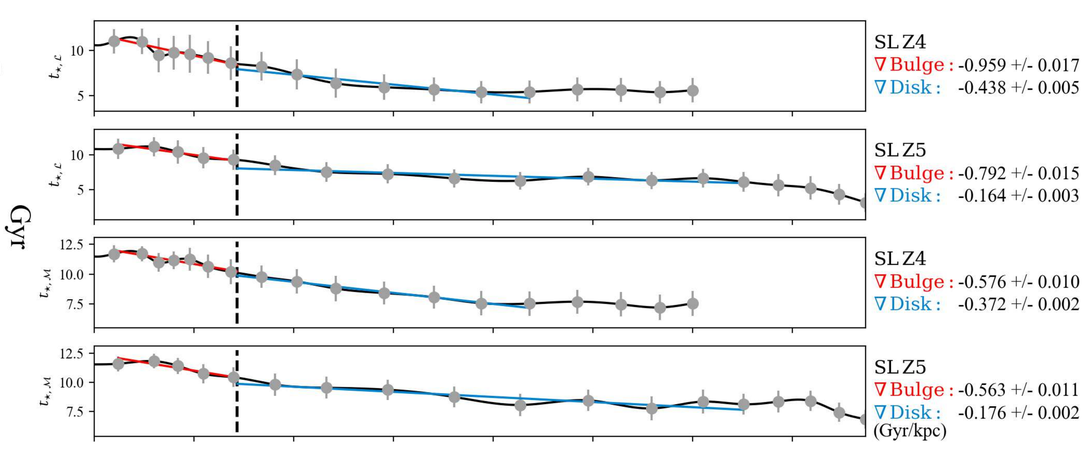

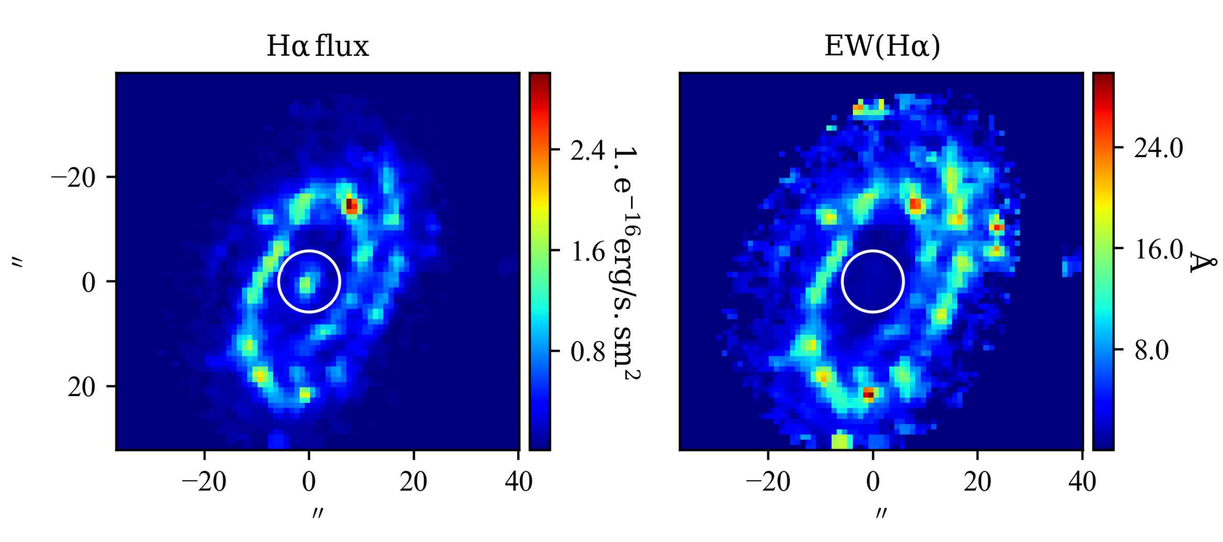

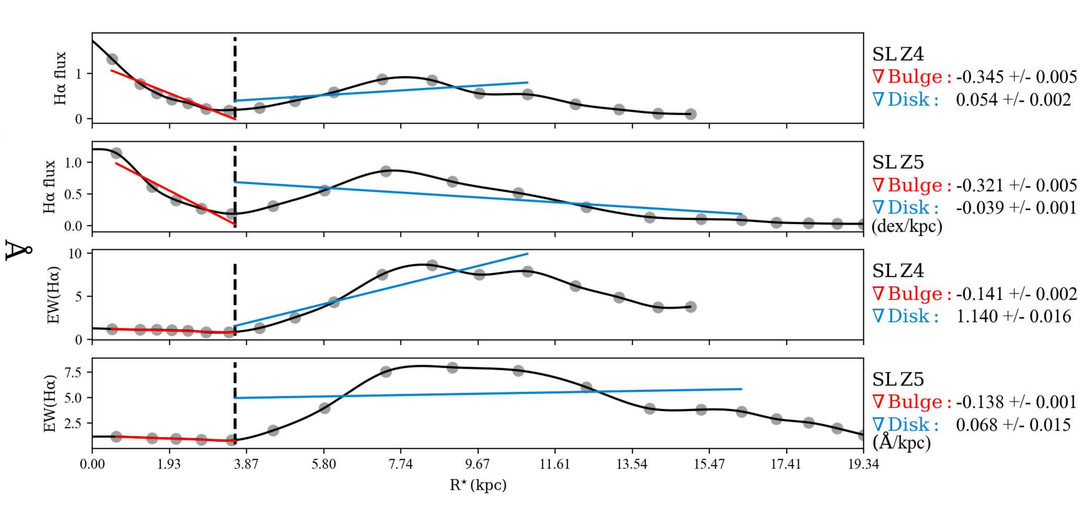

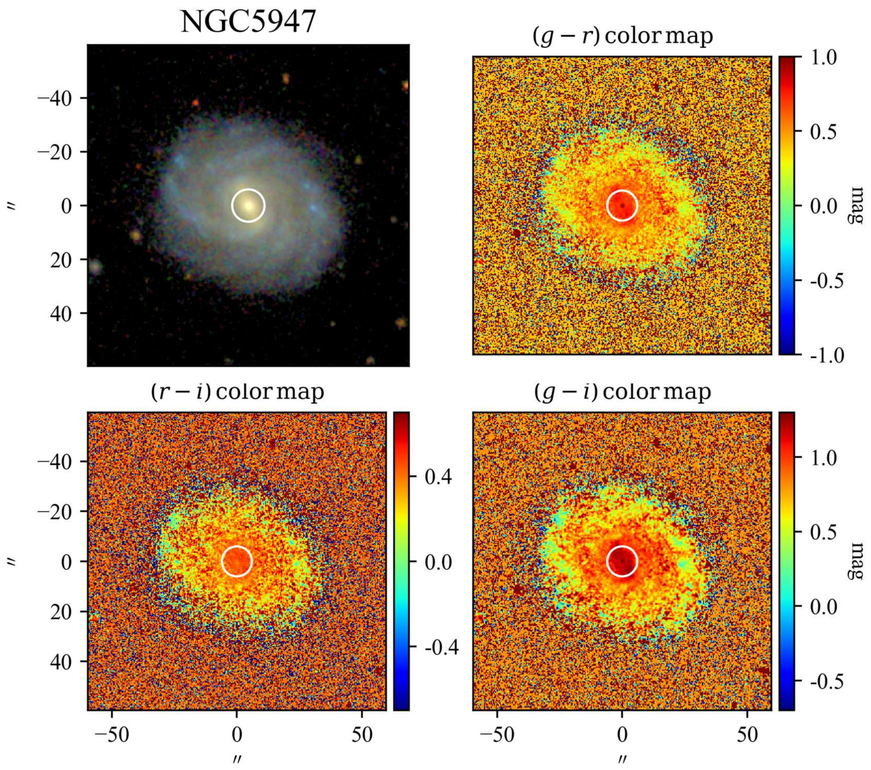

SBP decomposition of SDSS r band

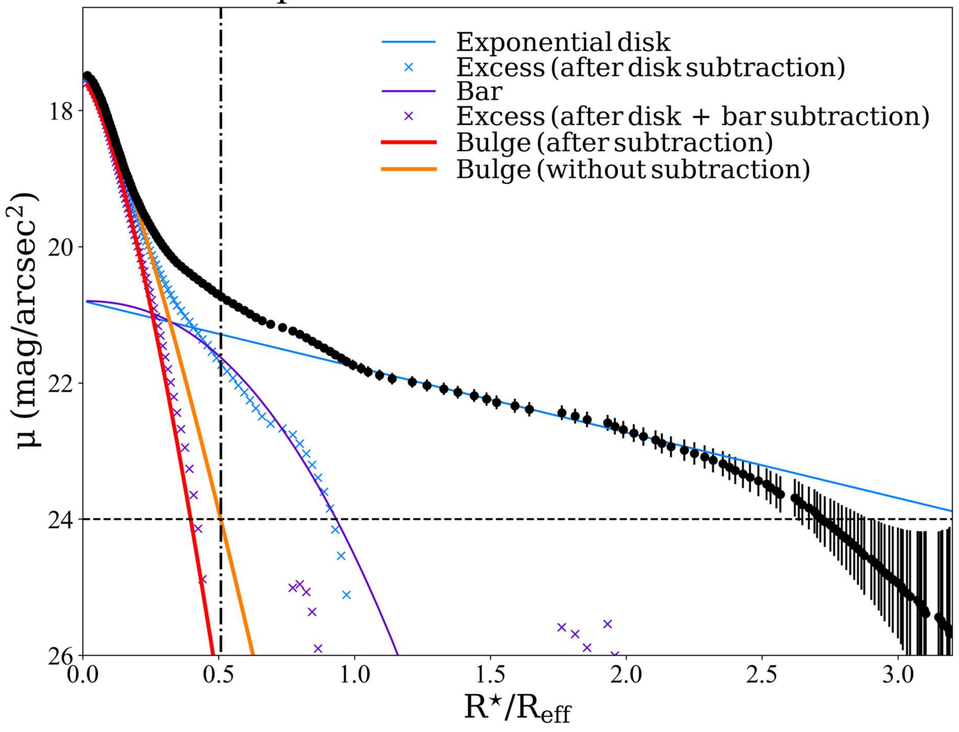

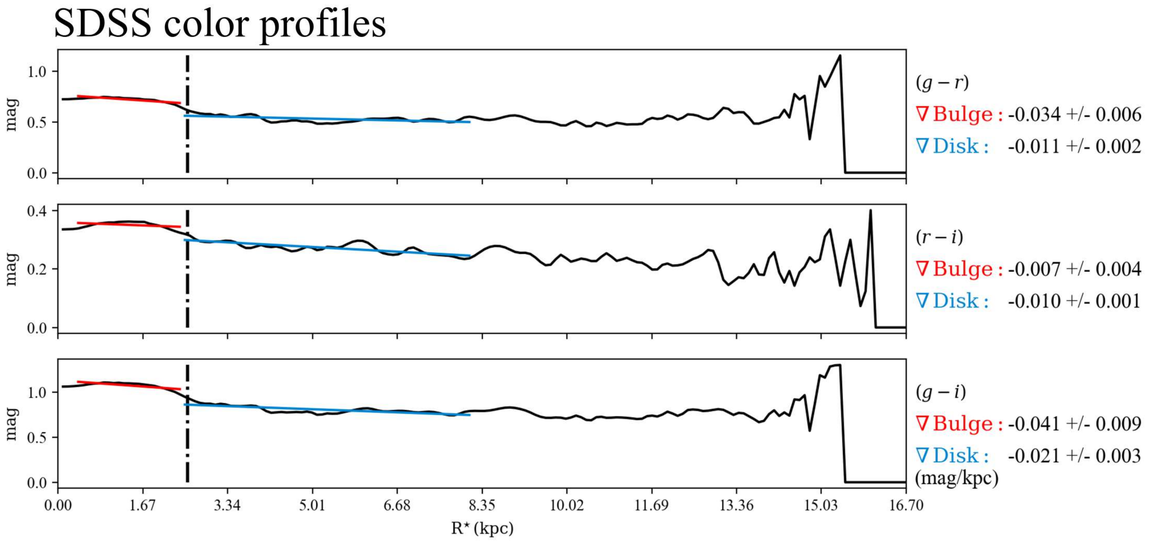

$\mathcal{RY}$ SBPs

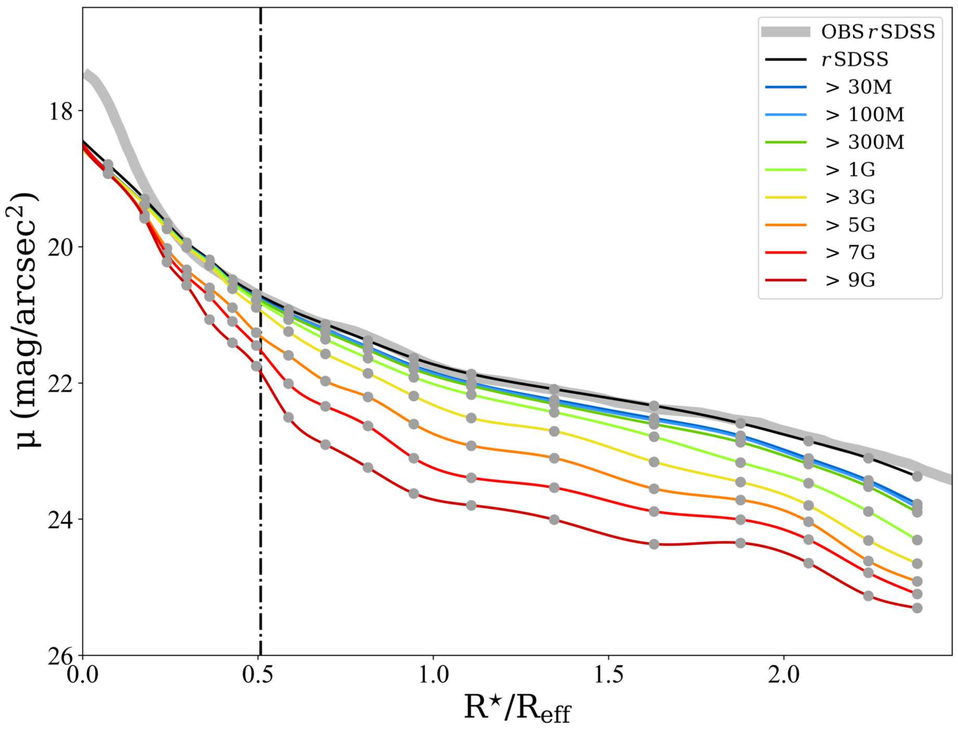

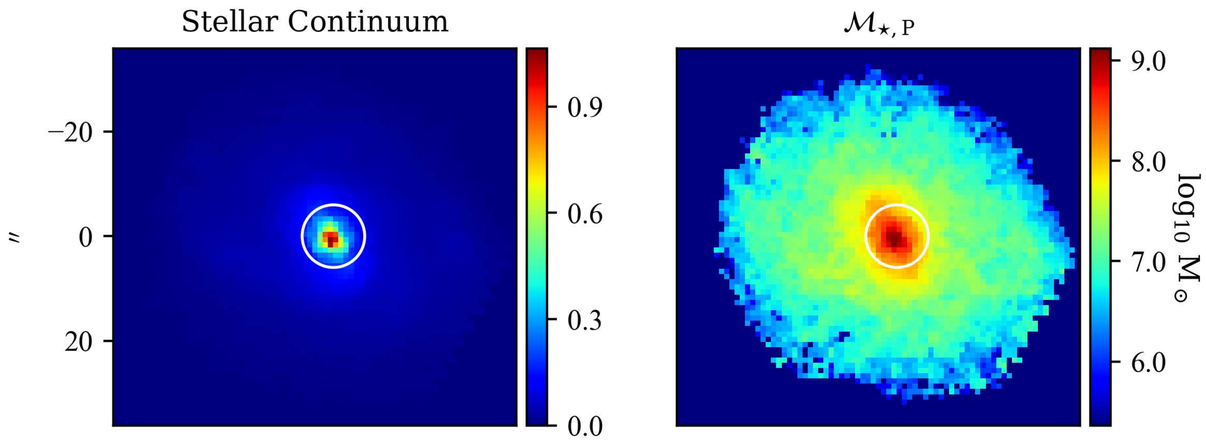

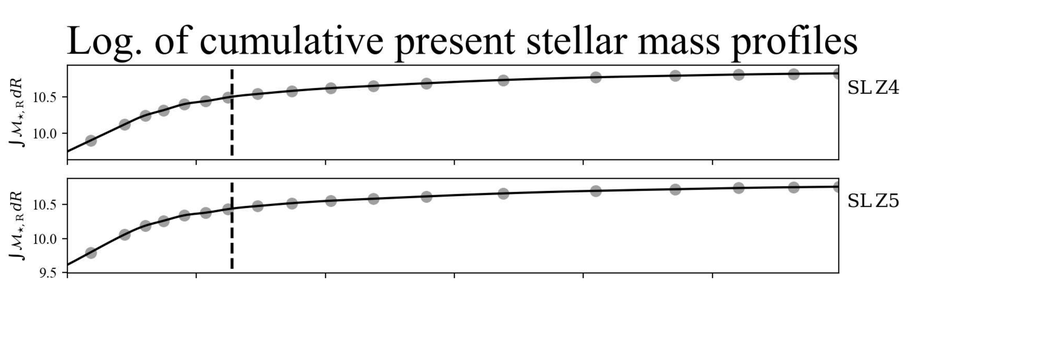

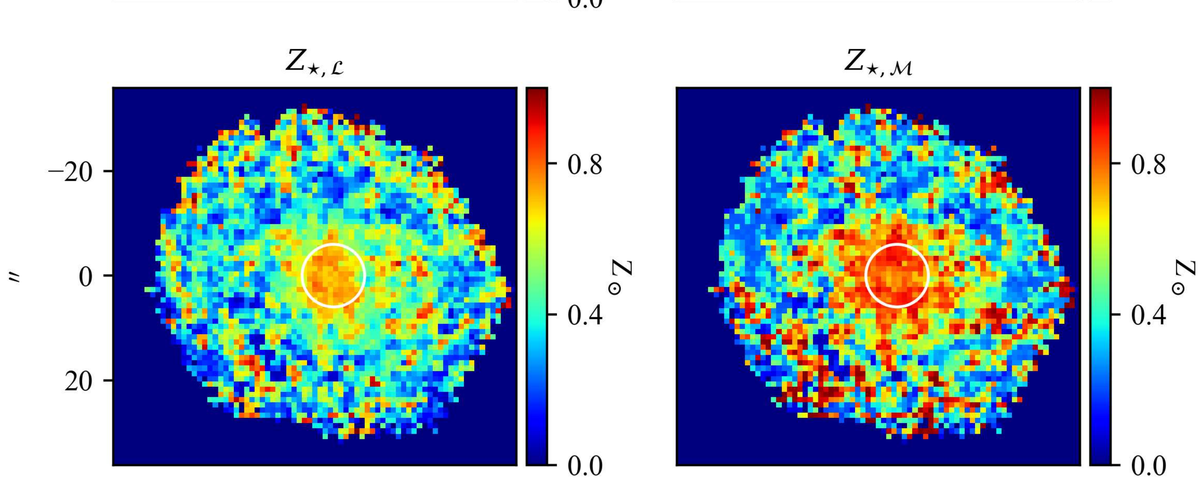

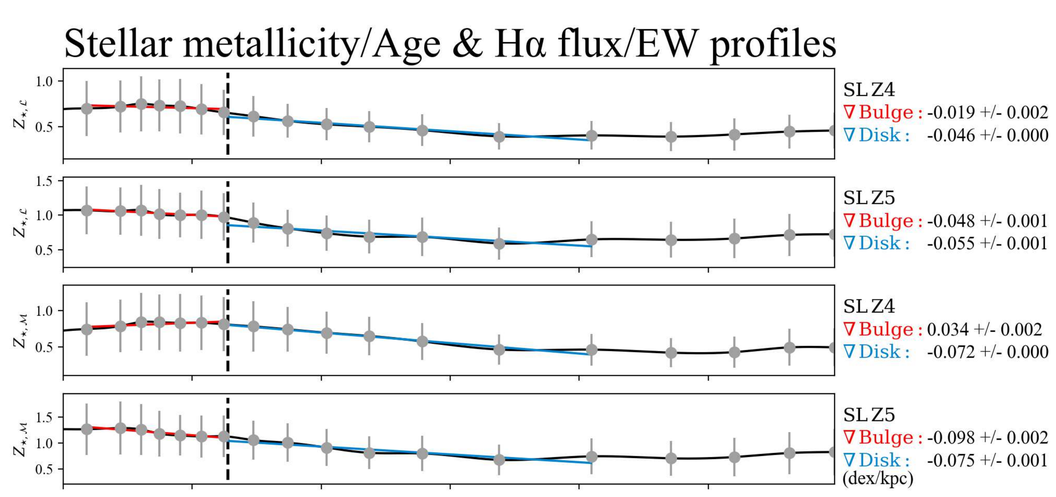

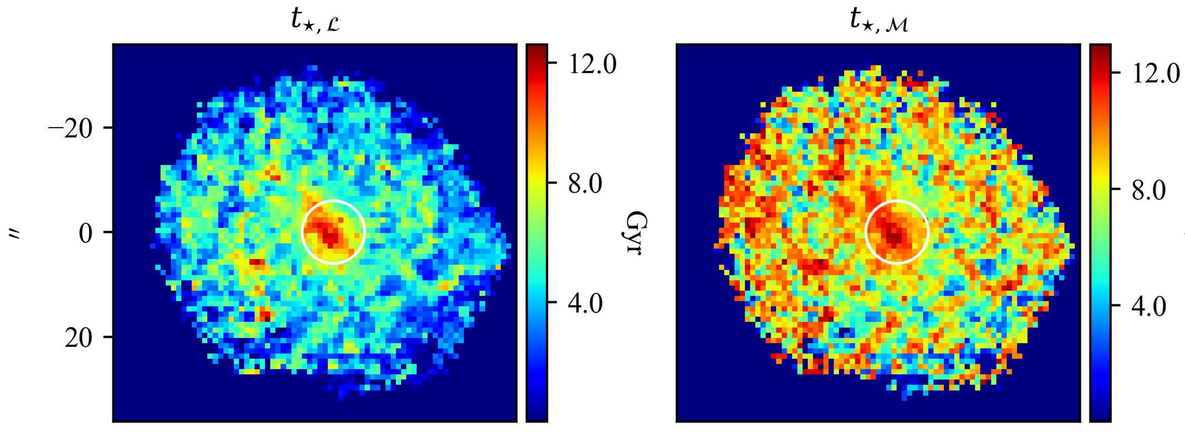

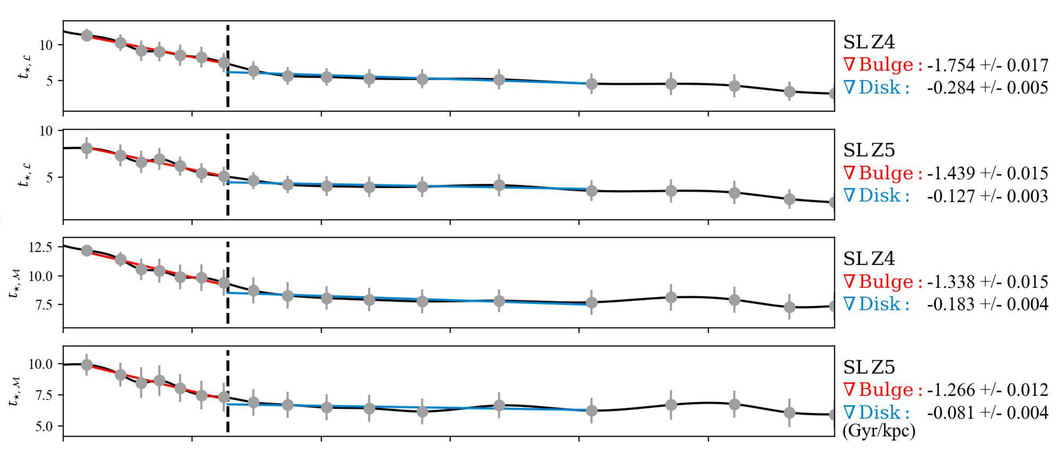

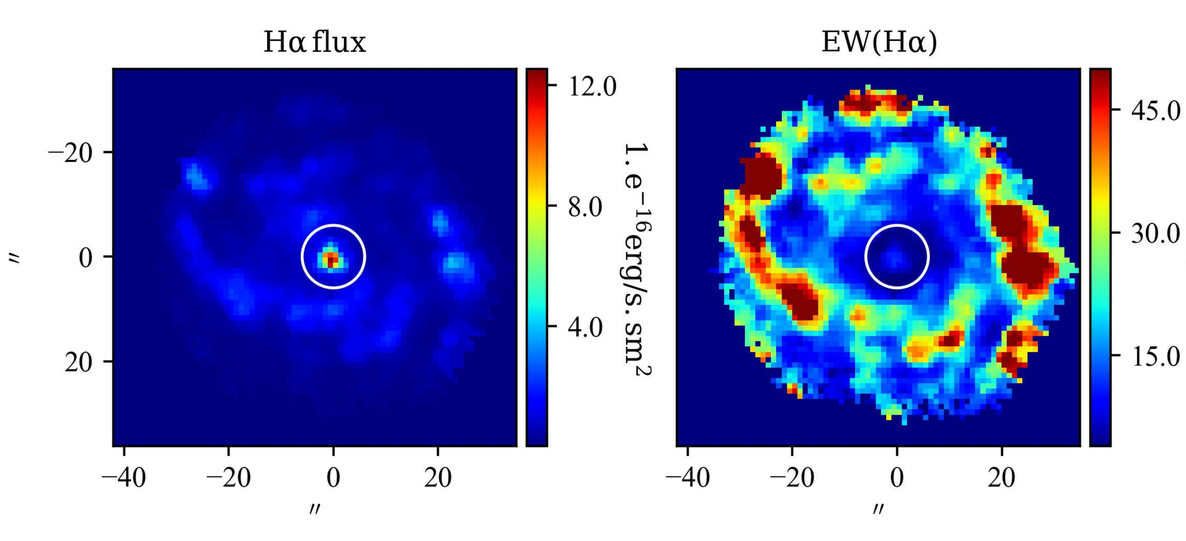

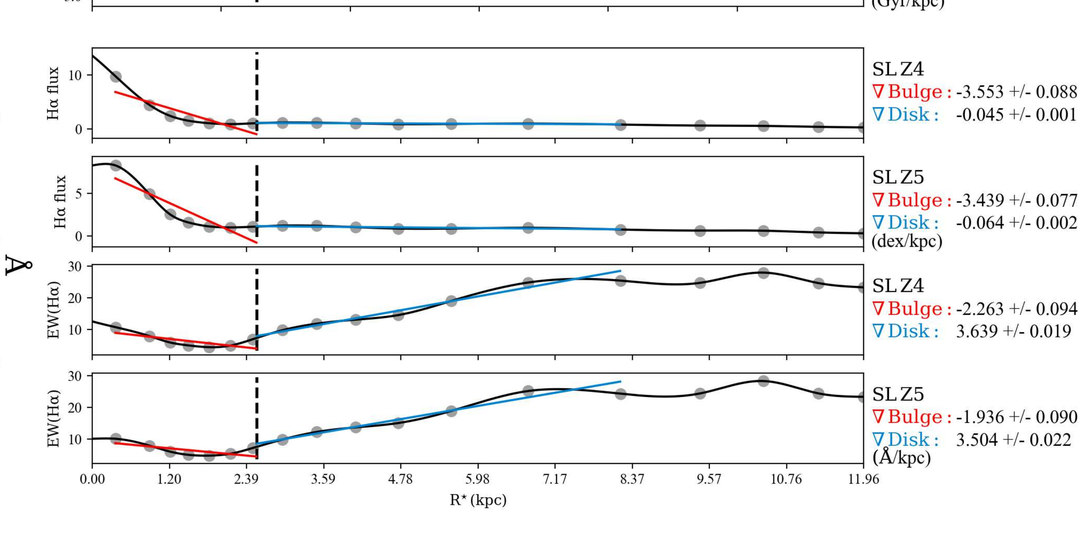

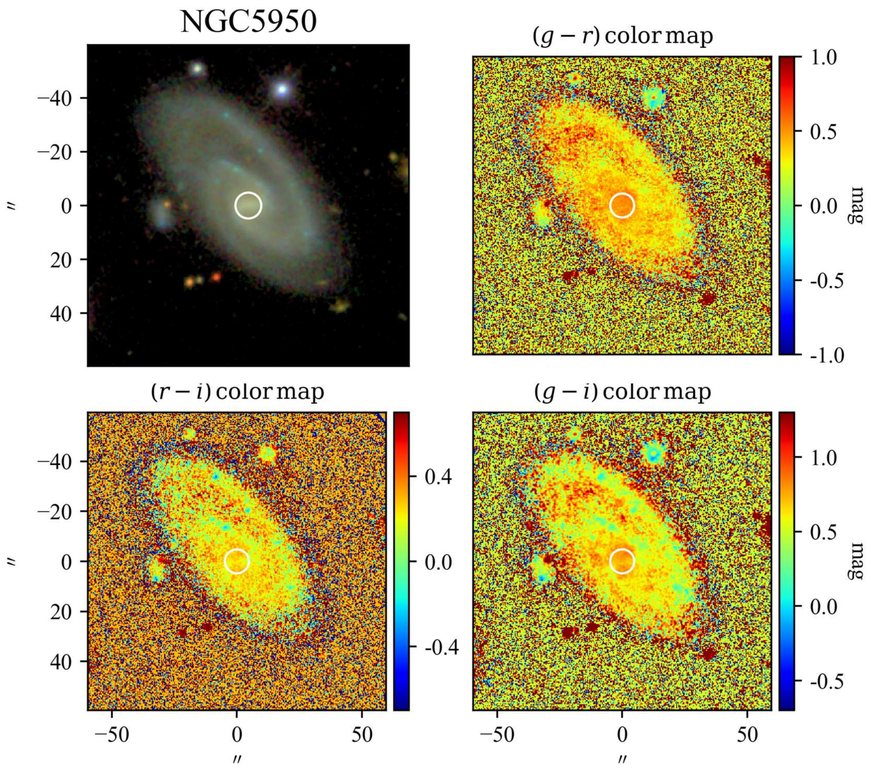

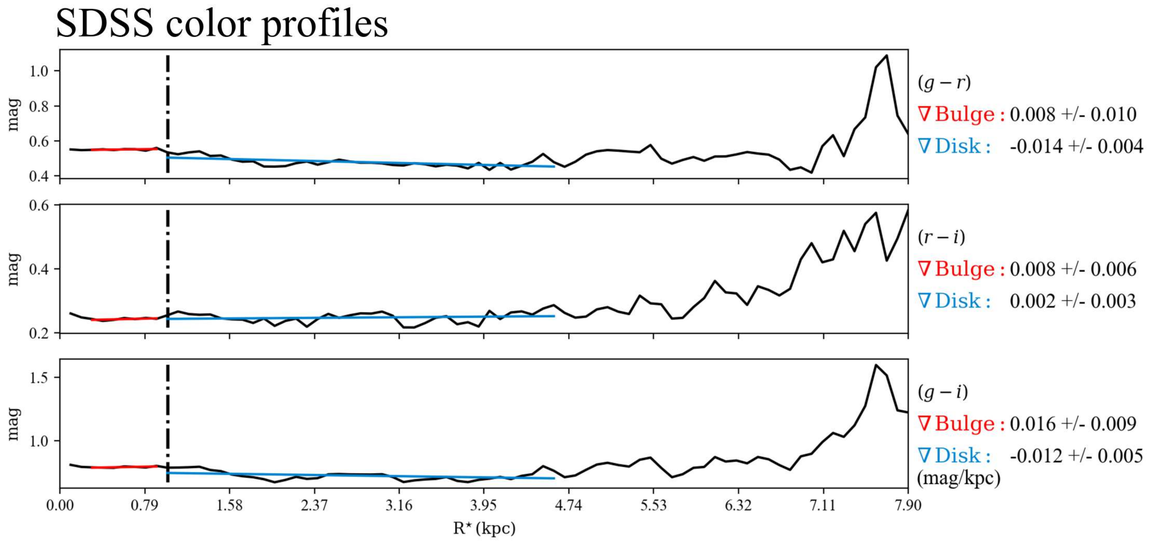

SBP decomposition of SDSS r band

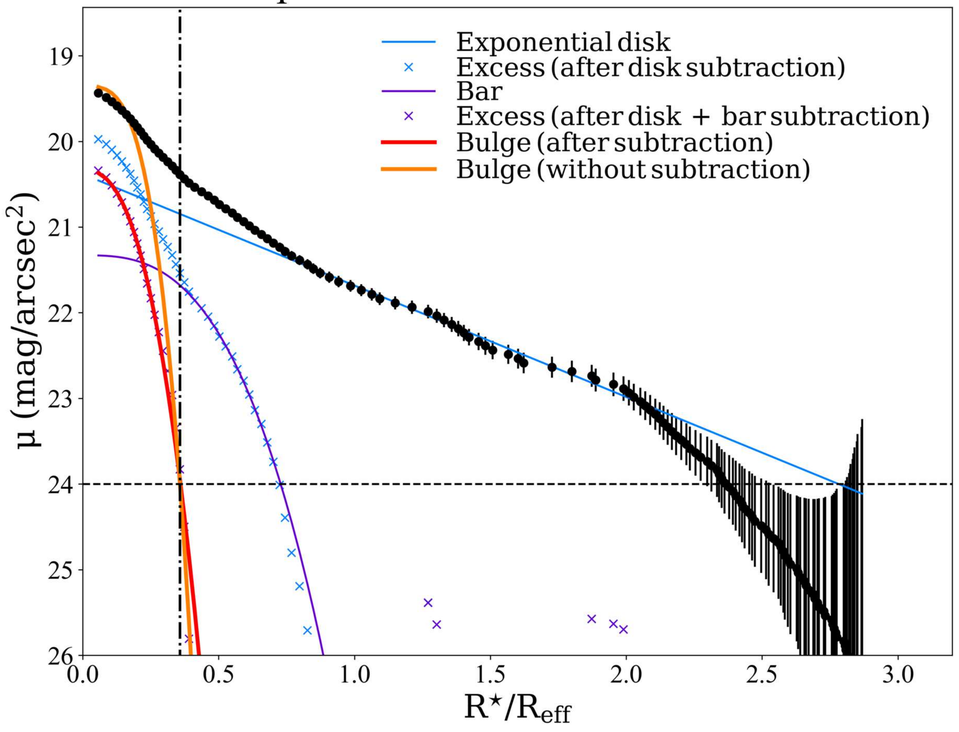

$\mathcal{RY}$ SBPs

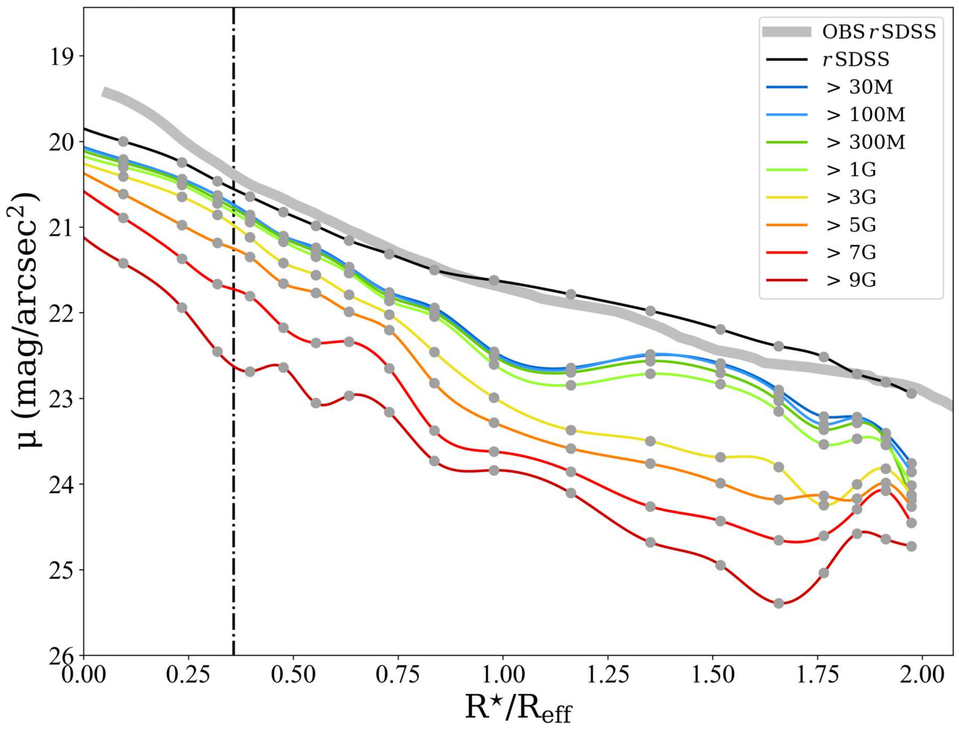

Stellar Continuum

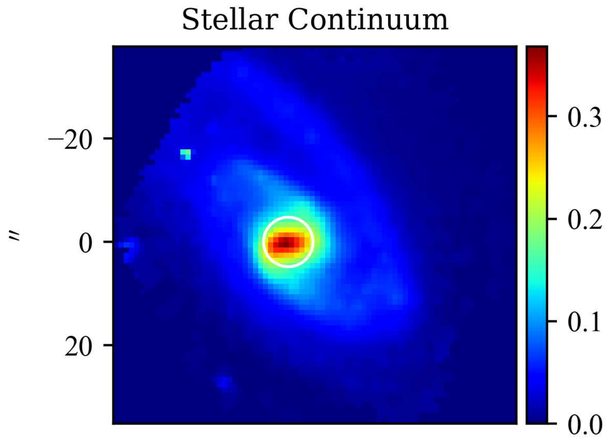

$\mathcal{M}_{\star,\mathrm{P}}$

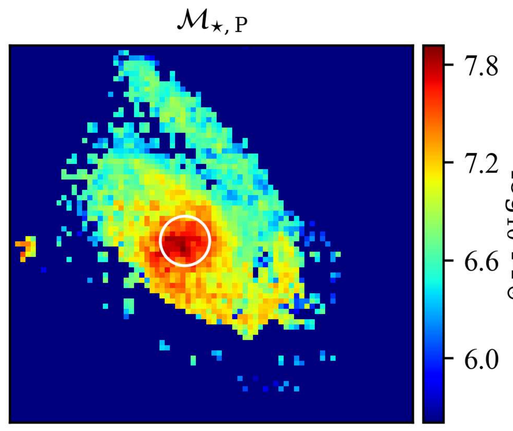

Log. of cumulative present stellar mass profiles

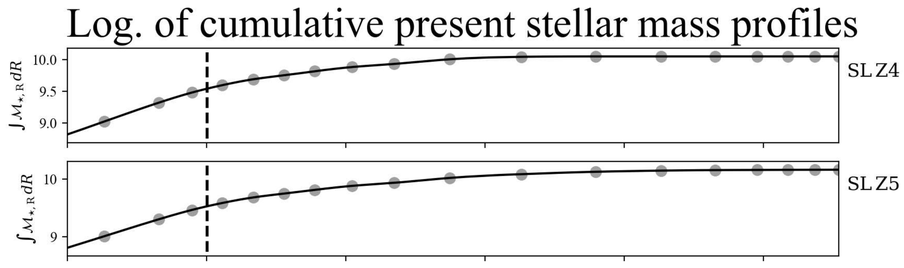

$Z_{\star,\mathcal{L}}$

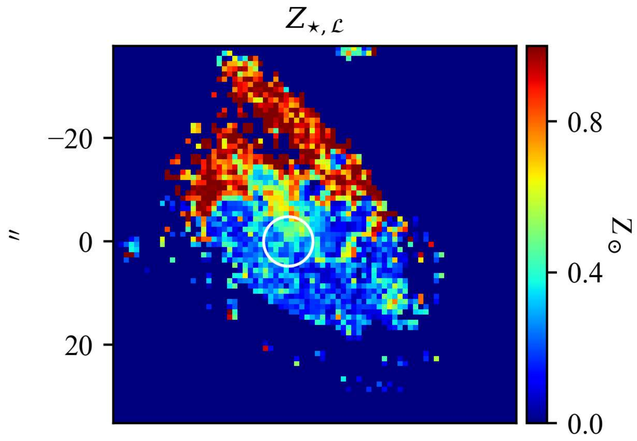

$Z_{\star,\mathcal{M}}$

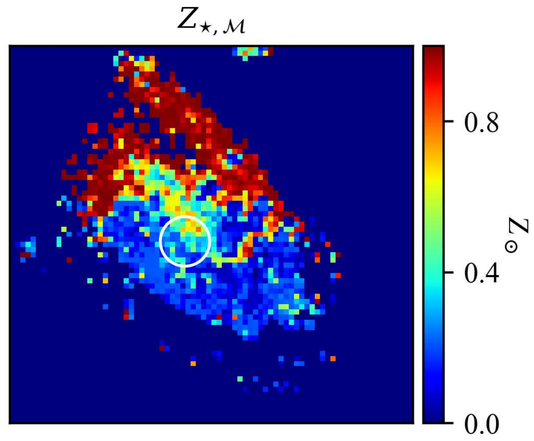

Stellar metallicity/Age & Hα flux/EW profiles

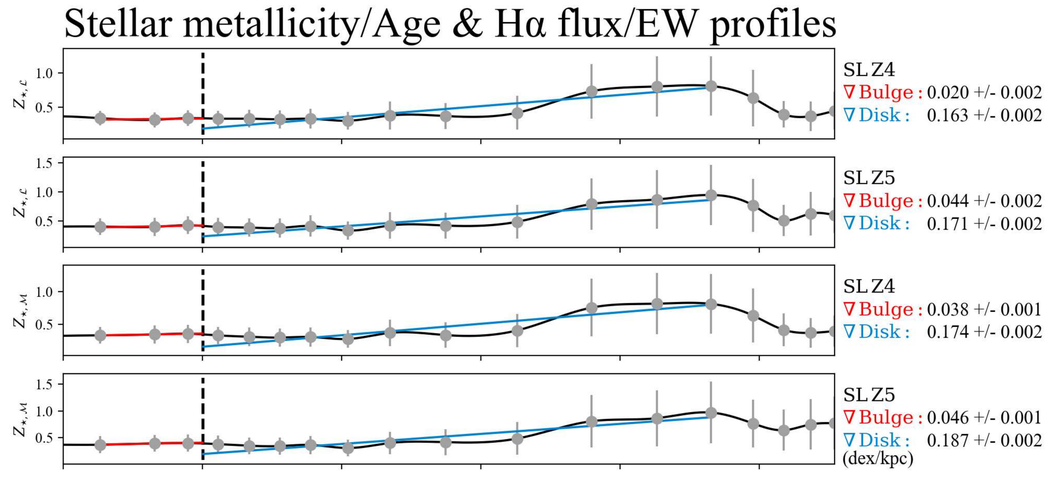

$t_{\star,\mathcal{L}}$

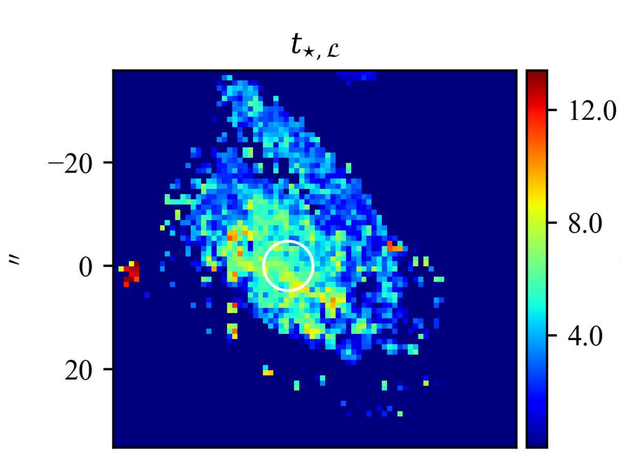

$t_{\star,\mathcal{M}}$

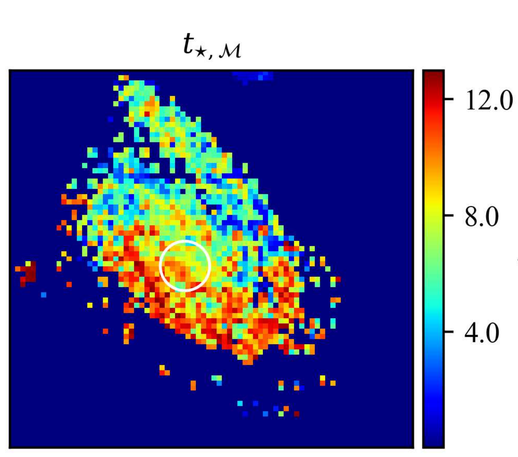

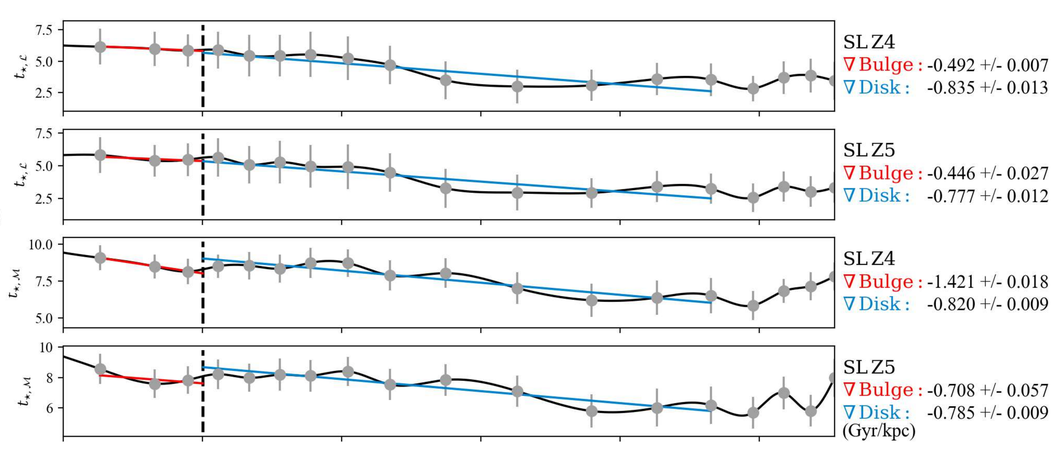

Hα flux

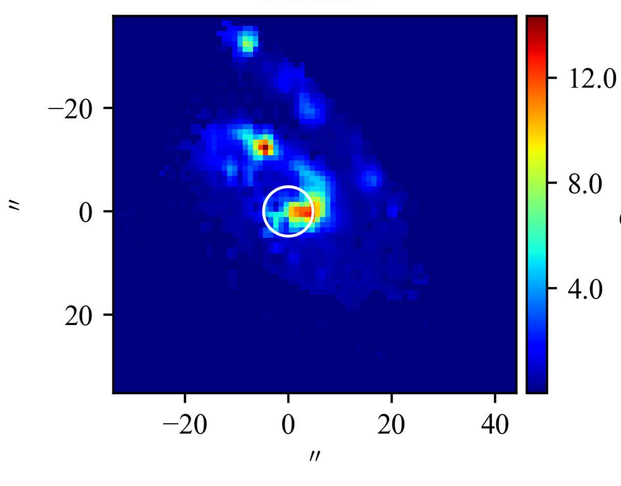

EW(Hα)

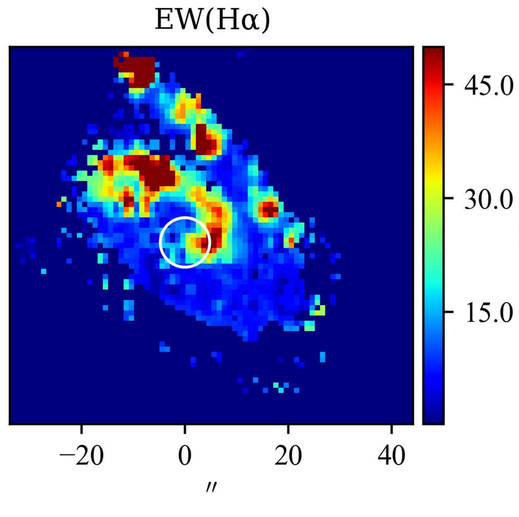

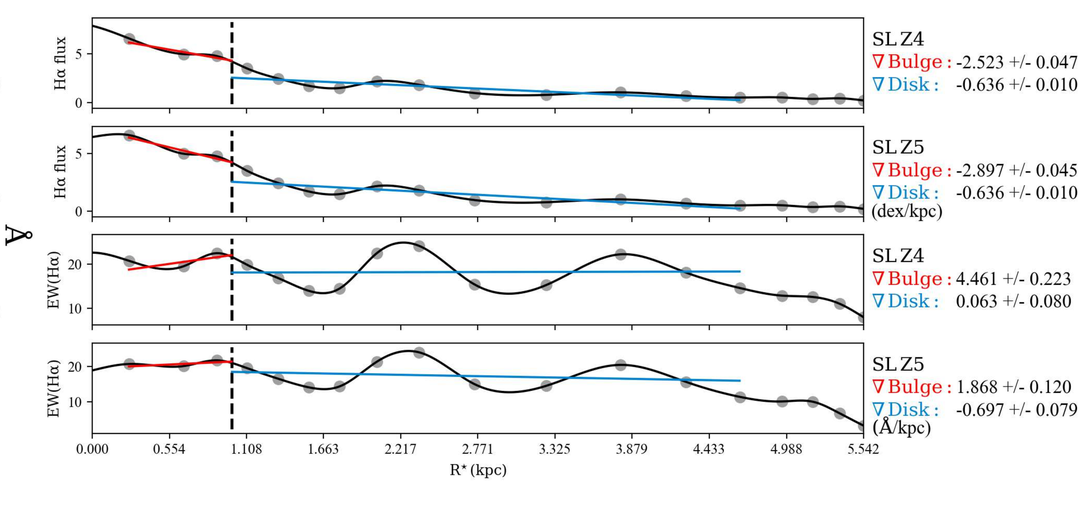

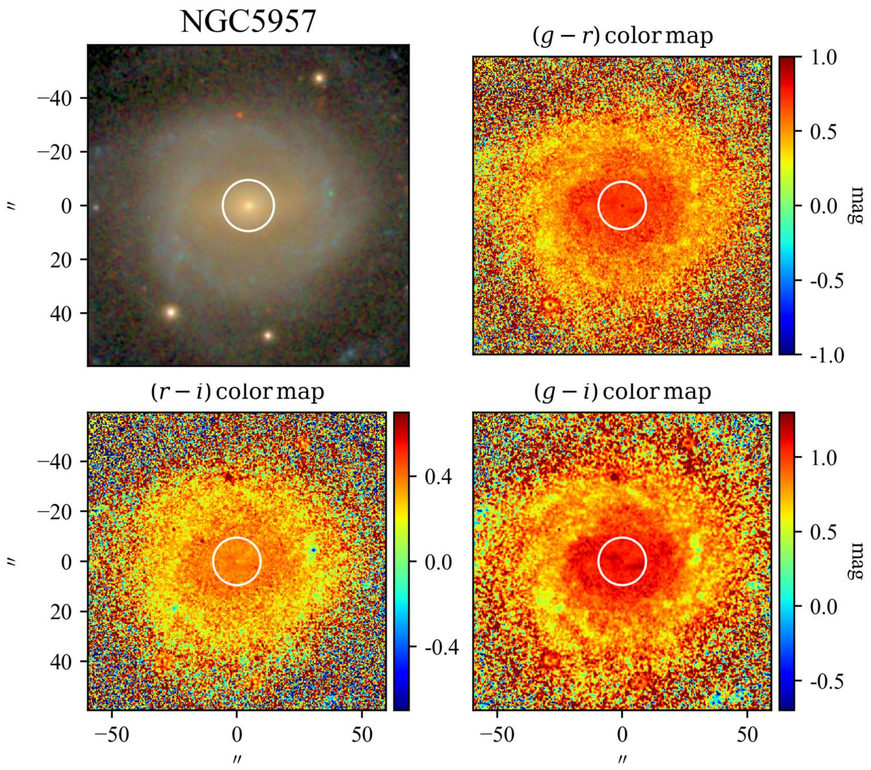

SBP decomposition of SDSS r band

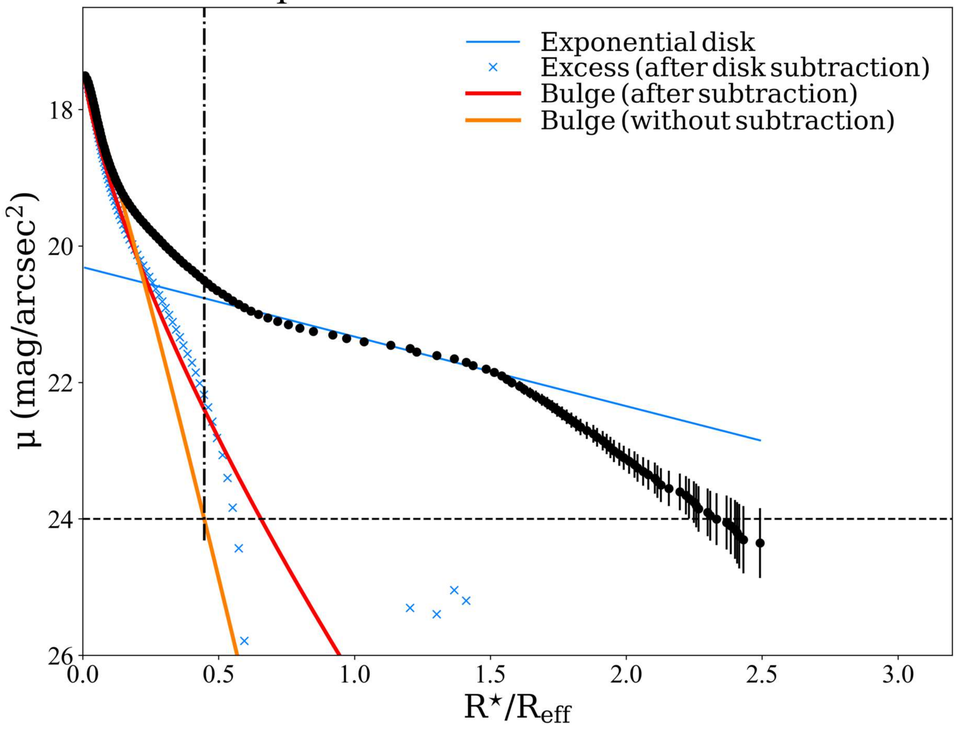

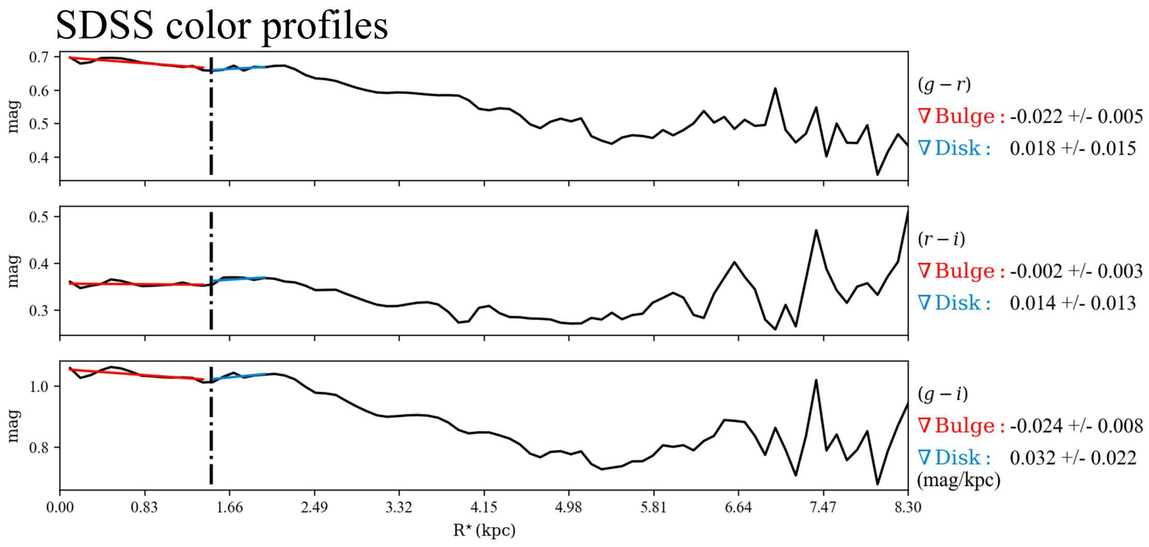

$\mathcal{RY}$ SBPs

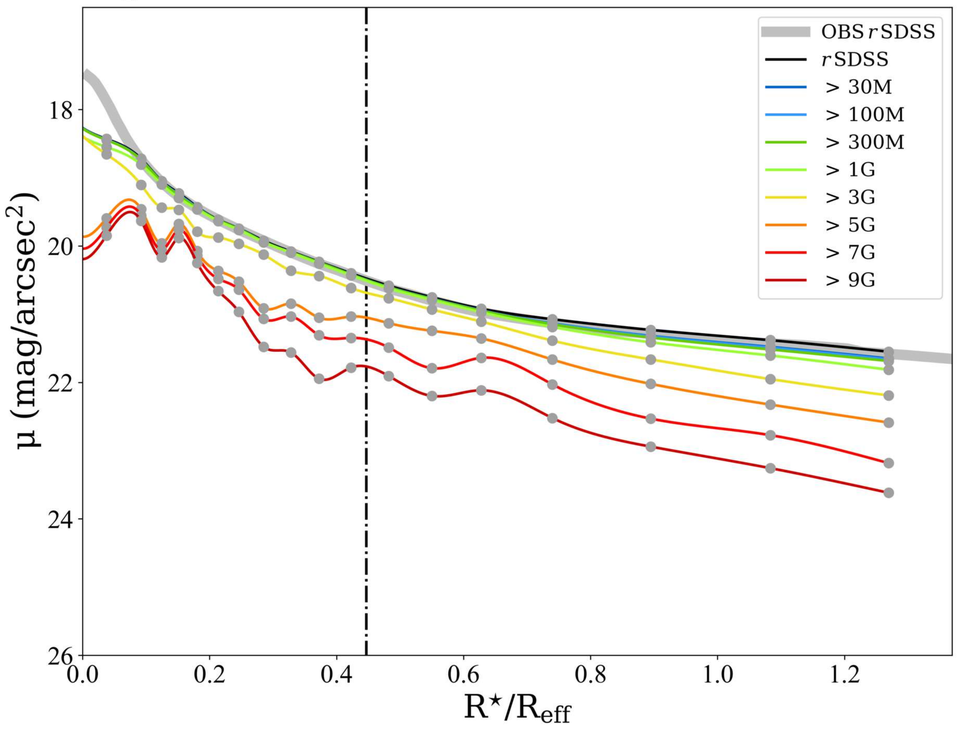

Stellar Continuum

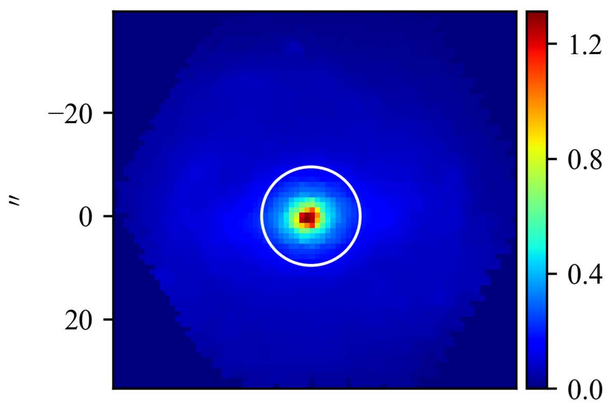

$\mathcal{M}_{\star,\mathrm{P}}$

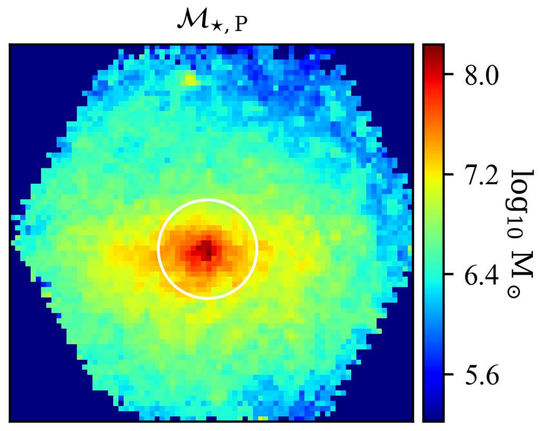

Log. of cumulative present stellar mass profiles

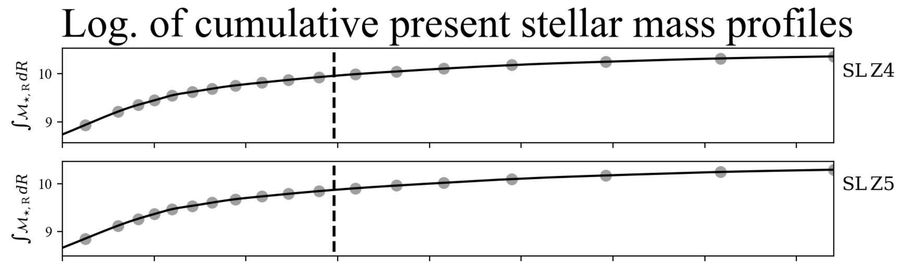

$Z_{\star,\mathcal{L}}$

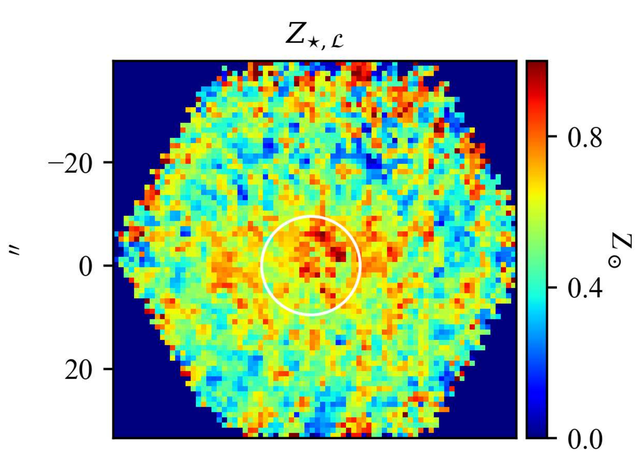

$Z_{\star,\mathcal{M}}$

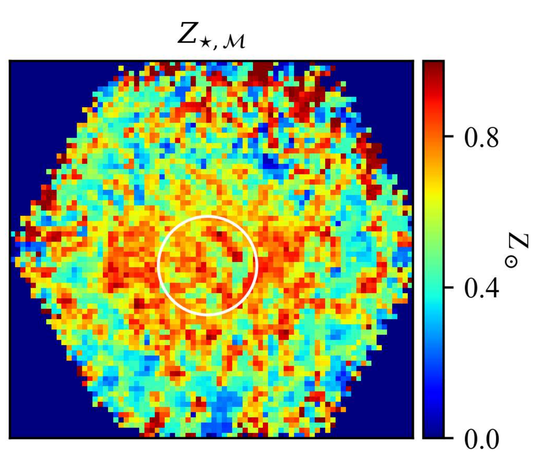

Stellar metallicity/Age & Hα flux/EW profiles

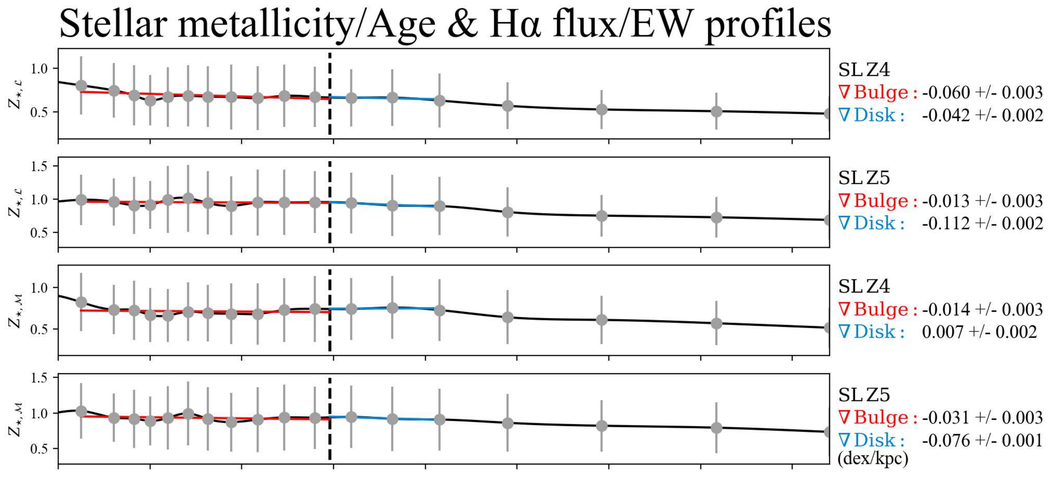

$t_{\star,\mathcal{L}}$

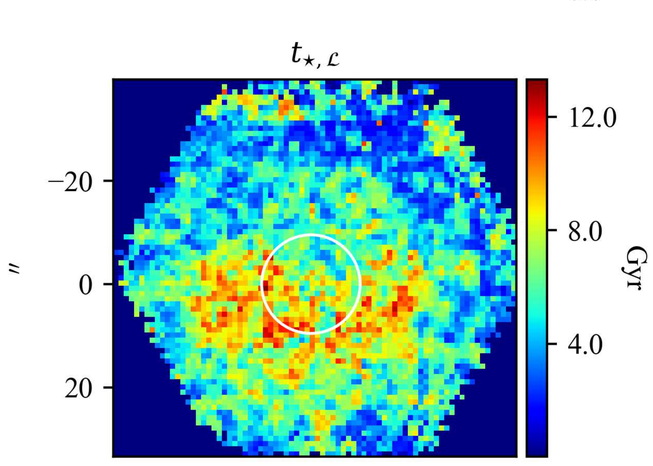

$t_{\star,\mathcal{M}}$

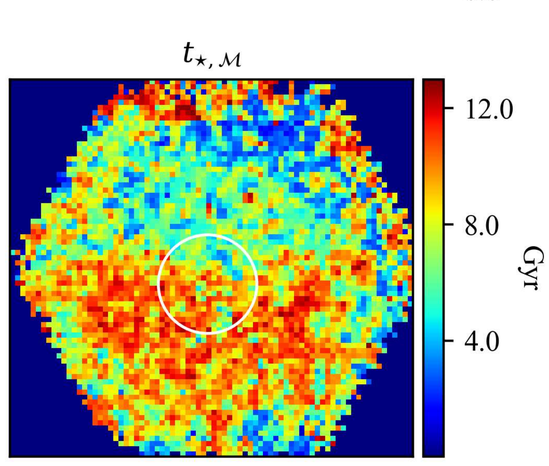

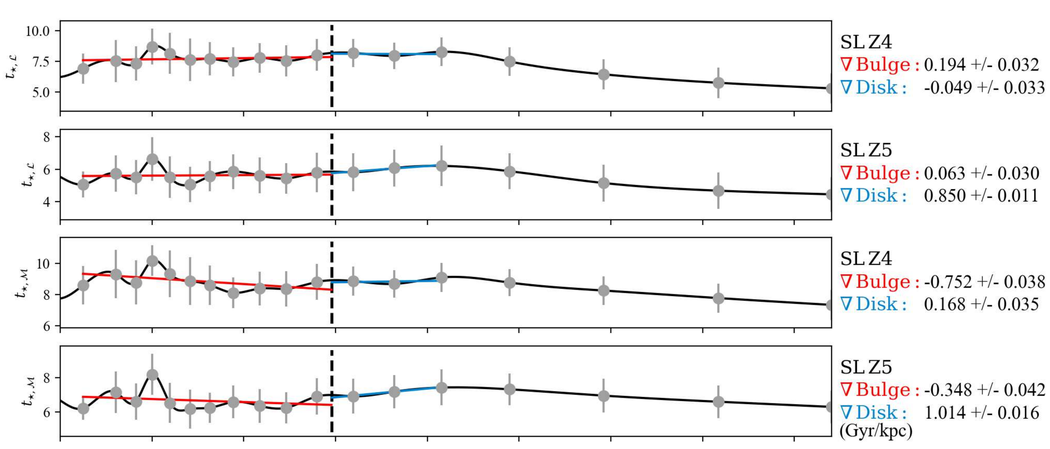

Hα flux

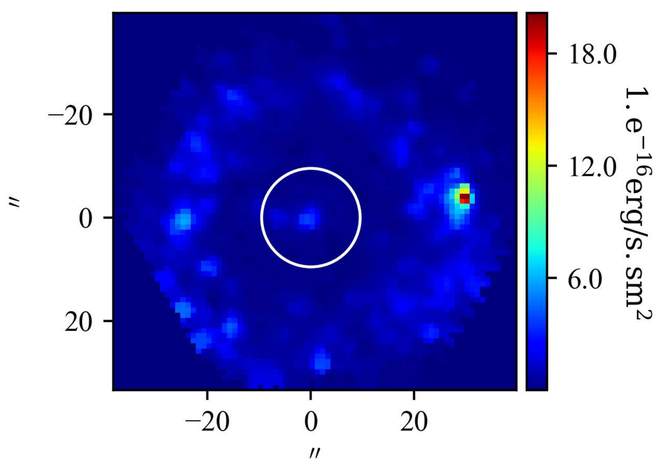

EW(Hα)

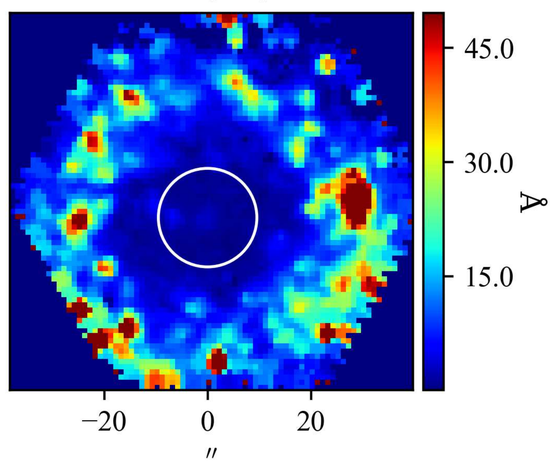

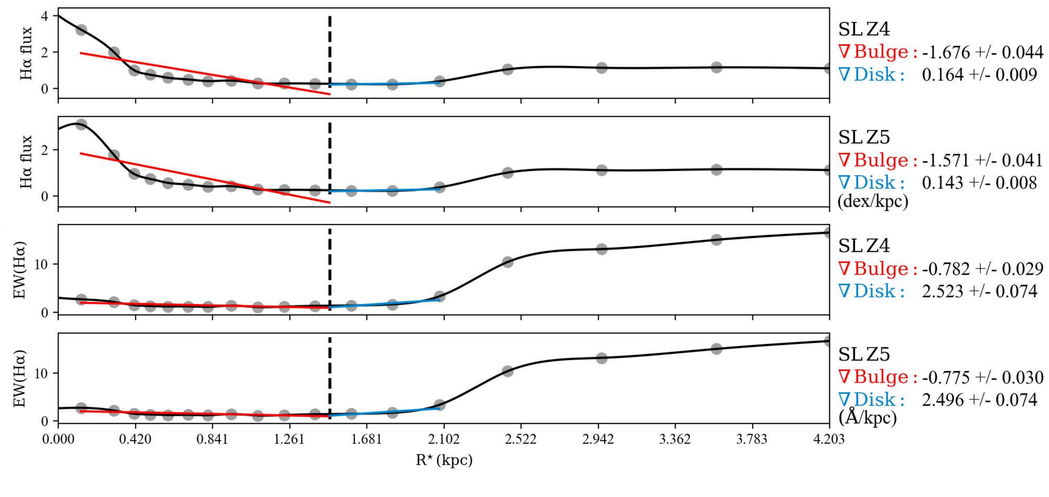

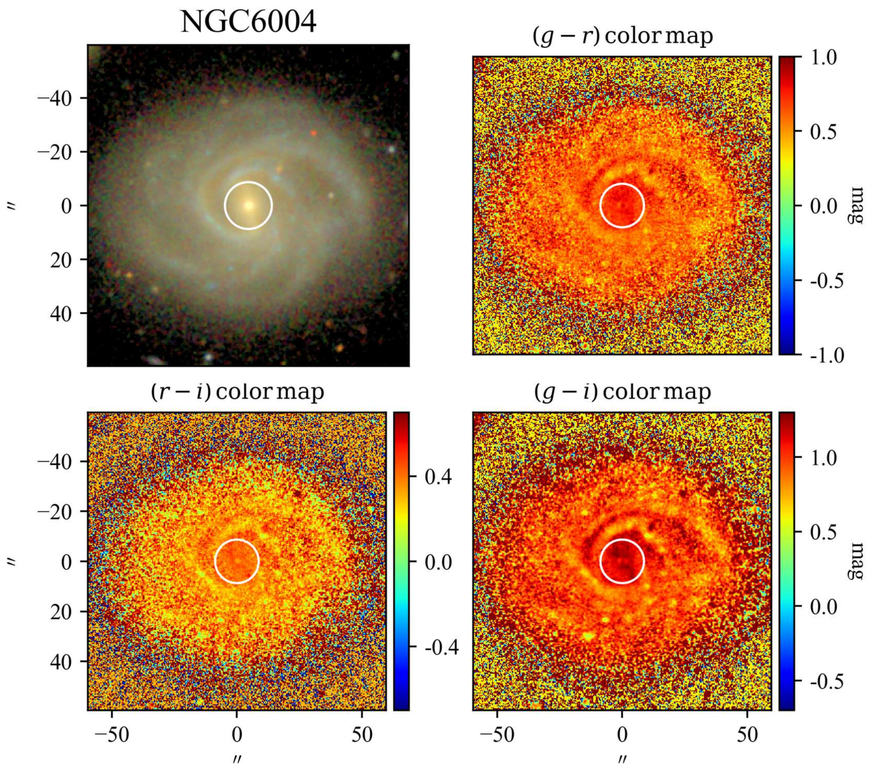

SBP decomposition of SDSS r band

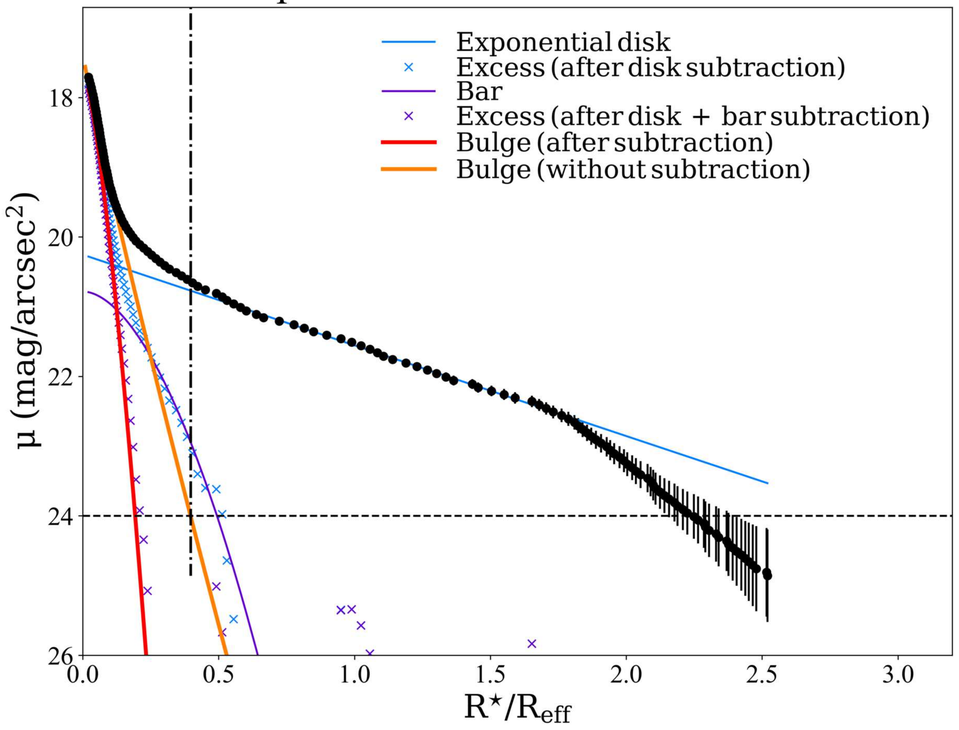

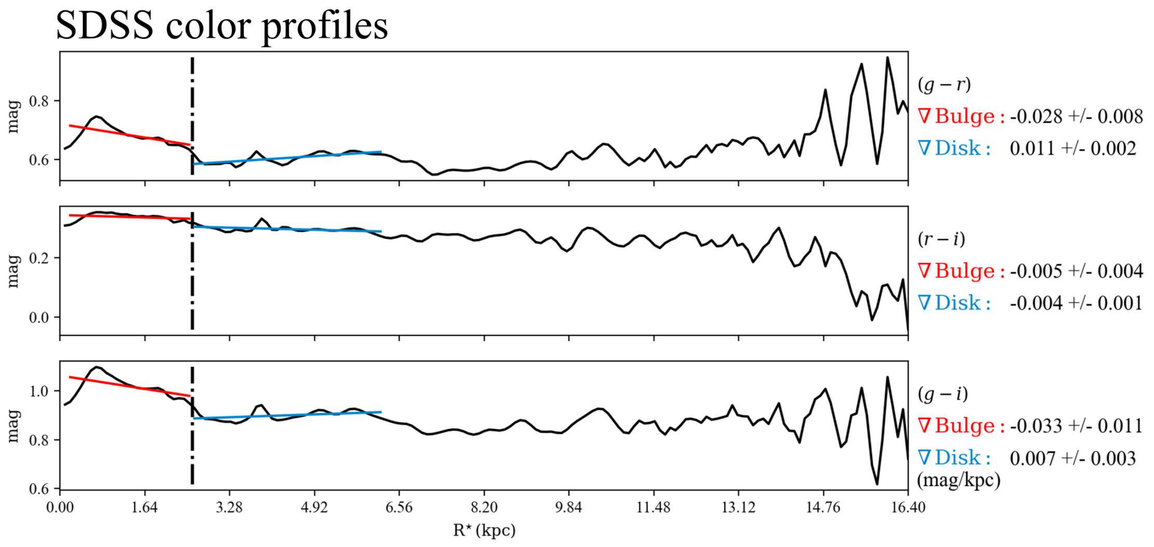

$\mathcal{RV}$ SBPs

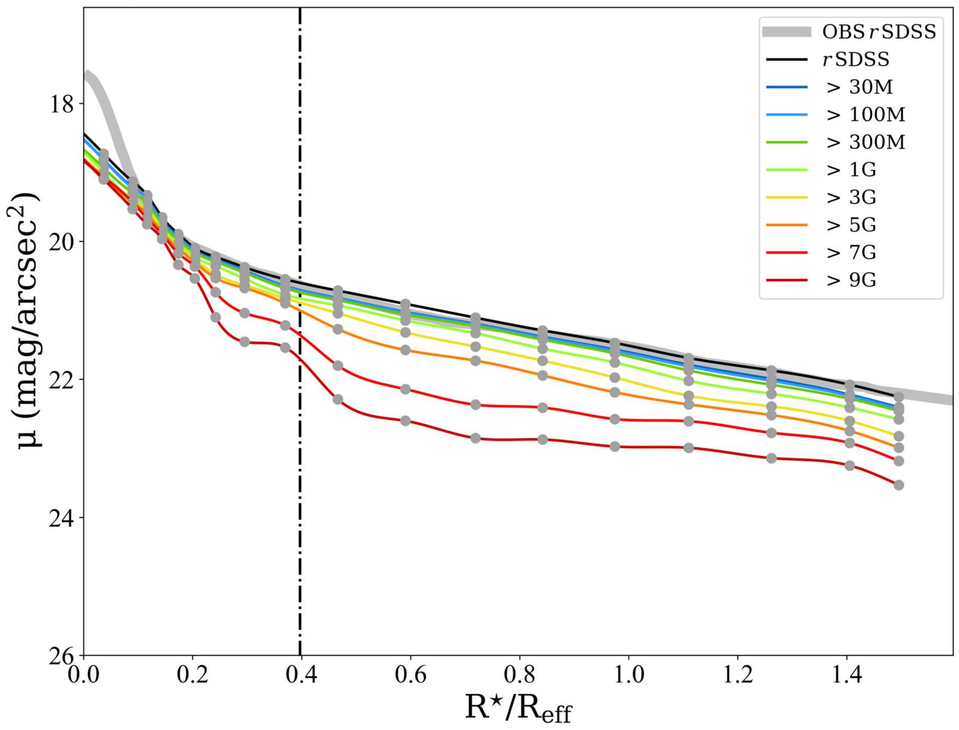

Stellar Continuum

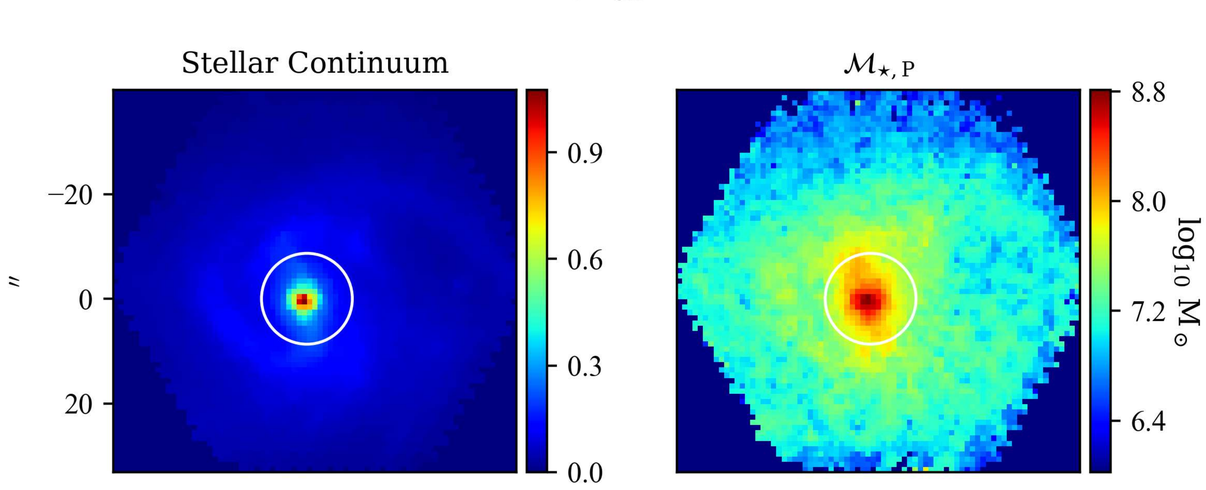

$\mathcal{M}_{\star,\mathrm{P}}$

Log. of cumulative present stellar mass profiles

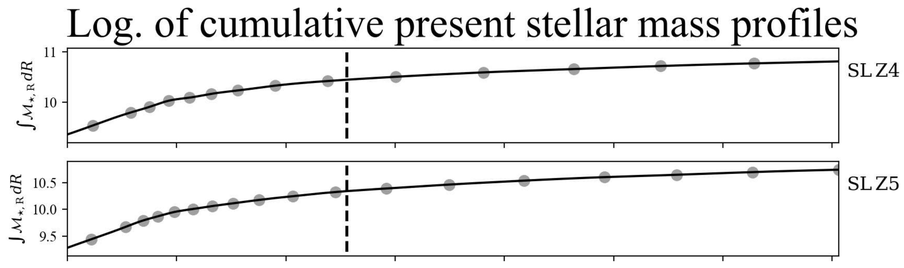

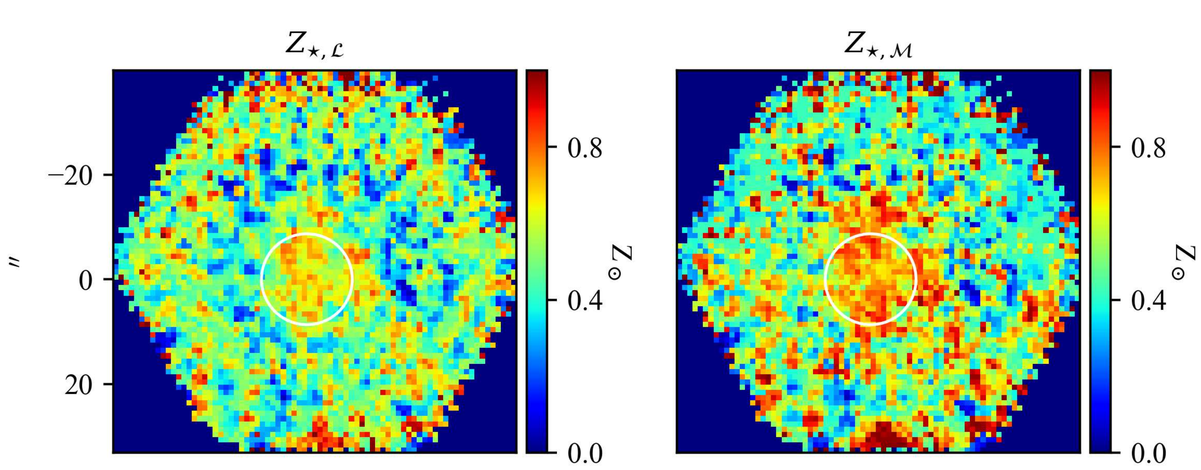

Stellar metallicity/Age & Hα flux/EW profiles

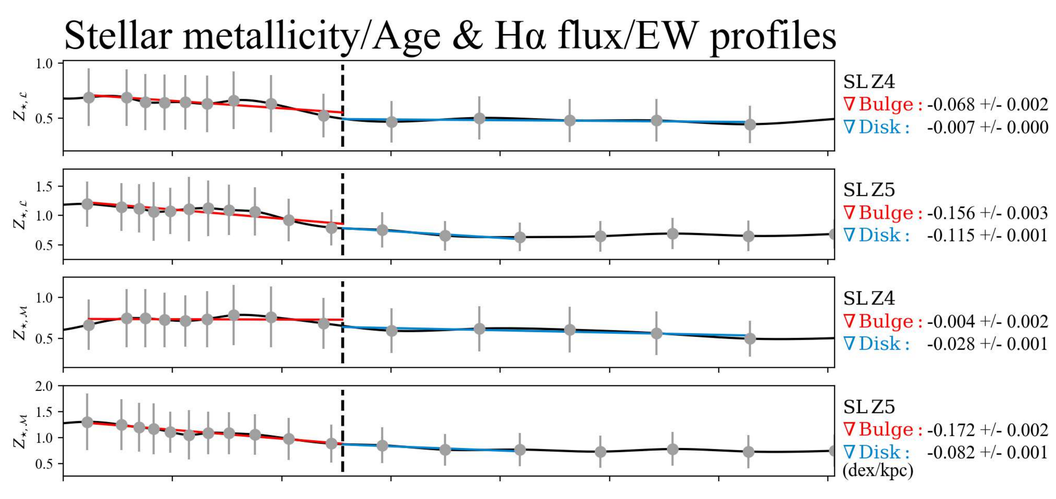

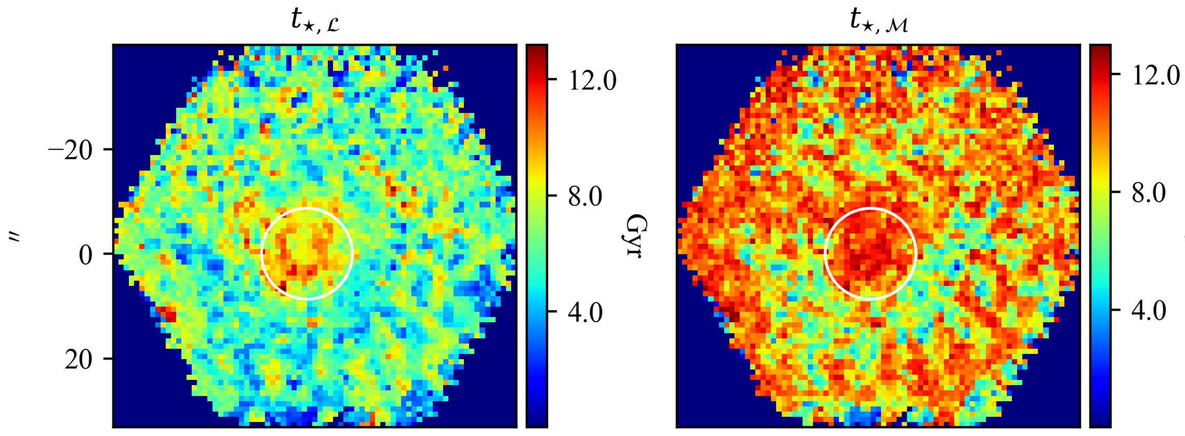

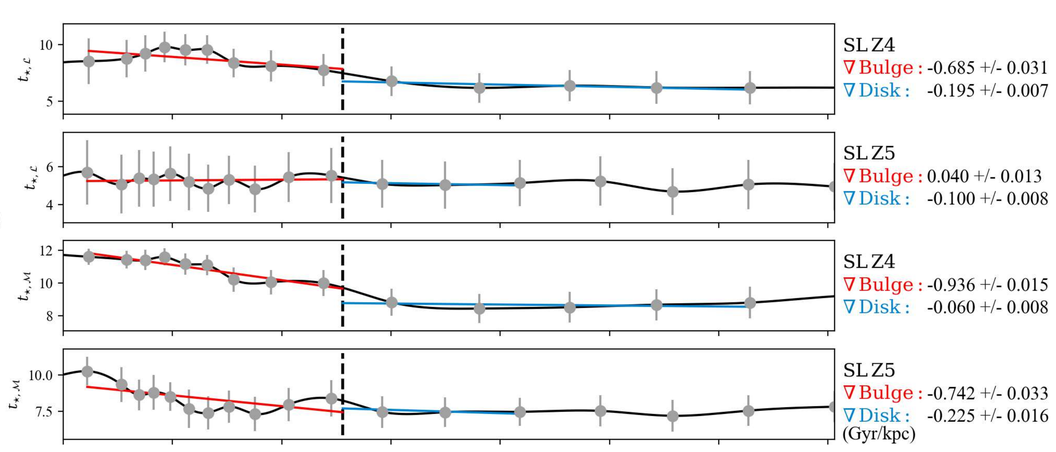

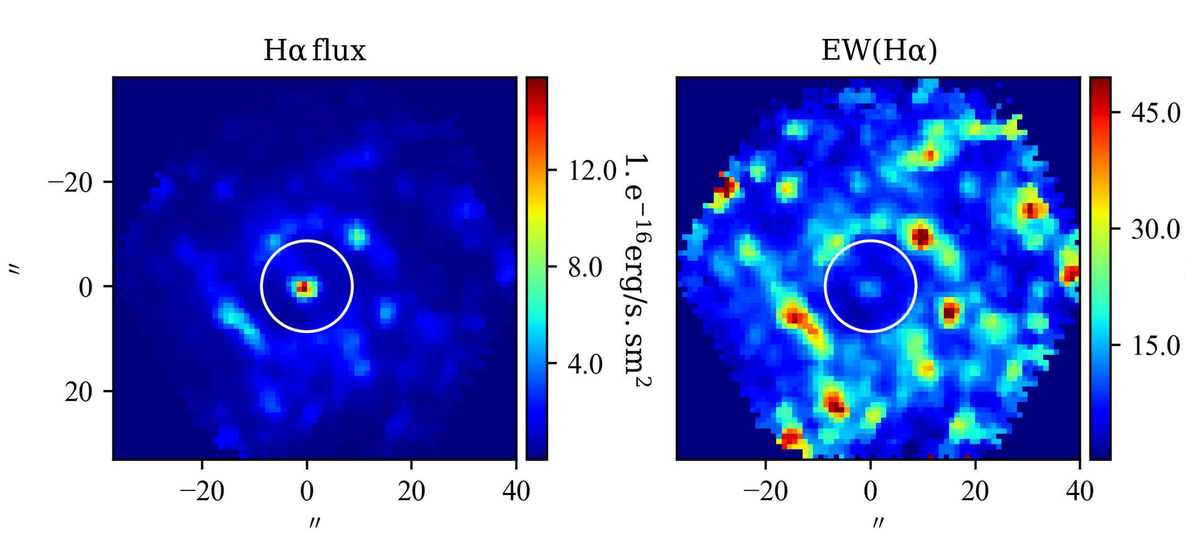

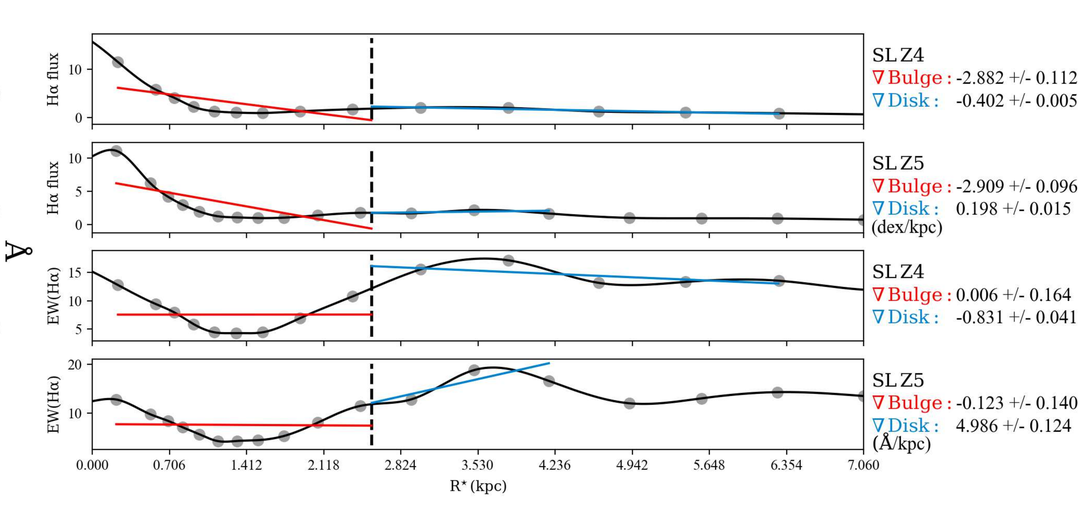

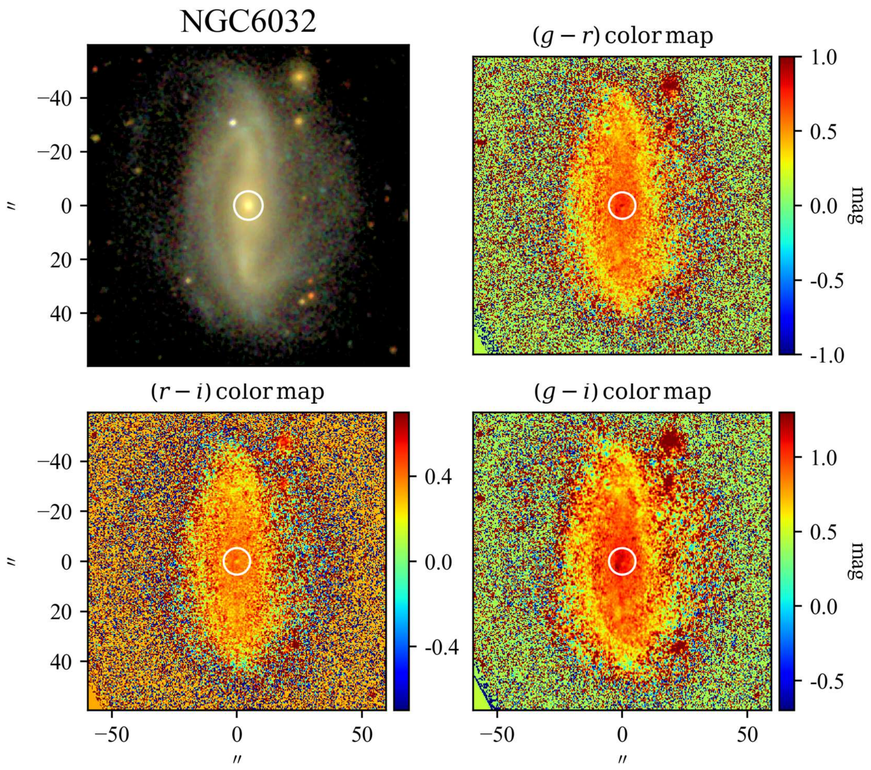

SBP decomposition of SDSS r band

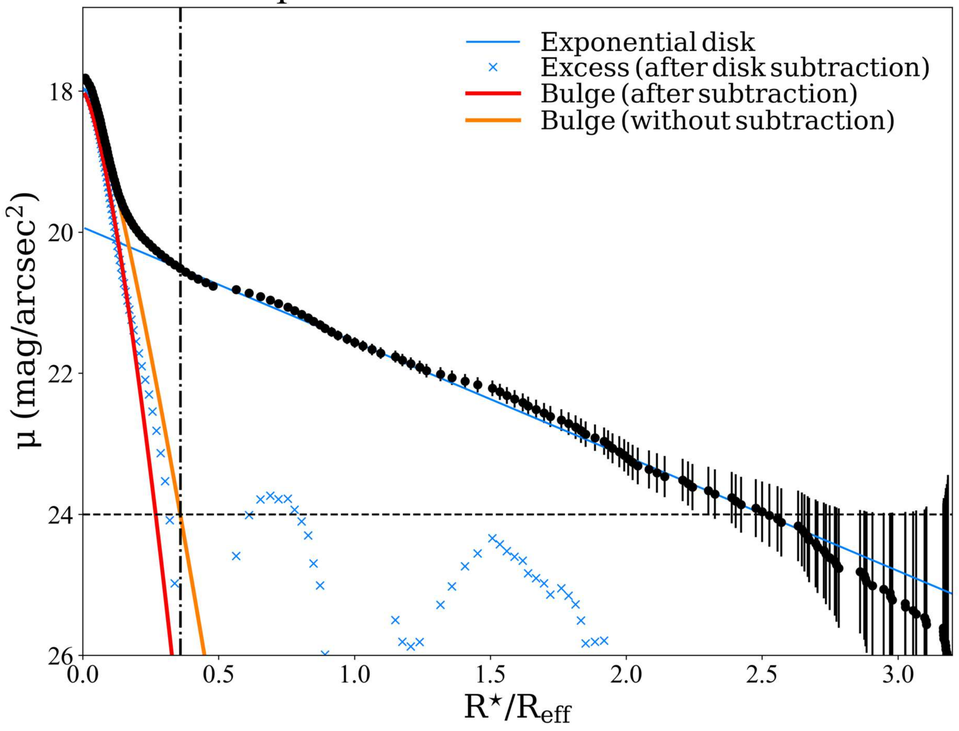

SDSS color profiles

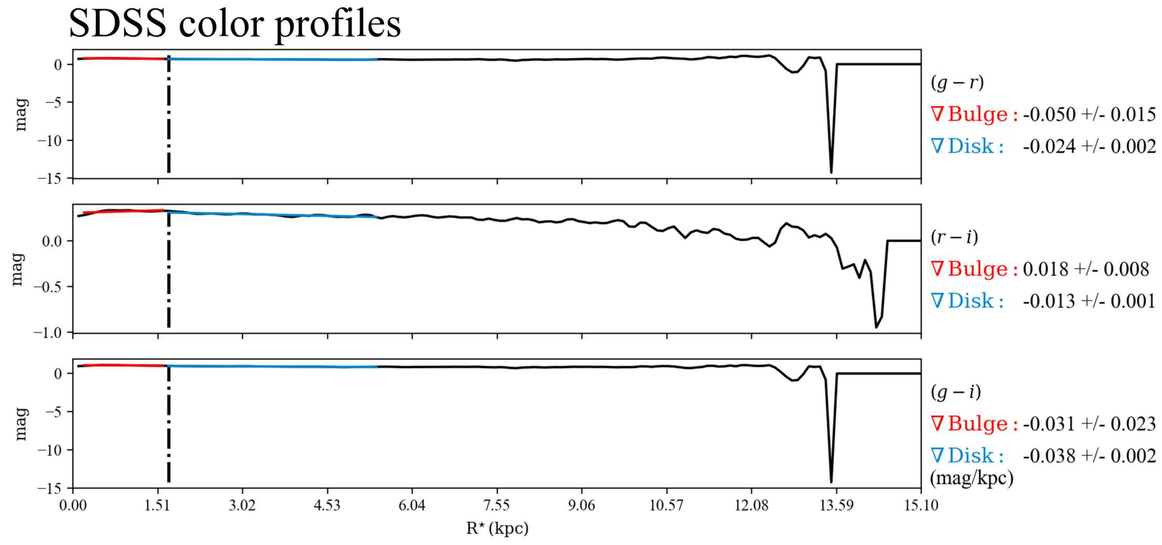

$\mathcal{RY}$ SBPs

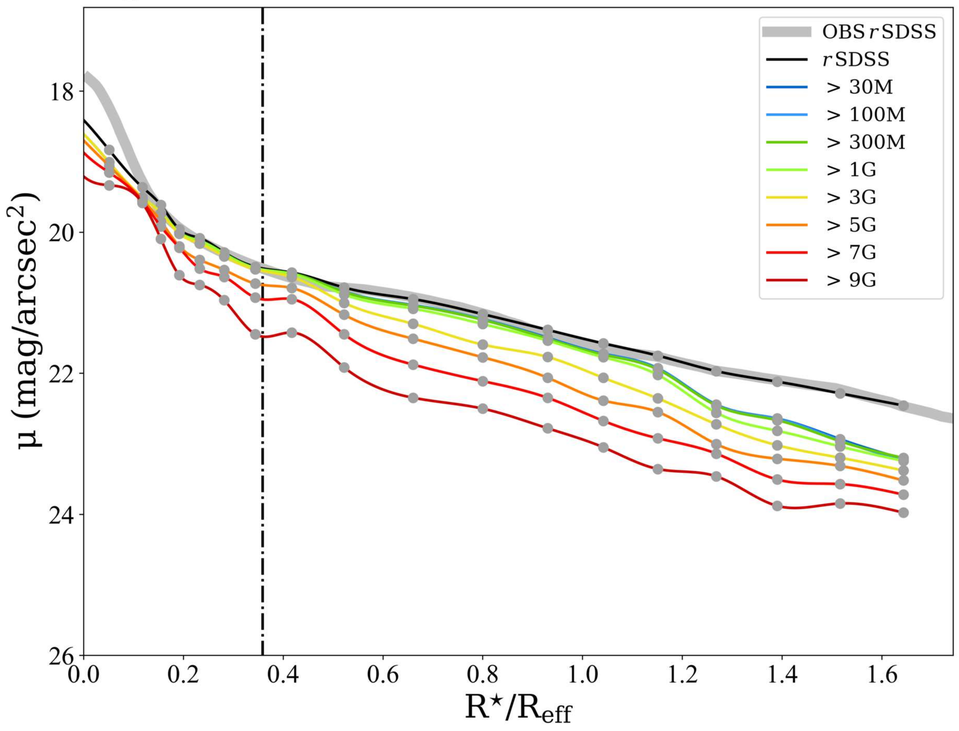

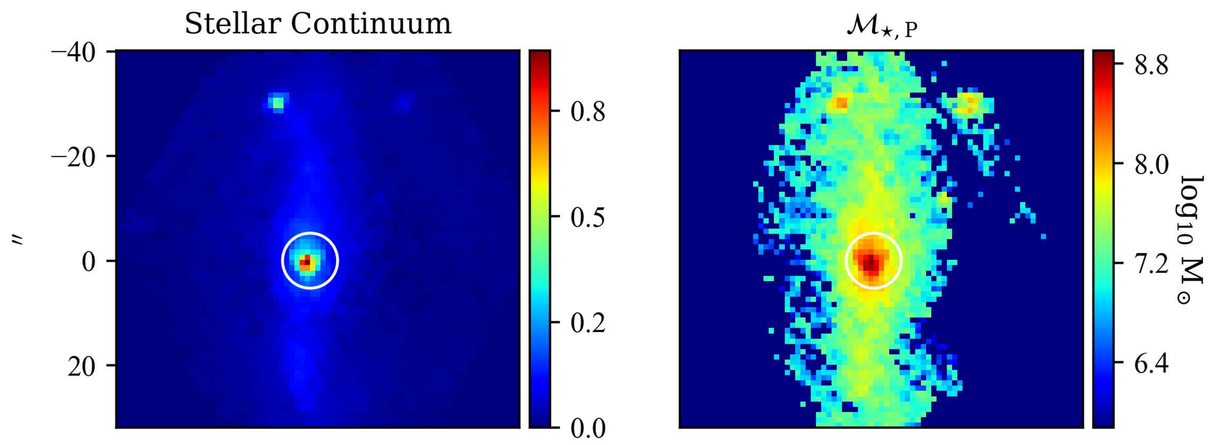

Log. of cumulative present stellar mass profiles

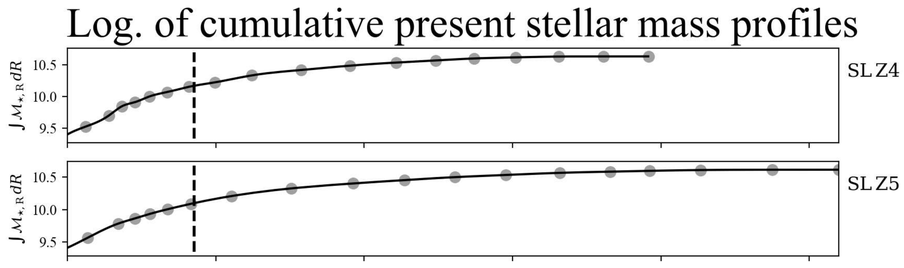

Stellar metallicity/Age & Hα flux/EW profiles

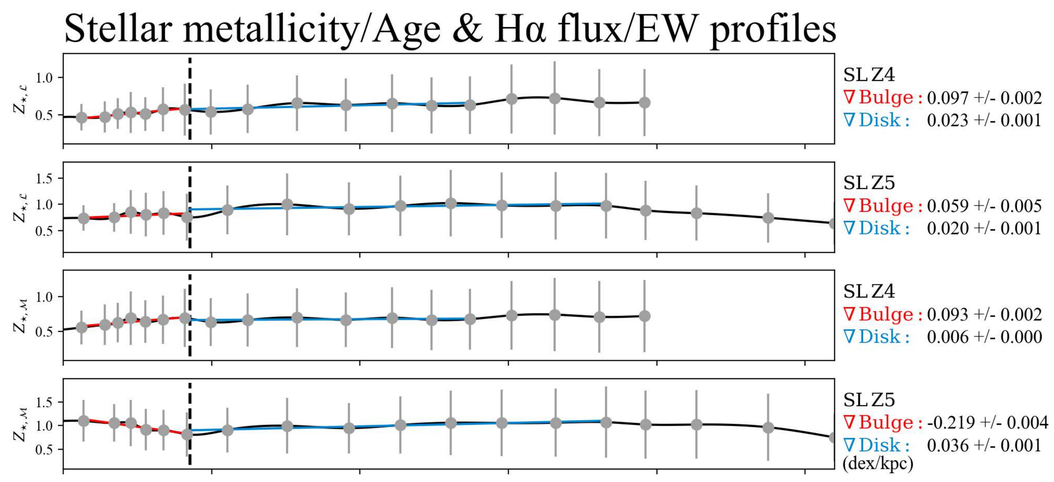

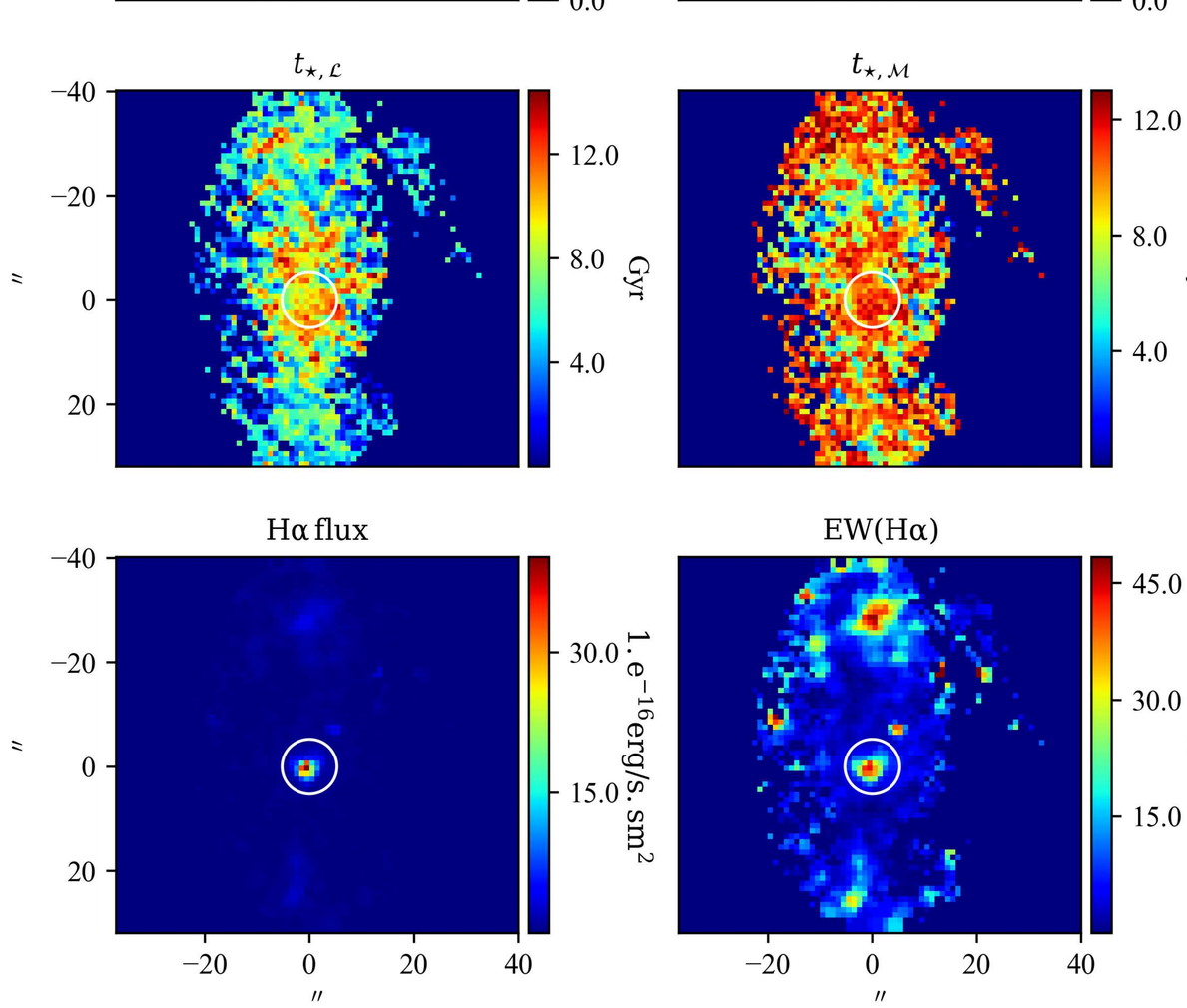

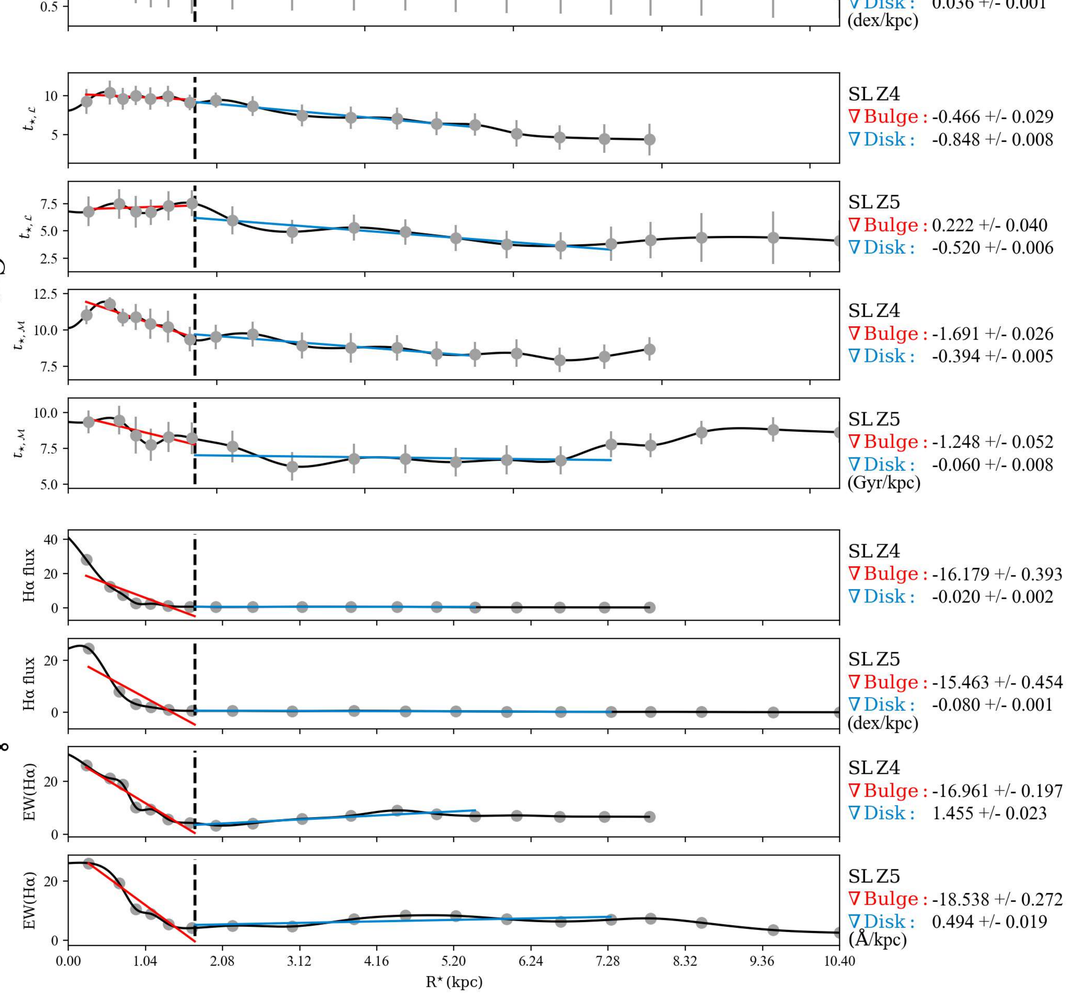

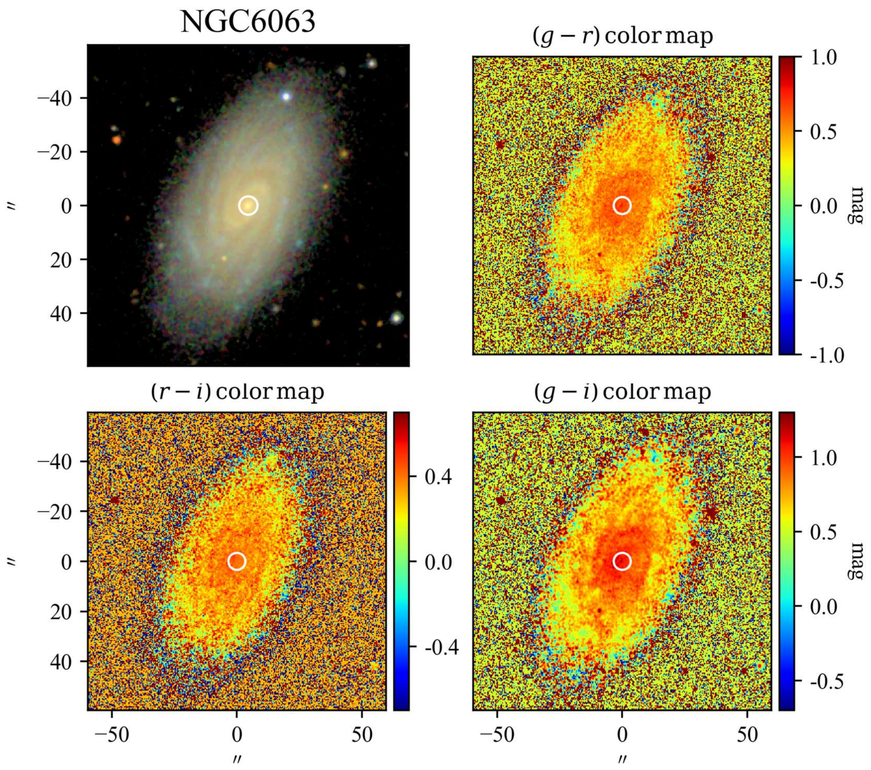

SBP decomposition of SDSS r band

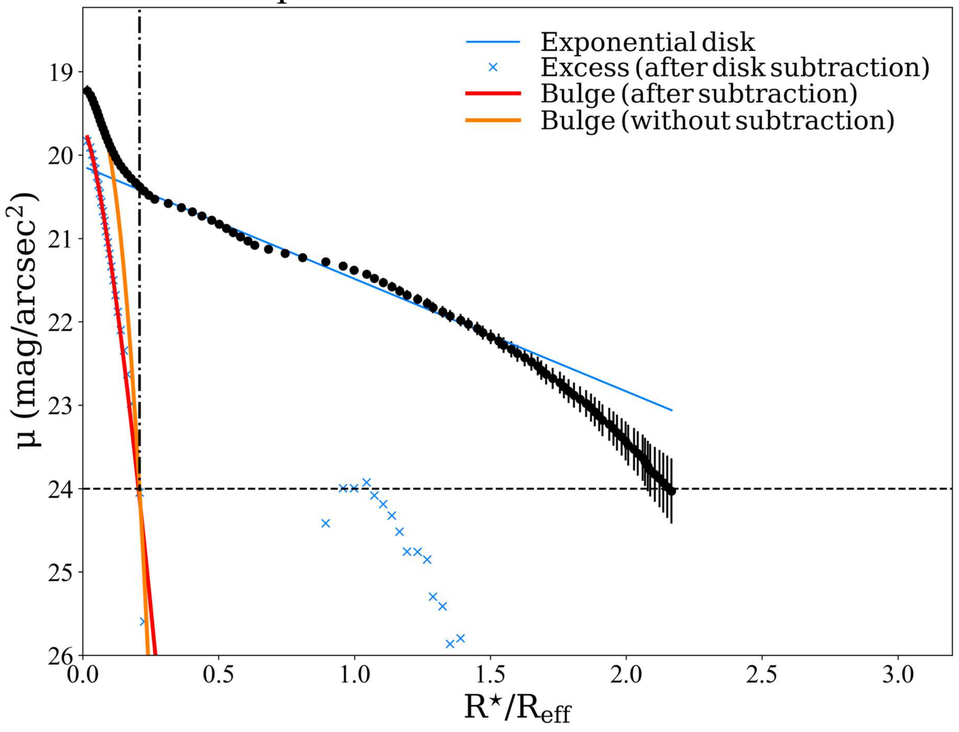

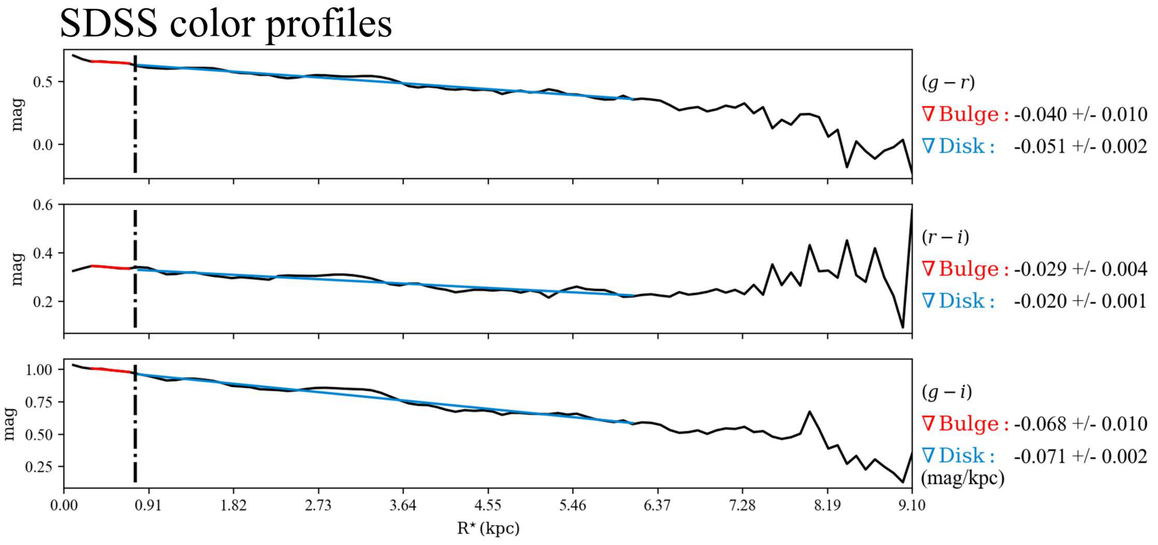

$\mathcal{RV}$ SBPs

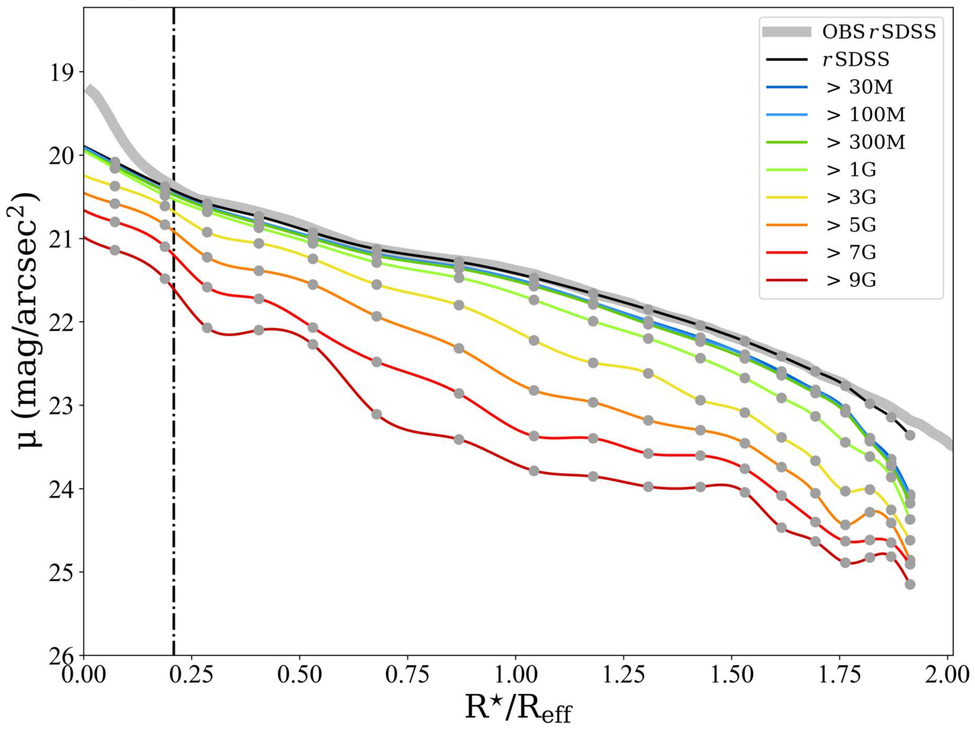

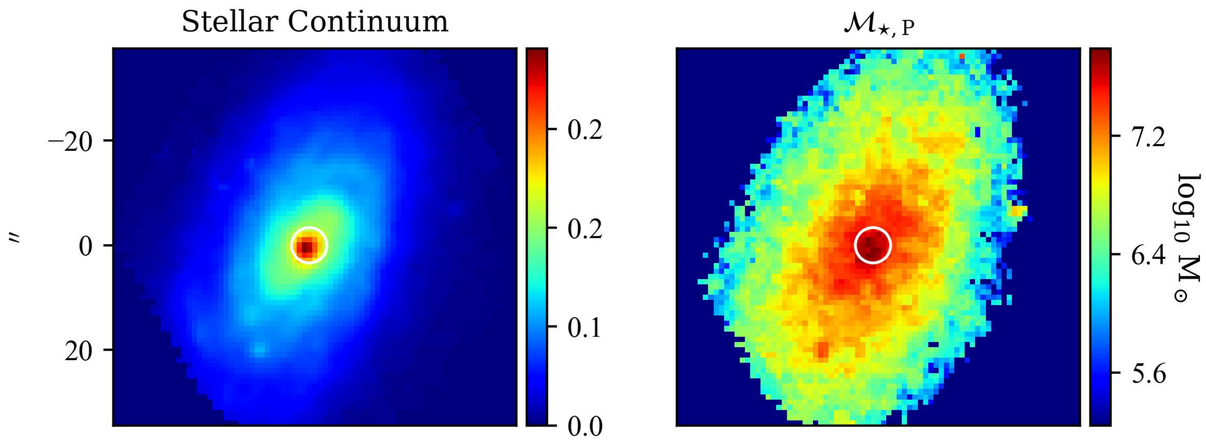

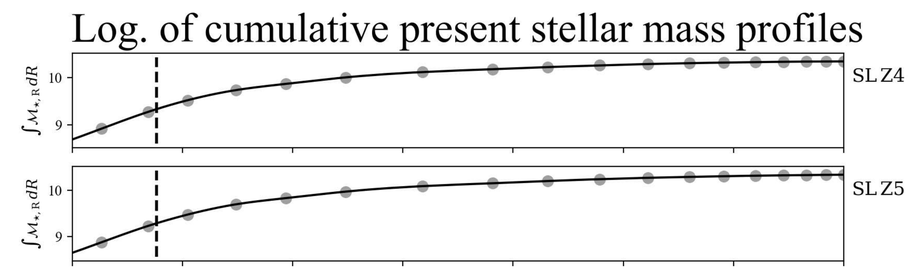

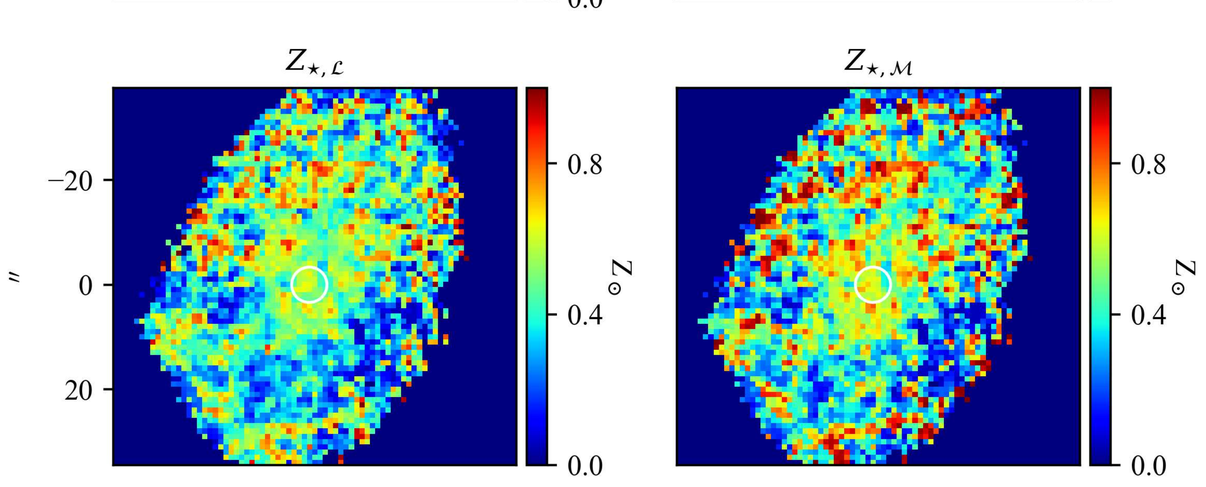

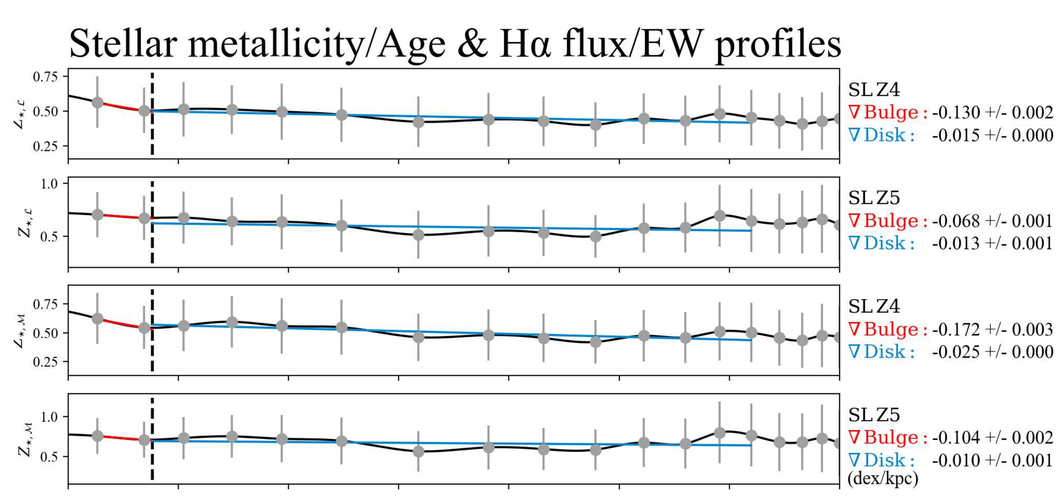

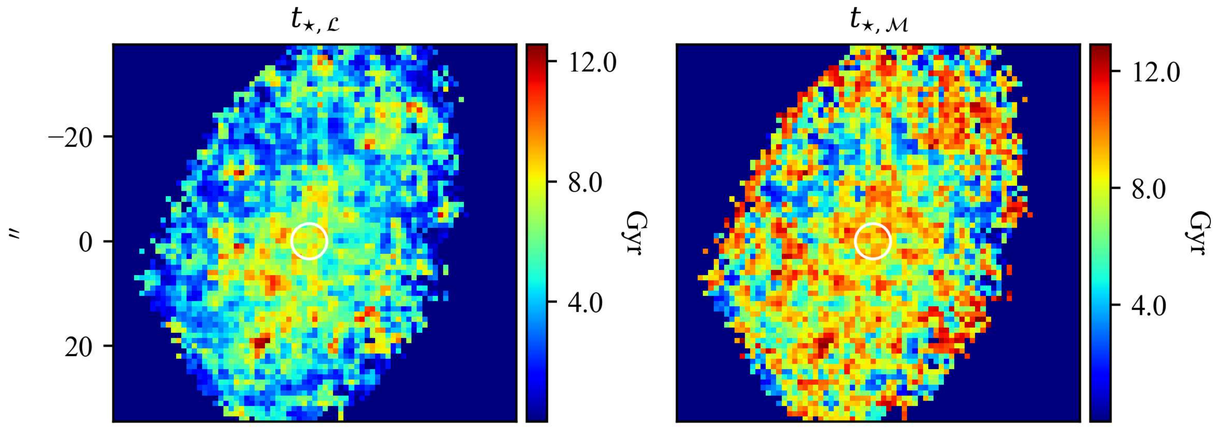

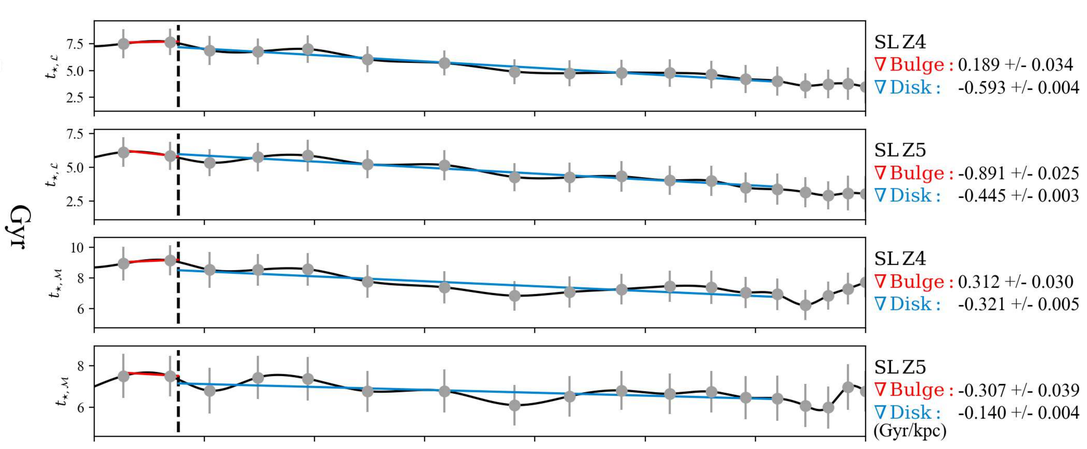

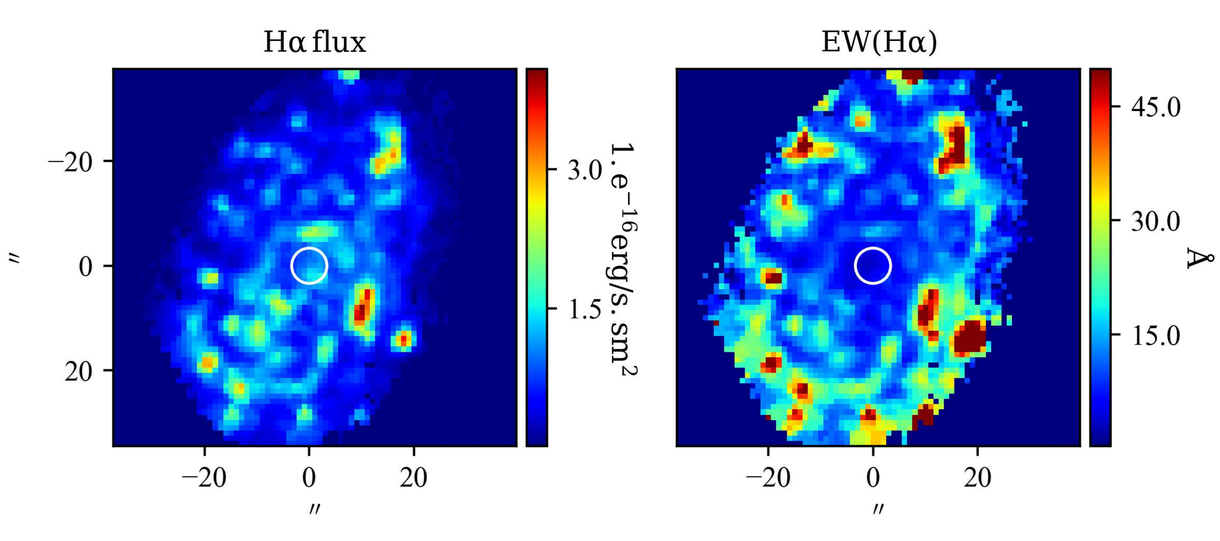

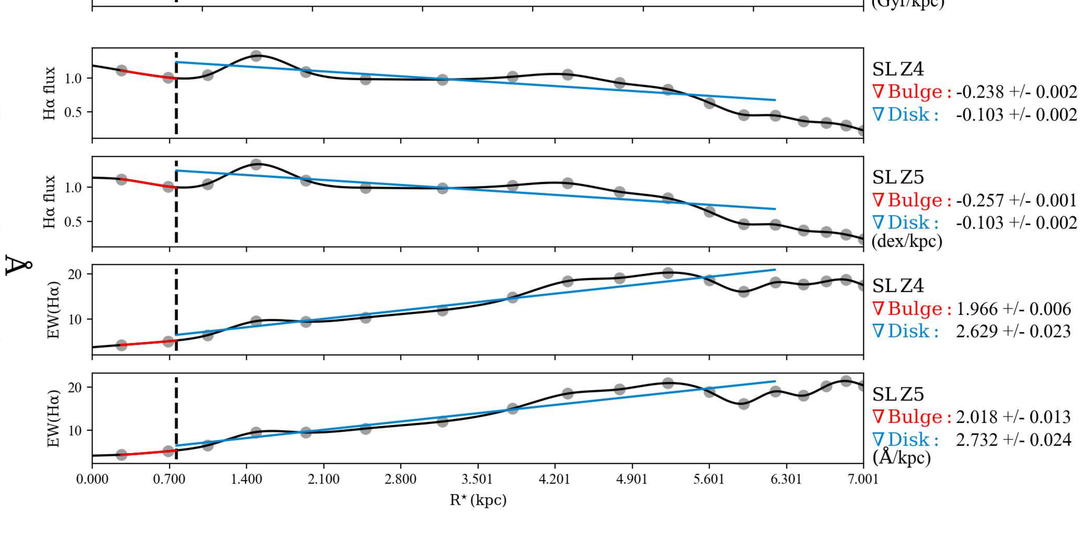

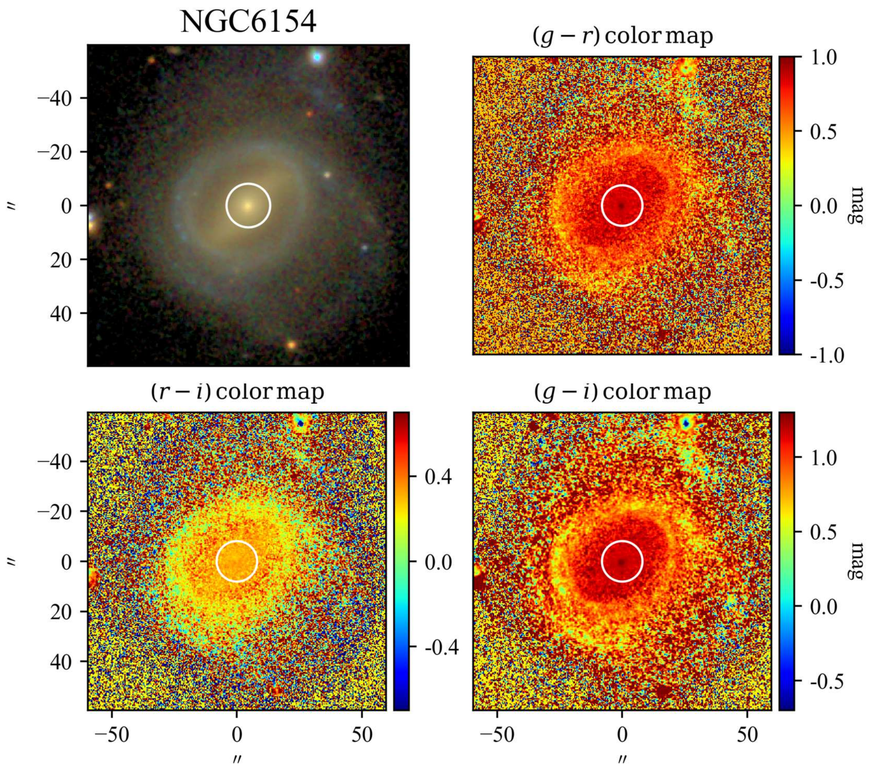

SBP decomposition of SDSS r band

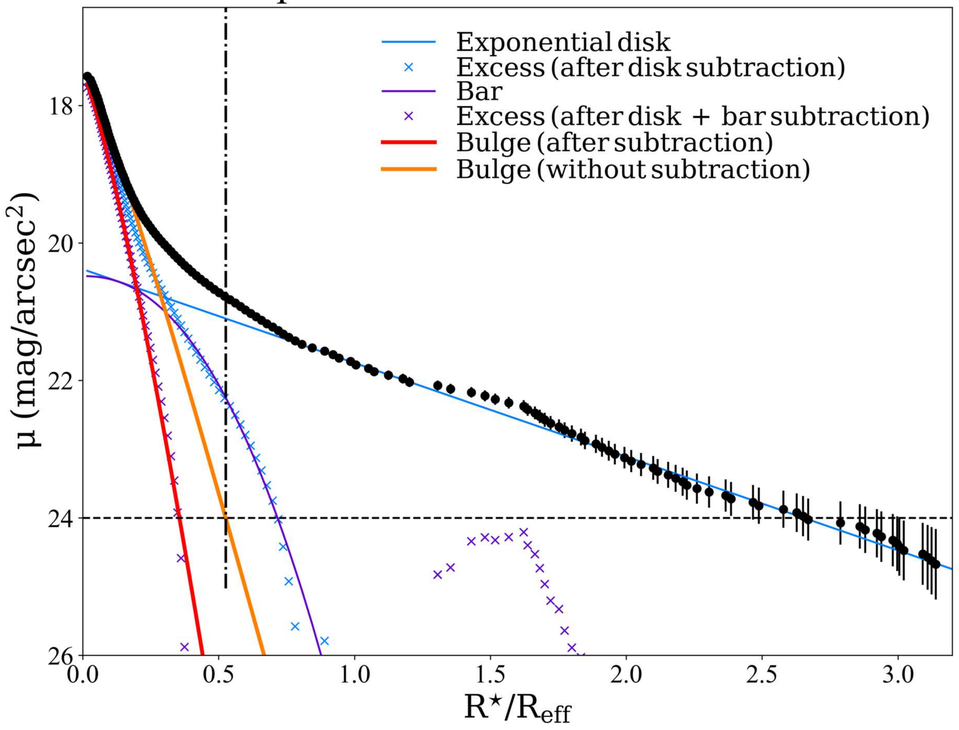

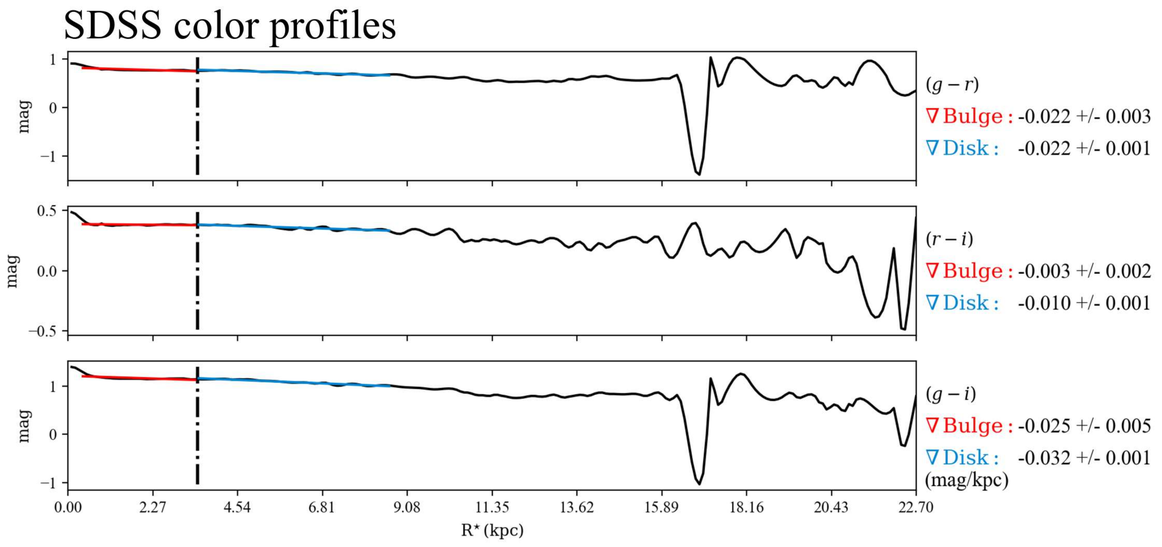

$\mathcal{RV}$ SBPs

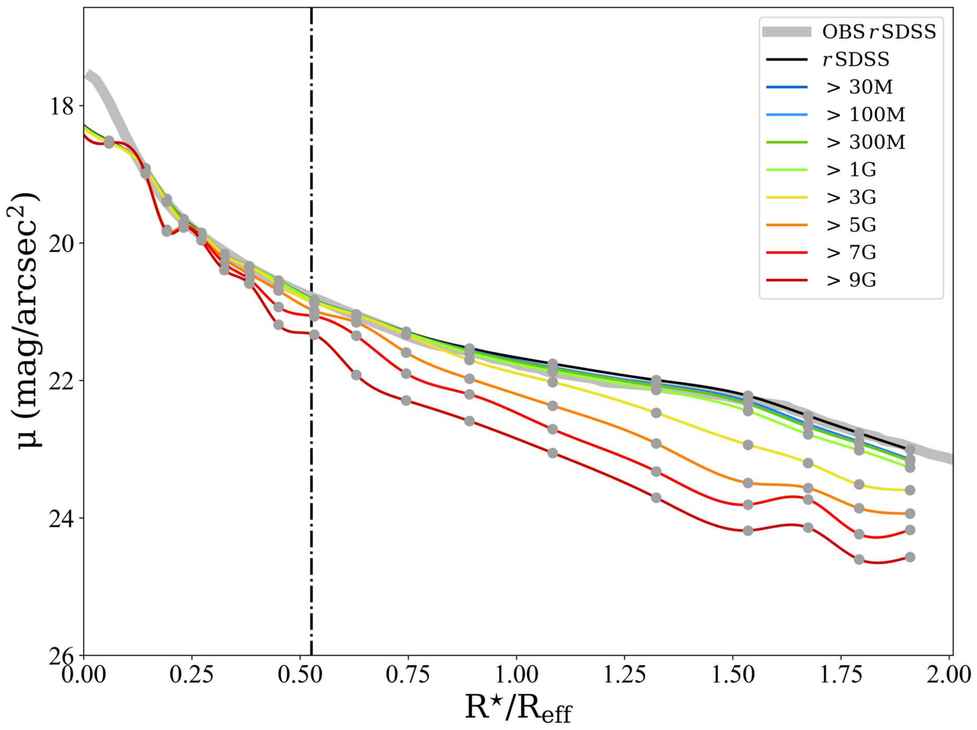

Stellar Continuum

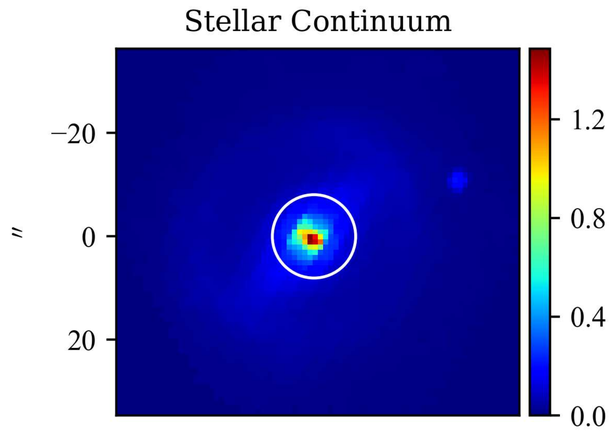

$\mathcal{M}_{\star,\mathrm{P}}$

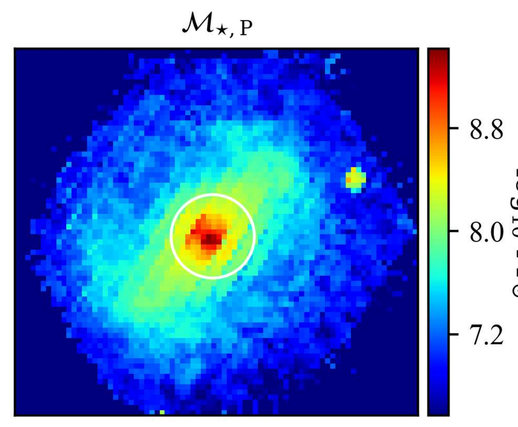

Log. of cumulative present stellar mass profiles

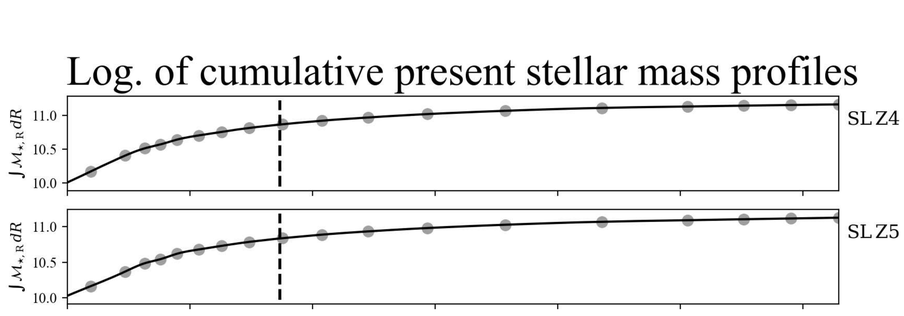

$Z_{\star,\mathcal{L}}$

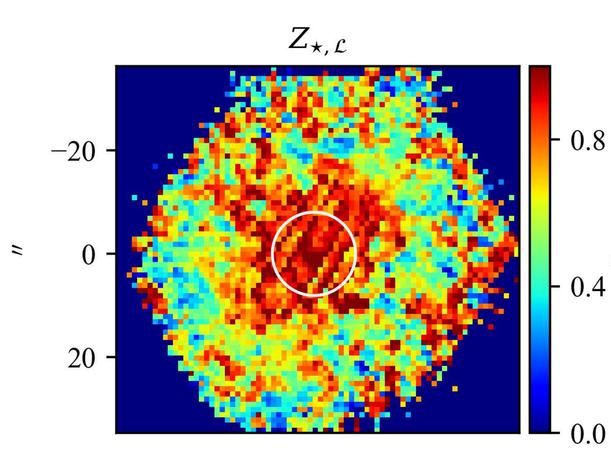

$Z_{\star,\mathcal{M}}$

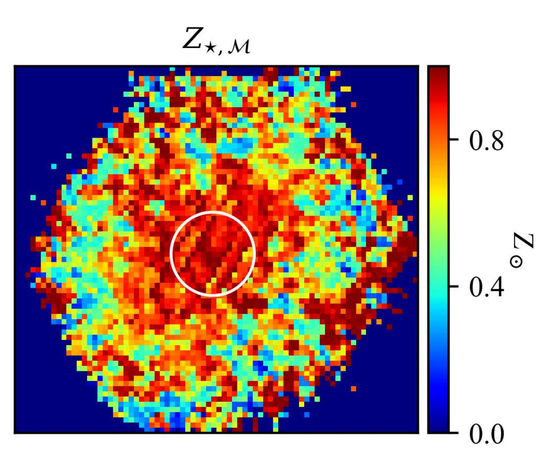

Stellar metallicity/Age & Hα flux/EW profiles

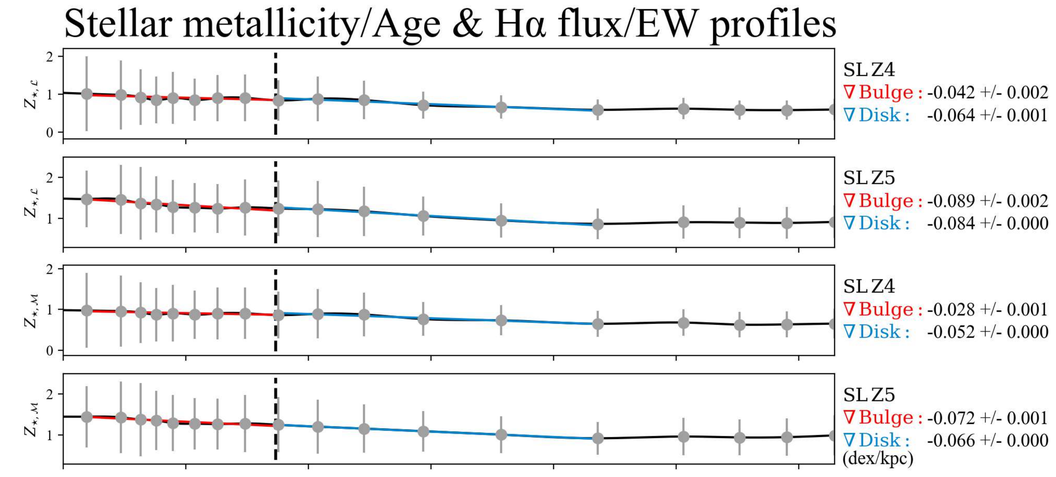

$t_{\star,\mathcal{L}}$

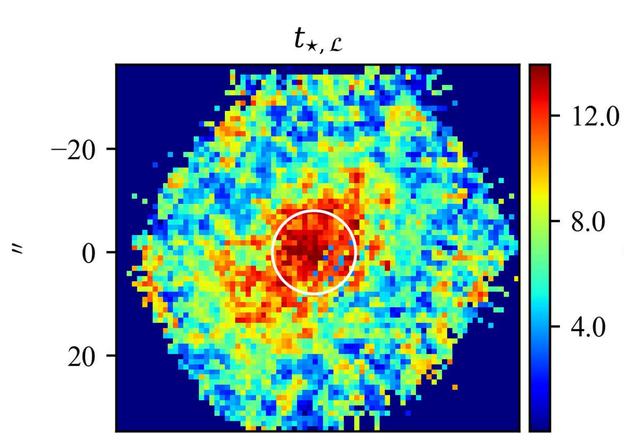

$t_{\star,\mathcal{M}}$

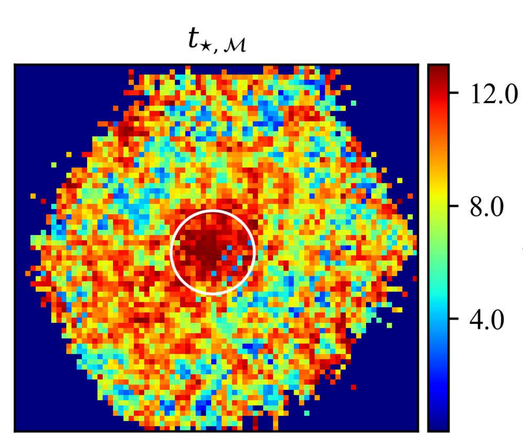

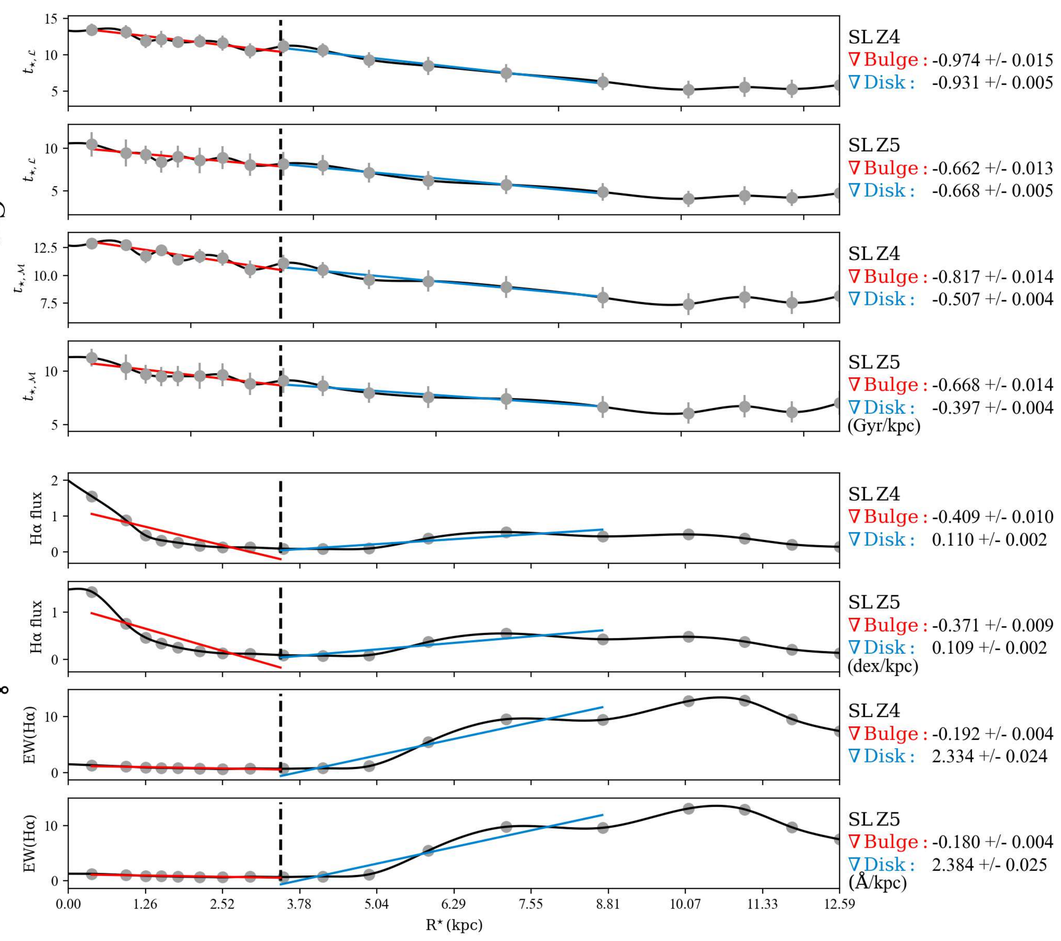

Hα flux

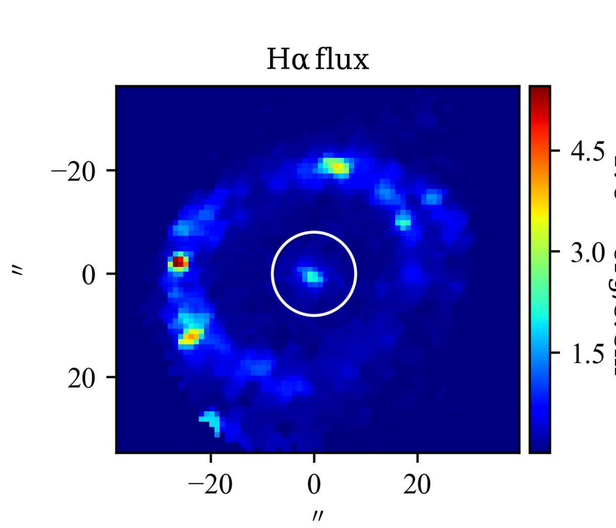

EW(Hα)

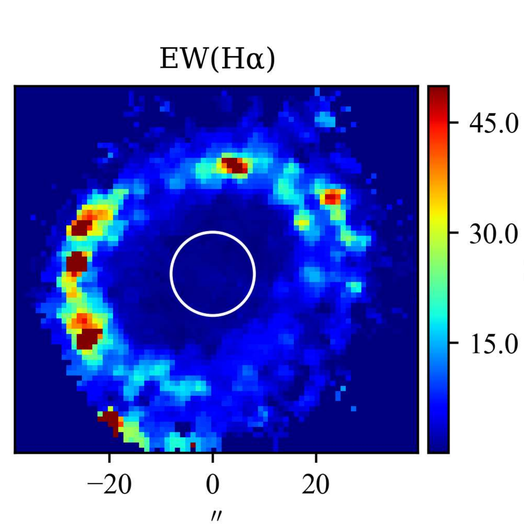

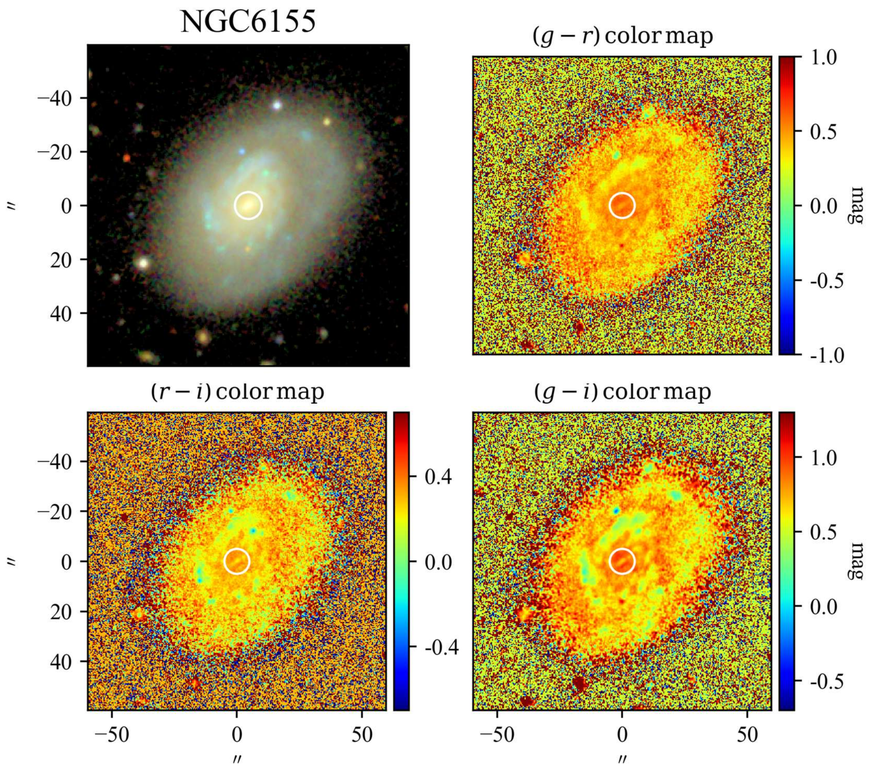

SBP decomposition of SDSS r band

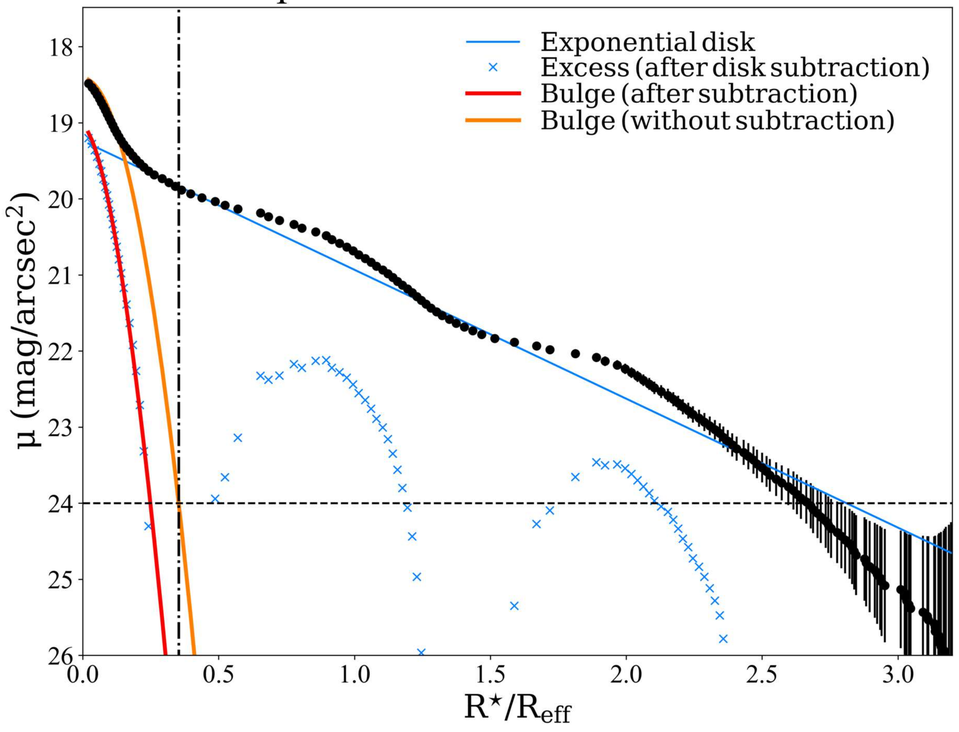

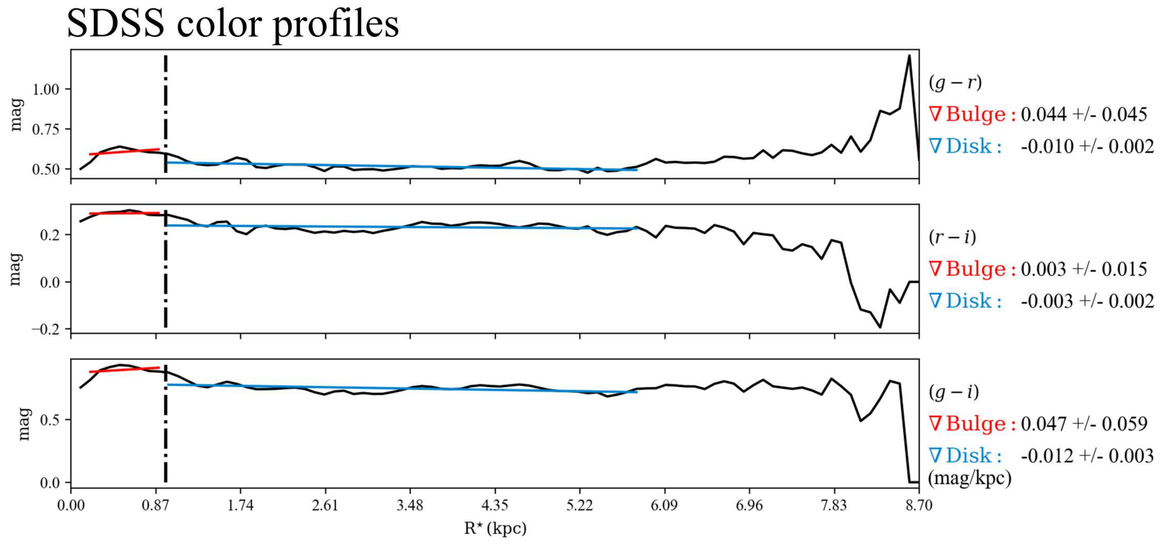

$\mathcal{RV}$ SBPs

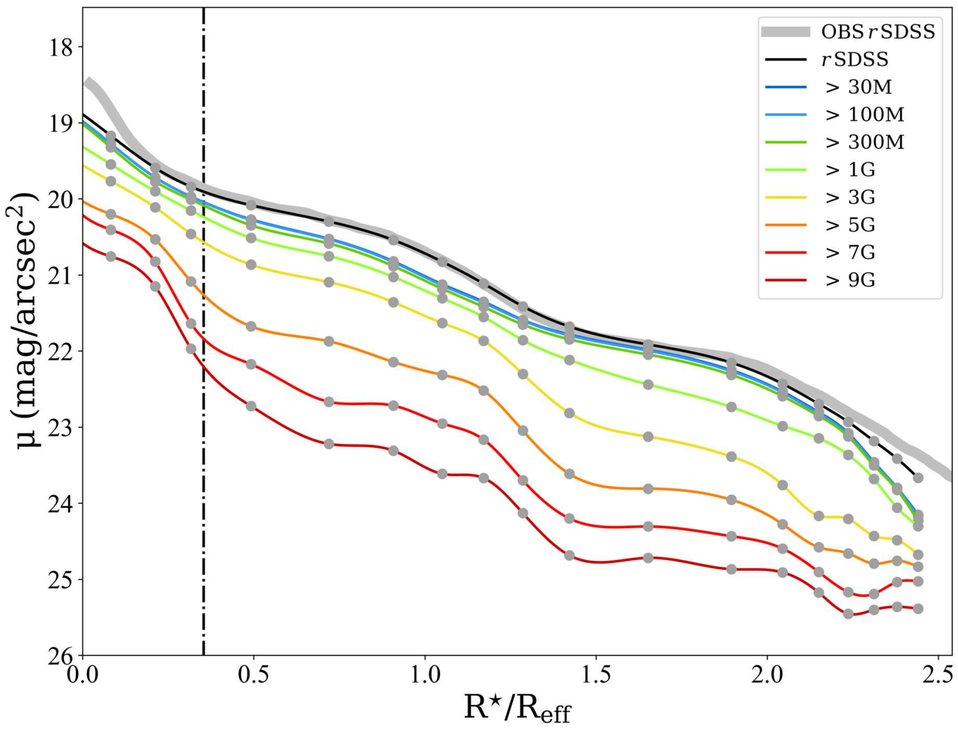

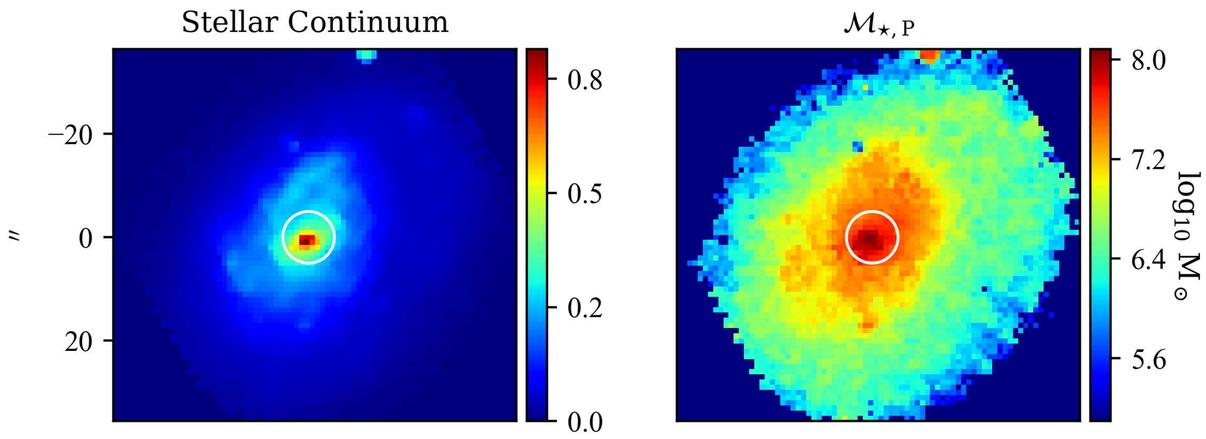

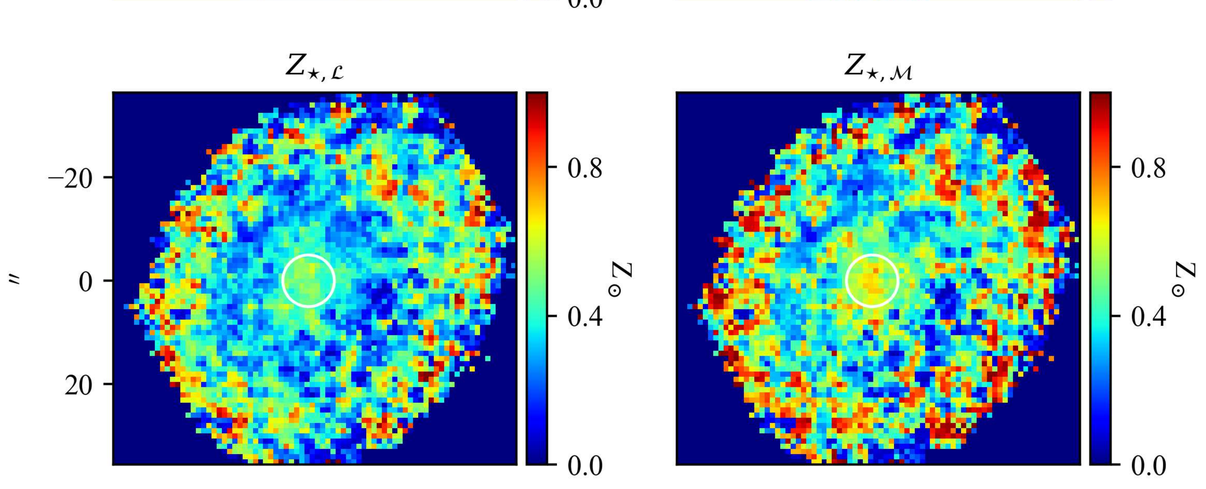

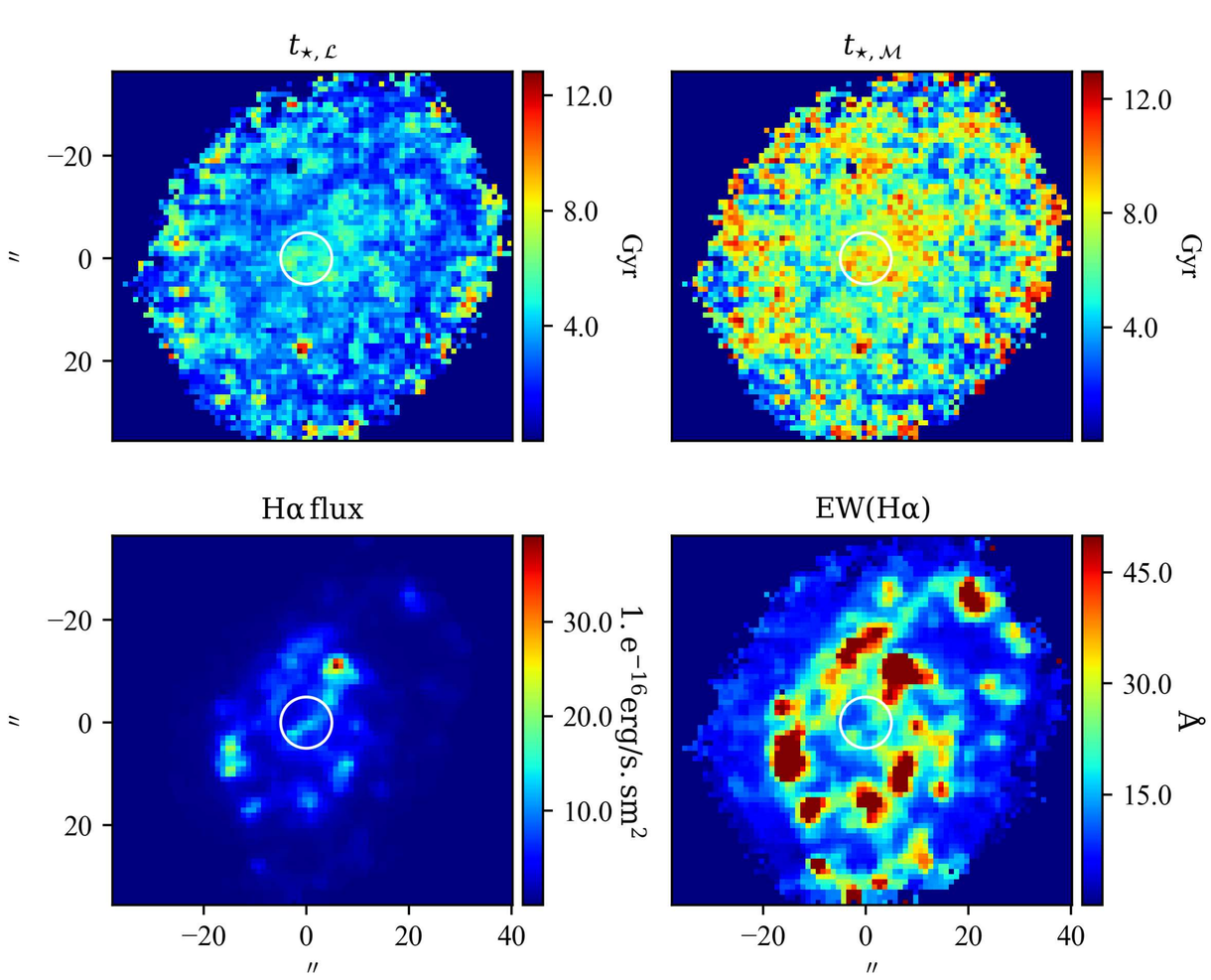

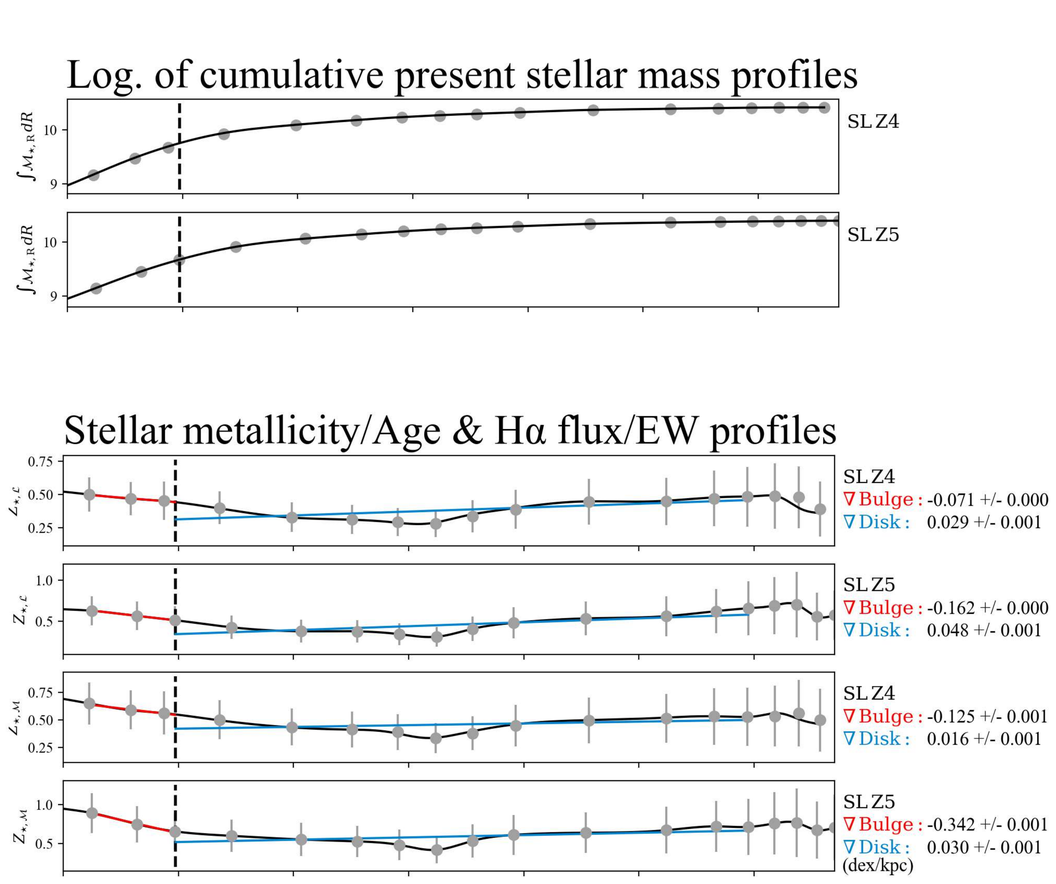

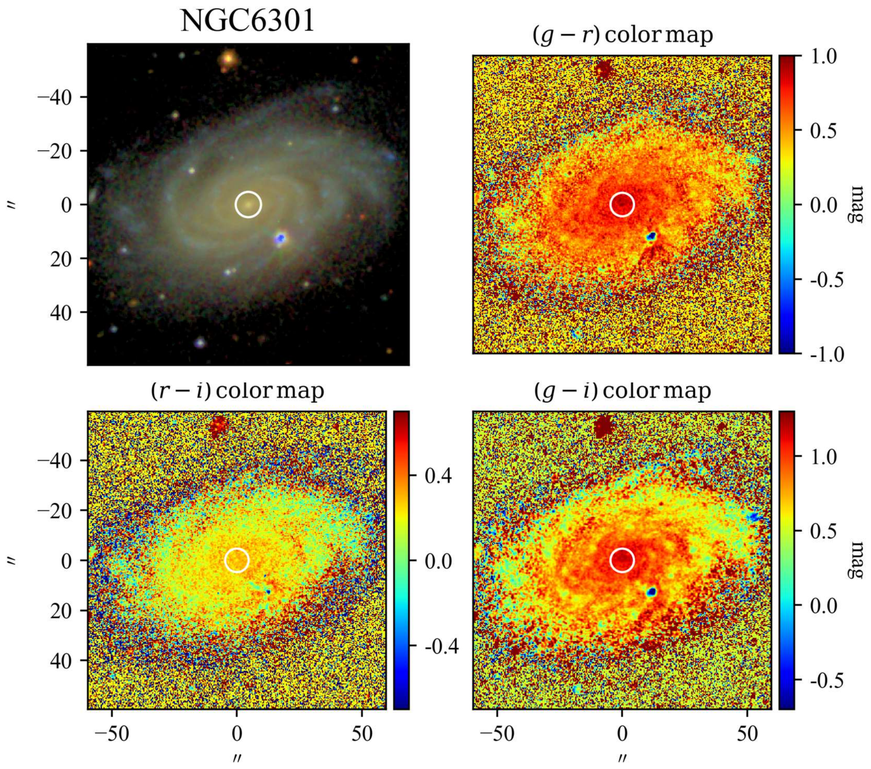
NGC6301
$(g-r)$ color map
$(r-i)$ color map
$(g-i)$ color map
mag
″

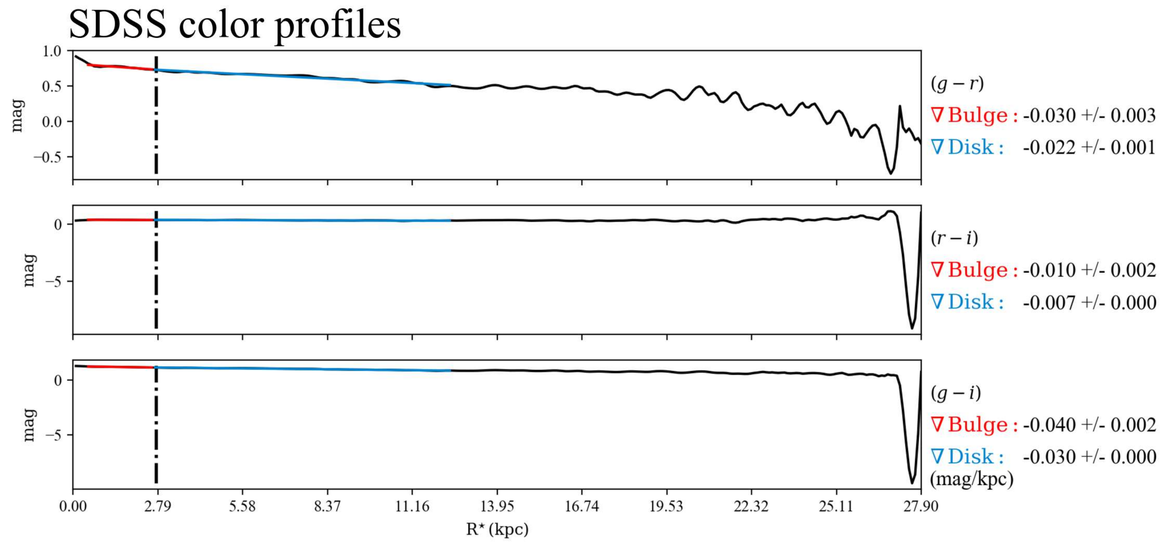
SDSS color profiles
$(g-r)$
∇ Bulge : -0.030 +/- 0.003
∇ Disk : -0.022 +/- 0.001
$(r-i)$
∇ Bulge : -0.010 +/- 0.002
∇ Disk : -0.007 +/- 0.000
$(g-i)$
∇ Bulge : -0.040 +/- 0.002
∇ Disk : -0.030 +/- 0.000
(mag/kpc)
mag
R* (kpc)

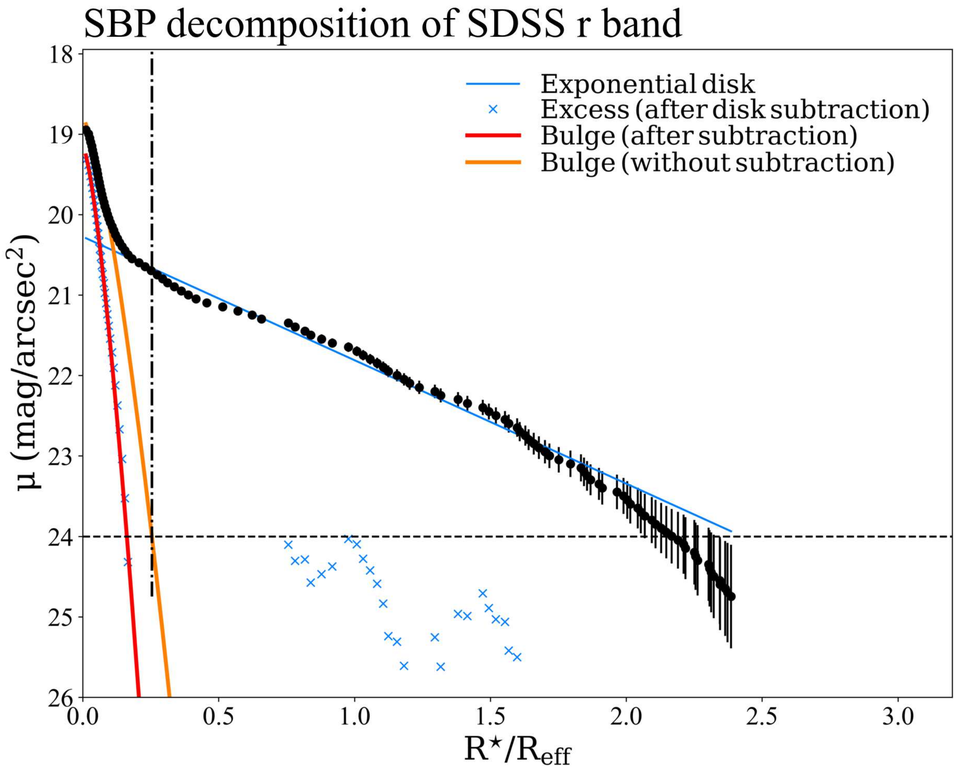
SBP decomposition of SDSS r band
Exponential disk
Excess (after disk subtraction)
Bulge (after subtraction)
Bulge (without subtraction)
μ (mag/arcsec²)
R*/Reff

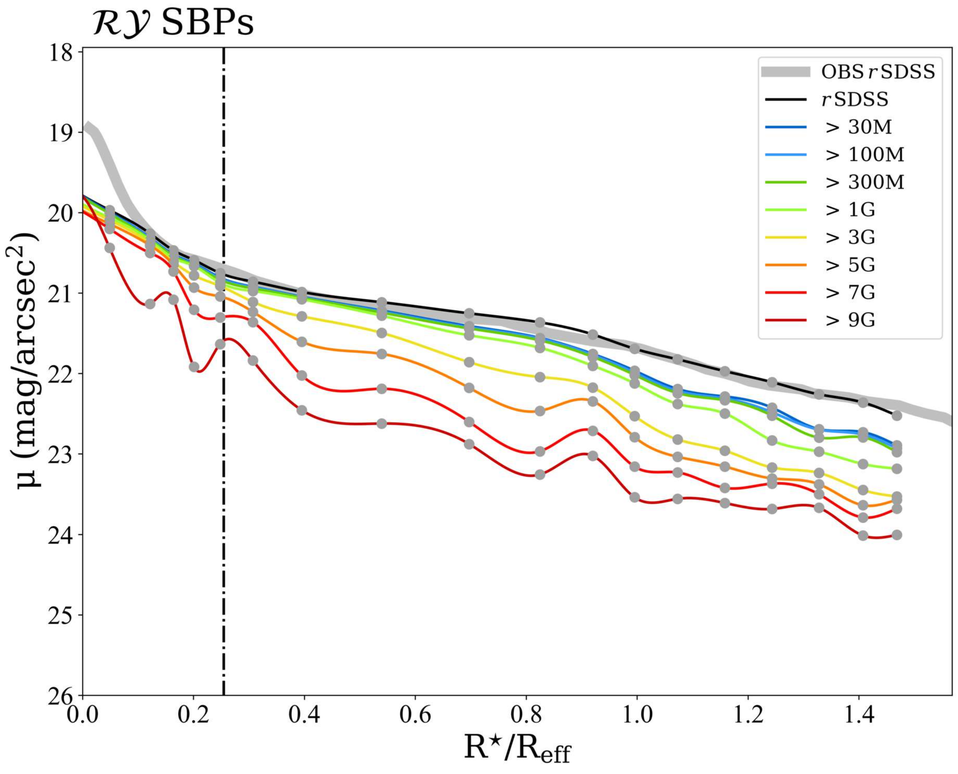
$\mathcal{RY}$ SBPs
OBS rSDSS
rSDSS
> 30M
> 100M
> 300M
> 1G
> 3G
> 5G
> 7G
> 9G
μ (mag/arcsec²)
R*/Reff

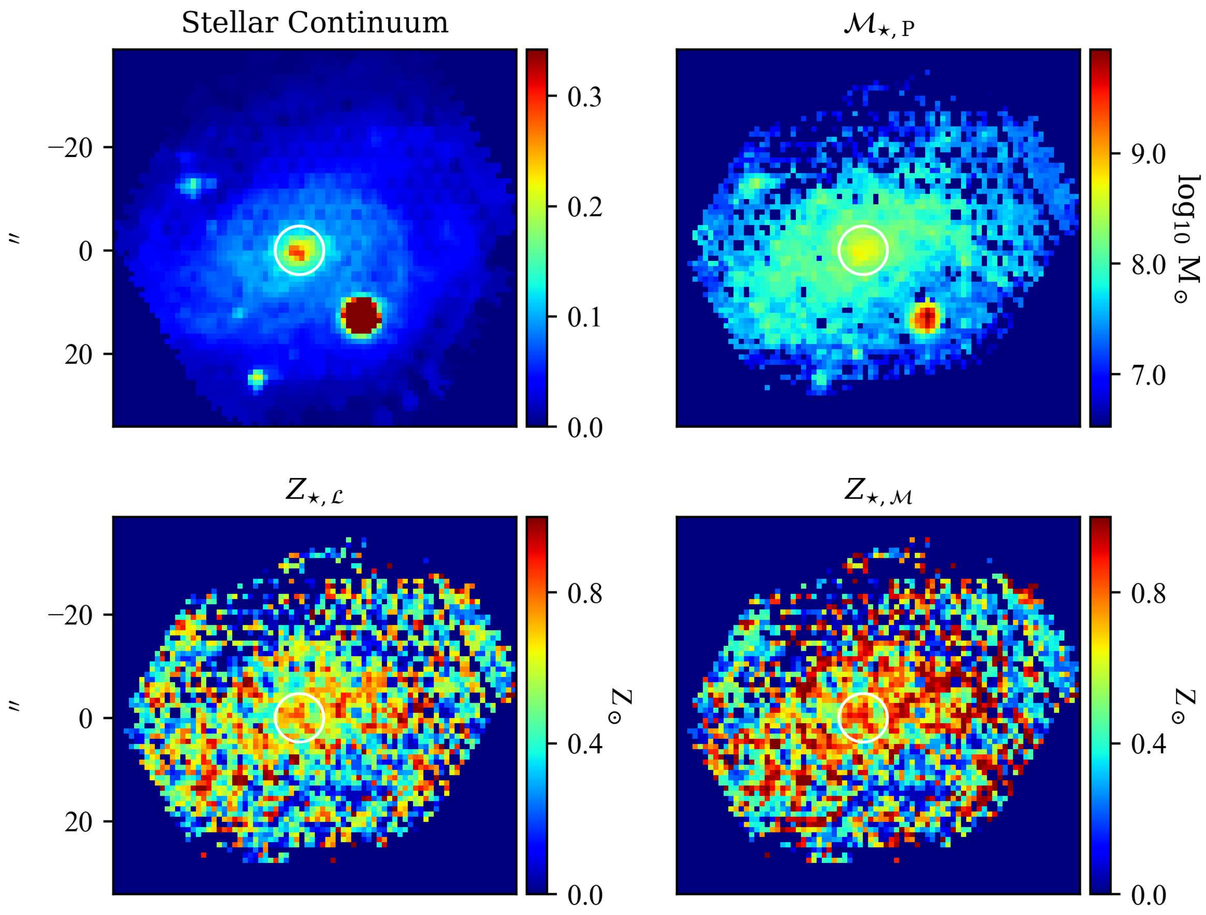
Stellar Continuum
$\mathcal{M}_{\star,\mathrm{P}}$
$Z_{\star,\mathcal{L}}$
$Z_{\star,\mathcal{M}}$
log10 M⊙
Z⊙
″

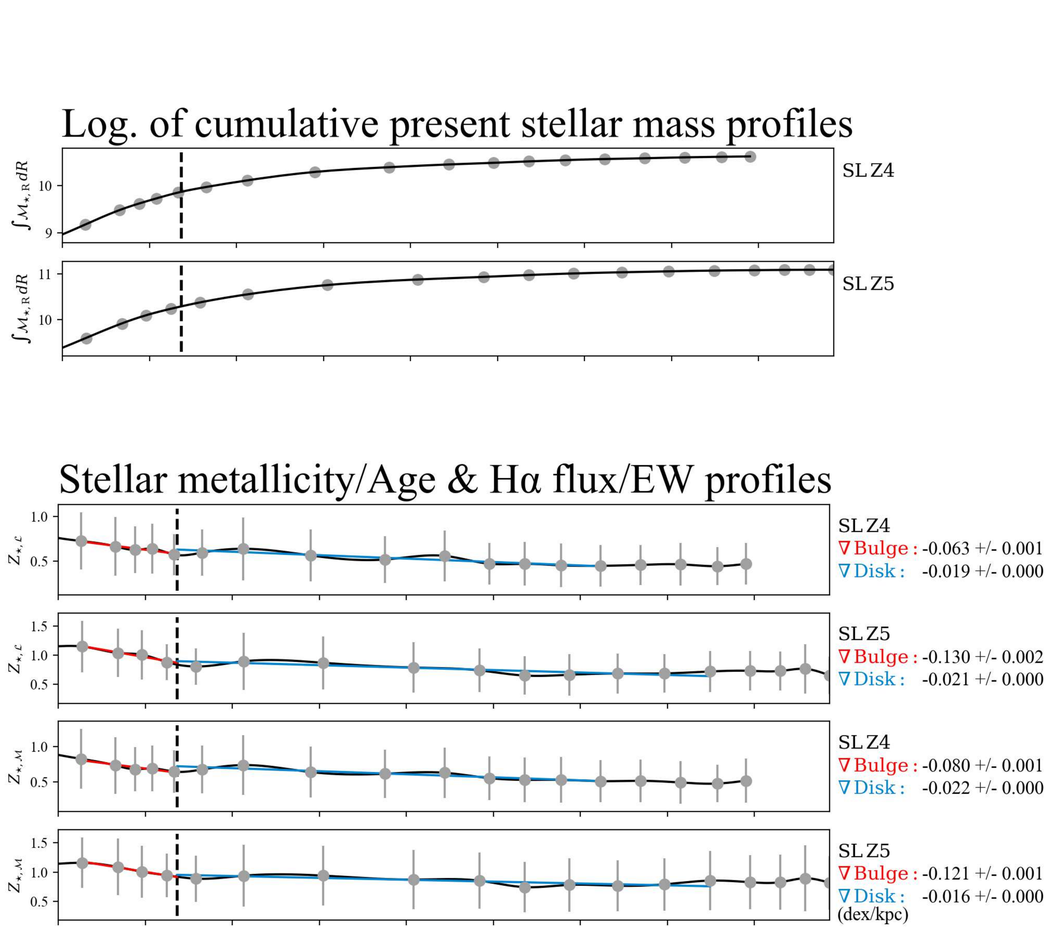
Log. of cumulative present stellar mass profiles
SL Z4
SL Z5
Stellar metallicity/Age & Hα flux/EW profiles
SL Z4
∇ Bulge : -0.063 +/- 0.001
∇ Disk : -0.019 +/- 0.000
SL Z5
∇ Bulge : -0.130 +/- 0.002
∇ Disk : -0.021 +/- 0.000
SL Z4
∇ Bulge : -0.080 +/- 0.001
∇ Disk : -0.022 +/- 0.000
SL Z5
∇ Bulge : -0.121 +/- 0.001
∇ Disk : -0.016 +/- 0.000
(dex/kpc)

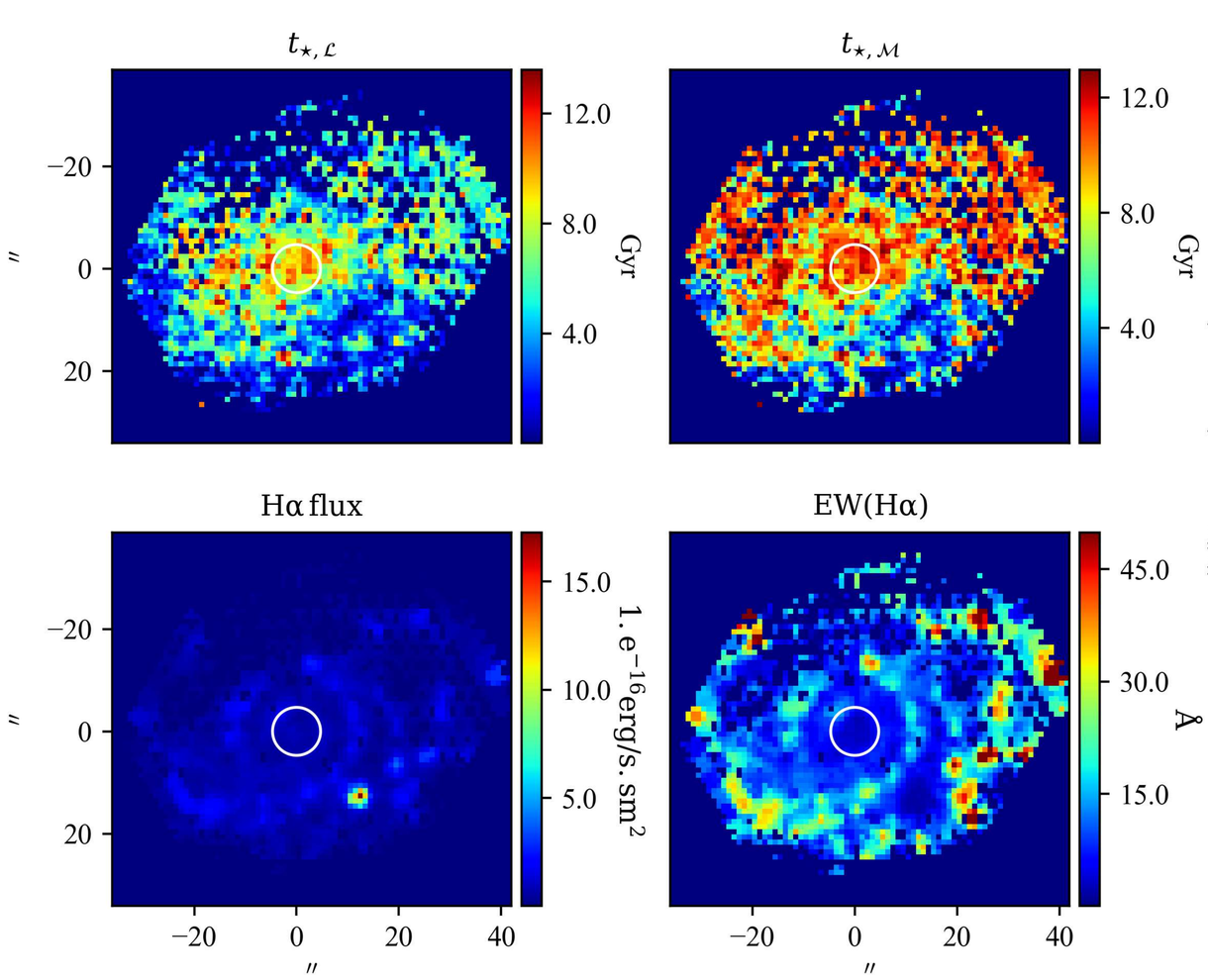
$t_{\star,\mathcal{L}}$
$t_{\star,\mathcal{M}}$
Gyr
Hα flux
EW(Hα)
1. e⁻¹⁶erg/s. sm²
Å
″

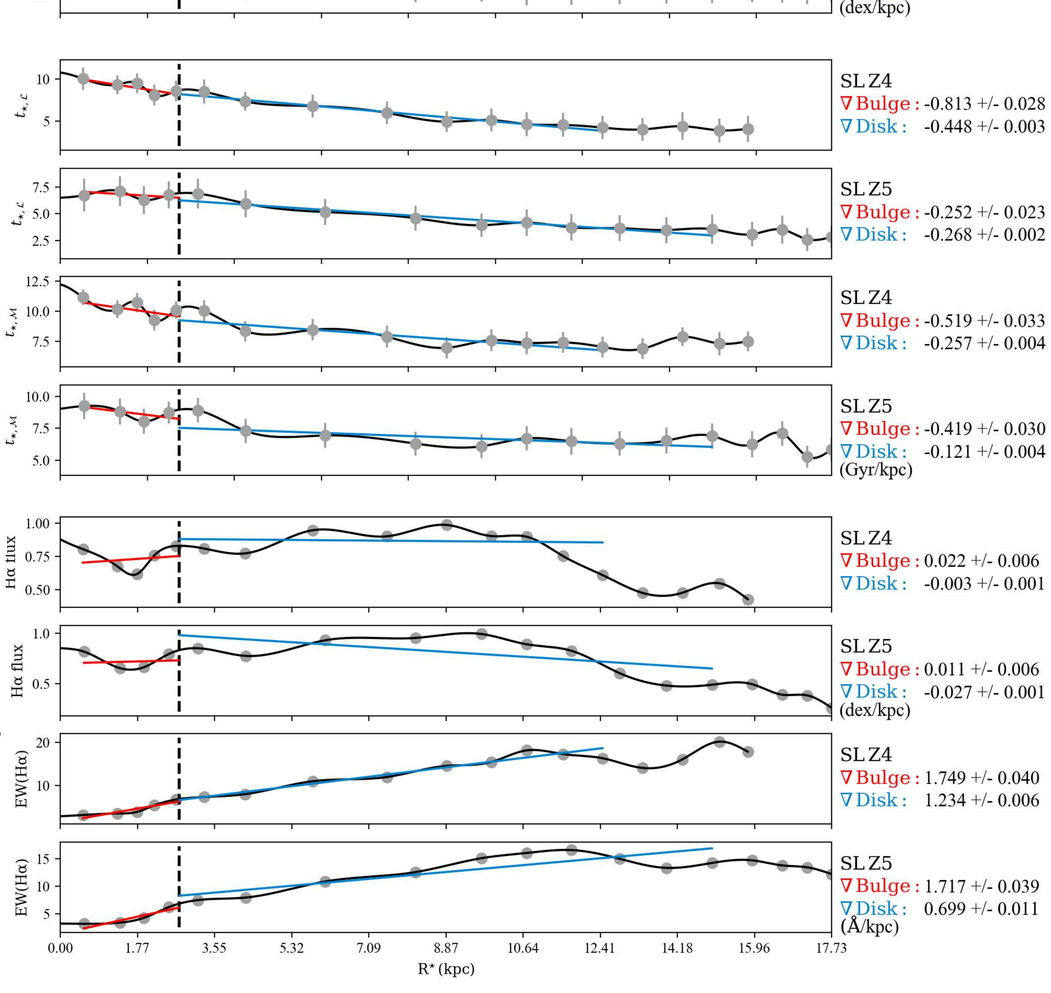
SL Z4
∇ Bulge : -0.813 +/- 0.028
∇ Disk : -0.448 +/- 0.003
SL Z5
∇ Bulge : -0.252 +/- 0.023
∇ Disk : -0.268 +/- 0.002
SL Z4
∇ Bulge : -0.519 +/- 0.033
∇ Disk : -0.257 +/- 0.004
SL Z5
∇ Bulge : -0.419 +/- 0.030
∇ Disk : -0.121 +/- 0.004
(Gyr/kpc)
SL Z4
∇ Bulge : 0.022 +/- 0.006
∇ Disk : -0.003 +/- 0.001
SL Z5
∇ Bulge : 0.011 +/- 0.006
∇ Disk : -0.027 +/- 0.001
(dex/kpc)
SL Z4
∇ Bulge : 1.749 +/- 0.040
∇ Disk : 1.234 +/- 0.006
SL Z5
∇ Bulge : 1.717 +/- 0.039
∇ Disk : 0.699 +/- 0.011
(Å/kpc)
R* (kpc)

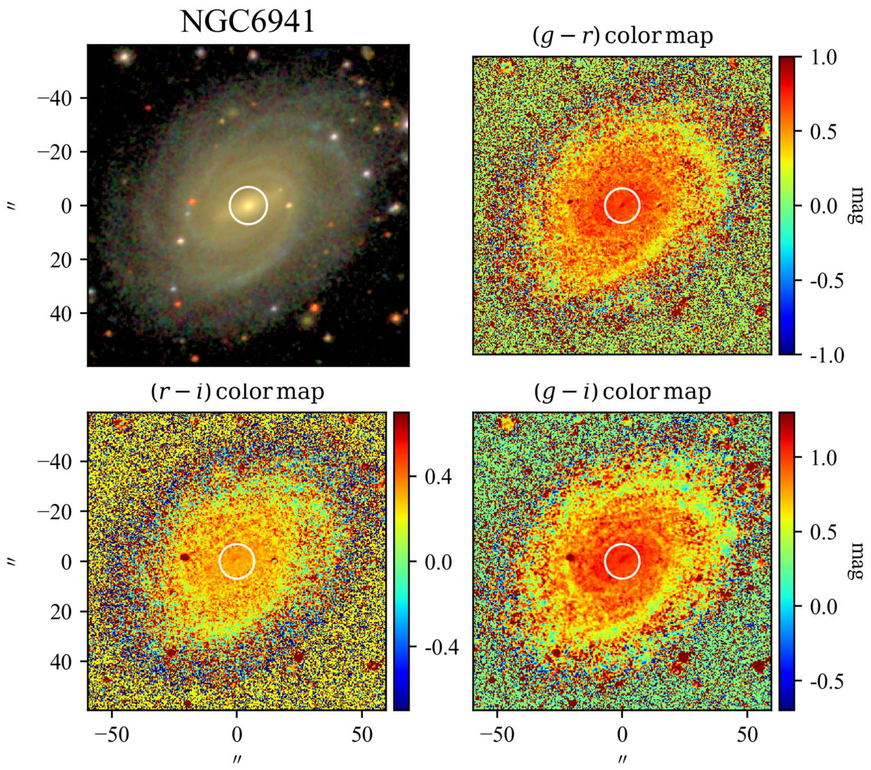

SBP decomposition of SDSS r band

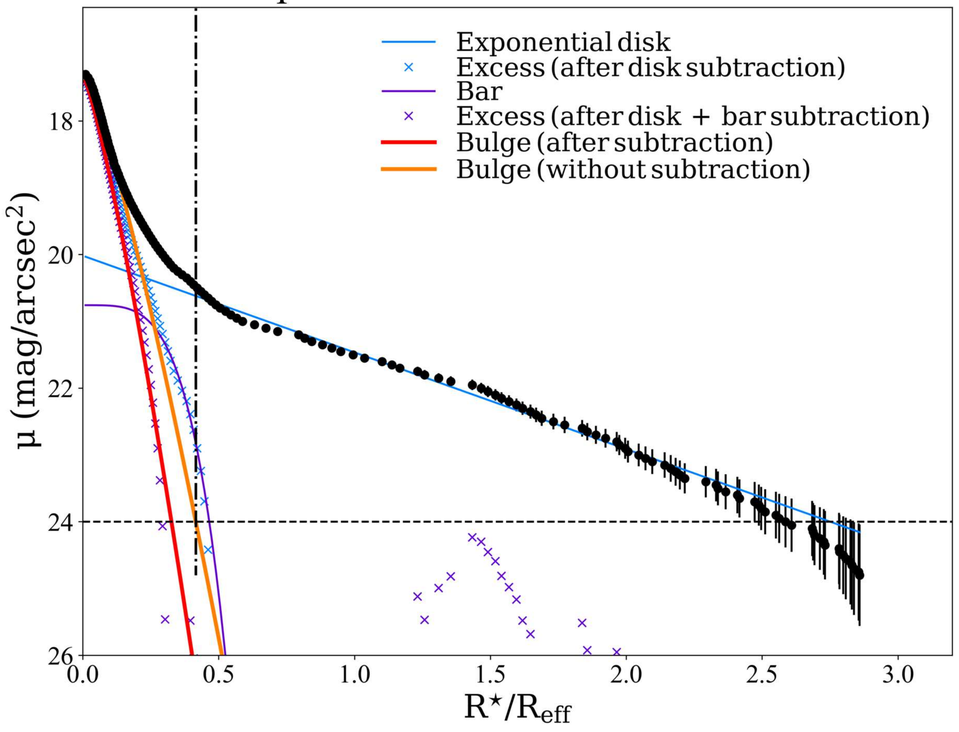

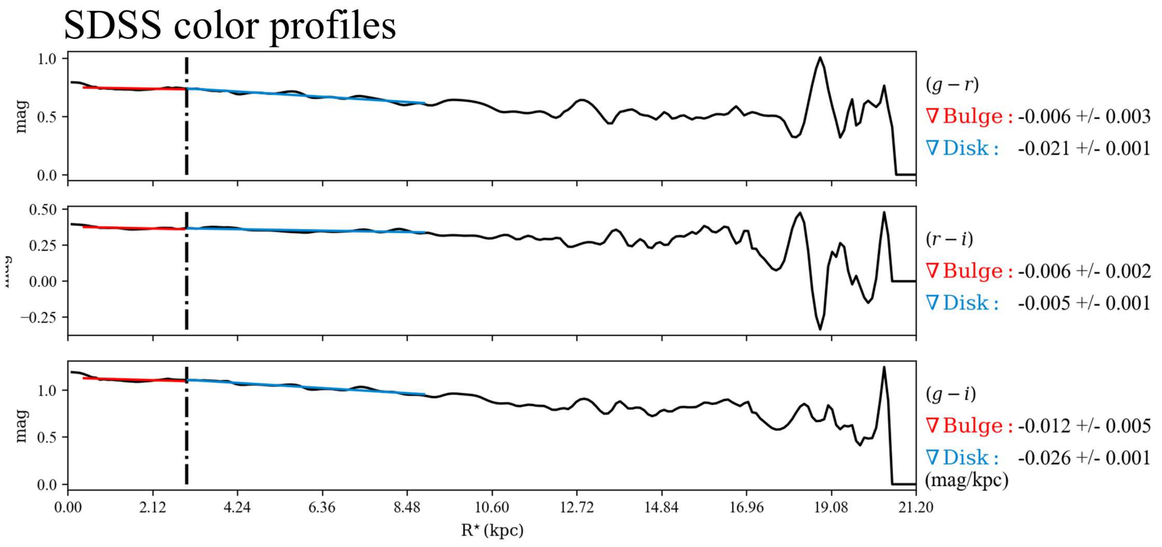

$\mathcal{RY}$ SBPs

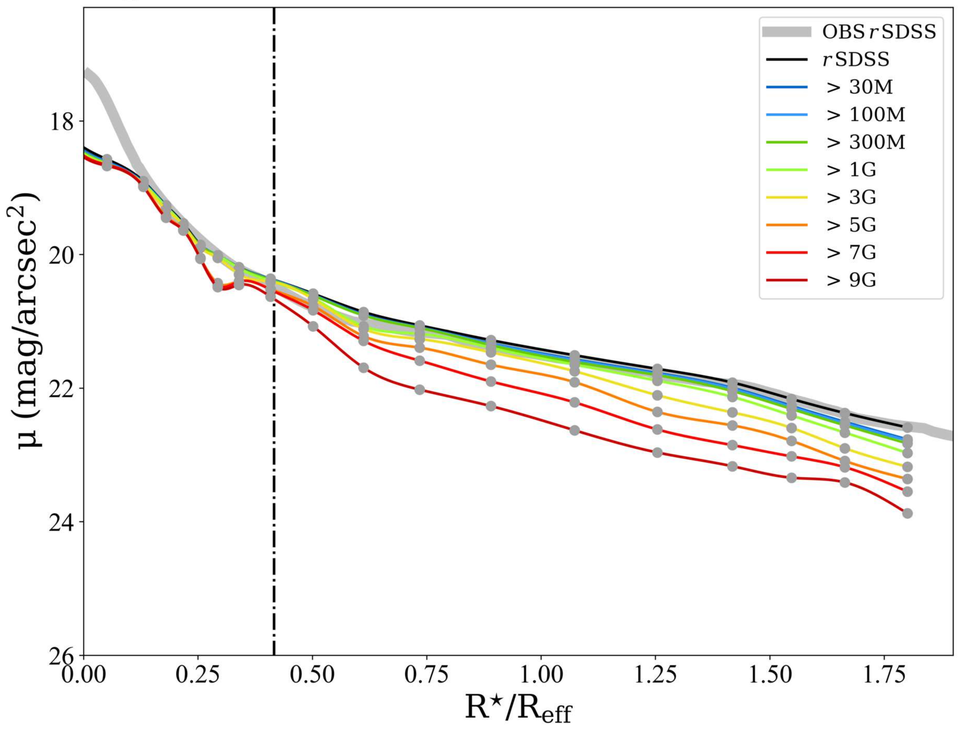

Stellar Continuum

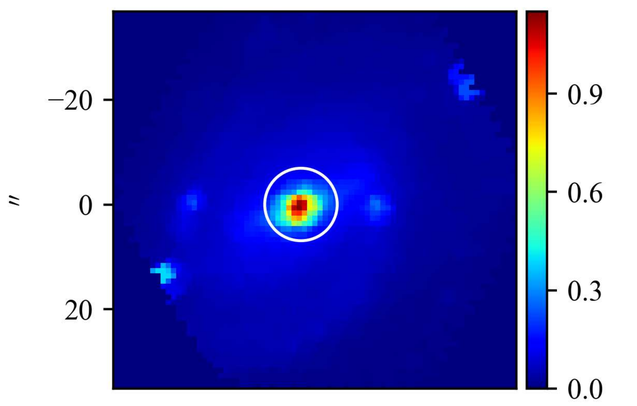

$\mathcal{M}_{\star,\mathrm{P}}$

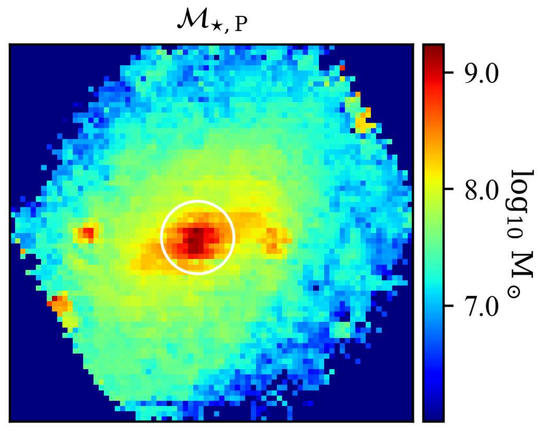

Log. of cumulative present stellar mass profiles

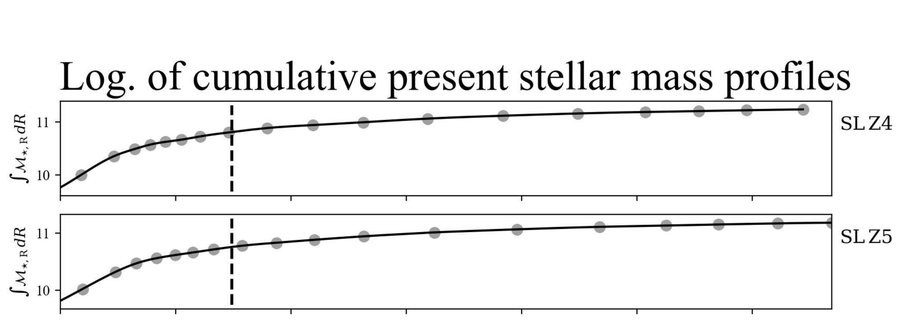

$Z_{\star,\mathcal{L}}$

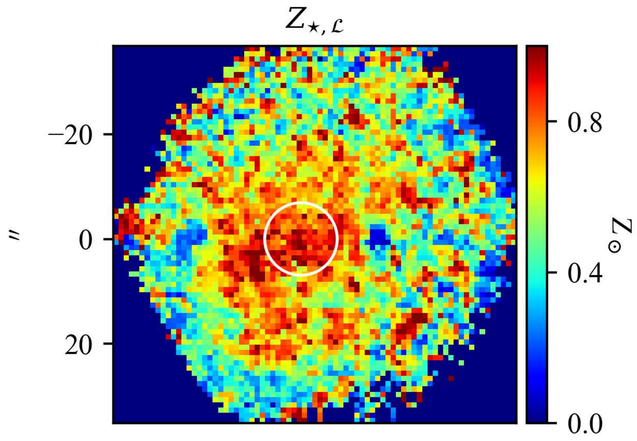

$Z_{\star,\mathcal{M}}$

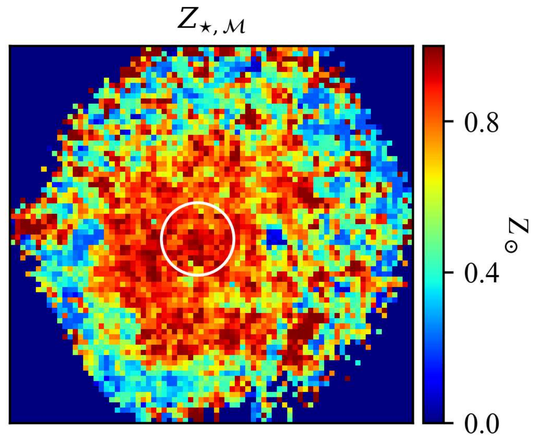

Stellar metallicity/Age & Hα flux/EW profiles

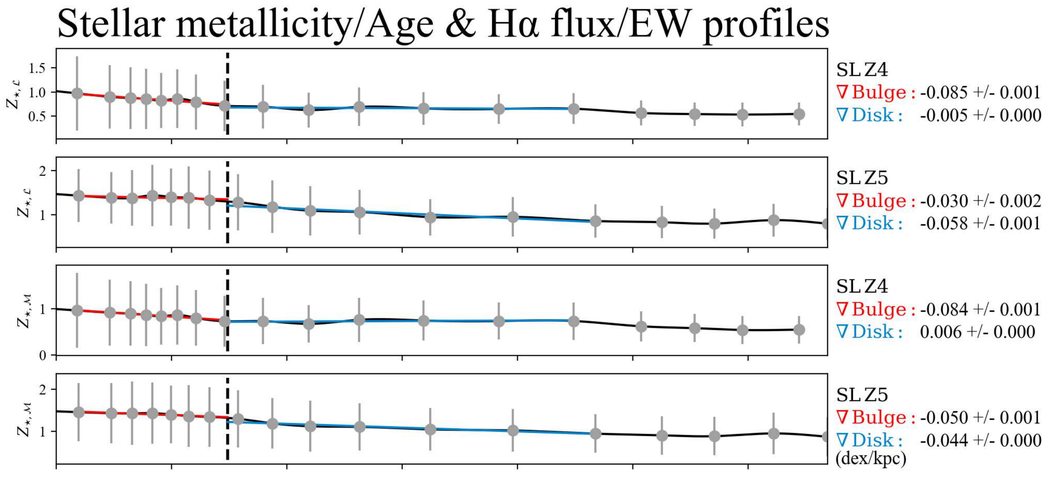

$t_{\star,\mathcal{L}}$

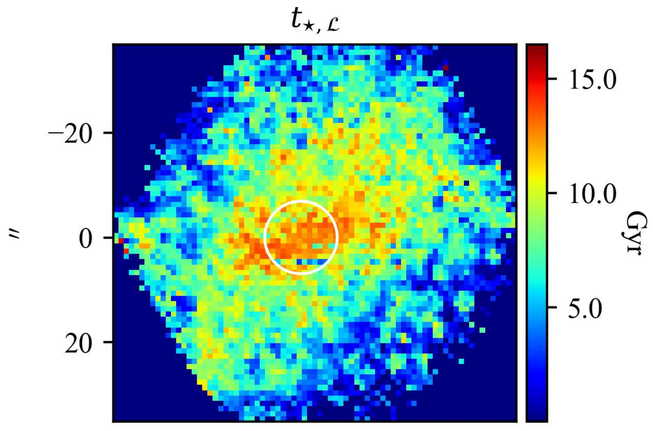

$t_{\star,\mathcal{M}}$

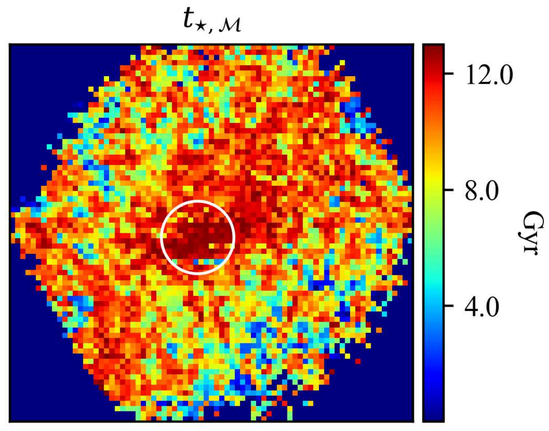

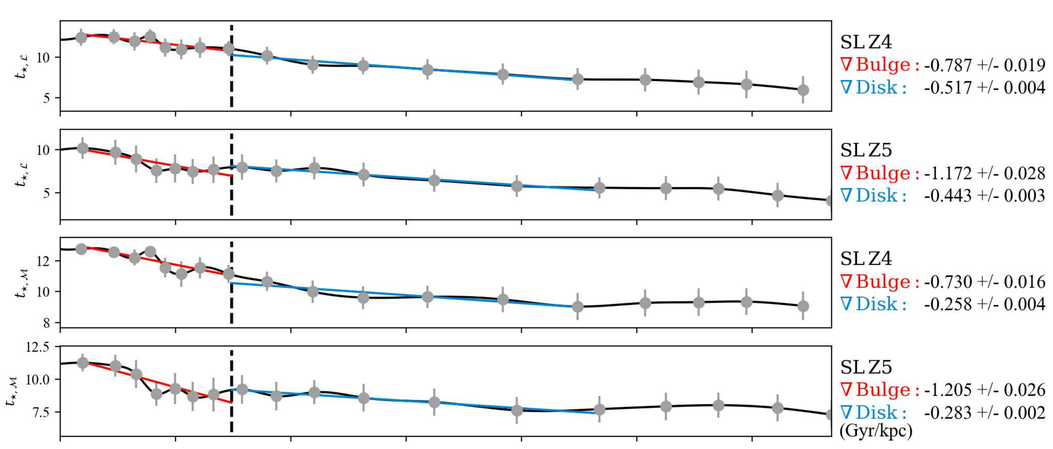

Hα flux

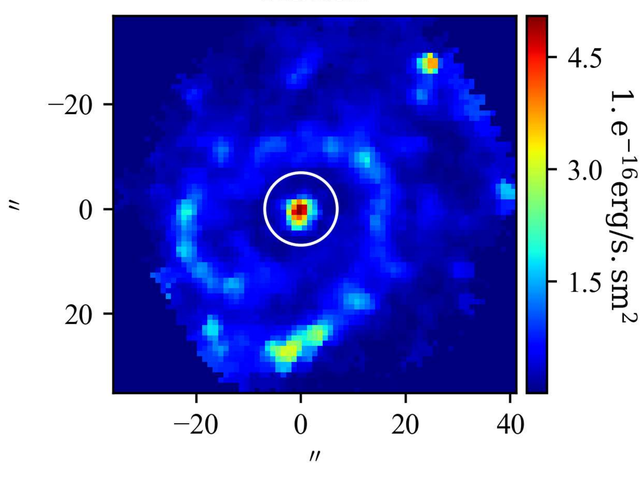

EW(Hα)

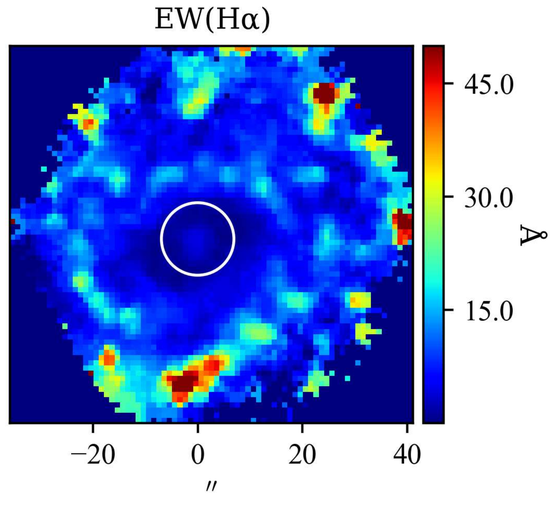

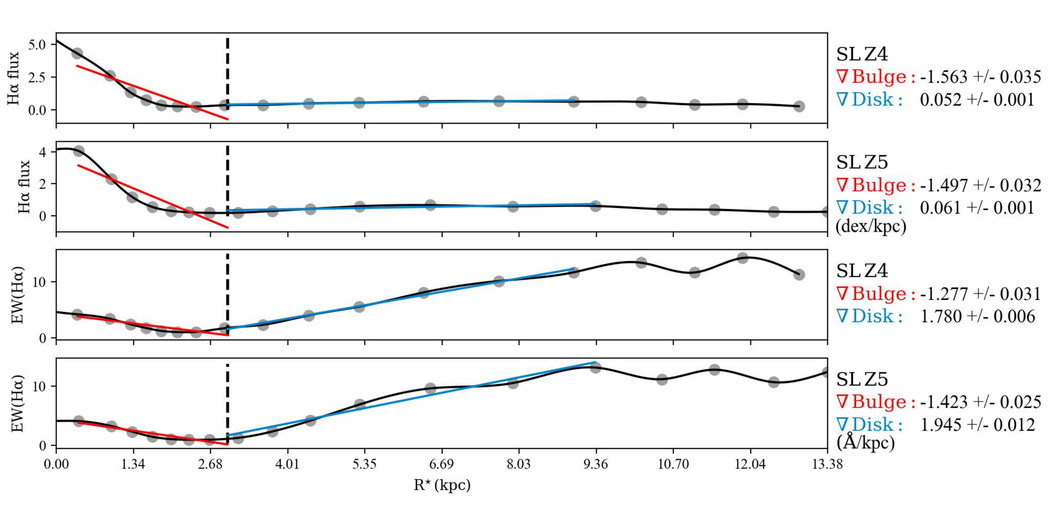

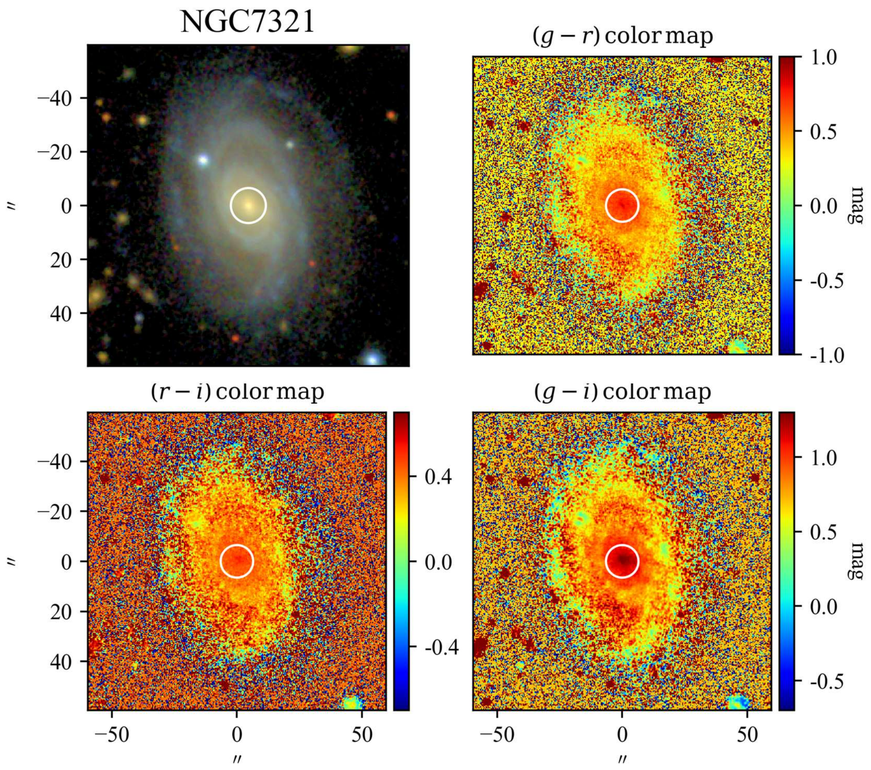

SBP decomposition of SDSS r band

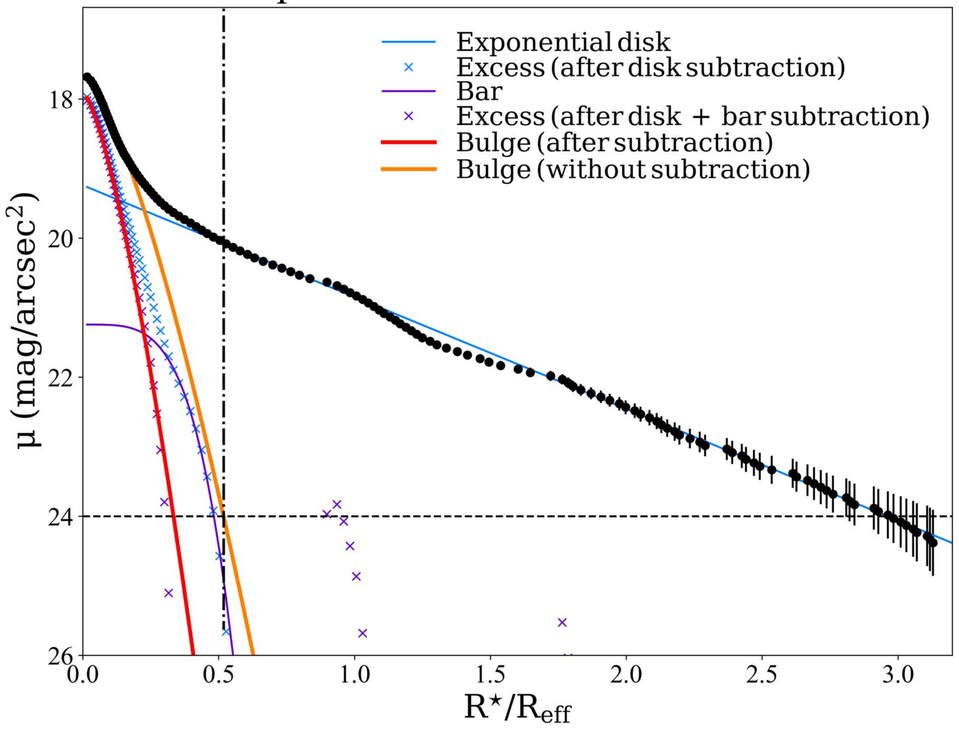

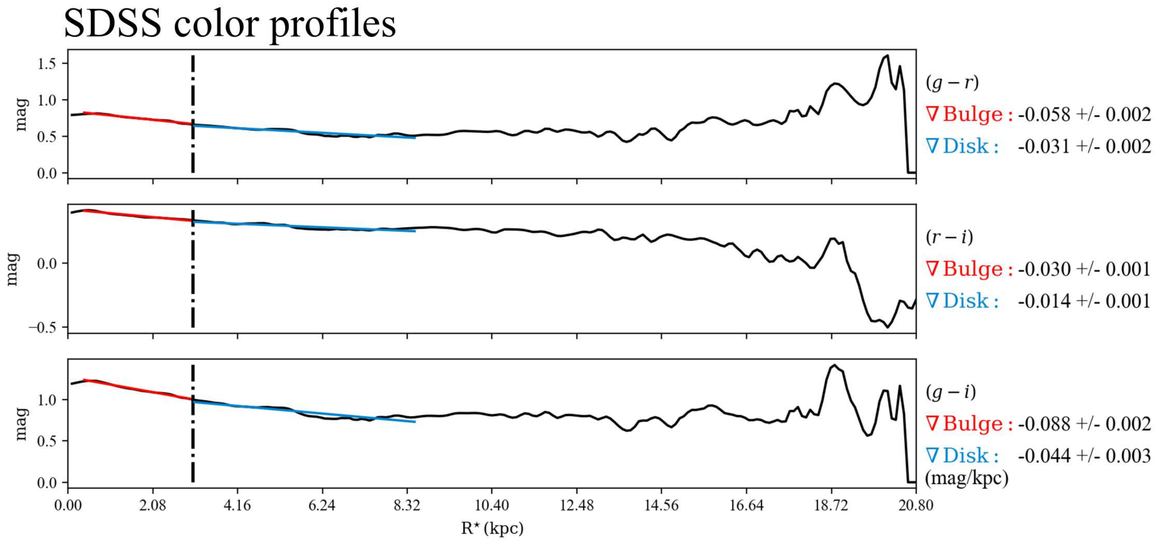

$\mathcal{RV}$ SBPs

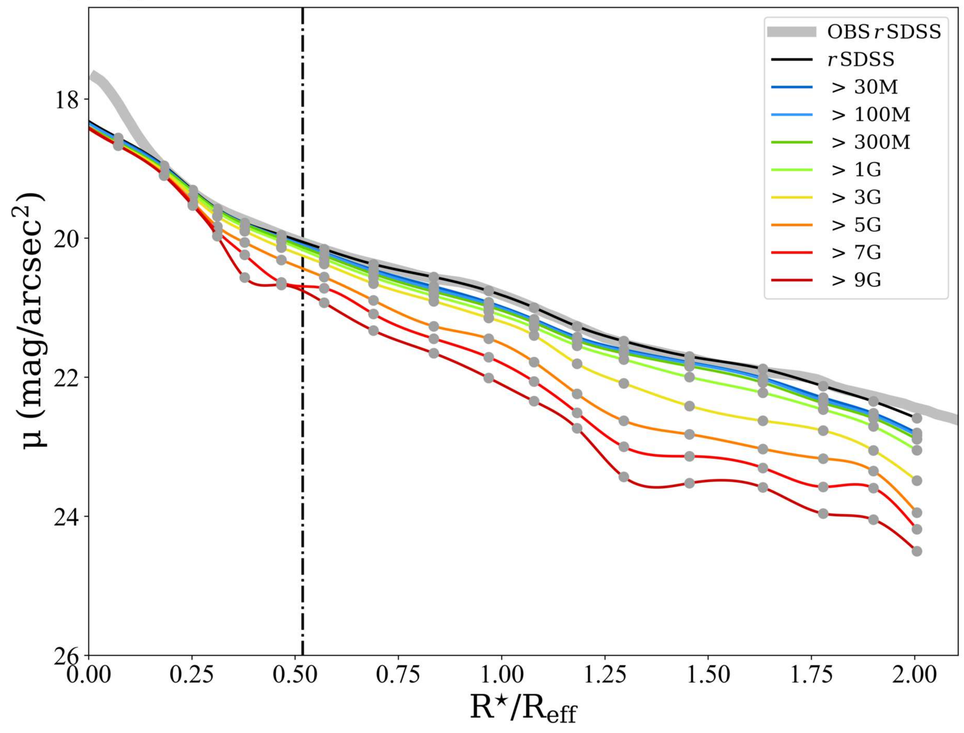

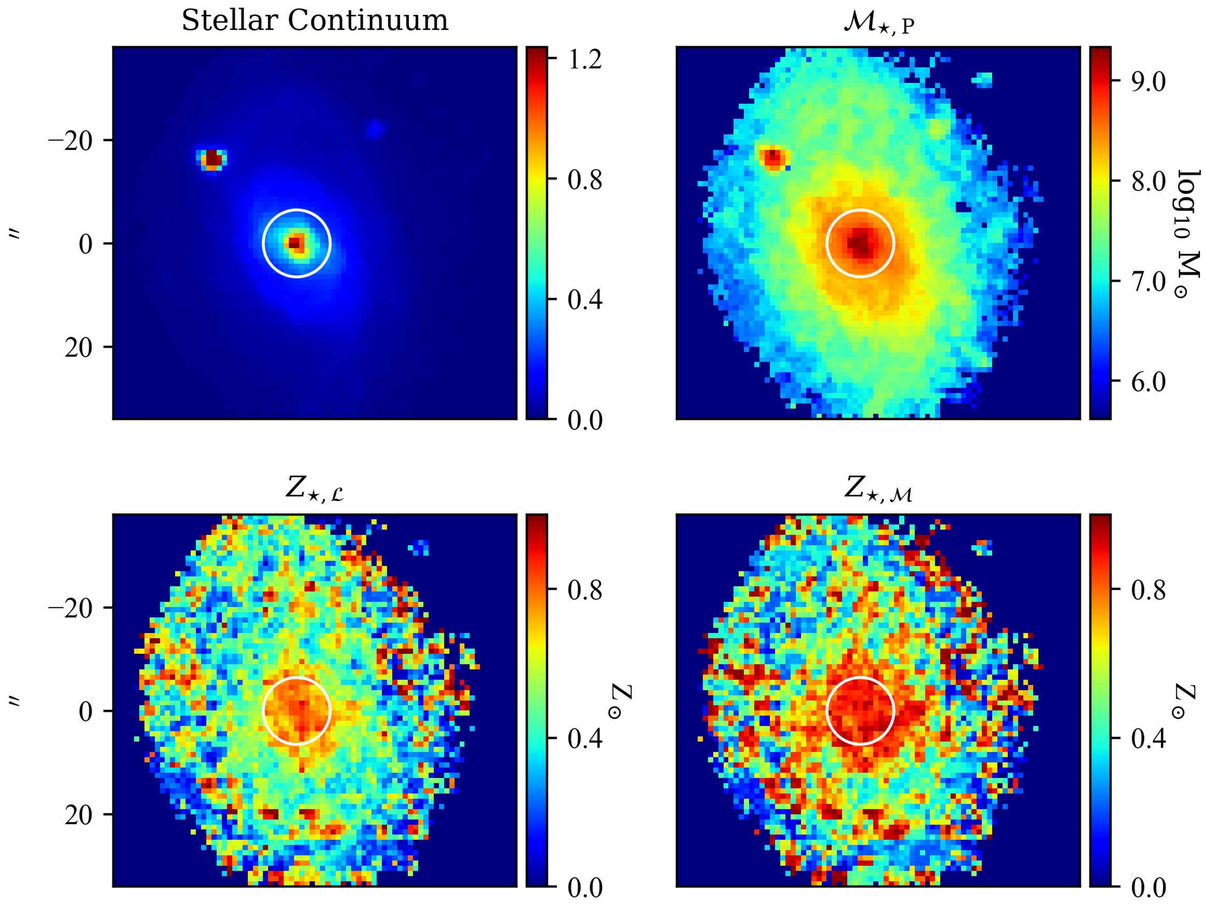

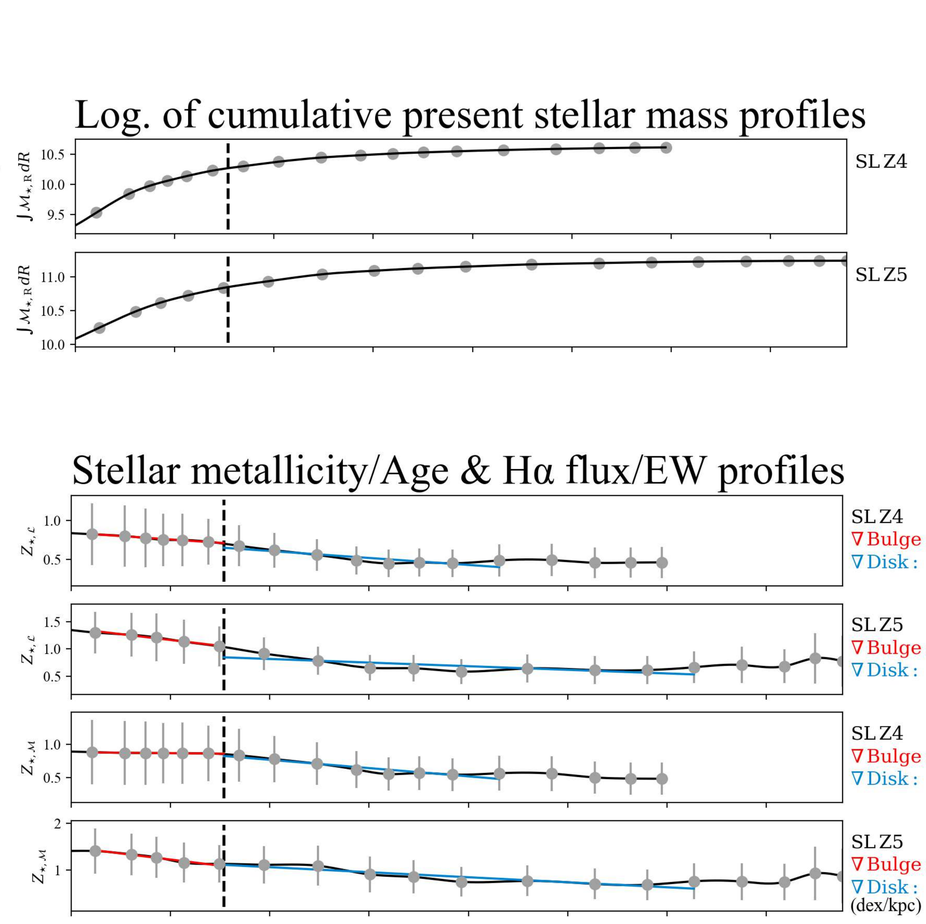

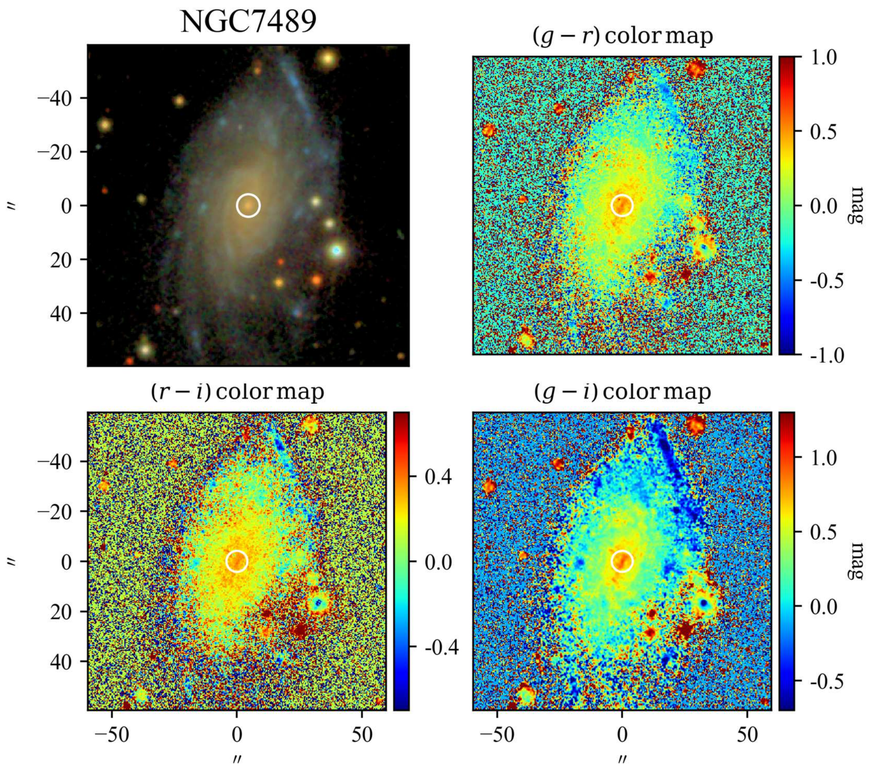

SBP decomposition of SDSS r band

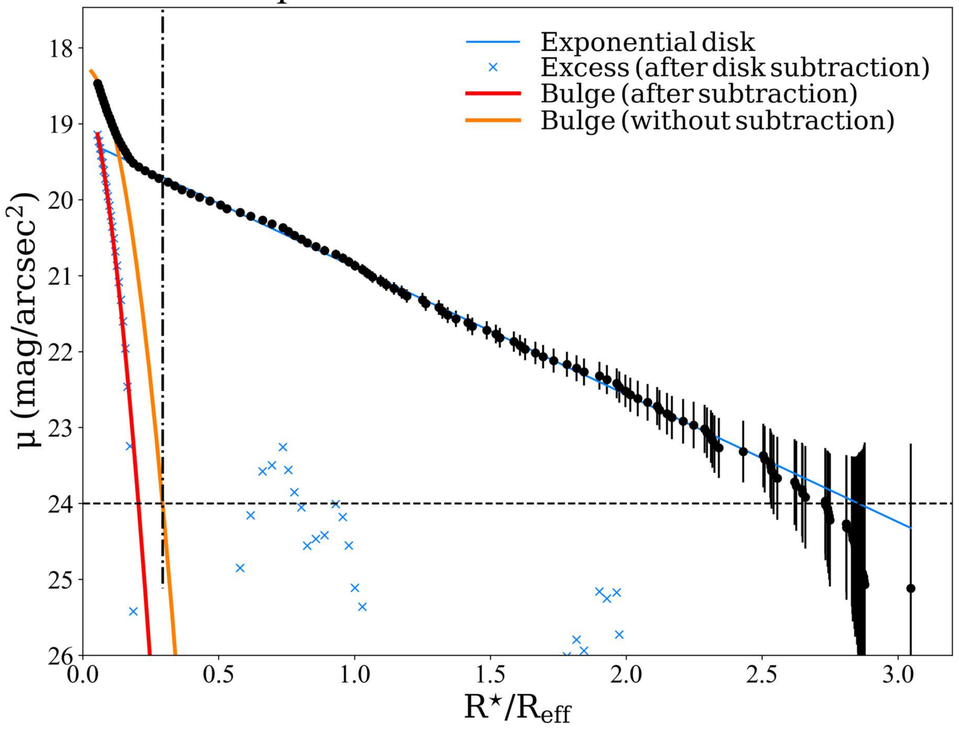

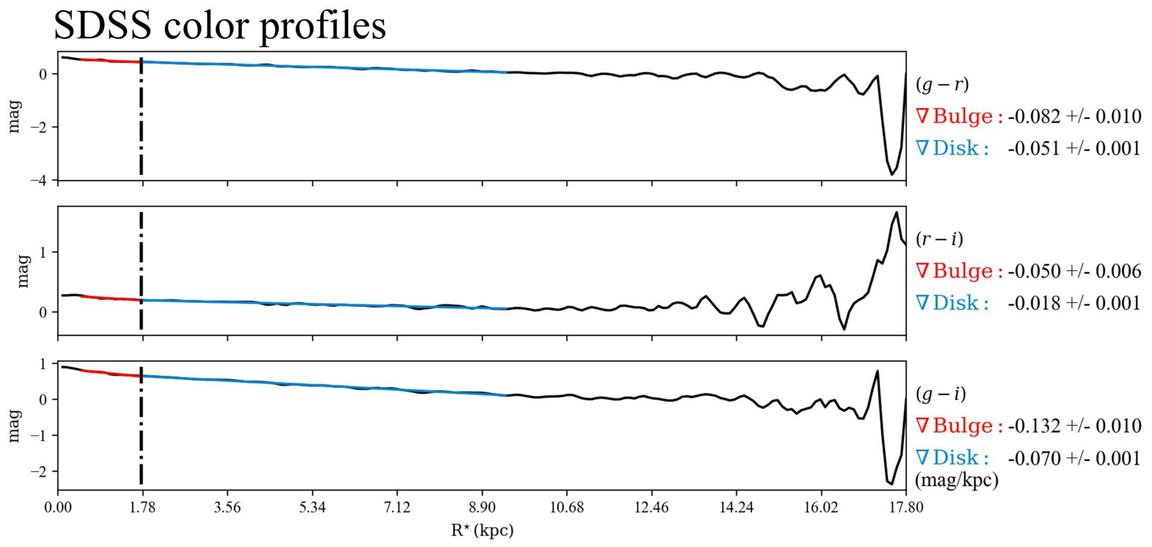

$\mathcal{RY}$ SBPs

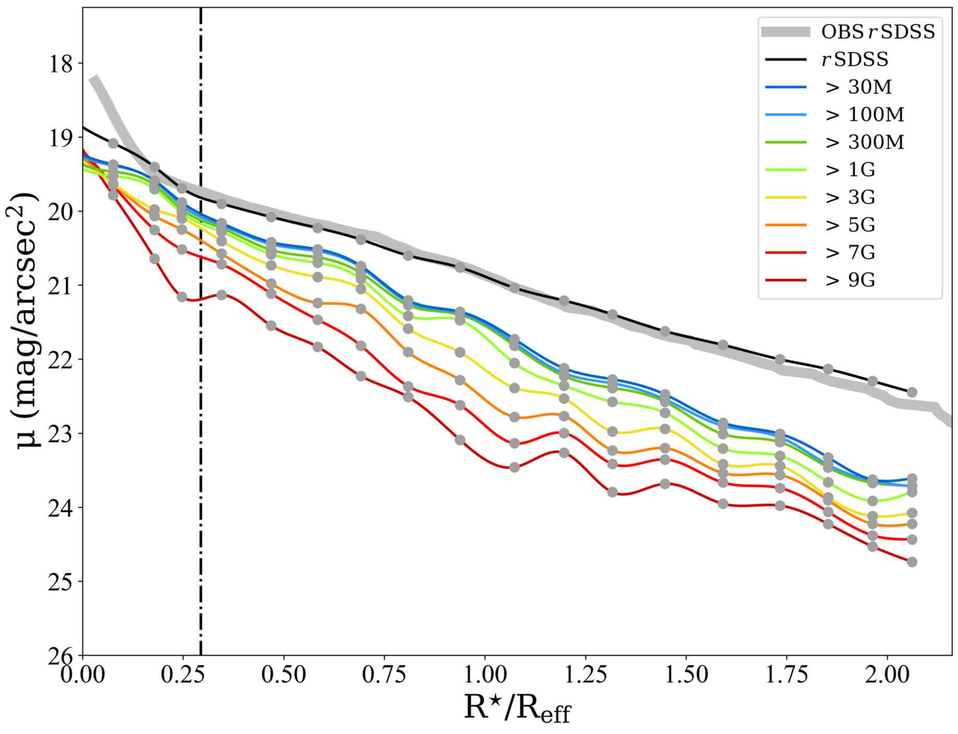

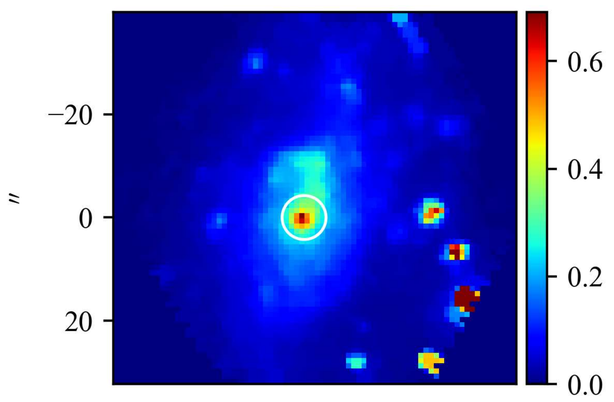

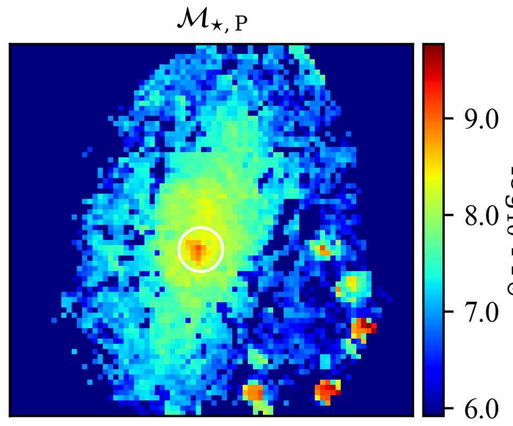

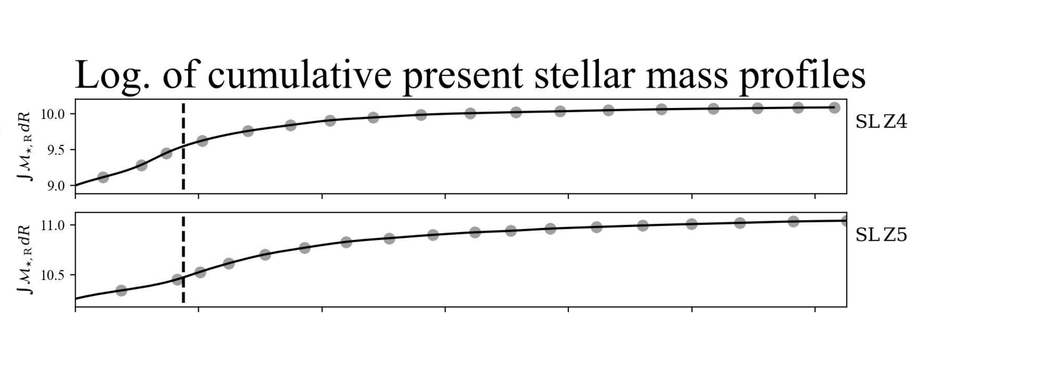

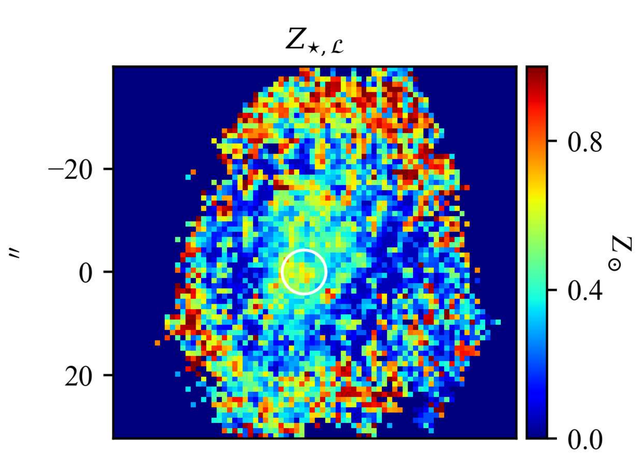

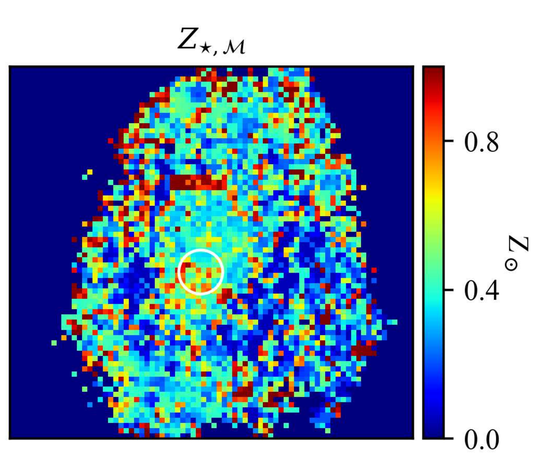

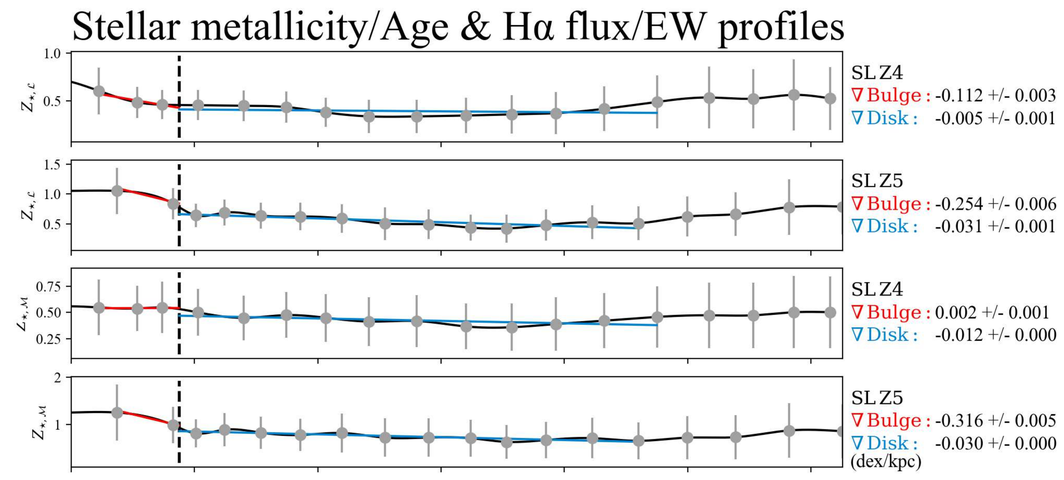

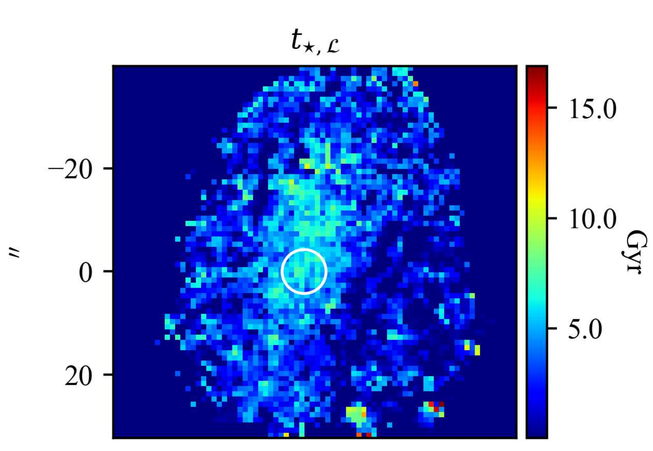

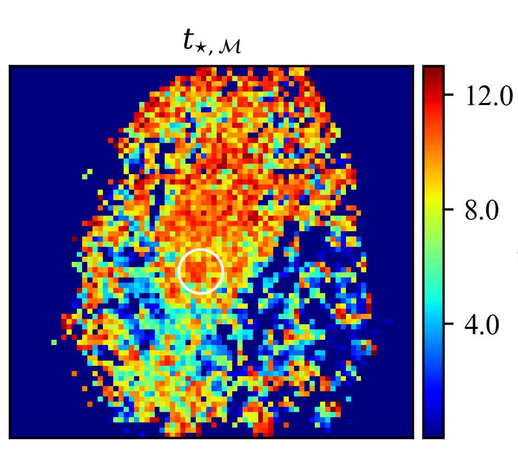

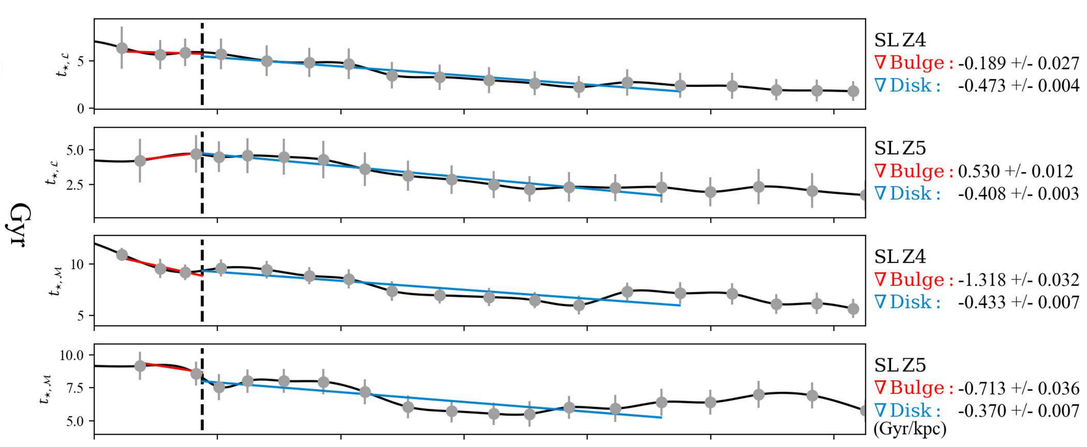

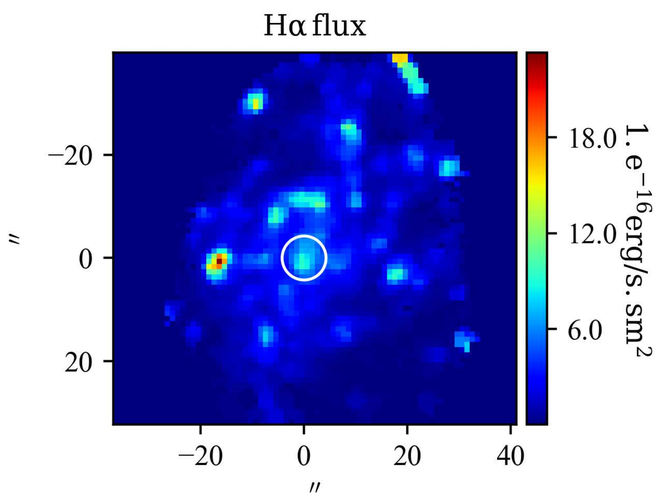

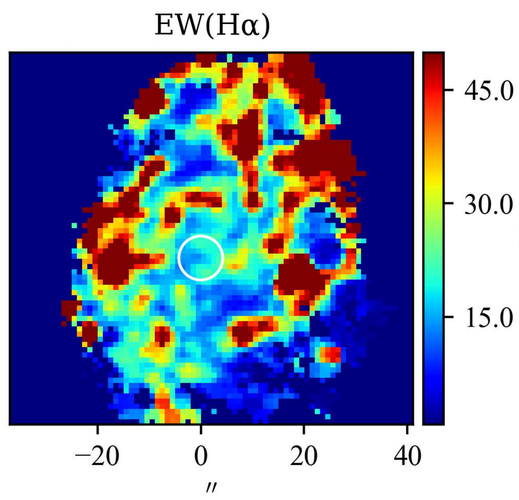

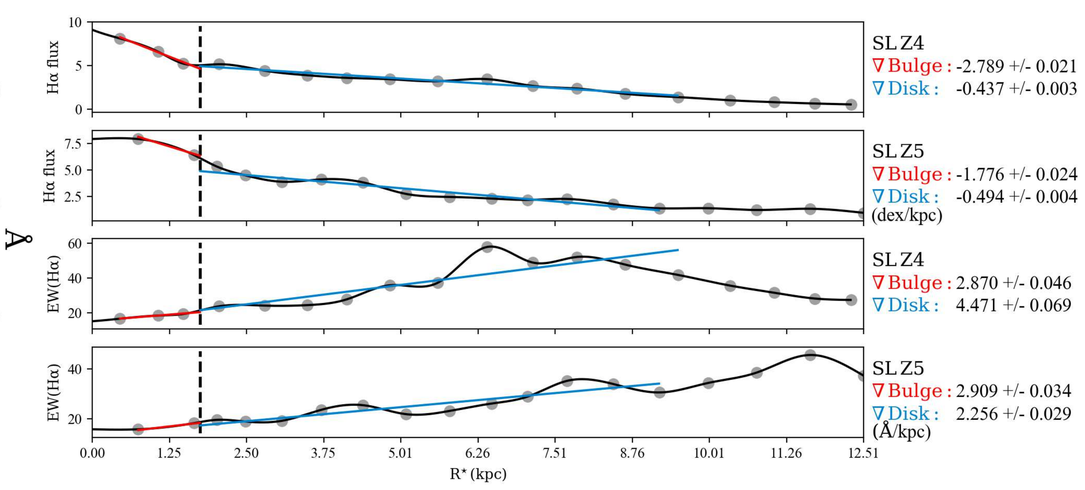

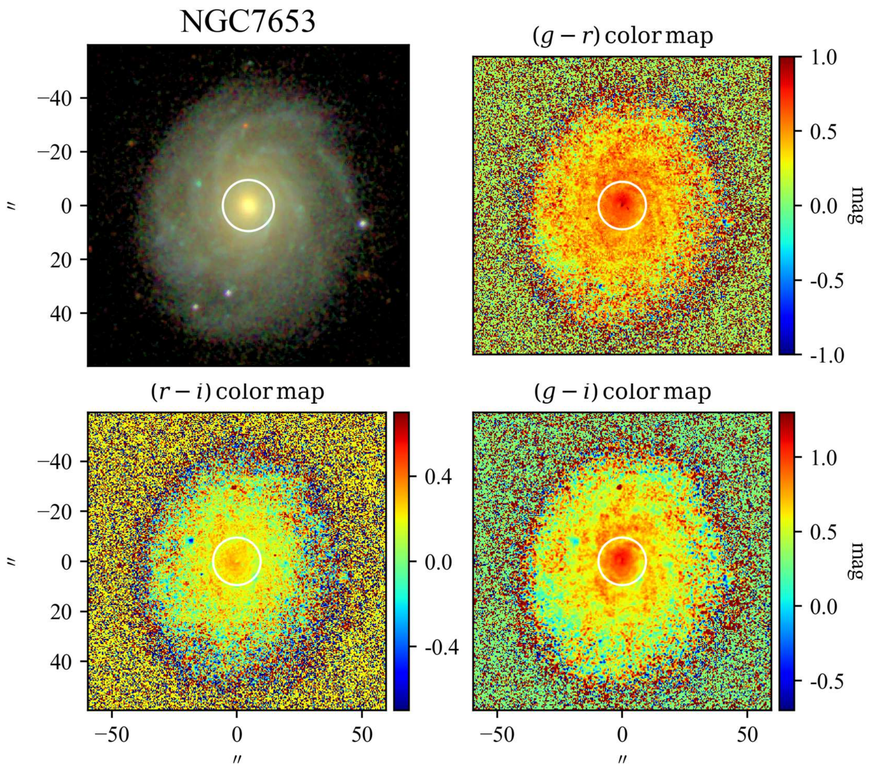

SBP decomposition of SDSS r band

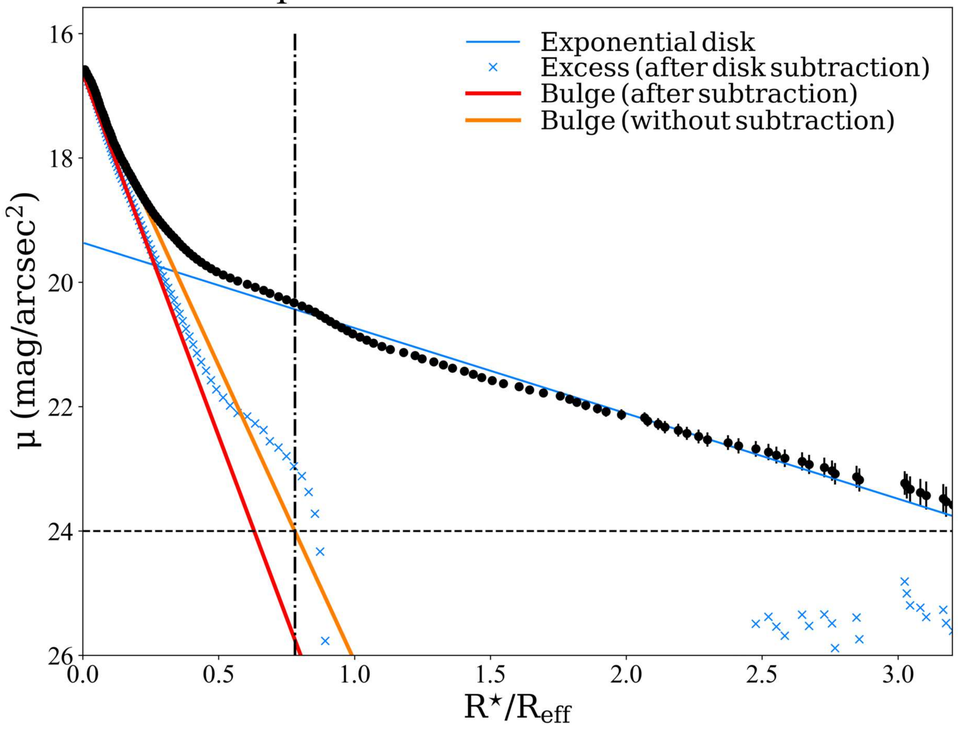

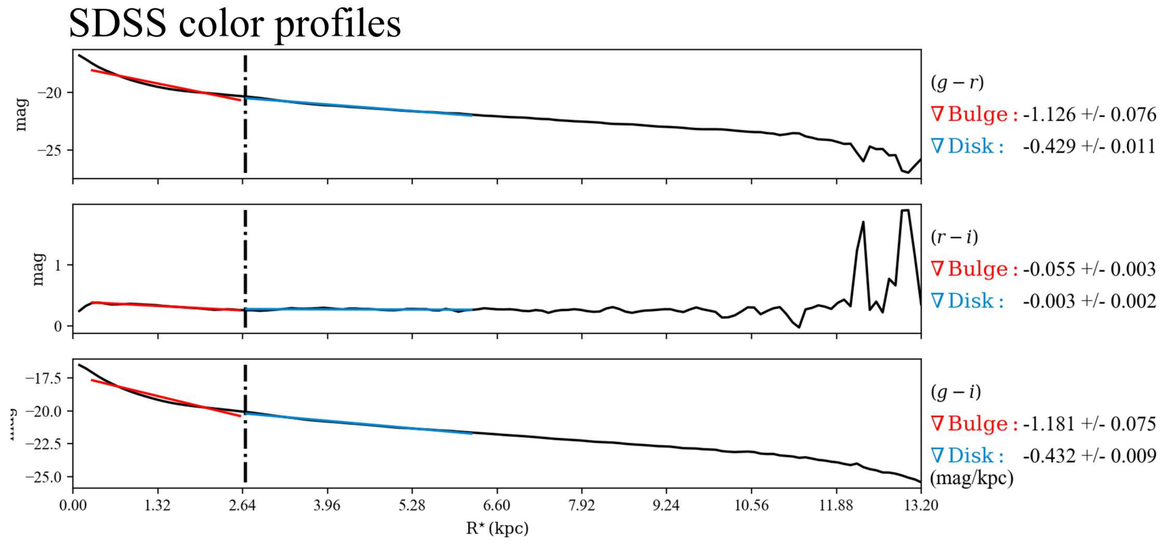

$\mathcal{RV}$ SBPs

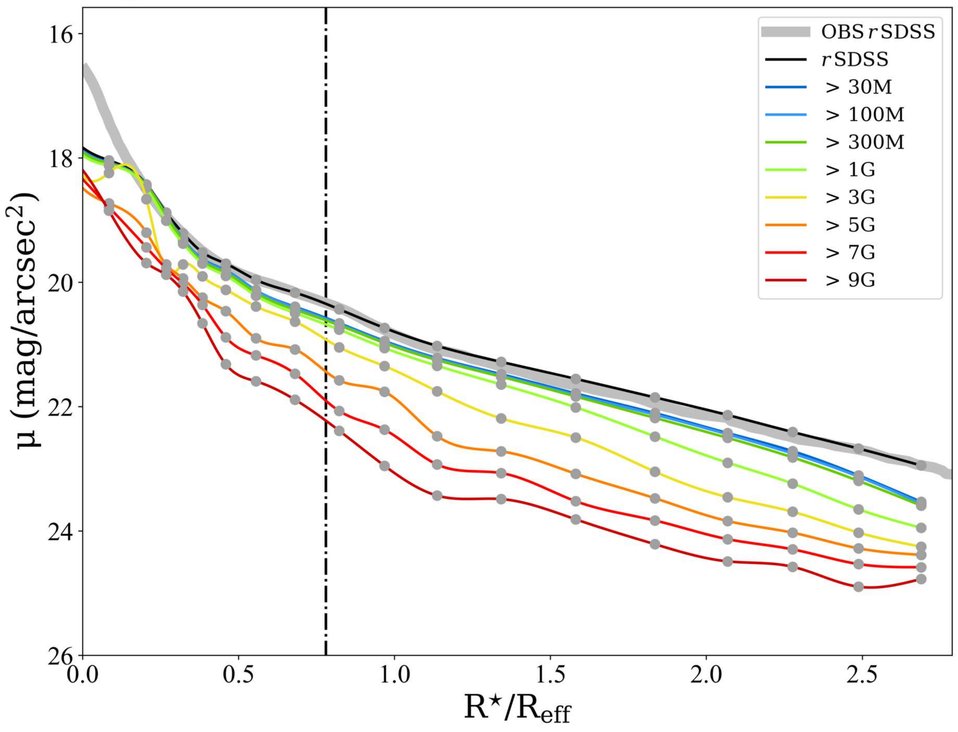

Stellar Continuum

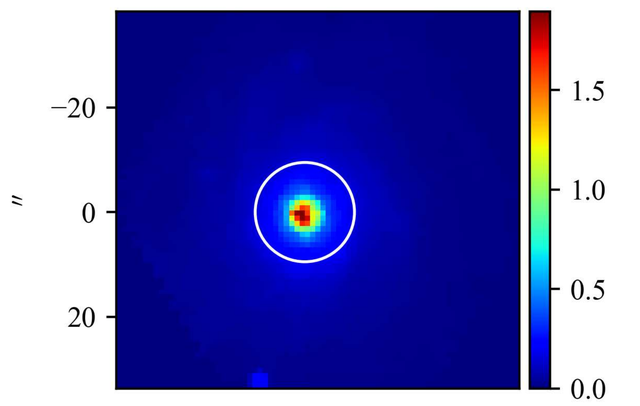

$\mathcal{M}_{\star,\mathrm{P}}$

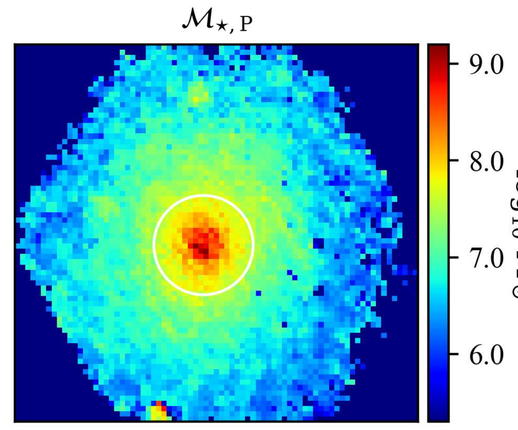

Log. of cumulative present stellar mass profiles

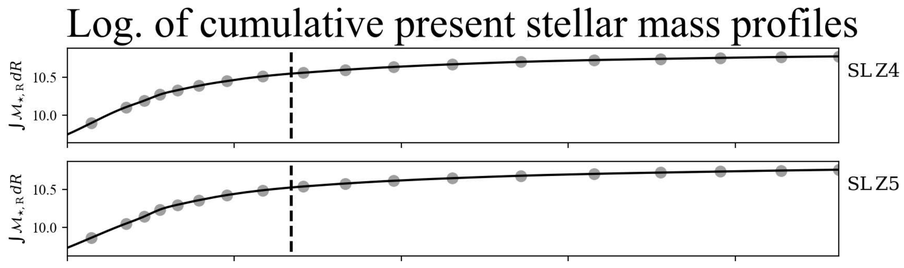

$Z_{\star,\mathcal{L}}$

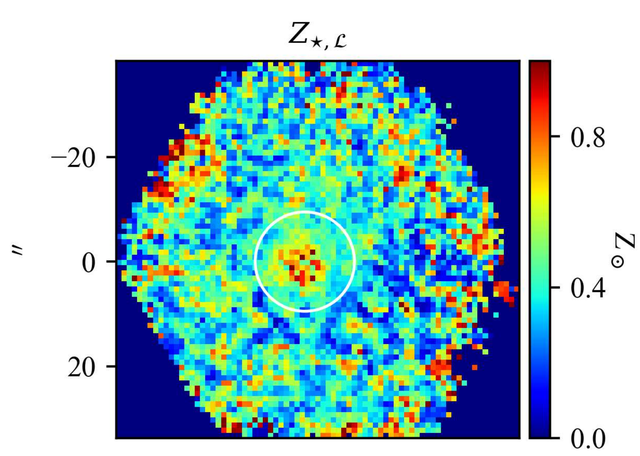

$Z_{\star,\mathcal{M}}$

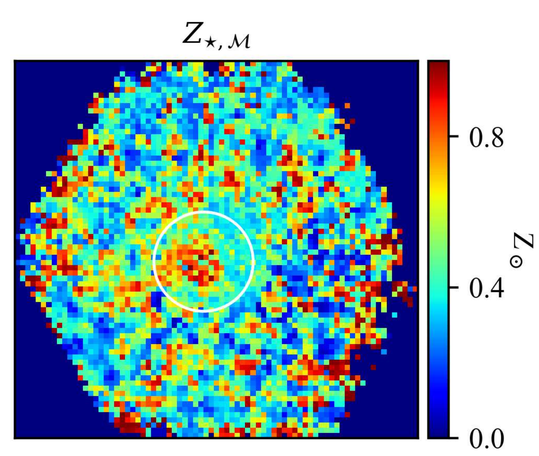

Stellar metallicity/Age & Hα flux/EW profiles

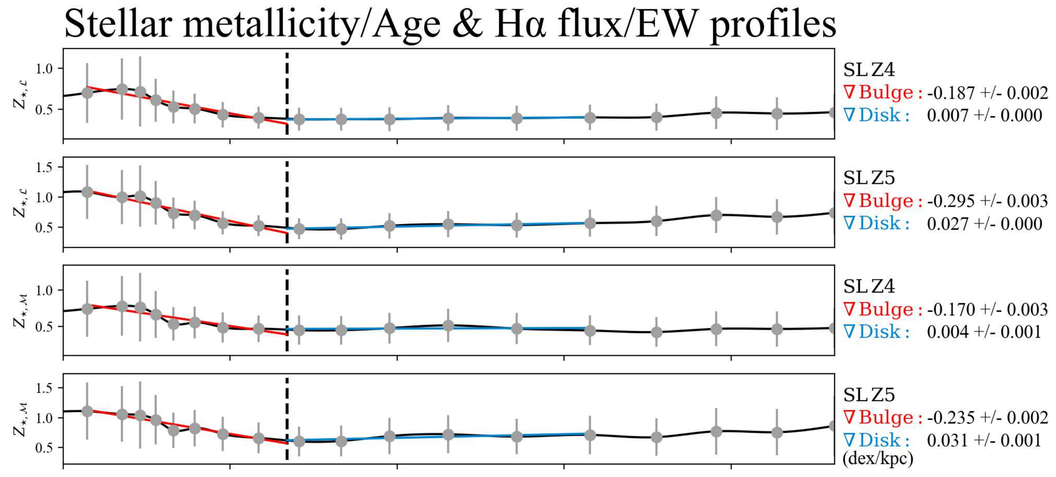

$t_{\star,\mathcal{L}}$

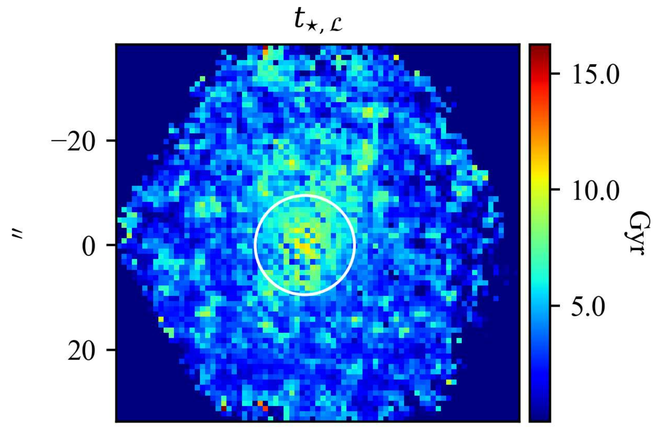

$t_{\star,\mathcal{M}}$

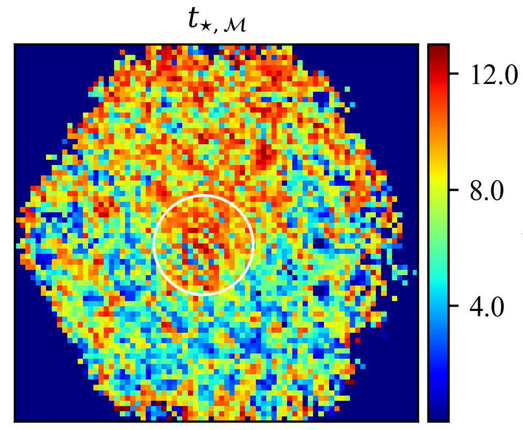

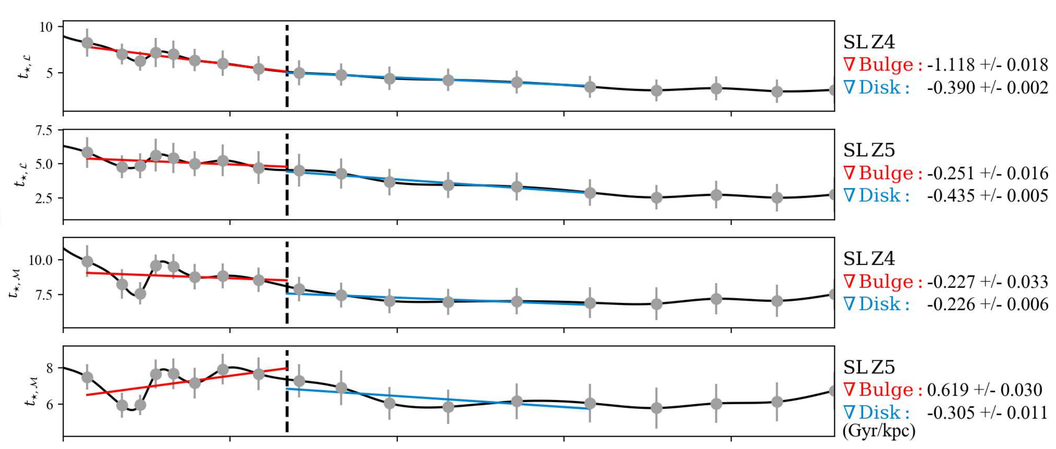

Hα flux

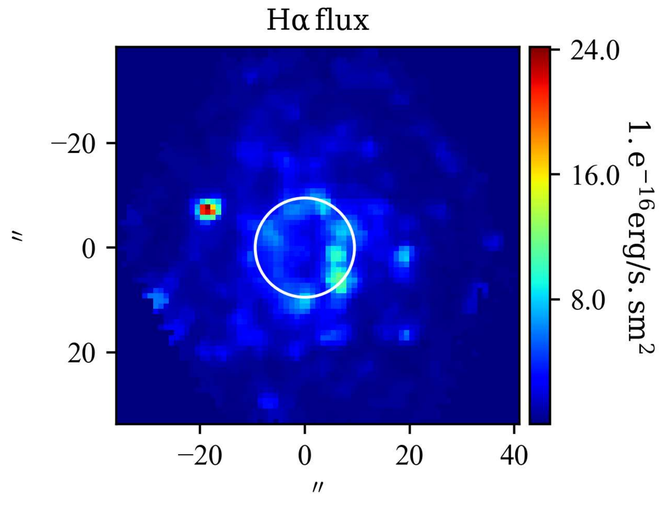

EW(Hα)

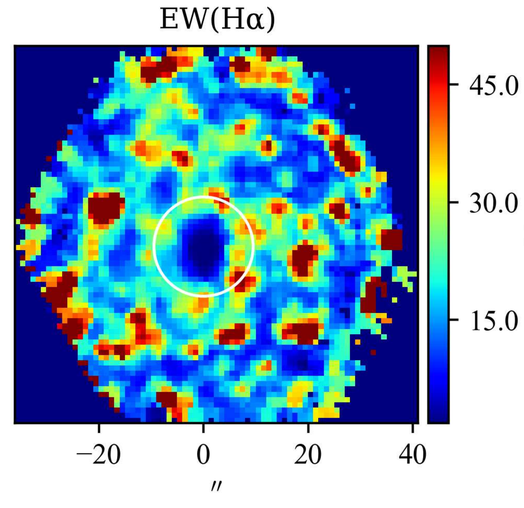

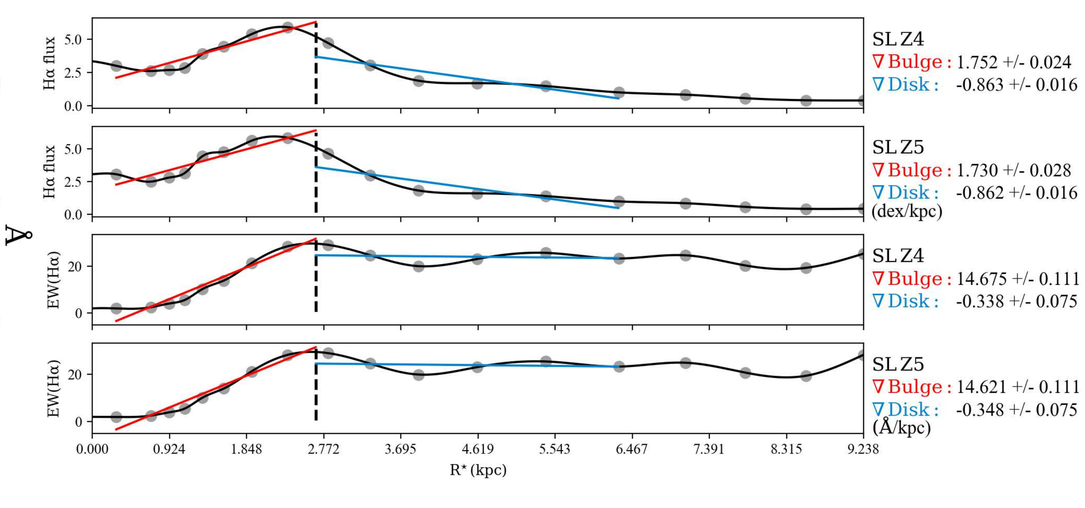

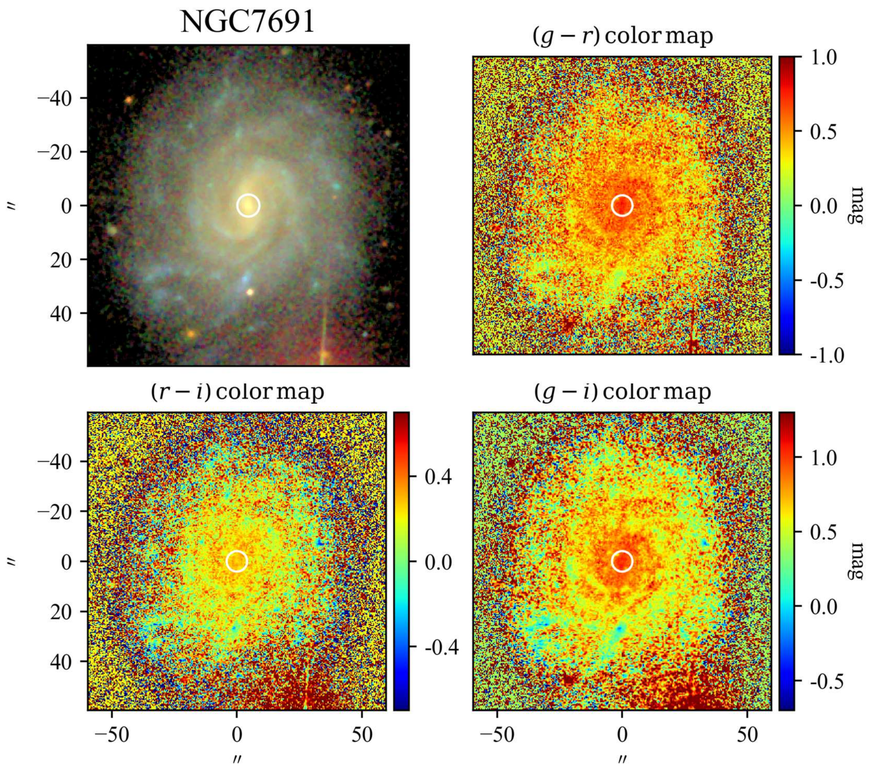

SBP decomposition of SDSS r band

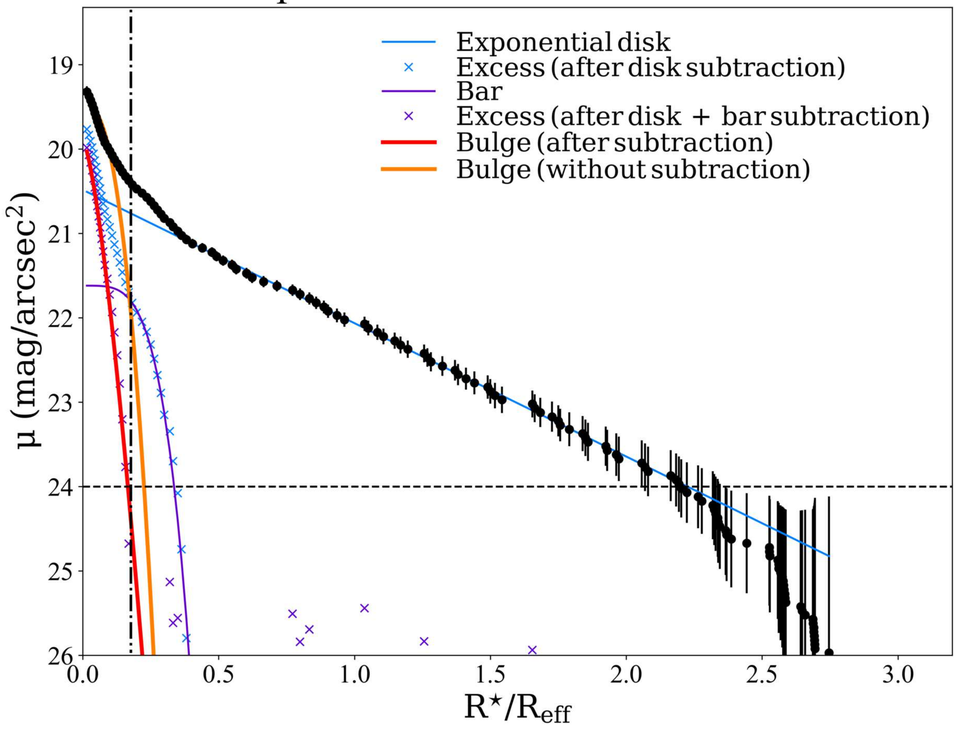

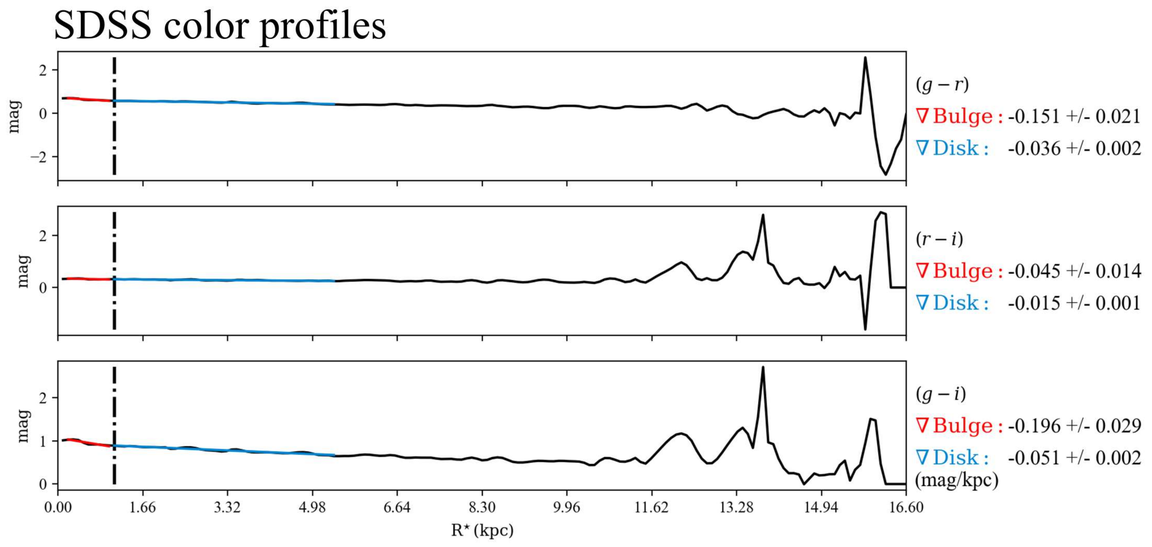

$\mathcal{RY}$ SBPs

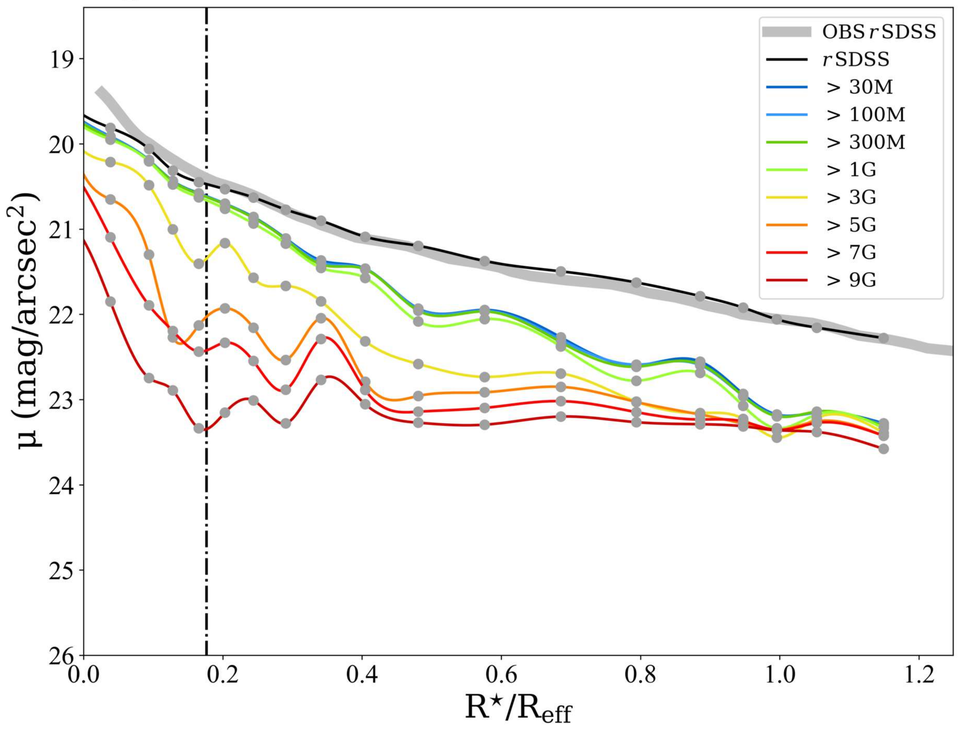

Stellar Continuum

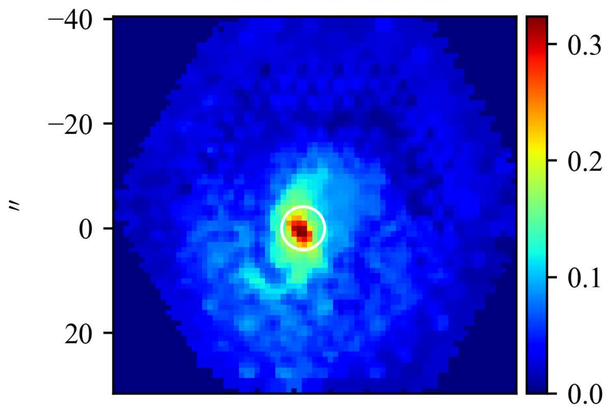

$\mathcal{M}_{\star,\mathrm{P}}$

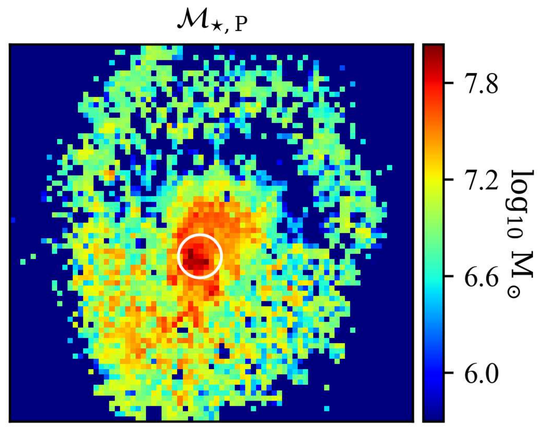

Log. of cumulative present stellar mass profiles

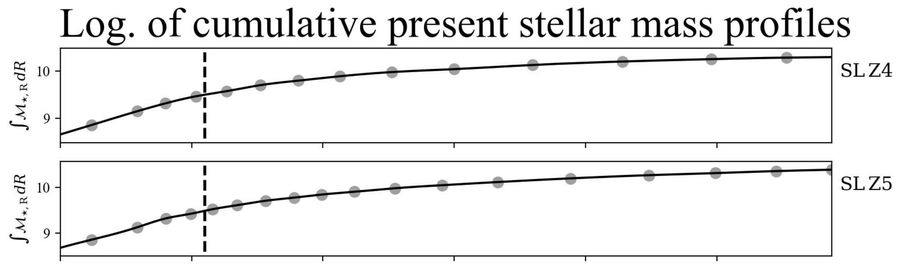

$Z_{\star,\mathcal{L}}$

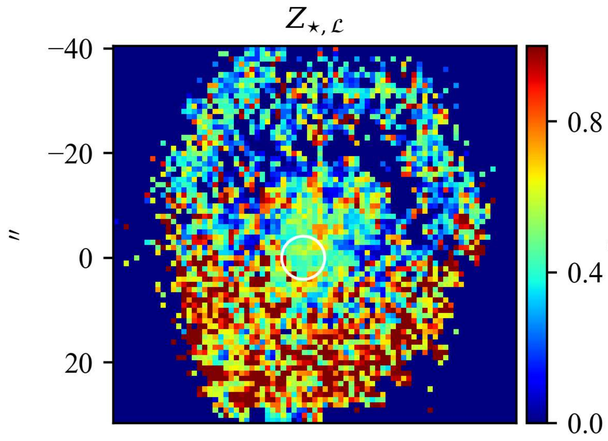

$Z_{\star,\mathcal{M}}$

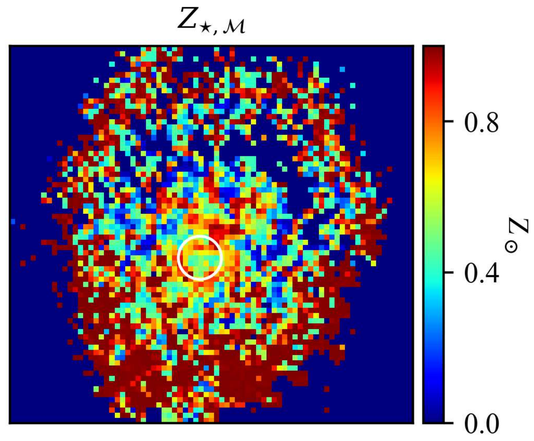

Stellar metallicity/Age & Hα flux/EW profiles

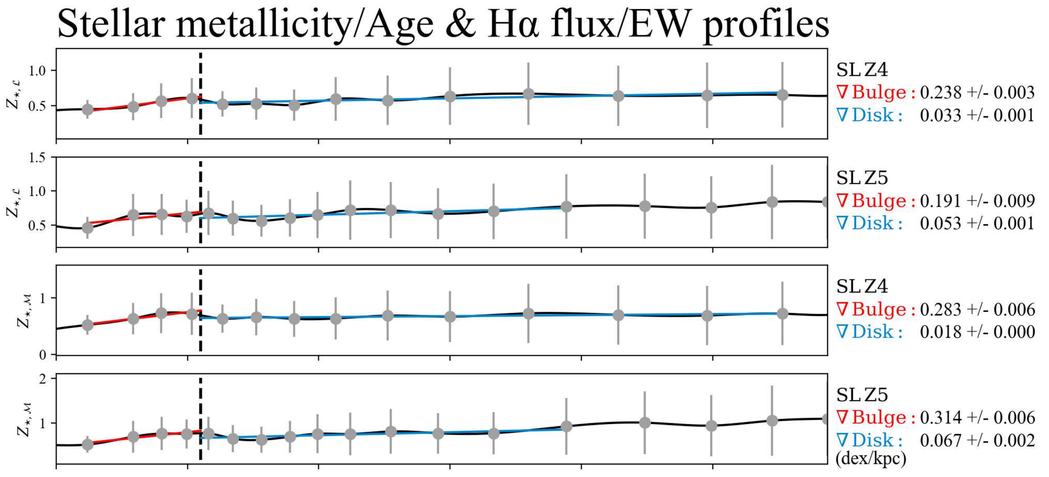

$t_{\star,\mathcal{L}}$

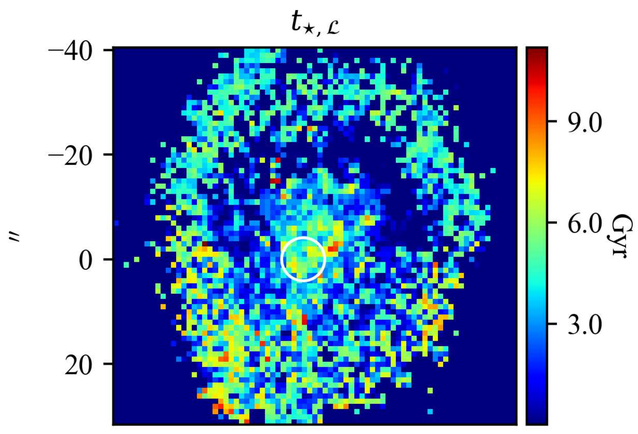

$t_{\star,\mathcal{M}}$

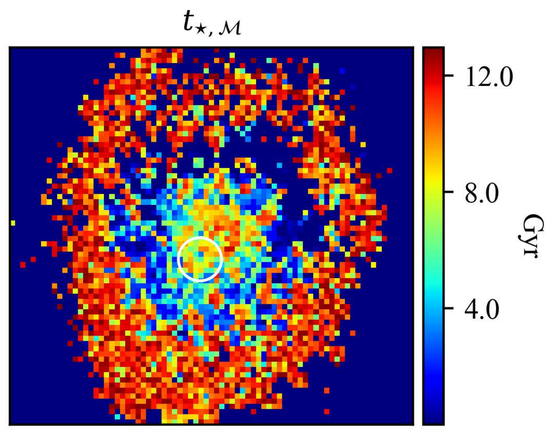

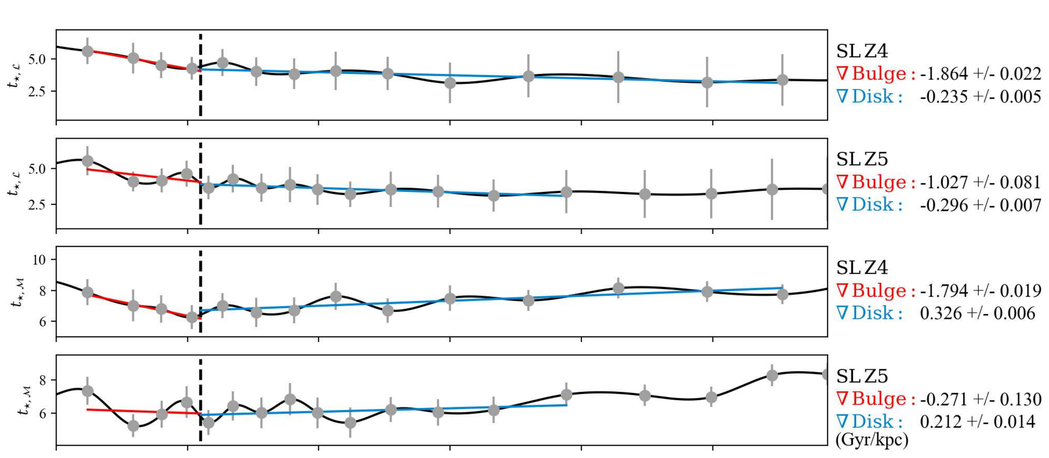

Hα flux

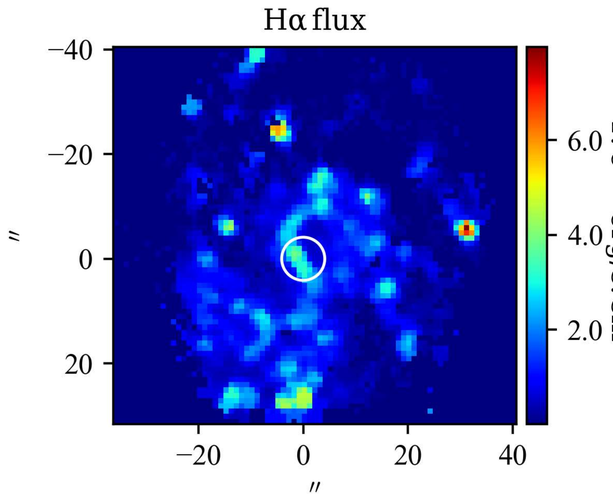

EW(Hα)

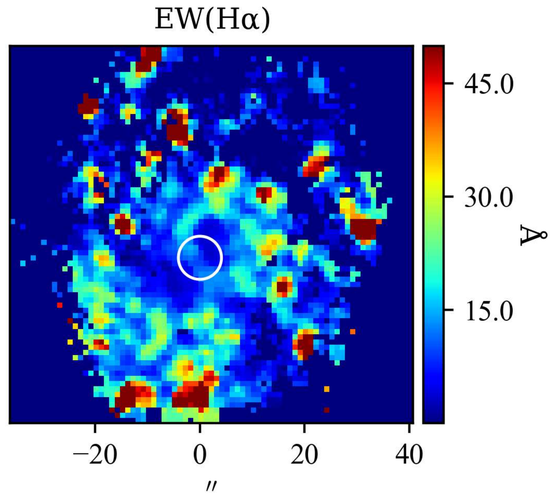

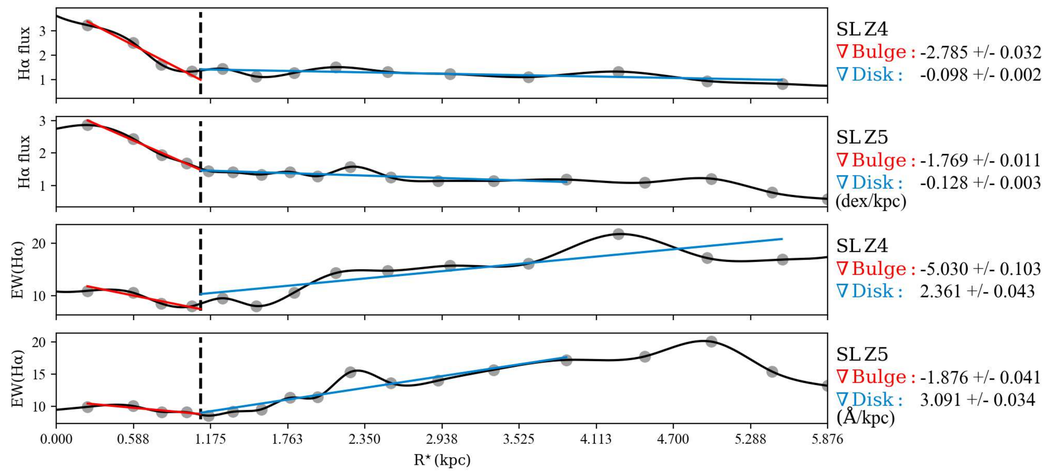

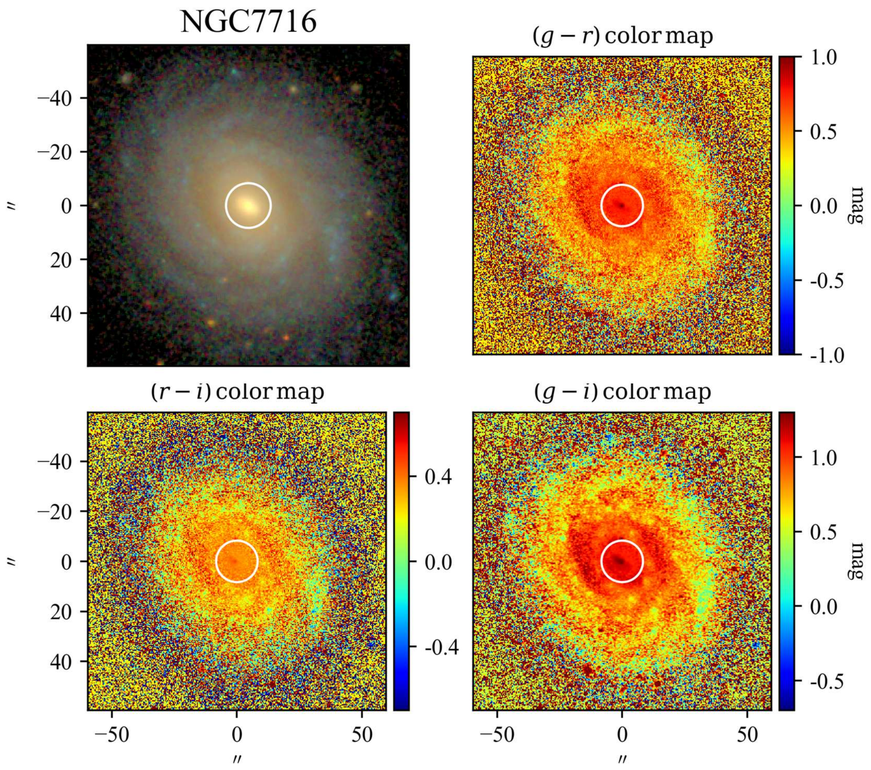

SBP decomposition of SDSS r band

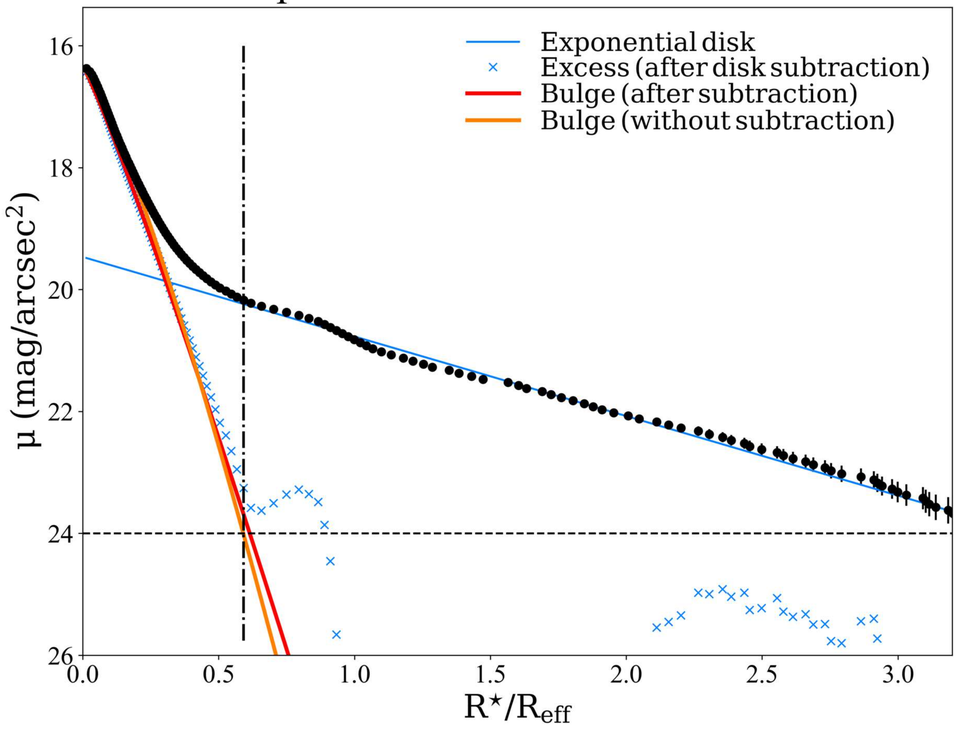

SDSS color profiles

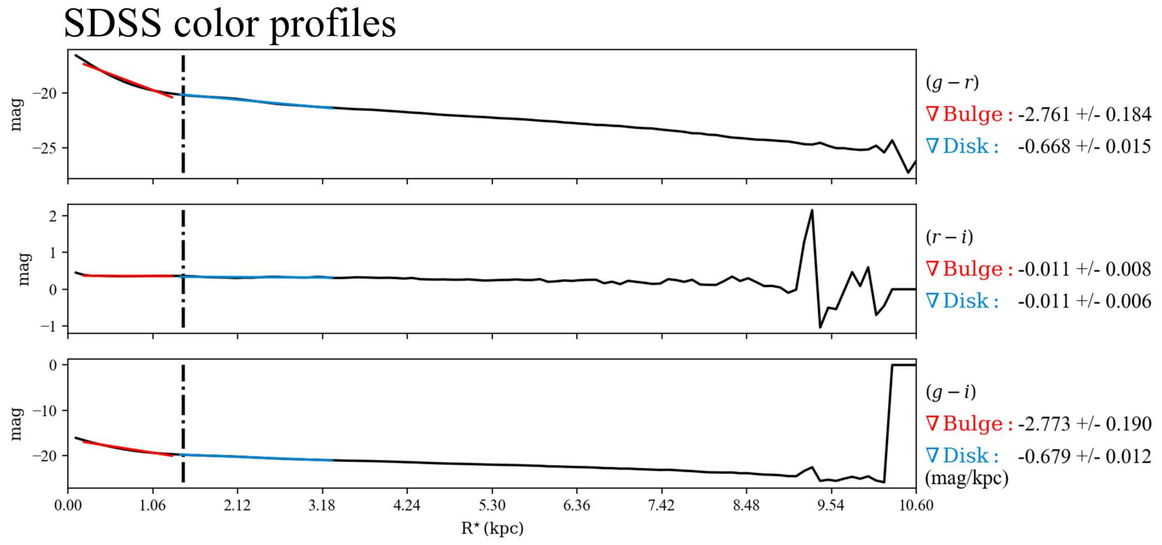

$\mathcal{RY}$ SBPs

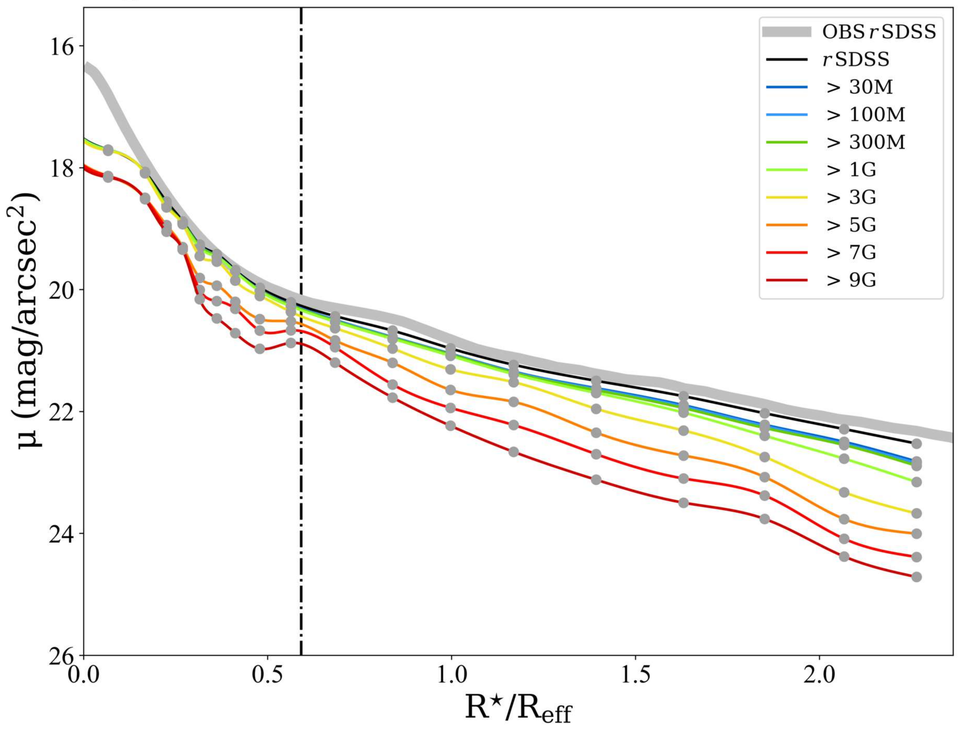

Stellar Continuum

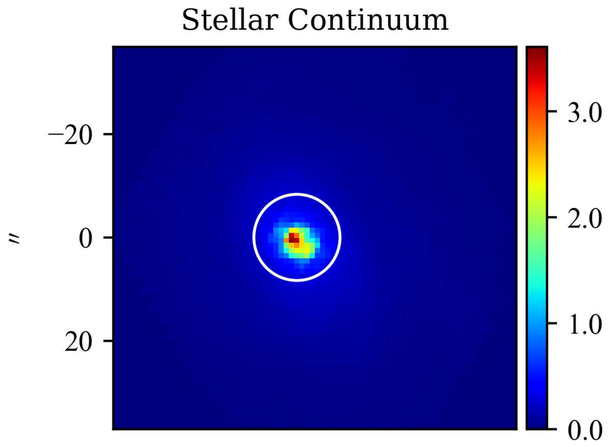

$\mathcal{M}_{\star,\,\mathrm{P}}$

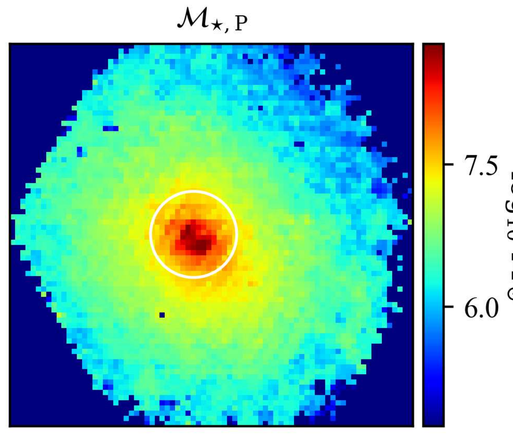

Log. of cumulative present stellar mass profiles

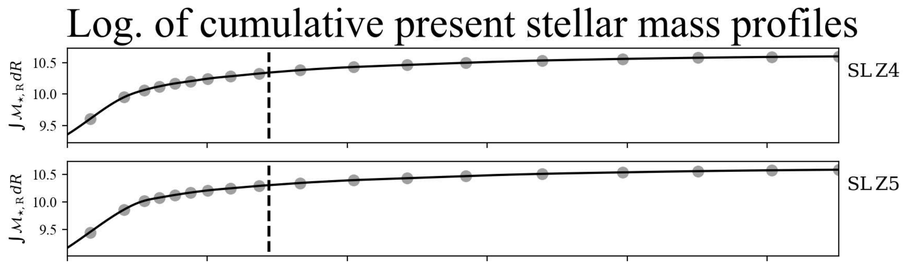

$Z_{\star,\,\mathcal{L}}$

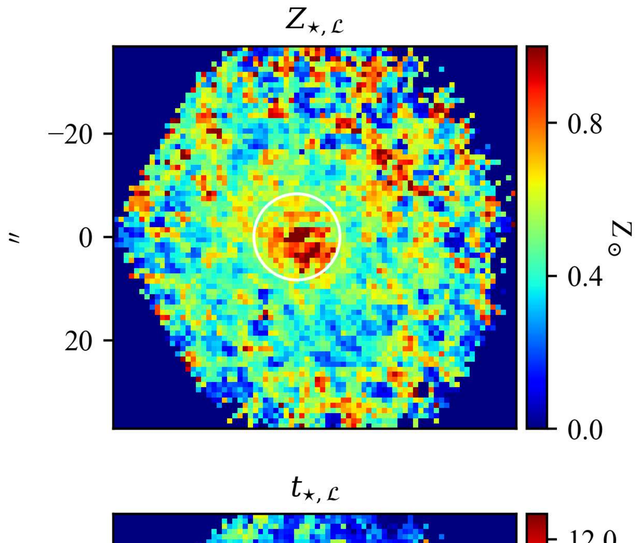

$Z_{\star,\,\mathcal{M}}$

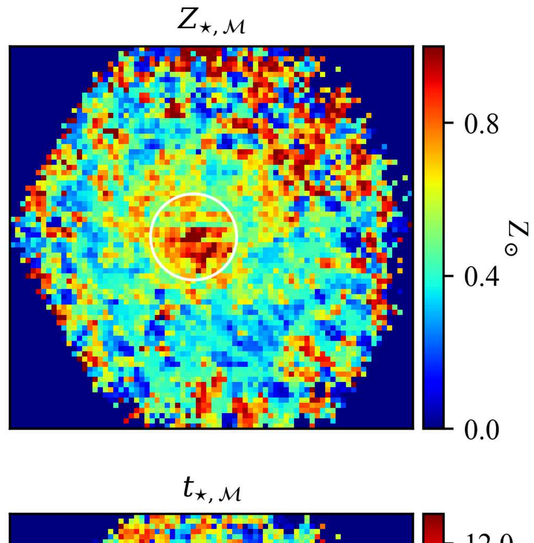

Stellar metallicity/Age & Hα flux/EW profiles

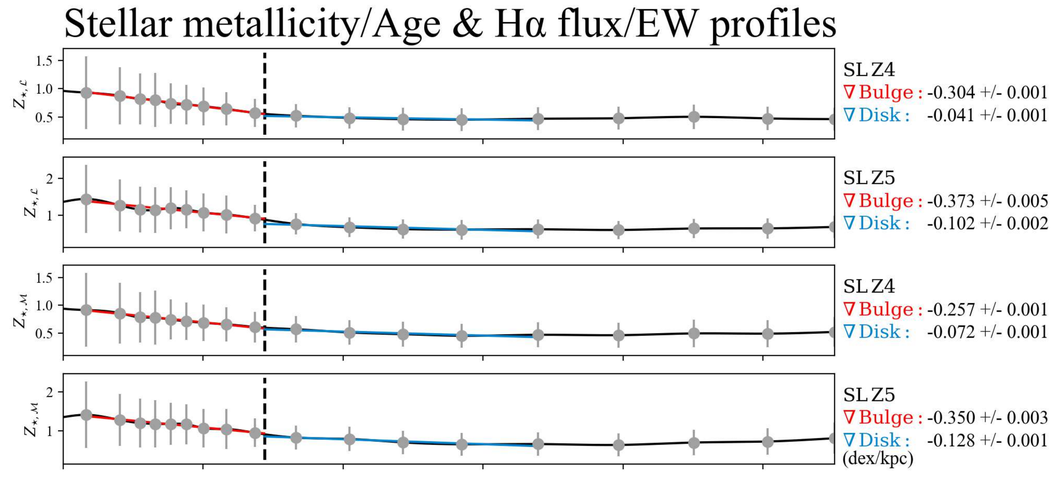

$t_{\star,\,\mathcal{L}}$

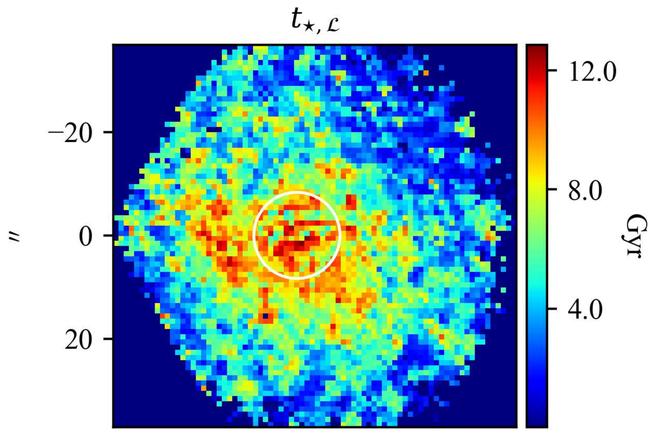

$t_{\star,\,\mathcal{M}}$

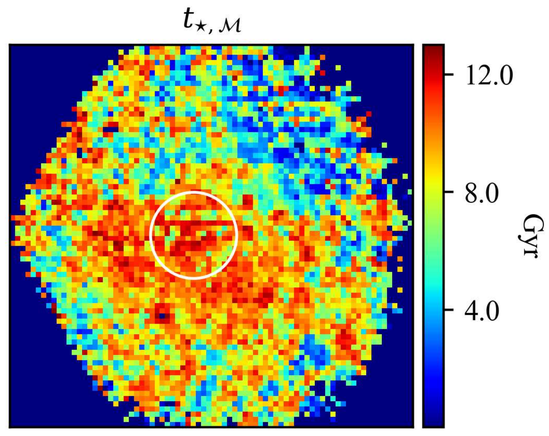

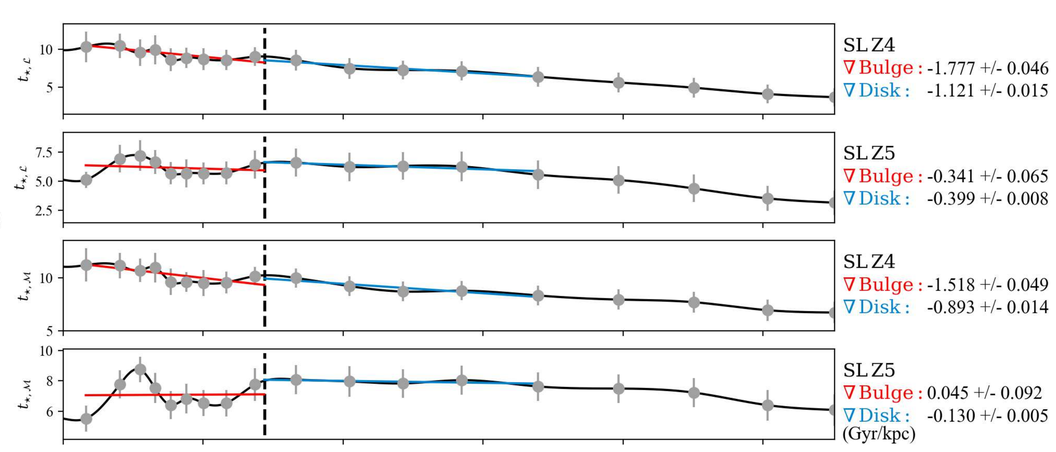

Hα flux

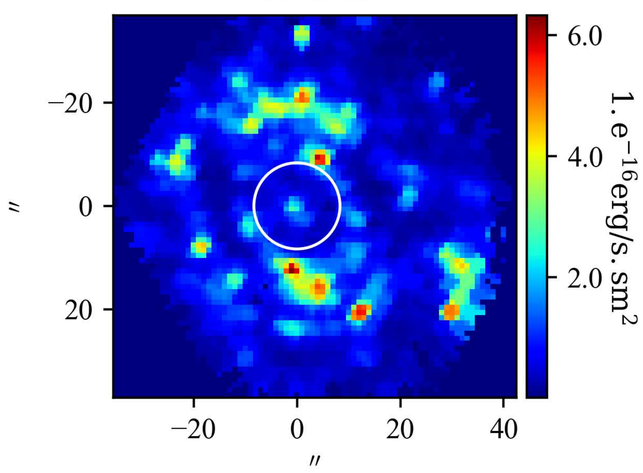

EW(Hα)

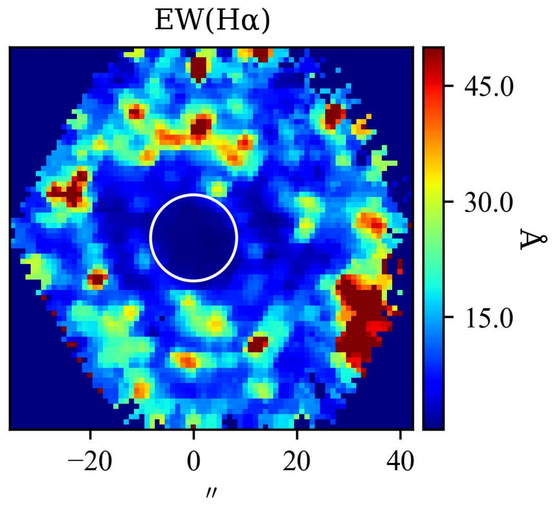

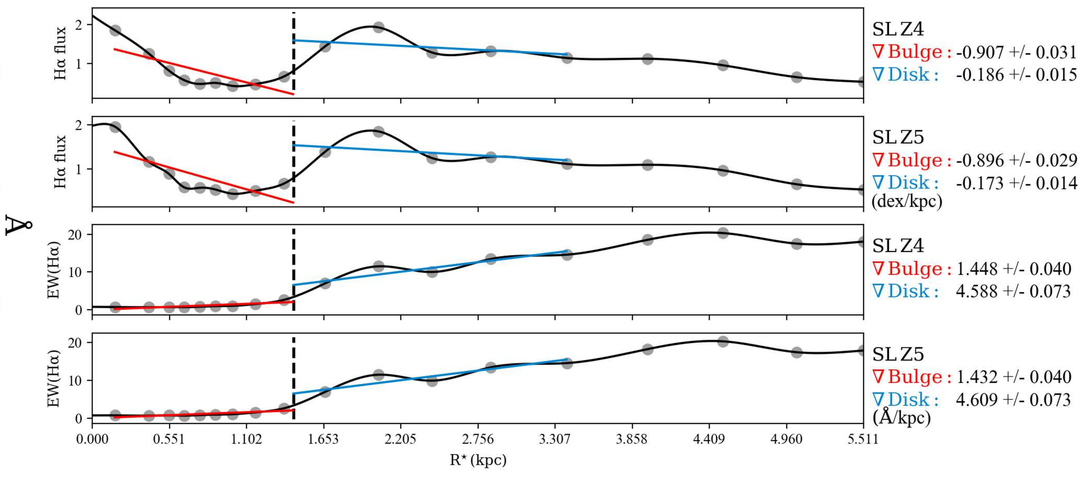

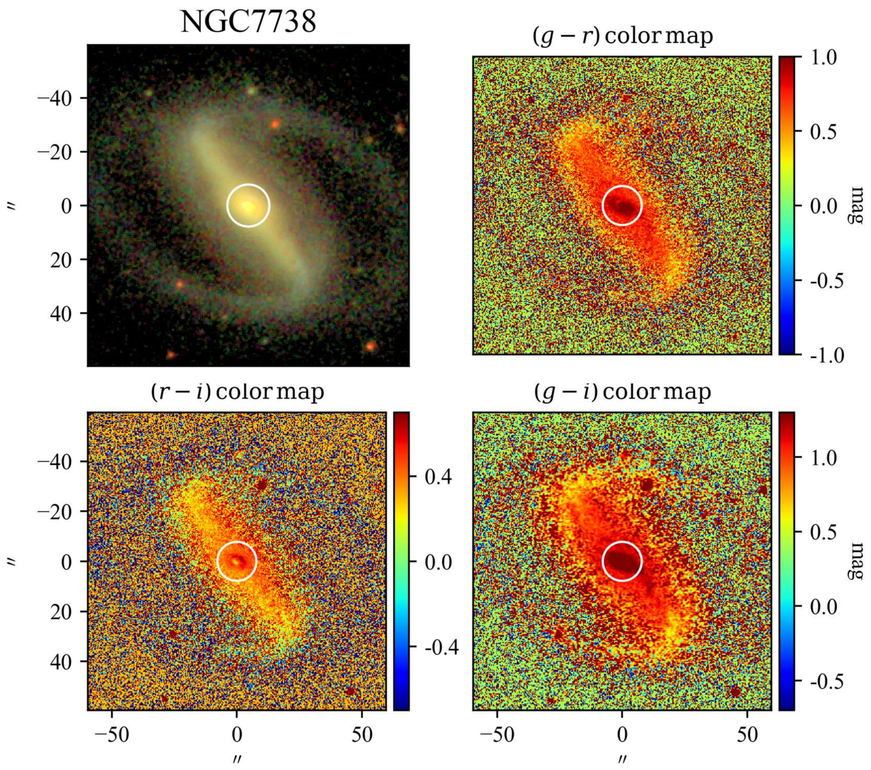

SBP decomposition of SDSS r band

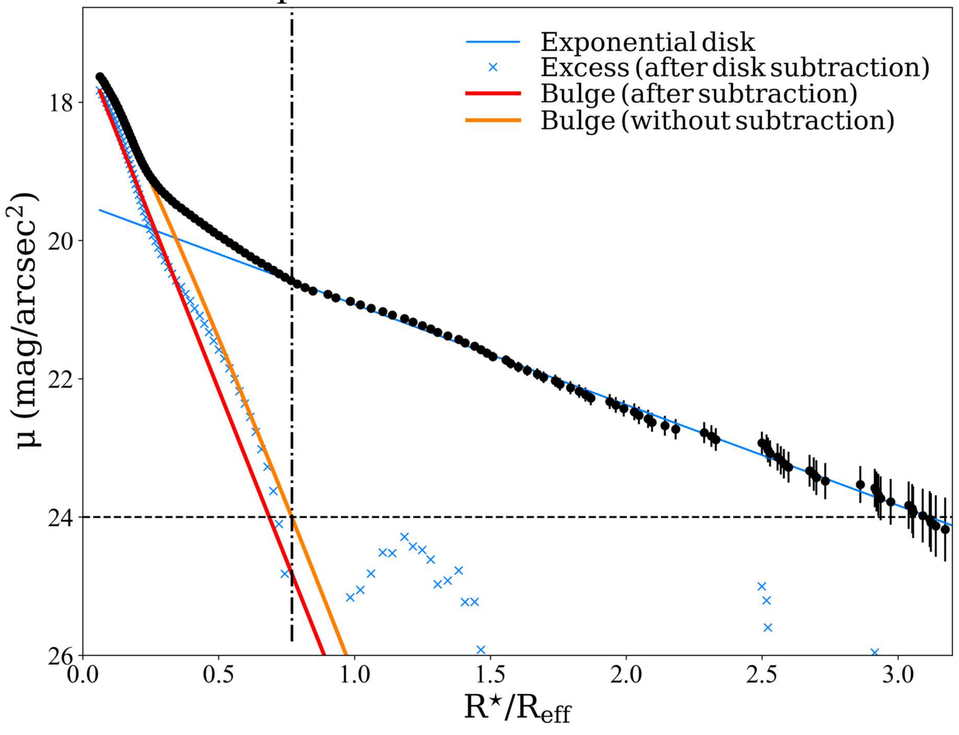

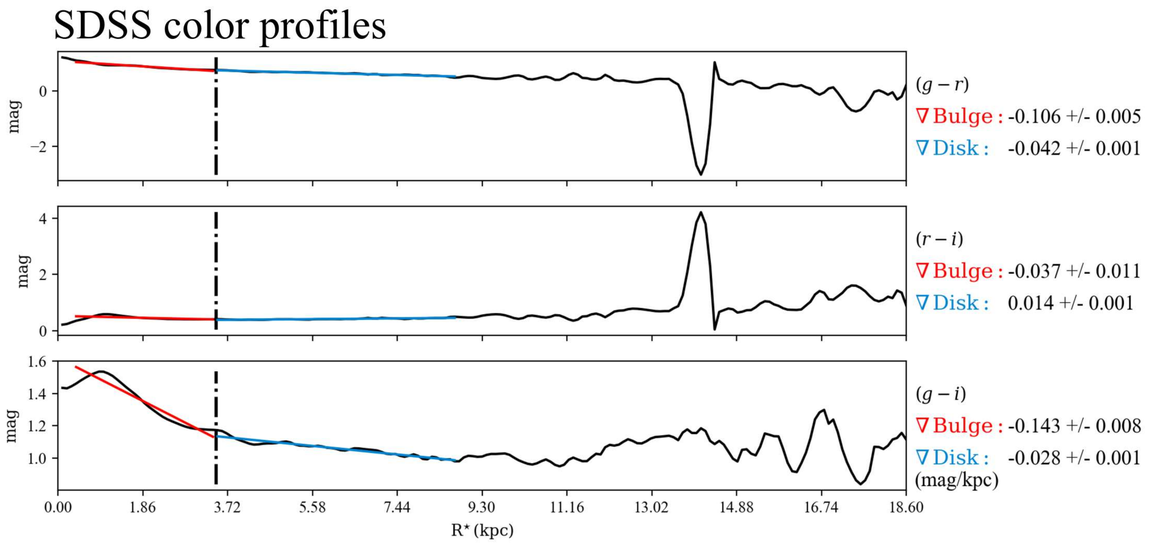

$\mathcal{RY}$ SBPs

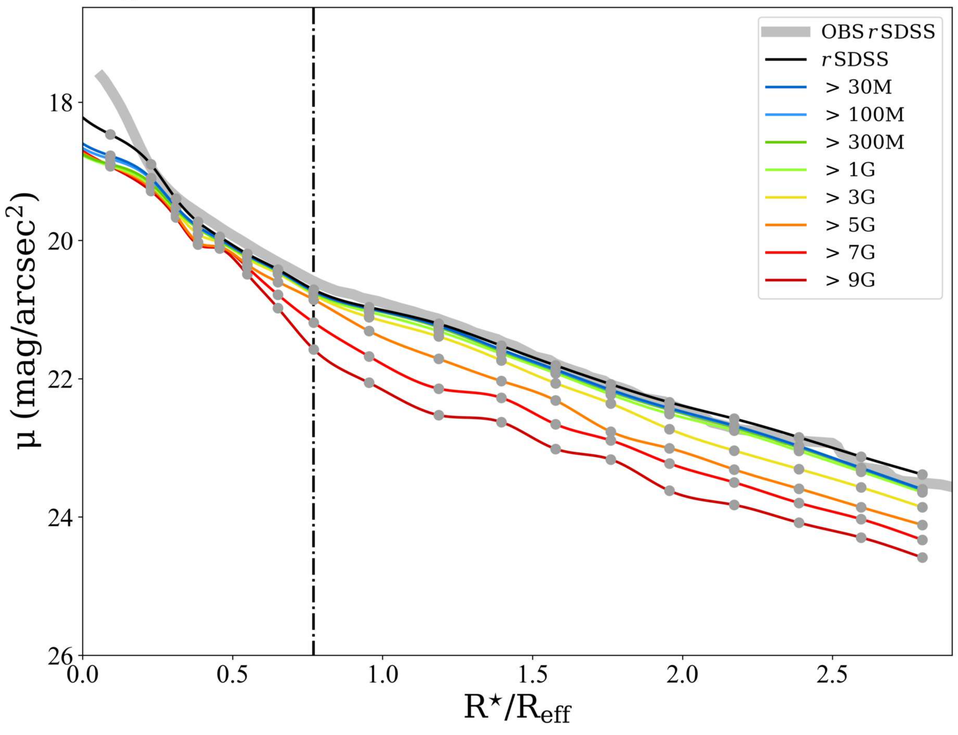

Stellar Continuum $\mathcal{M}_{\star,\mathrm{P}}$

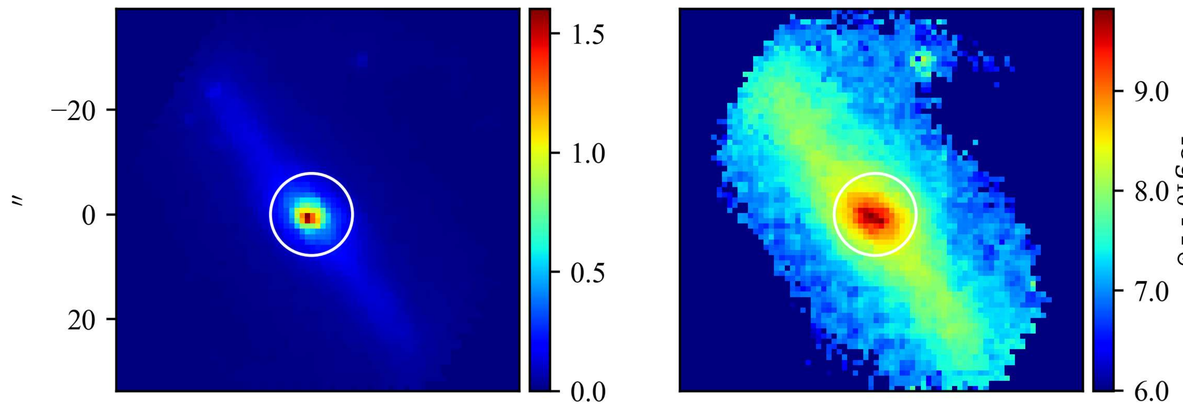

Log. of cumulative present stellar mass profiles

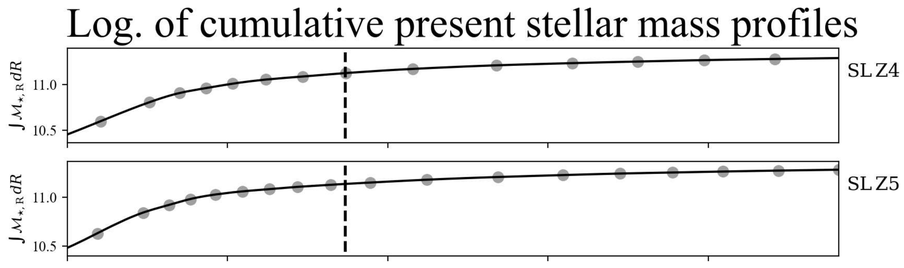

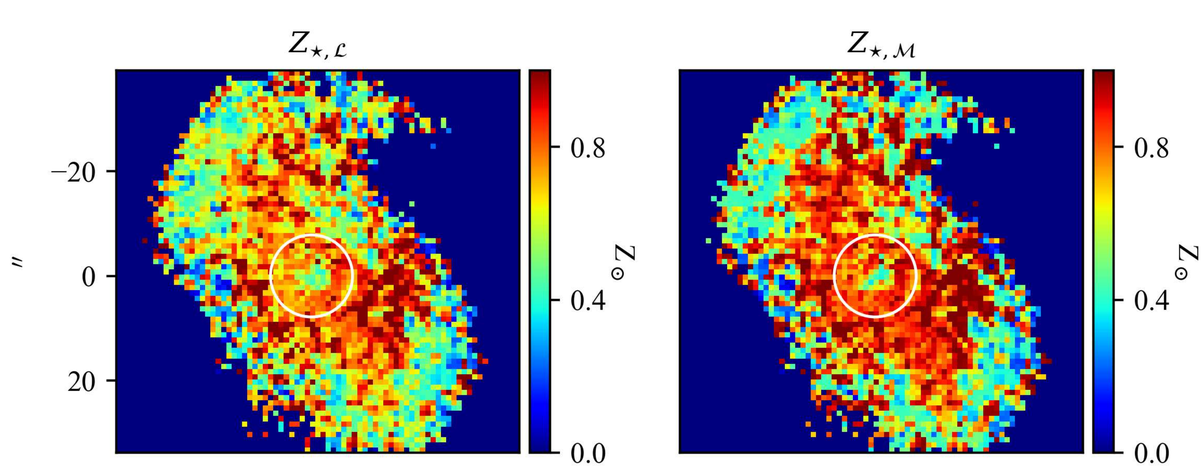

Stellar metallicity/Age & Hα flux/EW profiles

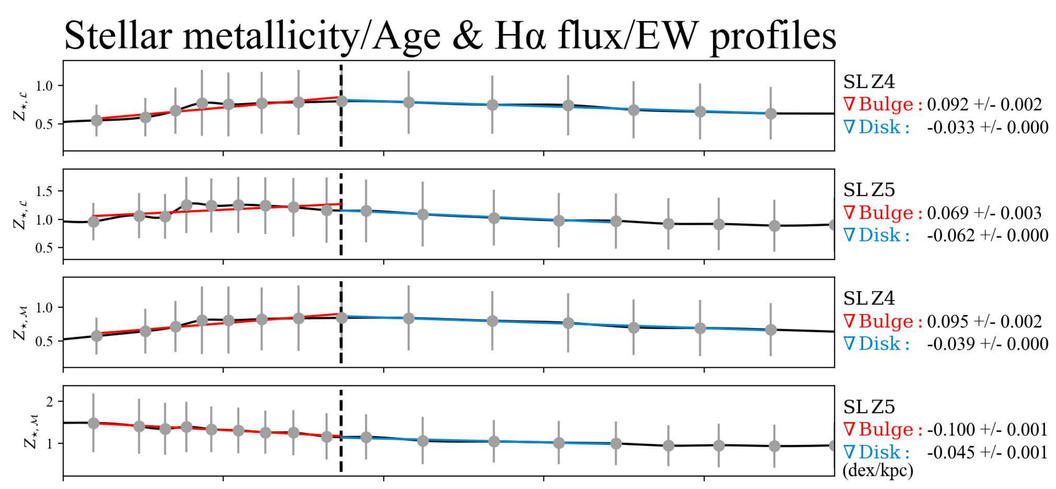

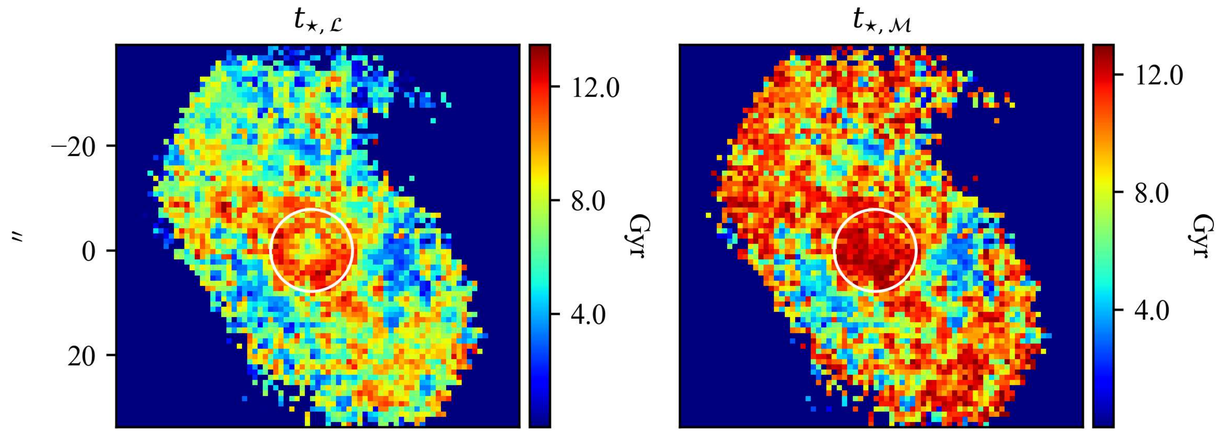

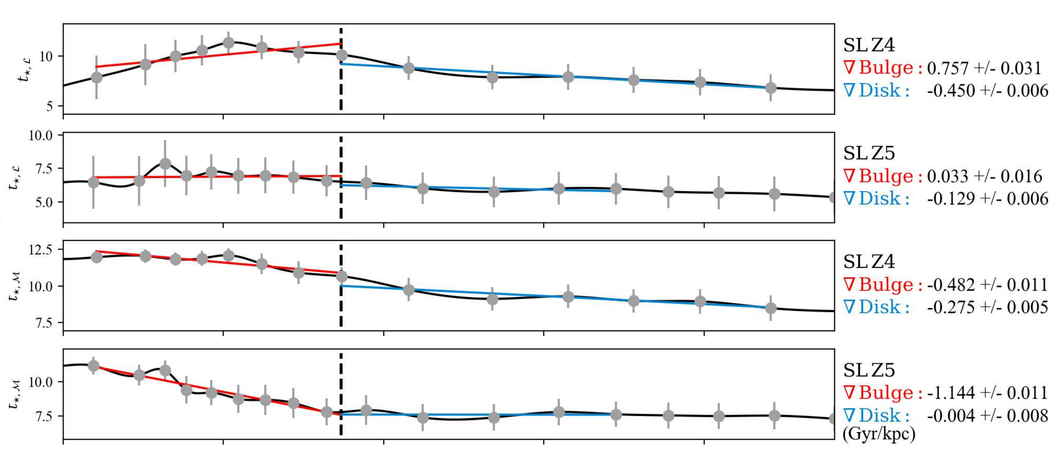

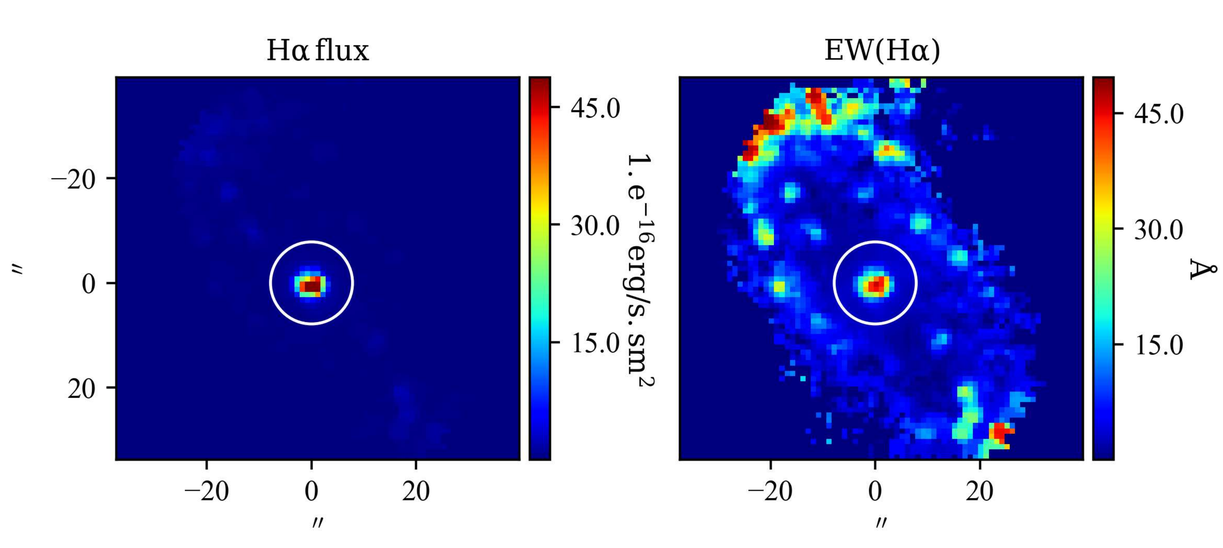

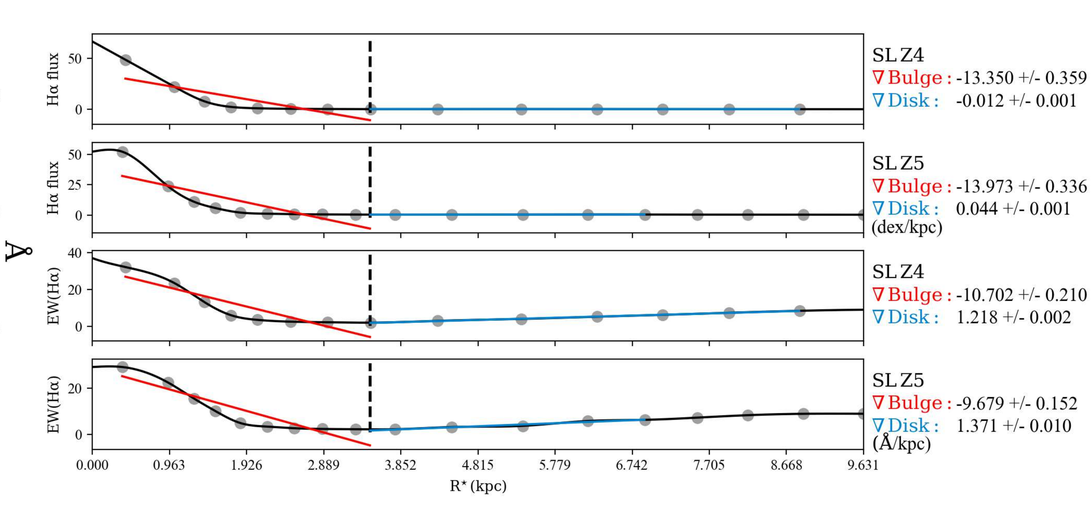

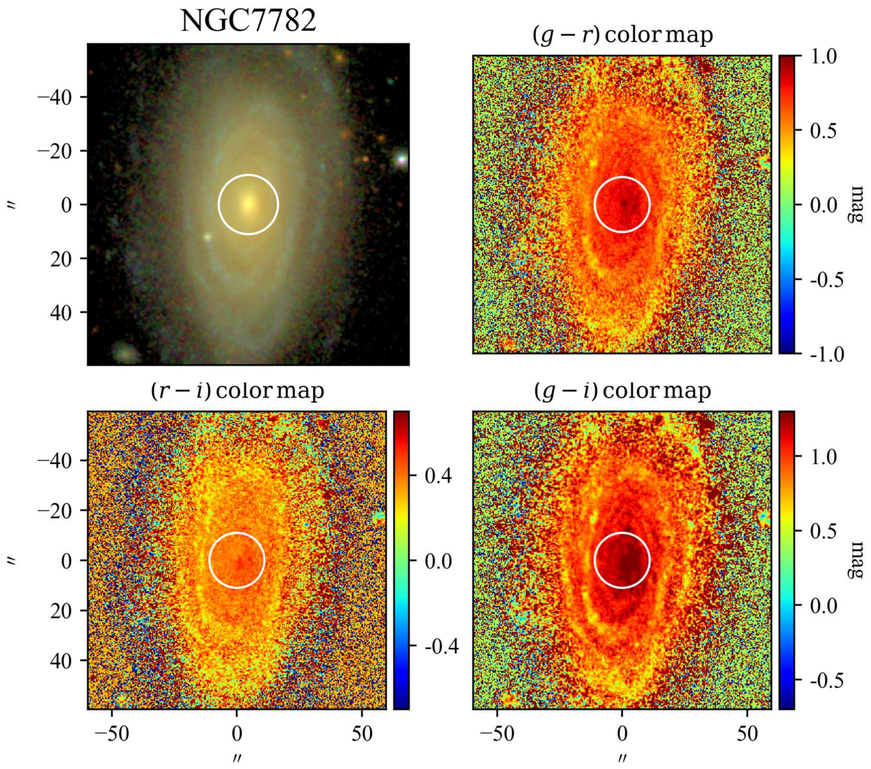
NGC7782
$(g-r)$ color map
$(r-i)$ color map
$(g-i)$ color map
mag
″

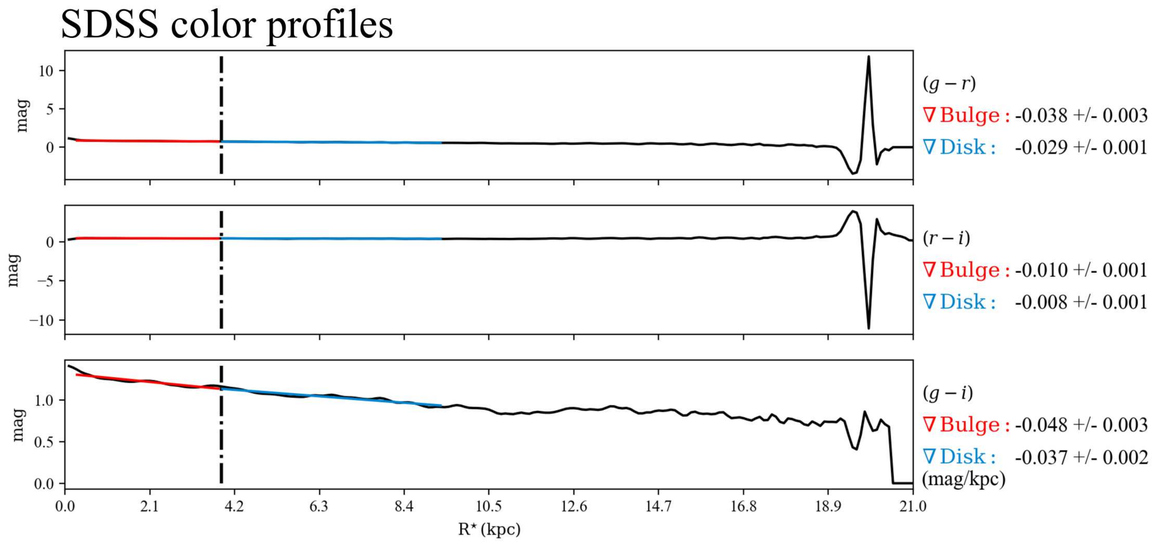
SDSS color profiles
$(g-r)$
∇ Bulge : -0.038 +/- 0.003
∇ Disk : -0.029 +/- 0.001
$(r-i)$
∇ Bulge : -0.010 +/- 0.001
∇ Disk : -0.008 +/- 0.001
$(g-i)$
∇ Bulge : -0.048 +/- 0.003
∇ Disk : -0.037 +/- 0.002
(mag/kpc)
mag
R* (kpc)

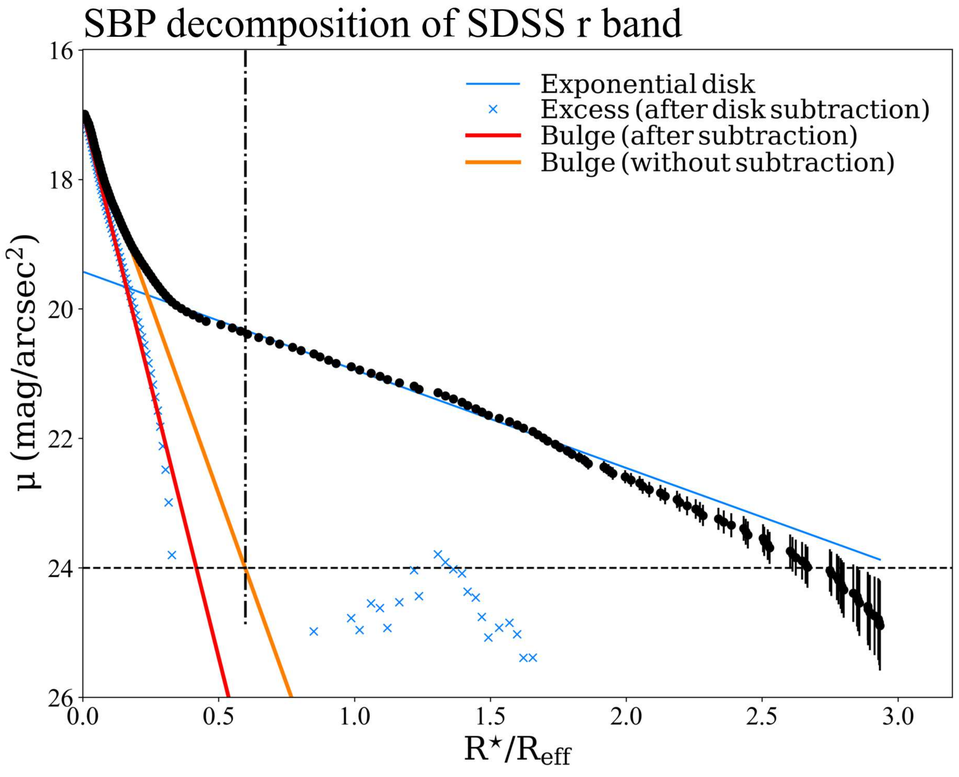
SBP decomposition of SDSS r band
Exponential disk
Excess (after disk subtraction)
Bulge (after subtraction)
Bulge (without subtraction)
μ (mag/arcsec^2)
R*/R$_{eff}$

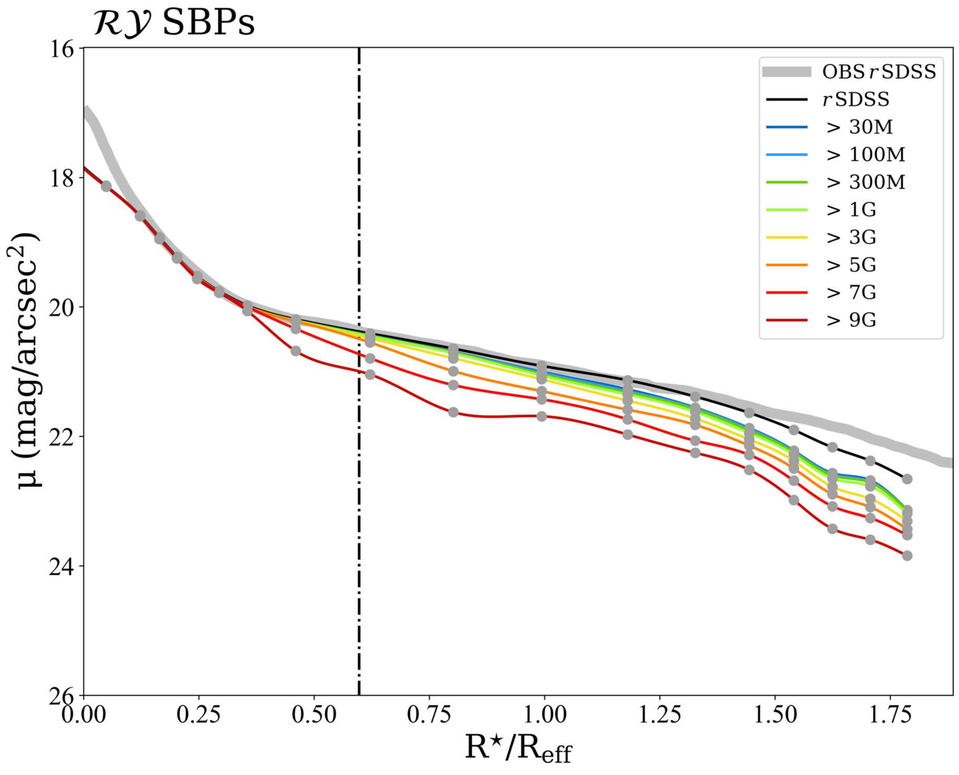
$\mathcal{RY}$ SBPs
OBS rSDSS
rSDSS
> 30M
> 100M
> 300M
> 1G
> 3G
> 5G
> 7G
> 9G
μ (mag/arcsec^2)
R*/R$_{eff}$

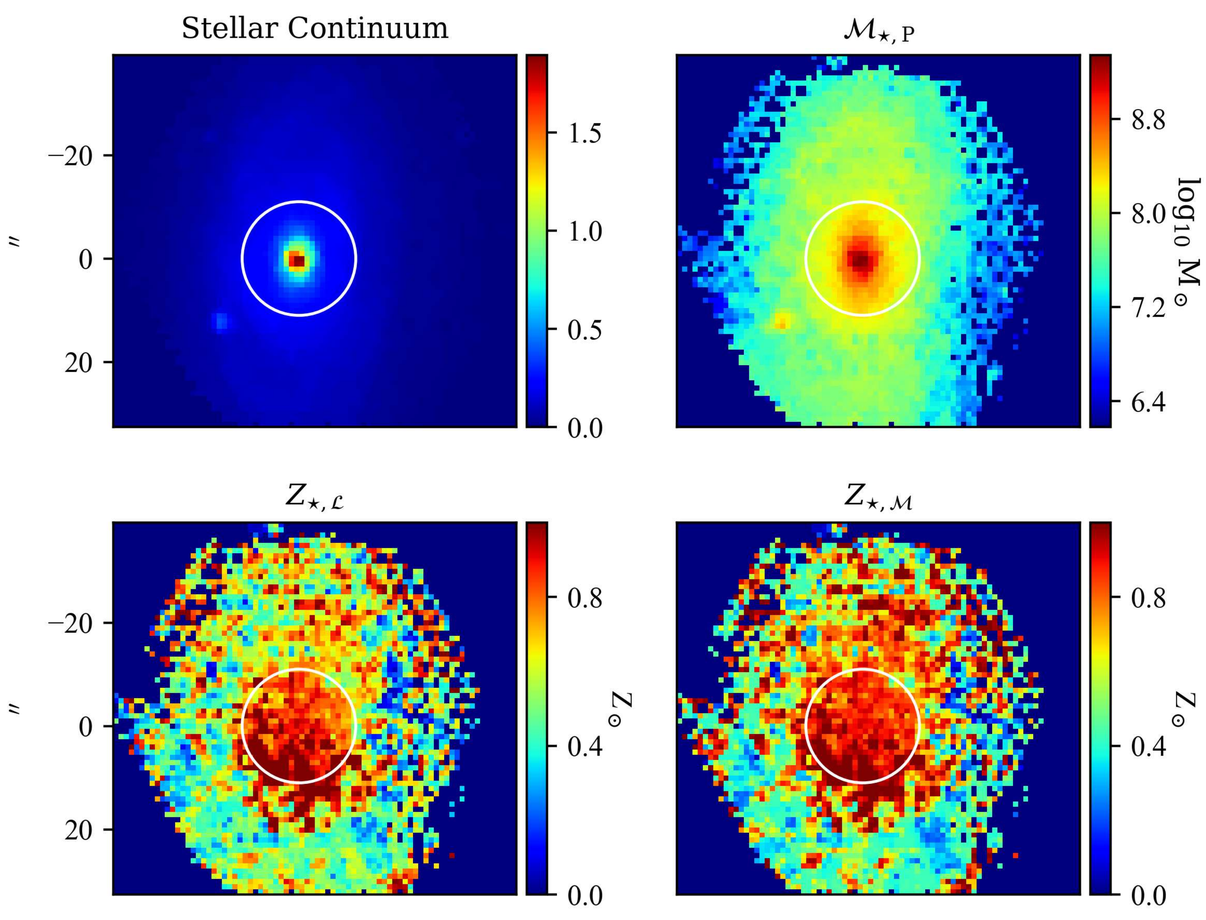
Stellar Continuum
$\mathcal{M}_{\star,\mathrm{P}}$
log10 M$_\odot$
″

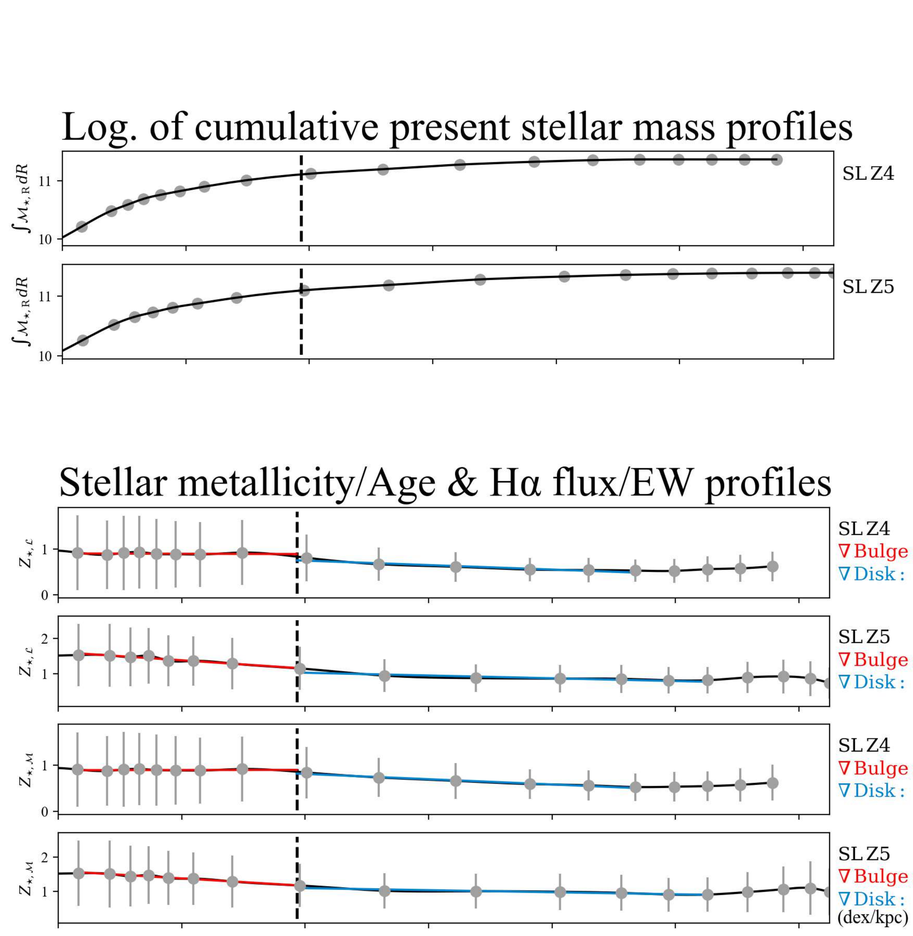
Log. of cumulative present stellar mass profiles
SL Z4
SL Z5

$Z_{\star,\mathcal{L}}$
$Z_{\star,\mathcal{M}}$
Z$_\odot$
″

Stellar metallicity/Age & Hα flux/EW profiles
SL Z4
∇ Bulge : -0.003 +/- 0.001
∇ Disk : -0.049 +/- 0.000
SL Z5
∇ Bulge : -0.117 +/- 0.001
∇ Disk : -0.039 +/- 0.001
SL Z4
∇ Bulge : 0.002 +/- 0.001
∇ Disk : -0.057 +/- 0.000
SL Z5
∇ Bulge : -0.108 +/- 0.001
∇ Disk : -0.030 +/- 0.000
(dex/kpc)

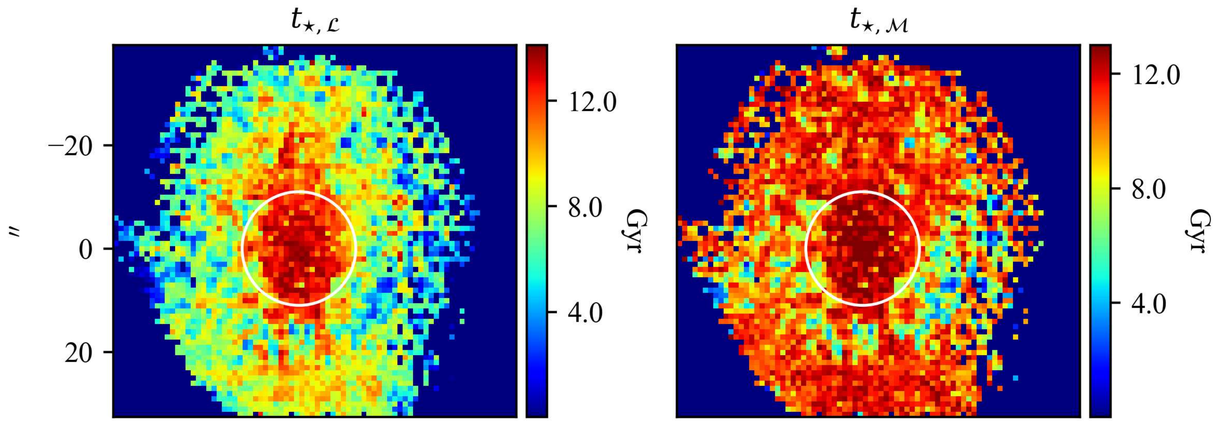
$t_{\star,\mathcal{L}}$
$t_{\star,\mathcal{M}}$
Gyr
″

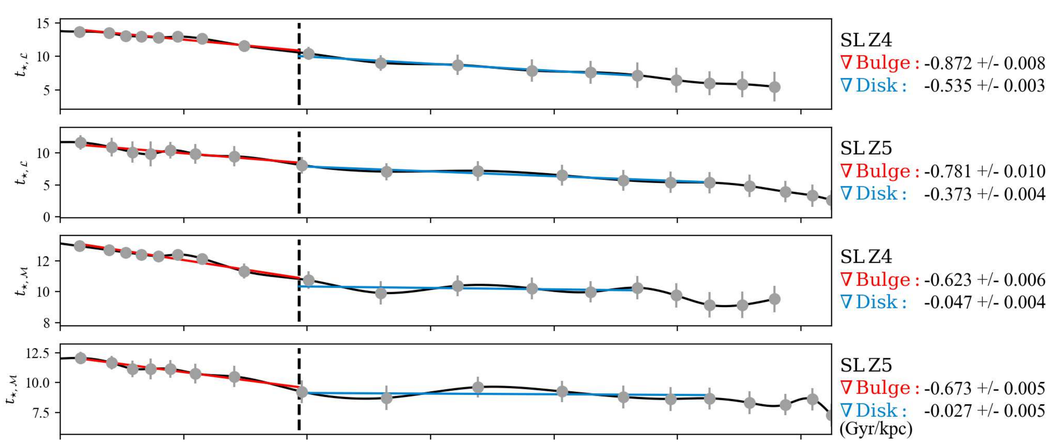
SL Z4
∇ Bulge : -0.872 +/- 0.008
∇ Disk : -0.535 +/- 0.003
SL Z5
∇ Bulge : -0.781 +/- 0.010
∇ Disk : -0.373 +/- 0.004
SL Z4
∇ Bulge : -0.623 +/- 0.006
∇ Disk : -0.047 +/- 0.004
SL Z5
∇ Bulge : -0.673 +/- 0.005
∇ Disk : -0.027 +/- 0.005
(Gyr/kpc)

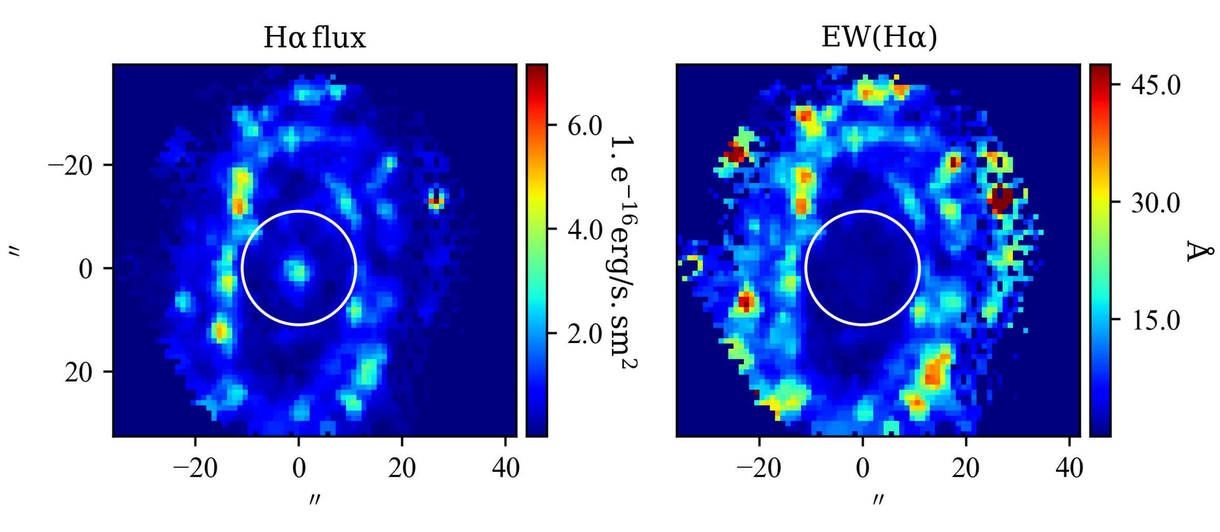
Hα flux
EW(Hα)
1. e^{-16}erg/s. sm^2
Å
″

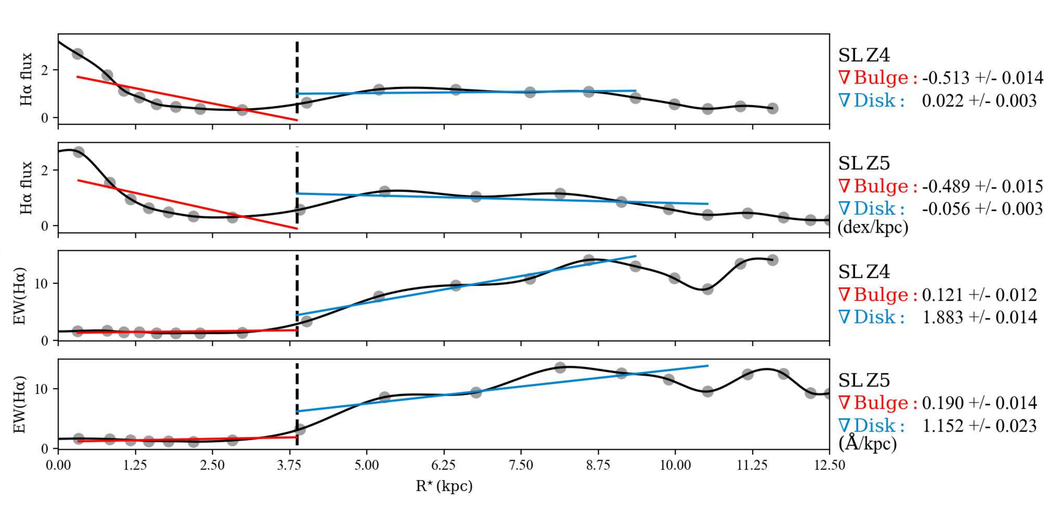
SL Z4
∇ Bulge : -0.513 +/- 0.014
∇ Disk : 0.022 +/- 0.003
SL Z5
∇ Bulge : -0.489 +/- 0.015
∇ Disk : -0.056 +/- 0.003
(dex/kpc)
SL Z4
∇ Bulge : 0.121 +/- 0.012
∇ Disk : 1.883 +/- 0.014
SL Z5
∇ Bulge : 0.190 +/- 0.014
∇ Disk : 1.152 +/- 0.023
(Å/kpc)
R* (kpc)

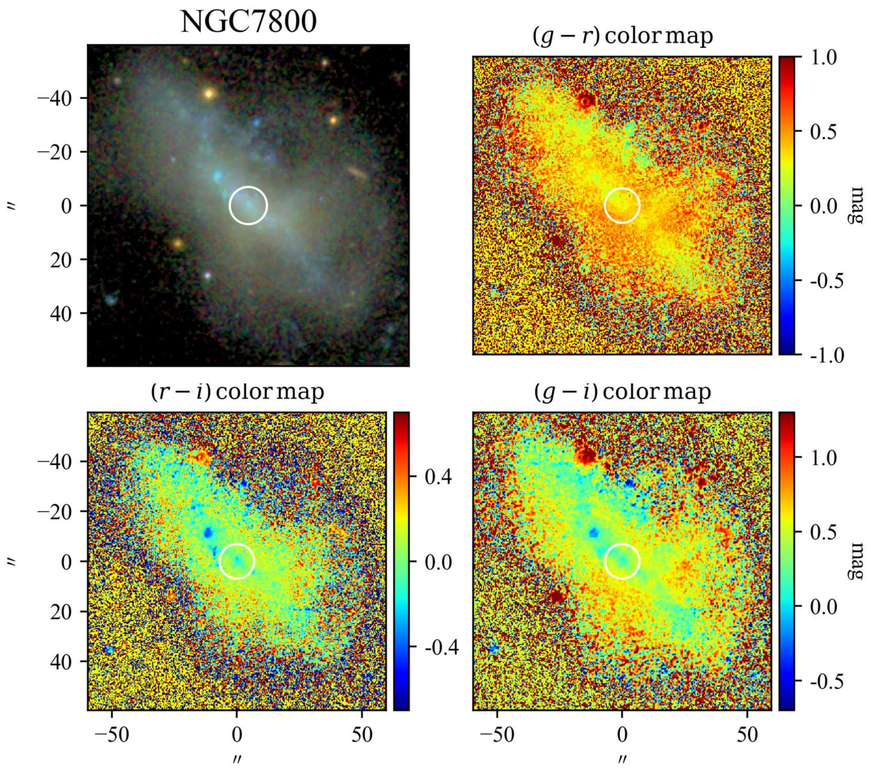

SBP decomposition of SDSS r band

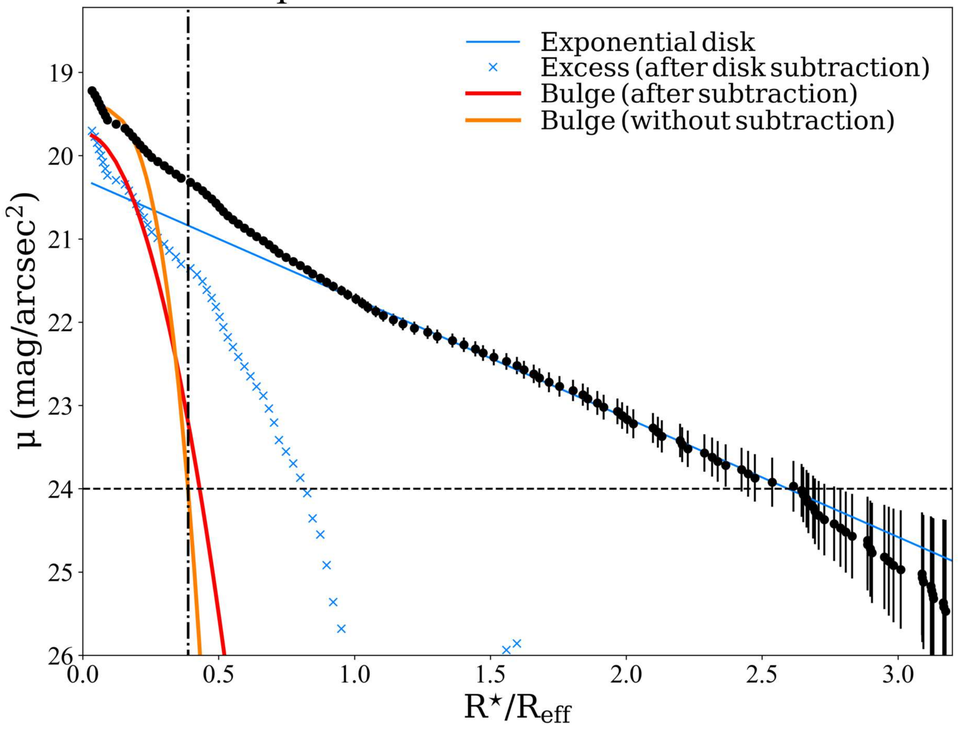

SDSS color profiles

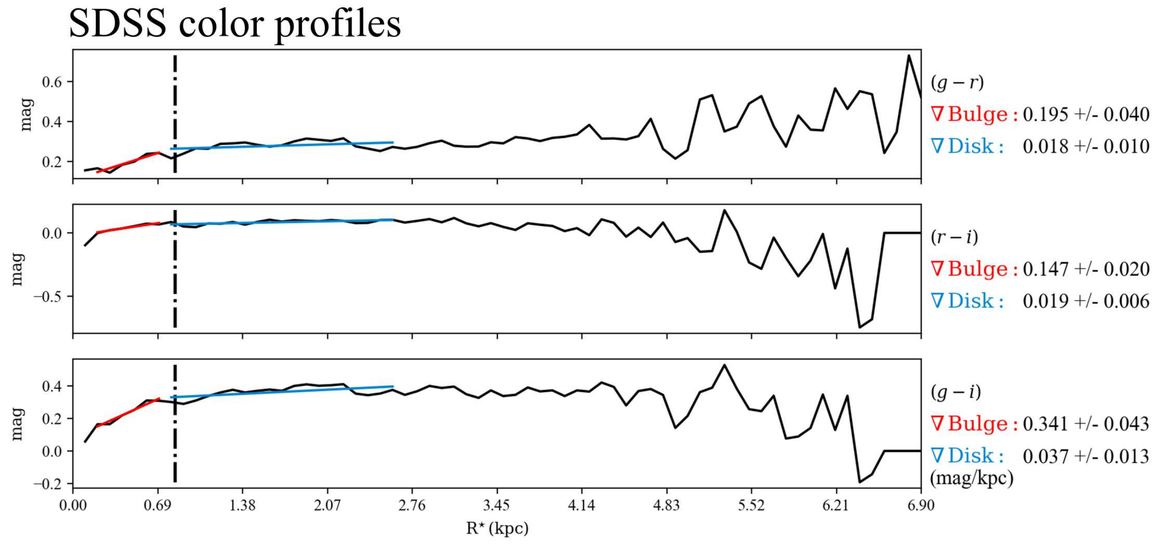

$\mathcal{RV}$ SBPs

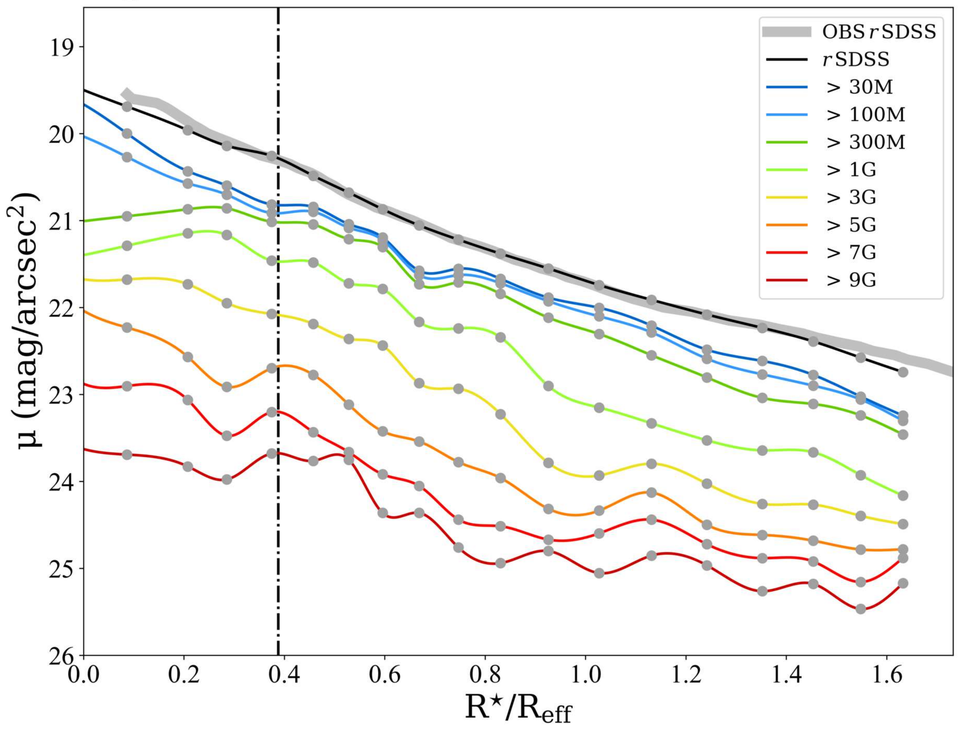

Stellar Continuum

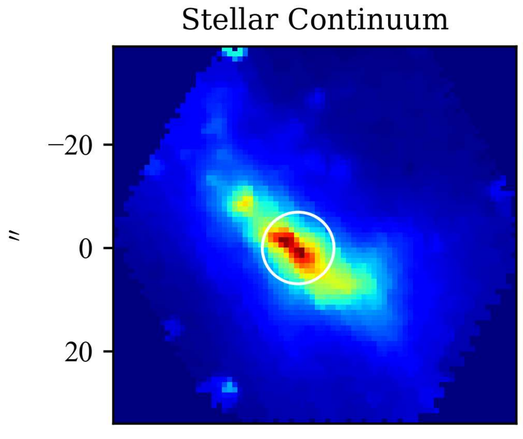

$\mathcal{M}_{\star,\rm P}$

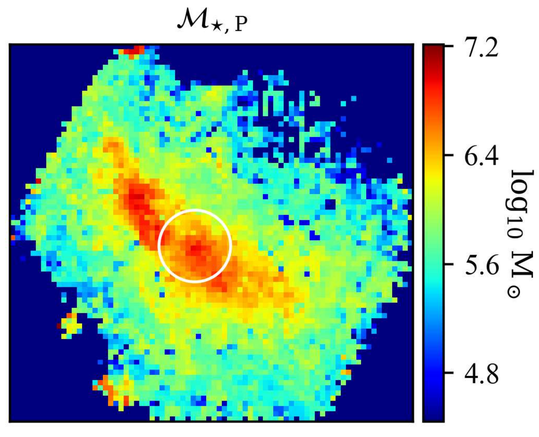

Log. of cumulative present stellar mass profiles

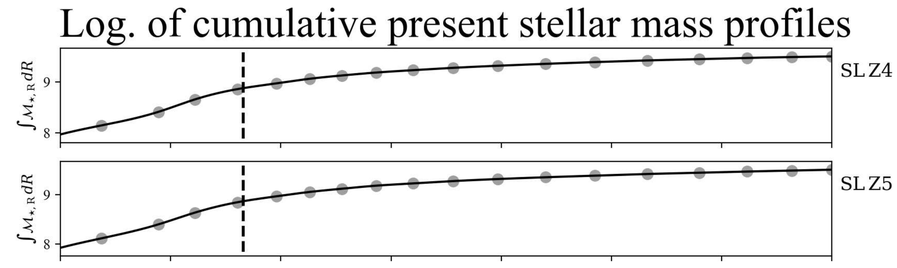

$Z_{\star,\mathcal{L}}$

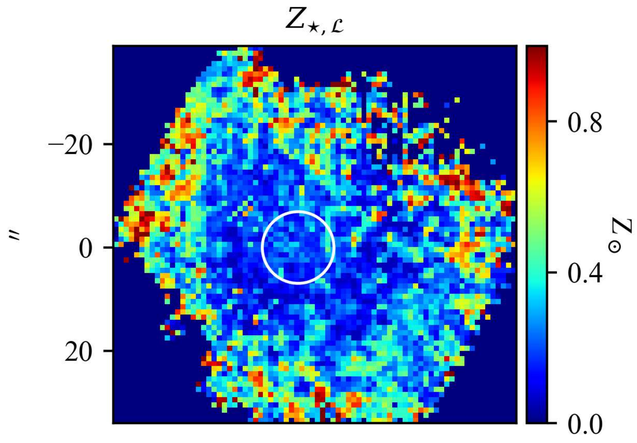

$Z_{\star,\mathcal{M}}$

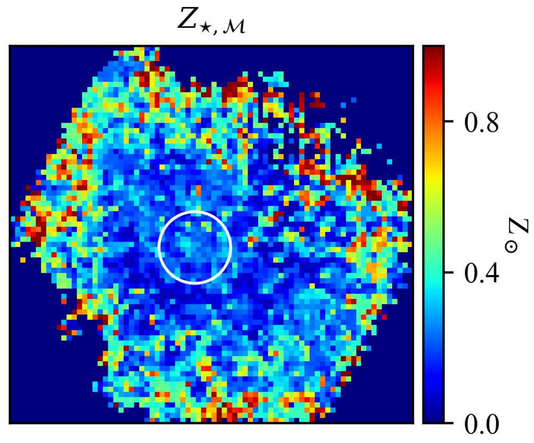

Stellar metallicity/Age & Hα flux/EW profiles

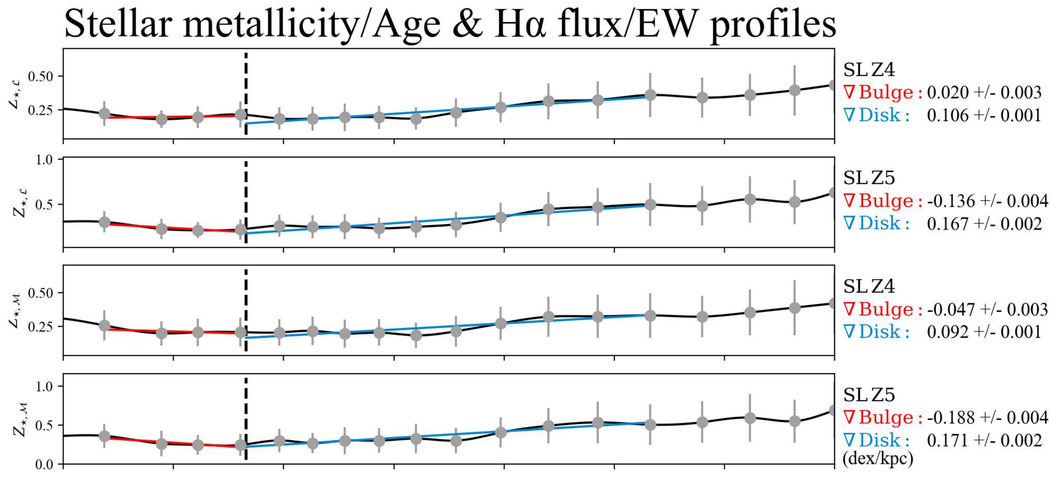

$t_{\star,\mathcal{L}}$

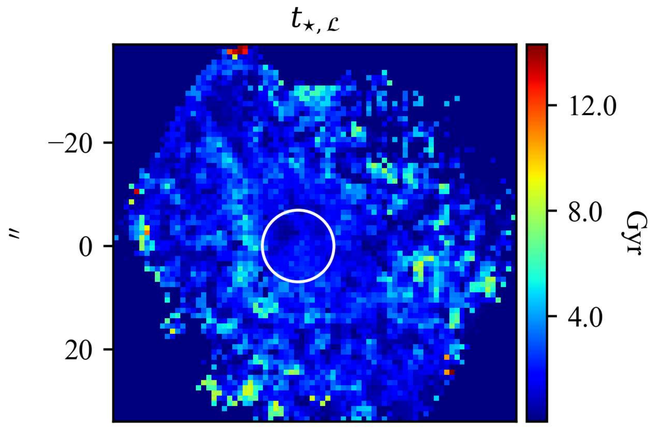

$t_{\star,\mathcal{M}}$

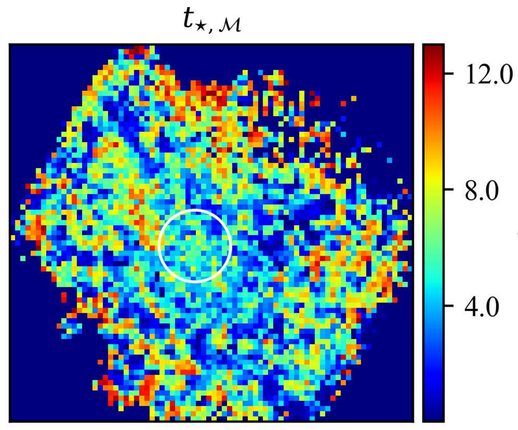

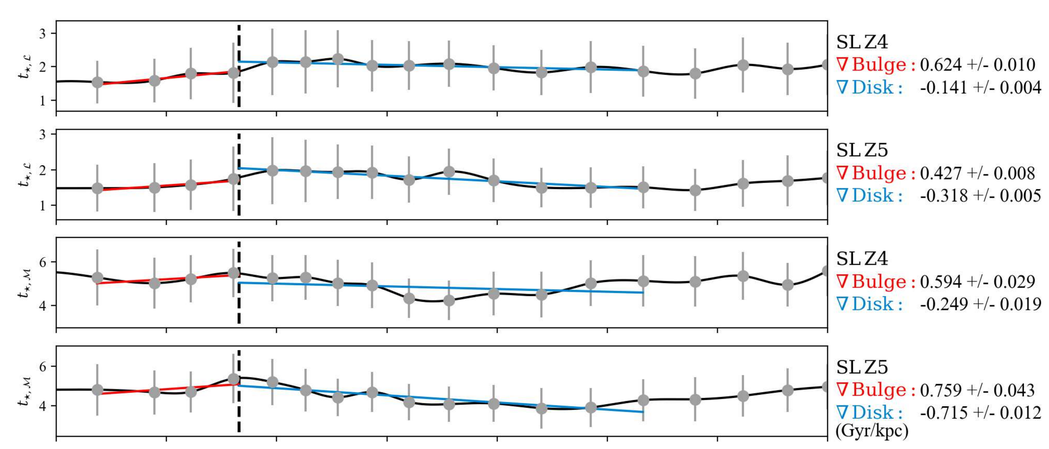

Hα flux

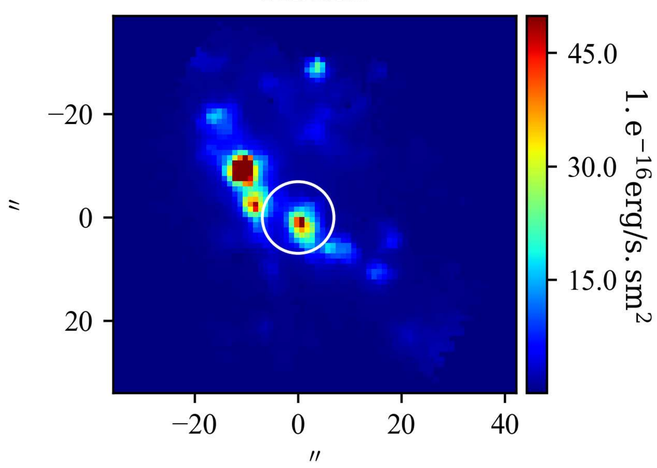

EW(Hα)

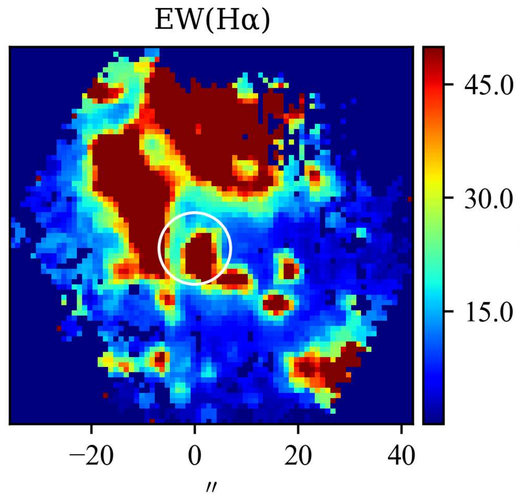

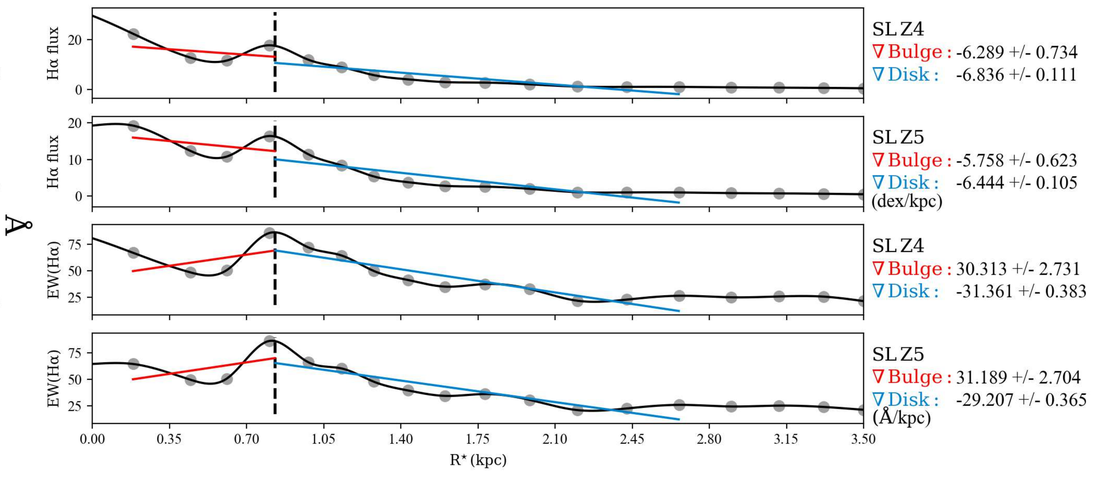

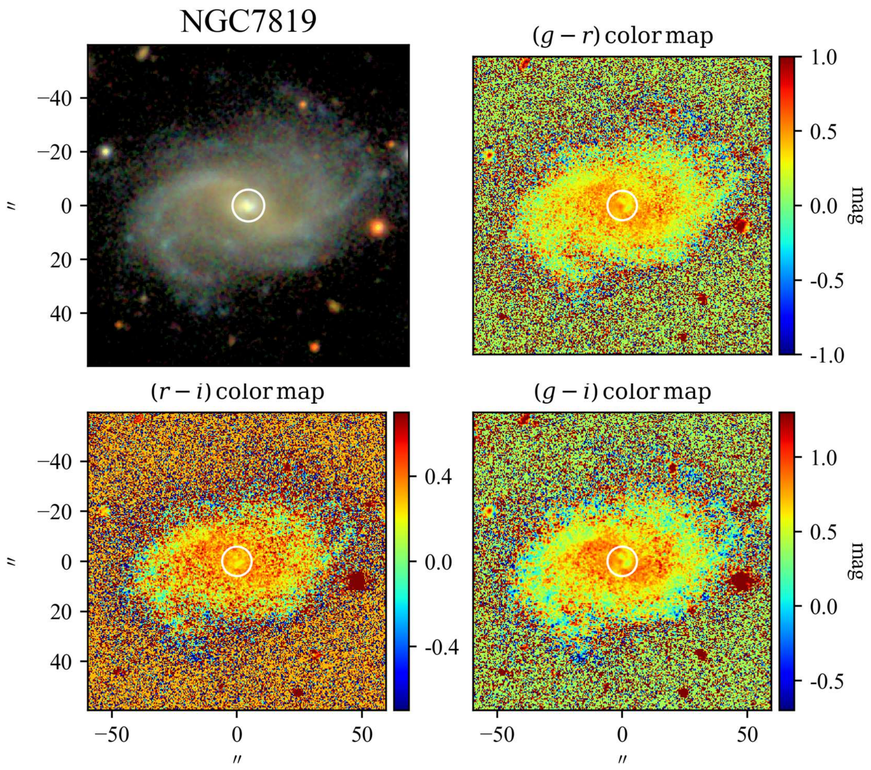

SBP decomposition of SDSS r band

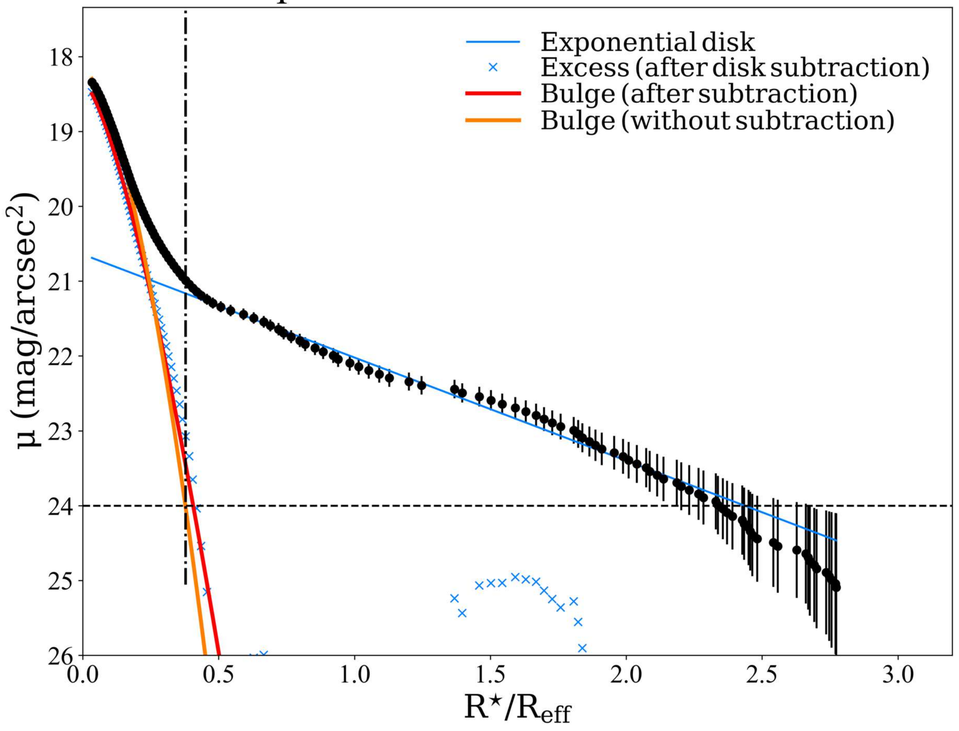

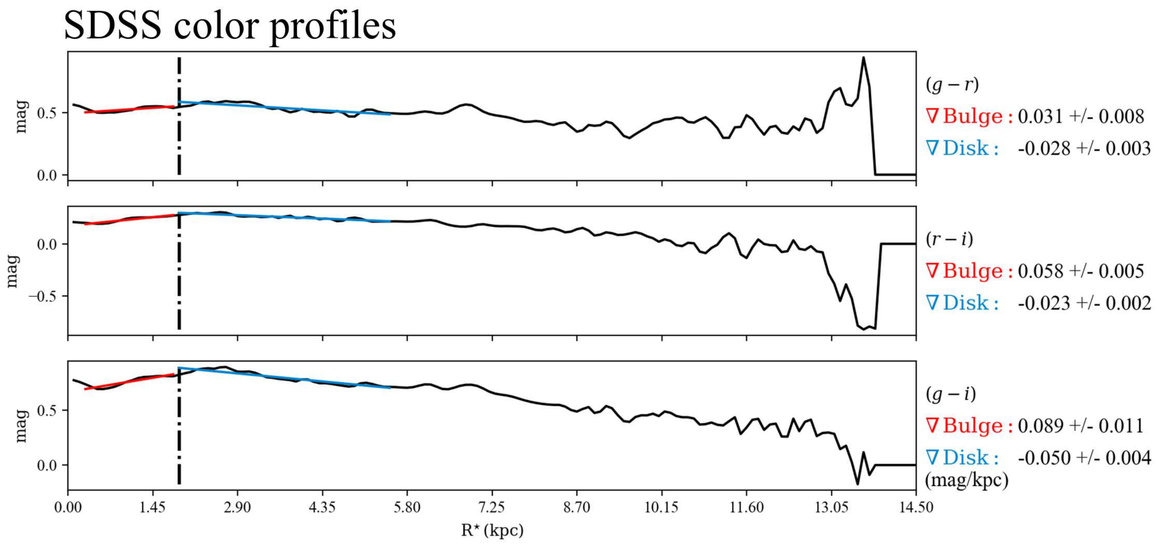

$\mathcal{RV}$ SBPs

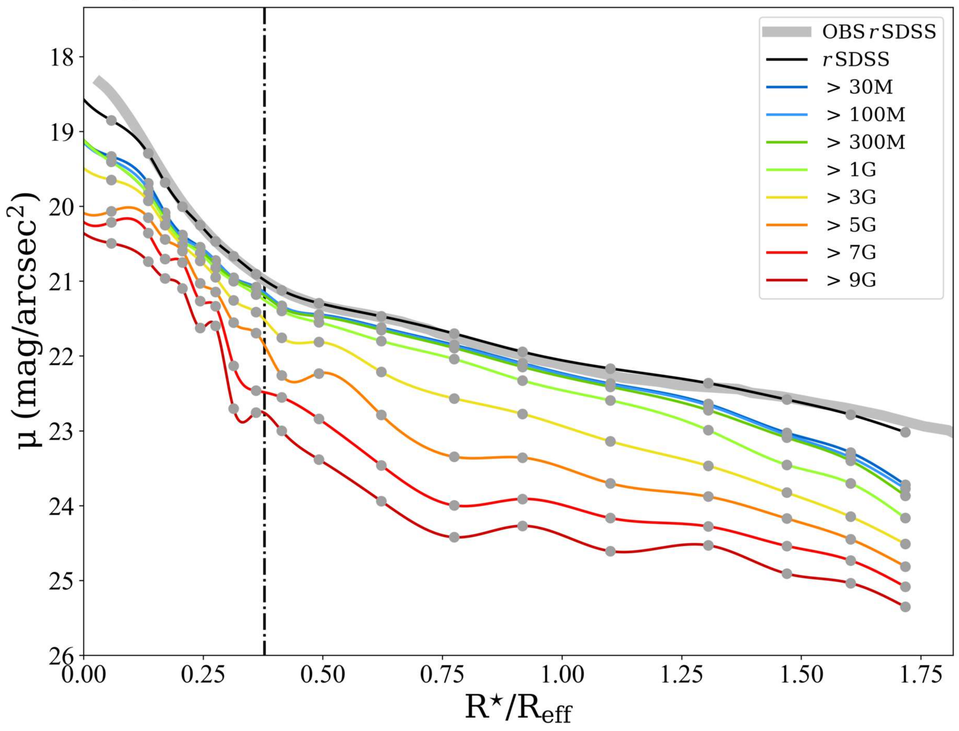

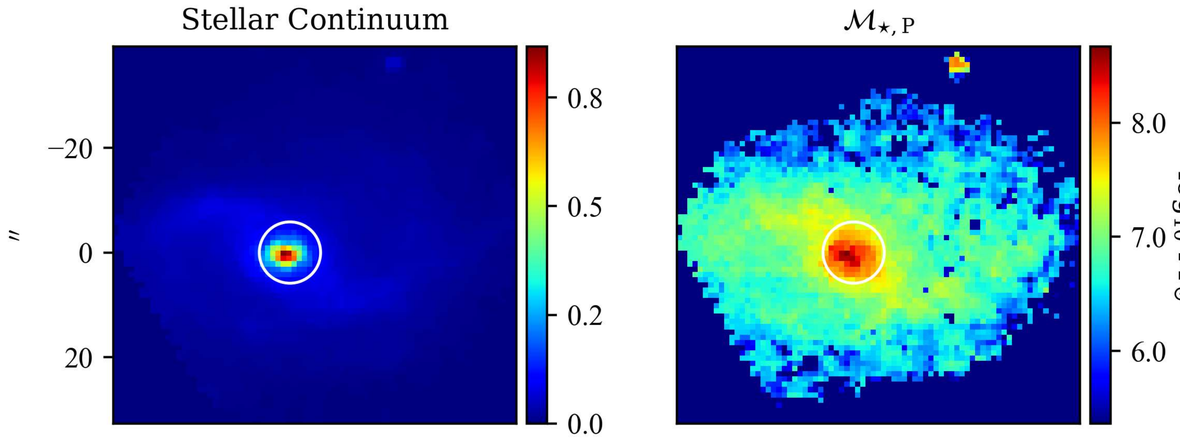

Log. of cumulative present stellar mass profiles

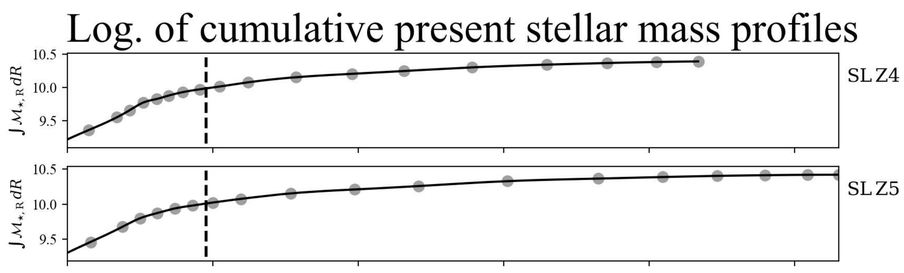

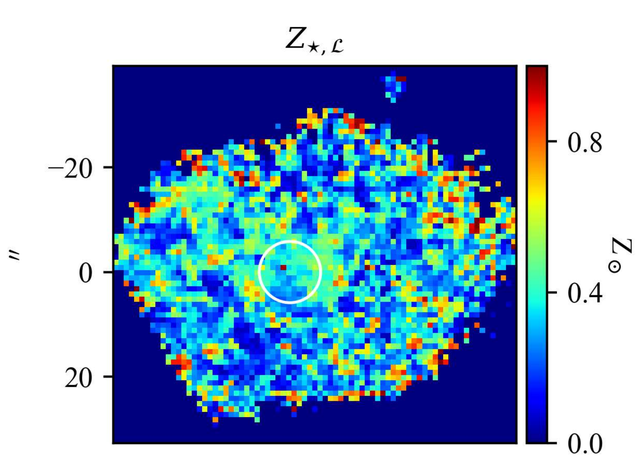

Stellar metallicity/Age & Hα flux/EW profiles

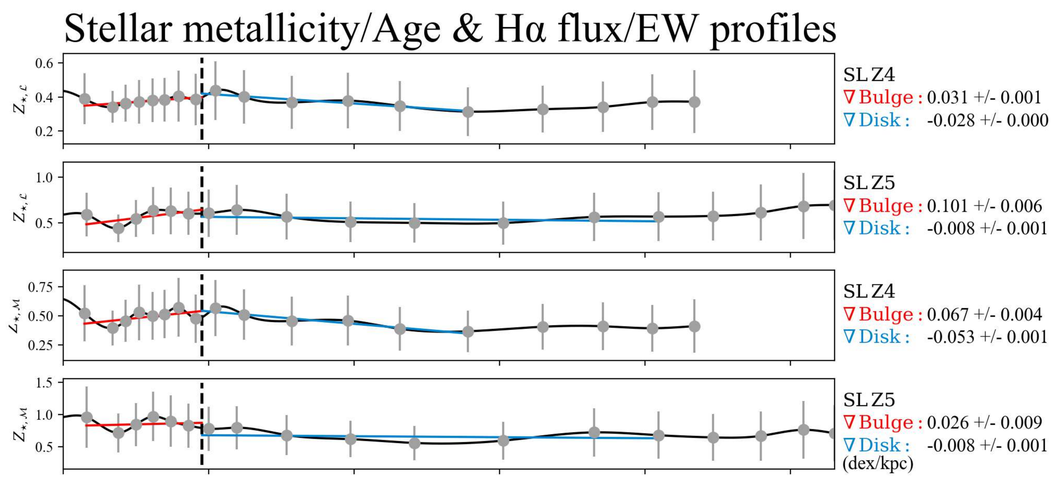

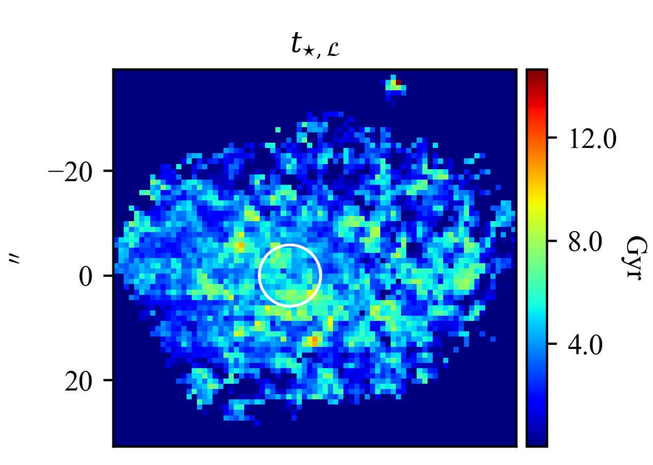

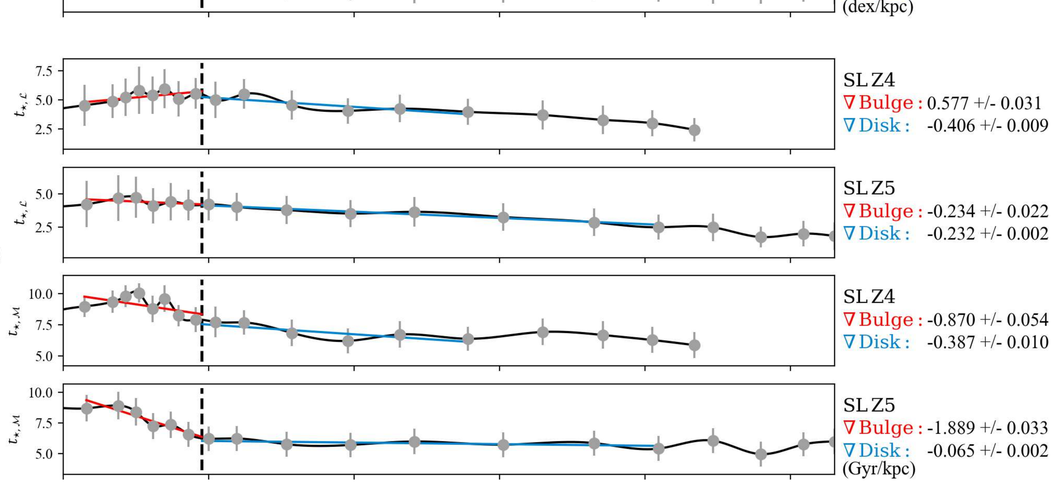

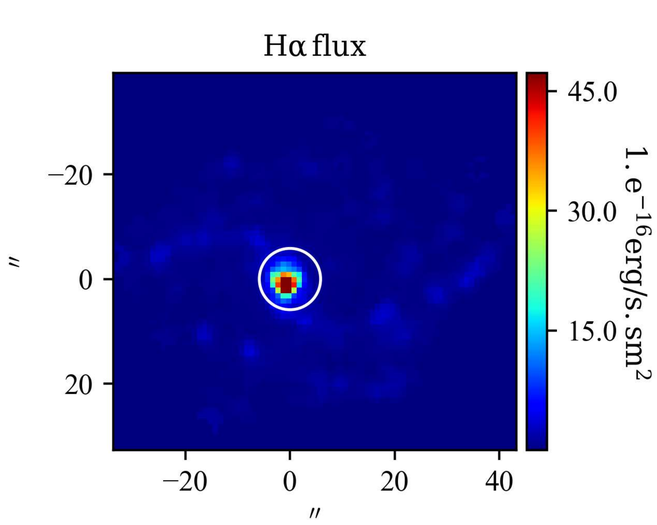

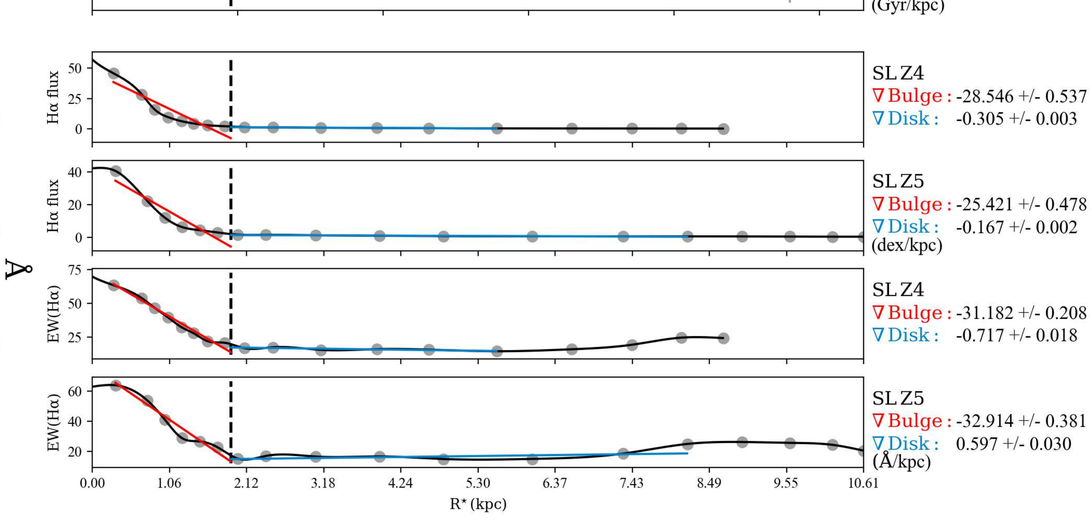

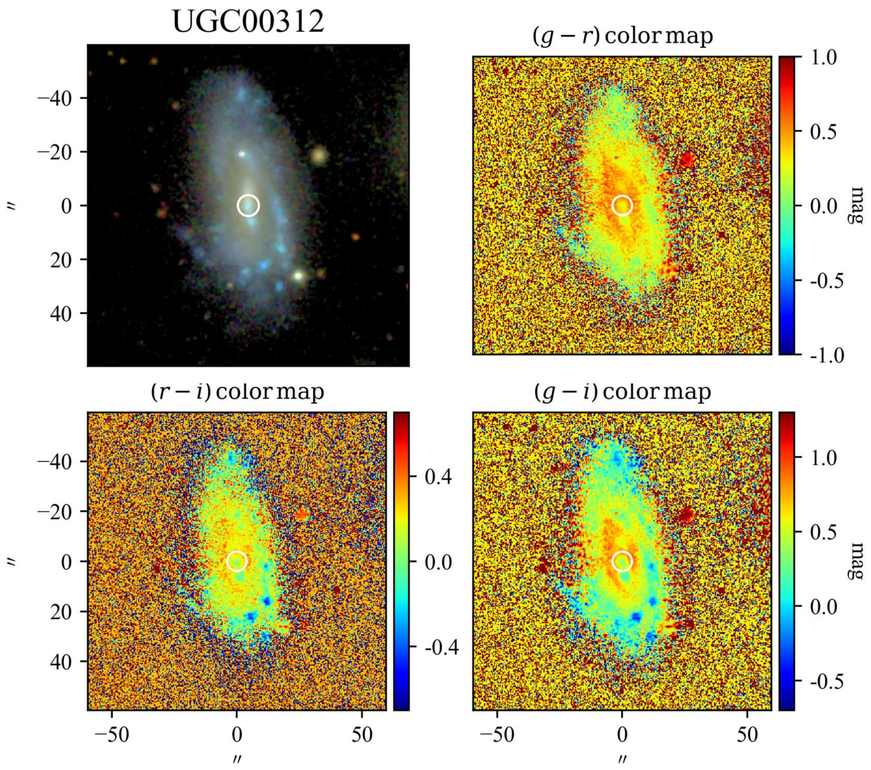

SBP decomposition of SDSS r band

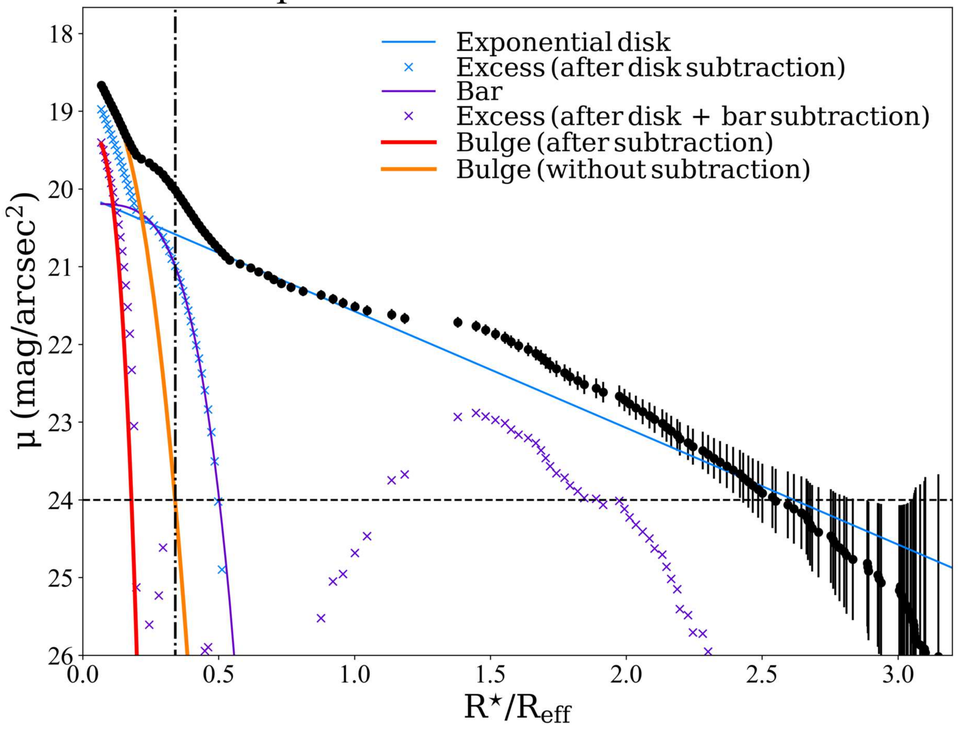

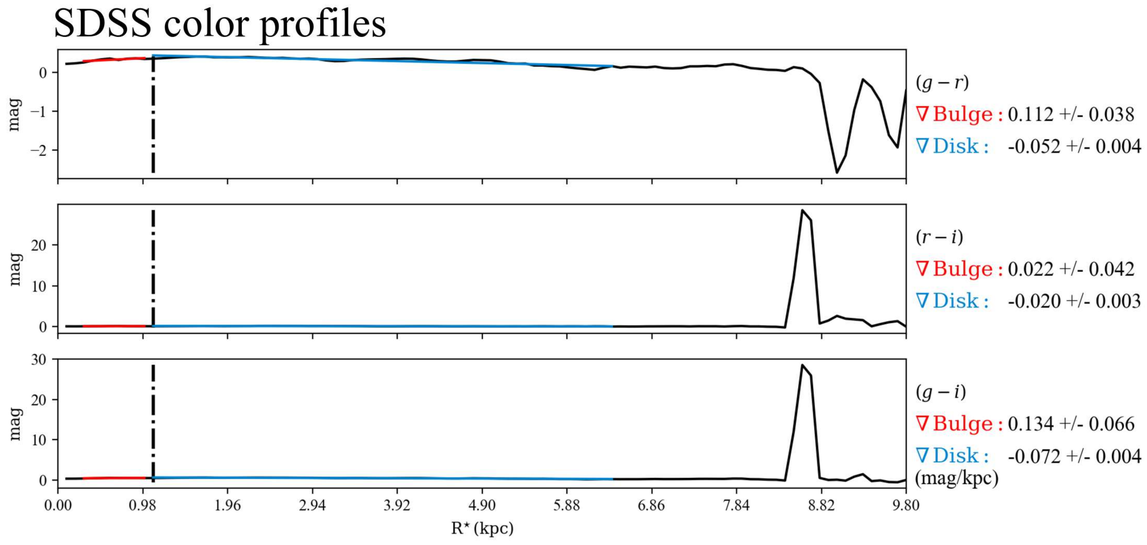

$\mathcal{RY}$ SBPs

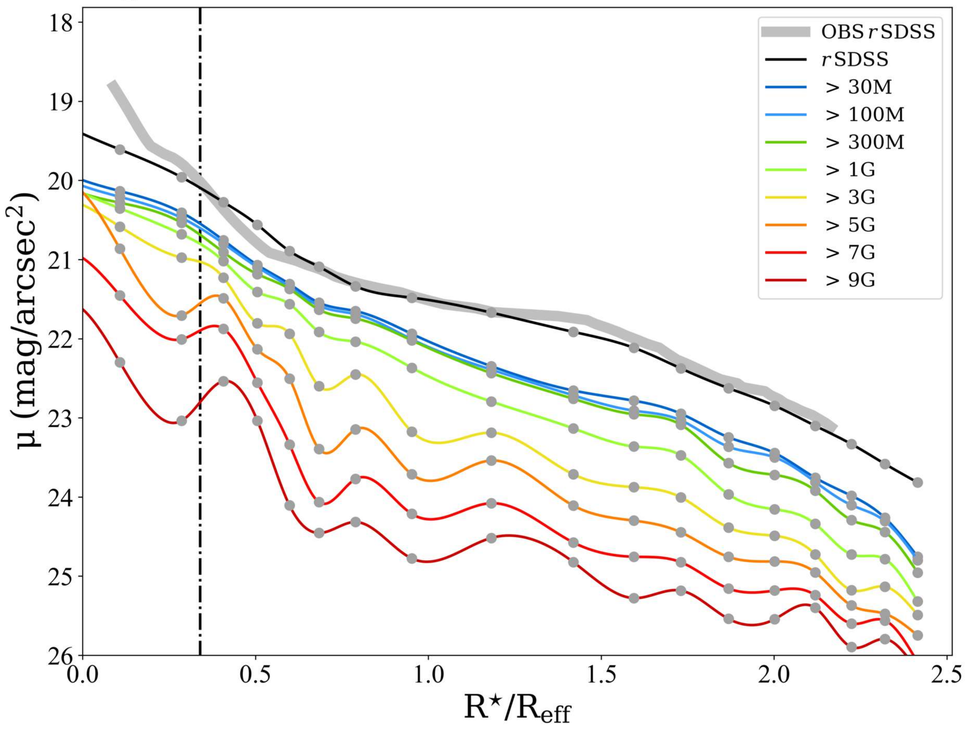

Stellar Continuum

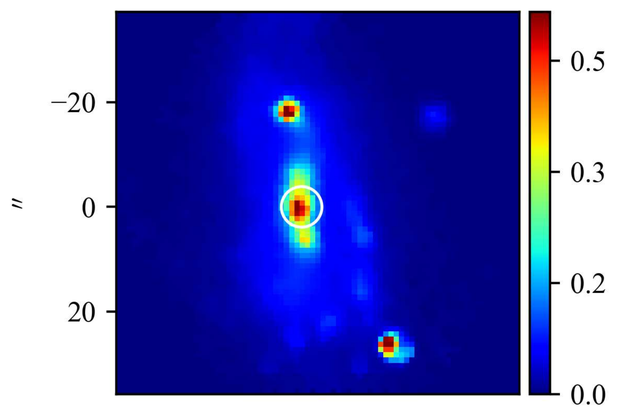

$\mathcal{M}_{\star,\mathrm{P}}$

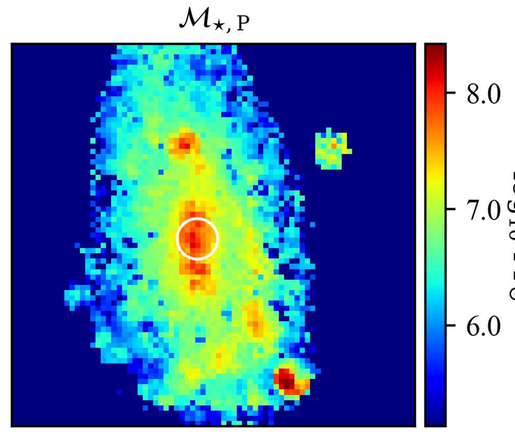

Log. of cumulative present stellar mass profiles

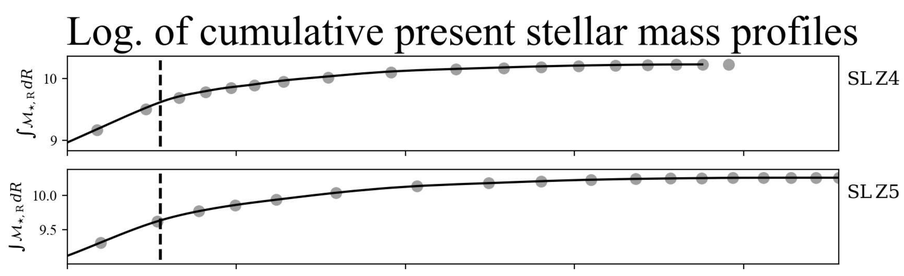

$Z_{\star,\mathcal{L}}$

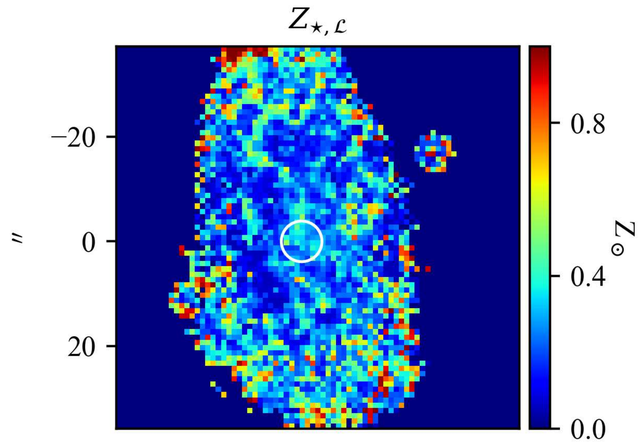

$Z_{\star,\mathcal{M}}$

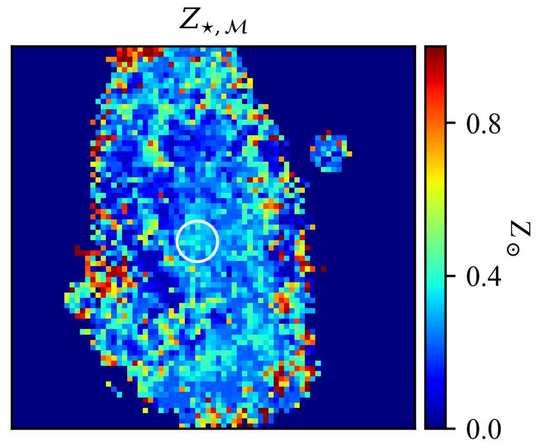

Stellar metallicity/Age & Hα flux/EW profiles

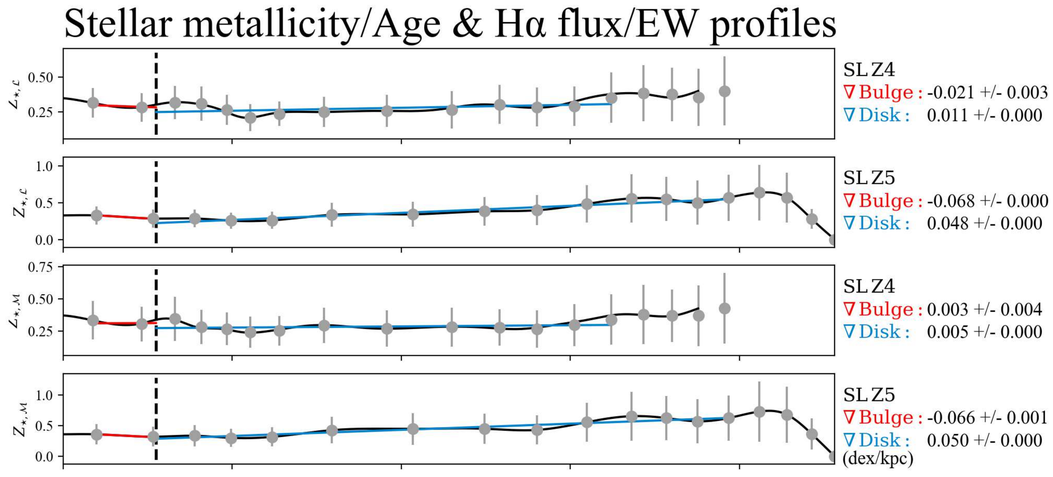

$t_{\star,\mathcal{L}}$

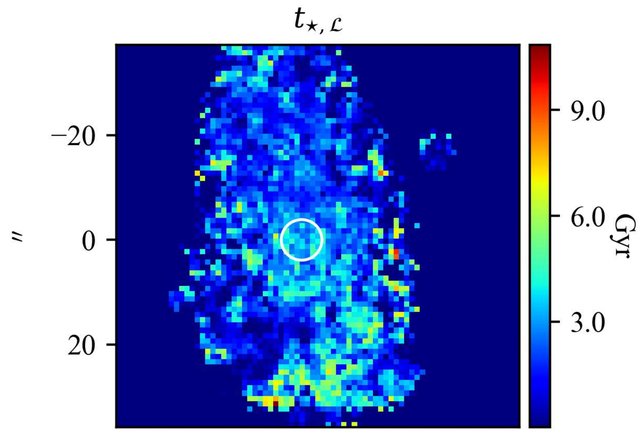

$t_{\star,\mathcal{M}}$

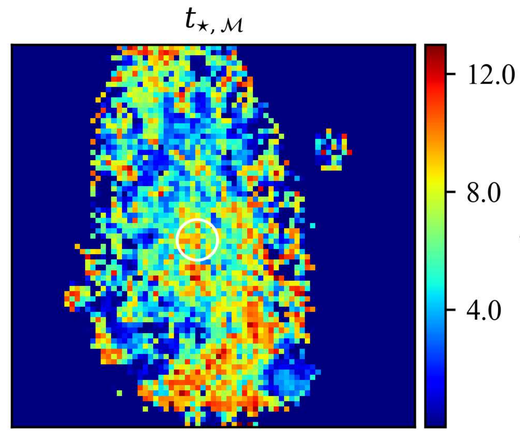

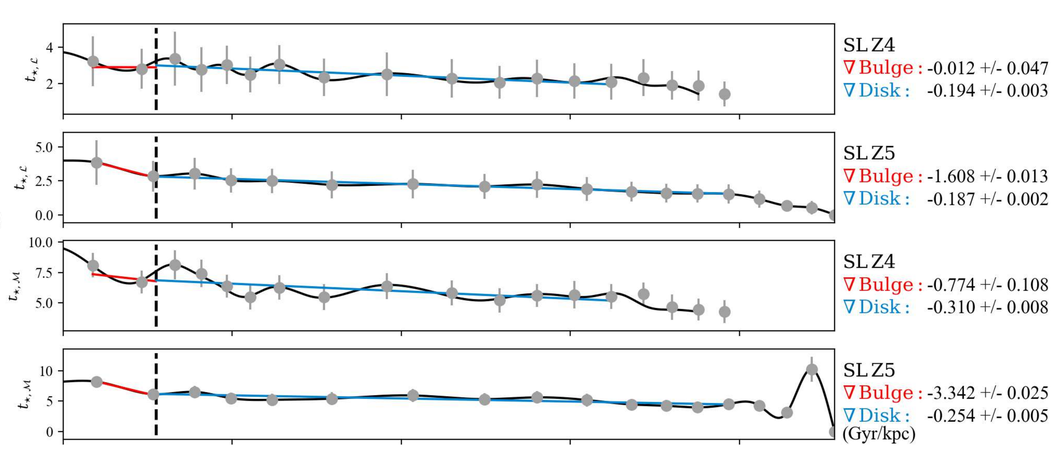

Hα flux

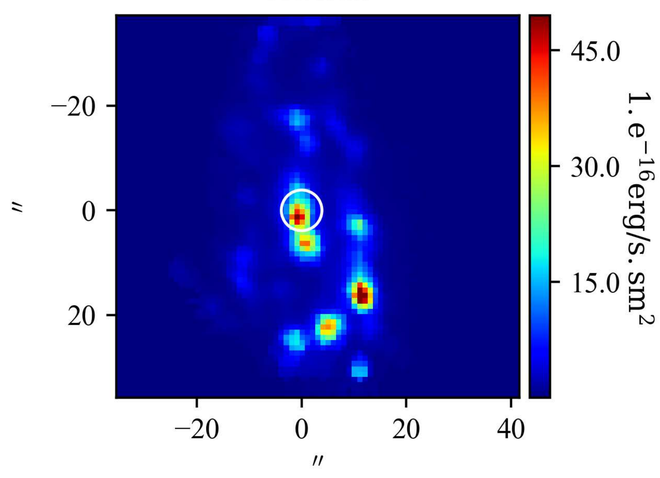

EW(Hα)

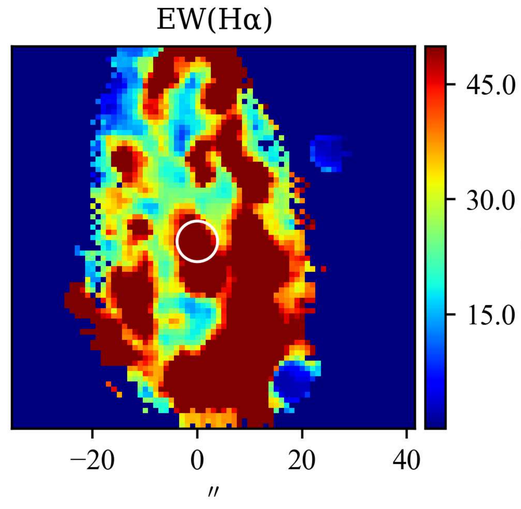

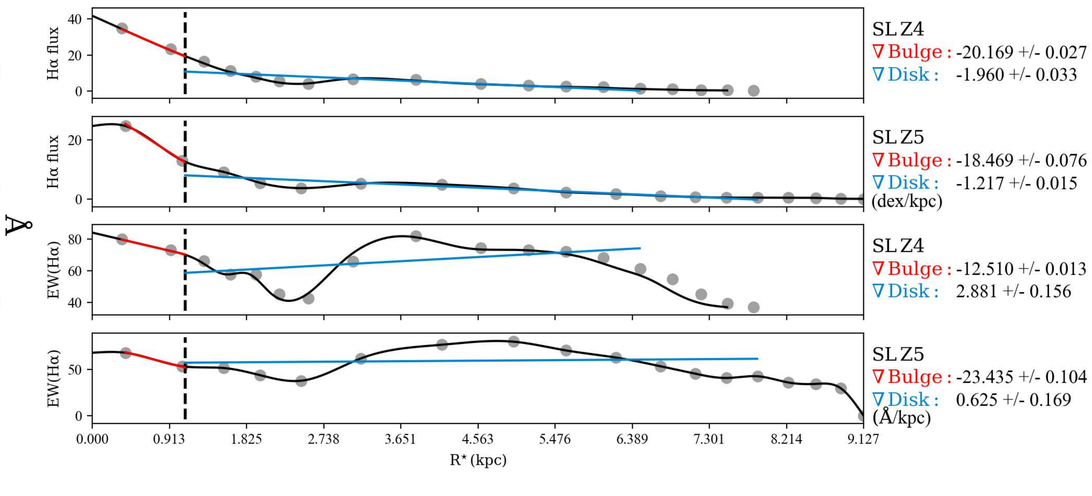

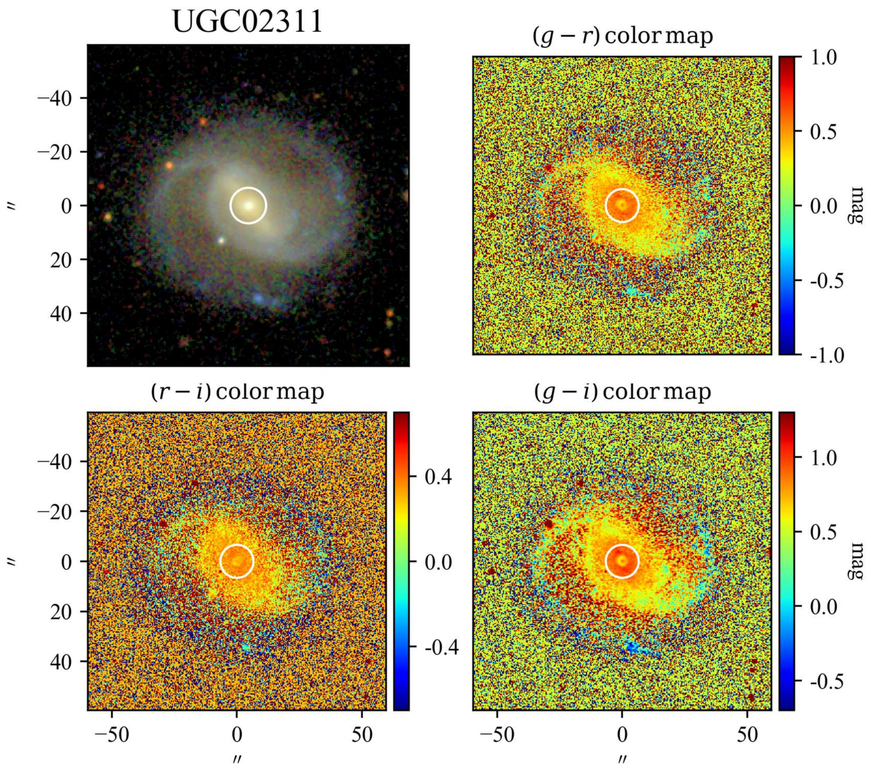

SBP decomposition of SDSS r band

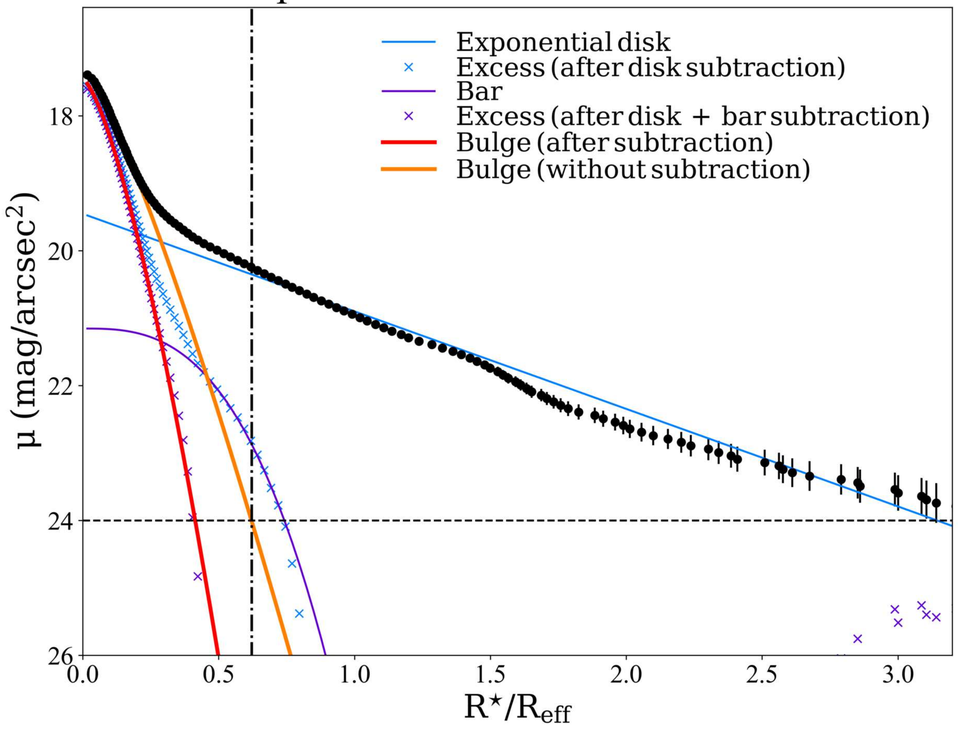

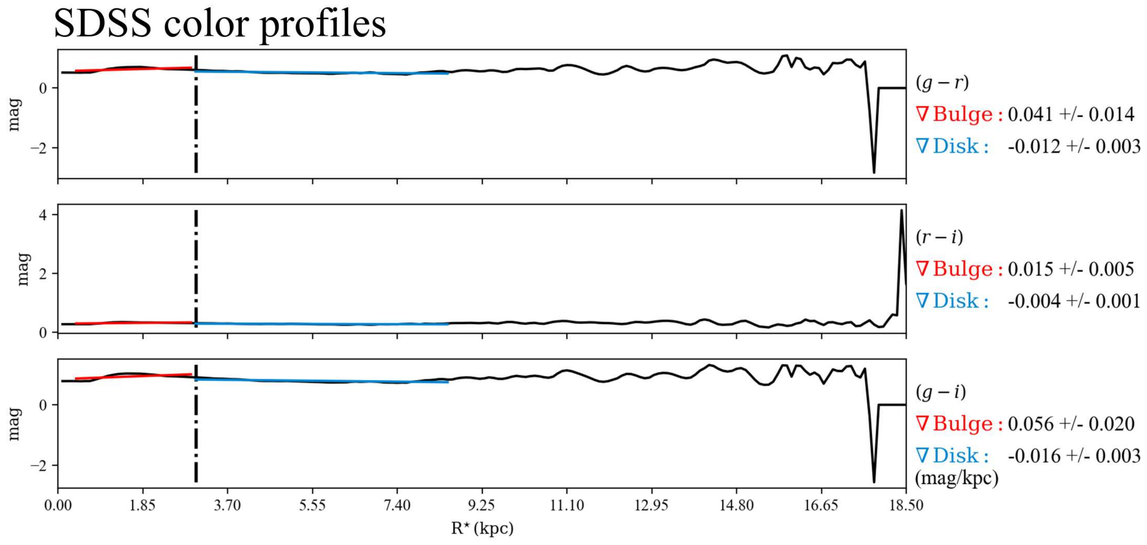

$\mathcal{RY}$ SBPs

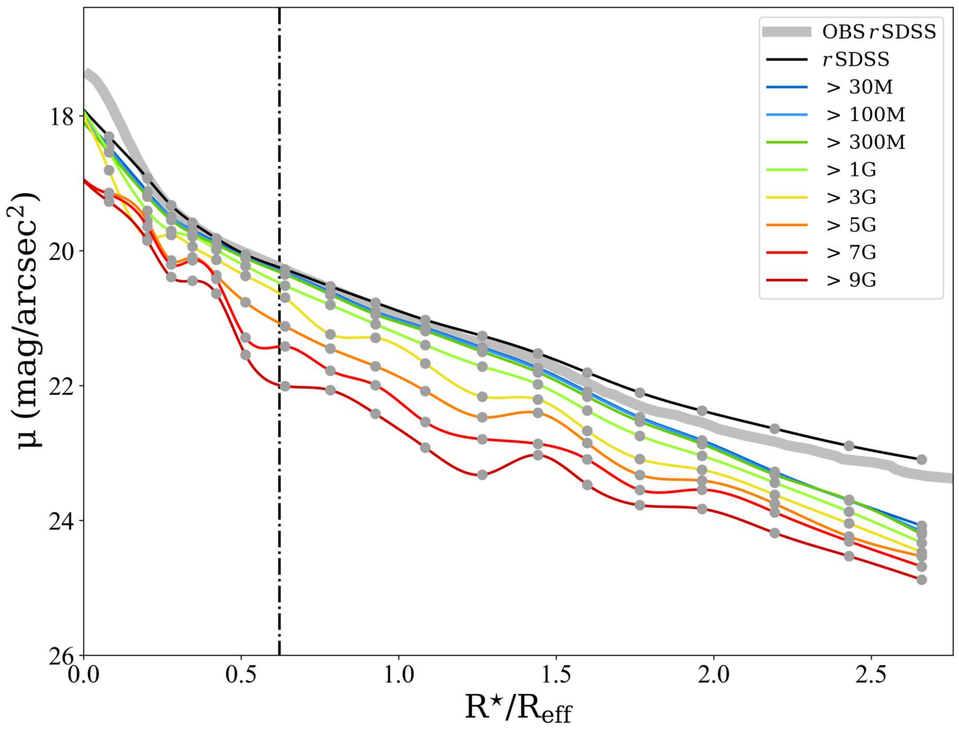

Stellar Continuum

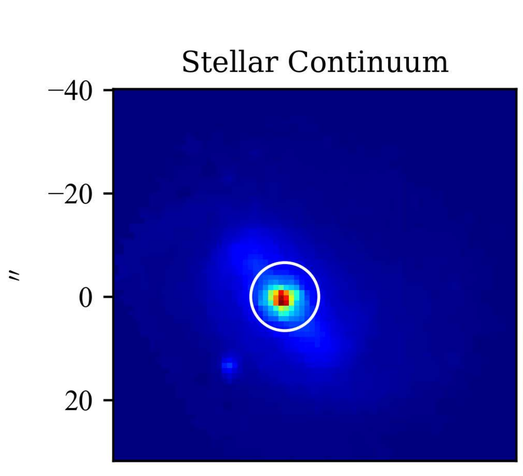

$\mathcal{M}_{\star,\mathrm{P}}$

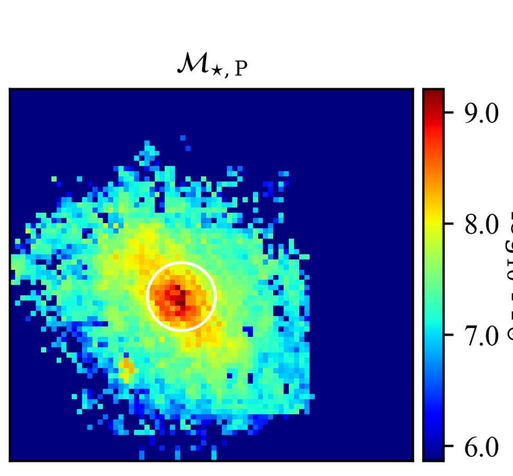

Log. of cumulative present stellar mass profiles

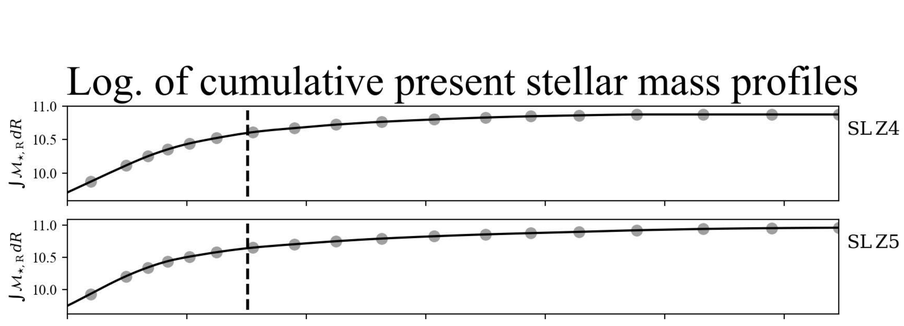

$Z_{\star,\mathcal{L}}$

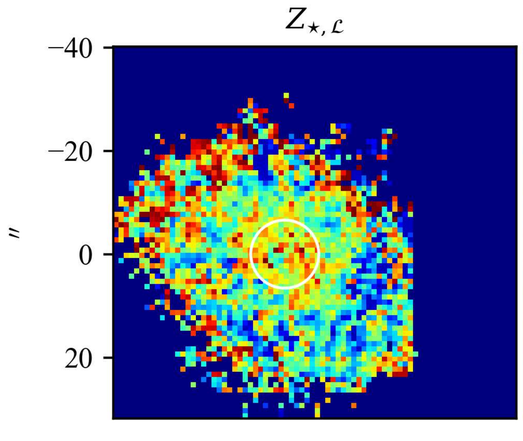

$Z_{\star,\mathcal{M}}$

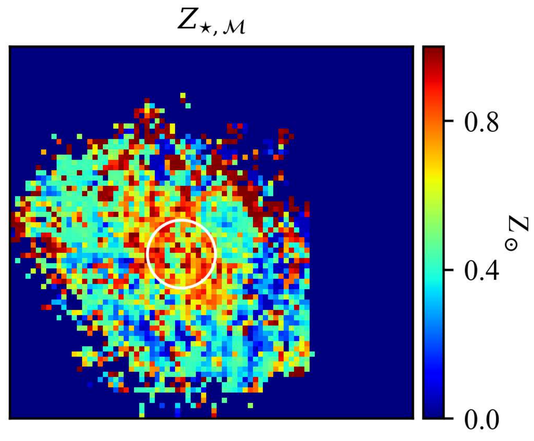

Stellar metallicity/Age & Hα flux/EW profiles

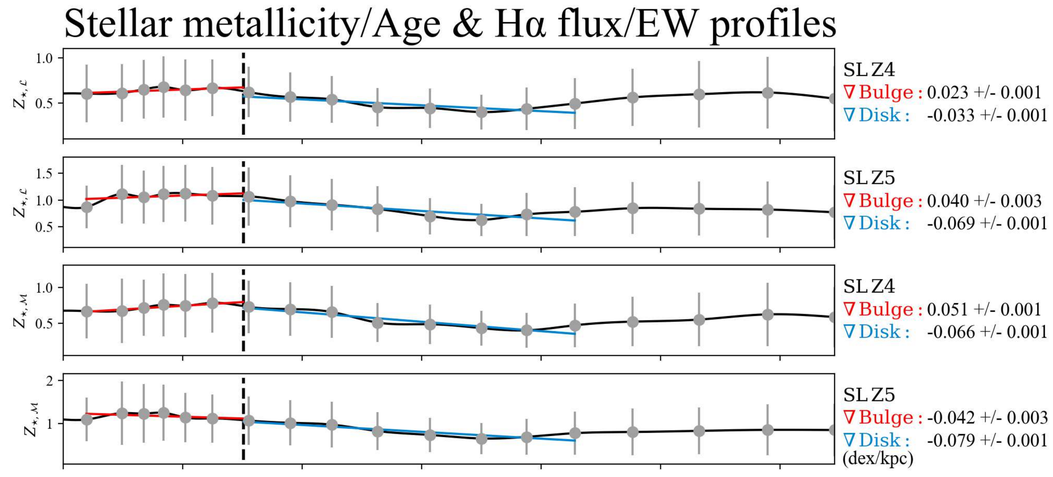

$t_{\star,\mathcal{L}}$

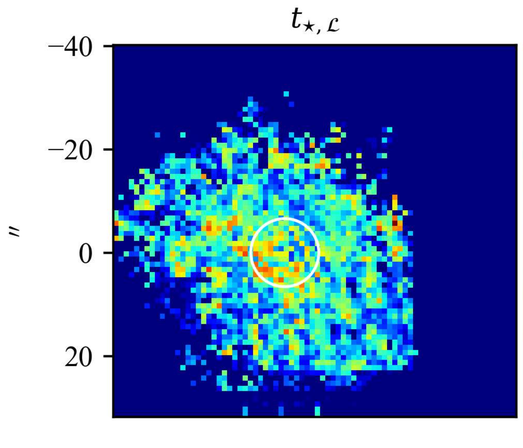

$t_{\star,\mathcal{M}}$

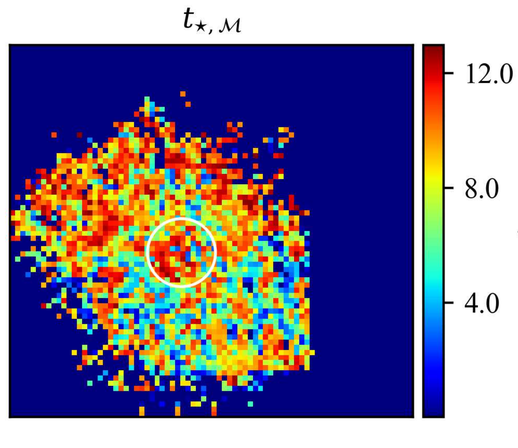

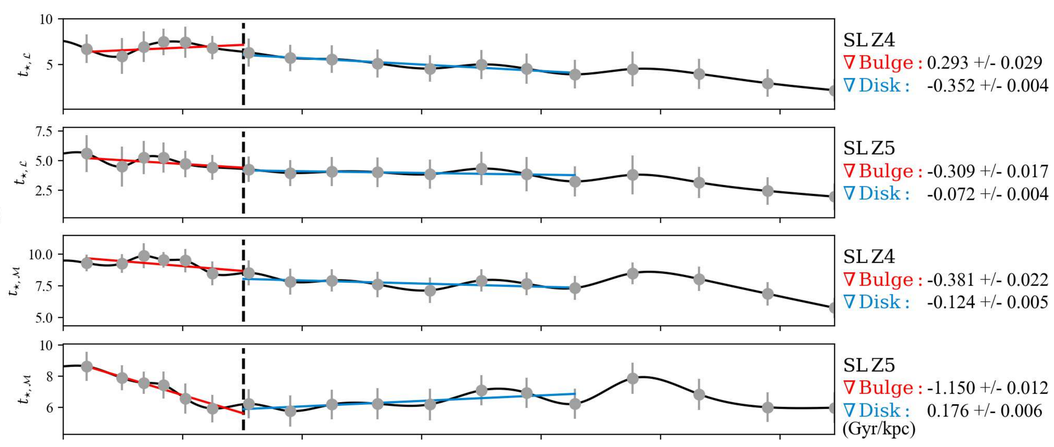

Hα flux

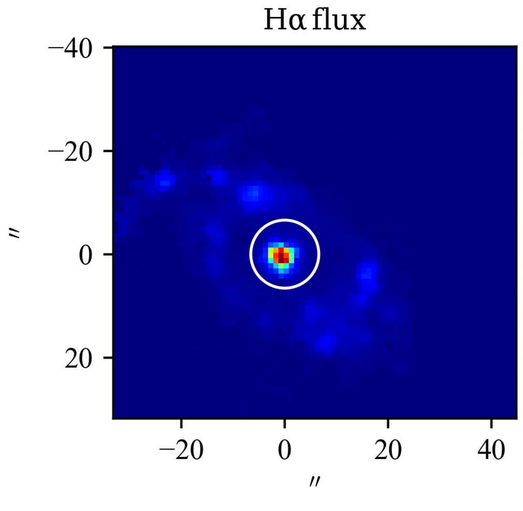

EW(Hα)

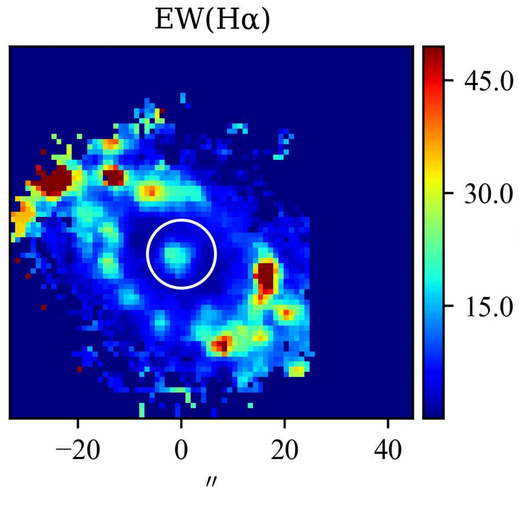

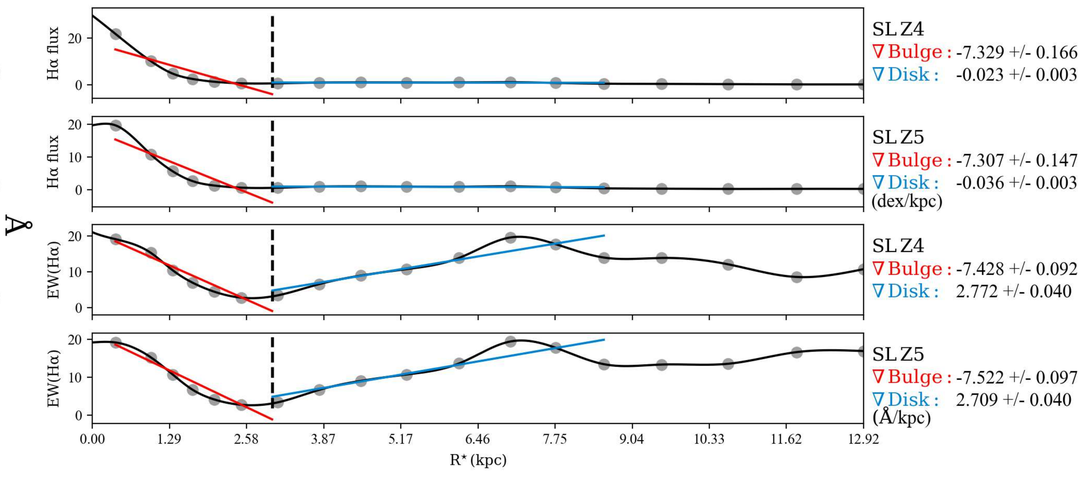

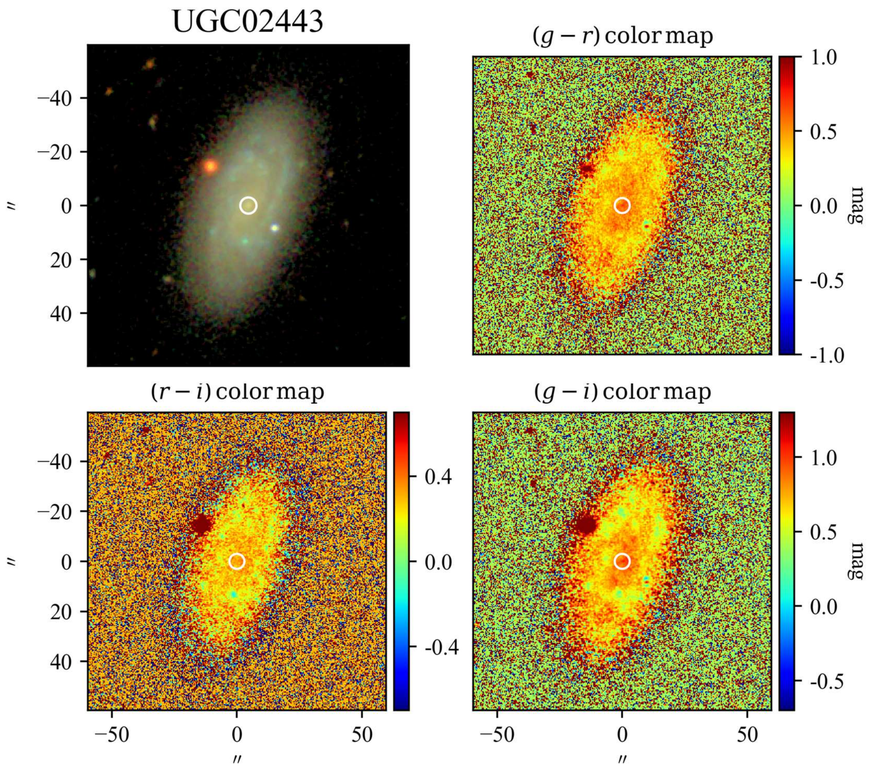

SBP decomposition of SDSS r band

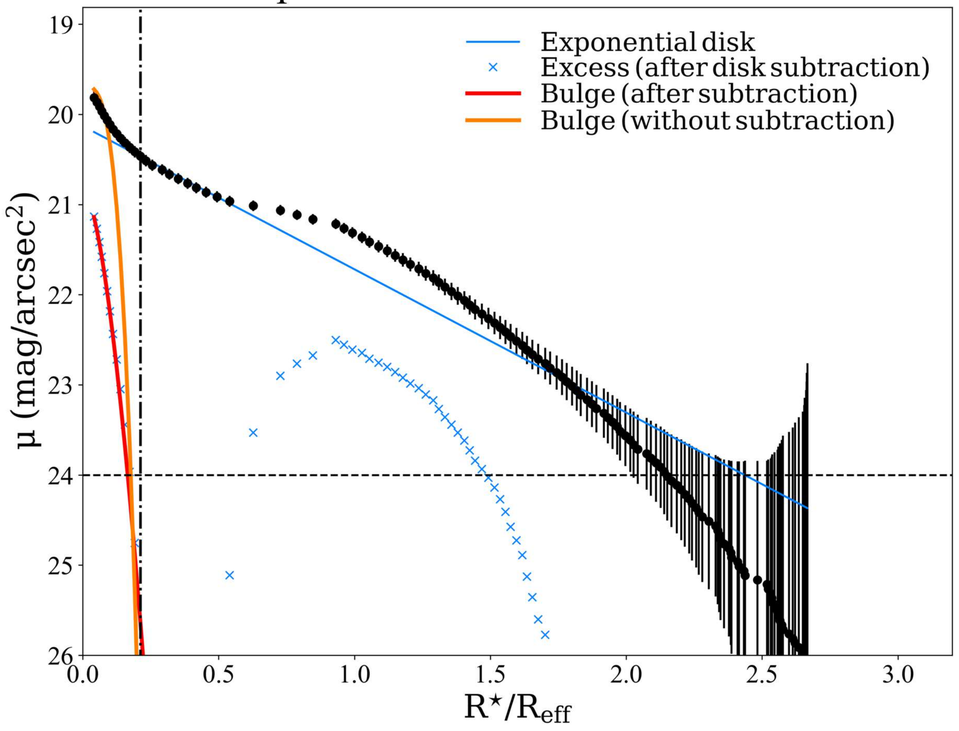

SDSS color profiles

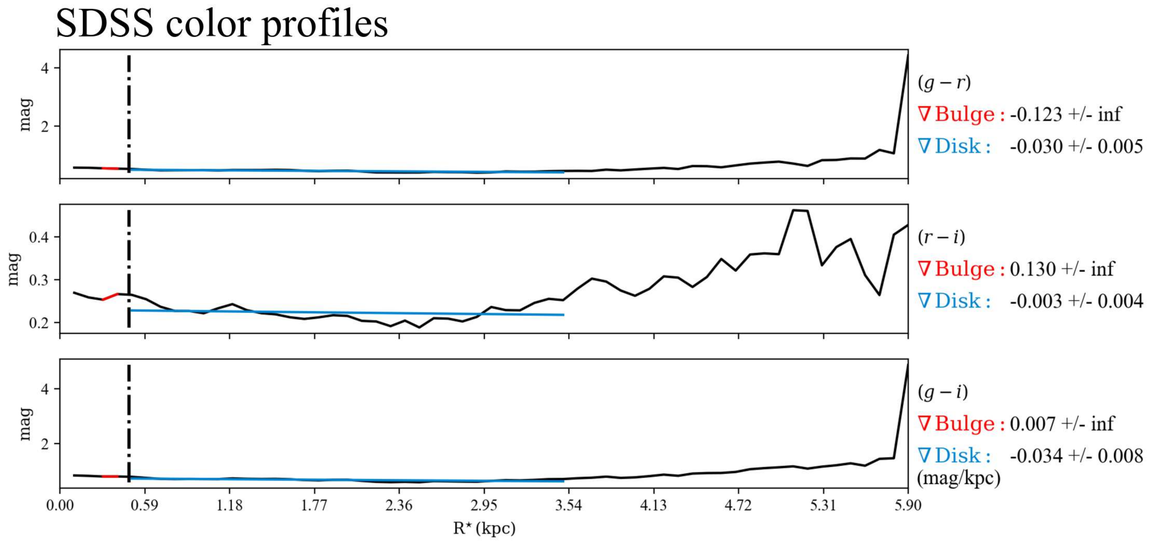

$\mathcal{RY}$ SBPs

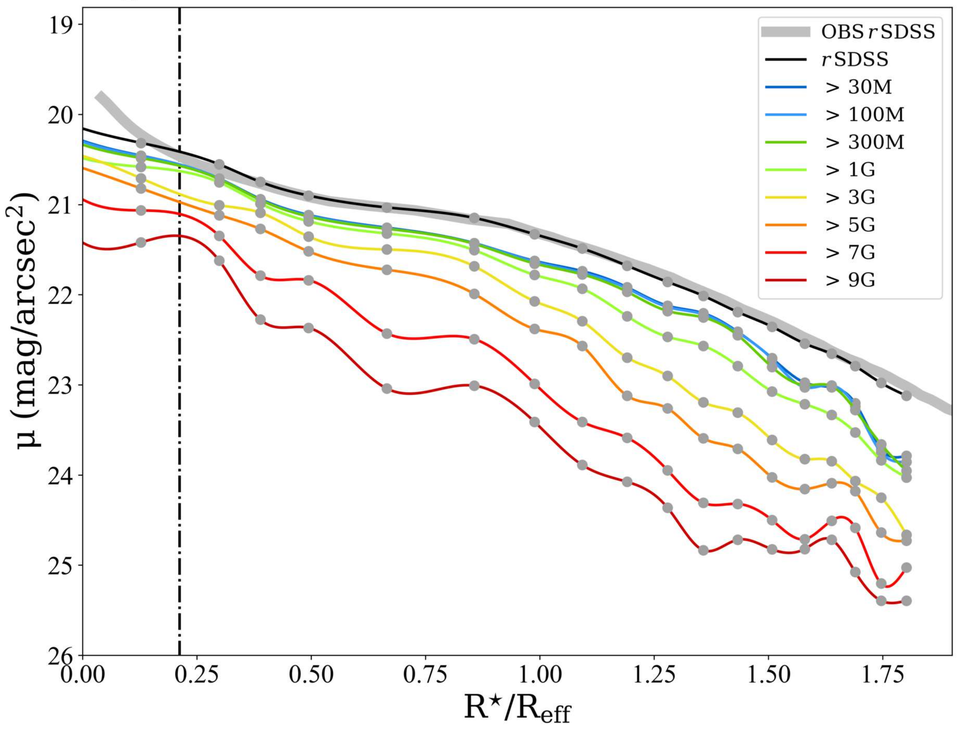

Stellar Continuum

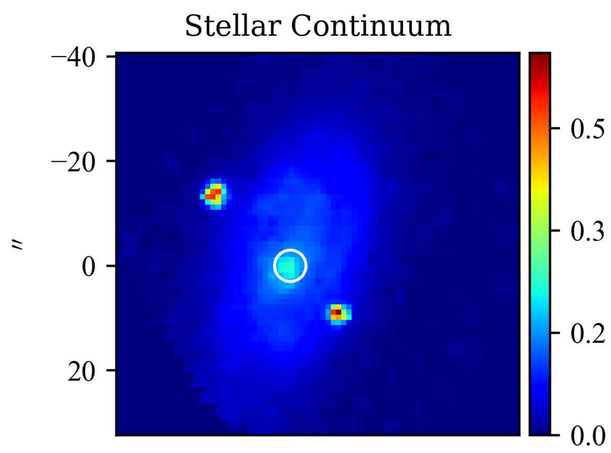

$\mathcal{M}_{\star,\mathrm{P}}$

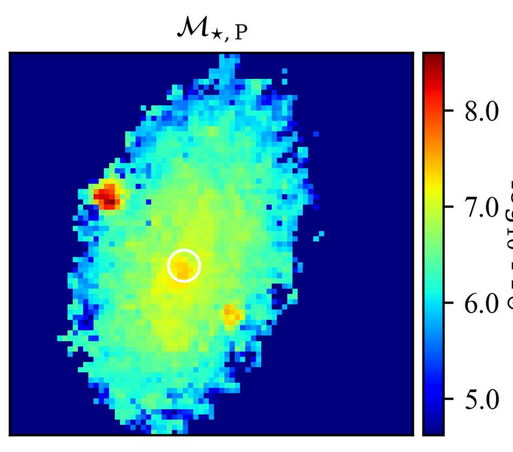

Log. of cumulative present stellar mass profiles

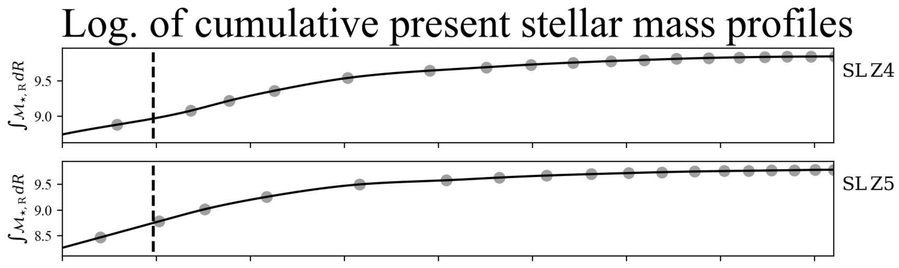

$Z_{\star,\mathcal{L}}$

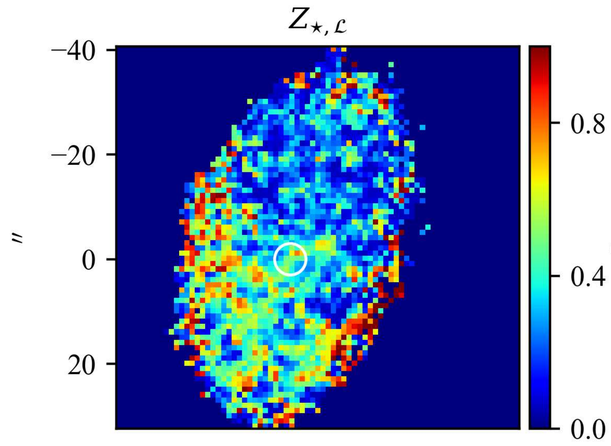

$Z_{\star,\mathcal{M}}$

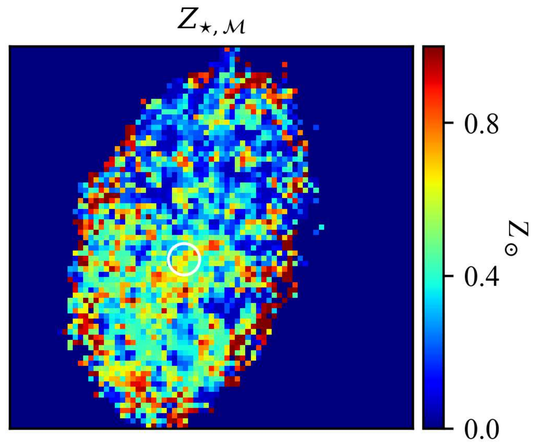

Stellar metallicity/Age & Hα flux/EW profiles

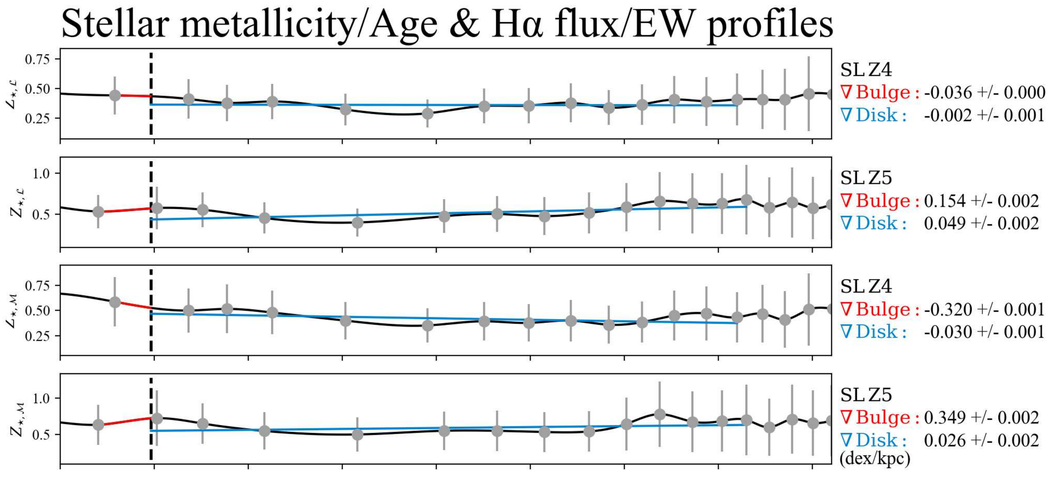

$t_{\star,\mathcal{L}}$

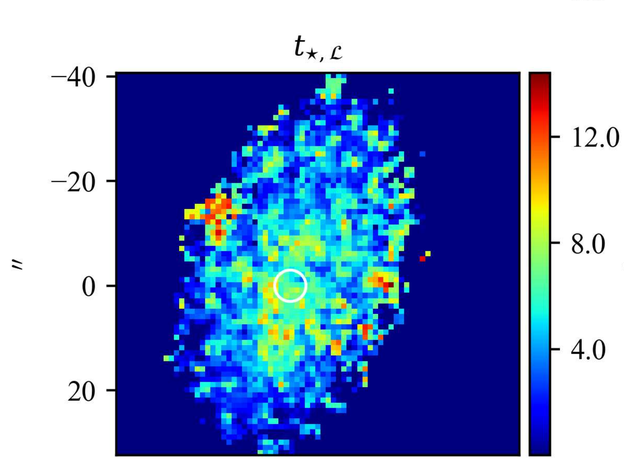

$t_{\star,\mathcal{M}}$

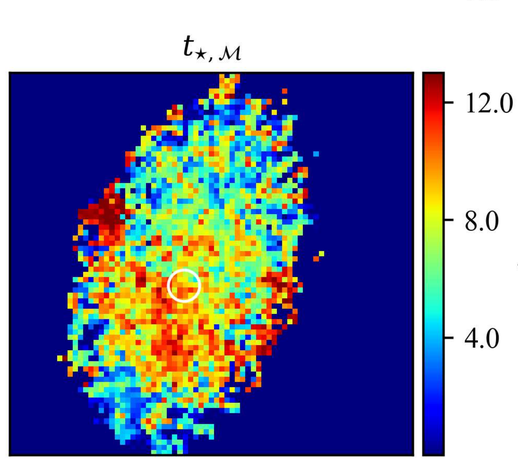

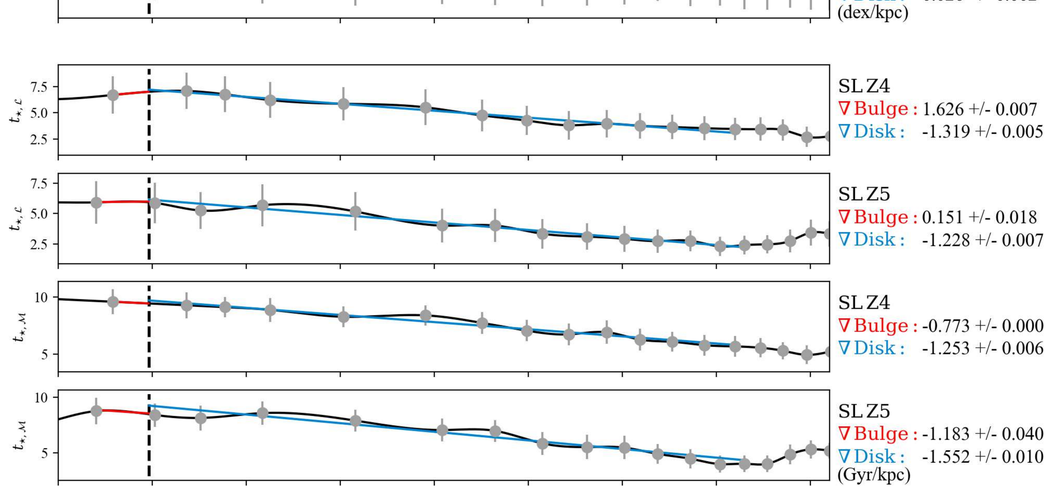

Hα flux

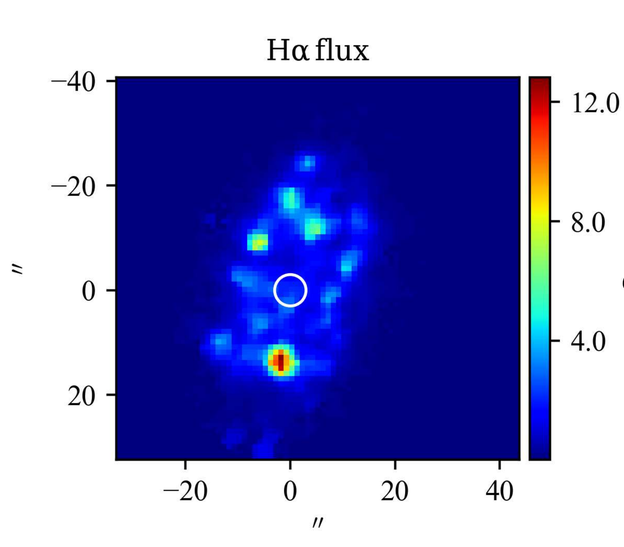

EW(Hα)

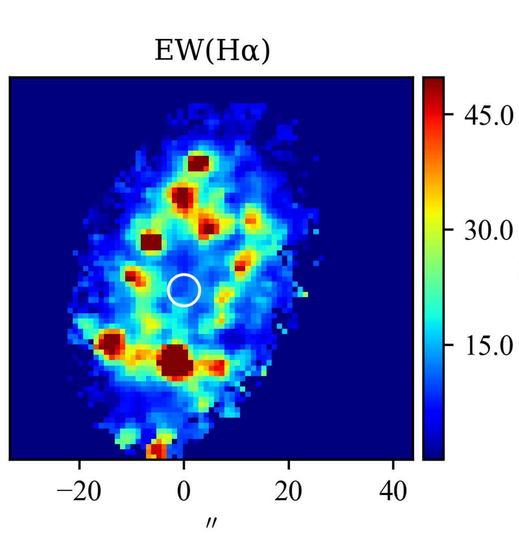

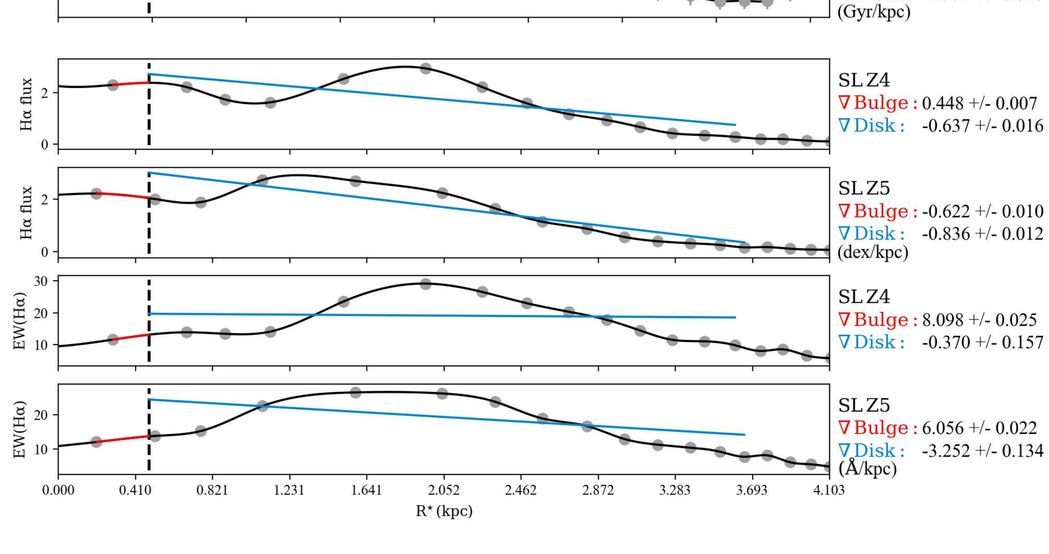

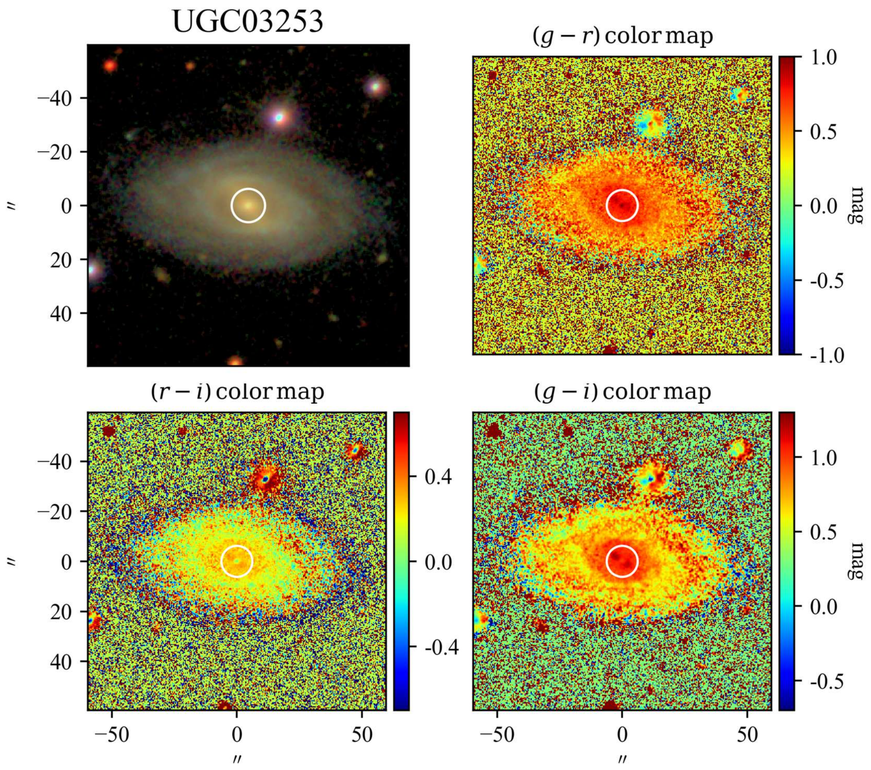

SBP decomposition of SDSS r band

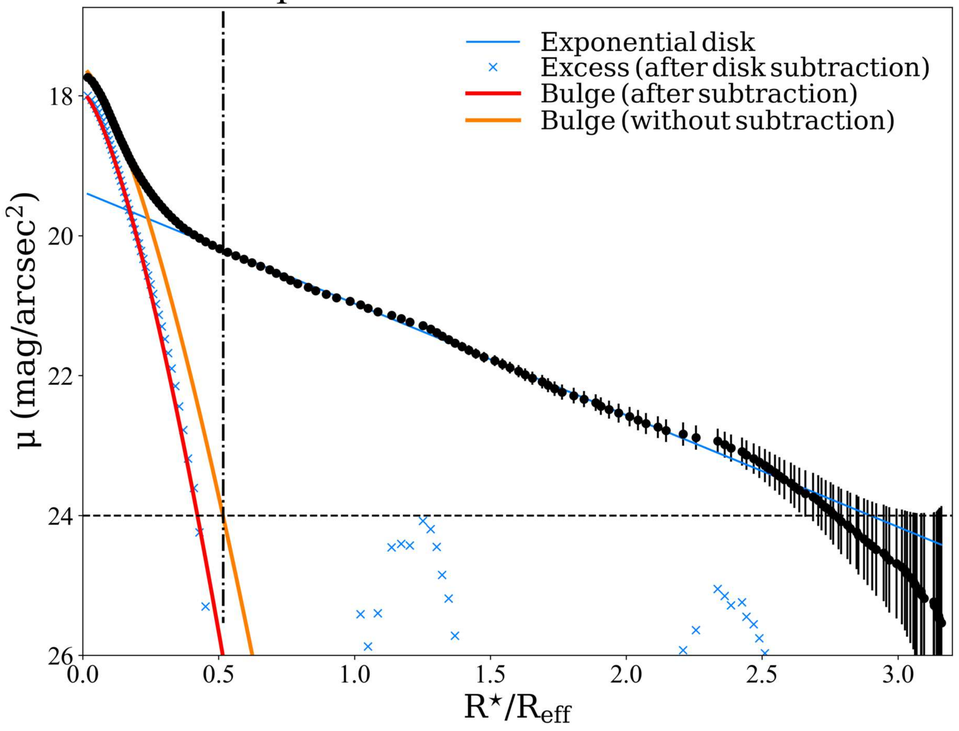

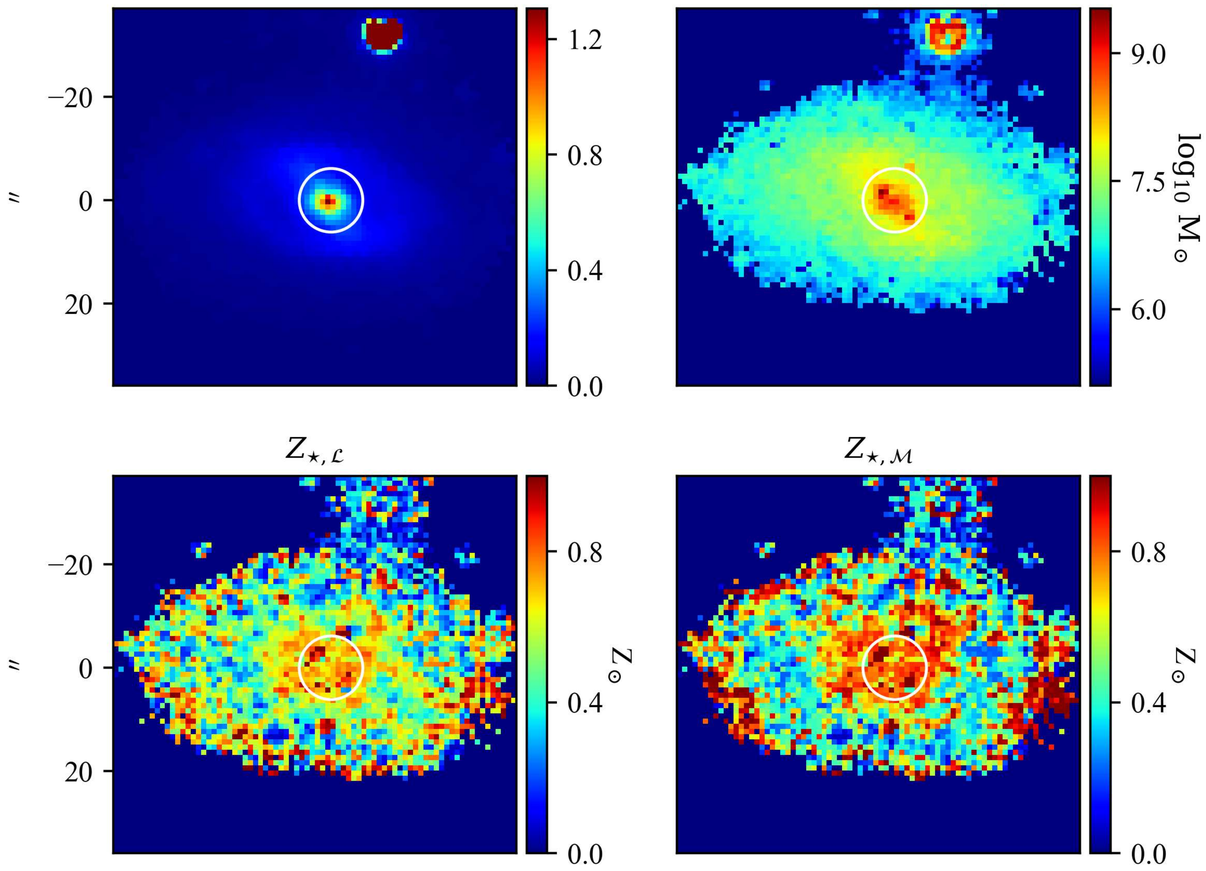

$\mathcal{RY}$ SBPs

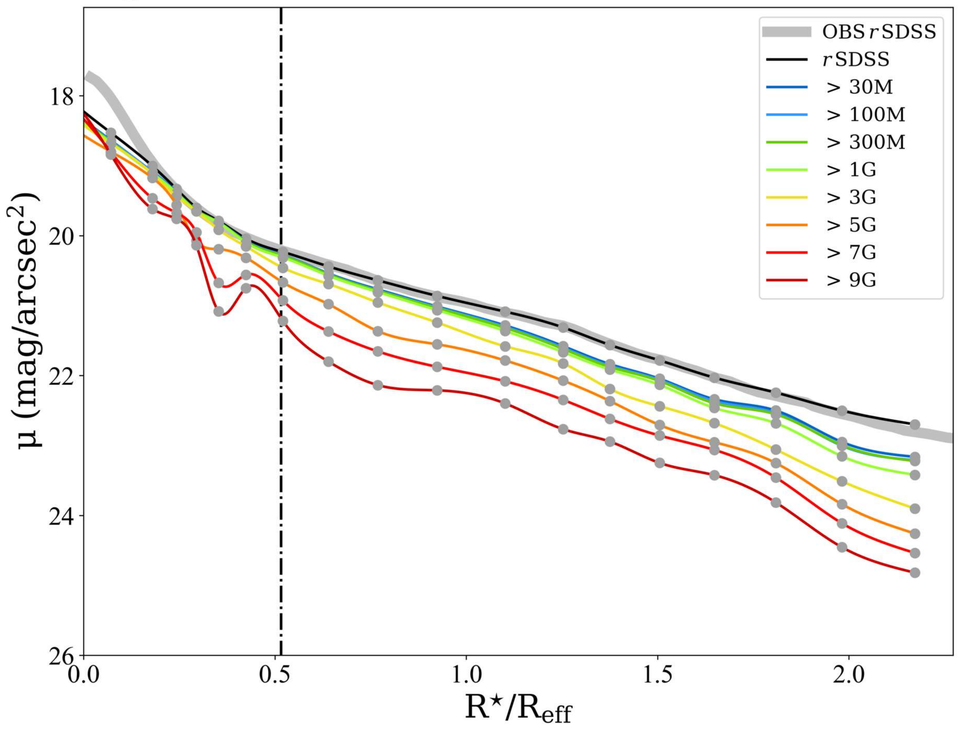

SDSS color profiles

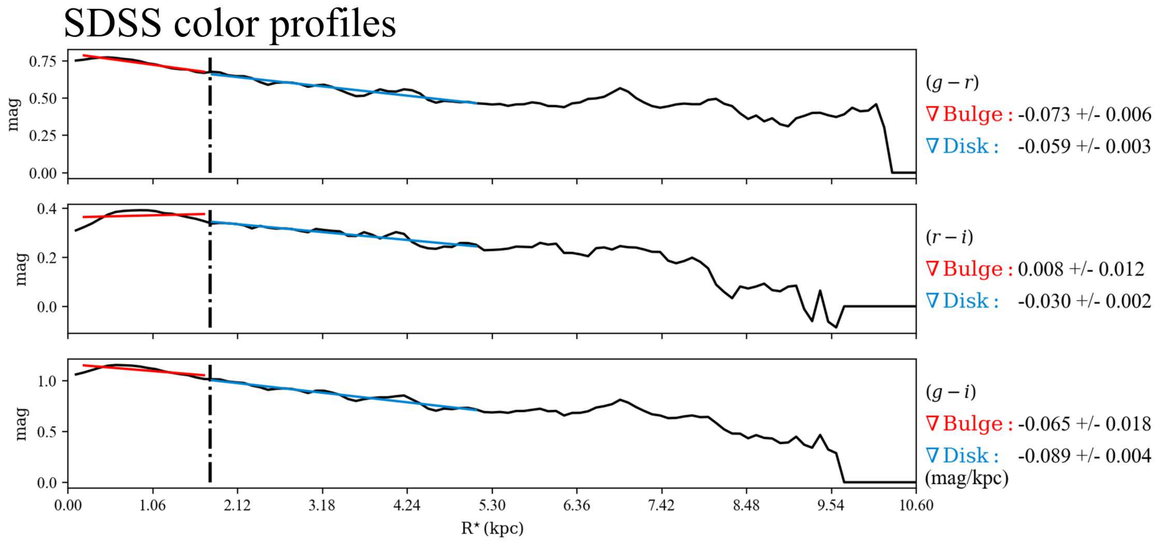

Log. of cumulative present stellar mass profiles

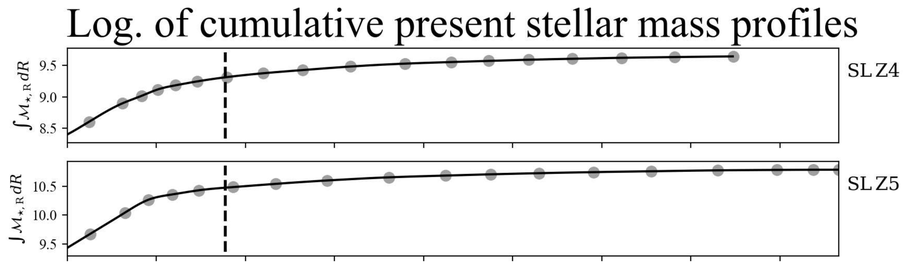

Stellar metallicity/Age & Hα flux/EW profiles

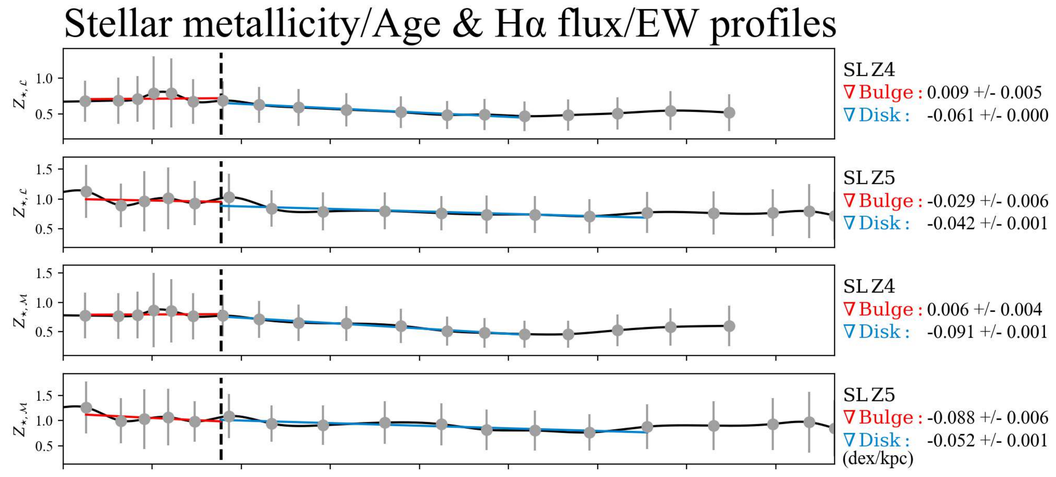

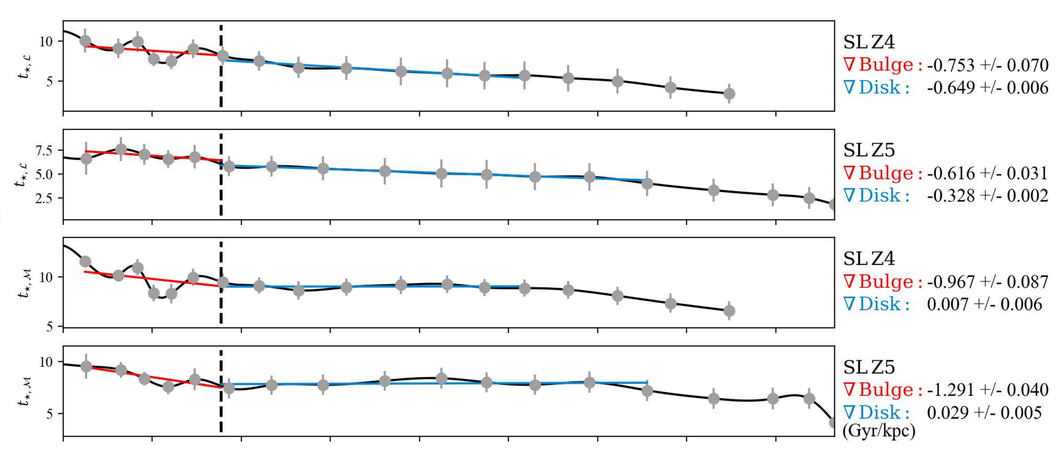

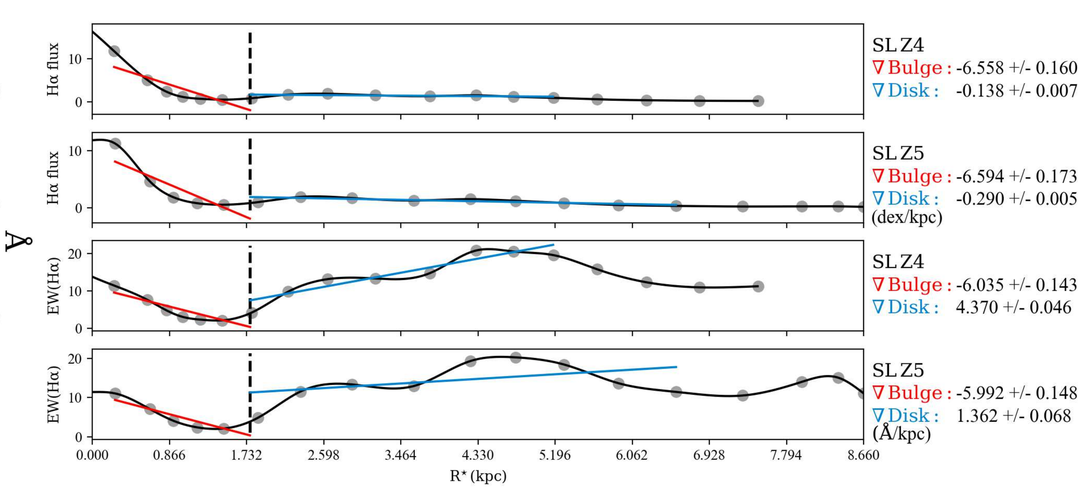

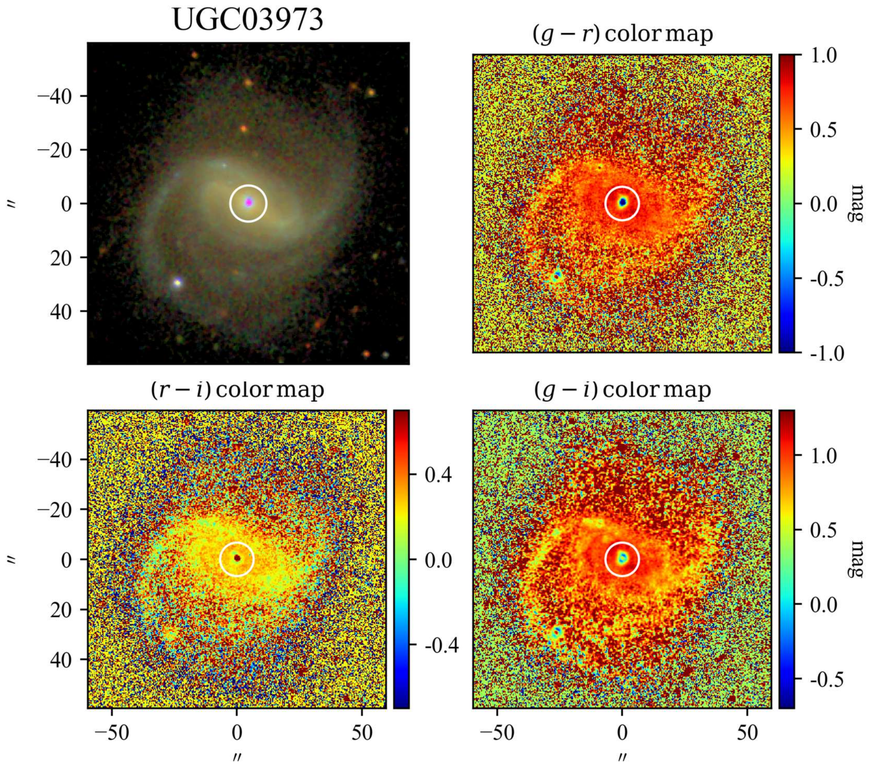

SBP decomposition of SDSS r band

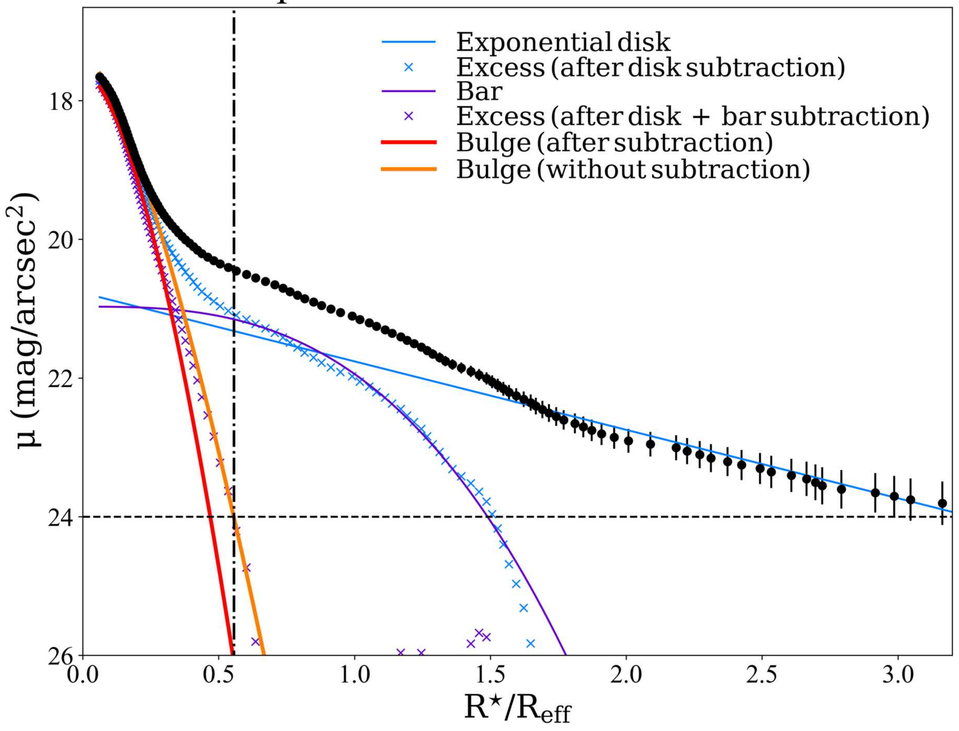

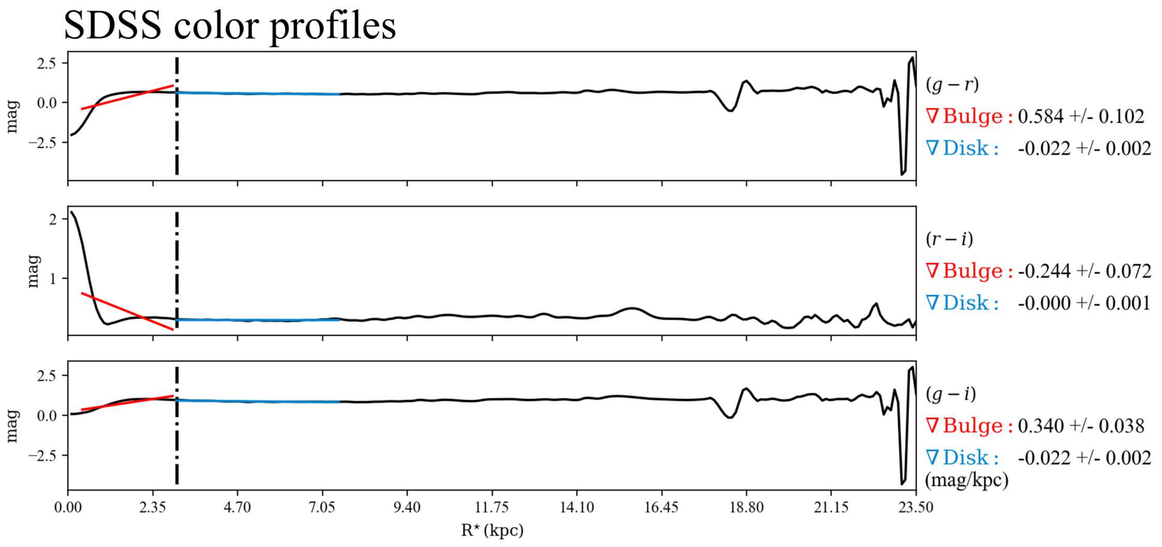

$\mathcal{RY}$ SBPs

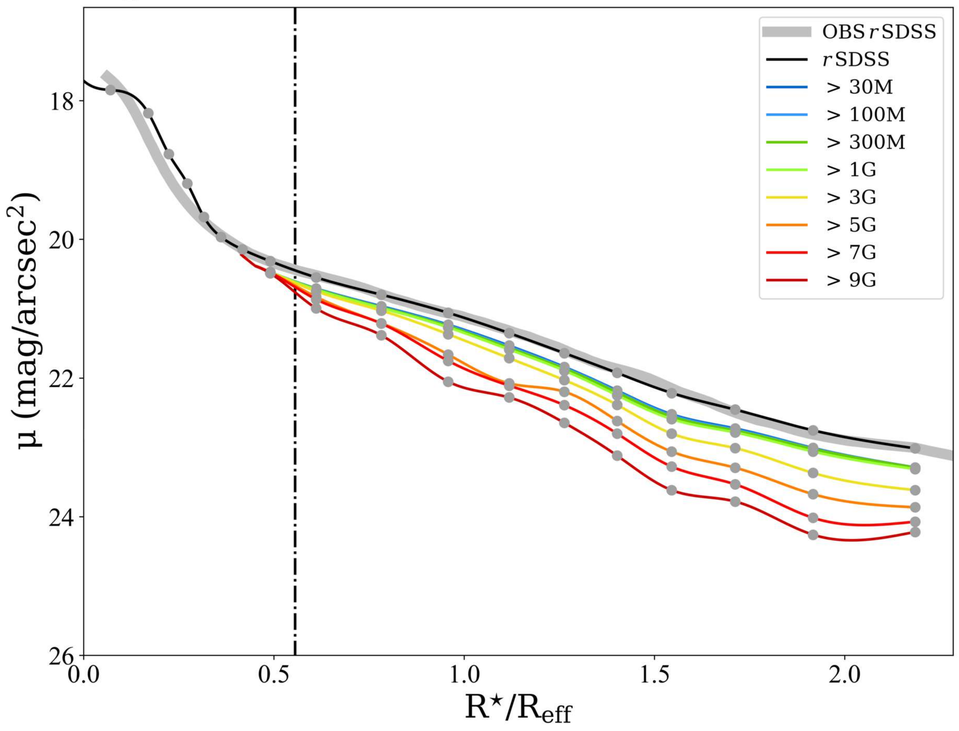

Stellar Continuum

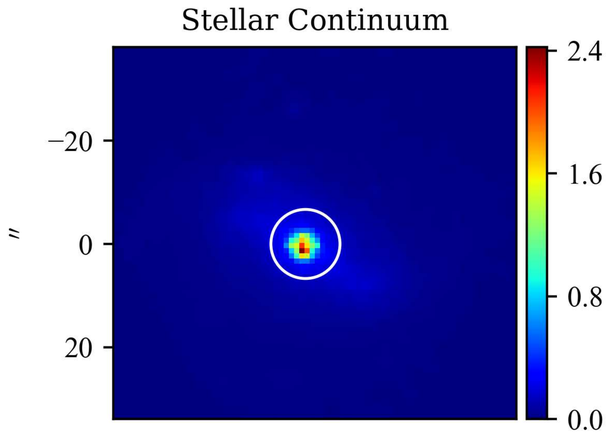

$\mathcal{M}_{\star,\mathrm{P}}$

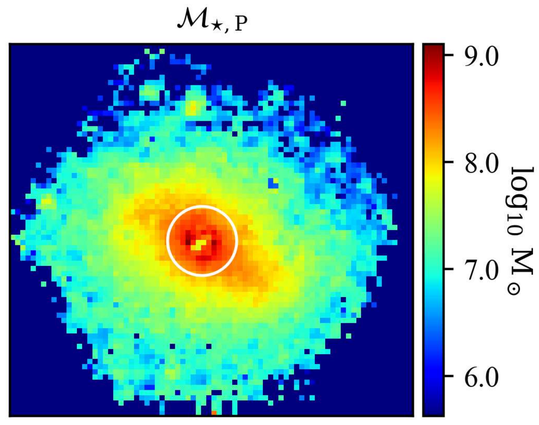

Log. of cumulative present stellar mass profiles

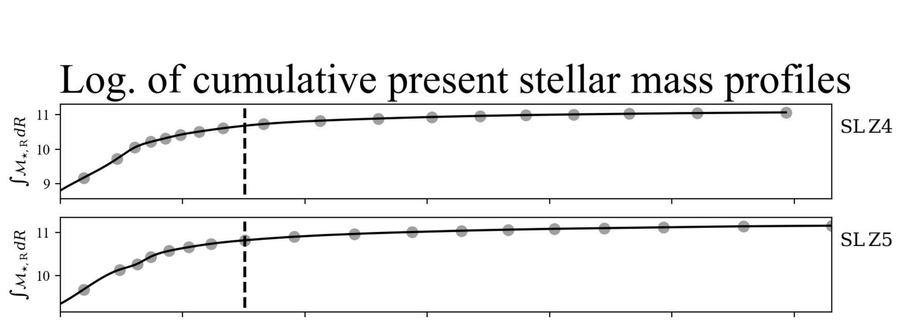

$Z_{\star,\mathcal{L}}$

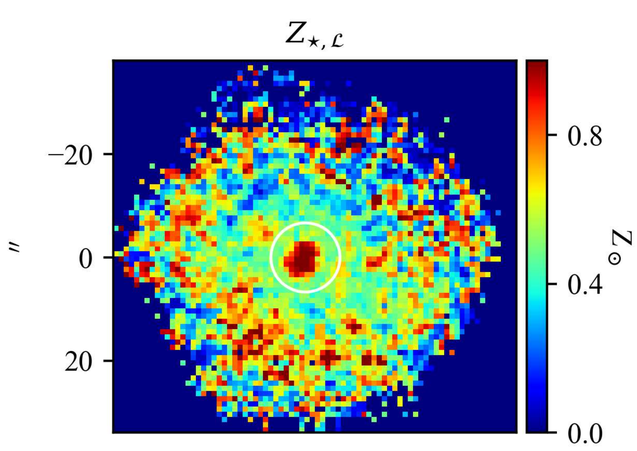

$Z_{\star,\mathcal{M}}$

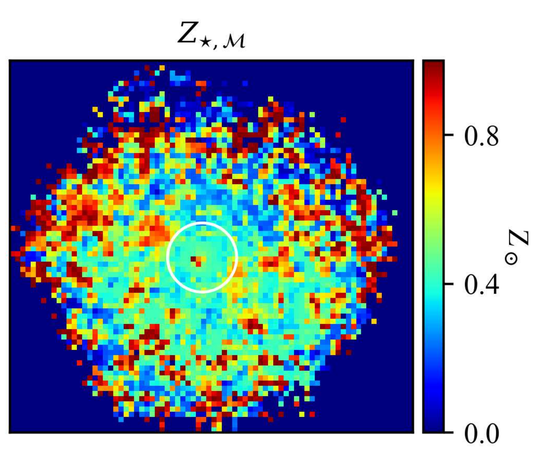

Stellar metallicity/Age & Hα flux/EW profiles

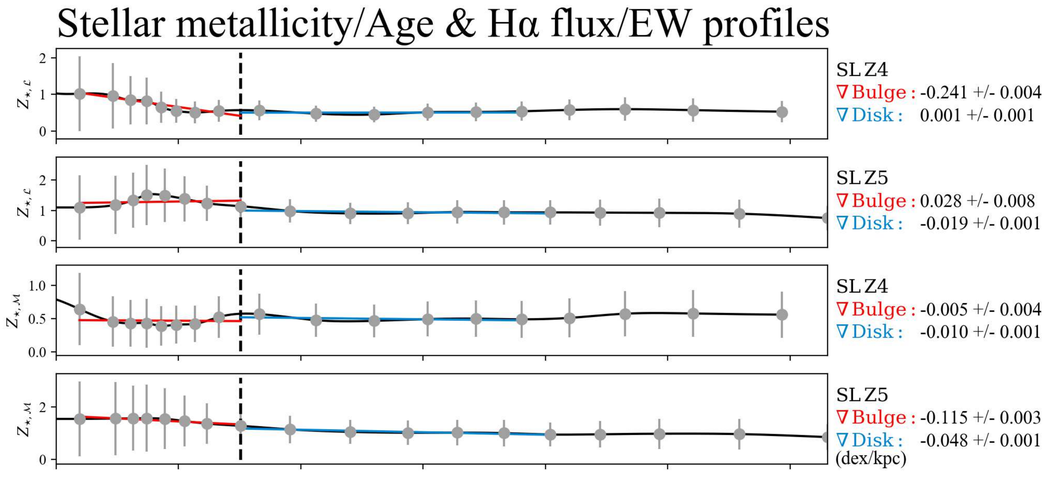

$t_{\star,\mathcal{L}}$

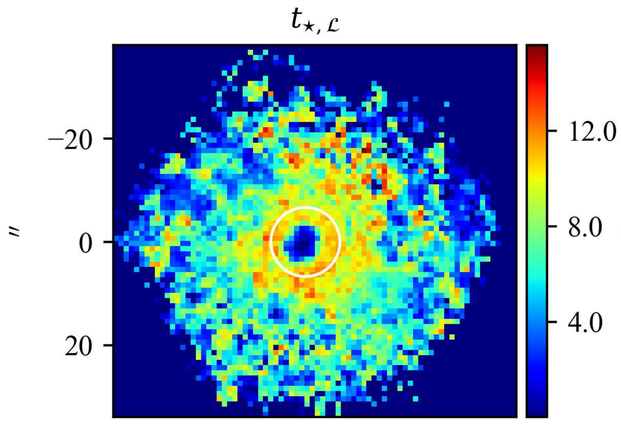

$t_{\star,\mathcal{M}}$

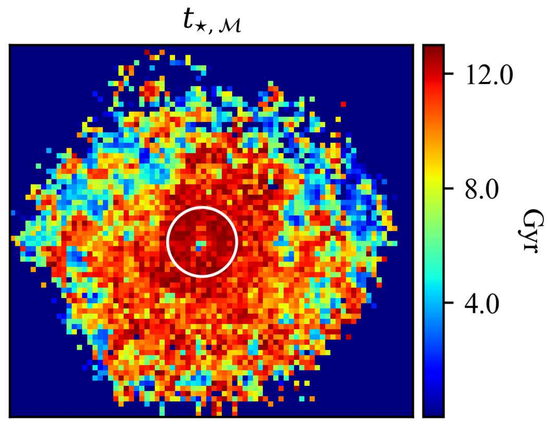

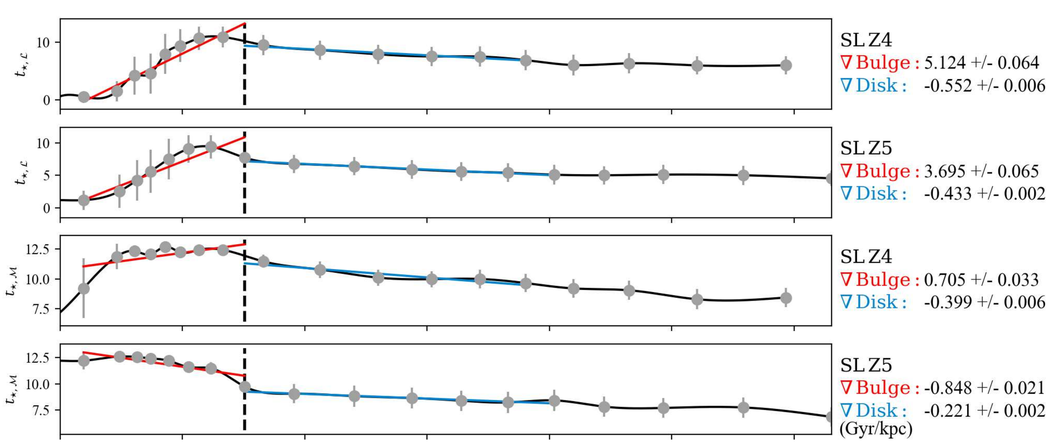

Hα flux

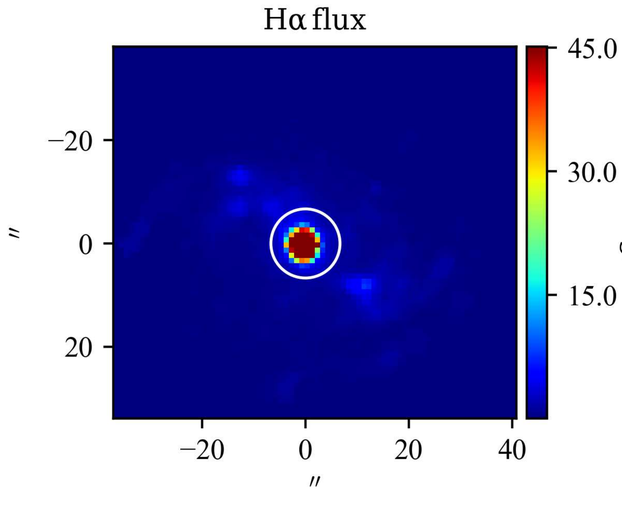

EW(Hα)

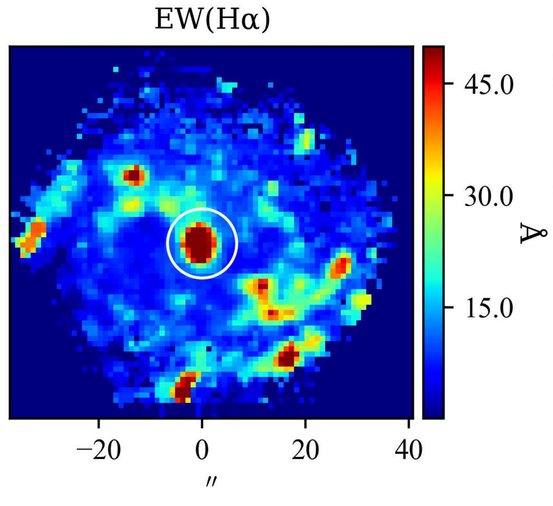

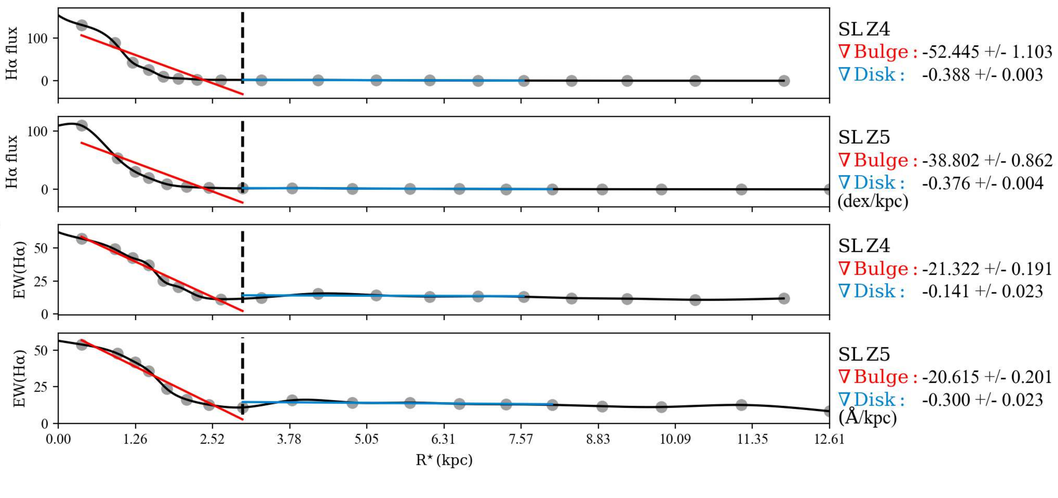

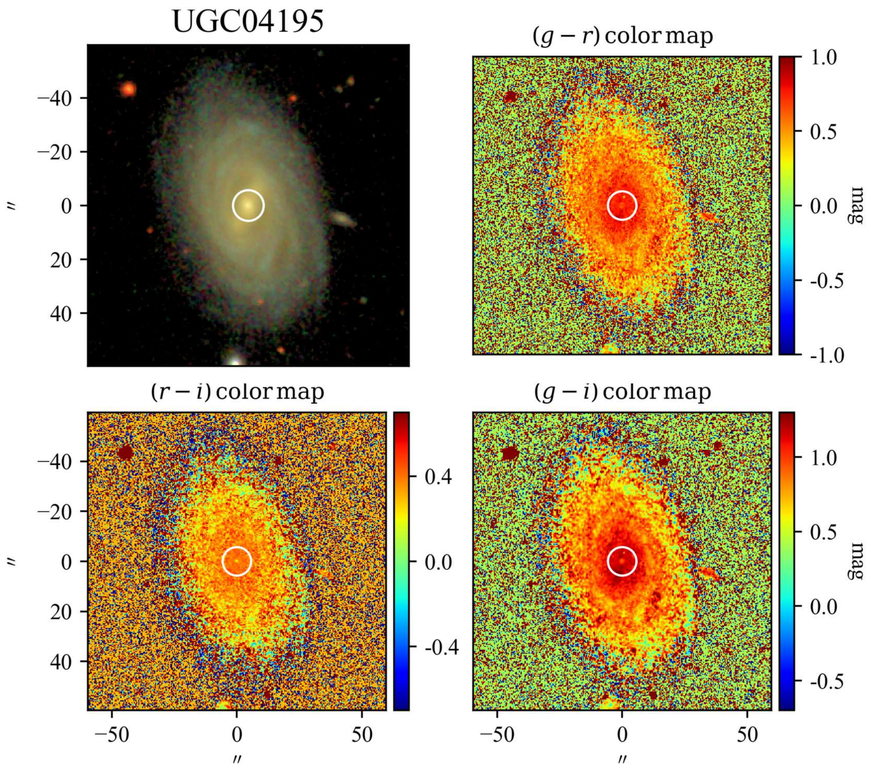

SBP decomposition of SDSS r band

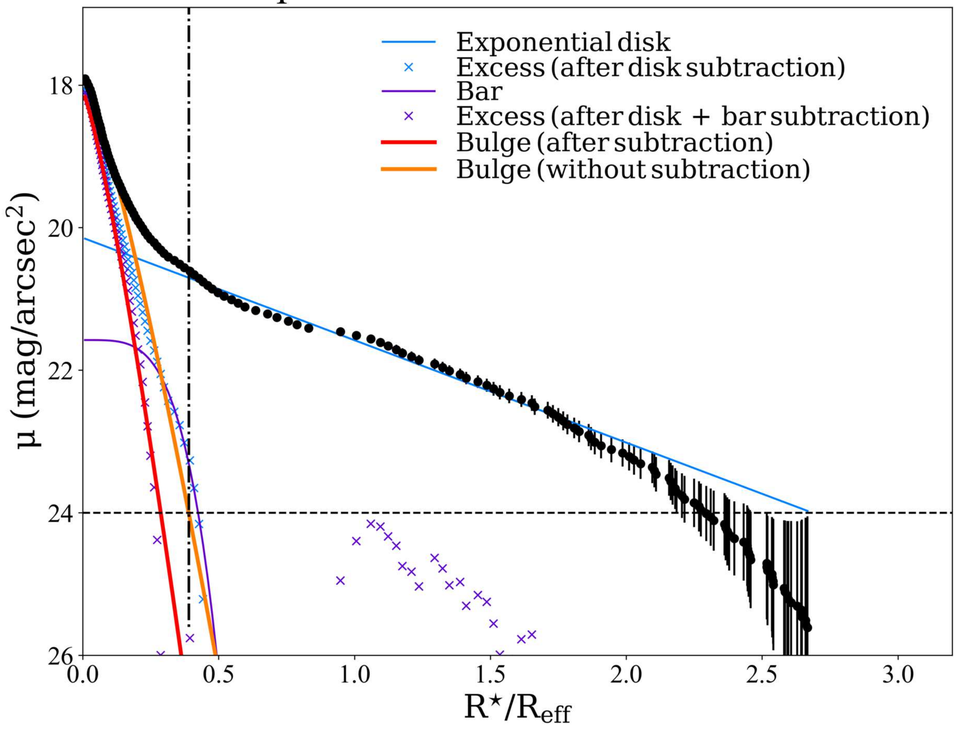

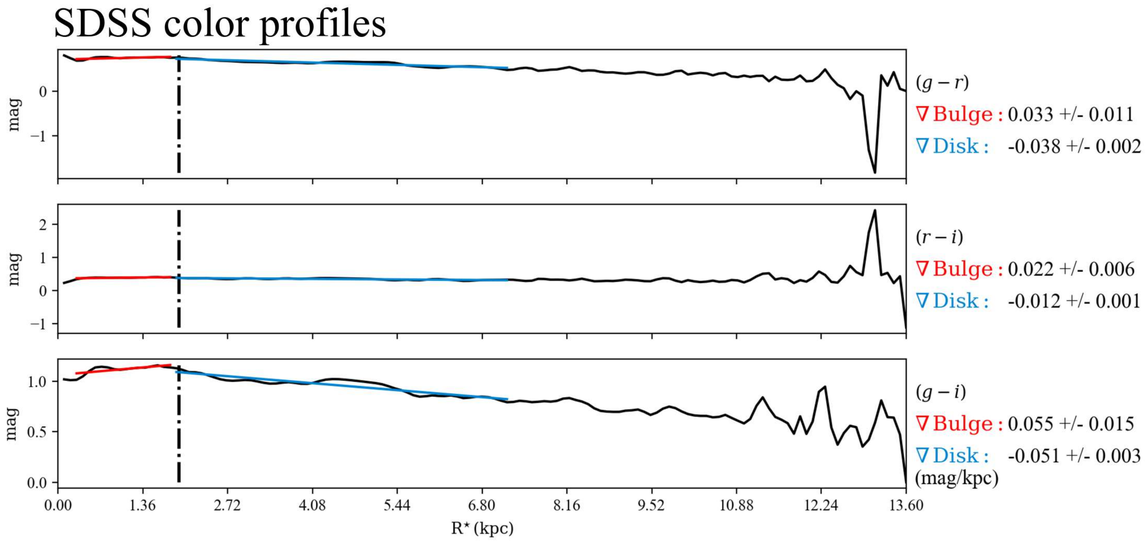

$\mathcal{RY}$ SBPs

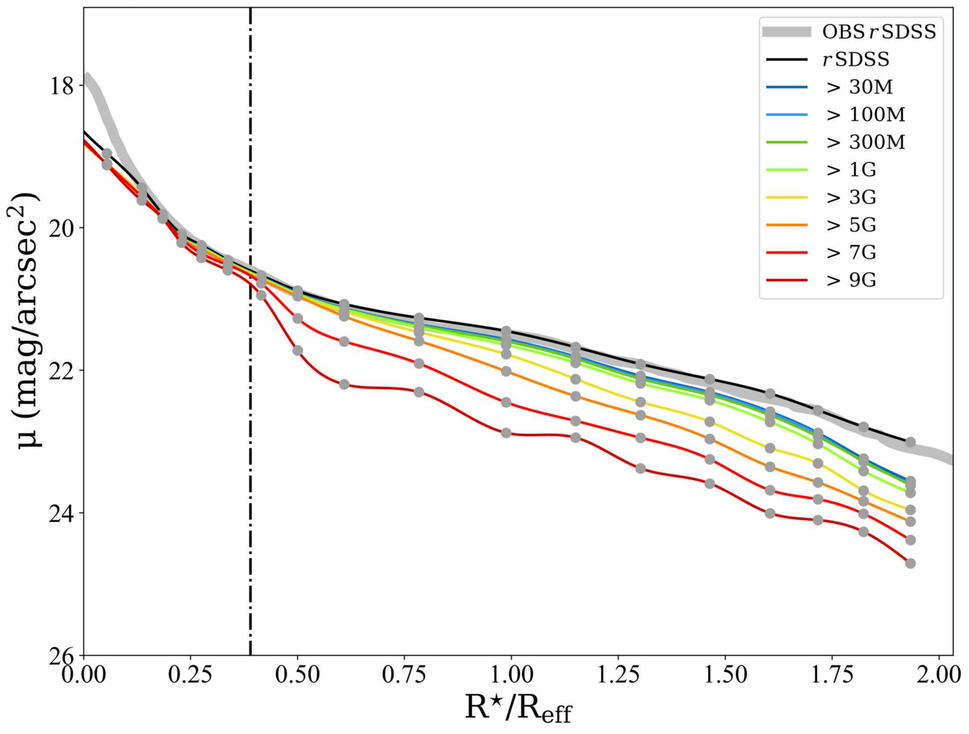

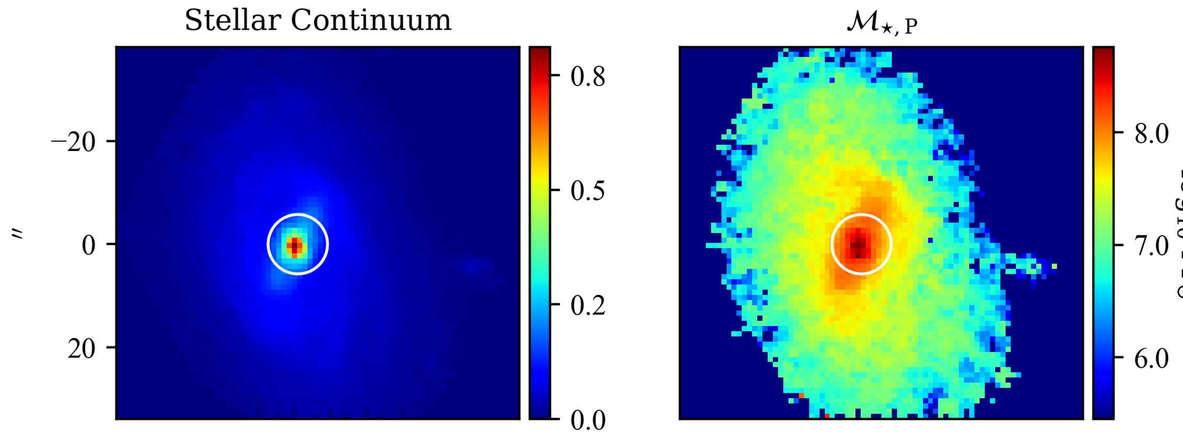

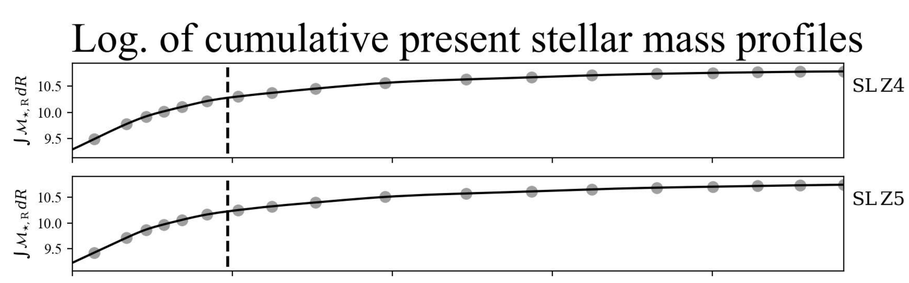

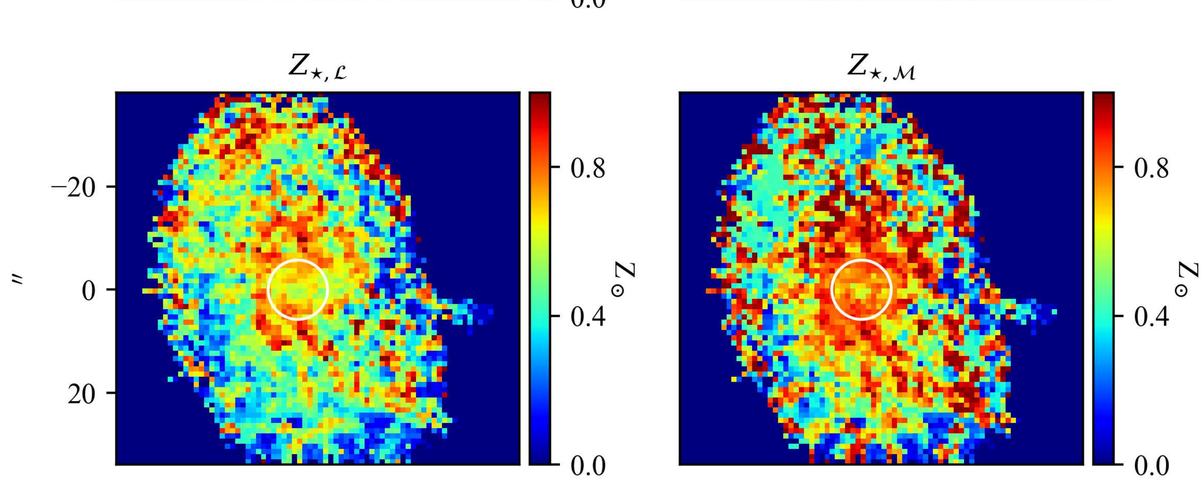

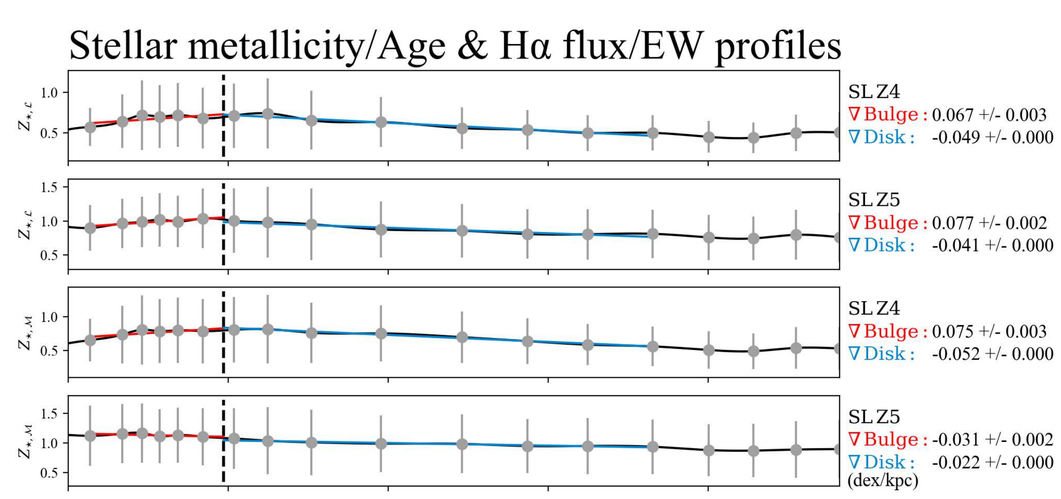

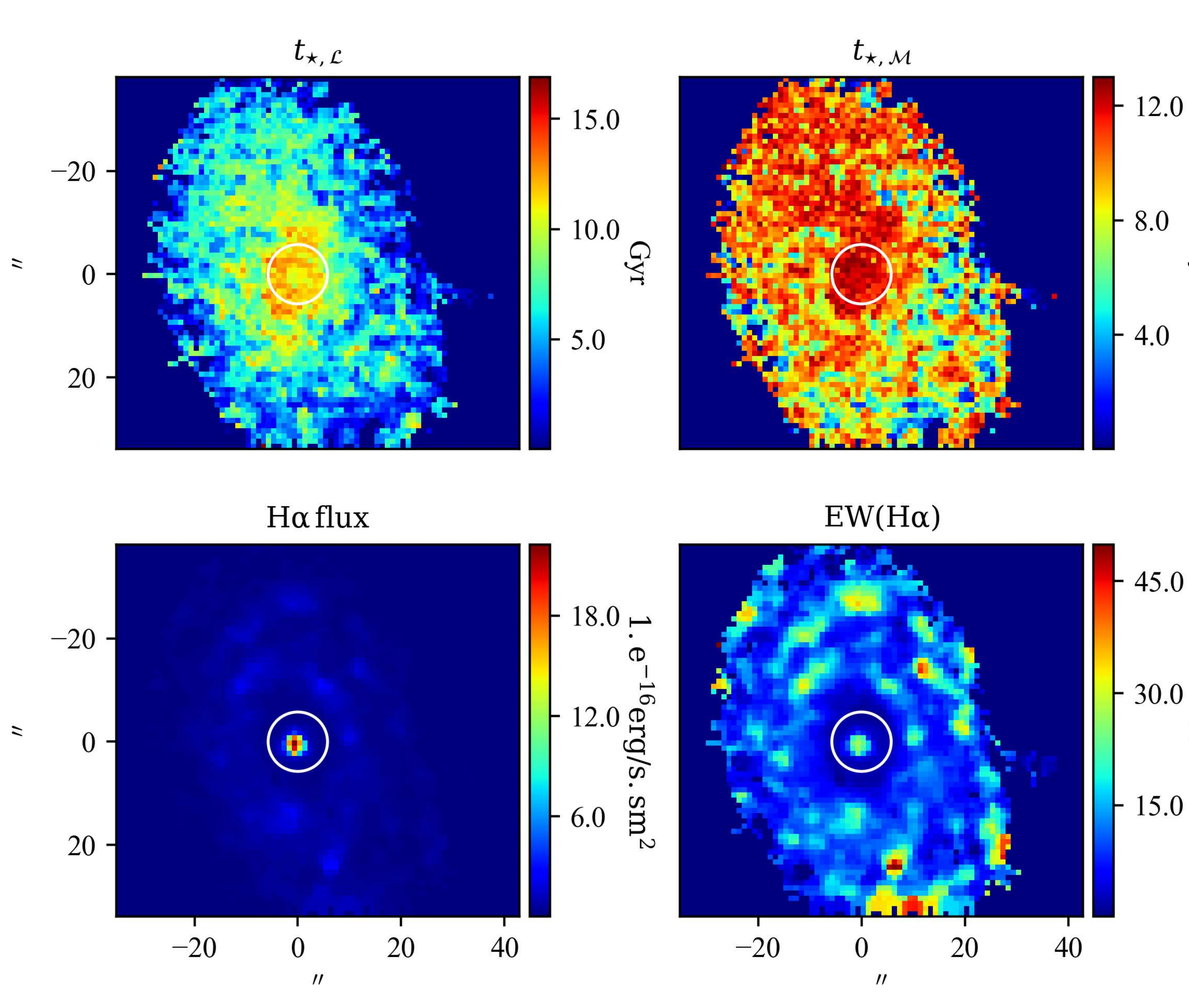

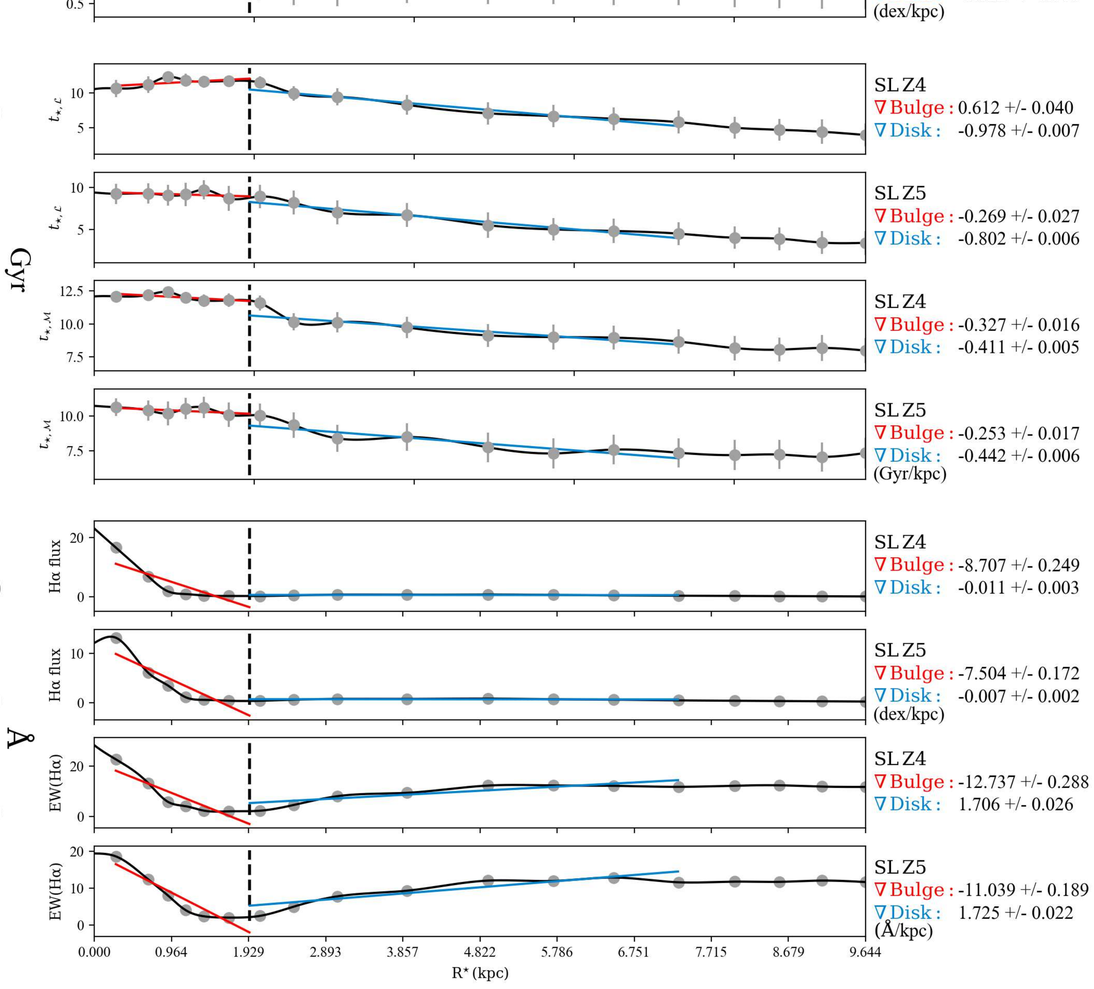

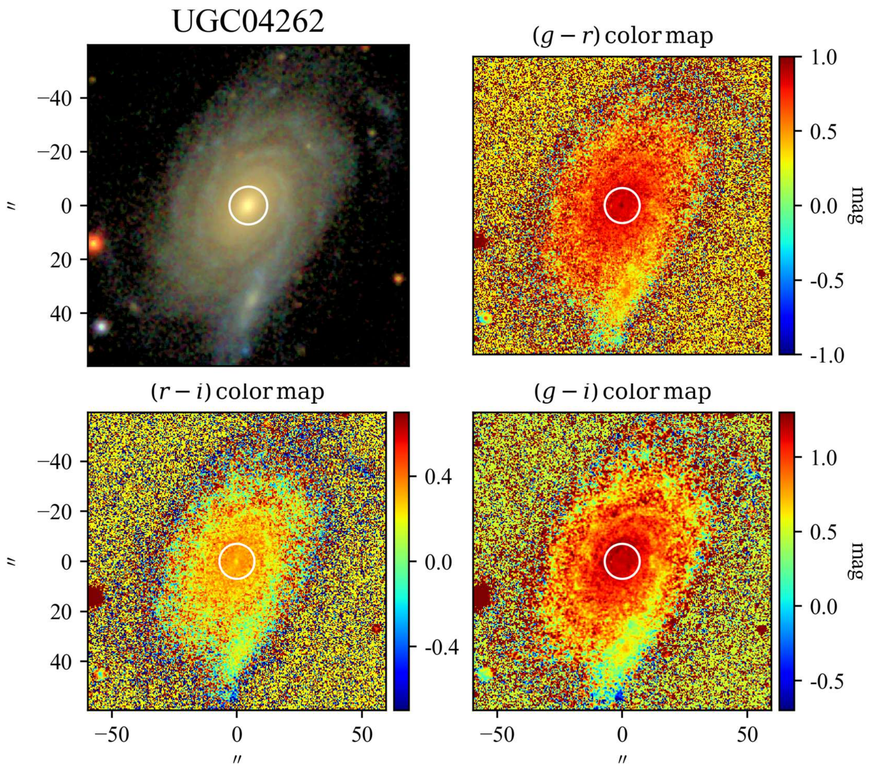

SBP decomposition of SDSS r band

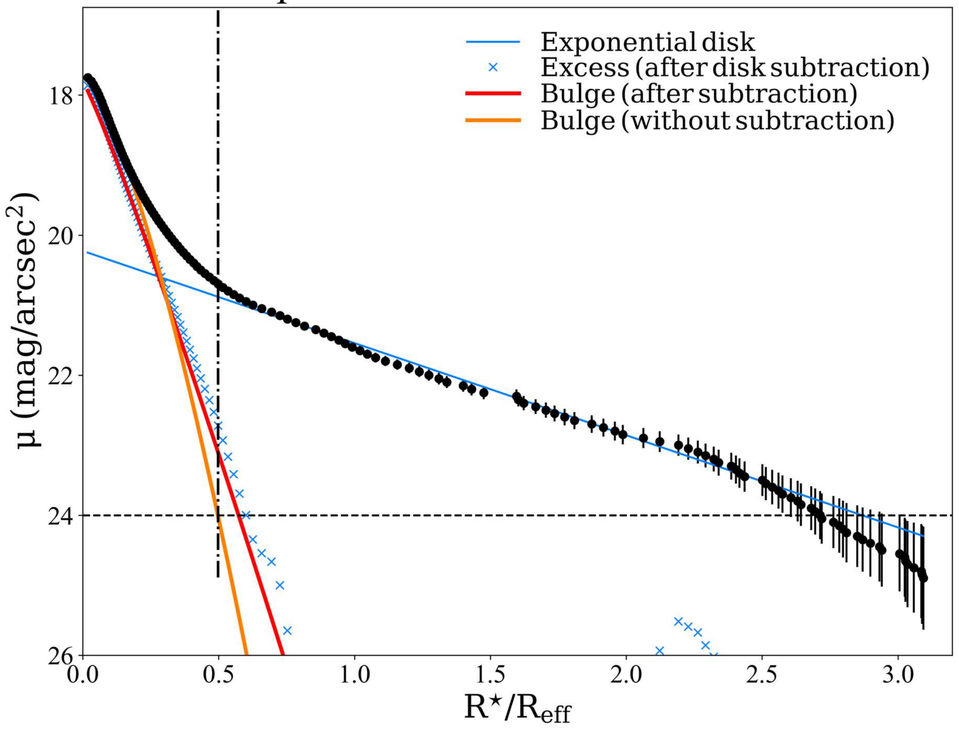

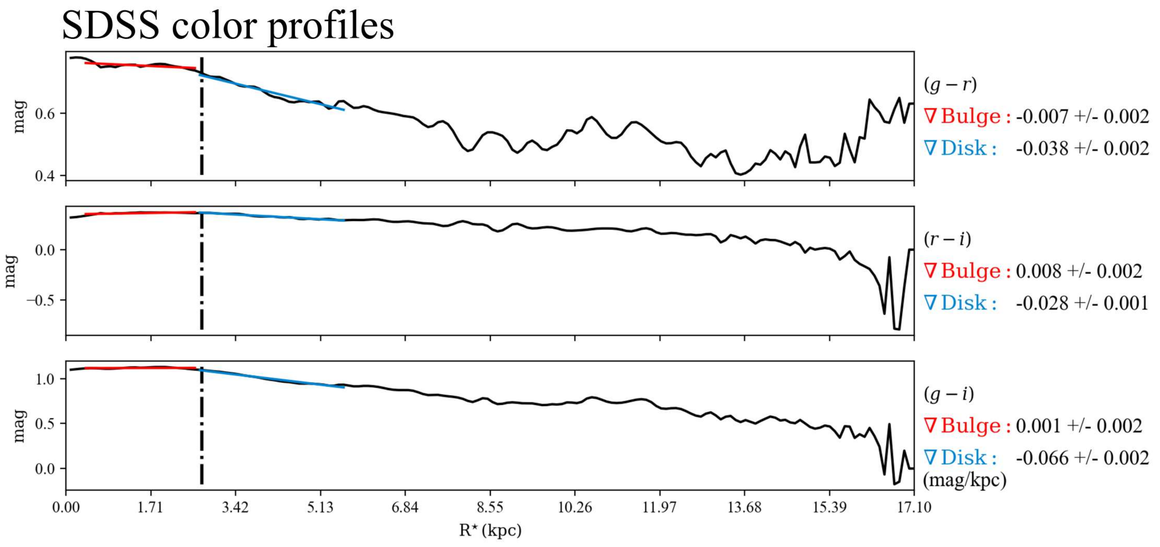

$\mathcal{RY}$ SBPs

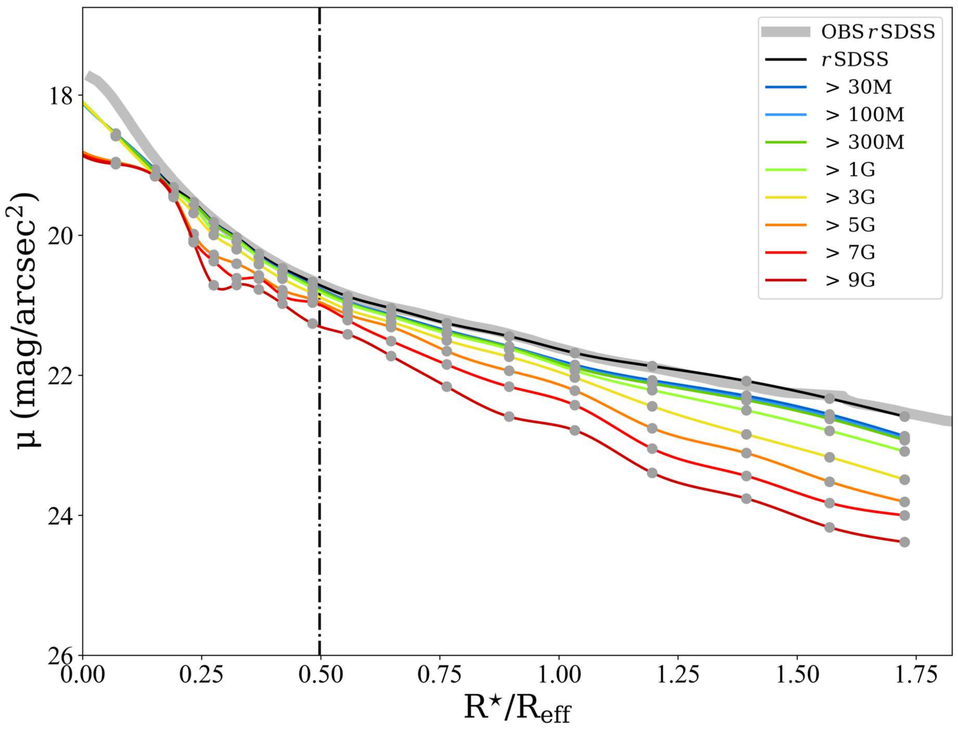

Stellar Continuum $\mathcal{M}_{\star,\mathrm{P}}$

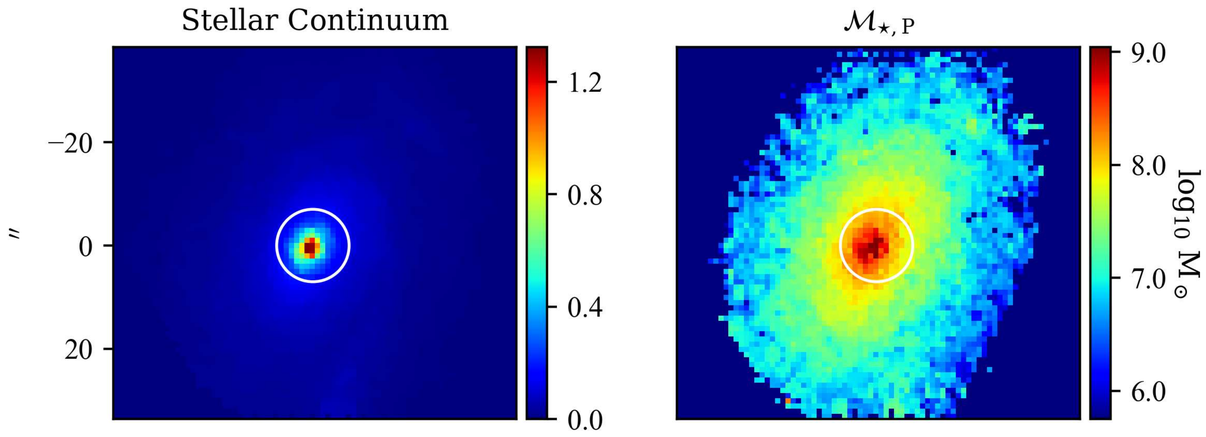

Log. of cumulative present stellar mass profiles

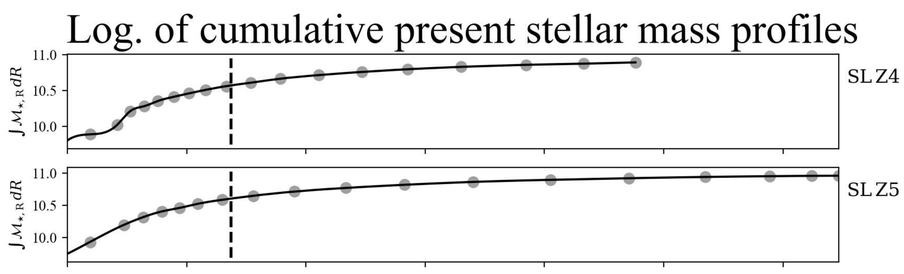

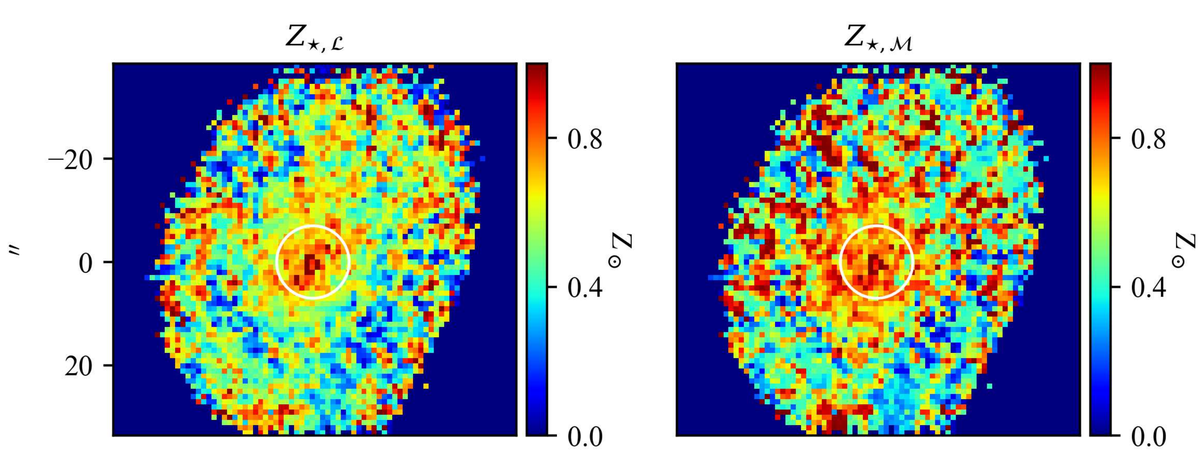

Stellar metallicity/Age & Hα flux/EW profiles

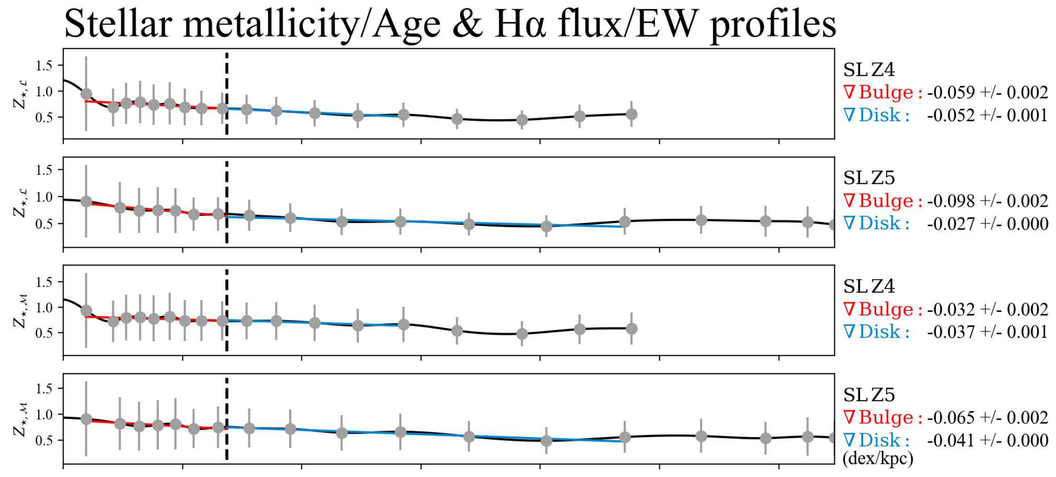

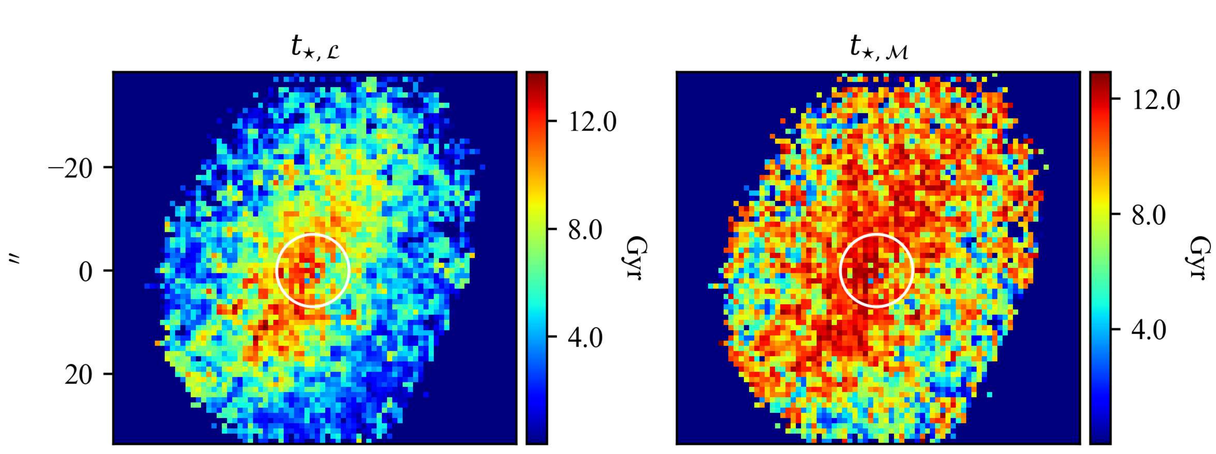

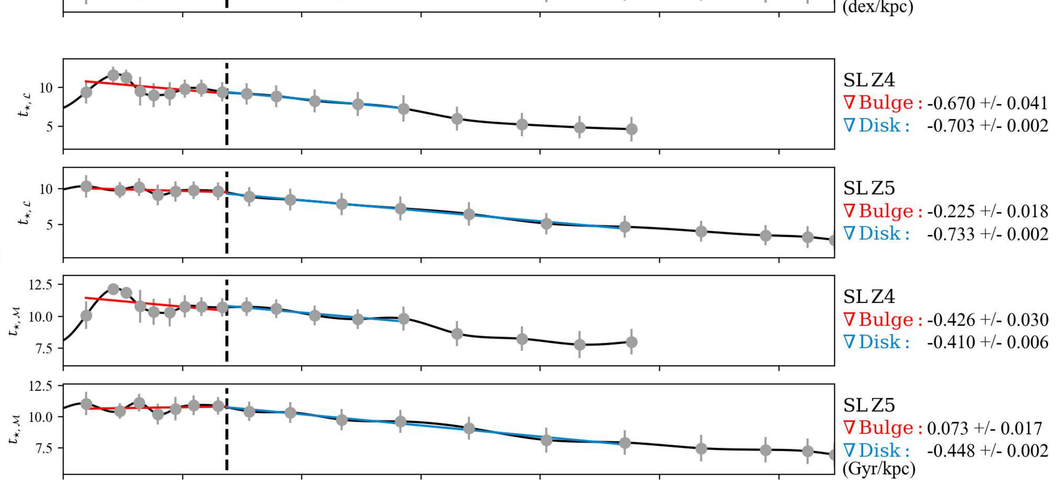

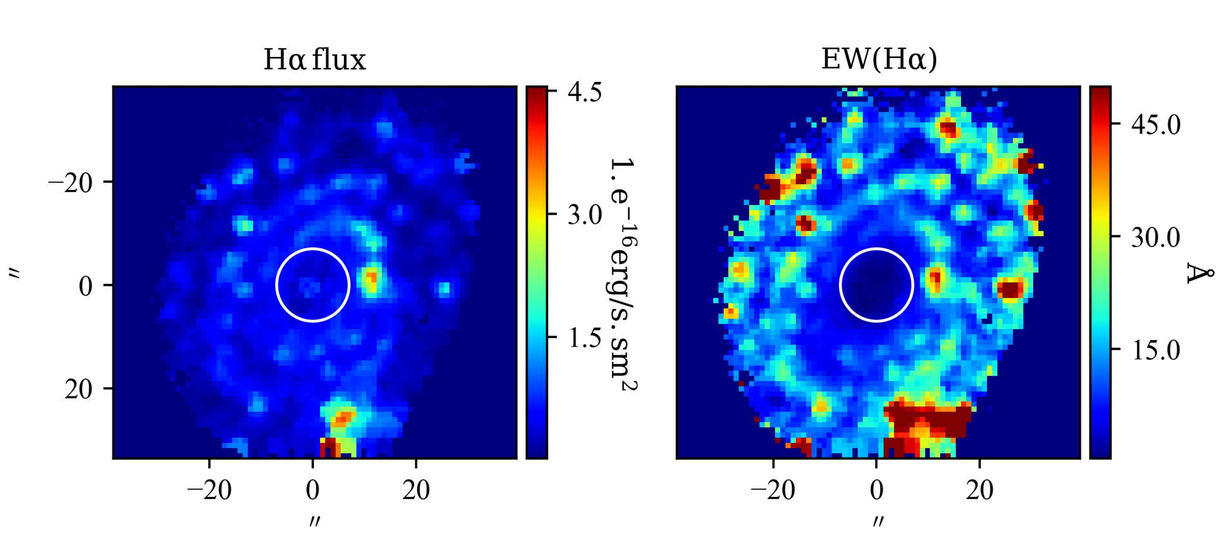

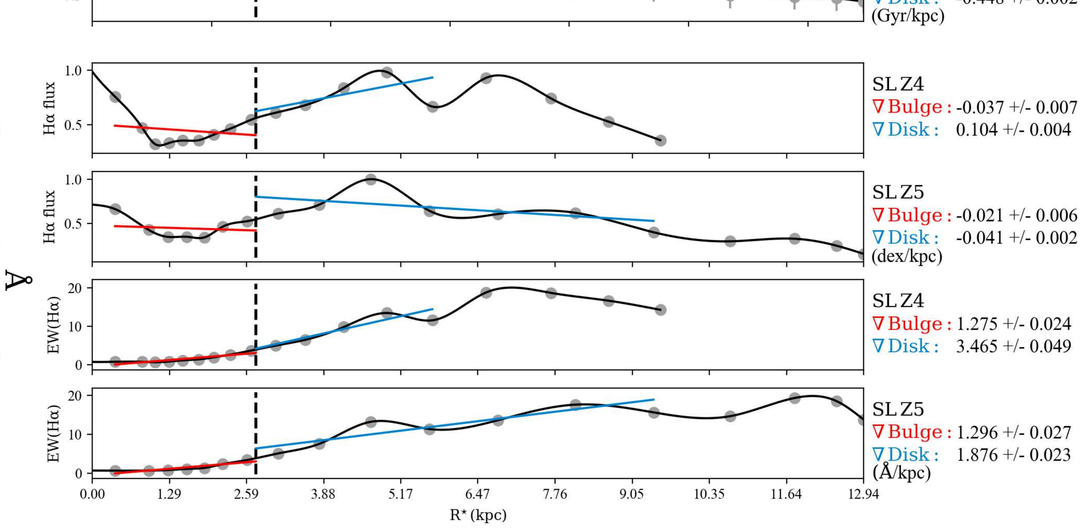

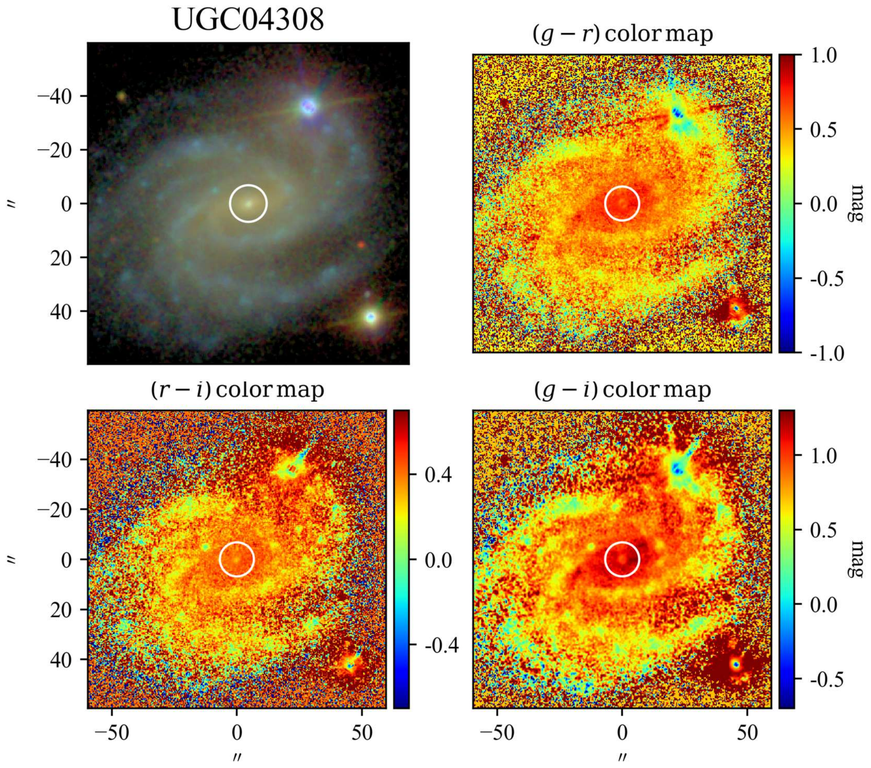

SBP decomposition of SDSS r band

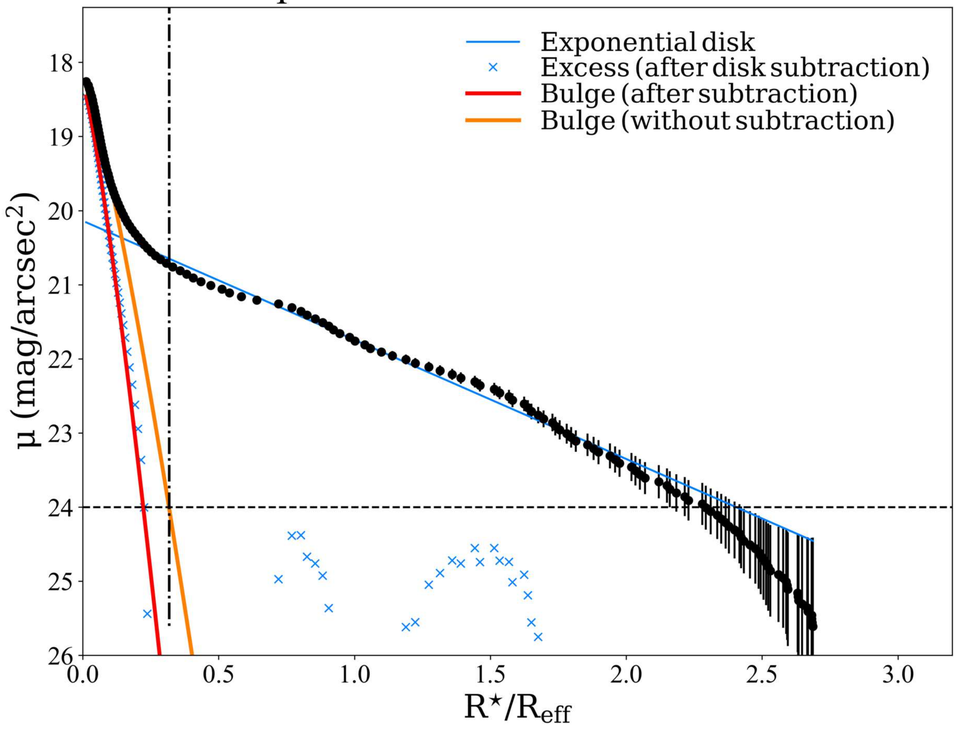

SDSS color profiles

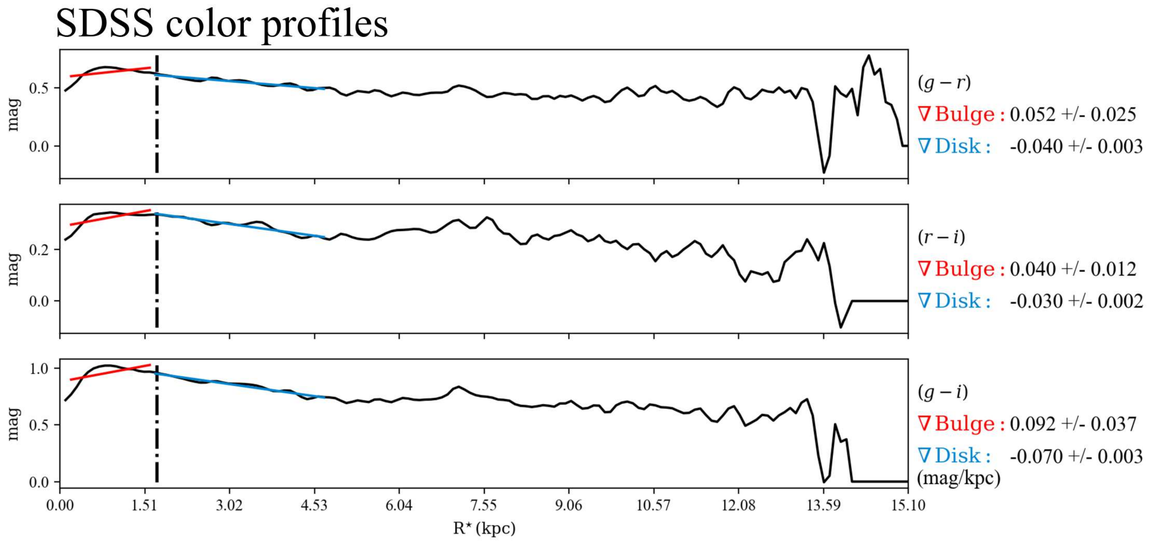

$\mathcal{RY}$ SBPs

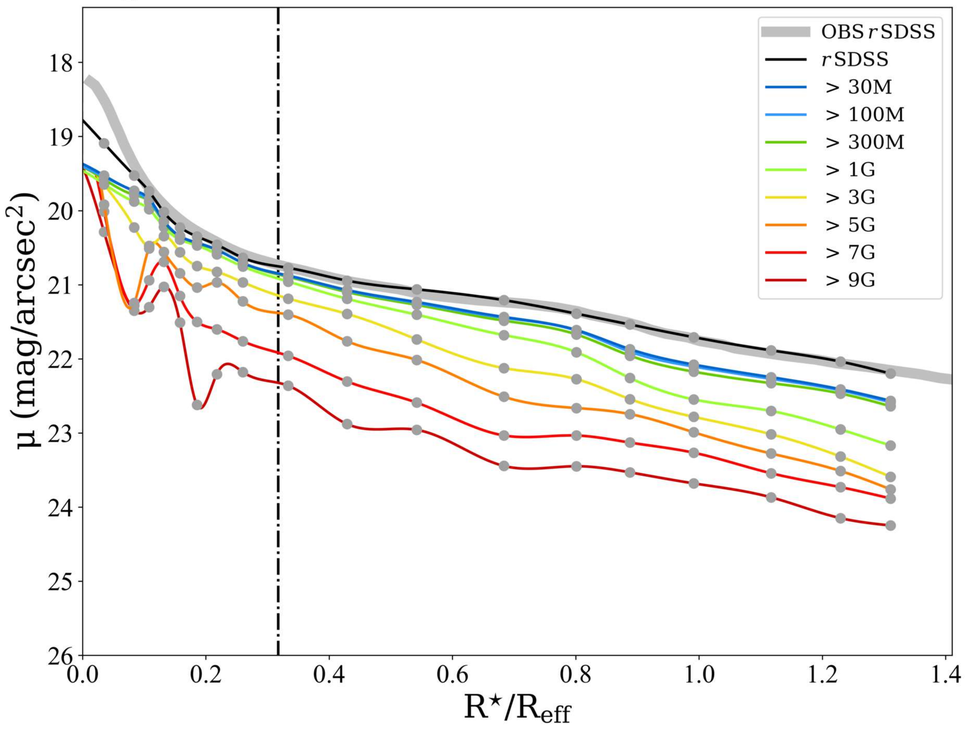

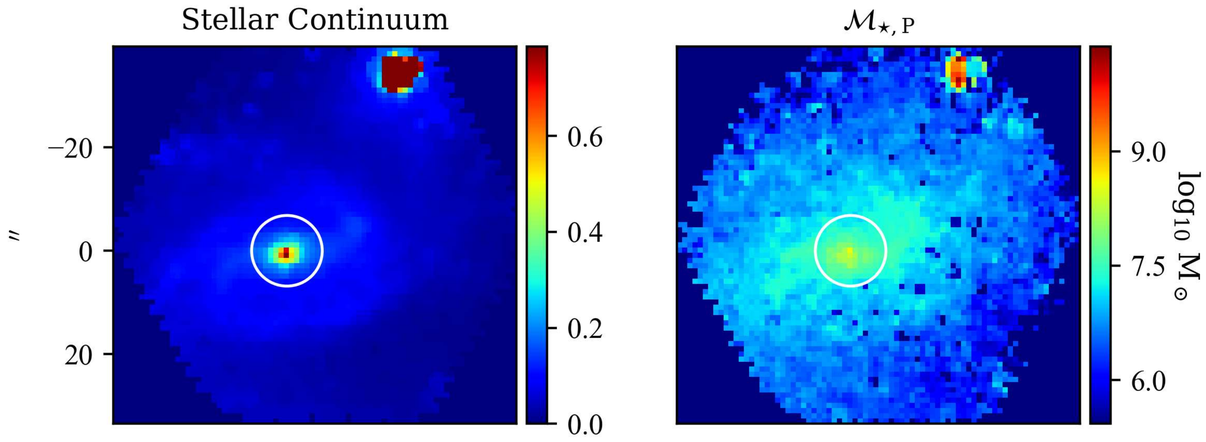

Log. of cumulative present stellar mass profiles

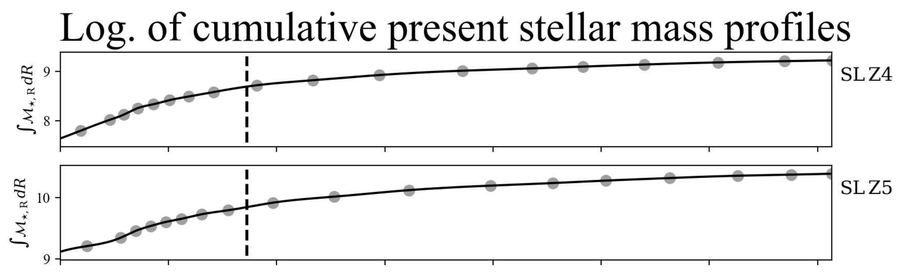

Stellar metallicity/Age & Hα flux/EW profiles

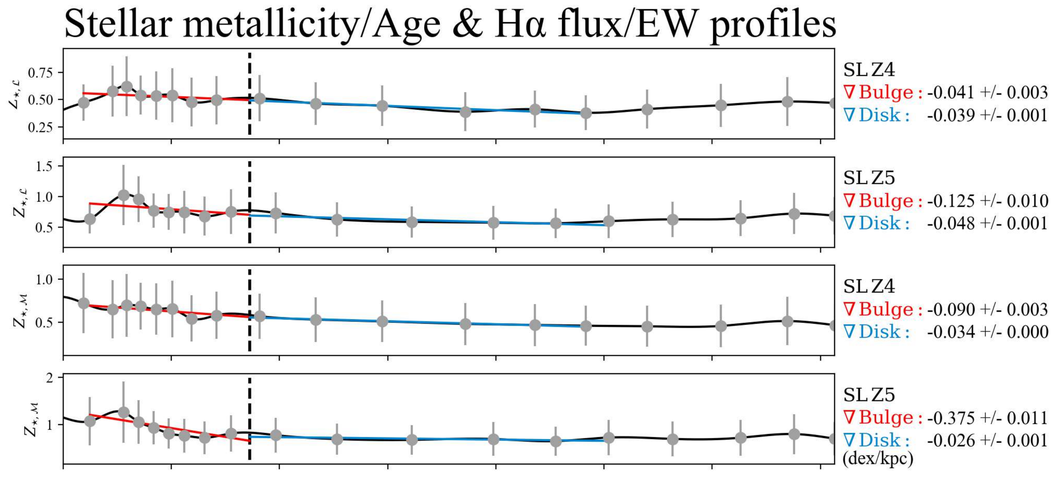

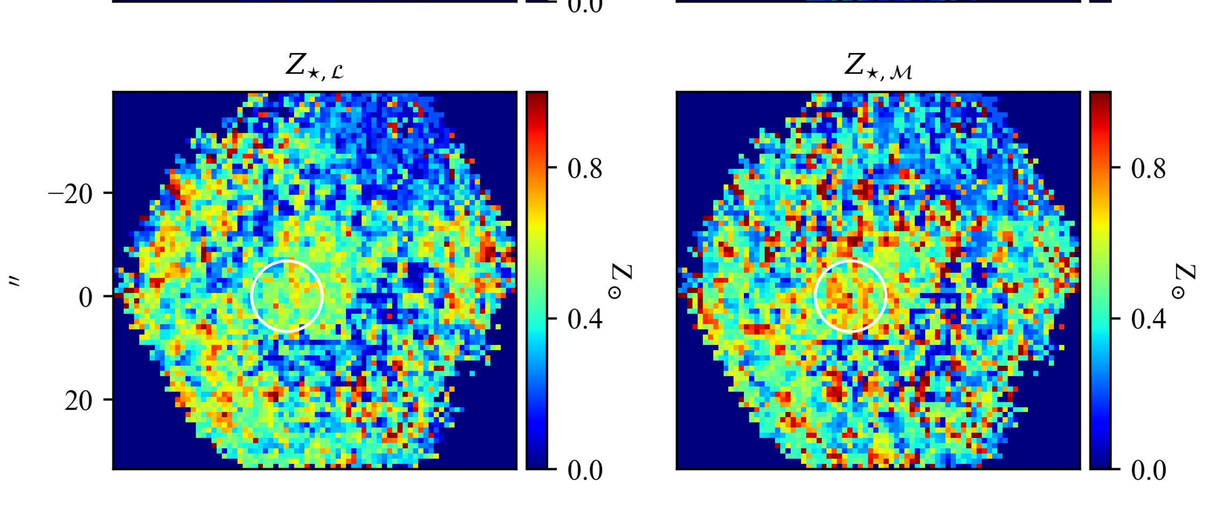

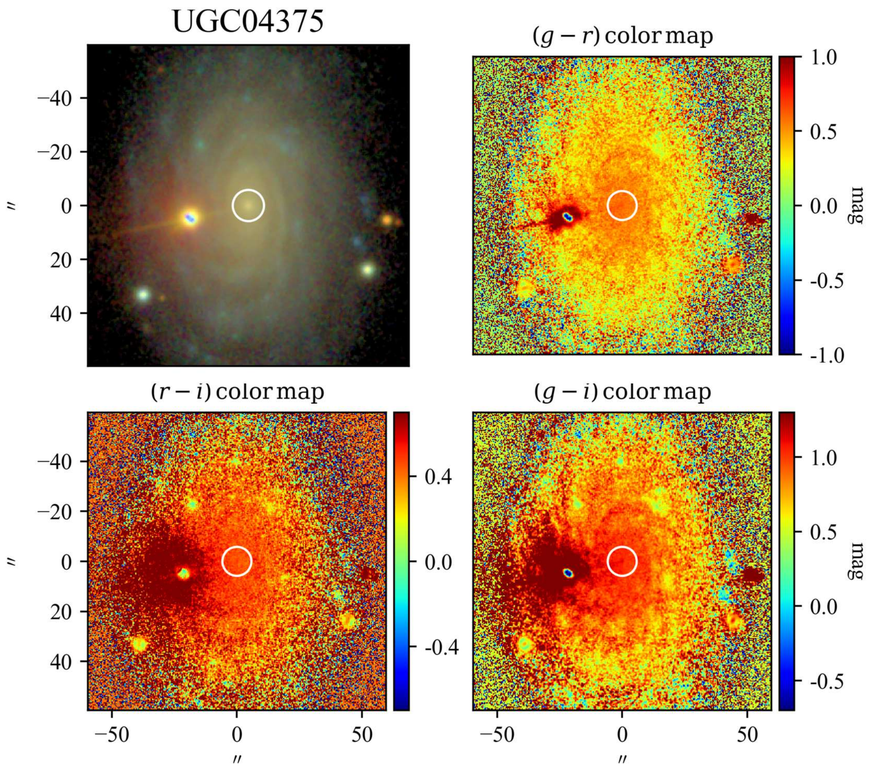

SBP decomposition of SDSS r band

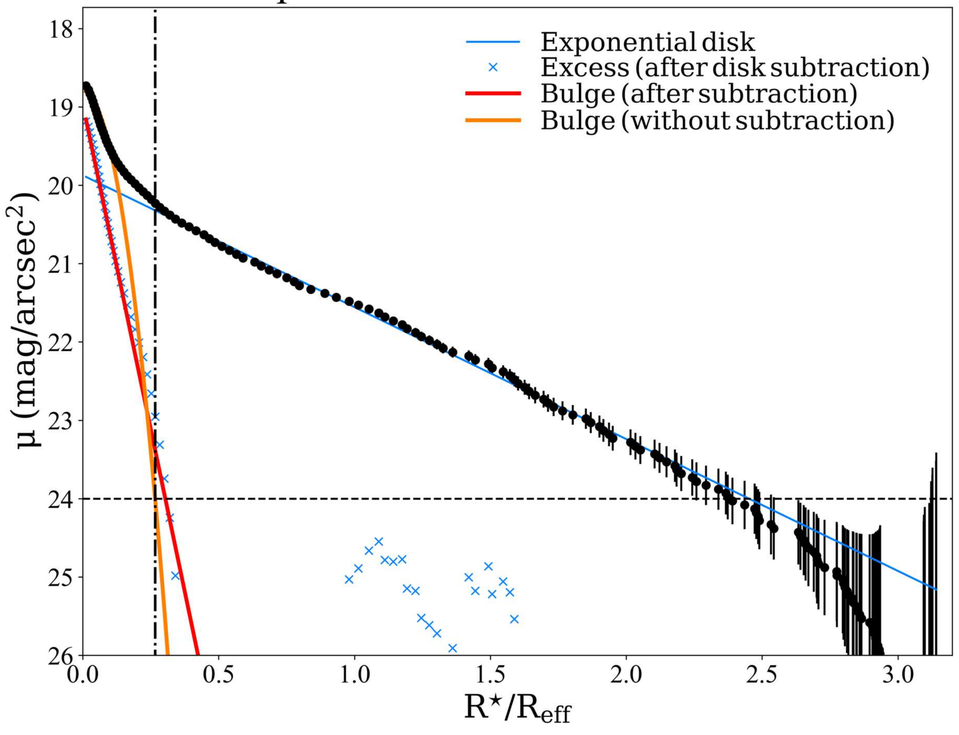

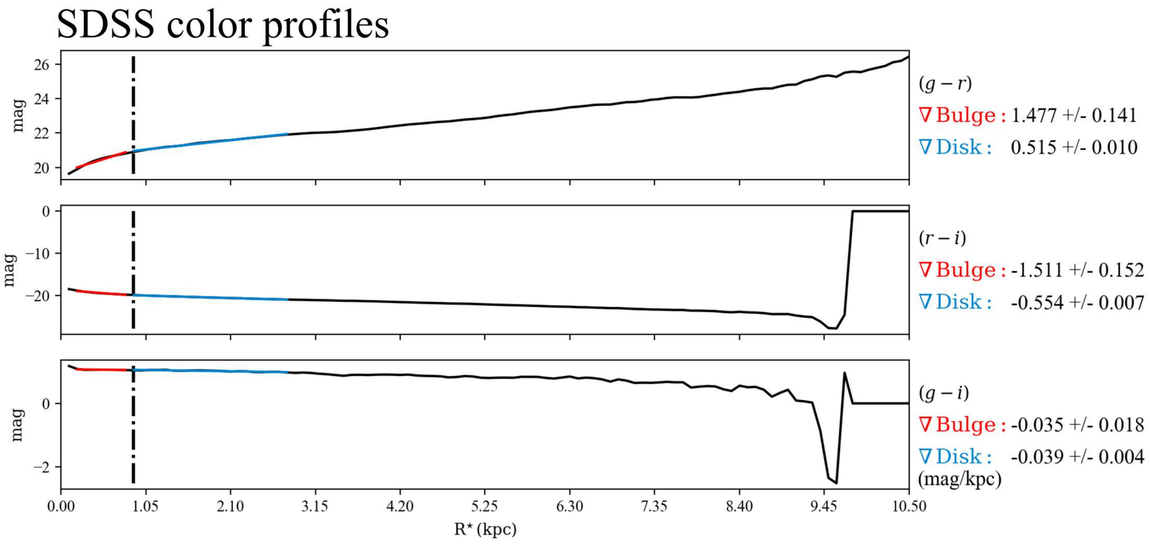

$\mathcal{RY}$ SBPs

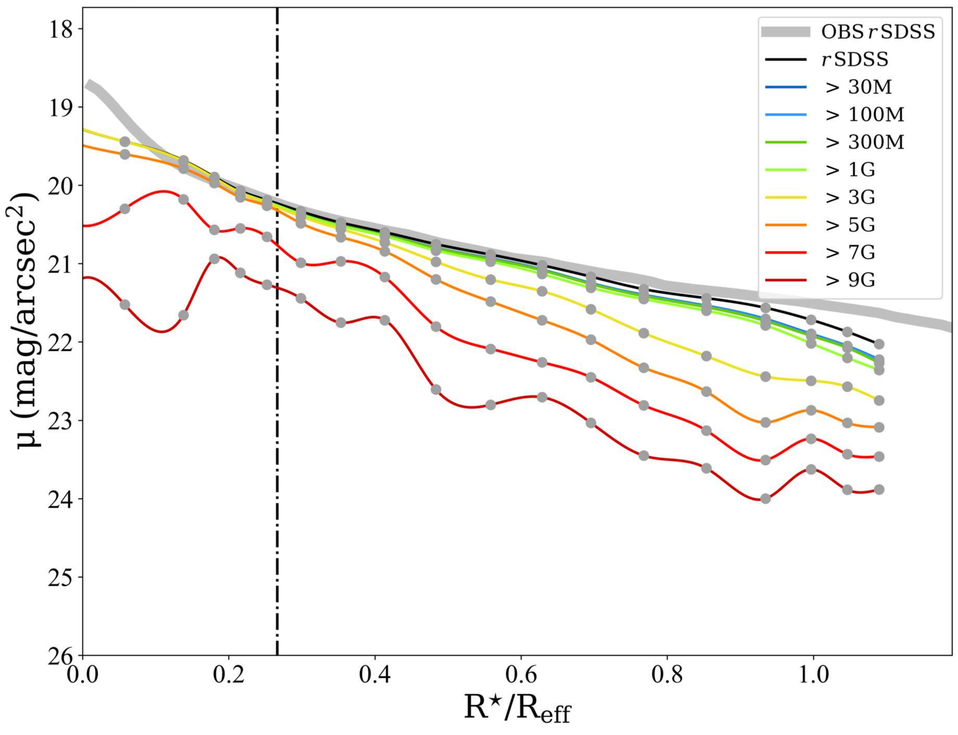

Stellar Continuum $\mathcal{M}_{\star,\mathrm{P}}$

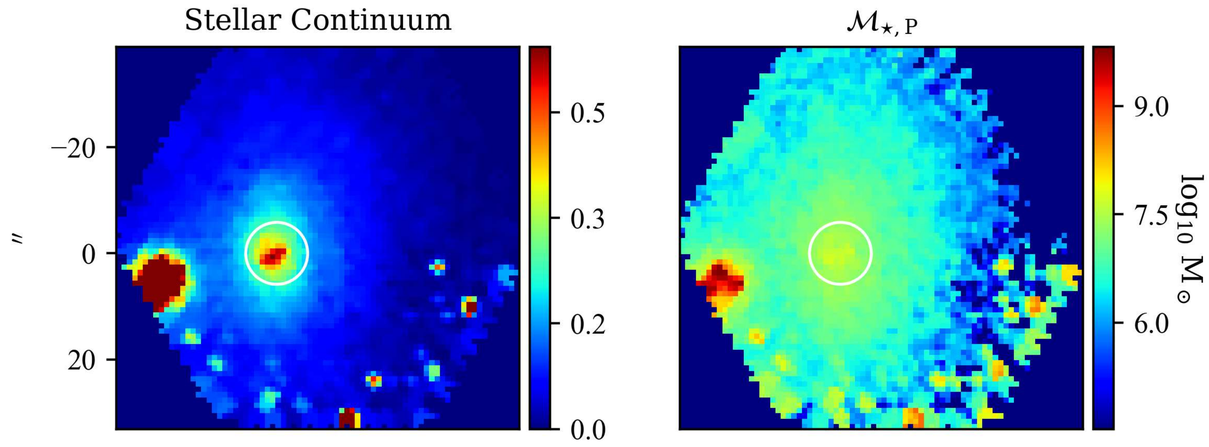

Log. of cumulative present stellar mass profiles

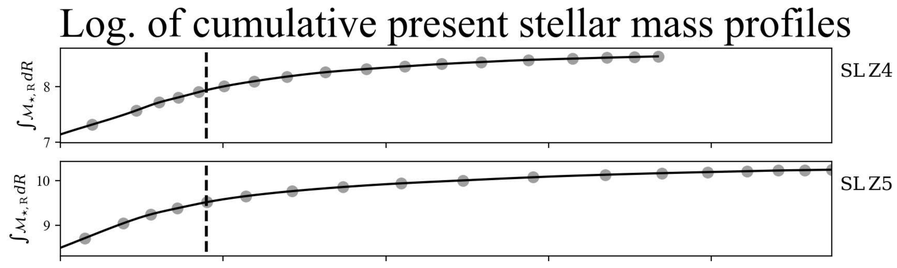

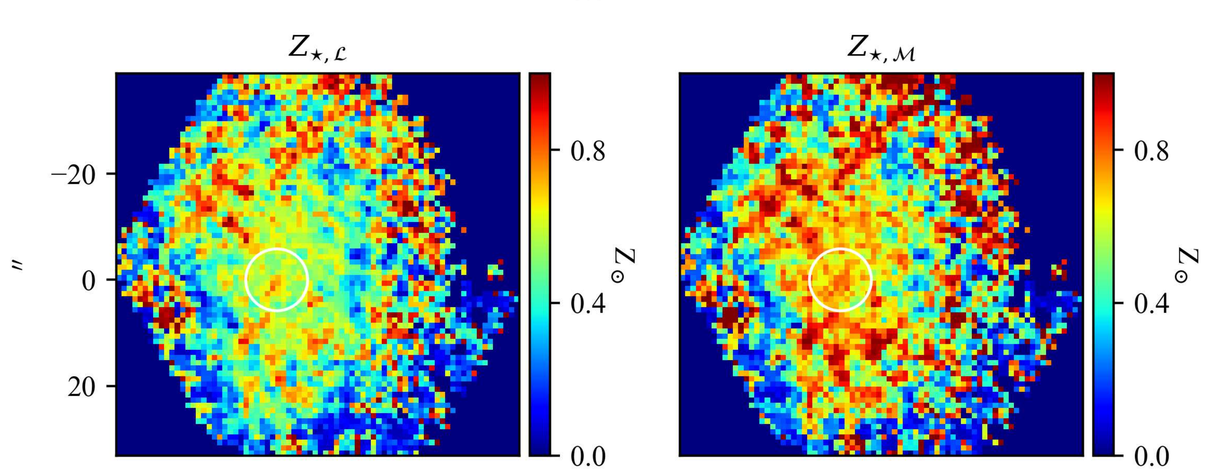

Stellar metallicity/Age & Hα flux/EW profiles

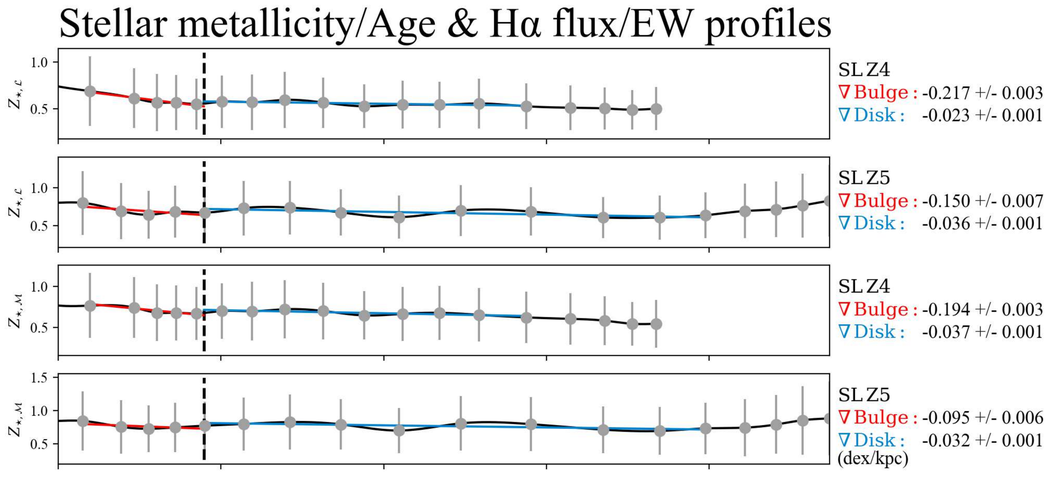

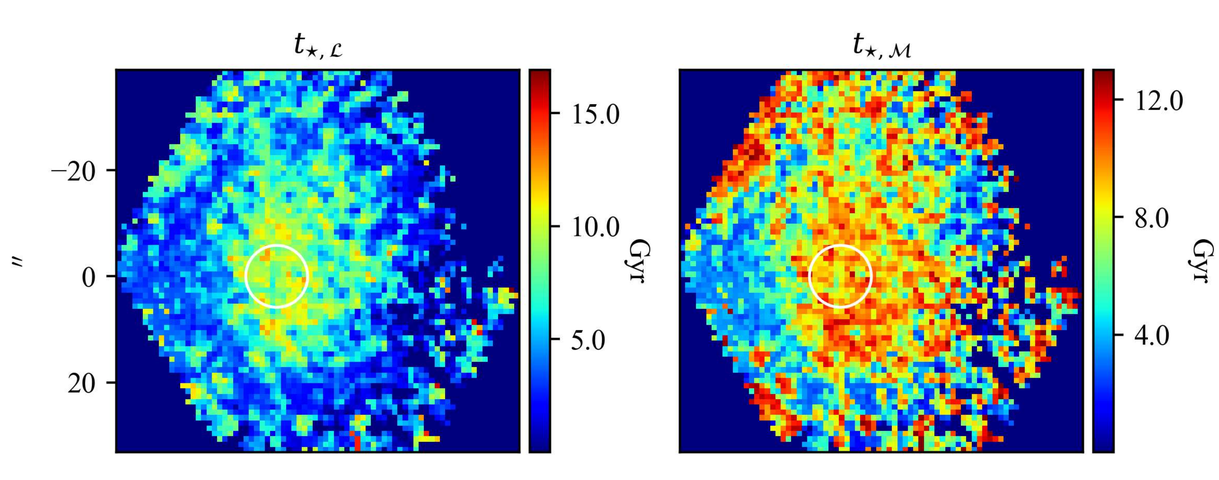

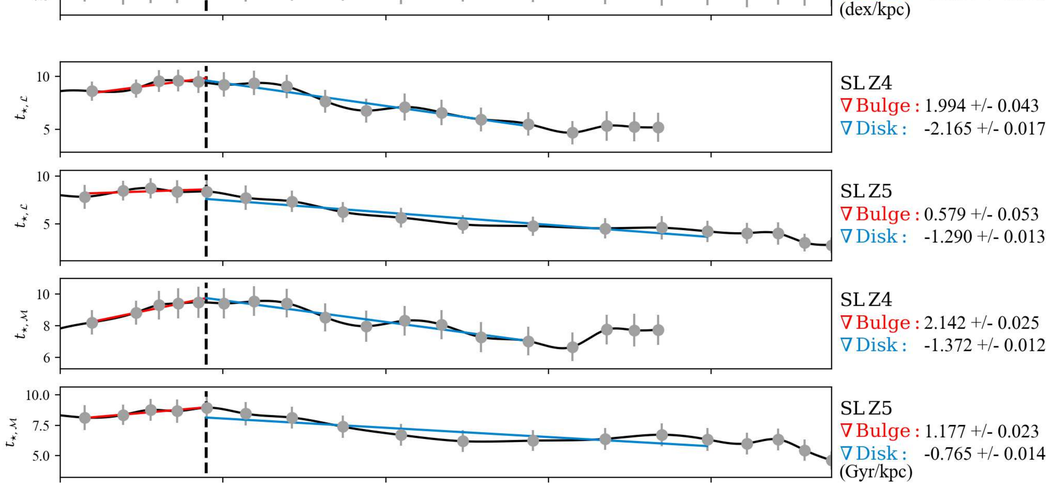

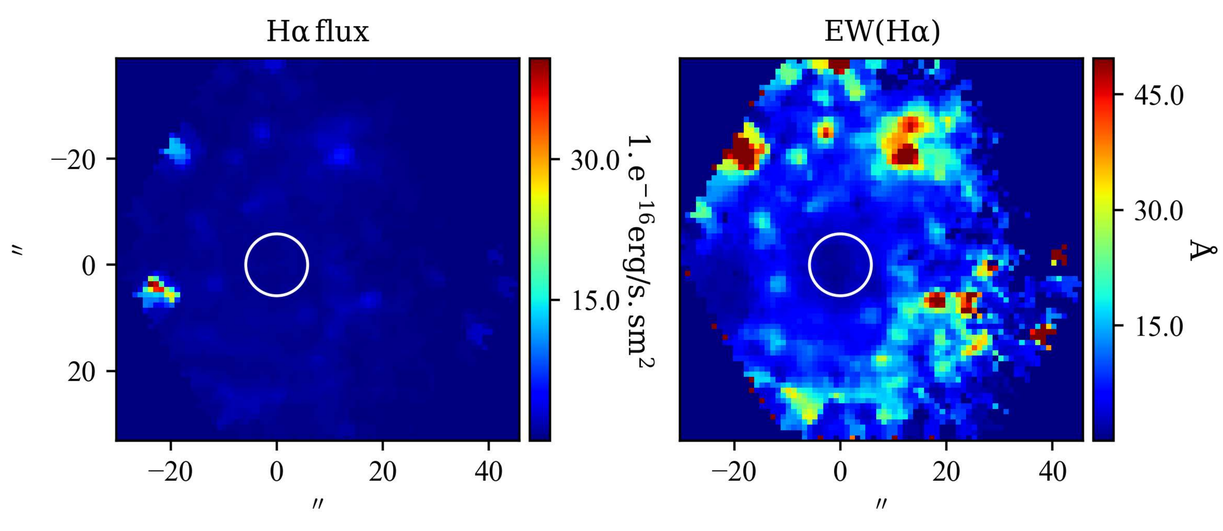

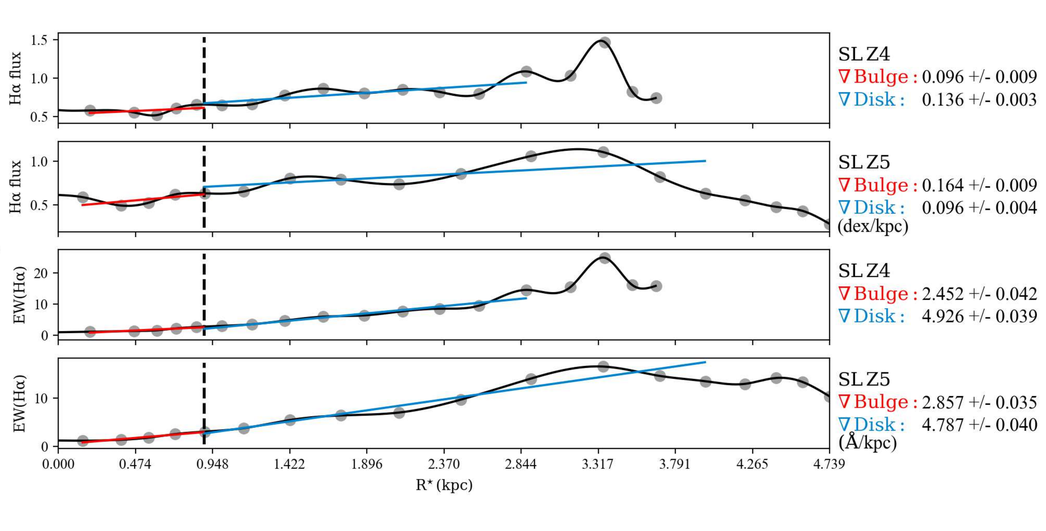

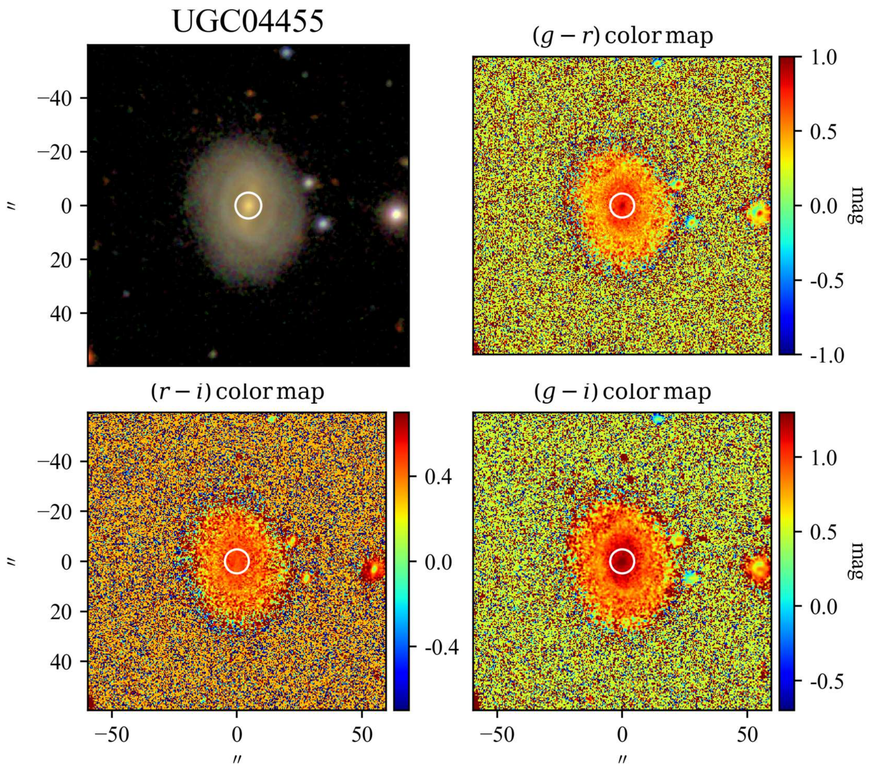

SBP decomposition of SDSS r band

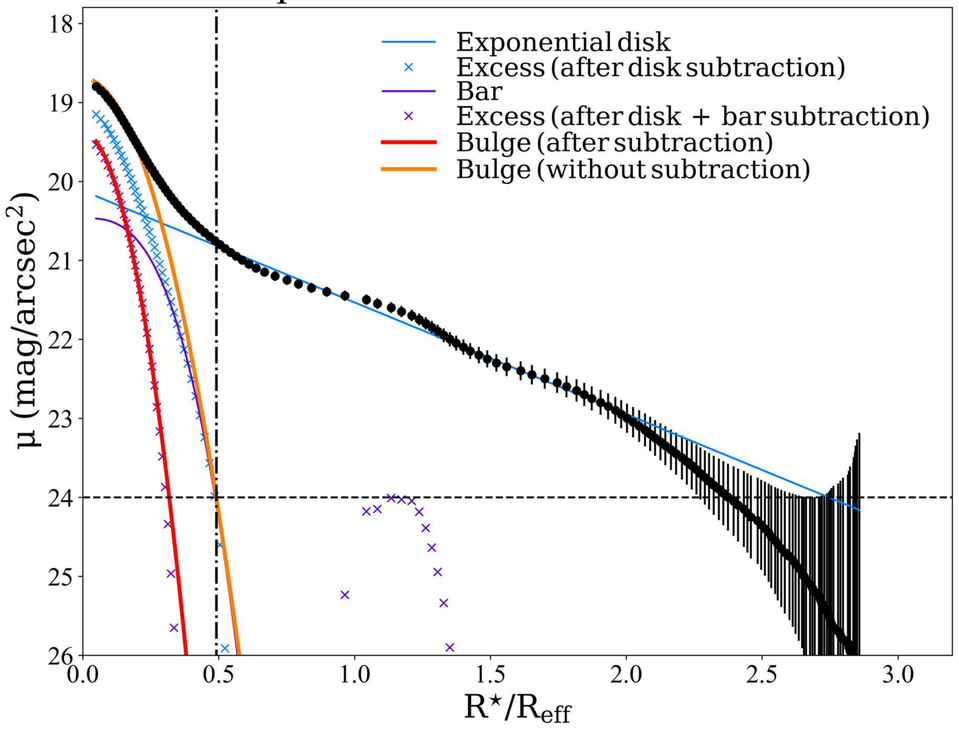

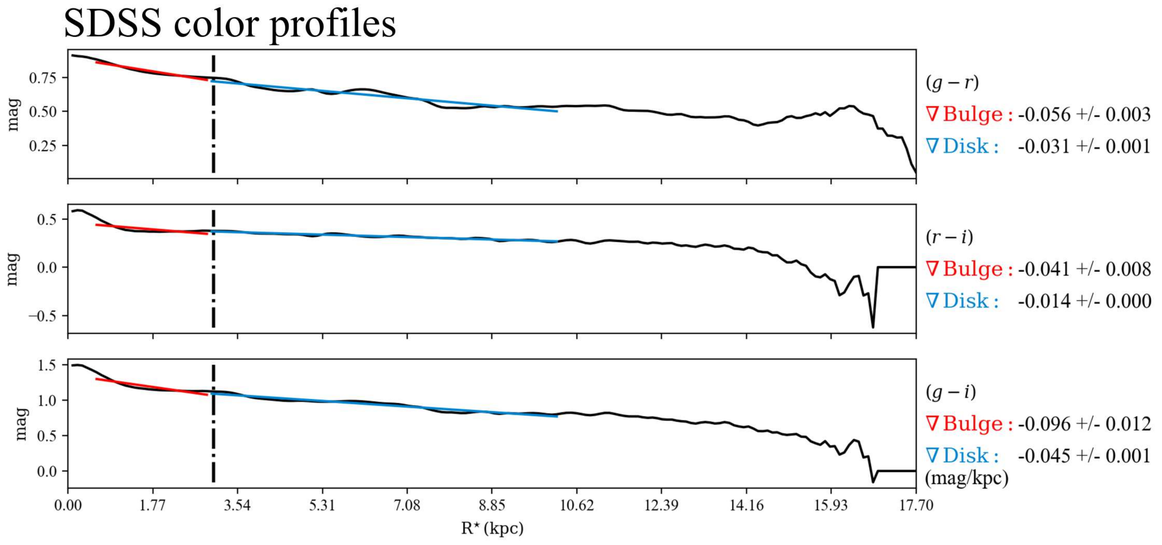

$\mathcal{RY}$ SBPs

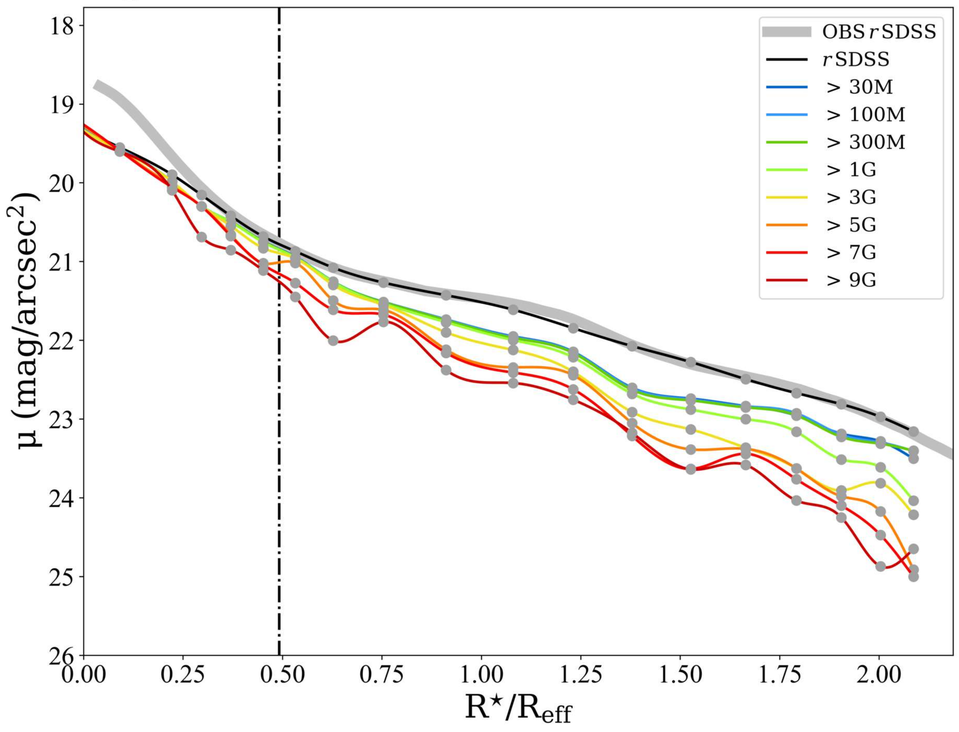

Stellar Continuum

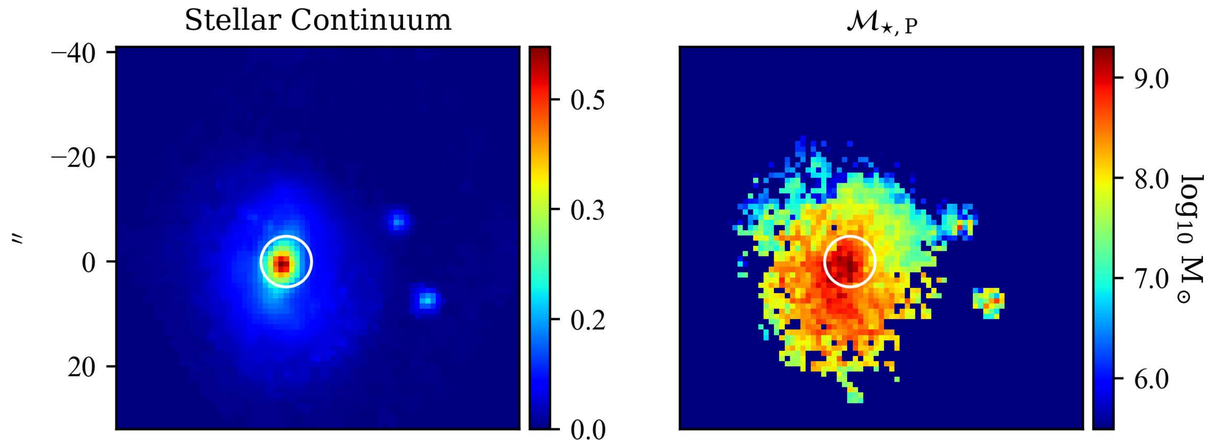

$\mathcal{M}_{\star,\mathrm{P}}$

Log. of cumulative present stellar mass profiles

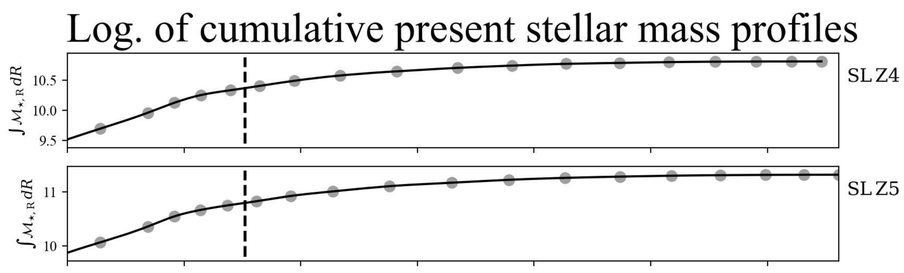

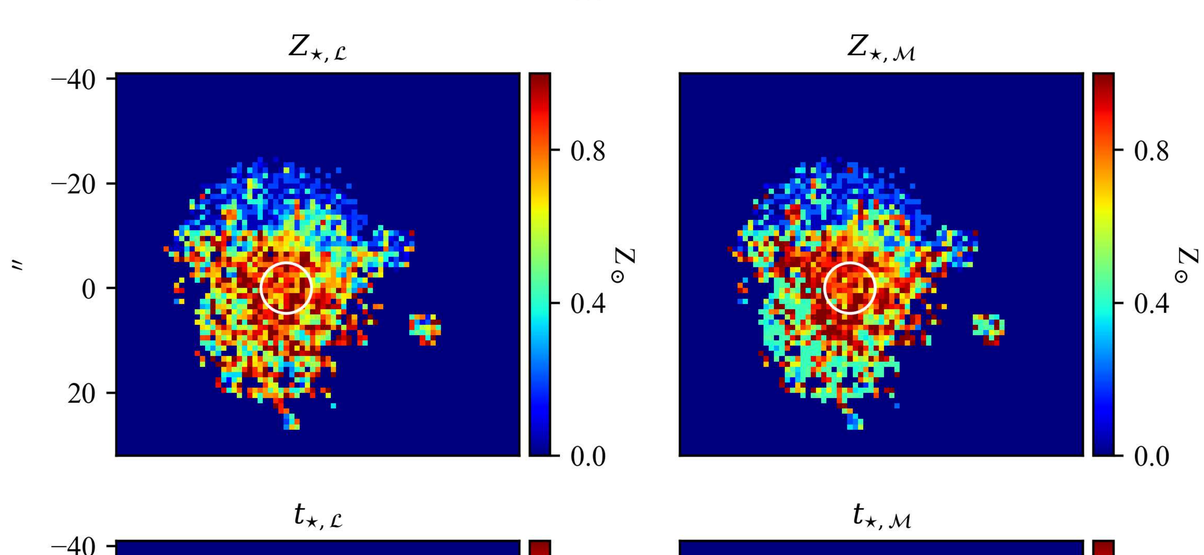

Stellar metallicity/Age & Hα flux/EW profiles

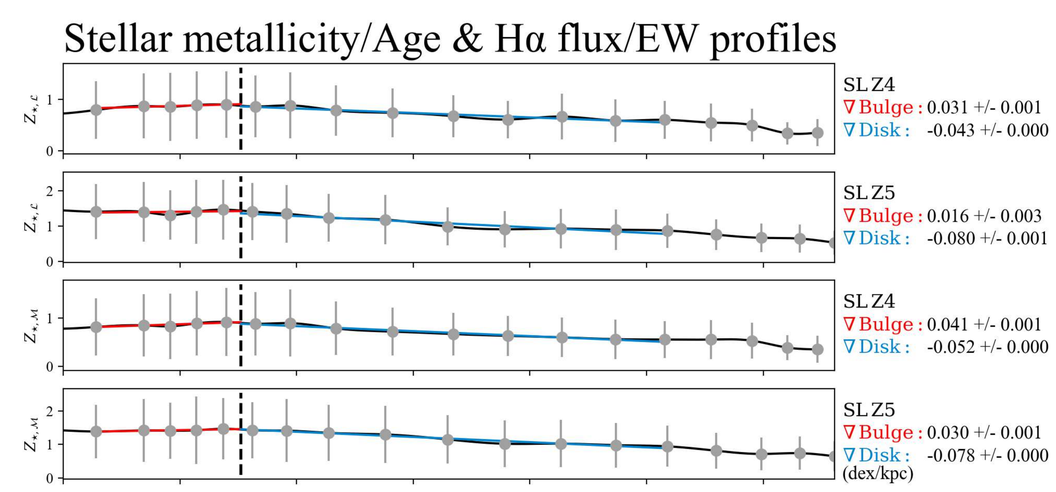

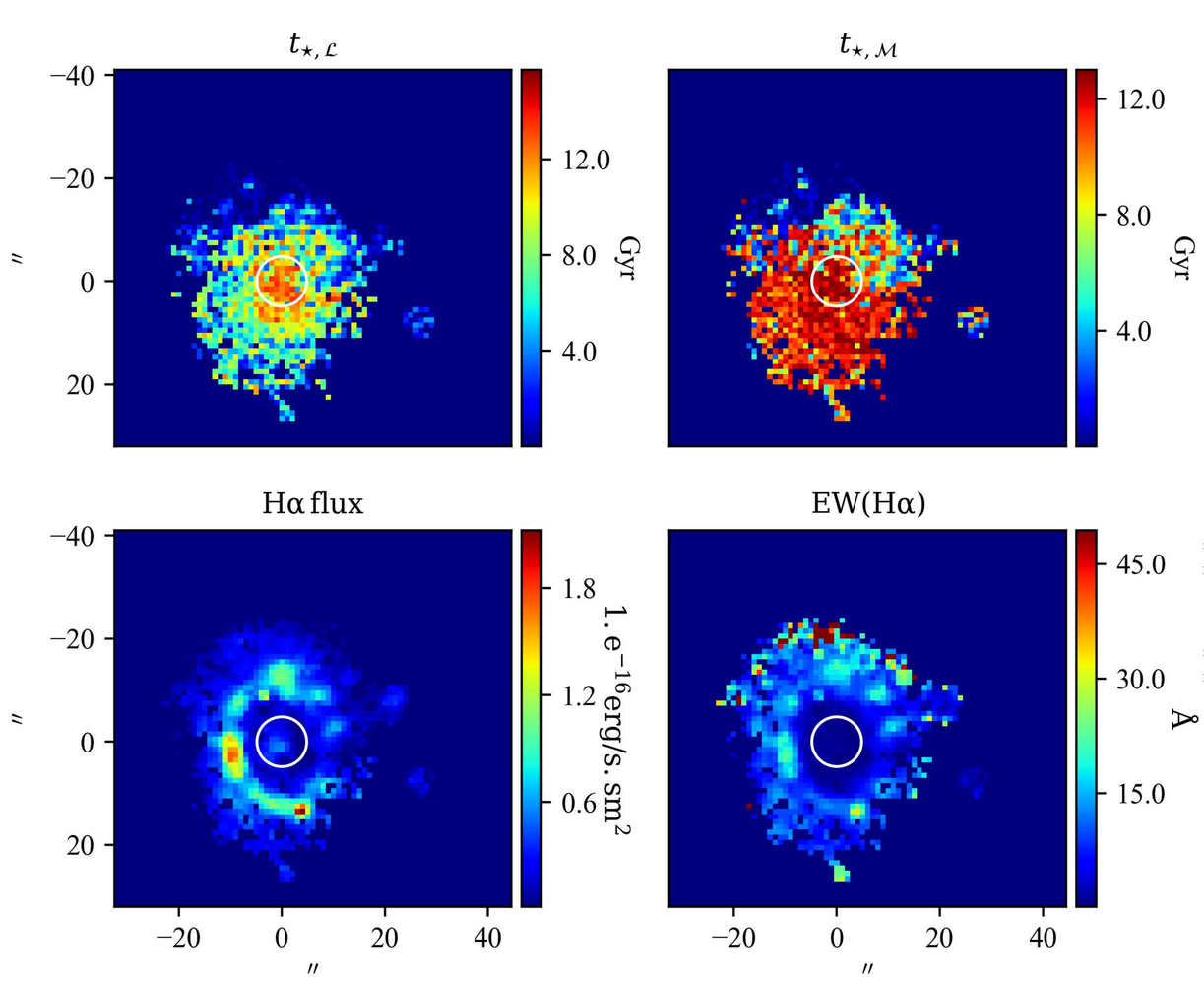

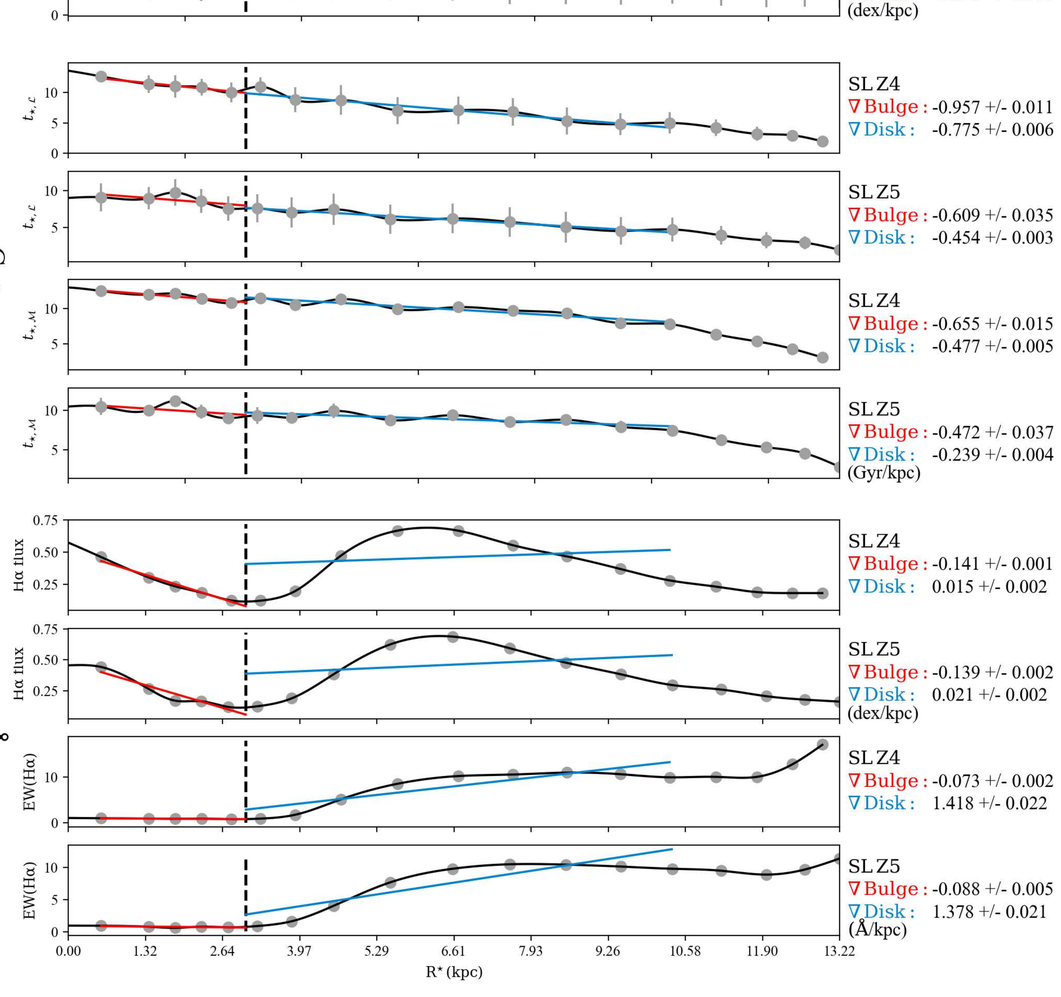

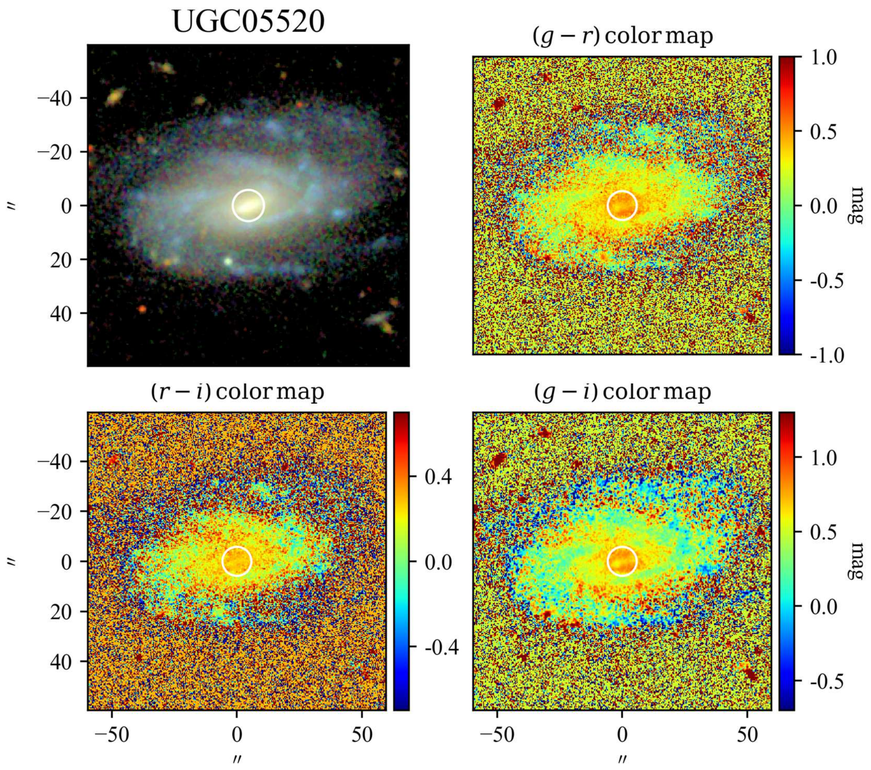

SBP decomposition of SDSS r band

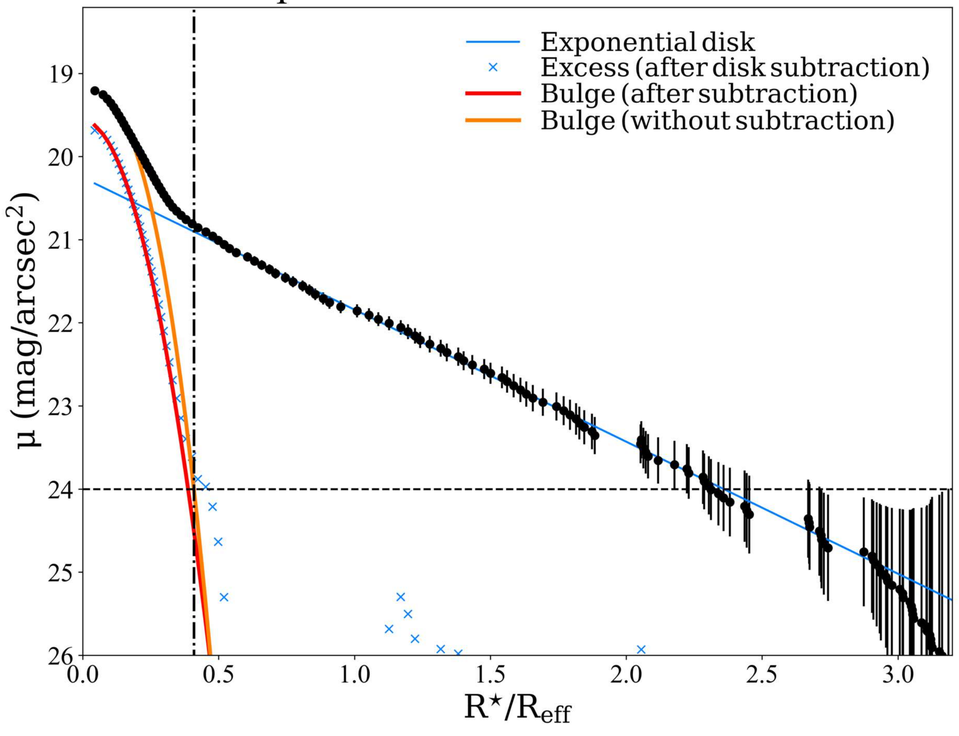

SDSS color profiles

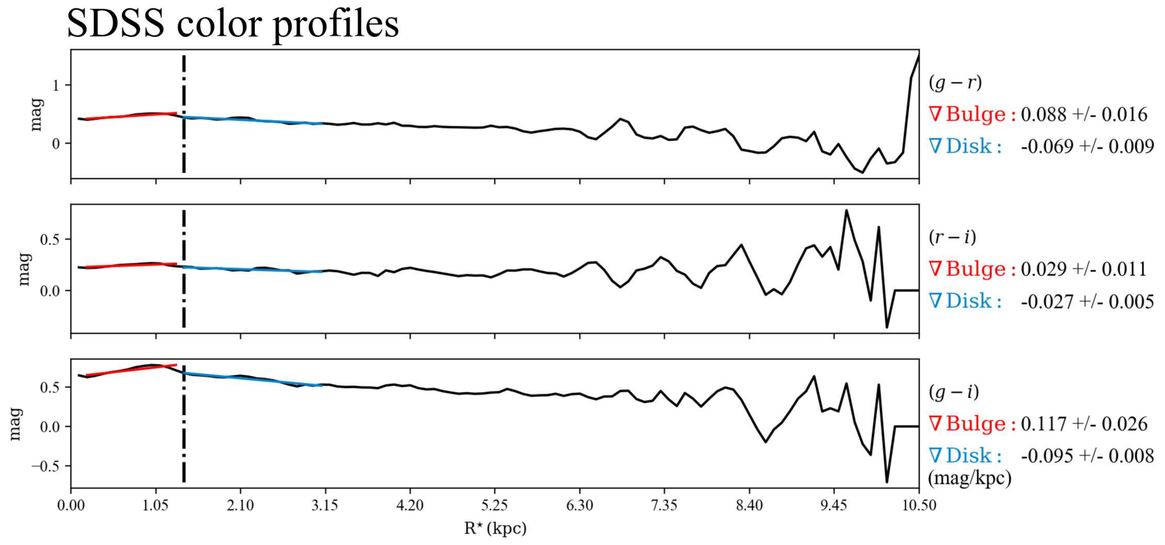

$\mathcal{RY}$ SBPs

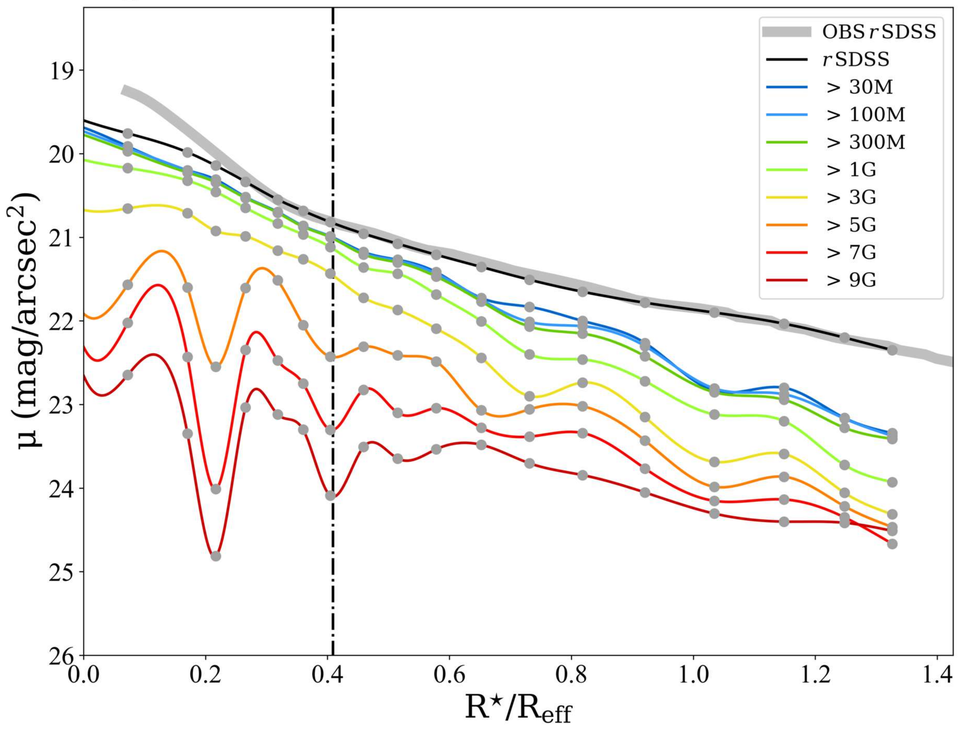

Stellar Continuum

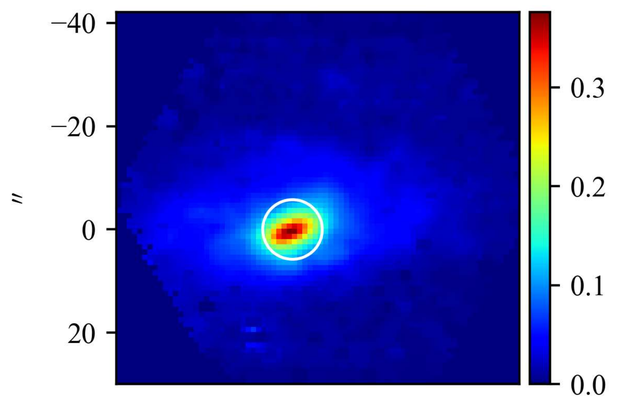

$\mathcal{M}_{\star,\mathrm{P}}$

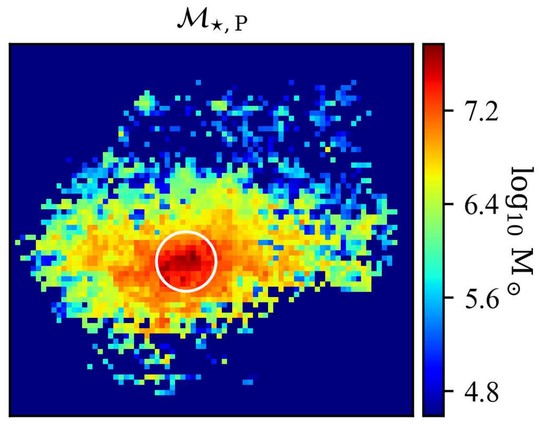

Log. of cumulative present stellar mass profiles

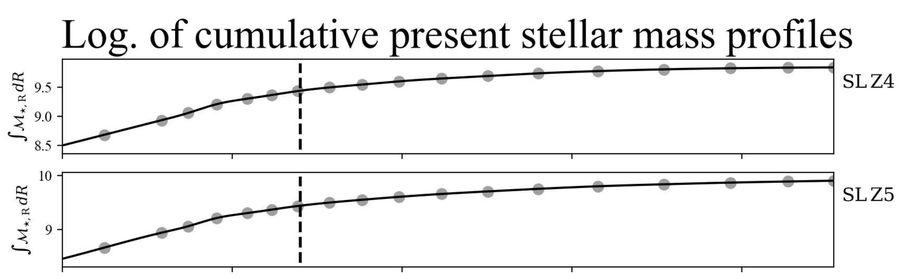

$Z_{\star,\mathcal{L}}$

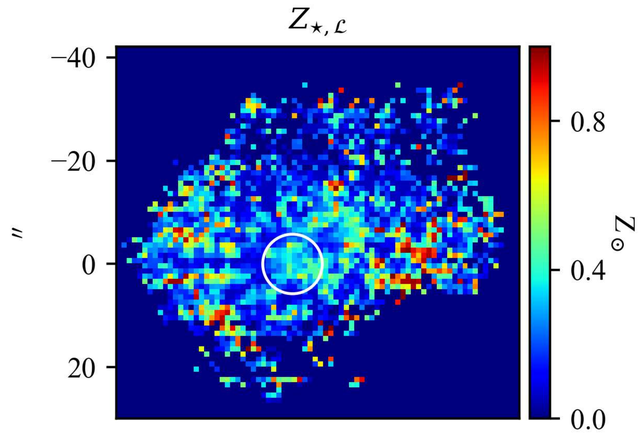

$Z_{\star,\mathcal{M}}$

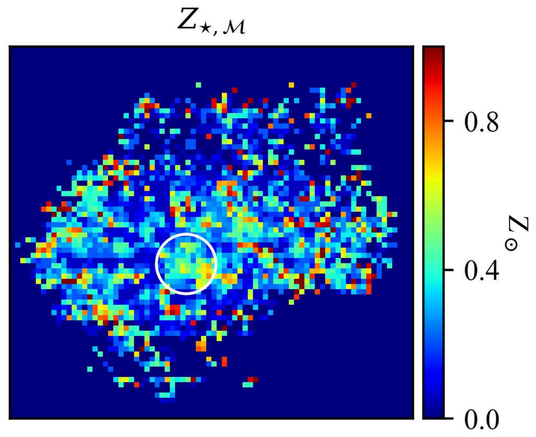

Stellar metallicity/Age & Hα flux/EW profiles

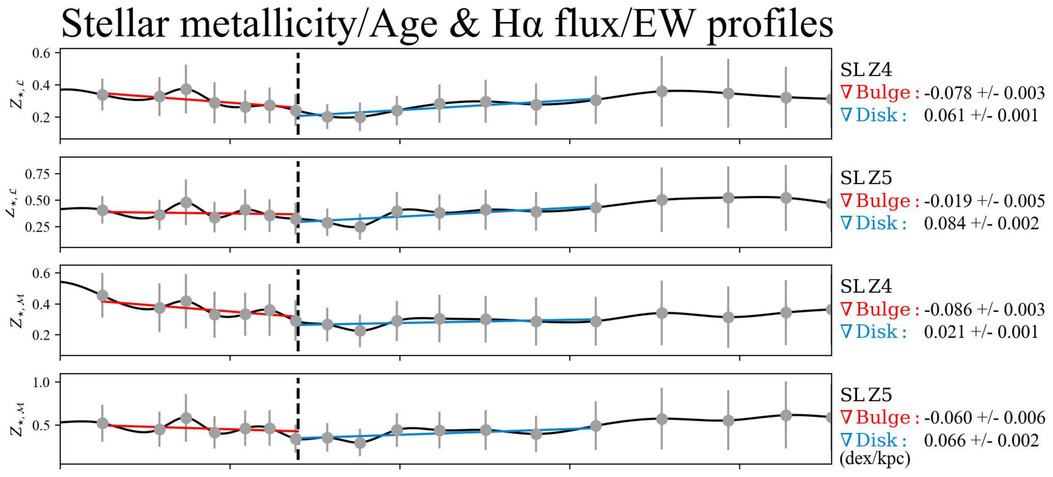

$t_{\star,\mathcal{L}}$

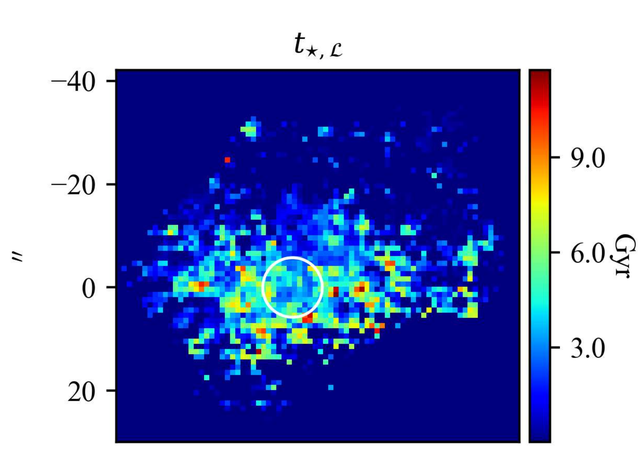

$t_{\star,\mathcal{M}}$

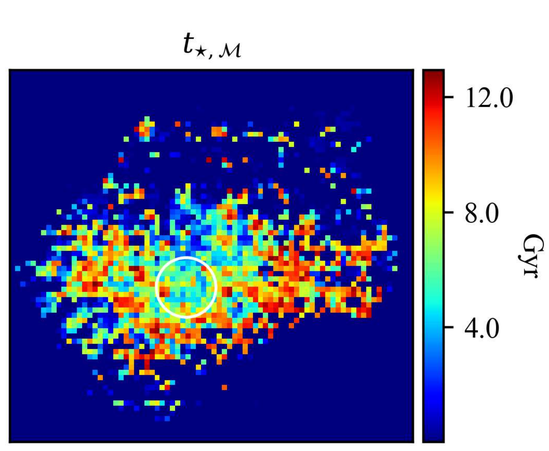

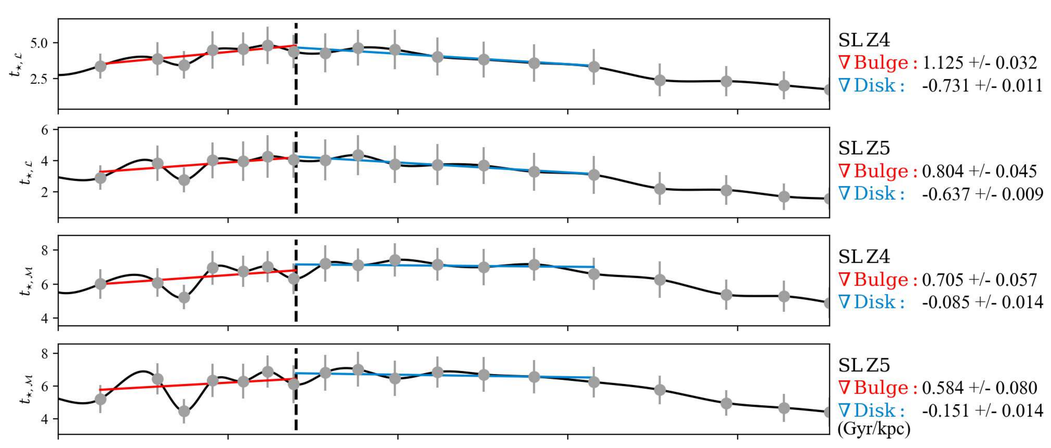

Hα flux

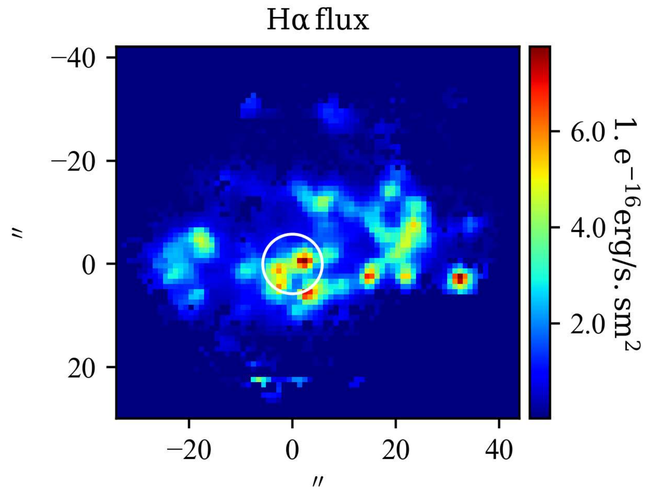

EW(Hα)

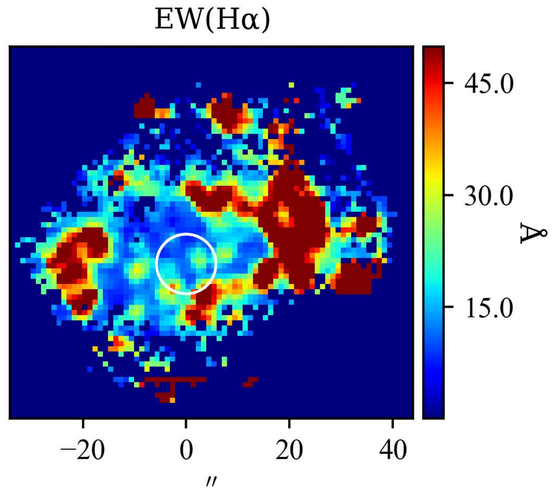

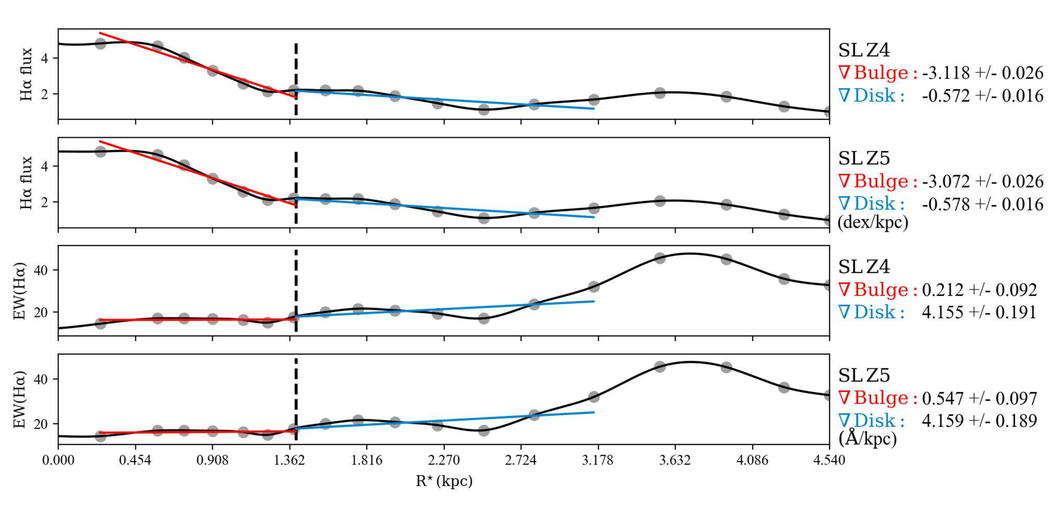

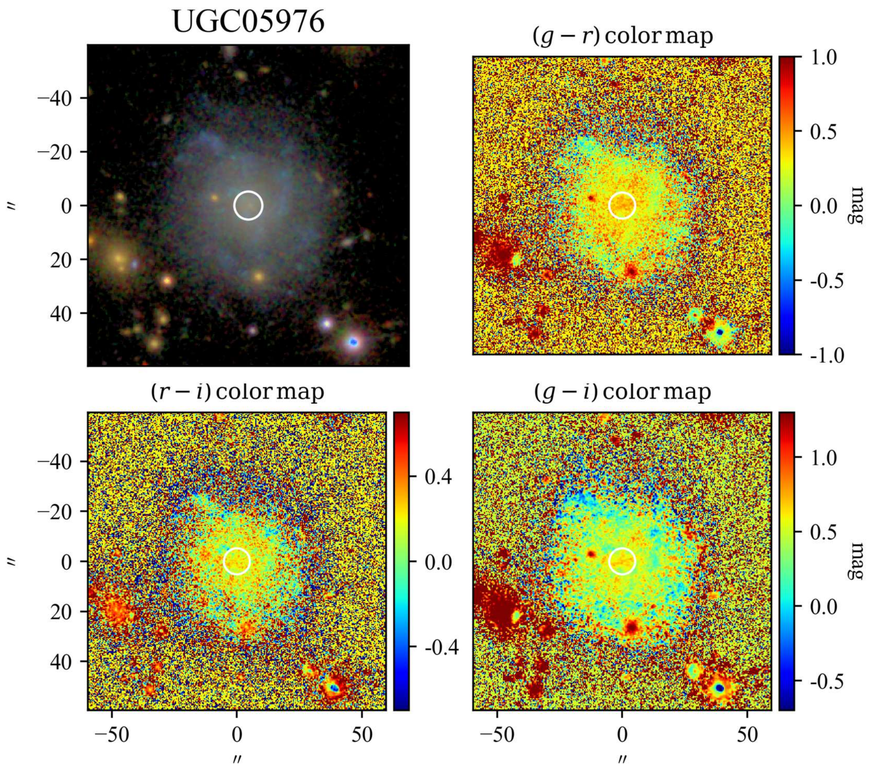

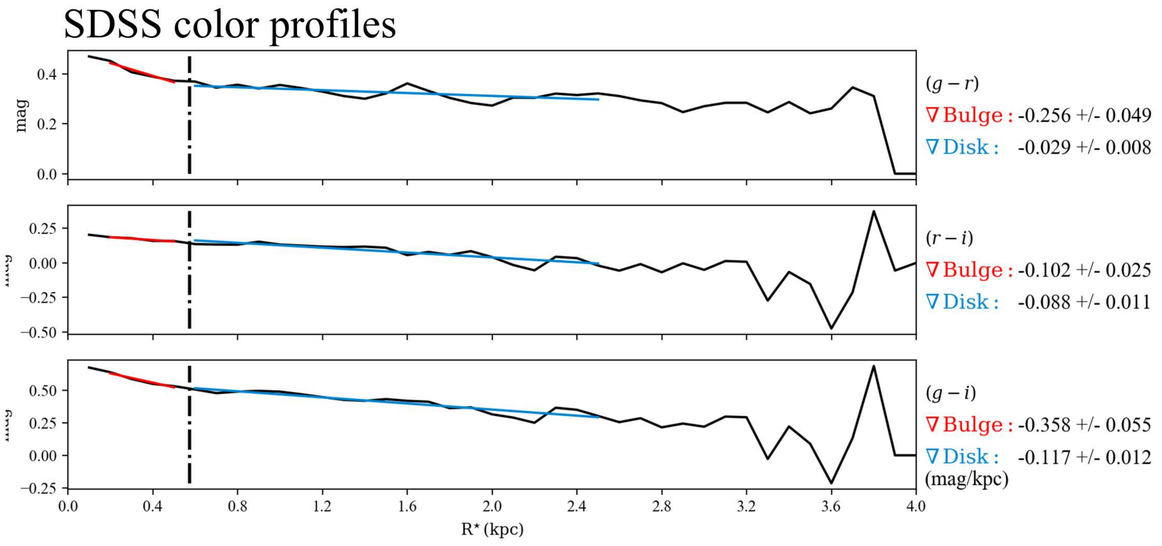

SBP decomposition of SDSS r band

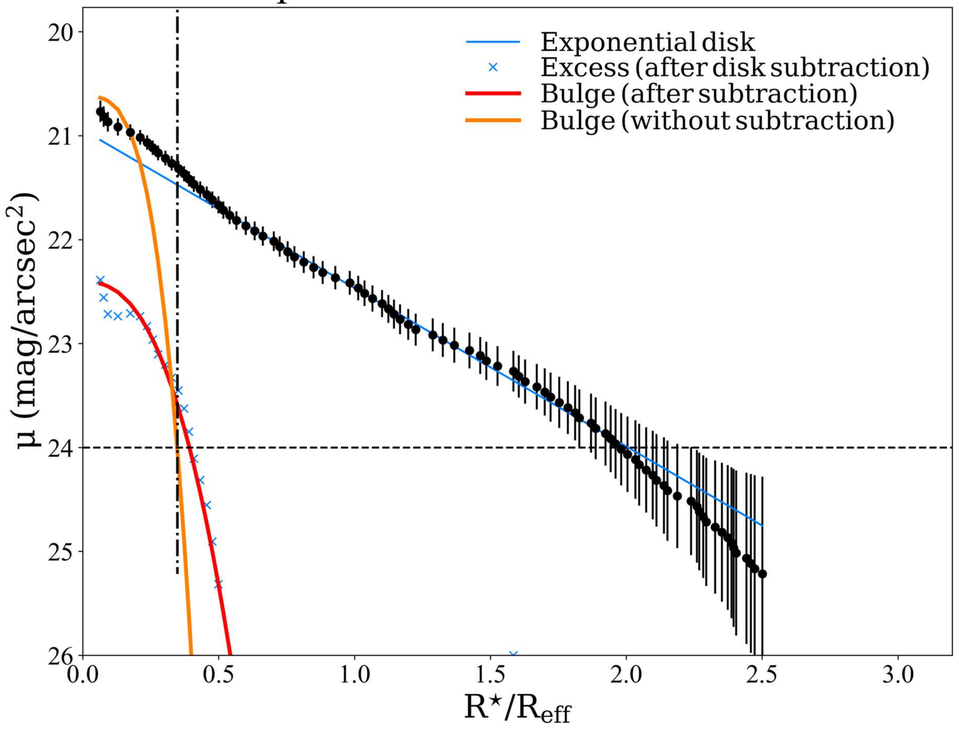

$\mathcal{RY}$ SBPs

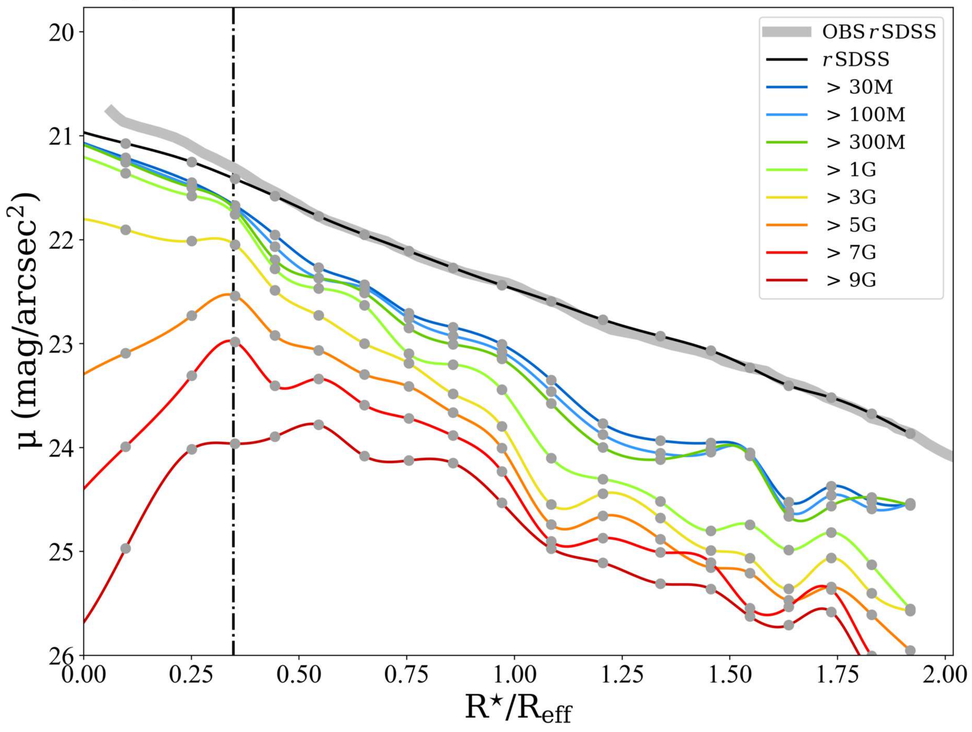

Stellar Continuum

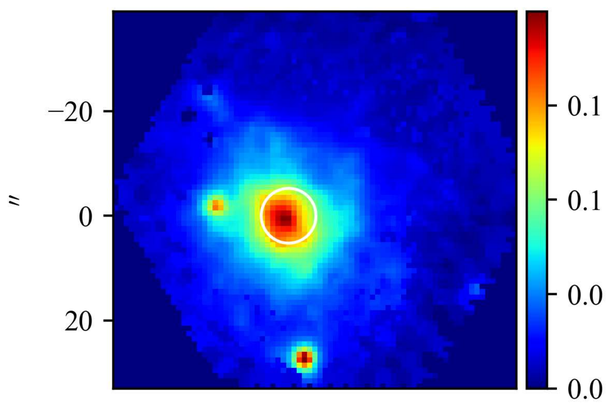

$\mathcal{M}_{\star,\mathrm{P}}$

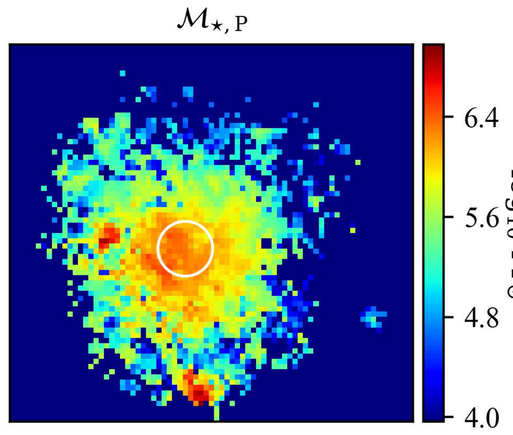

Log. of cumulative present stellar mass profiles

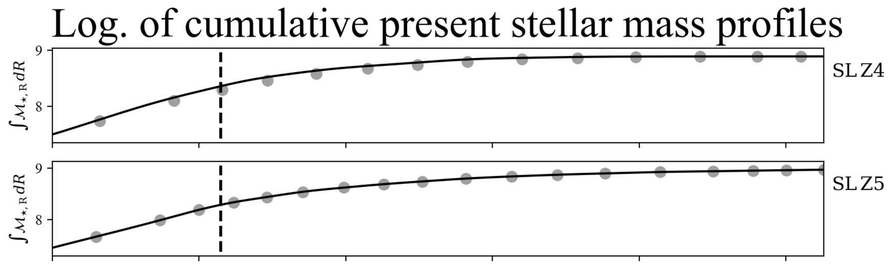

$Z_{\star,\mathcal{L}}$

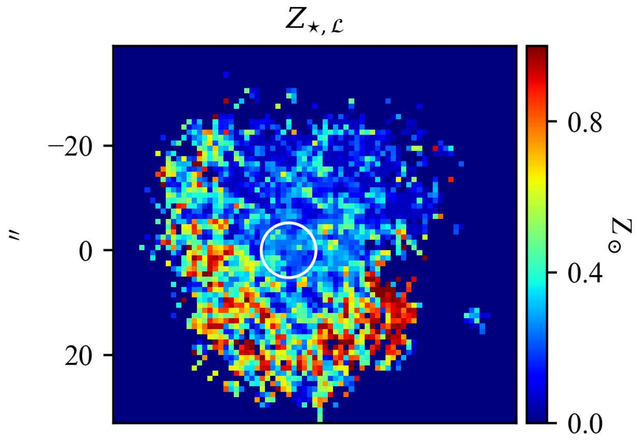

$Z_{\star,\mathcal{M}}$

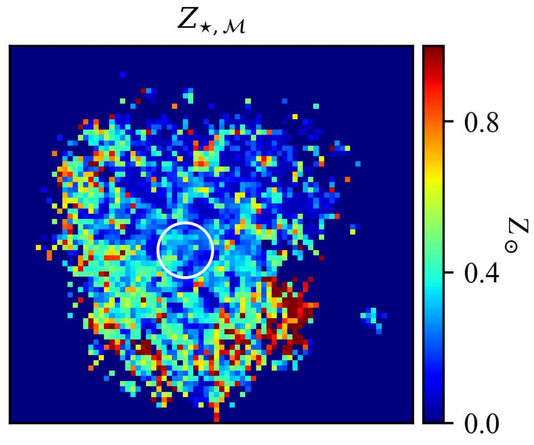

Stellar metallicity/Age & Hα flux/EW profiles

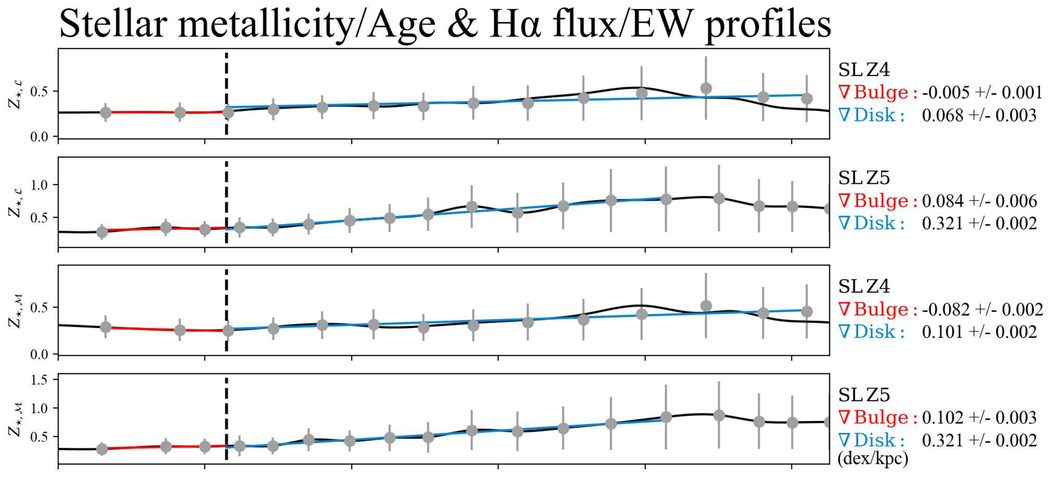

$t_{\star,\mathcal{L}}$

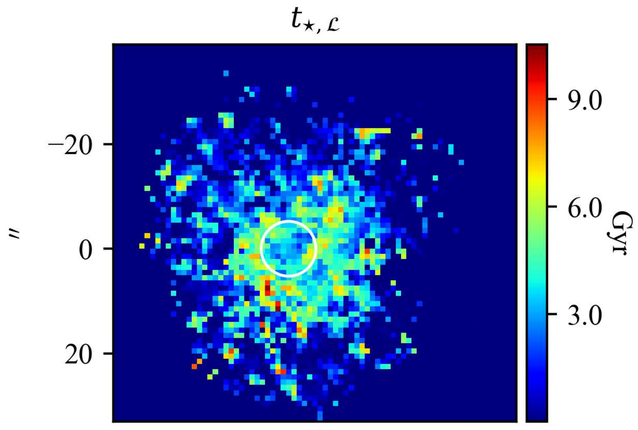

$t_{\star,\mathcal{M}}$

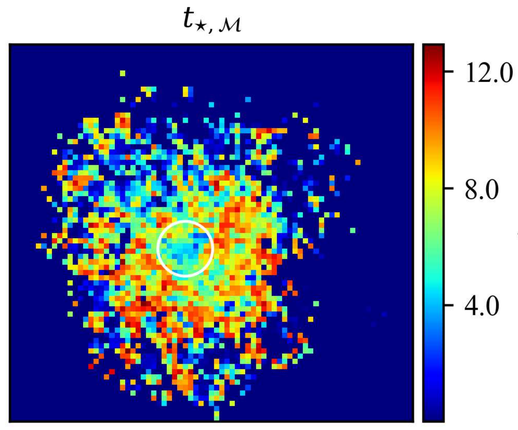

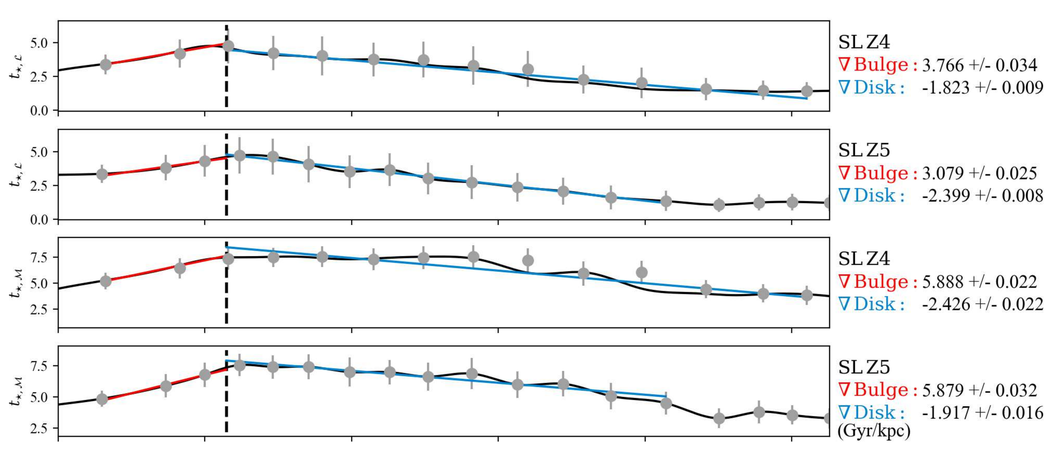

Hα flux

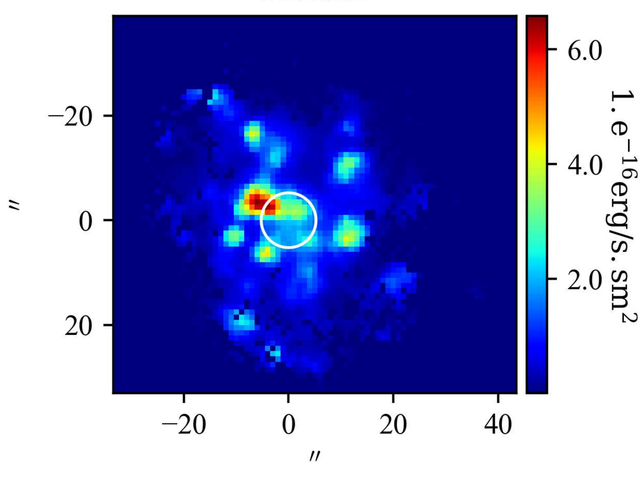

EW(Hα)

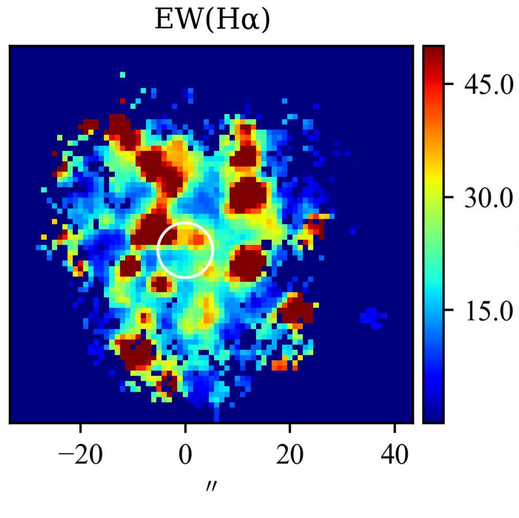

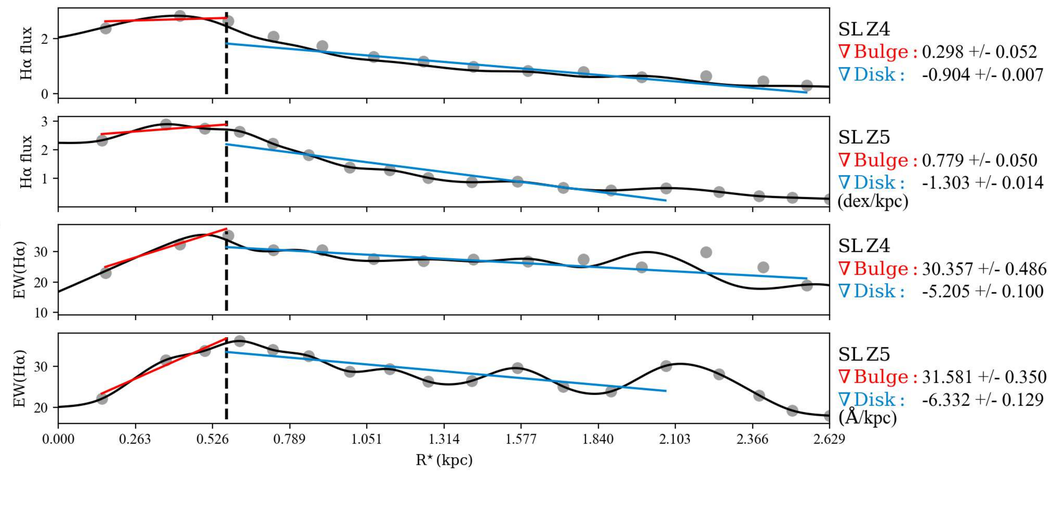

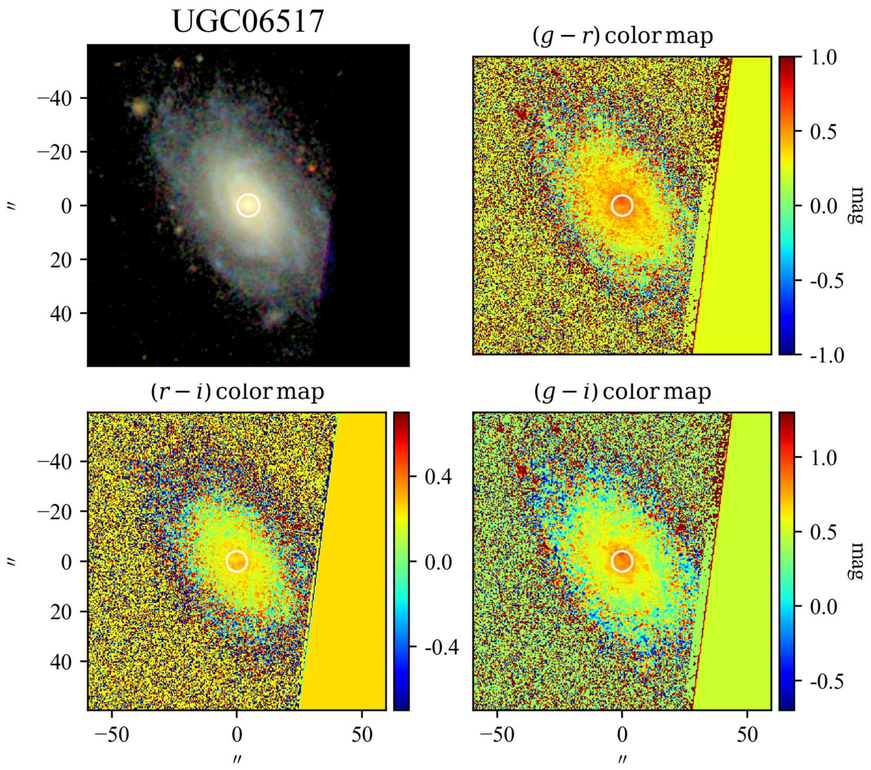

SBP decomposition of SDSS r band

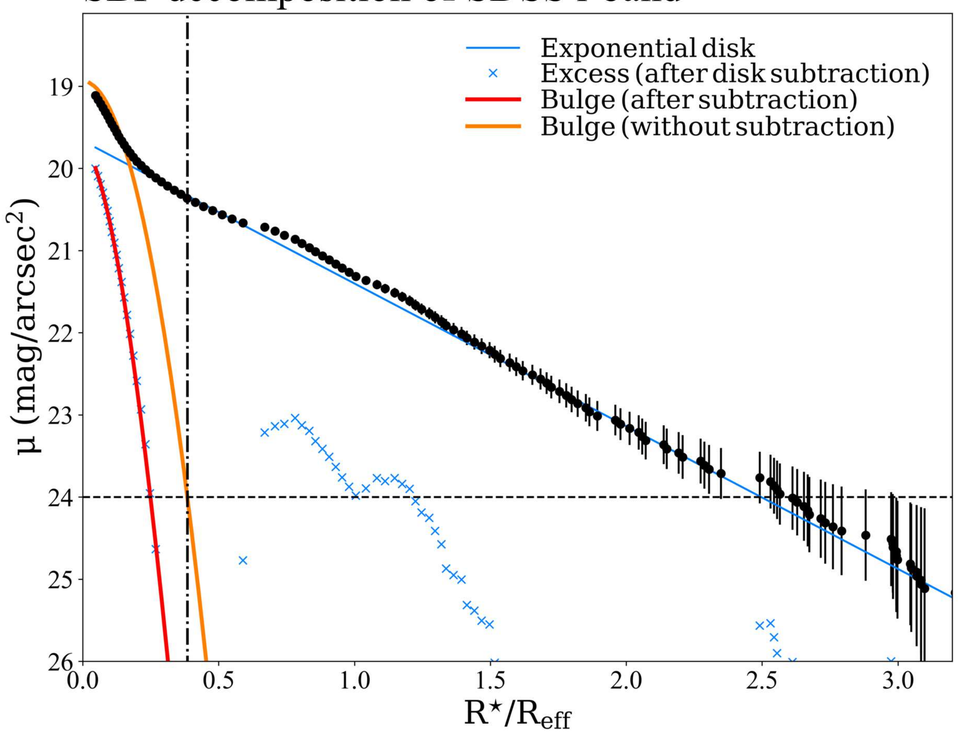

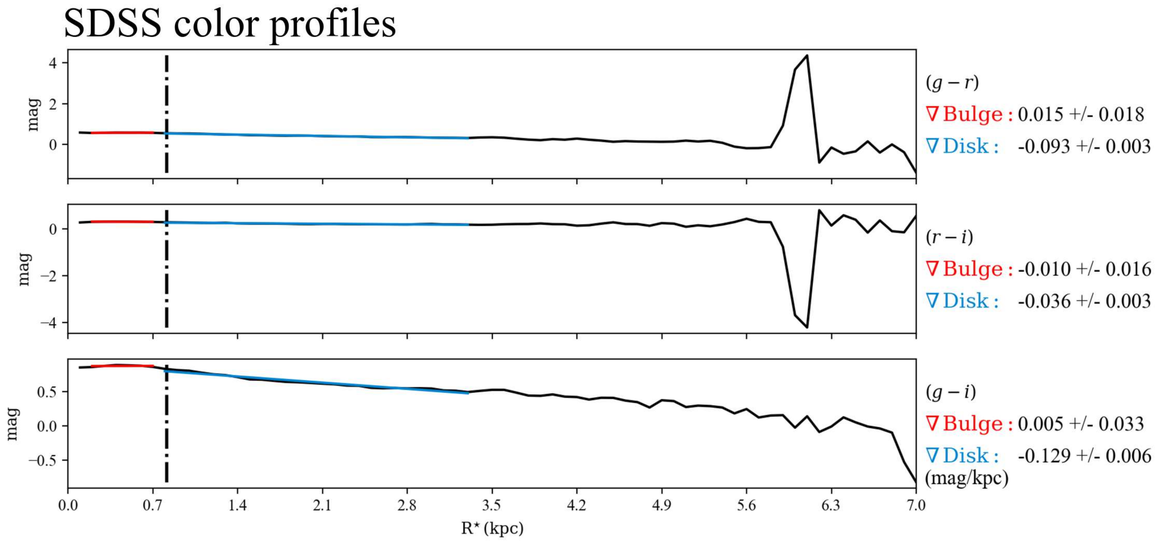

$\mathcal{RY}$ SBPs

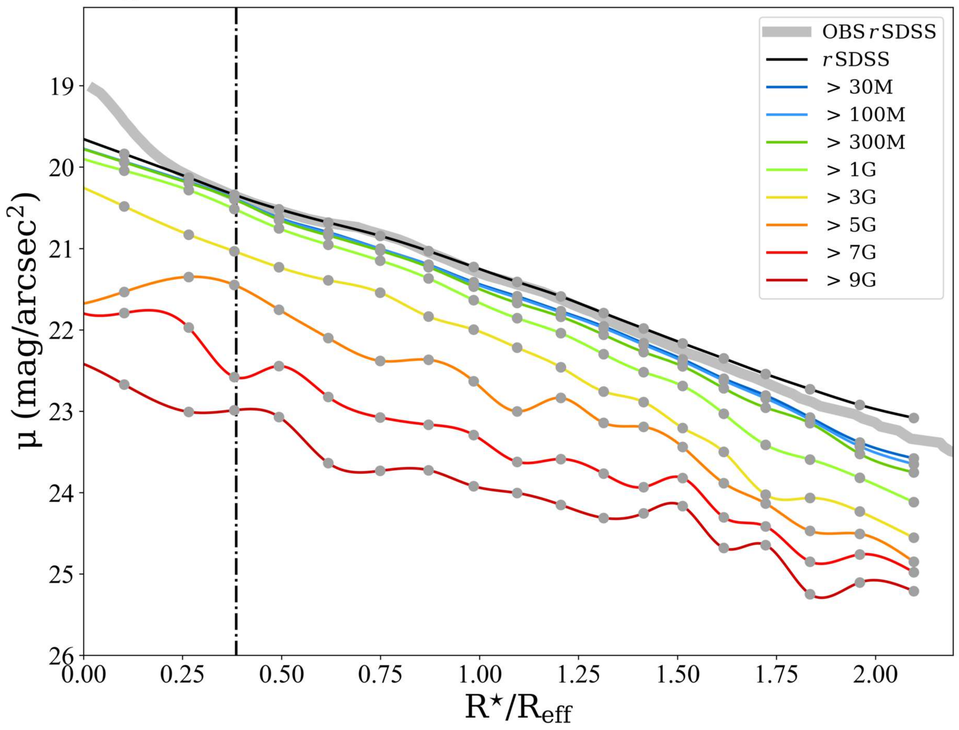

Stellar Continuum

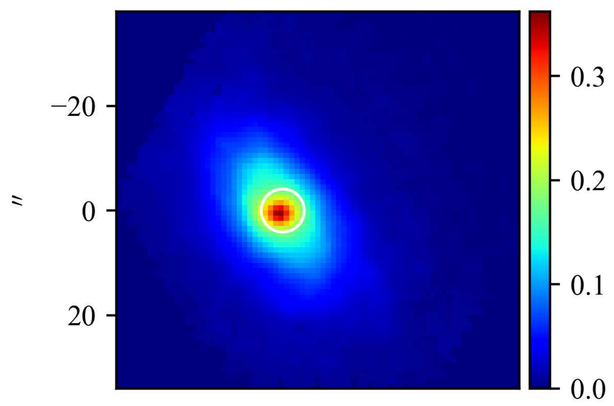

$\mathcal{M}_{\star,\mathrm{P}}$

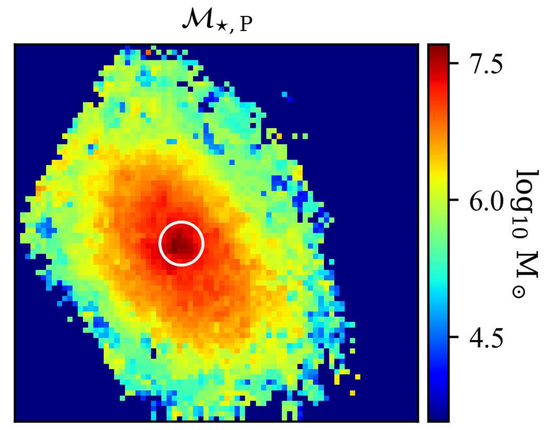

Log. of cumulative present stellar mass profiles

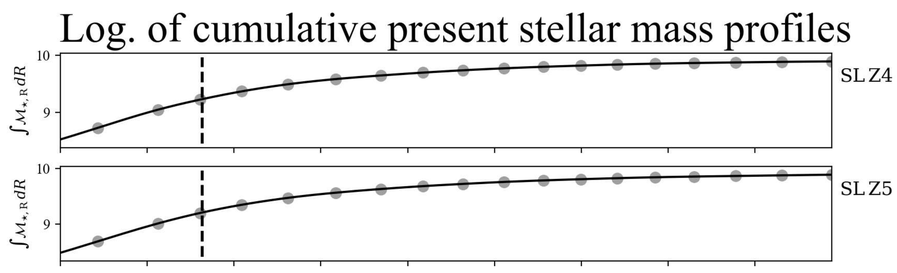

$Z_{\star,\mathcal{L}}$

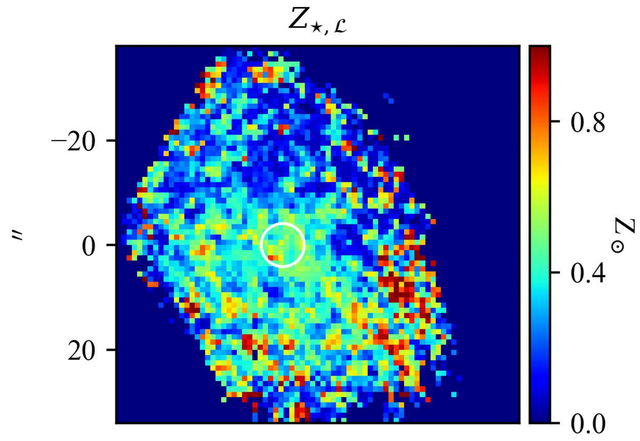

$Z_{\star,\mathcal{M}}$

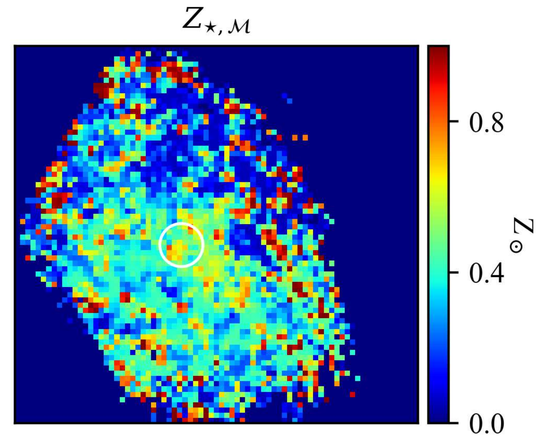

Stellar metallicity/Age & Hα flux/EW profiles

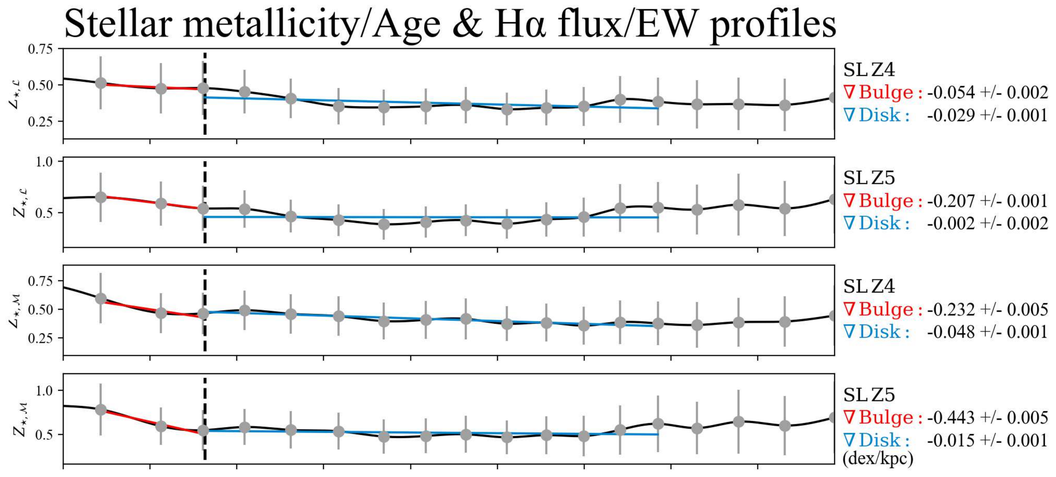

$t_{\star,\mathcal{L}}$

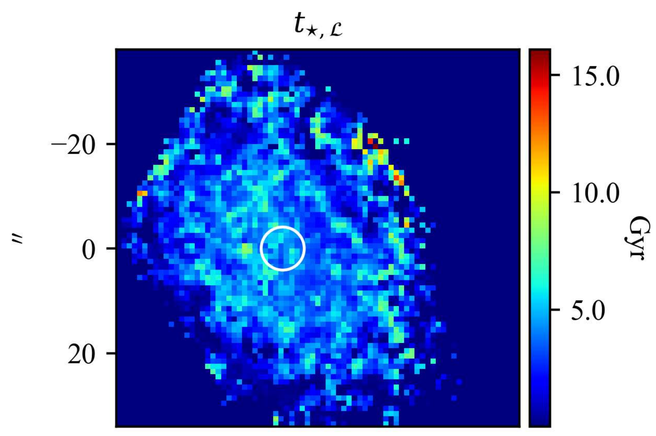

$t_{\star,\mathcal{M}}$

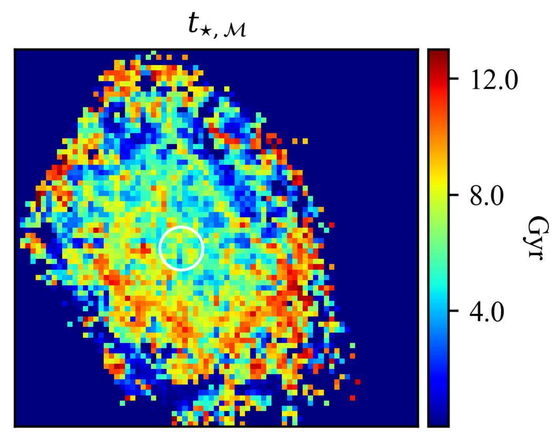

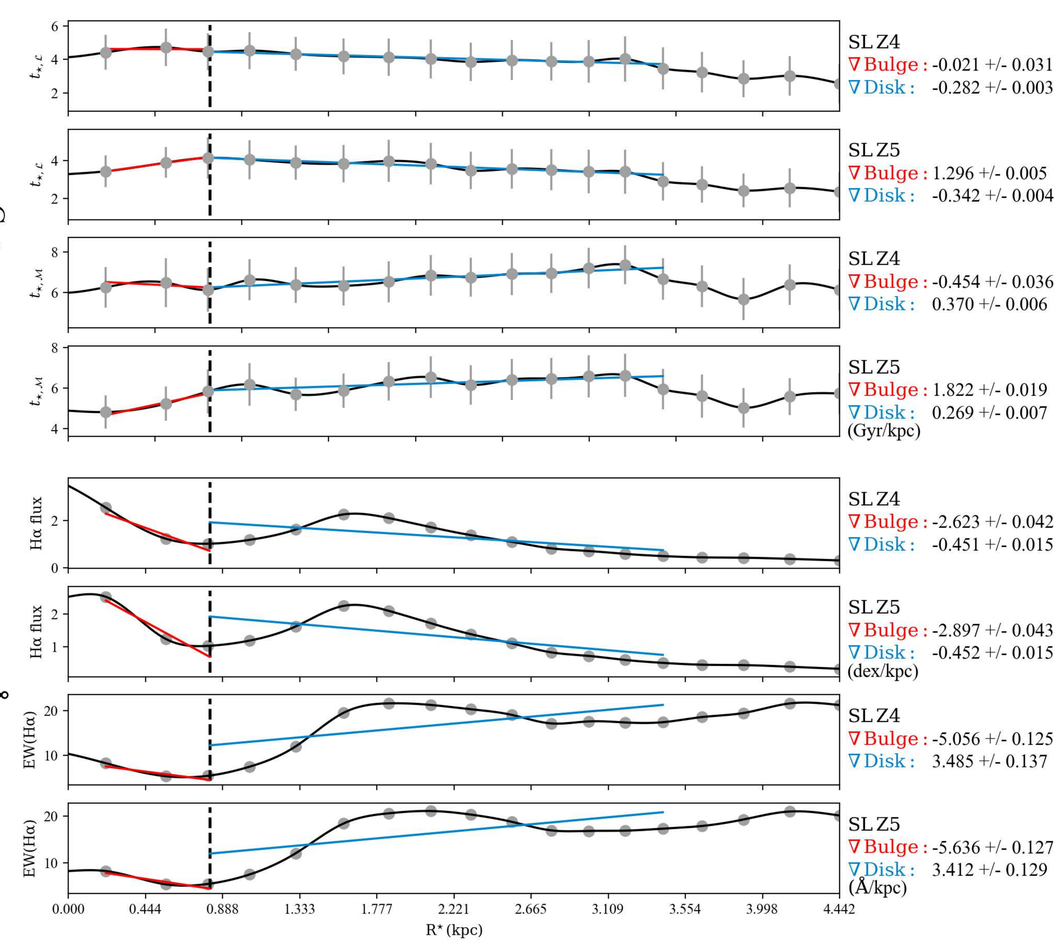

Hα flux

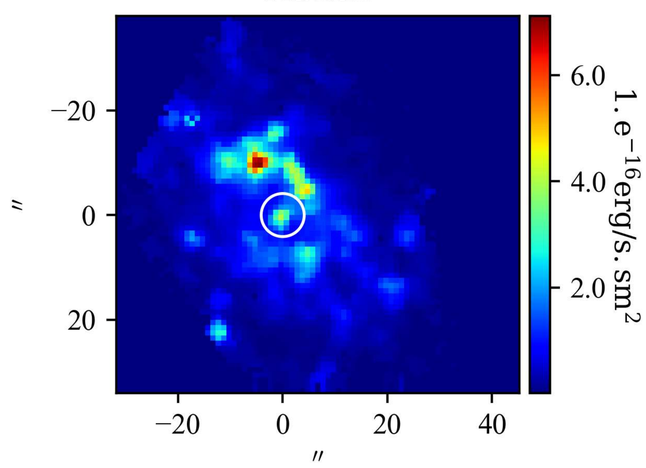

EW(Hα)

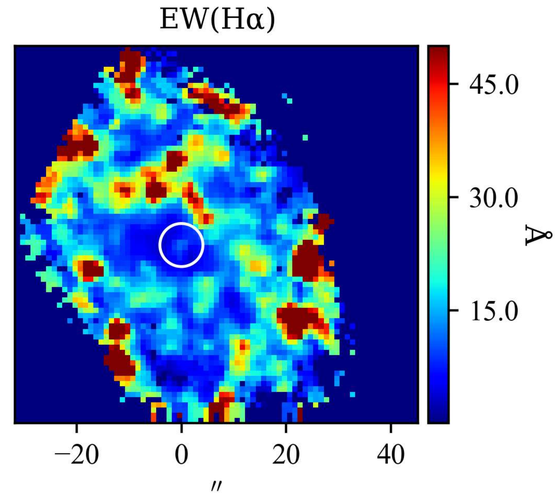

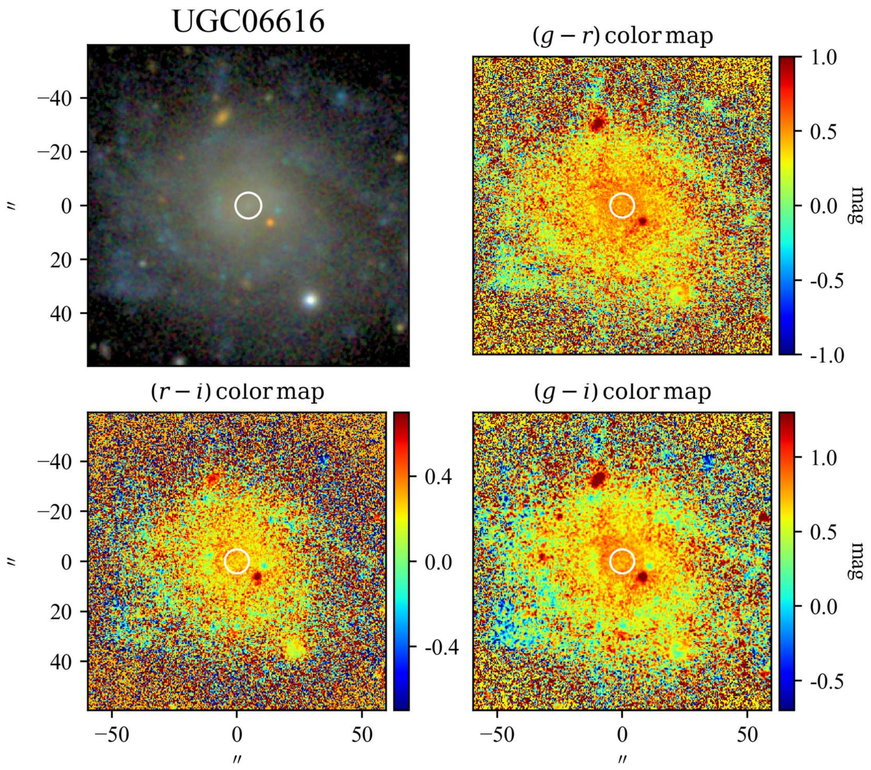

SBP decomposition of SDSS r band

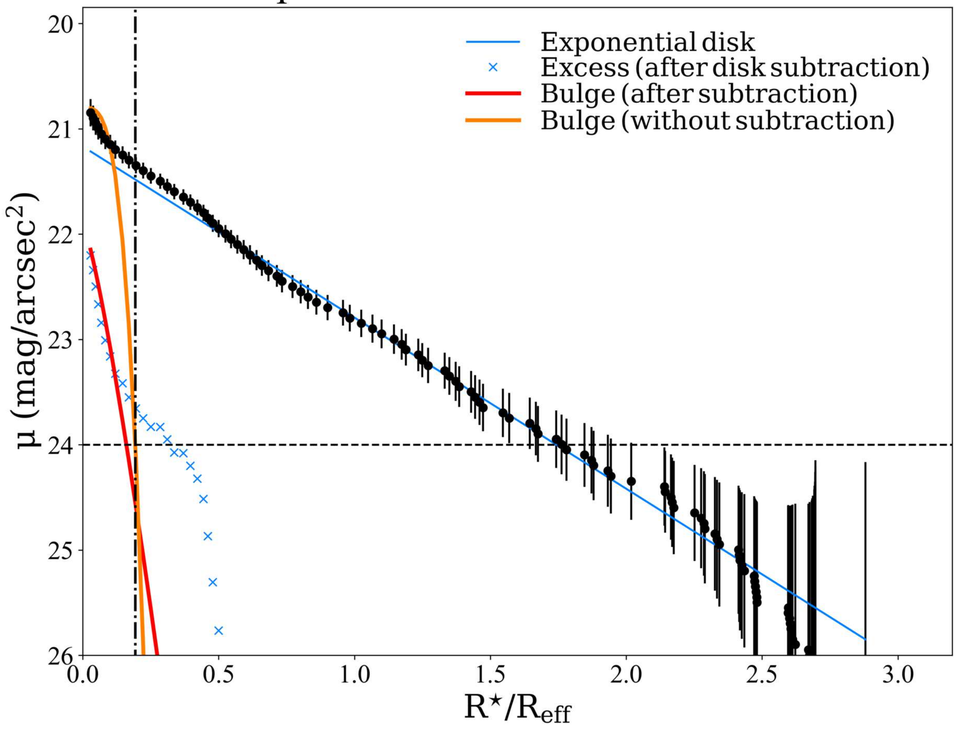

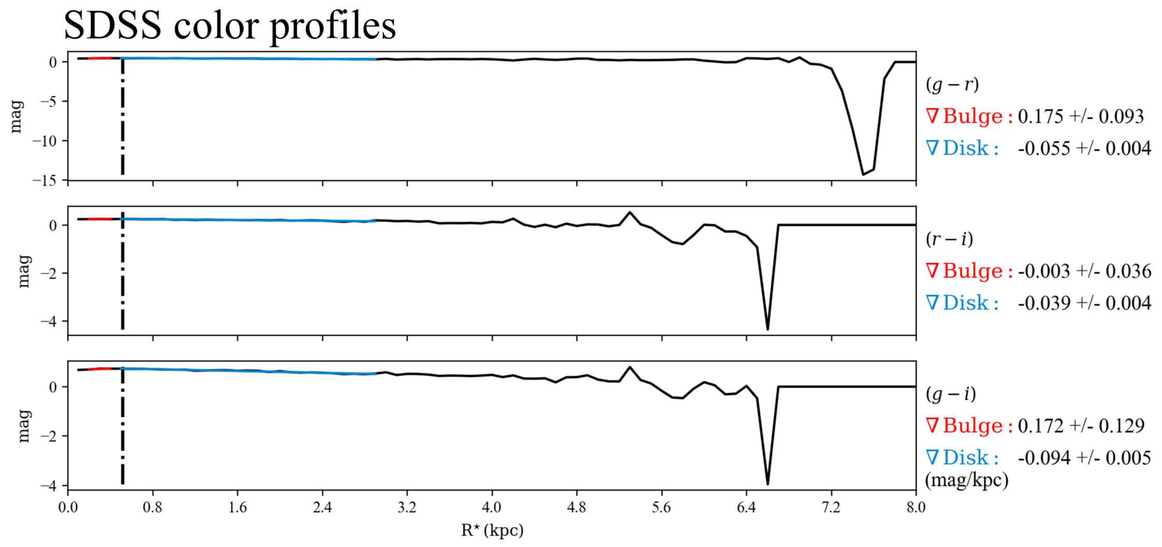

$\mathcal{RV}$ SBPs

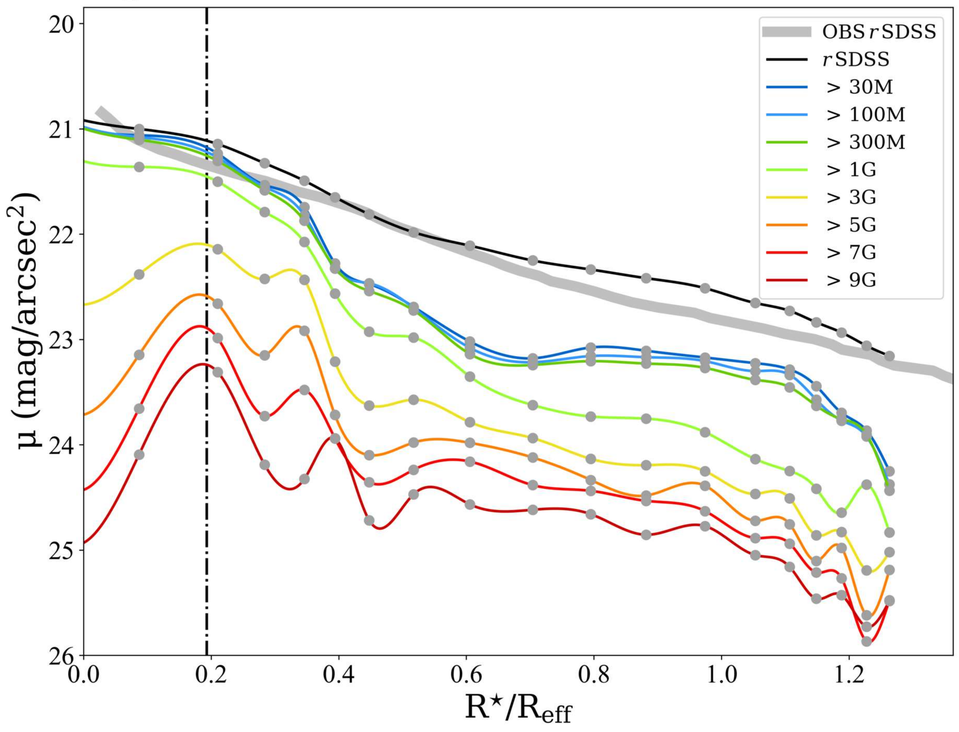

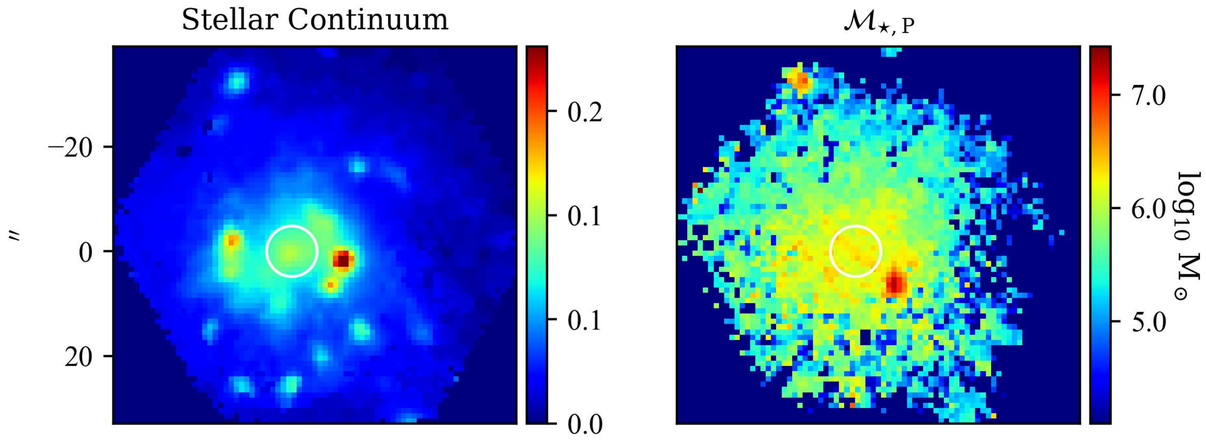

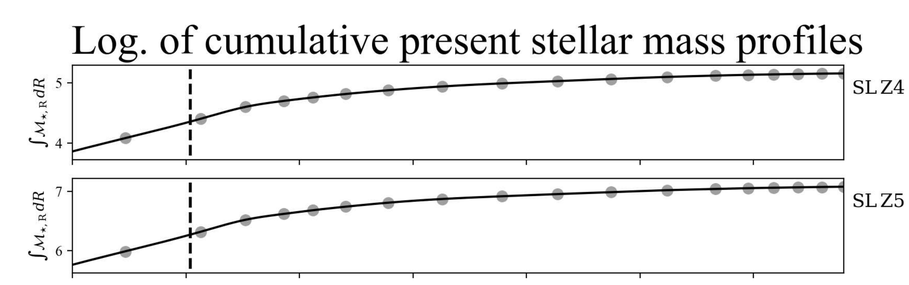

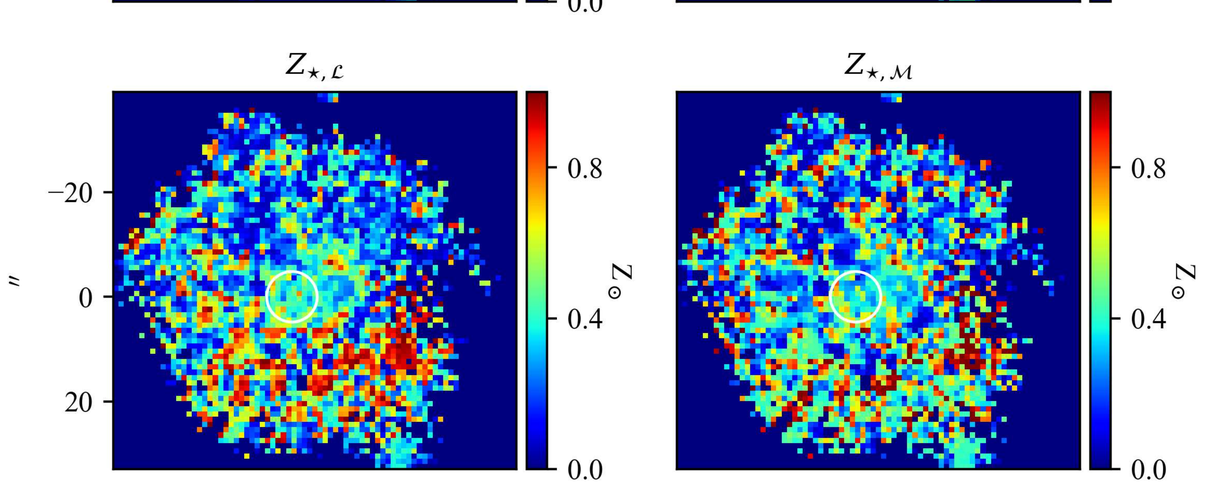

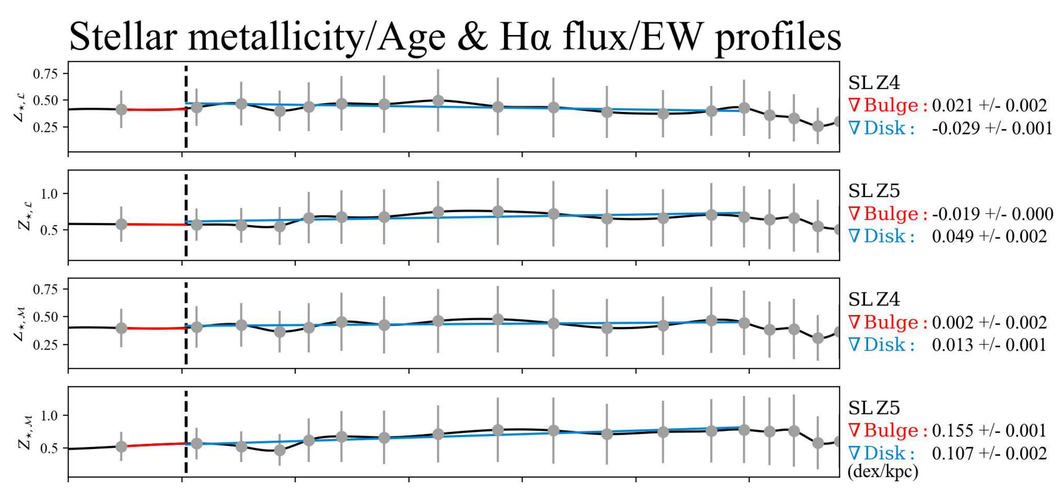

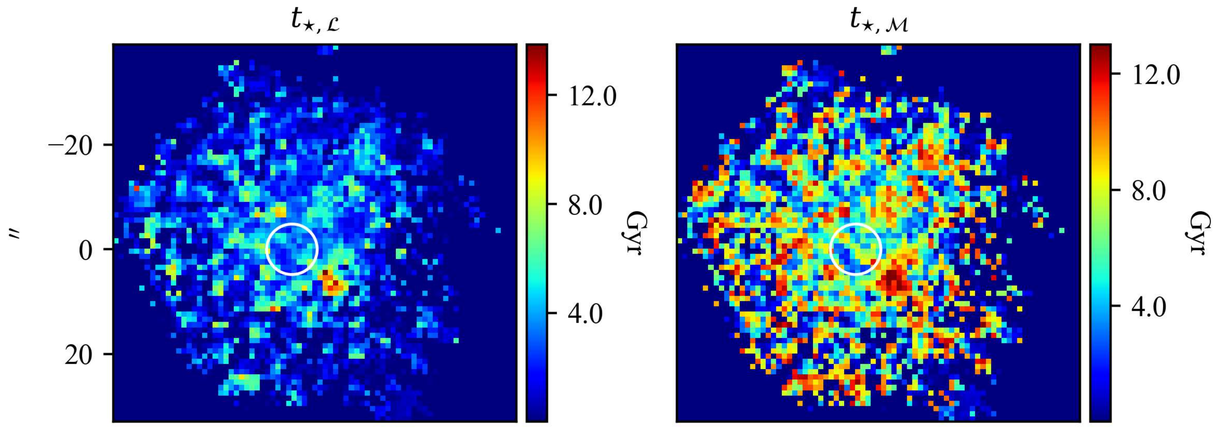

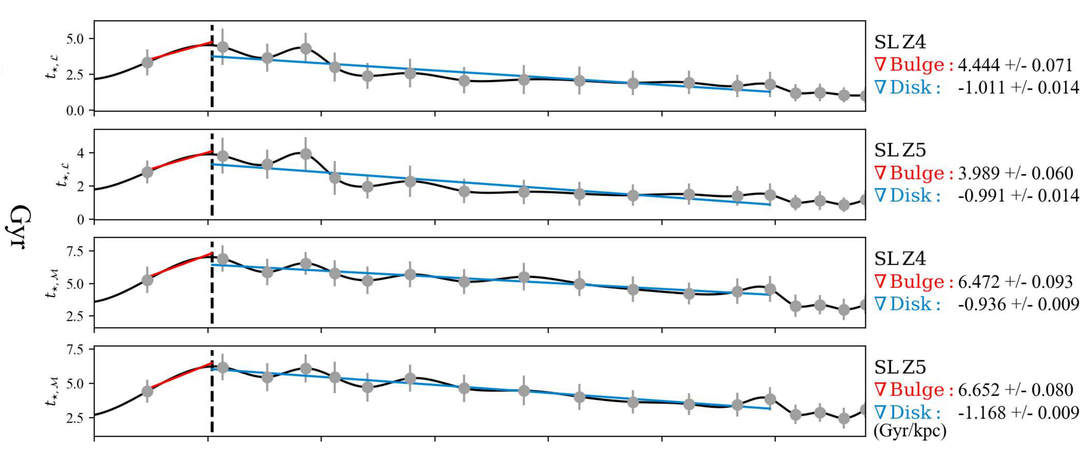

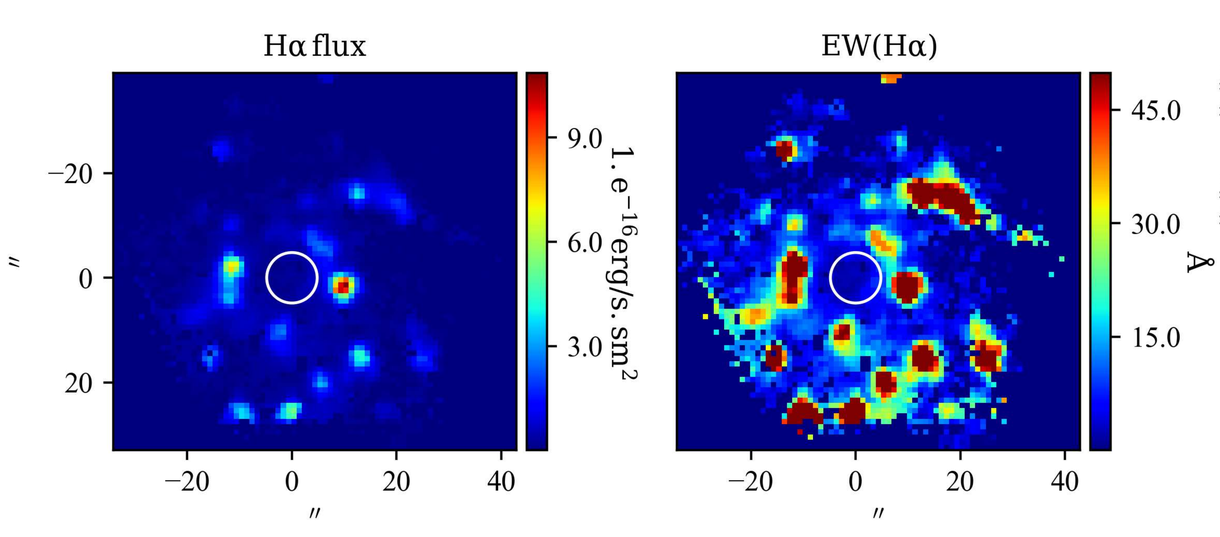

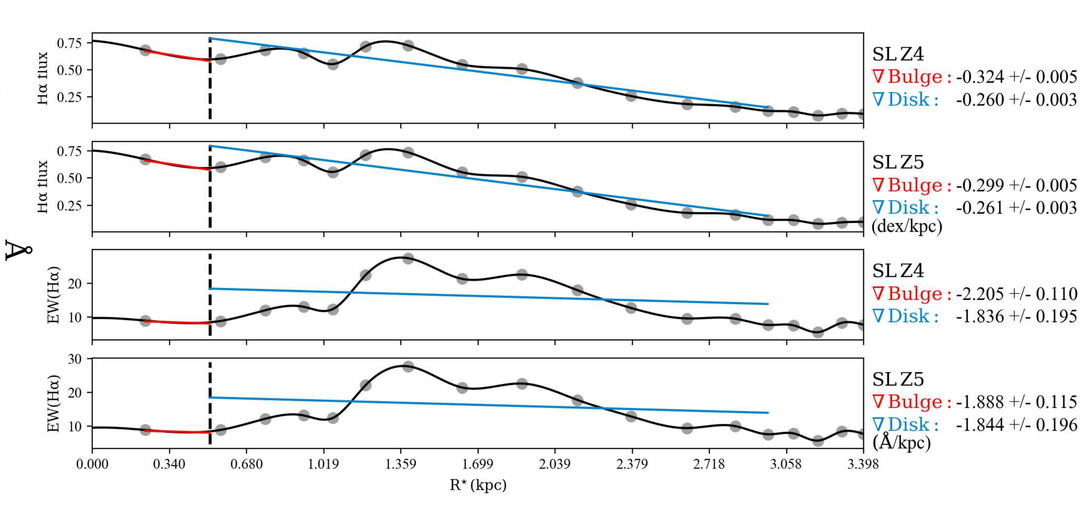

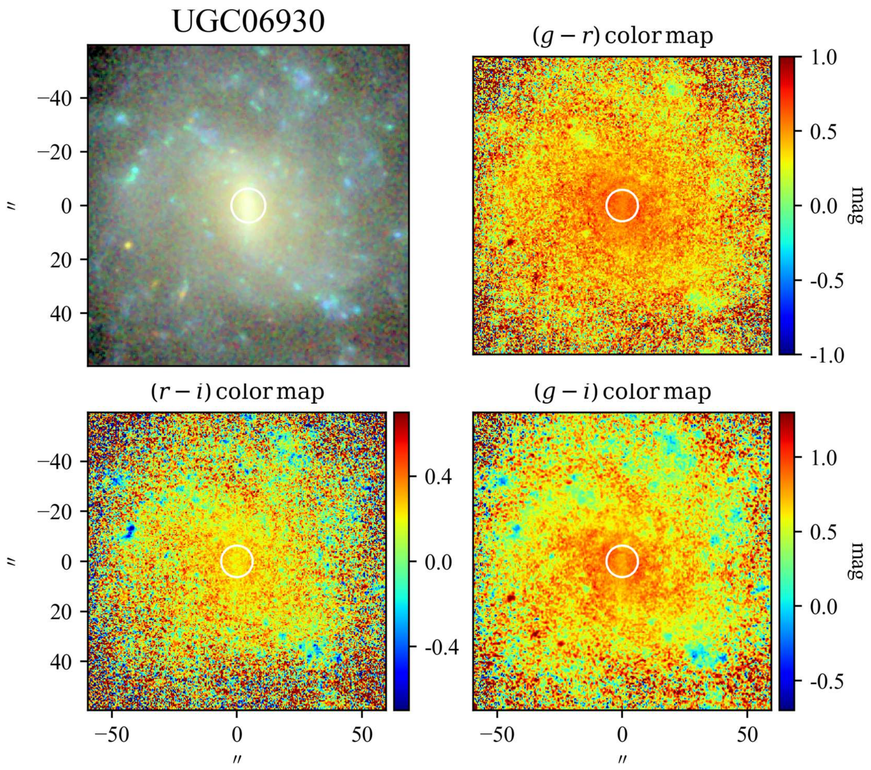

SBP decomposition of SDSS r band

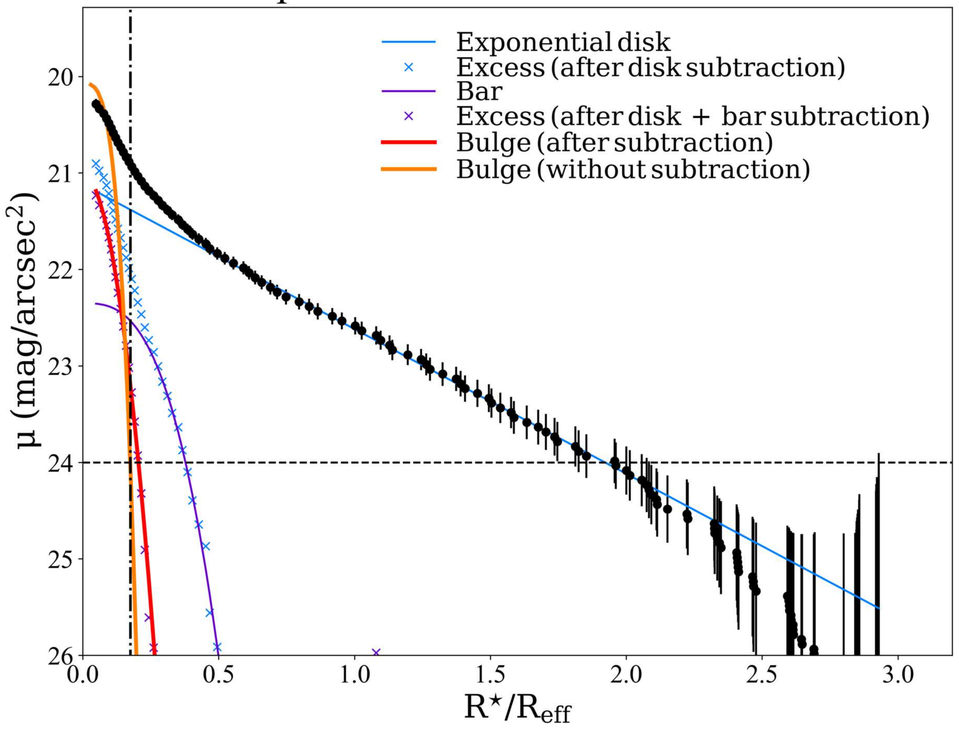

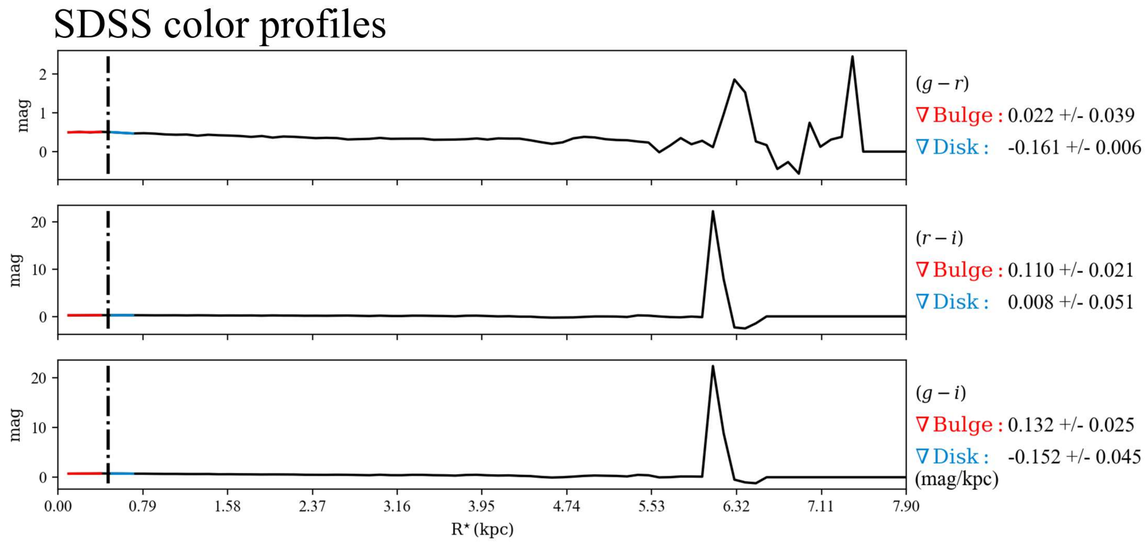

$\mathcal{RV}$ SBPs

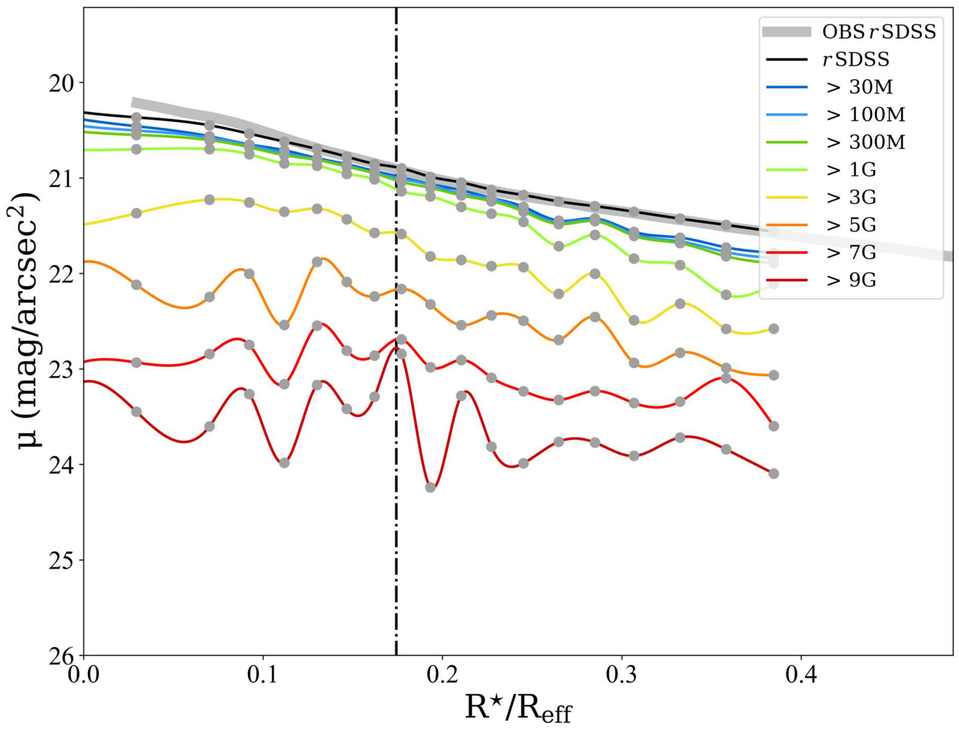

Stellar Continuum

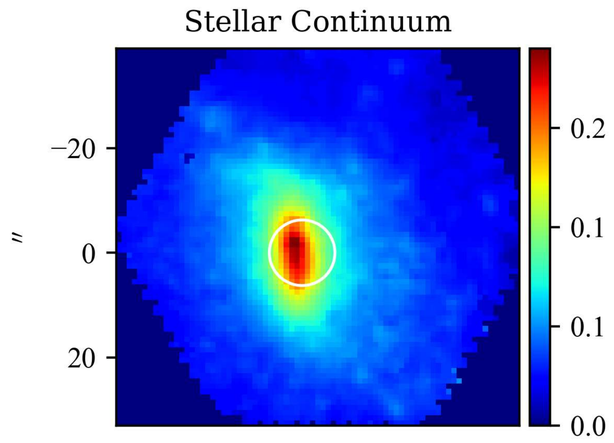

$\mathcal{M}_{\star,\mathrm{P}}$

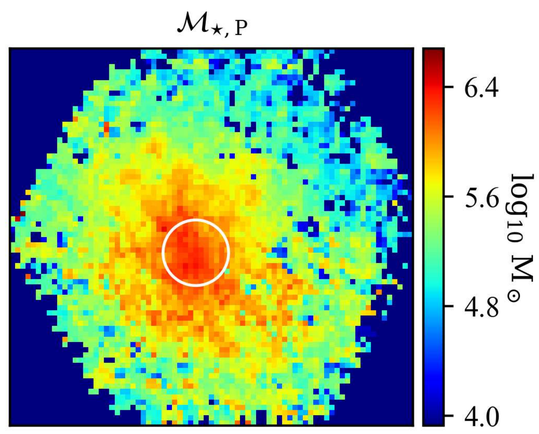

Log. of cumulative present stellar mass profiles

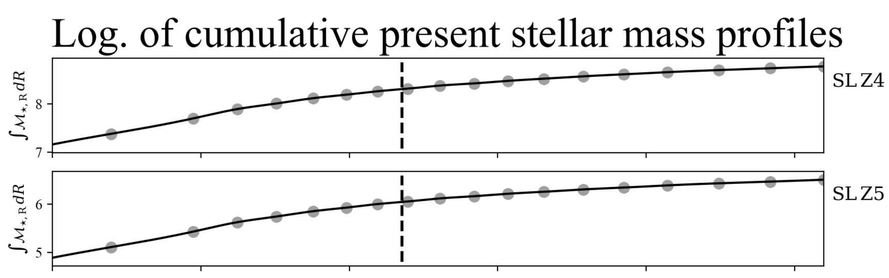

$Z_{\star,\mathcal{L}}$

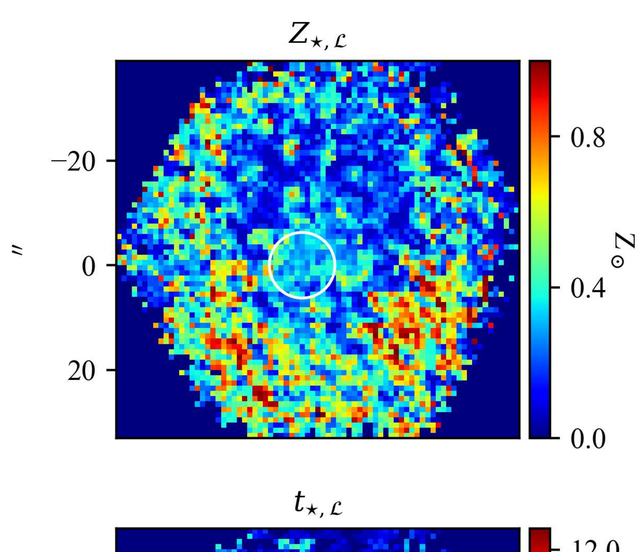

$Z_{\star,\mathcal{M}}$

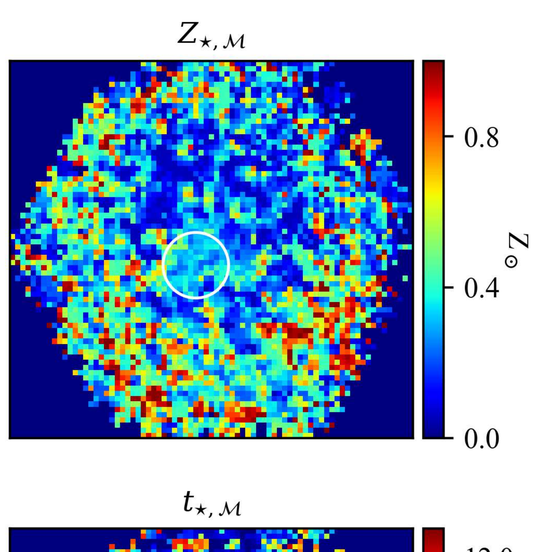

Stellar metallicity/Age & Hα flux/EW profiles

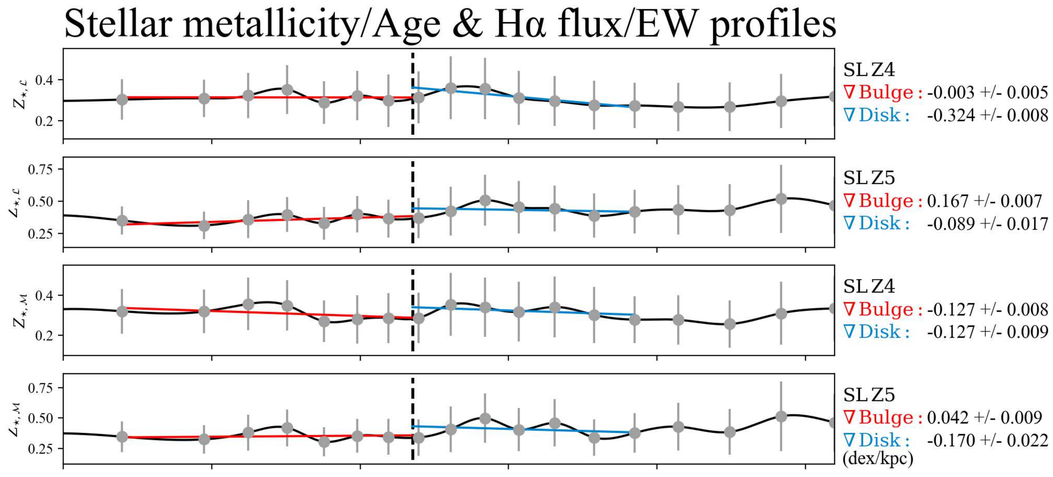

$t_{\star,\mathcal{L}}$

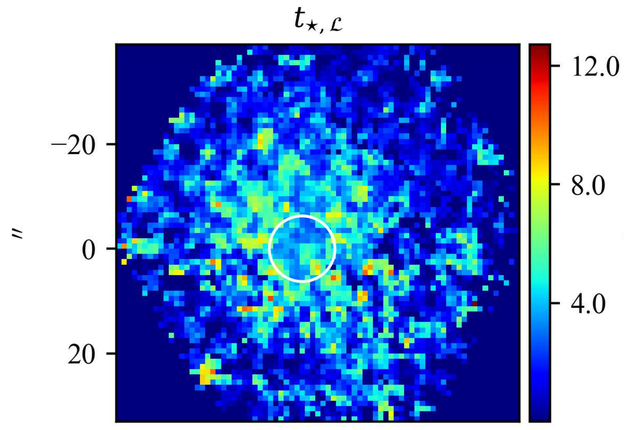

$t_{\star,\mathcal{M}}$

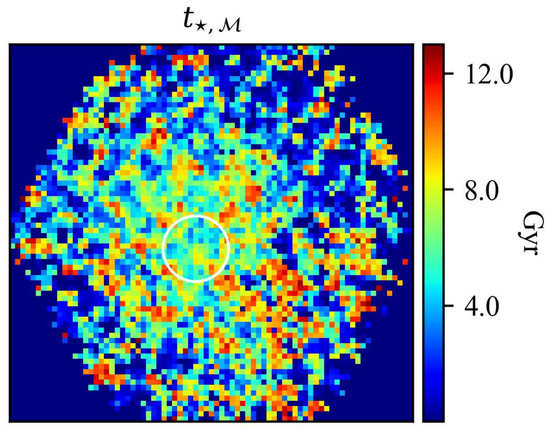

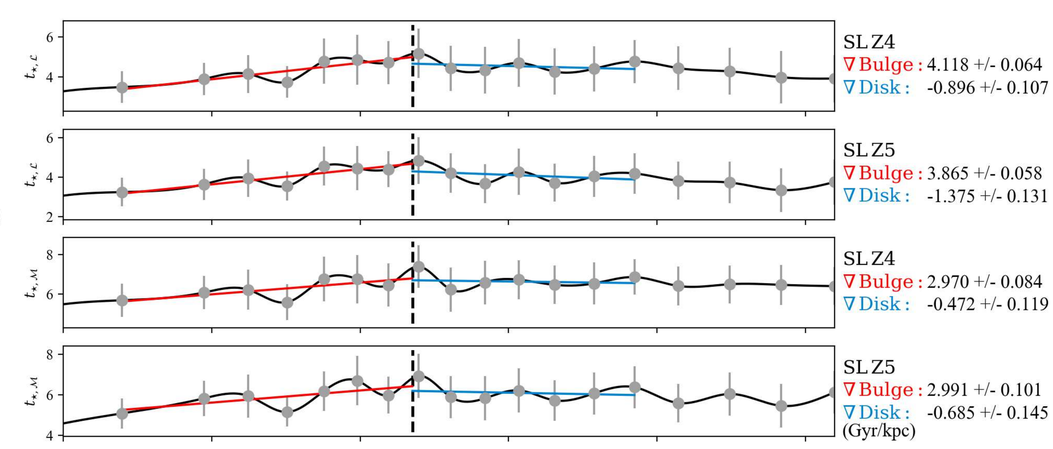

Hα flux

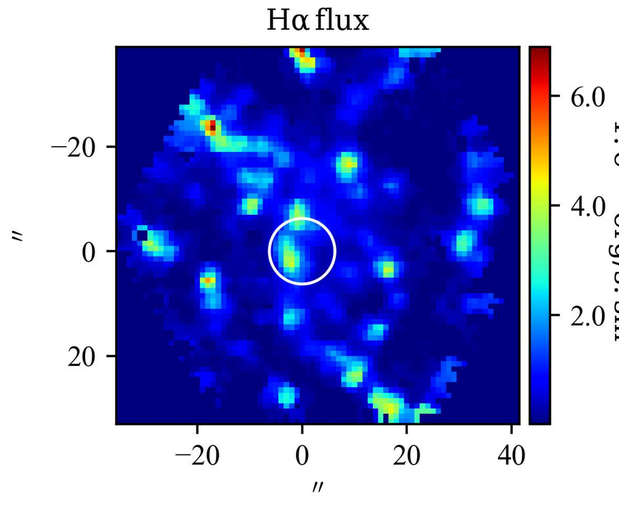

EW(Hα)

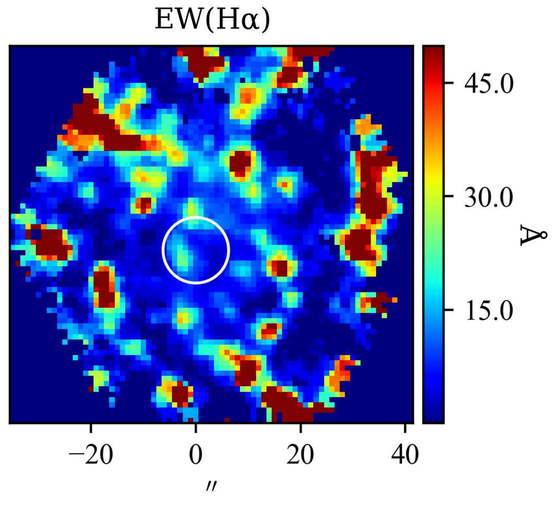

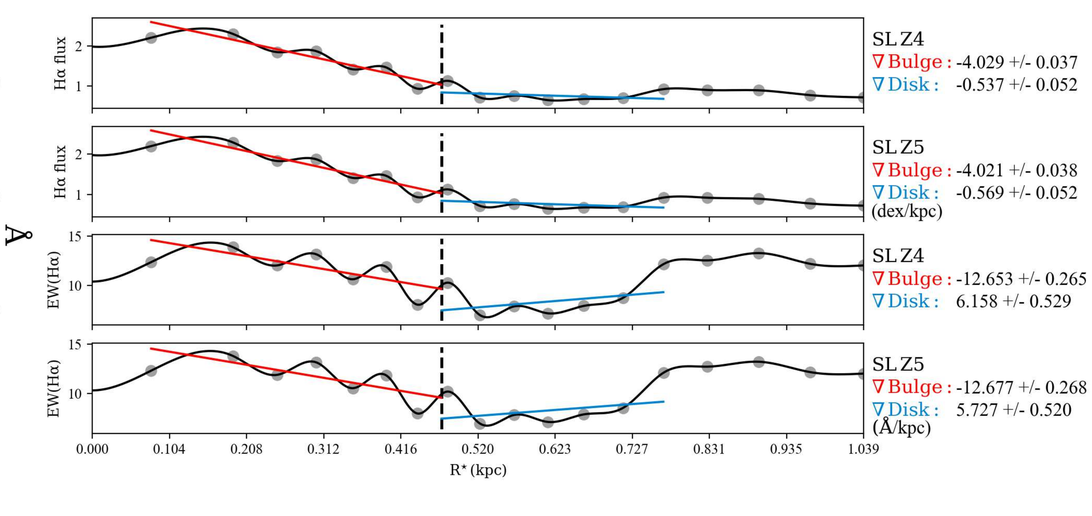

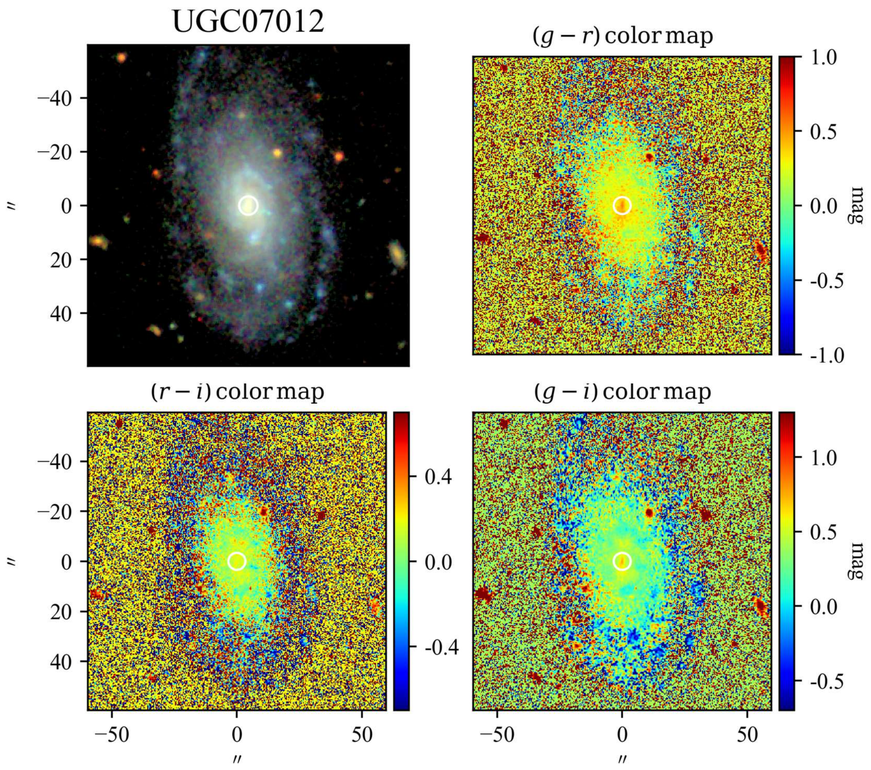

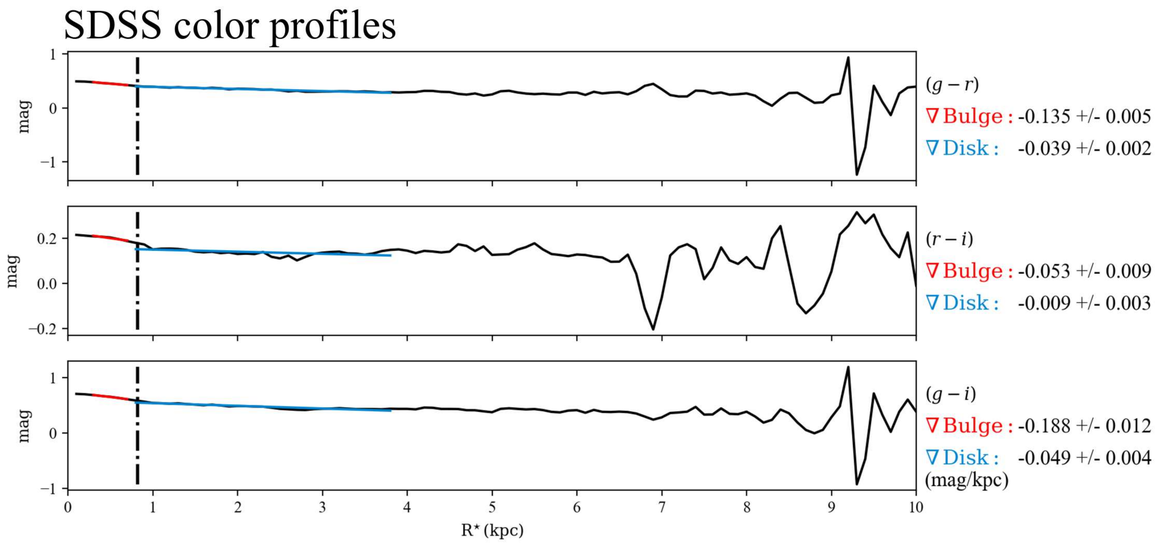

SBP decomposition of SDSS r band

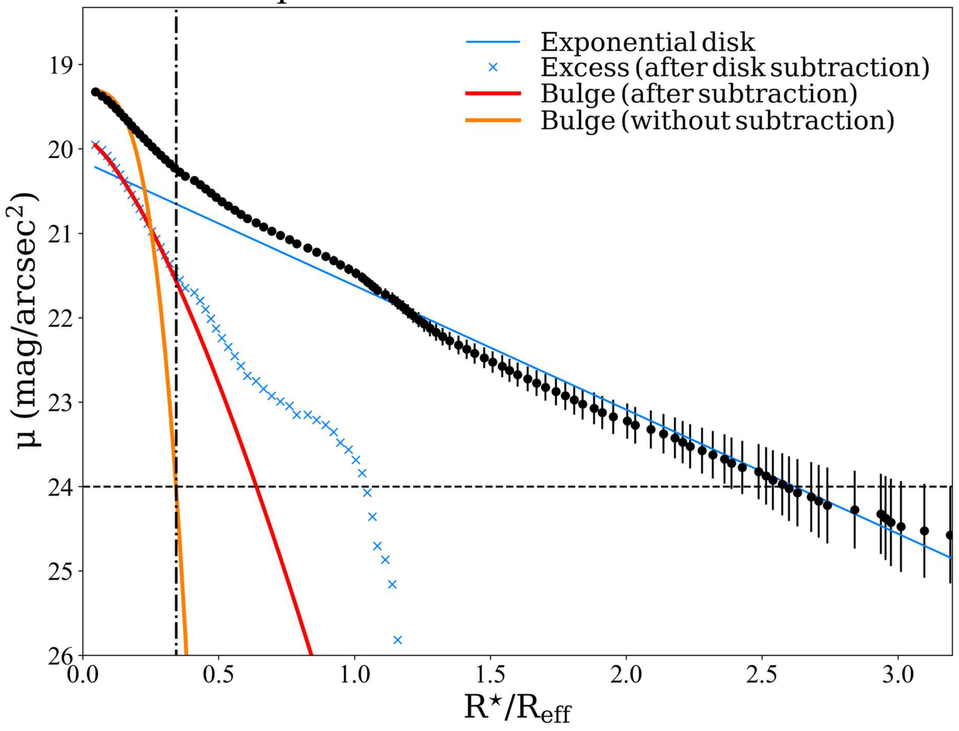

$\mathcal{RV}$ SBPs

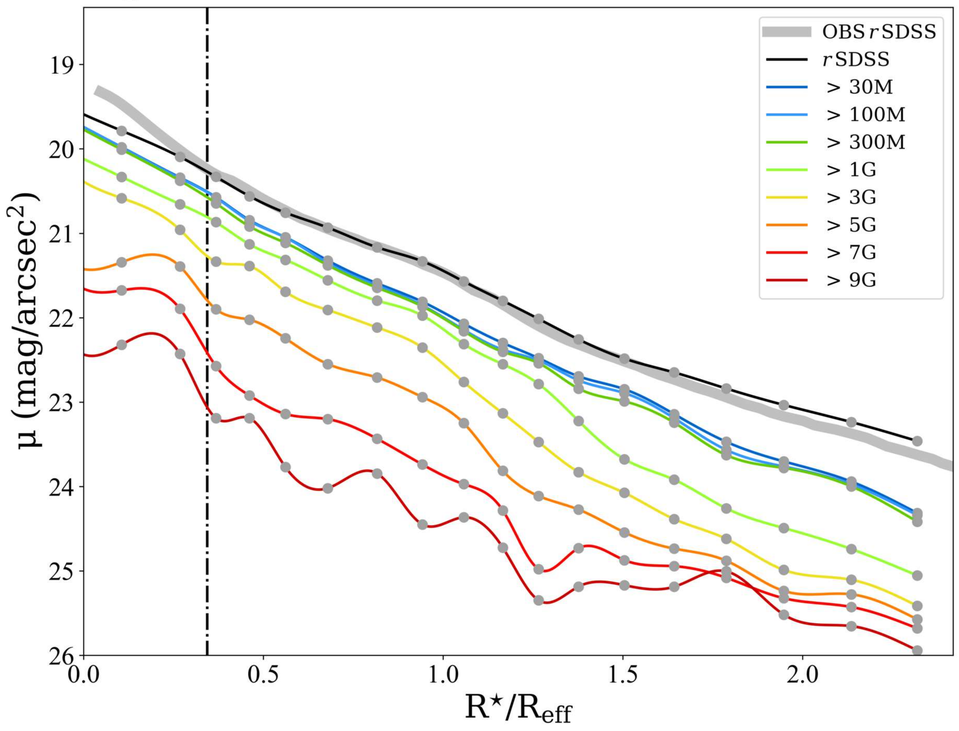

Stellar Continuum

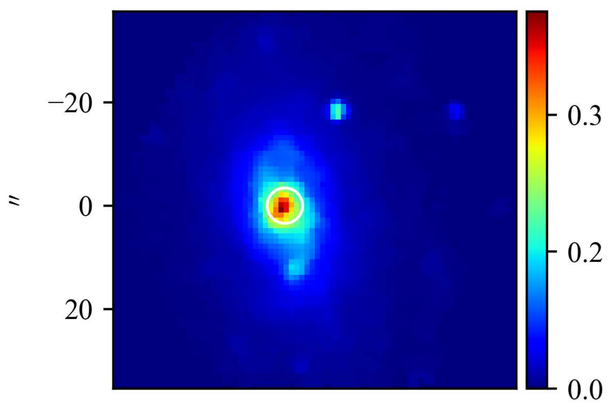

$\mathcal{M}_{\star,\mathrm{P}}$

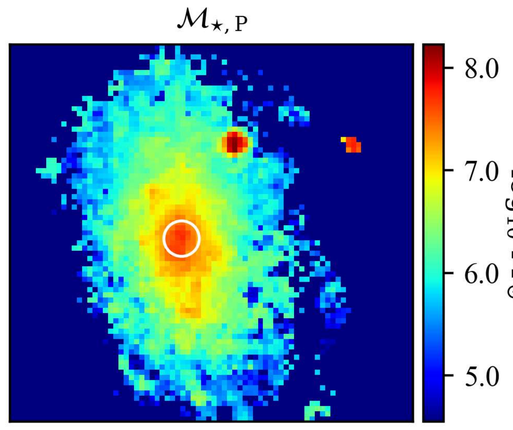

Log. of cumulative present stellar mass profiles

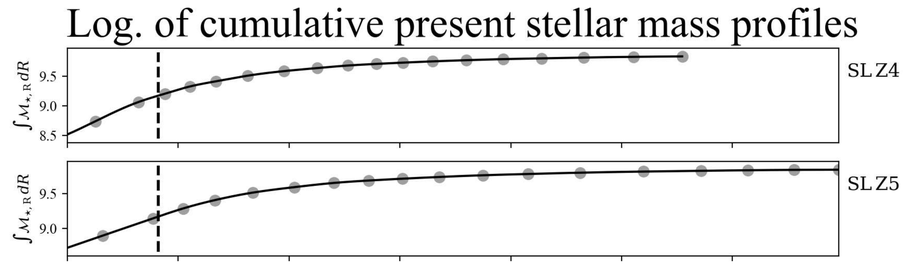

$Z_{\star,\mathcal{L}}$

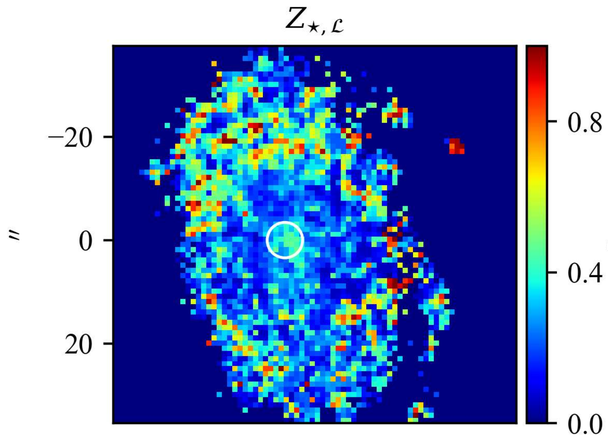

$Z_{\star,\mathcal{M}}$

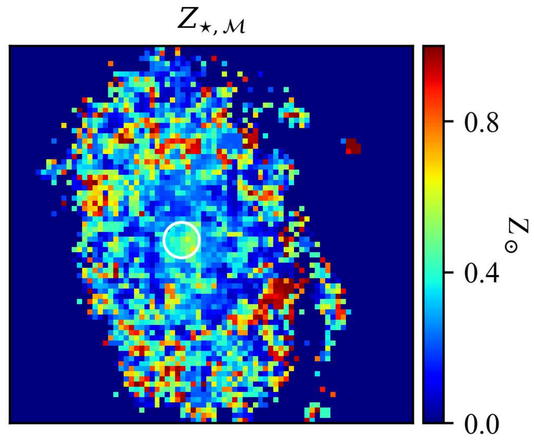

Stellar metallicity/Age & Hα flux/EW profiles

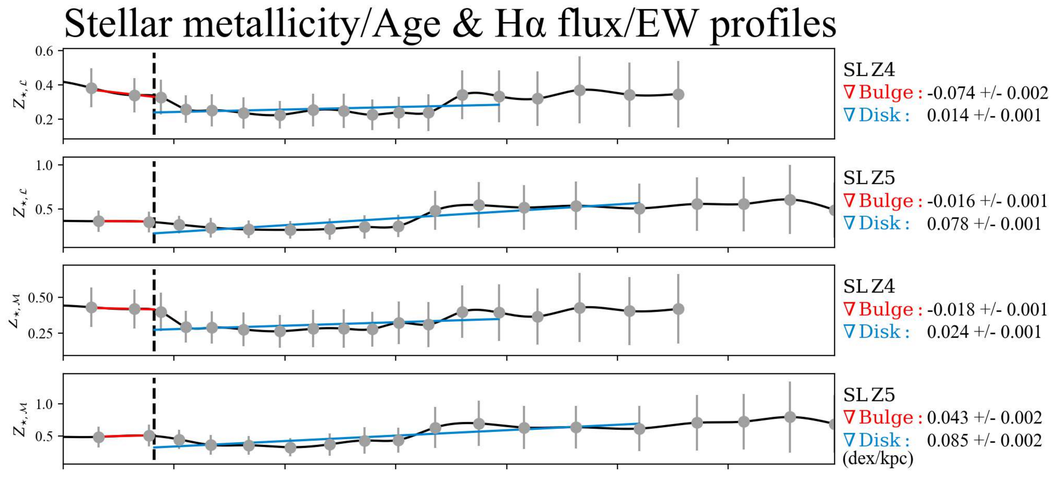

$t_{\star,\mathcal{L}}$

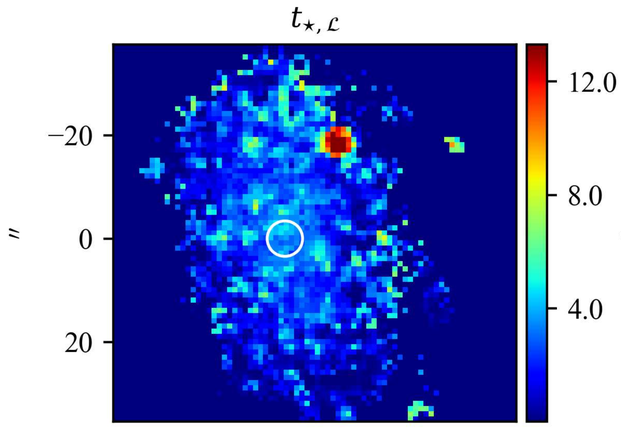

$t_{\star,\mathcal{M}}$

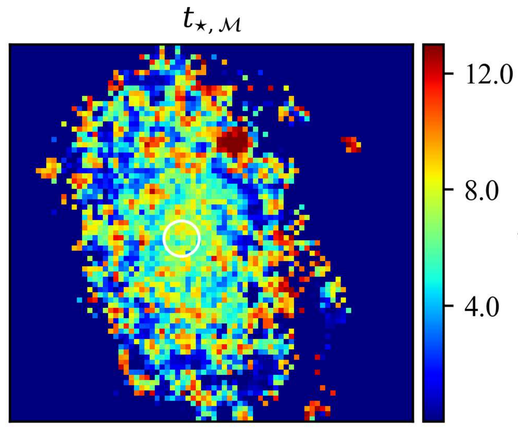

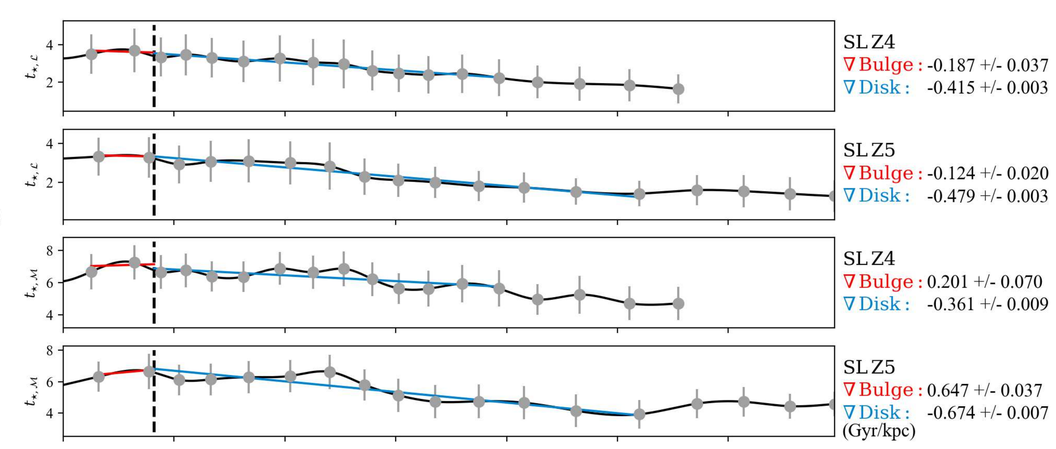

Hα flux

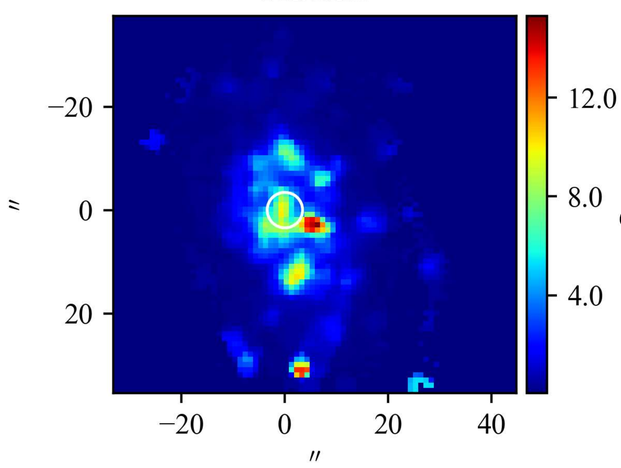

EW(Hα)

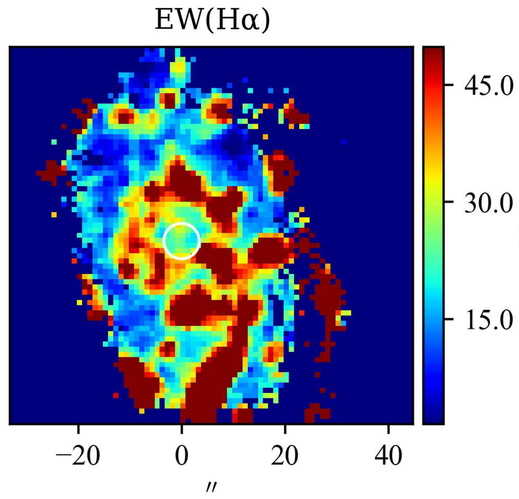

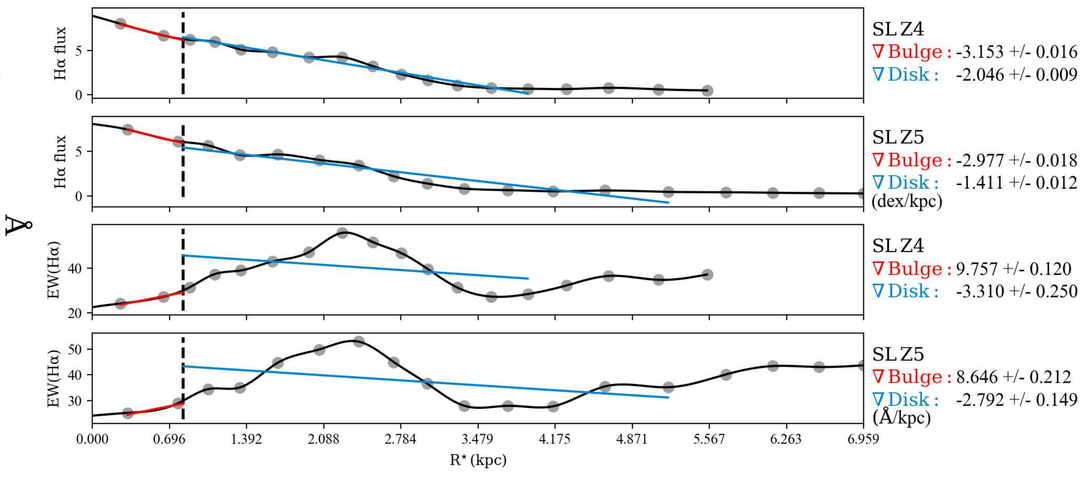

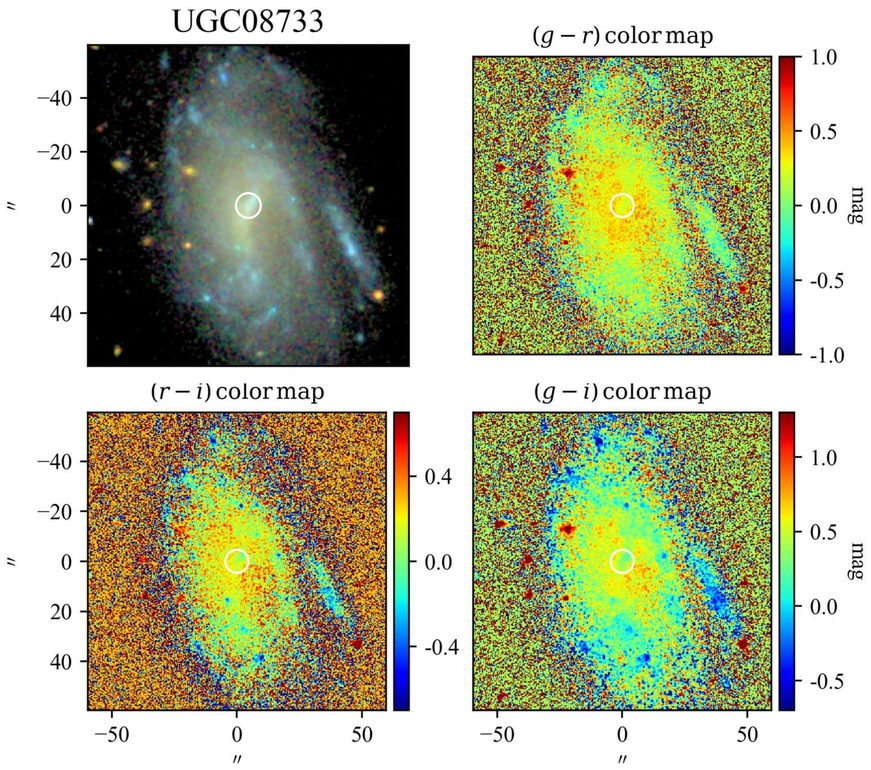

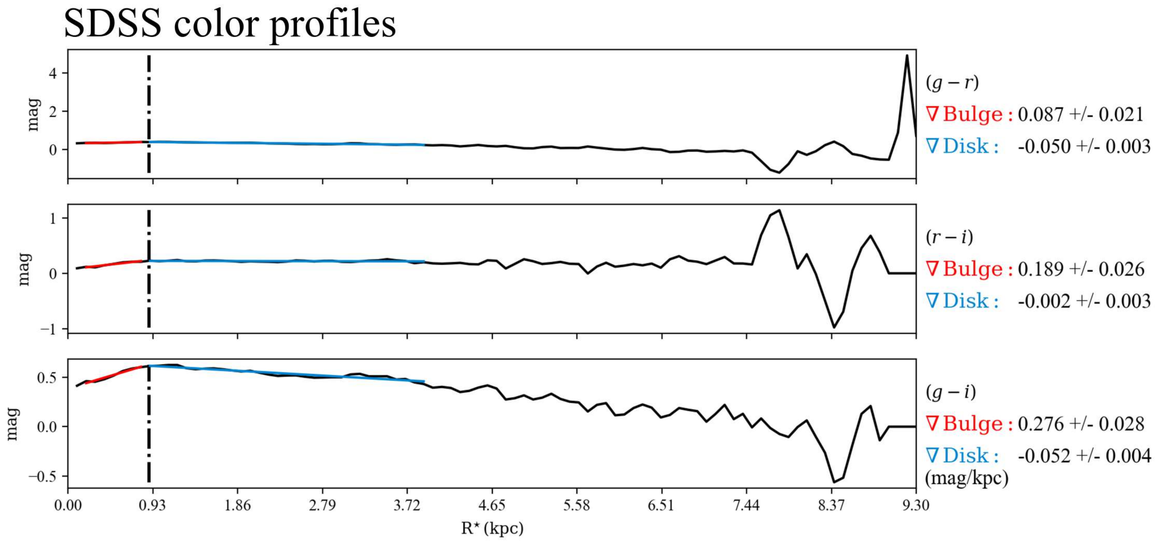

SBP decomposition of SDSS r band

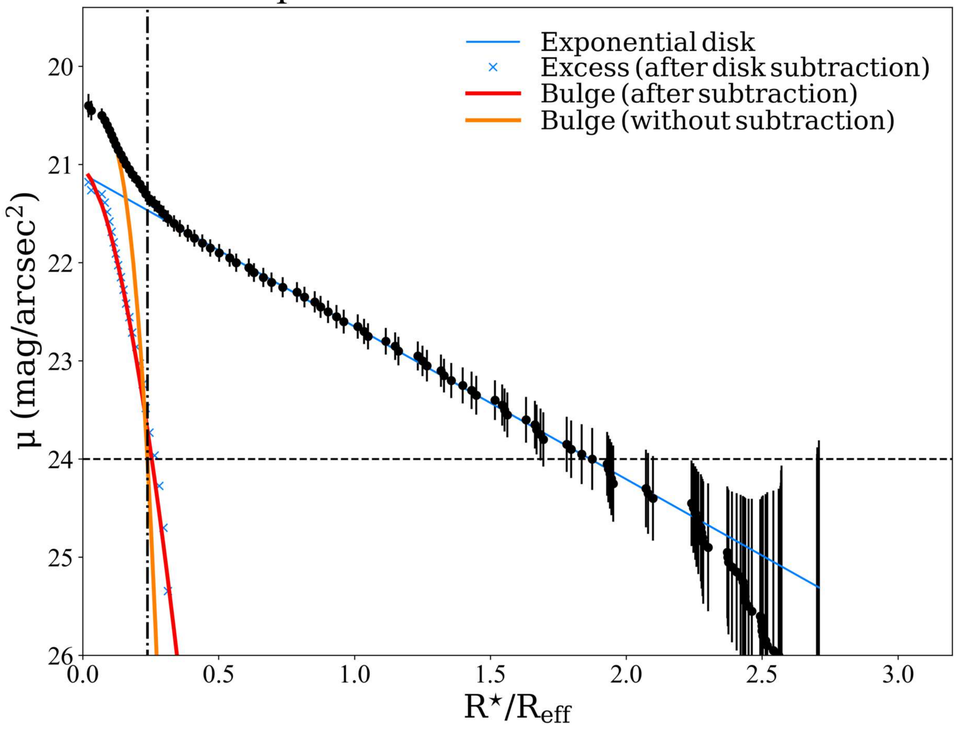

$\mathcal{RY}$ SBPs

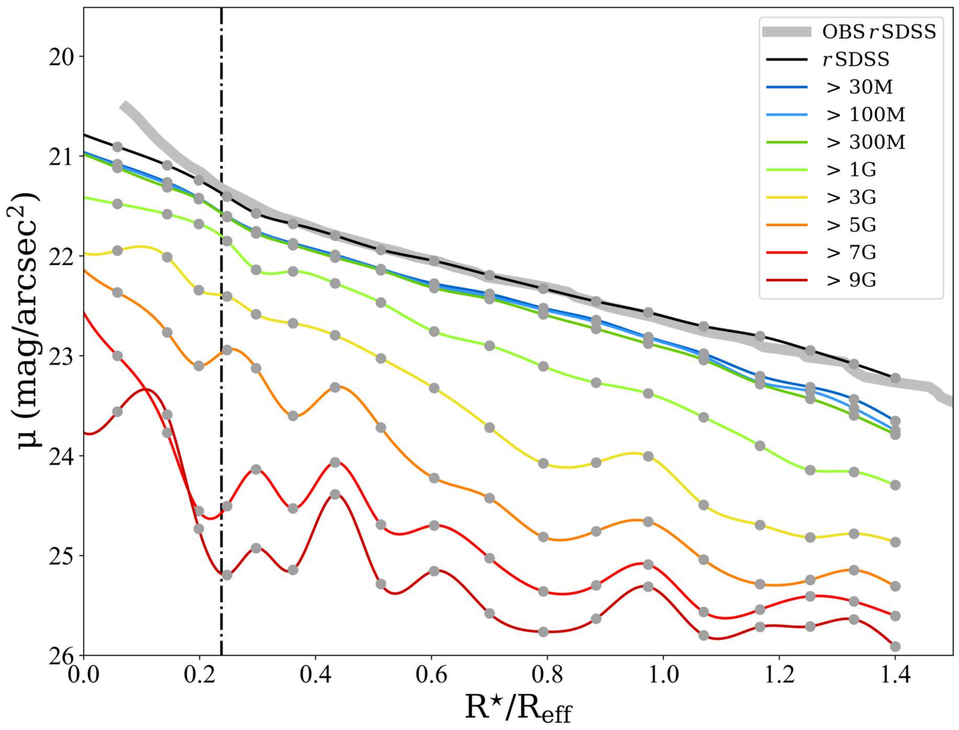

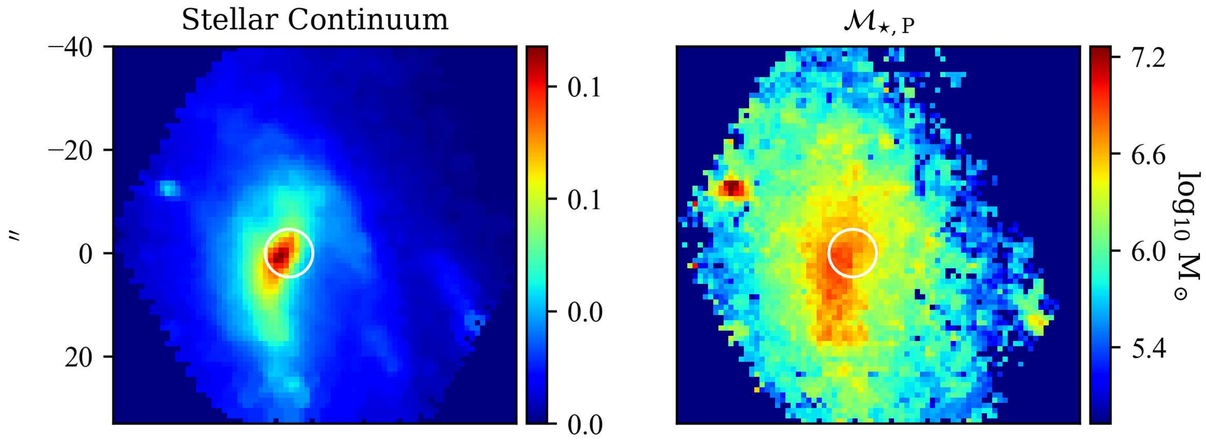

Log. of cumulative present stellar mass profiles

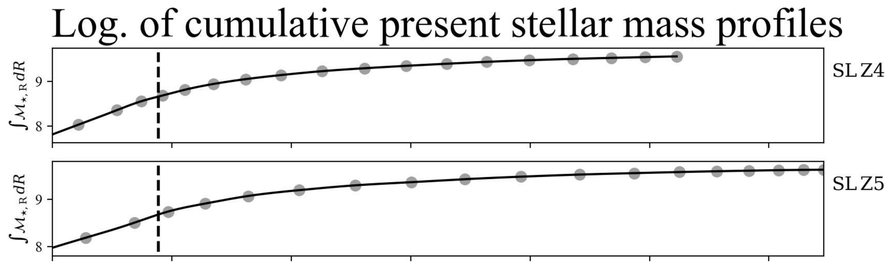

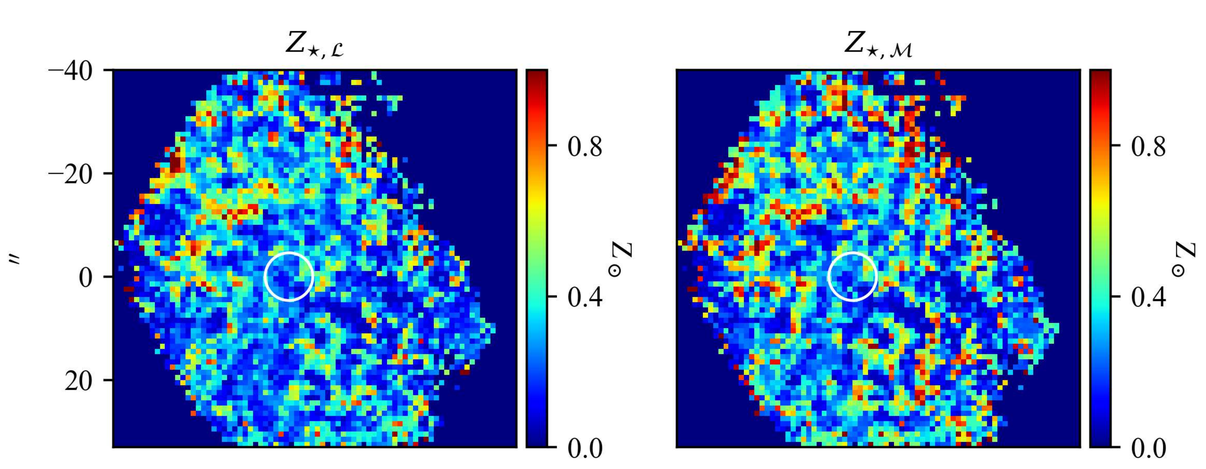

Stellar metallicity/Age & Hα flux/EW profiles

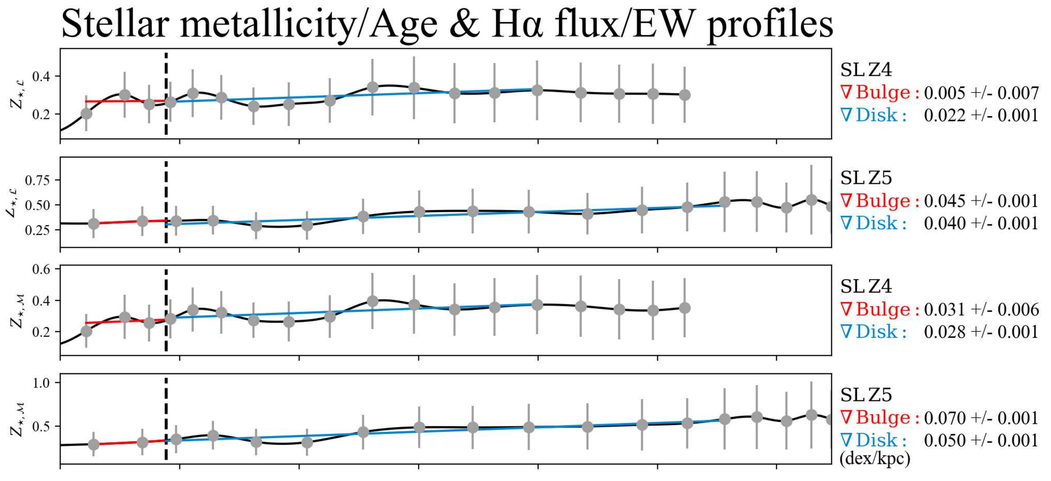

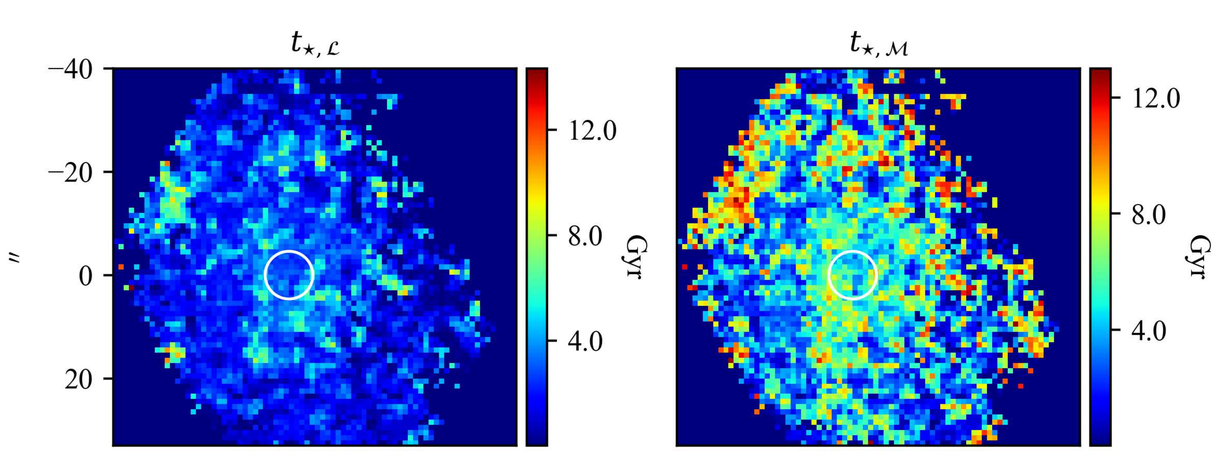

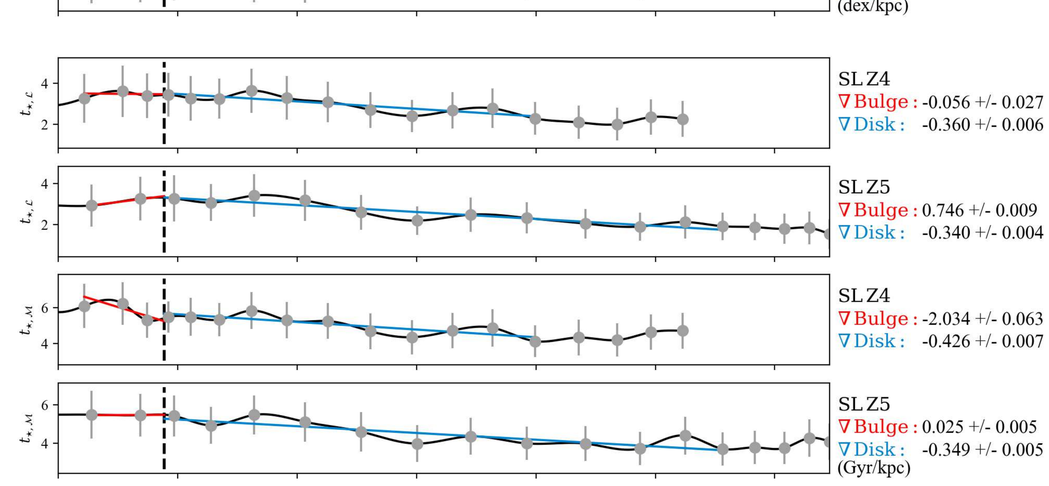

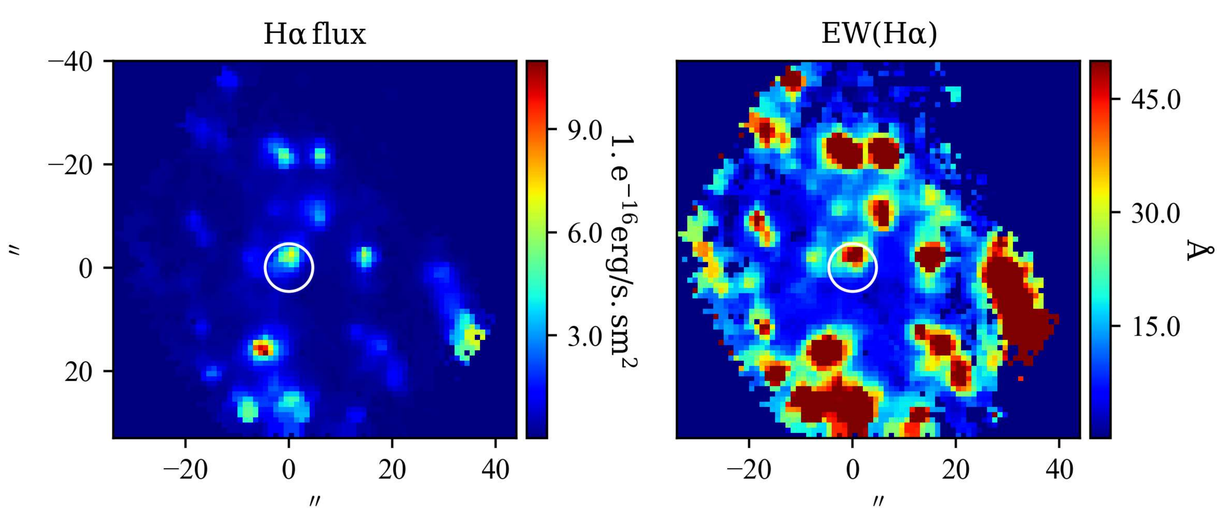

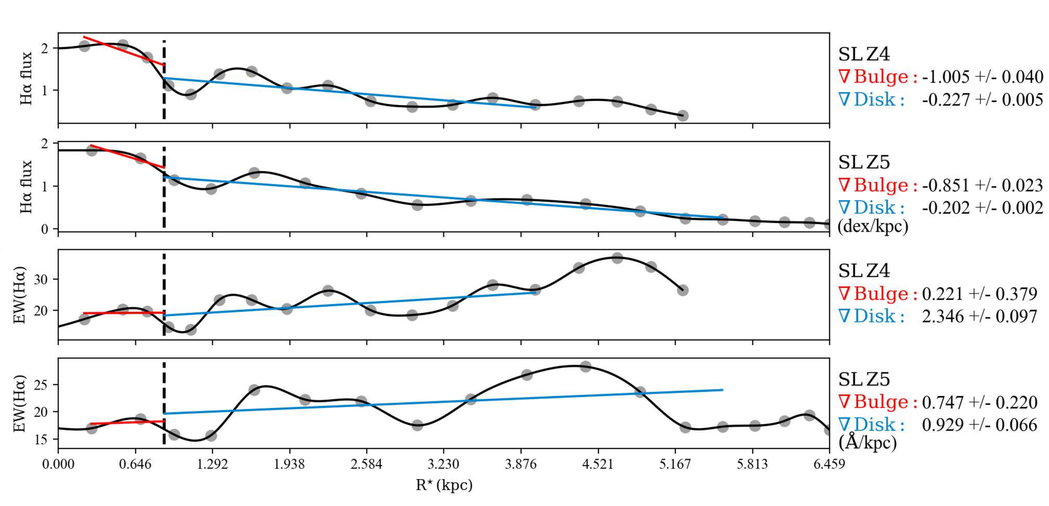

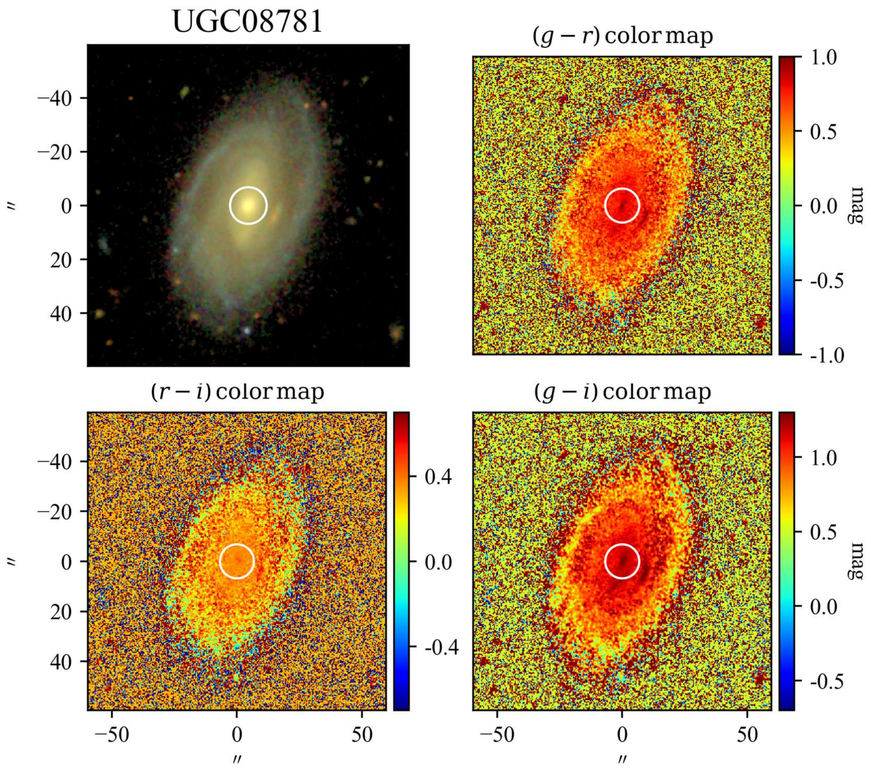

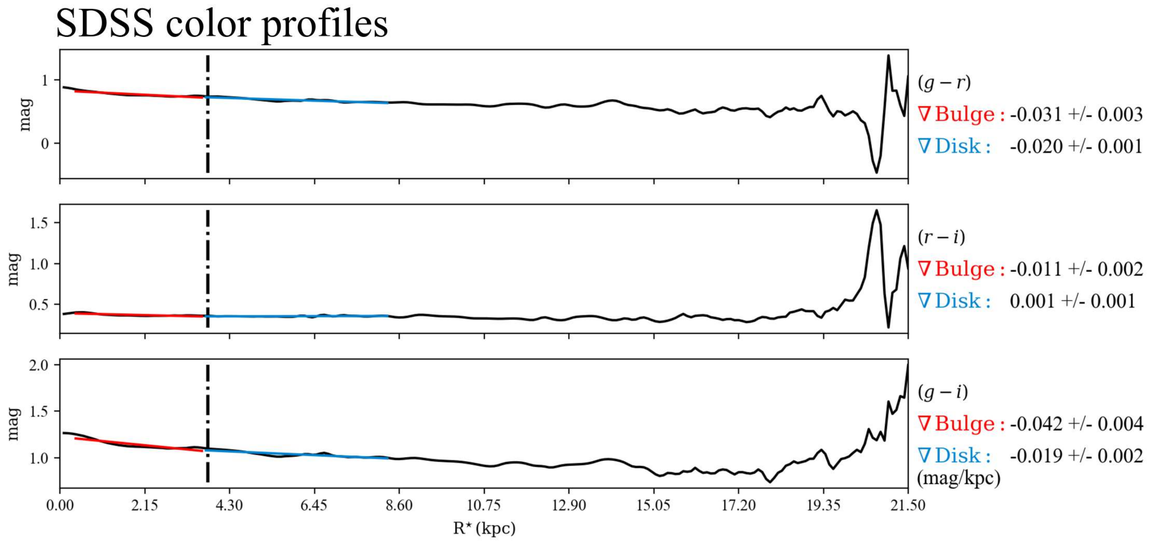

SBP decomposition of SDSS r band

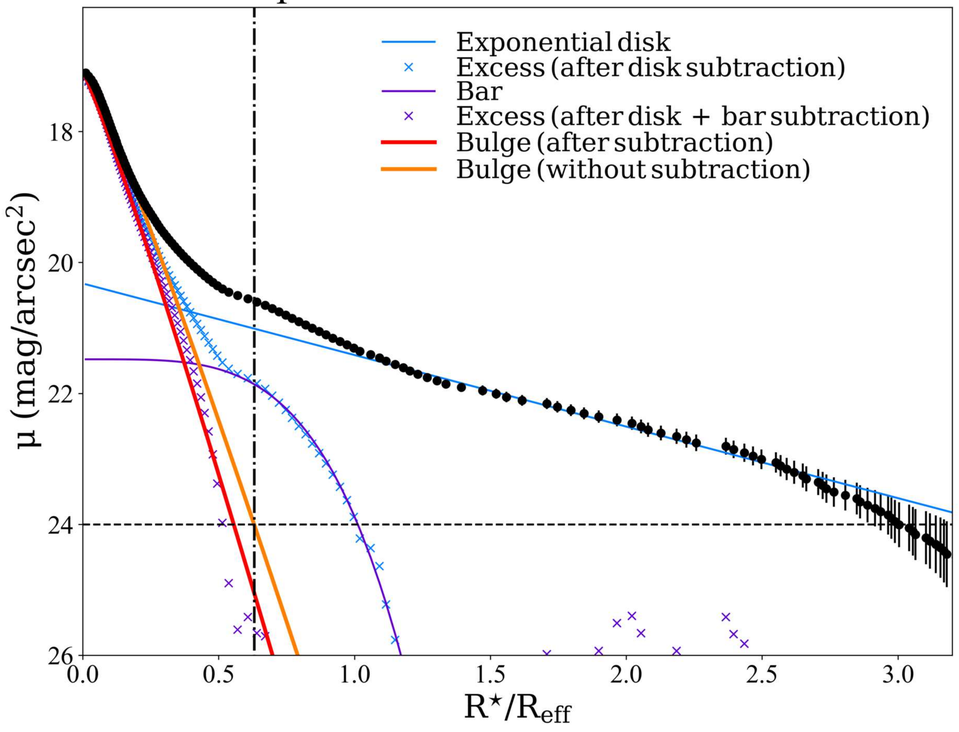

$\mathcal{RY}$ SBPs

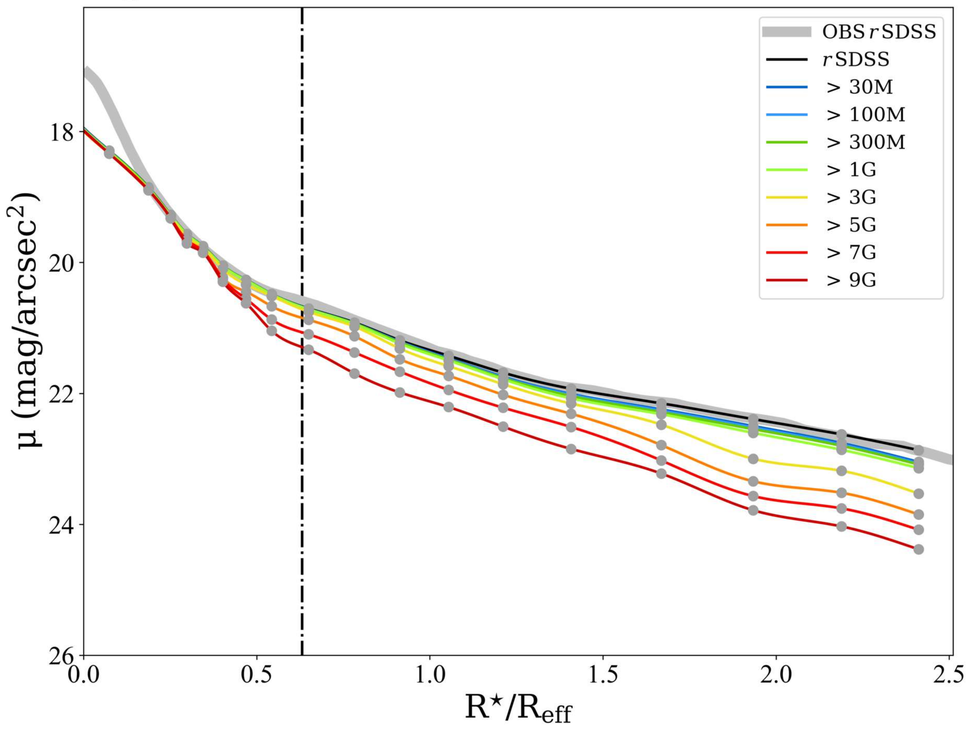

Stellar Continuum

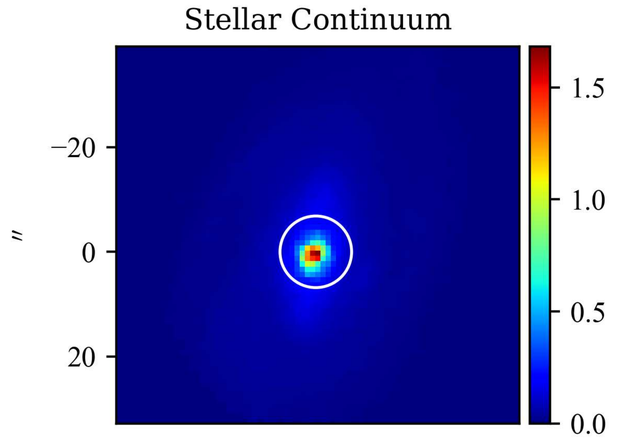

$\mathcal{M}_{\star,\mathrm{P}}$

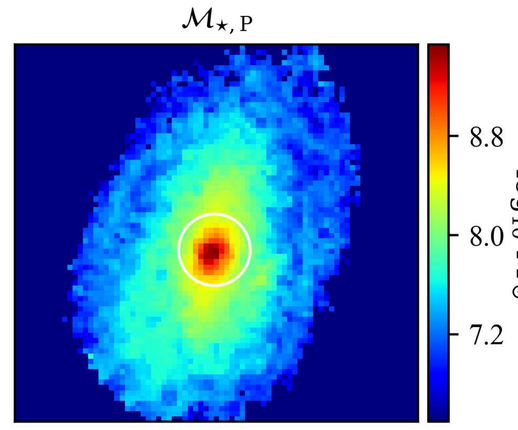

Log. of cumulative present stellar mass profiles

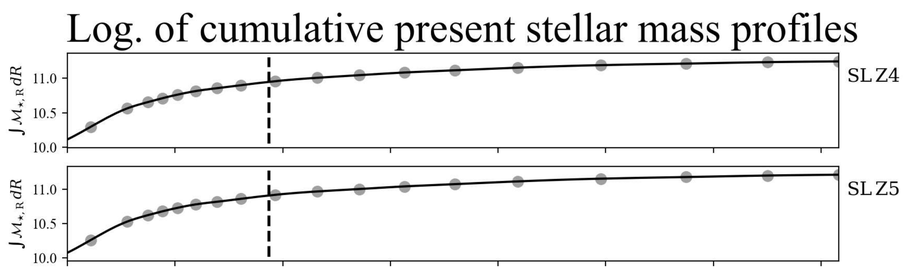

$Z_{\star,\mathcal{L}}$

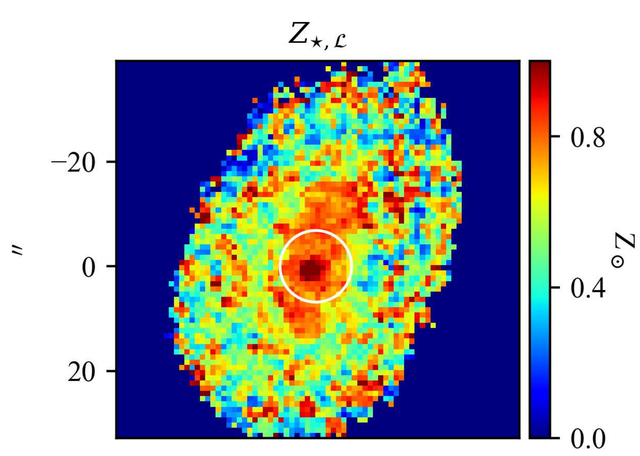

$Z_{\star,\mathcal{M}}$

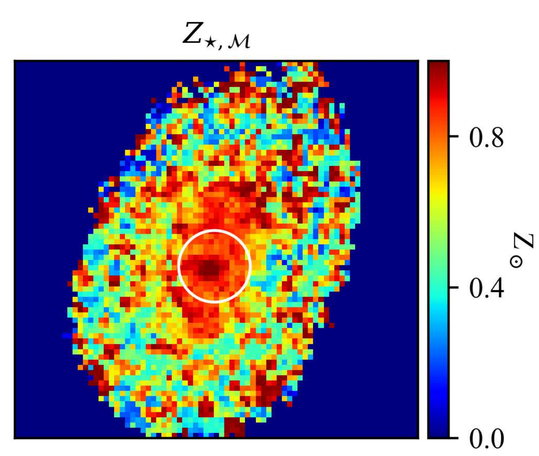

Stellar metallicity/Age & Hα flux/EW profiles

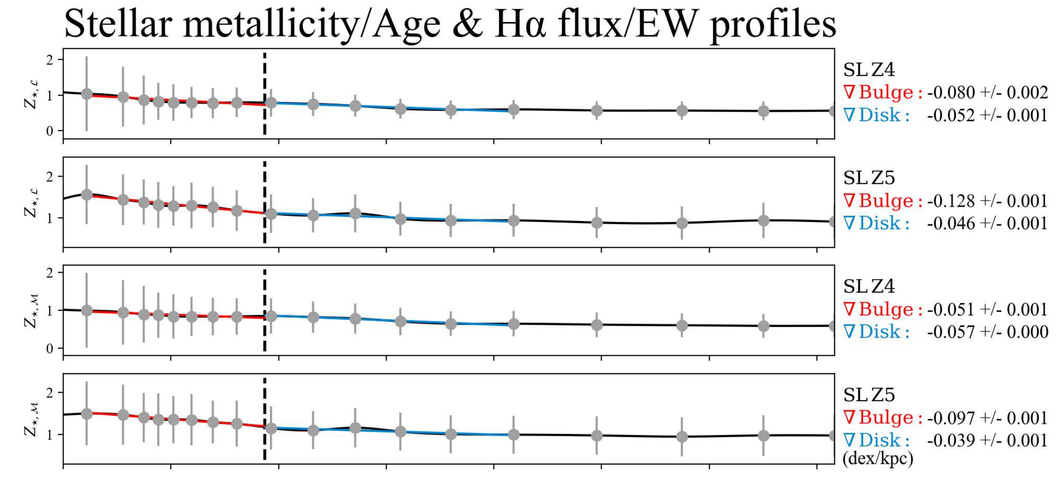

$t_{\star,\mathcal{L}}$

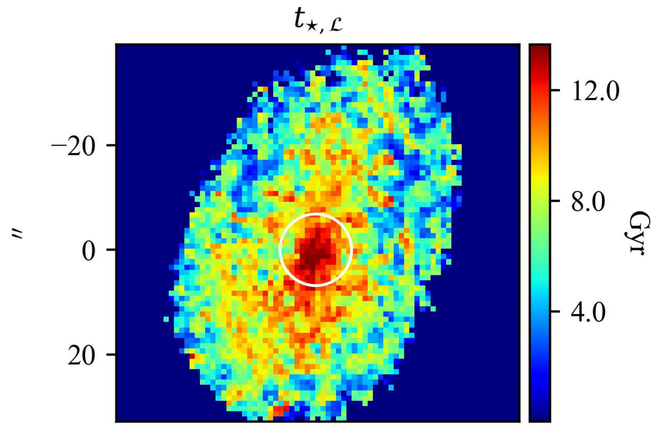

$t_{\star,\mathcal{M}}$

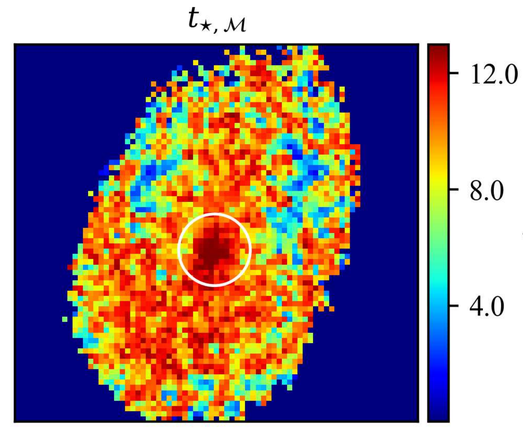

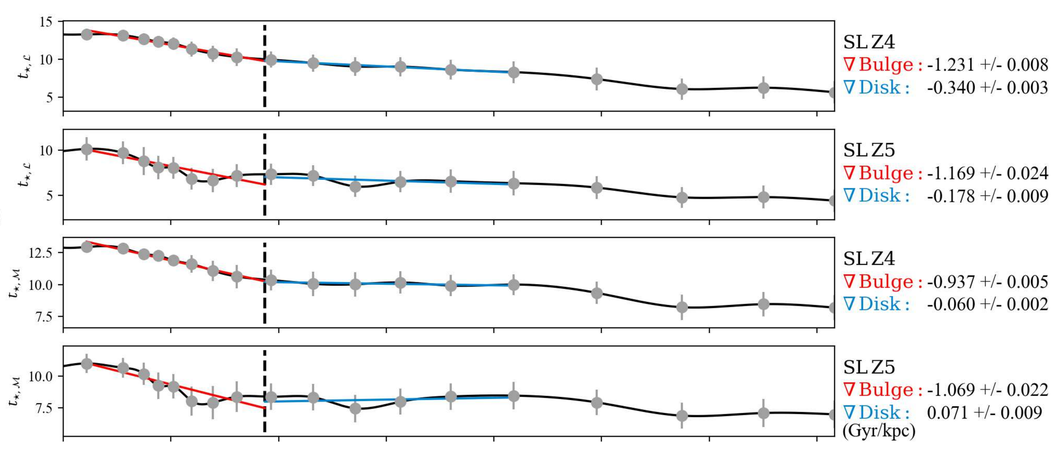

Hα flux

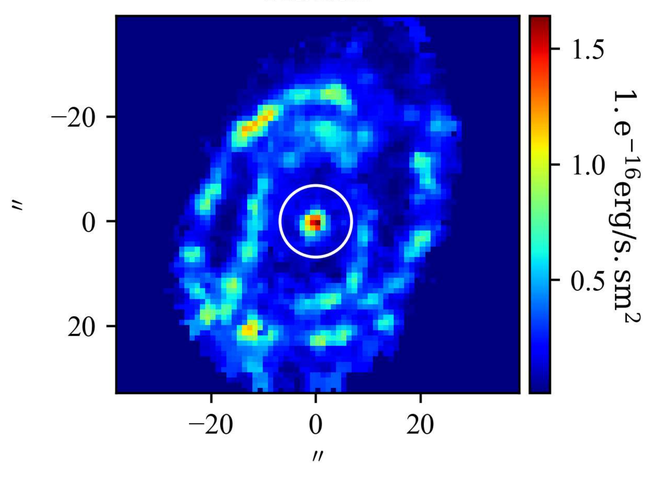

EW(Hα)

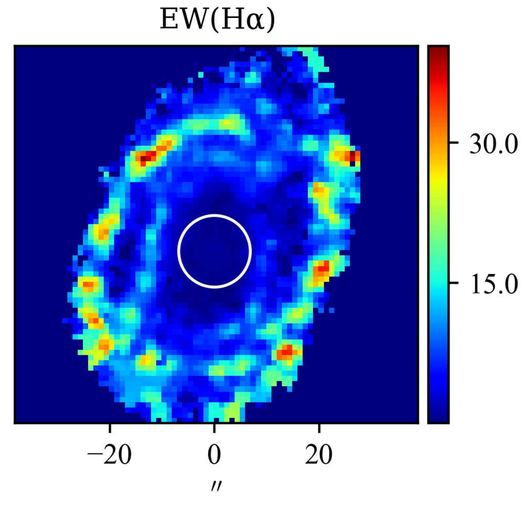

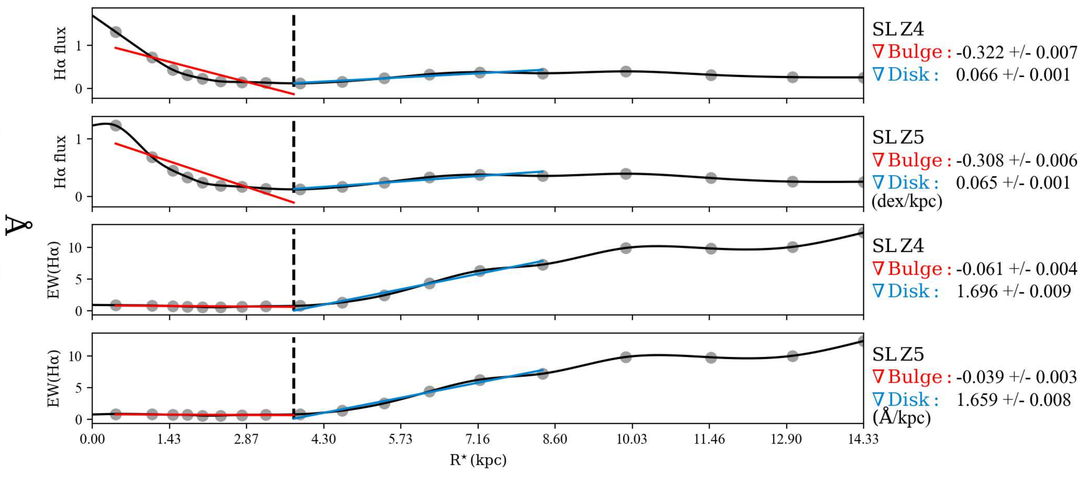

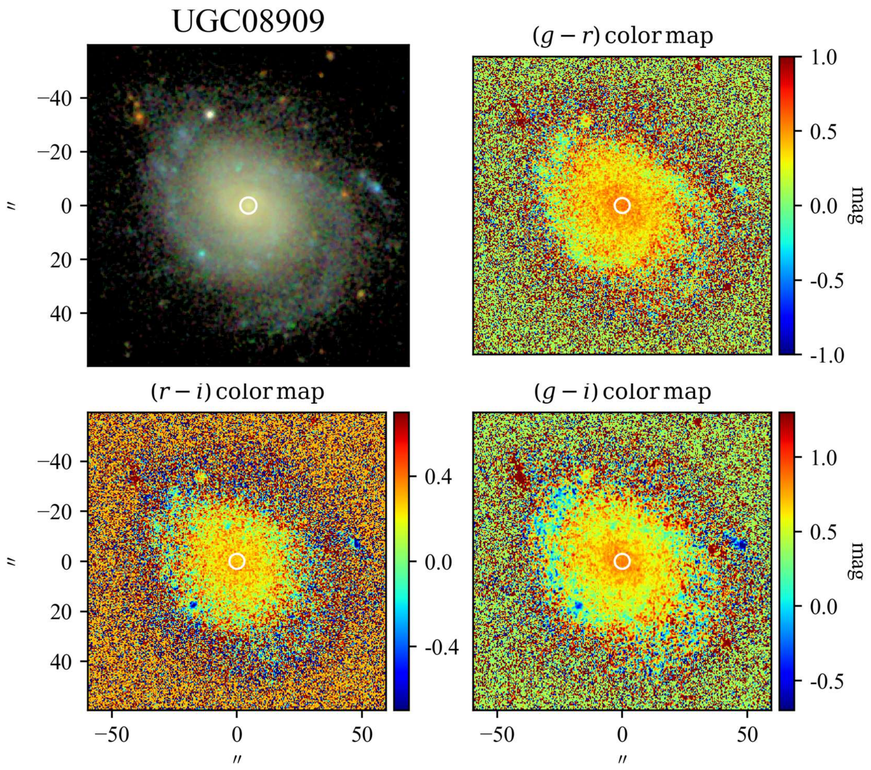

SBP decomposition of SDSS r band

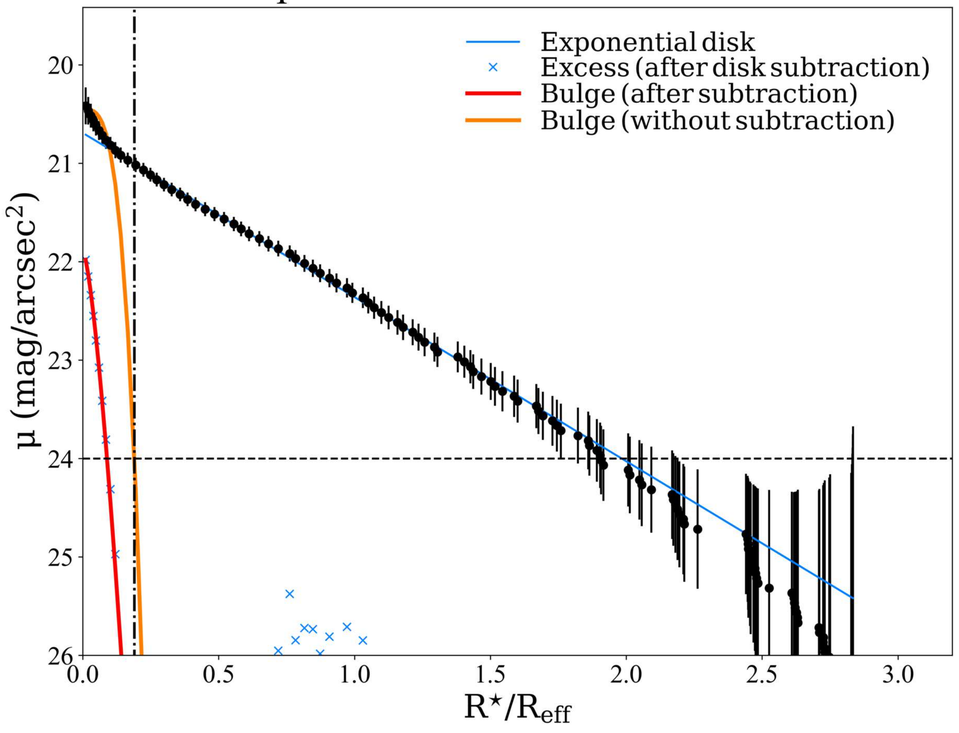

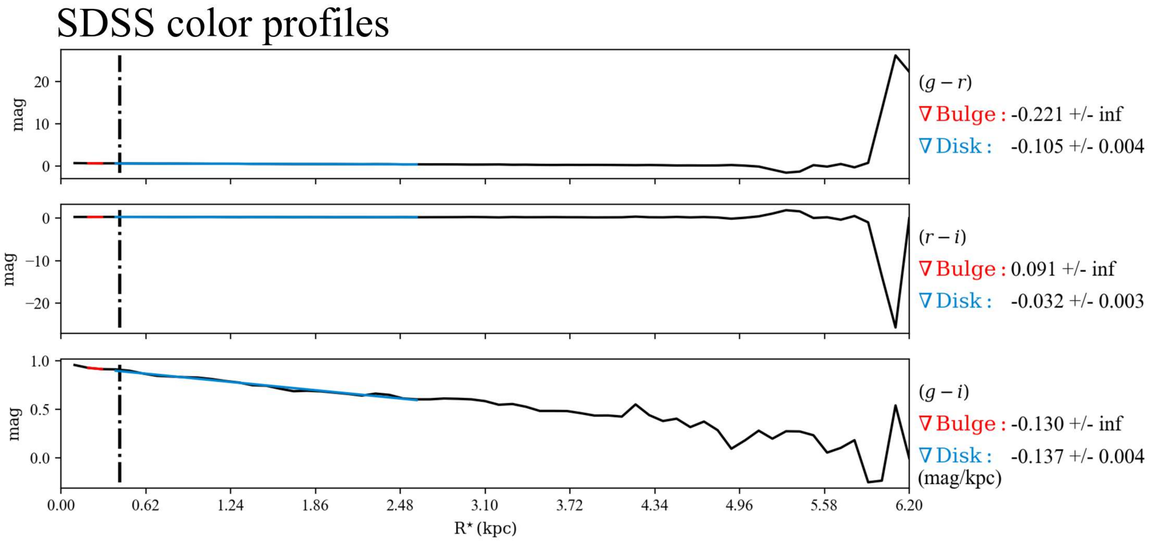

$\mathcal{RY}$ SBPs

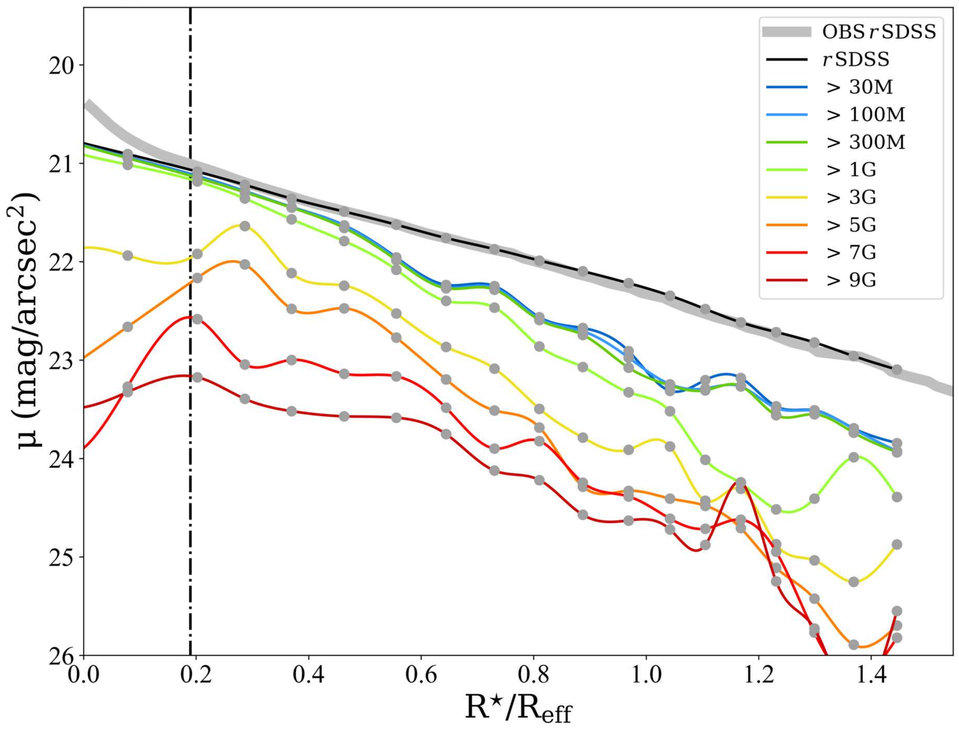

Stellar Continuum

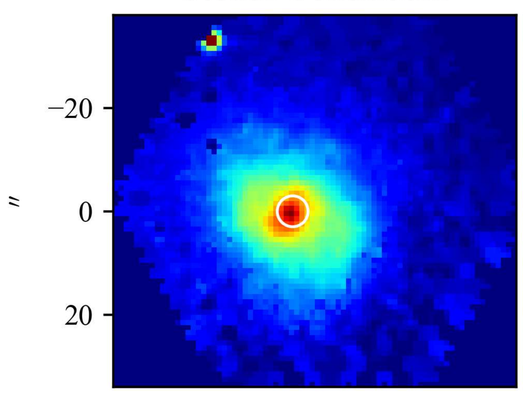

$\mathcal{M}_{\star,\,\rm P}$

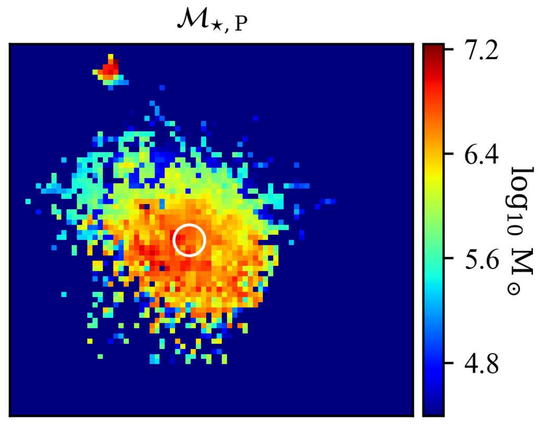

Log. of cumulative present stellar mass profiles

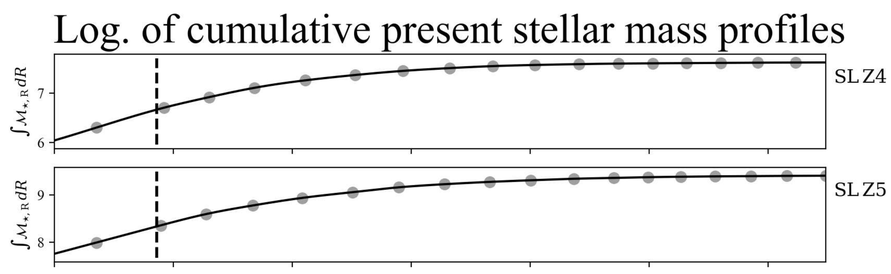

$Z_{\star,\,\mathcal{L}}$

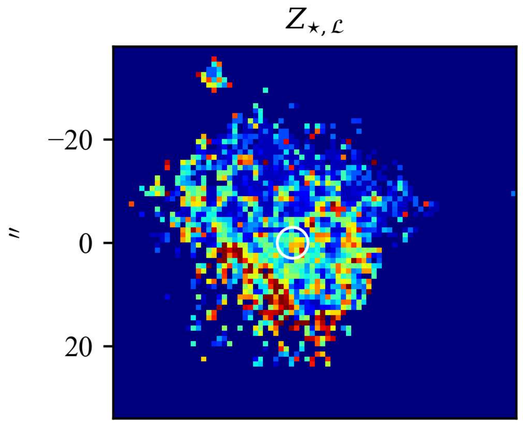

$Z_{\star,\,\mathcal{M}}$

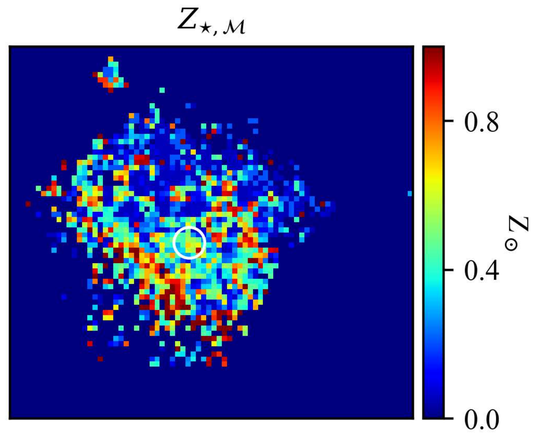

Stellar metallicity/Age & Hα flux/EW profiles

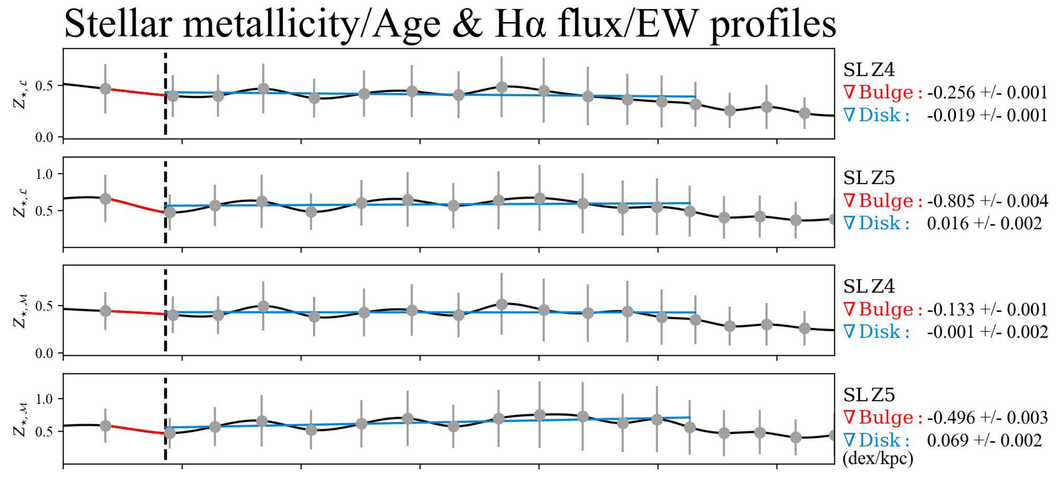

$t_{\star,\,\mathcal{L}}$

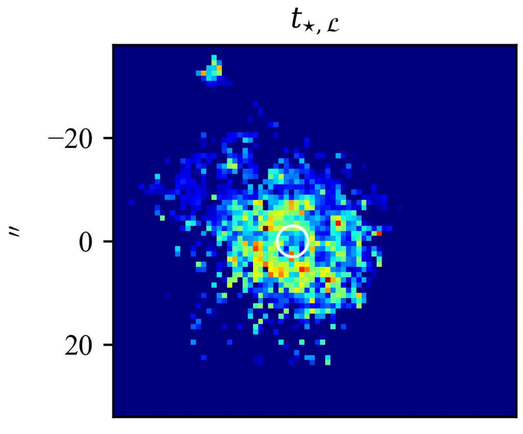

$t_{\star,\,\mathcal{M}}$

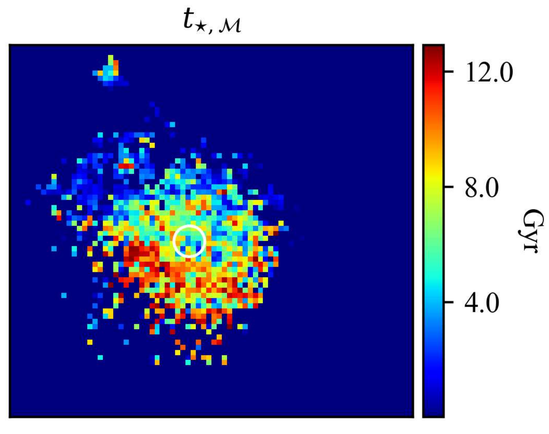

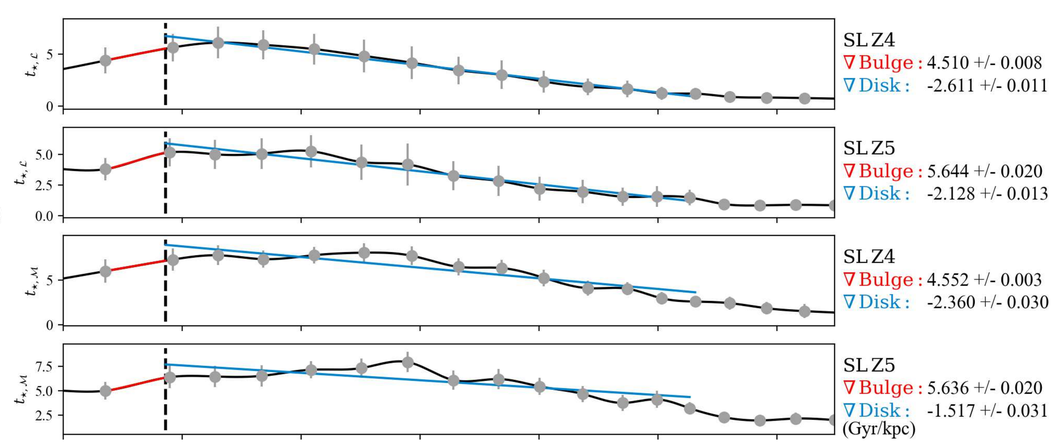

Hα flux

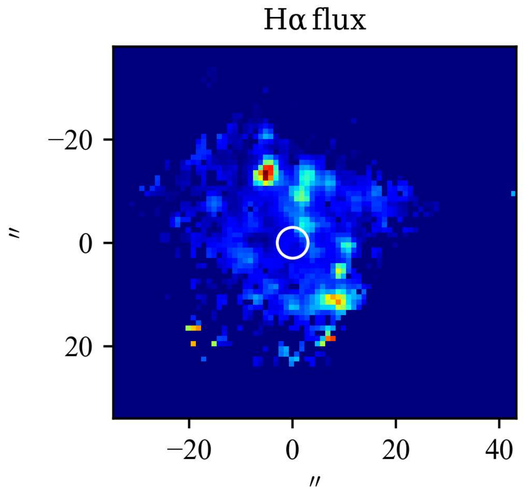

EW(Hα)

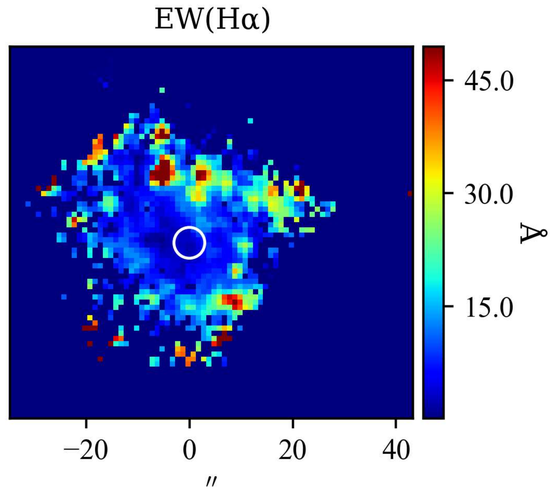

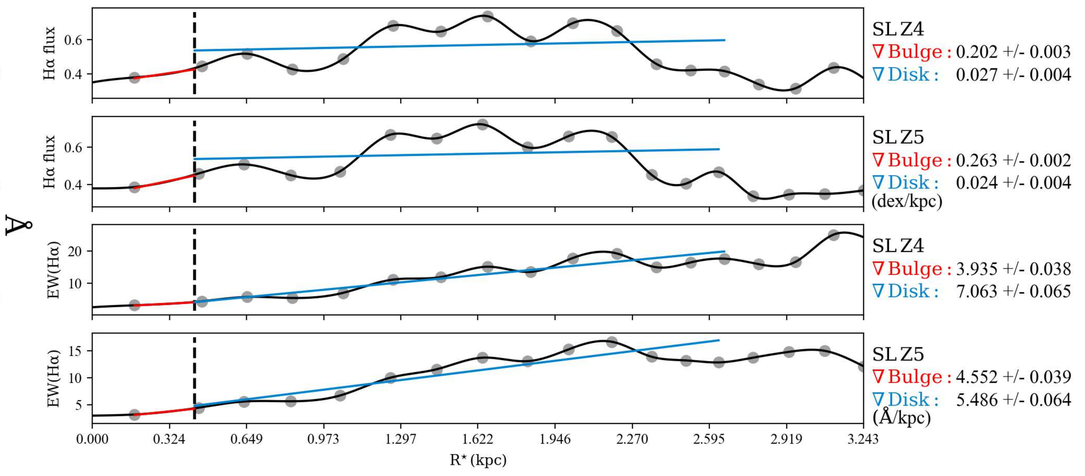

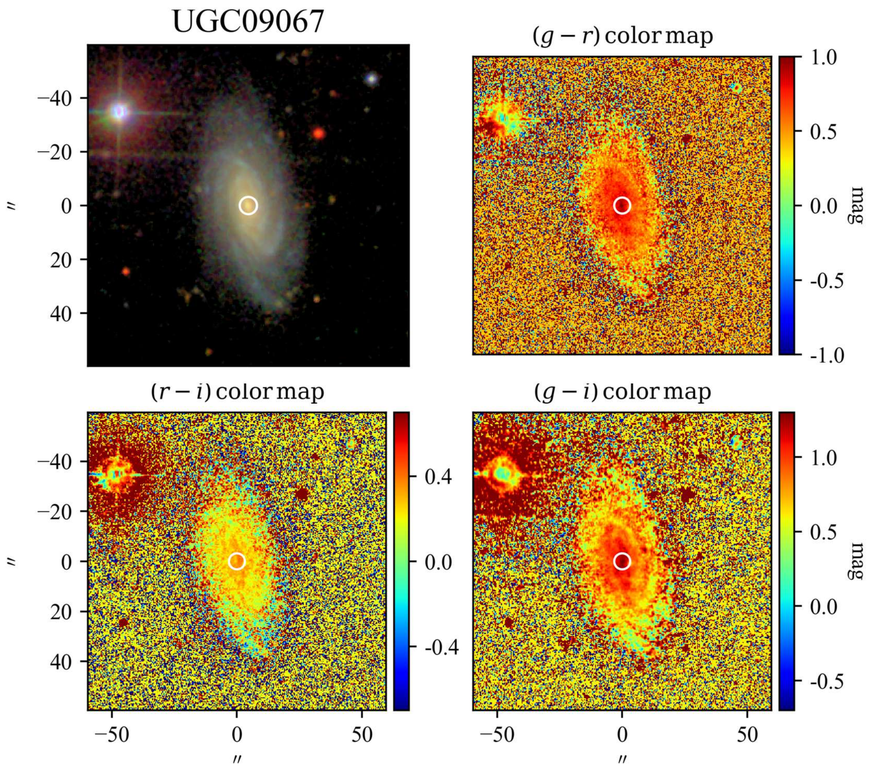

SBP decomposition of SDSS r band

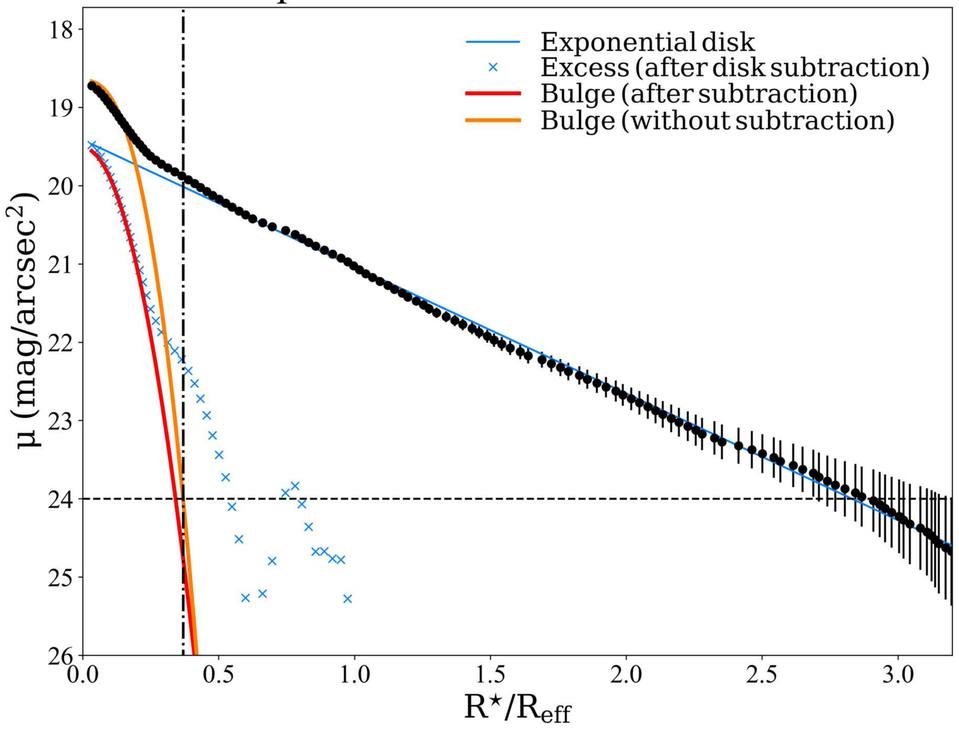

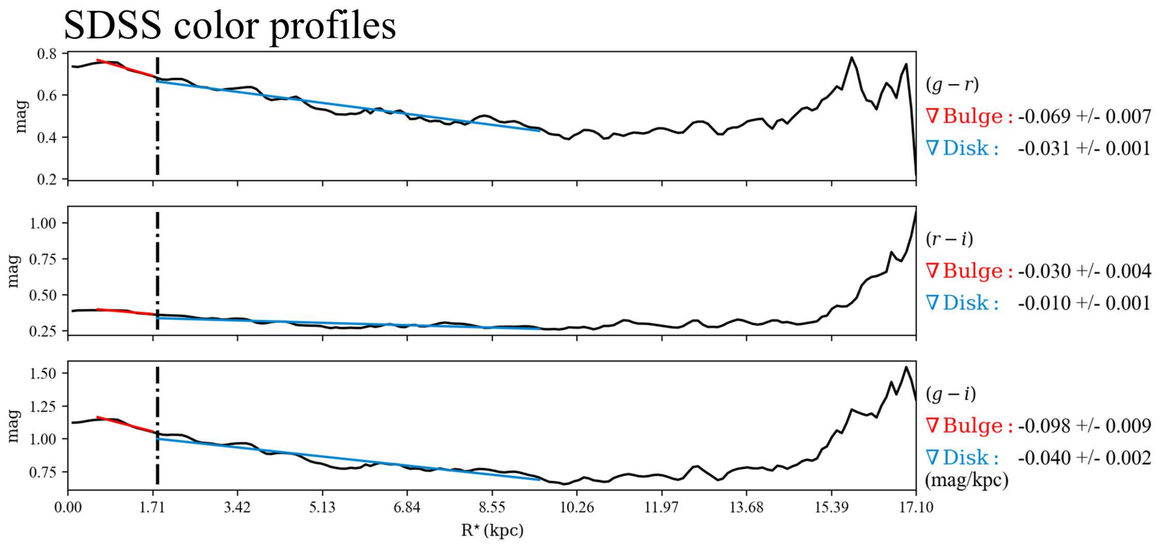

$\mathcal{RV}$ SBPs

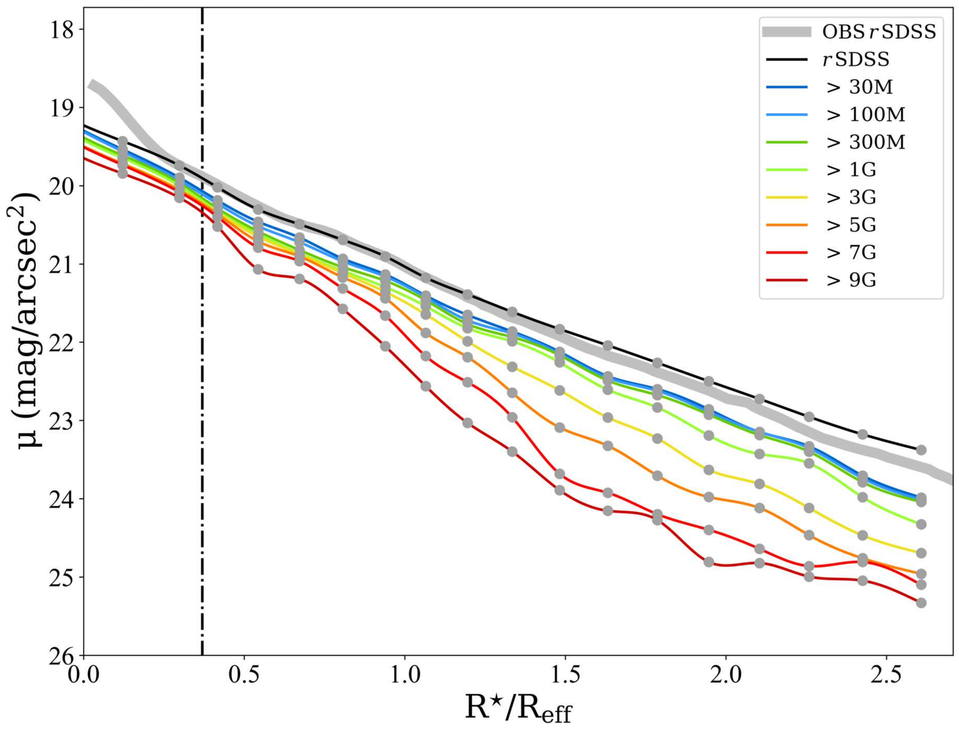

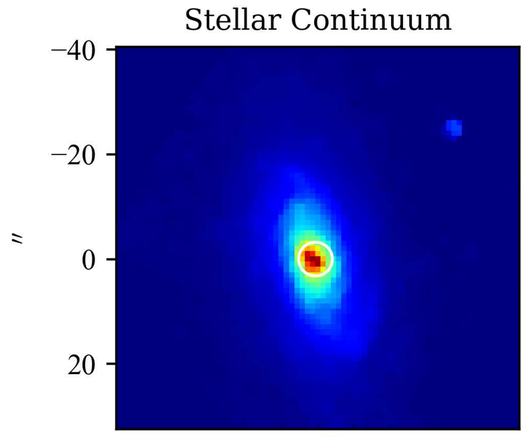

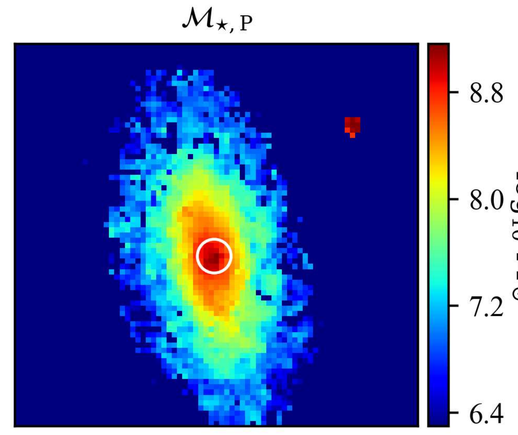

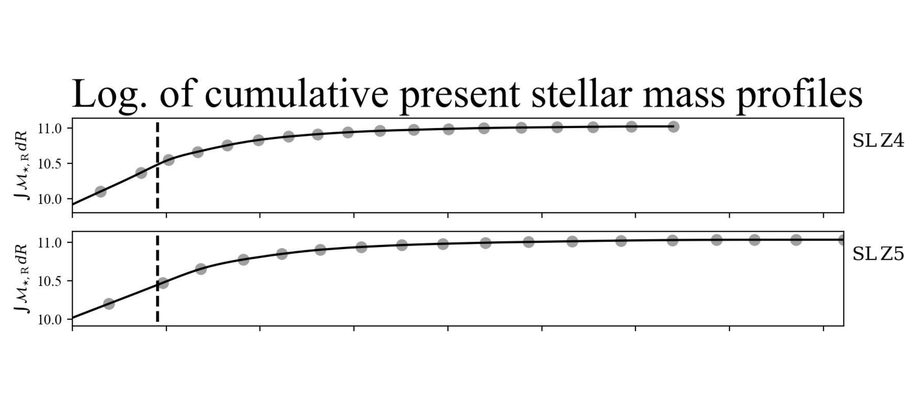

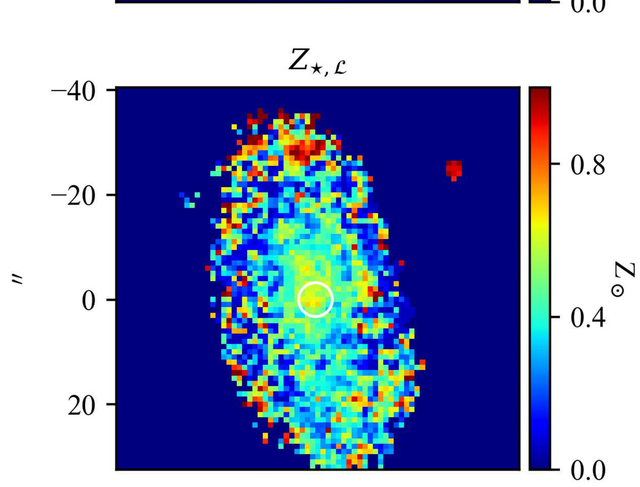

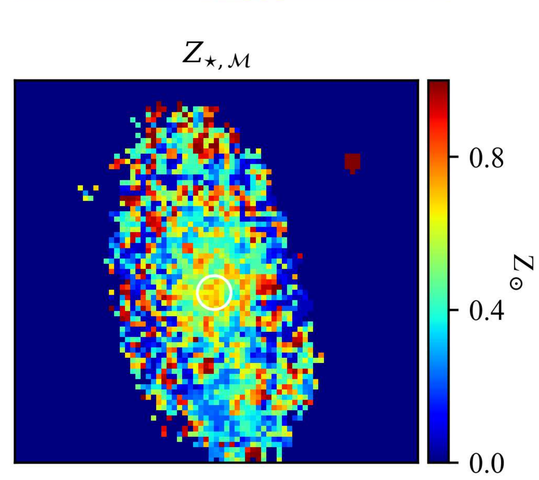

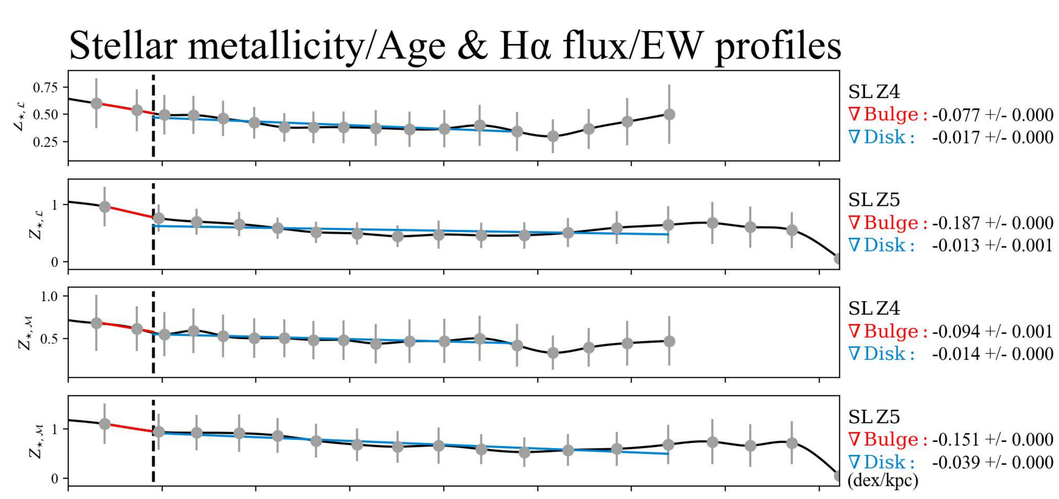

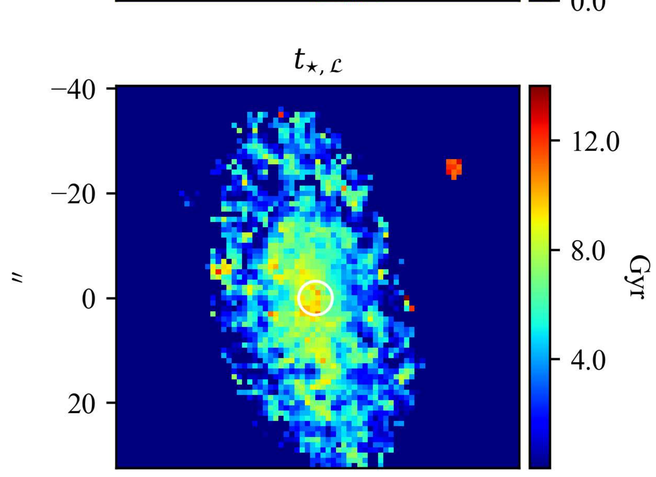

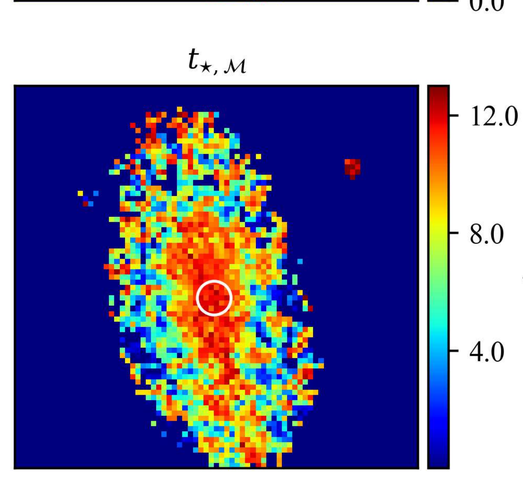

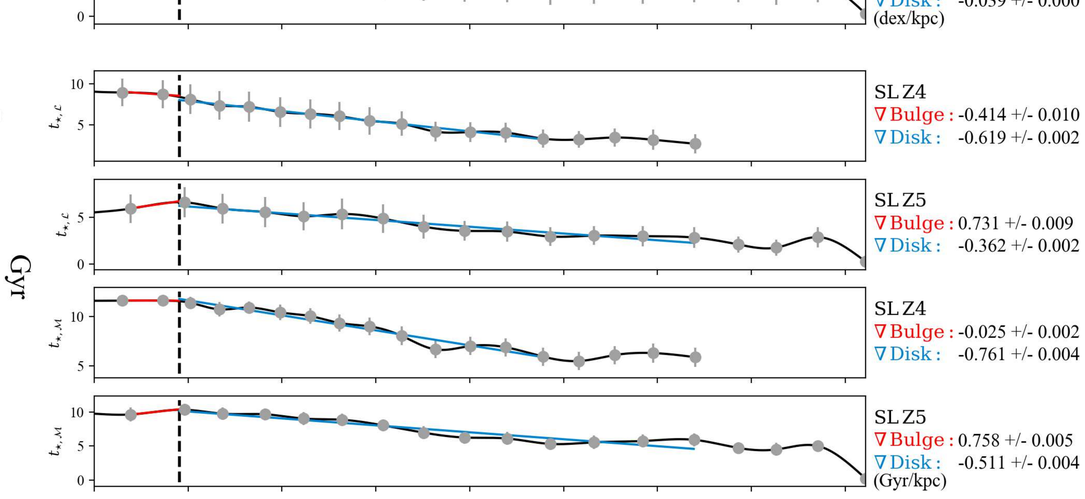

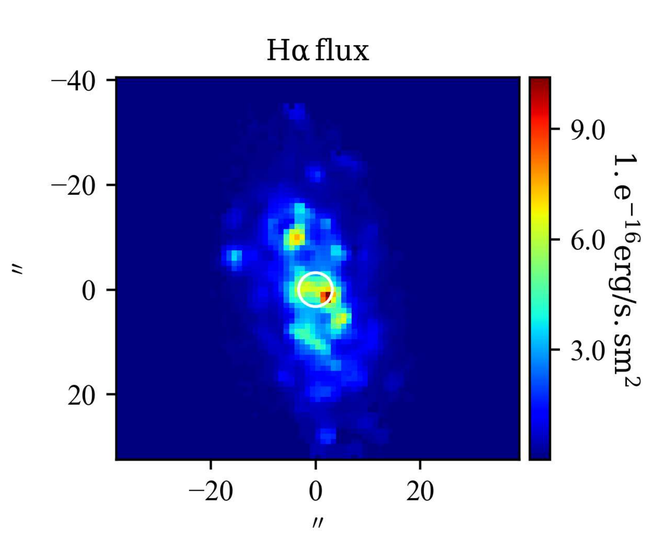

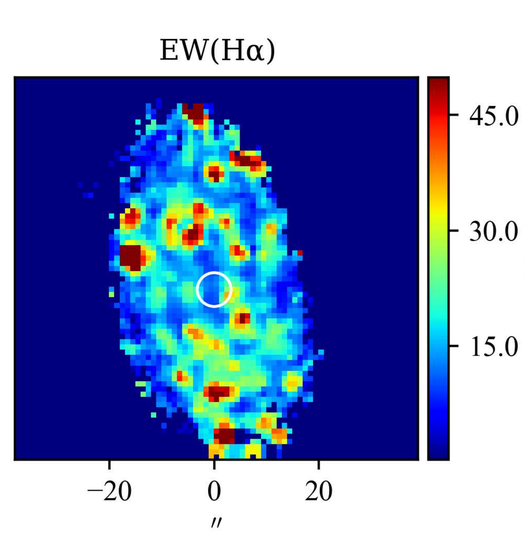

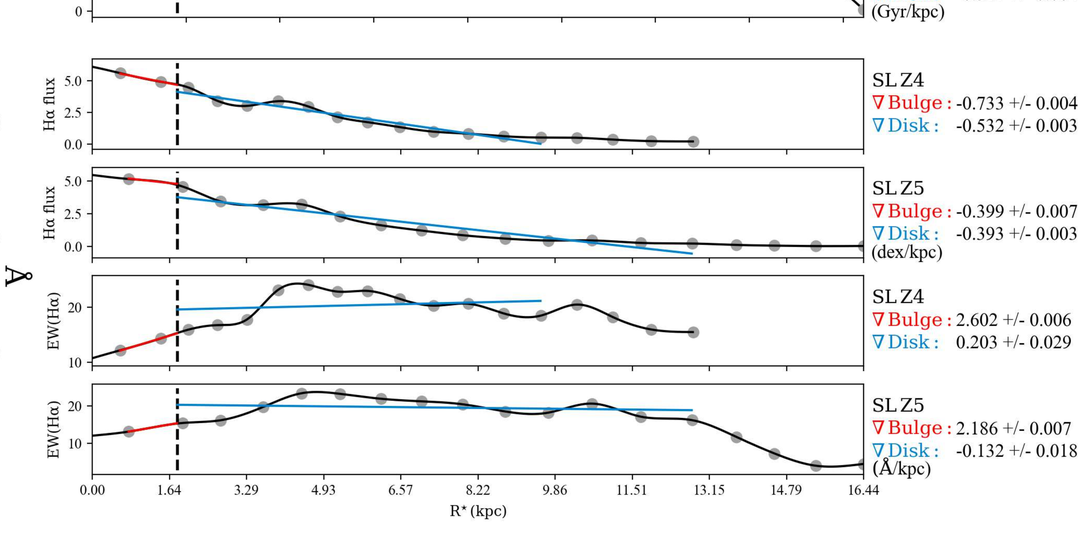

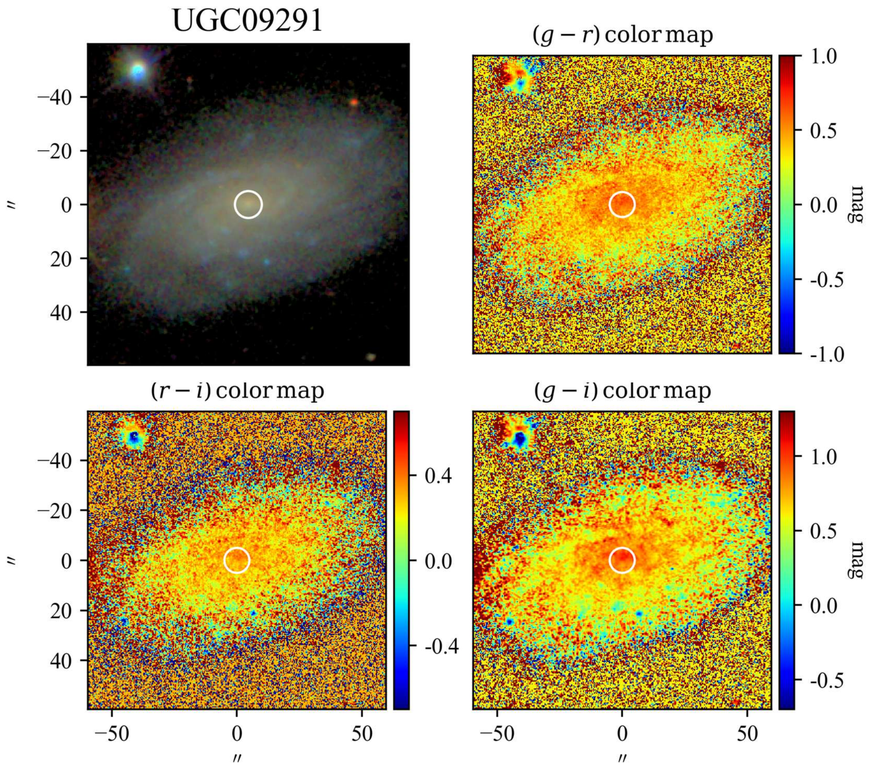
UGC09291
$(g-r)$ color map
$(r-i)$ color map
$(g-i)$ color map
mag
″

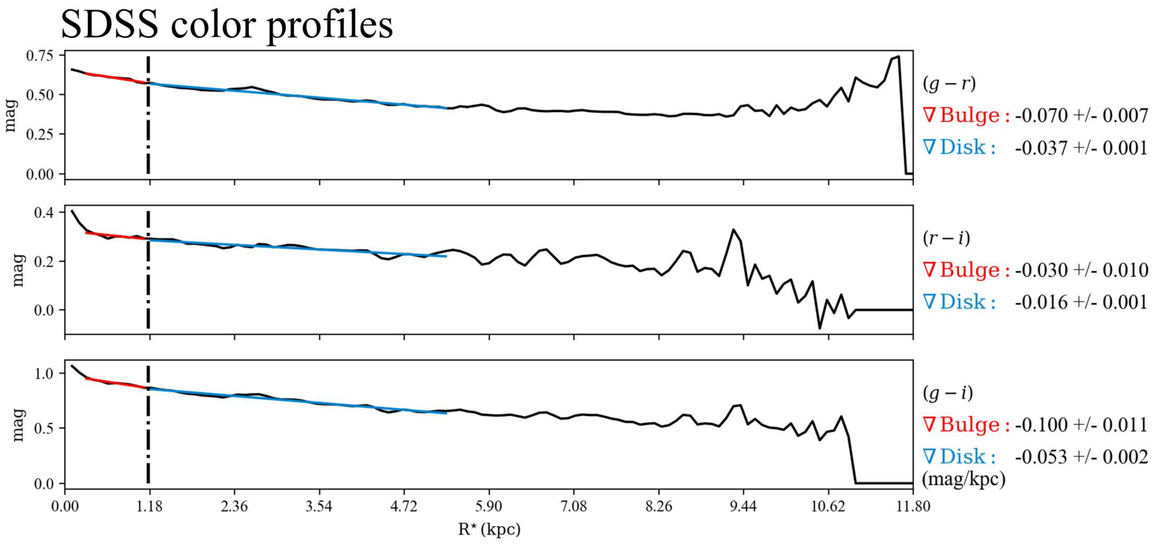
SDSS color profiles
$(g-r)$
∇ Bulge : -0.070 +/- 0.007
∇ Disk : -0.037 +/- 0.001
$(r-i)$
∇ Bulge : -0.030 +/- 0.010
∇ Disk : -0.016 +/- 0.001
$(g-i)$
∇ Bulge : -0.100 +/- 0.011
∇ Disk : -0.053 +/- 0.002
(mag/kpc)
mag
R* (kpc)

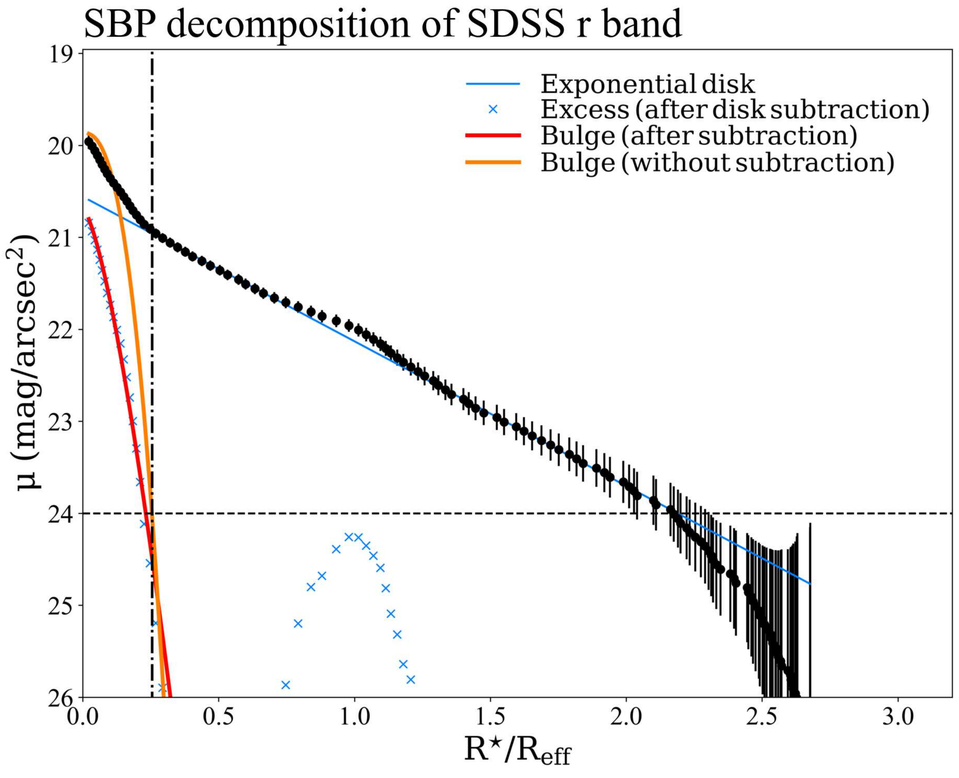
SBP decomposition of SDSS r band
Exponential disk
Excess (after disk subtraction)
Bulge (after subtraction)
Bulge (without subtraction)
μ (mag/arcsec²)
R*/Reff

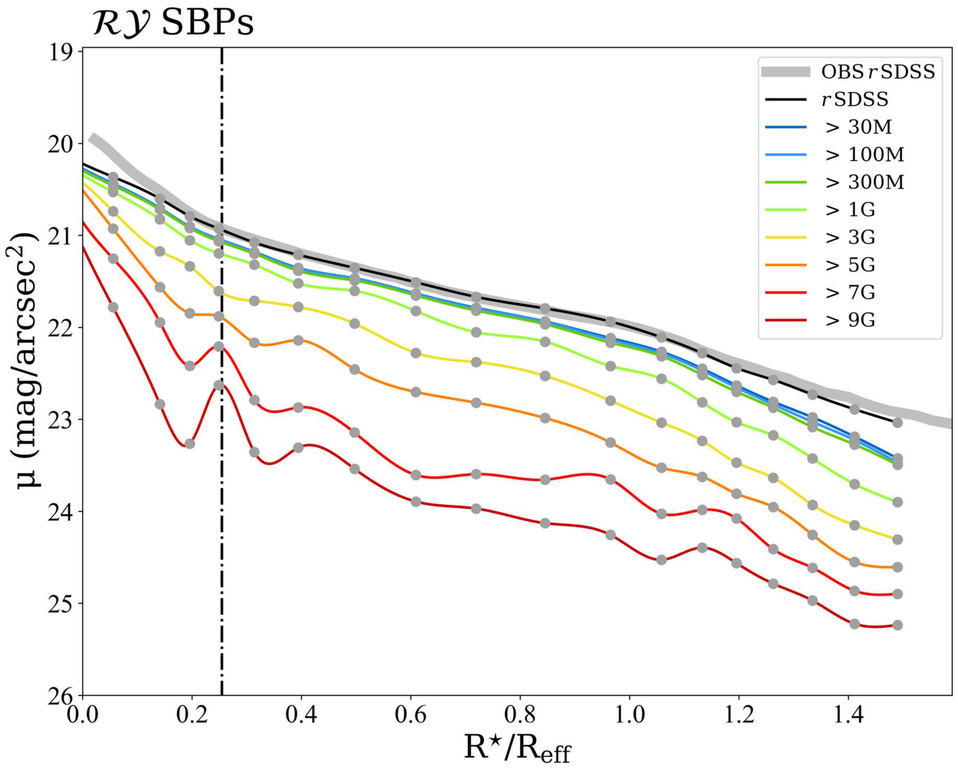
$\mathcal{RY}$ SBPs
OBS rSDSS
rSDSS
> 30M
> 100M
> 300M
> 1G
> 3G
> 5G
> 7G
> 9G
μ (mag/arcsec²)
R*/Reff

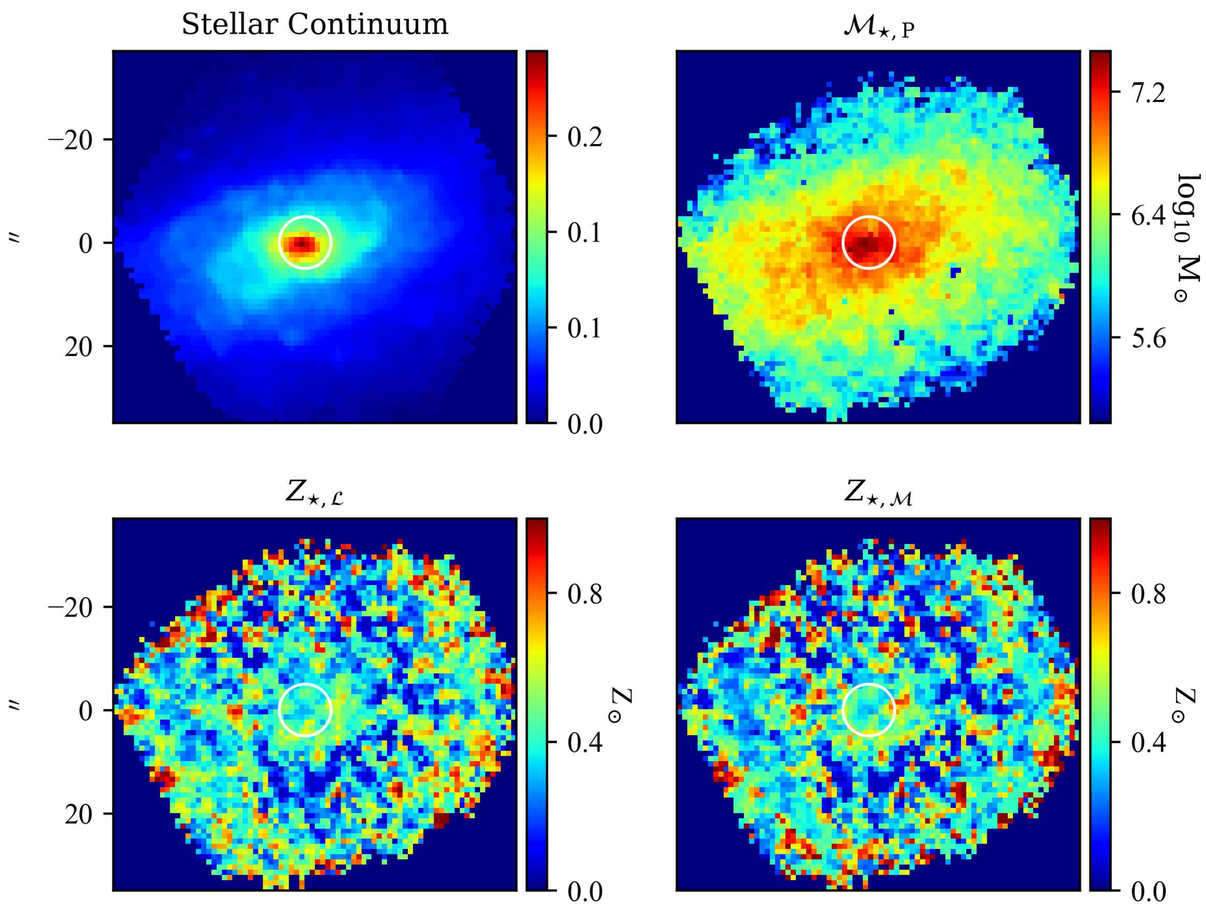
Stellar Continuum
$\mathcal{M}_{\star,\mathrm{P}}$
$Z_{\star,\mathcal{L}}$
$Z_{\star,\mathcal{M}}$
log10 M⊙
Z⊙
″

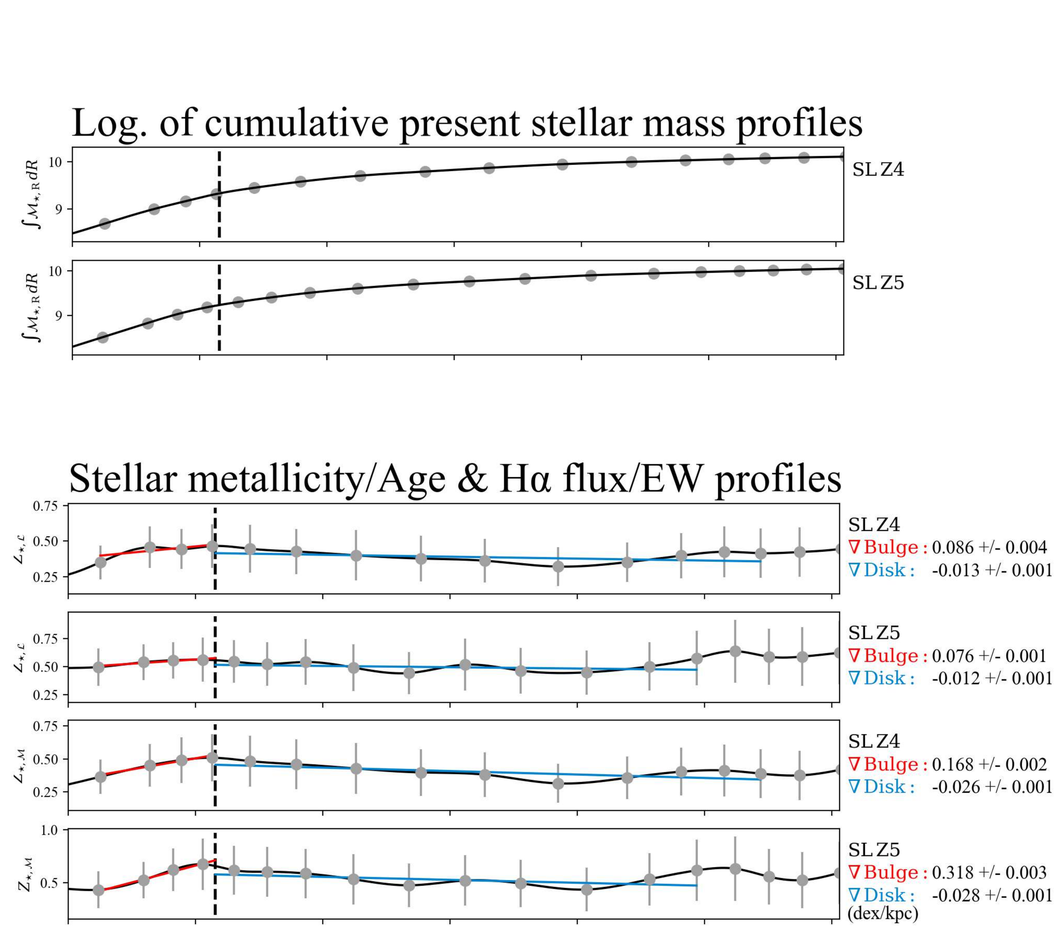
Log. of cumulative present stellar mass profiles
SL Z4
SL Z5
Stellar metallicity/Age & Hα flux/EW profiles
SL Z4
∇ Bulge : 0.086 +/- 0.004
∇ Disk : -0.013 +/- 0.001
SL Z5
∇ Bulge : 0.076 +/- 0.001
∇ Disk : -0.012 +/- 0.001
SL Z4
∇ Bulge : 0.168 +/- 0.002
∇ Disk : -0.026 +/- 0.001
SL Z5
∇ Bulge : 0.318 +/- 0.003
∇ Disk : -0.028 +/- 0.001
(dex/kpc)

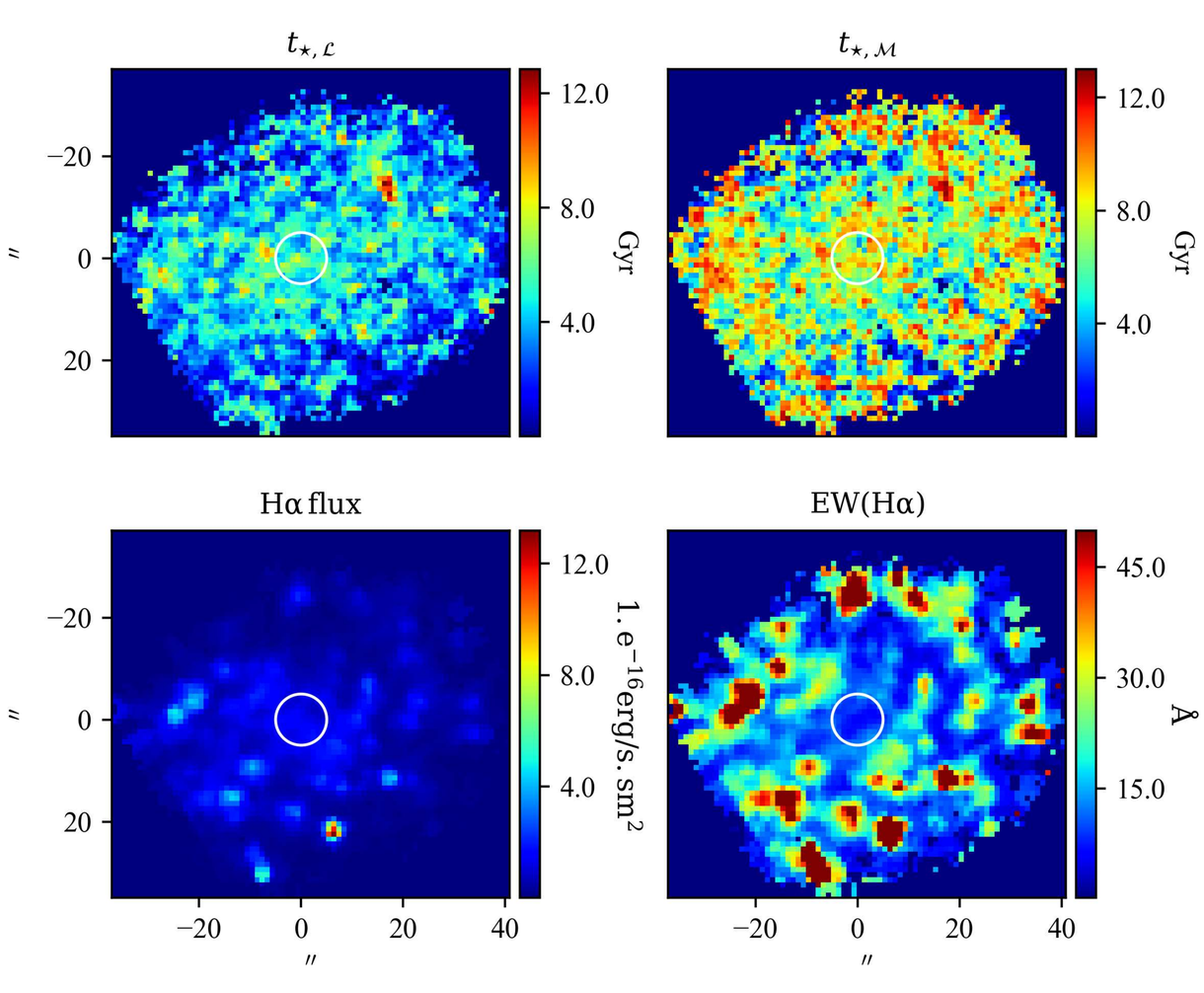
$t_{\star,\mathcal{L}}$
$t_{\star,\mathcal{M}}$
Gyr
″

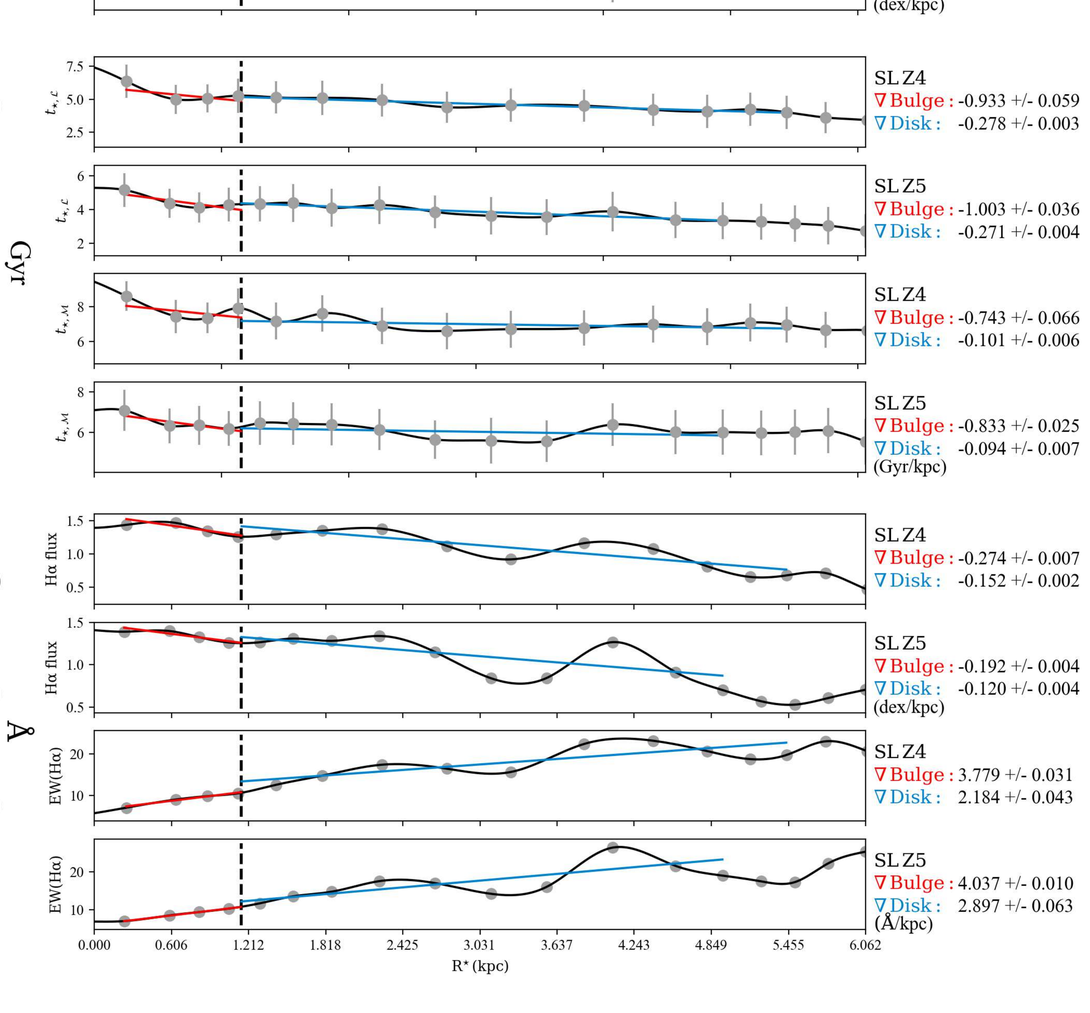
SL Z4
∇ Bulge : -0.933 +/- 0.059
∇ Disk : -0.278 +/- 0.003
SL Z5
∇ Bulge : -1.003 +/- 0.036
∇ Disk : -0.271 +/- 0.004
SL Z4
∇ Bulge : -0.743 +/- 0.066
∇ Disk : -0.101 +/- 0.006
SL Z5
∇ Bulge : -0.833 +/- 0.025
∇ Disk : -0.094 +/- 0.007
(Gyr/kpc)

Hα flux
EW(Hα)
1. e⁻¹⁶erg/s. sm²
Å
″

SL Z4
∇ Bulge : -0.274 +/- 0.007
∇ Disk : -0.152 +/- 0.002
SL Z5
∇ Bulge : -0.192 +/- 0.004
∇ Disk : -0.120 +/- 0.004
(dex/kpc)
SL Z4
∇ Bulge : 3.779 +/- 0.031
∇ Disk : 2.184 +/- 0.043
SL Z5
∇ Bulge : 4.037 +/- 0.010
∇ Disk : 2.897 +/- 0.063
(Å/kpc)
R* (kpc)

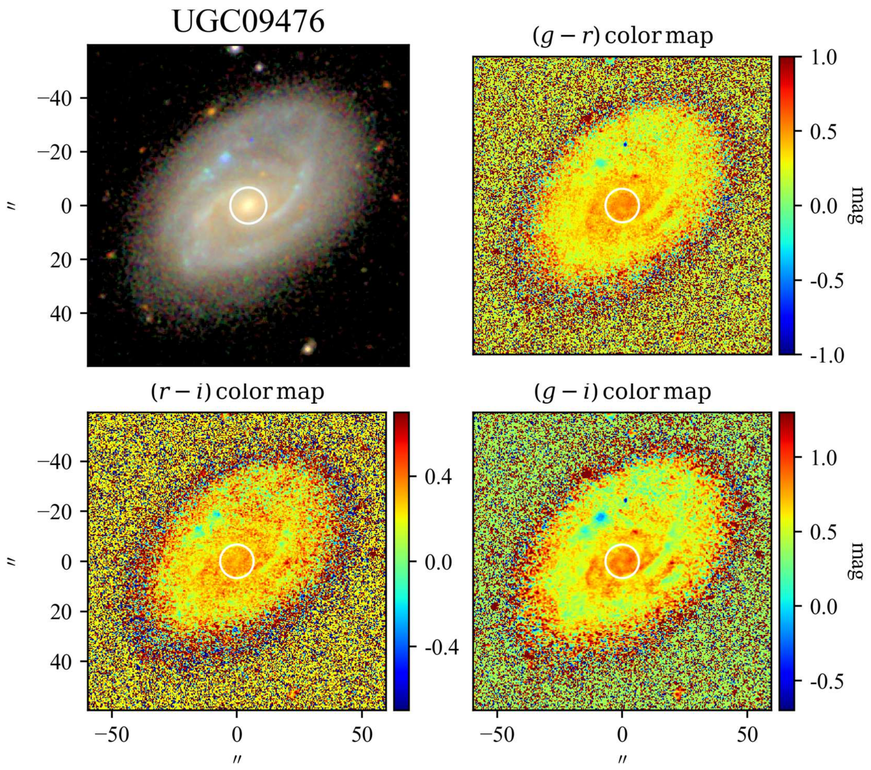

SBP decomposition of SDSS r band

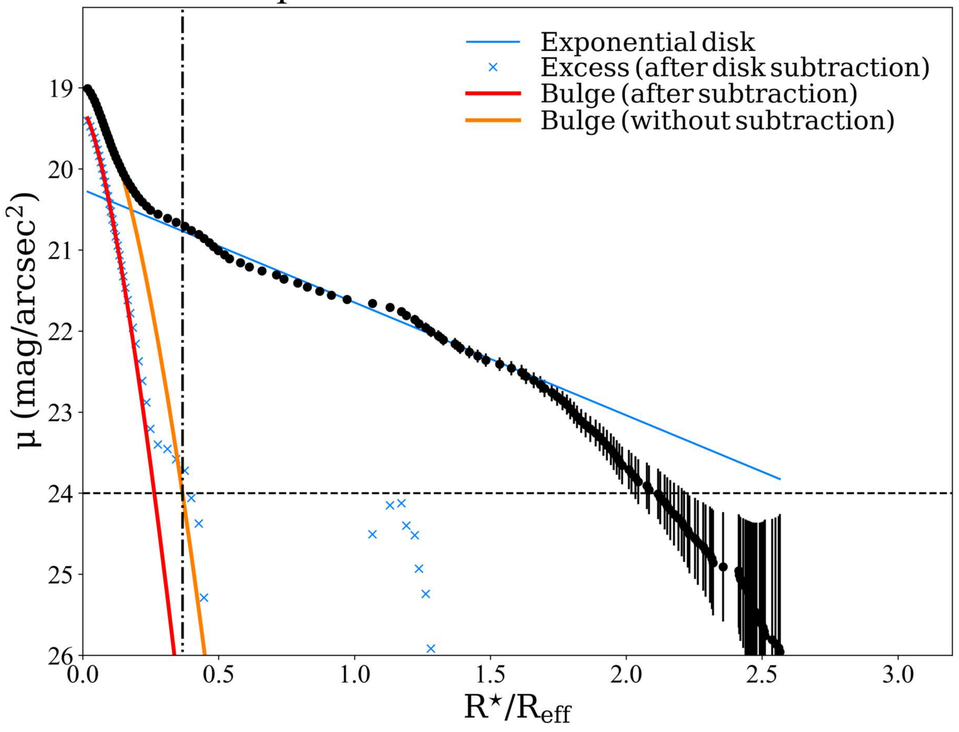

SDSS color profiles

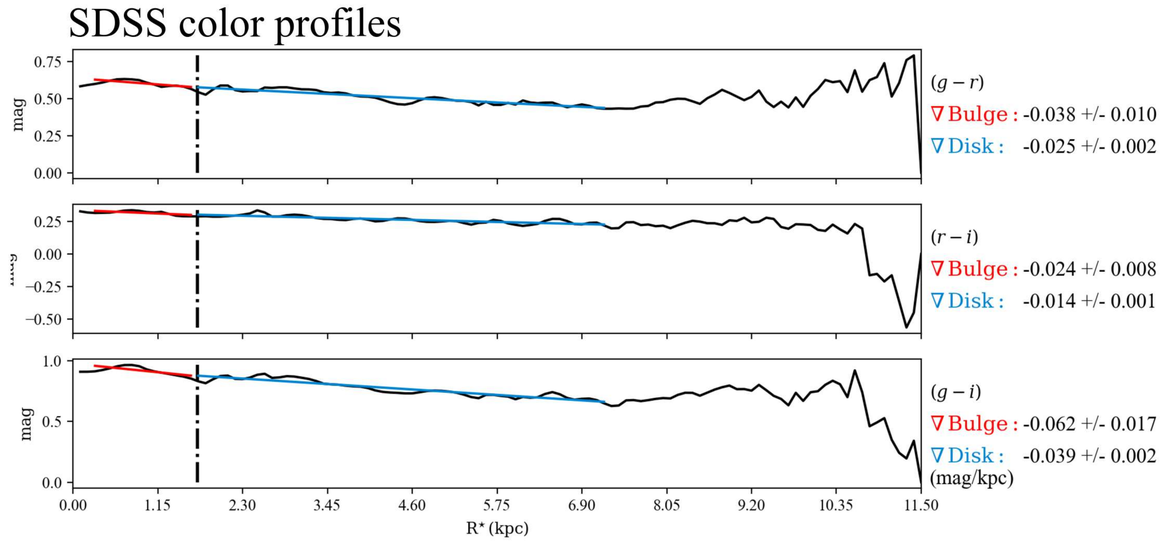

$\mathcal{RY}$ SBPs

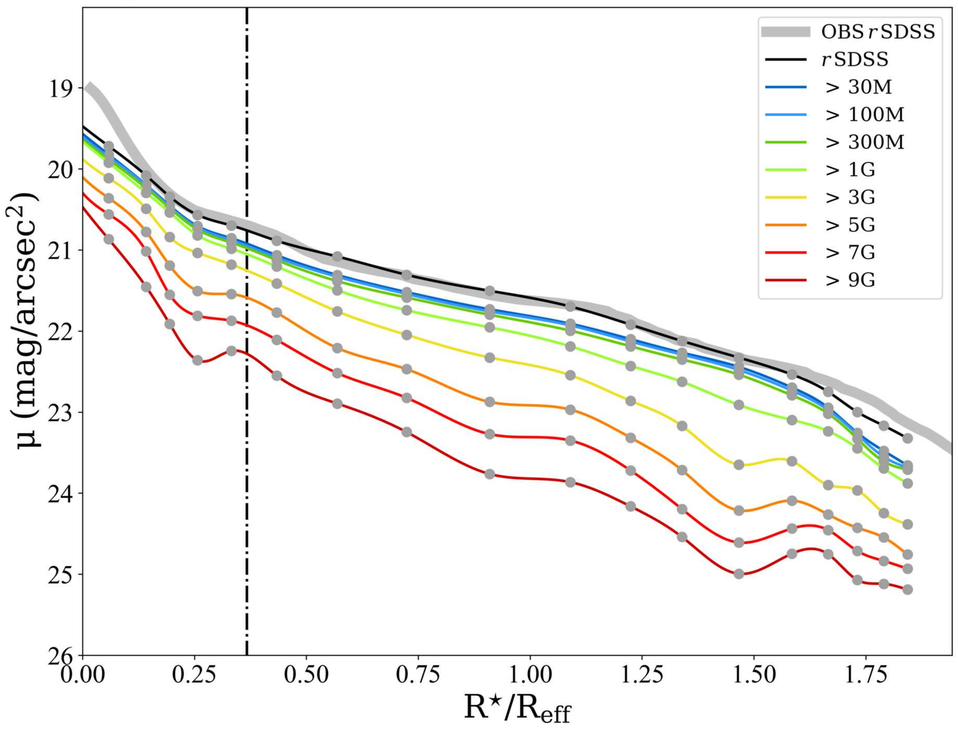

Stellar Continuum

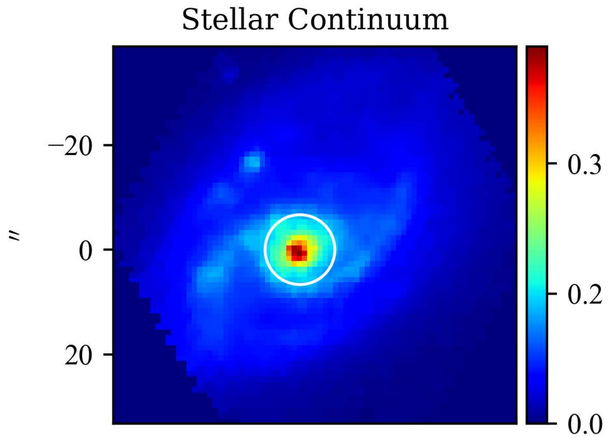

$\mathcal{M}_{\star,\mathrm{P}}$

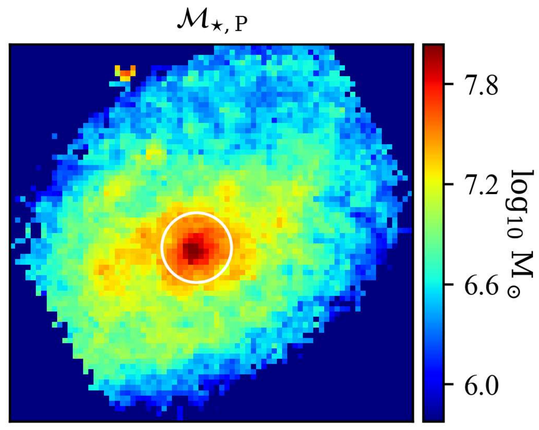

Log. of cumulative present stellar mass profiles

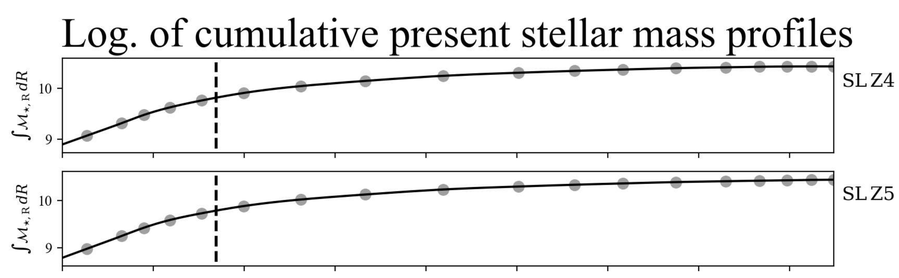

$Z_{\star,\mathcal{L}}$

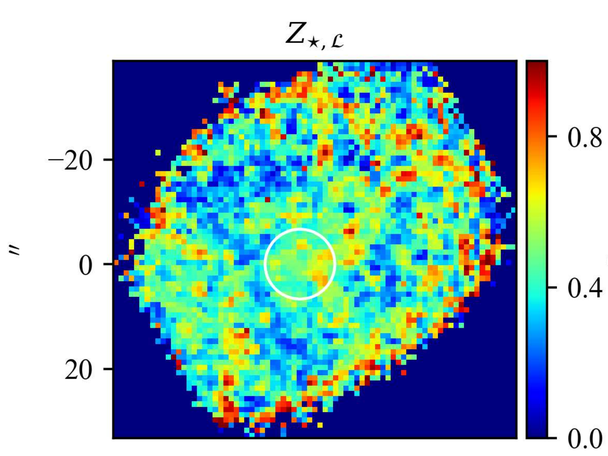

$Z_{\star,\mathcal{M}}$

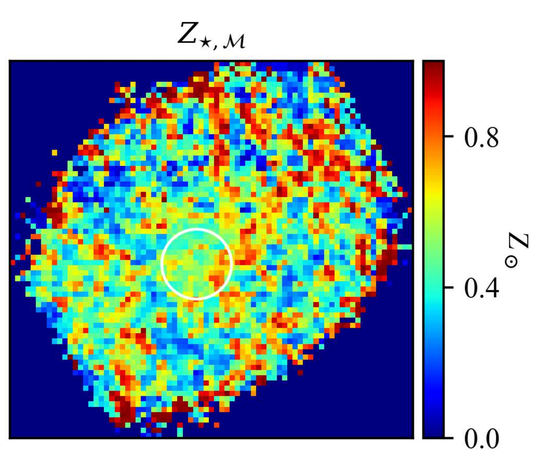

Stellar metallicity/Age & Hα flux/EW profiles

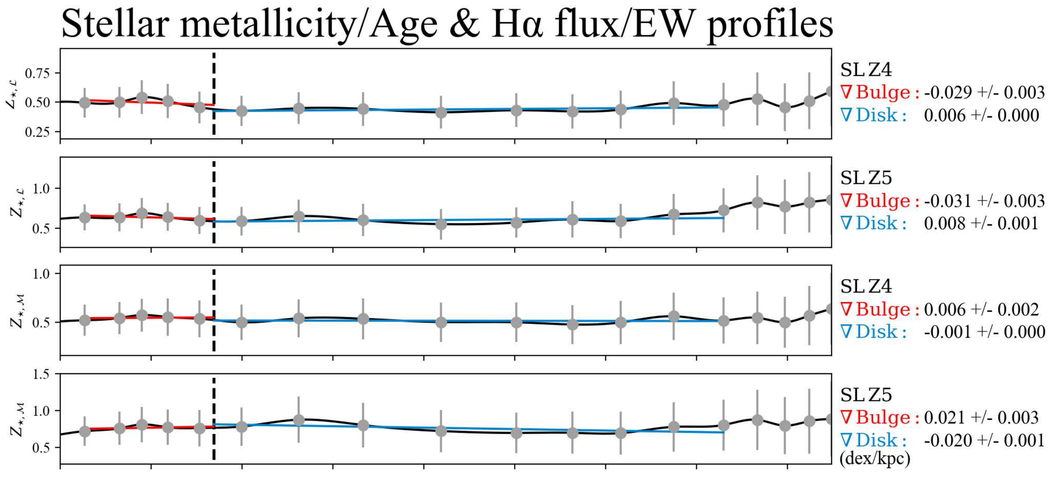

$t_{\star,\mathcal{L}}$

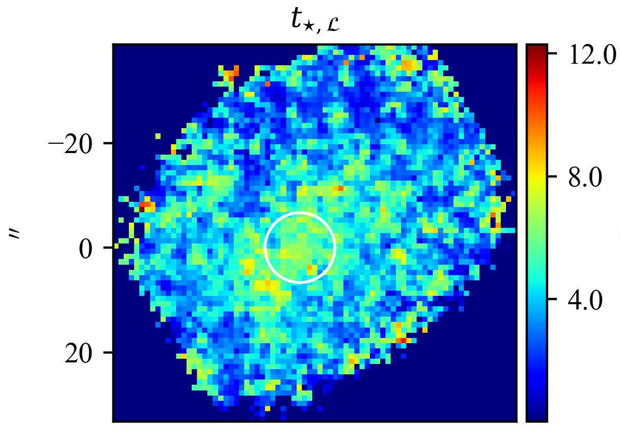

$t_{\star,\mathcal{M}}$

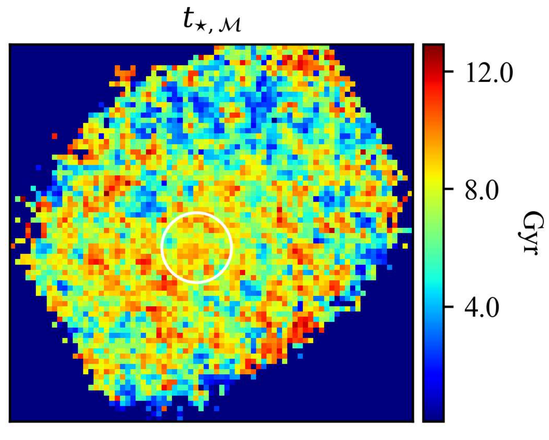

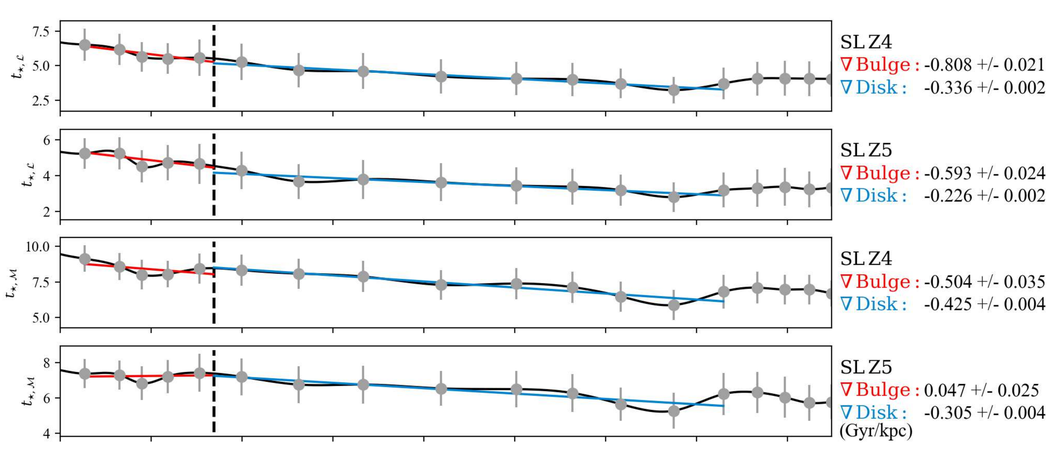

Hα flux

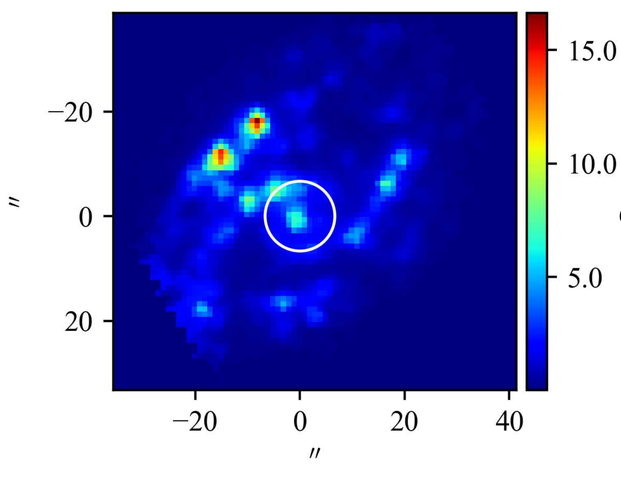

EW(Hα)

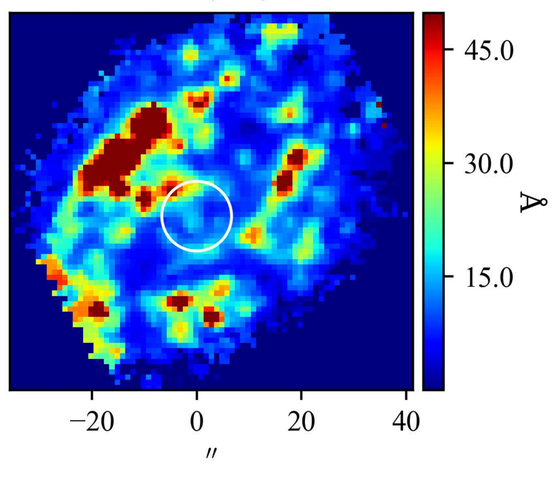

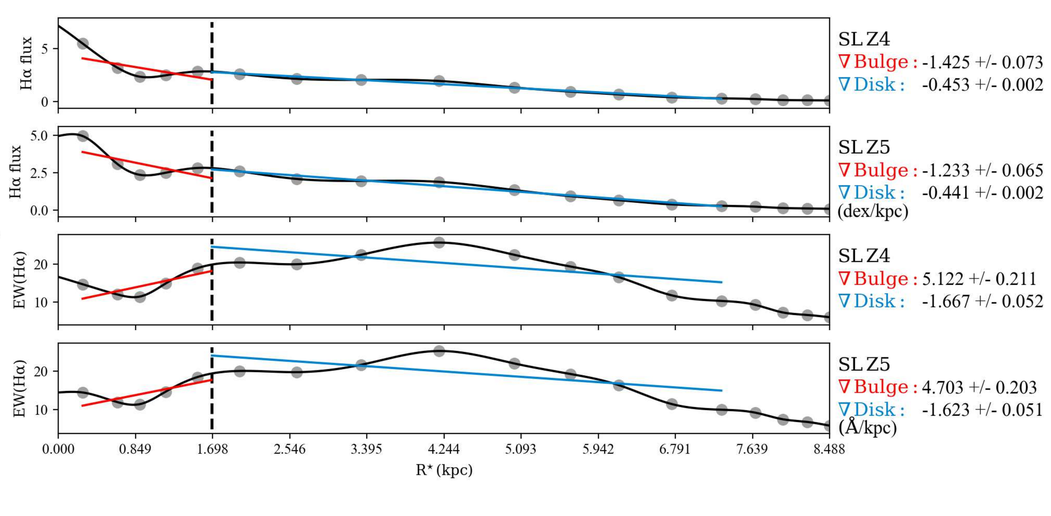

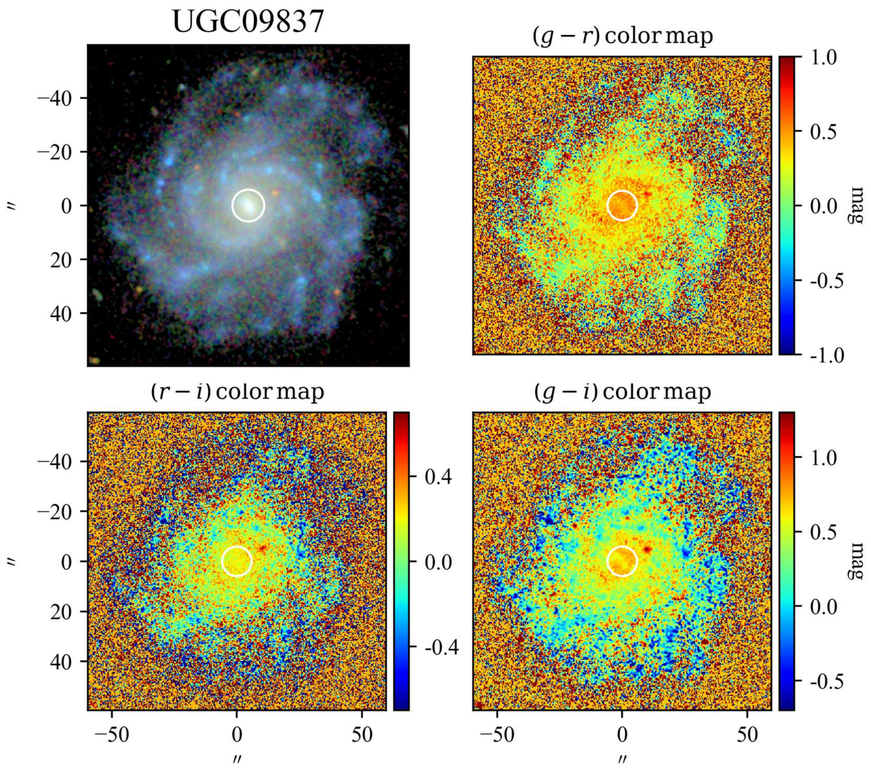

SBP decomposition of SDSS r band

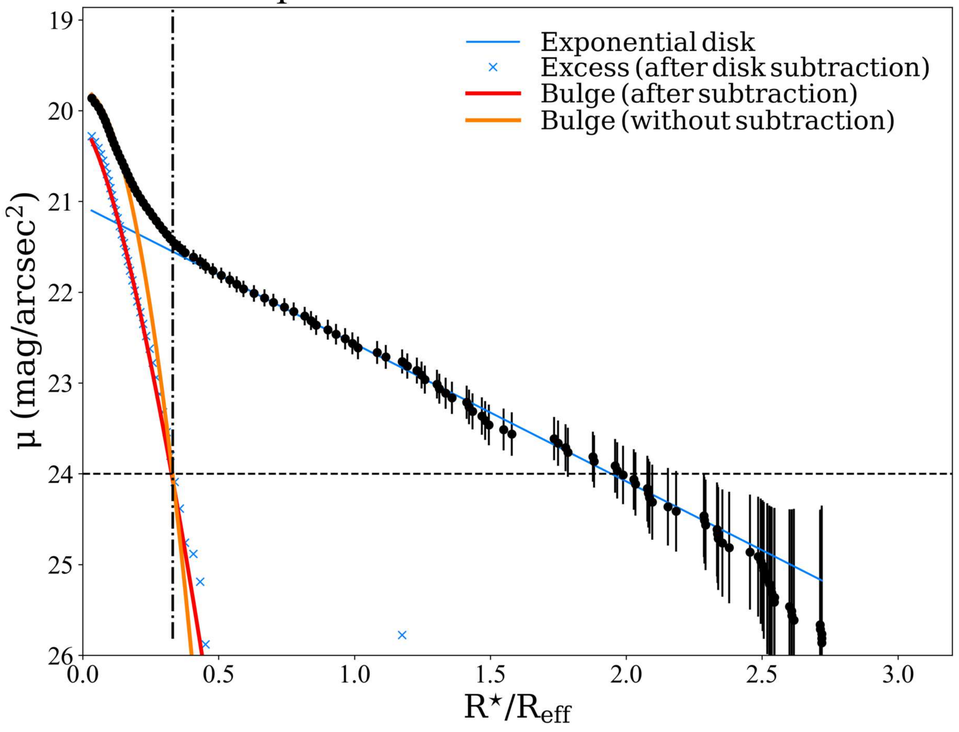

SDSS color profiles

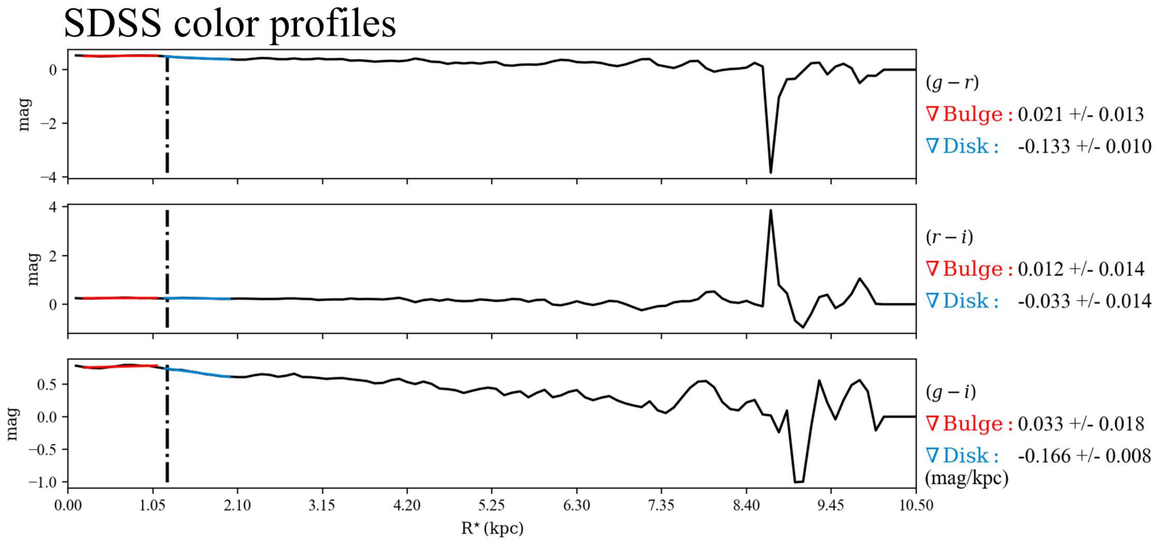

$\mathcal{RY}$ SBPs

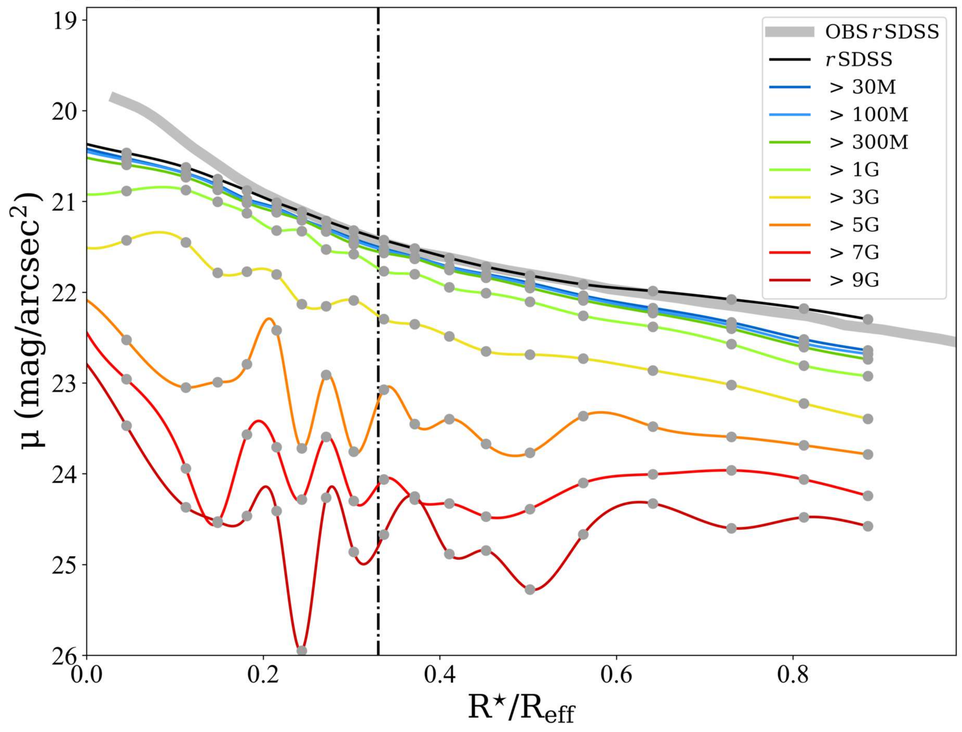

Stellar Continuum

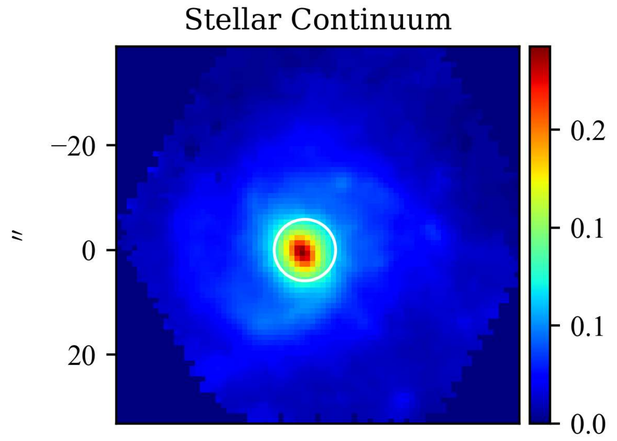

$\mathcal{M}_{\star,\mathrm{P}}$

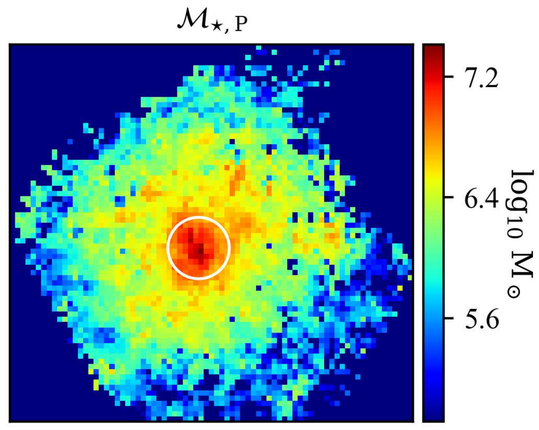

Log. of cumulative present stellar mass profiles

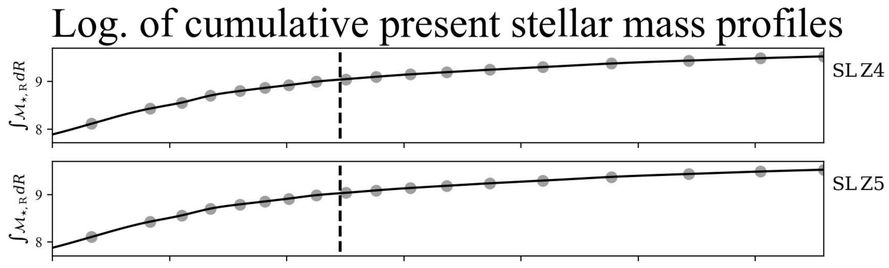

$Z_{\star,\mathcal{L}}$

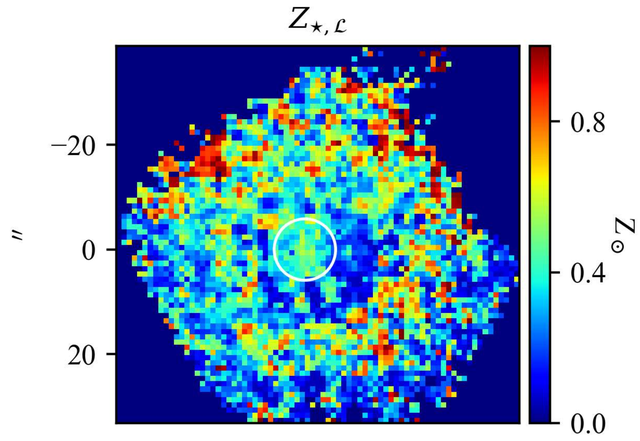

$Z_{\star,\mathcal{M}}$

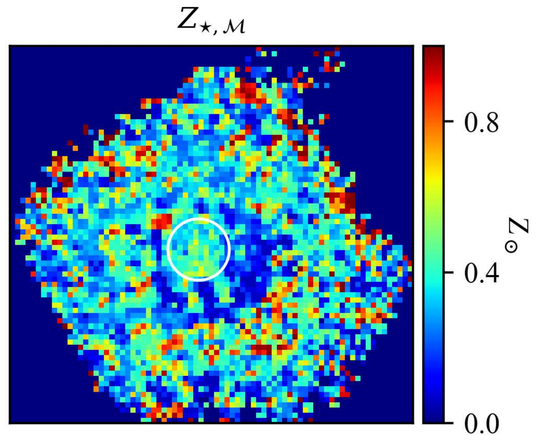

Stellar metallicity/Age & Hα flux/EW profiles

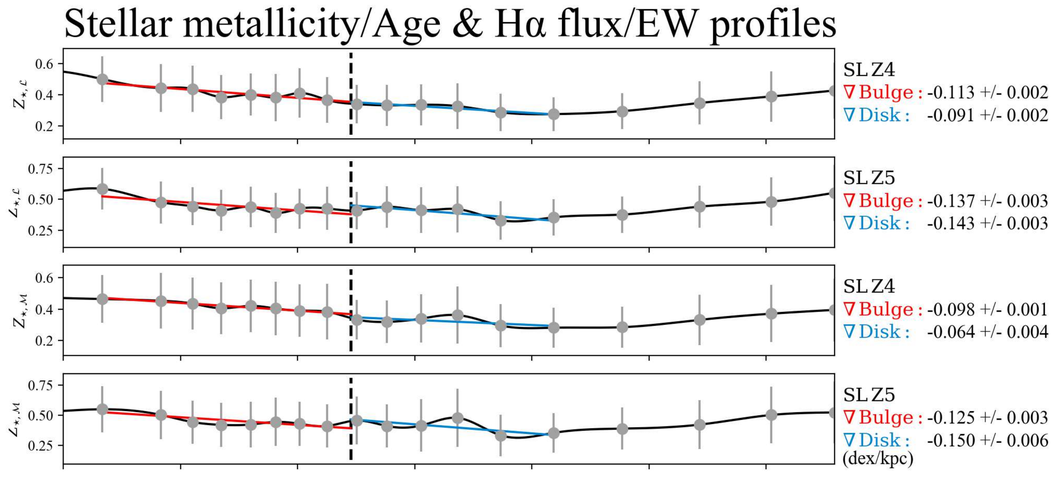

$t_{\star,\mathcal{L}}$

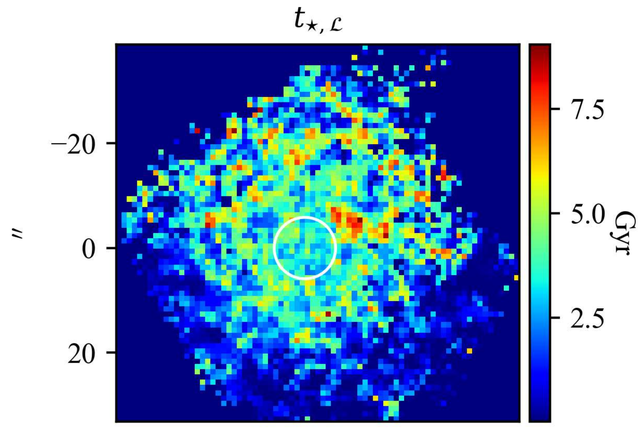

$t_{\star,\mathcal{M}}$

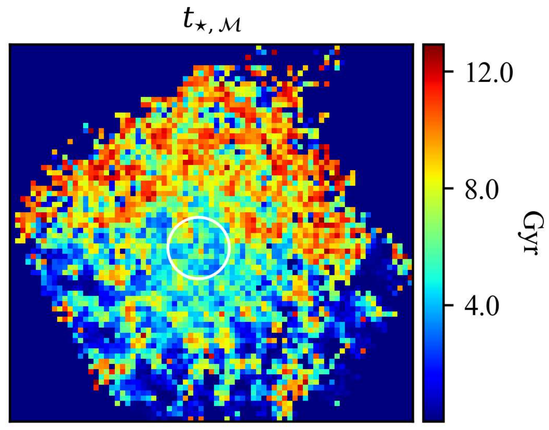

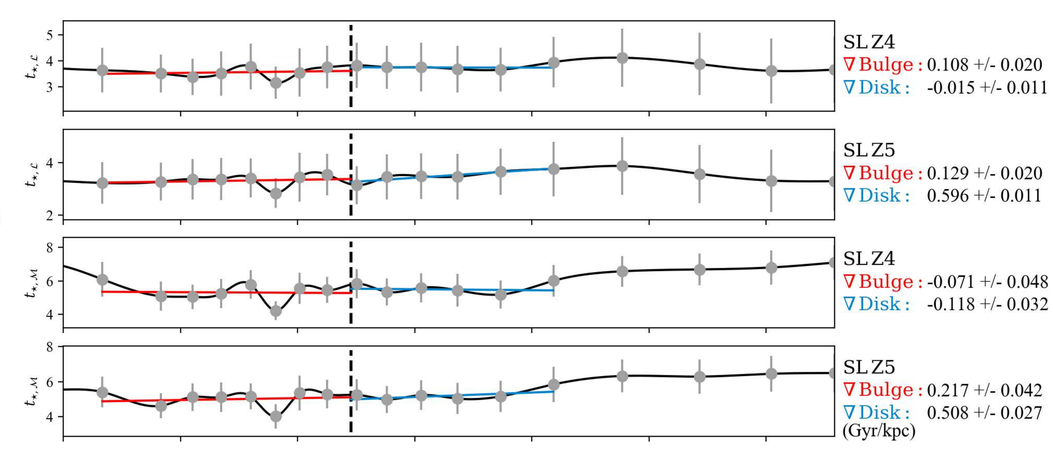

Hα flux

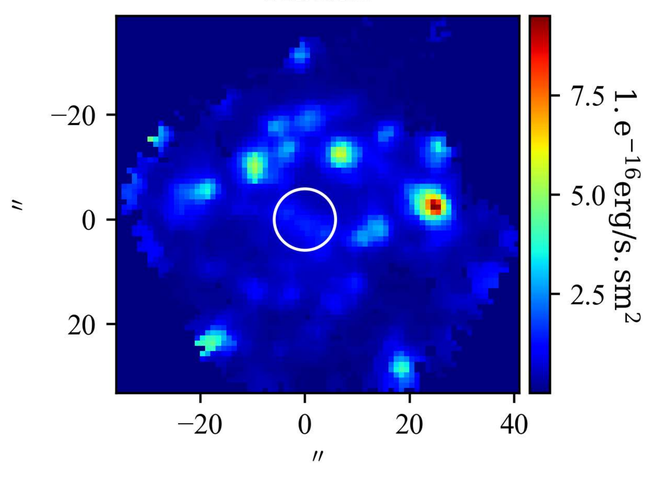

EW(Hα)

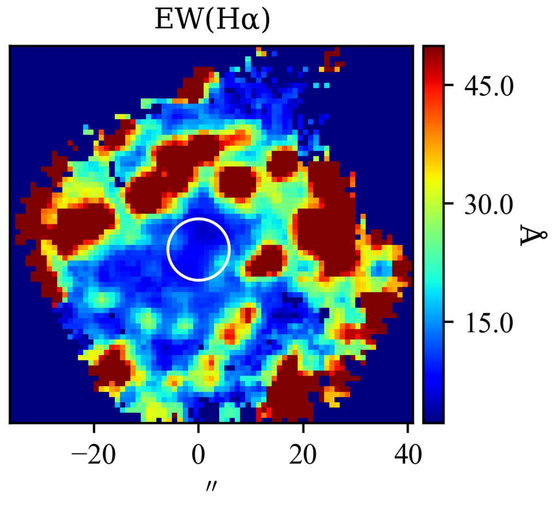

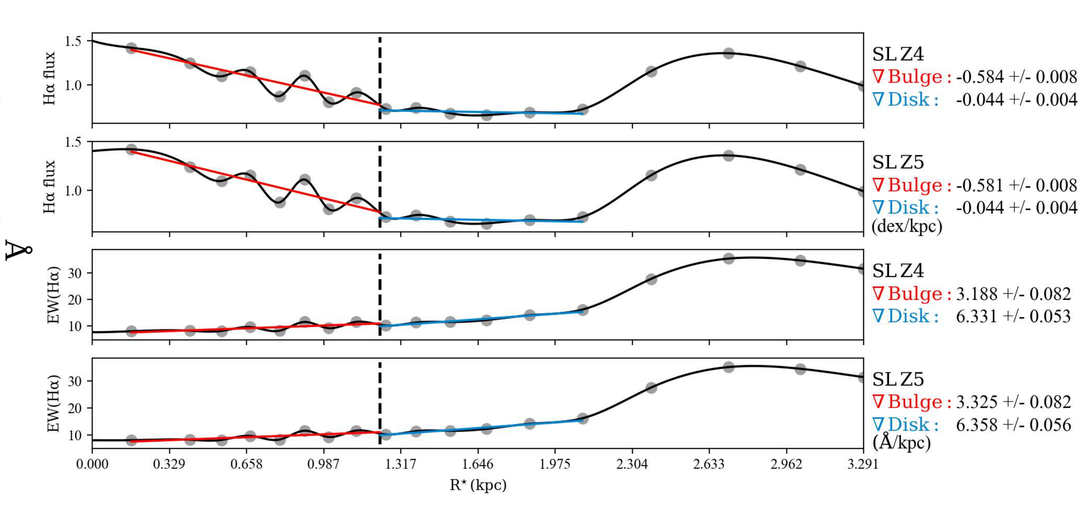

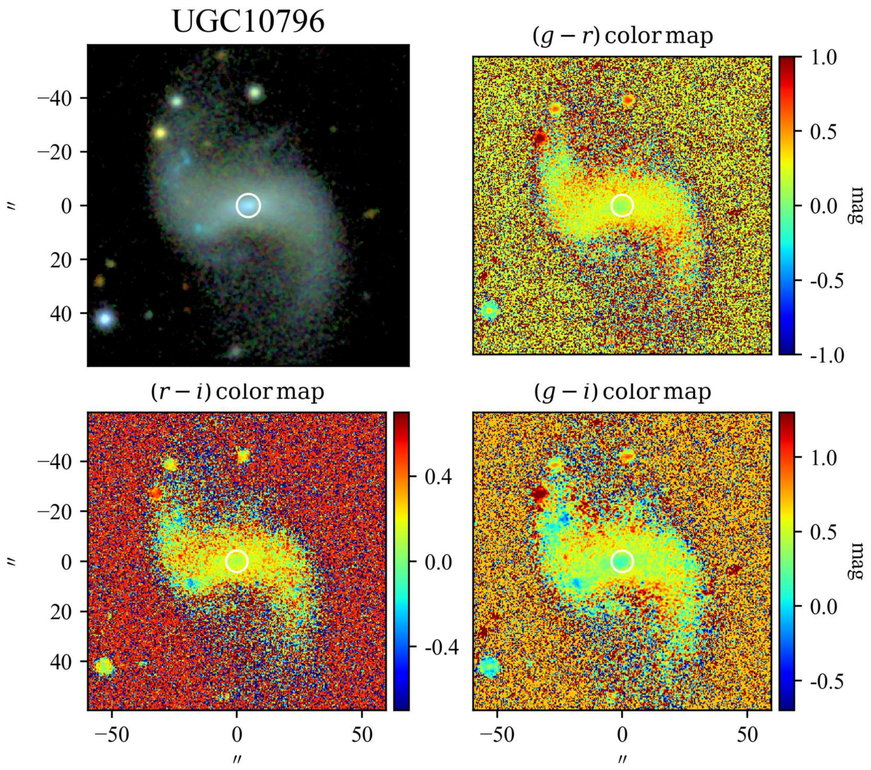

SBP decomposition of SDSS r band

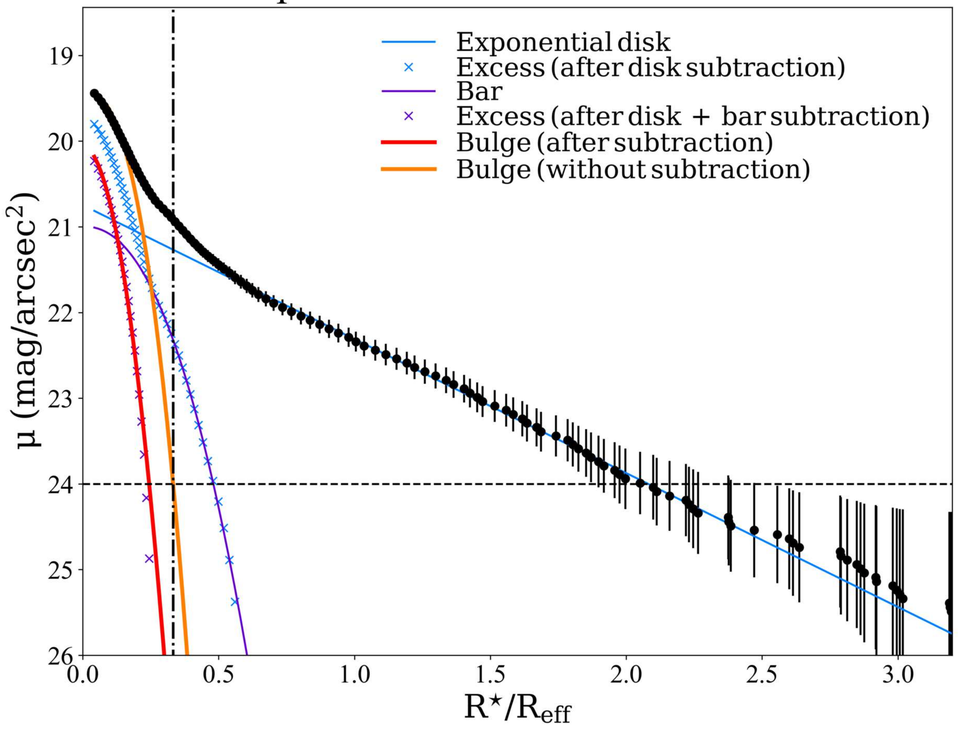

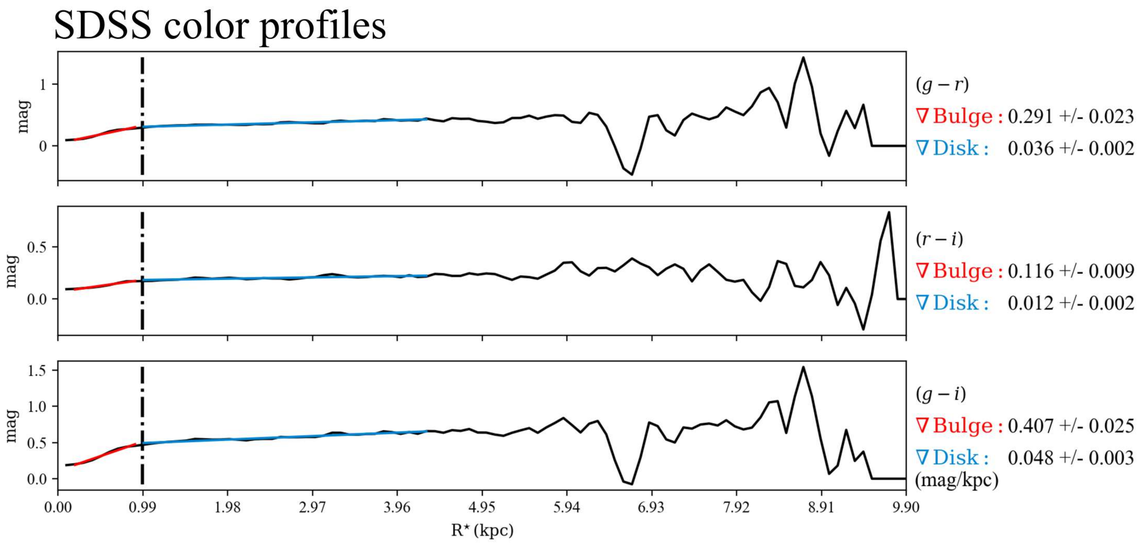

$\mathcal{RY}$ SBPs

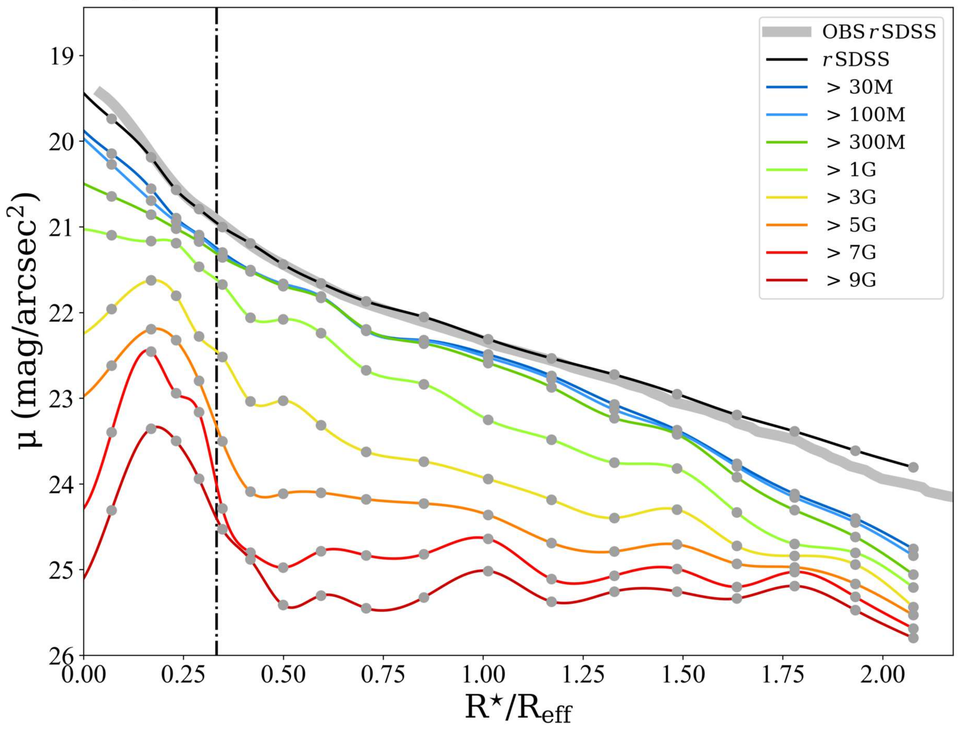

Stellar Continuum

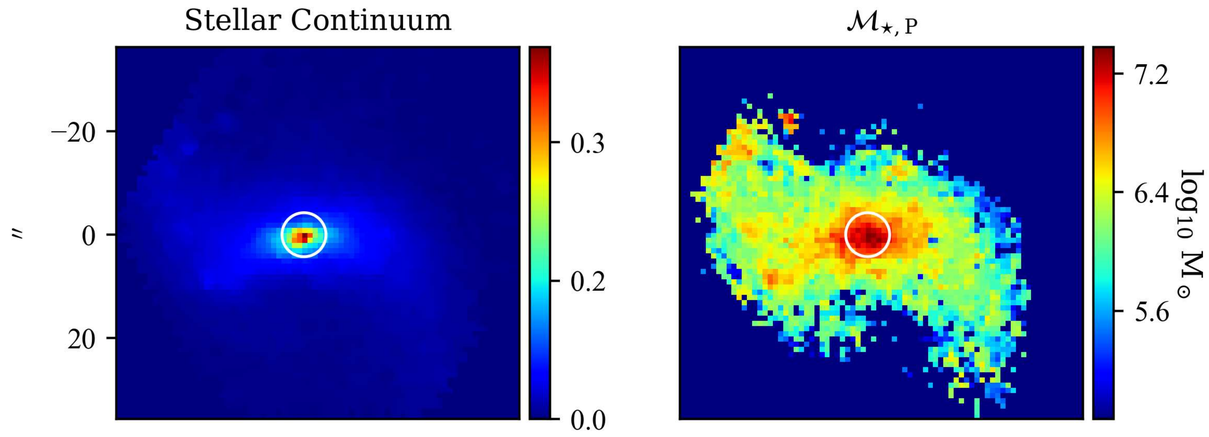

Log. of cumulative present stellar mass profiles

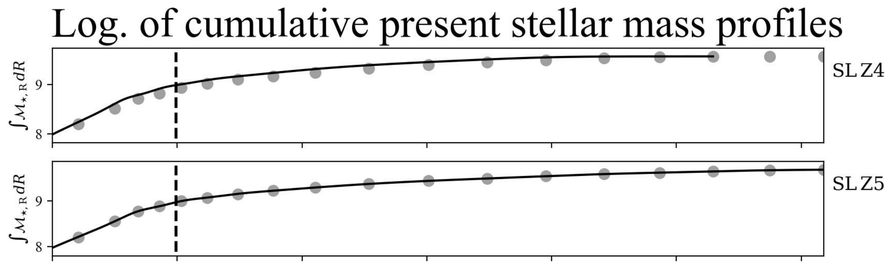

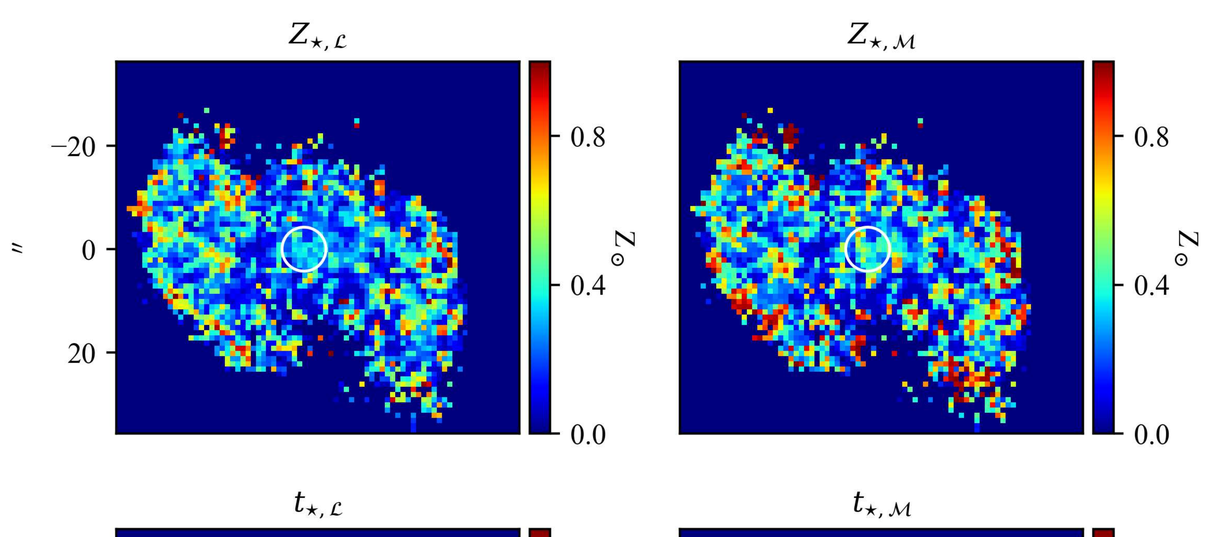

Stellar metallicity/Age & Hα flux/EW profiles

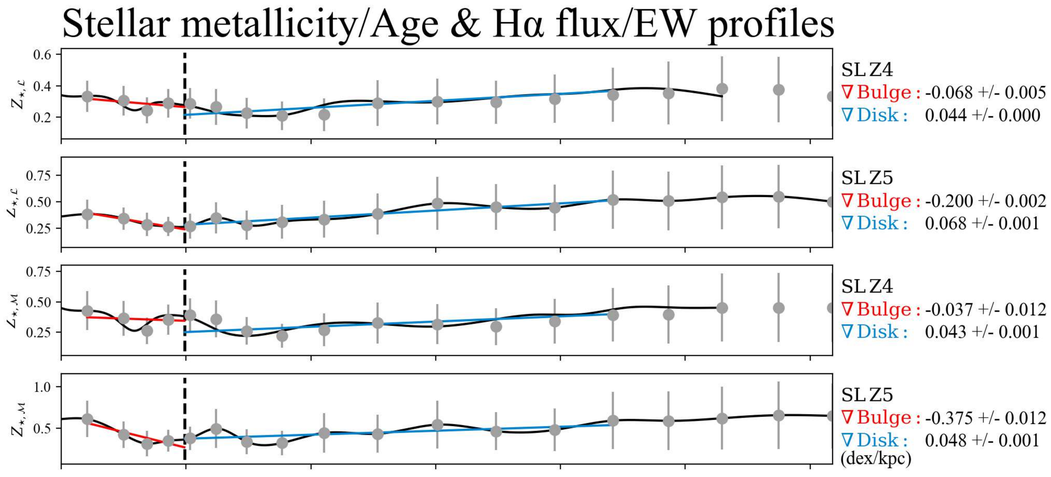

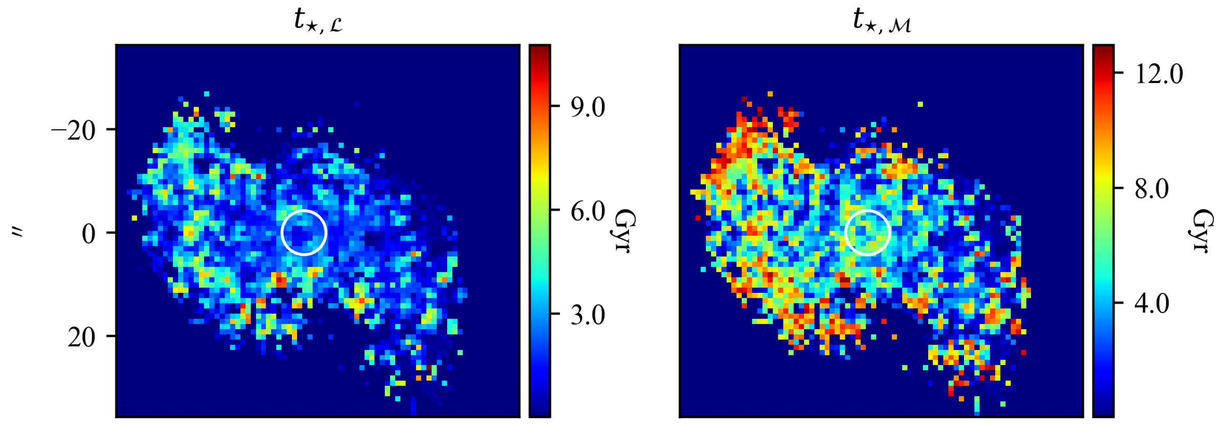

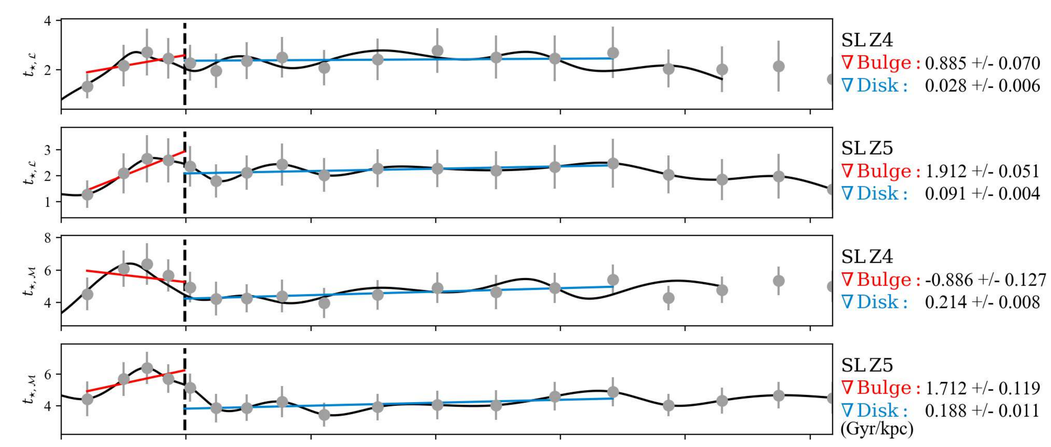

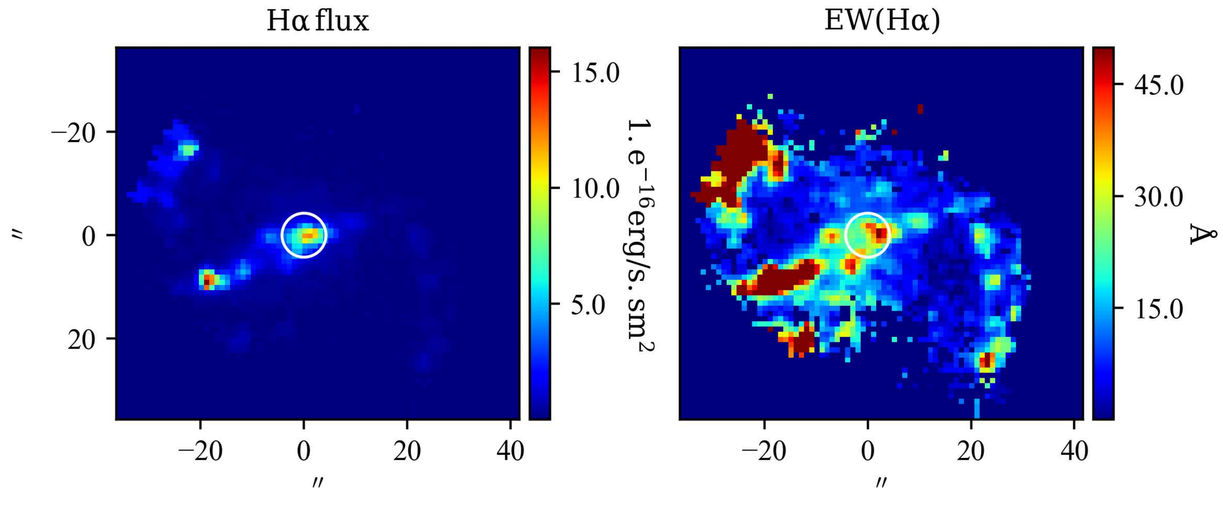

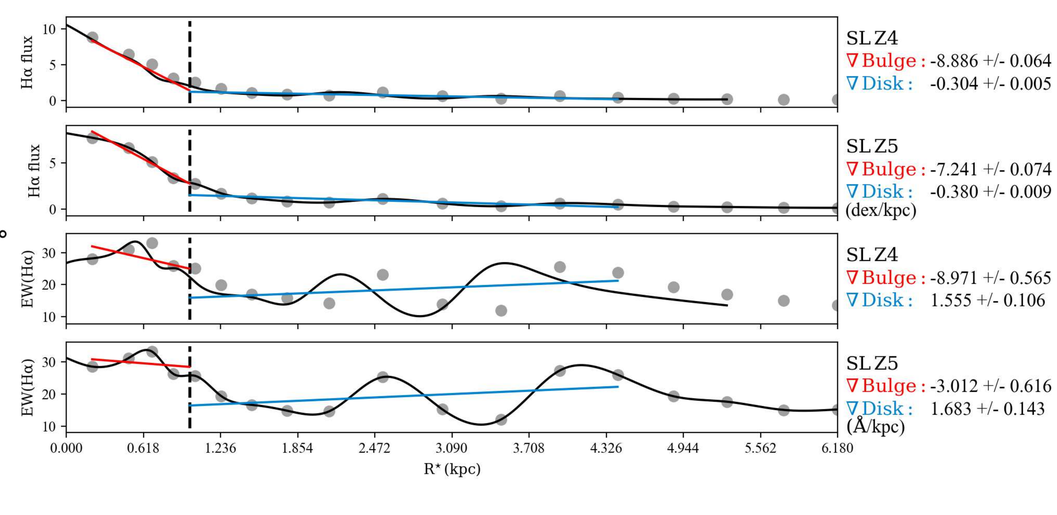

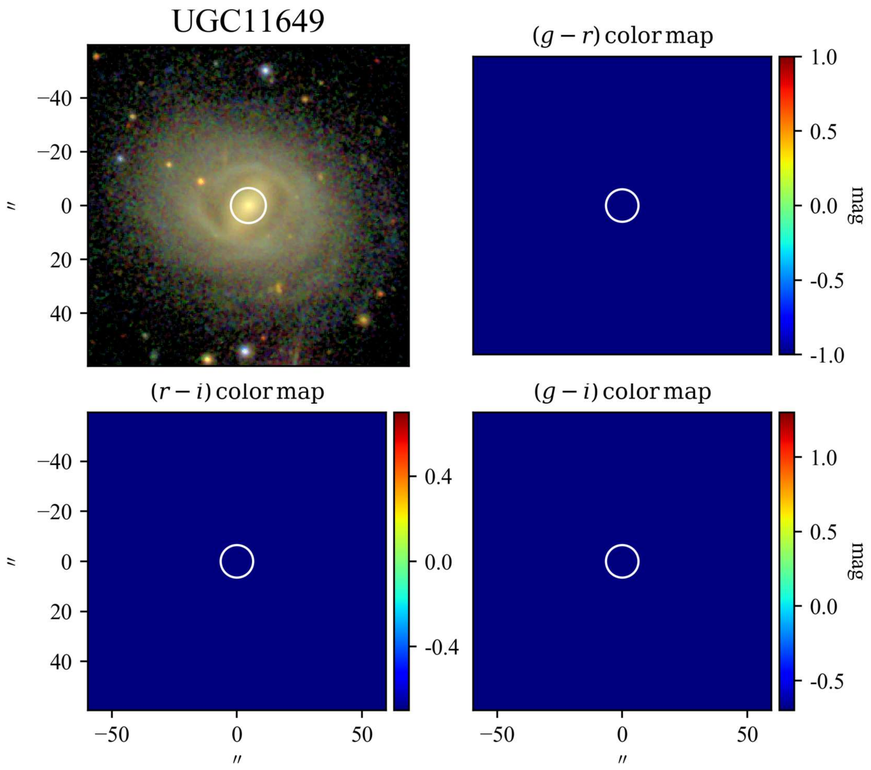

SBP decomposition of SDSS r band

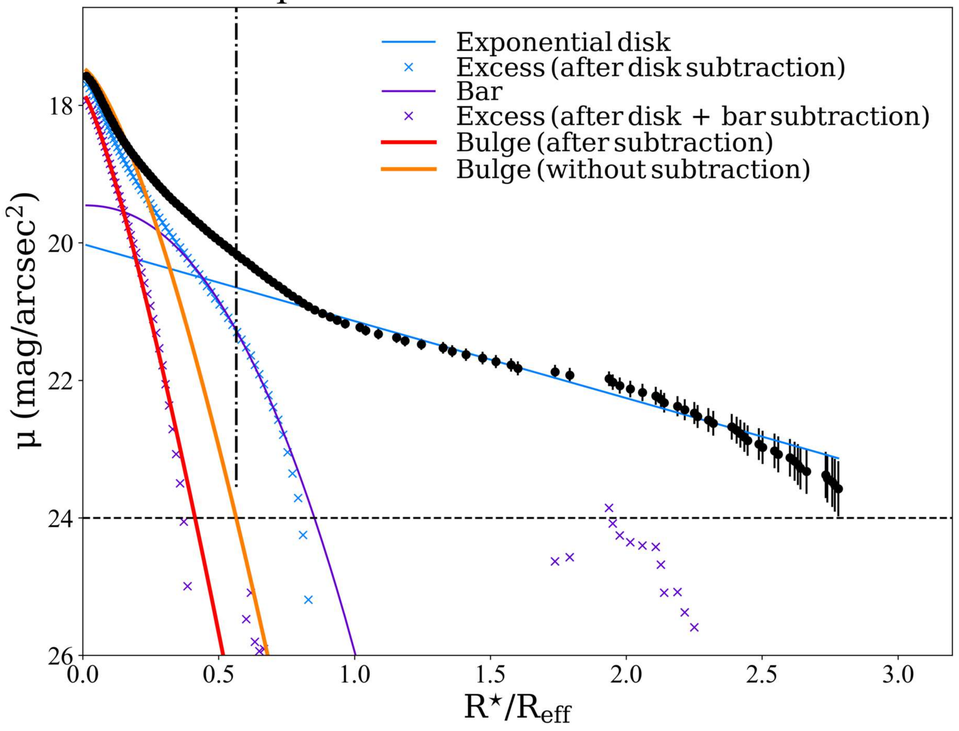

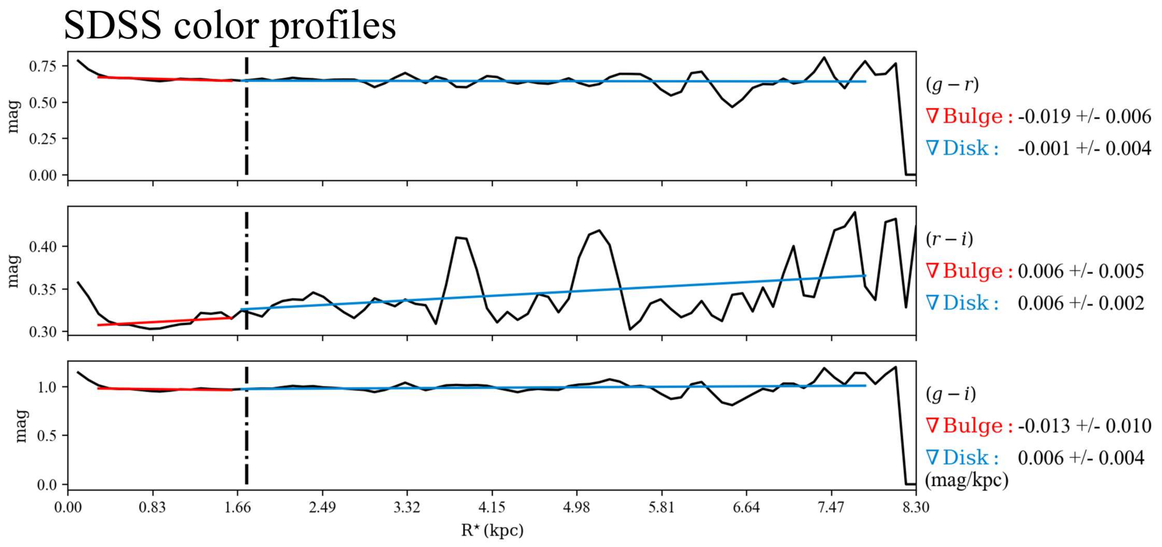

$\mathcal{RY}$ SBPs

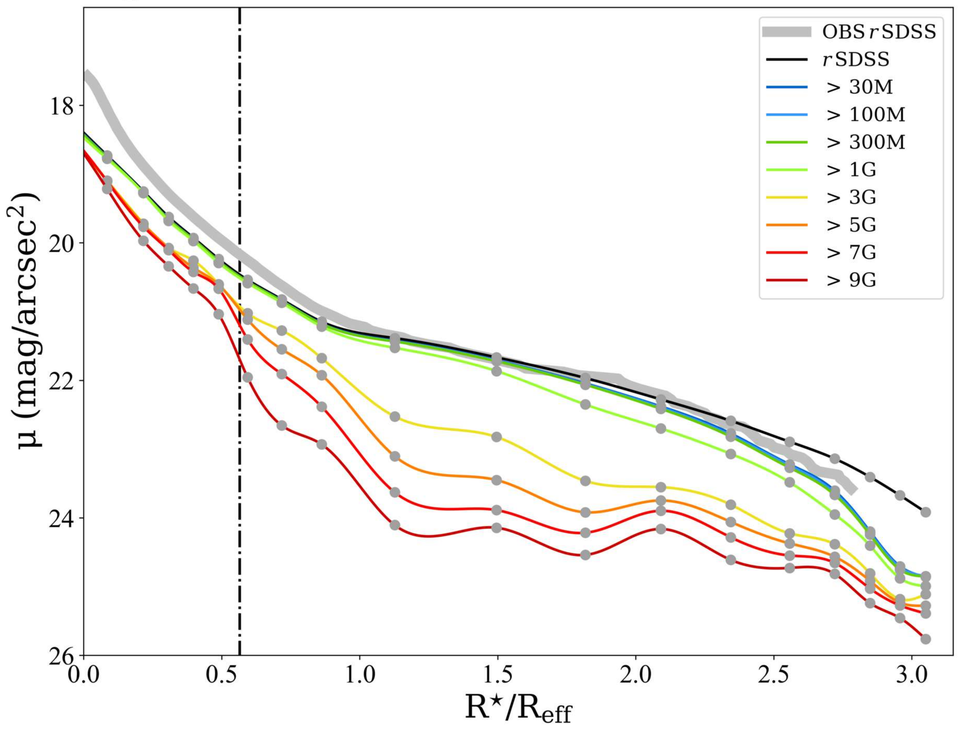

Stellar Continuum $\mathcal{M}_{\star,\mathrm{P}}$

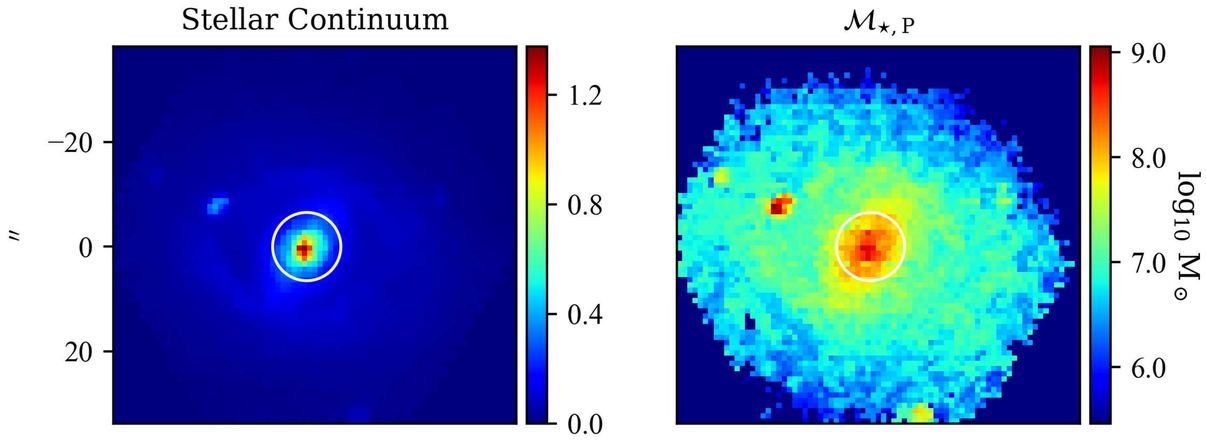

Log. of cumulative present stellar mass profiles

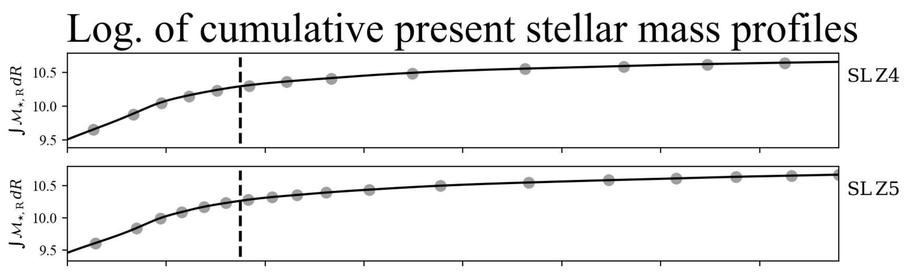

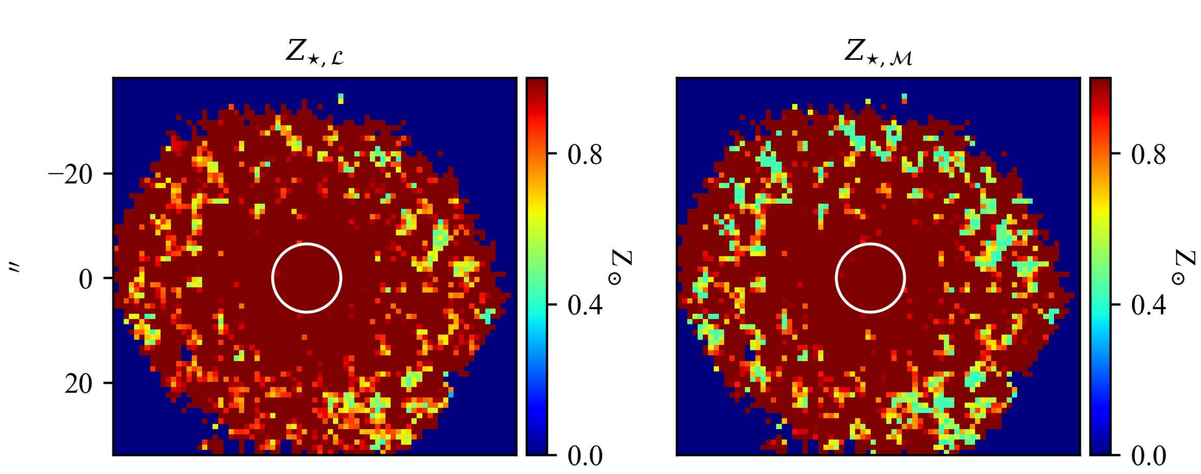

Stellar metallicity/Age & Hα flux/EW profiles

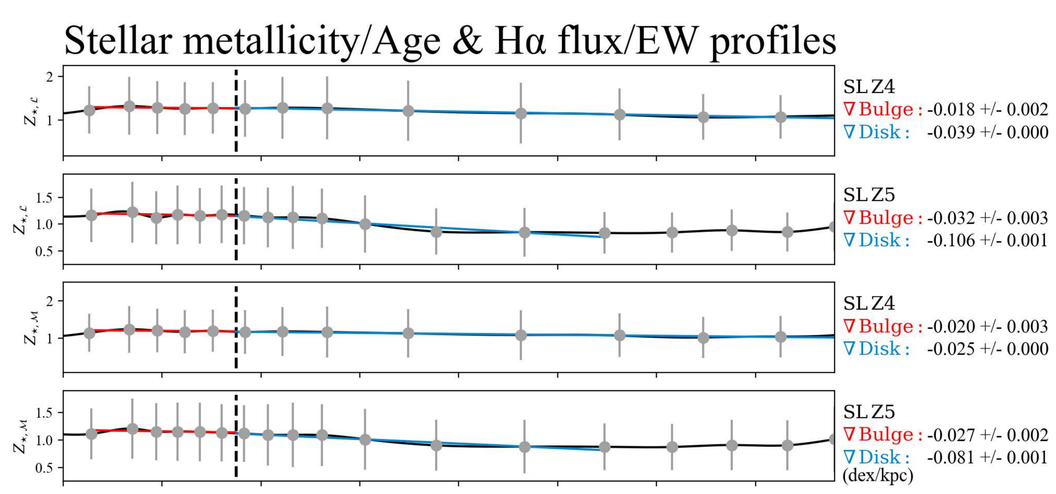

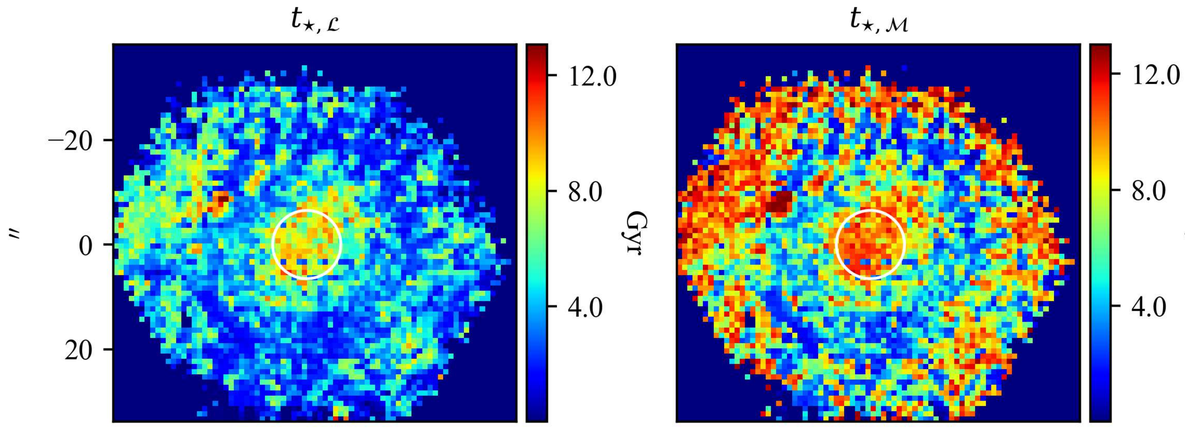

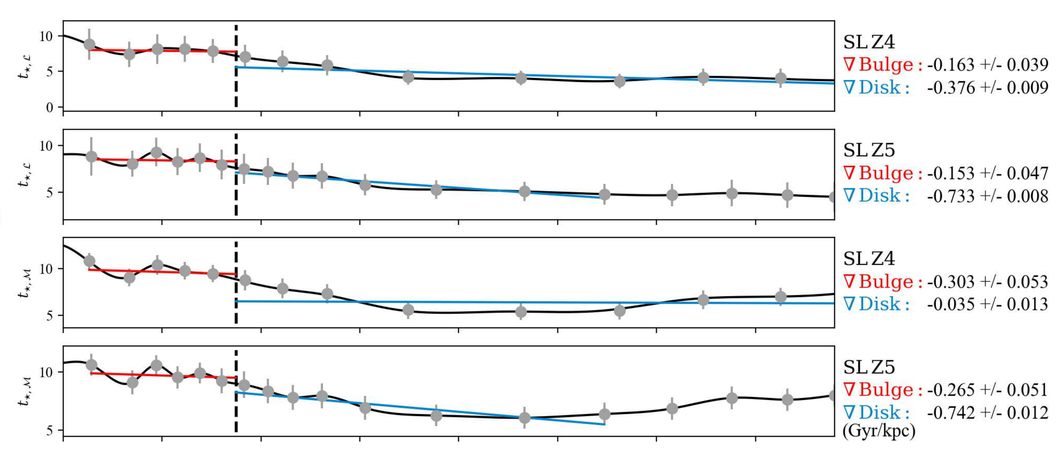

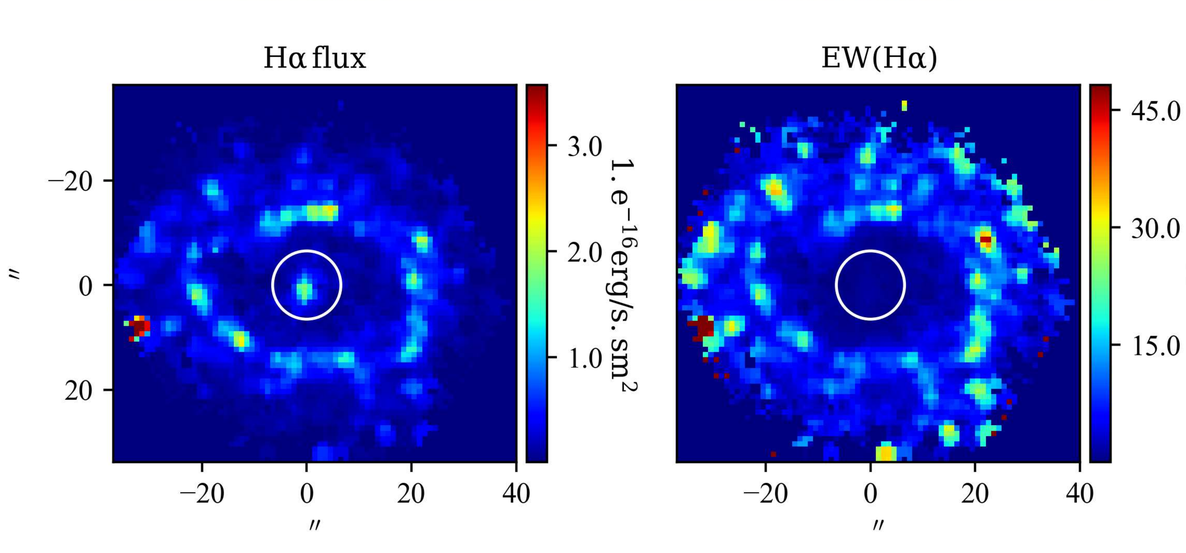

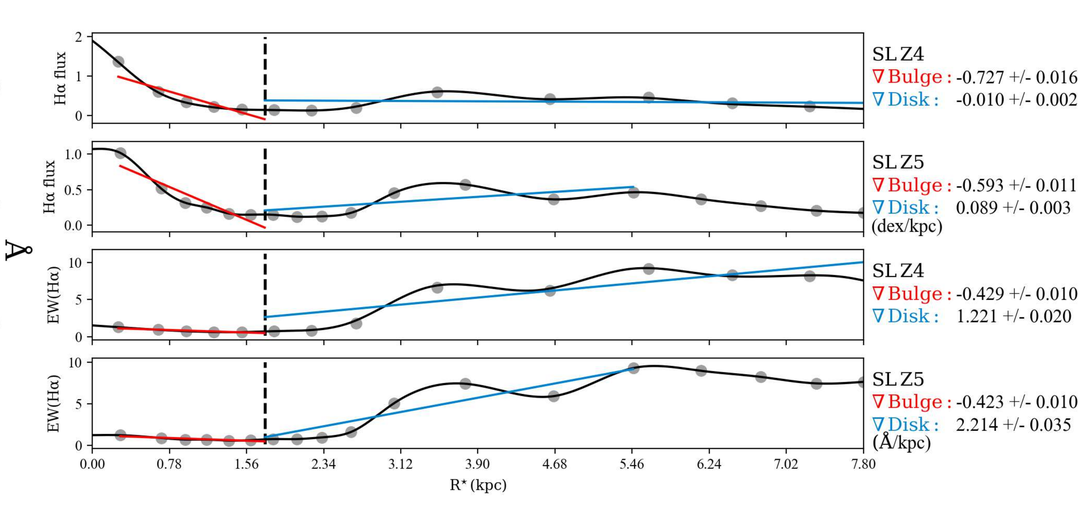

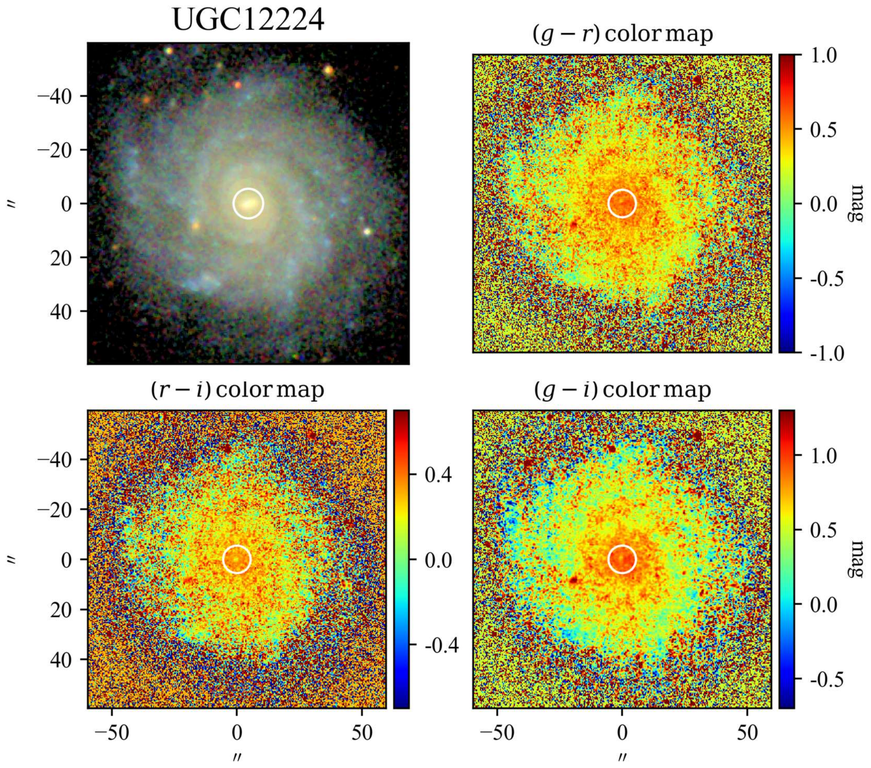

SBP decomposition of SDSS r band

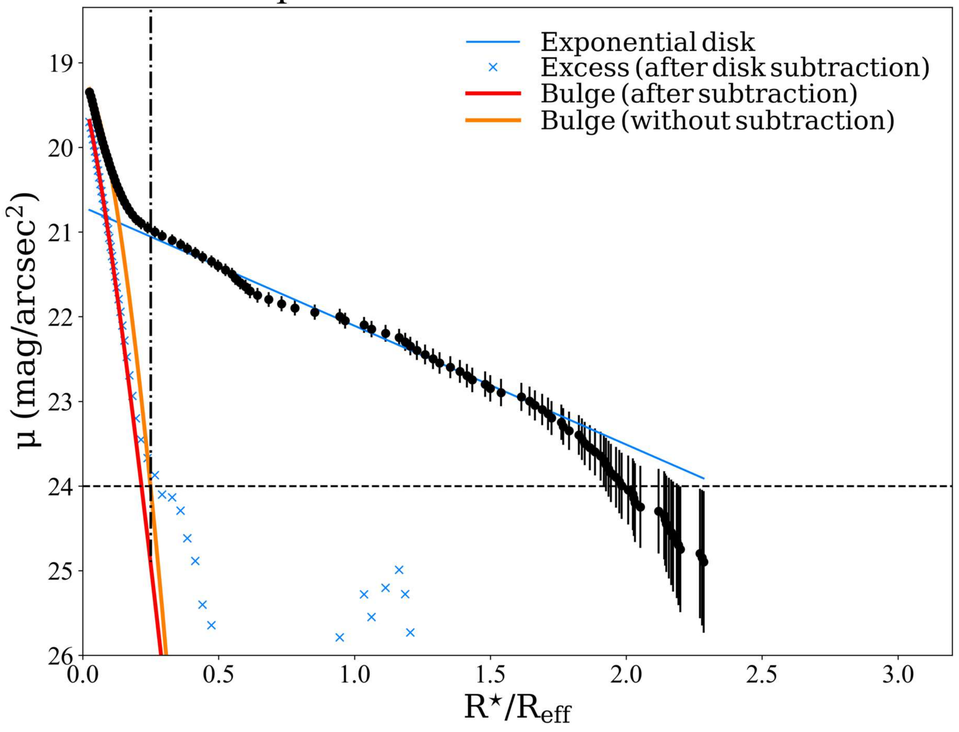

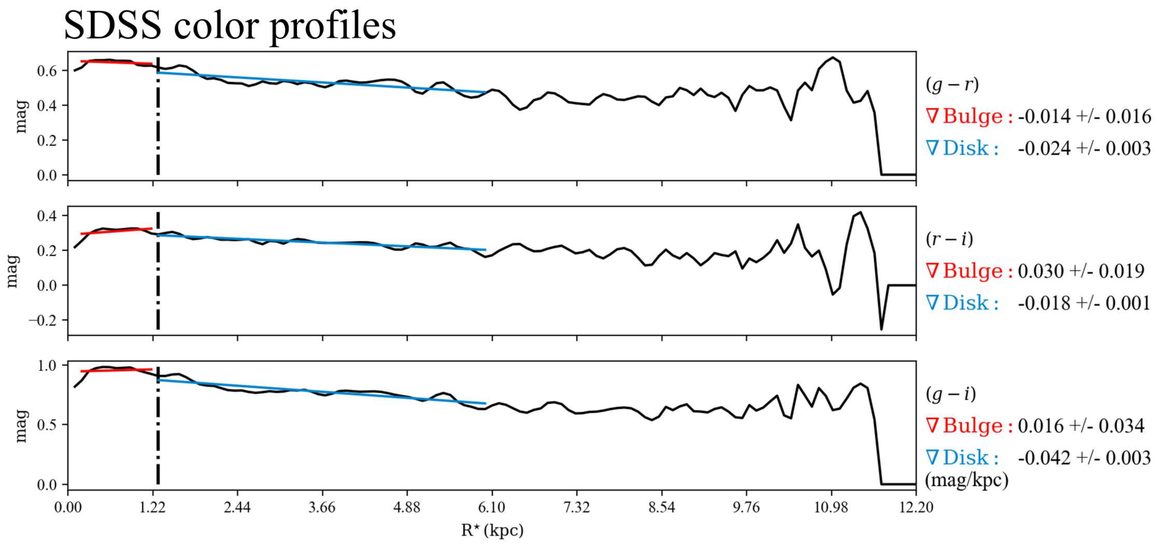

$\mathcal{RY}$ SBPs

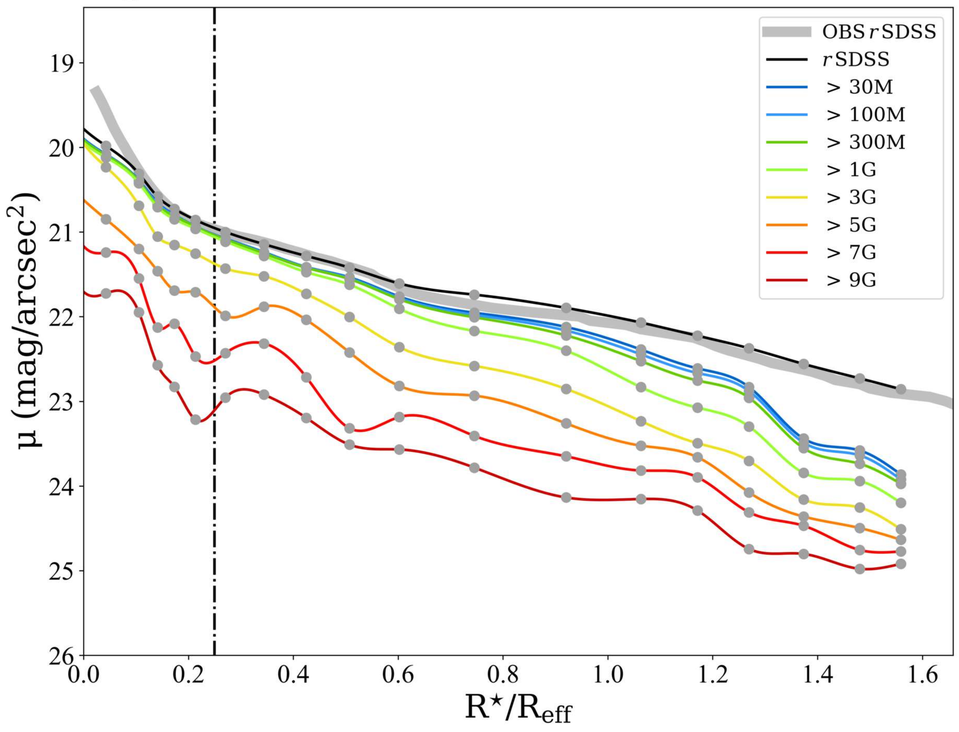

Stellar Continuum

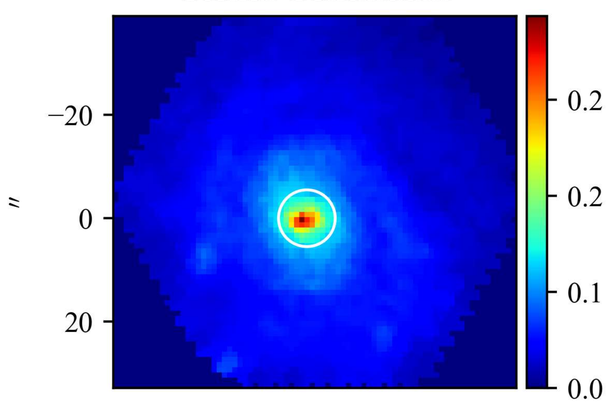

$\mathcal{M}_{\star,\mathrm{P}}$

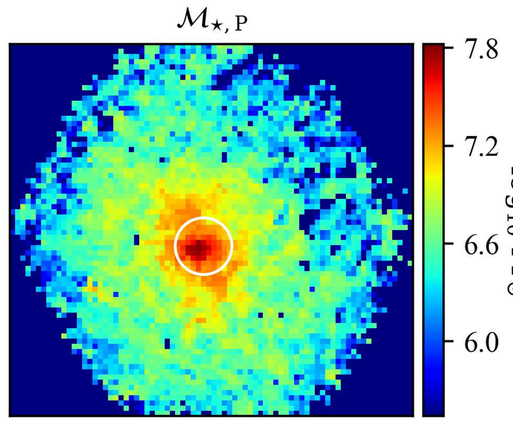

Log. of cumulative present stellar mass profiles

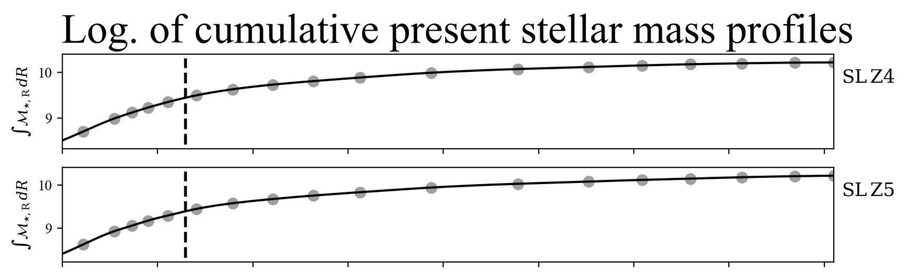

$Z_{\star,\mathcal{L}}$

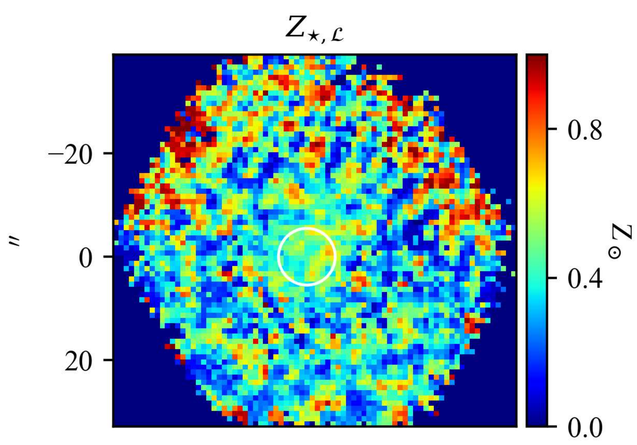

$Z_{\star,\mathcal{M}}$

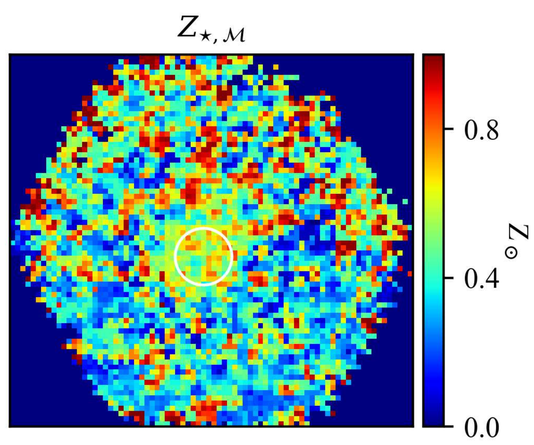

Stellar metallicity/Age & Hα flux/EW profiles

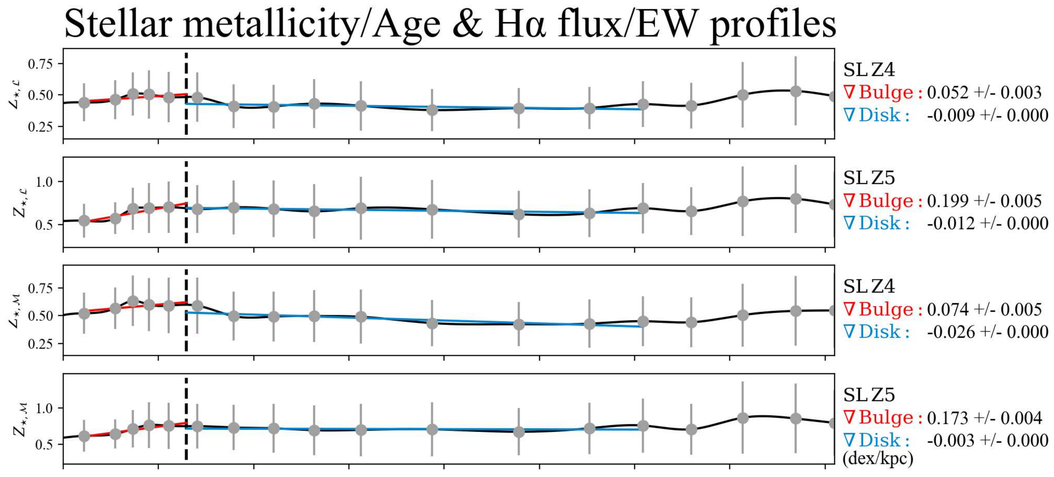

$t_{\star,\mathcal{L}}$

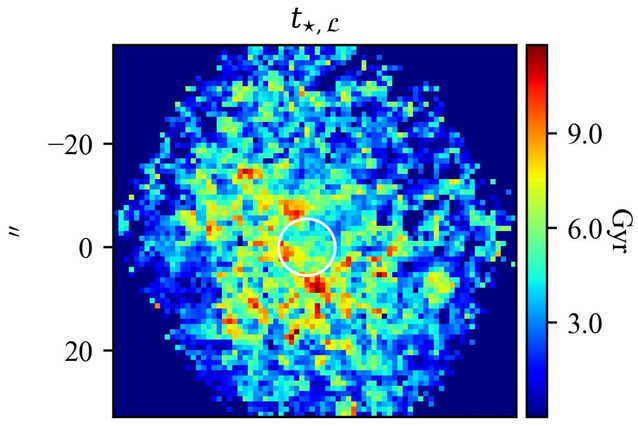

$t_{\star,\mathcal{M}}$

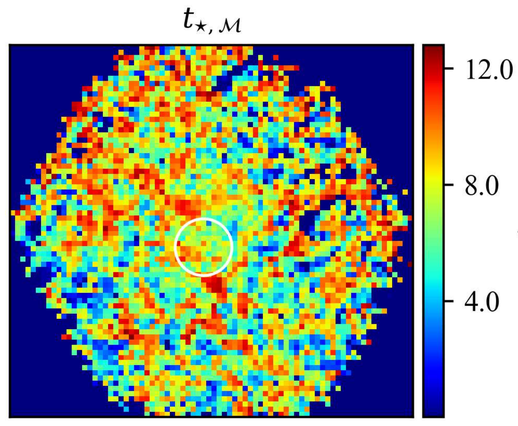

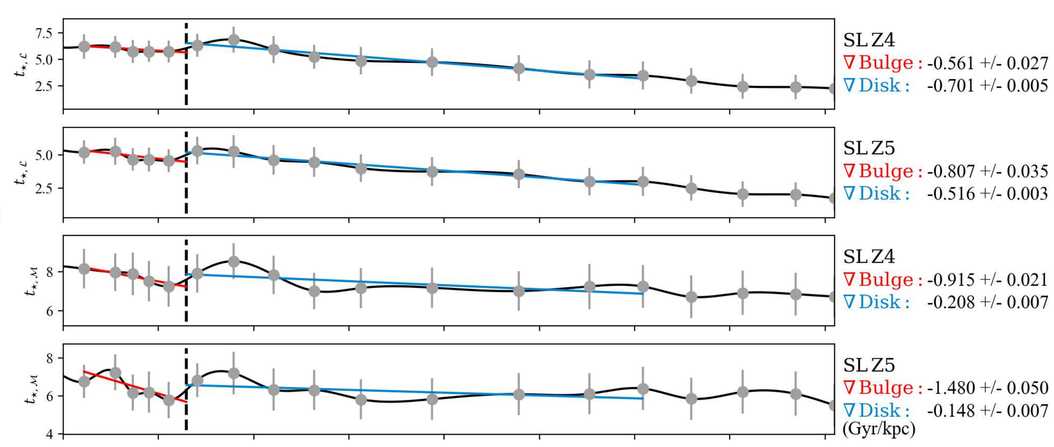

Hα flux

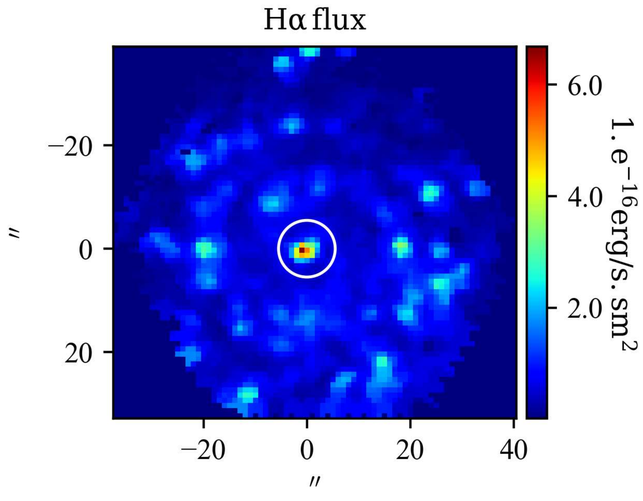

EW(Hα)

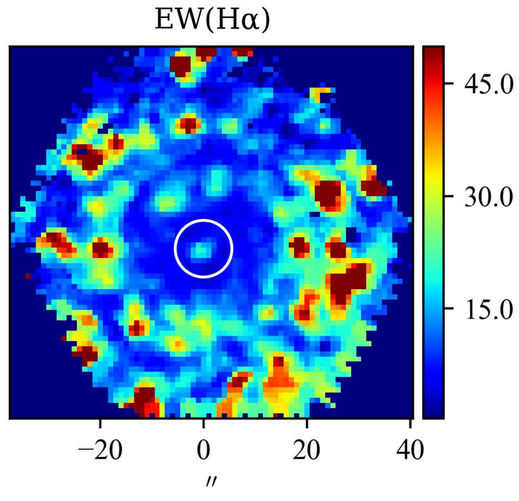

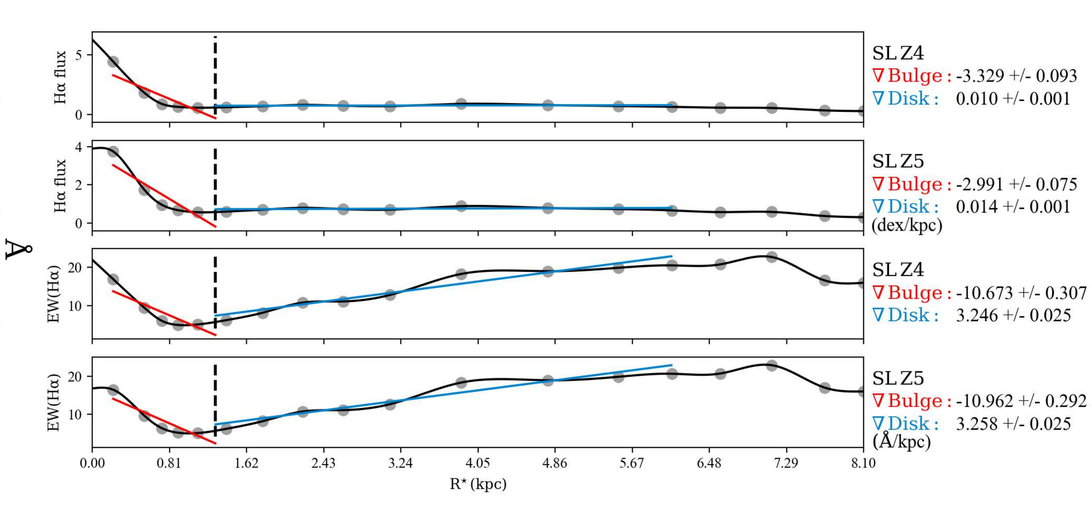

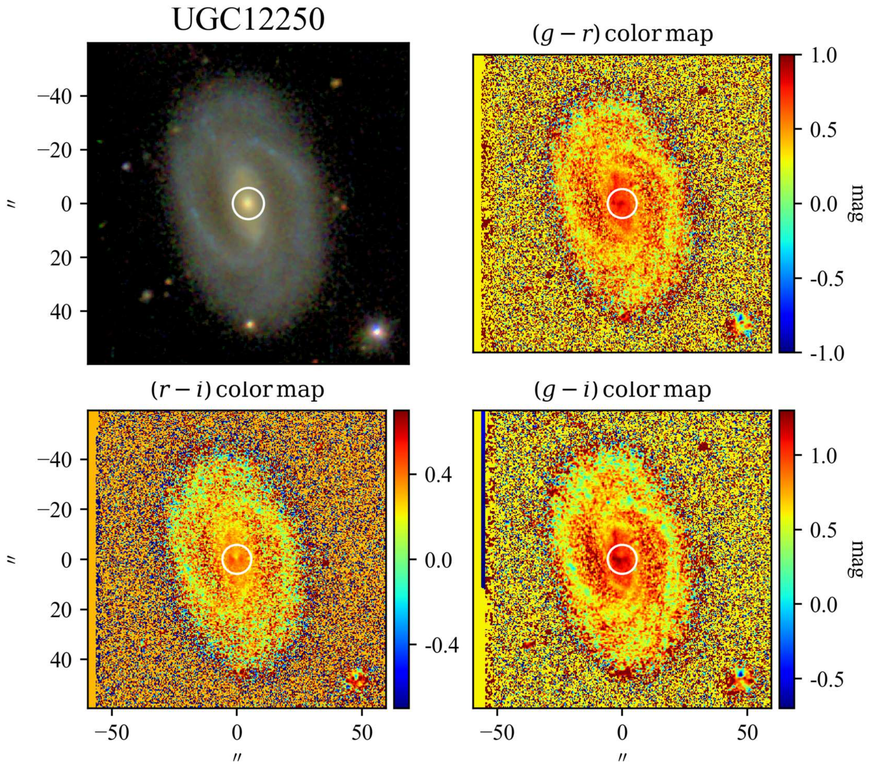

SBP decomposition of SDSS r band

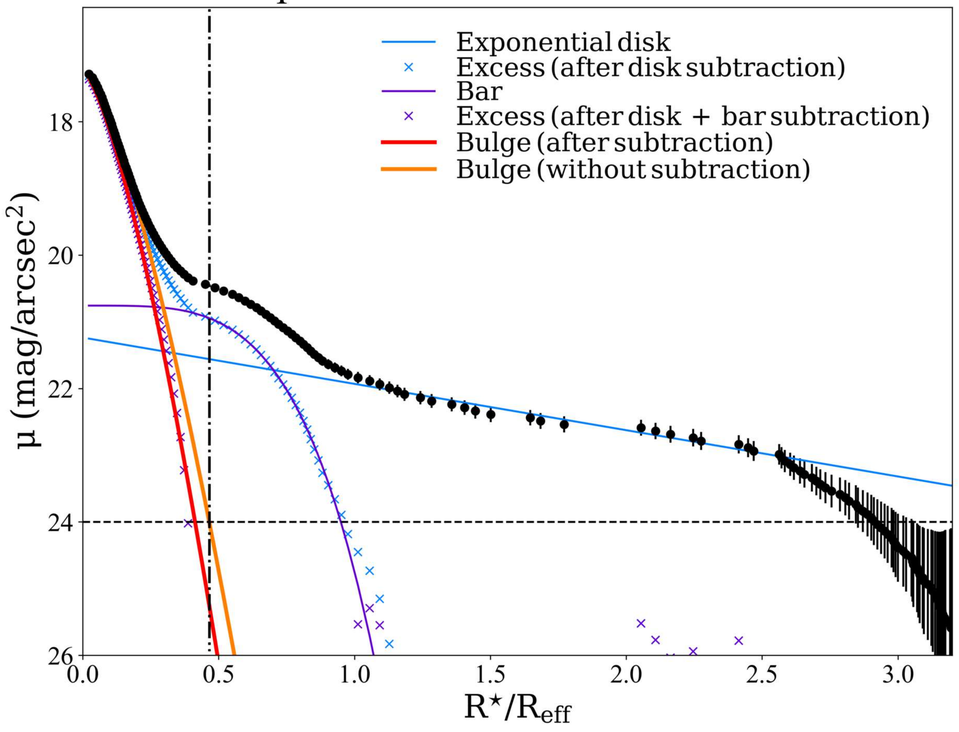

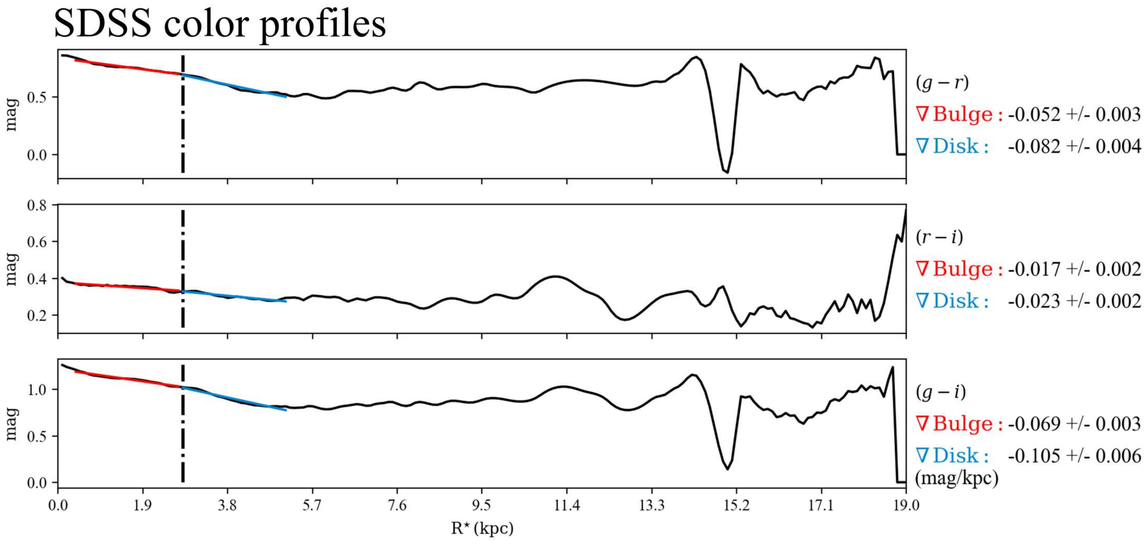

$\mathcal{RY}$ SBPs

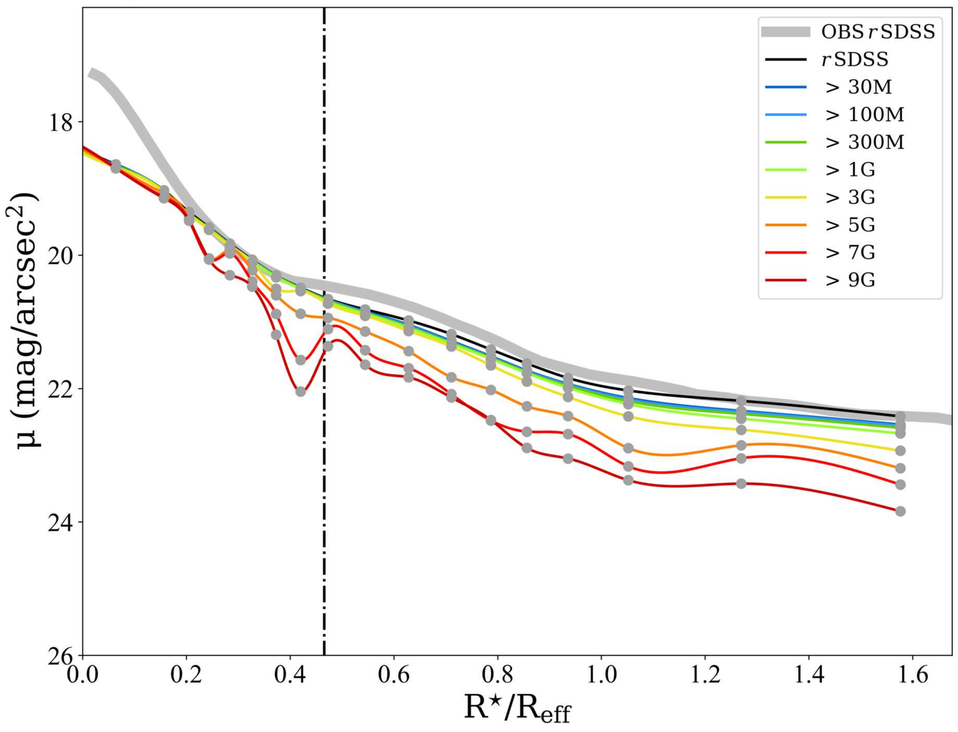

Stellar Continuum

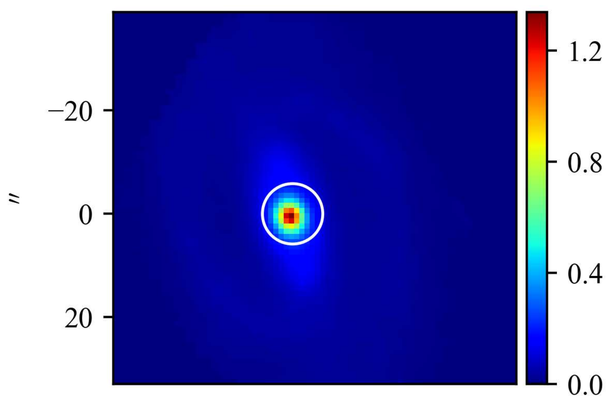

$\mathcal{M}_{\star,\,P}$

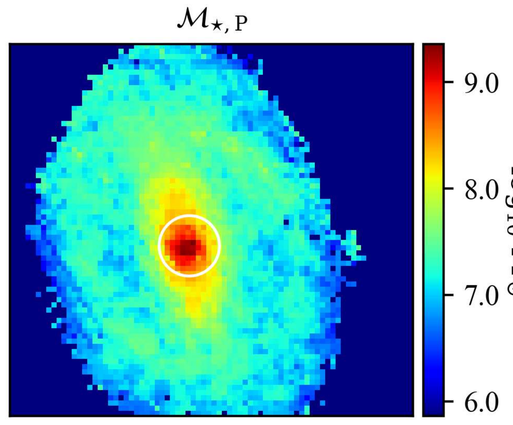

Log. of cumulative present stellar mass profiles

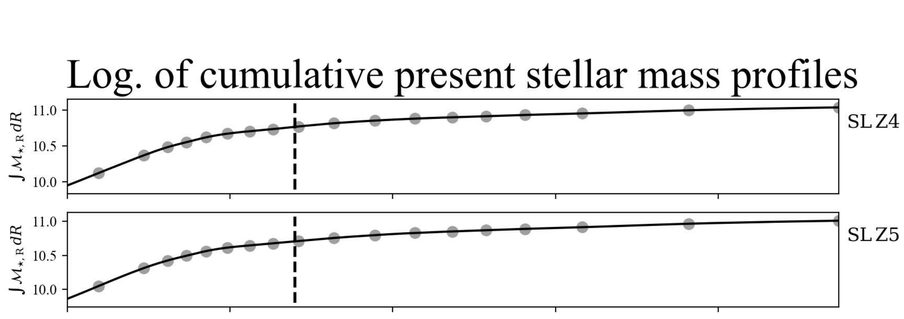

$Z_{\star,\,\mathcal{L}}$

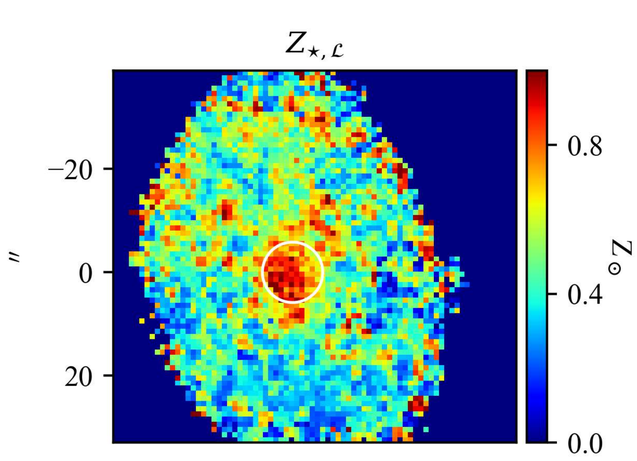

$Z_{\star,\,\mathcal{M}}$

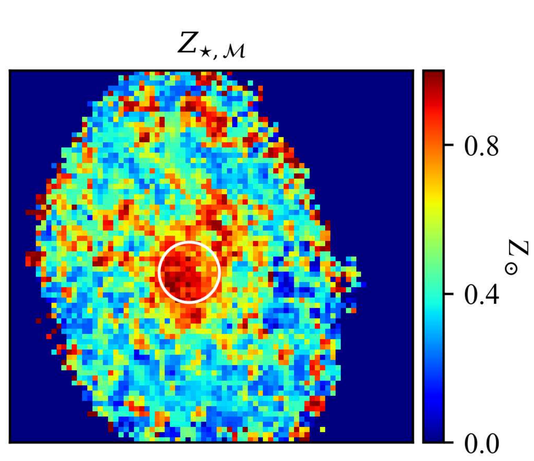

Stellar metallicity/Age & Hα flux/EW profiles

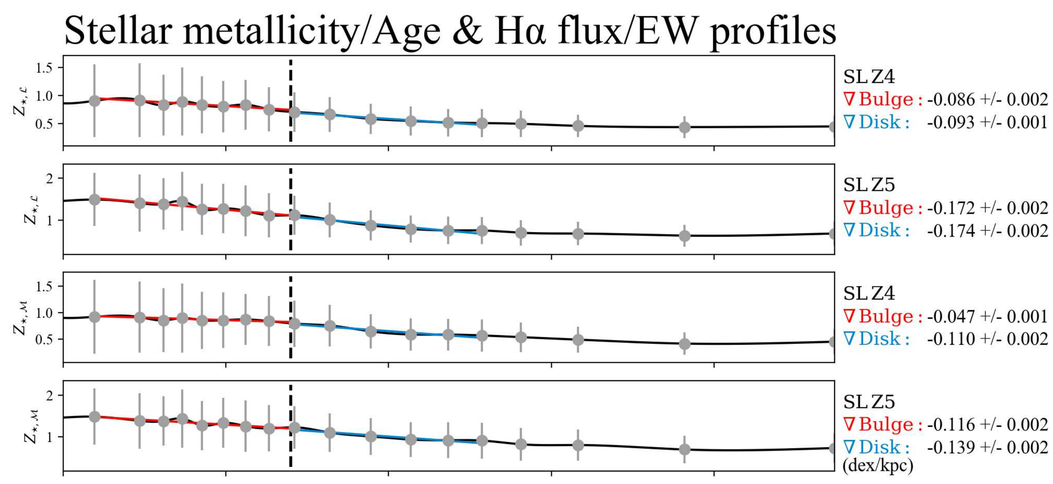

$t_{\star,\,\mathcal{L}}$

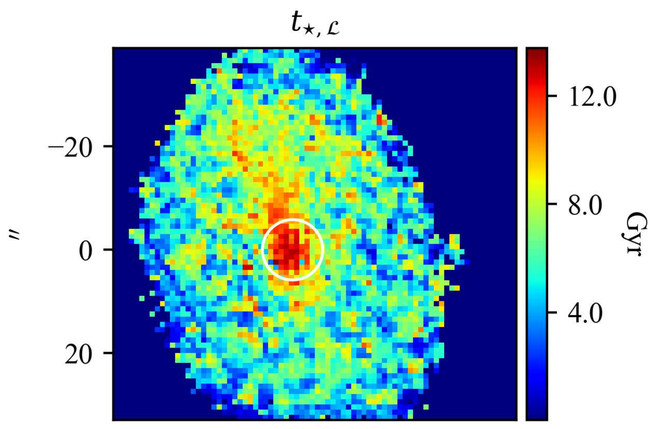

$t_{\star,\,\mathcal{M}}$

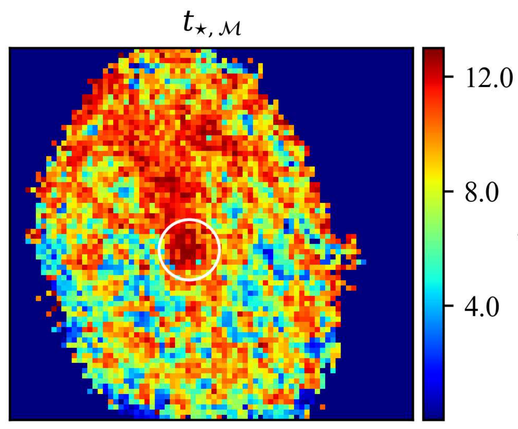

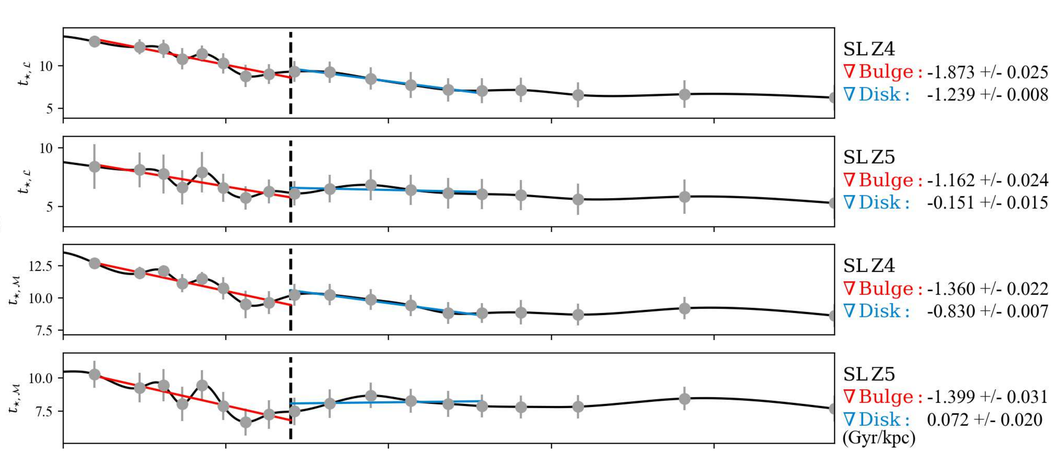

Hα flux

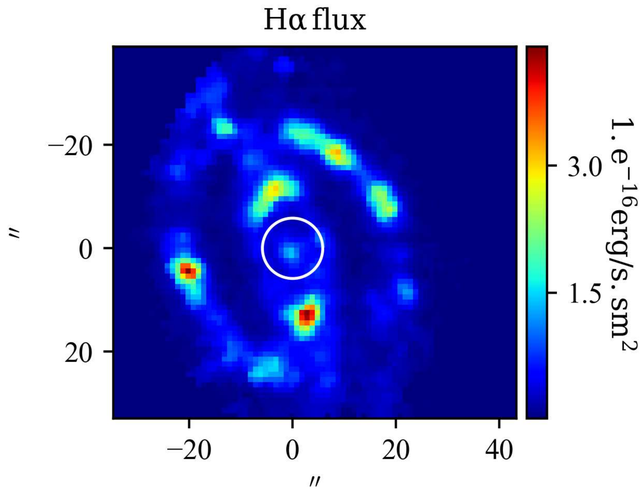

EW(Hα)

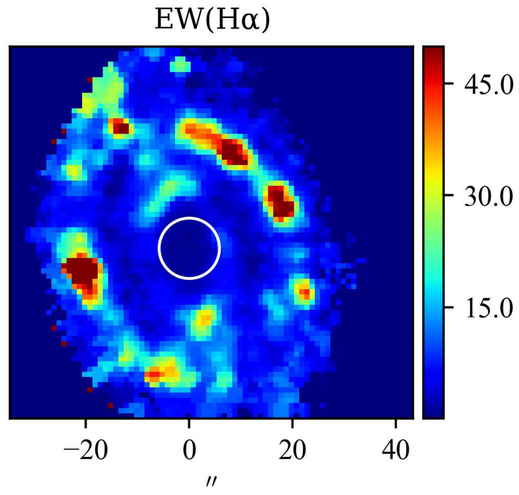

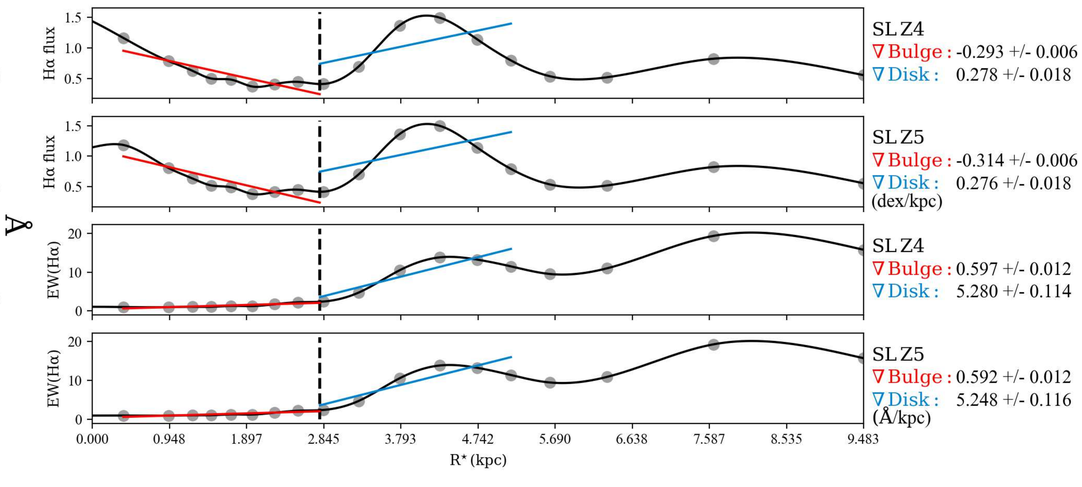

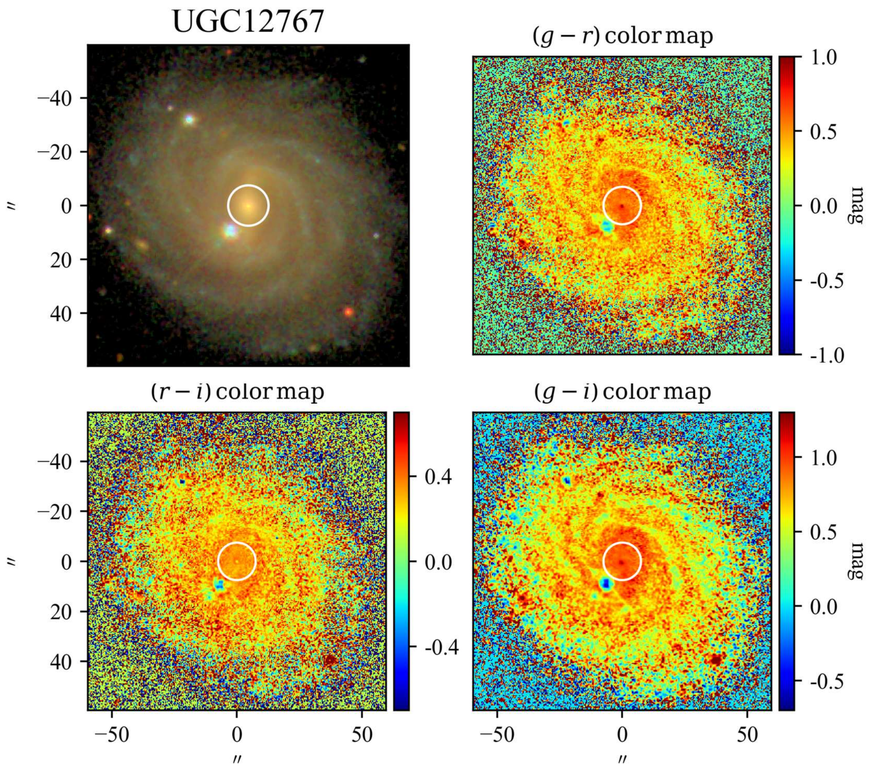

SBP decomposition of SDSS r band

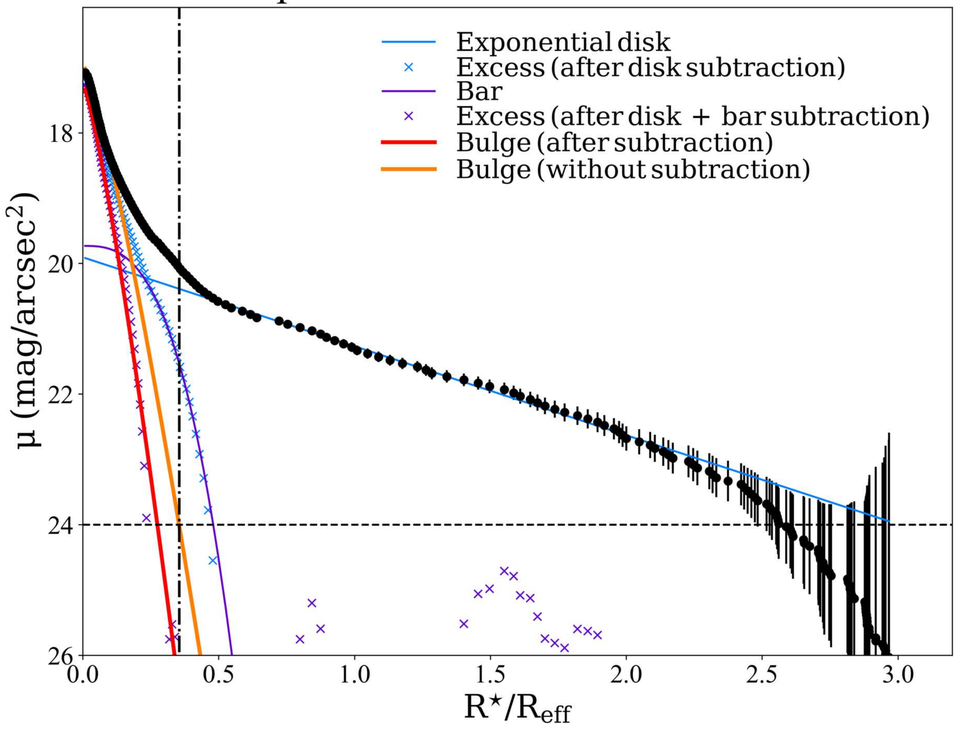

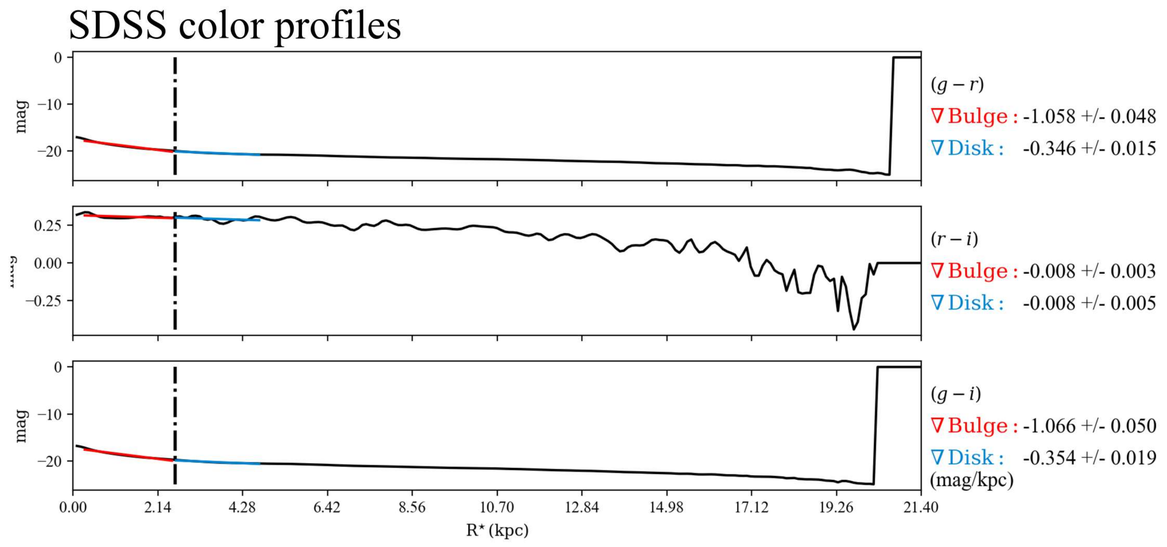

$\mathcal{RY}$ SBPs

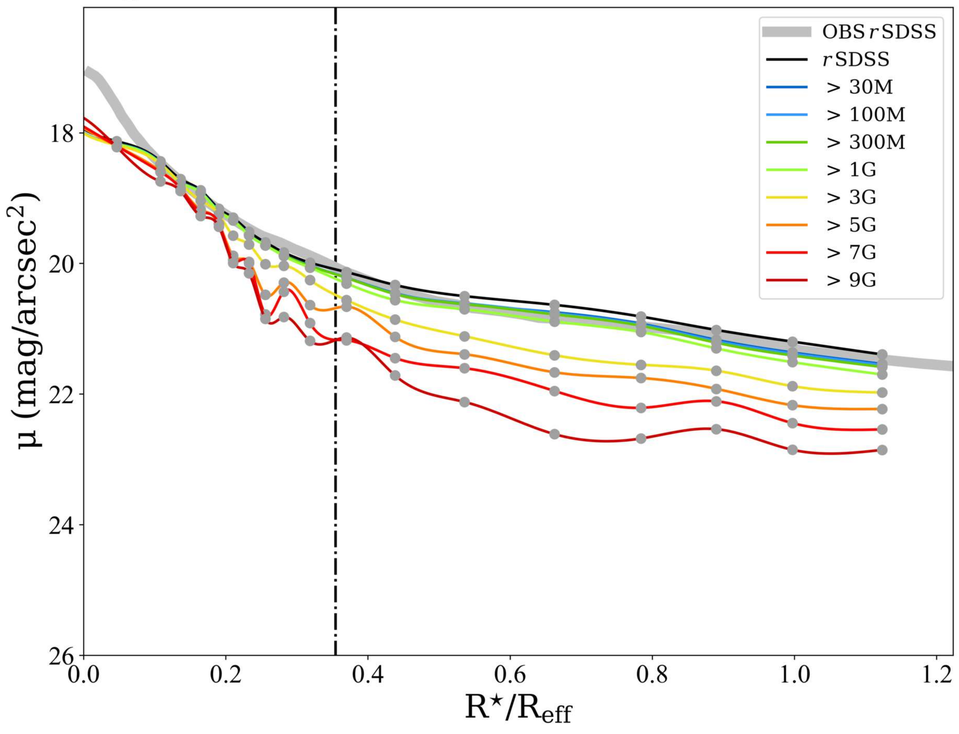

Stellar Continuum

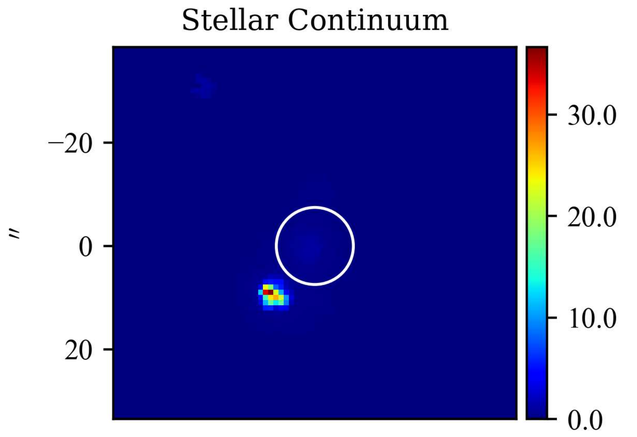

$\mathcal{M}_{\star,\mathrm{P}}$

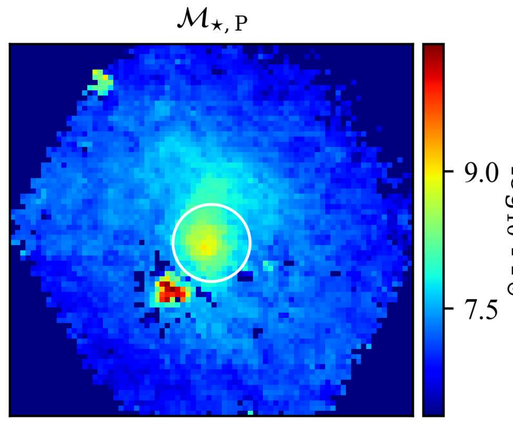

Log. of cumulative present stellar mass profiles

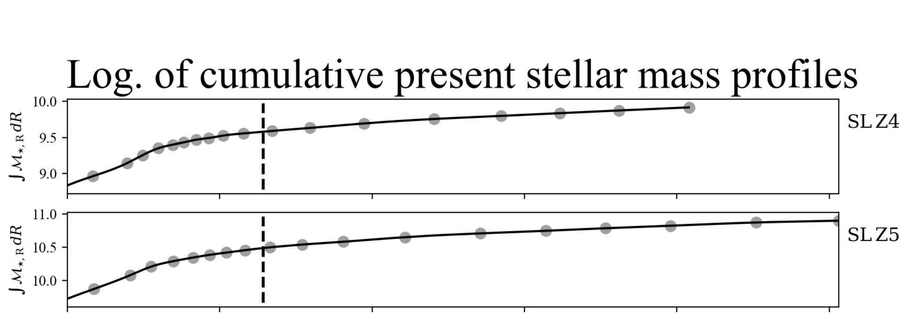

$Z_{\star,\mathcal{L}}$

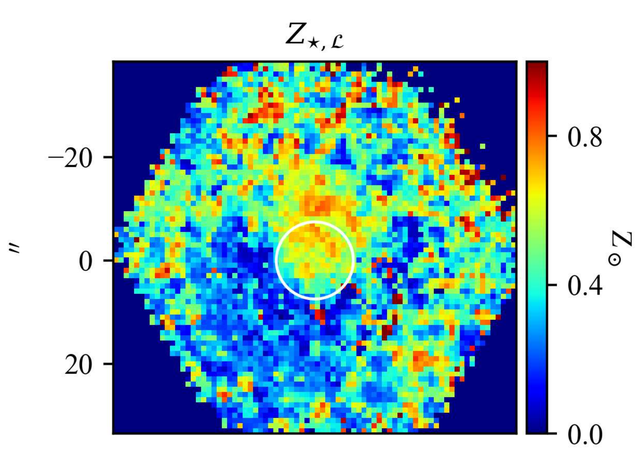

$Z_{\star,\mathcal{M}}$

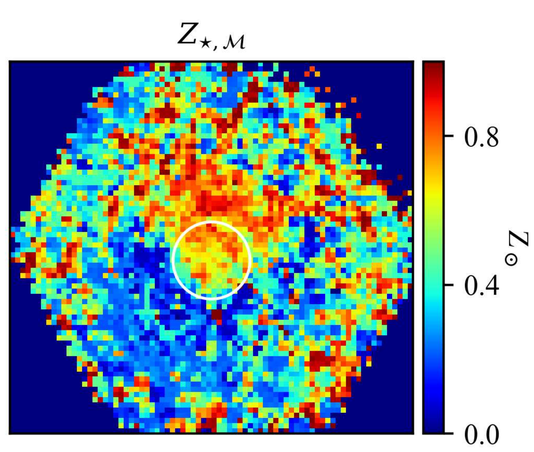

Stellar metallicity/Age & Hα flux/EW profiles

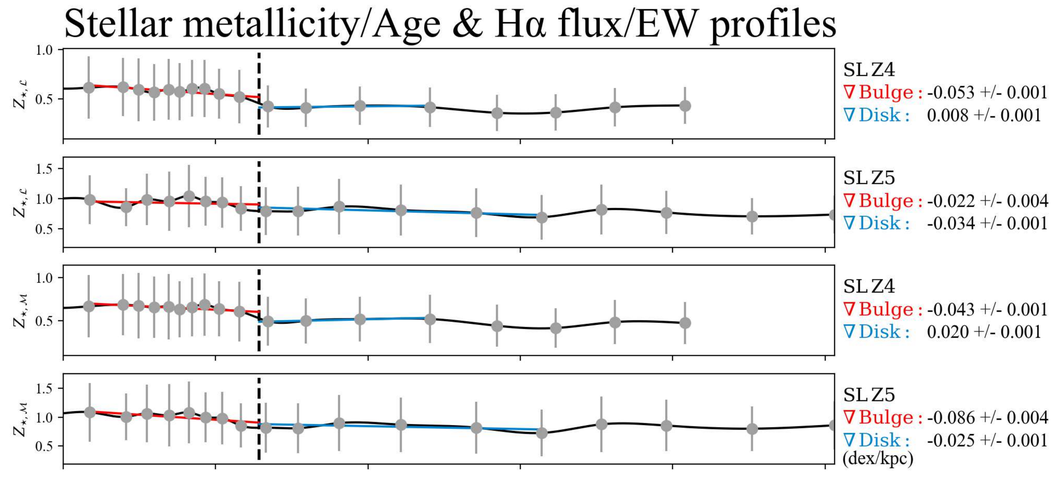

$t_{\star,\mathcal{L}}$

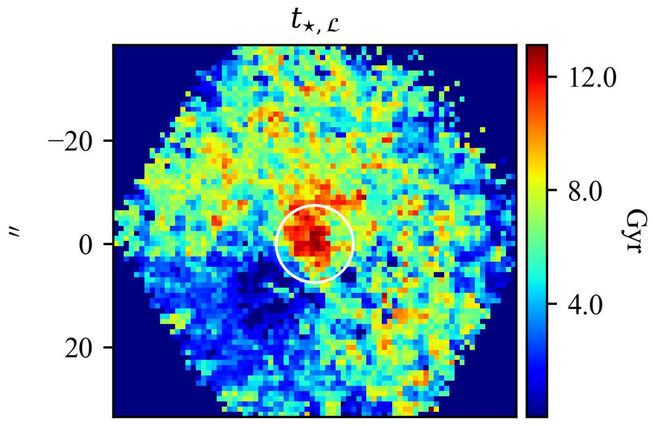

$t_{\star,\mathcal{M}}$

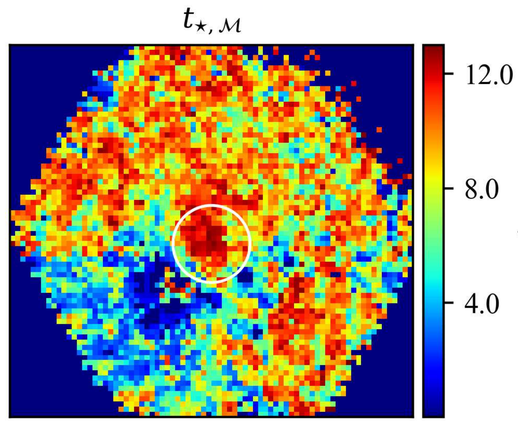

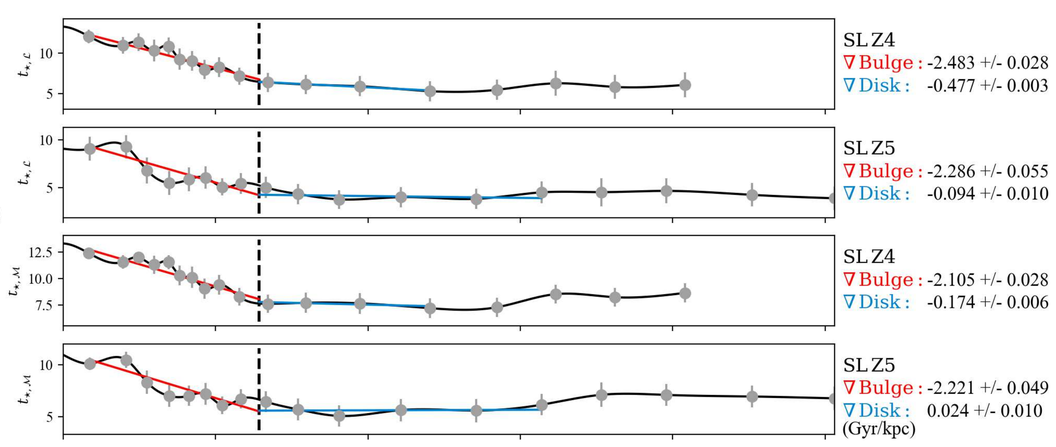

Hα flux

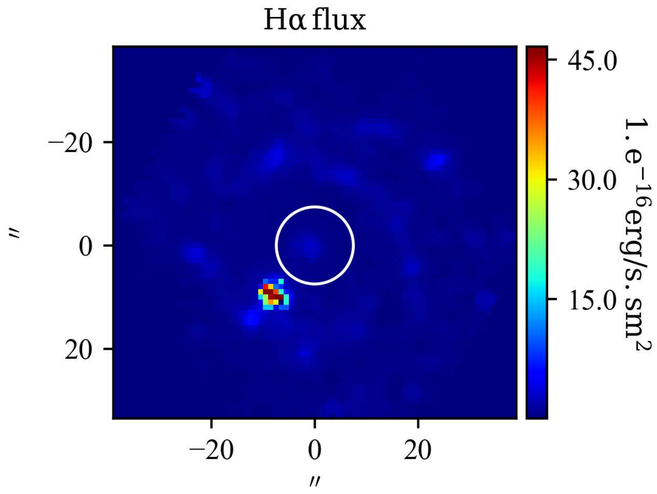

EW(Hα)

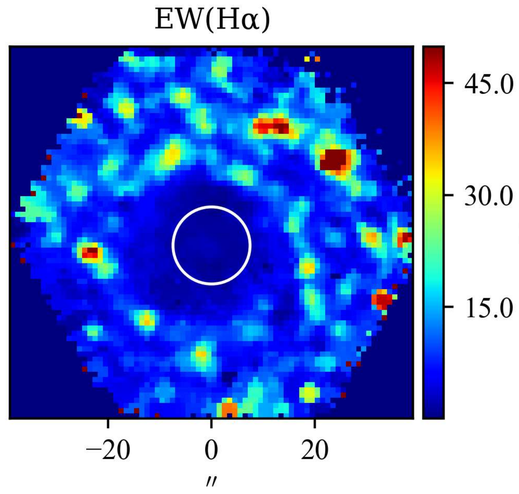

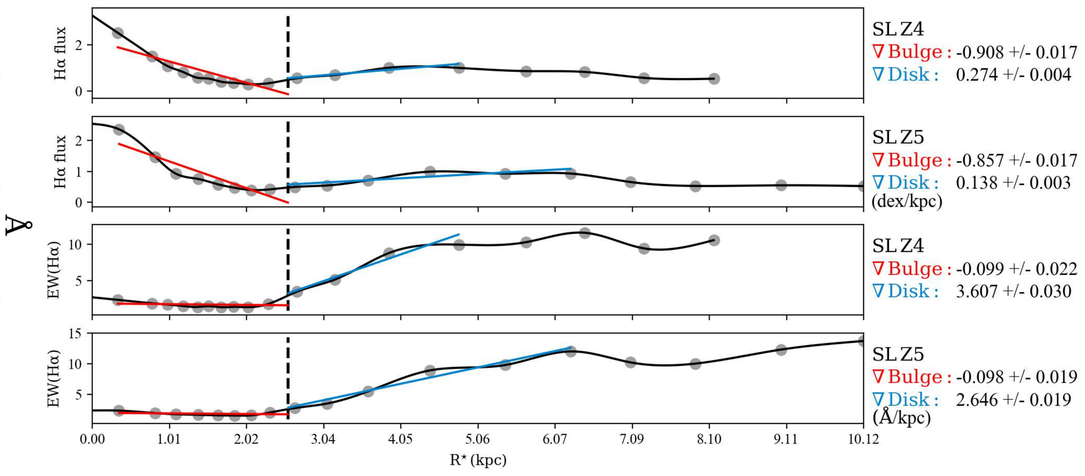

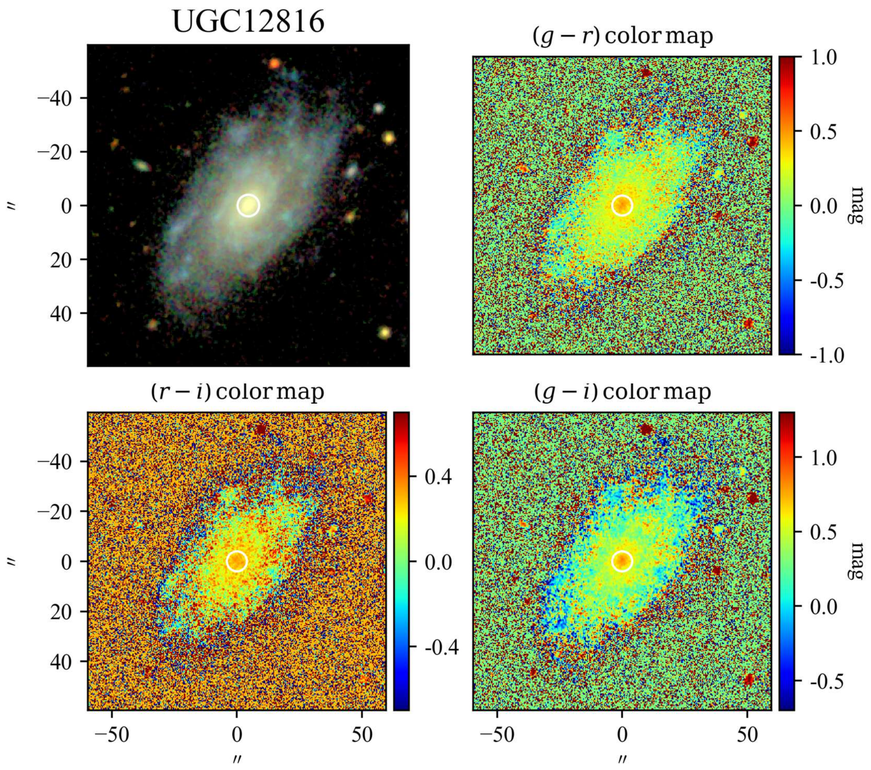

SBP decomposition of SDSS r band

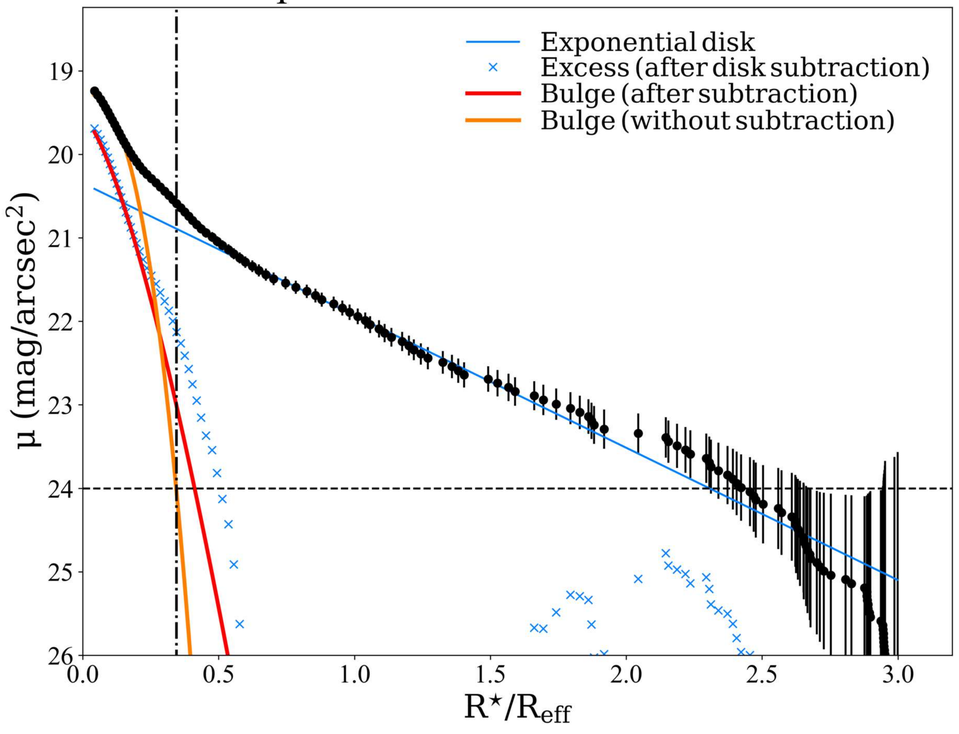

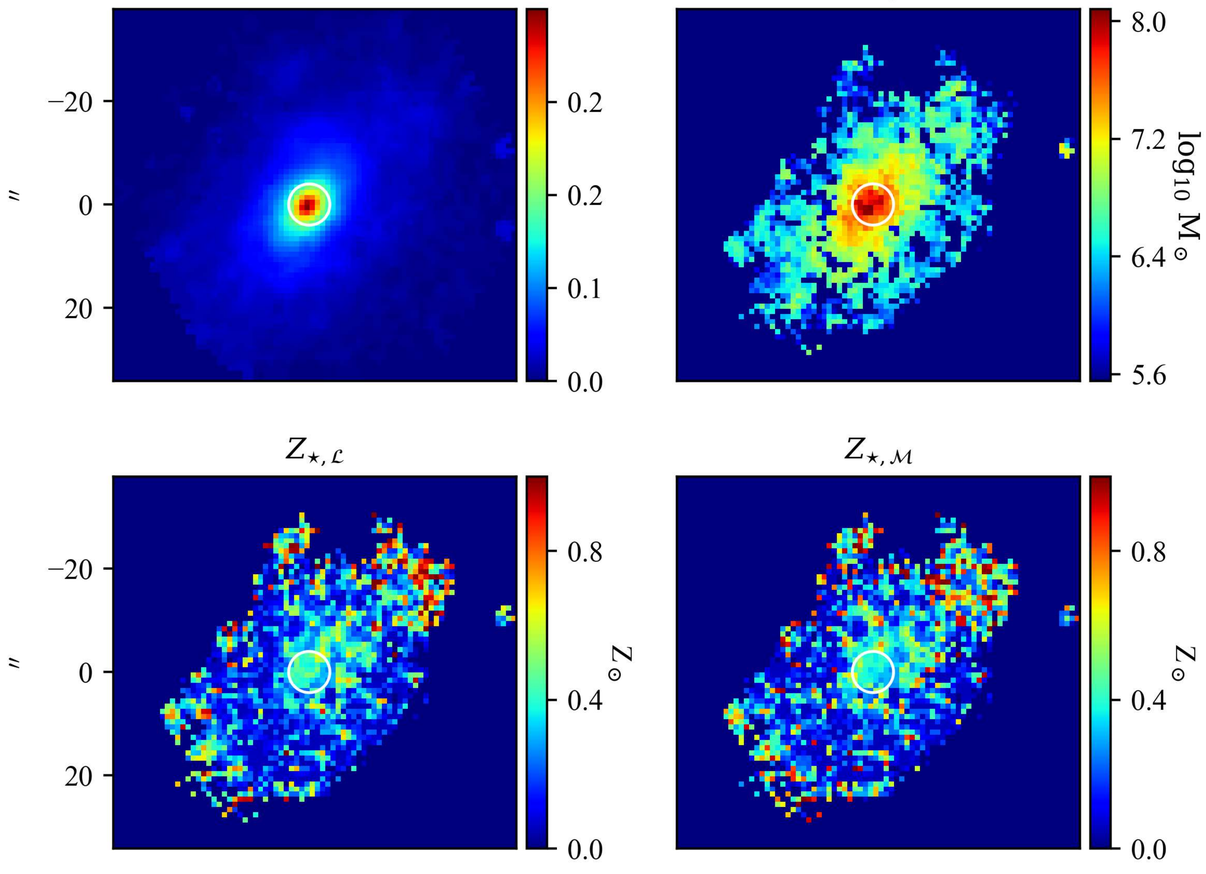

$\mathcal{RV}$ SBPs

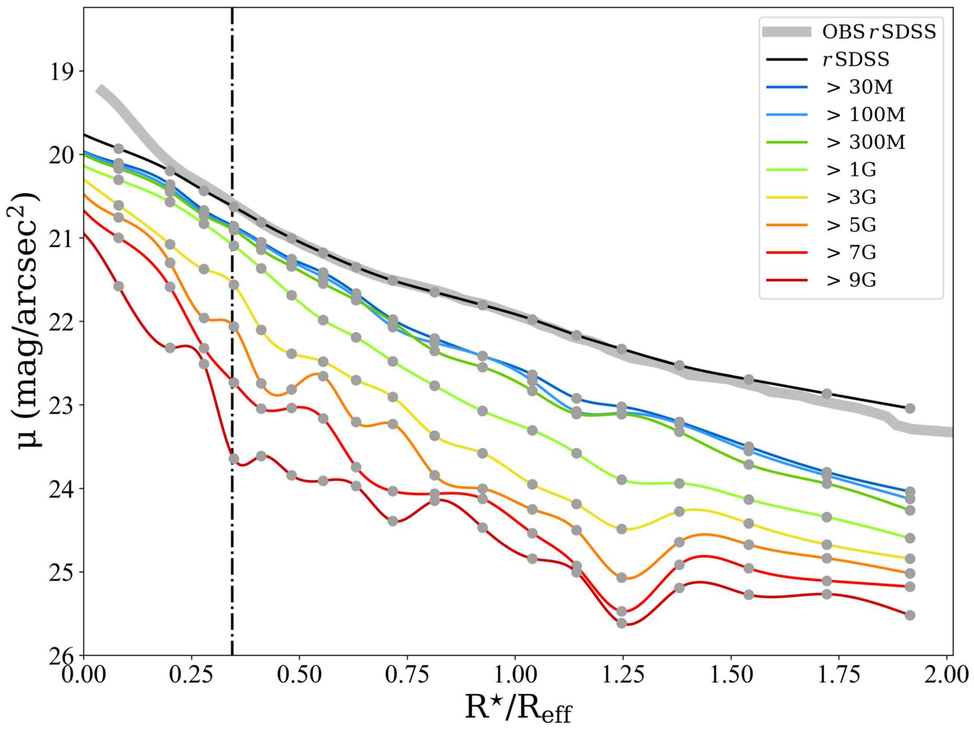

SDSS color profiles

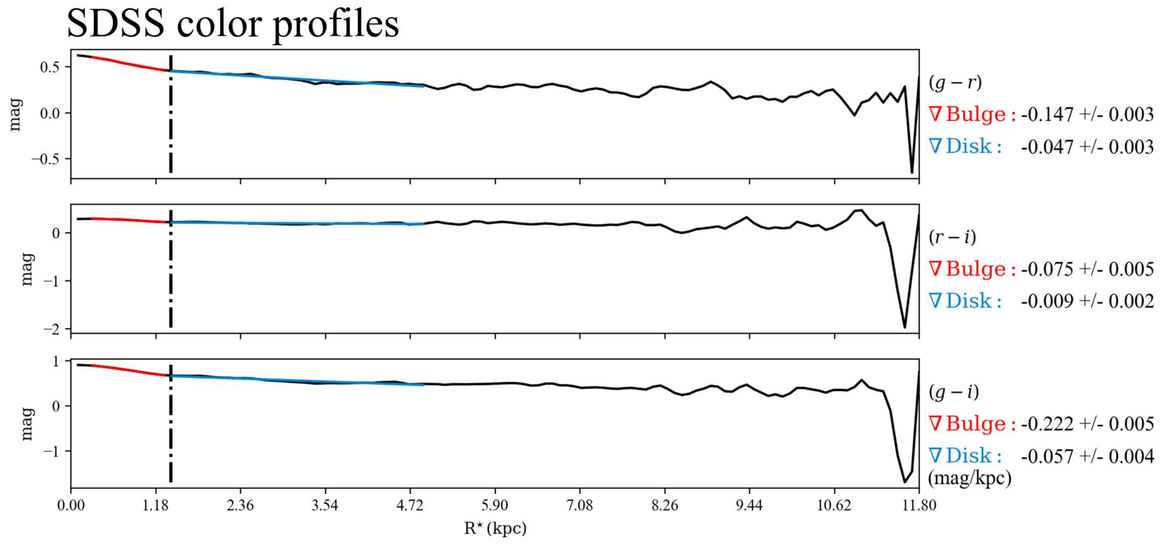

Log. of cumulative present stellar mass profiles

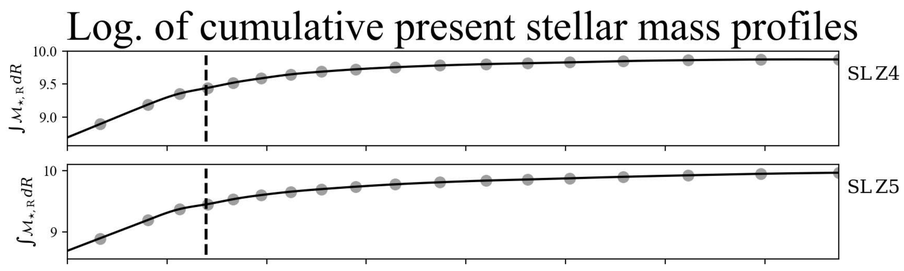

Stellar metallicity/Age & Hα flux/EW profiles

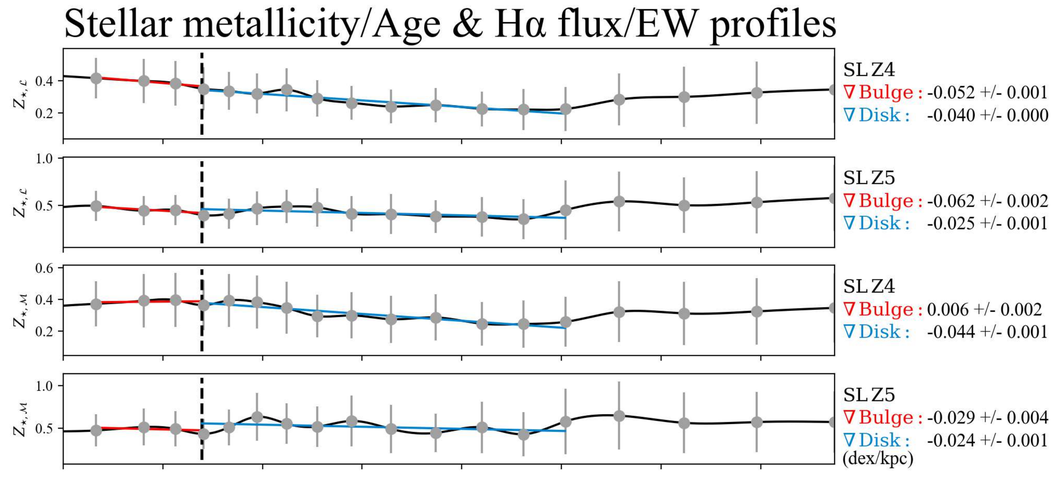

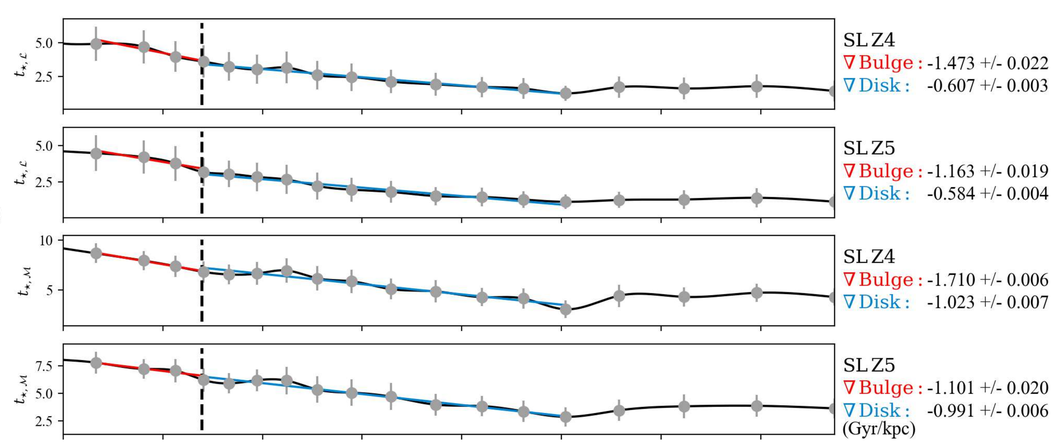

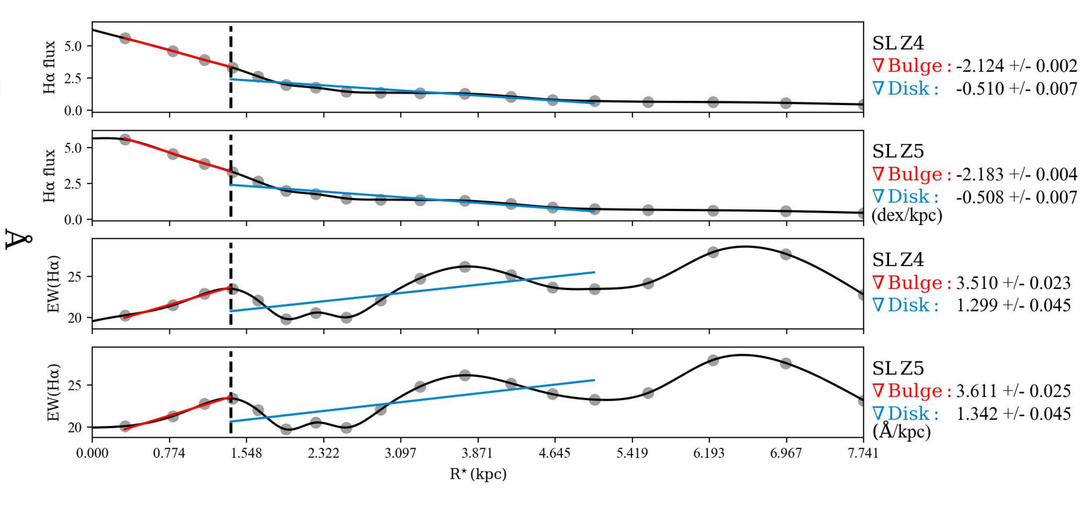

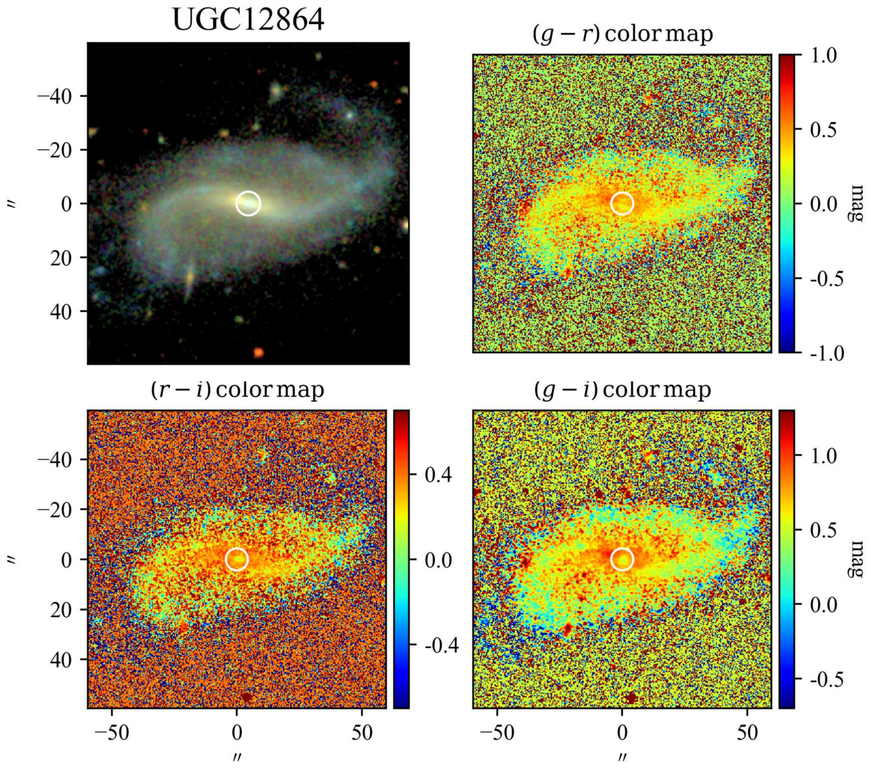

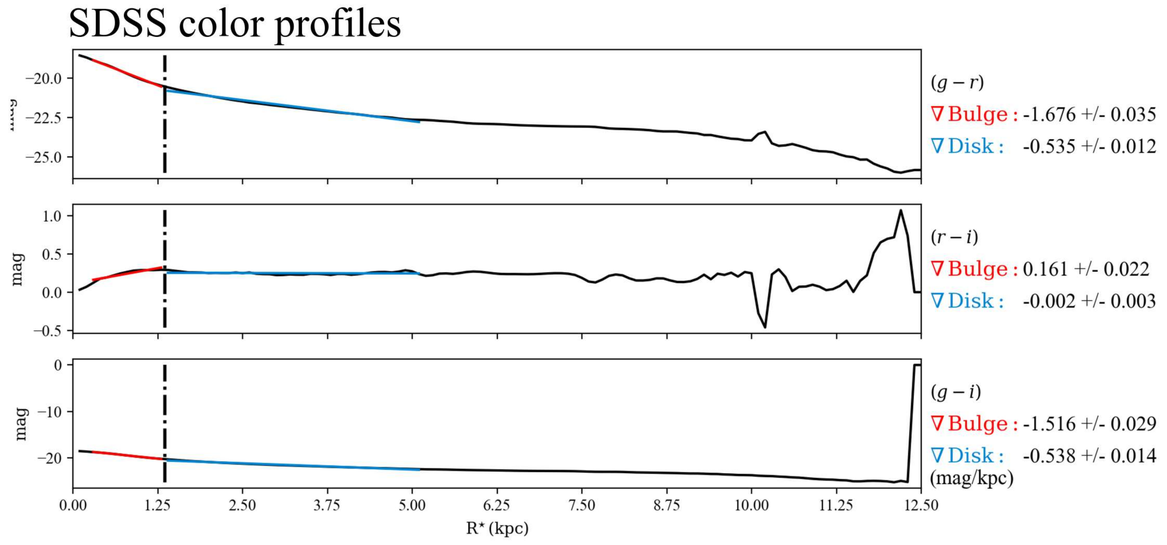

SBP decomposition of SDSS r band

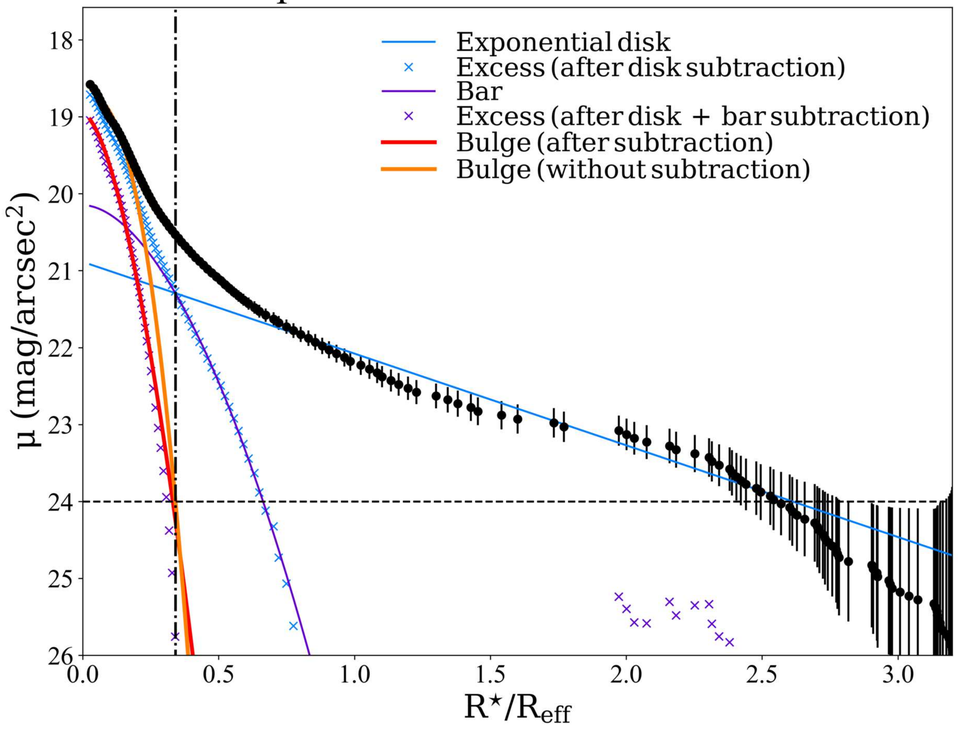

$\mathcal{RY}$ SBPs

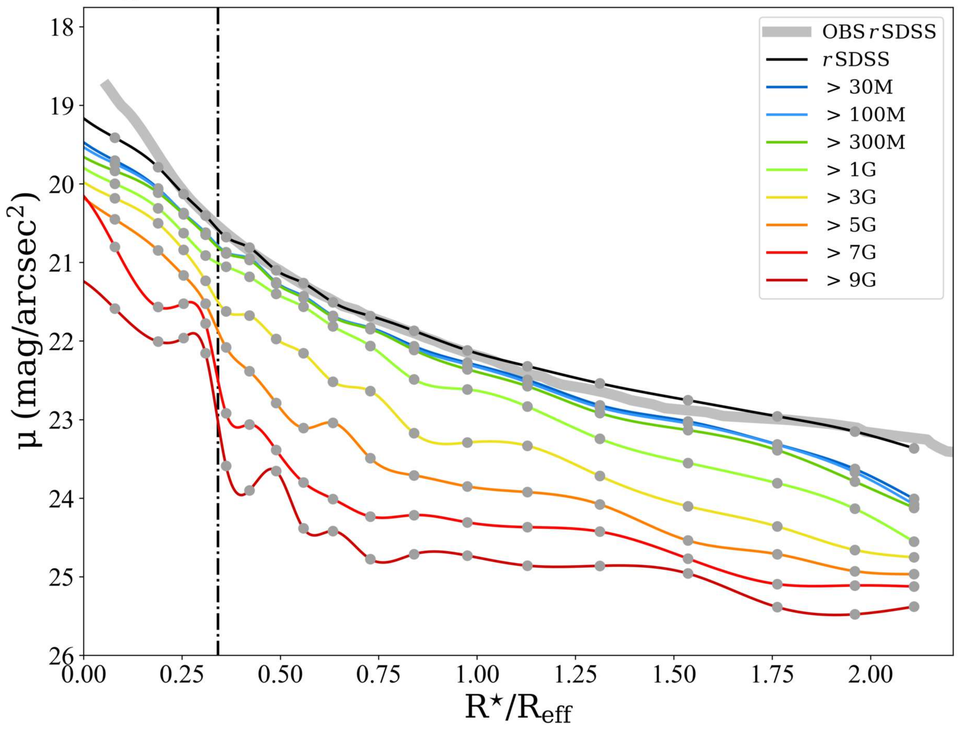

Stellar Continuum

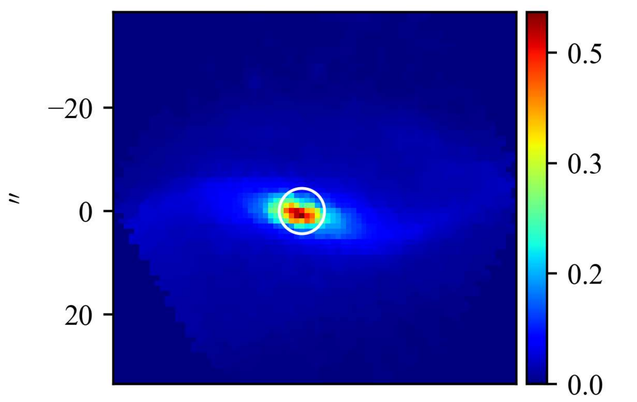

$\mathcal{M}_{\star,\mathrm{P}}$

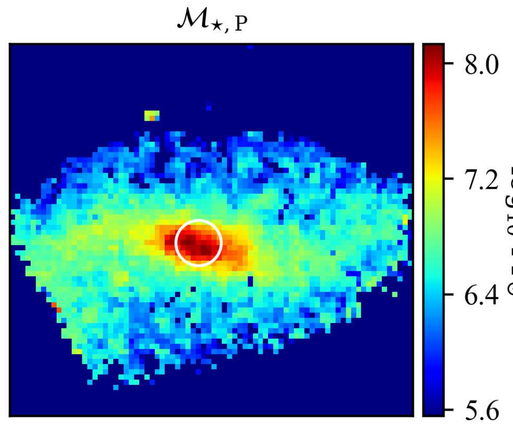

Log. of cumulative present stellar mass profiles

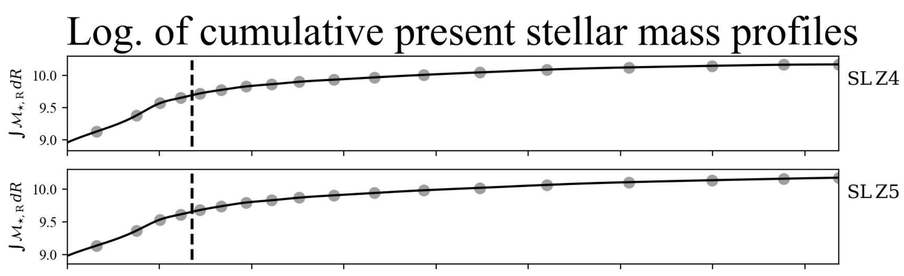

$Z_{\star,\mathcal{L}}$

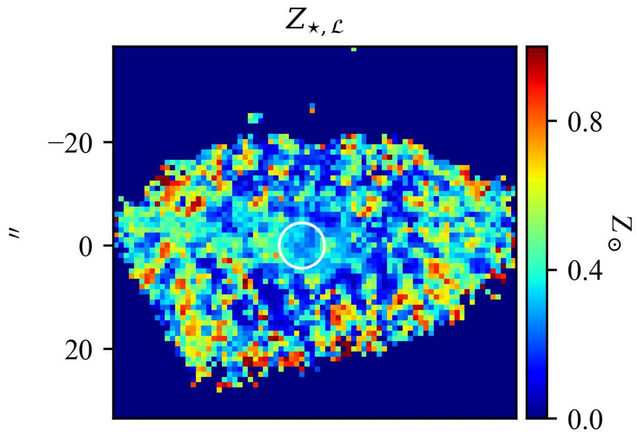

$Z_{\star,\mathcal{M}}$

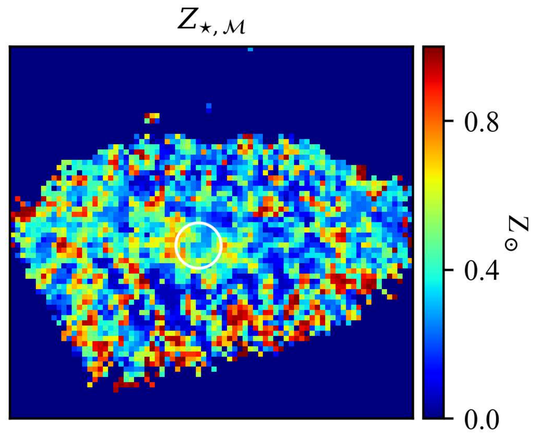

Stellar metallicity/Age & Hα flux/EW profiles

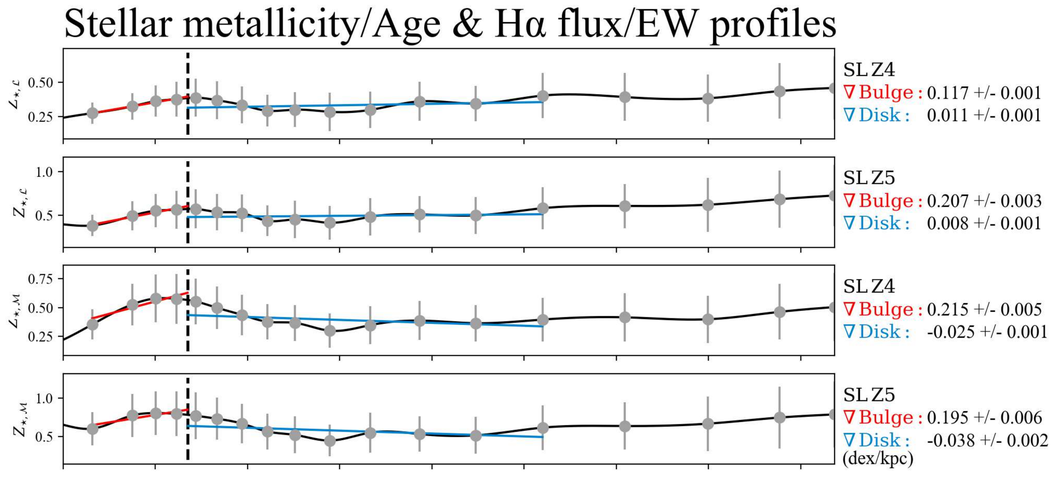

$t_{\star,\mathcal{L}}$

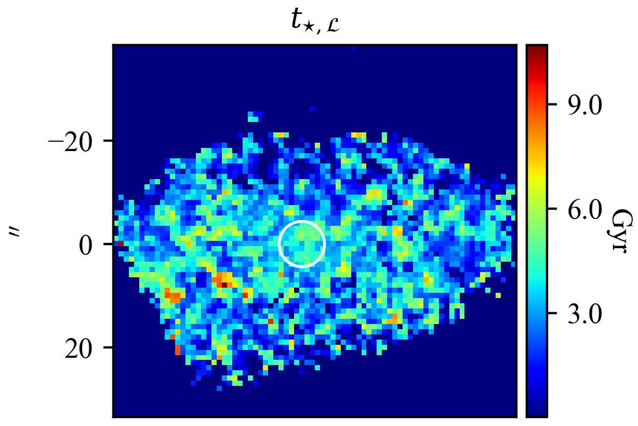

$t_{\star,\mathcal{M}}$

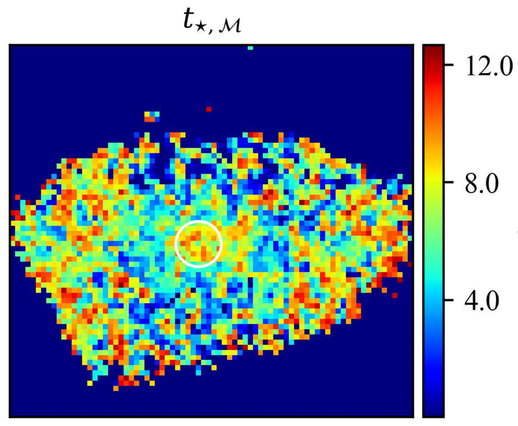

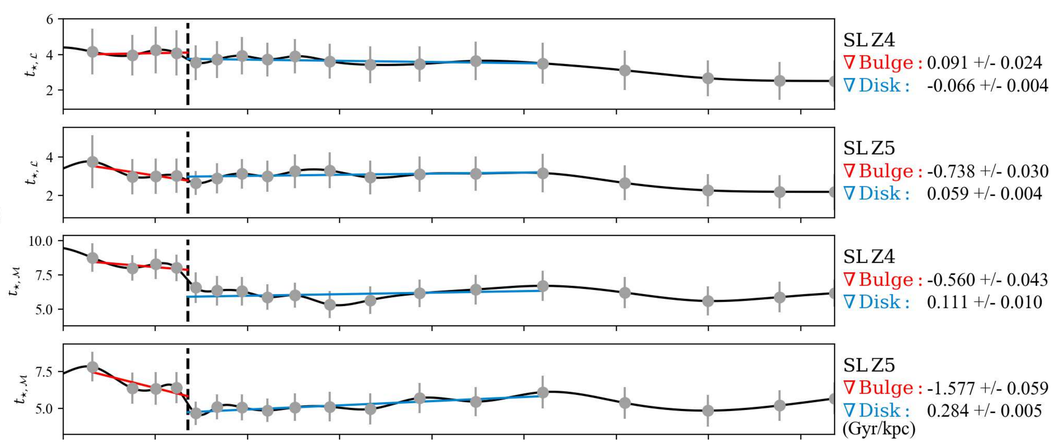

Hα flux

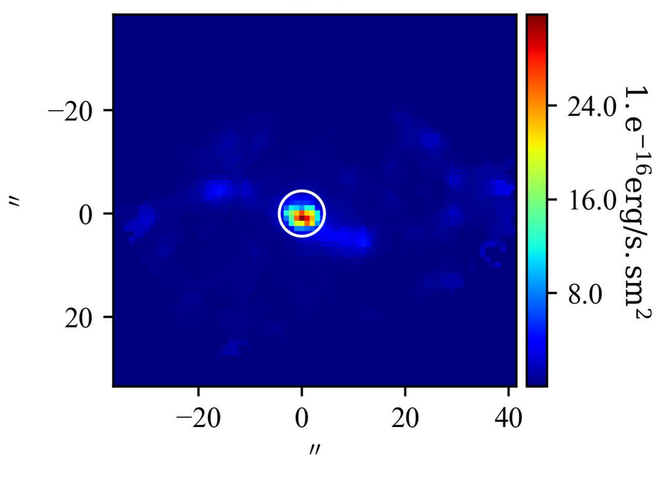

EW(Hα)

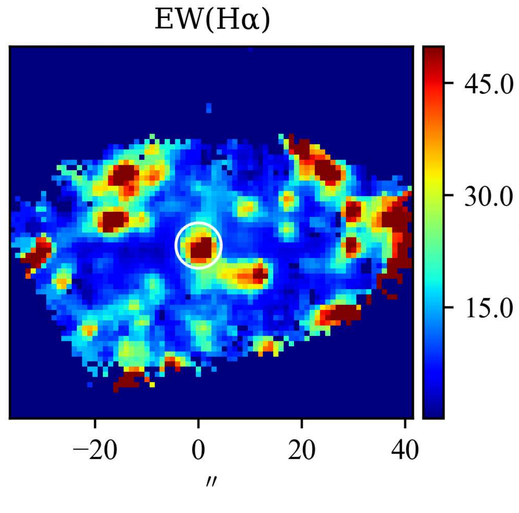

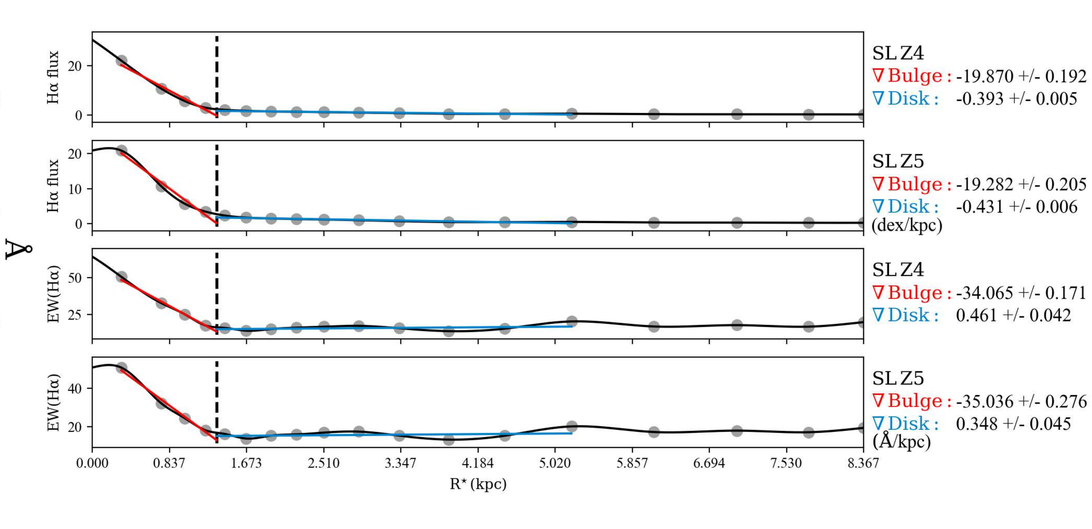

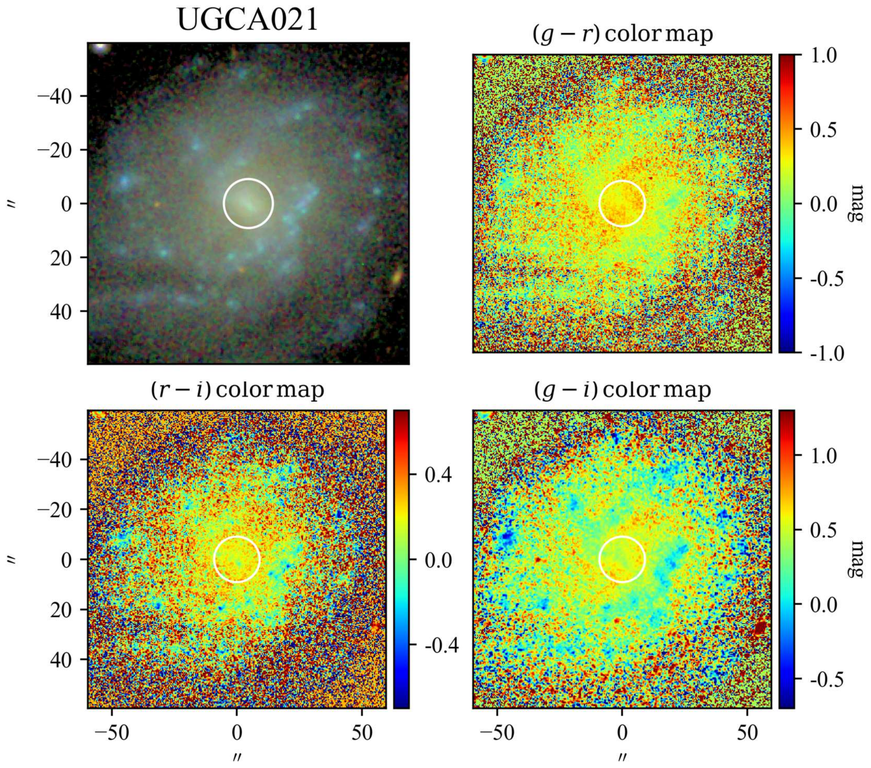

SBP decomposition of SDSS r band

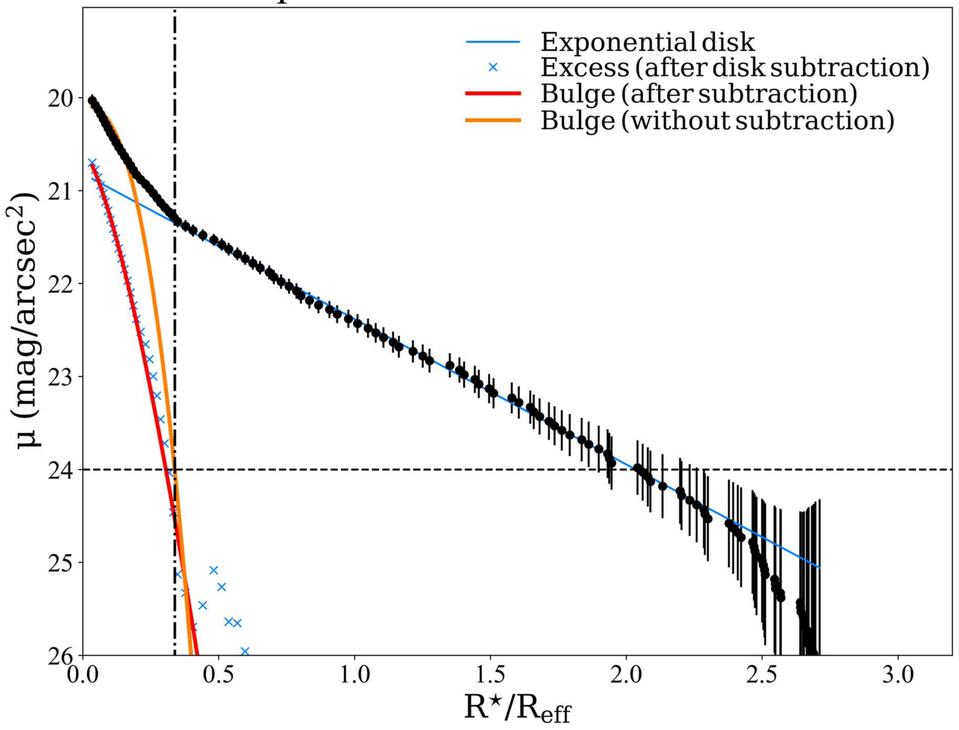

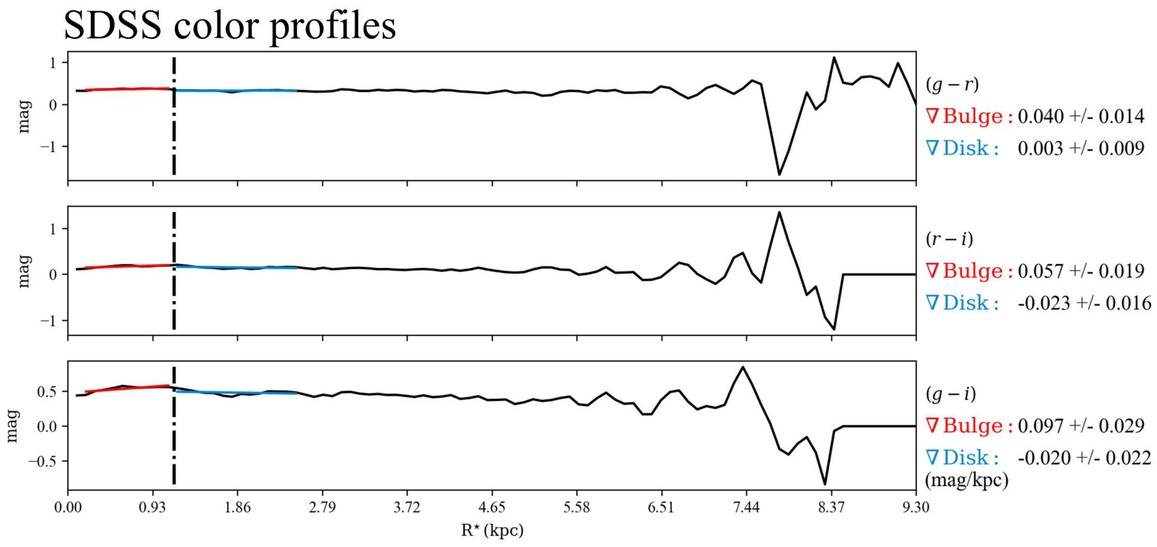

$\mathcal{RV}$ SBPs

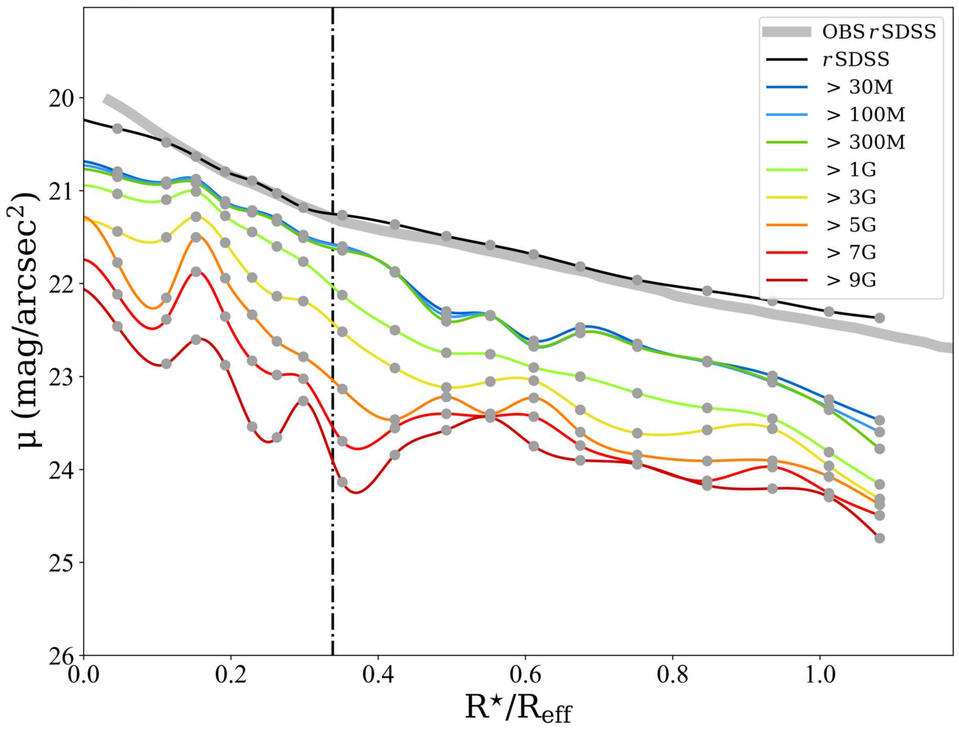

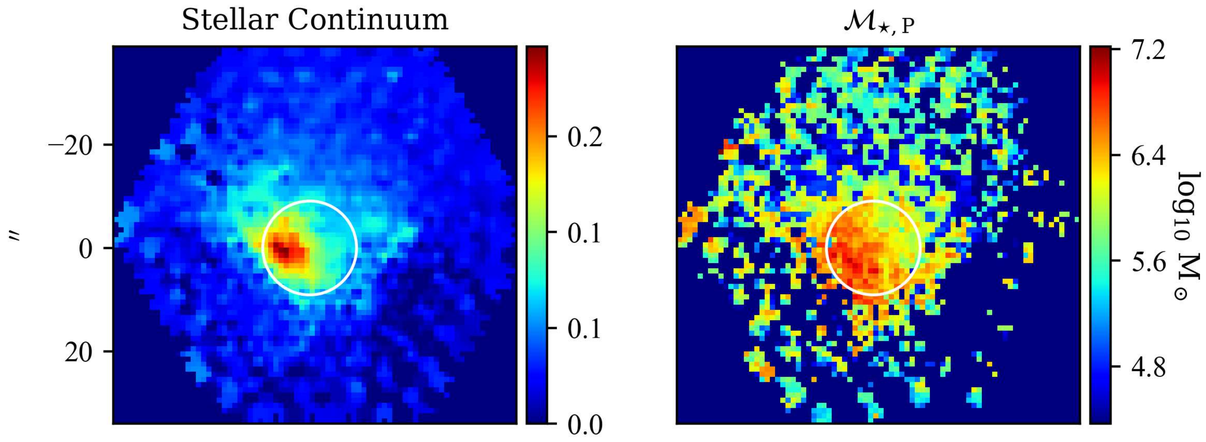

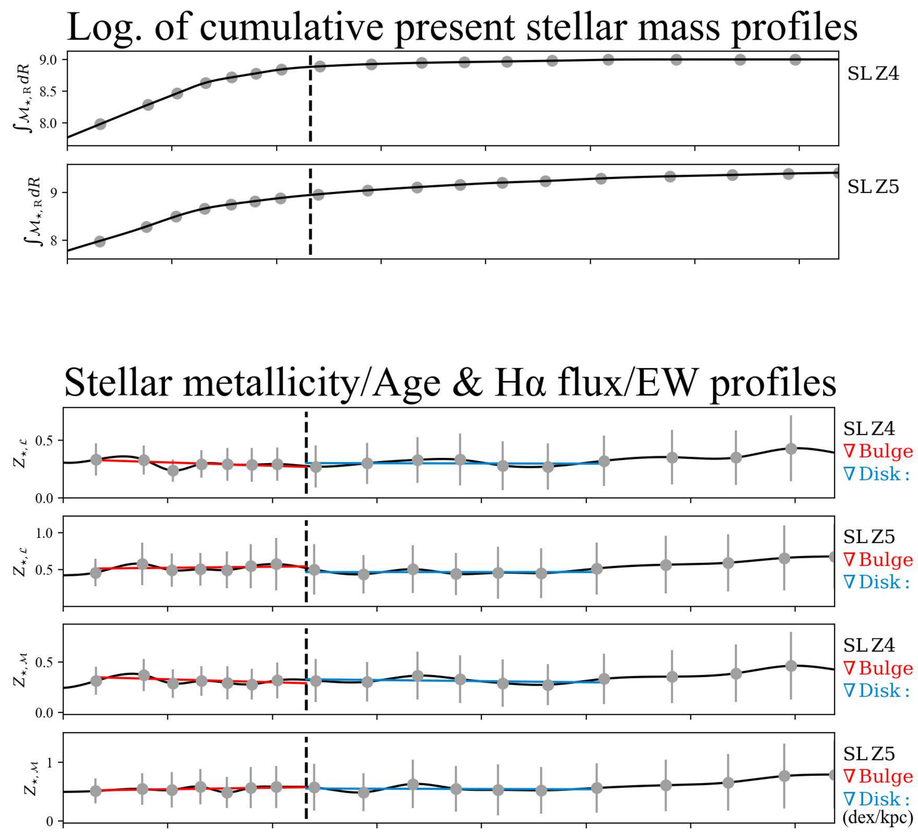

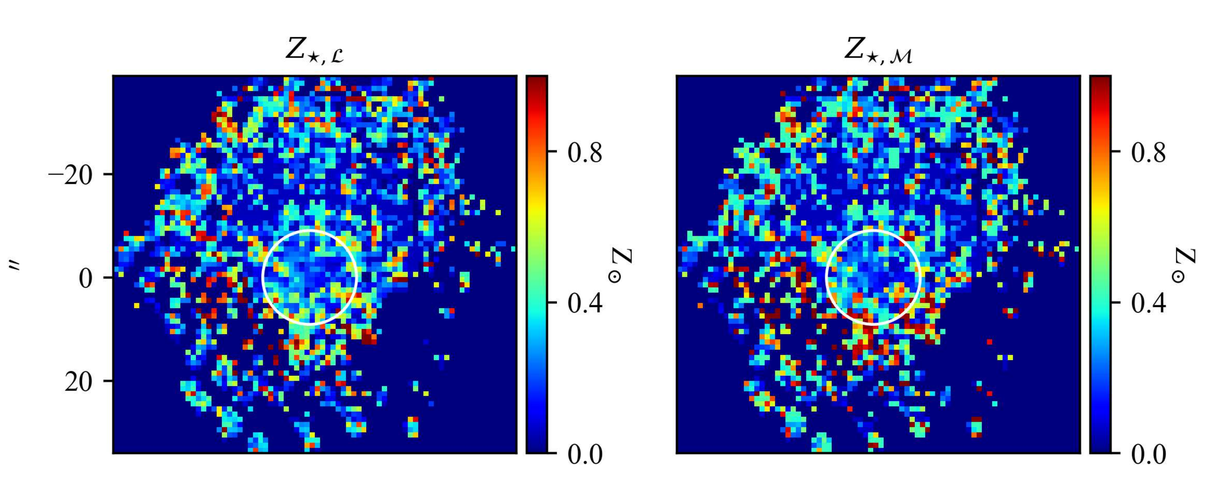

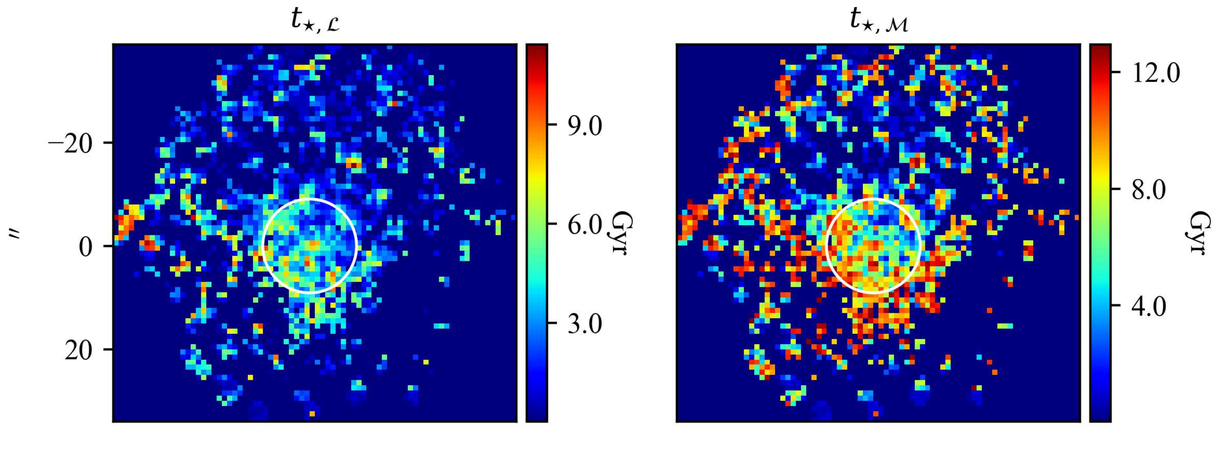

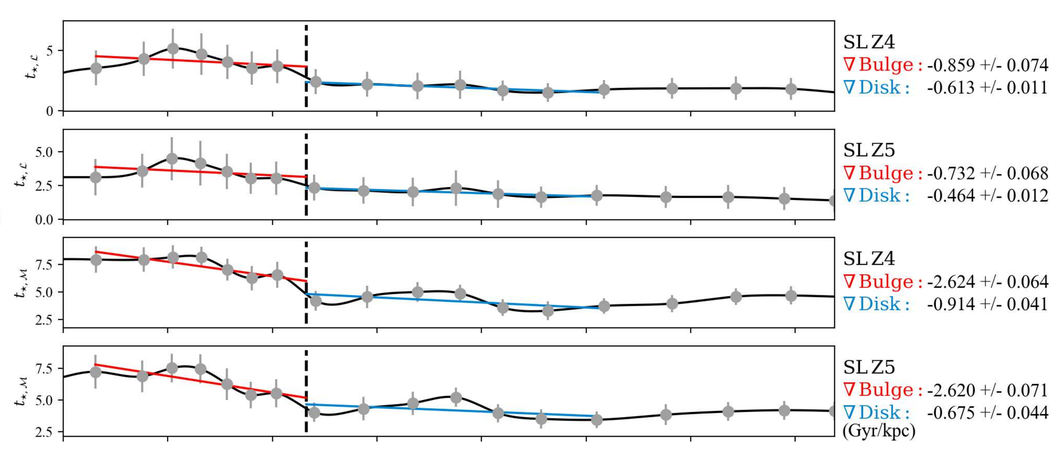

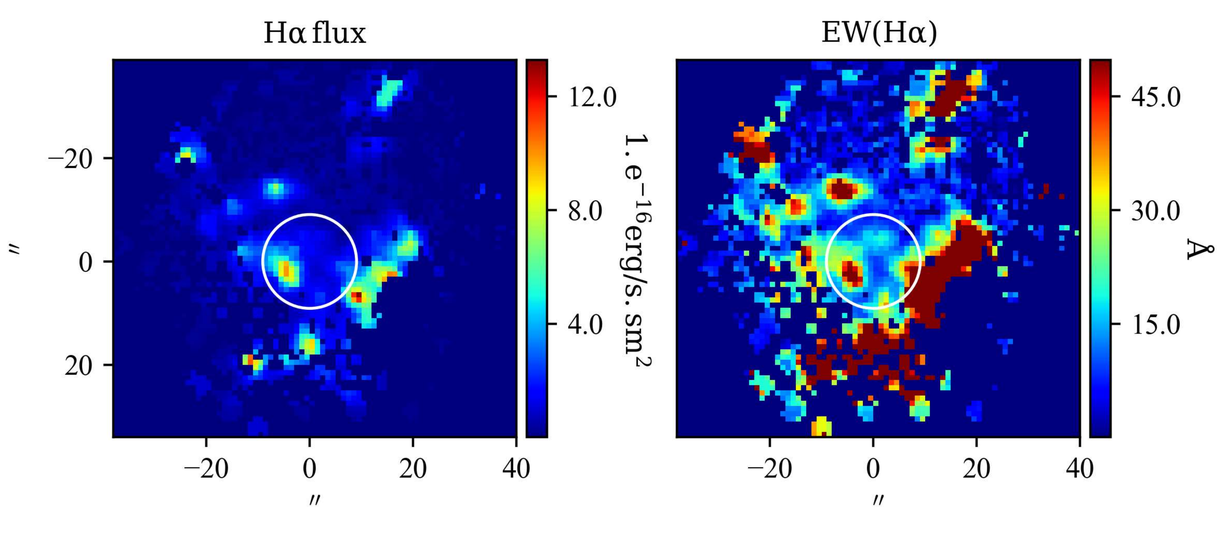

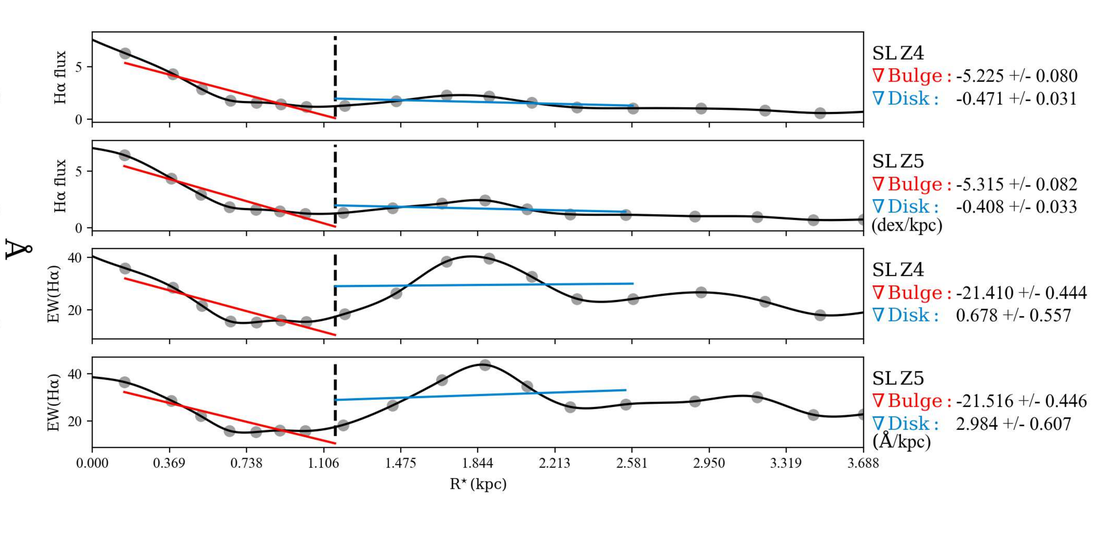

Appendix B

Outcome from the disk subtraction procedure for the LTG sample

From top to bottom, left to right, this appendix section presents:

i. The true-color image of the galaxy, with the overplotted small black circle depicting the diameter ($2{\cdot}R_C$) of the region from which the bulge spectrum was extracted, the white circle corresponding to $2{\cdot}R_B$, and the outer black circle showing the *equivalent* diameter ($2{\cdot}R_D$) of the region of the disk that was used to determine the average spectrum for the disk. In the right-hand side it is presented the observed SDSS g-band SBP (dark dots) with its uncertainties σ. The three radial surface brightness models tested for the disk are overlaid: blue solid line – standard exponential disk (**expD**); green solid line – inwardly flattening disk (**flatD**); red solid line – centrally depressed disk (**decrD**)). The vertical dashed line represents R_C, whereas the dashed-doted vertical line R_B. The grey vertical line depicts R_D.

ii. The resulting spectra and respective spectral fits for the galaxy: the top panel shows the normalized spectra of the bulge (red), disk (blue) and scaled spectrum of the disk (light-blue) according to the respective exponential disk model. The SDSS g-band transmission curve is overlaid in open-grey. The bottom panels display the resulting net spectrum of the bulge after subtraction of the three different models for the disk and the respective residuals. Labels on the r.h.s of the panel list the stellar mass $\log(\mathcal{M}_\star)$, and mass-weighted mean age and metallicity ($\langle t_{\star,B}\rangle_{\mathcal{M}}$ and $\langle Z_{\star,B}\rangle_{\mathcal{M}}$, respectively, for each of the fits, as obtained with STARLIGHT (with the SSP library Z4 and Z5; top-left and top-right, respectively) and FADO (with the SSP library Z4 and Z5; bottom-left and bottom-right, respectively).

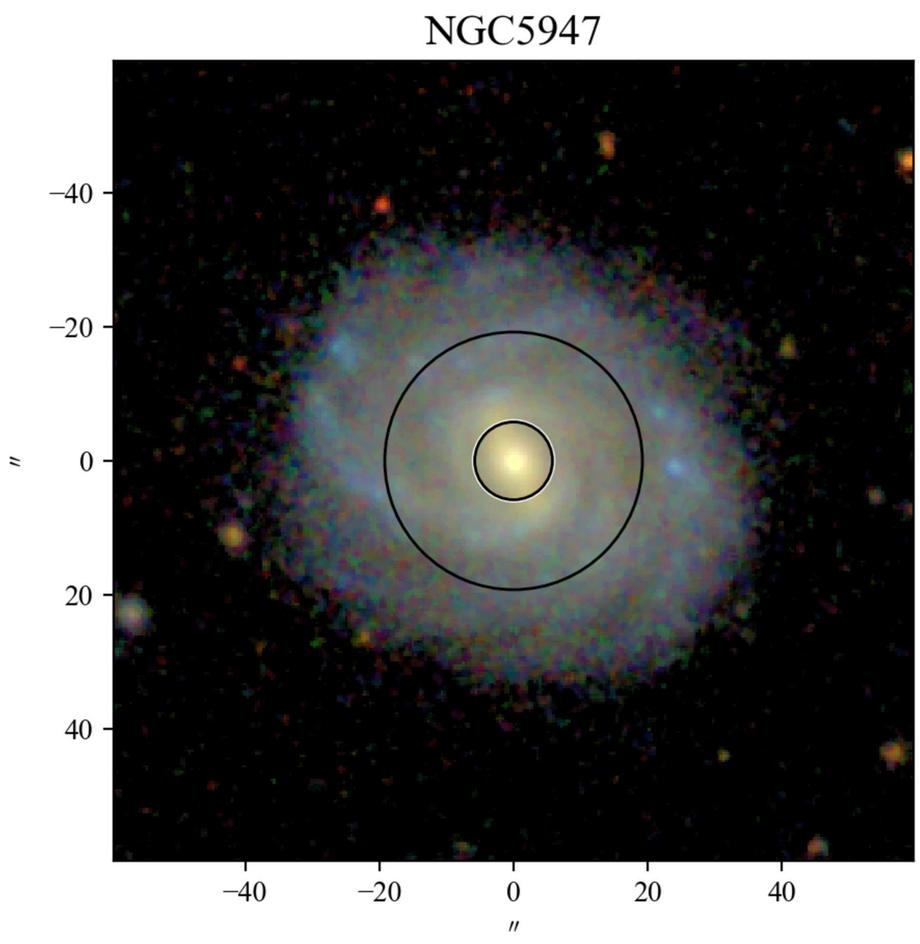
NGC5947
−40
−20
0
20
40
″
−40
−20
0
20
40
″

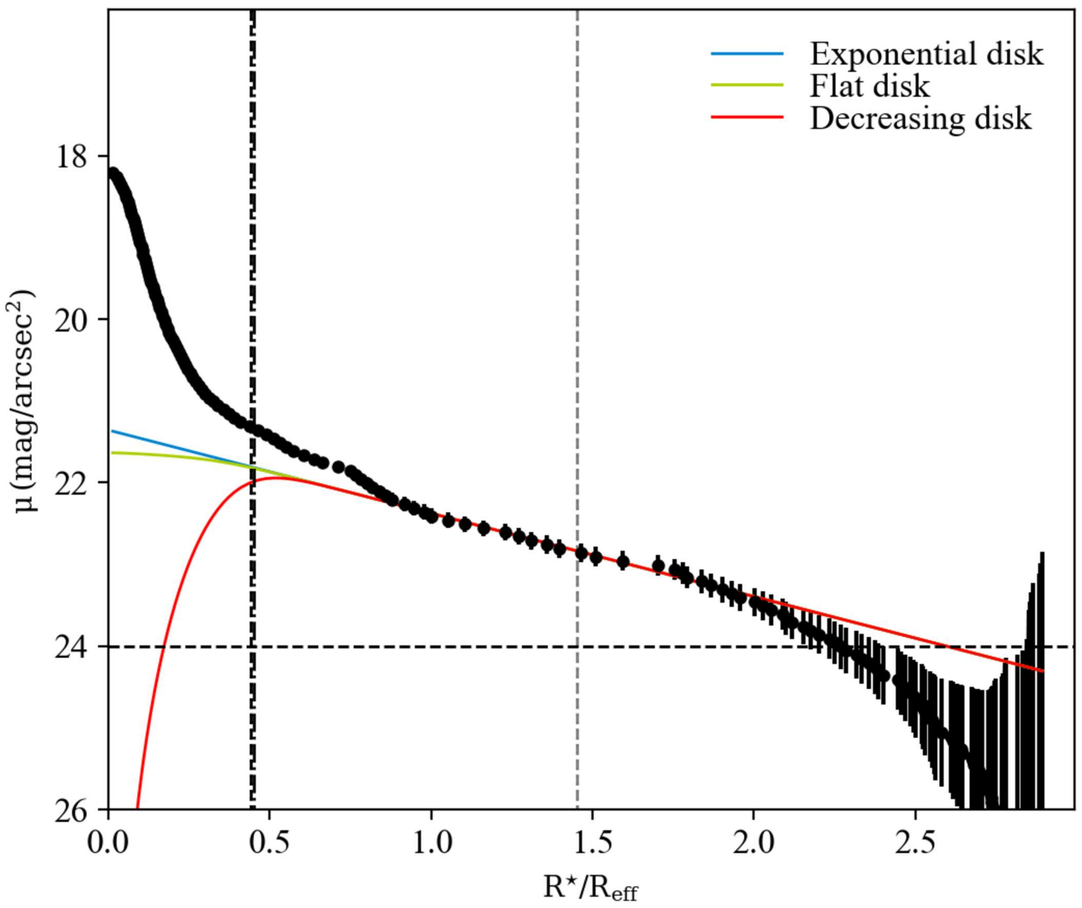
Exponential disk
Flat disk
Decreasing disk
μ (mag/arcsec²)
18
20
22
24
26
0.0
0.5
1.0
1.5
2.0
2.5
R⋆/Reff

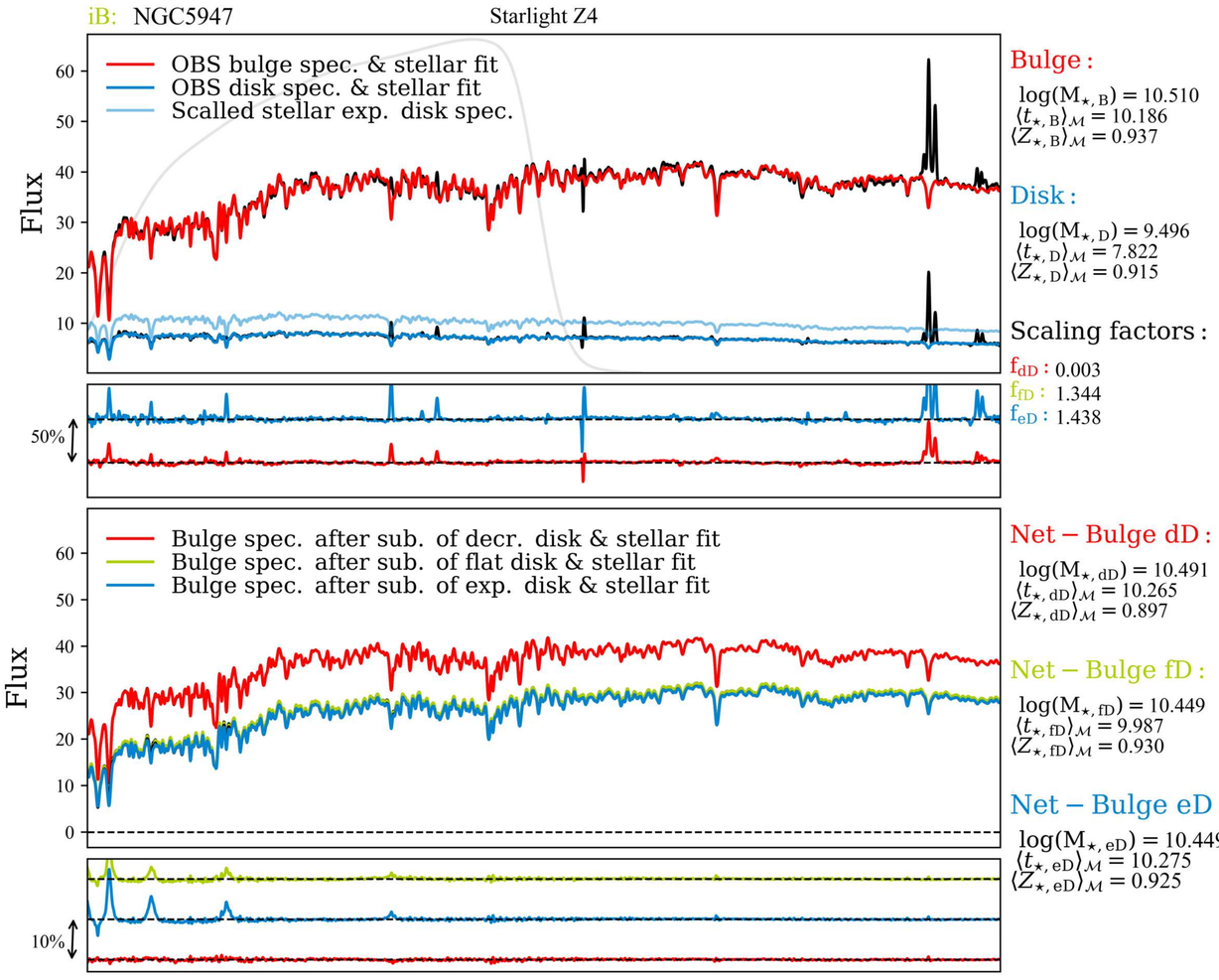
iB: NGC5947
Starlight Z4
OBS bulge spec. & stellar fit
OBS disk spec. & stellar fit
Scalled stellar exp. disk spec.
Flux
50%
Bulge :
log(M⋆, B) = 10.510
⟨t⋆, B⟩M = 10.186
⟨Z⋆, B⟩M = 0.937
Disk :
log(M⋆, D) = 9.496
⟨t⋆, D⟩M = 7.822
⟨Z⋆, D⟩M = 0.915
Scaling factors :
fdD : 0.003
ffD : 1.344
feD : 1.438
Bulge spec. after sub. of decr. disk & stellar fit
Bulge spec. after sub. of flat disk & stellar fit
Bulge spec. after sub. of exp. disk & stellar fit
10%
Net − Bulge dD :
log(M⋆, dD) = 10.491
⟨t⋆, dD⟩M = 10.265
⟨Z⋆, dD⟩M = 0.897
Net − Bulge fD :
log(M⋆, fD) = 10.449
⟨t⋆, fD⟩M = 9.987
⟨Z⋆, fD⟩M = 0.930
Net − Bulge eD :
log(M⋆, eD) = 10.449
⟨t⋆, eD⟩M = 10.275
⟨Z⋆, eD⟩M = 0.925

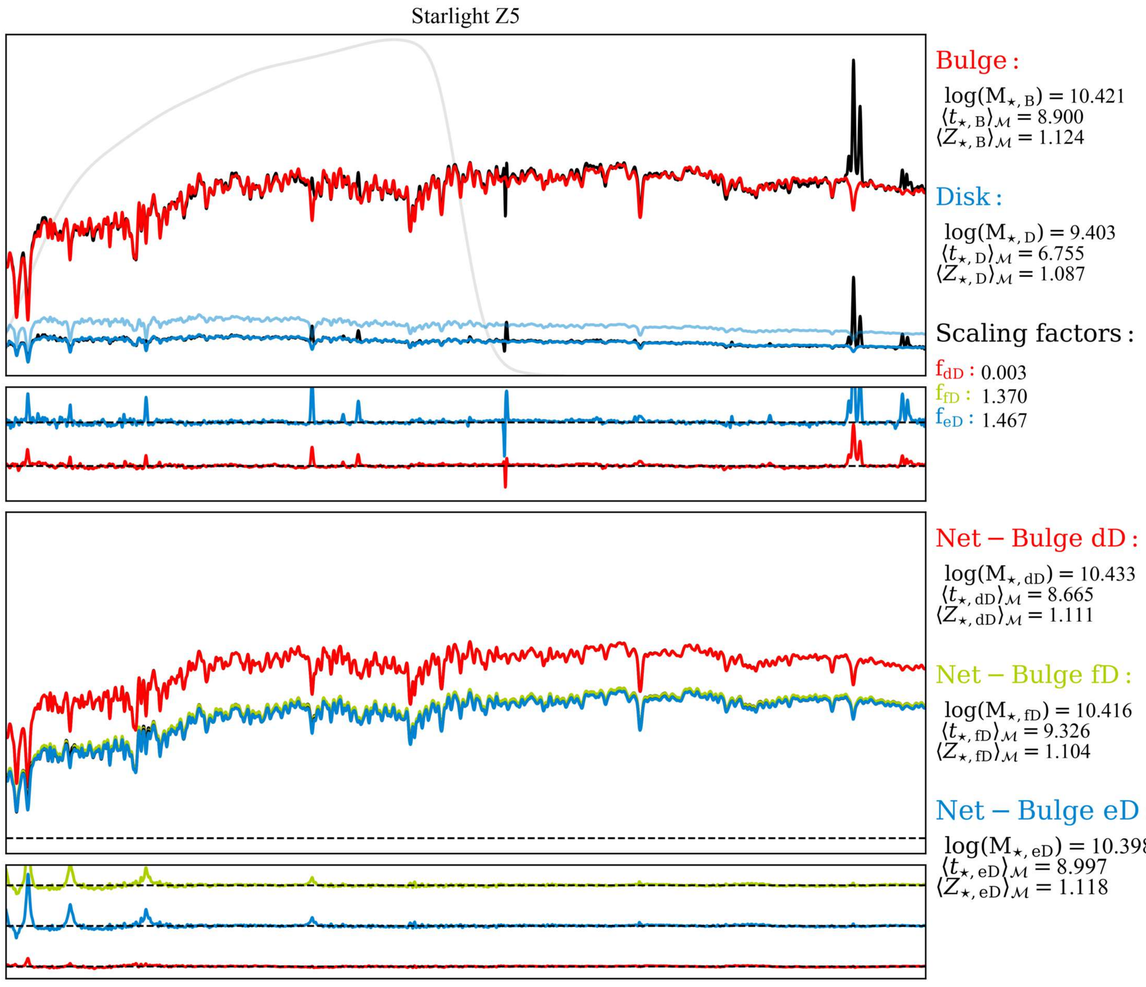
Starlight Z5
Bulge :
log(M⋆, B) = 10.421
⟨t⋆, B⟩M = 8.900
⟨Z⋆, B⟩M = 1.124
Disk :
log(M⋆, D) = 9.403
⟨t⋆, D⟩M = 6.755
⟨Z⋆, D⟩M = 1.087
Scaling factors :
fdD : 0.003
ffD : 1.370
feD : 1.467
Net − Bulge dD :
log(M⋆, dD) = 10.433
⟨t⋆, dD⟩M = 8.665
⟨Z⋆, dD⟩M = 1.111
Net − Bulge fD :
log(M⋆, fD) = 10.416
⟨t⋆, fD⟩M = 9.326
⟨Z⋆, fD⟩M = 1.104
Net − Bulge eD :
log(M⋆, eD) = 10.398
⟨t⋆, eD⟩M = 8.997
⟨Z⋆, eD⟩M = 1.118

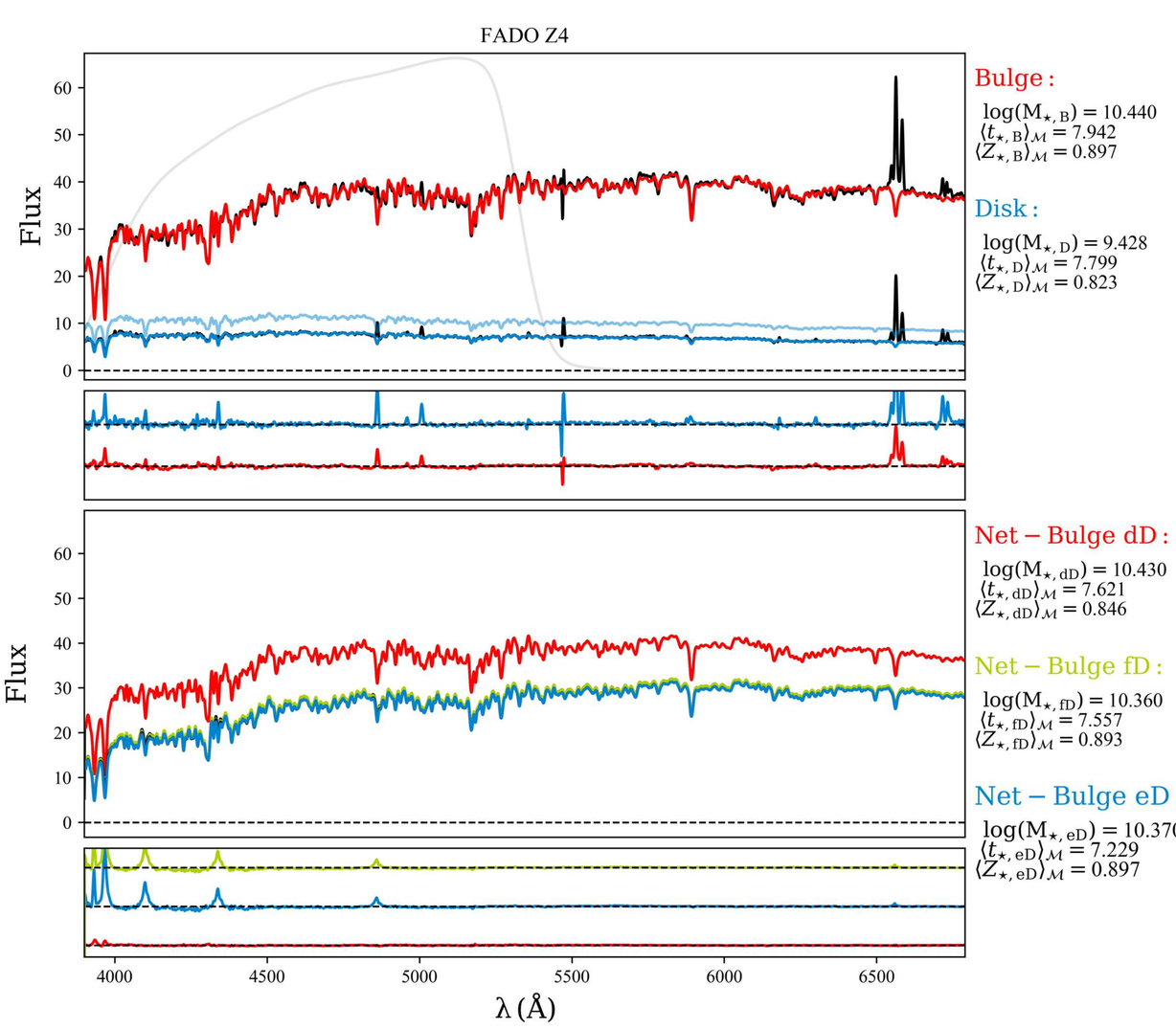
FADO Z4
Flux
Bulge :
log(M⋆, B) = 10.440
⟨t⋆, B⟩M = 7.942
⟨Z⋆, B⟩M = 0.897
Disk :
log(M⋆, D) = 9.428
⟨t⋆, D⟩M = 7.799
⟨Z⋆, D⟩M = 0.823
Net − Bulge dD :
log(M⋆, dD) = 10.430
⟨t⋆, dD⟩M = 7.621
⟨Z⋆, dD⟩M = 0.846
Net − Bulge fD :
log(M⋆, fD) = 10.360
⟨t⋆, fD⟩M = 7.557
⟨Z⋆, fD⟩M = 0.893
Net − Bulge eD :
log(M⋆, eD) = 10.370
⟨t⋆, eD⟩M = 7.229
⟨Z⋆, eD⟩M = 0.897
λ (Å)

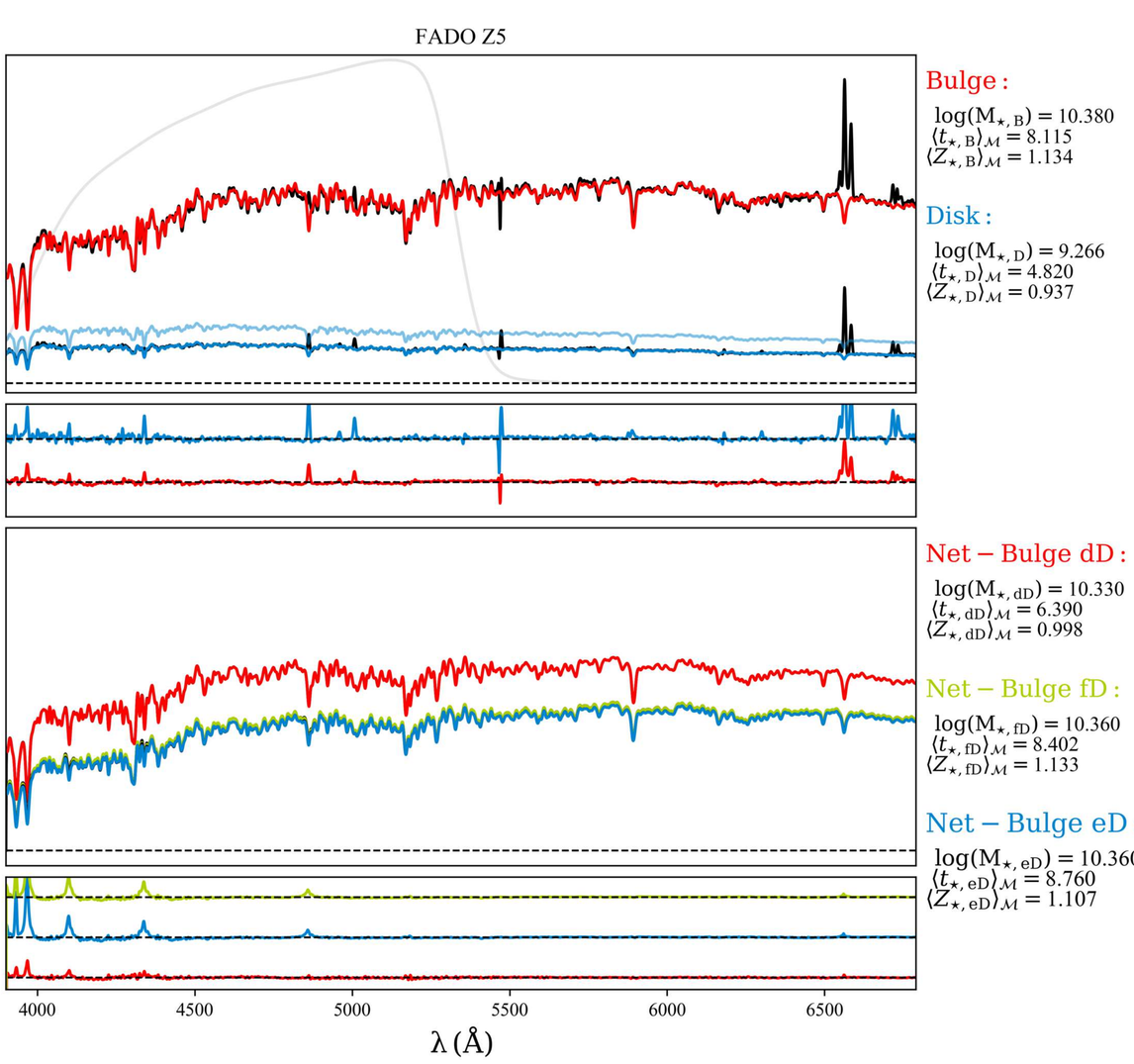
FADO Z5
Bulge :
log(M⋆, B) = 10.380
⟨t⋆, B⟩M = 8.115
⟨Z⋆, B⟩M = 1.134
Disk :
log(M⋆, D) = 9.266
⟨t⋆, D⟩M = 4.820
⟨Z⋆, D⟩M = 0.937
Net − Bulge dD :
log(M⋆, dD) = 10.330
⟨t⋆, dD⟩M = 6.390
⟨Z⋆, dD⟩M = 0.998
Net − Bulge fD :
log(M⋆, fD) = 10.360
⟨t⋆, fD⟩M = 8.402
⟨Z⋆, fD⟩M = 1.133
Net − Bulge eD :
log(M⋆, eD) = 10.360
⟨t⋆, eD⟩M = 8.760
⟨Z⋆, eD⟩M = 1.107
λ (Å)

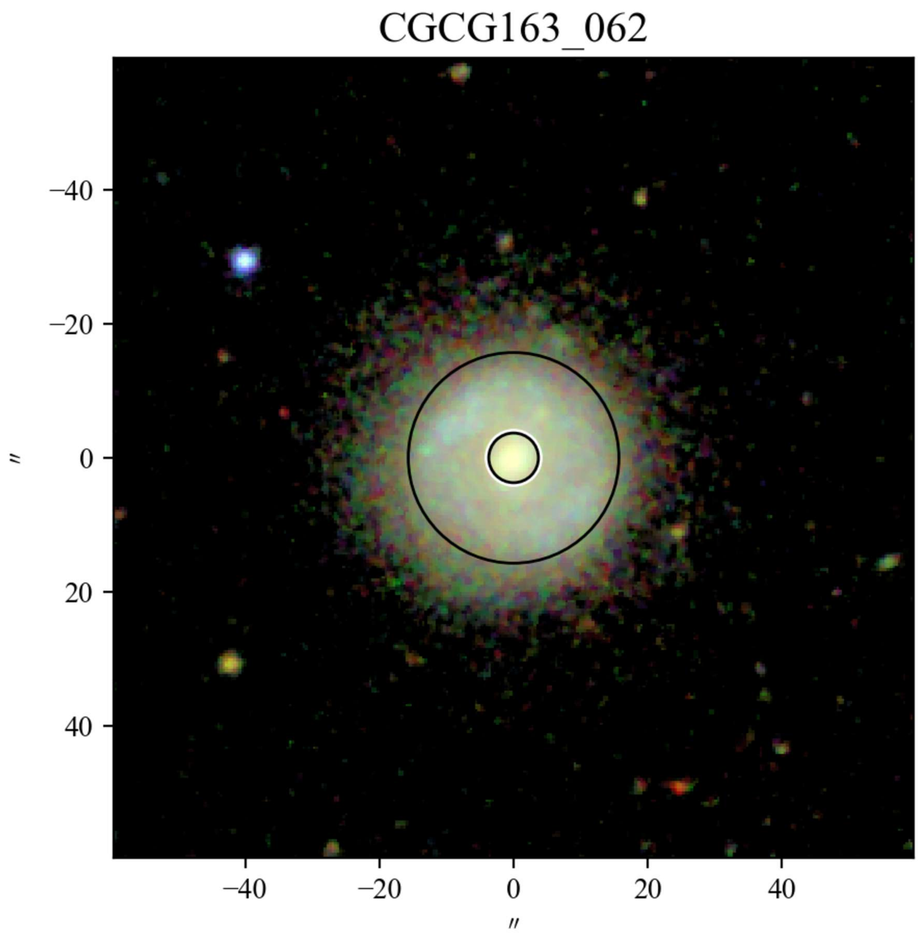
CGCG163_062
−40
−20
0
20
40
″
−40
−20
0
20
40
″

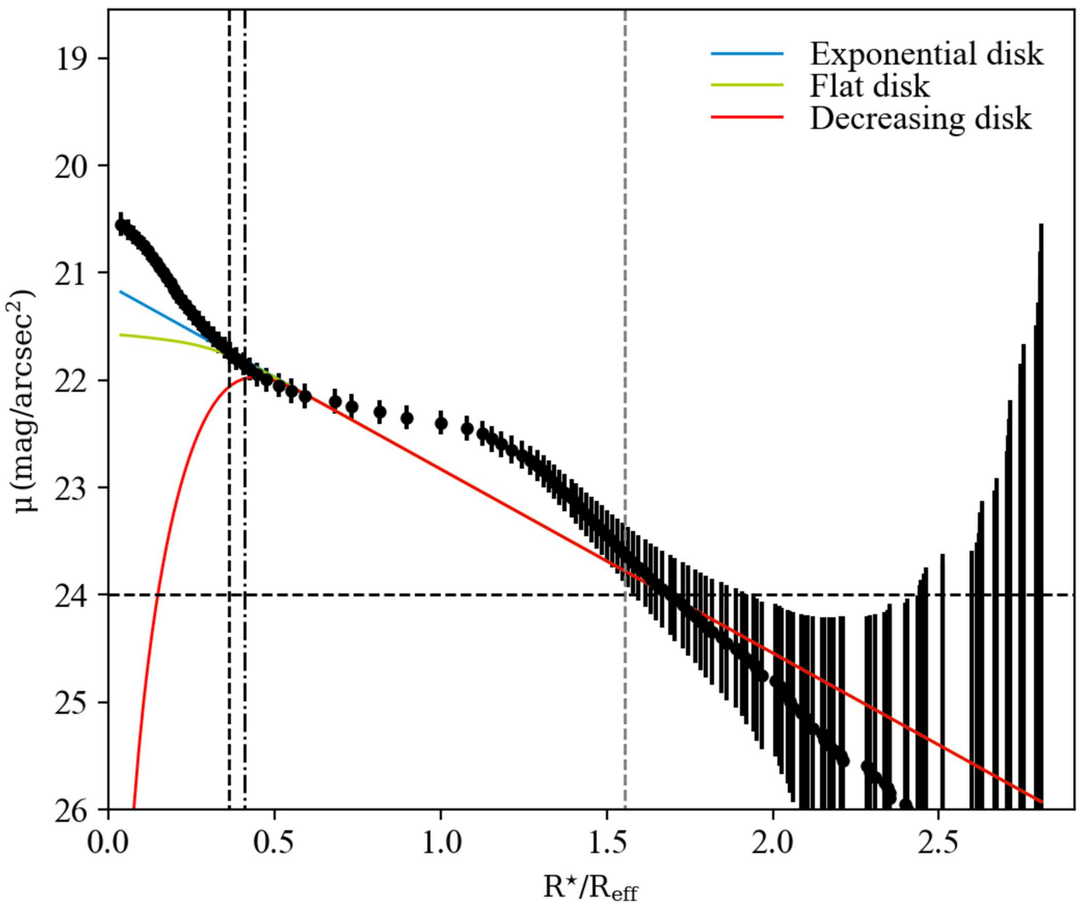
Exponential disk
Flat disk
Decreasing disk
μ (mag/arcsec²)
19
20
21
22
23
24
25
26
0.0
0.5
1.0
1.5
2.0
2.5
R⋆/Reff

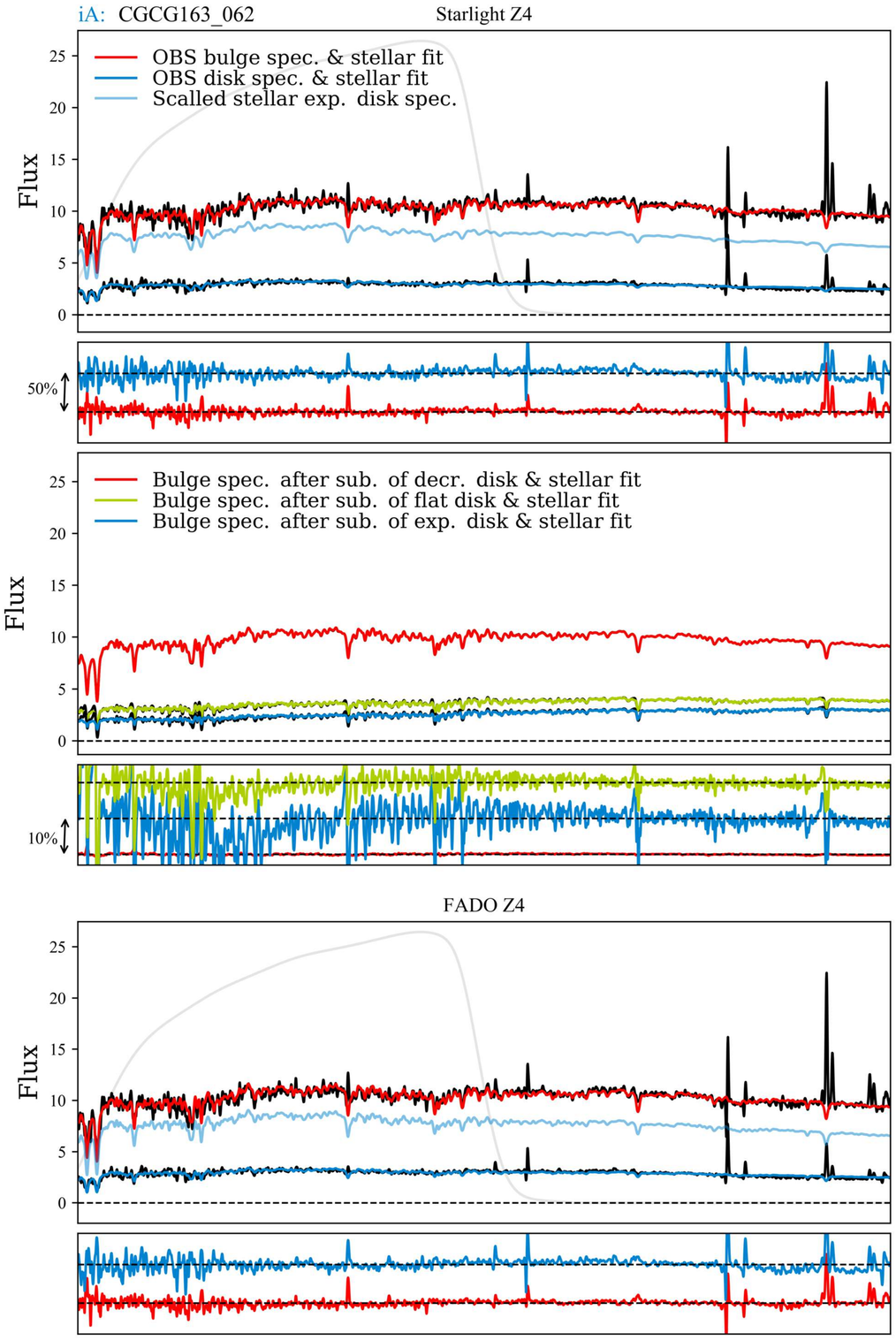
iA: CGCG163_062
Starlight Z4
OBS bulge spec. & stellar fit
OBS disk spec. & stellar fit
Scalled stellar exp. disk spec.
Flux
50%
Bulge :
log(M⋆, B) = 9.467
⟨t⋆, B⟩M = 6.421
⟨Z⋆, B⟩M = 0.728
Disk :
log(M⋆, D) = 8.606
⟨t⋆, D⟩M = 4.748
⟨Z⋆, D⟩M = 0.285
Scaling factors :
fdD : 0.153
ffD : 2.288
feD : 2.649
Bulge spec. after sub. of decr. disk & stellar fit
Bulge spec. after sub. of flat disk & stellar fit
Bulge spec. after sub. of exp. disk & stellar fit
10%
Net − Bulge dD :
log(M⋆, dD) = 9.439
⟨t⋆, dD⟩M = 6.654
⟨Z⋆, dD⟩M = 0.631
Net − Bulge fD :
log(M⋆, fD) = 9.602
⟨t⋆, fD⟩M = 11.625
⟨Z⋆, fD⟩M = 0.998
Net − Bulge eD :
log(M⋆, eD) = 9.641
⟨t⋆, eD⟩M = 12.545
⟨Z⋆, eD⟩M = 0.997

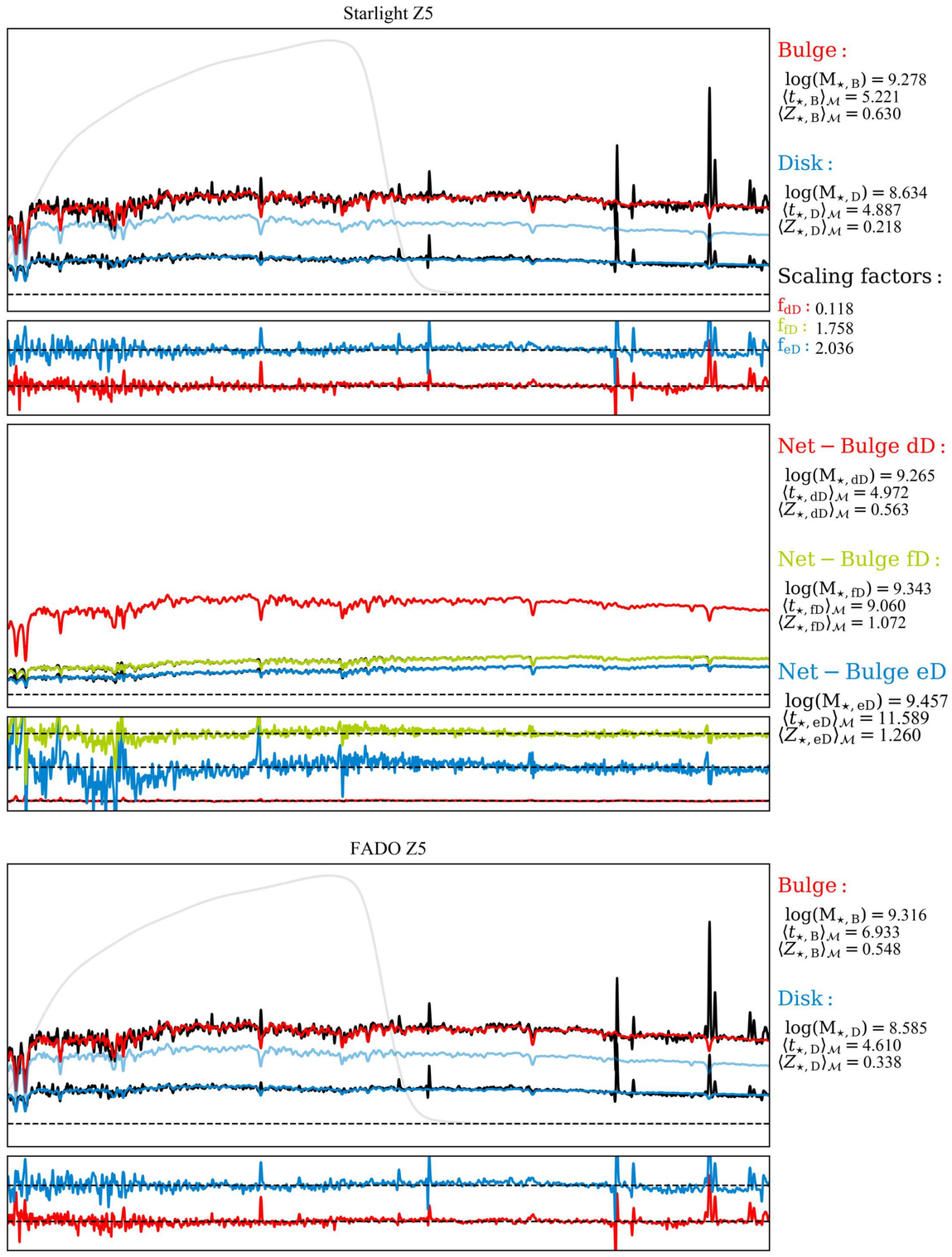
Starlight Z5
Bulge :
log(M⋆, B) = 9.278
⟨t⋆, B⟩M = 5.221
⟨Z⋆, B⟩M = 0.630
Disk :
log(M⋆, D) = 8.634
⟨t⋆, D⟩M = 4.887
⟨Z⋆, D⟩M = 0.218
Scaling factors :
fdD : 0.118
ffD : 1.758
feD : 2.036
Net − Bulge dD :
log(M⋆, dD) = 9.265
⟨t⋆, dD⟩M = 4.972
⟨Z⋆, dD⟩M = 0.563
Net − Bulge fD :
log(M⋆, fD) = 9.343
⟨t⋆, fD⟩M = 9.060
⟨Z⋆, fD⟩M = 1.072
Net − Bulge eD :
log(M⋆, eD) = 9.457
⟨t⋆, eD⟩M = 11.589
⟨Z⋆, eD⟩M = 1.260

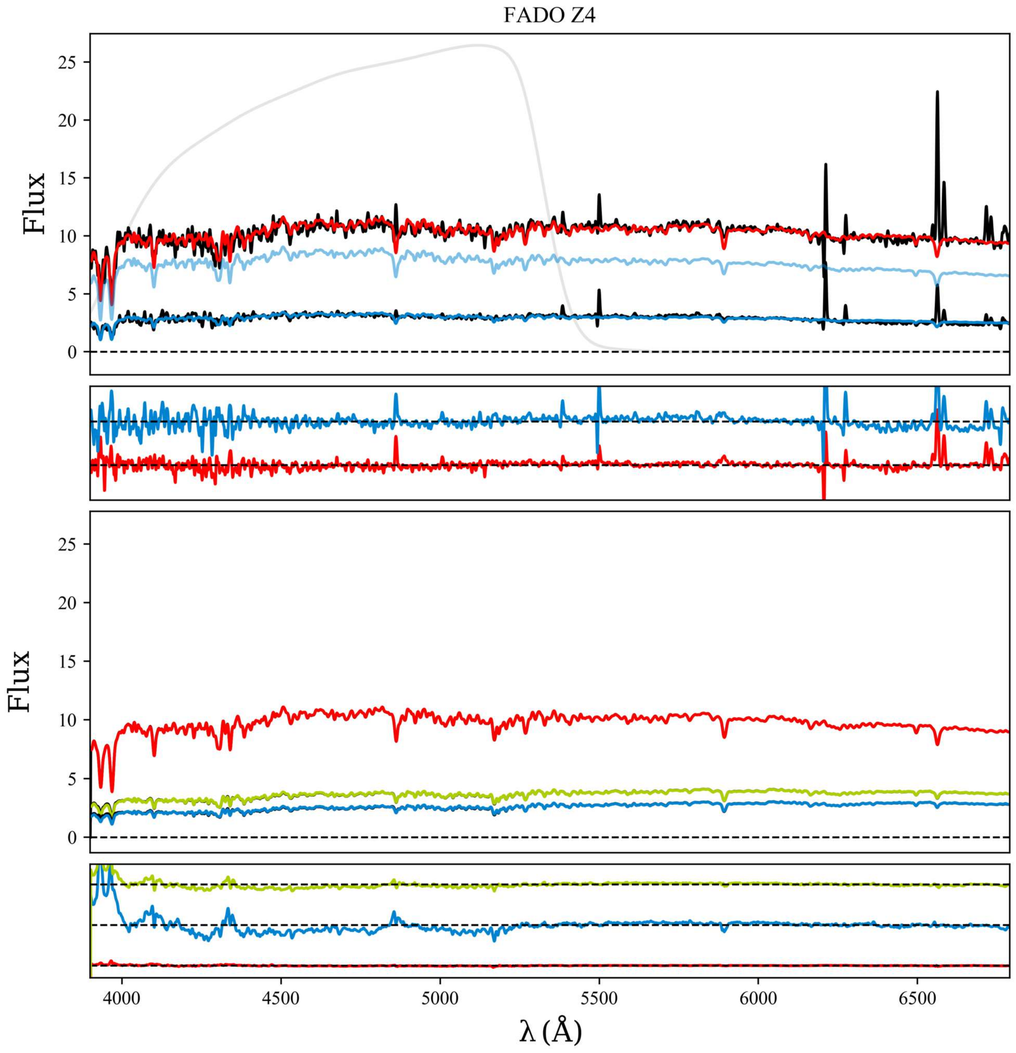
FADO Z4
Flux
Bulge :
log(M⋆, B) = 9.423
⟨t⋆, B⟩M = 6.380
⟨Z⋆, B⟩M = 0.639
Disk :
log(M⋆, D) = 8.544
⟨t⋆, D⟩M = 3.648
⟨Z⋆, D⟩M = 0.409
Net − Bulge dD :
log(M⋆, dD) = 9.384
⟨t⋆, dD⟩M = 5.596
⟨Z⋆, dD⟩M = 0.616
Net − Bulge fD :
log(M⋆, fD) = 9.425
⟨t⋆, fD⟩M = 11.350
⟨Z⋆, fD⟩M = 0.843
Net − Bulge eD :
log(M⋆, eD) = 9.467
⟨t⋆, eD⟩M = 12.970
⟨Z⋆, eD⟩M = 0.986
λ (Å)

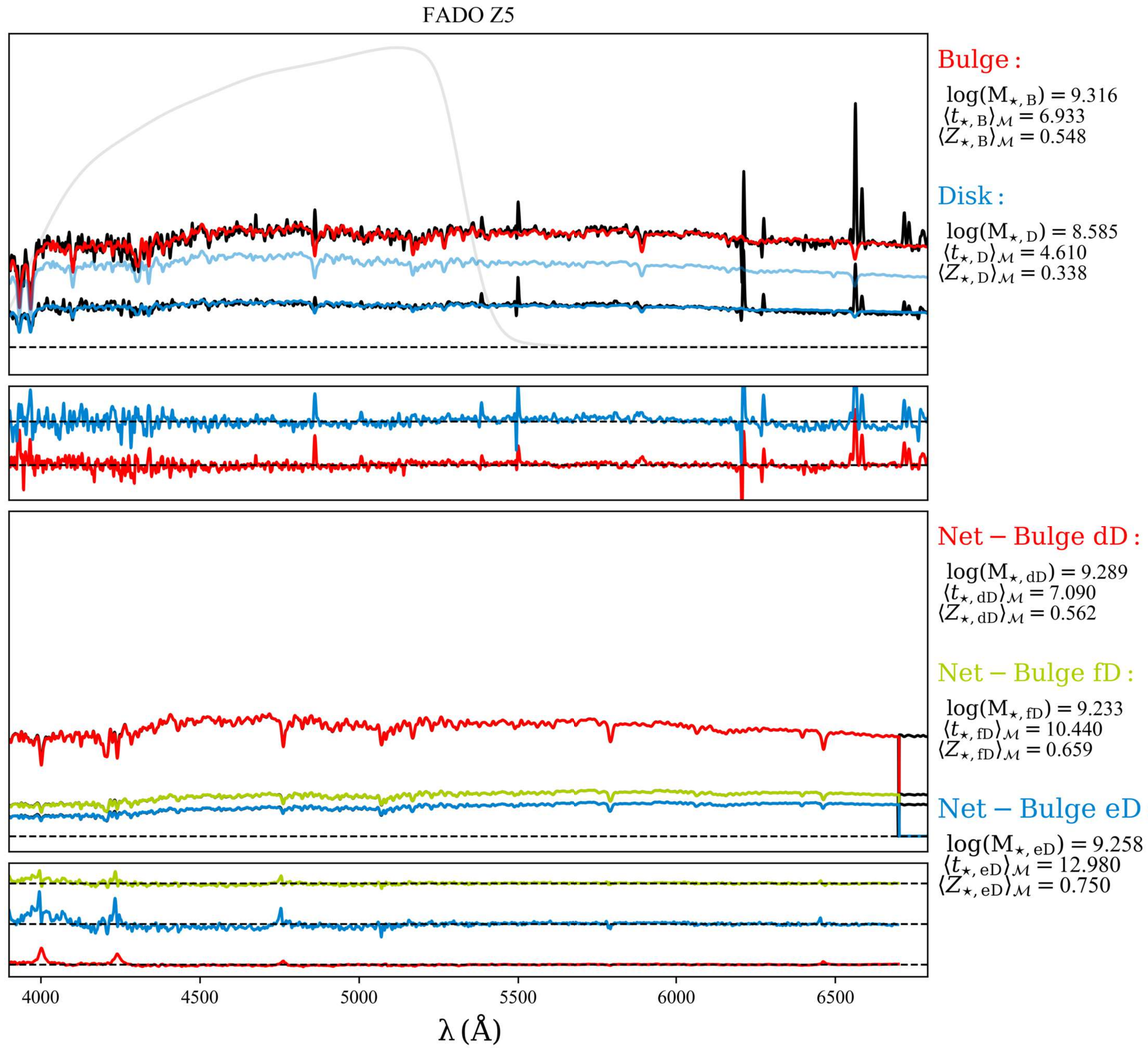
FADO Z5
Bulge :
log(M⋆, B) = 9.316
⟨t⋆, B⟩M = 6.933
⟨Z⋆, B⟩M = 0.548
Disk :
log(M⋆, D) = 8.585
⟨t⋆, D⟩M = 4.610
⟨Z⋆, D⟩M = 0.338
Net − Bulge dD :
log(M⋆, dD) = 9.289
⟨t⋆, dD⟩M = 7.090
⟨Z⋆, dD⟩M = 0.562
Net − Bulge fD :
log(M⋆, fD) = 9.233
⟨t⋆, fD⟩M = 10.440
⟨Z⋆, fD⟩M = 0.659
Net − Bulge eD :
log(M⋆, eD) = 9.258
⟨t⋆, eD⟩M = 12.980
⟨Z⋆, eD⟩M = 0.750
λ (Å)

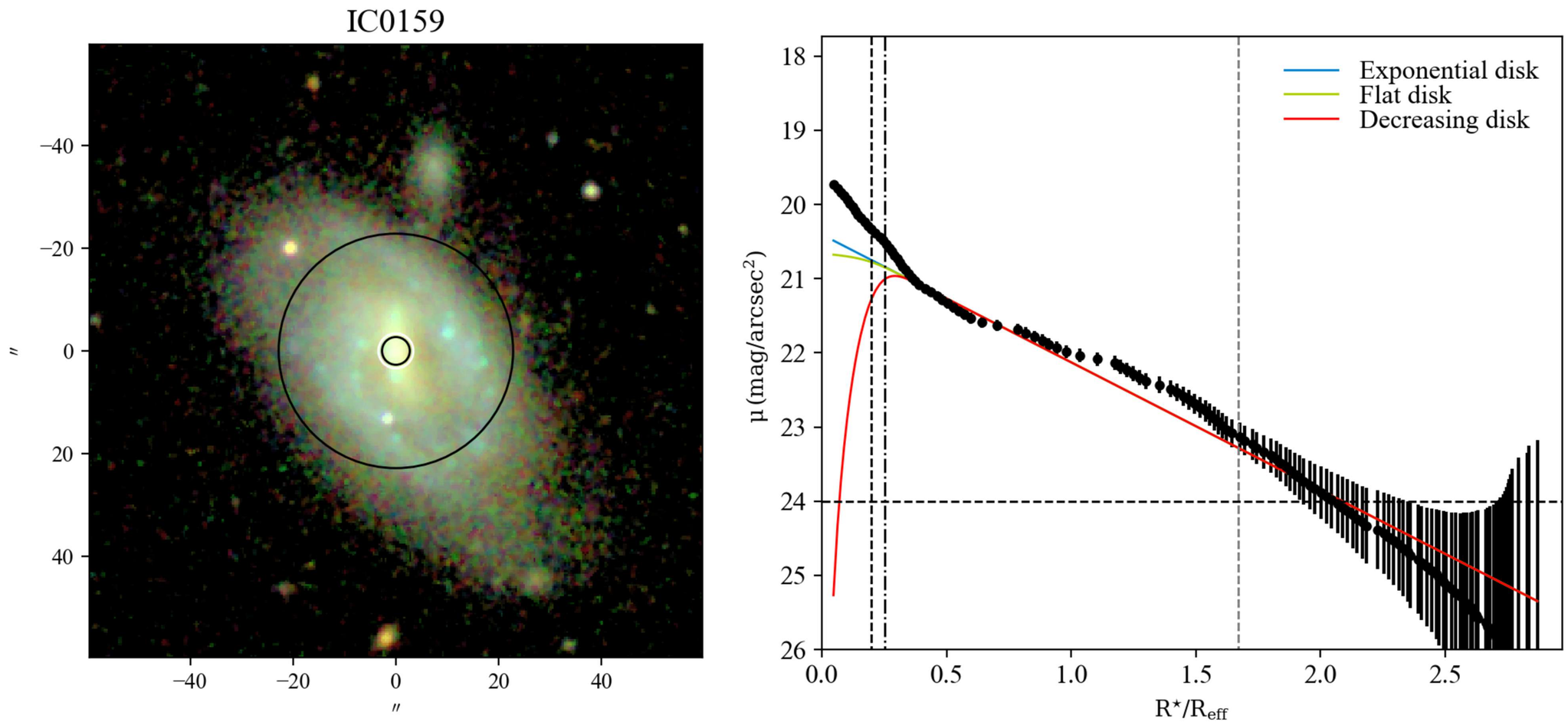
IC0159
Exponential disk
Flat disk
Decreasing disk
μ (mag/arcsec²)
R⋆/Reff
″

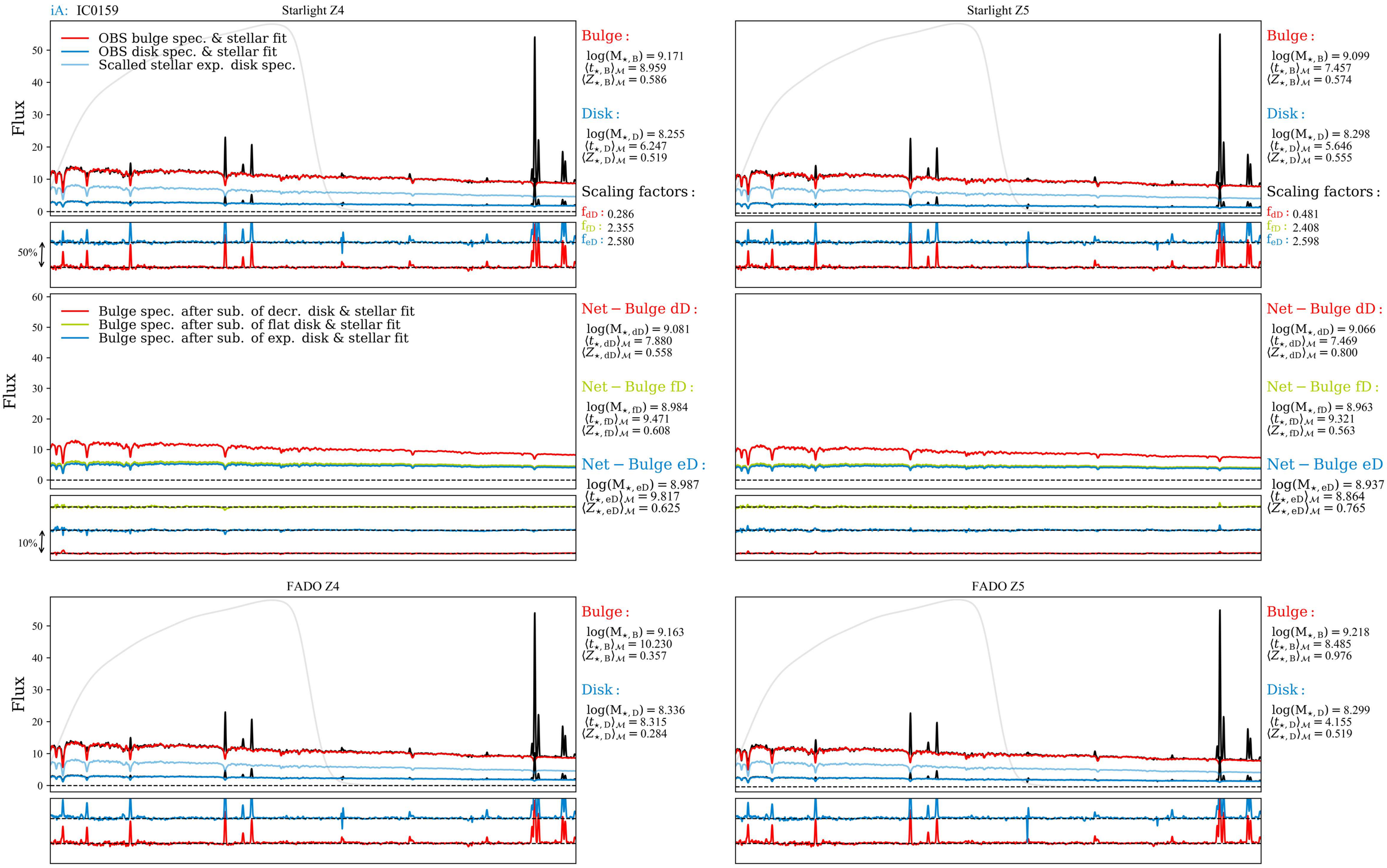
iA: IC0159
Starlight Z4
Starlight Z5
OBS bulge spec. & stellar fit
OBS disk spec. & stellar fit
Scalled stellar exp. disk spec.
Flux
Bulge :
log(M⋆, B) = 9.171
⟨t⋆, B⟩M = 8.959
⟨Z⋆, B⟩M = 0.586
Disk :
log(M⋆, D) = 8.255
⟨t⋆, D⟩M = 6.247
⟨Z⋆, D⟩M = 0.519
Scaling factors :
fdD : 0.286
ffD : 2.355
feD : 2.580
50%
Bulge :
log(M⋆, B) = 9.099
⟨t⋆, B⟩M = 7.457
⟨Z⋆, B⟩M = 0.574
Disk :
log(M⋆, D) = 8.298
⟨t⋆, D⟩M = 5.646
⟨Z⋆, D⟩M = 0.555
Scaling factors :
fdD : 0.481
ffD : 2.408
feD : 2.598
Bulge spec. after sub. of decr. disk & stellar fit
Bulge spec. after sub. of flat disk & stellar fit
Bulge spec. after sub. of exp. disk & stellar fit
Net − Bulge dD :
log(M⋆, dD) = 9.081
⟨t⋆, dD⟩M = 7.880
⟨Z⋆, dD⟩M = 0.558
Net − Bulge fD :
log(M⋆, fD) = 8.984
⟨t⋆, fD⟩M = 9.471
⟨Z⋆, fD⟩M = 0.608
Net − Bulge eD :
log(M⋆, eD) = 8.987
⟨t⋆, eD⟩M = 9.817
⟨Z⋆, eD⟩M = 0.625
10%
Net − Bulge dD :
log(M⋆, dD) = 9.066
⟨t⋆, dD⟩M = 7.469
⟨Z⋆, dD⟩M = 0.800
Net − Bulge fD :
log(M⋆, fD) = 8.963
⟨t⋆, fD⟩M = 9.321
⟨Z⋆, fD⟩M = 0.563
Net − Bulge eD :
log(M⋆, eD) = 8.937
⟨t⋆, eD⟩M = 8.864
⟨Z⋆, eD⟩M = 0.765
FADO Z4
FADO Z5
Bulge :
log(M⋆, B) = 9.163
⟨t⋆, B⟩M = 10.230
⟨Z⋆, B⟩M = 0.357
Disk :
log(M⋆, D) = 8.336
⟨t⋆, D⟩M = 8.315
⟨Z⋆, D⟩M = 0.284
Bulge :
log(M⋆, B) = 9.218
⟨t⋆, B⟩M = 8.485
⟨Z⋆, B⟩M = 0.976
Disk :
log(M⋆, D) = 8.299
⟨t⋆, D⟩M = 4.155
⟨Z⋆, D⟩M = 0.519
Net − Bulge dD :
log(M⋆, dD) = 9.111
⟨t⋆, dD⟩M = 9.090
⟨Z⋆, dD⟩M = 0.368
Net − Bulge fD :
log(M⋆, fD) = 8.986
⟨t⋆, fD⟩M = 12.060
⟨Z⋆, fD⟩M = 0.378
Net − Bulge eD :
log(M⋆, eD) = 8.954
⟨t⋆, eD⟩M = 11.820
⟨Z⋆, eD⟩M = 0.382
Net − Bulge dD :
log(M⋆, dD) = 9.170
⟨t⋆, dD⟩M = 8.836
⟨Z⋆, dD⟩M = 0.533
Net − Bulge fD :
log(M⋆, fD) = 8.987
⟨t⋆, fD⟩M = 9.432
⟨Z⋆, fD⟩M = 1.023
Net − Bulge eD :
log(M⋆, eD) = 8.903
⟨t⋆, eD⟩M = 7.564
⟨Z⋆, eD⟩M = 1.092
λ (Å)

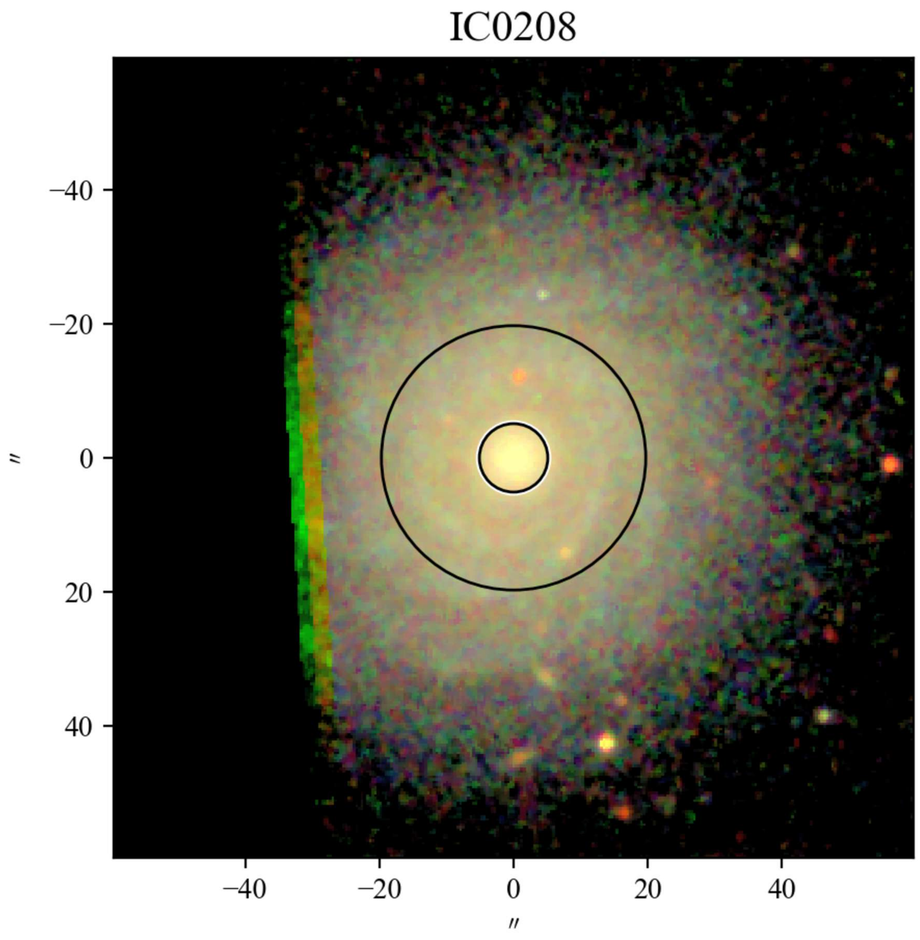
IC0208
−40
−20
0
20
40
″
−40
−20
0
20
40
″

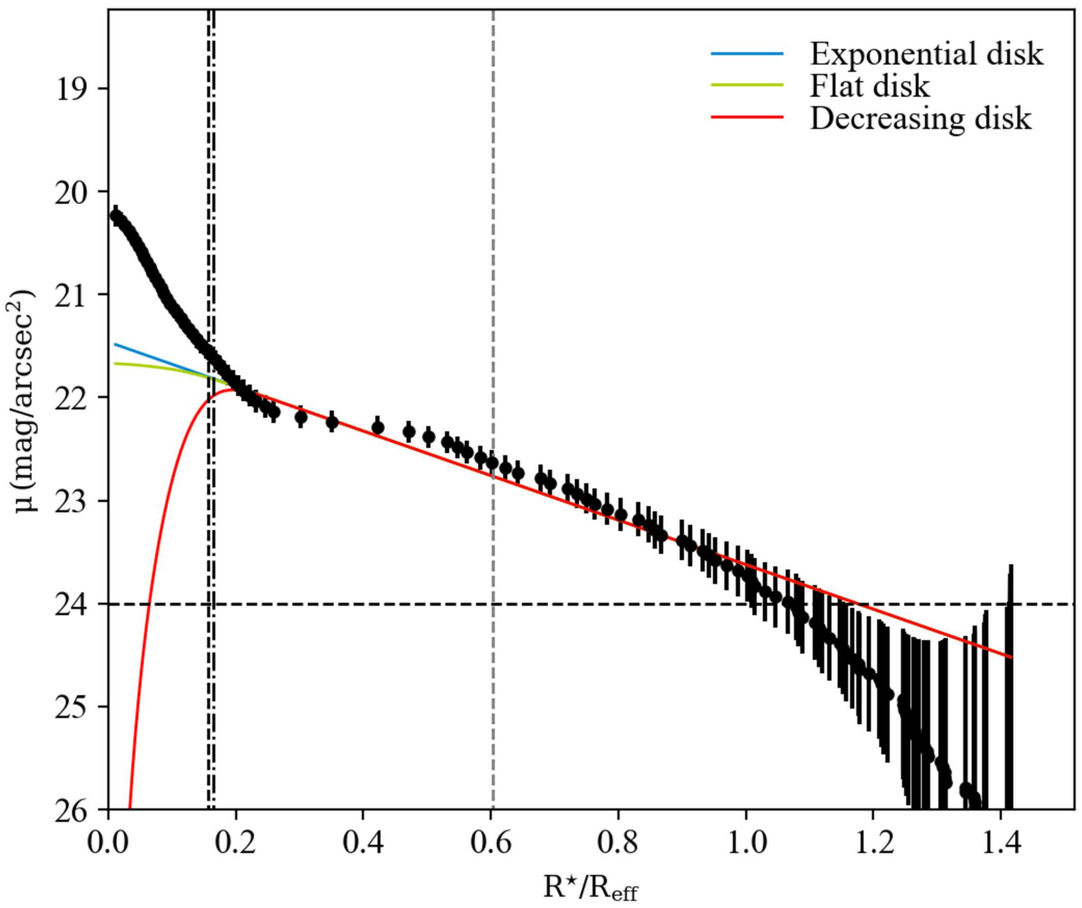
Exponential disk
Flat disk
Decreasing disk
μ (mag/arcsec²)
19
20
21
22
23
24
25
26
0.0
0.2
0.4
0.6
0.8
1.0
1.2
1.4
R⋆/Reff

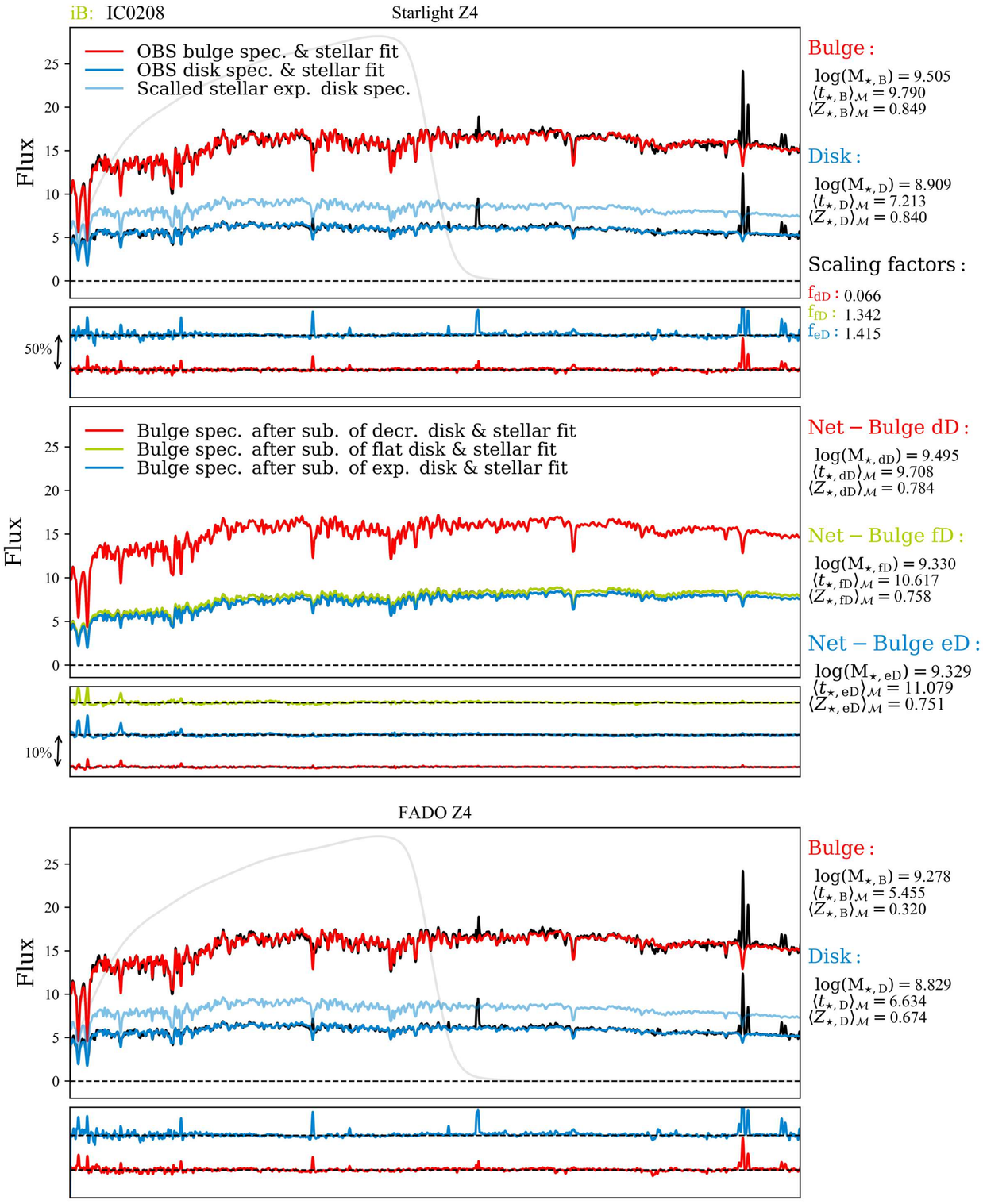
iB: IC0208
Starlight Z4
OBS bulge spec. & stellar fit
OBS disk spec. & stellar fit
Scalled stellar exp. disk spec.
Flux
Bulge :
log(M⋆, B) = 9.505
⟨t⋆, B⟩M = 9.790
⟨Z⋆, B⟩M = 0.849
Disk :
log(M⋆, D) = 8.909
⟨t⋆, D⟩M = 7.213
⟨Z⋆, D⟩M = 0.840
Scaling factors :
fdD : 0.066
ffD : 1.342
feD : 1.415
50%
Bulge spec. after sub. of decr. disk & stellar fit
Bulge spec. after sub. of flat disk & stellar fit
Bulge spec. after sub. of exp. disk & stellar fit
Net − Bulge dD :
log(M⋆, dD) = 9.495
⟨t⋆, dD⟩M = 9.708
⟨Z⋆, dD⟩M = 0.784
Net − Bulge fD :
log(M⋆, fD) = 9.330
⟨t⋆, fD⟩M = 10.617
⟨Z⋆, fD⟩M = 0.758
Net − Bulge eD :
log(M⋆, eD) = 9.329
⟨t⋆, eD⟩M = 11.079
⟨Z⋆, eD⟩M = 0.751
10%
FADO Z4
Bulge :
log(M⋆, B) = 9.278
⟨t⋆, B⟩M = 5.455
⟨Z⋆, B⟩M = 0.320
Disk :
log(M⋆, D) = 8.829
⟨t⋆, D⟩M = 6.634
⟨Z⋆, D⟩M = 0.674
Net − Bulge dD :
log(M⋆, dD) = 9.286
⟨t⋆, dD⟩M = 5.712
⟨Z⋆, dD⟩M = 0.325
Net − Bulge fD :
log(M⋆, fD) = 9.075
⟨t⋆, fD⟩M = 4.446
⟨Z⋆, fD⟩M = 0.359
Net − Bulge eD :
log(M⋆, eD) = 9.065
⟨t⋆, eD⟩M = 4.397
⟨Z⋆, eD⟩M = 0.359
4000
4500
5000
5500
6000
6500
λ (Å)

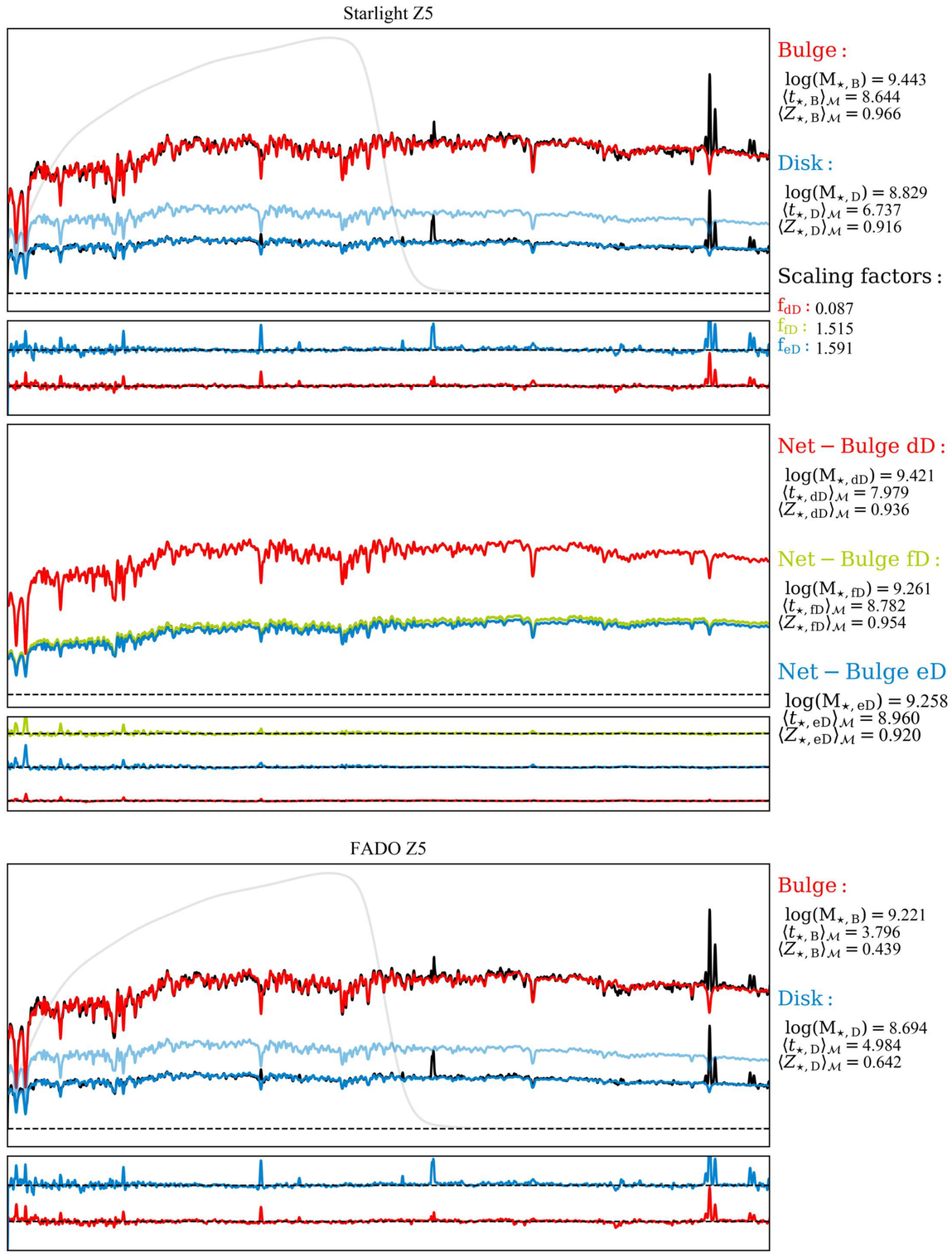
Starlight Z5
Bulge :
log(M⋆, B) = 9.443
⟨t⋆, B⟩M = 8.644
⟨Z⋆, B⟩M = 0.966
Disk :
log(M⋆, D) = 8.829
⟨t⋆, D⟩M = 6.737
⟨Z⋆, D⟩M = 0.916
Scaling factors :
fdD : 0.087
ffD : 1.515
feD : 1.591
Net − Bulge dD :
log(M⋆, dD) = 9.421
⟨t⋆, dD⟩M = 7.979
⟨Z⋆, dD⟩M = 0.936
Net − Bulge fD :
log(M⋆, fD) = 9.261
⟨t⋆, fD⟩M = 8.782
⟨Z⋆, fD⟩M = 0.954
Net − Bulge eD :
log(M⋆, eD) = 9.258
⟨t⋆, eD⟩M = 8.960
⟨Z⋆, eD⟩M = 0.920
FADO Z5
Bulge :
log(M⋆, B) = 9.221
⟨t⋆, B⟩M = 3.796
⟨Z⋆, B⟩M = 0.439
Disk :
log(M⋆, D) = 8.694
⟨t⋆, D⟩M = 4.984
⟨Z⋆, D⟩M = 0.642
Net − Bulge dD :
log(M⋆, dD) = 9.240
⟨t⋆, dD⟩M = 4.727
⟨Z⋆, dD⟩M = 0.421
Net − Bulge fD :
log(M⋆, fD) = 9.039
⟨t⋆, fD⟩M = 4.142
⟨Z⋆, fD⟩M = 0.370
Net − Bulge eD :
log(M⋆, eD) = 9.033
⟨t⋆, eD⟩M = 4.196
⟨Z⋆, eD⟩M = 0.371
4000
4500
5000
5500
6000
6500
λ (Å)

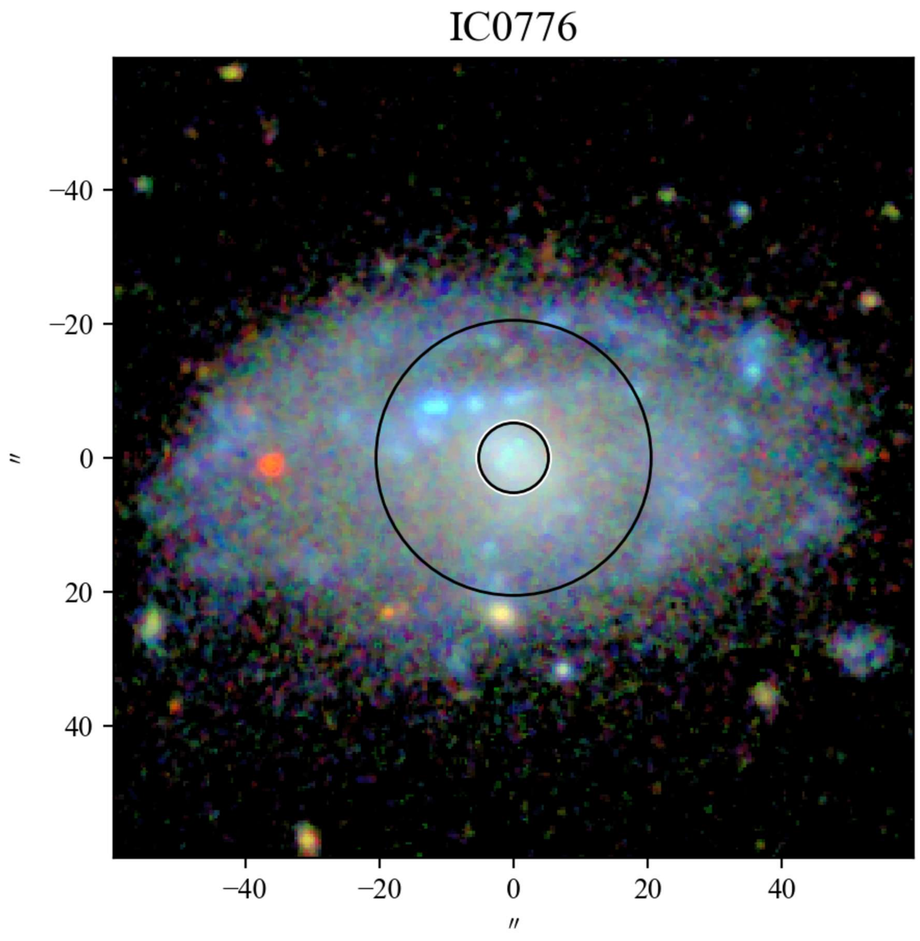
IC0776
−40
−20
0
20
40
″
−40
−20
0
20
40
″

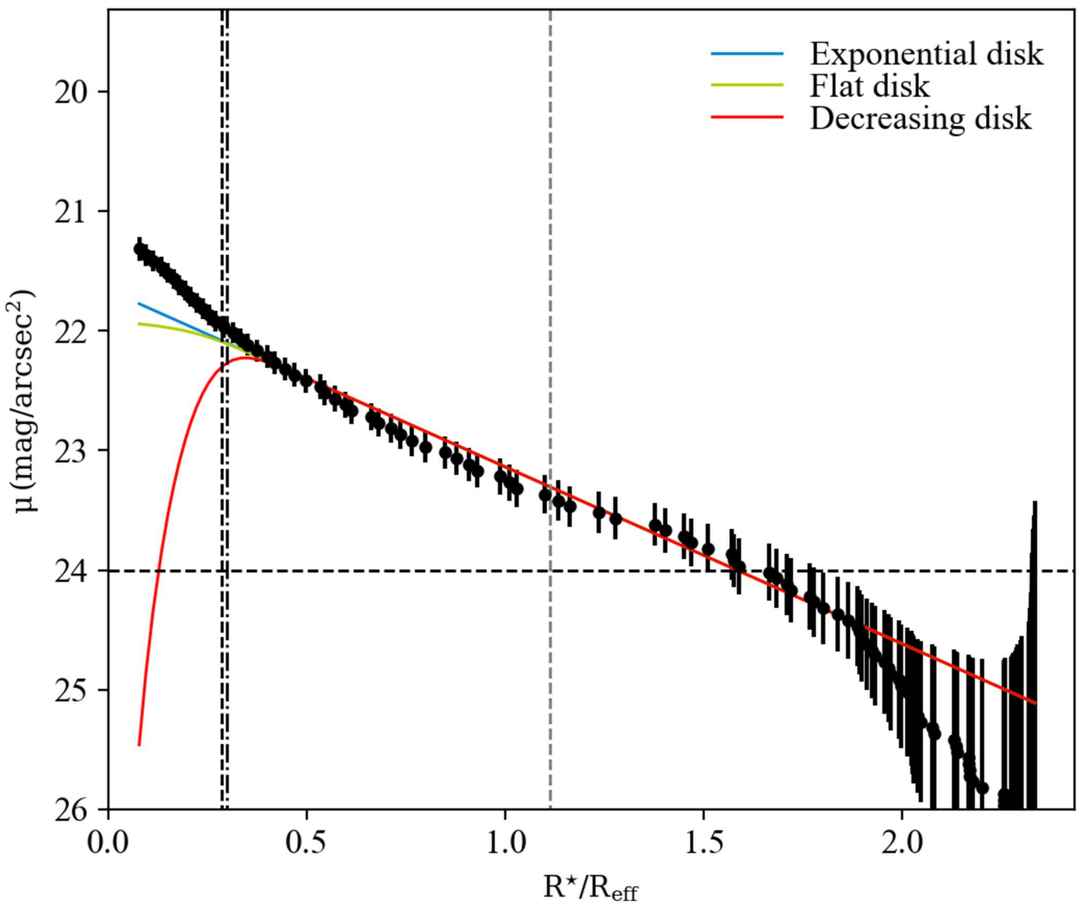
Exponential disk
Flat disk
Decreasing disk
μ (mag/arcsec²)
20
21
22
23
24
25
26
0.0
0.5
1.0
1.5
2.0
R⋆/Reff

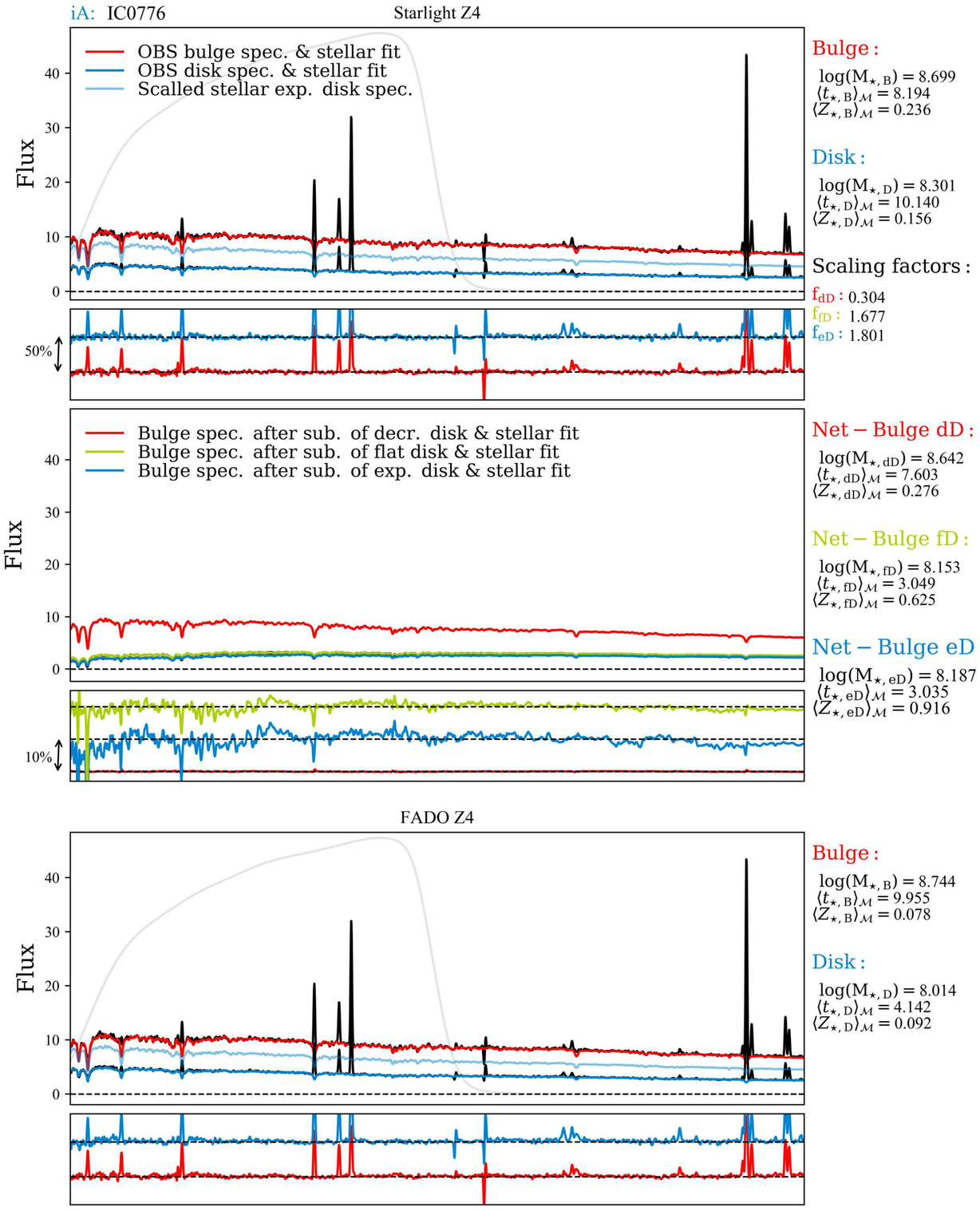
iA: IC0776
Starlight Z4
OBS bulge spec. & stellar fit
OBS disk spec. & stellar fit
Scalled stellar exp. disk spec.
Flux
50%
Bulge :
log(M⋆, B) = 8.699
⟨t⋆, B⟩M = 8.194
⟨Z⋆, B⟩M = 0.236
Disk :
log(M⋆, D) = 8.301
⟨t⋆, D⟩M = 10.140
⟨Z⋆, D⟩M = 0.156
Scaling factors :
fdD : 0.304
ffD : 1.677
feD : 1.801
Bulge spec. after sub. of decr. disk & stellar fit
Bulge spec. after sub. of flat disk & stellar fit
Bulge spec. after sub. of exp. disk & stellar fit
10%
Net − Bulge dD :
log(M⋆, dD) = 8.642
⟨t⋆, dD⟩M = 7.603
⟨Z⋆, dD⟩M = 0.276
Net − Bulge fD :
log(M⋆, fD) = 8.153
⟨t⋆, fD⟩M = 3.049
⟨Z⋆, fD⟩M = 0.625
Net − Bulge eD :
log(M⋆, eD) = 8.187
⟨t⋆, eD⟩M = 3.035
⟨Z⋆, eD⟩M = 0.916

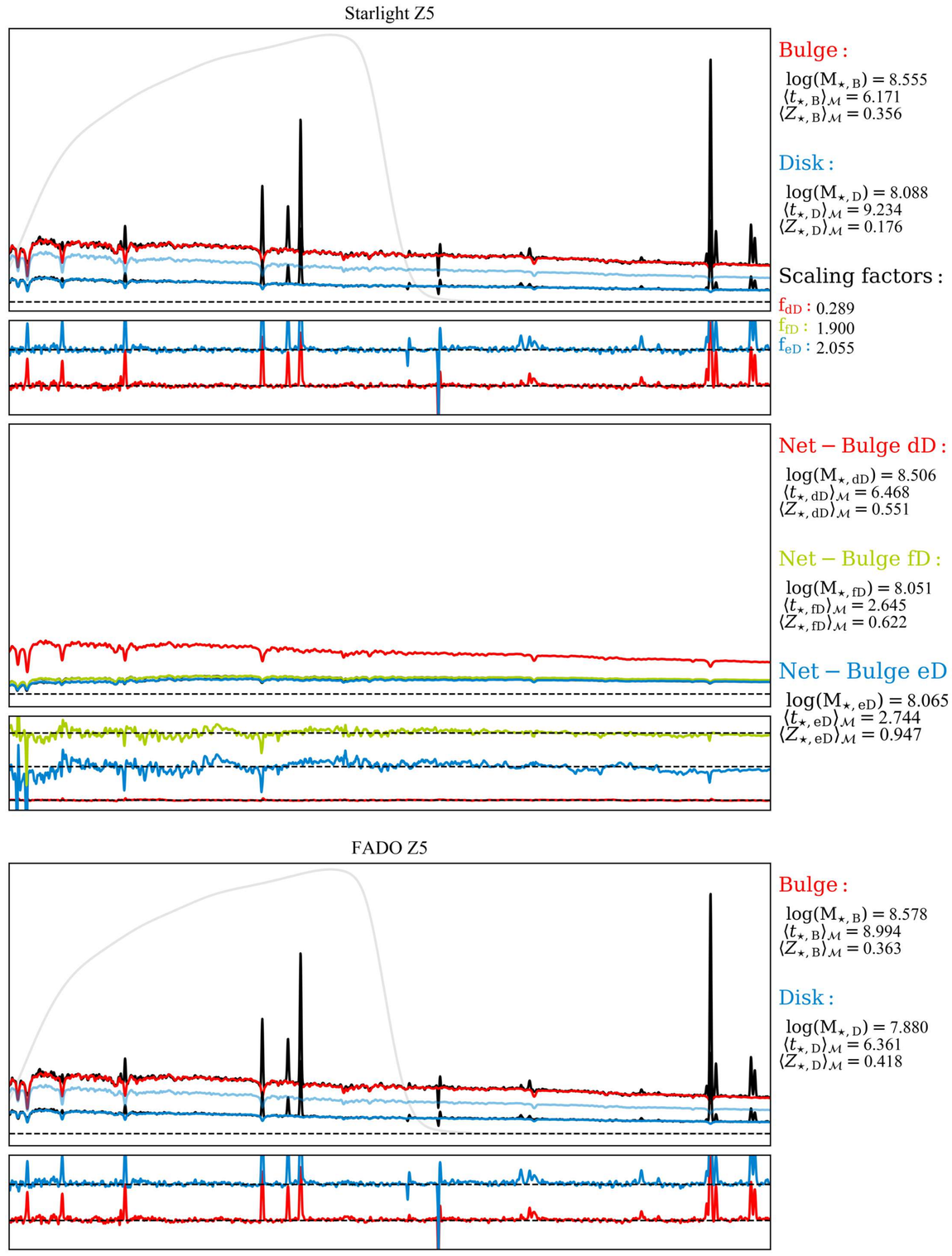
Starlight Z5
Bulge :
log(M⋆, B) = 8.555
⟨t⋆, B⟩M = 6.171
⟨Z⋆, B⟩M = 0.356
Disk :
log(M⋆, D) = 8.088
⟨t⋆, D⟩M = 9.234
⟨Z⋆, D⟩M = 0.176
Scaling factors :
fdD : 0.289
ffD : 1.900
feD : 2.055
Net − Bulge dD :
log(M⋆, dD) = 8.506
⟨t⋆, dD⟩M = 6.468
⟨Z⋆, dD⟩M = 0.551
Net − Bulge fD :
log(M⋆, fD) = 8.051
⟨t⋆, fD⟩M = 2.645
⟨Z⋆, fD⟩M = 0.622
Net − Bulge eD :
log(M⋆, eD) = 8.065
⟨t⋆, eD⟩M = 2.744
⟨Z⋆, eD⟩M = 0.947

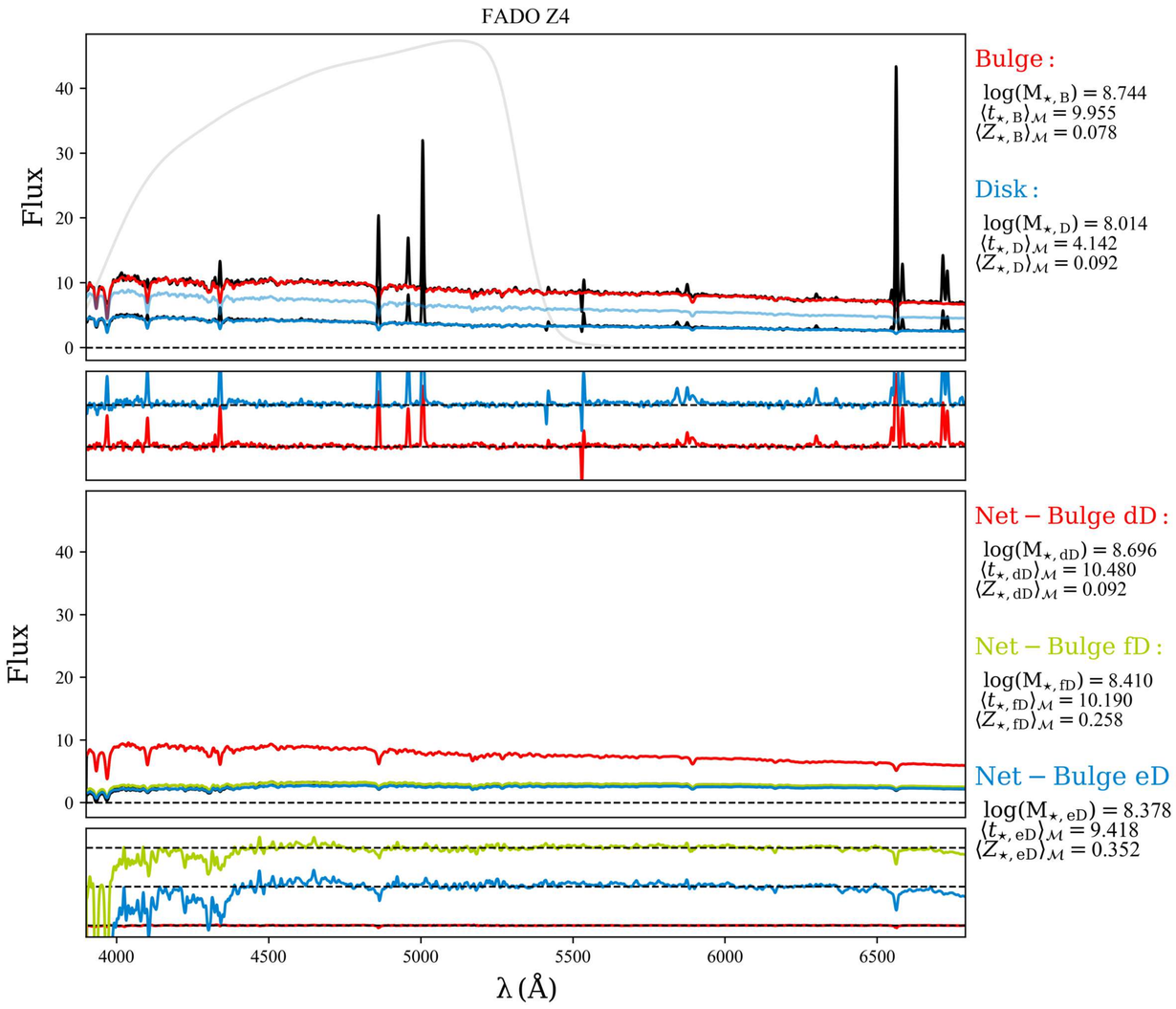
FADO Z4
Flux
Bulge :
log(M⋆, B) = 8.744
⟨t⋆, B⟩M = 9.955
⟨Z⋆, B⟩M = 0.078
Disk :
log(M⋆, D) = 8.014
⟨t⋆, D⟩M = 4.142
⟨Z⋆, D⟩M = 0.092
Net − Bulge dD :
log(M⋆, dD) = 8.696
⟨t⋆, dD⟩M = 10.480
⟨Z⋆, dD⟩M = 0.092
Net − Bulge fD :
log(M⋆, fD) = 8.410
⟨t⋆, fD⟩M = 10.190
⟨Z⋆, fD⟩M = 0.258
Net − Bulge eD :
log(M⋆, eD) = 8.378
⟨t⋆, eD⟩M = 9.418
⟨Z⋆, eD⟩M = 0.352
λ (Å)

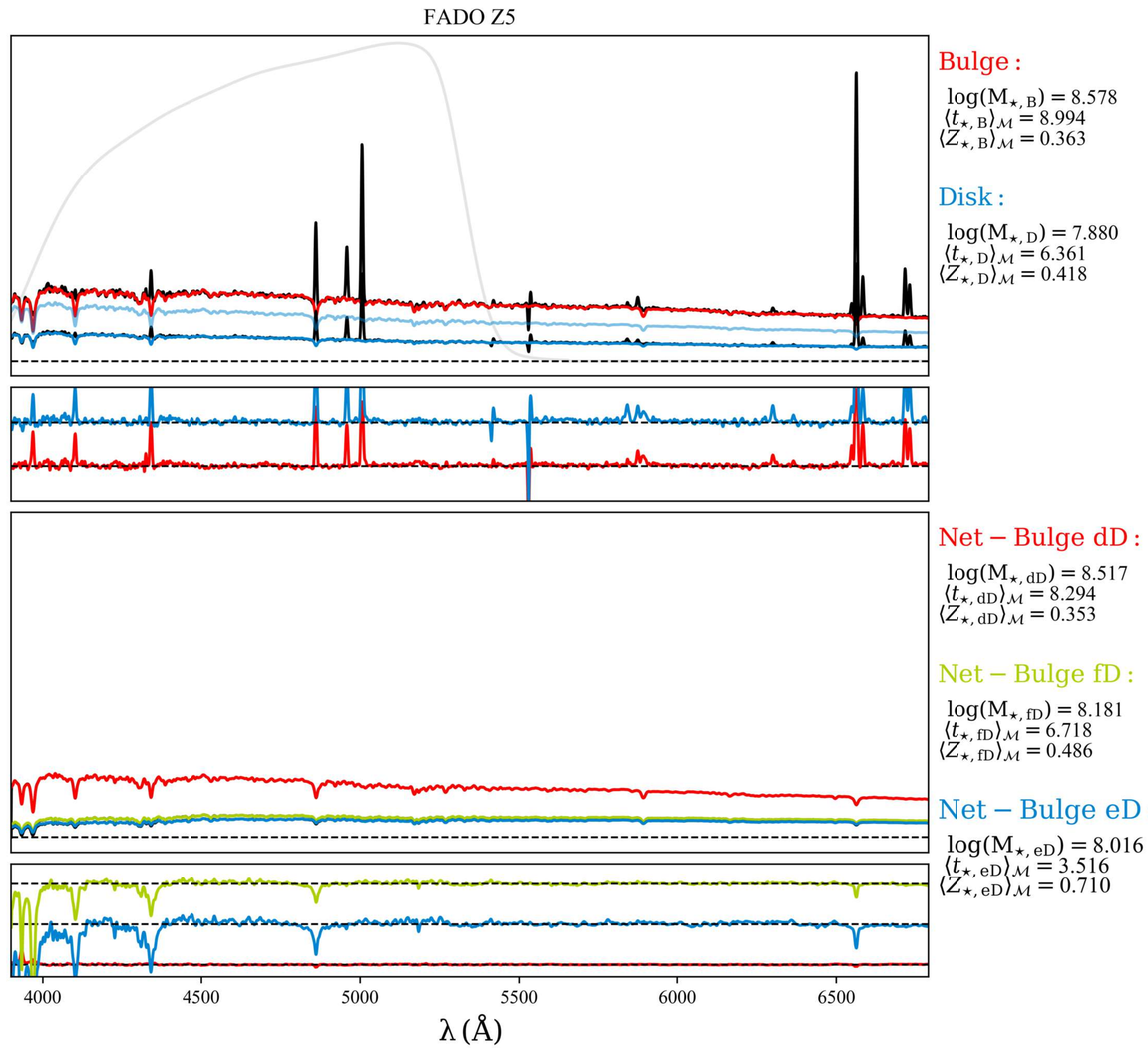
FADO Z5
Bulge :
log(M⋆, B) = 8.578
⟨t⋆, B⟩M = 8.994
⟨Z⋆, B⟩M = 0.363
Disk :
log(M⋆, D) = 7.880
⟨t⋆, D⟩M = 6.361
⟨Z⋆, D⟩M = 0.418
Net − Bulge dD :
log(M⋆, dD) = 8.517
⟨t⋆, dD⟩M = 8.294
⟨Z⋆, dD⟩M = 0.353
Net − Bulge fD :
log(M⋆, fD) = 8.181
⟨t⋆, fD⟩M = 6.718
⟨Z⋆, fD⟩M = 0.486
Net − Bulge eD :
log(M⋆, eD) = 8.016
⟨t⋆, eD⟩M = 3.516
⟨Z⋆, eD⟩M = 0.710
λ (Å)

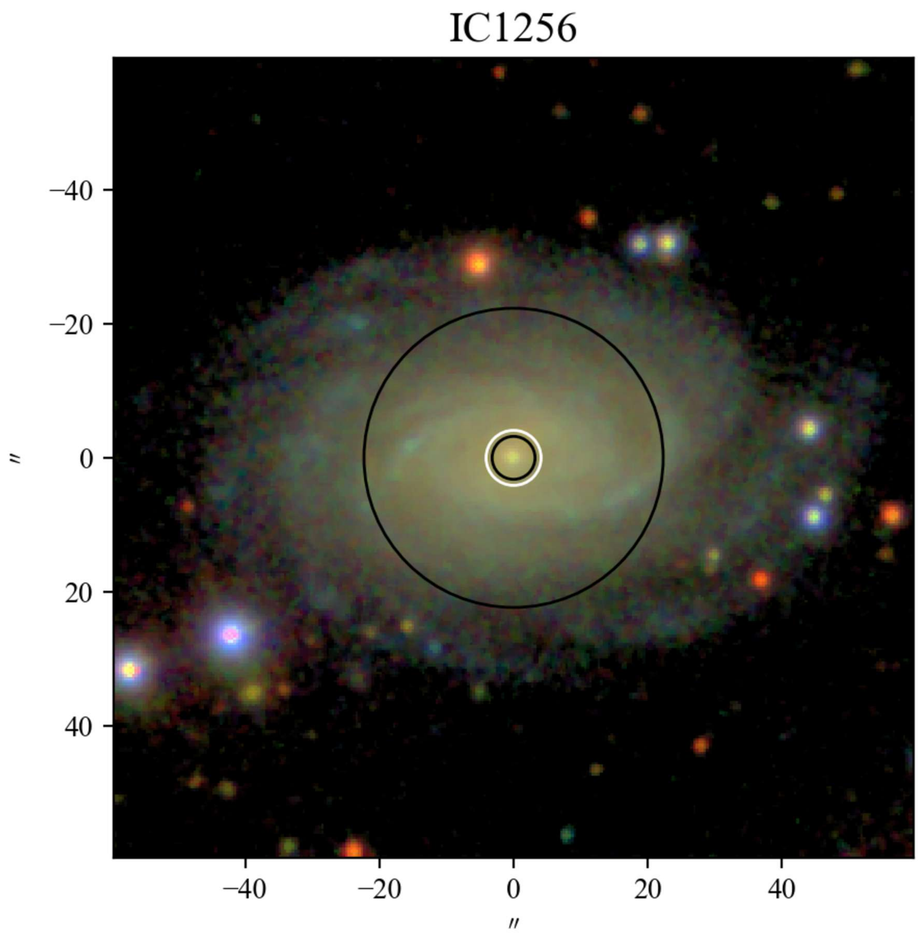
IC1256
−40
−20
0
20
40
″
−40
−20
0
20
40
″

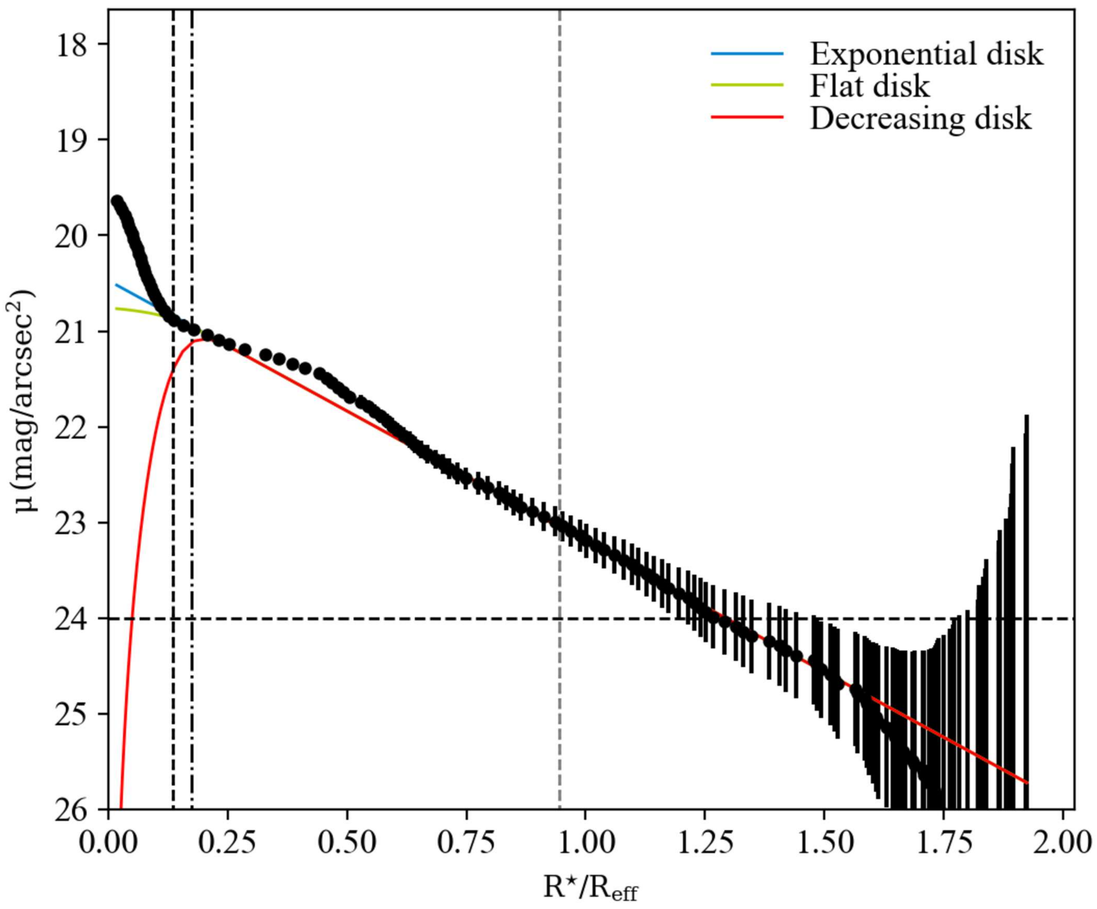
Exponential disk
Flat disk
Decreasing disk
μ (mag/arcsec²)
18
19
20
21
22
23
24
25
26
0.00
0.25
0.50
0.75
1.00
1.25
1.50
1.75
2.00
R⋆/Reff

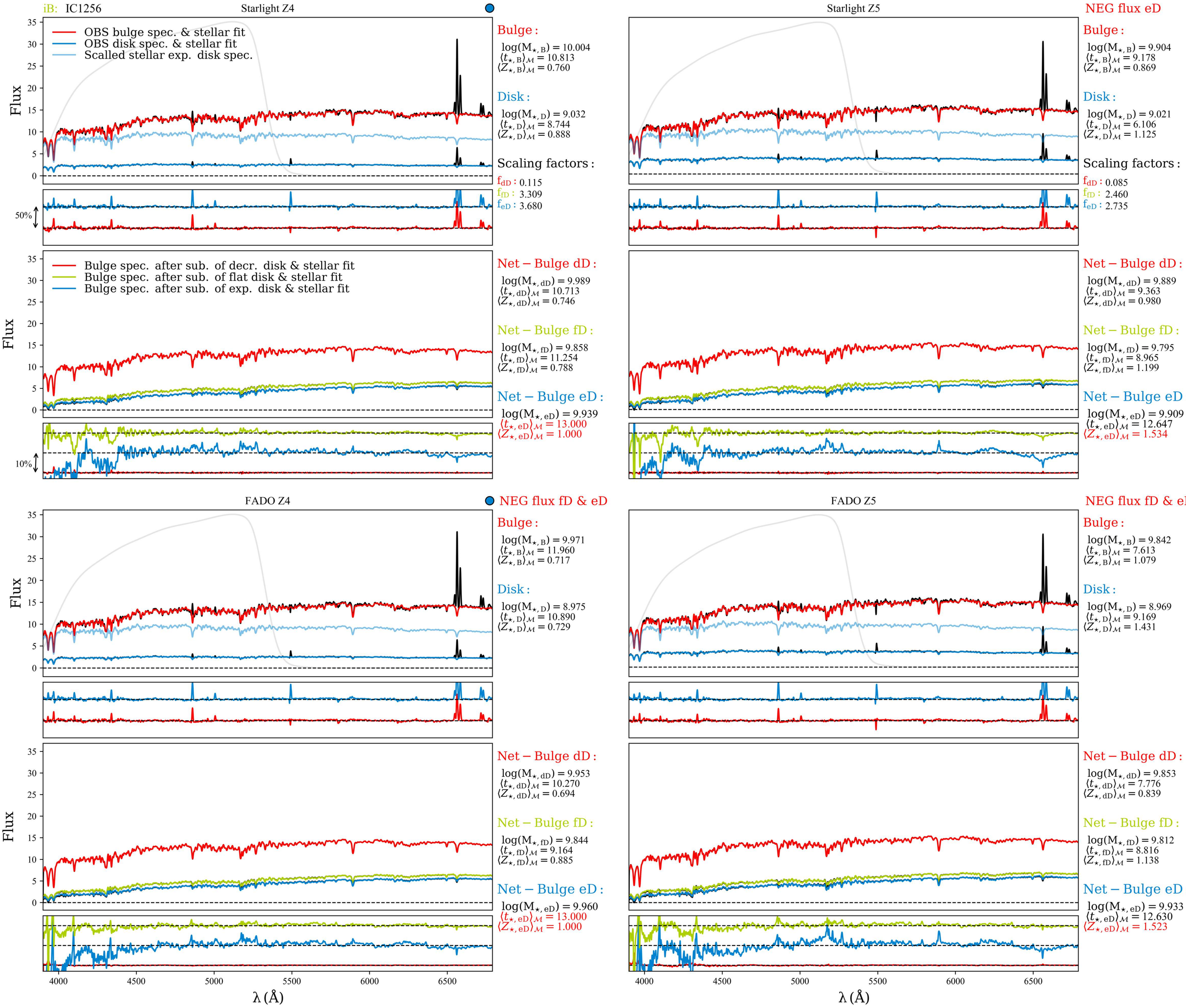
iB: IC1256
Starlight Z4
OBS bulge spec. & stellar fit
OBS disk spec. & stellar fit
Scalled stellar exp. disk spec.
Flux
Bulge :
log(M⋆, B) = 10.004
⟨t⋆, B⟩M = 10.813
⟨Z⋆, B⟩M = 0.760
Disk :
log(M⋆, D) = 9.032
⟨t⋆, D⟩M = 8.744
⟨Z⋆, D⟩M = 0.888
Scaling factors :
fdD : 0.115
ffD : 3.309
feD : 3.680
50%
Starlight Z5
NEG flux eD
Bulge :
log(M⋆, B) = 9.904
⟨t⋆, B⟩M = 9.178
⟨Z⋆, B⟩M = 0.869
Disk :
log(M⋆, D) = 9.021
⟨t⋆, D⟩M = 6.106
⟨Z⋆, D⟩M = 1.125
Scaling factors :
fdD : 0.085
ffD : 2.460
feD : 2.735
Bulge spec. after sub. of decr. disk & stellar fit
Bulge spec. after sub. of flat disk & stellar fit
Bulge spec. after sub. of exp. disk & stellar fit
Net − Bulge dD :
log(M⋆, dD) = 9.989
⟨t⋆, dD⟩M = 10.713
⟨Z⋆, dD⟩M = 0.746
Net − Bulge fD :
log(M⋆, fD) = 9.858
⟨t⋆, fD⟩M = 11.254
⟨Z⋆, fD⟩M = 0.788
Net − Bulge eD :
log(M⋆, eD) = 9.939
⟨t⋆, eD⟩M = 13.000
⟨Z⋆, eD⟩M = 1.000
10%
Net − Bulge dD :
log(M⋆, dD) = 9.889
⟨t⋆, dD⟩M = 9.363
⟨Z⋆, dD⟩M = 0.980
Net − Bulge fD :
log(M⋆, fD) = 9.795
⟨t⋆, fD⟩M = 8.965
⟨Z⋆, fD⟩M = 1.199
Net − Bulge eD :
log(M⋆, eD) = 9.909
⟨t⋆, eD⟩M = 12.647
⟨Z⋆, eD⟩M = 1.534
FADO Z4
NEG flux fD & eD
Bulge :
log(M⋆, B) = 9.971
⟨t⋆, B⟩M = 11.960
⟨Z⋆, B⟩M = 0.717
Disk :
log(M⋆, D) = 8.975
⟨t⋆, D⟩M = 10.890
⟨Z⋆, D⟩M = 0.729
FADO Z5
NEG flux fD & eD
Bulge :
log(M⋆, B) = 9.842
⟨t⋆, B⟩M = 7.613
⟨Z⋆, B⟩M = 1.079
Disk :
log(M⋆, D) = 8.969
⟨t⋆, D⟩M = 9.169
⟨Z⋆, D⟩M = 1.431
Net − Bulge dD :
log(M⋆, dD) = 9.953
⟨t⋆, dD⟩M = 10.270
⟨Z⋆, dD⟩M = 0.694
Net − Bulge fD :
log(M⋆, fD) = 9.844
⟨t⋆, fD⟩M = 9.164
⟨Z⋆, fD⟩M = 0.885
Net − Bulge eD :
log(M⋆, eD) = 9.960
⟨t⋆, eD⟩M = 13.000
⟨Z⋆, eD⟩M = 1.000
Net − Bulge dD :
log(M⋆, dD) = 9.853
⟨t⋆, dD⟩M = 7.776
⟨Z⋆, dD⟩M = 0.839
Net − Bulge fD :
log(M⋆, fD) = 9.812
⟨t⋆, fD⟩M = 8.816
⟨Z⋆, fD⟩M = 1.138
Net − Bulge eD :
log(M⋆, eD) = 9.933
⟨t⋆, eD⟩M = 12.630
⟨Z⋆, eD⟩M = 1.523
λ (Å)

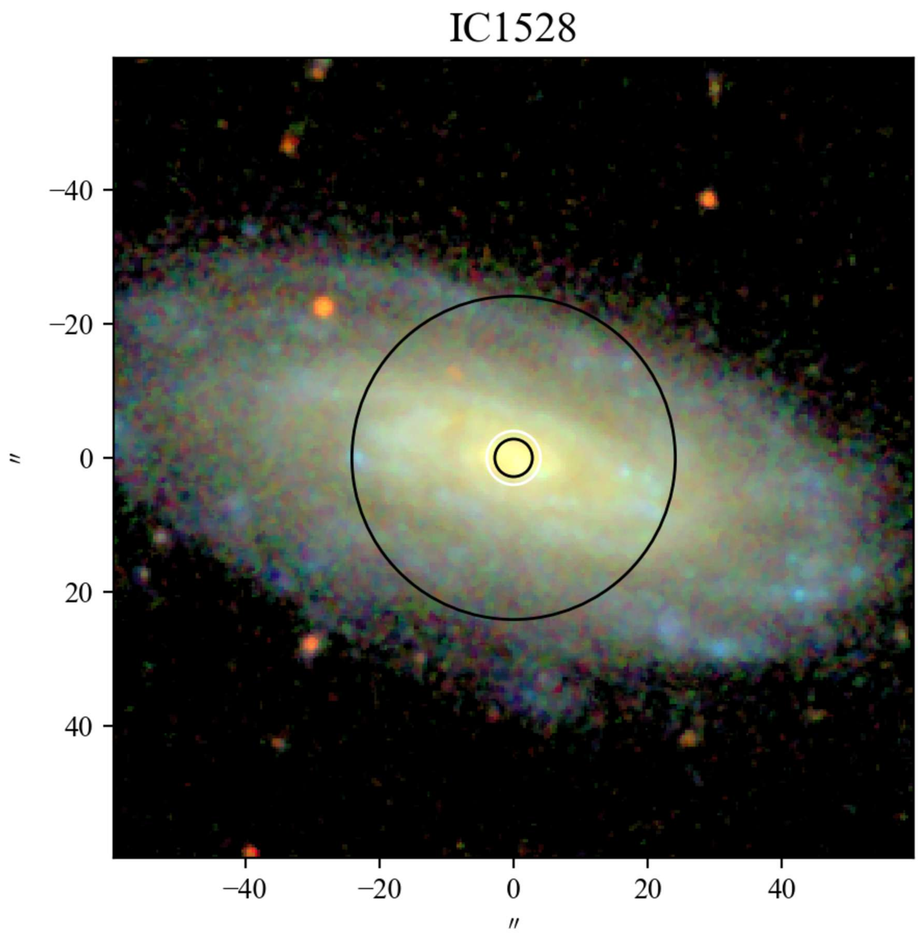
IC1528
−40
−20
0
20
40
″
−40
−20
0
20
40
″

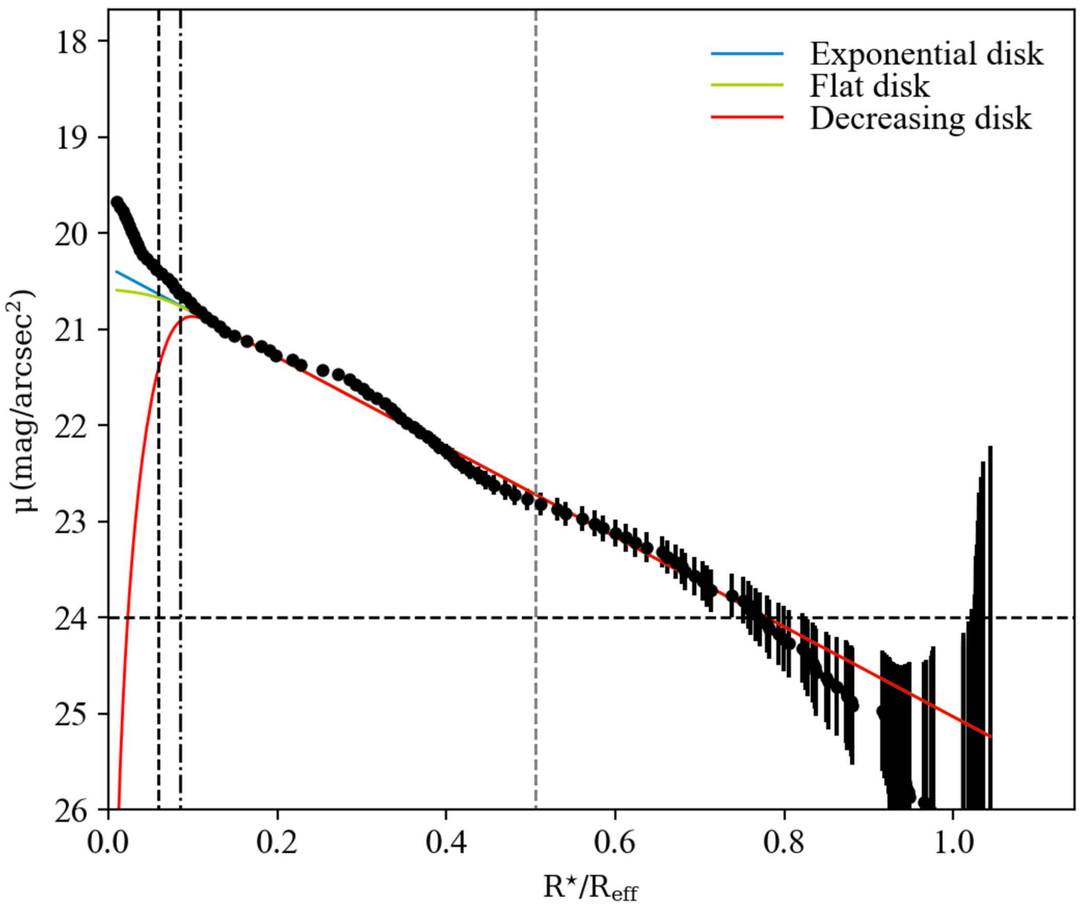
Exponential disk
Flat disk
Decreasing disk
μ (mag/arcsec²)
18
19
20
21
22
23
24
25
26
0.0
0.2
0.4
0.6
0.8
1.0
R⋆/Reff

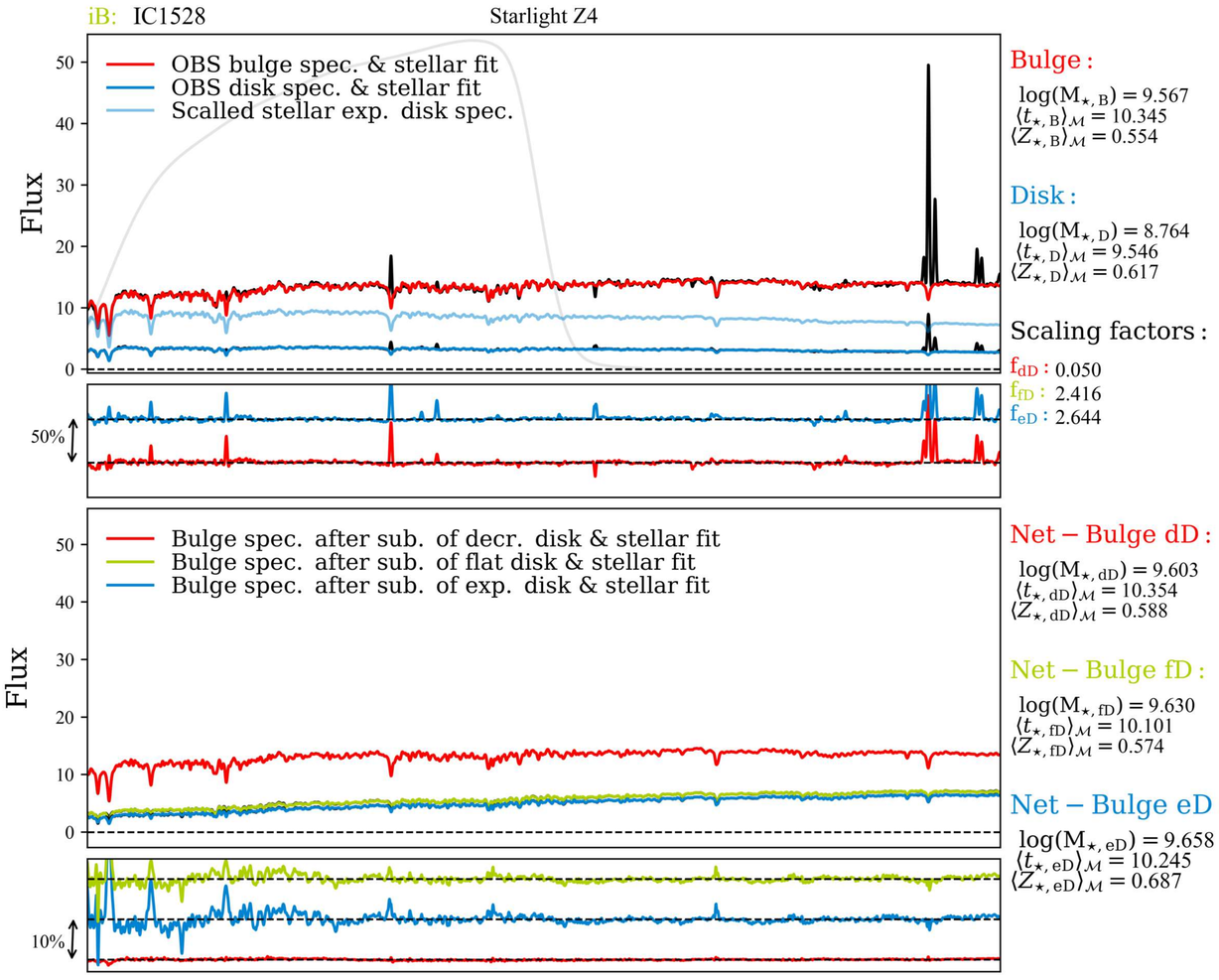
iB: IC1528
Starlight Z4
OBS bulge spec. & stellar fit
OBS disk spec. & stellar fit
Scalled stellar exp. disk spec.
Flux
50%
Bulge :
log(M⋆, B) = 9.567
⟨t⋆, B⟩M = 10.345
⟨Z⋆, B⟩M = 0.554
Disk :
log(M⋆, D) = 8.764
⟨t⋆, D⟩M = 9.546
⟨Z⋆, D⟩M = 0.617
Scaling factors :
fdD : 0.050
ffD : 2.416
feD : 2.644
Bulge spec. after sub. of decr. disk & stellar fit
Bulge spec. after sub. of flat disk & stellar fit
Bulge spec. after sub. of exp. disk & stellar fit
10%
Net − Bulge dD :
log(M⋆, dD) = 9.603
⟨t⋆, dD⟩M = 10.354
⟨Z⋆, dD⟩M = 0.588
Net − Bulge fD :
log(M⋆, fD) = 9.630
⟨t⋆, fD⟩M = 10.101
⟨Z⋆, fD⟩M = 0.574
Net − Bulge eD :
log(M⋆, eD) = 9.658
⟨t⋆, eD⟩M = 10.245
⟨Z⋆, eD⟩M = 0.687

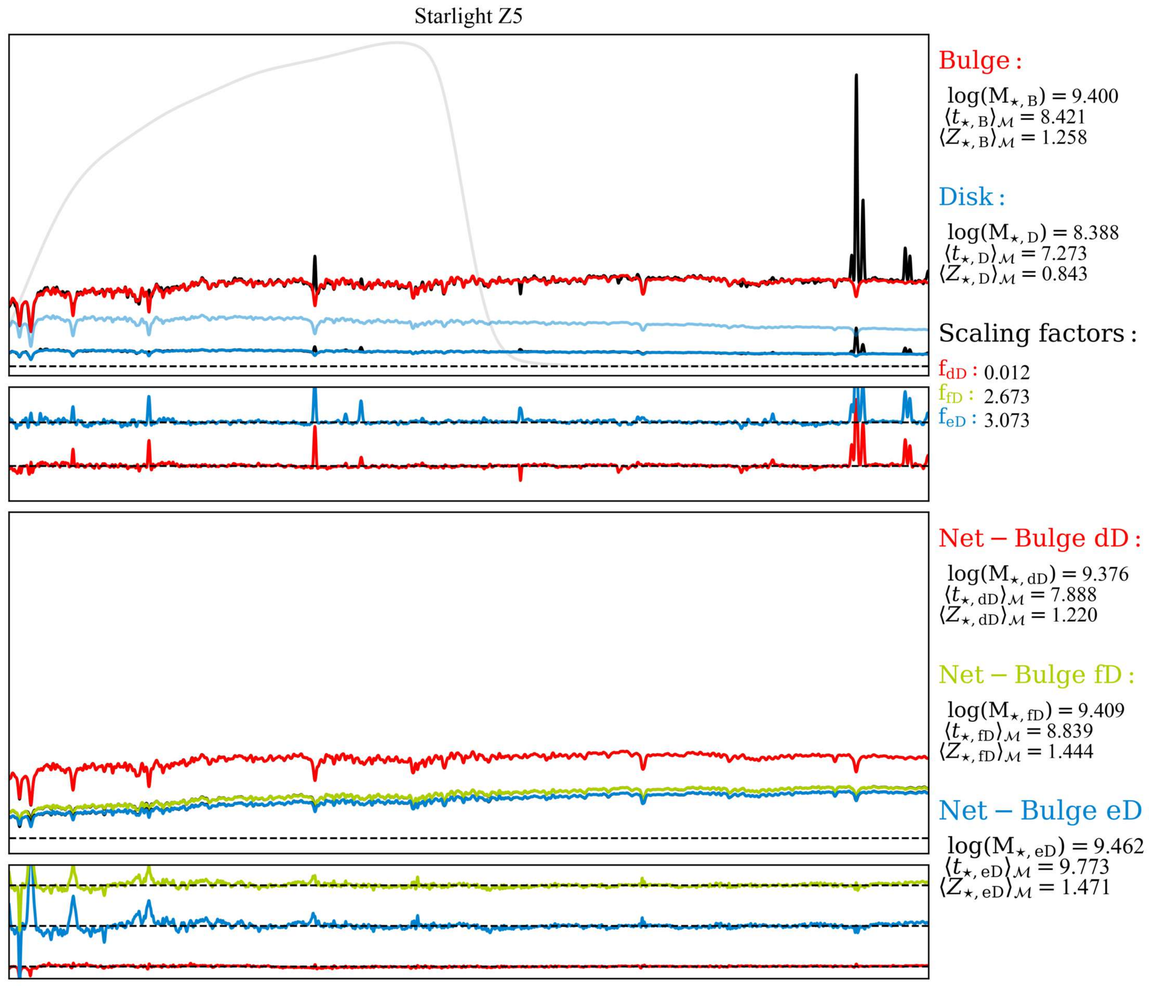
Starlight Z5
Bulge :
log(M⋆, B) = 9.400
⟨t⋆, B⟩M = 8.421
⟨Z⋆, B⟩M = 1.258
Disk :
log(M⋆, D) = 8.388
⟨t⋆, D⟩M = 7.273
⟨Z⋆, D⟩M = 0.843
Scaling factors :
fdD : 0.012
ffD : 2.673
feD : 3.073
Net − Bulge dD :
log(M⋆, dD) = 9.376
⟨t⋆, dD⟩M = 7.888
⟨Z⋆, dD⟩M = 1.220
Net − Bulge fD :
log(M⋆, fD) = 9.409
⟨t⋆, fD⟩M = 8.839
⟨Z⋆, fD⟩M = 1.444
Net − Bulge eD :
log(M⋆, eD) = 9.462
⟨t⋆, eD⟩M = 9.773
⟨Z⋆, eD⟩M = 1.471

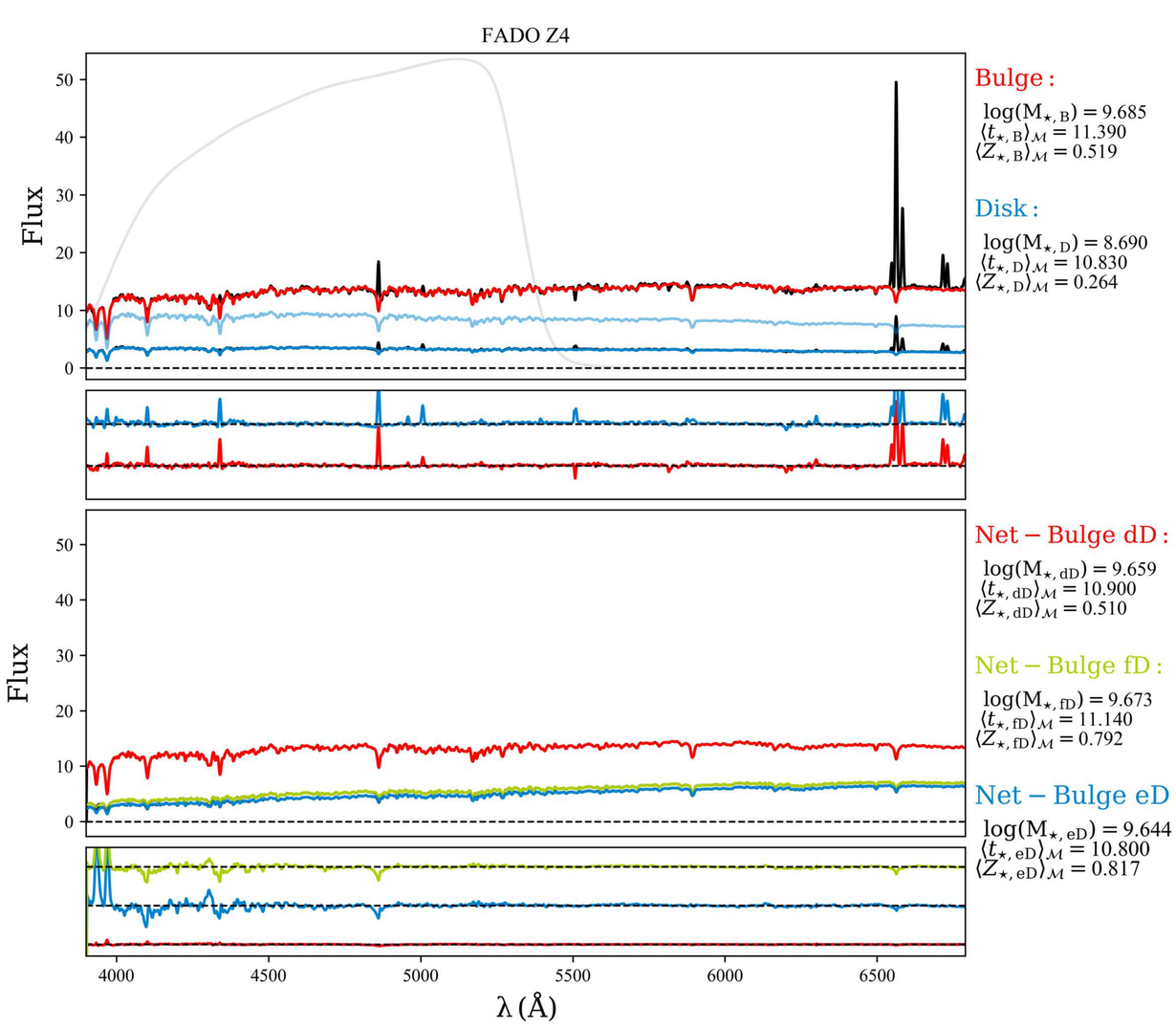
FADO Z4
Flux
Bulge :
log(M⋆, B) = 9.685
⟨t⋆, B⟩M = 11.390
⟨Z⋆, B⟩M = 0.519
Disk :
log(M⋆, D) = 8.690
⟨t⋆, D⟩M = 10.830
⟨Z⋆, D⟩M = 0.264
Net − Bulge dD :
log(M⋆, dD) = 9.659
⟨t⋆, dD⟩M = 10.900
⟨Z⋆, dD⟩M = 0.510
Net − Bulge fD :
log(M⋆, fD) = 9.673
⟨t⋆, fD⟩M = 11.140
⟨Z⋆, fD⟩M = 0.792
Net − Bulge eD :
log(M⋆, eD) = 9.644
⟨t⋆, eD⟩M = 10.800
⟨Z⋆, eD⟩M = 0.817
4000
4500
5000
5500
6000
6500
λ (Å)

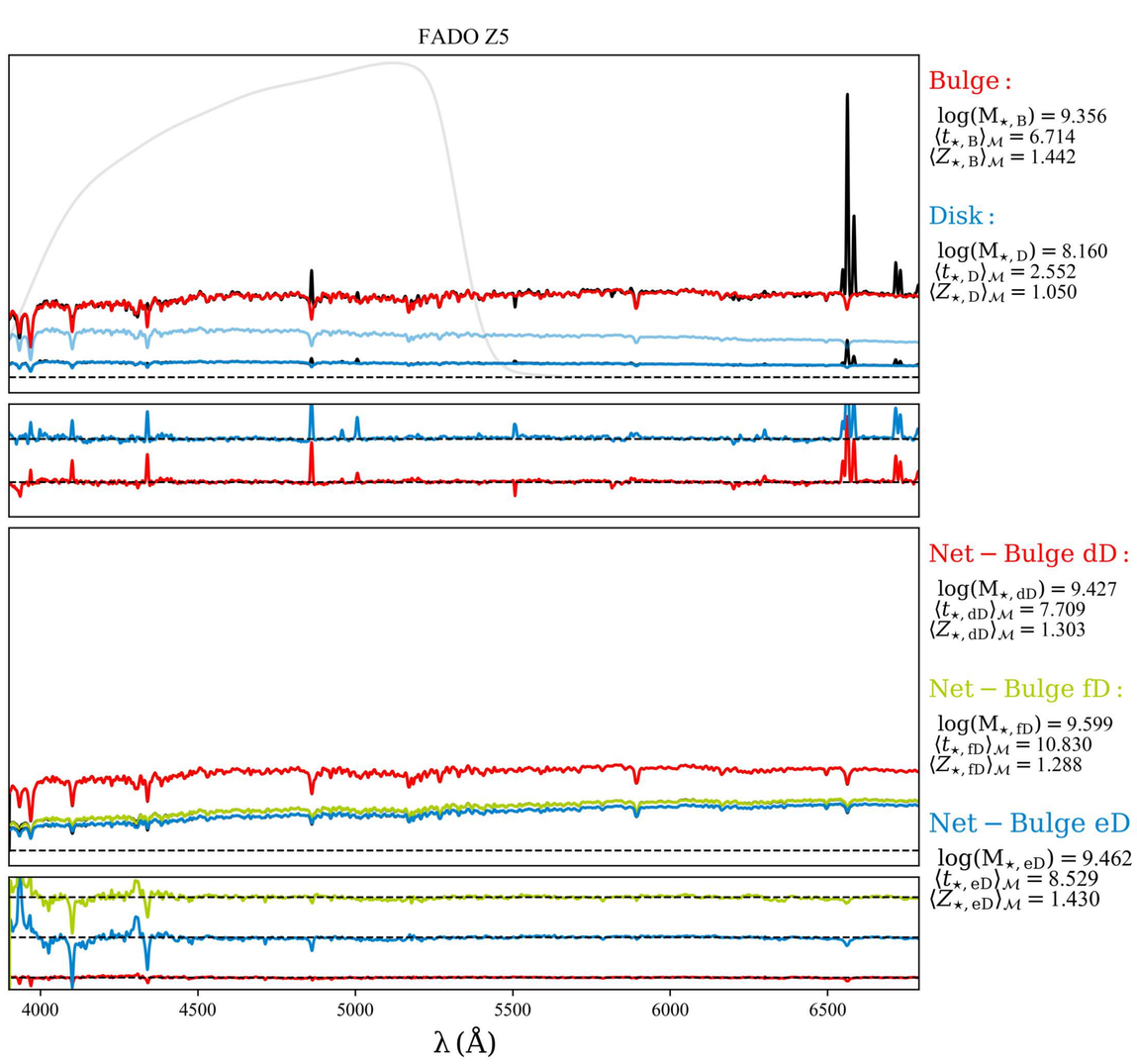
FADO Z5
Bulge :
log(M⋆, B) = 9.356
⟨t⋆, B⟩M = 6.714
⟨Z⋆, B⟩M = 1.442
Disk :
log(M⋆, D) = 8.160
⟨t⋆, D⟩M = 2.552
⟨Z⋆, D⟩M = 1.050
Net − Bulge dD :
log(M⋆, dD) = 9.427
⟨t⋆, dD⟩M = 7.709
⟨Z⋆, dD⟩M = 1.303
Net − Bulge fD :
log(M⋆, fD) = 9.599
⟨t⋆, fD⟩M = 10.830
⟨Z⋆, fD⟩M = 1.288
Net − Bulge eD :
log(M⋆, eD) = 9.462
⟨t⋆, eD⟩M = 8.529
⟨Z⋆, eD⟩M = 1.430
4000
4500
5000
5500
6000
6500
λ (Å)

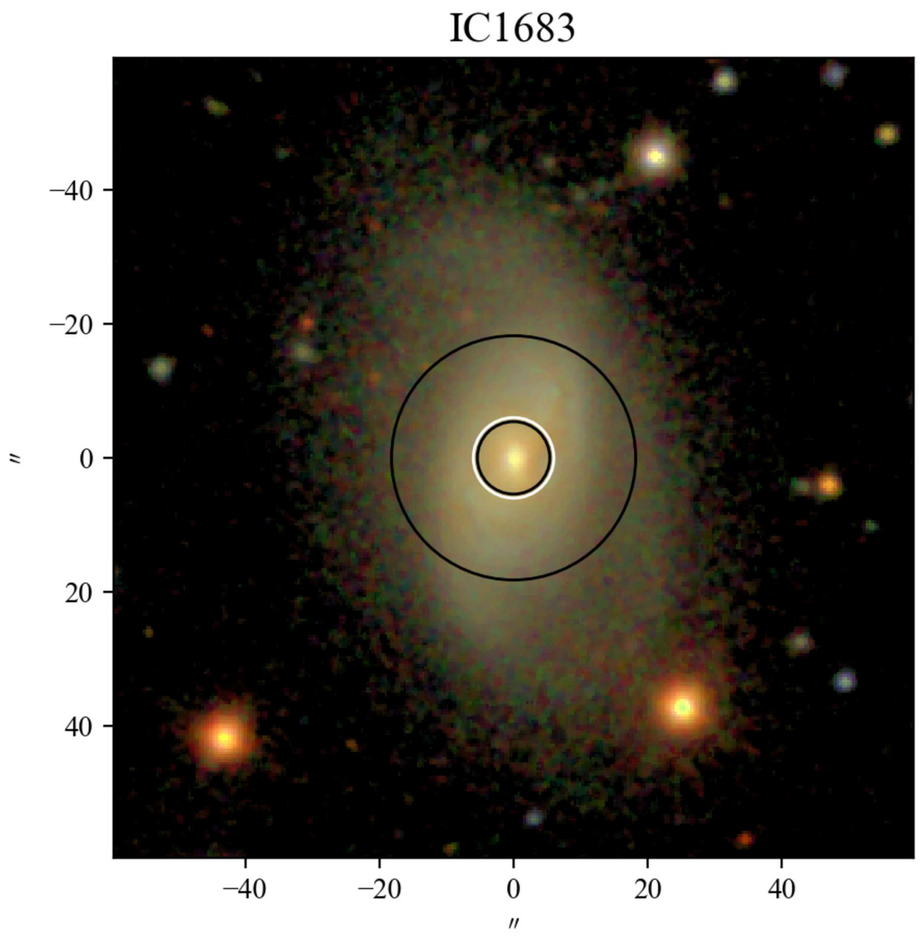
IC1683
−40
−20
0
20
40
″
−40
−20
0
20
40
″

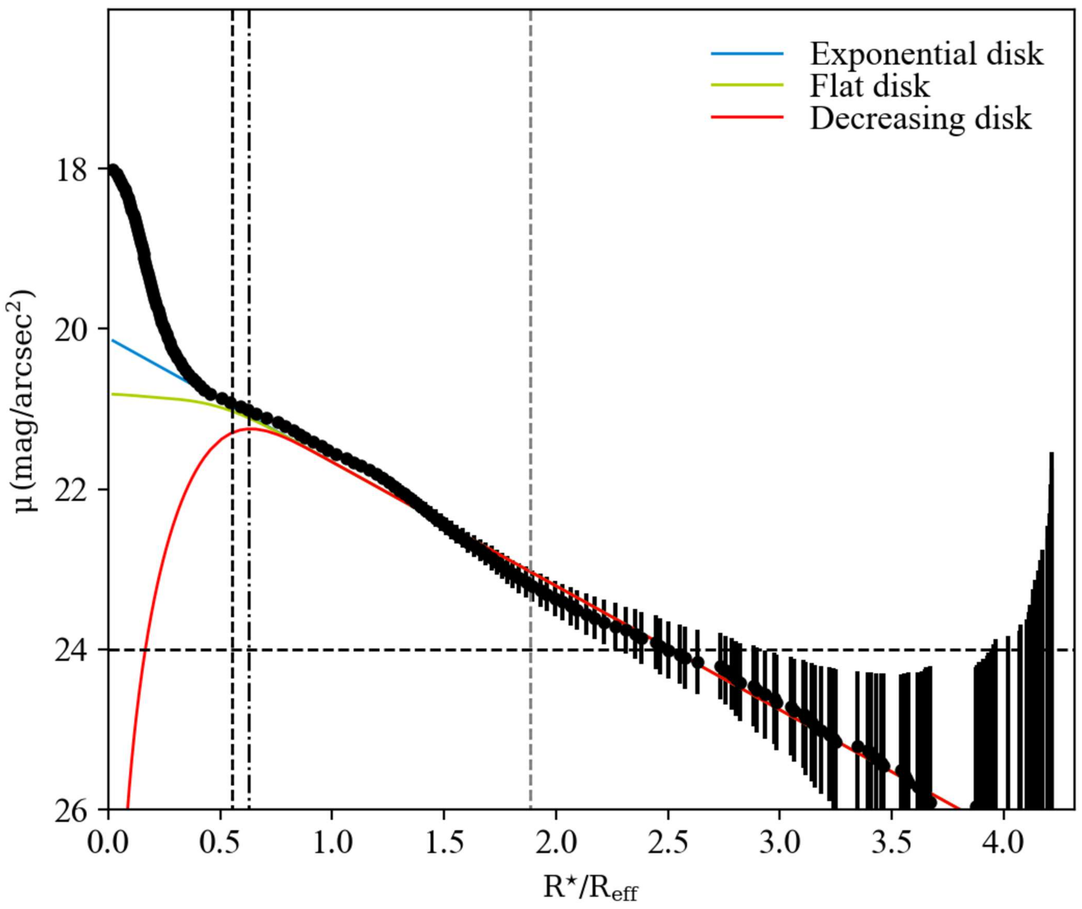
Exponential disk
Flat disk
Decreasing disk
μ (mag/arcsec²)
18
20
22
24
26
0.0
0.5
1.0
1.5
2.0
2.5
3.0
3.5
4.0
R⋆/Reff

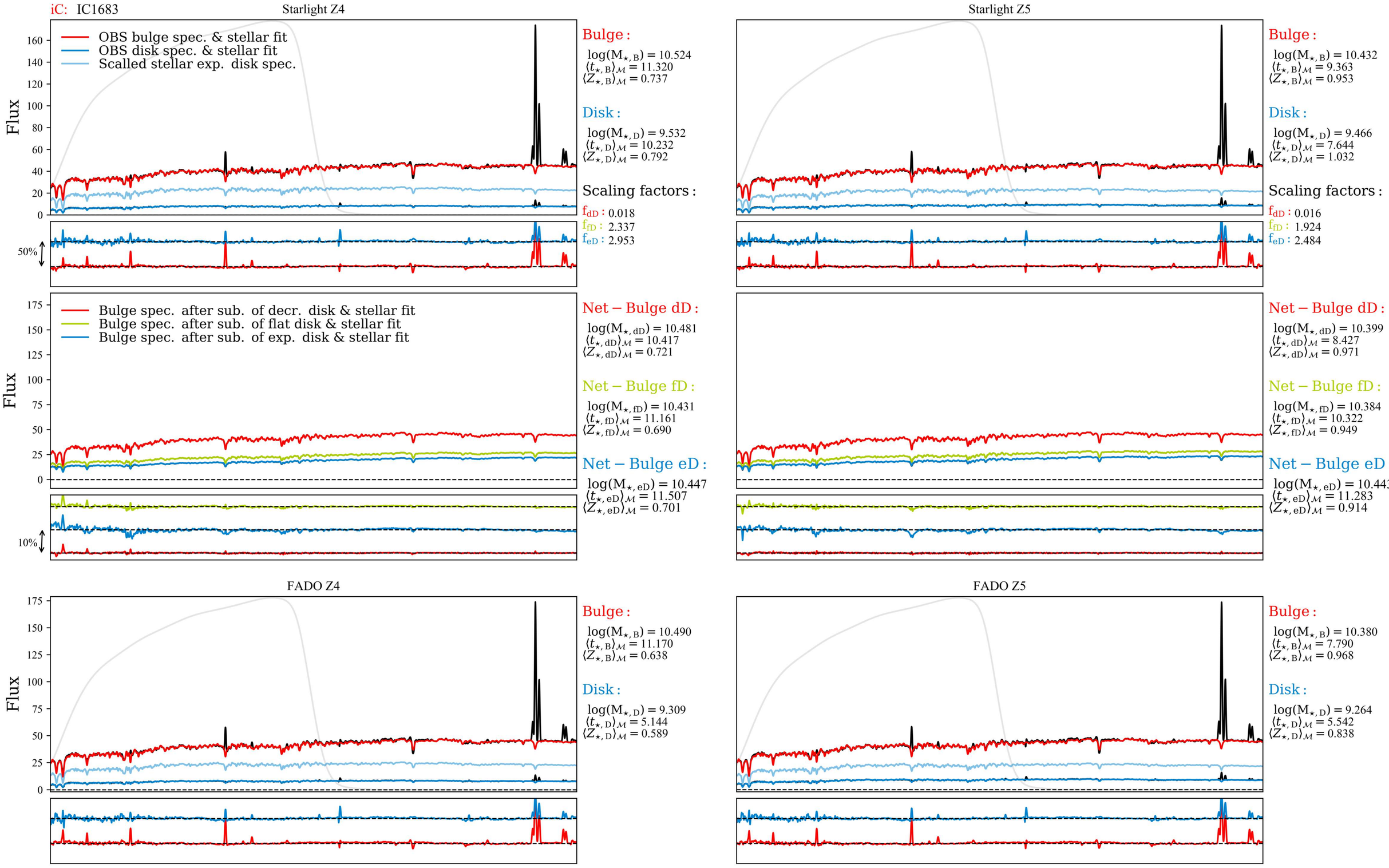
iC: IC1683
Starlight Z4
OBS bulge spec. & stellar fit
OBS disk spec. & stellar fit
Scalled stellar exp. disk spec.
Flux
50%
Bulge :
log(M⋆, B) = 10.524
⟨t⋆, B⟩M = 11.320
⟨Z⋆, B⟩M = 0.737
Disk :
log(M⋆, D) = 9.532
⟨t⋆, D⟩M = 10.232
⟨Z⋆, D⟩M = 0.792
Scaling factors :
fdD : 0.018
ffD : 2.337
feD : 2.953
Bulge spec. after sub. of decr. disk & stellar fit
Bulge spec. after sub. of flat disk & stellar fit
Bulge spec. after sub. of exp. disk & stellar fit
10%
Net − Bulge dD :
log(M⋆, dD) = 10.481
⟨t⋆, dD⟩M = 10.417
⟨Z⋆, dD⟩M = 0.721
Net − Bulge fD :
log(M⋆, fD) = 10.431
⟨t⋆, fD⟩M = 11.161
⟨Z⋆, fD⟩M = 0.690
Net − Bulge eD :
log(M⋆, eD) = 10.447
⟨t⋆, eD⟩M = 11.507
⟨Z⋆, eD⟩M = 0.701
Starlight Z5
Bulge :
log(M⋆, B) = 10.432
⟨t⋆, B⟩M = 9.363
⟨Z⋆, B⟩M = 0.953
Disk :
log(M⋆, D) = 9.466
⟨t⋆, D⟩M = 7.644
⟨Z⋆, D⟩M = 1.032
Scaling factors :
fdD : 0.016
ffD : 1.924
feD : 2.484
Net − Bulge dD :
log(M⋆, dD) = 10.399
⟨t⋆, dD⟩M = 8.427
⟨Z⋆, dD⟩M = 0.971
Net − Bulge fD :
log(M⋆, fD) = 10.384
⟨t⋆, fD⟩M = 10.322
⟨Z⋆, fD⟩M = 0.949
Net − Bulge eD :
log(M⋆, eD) = 10.443
⟨t⋆, eD⟩M = 11.283
⟨Z⋆, eD⟩M = 0.914
FADO Z4
Bulge :
log(M⋆, B) = 10.490
⟨t⋆, B⟩M = 11.170
⟨Z⋆, B⟩M = 0.638
Disk :
log(M⋆, D) = 9.309
⟨t⋆, D⟩M = 5.144
⟨Z⋆, D⟩M = 0.589
Net − Bulge dD :
log(M⋆, dD) = 10.470
⟨t⋆, dD⟩M = 10.190
⟨Z⋆, dD⟩M = 0.641
Net − Bulge fD :
log(M⋆, fD) = 10.430
⟨t⋆, fD⟩M = 12.840
⟨Z⋆, fD⟩M = 0.642
Net − Bulge eD :
log(M⋆, eD) = 10.420
⟨t⋆, eD⟩M = 12.970
⟨Z⋆, eD⟩M = 0.638
FADO Z5
Bulge :
log(M⋆, B) = 10.380
⟨t⋆, B⟩M = 7.790
⟨Z⋆, B⟩M = 0.968
Disk :
log(M⋆, D) = 9.264
⟨t⋆, D⟩M = 5.542
⟨Z⋆, D⟩M = 0.838
Net − Bulge dD :
log(M⋆, dD) = 10.390
⟨t⋆, dD⟩M = 8.713
⟨Z⋆, dD⟩M = 0.879
Net − Bulge fD :
log(M⋆, fD) = 10.430
⟨t⋆, fD⟩M = 11.660
⟨Z⋆, fD⟩M = 0.968
Net − Bulge eD :
log(M⋆, eD) = 10.420
⟨t⋆, eD⟩M = 12.200
⟨Z⋆, eD⟩M = 0.904
λ (Å)

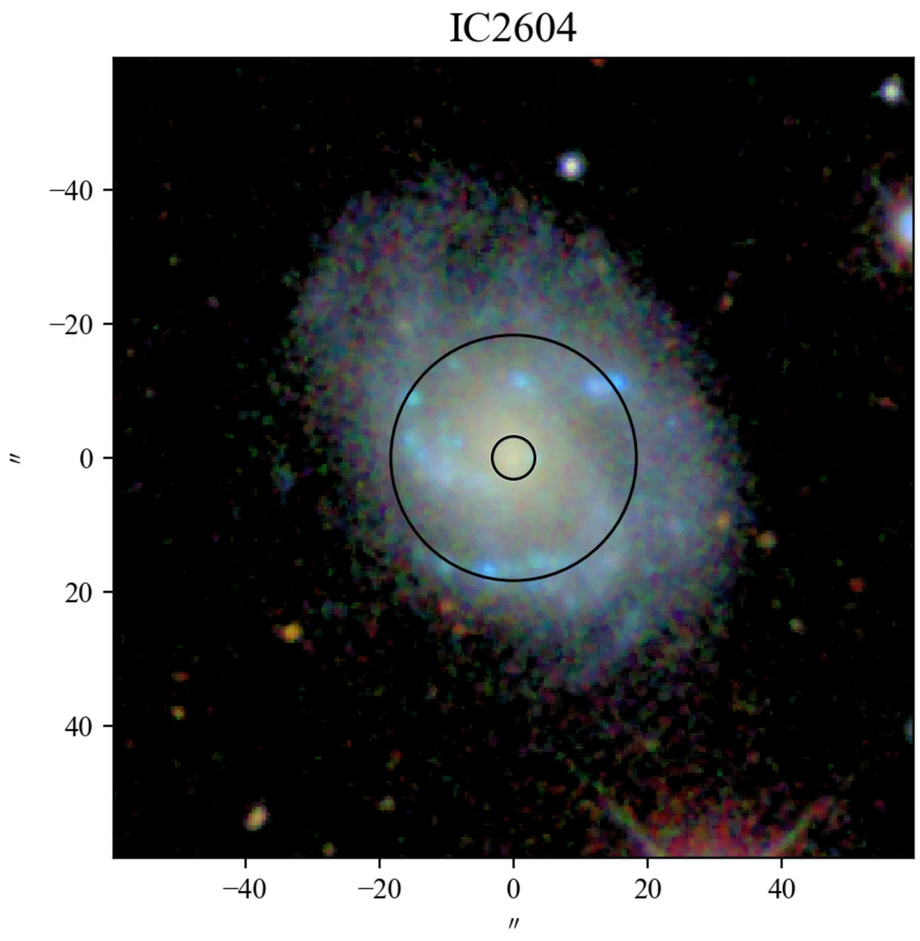
IC2604
−40
−20
0
20
40
″
−40
−20
0
20
40
″

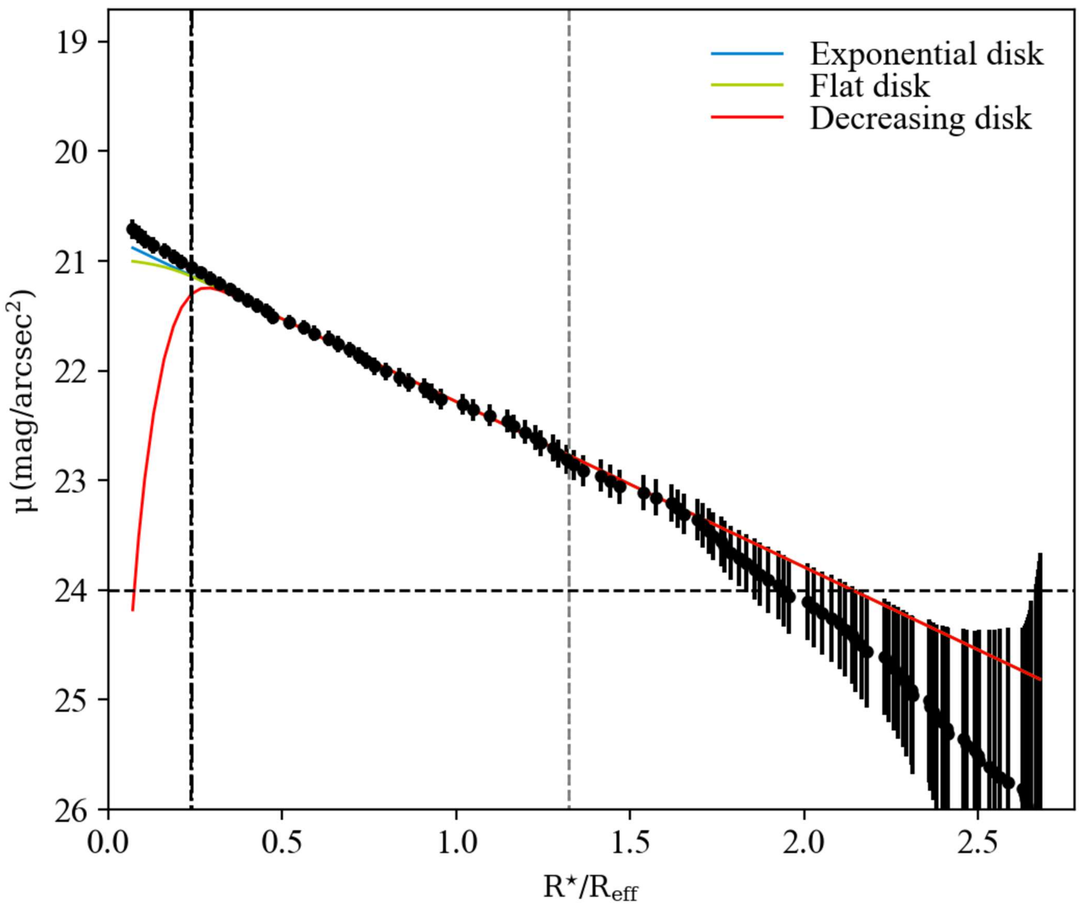
Exponential disk
Flat disk
Decreasing disk
μ (mag/arcsec²)
19
20
21
22
23
24
25
26
0.0
0.5
1.0
1.5
2.0
2.5
R⋆/Reff

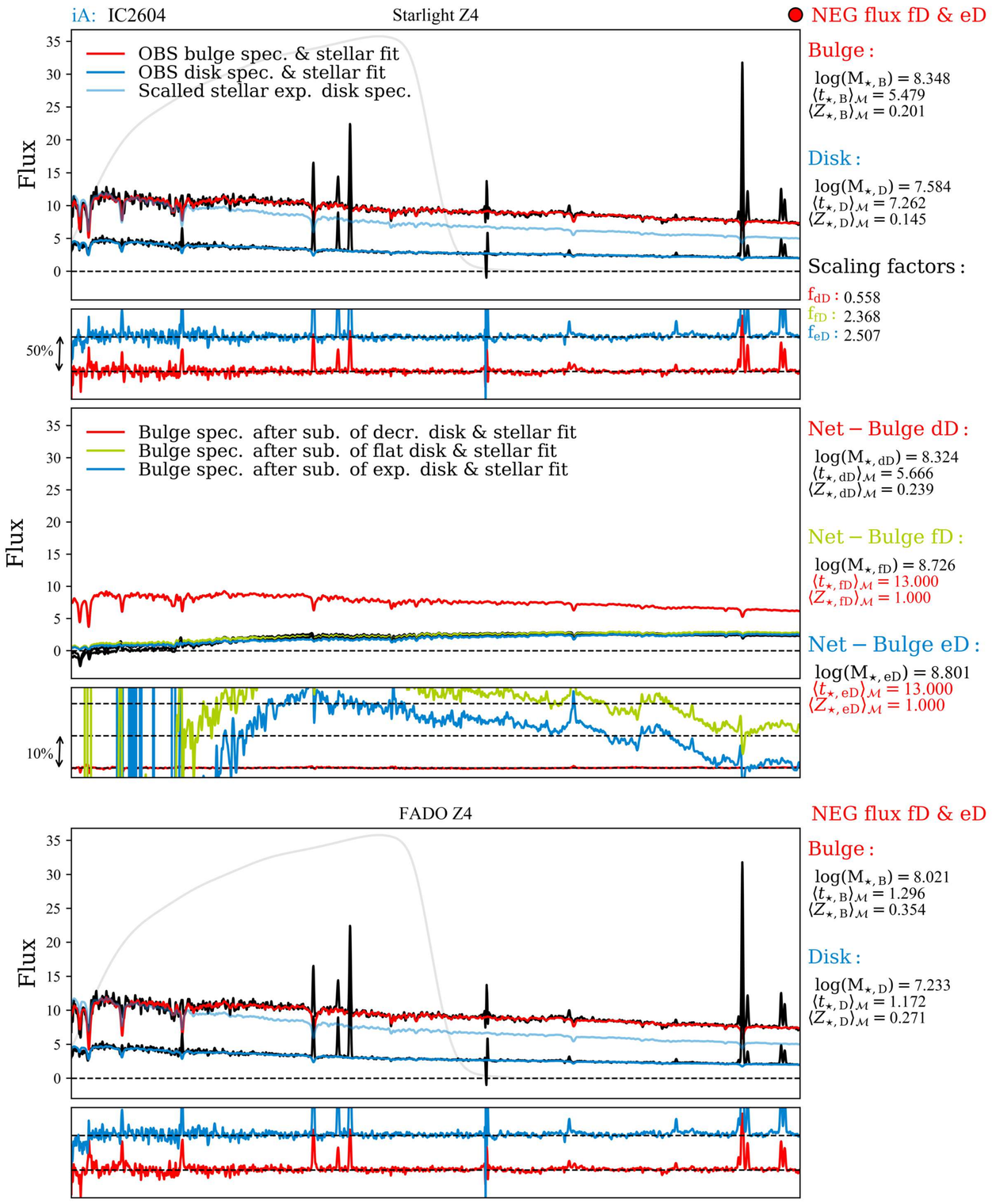
iA: IC2604
Starlight Z4
NEG flux fD & eD
OBS bulge spec. & stellar fit
OBS disk spec. & stellar fit
Scalled stellar exp. disk spec.
Flux
Bulge :
log(M⋆, B) = 8.348
⟨t⋆, B⟩M = 5.479
⟨Z⋆, B⟩M = 0.201
Disk :
log(M⋆, D) = 7.584
⟨t⋆, D⟩M = 7.262
⟨Z⋆, D⟩M = 0.145
Scaling factors :
fdD : 0.558
ffD : 2.368
feD : 2.507
50%
Bulge spec. after sub. of decr. disk & stellar fit
Bulge spec. after sub. of flat disk & stellar fit
Bulge spec. after sub. of exp. disk & stellar fit
Net − Bulge dD :
log(M⋆, dD) = 8.324
⟨t⋆, dD⟩M = 5.666
⟨Z⋆, dD⟩M = 0.239
Net − Bulge fD :
log(M⋆, fD) = 8.726
⟨t⋆, fD⟩M = 13.000
⟨Z⋆, fD⟩M = 1.000
Net − Bulge eD :
log(M⋆, eD) = 8.801
⟨t⋆, eD⟩M = 13.000
⟨Z⋆, eD⟩M = 1.000
10%
FADO Z4
NEG flux fD & eD
Bulge :
log(M⋆, B) = 8.021
⟨t⋆, B⟩M = 1.296
⟨Z⋆, B⟩M = 0.354
Disk :
log(M⋆, D) = 7.233
⟨t⋆, D⟩M = 1.172
⟨Z⋆, D⟩M = 0.271
Net − Bulge dD :
log(M⋆, dD) = 8.000
⟨t⋆, dD⟩M = 1.170
⟨Z⋆, dD⟩M = 0.378
Net − Bulge fD :
log(M⋆, fD) = 8.016
⟨t⋆, fD⟩M = 1.434
⟨Z⋆, fD⟩M = 1.000
Net − Bulge eD :
log(M⋆, eD) = 8.107
⟨t⋆, eD⟩M = 1.786
⟨Z⋆, eD⟩M = 1.000
λ (Å)

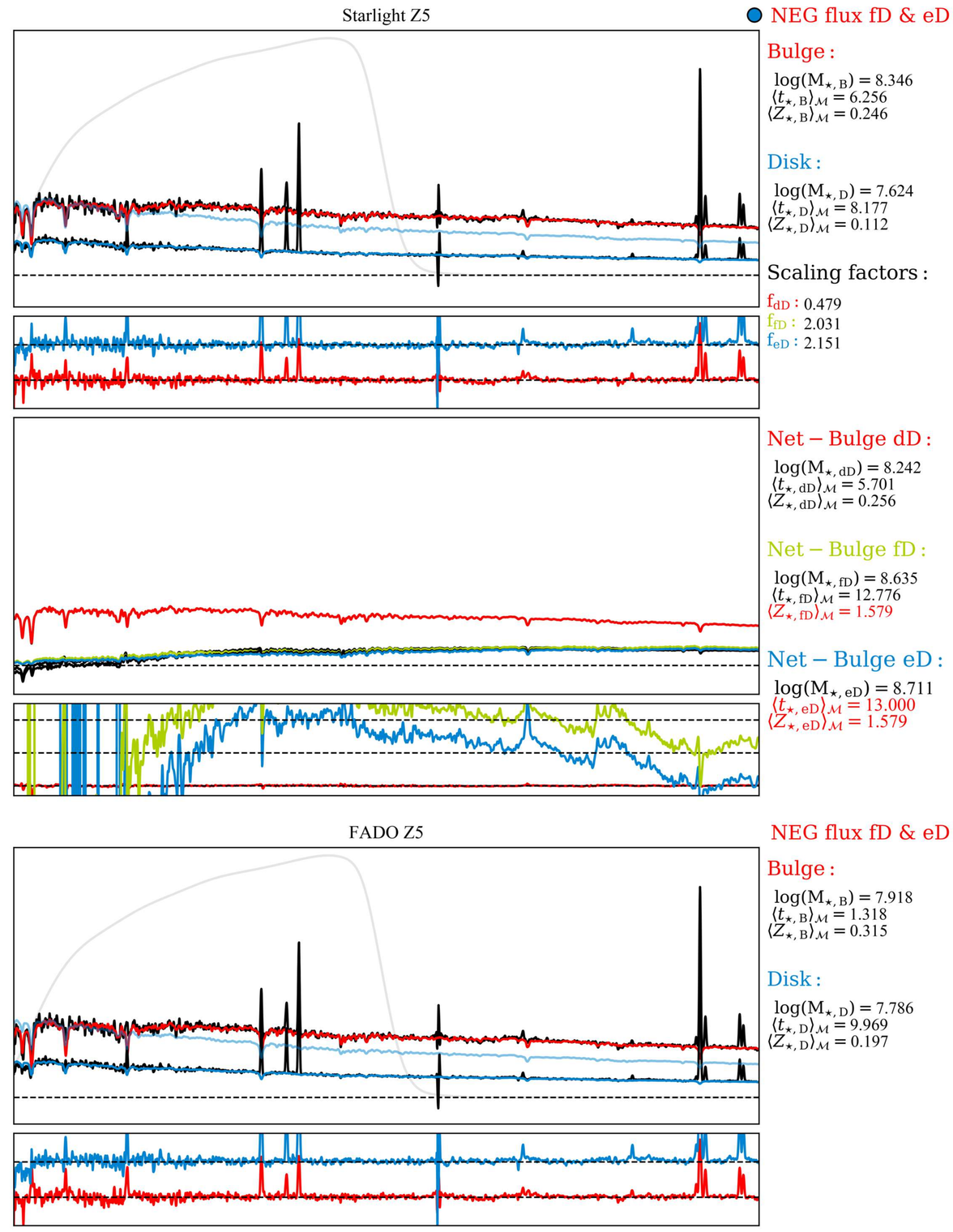
Starlight Z5
NEG flux fD & eD
Bulge :
log(M⋆, B) = 8.346
⟨t⋆, B⟩M = 6.256
⟨Z⋆, B⟩M = 0.246
Disk :
log(M⋆, D) = 7.624
⟨t⋆, D⟩M = 8.177
⟨Z⋆, D⟩M = 0.112
Scaling factors :
fdD : 0.479
ffD : 2.031
feD : 2.151
Net − Bulge dD :
log(M⋆, dD) = 8.242
⟨t⋆, dD⟩M = 5.701
⟨Z⋆, dD⟩M = 0.256
Net − Bulge fD :
log(M⋆, fD) = 8.635
⟨t⋆, fD⟩M = 12.776
⟨Z⋆, fD⟩M = 1.579
Net − Bulge eD :
log(M⋆, eD) = 8.711
⟨t⋆, eD⟩M = 13.000
⟨Z⋆, eD⟩M = 1.579
FADO Z5
NEG flux fD & eD
Bulge :
log(M⋆, B) = 7.918
⟨t⋆, B⟩M = 1.318
⟨Z⋆, B⟩M = 0.315
Disk :
log(M⋆, D) = 7.786
⟨t⋆, D⟩M = 9.969
⟨Z⋆, D⟩M = 0.197
Net − Bulge dD :
log(M⋆, dD) = 7.987
⟨t⋆, dD⟩M = 1.583
⟨Z⋆, dD⟩M = 0.442
Net − Bulge fD :
log(M⋆, fD) = 7.981
⟨t⋆, fD⟩M = 2.176
⟨Z⋆, fD⟩M = 1.000
Net − Bulge eD :
log(M⋆, eD) = 8.236
⟨t⋆, eD⟩M = 3.790
⟨Z⋆, eD⟩M = 0.757
λ (Å)

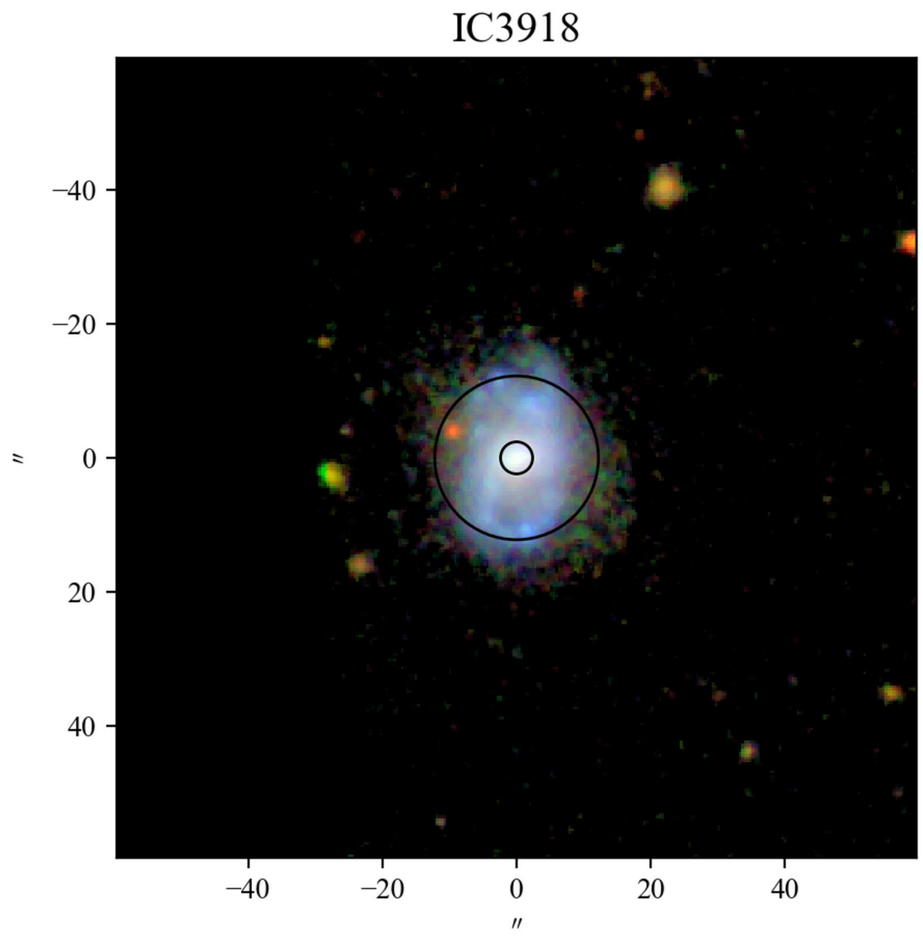
IC3918
−40
−20
0
20
40
″
−40
−20
0
20
40
″

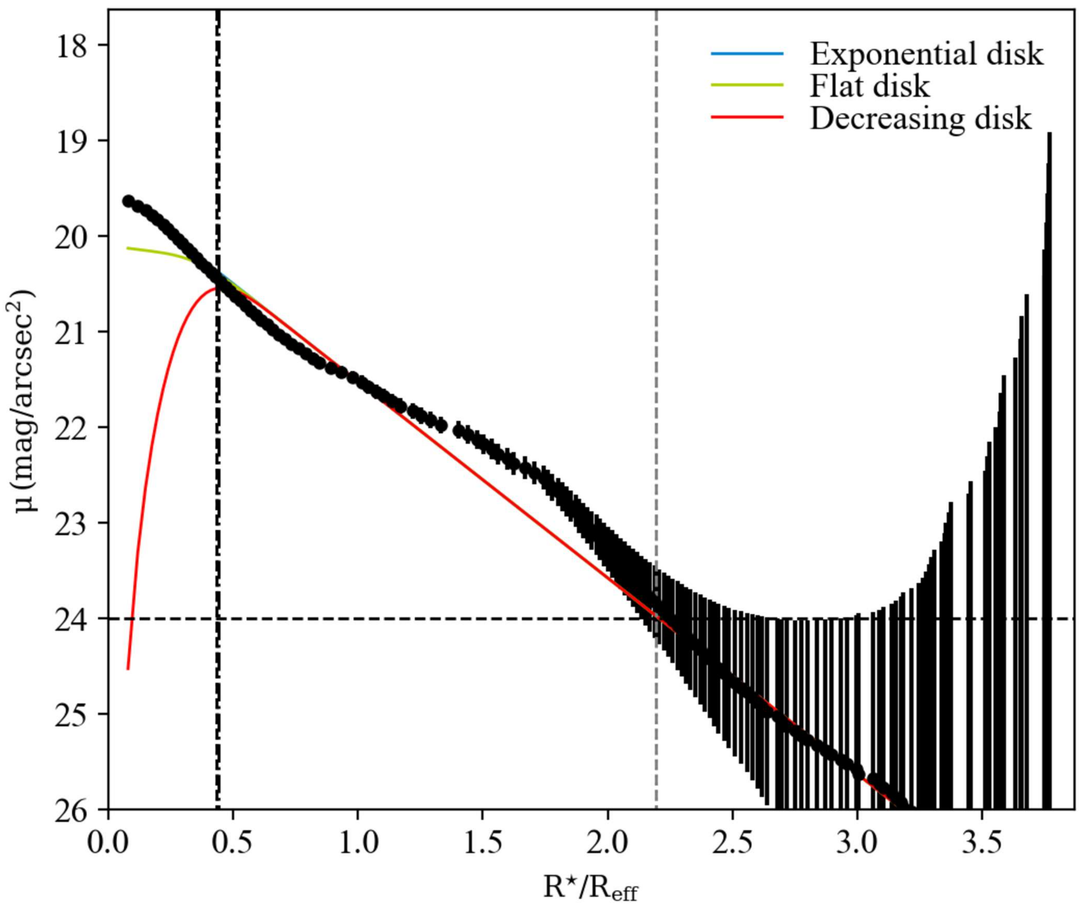
Exponential disk
Flat disk
Decreasing disk
μ (mag/arcsec²)
18
19
20
21
22
23
24
25
26
0.0
0.5
1.0
1.5
2.0
2.5
3.0
3.5
R⋆/Reff

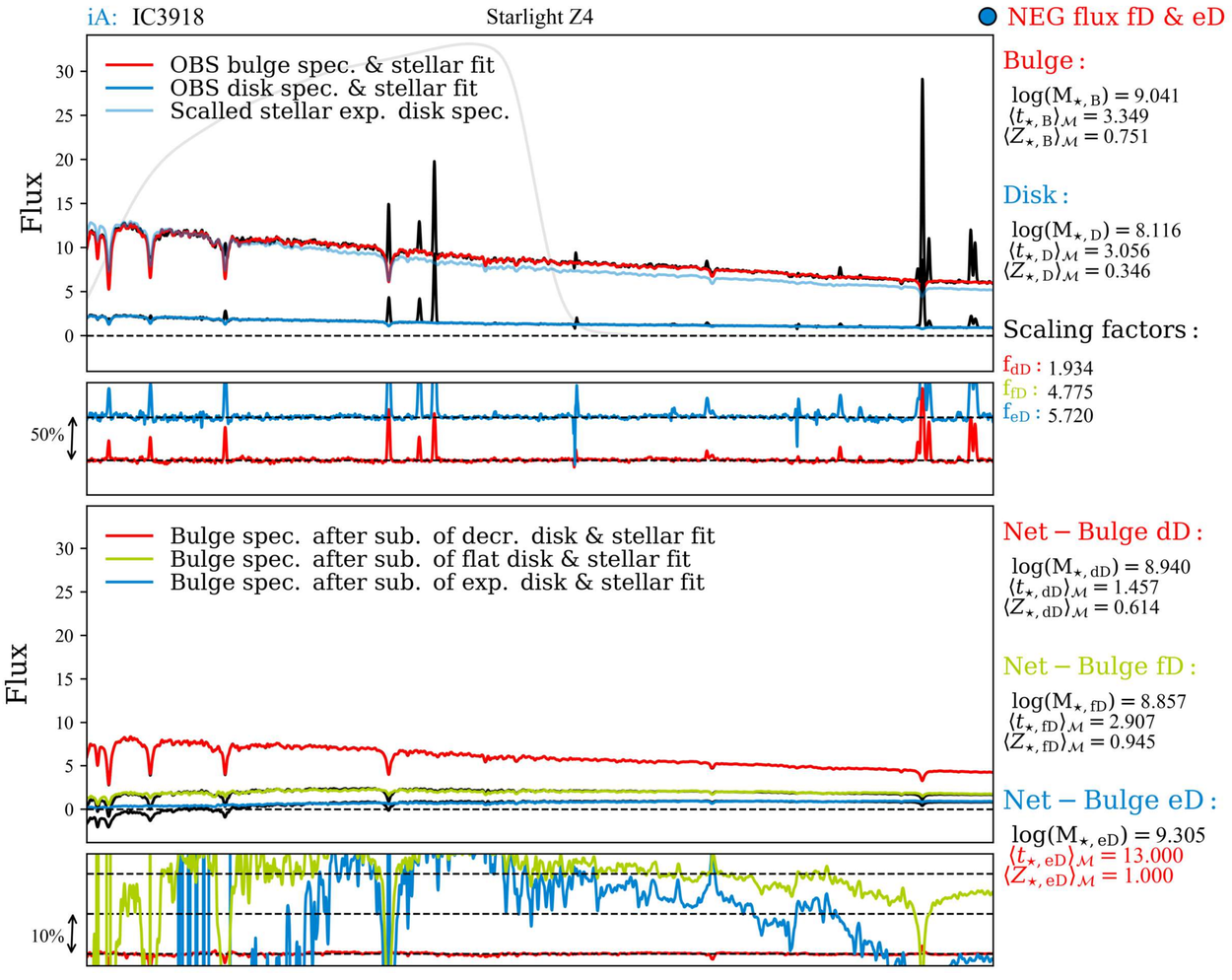
iA: IC3918
Starlight Z4
NEG flux fD & eD
OBS bulge spec. & stellar fit
OBS disk spec. & stellar fit
Scalled stellar exp. disk spec.
Flux
50%
Bulge :
log(M⋆, B) = 9.041
⟨t⋆, B⟩M = 3.349
⟨Z⋆, B⟩M = 0.751
Disk :
log(M⋆, D) = 8.116
⟨t⋆, D⟩M = 3.056
⟨Z⋆, D⟩M = 0.346
Scaling factors :
fdD : 1.934
ffD : 4.775
feD : 5.720
Bulge spec. after sub. of decr. disk & stellar fit
Bulge spec. after sub. of flat disk & stellar fit
Bulge spec. after sub. of exp. disk & stellar fit
10%
Net − Bulge dD :
log(M⋆, dD) = 8.940
⟨t⋆, dD⟩M = 1.457
⟨Z⋆, dD⟩M = 0.614
Net − Bulge fD :
log(M⋆, fD) = 8.857
⟨t⋆, fD⟩M = 2.907
⟨Z⋆, fD⟩M = 0.945
Net − Bulge eD :
log(M⋆, eD) = 9.305
⟨t⋆, eD⟩M = 13.000
⟨Z⋆, eD⟩M = 1.000

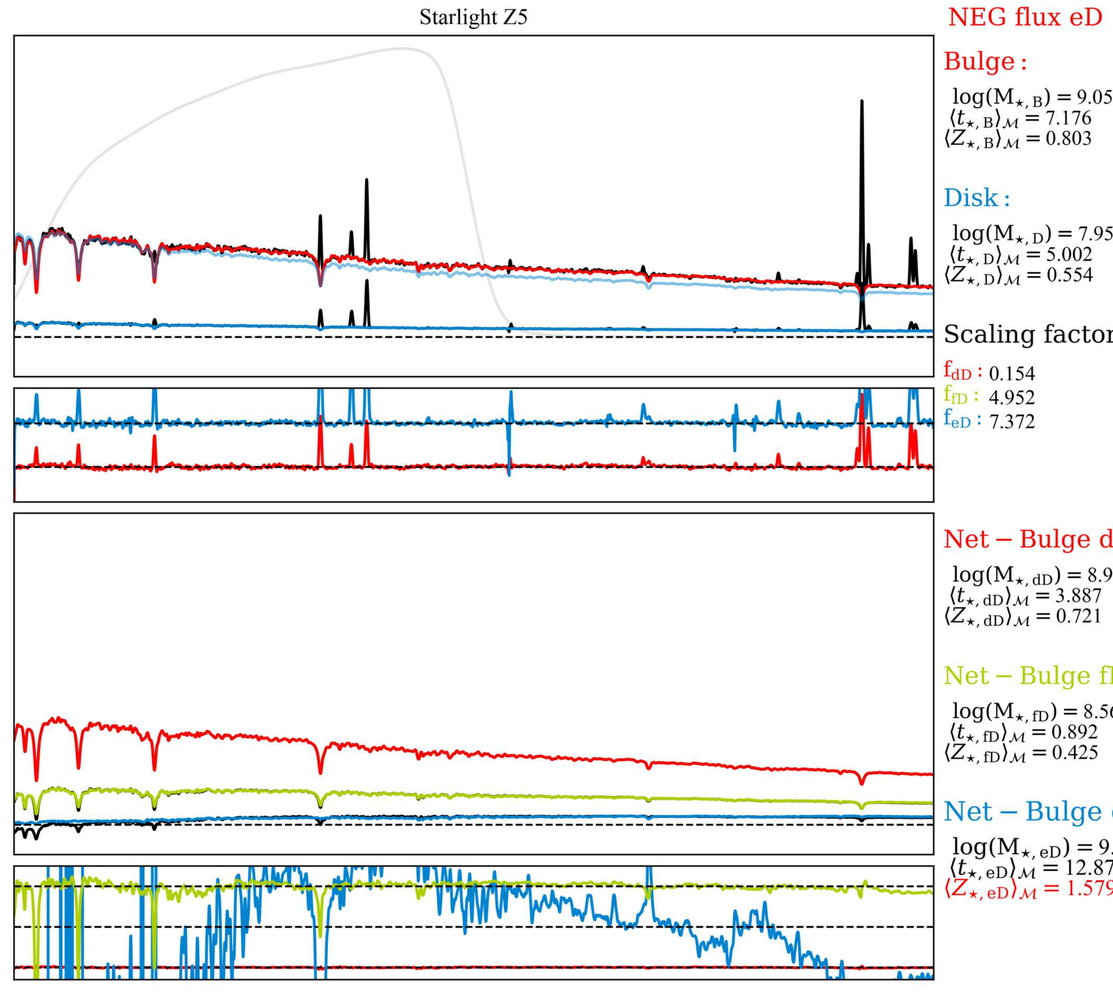
Starlight Z5
NEG flux eD
Bulge :
log(M⋆, B) = 9.058
⟨t⋆, B⟩M = 7.176
⟨Z⋆, B⟩M = 0.803
Disk :
log(M⋆, D) = 7.952
⟨t⋆, D⟩M = 5.002
⟨Z⋆, D⟩M = 0.554
Scaling factors :
fdD : 0.154
ffD : 4.952
feD : 7.372
Net − Bulge dD :
log(M⋆, dD) = 8.925
⟨t⋆, dD⟩M = 3.887
⟨Z⋆, dD⟩M = 0.721
Net − Bulge fD :
log(M⋆, fD) = 8.567
⟨t⋆, fD⟩M = 0.892
⟨Z⋆, fD⟩M = 0.425
Net − Bulge eD :
log(M⋆, eD) = 9.047
⟨t⋆, eD⟩M = 12.878
⟨Z⋆, eD⟩M = 1.579

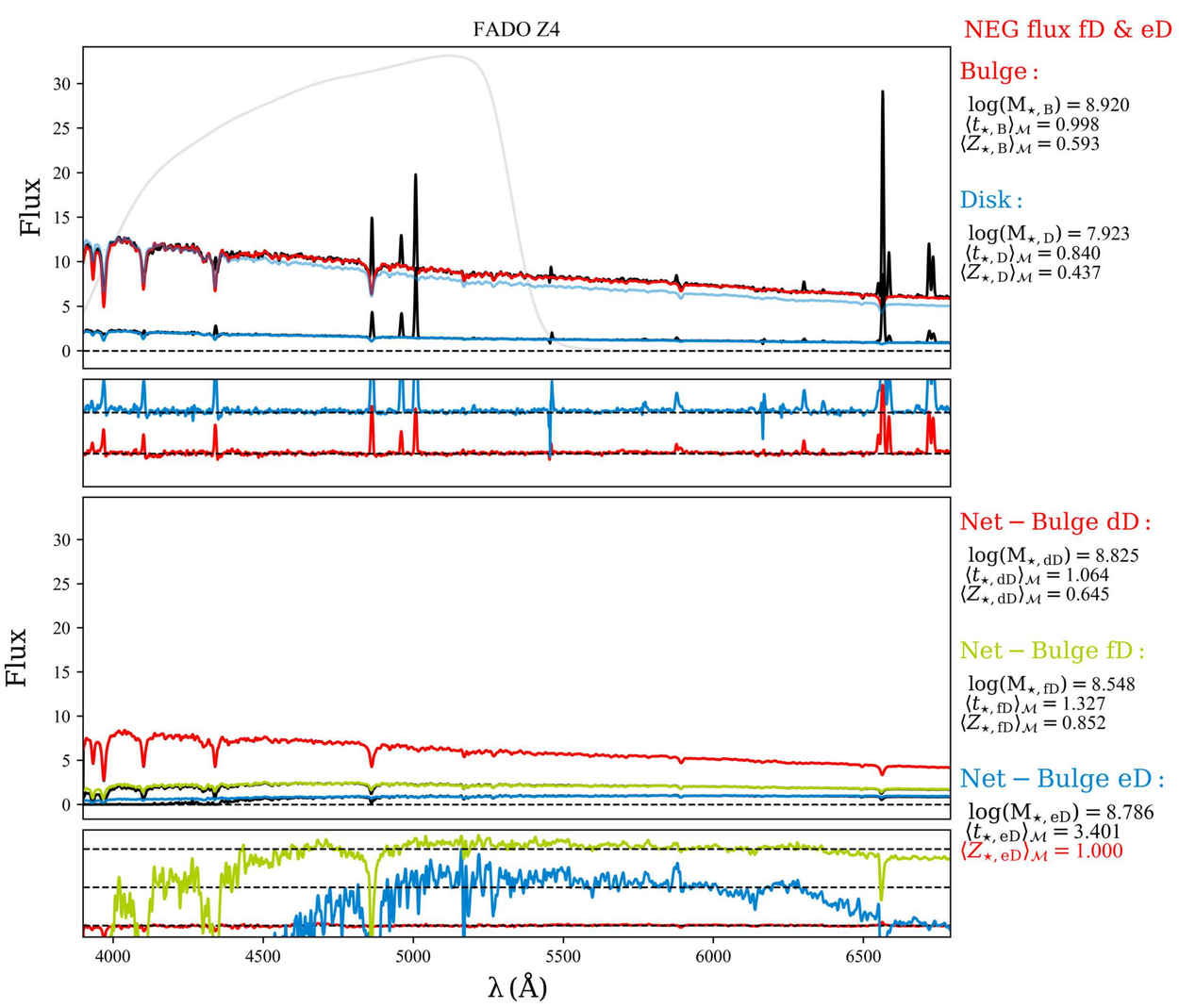
FADO Z4
NEG flux fD & eD
Flux
Bulge :
log(M⋆, B) = 8.920
⟨t⋆, B⟩M = 0.998
⟨Z⋆, B⟩M = 0.593
Disk :
log(M⋆, D) = 7.923
⟨t⋆, D⟩M = 0.840
⟨Z⋆, D⟩M = 0.437
Net − Bulge dD :
log(M⋆, dD) = 8.825
⟨t⋆, dD⟩M = 1.064
⟨Z⋆, dD⟩M = 0.645
Net − Bulge fD :
log(M⋆, fD) = 8.548
⟨t⋆, fD⟩M = 1.327
⟨Z⋆, fD⟩M = 0.852
Net − Bulge eD :
log(M⋆, eD) = 8.786
⟨t⋆, eD⟩M = 3.401
⟨Z⋆, eD⟩M = 1.000
4000
4500
5000
5500
6000
6500
λ (Å)

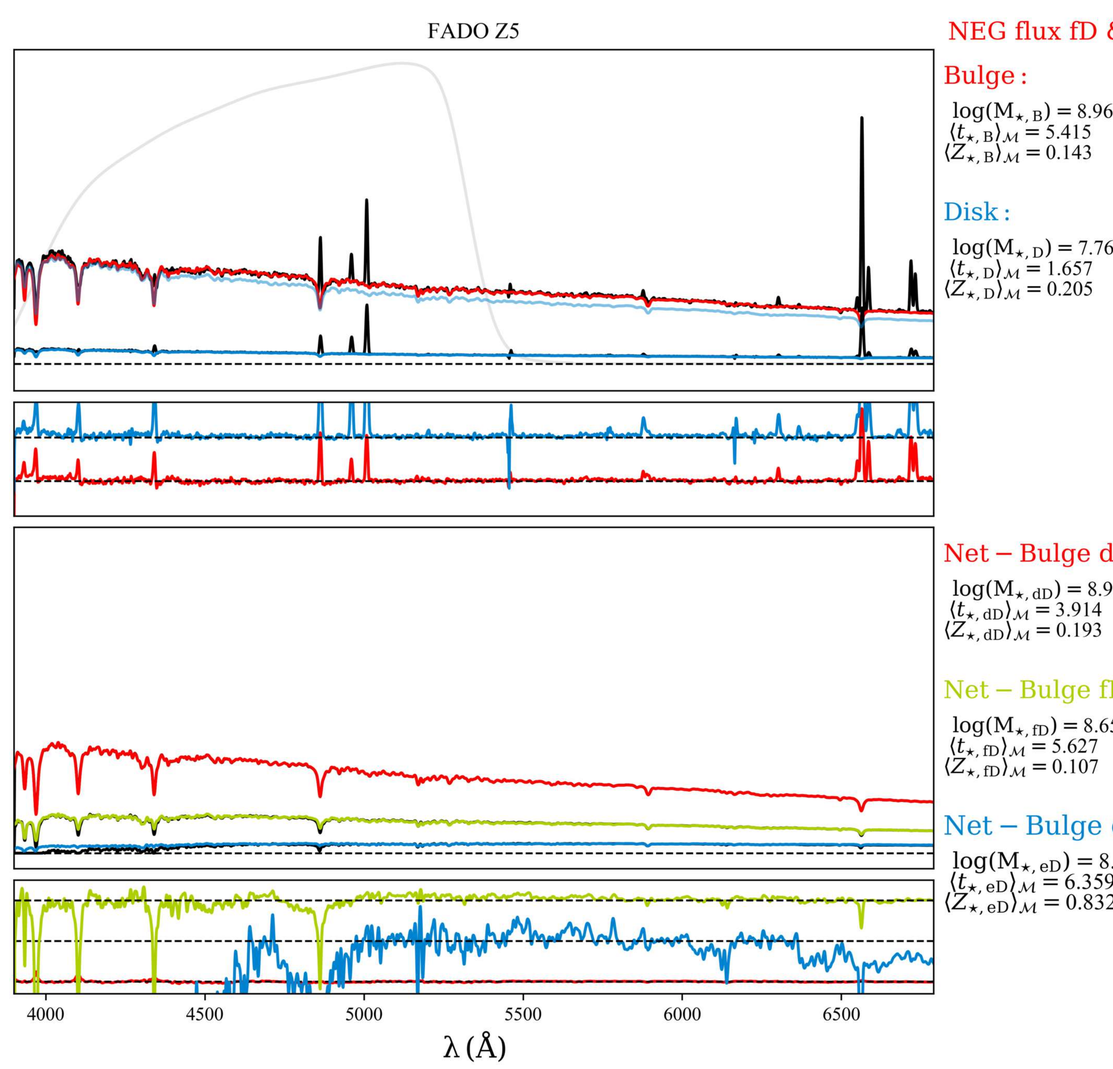
FADO Z5
NEG flux fD & eD
Bulge :
log(M⋆, B) = 8.960
⟨t⋆, B⟩M = 5.415
⟨Z⋆, B⟩M = 0.143
Disk :
log(M⋆, D) = 7.762
⟨t⋆, D⟩M = 1.657
⟨Z⋆, D⟩M = 0.205
Net − Bulge dD :
log(M⋆, dD) = 8.922
⟨t⋆, dD⟩M = 3.914
⟨Z⋆, dD⟩M = 0.193
Net − Bulge fD :
log(M⋆, fD) = 8.659
⟨t⋆, fD⟩M = 5.627
⟨Z⋆, fD⟩M = 0.107
Net − Bulge eD :
log(M⋆, eD) = 8.572
⟨t⋆, eD⟩M = 6.359
⟨Z⋆, eD⟩M = 0.832
4000
4500
5000
5500
6000
6500
λ (Å)

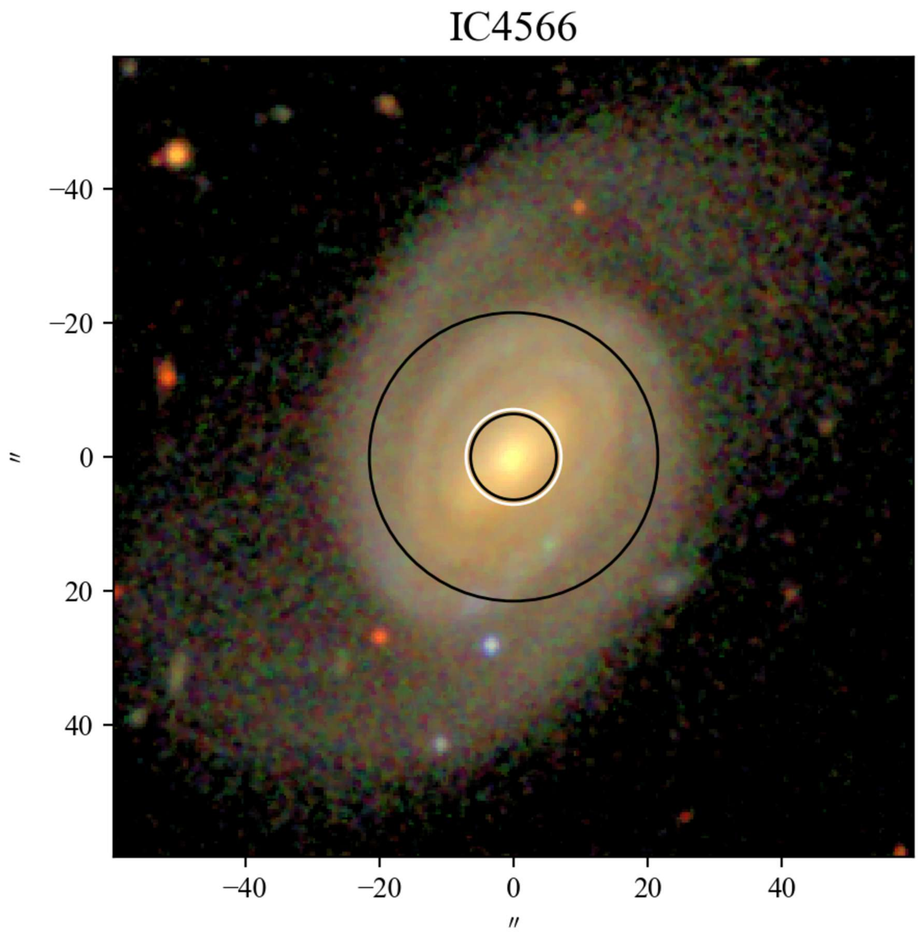
IC4566
−40
−20
0
20
40
″
−40
−20
0
20
40
″

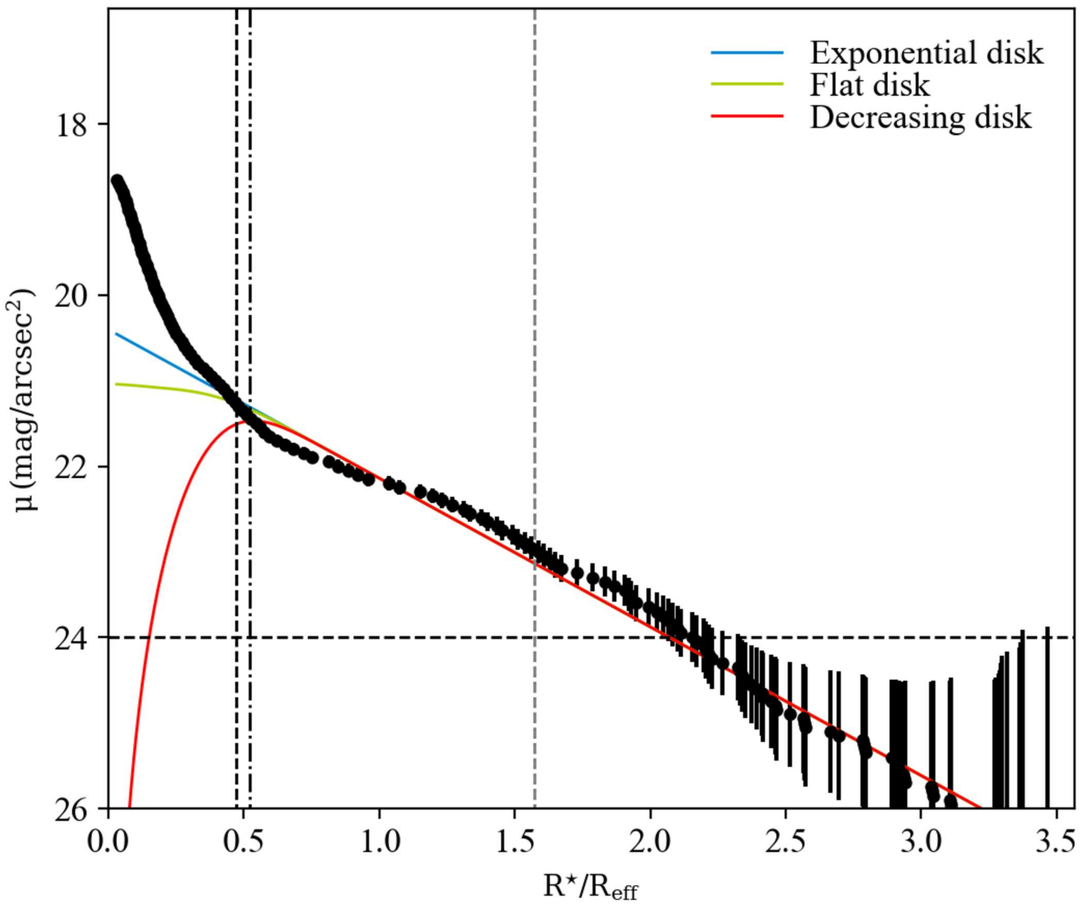
Exponential disk
Flat disk
Decreasing disk
μ (mag/arcsec²)
18
20
22
24
26
0.0
0.5
1.0
1.5
2.0
2.5
3.0
3.5
R⋆/Reff

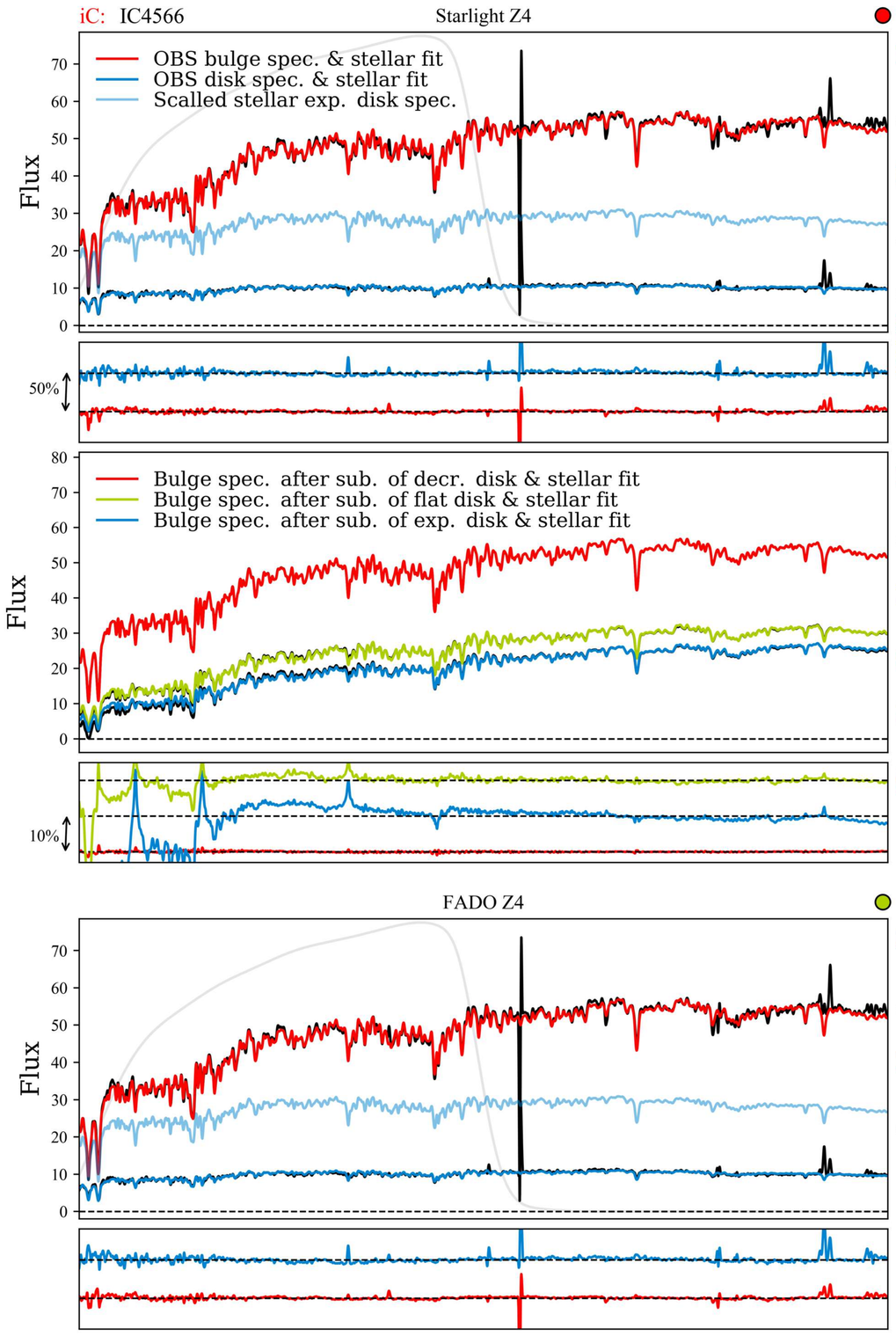
iC: IC4566
Starlight Z4
OBS bulge spec. & stellar fit
OBS disk spec. & stellar fit
Scalled stellar exp. disk spec.
Flux
50%
Bulge spec. after sub. of decr. disk & stellar fit
Bulge spec. after sub. of flat disk & stellar fit
Bulge spec. after sub. of exp. disk & stellar fit
10%
Bulge :
log(M⋆, B) = 10.773
⟨t⋆, B⟩M = 12.519
⟨Z⋆, B⟩M = 0.783
Disk :
log(M⋆, D) = 9.914
⟨t⋆, D⟩M = 10.575
⟨Z⋆, D⟩M = 0.703
Scaling factors :
fdD : 0.030
ffD : 2.289
feD : 2.797
Net − Bulge dD :
log(M⋆, dD) = 10.765
⟨t⋆, dD⟩M = 11.871
⟨Z⋆, dD⟩M = 0.767
Net − Bulge fD :
log(M⋆, fD) = 10.660
⟨t⋆, fD⟩M = 13.000
⟨Z⋆, fD⟩M = 1.000
Net − Bulge eD :
log(M⋆, eD) = 10.668
⟨t⋆, eD⟩M = 13.000
⟨Z⋆, eD⟩M = 1.000

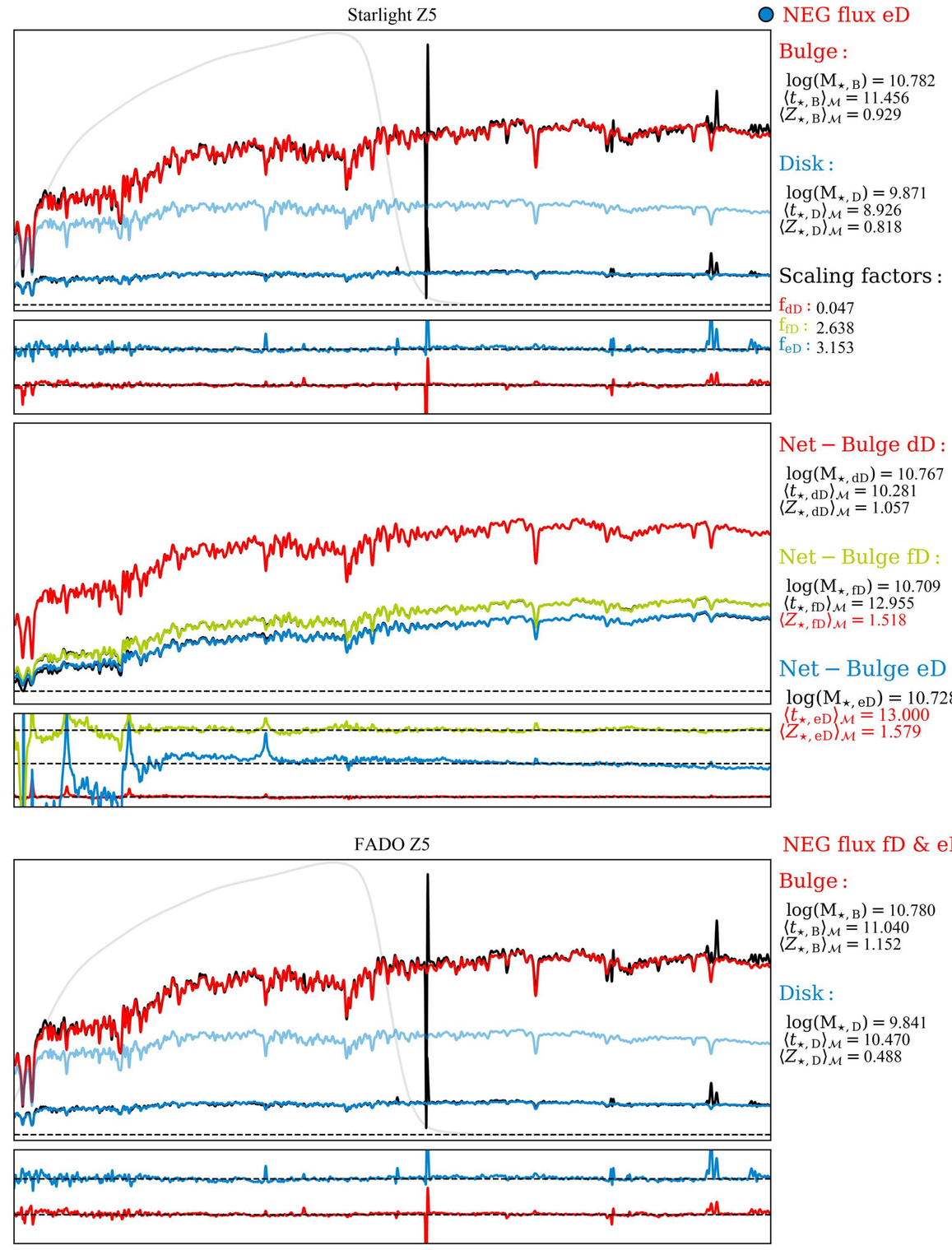
Starlight Z5
NEG flux eD
Bulge :
log(M⋆, B) = 10.782
⟨t⋆, B⟩M = 11.456
⟨Z⋆, B⟩M = 0.929
Disk :
log(M⋆, D) = 9.871
⟨t⋆, D⟩M = 8.926
⟨Z⋆, D⟩M = 0.818
Scaling factors :
fdD : 0.047
ffD : 2.638
feD : 3.153
Net − Bulge dD :
log(M⋆, dD) = 10.767
⟨t⋆, dD⟩M = 10.281
⟨Z⋆, dD⟩M = 1.057
Net − Bulge fD :
log(M⋆, fD) = 10.709
⟨t⋆, fD⟩M = 12.955
⟨Z⋆, fD⟩M = 1.518
Net − Bulge eD :
log(M⋆, eD) = 10.728
⟨t⋆, eD⟩M = 13.000
⟨Z⋆, eD⟩M = 1.579

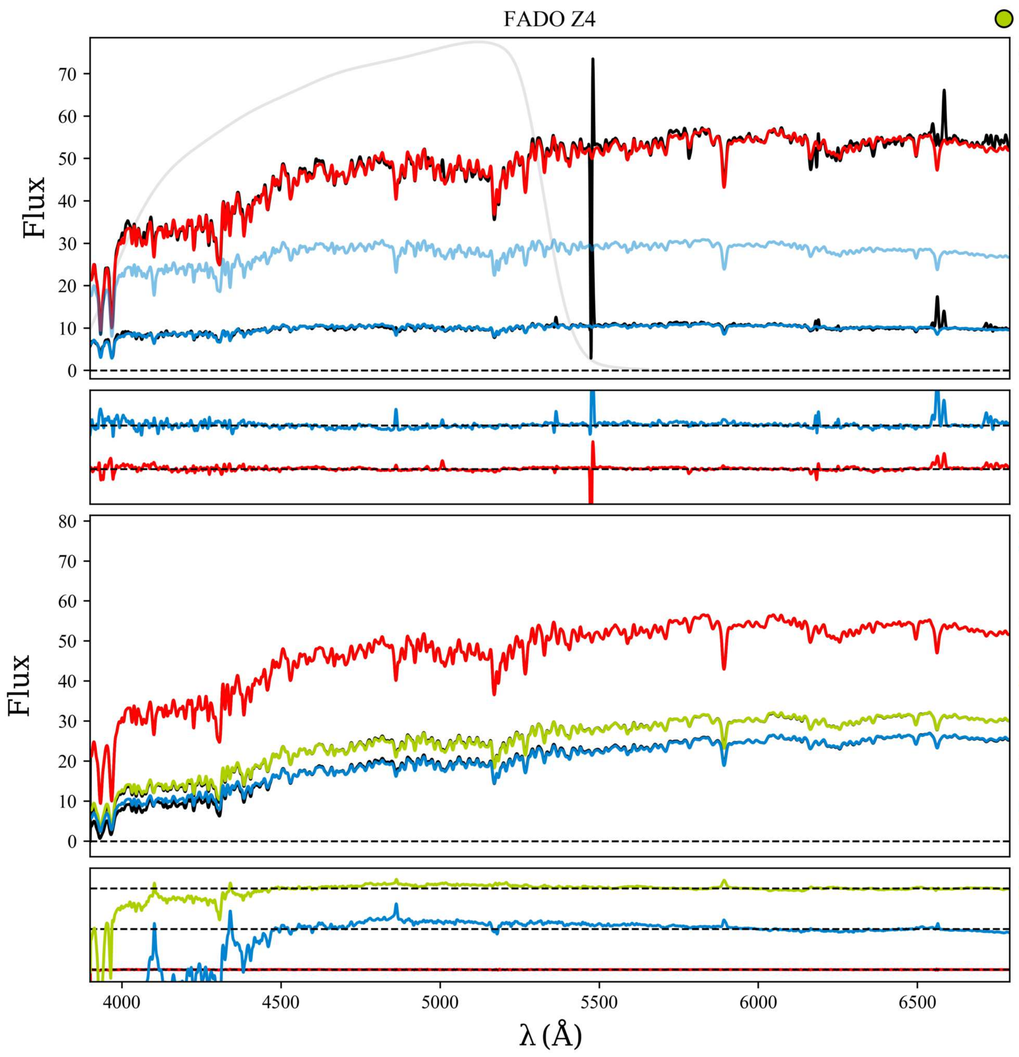
FADO Z4
Flux
Bulge :
log(M⋆, B) = 10.770
⟨t⋆, B⟩M = 12.160
⟨Z⋆, B⟩M = 0.683
Disk :
log(M⋆, D) = 9.852
⟨t⋆, D⟩M = 10.970
⟨Z⋆, D⟩M = 0.436
Net − Bulge dD :
log(M⋆, dD) = 10.760
⟨t⋆, dD⟩M = 12.110
⟨Z⋆, dD⟩M = 0.688
Net − Bulge fD :
log(M⋆, fD) = 10.680
⟨t⋆, fD⟩M = 13.000
⟨Z⋆, fD⟩M = 0.944
Net − Bulge eD :
log(M⋆, eD) = 10.660
⟨t⋆, eD⟩M = 11.000
⟨Z⋆, eD⟩M = 1.000
λ (Å)

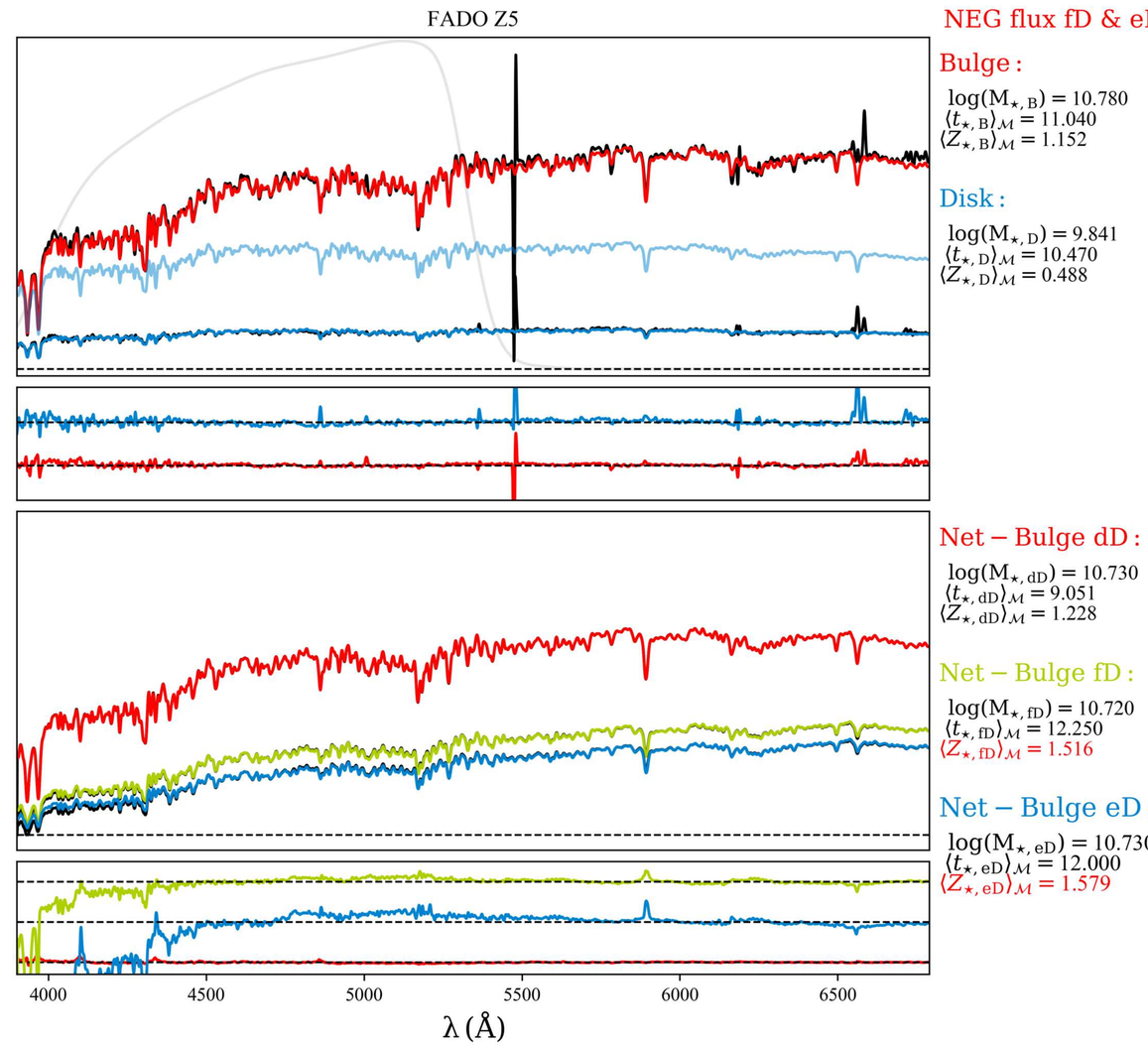
FADO Z5
NEG flux fD & eD
Bulge :
log(M⋆, B) = 10.780
⟨t⋆, B⟩M = 11.040
⟨Z⋆, B⟩M = 1.152
Disk :
log(M⋆, D) = 9.841
⟨t⋆, D⟩M = 10.470
⟨Z⋆, D⟩M = 0.488
Net − Bulge dD :
log(M⋆, dD) = 10.730
⟨t⋆, dD⟩M = 9.051
⟨Z⋆, dD⟩M = 1.228
Net − Bulge fD :
log(M⋆, fD) = 10.720
⟨t⋆, fD⟩M = 12.250
⟨Z⋆, fD⟩M = 1.516
Net − Bulge eD :
log(M⋆, eD) = 10.730
⟨t⋆, eD⟩M = 12.000
⟨Z⋆, eD⟩M = 1.579
λ (Å)

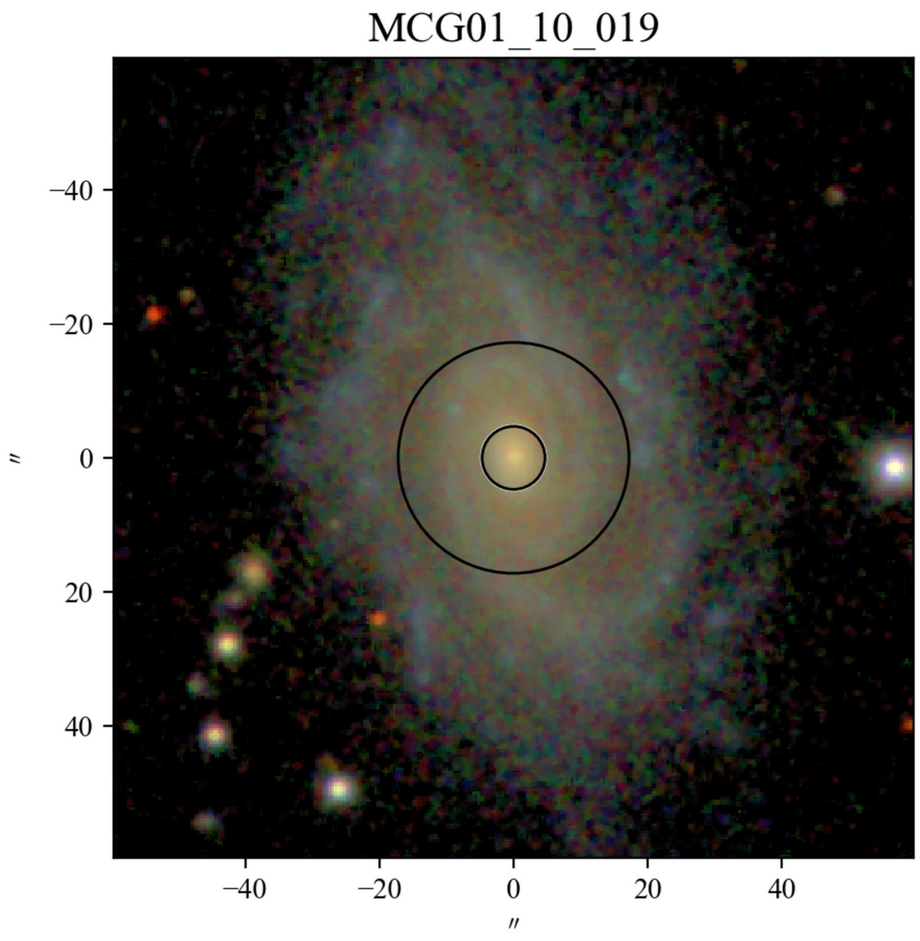
MCG01_10_019
−40
−20
0
20
40
″
−40
−20
0
20
40
″

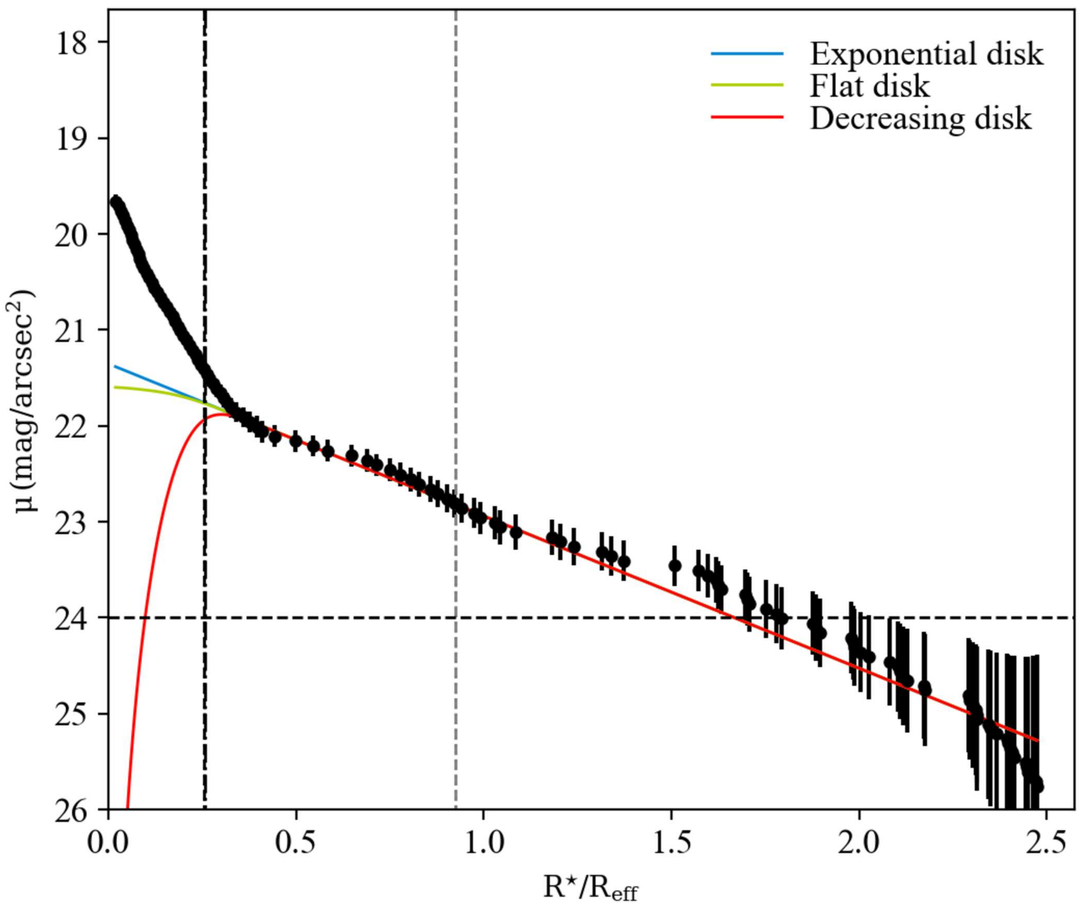
Exponential disk
Flat disk
Decreasing disk
μ (mag/arcsec²)
18
19
20
21
22
23
24
25
26
0.0
0.5
1.0
1.5
2.0
2.5
R⋆/Reff

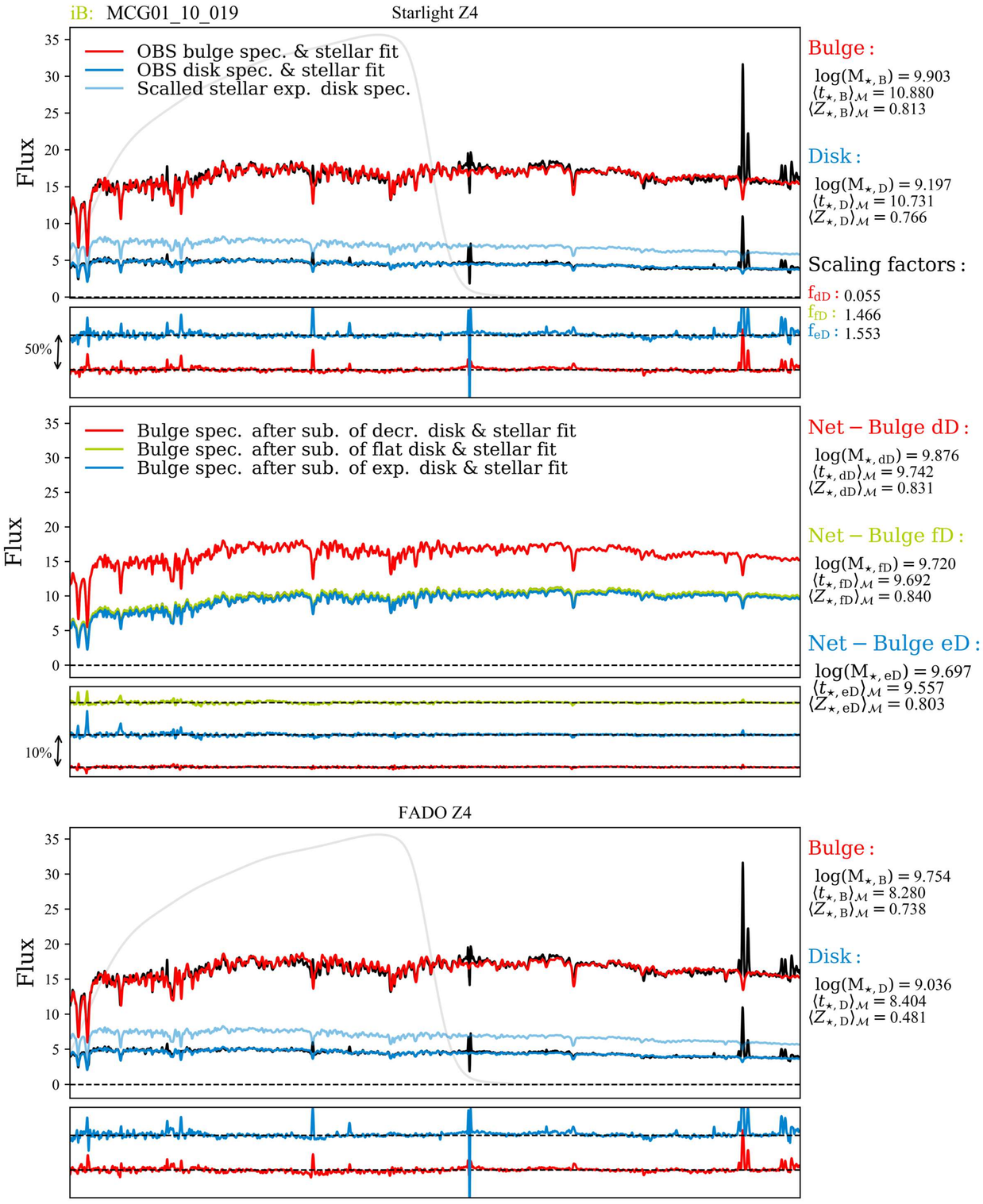
iB: MCG01_10_019
Starlight Z4
OBS bulge spec. & stellar fit
OBS disk spec. & stellar fit
Scalled stellar exp. disk spec.
Flux
50%
Bulge spec. after sub. of decr. disk & stellar fit
Bulge spec. after sub. of flat disk & stellar fit
Bulge spec. after sub. of exp. disk & stellar fit
10%
λ (Å)
Bulge :
log(M⋆, B) = 9.903
⟨t⋆, B⟩M = 10.880
⟨Z⋆, B⟩M = 0.813
Disk :
log(M⋆, D) = 9.197
⟨t⋆, D⟩M = 10.731
⟨Z⋆, D⟩M = 0.766
Scaling factors :
fdD : 0.055
ffD : 1.466
feD : 1.553
Net − Bulge dD :
log(M⋆, dD) = 9.876
⟨t⋆, dD⟩M = 9.742
⟨Z⋆, dD⟩M = 0.831
Net − Bulge fD :
log(M⋆, fD) = 9.720
⟨t⋆, fD⟩M = 9.692
⟨Z⋆, fD⟩M = 0.840
Net − Bulge eD :
log(M⋆, eD) = 9.697
⟨t⋆, eD⟩M = 9.557
⟨Z⋆, eD⟩M = 0.803

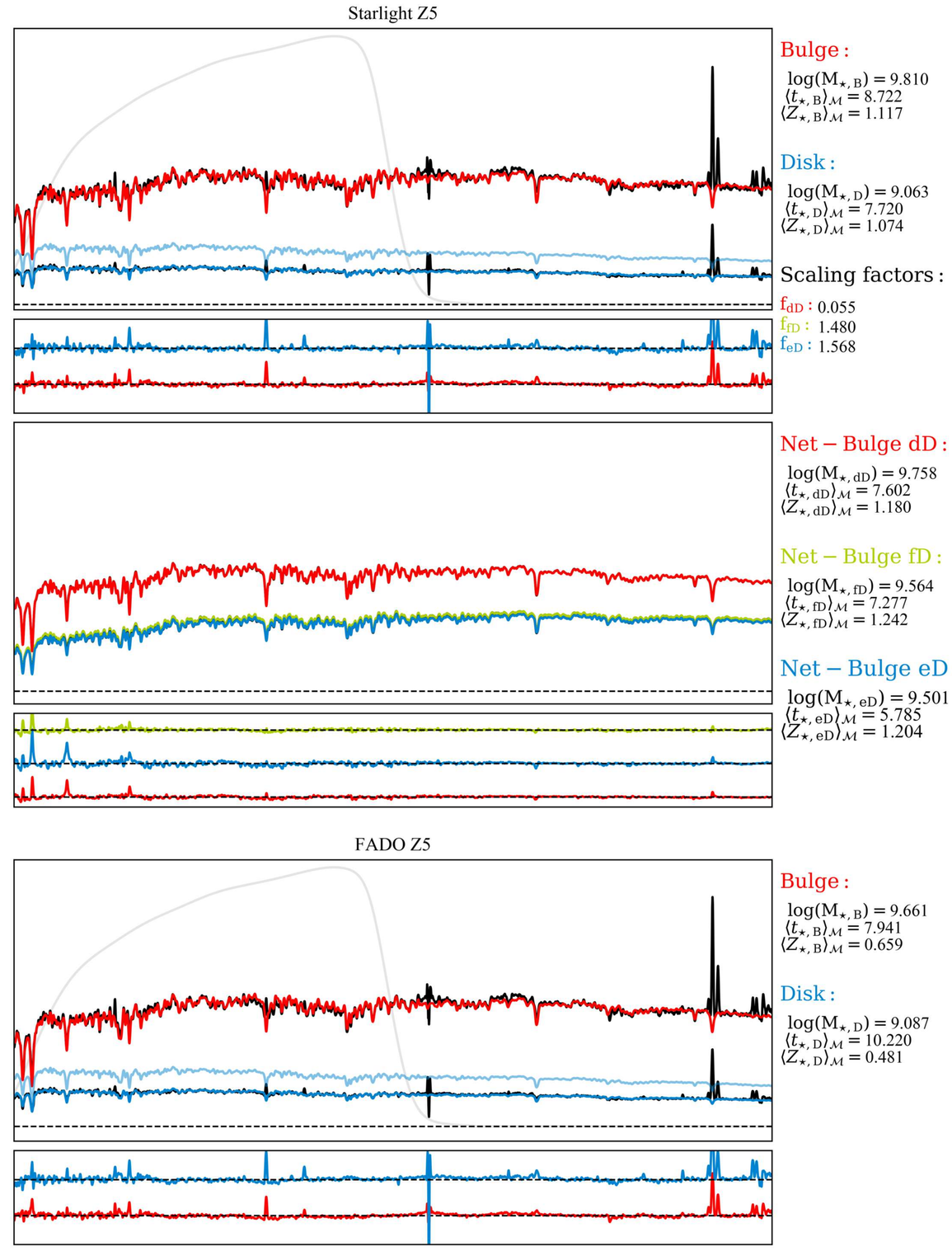
Starlight Z5
Bulge :
log(M⋆, B) = 9.810
⟨t⋆, B⟩M = 8.722
⟨Z⋆, B⟩M = 1.117
Disk :
log(M⋆, D) = 9.063
⟨t⋆, D⟩M = 7.720
⟨Z⋆, D⟩M = 1.074
Scaling factors :
fdD : 0.055
ffD : 1.480
feD : 1.568
Net − Bulge dD :
log(M⋆, dD) = 9.758
⟨t⋆, dD⟩M = 7.602
⟨Z⋆, dD⟩M = 1.180
Net − Bulge fD :
log(M⋆, fD) = 9.564
⟨t⋆, fD⟩M = 7.277
⟨Z⋆, fD⟩M = 1.242
Net − Bulge eD :
log(M⋆, eD) = 9.501
⟨t⋆, eD⟩M = 5.785
⟨Z⋆, eD⟩M = 1.204

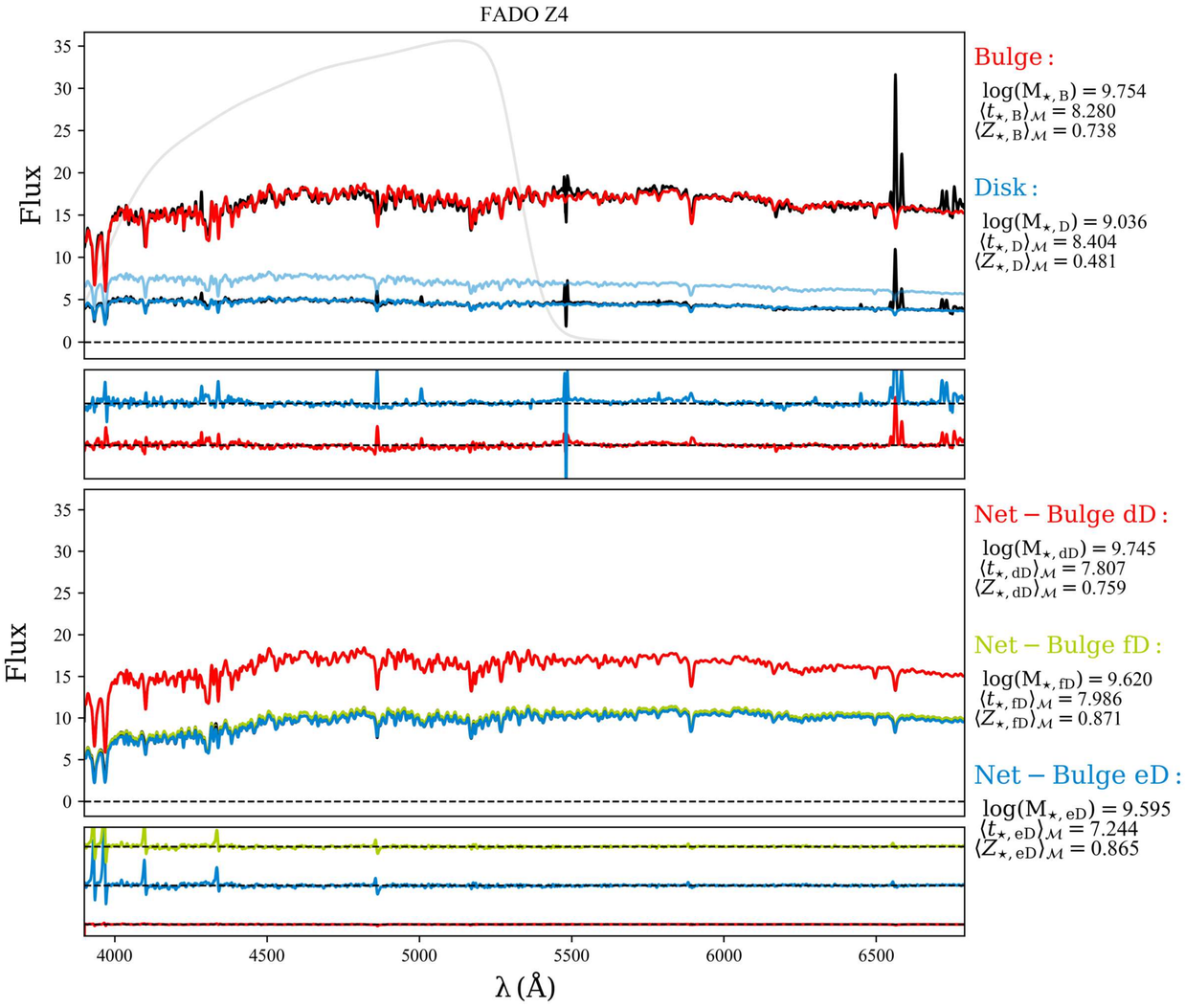
FADO Z4
Flux
λ (Å)
Bulge :
log(M⋆, B) = 9.754
⟨t⋆, B⟩M = 8.280
⟨Z⋆, B⟩M = 0.738
Disk :
log(M⋆, D) = 9.036
⟨t⋆, D⟩M = 8.404
⟨Z⋆, D⟩M = 0.481
Net − Bulge dD :
log(M⋆, dD) = 9.745
⟨t⋆, dD⟩M = 7.807
⟨Z⋆, dD⟩M = 0.759
Net − Bulge fD :
log(M⋆, fD) = 9.620
⟨t⋆, fD⟩M = 7.986
⟨Z⋆, fD⟩M = 0.871
Net − Bulge eD :
log(M⋆, eD) = 9.595
⟨t⋆, eD⟩M = 7.244
⟨Z⋆, eD⟩M = 0.865

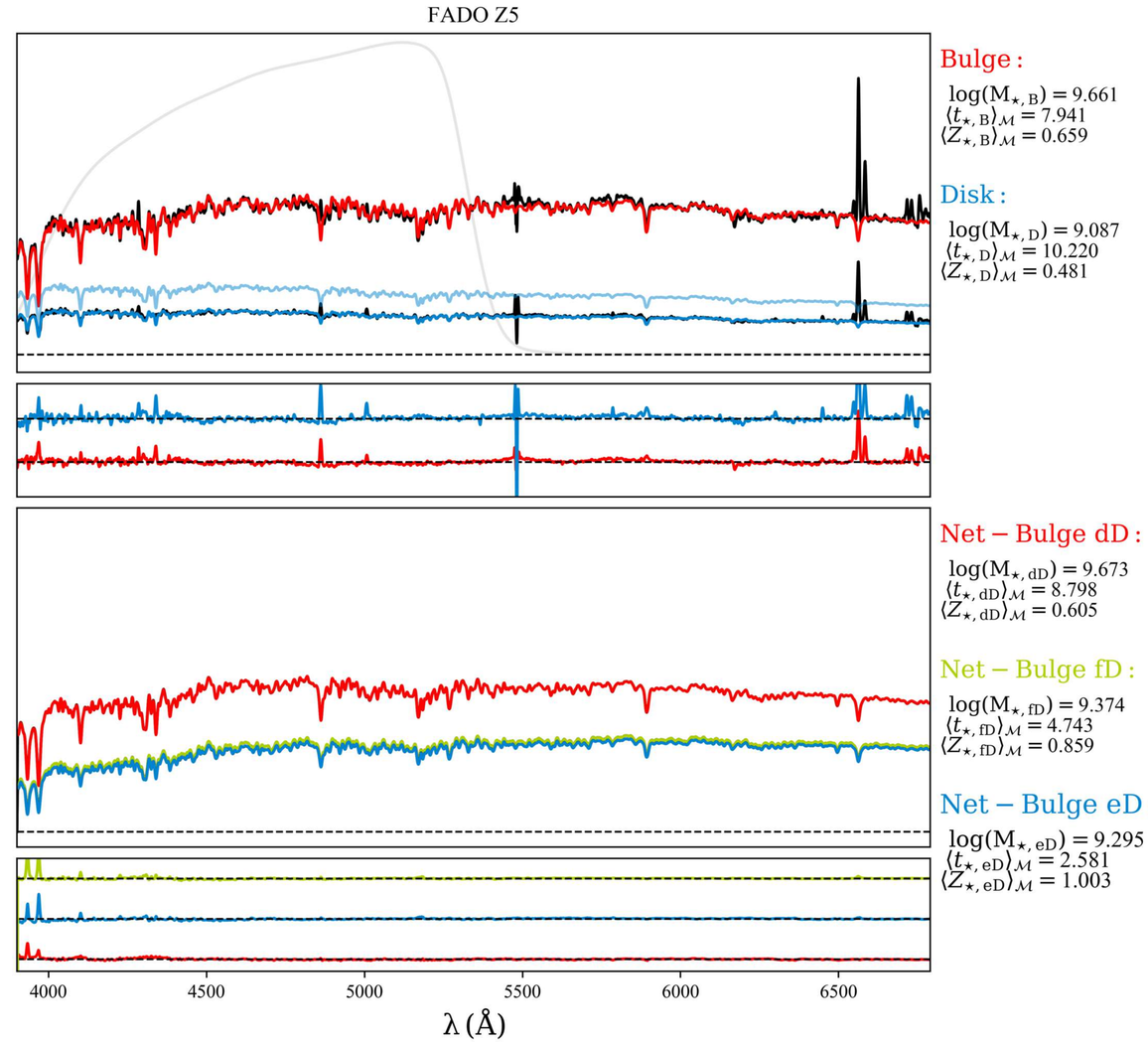
FADO Z5
λ (Å)
Bulge :
log(M⋆, B) = 9.661
⟨t⋆, B⟩M = 7.941
⟨Z⋆, B⟩M = 0.659
Disk :
log(M⋆, D) = 9.087
⟨t⋆, D⟩M = 10.220
⟨Z⋆, D⟩M = 0.481
Net − Bulge dD :
log(M⋆, dD) = 9.673
⟨t⋆, dD⟩M = 8.798
⟨Z⋆, dD⟩M = 0.605
Net − Bulge fD :
log(M⋆, fD) = 9.374
⟨t⋆, fD⟩M = 4.743
⟨Z⋆, fD⟩M = 0.859
Net − Bulge eD :
log(M⋆, eD) = 9.295
⟨t⋆, eD⟩M = 2.581
⟨Z⋆, eD⟩M = 1.003

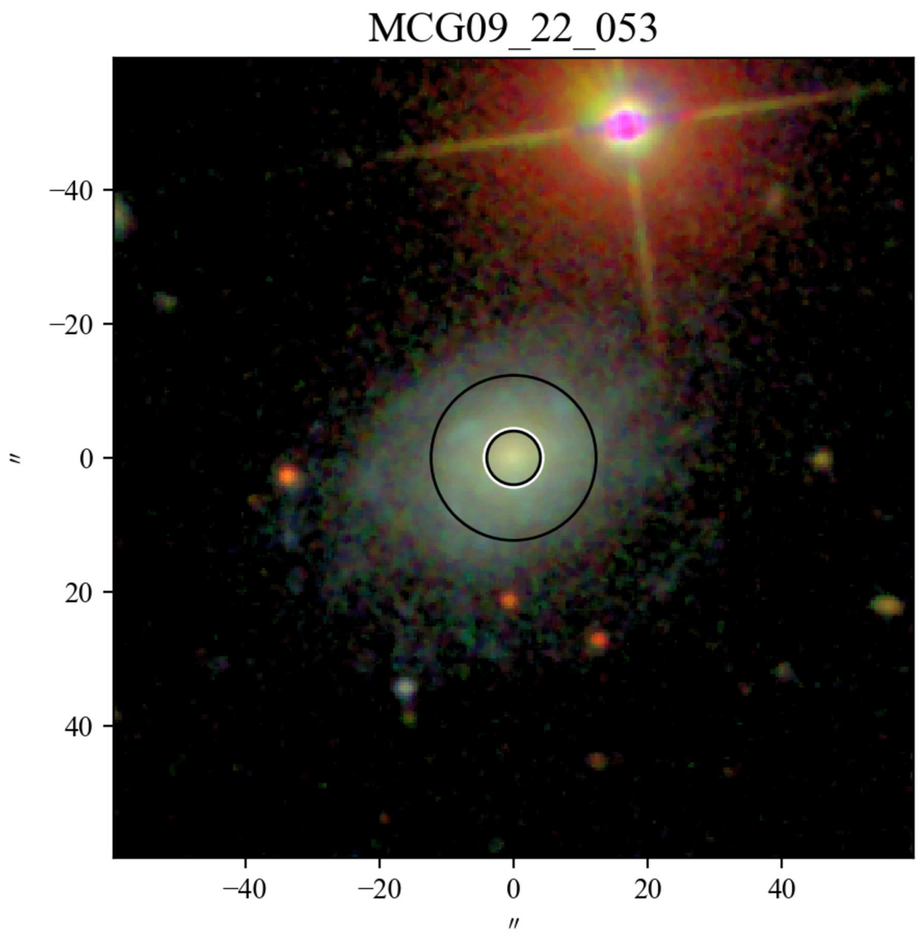
MCG09_22_053
−40
−20
0
20
40
″
−40
−20
0
20
40
″

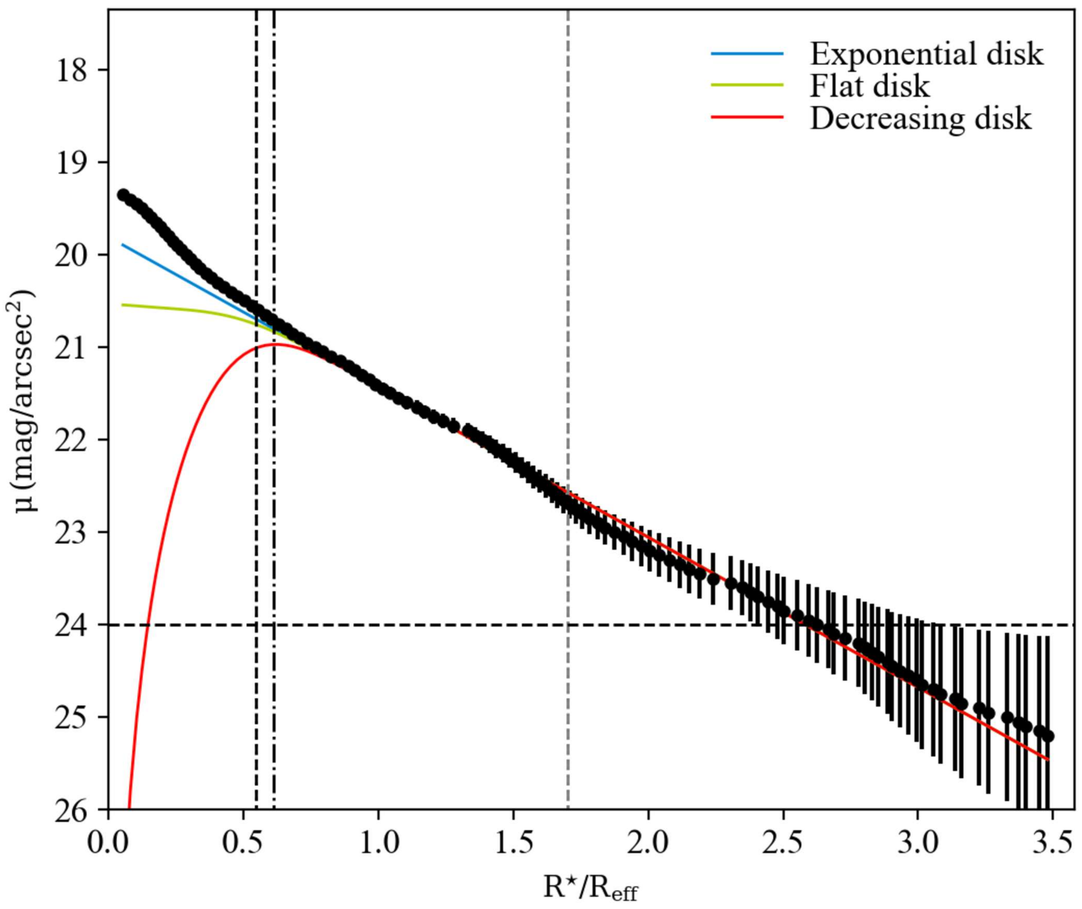
Exponential disk
Flat disk
Decreasing disk
μ (mag/arcsec²)
18
19
20
21
22
23
24
25
26
0.0
0.5
1.0
1.5
2.0
2.5
3.0
3.5
R⋆/Reff

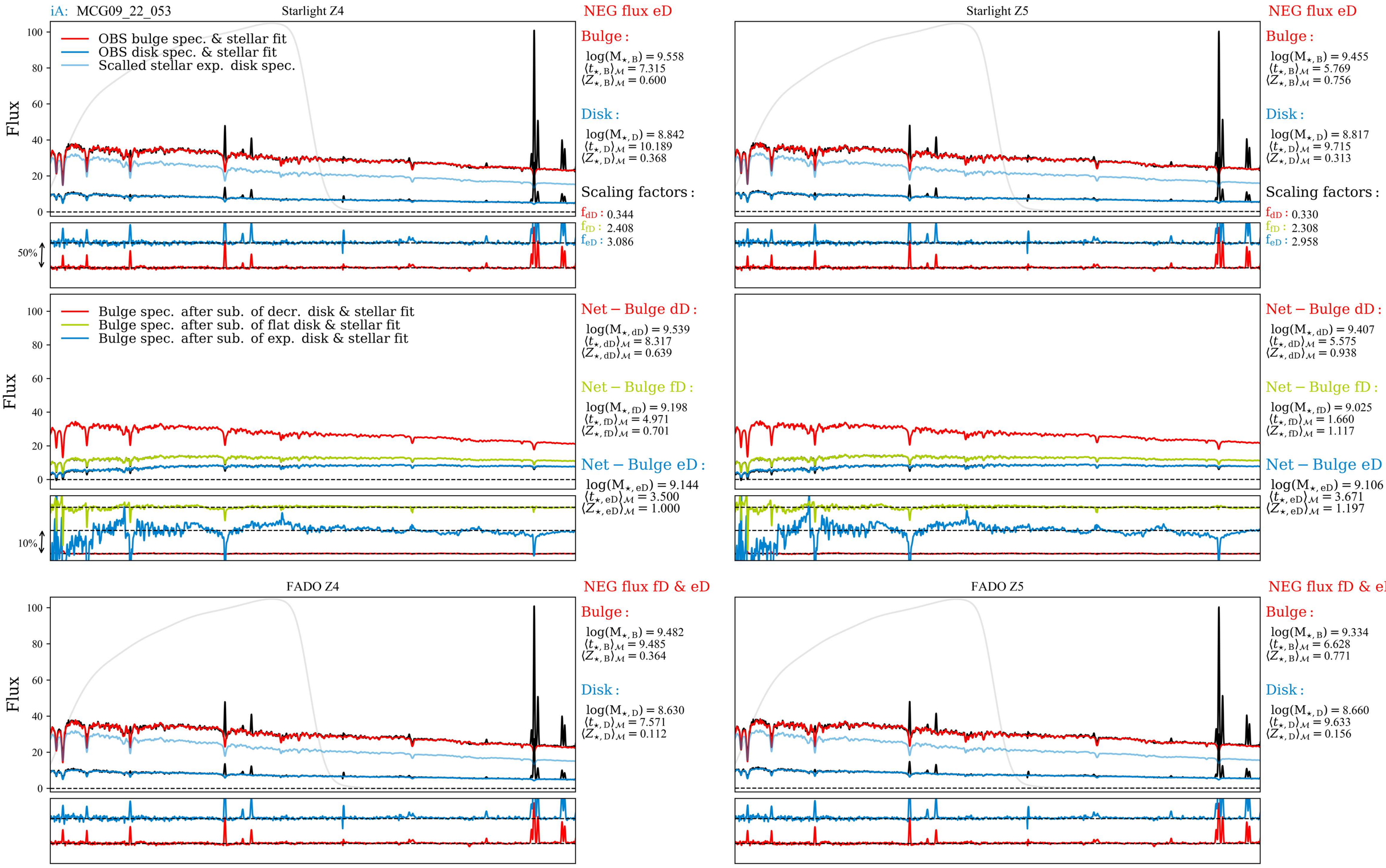
iA: MCG09_22_053
Starlight Z4
NEG flux eD
OBS bulge spec. & stellar fit
OBS disk spec. & stellar fit
Scalled stellar exp. disk spec.
Flux
50%
Bulge :
log(M⋆, B) = 9.558
⟨t⋆, B⟩M = 7.315
⟨Z⋆, B⟩M = 0.600
Disk :
log(M⋆, D) = 8.842
⟨t⋆, D⟩M = 10.189
⟨Z⋆, D⟩M = 0.368
Scaling factors :
fdD : 0.344
ffD : 2.408
feD : 3.086
Starlight Z5
NEG flux eD
Bulge :
log(M⋆, B) = 9.455
⟨t⋆, B⟩M = 5.769
⟨Z⋆, B⟩M = 0.756
Disk :
log(M⋆, D) = 8.817
⟨t⋆, D⟩M = 9.715
⟨Z⋆, D⟩M = 0.313
Scaling factors :
fdD : 0.330
ffD : 2.308
feD : 2.958
Bulge spec. after sub. of decr. disk & stellar fit
Bulge spec. after sub. of flat disk & stellar fit
Bulge spec. after sub. of exp. disk & stellar fit
10%
Net − Bulge dD :
log(M⋆, dD) = 9.539
⟨t⋆, dD⟩M = 8.317
⟨Z⋆, dD⟩M = 0.639
Net − Bulge fD :
log(M⋆, fD) = 9.198
⟨t⋆, fD⟩M = 4.971
⟨Z⋆, fD⟩M = 0.701
Net − Bulge eD :
log(M⋆, eD) = 9.144
⟨t⋆, eD⟩M = 3.500
⟨Z⋆, eD⟩M = 1.000
Net − Bulge dD :
log(M⋆, dD) = 9.407
⟨t⋆, dD⟩M = 5.575
⟨Z⋆, dD⟩M = 0.938
Net − Bulge fD :
log(M⋆, fD) = 9.025
⟨t⋆, fD⟩M = 1.660
⟨Z⋆, fD⟩M = 1.117
Net − Bulge eD :
log(M⋆, eD) = 9.106
⟨t⋆, eD⟩M = 3.671
⟨Z⋆, eD⟩M = 1.197
FADO Z4
NEG flux fD & eD
Bulge :
log(M⋆, B) = 9.482
⟨t⋆, B⟩M = 9.485
⟨Z⋆, B⟩M = 0.364
Disk :
log(M⋆, D) = 8.630
⟨t⋆, D⟩M = 7.571
⟨Z⋆, D⟩M = 0.112
FADO Z5
NEG flux fD & eD
Bulge :
log(M⋆, B) = 9.334
⟨t⋆, B⟩M = 6.628
⟨Z⋆, B⟩M = 0.771
Disk :
log(M⋆, D) = 8.660
⟨t⋆, D⟩M = 9.633
⟨Z⋆, D⟩M = 0.156
Net − Bulge dD :
log(M⋆, dD) = 9.482
⟨t⋆, dD⟩M = 8.472
⟨Z⋆, dD⟩M = 0.452
Net − Bulge fD :
log(M⋆, fD) = 9.318
⟨t⋆, fD⟩M = 7.881
⟨Z⋆, fD⟩M = 0.636
Net − Bulge eD :
log(M⋆, eD) = 9.130
⟨t⋆, eD⟩M = 4.000
⟨Z⋆, eD⟩M = 1.000
Net − Bulge dD :
log(M⋆, dD) = 9.407
⟨t⋆, dD⟩M = 5.919
⟨Z⋆, dD⟩M = 0.780
Net − Bulge fD :
log(M⋆, fD) = 8.957
⟨t⋆, fD⟩M = 1.931
⟨Z⋆, fD⟩M = 1.197
Net − Bulge eD :
log(M⋆, eD) = 9.044
⟨t⋆, eD⟩M = 3.612
⟨Z⋆, eD⟩M = 1.177
λ (Å)

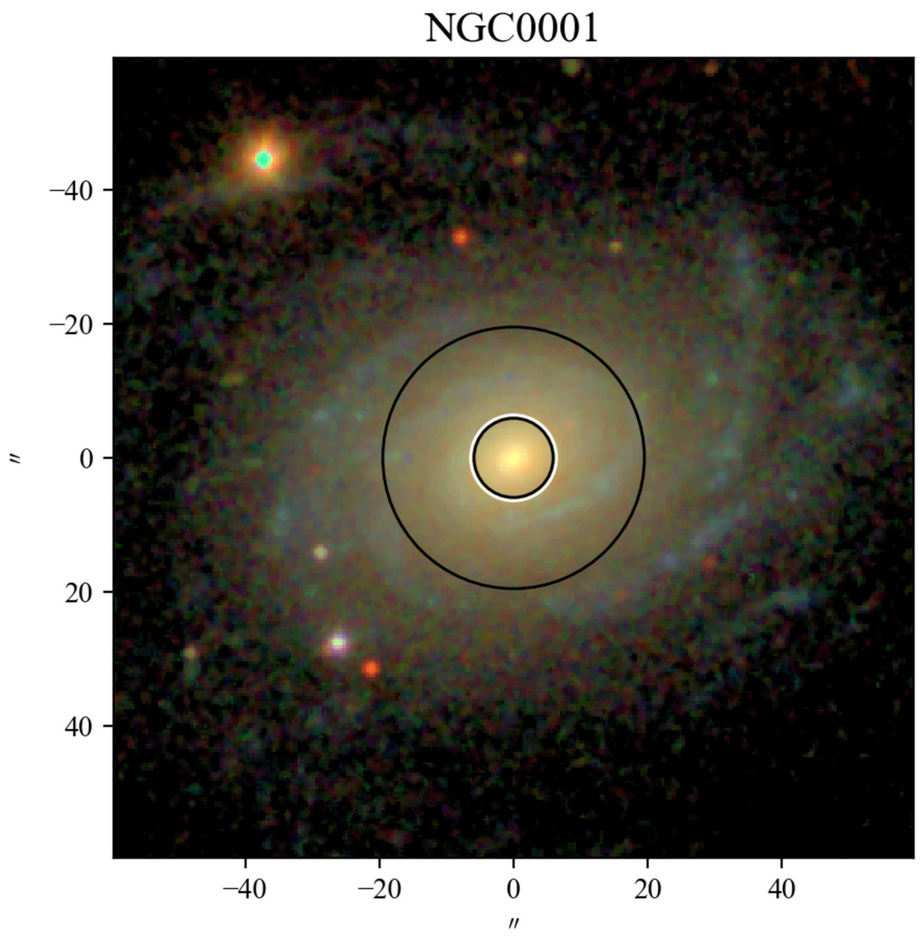
NGC0001
−40
−20
0
20
40
″
−40
−20
0
20
40
″

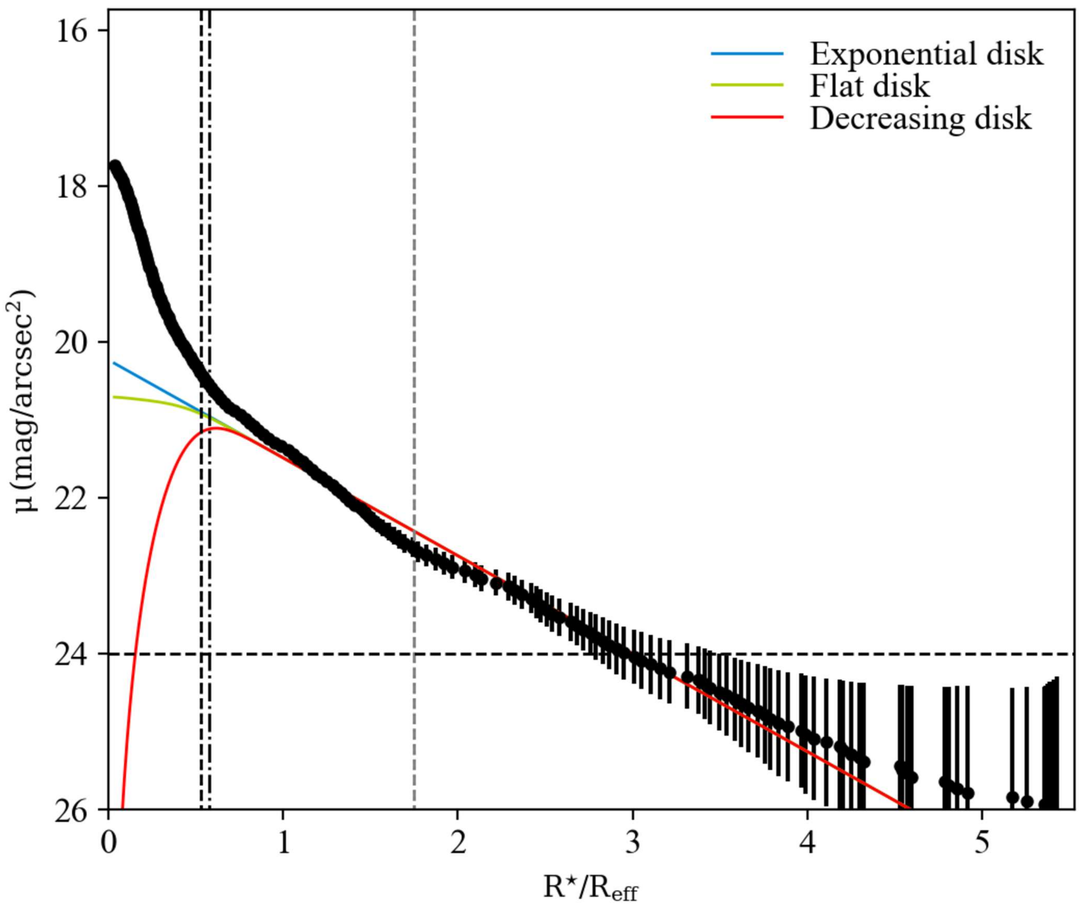
Exponential disk
Flat disk
Decreasing disk
μ (mag/arcsec²)
16
18
20
22
24
26
0
1
2
3
4
5
R⋆/Reff

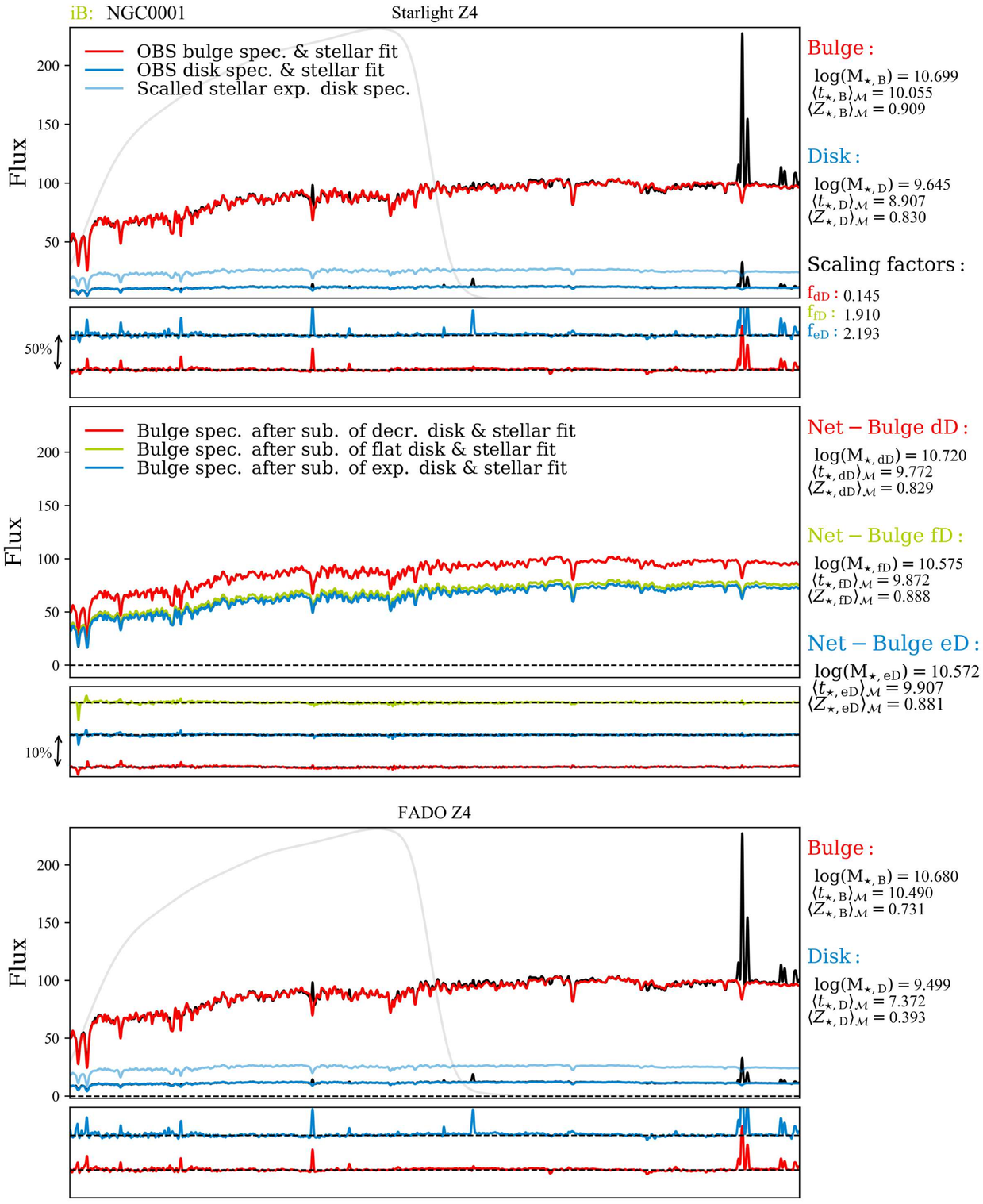
iB: NGC0001
Starlight Z4
OBS bulge spec. & stellar fit
OBS disk spec. & stellar fit
Scalled stellar exp. disk spec.
Flux
50%
Bulge :
log(M⋆, B) = 10.699
⟨t⋆, B⟩M = 10.055
⟨Z⋆, B⟩M = 0.909
Disk :
log(M⋆, D) = 9.645
⟨t⋆, D⟩M = 8.907
⟨Z⋆, D⟩M = 0.830
Scaling factors :
fdD : 0.145
ffD : 1.910
feD : 2.193
Bulge spec. after sub. of decr. disk & stellar fit
Bulge spec. after sub. of flat disk & stellar fit
Bulge spec. after sub. of exp. disk & stellar fit
10%
Net − Bulge dD :
log(M⋆, dD) = 10.720
⟨t⋆, dD⟩M = 9.772
⟨Z⋆, dD⟩M = 0.829
Net − Bulge fD :
log(M⋆, fD) = 10.575
⟨t⋆, fD⟩M = 9.872
⟨Z⋆, fD⟩M = 0.888
Net − Bulge eD :
log(M⋆, eD) = 10.572
⟨t⋆, eD⟩M = 9.907
⟨Z⋆, eD⟩M = 0.881

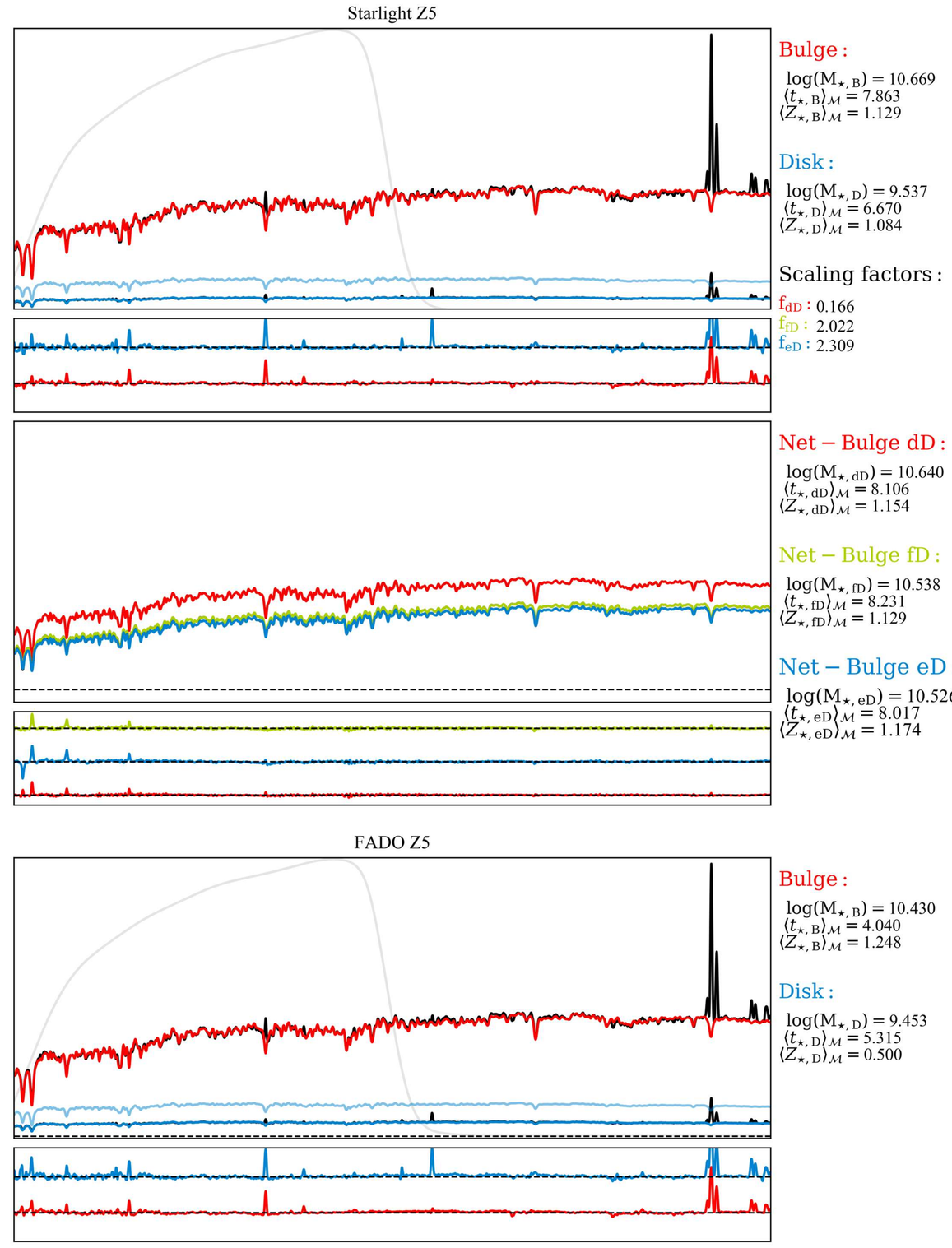
Starlight Z5
Bulge :
log(M⋆, B) = 10.669
⟨t⋆, B⟩M = 7.863
⟨Z⋆, B⟩M = 1.129
Disk :
log(M⋆, D) = 9.537
⟨t⋆, D⟩M = 6.670
⟨Z⋆, D⟩M = 1.084
Scaling factors :
fdD : 0.166
ffD : 2.022
feD : 2.309
Net − Bulge dD :
log(M⋆, dD) = 10.640
⟨t⋆, dD⟩M = 8.106
⟨Z⋆, dD⟩M = 1.154
Net − Bulge fD :
log(M⋆, fD) = 10.538
⟨t⋆, fD⟩M = 8.231
⟨Z⋆, fD⟩M = 1.129
Net − Bulge eD :
log(M⋆, eD) = 10.526
⟨t⋆, eD⟩M = 8.017
⟨Z⋆, eD⟩M = 1.174

FADO Z4
Flux
Bulge :
log(M⋆, B) = 10.680
⟨t⋆, B⟩M = 10.490
⟨Z⋆, B⟩M = 0.731
Disk :
log(M⋆, D) = 9.499
⟨t⋆, D⟩M = 7.372
⟨Z⋆, D⟩M = 0.393
Net − Bulge dD :
log(M⋆, dD) = 10.680
⟨t⋆, dD⟩M = 10.710
⟨Z⋆, dD⟩M = 0.669
Net − Bulge fD :
log(M⋆, fD) = 10.620
⟨t⋆, fD⟩M = 8.603
⟨Z⋆, fD⟩M = 0.742
Net − Bulge eD :
log(M⋆, eD) = 10.630
⟨t⋆, eD⟩M = 11.100
⟨Z⋆, eD⟩M = 0.778
λ (Å)

FADO Z5
Bulge :
log(M⋆, B) = 10.430
⟨t⋆, B⟩M = 4.040
⟨Z⋆, B⟩M = 1.248
Disk :
log(M⋆, D) = 9.453
⟨t⋆, D⟩M = 5.315
⟨Z⋆, D⟩M = 0.500
Net − Bulge dD :
log(M⋆, dD) = 10.550
⟨t⋆, dD⟩M = 5.723
⟨Z⋆, dD⟩M = 1.065
Net − Bulge fD :
log(M⋆, fD) = 10.480
⟨t⋆, fD⟩M = 7.302
⟨Z⋆, fD⟩M = 1.294
Net − Bulge eD :
log(M⋆, eD) = 10.420
⟨t⋆, eD⟩M = 5.868
⟨Z⋆, eD⟩M = 1.267
λ (Å)

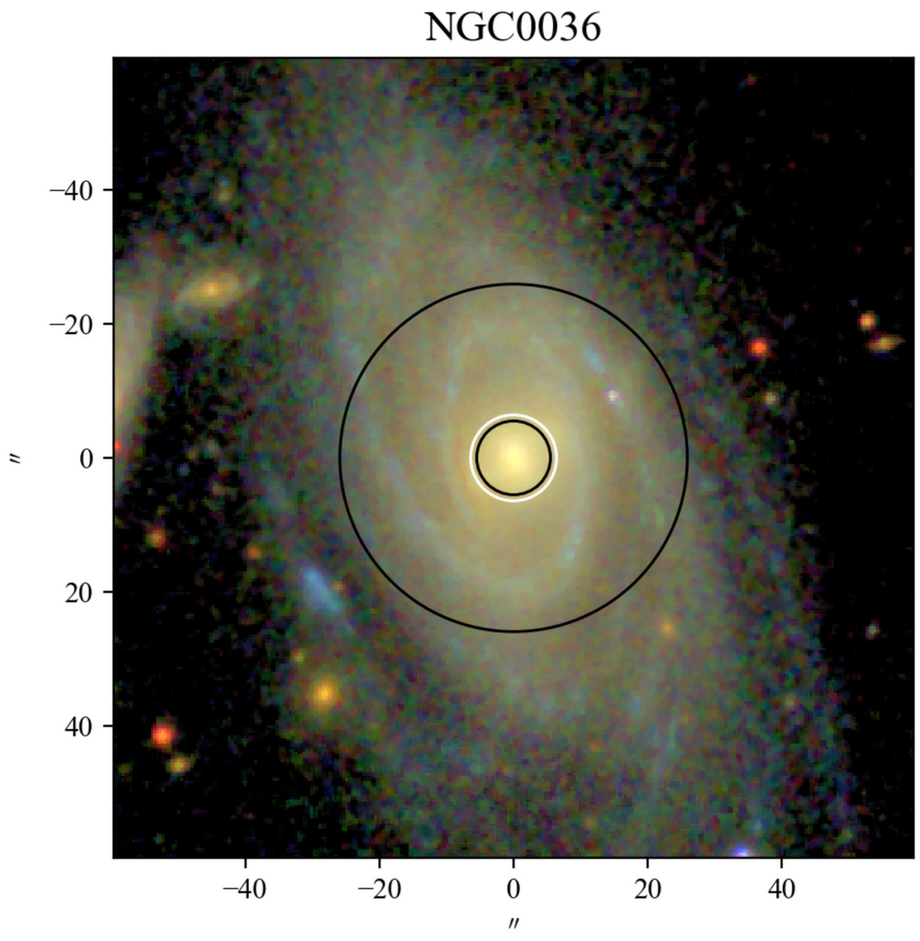
NGC0036
−40
−20
0
20
40
″
−40
−20
0
20
40
″

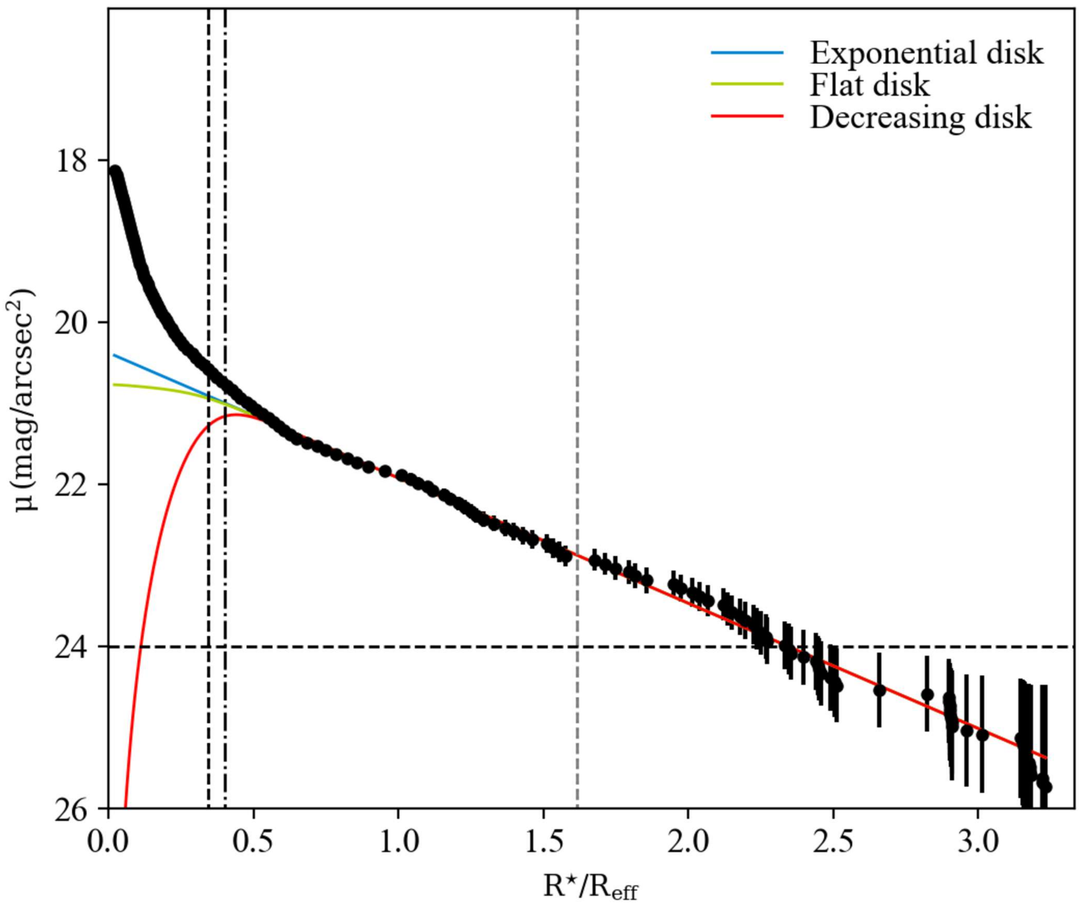
Exponential disk
Flat disk
Decreasing disk
μ (mag/arcsec²)
18
20
22
24
26
0.0
0.5
1.0
1.5
2.0
2.5
3.0
R⋆/Reff

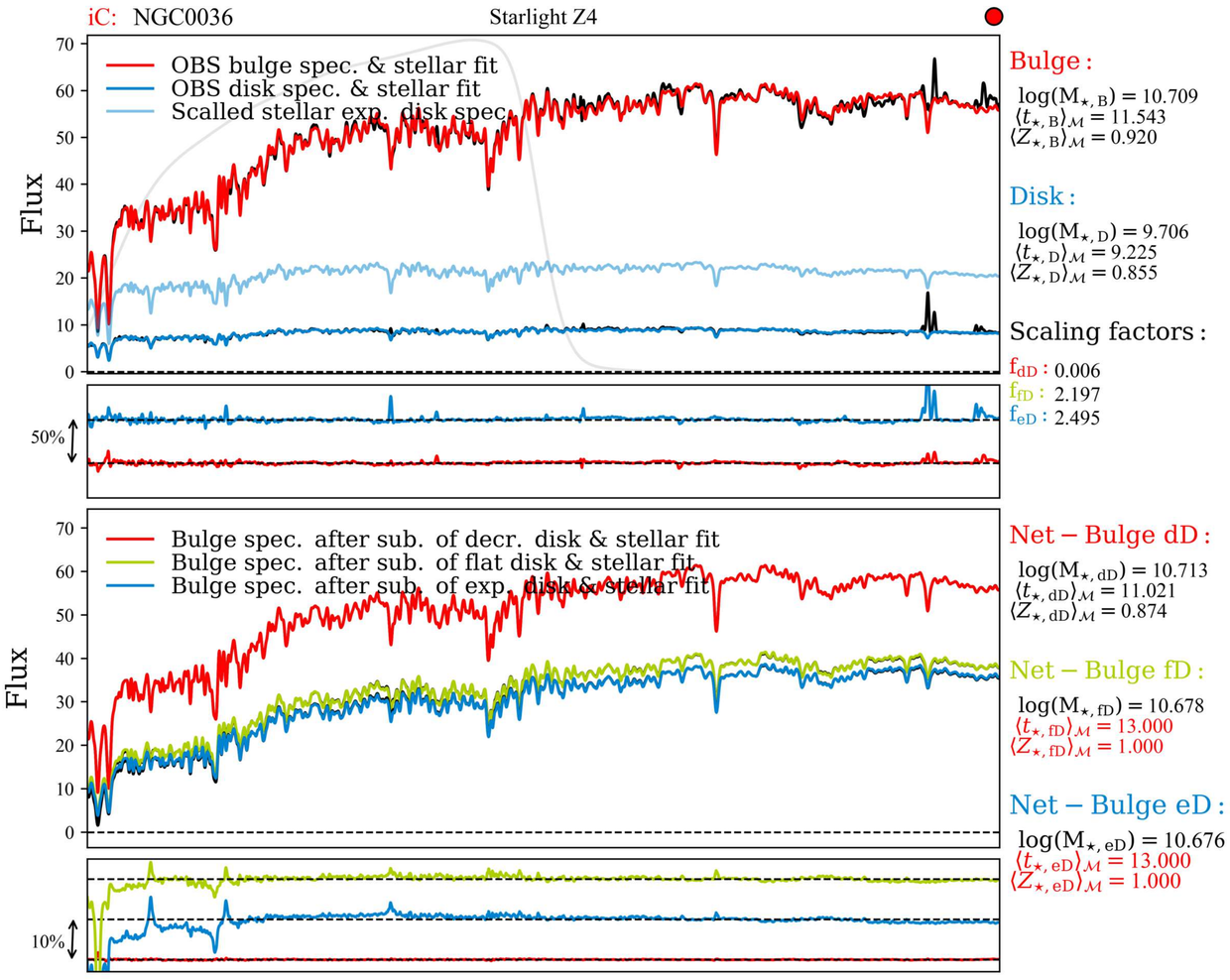
iC: NGC0036
Starlight Z4
OBS bulge spec. & stellar fit
OBS disk spec. & stellar fit
Scalled stellar exp. disk spec.
Flux
Bulge :
log(M⋆, B) = 10.709
⟨t⋆, B⟩M = 11.543
⟨Z⋆, B⟩M = 0.920
Disk :
log(M⋆, D) = 9.706
⟨t⋆, D⟩M = 9.225
⟨Z⋆, D⟩M = 0.855
Scaling factors :
fdD : 0.006
ffD : 2.197
feD : 2.495
50%
Bulge spec. after sub. of decr. disk & stellar fit
Bulge spec. after sub. of flat disk & stellar fit
Bulge spec. after sub. of exp. disk & stellar fit
Net − Bulge dD :
log(M⋆, dD) = 10.713
⟨t⋆, dD⟩M = 11.021
⟨Z⋆, dD⟩M = 0.874
Net − Bulge fD :
log(M⋆, fD) = 10.678
⟨t⋆, fD⟩M = 13.000
⟨Z⋆, fD⟩M = 1.000
Net − Bulge eD :
log(M⋆, eD) = 10.676
⟨t⋆, eD⟩M = 13.000
⟨Z⋆, eD⟩M = 1.000
10%

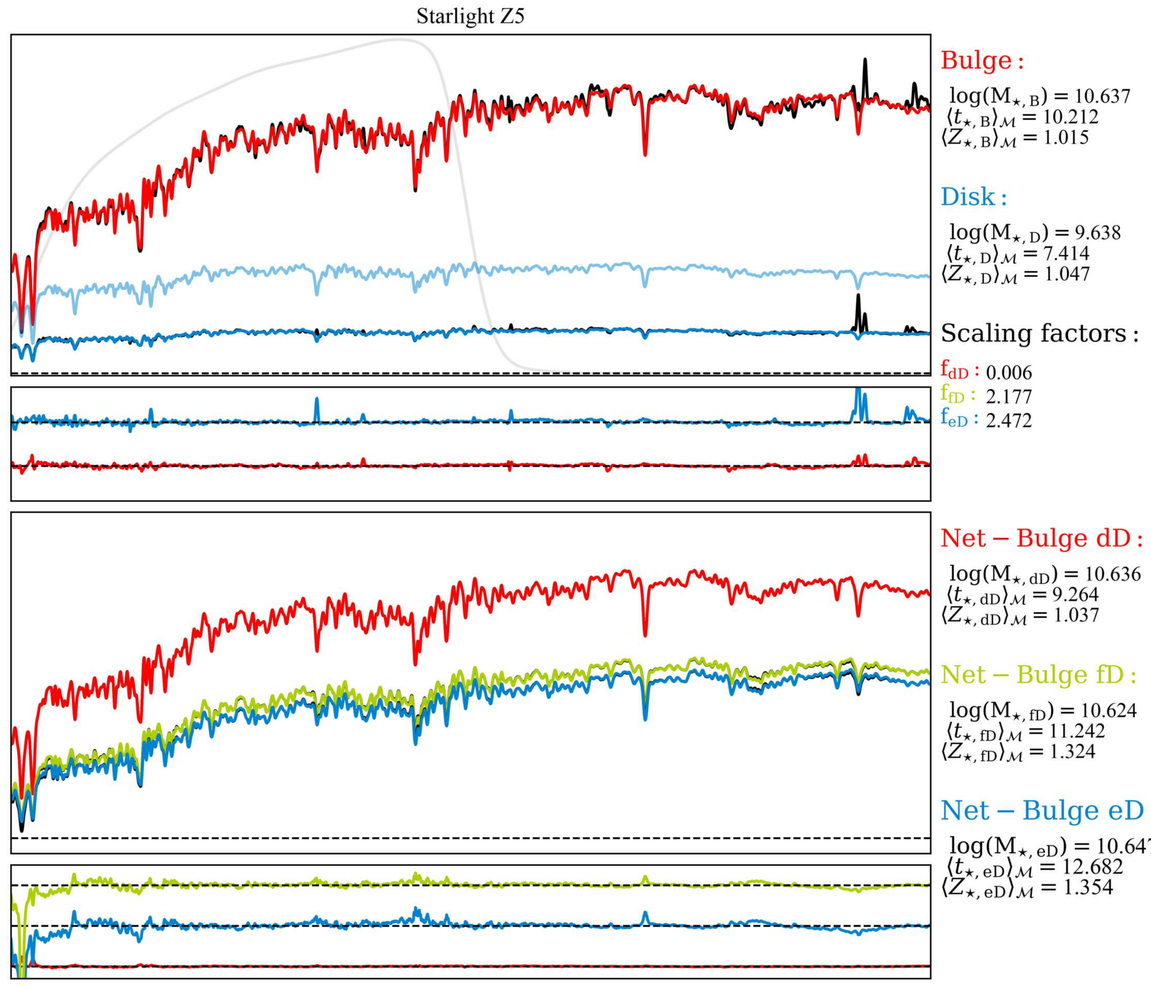
Starlight Z5
Bulge :
log(M⋆, B) = 10.637
⟨t⋆, B⟩M = 10.212
⟨Z⋆, B⟩M = 1.015
Disk :
log(M⋆, D) = 9.638
⟨t⋆, D⟩M = 7.414
⟨Z⋆, D⟩M = 1.047
Scaling factors :
fdD : 0.006
ffD : 2.177
feD : 2.472
Net − Bulge dD :
log(M⋆, dD) = 10.636
⟨t⋆, dD⟩M = 9.264
⟨Z⋆, dD⟩M = 1.037
Net − Bulge fD :
log(M⋆, fD) = 10.624
⟨t⋆, fD⟩M = 11.242
⟨Z⋆, fD⟩M = 1.324
Net − Bulge eD :
log(M⋆, eD) = 10.647
⟨t⋆, eD⟩M = 12.682
⟨Z⋆, eD⟩M = 1.354

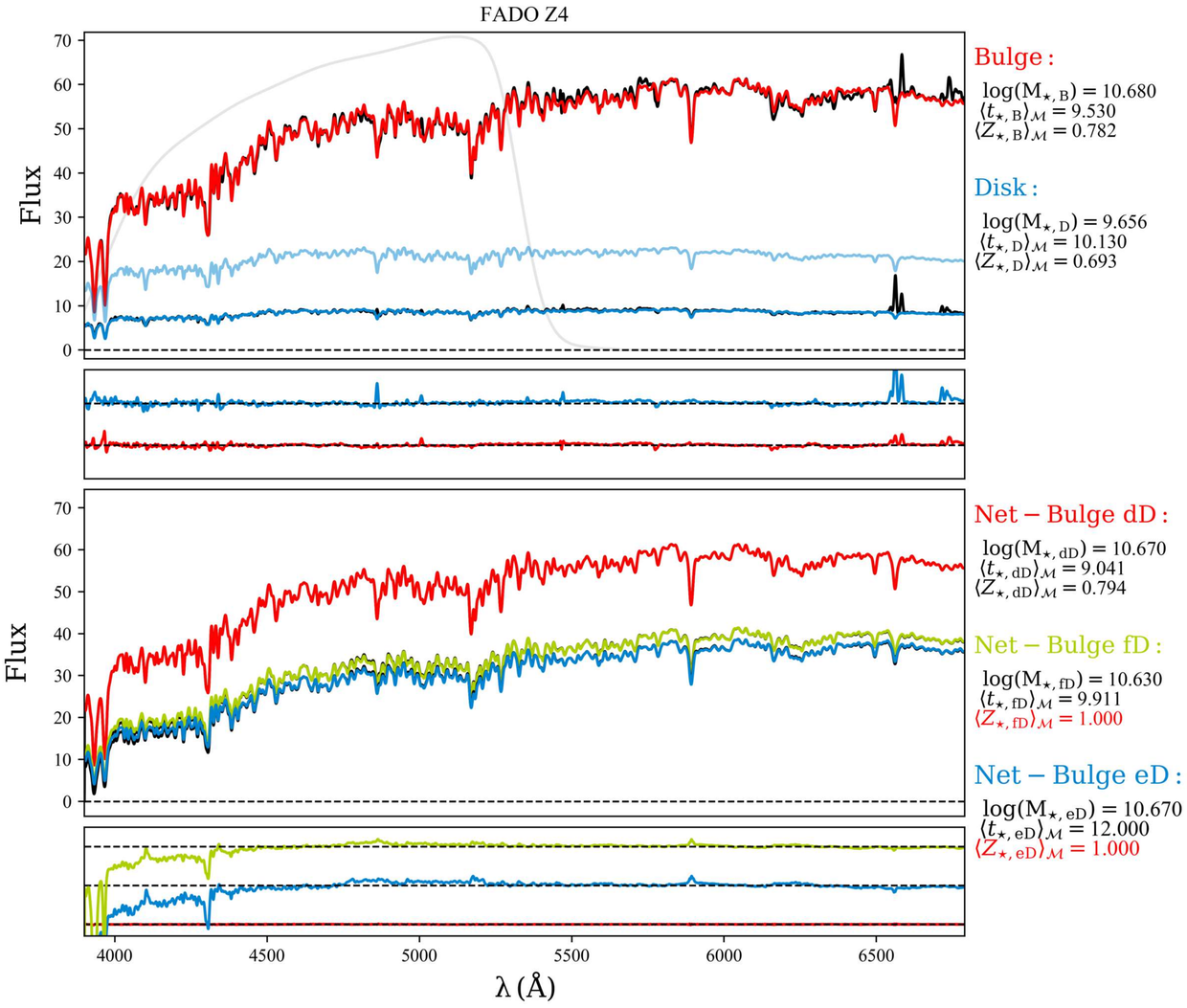
FADO Z4
Flux
Bulge :
log(M⋆, B) = 10.680
⟨t⋆, B⟩M = 9.530
⟨Z⋆, B⟩M = 0.782
Disk :
log(M⋆, D) = 9.656
⟨t⋆, D⟩M = 10.130
⟨Z⋆, D⟩M = 0.693
Net − Bulge dD :
log(M⋆, dD) = 10.670
⟨t⋆, dD⟩M = 9.041
⟨Z⋆, dD⟩M = 0.794
Net − Bulge fD :
log(M⋆, fD) = 10.630
⟨t⋆, fD⟩M = 9.911
⟨Z⋆, fD⟩M = 1.000
Net − Bulge eD :
log(M⋆, eD) = 10.670
⟨t⋆, eD⟩M = 12.000
⟨Z⋆, eD⟩M = 1.000
λ (Å)

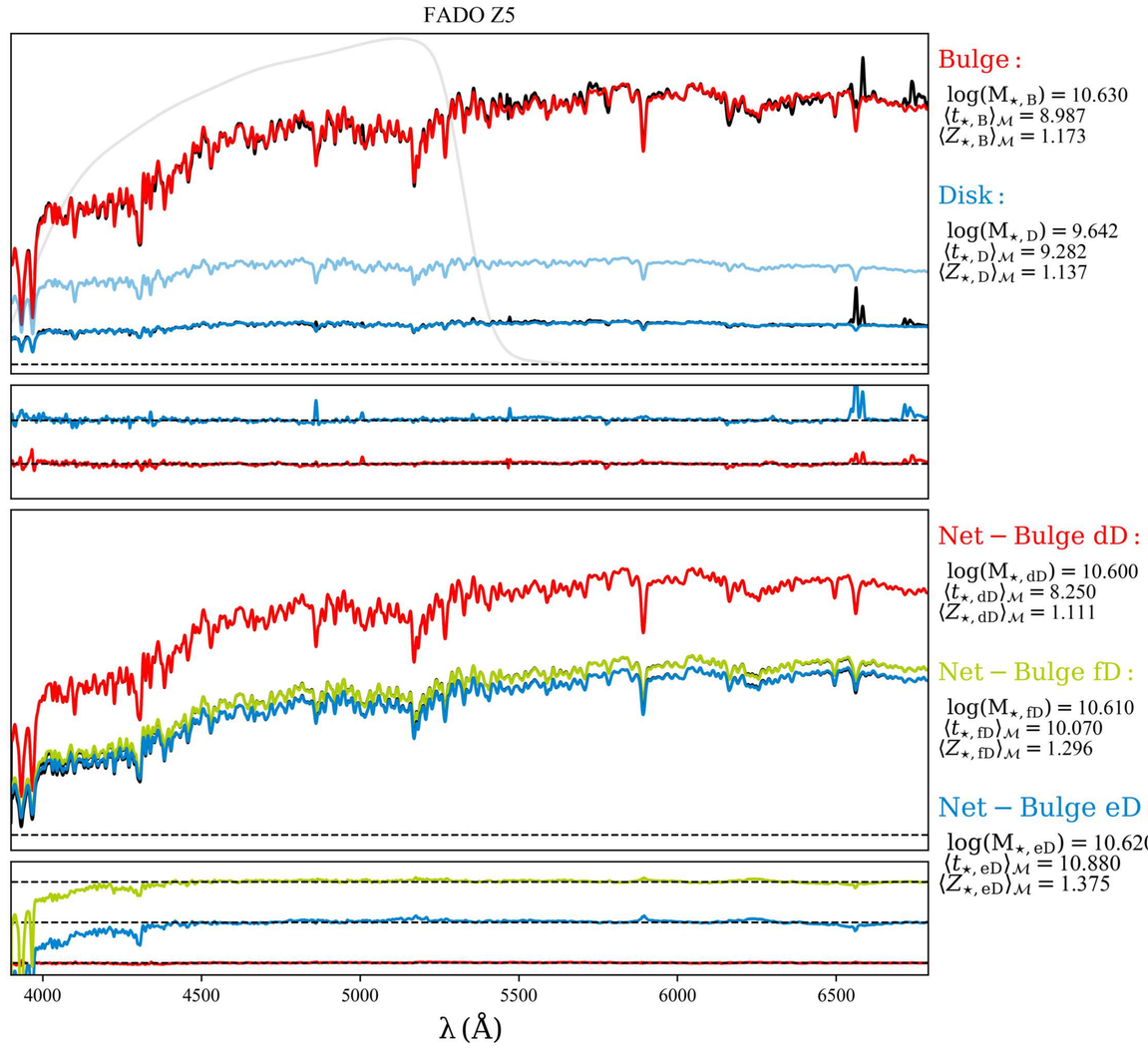
FADO Z5
Bulge :
log(M⋆, B) = 10.630
⟨t⋆, B⟩M = 8.987
⟨Z⋆, B⟩M = 1.173
Disk :
log(M⋆, D) = 9.642
⟨t⋆, D⟩M = 9.282
⟨Z⋆, D⟩M = 1.137
Net − Bulge dD :
log(M⋆, dD) = 10.600
⟨t⋆, dD⟩M = 8.250
⟨Z⋆, dD⟩M = 1.111
Net − Bulge fD :
log(M⋆, fD) = 10.610
⟨t⋆, fD⟩M = 10.070
⟨Z⋆, fD⟩M = 1.296
Net − Bulge eD :
log(M⋆, eD) = 10.620
⟨t⋆, eD⟩M = 10.880
⟨Z⋆, eD⟩M = 1.375
λ (Å)

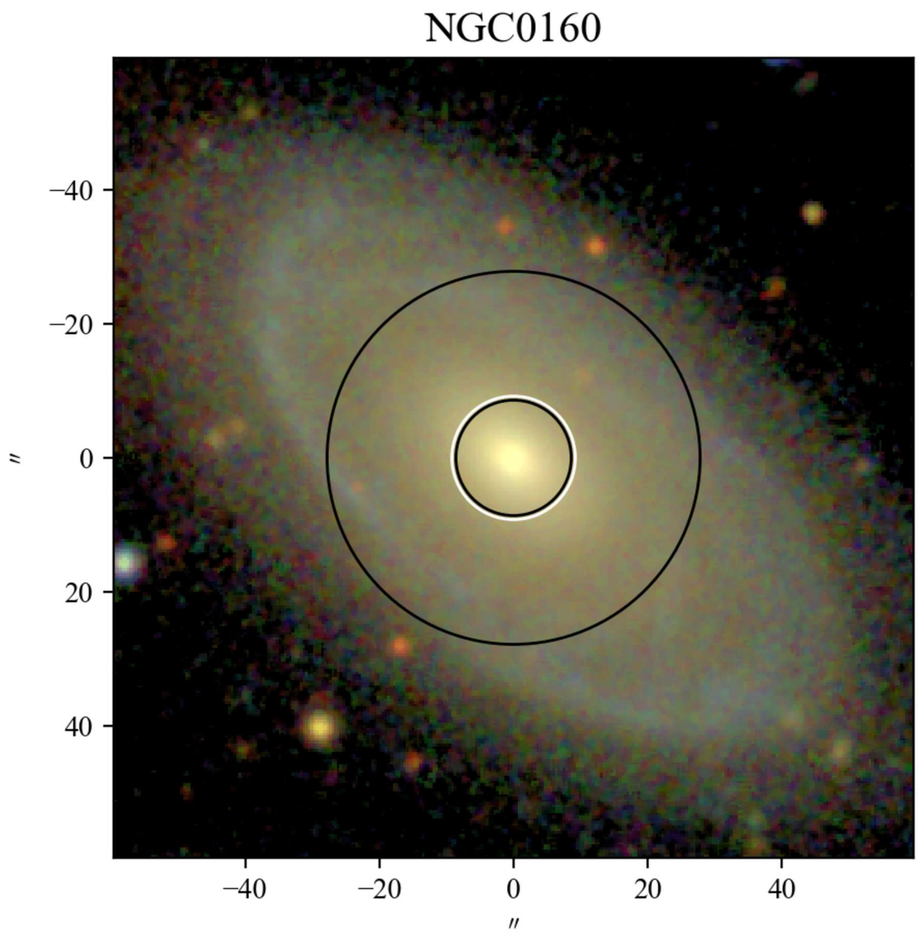
NGC0160
−40
−20
0
20
40
″
−40
−20
0
20
40
″

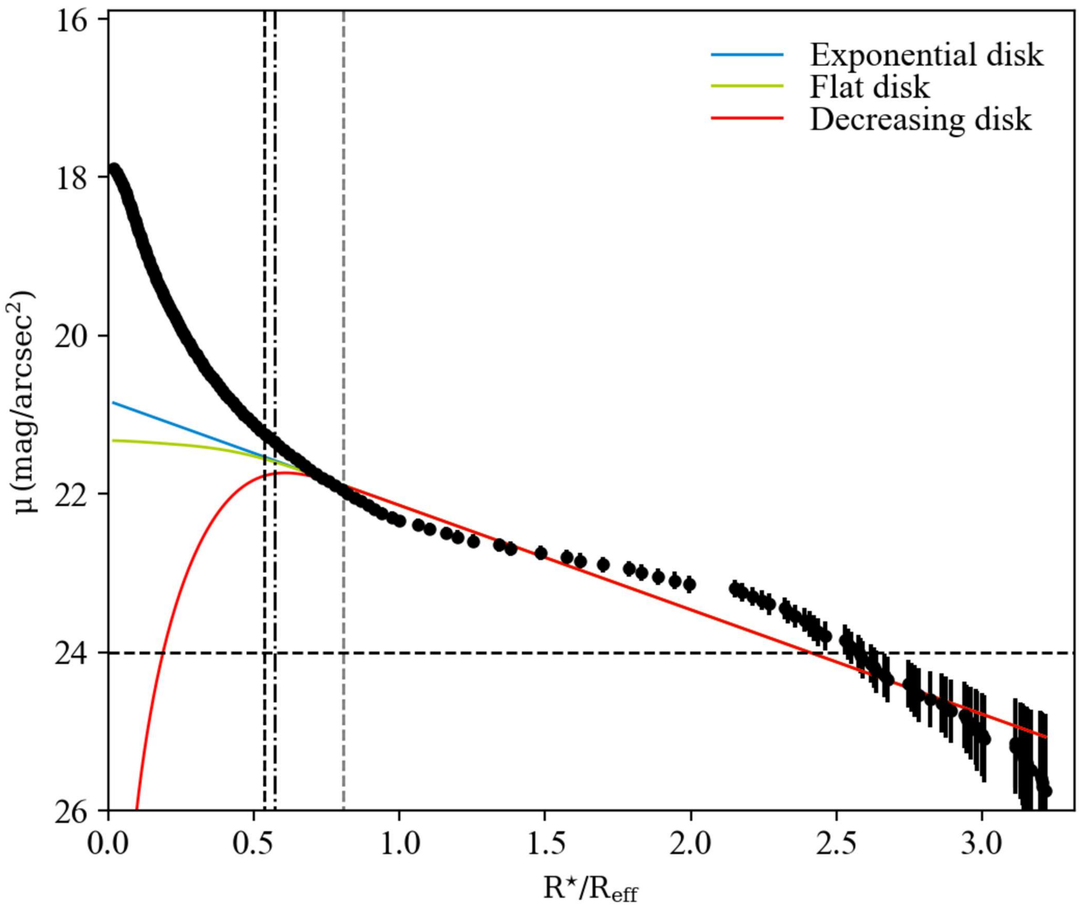
Exponential disk
Flat disk
Decreasing disk
μ (mag/arcsec²)
16
18
20
22
24
26
0.0
0.5
1.0
1.5
2.0
2.5
3.0
R⋆/Reff

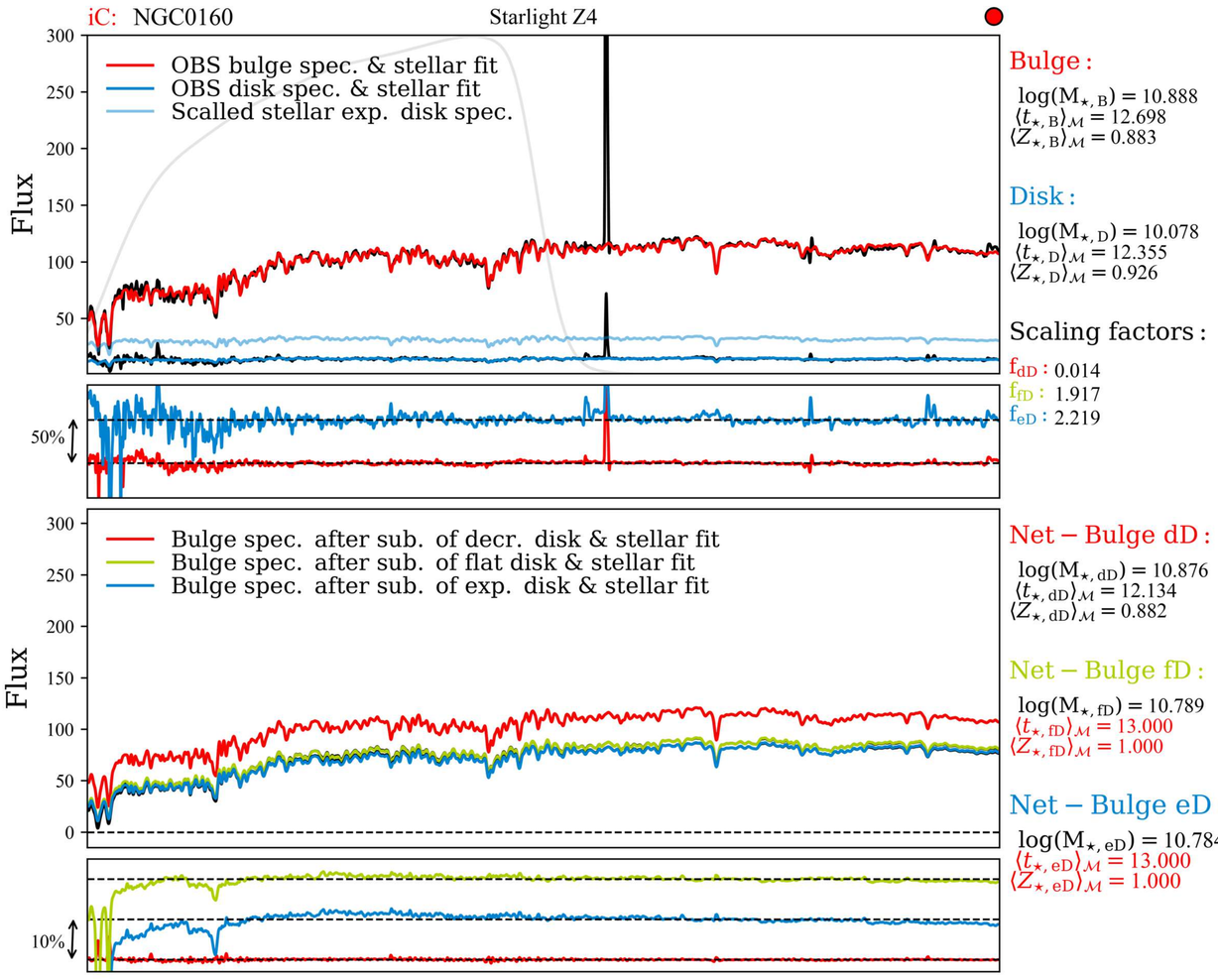
iC: NGC0160
Starlight Z4
OBS bulge spec. & stellar fit
OBS disk spec. & stellar fit
Scalled stellar exp. disk spec.
Flux
50%
Bulge spec. after sub. of decr. disk & stellar fit
Bulge spec. after sub. of flat disk & stellar fit
Bulge spec. after sub. of exp. disk & stellar fit
10%
Bulge :
log(M⋆, B) = 10.888
⟨t⋆, B⟩M = 12.698
⟨Z⋆, B⟩M = 0.883
Disk :
log(M⋆, D) = 10.078
⟨t⋆, D⟩M = 12.355
⟨Z⋆, D⟩M = 0.926
Scaling factors :
fdD : 0.014
ffD : 1.917
feD : 2.219
Net − Bulge dD :
log(M⋆, dD) = 10.876
⟨t⋆, dD⟩M = 12.134
⟨Z⋆, dD⟩M = 0.882
Net − Bulge fD :
log(M⋆, fD) = 10.789
⟨t⋆, fD⟩M = 13.000
⟨Z⋆, fD⟩M = 1.000
Net − Bulge eD :
log(M⋆, eD) = 10.784
⟨t⋆, eD⟩M = 13.000
⟨Z⋆, eD⟩M = 1.000

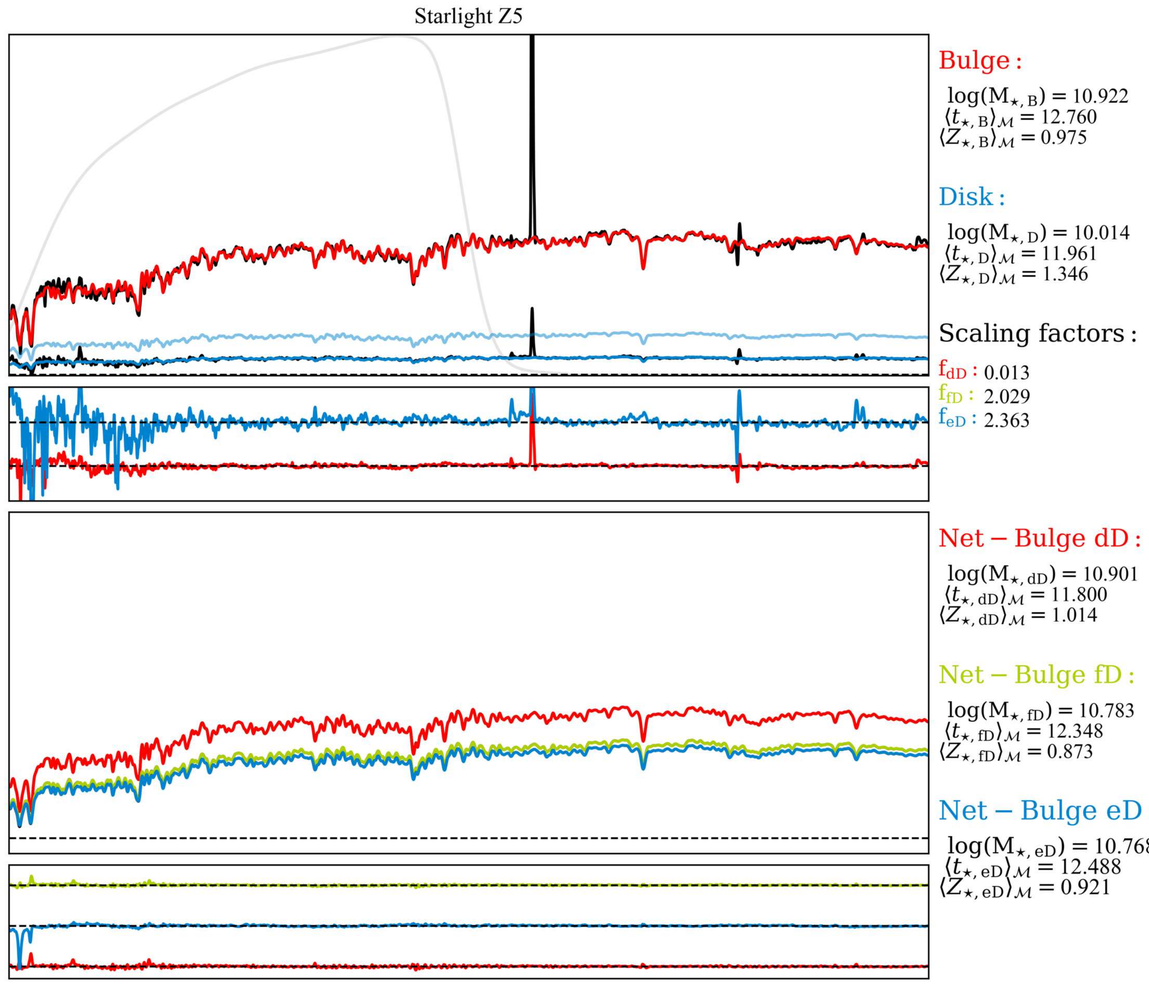
Starlight Z5
Bulge :
log(M⋆, B) = 10.922
⟨t⋆, B⟩M = 12.760
⟨Z⋆, B⟩M = 0.975
Disk :
log(M⋆, D) = 10.014
⟨t⋆, D⟩M = 11.961
⟨Z⋆, D⟩M = 1.346
Scaling factors :
fdD : 0.013
ffD : 2.029
feD : 2.363
Net − Bulge dD :
log(M⋆, dD) = 10.901
⟨t⋆, dD⟩M = 11.800
⟨Z⋆, dD⟩M = 1.014
Net − Bulge fD :
log(M⋆, fD) = 10.783
⟨t⋆, fD⟩M = 12.348
⟨Z⋆, fD⟩M = 0.873
Net − Bulge eD :
log(M⋆, eD) = 10.768
⟨t⋆, eD⟩M = 12.488
⟨Z⋆, eD⟩M = 0.921

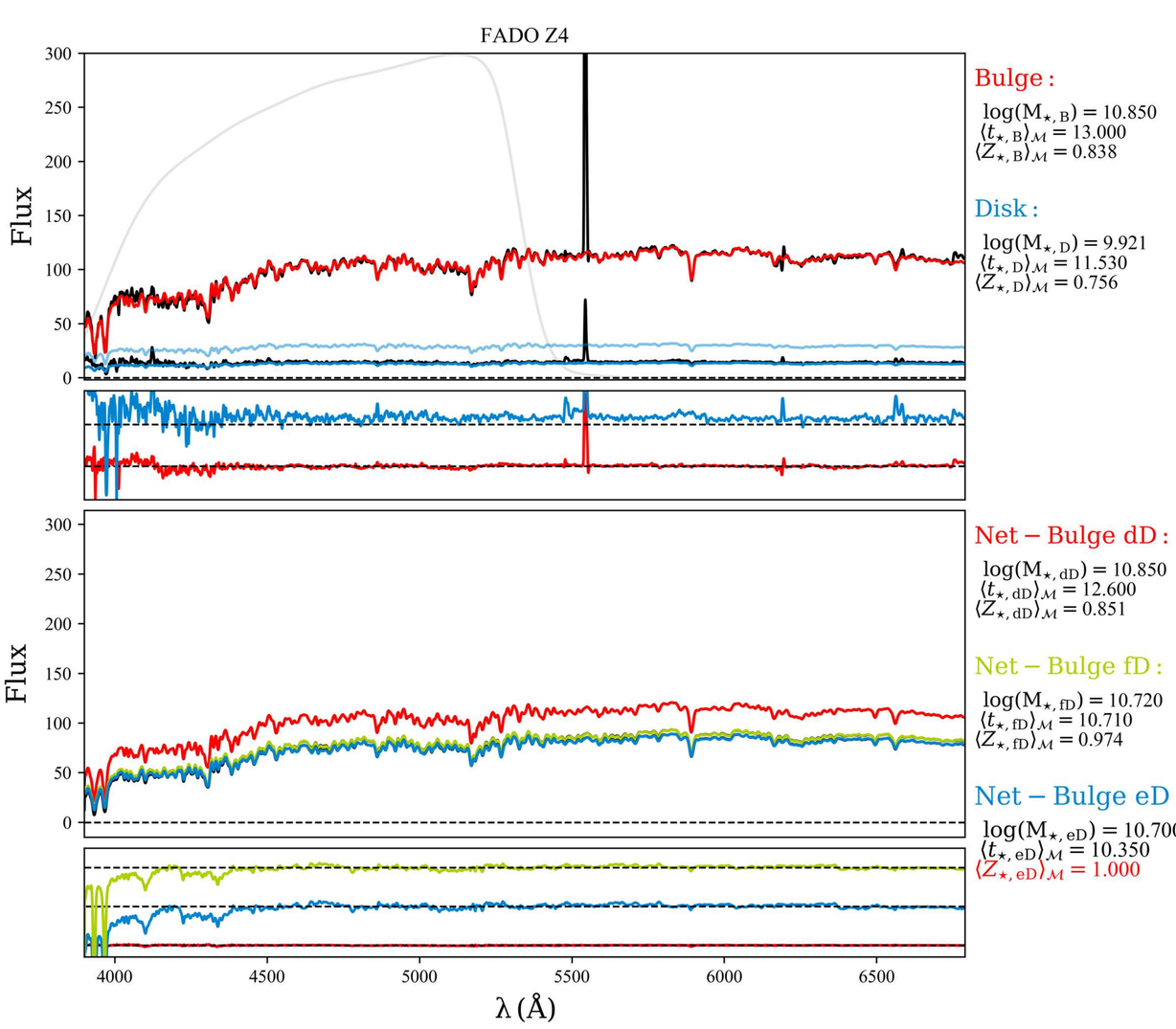
FADO Z4
Flux
Bulge :
log(M⋆, B) = 10.850
⟨t⋆, B⟩M = 13.000
⟨Z⋆, B⟩M = 0.838
Disk :
log(M⋆, D) = 9.921
⟨t⋆, D⟩M = 11.530
⟨Z⋆, D⟩M = 0.756
Net − Bulge dD :
log(M⋆, dD) = 10.850
⟨t⋆, dD⟩M = 12.600
⟨Z⋆, dD⟩M = 0.851
Net − Bulge fD :
log(M⋆, fD) = 10.720
⟨t⋆, fD⟩M = 10.710
⟨Z⋆, fD⟩M = 0.974
Net − Bulge eD :
log(M⋆, eD) = 10.700
⟨t⋆, eD⟩M = 10.350
⟨Z⋆, eD⟩M = 1.000
λ (Å)

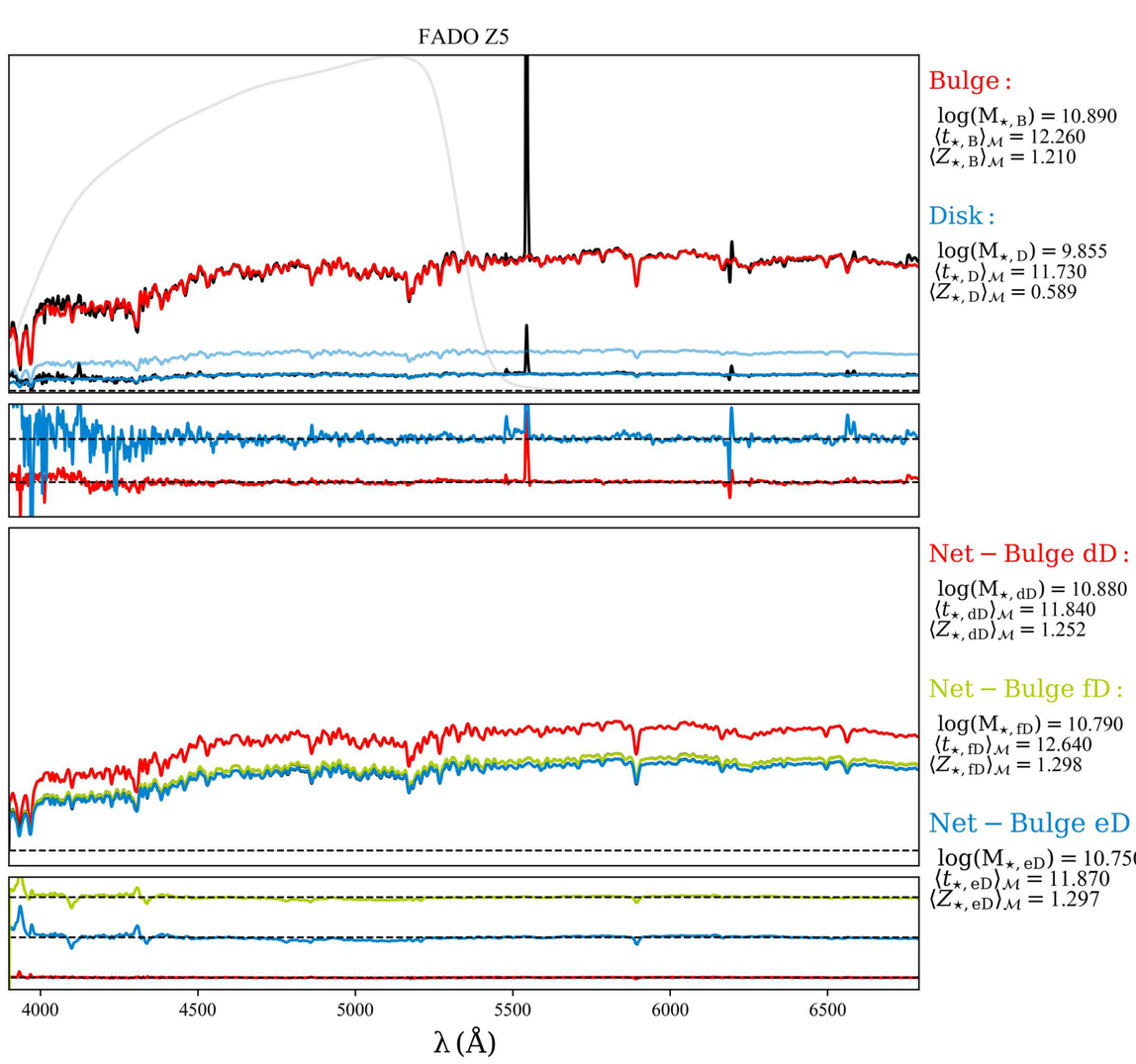
FADO Z5
Bulge :
log(M⋆, B) = 10.890
⟨t⋆, B⟩M = 12.260
⟨Z⋆, B⟩M = 1.210
Disk :
log(M⋆, D) = 9.855
⟨t⋆, D⟩M = 11.730
⟨Z⋆, D⟩M = 0.589
Net − Bulge dD :
log(M⋆, dD) = 10.880
⟨t⋆, dD⟩M = 11.840
⟨Z⋆, dD⟩M = 1.252
Net − Bulge fD :
log(M⋆, fD) = 10.790
⟨t⋆, fD⟩M = 12.640
⟨Z⋆, fD⟩M = 1.298
Net − Bulge eD :
log(M⋆, eD) = 10.750
⟨t⋆, eD⟩M = 11.870
⟨Z⋆, eD⟩M = 1.297
λ (Å)

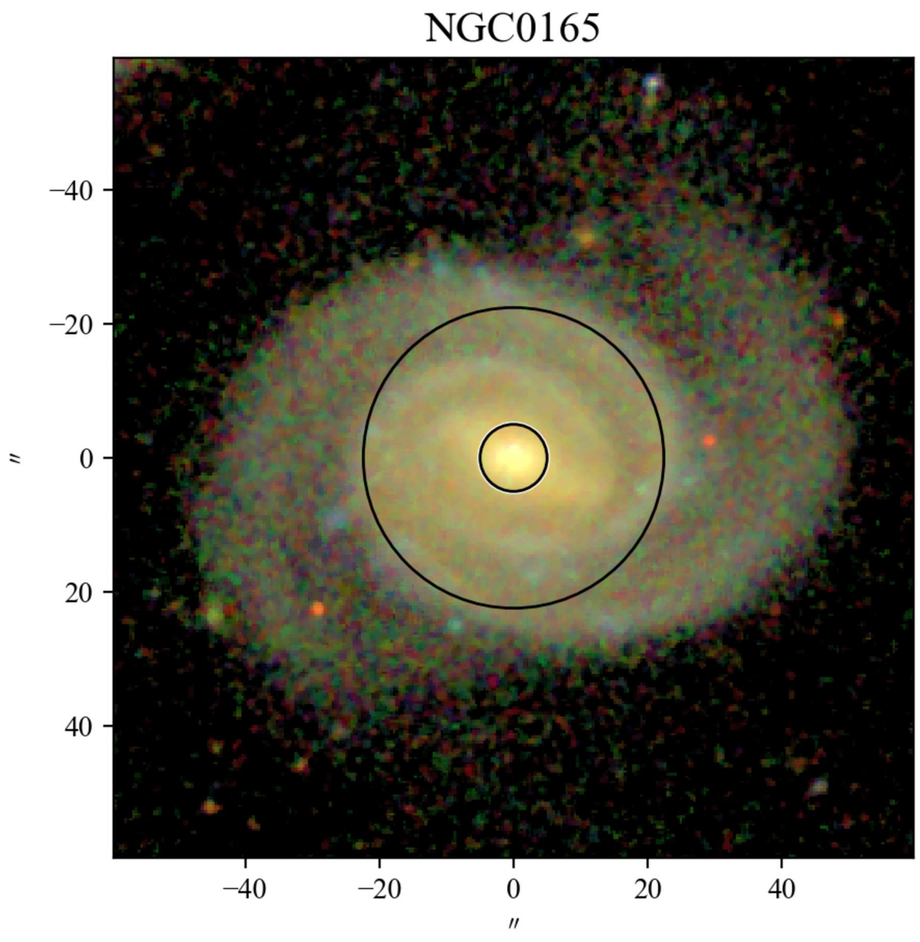
NGC0165
−40
−20
0
20
40
″
−40
−20
0
20
40
″

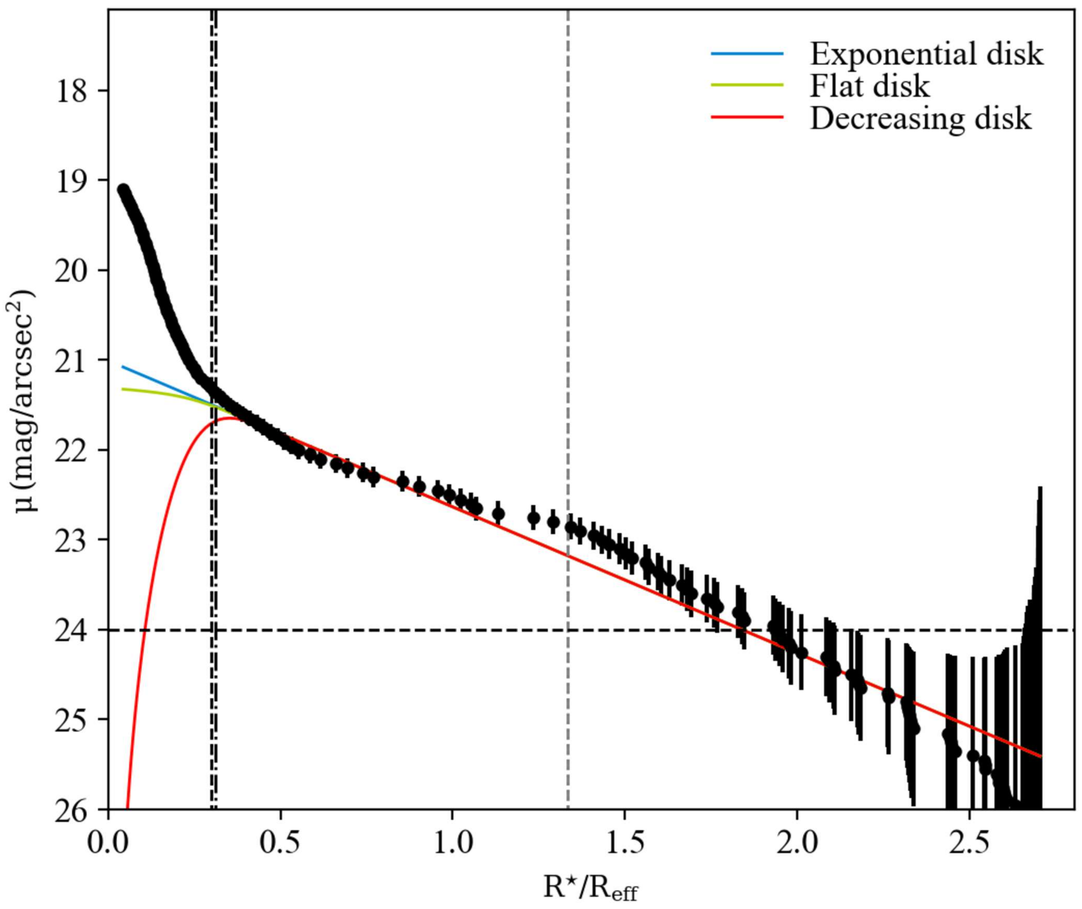
Exponential disk
Flat disk
Decreasing disk
μ (mag/arcsec²)
18
19
20
21
22
23
24
25
26
0.0
0.5
1.0
1.5
2.0
2.5
R⋆/Reff

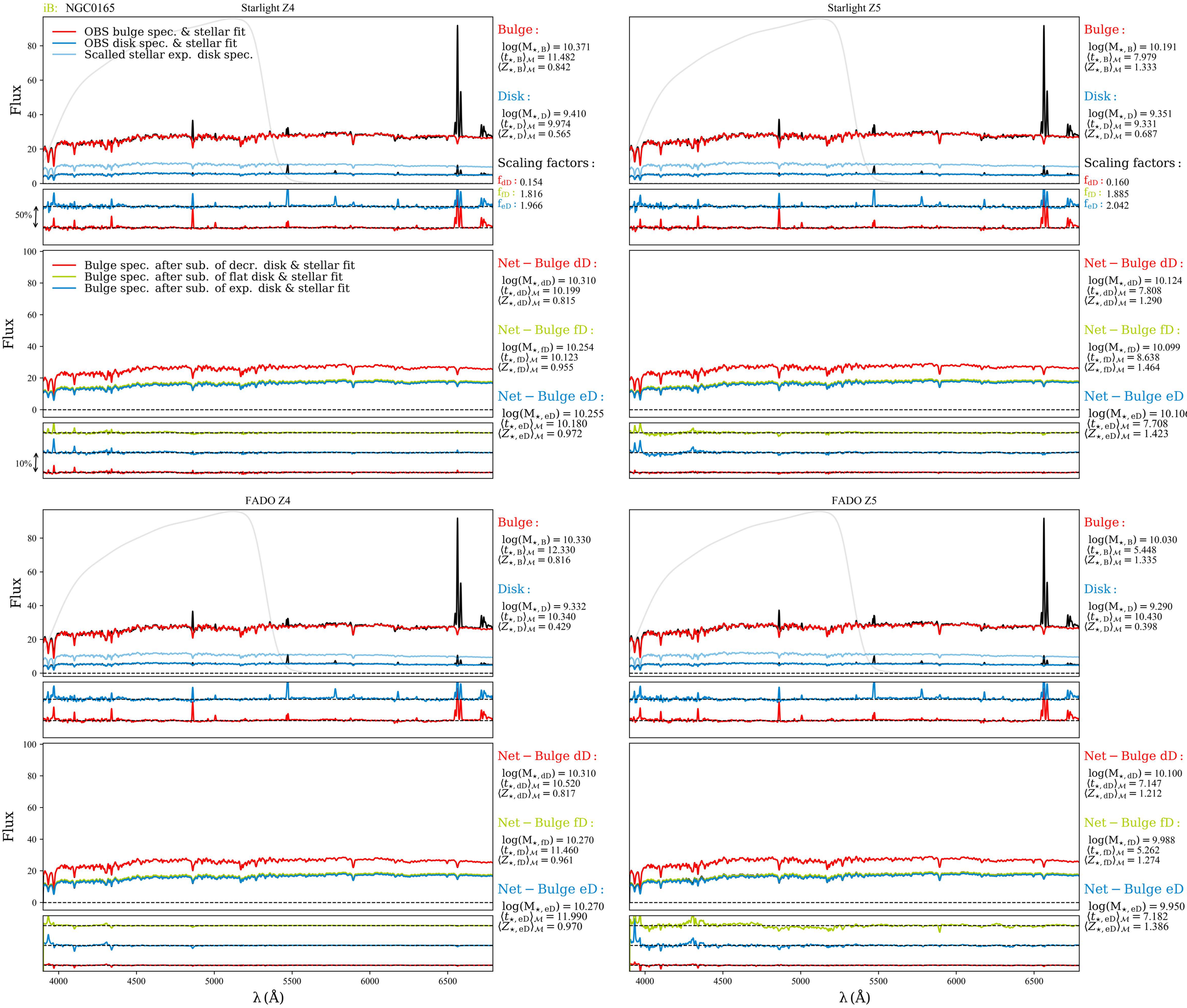
iB: NGC0165
Starlight Z4
OBS bulge spec. & stellar fit
OBS disk spec. & stellar fit
Scalled stellar exp. disk spec.
Flux
Bulge :
log(M⋆, B) = 10.371
⟨t⋆, B⟩M = 11.482
⟨Z⋆, B⟩M = 0.842
Disk :
log(M⋆, D) = 9.410
⟨t⋆, D⟩M = 9.974
⟨Z⋆, D⟩M = 0.565
Scaling factors :
fdD : 0.154
ffD : 1.816
feD : 1.966
50%
Bulge spec. after sub. of decr. disk & stellar fit
Bulge spec. after sub. of flat disk & stellar fit
Bulge spec. after sub. of exp. disk & stellar fit
Net − Bulge dD :
log(M⋆, dD) = 10.310
⟨t⋆, dD⟩M = 10.199
⟨Z⋆, dD⟩M = 0.815
Net − Bulge fD :
log(M⋆, fD) = 10.254
⟨t⋆, fD⟩M = 10.123
⟨Z⋆, fD⟩M = 0.955
Net − Bulge eD :
log(M⋆, eD) = 10.255
⟨t⋆, eD⟩M = 10.180
⟨Z⋆, eD⟩M = 0.972
10%
FADO Z4
Bulge :
log(M⋆, B) = 10.330
⟨t⋆, B⟩M = 12.330
⟨Z⋆, B⟩M = 0.816
Disk :
log(M⋆, D) = 9.332
⟨t⋆, D⟩M = 10.340
⟨Z⋆, D⟩M = 0.429
Net − Bulge dD :
log(M⋆, dD) = 10.310
⟨t⋆, dD⟩M = 10.520
⟨Z⋆, dD⟩M = 0.817
Net − Bulge fD :
log(M⋆, fD) = 10.270
⟨t⋆, fD⟩M = 11.460
⟨Z⋆, fD⟩M = 0.961
Net − Bulge eD :
log(M⋆, eD) = 10.270
⟨t⋆, eD⟩M = 11.990
⟨Z⋆, eD⟩M = 0.970
λ (Å)

Starlight Z5
Bulge :
log(M⋆, B) = 10.191
⟨t⋆, B⟩M = 7.979
⟨Z⋆, B⟩M = 1.333
Disk :
log(M⋆, D) = 9.351
⟨t⋆, D⟩M = 9.331
⟨Z⋆, D⟩M = 0.687
Scaling factors :
fdD : 0.160
ffD : 1.885
feD : 2.042
Net − Bulge dD :
log(M⋆, dD) = 10.124
⟨t⋆, dD⟩M = 7.808
⟨Z⋆, dD⟩M = 1.290
Net − Bulge fD :
log(M⋆, fD) = 10.099
⟨t⋆, fD⟩M = 8.638
⟨Z⋆, fD⟩M = 1.464
Net − Bulge eD :
log(M⋆, eD) = 10.106
⟨t⋆, eD⟩M = 7.708
⟨Z⋆, eD⟩M = 1.423
FADO Z5
Bulge :
log(M⋆, B) = 10.030
⟨t⋆, B⟩M = 5.448
⟨Z⋆, B⟩M = 1.335
Disk :
log(M⋆, D) = 9.290
⟨t⋆, D⟩M = 10.430
⟨Z⋆, D⟩M = 0.398
Net − Bulge dD :
log(M⋆, dD) = 10.100
⟨t⋆, dD⟩M = 7.147
⟨Z⋆, dD⟩M = 1.212
Net − Bulge fD :
log(M⋆, fD) = 9.988
⟨t⋆, fD⟩M = 5.262
⟨Z⋆, fD⟩M = 1.274
Net − Bulge eD :
log(M⋆, eD) = 9.950
⟨t⋆, eD⟩M = 7.182
⟨Z⋆, eD⟩M = 1.386
λ (Å)

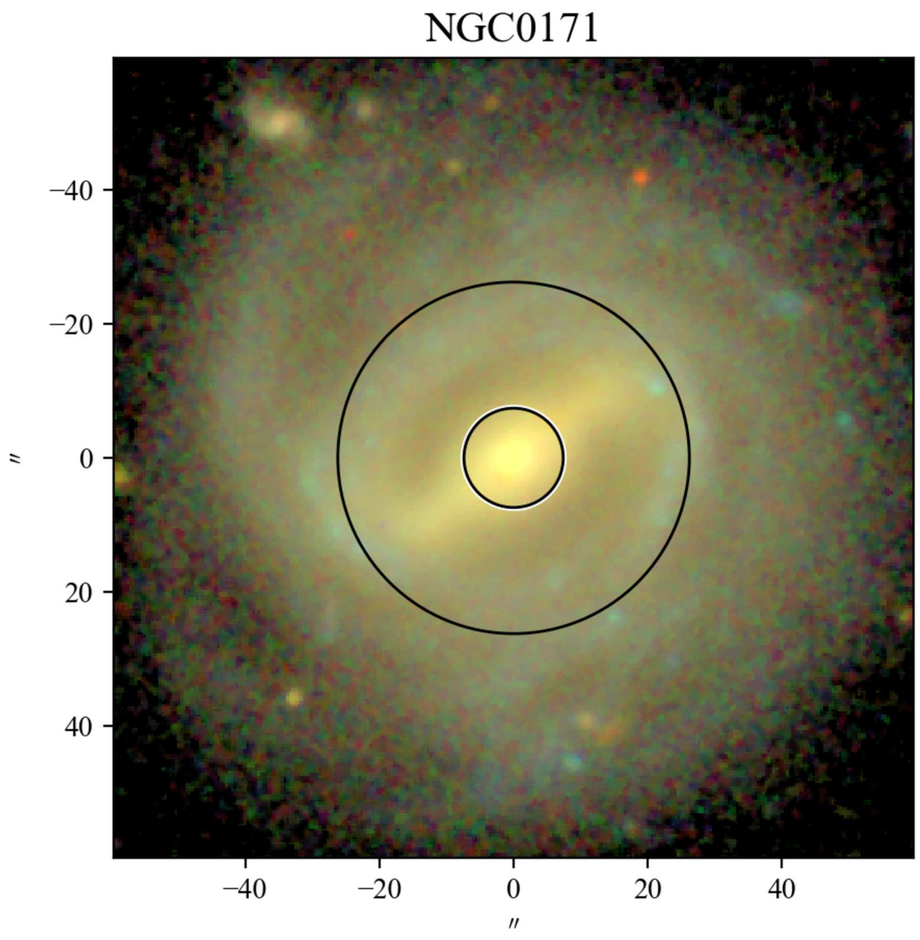
NGC0171
−40
−20
0
20
40
″
−40
−20
0
20
40
″

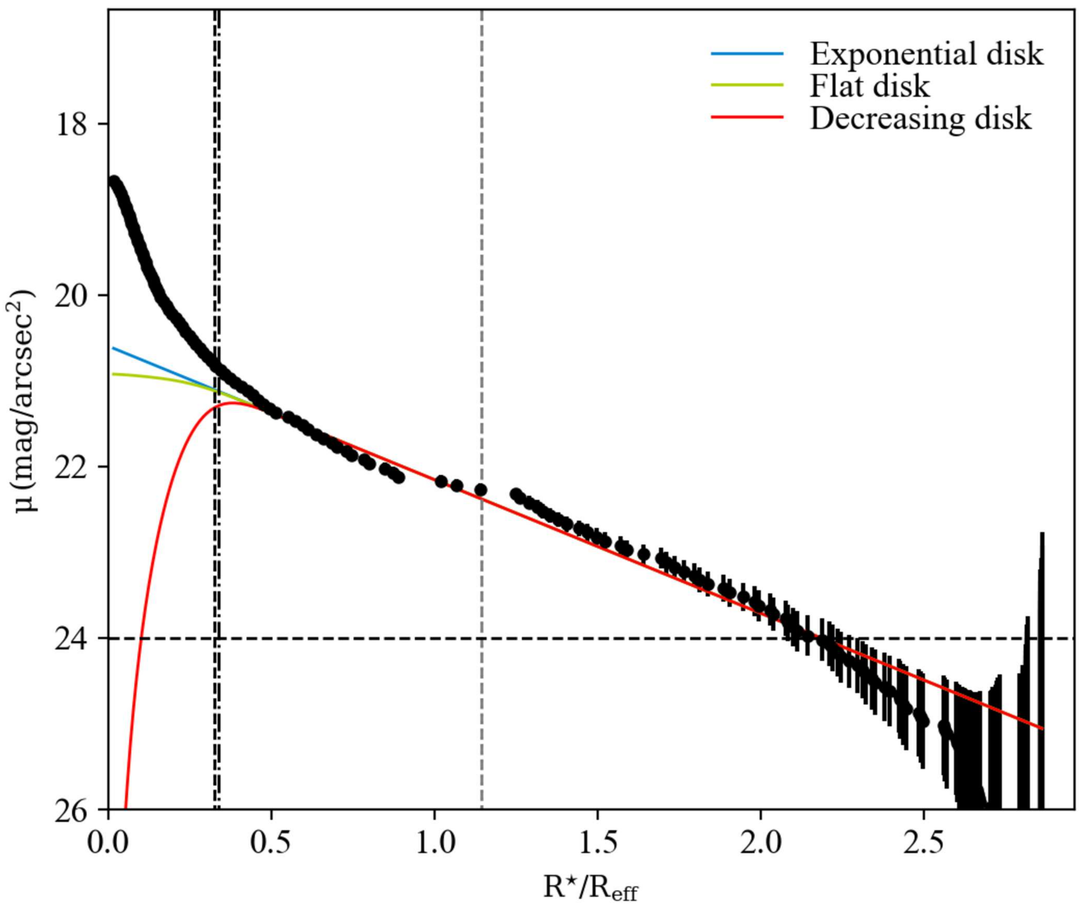
Exponential disk
Flat disk
Decreasing disk
μ (mag/arcsec²)
18
20
22
24
26
0.0
0.5
1.0
1.5
2.0
2.5
R⋆/Reff

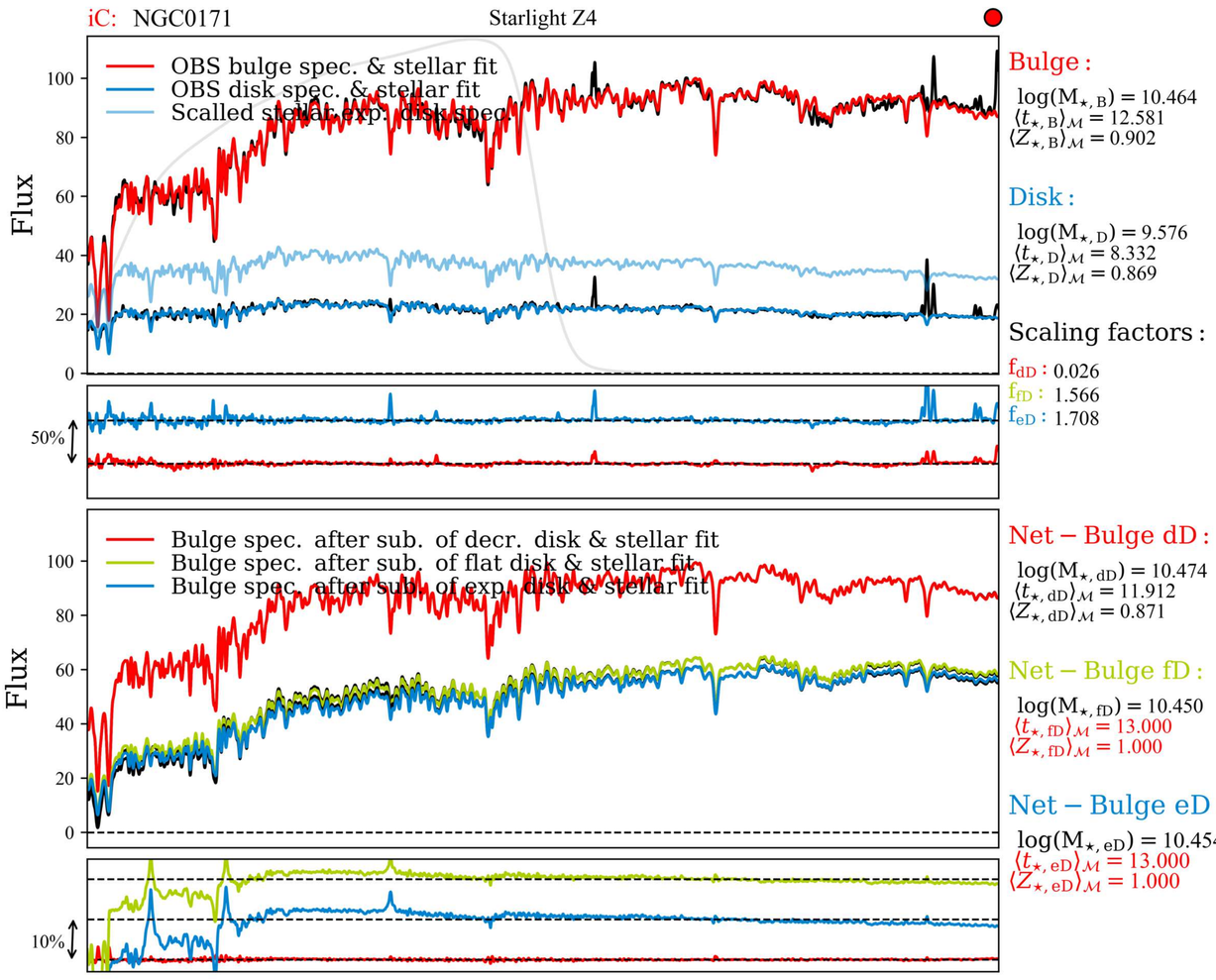
iC: NGC0171
Starlight Z4
OBS bulge spec. & stellar fit
OBS disk spec. & stellar fit
Scalled stellar exp. disk spec.
Flux
Bulge :
log(M⋆, B) = 10.464
⟨t⋆, B⟩M = 12.581
⟨Z⋆, B⟩M = 0.902
Disk :
log(M⋆, D) = 9.576
⟨t⋆, D⟩M = 8.332
⟨Z⋆, D⟩M = 0.869
Scaling factors :
fdD : 0.026
ffD : 1.566
feD : 1.708
50%
Bulge spec. after sub. of decr. disk & stellar fit
Bulge spec. after sub. of flat disk & stellar fit
Bulge spec. after sub. of exp. disk & stellar fit
Net − Bulge dD :
log(M⋆, dD) = 10.474
⟨t⋆, dD⟩M = 11.912
⟨Z⋆, dD⟩M = 0.871
Net − Bulge fD :
log(M⋆, fD) = 10.450
⟨t⋆, fD⟩M = 13.000
⟨Z⋆, fD⟩M = 1.000
Net − Bulge eD :
log(M⋆, eD) = 10.454
⟨t⋆, eD⟩M = 13.000
⟨Z⋆, eD⟩M = 1.000
10%

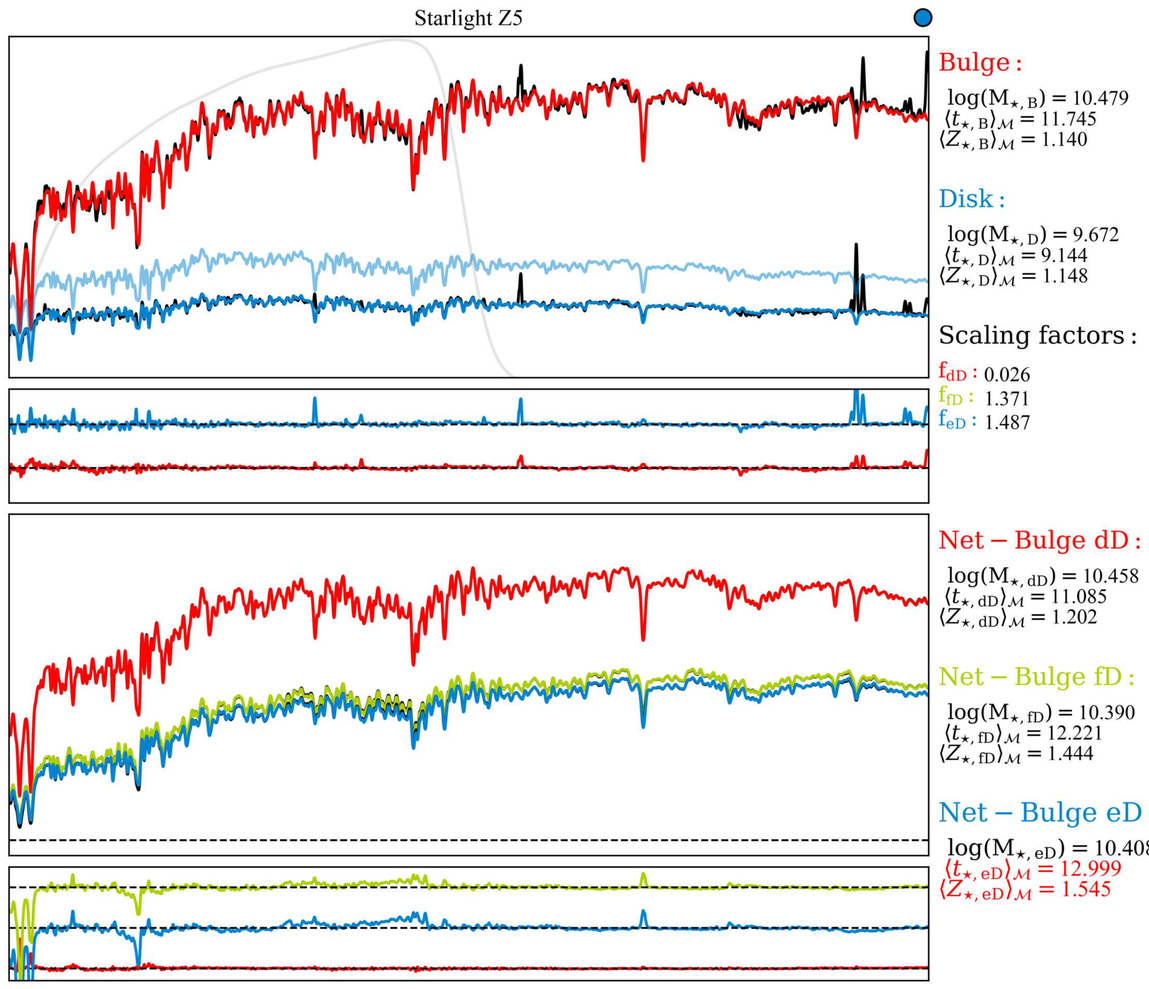
Starlight Z5
Bulge :
log(M⋆, B) = 10.479
⟨t⋆, B⟩M = 11.745
⟨Z⋆, B⟩M = 1.140
Disk :
log(M⋆, D) = 9.672
⟨t⋆, D⟩M = 9.144
⟨Z⋆, D⟩M = 1.148
Scaling factors :
fdD : 0.026
ffD : 1.371
feD : 1.487
Net − Bulge dD :
log(M⋆, dD) = 10.458
⟨t⋆, dD⟩M = 11.085
⟨Z⋆, dD⟩M = 1.202
Net − Bulge fD :
log(M⋆, fD) = 10.390
⟨t⋆, fD⟩M = 12.221
⟨Z⋆, fD⟩M = 1.444
Net − Bulge eD :
log(M⋆, eD) = 10.408
⟨t⋆, eD⟩M = 12.999
⟨Z⋆, eD⟩M = 1.545

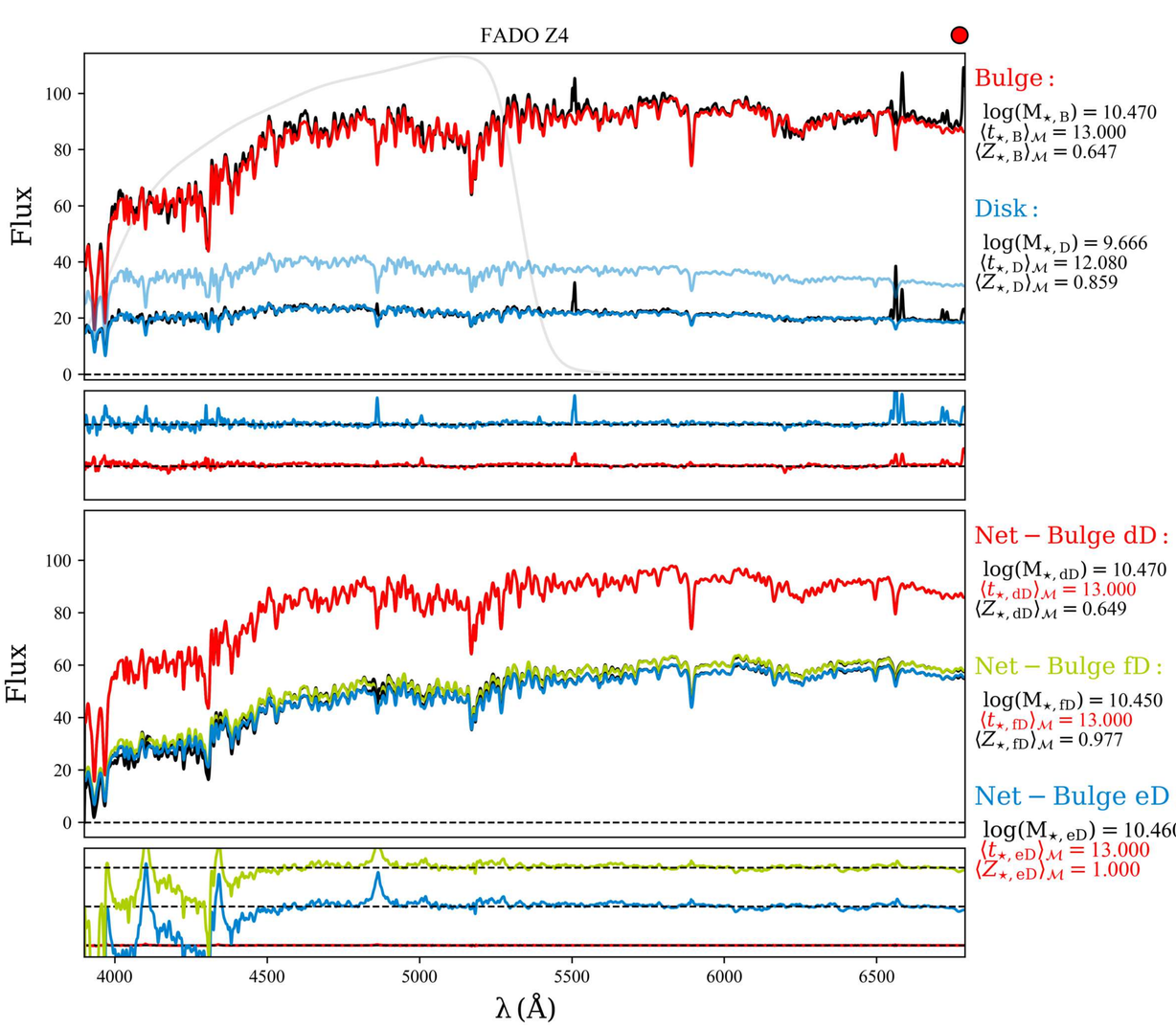
FADO Z4
Flux
Bulge :
log(M⋆, B) = 10.470
⟨t⋆, B⟩M = 13.000
⟨Z⋆, B⟩M = 0.647
Disk :
log(M⋆, D) = 9.666
⟨t⋆, D⟩M = 12.080
⟨Z⋆, D⟩M = 0.859
Net − Bulge dD :
log(M⋆, dD) = 10.470
⟨t⋆, dD⟩M = 13.000
⟨Z⋆, dD⟩M = 0.649
Net − Bulge fD :
log(M⋆, fD) = 10.450
⟨t⋆, fD⟩M = 13.000
⟨Z⋆, fD⟩M = 0.977
Net − Bulge eD :
log(M⋆, eD) = 10.460
⟨t⋆, eD⟩M = 13.000
⟨Z⋆, eD⟩M = 1.000
λ (Å)

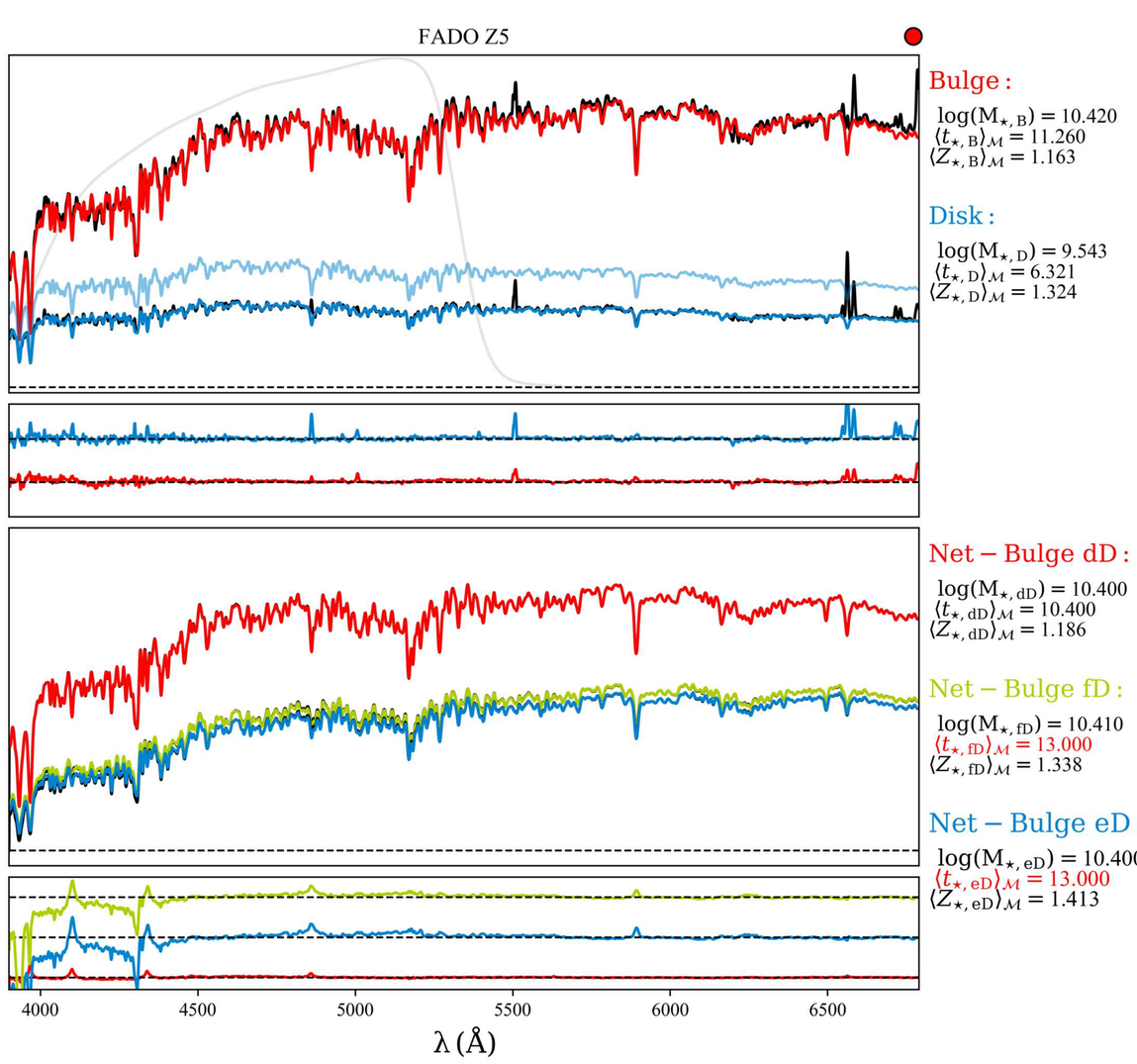
FADO Z5
Bulge :
log(M⋆, B) = 10.420
⟨t⋆, B⟩M = 11.260
⟨Z⋆, B⟩M = 1.163
Disk :
log(M⋆, D) = 9.543
⟨t⋆, D⟩M = 6.321
⟨Z⋆, D⟩M = 1.324
Net − Bulge dD :
log(M⋆, dD) = 10.400
⟨t⋆, dD⟩M = 10.400
⟨Z⋆, dD⟩M = 1.186
Net − Bulge fD :
log(M⋆, fD) = 10.410
⟨t⋆, fD⟩M = 13.000
⟨Z⋆, fD⟩M = 1.338
Net − Bulge eD :
log(M⋆, eD) = 10.400
⟨t⋆, eD⟩M = 13.000
⟨Z⋆, eD⟩M = 1.413
λ (Å)

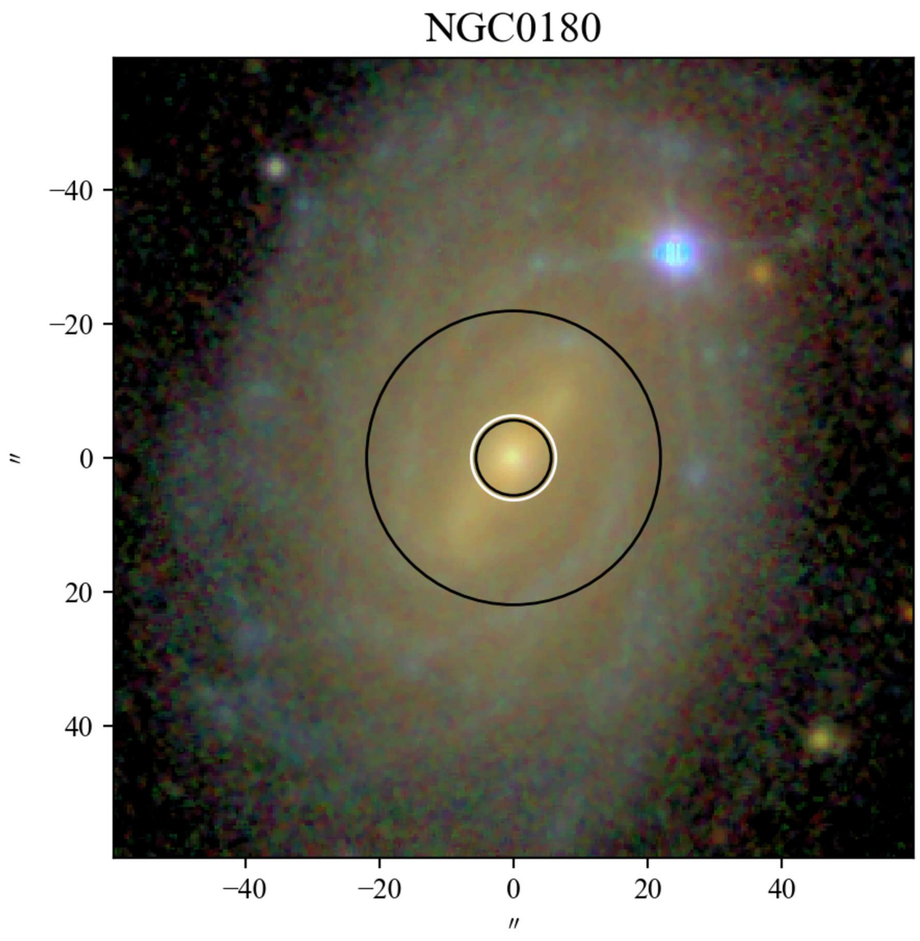
NGC0180
−40
−20
0
20
40
″
−40
−20
0
20
40
″

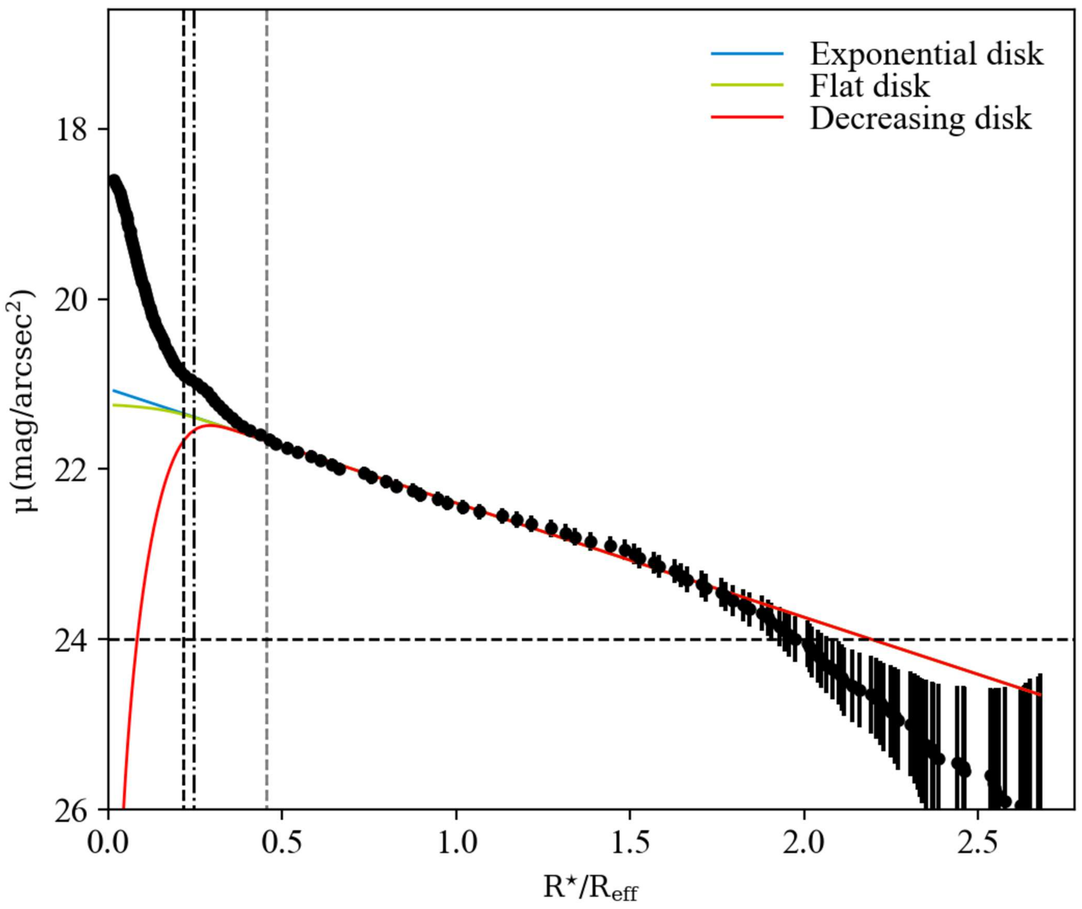
Exponential disk
Flat disk
Decreasing disk
μ (mag/arcsec²)
18
20
22
24
26
0.0
0.5
1.0
1.5
2.0
2.5
R⋆/Reff

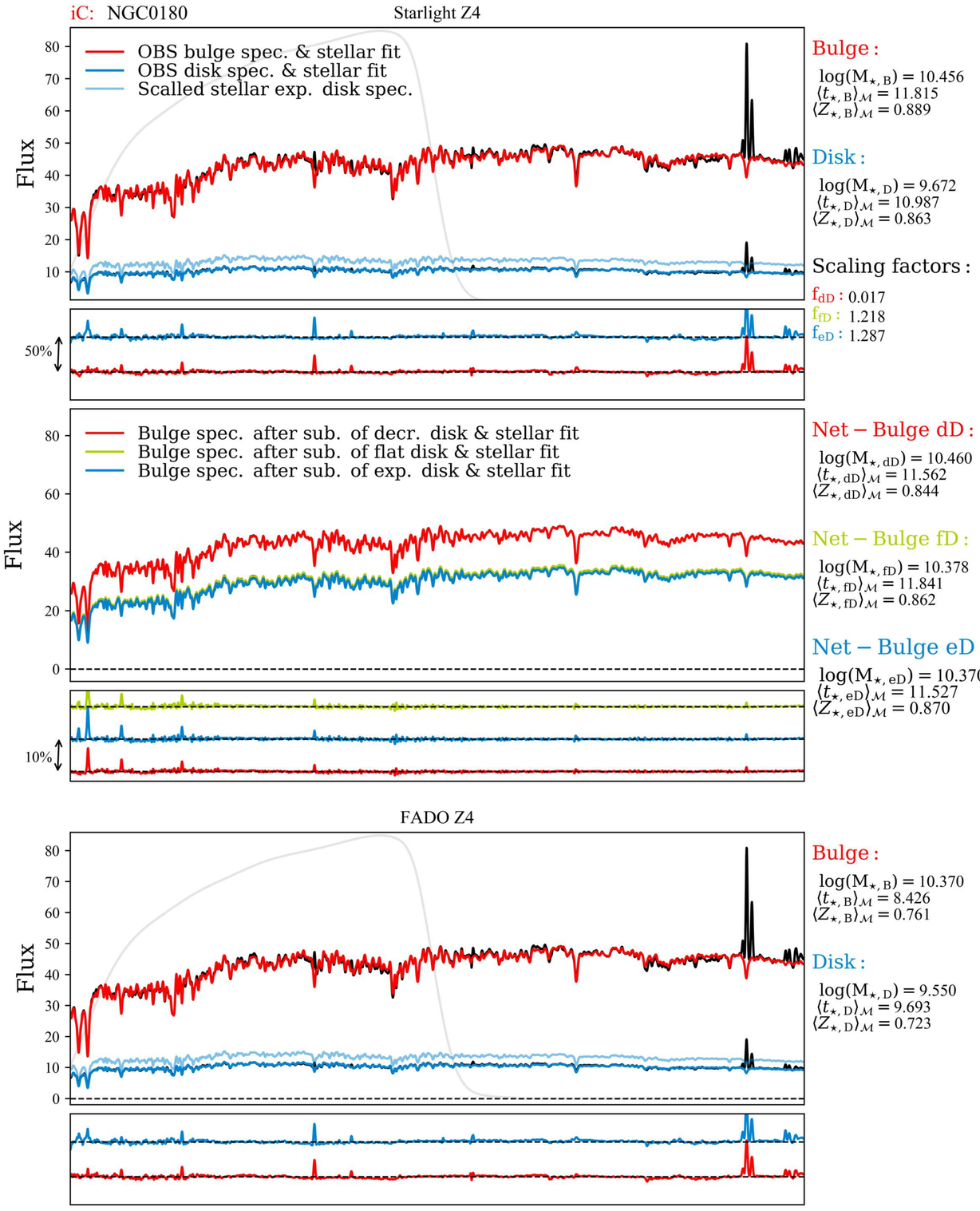
iC: NGC0180
Starlight Z4
OBS bulge spec. & stellar fit
OBS disk spec. & stellar fit
Scalled stellar exp. disk spec.
Flux
50%
Bulge :
log(M⋆, B) = 10.456
⟨t⋆, B⟩M = 11.815
⟨Z⋆, B⟩M = 0.889
Disk :
log(M⋆, D) = 9.672
⟨t⋆, D⟩M = 10.987
⟨Z⋆, D⟩M = 0.863
Scaling factors :
fdD : 0.017
ffD : 1.218
feD : 1.287
Bulge spec. after sub. of decr. disk & stellar fit
Bulge spec. after sub. of flat disk & stellar fit
Bulge spec. after sub. of exp. disk & stellar fit
10%
Net − Bulge dD :
log(M⋆, dD) = 10.460
⟨t⋆, dD⟩M = 11.562
⟨Z⋆, dD⟩M = 0.844
Net − Bulge fD :
log(M⋆, fD) = 10.378
⟨t⋆, fD⟩M = 11.841
⟨Z⋆, fD⟩M = 0.862
Net − Bulge eD :
log(M⋆, eD) = 10.370
⟨t⋆, eD⟩M = 11.527
⟨Z⋆, eD⟩M = 0.870

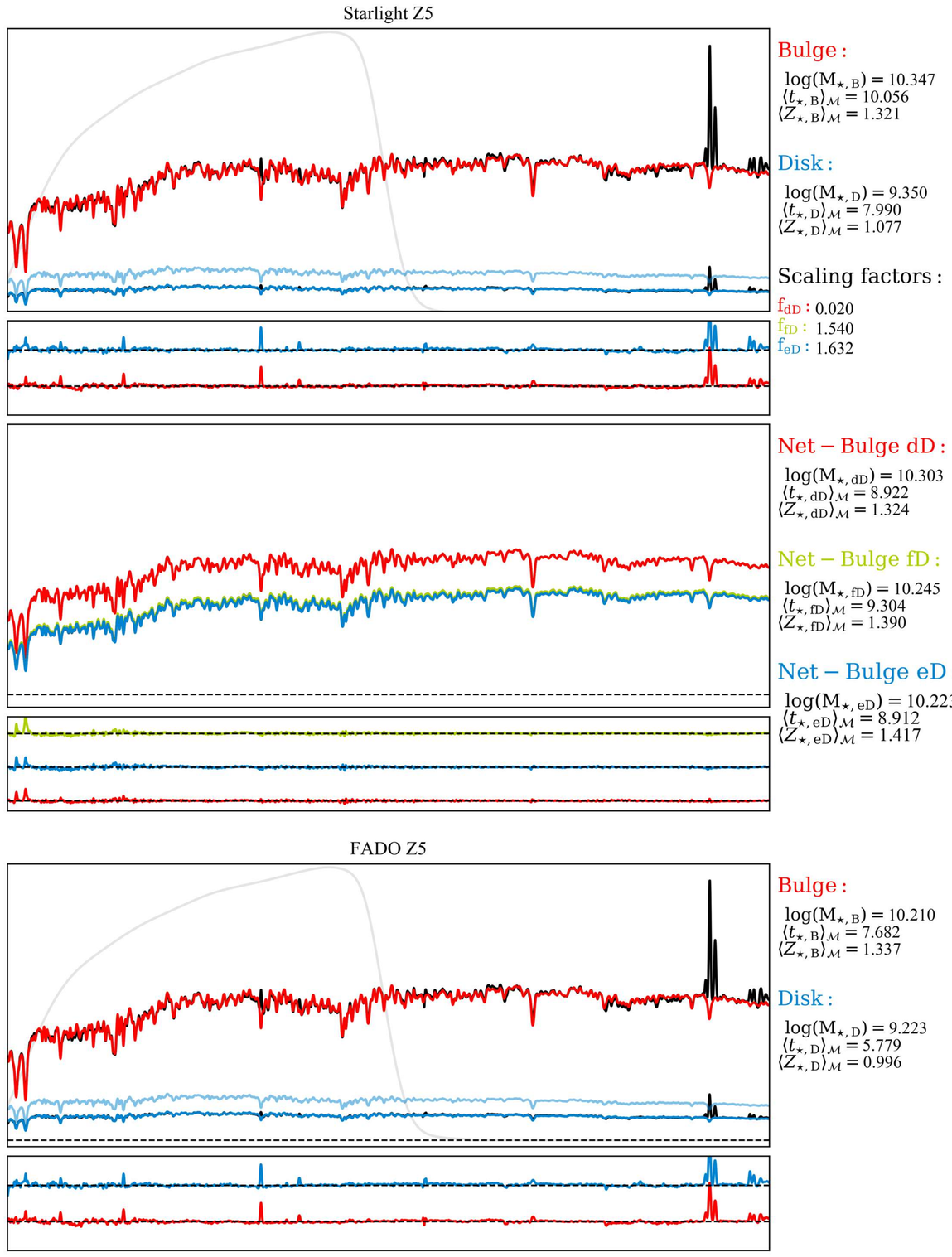
Starlight Z5
Bulge :
log(M⋆, B) = 10.347
⟨t⋆, B⟩M = 10.056
⟨Z⋆, B⟩M = 1.321
Disk :
log(M⋆, D) = 9.350
⟨t⋆, D⟩M = 7.990
⟨Z⋆, D⟩M = 1.077
Scaling factors :
fdD : 0.020
ffD : 1.540
feD : 1.632
Net − Bulge dD :
log(M⋆, dD) = 10.303
⟨t⋆, dD⟩M = 8.922
⟨Z⋆, dD⟩M = 1.324
Net − Bulge fD :
log(M⋆, fD) = 10.245
⟨t⋆, fD⟩M = 9.304
⟨Z⋆, fD⟩M = 1.390
Net − Bulge eD :
log(M⋆, eD) = 10.223
⟨t⋆, eD⟩M = 8.912
⟨Z⋆, eD⟩M = 1.417

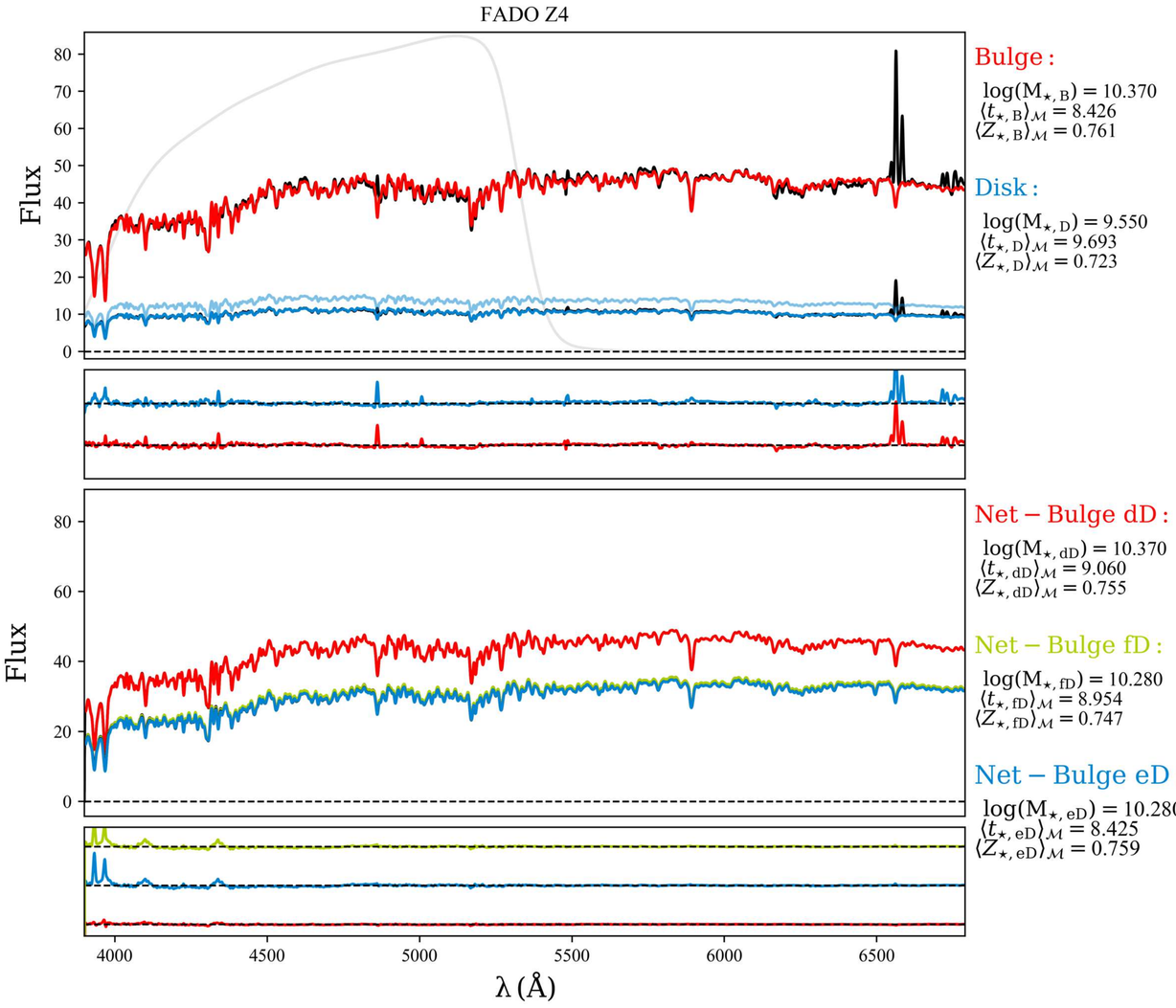
FADO Z4
Flux
Bulge :
log(M⋆, B) = 10.370
⟨t⋆, B⟩M = 8.426
⟨Z⋆, B⟩M = 0.761
Disk :
log(M⋆, D) = 9.550
⟨t⋆, D⟩M = 9.693
⟨Z⋆, D⟩M = 0.723
Net − Bulge dD :
log(M⋆, dD) = 10.370
⟨t⋆, dD⟩M = 9.060
⟨Z⋆, dD⟩M = 0.755
Net − Bulge fD :
log(M⋆, fD) = 10.280
⟨t⋆, fD⟩M = 8.954
⟨Z⋆, fD⟩M = 0.747
Net − Bulge eD :
log(M⋆, eD) = 10.280
⟨t⋆, eD⟩M = 8.425
⟨Z⋆, eD⟩M = 0.759
4000
4500
5000
5500
6000
6500
λ (Å)

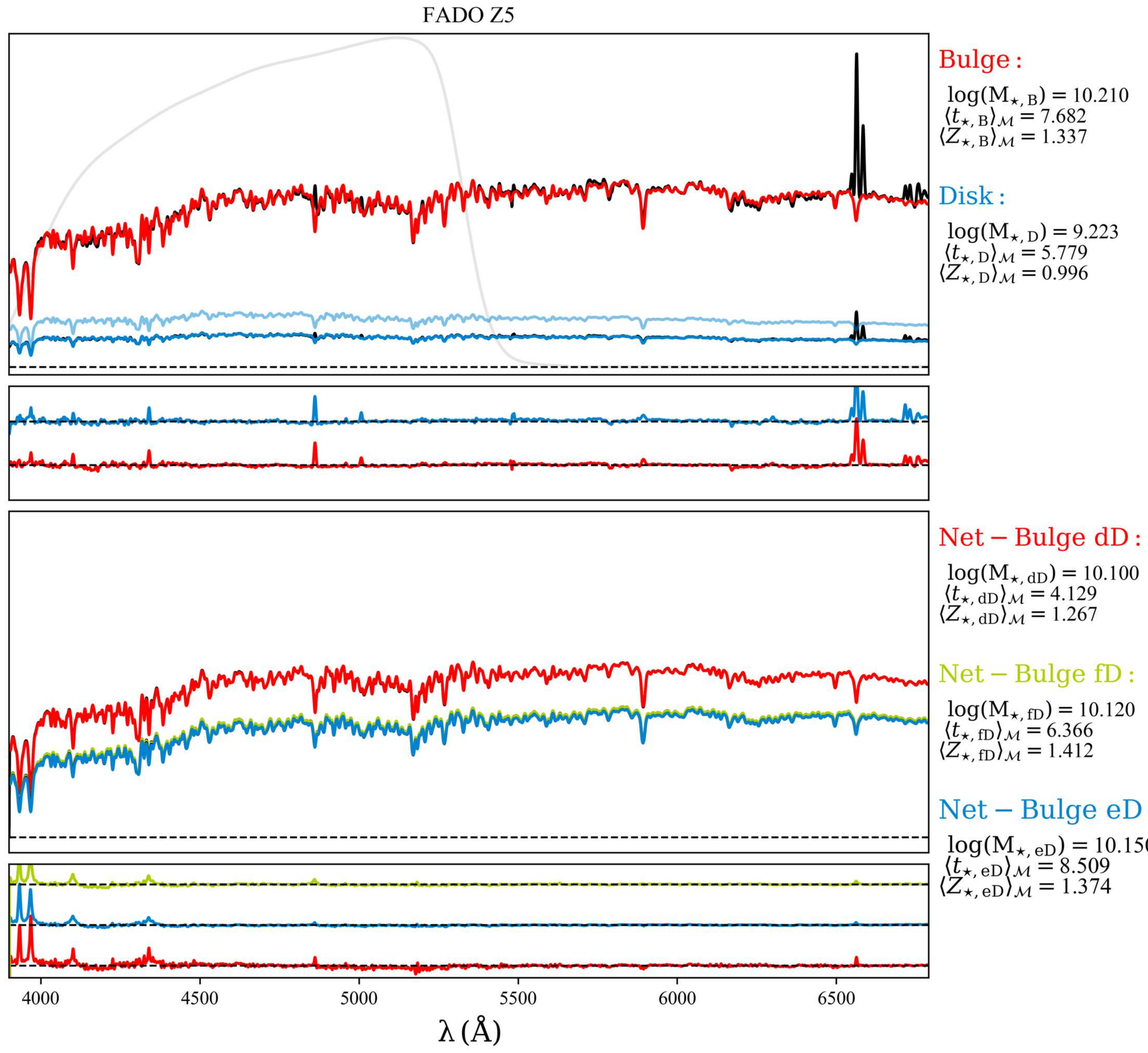
FADO Z5
Bulge :
log(M⋆, B) = 10.210
⟨t⋆, B⟩M = 7.682
⟨Z⋆, B⟩M = 1.337
Disk :
log(M⋆, D) = 9.223
⟨t⋆, D⟩M = 5.779
⟨Z⋆, D⟩M = 0.996
Net − Bulge dD :
log(M⋆, dD) = 10.100
⟨t⋆, dD⟩M = 4.129
⟨Z⋆, dD⟩M = 1.267
Net − Bulge fD :
log(M⋆, fD) = 10.120
⟨t⋆, fD⟩M = 6.366
⟨Z⋆, fD⟩M = 1.412
Net − Bulge eD :
log(M⋆, eD) = 10.150
⟨t⋆, eD⟩M = 8.509
⟨Z⋆, eD⟩M = 1.374
4000
4500
5000
5500
6000
6500
λ (Å)

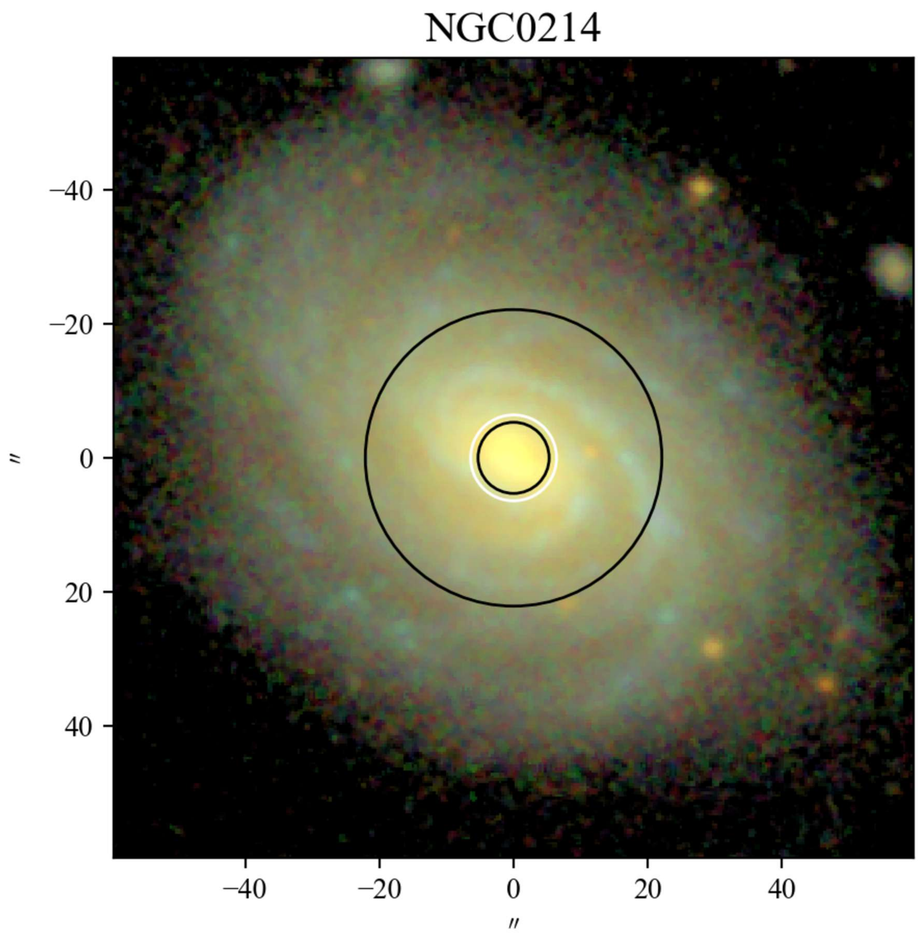
NGC0214
−40
−20
0
20
40
″
−40
−20
0
20
40
″

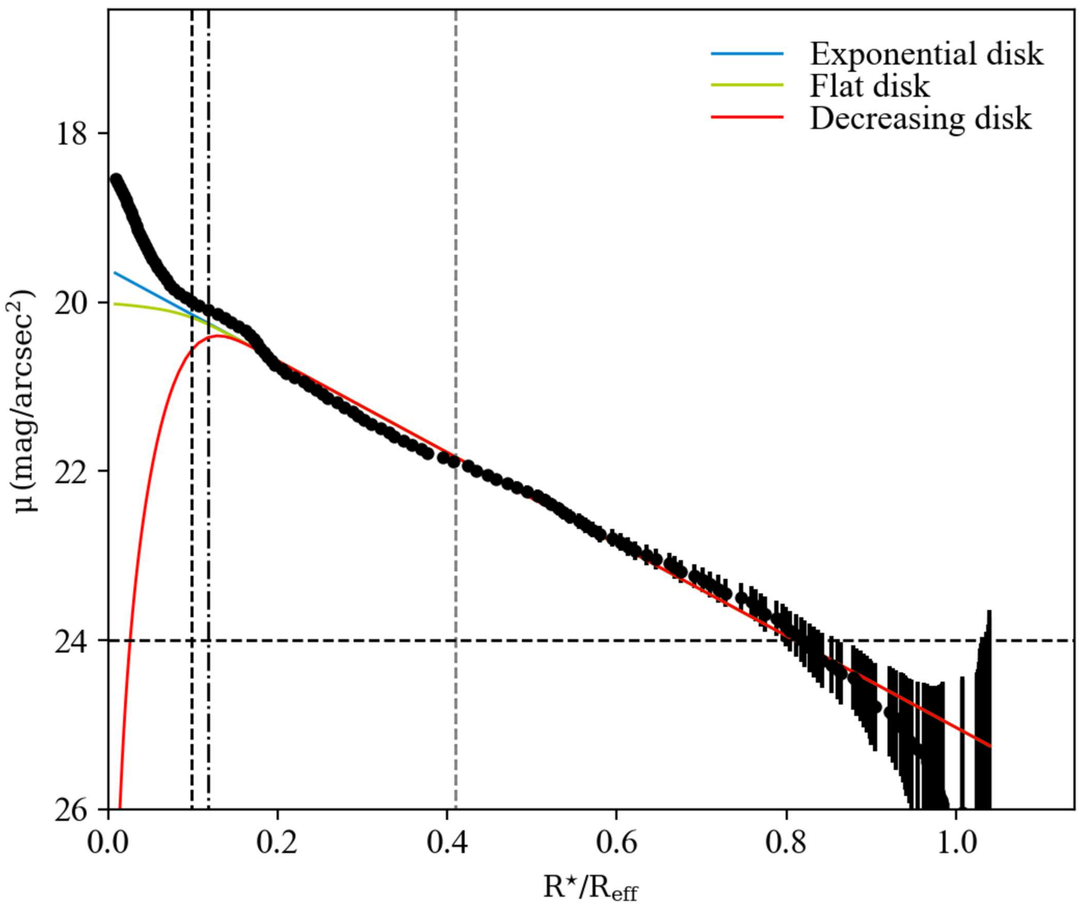
Exponential disk
Flat disk
Decreasing disk
μ (mag/arcsec²)
18
20
22
24
26
0.0
0.2
0.4
0.6
0.8
1.0
R⋆/Reff

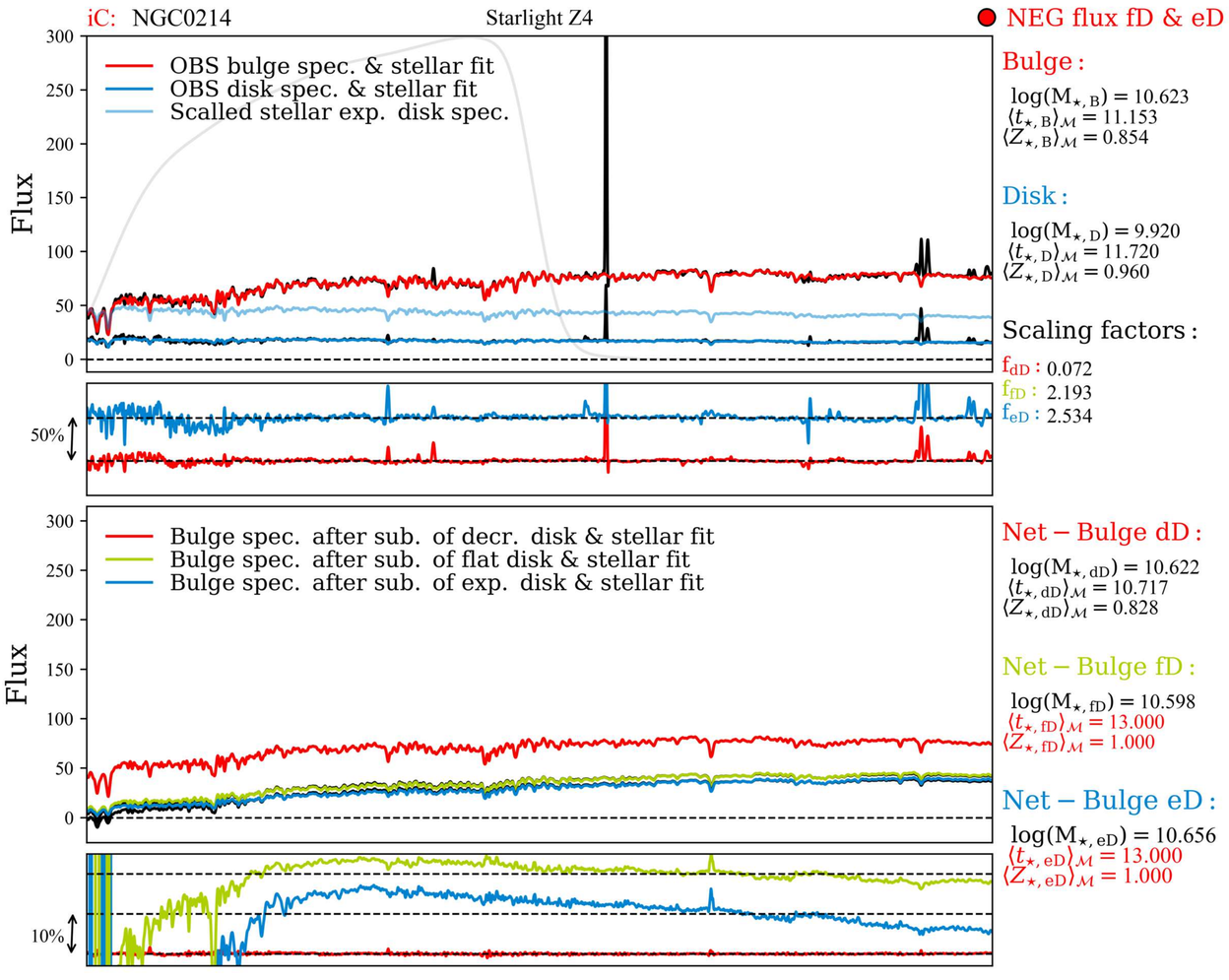
iC: NGC0214
Starlight Z4
NEG flux fD & eD
OBS bulge spec. & stellar fit
OBS disk spec. & stellar fit
Scalled stellar exp. disk spec.
Flux
50%
Bulge :
log(M⋆, B) = 10.623
⟨t⋆, B⟩M = 11.153
⟨Z⋆, B⟩M = 0.854
Disk :
log(M⋆, D) = 9.920
⟨t⋆, D⟩M = 11.720
⟨Z⋆, D⟩M = 0.960
Scaling factors :
fdD : 0.072
ffD : 2.193
feD : 2.534
Bulge spec. after sub. of decr. disk & stellar fit
Bulge spec. after sub. of flat disk & stellar fit
Bulge spec. after sub. of exp. disk & stellar fit
10%
Net − Bulge dD :
log(M⋆, dD) = 10.622
⟨t⋆, dD⟩M = 10.717
⟨Z⋆, dD⟩M = 0.828
Net − Bulge fD :
log(M⋆, fD) = 10.598
⟨t⋆, fD⟩M = 13.000
⟨Z⋆, fD⟩M = 1.000
Net − Bulge eD :
log(M⋆, eD) = 10.656
⟨t⋆, eD⟩M = 13.000
⟨Z⋆, eD⟩M = 1.000

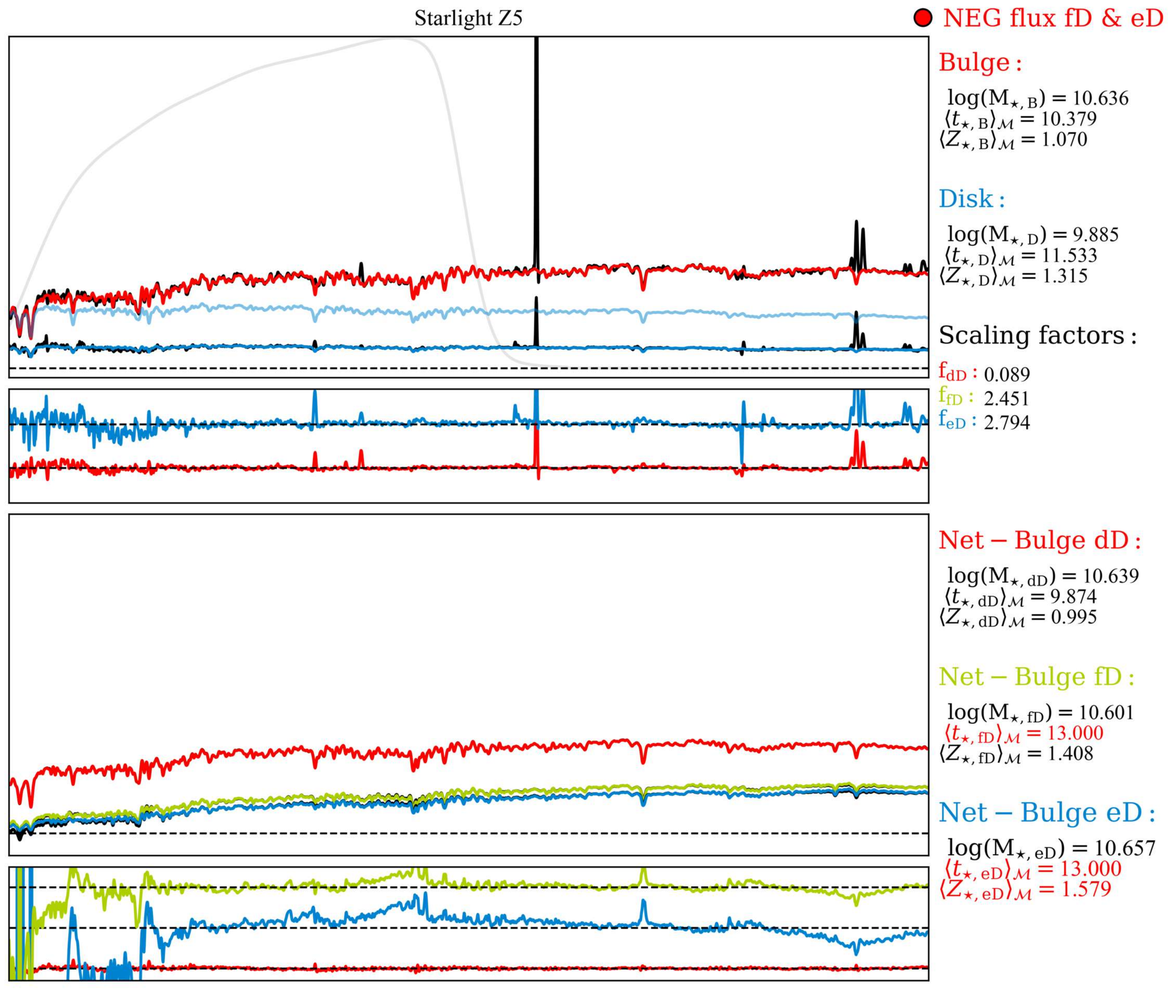
Starlight Z5
NEG flux fD & eD
Bulge :
log(M⋆, B) = 10.636
⟨t⋆, B⟩M = 10.379
⟨Z⋆, B⟩M = 1.070
Disk :
log(M⋆, D) = 9.885
⟨t⋆, D⟩M = 11.533
⟨Z⋆, D⟩M = 1.315
Scaling factors :
fdD : 0.089
ffD : 2.451
feD : 2.794
Net − Bulge dD :
log(M⋆, dD) = 10.639
⟨t⋆, dD⟩M = 9.874
⟨Z⋆, dD⟩M = 0.995
Net − Bulge fD :
log(M⋆, fD) = 10.601
⟨t⋆, fD⟩M = 13.000
⟨Z⋆, fD⟩M = 1.408
Net − Bulge eD :
log(M⋆, eD) = 10.657
⟨t⋆, eD⟩M = 13.000
⟨Z⋆, eD⟩M = 1.579

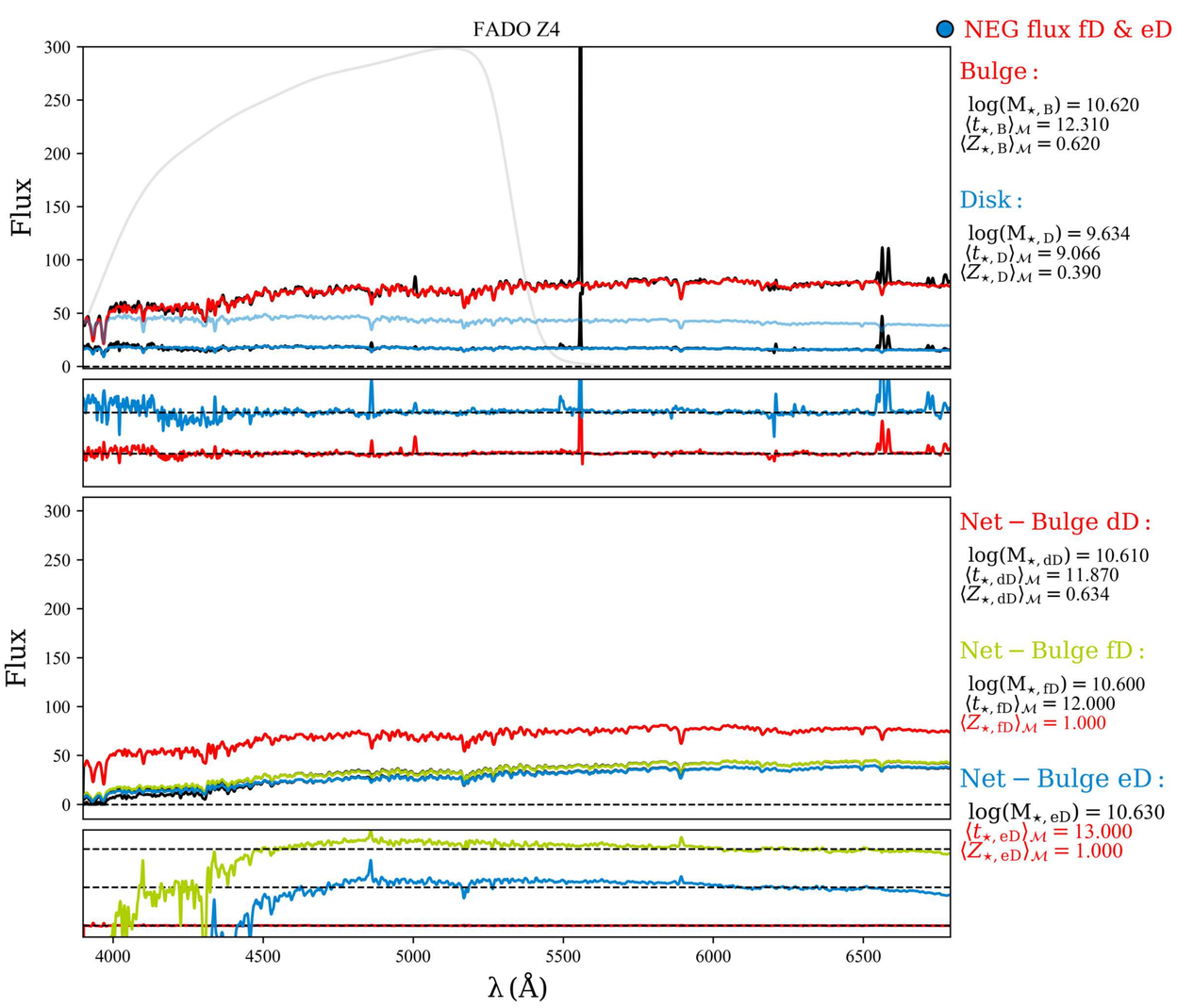
FADO Z4
NEG flux fD & eD
Flux
Bulge :
log(M⋆, B) = 10.620
⟨t⋆, B⟩M = 12.310
⟨Z⋆, B⟩M = 0.620
Disk :
log(M⋆, D) = 9.634
⟨t⋆, D⟩M = 9.066
⟨Z⋆, D⟩M = 0.390
Net − Bulge dD :
log(M⋆, dD) = 10.610
⟨t⋆, dD⟩M = 11.870
⟨Z⋆, dD⟩M = 0.634
Net − Bulge fD :
log(M⋆, fD) = 10.600
⟨t⋆, fD⟩M = 12.000
⟨Z⋆, fD⟩M = 1.000
Net − Bulge eD :
log(M⋆, eD) = 10.630
⟨t⋆, eD⟩M = 13.000
⟨Z⋆, eD⟩M = 1.000
λ (Å)

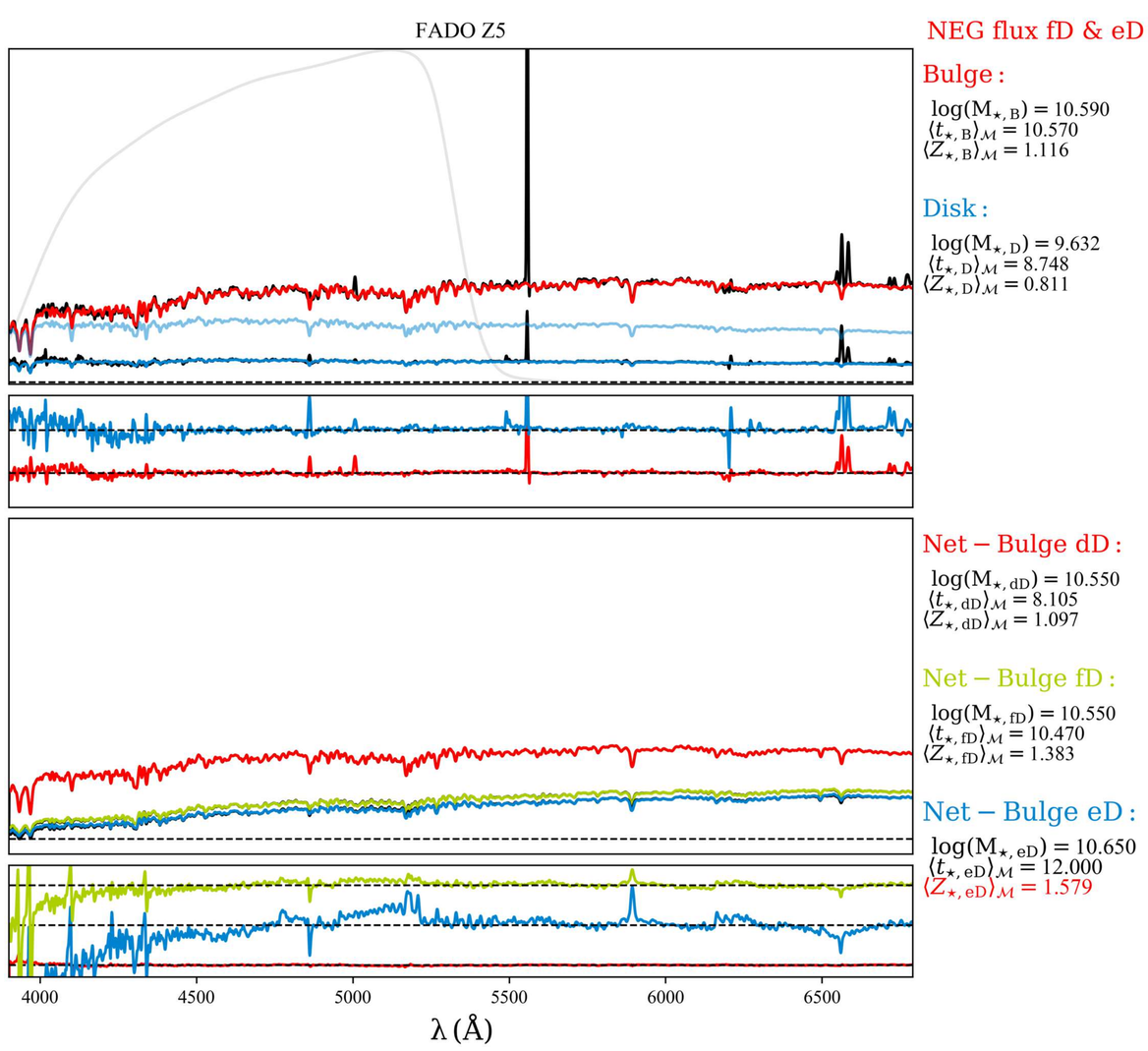
FADO Z5
NEG flux fD & eD
Bulge :
log(M⋆, B) = 10.590
⟨t⋆, B⟩M = 10.570
⟨Z⋆, B⟩M = 1.116
Disk :
log(M⋆, D) = 9.632
⟨t⋆, D⟩M = 8.748
⟨Z⋆, D⟩M = 0.811
Net − Bulge dD :
log(M⋆, dD) = 10.550
⟨t⋆, dD⟩M = 8.105
⟨Z⋆, dD⟩M = 1.097
Net − Bulge fD :
log(M⋆, fD) = 10.550
⟨t⋆, fD⟩M = 10.470
⟨Z⋆, fD⟩M = 1.383
Net − Bulge eD :
log(M⋆, eD) = 10.650
⟨t⋆, eD⟩M = 12.000
⟨Z⋆, eD⟩M = 1.579
λ (Å)

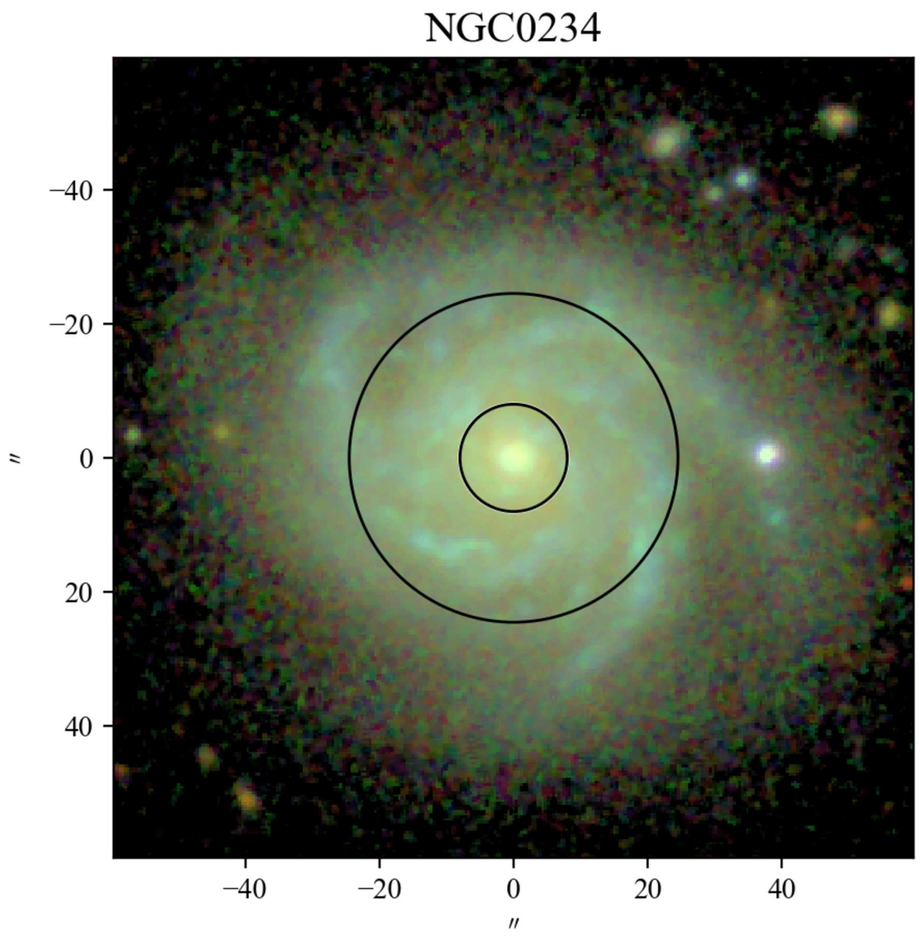
NGC0234
−40
−20
0
20
40
″
−40
−20
0
20
40
″

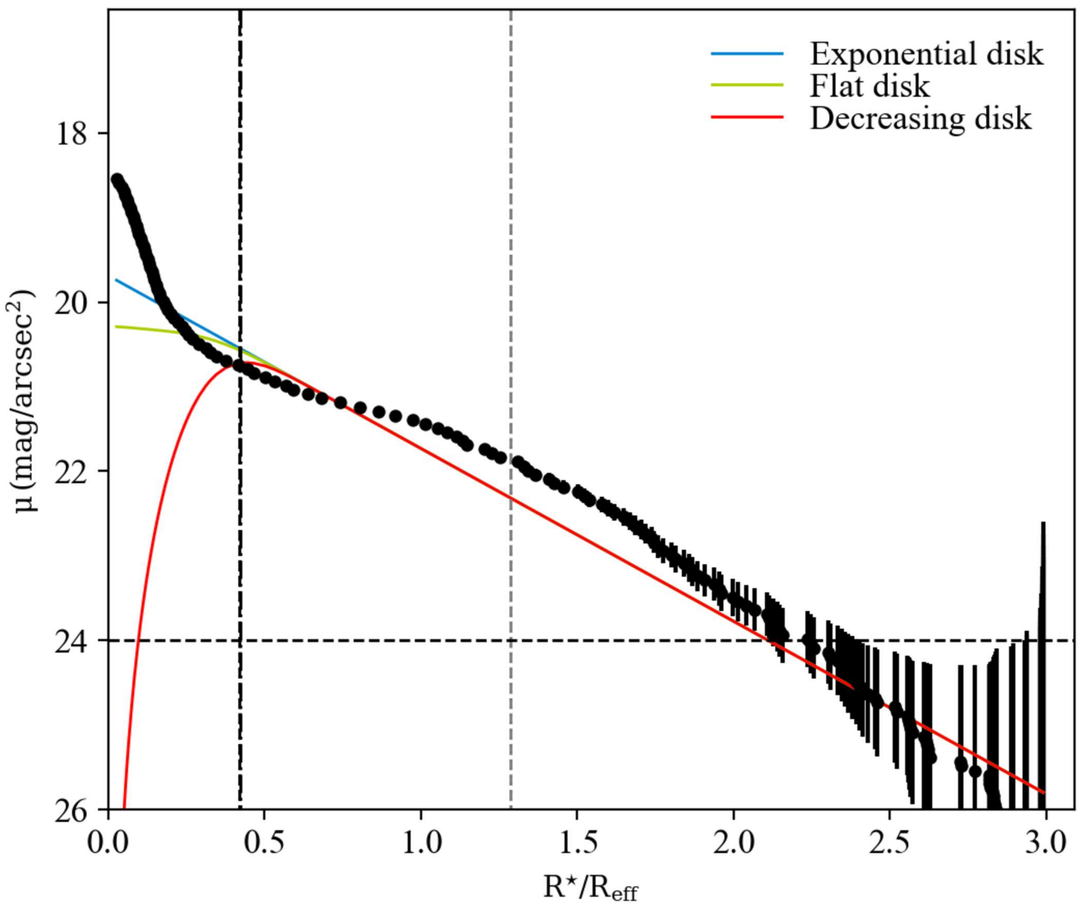
Exponential disk
Flat disk
Decreasing disk
18
20
22
24
26
μ (mag/arcsec²)
0.0
0.5
1.0
1.5
2.0
2.5
3.0
R⋆/Reff

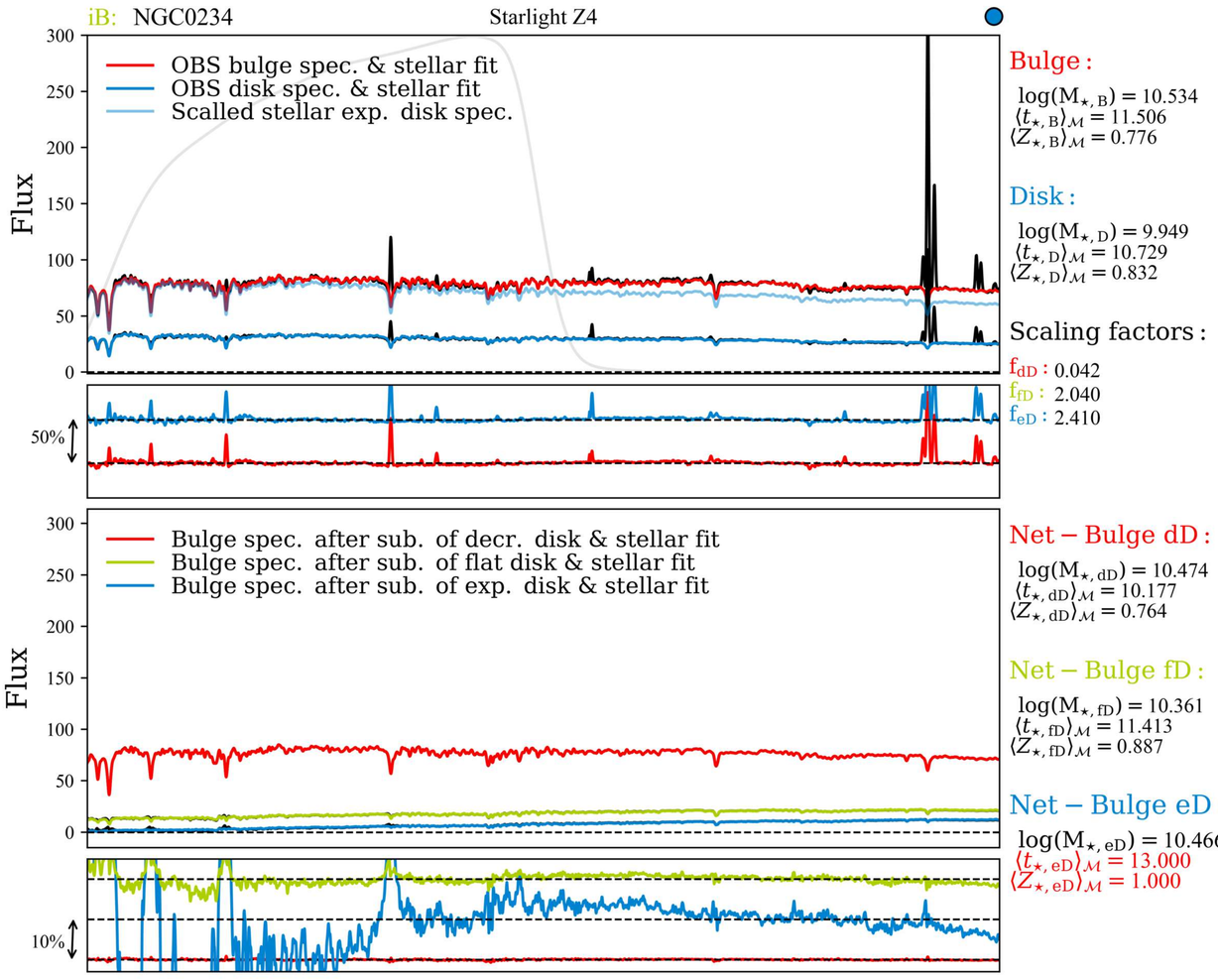
iB: NGC0234
Starlight Z4
OBS bulge spec. & stellar fit
OBS disk spec. & stellar fit
Scalled stellar exp. disk spec.
Flux
50%
Bulge :
log(M⋆, B) = 10.534
⟨t⋆, B⟩M = 11.506
⟨Z⋆, B⟩M = 0.776
Disk :
log(M⋆, D) = 9.949
⟨t⋆, D⟩M = 10.729
⟨Z⋆, D⟩M = 0.832
Scaling factors :
fdD : 0.042
ffD : 2.040
feD : 2.410
Bulge spec. after sub. of decr. disk & stellar fit
Bulge spec. after sub. of flat disk & stellar fit
Bulge spec. after sub. of exp. disk & stellar fit
10%
Net − Bulge dD :
log(M⋆, dD) = 10.474
⟨t⋆, dD⟩M = 10.177
⟨Z⋆, dD⟩M = 0.764
Net − Bulge fD :
log(M⋆, fD) = 10.361
⟨t⋆, fD⟩M = 11.413
⟨Z⋆, fD⟩M = 0.887
Net − Bulge eD :
log(M⋆, eD) = 10.466
⟨t⋆, eD⟩M = 13.000
⟨Z⋆, eD⟩M = 1.000

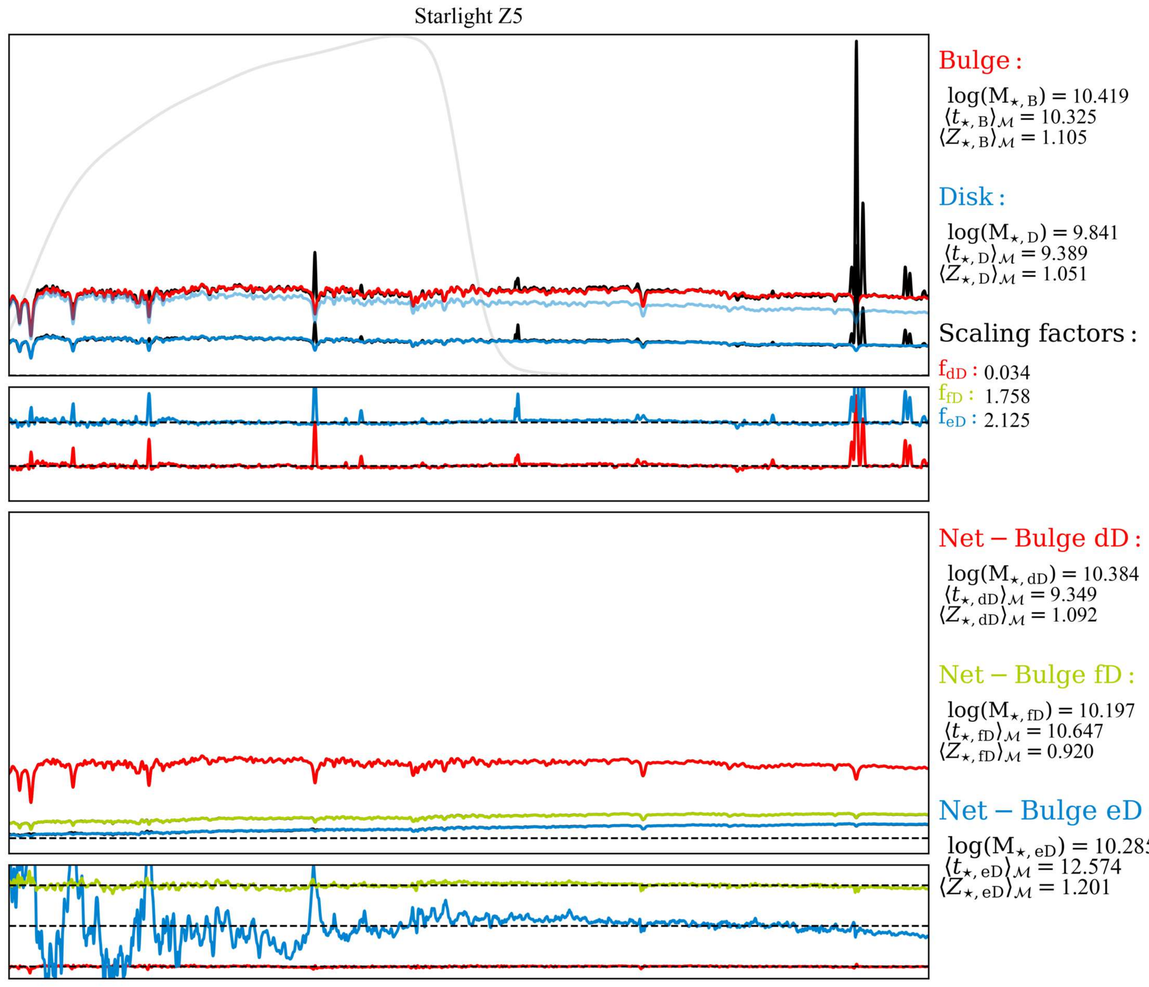
Starlight Z5
Bulge :
log(M⋆, B) = 10.419
⟨t⋆, B⟩M = 10.325
⟨Z⋆, B⟩M = 1.105
Disk :
log(M⋆, D) = 9.841
⟨t⋆, D⟩M = 9.389
⟨Z⋆, D⟩M = 1.051
Scaling factors :
fdD : 0.034
ffD : 1.758
feD : 2.125
Net − Bulge dD :
log(M⋆, dD) = 10.384
⟨t⋆, dD⟩M = 9.349
⟨Z⋆, dD⟩M = 1.092
Net − Bulge fD :
log(M⋆, fD) = 10.197
⟨t⋆, fD⟩M = 10.647
⟨Z⋆, fD⟩M = 0.920
Net − Bulge eD :
log(M⋆, eD) = 10.285
⟨t⋆, eD⟩M = 12.574
⟨Z⋆, eD⟩M = 1.201

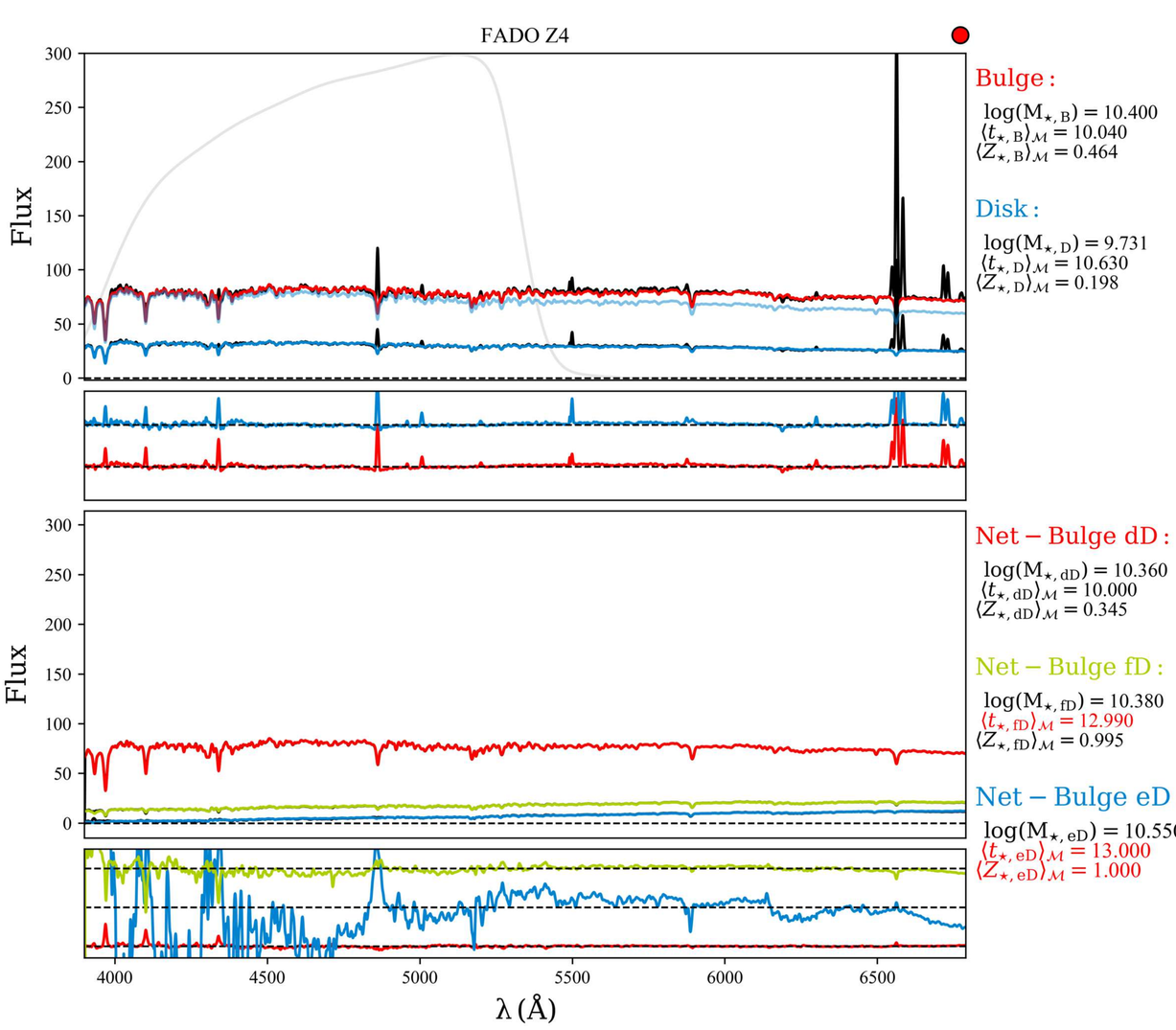
FADO Z4
Flux
Bulge :
log(M⋆, B) = 10.400
⟨t⋆, B⟩M = 10.040
⟨Z⋆, B⟩M = 0.464
Disk :
log(M⋆, D) = 9.731
⟨t⋆, D⟩M = 10.630
⟨Z⋆, D⟩M = 0.198
Net − Bulge dD :
log(M⋆, dD) = 10.360
⟨t⋆, dD⟩M = 10.000
⟨Z⋆, dD⟩M = 0.345
Net − Bulge fD :
log(M⋆, fD) = 10.380
⟨t⋆, fD⟩M = 12.990
⟨Z⋆, fD⟩M = 0.995
Net − Bulge eD :
log(M⋆, eD) = 10.550
⟨t⋆, eD⟩M = 13.000
⟨Z⋆, eD⟩M = 1.000
λ (Å)

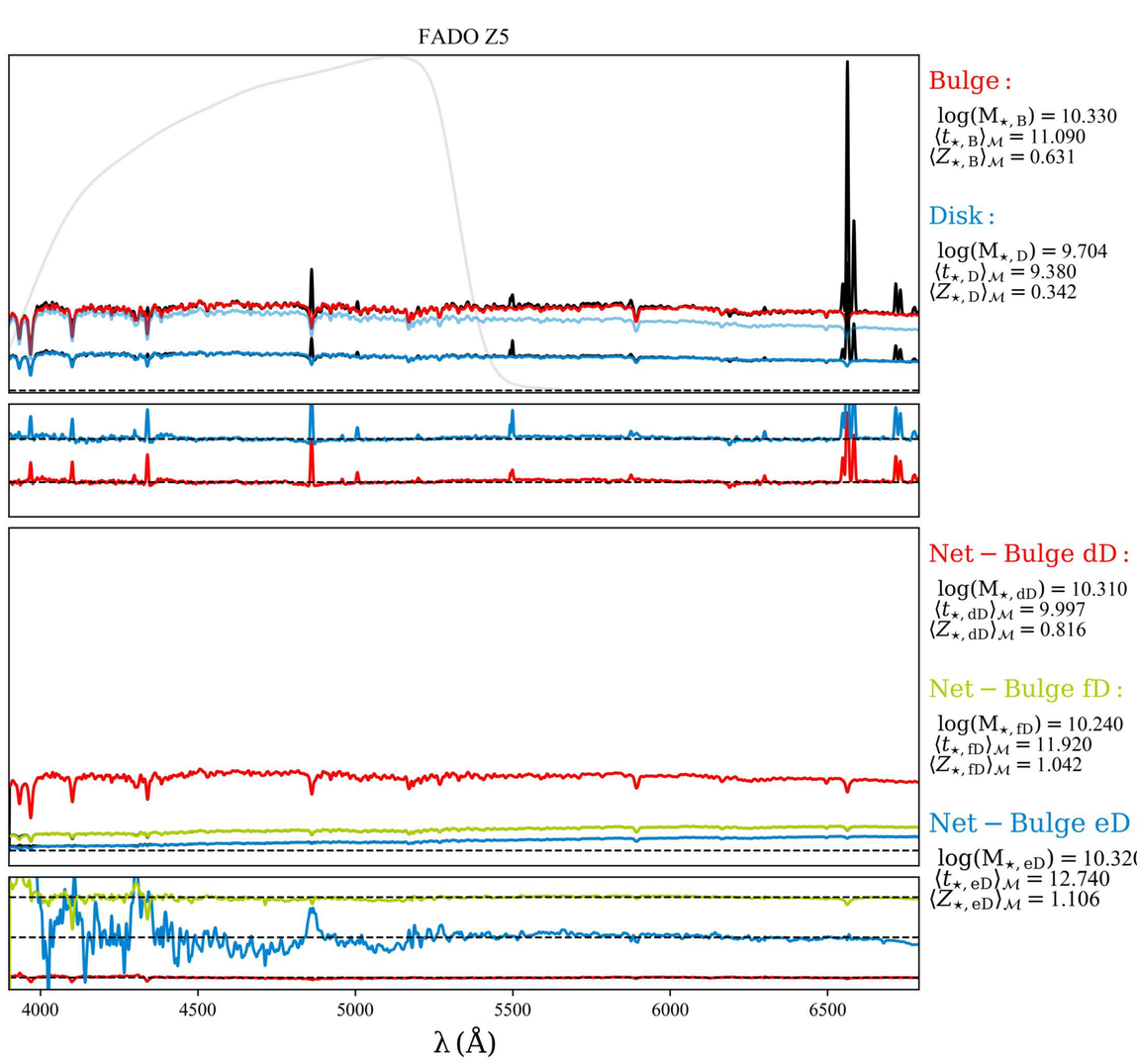
FADO Z5
Bulge :
log(M⋆, B) = 10.330
⟨t⋆, B⟩M = 11.090
⟨Z⋆, B⟩M = 0.631
Disk :
log(M⋆, D) = 9.704
⟨t⋆, D⟩M = 9.380
⟨Z⋆, D⟩M = 0.342
Net − Bulge dD :
log(M⋆, dD) = 10.310
⟨t⋆, dD⟩M = 9.997
⟨Z⋆, dD⟩M = 0.816
Net − Bulge fD :
log(M⋆, fD) = 10.240
⟨t⋆, fD⟩M = 11.920
⟨Z⋆, fD⟩M = 1.042
Net − Bulge eD :
log(M⋆, eD) = 10.320
⟨t⋆, eD⟩M = 12.740
⟨Z⋆, eD⟩M = 1.106
λ (Å)

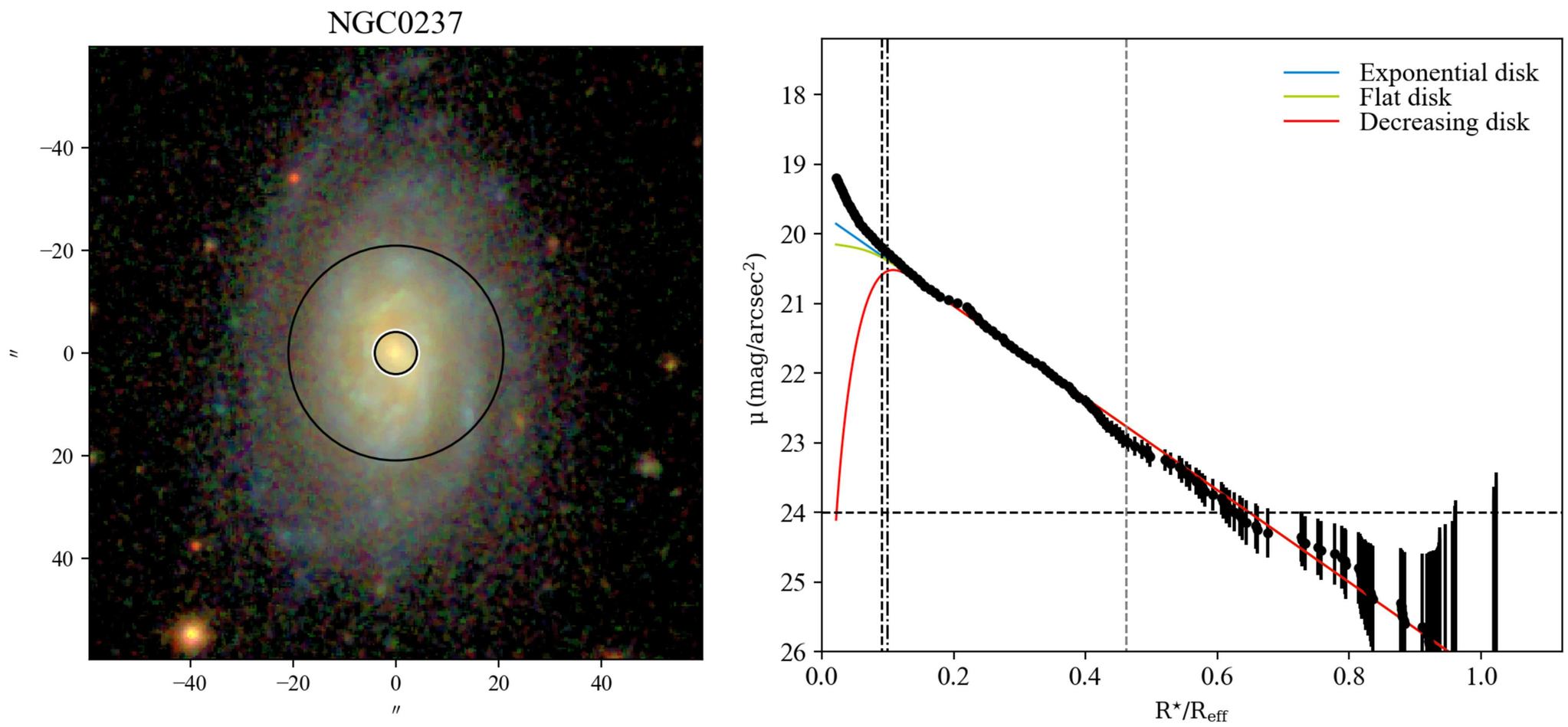
NGC0237
Exponential disk
Flat disk
Decreasing disk
μ (mag/arcsec²)
R⋆/R_eff

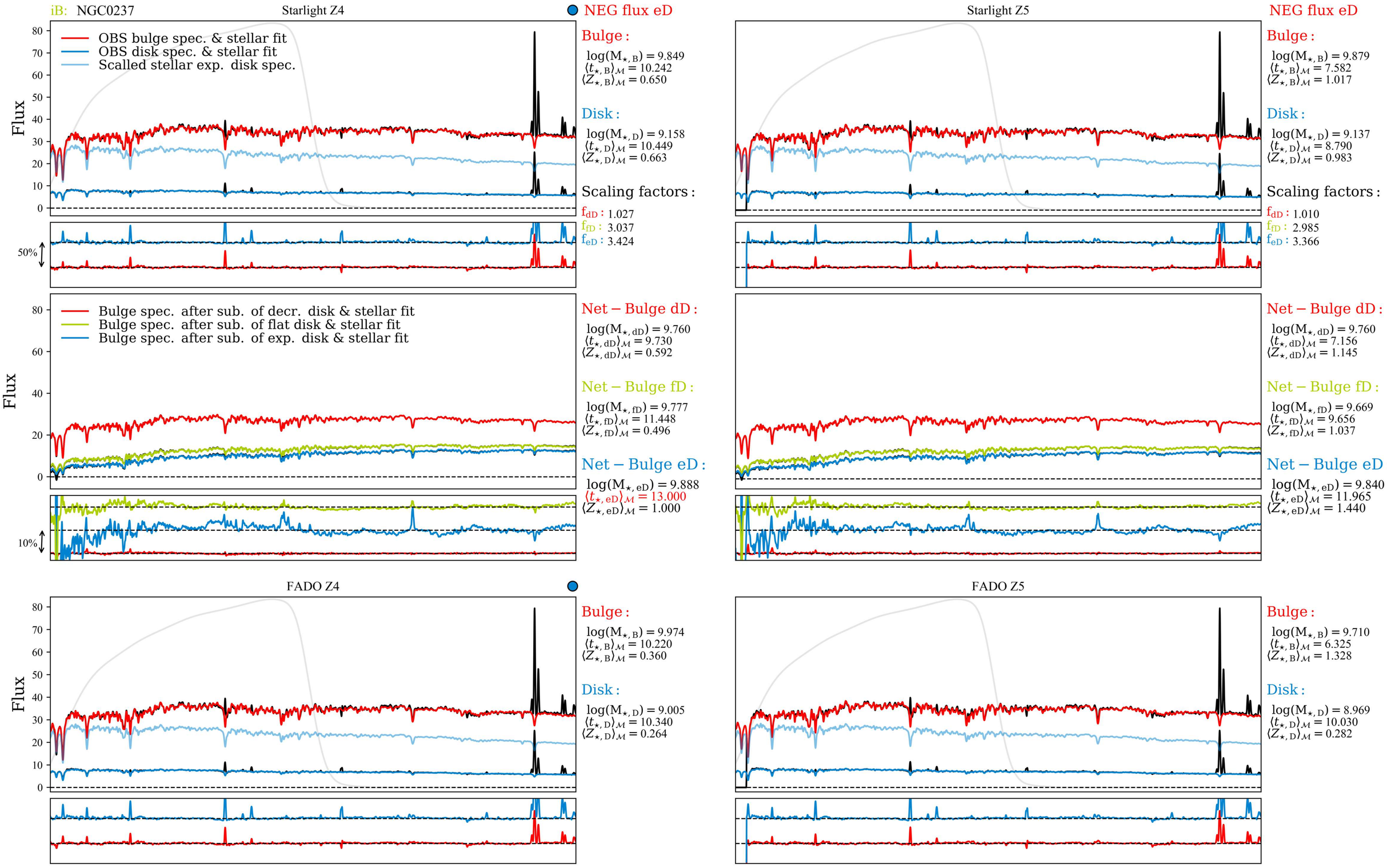
iB: NGC0237
Starlight Z4
NEG flux eD
OBS bulge spec. & stellar fit
OBS disk spec. & stellar fit
Scalled stellar exp. disk spec.
Flux
50%
Bulge :
log(M⋆, B) = 9.849
⟨t⋆, B⟩M = 10.242
⟨Z⋆, B⟩M = 0.650
Disk :
log(M⋆, D) = 9.158
⟨t⋆, D⟩M = 10.449
⟨Z⋆, D⟩M = 0.663
Scaling factors :
fdD : 1.027
ffD : 3.037
feD : 3.424
Starlight Z5
NEG flux eD
Bulge :
log(M⋆, B) = 9.879
⟨t⋆, B⟩M = 7.582
⟨Z⋆, B⟩M = 1.017
Disk :
log(M⋆, D) = 9.137
⟨t⋆, D⟩M = 8.790
⟨Z⋆, D⟩M = 0.983
Scaling factors :
fdD : 1.010
ffD : 2.985
feD : 3.366
Bulge spec. after sub. of decr. disk & stellar fit
Bulge spec. after sub. of flat disk & stellar fit
Bulge spec. after sub. of exp. disk & stellar fit
10%
Net − Bulge dD :
log(M⋆, dD) = 9.760
⟨t⋆, dD⟩M = 9.730
⟨Z⋆, dD⟩M = 0.592
Net − Bulge fD :
log(M⋆, fD) = 9.777
⟨t⋆, fD⟩M = 11.448
⟨Z⋆, fD⟩M = 0.496
Net − Bulge eD :
log(M⋆, eD) = 9.888
⟨t⋆, eD⟩M = 13.000
⟨Z⋆, eD⟩M = 1.000
Net − Bulge dD :
log(M⋆, dD) = 9.760
⟨t⋆, dD⟩M = 7.156
⟨Z⋆, dD⟩M = 1.145
Net − Bulge fD :
log(M⋆, fD) = 9.669
⟨t⋆, fD⟩M = 9.656
⟨Z⋆, fD⟩M = 1.037
Net − Bulge eD :
log(M⋆, eD) = 9.840
⟨t⋆, eD⟩M = 11.965
⟨Z⋆, eD⟩M = 1.440
FADO Z4
Bulge :
log(M⋆, B) = 9.974
⟨t⋆, B⟩M = 10.220
⟨Z⋆, B⟩M = 0.360
Disk :
log(M⋆, D) = 9.005
⟨t⋆, D⟩M = 10.340
⟨Z⋆, D⟩M = 0.264
FADO Z5
Bulge :
log(M⋆, B) = 9.710
⟨t⋆, B⟩M = 6.325
⟨Z⋆, B⟩M = 1.328
Disk :
log(M⋆, D) = 8.969
⟨t⋆, D⟩M = 10.030
⟨Z⋆, D⟩M = 0.282
Net − Bulge dD :
log(M⋆, dD) = 9.935
⟨t⋆, dD⟩M = 10.550
⟨Z⋆, dD⟩M = 0.393
Net − Bulge fD :
log(M⋆, fD) = 9.821
⟨t⋆, fD⟩M = 10.880
⟨Z⋆, fD⟩M = 0.421
Net − Bulge eD :
log(M⋆, eD) = 9.896
⟨t⋆, eD⟩M = 13.000
⟨Z⋆, eD⟩M = 0.593
Net − Bulge dD :
log(M⋆, dD) = 9.590
⟨t⋆, dD⟩M = 4.198
⟨Z⋆, dD⟩M = 1.206
Net − Bulge fD :
log(M⋆, fD) = 9.634
⟨t⋆, fD⟩M = 7.856
⟨Z⋆, fD⟩M = 1.577
Net − Bulge eD :
log(M⋆, eD) = 9.818
⟨t⋆, eD⟩M = 11.600
⟨Z⋆, eD⟩M = 1.579
λ (Å)

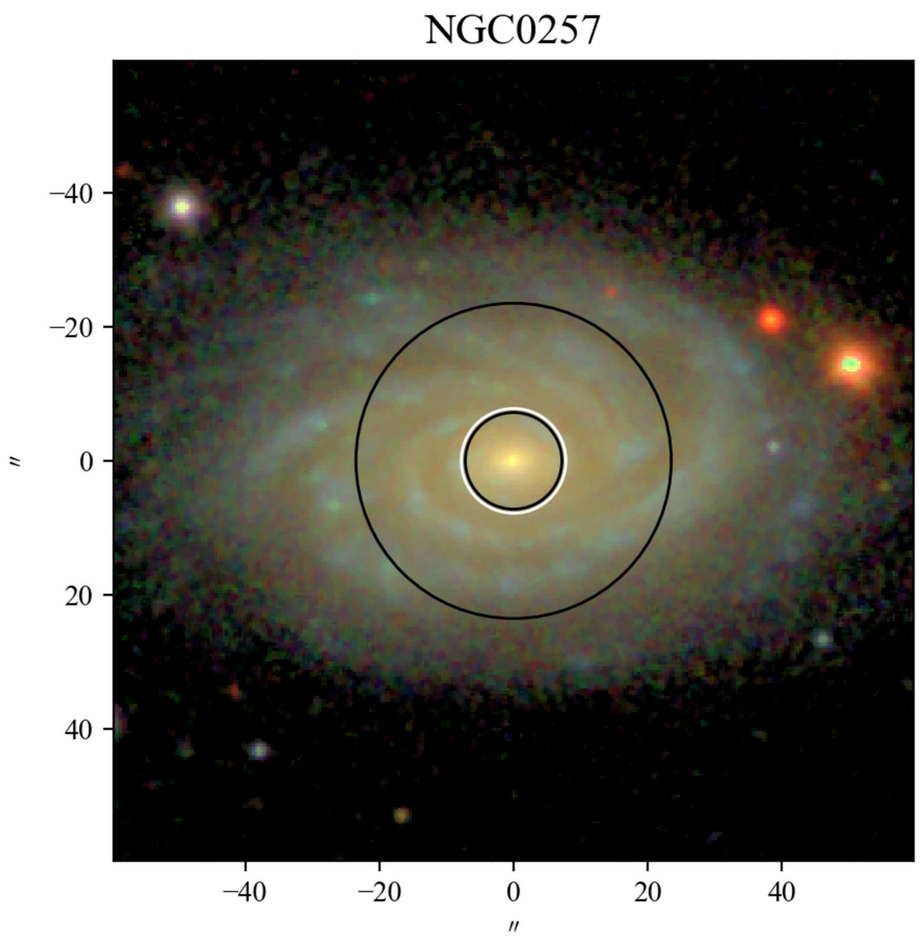
NGC0257
−40
−20
0
20
40
″
−40
−20
0
20
40
″

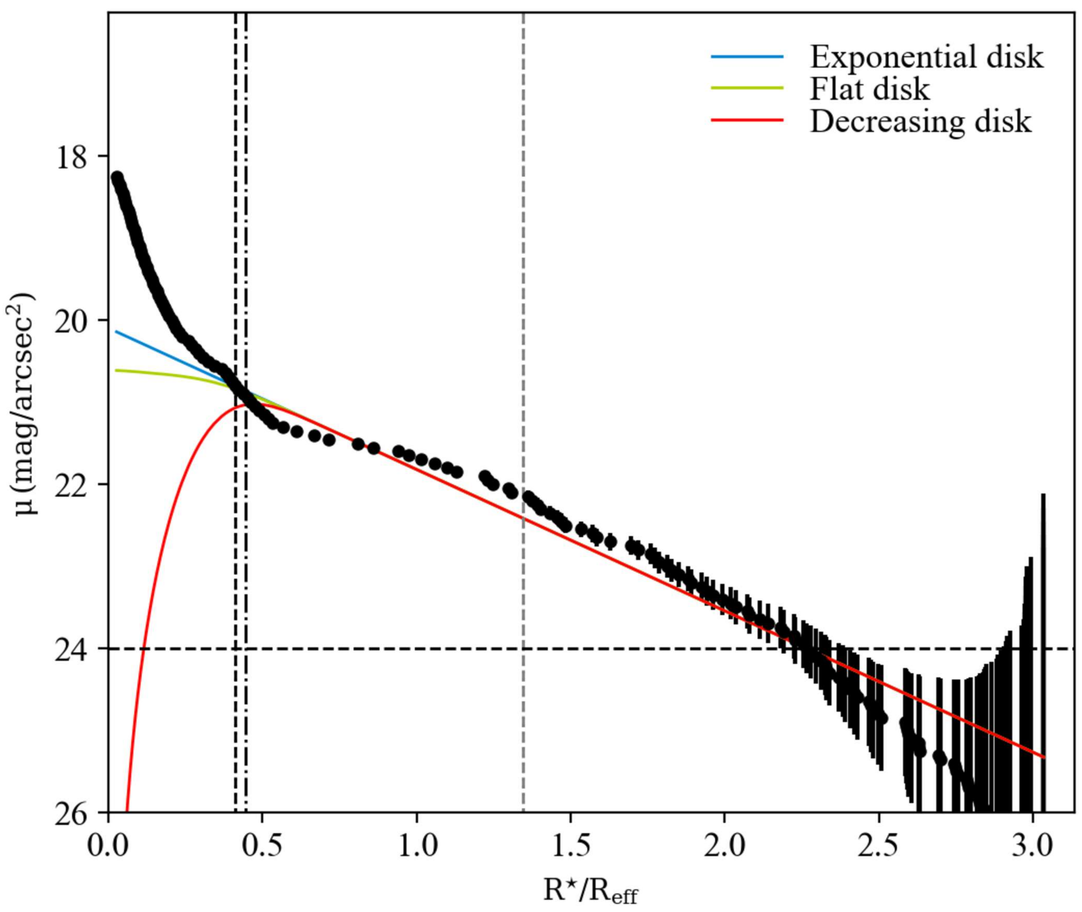
Exponential disk
Flat disk
Decreasing disk
μ (mag/arcsec²)
18
20
22
24
26
0.0
0.5
1.0
1.5
2.0
2.5
3.0
R⋆/Reff

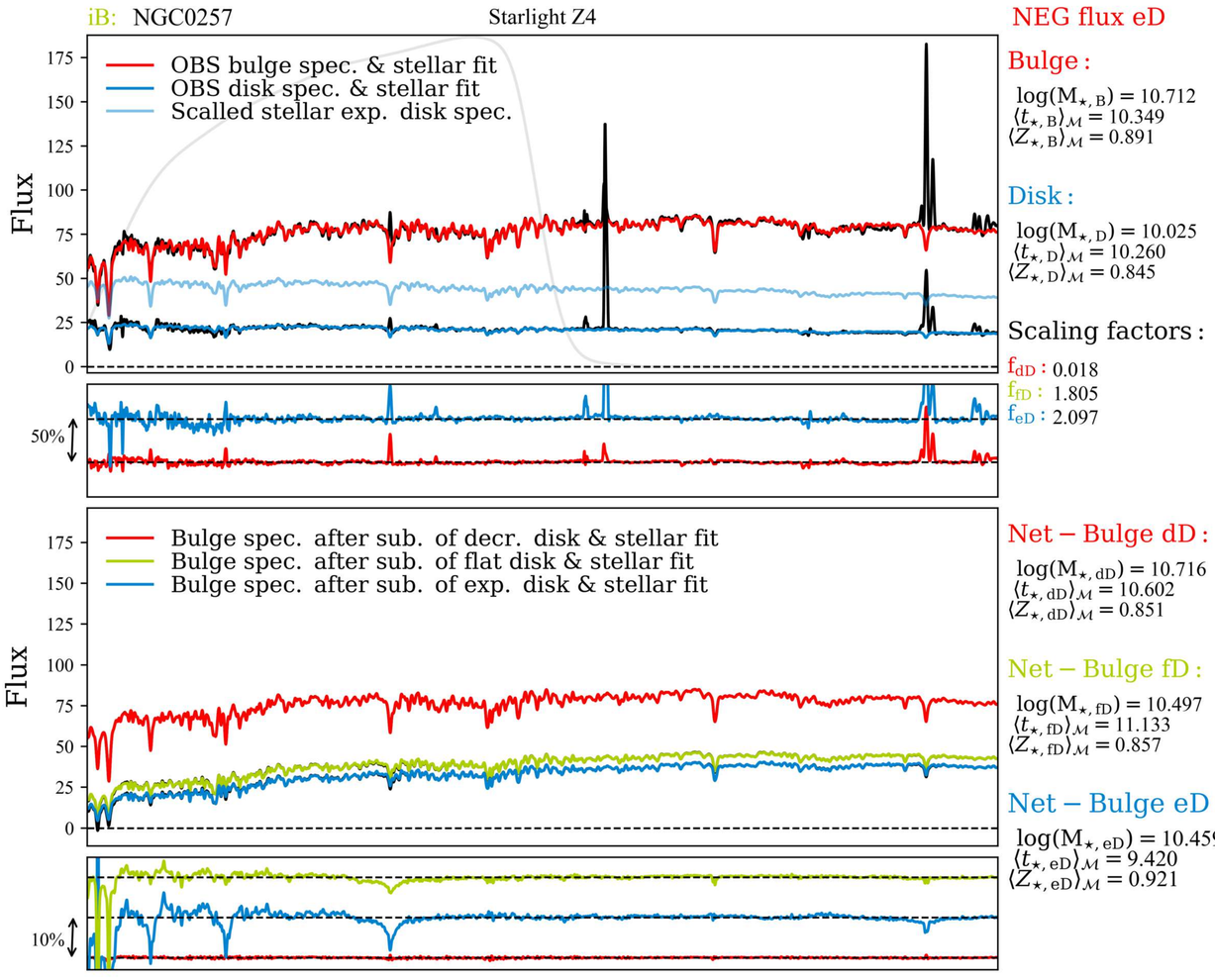
iB: NGC0257
Starlight Z4
OBS bulge spec. & stellar fit
OBS disk spec. & stellar fit
Scalled stellar exp. disk spec.
Flux
50%
Bulge spec. after sub. of decr. disk & stellar fit
Bulge spec. after sub. of flat disk & stellar fit
Bulge spec. after sub. of exp. disk & stellar fit
10%
NEG flux eD
Bulge :
log(M⋆, B) = 10.712
⟨t⋆, B⟩M = 10.349
⟨Z⋆, B⟩M = 0.891
Disk :
log(M⋆, D) = 10.025
⟨t⋆, D⟩M = 10.260
⟨Z⋆, D⟩M = 0.845
Scaling factors :
fdD : 0.018
ffD : 1.805
feD : 2.097
Net − Bulge dD :
log(M⋆, dD) = 10.716
⟨t⋆, dD⟩M = 10.602
⟨Z⋆, dD⟩M = 0.851
Net − Bulge fD :
log(M⋆, fD) = 10.497
⟨t⋆, fD⟩M = 11.133
⟨Z⋆, fD⟩M = 0.857
Net − Bulge eD :
log(M⋆, eD) = 10.459
⟨t⋆, eD⟩M = 9.420
⟨Z⋆, eD⟩M = 0.921

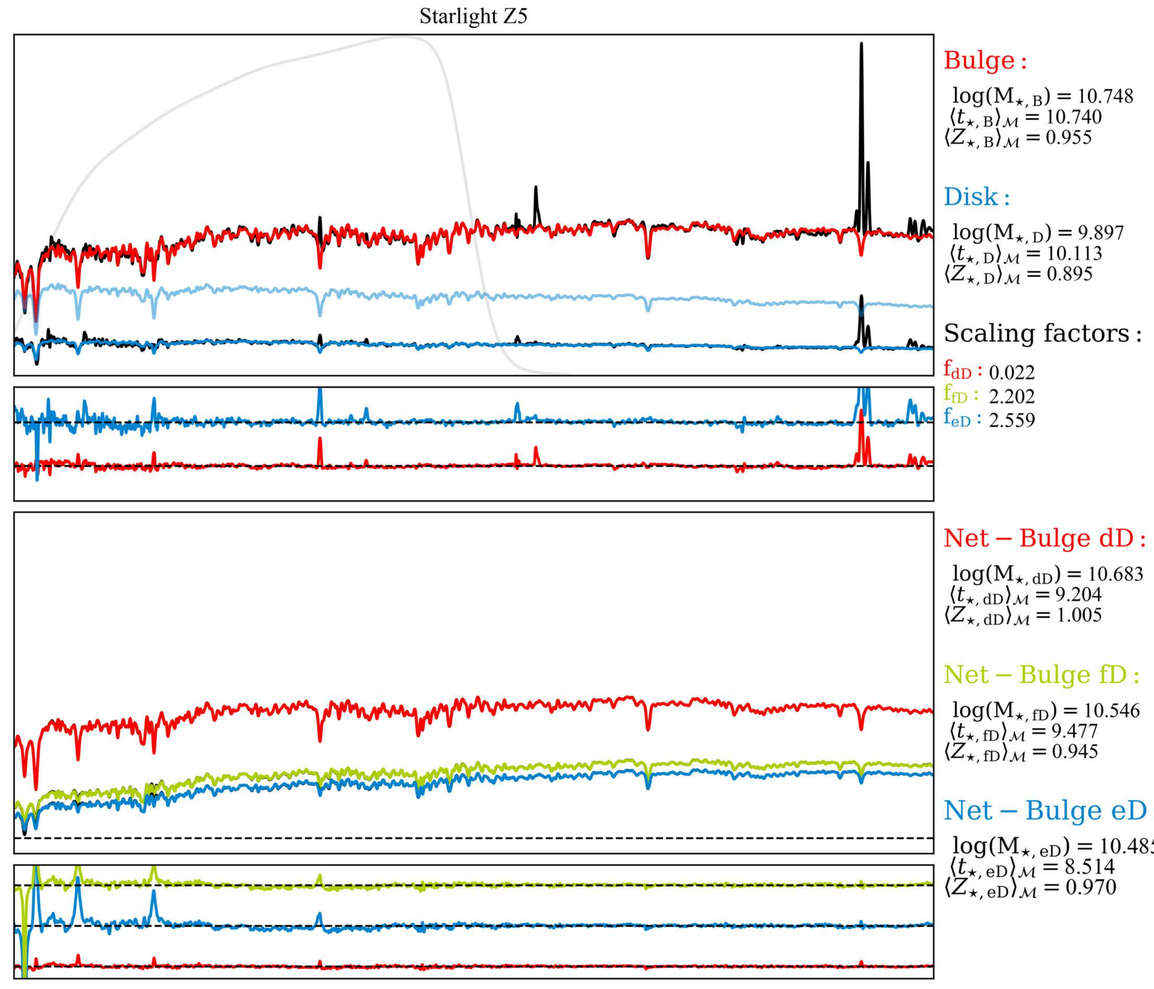
Starlight Z5
Bulge :
log(M⋆, B) = 10.748
⟨t⋆, B⟩M = 10.740
⟨Z⋆, B⟩M = 0.955
Disk :
log(M⋆, D) = 9.897
⟨t⋆, D⟩M = 10.113
⟨Z⋆, D⟩M = 0.895
Scaling factors :
fdD : 0.022
ffD : 2.202
feD : 2.559
Net − Bulge dD :
log(M⋆, dD) = 10.683
⟨t⋆, dD⟩M = 9.204
⟨Z⋆, dD⟩M = 1.005
Net − Bulge fD :
log(M⋆, fD) = 10.546
⟨t⋆, fD⟩M = 9.477
⟨Z⋆, fD⟩M = 0.945
Net − Bulge eD :
log(M⋆, eD) = 10.485
⟨t⋆, eD⟩M = 8.514
⟨Z⋆, eD⟩M = 0.970

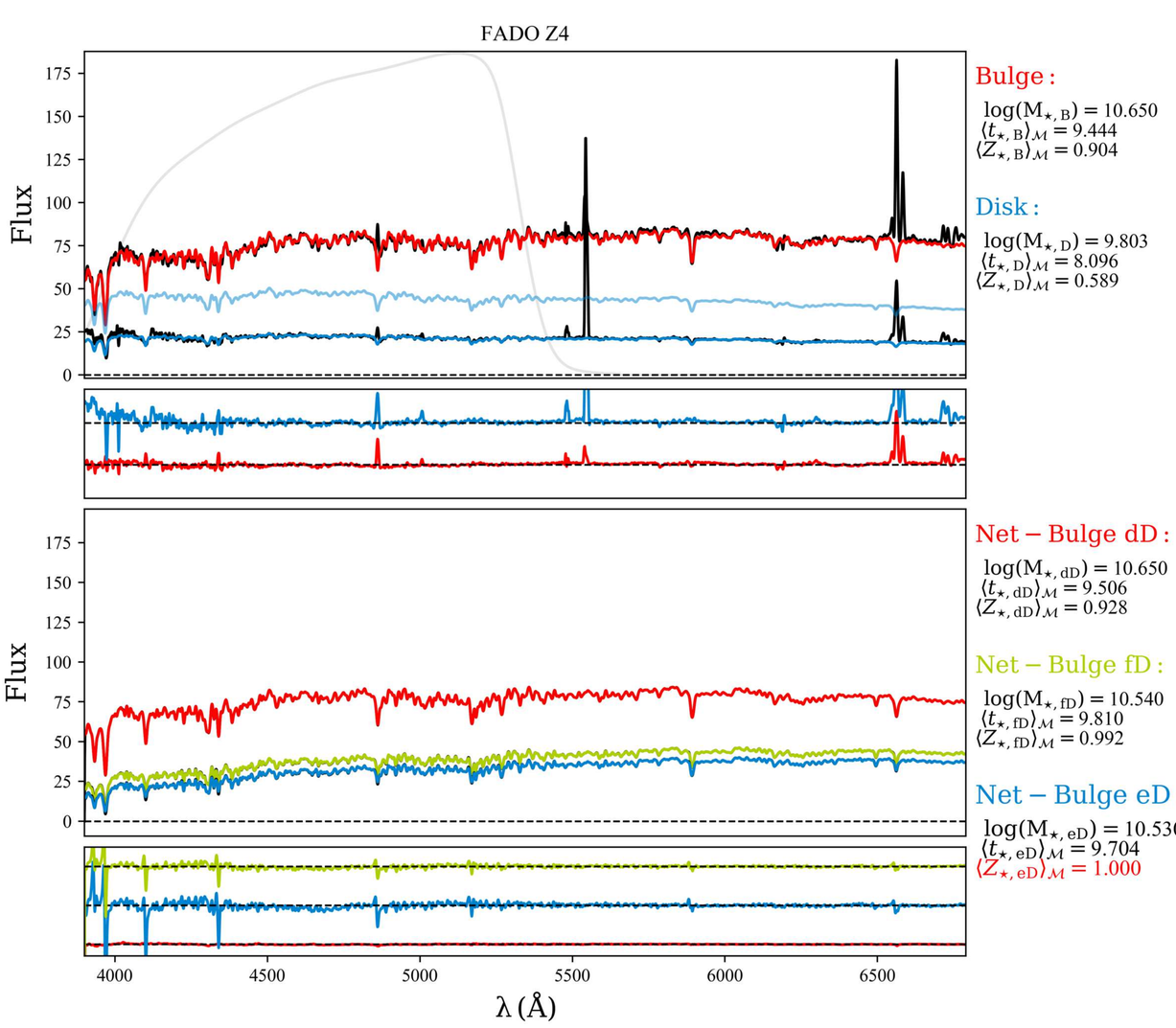
FADO Z4
Flux
Bulge :
log(M⋆, B) = 10.650
⟨t⋆, B⟩M = 9.444
⟨Z⋆, B⟩M = 0.904
Disk :
log(M⋆, D) = 9.803
⟨t⋆, D⟩M = 8.096
⟨Z⋆, D⟩M = 0.589
Net − Bulge dD :
log(M⋆, dD) = 10.650
⟨t⋆, dD⟩M = 9.506
⟨Z⋆, dD⟩M = 0.928
Net − Bulge fD :
log(M⋆, fD) = 10.540
⟨t⋆, fD⟩M = 9.810
⟨Z⋆, fD⟩M = 0.992
Net − Bulge eD :
log(M⋆, eD) = 10.530
⟨t⋆, eD⟩M = 9.704
⟨Z⋆, eD⟩M = 1.000
λ (Å)

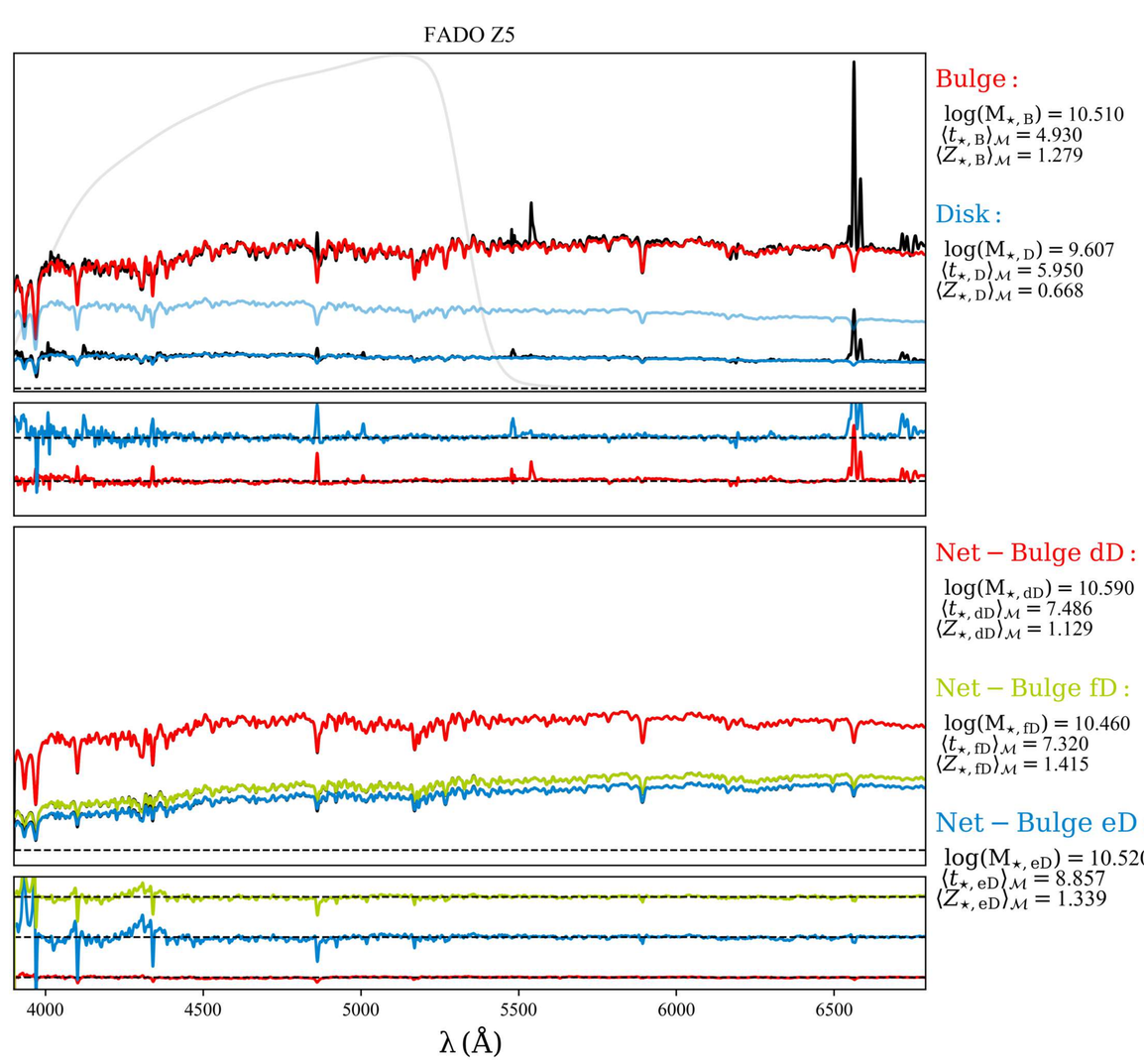
FADO Z5
Bulge :
log(M⋆, B) = 10.510
⟨t⋆, B⟩M = 4.930
⟨Z⋆, B⟩M = 1.279
Disk :
log(M⋆, D) = 9.607
⟨t⋆, D⟩M = 5.950
⟨Z⋆, D⟩M = 0.668
Net − Bulge dD :
log(M⋆, dD) = 10.590
⟨t⋆, dD⟩M = 7.486
⟨Z⋆, dD⟩M = 1.129
Net − Bulge fD :
log(M⋆, fD) = 10.460
⟨t⋆, fD⟩M = 7.320
⟨Z⋆, fD⟩M = 1.415
Net − Bulge eD :
log(M⋆, eD) = 10.520
⟨t⋆, eD⟩M = 8.857
⟨Z⋆, eD⟩M = 1.339
λ (Å)

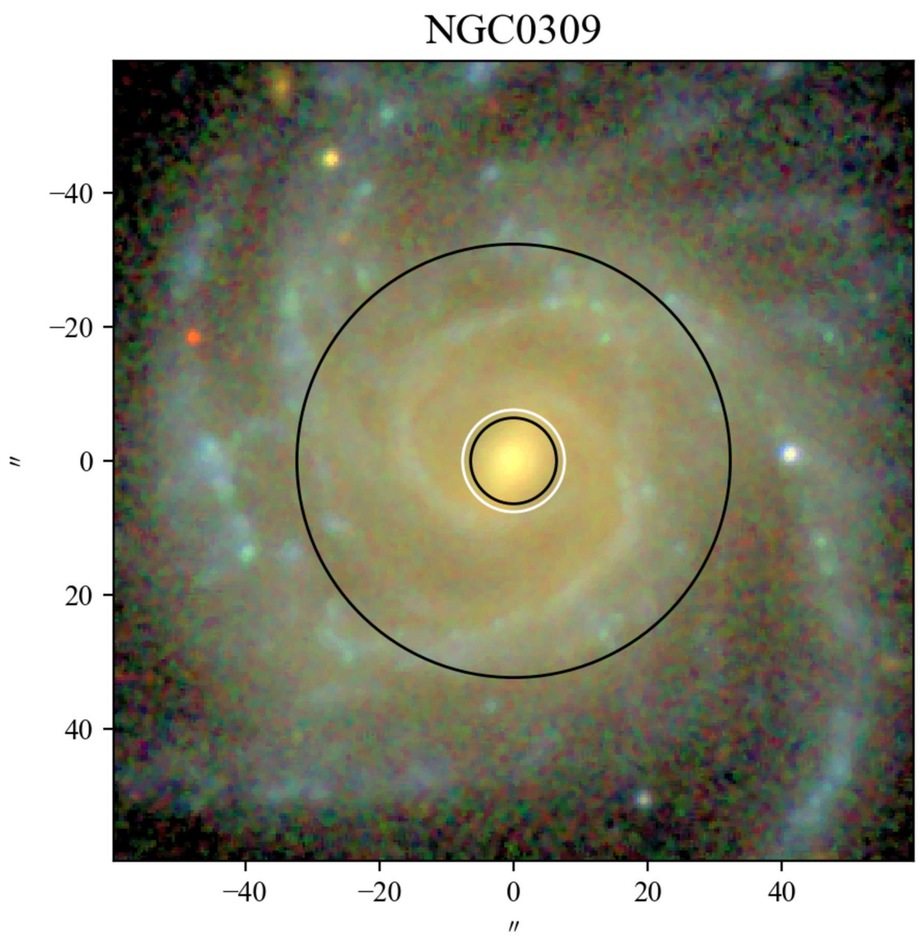
NGC0309
−40
−20
0
20
40
″
−40
−20
0
20
40
″

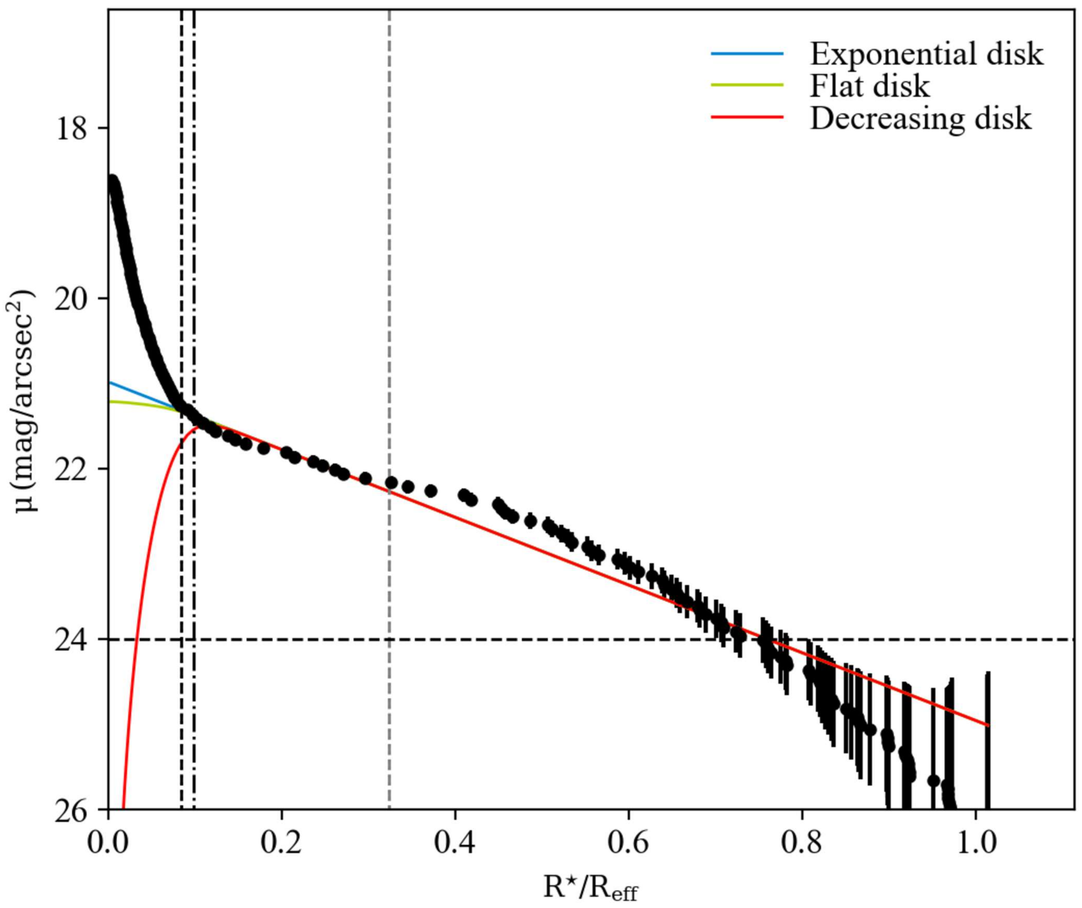
Exponential disk
Flat disk
Decreasing disk
μ (mag/arcsec²)
18
20
22
24
26
0.0
0.2
0.4
0.6
0.8
1.0
R⋆/Reff

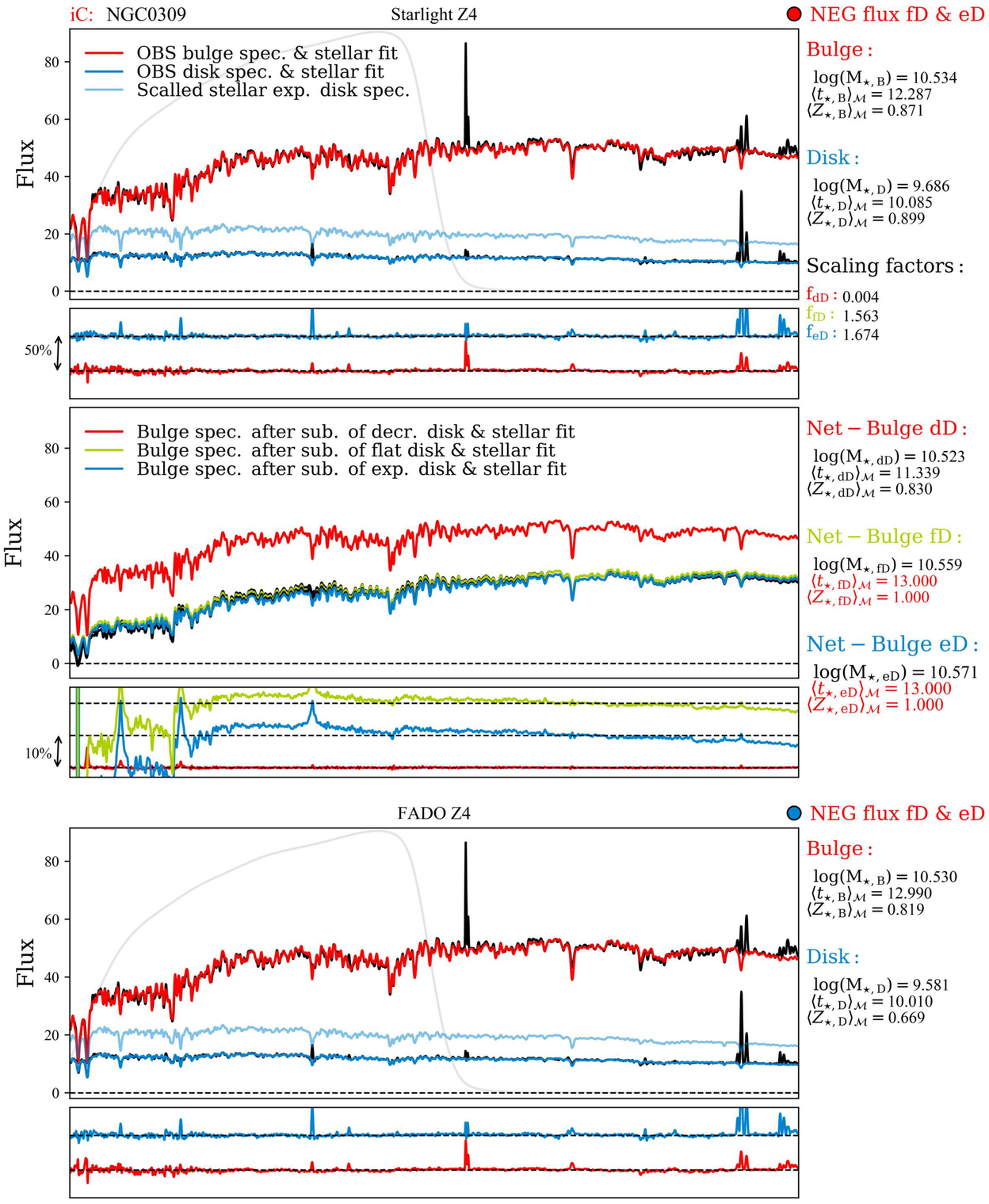
iC: NGC0309
Starlight Z4
NEG flux fD & eD
OBS bulge spec. & stellar fit
OBS disk spec. & stellar fit
Scalled stellar exp. disk spec.
Flux
50%
Bulge :
log(M⋆, B) = 10.534
⟨t⋆, B⟩M = 12.287
⟨Z⋆, B⟩M = 0.871
Disk :
log(M⋆, D) = 9.686
⟨t⋆, D⟩M = 10.085
⟨Z⋆, D⟩M = 0.899
Scaling factors :
fdD : 0.004
ffD : 1.563
feD : 1.674
Bulge spec. after sub. of decr. disk & stellar fit
Bulge spec. after sub. of flat disk & stellar fit
Bulge spec. after sub. of exp. disk & stellar fit
10%
Net − Bulge dD :
log(M⋆, dD) = 10.523
⟨t⋆, dD⟩M = 11.339
⟨Z⋆, dD⟩M = 0.830
Net − Bulge fD :
log(M⋆, fD) = 10.559
⟨t⋆, fD⟩M = 13.000
⟨Z⋆, fD⟩M = 1.000
Net − Bulge eD :
log(M⋆, eD) = 10.571
⟨t⋆, eD⟩M = 13.000
⟨Z⋆, eD⟩M = 1.000

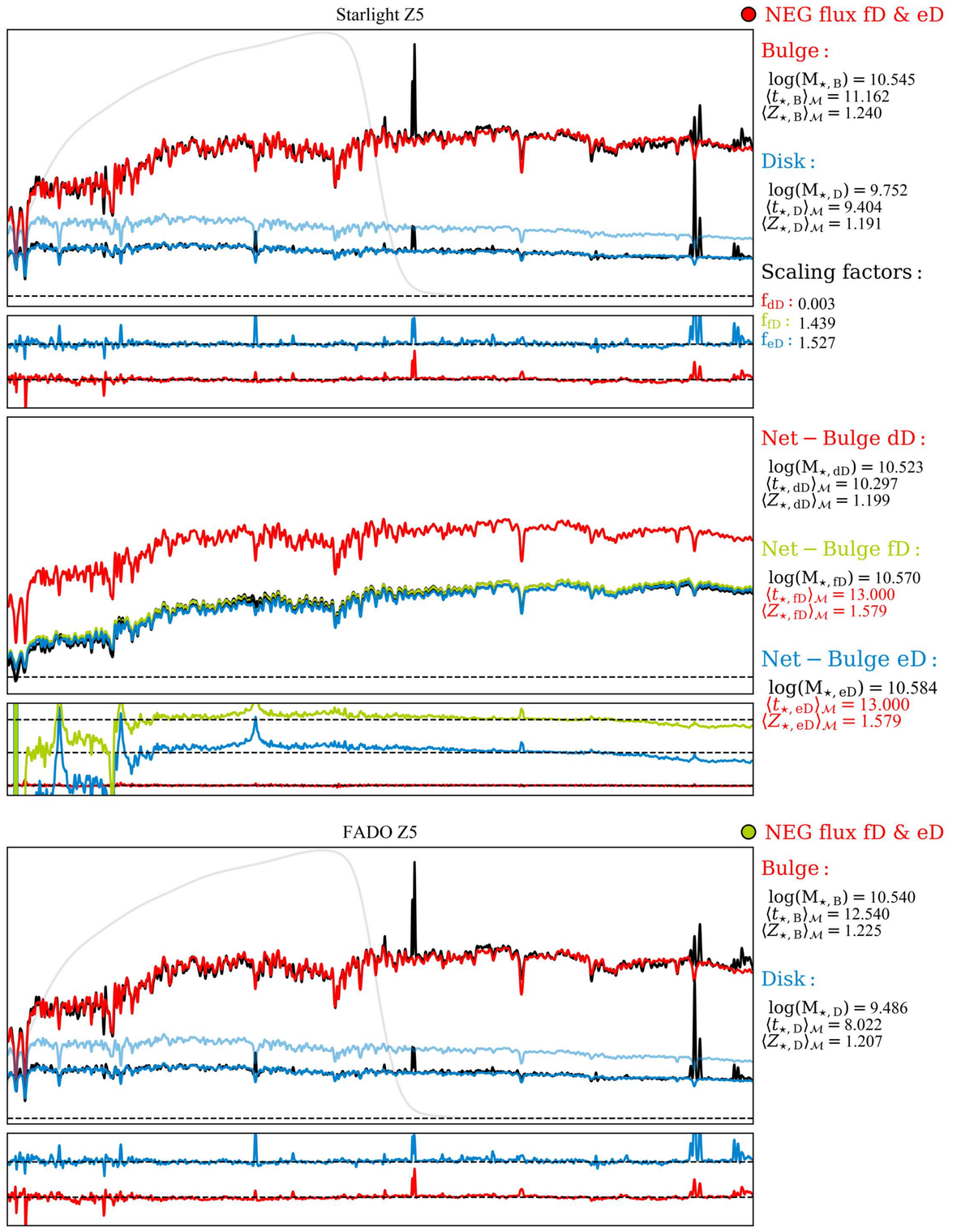
Starlight Z5
NEG flux fD & eD
Bulge :
log(M⋆, B) = 10.545
⟨t⋆, B⟩M = 11.162
⟨Z⋆, B⟩M = 1.240
Disk :
log(M⋆, D) = 9.752
⟨t⋆, D⟩M = 9.404
⟨Z⋆, D⟩M = 1.191
Scaling factors :
fdD : 0.003
ffD : 1.439
feD : 1.527
Net − Bulge dD :
log(M⋆, dD) = 10.523
⟨t⋆, dD⟩M = 10.297
⟨Z⋆, dD⟩M = 1.199
Net − Bulge fD :
log(M⋆, fD) = 10.570
⟨t⋆, fD⟩M = 13.000
⟨Z⋆, fD⟩M = 1.579
Net − Bulge eD :
log(M⋆, eD) = 10.584
⟨t⋆, eD⟩M = 13.000
⟨Z⋆, eD⟩M = 1.579

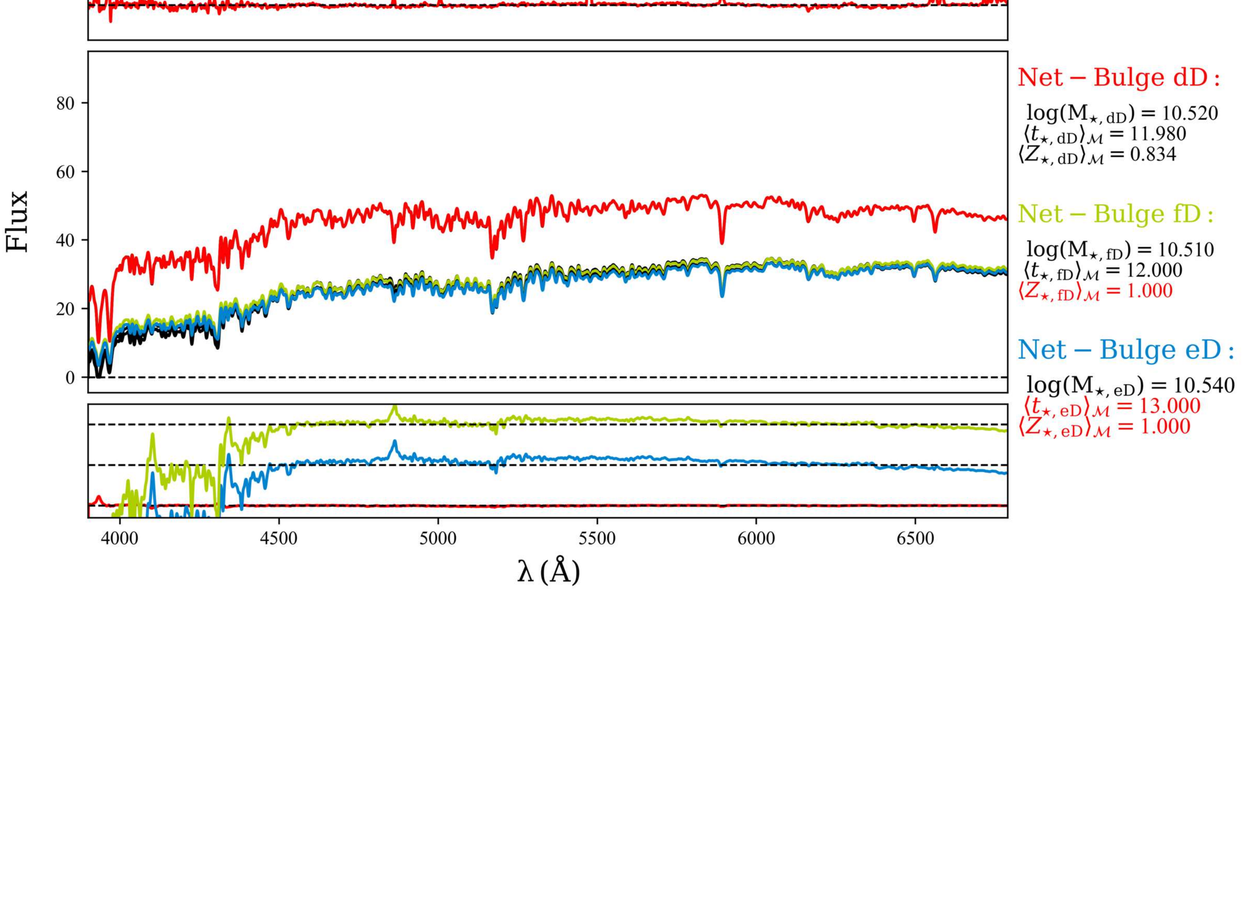
FADO Z4
NEG flux fD & eD
Flux
Bulge :
log(M⋆, B) = 10.530
⟨t⋆, B⟩M = 12.990
⟨Z⋆, B⟩M = 0.819
Disk :
log(M⋆, D) = 9.581
⟨t⋆, D⟩M = 10.010
⟨Z⋆, D⟩M = 0.669
Net − Bulge dD :
log(M⋆, dD) = 10.520
⟨t⋆, dD⟩M = 11.980
⟨Z⋆, dD⟩M = 0.834
Net − Bulge fD :
log(M⋆, fD) = 10.510
⟨t⋆, fD⟩M = 12.000
⟨Z⋆, fD⟩M = 1.000
Net − Bulge eD :
log(M⋆, eD) = 10.540
⟨t⋆, eD⟩M = 13.000
⟨Z⋆, eD⟩M = 1.000
λ (Å)

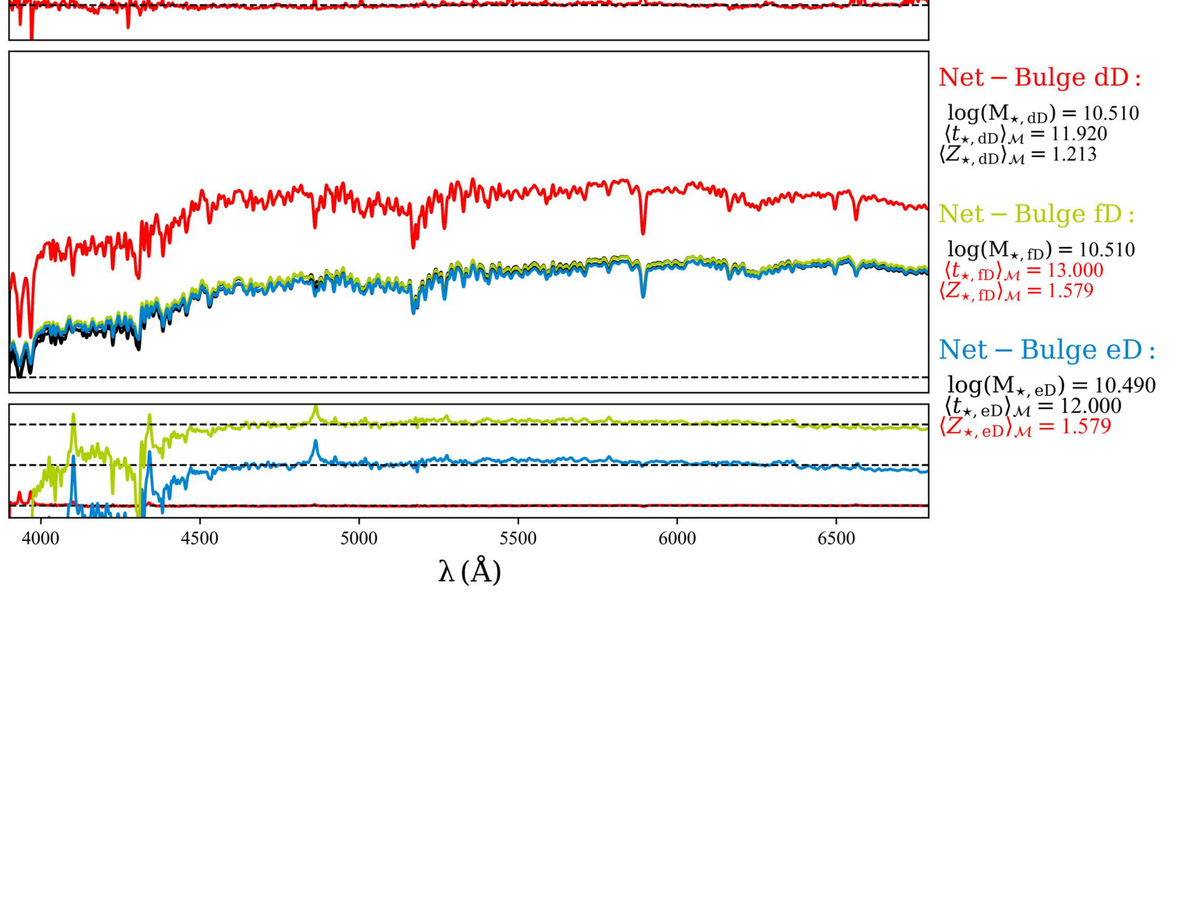
FADO Z5
NEG flux fD & eD
Bulge :
log(M⋆, B) = 10.540
⟨t⋆, B⟩M = 12.540
⟨Z⋆, B⟩M = 1.225
Disk :
log(M⋆, D) = 9.486
⟨t⋆, D⟩M = 8.022
⟨Z⋆, D⟩M = 1.207
Net − Bulge dD :
log(M⋆, dD) = 10.510
⟨t⋆, dD⟩M = 11.920
⟨Z⋆, dD⟩M = 1.213
Net − Bulge fD :
log(M⋆, fD) = 10.510
⟨t⋆, fD⟩M = 13.000
⟨Z⋆, fD⟩M = 1.579
Net − Bulge eD :
log(M⋆, eD) = 10.490
⟨t⋆, eD⟩M = 12.000
⟨Z⋆, eD⟩M = 1.579
λ (Å)

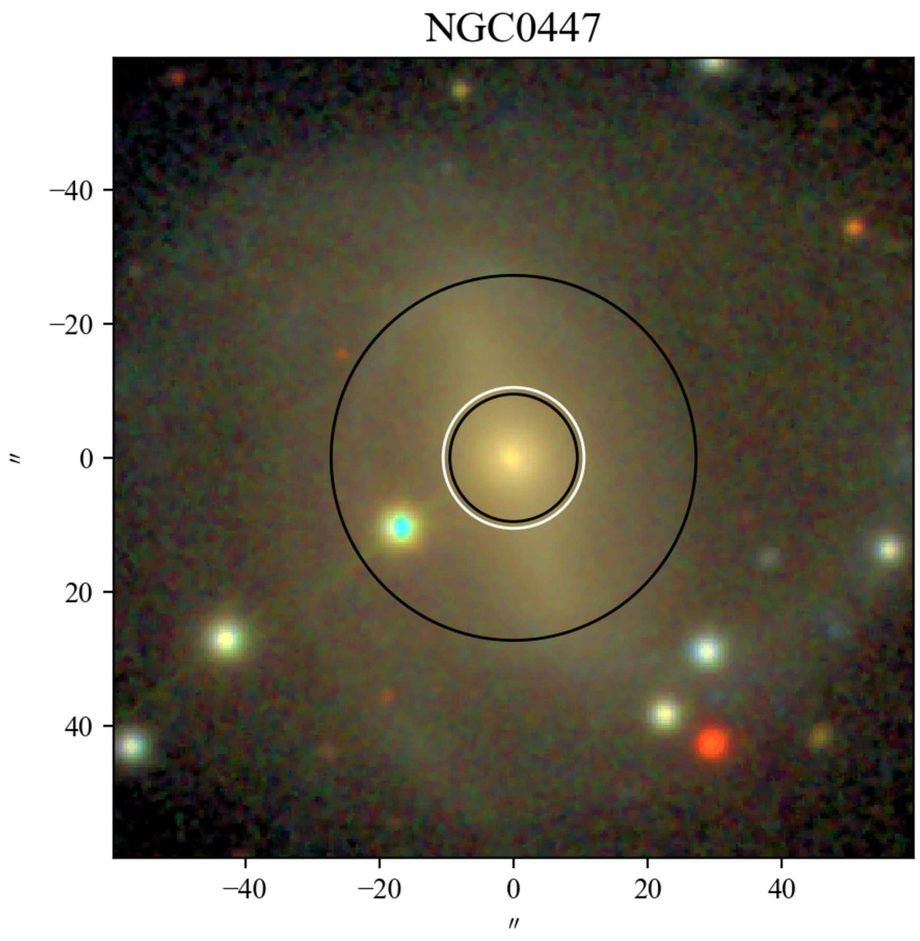
NGC0447
−40
−20
0
20
40
″
−40
−20
0
20
40
″

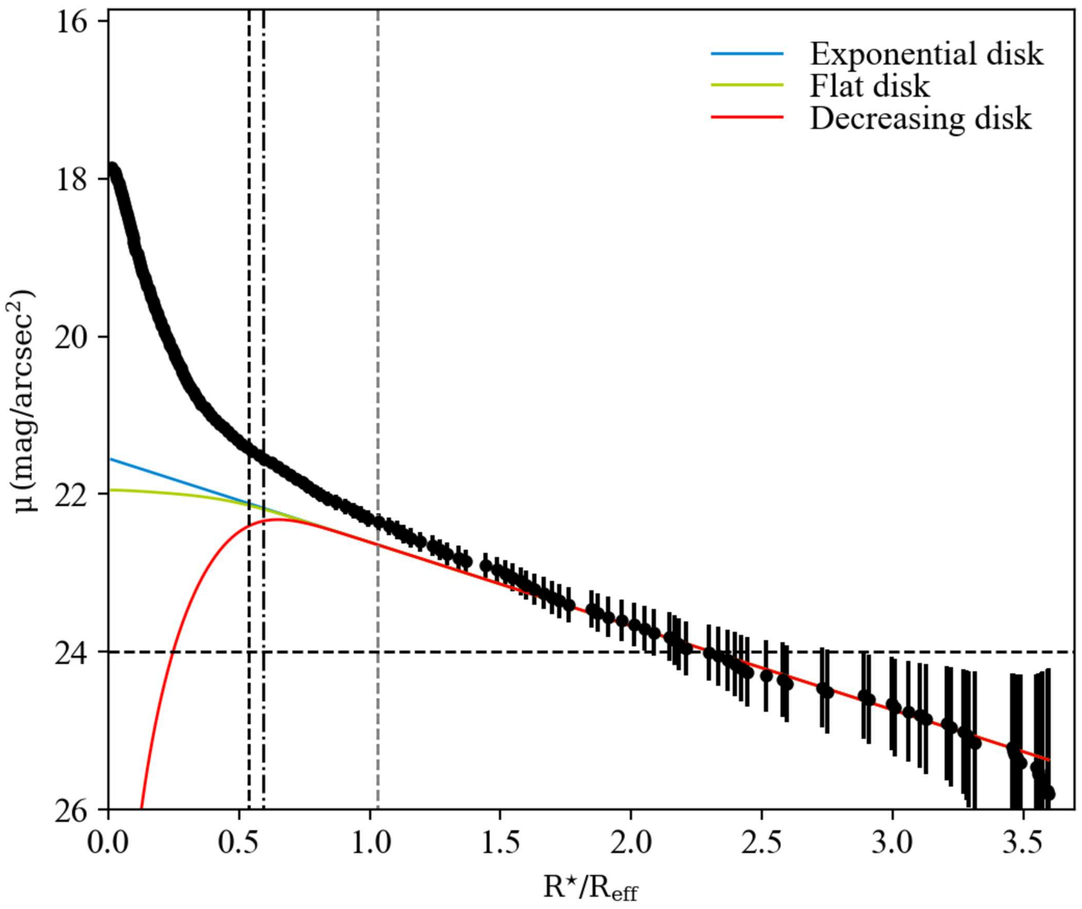
Exponential disk
Flat disk
Decreasing disk
μ (mag/arcsec²)
16
18
20
22
24
26
0.0
0.5
1.0
1.5
2.0
2.5
3.0
3.5
R⋆/Reff

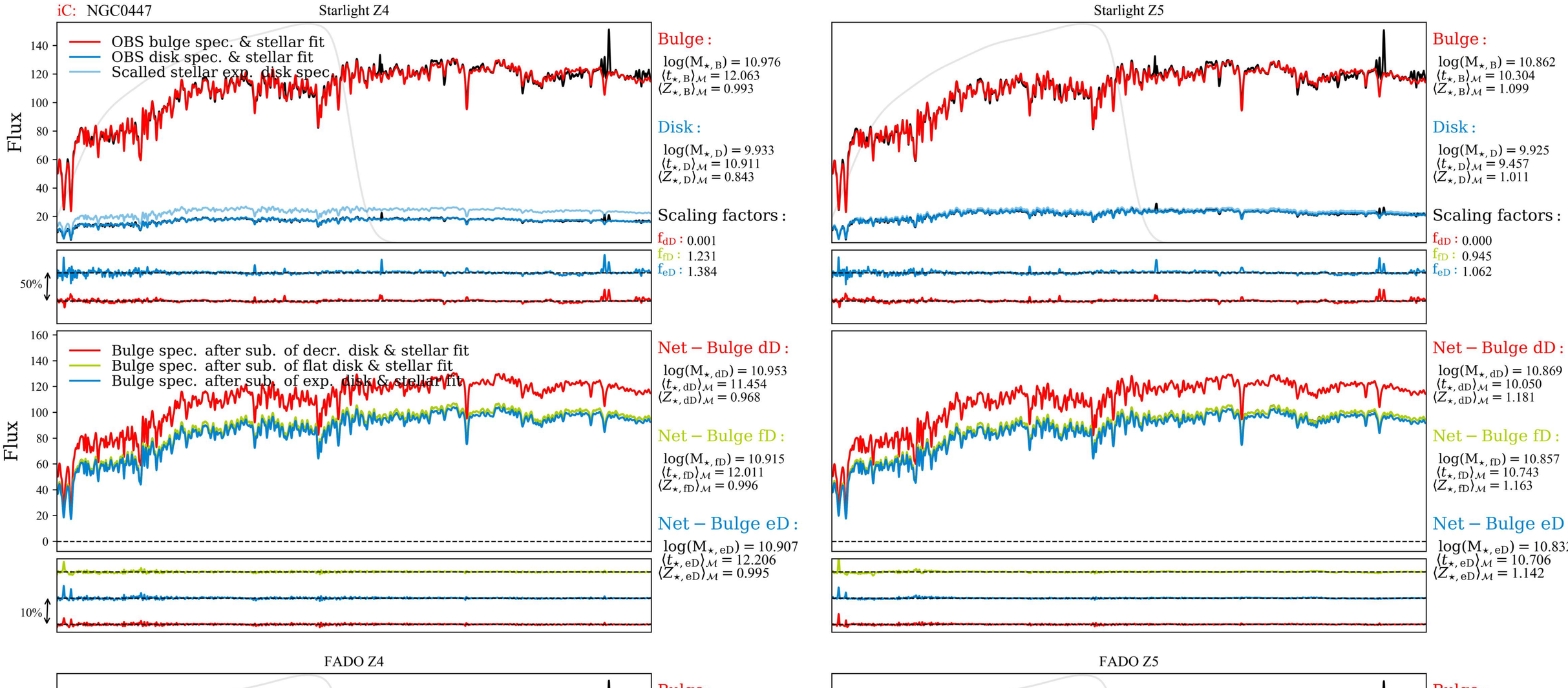
iC: NGC0447
Starlight Z4
OBS bulge spec. & stellar fit
OBS disk spec. & stellar fit
Scalled stellar exp. disk spec.
Flux
50%
Bulge spec. after sub. of decr. disk & stellar fit
Bulge spec. after sub. of flat disk & stellar fit
Bulge spec. after sub. of exp. disk & stellar fit
10%
Bulge :
log(M⋆, B) = 10.976
⟨t⋆, B⟩M = 12.063
⟨Z⋆, B⟩M = 0.993
Disk :
log(M⋆, D) = 9.933
⟨t⋆, D⟩M = 10.911
⟨Z⋆, D⟩M = 0.843
Scaling factors :
fdD : 0.001
ffD : 1.231
feD : 1.384
Net − Bulge dD :
log(M⋆, dD) = 10.953
⟨t⋆, dD⟩M = 11.454
⟨Z⋆, dD⟩M = 0.968
Net − Bulge fD :
log(M⋆, fD) = 10.915
⟨t⋆, fD⟩M = 12.011
⟨Z⋆, fD⟩M = 0.996
Net − Bulge eD :
log(M⋆, eD) = 10.907
⟨t⋆, eD⟩M = 12.206
⟨Z⋆, eD⟩M = 0.995

Starlight Z5
Bulge :
log(M⋆, B) = 10.862
⟨t⋆, B⟩M = 10.304
⟨Z⋆, B⟩M = 1.099
Disk :
log(M⋆, D) = 9.925
⟨t⋆, D⟩M = 9.457
⟨Z⋆, D⟩M = 1.011
Scaling factors :
fdD : 0.000
ffD : 0.945
feD : 1.062
Net − Bulge dD :
log(M⋆, dD) = 10.869
⟨t⋆, dD⟩M = 10.050
⟨Z⋆, dD⟩M = 1.181
Net − Bulge fD :
log(M⋆, fD) = 10.857
⟨t⋆, fD⟩M = 10.743
⟨Z⋆, fD⟩M = 1.163
Net − Bulge eD :
log(M⋆, eD) = 10.832
⟨t⋆, eD⟩M = 10.706
⟨Z⋆, eD⟩M = 1.142

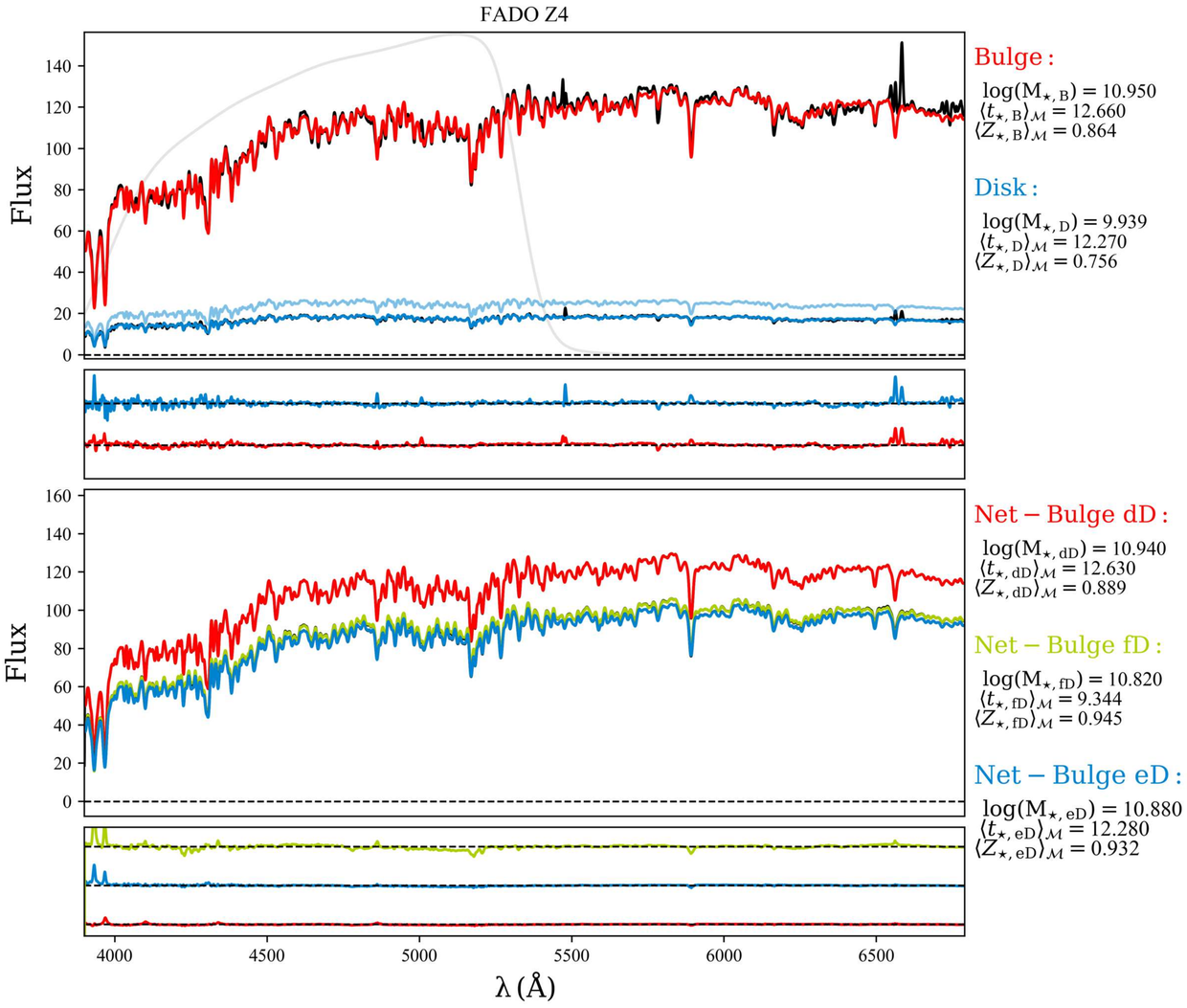
FADO Z4
Flux
Bulge :
log(M⋆, B) = 10.950
⟨t⋆, B⟩M = 12.660
⟨Z⋆, B⟩M = 0.864
Disk :
log(M⋆, D) = 9.939
⟨t⋆, D⟩M = 12.270
⟨Z⋆, D⟩M = 0.756
Net − Bulge dD :
log(M⋆, dD) = 10.940
⟨t⋆, dD⟩M = 12.630
⟨Z⋆, dD⟩M = 0.889
Net − Bulge fD :
log(M⋆, fD) = 10.820
⟨t⋆, fD⟩M = 9.344
⟨Z⋆, fD⟩M = 0.945
Net − Bulge eD :
log(M⋆, eD) = 10.880
⟨t⋆, eD⟩M = 12.280
⟨Z⋆, eD⟩M = 0.932
λ (Å)

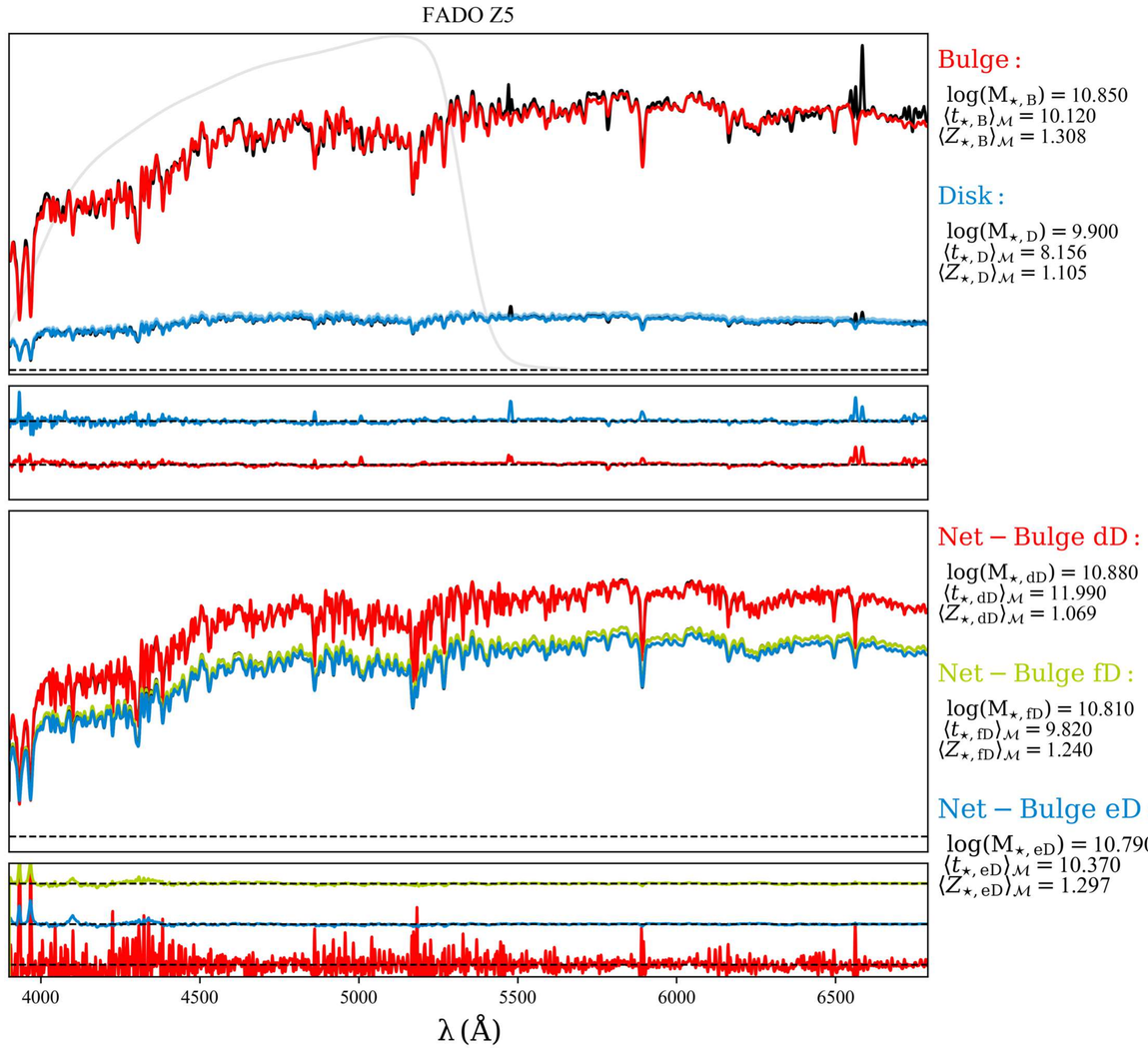
FADO Z5
Bulge :
log(M⋆, B) = 10.850
⟨t⋆, B⟩M = 10.120
⟨Z⋆, B⟩M = 1.308
Disk :
log(M⋆, D) = 9.900
⟨t⋆, D⟩M = 8.156
⟨Z⋆, D⟩M = 1.105
Net − Bulge dD :
log(M⋆, dD) = 10.880
⟨t⋆, dD⟩M = 11.990
⟨Z⋆, dD⟩M = 1.069
Net − Bulge fD :
log(M⋆, fD) = 10.810
⟨t⋆, fD⟩M = 9.820
⟨Z⋆, fD⟩M = 1.240
Net − Bulge eD :
log(M⋆, eD) = 10.790
⟨t⋆, eD⟩M = 10.370
⟨Z⋆, eD⟩M = 1.297
λ (Å)

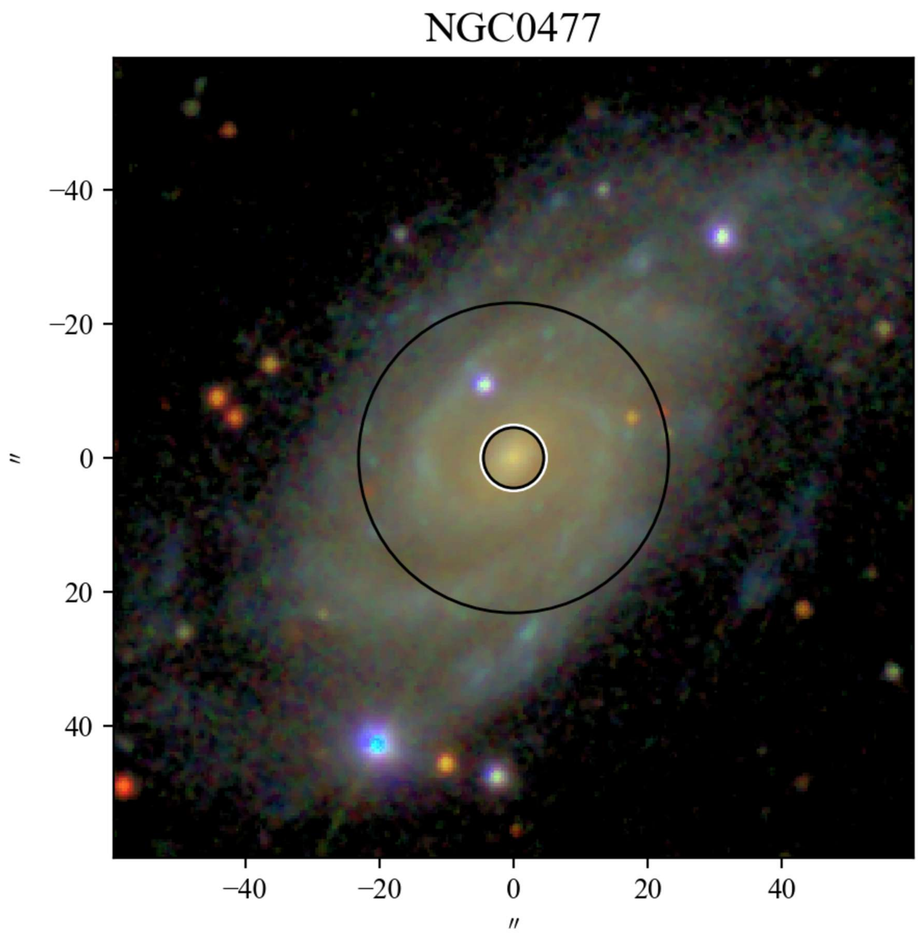
NGC0477
−40
−20
0
20
40
″
−40
−20
0
20
40
″

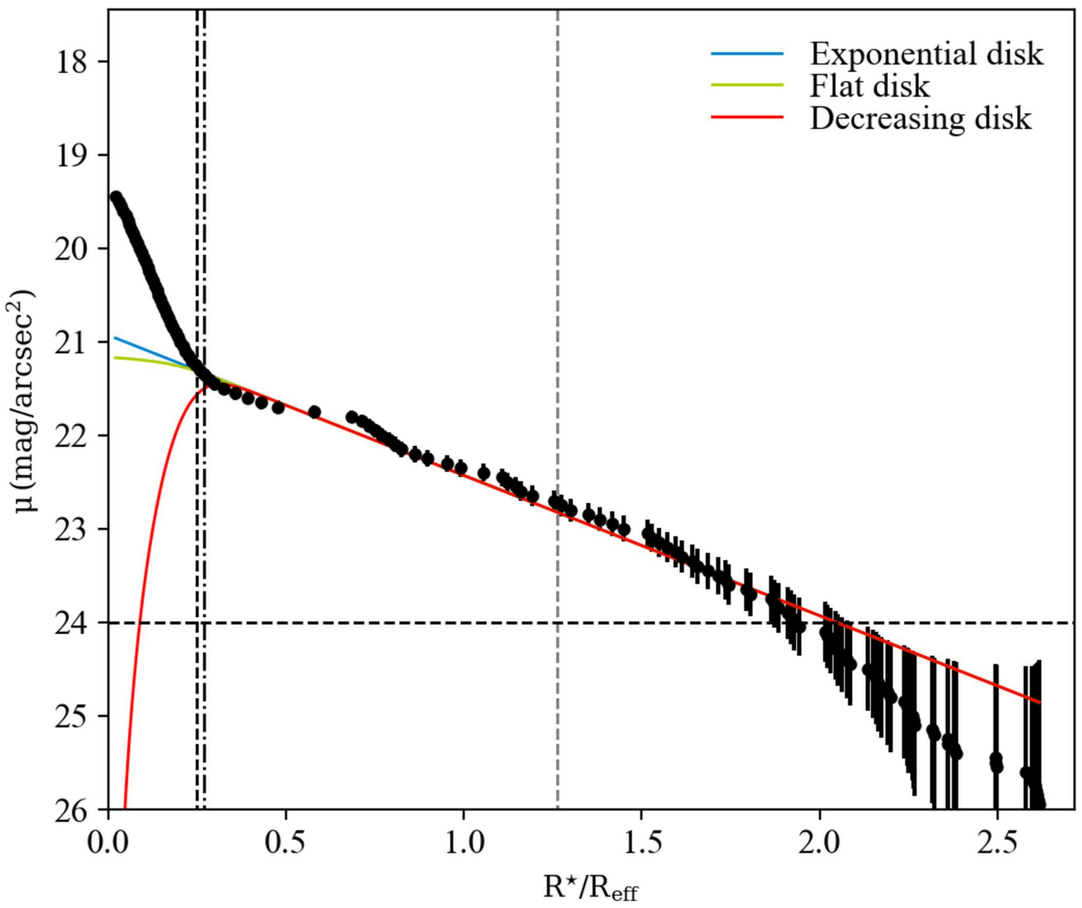
Exponential disk
Flat disk
Decreasing disk
μ (mag/arcsec²)
18
19
20
21
22
23
24
25
26
0.0
0.5
1.0
1.5
2.0
2.5
R⋆/Reff

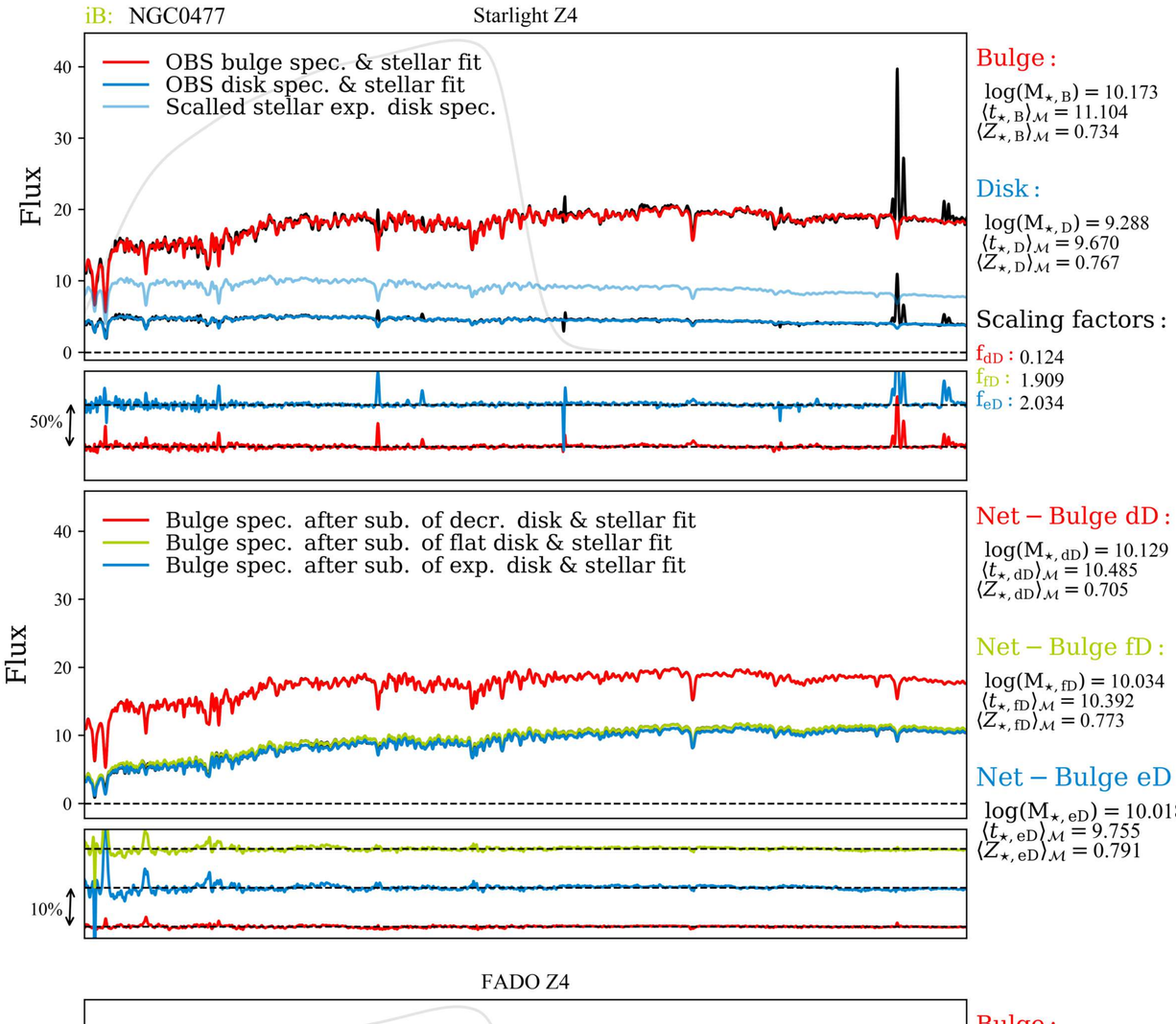
iB: NGC0477
Starlight Z4
OBS bulge spec. & stellar fit
OBS disk spec. & stellar fit
Scalled stellar exp. disk spec.
Flux
50%
Bulge :
log(M⋆, B) = 10.173
⟨t⋆, B⟩M = 11.104
⟨Z⋆, B⟩M = 0.734
Disk :
log(M⋆, D) = 9.288
⟨t⋆, D⟩M = 9.670
⟨Z⋆, D⟩M = 0.767
Scaling factors :
fdD : 0.124
ffD : 1.909
feD : 2.034
Bulge spec. after sub. of decr. disk & stellar fit
Bulge spec. after sub. of flat disk & stellar fit
Bulge spec. after sub. of exp. disk & stellar fit
10%
Net − Bulge dD :
log(M⋆, dD) = 10.129
⟨t⋆, dD⟩M = 10.485
⟨Z⋆, dD⟩M = 0.705
Net − Bulge fD :
log(M⋆, fD) = 10.034
⟨t⋆, fD⟩M = 10.392
⟨Z⋆, fD⟩M = 0.773
Net − Bulge eD :
log(M⋆, eD) = 10.018
⟨t⋆, eD⟩M = 9.755
⟨Z⋆, eD⟩M = 0.791

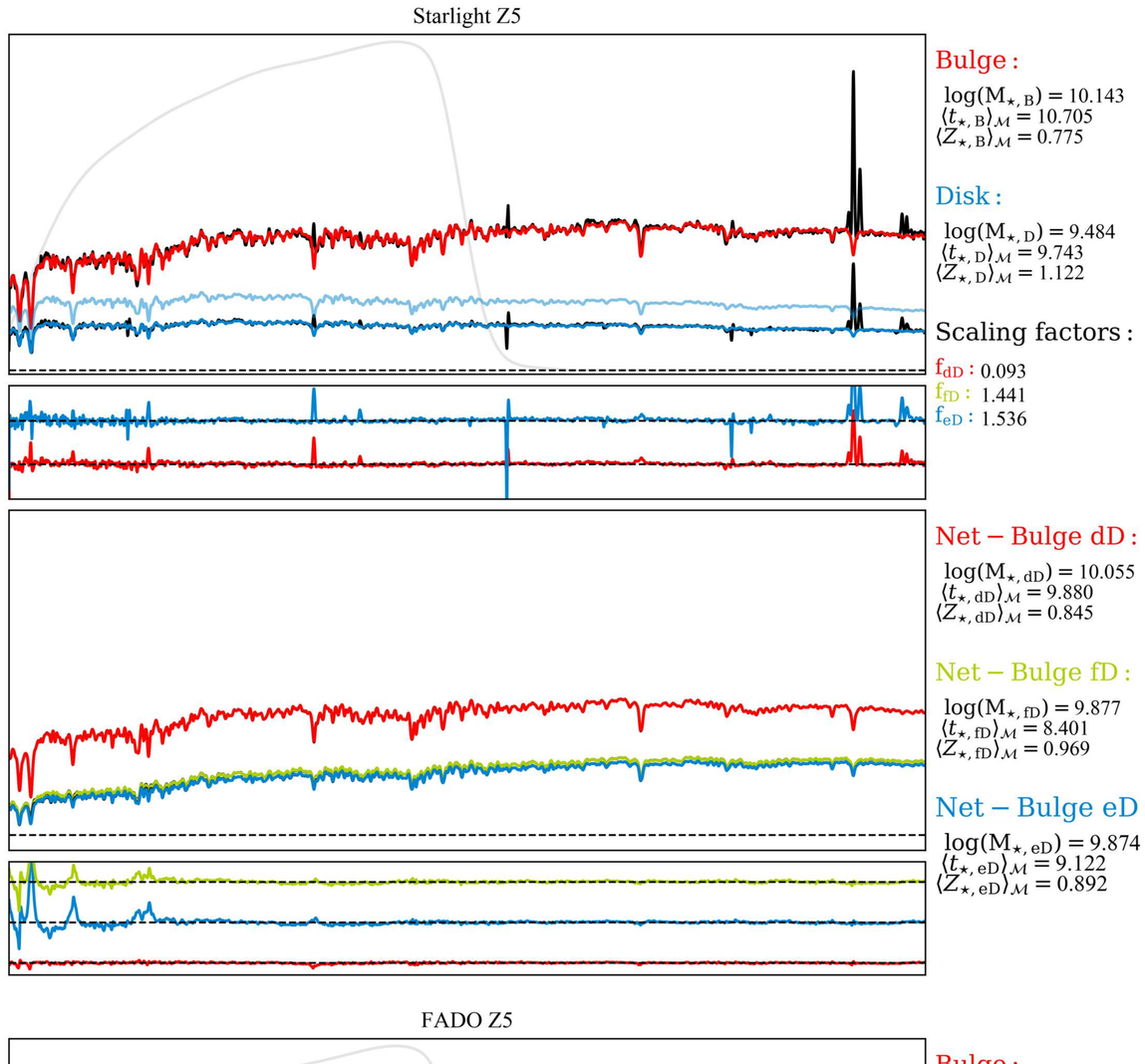
Starlight Z5
Bulge :
log(M⋆, B) = 10.143
⟨t⋆, B⟩M = 10.705
⟨Z⋆, B⟩M = 0.775
Disk :
log(M⋆, D) = 9.484
⟨t⋆, D⟩M = 9.743
⟨Z⋆, D⟩M = 1.122
Scaling factors :
fdD : 0.093
ffD : 1.441
feD : 1.536
Net − Bulge dD :
log(M⋆, dD) = 10.055
⟨t⋆, dD⟩M = 9.880
⟨Z⋆, dD⟩M = 0.845
Net − Bulge fD :
log(M⋆, fD) = 9.877
⟨t⋆, fD⟩M = 8.401
⟨Z⋆, fD⟩M = 0.969
Net − Bulge eD :
log(M⋆, eD) = 9.874
⟨t⋆, eD⟩M = 9.122
⟨Z⋆, eD⟩M = 0.892

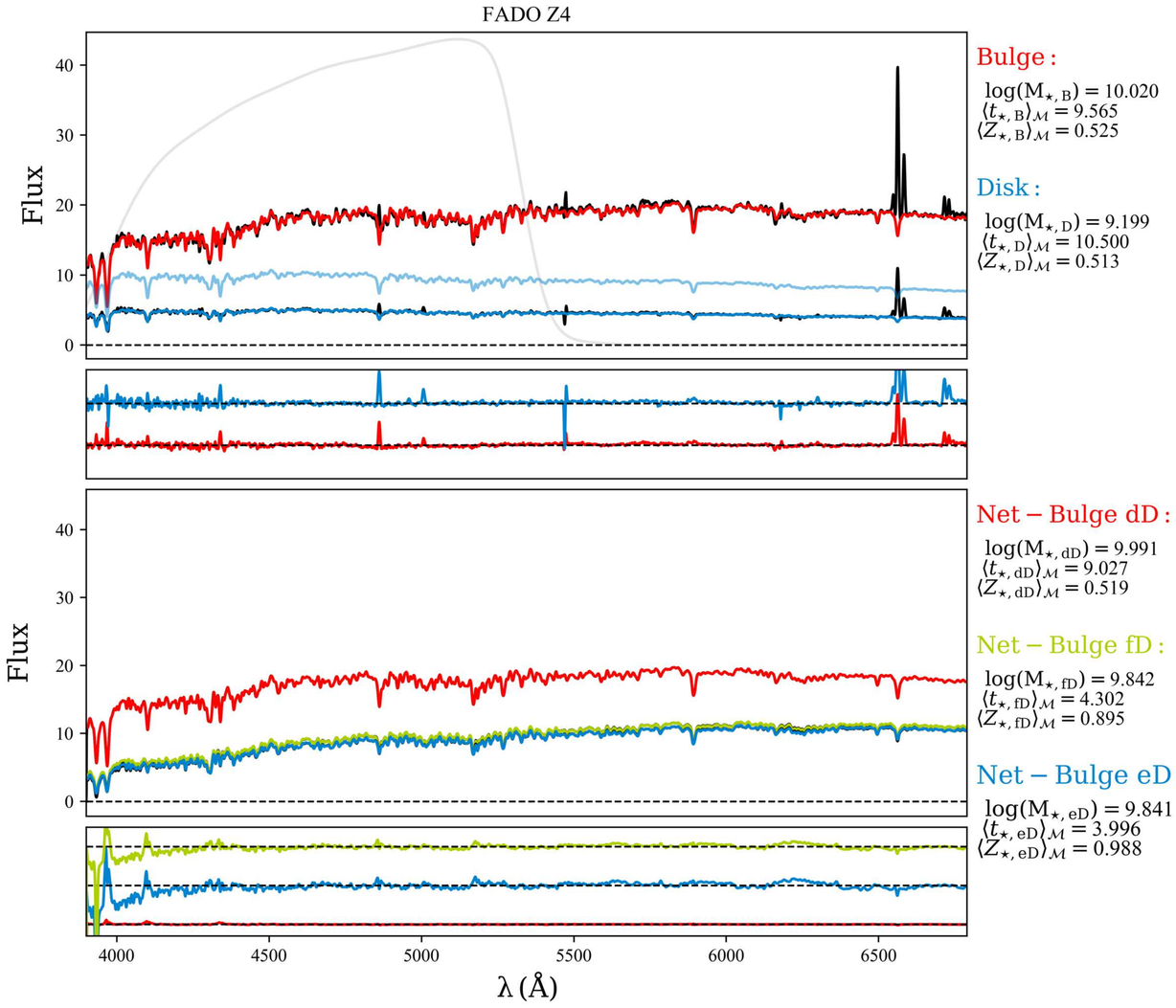
FADO Z4
Flux
Bulge :
log(M⋆, B) = 10.020
⟨t⋆, B⟩M = 9.565
⟨Z⋆, B⟩M = 0.525
Disk :
log(M⋆, D) = 9.199
⟨t⋆, D⟩M = 10.500
⟨Z⋆, D⟩M = 0.513
Net − Bulge dD :
log(M⋆, dD) = 9.991
⟨t⋆, dD⟩M = 9.027
⟨Z⋆, dD⟩M = 0.519
Net − Bulge fD :
log(M⋆, fD) = 9.842
⟨t⋆, fD⟩M = 4.302
⟨Z⋆, fD⟩M = 0.895
Net − Bulge eD :
log(M⋆, eD) = 9.841
⟨t⋆, eD⟩M = 3.996
⟨Z⋆, eD⟩M = 0.988
4000
4500
5000
5500
6000
6500
λ (Å)

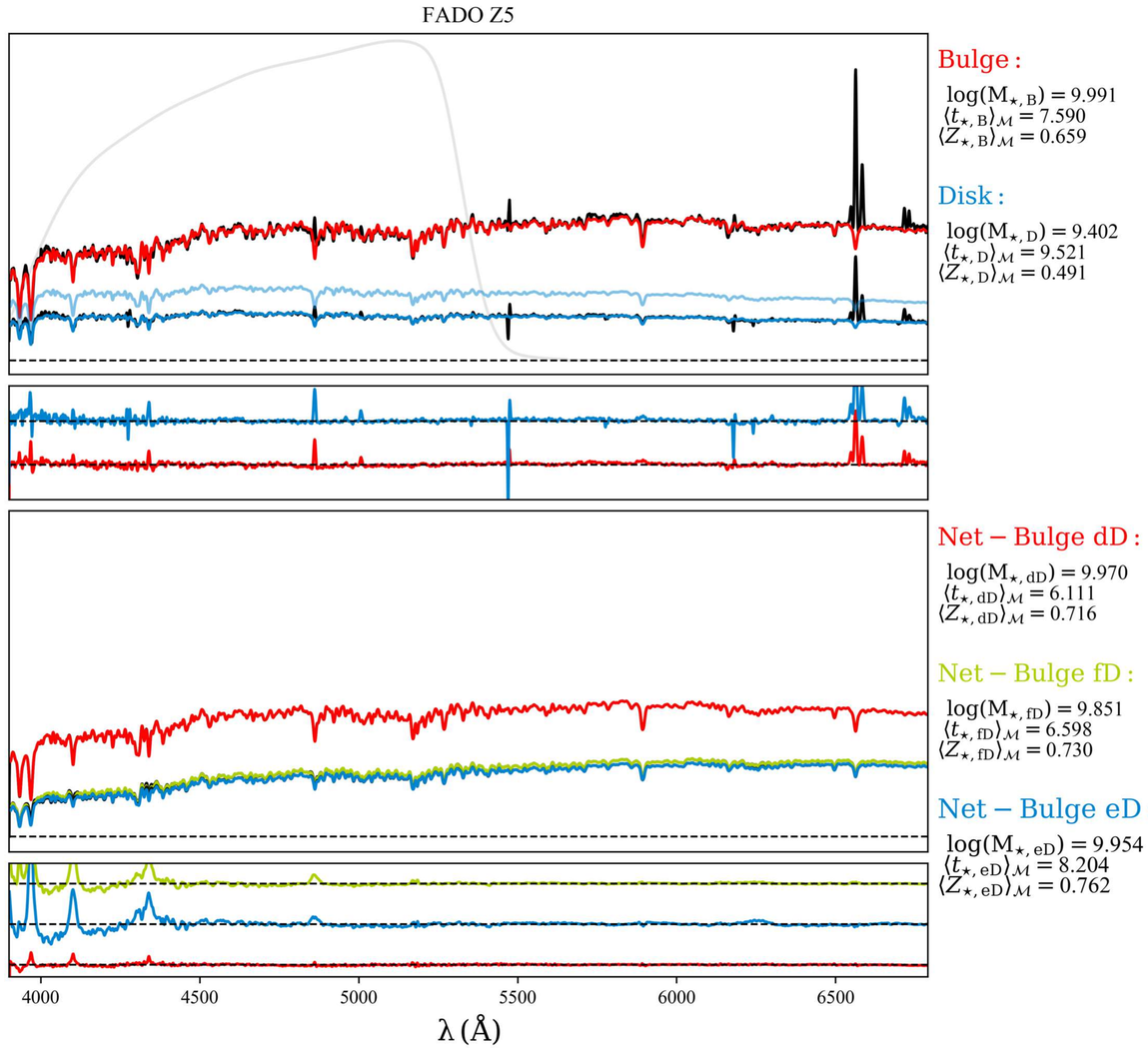
FADO Z5
Bulge :
log(M⋆, B) = 9.991
⟨t⋆, B⟩M = 7.590
⟨Z⋆, B⟩M = 0.659
Disk :
log(M⋆, D) = 9.402
⟨t⋆, D⟩M = 9.521
⟨Z⋆, D⟩M = 0.491
Net − Bulge dD :
log(M⋆, dD) = 9.970
⟨t⋆, dD⟩M = 6.111
⟨Z⋆, dD⟩M = 0.716
Net − Bulge fD :
log(M⋆, fD) = 9.851
⟨t⋆, fD⟩M = 6.598
⟨Z⋆, fD⟩M = 0.730
Net − Bulge eD :
log(M⋆, eD) = 9.954
⟨t⋆, eD⟩M = 8.204
⟨Z⋆, eD⟩M = 0.762
4000
4500
5000
5500
6000
6500
λ (Å)

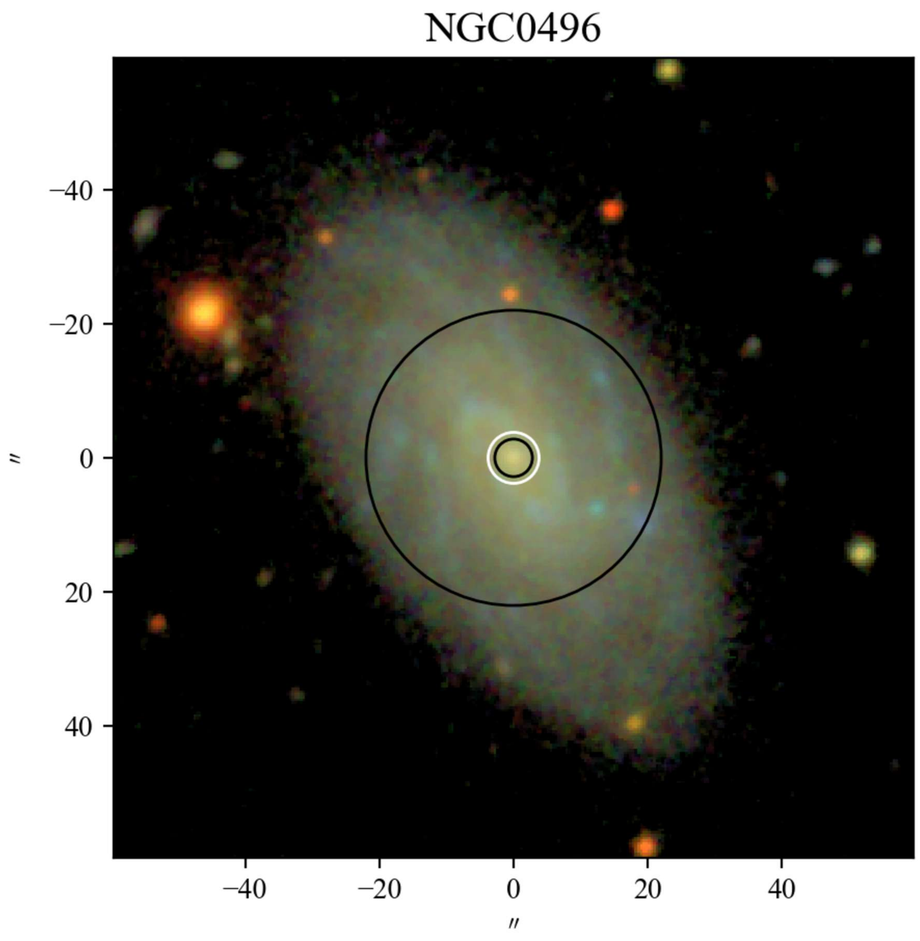
NGC0496
−40
−20
0
20
40
″
−40
−20
0
20
40
″

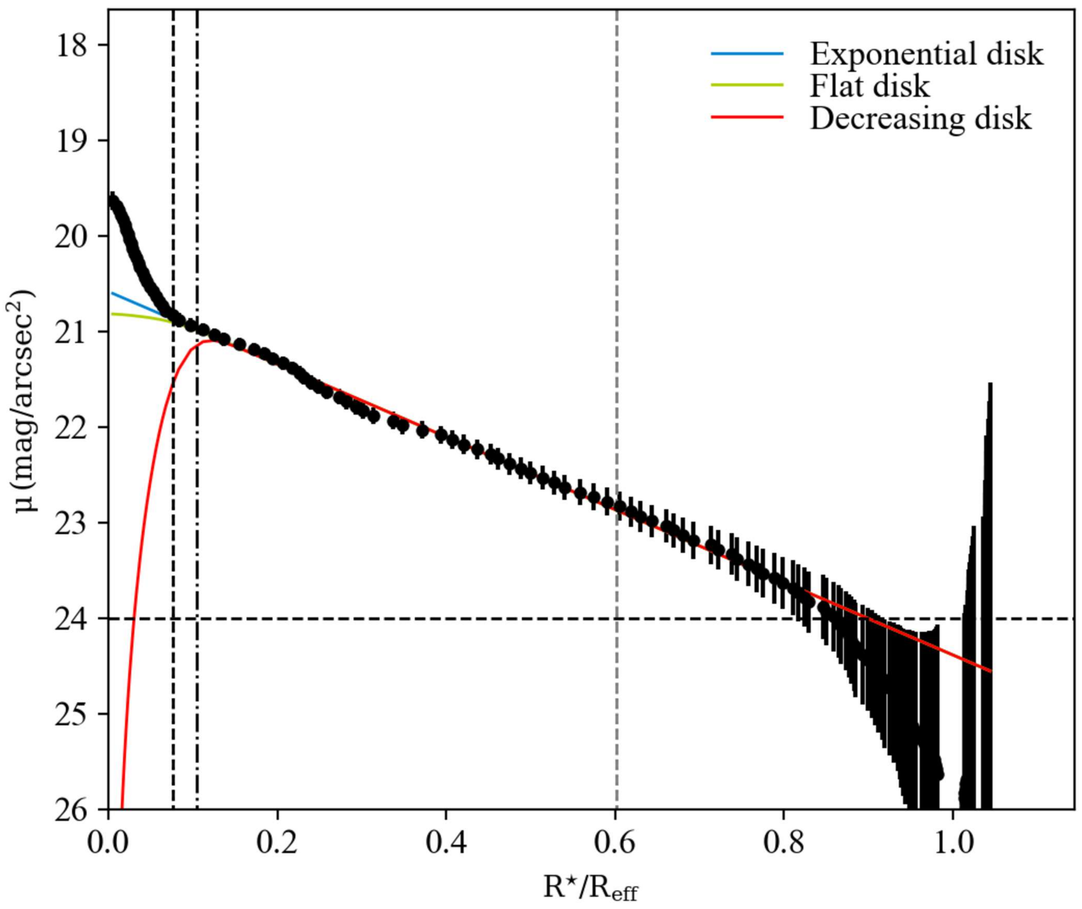
Exponential disk
Flat disk
Decreasing disk
μ (mag/arcsec²)
18
19
20
21
22
23
24
25
26
0.0
0.2
0.4
0.6
0.8
1.0
R⋆/Reff

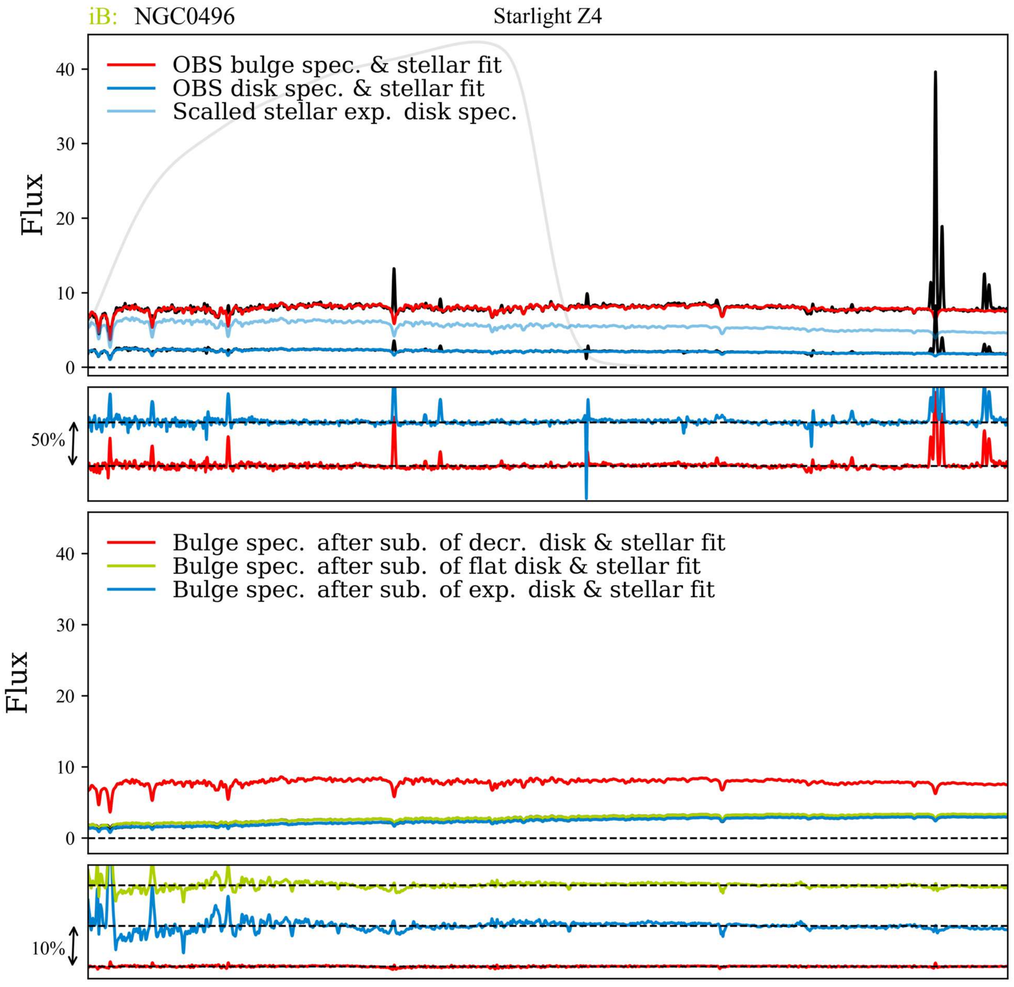
iB: NGC0496
Starlight Z4
OBS bulge spec. & stellar fit
OBS disk spec. & stellar fit
Scalled stellar exp. disk spec.
Flux
50%
Bulge :
log(M⋆, B) = 9.808
⟨t⋆, B⟩M = 11.107
⟨Z⋆, B⟩M = 0.711
Disk :
log(M⋆, D) = 8.983
⟨t⋆, D⟩M = 9.814
⟨Z⋆, D⟩M = 0.774
Scaling factors :
fdD : 0.018
ffD : 2.389
feD : 2.595
Bulge spec. after sub. of decr. disk & stellar fit
Bulge spec. after sub. of flat disk & stellar fit
Bulge spec. after sub. of exp. disk & stellar fit
10%
Net − Bulge dD :
log(M⋆, dD) = 9.771
⟨t⋆, dD⟩M = 10.277
⟨Z⋆, dD⟩M = 0.673
Net − Bulge fD :
log(M⋆, fD) = 9.605
⟨t⋆, fD⟩M = 8.517
⟨Z⋆, fD⟩M = 0.669
Net − Bulge eD :
log(M⋆, eD) = 9.547
⟨t⋆, eD⟩M = 6.872
⟨Z⋆, eD⟩M = 0.637

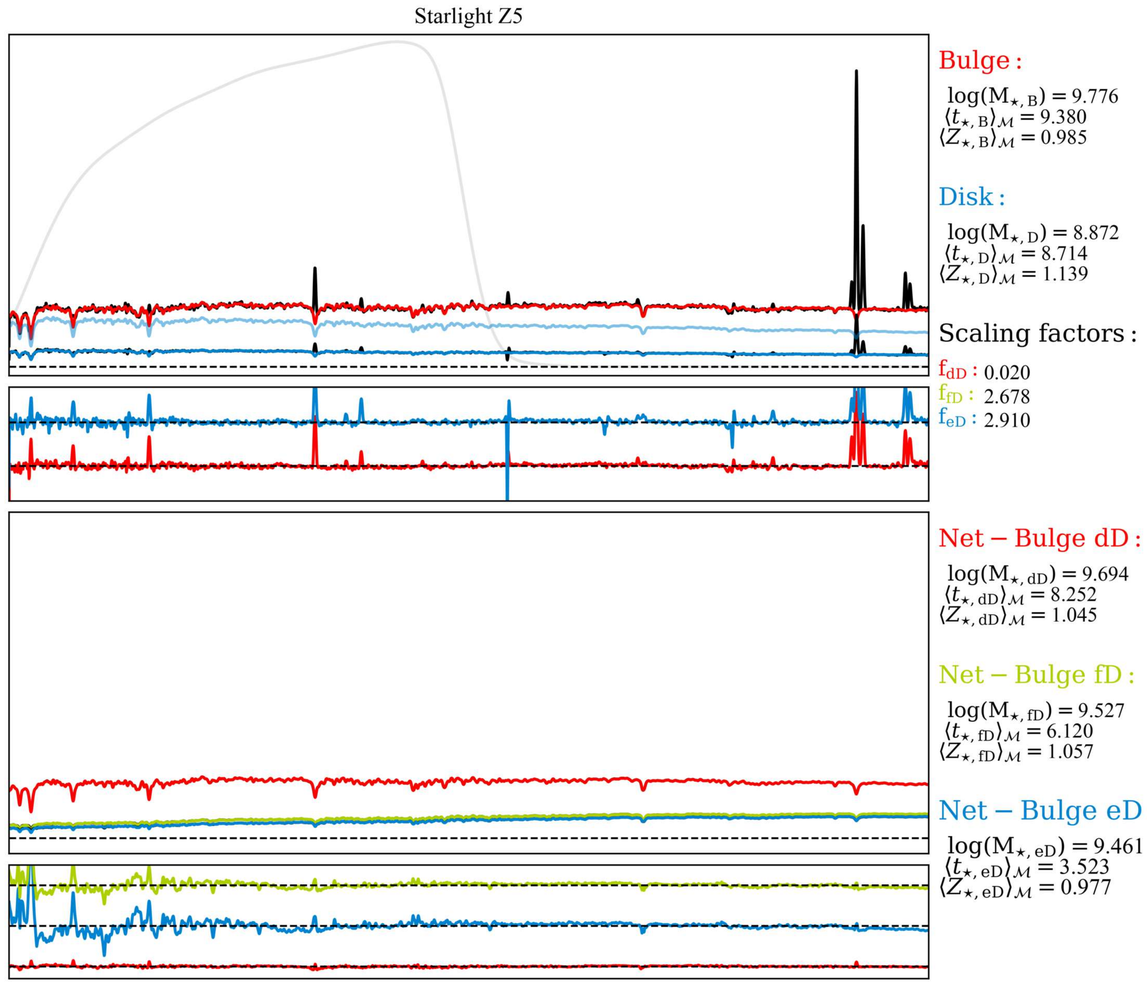
Starlight Z5
Bulge :
log(M⋆, B) = 9.776
⟨t⋆, B⟩M = 9.380
⟨Z⋆, B⟩M = 0.985
Disk :
log(M⋆, D) = 8.872
⟨t⋆, D⟩M = 8.714
⟨Z⋆, D⟩M = 1.139
Scaling factors :
fdD : 0.020
ffD : 2.678
feD : 2.910
Net − Bulge dD :
log(M⋆, dD) = 9.694
⟨t⋆, dD⟩M = 8.252
⟨Z⋆, dD⟩M = 1.045
Net − Bulge fD :
log(M⋆, fD) = 9.527
⟨t⋆, fD⟩M = 6.120
⟨Z⋆, fD⟩M = 1.057
Net − Bulge eD :
log(M⋆, eD) = 9.461
⟨t⋆, eD⟩M = 3.523
⟨Z⋆, eD⟩M = 0.977

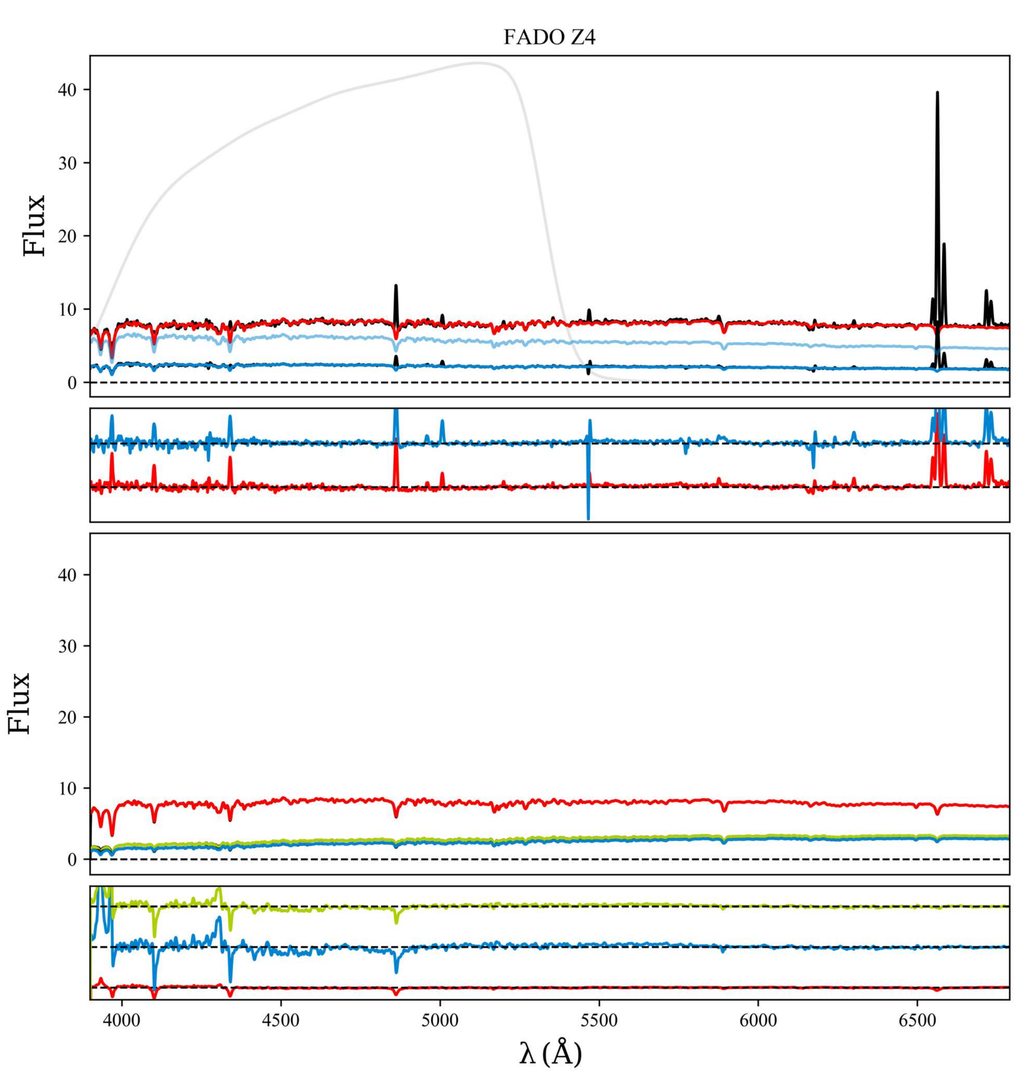
FADO Z4
Flux
Bulge :
log(M⋆, B) = 9.768
⟨t⋆, B⟩M = 11.890
⟨Z⋆, B⟩M = 0.641
Disk :
log(M⋆, D) = 8.900
⟨t⋆, D⟩M = 9.131
⟨Z⋆, D⟩M = 0.488
Net − Bulge dD :
log(M⋆, dD) = 9.734
⟨t⋆, dD⟩M = 11.000
⟨Z⋆, dD⟩M = 0.615
Net − Bulge fD :
log(M⋆, fD) = 9.593
⟨t⋆, fD⟩M = 10.080
⟨Z⋆, fD⟩M = 0.696
Net − Bulge eD :
log(M⋆, eD) = 9.565
⟨t⋆, eD⟩M = 9.106
⟨Z⋆, eD⟩M = 0.695
λ (Å)

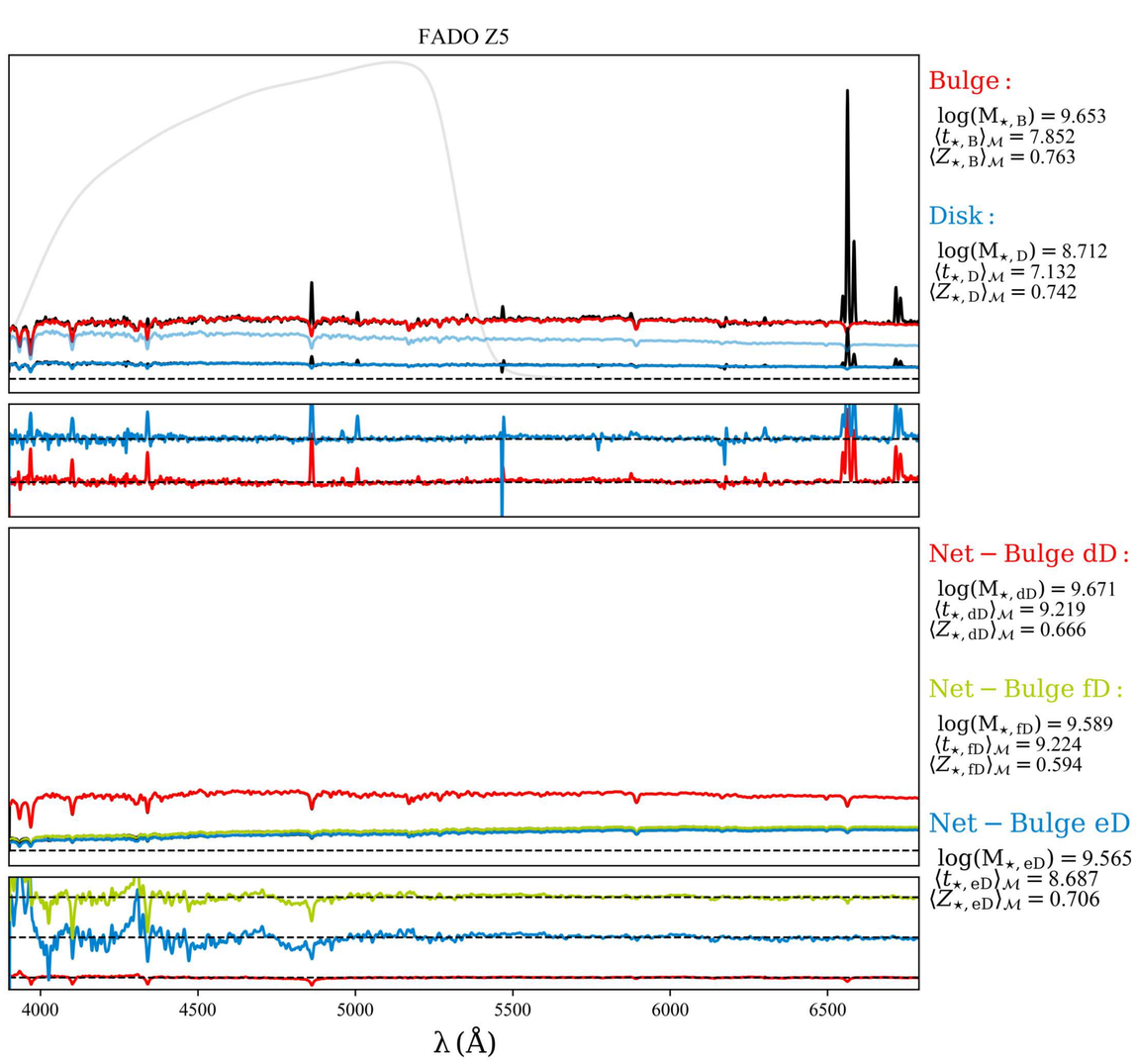
FADO Z5
Bulge :
log(M⋆, B) = 9.653
⟨t⋆, B⟩M = 7.852
⟨Z⋆, B⟩M = 0.763
Disk :
log(M⋆, D) = 8.712
⟨t⋆, D⟩M = 7.132
⟨Z⋆, D⟩M = 0.742
Net − Bulge dD :
log(M⋆, dD) = 9.671
⟨t⋆, dD⟩M = 9.219
⟨Z⋆, dD⟩M = 0.666
Net − Bulge fD :
log(M⋆, fD) = 9.589
⟨t⋆, fD⟩M = 9.224
⟨Z⋆, fD⟩M = 0.594
Net − Bulge eD :
log(M⋆, eD) = 9.565
⟨t⋆, eD⟩M = 8.687
⟨Z⋆, eD⟩M = 0.706
λ (Å)

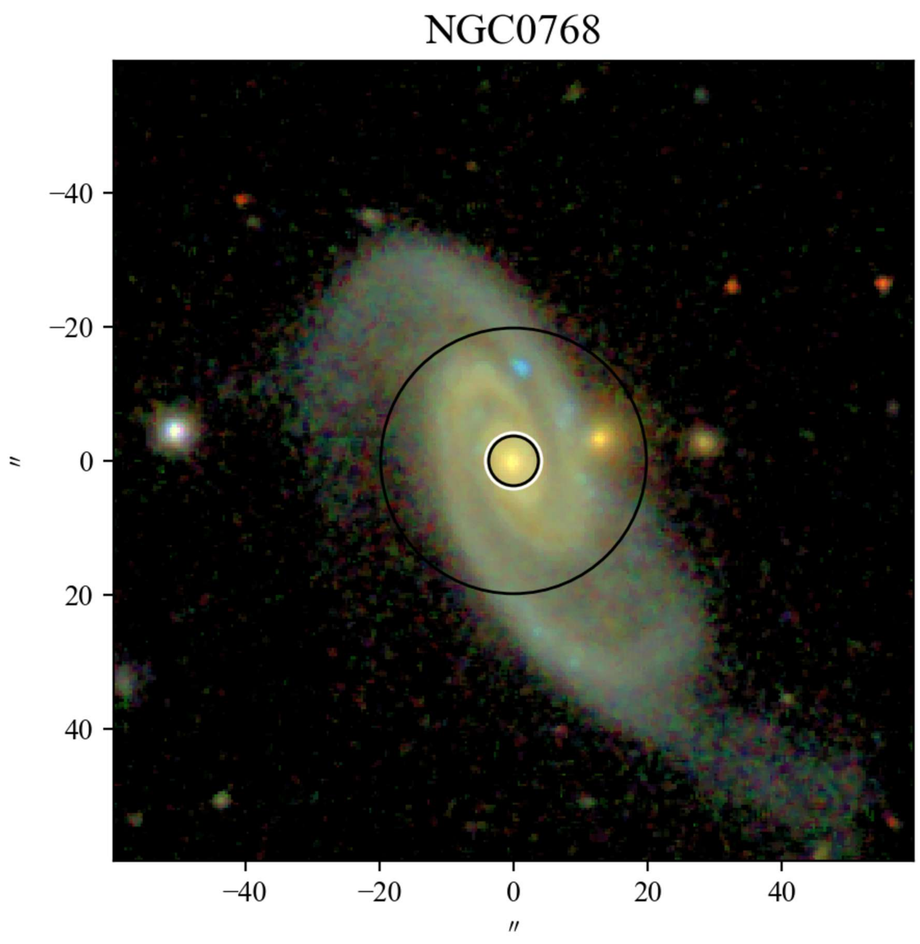
NGC0768
−40
−20
0
20
40
″
−40
−20
0
20
40
″

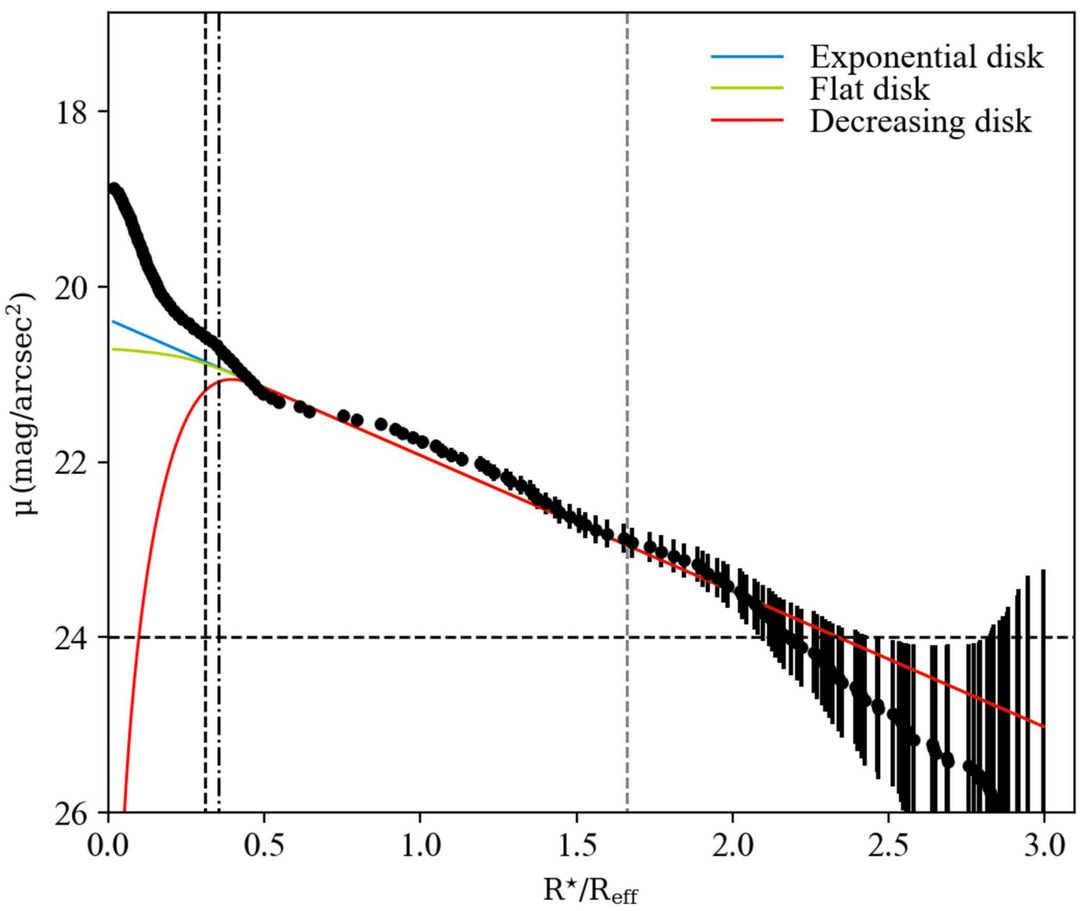
Exponential disk
Flat disk
Decreasing disk
18
20
22
24
26
μ (mag/arcsec²)
0.0
0.5
1.0
1.5
2.0
2.5
3.0
R⋆/Reff

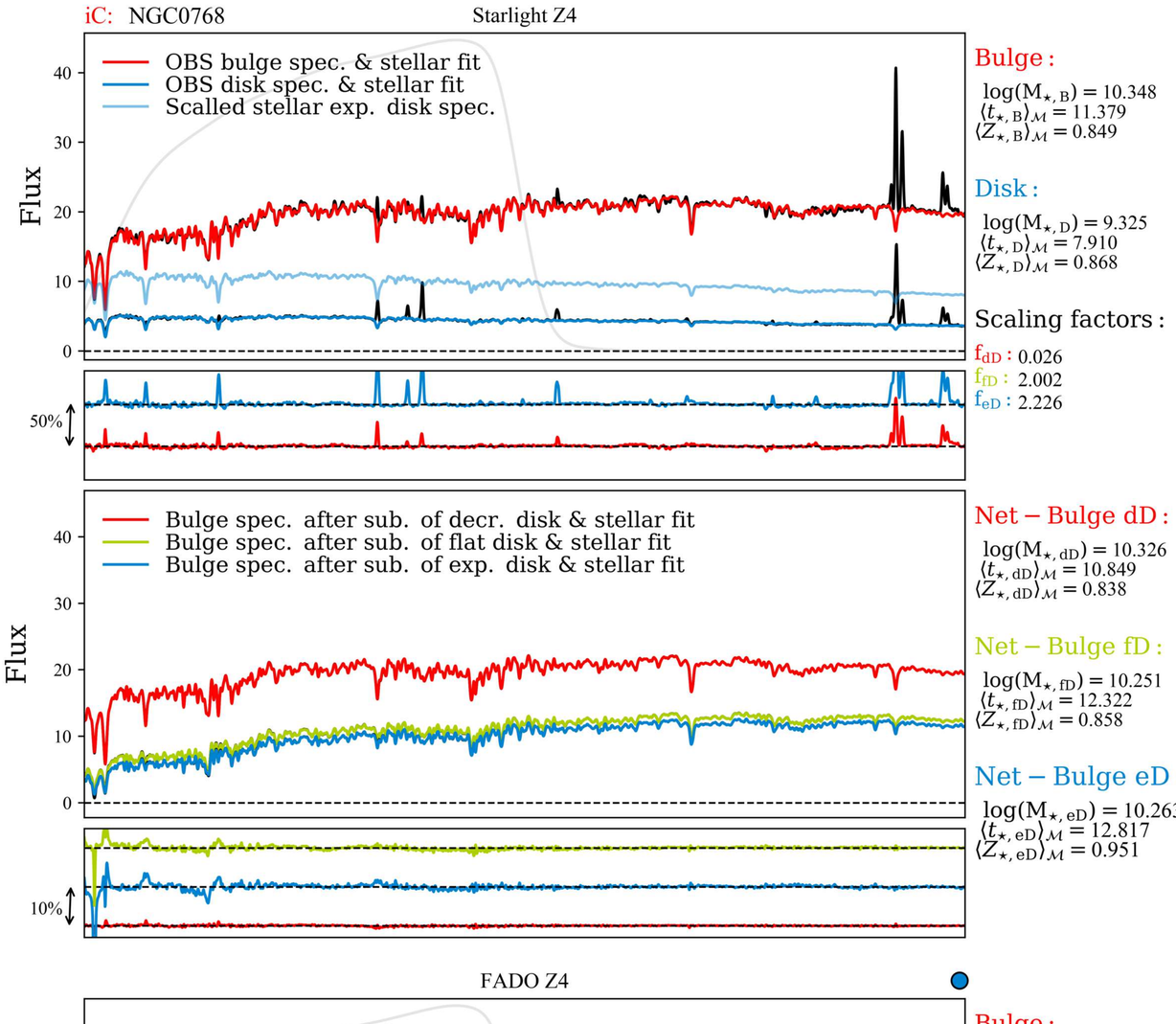
iC: NGC0768
Starlight Z4
OBS bulge spec. & stellar fit
OBS disk spec. & stellar fit
Scalled stellar exp. disk spec.
Flux
50%
Bulge :
log(M⋆, B) = 10.348
⟨t⋆, B⟩M = 11.379
⟨Z⋆, B⟩M = 0.849
Disk :
log(M⋆, D) = 9.325
⟨t⋆, D⟩M = 7.910
⟨Z⋆, D⟩M = 0.868
Scaling factors :
fdD : 0.026
ffD : 2.002
feD : 2.226
Bulge spec. after sub. of decr. disk & stellar fit
Bulge spec. after sub. of flat disk & stellar fit
Bulge spec. after sub. of exp. disk & stellar fit
10%
Net − Bulge dD :
log(M⋆, dD) = 10.326
⟨t⋆, dD⟩M = 10.849
⟨Z⋆, dD⟩M = 0.838
Net − Bulge fD :
log(M⋆, fD) = 10.251
⟨t⋆, fD⟩M = 12.322
⟨Z⋆, fD⟩M = 0.858
Net − Bulge eD :
log(M⋆, eD) = 10.263
⟨t⋆, eD⟩M = 12.817
⟨Z⋆, eD⟩M = 0.951

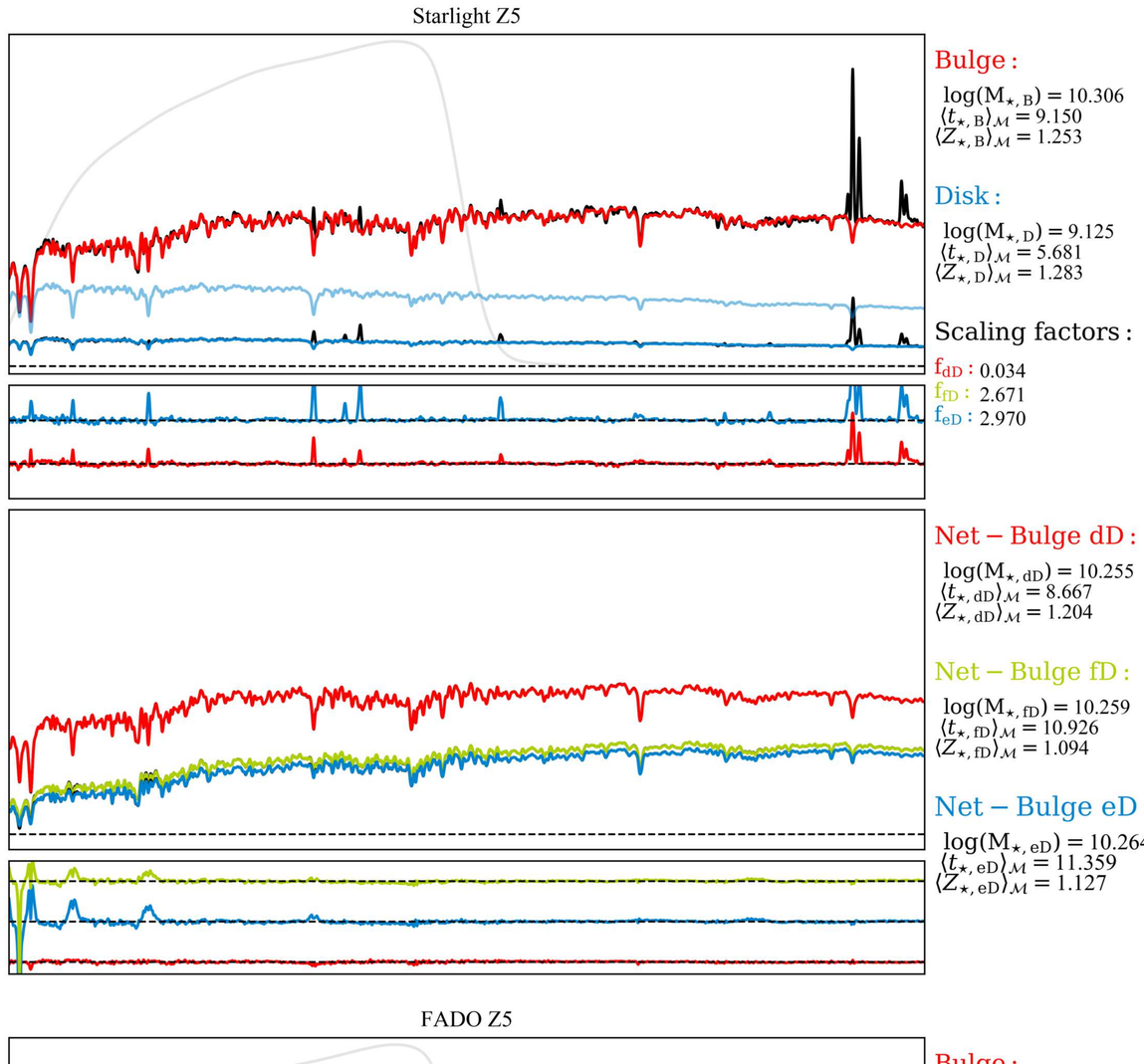
Starlight Z5
Bulge :
log(M⋆, B) = 10.306
⟨t⋆, B⟩M = 9.150
⟨Z⋆, B⟩M = 1.253
Disk :
log(M⋆, D) = 9.125
⟨t⋆, D⟩M = 5.681
⟨Z⋆, D⟩M = 1.283
Scaling factors :
fdD : 0.034
ffD : 2.671
feD : 2.970
Net − Bulge dD :
log(M⋆, dD) = 10.255
⟨t⋆, dD⟩M = 8.667
⟨Z⋆, dD⟩M = 1.204
Net − Bulge fD :
log(M⋆, fD) = 10.259
⟨t⋆, fD⟩M = 10.926
⟨Z⋆, fD⟩M = 1.094
Net − Bulge eD :
log(M⋆, eD) = 10.264
⟨t⋆, eD⟩M = 11.359
⟨Z⋆, eD⟩M = 1.127

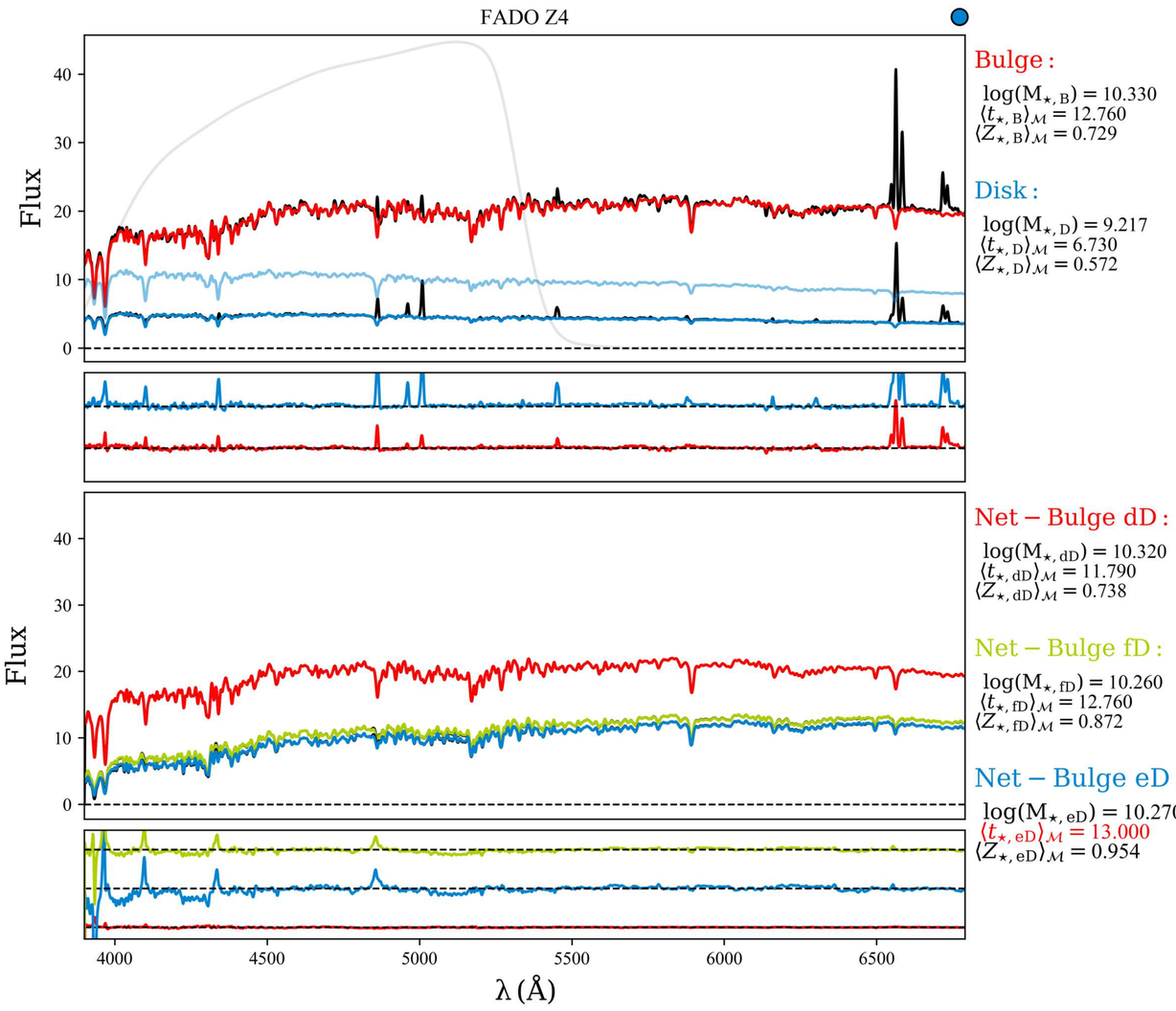
FADO Z4
Flux
Bulge :
log(M⋆, B) = 10.330
⟨t⋆, B⟩M = 12.760
⟨Z⋆, B⟩M = 0.729
Disk :
log(M⋆, D) = 9.217
⟨t⋆, D⟩M = 6.730
⟨Z⋆, D⟩M = 0.572
Net − Bulge dD :
log(M⋆, dD) = 10.320
⟨t⋆, dD⟩M = 11.790
⟨Z⋆, dD⟩M = 0.738
Net − Bulge fD :
log(M⋆, fD) = 10.260
⟨t⋆, fD⟩M = 12.760
⟨Z⋆, fD⟩M = 0.872
Net − Bulge eD :
log(M⋆, eD) = 10.270
⟨t⋆, eD⟩M = 13.000
⟨Z⋆, eD⟩M = 0.954
4000
4500
5000
5500
6000
6500
λ (Å)

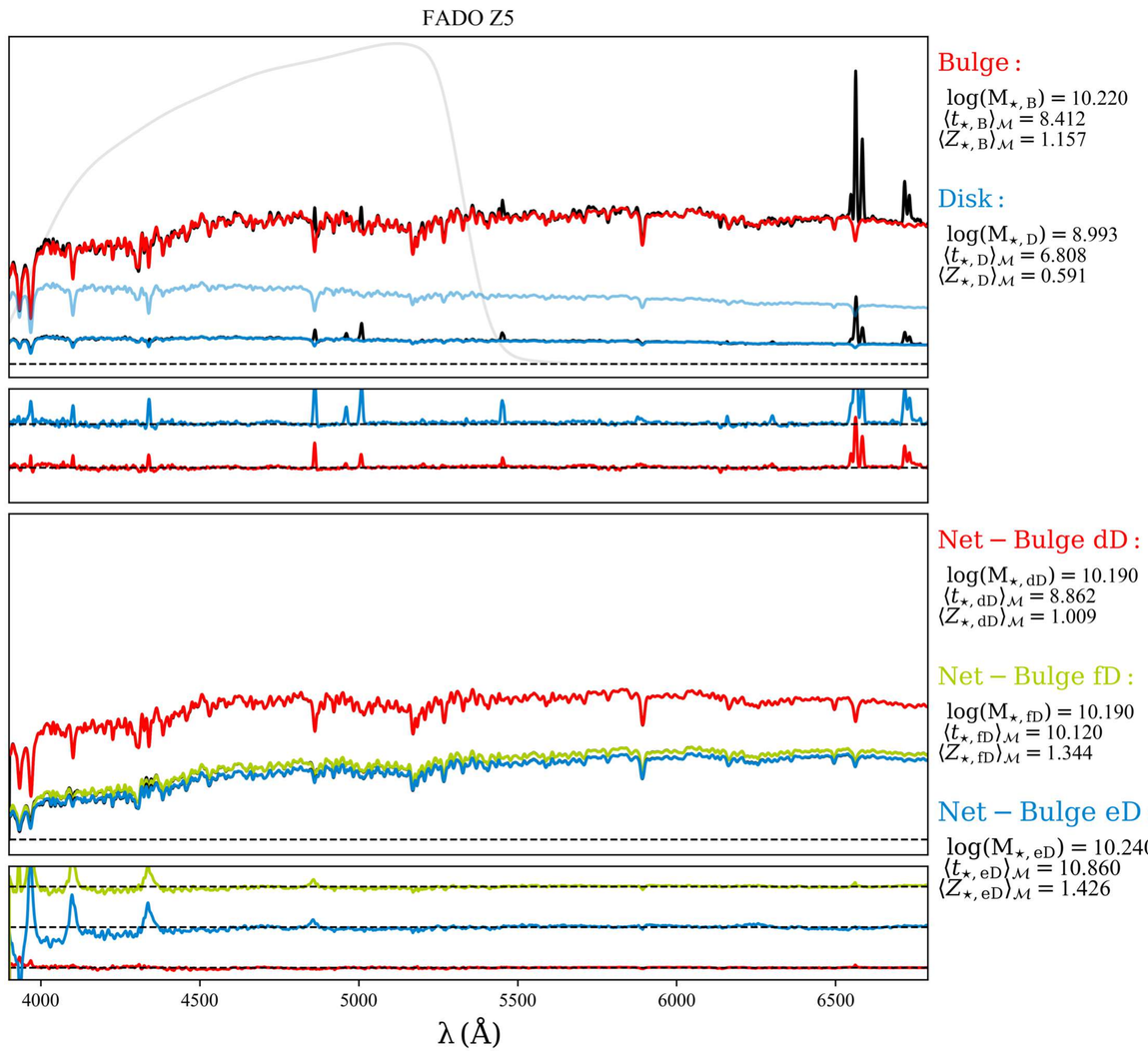
FADO Z5
Bulge :
log(M⋆, B) = 10.220
⟨t⋆, B⟩M = 8.412
⟨Z⋆, B⟩M = 1.157
Disk :
log(M⋆, D) = 8.993
⟨t⋆, D⟩M = 6.808
⟨Z⋆, D⟩M = 0.591
Net − Bulge dD :
log(M⋆, dD) = 10.190
⟨t⋆, dD⟩M = 8.862
⟨Z⋆, dD⟩M = 1.009
Net − Bulge fD :
log(M⋆, fD) = 10.190
⟨t⋆, fD⟩M = 10.120
⟨Z⋆, fD⟩M = 1.344
Net − Bulge eD :
log(M⋆, eD) = 10.240
⟨t⋆, eD⟩M = 10.860
⟨Z⋆, eD⟩M = 1.426
4000
4500
5000
5500
6000
6500
λ (Å)

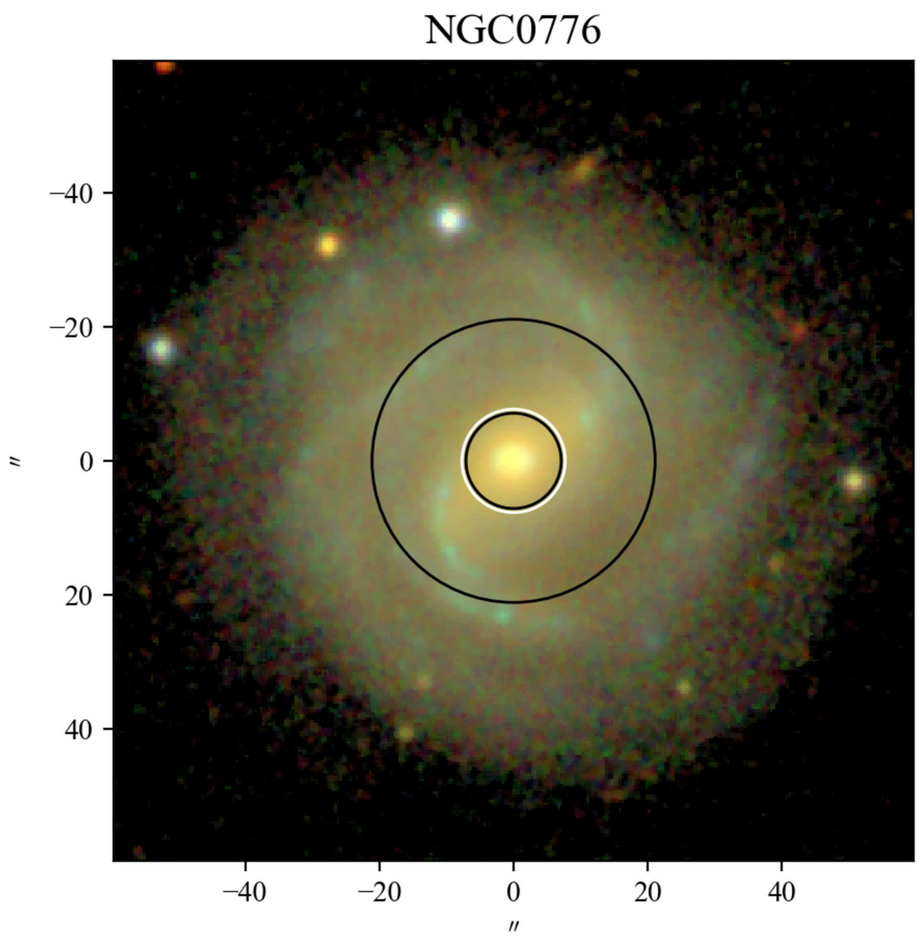
NGC0776
−40
−20
0
20
40
″
−40
−20
0
20
40
″

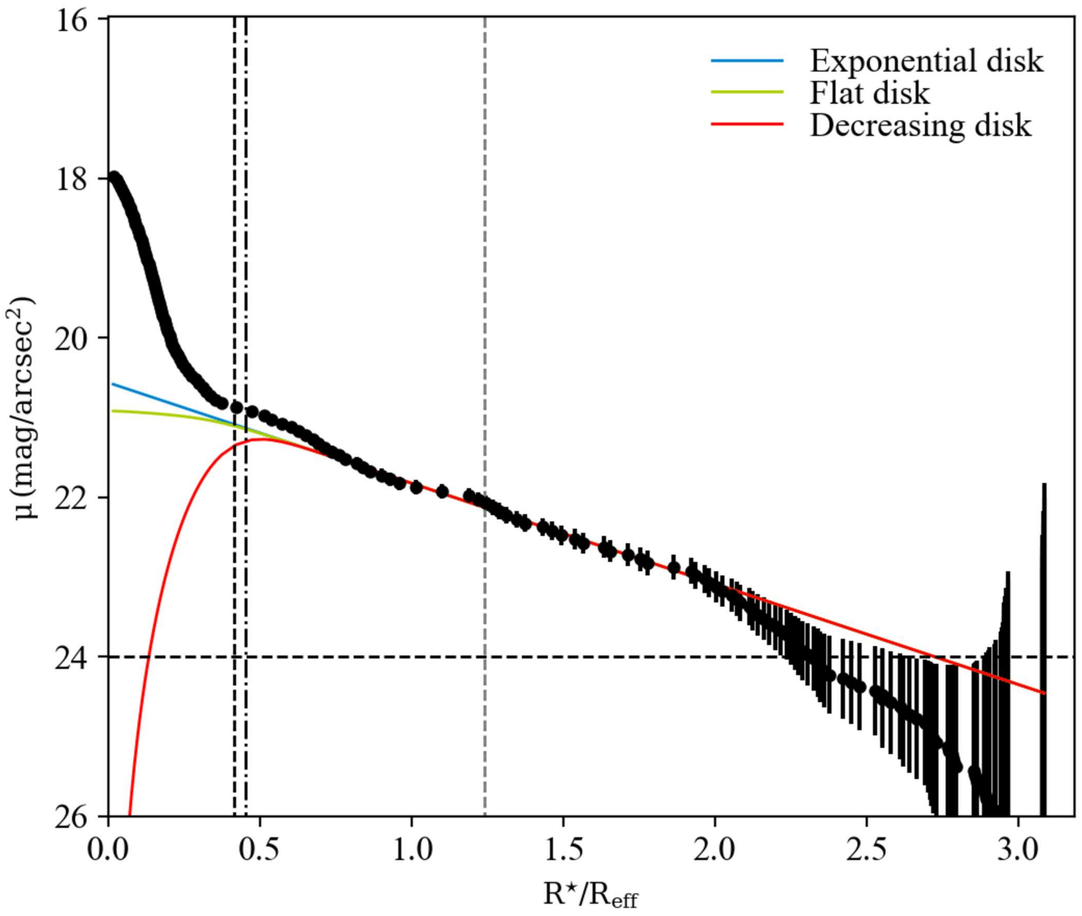
Exponential disk
Flat disk
Decreasing disk
μ (mag/arcsec²)
16
18
20
22
24
26
0.0
0.5
1.0
1.5
2.0
2.5
3.0
R⋆/Reff

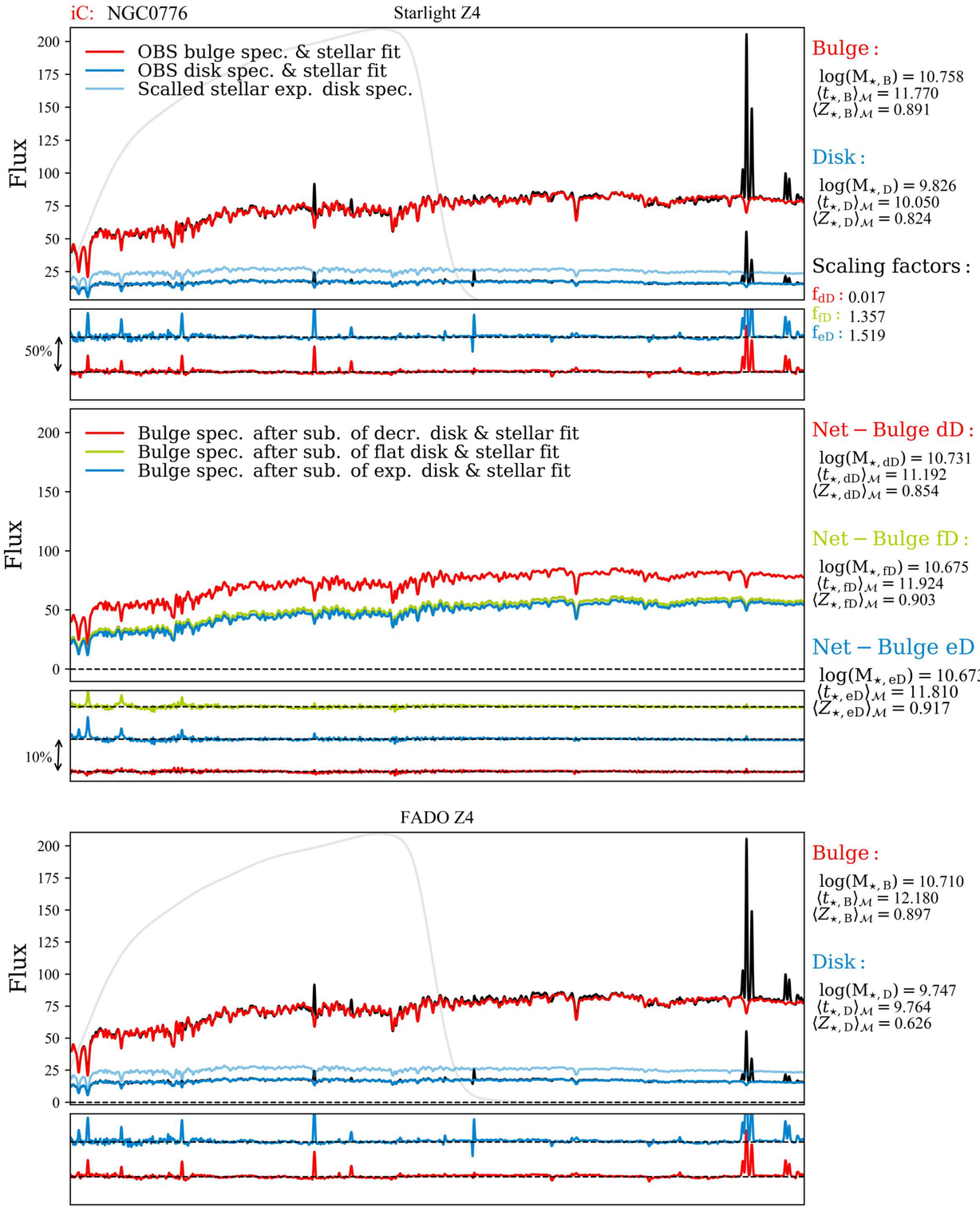
iC: NGC0776
Starlight Z4
OBS bulge spec. & stellar fit
OBS disk spec. & stellar fit
Scalled stellar exp. disk spec.
Flux
50%
Bulge :
log(M⋆, B) = 10.758
⟨t⋆, B⟩M = 11.770
⟨Z⋆, B⟩M = 0.891
Disk :
log(M⋆, D) = 9.826
⟨t⋆, D⟩M = 10.050
⟨Z⋆, D⟩M = 0.824
Scaling factors :
fdD : 0.017
ffD : 1.357
feD : 1.519
Bulge spec. after sub. of decr. disk & stellar fit
Bulge spec. after sub. of flat disk & stellar fit
Bulge spec. after sub. of exp. disk & stellar fit
10%
Net − Bulge dD :
log(M⋆, dD) = 10.731
⟨t⋆, dD⟩M = 11.192
⟨Z⋆, dD⟩M = 0.854
Net − Bulge fD :
log(M⋆, fD) = 10.675
⟨t⋆, fD⟩M = 11.924
⟨Z⋆, fD⟩M = 0.903
Net − Bulge eD :
log(M⋆, eD) = 10.673
⟨t⋆, eD⟩M = 11.810
⟨Z⋆, eD⟩M = 0.917

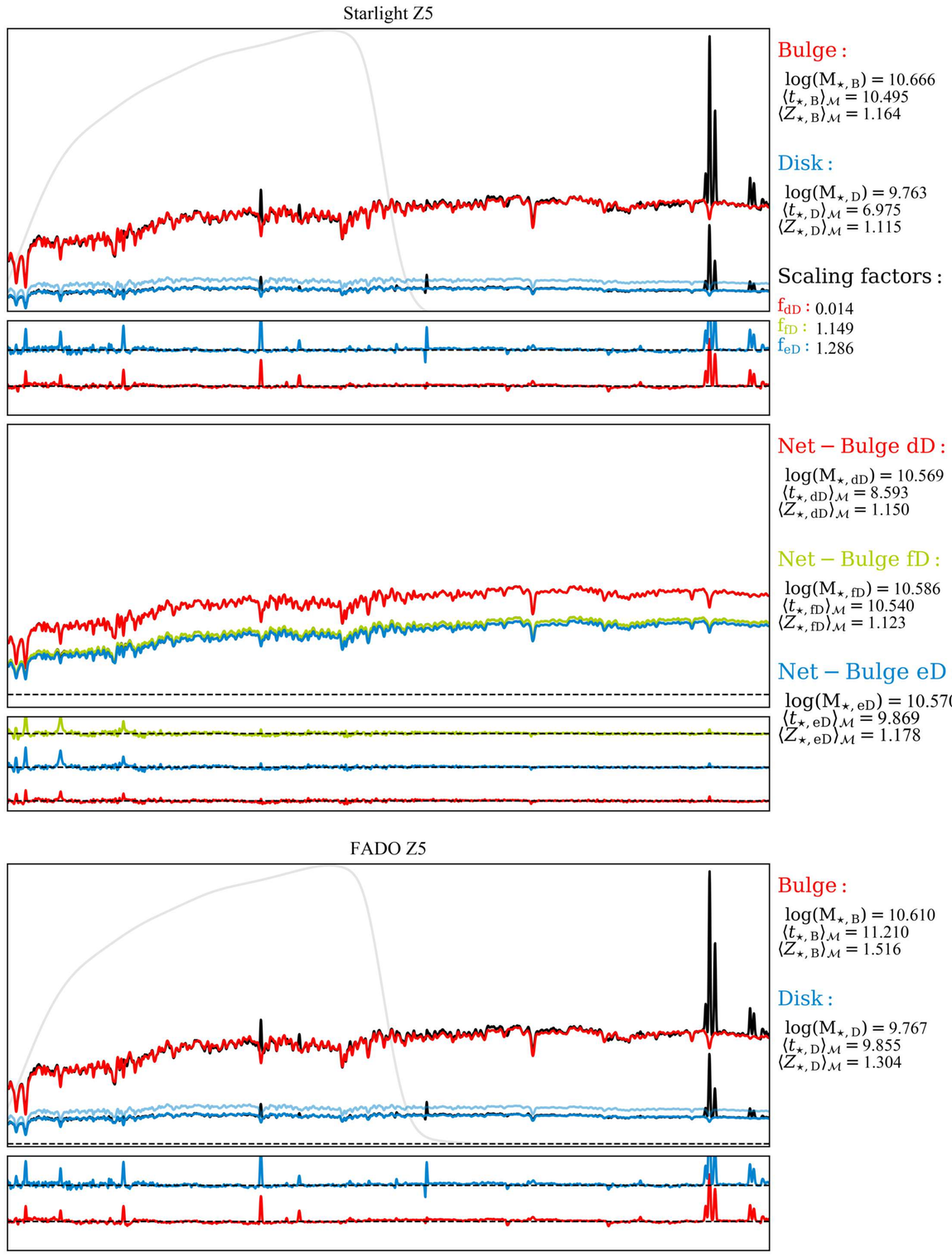
Starlight Z5
Bulge :
log(M⋆, B) = 10.666
⟨t⋆, B⟩M = 10.495
⟨Z⋆, B⟩M = 1.164
Disk :
log(M⋆, D) = 9.763
⟨t⋆, D⟩M = 6.975
⟨Z⋆, D⟩M = 1.115
Scaling factors :
fdD : 0.014
ffD : 1.149
feD : 1.286
Net − Bulge dD :
log(M⋆, dD) = 10.569
⟨t⋆, dD⟩M = 8.593
⟨Z⋆, dD⟩M = 1.150
Net − Bulge fD :
log(M⋆, fD) = 10.586
⟨t⋆, fD⟩M = 10.540
⟨Z⋆, fD⟩M = 1.123
Net − Bulge eD :
log(M⋆, eD) = 10.570
⟨t⋆, eD⟩M = 9.869
⟨Z⋆, eD⟩M = 1.178

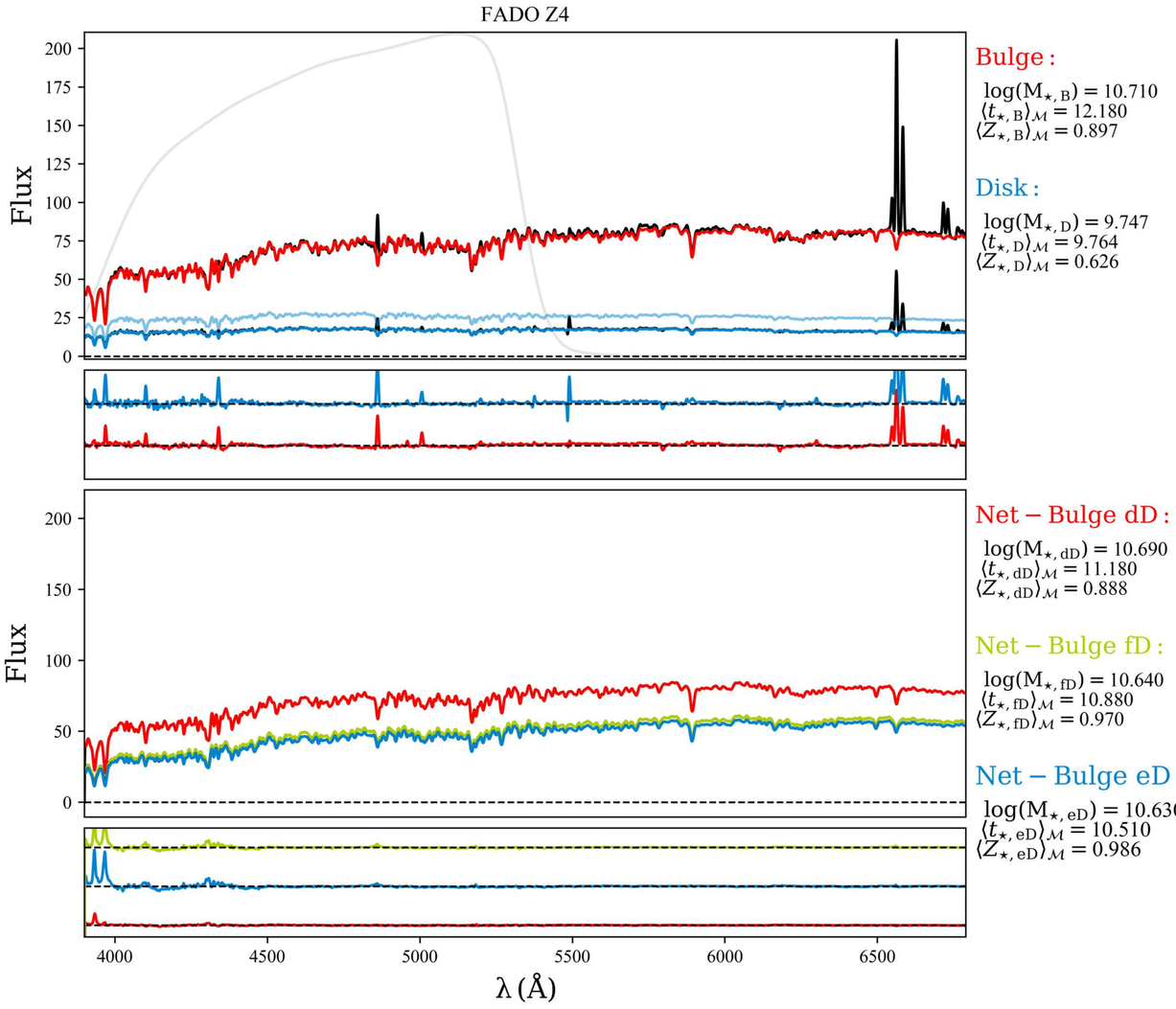
FADO Z4
Flux
Bulge :
log(M⋆, B) = 10.710
⟨t⋆, B⟩M = 12.180
⟨Z⋆, B⟩M = 0.897
Disk :
log(M⋆, D) = 9.747
⟨t⋆, D⟩M = 9.764
⟨Z⋆, D⟩M = 0.626
Net − Bulge dD :
log(M⋆, dD) = 10.690
⟨t⋆, dD⟩M = 11.180
⟨Z⋆, dD⟩M = 0.888
Net − Bulge fD :
log(M⋆, fD) = 10.640
⟨t⋆, fD⟩M = 10.880
⟨Z⋆, fD⟩M = 0.970
Net − Bulge eD :
log(M⋆, eD) = 10.630
⟨t⋆, eD⟩M = 10.510
⟨Z⋆, eD⟩M = 0.986
λ (Å)

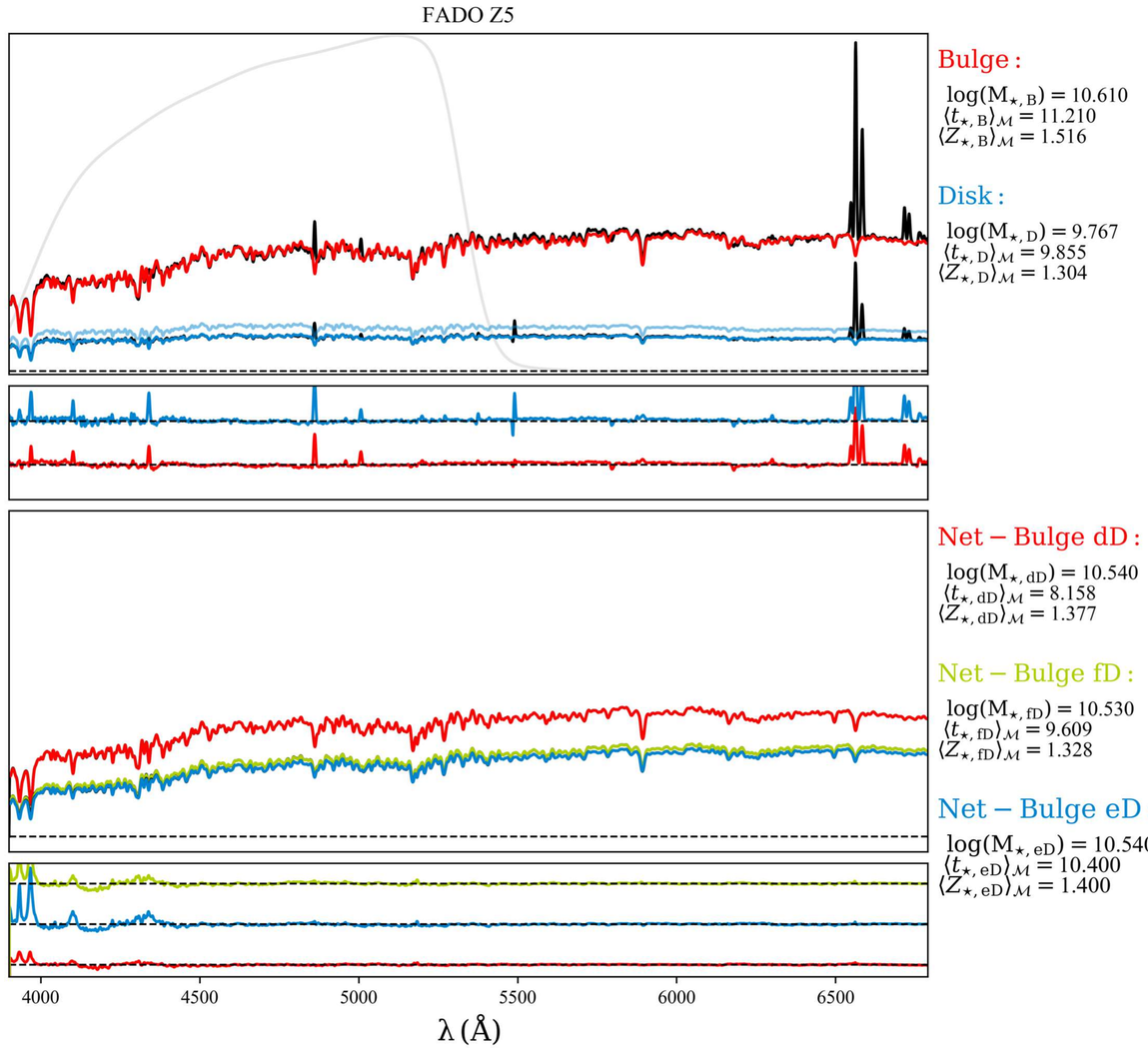
FADO Z5
Bulge :
log(M⋆, B) = 10.610
⟨t⋆, B⟩M = 11.210
⟨Z⋆, B⟩M = 1.516
Disk :
log(M⋆, D) = 9.767
⟨t⋆, D⟩M = 9.855
⟨Z⋆, D⟩M = 1.304
Net − Bulge dD :
log(M⋆, dD) = 10.540
⟨t⋆, dD⟩M = 8.158
⟨Z⋆, dD⟩M = 1.377
Net − Bulge fD :
log(M⋆, fD) = 10.530
⟨t⋆, fD⟩M = 9.609
⟨Z⋆, fD⟩M = 1.328
Net − Bulge eD :
log(M⋆, eD) = 10.540
⟨t⋆, eD⟩M = 10.400
⟨Z⋆, eD⟩M = 1.400
λ (Å)

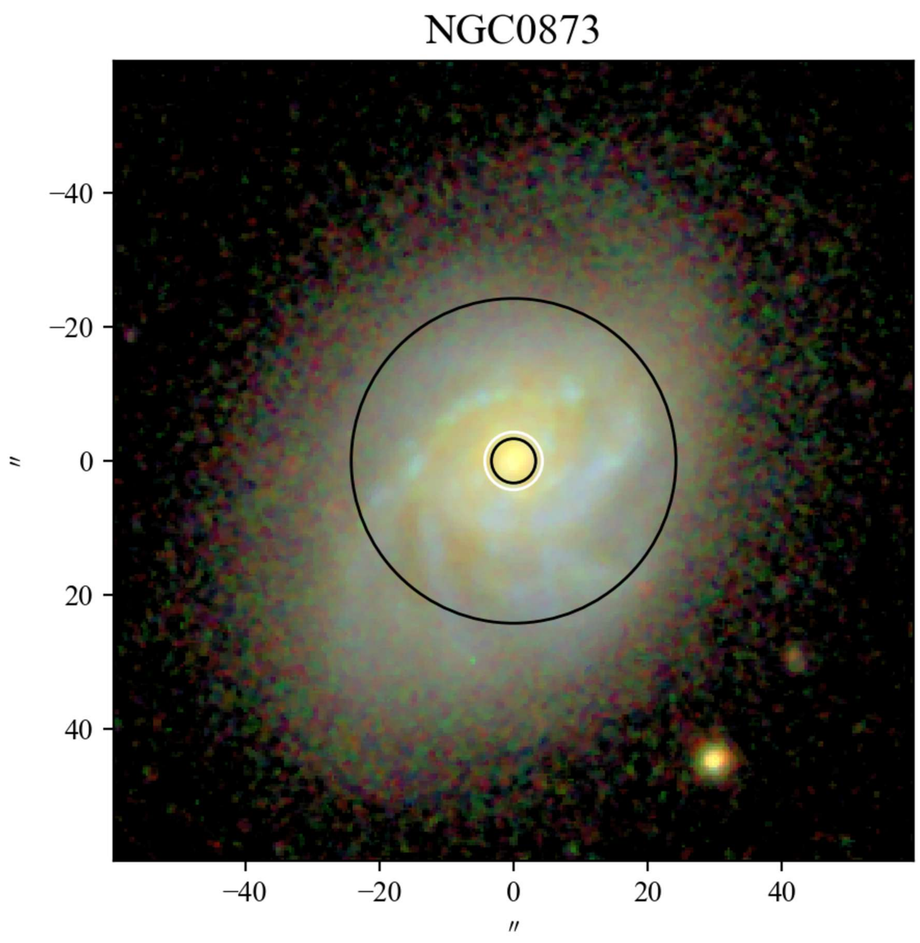
NGC0873
−40
−20
0
20
40
″
−40
−20
0
20
40
″

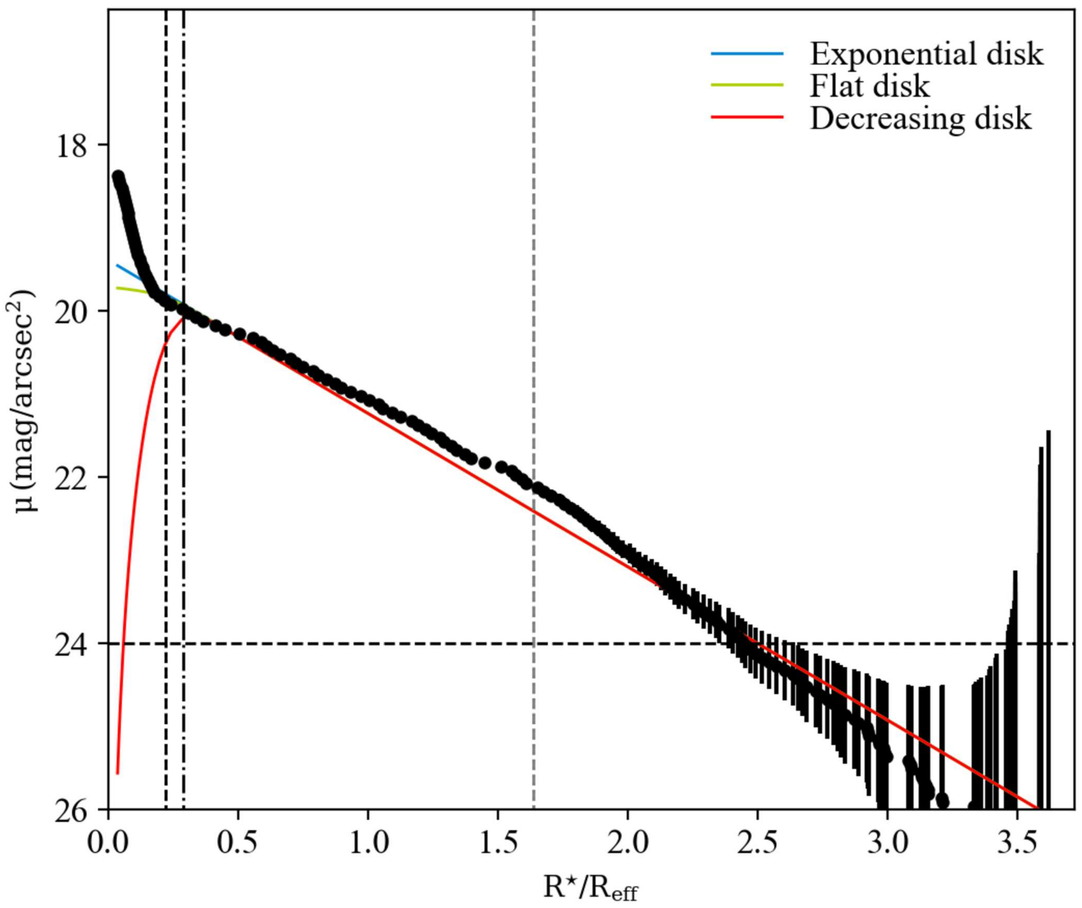
Exponential disk
Flat disk
Decreasing disk
μ (mag/arcsec²)
18
20
22
24
26
0.0
0.5
1.0
1.5
2.0
2.5
3.0
3.5
R⋆/Reff

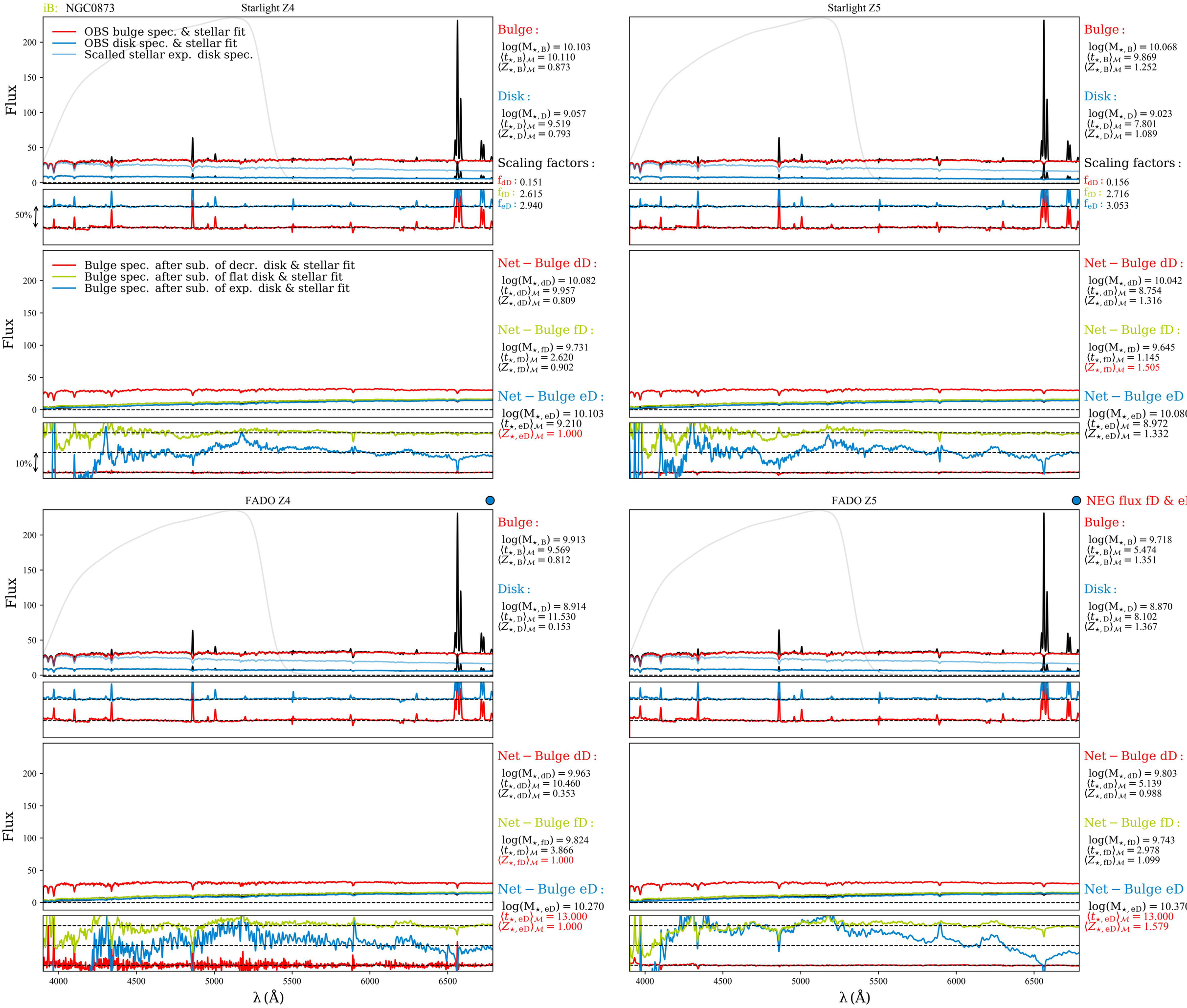
iB: NGC0873
Starlight Z4
OBS bulge spec. & stellar fit
OBS disk spec. & stellar fit
Scalled stellar exp. disk spec.
Flux
Bulge :
log(M⋆, B) = 10.103
⟨t⋆, B⟩M = 10.110
⟨Z⋆, B⟩M = 0.873
Disk :
log(M⋆, D) = 9.057
⟨t⋆, D⟩M = 9.519
⟨Z⋆, D⟩M = 0.793
Scaling factors :
fdD : 0.151
ffD : 2.615
feD : 2.940
50%
Bulge spec. after sub. of decr. disk & stellar fit
Bulge spec. after sub. of flat disk & stellar fit
Bulge spec. after sub. of exp. disk & stellar fit
Net − Bulge dD :
log(M⋆, dD) = 10.082
⟨t⋆, dD⟩M = 9.957
⟨Z⋆, dD⟩M = 0.809
Net − Bulge fD :
log(M⋆, fD) = 9.731
⟨t⋆, fD⟩M = 2.620
⟨Z⋆, fD⟩M = 0.902
Net − Bulge eD :
log(M⋆, eD) = 10.103
⟨t⋆, eD⟩M = 9.210
⟨Z⋆, eD⟩M = 1.000
10%
FADO Z4
Bulge :
log(M⋆, B) = 9.913
⟨t⋆, B⟩M = 9.569
⟨Z⋆, B⟩M = 0.812
Disk :
log(M⋆, D) = 8.914
⟨t⋆, D⟩M = 11.530
⟨Z⋆, D⟩M = 0.153
Net − Bulge dD :
log(M⋆, dD) = 9.963
⟨t⋆, dD⟩M = 10.460
⟨Z⋆, dD⟩M = 0.353
Net − Bulge fD :
log(M⋆, fD) = 9.824
⟨t⋆, fD⟩M = 3.866
⟨Z⋆, fD⟩M = 1.000
Net − Bulge eD :
log(M⋆, eD) = 10.270
⟨t⋆, eD⟩M = 13.000
⟨Z⋆, eD⟩M = 1.000
λ (Å)

Starlight Z5
Bulge :
log(M⋆, B) = 10.068
⟨t⋆, B⟩M = 9.869
⟨Z⋆, B⟩M = 1.252
Disk :
log(M⋆, D) = 9.023
⟨t⋆, D⟩M = 7.801
⟨Z⋆, D⟩M = 1.089
Scaling factors :
fdD : 0.156
ffD : 2.716
feD : 3.053
Net − Bulge dD :
log(M⋆, dD) = 10.042
⟨t⋆, dD⟩M = 8.754
⟨Z⋆, dD⟩M = 1.316
Net − Bulge fD :
log(M⋆, fD) = 9.645
⟨t⋆, fD⟩M = 1.145
⟨Z⋆, fD⟩M = 1.505
Net − Bulge eD :
log(M⋆, eD) = 10.080
⟨t⋆, eD⟩M = 8.972
⟨Z⋆, eD⟩M = 1.332
FADO Z5
NEG flux fD & eD
Bulge :
log(M⋆, B) = 9.718
⟨t⋆, B⟩M = 5.474
⟨Z⋆, B⟩M = 1.351
Disk :
log(M⋆, D) = 8.870
⟨t⋆, D⟩M = 8.102
⟨Z⋆, D⟩M = 1.367
Net − Bulge dD :
log(M⋆, dD) = 9.803
⟨t⋆, dD⟩M = 5.139
⟨Z⋆, dD⟩M = 0.988
Net − Bulge fD :
log(M⋆, fD) = 9.743
⟨t⋆, fD⟩M = 2.978
⟨Z⋆, fD⟩M = 1.099
Net − Bulge eD :
log(M⋆, eD) = 10.370
⟨t⋆, eD⟩M = 13.000
⟨Z⋆, eD⟩M = 1.579
λ (Å)

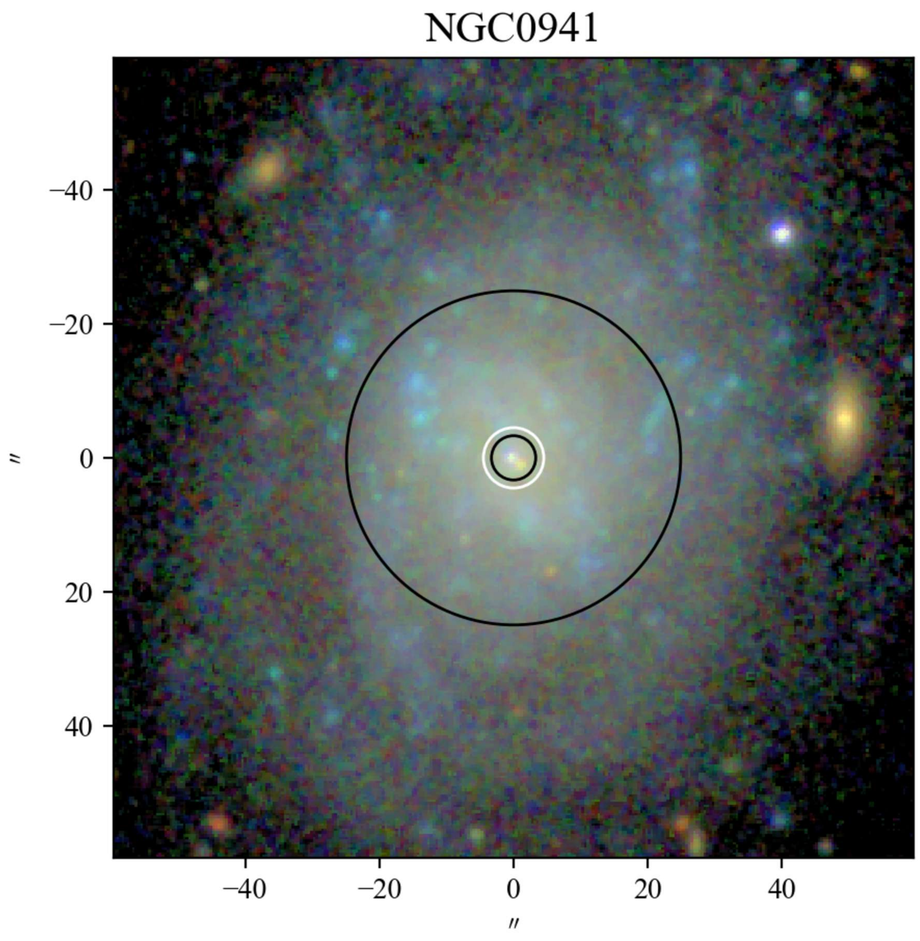
NGC0941
−40
−20
0
20
40
″
−40
−20
0
20
40
″

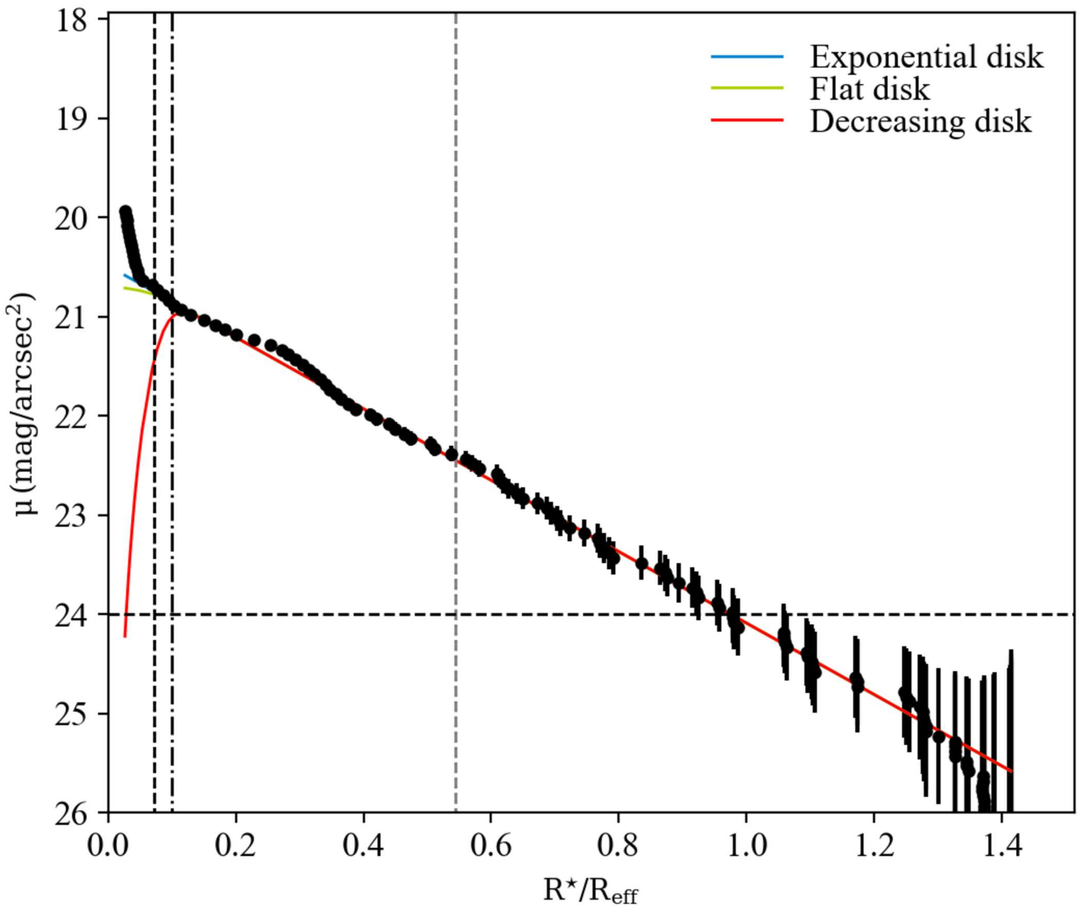
Exponential disk
Flat disk
Decreasing disk
μ (mag/arcsec²)
18
19
20
21
22
23
24
25
26
0.0
0.2
0.4
0.6
0.8
1.0
1.2
1.4
R⋆/Reff

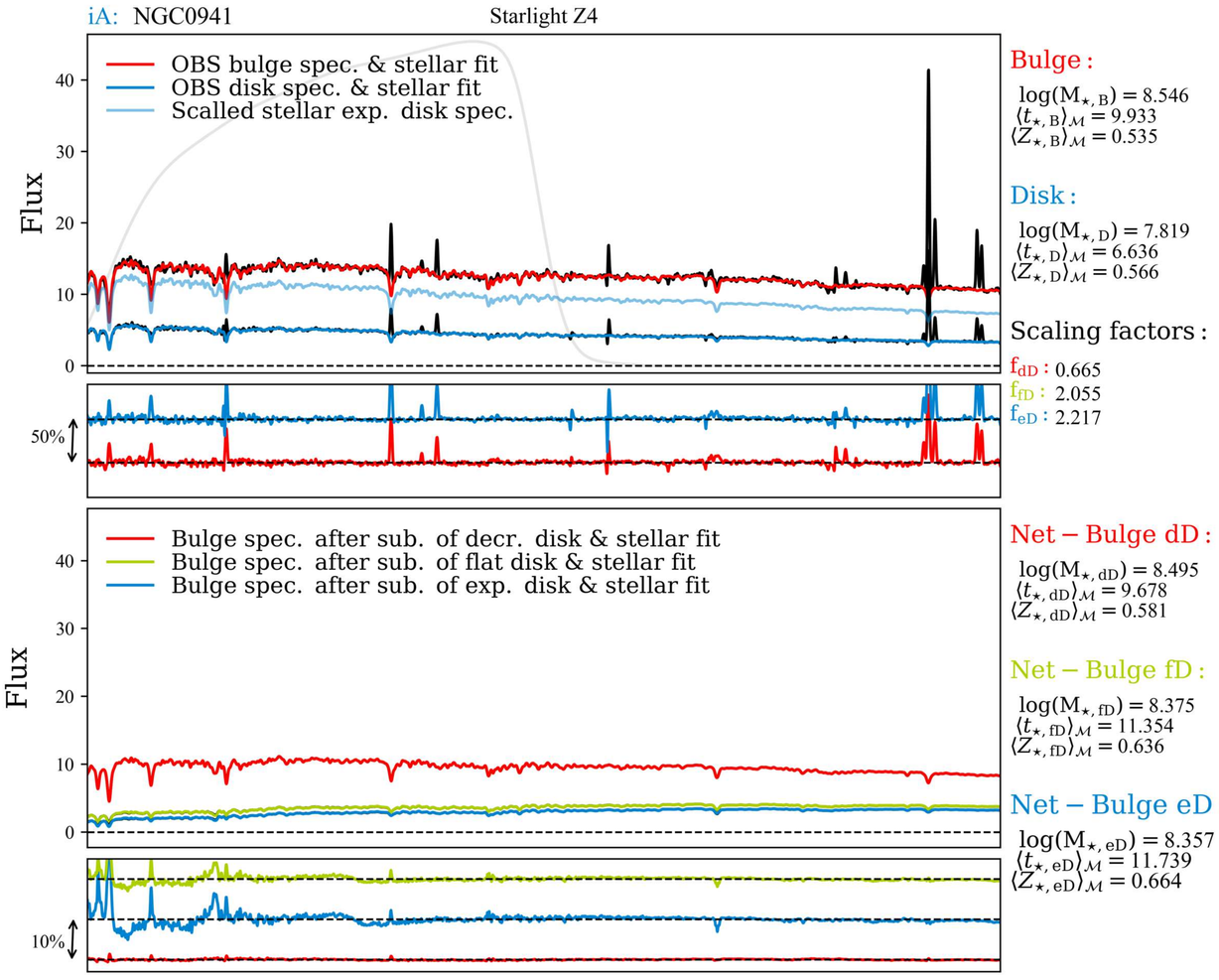
iA: NGC0941
Starlight Z4
OBS bulge spec. & stellar fit
OBS disk spec. & stellar fit
Scalled stellar exp. disk spec.
Flux
50%
Bulge :
log(M⋆, B) = 8.546
⟨t⋆, B⟩M = 9.933
⟨Z⋆, B⟩M = 0.535
Disk :
log(M⋆, D) = 7.819
⟨t⋆, D⟩M = 6.636
⟨Z⋆, D⟩M = 0.566
Scaling factors :
fdD : 0.665
ffD : 2.055
feD : 2.217
Bulge spec. after sub. of decr. disk & stellar fit
Bulge spec. after sub. of flat disk & stellar fit
Bulge spec. after sub. of exp. disk & stellar fit
10%
Net − Bulge dD :
log(M⋆, dD) = 8.495
⟨t⋆, dD⟩M = 9.678
⟨Z⋆, dD⟩M = 0.581
Net − Bulge fD :
log(M⋆, fD) = 8.375
⟨t⋆, fD⟩M = 11.354
⟨Z⋆, fD⟩M = 0.636
Net − Bulge eD :
log(M⋆, eD) = 8.357
⟨t⋆, eD⟩M = 11.739
⟨Z⋆, eD⟩M = 0.664

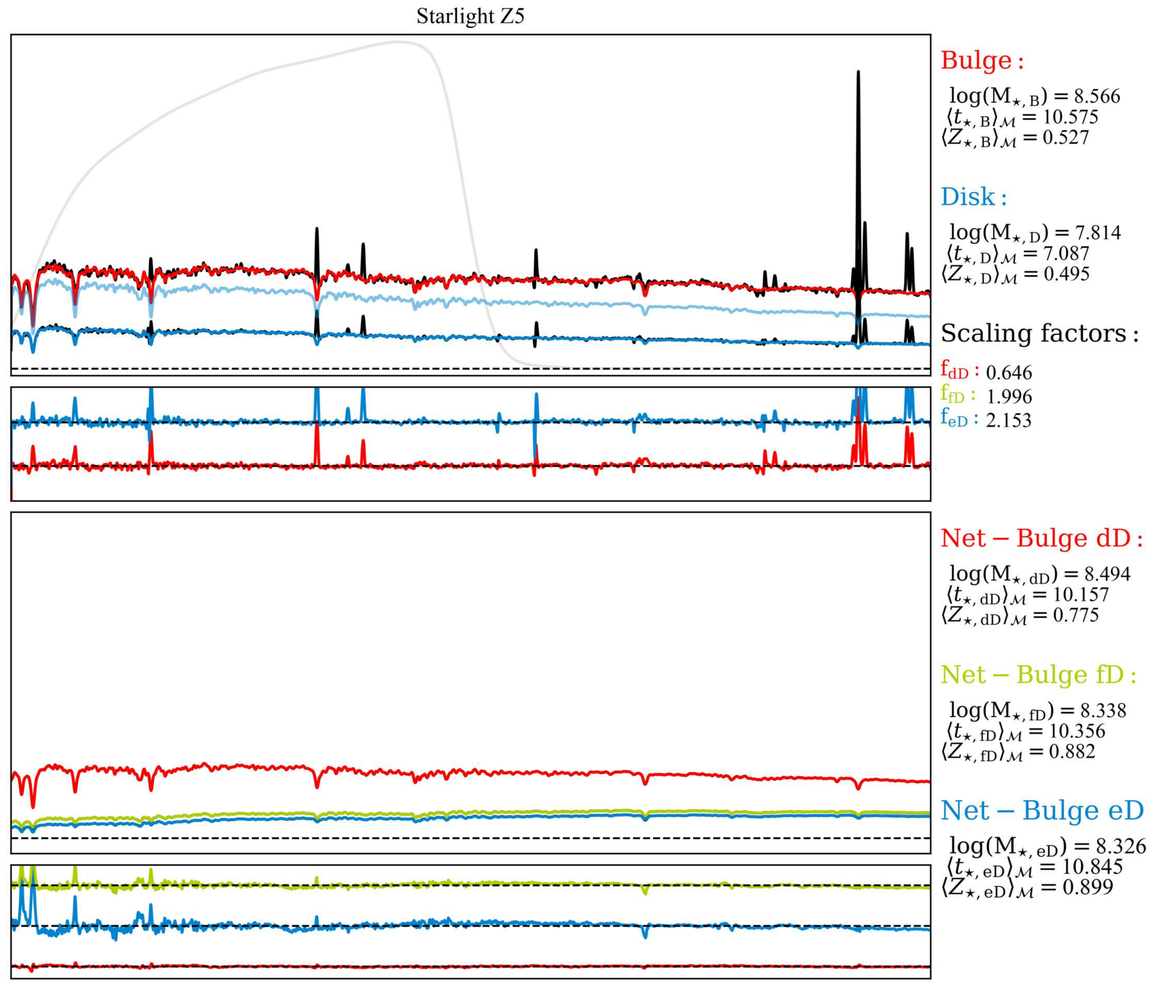
Starlight Z5
Bulge :
log(M⋆, B) = 8.566
⟨t⋆, B⟩M = 10.575
⟨Z⋆, B⟩M = 0.527
Disk :
log(M⋆, D) = 7.814
⟨t⋆, D⟩M = 7.087
⟨Z⋆, D⟩M = 0.495
Scaling factors :
fdD : 0.646
ffD : 1.996
feD : 2.153
Net − Bulge dD :
log(M⋆, dD) = 8.494
⟨t⋆, dD⟩M = 10.157
⟨Z⋆, dD⟩M = 0.775
Net − Bulge fD :
log(M⋆, fD) = 8.338
⟨t⋆, fD⟩M = 10.356
⟨Z⋆, fD⟩M = 0.882
Net − Bulge eD :
log(M⋆, eD) = 8.326
⟨t⋆, eD⟩M = 10.845
⟨Z⋆, eD⟩M = 0.899

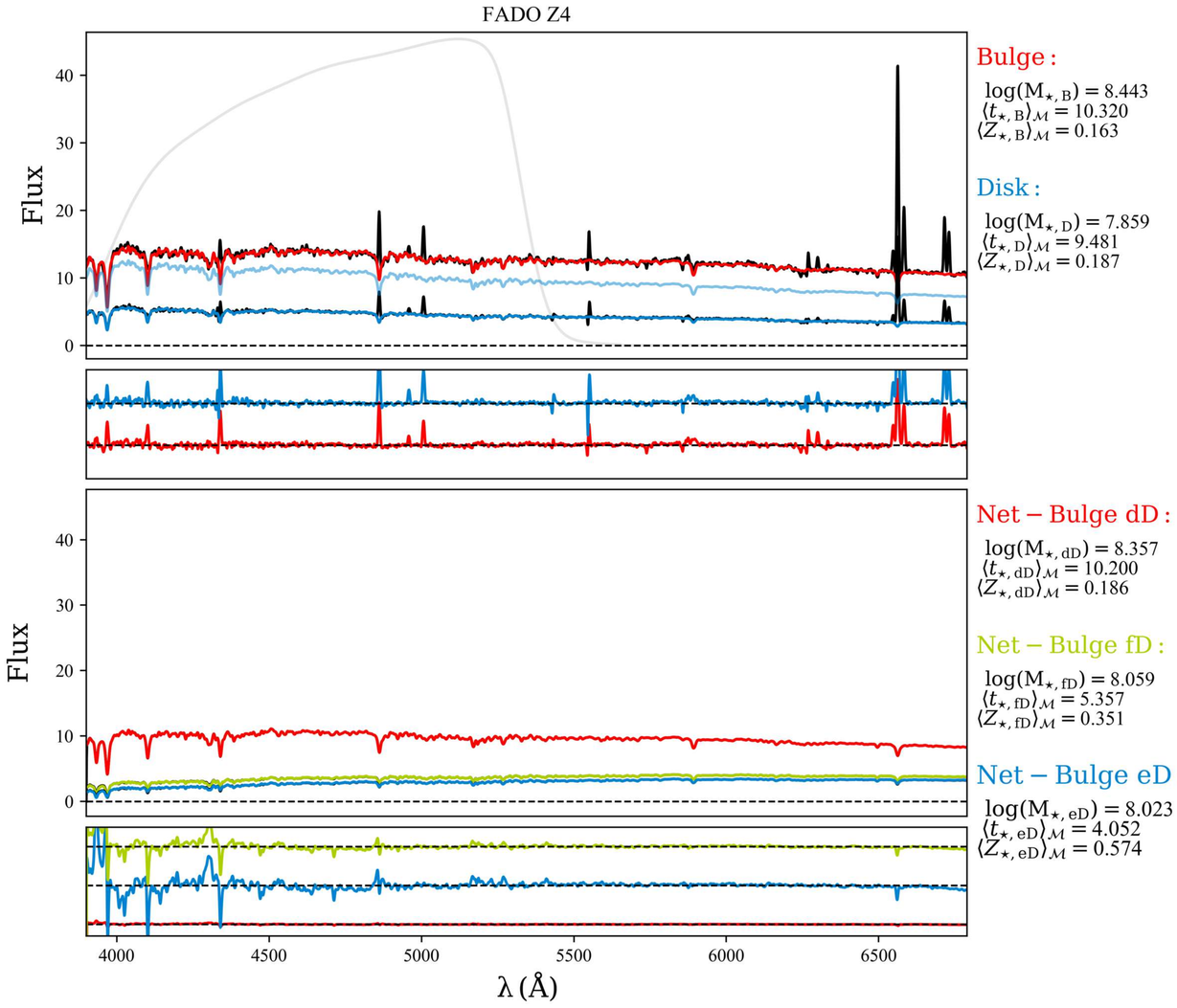
FADO Z4
Flux
Bulge :
log(M⋆, B) = 8.443
⟨t⋆, B⟩M = 10.320
⟨Z⋆, B⟩M = 0.163
Disk :
log(M⋆, D) = 7.859
⟨t⋆, D⟩M = 9.481
⟨Z⋆, D⟩M = 0.187
Net − Bulge dD :
log(M⋆, dD) = 8.357
⟨t⋆, dD⟩M = 10.200
⟨Z⋆, dD⟩M = 0.186
Net − Bulge fD :
log(M⋆, fD) = 8.059
⟨t⋆, fD⟩M = 5.357
⟨Z⋆, fD⟩M = 0.351
Net − Bulge eD :
log(M⋆, eD) = 8.023
⟨t⋆, eD⟩M = 4.052
⟨Z⋆, eD⟩M = 0.574
λ (Å)

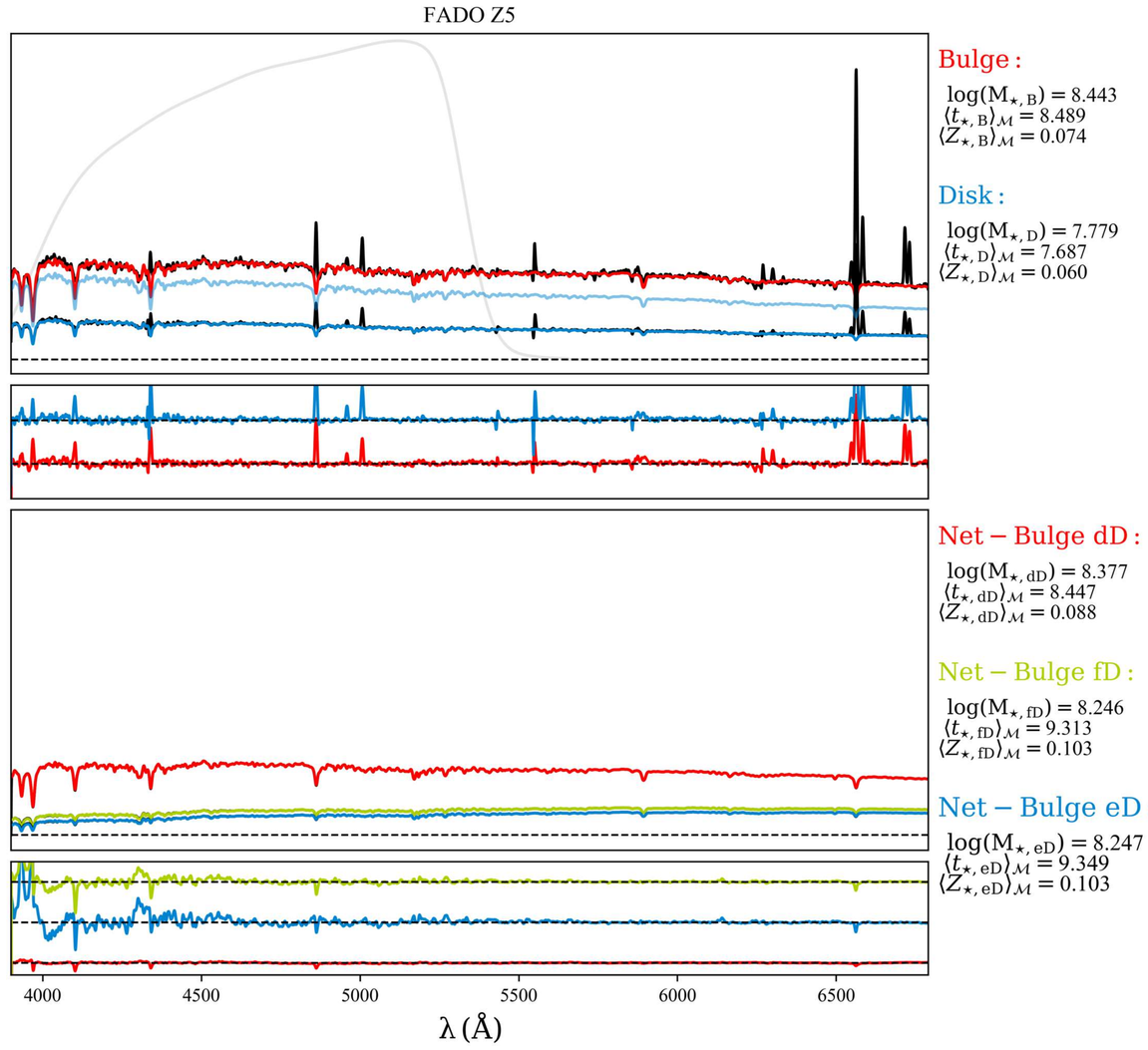
FADO Z5
Bulge :
log(M⋆, B) = 8.443
⟨t⋆, B⟩M = 8.489
⟨Z⋆, B⟩M = 0.074
Disk :
log(M⋆, D) = 7.779
⟨t⋆, D⟩M = 7.687
⟨Z⋆, D⟩M = 0.060
Net − Bulge dD :
log(M⋆, dD) = 8.377
⟨t⋆, dD⟩M = 8.447
⟨Z⋆, dD⟩M = 0.088
Net − Bulge fD :
log(M⋆, fD) = 8.246
⟨t⋆, fD⟩M = 9.313
⟨Z⋆, fD⟩M = 0.103
Net − Bulge eD :
log(M⋆, eD) = 8.247
⟨t⋆, eD⟩M = 9.349
⟨Z⋆, eD⟩M = 0.103
λ (Å)

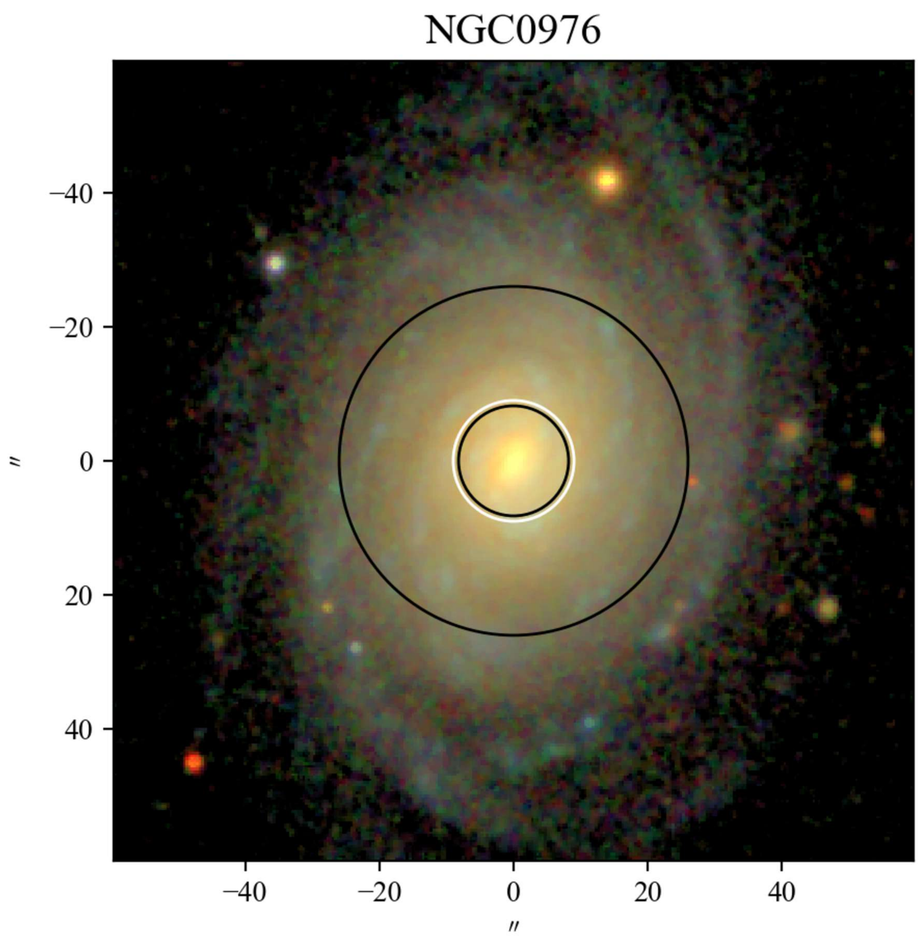
NGC0976
−40
−20
0
20
40
″
−40
−20
0
20
40
″

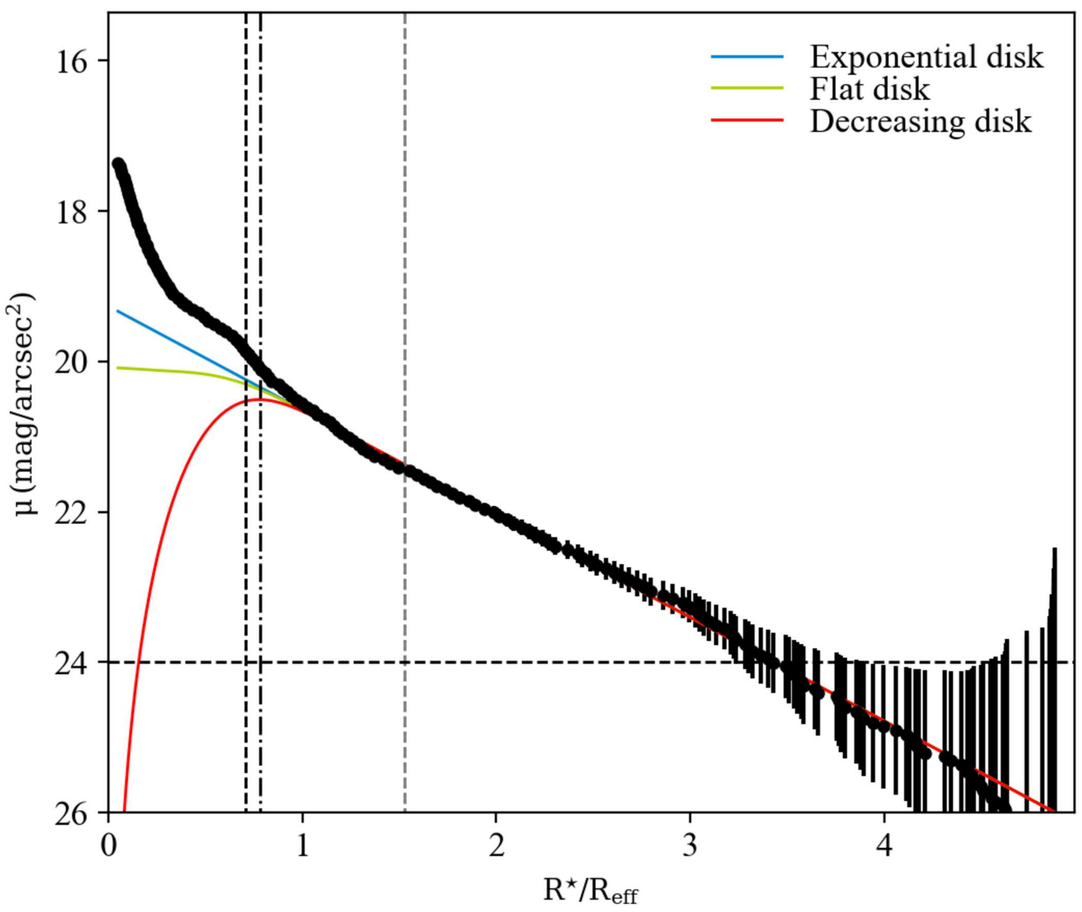
Exponential disk
Flat disk
Decreasing disk
μ (mag/arcsec²)
16
18
20
22
24
26
0
1
2
3
4
R⋆/Reff

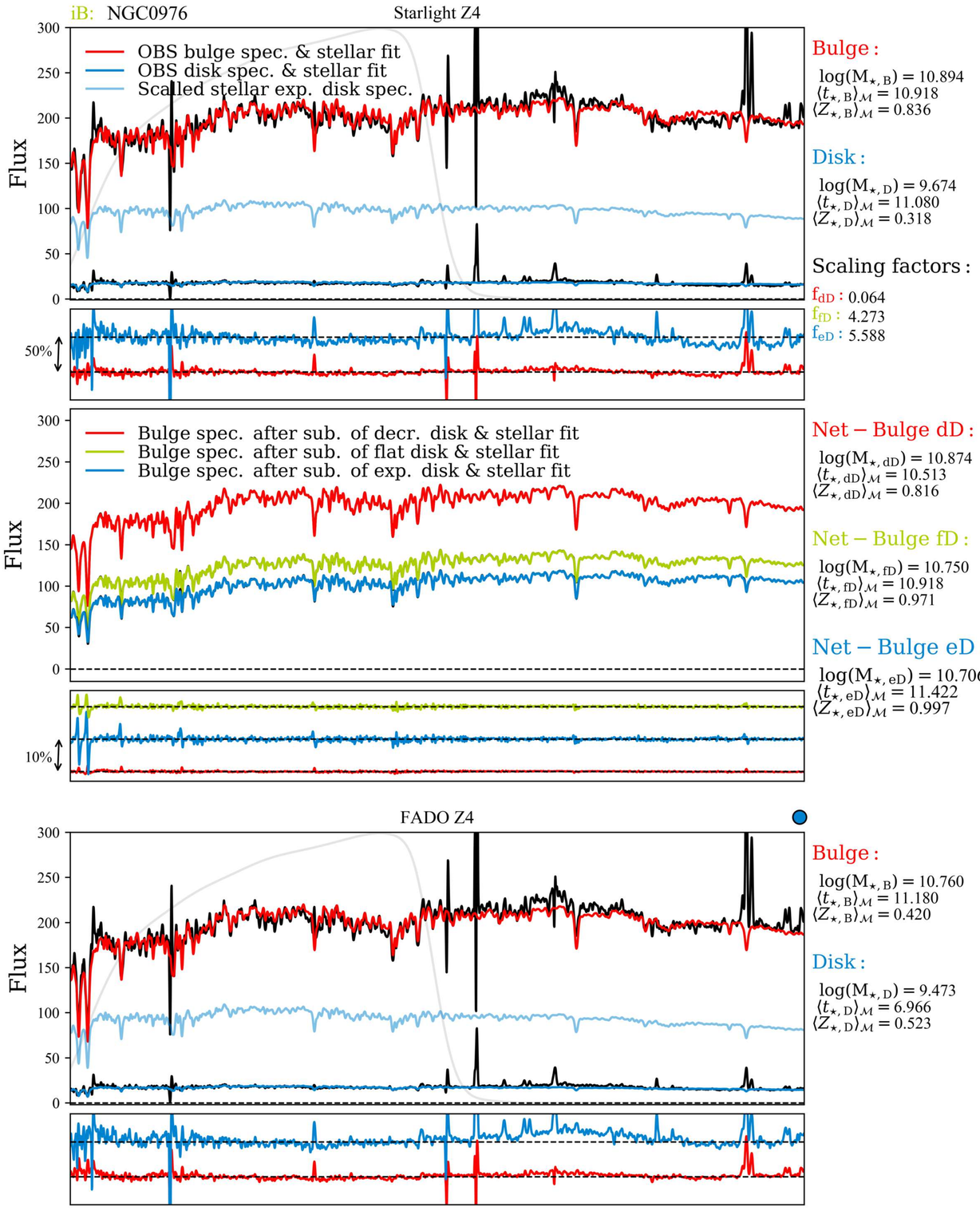
iB: NGC0976
Starlight Z4
OBS bulge spec. & stellar fit
OBS disk spec. & stellar fit
Scalled stellar exp. disk spec.
Flux
300
250
200
150
100
50
0
50%
Bulge :
log(M⋆, B) = 10.894
⟨t⋆, B⟩M = 10.918
⟨Z⋆, B⟩M = 0.836
Disk :
log(M⋆, D) = 9.674
⟨t⋆, D⟩M = 11.080
⟨Z⋆, D⟩M = 0.318
Scaling factors :
fdD : 0.064
ffD : 4.273
feD : 5.588
Bulge spec. after sub. of decr. disk & stellar fit
Bulge spec. after sub. of flat disk & stellar fit
Bulge spec. after sub. of exp. disk & stellar fit
10%
Net − Bulge dD :
log(M⋆, dD) = 10.874
⟨t⋆, dD⟩M = 10.513
⟨Z⋆, dD⟩M = 0.816
Net − Bulge fD :
log(M⋆, fD) = 10.750
⟨t⋆, fD⟩M = 10.918
⟨Z⋆, fD⟩M = 0.971
Net − Bulge eD :
log(M⋆, eD) = 10.706
⟨t⋆, eD⟩M = 11.422
⟨Z⋆, eD⟩M = 0.997

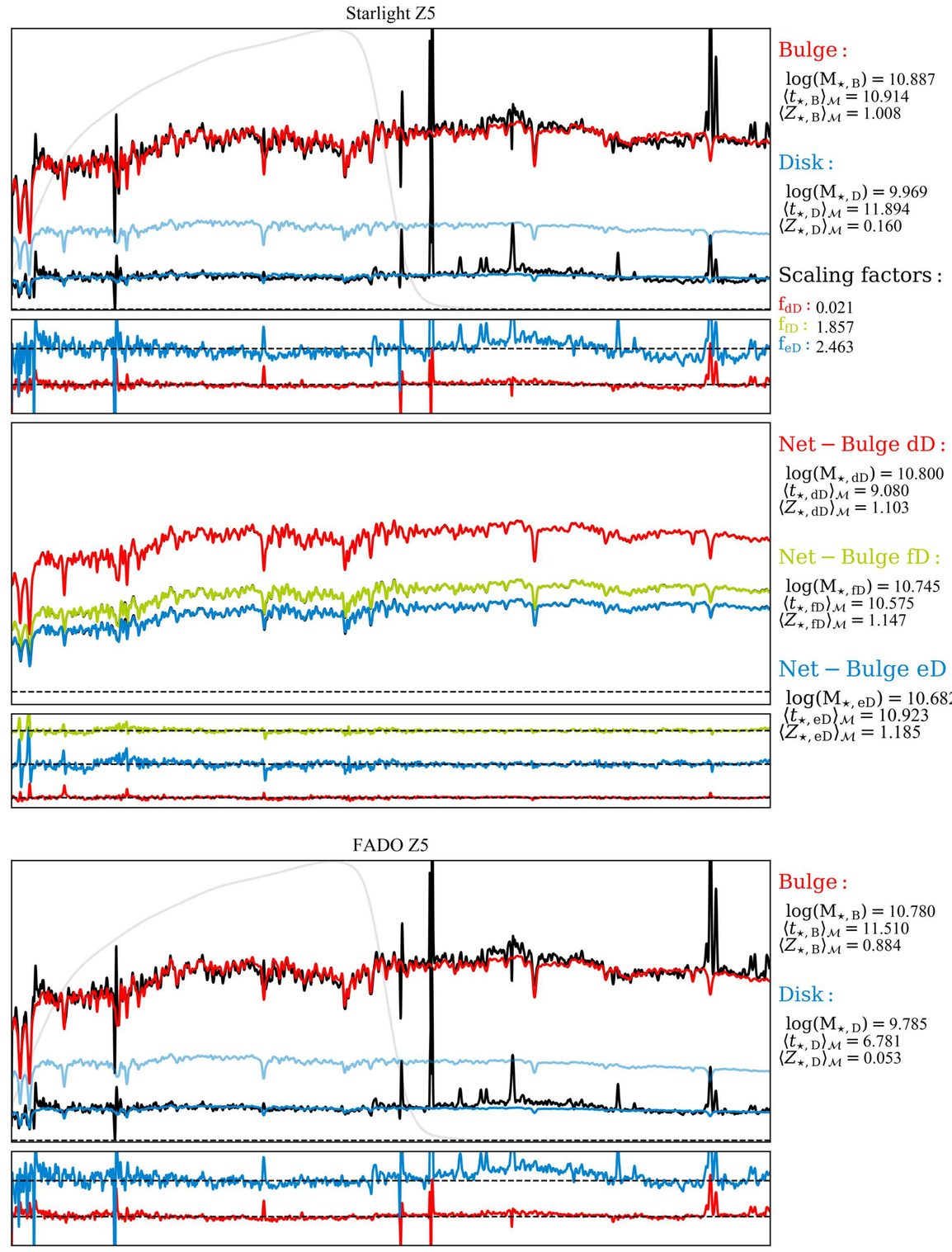
Starlight Z5
Bulge :
log(M⋆, B) = 10.887
⟨t⋆, B⟩M = 10.914
⟨Z⋆, B⟩M = 1.008
Disk :
log(M⋆, D) = 9.969
⟨t⋆, D⟩M = 11.894
⟨Z⋆, D⟩M = 0.160
Scaling factors :
fdD : 0.021
ffD : 1.857
feD : 2.463
Net − Bulge dD :
log(M⋆, dD) = 10.800
⟨t⋆, dD⟩M = 9.080
⟨Z⋆, dD⟩M = 1.103
Net − Bulge fD :
log(M⋆, fD) = 10.745
⟨t⋆, fD⟩M = 10.575
⟨Z⋆, fD⟩M = 1.147
Net − Bulge eD :
log(M⋆, eD) = 10.682
⟨t⋆, eD⟩M = 10.923
⟨Z⋆, eD⟩M = 1.185

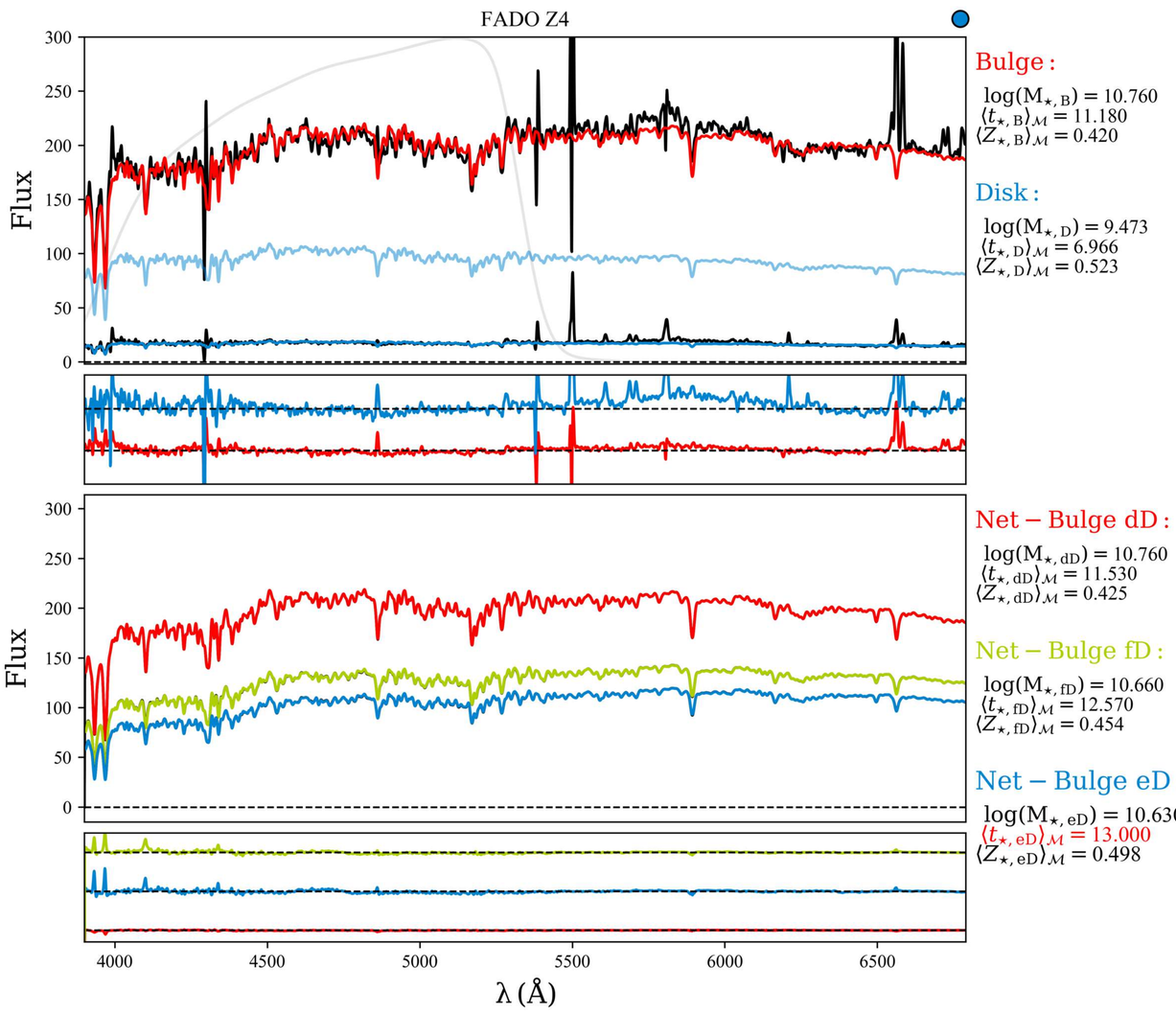
FADO Z4
Flux
300
250
200
150
100
50
0
Bulge :
log(M⋆, B) = 10.760
⟨t⋆, B⟩M = 11.180
⟨Z⋆, B⟩M = 0.420
Disk :
log(M⋆, D) = 9.473
⟨t⋆, D⟩M = 6.966
⟨Z⋆, D⟩M = 0.523
Net − Bulge dD :
log(M⋆, dD) = 10.760
⟨t⋆, dD⟩M = 11.530
⟨Z⋆, dD⟩M = 0.425
Net − Bulge fD :
log(M⋆, fD) = 10.660
⟨t⋆, fD⟩M = 12.570
⟨Z⋆, fD⟩M = 0.454
Net − Bulge eD :
log(M⋆, eD) = 10.630
⟨t⋆, eD⟩M = 13.000
⟨Z⋆, eD⟩M = 0.498
4000
4500
5000
5500
6000
6500
λ (Å)

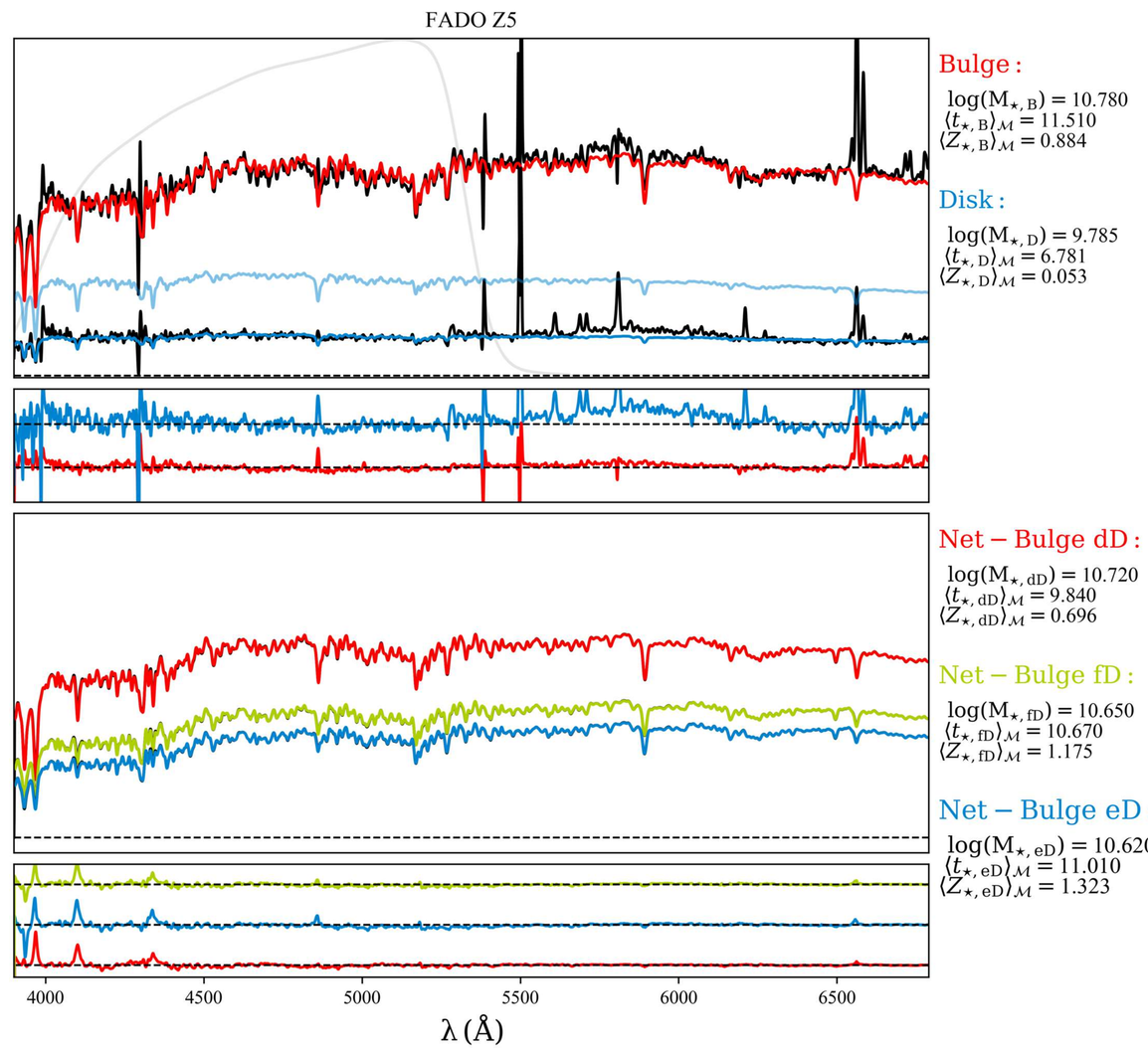
FADO Z5
Bulge :
log(M⋆, B) = 10.780
⟨t⋆, B⟩M = 11.510
⟨Z⋆, B⟩M = 0.884
Disk :
log(M⋆, D) = 9.785
⟨t⋆, D⟩M = 6.781
⟨Z⋆, D⟩M = 0.053
Net − Bulge dD :
log(M⋆, dD) = 10.720
⟨t⋆, dD⟩M = 9.840
⟨Z⋆, dD⟩M = 0.696
Net − Bulge fD :
log(M⋆, fD) = 10.650
⟨t⋆, fD⟩M = 10.670
⟨Z⋆, fD⟩M = 1.175
Net − Bulge eD :
log(M⋆, eD) = 10.620
⟨t⋆, eD⟩M = 11.010
⟨Z⋆, eD⟩M = 1.323
4000
4500
5000
5500
6000
6500
λ (Å)

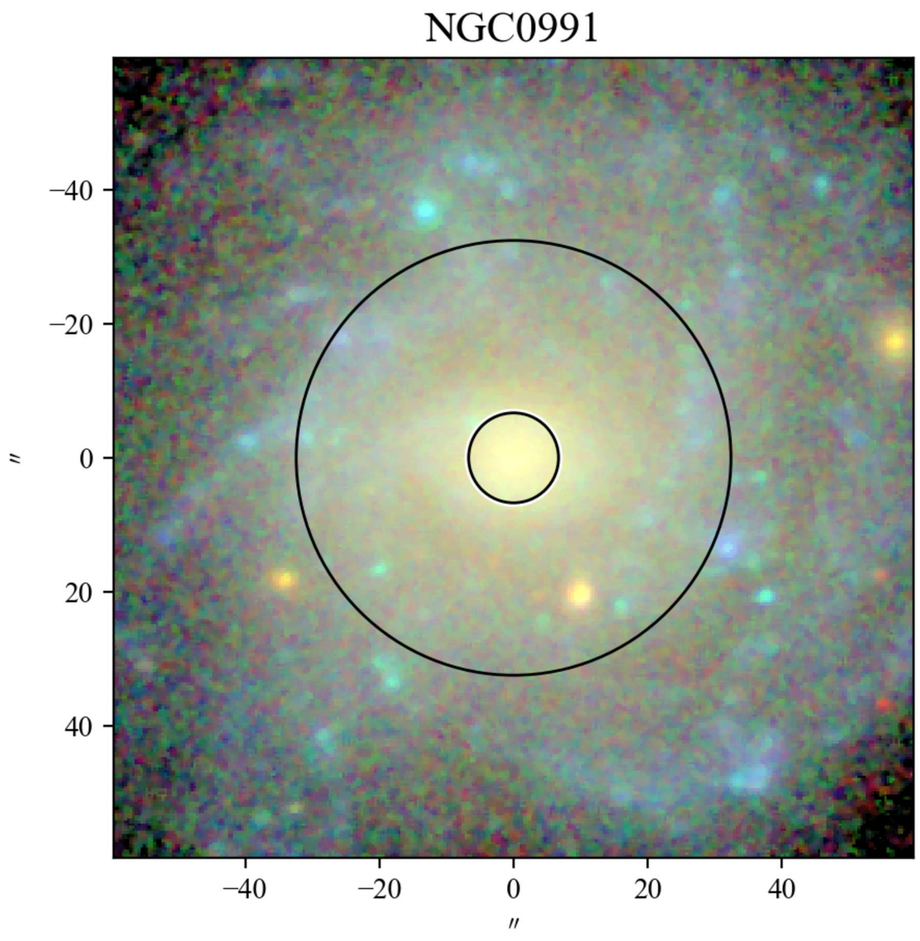
NGC0991
−40
−20
0
20
40
″
−40
−20
0
20
40
″

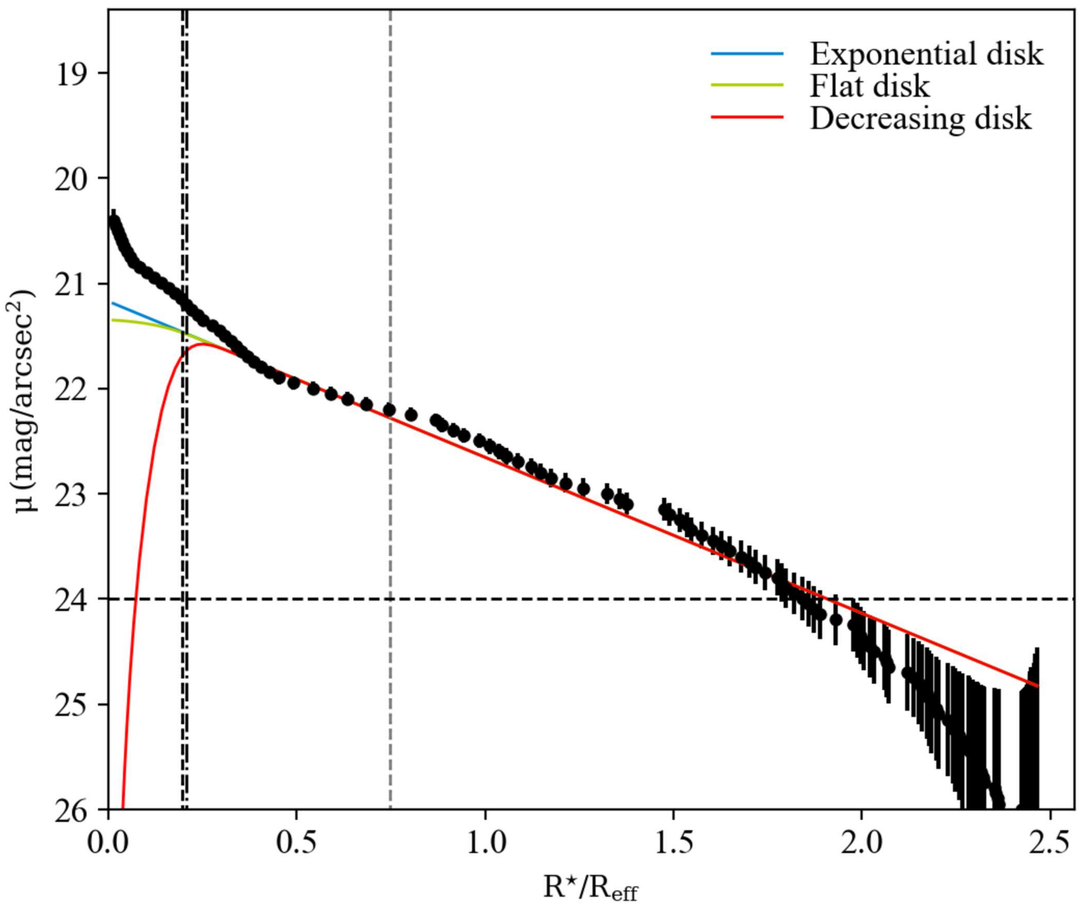
Exponential disk
Flat disk
Decreasing disk
μ (mag/arcsec²)
19
20
21
22
23
24
25
26
0.0
0.5
1.0
1.5
2.0
2.5
R⋆/Reff

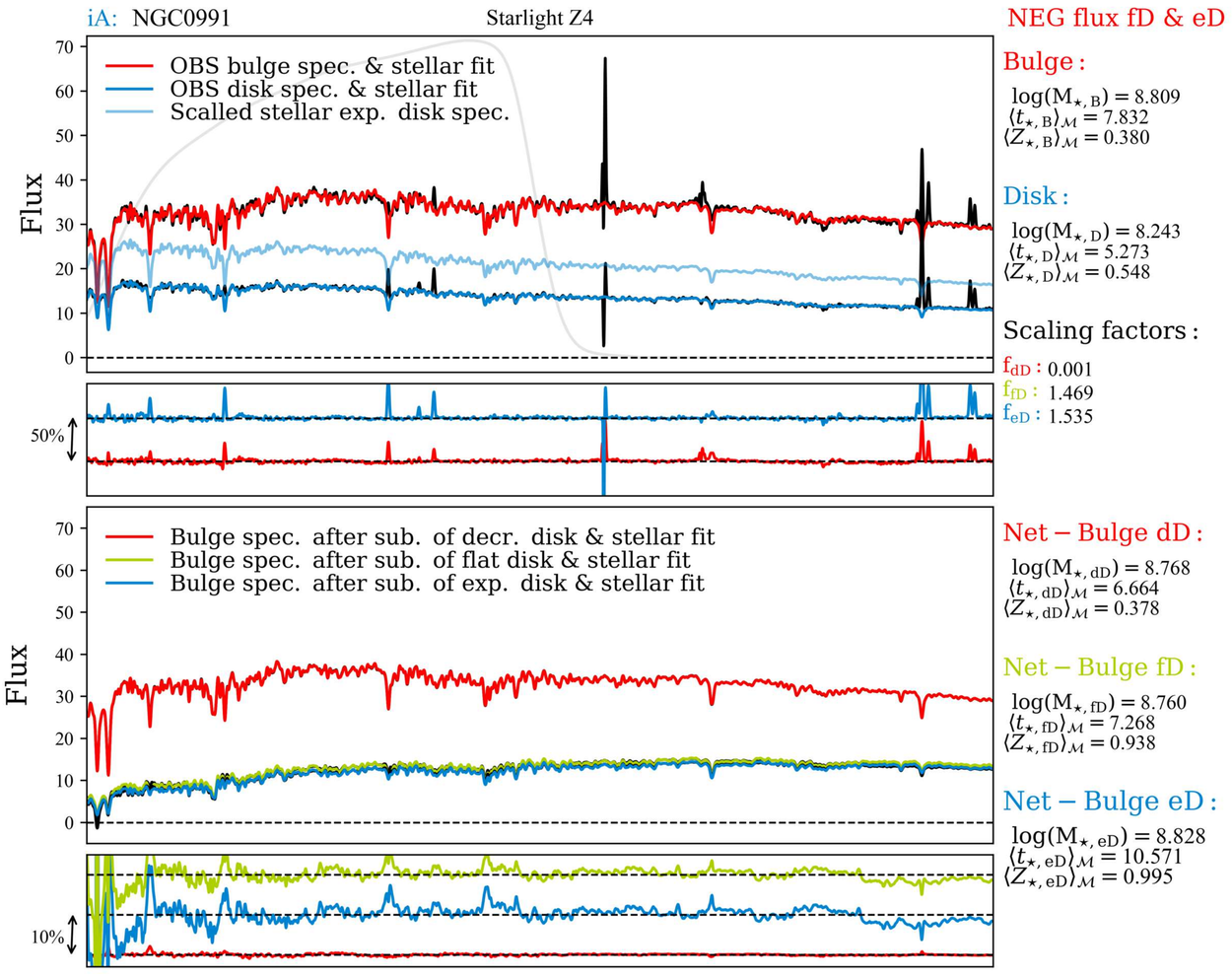
iA: NGC0991
Starlight Z4
OBS bulge spec. & stellar fit
OBS disk spec. & stellar fit
Scalled stellar exp. disk spec.
Flux
50%
NEG flux fD & eD
Bulge :
log(M⋆, B) = 8.809
⟨t⋆, B⟩M = 7.832
⟨Z⋆, B⟩M = 0.380
Disk :
log(M⋆, D) = 8.243
⟨t⋆, D⟩M = 5.273
⟨Z⋆, D⟩M = 0.548
Scaling factors :
fdD : 0.001
ffD : 1.469
feD : 1.535
Bulge spec. after sub. of decr. disk & stellar fit
Bulge spec. after sub. of flat disk & stellar fit
Bulge spec. after sub. of exp. disk & stellar fit
10%
Net − Bulge dD :
log(M⋆, dD) = 8.768
⟨t⋆, dD⟩M = 6.664
⟨Z⋆, dD⟩M = 0.378
Net − Bulge fD :
log(M⋆, fD) = 8.760
⟨t⋆, fD⟩M = 7.268
⟨Z⋆, fD⟩M = 0.938
Net − Bulge eD :
log(M⋆, eD) = 8.828
⟨t⋆, eD⟩M = 10.571
⟨Z⋆, eD⟩M = 0.995

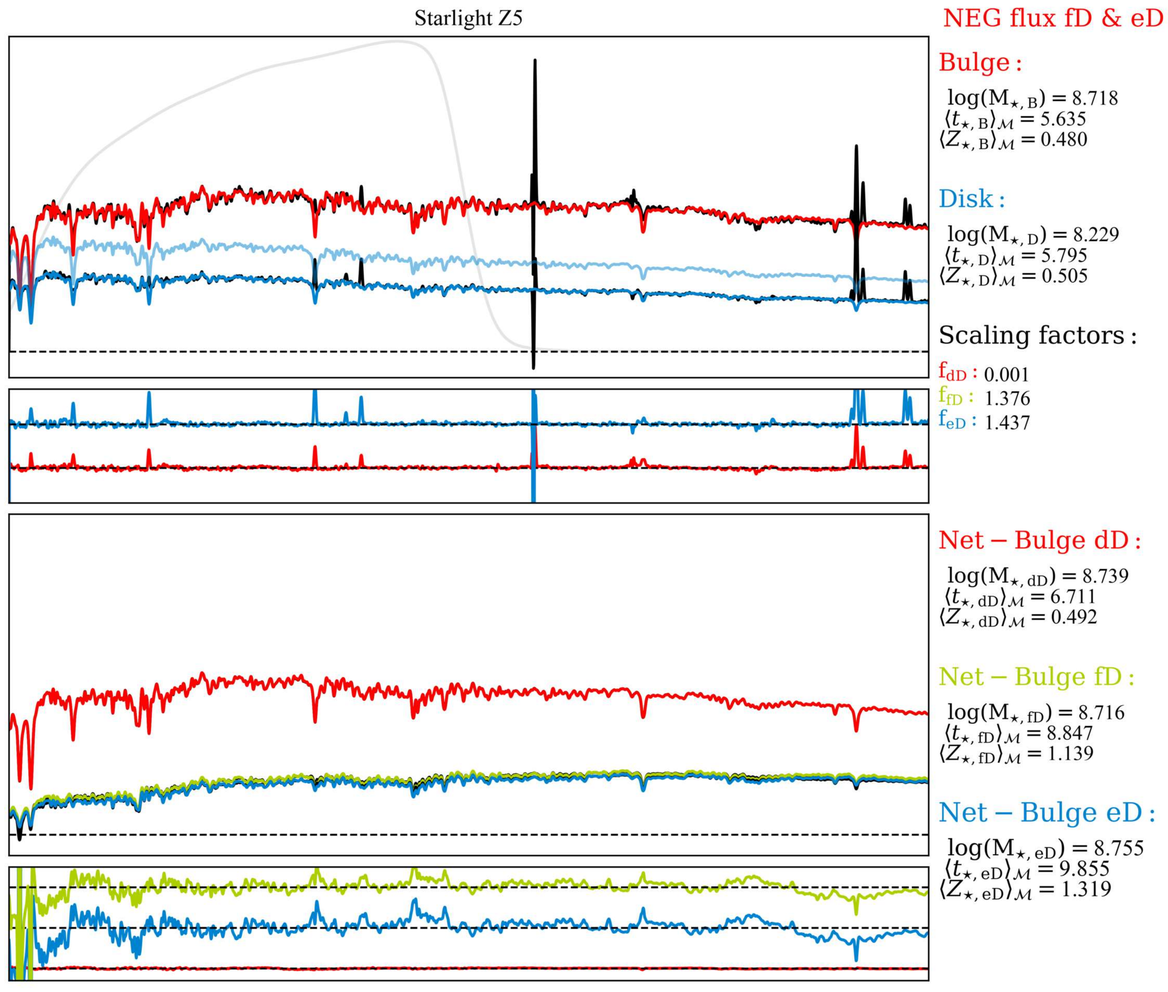
Starlight Z5
NEG flux fD & eD
Bulge :
log(M⋆, B) = 8.718
⟨t⋆, B⟩M = 5.635
⟨Z⋆, B⟩M = 0.480
Disk :
log(M⋆, D) = 8.229
⟨t⋆, D⟩M = 5.795
⟨Z⋆, D⟩M = 0.505
Scaling factors :
fdD : 0.001
ffD : 1.376
feD : 1.437
Net − Bulge dD :
log(M⋆, dD) = 8.739
⟨t⋆, dD⟩M = 6.711
⟨Z⋆, dD⟩M = 0.492
Net − Bulge fD :
log(M⋆, fD) = 8.716
⟨t⋆, fD⟩M = 8.847
⟨Z⋆, fD⟩M = 1.139
Net − Bulge eD :
log(M⋆, eD) = 8.755
⟨t⋆, eD⟩M = 9.855
⟨Z⋆, eD⟩M = 1.319

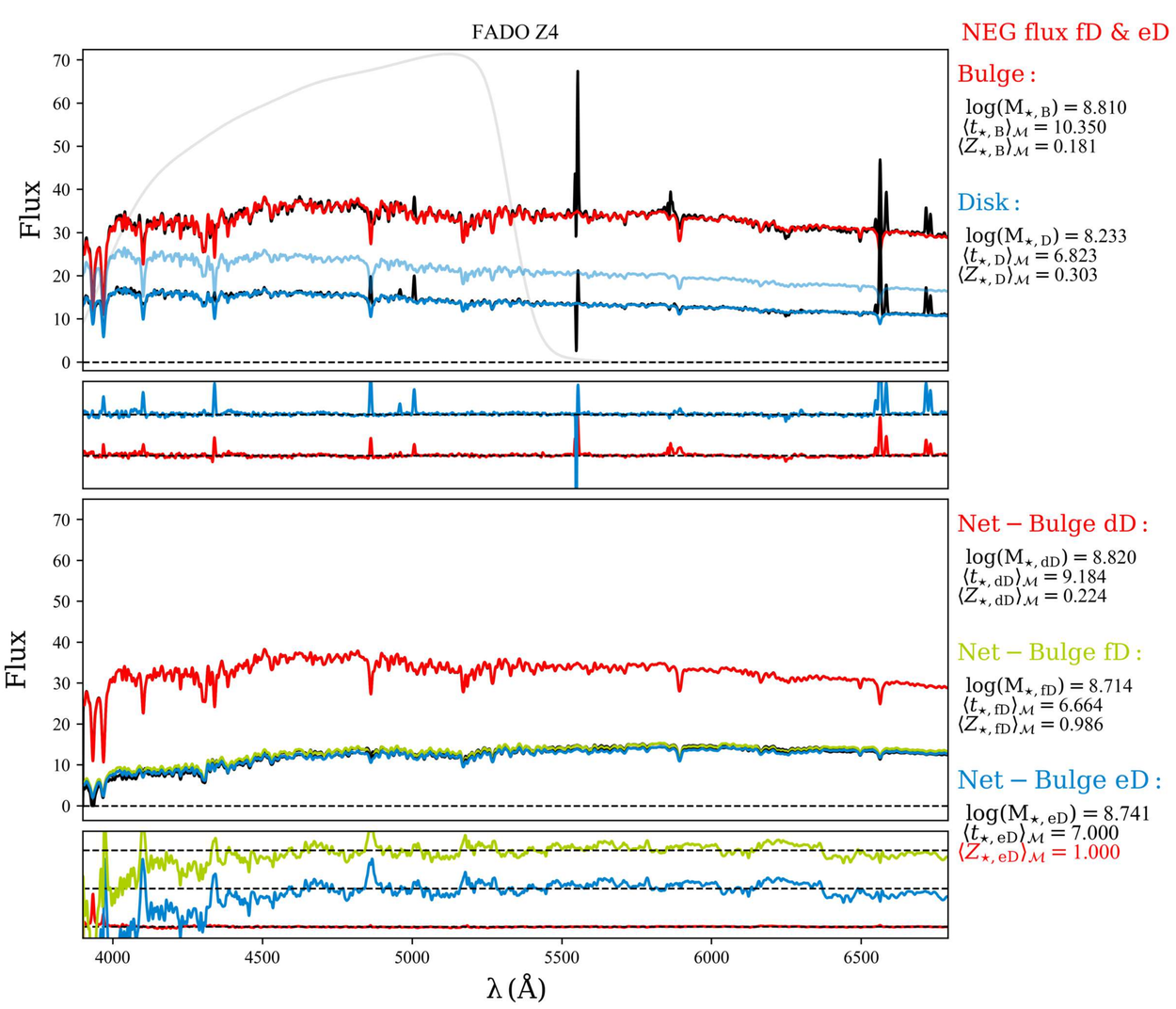
FADO Z4
NEG flux fD & eD
Bulge :
log(M⋆, B) = 8.810
⟨t⋆, B⟩M = 10.350
⟨Z⋆, B⟩M = 0.181
Disk :
log(M⋆, D) = 8.233
⟨t⋆, D⟩M = 6.823
⟨Z⋆, D⟩M = 0.303
Net − Bulge dD :
log(M⋆, dD) = 8.820
⟨t⋆, dD⟩M = 9.184
⟨Z⋆, dD⟩M = 0.224
Net − Bulge fD :
log(M⋆, fD) = 8.714
⟨t⋆, fD⟩M = 6.664
⟨Z⋆, fD⟩M = 0.986
Net − Bulge eD :
log(M⋆, eD) = 8.741
⟨t⋆, eD⟩M = 7.000
⟨Z⋆, eD⟩M = 1.000
Flux
λ (Å)

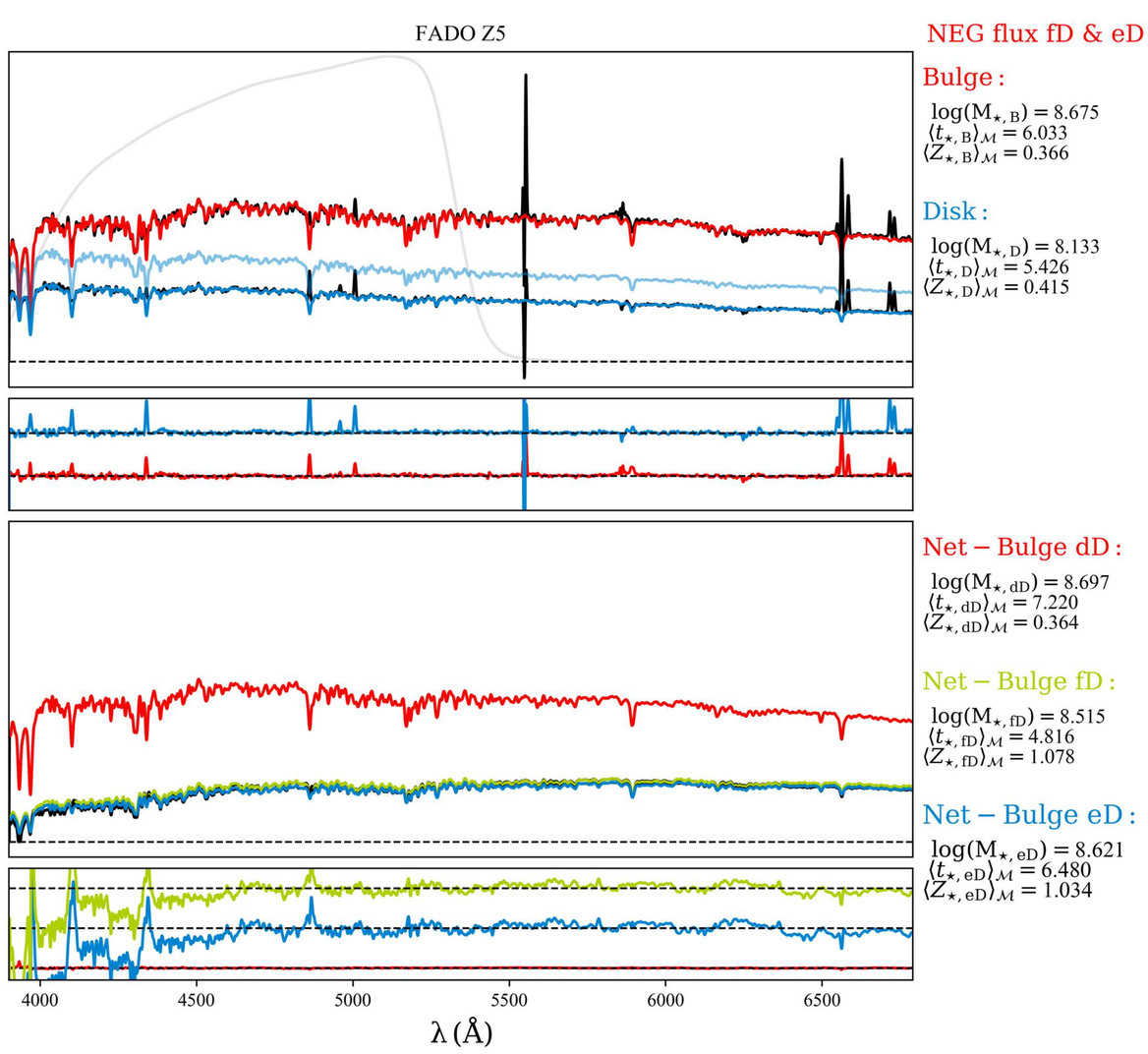
FADO Z5
NEG flux fD & eD
Bulge :
log(M⋆, B) = 8.675
⟨t⋆, B⟩M = 6.033
⟨Z⋆, B⟩M = 0.366
Disk :
log(M⋆, D) = 8.133
⟨t⋆, D⟩M = 5.426
⟨Z⋆, D⟩M = 0.415
Net − Bulge dD :
log(M⋆, dD) = 8.697
⟨t⋆, dD⟩M = 7.220
⟨Z⋆, dD⟩M = 0.364
Net − Bulge fD :
log(M⋆, fD) = 8.515
⟨t⋆, fD⟩M = 4.816
⟨Z⋆, fD⟩M = 1.078
Net − Bulge eD :
log(M⋆, eD) = 8.621
⟨t⋆, eD⟩M = 6.480
⟨Z⋆, eD⟩M = 1.034
λ (Å)

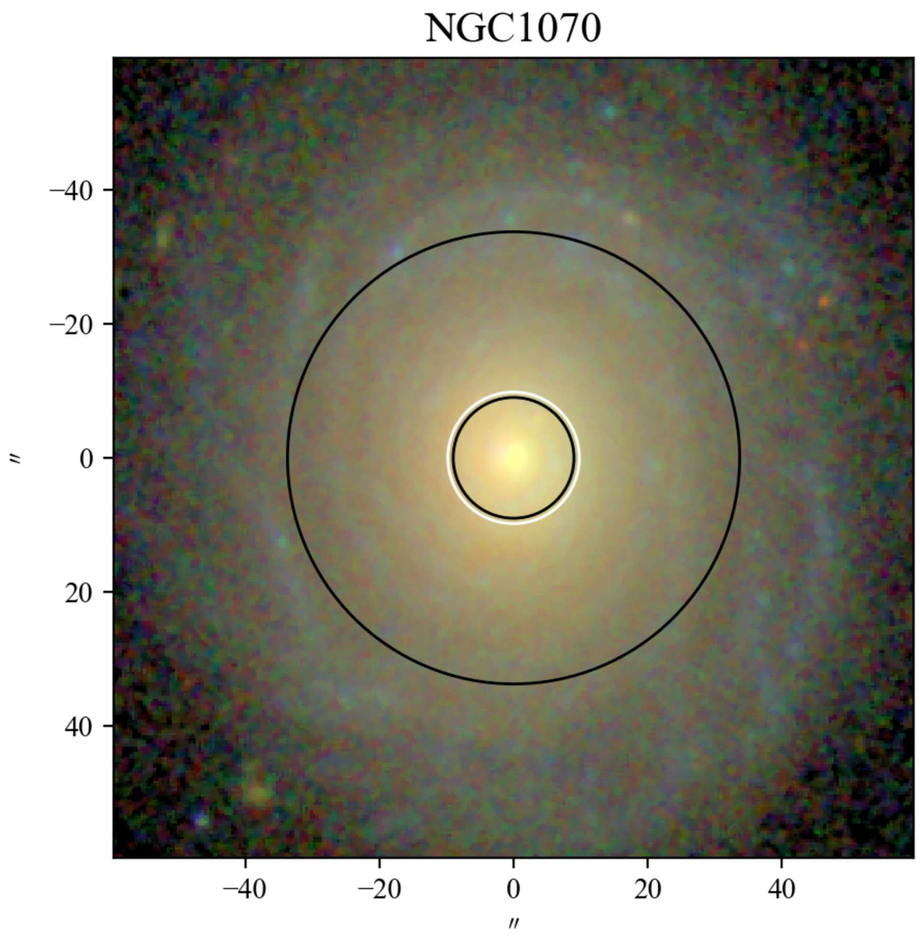

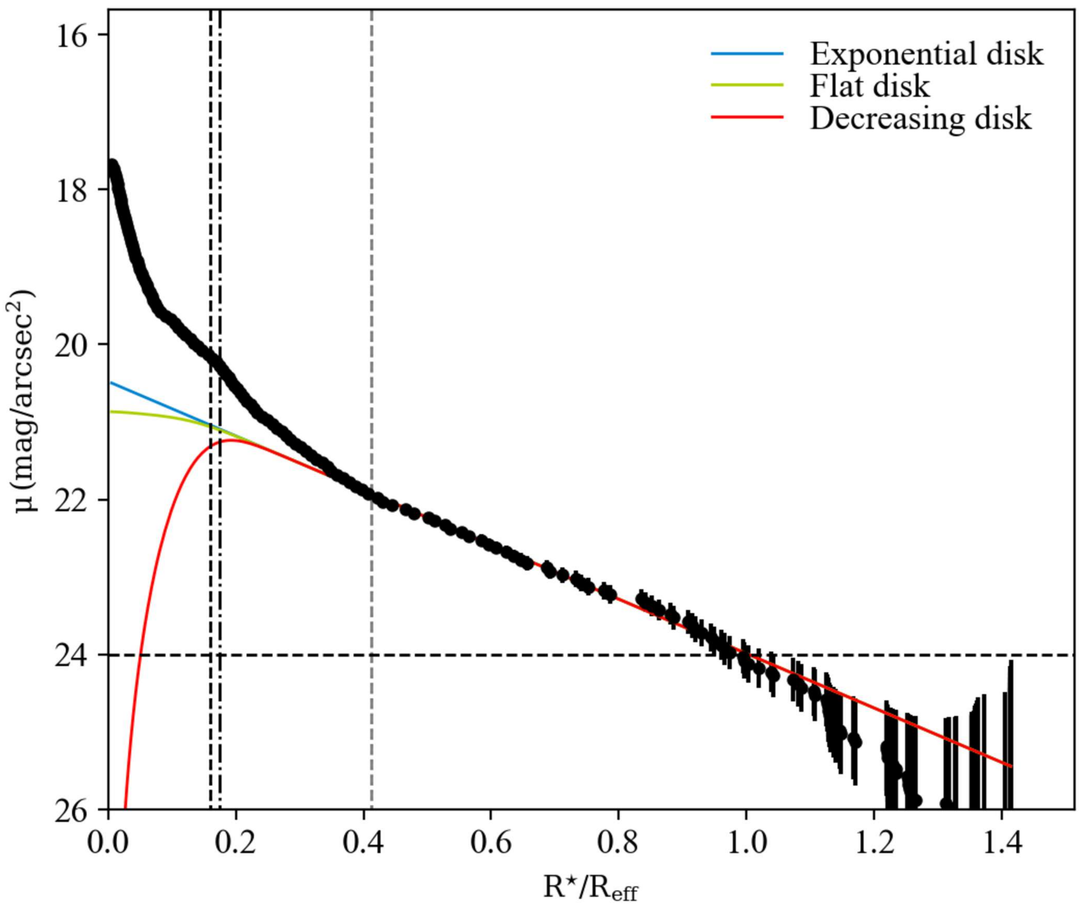

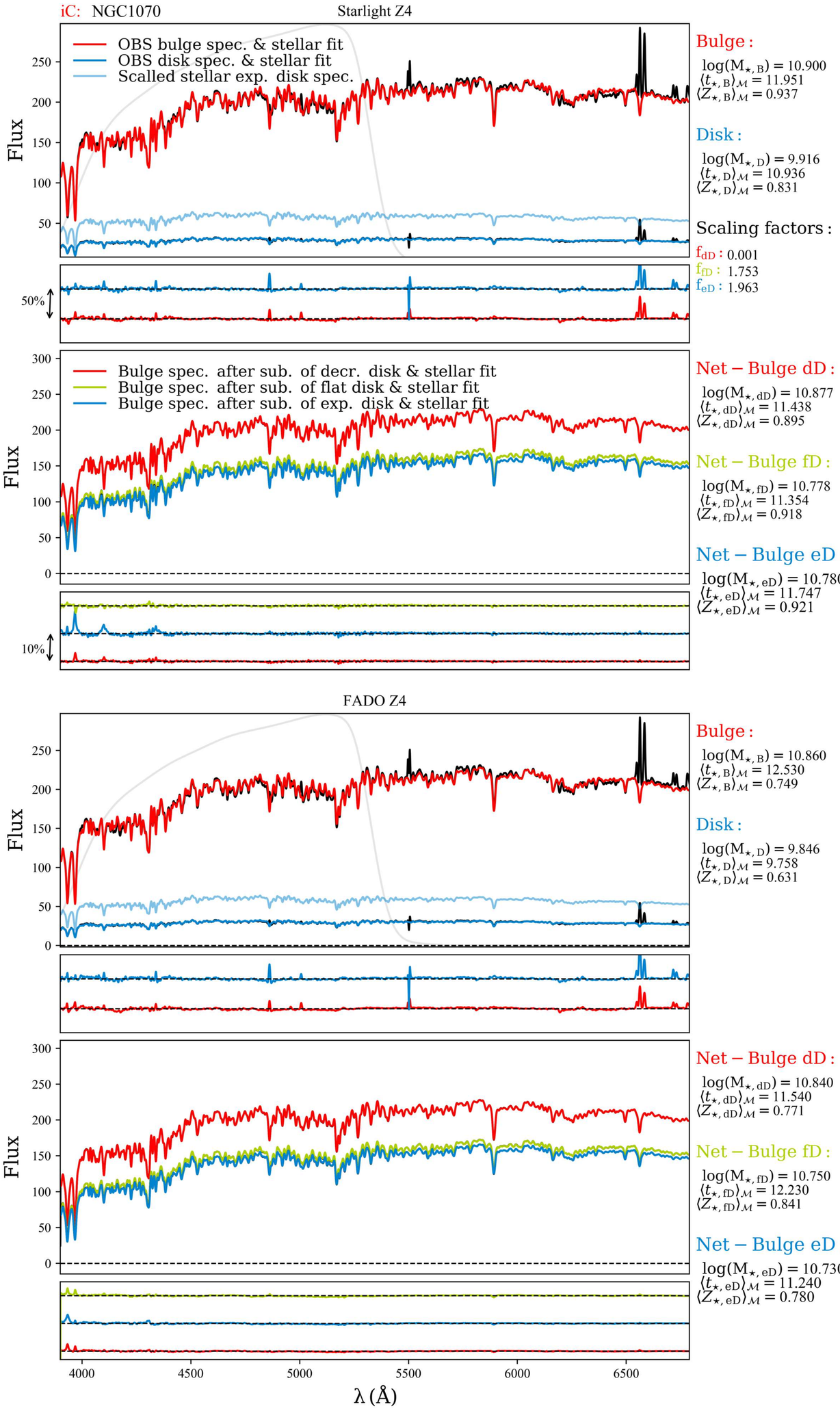

Bulge :
$\log(M_{\star,B}) = 10.900$
$\langle t_{\star,B}\rangle_{\mathcal{M}} = 11.951$
$\langle Z_{\star,B}\rangle_{\mathcal{M}} = 0.937$

Disk :
$\log(M_{\star,D}) = 9.916$
$\langle t_{\star,D}\rangle_{\mathcal{M}} = 10.936$
$\langle Z_{\star,D}\rangle_{\mathcal{M}} = 0.831$

Scaling factors :
f_{dD} : 0.001
f_{fD} : 1.753
f_{eD} : 1.963

Net − Bulge dD :
$\log(M_{\star,dD}) = 10.877$
$\langle t_{\star,dD}\rangle_{\mathcal{M}} = 11.438$
$\langle Z_{\star,dD}\rangle_{\mathcal{M}} = 0.895$

Net − Bulge fD :
$\log(M_{\star,fD}) = 10.778$
$\langle t_{\star,fD}\rangle_{\mathcal{M}} = 11.354$
$\langle Z_{\star,fD}\rangle_{\mathcal{M}} = 0.918$

Net − Bulge eD :
$\log(M_{\star,eD}) = 10.780$
$\langle t_{\star,eD}\rangle_{\mathcal{M}} = 11.747$
$\langle Z_{\star,eD}\rangle_{\mathcal{M}} = 0.921$

Bulge :
$\log(M_{\star,B}) = 12.530$
$\langle t_{\star,B}\rangle_{\mathcal{M}} = 0.749$

Disk :
$\log(M_{\star,D}) = 9.846$
$\langle t_{\star,D}\rangle_{\mathcal{M}} = 9.758$
$\langle Z_{\star,D}\rangle_{\mathcal{M}} = 0.631$

Net − Bulge dD :
$\log(M_{\star,dD}) = 10.840$
$\langle t_{\star,dD}\rangle_{\mathcal{M}} = 11.540$
$\langle Z_{\star,dD}\rangle_{\mathcal{M}} = 0.771$

Net − Bulge fD :
$\log(M_{\star,fD}) = 10.750$
$\langle t_{\star,fD}\rangle_{\mathcal{M}} = 12.230$
$\langle Z_{\star,fD}\rangle_{\mathcal{M}} = 0.841$

Net − Bulge eD :
$\log(M_{\star,eD}) = 10.730$
$\langle t_{\star,eD}\rangle_{\mathcal{M}} = 11.240$
$\langle Z_{\star,eD}\rangle_{\mathcal{M}} = 0.780$

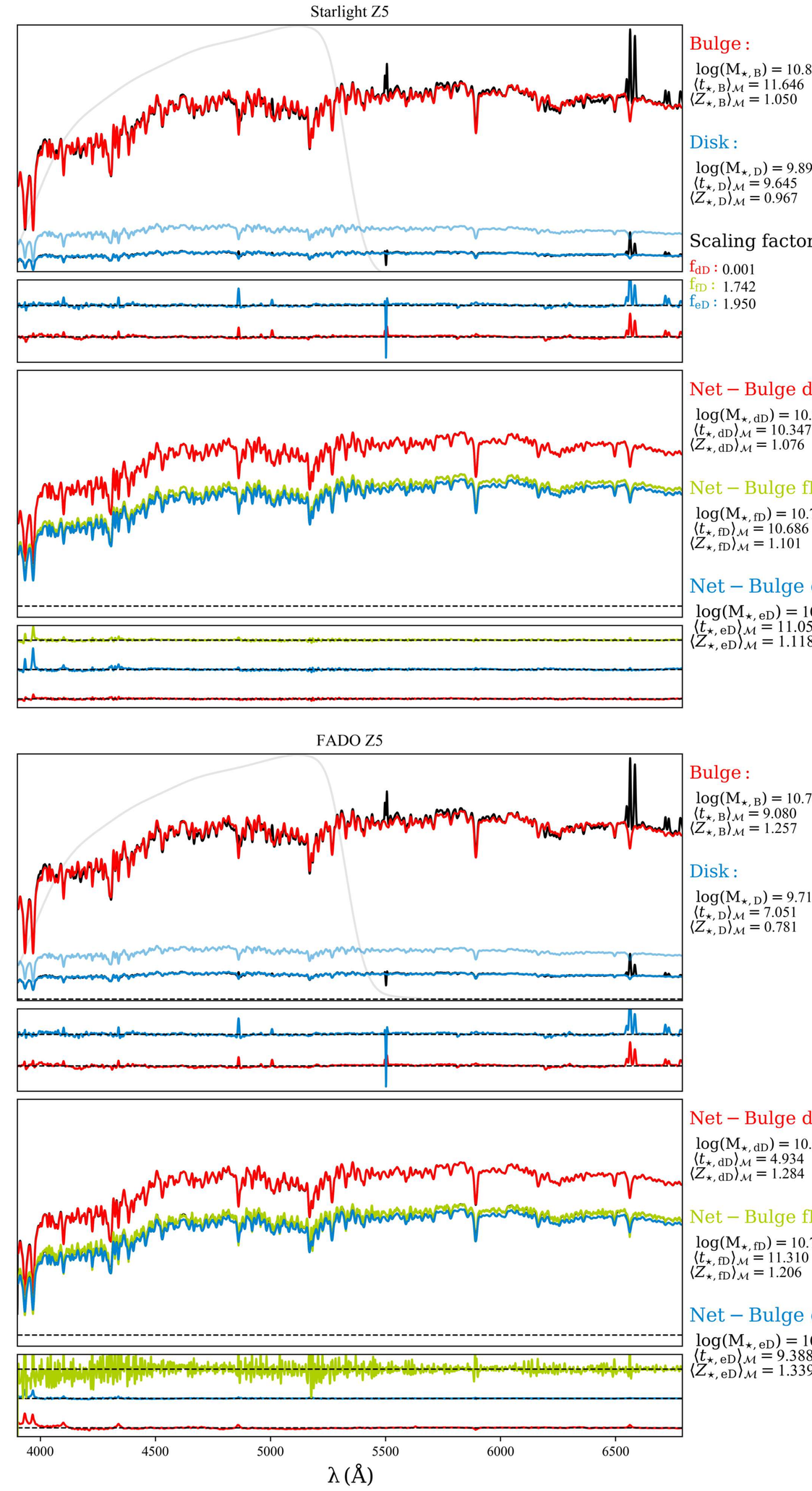

Bulge :
$\log(M_{\star,B}) = 10.864$
$\langle t_{\star,B}\rangle_{\mathcal{M}} = 11.646$
$\langle Z_{\star,B}\rangle_{\mathcal{M}} = 1.050$

Disk :
$\log(M_{\star,D}) = 9.894$
$\langle t_{\star,D}\rangle_{\mathcal{M}} = 9.645$
$\langle Z_{\star,D}\rangle_{\mathcal{M}} = 0.967$

Scaling factors :
f_{dD} : 0.001
f_{fD} : 1.742
f_{eD} : 1.950

Net − Bulge dD :
$\log(M_{\star,dD}) = 10.801$
$\langle t_{\star,dD}\rangle_{\mathcal{M}} = 10.347$
$\langle Z_{\star,dD}\rangle_{\mathcal{M}} = 1.076$

Net − Bulge fD :
$\log(M_{\star,fD}) = 10.729$
$\langle t_{\star,fD}\rangle_{\mathcal{M}} = 10.686$
$\langle Z_{\star,fD}\rangle_{\mathcal{M}} = 1.101$

Net − Bulge eD :
$\log(M_{\star,eD}) = 10.729$
$\langle t_{\star,eD}\rangle_{\mathcal{M}} = 11.056$
$\langle Z_{\star,eD}\rangle_{\mathcal{M}} = 1.118$

Bulge :
$\log(M_{\star,B}) = 10.700$
$\langle t_{\star,B}\rangle_{\mathcal{M}} = 9.080$
$\langle Z_{\star,B}\rangle_{\mathcal{M}} = 1.257$

Disk :
$\log(M_{\star,D}) = 9.716$
$\langle t_{\star,D}\rangle_{\mathcal{M}} = 7.051$
$\langle Z_{\star,D}\rangle_{\mathcal{M}} = 0.781$

Net − Bulge dD :
$\log(M_{\star,dD}) = 10.560$
$\langle t_{\star,dD}\rangle_{\mathcal{M}} = 4.934$
$\langle Z_{\star,dD}\rangle_{\mathcal{M}} = 1.284$

Net − Bulge fD :
$\log(M_{\star,fD}) = 10.700$
$\langle t_{\star,fD}\rangle_{\mathcal{M}} = 11.310$
$\langle Z_{\star,fD}\rangle_{\mathcal{M}} = 1.206$

Net − Bulge eD :
$\log(M_{\star,eD}) = 10.610$
$\langle t_{\star,eD}\rangle_{\mathcal{M}} = 9.388$
$\langle Z_{\star,eD}\rangle_{\mathcal{M}} = 1.339$

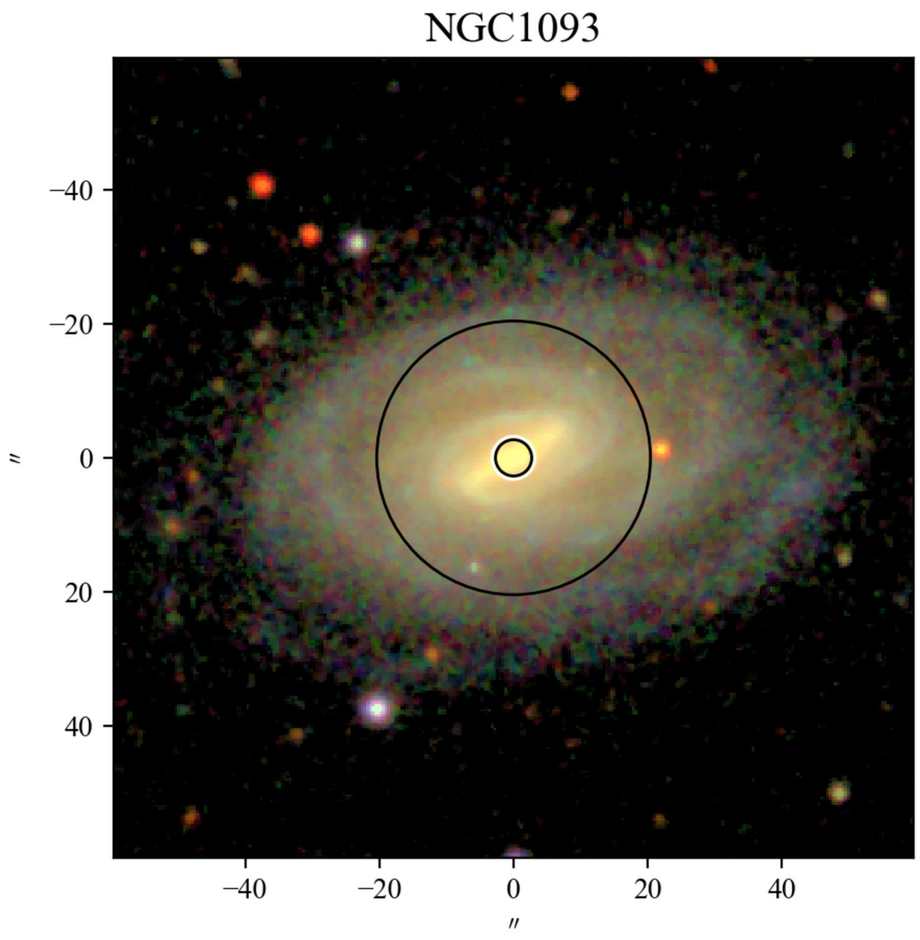
NGC1093
−40
−20
0
20
40
″
−40
−20
0
20
40
″

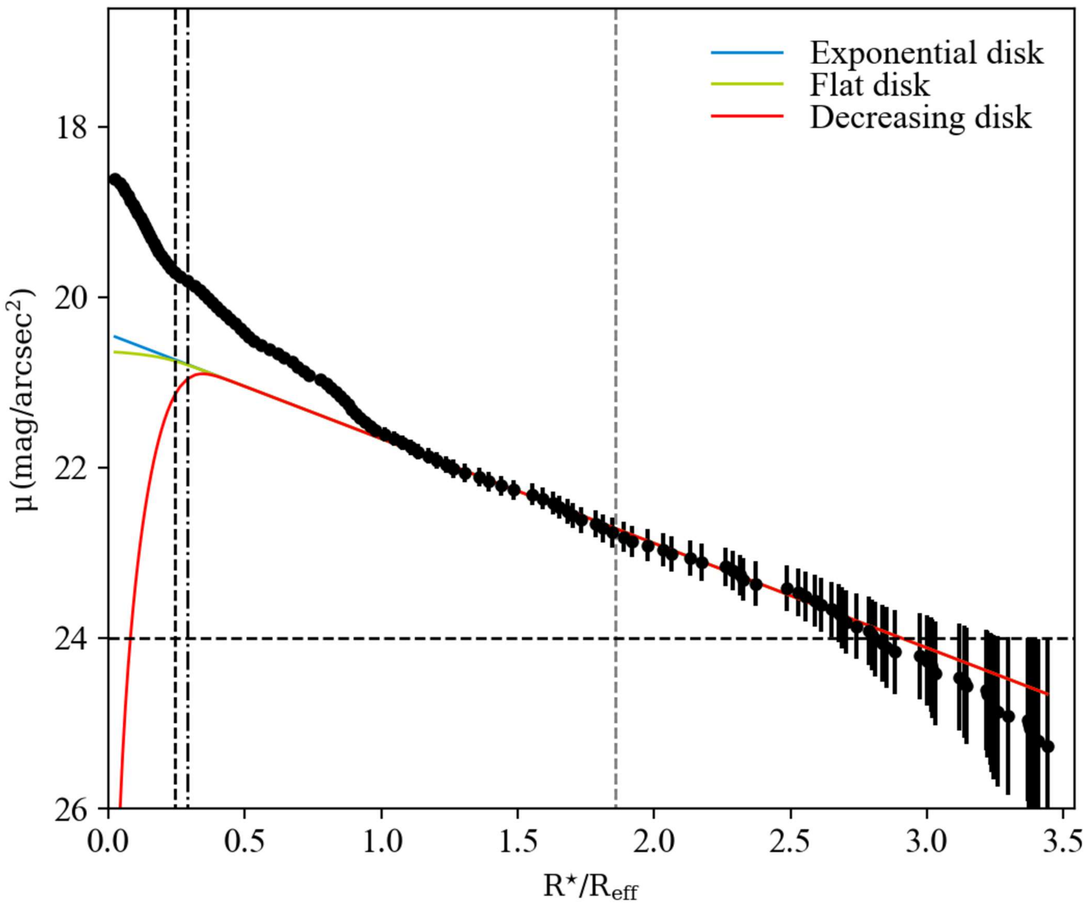
Exponential disk
Flat disk
Decreasing disk
μ (mag/arcsec²)
18
20
22
24
26
0.0
0.5
1.0
1.5
2.0
2.5
3.0
3.5
R⋆/Reff

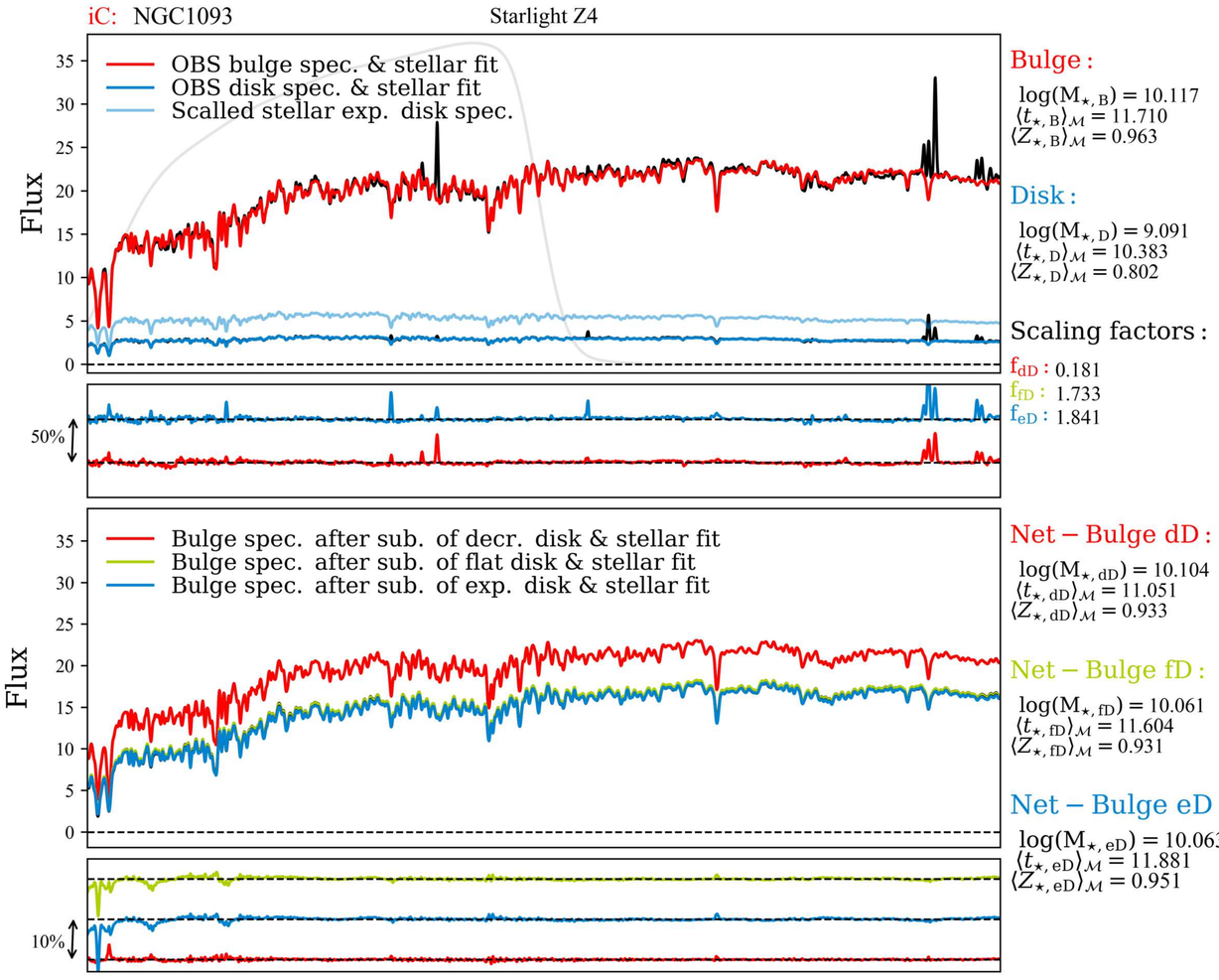
iC: NGC1093
Starlight Z4
OBS bulge spec. & stellar fit
OBS disk spec. & stellar fit
Scalled stellar exp. disk spec.
Flux
50%
Bulge spec. after sub. of decr. disk & stellar fit
Bulge spec. after sub. of flat disk & stellar fit
Bulge spec. after sub. of exp. disk & stellar fit
10%
Bulge :
log(M⋆, B) = 10.117
⟨t⋆, B⟩M = 11.710
⟨Z⋆, B⟩M = 0.963
Disk :
log(M⋆, D) = 9.091
⟨t⋆, D⟩M = 10.383
⟨Z⋆, D⟩M = 0.802
Scaling factors :
fdD : 0.181
ffD : 1.733
feD : 1.841
Net − Bulge dD :
log(M⋆, dD) = 10.104
⟨t⋆, dD⟩M = 11.051
⟨Z⋆, dD⟩M = 0.933
Net − Bulge fD :
log(M⋆, fD) = 10.061
⟨t⋆, fD⟩M = 11.604
⟨Z⋆, fD⟩M = 0.931
Net − Bulge eD :
log(M⋆, eD) = 10.063
⟨t⋆, eD⟩M = 11.881
⟨Z⋆, eD⟩M = 0.951

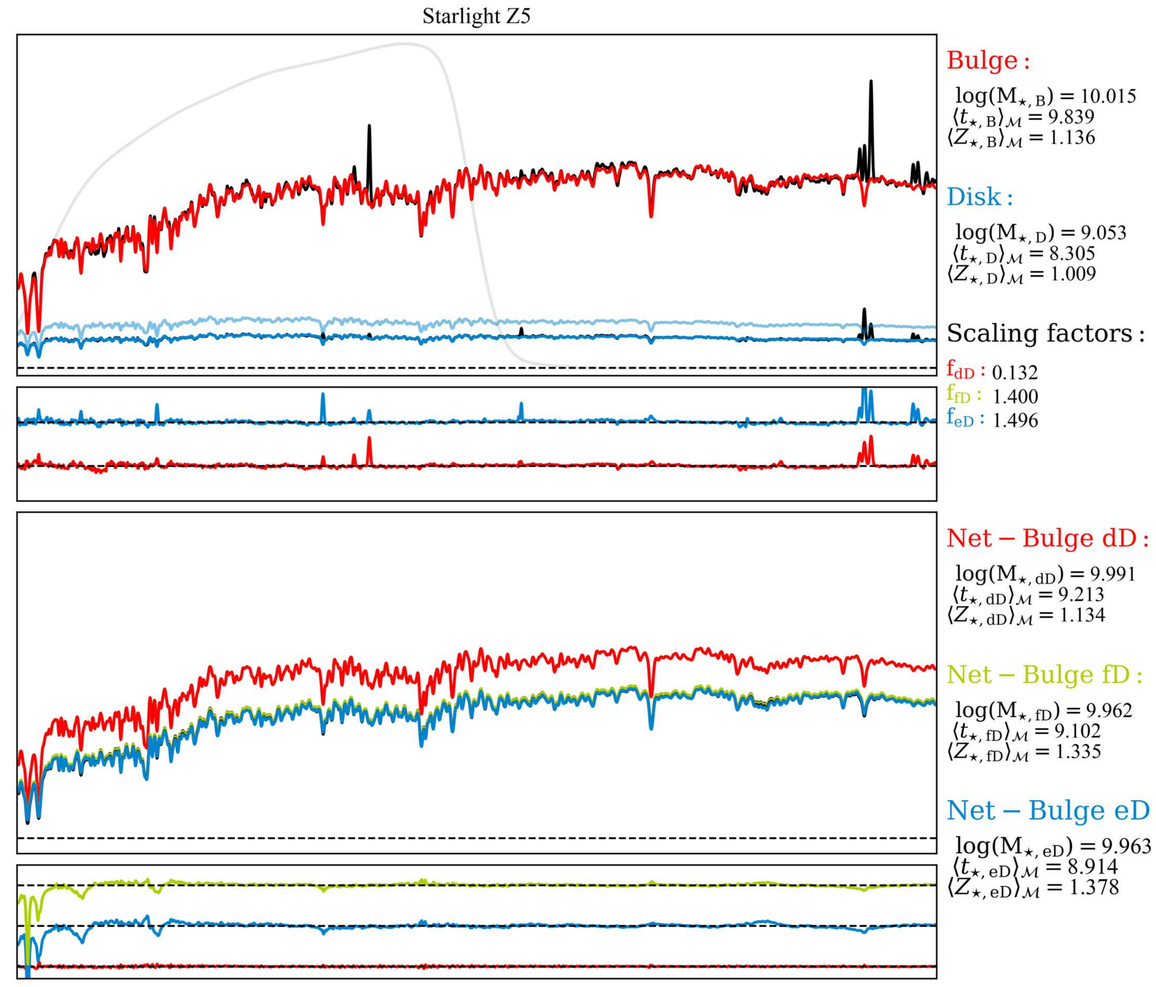
Starlight Z5
Bulge :
log(M⋆, B) = 10.015
⟨t⋆, B⟩M = 9.839
⟨Z⋆, B⟩M = 1.136
Disk :
log(M⋆, D) = 9.053
⟨t⋆, D⟩M = 8.305
⟨Z⋆, D⟩M = 1.009
Scaling factors :
fdD : 0.132
ffD : 1.400
feD : 1.496
Net − Bulge dD :
log(M⋆, dD) = 9.991
⟨t⋆, dD⟩M = 9.213
⟨Z⋆, dD⟩M = 1.134
Net − Bulge fD :
log(M⋆, fD) = 9.962
⟨t⋆, fD⟩M = 9.102
⟨Z⋆, fD⟩M = 1.335
Net − Bulge eD :
log(M⋆, eD) = 9.963
⟨t⋆, eD⟩M = 8.914
⟨Z⋆, eD⟩M = 1.378

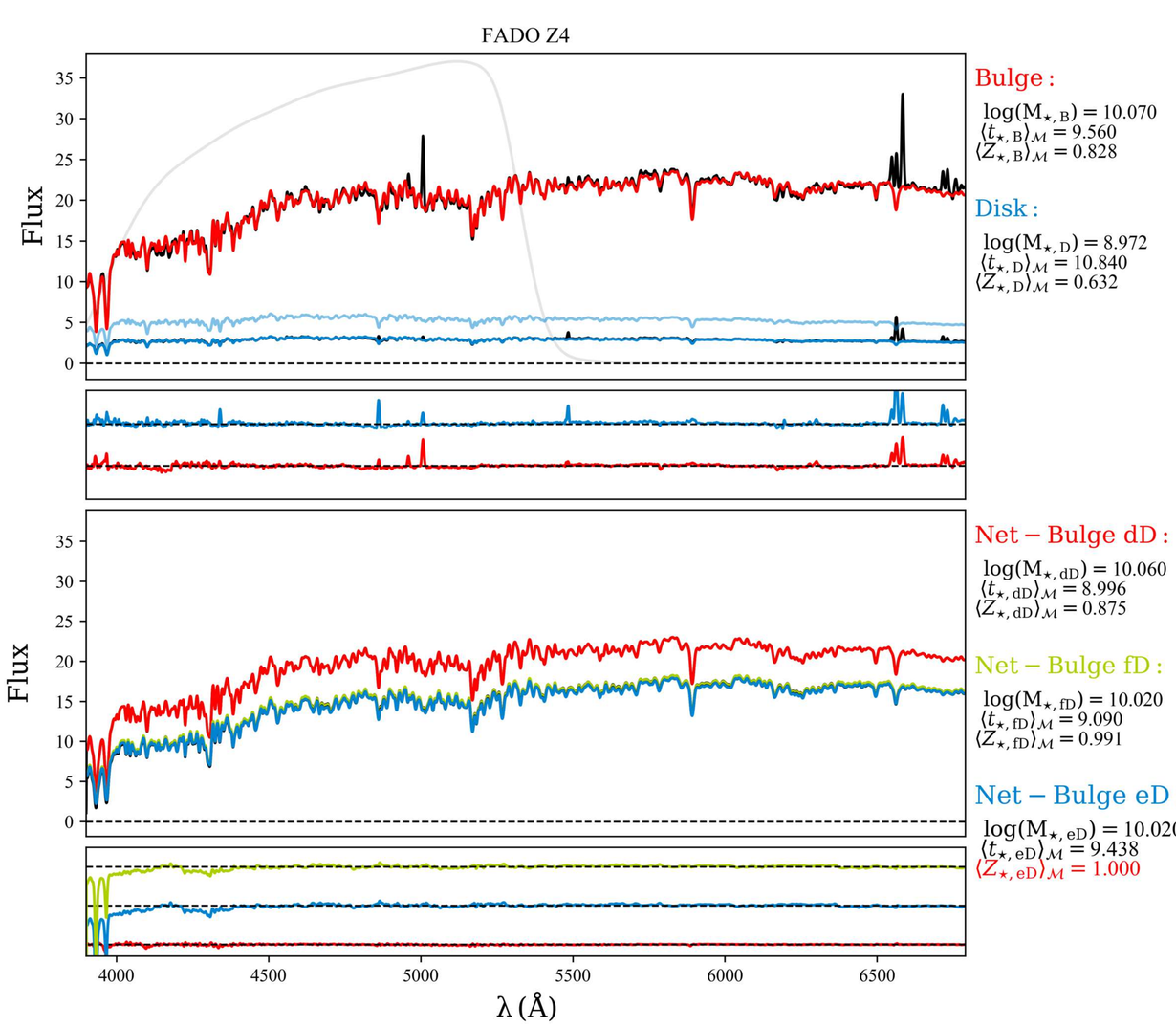
FADO Z4
Flux
Bulge :
log(M⋆, B) = 10.070
⟨t⋆, B⟩M = 9.560
⟨Z⋆, B⟩M = 0.828
Disk :
log(M⋆, D) = 8.972
⟨t⋆, D⟩M = 10.840
⟨Z⋆, D⟩M = 0.632
Net − Bulge dD :
log(M⋆, dD) = 10.060
⟨t⋆, dD⟩M = 8.996
⟨Z⋆, dD⟩M = 0.875
Net − Bulge fD :
log(M⋆, fD) = 10.020
⟨t⋆, fD⟩M = 9.090
⟨Z⋆, fD⟩M = 0.991
Net − Bulge eD :
log(M⋆, eD) = 10.020
⟨t⋆, eD⟩M = 9.438
⟨Z⋆, eD⟩M = 1.000
4000
4500
5000
5500
6000
6500
λ (Å)

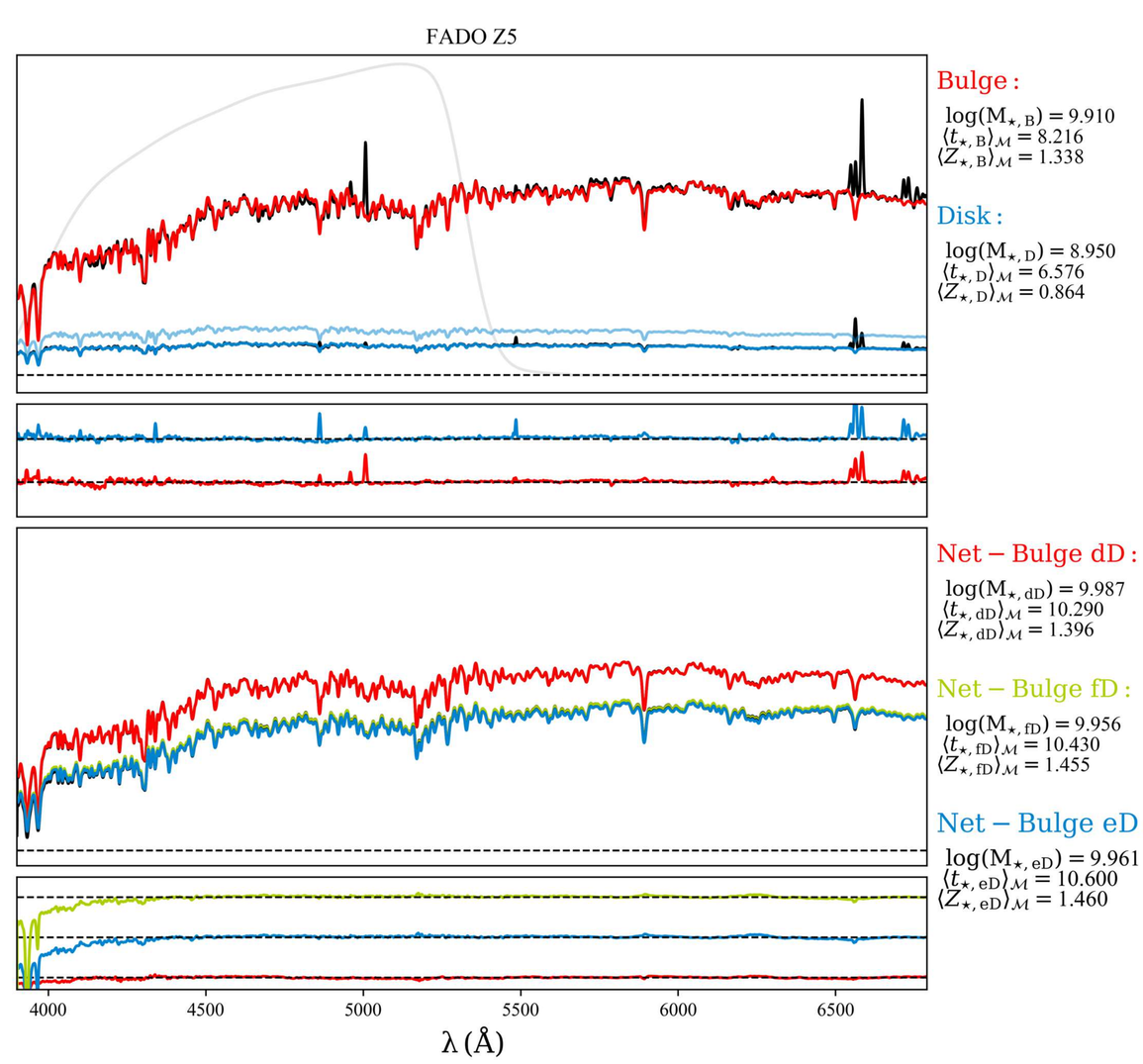
FADO Z5
Bulge :
log(M⋆, B) = 9.910
⟨t⋆, B⟩M = 8.216
⟨Z⋆, B⟩M = 1.338
Disk :
log(M⋆, D) = 8.950
⟨t⋆, D⟩M = 6.576
⟨Z⋆, D⟩M = 0.864
Net − Bulge dD :
log(M⋆, dD) = 9.987
⟨t⋆, dD⟩M = 10.290
⟨Z⋆, dD⟩M = 1.396
Net − Bulge fD :
log(M⋆, fD) = 9.956
⟨t⋆, fD⟩M = 10.430
⟨Z⋆, fD⟩M = 1.455
Net − Bulge eD :
log(M⋆, eD) = 9.961
⟨t⋆, eD⟩M = 10.600
⟨Z⋆, eD⟩M = 1.460
4000
4500
5000
5500
6000
6500
λ (Å)

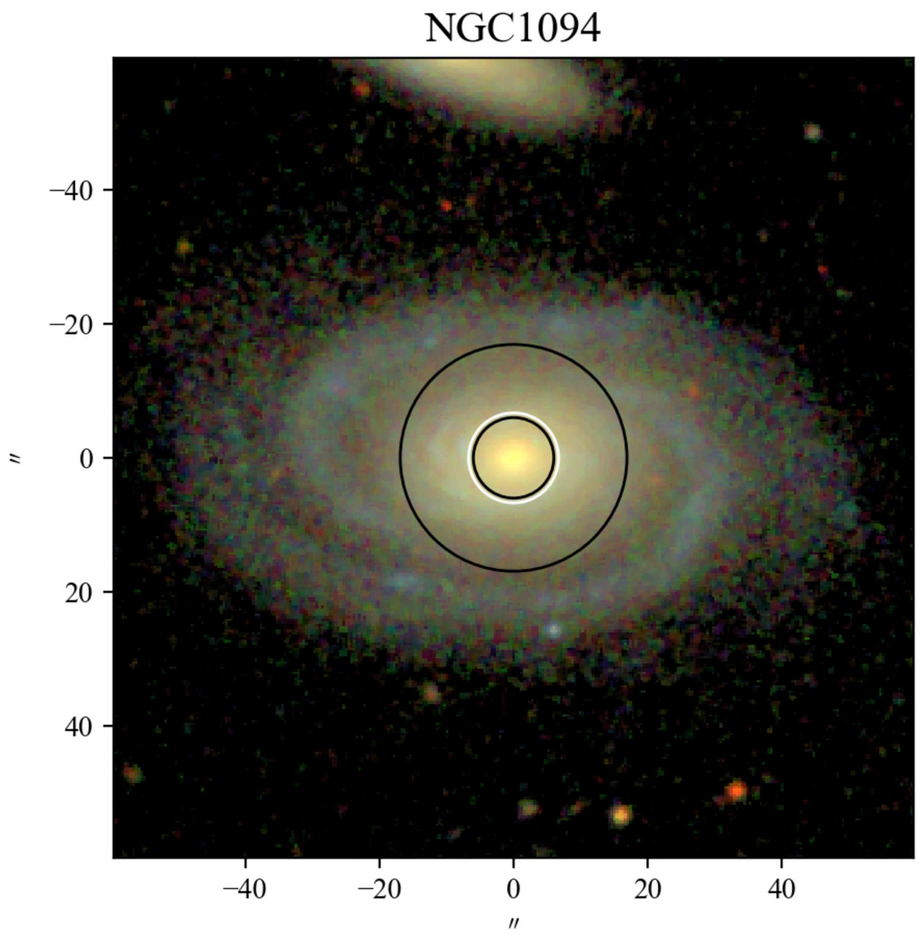
NGC1094
−40
−20
0
20
40
″
−40
−20
0
20
40
″

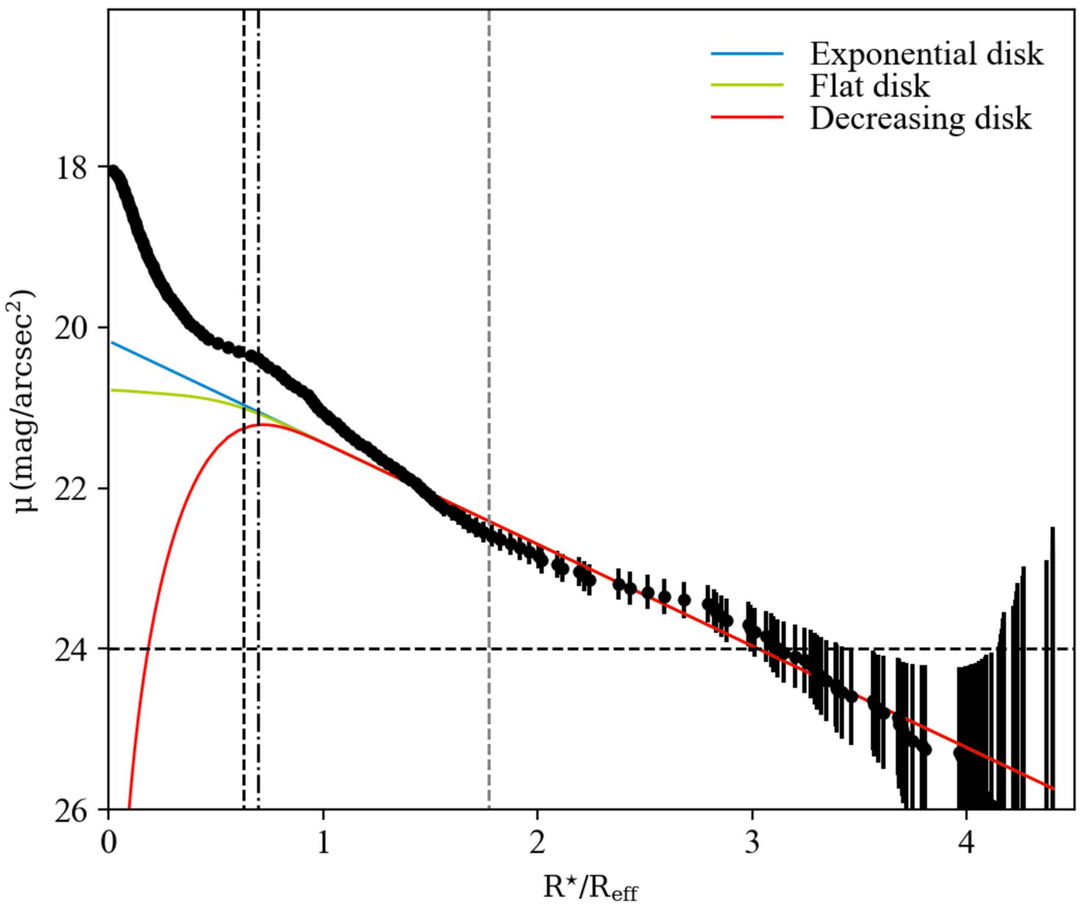
Exponential disk
Flat disk
Decreasing disk
μ (mag/arcsec²)
18
20
22
24
26
0
1
2
3
4
R⋆/Reff

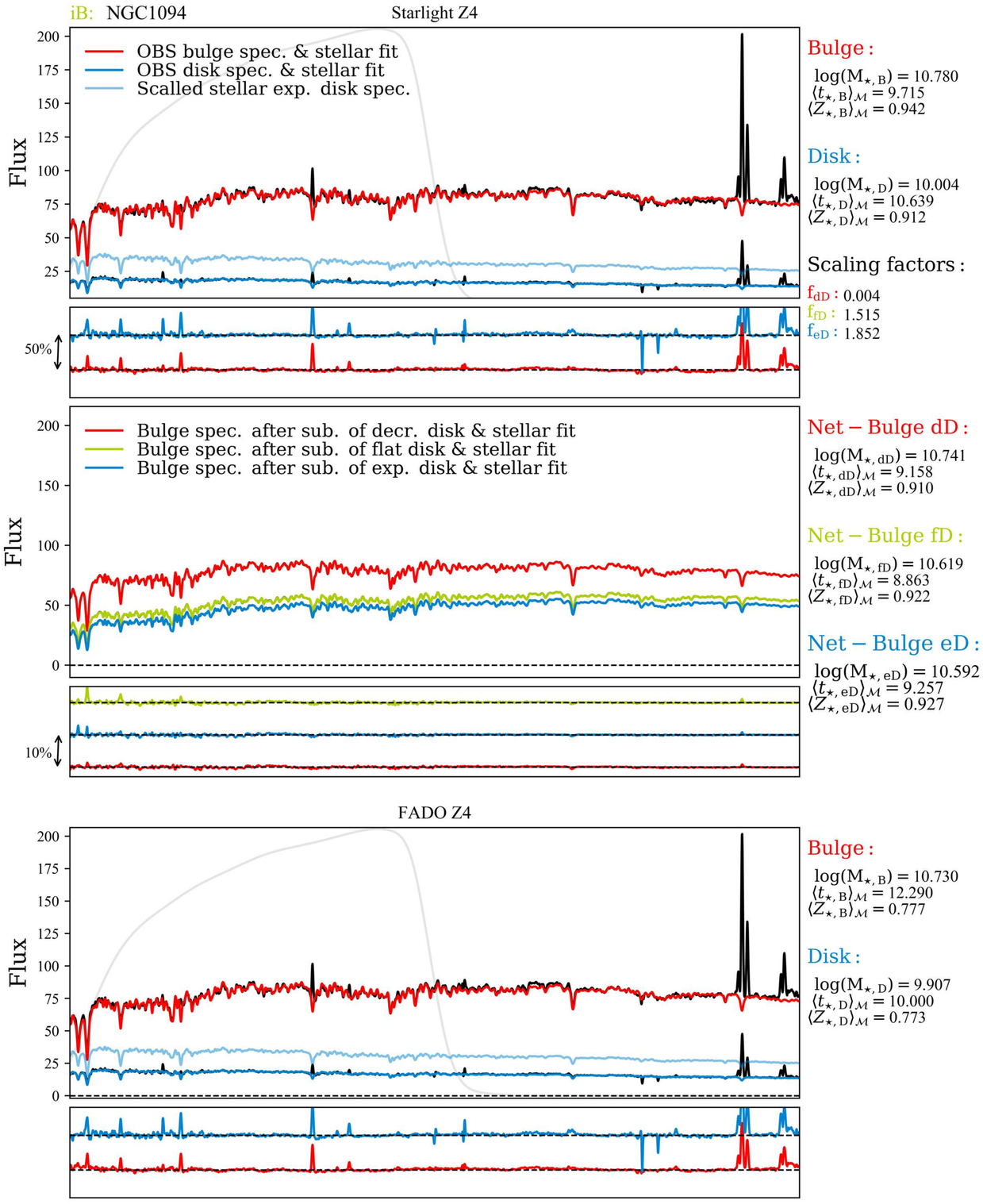
iB: NGC1094
Starlight Z4
OBS bulge spec. & stellar fit
OBS disk spec. & stellar fit
Scalled stellar exp. disk spec.
Flux
50%
Bulge :
log(M⋆, B) = 10.780
⟨t⋆, B⟩M = 9.715
⟨Z⋆, B⟩M = 0.942
Disk :
log(M⋆, D) = 10.004
⟨t⋆, D⟩M = 10.639
⟨Z⋆, D⟩M = 0.912
Scaling factors :
fdD : 0.004
ffD : 1.515
feD : 1.852
Bulge spec. after sub. of decr. disk & stellar fit
Bulge spec. after sub. of flat disk & stellar fit
Bulge spec. after sub. of exp. disk & stellar fit
10%
Net − Bulge dD :
log(M⋆, dD) = 10.741
⟨t⋆, dD⟩M = 9.158
⟨Z⋆, dD⟩M = 0.910
Net − Bulge fD :
log(M⋆, fD) = 10.619
⟨t⋆, fD⟩M = 8.863
⟨Z⋆, fD⟩M = 0.922
Net − Bulge eD :
log(M⋆, eD) = 10.592
⟨t⋆, eD⟩M = 9.257
⟨Z⋆, eD⟩M = 0.927

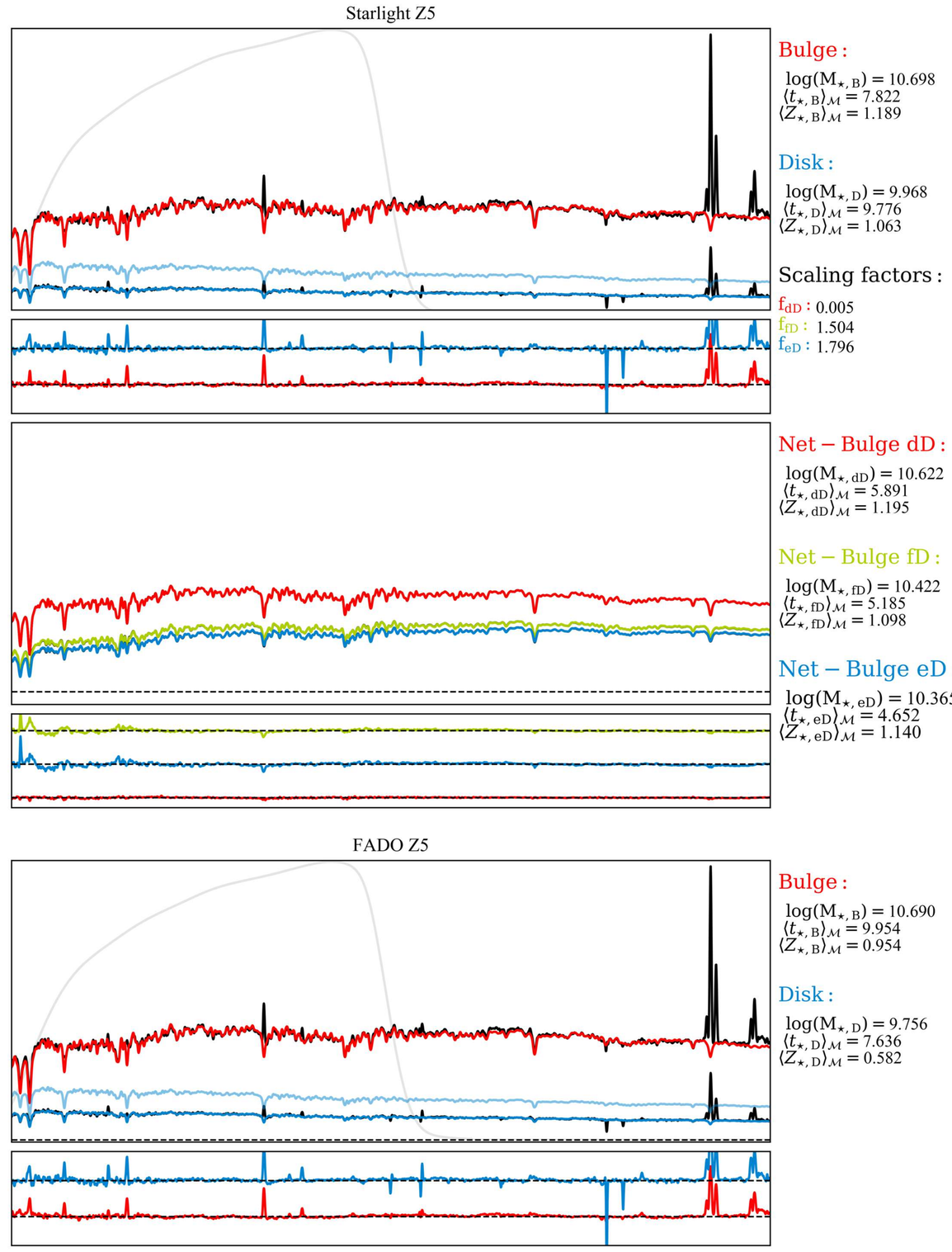
Starlight Z5
Bulge :
log(M⋆, B) = 10.698
⟨t⋆, B⟩M = 7.822
⟨Z⋆, B⟩M = 1.189
Disk :
log(M⋆, D) = 9.968
⟨t⋆, D⟩M = 9.776
⟨Z⋆, D⟩M = 1.063
Scaling factors :
fdD : 0.005
ffD : 1.504
feD : 1.796
Net − Bulge dD :
log(M⋆, dD) = 10.622
⟨t⋆, dD⟩M = 5.891
⟨Z⋆, dD⟩M = 1.195
Net − Bulge fD :
log(M⋆, fD) = 10.422
⟨t⋆, fD⟩M = 5.185
⟨Z⋆, fD⟩M = 1.098
Net − Bulge eD :
log(M⋆, eD) = 10.365
⟨t⋆, eD⟩M = 4.652
⟨Z⋆, eD⟩M = 1.140

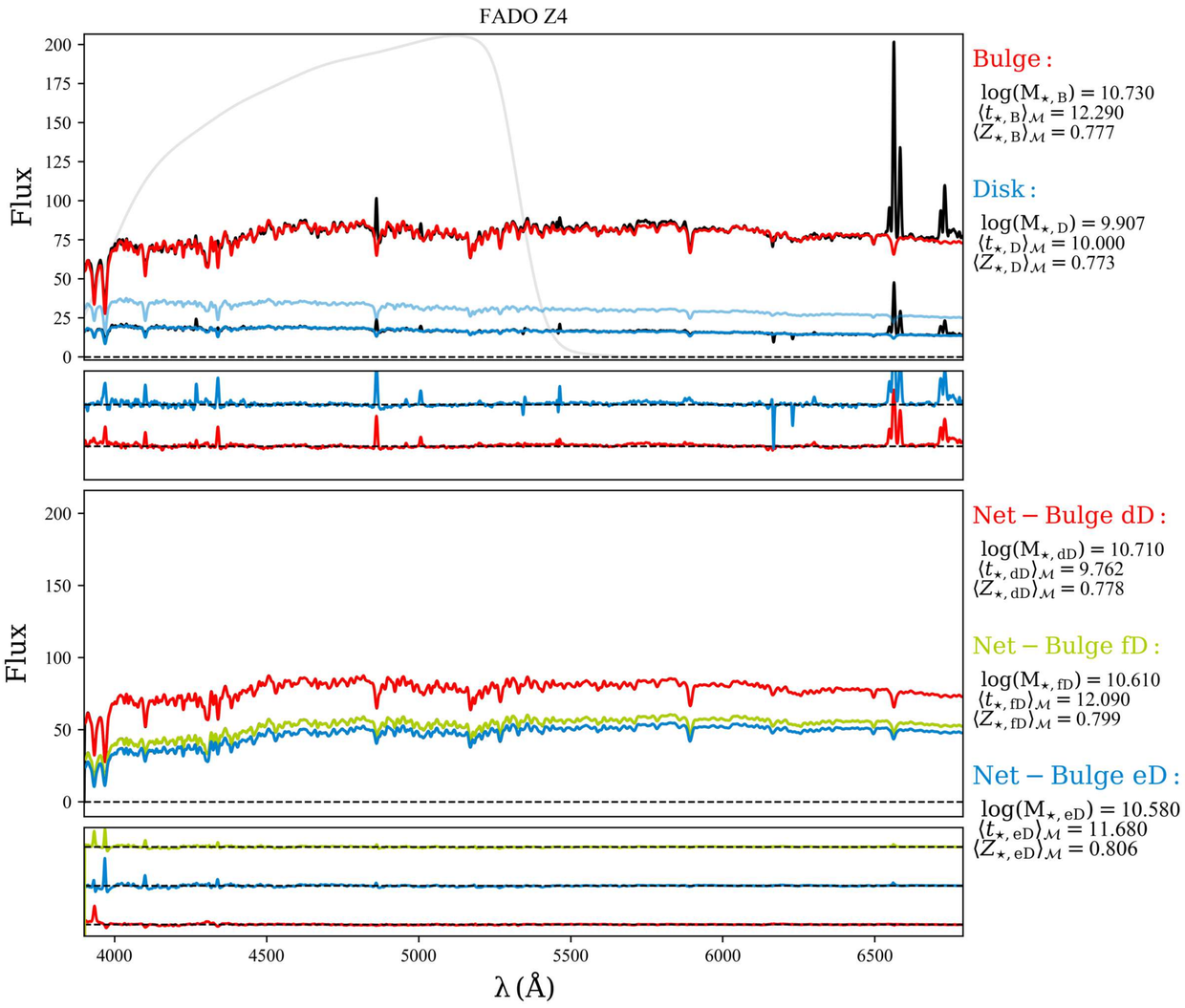
FADO Z4
Flux
Bulge :
log(M⋆, B) = 10.730
⟨t⋆, B⟩M = 12.290
⟨Z⋆, B⟩M = 0.777
Disk :
log(M⋆, D) = 9.907
⟨t⋆, D⟩M = 10.000
⟨Z⋆, D⟩M = 0.773
Net − Bulge dD :
log(M⋆, dD) = 10.710
⟨t⋆, dD⟩M = 9.762
⟨Z⋆, dD⟩M = 0.778
Net − Bulge fD :
log(M⋆, fD) = 10.610
⟨t⋆, fD⟩M = 12.090
⟨Z⋆, fD⟩M = 0.799
Net − Bulge eD :
log(M⋆, eD) = 10.580
⟨t⋆, eD⟩M = 11.680
⟨Z⋆, eD⟩M = 0.806
λ (Å)

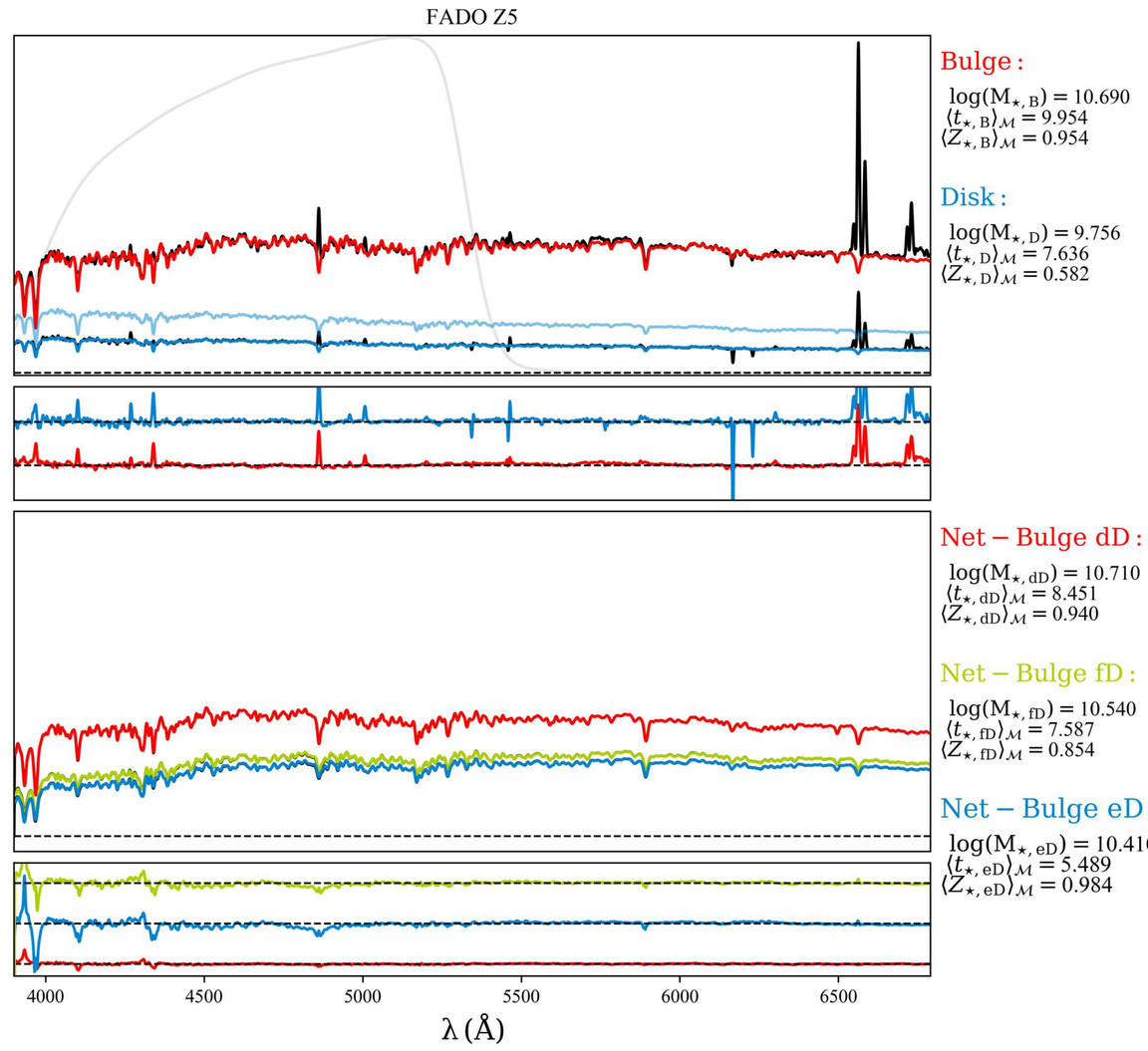
FADO Z5
Bulge :
log(M⋆, B) = 10.690
⟨t⋆, B⟩M = 9.954
⟨Z⋆, B⟩M = 0.954
Disk :
log(M⋆, D) = 9.756
⟨t⋆, D⟩M = 7.636
⟨Z⋆, D⟩M = 0.582
Net − Bulge dD :
log(M⋆, dD) = 10.710
⟨t⋆, dD⟩M = 8.451
⟨Z⋆, dD⟩M = 0.940
Net − Bulge fD :
log(M⋆, fD) = 10.540
⟨t⋆, fD⟩M = 7.587
⟨Z⋆, fD⟩M = 0.854
Net − Bulge eD :
log(M⋆, eD) = 10.410
⟨t⋆, eD⟩M = 5.489
⟨Z⋆, eD⟩M = 0.984
λ (Å)

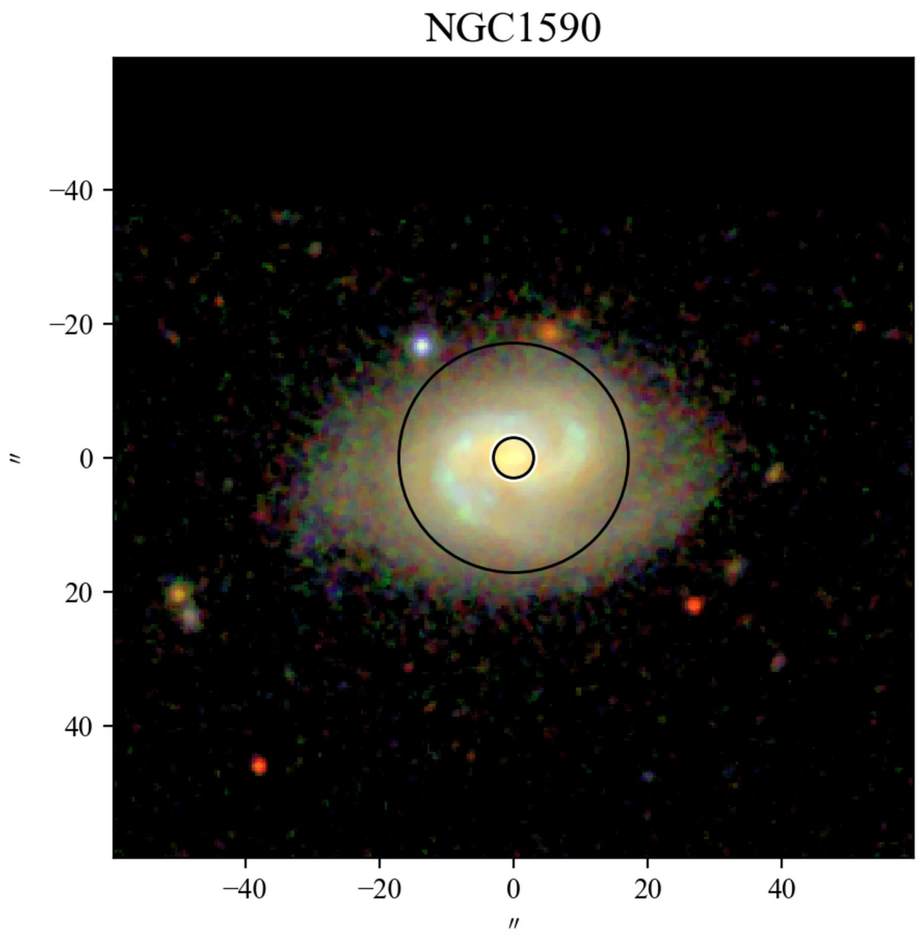
NGC1590
−40
−20
0
20
40
″
−40
−20
0
20
40
″

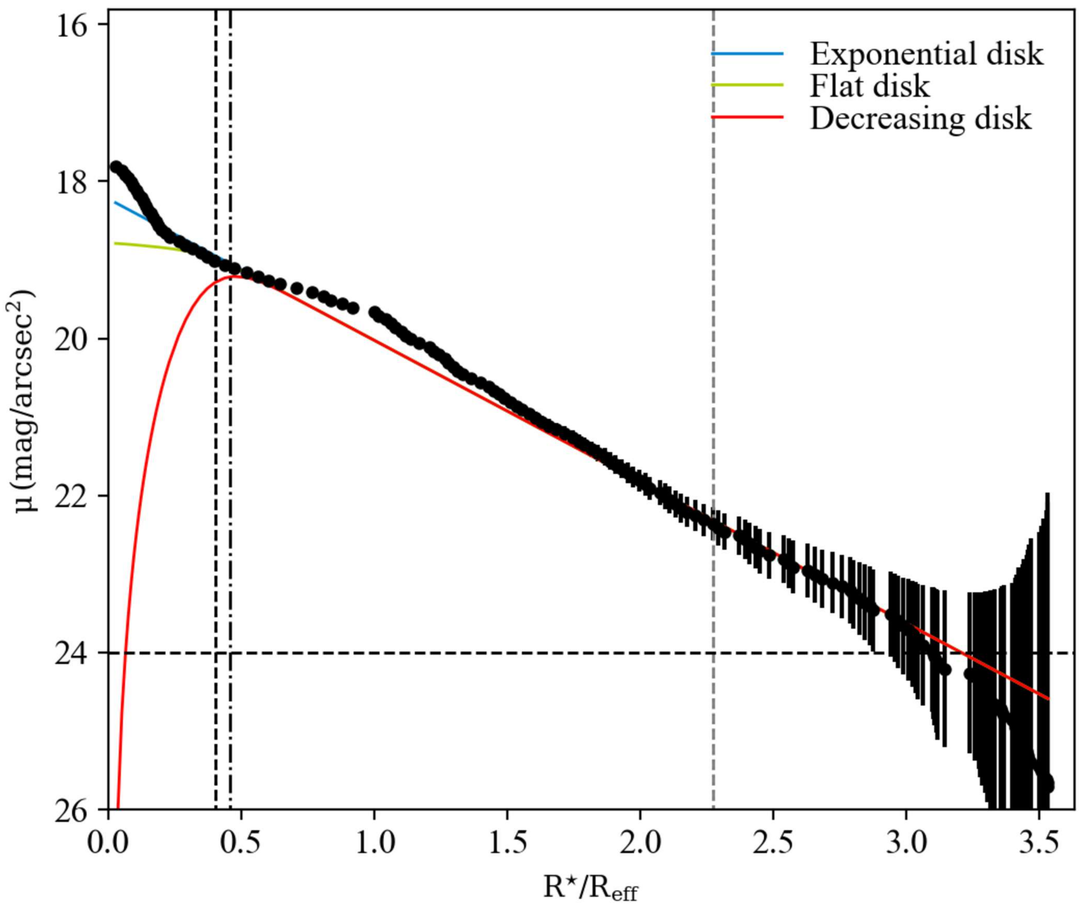
Exponential disk
Flat disk
Decreasing disk
μ (mag/arcsec²)
16
18
20
22
24
26
0.0
0.5
1.0
1.5
2.0
2.5
3.0
3.5
R⋆/Reff

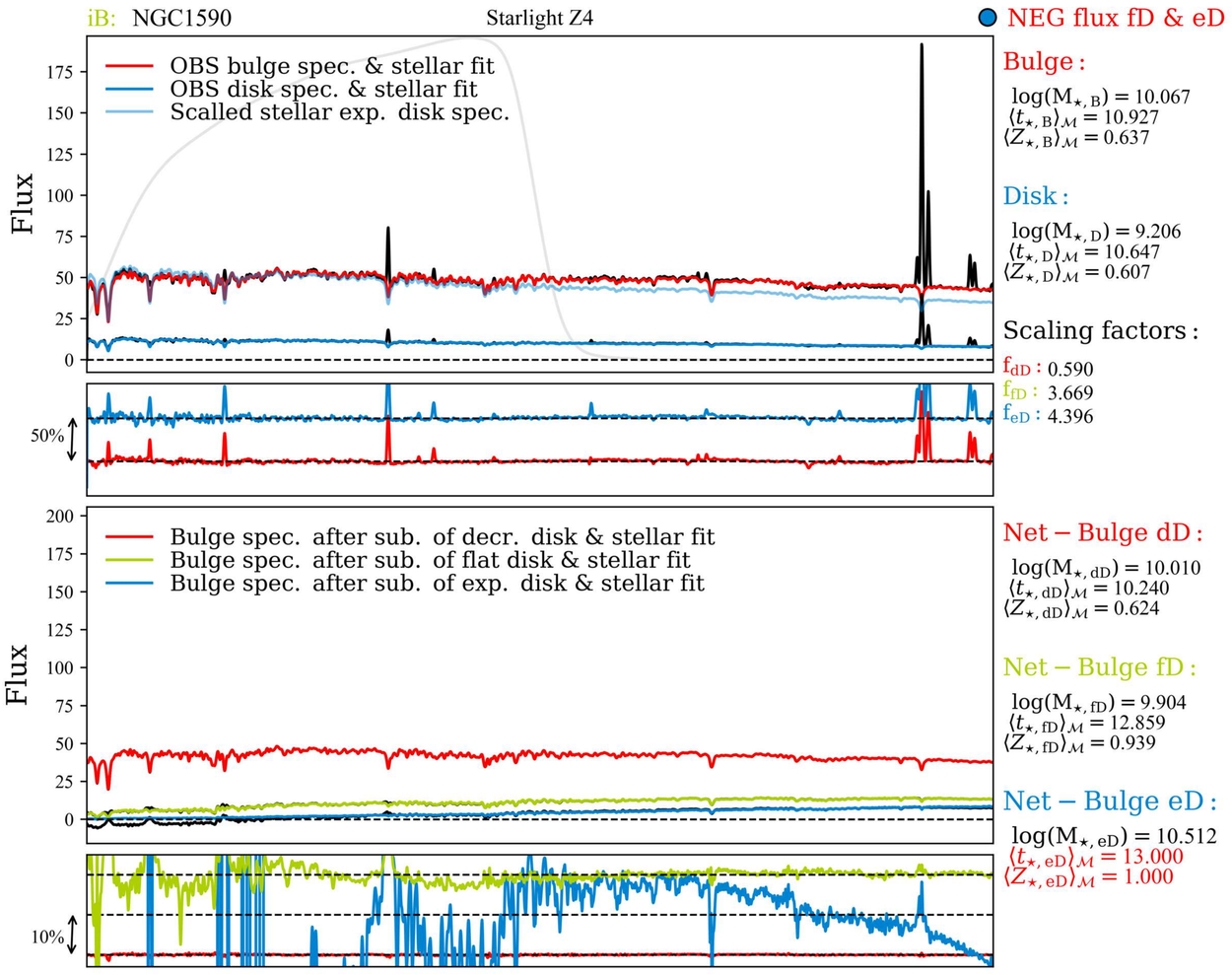
iB: NGC1590
Starlight Z4
NEG flux fD & eD
OBS bulge spec. & stellar fit
OBS disk spec. & stellar fit
Scalled stellar exp. disk spec.
Flux
Bulge :
log(M⋆, B) = 10.067
⟨t⋆, B⟩M = 10.927
⟨Z⋆, B⟩M = 0.637
Disk :
log(M⋆, D) = 9.206
⟨t⋆, D⟩M = 10.647
⟨Z⋆, D⟩M = 0.607
Scaling factors :
fdD : 0.590
ffD : 3.669
feD : 4.396
50%
Bulge spec. after sub. of decr. disk & stellar fit
Bulge spec. after sub. of flat disk & stellar fit
Bulge spec. after sub. of exp. disk & stellar fit
Net − Bulge dD :
log(M⋆, dD) = 10.010
⟨t⋆, dD⟩M = 10.240
⟨Z⋆, dD⟩M = 0.624
Net − Bulge fD :
log(M⋆, fD) = 9.904
⟨t⋆, fD⟩M = 12.859
⟨Z⋆, fD⟩M = 0.939
Net − Bulge eD :
log(M⋆, eD) = 10.512
⟨t⋆, eD⟩M = 13.000
⟨Z⋆, eD⟩M = 1.000
10%

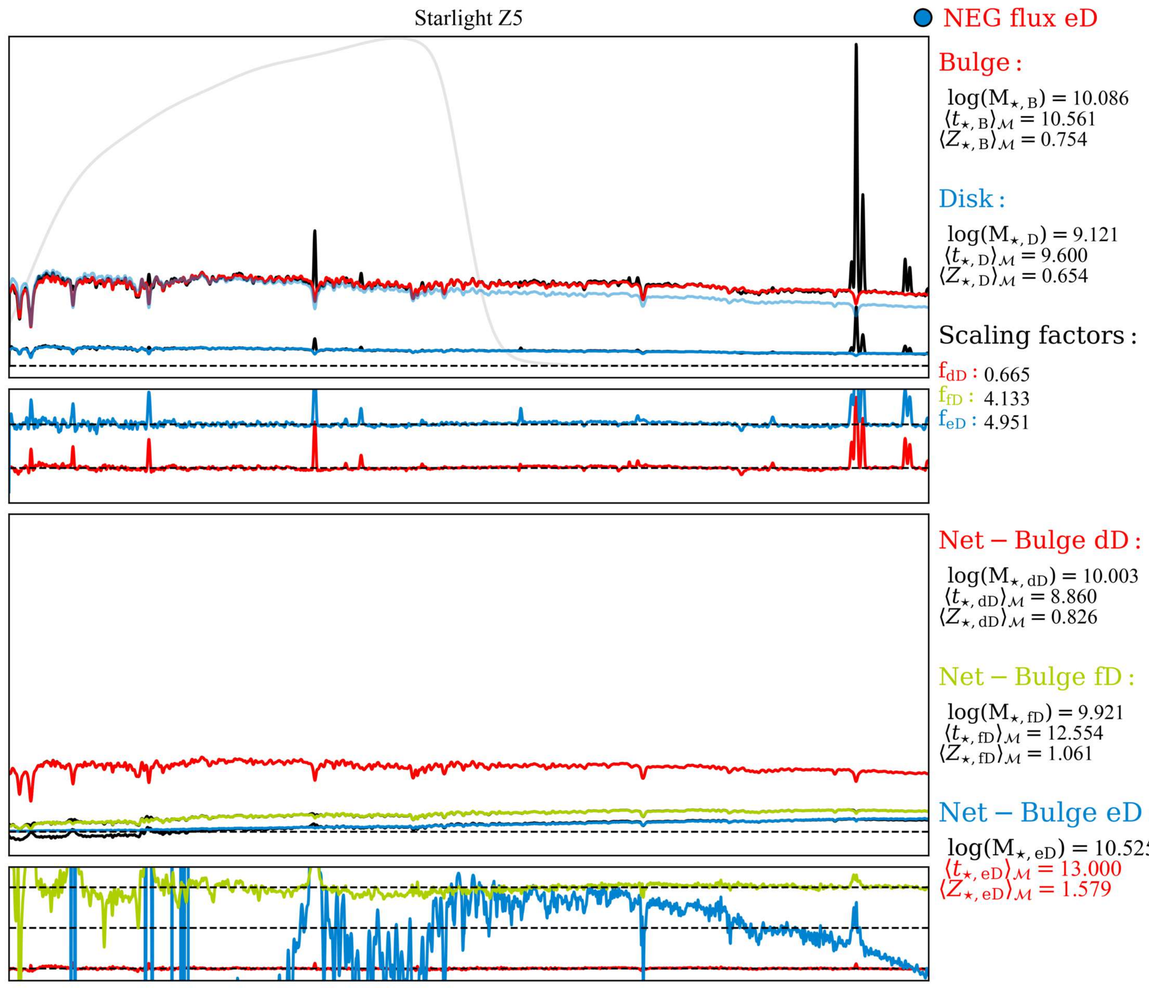
Starlight Z5
NEG flux eD
Bulge :
log(M⋆, B) = 10.086
⟨t⋆, B⟩M = 10.561
⟨Z⋆, B⟩M = 0.754
Disk :
log(M⋆, D) = 9.121
⟨t⋆, D⟩M = 9.600
⟨Z⋆, D⟩M = 0.654
Scaling factors :
fdD : 0.665
ffD : 4.133
feD : 4.951
Net − Bulge dD :
log(M⋆, dD) = 10.003
⟨t⋆, dD⟩M = 8.860
⟨Z⋆, dD⟩M = 0.826
Net − Bulge fD :
log(M⋆, fD) = 9.921
⟨t⋆, fD⟩M = 12.554
⟨Z⋆, fD⟩M = 1.061
Net − Bulge eD :
log(M⋆, eD) = 10.525
⟨t⋆, eD⟩M = 13.000
⟨Z⋆, eD⟩M = 1.579

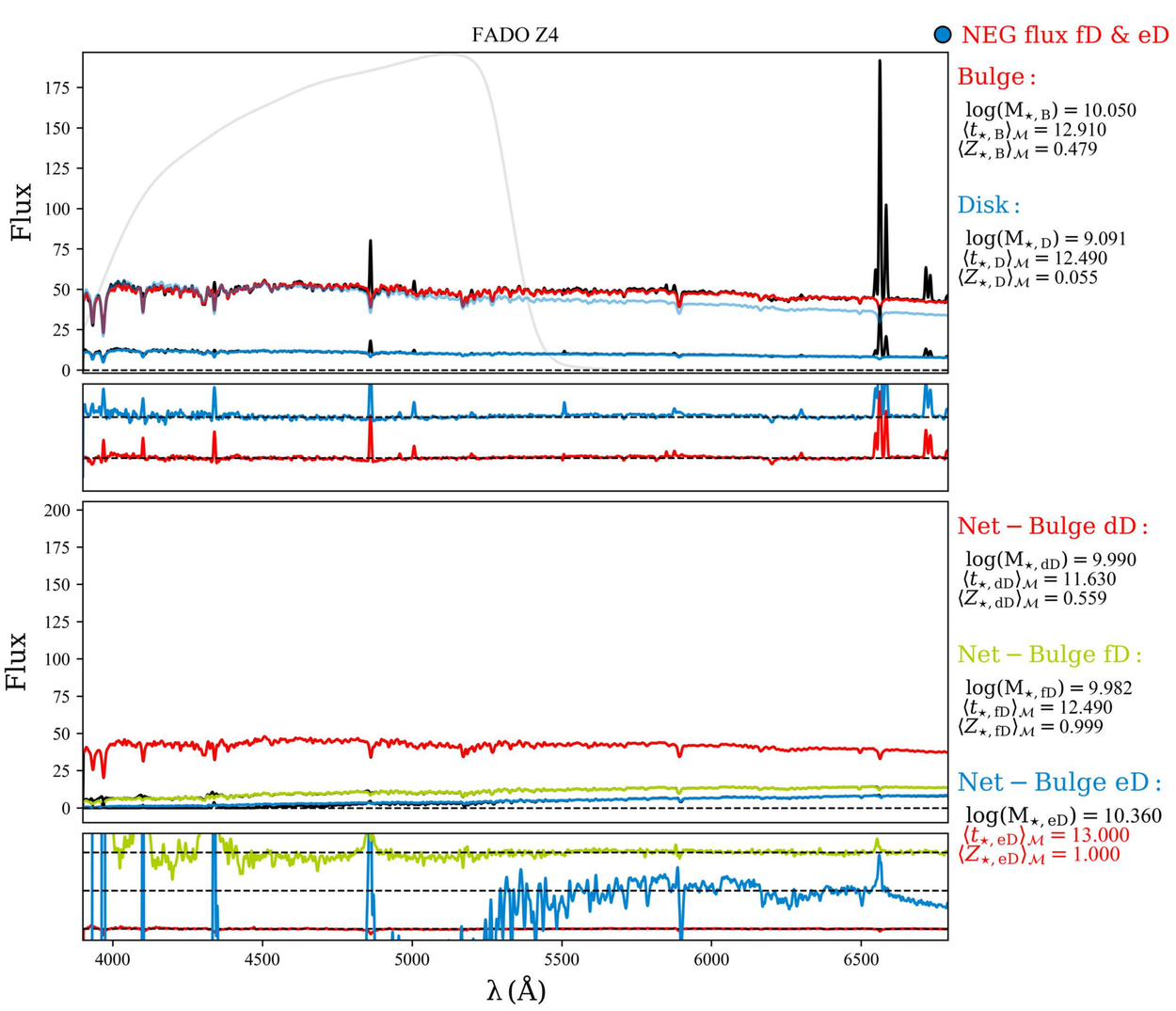
FADO Z4
NEG flux fD & eD
Flux
Bulge :
log(M⋆, B) = 10.050
⟨t⋆, B⟩M = 12.910
⟨Z⋆, B⟩M = 0.479
Disk :
log(M⋆, D) = 9.091
⟨t⋆, D⟩M = 12.490
⟨Z⋆, D⟩M = 0.055
Net − Bulge dD :
log(M⋆, dD) = 9.990
⟨t⋆, dD⟩M = 11.630
⟨Z⋆, dD⟩M = 0.559
Net − Bulge fD :
log(M⋆, fD) = 9.982
⟨t⋆, fD⟩M = 12.490
⟨Z⋆, fD⟩M = 0.999
Net − Bulge eD :
log(M⋆, eD) = 10.360
⟨t⋆, eD⟩M = 13.000
⟨Z⋆, eD⟩M = 1.000
λ (Å)

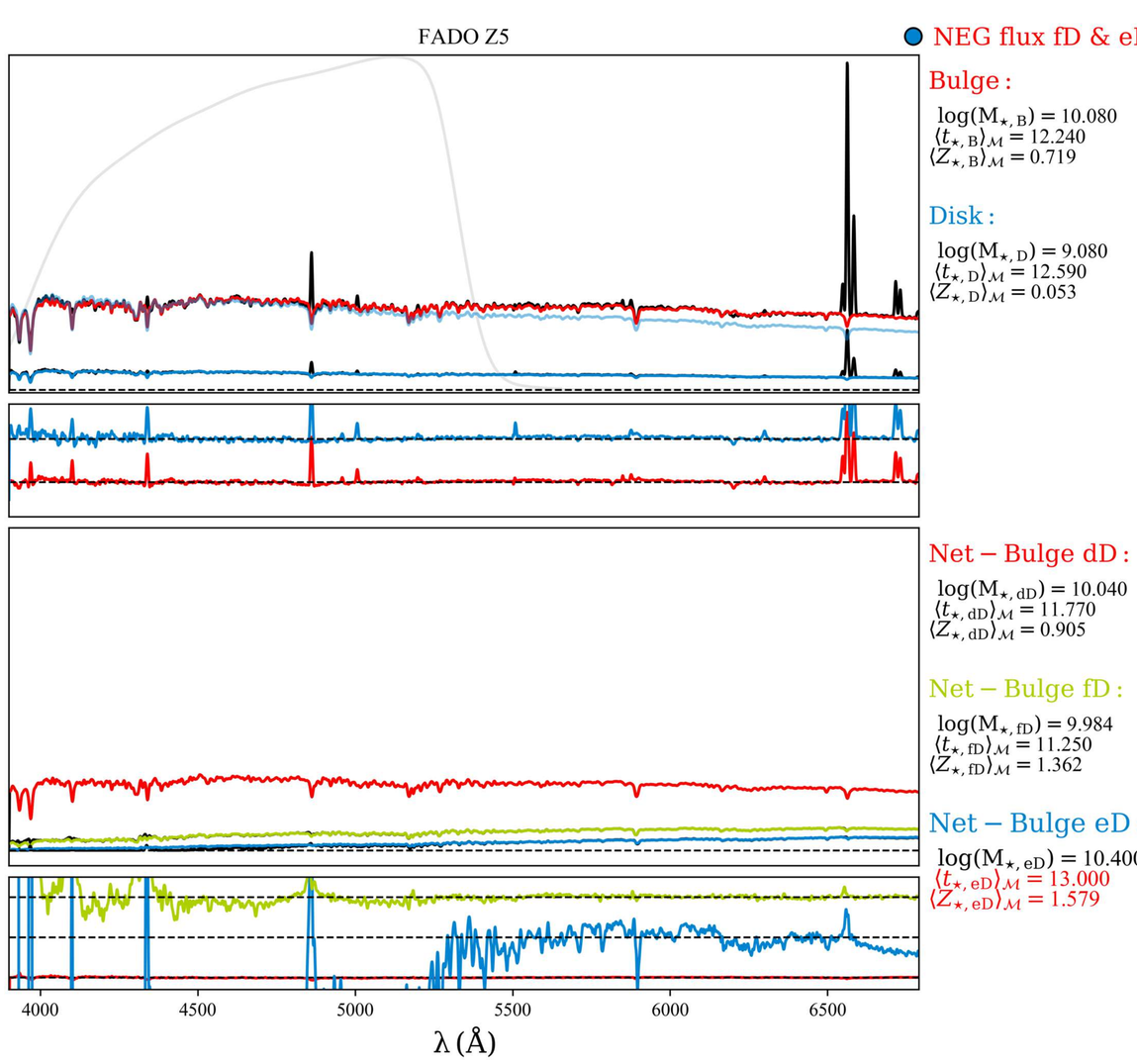
FADO Z5
NEG flux fD & eD
Bulge :
log(M⋆, B) = 10.080
⟨t⋆, B⟩M = 12.240
⟨Z⋆, B⟩M = 0.719
Disk :
log(M⋆, D) = 9.080
⟨t⋆, D⟩M = 12.590
⟨Z⋆, D⟩M = 0.053
Net − Bulge dD :
log(M⋆, dD) = 10.040
⟨t⋆, dD⟩M = 11.770
⟨Z⋆, dD⟩M = 0.905
Net − Bulge fD :
log(M⋆, fD) = 9.984
⟨t⋆, fD⟩M = 11.250
⟨Z⋆, fD⟩M = 1.362
Net − Bulge eD :
log(M⋆, eD) = 10.400
⟨t⋆, eD⟩M = 13.000
⟨Z⋆, eD⟩M = 1.579
λ (Å)

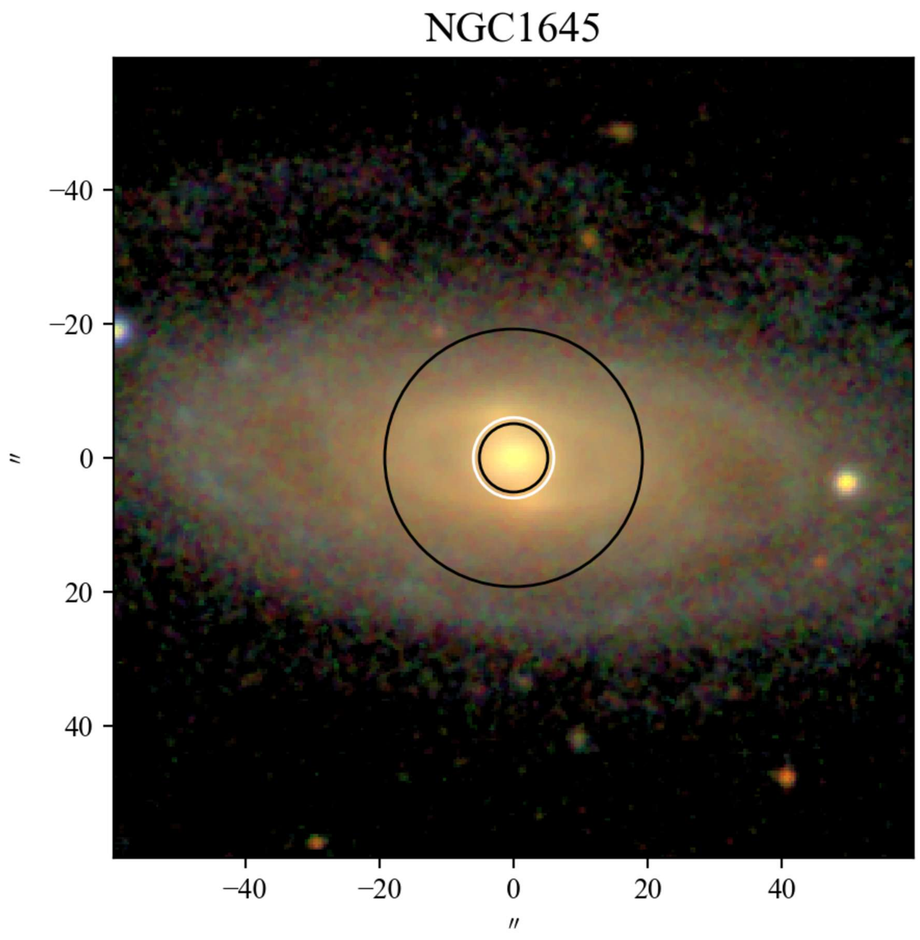
NGC1645
−40
−20
0
20
40
″
−40
−20
0
20
40
″

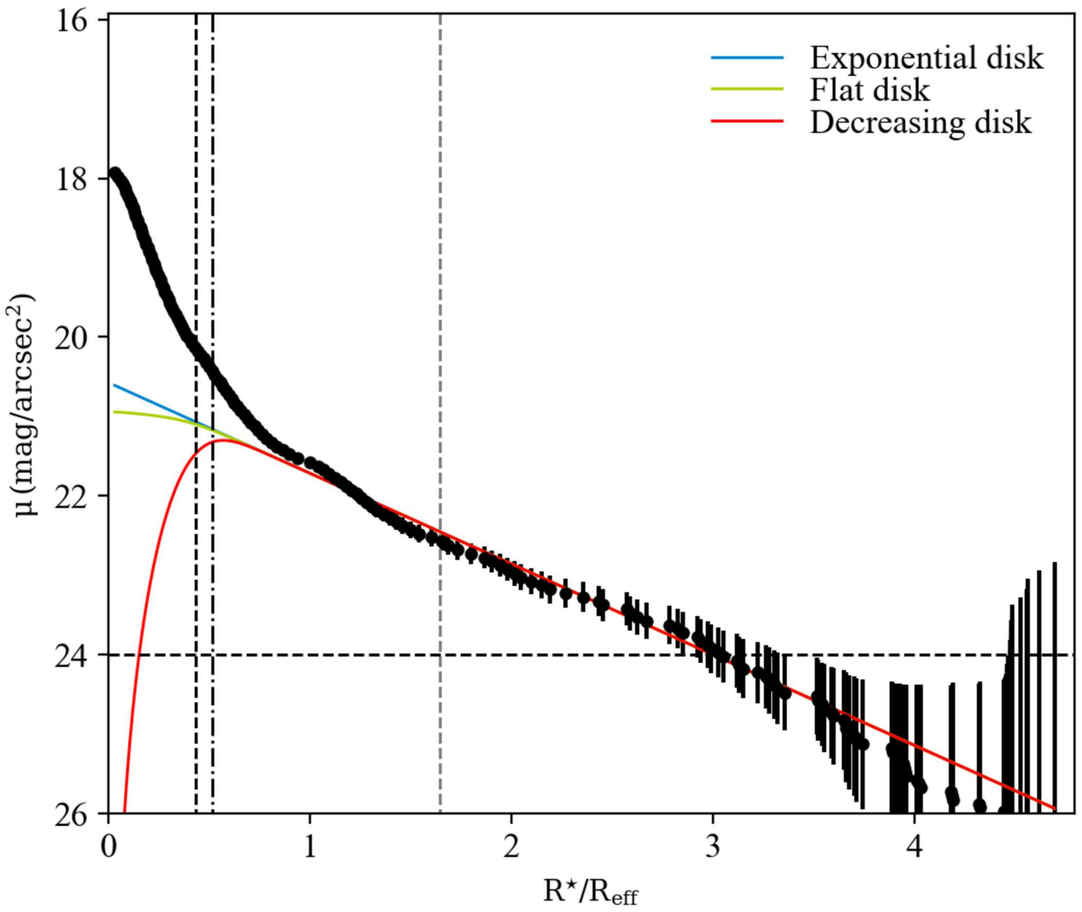
Exponential disk
Flat disk
Decreasing disk
μ (mag/arcsec²)
16
18
20
22
24
26
0
1
2
3
4
R⋆/Reff

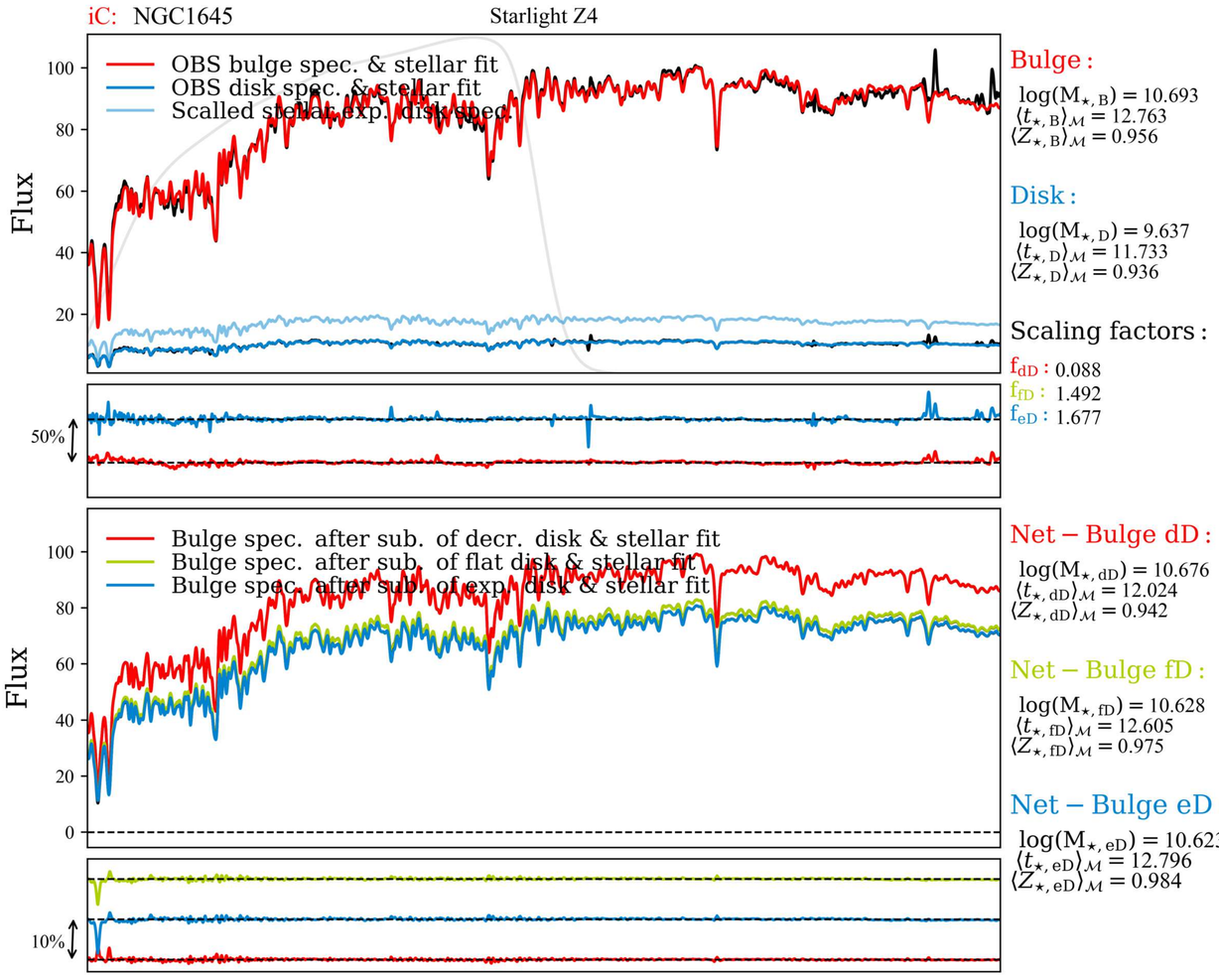
iC: NGC1645
Starlight Z4
OBS bulge spec. & stellar fit
OBS disk spec. & stellar fit
Scalled stellar exp. disk spec.
Flux
100
80
60
40
20
50%
Bulge spec. after sub. of decr. disk & stellar fit
Bulge spec. after sub. of flat disk & stellar fit
Bulge spec. after sub. of exp. disk & stellar fit
100
80
60
40
20
0
10%
Bulge :
log(M⋆, B) = 10.693
⟨t⋆, B⟩M = 12.763
⟨Z⋆, B⟩M = 0.956
Disk :
log(M⋆, D) = 9.637
⟨t⋆, D⟩M = 11.733
⟨Z⋆, D⟩M = 0.936
Scaling factors :
fdD : 0.088
ffD : 1.492
feD : 1.677
Net − Bulge dD :
log(M⋆, dD) = 10.676
⟨t⋆, dD⟩M = 12.024
⟨Z⋆, dD⟩M = 0.942
Net − Bulge fD :
log(M⋆, fD) = 10.628
⟨t⋆, fD⟩M = 12.605
⟨Z⋆, fD⟩M = 0.975
Net − Bulge eD :
log(M⋆, eD) = 10.623
⟨t⋆, eD⟩M = 12.796
⟨Z⋆, eD⟩M = 0.984

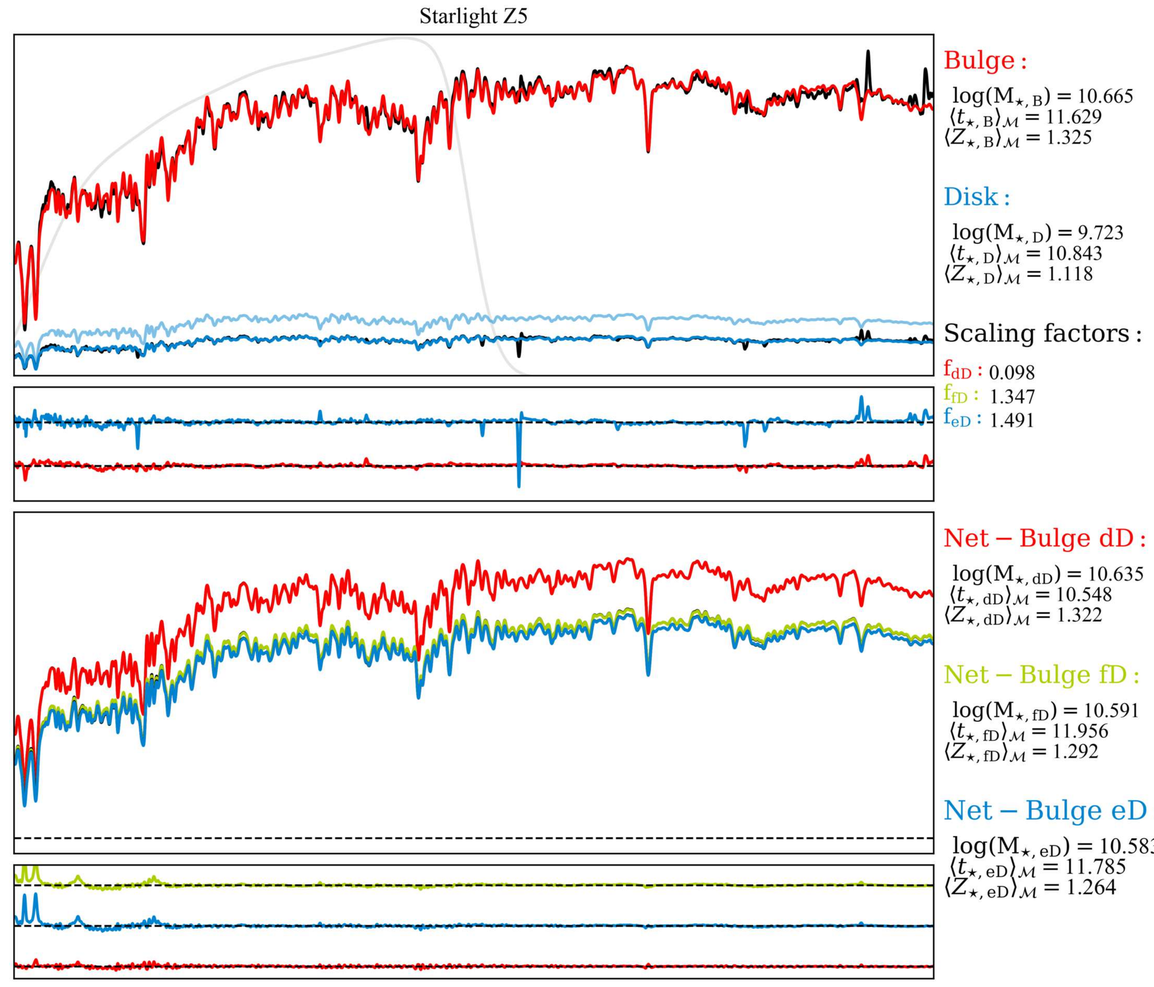
Starlight Z5
Bulge :
log(M⋆, B) = 10.665
⟨t⋆, B⟩M = 11.629
⟨Z⋆, B⟩M = 1.325
Disk :
log(M⋆, D) = 9.723
⟨t⋆, D⟩M = 10.843
⟨Z⋆, D⟩M = 1.118
Scaling factors :
fdD : 0.098
ffD : 1.347
feD : 1.491
Net − Bulge dD :
log(M⋆, dD) = 10.635
⟨t⋆, dD⟩M = 10.548
⟨Z⋆, dD⟩M = 1.322
Net − Bulge fD :
log(M⋆, fD) = 10.591
⟨t⋆, fD⟩M = 11.956
⟨Z⋆, fD⟩M = 1.292
Net − Bulge eD :
log(M⋆, eD) = 10.583
⟨t⋆, eD⟩M = 11.785
⟨Z⋆, eD⟩M = 1.264

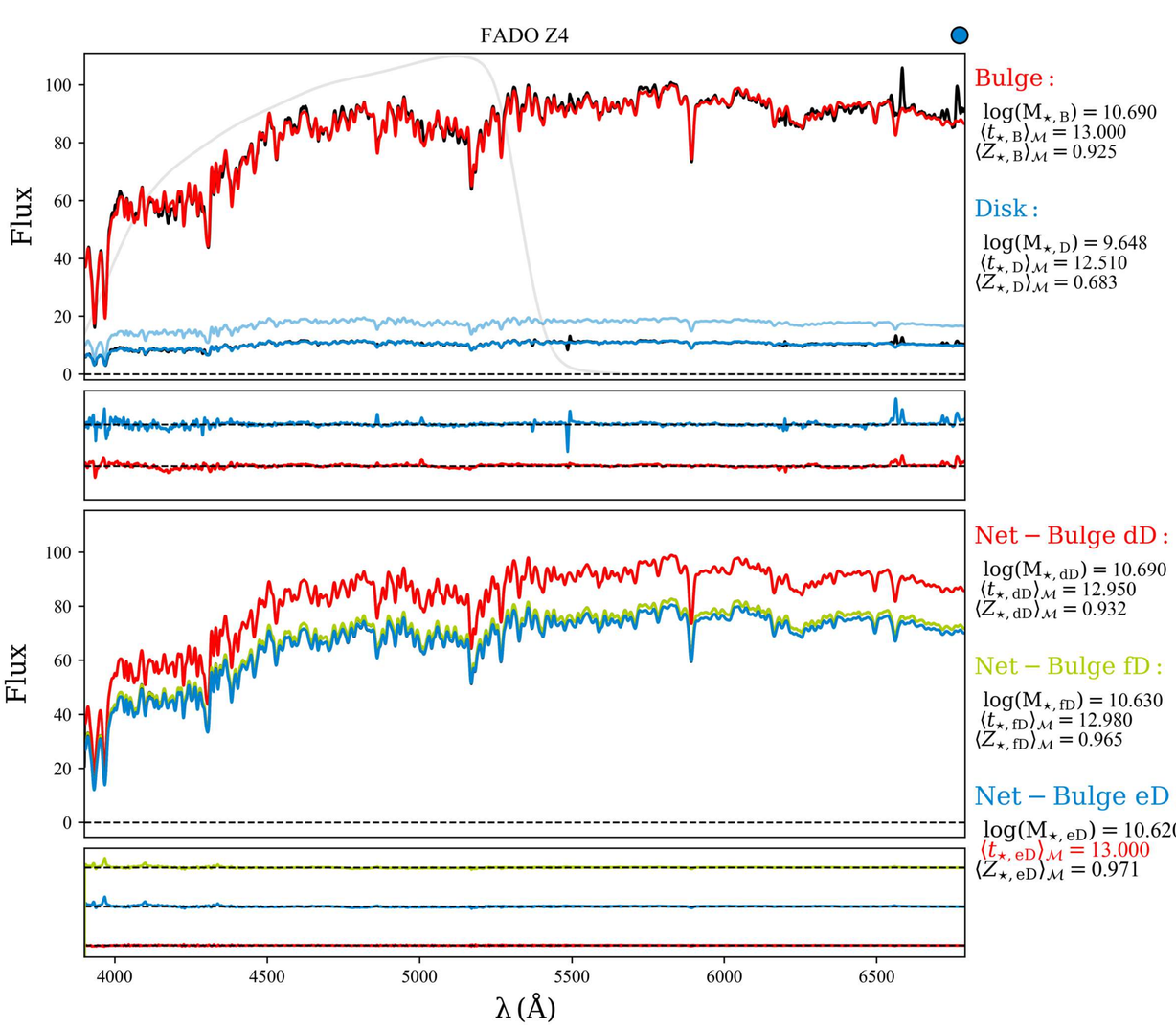
FADO Z4
Flux
100
80
60
40
20
0
Bulge :
log(M⋆, B) = 10.690
⟨t⋆, B⟩M = 13.000
⟨Z⋆, B⟩M = 0.925
Disk :
log(M⋆, D) = 9.648
⟨t⋆, D⟩M = 12.510
⟨Z⋆, D⟩M = 0.683
Net − Bulge dD :
log(M⋆, dD) = 10.690
⟨t⋆, dD⟩M = 12.950
⟨Z⋆, dD⟩M = 0.932
Net − Bulge fD :
log(M⋆, fD) = 10.630
⟨t⋆, fD⟩M = 12.980
⟨Z⋆, fD⟩M = 0.965
Net − Bulge eD :
log(M⋆, eD) = 10.620
⟨t⋆, eD⟩M = 13.000
⟨Z⋆, eD⟩M = 0.971
4000
4500
5000
5500
6000
6500
λ (Å)

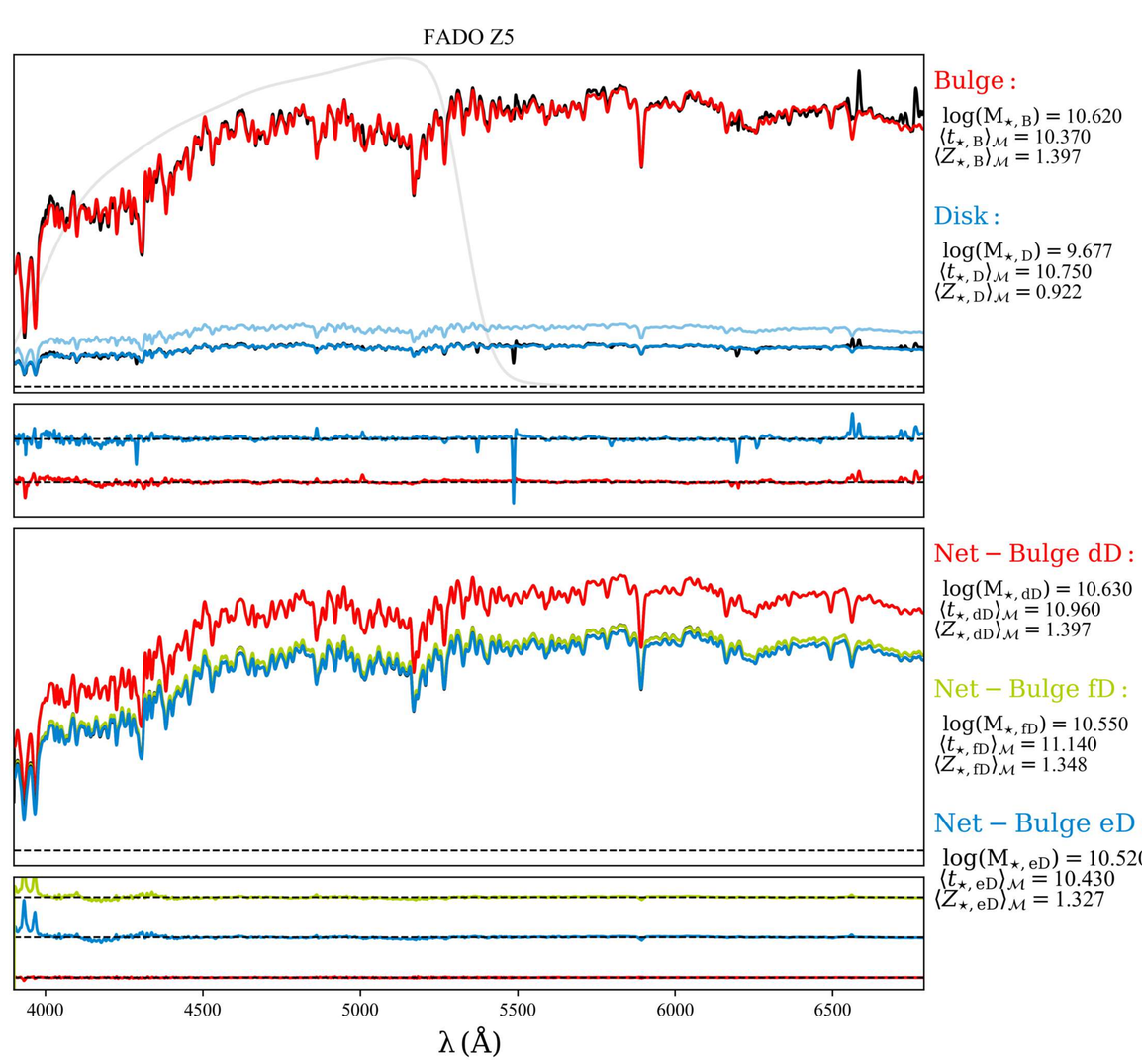
FADO Z5
Bulge :
log(M⋆, B) = 10.620
⟨t⋆, B⟩M = 10.370
⟨Z⋆, B⟩M = 1.397
Disk :
log(M⋆, D) = 9.677
⟨t⋆, D⟩M = 10.750
⟨Z⋆, D⟩M = 0.922
Net − Bulge dD :
log(M⋆, dD) = 10.630
⟨t⋆, dD⟩M = 10.960
⟨Z⋆, dD⟩M = 1.397
Net − Bulge fD :
log(M⋆, fD) = 10.550
⟨t⋆, fD⟩M = 11.140
⟨Z⋆, fD⟩M = 1.348
Net − Bulge eD :
log(M⋆, eD) = 10.520
⟨t⋆, eD⟩M = 10.430
⟨Z⋆, eD⟩M = 1.327
4000
4500
5000
5500
6000
6500
λ (Å)

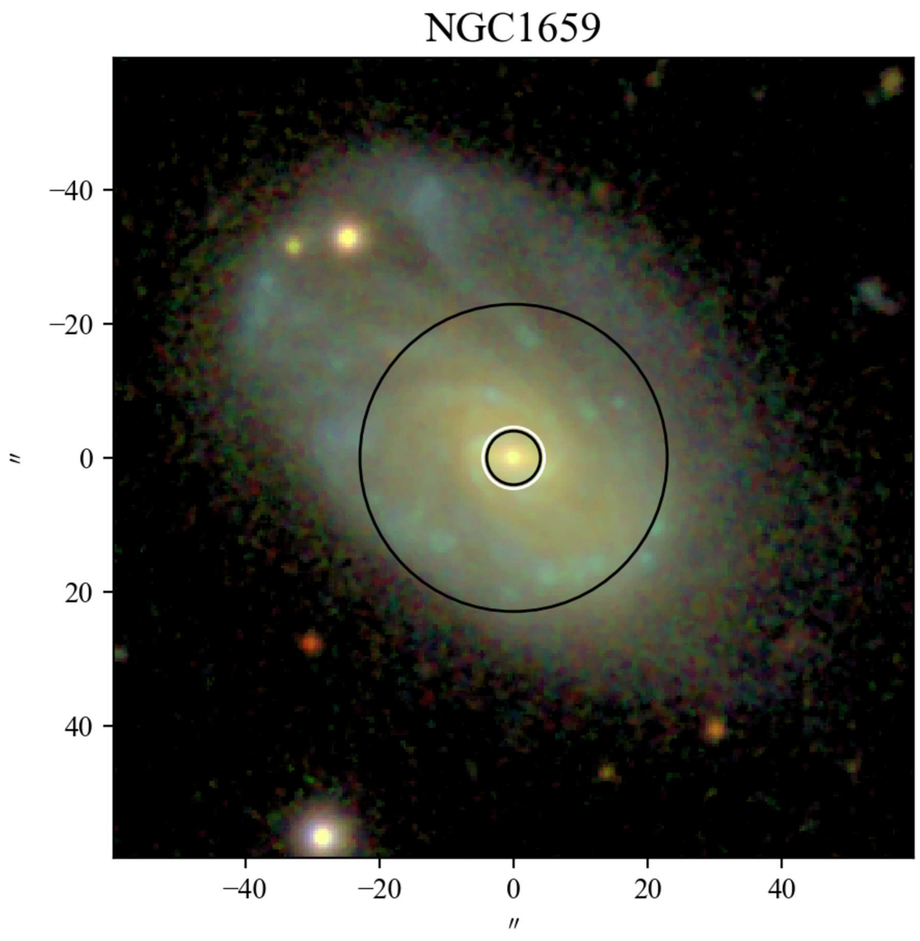
NGC1659
−40
−20
0
20
40
″
−40
−20
0
20
40
″

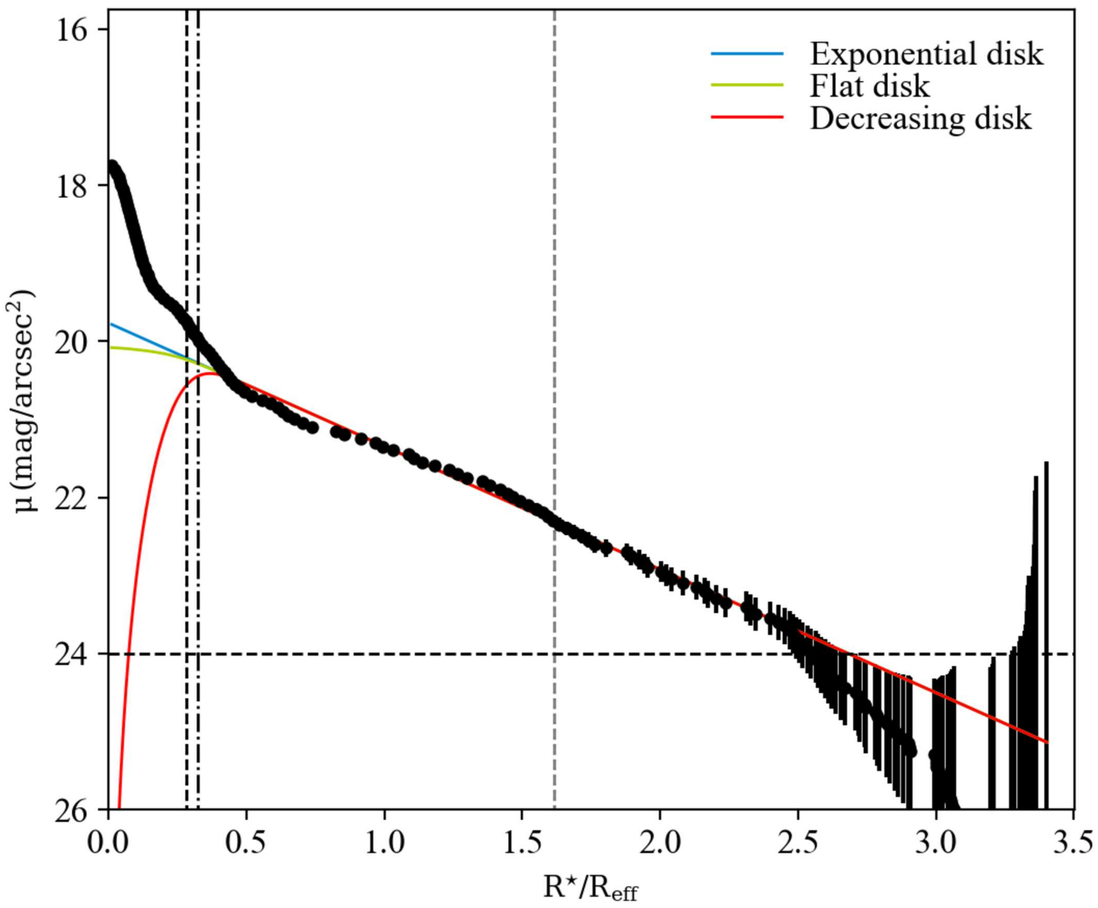
Exponential disk
Flat disk
Decreasing disk
μ (mag/arcsec²)
16
18
20
22
24
26
0.0
0.5
1.0
1.5
2.0
2.5
3.0
3.5
R⋆/Reff

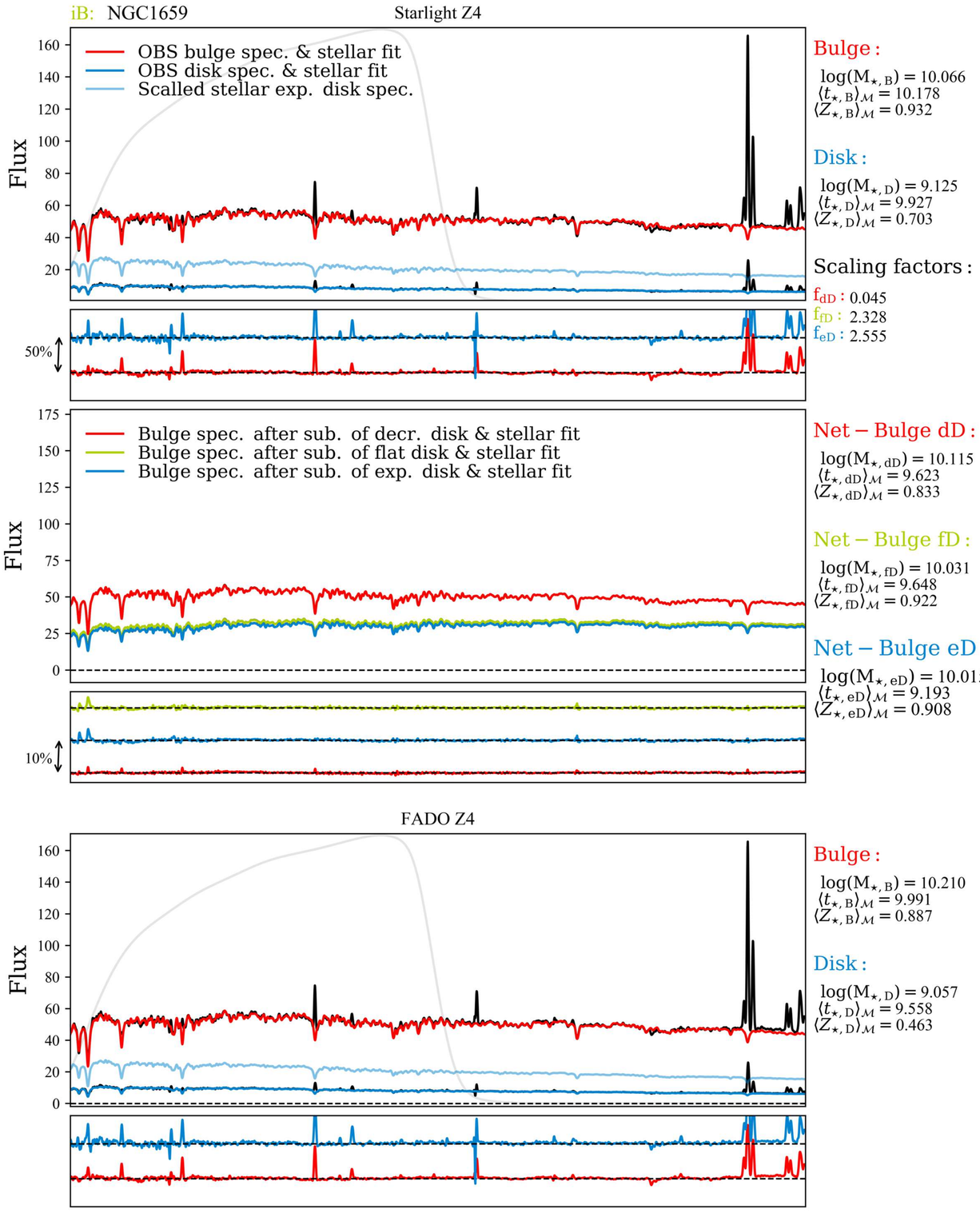
iB: NGC1659
Starlight Z4
OBS bulge spec. & stellar fit
OBS disk spec. & stellar fit
Scalled stellar exp. disk spec.
Flux
50%
Bulge spec. after sub. of decr. disk & stellar fit
Bulge spec. after sub. of flat disk & stellar fit
Bulge spec. after sub. of exp. disk & stellar fit
10%
Bulge :
log(M⋆, B) = 10.066
⟨t⋆, B⟩M = 10.178
⟨Z⋆, B⟩M = 0.932
Disk :
log(M⋆, D) = 9.125
⟨t⋆, D⟩M = 9.927
⟨Z⋆, D⟩M = 0.703
Scaling factors :
fdD : 0.045
ffD : 2.328
feD : 2.555
Net − Bulge dD :
log(M⋆, dD) = 10.115
⟨t⋆, dD⟩M = 9.623
⟨Z⋆, dD⟩M = 0.833
Net − Bulge fD :
log(M⋆, fD) = 10.031
⟨t⋆, fD⟩M = 9.648
⟨Z⋆, fD⟩M = 0.922
Net − Bulge eD :
log(M⋆, eD) = 10.015
⟨t⋆, eD⟩M = 9.193
⟨Z⋆, eD⟩M = 0.908

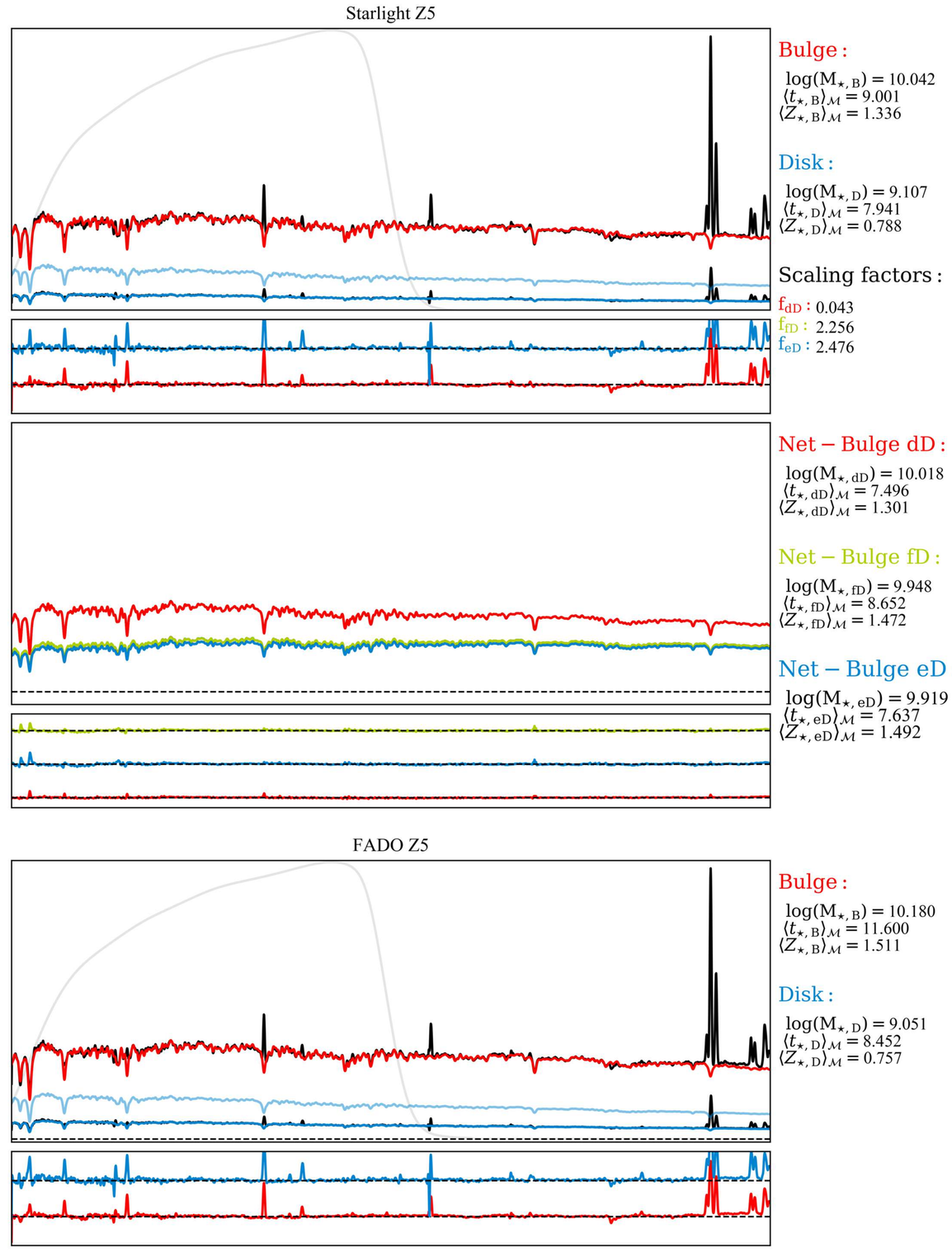
Starlight Z5
Bulge :
log(M⋆, B) = 10.042
⟨t⋆, B⟩M = 9.001
⟨Z⋆, B⟩M = 1.336
Disk :
log(M⋆, D) = 9.107
⟨t⋆, D⟩M = 7.941
⟨Z⋆, D⟩M = 0.788
Scaling factors :
fdD : 0.043
ffD : 2.256
feD : 2.476
Net − Bulge dD :
log(M⋆, dD) = 10.018
⟨t⋆, dD⟩M = 7.496
⟨Z⋆, dD⟩M = 1.301
Net − Bulge fD :
log(M⋆, fD) = 9.948
⟨t⋆, fD⟩M = 8.652
⟨Z⋆, fD⟩M = 1.472
Net − Bulge eD :
log(M⋆, eD) = 9.919
⟨t⋆, eD⟩M = 7.637
⟨Z⋆, eD⟩M = 1.492

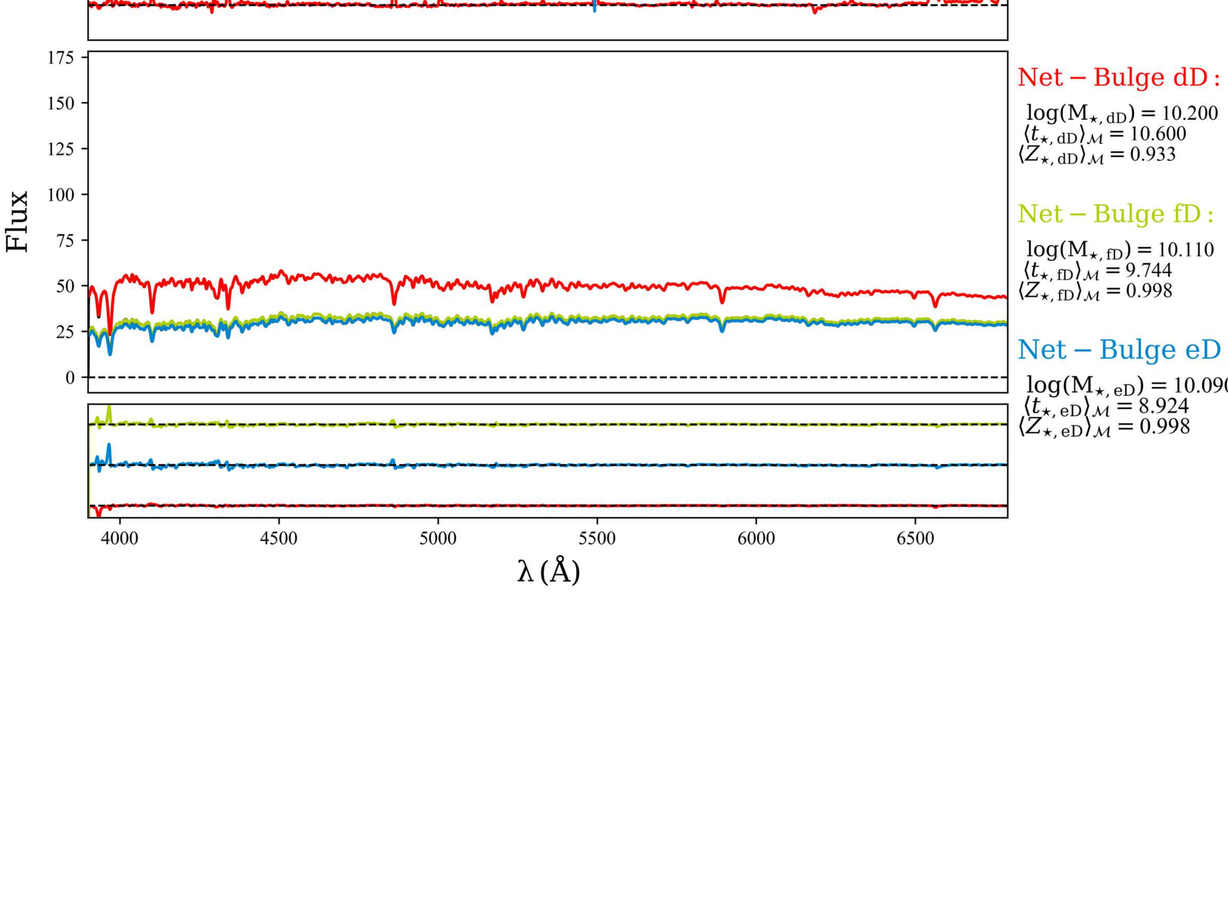
FADO Z4
Flux
Bulge :
log(M⋆, B) = 10.210
⟨t⋆, B⟩M = 9.991
⟨Z⋆, B⟩M = 0.887
Disk :
log(M⋆, D) = 9.057
⟨t⋆, D⟩M = 9.558
⟨Z⋆, D⟩M = 0.463
Net − Bulge dD :
log(M⋆, dD) = 10.200
⟨t⋆, dD⟩M = 10.600
⟨Z⋆, dD⟩M = 0.933
Net − Bulge fD :
log(M⋆, fD) = 10.110
⟨t⋆, fD⟩M = 9.744
⟨Z⋆, fD⟩M = 0.998
Net − Bulge eD :
log(M⋆, eD) = 10.090
⟨t⋆, eD⟩M = 8.924
⟨Z⋆, eD⟩M = 0.998
λ (Å)

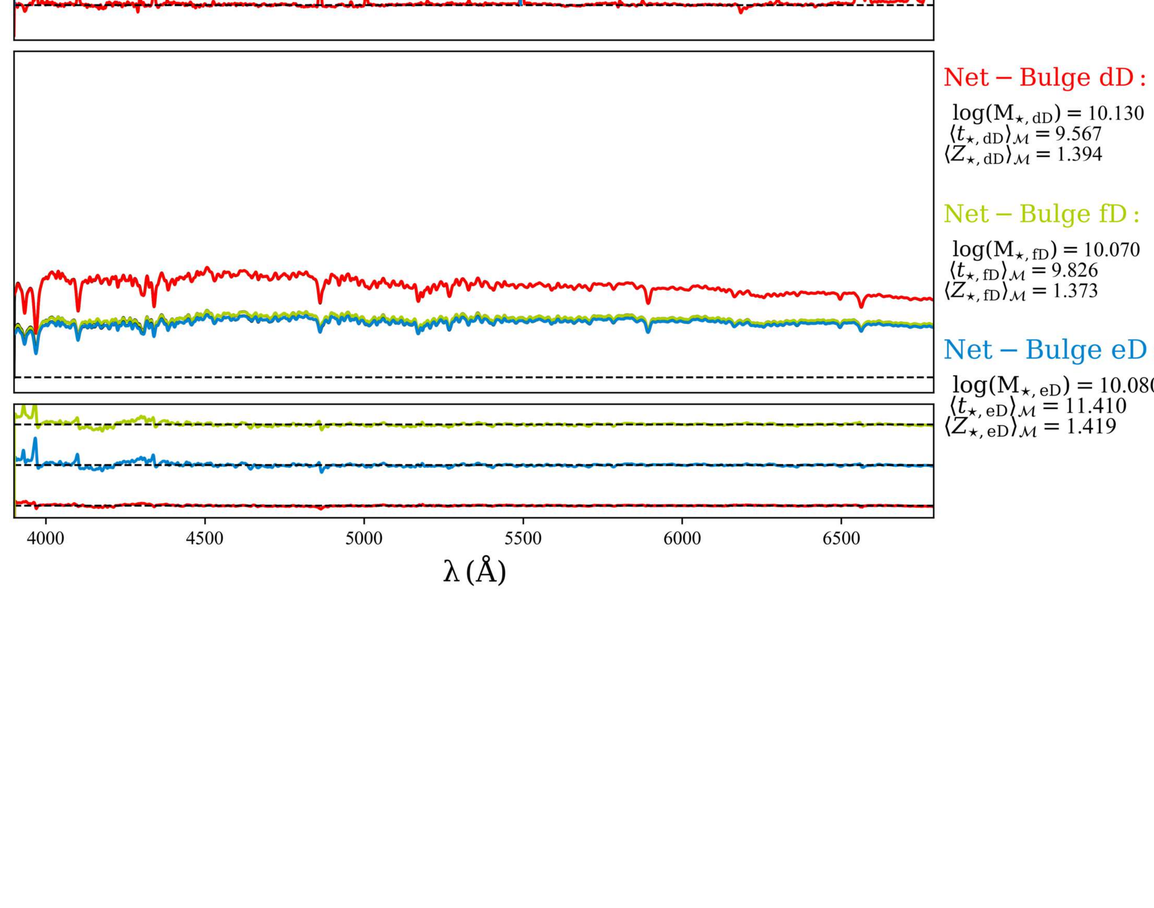
FADO Z5
Bulge :
log(M⋆, B) = 10.180
⟨t⋆, B⟩M = 11.600
⟨Z⋆, B⟩M = 1.511
Disk :
log(M⋆, D) = 9.051
⟨t⋆, D⟩M = 8.452
⟨Z⋆, D⟩M = 0.757
Net − Bulge dD :
log(M⋆, dD) = 10.130
⟨t⋆, dD⟩M = 9.567
⟨Z⋆, dD⟩M = 1.394
Net − Bulge fD :
log(M⋆, fD) = 10.070
⟨t⋆, fD⟩M = 9.826
⟨Z⋆, fD⟩M = 1.373
Net − Bulge eD :
log(M⋆, eD) = 10.080
⟨t⋆, eD⟩M = 11.410
⟨Z⋆, eD⟩M = 1.419
λ (Å)

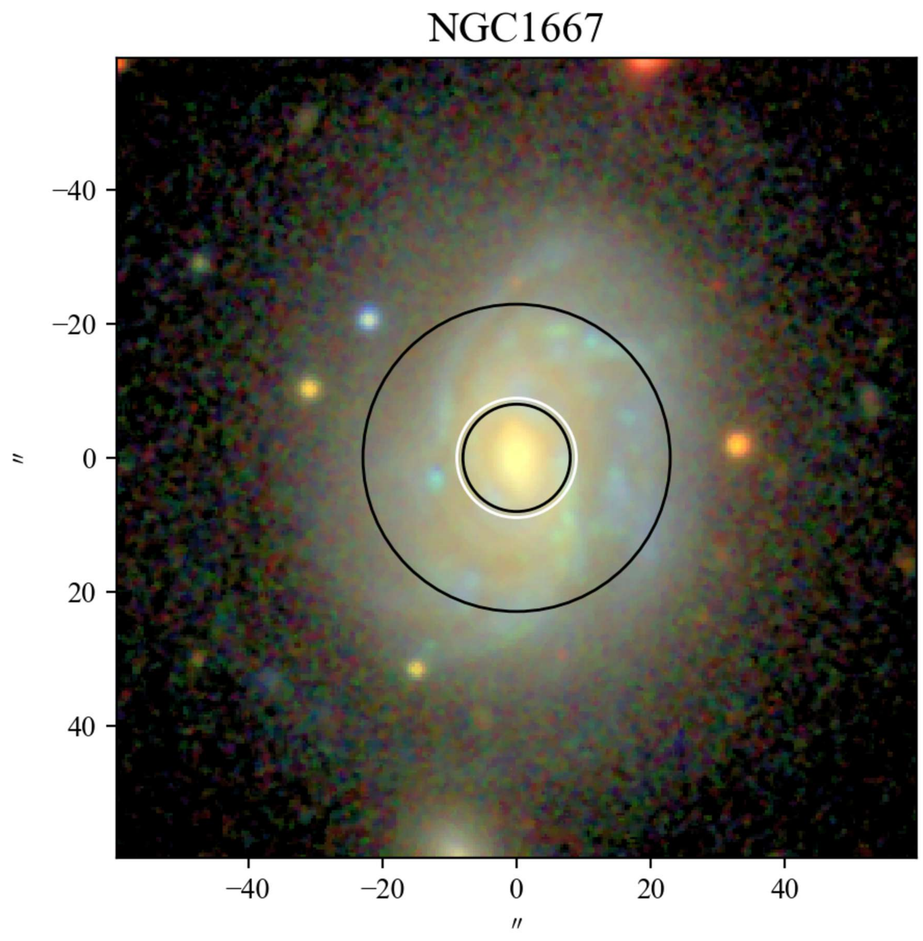
NGC1667
−40
−20
0
20
40
″
−40
−20
0
20
40
″

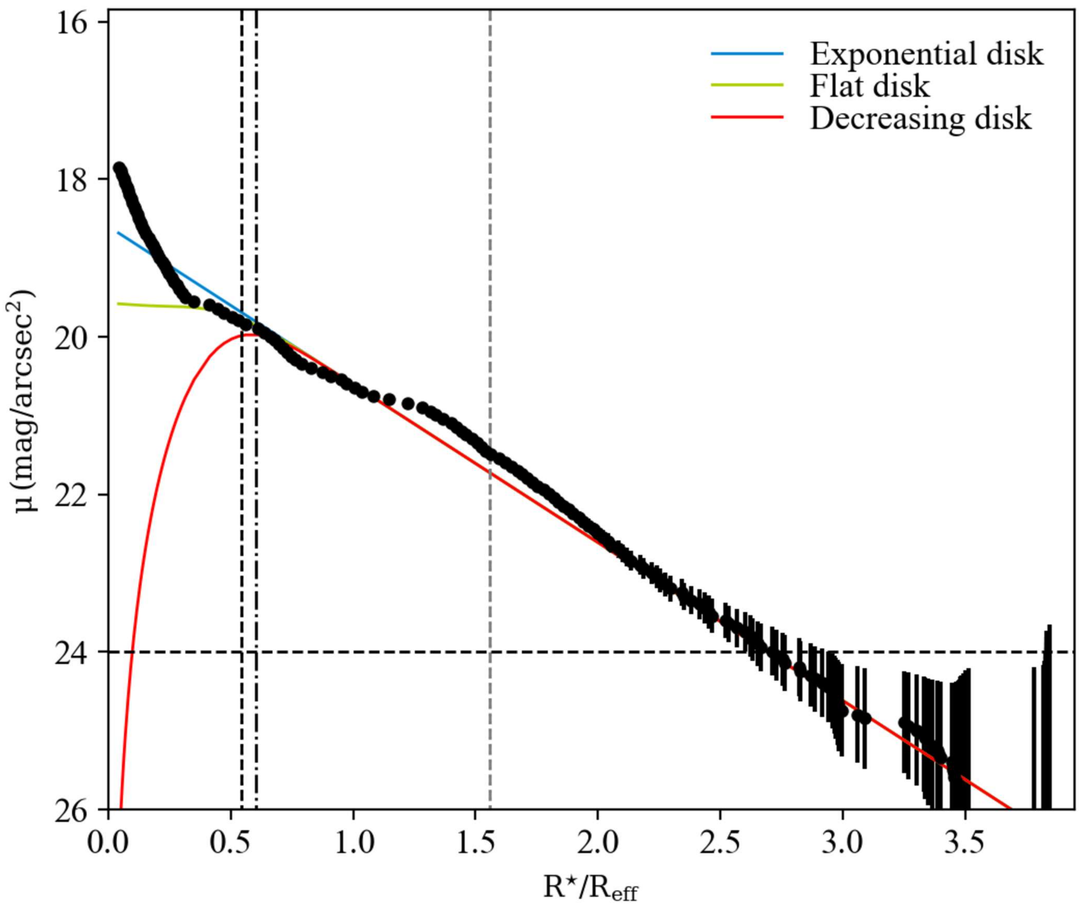
Exponential disk
Flat disk
Decreasing disk
μ (mag/arcsec²)
16
18
20
22
24
26
0.0
0.5
1.0
1.5
2.0
2.5
3.0
3.5
R⋆/Reff

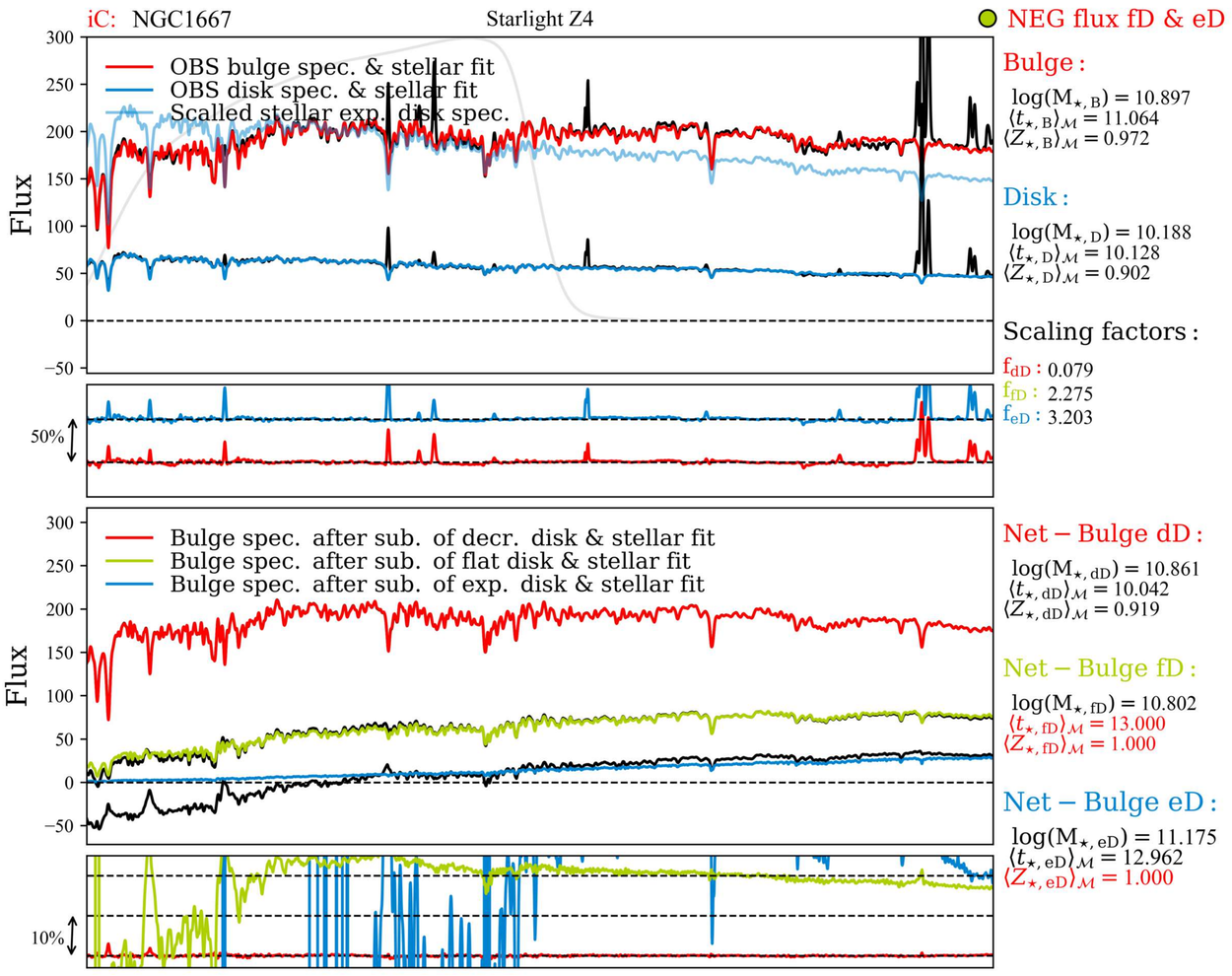
iC: NGC1667
Starlight Z4
NEG flux fD & eD
OBS bulge spec. & stellar fit
OBS disk spec. & stellar fit
Scalled stellar exp. disk spec.
Flux
Bulge :
log(M⋆, B) = 10.897
⟨t⋆, B⟩M = 11.064
⟨Z⋆, B⟩M = 0.972
Disk :
log(M⋆, D) = 10.188
⟨t⋆, D⟩M = 10.128
⟨Z⋆, D⟩M = 0.902
Scaling factors :
fdD : 0.079
ffD : 2.275
feD : 3.203
50%
Bulge spec. after sub. of decr. disk & stellar fit
Bulge spec. after sub. of flat disk & stellar fit
Bulge spec. after sub. of exp. disk & stellar fit
Net − Bulge dD :
log(M⋆, dD) = 10.861
⟨t⋆, dD⟩M = 10.042
⟨Z⋆, dD⟩M = 0.919
Net − Bulge fD :
log(M⋆, fD) = 10.802
⟨t⋆, fD⟩M = 13.000
⟨Z⋆, fD⟩M = 1.000
Net − Bulge eD :
log(M⋆, eD) = 11.175
⟨t⋆, eD⟩M = 12.962
⟨Z⋆, eD⟩M = 1.000
10%

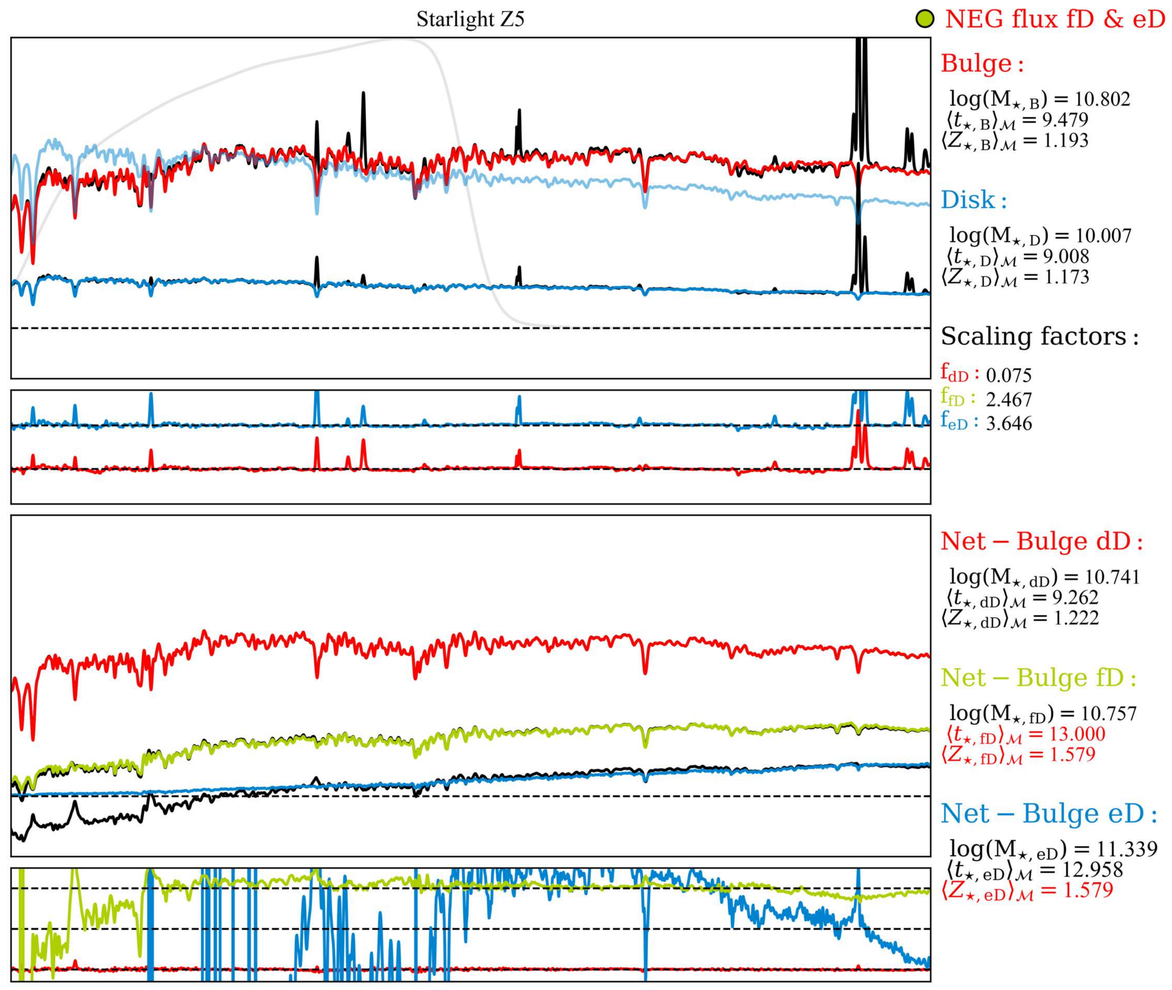
Starlight Z5
NEG flux fD & eD
Bulge :
log(M⋆, B) = 10.802
⟨t⋆, B⟩M = 9.479
⟨Z⋆, B⟩M = 1.193
Disk :
log(M⋆, D) = 10.007
⟨t⋆, D⟩M = 9.008
⟨Z⋆, D⟩M = 1.173
Scaling factors :
fdD : 0.075
ffD : 2.467
feD : 3.646
Net − Bulge dD :
log(M⋆, dD) = 10.741
⟨t⋆, dD⟩M = 9.262
⟨Z⋆, dD⟩M = 1.222
Net − Bulge fD :
log(M⋆, fD) = 10.757
⟨t⋆, fD⟩M = 13.000
⟨Z⋆, fD⟩M = 1.579
Net − Bulge eD :
log(M⋆, eD) = 11.339
⟨t⋆, eD⟩M = 12.958
⟨Z⋆, eD⟩M = 1.579

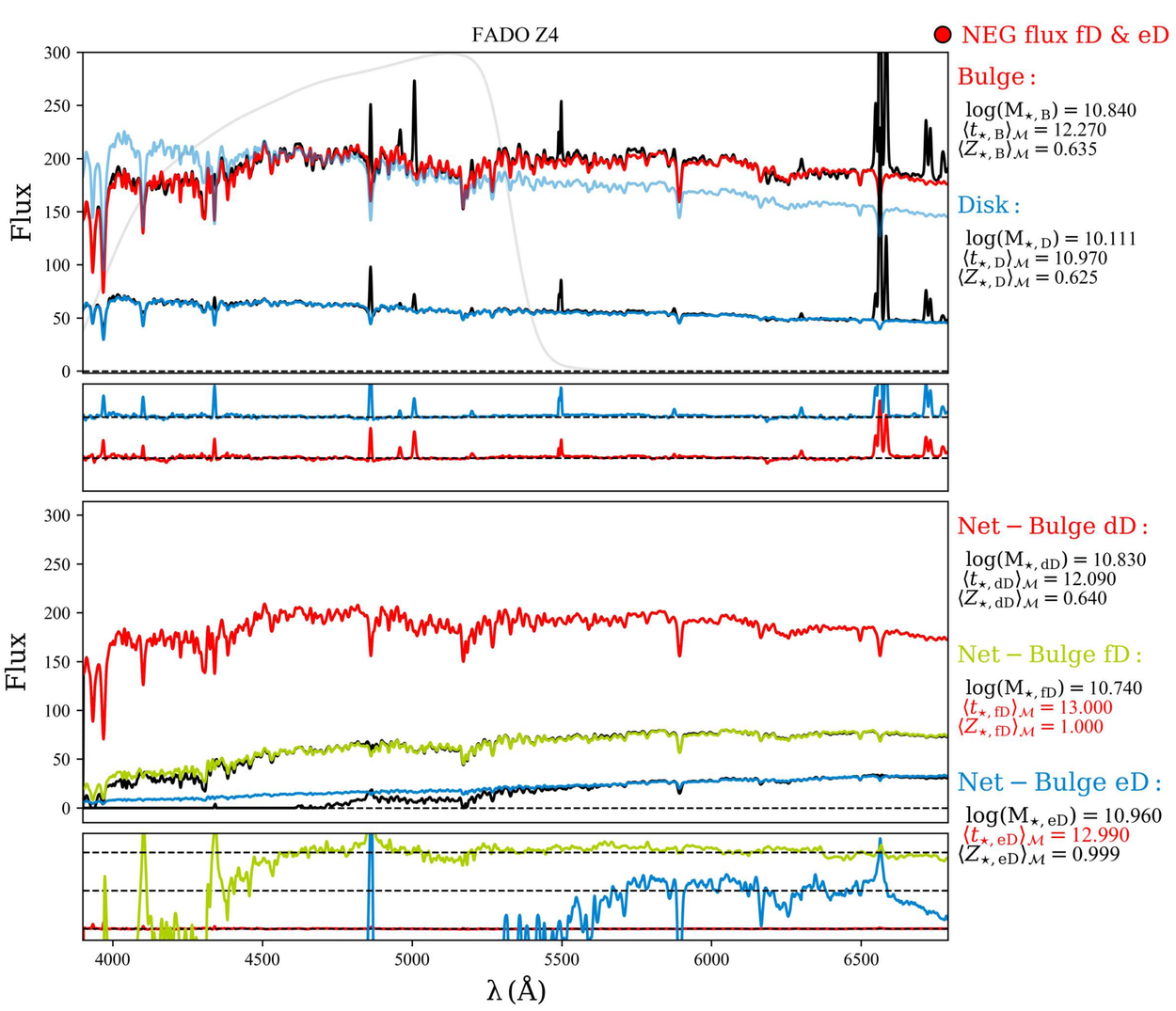
FADO Z4
NEG flux fD & eD
Flux
Bulge :
log(M⋆, B) = 10.840
⟨t⋆, B⟩M = 12.270
⟨Z⋆, B⟩M = 0.635
Disk :
log(M⋆, D) = 10.111
⟨t⋆, D⟩M = 10.970
⟨Z⋆, D⟩M = 0.625
Net − Bulge dD :
log(M⋆, dD) = 10.830
⟨t⋆, dD⟩M = 12.090
⟨Z⋆, dD⟩M = 0.640
Net − Bulge fD :
log(M⋆, fD) = 10.740
⟨t⋆, fD⟩M = 13.000
⟨Z⋆, fD⟩M = 1.000
Net − Bulge eD :
log(M⋆, eD) = 10.960
⟨t⋆, eD⟩M = 12.990
⟨Z⋆, eD⟩M = 0.999
4000
4500
5000
5500
6000
6500
λ (Å)

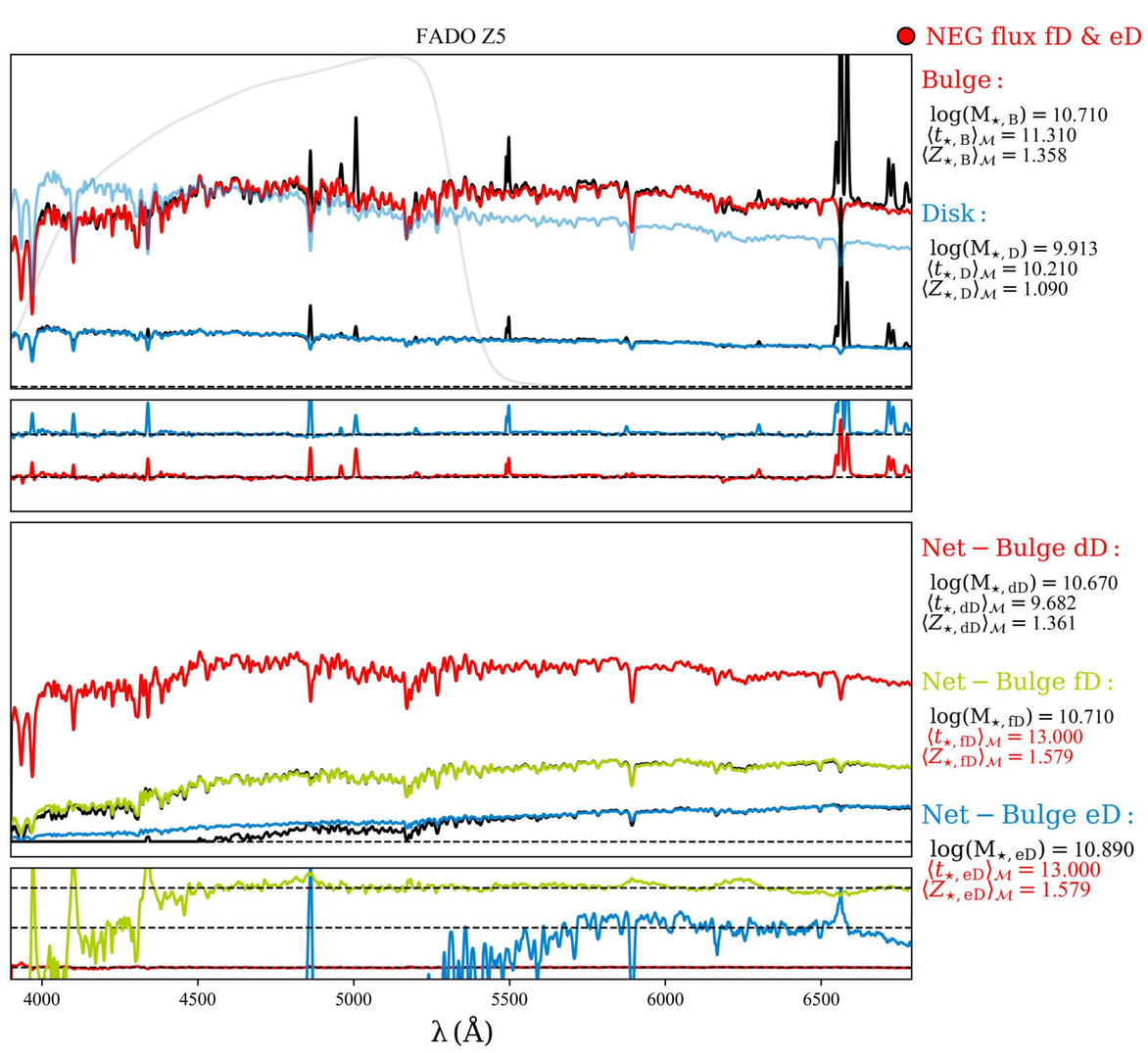
FADO Z5
NEG flux fD & eD
Bulge :
log(M⋆, B) = 10.710
⟨t⋆, B⟩M = 11.310
⟨Z⋆, B⟩M = 1.358
Disk :
log(M⋆, D) = 9.913
⟨t⋆, D⟩M = 10.210
⟨Z⋆, D⟩M = 1.090
Net − Bulge dD :
log(M⋆, dD) = 10.670
⟨t⋆, dD⟩M = 9.682
⟨Z⋆, dD⟩M = 1.361
Net − Bulge fD :
log(M⋆, fD) = 10.710
⟨t⋆, fD⟩M = 13.000
⟨Z⋆, fD⟩M = 1.579
Net − Bulge eD :
log(M⋆, eD) = 10.890
⟨t⋆, eD⟩M = 13.000
⟨Z⋆, eD⟩M = 1.579
4000
4500
5000
5500
6000
6500
λ (Å)

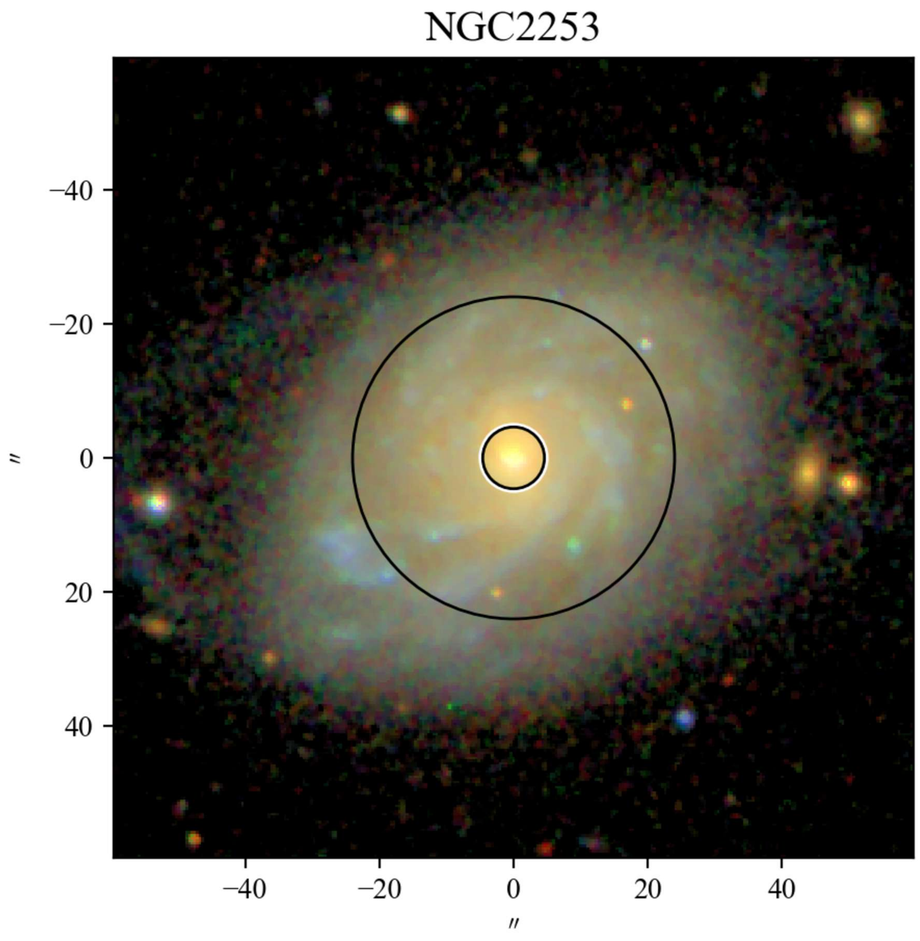
NGC2253
−40
−20
0
20
40
″
−40
−20
0
20
40
″

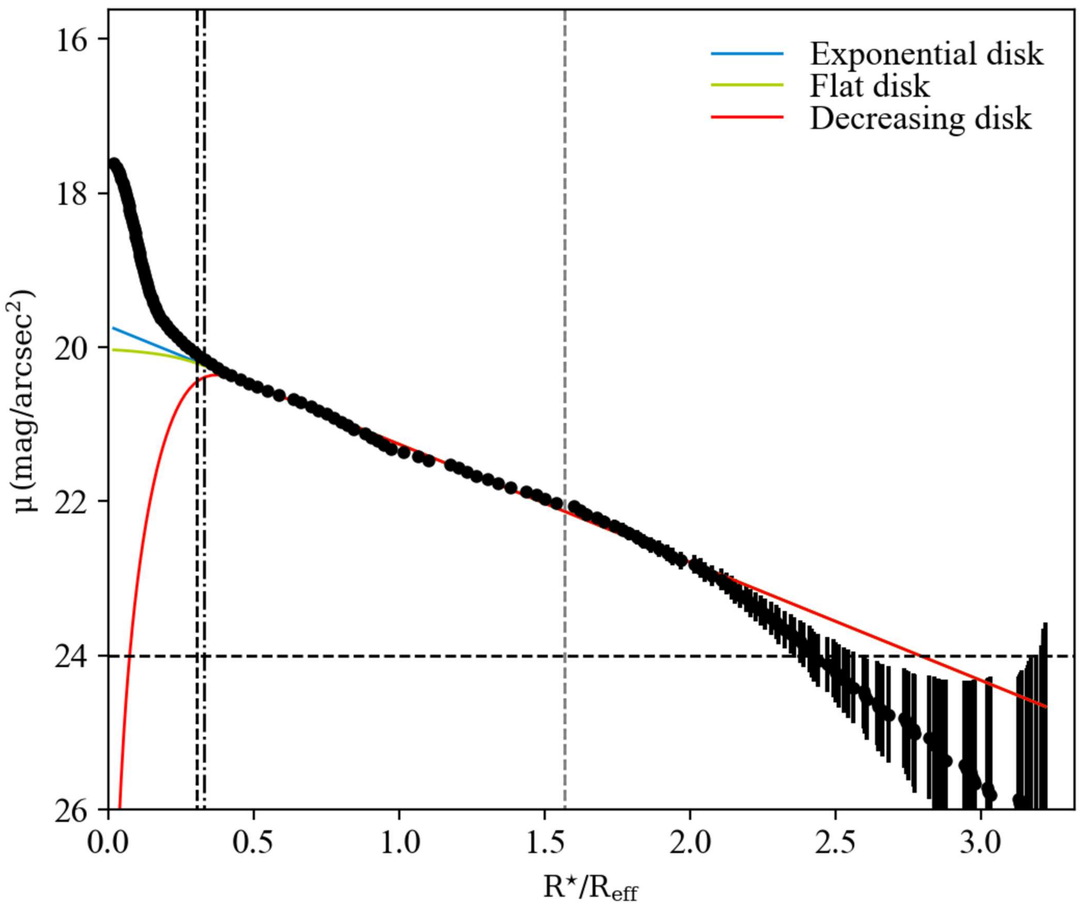
Exponential disk
Flat disk
Decreasing disk
μ (mag/arcsec²)
16
18
20
22
24
26
0.0
0.5
1.0
1.5
2.0
2.5
3.0
R⋆/Reff

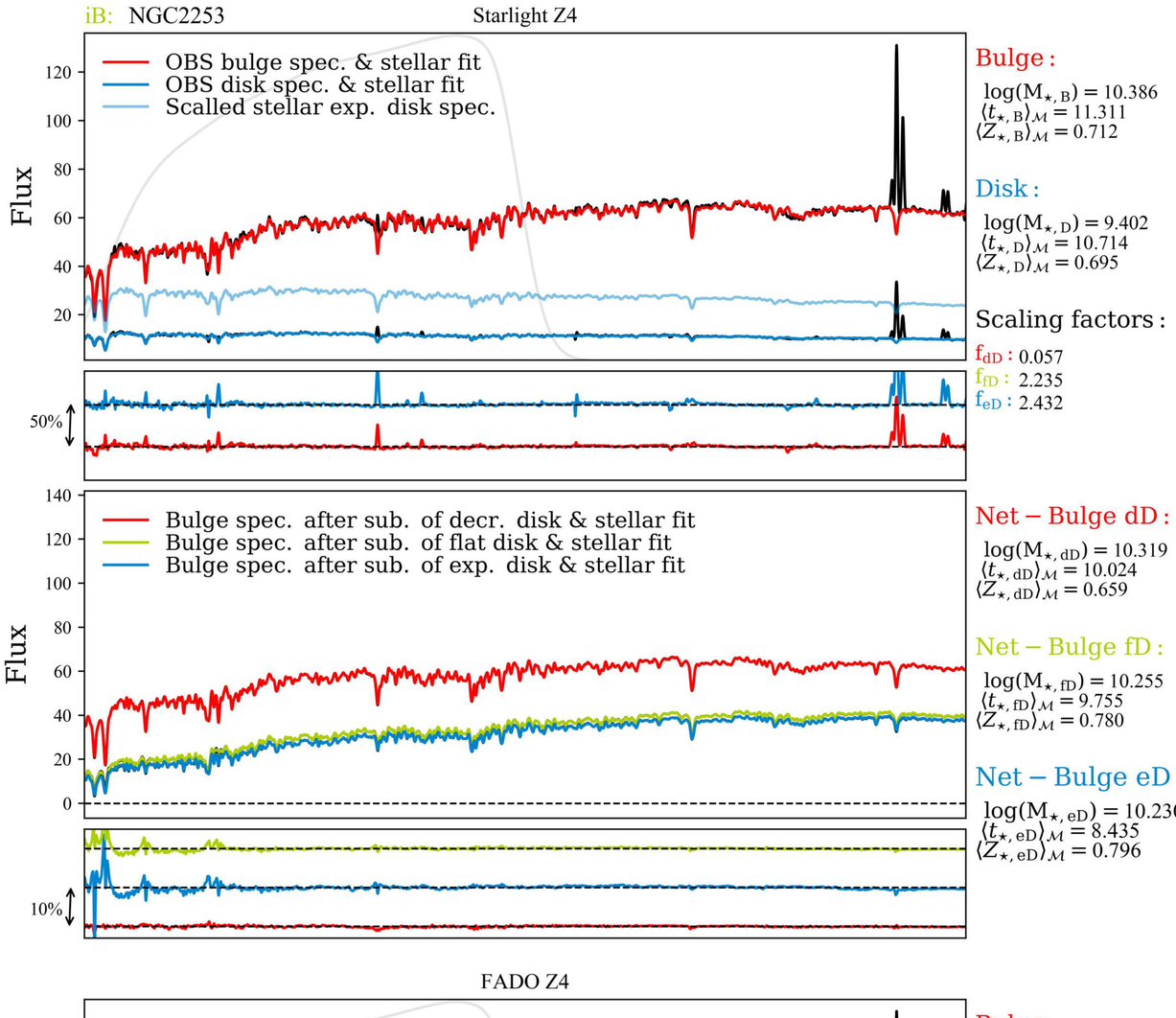
iB: NGC2253
Starlight Z4
OBS bulge spec. & stellar fit
OBS disk spec. & stellar fit
Scalled stellar exp. disk spec.
Flux
120
100
80
60
40
20
50%
Bulge :
log(M⋆, B) = 10.386
⟨t⋆, B⟩M = 11.311
⟨Z⋆, B⟩M = 0.712
Disk :
log(M⋆, D) = 9.402
⟨t⋆, D⟩M = 10.714
⟨Z⋆, D⟩M = 0.695
Scaling factors :
fdD : 0.057
ffD : 2.235
feD : 2.432
Bulge spec. after sub. of decr. disk & stellar fit
Bulge spec. after sub. of flat disk & stellar fit
Bulge spec. after sub. of exp. disk & stellar fit
140
120
100
80
60
40
20
0
10%
Net − Bulge dD :
log(M⋆, dD) = 10.319
⟨t⋆, dD⟩M = 10.024
⟨Z⋆, dD⟩M = 0.659
Net − Bulge fD :
log(M⋆, fD) = 10.255
⟨t⋆, fD⟩M = 9.755
⟨Z⋆, fD⟩M = 0.780
Net − Bulge eD :
log(M⋆, eD) = 10.230
⟨t⋆, eD⟩M = 8.435
⟨Z⋆, eD⟩M = 0.796

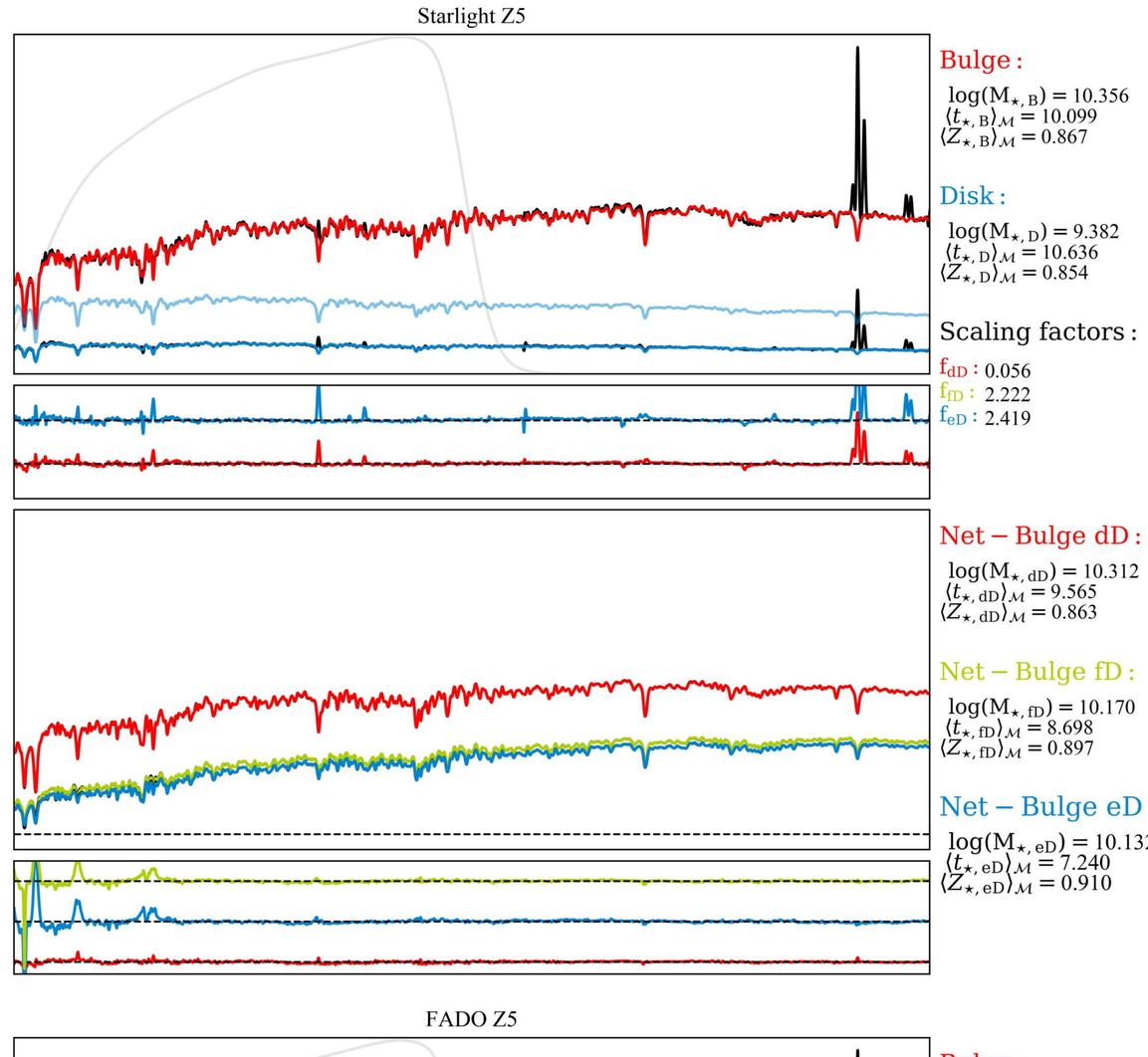
Starlight Z5
Bulge :
log(M⋆, B) = 10.356
⟨t⋆, B⟩M = 10.099
⟨Z⋆, B⟩M = 0.867
Disk :
log(M⋆, D) = 9.382
⟨t⋆, D⟩M = 10.636
⟨Z⋆, D⟩M = 0.854
Scaling factors :
fdD : 0.056
ffD : 2.222
feD : 2.419
Net − Bulge dD :
log(M⋆, dD) = 10.312
⟨t⋆, dD⟩M = 9.565
⟨Z⋆, dD⟩M = 0.863
Net − Bulge fD :
log(M⋆, fD) = 10.170
⟨t⋆, fD⟩M = 8.698
⟨Z⋆, fD⟩M = 0.897
Net − Bulge eD :
log(M⋆, eD) = 10.132
⟨t⋆, eD⟩M = 7.240
⟨Z⋆, eD⟩M = 0.910

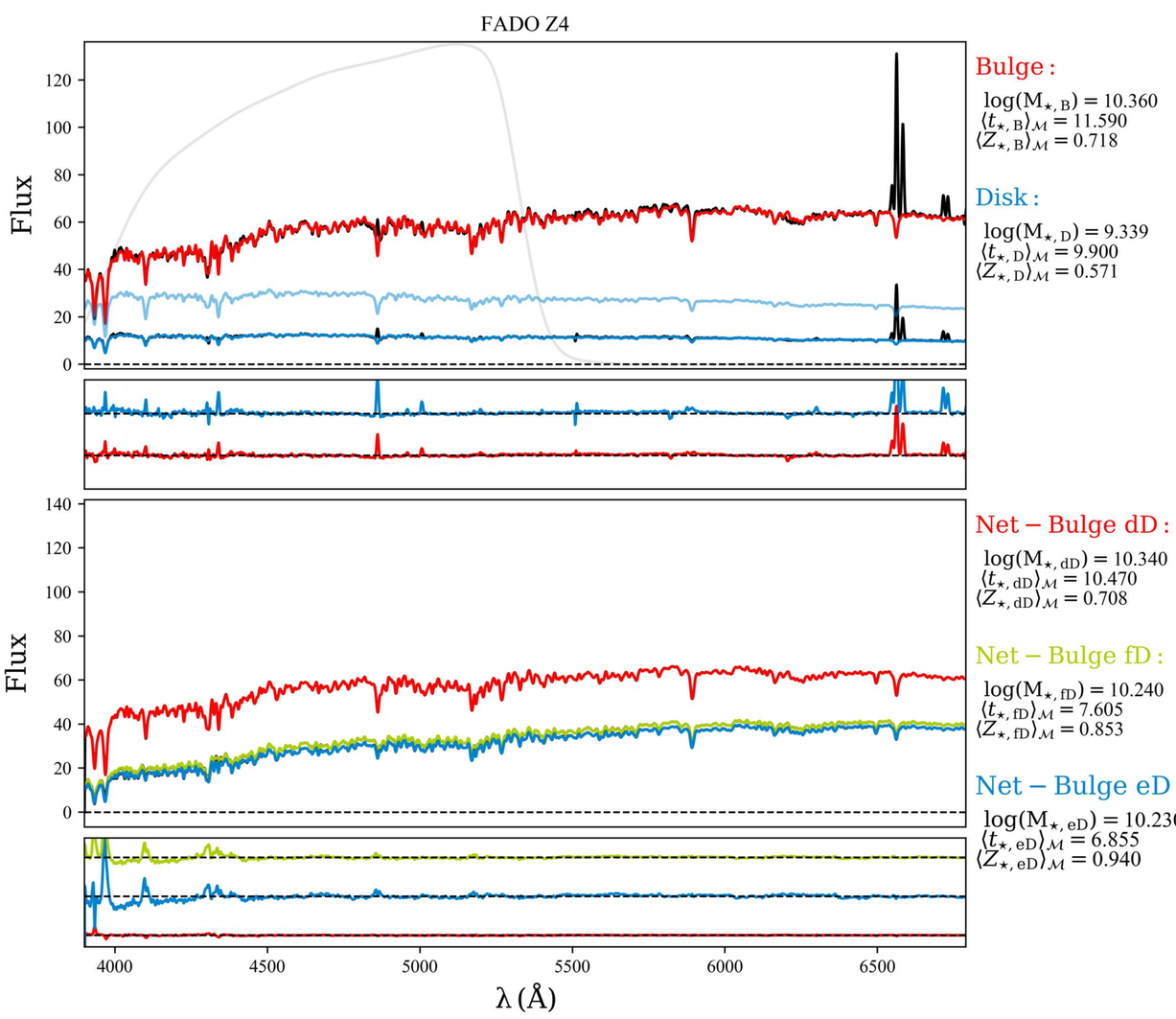
FADO Z4
Flux
120
100
80
60
40
20
0
Bulge :
log(M⋆, B) = 10.360
⟨t⋆, B⟩M = 11.590
⟨Z⋆, B⟩M = 0.718
Disk :
log(M⋆, D) = 9.339
⟨t⋆, D⟩M = 9.900
⟨Z⋆, D⟩M = 0.571
Net − Bulge dD :
log(M⋆, dD) = 10.340
⟨t⋆, dD⟩M = 10.470
⟨Z⋆, dD⟩M = 0.708
Net − Bulge fD :
log(M⋆, fD) = 10.240
⟨t⋆, fD⟩M = 7.605
⟨Z⋆, fD⟩M = 0.853
Net − Bulge eD :
log(M⋆, eD) = 10.230
⟨t⋆, eD⟩M = 6.855
⟨Z⋆, eD⟩M = 0.940
4000
4500
5000
5500
6000
6500
λ (Å)

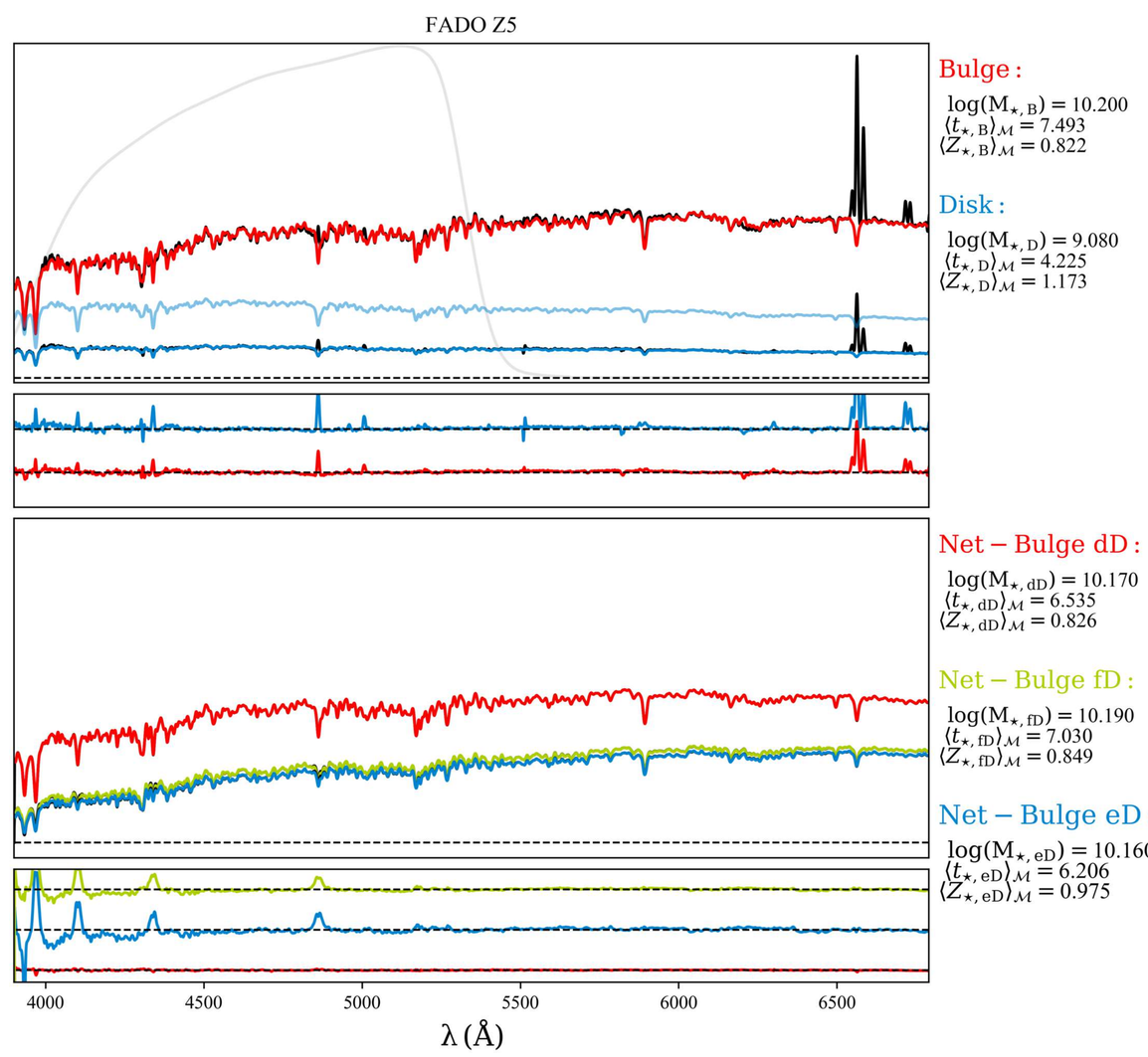
FADO Z5
Bulge :
log(M⋆, B) = 10.200
⟨t⋆, B⟩M = 7.493
⟨Z⋆, B⟩M = 0.822
Disk :
log(M⋆, D) = 9.080
⟨t⋆, D⟩M = 4.225
⟨Z⋆, D⟩M = 1.173
Net − Bulge dD :
log(M⋆, dD) = 10.170
⟨t⋆, dD⟩M = 6.535
⟨Z⋆, dD⟩M = 0.826
Net − Bulge fD :
log(M⋆, fD) = 10.190
⟨t⋆, fD⟩M = 7.030
⟨Z⋆, fD⟩M = 0.849
Net − Bulge eD :
log(M⋆, eD) = 10.160
⟨t⋆, eD⟩M = 6.206
⟨Z⋆, eD⟩M = 0.975
4000
4500
5000
5500
6000
6500
λ (Å)

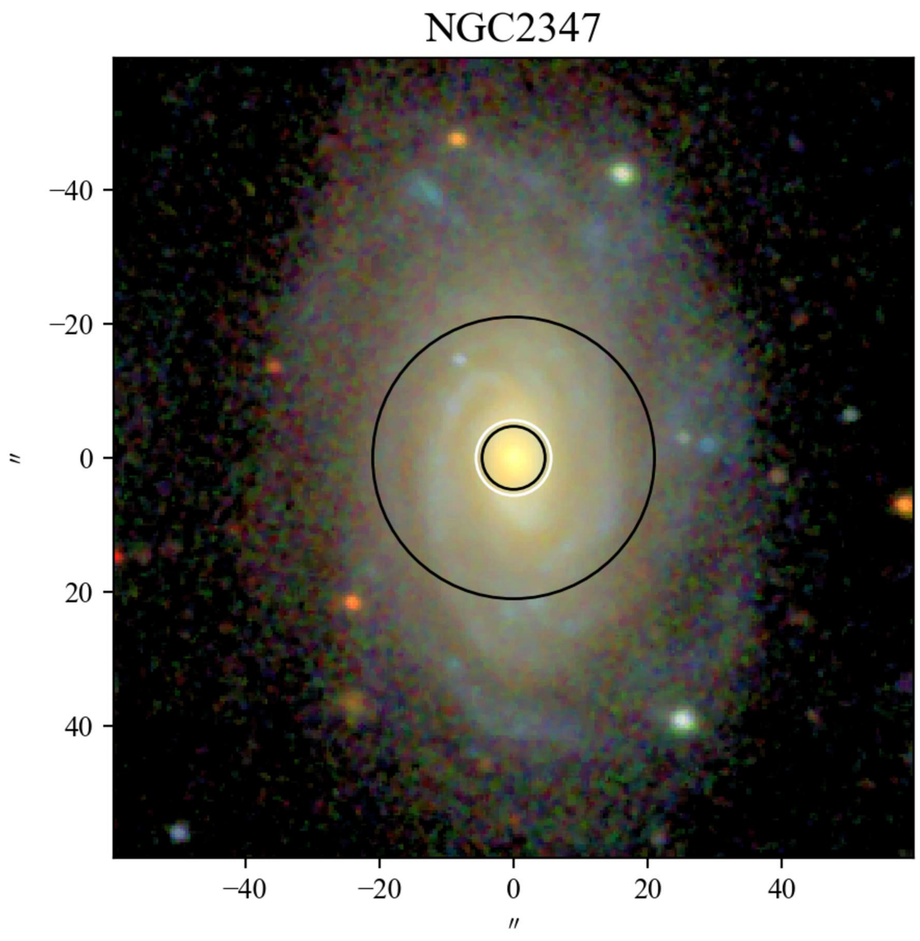
NGC2347
−40
−20
0
20
40
″
−40
−20
0
20
40
″

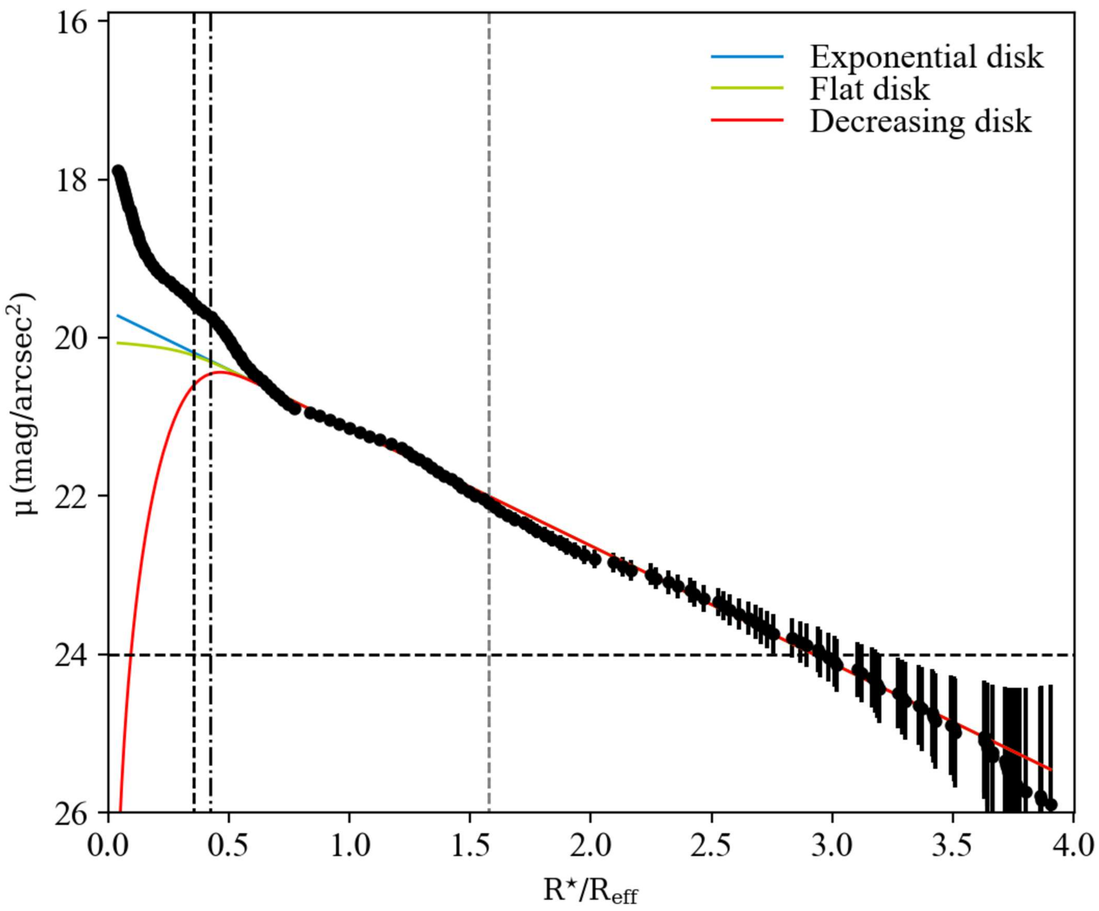
Exponential disk
Flat disk
Decreasing disk
μ (mag/arcsec²)
16
18
20
22
24
26
0.0
0.5
1.0
1.5
2.0
2.5
3.0
3.5
4.0
R⋆/Reff

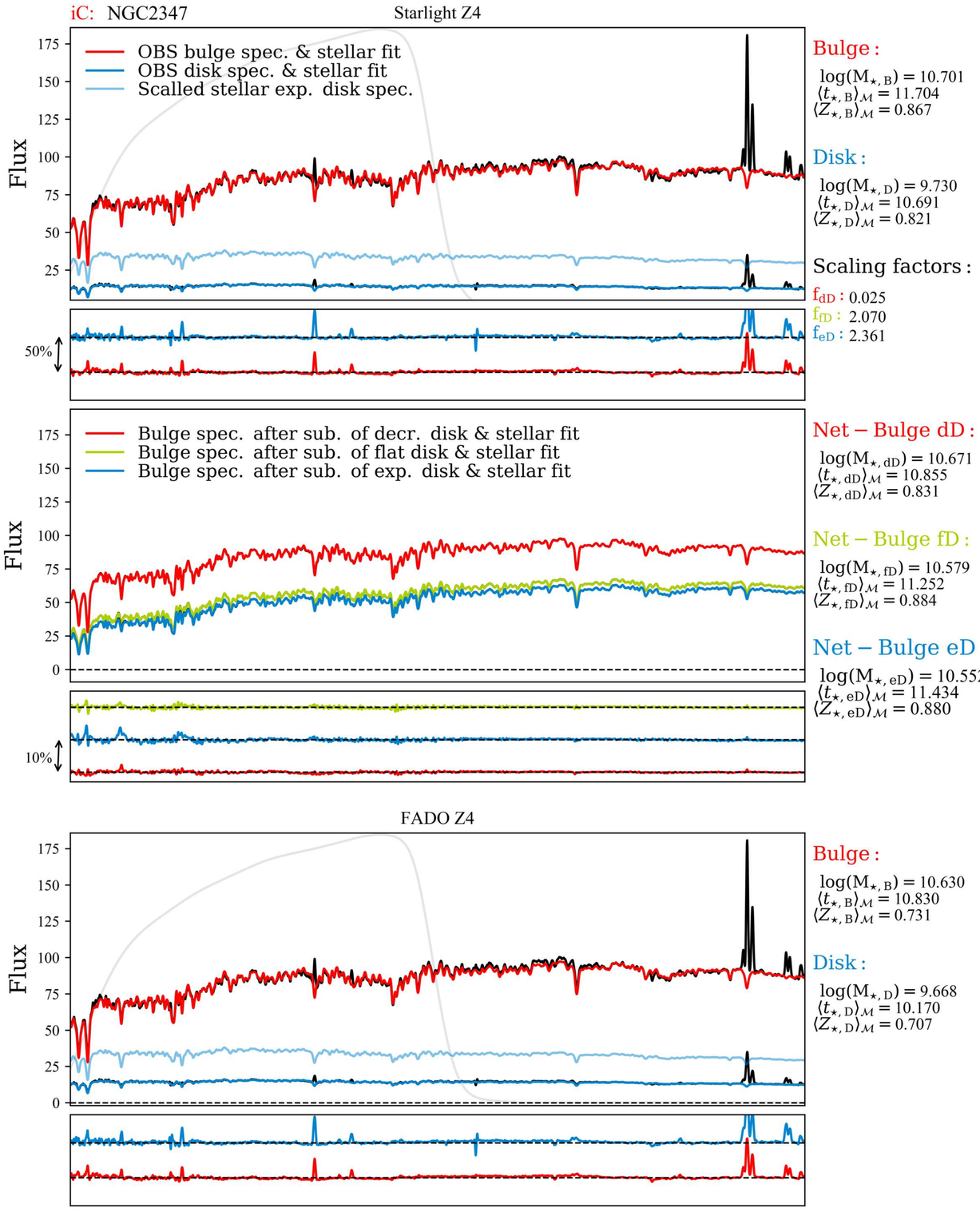
iC: NGC2347
Starlight Z4
OBS bulge spec. & stellar fit
OBS disk spec. & stellar fit
Scalled stellar exp. disk spec.
Flux
175
150
125
100
75
50
25
50%
Bulge :
log(M⋆, B) = 10.701
⟨t⋆, B⟩M = 11.704
⟨Z⋆, B⟩M = 0.867
Disk :
log(M⋆, D) = 9.730
⟨t⋆, D⟩M = 10.691
⟨Z⋆, D⟩M = 0.821
Scaling factors :
fdD : 0.025
ffD : 2.070
feD : 2.361
Bulge spec. after sub. of decr. disk & stellar fit
Bulge spec. after sub. of flat disk & stellar fit
Bulge spec. after sub. of exp. disk & stellar fit
0
10%
Net − Bulge dD :
log(M⋆, dD) = 10.671
⟨t⋆, dD⟩M = 10.855
⟨Z⋆, dD⟩M = 0.831
Net − Bulge fD :
log(M⋆, fD) = 10.579
⟨t⋆, fD⟩M = 11.252
⟨Z⋆, fD⟩M = 0.884
Net − Bulge eD :
log(M⋆, eD) = 10.552
⟨t⋆, eD⟩M = 11.434
⟨Z⋆, eD⟩M = 0.880

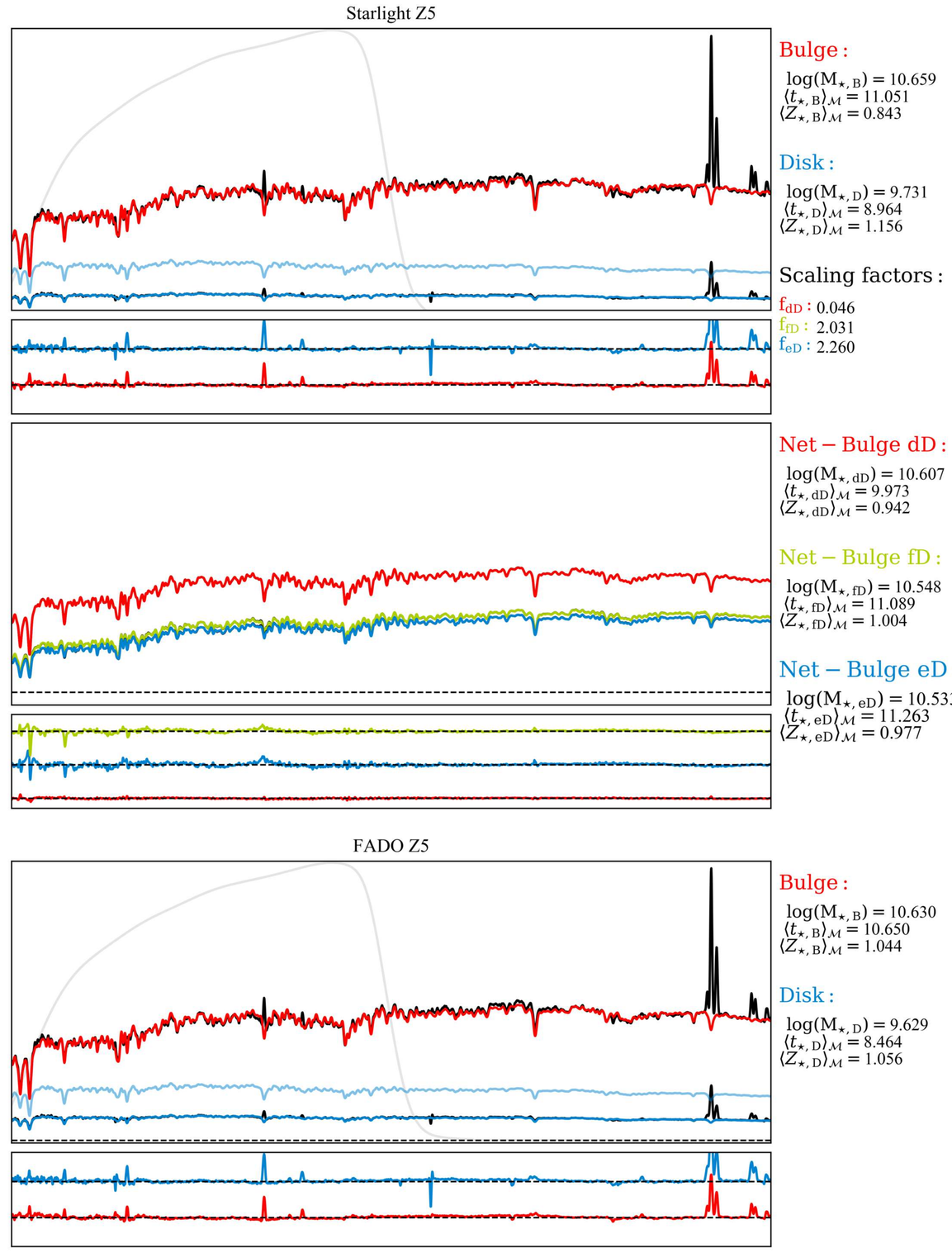
Starlight Z5
Bulge :
log(M⋆, B) = 10.659
⟨t⋆, B⟩M = 11.051
⟨Z⋆, B⟩M = 0.843
Disk :
log(M⋆, D) = 9.731
⟨t⋆, D⟩M = 8.964
⟨Z⋆, D⟩M = 1.156
Scaling factors :
fdD : 0.046
ffD : 2.031
feD : 2.260
Net − Bulge dD :
log(M⋆, dD) = 10.607
⟨t⋆, dD⟩M = 9.973
⟨Z⋆, dD⟩M = 0.942
Net − Bulge fD :
log(M⋆, fD) = 10.548
⟨t⋆, fD⟩M = 11.089
⟨Z⋆, fD⟩M = 1.004
Net − Bulge eD :
log(M⋆, eD) = 10.533
⟨t⋆, eD⟩M = 11.263
⟨Z⋆, eD⟩M = 0.977

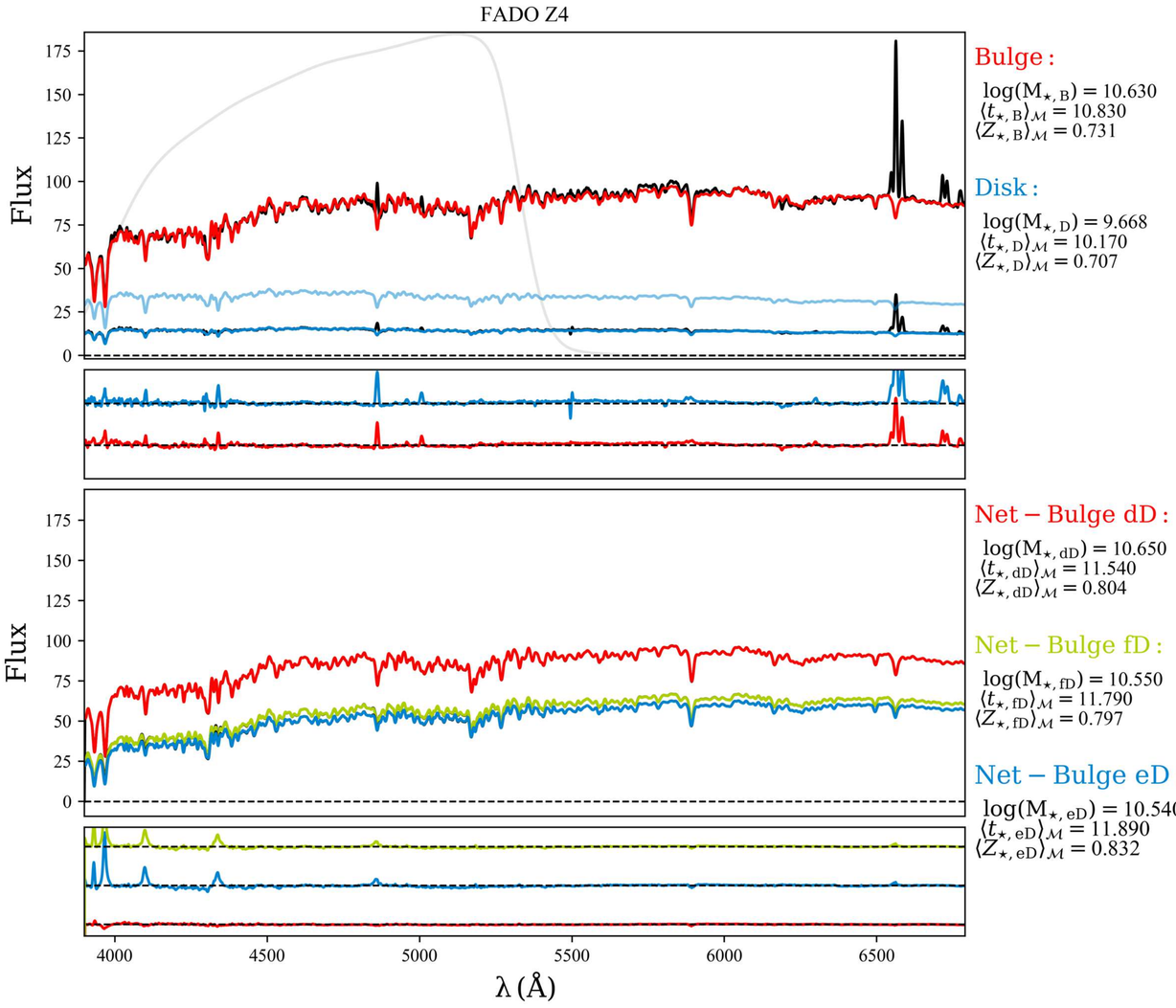
FADO Z4
Flux
175
150
125
100
75
50
25
0
Bulge :
log(M⋆, B) = 10.630
⟨t⋆, B⟩M = 10.830
⟨Z⋆, B⟩M = 0.731
Disk :
log(M⋆, D) = 9.668
⟨t⋆, D⟩M = 10.170
⟨Z⋆, D⟩M = 0.707
Net − Bulge dD :
log(M⋆, dD) = 10.650
⟨t⋆, dD⟩M = 11.540
⟨Z⋆, dD⟩M = 0.804
Net − Bulge fD :
log(M⋆, fD) = 10.550
⟨t⋆, fD⟩M = 11.790
⟨Z⋆, fD⟩M = 0.797
Net − Bulge eD :
log(M⋆, eD) = 10.540
⟨t⋆, eD⟩M = 11.890
⟨Z⋆, eD⟩M = 0.832
4000
4500
5000
5500
6000
6500
λ (Å)

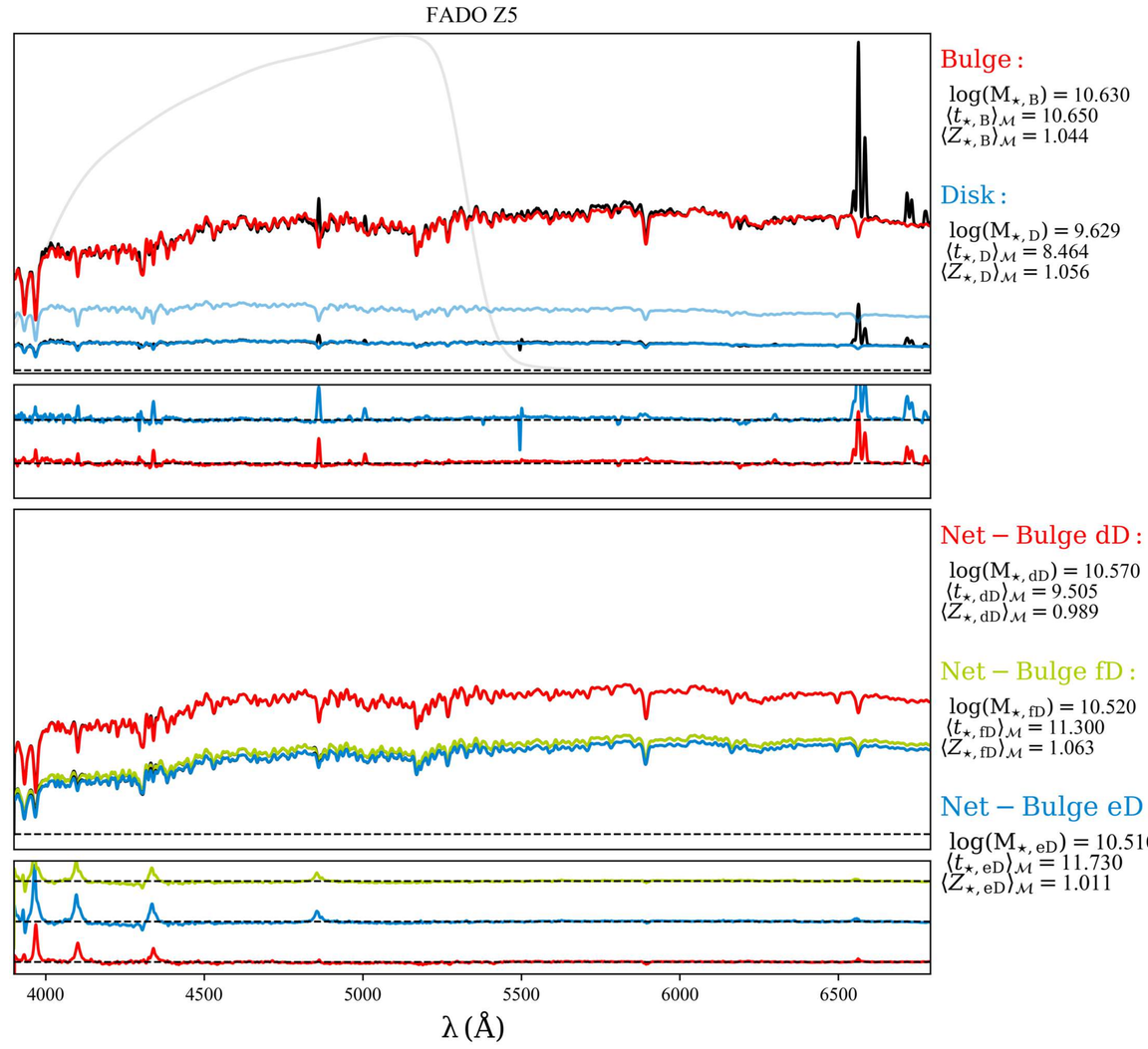
FADO Z5
Bulge :
log(M⋆, B) = 10.630
⟨t⋆, B⟩M = 10.650
⟨Z⋆, B⟩M = 1.044
Disk :
log(M⋆, D) = 9.629
⟨t⋆, D⟩M = 8.464
⟨Z⋆, D⟩M = 1.056
Net − Bulge dD :
log(M⋆, dD) = 10.570
⟨t⋆, dD⟩M = 9.505
⟨Z⋆, dD⟩M = 0.989
Net − Bulge fD :
log(M⋆, fD) = 10.520
⟨t⋆, fD⟩M = 11.300
⟨Z⋆, fD⟩M = 1.063
Net − Bulge eD :
log(M⋆, eD) = 10.510
⟨t⋆, eD⟩M = 11.730
⟨Z⋆, eD⟩M = 1.011
4000
4500
5000
5500
6000
6500
λ (Å)

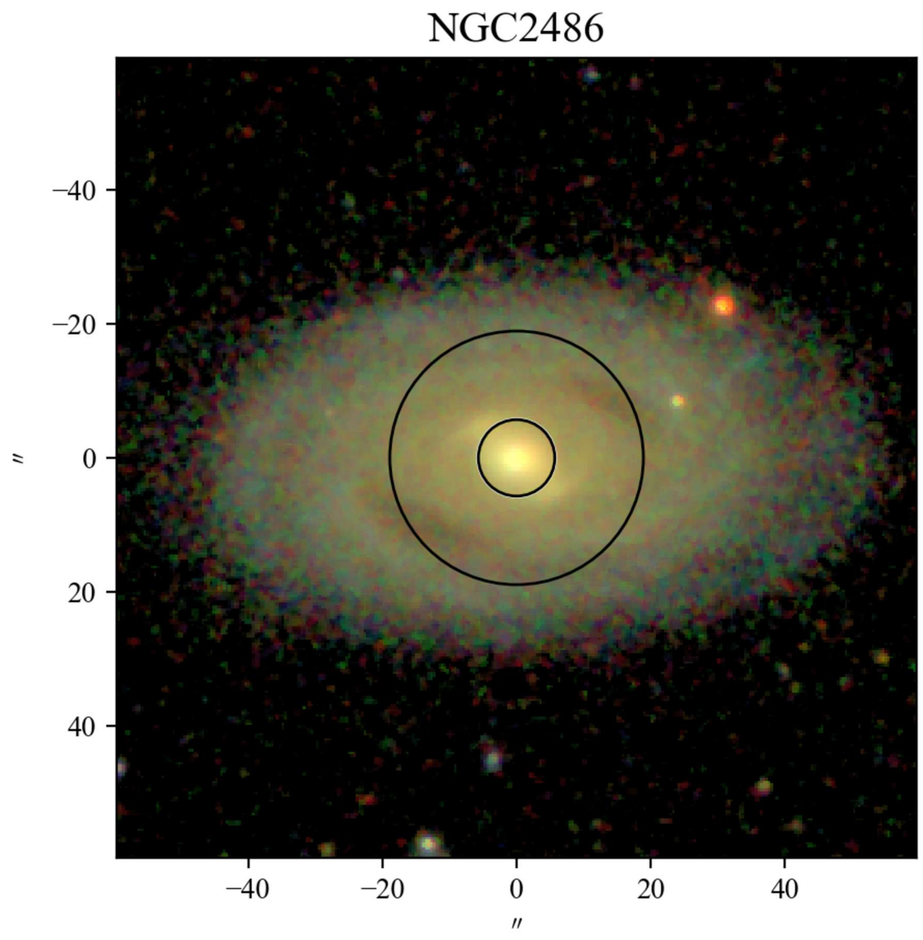
NGC2486
−40
−20
0
20
40
″
−40
−20
0
20
40
″

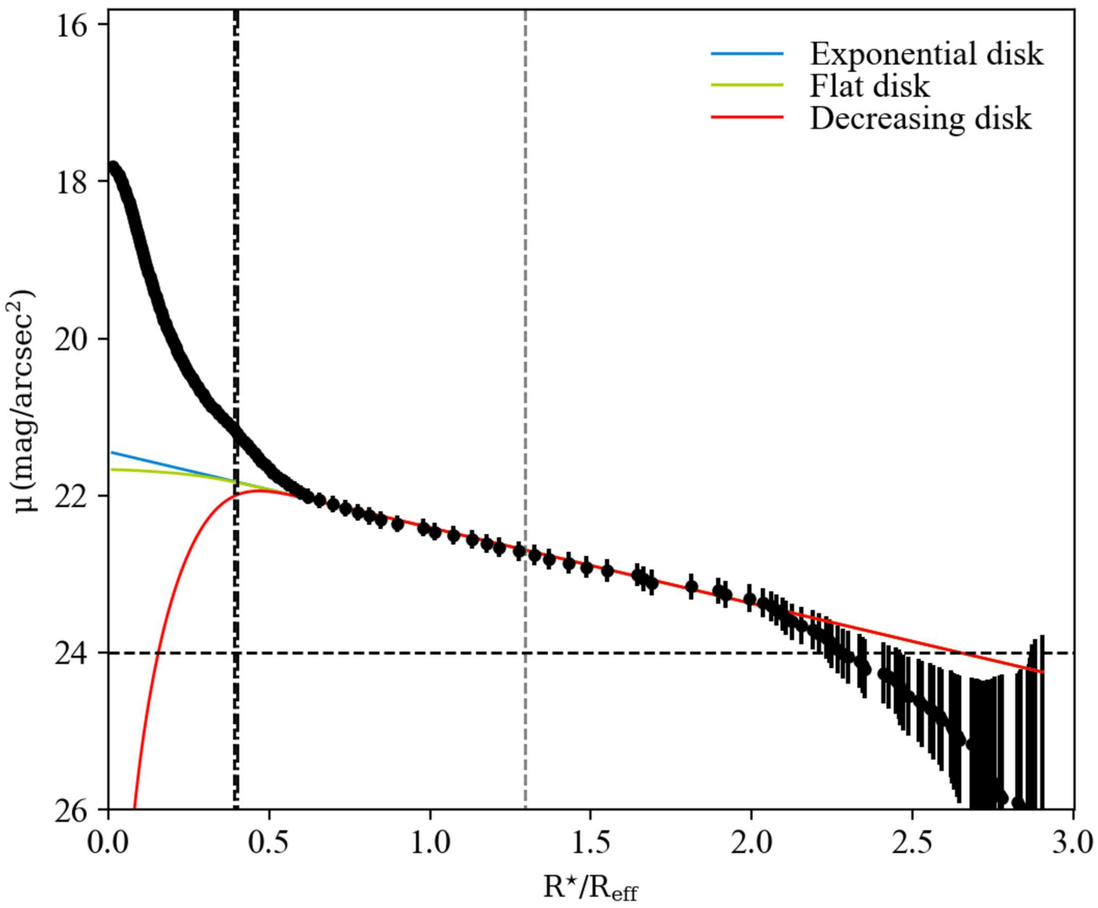
Exponential disk
Flat disk
Decreasing disk
μ (mag/arcsec²)
16
18
20
22
24
26
0.0
0.5
1.0
1.5
2.0
2.5
3.0
R⋆/Reff

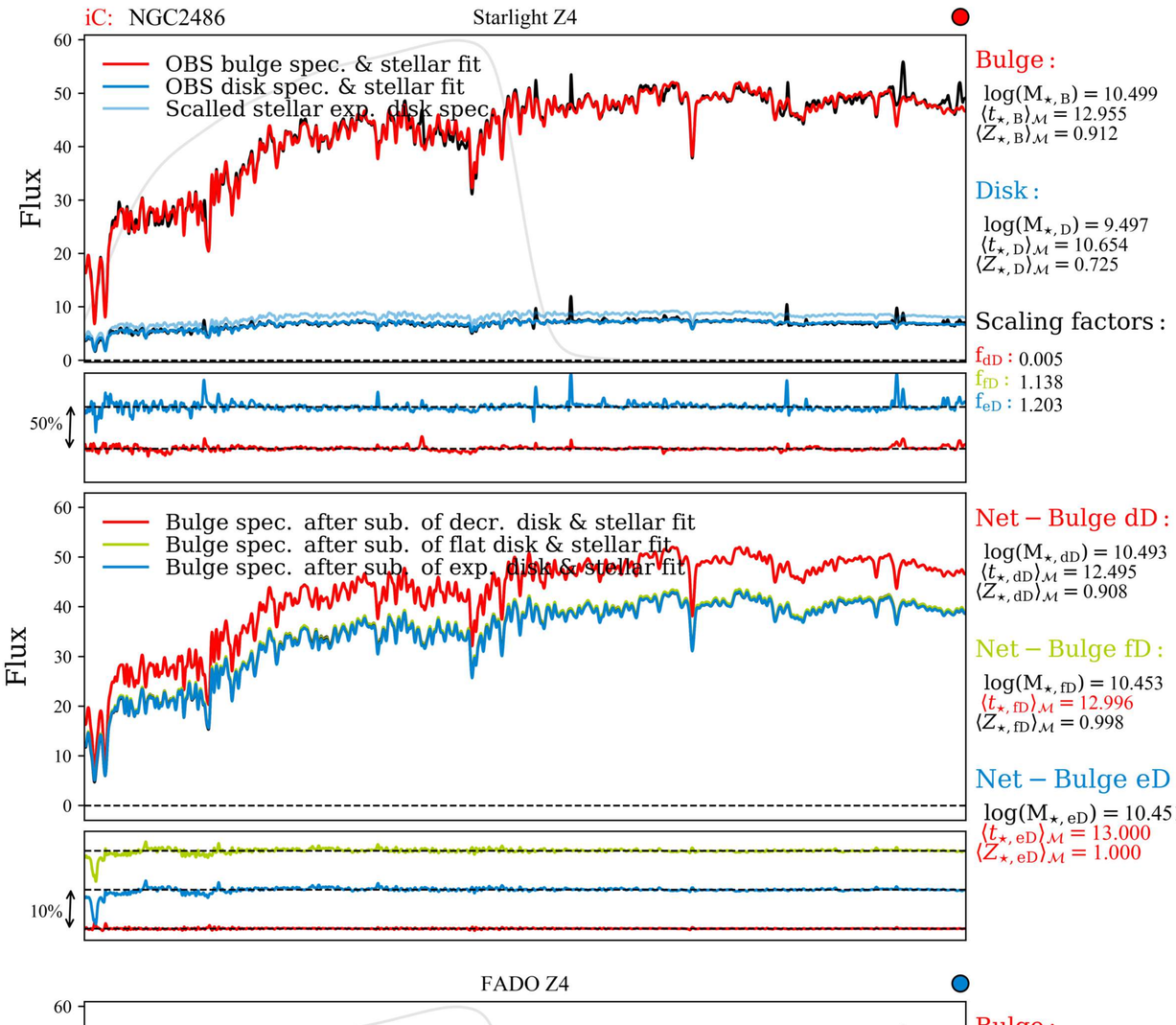
iC: NGC2486
Starlight Z4
OBS bulge spec. & stellar fit
OBS disk spec. & stellar fit
Scalled stellar exp. disk spec.
Flux
Bulge :
log(M⋆, B) = 10.499
⟨t⋆, B⟩M = 12.955
⟨Z⋆, B⟩M = 0.912
Disk :
log(M⋆, D) = 9.497
⟨t⋆, D⟩M = 10.654
⟨Z⋆, D⟩M = 0.725
Scaling factors :
fdD : 0.005
ffD : 1.138
feD : 1.203
50%
Bulge spec. after sub. of decr. disk & stellar fit
Bulge spec. after sub. of flat disk & stellar fit
Bulge spec. after sub. of exp. disk & stellar fit
Net − Bulge dD :
log(M⋆, dD) = 10.493
⟨t⋆, dD⟩M = 12.495
⟨Z⋆, dD⟩M = 0.908
Net − Bulge fD :
log(M⋆, fD) = 10.453
⟨t⋆, fD⟩M = 12.996
⟨Z⋆, fD⟩M = 0.998
Net − Bulge eD :
log(M⋆, eD) = 10.451
⟨t⋆, eD⟩M = 13.000
⟨Z⋆, eD⟩M = 1.000
10%

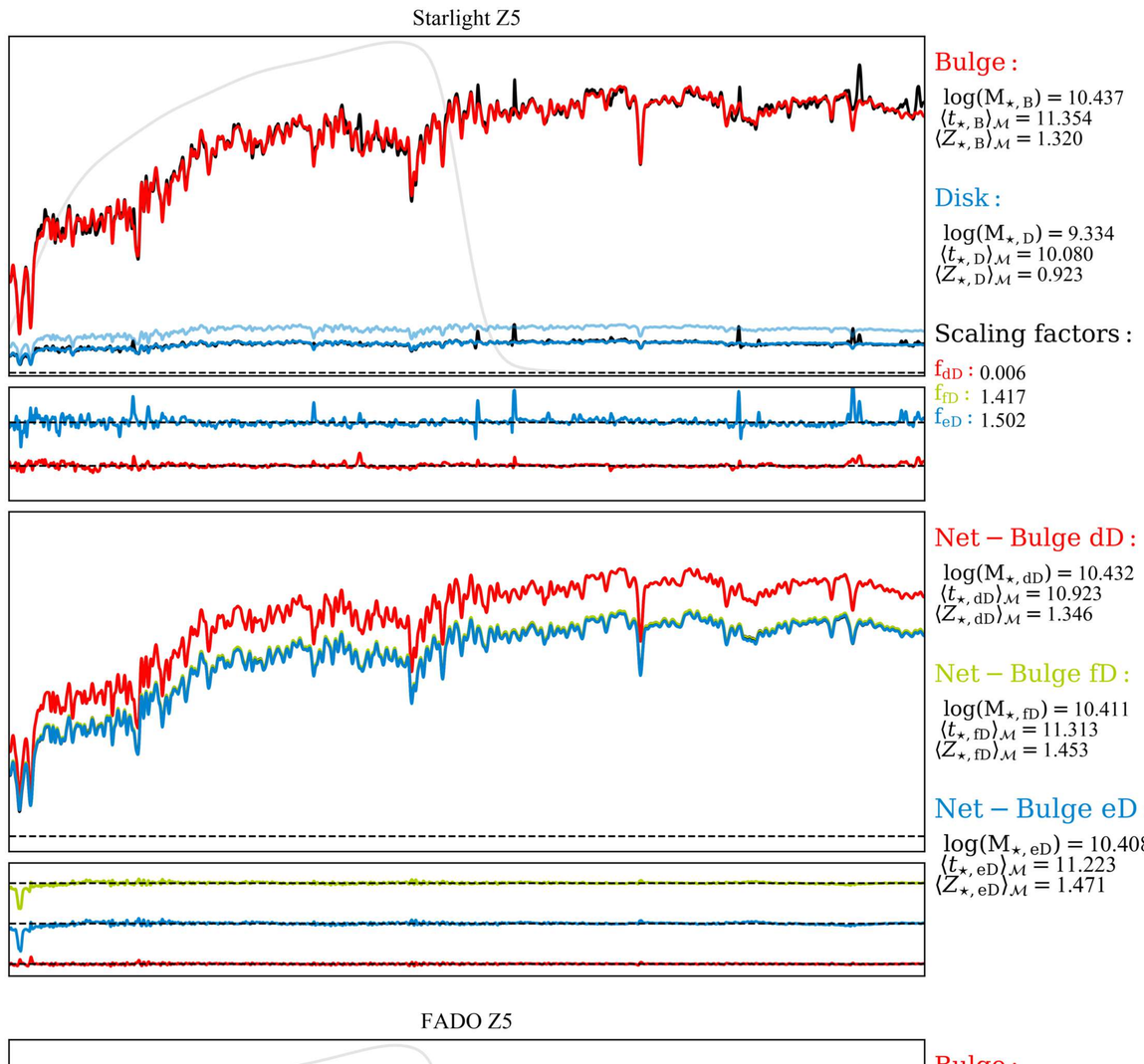
Starlight Z5
Bulge :
log(M⋆, B) = 10.437
⟨t⋆, B⟩M = 11.354
⟨Z⋆, B⟩M = 1.320
Disk :
log(M⋆, D) = 9.334
⟨t⋆, D⟩M = 10.080
⟨Z⋆, D⟩M = 0.923
Scaling factors :
fdD : 0.006
ffD : 1.417
feD : 1.502
Net − Bulge dD :
log(M⋆, dD) = 10.432
⟨t⋆, dD⟩M = 10.923
⟨Z⋆, dD⟩M = 1.346
Net − Bulge fD :
log(M⋆, fD) = 10.411
⟨t⋆, fD⟩M = 11.313
⟨Z⋆, fD⟩M = 1.453
Net − Bulge eD :
log(M⋆, eD) = 10.408
⟨t⋆, eD⟩M = 11.223
⟨Z⋆, eD⟩M = 1.471

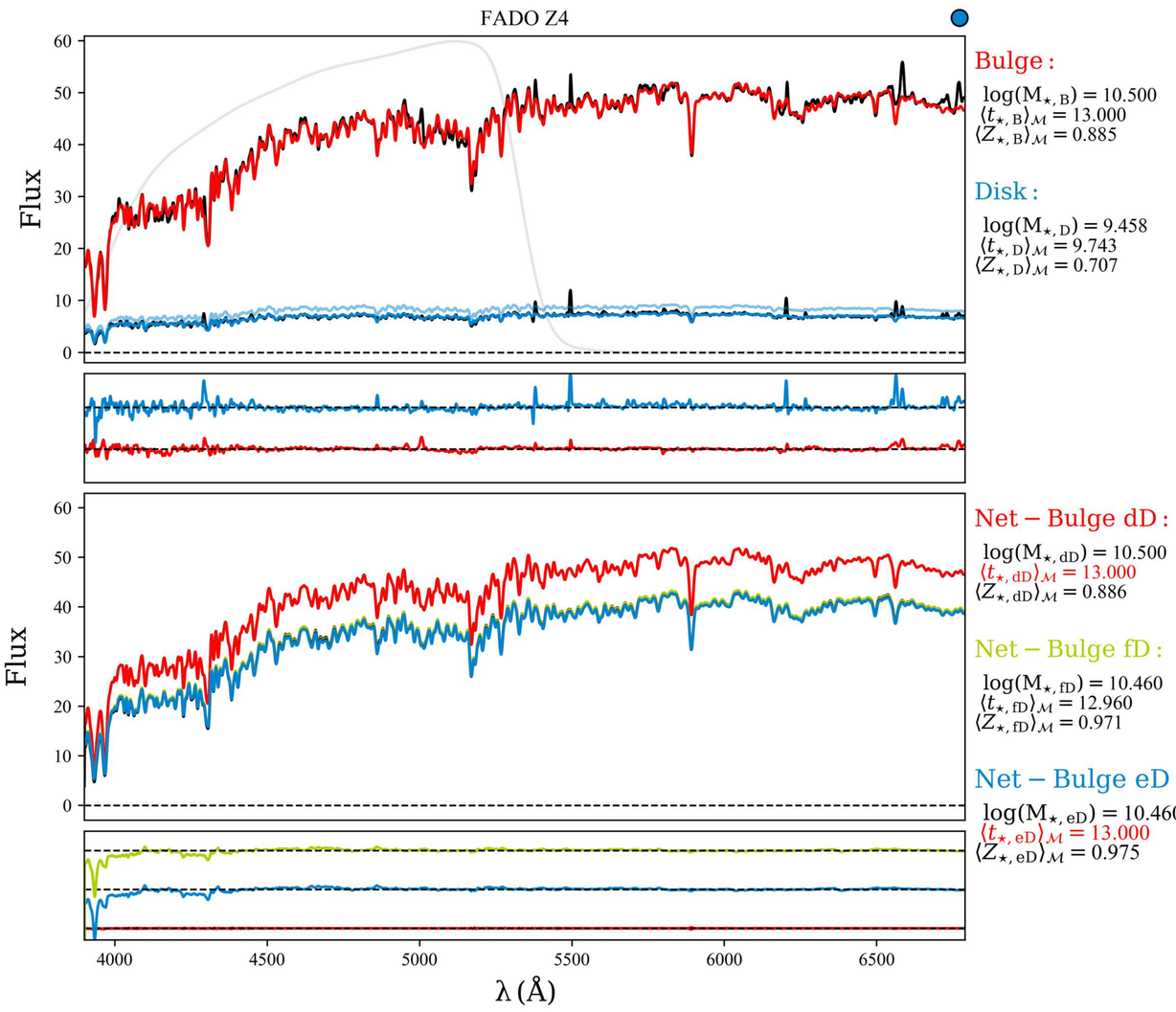
FADO Z4
Flux
Bulge :
log(M⋆, B) = 10.500
⟨t⋆, B⟩M = 13.000
⟨Z⋆, B⟩M = 0.885
Disk :
log(M⋆, D) = 9.458
⟨t⋆, D⟩M = 9.743
⟨Z⋆, D⟩M = 0.707
Net − Bulge dD :
log(M⋆, dD) = 10.500
⟨t⋆, dD⟩M = 13.000
⟨Z⋆, dD⟩M = 0.886
Net − Bulge fD :
log(M⋆, fD) = 10.460
⟨t⋆, fD⟩M = 12.960
⟨Z⋆, fD⟩M = 0.971
Net − Bulge eD :
log(M⋆, eD) = 10.460
⟨t⋆, eD⟩M = 13.000
⟨Z⋆, eD⟩M = 0.975
λ (Å)

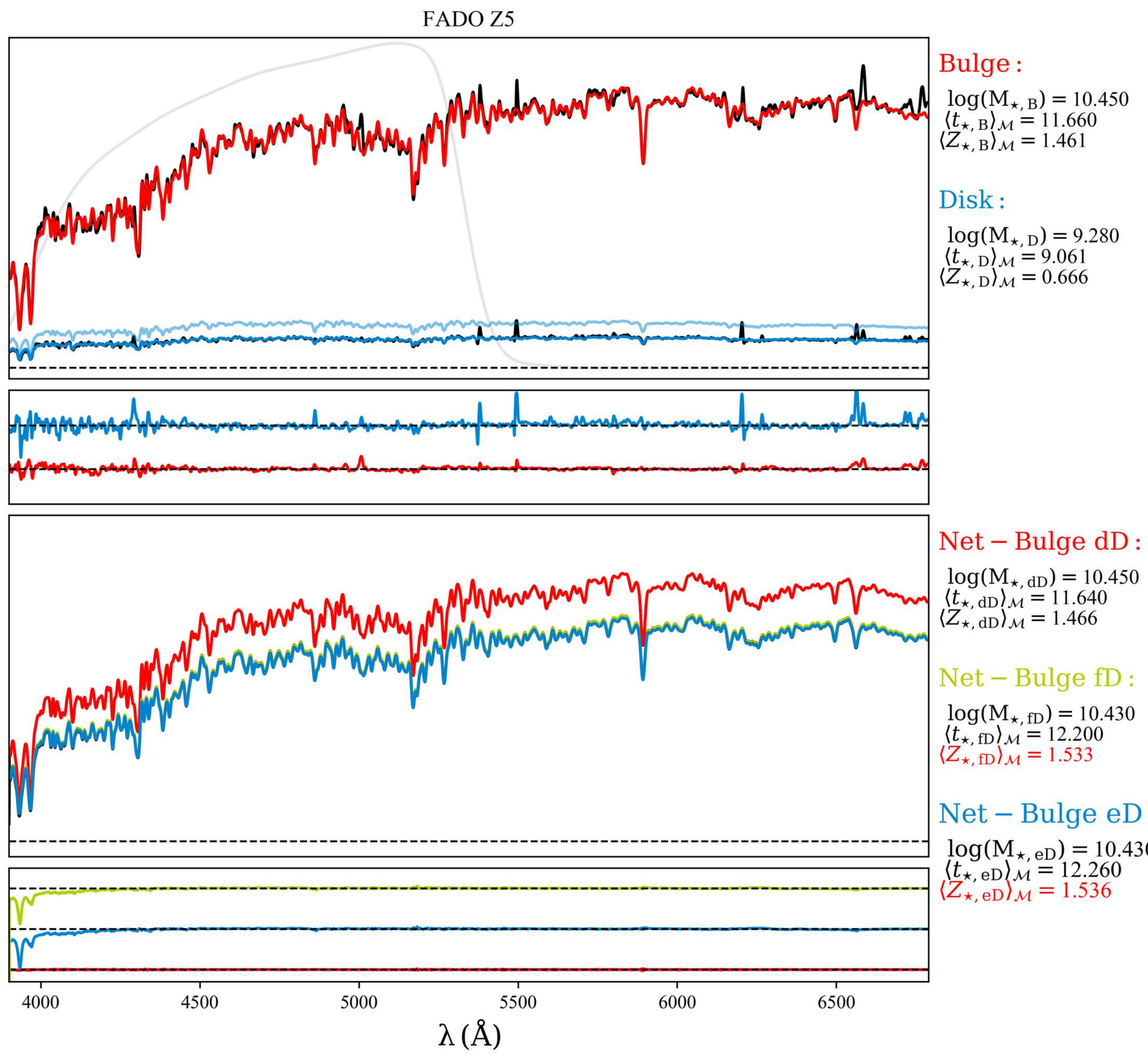
FADO Z5
Bulge :
log(M⋆, B) = 10.450
⟨t⋆, B⟩M = 11.660
⟨Z⋆, B⟩M = 1.461
Disk :
log(M⋆, D) = 9.280
⟨t⋆, D⟩M = 9.061
⟨Z⋆, D⟩M = 0.666
Net − Bulge dD :
log(M⋆, dD) = 10.450
⟨t⋆, dD⟩M = 11.640
⟨Z⋆, dD⟩M = 1.466
Net − Bulge fD :
log(M⋆, fD) = 10.430
⟨t⋆, fD⟩M = 12.200
⟨Z⋆, fD⟩M = 1.533
Net − Bulge eD :
log(M⋆, eD) = 10.430
⟨t⋆, eD⟩M = 12.260
⟨Z⋆, eD⟩M = 1.536
λ (Å)

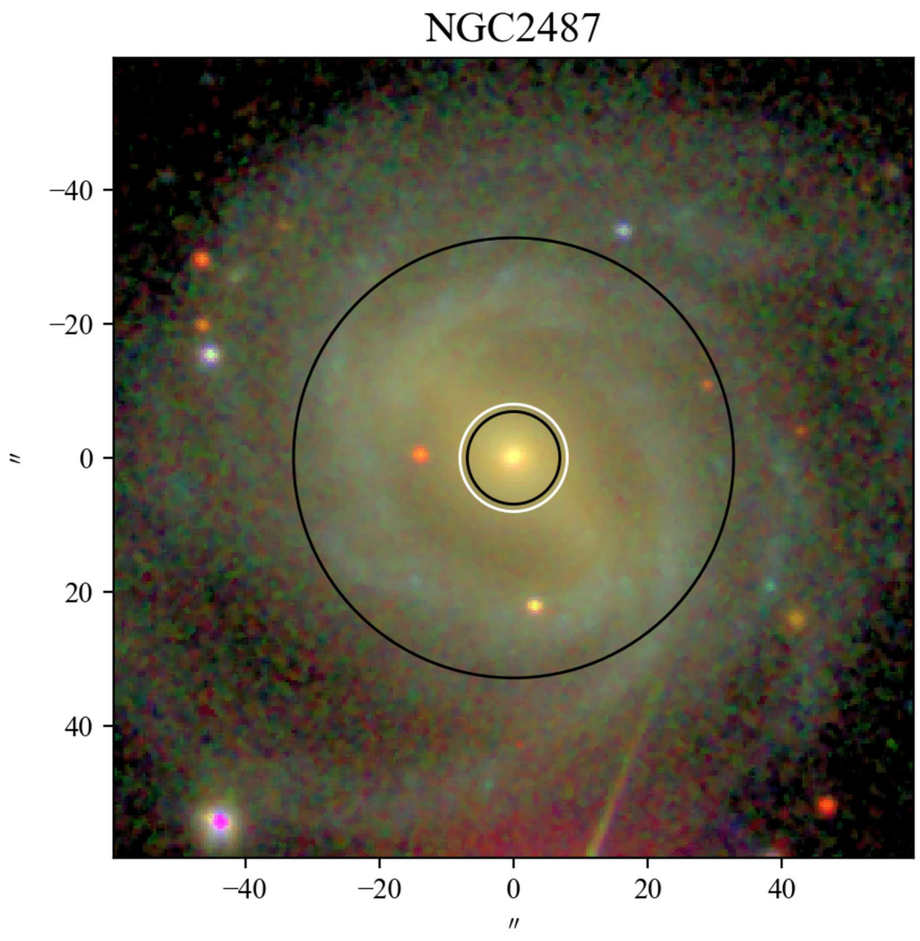
NGC2487
−40
−20
0
20
40
″
−40
−20
0
20
40
″

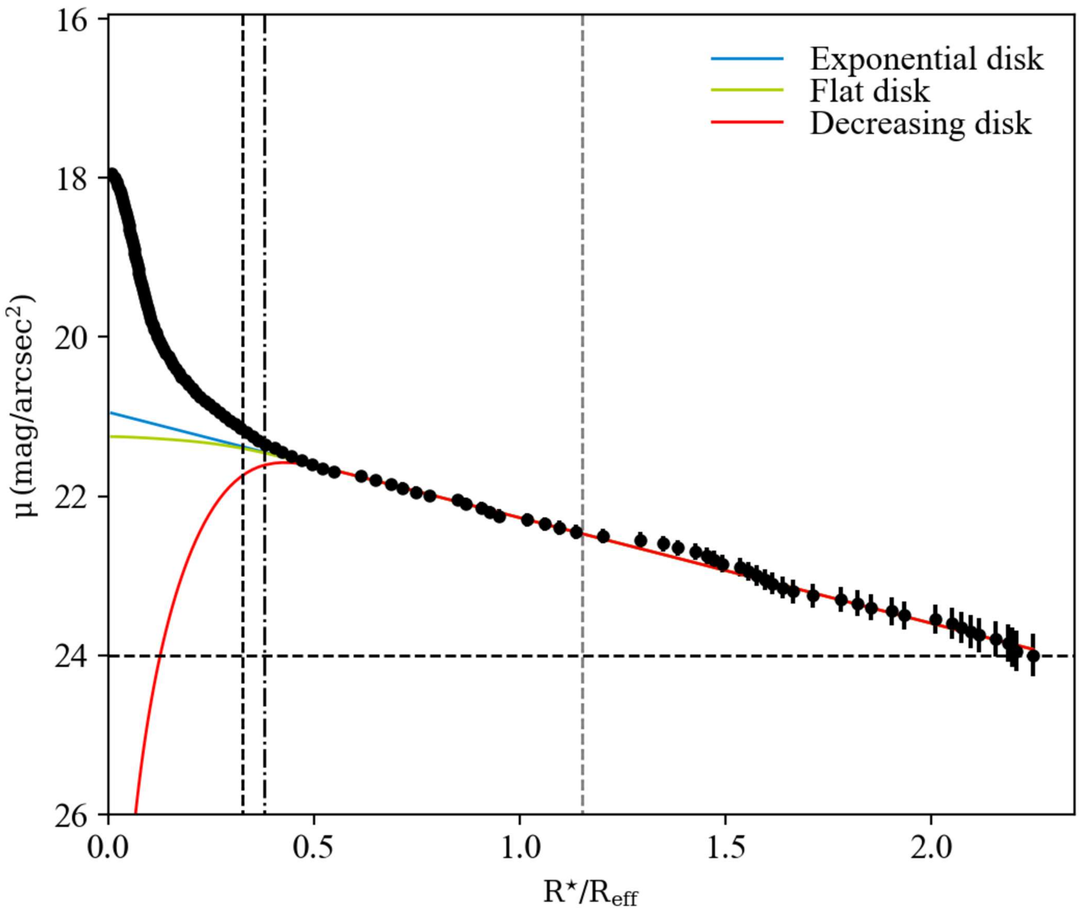
Exponential disk
Flat disk
Decreasing disk
μ (mag/arcsec²)
16
18
20
22
24
26
0.0
0.5
1.0
1.5
2.0
R⋆/Reff

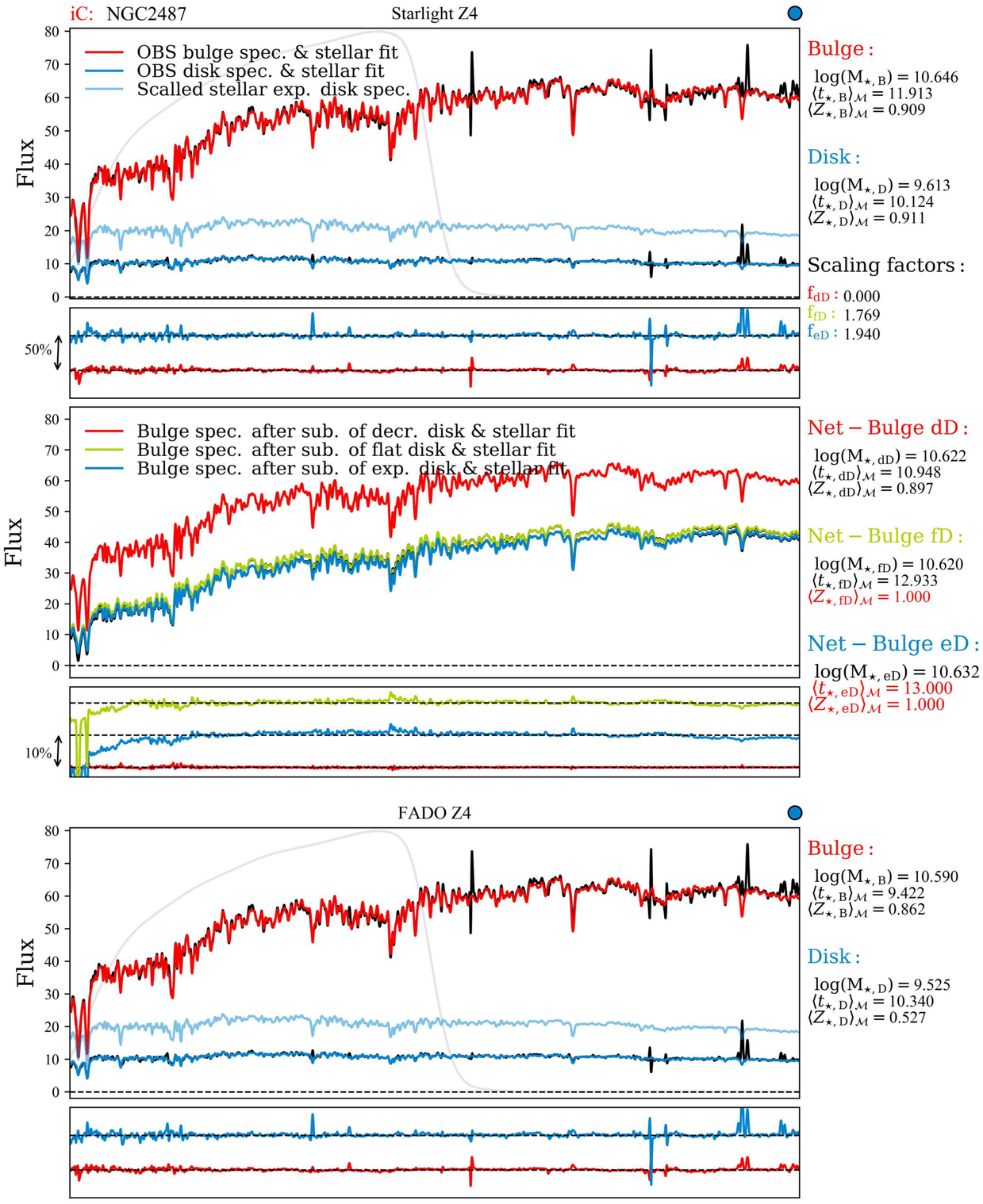
iC: NGC2487
Starlight Z4
OBS bulge spec. & stellar fit
OBS disk spec. & stellar fit
Scalled stellar exp. disk spec.
Flux
50%
Bulge :
log(M⋆, B) = 10.646
⟨t⋆, B⟩M = 11.913
⟨Z⋆, B⟩M = 0.909
Disk :
log(M⋆, D) = 9.613
⟨t⋆, D⟩M = 10.124
⟨Z⋆, D⟩M = 0.911
Scaling factors :
fdD : 0.000
ffD : 1.769
feD : 1.940
Bulge spec. after sub. of decr. disk & stellar fit
Bulge spec. after sub. of flat disk & stellar fit
Bulge spec. after sub. of exp. disk & stellar fit
10%
Net − Bulge dD :
log(M⋆, dD) = 10.622
⟨t⋆, dD⟩M = 10.948
⟨Z⋆, dD⟩M = 0.897
Net − Bulge fD :
log(M⋆, fD) = 10.620
⟨t⋆, fD⟩M = 12.933
⟨Z⋆, fD⟩M = 1.000
Net − Bulge eD :
log(M⋆, eD) = 10.632
⟨t⋆, eD⟩M = 13.000
⟨Z⋆, eD⟩M = 1.000

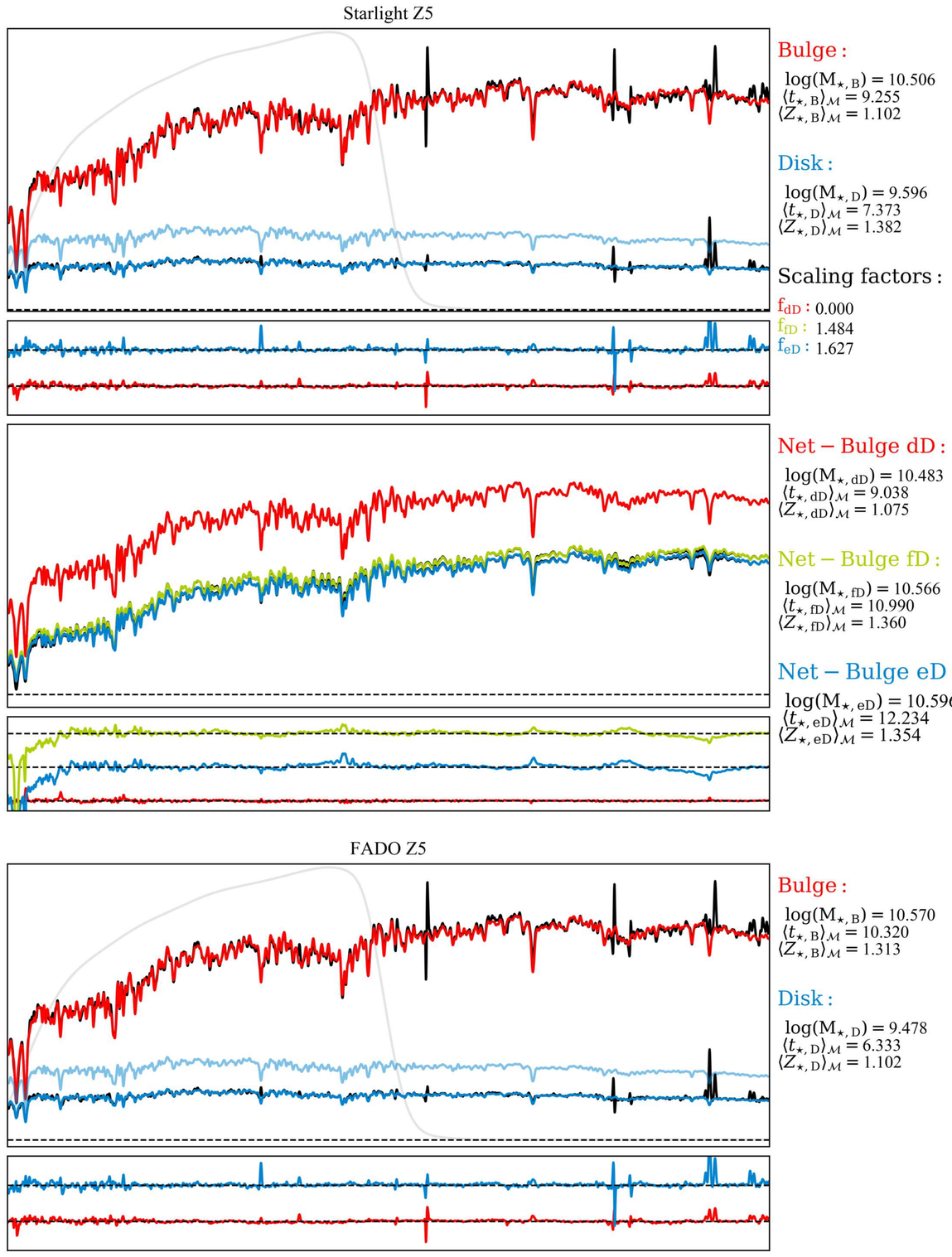
Starlight Z5
Bulge :
log(M⋆, B) = 10.506
⟨t⋆, B⟩M = 9.255
⟨Z⋆, B⟩M = 1.102
Disk :
log(M⋆, D) = 9.596
⟨t⋆, D⟩M = 7.373
⟨Z⋆, D⟩M = 1.382
Scaling factors :
fdD : 0.000
ffD : 1.484
feD : 1.627
Net − Bulge dD :
log(M⋆, dD) = 10.483
⟨t⋆, dD⟩M = 9.038
⟨Z⋆, dD⟩M = 1.075
Net − Bulge fD :
log(M⋆, fD) = 10.566
⟨t⋆, fD⟩M = 10.990
⟨Z⋆, fD⟩M = 1.360
Net − Bulge eD :
log(M⋆, eD) = 10.596
⟨t⋆, eD⟩M = 12.234
⟨Z⋆, eD⟩M = 1.354

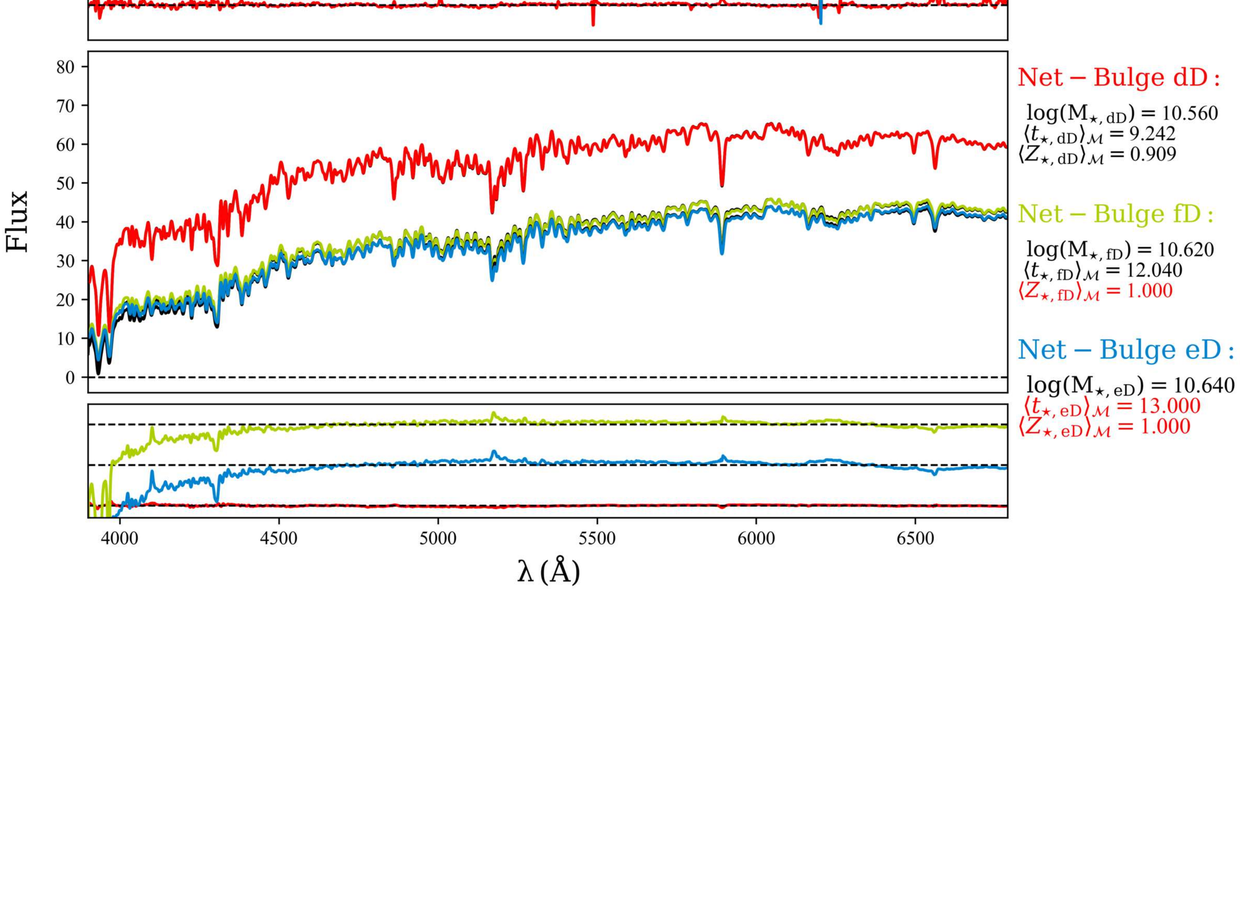
FADO Z4
Flux
Bulge :
log(M⋆, B) = 10.590
⟨t⋆, B⟩M = 9.422
⟨Z⋆, B⟩M = 0.862
Disk :
log(M⋆, D) = 9.525
⟨t⋆, D⟩M = 10.340
⟨Z⋆, D⟩M = 0.527
Net − Bulge dD :
log(M⋆, dD) = 10.560
⟨t⋆, dD⟩M = 9.242
⟨Z⋆, dD⟩M = 0.909
Net − Bulge fD :
log(M⋆, fD) = 10.620
⟨t⋆, fD⟩M = 12.040
⟨Z⋆, fD⟩M = 1.000
Net − Bulge eD :
log(M⋆, eD) = 10.640
⟨t⋆, eD⟩M = 13.000
⟨Z⋆, eD⟩M = 1.000
λ (Å)

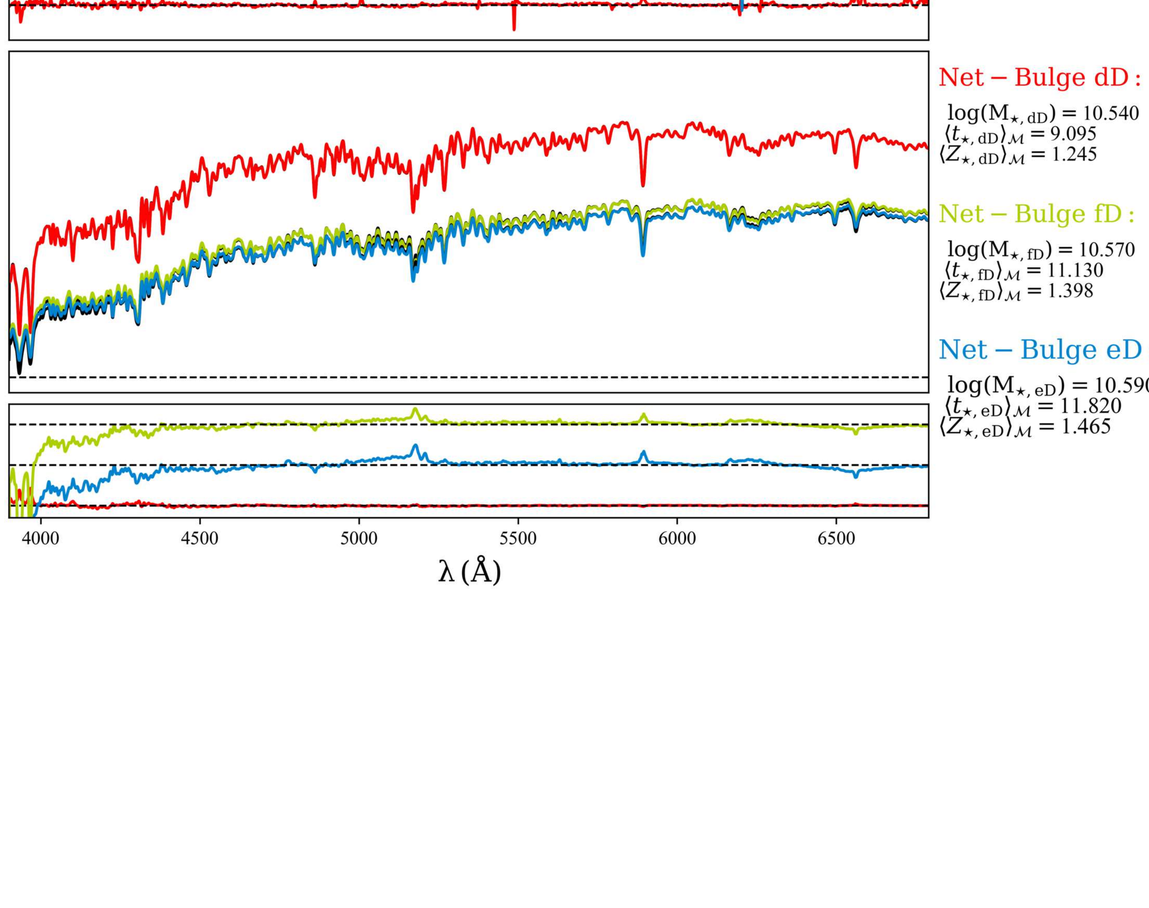
FADO Z5
Bulge :
log(M⋆, B) = 10.570
⟨t⋆, B⟩M = 10.320
⟨Z⋆, B⟩M = 1.313
Disk :
log(M⋆, D) = 9.478
⟨t⋆, D⟩M = 6.333
⟨Z⋆, D⟩M = 1.102
Net − Bulge dD :
log(M⋆, dD) = 10.540
⟨t⋆, dD⟩M = 9.095
⟨Z⋆, dD⟩M = 1.245
Net − Bulge fD :
log(M⋆, fD) = 10.570
⟨t⋆, fD⟩M = 11.130
⟨Z⋆, fD⟩M = 1.398
Net − Bulge eD :
log(M⋆, eD) = 10.590
⟨t⋆, eD⟩M = 11.820
⟨Z⋆, eD⟩M = 1.465
λ (Å)

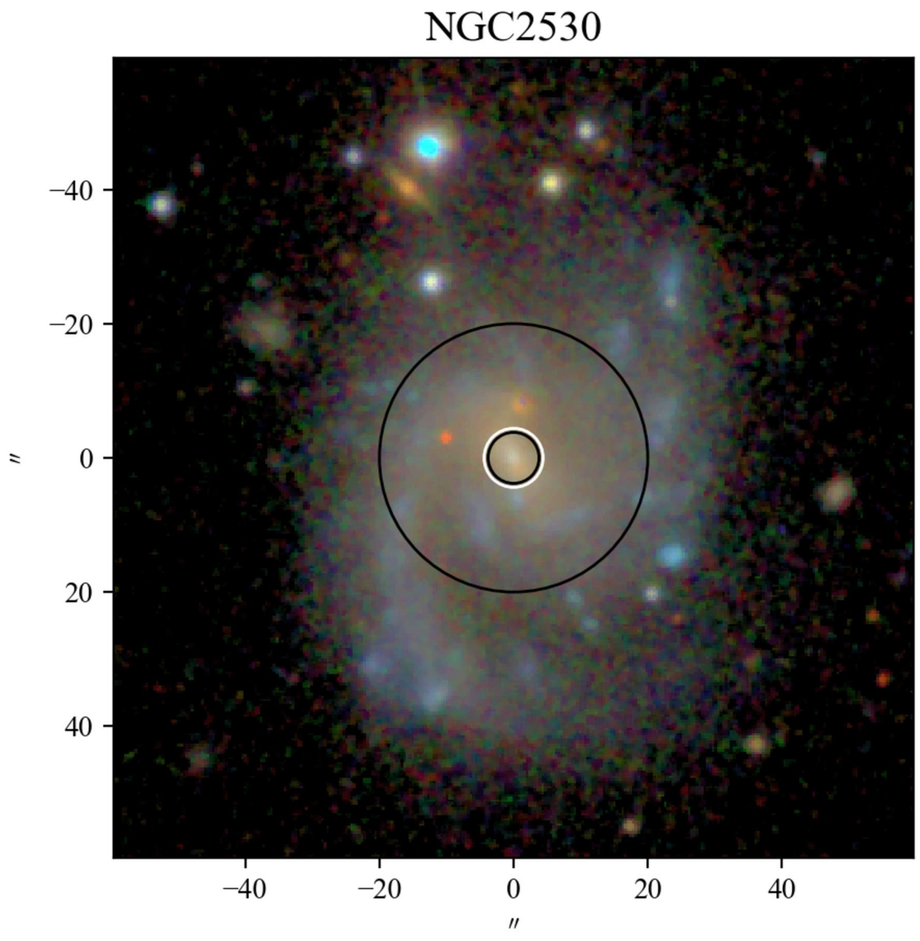
NGC2530
−40
−20
0
20
40
″
−40
−20
0
20
40
″

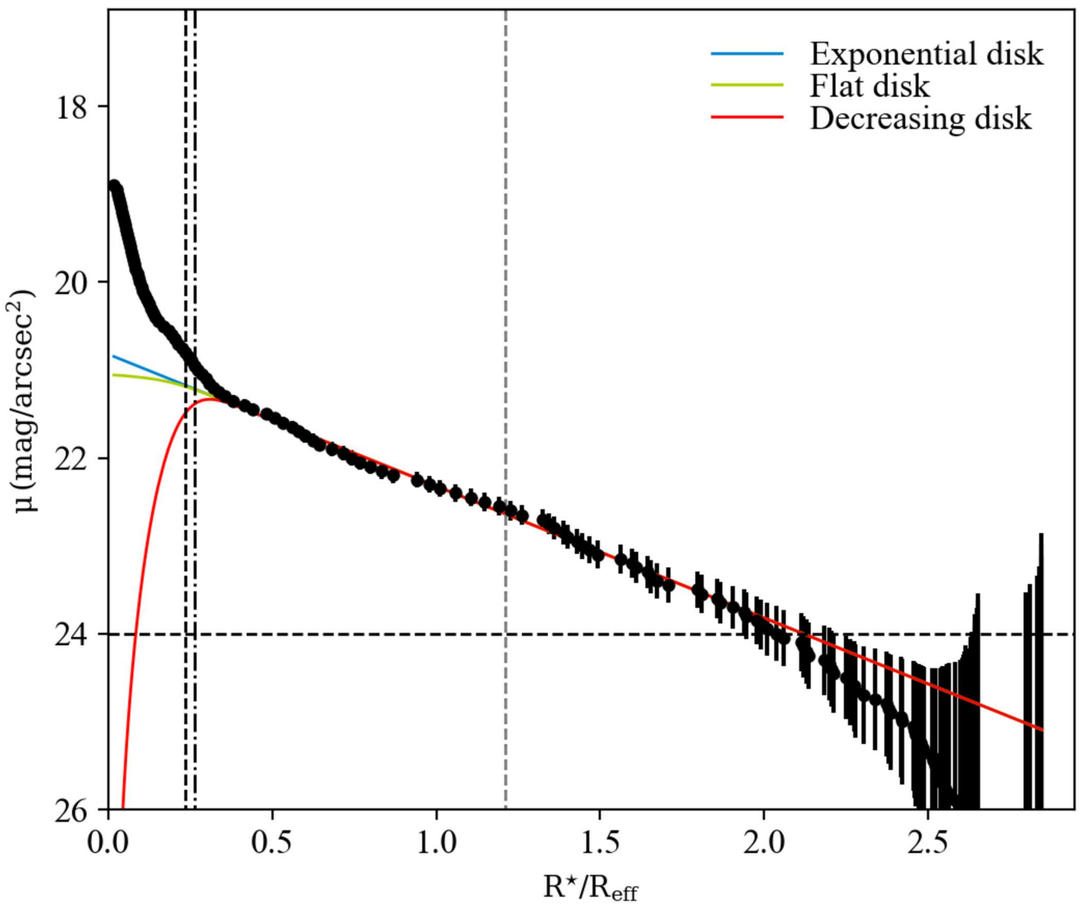
Exponential disk
Flat disk
Decreasing disk
μ (mag/arcsec²)
18
20
22
24
26
0.0
0.5
1.0
1.5
2.0
2.5
R⋆/Reff

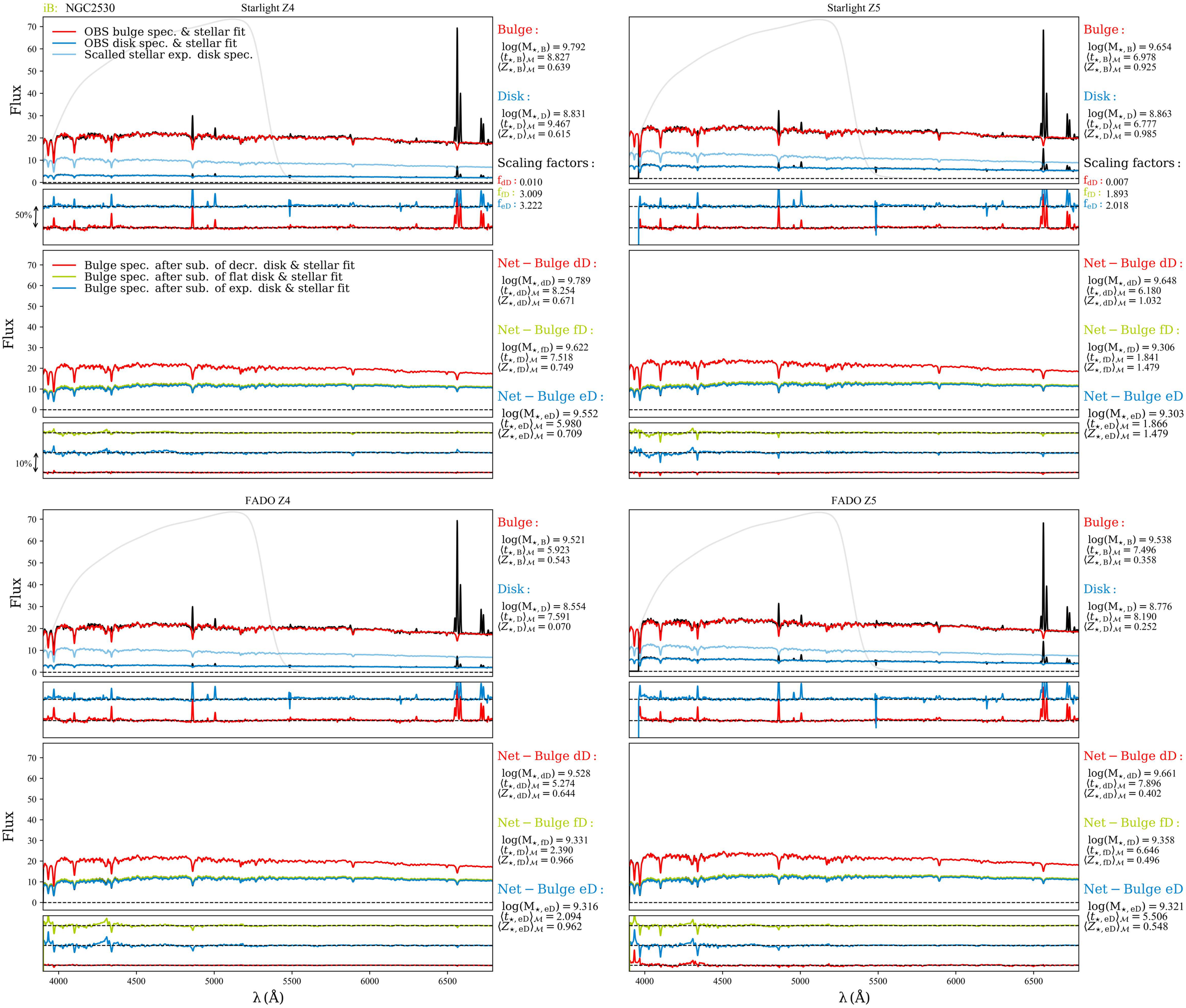
iB: NGC2530
Starlight Z4
OBS bulge spec. & stellar fit
OBS disk spec. & stellar fit
Scalled stellar exp. disk spec.
Flux
50%
Bulge :
log(M⋆, B) = 9.792
⟨t⋆, B⟩M = 8.827
⟨Z⋆, B⟩M = 0.639
Disk :
log(M⋆, D) = 8.831
⟨t⋆, D⟩M = 9.467
⟨Z⋆, D⟩M = 0.615
Scaling factors :
fdD : 0.010
ffD : 3.009
feD : 3.222
Bulge spec. after sub. of decr. disk & stellar fit
Bulge spec. after sub. of flat disk & stellar fit
Bulge spec. after sub. of exp. disk & stellar fit
10%
Net − Bulge dD :
log(M⋆, dD) = 9.789
⟨t⋆, dD⟩M = 8.254
⟨Z⋆, dD⟩M = 0.671
Net − Bulge fD :
log(M⋆, fD) = 9.622
⟨t⋆, fD⟩M = 7.518
⟨Z⋆, fD⟩M = 0.749
Net − Bulge eD :
log(M⋆, eD) = 9.552
⟨t⋆, eD⟩M = 5.980
⟨Z⋆, eD⟩M = 0.709
FADO Z4
Bulge :
log(M⋆, B) = 9.521
⟨t⋆, B⟩M = 5.923
⟨Z⋆, B⟩M = 0.543
Disk :
log(M⋆, D) = 8.554
⟨t⋆, D⟩M = 7.591
⟨Z⋆, D⟩M = 0.070
Net − Bulge dD :
log(M⋆, dD) = 9.528
⟨t⋆, dD⟩M = 5.274
⟨Z⋆, dD⟩M = 0.644
Net − Bulge fD :
log(M⋆, fD) = 9.331
⟨t⋆, fD⟩M = 2.390
⟨Z⋆, fD⟩M = 0.966
Net − Bulge eD :
log(M⋆, eD) = 9.316
⟨t⋆, eD⟩M = 2.094
⟨Z⋆, eD⟩M = 0.962
λ (Å)

Starlight Z5
Bulge :
log(M⋆, B) = 9.654
⟨t⋆, B⟩M = 6.978
⟨Z⋆, B⟩M = 0.925
Disk :
log(M⋆, D) = 8.863
⟨t⋆, D⟩M = 6.777
⟨Z⋆, D⟩M = 0.985
Scaling factors :
fdD : 0.007
ffD : 1.893
feD : 2.018
Net − Bulge dD :
log(M⋆, dD) = 9.648
⟨t⋆, dD⟩M = 6.180
⟨Z⋆, dD⟩M = 1.032
Net − Bulge fD :
log(M⋆, fD) = 9.306
⟨t⋆, fD⟩M = 1.841
⟨Z⋆, fD⟩M = 1.479
Net − Bulge eD :
log(M⋆, eD) = 9.303
⟨t⋆, eD⟩M = 1.866
⟨Z⋆, eD⟩M = 1.479
FADO Z5
Bulge :
log(M⋆, B) = 9.538
⟨t⋆, B⟩M = 7.496
⟨Z⋆, B⟩M = 0.358
Disk :
log(M⋆, D) = 8.776
⟨t⋆, D⟩M = 8.190
⟨Z⋆, D⟩M = 0.252
Net − Bulge dD :
log(M⋆, dD) = 9.661
⟨t⋆, dD⟩M = 7.896
⟨Z⋆, dD⟩M = 0.402
Net − Bulge fD :
log(M⋆, fD) = 9.358
⟨t⋆, fD⟩M = 6.646
⟨Z⋆, fD⟩M = 0.496
Net − Bulge eD :
log(M⋆, eD) = 9.321
⟨t⋆, eD⟩M = 5.506
⟨Z⋆, eD⟩M = 0.548
λ (Å)

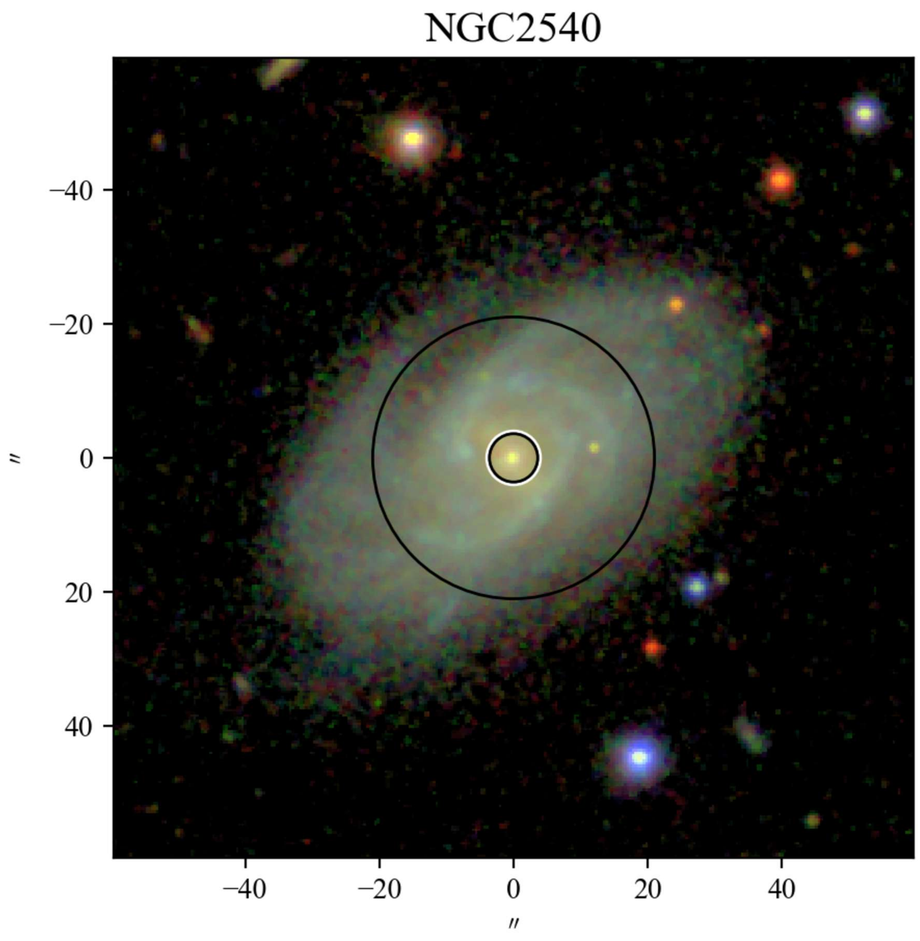
NGC2540
−40
−20
0
20
40
″
−40
−20
0
20
40
″

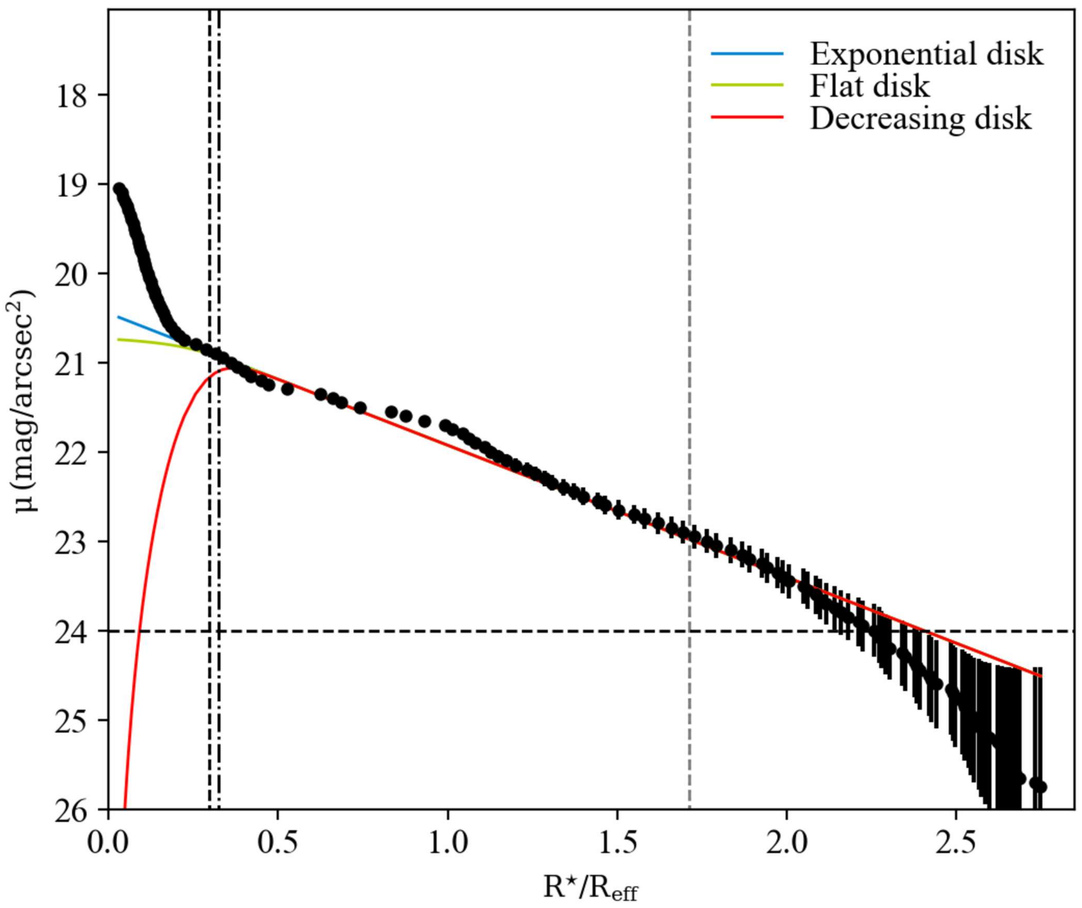
Exponential disk
Flat disk
Decreasing disk
μ (mag/arcsec²)
18
19
20
21
22
23
24
25
26
0.0
0.5
1.0
1.5
2.0
2.5
R⋆/Reff

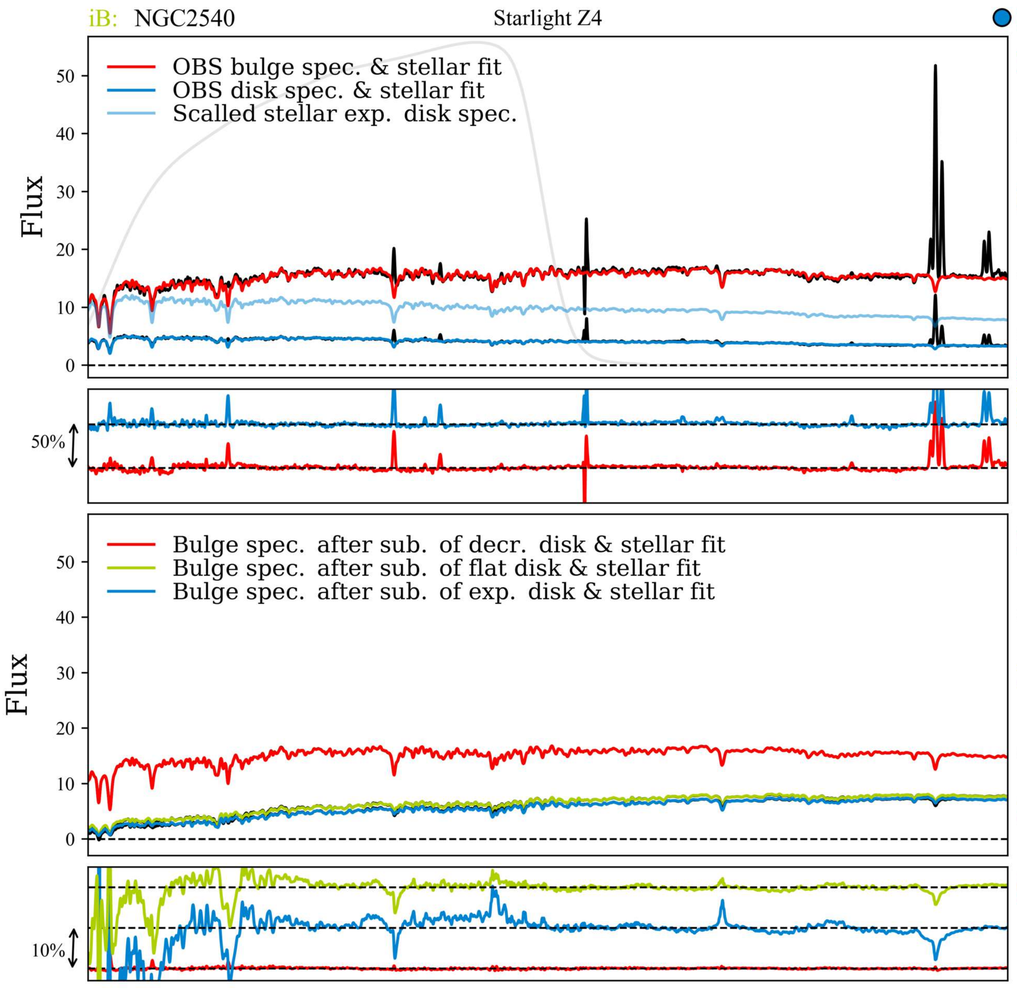
iB: NGC2540
Starlight Z4
NEG flux eD
OBS bulge spec. & stellar fit
OBS disk spec. & stellar fit
Scalled stellar exp. disk spec.
Flux
50%
Bulge spec. after sub. of decr. disk & stellar fit
Bulge spec. after sub. of flat disk & stellar fit
Bulge spec. after sub. of exp. disk & stellar fit
10%
Bulge :
log(M⋆, B) = 10.145
⟨t⋆, B⟩M = 10.455
⟨Z⋆, B⟩M = 0.847
Disk :
log(M⋆, D) = 9.264
⟨t⋆, D⟩M = 9.313
⟨Z⋆, D⟩M = 0.703
Scaling factors :
fdD : 0.026
ffD : 2.194
feD : 2.383
Net − Bulge dD :
log(M⋆, dD) = 10.100
⟨t⋆, dD⟩M = 9.734
⟨Z⋆, dD⟩M = 0.807
Net − Bulge fD :
log(M⋆, fD) = 9.933
⟨t⋆, fD⟩M = 7.891
⟨Z⋆, fD⟩M = 1.000
Net − Bulge eD :
log(M⋆, eD) = 10.153
⟨t⋆, eD⟩M = 13.000
⟨Z⋆, eD⟩M = 1.000

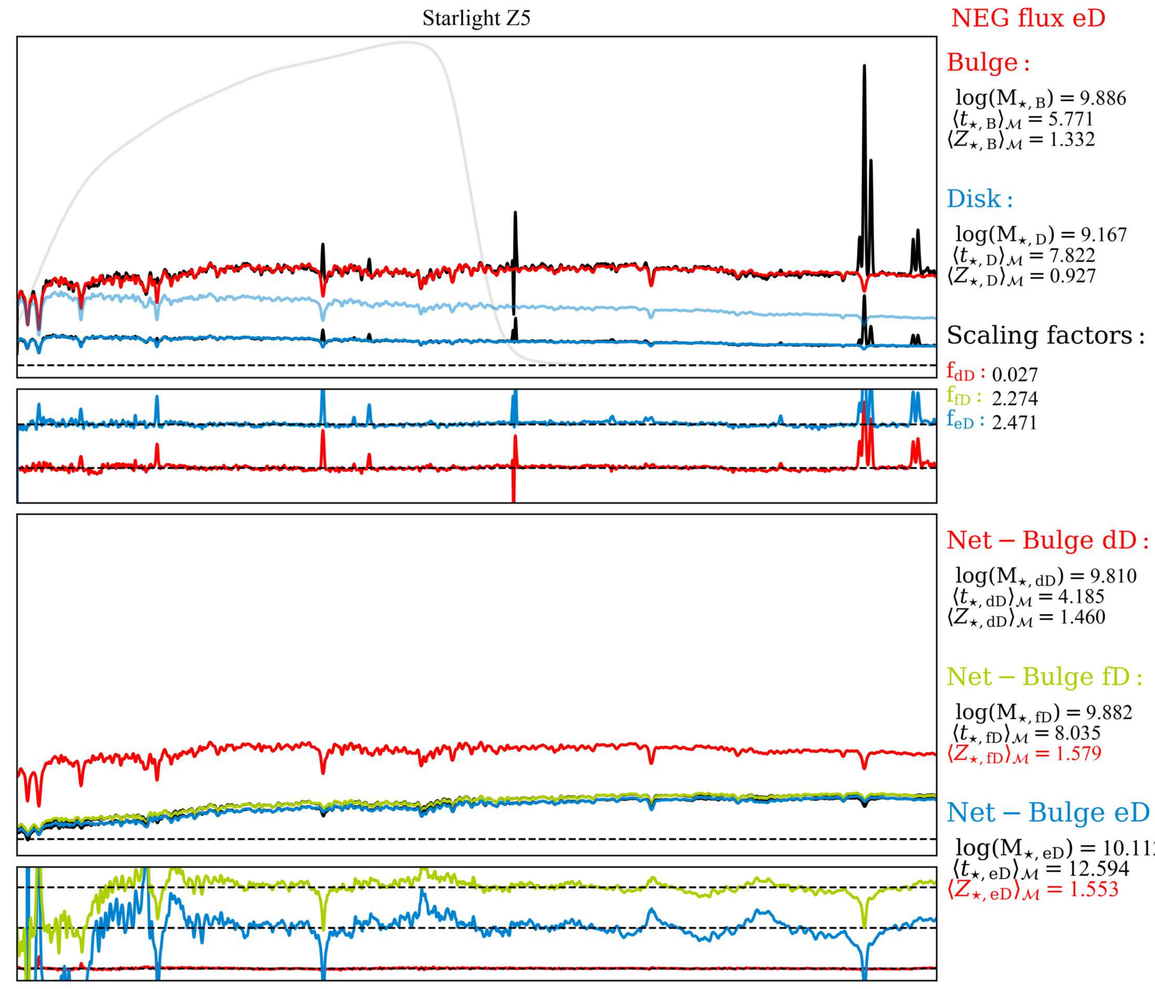
Starlight Z5
NEG flux eD
Bulge :
log(M⋆, B) = 9.886
⟨t⋆, B⟩M = 5.771
⟨Z⋆, B⟩M = 1.332
Disk :
log(M⋆, D) = 9.167
⟨t⋆, D⟩M = 7.822
⟨Z⋆, D⟩M = 0.927
Scaling factors :
fdD : 0.027
ffD : 2.274
feD : 2.471
Net − Bulge dD :
log(M⋆, dD) = 9.810
⟨t⋆, dD⟩M = 4.185
⟨Z⋆, dD⟩M = 1.460
Net − Bulge fD :
log(M⋆, fD) = 9.882
⟨t⋆, fD⟩M = 8.035
⟨Z⋆, fD⟩M = 1.579
Net − Bulge eD :
log(M⋆, eD) = 10.112
⟨t⋆, eD⟩M = 12.594
⟨Z⋆, eD⟩M = 1.553

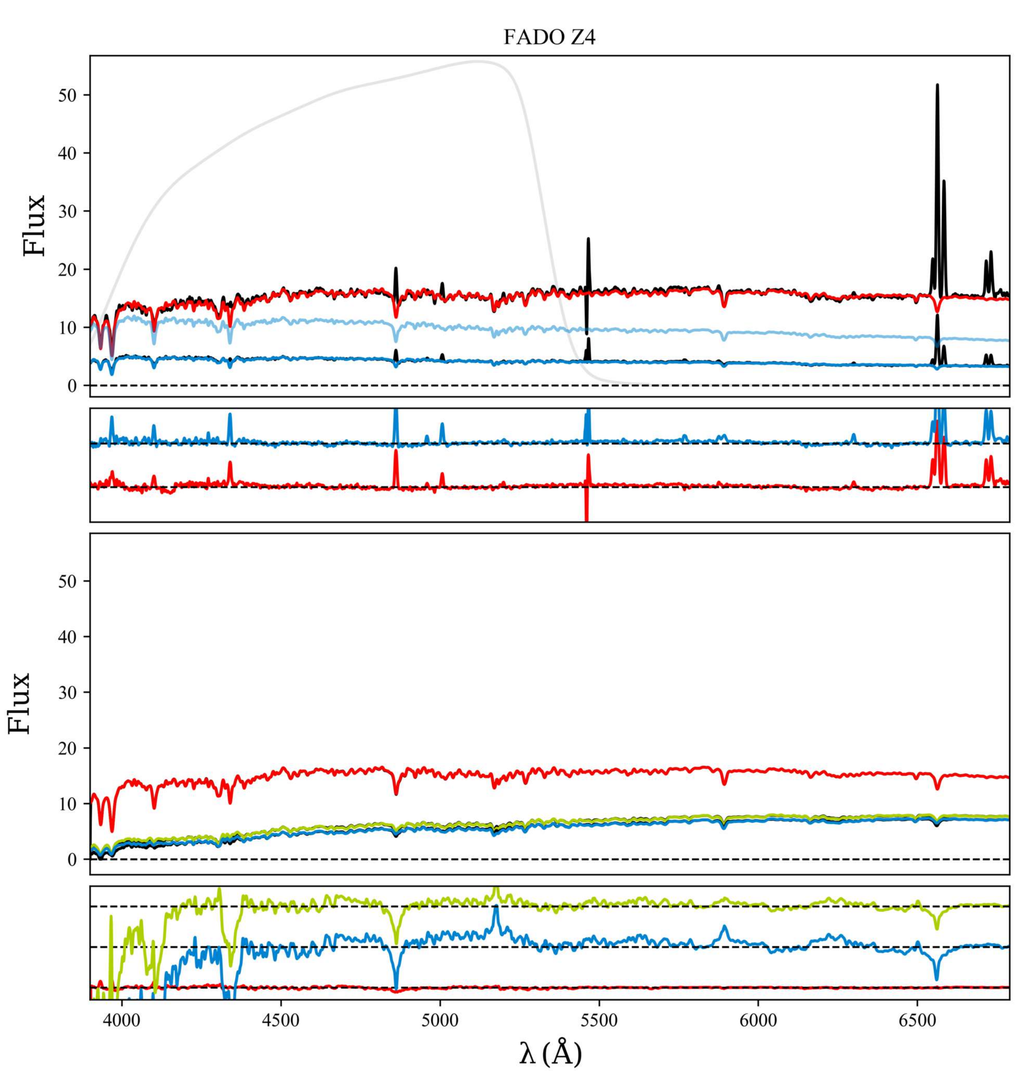
FADO Z4
NEG flux fD & eD
Flux
Bulge :
log(M⋆, B) = 10.150
⟨t⋆, B⟩M = 12.030
⟨Z⋆, B⟩M = 0.566
Disk :
log(M⋆, D) = 9.204
⟨t⋆, D⟩M = 10.130
⟨Z⋆, D⟩M = 0.357
Net − Bulge dD :
log(M⋆, dD) = 10.110
⟨t⋆, dD⟩M = 11.240
⟨Z⋆, dD⟩M = 0.543
Net − Bulge fD :
log(M⋆, fD) = 9.907
⟨t⋆, fD⟩M = 6.350
⟨Z⋆, fD⟩M = 0.846
Net − Bulge eD :
log(M⋆, eD) = 10.090
⟨t⋆, eD⟩M = 10.550
⟨Z⋆, eD⟩M = 1.000
4000
4500
5000
5500
6000
6500
λ (Å)

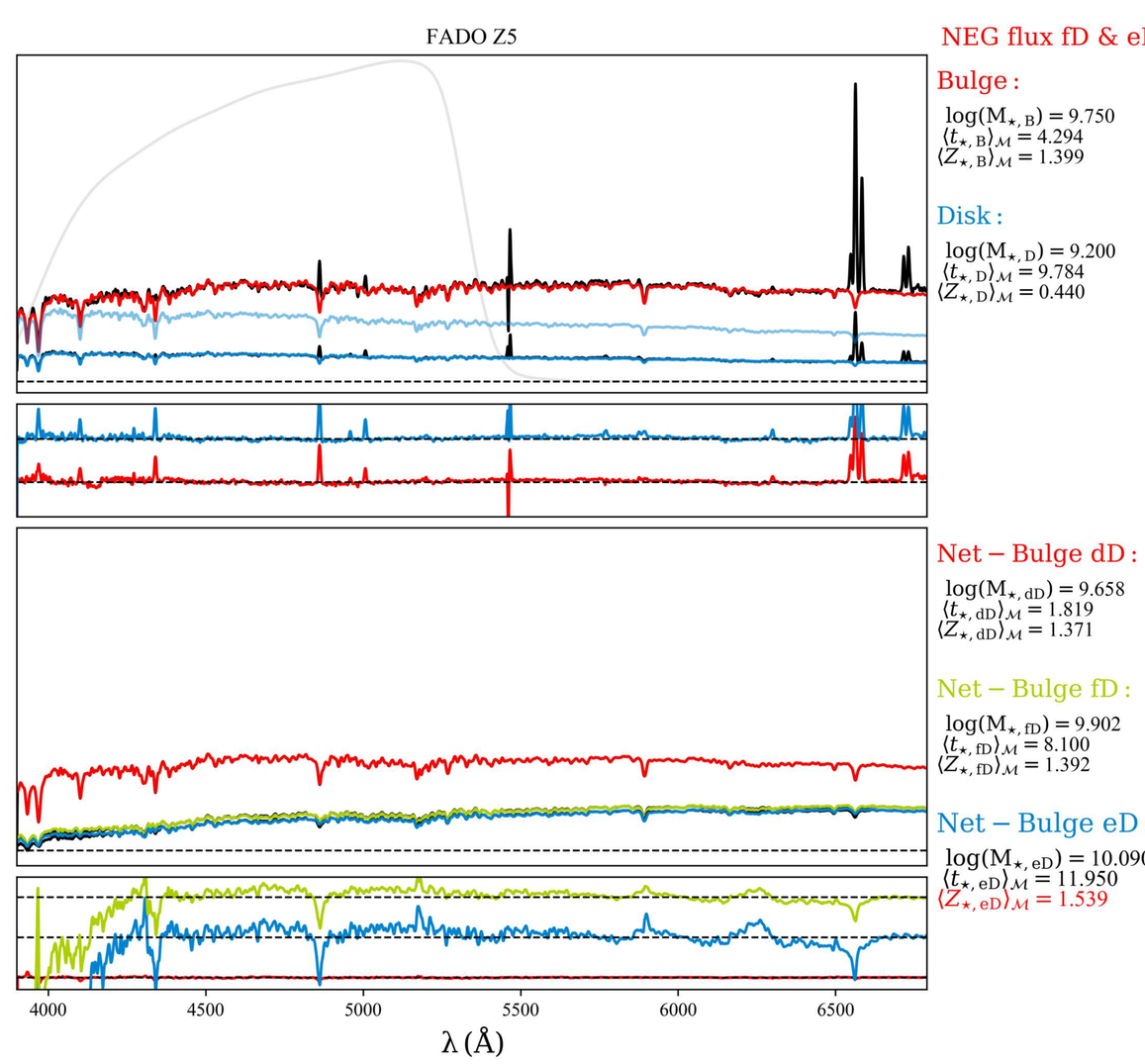
FADO Z5
NEG flux fD & eD
Bulge :
log(M⋆, B) = 9.750
⟨t⋆, B⟩M = 4.294
⟨Z⋆, B⟩M = 1.399
Disk :
log(M⋆, D) = 9.200
⟨t⋆, D⟩M = 9.784
⟨Z⋆, D⟩M = 0.440
Net − Bulge dD :
log(M⋆, dD) = 9.658
⟨t⋆, dD⟩M = 1.819
⟨Z⋆, dD⟩M = 1.371
Net − Bulge fD :
log(M⋆, fD) = 9.902
⟨t⋆, fD⟩M = 8.100
⟨Z⋆, fD⟩M = 1.392
Net − Bulge eD :
log(M⋆, eD) = 10.090
⟨t⋆, eD⟩M = 11.950
⟨Z⋆, eD⟩M = 1.539
4000
4500
5000
5500
6000
6500
λ (Å)

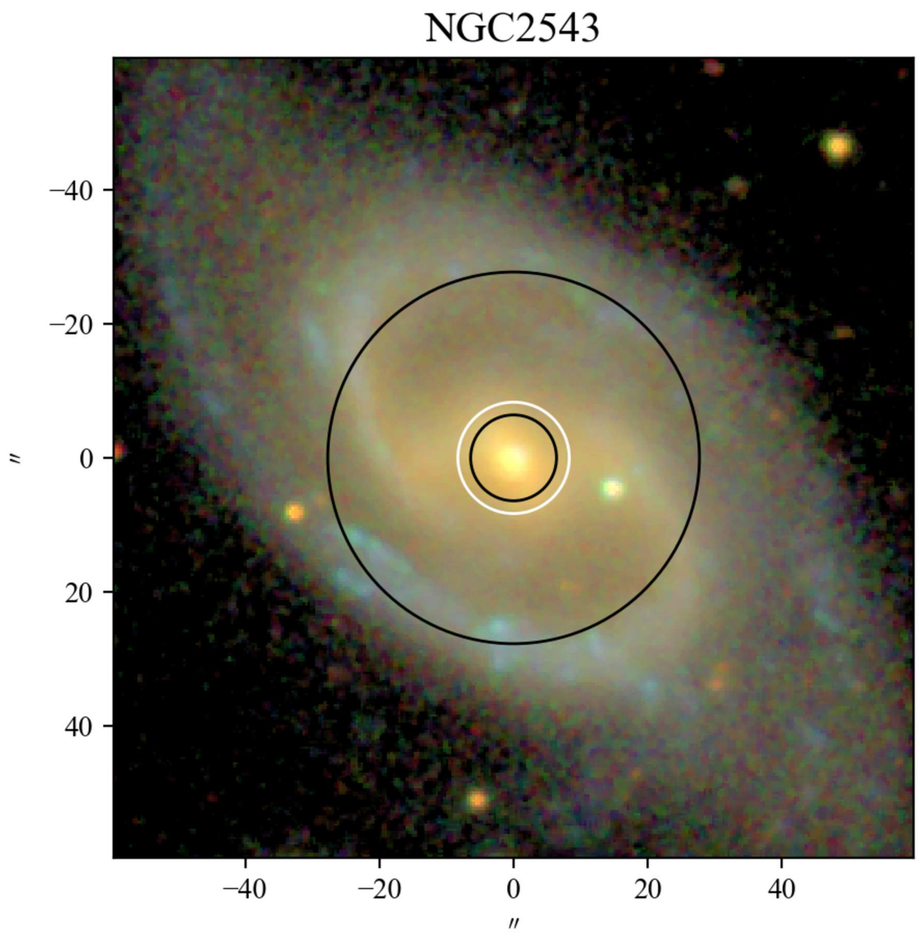
NGC2543
−40
−20
0
20
40
″

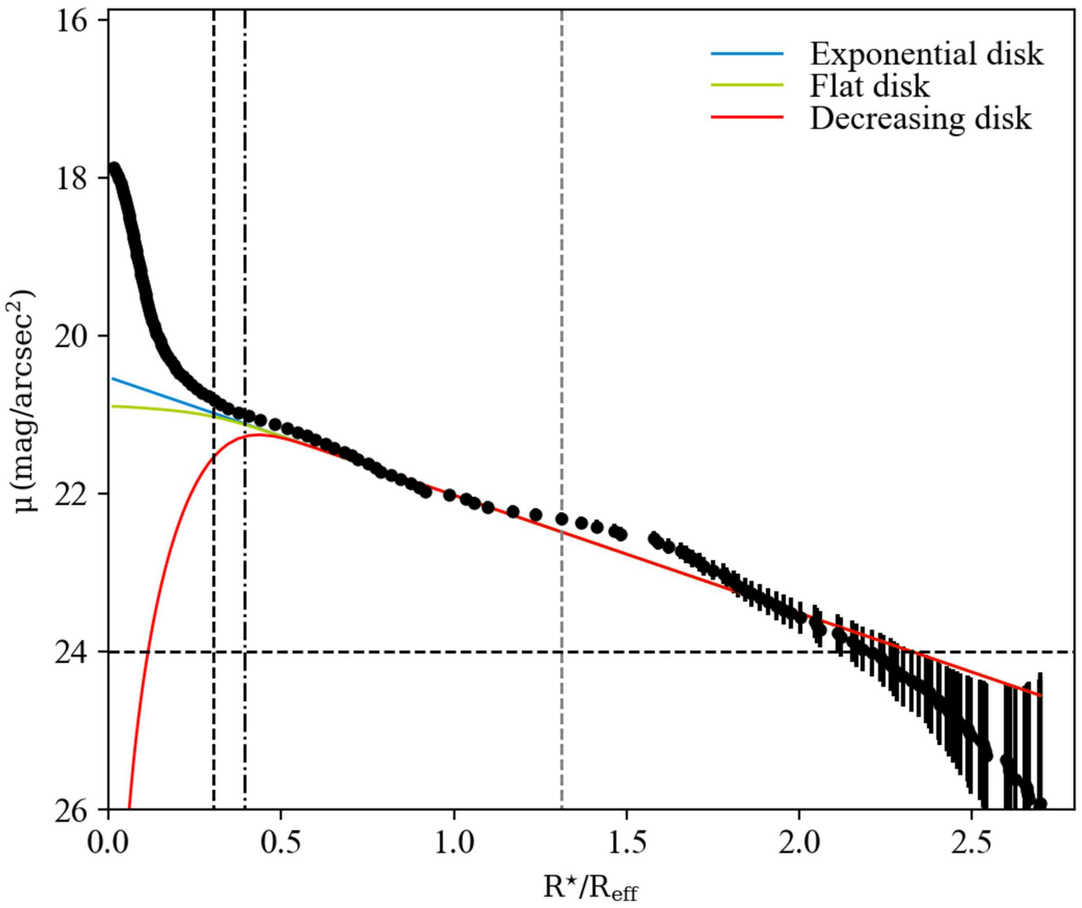
Exponential disk
Flat disk
Decreasing disk
μ (mag/arcsec²)
R⋆/Reff

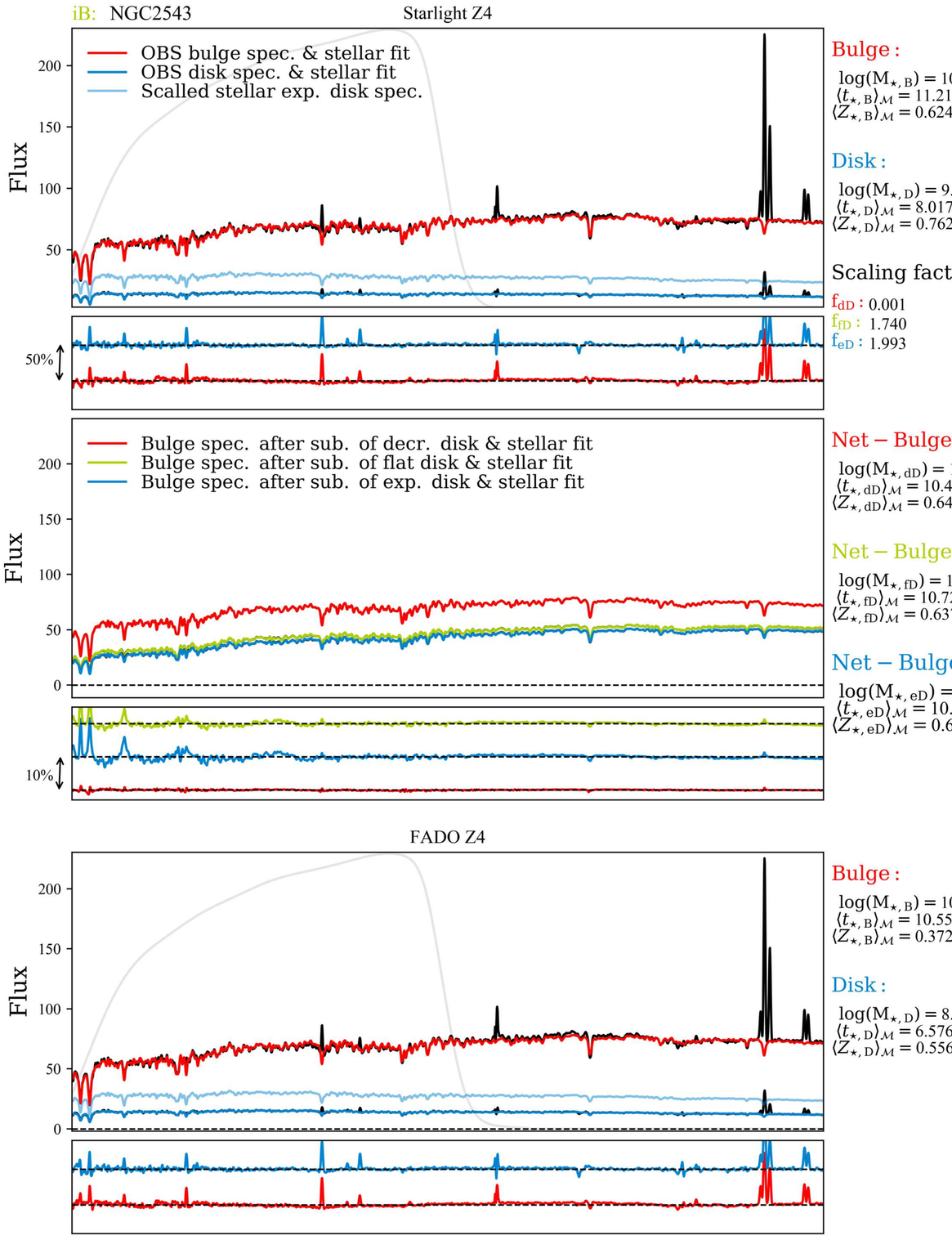
iB: NGC2543
Starlight Z4
OBS bulge spec. & stellar fit
OBS disk spec. & stellar fit
Scalled stellar exp. disk spec.
Flux
50%
Bulge :
log(M⋆, B) = 10.162
⟨t⋆, B⟩M = 11.218
⟨Z⋆, B⟩M = 0.624
Disk :
log(M⋆, D) = 9.069
⟨t⋆, D⟩M = 8.017
⟨Z⋆, D⟩M = 0.762
Scaling factors :
fdD : 0.001
ffD : 1.740
feD : 1.993

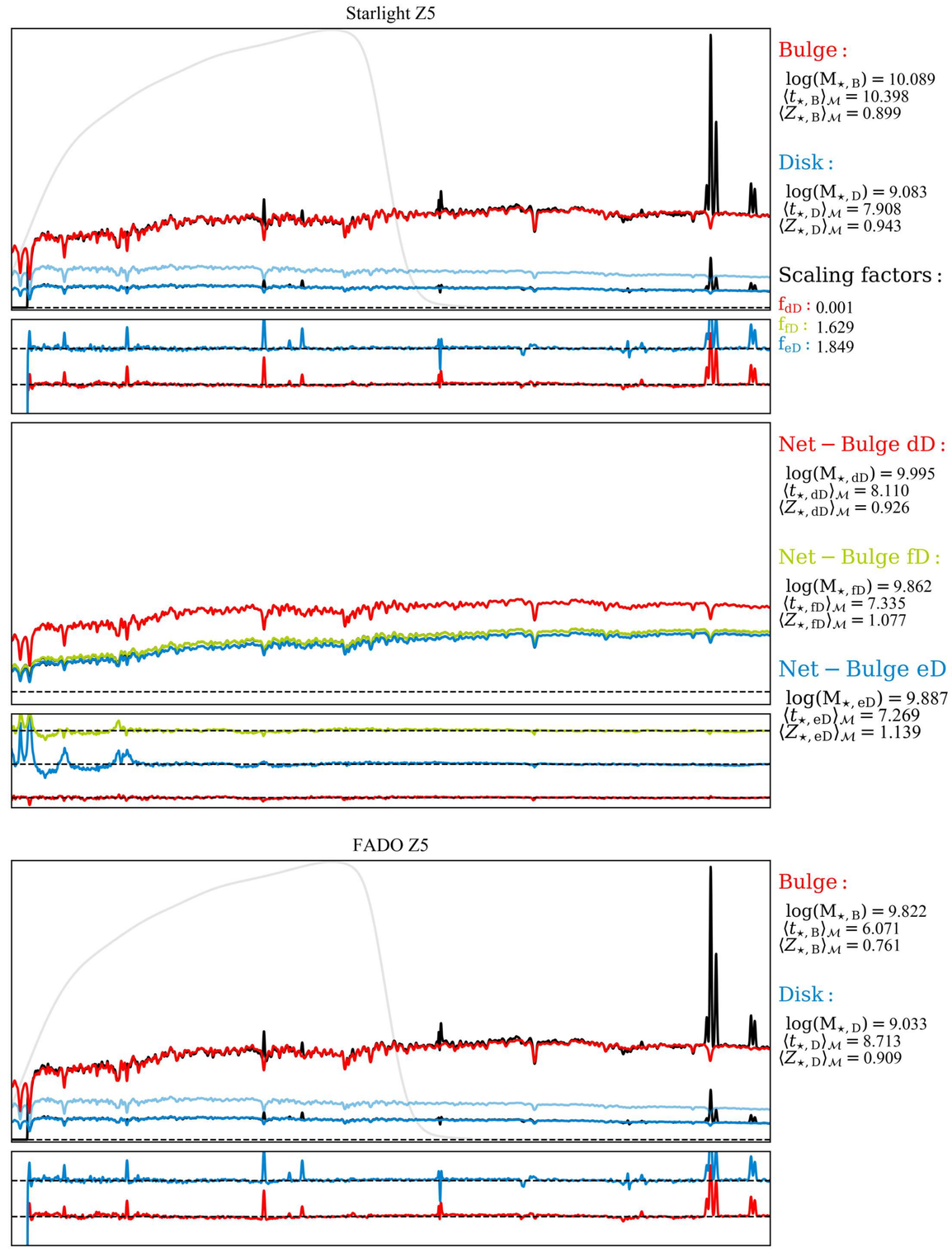
Starlight Z5
Bulge :
log(M⋆, B) = 10.089
⟨t⋆, B⟩M = 10.398
⟨Z⋆, B⟩M = 0.899
Disk :
log(M⋆, D) = 9.083
⟨t⋆, D⟩M = 7.908
⟨Z⋆, D⟩M = 0.943
Scaling factors :
fdD : 0.001
ffD : 1.629
feD : 1.849

Bulge spec. after sub. of decr. disk & stellar fit
Bulge spec. after sub. of flat disk & stellar fit
Bulge spec. after sub. of exp. disk & stellar fit
Flux
10%
Net − Bulge dD :
log(M⋆, dD) = 10.148
⟨t⋆, dD⟩M = 10.454
⟨Z⋆, dD⟩M = 0.642
Net − Bulge fD :
log(M⋆, fD) = 10.099
⟨t⋆, fD⟩M = 10.722
⟨Z⋆, fD⟩M = 0.637
Net − Bulge eD :
log(M⋆, eD) = 10.071
⟨t⋆, eD⟩M = 10.122
⟨Z⋆, eD⟩M = 0.620

Net − Bulge dD :
log(M⋆, dD) = 9.995
⟨t⋆, dD⟩M = 8.110
⟨Z⋆, dD⟩M = 0.926
Net − Bulge fD :
log(M⋆, fD) = 9.862
⟨t⋆, fD⟩M = 7.335
⟨Z⋆, fD⟩M = 1.077
Net − Bulge eD :
log(M⋆, eD) = 9.887
⟨t⋆, eD⟩M = 7.269
⟨Z⋆, eD⟩M = 1.139

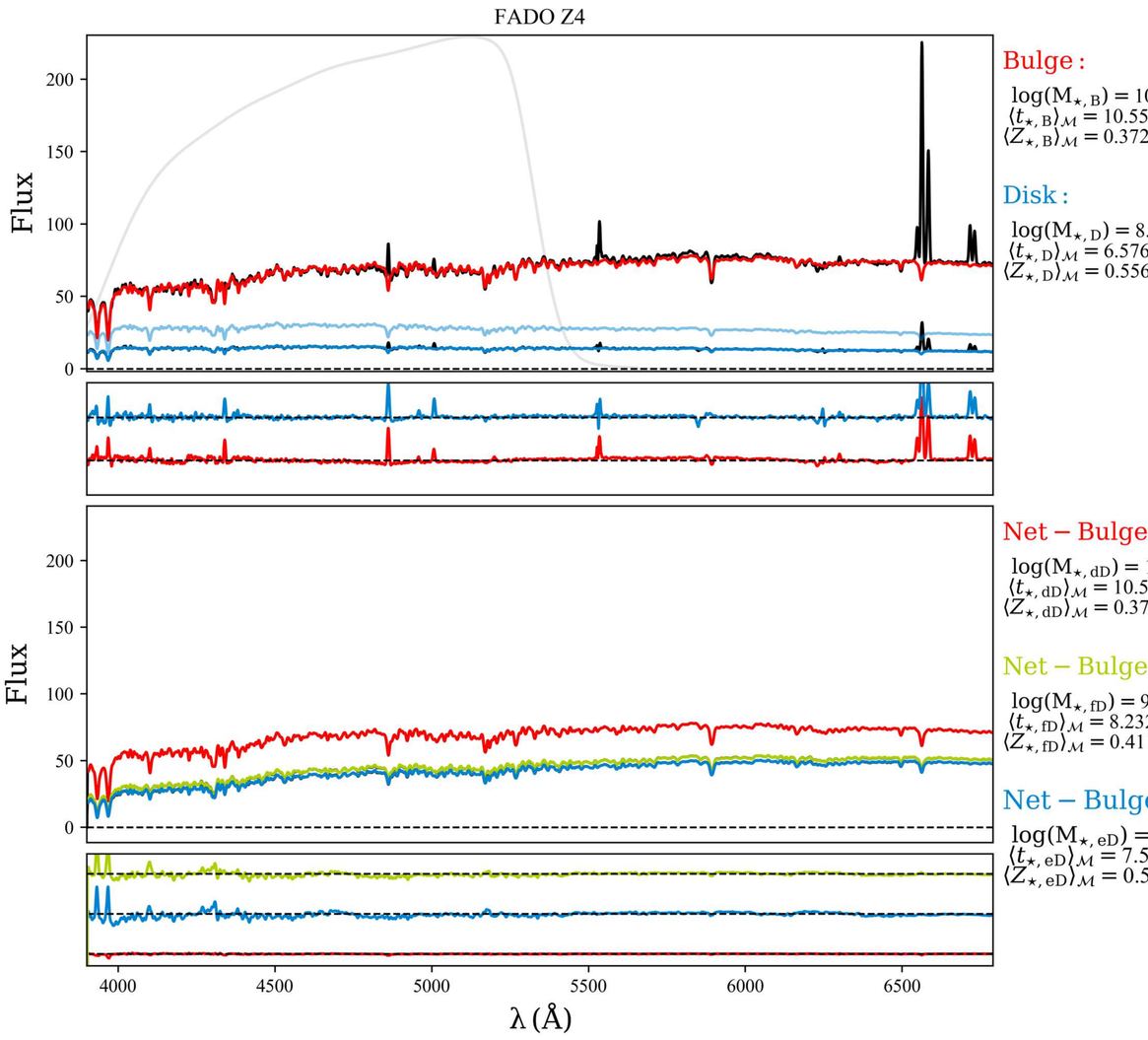
FADO Z4
Flux
Bulge :
log(M⋆, B) = 10.030
⟨t⋆, B⟩M = 10.550
⟨Z⋆, B⟩M = 0.372
Disk :
log(M⋆, D) = 8.952
⟨t⋆, D⟩M = 6.576
⟨Z⋆, D⟩M = 0.556

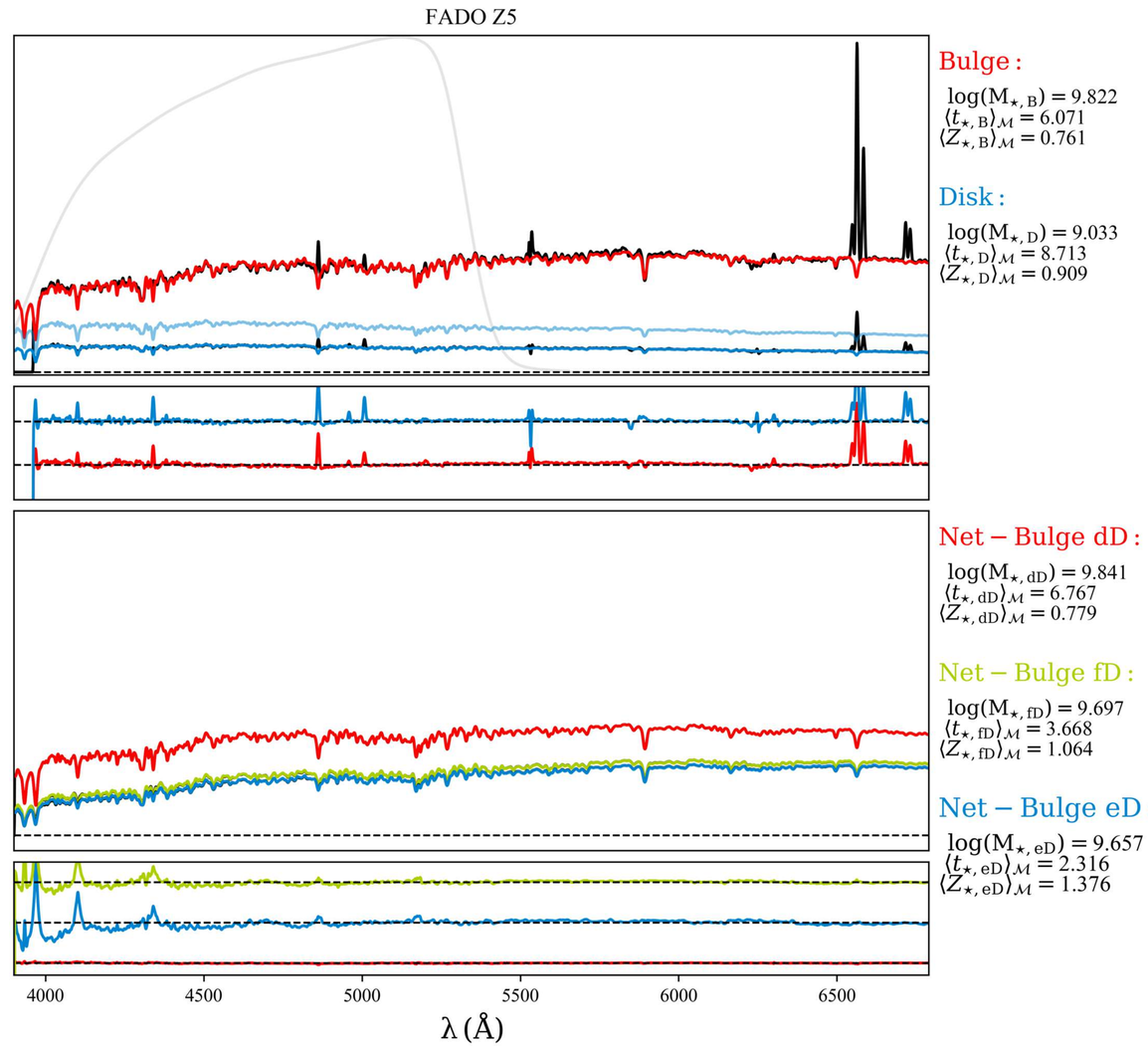
FADO Z5
Bulge :
log(M⋆, B) = 9.822
⟨t⋆, B⟩M = 6.071
⟨Z⋆, B⟩M = 0.761
Disk :
log(M⋆, D) = 9.033
⟨t⋆, D⟩M = 8.713
⟨Z⋆, D⟩M = 0.909

Flux
Net − Bulge dD :
log(M⋆, dD) = 10.030
⟨t⋆, dD⟩M = 10.530
⟨Z⋆, dD⟩M = 0.376
Net − Bulge fD :
log(M⋆, fD) = 9.940
⟨t⋆, fD⟩M = 8.232
⟨Z⋆, fD⟩M = 0.411
Net − Bulge eD :
log(M⋆, eD) = 9.958
⟨t⋆, eD⟩M = 7.526
⟨Z⋆, eD⟩M = 0.523
λ (Å)

Net − Bulge dD :
log(M⋆, dD) = 9.841
⟨t⋆, dD⟩M = 6.767
⟨Z⋆, dD⟩M = 0.779
Net − Bulge fD :
log(M⋆, fD) = 9.697
⟨t⋆, fD⟩M = 3.668
⟨Z⋆, fD⟩M = 1.064
Net − Bulge eD :
log(M⋆, eD) = 9.657
⟨t⋆, eD⟩M = 2.316
⟨Z⋆, eD⟩M = 1.376
λ (Å)

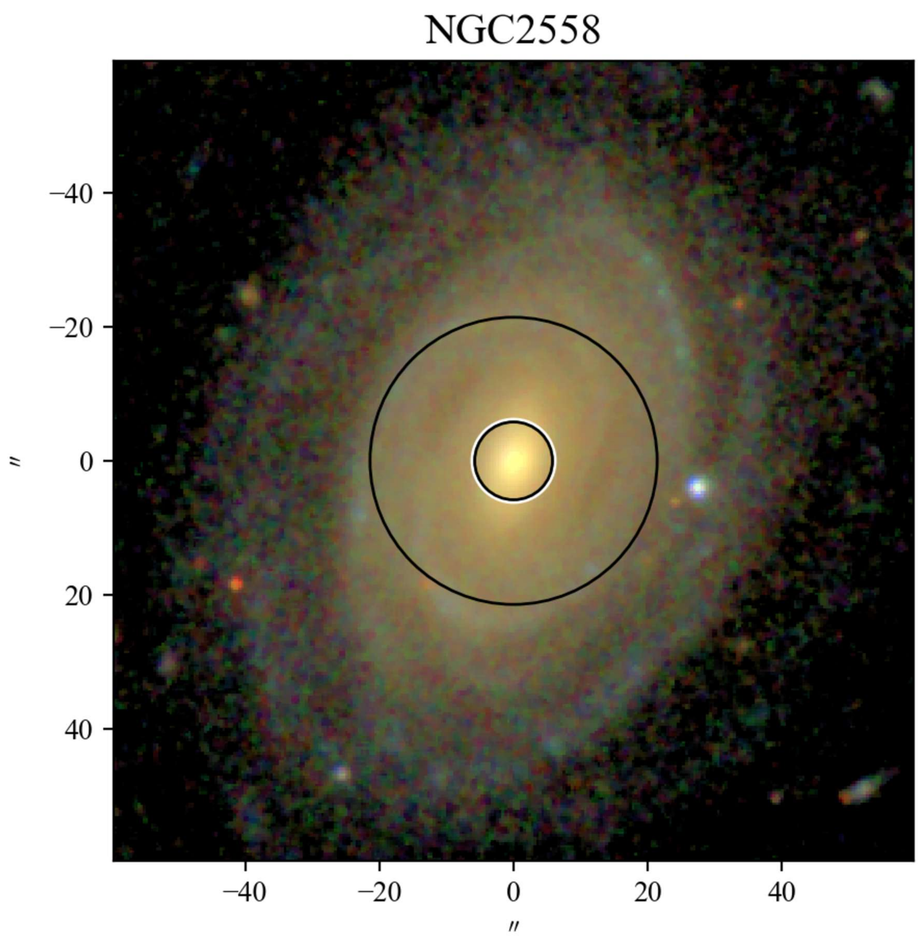
NGC2558
−40
−20
0
20
40
″
−40
−20
0
20
40
″

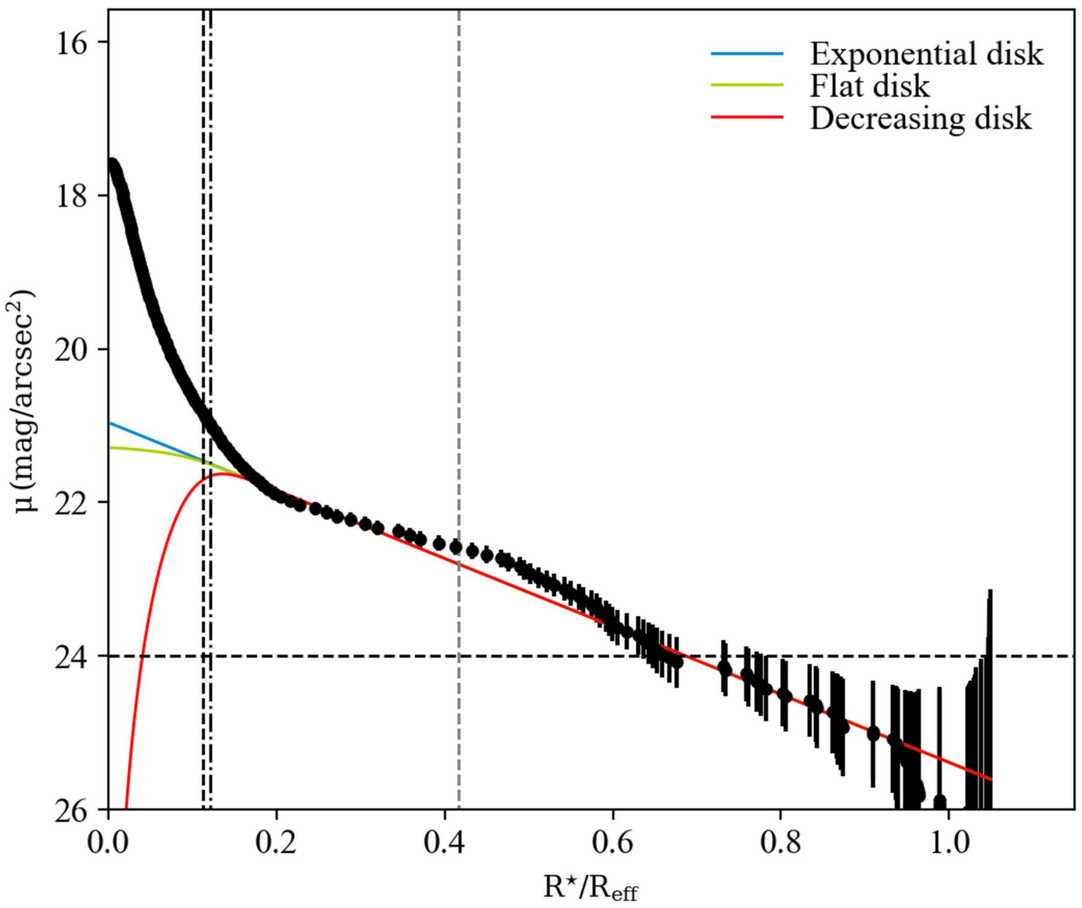
Exponential disk
Flat disk
Decreasing disk
μ (mag/arcsec²)
16
18
20
22
24
26
0.0
0.2
0.4
0.6
0.8
1.0
R⋆/Reff

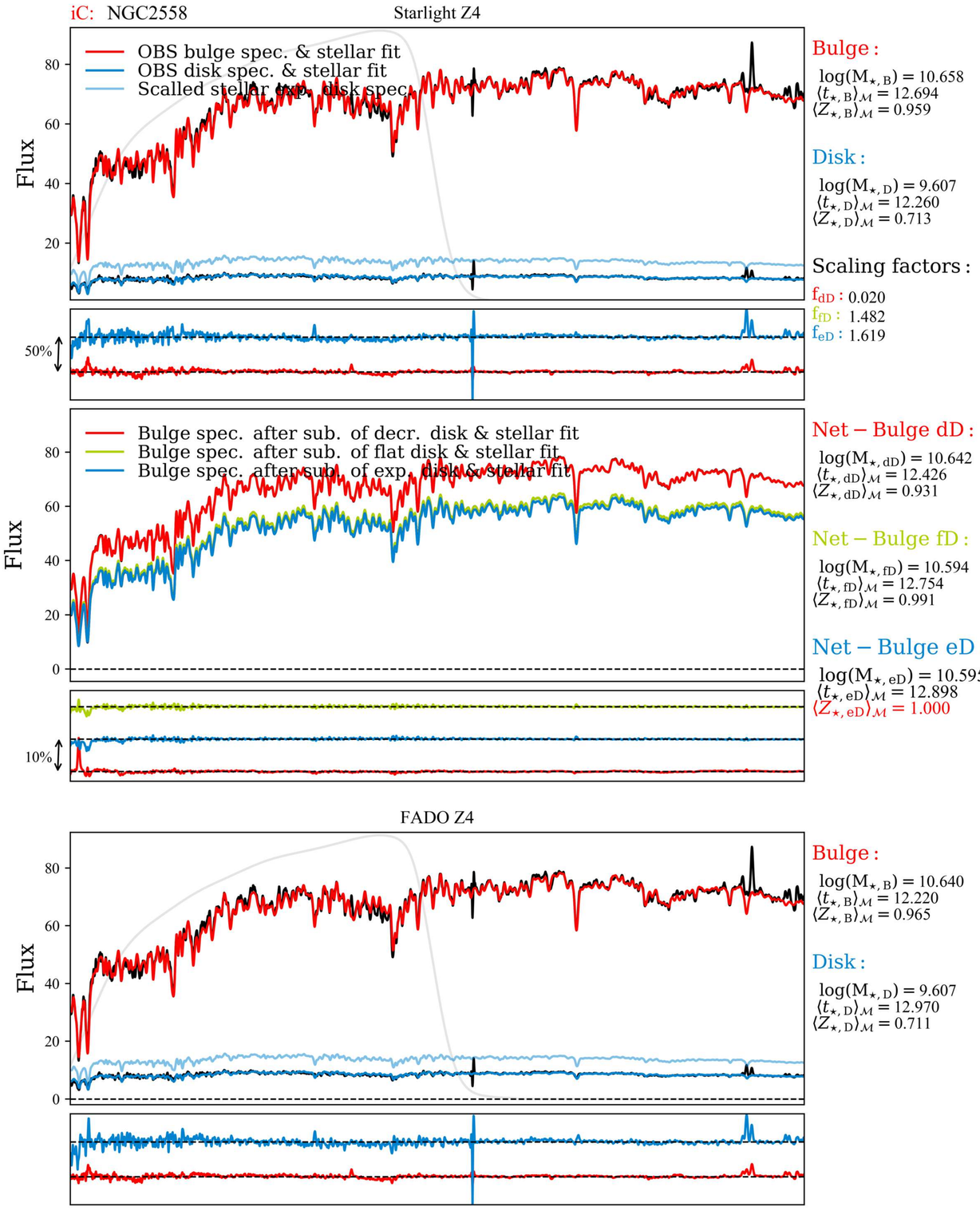
iC: NGC2558
Starlight Z4
OBS bulge spec. & stellar fit
OBS disk spec. & stellar fit
Scalled stellar exp. disk spec.
Flux
50%
Bulge :
log(M⋆, B) = 10.658
⟨t⋆, B⟩M = 12.694
⟨Z⋆, B⟩M = 0.959
Disk :
log(M⋆, D) = 9.607
⟨t⋆, D⟩M = 12.260
⟨Z⋆, D⟩M = 0.713
Scaling factors :
fdD : 0.020
ffD : 1.482
feD : 1.619
Bulge spec. after sub. of decr. disk & stellar fit
Bulge spec. after sub. of flat disk & stellar fit
Bulge spec. after sub. of exp. disk & stellar fit
10%
Net − Bulge dD :
log(M⋆, dD) = 10.642
⟨t⋆, dD⟩M = 12.426
⟨Z⋆, dD⟩M = 0.931
Net − Bulge fD :
log(M⋆, fD) = 10.594
⟨t⋆, fD⟩M = 12.754
⟨Z⋆, fD⟩M = 0.991
Net − Bulge eD :
log(M⋆, eD) = 10.595
⟨t⋆, eD⟩M = 12.898
⟨Z⋆, eD⟩M = 1.000

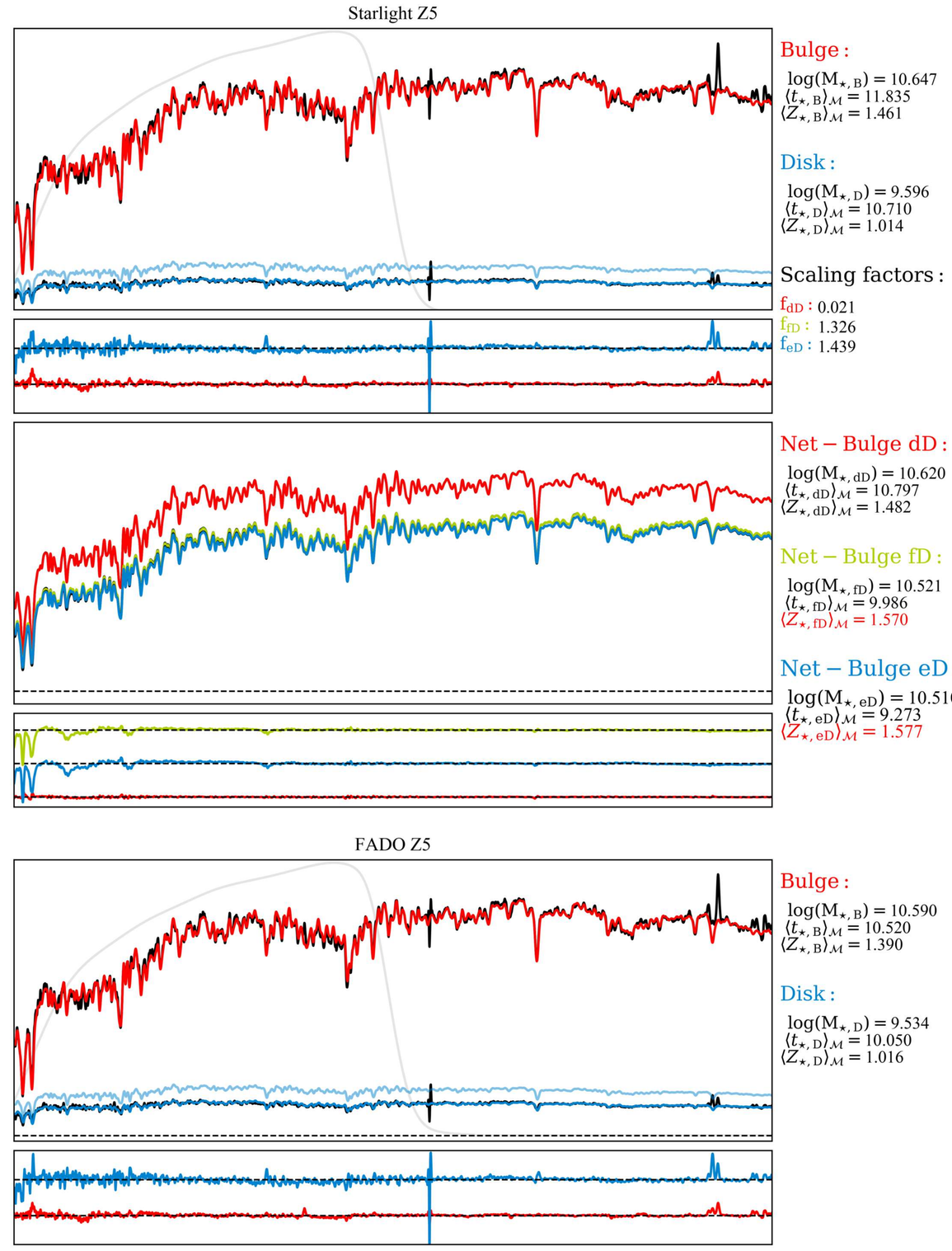
Starlight Z5
Bulge :
log(M⋆, B) = 10.647
⟨t⋆, B⟩M = 11.835
⟨Z⋆, B⟩M = 1.461
Disk :
log(M⋆, D) = 9.596
⟨t⋆, D⟩M = 10.710
⟨Z⋆, D⟩M = 1.014
Scaling factors :
fdD : 0.021
ffD : 1.326
feD : 1.439
Net − Bulge dD :
log(M⋆, dD) = 10.620
⟨t⋆, dD⟩M = 10.797
⟨Z⋆, dD⟩M = 1.482
Net − Bulge fD :
log(M⋆, fD) = 10.521
⟨t⋆, fD⟩M = 9.986
⟨Z⋆, fD⟩M = 1.570
Net − Bulge eD :
log(M⋆, eD) = 10.510
⟨t⋆, eD⟩M = 9.273
⟨Z⋆, eD⟩M = 1.577

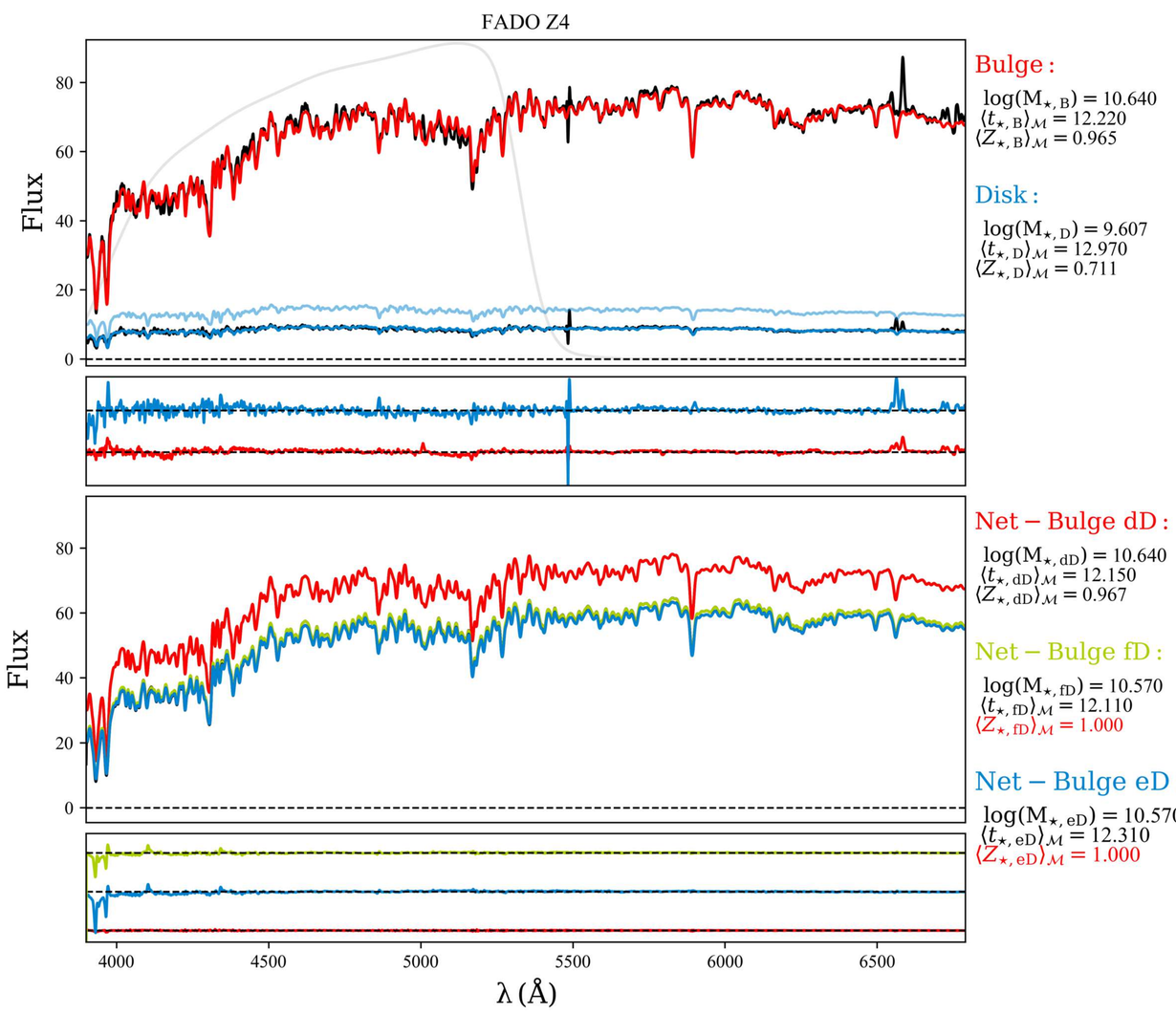
FADO Z4
Flux
Bulge :
log(M⋆, B) = 10.640
⟨t⋆, B⟩M = 12.220
⟨Z⋆, B⟩M = 0.965
Disk :
log(M⋆, D) = 9.607
⟨t⋆, D⟩M = 12.970
⟨Z⋆, D⟩M = 0.711
Net − Bulge dD :
log(M⋆, dD) = 10.640
⟨t⋆, dD⟩M = 12.150
⟨Z⋆, dD⟩M = 0.967
Net − Bulge fD :
log(M⋆, fD) = 10.570
⟨t⋆, fD⟩M = 12.110
⟨Z⋆, fD⟩M = 1.000
Net − Bulge eD :
log(M⋆, eD) = 10.570
⟨t⋆, eD⟩M = 12.310
⟨Z⋆, eD⟩M = 1.000
λ (Å)

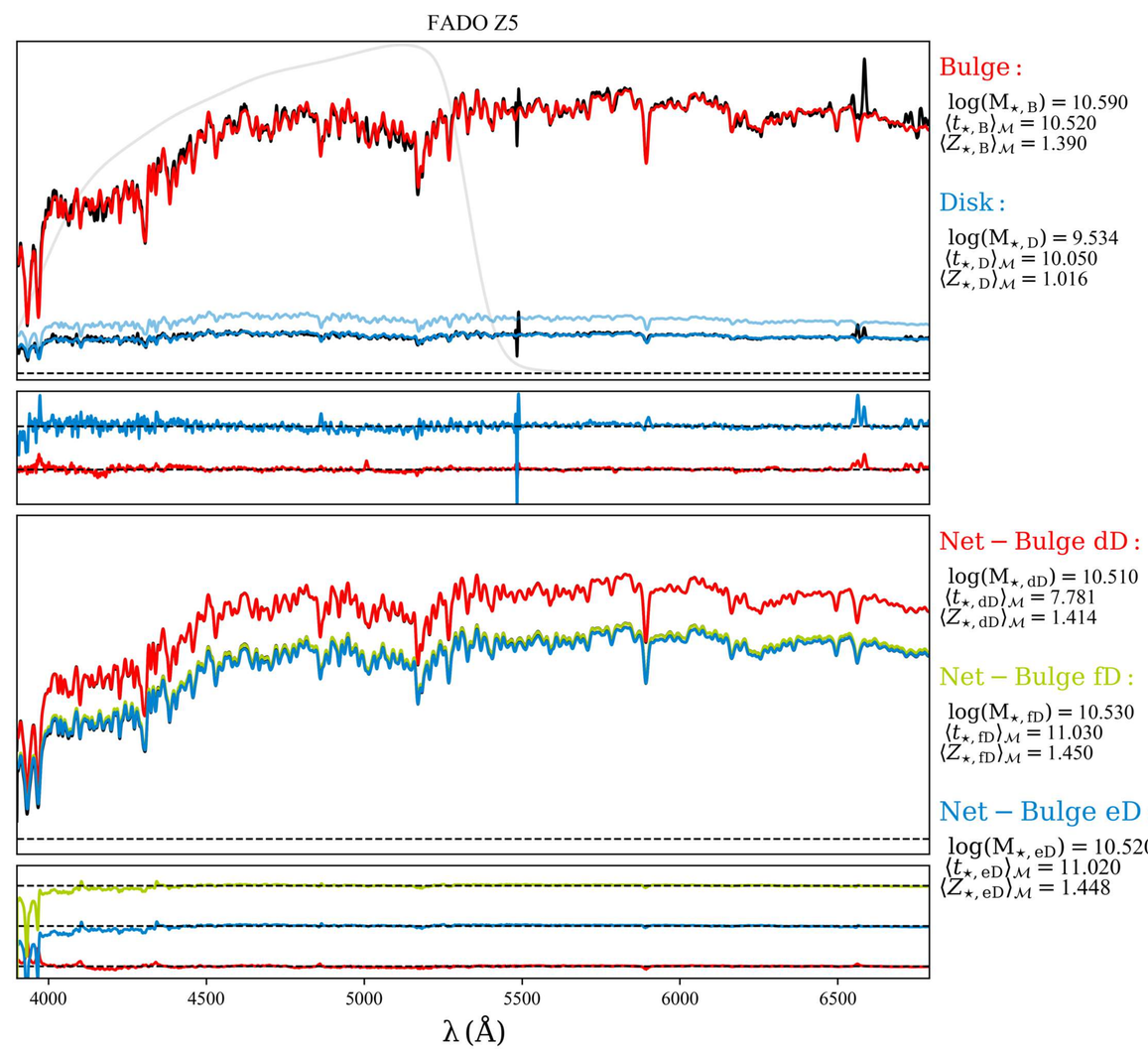
FADO Z5
Bulge :
log(M⋆, B) = 10.590
⟨t⋆, B⟩M = 10.520
⟨Z⋆, B⟩M = 1.390
Disk :
log(M⋆, D) = 9.534
⟨t⋆, D⟩M = 10.050
⟨Z⋆, D⟩M = 1.016
Net − Bulge dD :
log(M⋆, dD) = 10.510
⟨t⋆, dD⟩M = 7.781
⟨Z⋆, dD⟩M = 1.414
Net − Bulge fD :
log(M⋆, fD) = 10.530
⟨t⋆, fD⟩M = 11.030
⟨Z⋆, fD⟩M = 1.450
Net − Bulge eD :
log(M⋆, eD) = 10.520
⟨t⋆, eD⟩M = 11.020
⟨Z⋆, eD⟩M = 1.448
λ (Å)

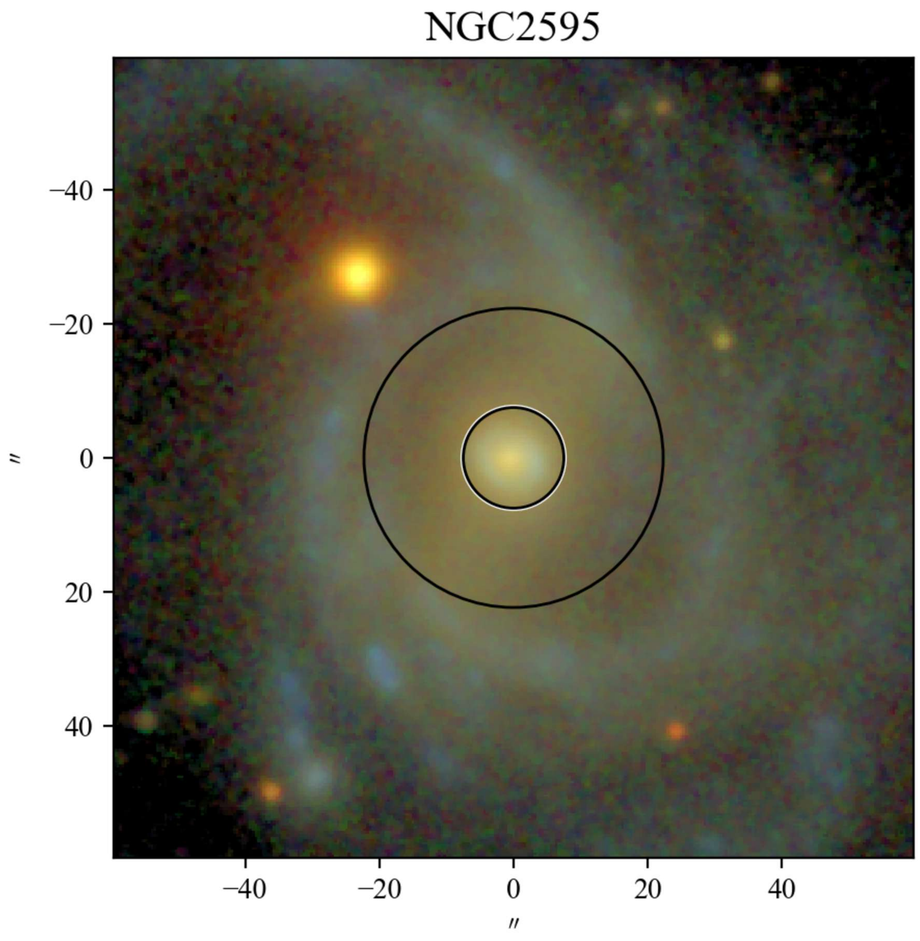
NGC2595
−40
−20
0
20
40
″
−40
−20
0
20
40
″

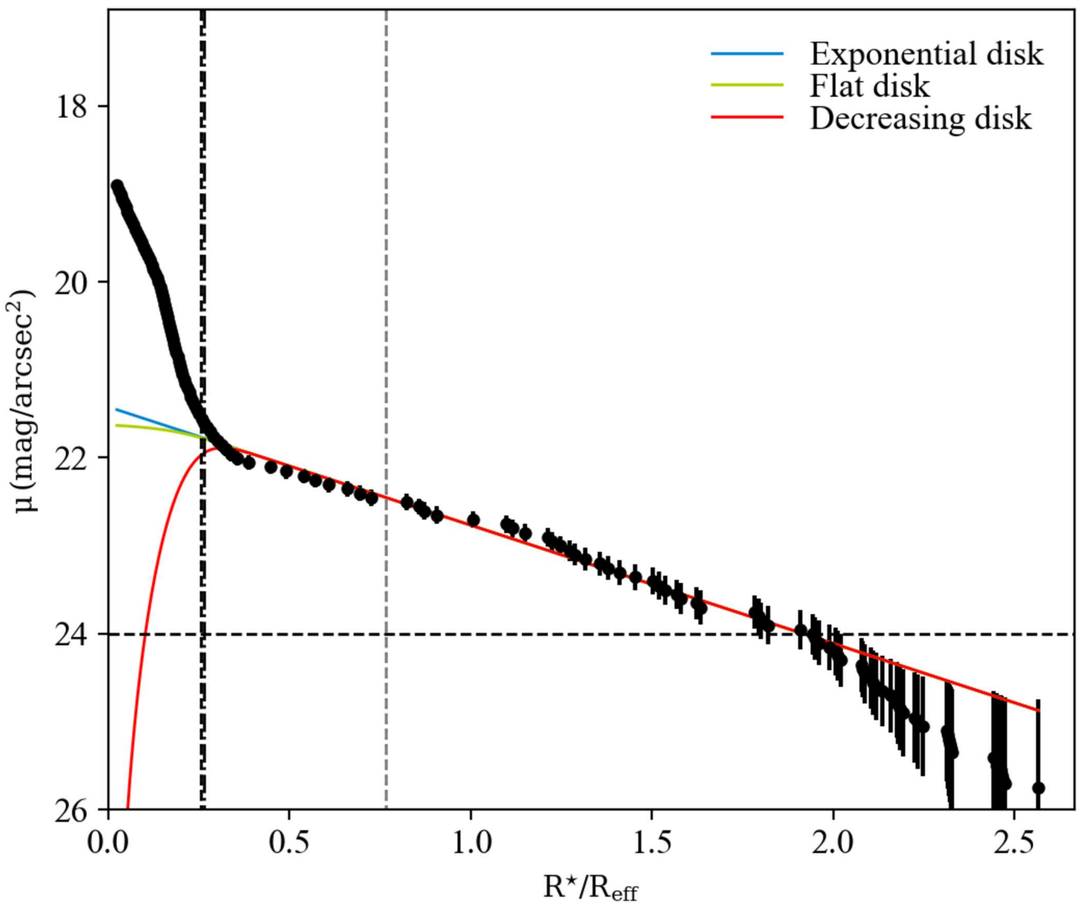
Exponential disk
Flat disk
Decreasing disk
18
20
22
24
26
μ (mag/arcsec²)
0.0
0.5
1.0
1.5
2.0
2.5
R⋆/Reff

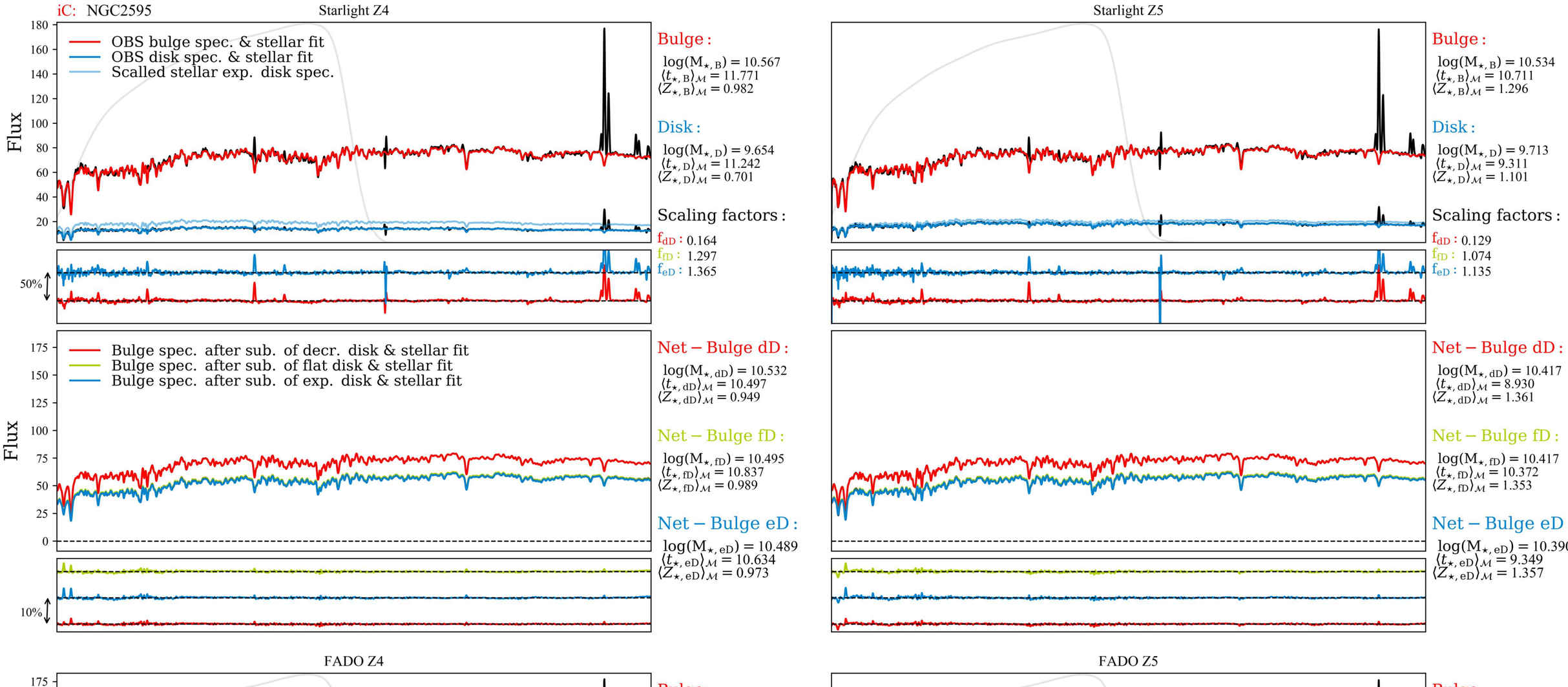
iC: NGC2595
Starlight Z4
OBS bulge spec. & stellar fit
OBS disk spec. & stellar fit
Scalled stellar exp. disk spec.
Flux
50%
Bulge :
log(M⋆, B) = 10.567
⟨t⋆, B⟩M = 11.771
⟨Z⋆, B⟩M = 0.982
Disk :
log(M⋆, D) = 9.654
⟨t⋆, D⟩M = 11.242
⟨Z⋆, D⟩M = 0.701
Scaling factors :
fdD : 0.164
ffD : 1.297
feD : 1.365
Starlight Z5
Bulge :
log(M⋆, B) = 10.534
⟨t⋆, B⟩M = 10.711
⟨Z⋆, B⟩M = 1.296
Disk :
log(M⋆, D) = 9.713
⟨t⋆, D⟩M = 9.311
⟨Z⋆, D⟩M = 1.101
Scaling factors :
fdD : 0.129
ffD : 1.074
feD : 1.135
Bulge spec. after sub. of decr. disk & stellar fit
Bulge spec. after sub. of flat disk & stellar fit
Bulge spec. after sub. of exp. disk & stellar fit
10%
Net − Bulge dD :
log(M⋆, dD) = 10.532
⟨t⋆, dD⟩M = 10.497
⟨Z⋆, dD⟩M = 0.949
Net − Bulge fD :
log(M⋆, fD) = 10.495
⟨t⋆, fD⟩M = 10.837
⟨Z⋆, fD⟩M = 0.989
Net − Bulge eD :
log(M⋆, eD) = 10.489
⟨t⋆, eD⟩M = 10.634
⟨Z⋆, eD⟩M = 0.973
Net − Bulge dD :
log(M⋆, dD) = 10.417
⟨t⋆, dD⟩M = 8.930
⟨Z⋆, dD⟩M = 1.361
Net − Bulge fD :
log(M⋆, fD) = 10.417
⟨t⋆, fD⟩M = 10.372
⟨Z⋆, fD⟩M = 1.353
Net − Bulge eD :
log(M⋆, eD) = 10.390
⟨t⋆, eD⟩M = 9.349
⟨Z⋆, eD⟩M = 1.357
FADO Z4
Bulge :
log(M⋆, B) = 10.610
⟨t⋆, B⟩M = 11.860
⟨Z⋆, B⟩M = 0.946
Disk :
log(M⋆, D) = 9.628
⟨t⋆, D⟩M = 11.400
⟨Z⋆, D⟩M = 0.622
FADO Z5
Bulge :
log(M⋆, B) = 10.470
⟨t⋆, B⟩M = 10.850
⟨Z⋆, B⟩M = 1.475
Disk :
log(M⋆, D) = 9.734
⟨t⋆, D⟩M = 11.760
⟨Z⋆, D⟩M = 1.179
Net − Bulge dD :
log(M⋆, dD) = 10.610
⟨t⋆, dD⟩M = 11.950
⟨Z⋆, dD⟩M = 0.964
Net − Bulge fD :
log(M⋆, fD) = 10.550
⟨t⋆, fD⟩M = 12.320
⟨Z⋆, fD⟩M = 0.992
Net − Bulge eD :
log(M⋆, eD) = 10.540
⟨t⋆, eD⟩M = 11.890
⟨Z⋆, eD⟩M = 0.999
Net − Bulge dD :
log(M⋆, dD) = 10.470
⟨t⋆, dD⟩M = 10.220
⟨Z⋆, dD⟩M = 1.384
Net − Bulge fD :
log(M⋆, fD) = 10.300
⟨t⋆, fD⟩M = 7.699
⟨Z⋆, fD⟩M = 1.393
Net − Bulge eD :
log(M⋆, eD) = 10.360
⟨t⋆, eD⟩M = 8.938
⟨Z⋆, eD⟩M = 1.390
4000
4500
5000
5500
6000
6500
λ (Å)

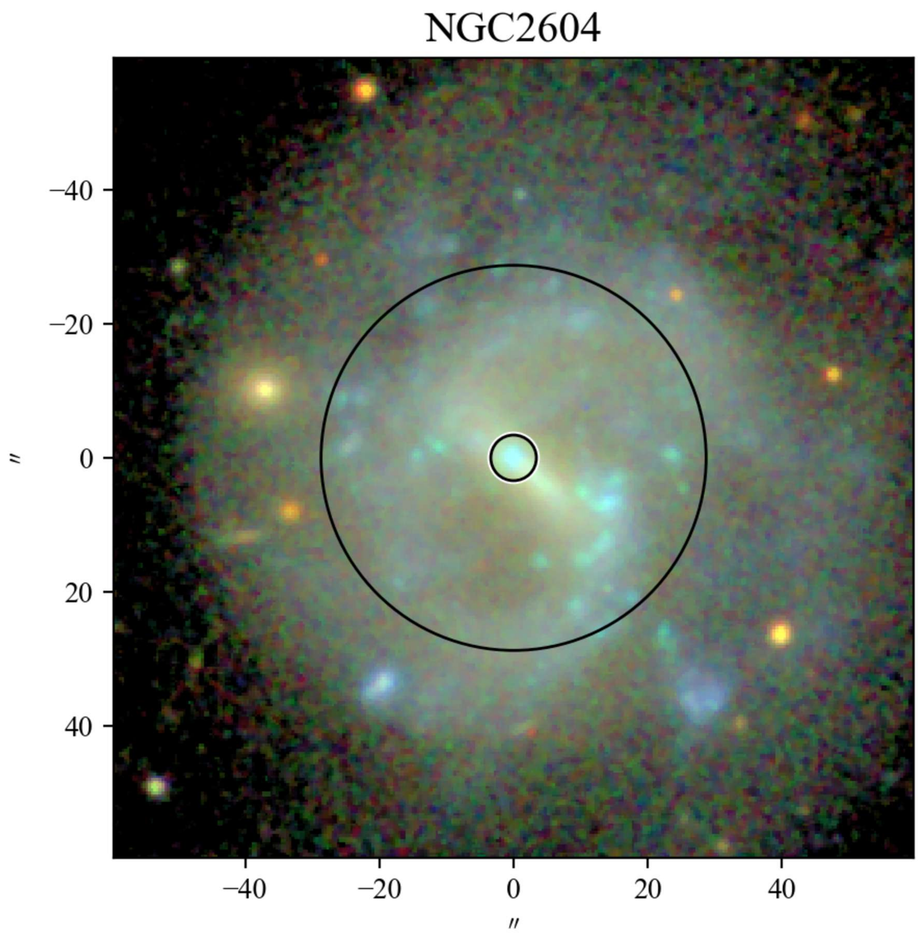
NGC2604
−40
−20
0
20
40
″
−40
−20
0
20
40
″

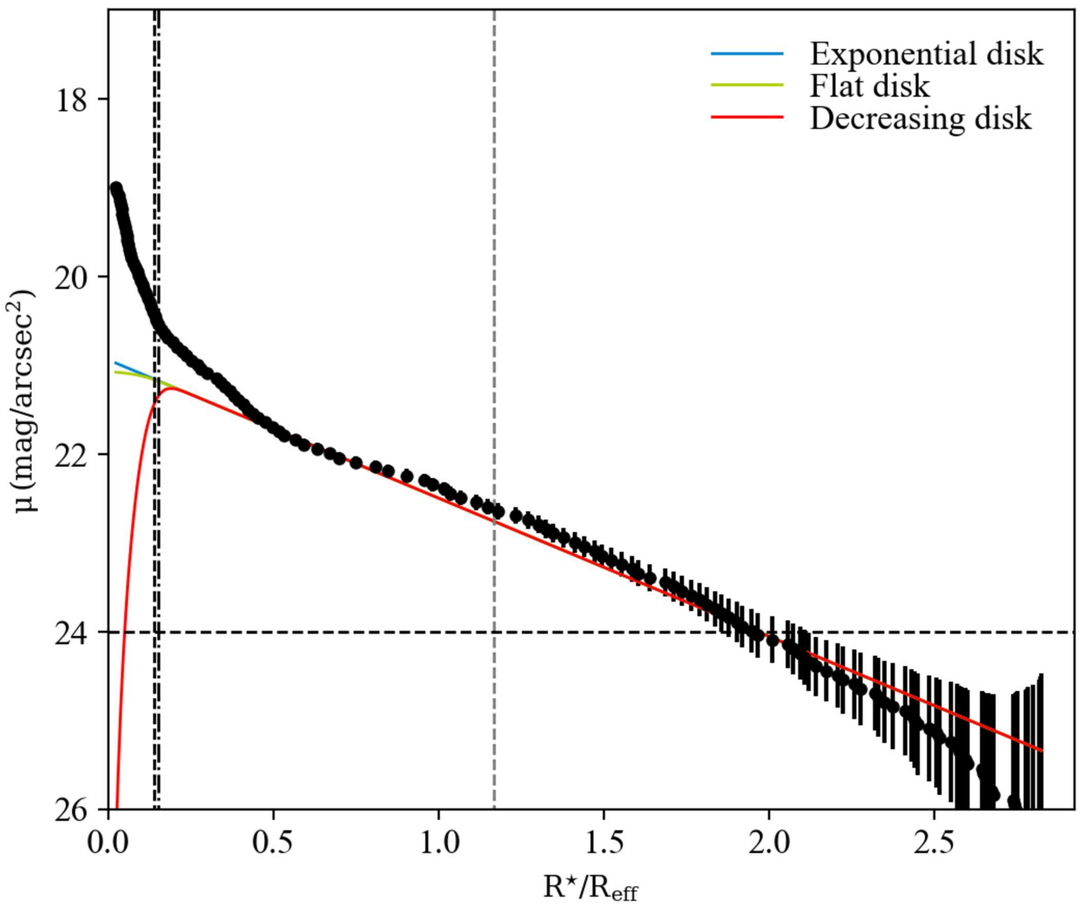
Exponential disk
Flat disk
Decreasing disk
μ (mag/arcsec²)
18
20
22
24
26
0.0
0.5
1.0
1.5
2.0
2.5
R⋆/Reff

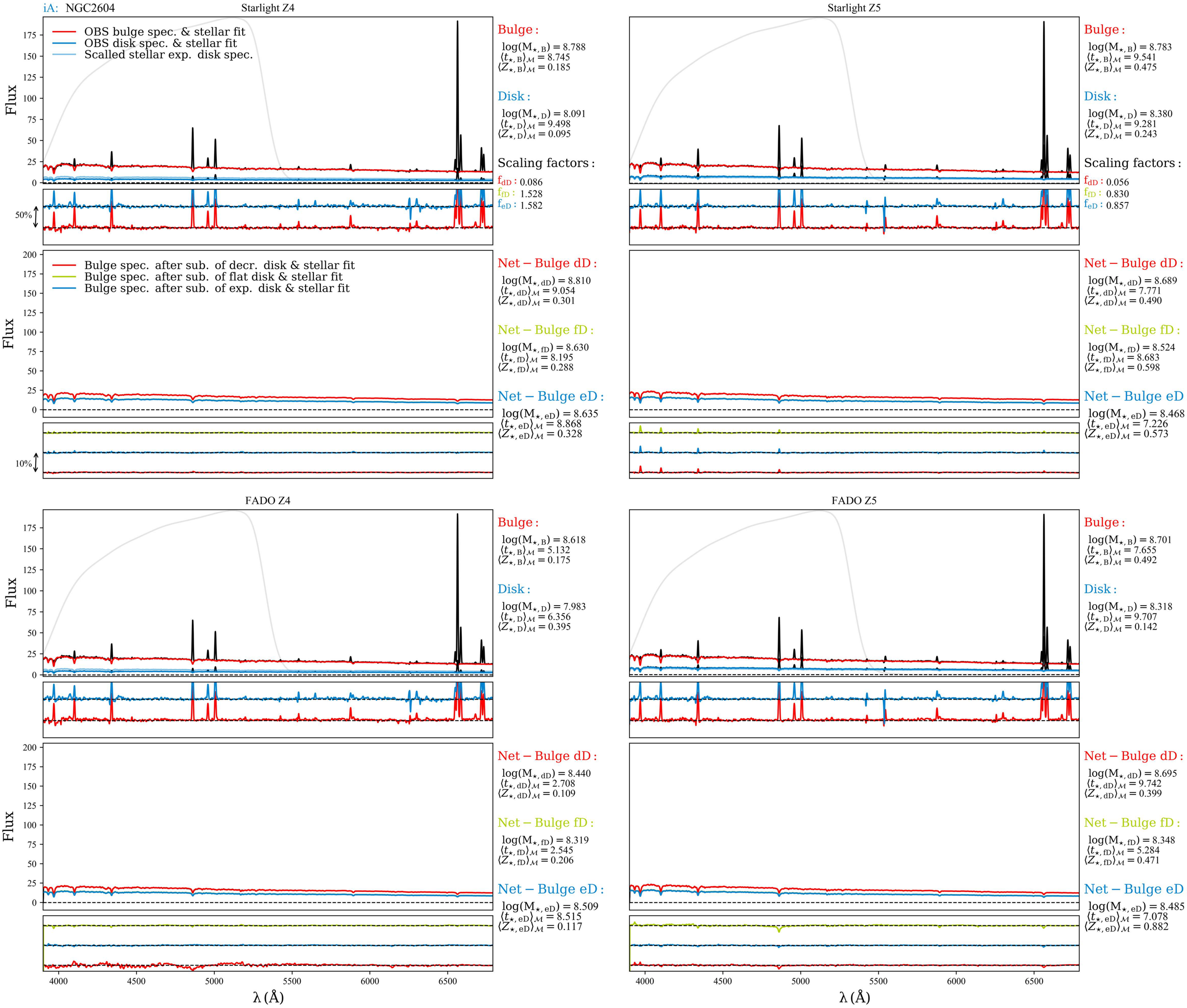
iA: NGC2604
Starlight Z4
OBS bulge spec. & stellar fit
OBS disk spec. & stellar fit
Scalled stellar exp. disk spec.
Flux
Bulge :
log(M⋆, B) = 8.788
⟨t⋆, B⟩M = 8.745
⟨Z⋆, B⟩M = 0.185
Disk :
log(M⋆, D) = 8.091
⟨t⋆, D⟩M = 9.498
⟨Z⋆, D⟩M = 0.095
Scaling factors :
fdD : 0.086
ffD : 1.528
feD : 1.582
50%
Bulge spec. after sub. of decr. disk & stellar fit
Bulge spec. after sub. of flat disk & stellar fit
Bulge spec. after sub. of exp. disk & stellar fit
Net − Bulge dD :
log(M⋆, dD) = 8.810
⟨t⋆, dD⟩M = 9.054
⟨Z⋆, dD⟩M = 0.301
Net − Bulge fD :
log(M⋆, fD) = 8.630
⟨t⋆, fD⟩M = 8.195
⟨Z⋆, fD⟩M = 0.288
Net − Bulge eD :
log(M⋆, eD) = 8.635
⟨t⋆, eD⟩M = 8.868
⟨Z⋆, eD⟩M = 0.328
10%
FADO Z4
Bulge :
log(M⋆, B) = 8.618
⟨t⋆, B⟩M = 5.132
⟨Z⋆, B⟩M = 0.175
Disk :
log(M⋆, D) = 7.983
⟨t⋆, D⟩M = 6.356
⟨Z⋆, D⟩M = 0.395
Net − Bulge dD :
log(M⋆, dD) = 8.440
⟨t⋆, dD⟩M = 2.708
⟨Z⋆, dD⟩M = 0.109
Net − Bulge fD :
log(M⋆, fD) = 8.319
⟨t⋆, fD⟩M = 2.545
⟨Z⋆, fD⟩M = 0.206
Net − Bulge eD :
log(M⋆, eD) = 8.509
⟨t⋆, eD⟩M = 8.515
⟨Z⋆, eD⟩M = 0.117
λ (Å)

Starlight Z5
Bulge :
log(M⋆, B) = 8.783
⟨t⋆, B⟩M = 9.541
⟨Z⋆, B⟩M = 0.475
Disk :
log(M⋆, D) = 8.380
⟨t⋆, D⟩M = 9.281
⟨Z⋆, D⟩M = 0.243
Scaling factors :
fdD : 0.056
ffD : 0.830
feD : 0.857
Net − Bulge dD :
log(M⋆, dD) = 8.689
⟨t⋆, dD⟩M = 7.771
⟨Z⋆, dD⟩M = 0.490
Net − Bulge fD :
log(M⋆, fD) = 8.524
⟨t⋆, fD⟩M = 8.683
⟨Z⋆, fD⟩M = 0.598
Net − Bulge eD :
log(M⋆, eD) = 8.468
⟨t⋆, eD⟩M = 7.226
⟨Z⋆, eD⟩M = 0.573
FADO Z5
Bulge :
log(M⋆, B) = 8.701
⟨t⋆, B⟩M = 7.655
⟨Z⋆, B⟩M = 0.492
Disk :
log(M⋆, D) = 8.318
⟨t⋆, D⟩M = 9.707
⟨Z⋆, D⟩M = 0.142
Net − Bulge dD :
log(M⋆, dD) = 8.695
⟨t⋆, dD⟩M = 9.742
⟨Z⋆, dD⟩M = 0.399
Net − Bulge fD :
log(M⋆, fD) = 8.348
⟨t⋆, fD⟩M = 5.284
⟨Z⋆, fD⟩M = 0.471
Net − Bulge eD :
log(M⋆, eD) = 8.485
⟨t⋆, eD⟩M = 7.078
⟨Z⋆, eD⟩M = 0.882
λ (Å)

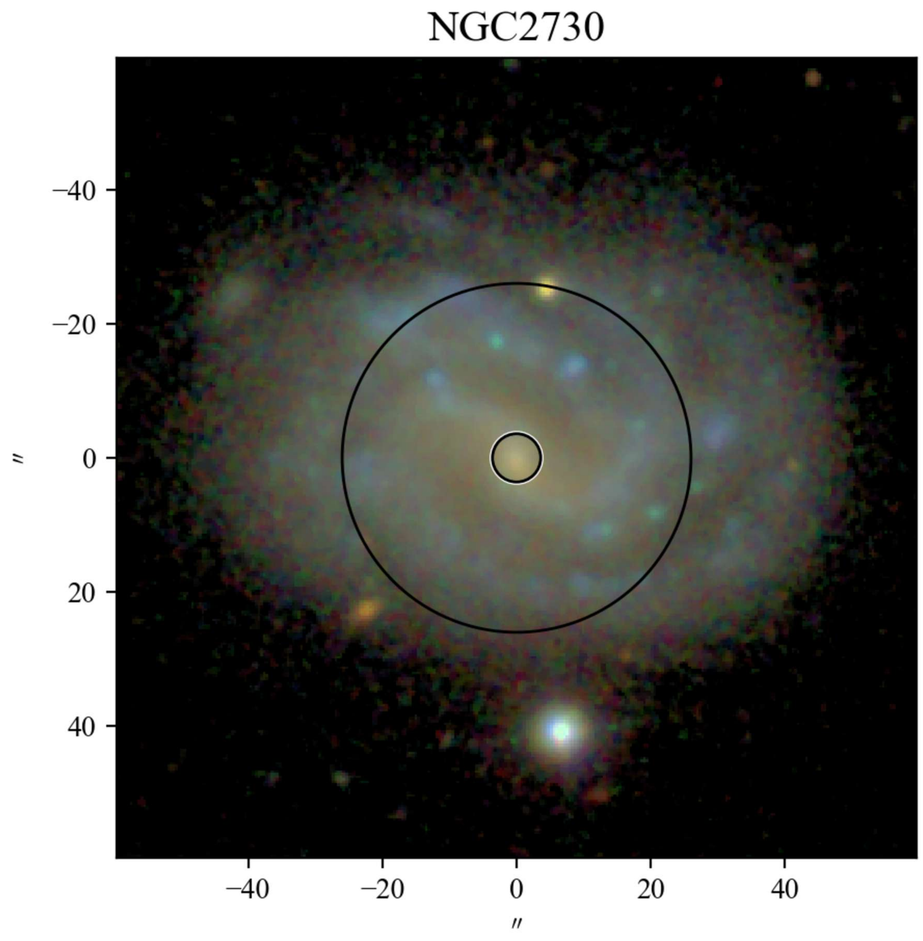
NGC2730
−40
−20
0
20
40
″
−40
−20
0
20
40
″

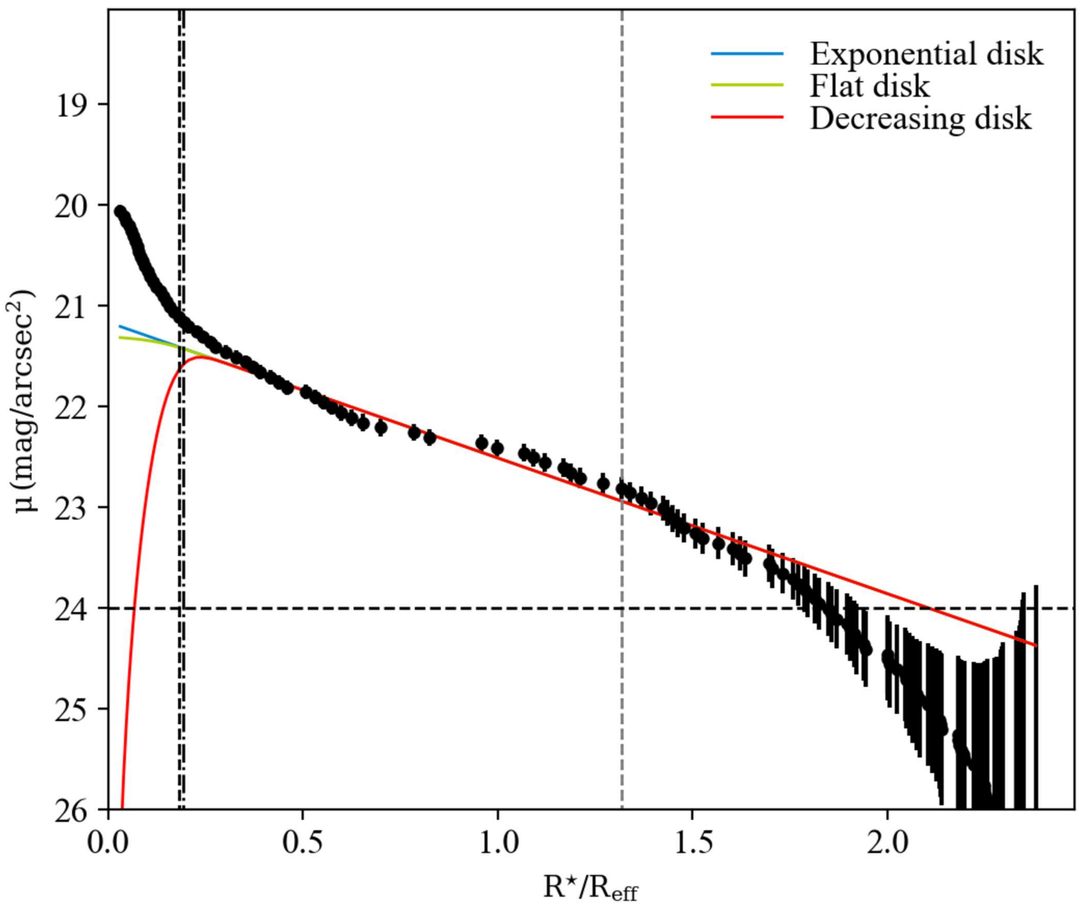
Exponential disk
Flat disk
Decreasing disk
μ (mag/arcsec²)
19
20
21
22
23
24
25
26
0.0
0.5
1.0
1.5
2.0
R⋆/Reff

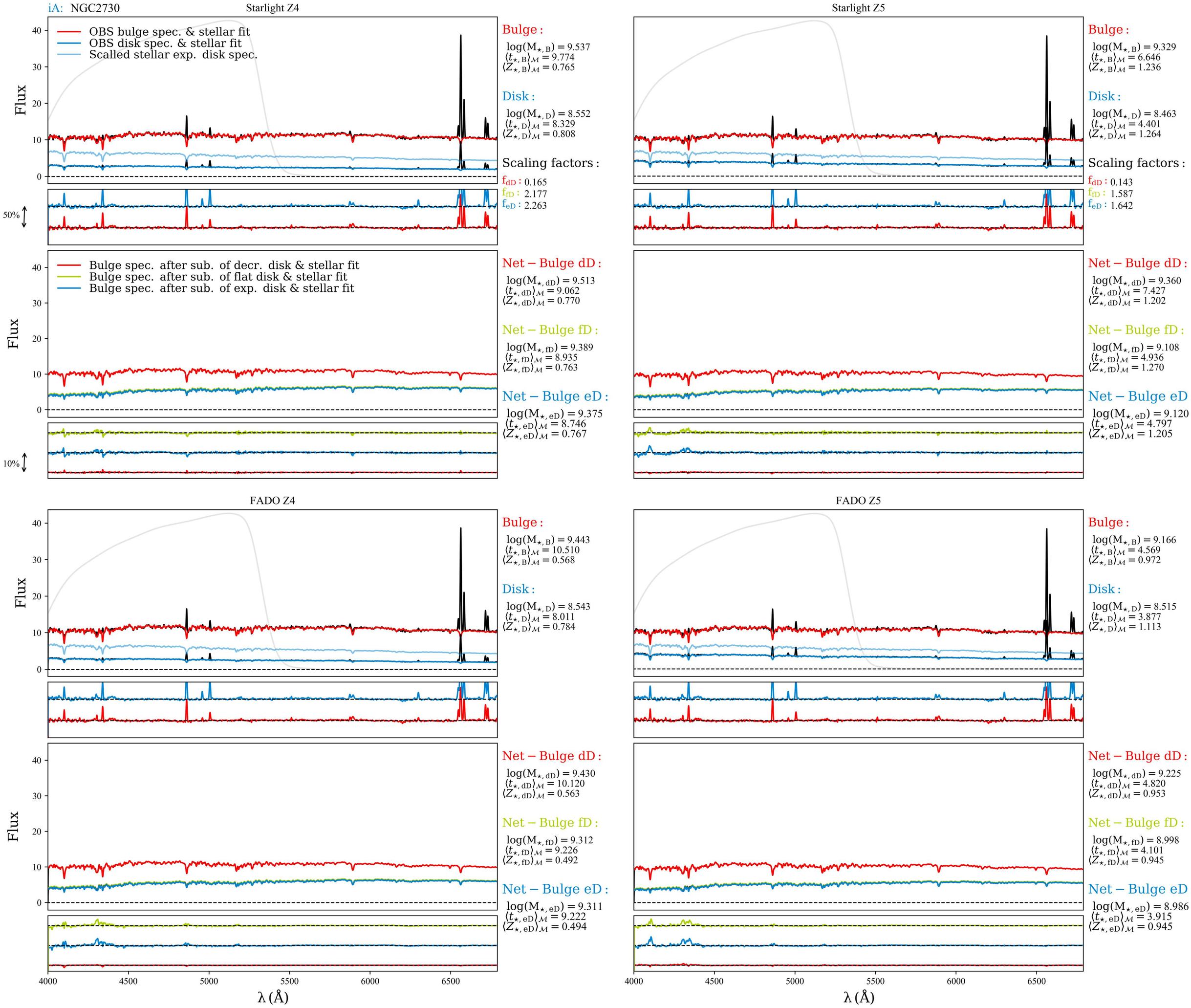
iA: NGC2730
Starlight Z4
OBS bulge spec. & stellar fit
OBS disk spec. & stellar fit
Scalled stellar exp. disk spec.
Flux
50%
Bulge :
log(M⋆, B) = 9.537
⟨t⋆, B⟩M = 9.774
⟨Z⋆, B⟩M = 0.765
Disk :
log(M⋆, D) = 8.552
⟨t⋆, D⟩M = 8.329
⟨Z⋆, D⟩M = 0.808
Scaling factors :
fdD : 0.165
ffD : 2.177
feD : 2.263
Starlight Z5
Bulge :
log(M⋆, B) = 9.329
⟨t⋆, B⟩M = 6.646
⟨Z⋆, B⟩M = 1.236
Disk :
log(M⋆, D) = 8.463
⟨t⋆, D⟩M = 4.401
⟨Z⋆, D⟩M = 1.264
Scaling factors :
fdD : 0.143
ffD : 1.587
feD : 1.642
Bulge spec. after sub. of decr. disk & stellar fit
Bulge spec. after sub. of flat disk & stellar fit
Bulge spec. after sub. of exp. disk & stellar fit
10%
Net − Bulge dD :
log(M⋆, dD) = 9.513
⟨t⋆, dD⟩M = 9.062
⟨Z⋆, dD⟩M = 0.770
Net − Bulge fD :
log(M⋆, fD) = 9.389
⟨t⋆, fD⟩M = 8.935
⟨Z⋆, fD⟩M = 0.763
Net − Bulge eD :
log(M⋆, eD) = 9.375
⟨t⋆, eD⟩M = 8.746
⟨Z⋆, eD⟩M = 0.767
Net − Bulge dD :
log(M⋆, dD) = 9.360
⟨t⋆, dD⟩M = 7.427
⟨Z⋆, dD⟩M = 1.202
Net − Bulge fD :
log(M⋆, fD) = 9.108
⟨t⋆, fD⟩M = 4.936
⟨Z⋆, fD⟩M = 1.270
Net − Bulge eD :
log(M⋆, eD) = 9.120
⟨t⋆, eD⟩M = 4.797
⟨Z⋆, eD⟩M = 1.205
FADO Z4
Bulge :
log(M⋆, B) = 9.443
⟨t⋆, B⟩M = 10.510
⟨Z⋆, B⟩M = 0.568
Disk :
log(M⋆, D) = 8.543
⟨t⋆, D⟩M = 8.011
⟨Z⋆, D⟩M = 0.784
FADO Z5
Bulge :
log(M⋆, B) = 9.166
⟨t⋆, B⟩M = 4.569
⟨Z⋆, B⟩M = 0.972
Disk :
log(M⋆, D) = 8.515
⟨t⋆, D⟩M = 3.877
⟨Z⋆, D⟩M = 1.113
Net − Bulge dD :
log(M⋆, dD) = 9.430
⟨t⋆, dD⟩M = 10.120
⟨Z⋆, dD⟩M = 0.563
Net − Bulge fD :
log(M⋆, fD) = 9.312
⟨t⋆, fD⟩M = 9.226
⟨Z⋆, fD⟩M = 0.492
Net − Bulge eD :
log(M⋆, eD) = 9.311
⟨t⋆, eD⟩M = 9.222
⟨Z⋆, eD⟩M = 0.494
Net − Bulge dD :
log(M⋆, dD) = 9.225
⟨t⋆, dD⟩M = 4.820
⟨Z⋆, dD⟩M = 0.953
Net − Bulge fD :
log(M⋆, fD) = 8.998
⟨t⋆, fD⟩M = 4.101
⟨Z⋆, fD⟩M = 0.945
Net − Bulge eD :
log(M⋆, eD) = 8.986
⟨t⋆, eD⟩M = 3.915
⟨Z⋆, eD⟩M = 0.945
Flux
0
10
20
30
40
4000
4500
5000
5500
6000
6500
λ (Å)

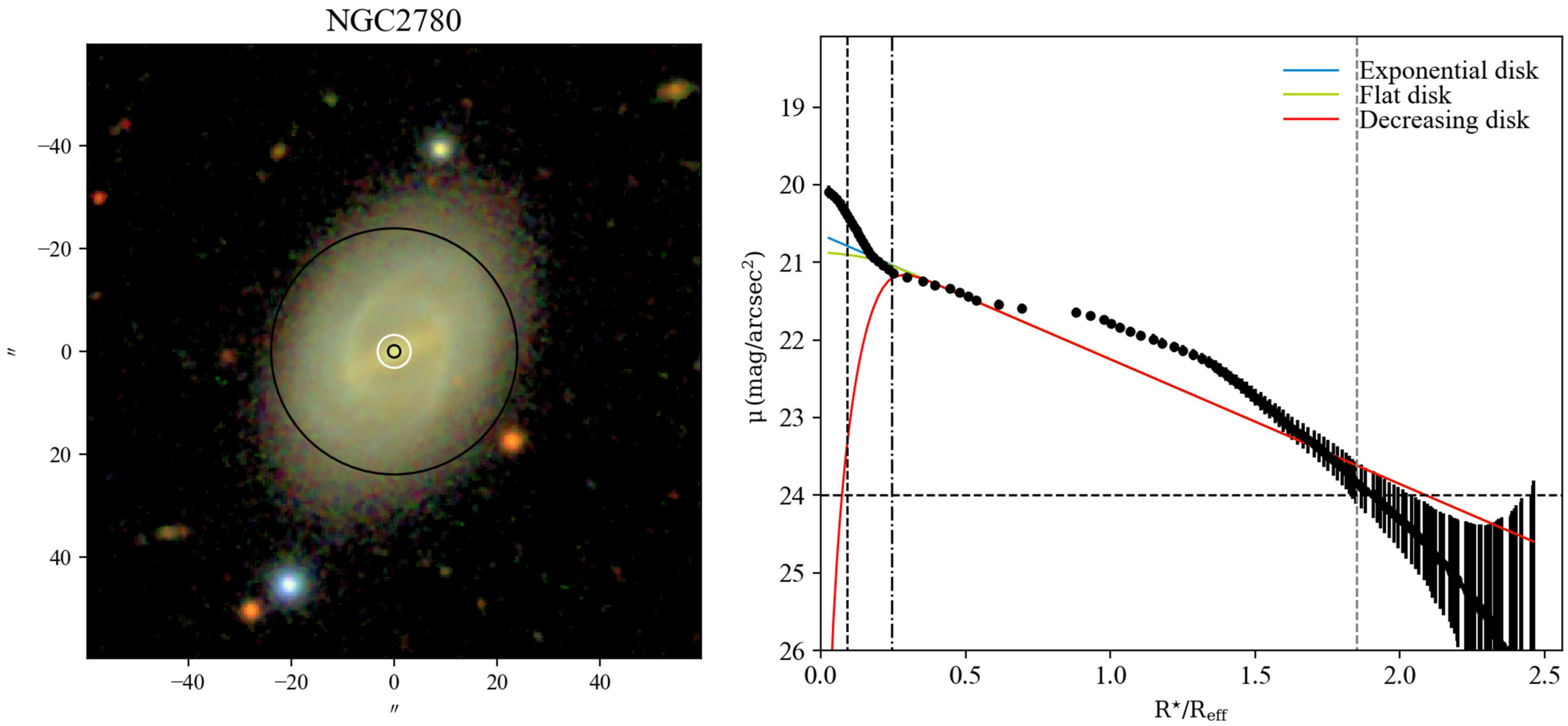
NGC2780
Exponential disk
Flat disk
Decreasing disk
μ (mag/arcsec²)
R⋆/Reff

iB: NGC2780
Starlight Z4
OBS bulge spec. & stellar fit
OBS disk spec. & stellar fit
Scalled stellar exp. disk spec.
Flux
Bulge :
log(M⋆, B) = 8.819
⟨t⋆, B⟩M = 11.065
⟨Z⋆, B⟩M = 0.829
Disk :
log(M⋆, D) = 8.008
⟨t⋆, D⟩M = 9.406
⟨Z⋆, D⟩M = 0.778
Scaling factors :
fdD : 0.003
ffD : 2.316
feD : 2.677
50%
Bulge spec. after sub. of decr. disk & stellar fit
Bulge spec. after sub. of flat disk & stellar fit
Bulge spec. after sub. of exp. disk & stellar fit
Net − Bulge dD :
log(M⋆, dD) = 8.789
⟨t⋆, dD⟩M = 9.318
⟨Z⋆, dD⟩M = 0.789
Net − Bulge fD :
log(M⋆, fD) = 8.653
⟨t⋆, fD⟩M = 8.572
⟨Z⋆, fD⟩M = 0.902
Net − Bulge eD :
log(M⋆, eD) = 8.648
⟨t⋆, eD⟩M = 8.580
⟨Z⋆, eD⟩M = 0.904
10%
FADO Z4
Bulge :
log(M⋆, B) = 8.721
⟨t⋆, B⟩M = 11.010
⟨Z⋆, B⟩M = 0.577
Disk :
log(M⋆, D) = 7.883
⟨t⋆, D⟩M = 8.876
⟨Z⋆, D⟩M = 0.638
Net − Bulge dD :
log(M⋆, dD) = 8.728
⟨t⋆, dD⟩M = 10.270
⟨Z⋆, dD⟩M = 0.591
Net − Bulge fD :
log(M⋆, fD) = 8.567
⟨t⋆, fD⟩M = 8.007
⟨Z⋆, fD⟩M = 0.545
Net − Bulge eD :
log(M⋆, eD) = 8.523
⟨t⋆, eD⟩M = 8.035
⟨Z⋆, eD⟩M = 0.474
λ (Å)
Starlight Z5
Bulge :
log(M⋆, B) = 8.478
⟨t⋆, B⟩M = 4.775
⟨Z⋆, B⟩M = 1.195
Disk :
log(M⋆, D) = 7.771
⟨t⋆, D⟩M = 6.088
⟨Z⋆, D⟩M = 1.004
Scaling factors :
fdD : 0.003
ffD : 2.187
feD : 2.528
Net − Bulge dD :
log(M⋆, dD) = 8.489
⟨t⋆, dD⟩M = 4.107
⟨Z⋆, dD⟩M = 1.211
Net − Bulge fD :
log(M⋆, fD) = 8.324
⟨t⋆, fD⟩M = 4.977
⟨Z⋆, fD⟩M = 1.251
Net − Bulge eD :
log(M⋆, eD) = 8.313
⟨t⋆, eD⟩M = 4.112
⟨Z⋆, eD⟩M = 1.230
FADO Z5
Bulge :
log(M⋆, B) = 8.662
⟨t⋆, B⟩M = 8.836
⟨Z⋆, B⟩M = 1.263
Disk :
log(M⋆, D) = 7.653
⟨t⋆, D⟩M = 3.641
⟨Z⋆, D⟩M = 0.873
Net − Bulge dD :
log(M⋆, dD) = 8.667
⟨t⋆, dD⟩M = 8.807
⟨Z⋆, dD⟩M = 1.238
Net − Bulge fD :
log(M⋆, fD) = 8.571
⟨t⋆, fD⟩M = 9.978
⟨Z⋆, fD⟩M = 1.286
Net − Bulge eD :
log(M⋆, eD) = 8.572
⟨t⋆, eD⟩M = 10.240
⟨Z⋆, eD⟩M = 1.287
λ (Å)

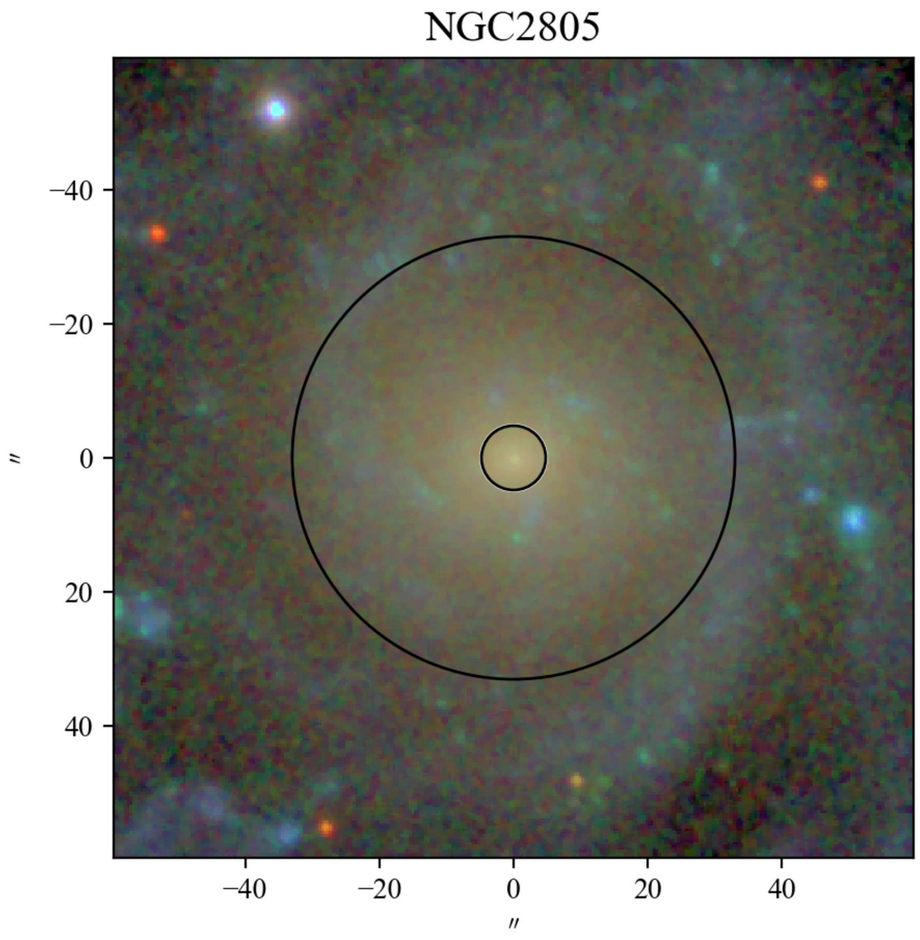
NGC2805
−40
−20
0
20
40
″
−40
−20
0
20
40
″

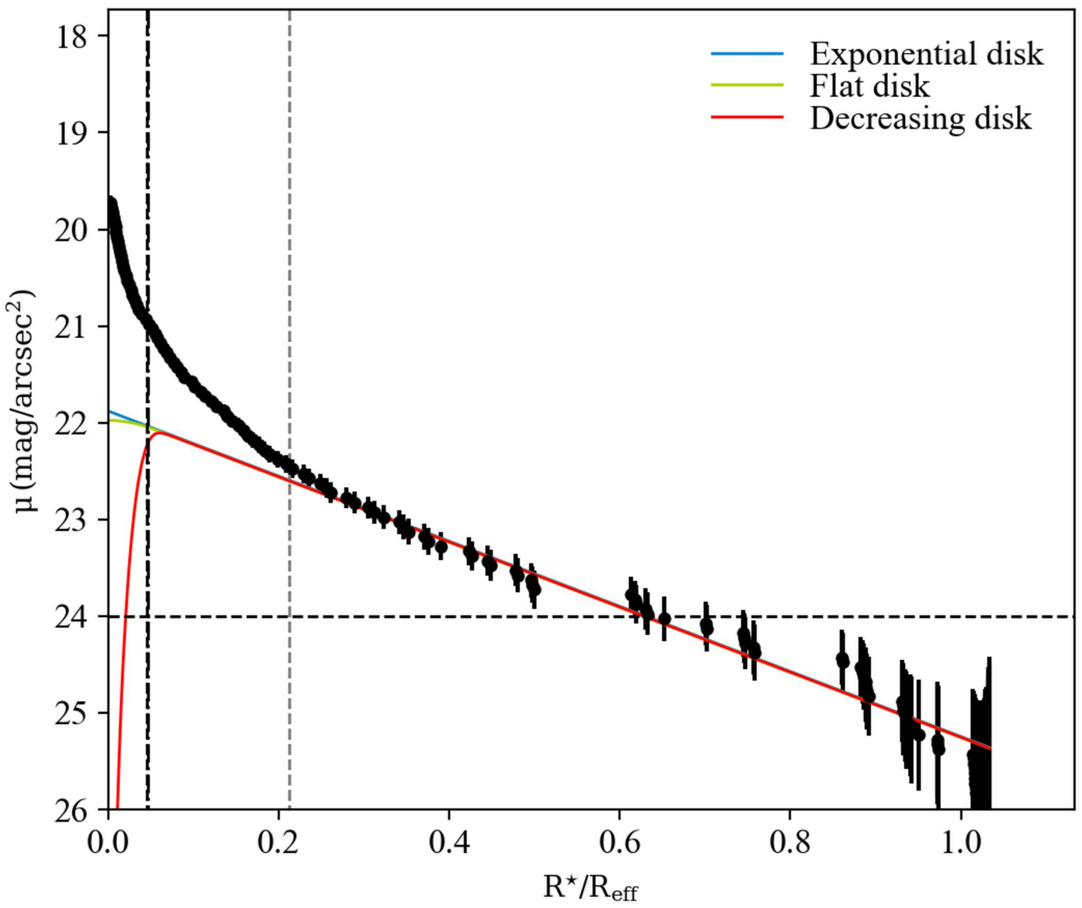
Exponential disk
Flat disk
Decreasing disk
μ (mag/arcsec²)
18
19
20
21
22
23
24
25
26
0.0
0.2
0.4
0.6
0.8
1.0
R⋆/Reff

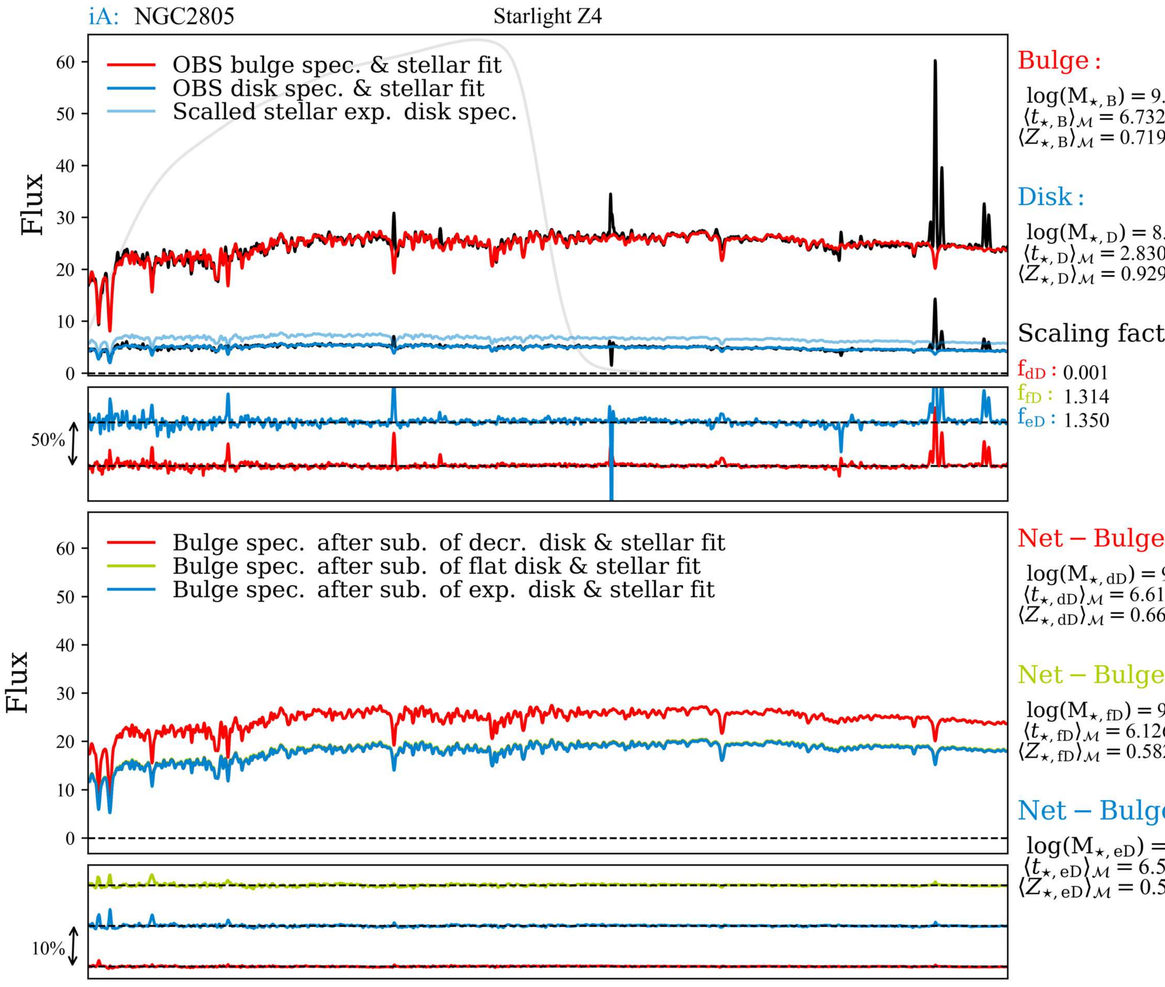
iA: NGC2805
Starlight Z4
OBS bulge spec. & stellar fit
OBS disk spec. & stellar fit
Scalled stellar exp. disk spec.
Flux
50%
Bulge :
log(M⋆, B) = 9.155
⟨t⋆, B⟩M = 6.732
⟨Z⋆, B⟩M = 0.719
Disk :
log(M⋆, D) = 8.196
⟨t⋆, D⟩M = 2.830
⟨Z⋆, D⟩M = 0.929
Scaling factors :
fdD : 0.001
ffD : 1.314
feD : 1.350
Bulge spec. after sub. of decr. disk & stellar fit
Bulge spec. after sub. of flat disk & stellar fit
Bulge spec. after sub. of exp. disk & stellar fit
10%
Net − Bulge dD :
log(M⋆, dD) = 9.147
⟨t⋆, dD⟩M = 6.611
⟨Z⋆, dD⟩M = 0.664
Net − Bulge fD :
log(M⋆, fD) = 9.051
⟨t⋆, fD⟩M = 6.126
⟨Z⋆, fD⟩M = 0.582
Net − Bulge eD :
log(M⋆, eD) = 9.072
⟨t⋆, eD⟩M = 6.534
⟨Z⋆, eD⟩M = 0.577

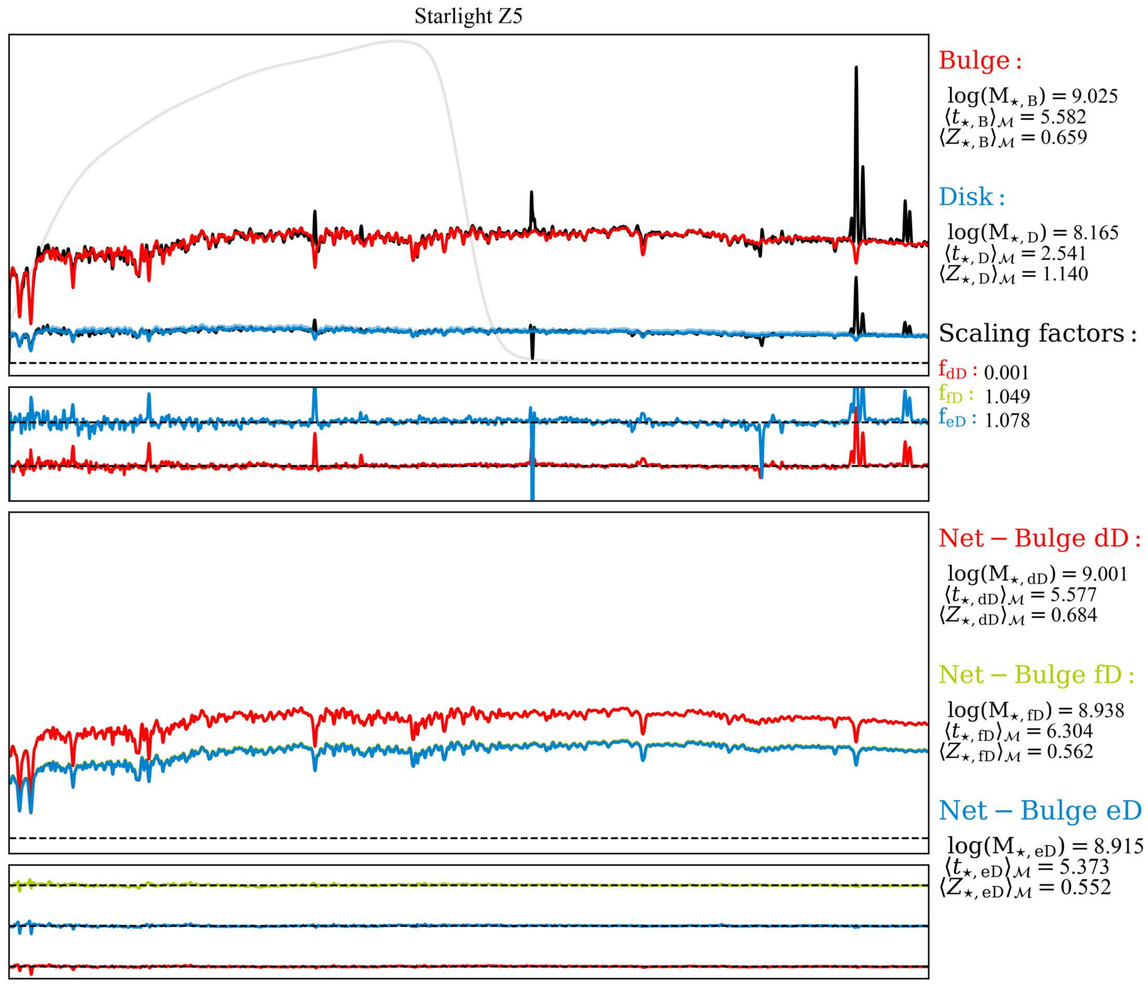
Starlight Z5
Bulge :
log(M⋆, B) = 9.025
⟨t⋆, B⟩M = 5.582
⟨Z⋆, B⟩M = 0.659
Disk :
log(M⋆, D) = 8.165
⟨t⋆, D⟩M = 2.541
⟨Z⋆, D⟩M = 1.140
Scaling factors :
fdD : 0.001
ffD : 1.049
feD : 1.078
Net − Bulge dD :
log(M⋆, dD) = 9.001
⟨t⋆, dD⟩M = 5.577
⟨Z⋆, dD⟩M = 0.684
Net − Bulge fD :
log(M⋆, fD) = 8.938
⟨t⋆, fD⟩M = 6.304
⟨Z⋆, fD⟩M = 0.562
Net − Bulge eD :
log(M⋆, eD) = 8.915
⟨t⋆, eD⟩M = 5.373
⟨Z⋆, eD⟩M = 0.552

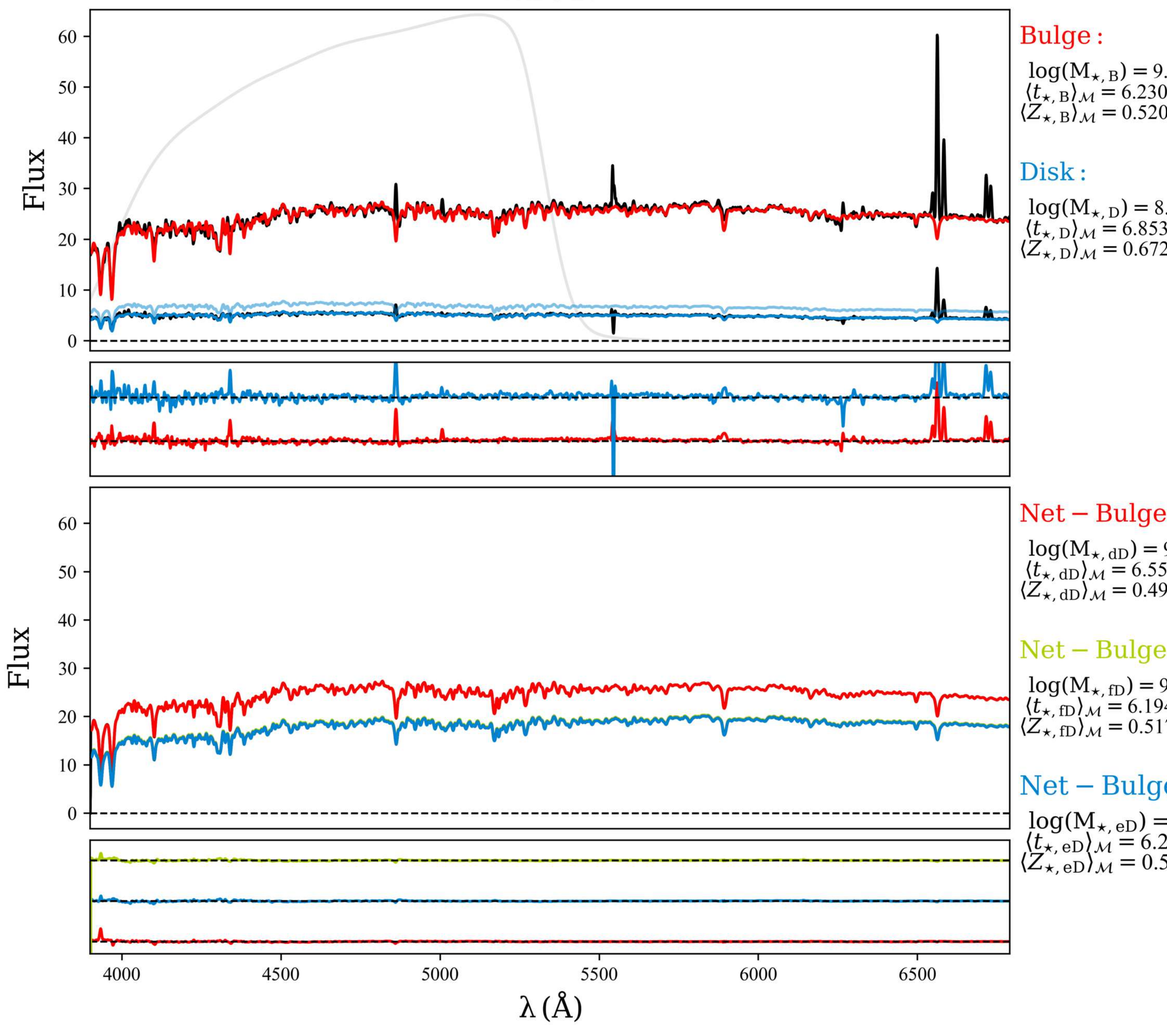
FADO Z4
Flux
Bulge :
log(M⋆, B) = 9.123
⟨t⋆, B⟩M = 6.230
⟨Z⋆, B⟩M = 0.520
Disk :
log(M⋆, D) = 8.259
⟨t⋆, D⟩M = 6.853
⟨Z⋆, D⟩M = 0.672
Net − Bulge dD :
log(M⋆, dD) = 9.127
⟨t⋆, dD⟩M = 6.550
⟨Z⋆, dD⟩M = 0.495
Net − Bulge fD :
log(M⋆, fD) = 9.042
⟨t⋆, fD⟩M = 6.194
⟨Z⋆, fD⟩M = 0.517
Net − Bulge eD :
log(M⋆, eD) = 9.054
⟨t⋆, eD⟩M = 6.237
⟨Z⋆, eD⟩M = 0.541
λ (Å)

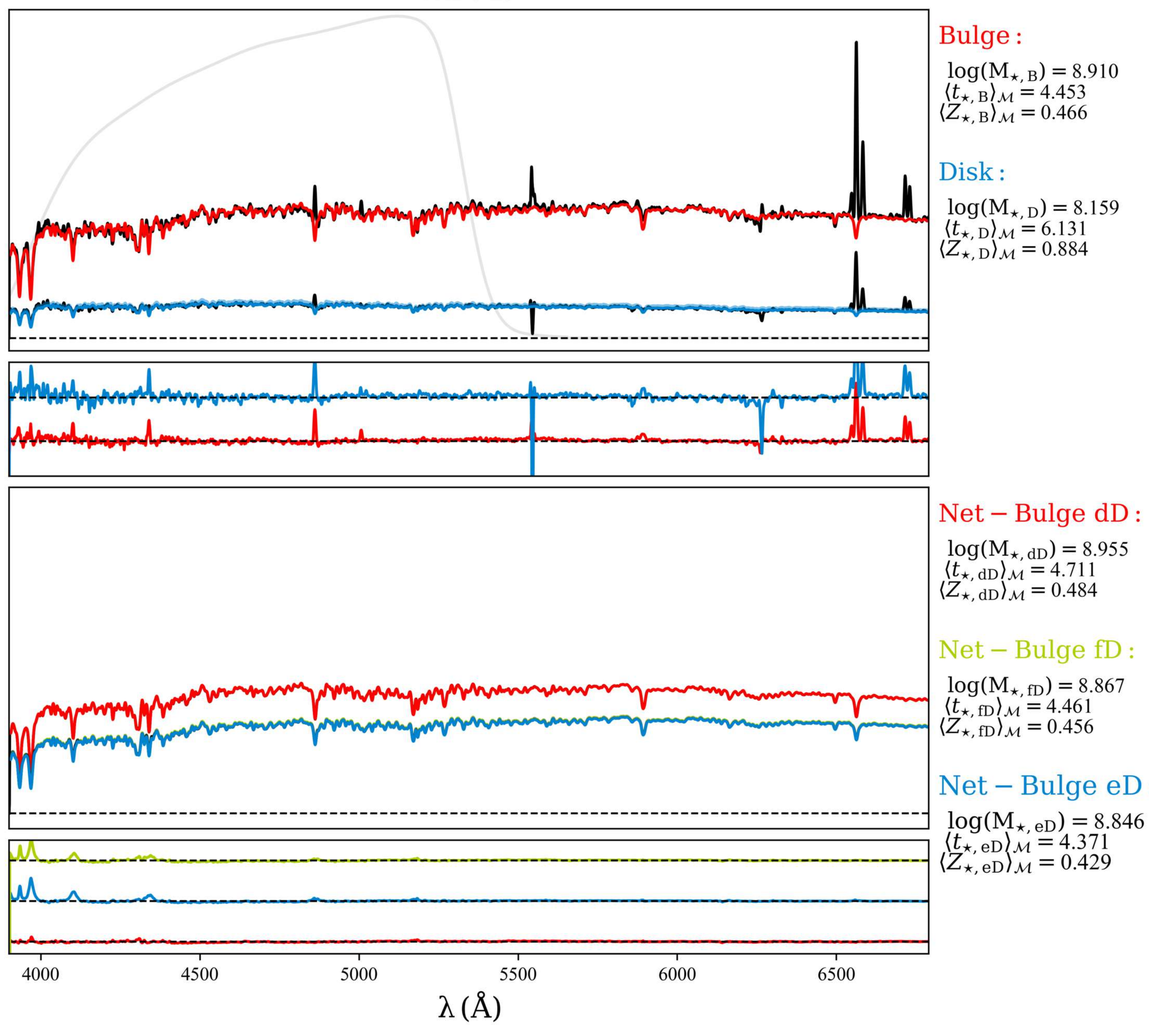
FADO Z5
Bulge :
log(M⋆, B) = 8.910
⟨t⋆, B⟩M = 4.453
⟨Z⋆, B⟩M = 0.466
Disk :
log(M⋆, D) = 8.159
⟨t⋆, D⟩M = 6.131
⟨Z⋆, D⟩M = 0.884
Net − Bulge dD :
log(M⋆, dD) = 8.955
⟨t⋆, dD⟩M = 4.711
⟨Z⋆, dD⟩M = 0.484
Net − Bulge fD :
log(M⋆, fD) = 8.867
⟨t⋆, fD⟩M = 4.461
⟨Z⋆, fD⟩M = 0.456
Net − Bulge eD :
log(M⋆, eD) = 8.846
⟨t⋆, eD⟩M = 4.371
⟨Z⋆, eD⟩M = 0.429
λ (Å)

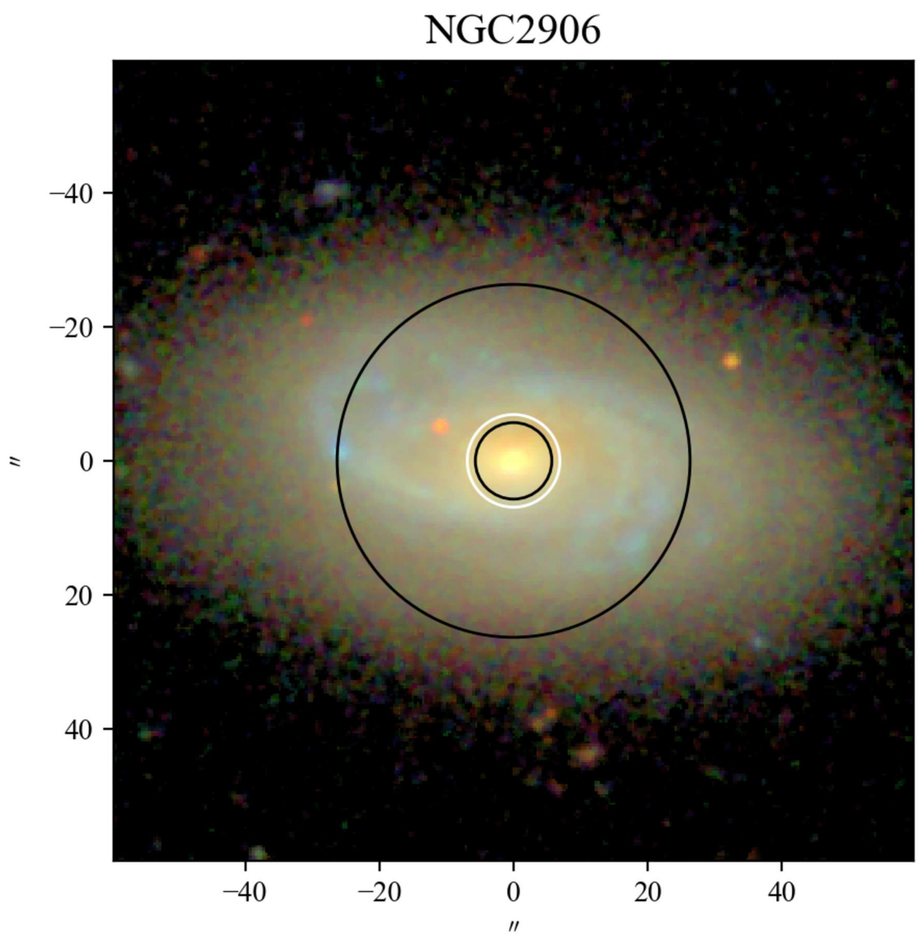
NGC2906
−40
−20
0
20
40
″
−40
−20
0
20
40
″

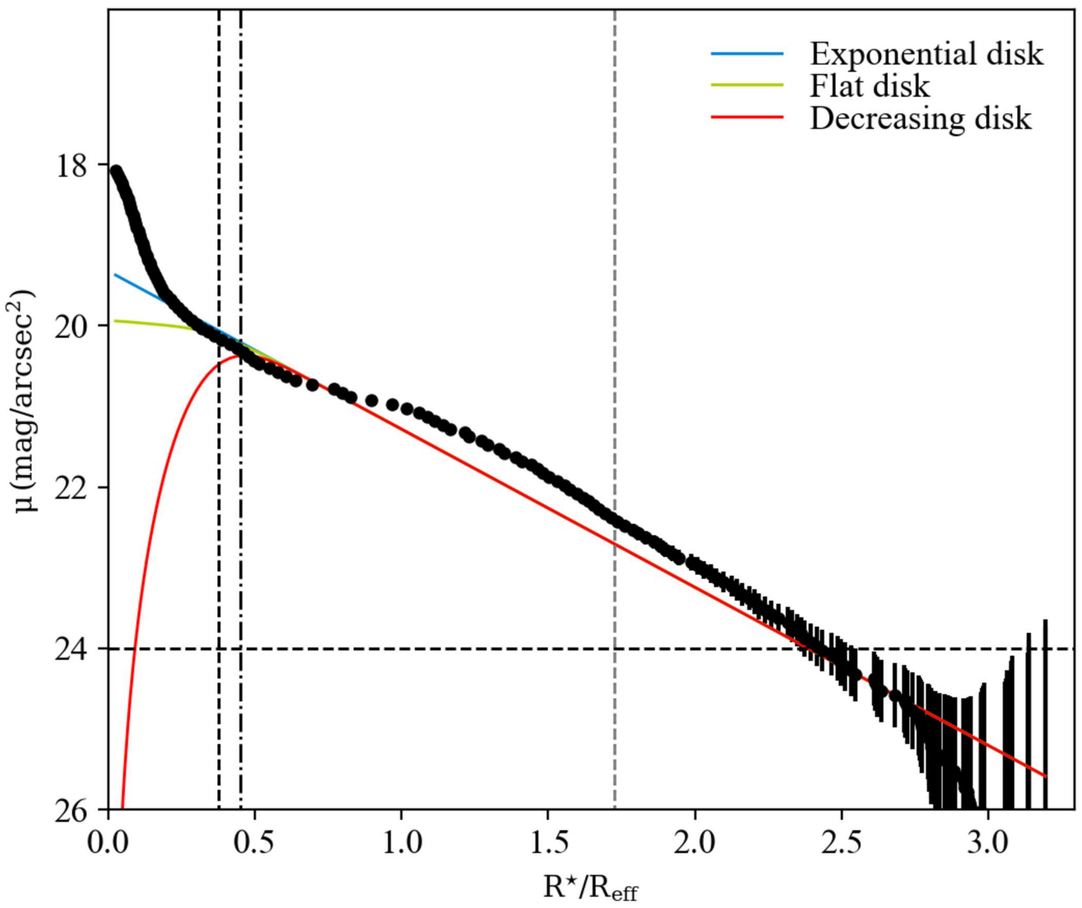
Exponential disk
Flat disk
Decreasing disk
μ (mag/arcsec²)
18
20
22
24
26
0.0
0.5
1.0
1.5
2.0
2.5
3.0
R⋆/Reff

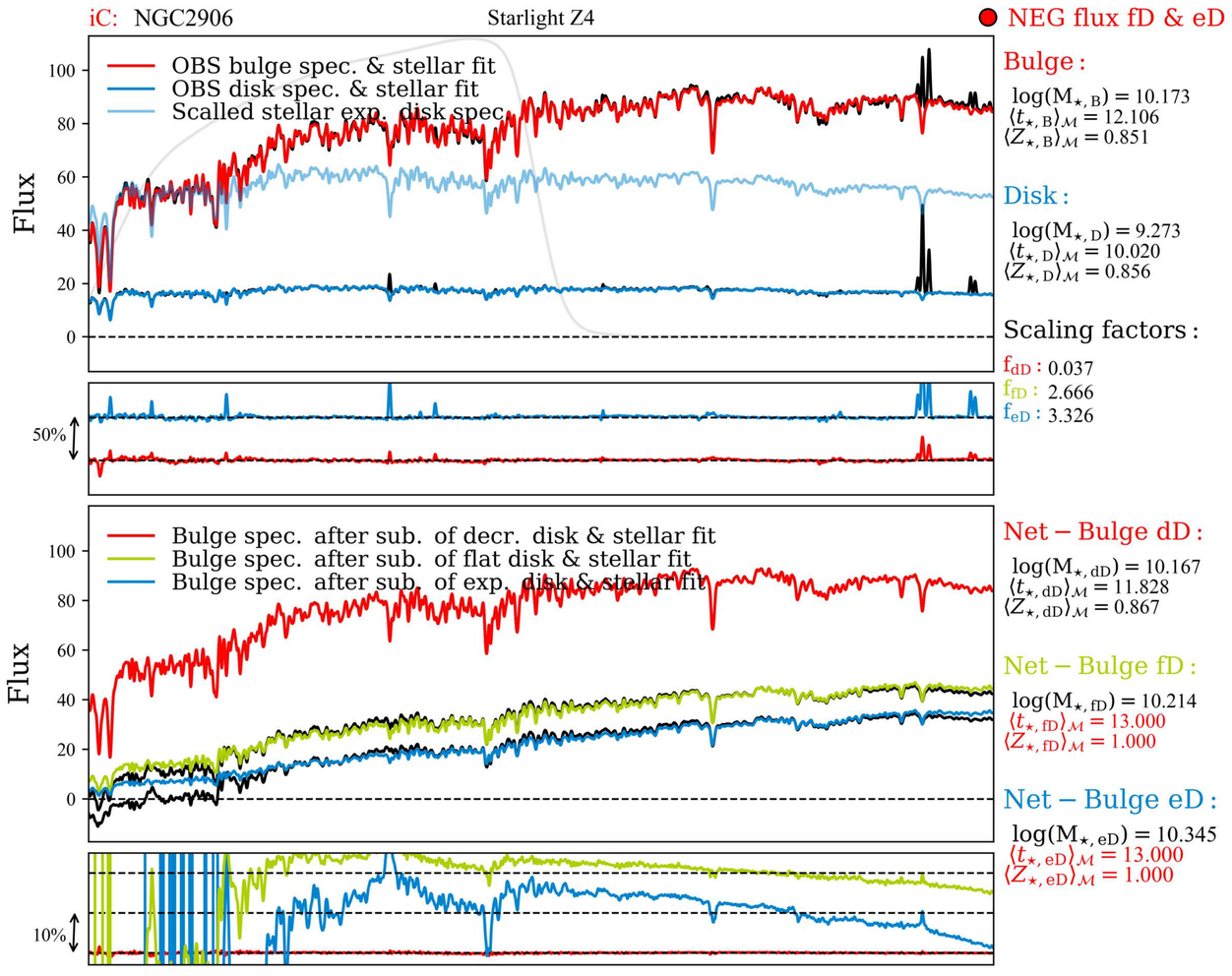
iC: NGC2906
Starlight Z4
NEG flux fD & eD
OBS bulge spec. & stellar fit
OBS disk spec. & stellar fit
Scalled stellar exp. disk spec.
Flux
50%
Bulge :
log(M⋆, B) = 10.173
⟨t⋆, B⟩M = 12.106
⟨Z⋆, B⟩M = 0.851
Disk :
log(M⋆, D) = 9.273
⟨t⋆, D⟩M = 10.020
⟨Z⋆, D⟩M = 0.856
Scaling factors :
fdD : 0.037
ffD : 2.666
feD : 3.326
Bulge spec. after sub. of decr. disk & stellar fit
Bulge spec. after sub. of flat disk & stellar fit
Bulge spec. after sub. of exp. disk & stellar fit
10%
Net − Bulge dD :
log(M⋆, dD) = 10.167
⟨t⋆, dD⟩M = 11.828
⟨Z⋆, dD⟩M = 0.867
Net − Bulge fD :
log(M⋆, fD) = 10.214
⟨t⋆, fD⟩M = 13.000
⟨Z⋆, fD⟩M = 1.000
Net − Bulge eD :
log(M⋆, eD) = 10.345
⟨t⋆, eD⟩M = 13.000
⟨Z⋆, eD⟩M = 1.000

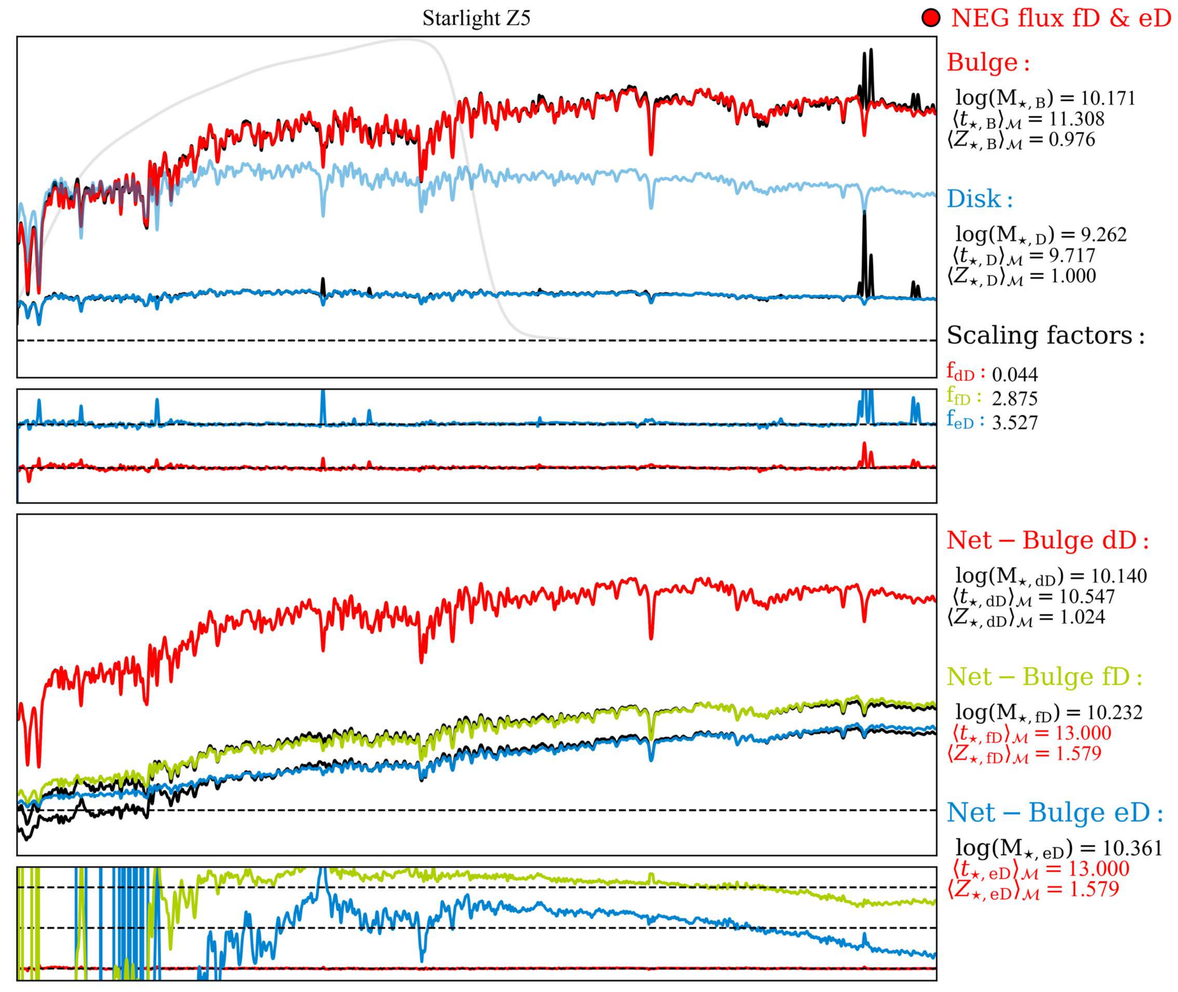
Starlight Z5
NEG flux fD & eD
Bulge :
log(M⋆, B) = 10.171
⟨t⋆, B⟩M = 11.308
⟨Z⋆, B⟩M = 0.976
Disk :
log(M⋆, D) = 9.262
⟨t⋆, D⟩M = 9.717
⟨Z⋆, D⟩M = 1.000
Scaling factors :
fdD : 0.044
ffD : 2.875
feD : 3.527
Net − Bulge dD :
log(M⋆, dD) = 10.140
⟨t⋆, dD⟩M = 10.547
⟨Z⋆, dD⟩M = 1.024
Net − Bulge fD :
log(M⋆, fD) = 10.232
⟨t⋆, fD⟩M = 13.000
⟨Z⋆, fD⟩M = 1.579
Net − Bulge eD :
log(M⋆, eD) = 10.361
⟨t⋆, eD⟩M = 13.000
⟨Z⋆, eD⟩M = 1.579

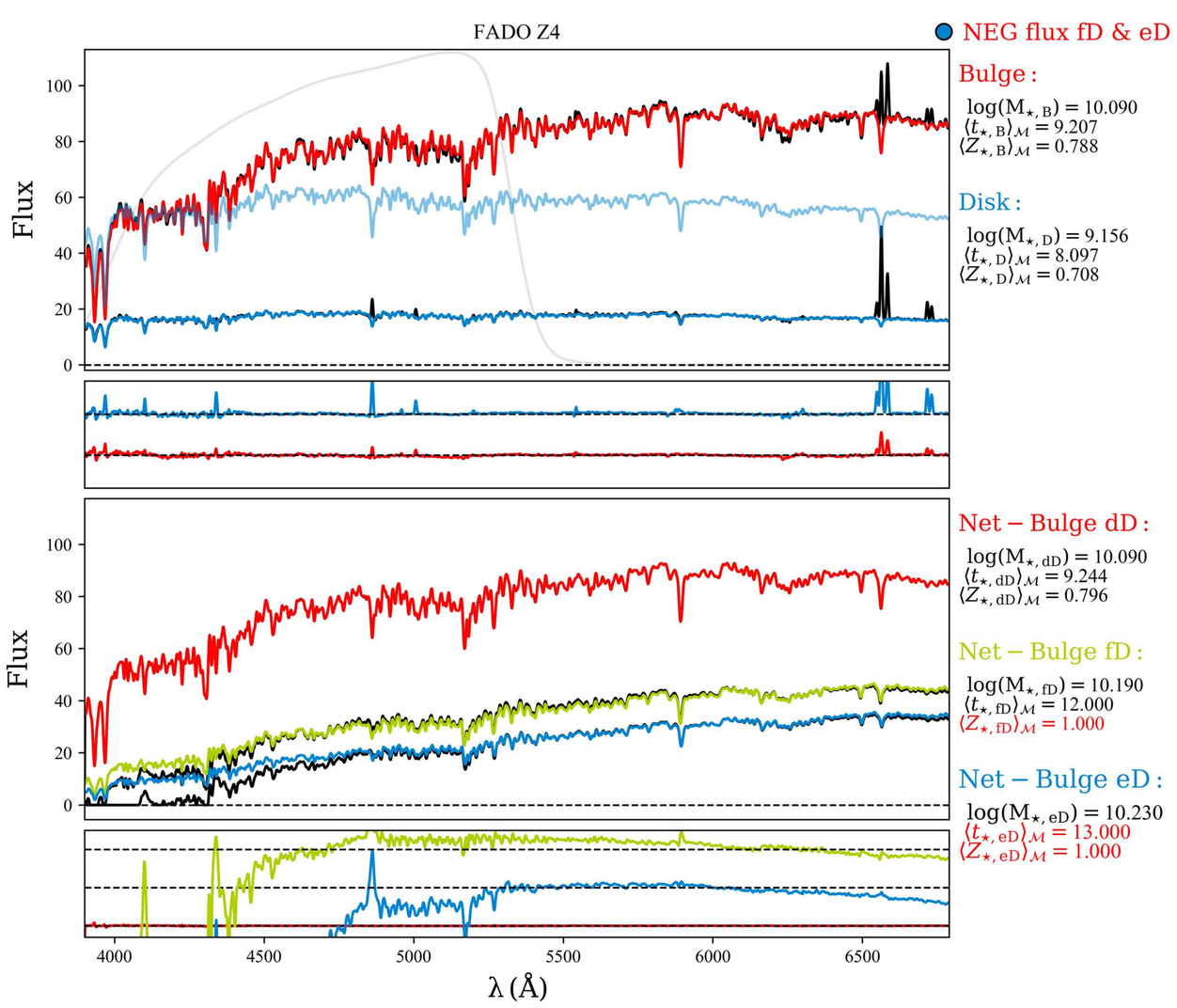
FADO Z4
NEG flux fD & eD
Flux
Bulge :
log(M⋆, B) = 10.090
⟨t⋆, B⟩M = 9.207
⟨Z⋆, B⟩M = 0.788
Disk :
log(M⋆, D) = 9.156
⟨t⋆, D⟩M = 8.097
⟨Z⋆, D⟩M = 0.708
Net − Bulge dD :
log(M⋆, dD) = 10.090
⟨t⋆, dD⟩M = 9.244
⟨Z⋆, dD⟩M = 0.796
Net − Bulge fD :
log(M⋆, fD) = 10.190
⟨t⋆, fD⟩M = 12.000
⟨Z⋆, fD⟩M = 1.000
Net − Bulge eD :
log(M⋆, eD) = 10.230
⟨t⋆, eD⟩M = 13.000
⟨Z⋆, eD⟩M = 1.000
λ (Å)

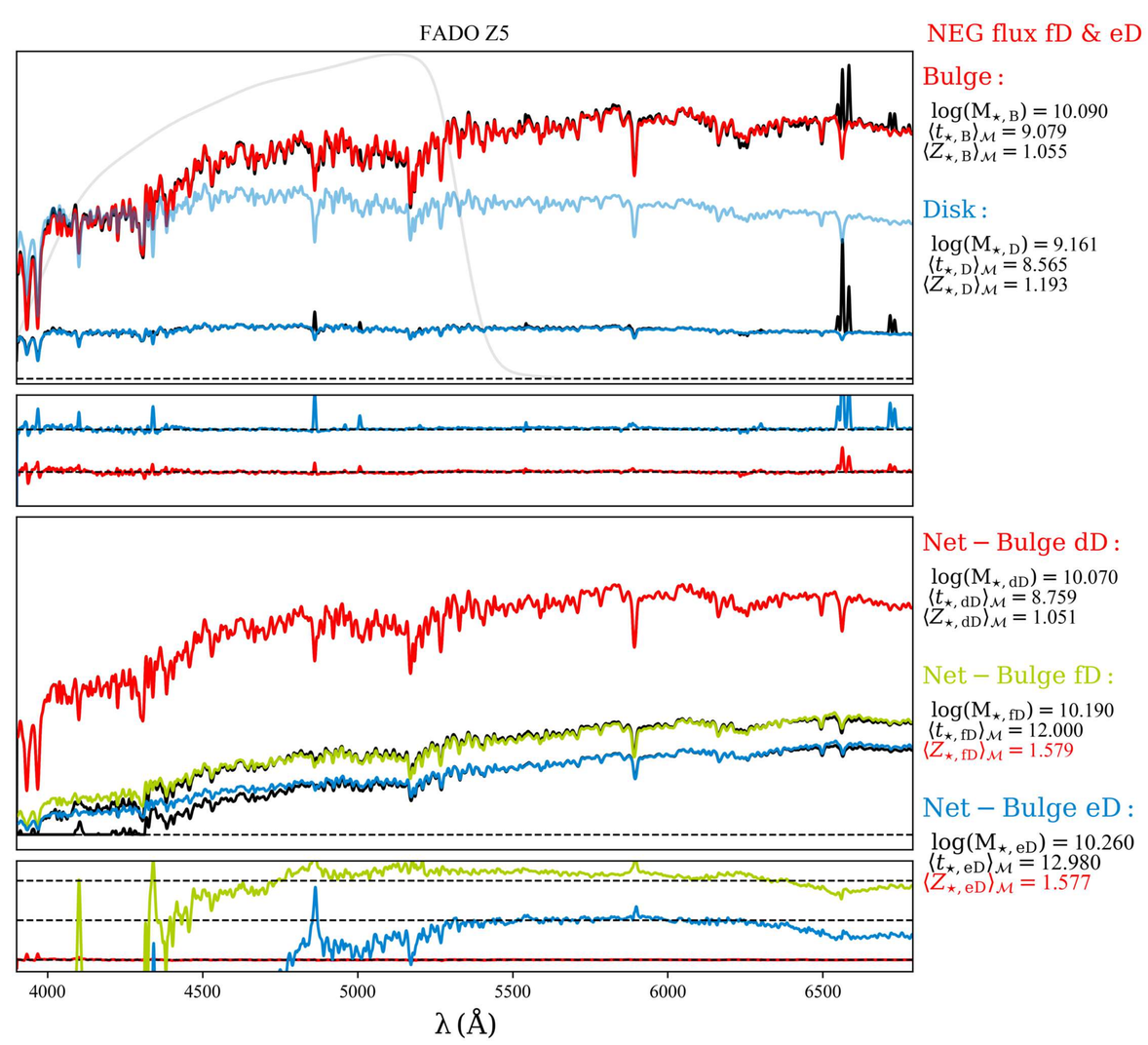
FADO Z5
NEG flux fD & eD
Bulge :
log(M⋆, B) = 10.090
⟨t⋆, B⟩M = 9.079
⟨Z⋆, B⟩M = 1.055
Disk :
log(M⋆, D) = 9.161
⟨t⋆, D⟩M = 8.565
⟨Z⋆, D⟩M = 1.193
Net − Bulge dD :
log(M⋆, dD) = 10.070
⟨t⋆, dD⟩M = 8.759
⟨Z⋆, dD⟩M = 1.051
Net − Bulge fD :
log(M⋆, fD) = 10.190
⟨t⋆, fD⟩M = 12.000
⟨Z⋆, fD⟩M = 1.579
Net − Bulge eD :
log(M⋆, eD) = 10.260
⟨t⋆, eD⟩M = 12.980
⟨Z⋆, eD⟩M = 1.577
λ (Å)

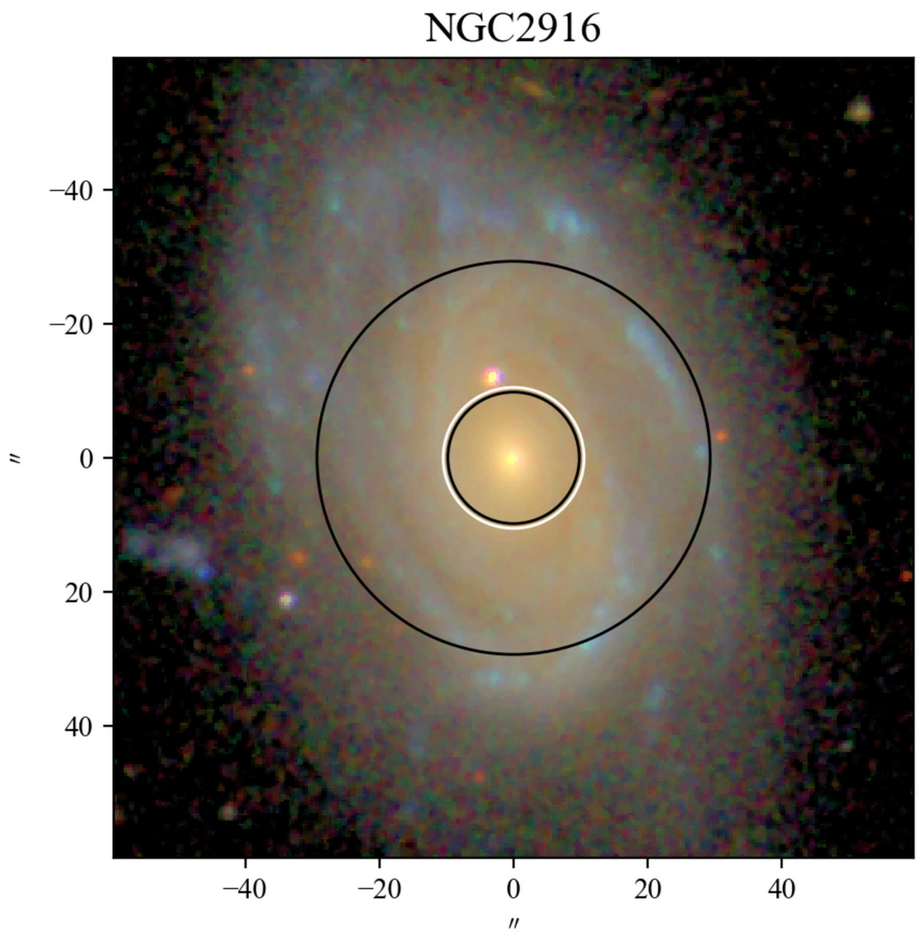
NGC2916
−40
−20
0
20
40
″
−40
−20
0
20
40
″

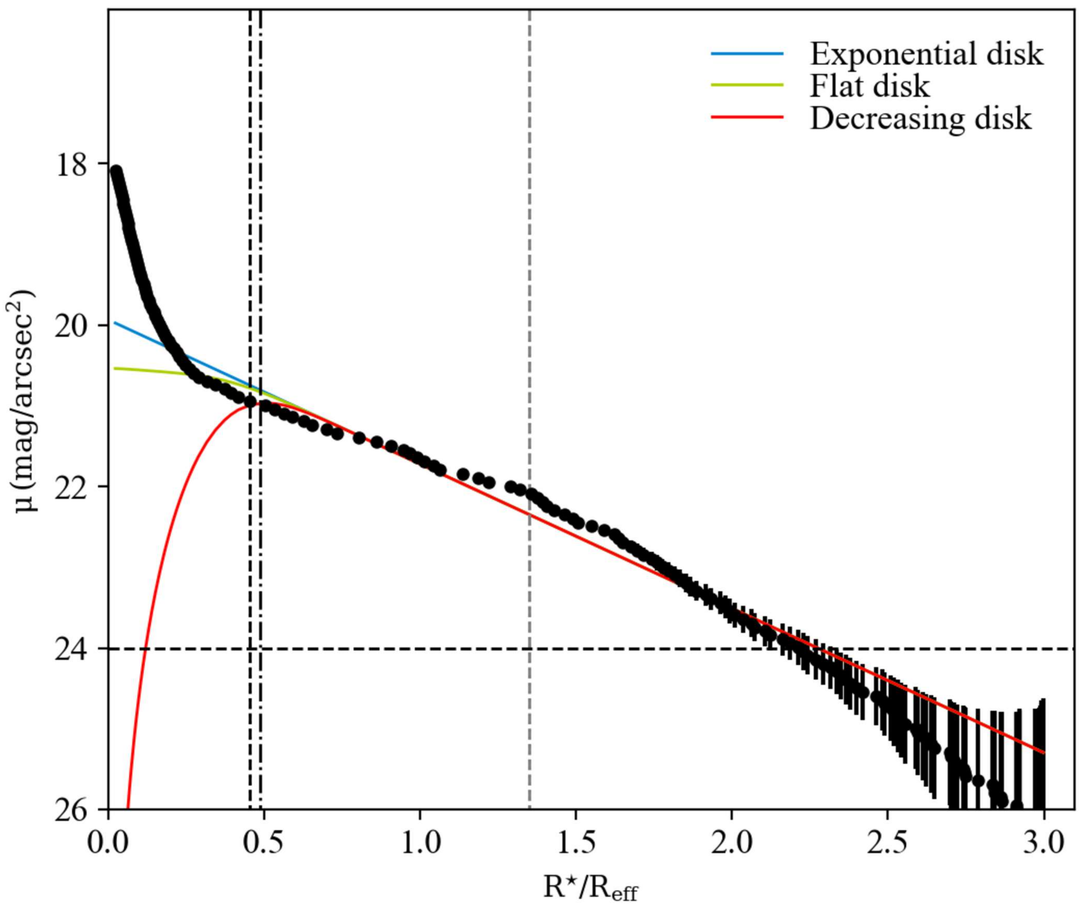
Exponential disk
Flat disk
Decreasing disk
μ (mag/arcsec²)
18
20
22
24
26
0.0
0.5
1.0
1.5
2.0
2.5
3.0
R⋆/Reff

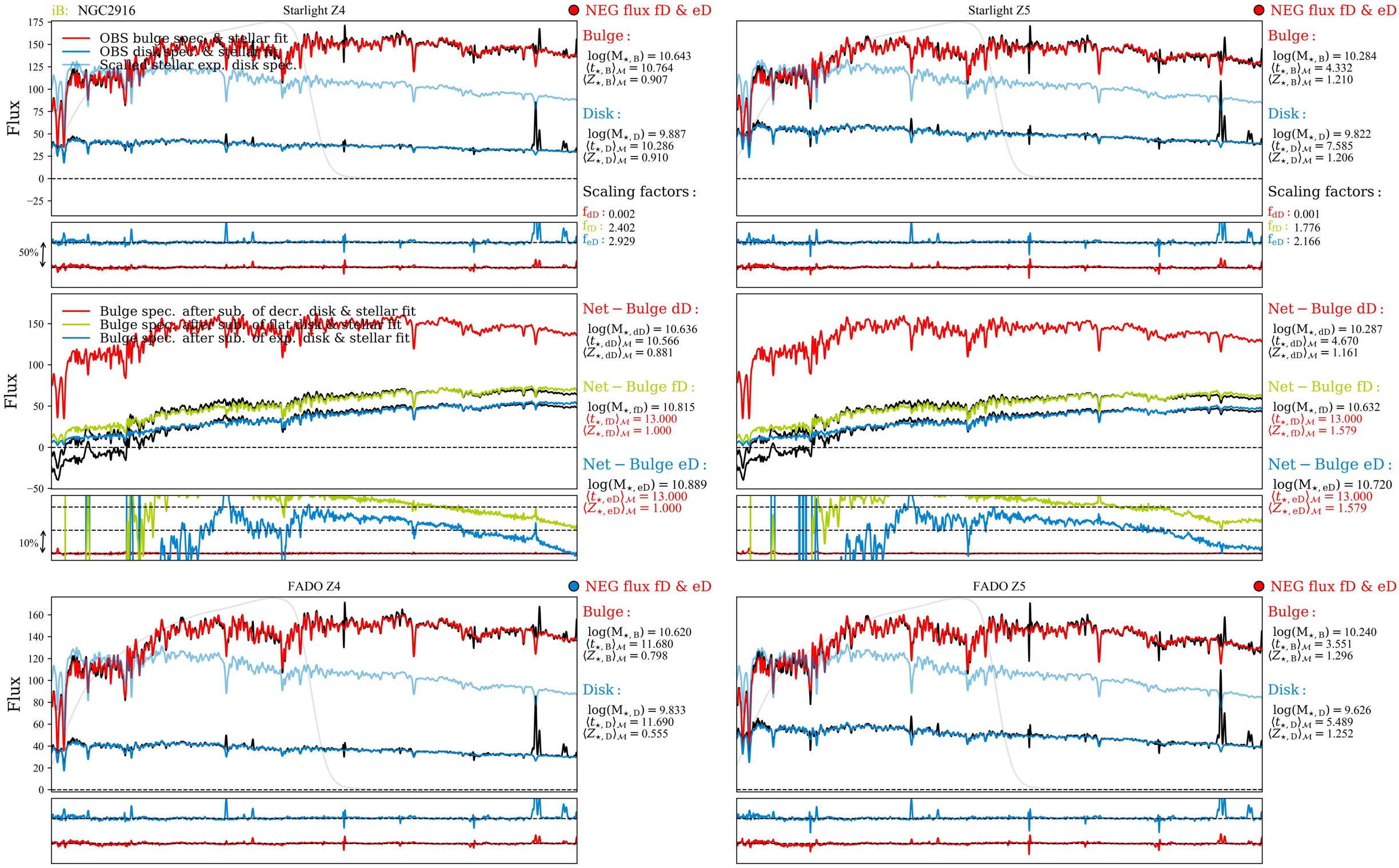
iB: NGC2916
Starlight Z4
NEG flux fD & eD
OBS bulge spec. & stellar fit
OBS disk spec. & stellar fit
Scalled stellar exp. disk spec.
Flux
Bulge :
log(M⋆, B) = 10.643
⟨t⋆, B⟩M = 10.764
⟨Z⋆, B⟩M = 0.907
Disk :
log(M⋆, D) = 9.887
⟨t⋆, D⟩M = 10.286
⟨Z⋆, D⟩M = 0.910
Scaling factors :
fdD : 0.002
ffD : 2.402
feD : 2.929
50%
Starlight Z5
NEG flux fD & eD
Bulge :
log(M⋆, B) = 10.284
⟨t⋆, B⟩M = 4.332
⟨Z⋆, B⟩M = 1.210
Disk :
log(M⋆, D) = 9.822
⟨t⋆, D⟩M = 7.585
⟨Z⋆, D⟩M = 1.206
Scaling factors :
fdD : 0.001
ffD : 1.776
feD : 2.166
Bulge spec. after sub. of decr. disk & stellar fit
Bulge spec. after sub. of flat. disk & stellar fit
Bulge spec. after sub. of exp. disk & stellar fit
Flux
Net − Bulge dD :
log(M⋆, dD) = 10.636
⟨t⋆, dD⟩M = 10.566
⟨Z⋆, dD⟩M = 0.881
Net − Bulge fD :
log(M⋆, fD) = 10.815
⟨t⋆, fD⟩M = 13.000
⟨Z⋆, fD⟩M = 1.000
Net − Bulge eD :
log(M⋆, eD) = 10.889
⟨t⋆, eD⟩M = 13.000
⟨Z⋆, eD⟩M = 1.000
10%
Net − Bulge dD :
log(M⋆, dD) = 10.287
⟨t⋆, dD⟩M = 4.670
⟨Z⋆, dD⟩M = 1.161
Net − Bulge fD :
log(M⋆, fD) = 10.632
⟨t⋆, fD⟩M = 13.000
⟨Z⋆, fD⟩M = 1.579
Net − Bulge eD :
log(M⋆, eD) = 10.720
⟨t⋆, eD⟩M = 13.000
⟨Z⋆, eD⟩M = 1.579
FADO Z4
NEG flux fD & eD
Flux
Bulge :
log(M⋆, B) = 10.620
⟨t⋆, B⟩M = 11.680
⟨Z⋆, B⟩M = 0.798
Disk :
log(M⋆, D) = 9.833
⟨t⋆, D⟩M = 11.690
⟨Z⋆, D⟩M = 0.555
FADO Z5
NEG flux fD & eD
Bulge :
log(M⋆, B) = 10.240
⟨t⋆, B⟩M = 3.551
⟨Z⋆, B⟩M = 1.296
Disk :
log(M⋆, D) = 9.626
⟨t⋆, D⟩M = 5.489
⟨Z⋆, D⟩M = 1.252
Net − Bulge dD :
log(M⋆, dD) = 10.610
⟨t⋆, dD⟩M = 10.910
⟨Z⋆, dD⟩M = 0.796
Net − Bulge fD :
log(M⋆, fD) = 10.710
⟨t⋆, fD⟩M = 12.000
⟨Z⋆, fD⟩M = 1.000
Net − Bulge eD :
log(M⋆, eD) = 10.700
⟨t⋆, eD⟩M = 13.000
⟨Z⋆, eD⟩M = 1.000
Net − Bulge dD :
log(M⋆, dD) = 10.250
⟨t⋆, dD⟩M = 3.746
⟨Z⋆, dD⟩M = 1.301
Net − Bulge fD :
log(M⋆, fD) = 10.520
⟨t⋆, fD⟩M = 13.000
⟨Z⋆, fD⟩M = 1.579
Net − Bulge eD :
log(M⋆, eD) = 10.520
⟨t⋆, eD⟩M = 13.000
⟨Z⋆, eD⟩M = 1.272
λ (Å)
λ (Å)

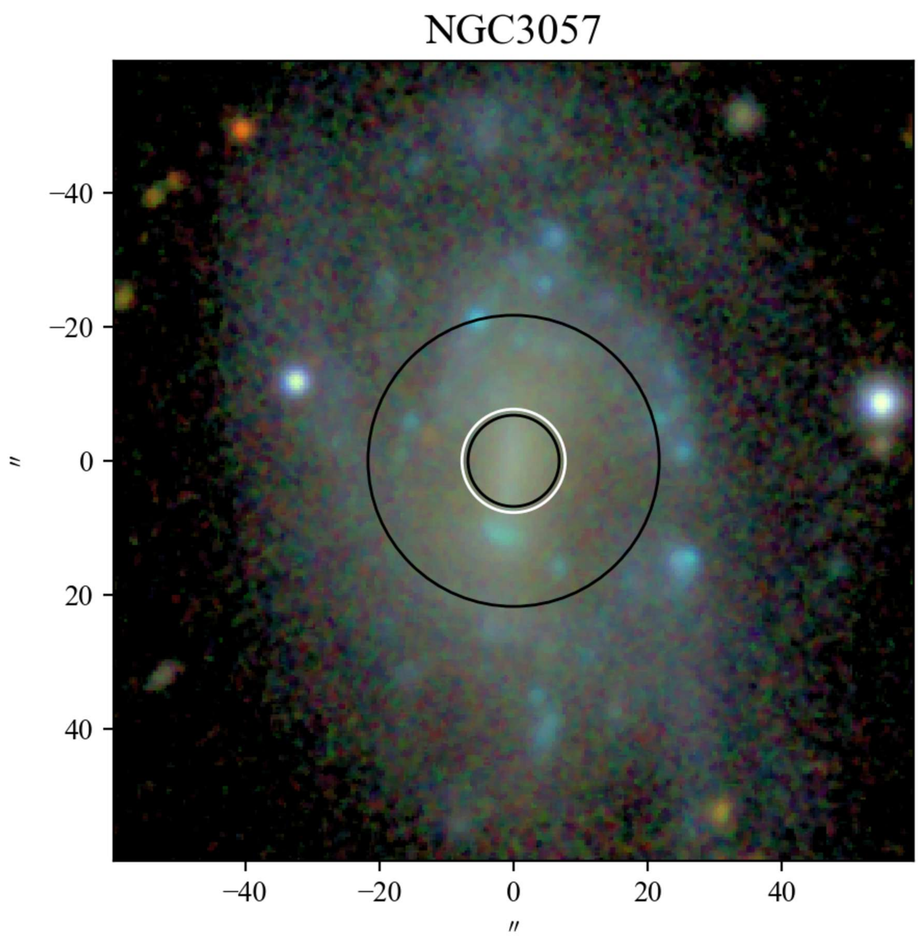
NGC3057
−40
−20
0
20
40
″
−40
−20
0
20
40
″

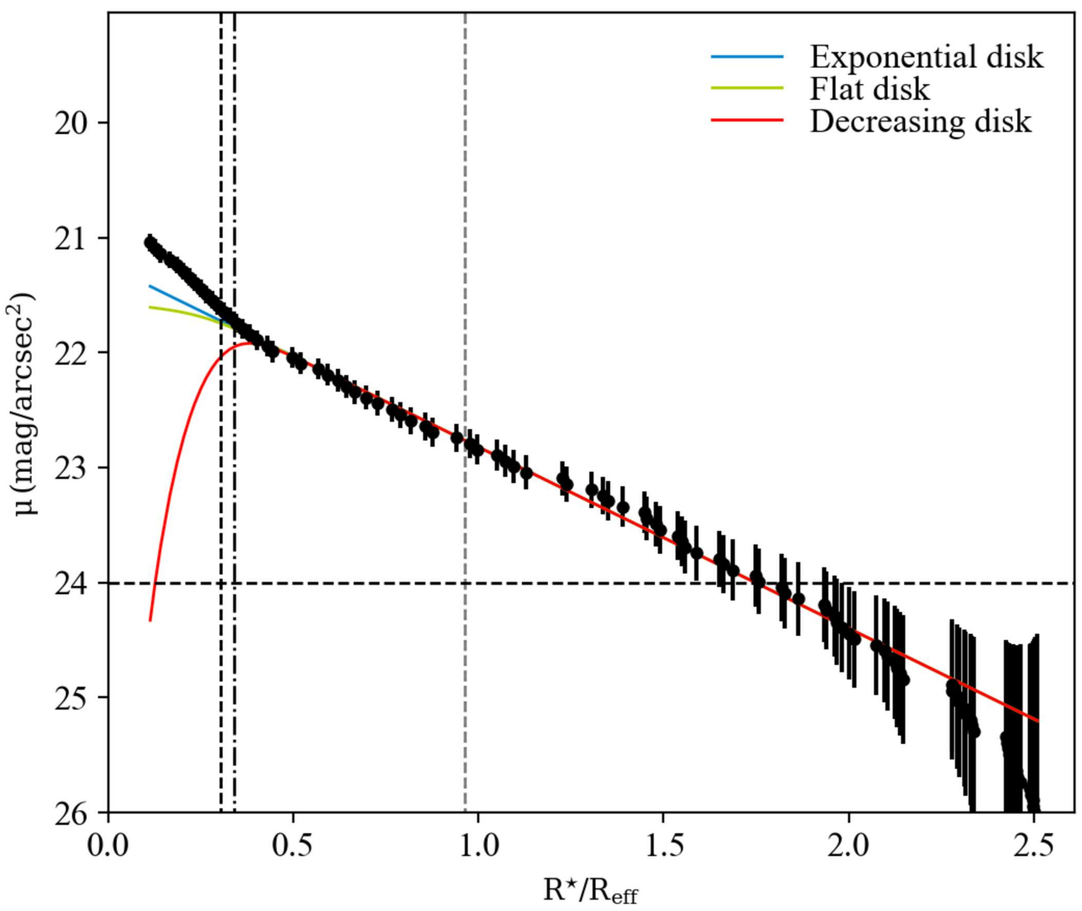
Exponential disk
Flat disk
Decreasing disk
μ (mag/arcsec²)
20
21
22
23
24
25
26
0.0
0.5
1.0
1.5
2.0
2.5
R⋆/Reff

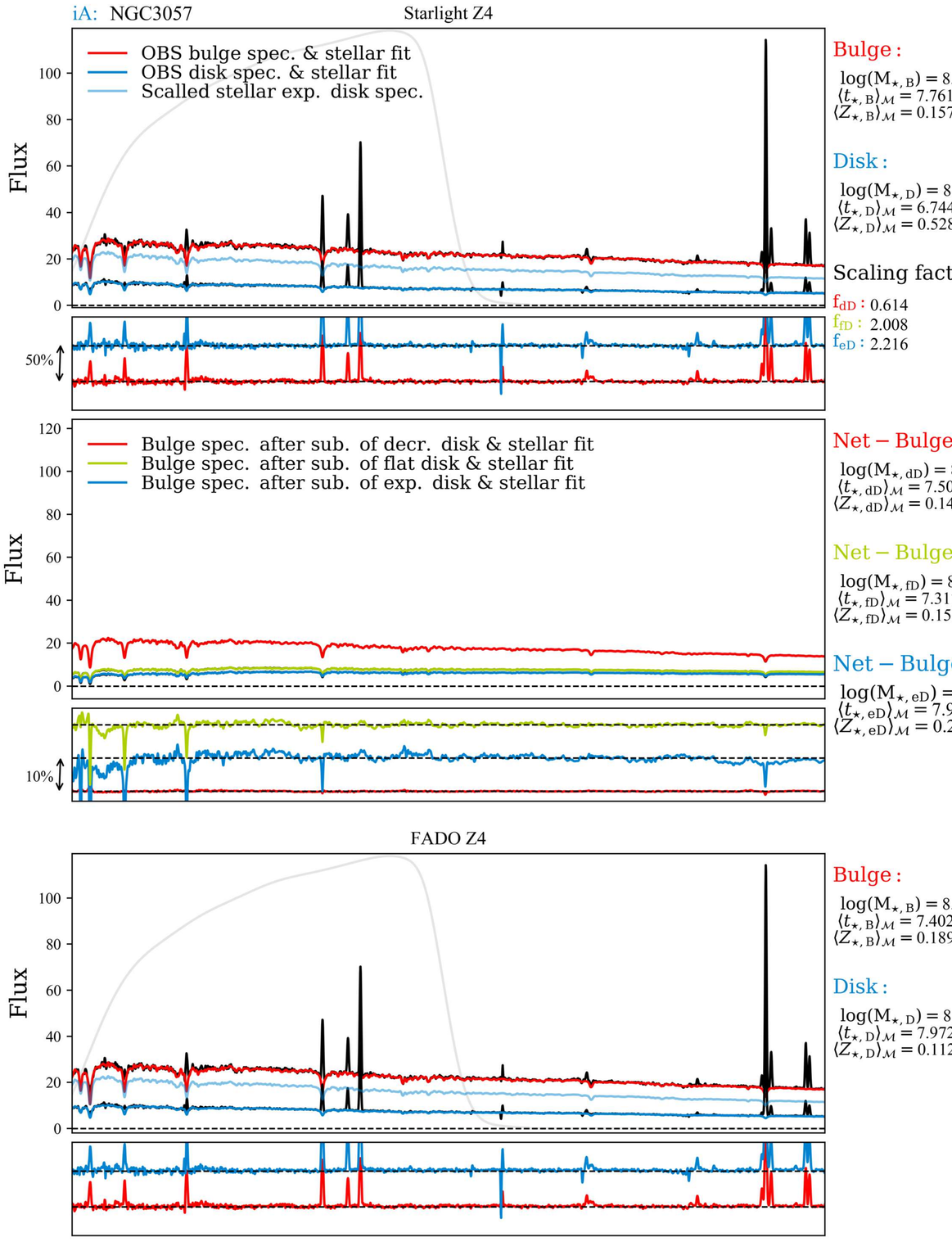
iA: NGC3057
Starlight Z4
OBS bulge spec. & stellar fit
OBS disk spec. & stellar fit
Scalled stellar exp. disk spec.
Flux
50%
Bulge spec. after sub. of decr. disk & stellar fit
Bulge spec. after sub. of flat disk & stellar fit
Bulge spec. after sub. of exp. disk & stellar fit
10%
Bulge :
log(M⋆, B) = 8.731
⟨t⋆, B⟩M = 7.761
⟨Z⋆, B⟩M = 0.157
Disk :
log(M⋆, D) = 8.137
⟨t⋆, D⟩M = 6.744
⟨Z⋆, D⟩M = 0.528
Scaling factors :
fdD : 0.614
ffD : 2.008
feD : 2.216
Net − Bulge dD :
log(M⋆, dD) = 8.612
⟨t⋆, dD⟩M = 7.508
⟨Z⋆, dD⟩M = 0.143
Net − Bulge fD :
log(M⋆, fD) = 8.378
⟨t⋆, fD⟩M = 7.317
⟨Z⋆, fD⟩M = 0.159
Net − Bulge eD :
log(M⋆, eD) = 8.402
⟨t⋆, eD⟩M = 7.916
⟨Z⋆, eD⟩M = 0.258

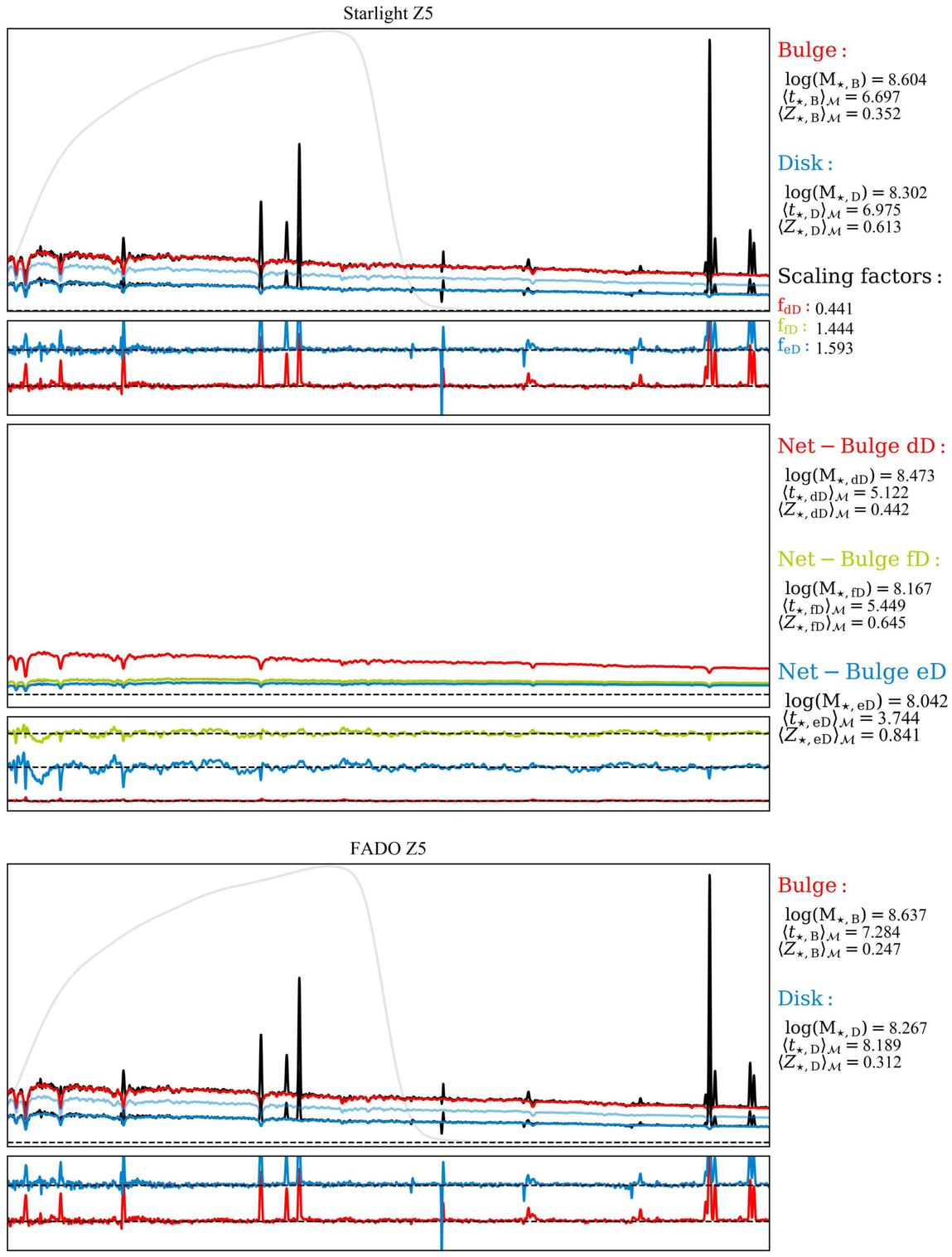
Starlight Z5
Bulge :
log(M⋆, B) = 8.604
⟨t⋆, B⟩M = 6.697
⟨Z⋆, B⟩M = 0.352
Disk :
log(M⋆, D) = 8.302
⟨t⋆, D⟩M = 6.975
⟨Z⋆, D⟩M = 0.613
Scaling factors :
fdD : 0.441
ffD : 1.444
feD : 1.593
Net − Bulge dD :
log(M⋆, dD) = 8.473
⟨t⋆, dD⟩M = 5.122
⟨Z⋆, dD⟩M = 0.442
Net − Bulge fD :
log(M⋆, fD) = 8.167
⟨t⋆, fD⟩M = 5.449
⟨Z⋆, fD⟩M = 0.645
Net − Bulge eD :
log(M⋆, eD) = 8.042
⟨t⋆, eD⟩M = 3.744
⟨Z⋆, eD⟩M = 0.841

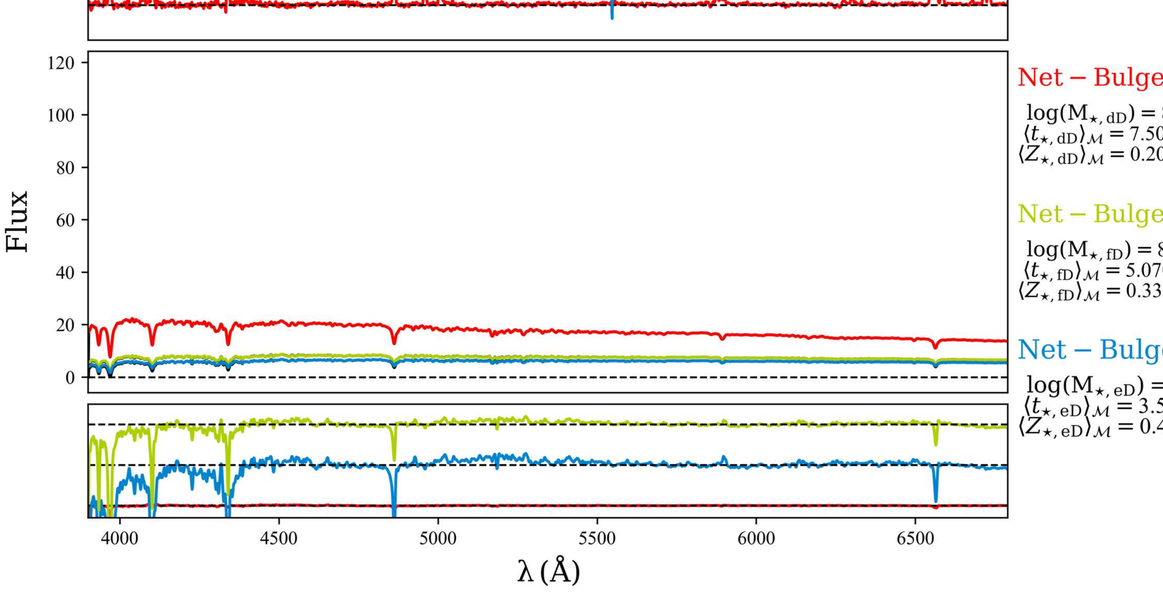
FADO Z4
Flux
Bulge :
log(M⋆, B) = 8.710
⟨t⋆, B⟩M = 7.402
⟨Z⋆, B⟩M = 0.189
Disk :
log(M⋆, D) = 8.081
⟨t⋆, D⟩M = 7.972
⟨Z⋆, D⟩M = 0.112
Net − Bulge dD :
log(M⋆, dD) = 8.623
⟨t⋆, dD⟩M = 7.509
⟨Z⋆, dD⟩M = 0.206
Net − Bulge fD :
log(M⋆, fD) = 8.352
⟨t⋆, fD⟩M = 5.070
⟨Z⋆, fD⟩M = 0.330
Net − Bulge eD :
log(M⋆, eD) = 8.262
⟨t⋆, eD⟩M = 3.584
⟨Z⋆, eD⟩M = 0.467
4000
4500
5000
5500
6000
6500
λ (Å)

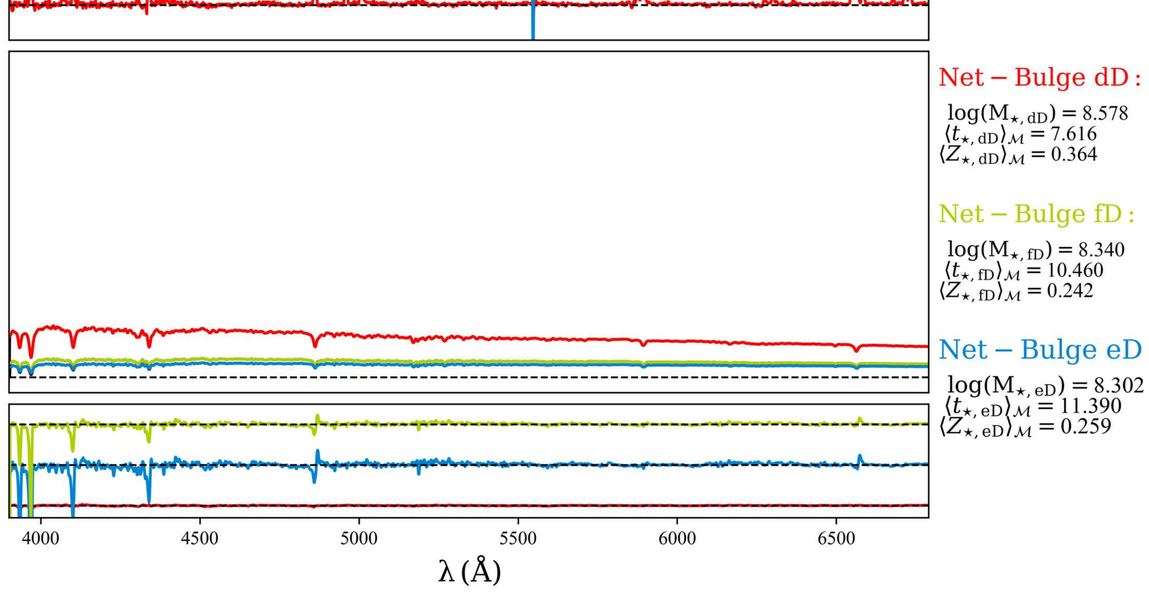
FADO Z5
Bulge :
log(M⋆, B) = 8.637
⟨t⋆, B⟩M = 7.284
⟨Z⋆, B⟩M = 0.247
Disk :
log(M⋆, D) = 8.267
⟨t⋆, D⟩M = 8.189
⟨Z⋆, D⟩M = 0.312
Net − Bulge dD :
log(M⋆, dD) = 8.578
⟨t⋆, dD⟩M = 7.616
⟨Z⋆, dD⟩M = 0.364
Net − Bulge fD :
log(M⋆, fD) = 8.340
⟨t⋆, fD⟩M = 10.460
⟨Z⋆, fD⟩M = 0.242
Net − Bulge eD :
log(M⋆, eD) = 8.302
⟨t⋆, eD⟩M = 11.390
⟨Z⋆, eD⟩M = 0.259
4000
4500
5000
5500
6000
6500
λ (Å)

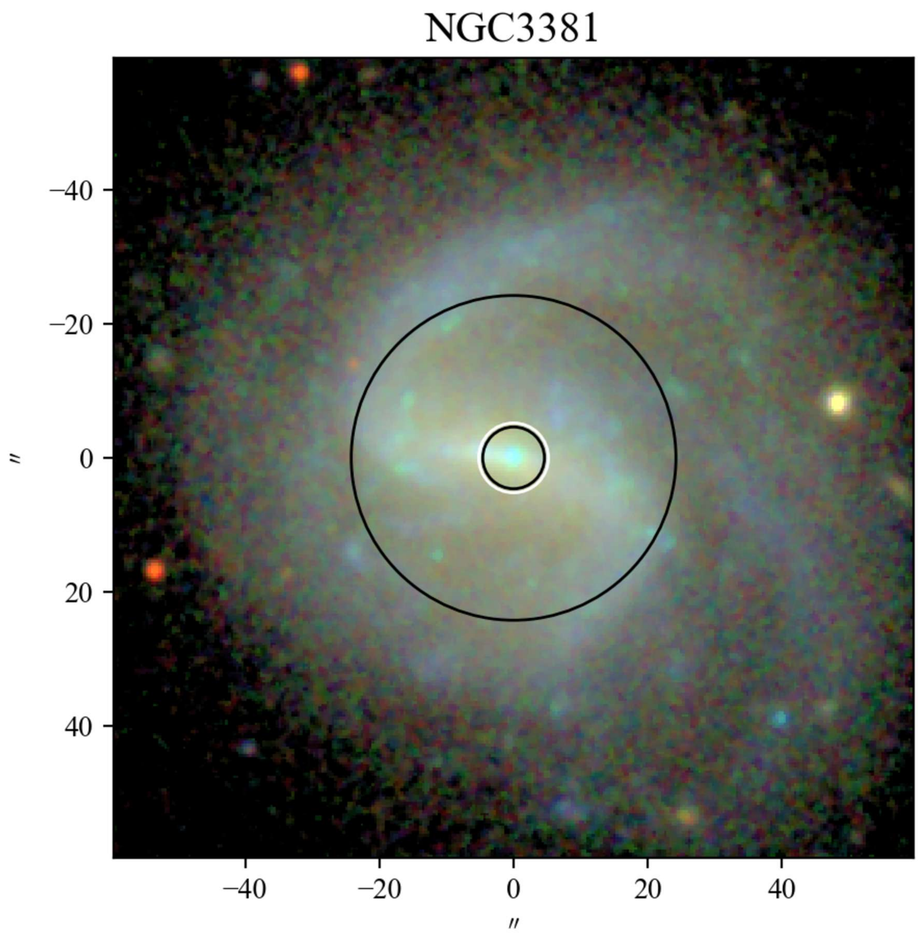
NGC3381
−40
−20
0
20
40
″
−40
−20
0
20
40
″

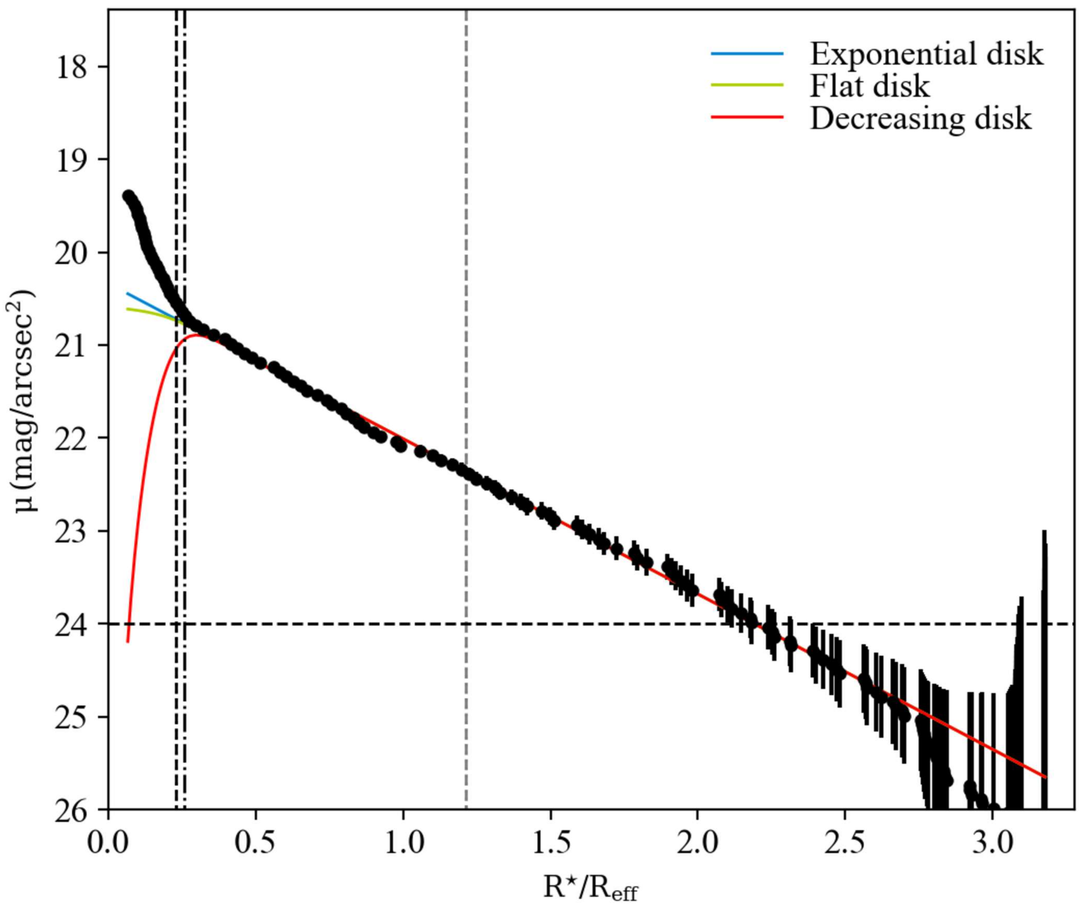
Exponential disk
Flat disk
Decreasing disk
μ (mag/arcsec²)
18
19
20
21
22
23
24
25
26
0.0
0.5
1.0
1.5
2.0
2.5
3.0
R⋆/Reff

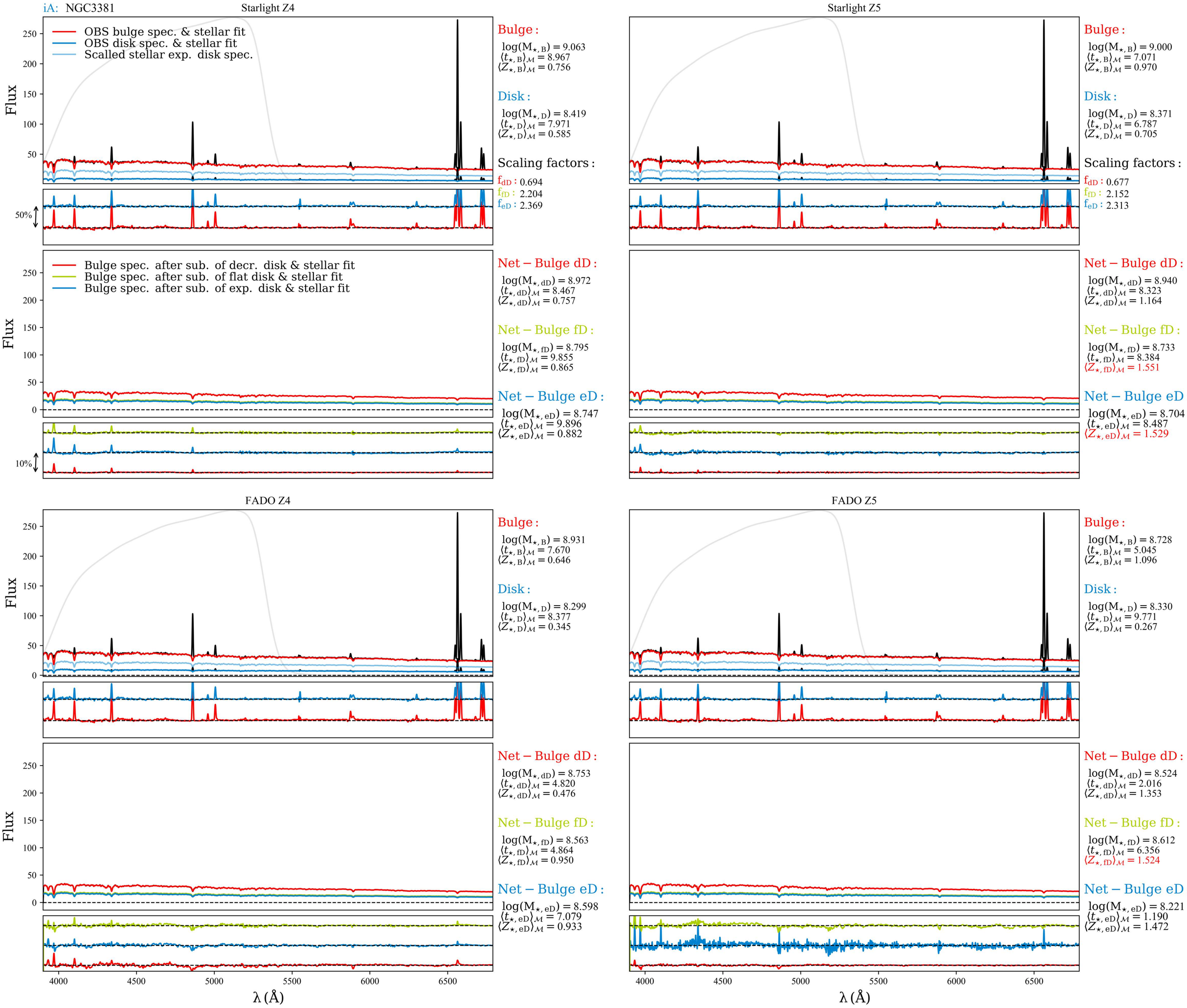
iA: NGC3381
Starlight Z4
OBS bulge spec. & stellar fit
OBS disk spec. & stellar fit
Scalled stellar exp. disk spec.
Flux
50%
Bulge :
log(M⋆, B) = 9.063
⟨t⋆, B⟩M = 8.967
⟨Z⋆, B⟩M = 0.756
Disk :
log(M⋆, D) = 8.419
⟨t⋆, D⟩M = 7.971
⟨Z⋆, D⟩M = 0.585
Scaling factors :
fdD : 0.694
ffD : 2.204
feD : 2.369
Starlight Z5
Bulge :
log(M⋆, B) = 9.000
⟨t⋆, B⟩M = 7.071
⟨Z⋆, B⟩M = 0.970
Disk :
log(M⋆, D) = 8.371
⟨t⋆, D⟩M = 6.787
⟨Z⋆, D⟩M = 0.705
Scaling factors :
fdD : 0.677
ffD : 2.152
feD : 2.313
Bulge spec. after sub. of decr. disk & stellar fit
Bulge spec. after sub. of flat disk & stellar fit
Bulge spec. after sub. of exp. disk & stellar fit
10%
Net − Bulge dD :
log(M⋆, dD) = 8.972
⟨t⋆, dD⟩M = 8.467
⟨Z⋆, dD⟩M = 0.757
Net − Bulge fD :
log(M⋆, fD) = 8.795
⟨t⋆, fD⟩M = 9.855
⟨Z⋆, fD⟩M = 0.865
Net − Bulge eD :
log(M⋆, eD) = 8.747
⟨t⋆, eD⟩M = 9.896
⟨Z⋆, eD⟩M = 0.882
Net − Bulge dD :
log(M⋆, dD) = 8.940
⟨t⋆, dD⟩M = 8.323
⟨Z⋆, dD⟩M = 1.164
Net − Bulge fD :
log(M⋆, fD) = 8.733
⟨t⋆, fD⟩M = 8.384
⟨Z⋆, fD⟩M = 1.551
Net − Bulge eD :
log(M⋆, eD) = 8.704
⟨t⋆, eD⟩M = 8.487
⟨Z⋆, eD⟩M = 1.529
FADO Z4
Bulge :
log(M⋆, B) = 8.931
⟨t⋆, B⟩M = 7.670
⟨Z⋆, B⟩M = 0.646
Disk :
log(M⋆, D) = 8.299
⟨t⋆, D⟩M = 8.377
⟨Z⋆, D⟩M = 0.345
FADO Z5
Bulge :
log(M⋆, B) = 8.728
⟨t⋆, B⟩M = 5.045
⟨Z⋆, B⟩M = 1.096
Disk :
log(M⋆, D) = 8.330
⟨t⋆, D⟩M = 9.771
⟨Z⋆, D⟩M = 0.267
Net − Bulge dD :
log(M⋆, dD) = 8.753
⟨t⋆, dD⟩M = 4.820
⟨Z⋆, dD⟩M = 0.476
Net − Bulge fD :
log(M⋆, fD) = 8.563
⟨t⋆, fD⟩M = 4.864
⟨Z⋆, fD⟩M = 0.950
Net − Bulge eD :
log(M⋆, eD) = 8.598
⟨t⋆, eD⟩M = 7.079
⟨Z⋆, eD⟩M = 0.933
Net − Bulge dD :
log(M⋆, dD) = 8.524
⟨t⋆, dD⟩M = 2.016
⟨Z⋆, dD⟩M = 1.353
Net − Bulge fD :
log(M⋆, fD) = 8.612
⟨t⋆, fD⟩M = 6.356
⟨Z⋆, fD⟩M = 1.524
Net − Bulge eD :
log(M⋆, eD) = 8.221
⟨t⋆, eD⟩M = 1.190
⟨Z⋆, eD⟩M = 1.472
Flux
0
50
100
150
200
250
4000
4500
5000
5500
6000
6500
λ (Å)

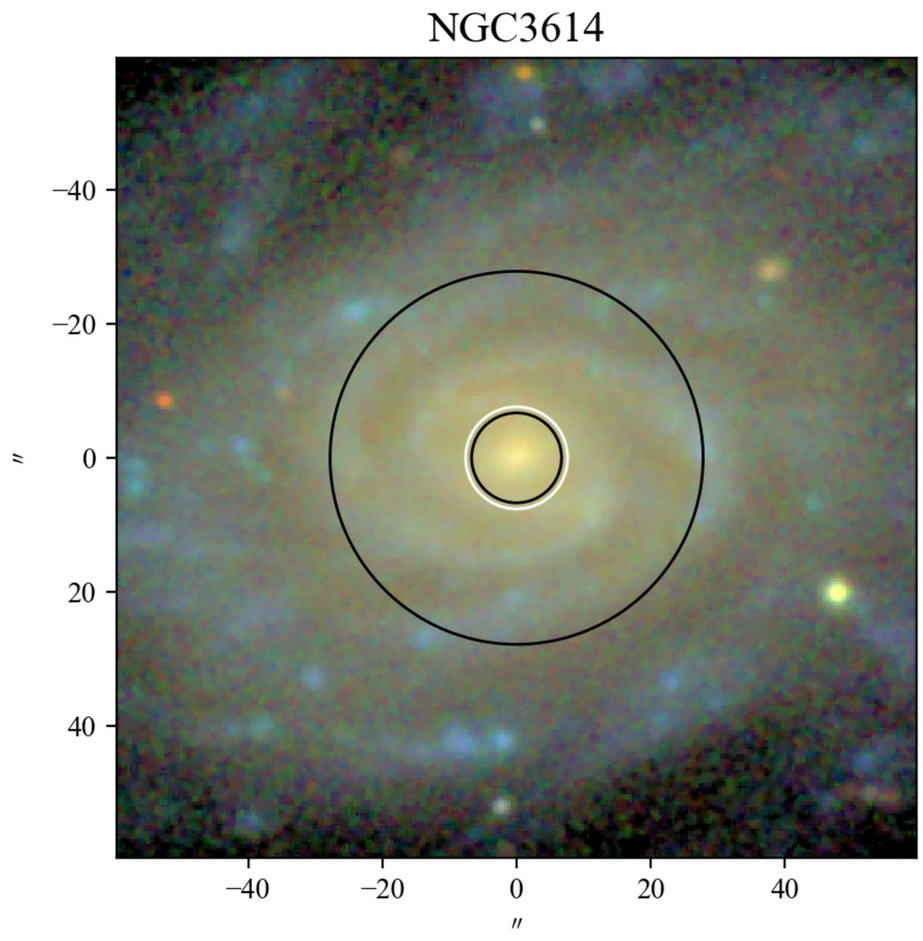
NGC3614
″
−40
−20
0
20
40

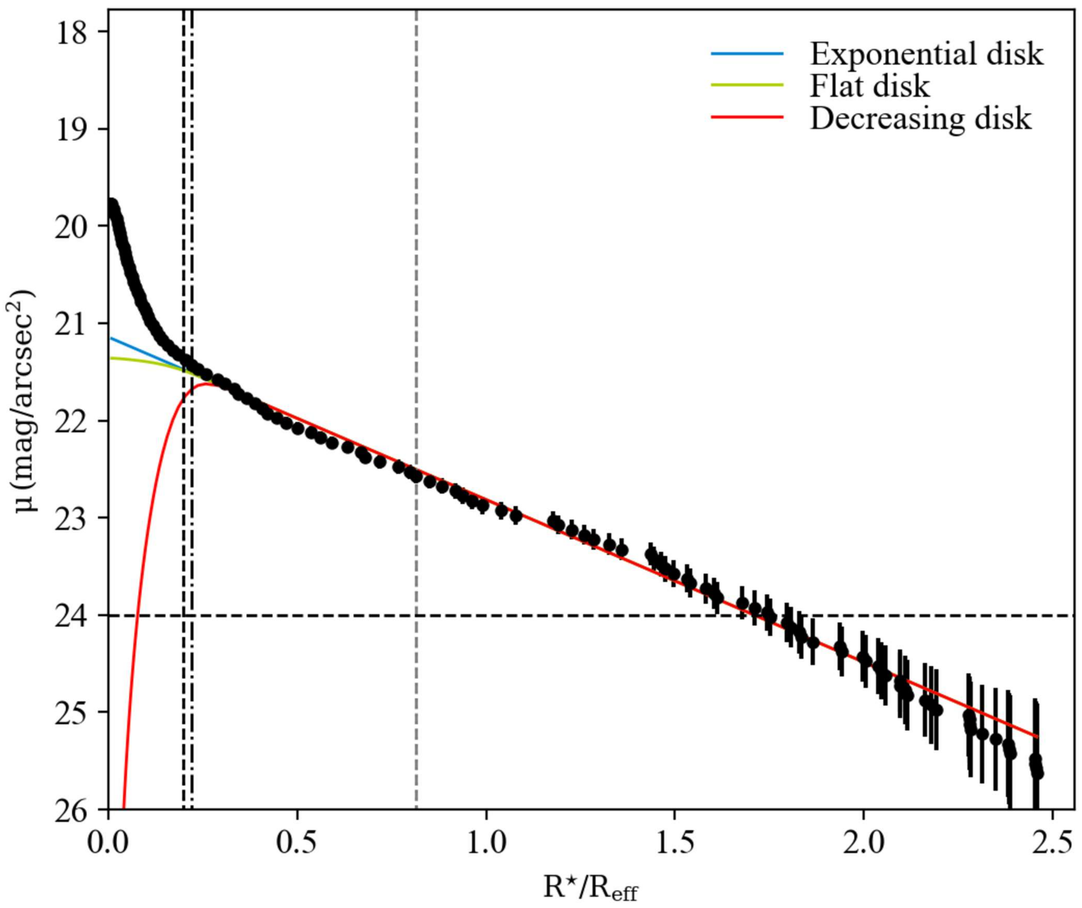
Exponential disk
Flat disk
Decreasing disk
μ (mag/arcsec²)
R⋆/R_eff

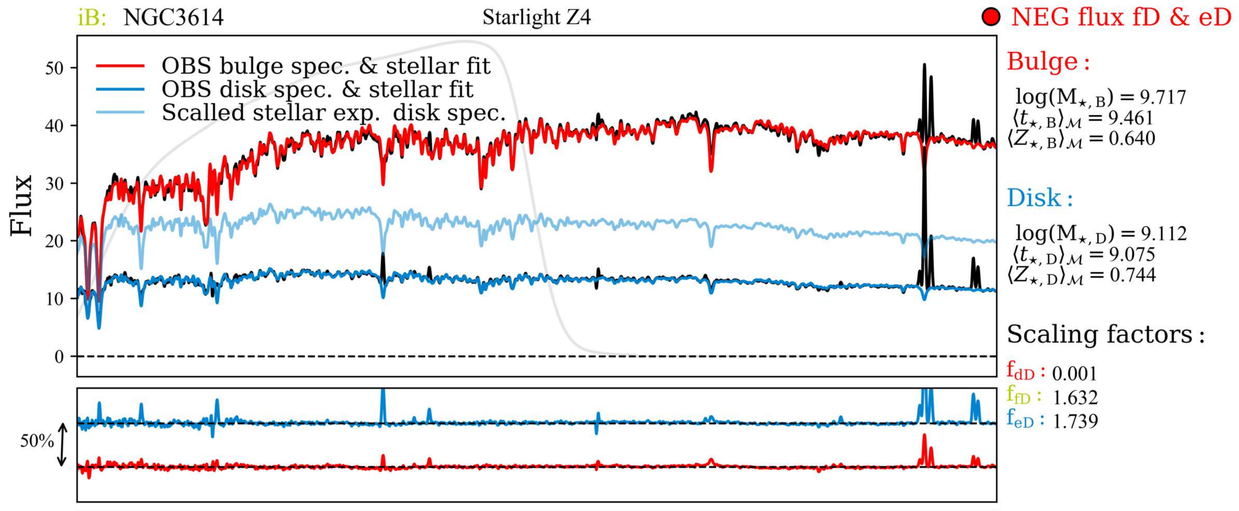
iB: NGC3614
Starlight Z4
NEG flux fD & eD
OBS bulge spec. & stellar fit
OBS disk spec. & stellar fit
Scalled stellar exp. disk spec.
Flux
50%
Bulge :
log(M⋆, B) = 9.717
⟨t⋆, B⟩M = 9.461
⟨Z⋆, B⟩M = 0.640
Disk :
log(M⋆, D) = 9.112
⟨t⋆, D⟩M = 9.075
⟨Z⋆, D⟩M = 0.744
Scaling factors :
fdD : 0.001
ffD : 1.632
feD : 1.739

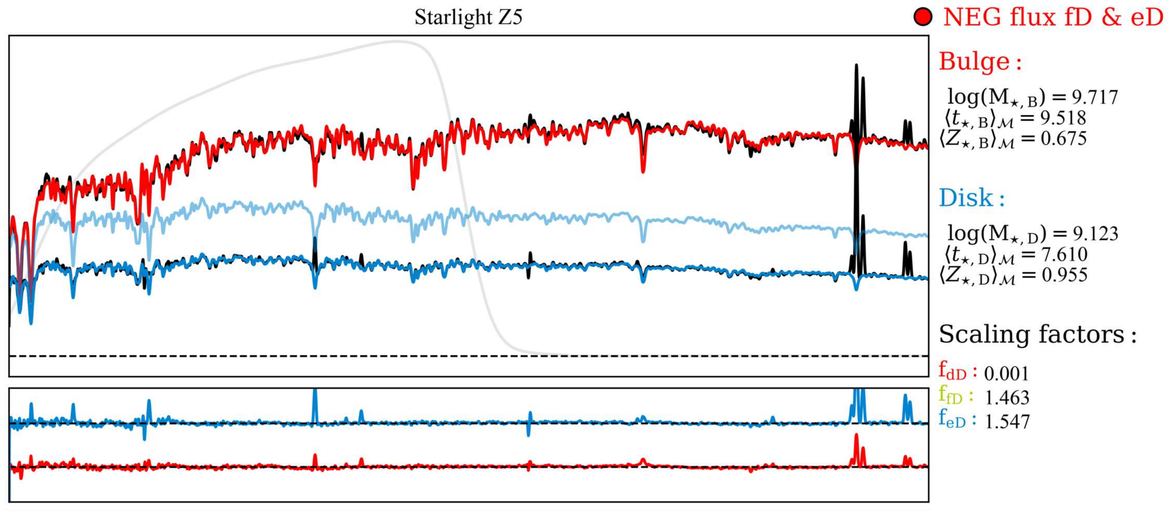
Starlight Z5
NEG flux fD & eD
Bulge :
log(M⋆, B) = 9.717
⟨t⋆, B⟩M = 9.518
⟨Z⋆, B⟩M = 0.675
Disk :
log(M⋆, D) = 9.123
⟨t⋆, D⟩M = 7.610
⟨Z⋆, D⟩M = 0.955
Scaling factors :
fdD : 0.001
ffD : 1.463
feD : 1.547

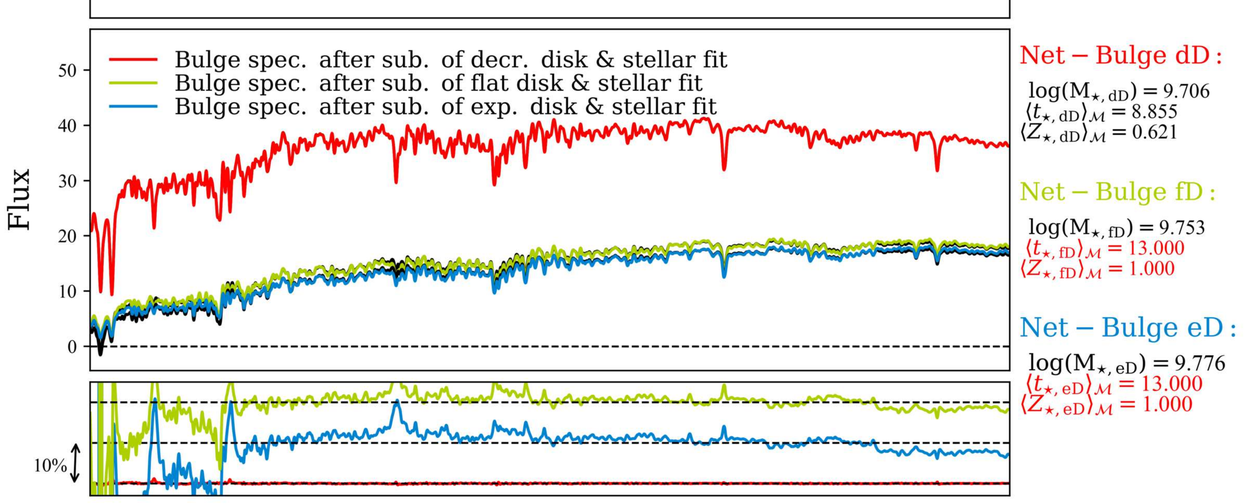
Bulge spec. after sub. of decr. disk & stellar fit
Bulge spec. after sub. of flat disk & stellar fit
Bulge spec. after sub. of exp. disk & stellar fit
Flux
10%
Net − Bulge dD :
log(M⋆, dD) = 9.706
⟨t⋆, dD⟩M = 8.855
⟨Z⋆, dD⟩M = 0.621
Net − Bulge fD :
log(M⋆, fD) = 9.753
⟨t⋆, fD⟩M = 13.000
⟨Z⋆, fD⟩M = 1.000
Net − Bulge eD :
log(M⋆, eD) = 9.776
⟨t⋆, eD⟩M = 13.000
⟨Z⋆, eD⟩M = 1.000

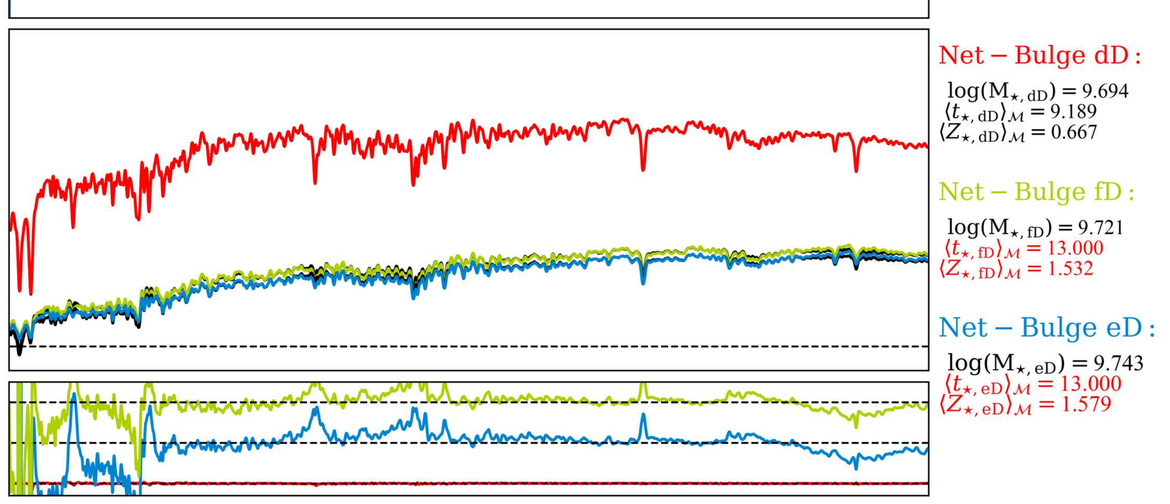
Net − Bulge dD :
log(M⋆, dD) = 9.694
⟨t⋆, dD⟩M = 9.189
⟨Z⋆, dD⟩M = 0.667
Net − Bulge fD :
log(M⋆, fD) = 9.721
⟨t⋆, fD⟩M = 13.000
⟨Z⋆, fD⟩M = 1.532
Net − Bulge eD :
log(M⋆, eD) = 9.743
⟨t⋆, eD⟩M = 13.000
⟨Z⋆, eD⟩M = 1.579

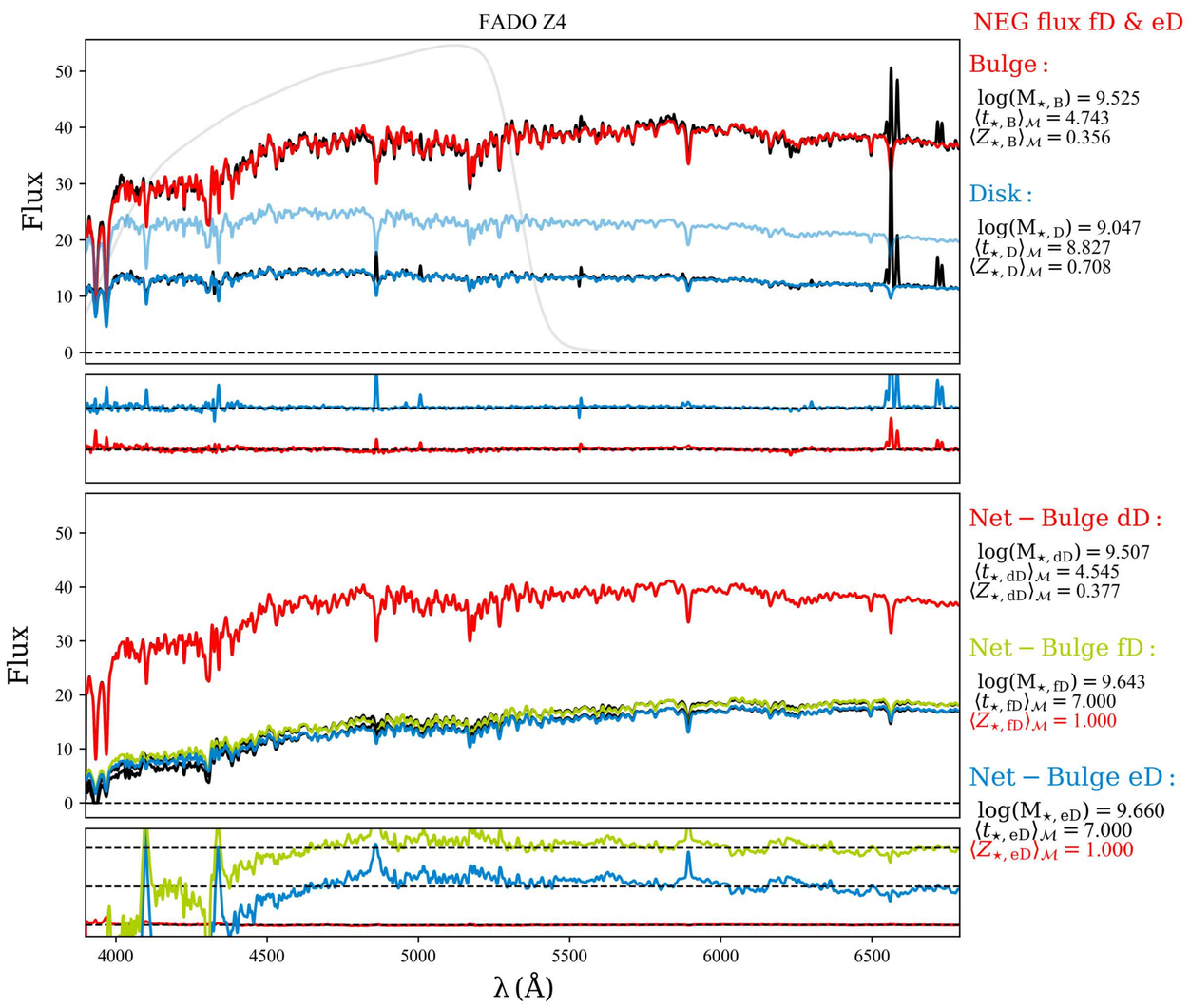
FADO Z4
NEG flux fD & eD
Flux
Bulge :
log(M⋆, B) = 9.525
⟨t⋆, B⟩M = 4.743
⟨Z⋆, B⟩M = 0.356
Disk :
log(M⋆, D) = 9.047
⟨t⋆, D⟩M = 8.827
⟨Z⋆, D⟩M = 0.708
Net − Bulge dD :
log(M⋆, dD) = 9.507
⟨t⋆, dD⟩M = 4.545
⟨Z⋆, dD⟩M = 0.377
Net − Bulge fD :
log(M⋆, fD) = 9.643
⟨t⋆, fD⟩M = 7.000
⟨Z⋆, fD⟩M = 1.000
Net − Bulge eD :
log(M⋆, eD) = 9.660
⟨t⋆, eD⟩M = 7.000
⟨Z⋆, eD⟩M = 1.000
λ (Å)

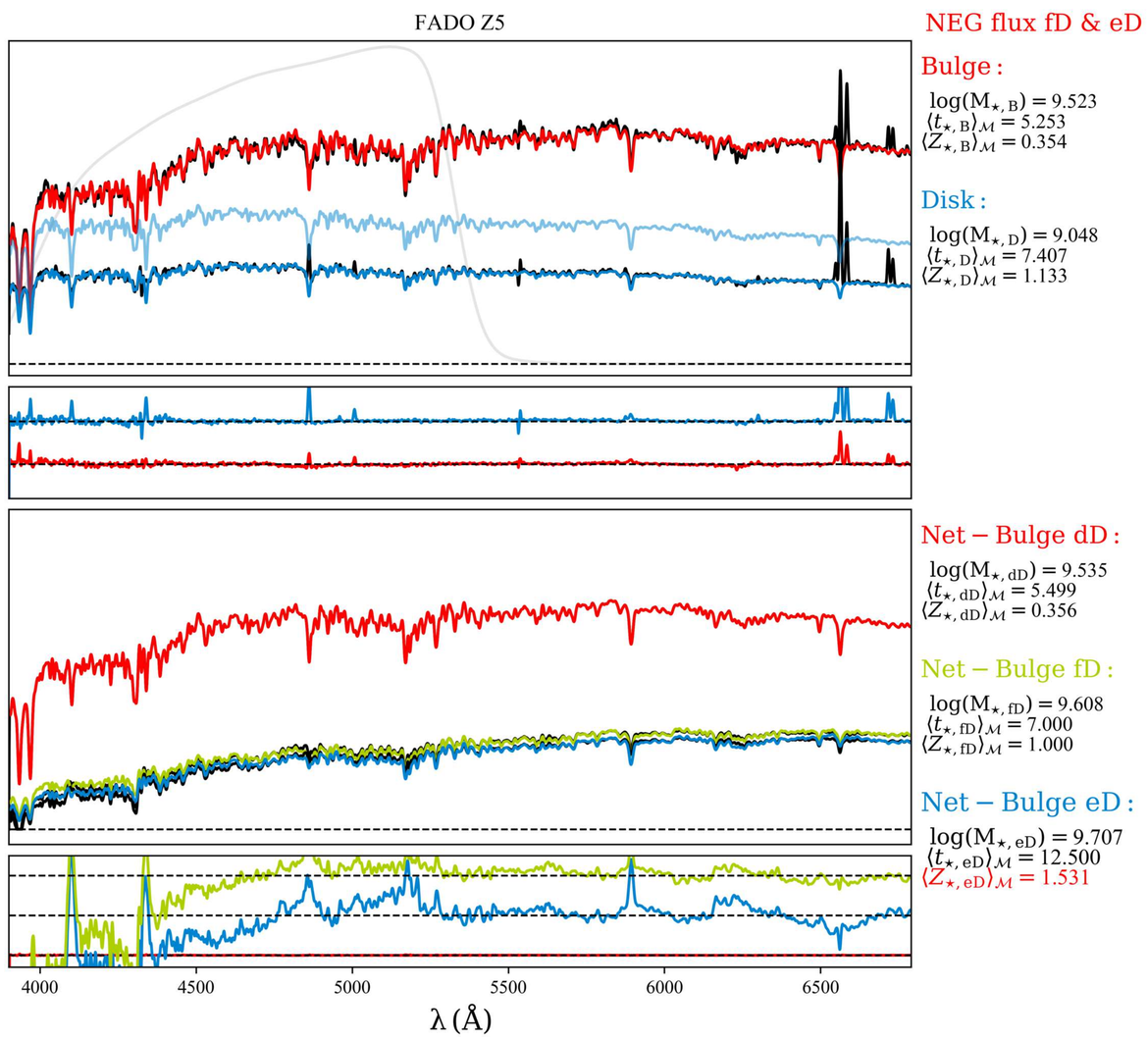
FADO Z5
NEG flux fD & eD
Bulge :
log(M⋆, B) = 9.523
⟨t⋆, B⟩M = 5.253
⟨Z⋆, B⟩M = 0.354
Disk :
log(M⋆, D) = 9.048
⟨t⋆, D⟩M = 7.407
⟨Z⋆, D⟩M = 1.133
Net − Bulge dD :
log(M⋆, dD) = 9.535
⟨t⋆, dD⟩M = 5.499
⟨Z⋆, dD⟩M = 0.356
Net − Bulge fD :
log(M⋆, fD) = 9.608
⟨t⋆, fD⟩M = 7.000
⟨Z⋆, fD⟩M = 1.000
Net − Bulge eD :
log(M⋆, eD) = 9.707
⟨t⋆, eD⟩M = 12.500
⟨Z⋆, eD⟩M = 1.531
λ (Å)

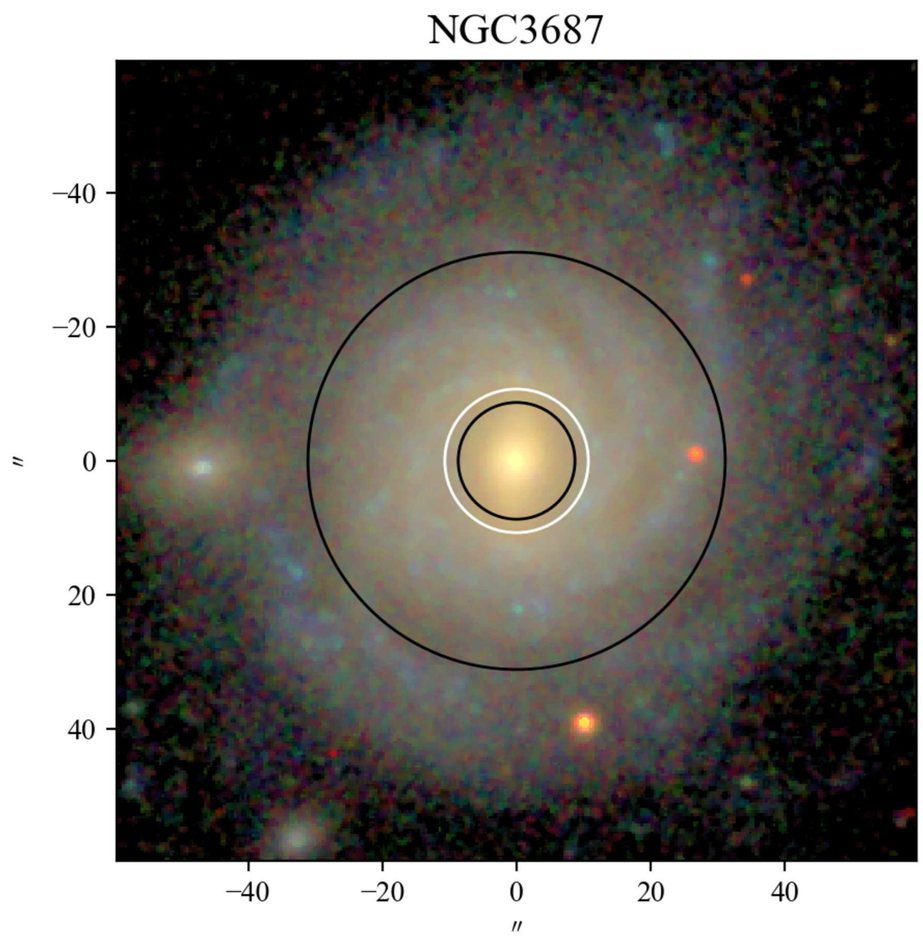
NGC3687
−40
−20
0
20
40
″
−40
−20
0
20
40
″

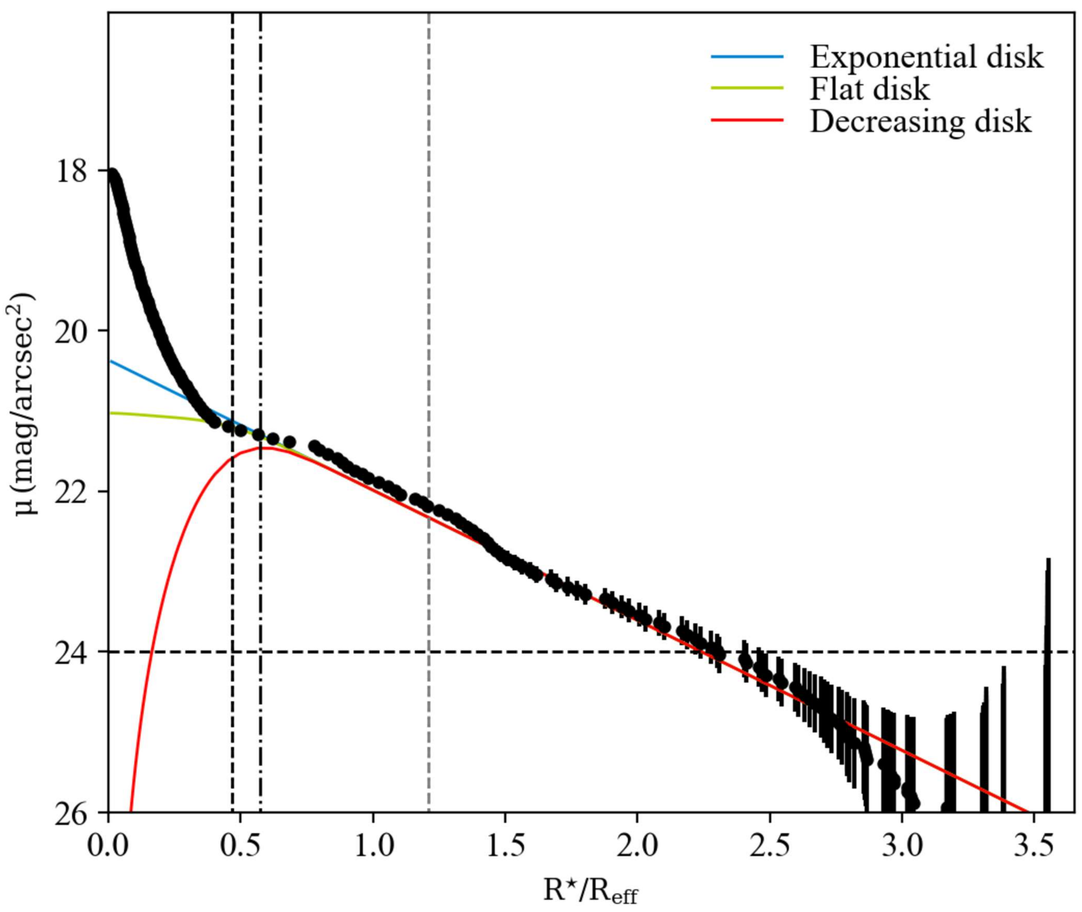
Exponential disk
Flat disk
Decreasing disk
μ (mag/arcsec²)
18
20
22
24
26
0.0
0.5
1.0
1.5
2.0
2.5
3.0
3.5
R⋆/Reff

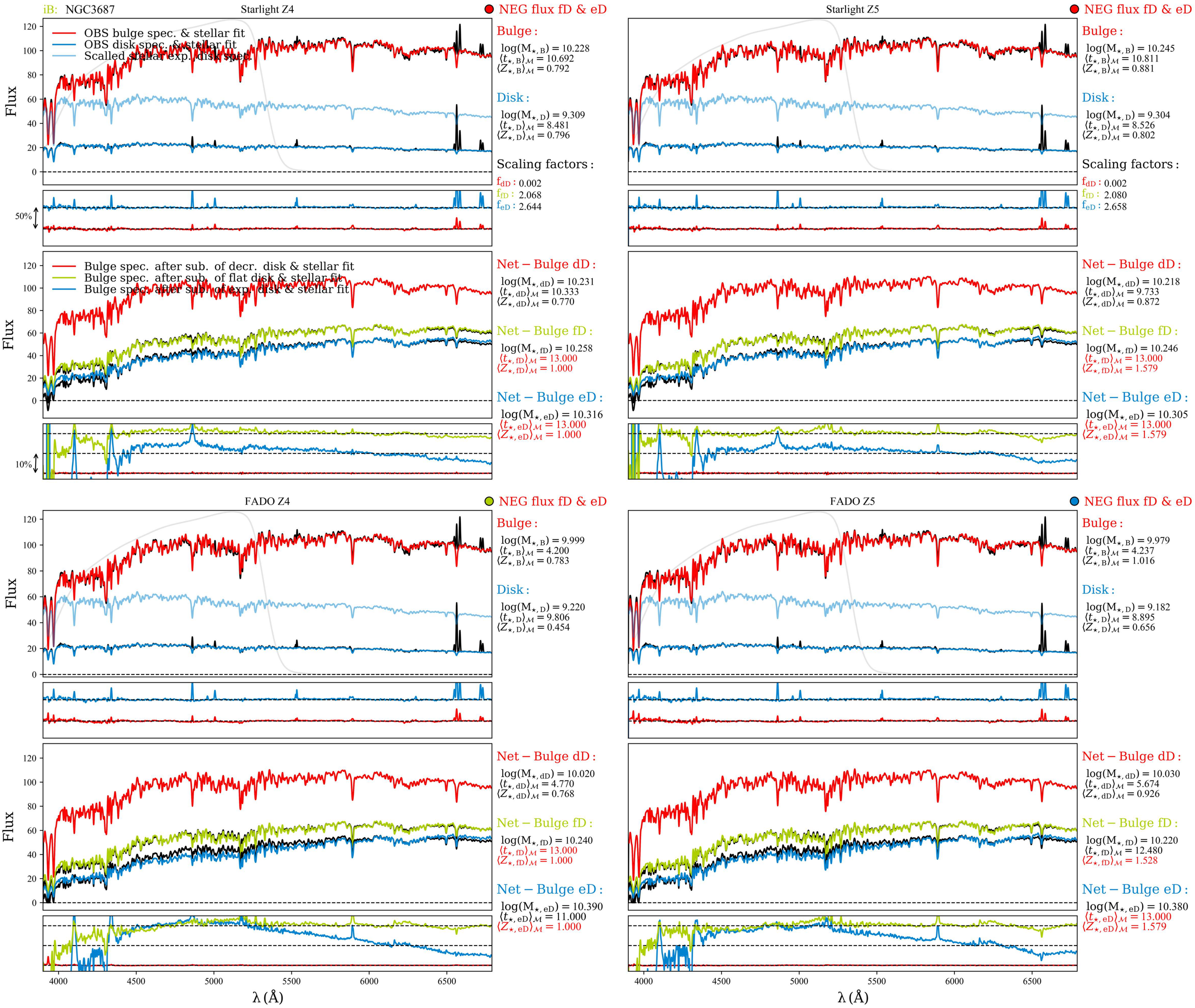
iB: NGC3687
Starlight Z4
NEG flux fD & eD
OBS bulge spec. & stellar fit
OBS disk spec. & stellar fit
Scalled stellar exp. disk spec.
Flux
50%
Bulge :
log(M⋆, B) = 10.228
⟨t⋆, B⟩M = 10.692
⟨Z⋆, B⟩M = 0.792
Disk :
log(M⋆, D) = 9.309
⟨t⋆, D⟩M = 8.481
⟨Z⋆, D⟩M = 0.796
Scaling factors :
fdD : 0.002
ffD : 2.068
feD : 2.644
Bulge spec. after sub. of decr. disk & stellar fit
Bulge spec. after sub. of flat disk & stellar fit
Bulge spec. after sub. of exp. disk & stellar fit
10%
Net − Bulge dD :
log(M⋆, dD) = 10.231
⟨t⋆, dD⟩M = 10.333
⟨Z⋆, dD⟩M = 0.770
Net − Bulge fD :
log(M⋆, fD) = 10.258
⟨t⋆, fD⟩M = 13.000
⟨Z⋆, fD⟩M = 1.000
Net − Bulge eD :
log(M⋆, eD) = 10.316
⟨t⋆, eD⟩M = 13.000
⟨Z⋆, eD⟩M = 1.000
Starlight Z5
NEG flux fD & eD
Bulge :
log(M⋆, B) = 10.245
⟨t⋆, B⟩M = 10.811
⟨Z⋆, B⟩M = 0.881
Disk :
log(M⋆, D) = 9.304
⟨t⋆, D⟩M = 8.526
⟨Z⋆, D⟩M = 0.802
Scaling factors :
fdD : 0.002
ffD : 2.080
feD : 2.658
Net − Bulge dD :
log(M⋆, dD) = 10.218
⟨t⋆, dD⟩M = 9.733
⟨Z⋆, dD⟩M = 0.872
Net − Bulge fD :
log(M⋆, fD) = 10.246
⟨t⋆, fD⟩M = 13.000
⟨Z⋆, fD⟩M = 1.579
Net − Bulge eD :
log(M⋆, eD) = 10.305
⟨t⋆, eD⟩M = 13.000
⟨Z⋆, eD⟩M = 1.579
FADO Z4
NEG flux fD & eD
Bulge :
log(M⋆, B) = 9.999
⟨t⋆, B⟩M = 4.200
⟨Z⋆, B⟩M = 0.783
Disk :
log(M⋆, D) = 9.220
⟨t⋆, D⟩M = 9.806
⟨Z⋆, D⟩M = 0.454
Net − Bulge dD :
log(M⋆, dD) = 10.020
⟨t⋆, dD⟩M = 4.770
⟨Z⋆, dD⟩M = 0.768
Net − Bulge fD :
log(M⋆, fD) = 10.240
⟨t⋆, fD⟩M = 13.000
⟨Z⋆, fD⟩M = 1.000
Net − Bulge eD :
log(M⋆, eD) = 10.390
⟨t⋆, eD⟩M = 11.000
⟨Z⋆, eD⟩M = 1.000
FADO Z5
NEG flux fD & eD
Bulge :
log(M⋆, B) = 9.979
⟨t⋆, B⟩M = 4.237
⟨Z⋆, B⟩M = 1.016
Disk :
log(M⋆, D) = 9.182
⟨t⋆, D⟩M = 8.895
⟨Z⋆, D⟩M = 0.656
Net − Bulge dD :
log(M⋆, dD) = 10.030
⟨t⋆, dD⟩M = 5.674
⟨Z⋆, dD⟩M = 0.926
Net − Bulge fD :
log(M⋆, fD) = 10.220
⟨t⋆, fD⟩M = 12.480
⟨Z⋆, fD⟩M = 1.528
Net − Bulge eD :
log(M⋆, eD) = 10.380
⟨t⋆, eD⟩M = 13.000
⟨Z⋆, eD⟩M = 1.579
4000
4500
5000
5500
6000
6500
λ (Å)

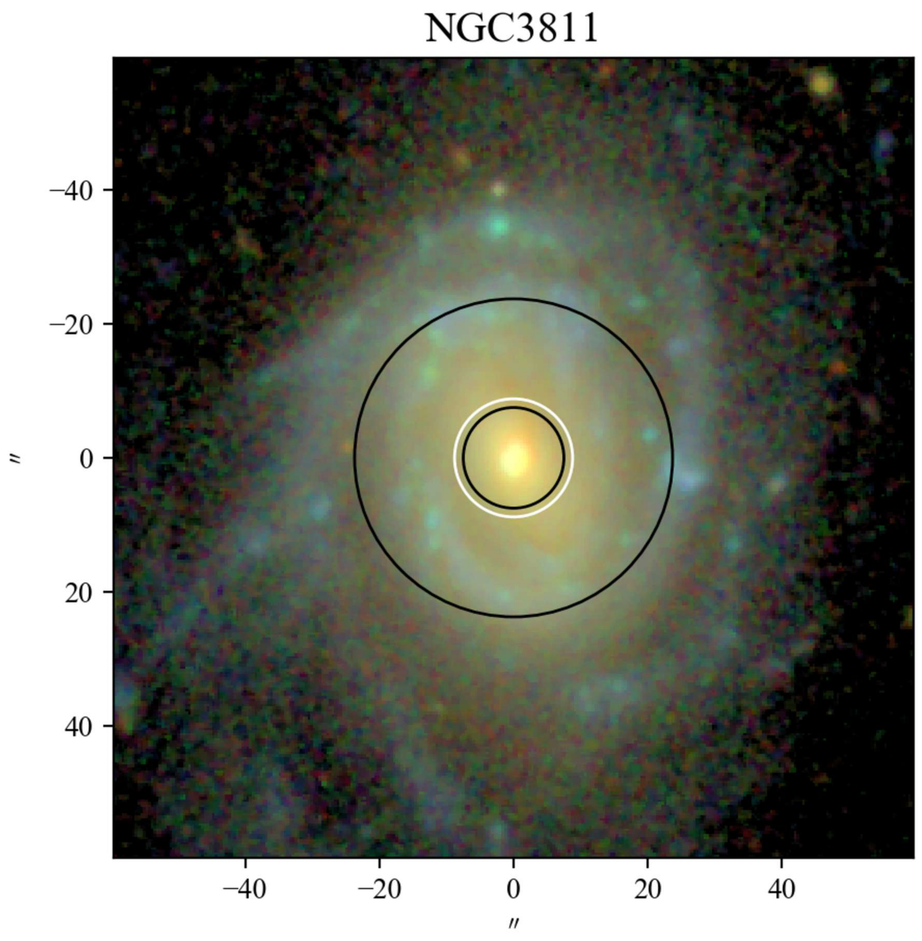
NGC3811
−40
−20
0
20
40
″
−40
−20
0
20
40
″

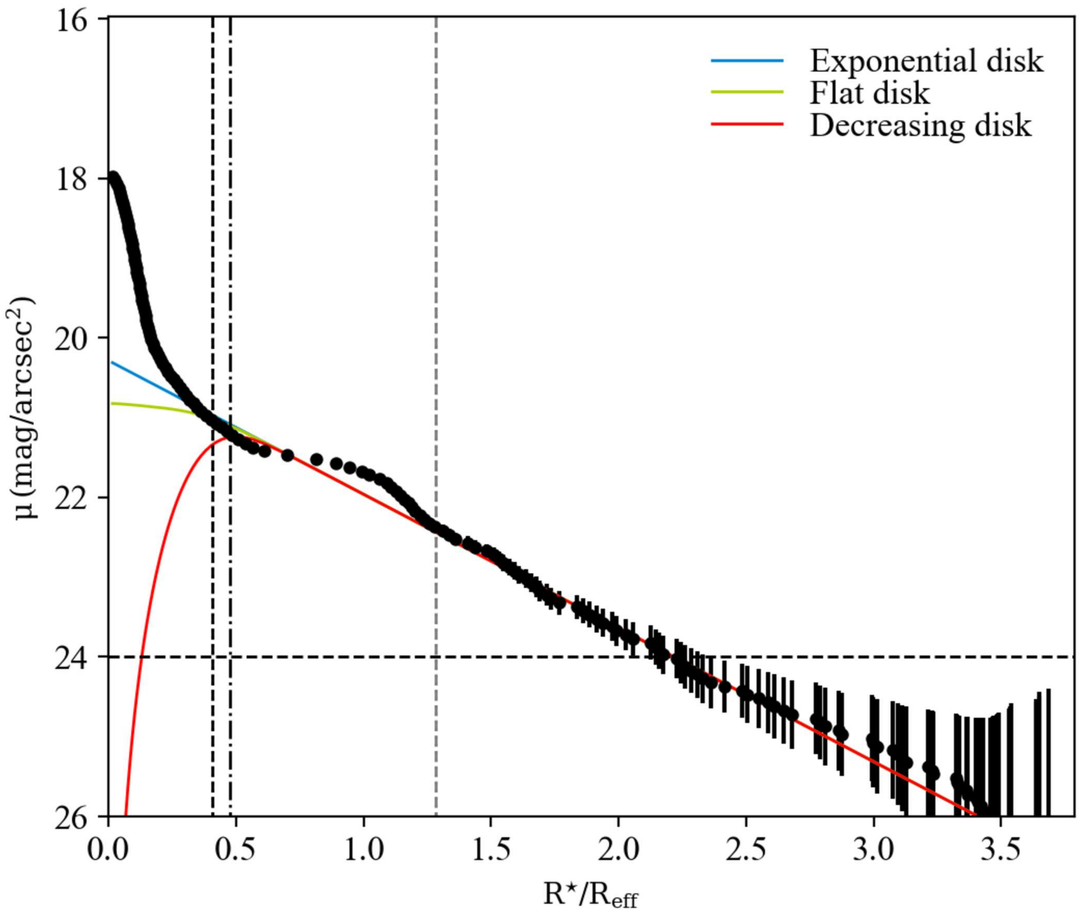
Exponential disk
Flat disk
Decreasing disk
μ (mag/arcsec²)
16
18
20
22
24
26
0.0
0.5
1.0
1.5
2.0
2.5
3.0
3.5
R⋆/Reff

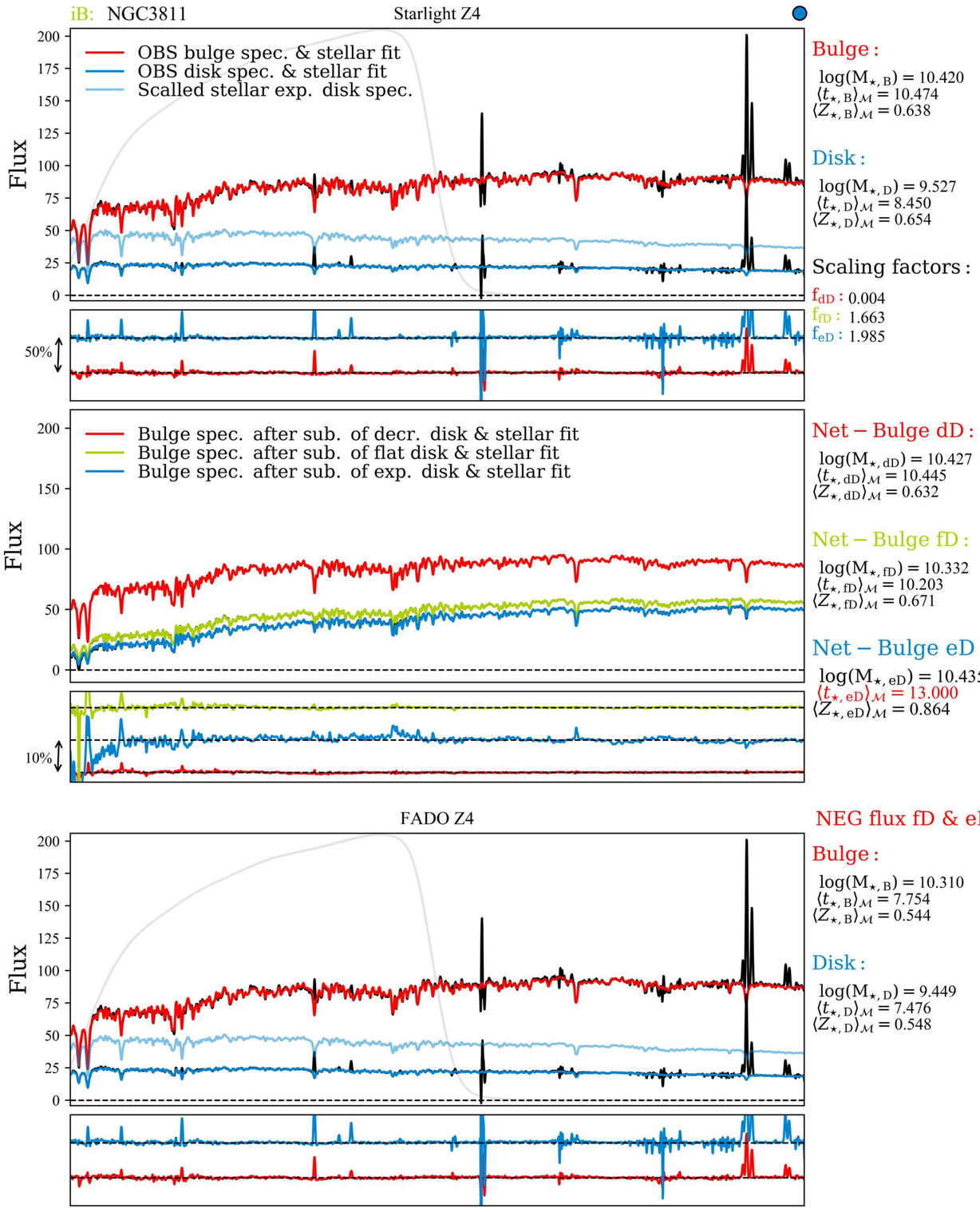
iB: NGC3811
Starlight Z4
OBS bulge spec. & stellar fit
OBS disk spec. & stellar fit
Scalled stellar exp. disk spec.
Flux
50%
Bulge spec. after sub. of decr. disk & stellar fit
Bulge spec. after sub. of flat disk & stellar fit
Bulge spec. after sub. of exp. disk & stellar fit
10%
Bulge :
log(M⋆, B) = 10.420
⟨t⋆, B⟩M = 10.474
⟨Z⋆, B⟩M = 0.638
Disk :
log(M⋆, D) = 9.527
⟨t⋆, D⟩M = 8.450
⟨Z⋆, D⟩M = 0.654
Scaling factors :
fdD : 0.004
ffD : 1.663
feD : 1.985
Net − Bulge dD :
log(M⋆, dD) = 10.427
⟨t⋆, dD⟩M = 10.445
⟨Z⋆, dD⟩M = 0.632
Net − Bulge fD :
log(M⋆, fD) = 10.332
⟨t⋆, fD⟩M = 10.203
⟨Z⋆, fD⟩M = 0.671
Net − Bulge eD :
log(M⋆, eD) = 10.435
⟨t⋆, eD⟩M = 13.000
⟨Z⋆, eD⟩M = 0.864

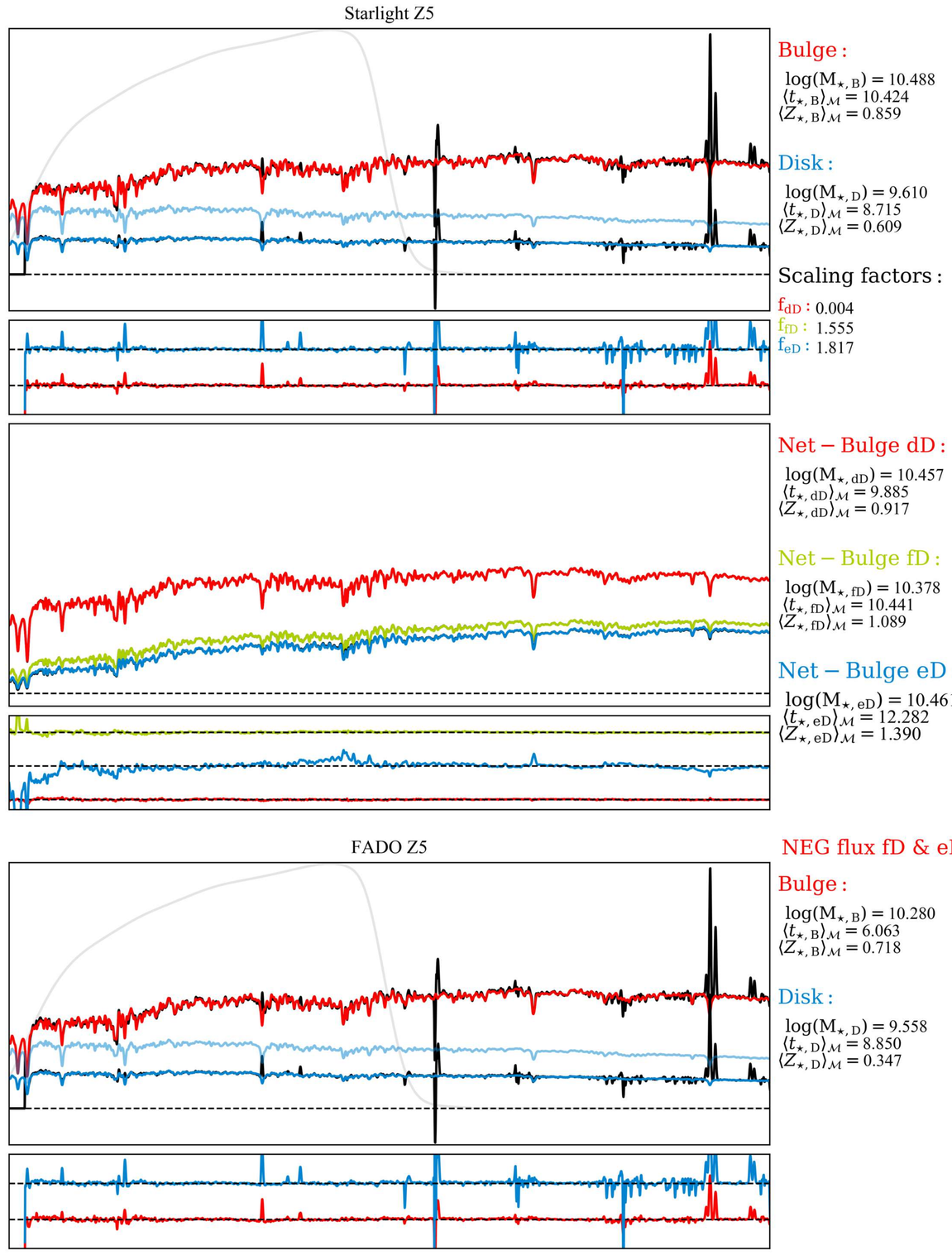
Starlight Z5
Bulge :
log(M⋆, B) = 10.488
⟨t⋆, B⟩M = 10.424
⟨Z⋆, B⟩M = 0.859
Disk :
log(M⋆, D) = 9.610
⟨t⋆, D⟩M = 8.715
⟨Z⋆, D⟩M = 0.609
Scaling factors :
fdD : 0.004
ffD : 1.555
feD : 1.817
Net − Bulge dD :
log(M⋆, dD) = 10.457
⟨t⋆, dD⟩M = 9.885
⟨Z⋆, dD⟩M = 0.917
Net − Bulge fD :
log(M⋆, fD) = 10.378
⟨t⋆, fD⟩M = 10.441
⟨Z⋆, fD⟩M = 1.089
Net − Bulge eD :
log(M⋆, eD) = 10.461
⟨t⋆, eD⟩M = 12.282
⟨Z⋆, eD⟩M = 1.390

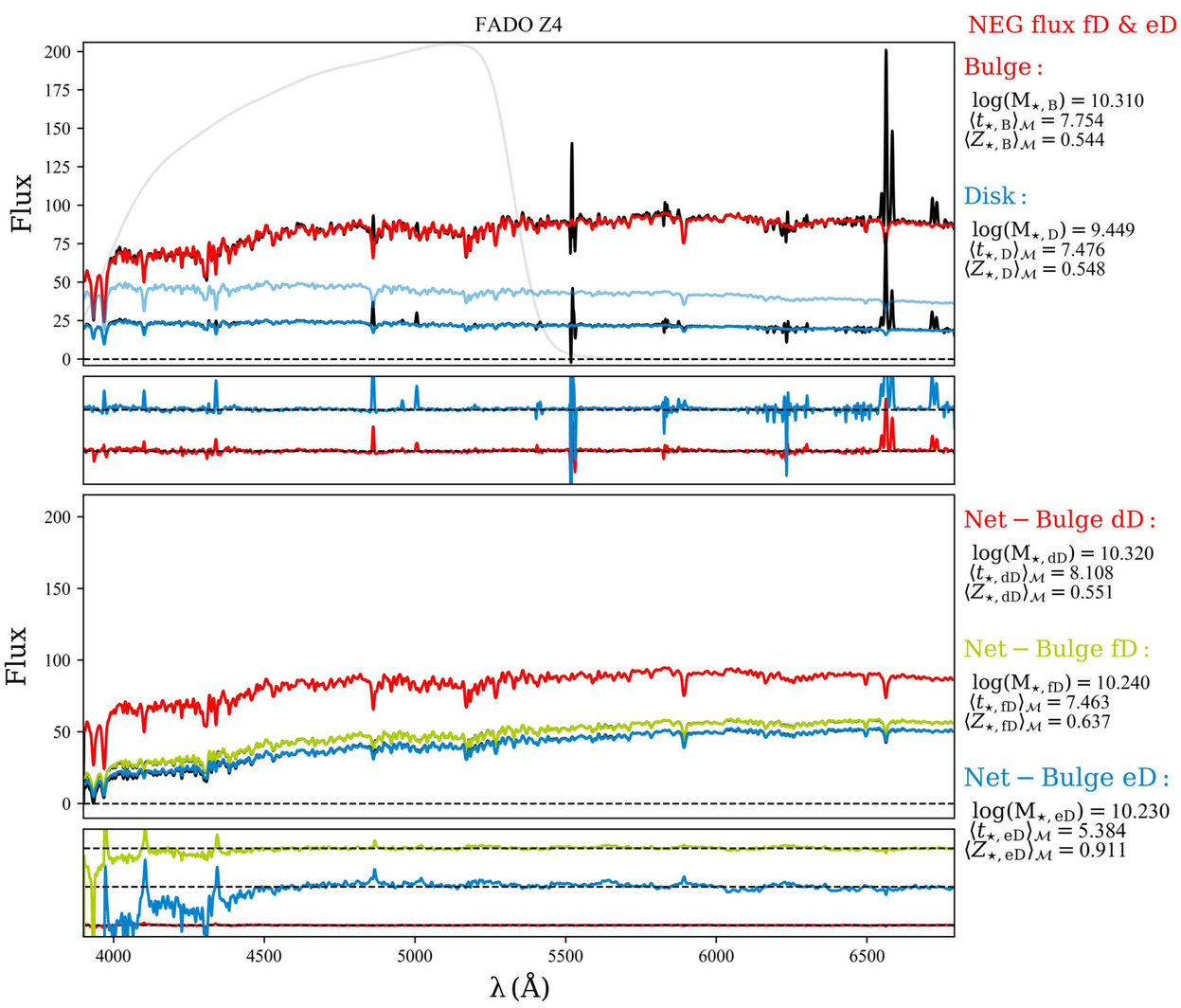
FADO Z4
NEG flux fD & eD
Flux
Bulge :
log(M⋆, B) = 10.310
⟨t⋆, B⟩M = 7.754
⟨Z⋆, B⟩M = 0.544
Disk :
log(M⋆, D) = 9.449
⟨t⋆, D⟩M = 7.476
⟨Z⋆, D⟩M = 0.548
Net − Bulge dD :
log(M⋆, dD) = 10.320
⟨t⋆, dD⟩M = 8.108
⟨Z⋆, dD⟩M = 0.551
Net − Bulge fD :
log(M⋆, fD) = 10.240
⟨t⋆, fD⟩M = 7.463
⟨Z⋆, fD⟩M = 0.637
Net − Bulge eD :
log(M⋆, eD) = 10.230
⟨t⋆, eD⟩M = 5.384
⟨Z⋆, eD⟩M = 0.911
λ (Å)

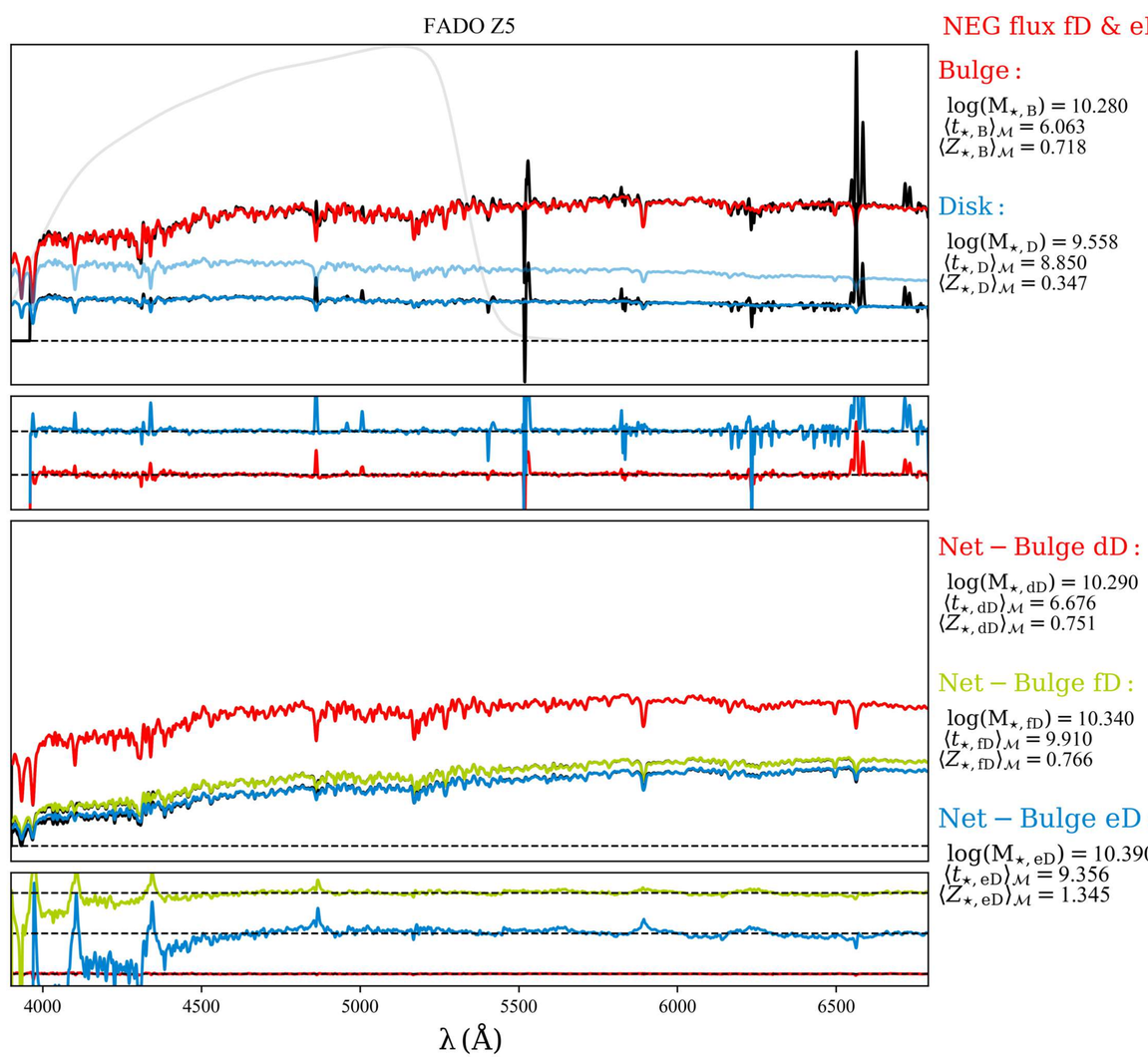
FADO Z5
NEG flux fD & eD
Bulge :
log(M⋆, B) = 10.280
⟨t⋆, B⟩M = 6.063
⟨Z⋆, B⟩M = 0.718
Disk :
log(M⋆, D) = 9.558
⟨t⋆, D⟩M = 8.850
⟨Z⋆, D⟩M = 0.347
Net − Bulge dD :
log(M⋆, dD) = 10.290
⟨t⋆, dD⟩M = 6.676
⟨Z⋆, dD⟩M = 0.751
Net − Bulge fD :
log(M⋆, fD) = 10.340
⟨t⋆, fD⟩M = 9.910
⟨Z⋆, fD⟩M = 0.766
Net − Bulge eD :
log(M⋆, eD) = 10.390
⟨t⋆, eD⟩M = 9.356
⟨Z⋆, eD⟩M = 1.345
λ (Å)

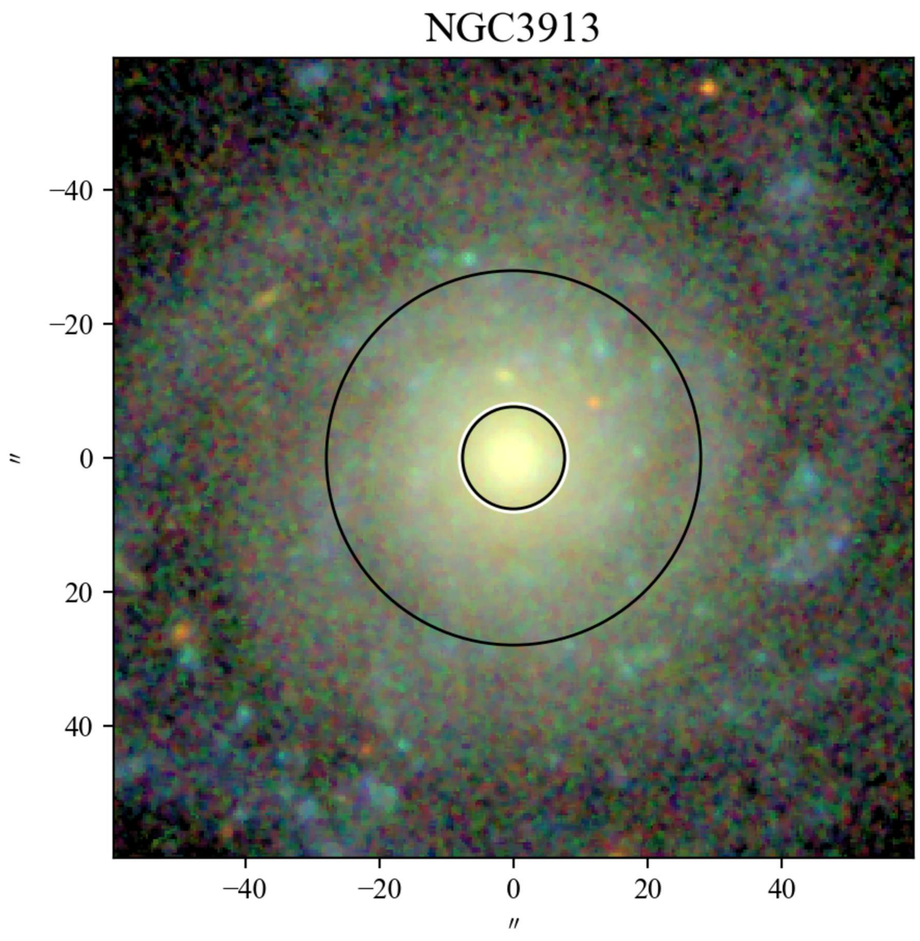
NGC3913
−40
−20
0
20
40
″

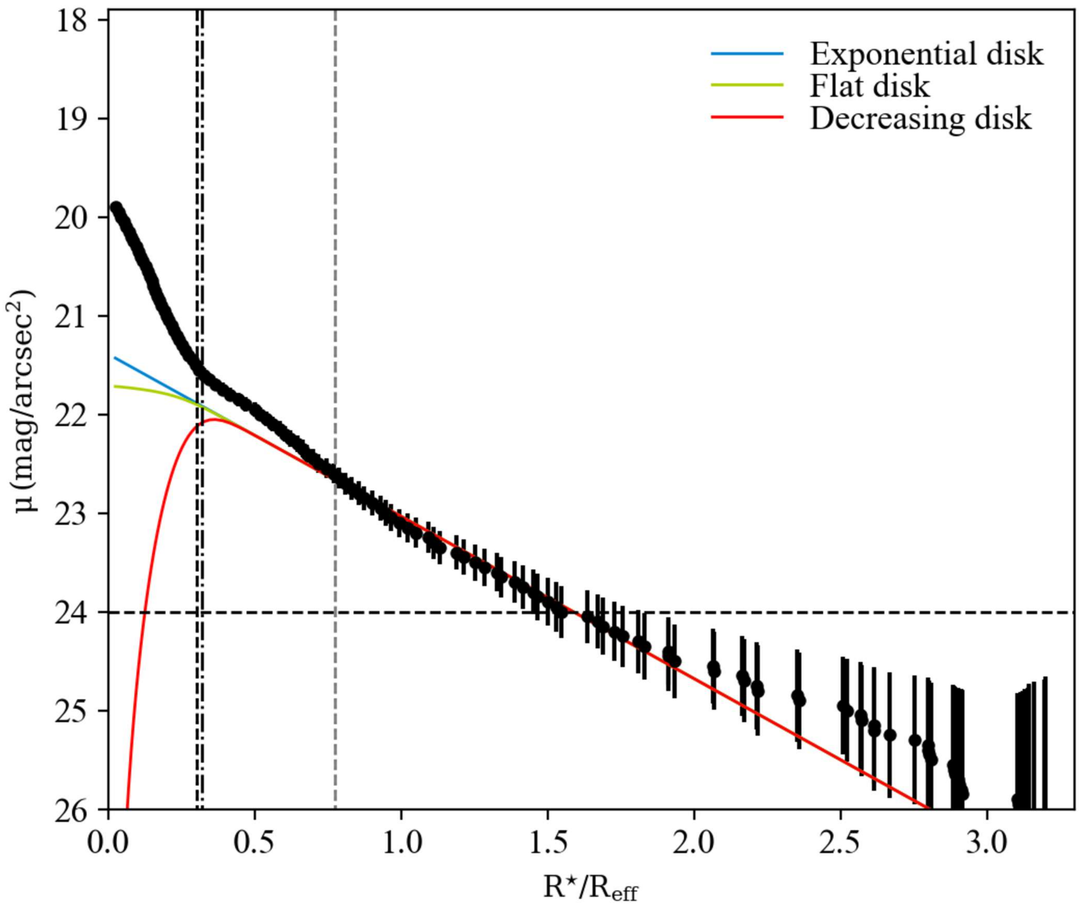
Exponential disk
Flat disk
Decreasing disk
μ (mag/arcsec²)
R⋆/Reff

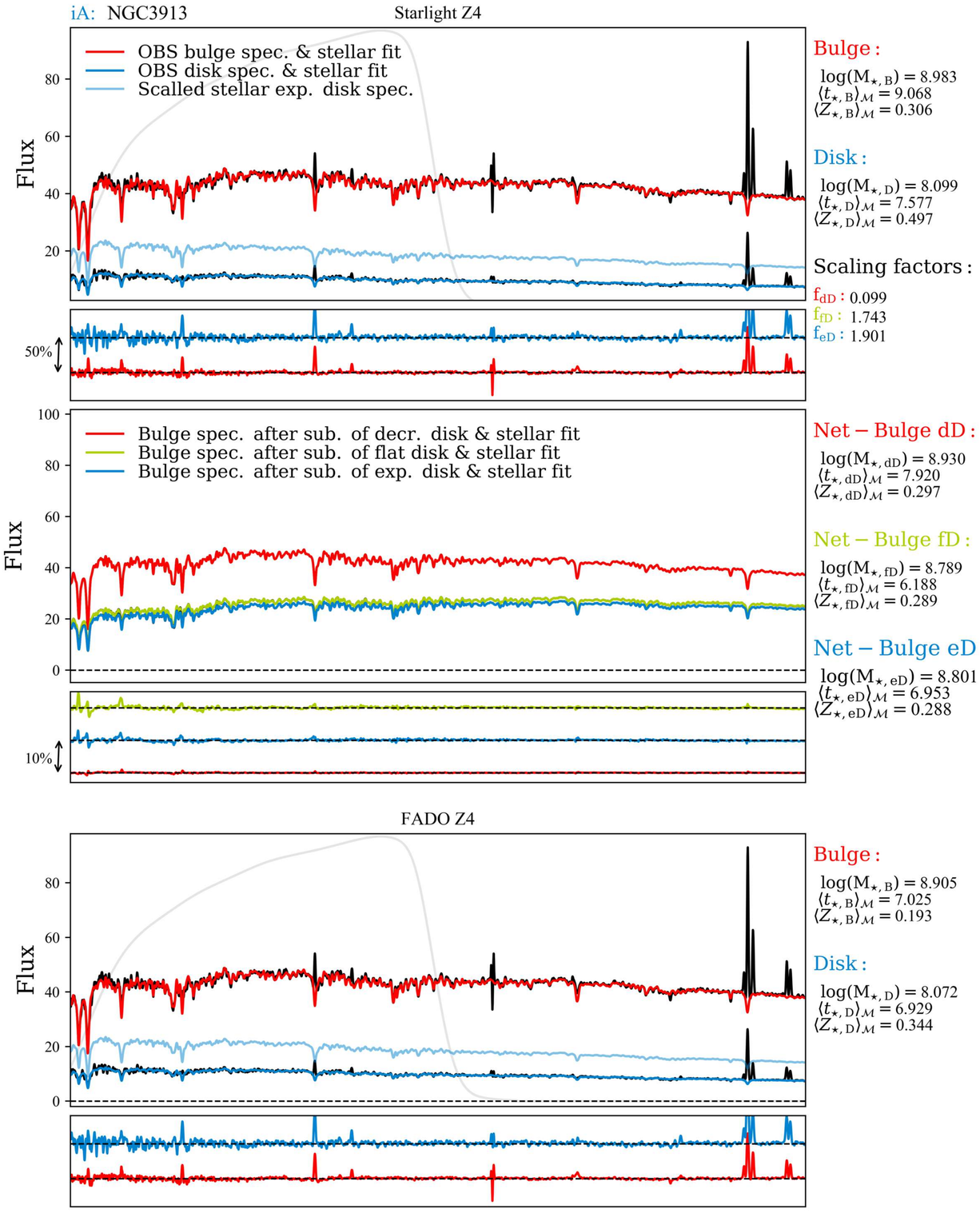
iA: NGC3913
Starlight Z4
OBS bulge spec. & stellar fit
OBS disk spec. & stellar fit
Scalled stellar exp. disk spec.
Flux
50%
Bulge spec. after sub. of decr. disk & stellar fit
Bulge spec. after sub. of flat disk & stellar fit
Bulge spec. after sub. of exp. disk & stellar fit
10%
Bulge :
log(M⋆, B) = 8.983
⟨t⋆, B⟩M = 9.068
⟨Z⋆, B⟩M = 0.306
Disk :
log(M⋆, D) = 8.099
⟨t⋆, D⟩M = 7.577
⟨Z⋆, D⟩M = 0.497
Scaling factors :
fdD : 0.099
ffD : 1.743
feD : 1.901
Net − Bulge dD :
log(M⋆, dD) = 8.930
⟨t⋆, dD⟩M = 7.920
⟨Z⋆, dD⟩M = 0.297
Net − Bulge fD :
log(M⋆, fD) = 8.789
⟨t⋆, fD⟩M = 6.188
⟨Z⋆, fD⟩M = 0.289
Net − Bulge eD :
log(M⋆, eD) = 8.801
⟨t⋆, eD⟩M = 6.953
⟨Z⋆, eD⟩M = 0.288

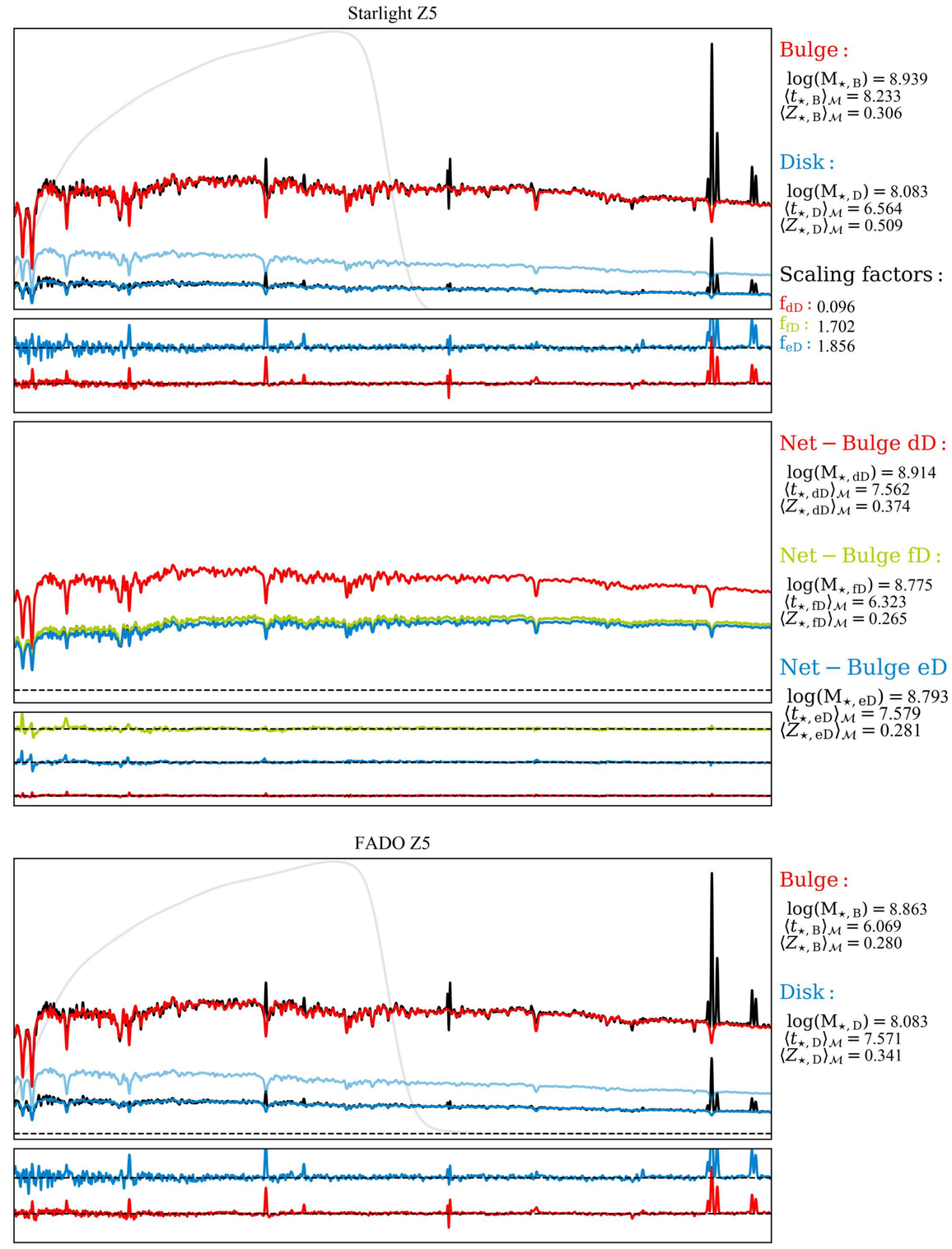
Starlight Z5
Bulge :
log(M⋆, B) = 8.939
⟨t⋆, B⟩M = 8.233
⟨Z⋆, B⟩M = 0.306
Disk :
log(M⋆, D) = 8.083
⟨t⋆, D⟩M = 6.564
⟨Z⋆, D⟩M = 0.509
Scaling factors :
fdD : 0.096
ffD : 1.702
feD : 1.856
Net − Bulge dD :
log(M⋆, dD) = 8.914
⟨t⋆, dD⟩M = 7.562
⟨Z⋆, dD⟩M = 0.374
Net − Bulge fD :
log(M⋆, fD) = 8.775
⟨t⋆, fD⟩M = 6.323
⟨Z⋆, fD⟩M = 0.265
Net − Bulge eD :
log(M⋆, eD) = 8.793
⟨t⋆, eD⟩M = 7.579
⟨Z⋆, eD⟩M = 0.281

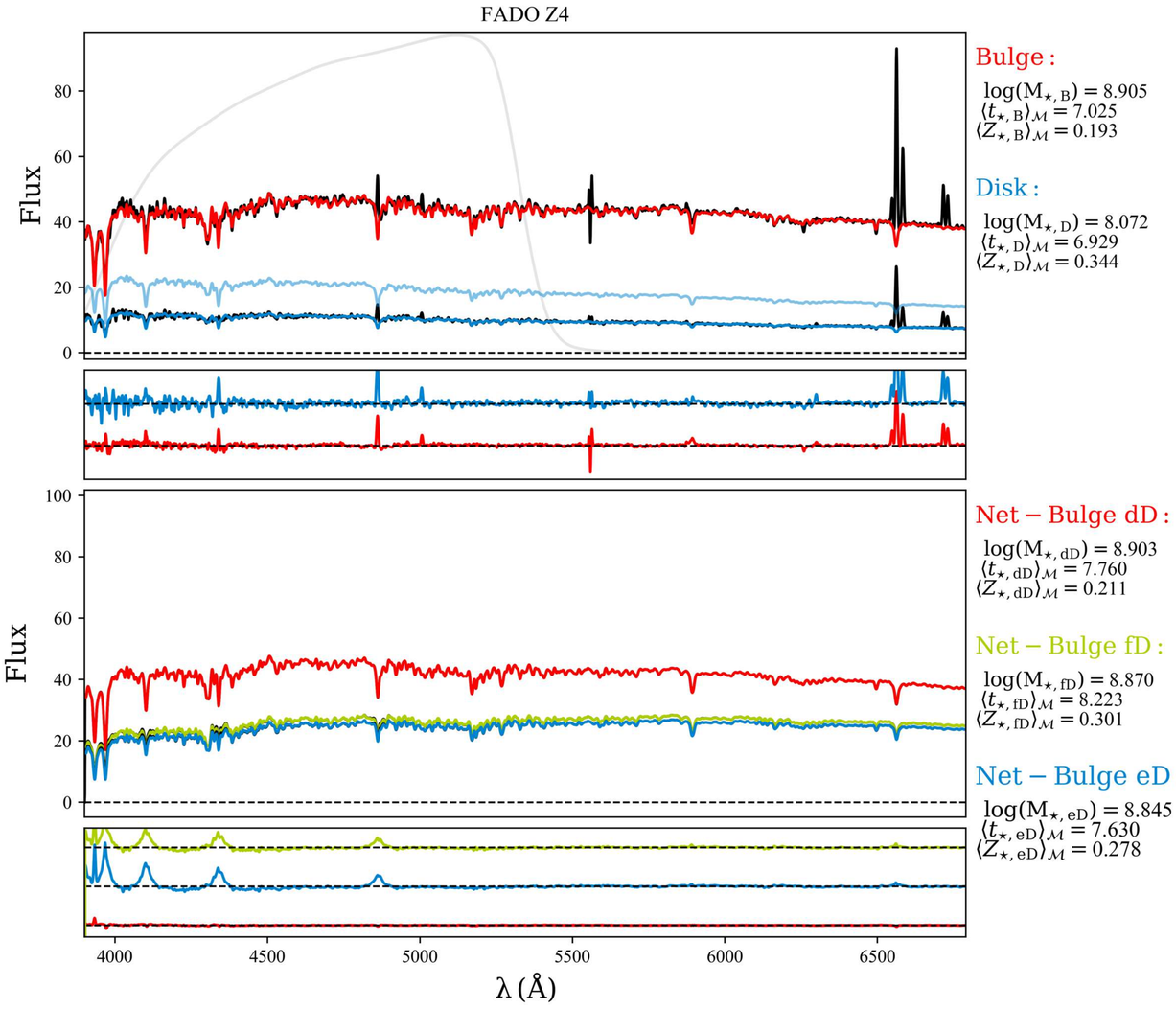
FADO Z4
Flux
Bulge :
log(M⋆, B) = 8.905
⟨t⋆, B⟩M = 7.025
⟨Z⋆, B⟩M = 0.193
Disk :
log(M⋆, D) = 8.072
⟨t⋆, D⟩M = 6.929
⟨Z⋆, D⟩M = 0.344
Net − Bulge dD :
log(M⋆, dD) = 8.903
⟨t⋆, dD⟩M = 7.760
⟨Z⋆, dD⟩M = 0.211
Net − Bulge fD :
log(M⋆, fD) = 8.870
⟨t⋆, fD⟩M = 8.223
⟨Z⋆, fD⟩M = 0.301
Net − Bulge eD :
log(M⋆, eD) = 8.845
⟨t⋆, eD⟩M = 7.630
⟨Z⋆, eD⟩M = 0.278
λ (Å)

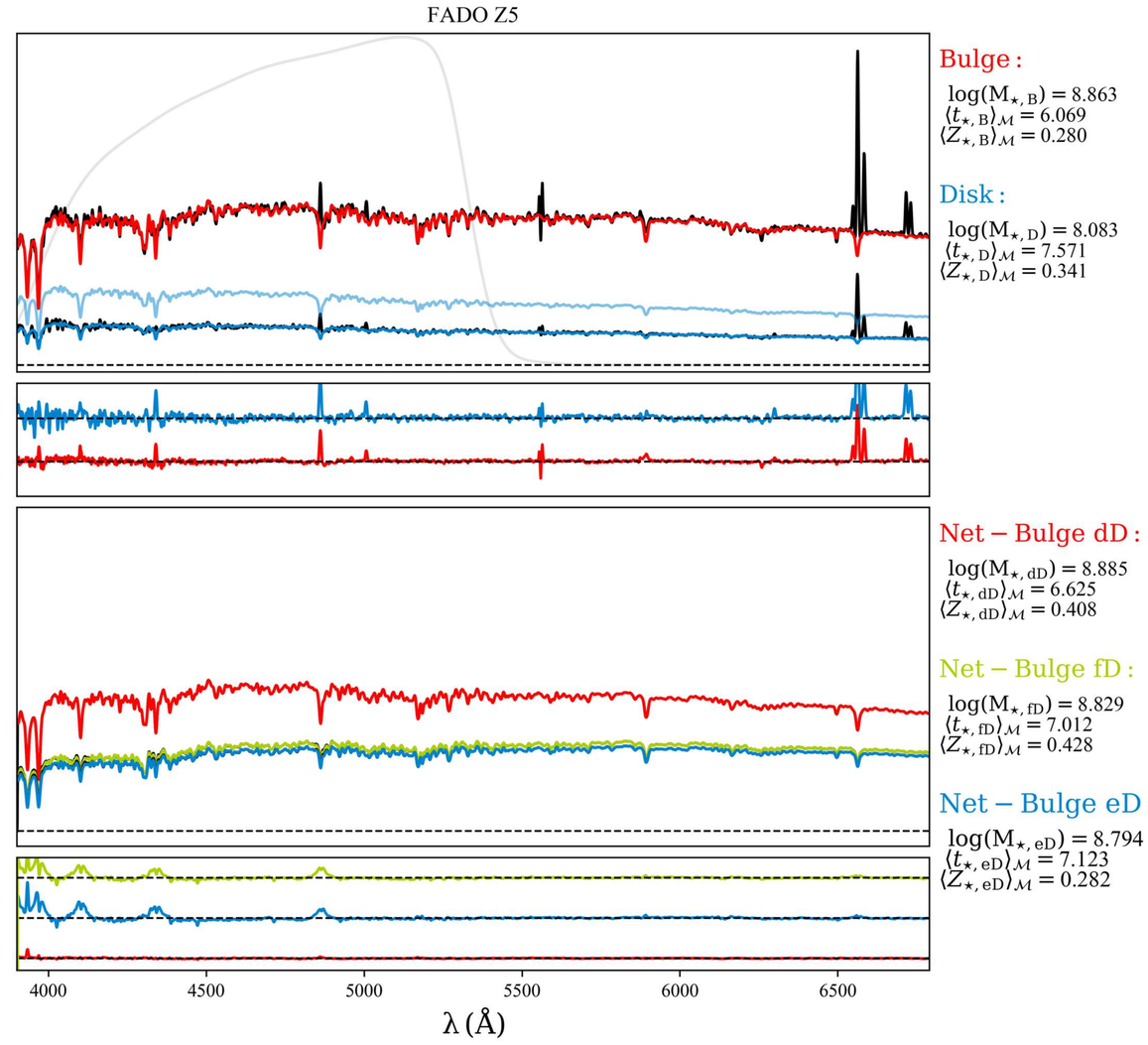
FADO Z5
Bulge :
log(M⋆, B) = 8.863
⟨t⋆, B⟩M = 6.069
⟨Z⋆, B⟩M = 0.280
Disk :
log(M⋆, D) = 8.083
⟨t⋆, D⟩M = 7.571
⟨Z⋆, D⟩M = 0.341
Net − Bulge dD :
log(M⋆, dD) = 8.885
⟨t⋆, dD⟩M = 6.625
⟨Z⋆, dD⟩M = 0.408
Net − Bulge fD :
log(M⋆, fD) = 8.829
⟨t⋆, fD⟩M = 7.012
⟨Z⋆, fD⟩M = 0.428
Net − Bulge eD :
log(M⋆, eD) = 8.794
⟨t⋆, eD⟩M = 7.123
⟨Z⋆, eD⟩M = 0.282
λ (Å)

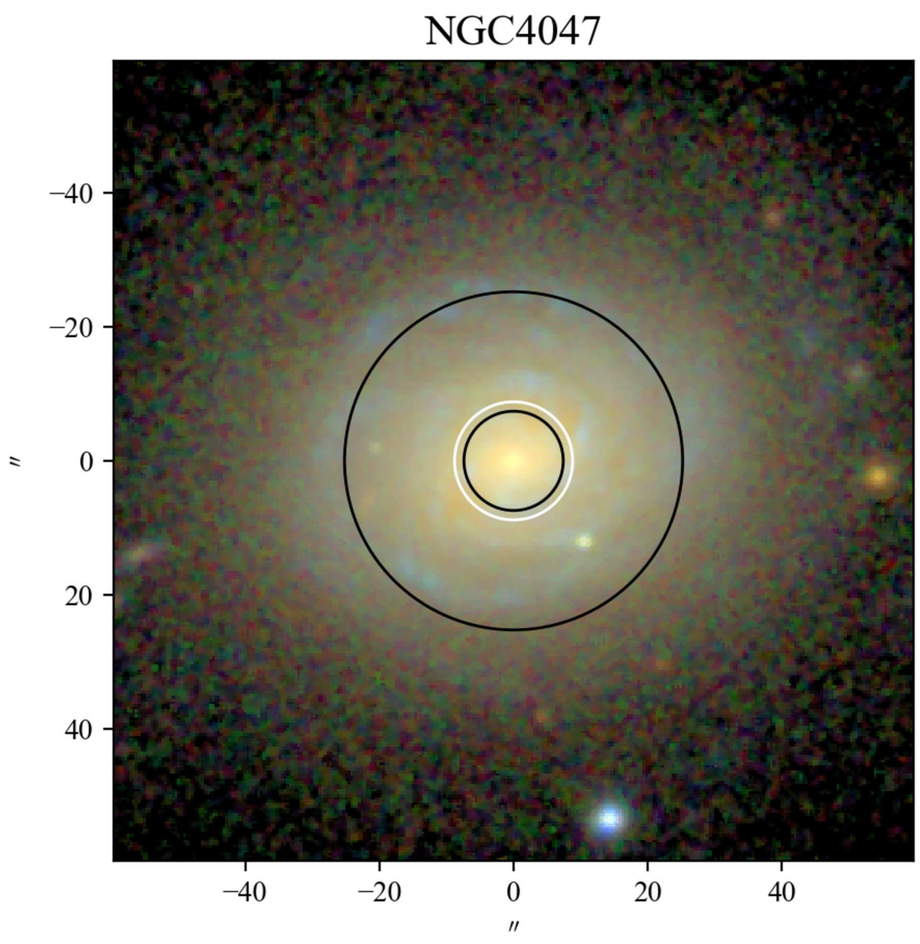
NGC4047
−40
−20
0
20
40
″
−40
−20
0
20
40
″

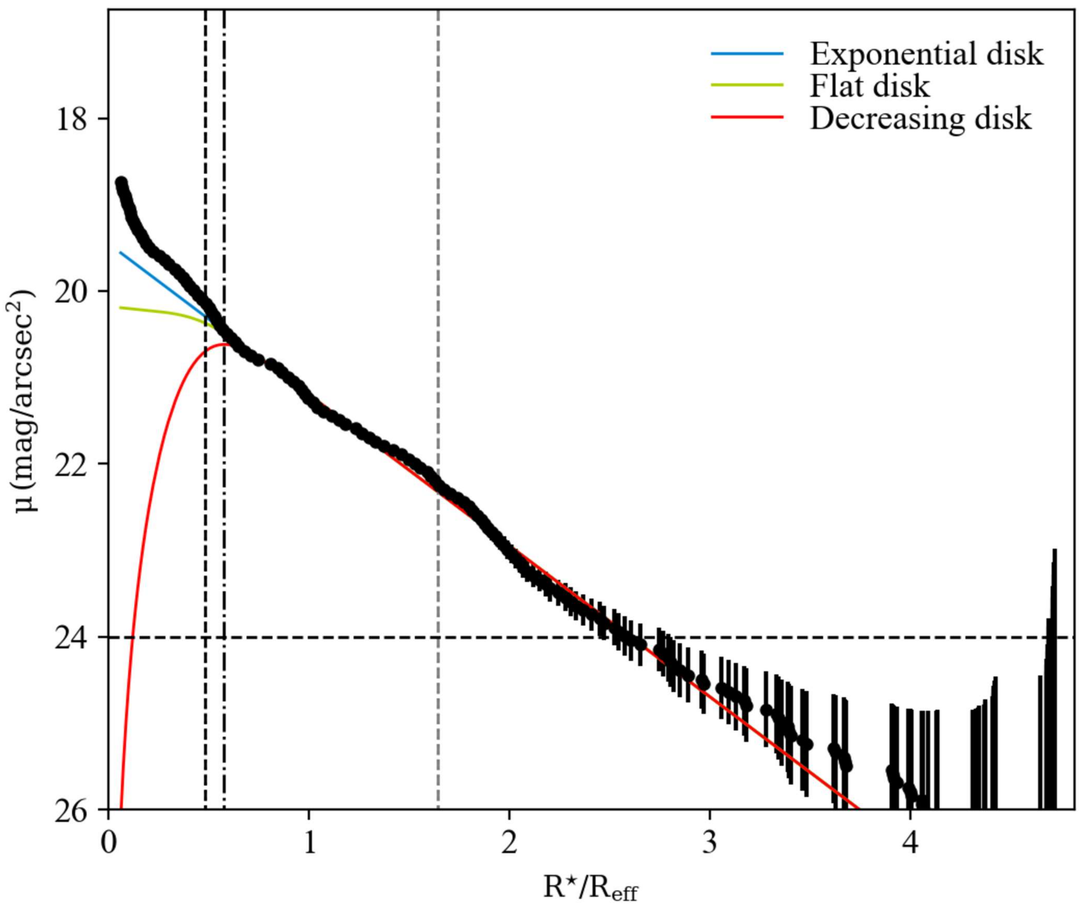
Exponential disk
Flat disk
Decreasing disk
μ (mag/arcsec²)
18
20
22
24
26
0
1
2
3
4
R⋆/Reff

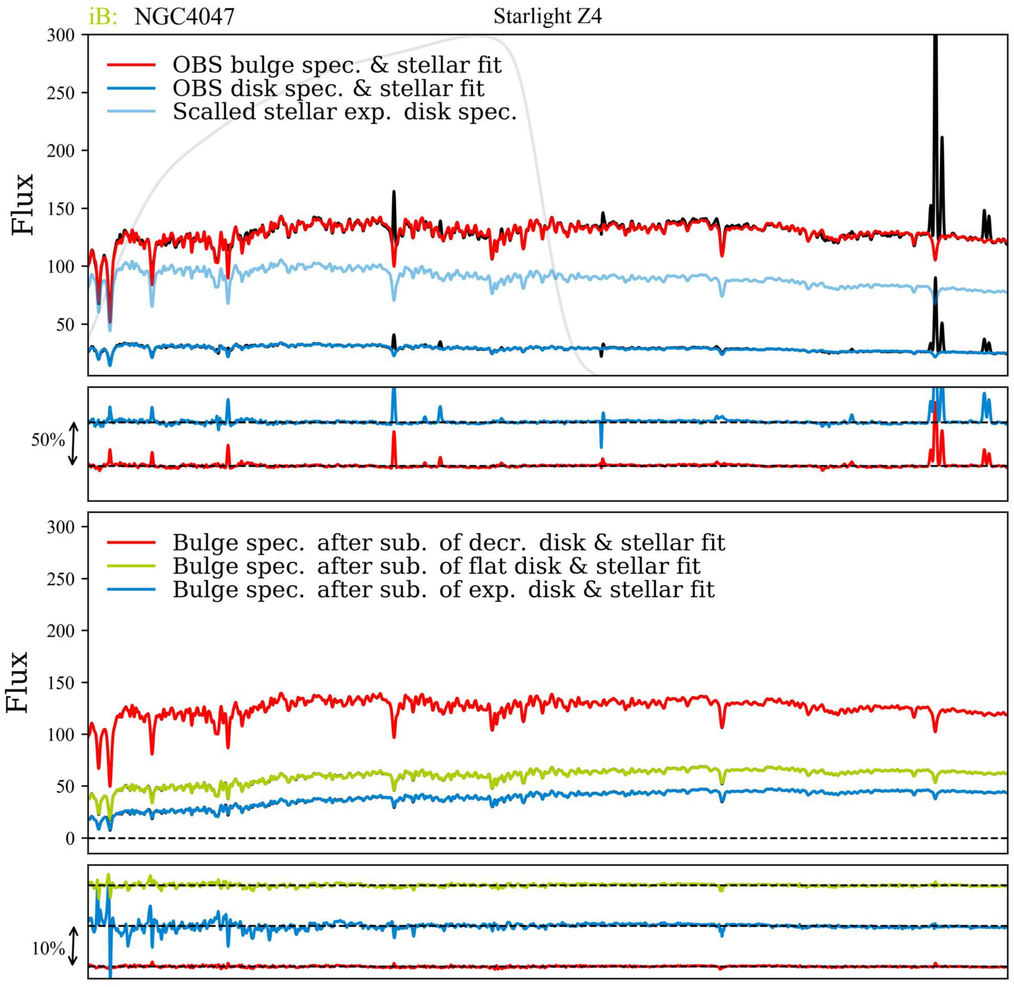
iB: NGC4047
Starlight Z4
OBS bulge spec. & stellar fit
OBS disk spec. & stellar fit
Scalled stellar exp. disk spec.
Flux
50%
Bulge :
log(M⋆, B) = 10.609
⟨t⋆, B⟩M = 10.495
⟨Z⋆, B⟩M = 0.799
Disk :
log(M⋆, D) = 9.844
⟨t⋆, D⟩M = 10.556
⟨Z⋆, D⟩M = 0.777
Scaling factors :
fdD : 0.104
ffD : 2.388
feD : 3.120
Bulge spec. after sub. of decr. disk & stellar fit
Bulge spec. after sub. of flat disk & stellar fit
Bulge spec. after sub. of exp. disk & stellar fit
10%
Net − Bulge dD :
log(M⋆, dD) = 10.580
⟨t⋆, dD⟩M = 9.953
⟨Z⋆, dD⟩M = 0.802
Net − Bulge fD :
log(M⋆, fD) = 10.320
⟨t⋆, fD⟩M = 9.164
⟨Z⋆, fD⟩M = 0.808
Net − Bulge eD :
log(M⋆, eD) = 10.203
⟨t⋆, eD⟩M = 8.192
⟨Z⋆, eD⟩M = 0.851

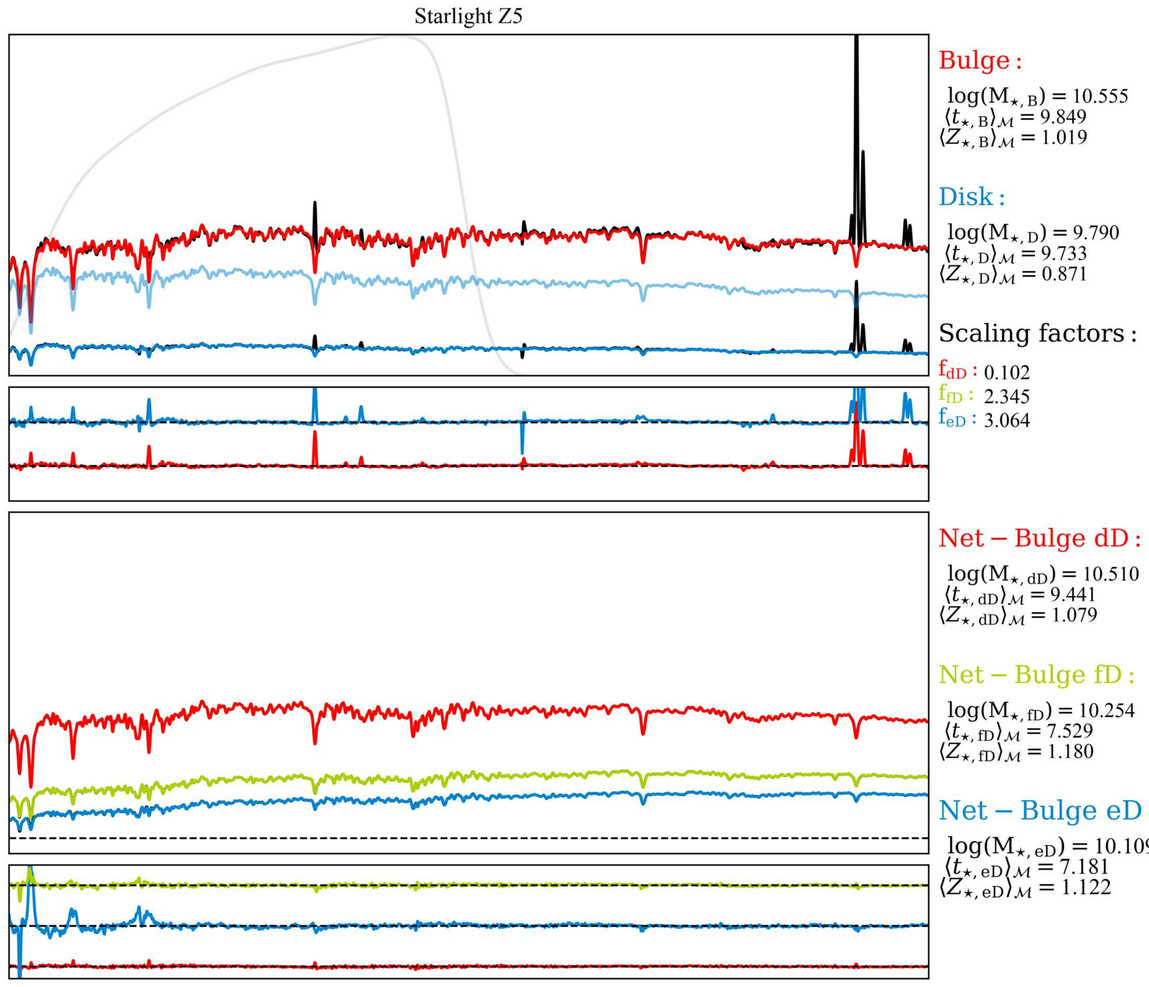
Starlight Z5
Bulge :
log(M⋆, B) = 10.555
⟨t⋆, B⟩M = 9.849
⟨Z⋆, B⟩M = 1.019
Disk :
log(M⋆, D) = 9.790
⟨t⋆, D⟩M = 9.733
⟨Z⋆, D⟩M = 0.871
Scaling factors :
fdD : 0.102
ffD : 2.345
feD : 3.064
Net − Bulge dD :
log(M⋆, dD) = 10.510
⟨t⋆, dD⟩M = 9.441
⟨Z⋆, dD⟩M = 1.079
Net − Bulge fD :
log(M⋆, fD) = 10.254
⟨t⋆, fD⟩M = 7.529
⟨Z⋆, fD⟩M = 1.180
Net − Bulge eD :
log(M⋆, eD) = 10.109
⟨t⋆, eD⟩M = 7.181
⟨Z⋆, eD⟩M = 1.122

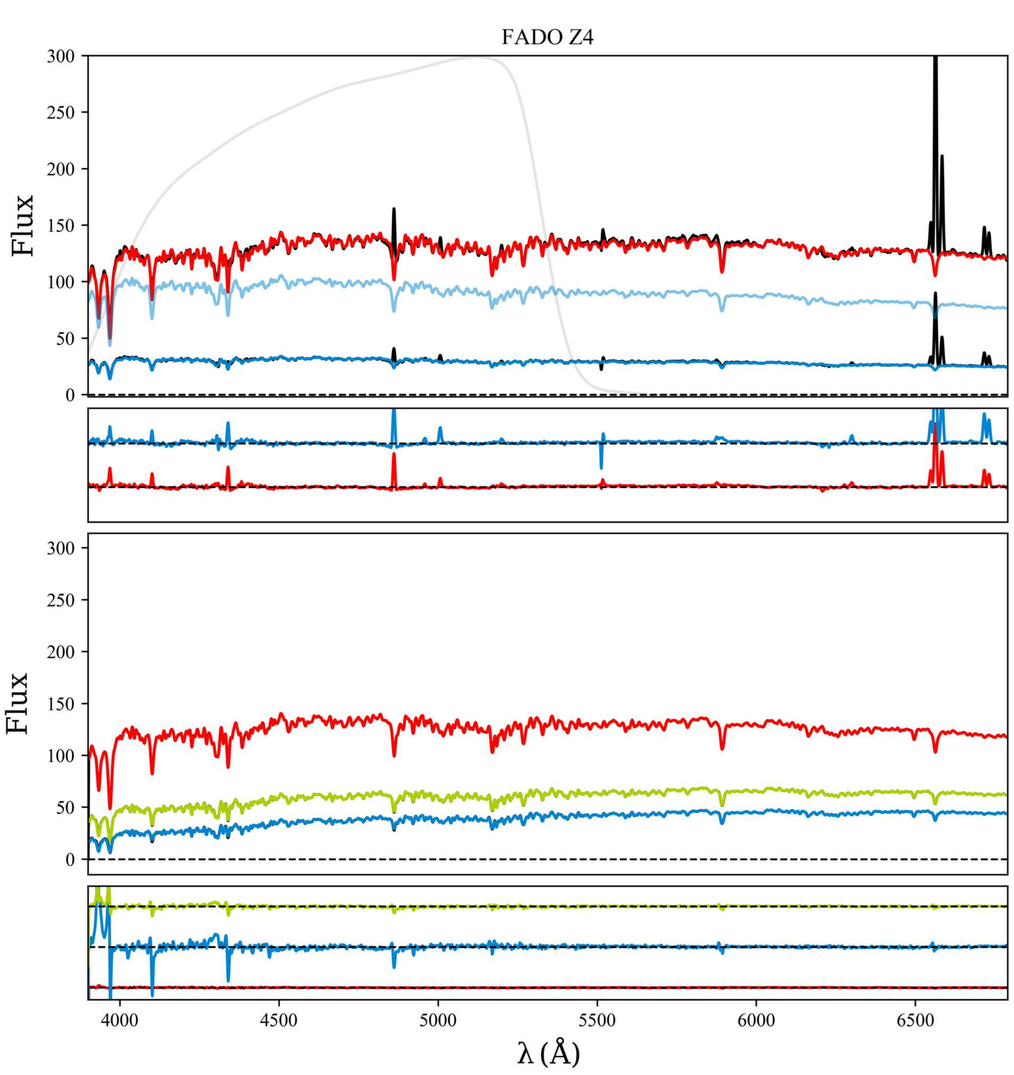
FADO Z4
Flux
Bulge :
log(M⋆, B) = 10.540
⟨t⋆, B⟩M = 8.513
⟨Z⋆, B⟩M = 0.756
Disk :
log(M⋆, D) = 9.683
⟨t⋆, D⟩M = 8.893
⟨Z⋆, D⟩M = 0.509
Net − Bulge dD :
log(M⋆, dD) = 10.520
⟨t⋆, dD⟩M = 9.130
⟨Z⋆, dD⟩M = 0.755
Net − Bulge fD :
log(M⋆, fD) = 10.320
⟨t⋆, fD⟩M = 7.968
⟨Z⋆, fD⟩M = 0.882
Net − Bulge eD :
log(M⋆, eD) = 10.310
⟨t⋆, eD⟩M = 8.607
⟨Z⋆, eD⟩M = 0.970
λ (Å)

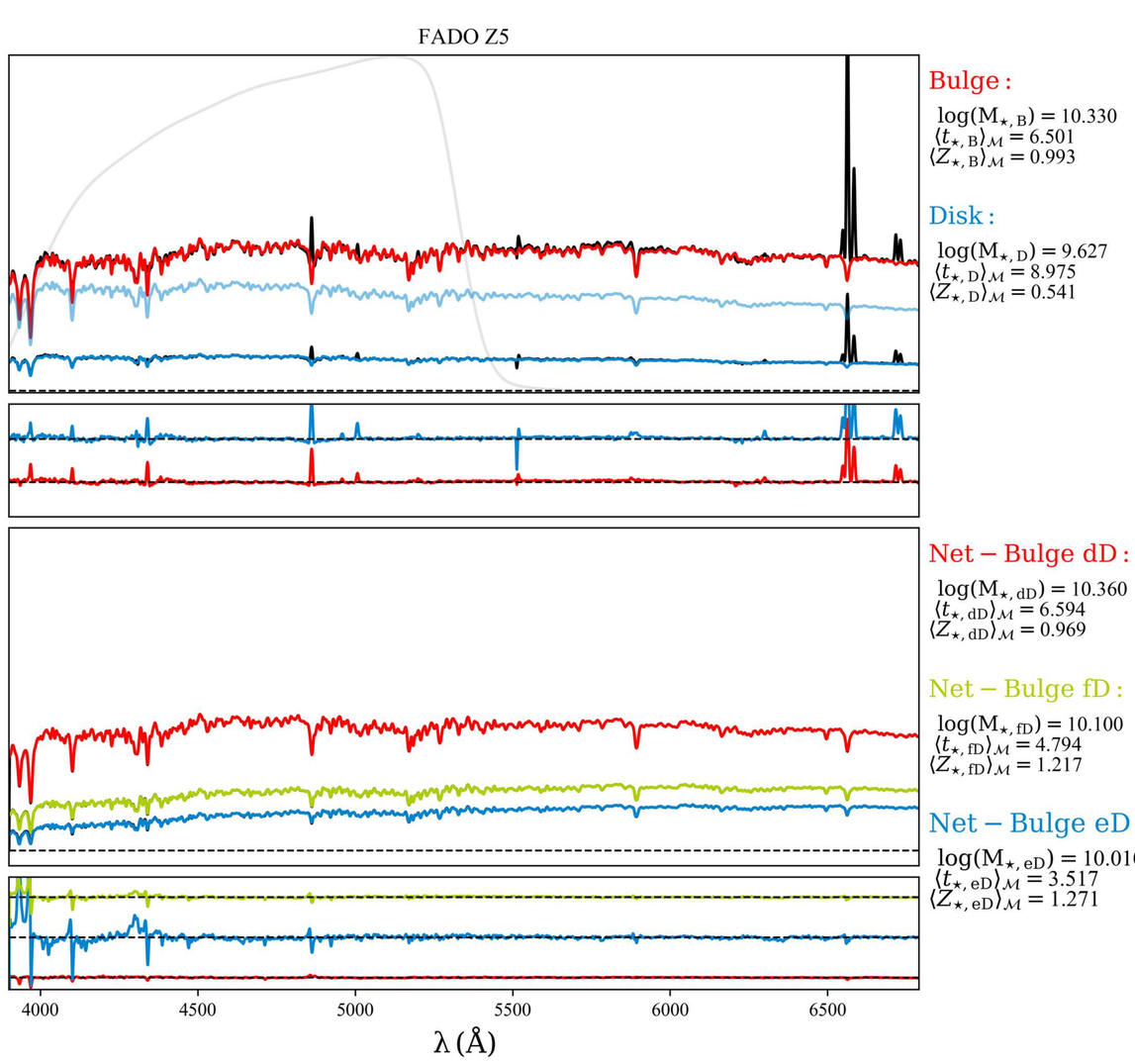
FADO Z5
Bulge :
log(M⋆, B) = 10.330
⟨t⋆, B⟩M = 6.501
⟨Z⋆, B⟩M = 0.993
Disk :
log(M⋆, D) = 9.627
⟨t⋆, D⟩M = 8.975
⟨Z⋆, D⟩M = 0.541
Net − Bulge dD :
log(M⋆, dD) = 10.360
⟨t⋆, dD⟩M = 6.594
⟨Z⋆, dD⟩M = 0.969
Net − Bulge fD :
log(M⋆, fD) = 10.100
⟨t⋆, fD⟩M = 4.794
⟨Z⋆, fD⟩M = 1.217
Net − Bulge eD :
log(M⋆, eD) = 10.010
⟨t⋆, eD⟩M = 3.517
⟨Z⋆, eD⟩M = 1.271
λ (Å)

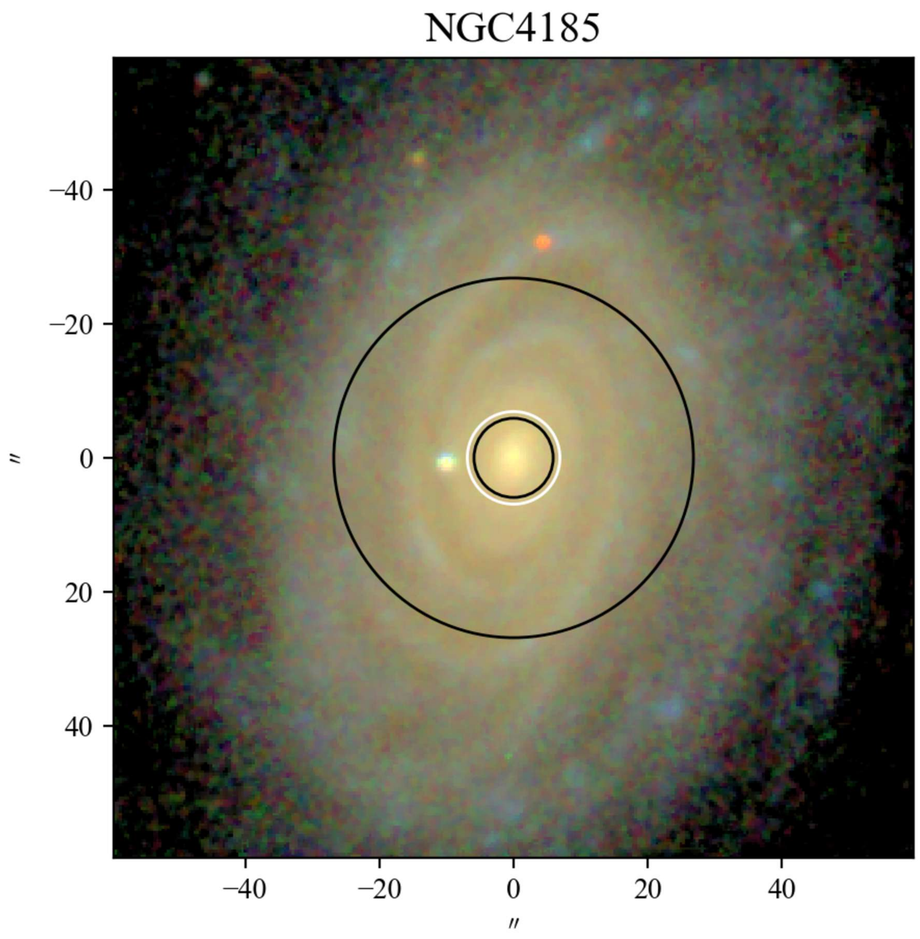
NGC4185
″
−40
−20
0
20
40

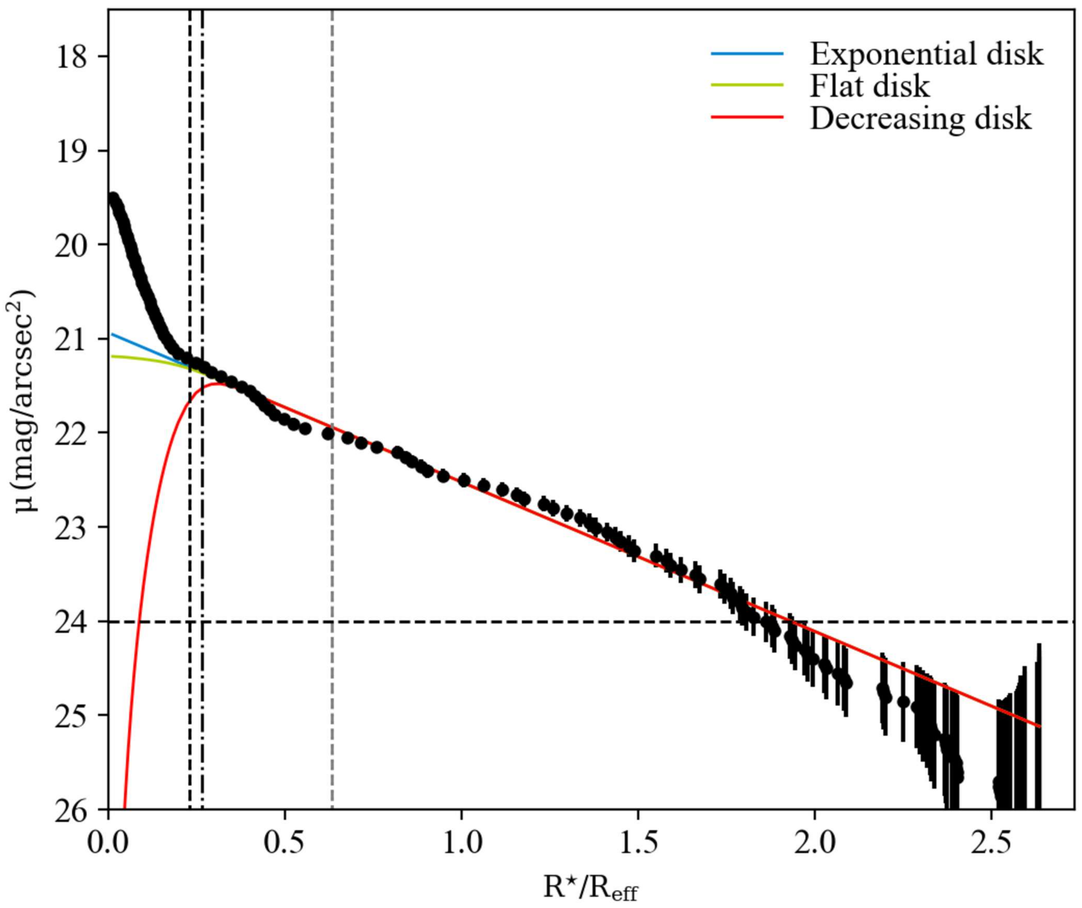
Exponential disk
Flat disk
Decreasing disk
μ (mag/arcsec²)
R⋆/R_eff

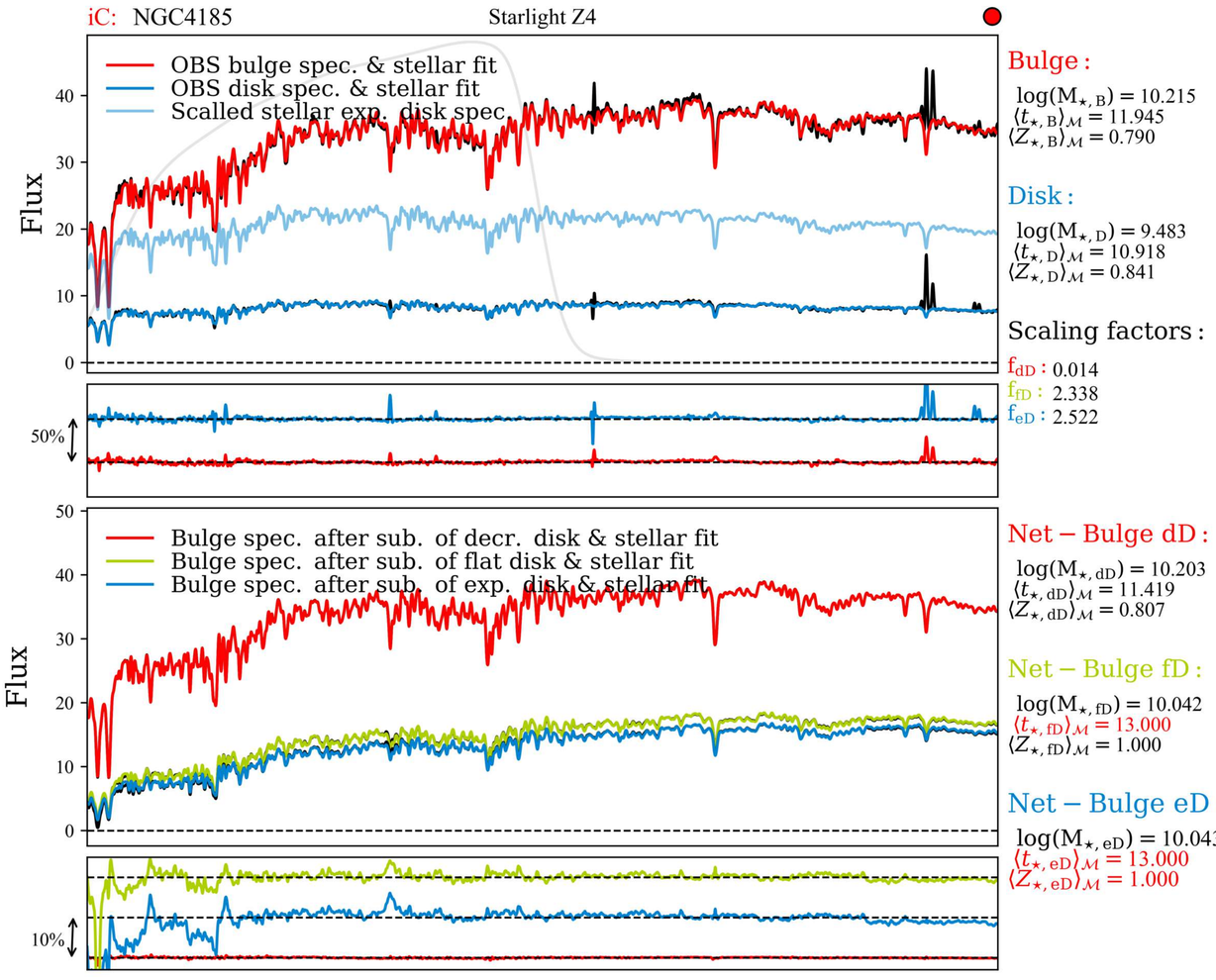
iC: NGC4185
Starlight Z4
OBS bulge spec. & stellar fit
OBS disk spec. & stellar fit
Scalled stellar exp. disk spec.
Flux
50%
Bulge spec. after sub. of decr. disk & stellar fit
Bulge spec. after sub. of flat disk & stellar fit
Bulge spec. after sub. of exp. disk & stellar fit
10%
Bulge :
log(M⋆, B) = 10.215
⟨t⋆, B⟩M = 11.945
⟨Z⋆, B⟩M = 0.790
Disk :
log(M⋆, D) = 9.483
⟨t⋆, D⟩M = 10.918
⟨Z⋆, D⟩M = 0.841
Scaling factors :
fdD : 0.014
ffD : 2.338
feD : 2.522
Net − Bulge dD :
log(M⋆, dD) = 10.203
⟨t⋆, dD⟩M = 11.419
⟨Z⋆, dD⟩M = 0.807
Net − Bulge fD :
log(M⋆, fD) = 10.042
⟨t⋆, fD⟩M = 13.000
⟨Z⋆, fD⟩M = 1.000
Net − Bulge eD :
log(M⋆, eD) = 10.043
⟨t⋆, eD⟩M = 13.000
⟨Z⋆, eD⟩M = 1.000

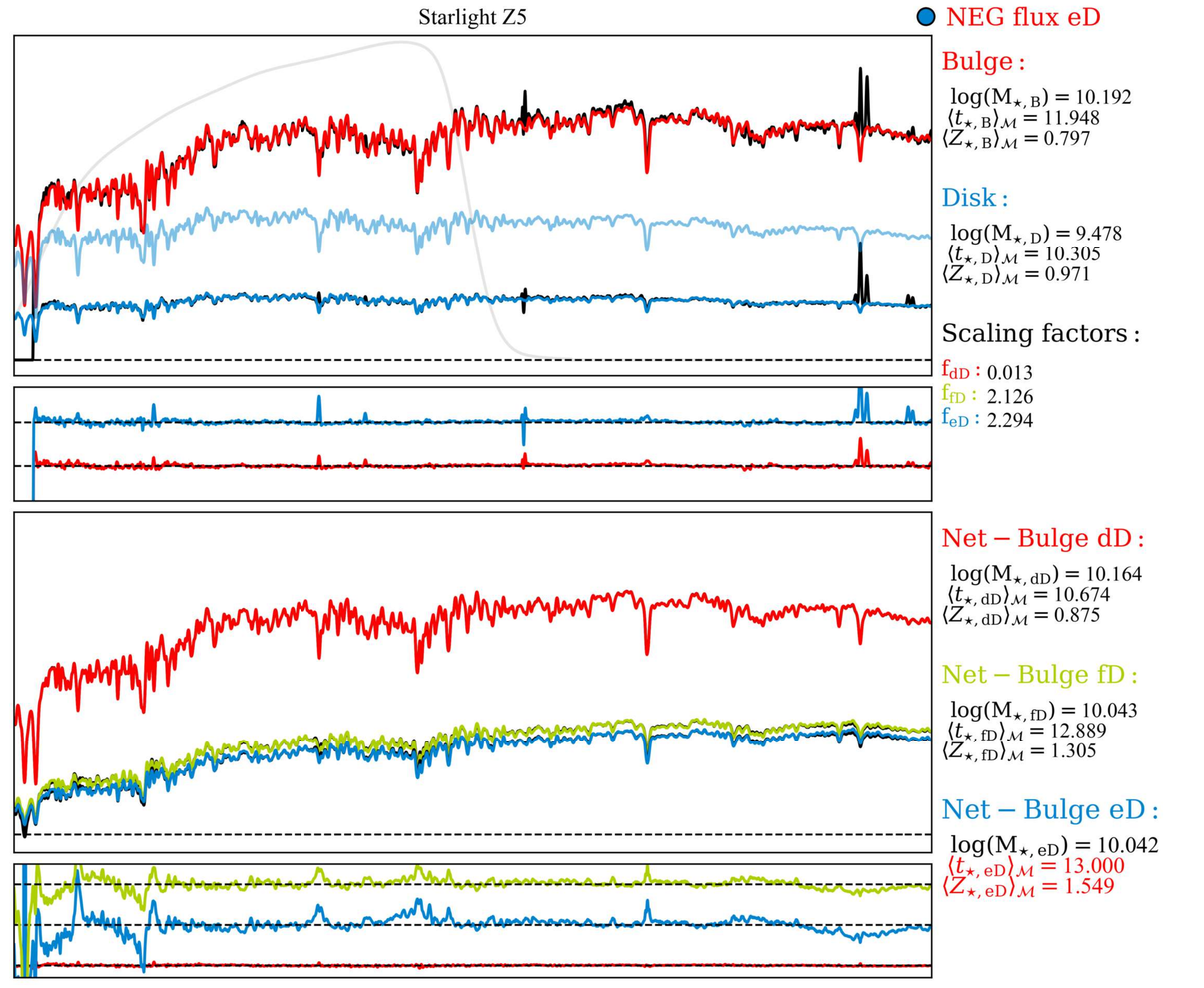
Starlight Z5
NEG flux eD
Bulge :
log(M⋆, B) = 10.192
⟨t⋆, B⟩M = 11.948
⟨Z⋆, B⟩M = 0.797
Disk :
log(M⋆, D) = 9.478
⟨t⋆, D⟩M = 10.305
⟨Z⋆, D⟩M = 0.971
Scaling factors :
fdD : 0.013
ffD : 2.126
feD : 2.294
Net − Bulge dD :
log(M⋆, dD) = 10.164
⟨t⋆, dD⟩M = 10.674
⟨Z⋆, dD⟩M = 0.875
Net − Bulge fD :
log(M⋆, fD) = 10.043
⟨t⋆, fD⟩M = 12.889
⟨Z⋆, fD⟩M = 1.305
Net − Bulge eD :
log(M⋆, eD) = 10.042
⟨t⋆, eD⟩M = 13.000
⟨Z⋆, eD⟩M = 1.549

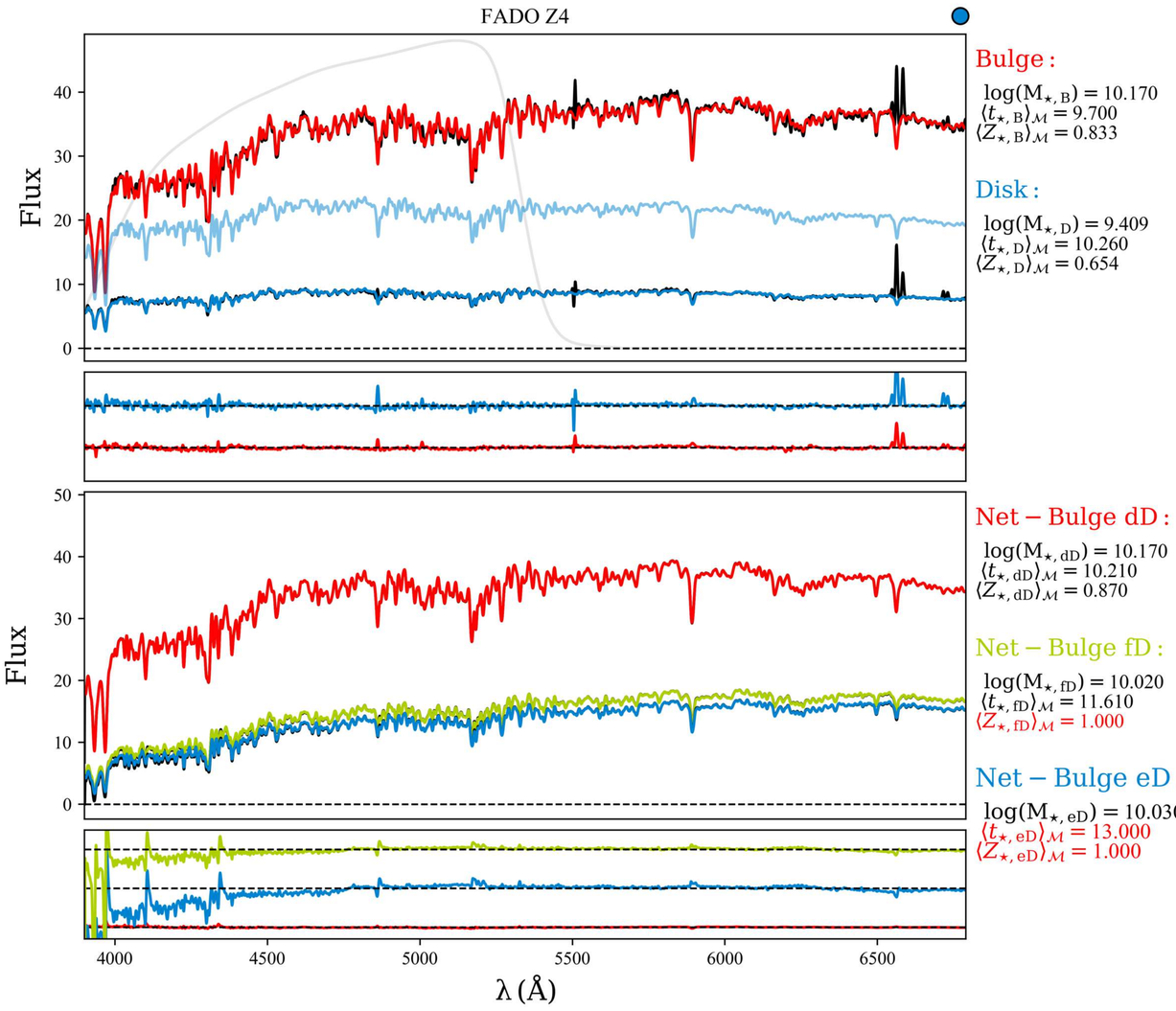
FADO Z4
Flux
Bulge :
log(M⋆, B) = 10.170
⟨t⋆, B⟩M = 9.700
⟨Z⋆, B⟩M = 0.833
Disk :
log(M⋆, D) = 9.409
⟨t⋆, D⟩M = 10.260
⟨Z⋆, D⟩M = 0.654
Net − Bulge dD :
log(M⋆, dD) = 10.170
⟨t⋆, dD⟩M = 10.210
⟨Z⋆, dD⟩M = 0.870
Net − Bulge fD :
log(M⋆, fD) = 10.020
⟨t⋆, fD⟩M = 11.610
⟨Z⋆, fD⟩M = 1.000
Net − Bulge eD :
log(M⋆, eD) = 10.030
⟨t⋆, eD⟩M = 13.000
⟨Z⋆, eD⟩M = 1.000
λ (Å)

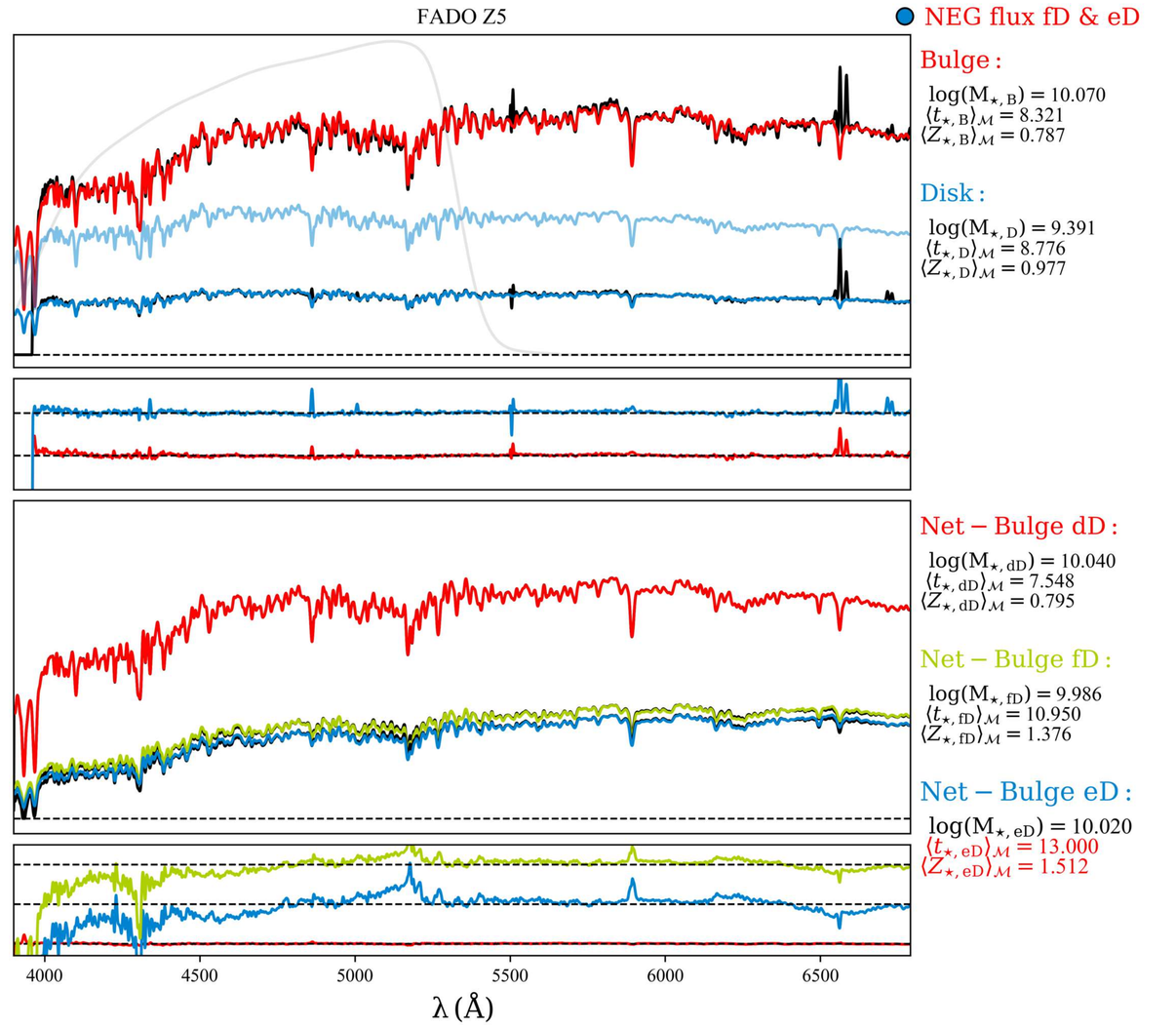
FADO Z5
NEG flux fD & eD
Bulge :
log(M⋆, B) = 10.070
⟨t⋆, B⟩M = 8.321
⟨Z⋆, B⟩M = 0.787
Disk :
log(M⋆, D) = 9.391
⟨t⋆, D⟩M = 8.776
⟨Z⋆, D⟩M = 0.977
Net − Bulge dD :
log(M⋆, dD) = 10.040
⟨t⋆, dD⟩M = 7.548
⟨Z⋆, dD⟩M = 0.795
Net − Bulge fD :
log(M⋆, fD) = 9.986
⟨t⋆, fD⟩M = 10.950
⟨Z⋆, fD⟩M = 1.376
Net − Bulge eD :
log(M⋆, eD) = 10.020
⟨t⋆, eD⟩M = 13.000
⟨Z⋆, eD⟩M = 1.512
λ (Å)

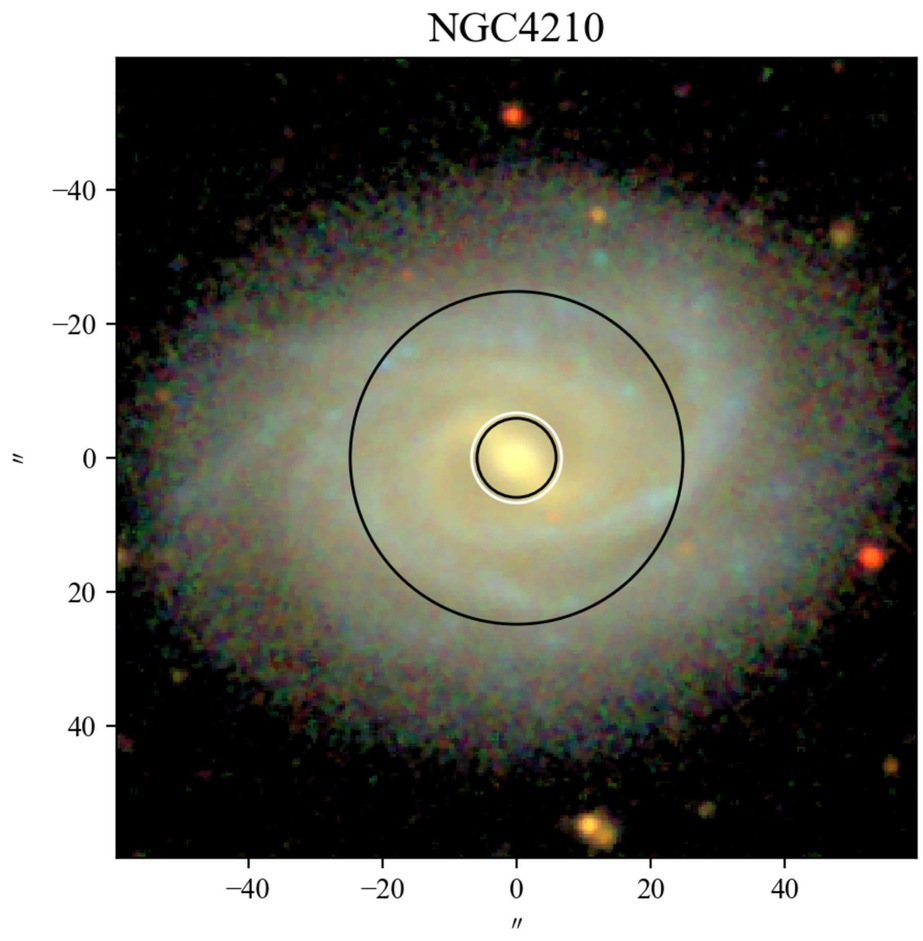
NGC4210
−40
−20
0
20
40
″
−40
−20
0
20
40
″

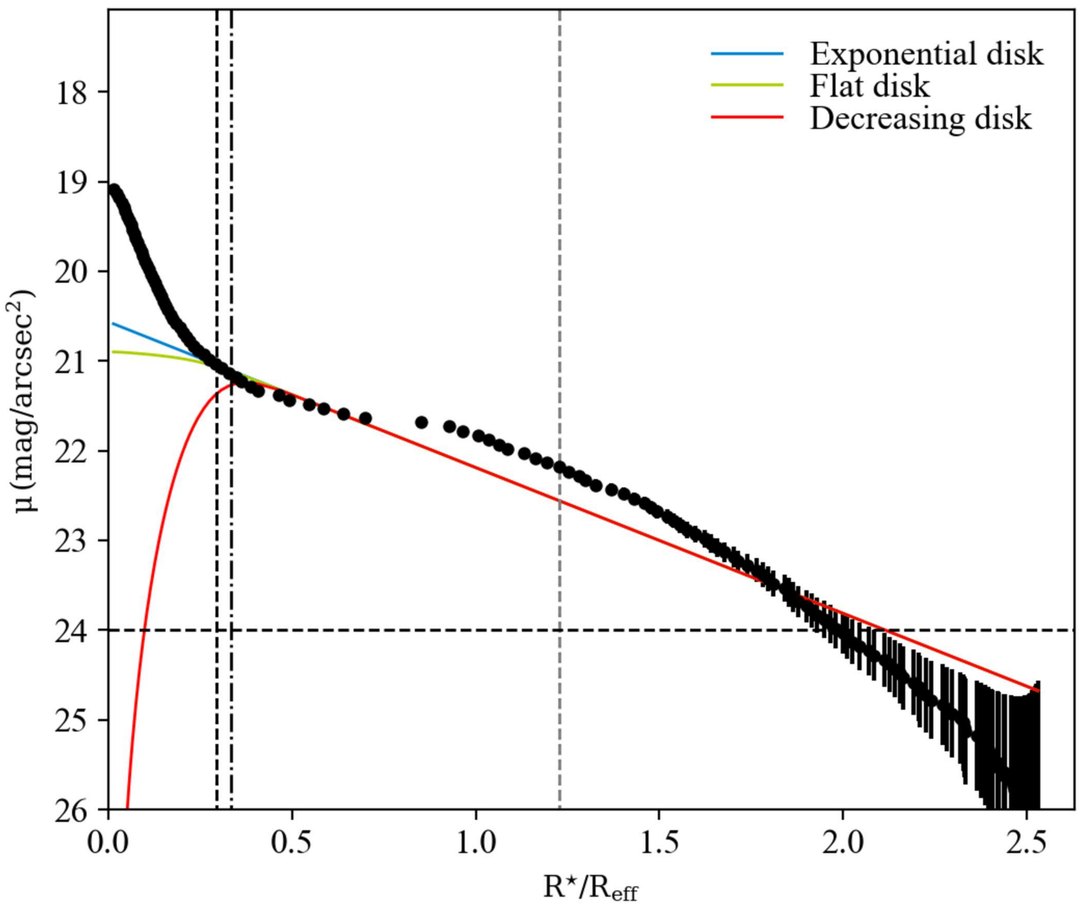
Exponential disk
Flat disk
Decreasing disk
μ (mag/arcsec²)
18
19
20
21
22
23
24
25
26
0.0
0.5
1.0
1.5
2.0
2.5
R⋆/Reff

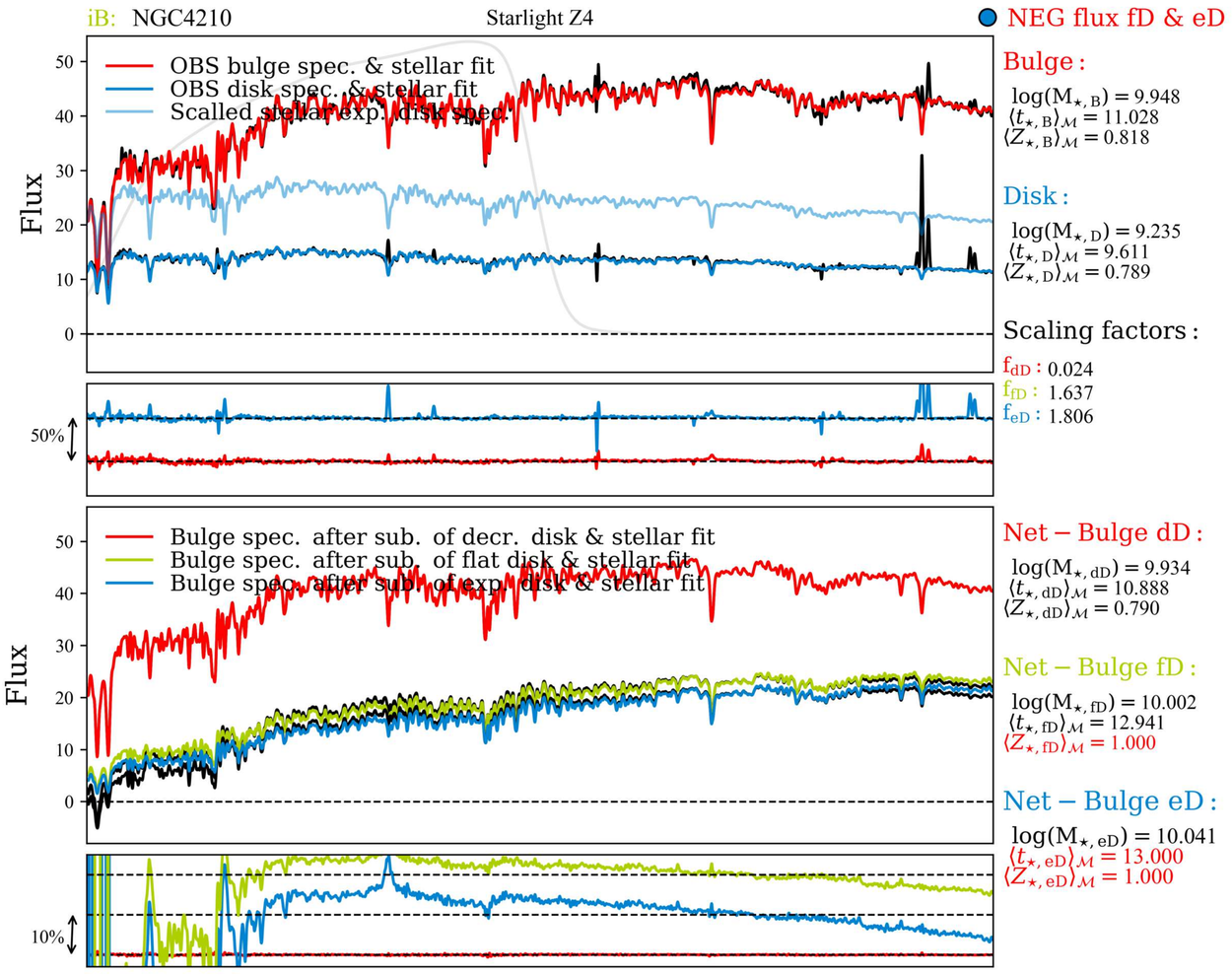
iB: NGC4210
Starlight Z4
NEG flux fD & eD
OBS bulge spec. & stellar fit
OBS disk spec. & stellar fit
Scalled stellar(exp) disk spec.
Flux
50%
Bulge :
log(M⋆, B) = 9.948
⟨t⋆, B⟩M = 11.028
⟨Z⋆, B⟩M = 0.818
Disk :
log(M⋆, D) = 9.235
⟨t⋆, D⟩M = 9.611
⟨Z⋆, D⟩M = 0.789
Scaling factors :
fdD : 0.024
ffD : 1.637
feD : 1.806
Bulge spec. after sub. of decr. disk & stellar fit
Bulge spec. after sub. of flat disk & stellar fit
Bulge spec. after sub. of exp. disk & stellar fit
10%
Net − Bulge dD :
log(M⋆, dD) = 9.934
⟨t⋆, dD⟩M = 10.888
⟨Z⋆, dD⟩M = 0.790
Net − Bulge fD :
log(M⋆, fD) = 10.002
⟨t⋆, fD⟩M = 12.941
⟨Z⋆, fD⟩M = 1.000
Net − Bulge eD :
log(M⋆, eD) = 10.041
⟨t⋆, eD⟩M = 13.000
⟨Z⋆, eD⟩M = 1.000

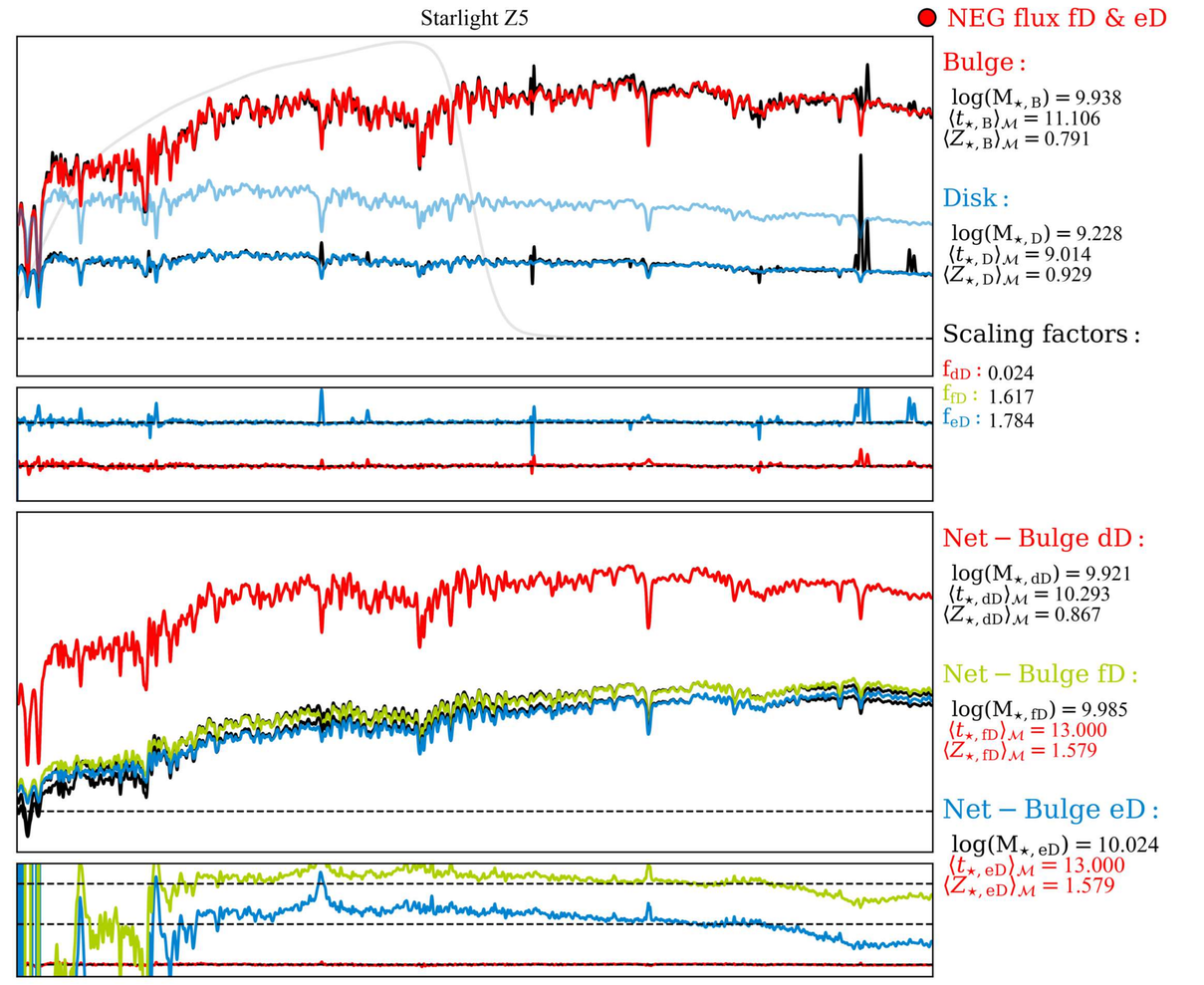
Starlight Z5
NEG flux fD & eD
Bulge :
log(M⋆, B) = 9.938
⟨t⋆, B⟩M = 11.106
⟨Z⋆, B⟩M = 0.791
Disk :
log(M⋆, D) = 9.228
⟨t⋆, D⟩M = 9.014
⟨Z⋆, D⟩M = 0.929
Scaling factors :
fdD : 0.024
ffD : 1.617
feD : 1.784
Net − Bulge dD :
log(M⋆, dD) = 9.921
⟨t⋆, dD⟩M = 10.293
⟨Z⋆, dD⟩M = 0.867
Net − Bulge fD :
log(M⋆, fD) = 9.985
⟨t⋆, fD⟩M = 13.000
⟨Z⋆, fD⟩M = 1.579
Net − Bulge eD :
log(M⋆, eD) = 10.024
⟨t⋆, eD⟩M = 13.000
⟨Z⋆, eD⟩M = 1.579

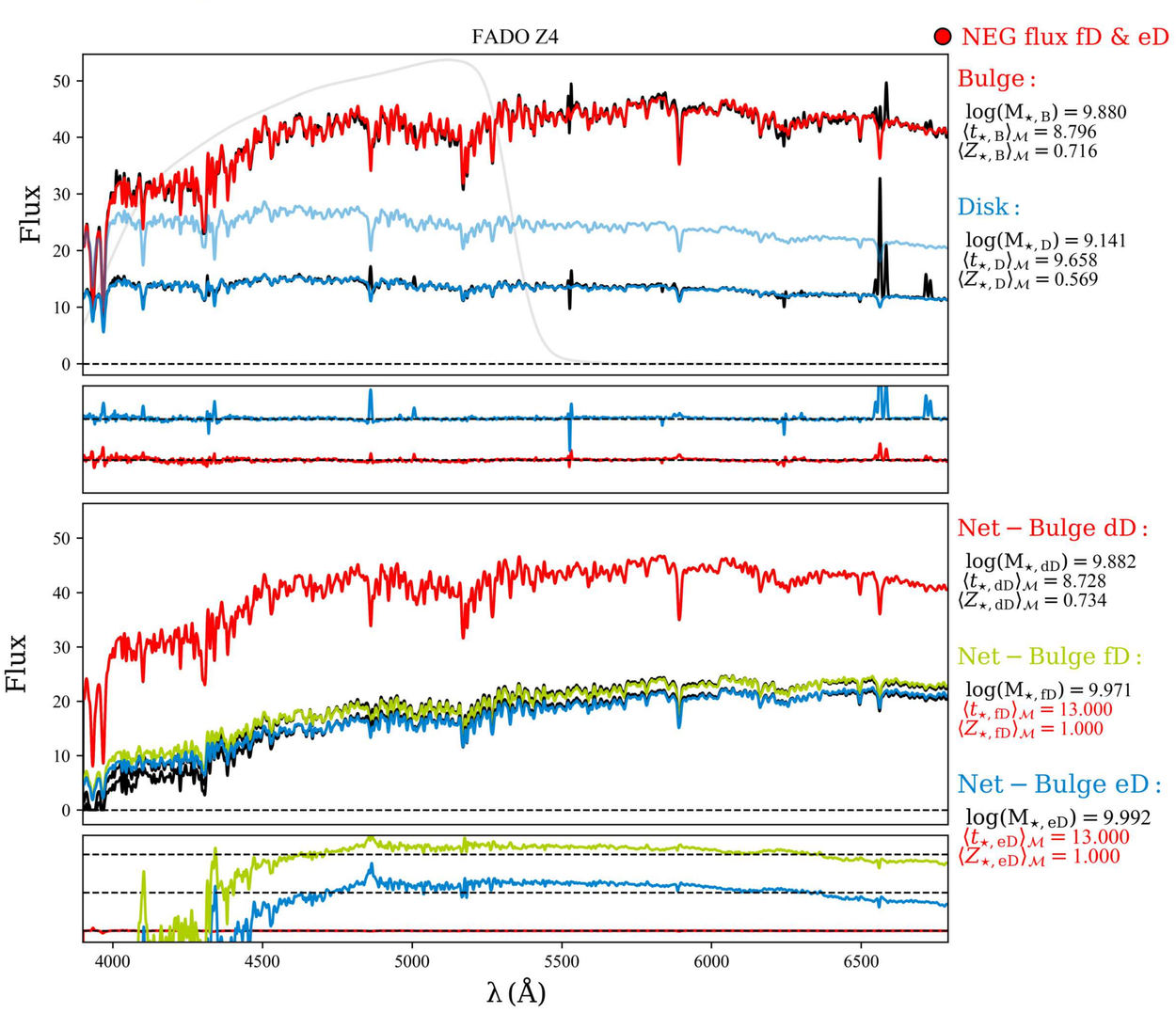
FADO Z4
NEG flux fD & eD
Flux
Bulge :
log(M⋆, B) = 9.880
⟨t⋆, B⟩M = 8.796
⟨Z⋆, B⟩M = 0.716
Disk :
log(M⋆, D) = 9.141
⟨t⋆, D⟩M = 9.658
⟨Z⋆, D⟩M = 0.569
Net − Bulge dD :
log(M⋆, dD) = 9.882
⟨t⋆, dD⟩M = 8.728
⟨Z⋆, dD⟩M = 0.734
Net − Bulge fD :
log(M⋆, fD) = 9.971
⟨t⋆, fD⟩M = 13.000
⟨Z⋆, fD⟩M = 1.000
Net − Bulge eD :
log(M⋆, eD) = 9.992
⟨t⋆, eD⟩M = 13.000
⟨Z⋆, eD⟩M = 1.000
λ (Å)

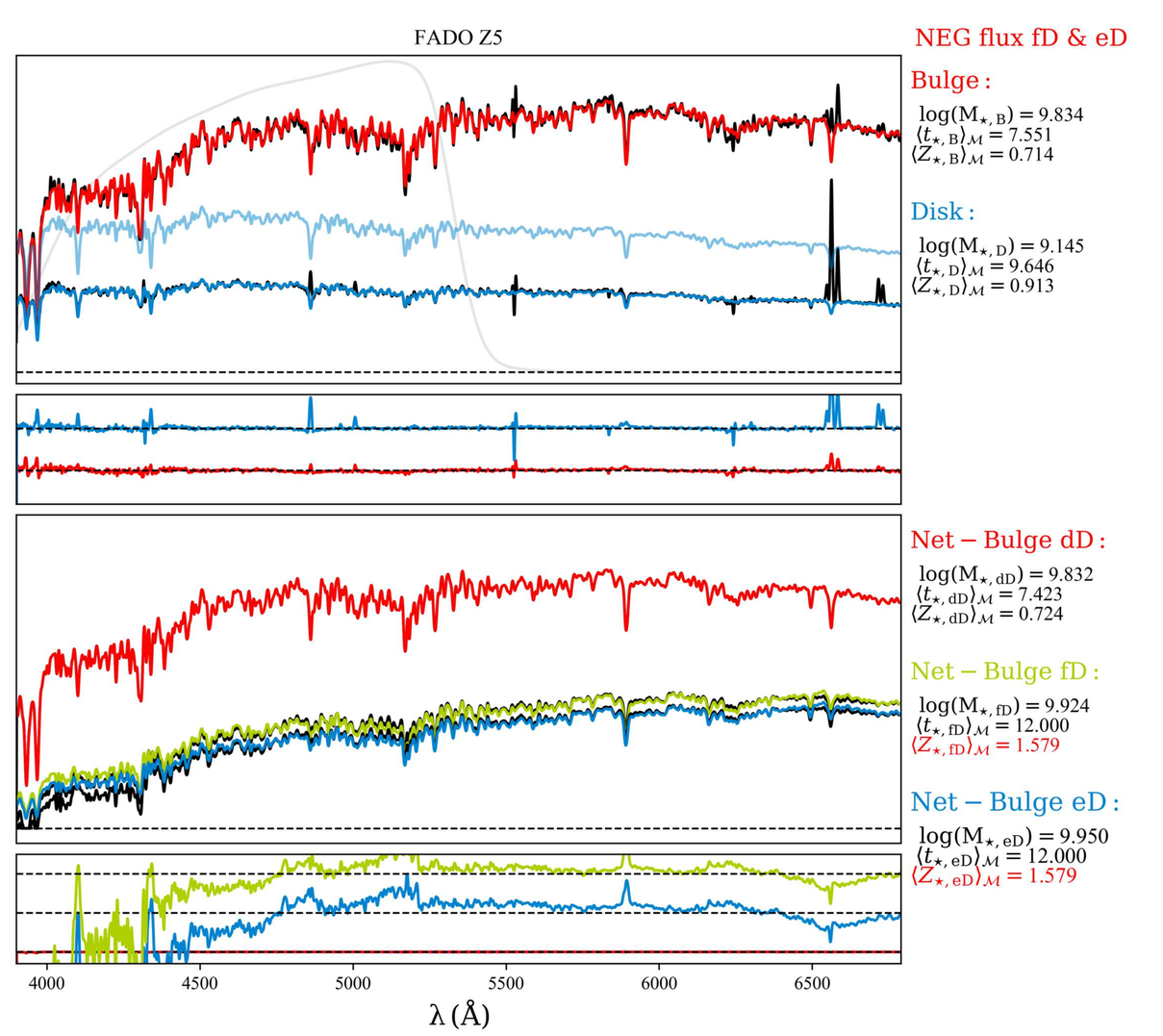
FADO Z5
NEG flux fD & eD
Bulge :
log(M⋆, B) = 9.834
⟨t⋆, B⟩M = 7.551
⟨Z⋆, B⟩M = 0.714
Disk :
log(M⋆, D) = 9.145
⟨t⋆, D⟩M = 9.646
⟨Z⋆, D⟩M = 0.913
Net − Bulge dD :
log(M⋆, dD) = 9.832
⟨t⋆, dD⟩M = 7.423
⟨Z⋆, dD⟩M = 0.724
Net − Bulge fD :
log(M⋆, fD) = 9.924
⟨t⋆, fD⟩M = 12.000
⟨Z⋆, fD⟩M = 1.579
Net − Bulge eD :
log(M⋆, eD) = 9.950
⟨t⋆, eD⟩M = 12.000
⟨Z⋆, eD⟩M = 1.579
λ (Å)

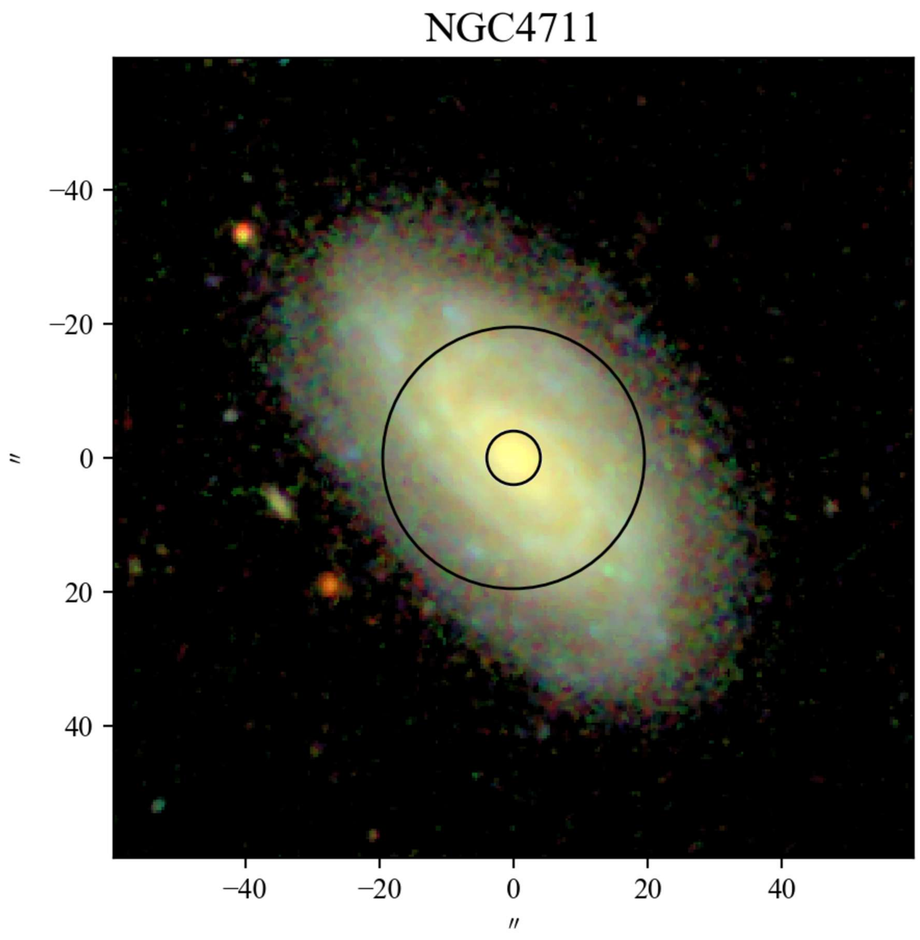
NGC4711
−40
−20
0
20
40
″
−40
−20
0
20
40
″

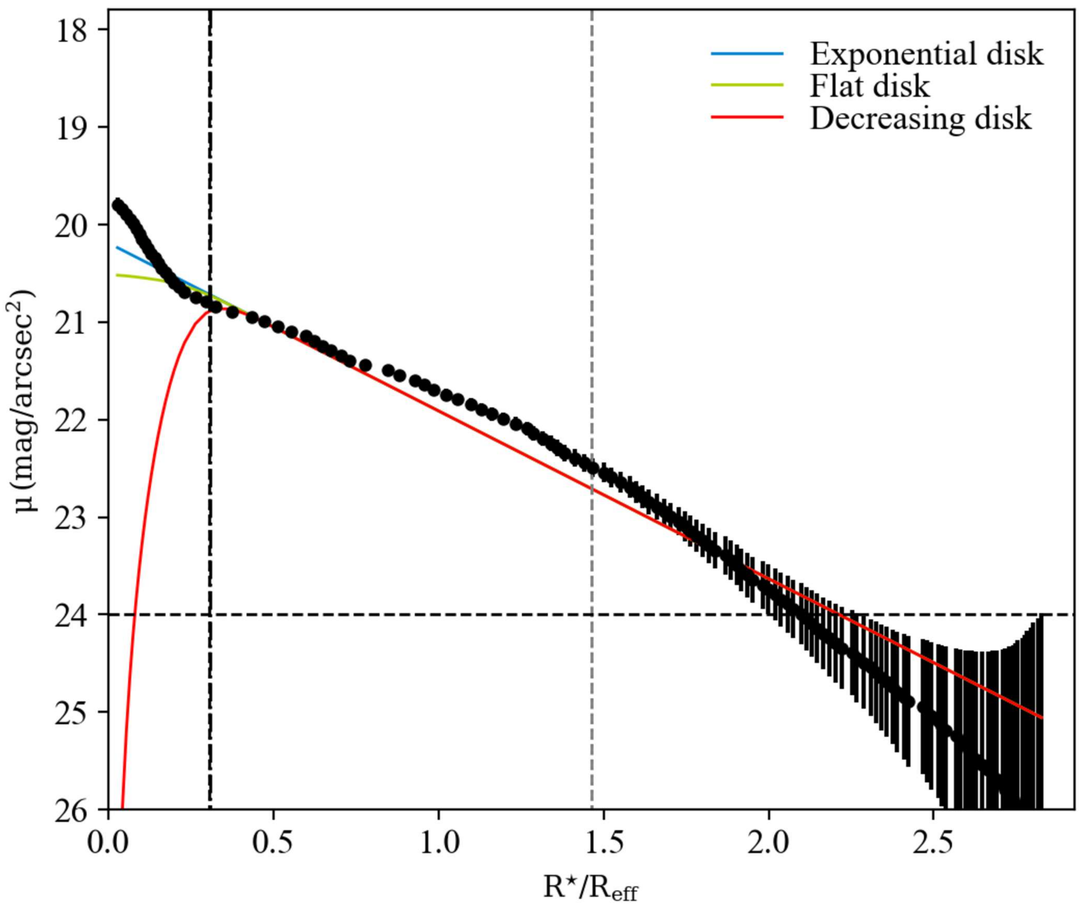
Exponential disk
Flat disk
Decreasing disk
μ (mag/arcsec²)
18
19
20
21
22
23
24
25
26
0.0
0.5
1.0
1.5
2.0
2.5
R⋆/Reff

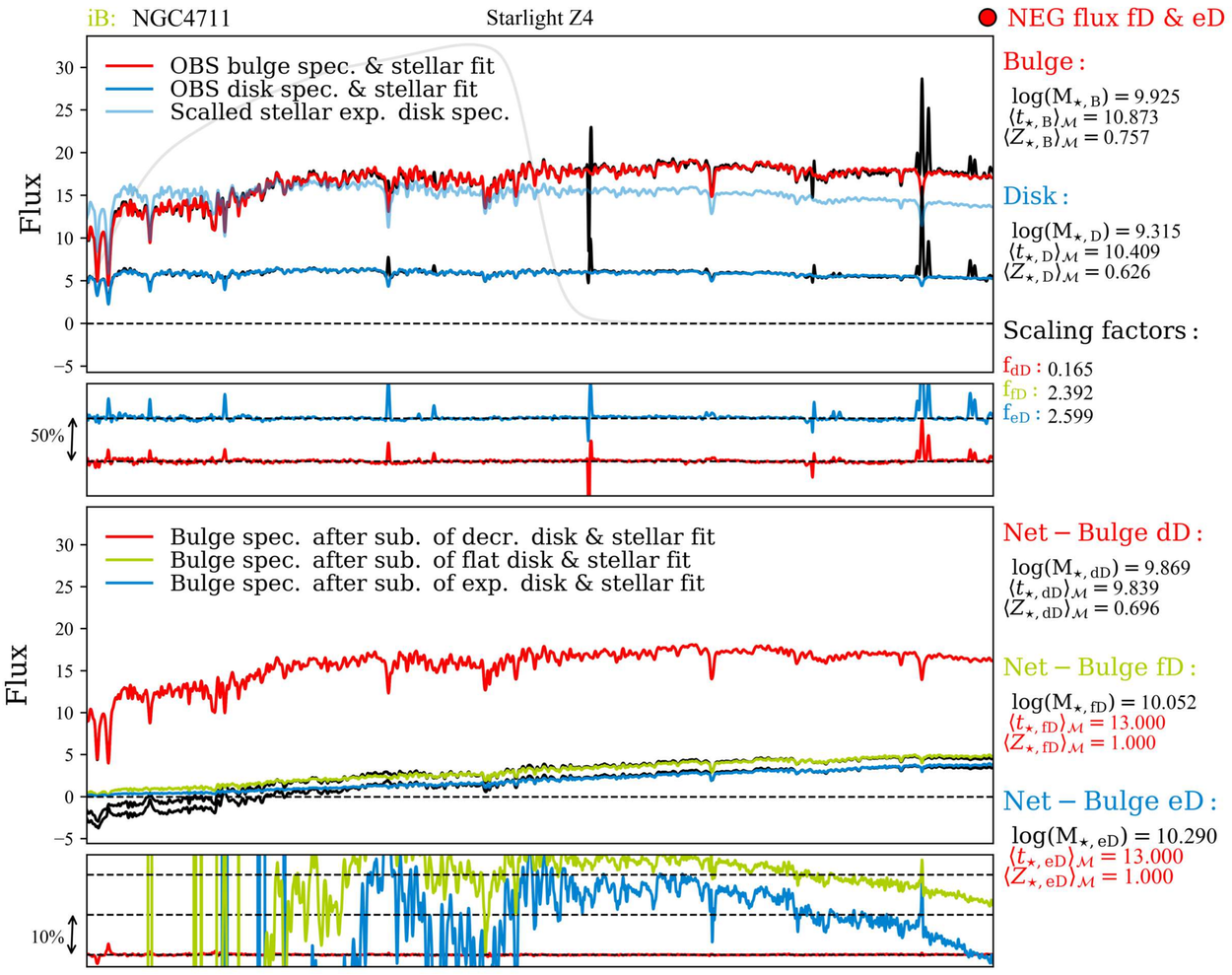
iB: NGC4711
Starlight Z4
NEG flux fD & eD
OBS bulge spec. & stellar fit
OBS disk spec. & stellar fit
Scalled stellar exp. disk spec.
Flux
50%
Bulge :
log(M⋆, B) = 9.925
⟨t⋆, B⟩M = 10.873
⟨Z⋆, B⟩M = 0.757
Disk :
log(M⋆, D) = 9.315
⟨t⋆, D⟩M = 10.409
⟨Z⋆, D⟩M = 0.626
Scaling factors :
fdD : 0.165
ffD : 2.392
feD : 2.599
Bulge spec. after sub. of decr. disk & stellar fit
Bulge spec. after sub. of flat disk & stellar fit
Bulge spec. after sub. of exp. disk & stellar fit
10%
Net − Bulge dD :
log(M⋆, dD) = 9.869
⟨t⋆, dD⟩M = 9.839
⟨Z⋆, dD⟩M = 0.696
Net − Bulge fD :
log(M⋆, fD) = 10.052
⟨t⋆, fD⟩M = 13.000
⟨Z⋆, fD⟩M = 1.000
Net − Bulge eD :
log(M⋆, eD) = 10.290
⟨t⋆, eD⟩M = 13.000
⟨Z⋆, eD⟩M = 1.000

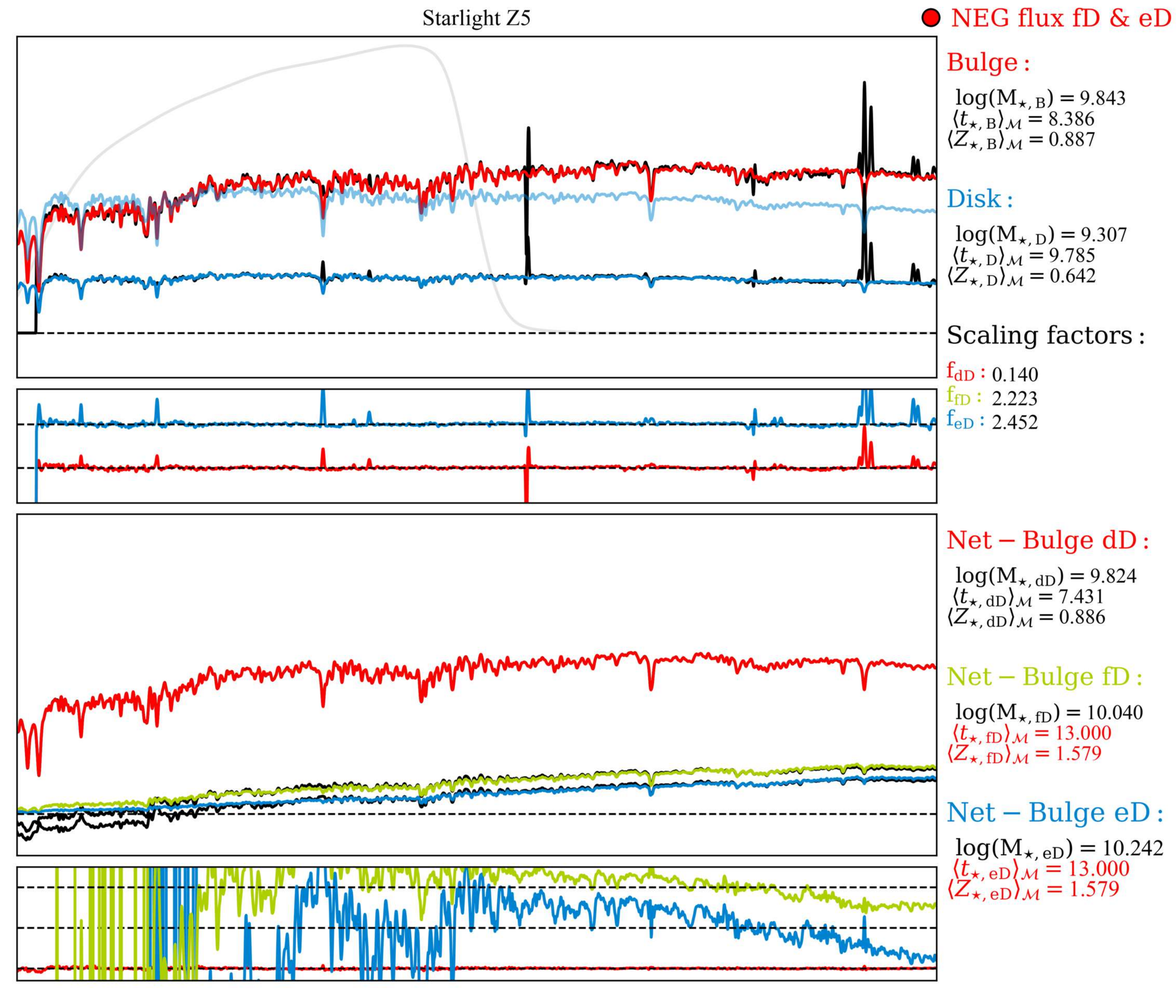
Starlight Z5
NEG flux fD & eD
Bulge :
log(M⋆, B) = 9.843
⟨t⋆, B⟩M = 8.386
⟨Z⋆, B⟩M = 0.887
Disk :
log(M⋆, D) = 9.307
⟨t⋆, D⟩M = 9.785
⟨Z⋆, D⟩M = 0.642
Scaling factors :
fdD : 0.140
ffD : 2.223
feD : 2.452
Net − Bulge dD :
log(M⋆, dD) = 9.824
⟨t⋆, dD⟩M = 7.431
⟨Z⋆, dD⟩M = 0.886
Net − Bulge fD :
log(M⋆, fD) = 10.040
⟨t⋆, fD⟩M = 13.000
⟨Z⋆, fD⟩M = 1.579
Net − Bulge eD :
log(M⋆, eD) = 10.242
⟨t⋆, eD⟩M = 13.000
⟨Z⋆, eD⟩M = 1.579

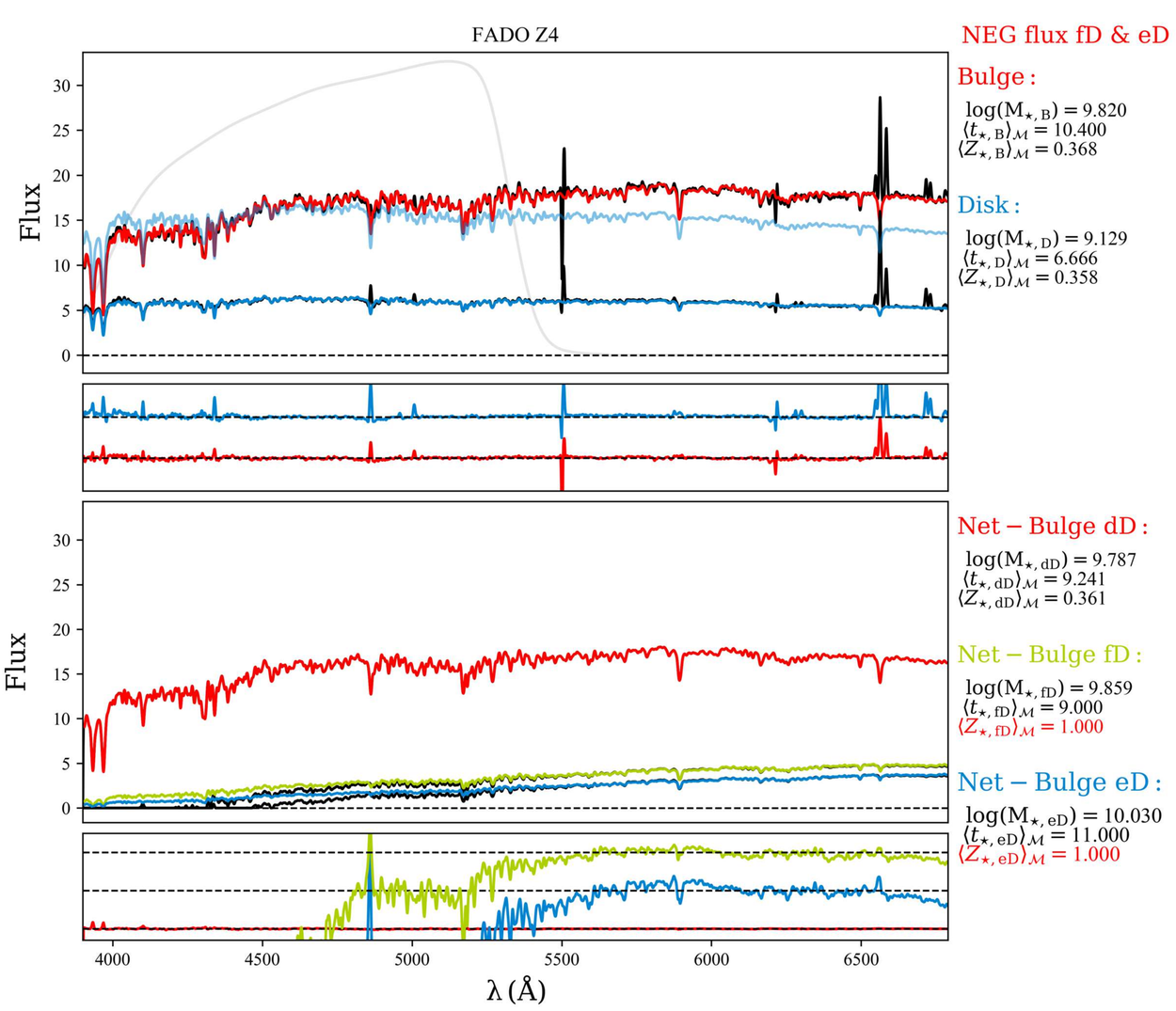
FADO Z4
NEG flux fD & eD
Flux
Bulge :
log(M⋆, B) = 9.820
⟨t⋆, B⟩M = 10.400
⟨Z⋆, B⟩M = 0.368
Disk :
log(M⋆, D) = 9.129
⟨t⋆, D⟩M = 6.666
⟨Z⋆, D⟩M = 0.358
Net − Bulge dD :
log(M⋆, dD) = 9.787
⟨t⋆, dD⟩M = 9.241
⟨Z⋆, dD⟩M = 0.361
Net − Bulge fD :
log(M⋆, fD) = 9.859
⟨t⋆, fD⟩M = 9.000
⟨Z⋆, fD⟩M = 1.000
Net − Bulge eD :
log(M⋆, eD) = 10.030
⟨t⋆, eD⟩M = 11.000
⟨Z⋆, eD⟩M = 1.000
4000
4500
5000
5500
6000
6500
λ (Å)

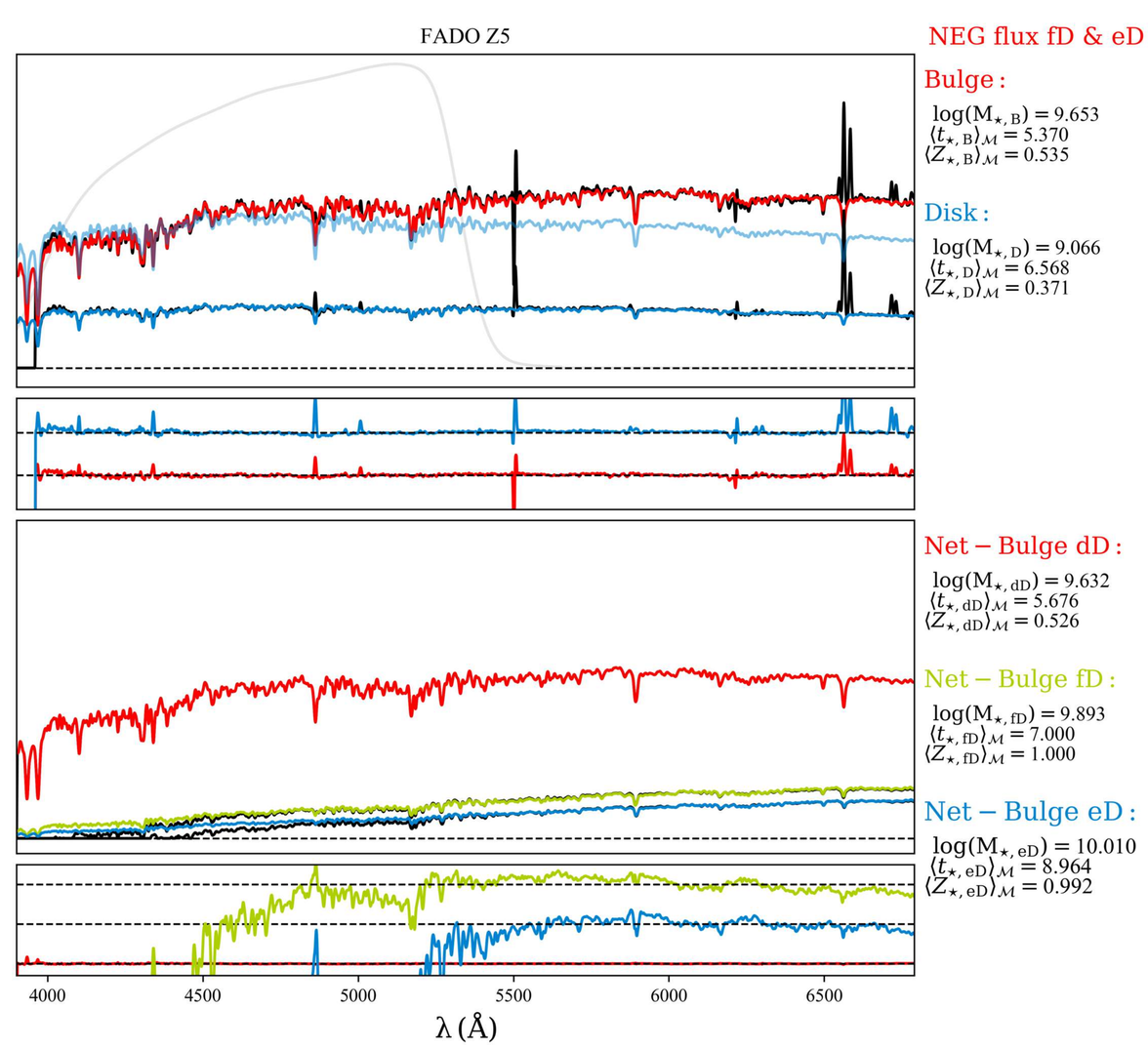
FADO Z5
NEG flux fD & eD
Bulge :
log(M⋆, B) = 9.653
⟨t⋆, B⟩M = 5.370
⟨Z⋆, B⟩M = 0.535
Disk :
log(M⋆, D) = 9.066
⟨t⋆, D⟩M = 6.568
⟨Z⋆, D⟩M = 0.371
Net − Bulge dD :
log(M⋆, dD) = 9.632
⟨t⋆, dD⟩M = 5.676
⟨Z⋆, dD⟩M = 0.526
Net − Bulge fD :
log(M⋆, fD) = 9.893
⟨t⋆, fD⟩M = 7.000
⟨Z⋆, fD⟩M = 1.000
Net − Bulge eD :
log(M⋆, eD) = 10.010
⟨t⋆, eD⟩M = 8.964
⟨Z⋆, eD⟩M = 0.992
4000
4500
5000
5500
6000
6500
λ (Å)

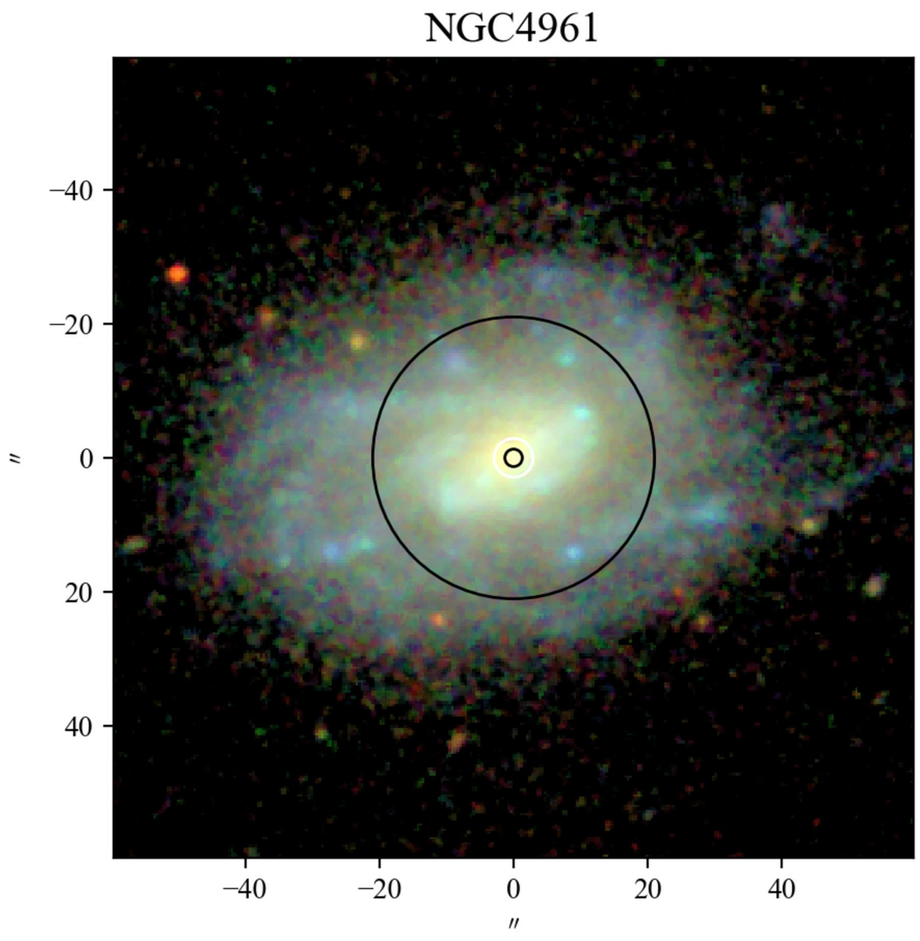
NGC4961
−40
−20
0
20
40
″
−40
−20
0
20
40
″

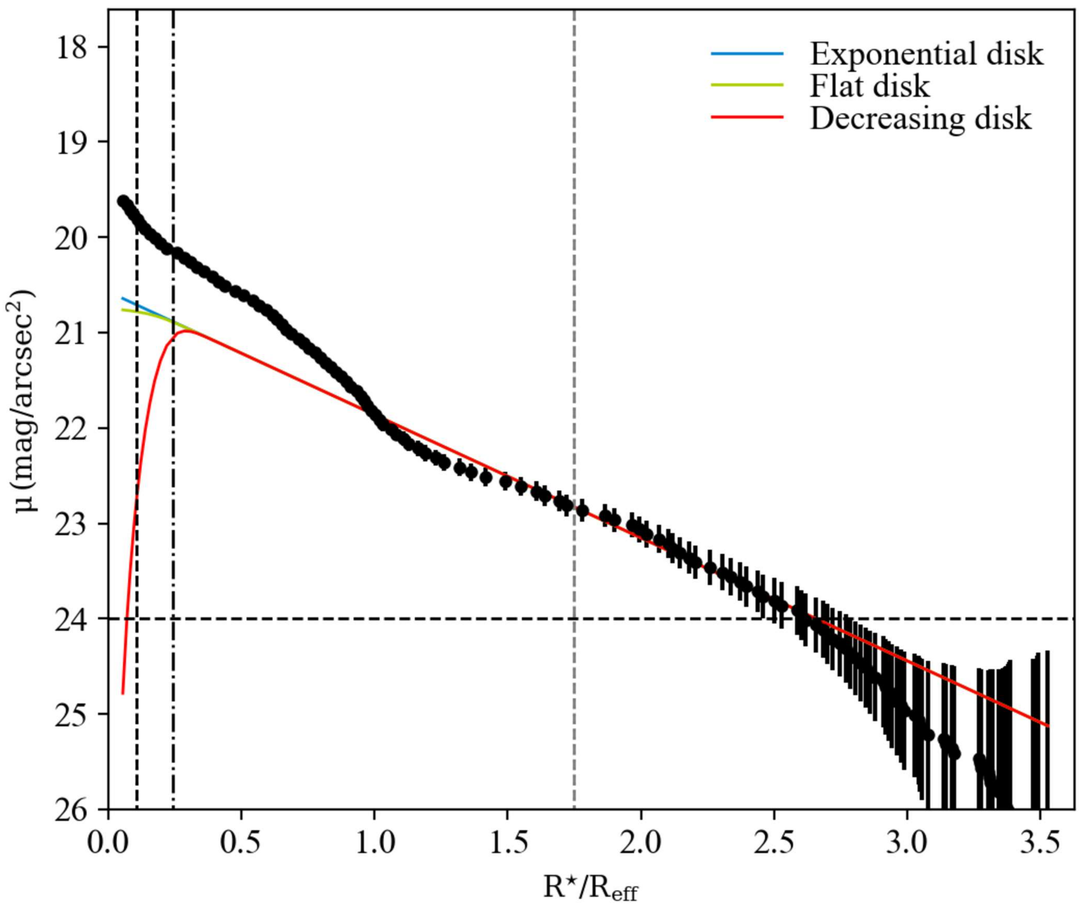
Exponential disk
Flat disk
Decreasing disk
μ (mag/arcsec²)
18
19
20
21
22
23
24
25
26
0.0
0.5
1.0
1.5
2.0
2.5
3.0
3.5
R⋆/Reff

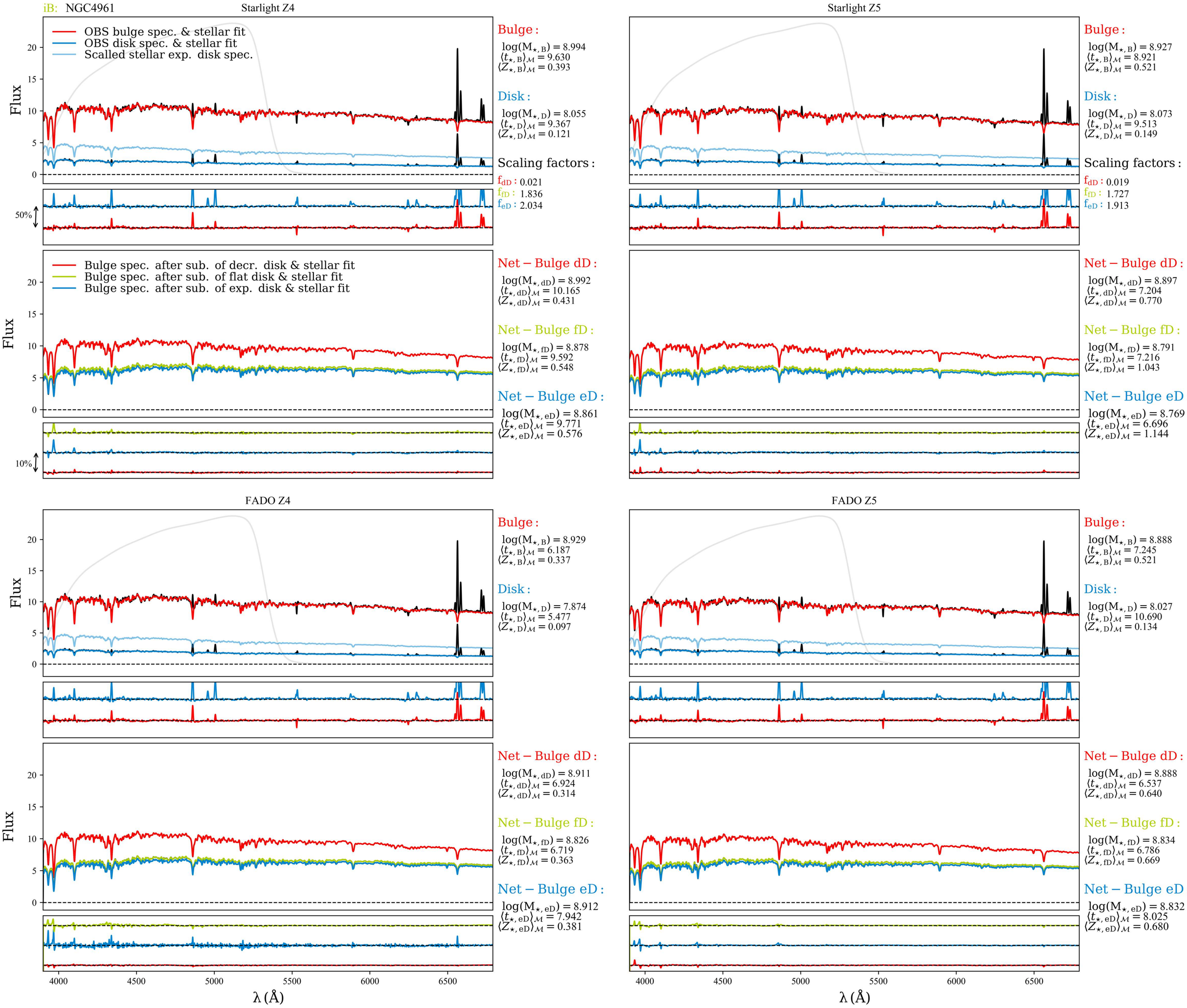
iB: NGC4961
Starlight Z4
OBS bulge spec. & stellar fit
OBS disk spec. & stellar fit
Scalled stellar exp. disk spec.
Flux
50%
Bulge :
log(M⋆, B) = 8.994
⟨t⋆, B⟩M = 9.630
⟨Z⋆, B⟩M = 0.393
Disk :
log(M⋆, D) = 8.055
⟨t⋆, D⟩M = 9.367
⟨Z⋆, D⟩M = 0.121
Scaling factors :
fdD : 0.021
ffD : 1.836
feD : 2.034
Starlight Z5
Bulge :
log(M⋆, B) = 8.927
⟨t⋆, B⟩M = 8.921
⟨Z⋆, B⟩M = 0.521
Disk :
log(M⋆, D) = 8.073
⟨t⋆, D⟩M = 9.513
⟨Z⋆, D⟩M = 0.149
Scaling factors :
fdD : 0.019
ffD : 1.727
feD : 1.913
Bulge spec. after sub. of decr. disk & stellar fit
Bulge spec. after sub. of flat disk & stellar fit
Bulge spec. after sub. of exp. disk & stellar fit
10%
Net − Bulge dD :
log(M⋆, dD) = 8.992
⟨t⋆, dD⟩M = 10.165
⟨Z⋆, dD⟩M = 0.431
Net − Bulge fD :
log(M⋆, fD) = 8.878
⟨t⋆, fD⟩M = 9.592
⟨Z⋆, fD⟩M = 0.548
Net − Bulge eD :
log(M⋆, eD) = 8.861
⟨t⋆, eD⟩M = 9.771
⟨Z⋆, eD⟩M = 0.576
Net − Bulge dD :
log(M⋆, dD) = 8.897
⟨t⋆, dD⟩M = 7.204
⟨Z⋆, dD⟩M = 0.770
Net − Bulge fD :
log(M⋆, fD) = 8.791
⟨t⋆, fD⟩M = 7.216
⟨Z⋆, fD⟩M = 1.043
Net − Bulge eD :
log(M⋆, eD) = 8.769
⟨t⋆, eD⟩M = 6.696
⟨Z⋆, eD⟩M = 1.144
FADO Z4
Bulge :
log(M⋆, B) = 8.929
⟨t⋆, B⟩M = 6.187
⟨Z⋆, B⟩M = 0.337
Disk :
log(M⋆, D) = 7.874
⟨t⋆, D⟩M = 5.477
⟨Z⋆, D⟩M = 0.097
FADO Z5
Bulge :
log(M⋆, B) = 8.888
⟨t⋆, B⟩M = 7.245
⟨Z⋆, B⟩M = 0.521
Disk :
log(M⋆, D) = 8.027
⟨t⋆, D⟩M = 10.690
⟨Z⋆, D⟩M = 0.134
Net − Bulge dD :
log(M⋆, dD) = 8.911
⟨t⋆, dD⟩M = 6.924
⟨Z⋆, dD⟩M = 0.314
Net − Bulge fD :
log(M⋆, fD) = 8.826
⟨t⋆, fD⟩M = 6.719
⟨Z⋆, fD⟩M = 0.363
Net − Bulge eD :
log(M⋆, eD) = 8.912
⟨t⋆, eD⟩M = 7.942
⟨Z⋆, eD⟩M = 0.381
Net − Bulge dD :
log(M⋆, dD) = 8.888
⟨t⋆, dD⟩M = 6.537
⟨Z⋆, dD⟩M = 0.640
Net − Bulge fD :
log(M⋆, fD) = 8.834
⟨t⋆, fD⟩M = 6.786
⟨Z⋆, fD⟩M = 0.669
Net − Bulge eD :
log(M⋆, eD) = 8.832
⟨t⋆, eD⟩M = 8.025
⟨Z⋆, eD⟩M = 0.680
Flux
0
5
10
15
20
4000
4500
5000
5500
6000
6500
λ (Å)

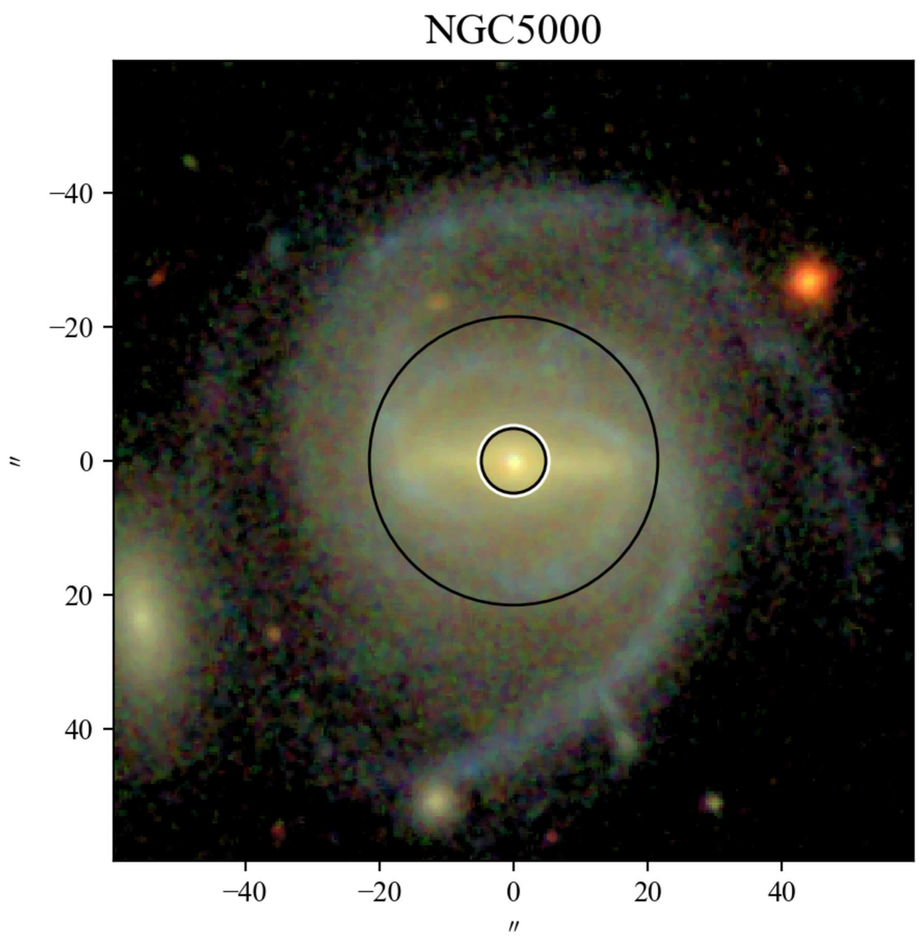
NGC5000
−40
−20
0
20
40
″
−40
−20
0
20
40
″

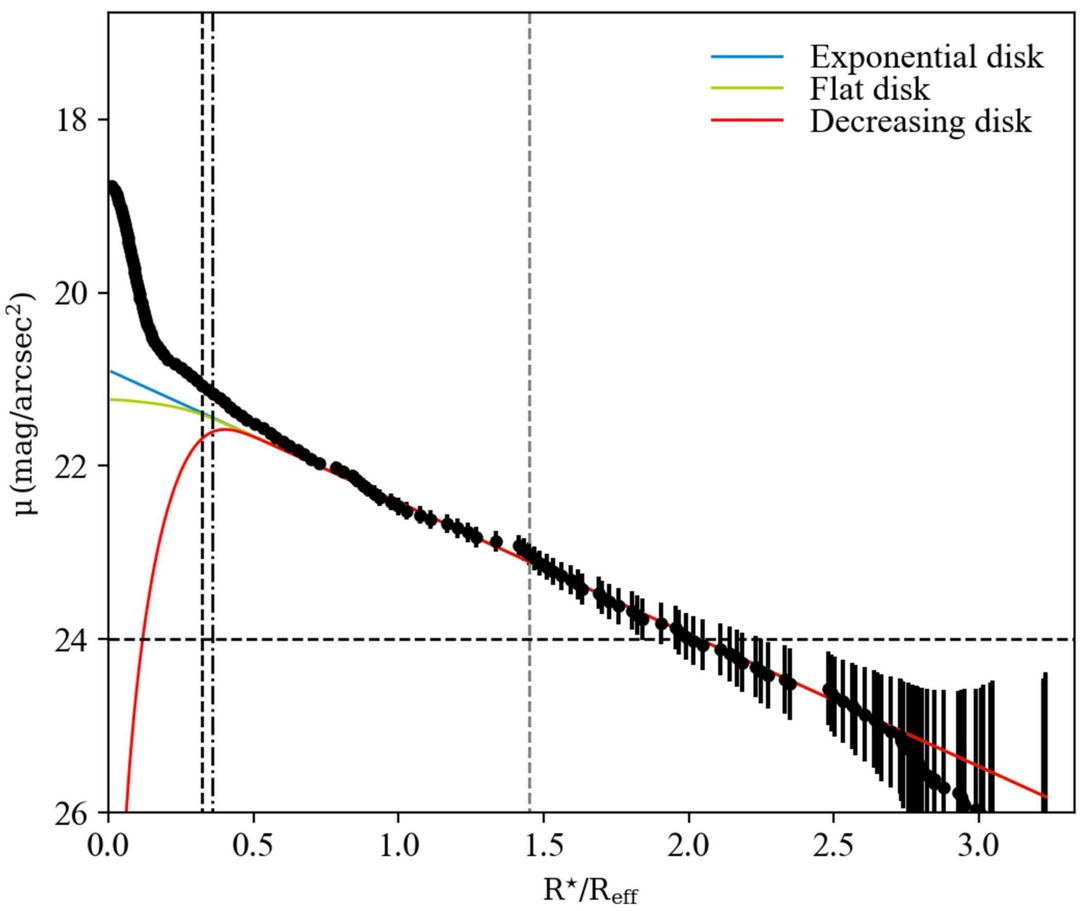
Exponential disk
Flat disk
Decreasing disk
18
20
22
24
26
μ (mag/arcsec²)
0.0
0.5
1.0
1.5
2.0
2.5
3.0
R⋆/Reff

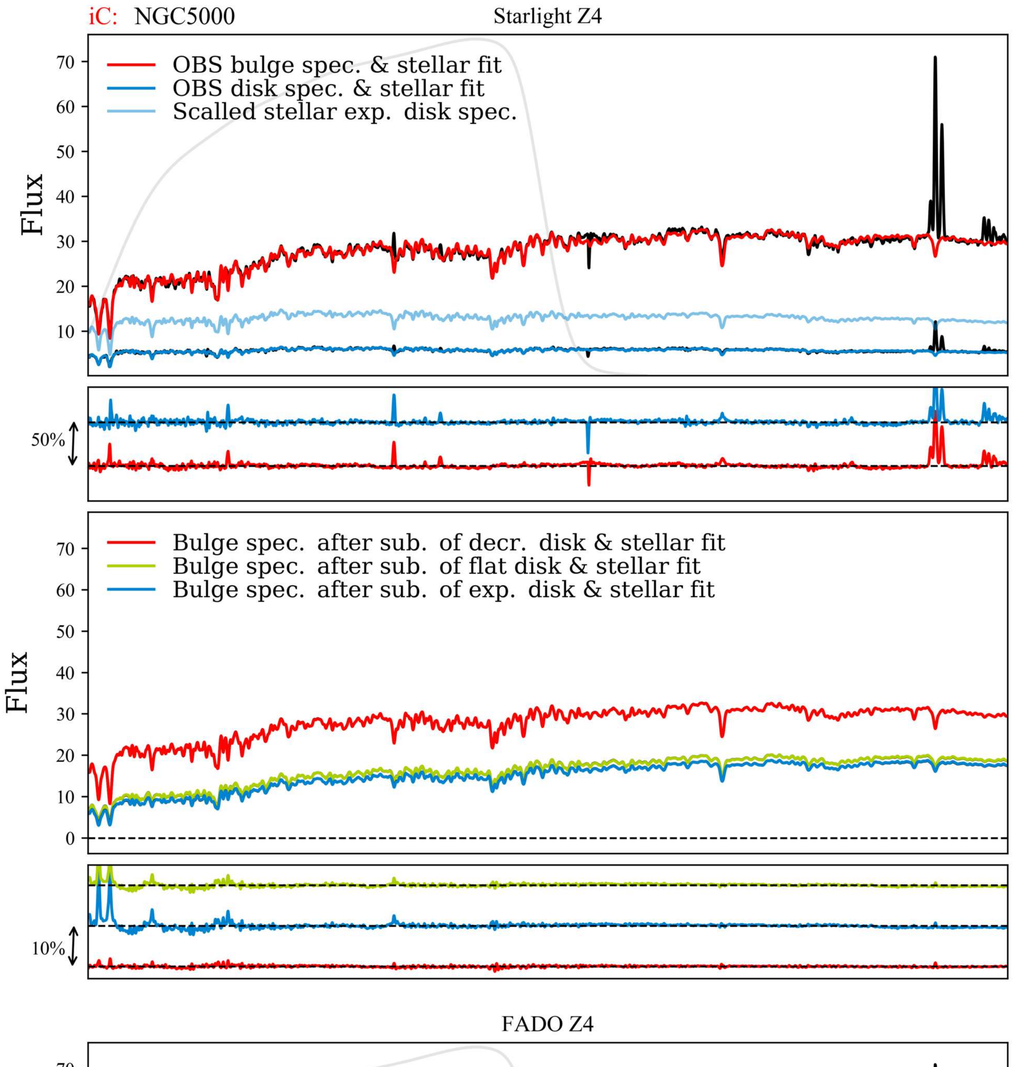
iC: NGC5000
Starlight Z4
OBS bulge spec. & stellar fit
OBS disk spec. & stellar fit
Scalled stellar exp. disk spec.
Flux
50%
Bulge spec. after sub. of decr. disk & stellar fit
Bulge spec. after sub. of flat disk & stellar fit
Bulge spec. after sub. of exp. disk & stellar fit
10%
Bulge :
log(M⋆, B) = 10.512
⟨t⋆, B⟩M = 11.787
⟨Z⋆, B⟩M = 0.837
Disk :
log(M⋆, D) = 9.570
⟨t⋆, D⟩M = 10.515
⟨Z⋆, D⟩M = 0.740
Scaling factors :
fdD : 0.002
ffD : 2.043
feD : 2.263
Net − Bulge dD :
log(M⋆, dD) = 10.484
⟨t⋆, dD⟩M = 11.100
⟨Z⋆, dD⟩M = 0.784
Net − Bulge fD :
log(M⋆, fD) = 10.411
⟨t⋆, fD⟩M = 11.580
⟨Z⋆, fD⟩M = 0.889
Net − Bulge eD :
log(M⋆, eD) = 10.405
⟨t⋆, eD⟩M = 11.843
⟨Z⋆, eD⟩M = 0.903

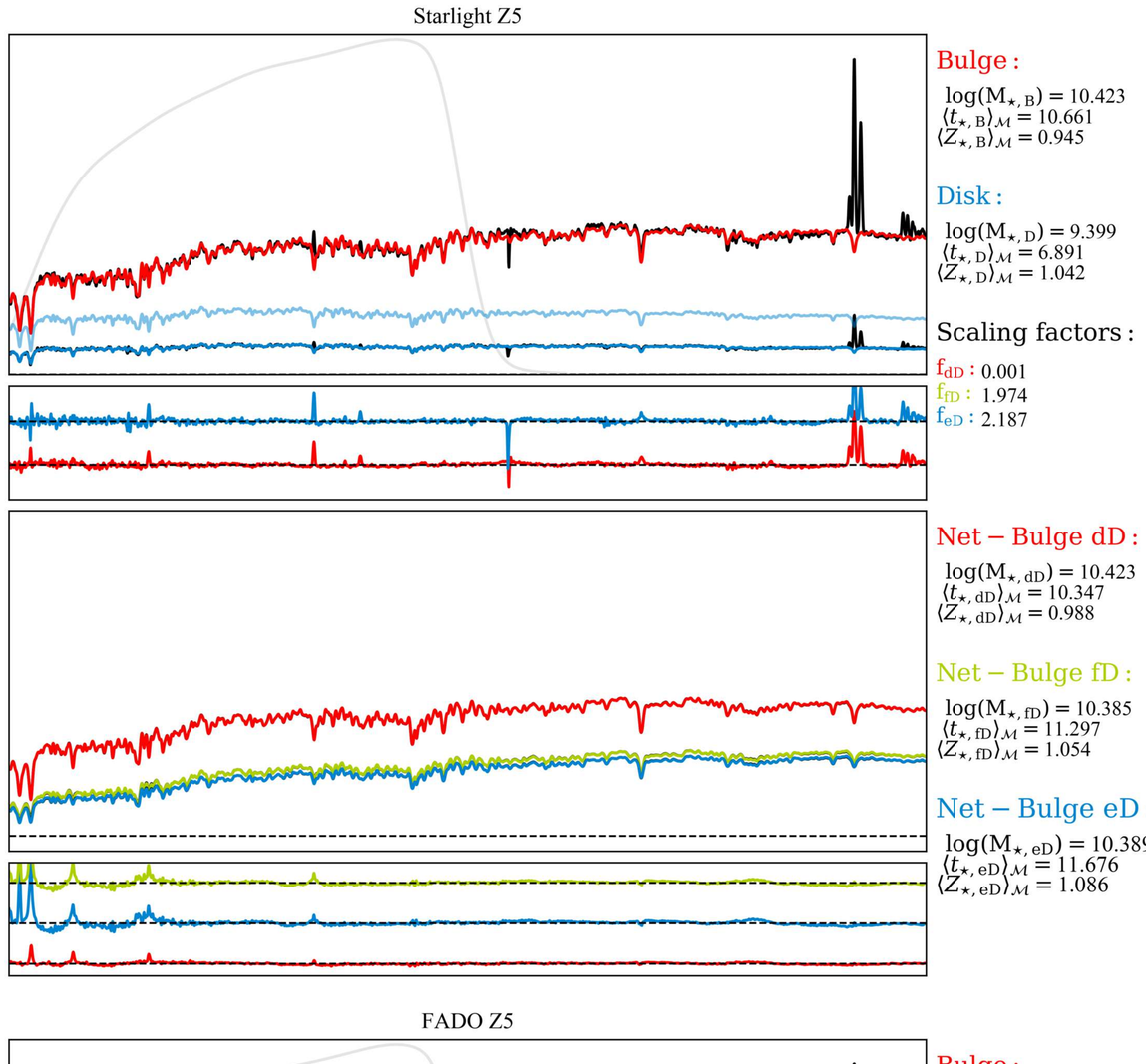
Starlight Z5
Bulge :
log(M⋆, B) = 10.423
⟨t⋆, B⟩M = 10.661
⟨Z⋆, B⟩M = 0.945
Disk :
log(M⋆, D) = 9.399
⟨t⋆, D⟩M = 6.891
⟨Z⋆, D⟩M = 1.042
Scaling factors :
fdD : 0.001
ffD : 1.974
feD : 2.187
Net − Bulge dD :
log(M⋆, dD) = 10.423
⟨t⋆, dD⟩M = 10.347
⟨Z⋆, dD⟩M = 0.988
Net − Bulge fD :
log(M⋆, fD) = 10.385
⟨t⋆, fD⟩M = 11.297
⟨Z⋆, fD⟩M = 1.054
Net − Bulge eD :
log(M⋆, eD) = 10.389
⟨t⋆, eD⟩M = 11.676
⟨Z⋆, eD⟩M = 1.086

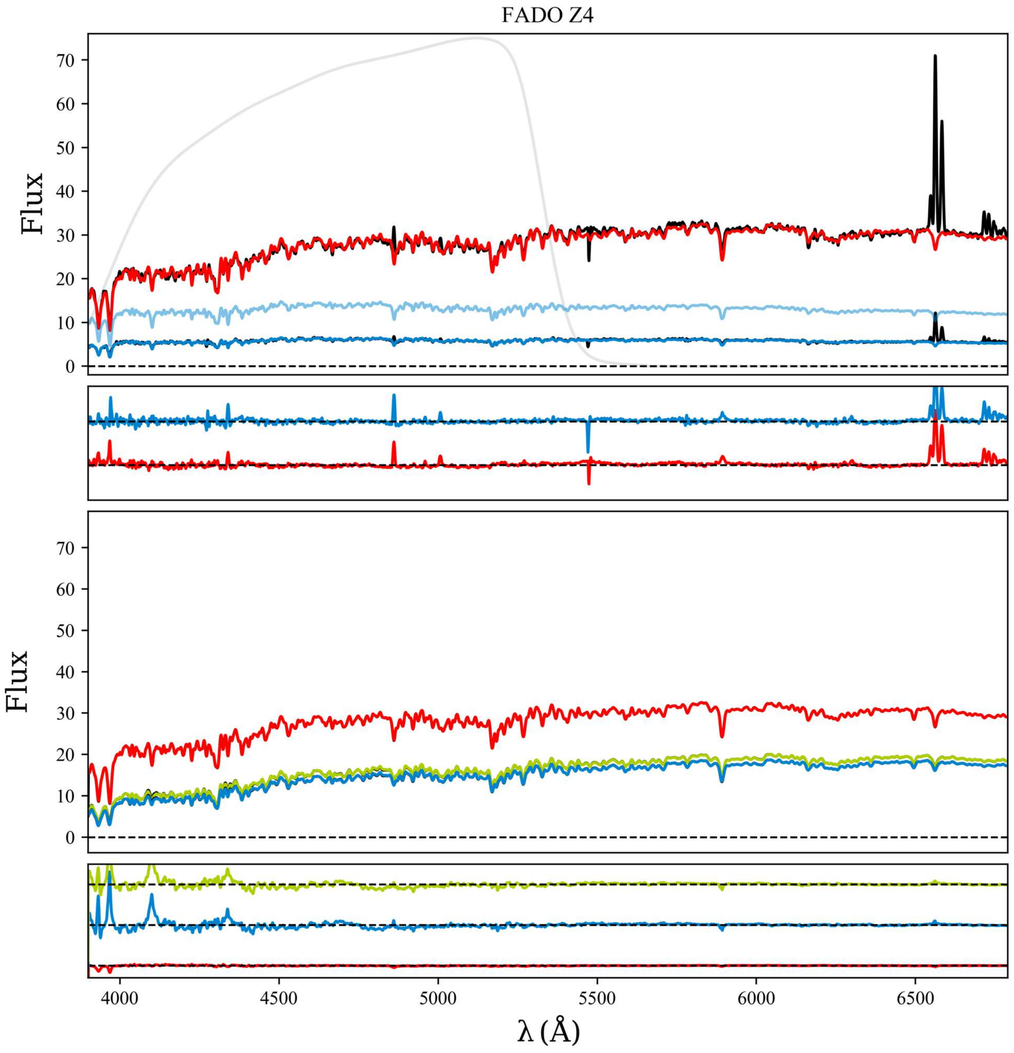
FADO Z4
Flux
Bulge :
log(M⋆, B) = 10.510
⟨t⋆, B⟩M = 12.150
⟨Z⋆, B⟩M = 0.854
Disk :
log(M⋆, D) = 9.493
⟨t⋆, D⟩M = 10.090
⟨Z⋆, D⟩M = 0.527
Net − Bulge dD :
log(M⋆, dD) = 10.510
⟨t⋆, dD⟩M = 12.690
⟨Z⋆, dD⟩M = 0.855
Net − Bulge fD :
log(M⋆, fD) = 10.390
⟨t⋆, fD⟩M = 12.540
⟨Z⋆, fD⟩M = 0.958
Net − Bulge eD :
log(M⋆, eD) = 10.390
⟨t⋆, eD⟩M = 12.000
⟨Z⋆, eD⟩M = 1.000
4000
4500
5000
5500
6000
6500
λ (Å)

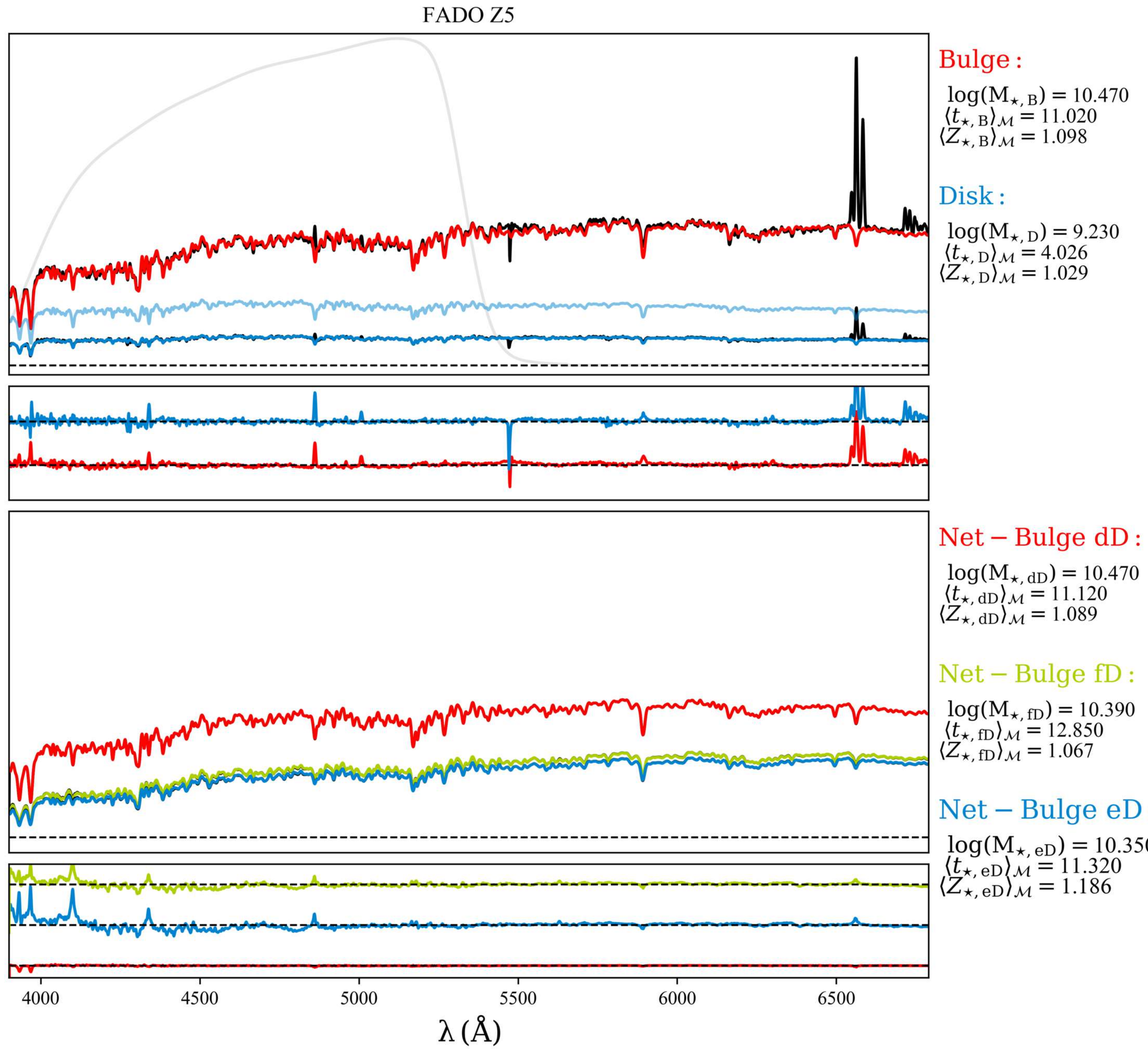
FADO Z5
Bulge :
log(M⋆, B) = 10.470
⟨t⋆, B⟩M = 11.020
⟨Z⋆, B⟩M = 1.098
Disk :
log(M⋆, D) = 9.230
⟨t⋆, D⟩M = 4.026
⟨Z⋆, D⟩M = 1.029
Net − Bulge dD :
log(M⋆, dD) = 10.470
⟨t⋆, dD⟩M = 11.120
⟨Z⋆, dD⟩M = 1.089
Net − Bulge fD :
log(M⋆, fD) = 10.390
⟨t⋆, fD⟩M = 12.850
⟨Z⋆, fD⟩M = 1.067
Net − Bulge eD :
log(M⋆, eD) = 10.350
⟨t⋆, eD⟩M = 11.320
⟨Z⋆, eD⟩M = 1.186
4000
4500
5000
5500
6000
6500
λ (Å)

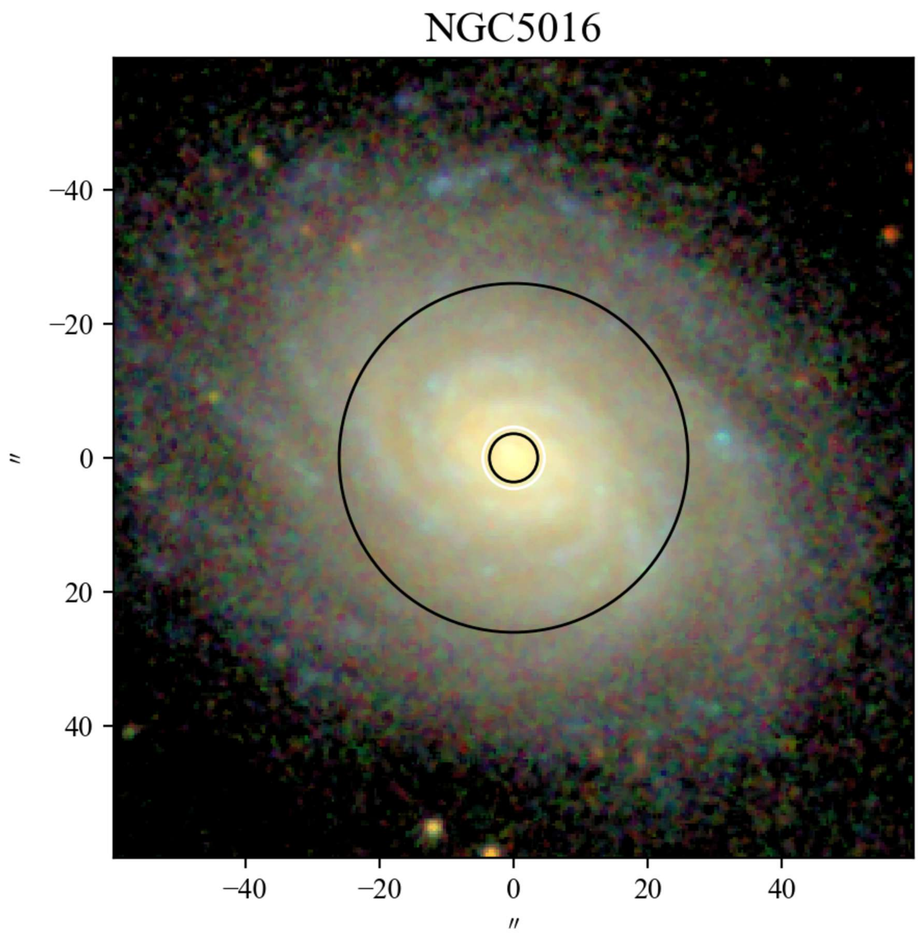
NGC5016
−40
−20
0
20
40
″
−40
−20
0
20
40
″

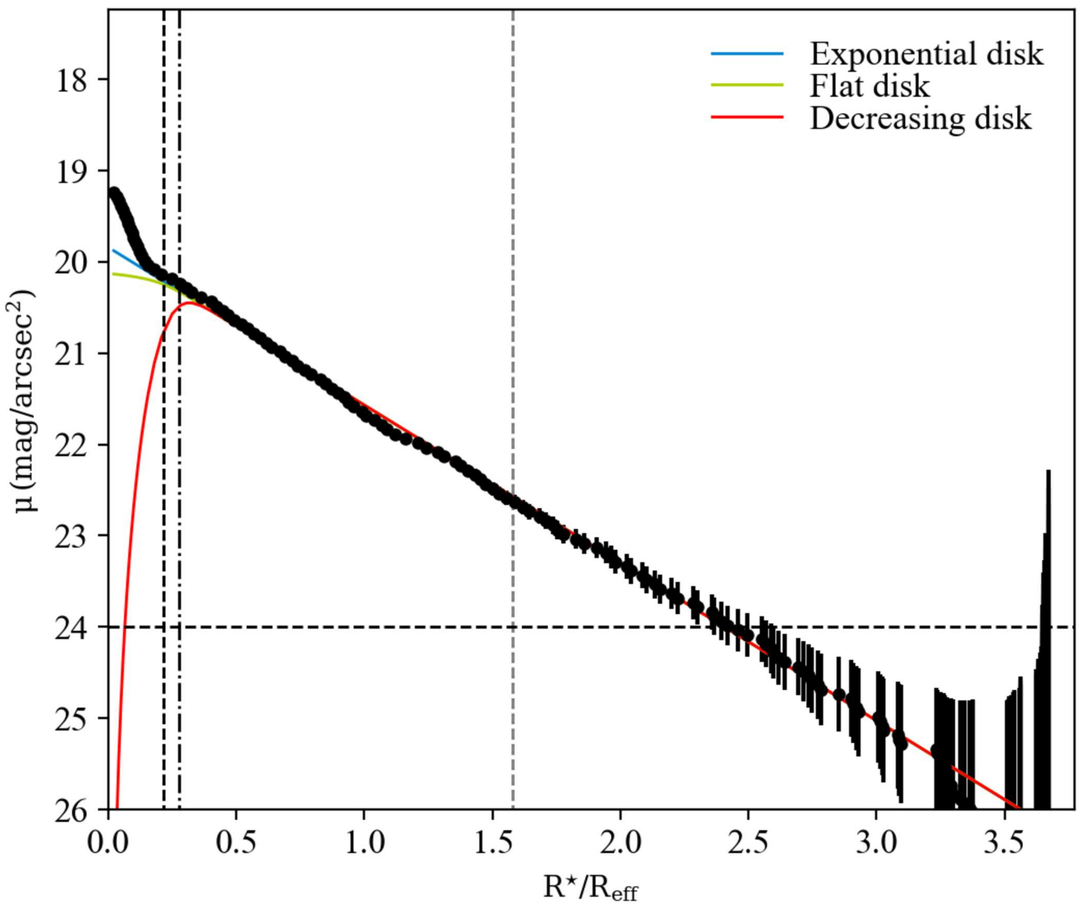
Exponential disk
Flat disk
Decreasing disk
μ (mag/arcsec²)
18
19
20
21
22
23
24
25
26
0.0
0.5
1.0
1.5
2.0
2.5
3.0
3.5
R⋆/Reff

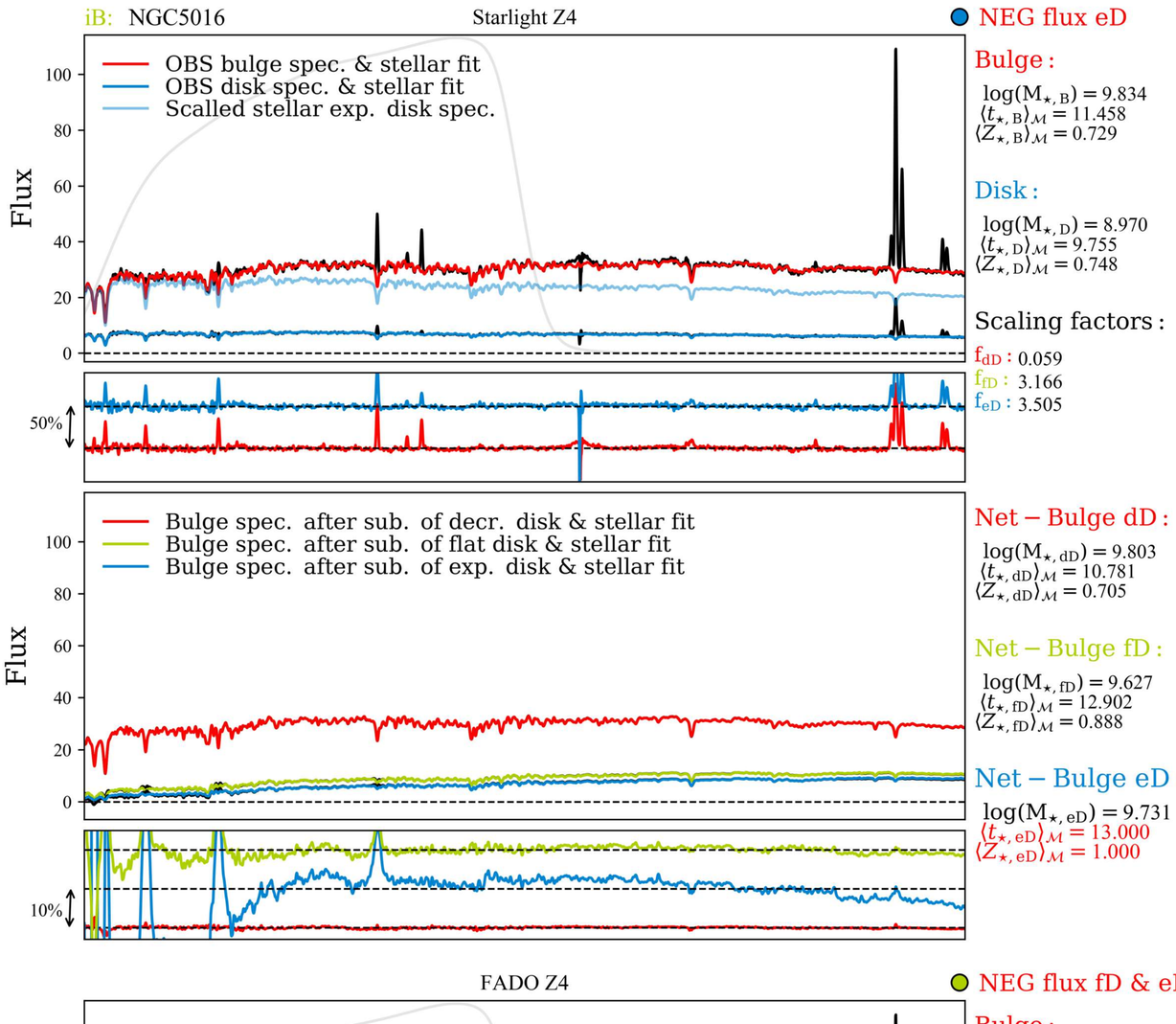
iB: NGC5016
Starlight Z4
NEG flux eD
OBS bulge spec. & stellar fit
OBS disk spec. & stellar fit
Scalled stellar exp. disk spec.
Flux
Bulge :
log(M⋆, B) = 9.834
⟨t⋆, B⟩M = 11.458
⟨Z⋆, B⟩M = 0.729
Disk :
log(M⋆, D) = 8.970
⟨t⋆, D⟩M = 9.755
⟨Z⋆, D⟩M = 0.748
Scaling factors :
fdD : 0.059
ffD : 3.166
feD : 3.505
50%
Bulge spec. after sub. of decr. disk & stellar fit
Bulge spec. after sub. of flat disk & stellar fit
Bulge spec. after sub. of exp. disk & stellar fit
Net − Bulge dD :
log(M⋆, dD) = 9.803
⟨t⋆, dD⟩M = 10.781
⟨Z⋆, dD⟩M = 0.705
Net − Bulge fD :
log(M⋆, fD) = 9.627
⟨t⋆, fD⟩M = 12.902
⟨Z⋆, fD⟩M = 0.888
Net − Bulge eD :
log(M⋆, eD) = 9.731
⟨t⋆, eD⟩M = 13.000
⟨Z⋆, eD⟩M = 1.000
10%

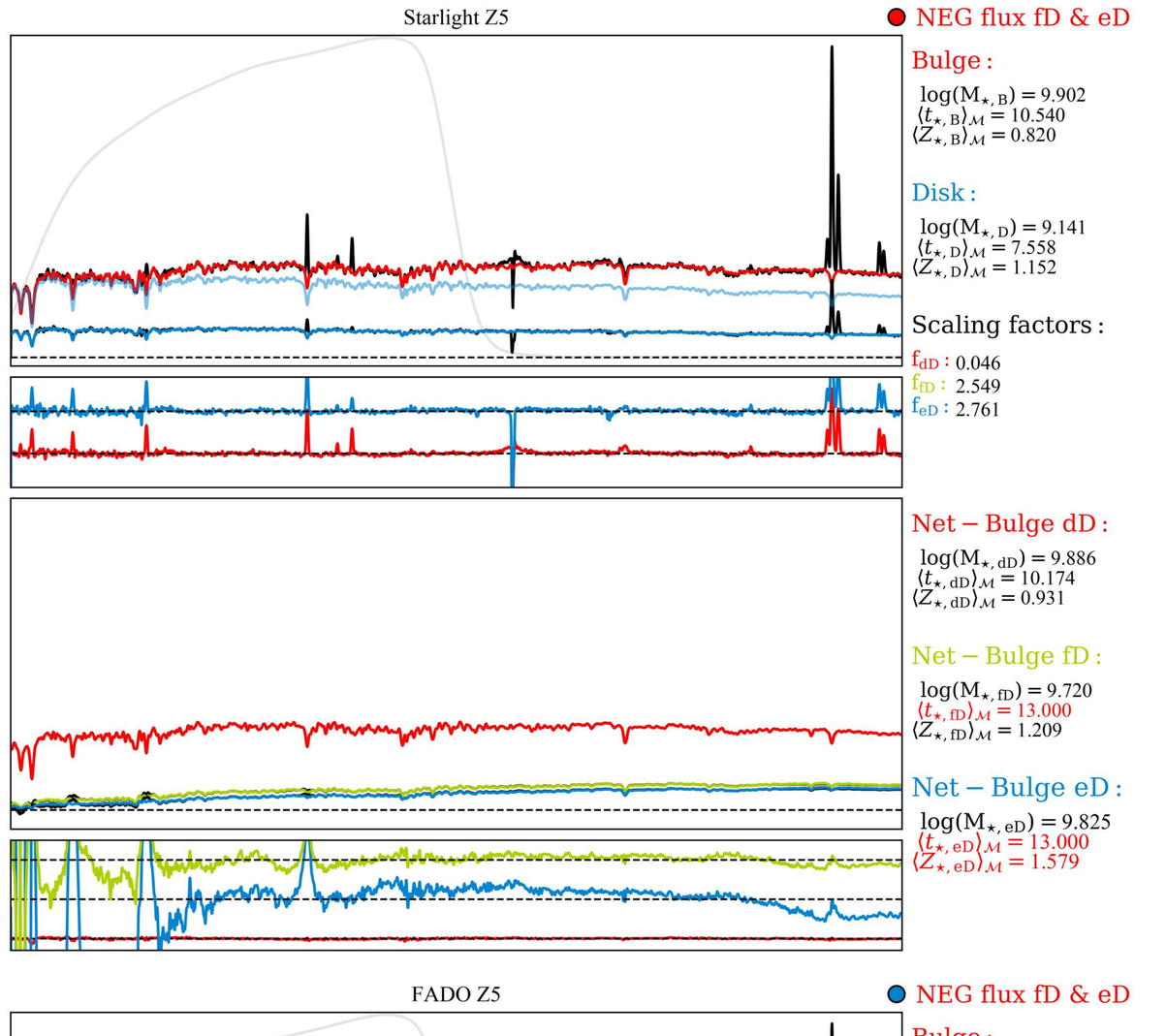
Starlight Z5
NEG flux fD & eD
Bulge :
log(M⋆, B) = 9.902
⟨t⋆, B⟩M = 10.540
⟨Z⋆, B⟩M = 0.820
Disk :
log(M⋆, D) = 9.141
⟨t⋆, D⟩M = 7.558
⟨Z⋆, D⟩M = 1.152
Scaling factors :
fdD : 0.046
ffD : 2.549
feD : 2.761
Net − Bulge dD :
log(M⋆, dD) = 9.886
⟨t⋆, dD⟩M = 10.174
⟨Z⋆, dD⟩M = 0.931
Net − Bulge fD :
log(M⋆, fD) = 9.720
⟨t⋆, fD⟩M = 13.000
⟨Z⋆, fD⟩M = 1.209
Net − Bulge eD :
log(M⋆, eD) = 9.825
⟨t⋆, eD⟩M = 13.000
⟨Z⋆, eD⟩M = 1.579

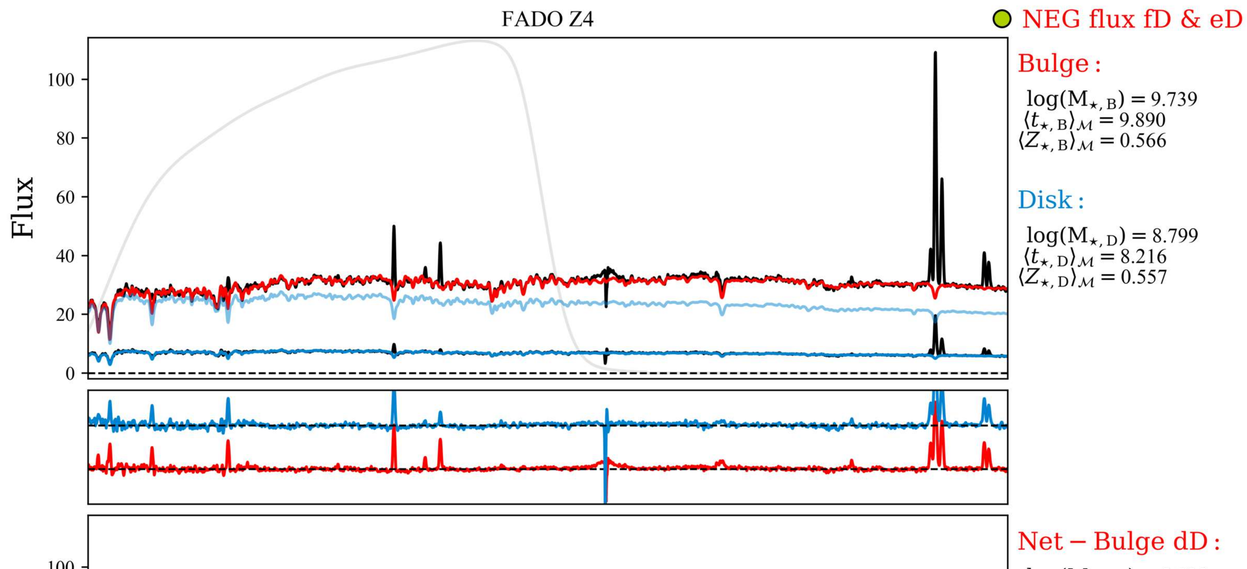
FADO Z4
NEG flux fD & eD
Flux
Bulge :
log(M⋆, B) = 9.739
⟨t⋆, B⟩M = 9.890
⟨Z⋆, B⟩M = 0.566
Disk :
log(M⋆, D) = 8.799
⟨t⋆, D⟩M = 8.216
⟨Z⋆, D⟩M = 0.557
Net − Bulge dD :
log(M⋆, dD) = 9.728
⟨t⋆, dD⟩M = 10.890
⟨Z⋆, dD⟩M = 0.561
Net − Bulge fD :
log(M⋆, fD) = 9.633
⟨t⋆, fD⟩M = 13.000
⟨Z⋆, fD⟩M = 0.941
Net − Bulge eD :
log(M⋆, eD) = 9.668
⟨t⋆, eD⟩M = 11.000
⟨Z⋆, eD⟩M = 1.000
λ (Å)

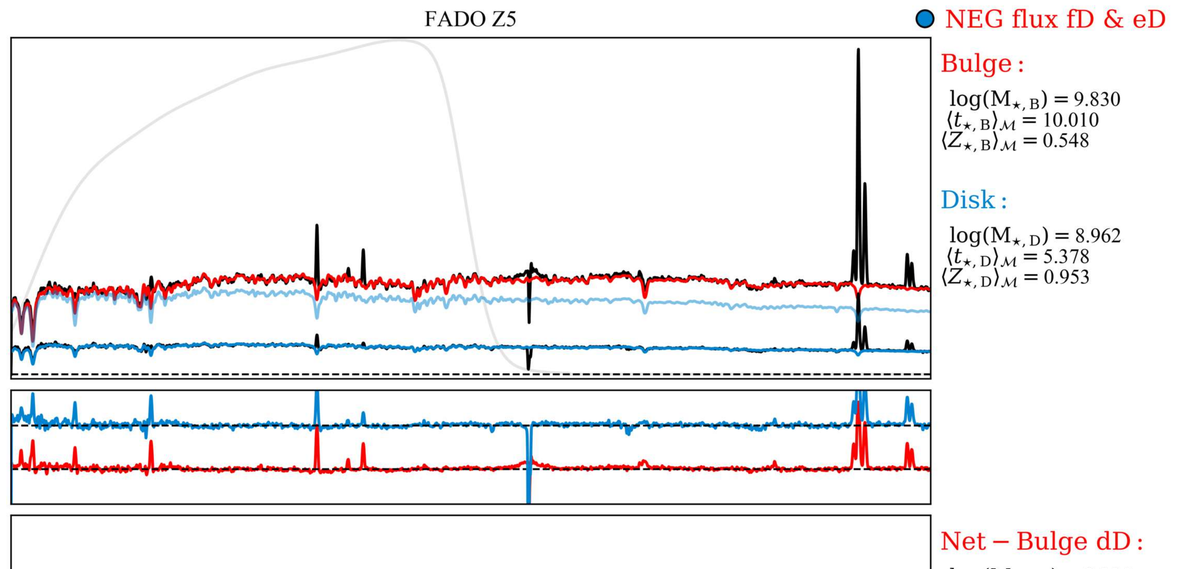
FADO Z5
NEG flux fD & eD
Bulge :
log(M⋆, B) = 9.830
⟨t⋆, B⟩M = 10.010
⟨Z⋆, B⟩M = 0.548
Disk :
log(M⋆, D) = 8.962
⟨t⋆, D⟩M = 5.378
⟨Z⋆, D⟩M = 0.953
Net − Bulge dD :
log(M⋆, dD) = 9.825
⟨t⋆, dD⟩M = 9.698
⟨Z⋆, dD⟩M = 0.613
Net − Bulge fD :
log(M⋆, fD) = 9.674
⟨t⋆, fD⟩M = 11.660
⟨Z⋆, fD⟩M = 1.385
Net − Bulge eD :
log(M⋆, eD) = 9.752
⟨t⋆, eD⟩M = 13.000
⟨Z⋆, eD⟩M = 1.579
λ (Å)

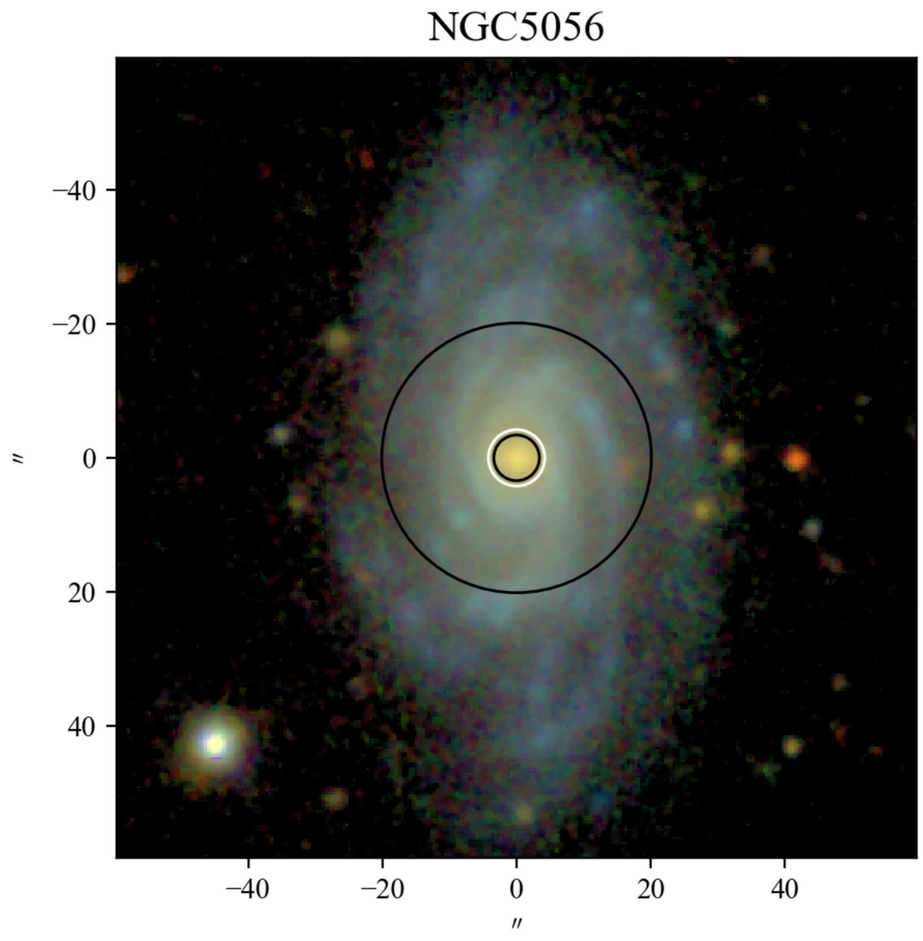
NGC5056
−40
−20
0
20
40
″
−40
−20
0
20
40
″

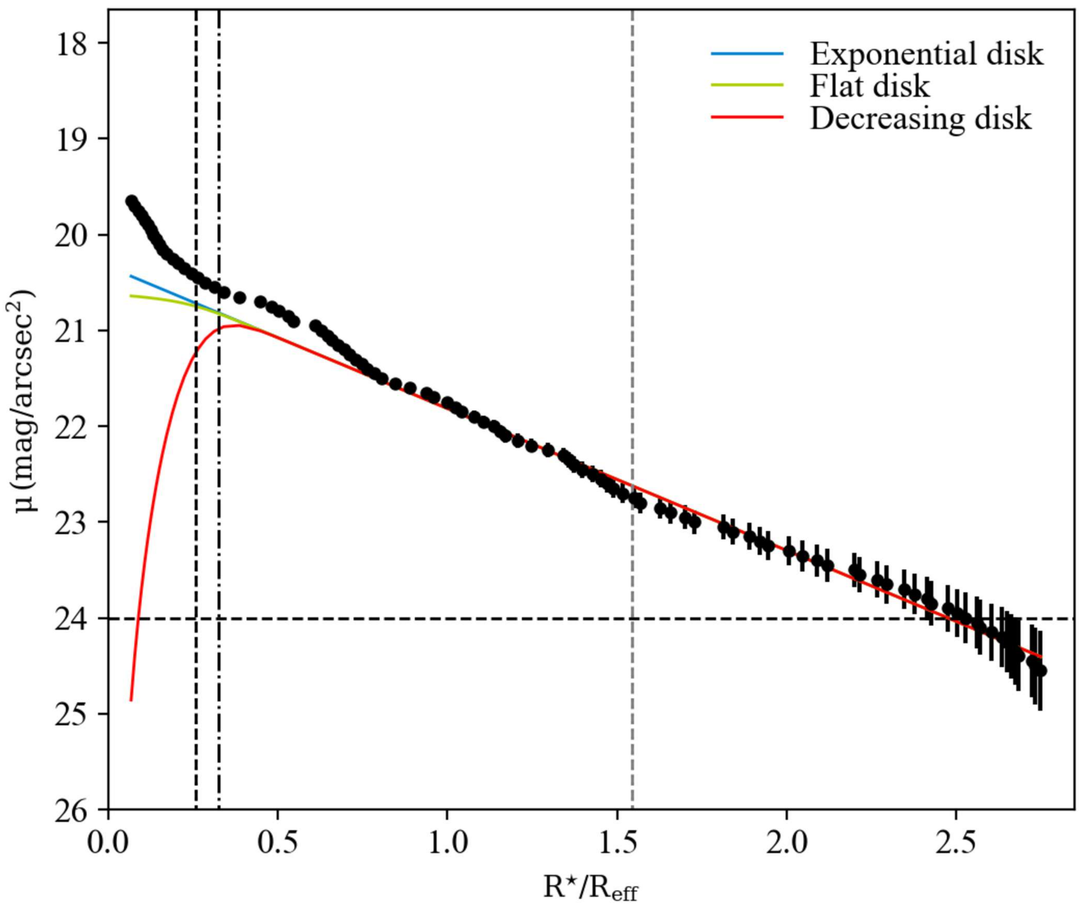
Exponential disk
Flat disk
Decreasing disk
μ (mag/arcsec²)
R⋆/Reff

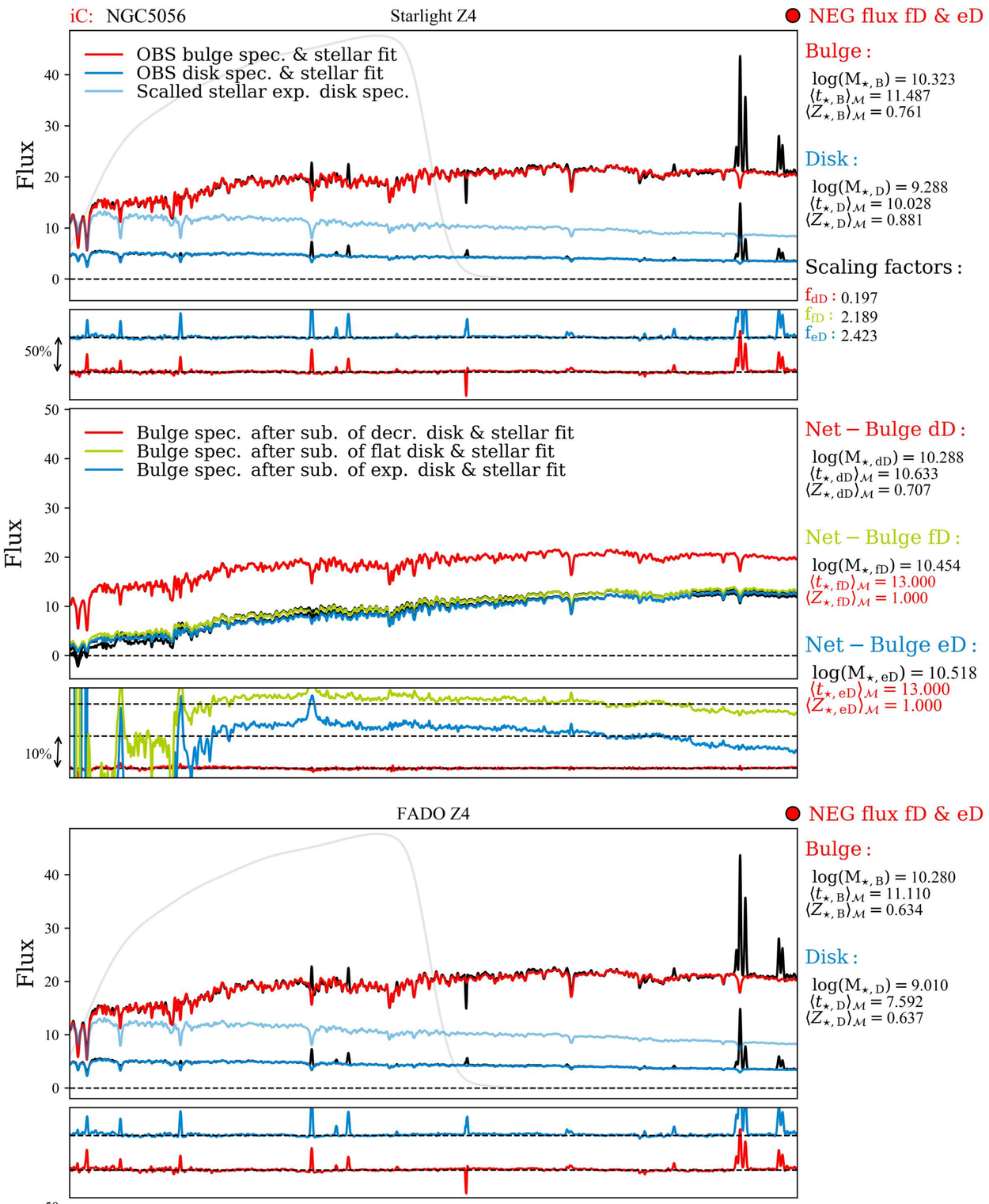
iC: NGC5056
Starlight Z4
NEG flux fD & eD
OBS bulge spec. & stellar fit
OBS disk spec. & stellar fit
Scalled stellar exp. disk spec.
Flux
50%
Bulge :
log(M⋆, B) = 10.323
⟨t⋆, B⟩M = 11.487
⟨Z⋆, B⟩M = 0.761
Disk :
log(M⋆, D) = 9.288
⟨t⋆, D⟩M = 10.028
⟨Z⋆, D⟩M = 0.881
Scaling factors :
fdD : 0.197
ffD : 2.189
feD : 2.423
Bulge spec. after sub. of decr. disk & stellar fit
Bulge spec. after sub. of flat disk & stellar fit
Bulge spec. after sub. of exp. disk & stellar fit
10%
Net − Bulge dD :
log(M⋆, dD) = 10.288
⟨t⋆, dD⟩M = 10.633
⟨Z⋆, dD⟩M = 0.707
Net − Bulge fD :
log(M⋆, fD) = 10.454
⟨t⋆, fD⟩M = 13.000
⟨Z⋆, fD⟩M = 1.000
Net − Bulge eD :
log(M⋆, eD) = 10.518
⟨t⋆, eD⟩M = 13.000
⟨Z⋆, eD⟩M = 1.000

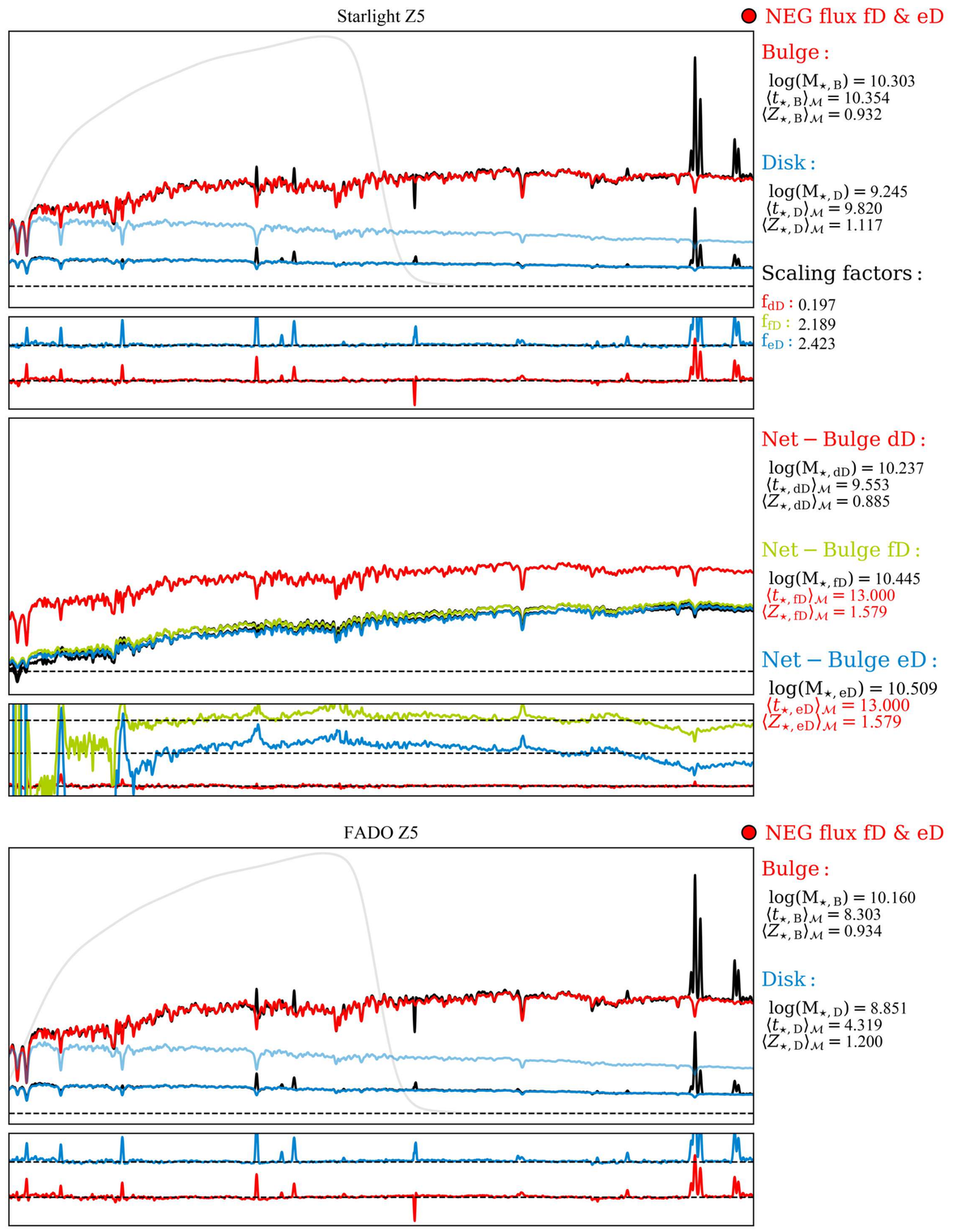
Starlight Z5
NEG flux fD & eD
Bulge :
log(M⋆, B) = 10.303
⟨t⋆, B⟩M = 10.354
⟨Z⋆, B⟩M = 0.932
Disk :
log(M⋆, D) = 9.245
⟨t⋆, D⟩M = 9.820
⟨Z⋆, D⟩M = 1.117
Scaling factors :
fdD : 0.197
ffD : 2.189
feD : 2.423
Net − Bulge dD :
log(M⋆, dD) = 10.237
⟨t⋆, dD⟩M = 9.553
⟨Z⋆, dD⟩M = 0.885
Net − Bulge fD :
log(M⋆, fD) = 10.445
⟨t⋆, fD⟩M = 13.000
⟨Z⋆, fD⟩M = 1.579
Net − Bulge eD :
log(M⋆, eD) = 10.509
⟨t⋆, eD⟩M = 13.000
⟨Z⋆, eD⟩M = 1.579

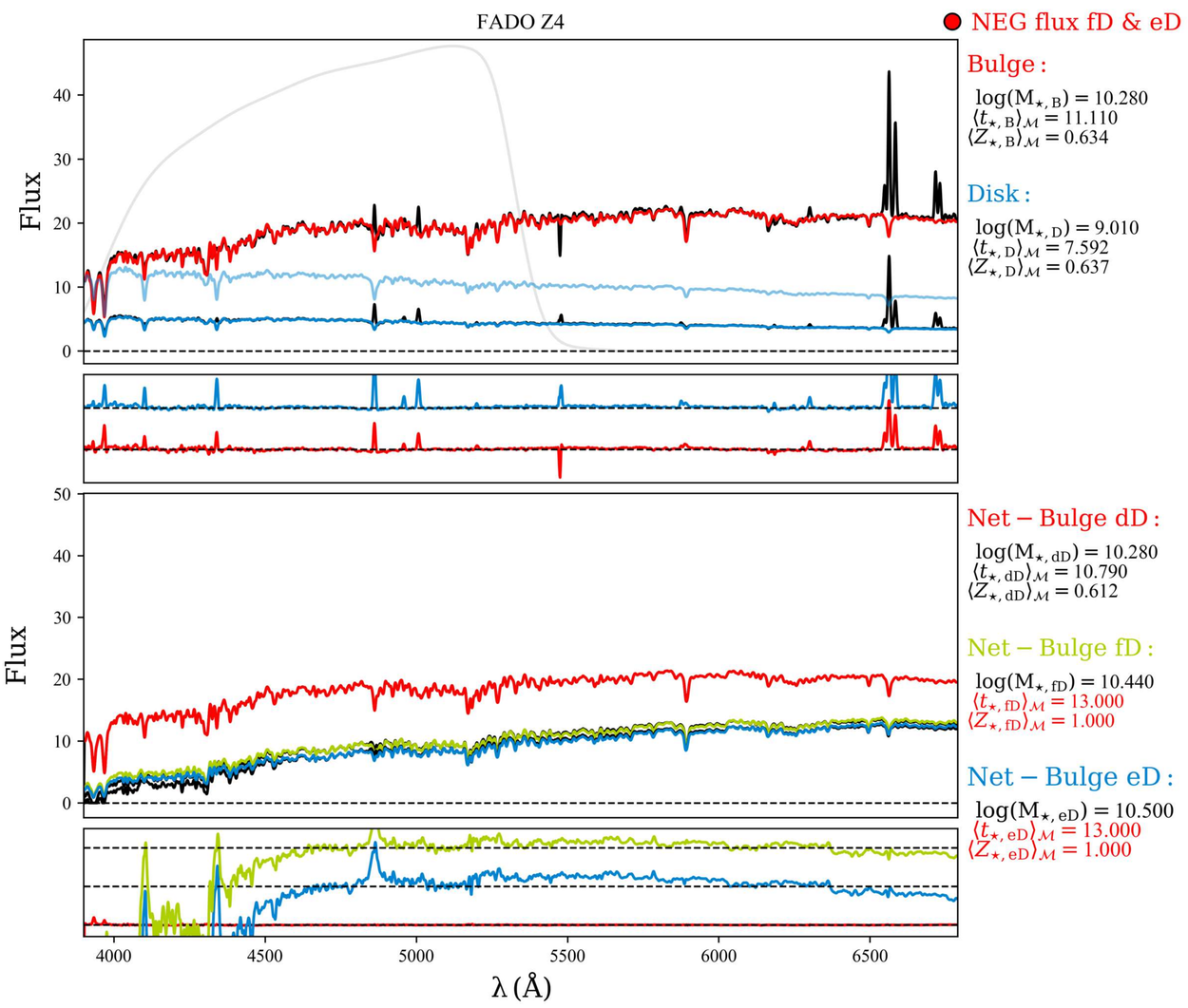
FADO Z4
NEG flux fD & eD
Flux
Bulge :
log(M⋆, B) = 10.280
⟨t⋆, B⟩M = 11.110
⟨Z⋆, B⟩M = 0.634
Disk :
log(M⋆, D) = 9.010
⟨t⋆, D⟩M = 7.592
⟨Z⋆, D⟩M = 0.637
Net − Bulge dD :
log(M⋆, dD) = 10.280
⟨t⋆, dD⟩M = 10.790
⟨Z⋆, dD⟩M = 0.612
Net − Bulge fD :
log(M⋆, fD) = 10.440
⟨t⋆, fD⟩M = 13.000
⟨Z⋆, fD⟩M = 1.000
Net − Bulge eD :
log(M⋆, eD) = 10.500
⟨t⋆, eD⟩M = 13.000
⟨Z⋆, eD⟩M = 1.000
λ (Å)

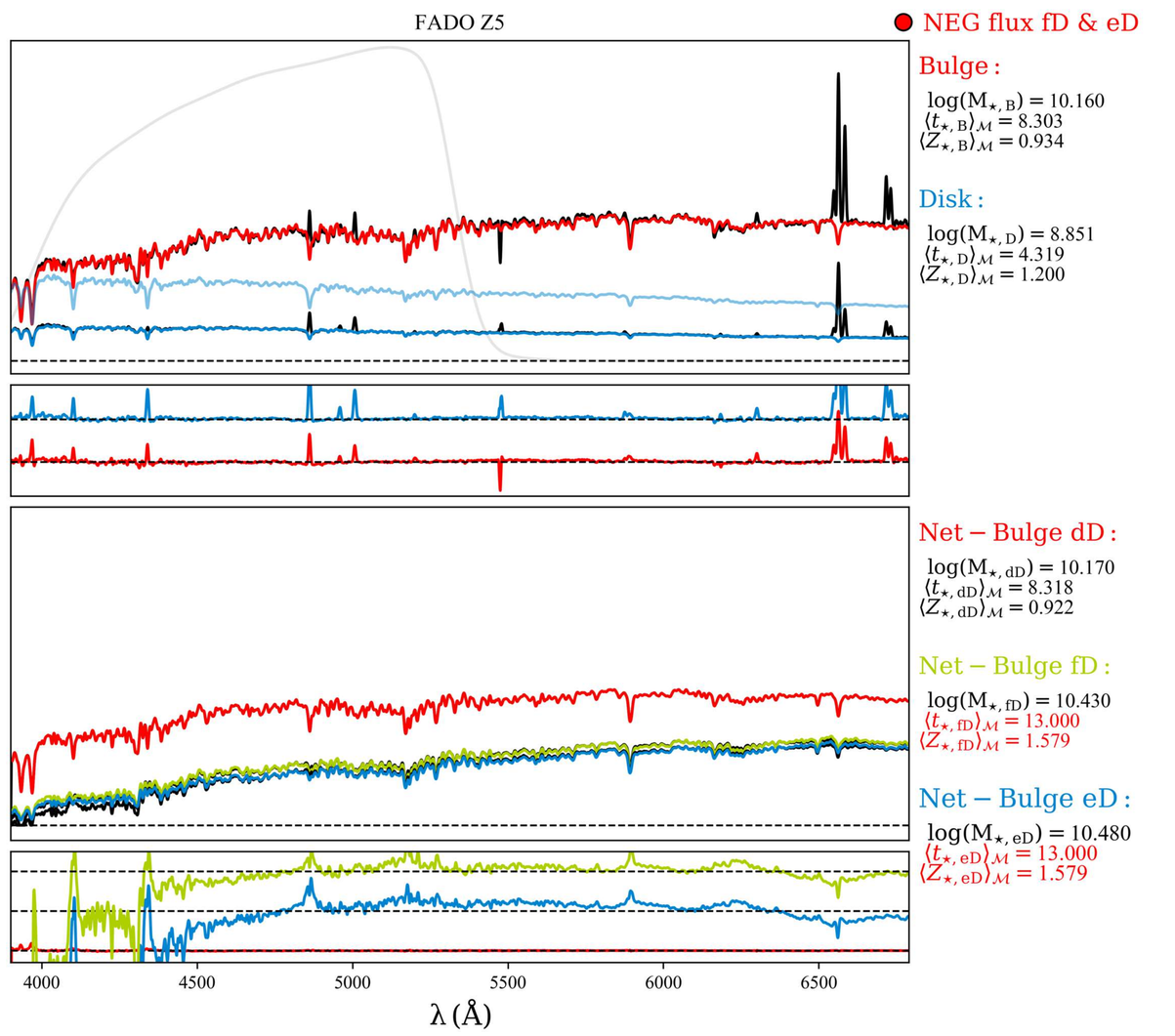
FADO Z5
NEG flux fD & eD
Bulge :
log(M⋆, B) = 10.160
⟨t⋆, B⟩M = 8.303
⟨Z⋆, B⟩M = 0.934
Disk :
log(M⋆, D) = 8.851
⟨t⋆, D⟩M = 4.319
⟨Z⋆, D⟩M = 1.200
Net − Bulge dD :
log(M⋆, dD) = 10.170
⟨t⋆, dD⟩M = 8.318
⟨Z⋆, dD⟩M = 0.922
Net − Bulge fD :
log(M⋆, fD) = 10.430
⟨t⋆, fD⟩M = 13.000
⟨Z⋆, fD⟩M = 1.579
Net − Bulge eD :
log(M⋆, eD) = 10.480
⟨t⋆, eD⟩M = 13.000
⟨Z⋆, eD⟩M = 1.579
λ (Å)

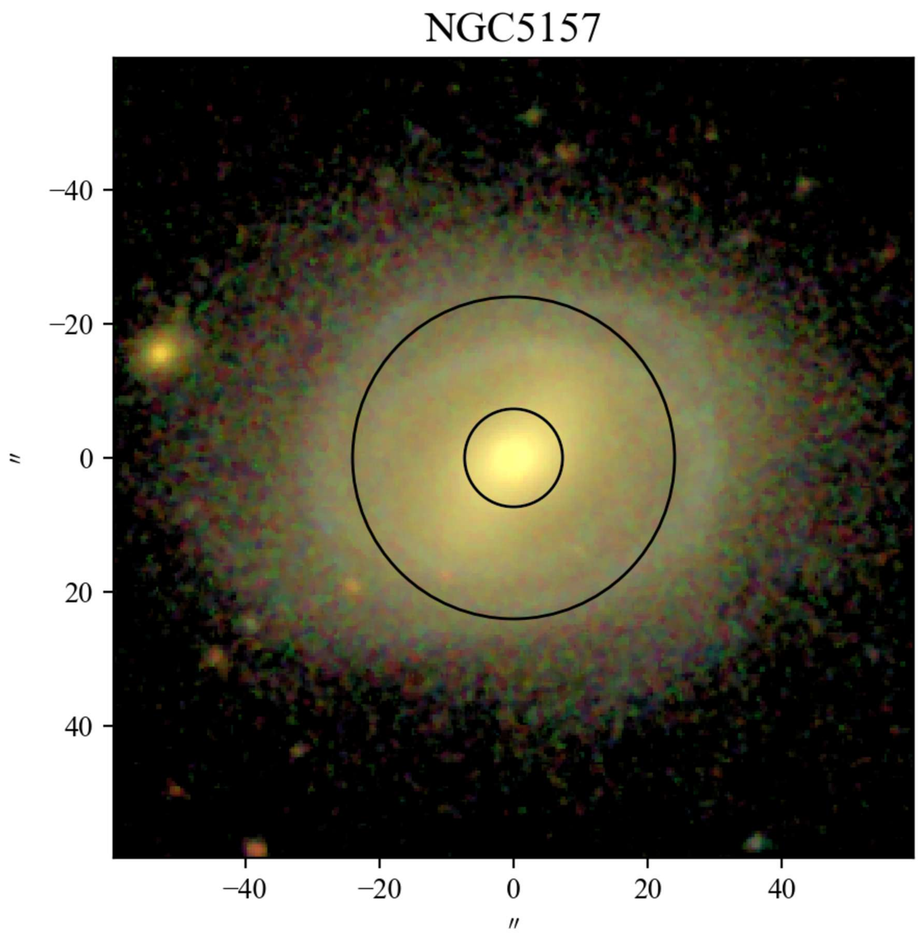
NGC5157
−40
−20
0
20
40
″
−40
−20
0
20
40
″

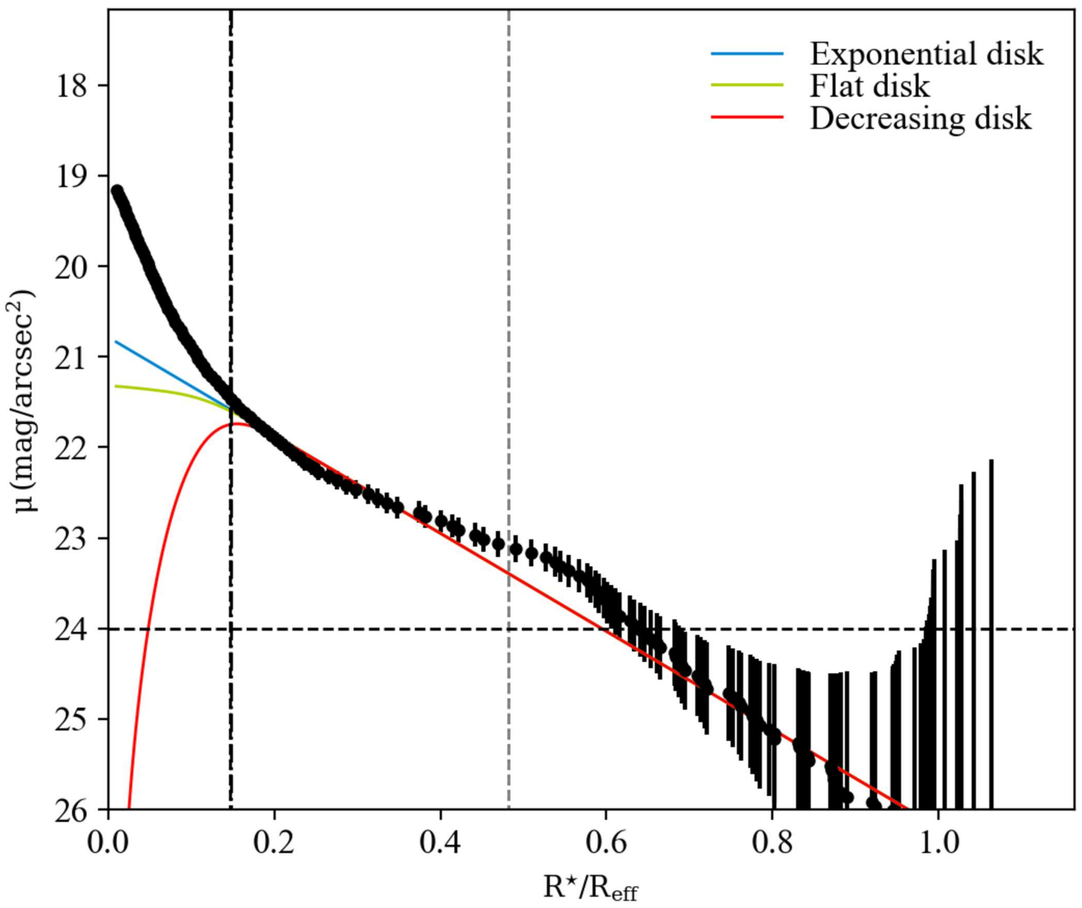
Exponential disk
Flat disk
Decreasing disk
μ (mag/arcsec²)
18
19
20
21
22
23
24
25
26
0.0
0.2
0.4
0.6
0.8
1.0
R⋆/Reff

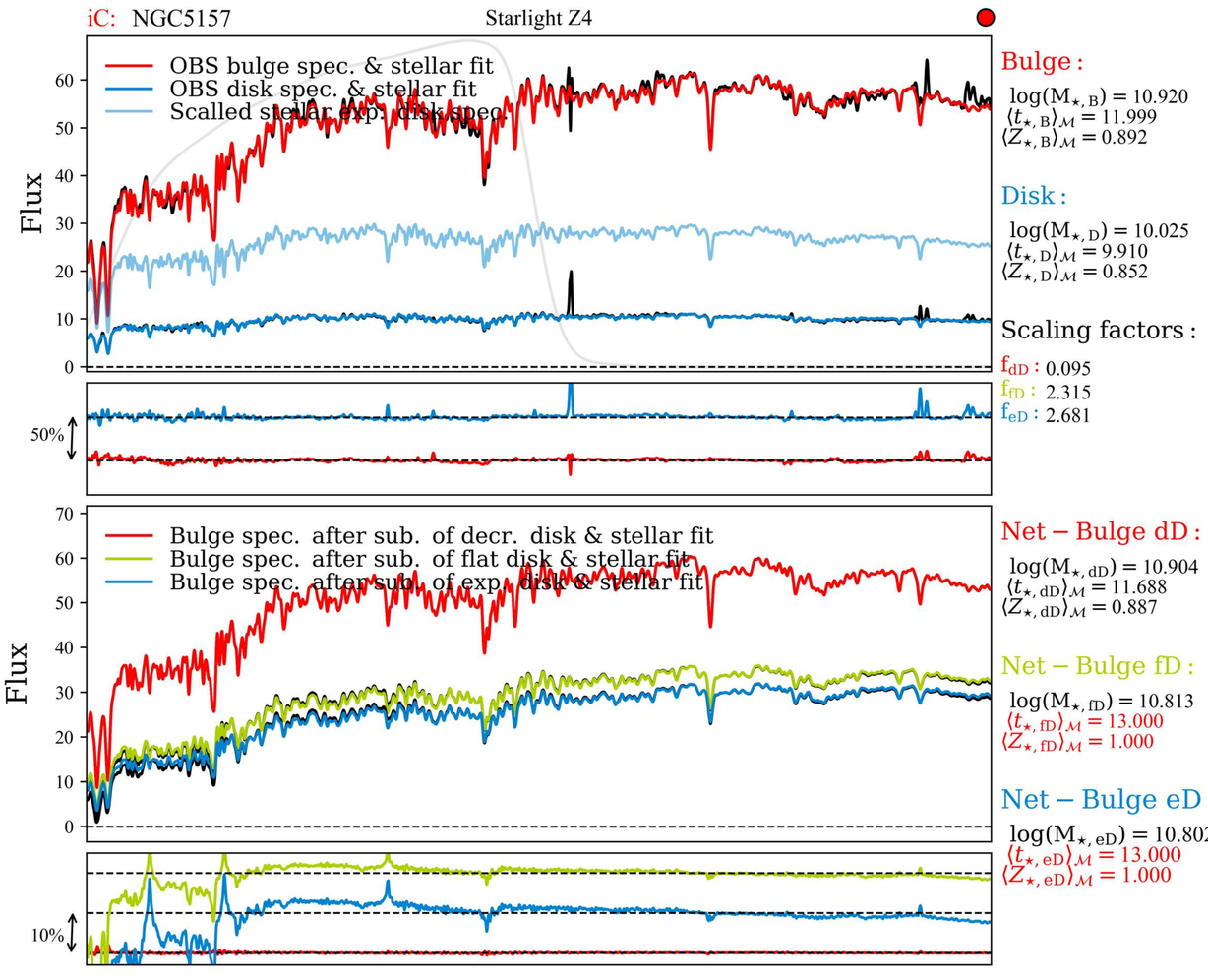
iC: NGC5157
Starlight Z4
OBS bulge spec. & stellar fit
OBS disk spec. & stellar fit
Scalled stellar exp. disk spec.
Flux
50%
Bulge spec. after sub. of decr. disk & stellar fit
Bulge spec. after sub. of flat disk & stellar fit
Bulge spec. after sub. of exp. disk & stellar fit
10%
Bulge :
log(M⋆, B) = 10.920
⟨t⋆, B⟩M = 11.999
⟨Z⋆, B⟩M = 0.892
Disk :
log(M⋆, D) = 10.025
⟨t⋆, D⟩M = 9.910
⟨Z⋆, D⟩M = 0.852
Scaling factors :
fdD : 0.095
ffD : 2.315
feD : 2.681
Net − Bulge dD :
log(M⋆, dD) = 10.904
⟨t⋆, dD⟩M = 11.688
⟨Z⋆, dD⟩M = 0.887
Net − Bulge fD :
log(M⋆, fD) = 10.813
⟨t⋆, fD⟩M = 13.000
⟨Z⋆, fD⟩M = 1.000
Net − Bulge eD :
log(M⋆, eD) = 10.802
⟨t⋆, eD⟩M = 13.000
⟨Z⋆, eD⟩M = 1.000

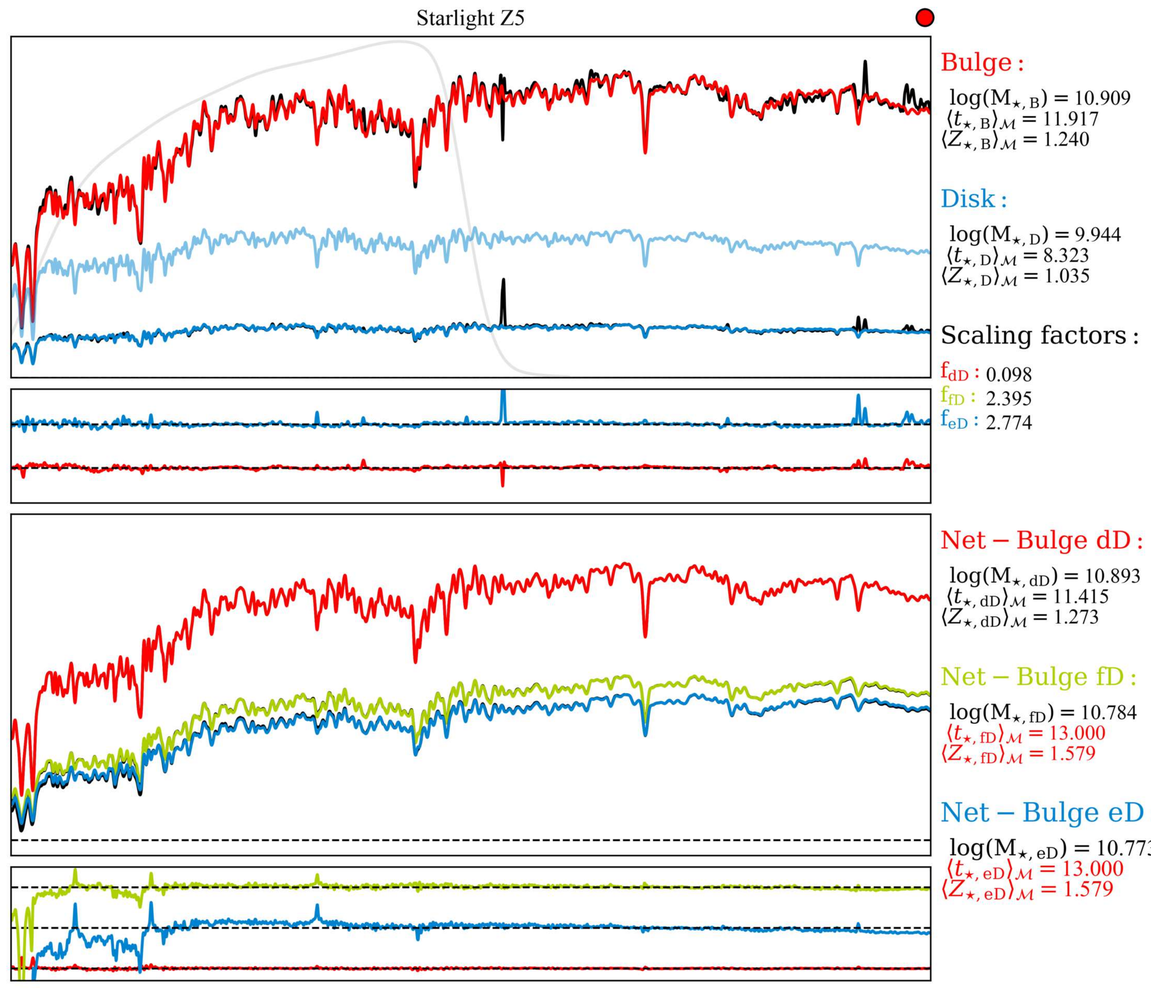
Starlight Z5
Bulge :
log(M⋆, B) = 10.909
⟨t⋆, B⟩M = 11.917
⟨Z⋆, B⟩M = 1.240
Disk :
log(M⋆, D) = 9.944
⟨t⋆, D⟩M = 8.323
⟨Z⋆, D⟩M = 1.035
Scaling factors :
fdD : 0.098
ffD : 2.395
feD : 2.774
Net − Bulge dD :
log(M⋆, dD) = 10.893
⟨t⋆, dD⟩M = 11.415
⟨Z⋆, dD⟩M = 1.273
Net − Bulge fD :
log(M⋆, fD) = 10.784
⟨t⋆, fD⟩M = 13.000
⟨Z⋆, fD⟩M = 1.579
Net − Bulge eD :
log(M⋆, eD) = 10.773
⟨t⋆, eD⟩M = 13.000
⟨Z⋆, eD⟩M = 1.579

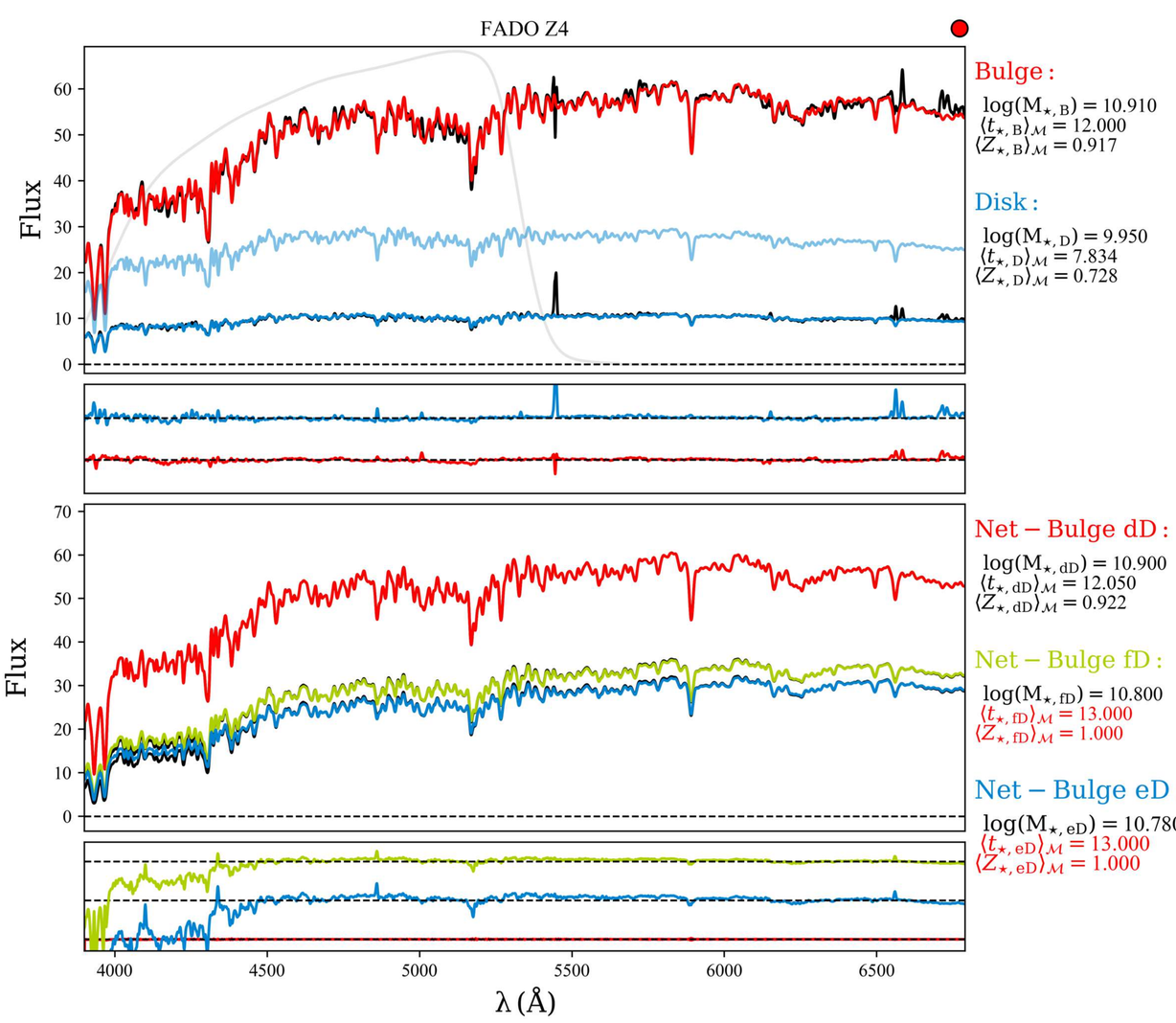
FADO Z4
Flux
Bulge :
log(M⋆, B) = 10.910
⟨t⋆, B⟩M = 12.000
⟨Z⋆, B⟩M = 0.917
Disk :
log(M⋆, D) = 9.950
⟨t⋆, D⟩M = 7.834
⟨Z⋆, D⟩M = 0.728
Net − Bulge dD :
log(M⋆, dD) = 10.900
⟨t⋆, dD⟩M = 12.050
⟨Z⋆, dD⟩M = 0.922
Net − Bulge fD :
log(M⋆, fD) = 10.800
⟨t⋆, fD⟩M = 13.000
⟨Z⋆, fD⟩M = 1.000
Net − Bulge eD :
log(M⋆, eD) = 10.780
⟨t⋆, eD⟩M = 13.000
⟨Z⋆, eD⟩M = 1.000
λ (Å)

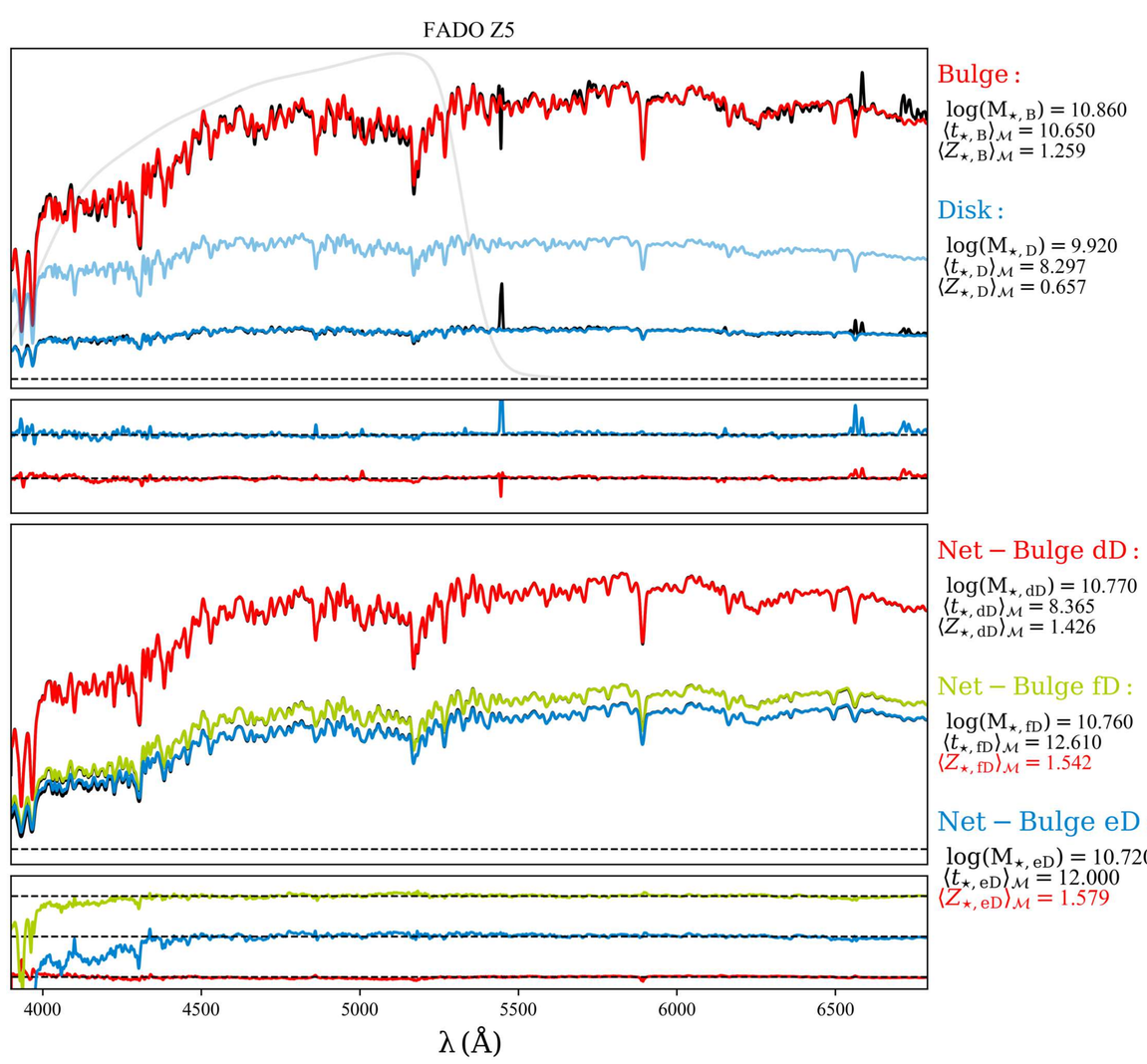
FADO Z5
Bulge :
log(M⋆, B) = 10.860
⟨t⋆, B⟩M = 10.650
⟨Z⋆, B⟩M = 1.259
Disk :
log(M⋆, D) = 9.920
⟨t⋆, D⟩M = 8.297
⟨Z⋆, D⟩M = 0.657
Net − Bulge dD :
log(M⋆, dD) = 10.770
⟨t⋆, dD⟩M = 8.365
⟨Z⋆, dD⟩M = 1.426
Net − Bulge fD :
log(M⋆, fD) = 10.760
⟨t⋆, fD⟩M = 12.610
⟨Z⋆, fD⟩M = 1.542
Net − Bulge eD :
log(M⋆, eD) = 10.720
⟨t⋆, eD⟩M = 12.000
⟨Z⋆, eD⟩M = 1.579
λ (Å)

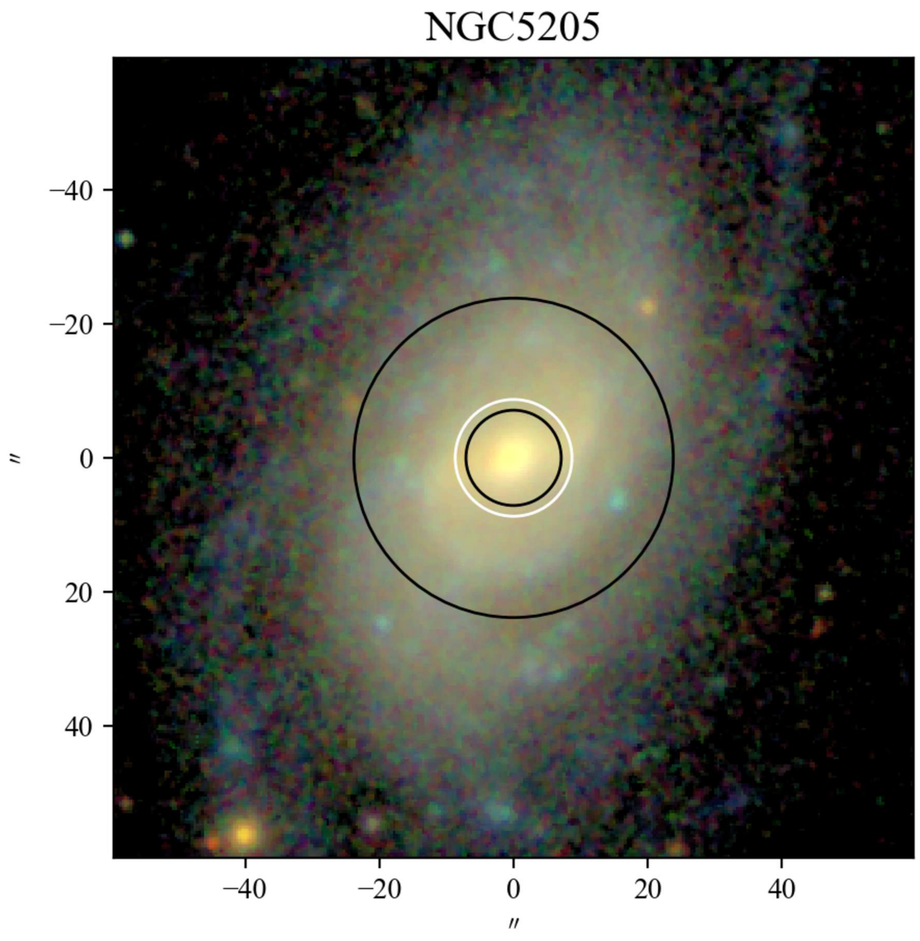
NGC5205
−40
−20
0
20
40
″
−40
−20
0
20
40
″

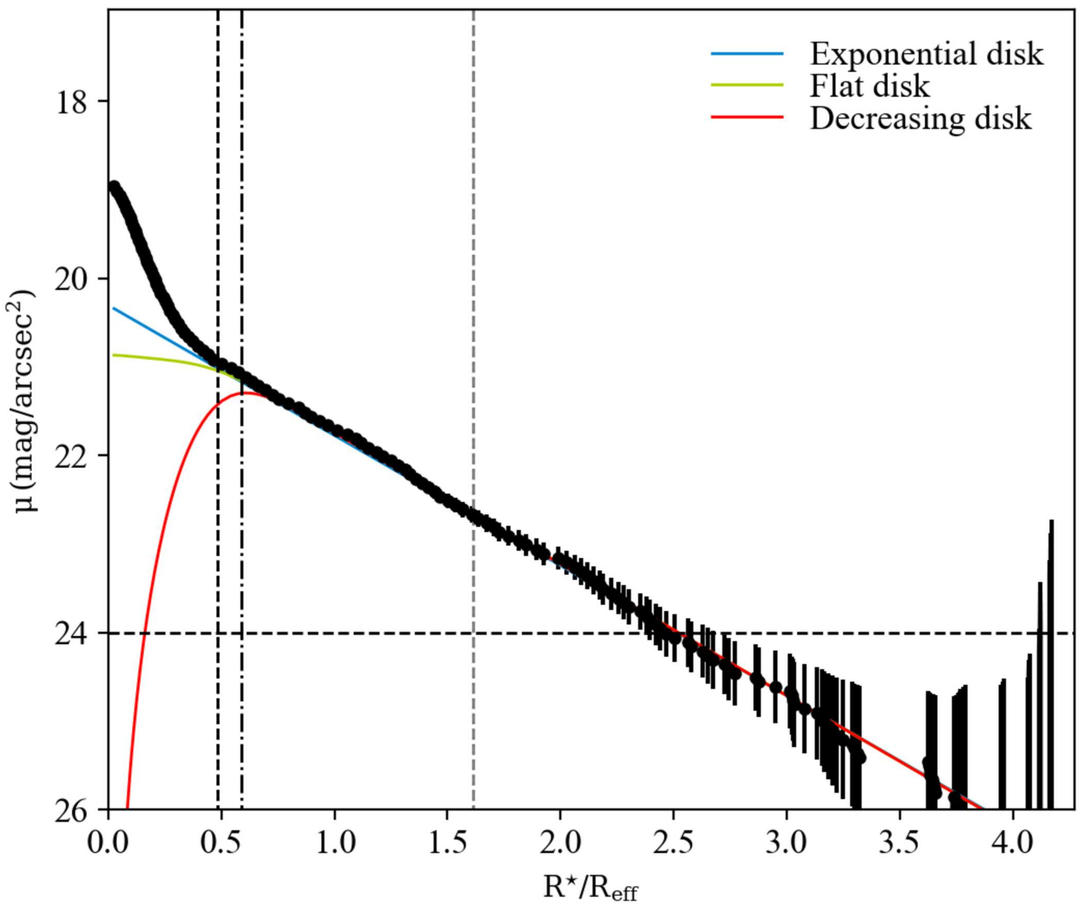
Exponential disk
Flat disk
Decreasing disk
μ (mag/arcsec²)
18
20
22
24
26
0.0
0.5
1.0
1.5
2.0
2.5
3.0
3.5
4.0
R⋆/Reff

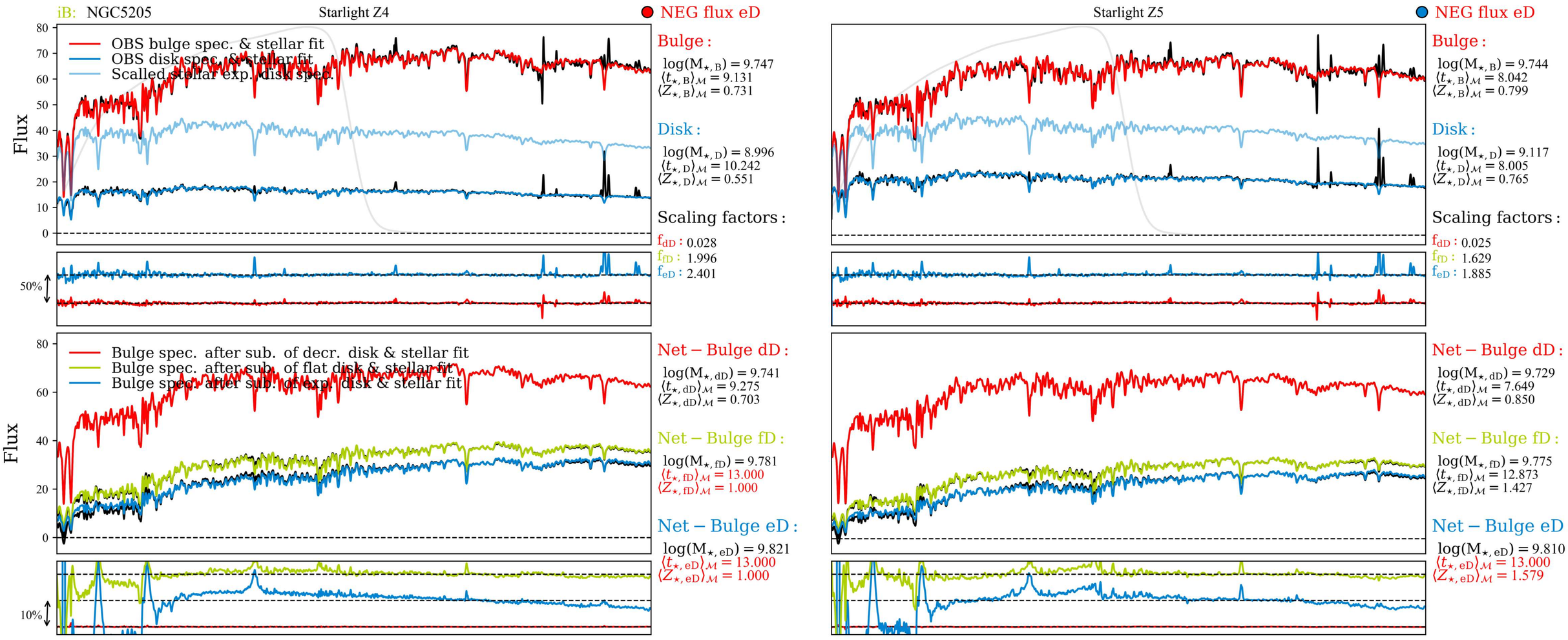
iB: NGC5205
Starlight Z4
NEG flux eD
OBS bulge spec. & stellar fit
OBS disk spec. & stellar fit
Scalled stellar exp. disk spec.
Flux
50%
Bulge :
log(M⋆, B) = 9.747
⟨t⋆, B⟩M = 9.131
⟨Z⋆, B⟩M = 0.731
Disk :
log(M⋆, D) = 8.996
⟨t⋆, D⟩M = 10.242
⟨Z⋆, D⟩M = 0.551
Scaling factors :
fdD : 0.028
ffD : 1.996
feD : 2.401
Starlight Z5
NEG flux eD
Bulge :
log(M⋆, B) = 9.744
⟨t⋆, B⟩M = 8.042
⟨Z⋆, B⟩M = 0.799
Disk :
log(M⋆, D) = 9.117
⟨t⋆, D⟩M = 8.005
⟨Z⋆, D⟩M = 0.765
Scaling factors :
fdD : 0.025
ffD : 1.629
feD : 1.885
Bulge spec. after sub. of decr. disk & stellar fit
Bulge spec. after sub. of flat disk & stellar fit
Bulge spec. after sub. of exp. disk & stellar fit
10%
Net − Bulge dD :
log(M⋆, dD) = 9.741
⟨t⋆, dD⟩M = 9.275
⟨Z⋆, dD⟩M = 0.703
Net − Bulge fD :
log(M⋆, fD) = 9.781
⟨t⋆, fD⟩M = 13.000
⟨Z⋆, fD⟩M = 1.000
Net − Bulge eD :
log(M⋆, eD) = 9.821
⟨t⋆, eD⟩M = 13.000
⟨Z⋆, eD⟩M = 1.000
Net − Bulge dD :
log(M⋆, dD) = 9.729
⟨t⋆, dD⟩M = 7.649
⟨Z⋆, dD⟩M = 0.850
Net − Bulge fD :
log(M⋆, fD) = 9.775
⟨t⋆, fD⟩M = 12.873
⟨Z⋆, fD⟩M = 1.427
Net − Bulge eD :
log(M⋆, eD) = 9.810
⟨t⋆, eD⟩M = 13.000
⟨Z⋆, eD⟩M = 1.579
FADO Z4
NEG flux fD & eD
Bulge :
log(M⋆, B) = 9.568
⟨t⋆, B⟩M = 4.240
⟨Z⋆, B⟩M = 0.615
Disk :
log(M⋆, D) = 8.744
⟨t⋆, D⟩M = 4.196
⟨Z⋆, D⟩M = 0.367
FADO Z5
NEG flux fD & eD
Bulge :
log(M⋆, B) = 9.608
⟨t⋆, B⟩M = 4.696
⟨Z⋆, B⟩M = 0.606
Disk :
log(M⋆, D) = 8.923
⟨t⋆, D⟩M = 4.623
⟨Z⋆, D⟩M = 0.364
Net − Bulge dD :
log(M⋆, dD) = 9.569
⟨t⋆, dD⟩M = 4.337
⟨Z⋆, dD⟩M = 0.617
Net − Bulge fD :
log(M⋆, fD) = 9.749
⟨t⋆, fD⟩M = 11.000
⟨Z⋆, fD⟩M = 1.000
Net − Bulge eD :
log(M⋆, eD) = 9.813
⟨t⋆, eD⟩M = 13.000
⟨Z⋆, eD⟩M = 1.000
Net − Bulge dD :
log(M⋆, dD) = 9.612
⟨t⋆, dD⟩M = 5.120
⟨Z⋆, dD⟩M = 0.622
Net − Bulge fD :
log(M⋆, fD) = 9.756
⟨t⋆, fD⟩M = 11.880
⟨Z⋆, fD⟩M = 1.471
Net − Bulge eD :
log(M⋆, eD) = 9.754
⟨t⋆, eD⟩M = 11.000
⟨Z⋆, eD⟩M = 1.579
λ (Å)

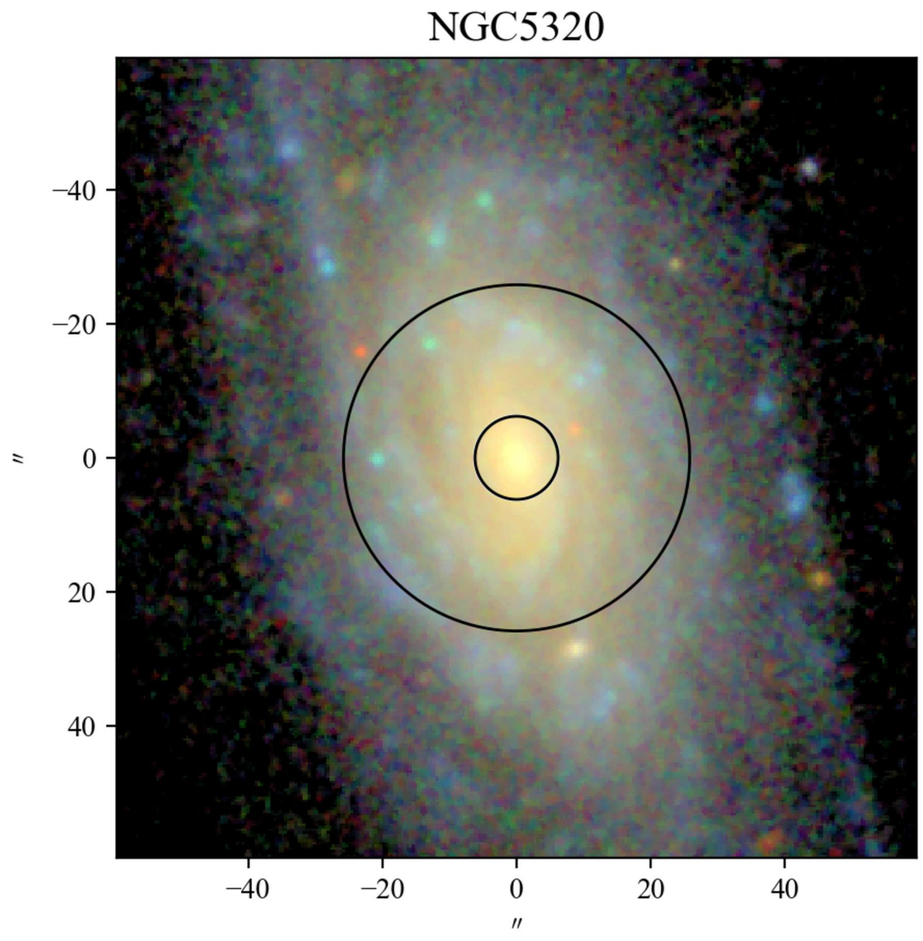
NGC5320
−40
−20
0
20
40
″
−40
−20
0
20
40
″

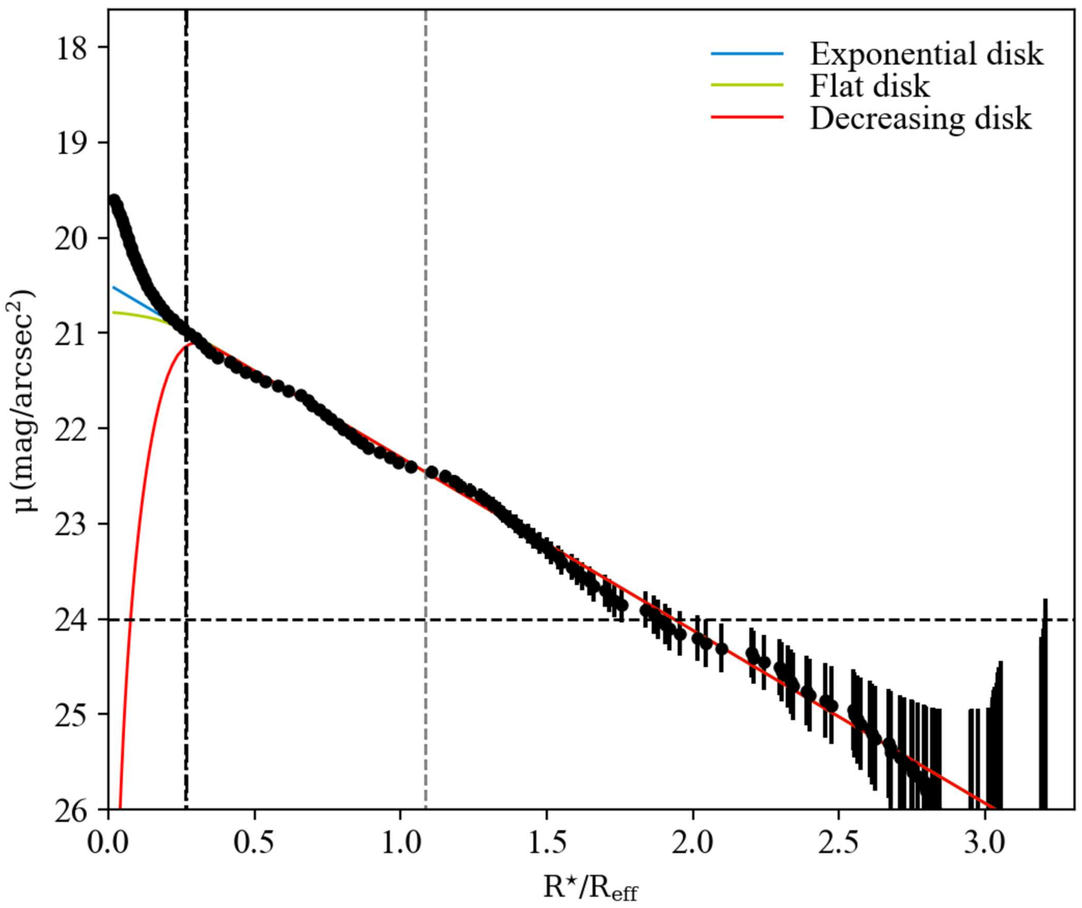
Exponential disk
Flat disk
Decreasing disk
μ (mag/arcsec²)
R⋆/Reff

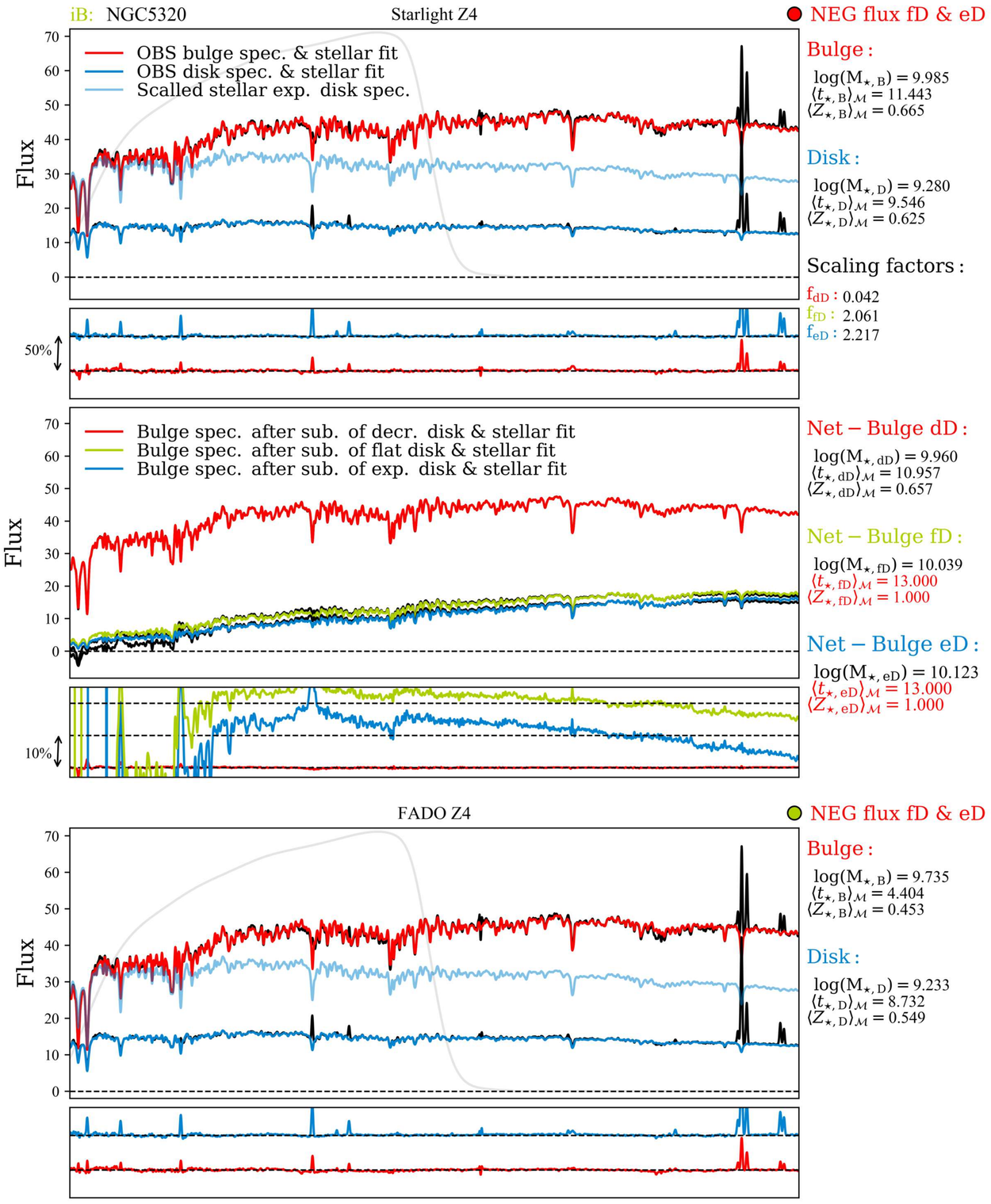
iB: NGC5320
Starlight Z4
NEG flux fD & eD
OBS bulge spec. & stellar fit
OBS disk spec. & stellar fit
Scalled stellar exp. disk spec.
Flux
Bulge :
log(M⋆, B) = 9.985
⟨t⋆, B⟩M = 11.443
⟨Z⋆, B⟩M = 0.665
Disk :
log(M⋆, D) = 9.280
⟨t⋆, D⟩M = 9.546
⟨Z⋆, D⟩M = 0.625
Scaling factors :
fdD : 0.042
ffD : 2.061
feD : 2.217
50%
Bulge spec. after sub. of decr. disk & stellar fit
Bulge spec. after sub. of flat disk & stellar fit
Bulge spec. after sub. of exp. disk & stellar fit
Net − Bulge dD :
log(M⋆, dD) = 9.960
⟨t⋆, dD⟩M = 10.957
⟨Z⋆, dD⟩M = 0.657
Net − Bulge fD :
log(M⋆, fD) = 10.039
⟨t⋆, fD⟩M = 13.000
⟨Z⋆, fD⟩M = 1.000
Net − Bulge eD :
log(M⋆, eD) = 10.123
⟨t⋆, eD⟩M = 13.000
⟨Z⋆, eD⟩M = 1.000
10%

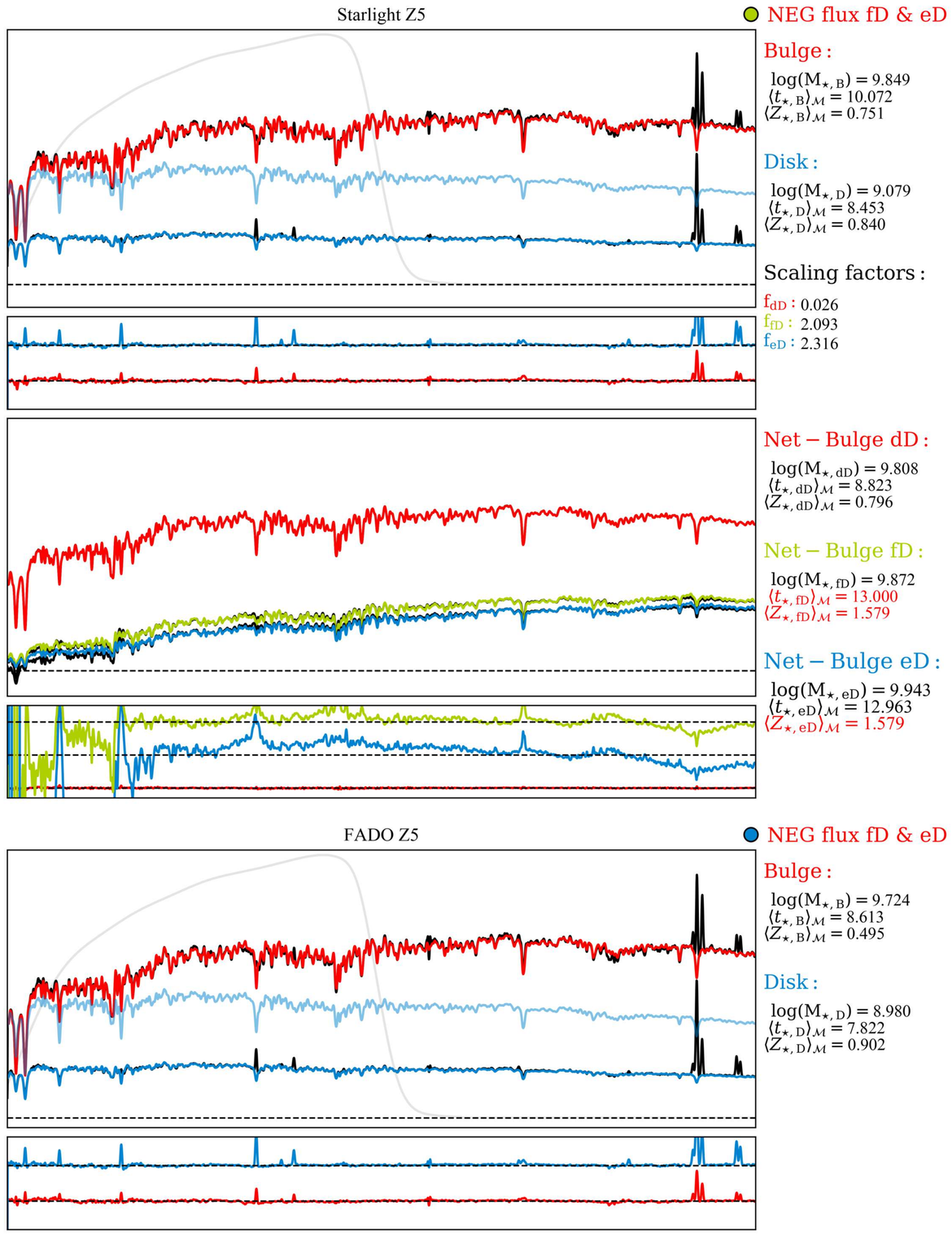
Starlight Z5
NEG flux fD & eD
Bulge :
log(M⋆, B) = 9.849
⟨t⋆, B⟩M = 10.072
⟨Z⋆, B⟩M = 0.751
Disk :
log(M⋆, D) = 9.079
⟨t⋆, D⟩M = 8.453
⟨Z⋆, D⟩M = 0.840
Scaling factors :
fdD : 0.026
ffD : 2.093
feD : 2.316
Net − Bulge dD :
log(M⋆, dD) = 9.808
⟨t⋆, dD⟩M = 8.823
⟨Z⋆, dD⟩M = 0.796
Net − Bulge fD :
log(M⋆, fD) = 9.872
⟨t⋆, fD⟩M = 13.000
⟨Z⋆, fD⟩M = 1.579
Net − Bulge eD :
log(M⋆, eD) = 9.943
⟨t⋆, eD⟩M = 12.963
⟨Z⋆, eD⟩M = 1.579

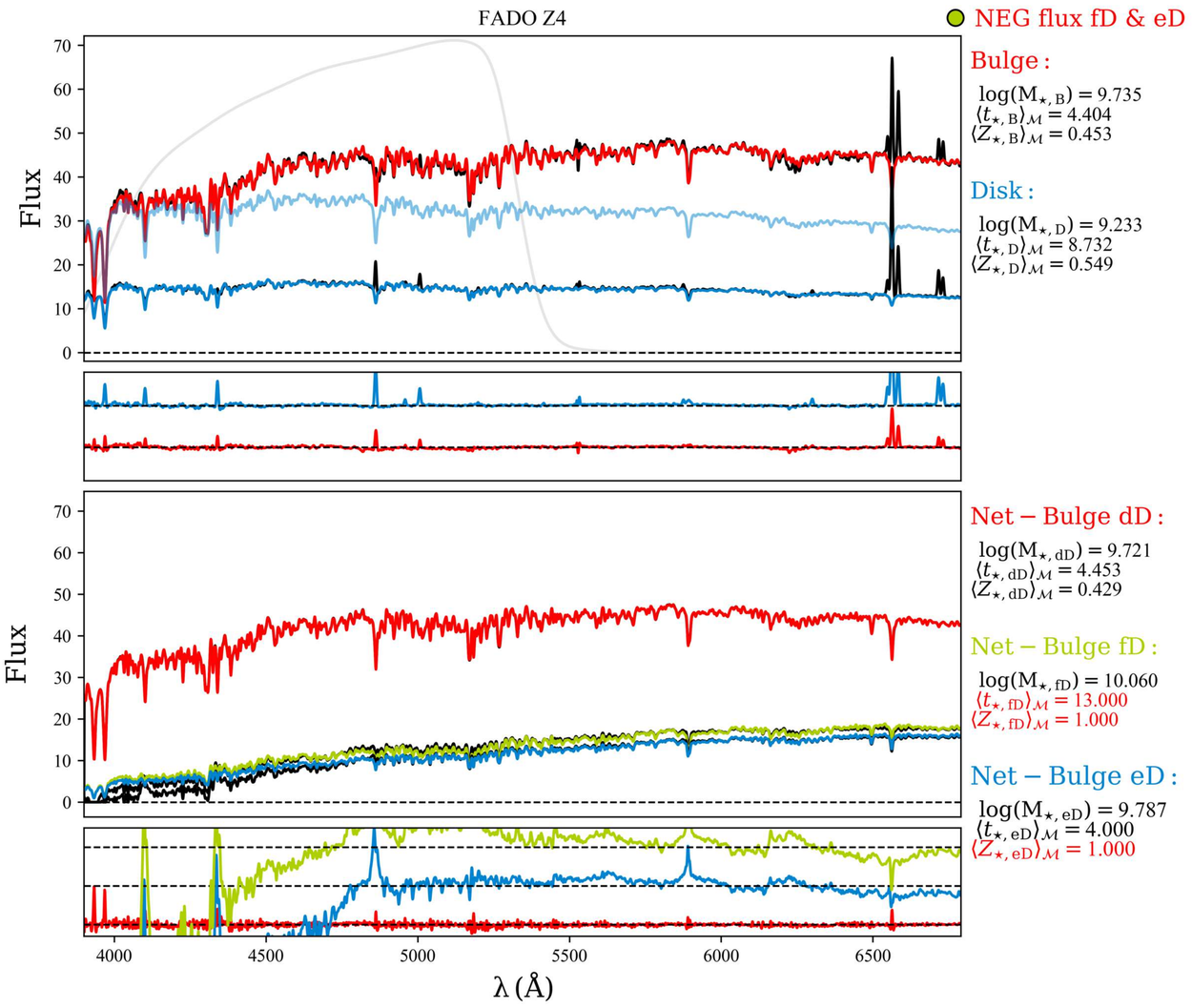
FADO Z4
NEG flux fD & eD
Flux
Bulge :
log(M⋆, B) = 9.735
⟨t⋆, B⟩M = 4.404
⟨Z⋆, B⟩M = 0.453
Disk :
log(M⋆, D) = 9.233
⟨t⋆, D⟩M = 8.732
⟨Z⋆, D⟩M = 0.549
Net − Bulge dD :
log(M⋆, dD) = 9.721
⟨t⋆, dD⟩M = 4.453
⟨Z⋆, dD⟩M = 0.429
Net − Bulge fD :
log(M⋆, fD) = 10.060
⟨t⋆, fD⟩M = 13.000
⟨Z⋆, fD⟩M = 1.000
Net − Bulge eD :
log(M⋆, eD) = 9.787
⟨t⋆, eD⟩M = 4.000
⟨Z⋆, eD⟩M = 1.000
λ (Å)

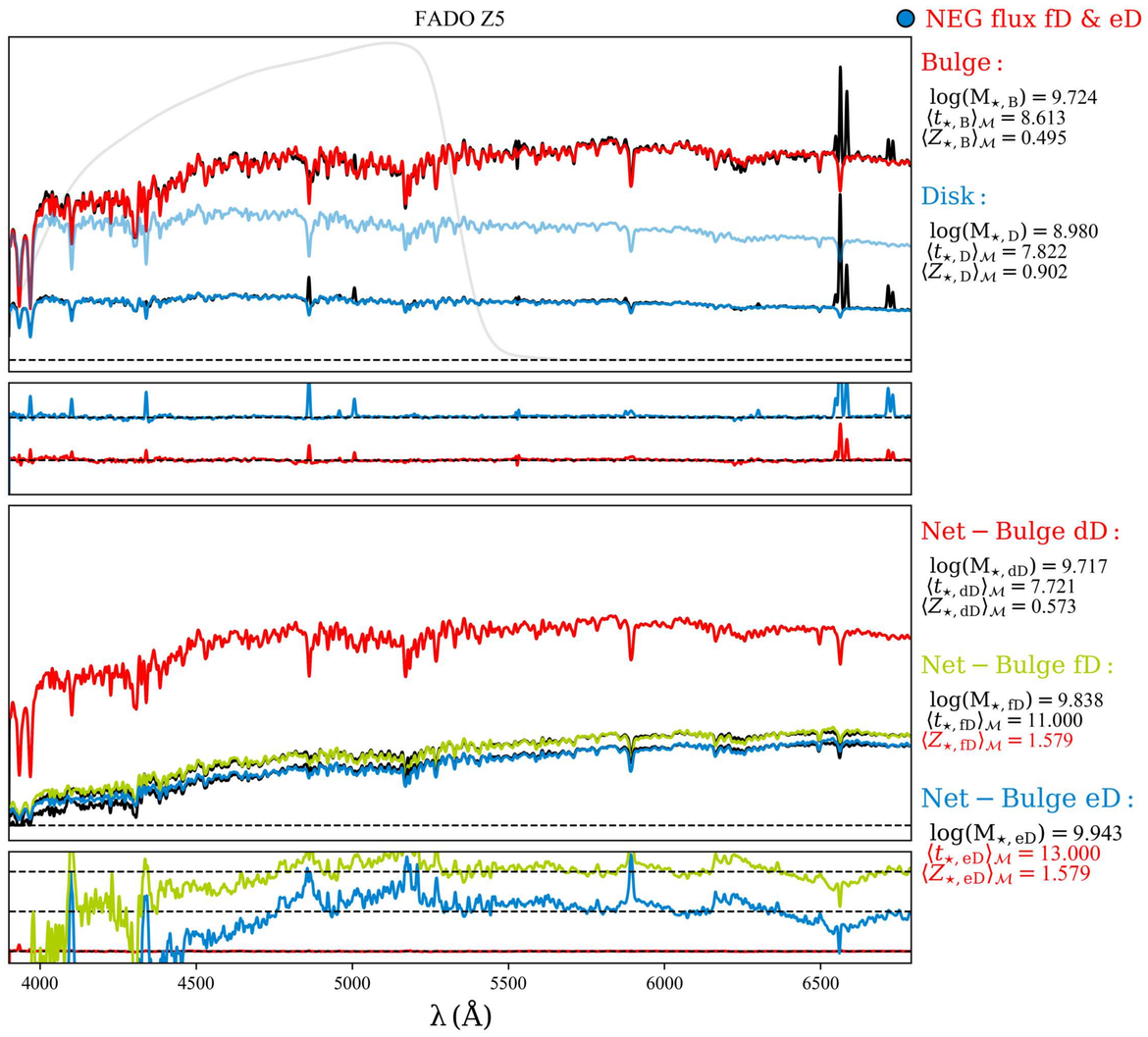
FADO Z5
NEG flux fD & eD
Bulge :
log(M⋆, B) = 9.724
⟨t⋆, B⟩M = 8.613
⟨Z⋆, B⟩M = 0.495
Disk :
log(M⋆, D) = 8.980
⟨t⋆, D⟩M = 7.822
⟨Z⋆, D⟩M = 0.902
Net − Bulge dD :
log(M⋆, dD) = 9.717
⟨t⋆, dD⟩M = 7.721
⟨Z⋆, dD⟩M = 0.573
Net − Bulge fD :
log(M⋆, fD) = 9.838
⟨t⋆, fD⟩M = 11.000
⟨Z⋆, fD⟩M = 1.579
Net − Bulge eD :
log(M⋆, eD) = 9.943
⟨t⋆, eD⟩M = 13.000
⟨Z⋆, eD⟩M = 1.579
λ (Å)

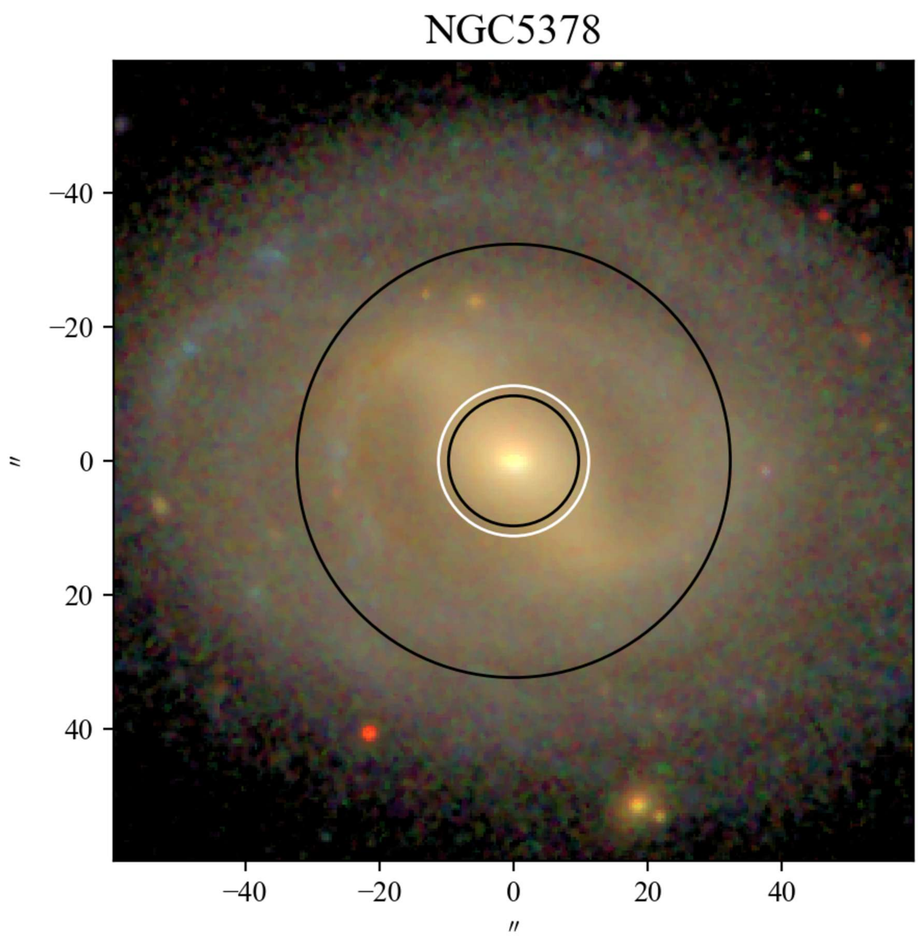
NGC5378
−40
−20
0
20
40
″
−40
−20
0
20
40
″

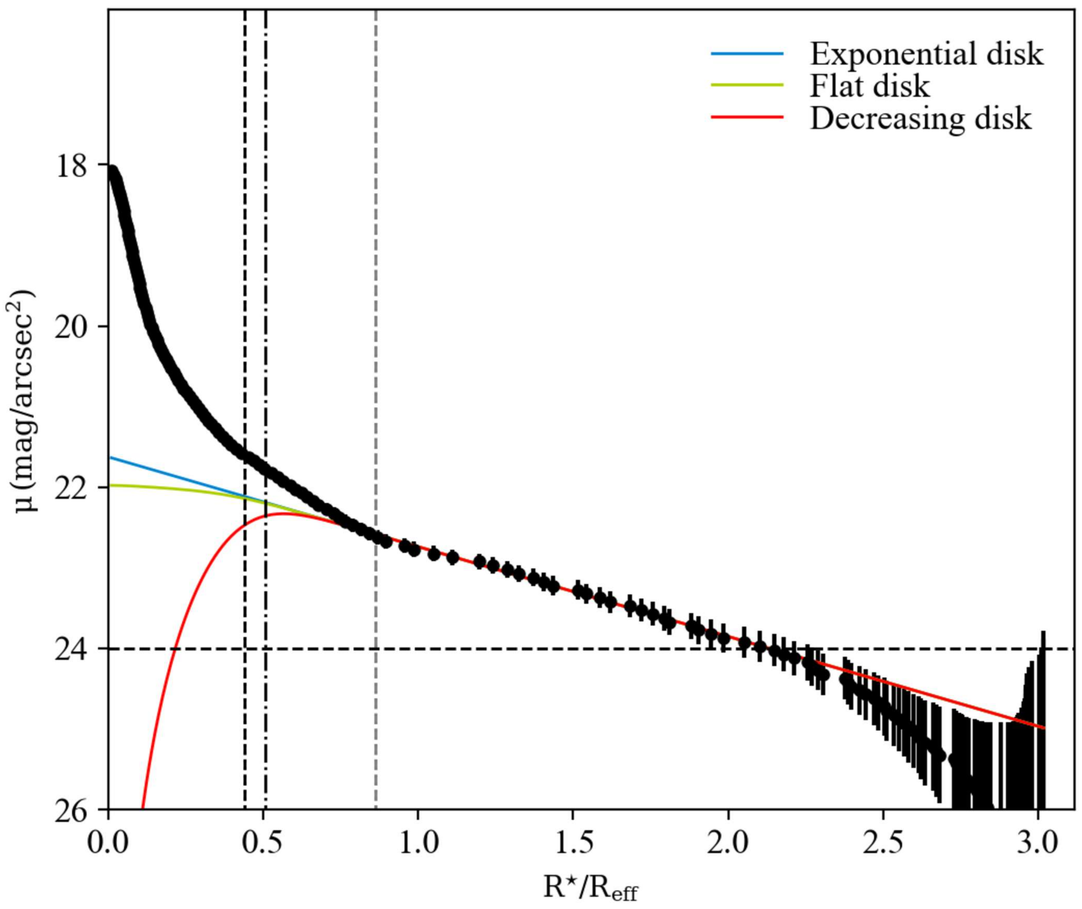
Exponential disk
Flat disk
Decreasing disk
μ (mag/arcsec²)
18
20
22
24
26
0.0
0.5
1.0
1.5
2.0
2.5
3.0
R⋆/Reff

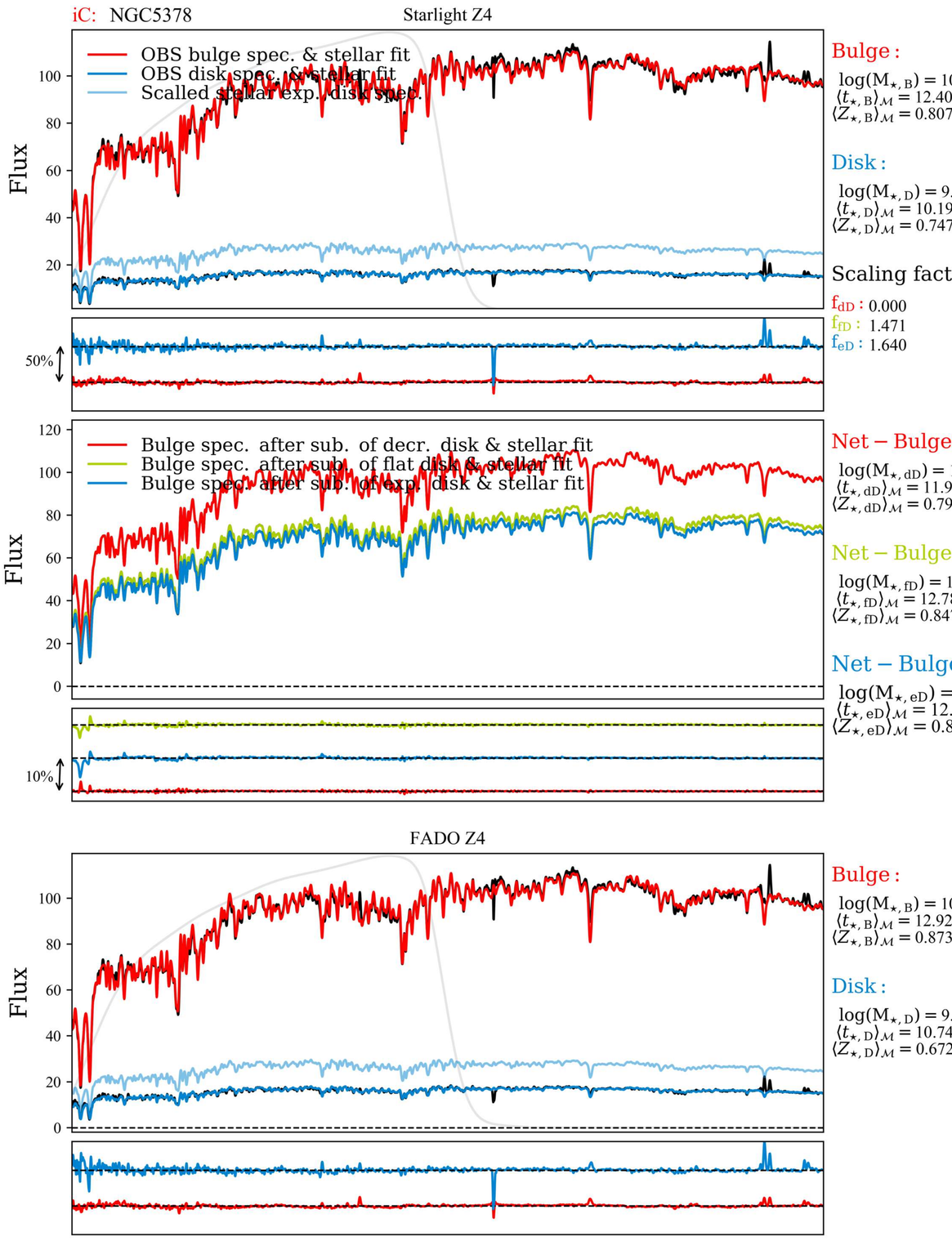
iC: NGC5378
Starlight Z4
OBS bulge spec. & stellar fit
OBS disk spec. & stellar fit
Scalled stellar exp. disk spec.
Flux
50%
Bulge spec. after sub. of decr. disk & stellar fit
Bulge spec. after sub. of flat disk & stellar fit
Bulge spec. after sub. of exp. disk & stellar fit
10%
Bulge :
log(M⋆, B) = 10.473
⟨t⋆, B⟩M = 12.400
⟨Z⋆, B⟩M = 0.807
Disk :
log(M⋆, D) = 9.538
⟨t⋆, D⟩M = 10.191
⟨Z⋆, D⟩M = 0.747
Scaling factors :
fdD : 0.000
ffD : 1.471
feD : 1.640
Net − Bulge dD :
log(M⋆, dD) = 10.465
⟨t⋆, dD⟩M = 11.987
⟨Z⋆, dD⟩M = 0.799
Net − Bulge fD :
log(M⋆, fD) = 10.389
⟨t⋆, fD⟩M = 12.781
⟨Z⋆, fD⟩M = 0.847
Net − Bulge eD :
log(M⋆, eD) = 10.380
⟨t⋆, eD⟩M = 12.848
⟨Z⋆, eD⟩M = 0.866

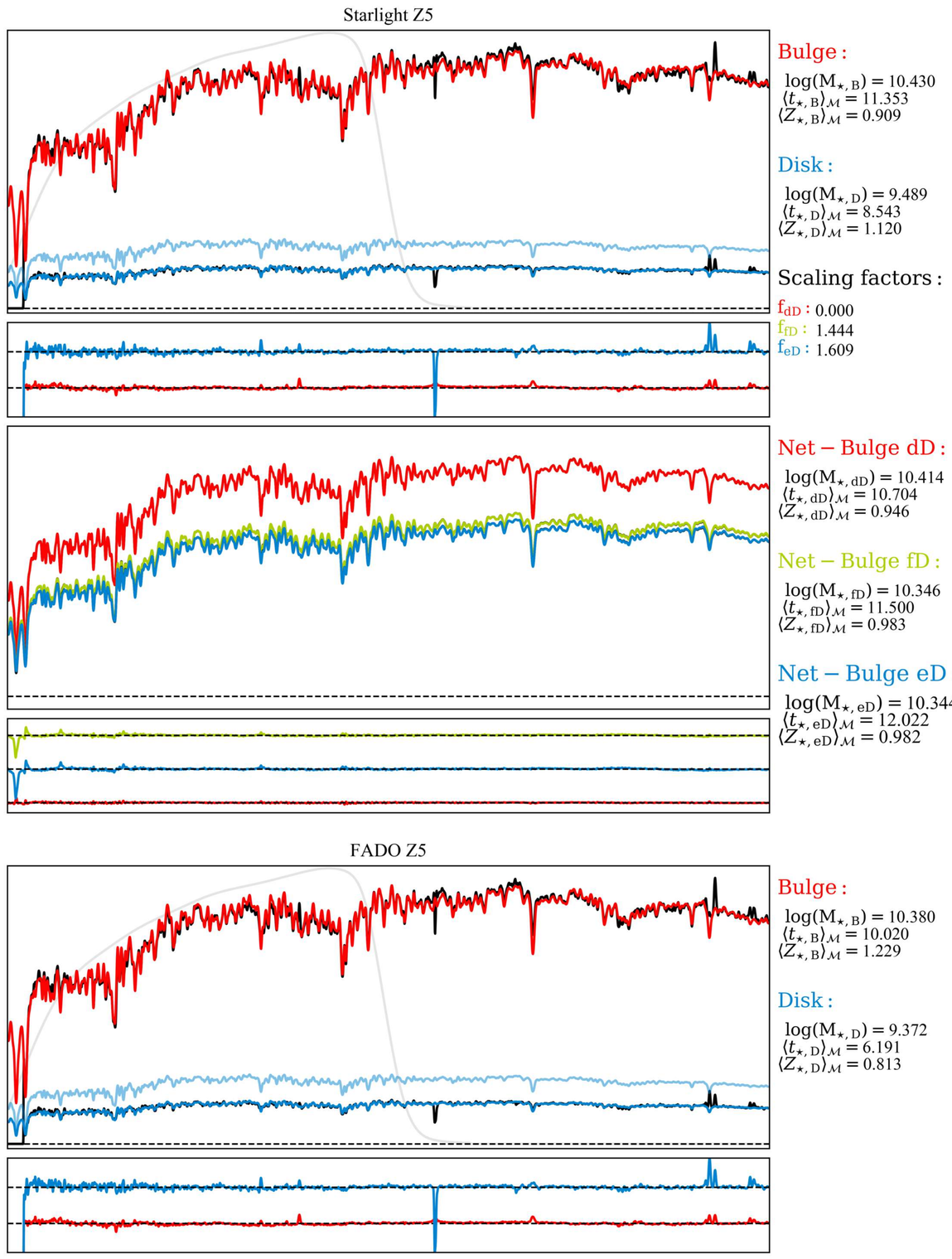
Starlight Z5
Bulge :
log(M⋆, B) = 10.430
⟨t⋆, B⟩M = 11.353
⟨Z⋆, B⟩M = 0.909
Disk :
log(M⋆, D) = 9.489
⟨t⋆, D⟩M = 8.543
⟨Z⋆, D⟩M = 1.120
Scaling factors :
fdD : 0.000
ffD : 1.444
feD : 1.609
Net − Bulge dD :
log(M⋆, dD) = 10.414
⟨t⋆, dD⟩M = 10.704
⟨Z⋆, dD⟩M = 0.946
Net − Bulge fD :
log(M⋆, fD) = 10.346
⟨t⋆, fD⟩M = 11.500
⟨Z⋆, fD⟩M = 0.983
Net − Bulge eD :
log(M⋆, eD) = 10.344
⟨t⋆, eD⟩M = 12.022
⟨Z⋆, eD⟩M = 0.982

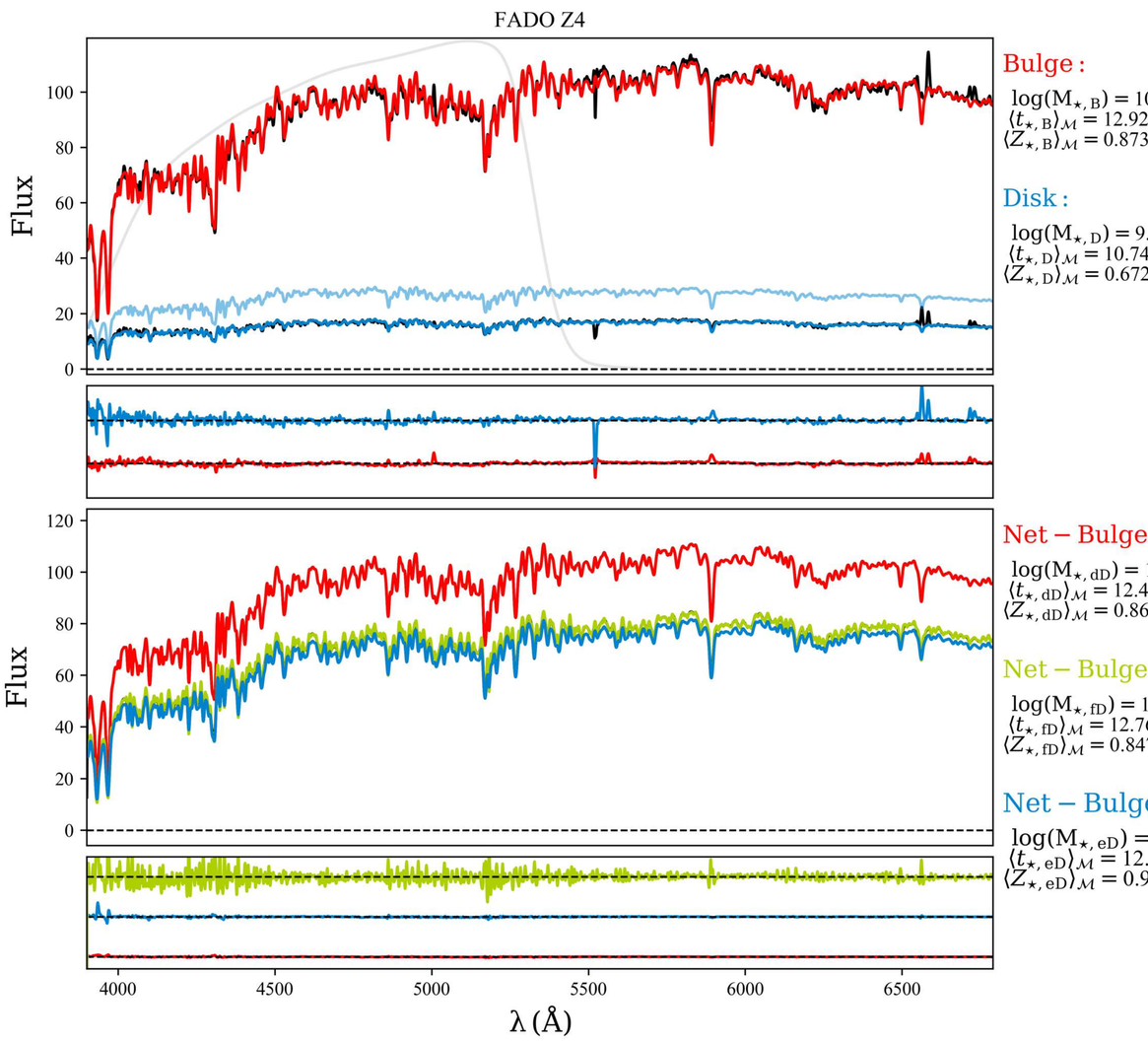
FADO Z4
Flux
Bulge :
log(M⋆, B) = 10.470
⟨t⋆, B⟩M = 12.920
⟨Z⋆, B⟩M = 0.873
Disk :
log(M⋆, D) = 9.531
⟨t⋆, D⟩M = 10.740
⟨Z⋆, D⟩M = 0.672
Net − Bulge dD :
log(M⋆, dD) = 10.460
⟨t⋆, dD⟩M = 12.470
⟨Z⋆, dD⟩M = 0.869
Net − Bulge fD :
log(M⋆, fD) = 10.370
⟨t⋆, fD⟩M = 12.760
⟨Z⋆, fD⟩M = 0.847
Net − Bulge eD :
log(M⋆, eD) = 10.370
⟨t⋆, eD⟩M = 12.940
⟨Z⋆, eD⟩M = 0.928
λ (Å)

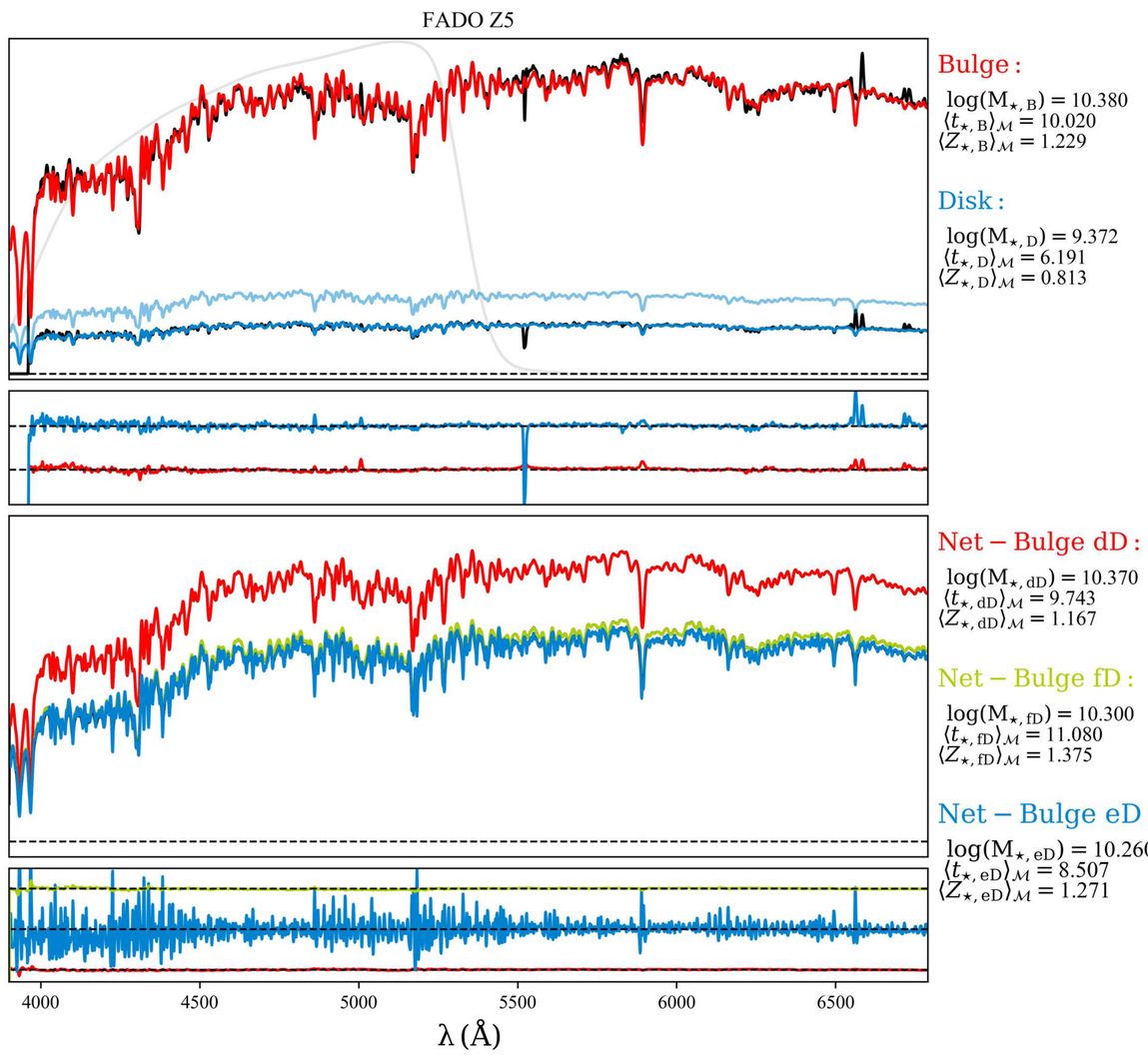
FADO Z5
Bulge :
log(M⋆, B) = 10.380
⟨t⋆, B⟩M = 10.020
⟨Z⋆, B⟩M = 1.229
Disk :
log(M⋆, D) = 9.372
⟨t⋆, D⟩M = 6.191
⟨Z⋆, D⟩M = 0.813
Net − Bulge dD :
log(M⋆, dD) = 10.370
⟨t⋆, dD⟩M = 9.743
⟨Z⋆, dD⟩M = 1.167
Net − Bulge fD :
log(M⋆, fD) = 10.300
⟨t⋆, fD⟩M = 11.080
⟨Z⋆, fD⟩M = 1.375
Net − Bulge eD :
log(M⋆, eD) = 10.260
⟨t⋆, eD⟩M = 8.507
⟨Z⋆, eD⟩M = 1.271
λ (Å)

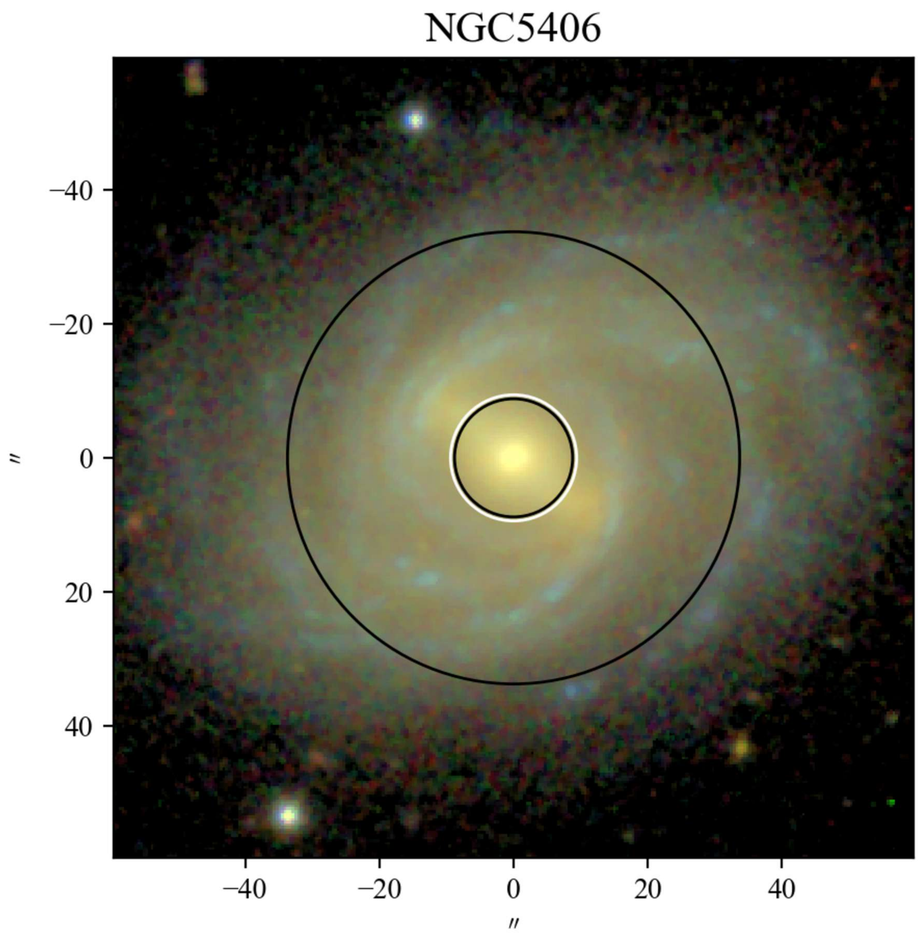
NGC5406
−40
−20
0
20
40
″
−40
−20
0
20
40
″

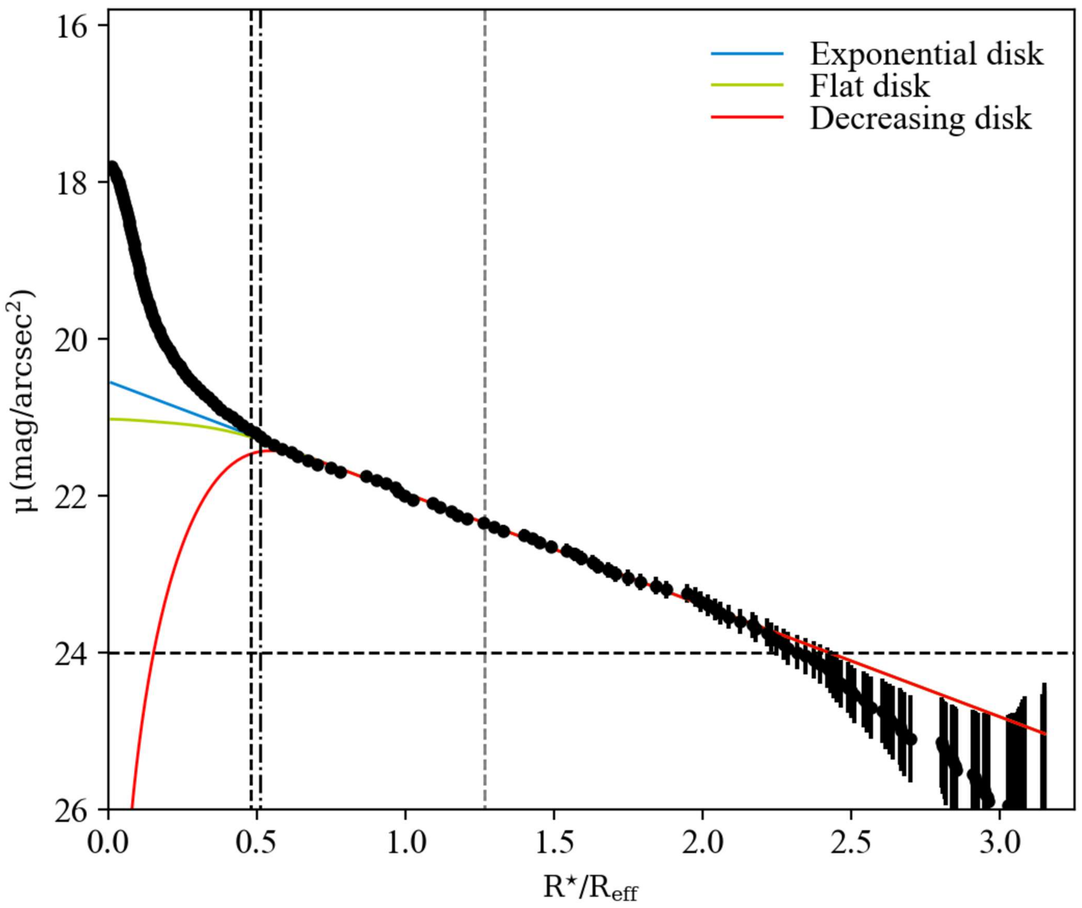
Exponential disk
Flat disk
Decreasing disk
μ (mag/arcsec²)
16
18
20
22
24
26
0.0
0.5
1.0
1.5
2.0
2.5
3.0
R⋆/Reff

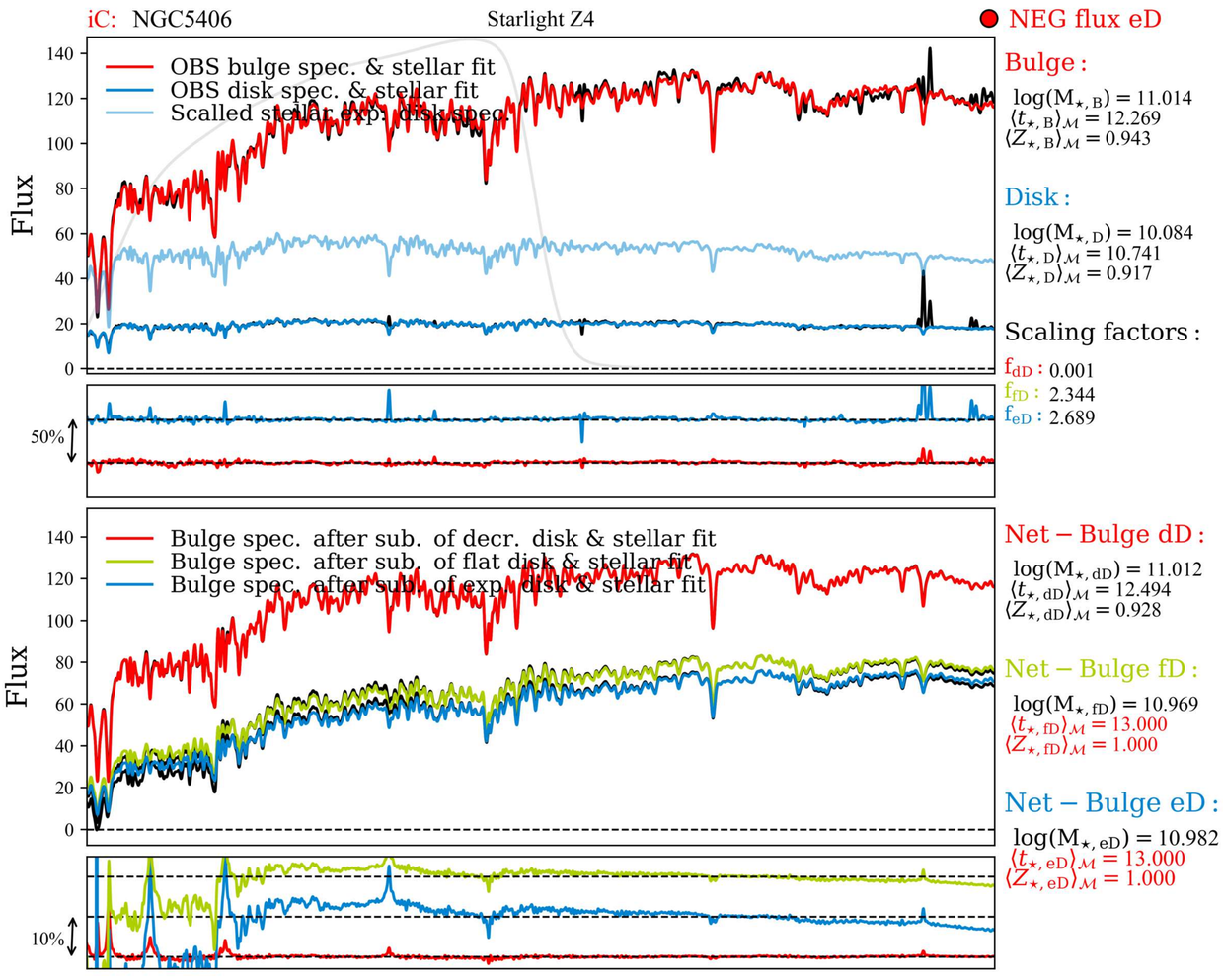
iC: NGC5406
Starlight Z4
NEG flux eD
OBS bulge spec. & stellar fit
OBS disk spec. & stellar fit
Scalled stellar exp. disk spec.
Flux
Bulge :
log(M⋆, B) = 11.014
⟨t⋆, B⟩M = 12.269
⟨Z⋆, B⟩M = 0.943
Disk :
log(M⋆, D) = 10.084
⟨t⋆, D⟩M = 10.741
⟨Z⋆, D⟩M = 0.917
Scaling factors :
fdD : 0.001
ffD : 2.344
feD : 2.689
50%
Bulge spec. after sub. of decr. disk & stellar fit
Bulge spec. after sub. of flat disk & stellar fit
Bulge spec. after sub. of exp. disk & stellar fit
Net − Bulge dD :
log(M⋆, dD) = 11.012
⟨t⋆, dD⟩M = 12.494
⟨Z⋆, dD⟩M = 0.928
Net − Bulge fD :
log(M⋆, fD) = 10.969
⟨t⋆, fD⟩M = 13.000
⟨Z⋆, fD⟩M = 1.000
Net − Bulge eD :
log(M⋆, eD) = 10.982
⟨t⋆, eD⟩M = 13.000
⟨Z⋆, eD⟩M = 1.000
10%

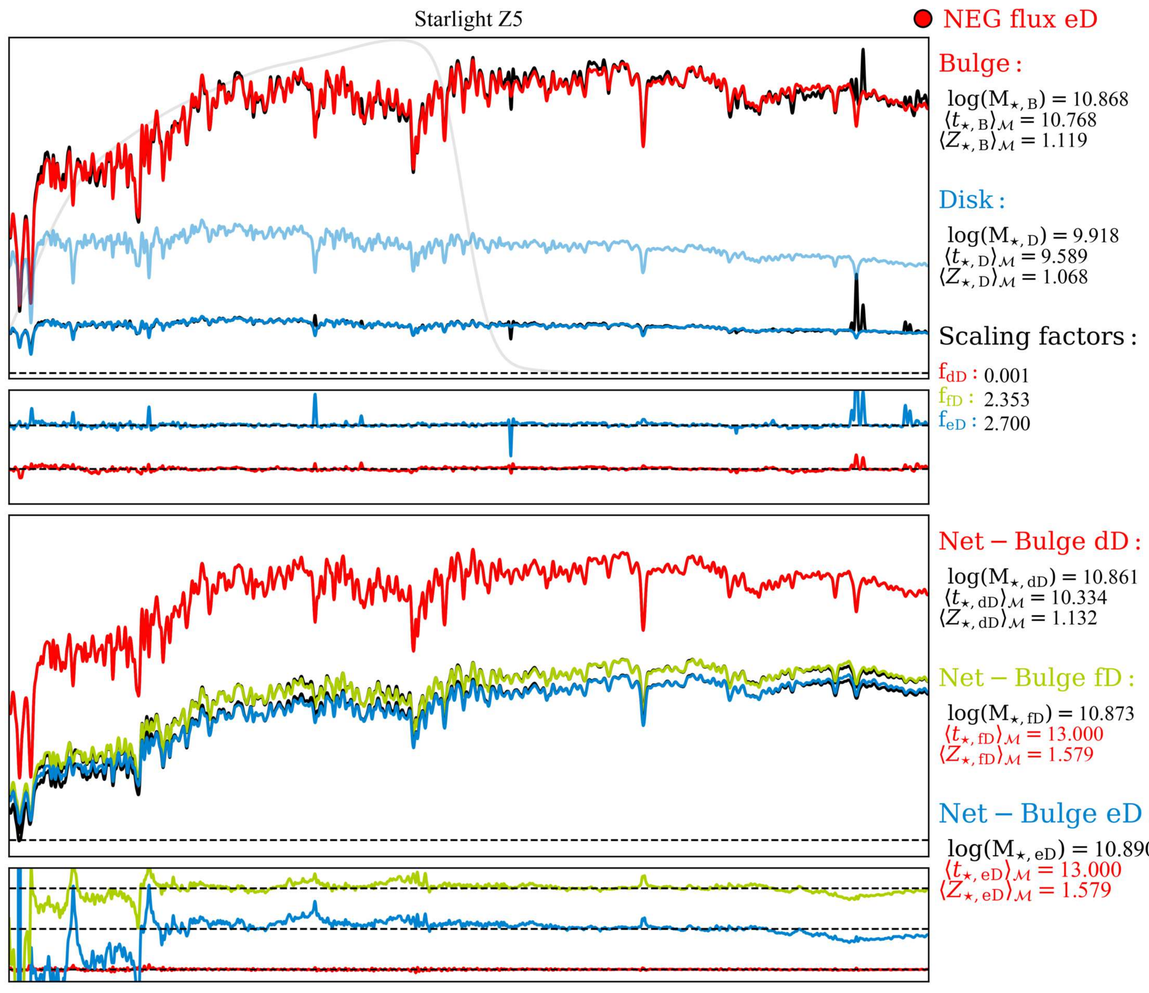
Starlight Z5
NEG flux eD
Bulge :
log(M⋆, B) = 10.868
⟨t⋆, B⟩M = 10.768
⟨Z⋆, B⟩M = 1.119
Disk :
log(M⋆, D) = 9.918
⟨t⋆, D⟩M = 9.589
⟨Z⋆, D⟩M = 1.068
Scaling factors :
fdD : 0.001
ffD : 2.353
feD : 2.700
Net − Bulge dD :
log(M⋆, dD) = 10.861
⟨t⋆, dD⟩M = 10.334
⟨Z⋆, dD⟩M = 1.132
Net − Bulge fD :
log(M⋆, fD) = 10.873
⟨t⋆, fD⟩M = 13.000
⟨Z⋆, fD⟩M = 1.579
Net − Bulge eD :
log(M⋆, eD) = 10.890
⟨t⋆, eD⟩M = 13.000
⟨Z⋆, eD⟩M = 1.579

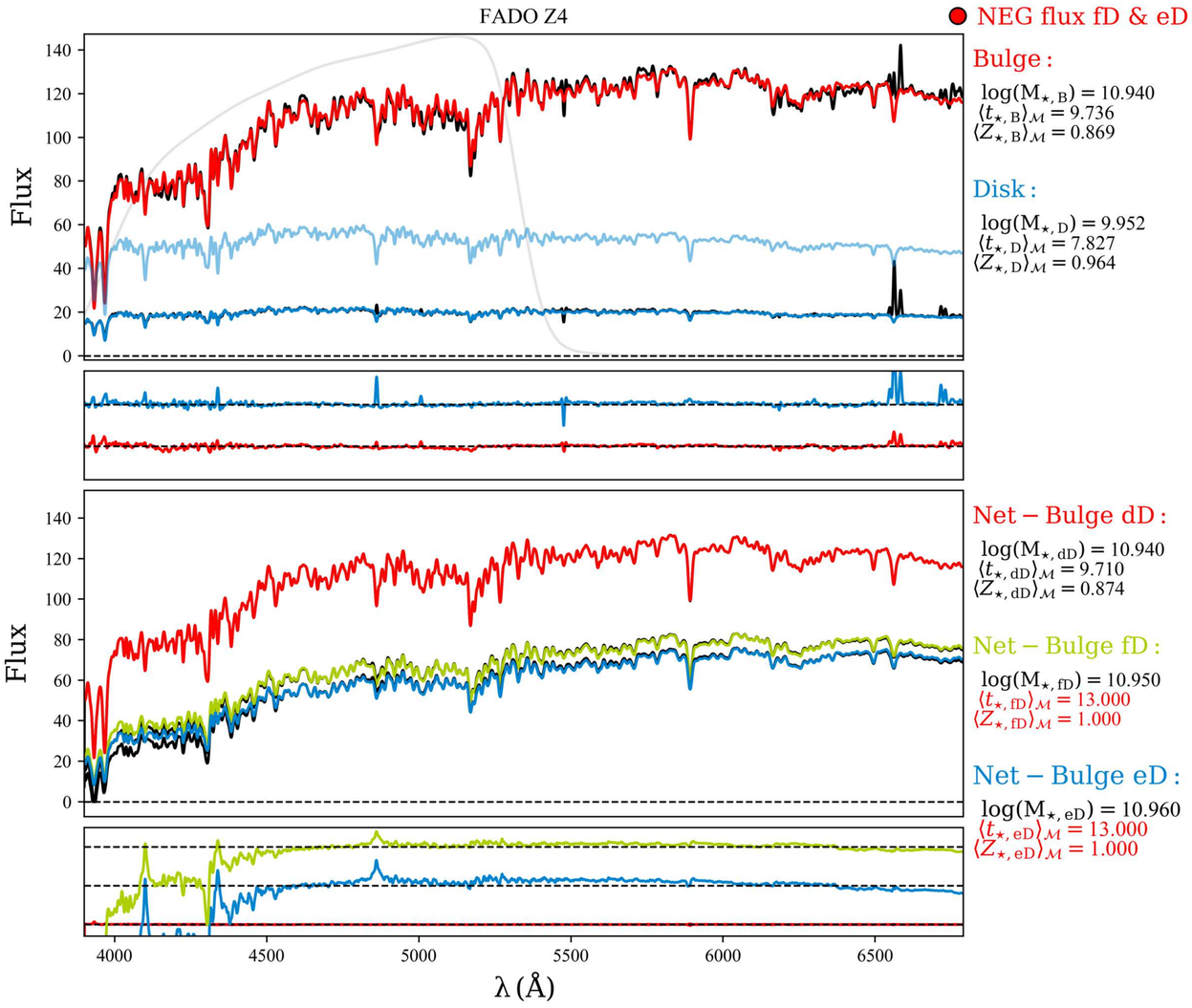
FADO Z4
NEG flux fD & eD
Flux
Bulge :
log(M⋆, B) = 10.940
⟨t⋆, B⟩M = 9.736
⟨Z⋆, B⟩M = 0.869
Disk :
log(M⋆, D) = 9.952
⟨t⋆, D⟩M = 7.827
⟨Z⋆, D⟩M = 0.964
Net − Bulge dD :
log(M⋆, dD) = 10.940
⟨t⋆, dD⟩M = 9.710
⟨Z⋆, dD⟩M = 0.874
Net − Bulge fD :
log(M⋆, fD) = 10.950
⟨t⋆, fD⟩M = 13.000
⟨Z⋆, fD⟩M = 1.000
Net − Bulge eD :
log(M⋆, eD) = 10.960
⟨t⋆, eD⟩M = 13.000
⟨Z⋆, eD⟩M = 1.000
4000
4500
5000
5500
6000
6500
λ (Å)

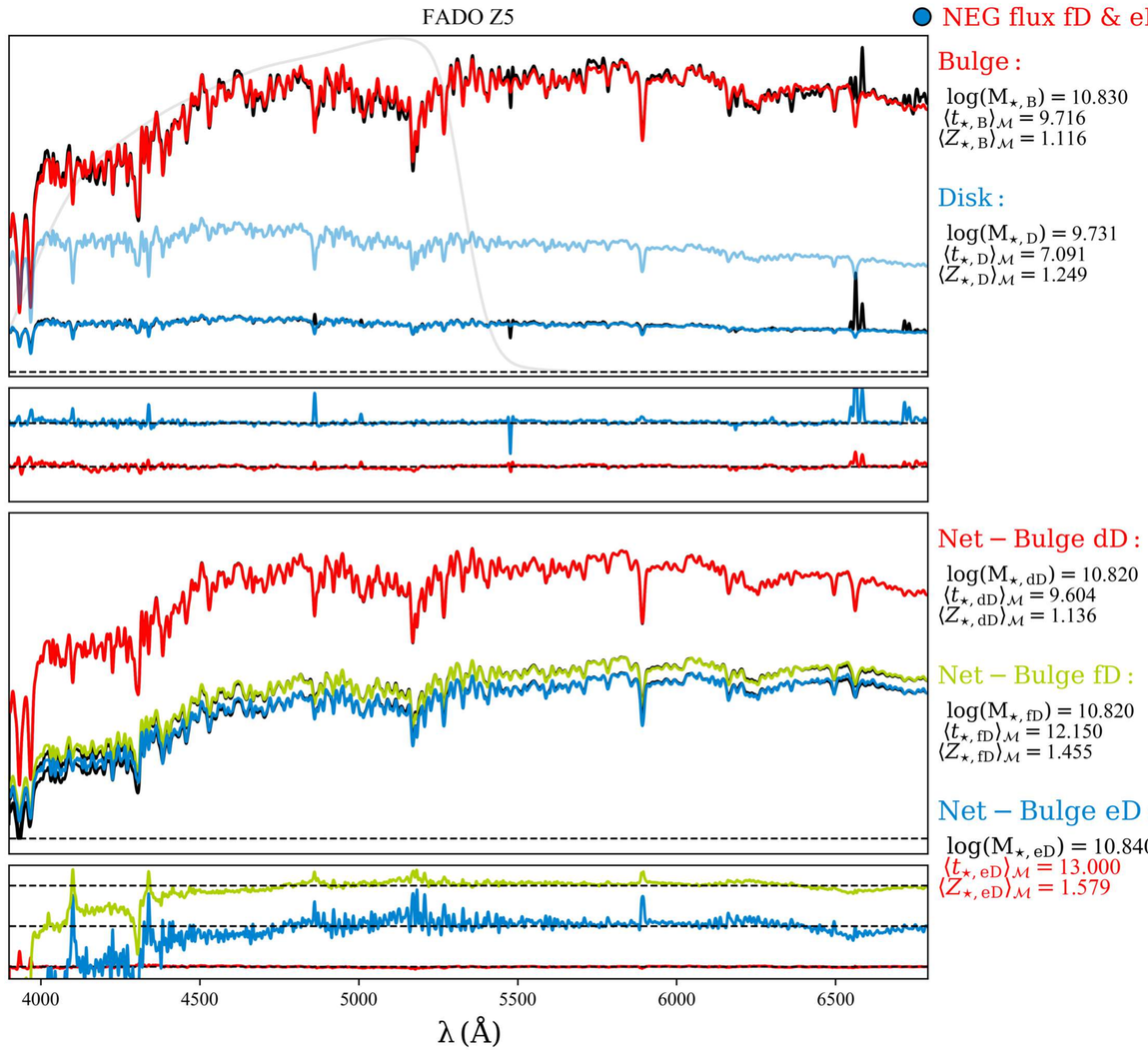
FADO Z5
NEG flux fD & eD
Bulge :
log(M⋆, B) = 10.830
⟨t⋆, B⟩M = 9.716
⟨Z⋆, B⟩M = 1.116
Disk :
log(M⋆, D) = 9.731
⟨t⋆, D⟩M = 7.091
⟨Z⋆, D⟩M = 1.249
Net − Bulge dD :
log(M⋆, dD) = 10.820
⟨t⋆, dD⟩M = 9.604
⟨Z⋆, dD⟩M = 1.136
Net − Bulge fD :
log(M⋆, fD) = 10.820
⟨t⋆, fD⟩M = 12.150
⟨Z⋆, fD⟩M = 1.455
Net − Bulge eD :
log(M⋆, eD) = 10.840
⟨t⋆, eD⟩M = 13.000
⟨Z⋆, eD⟩M = 1.579
4000
4500
5000
5500
6000
6500
λ (Å)

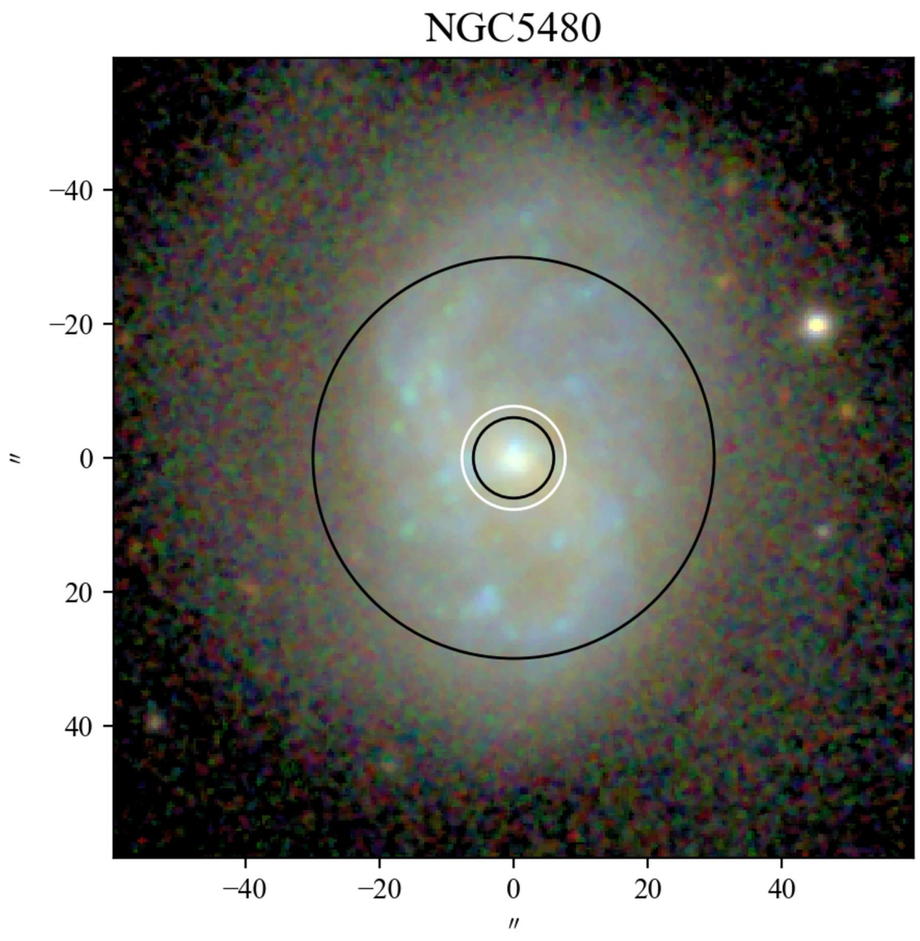
NGC5480
−40
−20
0
20
40
″
−40
−20
0
20
40
″

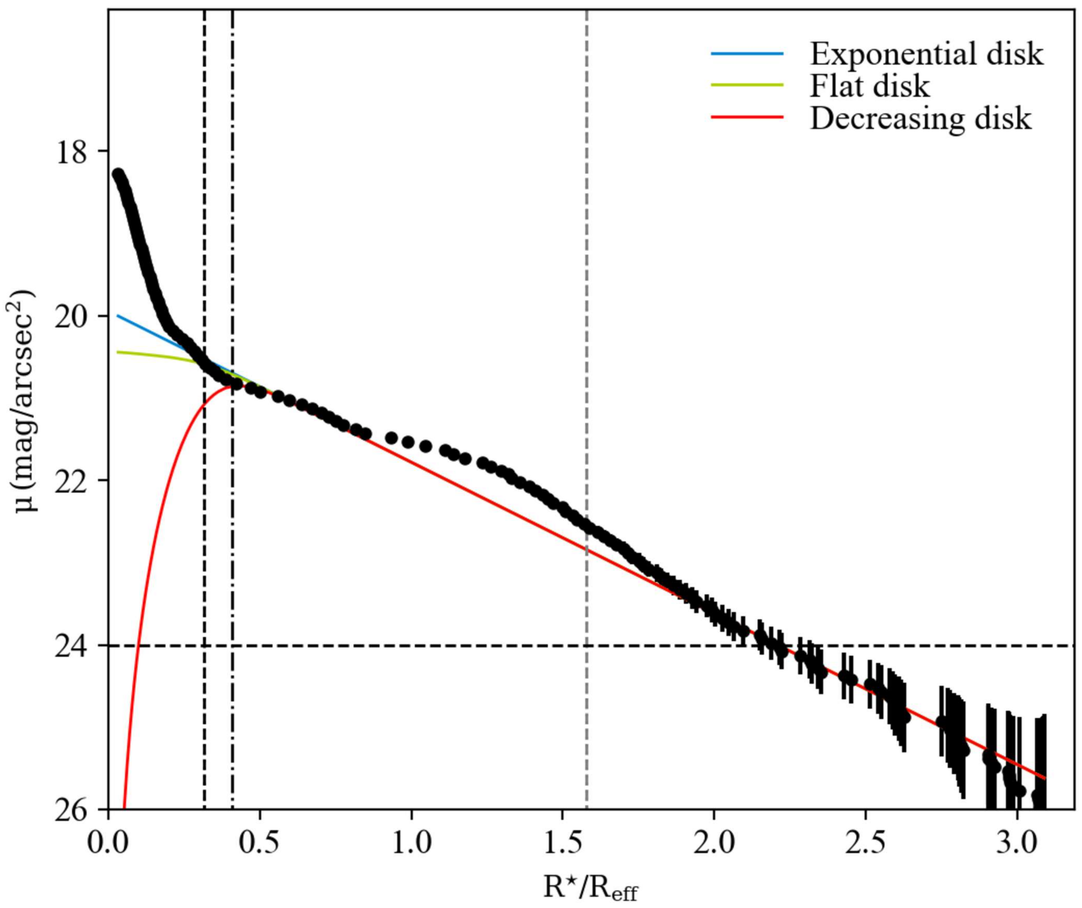
Exponential disk
Flat disk
Decreasing disk
μ (mag/arcsec²)
18
20
22
24
26
0.0
0.5
1.0
1.5
2.0
2.5
3.0
R⋆/Reff

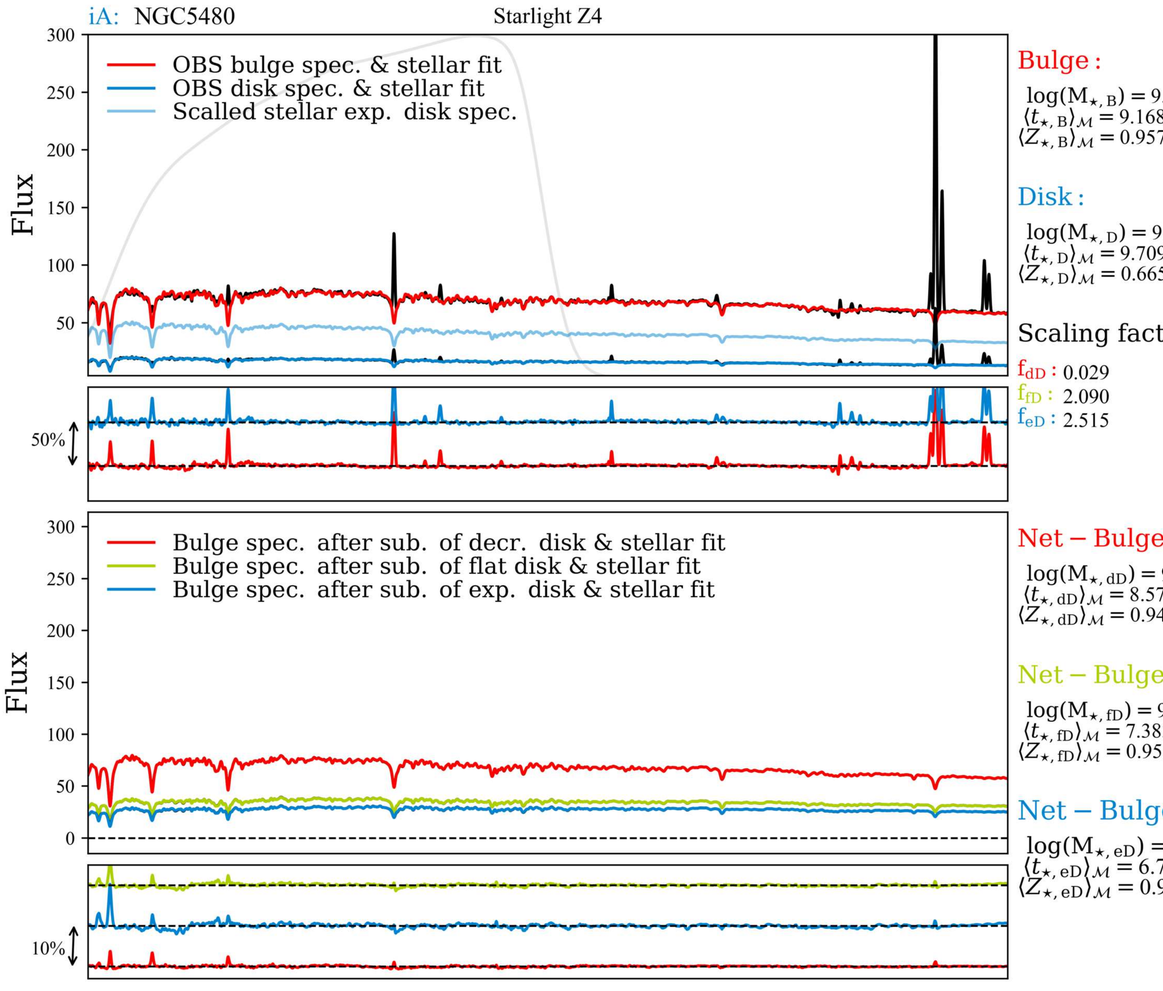
iA: NGC5480
Starlight Z4
OBS bulge spec. & stellar fit
OBS disk spec. & stellar fit
Scalled stellar exp. disk spec.
Flux
50%
Bulge :
log(M⋆, B) = 9.682
⟨t⋆, B⟩M = 9.168
⟨Z⋆, B⟩M = 0.957
Disk :
log(M⋆, D) = 9.013
⟨t⋆, D⟩M = 9.709
⟨Z⋆, D⟩M = 0.665
Scaling factors :
fdD : 0.029
ffD : 2.090
feD : 2.515
Bulge spec. after sub. of decr. disk & stellar fit
Bulge spec. after sub. of flat disk & stellar fit
Bulge spec. after sub. of exp. disk & stellar fit
10%
Net − Bulge dD :
log(M⋆, dD) = 9.667
⟨t⋆, dD⟩M = 8.579
⟨Z⋆, dD⟩M = 0.944
Net − Bulge fD :
log(M⋆, fD) = 9.369
⟨t⋆, fD⟩M = 7.383
⟨Z⋆, fD⟩M = 0.955
Net − Bulge eD :
log(M⋆, eD) = 9.269
⟨t⋆, eD⟩M = 6.780
⟨Z⋆, eD⟩M = 0.959

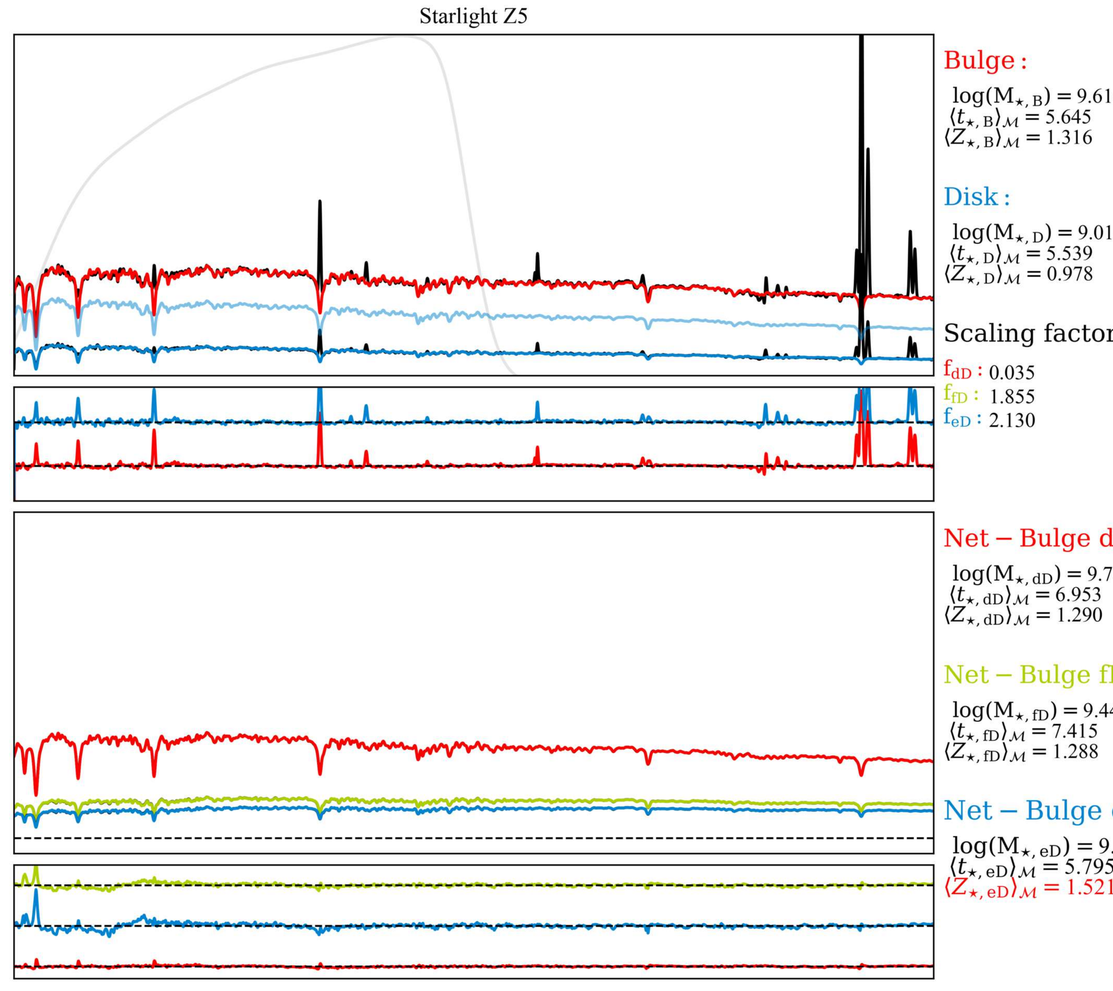
Starlight Z5
Bulge :
log(M⋆, B) = 9.616
⟨t⋆, B⟩M = 5.645
⟨Z⋆, B⟩M = 1.316
Disk :
log(M⋆, D) = 9.016
⟨t⋆, D⟩M = 5.539
⟨Z⋆, D⟩M = 0.978
Scaling factors :
fdD : 0.035
ffD : 1.855
feD : 2.130
Net − Bulge dD :
log(M⋆, dD) = 9.703
⟨t⋆, dD⟩M = 6.953
⟨Z⋆, dD⟩M = 1.290
Net − Bulge fD :
log(M⋆, fD) = 9.447
⟨t⋆, fD⟩M = 7.415
⟨Z⋆, fD⟩M = 1.288
Net − Bulge eD :
log(M⋆, eD) = 9.279
⟨t⋆, eD⟩M = 5.795
⟨Z⋆, eD⟩M = 1.521

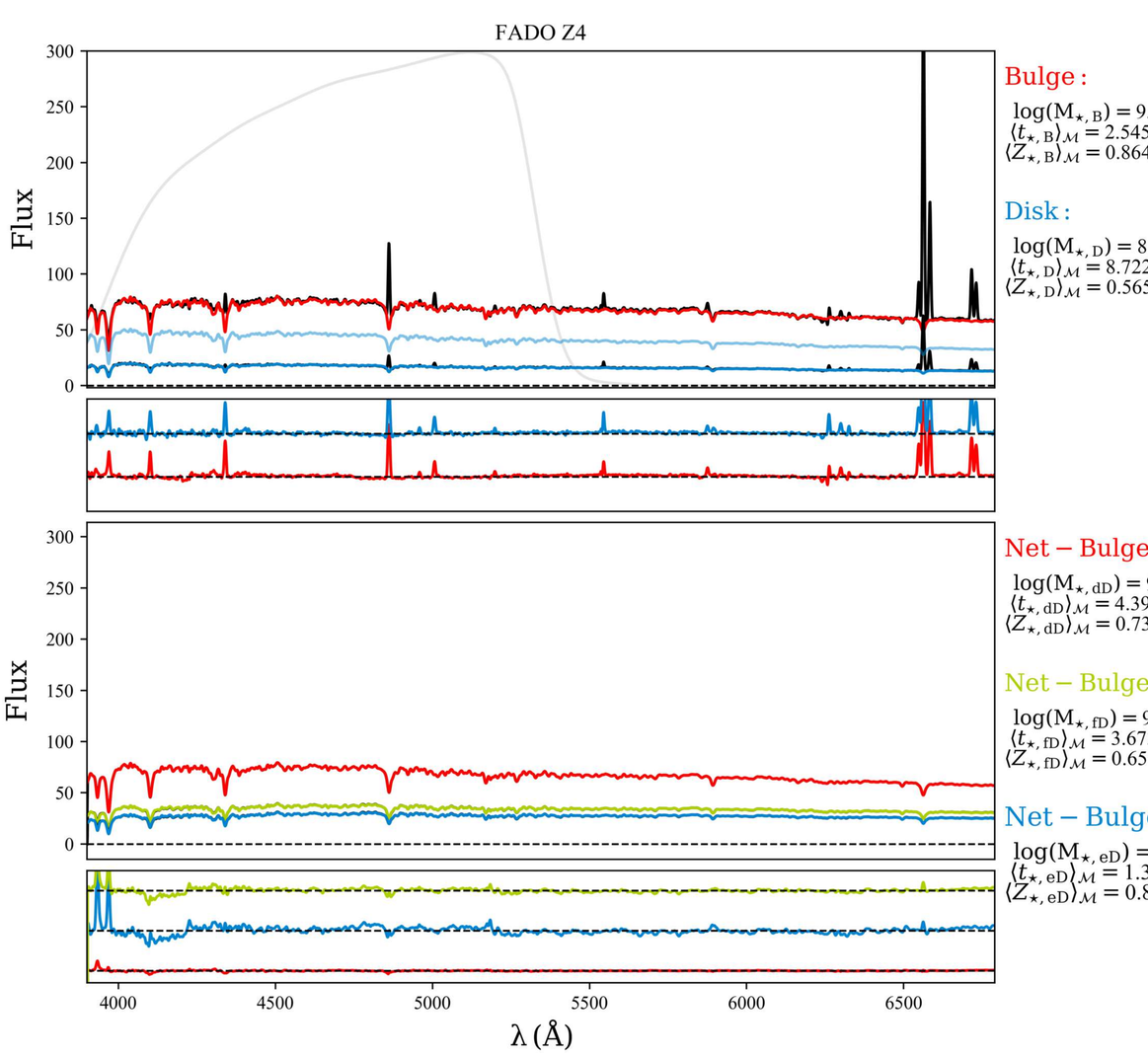
FADO Z4
Flux
Bulge :
log(M⋆, B) = 9.413
⟨t⋆, B⟩M = 2.545
⟨Z⋆, B⟩M = 0.864
Disk :
log(M⋆, D) = 8.958
⟨t⋆, D⟩M = 8.722
⟨Z⋆, D⟩M = 0.565
Net − Bulge dD :
log(M⋆, dD) = 9.419
⟨t⋆, dD⟩M = 4.393
⟨Z⋆, dD⟩M = 0.737
Net − Bulge fD :
log(M⋆, fD) = 9.132
⟨t⋆, fD⟩M = 3.673
⟨Z⋆, fD⟩M = 0.655
Net − Bulge eD :
log(M⋆, eD) = 8.929
⟨t⋆, eD⟩M = 1.327
⟨Z⋆, eD⟩M = 0.829
λ (Å)

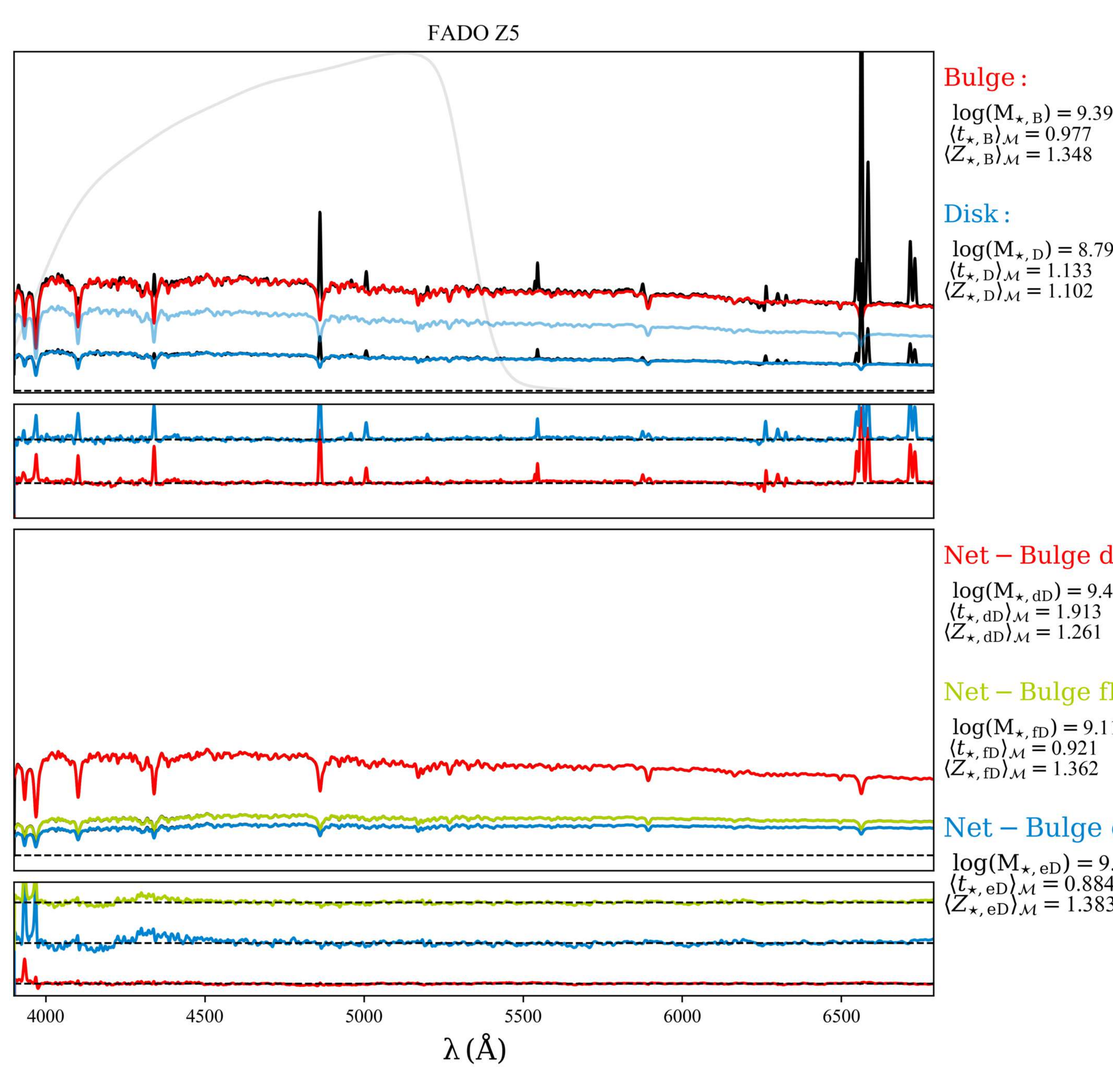
FADO Z5
Bulge :
log(M⋆, B) = 9.399
⟨t⋆, B⟩M = 0.977
⟨Z⋆, B⟩M = 1.348
Disk :
log(M⋆, D) = 8.793
⟨t⋆, D⟩M = 1.133
⟨Z⋆, D⟩M = 1.102
Net − Bulge dD :
log(M⋆, dD) = 9.415
⟨t⋆, dD⟩M = 1.913
⟨Z⋆, dD⟩M = 1.261
Net − Bulge fD :
log(M⋆, fD) = 9.114
⟨t⋆, fD⟩M = 0.921
⟨Z⋆, fD⟩M = 1.362
Net − Bulge eD :
log(M⋆, eD) = 9.056
⟨t⋆, eD⟩M = 0.884
⟨Z⋆, eD⟩M = 1.383
λ (Å)

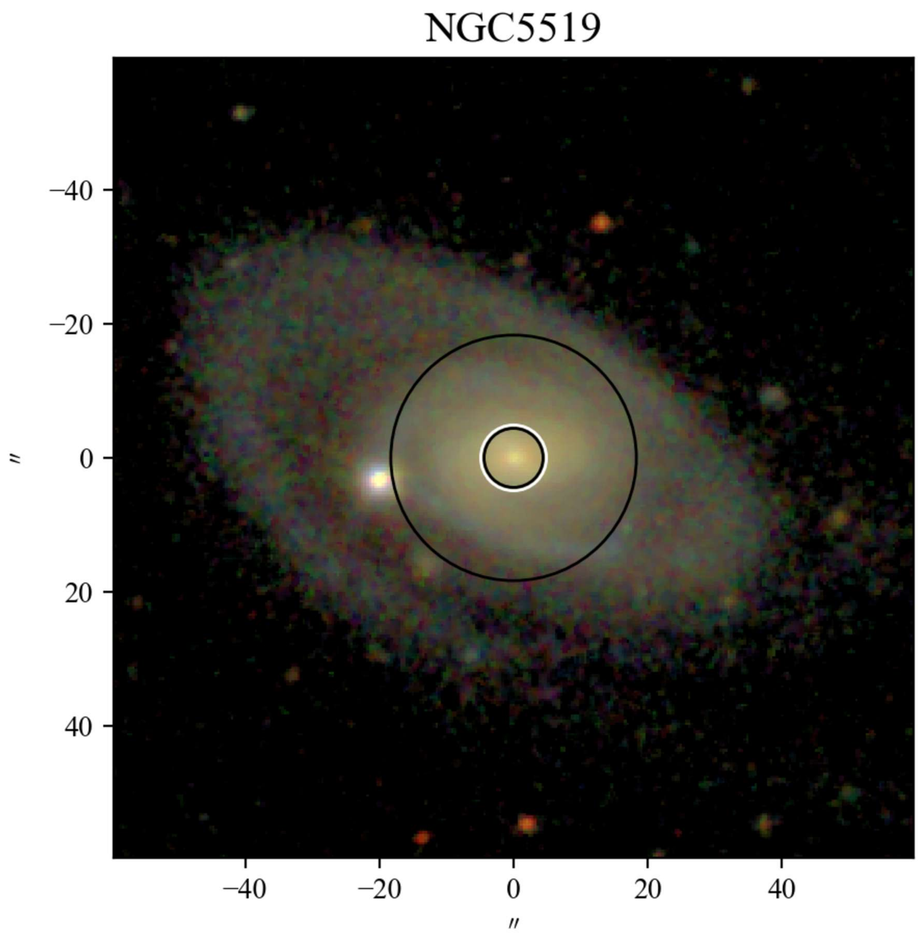
NGC5519
−40
−20
0
20
40
″
−40
−20
0
20
40
″

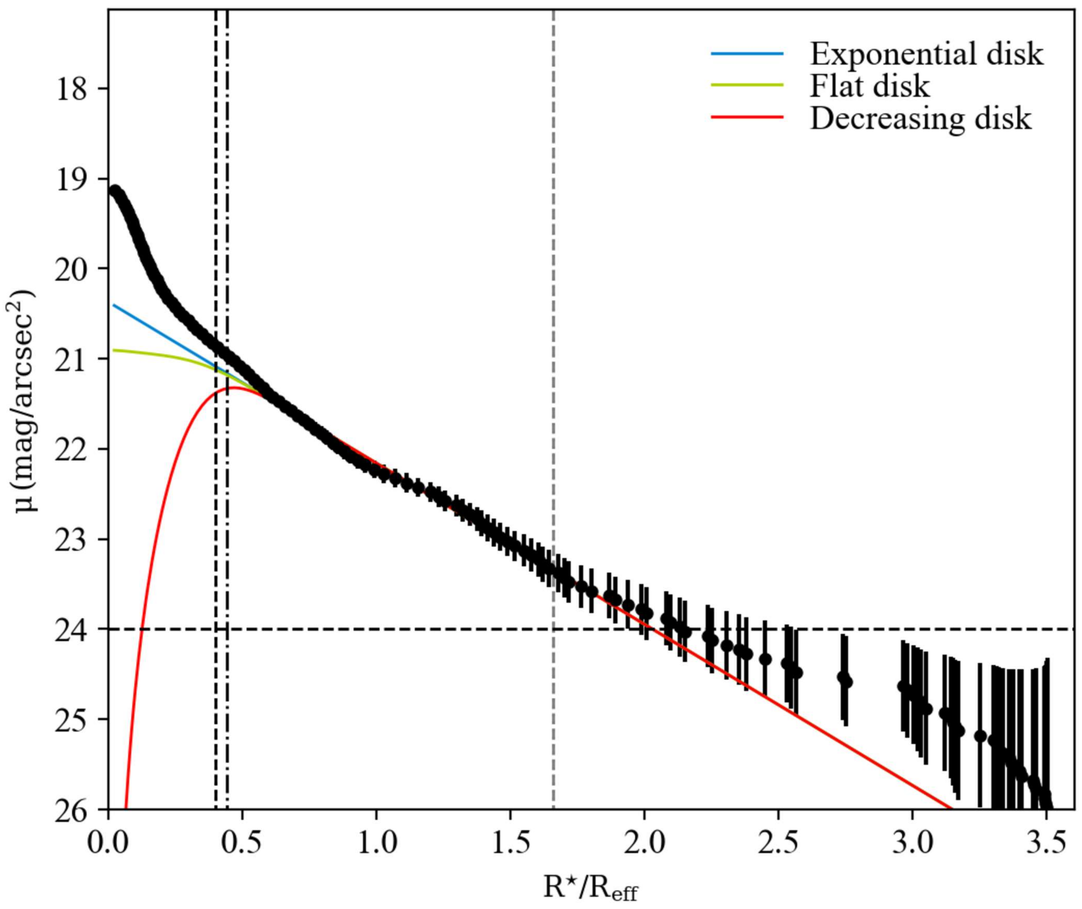
Exponential disk
Flat disk
Decreasing disk
μ (mag/arcsec²)
18
19
20
21
22
23
24
25
26
0.0
0.5
1.0
1.5
2.0
2.5
3.0
3.5
R⋆/Reff

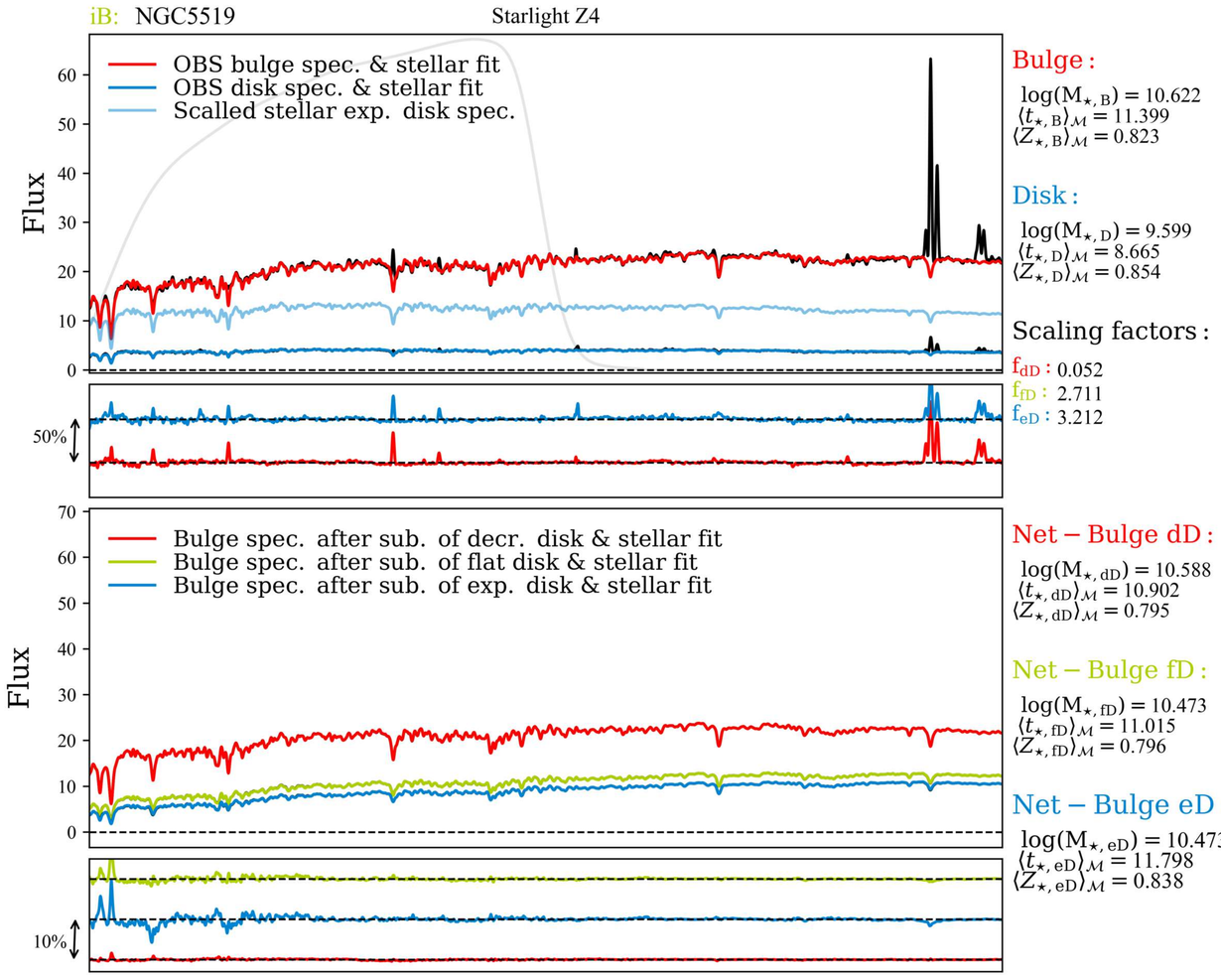
iB: NGC5519
Starlight Z4
OBS bulge spec. & stellar fit
OBS disk spec. & stellar fit
Scalled stellar exp. disk spec.
Flux
50%
Bulge :
log(M⋆, B) = 10.622
⟨t⋆, B⟩M = 11.399
⟨Z⋆, B⟩M = 0.823
Disk :
log(M⋆, D) = 9.599
⟨t⋆, D⟩M = 8.665
⟨Z⋆, D⟩M = 0.854
Scaling factors :
fdD : 0.052
ffD : 2.711
feD : 3.212
Bulge spec. after sub. of decr. disk & stellar fit
Bulge spec. after sub. of flat disk & stellar fit
Bulge spec. after sub. of exp. disk & stellar fit
10%
Net − Bulge dD :
log(M⋆, dD) = 10.588
⟨t⋆, dD⟩M = 10.902
⟨Z⋆, dD⟩M = 0.795
Net − Bulge fD :
log(M⋆, fD) = 10.473
⟨t⋆, fD⟩M = 11.015
⟨Z⋆, fD⟩M = 0.796
Net − Bulge eD :
log(M⋆, eD) = 10.473
⟨t⋆, eD⟩M = 11.798
⟨Z⋆, eD⟩M = 0.838

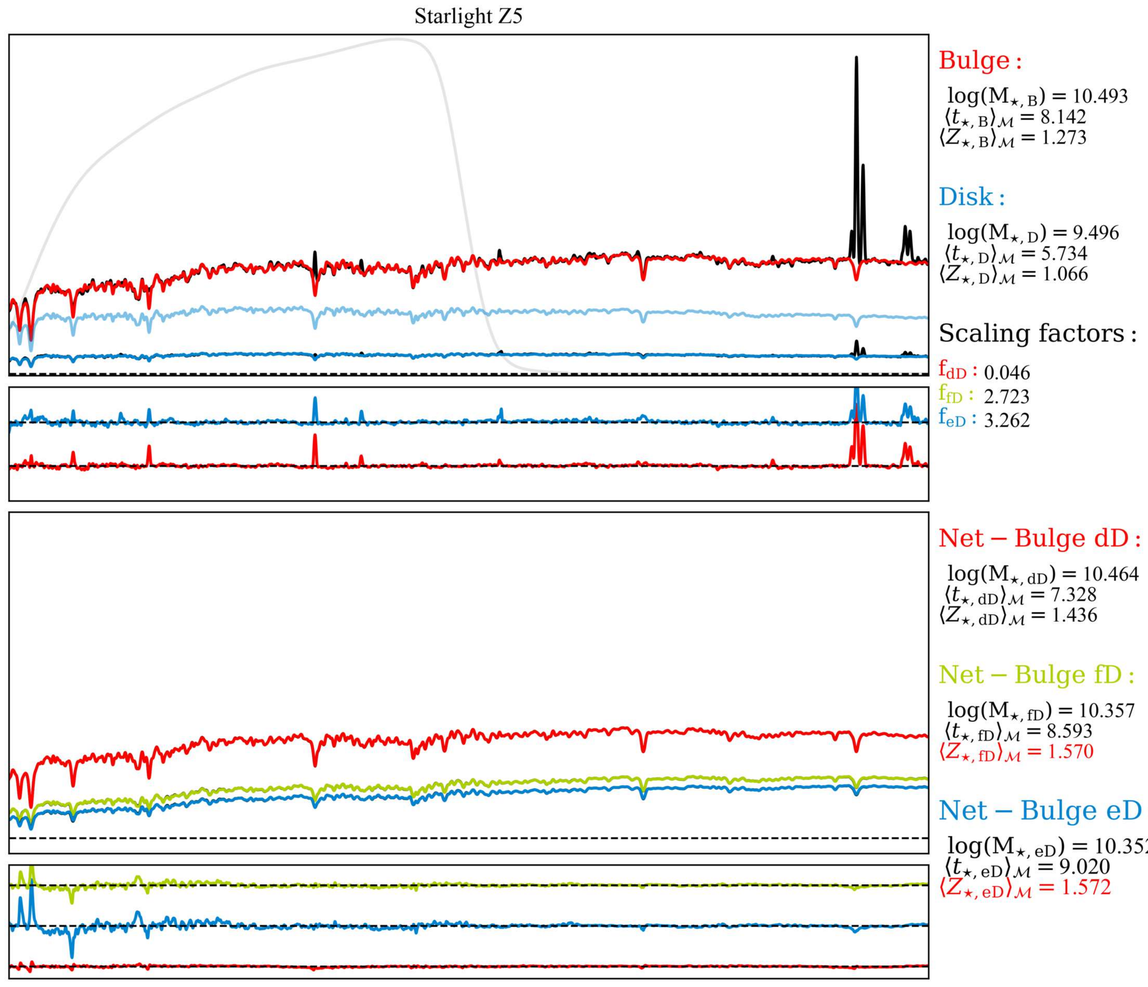
Starlight Z5
Bulge :
log(M⋆, B) = 10.493
⟨t⋆, B⟩M = 8.142
⟨Z⋆, B⟩M = 1.273
Disk :
log(M⋆, D) = 9.496
⟨t⋆, D⟩M = 5.734
⟨Z⋆, D⟩M = 1.066
Scaling factors :
fdD : 0.046
ffD : 2.723
feD : 3.262
Net − Bulge dD :
log(M⋆, dD) = 10.464
⟨t⋆, dD⟩M = 7.328
⟨Z⋆, dD⟩M = 1.436
Net − Bulge fD :
log(M⋆, fD) = 10.357
⟨t⋆, fD⟩M = 8.593
⟨Z⋆, fD⟩M = 1.570
Net − Bulge eD :
log(M⋆, eD) = 10.352
⟨t⋆, eD⟩M = 9.020
⟨Z⋆, eD⟩M = 1.572

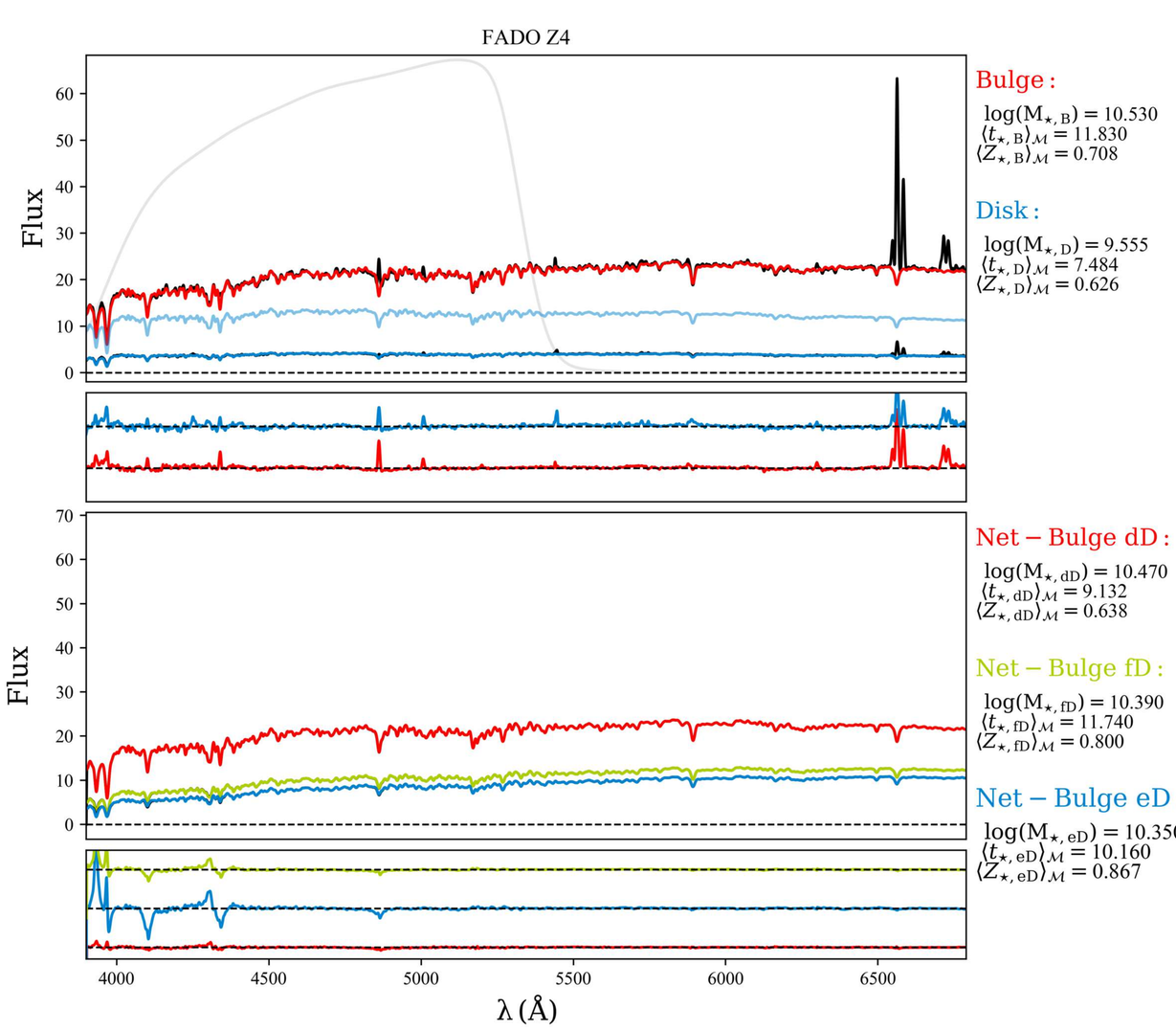
FADO Z4
Flux
Bulge :
log(M⋆, B) = 10.530
⟨t⋆, B⟩M = 11.830
⟨Z⋆, B⟩M = 0.708
Disk :
log(M⋆, D) = 9.555
⟨t⋆, D⟩M = 7.484
⟨Z⋆, D⟩M = 0.626
Net − Bulge dD :
log(M⋆, dD) = 10.470
⟨t⋆, dD⟩M = 9.132
⟨Z⋆, dD⟩M = 0.638
Net − Bulge fD :
log(M⋆, fD) = 10.390
⟨t⋆, fD⟩M = 11.740
⟨Z⋆, fD⟩M = 0.800
Net − Bulge eD :
log(M⋆, eD) = 10.350
⟨t⋆, eD⟩M = 10.160
⟨Z⋆, eD⟩M = 0.867
4000
4500
5000
5500
6000
6500
λ (Å)

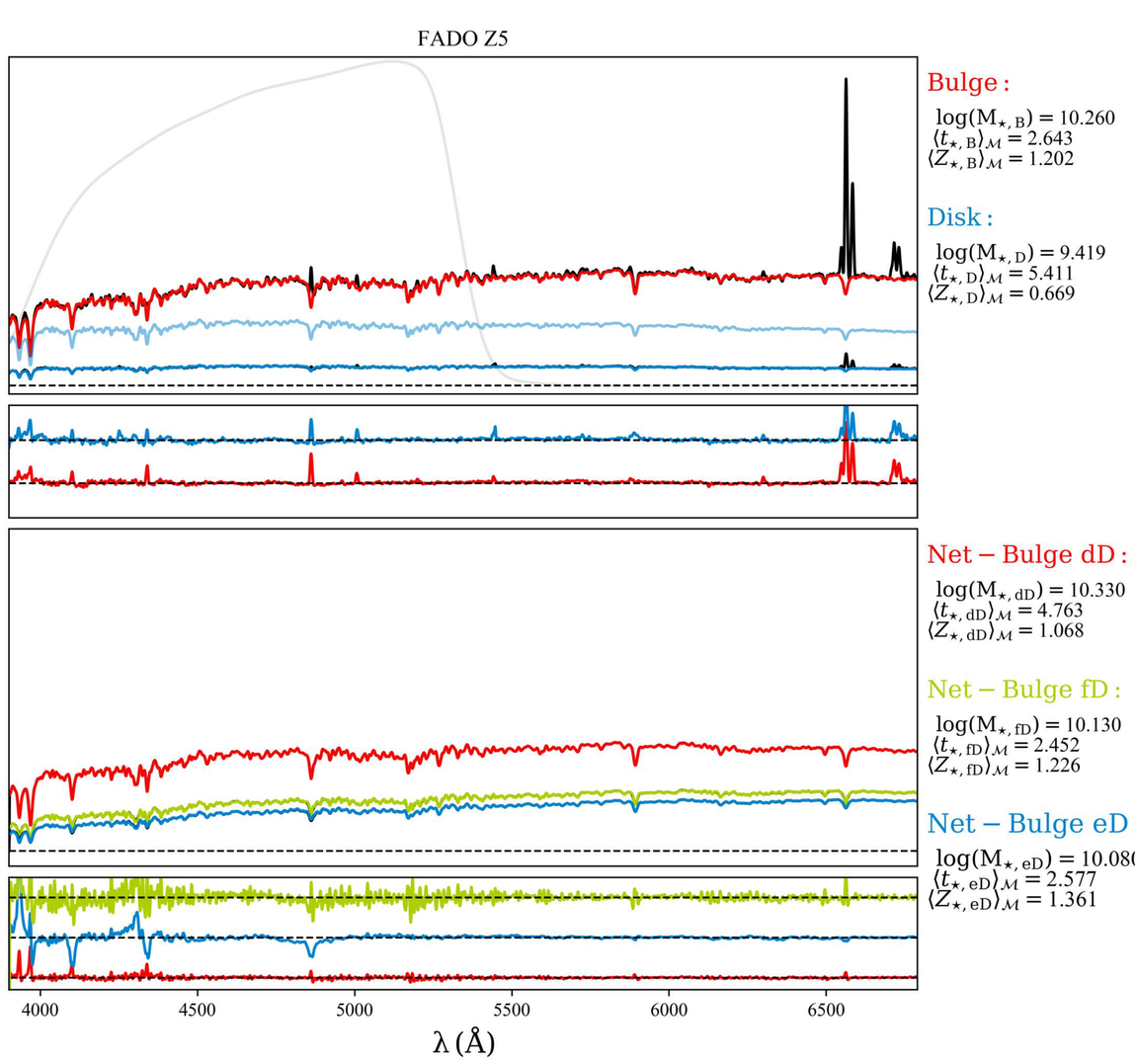
FADO Z5
Bulge :
log(M⋆, B) = 10.260
⟨t⋆, B⟩M = 2.643
⟨Z⋆, B⟩M = 1.202
Disk :
log(M⋆, D) = 9.419
⟨t⋆, D⟩M = 5.411
⟨Z⋆, D⟩M = 0.669
Net − Bulge dD :
log(M⋆, dD) = 10.330
⟨t⋆, dD⟩M = 4.763
⟨Z⋆, dD⟩M = 1.068
Net − Bulge fD :
log(M⋆, fD) = 10.130
⟨t⋆, fD⟩M = 2.452
⟨Z⋆, fD⟩M = 1.226
Net − Bulge eD :
log(M⋆, eD) = 10.080
⟨t⋆, eD⟩M = 2.577
⟨Z⋆, eD⟩M = 1.361
4000
4500
5000
5500
6000
6500
λ (Å)

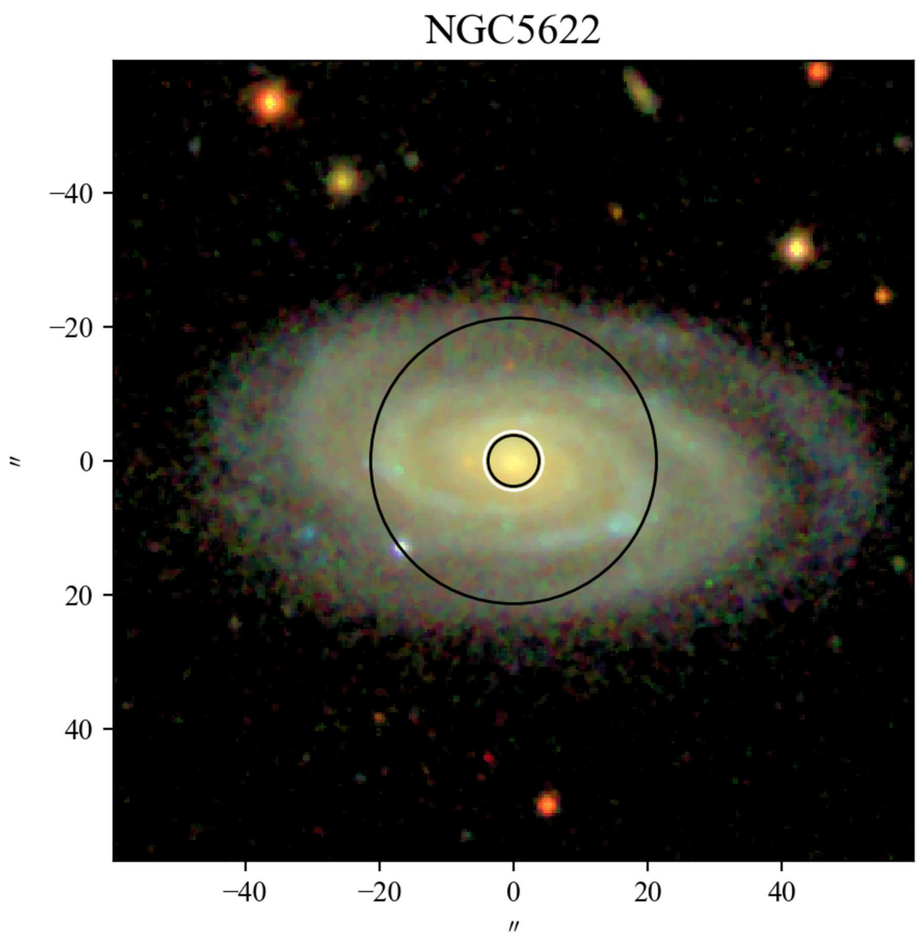
NGC5622
−40
−20
0
20
40
″
−40
−20
0
20
40
″

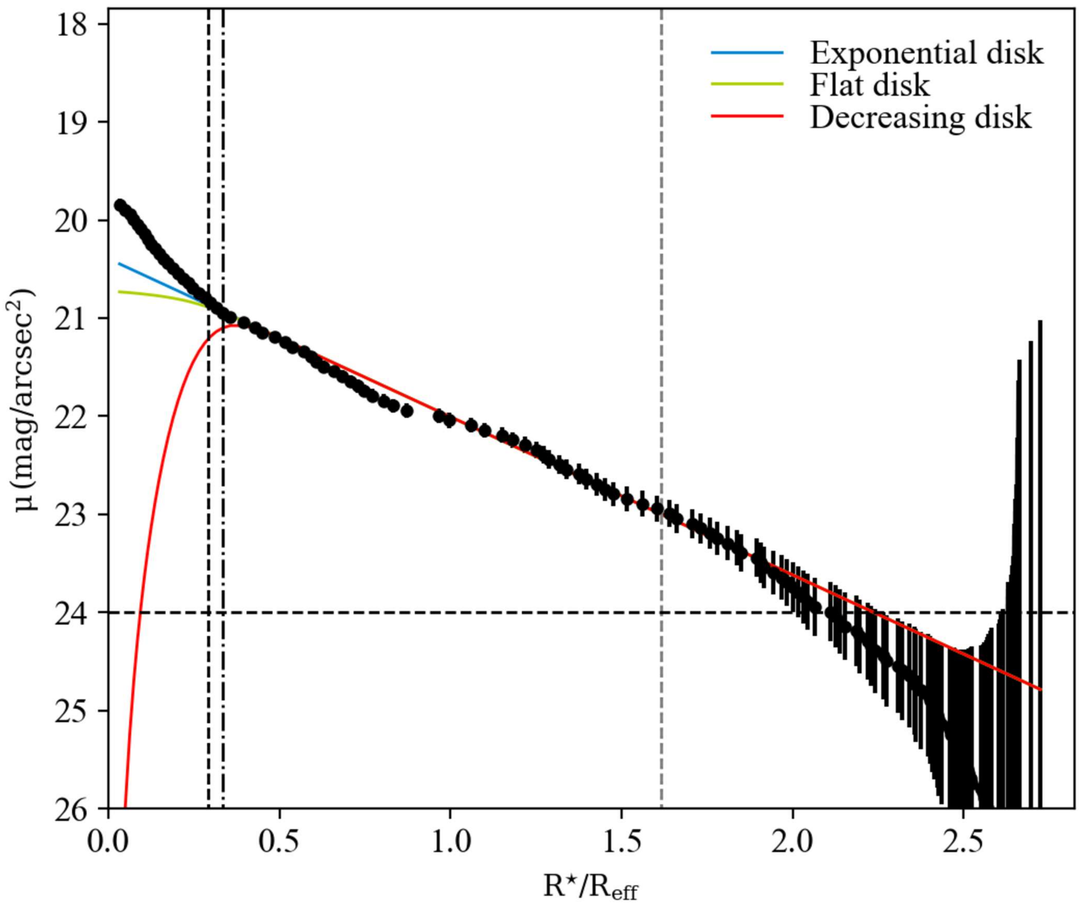
Exponential disk
Flat disk
Decreasing disk
μ (mag/arcsec²)
18
19
20
21
22
23
24
25
26
0.0
0.5
1.0
1.5
2.0
2.5
R*/Reff

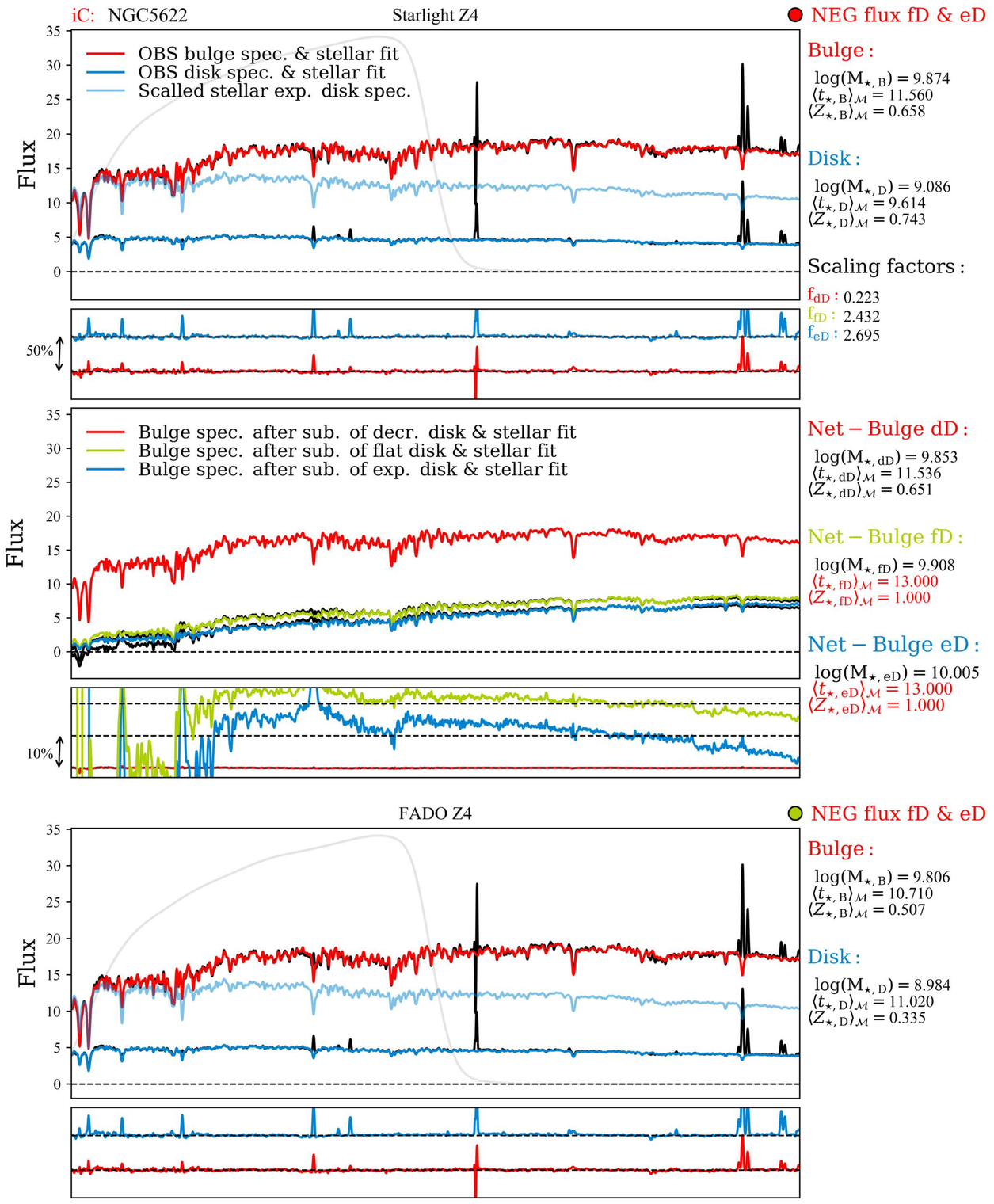
iC: NGC5622
Starlight Z4
NEG flux fD & eD
OBS bulge spec. & stellar fit
OBS disk spec. & stellar fit
Scalled stellar exp. disk spec.
Flux
50%
Bulge :
log(M⋆, B) = 9.874
⟨t⋆, B⟩M = 11.560
⟨Z⋆, B⟩M = 0.658
Disk :
log(M⋆, D) = 9.086
⟨t⋆, D⟩M = 9.614
⟨Z⋆, D⟩M = 0.743
Scaling factors :
fdD : 0.223
ffD : 2.432
feD : 2.695
Bulge spec. after sub. of decr. disk & stellar fit
Bulge spec. after sub. of flat disk & stellar fit
Bulge spec. after sub. of exp. disk & stellar fit
10%
Net − Bulge dD :
log(M⋆, dD) = 9.853
⟨t⋆, dD⟩M = 11.536
⟨Z⋆, dD⟩M = 0.651
Net − Bulge fD :
log(M⋆, fD) = 9.908
⟨t⋆, fD⟩M = 13.000
⟨Z⋆, fD⟩M = 1.000
Net − Bulge eD :
log(M⋆, eD) = 10.005
⟨t⋆, eD⟩M = 13.000
⟨Z⋆, eD⟩M = 1.000

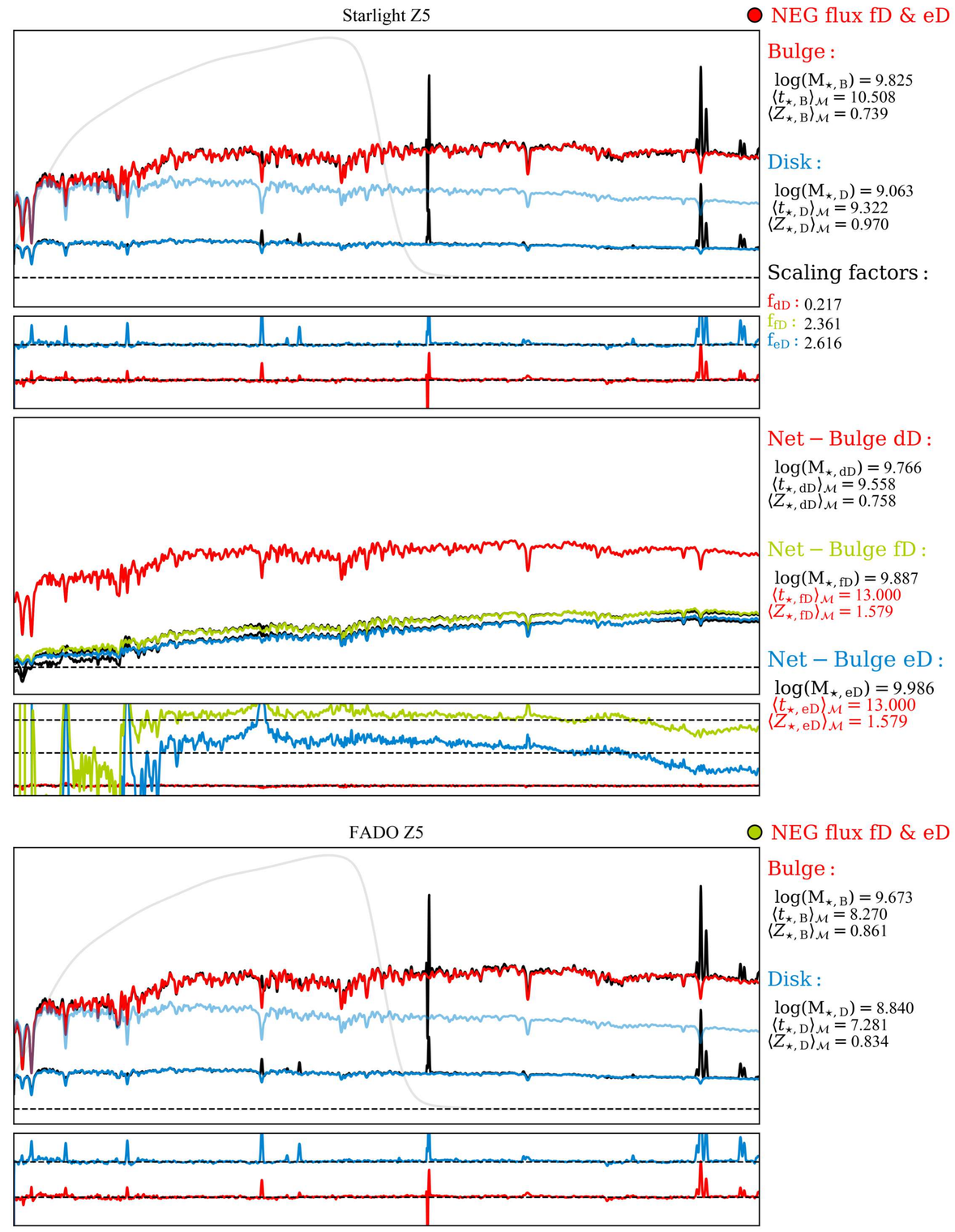
Starlight Z5
NEG flux fD & eD
Bulge :
log(M⋆, B) = 9.825
⟨t⋆, B⟩M = 10.508
⟨Z⋆, B⟩M = 0.739
Disk :
log(M⋆, D) = 9.063
⟨t⋆, D⟩M = 9.322
⟨Z⋆, D⟩M = 0.970
Scaling factors :
fdD : 0.217
ffD : 2.361
feD : 2.616
Net − Bulge dD :
log(M⋆, dD) = 9.766
⟨t⋆, dD⟩M = 9.558
⟨Z⋆, dD⟩M = 0.758
Net − Bulge fD :
log(M⋆, fD) = 9.887
⟨t⋆, fD⟩M = 13.000
⟨Z⋆, fD⟩M = 1.579
Net − Bulge eD :
log(M⋆, eD) = 9.986
⟨t⋆, eD⟩M = 13.000
⟨Z⋆, eD⟩M = 1.579

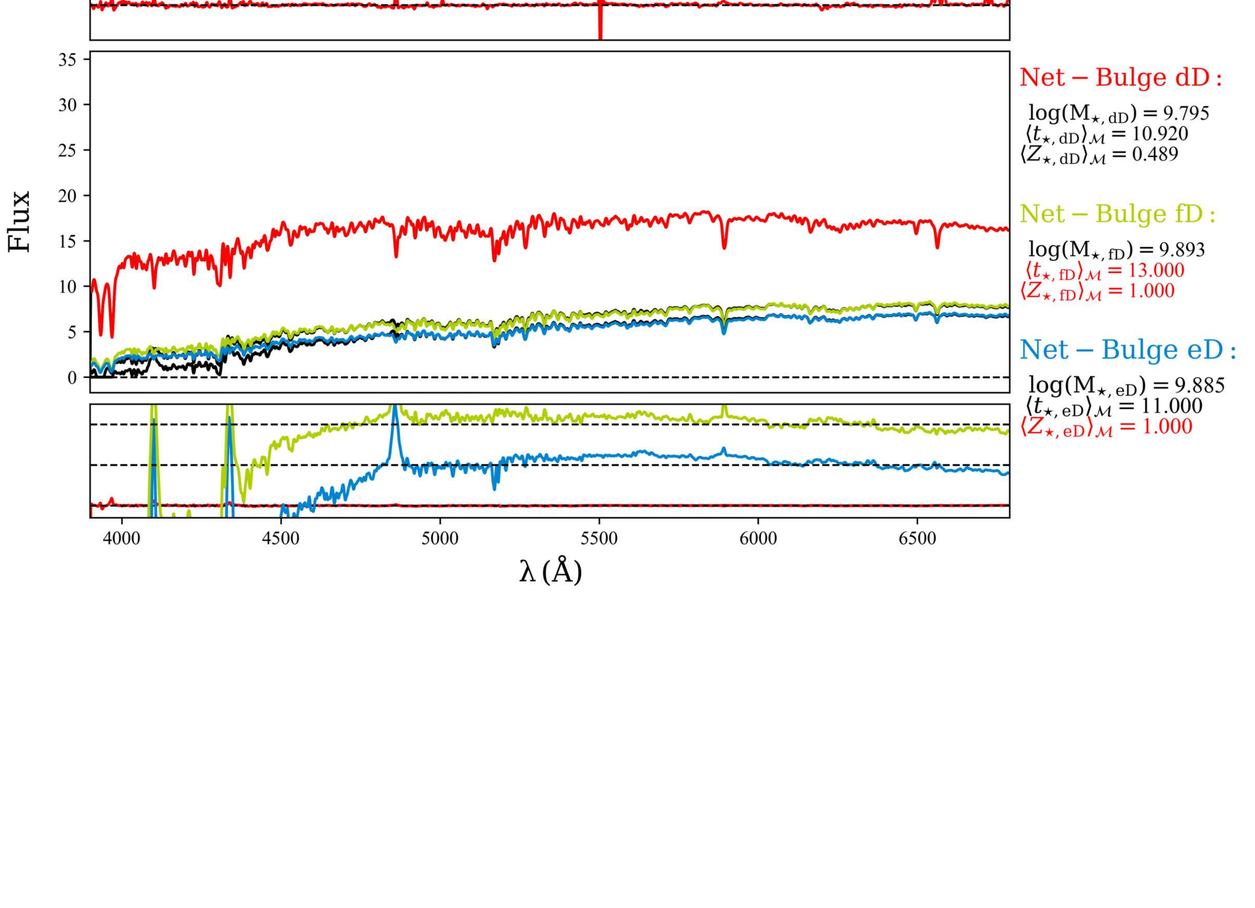
FADO Z4
NEG flux fD & eD
Flux
Bulge :
log(M⋆, B) = 9.806
⟨t⋆, B⟩M = 10.710
⟨Z⋆, B⟩M = 0.507
Disk :
log(M⋆, D) = 8.984
⟨t⋆, D⟩M = 11.020
⟨Z⋆, D⟩M = 0.335
Net − Bulge dD :
log(M⋆, dD) = 9.795
⟨t⋆, dD⟩M = 10.920
⟨Z⋆, dD⟩M = 0.489
Net − Bulge fD :
log(M⋆, fD) = 9.893
⟨t⋆, fD⟩M = 13.000
⟨Z⋆, fD⟩M = 1.000
Net − Bulge eD :
log(M⋆, eD) = 9.885
⟨t⋆, eD⟩M = 11.000
⟨Z⋆, eD⟩M = 1.000
λ (Å)

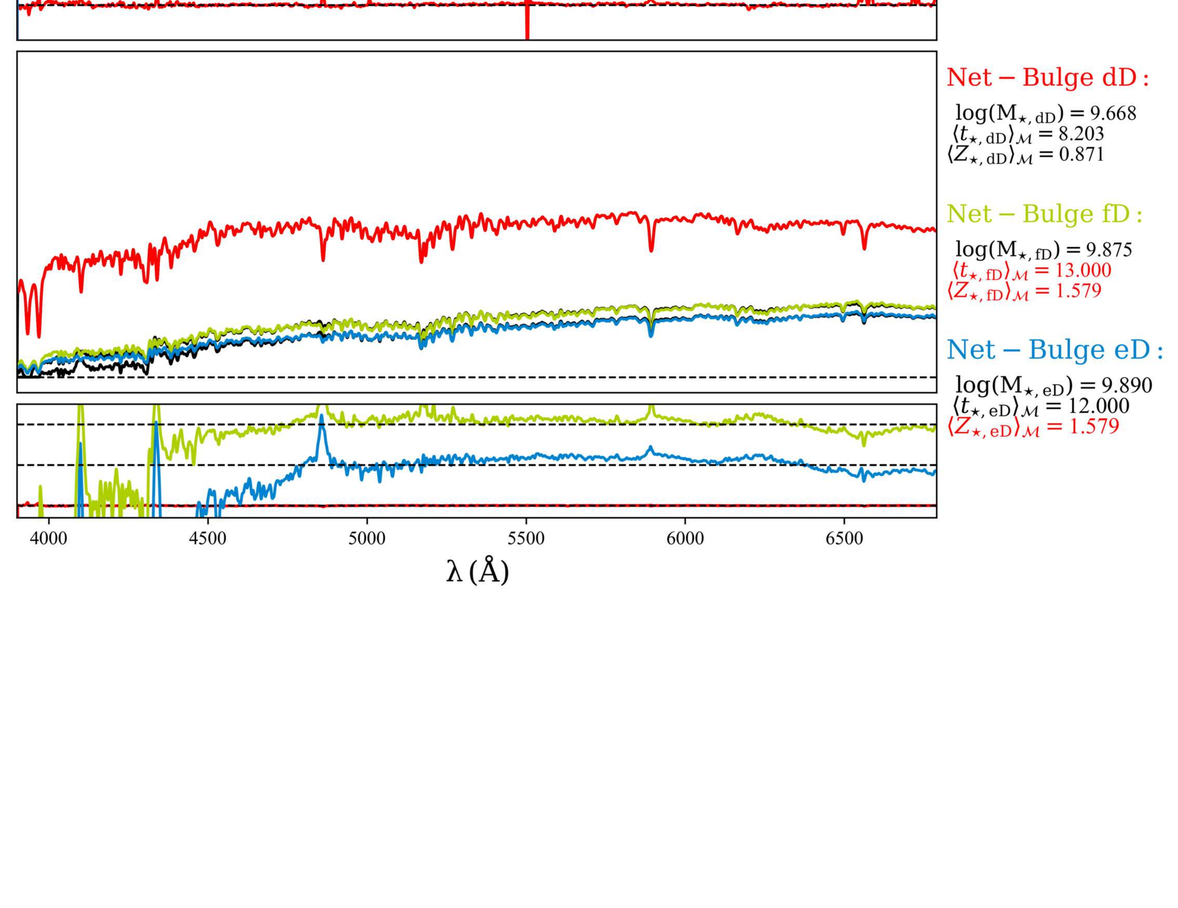
FADO Z5
NEG flux fD & eD
Bulge :
log(M⋆, B) = 9.673
⟨t⋆, B⟩M = 8.270
⟨Z⋆, B⟩M = 0.861
Disk :
log(M⋆, D) = 8.840
⟨t⋆, D⟩M = 7.281
⟨Z⋆, D⟩M = 0.834
Net − Bulge dD :
log(M⋆, dD) = 9.668
⟨t⋆, dD⟩M = 8.203
⟨Z⋆, dD⟩M = 0.871
Net − Bulge fD :
log(M⋆, fD) = 9.875
⟨t⋆, fD⟩M = 13.000
⟨Z⋆, fD⟩M = 1.579
Net − Bulge eD :
log(M⋆, eD) = 9.890
⟨t⋆, eD⟩M = 12.000
⟨Z⋆, eD⟩M = 1.579
λ (Å)

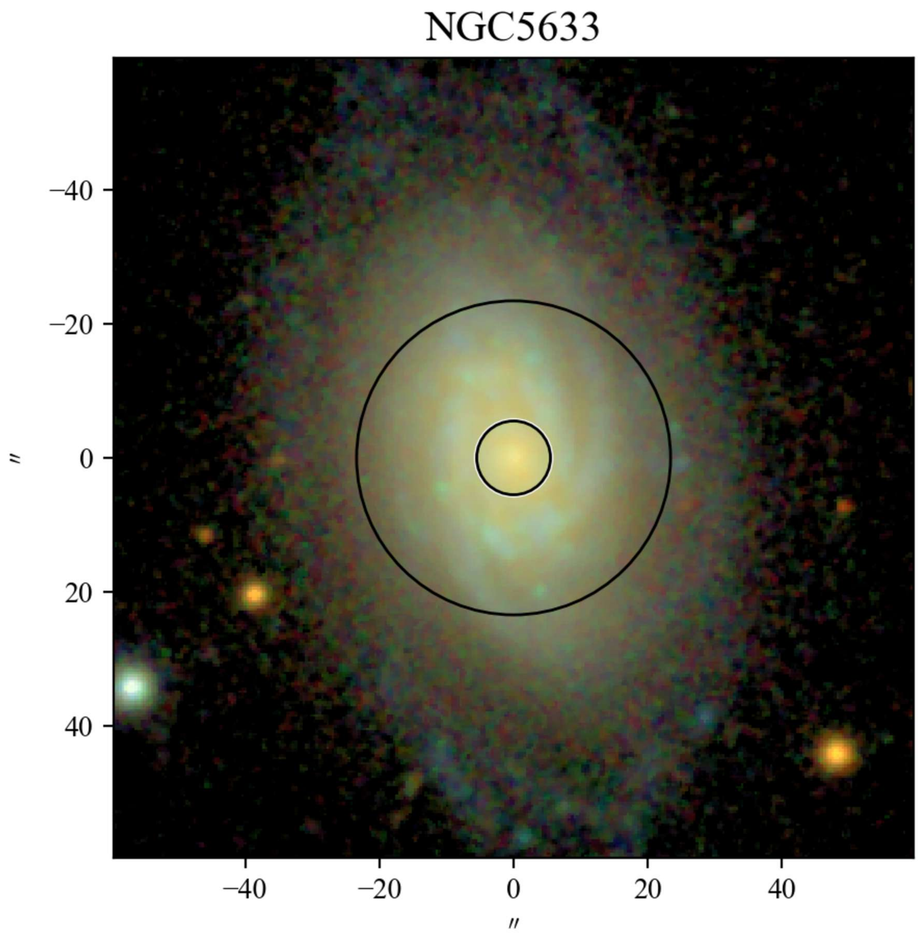
NGC5633
−40
−20
0
20
40
″
−40
−20
0
20
40
″

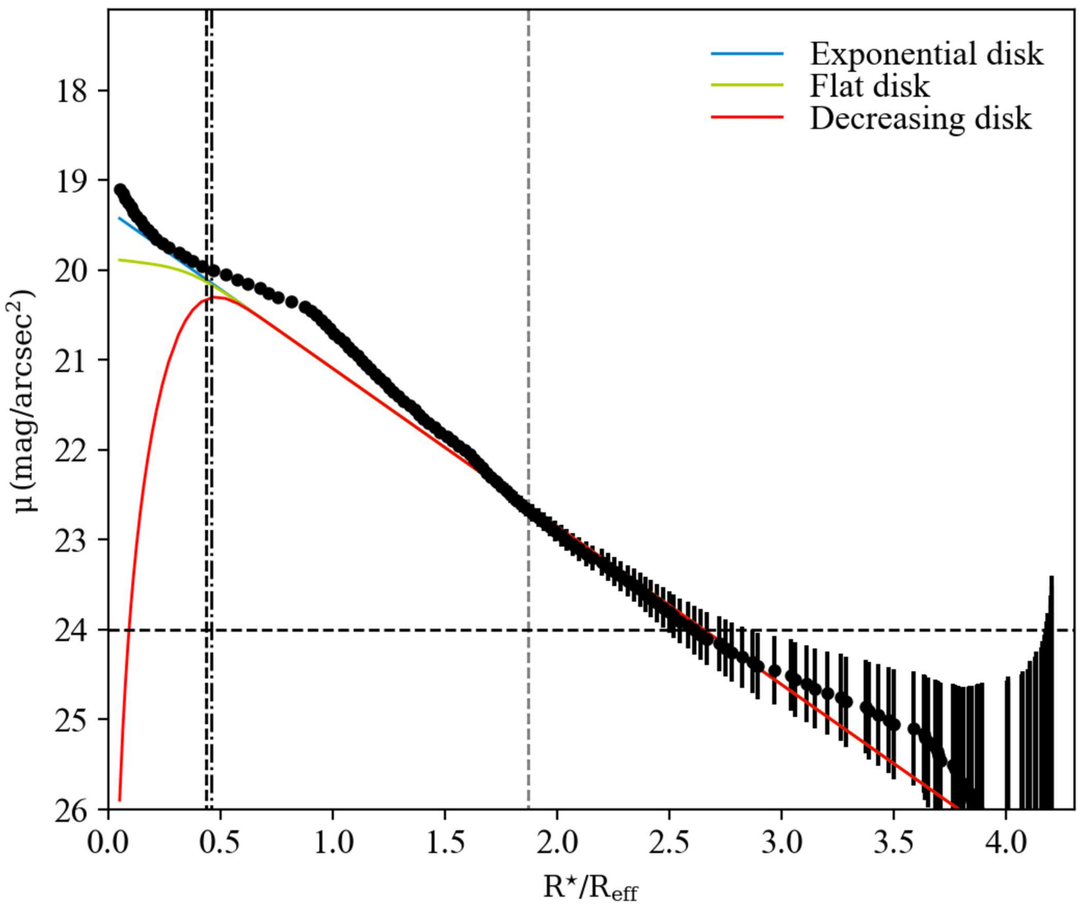
Exponential disk
Flat disk
Decreasing disk
μ (mag/arcsec²)
18
19
20
21
22
23
24
25
26
0.0
0.5
1.0
1.5
2.0
2.5
3.0
3.5
4.0
R⋆/Reff

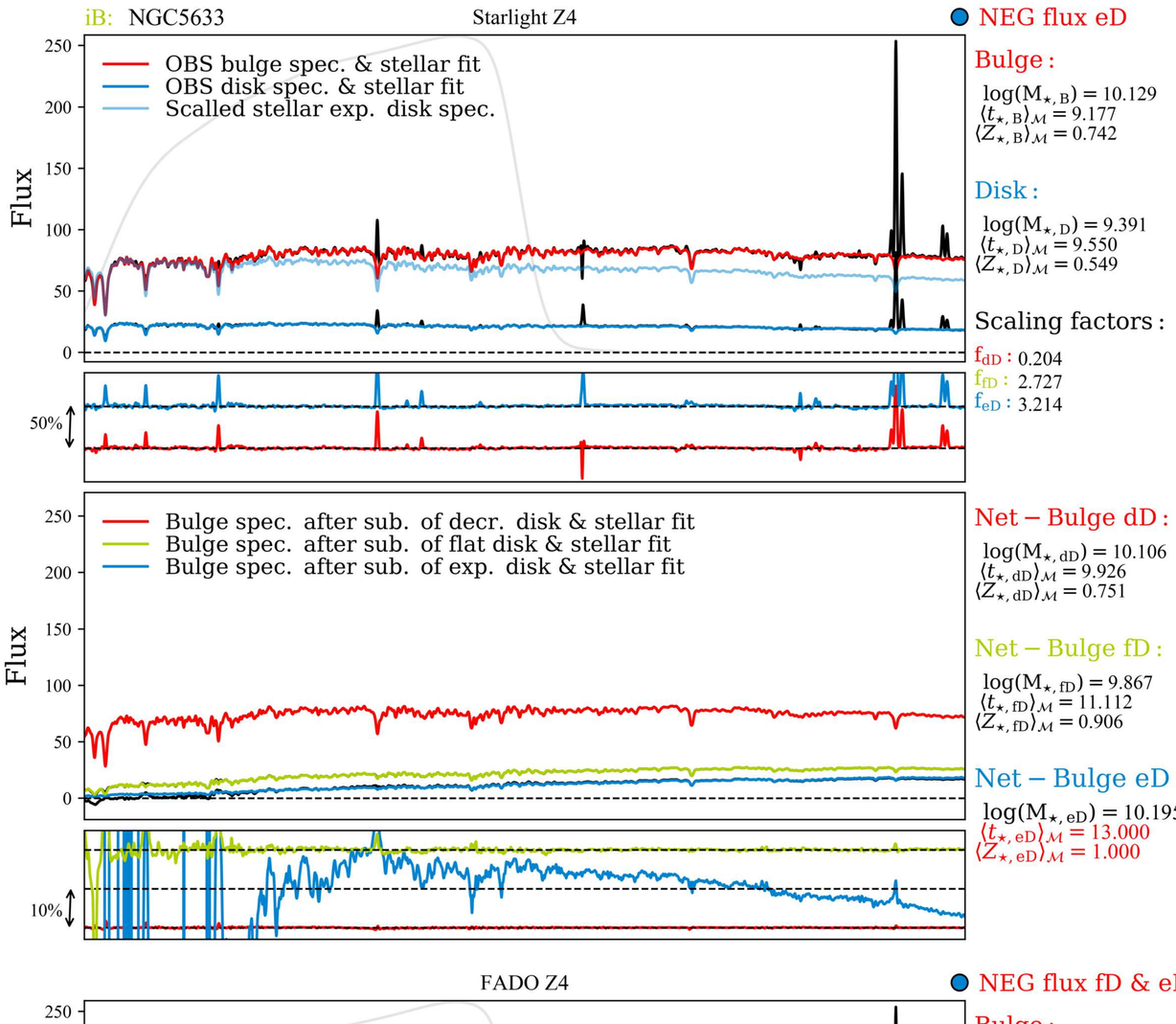
iB: NGC5633
Starlight Z4
NEG flux eD
OBS bulge spec. & stellar fit
OBS disk spec. & stellar fit
Scalled stellar exp. disk spec.
Flux
Bulge :
log(M⋆, B) = 10.129
⟨t⋆, B⟩M = 9.177
⟨Z⋆, B⟩M = 0.742
Disk :
log(M⋆, D) = 9.391
⟨t⋆, D⟩M = 9.550
⟨Z⋆, D⟩M = 0.549
Scaling factors :
fdD : 0.204
ffD : 2.727
feD : 3.214
50%
Bulge spec. after sub. of decr. disk & stellar fit
Bulge spec. after sub. of flat disk & stellar fit
Bulge spec. after sub. of exp. disk & stellar fit
Net − Bulge dD :
log(M⋆, dD) = 10.106
⟨t⋆, dD⟩M = 9.926
⟨Z⋆, dD⟩M = 0.751
Net − Bulge fD :
log(M⋆, fD) = 9.867
⟨t⋆, fD⟩M = 11.112
⟨Z⋆, fD⟩M = 0.906
Net − Bulge eD :
log(M⋆, eD) = 10.195
⟨t⋆, eD⟩M = 13.000
⟨Z⋆, eD⟩M = 1.000
10%

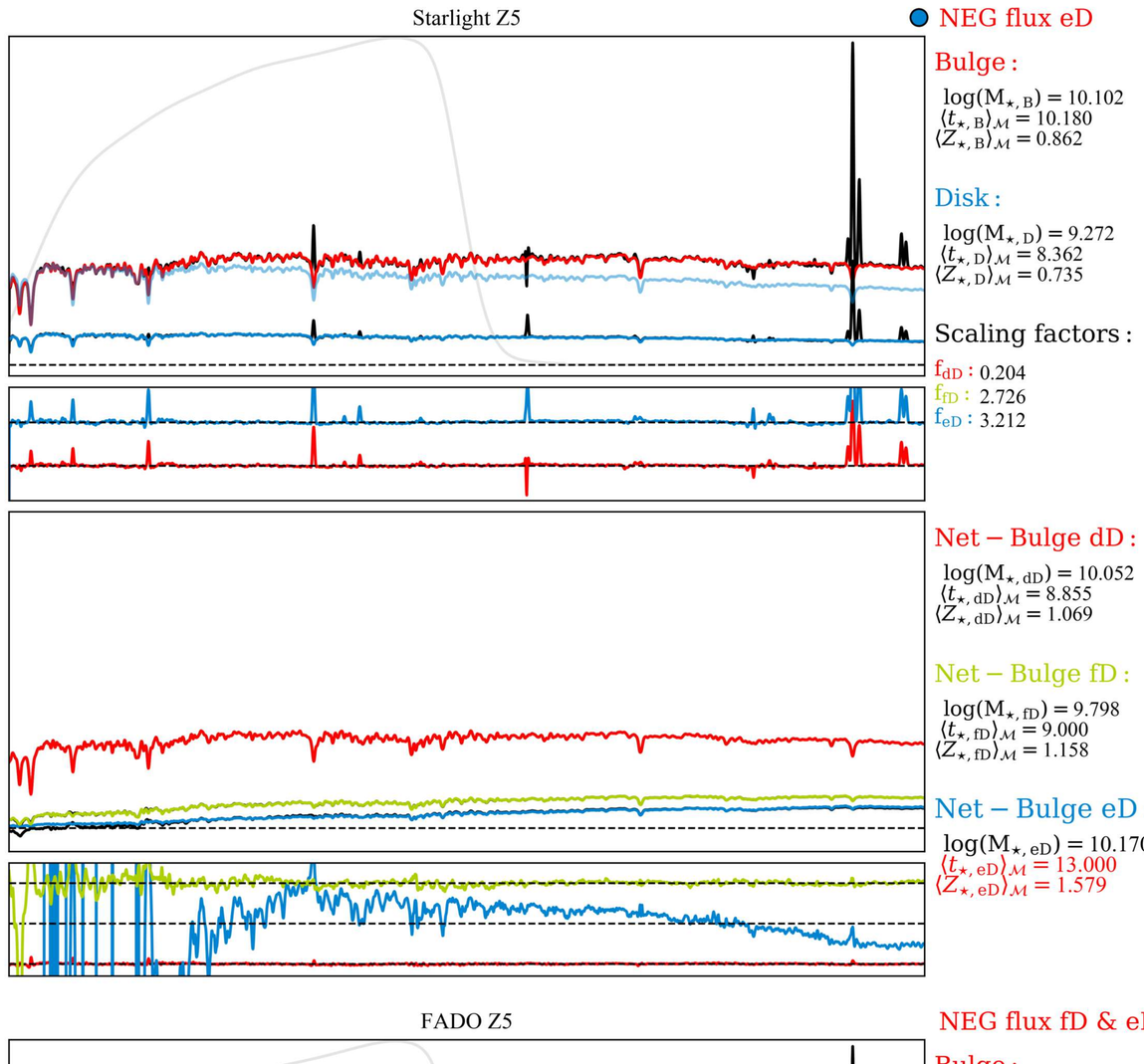
Starlight Z5
NEG flux eD
Bulge :
log(M⋆, B) = 10.102
⟨t⋆, B⟩M = 10.180
⟨Z⋆, B⟩M = 0.862
Disk :
log(M⋆, D) = 9.272
⟨t⋆, D⟩M = 8.362
⟨Z⋆, D⟩M = 0.735
Scaling factors :
fdD : 0.204
ffD : 2.726
feD : 3.212
Net − Bulge dD :
log(M⋆, dD) = 10.052
⟨t⋆, dD⟩M = 8.855
⟨Z⋆, dD⟩M = 1.069
Net − Bulge fD :
log(M⋆, fD) = 9.798
⟨t⋆, fD⟩M = 9.000
⟨Z⋆, fD⟩M = 1.158
Net − Bulge eD :
log(M⋆, eD) = 10.170
⟨t⋆, eD⟩M = 13.000
⟨Z⋆, eD⟩M = 1.579

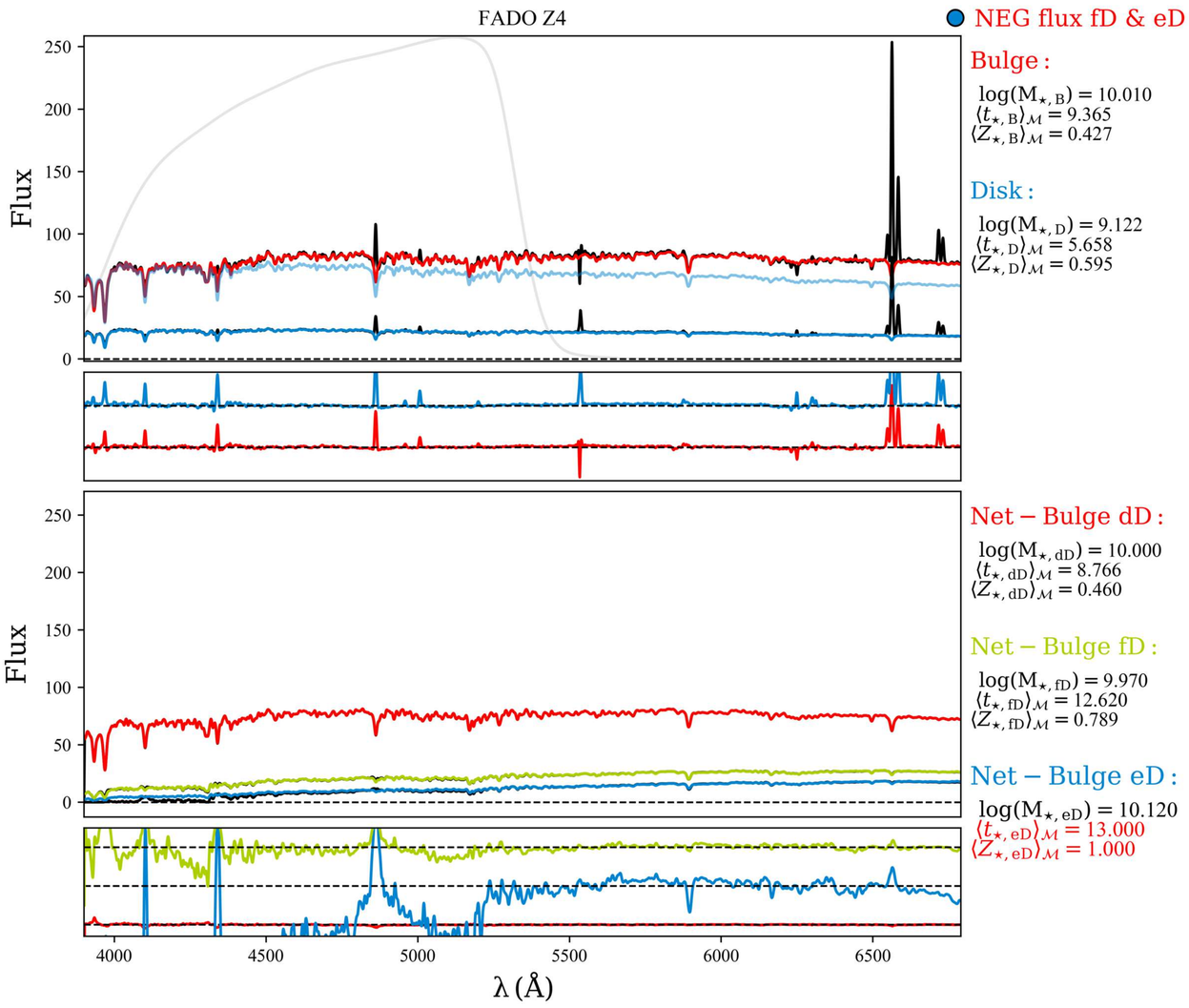
FADO Z4
NEG flux fD & eD
Flux
Bulge :
log(M⋆, B) = 10.010
⟨t⋆, B⟩M = 9.365
⟨Z⋆, B⟩M = 0.427
Disk :
log(M⋆, D) = 9.122
⟨t⋆, D⟩M = 5.658
⟨Z⋆, D⟩M = 0.595
Net − Bulge dD :
log(M⋆, dD) = 10.000
⟨t⋆, dD⟩M = 8.766
⟨Z⋆, dD⟩M = 0.460
Net − Bulge fD :
log(M⋆, fD) = 9.970
⟨t⋆, fD⟩M = 12.620
⟨Z⋆, fD⟩M = 0.789
Net − Bulge eD :
log(M⋆, eD) = 10.120
⟨t⋆, eD⟩M = 13.000
⟨Z⋆, eD⟩M = 1.000
λ (Å)

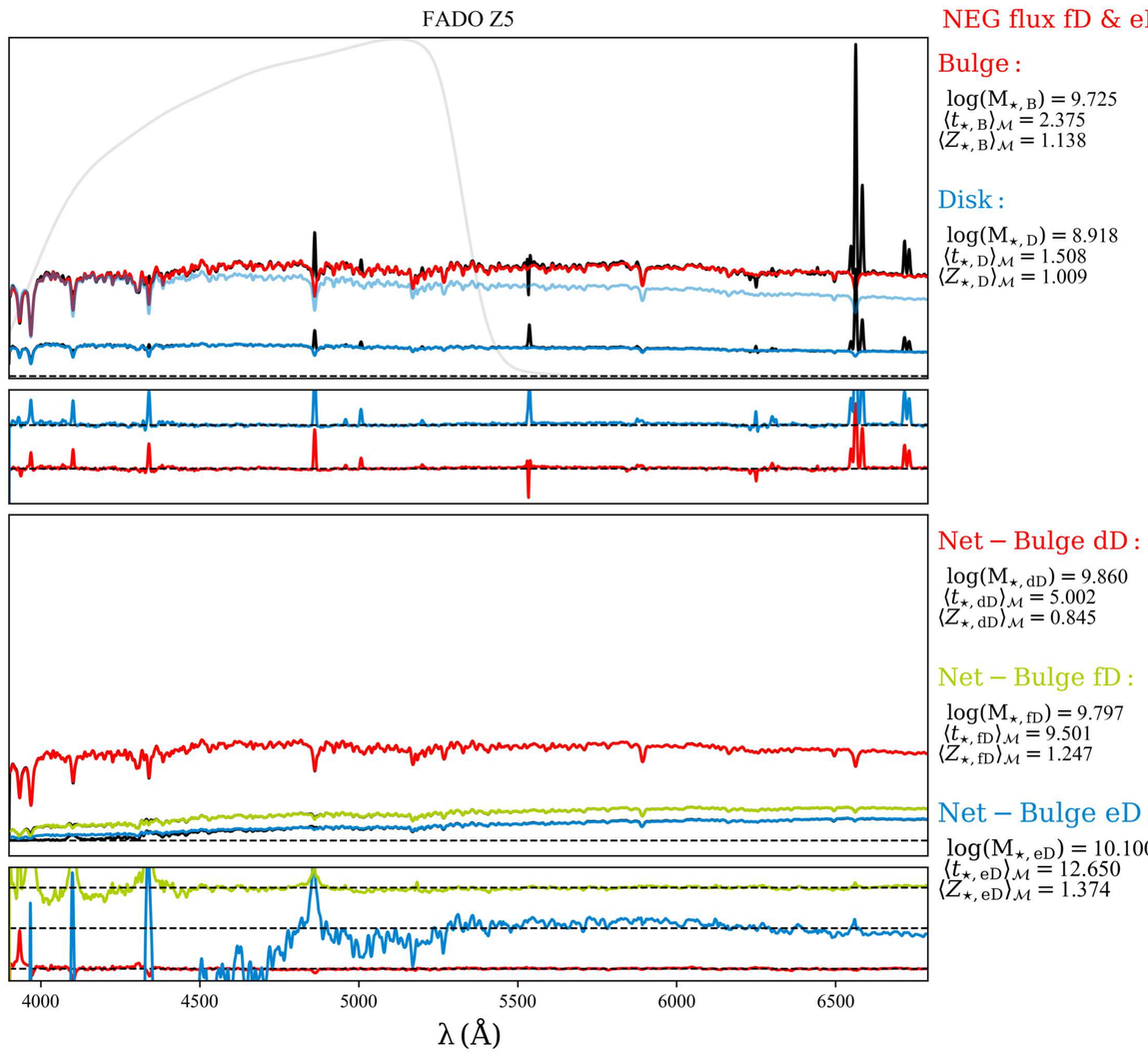
FADO Z5
NEG flux fD & eD
Bulge :
log(M⋆, B) = 9.725
⟨t⋆, B⟩M = 2.375
⟨Z⋆, B⟩M = 1.138
Disk :
log(M⋆, D) = 8.918
⟨t⋆, D⟩M = 1.508
⟨Z⋆, D⟩M = 1.009
Net − Bulge dD :
log(M⋆, dD) = 9.860
⟨t⋆, dD⟩M = 5.002
⟨Z⋆, dD⟩M = 0.845
Net − Bulge fD :
log(M⋆, fD) = 9.797
⟨t⋆, fD⟩M = 9.501
⟨Z⋆, fD⟩M = 1.247
Net − Bulge eD :
log(M⋆, eD) = 10.100
⟨t⋆, eD⟩M = 12.650
⟨Z⋆, eD⟩M = 1.374
λ (Å)

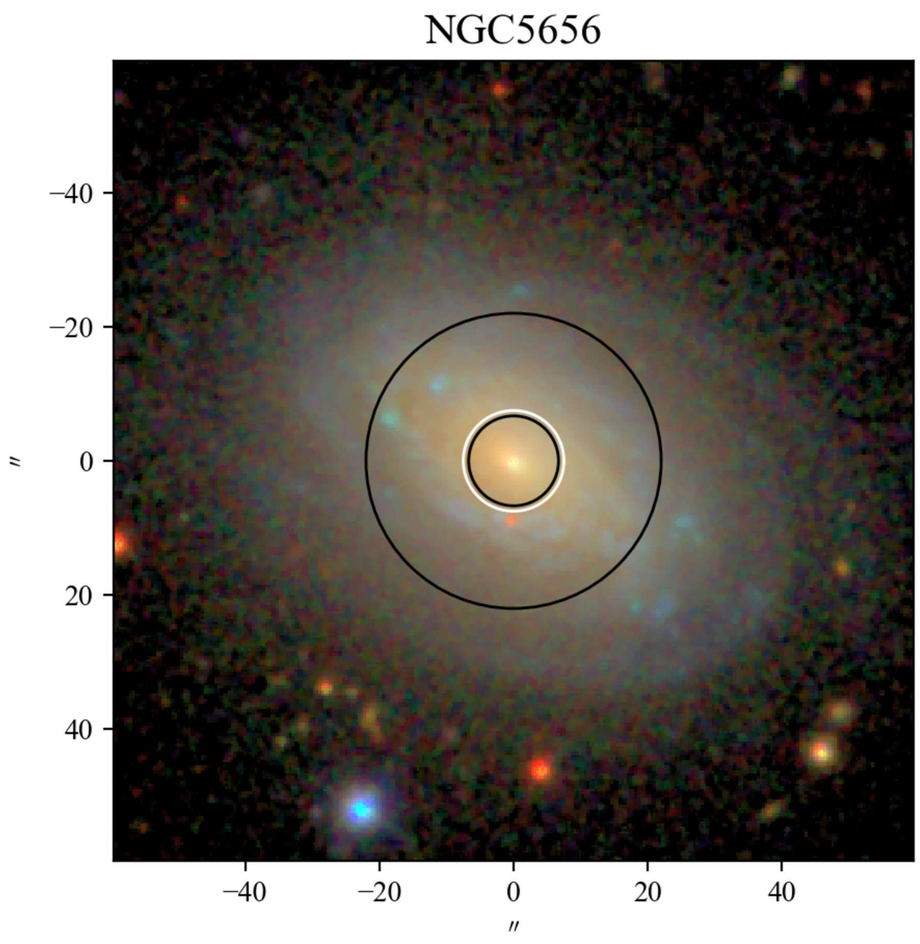
NGC5656
−40
−20
0
20
40
″
−40
−20
0
20
40
″

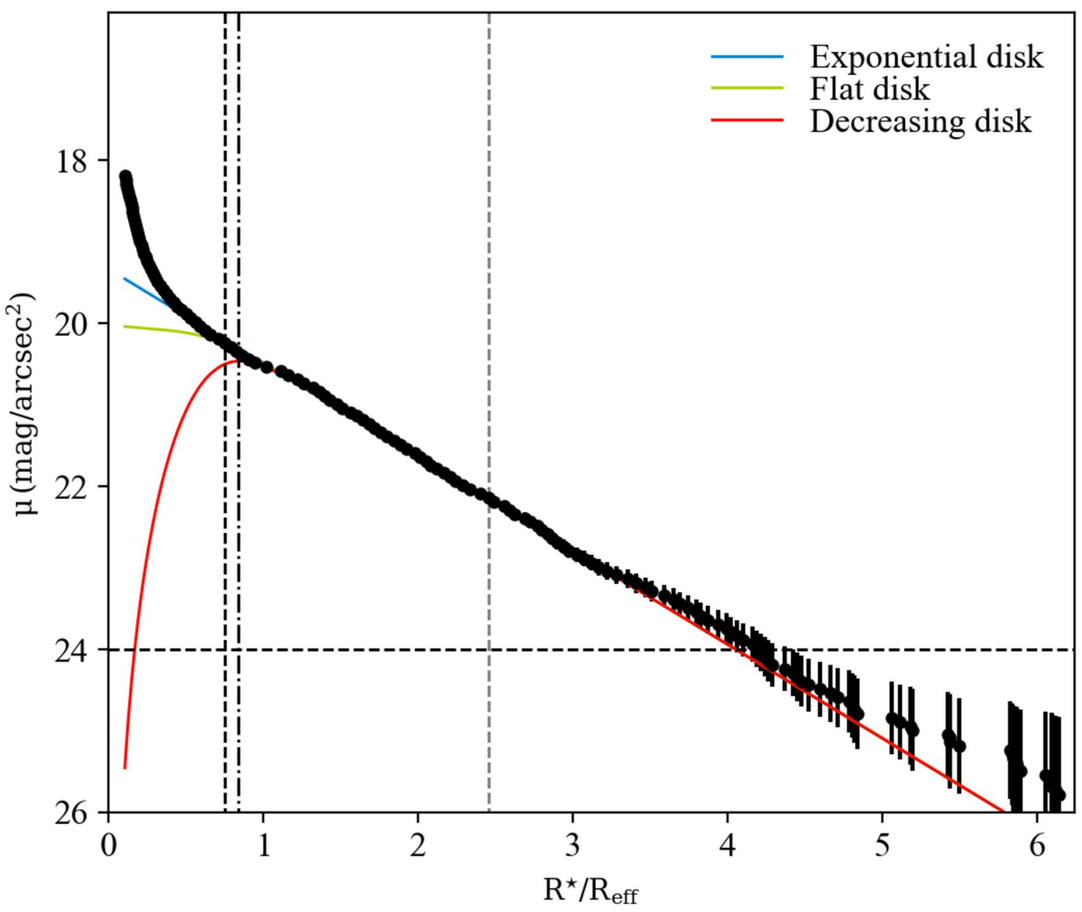
Exponential disk
Flat disk
Decreasing disk
μ (mag/arcsec²)
18
20
22
24
26
0
1
2
3
4
5
6
R⋆/Reff

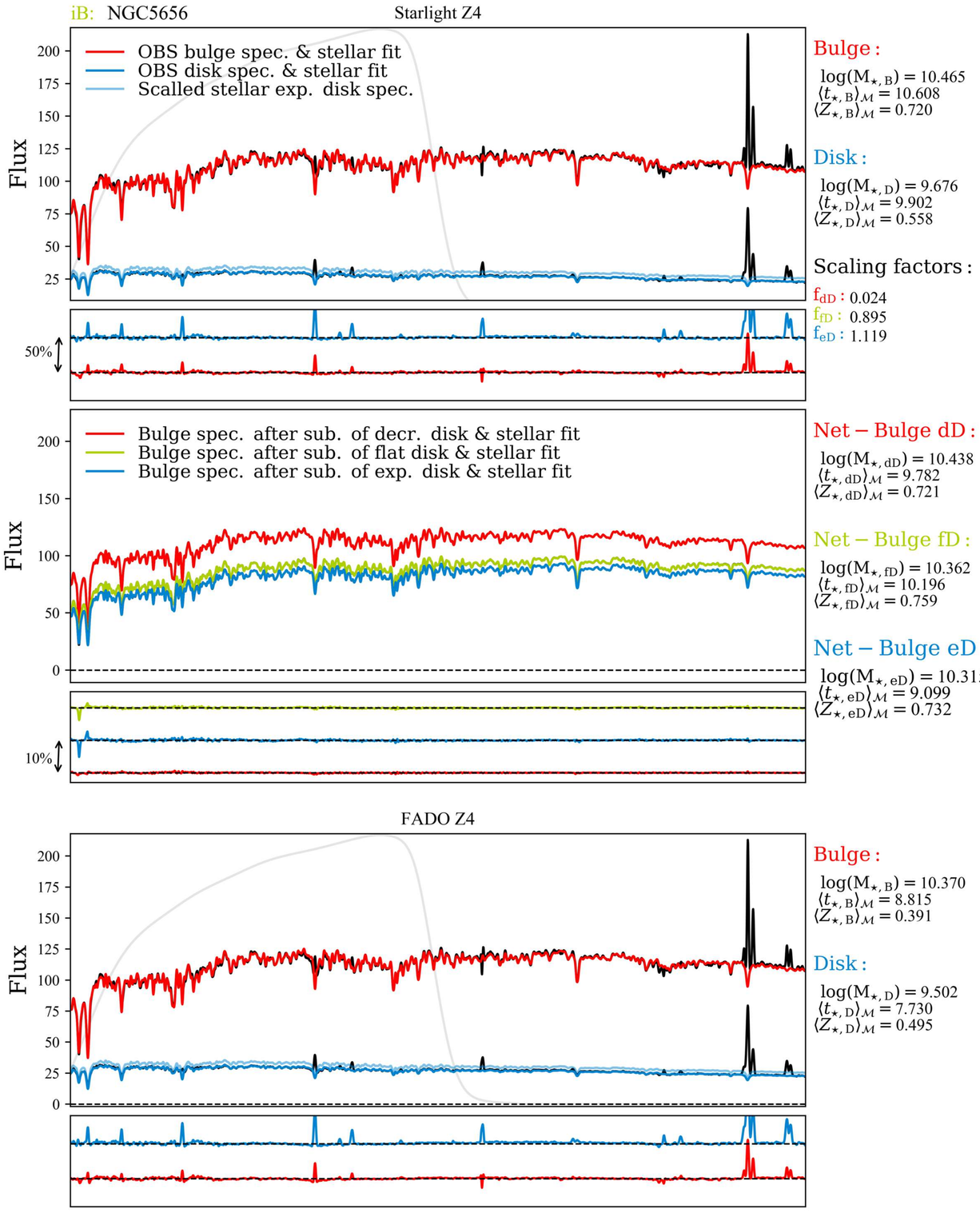
iB: NGC5656
Starlight Z4
OBS bulge spec. & stellar fit
OBS disk spec. & stellar fit
Scalled stellar exp. disk spec.
Flux
200
175
150
125
100
75
50
25
50%
Bulge :
log(M⋆, B) = 10.465
⟨t⋆, B⟩M = 10.608
⟨Z⋆, B⟩M = 0.720
Disk :
log(M⋆, D) = 9.676
⟨t⋆, D⟩M = 9.902
⟨Z⋆, D⟩M = 0.558
Scaling factors :
fdD : 0.024
ffD : 0.895
feD : 1.119
Bulge spec. after sub. of decr. disk & stellar fit
Bulge spec. after sub. of flat disk & stellar fit
Bulge spec. after sub. of exp. disk & stellar fit
Flux
200
150
100
50
0
10%
Net − Bulge dD :
log(M⋆, dD) = 10.438
⟨t⋆, dD⟩M = 9.782
⟨Z⋆, dD⟩M = 0.721
Net − Bulge fD :
log(M⋆, fD) = 10.362
⟨t⋆, fD⟩M = 10.196
⟨Z⋆, fD⟩M = 0.759
Net − Bulge eD :
log(M⋆, eD) = 10.315
⟨t⋆, eD⟩M = 9.099
⟨Z⋆, eD⟩M = 0.732

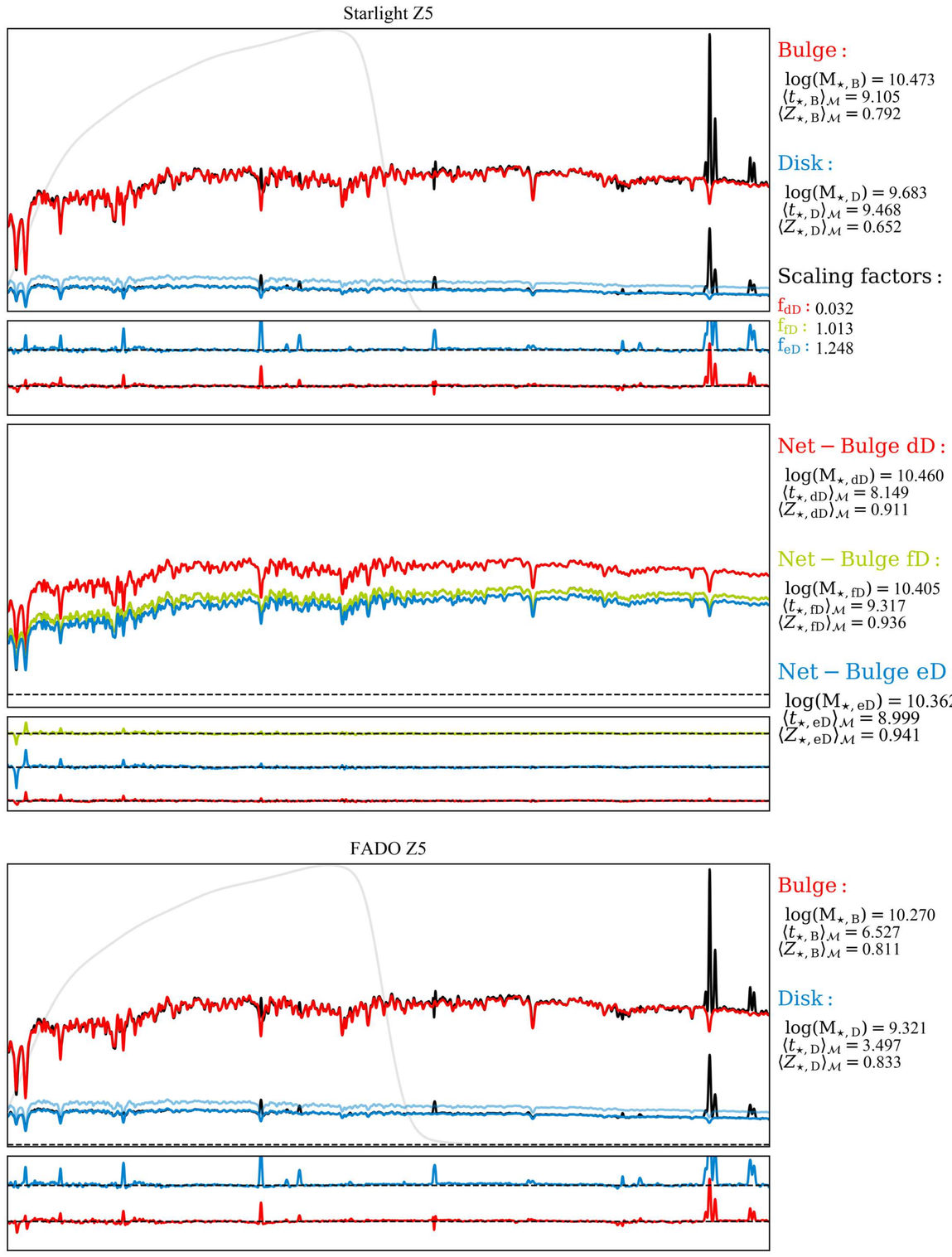
Starlight Z5
Bulge :
log(M⋆, B) = 10.473
⟨t⋆, B⟩M = 9.105
⟨Z⋆, B⟩M = 0.792
Disk :
log(M⋆, D) = 9.683
⟨t⋆, D⟩M = 9.468
⟨Z⋆, D⟩M = 0.652
Scaling factors :
fdD : 0.032
ffD : 1.013
feD : 1.248
Net − Bulge dD :
log(M⋆, dD) = 10.460
⟨t⋆, dD⟩M = 8.149
⟨Z⋆, dD⟩M = 0.911
Net − Bulge fD :
log(M⋆, fD) = 10.405
⟨t⋆, fD⟩M = 9.317
⟨Z⋆, fD⟩M = 0.936
Net − Bulge eD :
log(M⋆, eD) = 10.362
⟨t⋆, eD⟩M = 8.999
⟨Z⋆, eD⟩M = 0.941

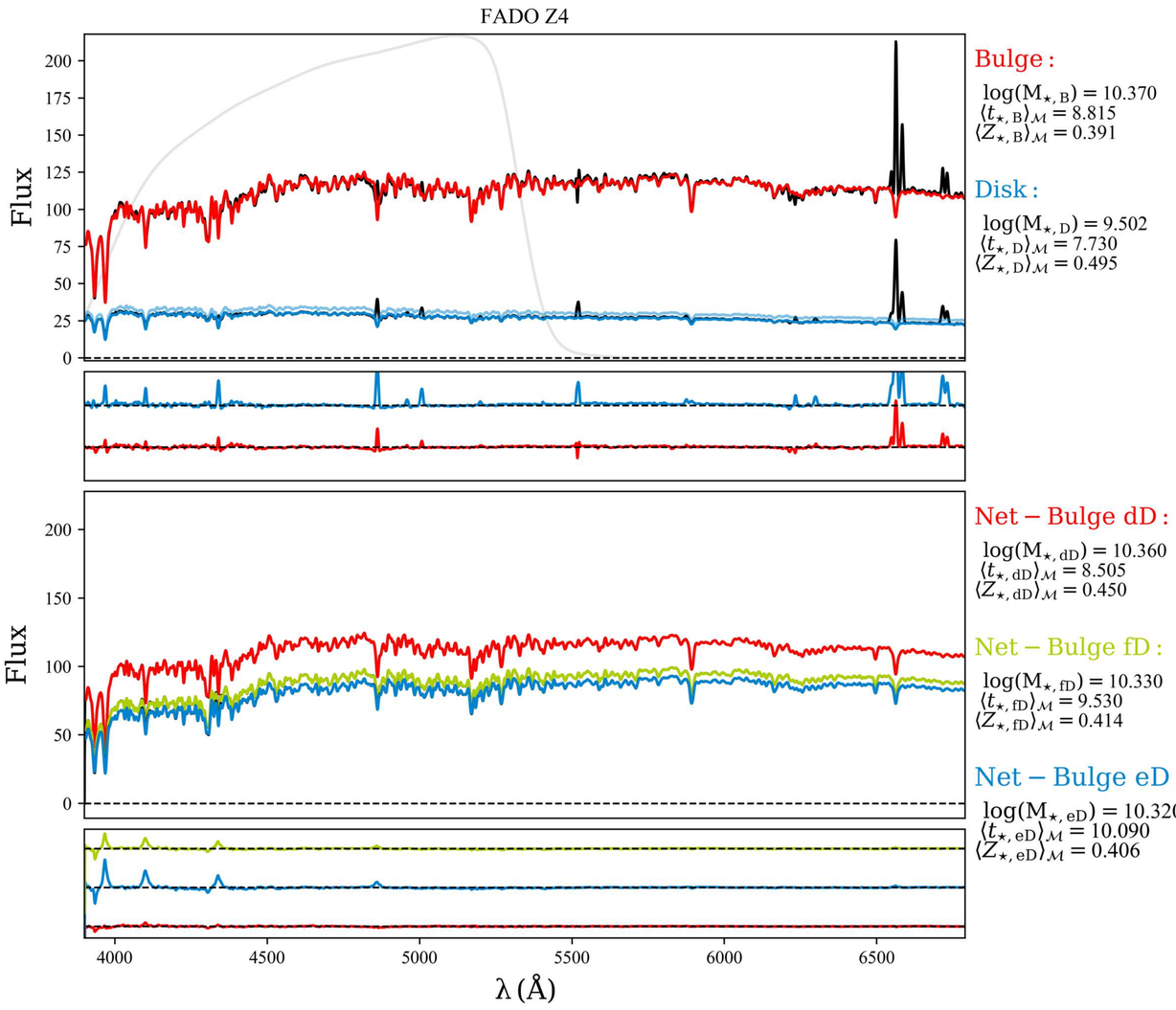
FADO Z4
Flux
200
175
150
125
100
75
50
25
0
Bulge :
log(M⋆, B) = 10.370
⟨t⋆, B⟩M = 8.815
⟨Z⋆, B⟩M = 0.391
Disk :
log(M⋆, D) = 9.502
⟨t⋆, D⟩M = 7.730
⟨Z⋆, D⟩M = 0.495
Flux
200
150
100
50
0
Net − Bulge dD :
log(M⋆, dD) = 10.360
⟨t⋆, dD⟩M = 8.505
⟨Z⋆, dD⟩M = 0.450
Net − Bulge fD :
log(M⋆, fD) = 10.330
⟨t⋆, fD⟩M = 9.530
⟨Z⋆, fD⟩M = 0.414
Net − Bulge eD :
log(M⋆, eD) = 10.320
⟨t⋆, eD⟩M = 10.090
⟨Z⋆, eD⟩M = 0.406
4000
4500
5000
5500
6000
6500
λ (Å)

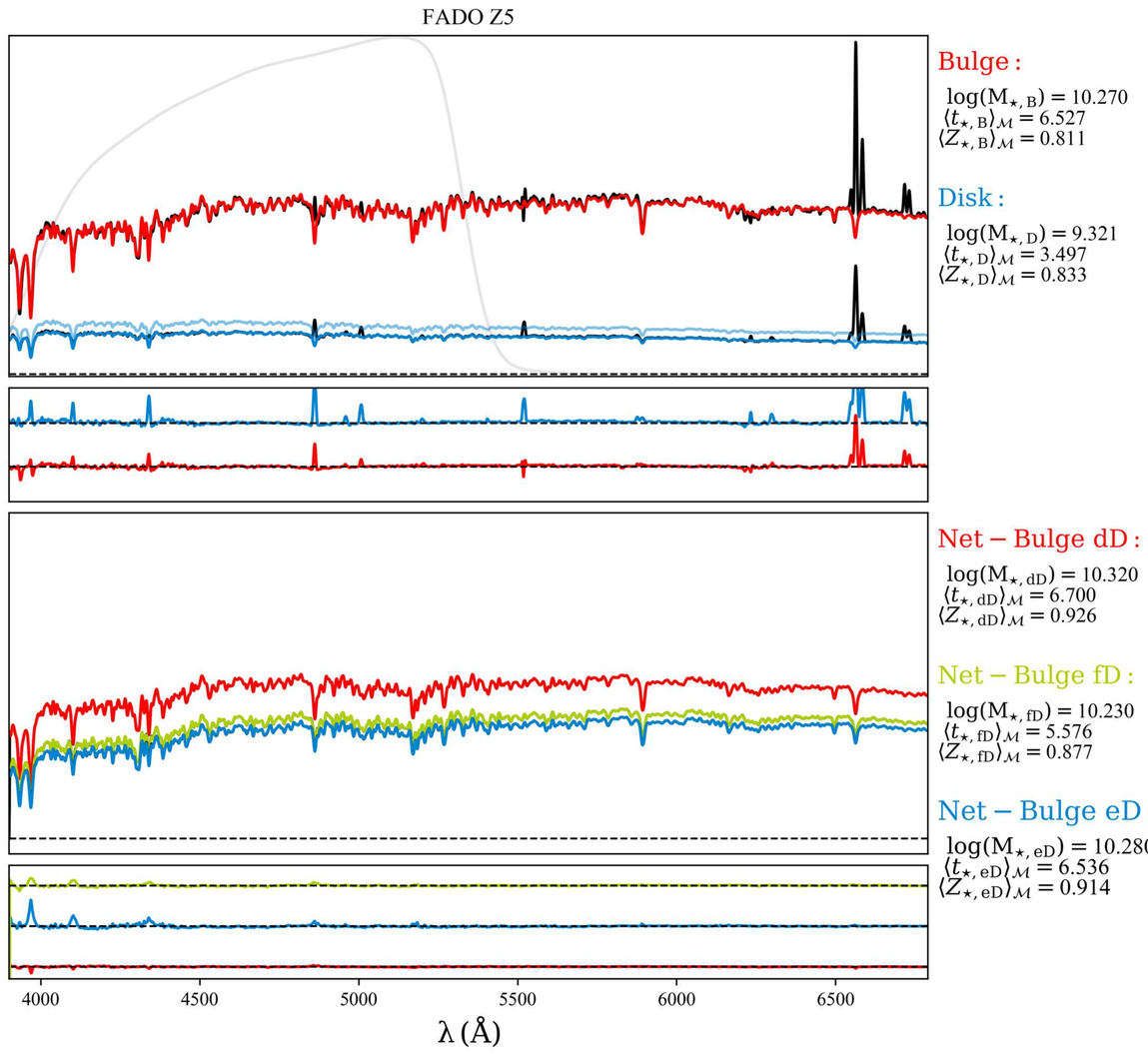
FADO Z5
Bulge :
log(M⋆, B) = 10.270
⟨t⋆, B⟩M = 6.527
⟨Z⋆, B⟩M = 0.811
Disk :
log(M⋆, D) = 9.321
⟨t⋆, D⟩M = 3.497
⟨Z⋆, D⟩M = 0.833
Net − Bulge dD :
log(M⋆, dD) = 10.320
⟨t⋆, dD⟩M = 6.700
⟨Z⋆, dD⟩M = 0.926
Net − Bulge fD :
log(M⋆, fD) = 10.230
⟨t⋆, fD⟩M = 5.576
⟨Z⋆, fD⟩M = 0.877
Net − Bulge eD :
log(M⋆, eD) = 10.280
⟨t⋆, eD⟩M = 6.536
⟨Z⋆, eD⟩M = 0.914
4000
4500
5000
5500
6000
6500
λ (Å)

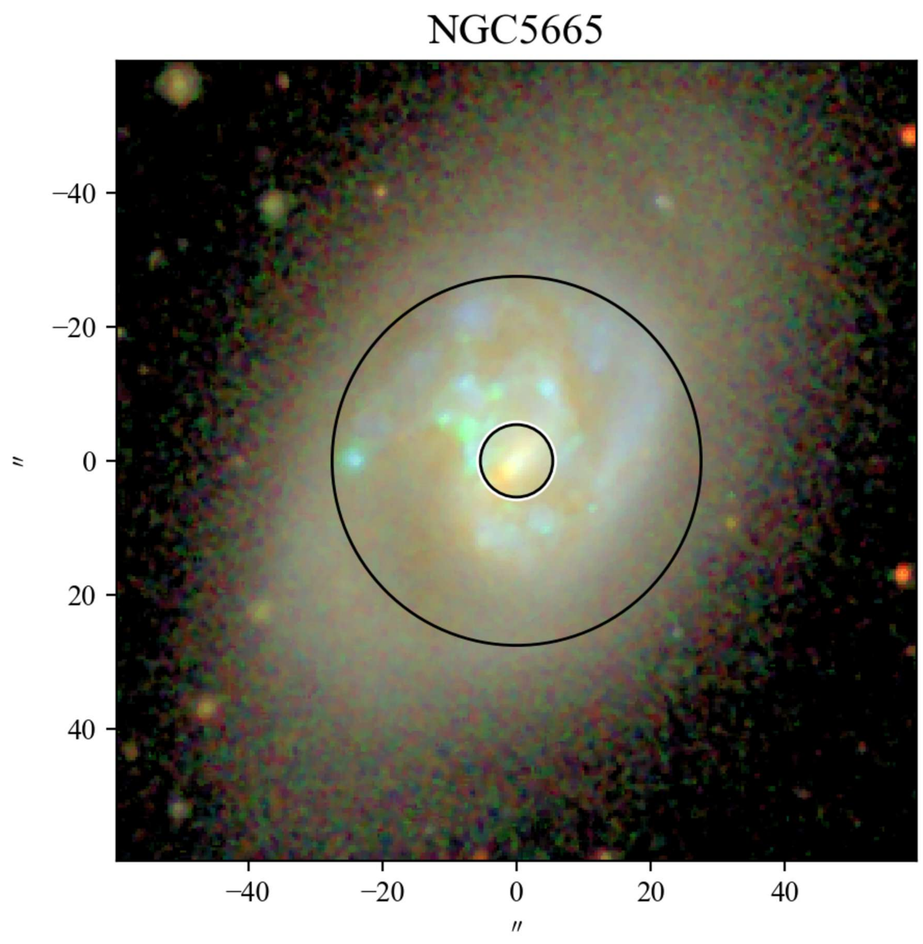
NGC5665
−40
−20
0
20
40
″
−40
−20
0
20
40
″

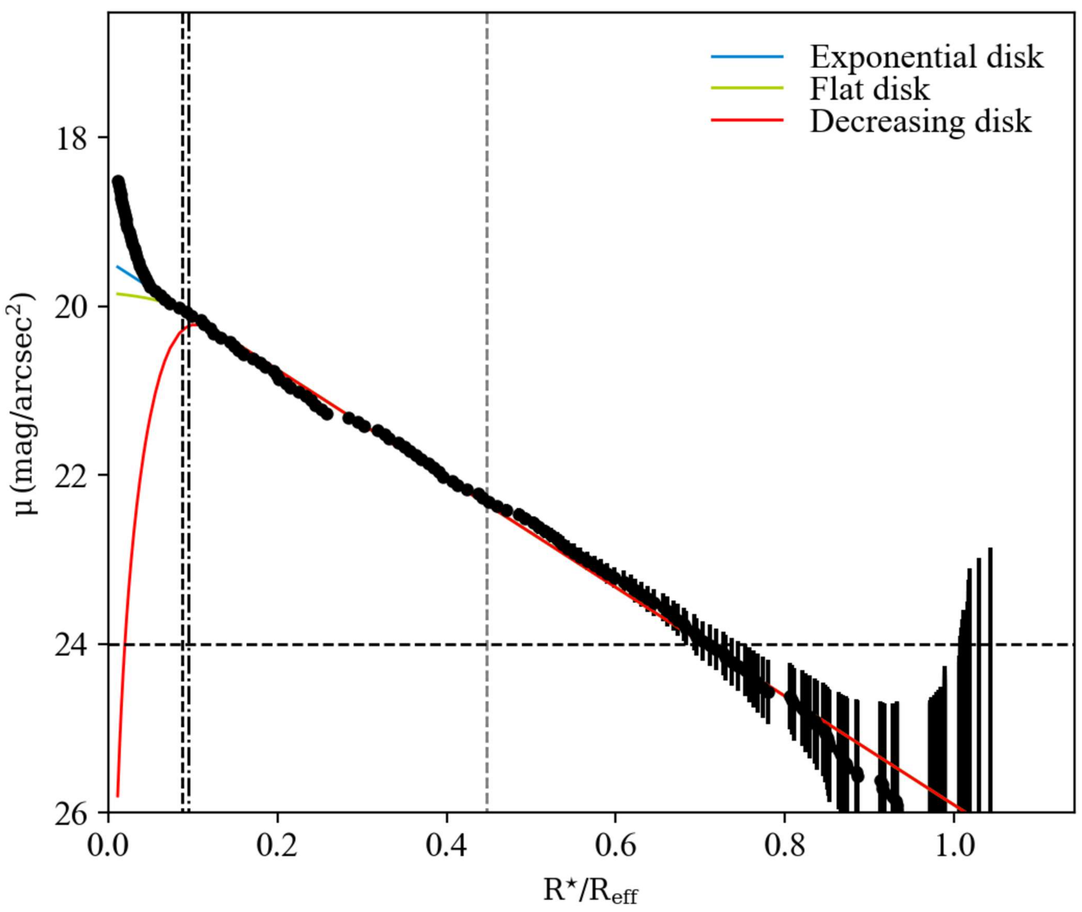
Exponential disk
Flat disk
Decreasing disk
μ (mag/arcsec²)
18
20
22
24
26
0.0
0.2
0.4
0.6
0.8
1.0
R⋆/Reff

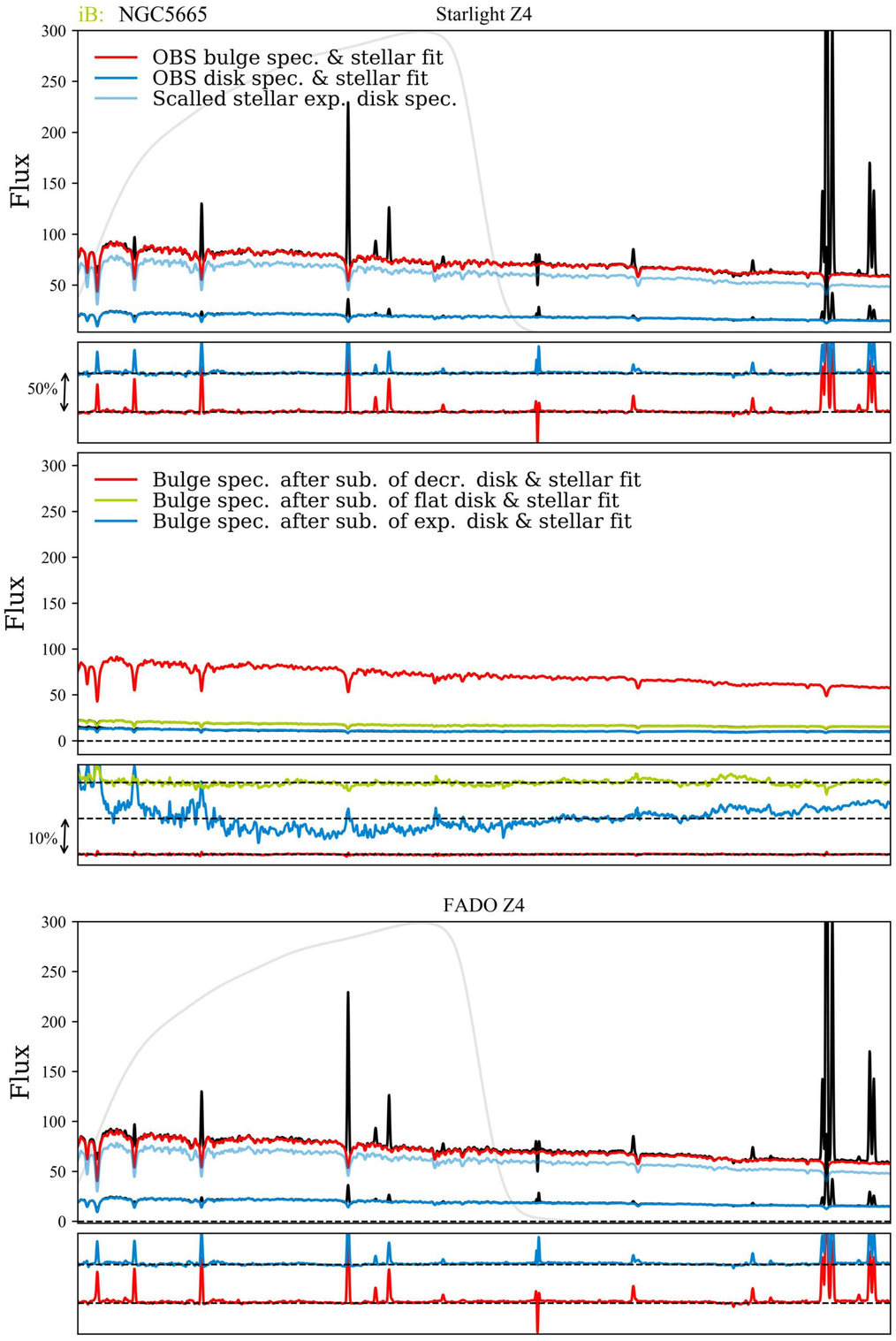
iB: NGC5665
Starlight Z4
OBS bulge spec. & stellar fit
OBS disk spec. & stellar fit
Scalled stellar exp. disk spec.
Flux
50%
Bulge :
log(M⋆, B) = 9.727
⟨t⋆, B⟩M = 10.201
⟨Z⋆, B⟩M = 0.483
Disk :
log(M⋆, D) = 9.151
⟨t⋆, D⟩M = 9.771
⟨Z⋆, D⟩M = 0.689
Scaling factors :
fdD : 0.044
ffD : 2.893
feD : 3.237
Bulge spec. after sub. of decr. disk & stellar fit
Bulge spec. after sub. of flat disk & stellar fit
Bulge spec. after sub. of exp. disk & stellar fit
10%
Net − Bulge dD :
log(M⋆, dD) = 9.684
⟨t⋆, dD⟩M = 8.748
⟨Z⋆, dD⟩M = 0.571
Net − Bulge fD :
log(M⋆, fD) = 8.955
⟨t⋆, fD⟩M = 10.727
⟨Z⋆, fD⟩M = 0.581
Net − Bulge eD :
log(M⋆, eD) = 7.603
⟨t⋆, eD⟩M = 0.010
⟨Z⋆, eD⟩M = 1.000

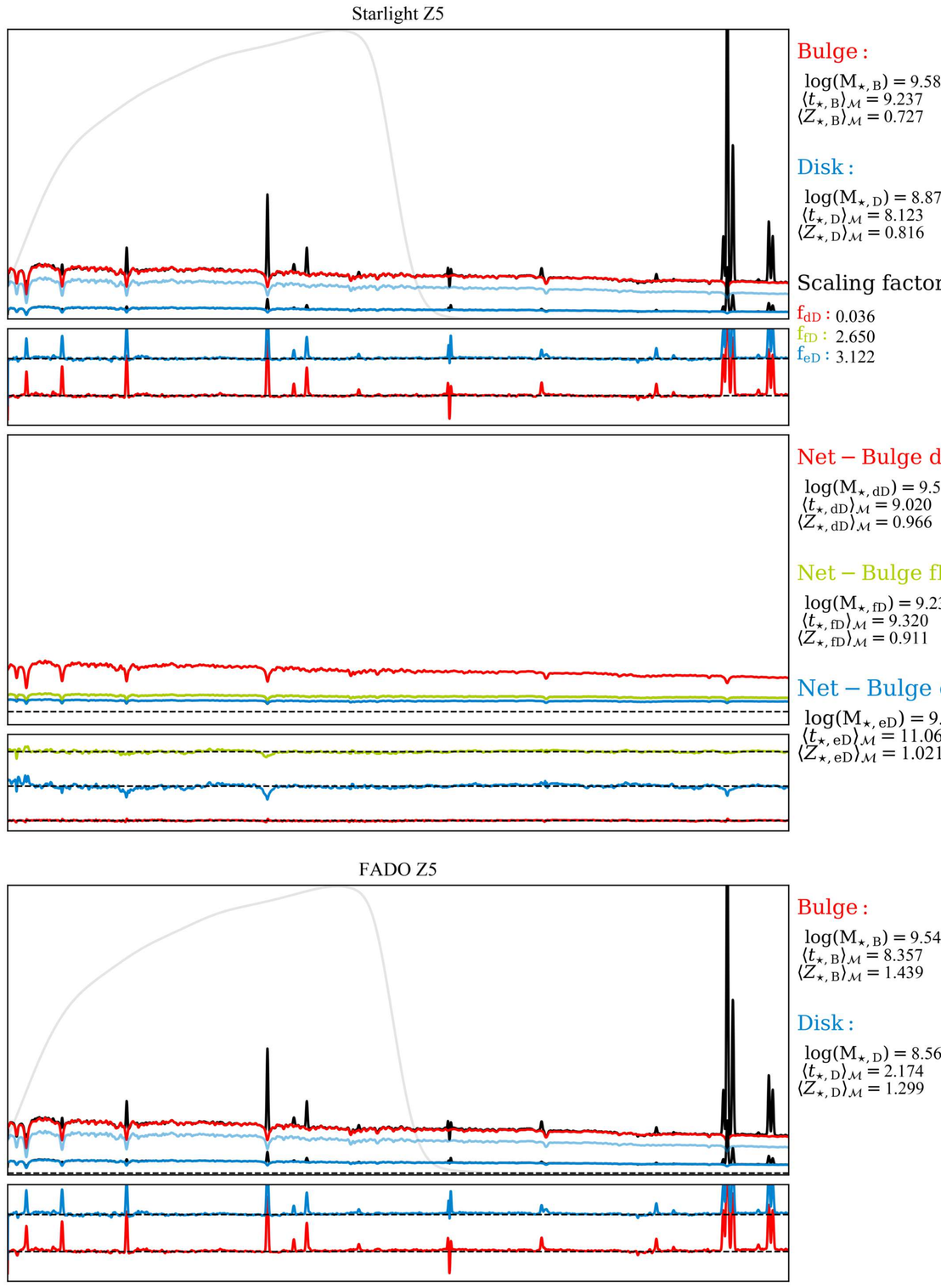
Starlight Z5
Bulge :
log(M⋆, B) = 9.587
⟨t⋆, B⟩M = 9.237
⟨Z⋆, B⟩M = 0.727
Disk :
log(M⋆, D) = 8.877
⟨t⋆, D⟩M = 8.123
⟨Z⋆, D⟩M = 0.816
Scaling factors :
fdD : 0.036
ffD : 2.650
feD : 3.122
Net − Bulge dD :
log(M⋆, dD) = 9.575
⟨t⋆, dD⟩M = 9.020
⟨Z⋆, dD⟩M = 0.966
Net − Bulge fD :
log(M⋆, fD) = 9.231
⟨t⋆, fD⟩M = 9.320
⟨Z⋆, fD⟩M = 0.911
Net − Bulge eD :
log(M⋆, eD) = 9.224
⟨t⋆, eD⟩M = 11.067
⟨Z⋆, eD⟩M = 1.021

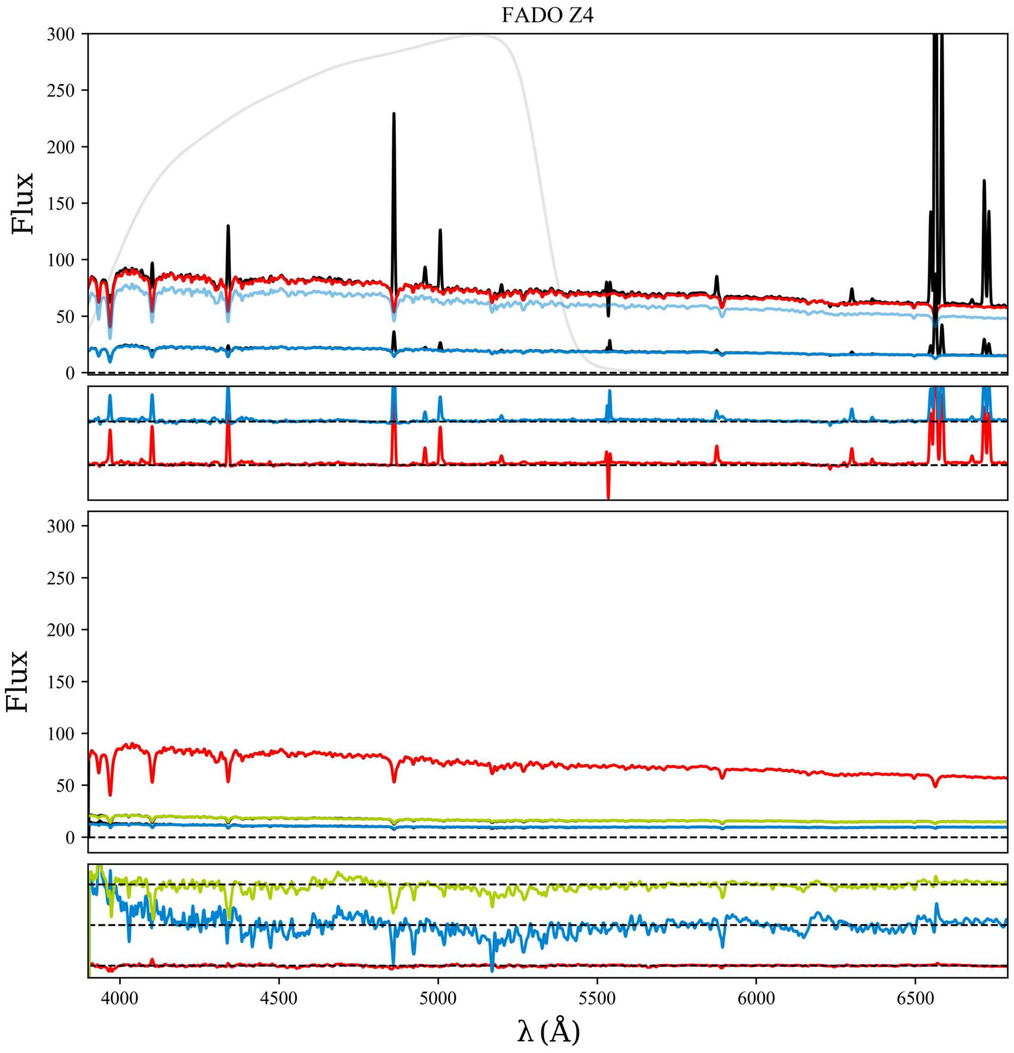
FADO Z4
Flux
Bulge :
log(M⋆, B) = 9.700
⟨t⋆, B⟩M = 8.369
⟨Z⋆, B⟩M = 0.426
Disk :
log(M⋆, D) = 8.980
⟨t⋆, D⟩M = 6.968
⟨Z⋆, D⟩M = 0.450
Net − Bulge dD :
log(M⋆, dD) = 9.708
⟨t⋆, dD⟩M = 10.980
⟨Z⋆, dD⟩M = 0.432
Net − Bulge fD :
log(M⋆, fD) = 9.243
⟨t⋆, fD⟩M = 9.703
⟨Z⋆, fD⟩M = 0.421
Net − Bulge eD :
log(M⋆, eD) = 7.740
⟨t⋆, eD⟩M = 0.007
⟨Z⋆, eD⟩M = 0.621
λ (Å)

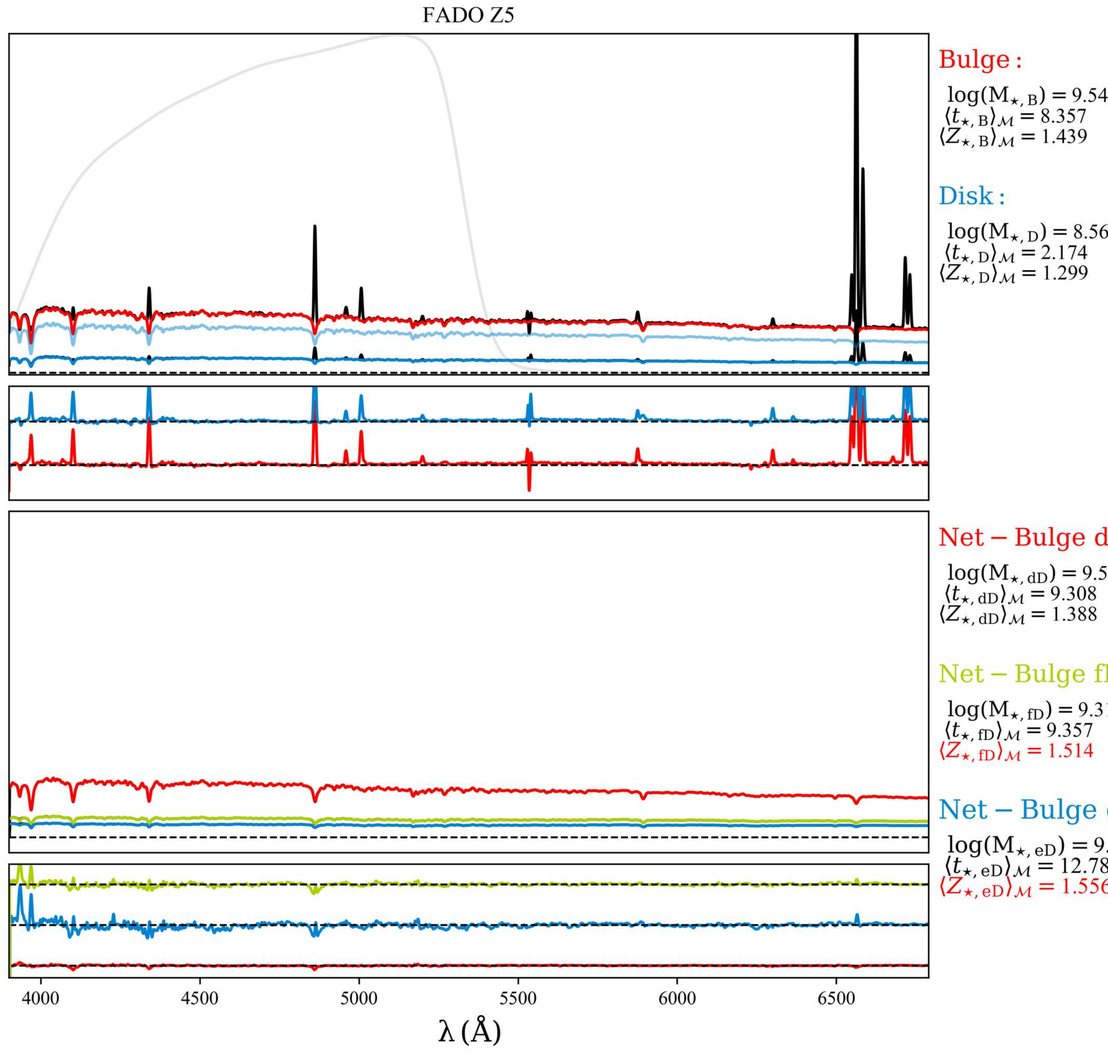
FADO Z5
Bulge :
log(M⋆, B) = 9.542
⟨t⋆, B⟩M = 8.357
⟨Z⋆, B⟩M = 1.439
Disk :
log(M⋆, D) = 8.564
⟨t⋆, D⟩M = 2.174
⟨Z⋆, D⟩M = 1.299
Net − Bulge dD :
log(M⋆, dD) = 9.579
⟨t⋆, dD⟩M = 9.308
⟨Z⋆, dD⟩M = 1.388
Net − Bulge fD :
log(M⋆, fD) = 9.313
⟨t⋆, fD⟩M = 9.357
⟨Z⋆, fD⟩M = 1.514
Net − Bulge eD :
log(M⋆, eD) = 9.432
⟨t⋆, eD⟩M = 12.780
⟨Z⋆, eD⟩M = 1.556
λ (Å)

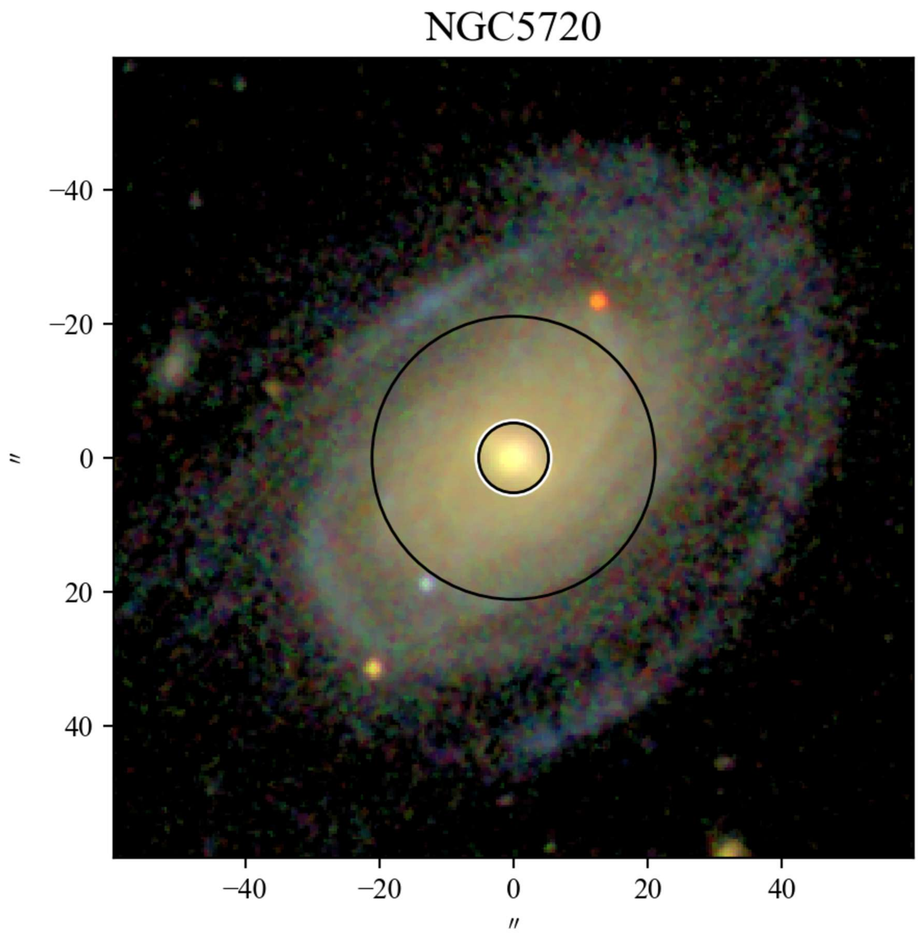
NGC5720
−40
−20
0
20
40
″
−40
−20
0
20
40
″

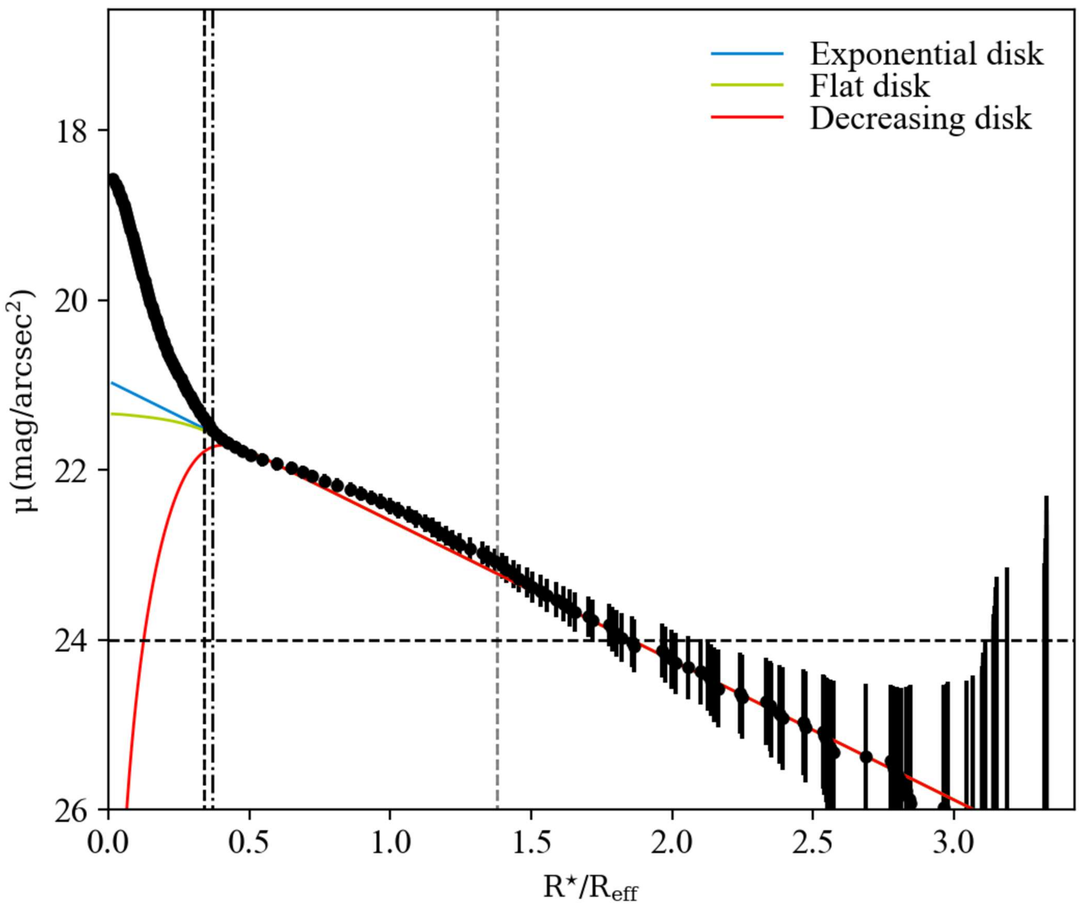
Exponential disk
Flat disk
Decreasing disk
μ (mag/arcsec²)
18
20
22
24
26
0.0
0.5
1.0
1.5
2.0
2.5
3.0
R⋆/Reff

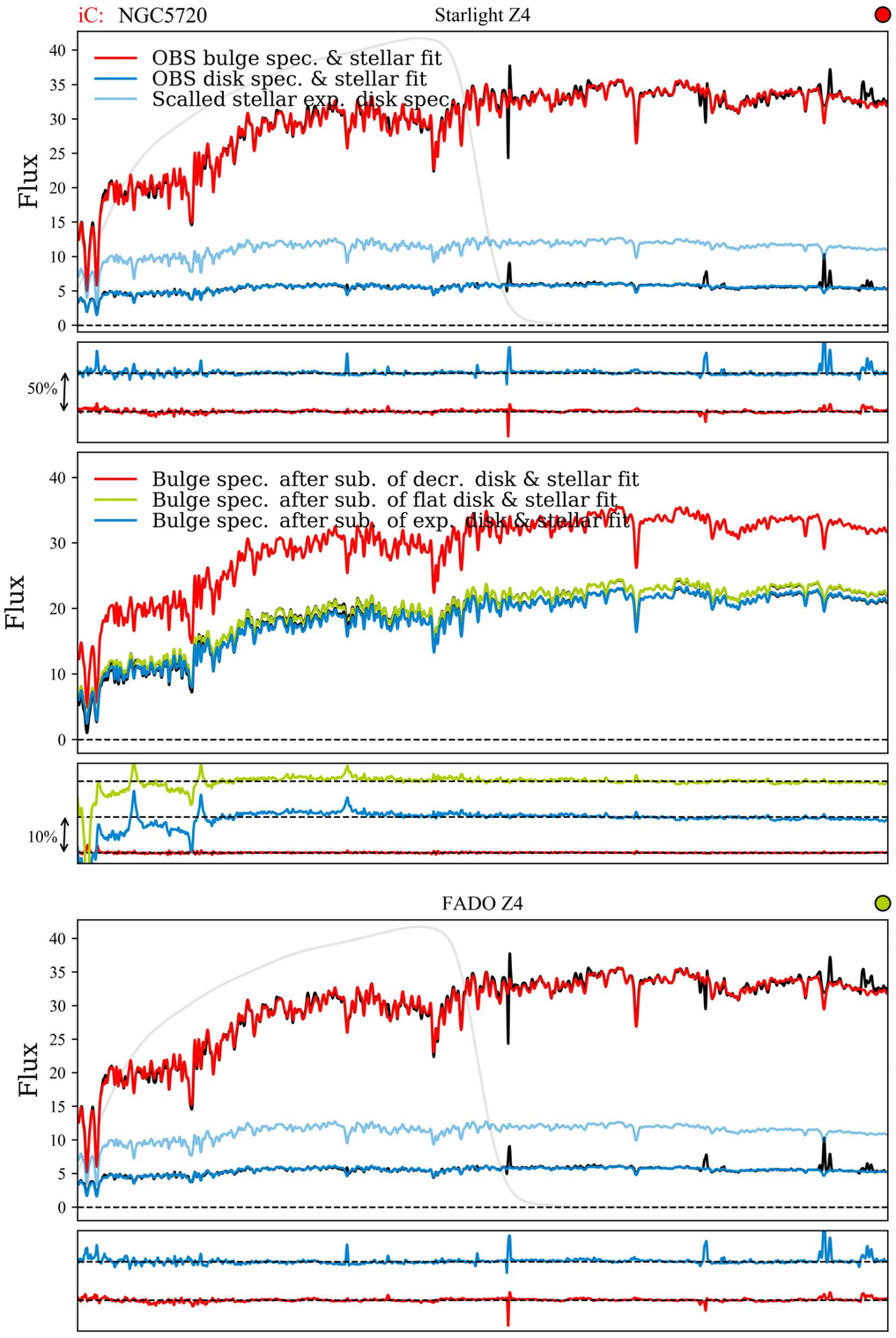
iC: NGC5720
Starlight Z4
OBS bulge spec. & stellar fit
OBS disk spec. & stellar fit
Scalled stellar exp. disk spec.
Flux
50%
Bulge :
log(M⋆, B) = 10.750
⟨t⋆, B⟩M = 12.193
⟨Z⋆, B⟩M = 0.891
Disk :
log(M⋆, D) = 9.841
⟨t⋆, D⟩M = 9.310
⟨Z⋆, D⟩M = 0.833
Scaling factors :
fdD : 0.035
ffD : 1.851
feD : 2.065
Bulge spec. after sub. of decr. disk & stellar fit
Bulge spec. after sub. of flat disk & stellar fit
Bulge spec. after sub. of exp. disk & stellar fit
10%
Net − Bulge dD :
log(M⋆, dD) = 10.736
⟨t⋆, dD⟩M = 11.197
⟨Z⋆, dD⟩M = 0.863
Net − Bulge fD :
log(M⋆, fD) = 10.693
⟨t⋆, fD⟩M = 13.000
⟨Z⋆, fD⟩M = 1.000
Net − Bulge eD :
log(M⋆, eD) = 10.687
⟨t⋆, eD⟩M = 13.000
⟨Z⋆, eD⟩M = 1.000

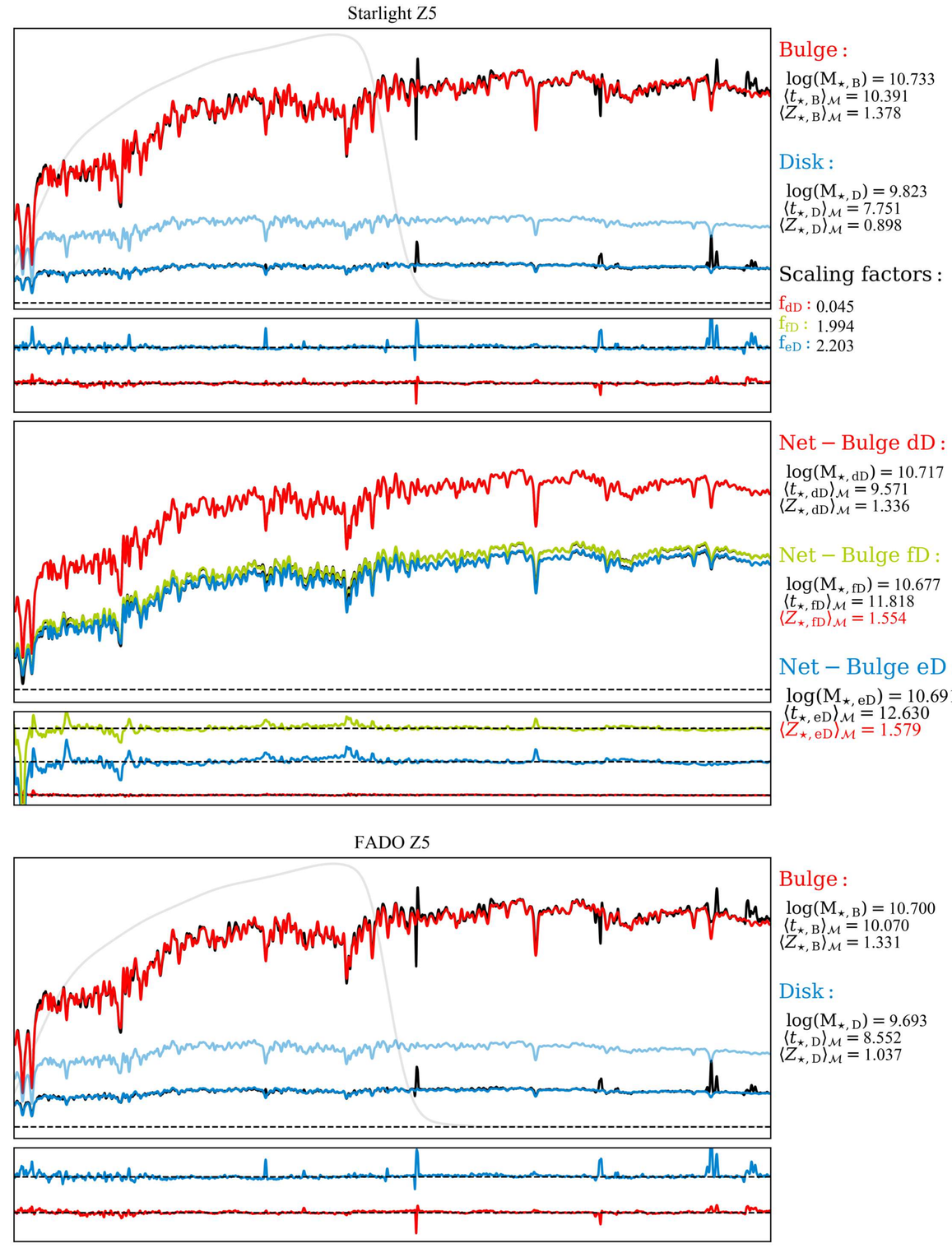
Starlight Z5
Bulge :
log(M⋆, B) = 10.733
⟨t⋆, B⟩M = 10.391
⟨Z⋆, B⟩M = 1.378
Disk :
log(M⋆, D) = 9.823
⟨t⋆, D⟩M = 7.751
⟨Z⋆, D⟩M = 0.898
Scaling factors :
fdD : 0.045
ffD : 1.994
feD : 2.203
Net − Bulge dD :
log(M⋆, dD) = 10.717
⟨t⋆, dD⟩M = 9.571
⟨Z⋆, dD⟩M = 1.336
Net − Bulge fD :
log(M⋆, fD) = 10.677
⟨t⋆, fD⟩M = 11.818
⟨Z⋆, fD⟩M = 1.554
Net − Bulge eD :
log(M⋆, eD) = 10.691
⟨t⋆, eD⟩M = 12.630
⟨Z⋆, eD⟩M = 1.579

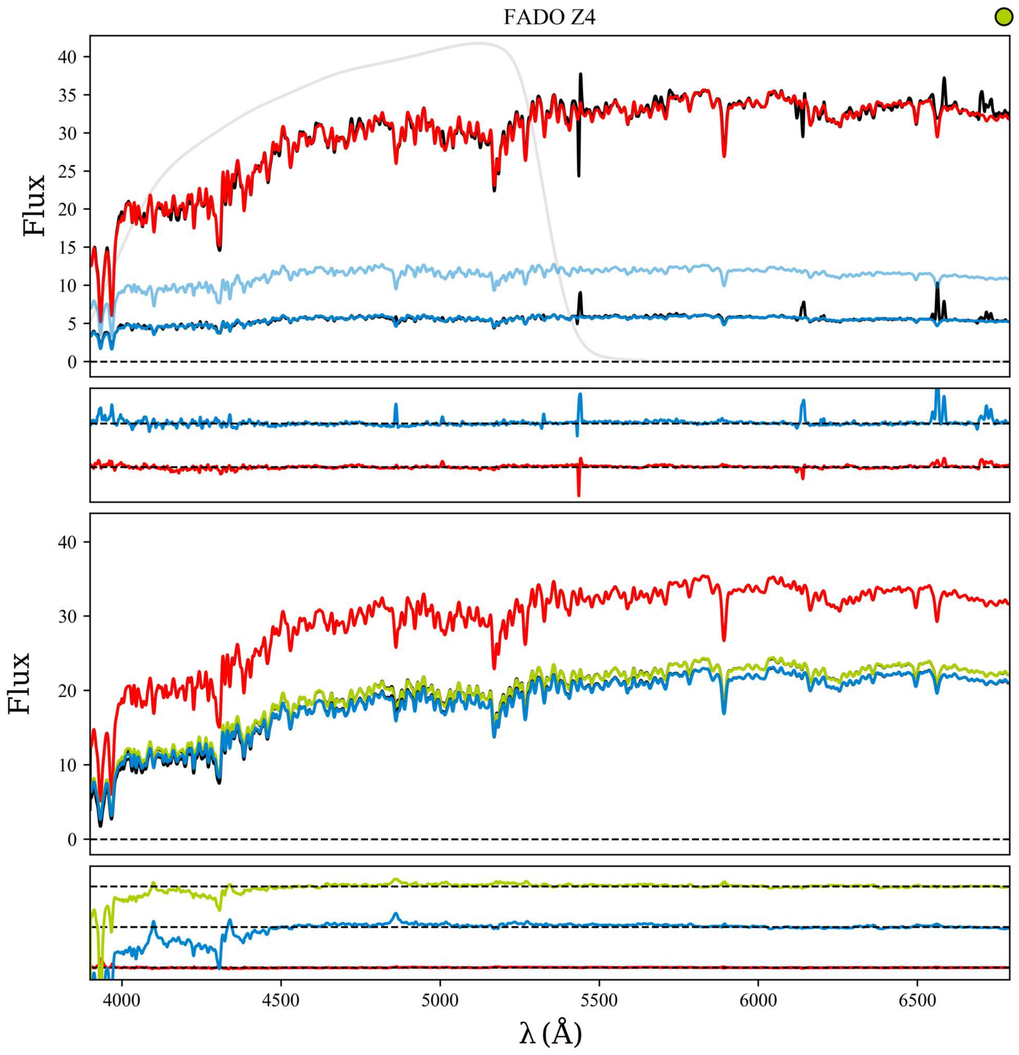
FADO Z4
Flux
Bulge :
log(M⋆, B) = 10.730
⟨t⋆, B⟩M = 12.120
⟨Z⋆, B⟩M = 0.888
Disk :
log(M⋆, D) = 9.782
⟨t⋆, D⟩M = 11.110
⟨Z⋆, D⟩M = 0.852
Net − Bulge dD :
log(M⋆, dD) = 10.720
⟨t⋆, dD⟩M = 11.770
⟨Z⋆, dD⟩M = 0.871
Net − Bulge fD :
log(M⋆, fD) = 10.690
⟨t⋆, fD⟩M = 13.000
⟨Z⋆, fD⟩M = 0.973
Net − Bulge eD :
log(M⋆, eD) = 10.650
⟨t⋆, eD⟩M = 11.000
⟨Z⋆, eD⟩M = 1.000
λ (Å)

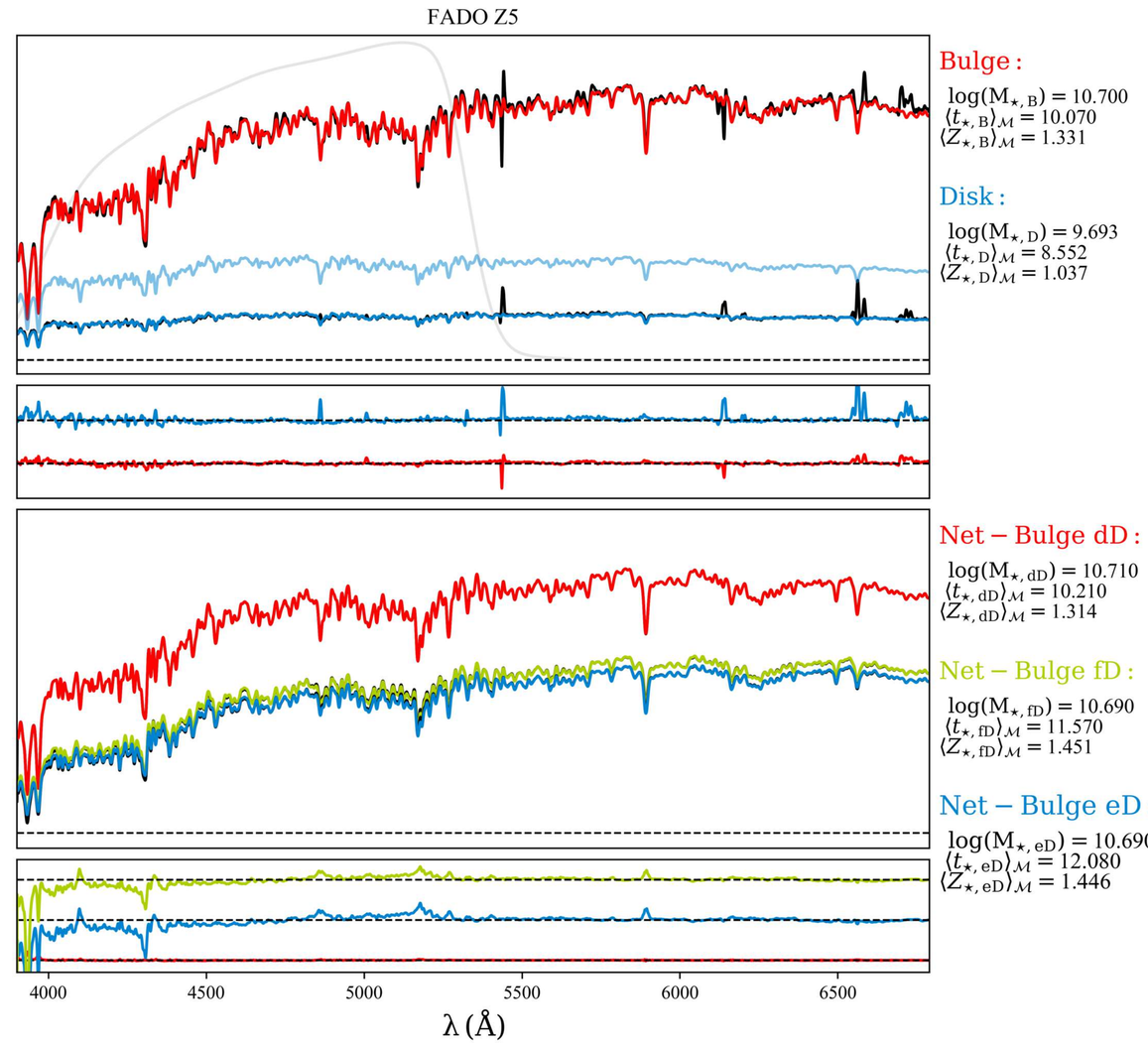
FADO Z5
Bulge :
log(M⋆, B) = 10.700
⟨t⋆, B⟩M = 10.070
⟨Z⋆, B⟩M = 1.331
Disk :
log(M⋆, D) = 9.693
⟨t⋆, D⟩M = 8.552
⟨Z⋆, D⟩M = 1.037
Net − Bulge dD :
log(M⋆, dD) = 10.710
⟨t⋆, dD⟩M = 10.210
⟨Z⋆, dD⟩M = 1.314
Net − Bulge fD :
log(M⋆, fD) = 10.690
⟨t⋆, fD⟩M = 11.570
⟨Z⋆, fD⟩M = 1.451
Net − Bulge eD :
log(M⋆, eD) = 10.690
⟨t⋆, eD⟩M = 12.080
⟨Z⋆, eD⟩M = 1.446
λ (Å)

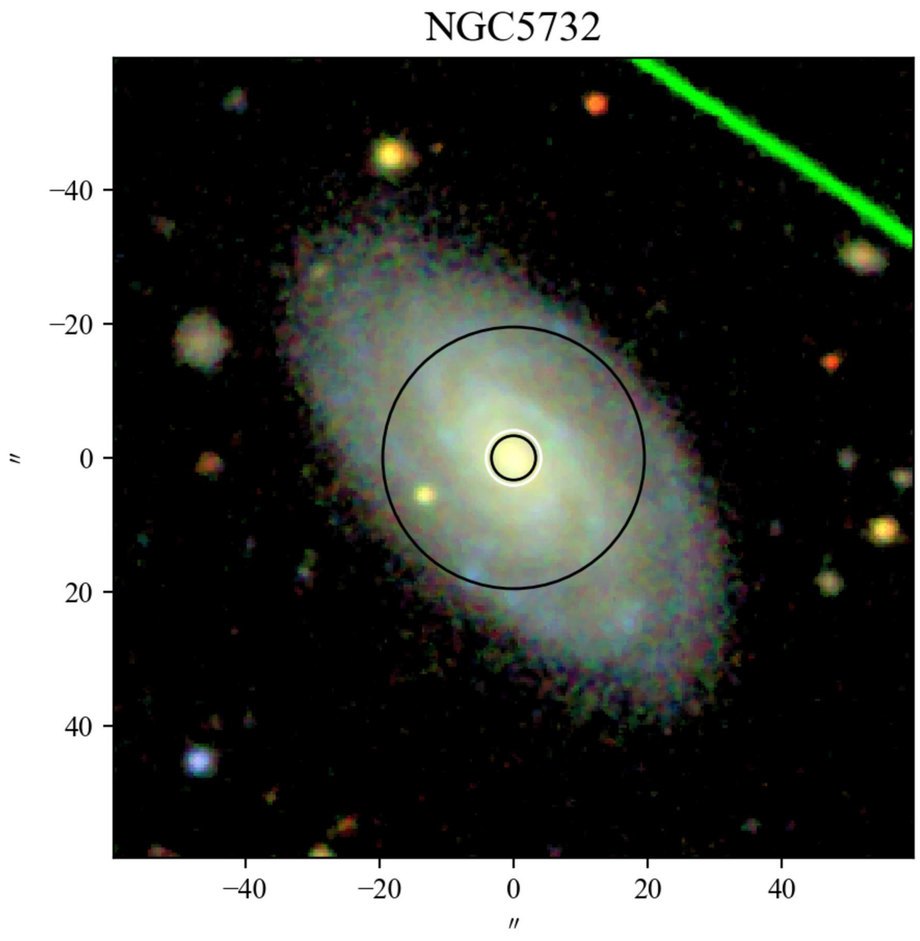
NGC5732
−40
−20
0
20
40
″
−40
−20
0
20
40
″

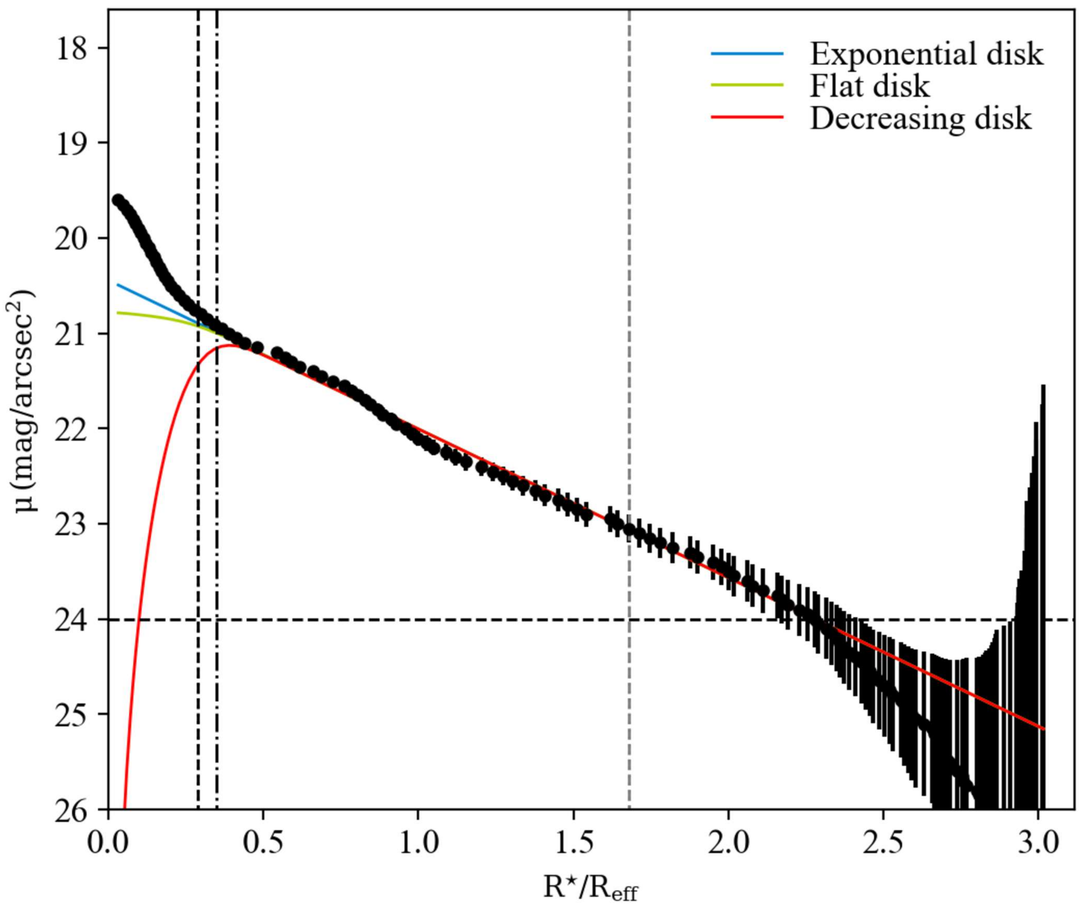
Exponential disk
Flat disk
Decreasing disk
μ (mag/arcsec²)
18
19
20
21
22
23
24
25
26
0.0
0.5
1.0
1.5
2.0
2.5
3.0
R⋆/Reff

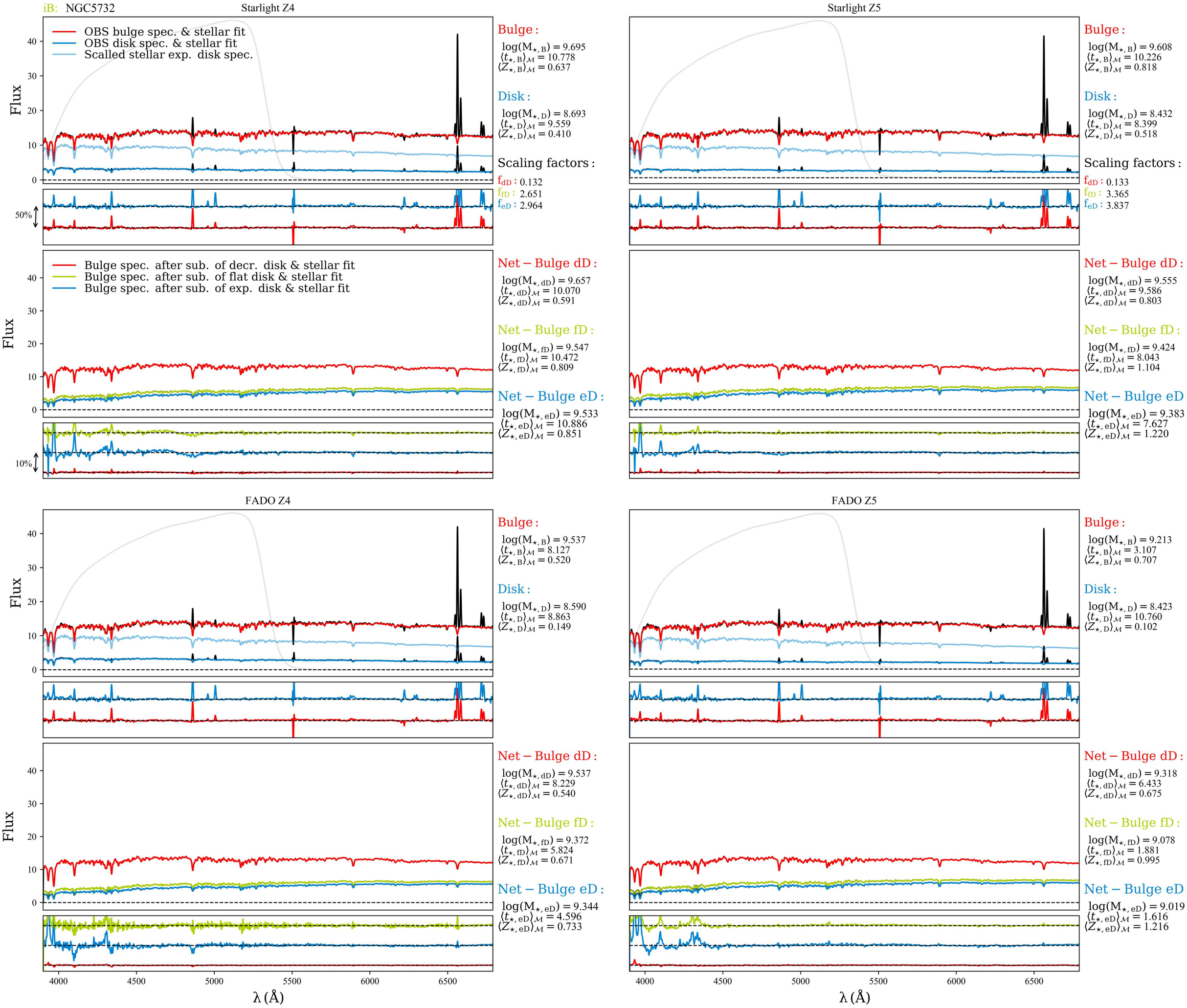
iB: NGC5732
Starlight Z4
OBS bulge spec. & stellar fit
OBS disk spec. & stellar fit
Scalled stellar exp. disk spec.
Flux
50%
Bulge :
log(M⋆, B) = 9.695
⟨t⋆, B⟩M = 10.778
⟨Z⋆, B⟩M = 0.637
Disk :
log(M⋆, D) = 8.693
⟨t⋆, D⟩M = 9.559
⟨Z⋆, D⟩M = 0.410
Scaling factors :
fdD : 0.132
ffD : 2.651
feD : 2.964
Starlight Z5
Bulge :
log(M⋆, B) = 9.608
⟨t⋆, B⟩M = 10.226
⟨Z⋆, B⟩M = 0.818
Disk :
log(M⋆, D) = 8.432
⟨t⋆, D⟩M = 8.399
⟨Z⋆, D⟩M = 0.518
Scaling factors :
fdD : 0.133
ffD : 3.365
feD : 3.837
Bulge spec. after sub. of decr. disk & stellar fit
Bulge spec. after sub. of flat disk & stellar fit
Bulge spec. after sub. of exp. disk & stellar fit
10%
Net − Bulge dD :
log(M⋆, dD) = 9.657
⟨t⋆, dD⟩M = 10.070
⟨Z⋆, dD⟩M = 0.591
Net − Bulge fD :
log(M⋆, fD) = 9.547
⟨t⋆, fD⟩M = 10.472
⟨Z⋆, fD⟩M = 0.809
Net − Bulge eD :
log(M⋆, eD) = 9.533
⟨t⋆, eD⟩M = 10.886
⟨Z⋆, eD⟩M = 0.851
Net − Bulge dD :
log(M⋆, dD) = 9.555
⟨t⋆, dD⟩M = 9.586
⟨Z⋆, dD⟩M = 0.803
Net − Bulge fD :
log(M⋆, fD) = 9.424
⟨t⋆, fD⟩M = 8.043
⟨Z⋆, fD⟩M = 1.104
Net − Bulge eD :
log(M⋆, eD) = 9.383
⟨t⋆, eD⟩M = 7.627
⟨Z⋆, eD⟩M = 1.220
FADO Z4
Bulge :
log(M⋆, B) = 9.537
⟨t⋆, B⟩M = 8.127
⟨Z⋆, B⟩M = 0.520
Disk :
log(M⋆, D) = 8.590
⟨t⋆, D⟩M = 8.863
⟨Z⋆, D⟩M = 0.149
FADO Z5
Bulge :
log(M⋆, B) = 9.213
⟨t⋆, B⟩M = 3.107
⟨Z⋆, B⟩M = 0.707
Disk :
log(M⋆, D) = 8.423
⟨t⋆, D⟩M = 10.760
⟨Z⋆, D⟩M = 0.102
Net − Bulge dD :
log(M⋆, dD) = 9.537
⟨t⋆, dD⟩M = 8.229
⟨Z⋆, dD⟩M = 0.540
Net − Bulge fD :
log(M⋆, fD) = 9.372
⟨t⋆, fD⟩M = 5.824
⟨Z⋆, fD⟩M = 0.671
Net − Bulge eD :
log(M⋆, eD) = 9.344
⟨t⋆, eD⟩M = 4.596
⟨Z⋆, eD⟩M = 0.733
Net − Bulge dD :
log(M⋆, dD) = 9.318
⟨t⋆, dD⟩M = 6.433
⟨Z⋆, dD⟩M = 0.675
Net − Bulge fD :
log(M⋆, fD) = 9.078
⟨t⋆, fD⟩M = 1.881
⟨Z⋆, fD⟩M = 0.995
Net − Bulge eD :
log(M⋆, eD) = 9.019
⟨t⋆, eD⟩M = 1.616
⟨Z⋆, eD⟩M = 1.216
0
10
20
30
40
4000
4500
5000
5500
6000
6500
λ (Å)

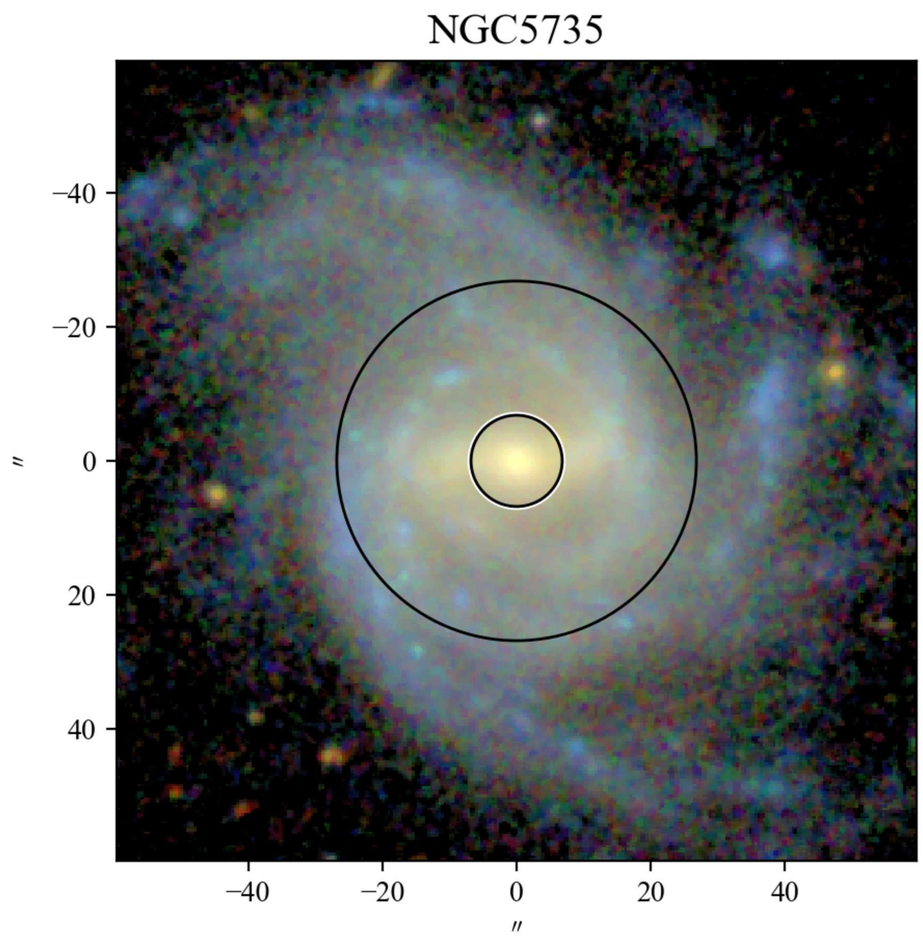
NGC5735
−40
−20
0
20
40
″
−40
−20
0
20
40
″

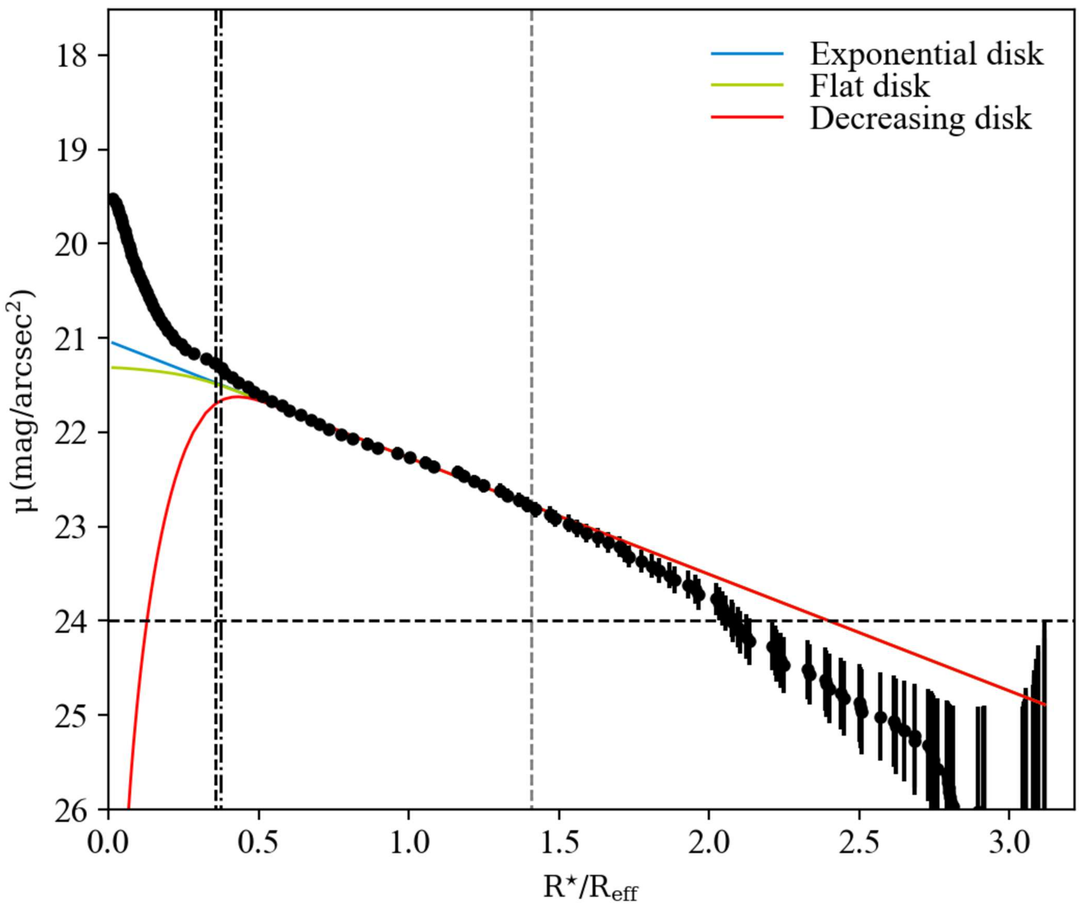
Exponential disk
Flat disk
Decreasing disk
μ (mag/arcsec²)
18
19
20
21
22
23
24
25
26
0.0
0.5
1.0
1.5
2.0
2.5
3.0
R⋆/Reff

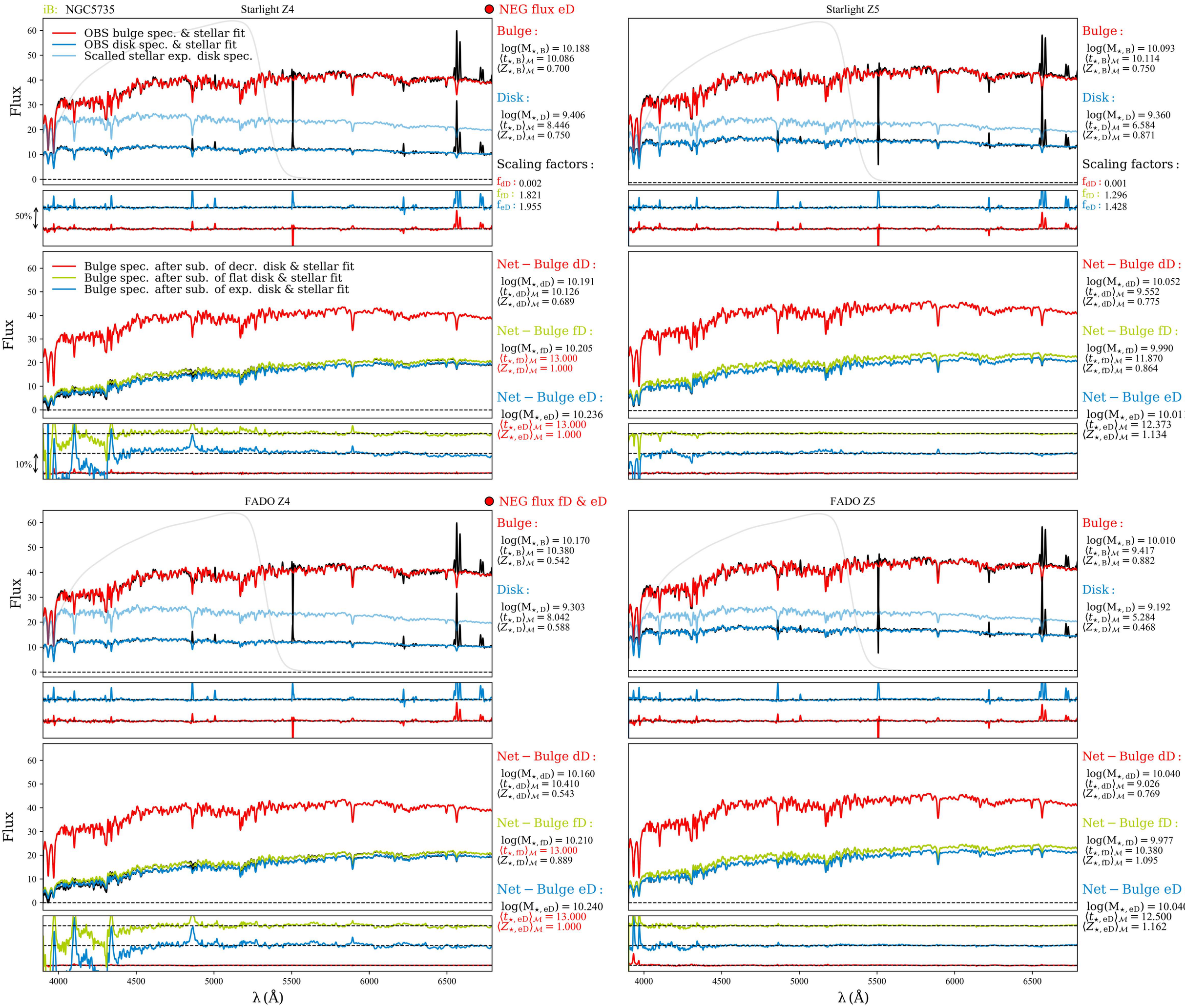
iB: NGC5735
Starlight Z4
NEG flux eD
OBS bulge spec. & stellar fit
OBS disk spec. & stellar fit
Scalled stellar exp. disk spec.
Flux
50%
Bulge :
log(M⋆, B) = 10.188
⟨t⋆, B⟩M = 10.086
⟨Z⋆, B⟩M = 0.700
Disk :
log(M⋆, D) = 9.406
⟨t⋆, D⟩M = 8.446
⟨Z⋆, D⟩M = 0.750
Scaling factors :
fdD : 0.002
ffD : 1.821
feD : 1.955
Starlight Z5
Bulge :
log(M⋆, B) = 10.093
⟨t⋆, B⟩M = 10.114
⟨Z⋆, B⟩M = 0.750
Disk :
log(M⋆, D) = 9.360
⟨t⋆, D⟩M = 6.584
⟨Z⋆, D⟩M = 0.871
Scaling factors :
fdD : 0.001
ffD : 1.296
feD : 1.428
Bulge spec. after sub. of decr. disk & stellar fit
Bulge spec. after sub. of flat disk & stellar fit
Bulge spec. after sub. of exp. disk & stellar fit
Flux
10%
Net − Bulge dD :
log(M⋆, dD) = 10.191
⟨t⋆, dD⟩M = 10.126
⟨Z⋆, dD⟩M = 0.689
Net − Bulge fD :
log(M⋆, fD) = 10.205
⟨t⋆, fD⟩M = 13.000
⟨Z⋆, fD⟩M = 1.000
Net − Bulge eD :
log(M⋆, eD) = 10.236
⟨t⋆, eD⟩M = 13.000
⟨Z⋆, eD⟩M = 1.000
Net − Bulge dD :
log(M⋆, dD) = 10.052
⟨t⋆, dD⟩M = 9.552
⟨Z⋆, dD⟩M = 0.775
Net − Bulge fD :
log(M⋆, fD) = 9.990
⟨t⋆, fD⟩M = 11.870
⟨Z⋆, fD⟩M = 0.864
Net − Bulge eD :
log(M⋆, eD) = 10.011
⟨t⋆, eD⟩M = 12.373
⟨Z⋆, eD⟩M = 1.134
FADO Z4
NEG flux fD & eD
Flux
Bulge :
log(M⋆, B) = 10.170
⟨t⋆, B⟩M = 10.380
⟨Z⋆, B⟩M = 0.542
Disk :
log(M⋆, D) = 9.303
⟨t⋆, D⟩M = 8.042
⟨Z⋆, D⟩M = 0.588
FADO Z5
Bulge :
log(M⋆, B) = 10.010
⟨t⋆, B⟩M = 9.417
⟨Z⋆, B⟩M = 0.882
Disk :
log(M⋆, D) = 9.192
⟨t⋆, D⟩M = 5.284
⟨Z⋆, D⟩M = 0.468
Flux
Net − Bulge dD :
log(M⋆, dD) = 10.160
⟨t⋆, dD⟩M = 10.410
⟨Z⋆, dD⟩M = 0.543
Net − Bulge fD :
log(M⋆, fD) = 10.210
⟨t⋆, fD⟩M = 13.000
⟨Z⋆, fD⟩M = 0.889
Net − Bulge eD :
log(M⋆, eD) = 10.240
⟨t⋆, eD⟩M = 13.000
⟨Z⋆, eD⟩M = 1.000
Net − Bulge dD :
log(M⋆, dD) = 10.040
⟨t⋆, dD⟩M = 9.026
⟨Z⋆, dD⟩M = 0.769
Net − Bulge fD :
log(M⋆, fD) = 9.977
⟨t⋆, fD⟩M = 10.380
⟨Z⋆, fD⟩M = 1.095
Net − Bulge eD :
log(M⋆, eD) = 10.040
⟨t⋆, eD⟩M = 12.500
⟨Z⋆, eD⟩M = 1.162
λ (Å)
λ (Å)

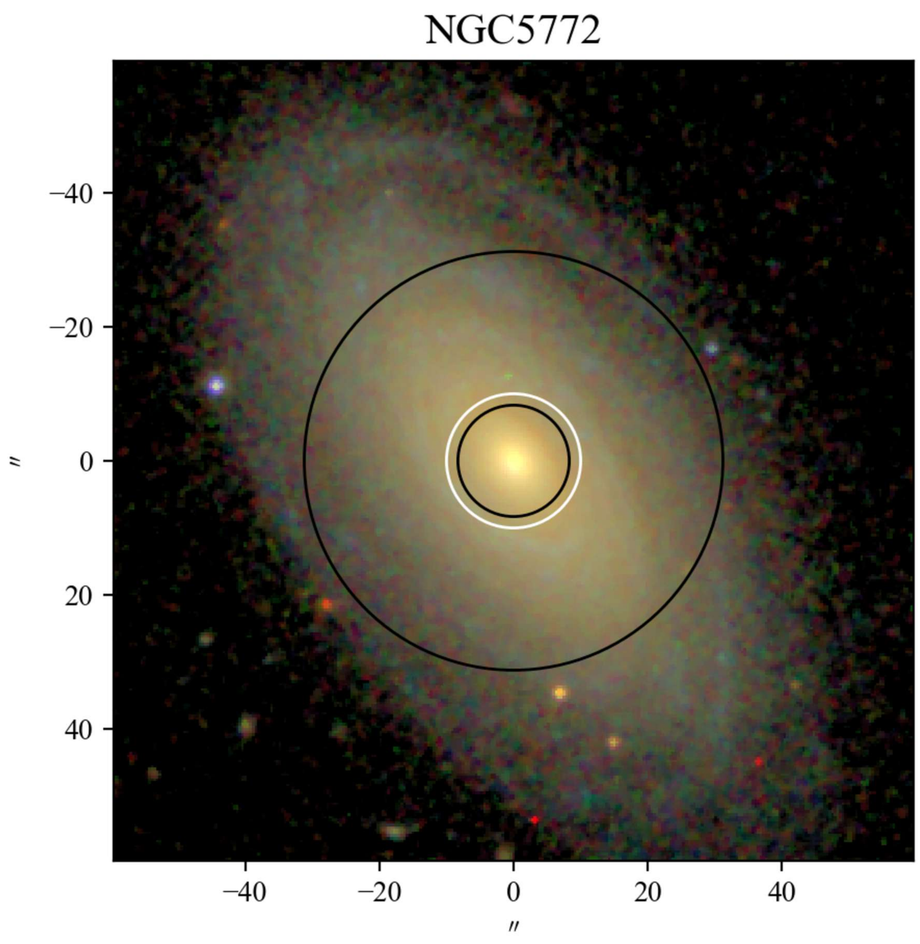
NGC5772
−40
−20
0
20
40
″
−40
−20
0
20
40
″

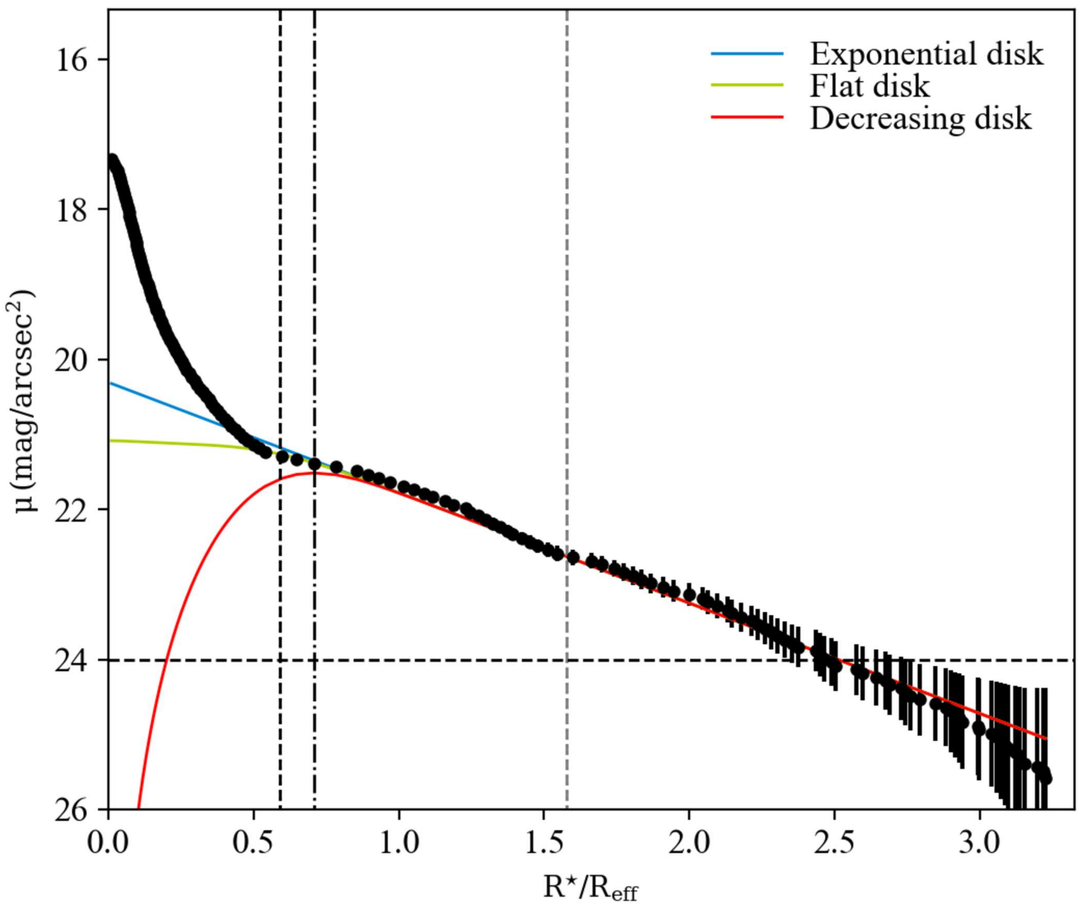
Exponential disk
Flat disk
Decreasing disk
μ (mag/arcsec²)
16
18
20
22
24
26
0.0
0.5
1.0
1.5
2.0
2.5
3.0
R⋆/Reff

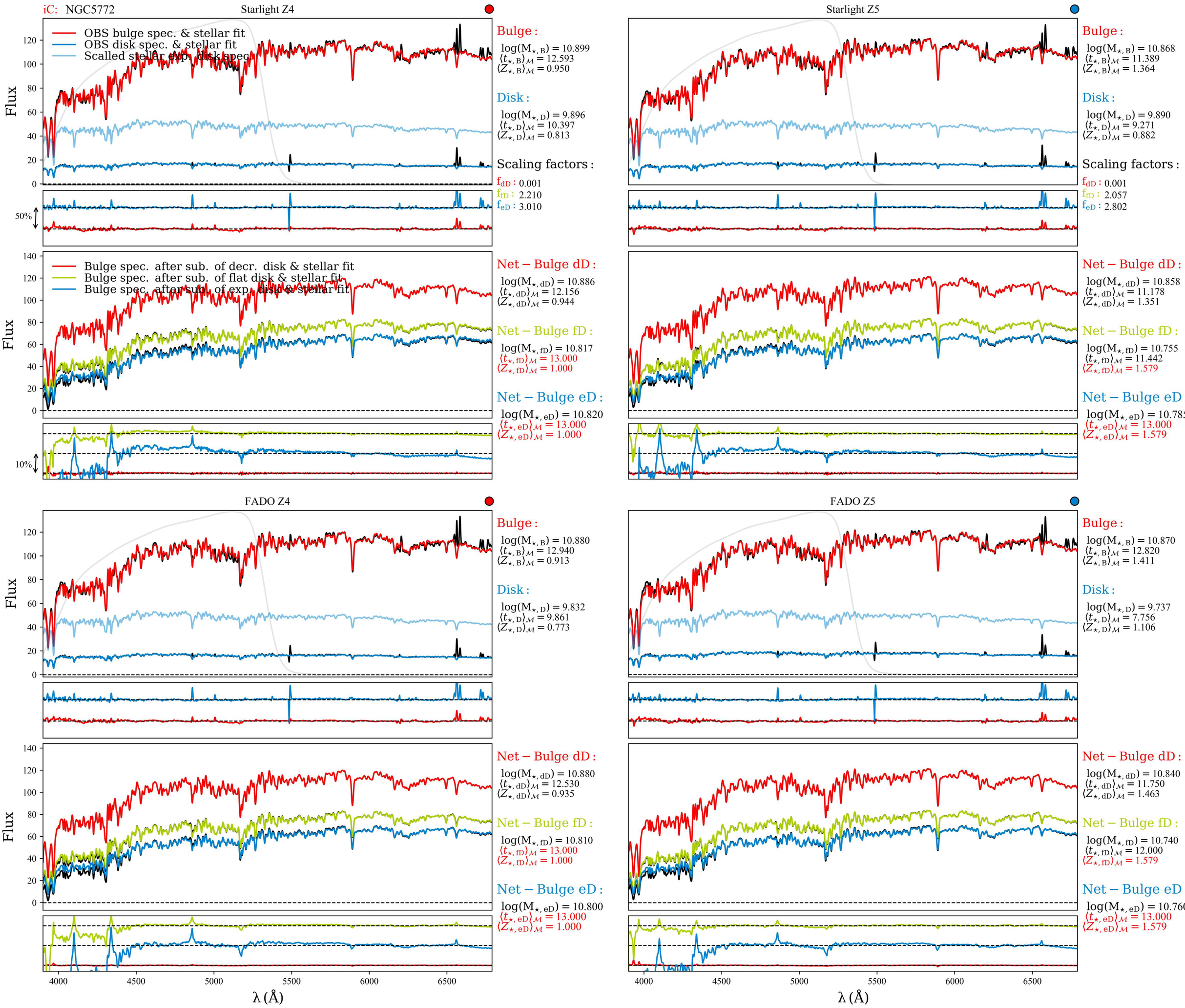
iC: NGC5772
Starlight Z4
OBS bulge spec. & stellar fit
OBS disk spec. & stellar fit
Scalled stellar exp. disk spec.
Flux
50%
Bulge :
log(M⋆, B) = 10.899
⟨t⋆, B⟩M = 12.593
⟨Z⋆, B⟩M = 0.950
Disk :
log(M⋆, D) = 9.896
⟨t⋆, D⟩M = 10.397
⟨Z⋆, D⟩M = 0.813
Scaling factors :
fdD : 0.001
ffD : 2.210
feD : 3.010
Starlight Z5
Bulge :
log(M⋆, B) = 10.868
⟨t⋆, B⟩M = 11.389
⟨Z⋆, B⟩M = 1.364
Disk :
log(M⋆, D) = 9.890
⟨t⋆, D⟩M = 9.271
⟨Z⋆, D⟩M = 0.882
Scaling factors :
fdD : 0.001
ffD : 2.057
feD : 2.802
Bulge spec. after sub. of decr. disk & stellar fit
Bulge spec. after sub. of flat disk & stellar fit
Bulge spec. after sub. of exp. disk & stellar fit
Flux
10%
Net − Bulge dD :
log(M⋆, dD) = 10.886
⟨t⋆, dD⟩M = 12.156
⟨Z⋆, dD⟩M = 0.944
Net − Bulge fD :
log(M⋆, fD) = 10.817
⟨t⋆, fD⟩M = 13.000
⟨Z⋆, fD⟩M = 1.000
Net − Bulge eD :
log(M⋆, eD) = 10.820
⟨t⋆, eD⟩M = 13.000
⟨Z⋆, eD⟩M = 1.000
Net − Bulge dD :
log(M⋆, dD) = 10.858
⟨t⋆, dD⟩M = 11.178
⟨Z⋆, dD⟩M = 1.351
Net − Bulge fD :
log(M⋆, fD) = 10.755
⟨t⋆, fD⟩M = 11.442
⟨Z⋆, fD⟩M = 1.579
Net − Bulge eD :
log(M⋆, eD) = 10.785
⟨t⋆, eD⟩M = 13.000
⟨Z⋆, eD⟩M = 1.579
FADO Z4
Flux
Bulge :
log(M⋆, B) = 10.880
⟨t⋆, B⟩M = 12.940
⟨Z⋆, B⟩M = 0.913
Disk :
log(M⋆, D) = 9.832
⟨t⋆, D⟩M = 9.861
⟨Z⋆, D⟩M = 0.773
FADO Z5
Bulge :
log(M⋆, B) = 10.870
⟨t⋆, B⟩M = 12.820
⟨Z⋆, B⟩M = 1.411
Disk :
log(M⋆, D) = 9.737
⟨t⋆, D⟩M = 7.756
⟨Z⋆, D⟩M = 1.106
Net − Bulge dD :
log(M⋆, dD) = 10.880
⟨t⋆, dD⟩M = 12.530
⟨Z⋆, dD⟩M = 0.935
Net − Bulge fD :
log(M⋆, fD) = 10.810
⟨t⋆, fD⟩M = 13.000
⟨Z⋆, fD⟩M = 1.000
Net − Bulge eD :
log(M⋆, eD) = 10.800
⟨t⋆, eD⟩M = 13.000
⟨Z⋆, eD⟩M = 1.000
Net − Bulge dD :
log(M⋆, dD) = 10.840
⟨t⋆, dD⟩M = 11.750
⟨Z⋆, dD⟩M = 1.463
Net − Bulge fD :
log(M⋆, fD) = 10.740
⟨t⋆, fD⟩M = 12.000
⟨Z⋆, fD⟩M = 1.579
Net − Bulge eD :
log(M⋆, eD) = 10.760
⟨t⋆, eD⟩M = 13.000
⟨Z⋆, eD⟩M = 1.579
λ (Å)
λ (Å)

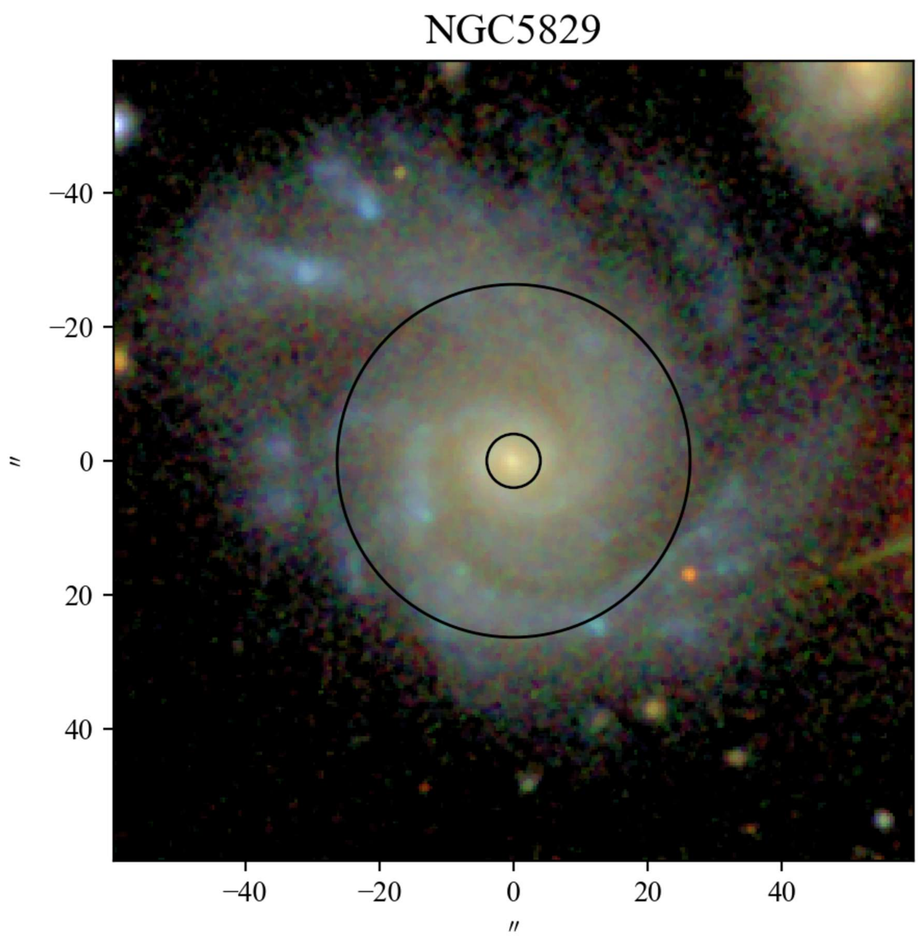
NGC5829
−40
−20
0
20
40
″
−40
−20
0
20
40
″

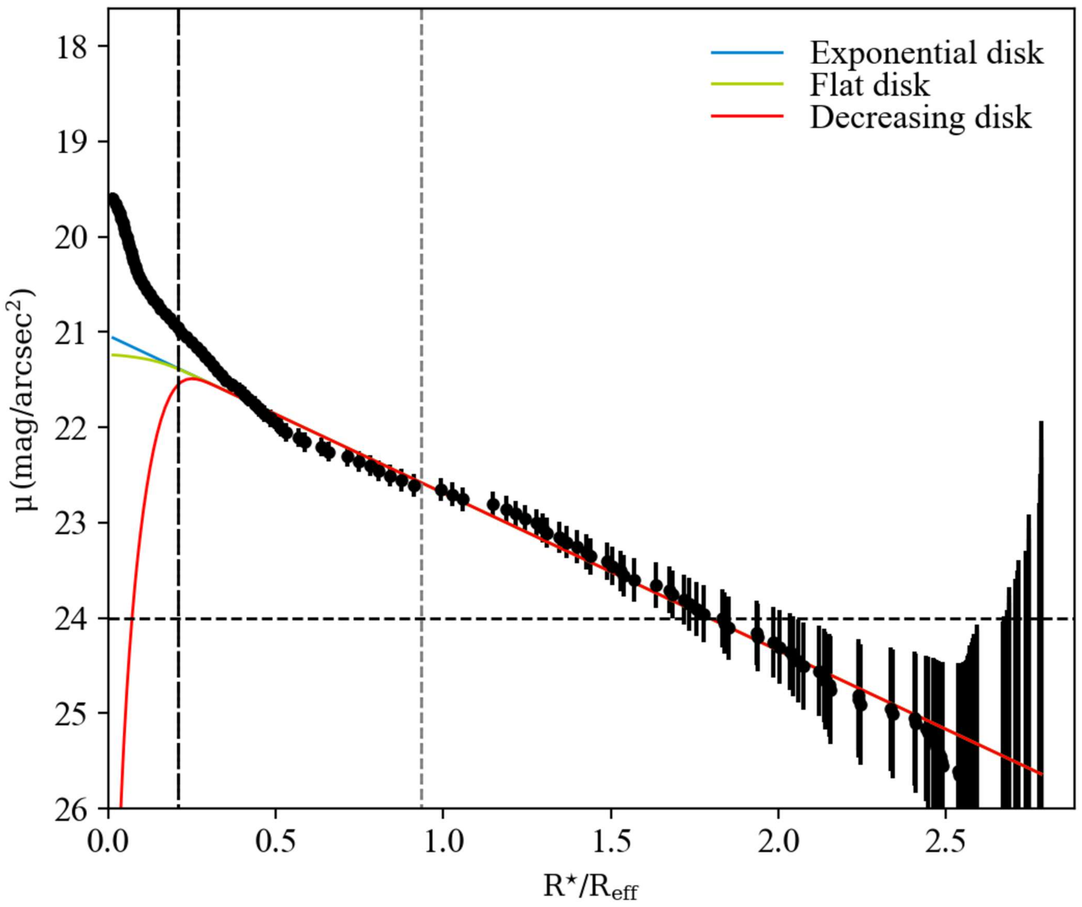
Exponential disk
Flat disk
Decreasing disk
μ (mag/arcsec²)
18
19
20
21
22
23
24
25
26
0.0
0.5
1.0
1.5
2.0
2.5
R⋆/Reff

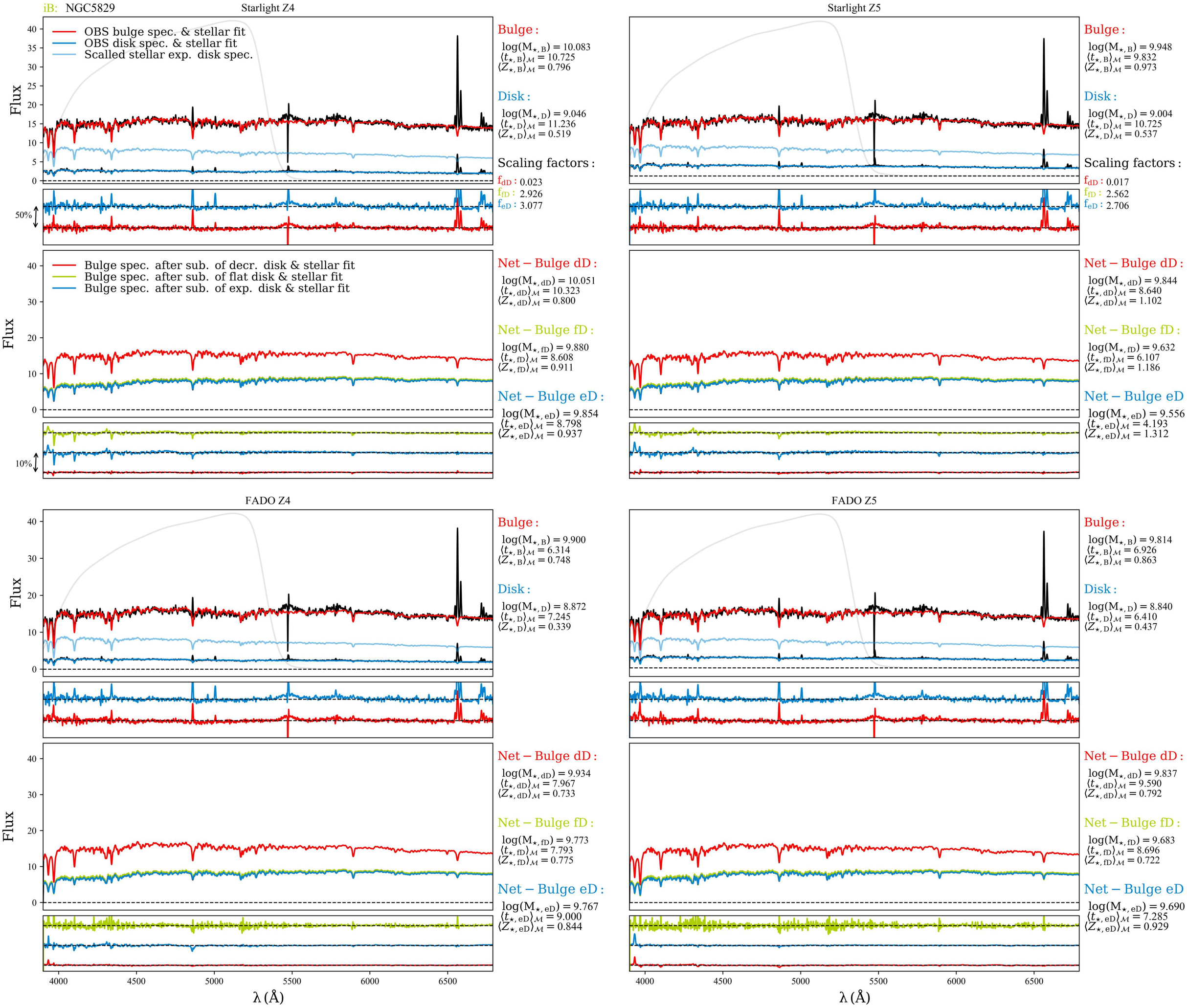
iB: NGC5829
Starlight Z4
OBS bulge spec. & stellar fit
OBS disk spec. & stellar fit
Scalled stellar exp. disk spec.
Flux
50%
Bulge :
log(M⋆, B) = 10.083
⟨t⋆, B⟩M = 10.725
⟨Z⋆, B⟩M = 0.796
Disk :
log(M⋆, D) = 9.046
⟨t⋆, D⟩M = 11.236
⟨Z⋆, D⟩M = 0.519
Scaling factors :
fdD : 0.023
ffD : 2.926
feD : 3.077
Starlight Z5
Bulge :
log(M⋆, B) = 9.948
⟨t⋆, B⟩M = 9.832
⟨Z⋆, B⟩M = 0.973
Disk :
log(M⋆, D) = 9.004
⟨t⋆, D⟩M = 10.725
⟨Z⋆, D⟩M = 0.537
Scaling factors :
fdD : 0.017
ffD : 2.562
feD : 2.706
Bulge spec. after sub. of decr. disk & stellar fit
Bulge spec. after sub. of flat disk & stellar fit
Bulge spec. after sub. of exp. disk & stellar fit
10%
Net − Bulge dD :
log(M⋆, dD) = 10.051
⟨t⋆, dD⟩M = 10.323
⟨Z⋆, dD⟩M = 0.800
Net − Bulge fD :
log(M⋆, fD) = 9.880
⟨t⋆, fD⟩M = 8.608
⟨Z⋆, fD⟩M = 0.911
Net − Bulge eD :
log(M⋆, eD) = 9.854
⟨t⋆, eD⟩M = 8.798
⟨Z⋆, eD⟩M = 0.937
Net − Bulge dD :
log(M⋆, dD) = 9.844
⟨t⋆, dD⟩M = 8.640
⟨Z⋆, dD⟩M = 1.102
Net − Bulge fD :
log(M⋆, fD) = 9.632
⟨t⋆, fD⟩M = 6.107
⟨Z⋆, fD⟩M = 1.186
Net − Bulge eD :
log(M⋆, eD) = 9.556
⟨t⋆, eD⟩M = 4.193
⟨Z⋆, eD⟩M = 1.312
FADO Z4
Bulge :
log(M⋆, B) = 9.900
⟨t⋆, B⟩M = 6.314
⟨Z⋆, B⟩M = 0.748
Disk :
log(M⋆, D) = 8.872
⟨t⋆, D⟩M = 7.245
⟨Z⋆, D⟩M = 0.339
FADO Z5
Bulge :
log(M⋆, B) = 9.814
⟨t⋆, B⟩M = 6.926
⟨Z⋆, B⟩M = 0.863
Disk :
log(M⋆, D) = 8.840
⟨t⋆, D⟩M = 6.410
⟨Z⋆, D⟩M = 0.437
Net − Bulge dD :
log(M⋆, dD) = 9.934
⟨t⋆, dD⟩M = 7.967
⟨Z⋆, dD⟩M = 0.733
Net − Bulge fD :
log(M⋆, fD) = 9.773
⟨t⋆, fD⟩M = 7.793
⟨Z⋆, fD⟩M = 0.775
Net − Bulge eD :
log(M⋆, eD) = 9.767
⟨t⋆, eD⟩M = 9.000
⟨Z⋆, eD⟩M = 0.844
Net − Bulge dD :
log(M⋆, dD) = 9.837
⟨t⋆, dD⟩M = 9.590
⟨Z⋆, dD⟩M = 0.792
Net − Bulge fD :
log(M⋆, fD) = 9.683
⟨t⋆, fD⟩M = 8.696
⟨Z⋆, fD⟩M = 0.722
Net − Bulge eD :
log(M⋆, eD) = 9.690
⟨t⋆, eD⟩M = 7.285
⟨Z⋆, eD⟩M = 0.929
λ (Å)

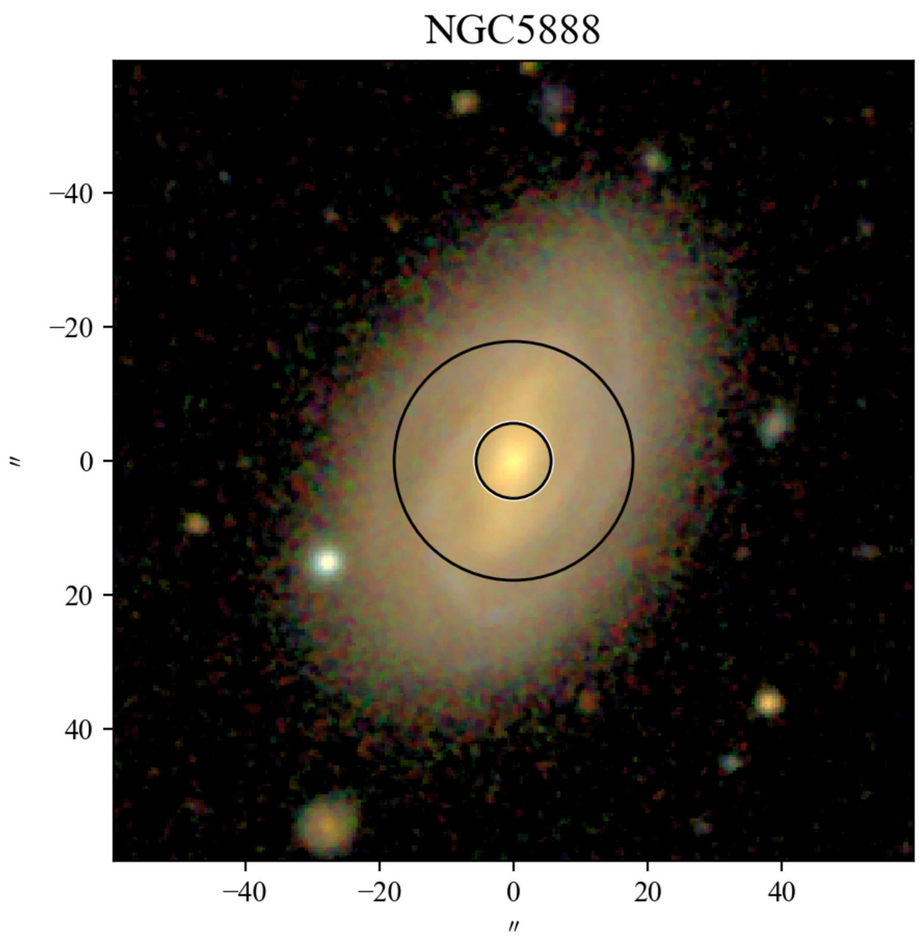
NGC5888
−40
−20
0
20
40
″
−40
−20
0
20
40
″

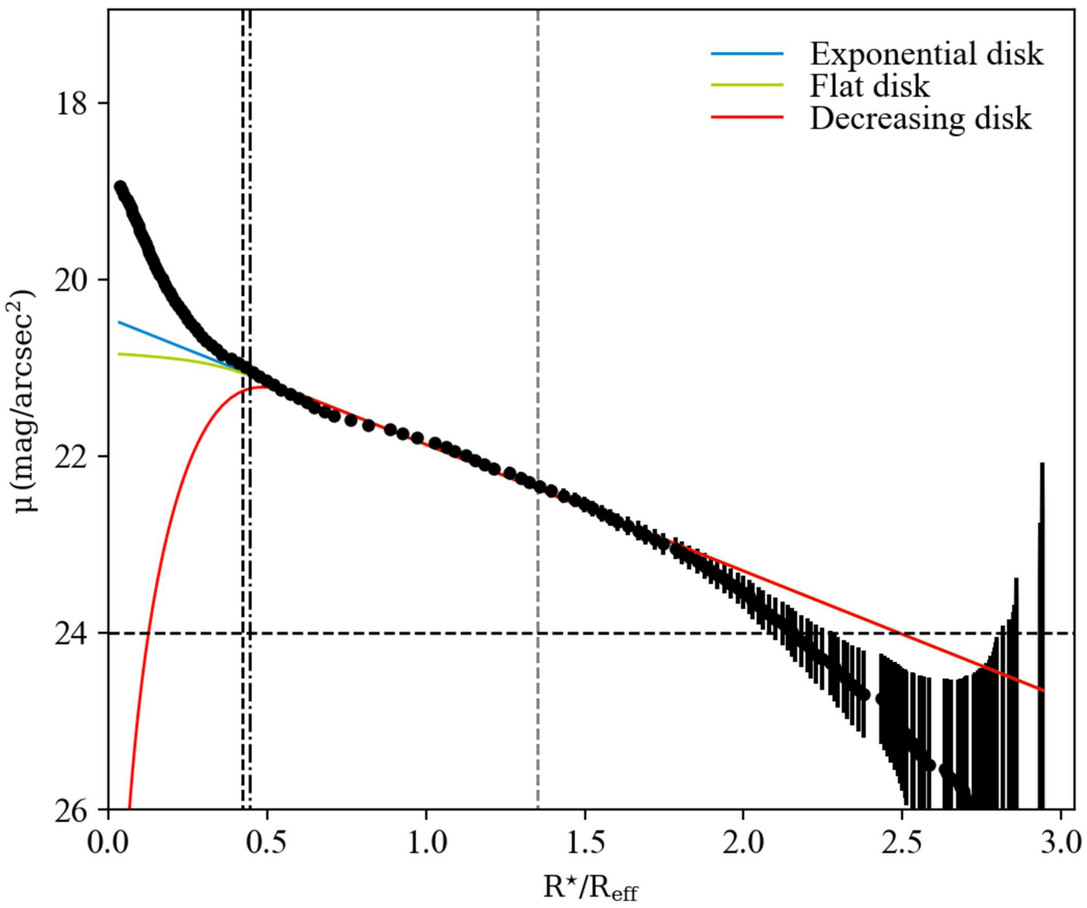
Exponential disk
Flat disk
Decreasing disk
μ (mag/arcsec²)
18
20
22
24
26
0.0
0.5
1.0
1.5
2.0
2.5
3.0
R⋆/Reff

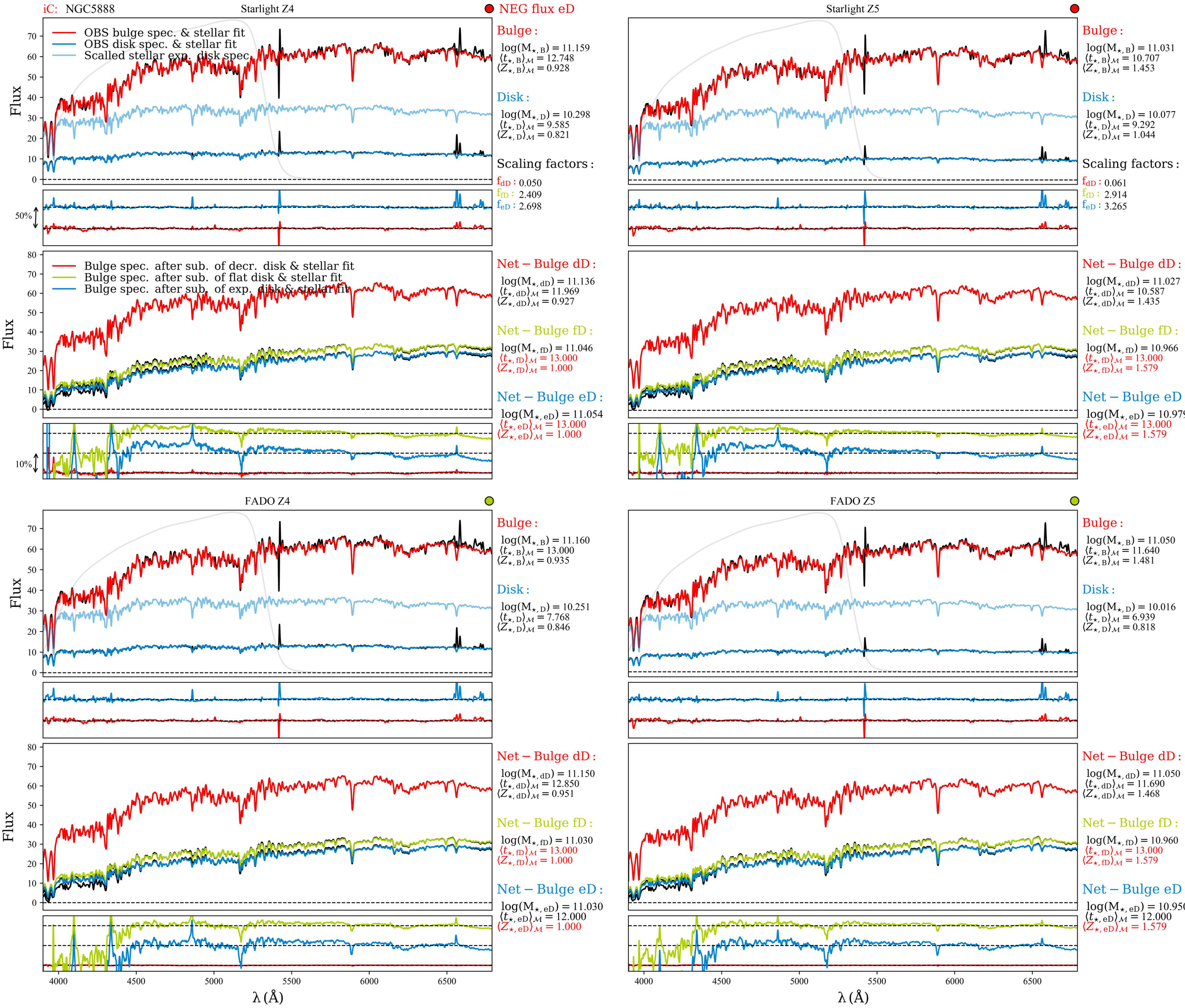
iC: NGC5888
Starlight Z4
NEG flux eD
OBS bulge spec. & stellar fit
OBS disk spec. & stellar fit
Scalled stellar exp. disk spec.
Flux
50%
Bulge :
log(M⋆, B) = 11.159
⟨t⋆, B⟩M = 12.748
⟨Z⋆, B⟩M = 0.928
Disk :
log(M⋆, D) = 10.298
⟨t⋆, D⟩M = 9.585
⟨Z⋆, D⟩M = 0.821
Scaling factors :
fdD : 0.050
ffD : 2.409
feD : 2.698
Starlight Z5
Bulge :
log(M⋆, B) = 11.031
⟨t⋆, B⟩M = 10.707
⟨Z⋆, B⟩M = 1.453
Disk :
log(M⋆, D) = 10.077
⟨t⋆, D⟩M = 9.292
⟨Z⋆, D⟩M = 1.044
Scaling factors :
fdD : 0.061
ffD : 2.914
feD : 3.265
Bulge spec. after sub. of decr. disk & stellar fit
Bulge spec. after sub. of flat disk & stellar fit
Bulge spec. after sub. of exp. disk & stellar fit
Flux
10%
Net − Bulge dD :
log(M⋆, dD) = 11.136
⟨t⋆, dD⟩M = 11.969
⟨Z⋆, dD⟩M = 0.927
Net − Bulge fD :
log(M⋆, fD) = 11.046
⟨t⋆, fD⟩M = 13.000
⟨Z⋆, fD⟩M = 1.000
Net − Bulge eD :
log(M⋆, eD) = 11.054
⟨t⋆, eD⟩M = 13.000
⟨Z⋆, eD⟩M = 1.000
Net − Bulge dD :
log(M⋆, dD) = 11.027
⟨t⋆, dD⟩M = 10.587
⟨Z⋆, dD⟩M = 1.435
Net − Bulge fD :
log(M⋆, fD) = 10.966
⟨t⋆, fD⟩M = 13.000
⟨Z⋆, fD⟩M = 1.579
Net − Bulge eD :
log(M⋆, eD) = 10.979
⟨t⋆, eD⟩M = 13.000
⟨Z⋆, eD⟩M = 1.579
FADO Z4
Flux
Bulge :
log(M⋆, B) = 11.160
⟨t⋆, B⟩M = 13.000
⟨Z⋆, B⟩M = 0.935
Disk :
log(M⋆, D) = 10.251
⟨t⋆, D⟩M = 7.768
⟨Z⋆, D⟩M = 0.846
FADO Z5
Bulge :
log(M⋆, B) = 11.050
⟨t⋆, B⟩M = 11.640
⟨Z⋆, B⟩M = 1.481
Disk :
log(M⋆, D) = 10.016
⟨t⋆, D⟩M = 6.939
⟨Z⋆, D⟩M = 0.818
Net − Bulge dD :
log(M⋆, dD) = 11.150
⟨t⋆, dD⟩M = 12.850
⟨Z⋆, dD⟩M = 0.951
Net − Bulge fD :
log(M⋆, fD) = 11.030
⟨t⋆, fD⟩M = 13.000
⟨Z⋆, fD⟩M = 1.000
Net − Bulge eD :
log(M⋆, eD) = 11.030
⟨t⋆, eD⟩M = 12.000
⟨Z⋆, eD⟩M = 1.000
Net − Bulge dD :
log(M⋆, dD) = 11.050
⟨t⋆, dD⟩M = 11.690
⟨Z⋆, dD⟩M = 1.468
Net − Bulge fD :
log(M⋆, fD) = 10.960
⟨t⋆, fD⟩M = 13.000
⟨Z⋆, fD⟩M = 1.579
Net − Bulge eD :
log(M⋆, eD) = 10.950
⟨t⋆, eD⟩M = 12.000
⟨Z⋆, eD⟩M = 1.579
λ (Å)

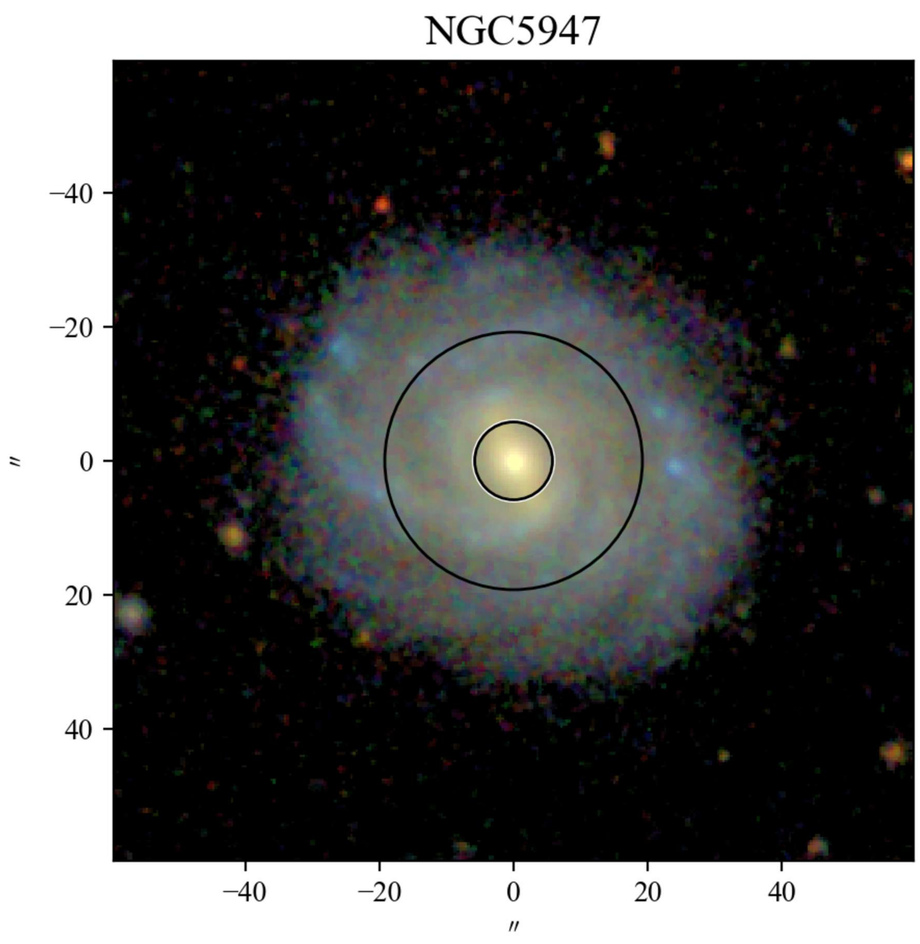
NGC5947
−40
−20
0
20
40
″
−40
−20
0
20
40
″

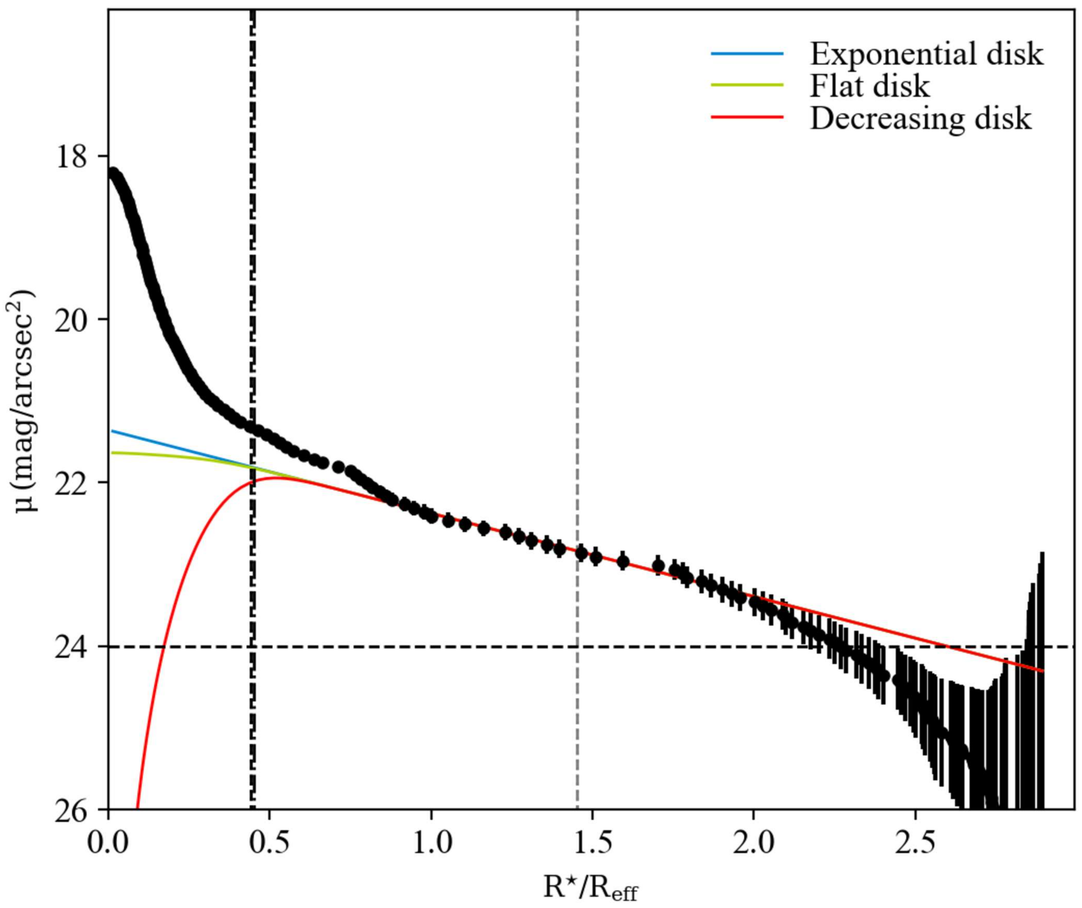
Exponential disk
Flat disk
Decreasing disk
μ (mag/arcsec²)
18
20
22
24
26
0.0
0.5
1.0
1.5
2.0
2.5
R⋆/Reff

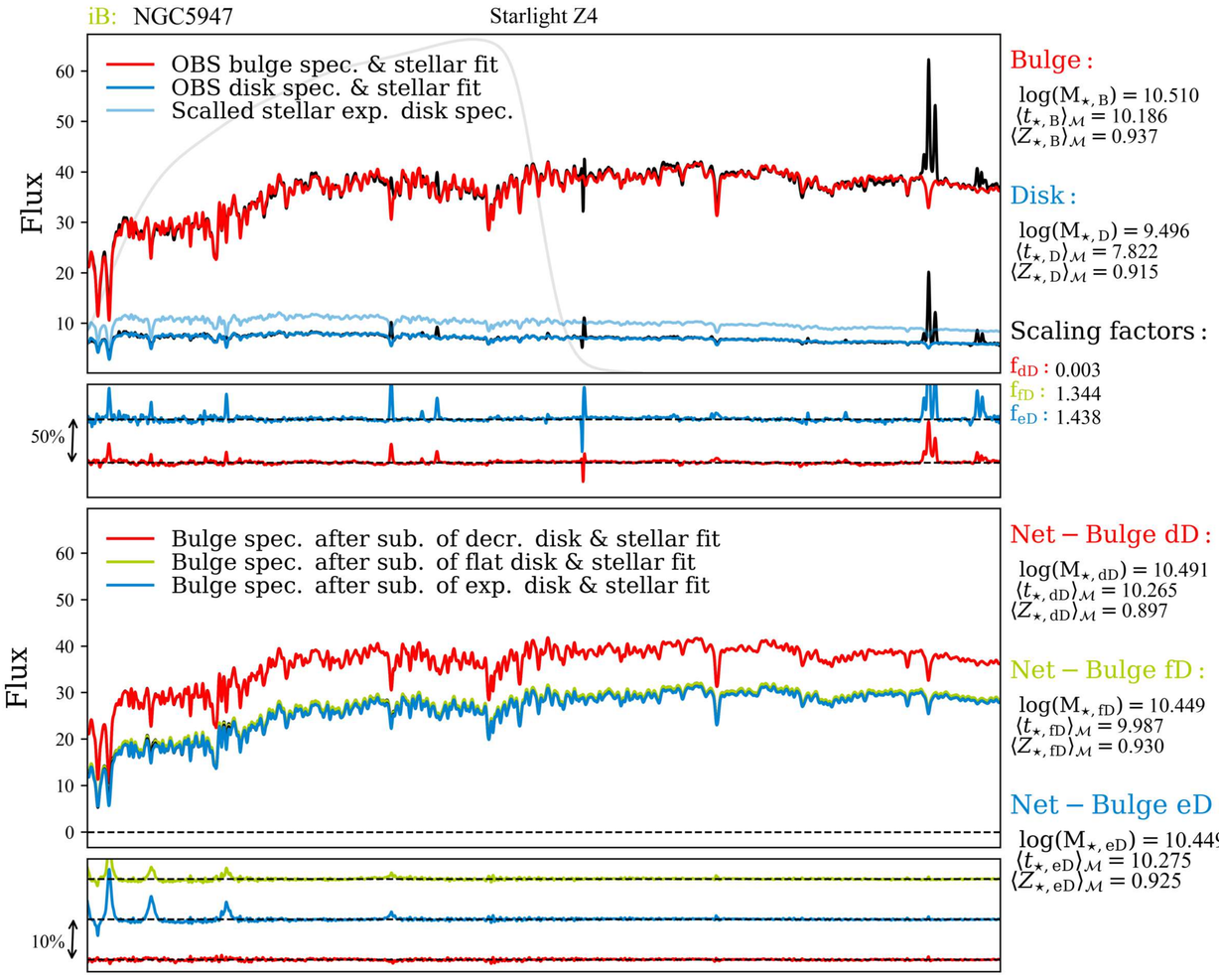
iB: NGC5947
Starlight Z4
OBS bulge spec. & stellar fit
OBS disk spec. & stellar fit
Scalled stellar exp. disk spec.
Flux
50%
Bulge :
log(M⋆, B) = 10.510
⟨t⋆, B⟩M = 10.186
⟨Z⋆, B⟩M = 0.937
Disk :
log(M⋆, D) = 9.496
⟨t⋆, D⟩M = 7.822
⟨Z⋆, D⟩M = 0.915
Scaling factors :
fdD : 0.003
ffD : 1.344
feD : 1.438
Bulge spec. after sub. of decr. disk & stellar fit
Bulge spec. after sub. of flat disk & stellar fit
Bulge spec. after sub. of exp. disk & stellar fit
10%
Net − Bulge dD :
log(M⋆, dD) = 10.491
⟨t⋆, dD⟩M = 10.265
⟨Z⋆, dD⟩M = 0.897
Net − Bulge fD :
log(M⋆, fD) = 10.449
⟨t⋆, fD⟩M = 9.987
⟨Z⋆, fD⟩M = 0.930
Net − Bulge eD :
log(M⋆, eD) = 10.449
⟨t⋆, eD⟩M = 10.275
⟨Z⋆, eD⟩M = 0.925

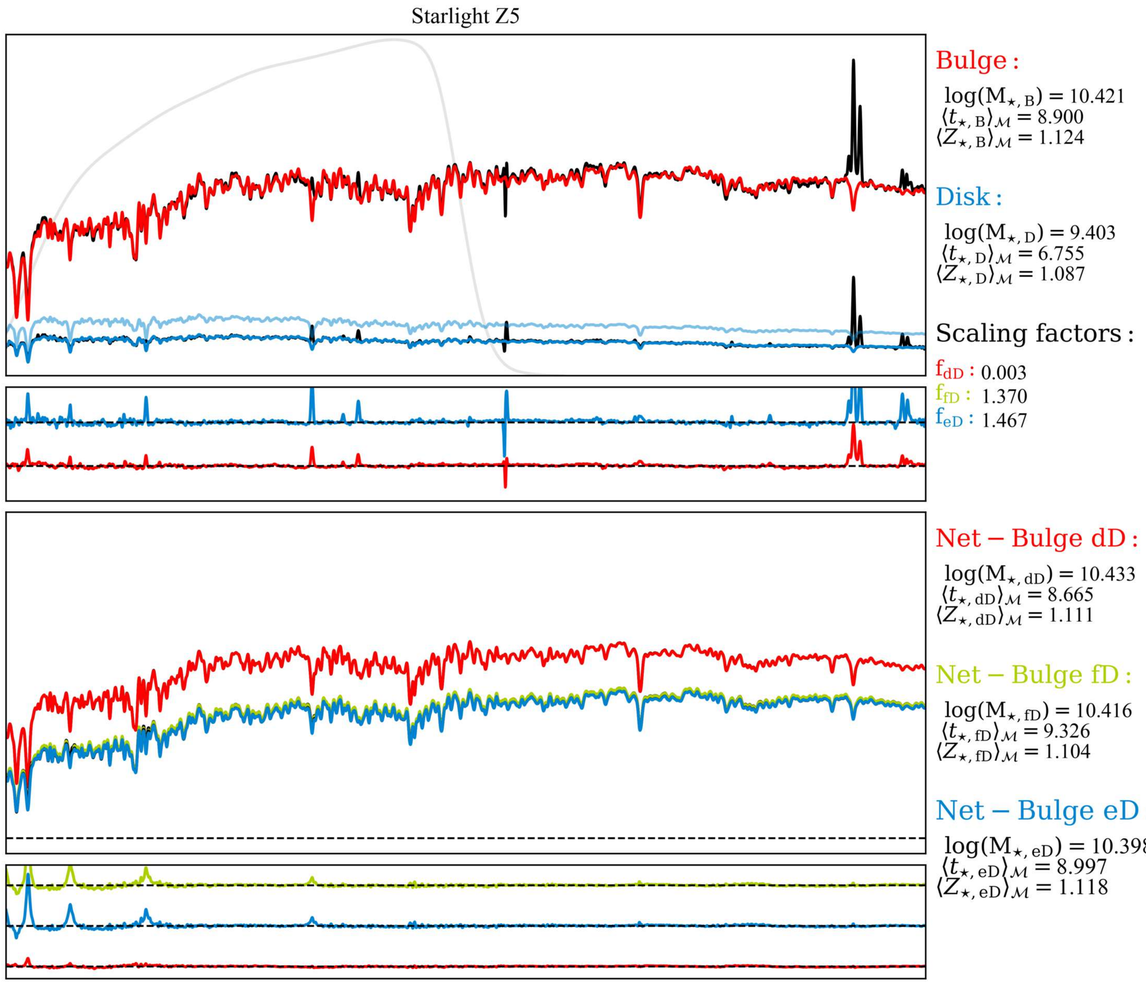
Starlight Z5
Bulge :
log(M⋆, B) = 10.421
⟨t⋆, B⟩M = 8.900
⟨Z⋆, B⟩M = 1.124
Disk :
log(M⋆, D) = 9.403
⟨t⋆, D⟩M = 6.755
⟨Z⋆, D⟩M = 1.087
Scaling factors :
fdD : 0.003
ffD : 1.370
feD : 1.467
Net − Bulge dD :
log(M⋆, dD) = 10.433
⟨t⋆, dD⟩M = 8.665
⟨Z⋆, dD⟩M = 1.111
Net − Bulge fD :
log(M⋆, fD) = 10.416
⟨t⋆, fD⟩M = 9.326
⟨Z⋆, fD⟩M = 1.104
Net − Bulge eD :
log(M⋆, eD) = 10.398
⟨t⋆, eD⟩M = 8.997
⟨Z⋆, eD⟩M = 1.118

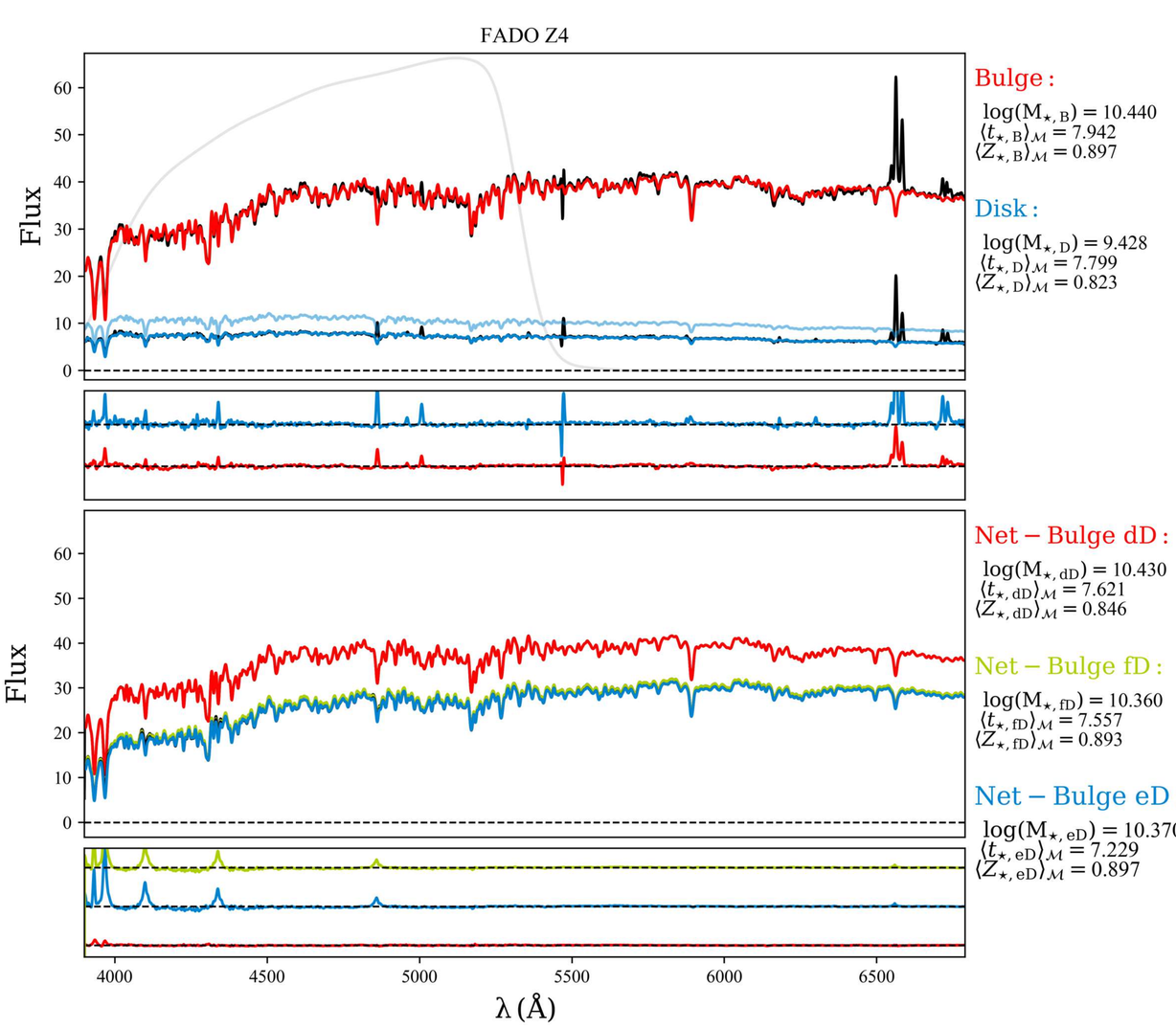
FADO Z4
Flux
Bulge :
log(M⋆, B) = 10.440
⟨t⋆, B⟩M = 7.942
⟨Z⋆, B⟩M = 0.897
Disk :
log(M⋆, D) = 9.428
⟨t⋆, D⟩M = 7.799
⟨Z⋆, D⟩M = 0.823
Net − Bulge dD :
log(M⋆, dD) = 10.430
⟨t⋆, dD⟩M = 7.621
⟨Z⋆, dD⟩M = 0.846
Net − Bulge fD :
log(M⋆, fD) = 10.360
⟨t⋆, fD⟩M = 7.557
⟨Z⋆, fD⟩M = 0.893
Net − Bulge eD :
log(M⋆, eD) = 10.370
⟨t⋆, eD⟩M = 7.229
⟨Z⋆, eD⟩M = 0.897
λ (Å)

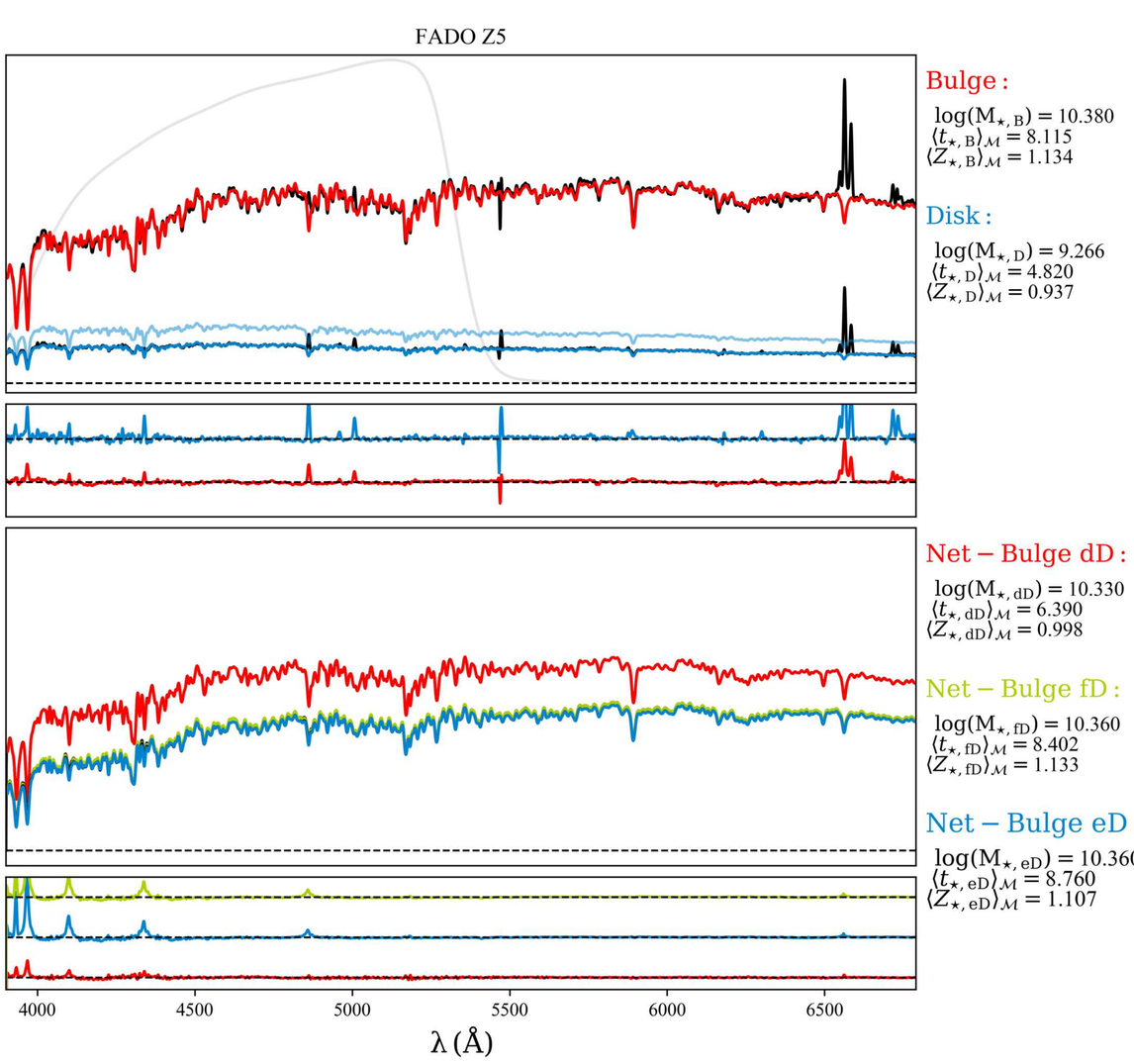
FADO Z5
Bulge :
log(M⋆, B) = 10.380
⟨t⋆, B⟩M = 8.115
⟨Z⋆, B⟩M = 1.134
Disk :
log(M⋆, D) = 9.266
⟨t⋆, D⟩M = 4.820
⟨Z⋆, D⟩M = 0.937
Net − Bulge dD :
log(M⋆, dD) = 10.330
⟨t⋆, dD⟩M = 6.390
⟨Z⋆, dD⟩M = 0.998
Net − Bulge fD :
log(M⋆, fD) = 10.360
⟨t⋆, fD⟩M = 8.402
⟨Z⋆, fD⟩M = 1.133
Net − Bulge eD :
log(M⋆, eD) = 10.360
⟨t⋆, eD⟩M = 8.760
⟨Z⋆, eD⟩M = 1.107
λ (Å)

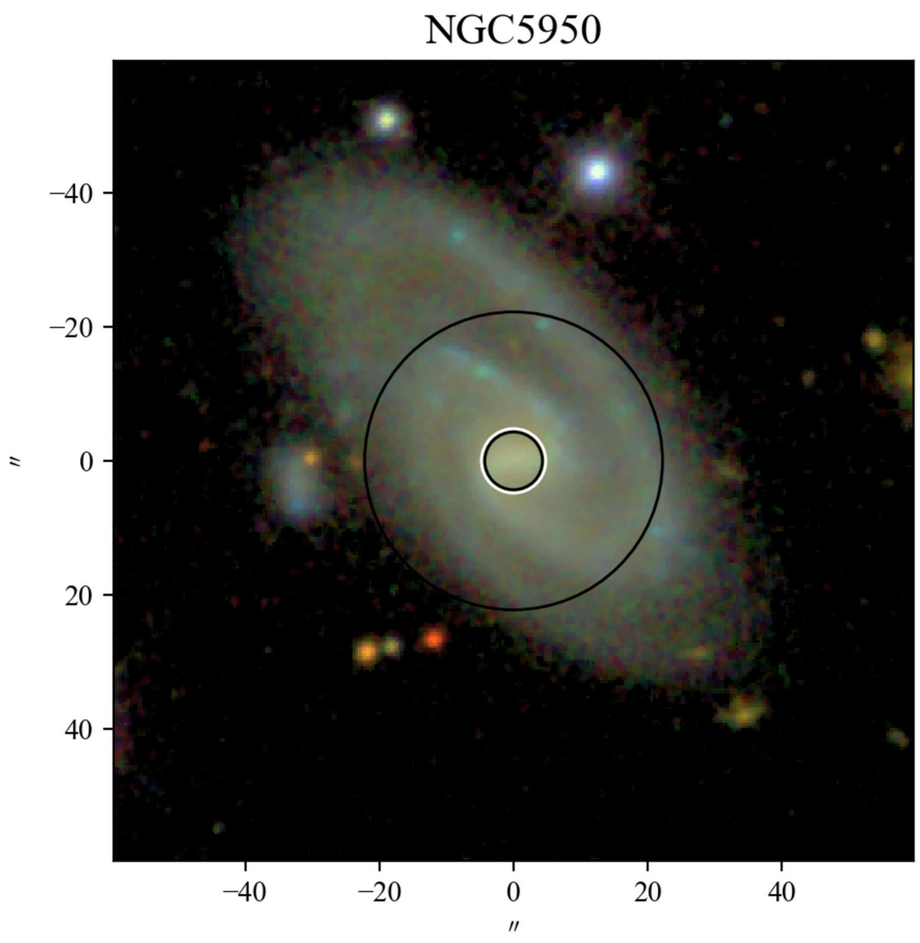
NGC5950
−40
−20
0
20
40
″
−40
−20
0
20
40
″

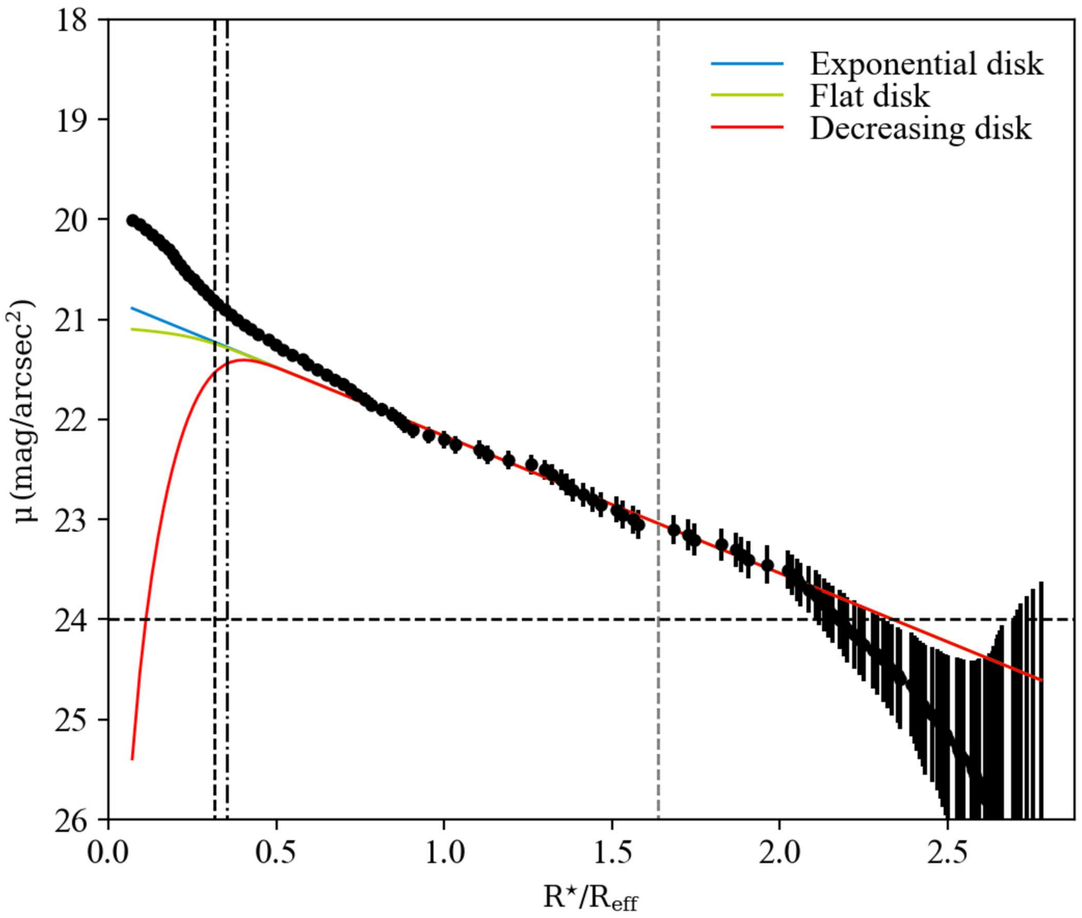
Exponential disk
Flat disk
Decreasing disk
μ (mag/arcsec²)
R⋆/R_eff

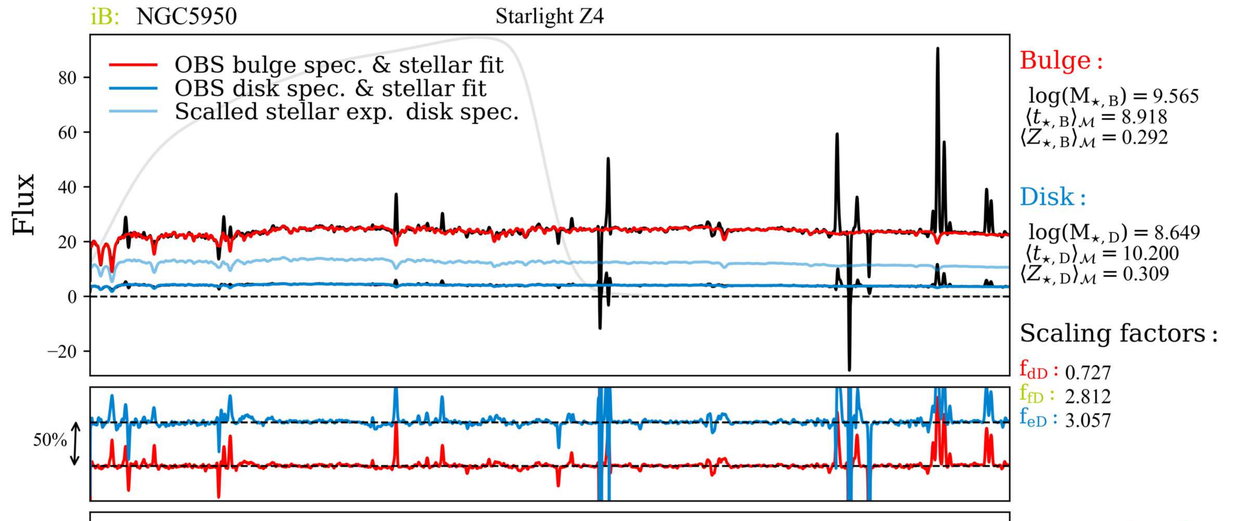
iB: NGC5950
Starlight Z4
OBS bulge spec. & stellar fit
OBS disk spec. & stellar fit
Scalled stellar exp. disk spec.
Flux
50%
Bulge :
log(M⋆, B) = 9.565
⟨t⋆, B⟩M = 8.918
⟨Z⋆, B⟩M = 0.292
Disk :
log(M⋆, D) = 8.649
⟨t⋆, D⟩M = 10.200
⟨Z⋆, D⟩M = 0.309
Scaling factors :
fdD : 0.727
ffD : 2.812
feD : 3.057

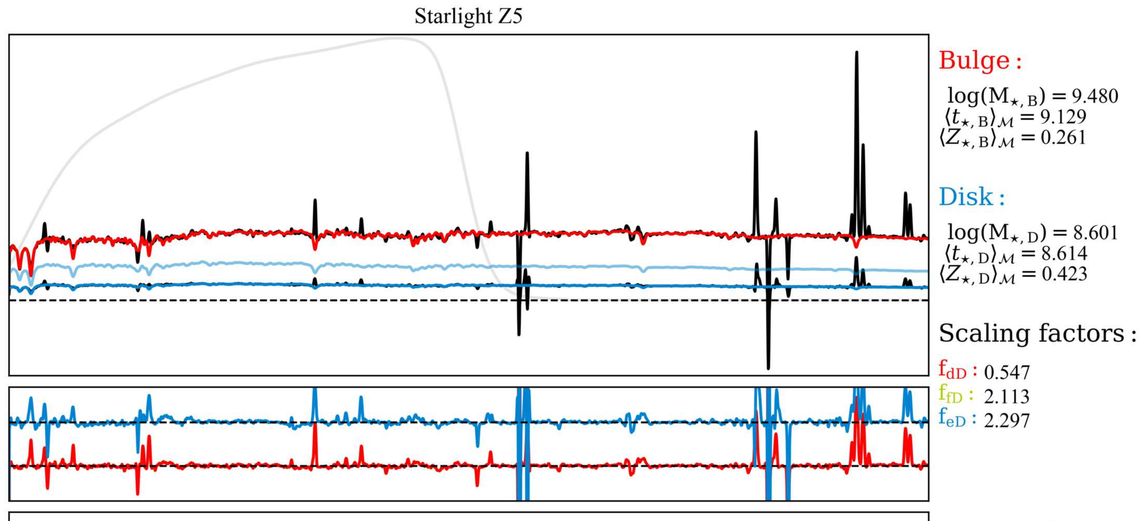
Starlight Z5
Bulge :
log(M⋆, B) = 9.480
⟨t⋆, B⟩M = 9.129
⟨Z⋆, B⟩M = 0.261
Disk :
log(M⋆, D) = 8.601
⟨t⋆, D⟩M = 8.614
⟨Z⋆, D⟩M = 0.423
Scaling factors :
fdD : 0.547
ffD : 2.113
feD : 2.297

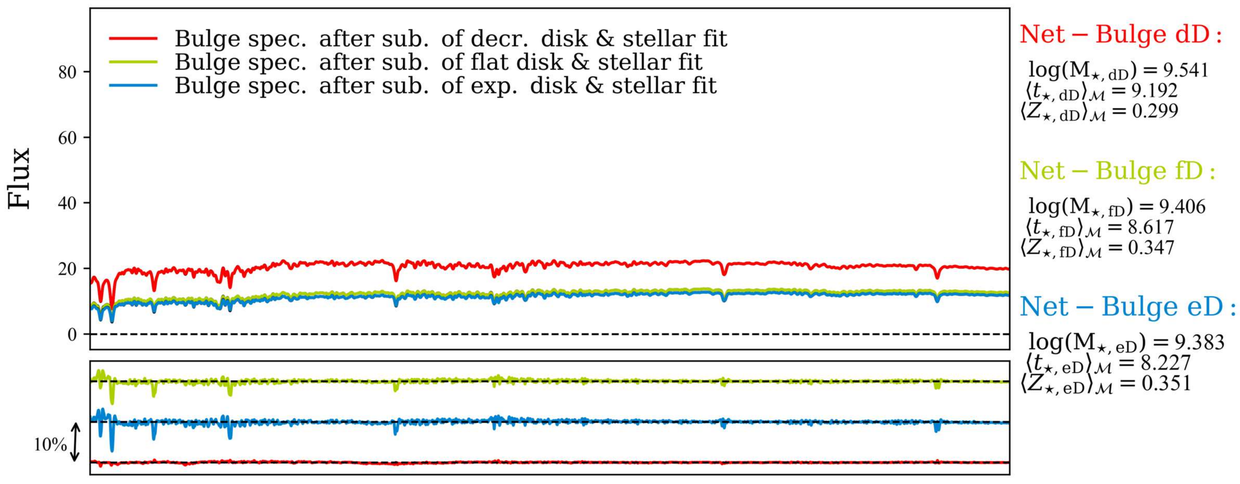
Bulge spec. after sub. of decr. disk & stellar fit
Bulge spec. after sub. of flat disk & stellar fit
Bulge spec. after sub. of exp. disk & stellar fit
Flux
10%
Net − Bulge dD :
log(M⋆, dD) = 9.541
⟨t⋆, dD⟩M = 9.192
⟨Z⋆, dD⟩M = 0.299
Net − Bulge fD :
log(M⋆, fD) = 9.406
⟨t⋆, fD⟩M = 8.617
⟨Z⋆, fD⟩M = 0.347
Net − Bulge eD :
log(M⋆, eD) = 9.383
⟨t⋆, eD⟩M = 8.227
⟨Z⋆, eD⟩M = 0.351

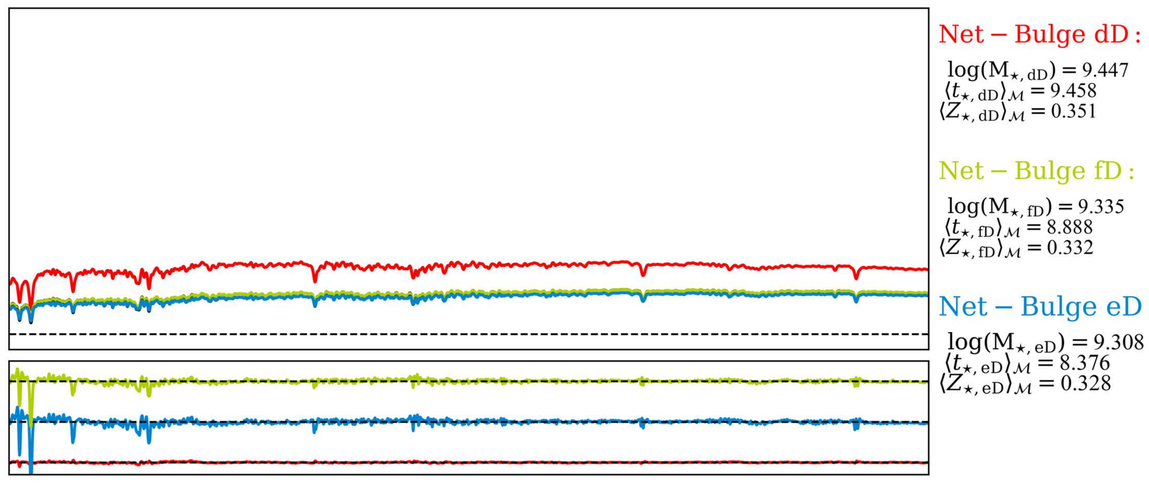
Net − Bulge dD :
log(M⋆, dD) = 9.447
⟨t⋆, dD⟩M = 9.458
⟨Z⋆, dD⟩M = 0.351
Net − Bulge fD :
log(M⋆, fD) = 9.335
⟨t⋆, fD⟩M = 8.888
⟨Z⋆, fD⟩M = 0.332
Net − Bulge eD :
log(M⋆, eD) = 9.308
⟨t⋆, eD⟩M = 8.376
⟨Z⋆, eD⟩M = 0.328

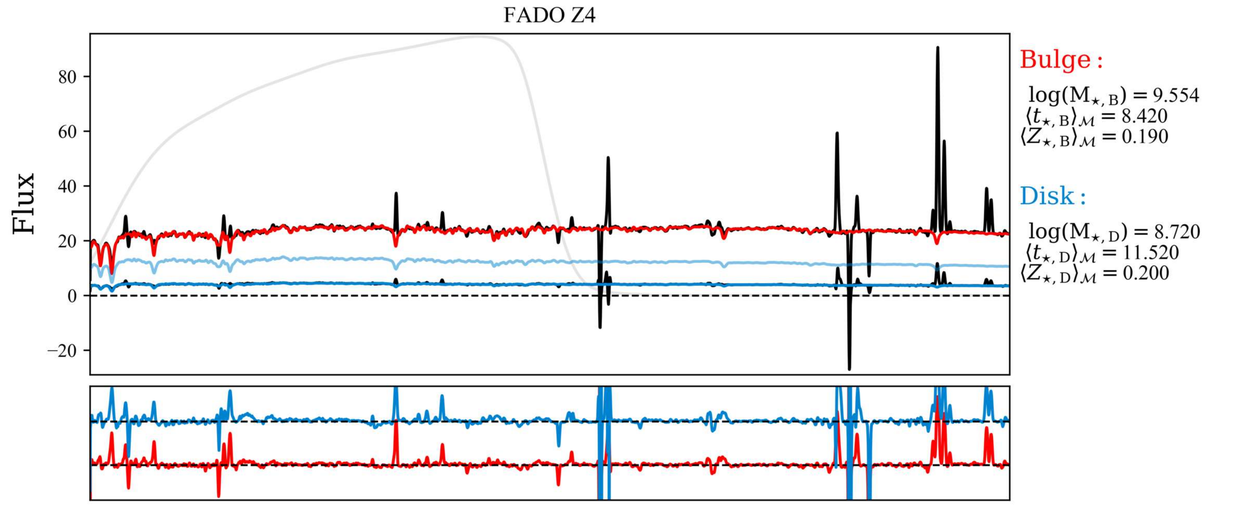
FADO Z4
Flux
Bulge :
log(M⋆, B) = 9.554
⟨t⋆, B⟩M = 8.420
⟨Z⋆, B⟩M = 0.190
Disk :
log(M⋆, D) = 8.720
⟨t⋆, D⟩M = 11.520
⟨Z⋆, D⟩M = 0.200

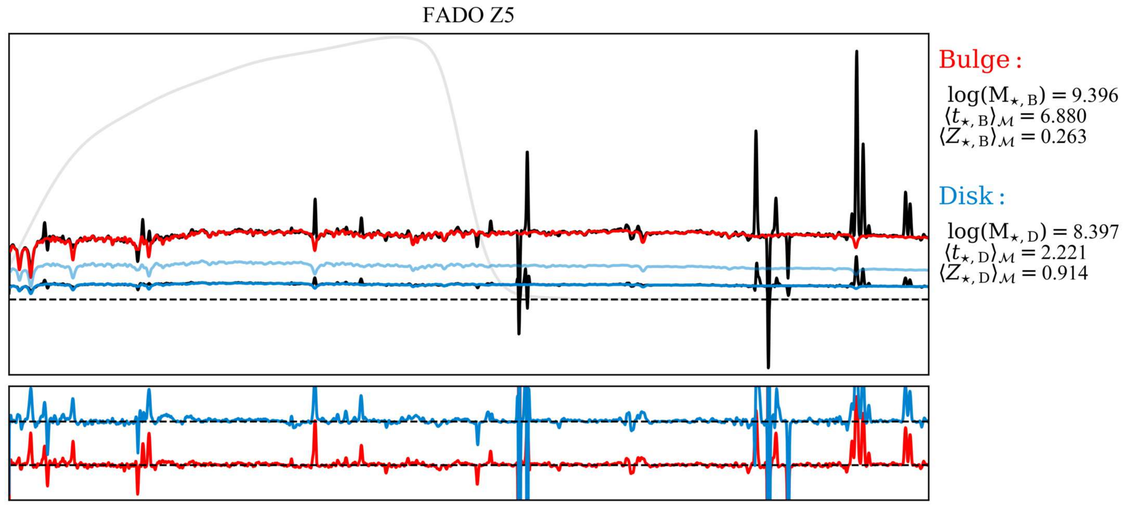
FADO Z5
Bulge :
log(M⋆, B) = 9.396
⟨t⋆, B⟩M = 6.880
⟨Z⋆, B⟩M = 0.263
Disk :
log(M⋆, D) = 8.397
⟨t⋆, D⟩M = 2.221
⟨Z⋆, D⟩M = 0.914

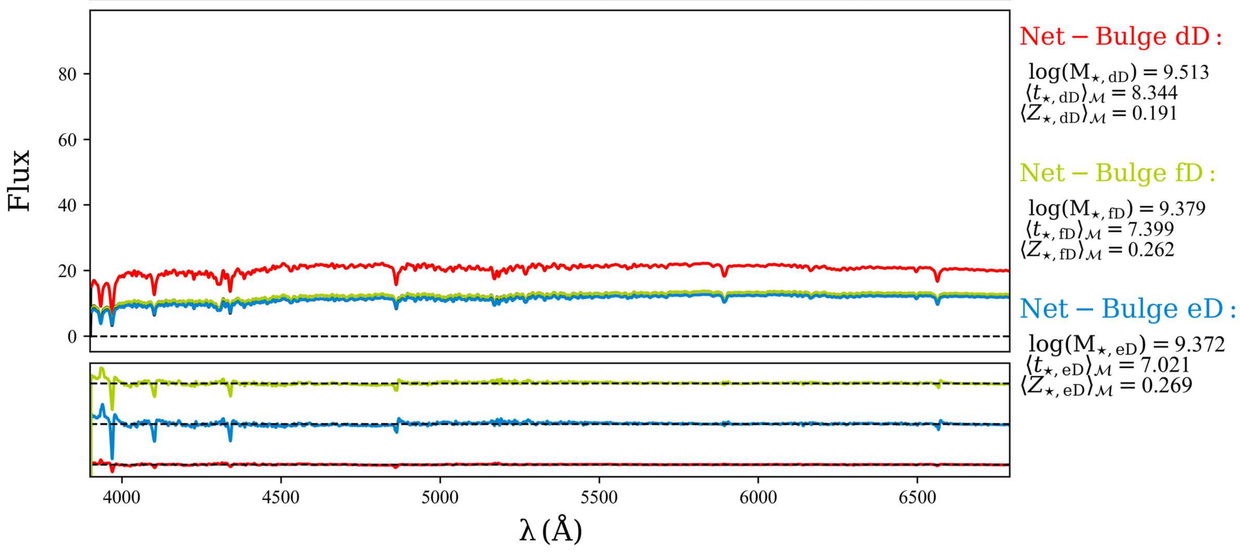
Flux
Net − Bulge dD :
log(M⋆, dD) = 9.513
⟨t⋆, dD⟩M = 8.344
⟨Z⋆, dD⟩M = 0.191
Net − Bulge fD :
log(M⋆, fD) = 9.379
⟨t⋆, fD⟩M = 7.399
⟨Z⋆, fD⟩M = 0.262
Net − Bulge eD :
log(M⋆, eD) = 9.372
⟨t⋆, eD⟩M = 7.021
⟨Z⋆, eD⟩M = 0.269
λ (Å)

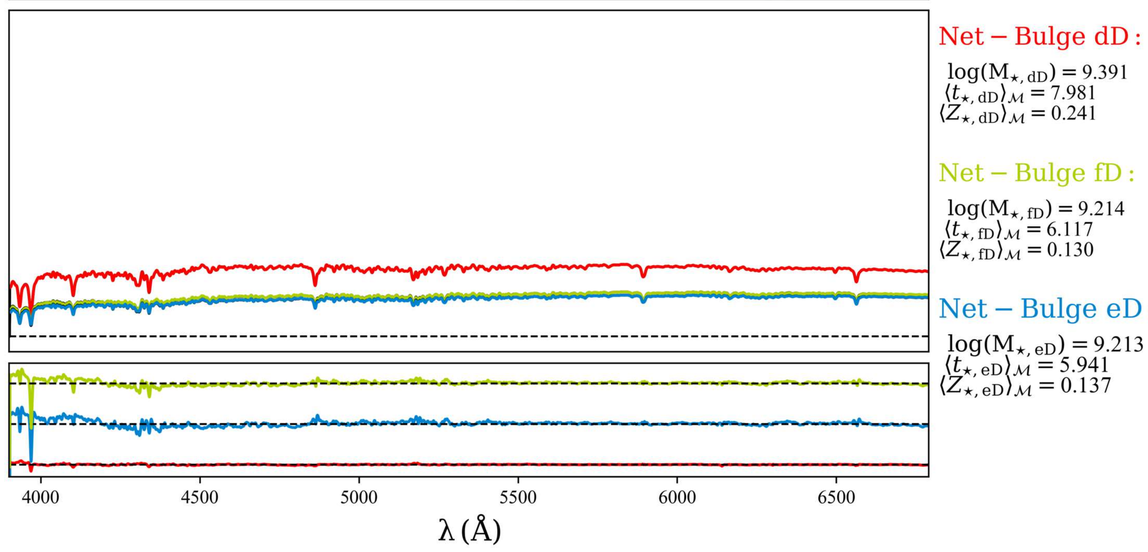
Net − Bulge dD :
log(M⋆, dD) = 9.391
⟨t⋆, dD⟩M = 7.981
⟨Z⋆, dD⟩M = 0.241
Net − Bulge fD :
log(M⋆, fD) = 9.214
⟨t⋆, fD⟩M = 6.117
⟨Z⋆, fD⟩M = 0.130
Net − Bulge eD :
log(M⋆, eD) = 9.213
⟨t⋆, eD⟩M = 5.941
⟨Z⋆, eD⟩M = 0.137
λ (Å)

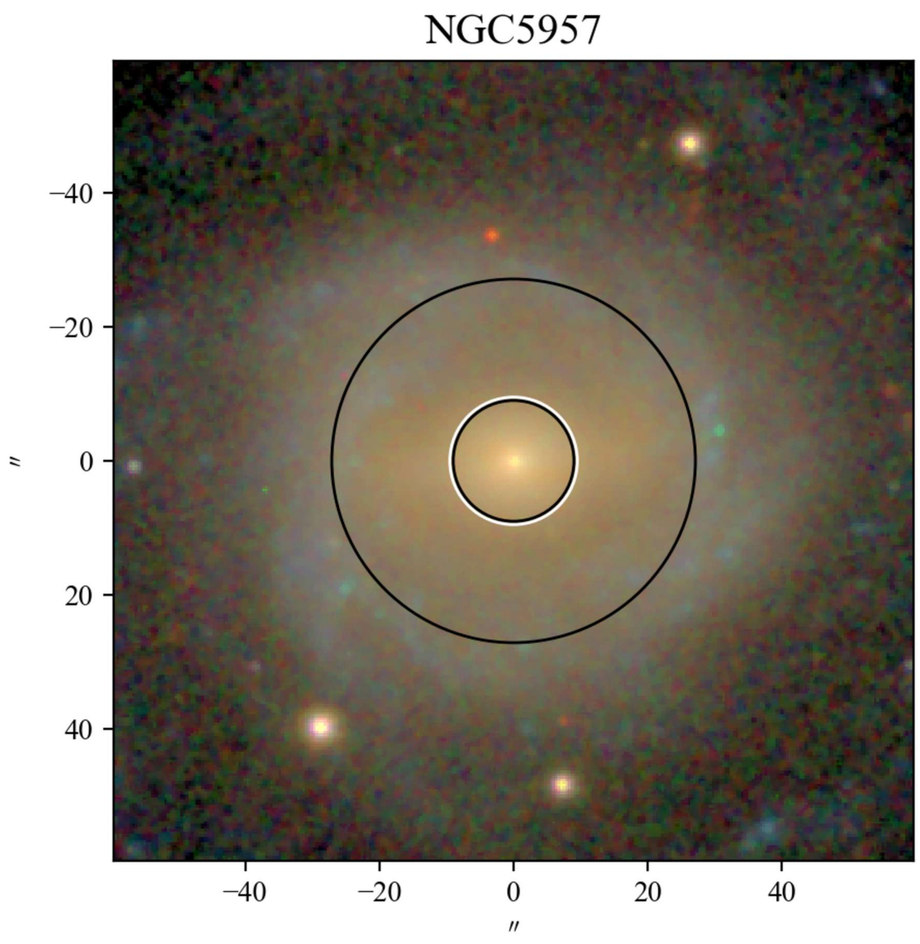
NGC5957
−40
−20
0
20
40
″
−40
−20
0
20
40
″

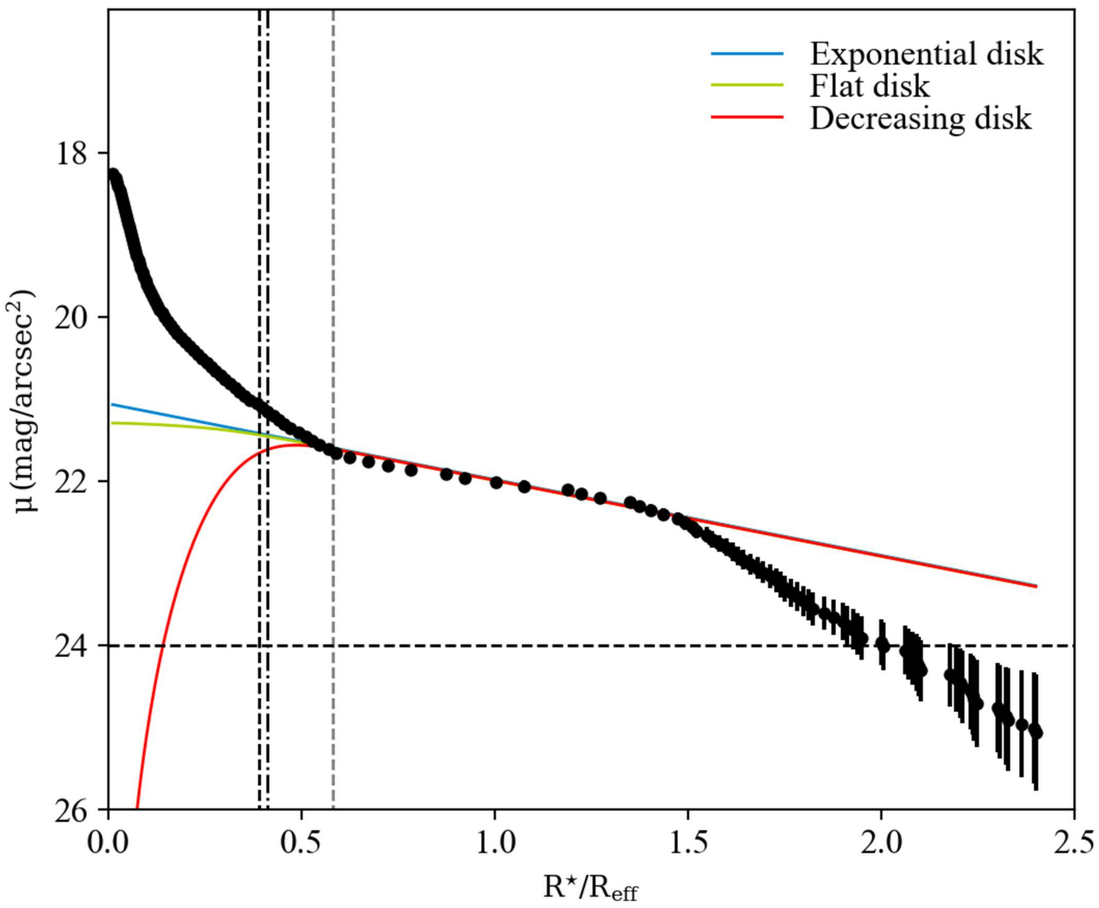
Exponential disk
Flat disk
Decreasing disk
μ (mag/arcsec²)
18
20
22
24
26
0.0
0.5
1.0
1.5
2.0
2.5
R⋆/Reff

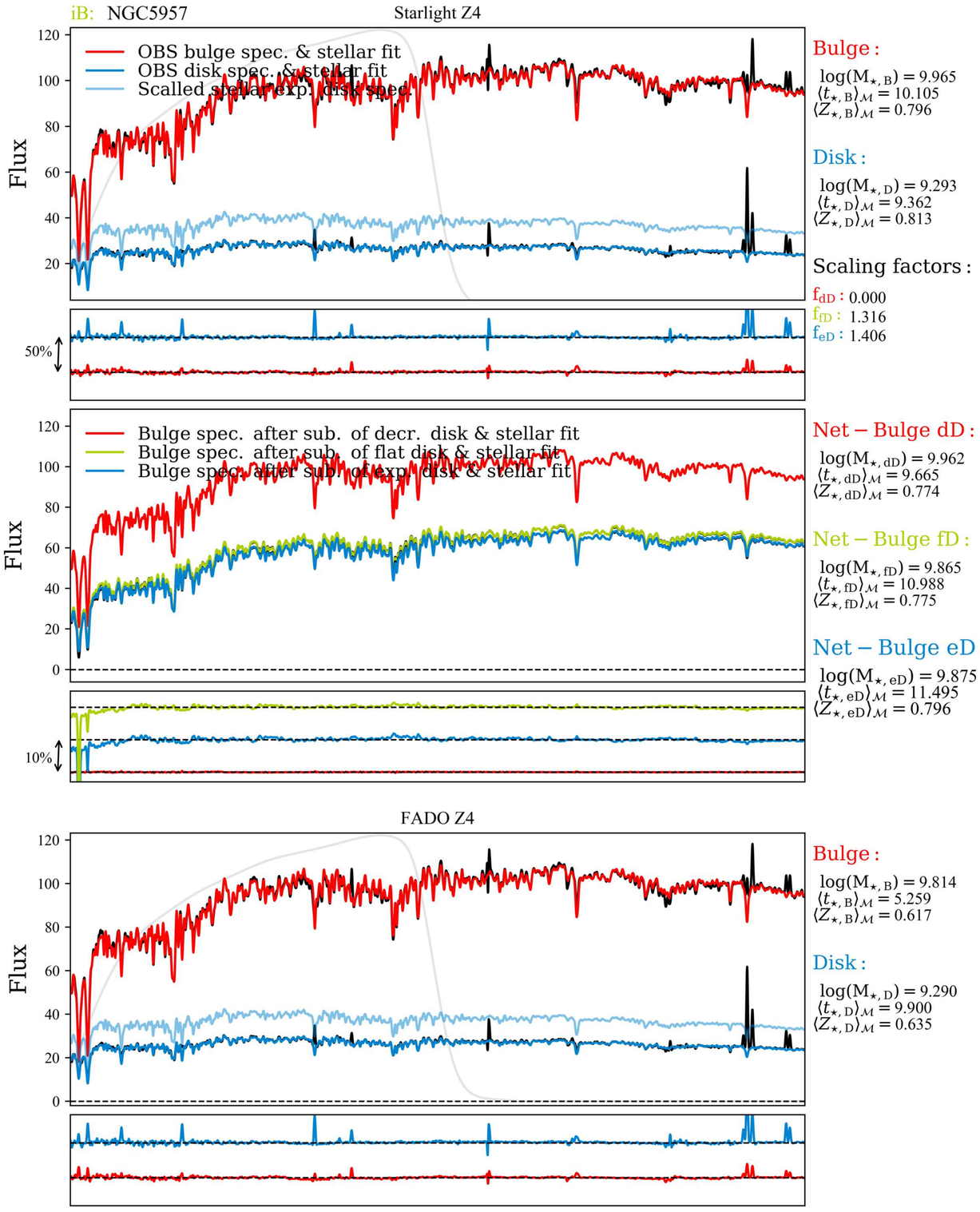
iB: NGC5957
Starlight Z4
OBS bulge spec. & stellar fit
OBS disk spec. & stellar fit
Scalled stellar exp. disk spec.
Flux
50%
Bulge :
log(M⋆, B) = 9.965
⟨t⋆, B⟩M = 10.105
⟨Z⋆, B⟩M = 0.796
Disk :
log(M⋆, D) = 9.293
⟨t⋆, D⟩M = 9.362
⟨Z⋆, D⟩M = 0.813
Scaling factors :
fdD : 0.000
ffD : 1.316
feD : 1.406
Bulge spec. after sub. of decr. disk & stellar fit
Bulge spec. after sub. of flat disk & stellar fit
Bulge spec. after sub. of exp. disk & stellar fit
10%
Net − Bulge dD :
log(M⋆, dD) = 9.962
⟨t⋆, dD⟩M = 9.665
⟨Z⋆, dD⟩M = 0.774
Net − Bulge fD :
log(M⋆, fD) = 9.865
⟨t⋆, fD⟩M = 10.988
⟨Z⋆, fD⟩M = 0.775
Net − Bulge eD :
log(M⋆, eD) = 9.875
⟨t⋆, eD⟩M = 11.495
⟨Z⋆, eD⟩M = 0.796

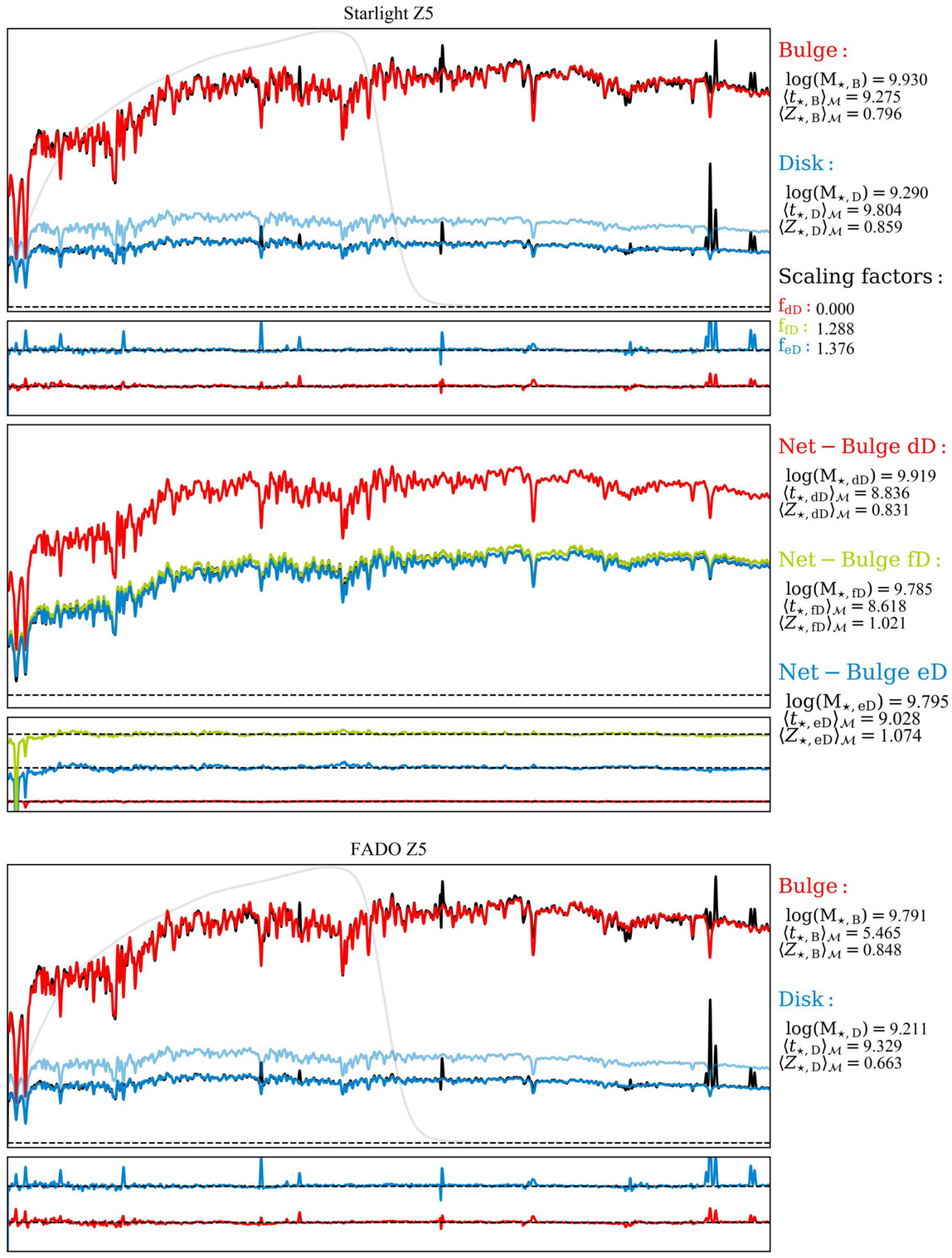
Starlight Z5
Bulge :
log(M⋆, B) = 9.930
⟨t⋆, B⟩M = 9.275
⟨Z⋆, B⟩M = 0.796
Disk :
log(M⋆, D) = 9.290
⟨t⋆, D⟩M = 9.804
⟨Z⋆, D⟩M = 0.859
Scaling factors :
fdD : 0.000
ffD : 1.288
feD : 1.376
Net − Bulge dD :
log(M⋆, dD) = 9.919
⟨t⋆, dD⟩M = 8.836
⟨Z⋆, dD⟩M = 0.831
Net − Bulge fD :
log(M⋆, fD) = 9.785
⟨t⋆, fD⟩M = 8.618
⟨Z⋆, fD⟩M = 1.021
Net − Bulge eD :
log(M⋆, eD) = 9.795
⟨t⋆, eD⟩M = 9.028
⟨Z⋆, eD⟩M = 1.074

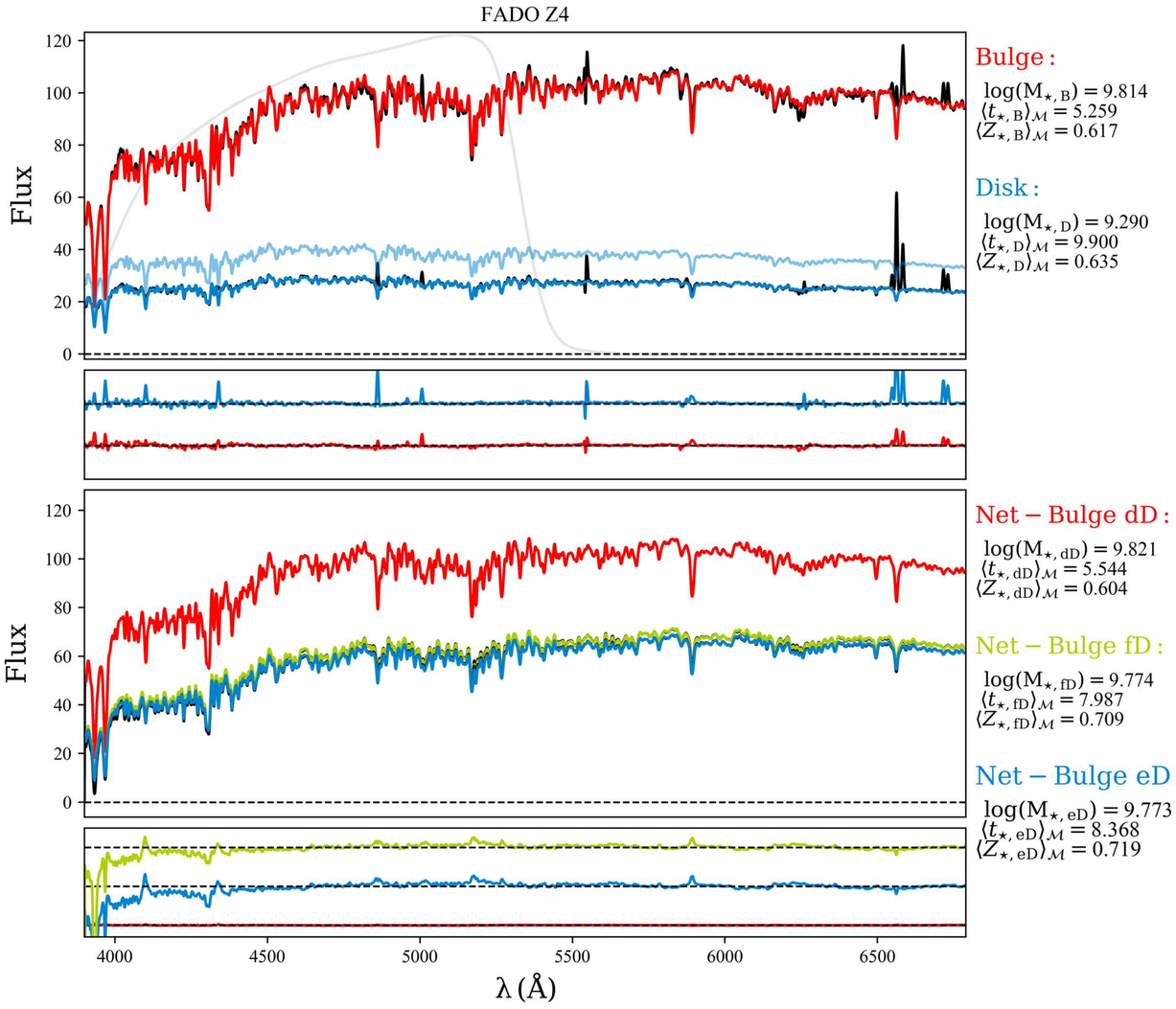
FADO Z4
Flux
Bulge :
log(M⋆, B) = 9.814
⟨t⋆, B⟩M = 5.259
⟨Z⋆, B⟩M = 0.617
Disk :
log(M⋆, D) = 9.290
⟨t⋆, D⟩M = 9.900
⟨Z⋆, D⟩M = 0.635
Net − Bulge dD :
log(M⋆, dD) = 9.821
⟨t⋆, dD⟩M = 5.544
⟨Z⋆, dD⟩M = 0.604
Net − Bulge fD :
log(M⋆, fD) = 9.774
⟨t⋆, fD⟩M = 7.987
⟨Z⋆, fD⟩M = 0.709
Net − Bulge eD :
log(M⋆, eD) = 9.773
⟨t⋆, eD⟩M = 8.368
⟨Z⋆, eD⟩M = 0.719
λ (Å)

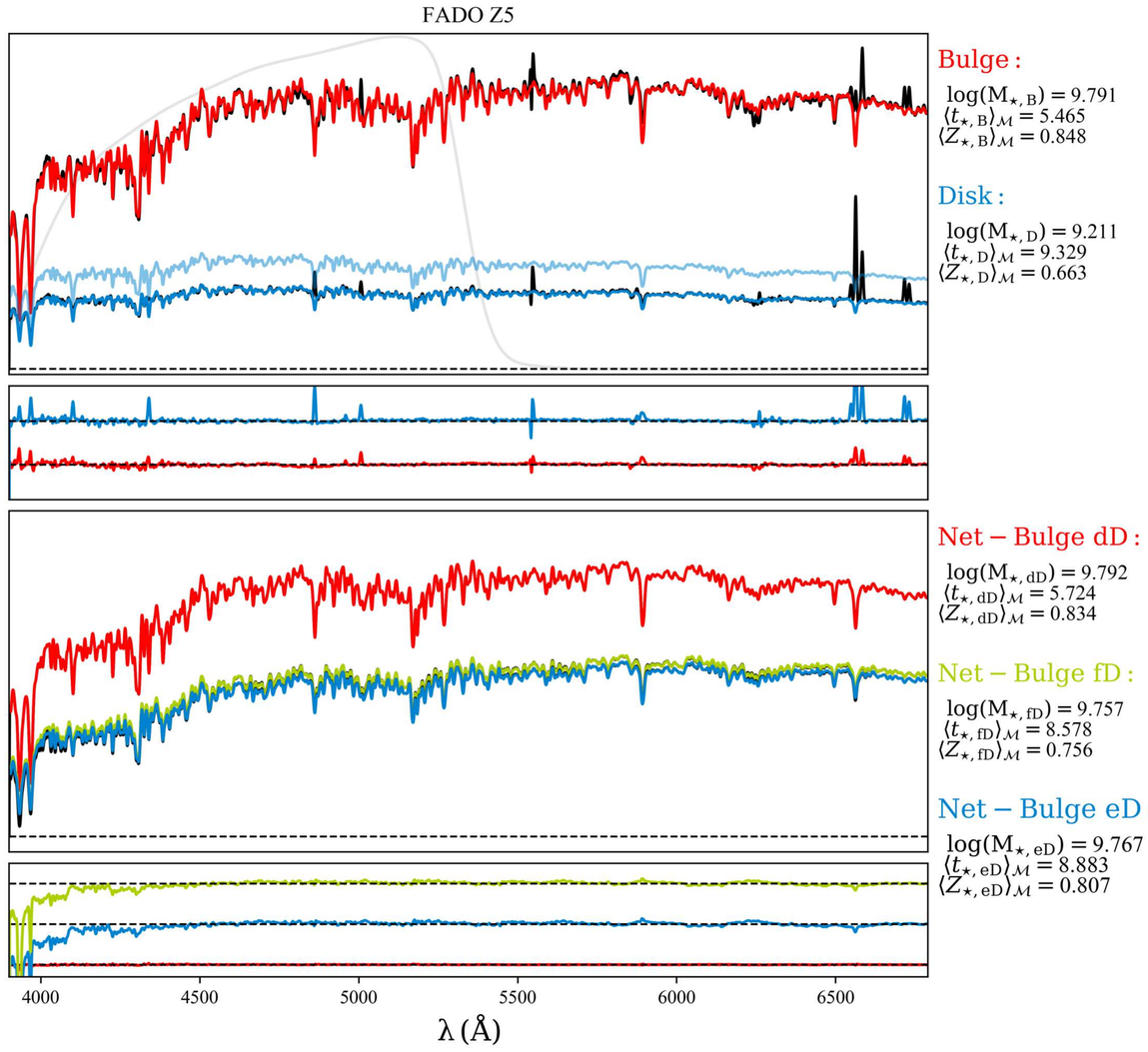
FADO Z5
Bulge :
log(M⋆, B) = 9.791
⟨t⋆, B⟩M = 5.465
⟨Z⋆, B⟩M = 0.848
Disk :
log(M⋆, D) = 9.211
⟨t⋆, D⟩M = 9.329
⟨Z⋆, D⟩M = 0.663
Net − Bulge dD :
log(M⋆, dD) = 9.792
⟨t⋆, dD⟩M = 5.724
⟨Z⋆, dD⟩M = 0.834
Net − Bulge fD :
log(M⋆, fD) = 9.757
⟨t⋆, fD⟩M = 8.578
⟨Z⋆, fD⟩M = 0.756
Net − Bulge eD :
log(M⋆, eD) = 9.767
⟨t⋆, eD⟩M = 8.883
⟨Z⋆, eD⟩M = 0.807
λ (Å)

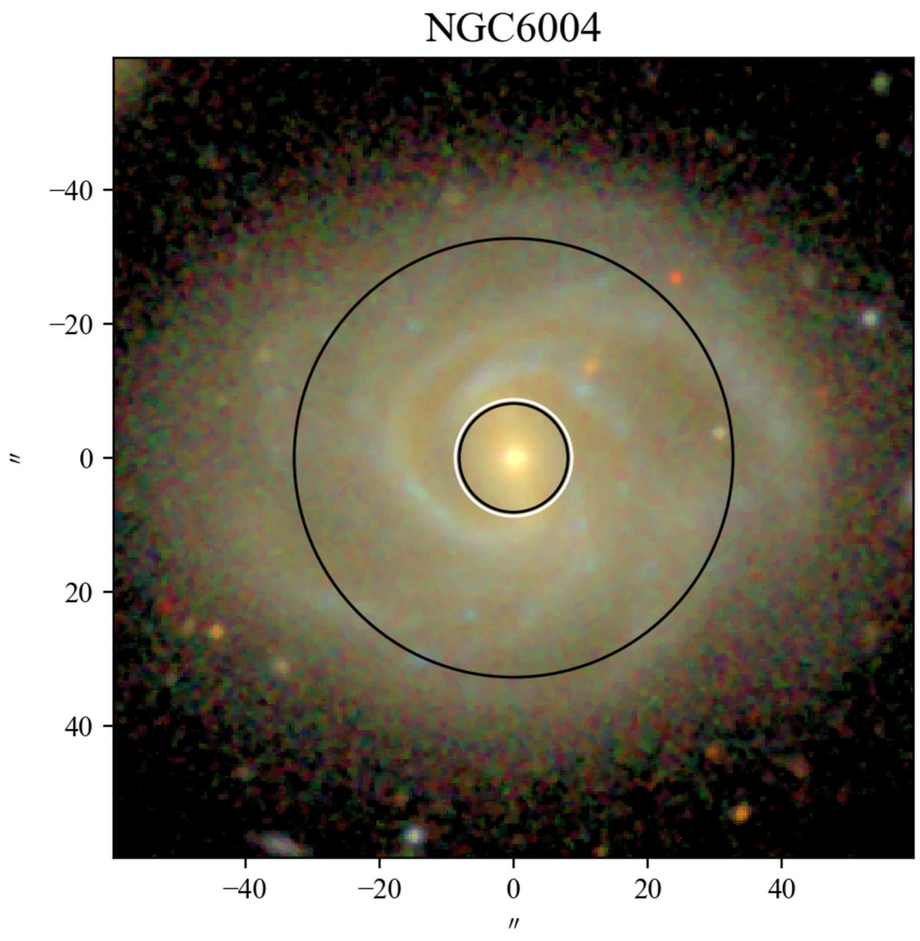
NGC6004
−40
−20
0
20
40
″
−40
−20
0
20
40
″

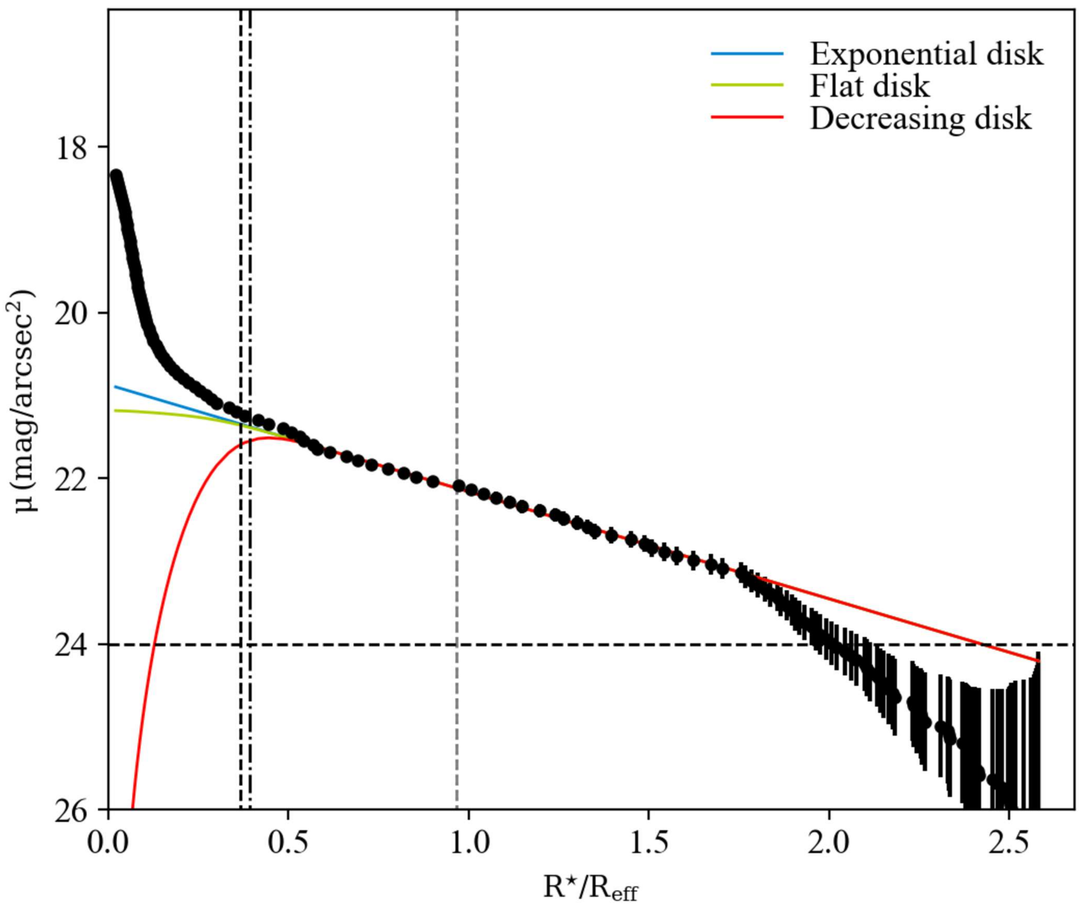
Exponential disk
Flat disk
Decreasing disk
μ (mag/arcsec²)
18
20
22
24
26
0.0
0.5
1.0
1.5
2.0
2.5
R⋆/Reff

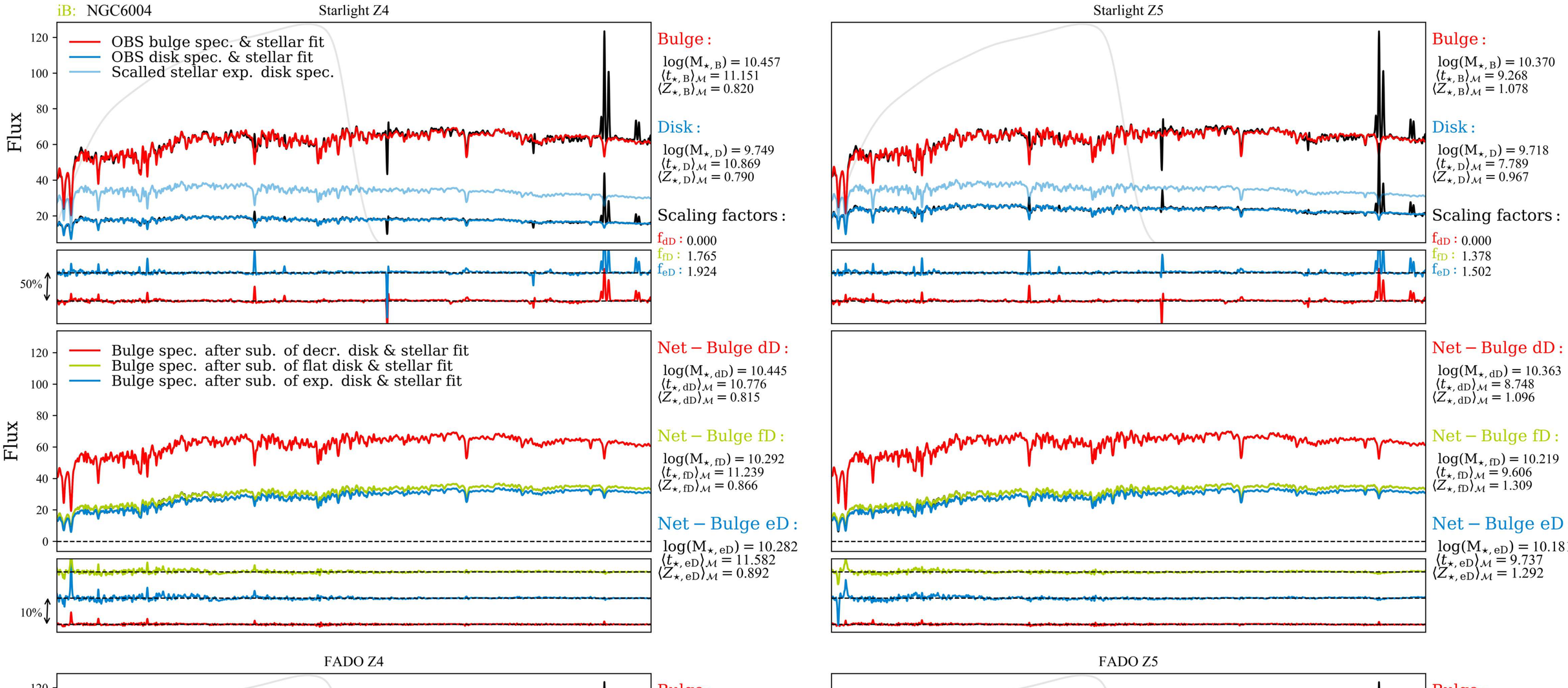
iB: NGC6004
Starlight Z4
OBS bulge spec. & stellar fit
OBS disk spec. & stellar fit
Scalled stellar exp. disk spec.
Flux
50%
Bulge :
log(M⋆, B) = 10.457
⟨t⋆, B⟩M = 11.151
⟨Z⋆, B⟩M = 0.820
Disk :
log(M⋆, D) = 9.749
⟨t⋆, D⟩M = 10.869
⟨Z⋆, D⟩M = 0.790
Scaling factors :
fdD : 0.000
ffD : 1.765
feD : 1.924
Starlight Z5
Bulge :
log(M⋆, B) = 10.370
⟨t⋆, B⟩M = 9.268
⟨Z⋆, B⟩M = 1.078
Disk :
log(M⋆, D) = 9.718
⟨t⋆, D⟩M = 7.789
⟨Z⋆, D⟩M = 0.967
Scaling factors :
fdD : 0.000
ffD : 1.378
feD : 1.502
Bulge spec. after sub. of decr. disk & stellar fit
Bulge spec. after sub. of flat disk & stellar fit
Bulge spec. after sub. of exp. disk & stellar fit
10%
Net − Bulge dD :
log(M⋆, dD) = 10.445
⟨t⋆, dD⟩M = 10.776
⟨Z⋆, dD⟩M = 0.815
Net − Bulge fD :
log(M⋆, fD) = 10.292
⟨t⋆, fD⟩M = 11.239
⟨Z⋆, fD⟩M = 0.866
Net − Bulge eD :
log(M⋆, eD) = 10.282
⟨t⋆, eD⟩M = 11.582
⟨Z⋆, eD⟩M = 0.892
Net − Bulge dD :
log(M⋆, dD) = 10.363
⟨t⋆, dD⟩M = 8.748
⟨Z⋆, dD⟩M = 1.096
Net − Bulge fD :
log(M⋆, fD) = 10.219
⟨t⋆, fD⟩M = 9.606
⟨Z⋆, fD⟩M = 1.309
Net − Bulge eD :
log(M⋆, eD) = 10.181
⟨t⋆, eD⟩M = 9.737
⟨Z⋆, eD⟩M = 1.292
FADO Z4
Bulge :
log(M⋆, B) = 10.350
⟨t⋆, B⟩M = 10.420
⟨Z⋆, B⟩M = 0.616
Disk :
log(M⋆, D) = 9.609
⟨t⋆, D⟩M = 9.443
⟨Z⋆, D⟩M = 0.497
FADO Z5
Bulge :
log(M⋆, B) = 10.090
⟨t⋆, B⟩M = 4.538
⟨Z⋆, B⟩M = 1.022
Disk :
log(M⋆, D) = 9.685
⟨t⋆, D⟩M = 6.477
⟨Z⋆, D⟩M = 0.738
Net − Bulge dD :
log(M⋆, dD) = 10.340
⟨t⋆, dD⟩M = 9.999
⟨Z⋆, dD⟩M = 0.604
Net − Bulge fD :
log(M⋆, fD) = 10.180
⟨t⋆, fD⟩M = 8.004
⟨Z⋆, fD⟩M = 0.702
Net − Bulge eD :
log(M⋆, eD) = 10.140
⟨t⋆, eD⟩M = 7.336
⟨Z⋆, eD⟩M = 0.705
Net − Bulge dD :
log(M⋆, dD) = 10.150
⟨t⋆, dD⟩M = 5.260
⟨Z⋆, dD⟩M = 1.009
Net − Bulge fD :
log(M⋆, fD) = 9.906
⟨t⋆, fD⟩M = 4.246
⟨Z⋆, fD⟩M = 1.352
Net − Bulge eD :
log(M⋆, eD) = 9.933
⟨t⋆, eD⟩M = 4.665
⟨Z⋆, eD⟩M = 1.294
λ (Å)

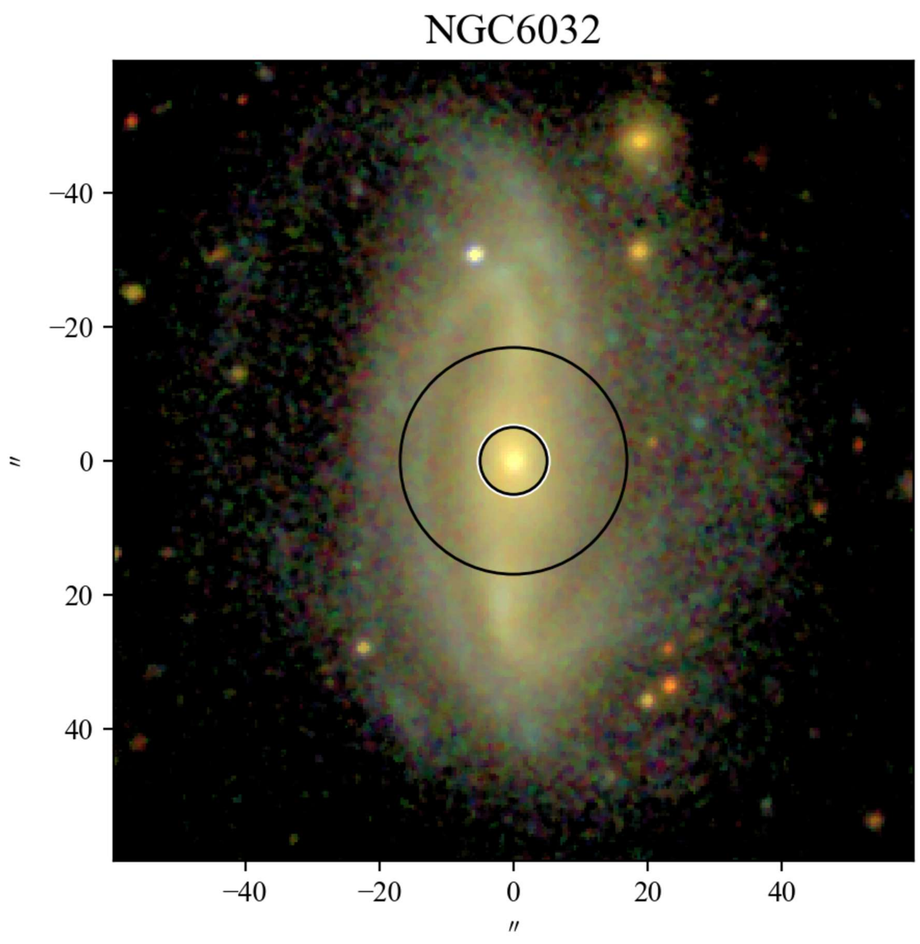
NGC6032
−40
−20
0
20
40
″
−40
−20
0
20
40
″

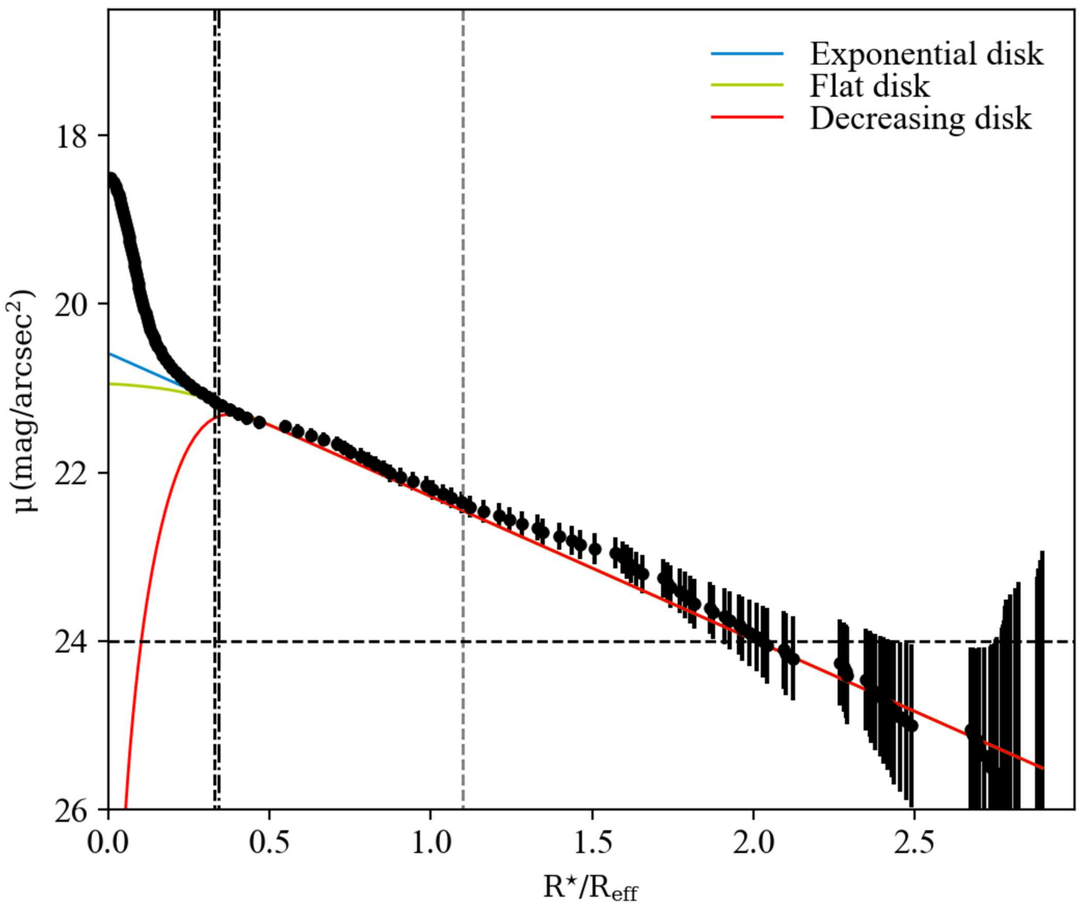
Exponential disk
Flat disk
Decreasing disk
μ (mag/arcsec²)
18
20
22
24
26
0.0
0.5
1.0
1.5
2.0
2.5
R⋆/Reff

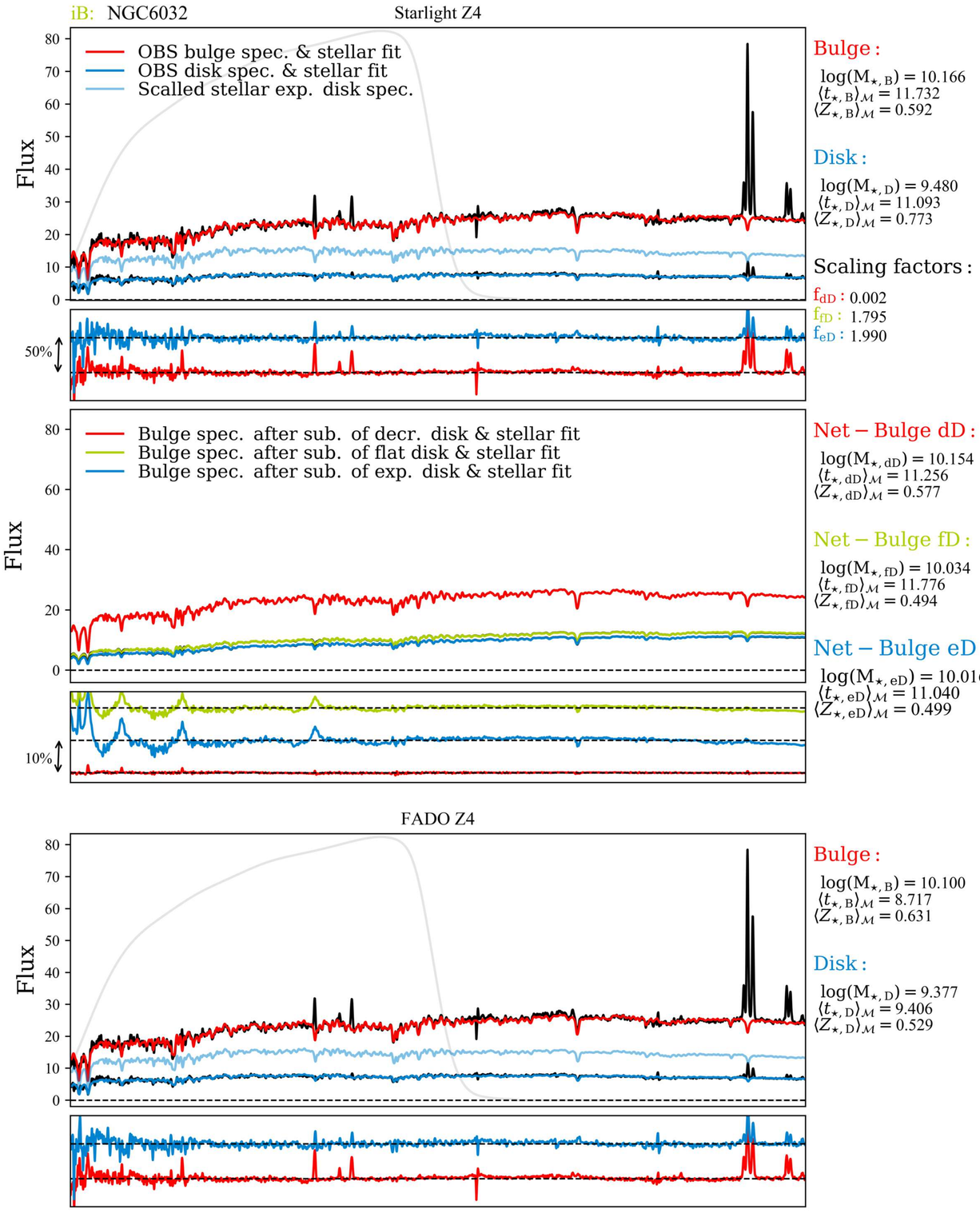
iB: NGC6032
Starlight Z4
OBS bulge spec. & stellar fit
OBS disk spec. & stellar fit
Scalled stellar exp. disk spec.
Flux
50%
Bulge :
log(M⋆, B) = 10.166
⟨t⋆, B⟩M = 11.732
⟨Z⋆, B⟩M = 0.592
Disk :
log(M⋆, D) = 9.480
⟨t⋆, D⟩M = 11.093
⟨Z⋆, D⟩M = 0.773
Scaling factors :
fdD : 0.002
ffD : 1.795
feD : 1.990
Bulge spec. after sub. of decr. disk & stellar fit
Bulge spec. after sub. of flat disk & stellar fit
Bulge spec. after sub. of exp. disk & stellar fit
10%
Net − Bulge dD :
log(M⋆, dD) = 10.154
⟨t⋆, dD⟩M = 11.256
⟨Z⋆, dD⟩M = 0.577
Net − Bulge fD :
log(M⋆, fD) = 10.034
⟨t⋆, fD⟩M = 11.776
⟨Z⋆, fD⟩M = 0.494
Net − Bulge eD :
log(M⋆, eD) = 10.016
⟨t⋆, eD⟩M = 11.040
⟨Z⋆, eD⟩M = 0.499

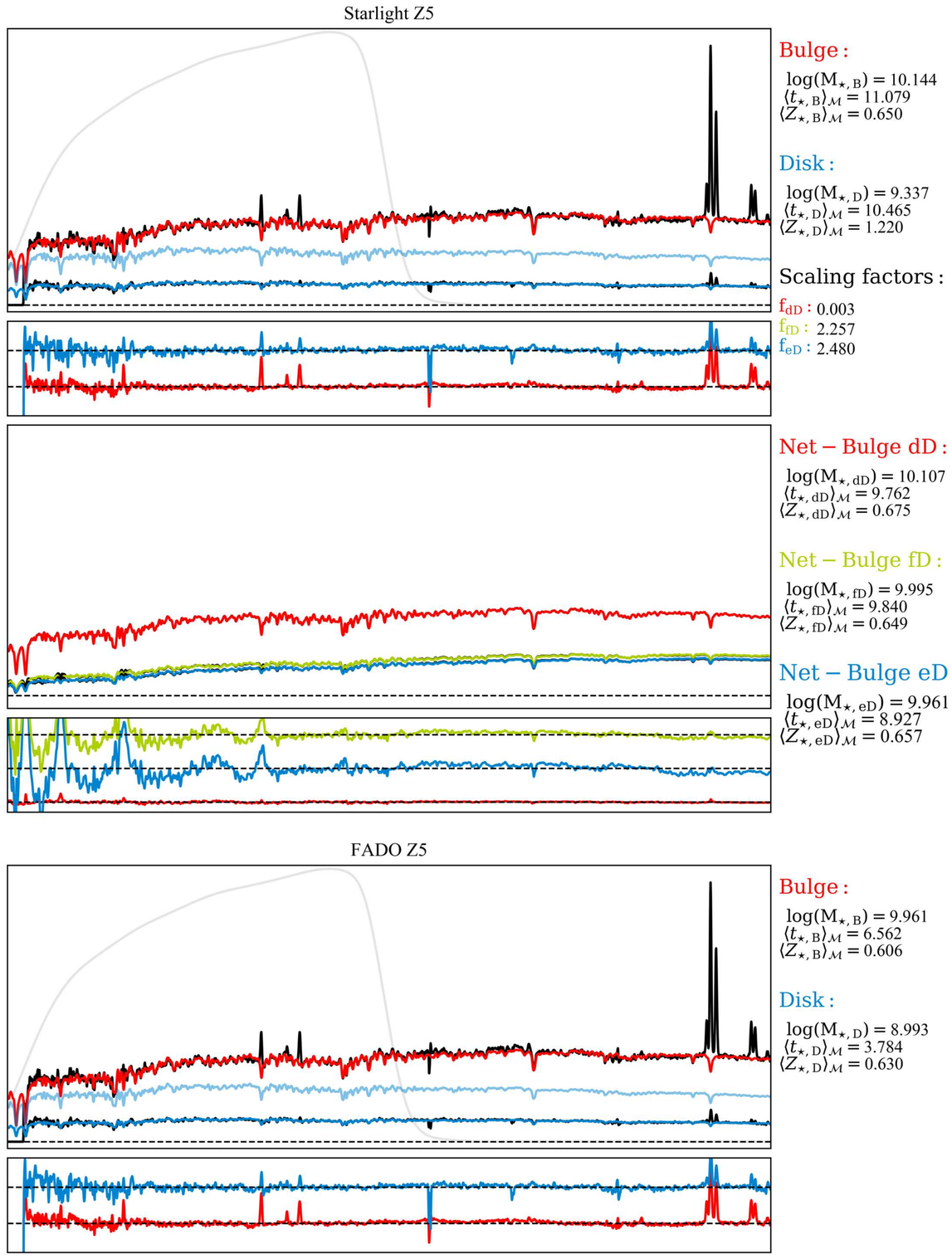
Starlight Z5
Bulge :
log(M⋆, B) = 10.144
⟨t⋆, B⟩M = 11.079
⟨Z⋆, B⟩M = 0.650
Disk :
log(M⋆, D) = 9.337
⟨t⋆, D⟩M = 10.465
⟨Z⋆, D⟩M = 1.220
Scaling factors :
fdD : 0.003
ffD : 2.257
feD : 2.480
Net − Bulge dD :
log(M⋆, dD) = 10.107
⟨t⋆, dD⟩M = 9.762
⟨Z⋆, dD⟩M = 0.675
Net − Bulge fD :
log(M⋆, fD) = 9.995
⟨t⋆, fD⟩M = 9.840
⟨Z⋆, fD⟩M = 0.649
Net − Bulge eD :
log(M⋆, eD) = 9.961
⟨t⋆, eD⟩M = 8.927
⟨Z⋆, eD⟩M = 0.657

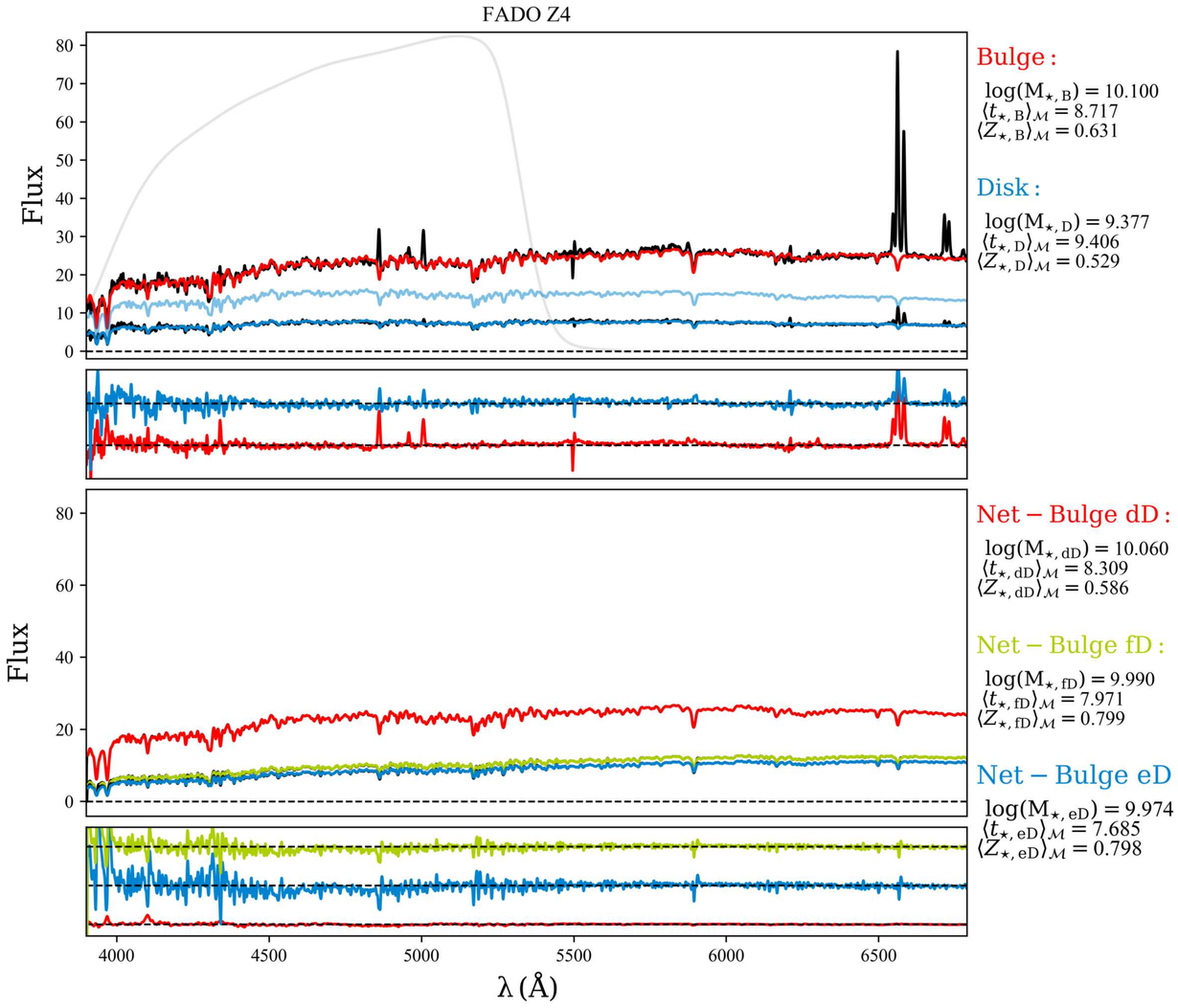
FADO Z4
Flux
Bulge :
log(M⋆, B) = 10.100
⟨t⋆, B⟩M = 8.717
⟨Z⋆, B⟩M = 0.631
Disk :
log(M⋆, D) = 9.377
⟨t⋆, D⟩M = 9.406
⟨Z⋆, D⟩M = 0.529
Net − Bulge dD :
log(M⋆, dD) = 10.060
⟨t⋆, dD⟩M = 8.309
⟨Z⋆, dD⟩M = 0.586
Net − Bulge fD :
log(M⋆, fD) = 9.990
⟨t⋆, fD⟩M = 7.971
⟨Z⋆, fD⟩M = 0.799
Net − Bulge eD :
log(M⋆, eD) = 9.974
⟨t⋆, eD⟩M = 7.685
⟨Z⋆, eD⟩M = 0.798
λ (Å)

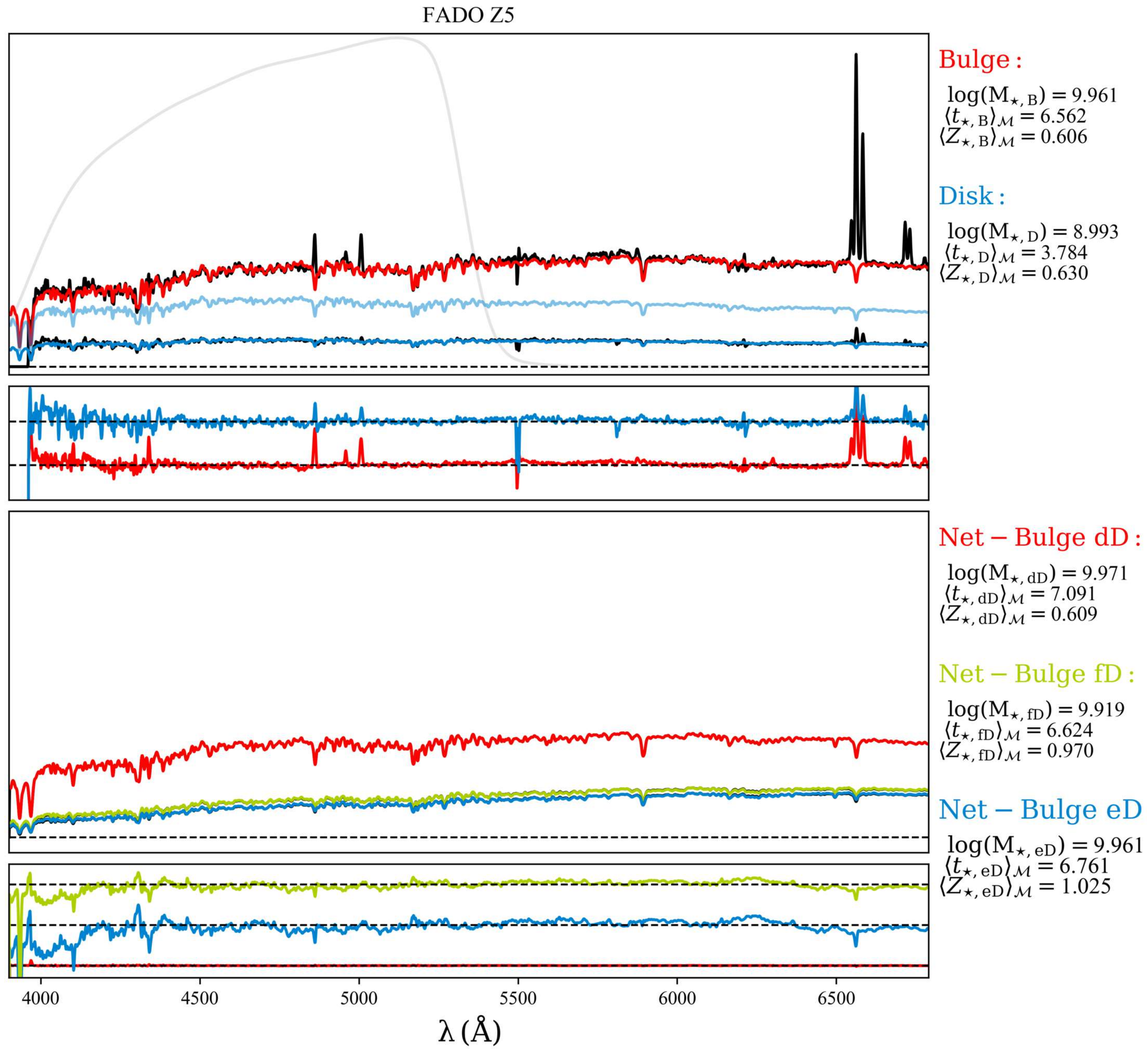
FADO Z5
Bulge :
log(M⋆, B) = 9.961
⟨t⋆, B⟩M = 6.562
⟨Z⋆, B⟩M = 0.606
Disk :
log(M⋆, D) = 8.993
⟨t⋆, D⟩M = 3.784
⟨Z⋆, D⟩M = 0.630
Net − Bulge dD :
log(M⋆, dD) = 9.971
⟨t⋆, dD⟩M = 7.091
⟨Z⋆, dD⟩M = 0.609
Net − Bulge fD :
log(M⋆, fD) = 9.919
⟨t⋆, fD⟩M = 6.624
⟨Z⋆, fD⟩M = 0.970
Net − Bulge eD :
log(M⋆, eD) = 9.961
⟨t⋆, eD⟩M = 6.761
⟨Z⋆, eD⟩M = 1.025
λ (Å)

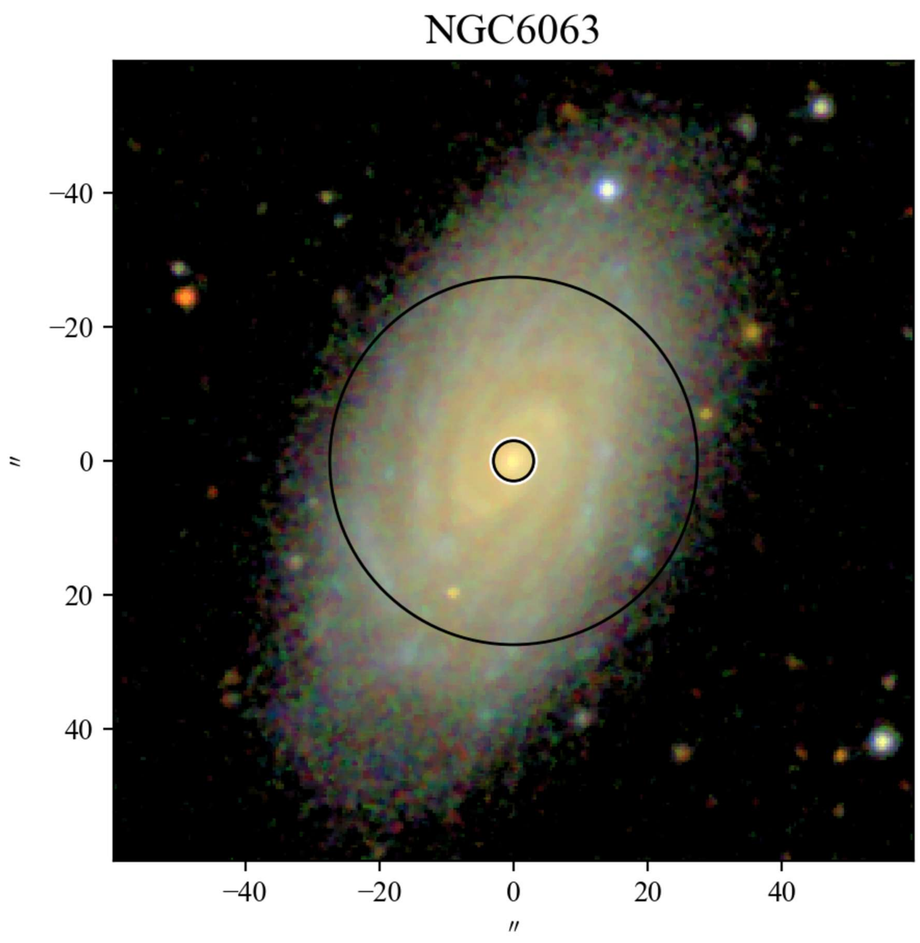
NGC6063
″
−40
−20
0
20
40

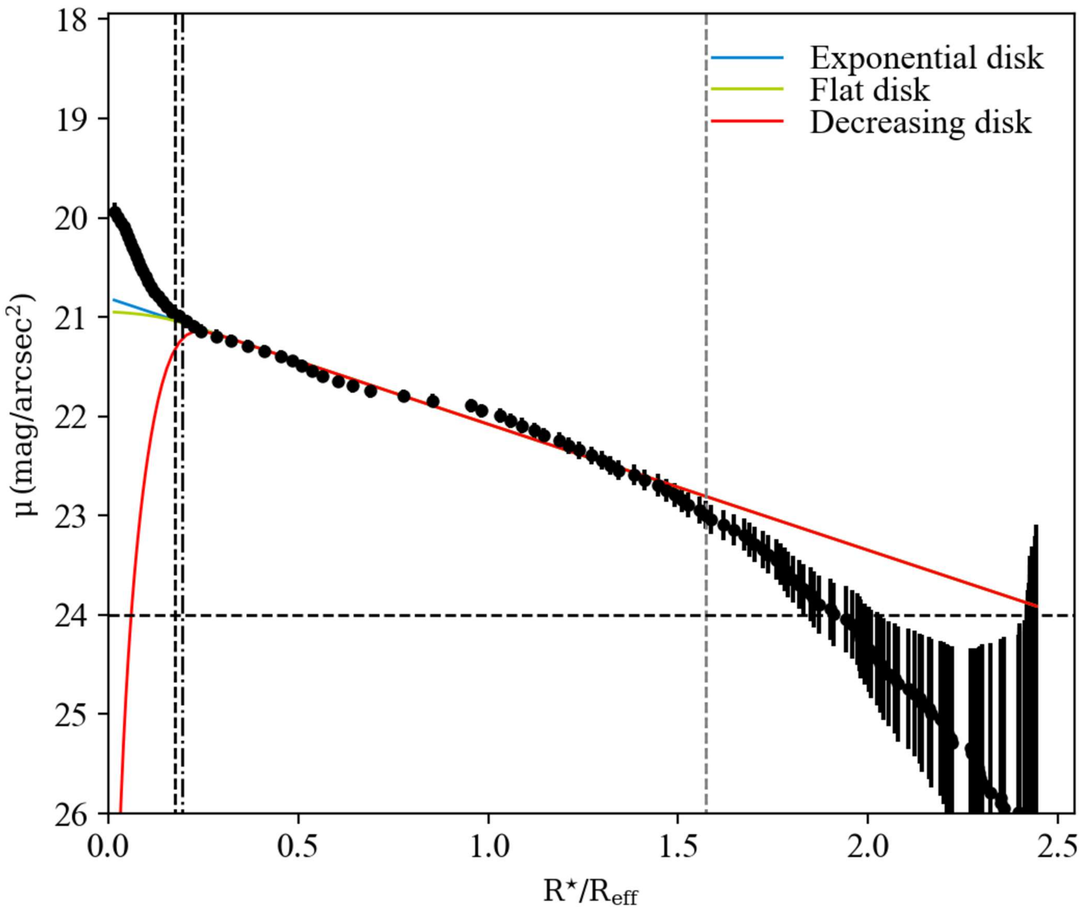
Exponential disk
Flat disk
Decreasing disk
μ (mag/arcsec²)
R⋆/R_eff

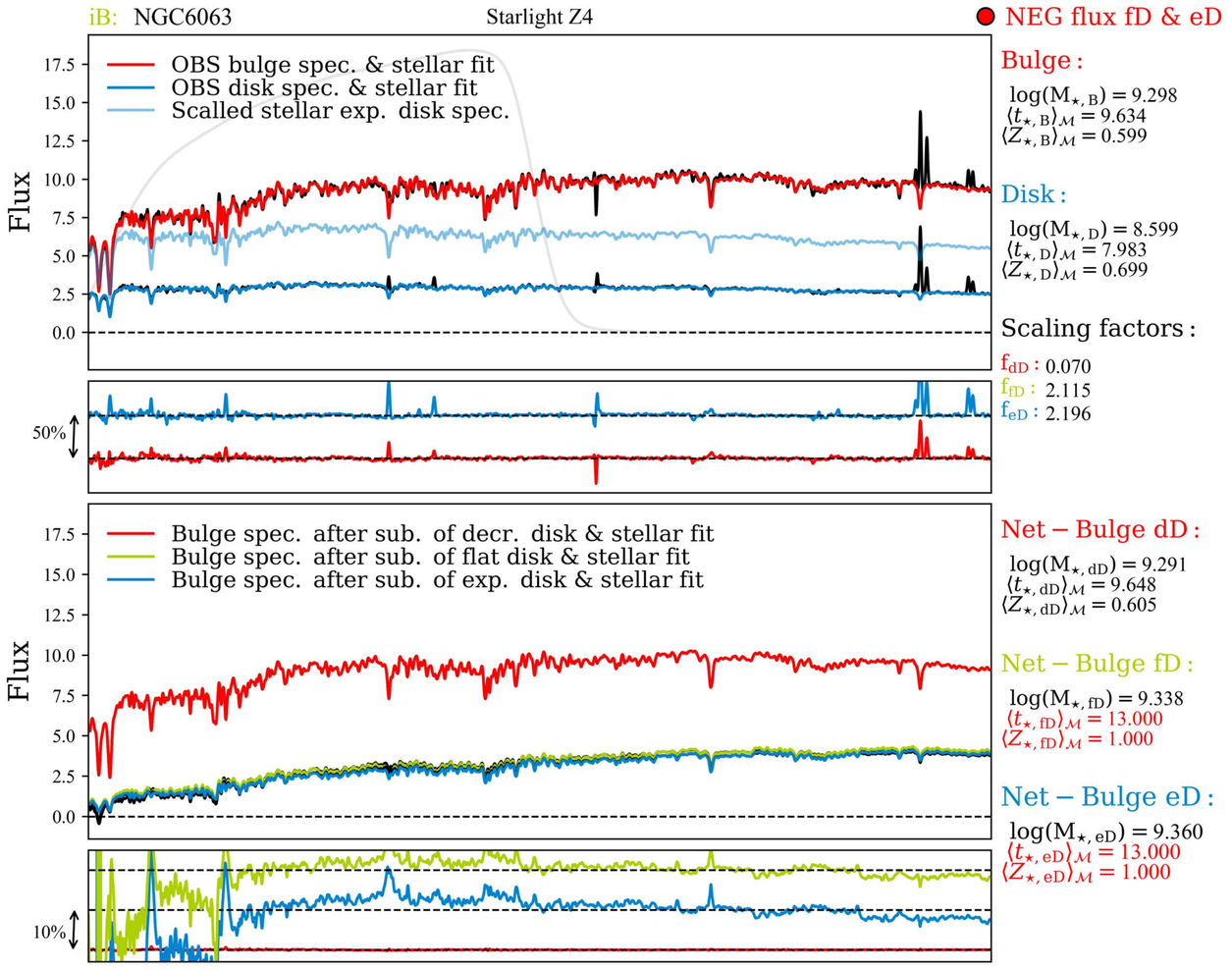
iB: NGC6063
Starlight Z4
NEG flux fD & eD
OBS bulge spec. & stellar fit
OBS disk spec. & stellar fit
Scalled stellar exp. disk spec.
Flux
Bulge :
log(M⋆, B) = 9.298
⟨t⋆, B⟩M = 9.634
⟨Z⋆, B⟩M = 0.599
Disk :
log(M⋆, D) = 8.599
⟨t⋆, D⟩M = 7.983
⟨Z⋆, D⟩M = 0.699
Scaling factors :
fdD : 0.070
ffD : 2.115
feD : 2.196
50%
Bulge spec. after sub. of decr. disk & stellar fit
Bulge spec. after sub. of flat disk & stellar fit
Bulge spec. after sub. of exp. disk & stellar fit
Net − Bulge dD :
log(M⋆, dD) = 9.291
⟨t⋆, dD⟩M = 9.648
⟨Z⋆, dD⟩M = 0.605
Net − Bulge fD :
log(M⋆, fD) = 9.338
⟨t⋆, fD⟩M = 13.000
⟨Z⋆, fD⟩M = 1.000
Net − Bulge eD :
log(M⋆, eD) = 9.360
⟨t⋆, eD⟩M = 13.000
⟨Z⋆, eD⟩M = 1.000
10%

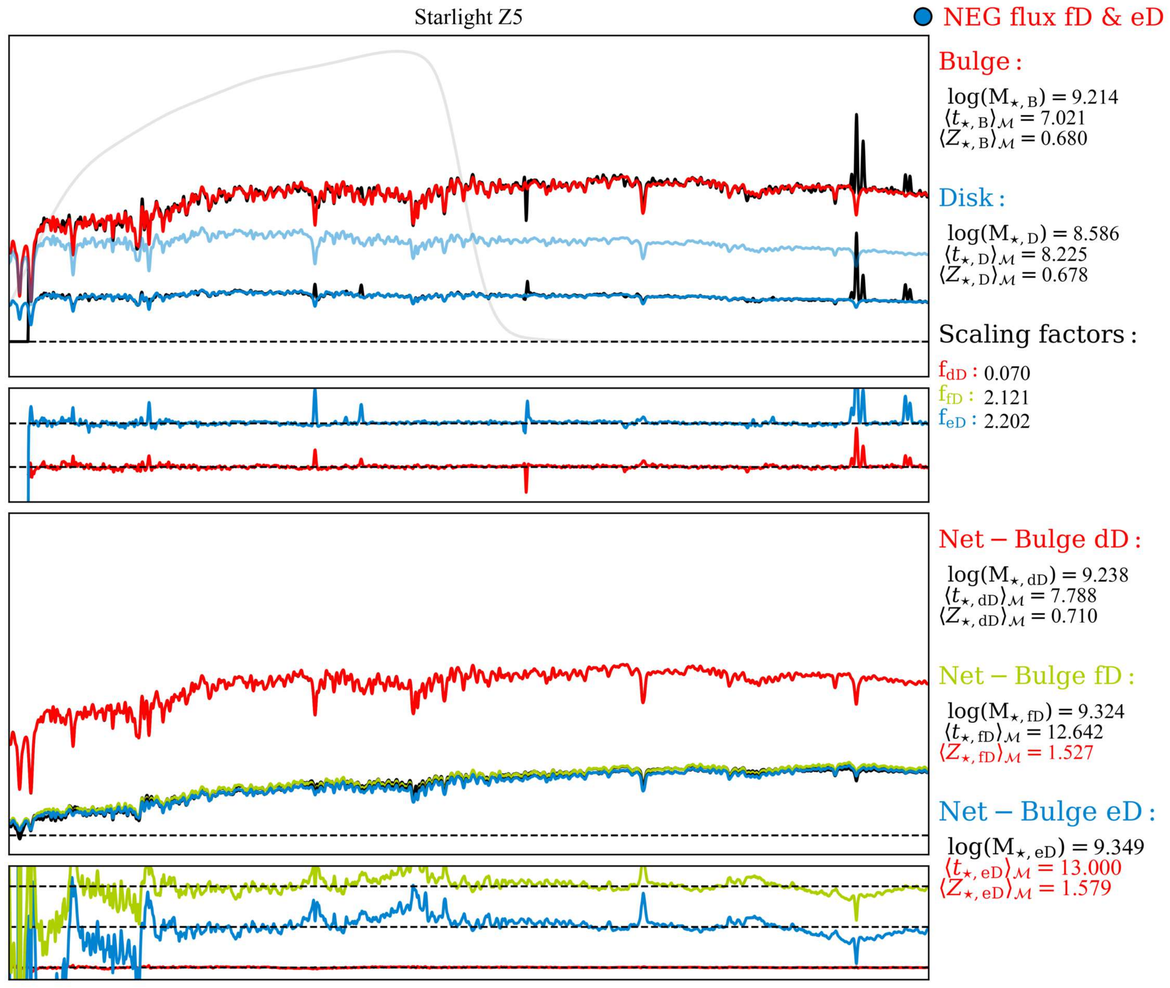
Starlight Z5
NEG flux fD & eD
Bulge :
log(M⋆, B) = 9.214
⟨t⋆, B⟩M = 7.021
⟨Z⋆, B⟩M = 0.680
Disk :
log(M⋆, D) = 8.586
⟨t⋆, D⟩M = 8.225
⟨Z⋆, D⟩M = 0.678
Scaling factors :
fdD : 0.070
ffD : 2.121
feD : 2.202
Net − Bulge dD :
log(M⋆, dD) = 9.238
⟨t⋆, dD⟩M = 7.788
⟨Z⋆, dD⟩M = 0.710
Net − Bulge fD :
log(M⋆, fD) = 9.324
⟨t⋆, fD⟩M = 12.642
⟨Z⋆, fD⟩M = 1.527
Net − Bulge eD :
log(M⋆, eD) = 9.349
⟨t⋆, eD⟩M = 13.000
⟨Z⋆, eD⟩M = 1.579

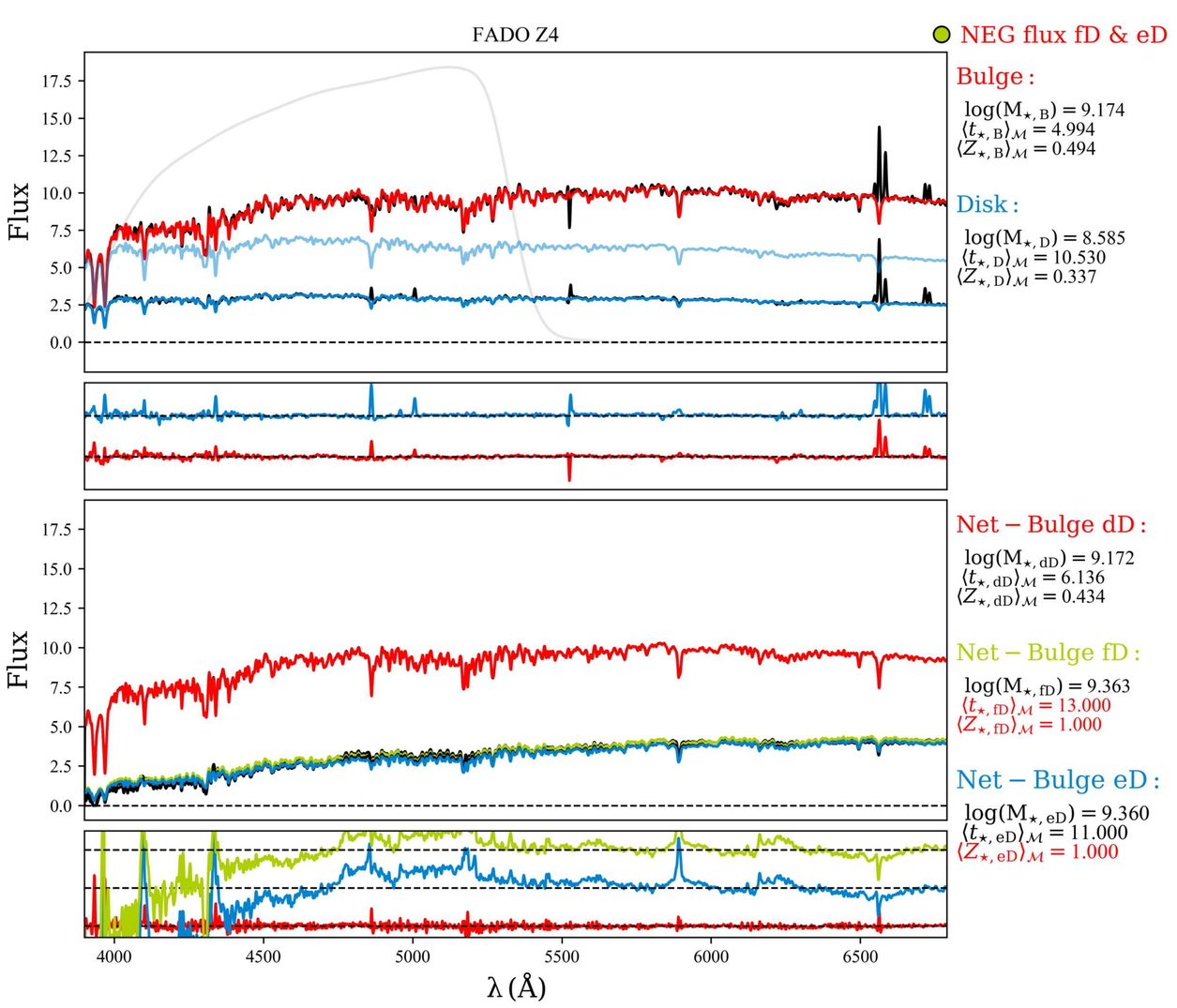
FADO Z4
NEG flux fD & eD
Flux
Bulge :
log(M⋆, B) = 9.174
⟨t⋆, B⟩M = 4.994
⟨Z⋆, B⟩M = 0.494
Disk :
log(M⋆, D) = 8.585
⟨t⋆, D⟩M = 10.530
⟨Z⋆, D⟩M = 0.337
Net − Bulge dD :
log(M⋆, dD) = 9.172
⟨t⋆, dD⟩M = 6.136
⟨Z⋆, dD⟩M = 0.434
Net − Bulge fD :
log(M⋆, fD) = 9.363
⟨t⋆, fD⟩M = 13.000
⟨Z⋆, fD⟩M = 1.000
Net − Bulge eD :
log(M⋆, eD) = 9.360
⟨t⋆, eD⟩M = 11.000
⟨Z⋆, eD⟩M = 1.000
λ (Å)

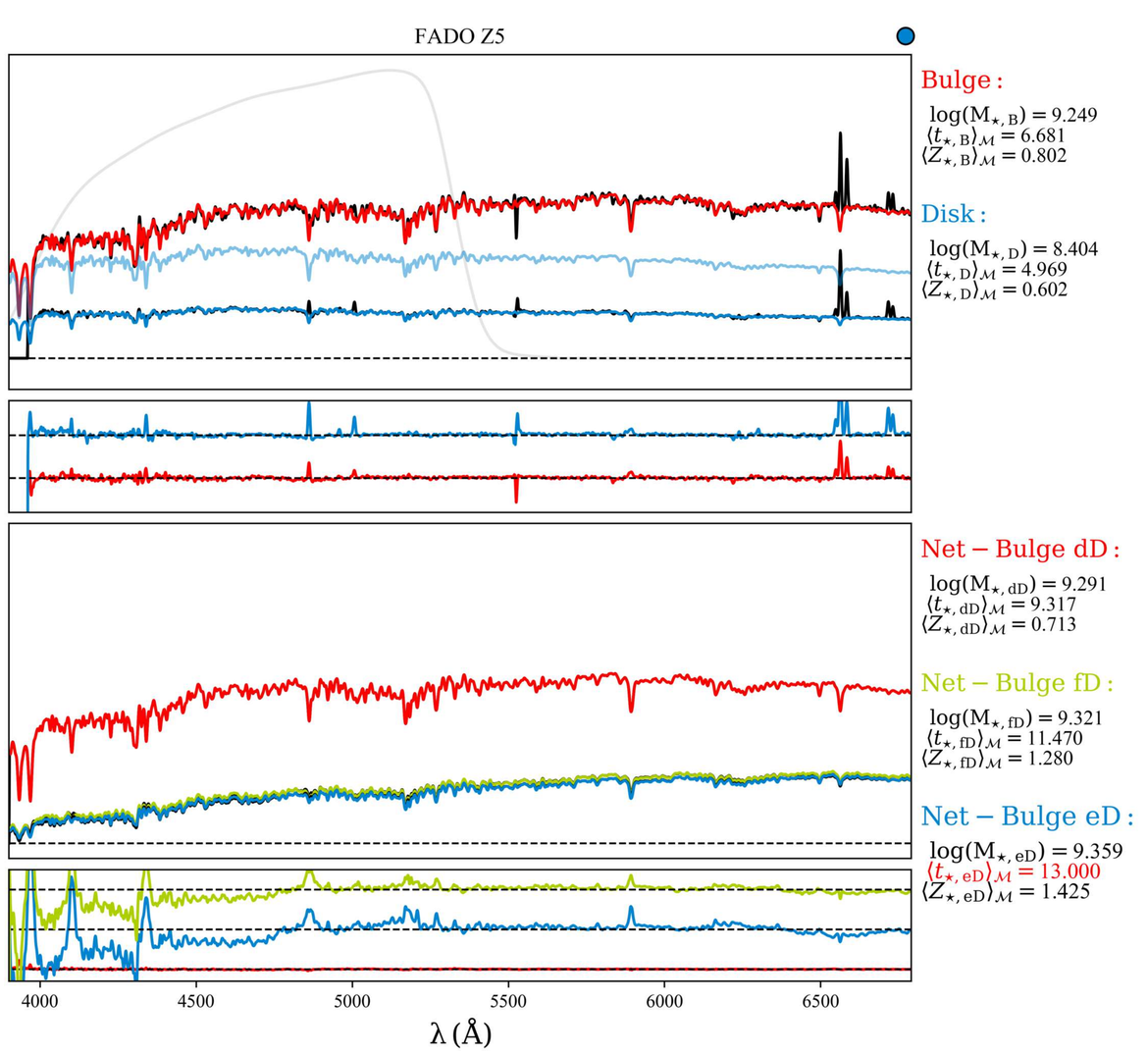
FADO Z5
Bulge :
log(M⋆, B) = 9.249
⟨t⋆, B⟩M = 6.681
⟨Z⋆, B⟩M = 0.802
Disk :
log(M⋆, D) = 8.404
⟨t⋆, D⟩M = 4.969
⟨Z⋆, D⟩M = 0.602
Net − Bulge dD :
log(M⋆, dD) = 9.291
⟨t⋆, dD⟩M = 9.317
⟨Z⋆, dD⟩M = 0.713
Net − Bulge fD :
log(M⋆, fD) = 9.321
⟨t⋆, fD⟩M = 11.470
⟨Z⋆, fD⟩M = 1.280
Net − Bulge eD :
log(M⋆, eD) = 9.359
⟨t⋆, eD⟩M = 13.000
⟨Z⋆, eD⟩M = 1.425
λ (Å)

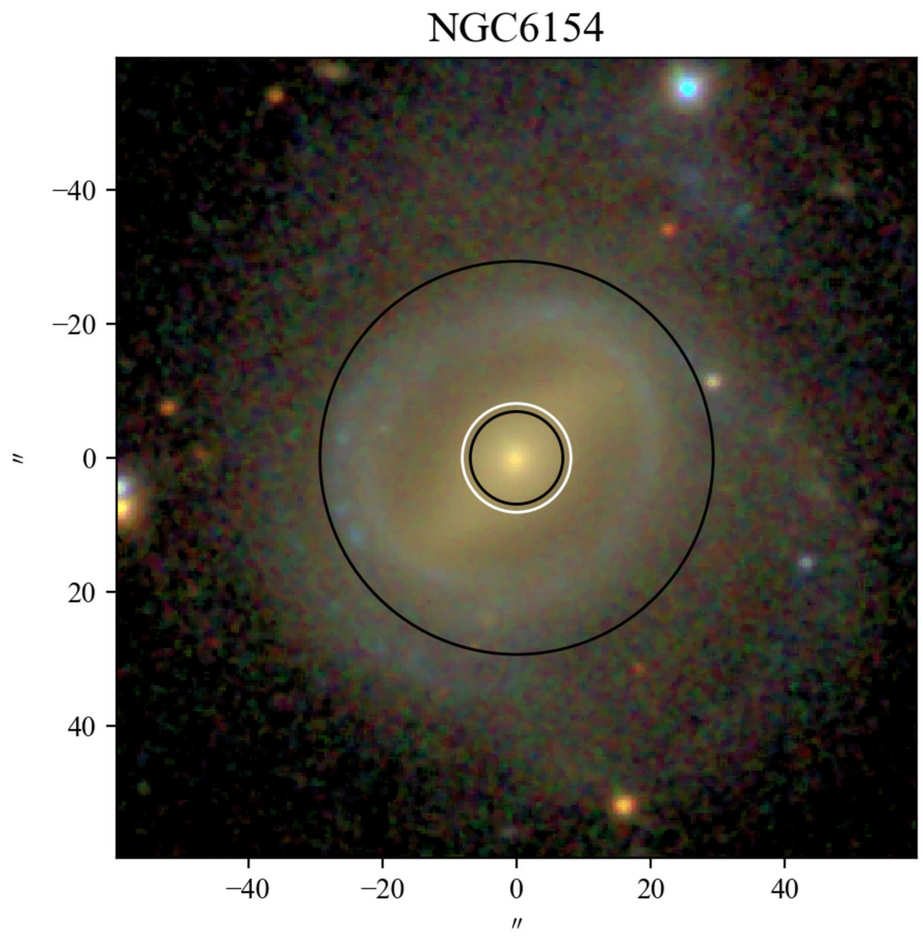
NGC6154
−40
−20
0
20
40
″
−40
−20
0
20
40
″

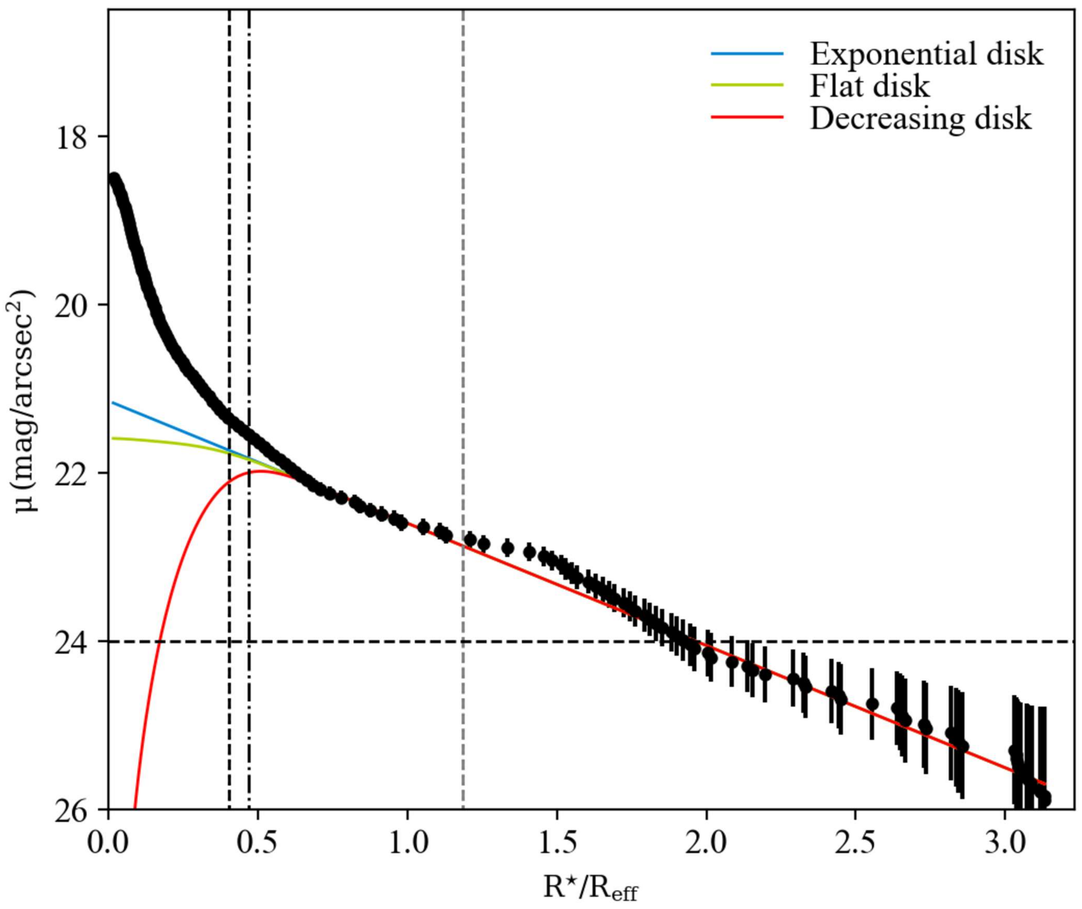
Exponential disk
Flat disk
Decreasing disk
μ (mag/arcsec²)
18
20
22
24
26
0.0
0.5
1.0
1.5
2.0
2.5
3.0
R⋆/Reff

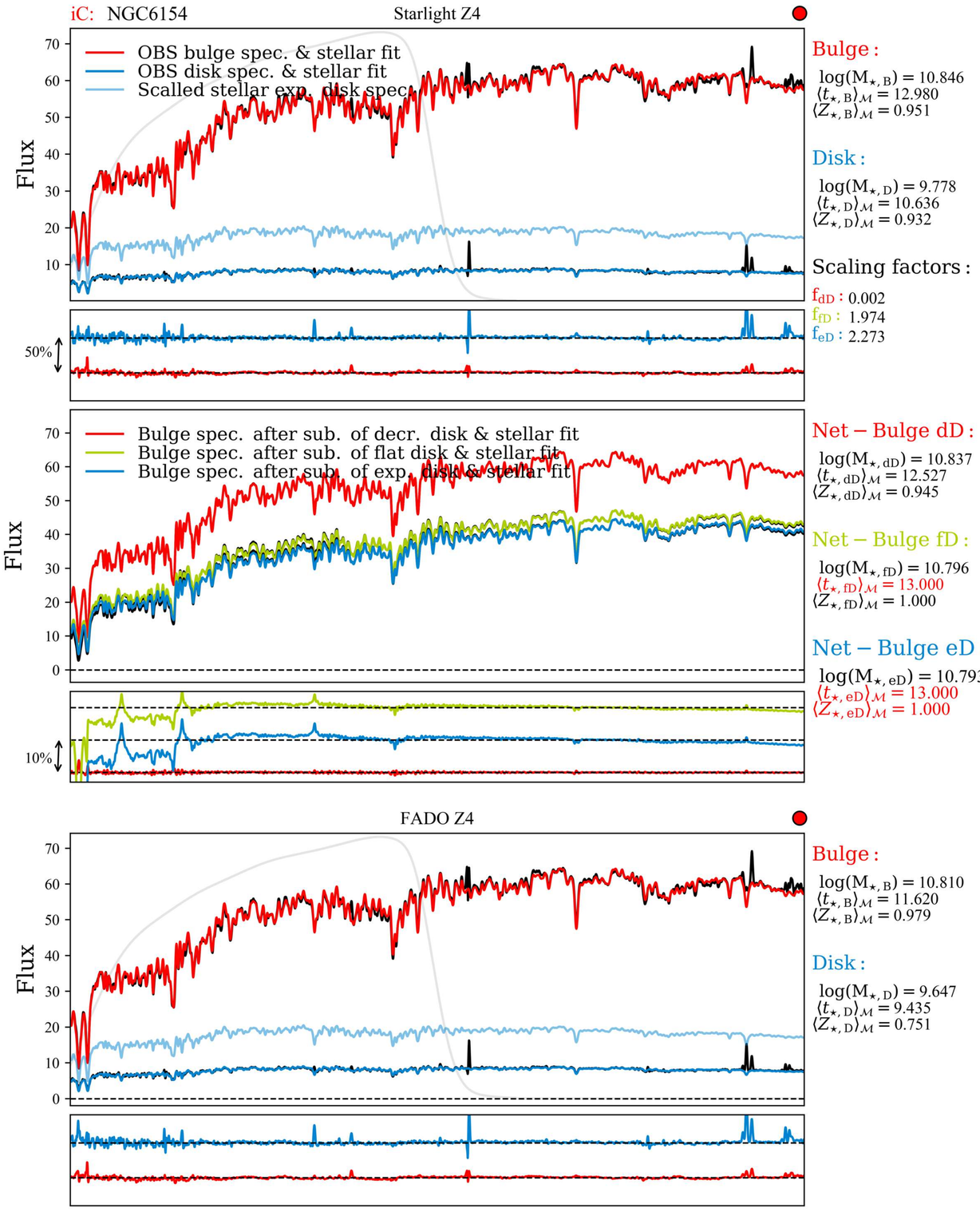
iC: NGC6154
Starlight Z4
OBS bulge spec. & stellar fit
OBS disk spec. & stellar fit
Scalled stellar exp. disk spec.
Flux
50%
Bulge :
log(M⋆, B) = 10.846
⟨t⋆, B⟩M = 12.980
⟨Z⋆, B⟩M = 0.951
Disk :
log(M⋆, D) = 9.778
⟨t⋆, D⟩M = 10.636
⟨Z⋆, D⟩M = 0.932
Scaling factors :
fdD : 0.002
ffD : 1.974
feD : 2.273
Bulge spec. after sub. of decr. disk & stellar fit
Bulge spec. after sub. of flat disk & stellar fit
Bulge spec. after sub. of exp. disk & stellar fit
10%
Net − Bulge dD :
log(M⋆, dD) = 10.837
⟨t⋆, dD⟩M = 12.527
⟨Z⋆, dD⟩M = 0.945
Net − Bulge fD :
log(M⋆, fD) = 10.796
⟨t⋆, fD⟩M = 13.000
⟨Z⋆, fD⟩M = 1.000
Net − Bulge eD :
log(M⋆, eD) = 10.793
⟨t⋆, eD⟩M = 13.000
⟨Z⋆, eD⟩M = 1.000

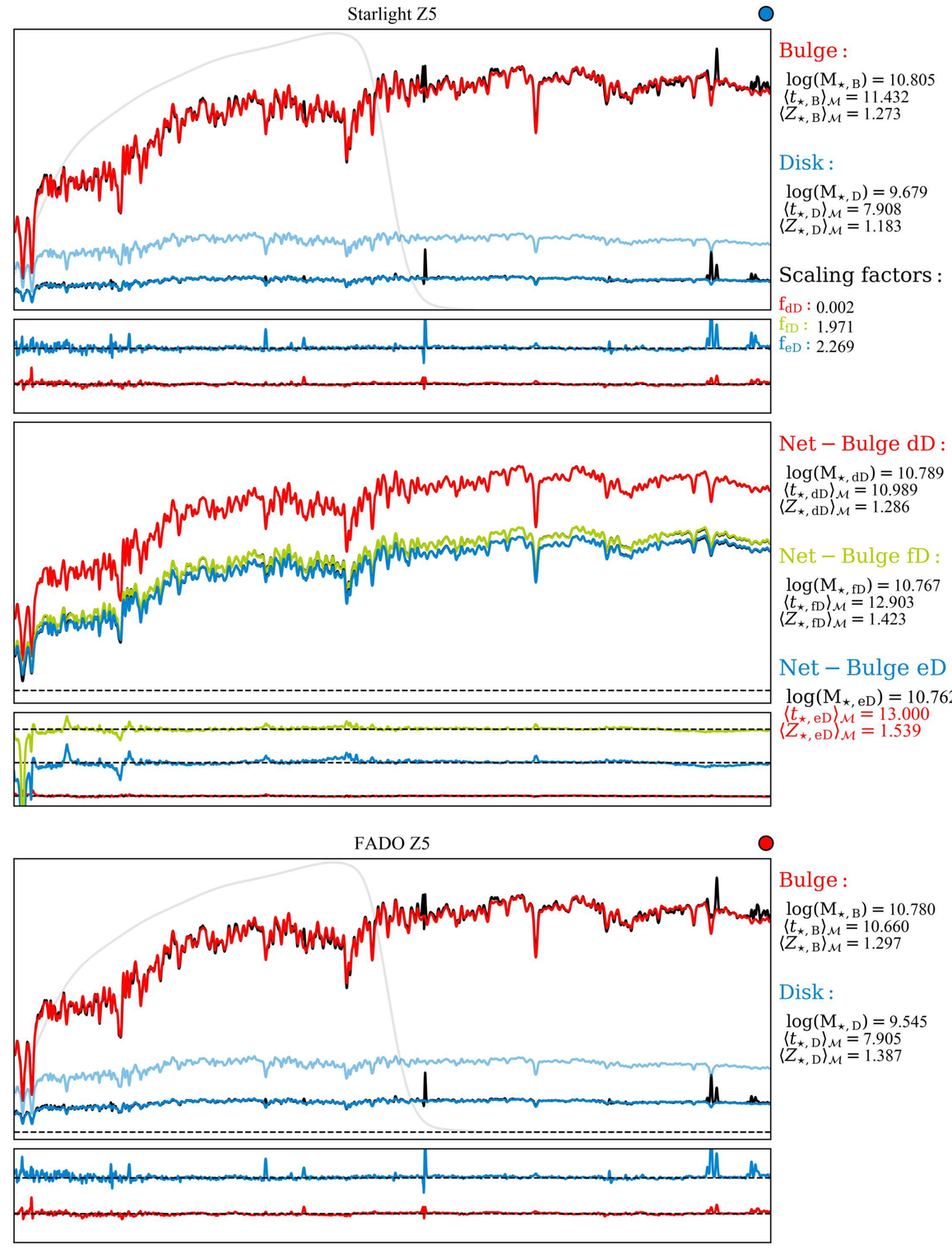
Starlight Z5
Bulge :
log(M⋆, B) = 10.805
⟨t⋆, B⟩M = 11.432
⟨Z⋆, B⟩M = 1.273
Disk :
log(M⋆, D) = 9.679
⟨t⋆, D⟩M = 7.908
⟨Z⋆, D⟩M = 1.183
Scaling factors :
fdD : 0.002
ffD : 1.971
feD : 2.269
Net − Bulge dD :
log(M⋆, dD) = 10.789
⟨t⋆, dD⟩M = 10.989
⟨Z⋆, dD⟩M = 1.286
Net − Bulge fD :
log(M⋆, fD) = 10.767
⟨t⋆, fD⟩M = 12.903
⟨Z⋆, fD⟩M = 1.423
Net − Bulge eD :
log(M⋆, eD) = 10.762
⟨t⋆, eD⟩M = 13.000
⟨Z⋆, eD⟩M = 1.539

FADO Z4
Flux
Bulge :
log(M⋆, B) = 10.810
⟨t⋆, B⟩M = 11.620
⟨Z⋆, B⟩M = 0.979
Disk :
log(M⋆, D) = 9.647
⟨t⋆, D⟩M = 9.435
⟨Z⋆, D⟩M = 0.751
Net − Bulge dD :
log(M⋆, dD) = 10.810
⟨t⋆, dD⟩M = 11.330
⟨Z⋆, dD⟩M = 0.982
Net − Bulge fD :
log(M⋆, fD) = 10.780
⟨t⋆, fD⟩M = 13.000
⟨Z⋆, fD⟩M = 1.000
Net − Bulge eD :
log(M⋆, eD) = 10.780
⟨t⋆, eD⟩M = 13.000
⟨Z⋆, eD⟩M = 1.000
4000
4500
5000
5500
6000
6500
λ (Å)

FADO Z5
Bulge :
log(M⋆, B) = 10.780
⟨t⋆, B⟩M = 10.660
⟨Z⋆, B⟩M = 1.297
Disk :
log(M⋆, D) = 9.545
⟨t⋆, D⟩M = 7.905
⟨Z⋆, D⟩M = 1.387
Net − Bulge dD :
log(M⋆, dD) = 10.730
⟨t⋆, dD⟩M = 9.096
⟨Z⋆, dD⟩M = 1.305
Net − Bulge fD :
log(M⋆, fD) = 10.760
⟨t⋆, fD⟩M = 13.000
⟨Z⋆, fD⟩M = 1.302
Net − Bulge eD :
log(M⋆, eD) = 10.750
⟨t⋆, eD⟩M = 13.000
⟨Z⋆, eD⟩M = 1.412
4000
4500
5000
5500
6000
6500
λ (Å)

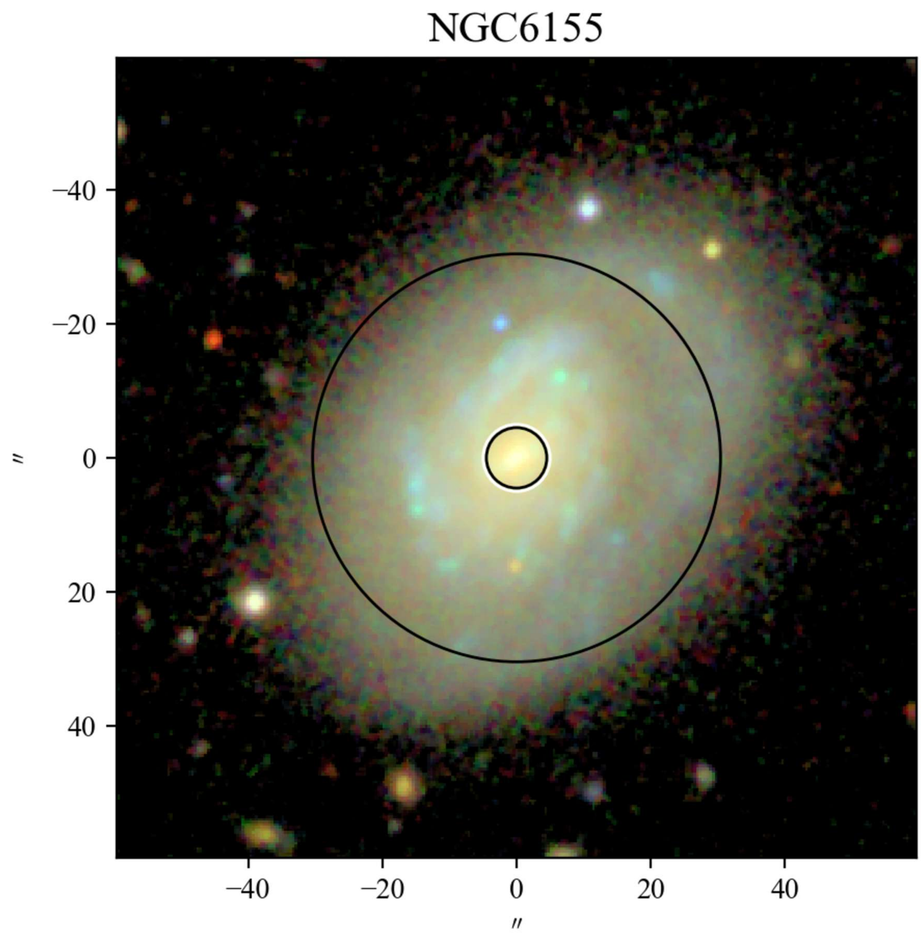
NGC6155
−40
−20
0
20
40
″
−40
−20
0
20
40
″

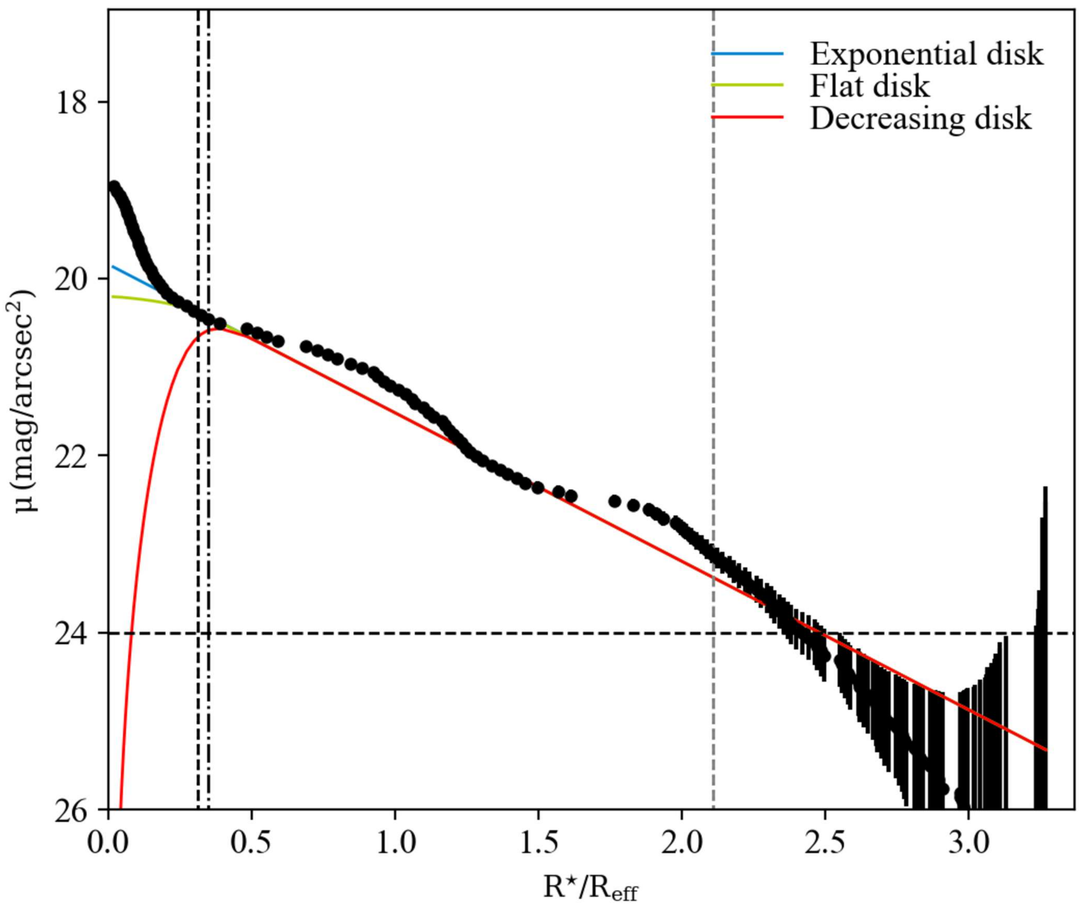
Exponential disk
Flat disk
Decreasing disk
μ (mag/arcsec²)
18
20
22
24
26
0.0
0.5
1.0
1.5
2.0
2.5
3.0
R⋆/Reff

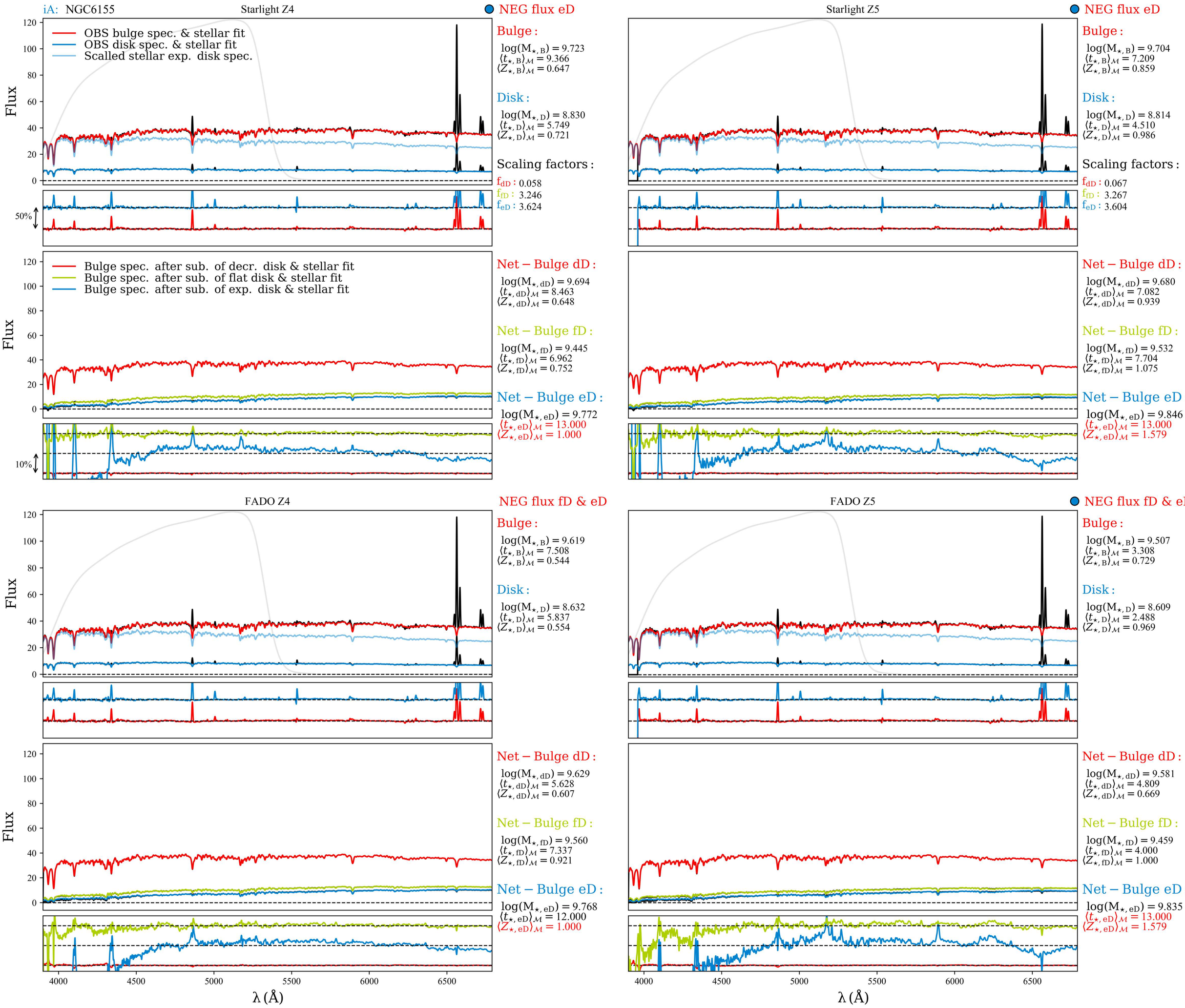
iA: NGC6155
Starlight Z4
NEG flux eD
OBS bulge spec. & stellar fit
OBS disk spec. & stellar fit
Scalled stellar exp. disk spec.
Flux
50%
Bulge :
log(M⋆, B) = 9.723
⟨t⋆, B⟩M = 9.366
⟨Z⋆, B⟩M = 0.647
Disk :
log(M⋆, D) = 8.830
⟨t⋆, D⟩M = 5.749
⟨Z⋆, D⟩M = 0.721
Scaling factors :
fdD : 0.058
ffD : 3.246
feD : 3.624
Starlight Z5
NEG flux eD
Bulge :
log(M⋆, B) = 9.704
⟨t⋆, B⟩M = 7.209
⟨Z⋆, B⟩M = 0.859
Disk :
log(M⋆, D) = 8.814
⟨t⋆, D⟩M = 4.510
⟨Z⋆, D⟩M = 0.986
Scaling factors :
fdD : 0.067
ffD : 3.267
feD : 3.604
Bulge spec. after sub. of decr. disk & stellar fit
Bulge spec. after sub. of flat disk & stellar fit
Bulge spec. after sub. of exp. disk & stellar fit
10%
Net − Bulge dD :
log(M⋆, dD) = 9.694
⟨t⋆, dD⟩M = 8.463
⟨Z⋆, dD⟩M = 0.648
Net − Bulge fD :
log(M⋆, fD) = 9.445
⟨t⋆, fD⟩M = 6.962
⟨Z⋆, fD⟩M = 0.752
Net − Bulge eD :
log(M⋆, eD) = 9.772
⟨t⋆, eD⟩M = 13.000
⟨Z⋆, eD⟩M = 1.000
Net − Bulge dD :
log(M⋆, dD) = 9.680
⟨t⋆, dD⟩M = 7.082
⟨Z⋆, dD⟩M = 0.939
Net − Bulge fD :
log(M⋆, fD) = 9.532
⟨t⋆, fD⟩M = 7.704
⟨Z⋆, fD⟩M = 1.075
Net − Bulge eD :
log(M⋆, eD) = 9.846
⟨t⋆, eD⟩M = 13.000
⟨Z⋆, eD⟩M = 1.579
FADO Z4
NEG flux fD & eD
Bulge :
log(M⋆, B) = 9.619
⟨t⋆, B⟩M = 7.508
⟨Z⋆, B⟩M = 0.544
Disk :
log(M⋆, D) = 8.632
⟨t⋆, D⟩M = 5.837
⟨Z⋆, D⟩M = 0.554
FADO Z5
NEG flux fD & eD
Bulge :
log(M⋆, B) = 9.507
⟨t⋆, B⟩M = 3.308
⟨Z⋆, B⟩M = 0.729
Disk :
log(M⋆, D) = 8.609
⟨t⋆, D⟩M = 2.488
⟨Z⋆, D⟩M = 0.969
Net − Bulge dD :
log(M⋆, dD) = 9.629
⟨t⋆, dD⟩M = 5.628
⟨Z⋆, dD⟩M = 0.607
Net − Bulge fD :
log(M⋆, fD) = 9.560
⟨t⋆, fD⟩M = 7.337
⟨Z⋆, fD⟩M = 0.921
Net − Bulge eD :
log(M⋆, eD) = 9.768
⟨t⋆, eD⟩M = 12.000
⟨Z⋆, eD⟩M = 1.000
Net − Bulge dD :
log(M⋆, dD) = 9.581
⟨t⋆, dD⟩M = 4.809
⟨Z⋆, dD⟩M = 0.669
Net − Bulge fD :
log(M⋆, fD) = 9.459
⟨t⋆, fD⟩M = 4.000
⟨Z⋆, fD⟩M = 1.000
Net − Bulge eD :
log(M⋆, eD) = 9.835
⟨t⋆, eD⟩M = 13.000
⟨Z⋆, eD⟩M = 1.579
λ (Å)

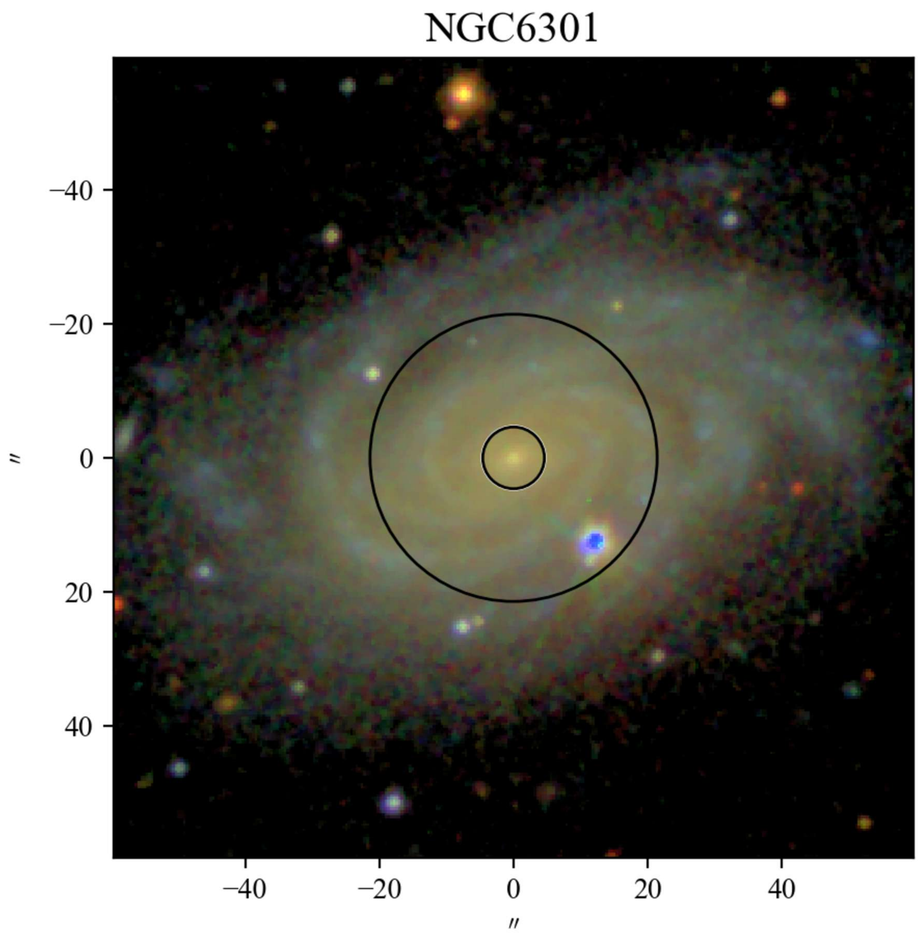
NGC6301
−40
−20
0
20
40
″
−40
−20
0
20
40
″

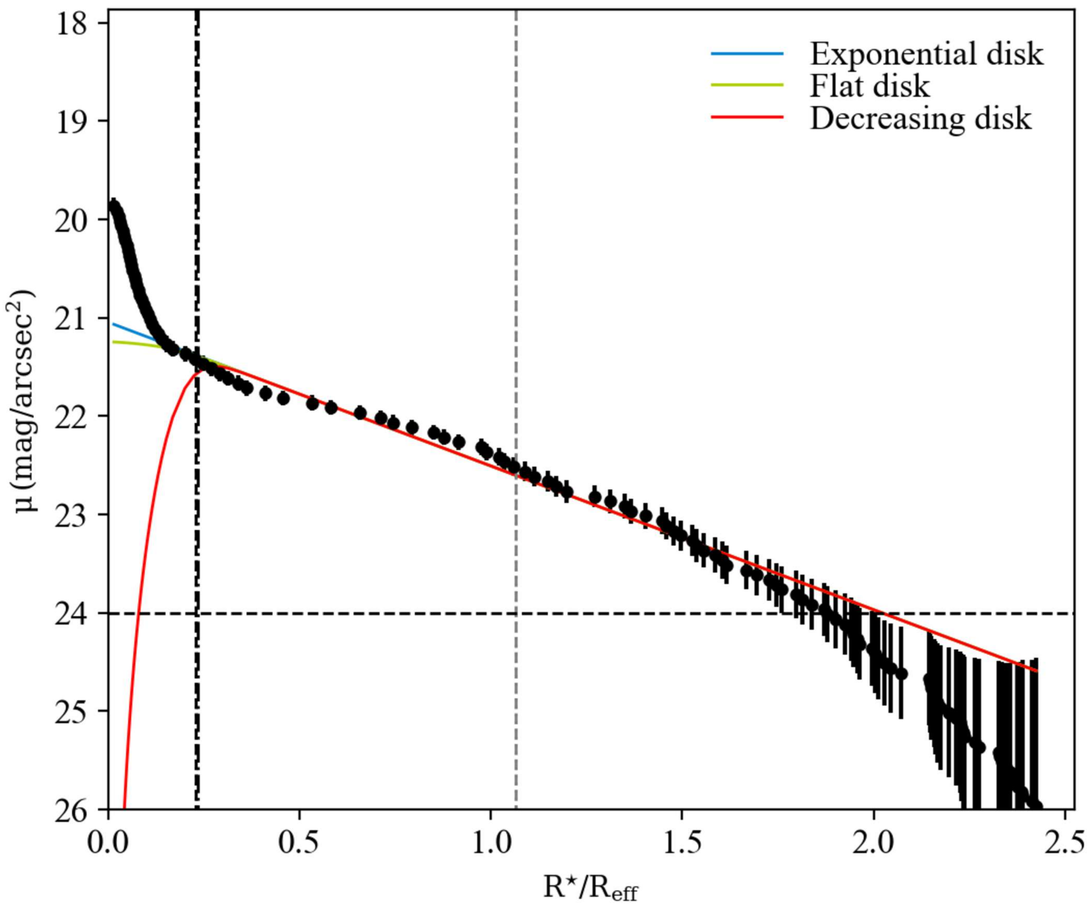
Exponential disk
Flat disk
Decreasing disk
μ (mag/arcsec²)
18
19
20
21
22
23
24
25
26
0.0
0.5
1.0
1.5
2.0
2.5
R⋆/Reff

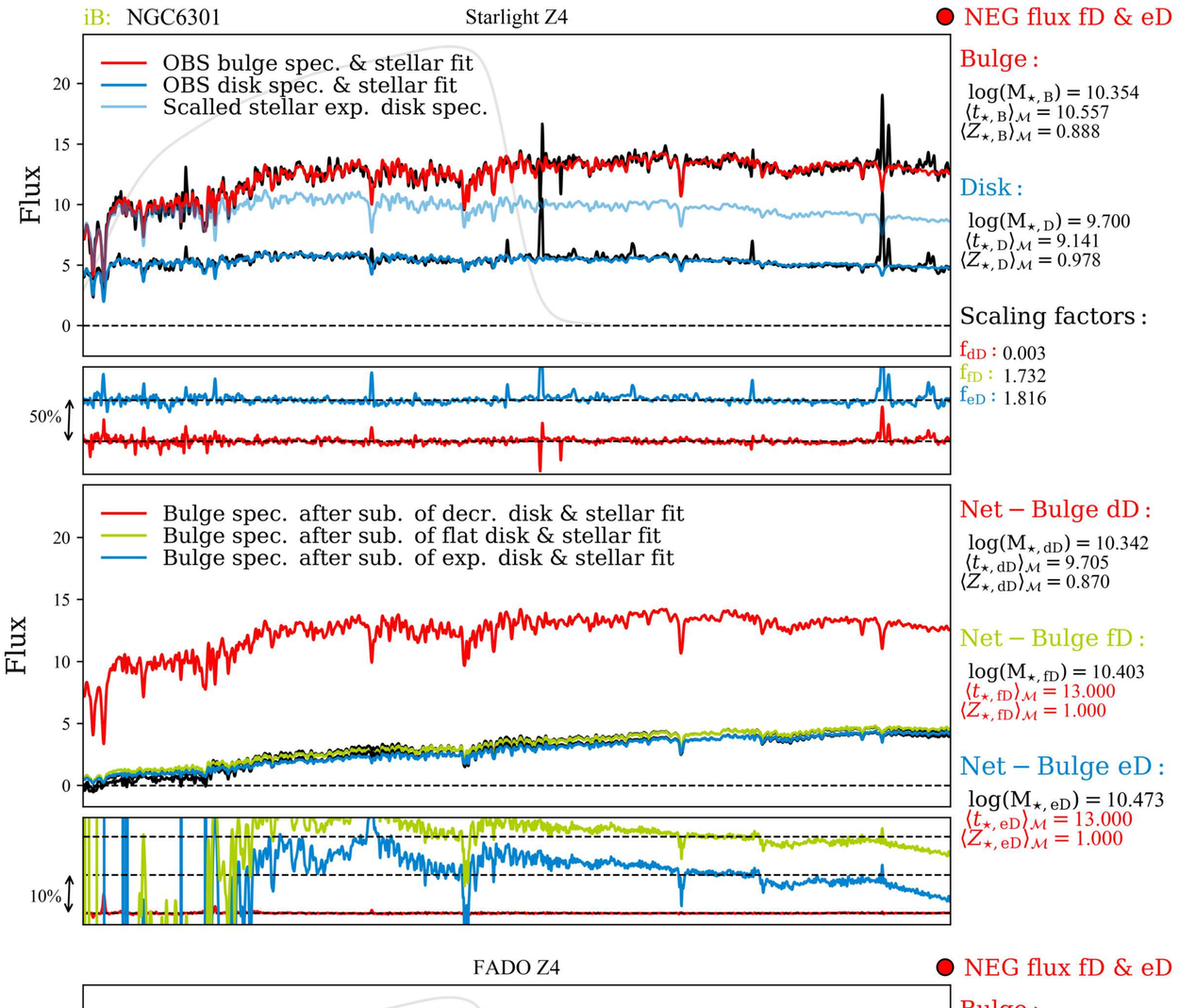
iB: NGC6301
Starlight Z4
NEG flux fD & eD
OBS bulge spec. & stellar fit
OBS disk spec. & stellar fit
Scalled stellar exp. disk spec.
Flux
50%
Bulge spec. after sub. of decr. disk & stellar fit
Bulge spec. after sub. of flat disk & stellar fit
Bulge spec. after sub. of exp. disk & stellar fit
10%
Bulge :
log(M⋆, B) = 10.354
⟨t⋆, B⟩M = 10.557
⟨Z⋆, B⟩M = 0.888
Disk :
log(M⋆, D) = 9.700
⟨t⋆, D⟩M = 9.141
⟨Z⋆, D⟩M = 0.978
Scaling factors :
fdD : 0.003
ffD : 1.732
feD : 1.816
Net − Bulge dD :
log(M⋆, dD) = 10.342
⟨t⋆, dD⟩M = 9.705
⟨Z⋆, dD⟩M = 0.870
Net − Bulge fD :
log(M⋆, fD) = 10.403
⟨t⋆, fD⟩M = 13.000
⟨Z⋆, fD⟩M = 1.000
Net − Bulge eD :
log(M⋆, eD) = 10.473
⟨t⋆, eD⟩M = 13.000
⟨Z⋆, eD⟩M = 1.000

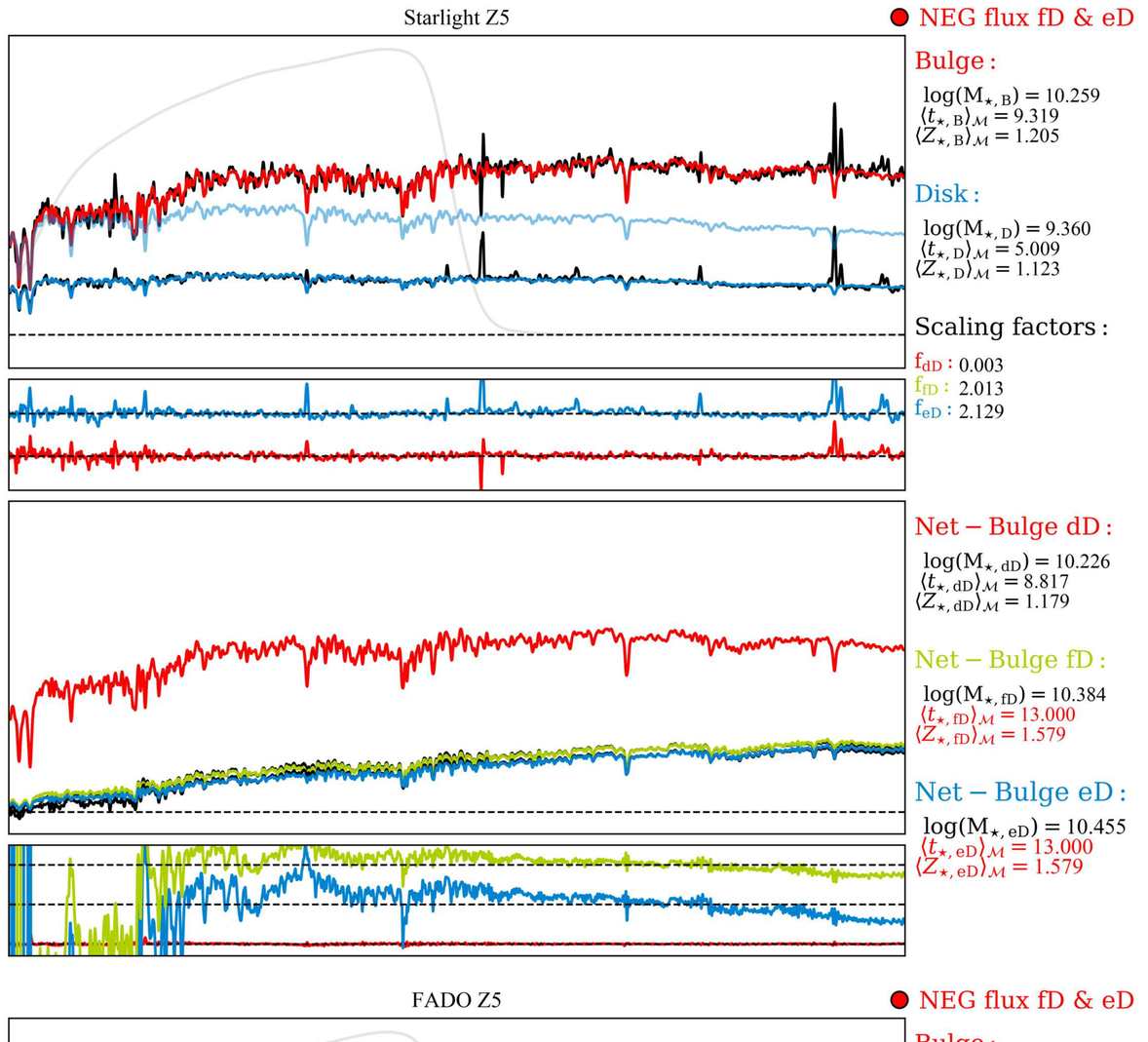
Starlight Z5
NEG flux fD & eD
Bulge :
log(M⋆, B) = 10.259
⟨t⋆, B⟩M = 9.319
⟨Z⋆, B⟩M = 1.205
Disk :
log(M⋆, D) = 9.360
⟨t⋆, D⟩M = 5.009
⟨Z⋆, D⟩M = 1.123
Scaling factors :
fdD : 0.003
ffD : 2.013
feD : 2.129
Net − Bulge dD :
log(M⋆, dD) = 10.226
⟨t⋆, dD⟩M = 8.817
⟨Z⋆, dD⟩M = 1.179
Net − Bulge fD :
log(M⋆, fD) = 10.384
⟨t⋆, fD⟩M = 13.000
⟨Z⋆, fD⟩M = 1.579
Net − Bulge eD :
log(M⋆, eD) = 10.455
⟨t⋆, eD⟩M = 13.000
⟨Z⋆, eD⟩M = 1.579

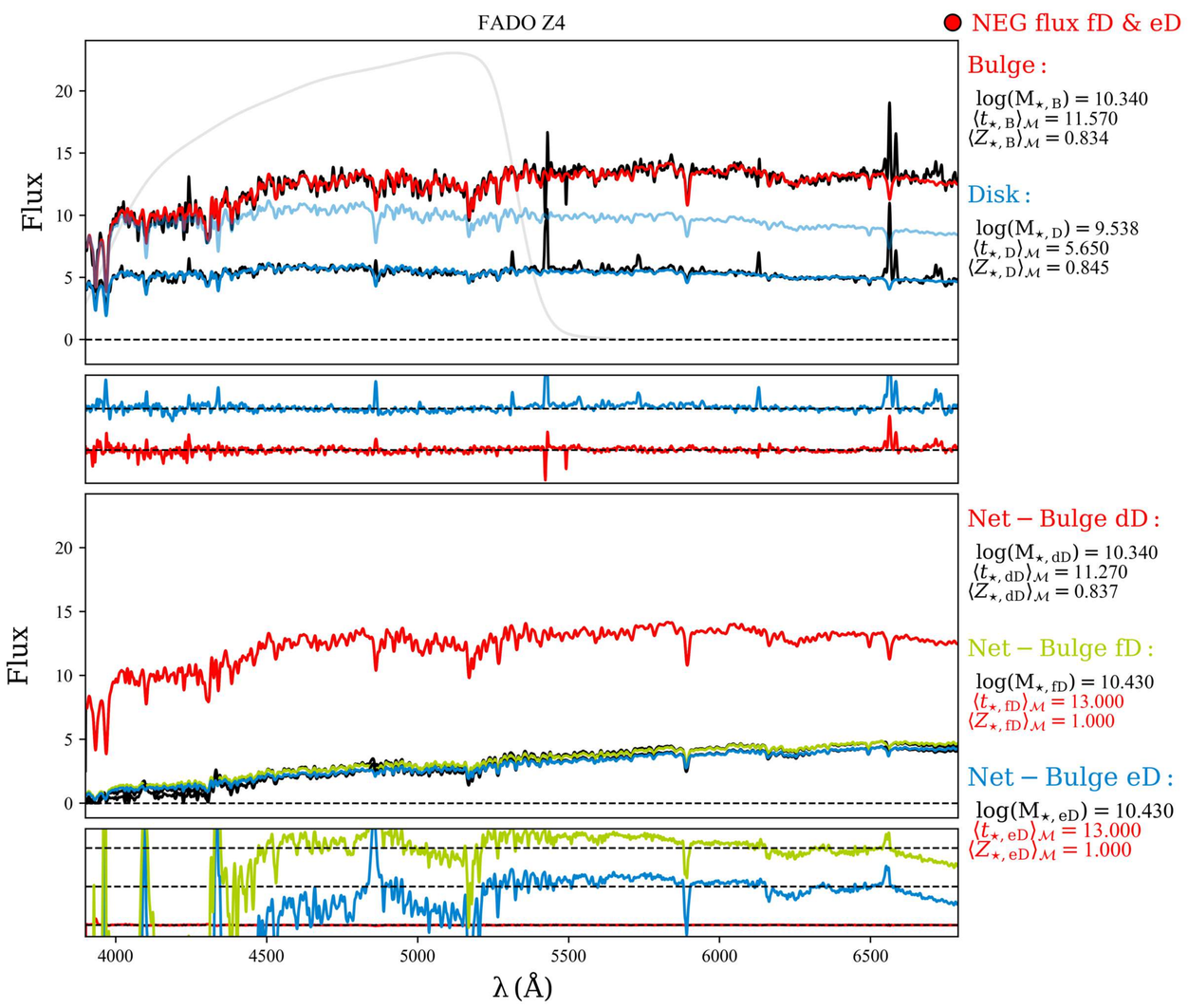
FADO Z4
NEG flux fD & eD
Flux
Bulge :
log(M⋆, B) = 10.340
⟨t⋆, B⟩M = 11.570
⟨Z⋆, B⟩M = 0.834
Disk :
log(M⋆, D) = 9.538
⟨t⋆, D⟩M = 5.650
⟨Z⋆, D⟩M = 0.845
Net − Bulge dD :
log(M⋆, dD) = 10.340
⟨t⋆, dD⟩M = 11.270
⟨Z⋆, dD⟩M = 0.837
Net − Bulge fD :
log(M⋆, fD) = 10.430
⟨t⋆, fD⟩M = 13.000
⟨Z⋆, fD⟩M = 1.000
Net − Bulge eD :
log(M⋆, eD) = 10.430
⟨t⋆, eD⟩M = 13.000
⟨Z⋆, eD⟩M = 1.000
λ (Å)

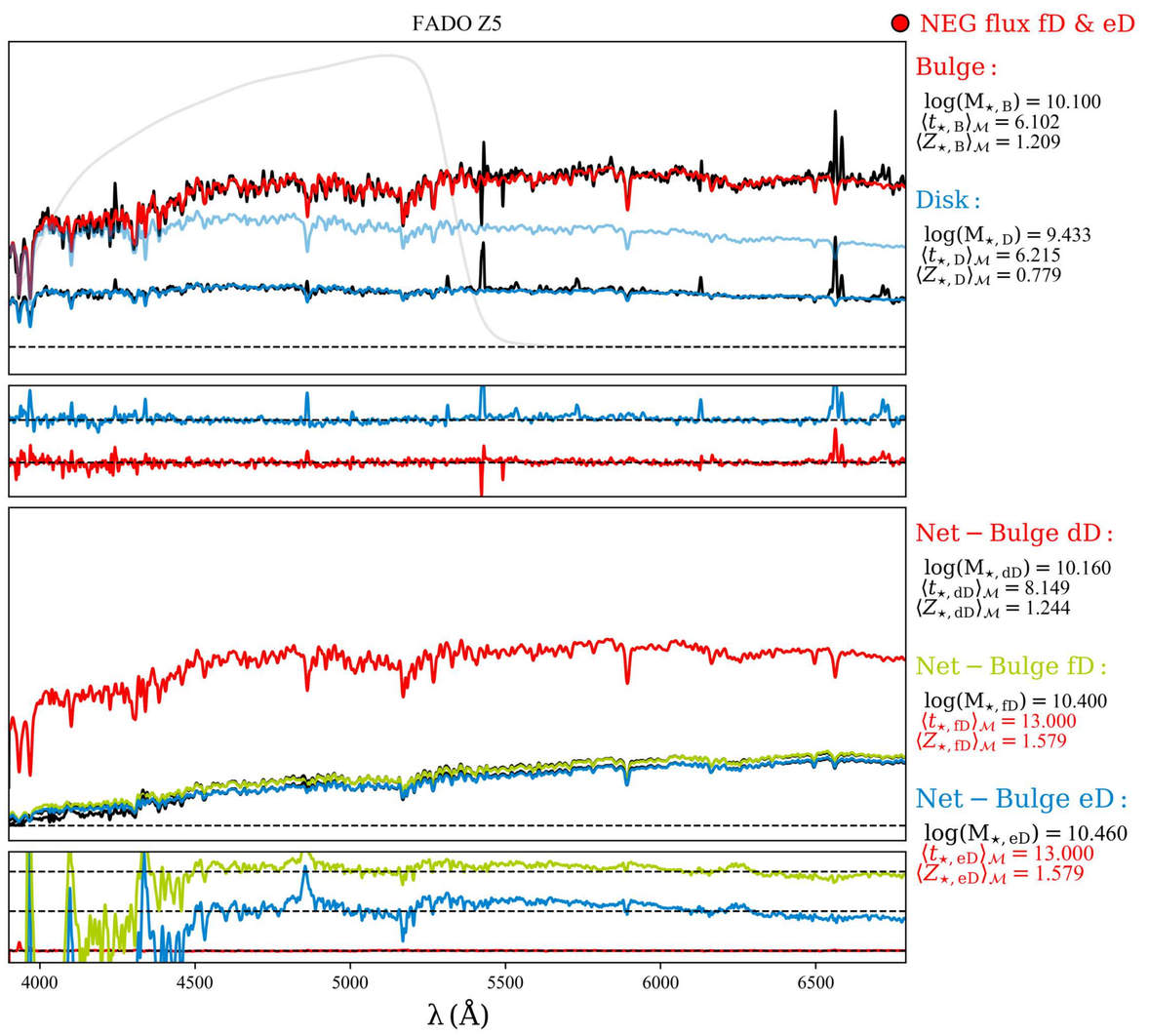
FADO Z5
NEG flux fD & eD
Bulge :
log(M⋆, B) = 10.100
⟨t⋆, B⟩M = 6.102
⟨Z⋆, B⟩M = 1.209
Disk :
log(M⋆, D) = 9.433
⟨t⋆, D⟩M = 6.215
⟨Z⋆, D⟩M = 0.779
Net − Bulge dD :
log(M⋆, dD) = 10.160
⟨t⋆, dD⟩M = 8.149
⟨Z⋆, dD⟩M = 1.244
Net − Bulge fD :
log(M⋆, fD) = 10.400
⟨t⋆, fD⟩M = 13.000
⟨Z⋆, fD⟩M = 1.579
Net − Bulge eD :
log(M⋆, eD) = 10.460
⟨t⋆, eD⟩M = 13.000
⟨Z⋆, eD⟩M = 1.579
λ (Å)

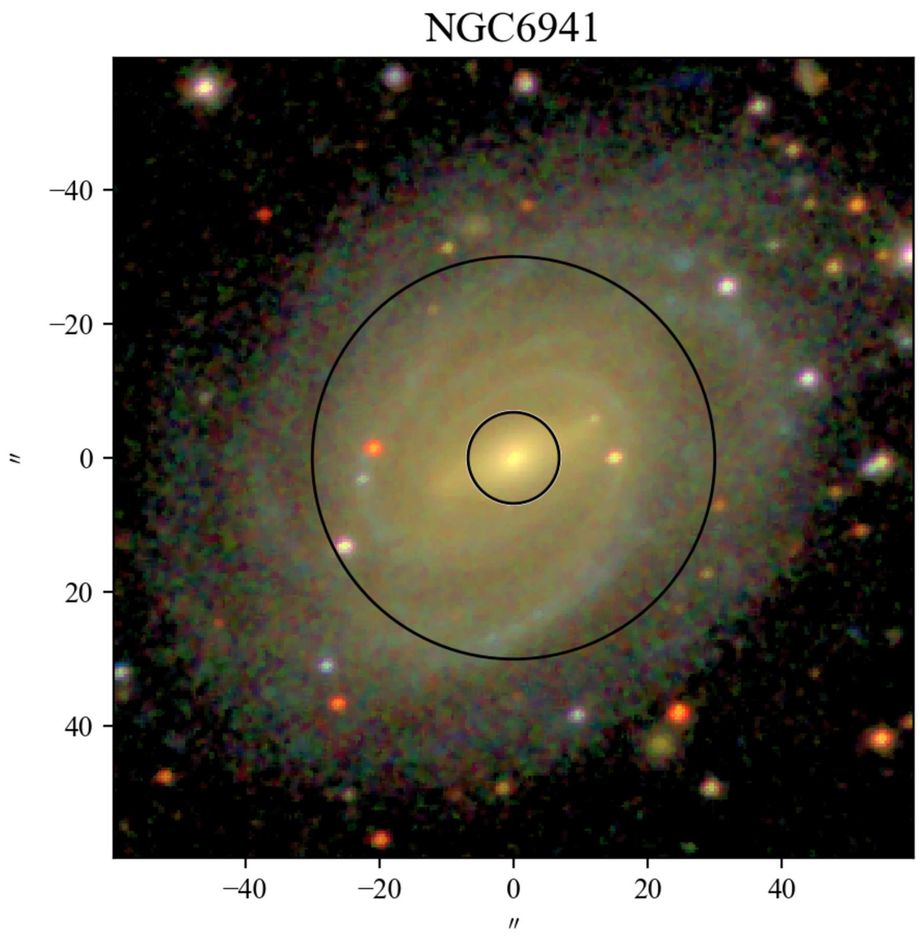
NGC6941
−40
−20
0
20
40
″
−40
−20
0
20
40
″

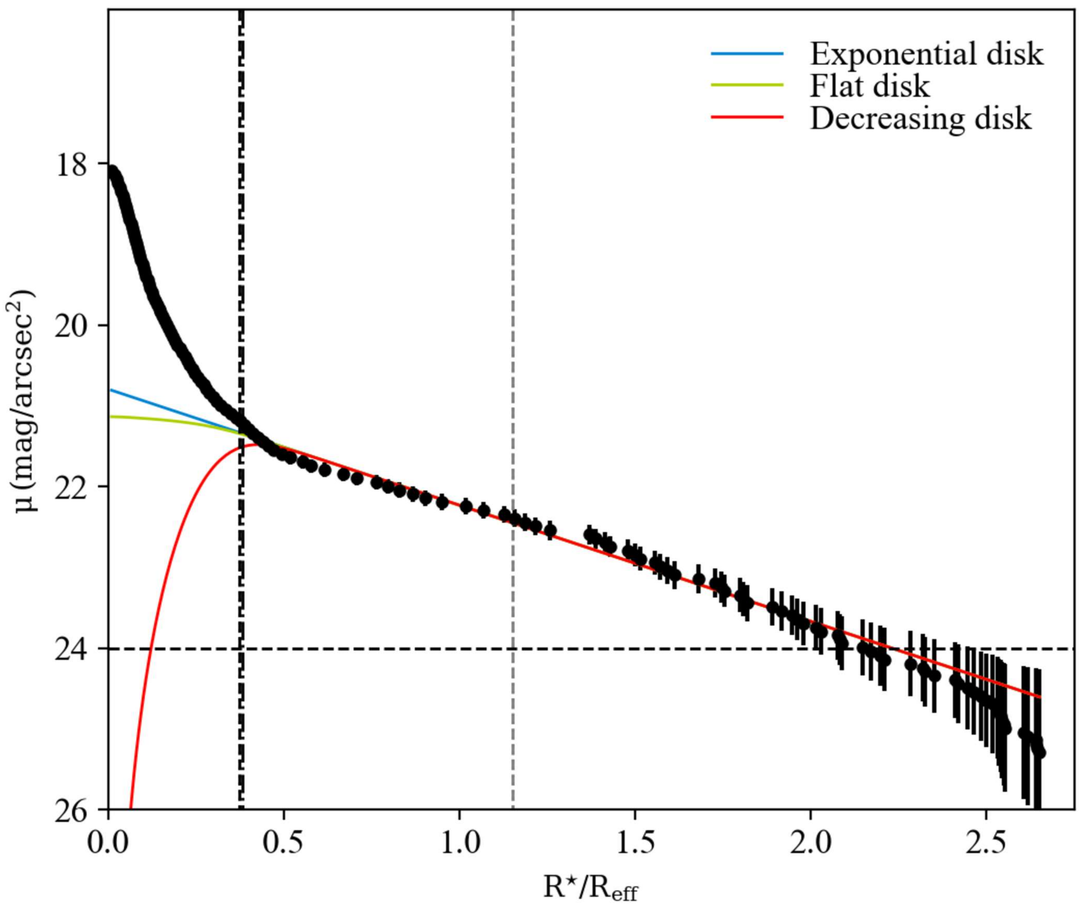
Exponential disk
Flat disk
Decreasing disk
μ (mag/arcsec²)
18
20
22
24
26
0.0
0.5
1.0
1.5
2.0
2.5
R⋆/Reff

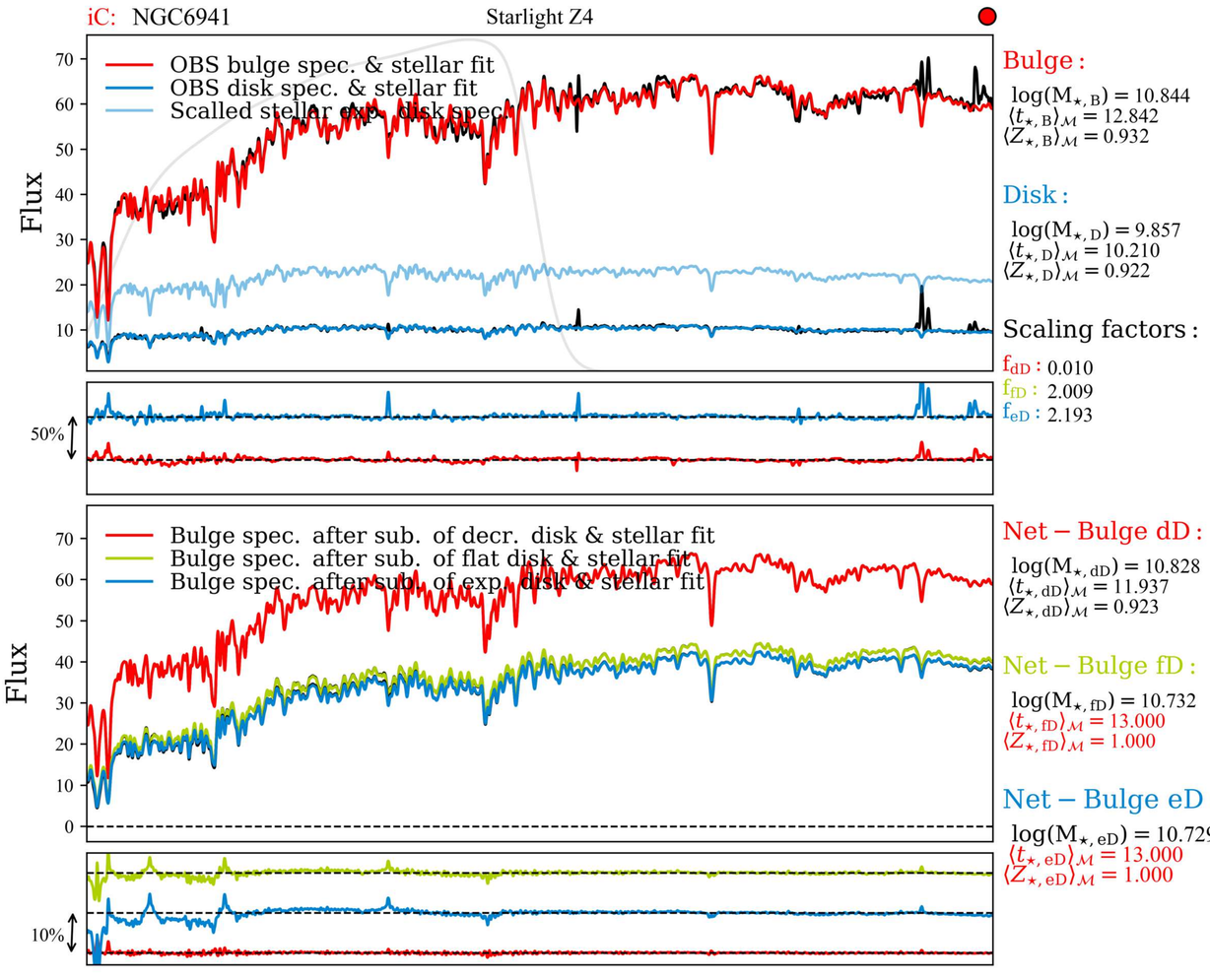
iC: NGC6941
Starlight Z4
OBS bulge spec. & stellar fit
OBS disk spec. & stellar fit
Scalled stellar exp. disk spec.
Flux
50%
Bulge spec. after sub. of decr. disk & stellar fit
Bulge spec. after sub. of flat disk & stellar fit
Bulge spec. after sub. of exp. disk & stellar fit
10%
Bulge :
log(M⋆, B) = 10.844
⟨t⋆, B⟩M = 12.842
⟨Z⋆, B⟩M = 0.932
Disk :
log(M⋆, D) = 9.857
⟨t⋆, D⟩M = 10.210
⟨Z⋆, D⟩M = 0.922
Scaling factors :
fdD : 0.010
ffD : 2.009
feD : 2.193
Net − Bulge dD :
log(M⋆, dD) = 10.828
⟨t⋆, dD⟩M = 11.937
⟨Z⋆, dD⟩M = 0.923
Net − Bulge fD :
log(M⋆, fD) = 10.732
⟨t⋆, fD⟩M = 13.000
⟨Z⋆, fD⟩M = 1.000
Net − Bulge eD :
log(M⋆, eD) = 10.729
⟨t⋆, eD⟩M = 13.000
⟨Z⋆, eD⟩M = 1.000

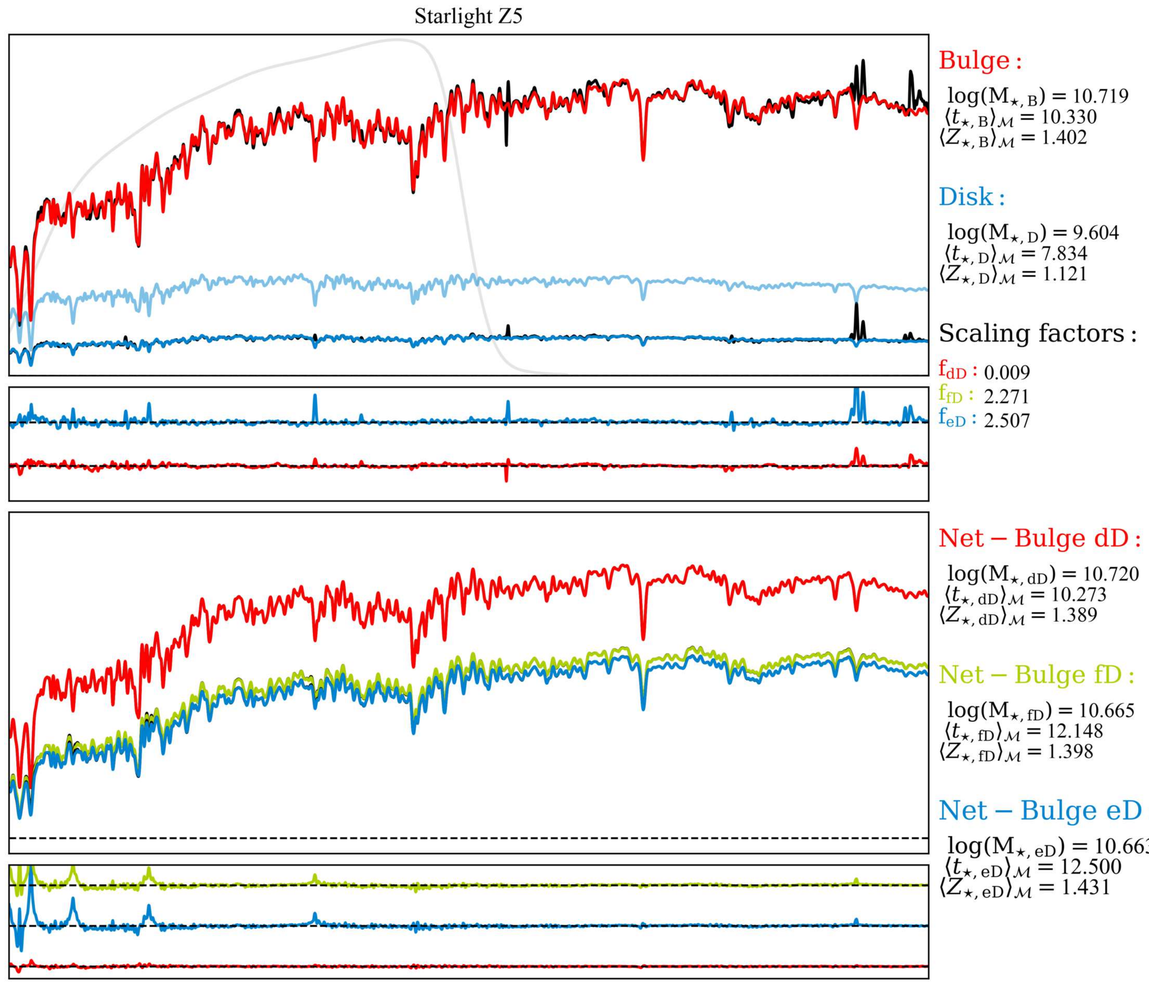
Starlight Z5
Bulge :
log(M⋆, B) = 10.719
⟨t⋆, B⟩M = 10.330
⟨Z⋆, B⟩M = 1.402
Disk :
log(M⋆, D) = 9.604
⟨t⋆, D⟩M = 7.834
⟨Z⋆, D⟩M = 1.121
Scaling factors :
fdD : 0.009
ffD : 2.271
feD : 2.507
Net − Bulge dD :
log(M⋆, dD) = 10.720
⟨t⋆, dD⟩M = 10.273
⟨Z⋆, dD⟩M = 1.389
Net − Bulge fD :
log(M⋆, fD) = 10.665
⟨t⋆, fD⟩M = 12.148
⟨Z⋆, fD⟩M = 1.398
Net − Bulge eD :
log(M⋆, eD) = 10.663
⟨t⋆, eD⟩M = 12.500
⟨Z⋆, eD⟩M = 1.431

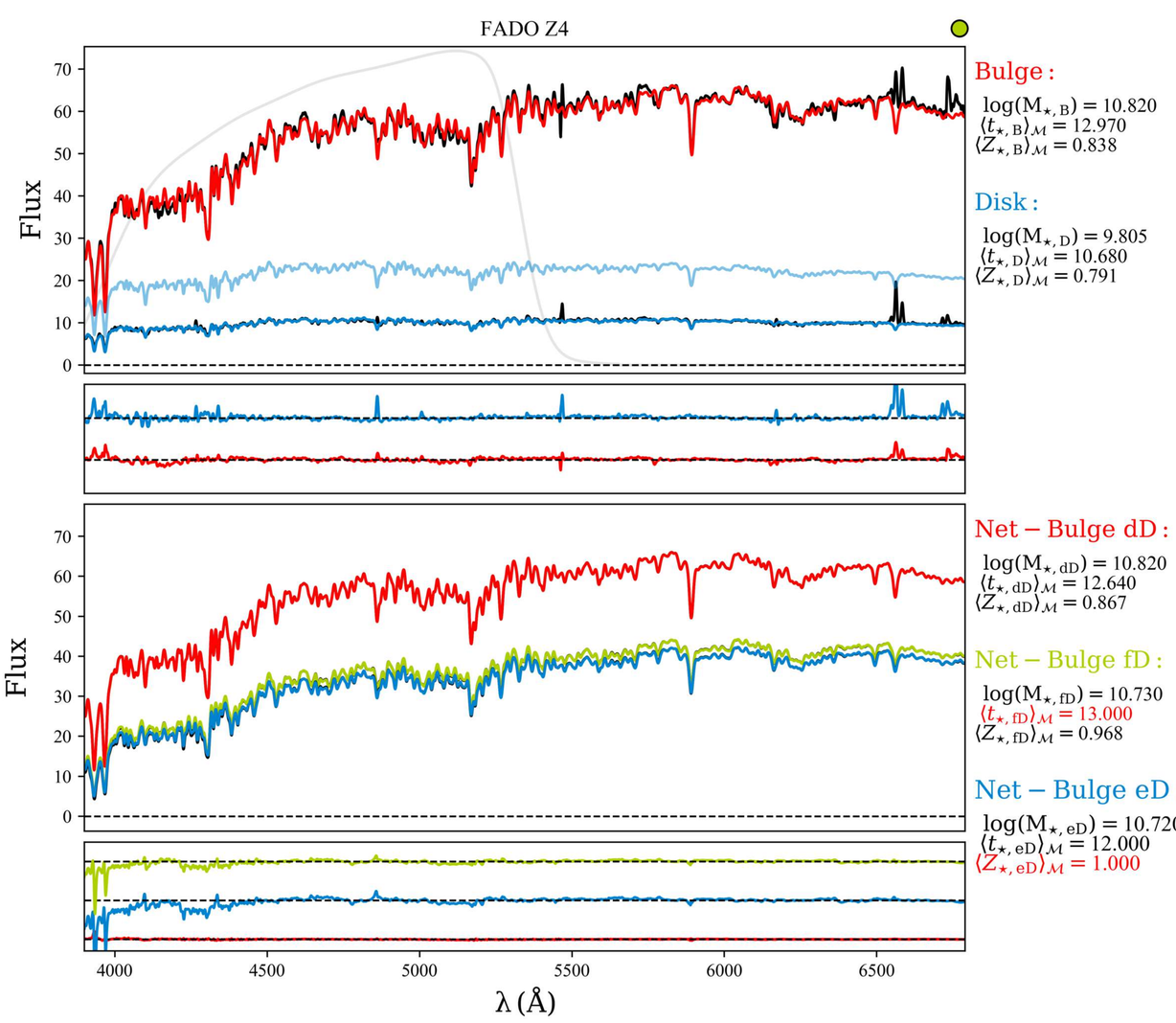
FADO Z4
Flux
Bulge :
log(M⋆, B) = 10.820
⟨t⋆, B⟩M = 12.970
⟨Z⋆, B⟩M = 0.838
Disk :
log(M⋆, D) = 9.805
⟨t⋆, D⟩M = 10.680
⟨Z⋆, D⟩M = 0.791
Net − Bulge dD :
log(M⋆, dD) = 10.820
⟨t⋆, dD⟩M = 12.640
⟨Z⋆, dD⟩M = 0.867
Net − Bulge fD :
log(M⋆, fD) = 10.730
⟨t⋆, fD⟩M = 13.000
⟨Z⋆, fD⟩M = 0.968
Net − Bulge eD :
log(M⋆, eD) = 10.720
⟨t⋆, eD⟩M = 12.000
⟨Z⋆, eD⟩M = 1.000
4000
4500
5000
5500
6000
6500
λ (Å)

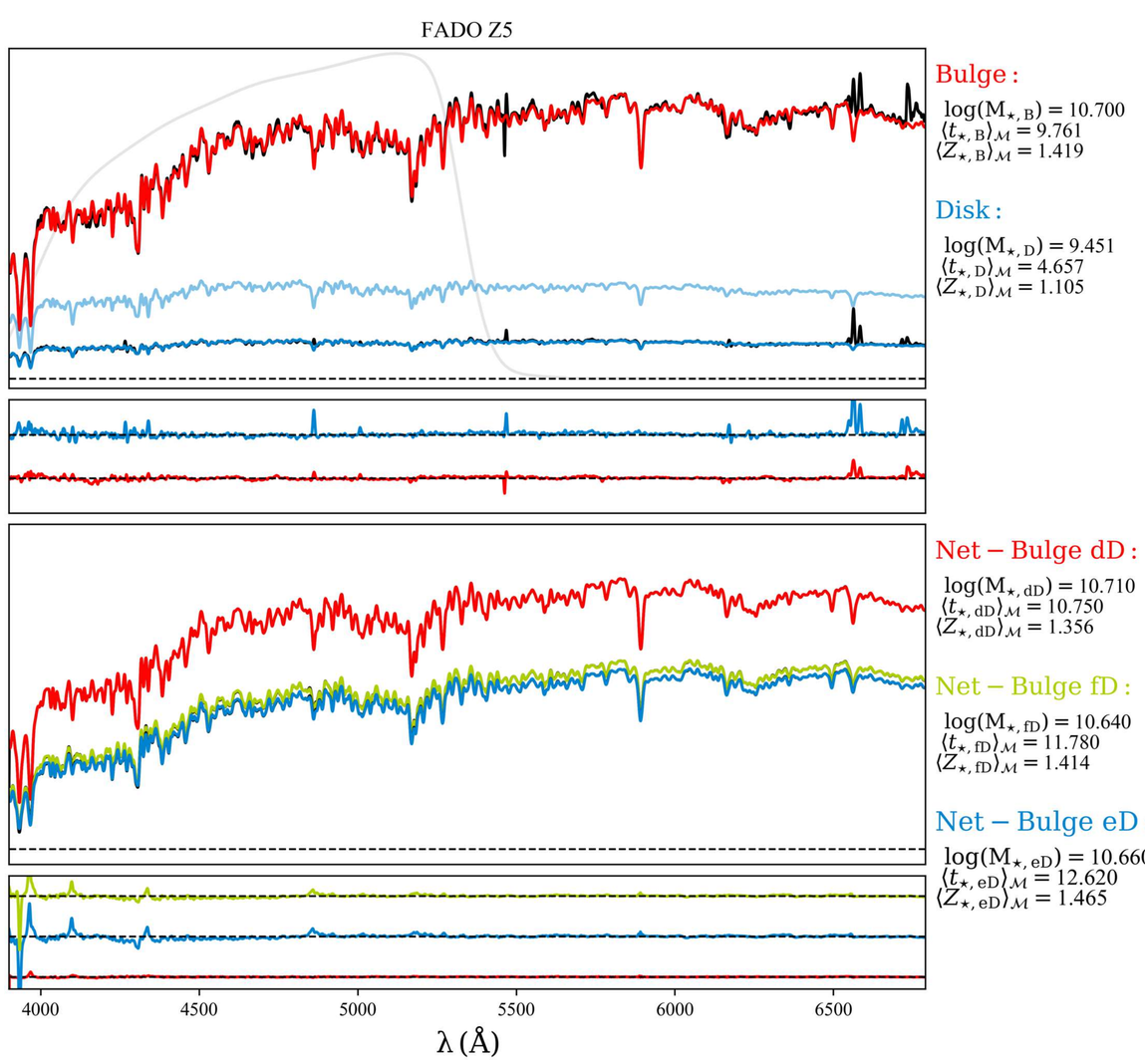
FADO Z5
Bulge :
log(M⋆, B) = 10.700
⟨t⋆, B⟩M = 9.761
⟨Z⋆, B⟩M = 1.419
Disk :
log(M⋆, D) = 9.451
⟨t⋆, D⟩M = 4.657
⟨Z⋆, D⟩M = 1.105
Net − Bulge dD :
log(M⋆, dD) = 10.710
⟨t⋆, dD⟩M = 10.750
⟨Z⋆, dD⟩M = 1.356
Net − Bulge fD :
log(M⋆, fD) = 10.640
⟨t⋆, fD⟩M = 11.780
⟨Z⋆, fD⟩M = 1.414
Net − Bulge eD :
log(M⋆, eD) = 10.660
⟨t⋆, eD⟩M = 12.620
⟨Z⋆, eD⟩M = 1.465
4000
4500
5000
5500
6000
6500
λ (Å)

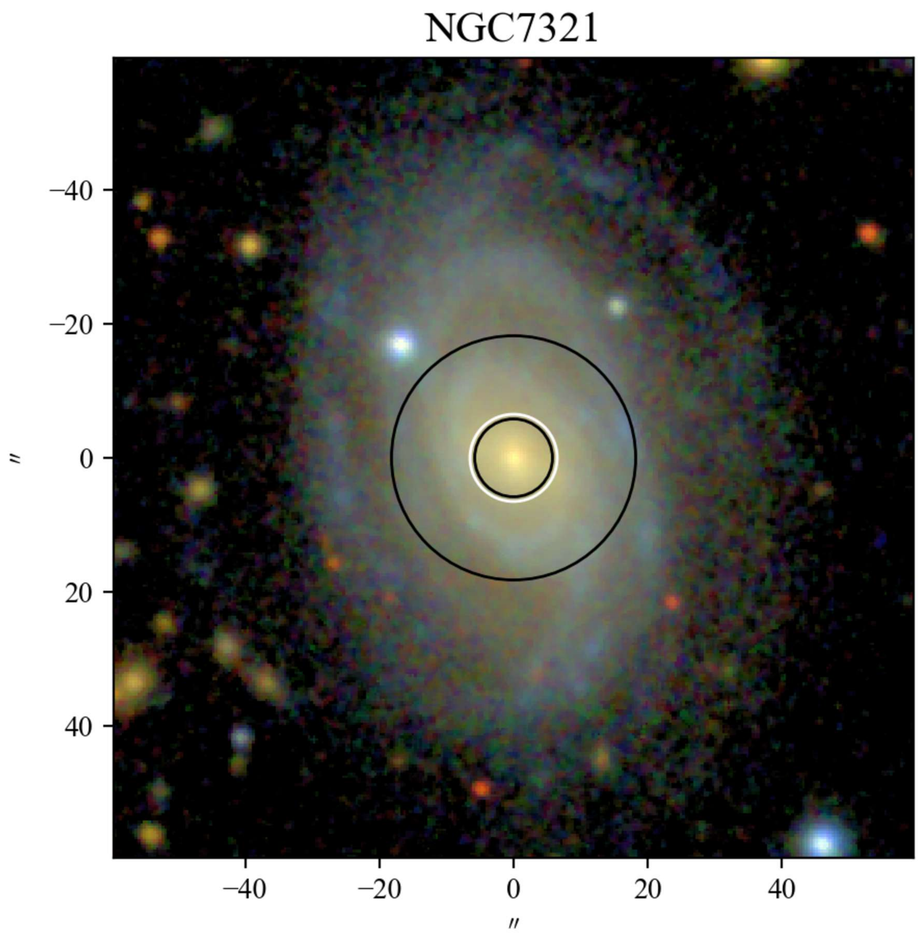
NGC7321
−40
−20
0
20
40
″
−40
−20
0
20
40
″

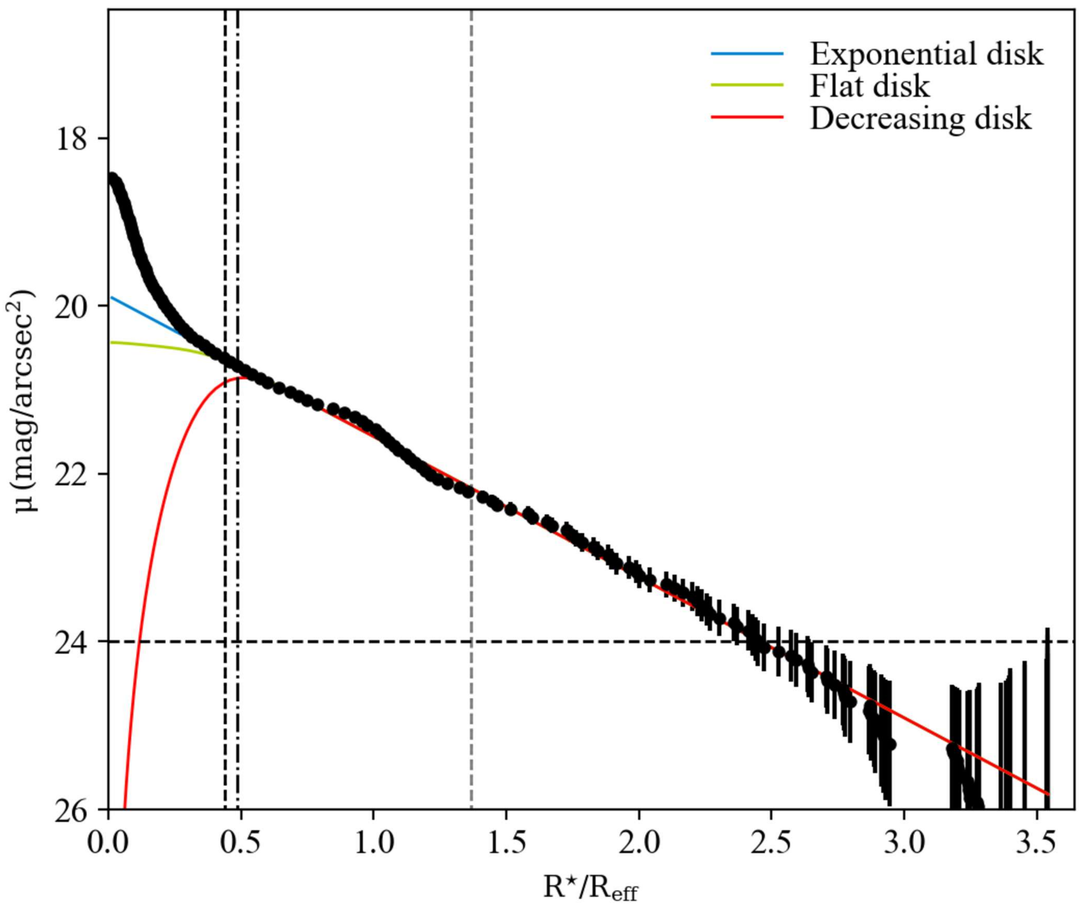
Exponential disk
Flat disk
Decreasing disk
μ (mag/arcsec²)
18
20
22
24
26
0.0
0.5
1.0
1.5
2.0
2.5
3.0
3.5
R⋆/Reff

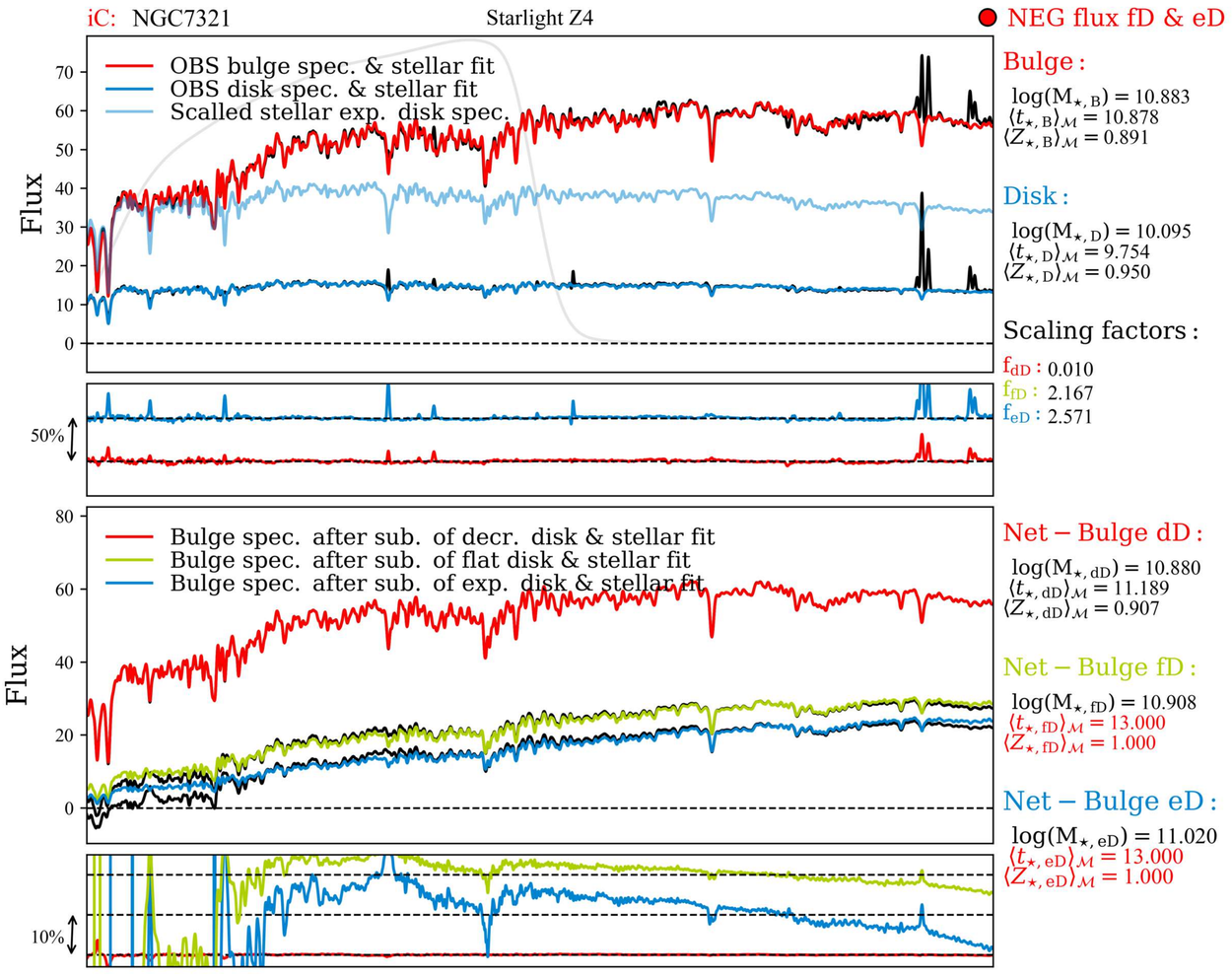
iC: NGC7321
Starlight Z4
NEG flux fD & eD
OBS bulge spec. & stellar fit
OBS disk spec. & stellar fit
Scalled stellar exp. disk spec.
Flux
50%
Bulge spec. after sub. of decr. disk & stellar fit
Bulge spec. after sub. of flat disk & stellar fit
Bulge spec. after sub. of exp. disk & stellar fit
10%
Bulge :
log(M⋆, B) = 10.883
⟨t⋆, B⟩M = 10.878
⟨Z⋆, B⟩M = 0.891
Disk :
log(M⋆, D) = 10.095
⟨t⋆, D⟩M = 9.754
⟨Z⋆, D⟩M = 0.950
Scaling factors :
fdD : 0.010
ffD : 2.167
feD : 2.571
Net − Bulge dD :
log(M⋆, dD) = 10.880
⟨t⋆, dD⟩M = 11.189
⟨Z⋆, dD⟩M = 0.907
Net − Bulge fD :
log(M⋆, fD) = 10.908
⟨t⋆, fD⟩M = 13.000
⟨Z⋆, fD⟩M = 1.000
Net − Bulge eD :
log(M⋆, eD) = 11.020
⟨t⋆, eD⟩M = 13.000
⟨Z⋆, eD⟩M = 1.000

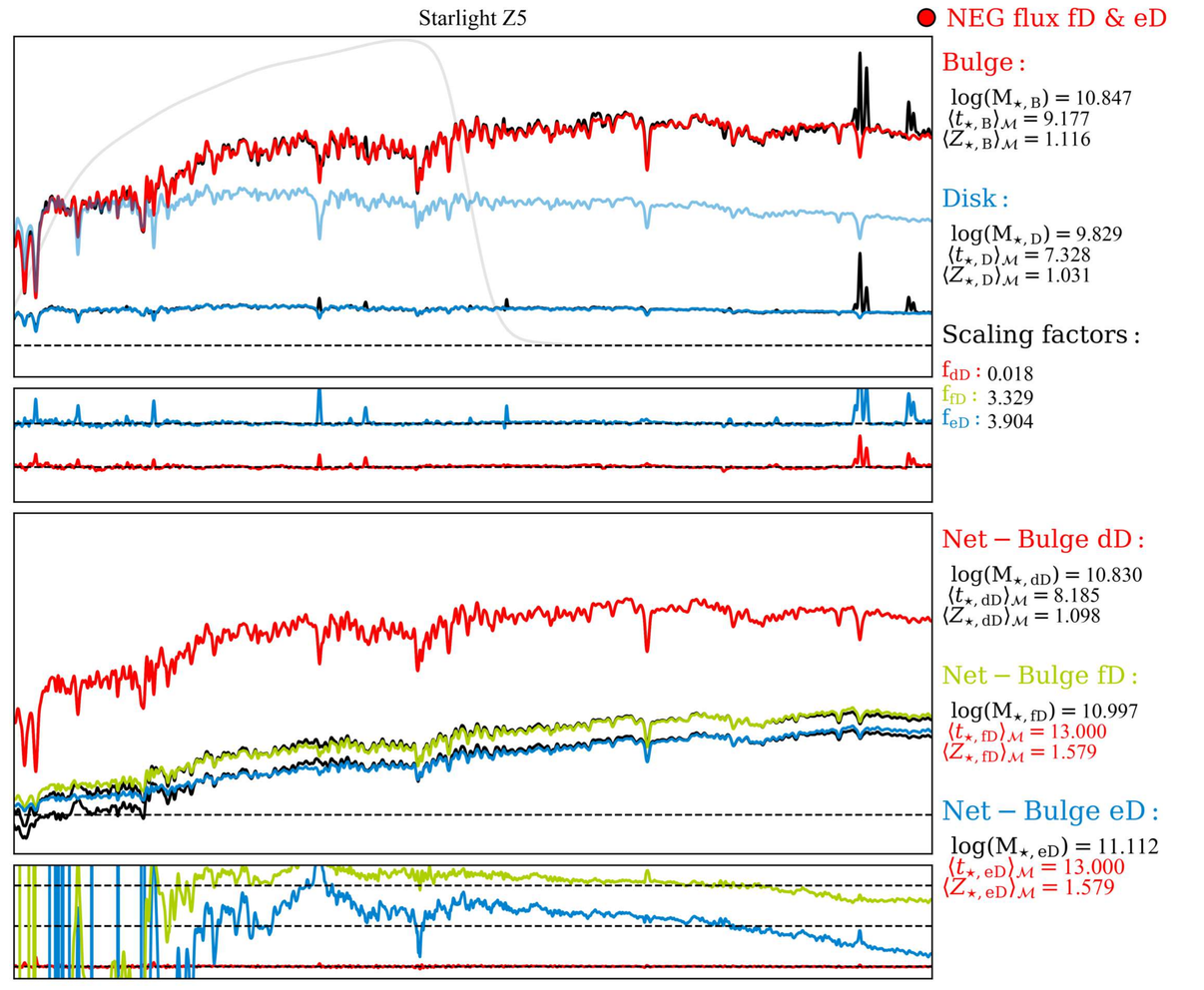
Starlight Z5
NEG flux fD & eD
Bulge :
log(M⋆, B) = 10.847
⟨t⋆, B⟩M = 9.177
⟨Z⋆, B⟩M = 1.116
Disk :
log(M⋆, D) = 9.829
⟨t⋆, D⟩M = 7.328
⟨Z⋆, D⟩M = 1.031
Scaling factors :
fdD : 0.018
ffD : 3.329
feD : 3.904
Net − Bulge dD :
log(M⋆, dD) = 10.830
⟨t⋆, dD⟩M = 8.185
⟨Z⋆, dD⟩M = 1.098
Net − Bulge fD :
log(M⋆, fD) = 10.997
⟨t⋆, fD⟩M = 13.000
⟨Z⋆, fD⟩M = 1.579
Net − Bulge eD :
log(M⋆, eD) = 11.112
⟨t⋆, eD⟩M = 13.000
⟨Z⋆, eD⟩M = 1.579

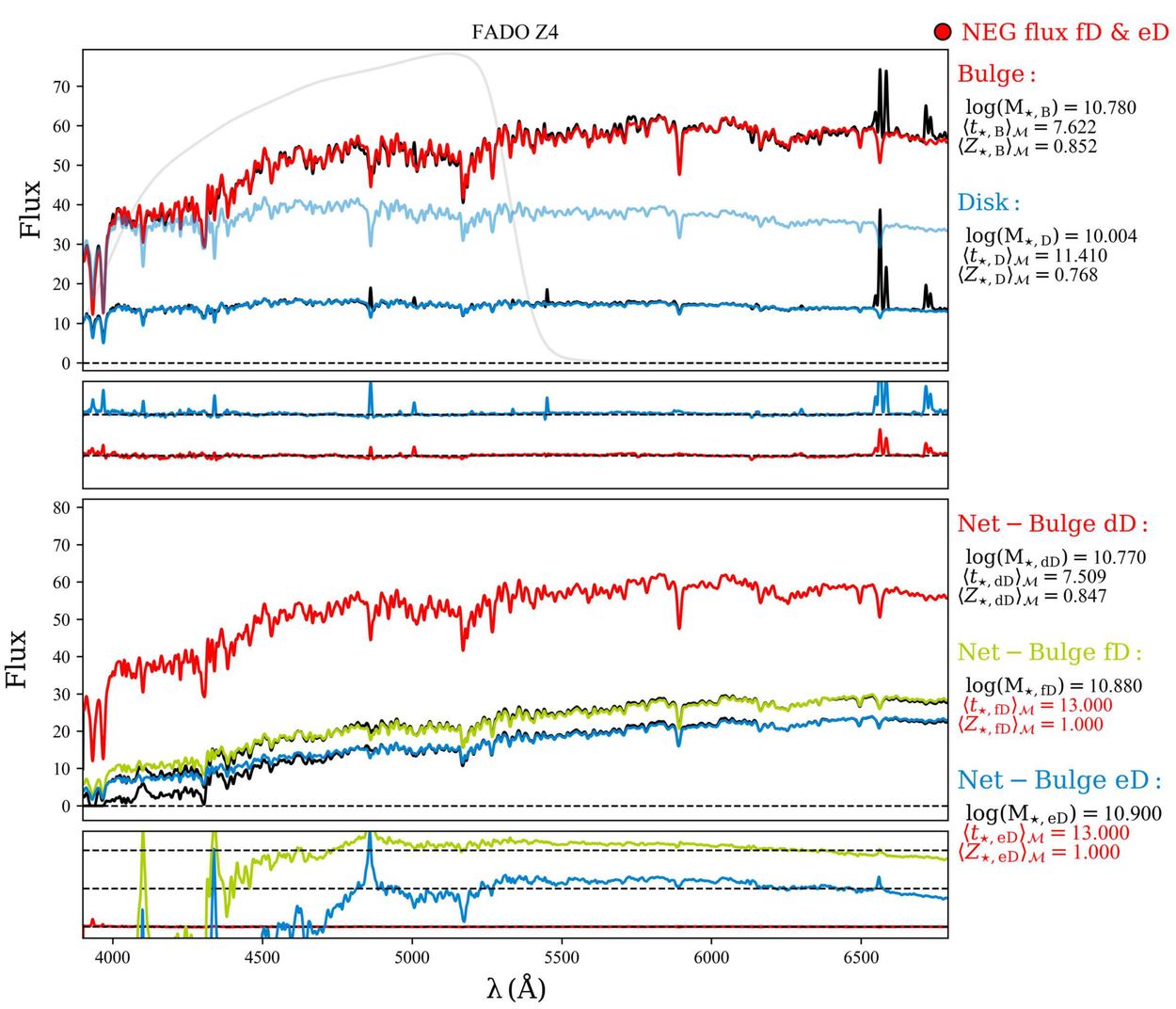
FADO Z4
NEG flux fD & eD
Flux
Bulge :
log(M⋆, B) = 10.780
⟨t⋆, B⟩M = 7.622
⟨Z⋆, B⟩M = 0.852
Disk :
log(M⋆, D) = 10.004
⟨t⋆, D⟩M = 11.410
⟨Z⋆, D⟩M = 0.768
Net − Bulge dD :
log(M⋆, dD) = 10.770
⟨t⋆, dD⟩M = 7.509
⟨Z⋆, dD⟩M = 0.847
Net − Bulge fD :
log(M⋆, fD) = 10.880
⟨t⋆, fD⟩M = 13.000
⟨Z⋆, fD⟩M = 1.000
Net − Bulge eD :
log(M⋆, eD) = 10.900
⟨t⋆, eD⟩M = 13.000
⟨Z⋆, eD⟩M = 1.000
λ (Å)

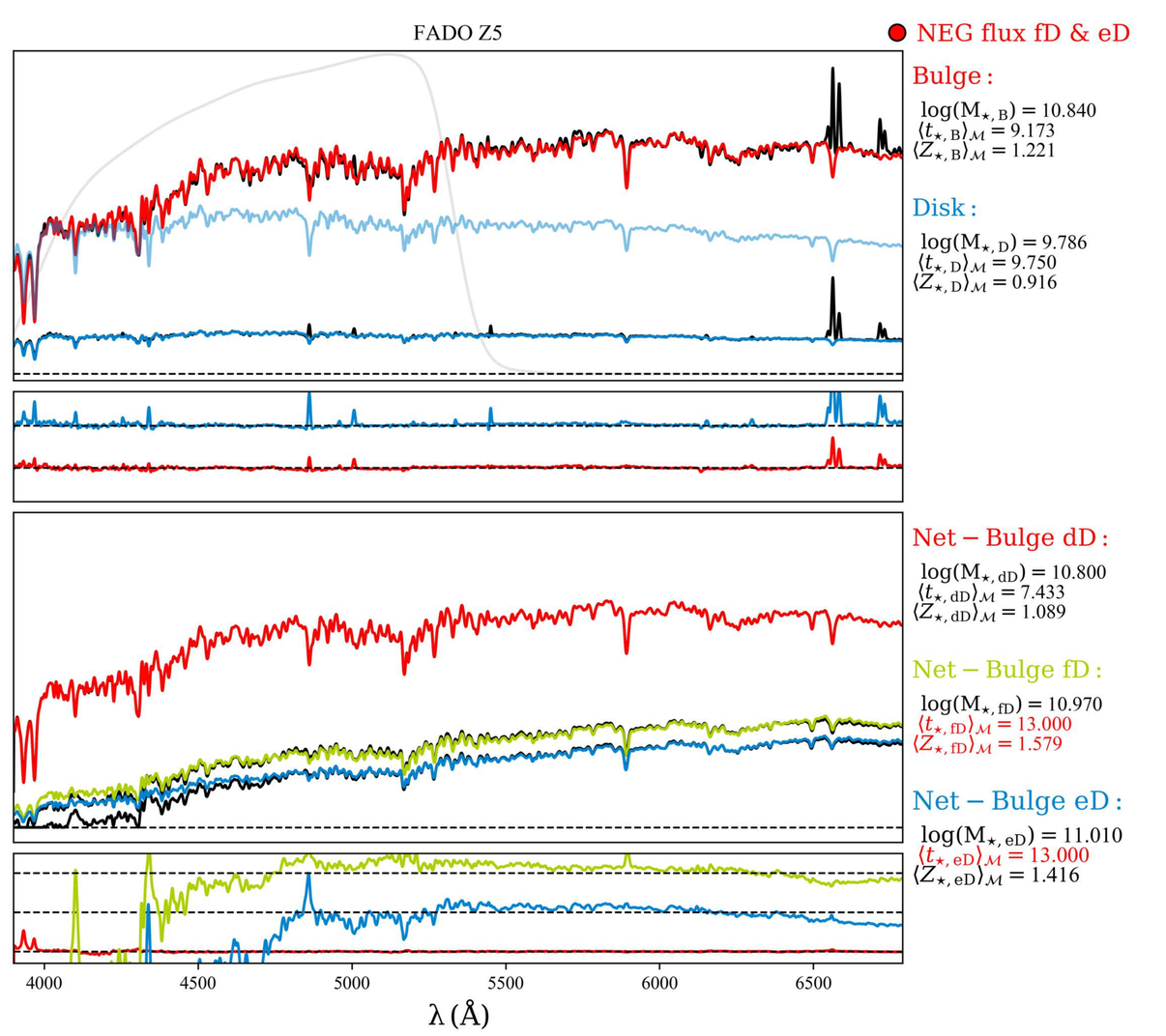
FADO Z5
NEG flux fD & eD
Bulge :
log(M⋆, B) = 10.840
⟨t⋆, B⟩M = 9.173
⟨Z⋆, B⟩M = 1.221
Disk :
log(M⋆, D) = 9.786
⟨t⋆, D⟩M = 9.750
⟨Z⋆, D⟩M = 0.916
Net − Bulge dD :
log(M⋆, dD) = 10.800
⟨t⋆, dD⟩M = 7.433
⟨Z⋆, dD⟩M = 1.089
Net − Bulge fD :
log(M⋆, fD) = 10.970
⟨t⋆, fD⟩M = 13.000
⟨Z⋆, fD⟩M = 1.579
Net − Bulge eD :
log(M⋆, eD) = 11.010
⟨t⋆, eD⟩M = 13.000
⟨Z⋆, eD⟩M = 1.416
λ (Å)

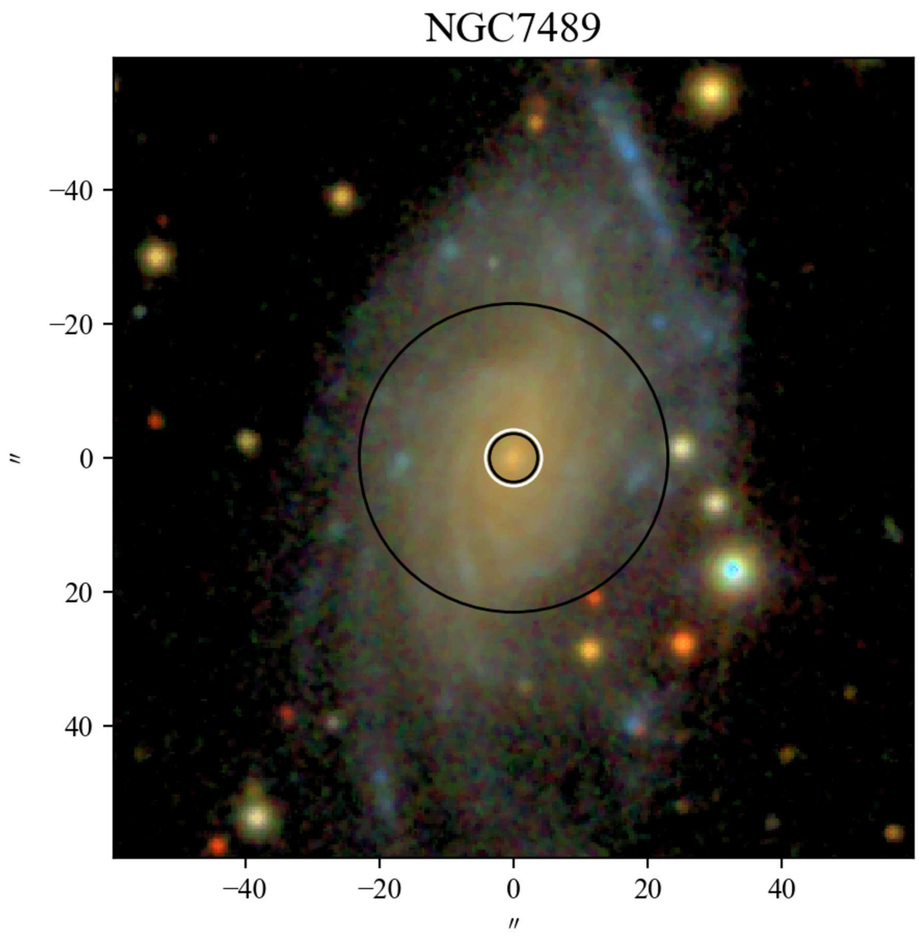
NGC7489
−40
−20
0
20
40
″
−40
−20
0
20
40
″

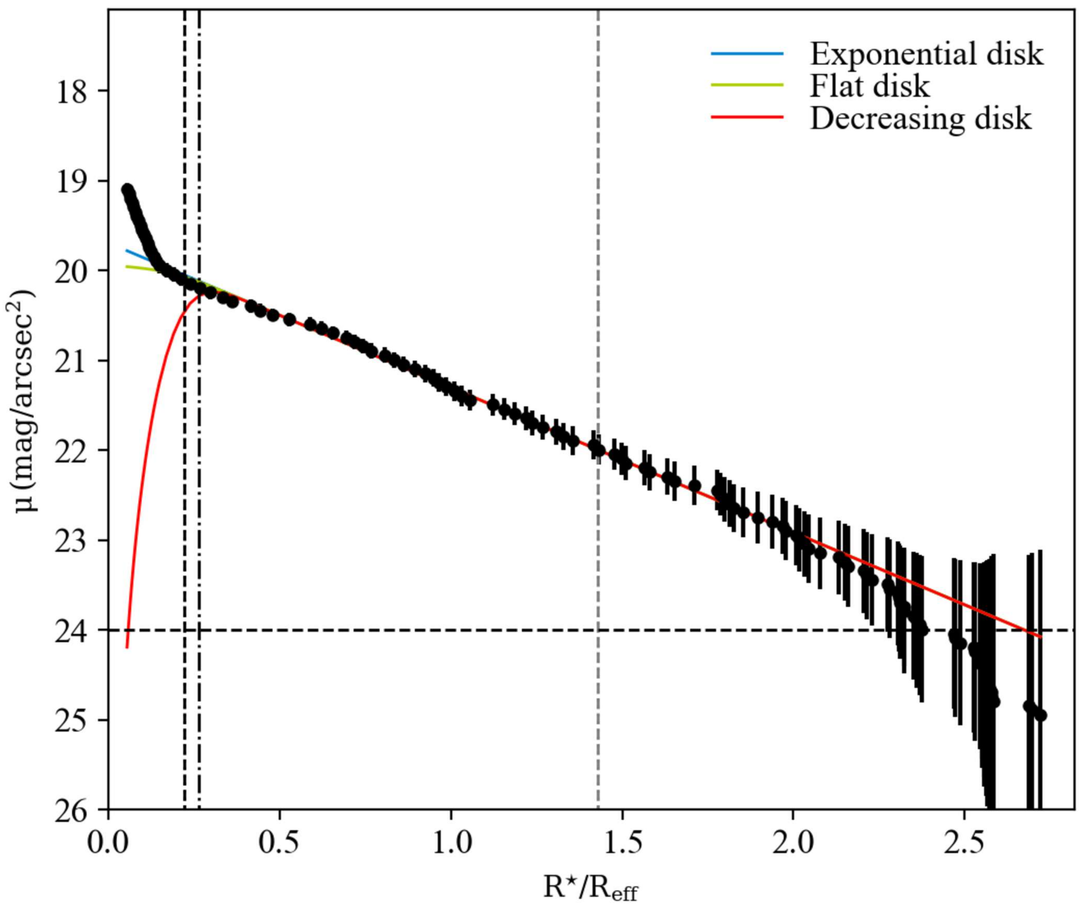
Exponential disk
Flat disk
Decreasing disk
μ (mag/arcsec²)
18
19
20
21
22
23
24
25
26
0.0
0.5
1.0
1.5
2.0
2.5
R⋆/Reff

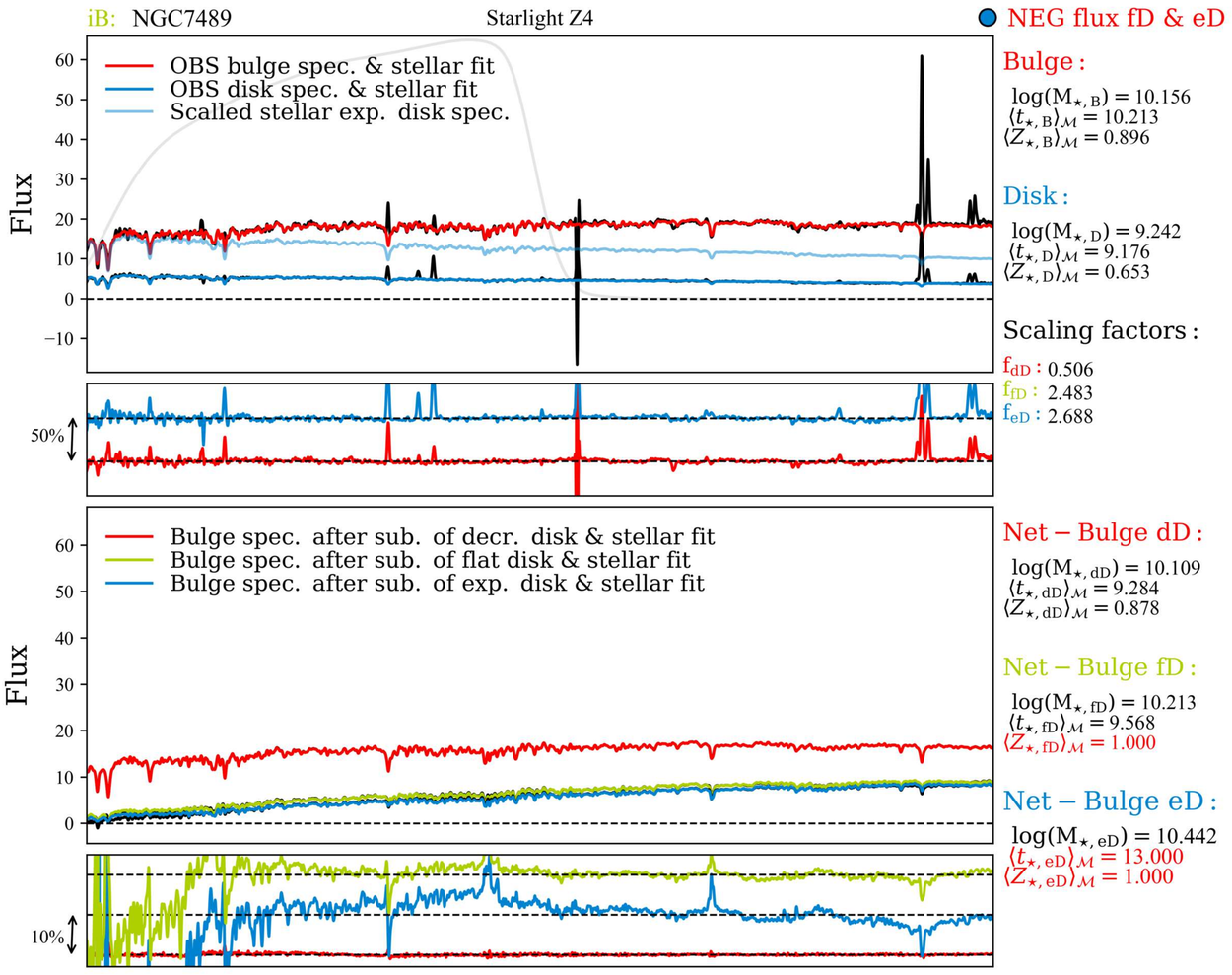
iB: NGC7489
Starlight Z4
NEG flux fD & eD
OBS bulge spec. & stellar fit
OBS disk spec. & stellar fit
Scalled stellar exp. disk spec.
Flux
50%
Bulge spec. after sub. of decr. disk & stellar fit
Bulge spec. after sub. of flat disk & stellar fit
Bulge spec. after sub. of exp. disk & stellar fit
10%
Bulge :
log(M⋆, B) = 10.156
⟨t⋆, B⟩M = 10.213
⟨Z⋆, B⟩M = 0.896
Disk :
log(M⋆, D) = 9.242
⟨t⋆, D⟩M = 9.176
⟨Z⋆, D⟩M = 0.653
Scaling factors :
fdD : 0.506
ffD : 2.483
feD : 2.688
Net − Bulge dD :
log(M⋆, dD) = 10.109
⟨t⋆, dD⟩M = 9.284
⟨Z⋆, dD⟩M = 0.878
Net − Bulge fD :
log(M⋆, fD) = 10.213
⟨t⋆, fD⟩M = 9.568
⟨Z⋆, fD⟩M = 1.000
Net − Bulge eD :
log(M⋆, eD) = 10.442
⟨t⋆, eD⟩M = 13.000
⟨Z⋆, eD⟩M = 1.000

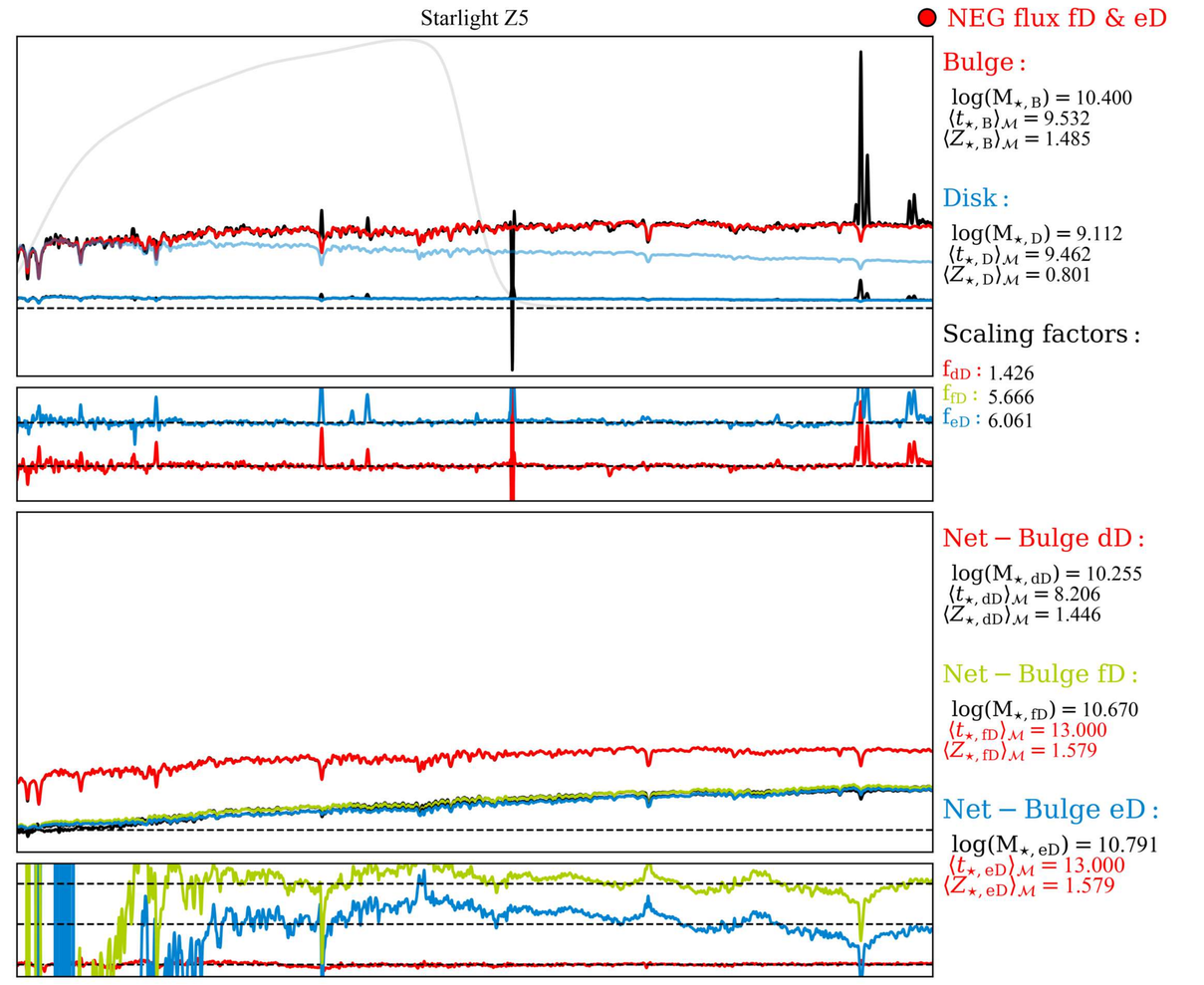
Starlight Z5
NEG flux fD & eD
Bulge :
log(M⋆, B) = 10.400
⟨t⋆, B⟩M = 9.532
⟨Z⋆, B⟩M = 1.485
Disk :
log(M⋆, D) = 9.112
⟨t⋆, D⟩M = 9.462
⟨Z⋆, D⟩M = 0.801
Scaling factors :
fdD : 1.426
ffD : 5.666
feD : 6.061
Net − Bulge dD :
log(M⋆, dD) = 10.255
⟨t⋆, dD⟩M = 8.206
⟨Z⋆, dD⟩M = 1.446
Net − Bulge fD :
log(M⋆, fD) = 10.670
⟨t⋆, fD⟩M = 13.000
⟨Z⋆, fD⟩M = 1.579
Net − Bulge eD :
log(M⋆, eD) = 10.791
⟨t⋆, eD⟩M = 13.000
⟨Z⋆, eD⟩M = 1.579

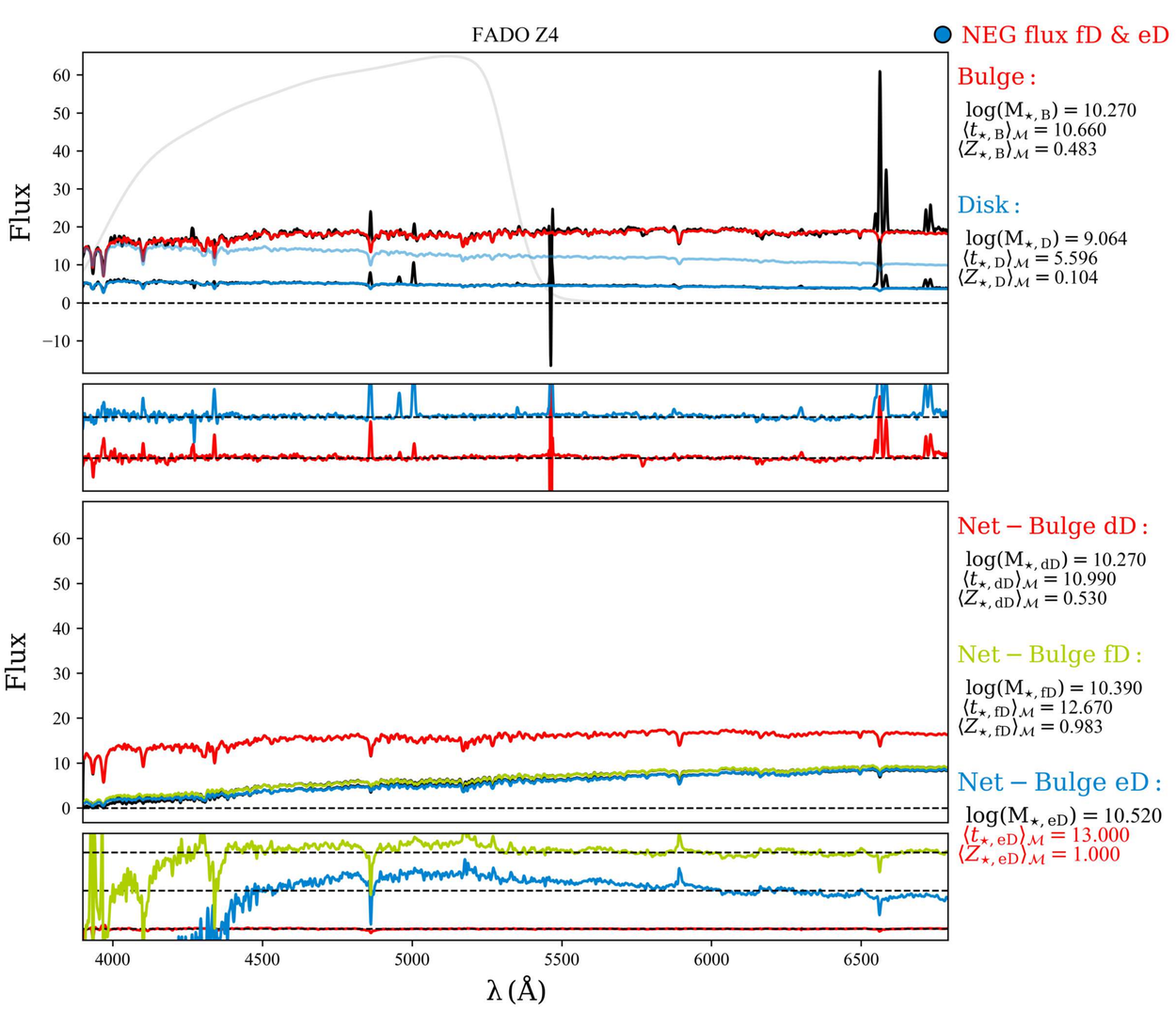
FADO Z4
NEG flux fD & eD
Flux
Bulge :
log(M⋆, B) = 10.270
⟨t⋆, B⟩M = 10.660
⟨Z⋆, B⟩M = 0.483
Disk :
log(M⋆, D) = 9.064
⟨t⋆, D⟩M = 5.596
⟨Z⋆, D⟩M = 0.104
Net − Bulge dD :
log(M⋆, dD) = 10.270
⟨t⋆, dD⟩M = 10.990
⟨Z⋆, dD⟩M = 0.530
Net − Bulge fD :
log(M⋆, fD) = 10.390
⟨t⋆, fD⟩M = 12.670
⟨Z⋆, fD⟩M = 0.983
Net − Bulge eD :
log(M⋆, eD) = 10.520
⟨t⋆, eD⟩M = 13.000
⟨Z⋆, eD⟩M = 1.000
λ (Å)

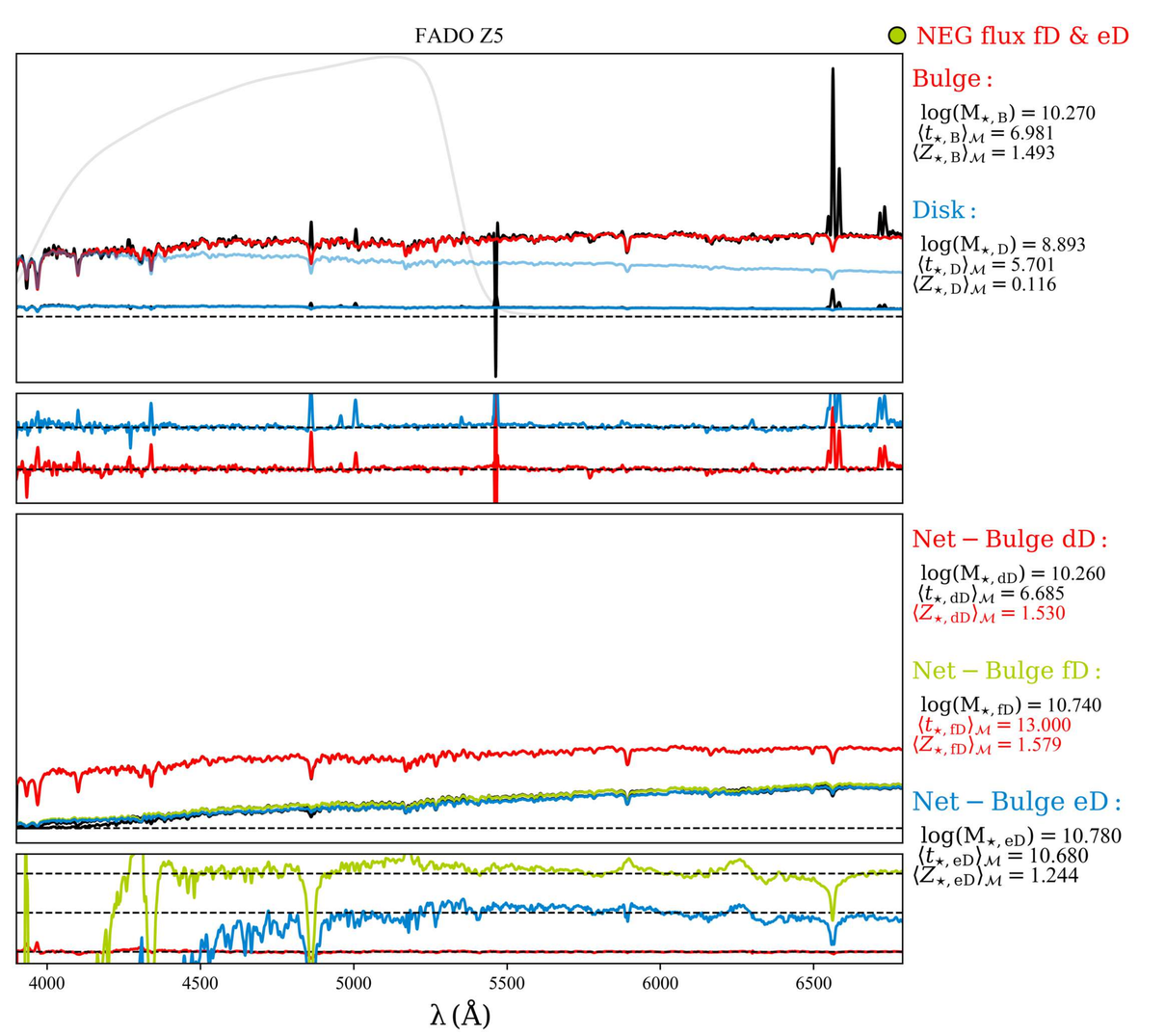
FADO Z5
NEG flux fD & eD
Bulge :
log(M⋆, B) = 10.270
⟨t⋆, B⟩M = 6.981
⟨Z⋆, B⟩M = 1.493
Disk :
log(M⋆, D) = 8.893
⟨t⋆, D⟩M = 5.701
⟨Z⋆, D⟩M = 0.116
Net − Bulge dD :
log(M⋆, dD) = 10.260
⟨t⋆, dD⟩M = 6.685
⟨Z⋆, dD⟩M = 1.530
Net − Bulge fD :
log(M⋆, fD) = 10.740
⟨t⋆, fD⟩M = 13.000
⟨Z⋆, fD⟩M = 1.579
Net − Bulge eD :
log(M⋆, eD) = 10.780
⟨t⋆, eD⟩M = 10.680
⟨Z⋆, eD⟩M = 1.244
λ (Å)

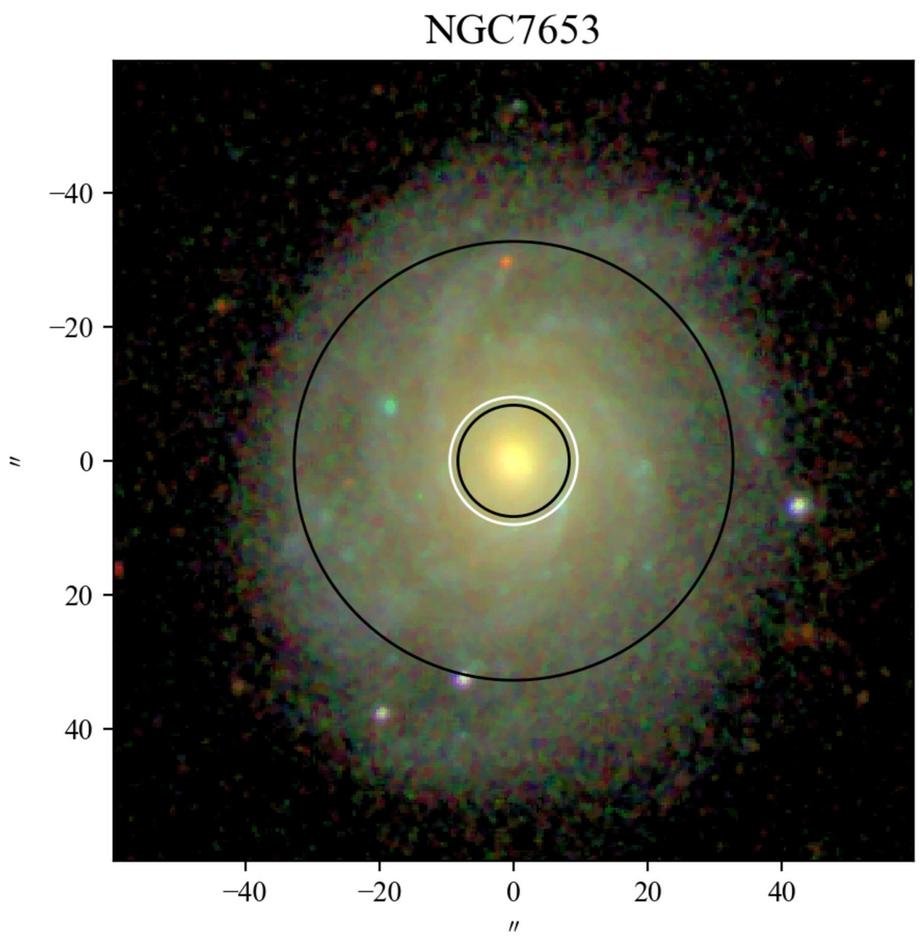
NGC7653
−40
−20
0
20
40
″

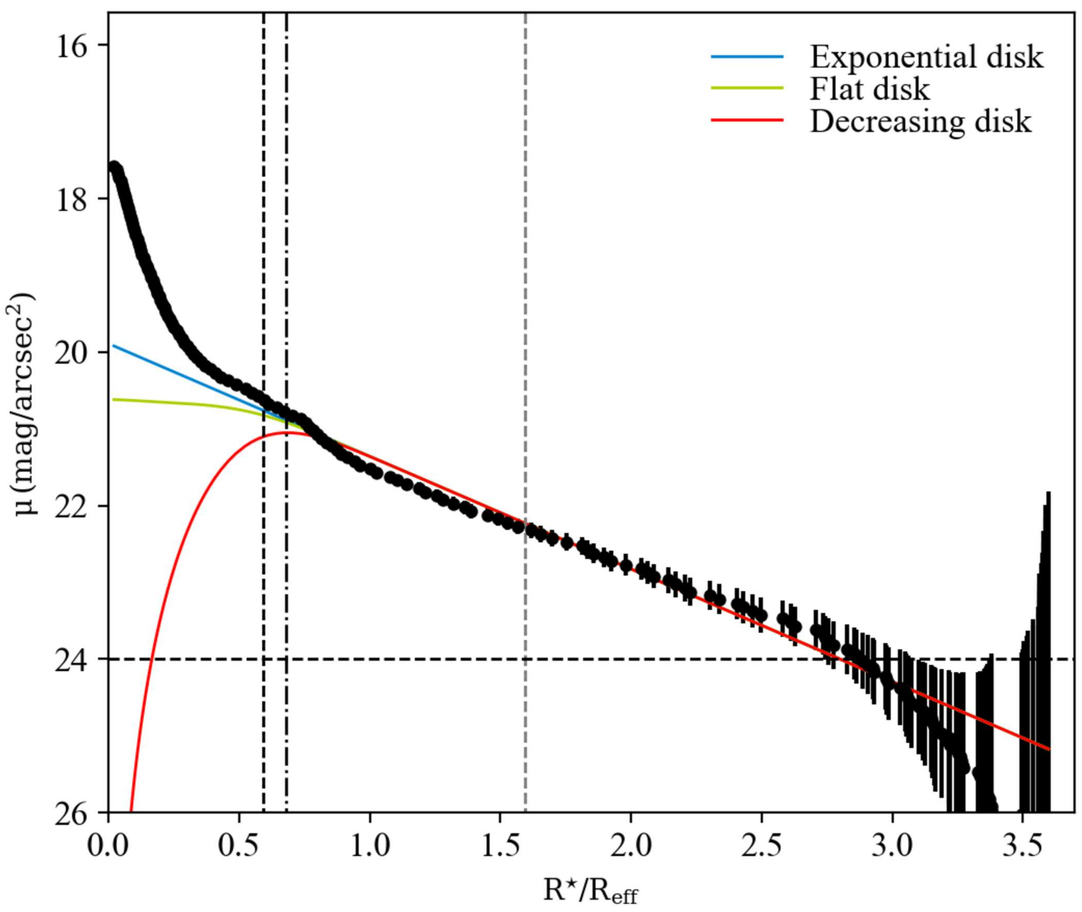
Exponential disk
Flat disk
Decreasing disk
μ (mag/arcsec²)
16
18
20
22
24
26
0.0
0.5
1.0
1.5
2.0
2.5
3.0
3.5
R⋆/Reff

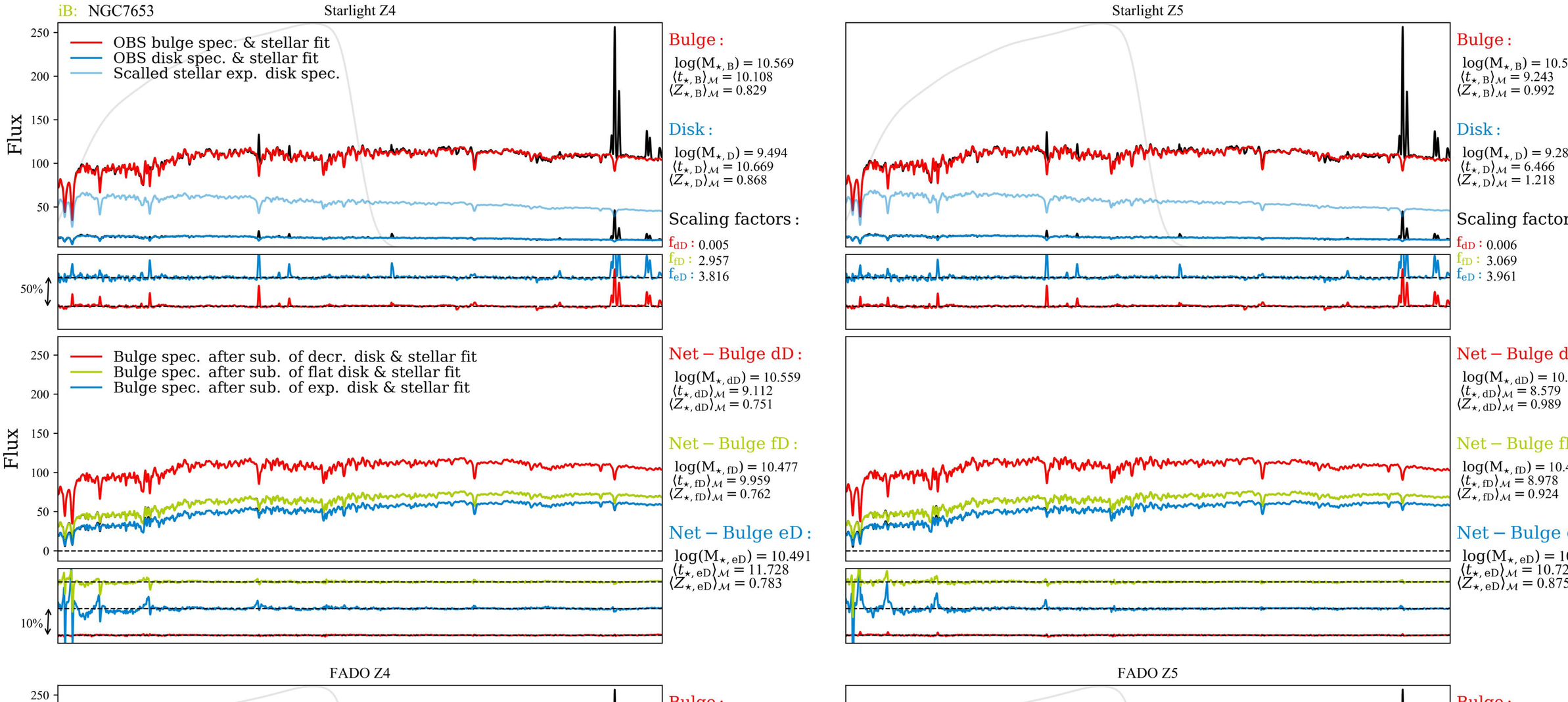
iB: NGC7653
Starlight Z4
OBS bulge spec. & stellar fit
OBS disk spec. & stellar fit
Scalled stellar exp. disk spec.
Flux
50%
Bulge :
log(M⋆, B) = 10.569
⟨t⋆, B⟩M = 10.108
⟨Z⋆, B⟩M = 0.829
Disk :
log(M⋆, D) = 9.494
⟨t⋆, D⟩M = 10.669
⟨Z⋆, D⟩M = 0.868
Scaling factors :
fdD : 0.005
ffD : 2.957
feD : 3.816
Bulge spec. after sub. of decr. disk & stellar fit
Bulge spec. after sub. of flat disk & stellar fit
Bulge spec. after sub. of exp. disk & stellar fit
10%
Net − Bulge dD :
log(M⋆, dD) = 10.559
⟨t⋆, dD⟩M = 9.112
⟨Z⋆, dD⟩M = 0.751
Net − Bulge fD :
log(M⋆, fD) = 10.477
⟨t⋆, fD⟩M = 9.959
⟨Z⋆, fD⟩M = 0.762
Net − Bulge eD :
log(M⋆, eD) = 10.491
⟨t⋆, eD⟩M = 11.728
⟨Z⋆, eD⟩M = 0.783

Starlight Z5
Bulge :
log(M⋆, B) = 10.561
⟨t⋆, B⟩M = 9.243
⟨Z⋆, B⟩M = 0.992
Disk :
log(M⋆, D) = 9.282
⟨t⋆, D⟩M = 6.466
⟨Z⋆, D⟩M = 1.218
Scaling factors :
fdD : 0.006
ffD : 3.069
feD : 3.961
Net − Bulge dD :
log(M⋆, dD) = 10.514
⟨t⋆, dD⟩M = 8.579
⟨Z⋆, dD⟩M = 0.989
Net − Bulge fD :
log(M⋆, fD) = 10.436
⟨t⋆, fD⟩M = 8.978
⟨Z⋆, fD⟩M = 0.924
Net − Bulge eD :
log(M⋆, eD) = 10.458
⟨t⋆, eD⟩M = 10.720
⟨Z⋆, eD⟩M = 0.875

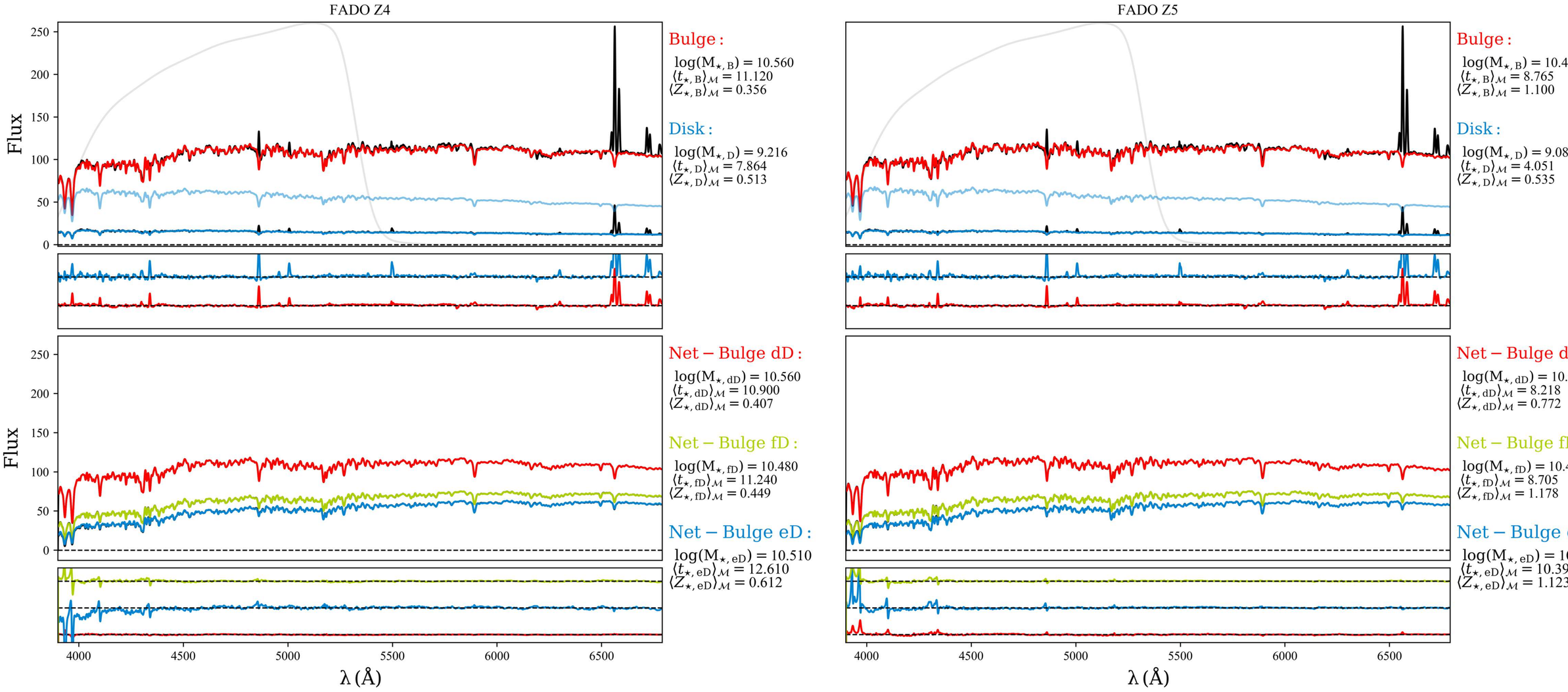
FADO Z4
Flux
Bulge :
log(M⋆, B) = 10.560
⟨t⋆, B⟩M = 11.120
⟨Z⋆, B⟩M = 0.356
Disk :
log(M⋆, D) = 9.216
⟨t⋆, D⟩M = 7.864
⟨Z⋆, D⟩M = 0.513
Net − Bulge dD :
log(M⋆, dD) = 10.560
⟨t⋆, dD⟩M = 10.900
⟨Z⋆, dD⟩M = 0.407
Net − Bulge fD :
log(M⋆, fD) = 10.480
⟨t⋆, fD⟩M = 11.240
⟨Z⋆, fD⟩M = 0.449
Net − Bulge eD :
log(M⋆, eD) = 10.510
⟨t⋆, eD⟩M = 12.610
⟨Z⋆, eD⟩M = 0.612
λ (Å)

FADO Z5
Bulge :
log(M⋆, B) = 10.480
⟨t⋆, B⟩M = 8.765
⟨Z⋆, B⟩M = 1.100
Disk :
log(M⋆, D) = 9.086
⟨t⋆, D⟩M = 4.051
⟨Z⋆, D⟩M = 0.535
Net − Bulge dD :
log(M⋆, dD) = 10.470
⟨t⋆, dD⟩M = 8.218
⟨Z⋆, dD⟩M = 0.772
Net − Bulge fD :
log(M⋆, fD) = 10.410
⟨t⋆, fD⟩M = 8.705
⟨Z⋆, fD⟩M = 1.178
Net − Bulge eD :
log(M⋆, eD) = 10.430
⟨t⋆, eD⟩M = 10.390
⟨Z⋆, eD⟩M = 1.123
λ (Å)

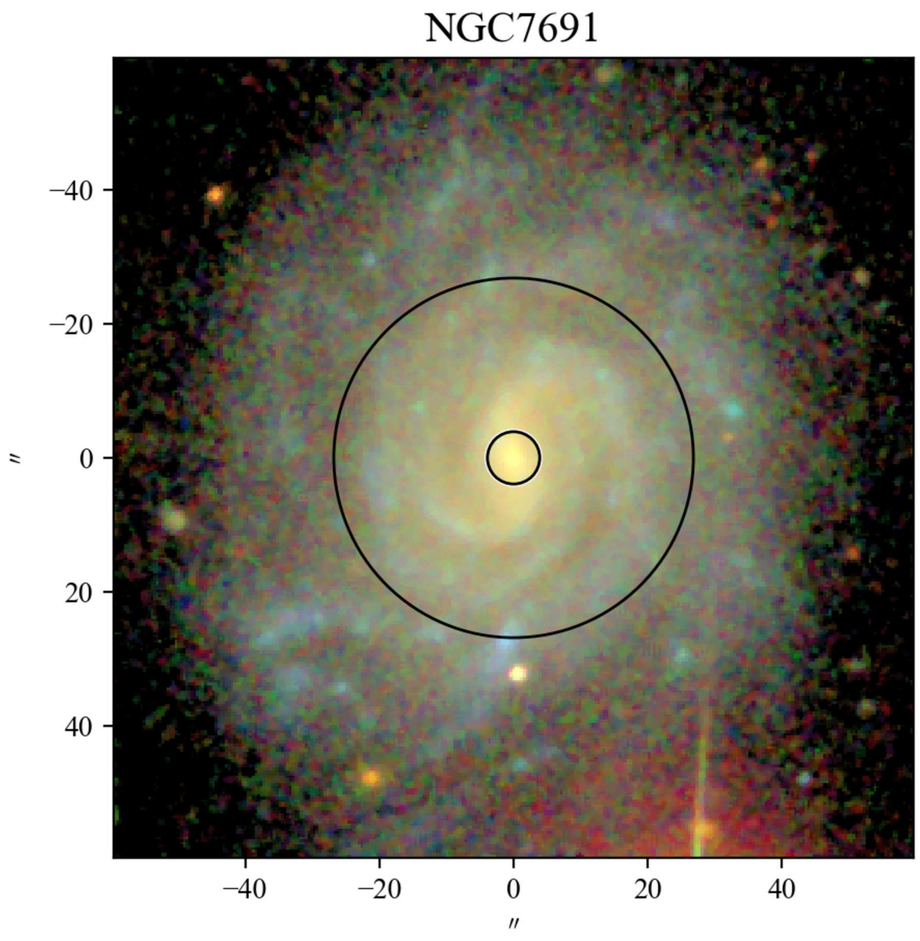
NGC7691
−40
−20
0
20
40
″
−40
−20
0
20
40
″

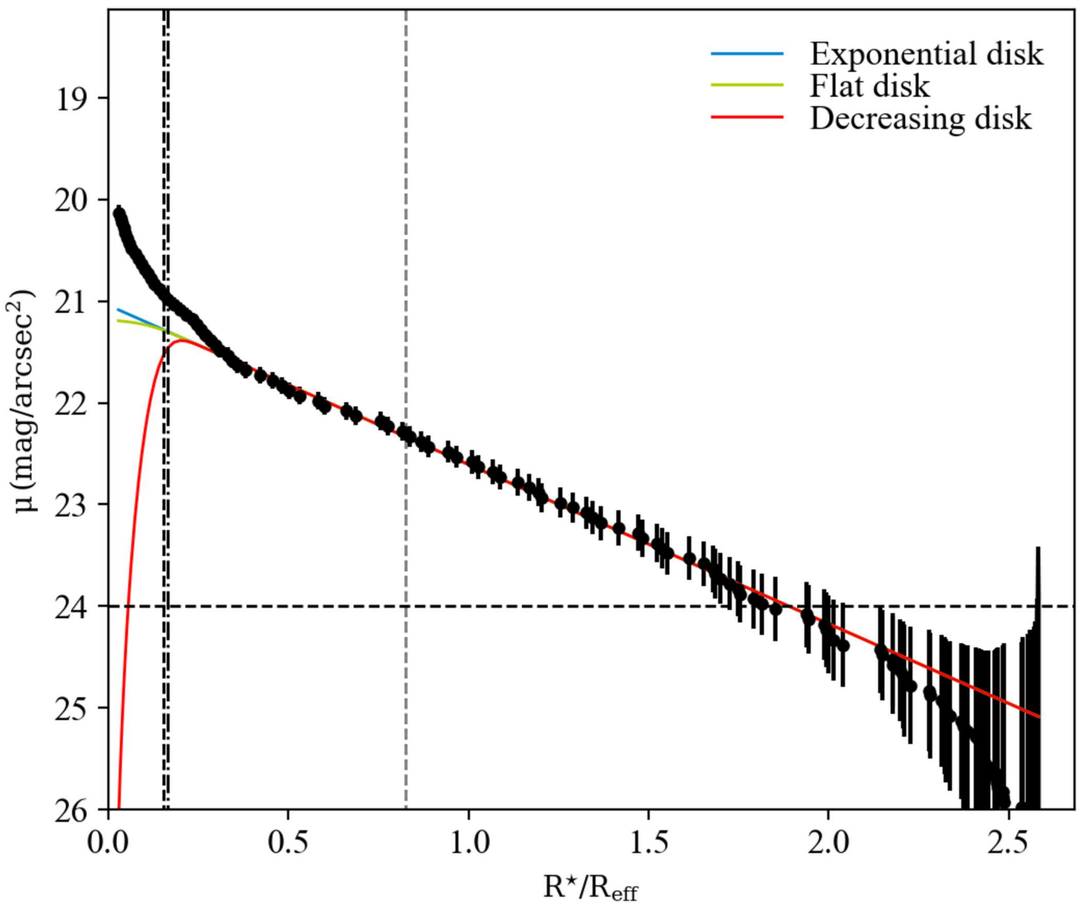
Exponential disk
Flat disk
Decreasing disk
μ (mag/arcsec²)
19
20
21
22
23
24
25
26
0.0
0.5
1.0
1.5
2.0
2.5
R⋆/Reff

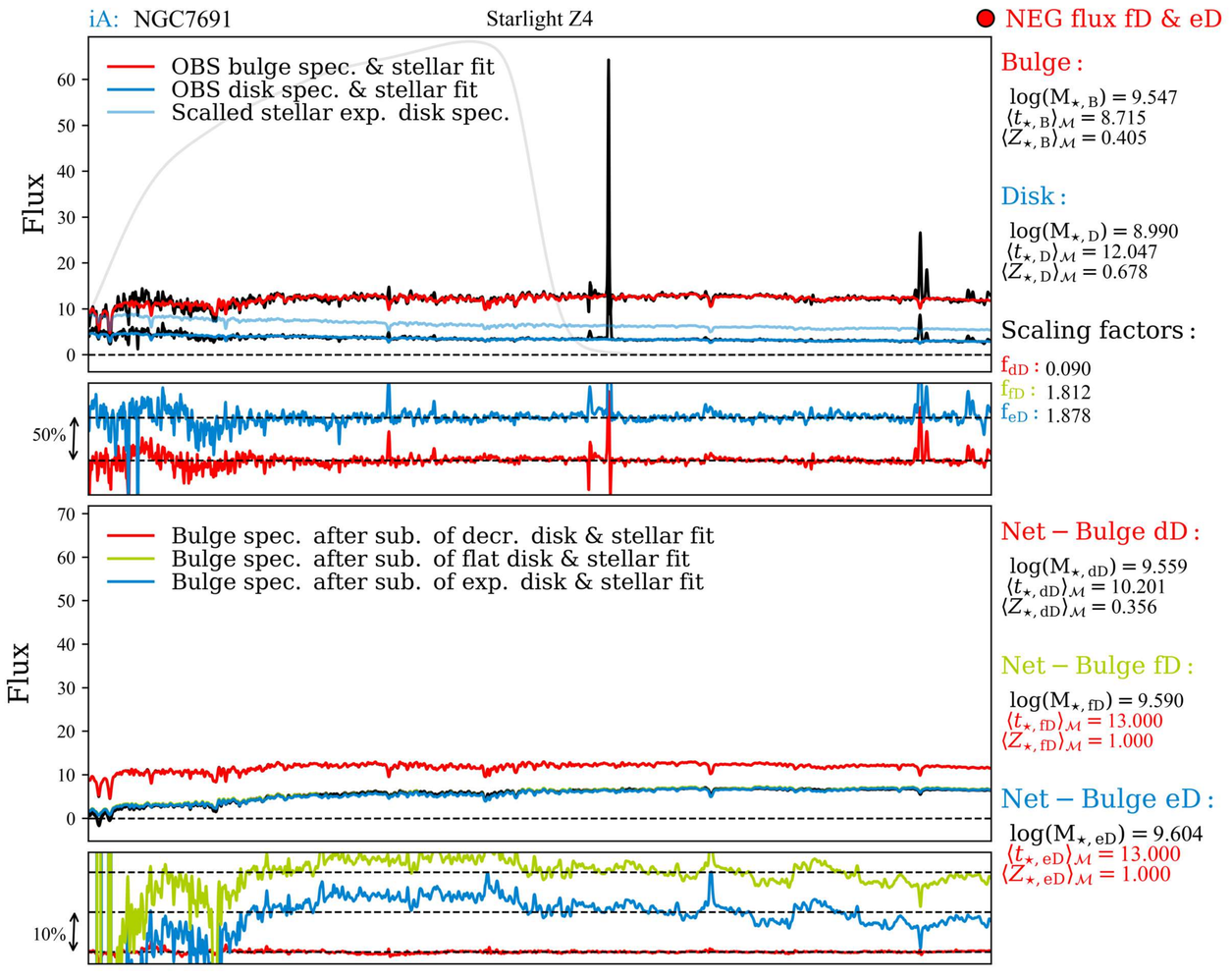
iA: NGC7691
Starlight Z4
NEG flux fD & eD
OBS bulge spec. & stellar fit
OBS disk spec. & stellar fit
Scalled stellar exp. disk spec.
Flux
50%
Bulge :
log(M⋆, B) = 9.547
⟨t⋆, B⟩M = 8.715
⟨Z⋆, B⟩M = 0.405
Disk :
log(M⋆, D) = 8.990
⟨t⋆, D⟩M = 12.047
⟨Z⋆, D⟩M = 0.678
Scaling factors :
fdD : 0.090
ffD : 1.812
feD : 1.878
Bulge spec. after sub. of decr. disk & stellar fit
Bulge spec. after sub. of flat disk & stellar fit
Bulge spec. after sub. of exp. disk & stellar fit
10%
Net − Bulge dD :
log(M⋆, dD) = 9.559
⟨t⋆, dD⟩M = 10.201
⟨Z⋆, dD⟩M = 0.356
Net − Bulge fD :
log(M⋆, fD) = 9.590
⟨t⋆, fD⟩M = 13.000
⟨Z⋆, fD⟩M = 1.000
Net − Bulge eD :
log(M⋆, eD) = 9.604
⟨t⋆, eD⟩M = 13.000
⟨Z⋆, eD⟩M = 1.000

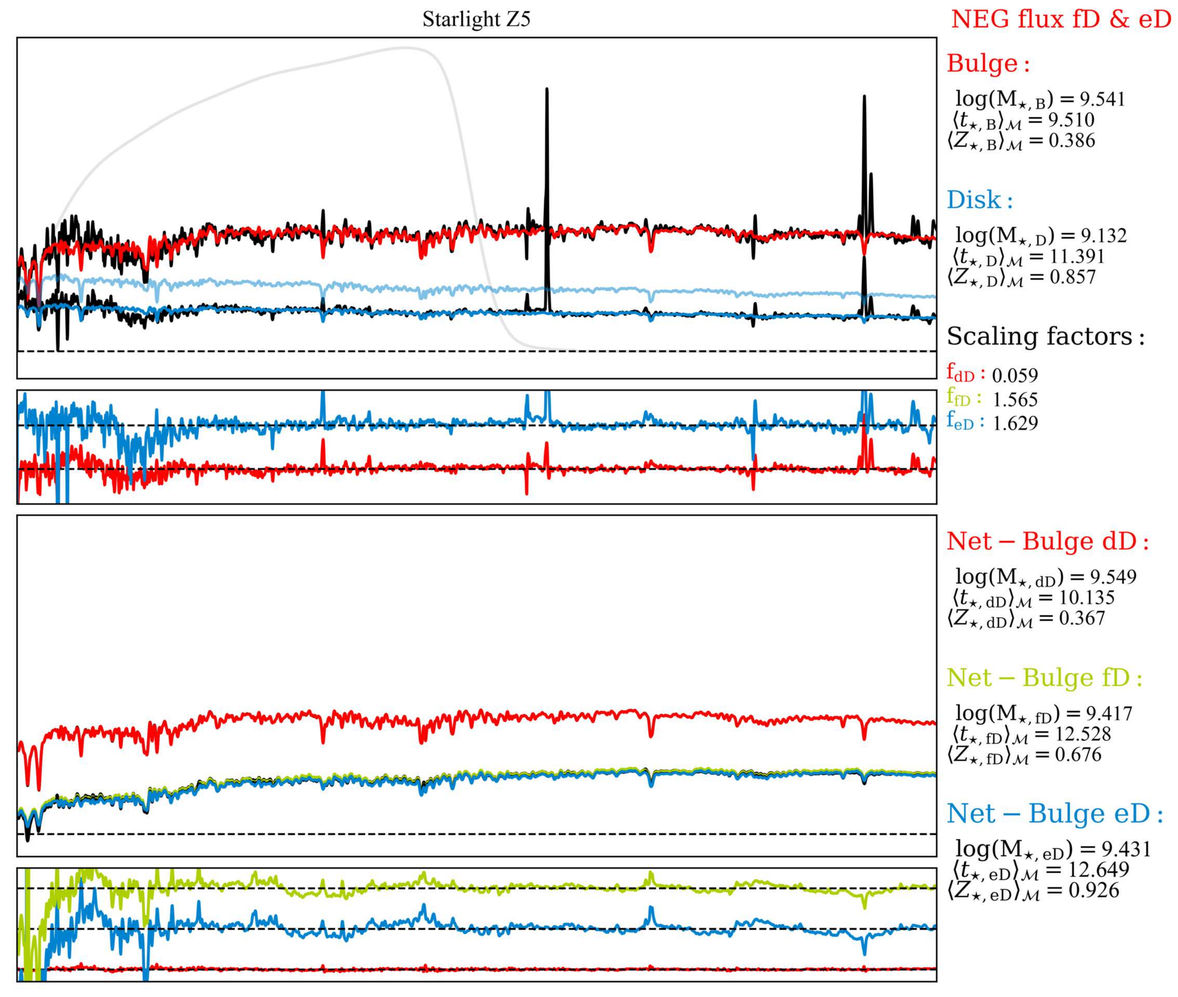
Starlight Z5
NEG flux fD & eD
Bulge :
log(M⋆, B) = 9.541
⟨t⋆, B⟩M = 9.510
⟨Z⋆, B⟩M = 0.386
Disk :
log(M⋆, D) = 9.132
⟨t⋆, D⟩M = 11.391
⟨Z⋆, D⟩M = 0.857
Scaling factors :
fdD : 0.059
ffD : 1.565
feD : 1.629
Net − Bulge dD :
log(M⋆, dD) = 9.549
⟨t⋆, dD⟩M = 10.135
⟨Z⋆, dD⟩M = 0.367
Net − Bulge fD :
log(M⋆, fD) = 9.417
⟨t⋆, fD⟩M = 12.528
⟨Z⋆, fD⟩M = 0.676
Net − Bulge eD :
log(M⋆, eD) = 9.431
⟨t⋆, eD⟩M = 12.649
⟨Z⋆, eD⟩M = 0.926

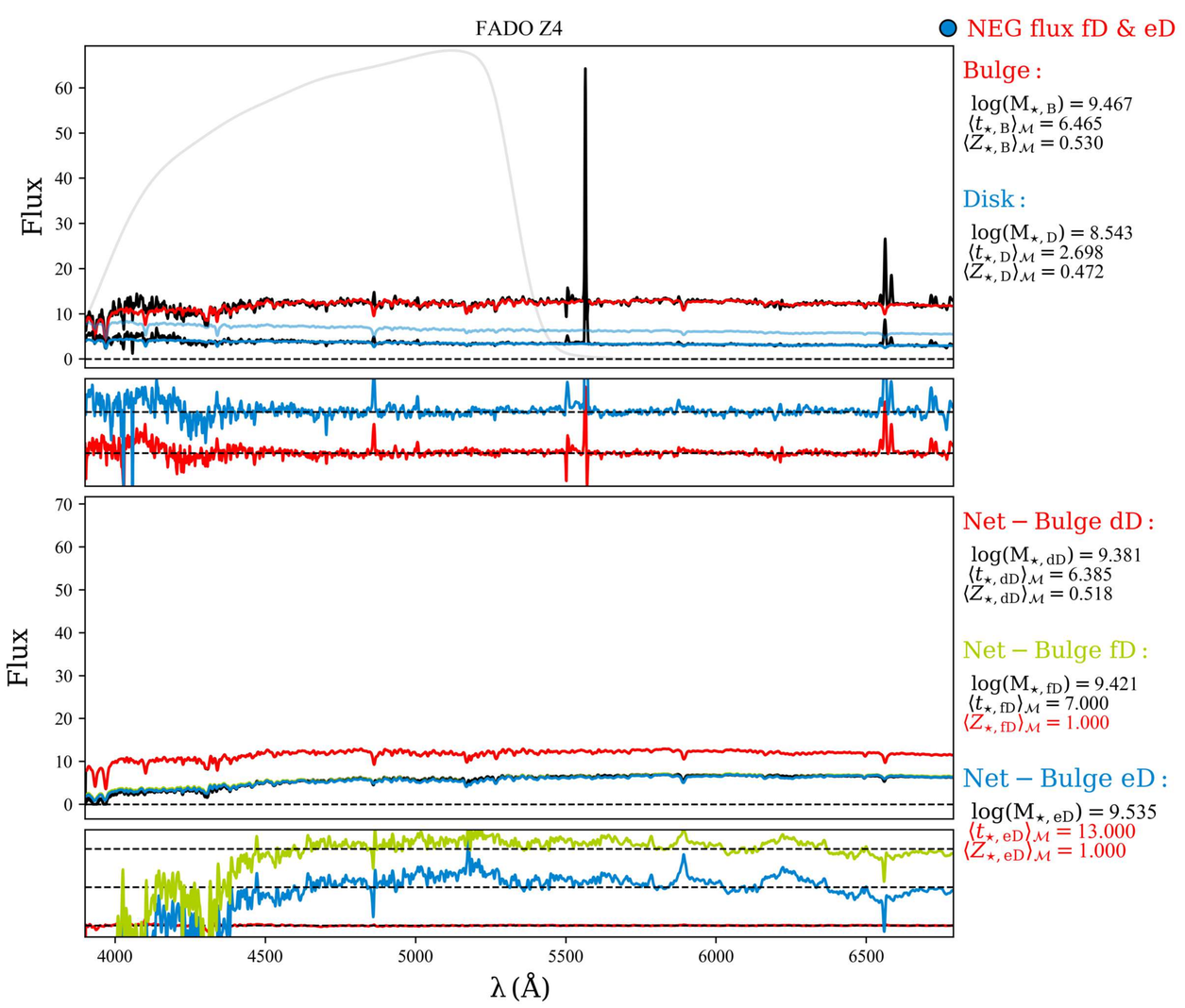
FADO Z4
NEG flux fD & eD
Flux
Bulge :
log(M⋆, B) = 9.467
⟨t⋆, B⟩M = 6.465
⟨Z⋆, B⟩M = 0.530
Disk :
log(M⋆, D) = 8.543
⟨t⋆, D⟩M = 2.698
⟨Z⋆, D⟩M = 0.472
Net − Bulge dD :
log(M⋆, dD) = 9.381
⟨t⋆, dD⟩M = 6.385
⟨Z⋆, dD⟩M = 0.518
Net − Bulge fD :
log(M⋆, fD) = 9.421
⟨t⋆, fD⟩M = 7.000
⟨Z⋆, fD⟩M = 1.000
Net − Bulge eD :
log(M⋆, eD) = 9.535
⟨t⋆, eD⟩M = 13.000
⟨Z⋆, eD⟩M = 1.000
λ (Å)

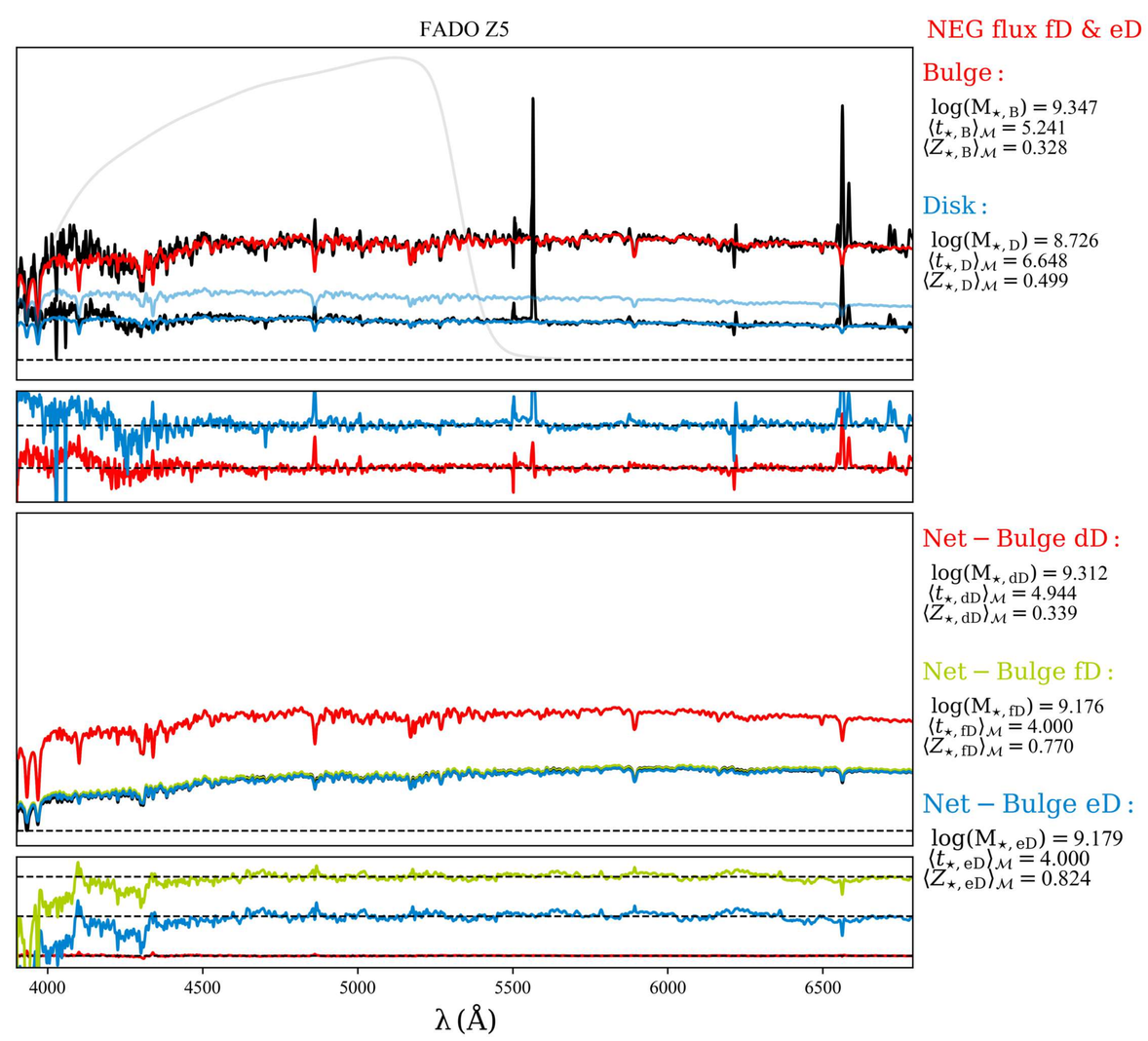
FADO Z5
NEG flux fD & eD
Bulge :
log(M⋆, B) = 9.347
⟨t⋆, B⟩M = 5.241
⟨Z⋆, B⟩M = 0.328
Disk :
log(M⋆, D) = 8.726
⟨t⋆, D⟩M = 6.648
⟨Z⋆, D⟩M = 0.499
Net − Bulge dD :
log(M⋆, dD) = 9.312
⟨t⋆, dD⟩M = 4.944
⟨Z⋆, dD⟩M = 0.339
Net − Bulge fD :
log(M⋆, fD) = 9.176
⟨t⋆, fD⟩M = 4.000
⟨Z⋆, fD⟩M = 0.770
Net − Bulge eD :
log(M⋆, eD) = 9.179
⟨t⋆, eD⟩M = 4.000
⟨Z⋆, eD⟩M = 0.824
λ (Å)

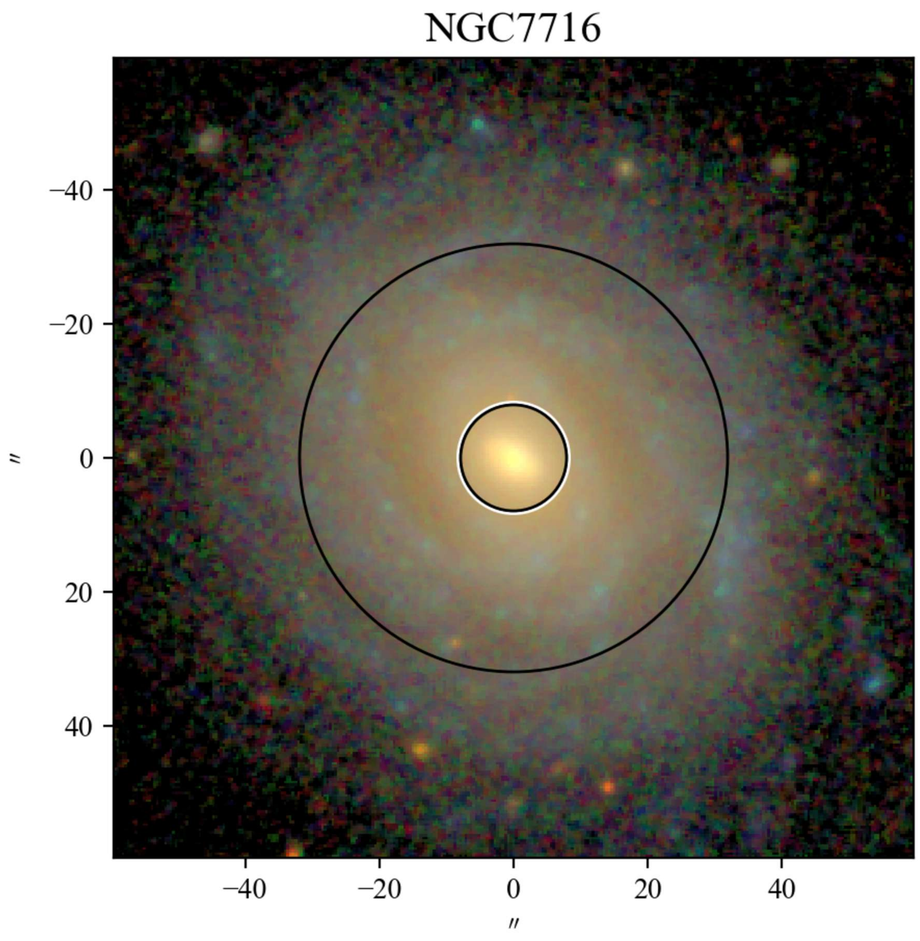
NGC7716
−40
−20
0
20
40
″
−40
−20
0
20
40
″

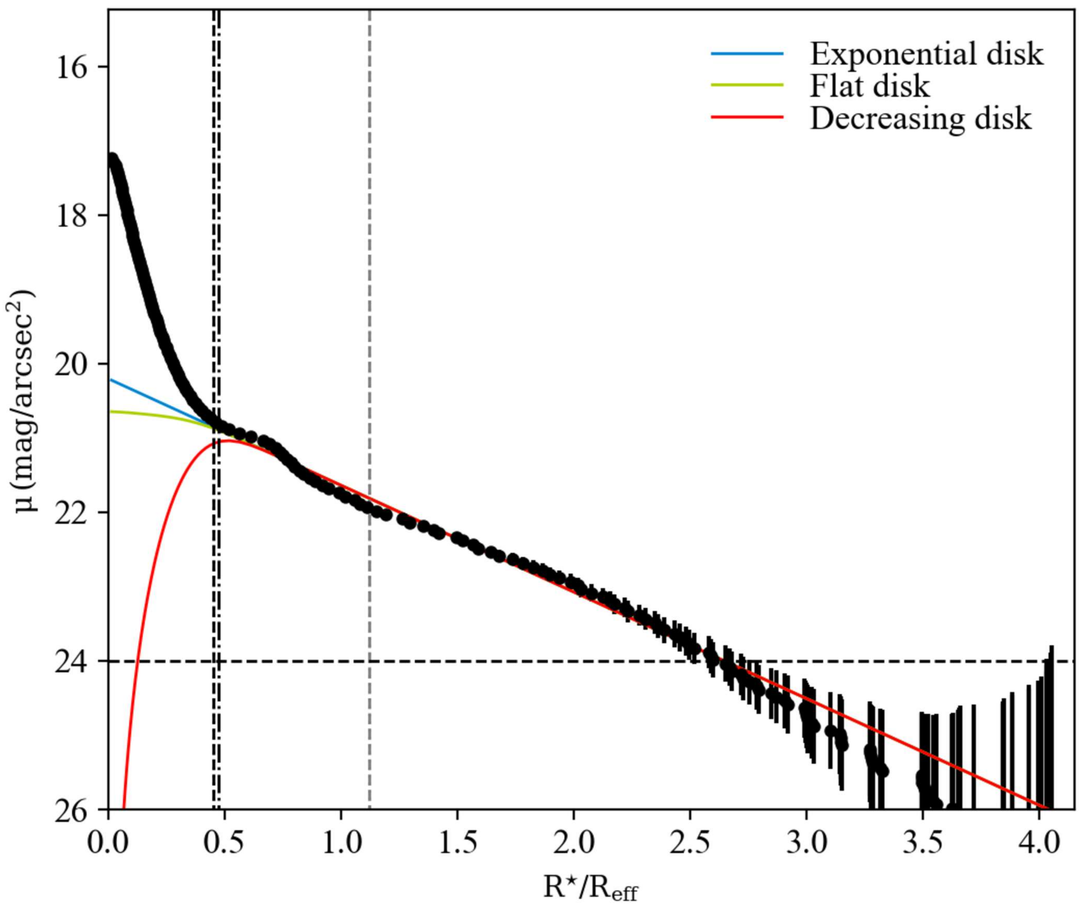
Exponential disk
Flat disk
Decreasing disk
μ (mag/arcsec²)
16
18
20
22
24
26
0.0
0.5
1.0
1.5
2.0
2.5
3.0
3.5
4.0
R⋆/Reff

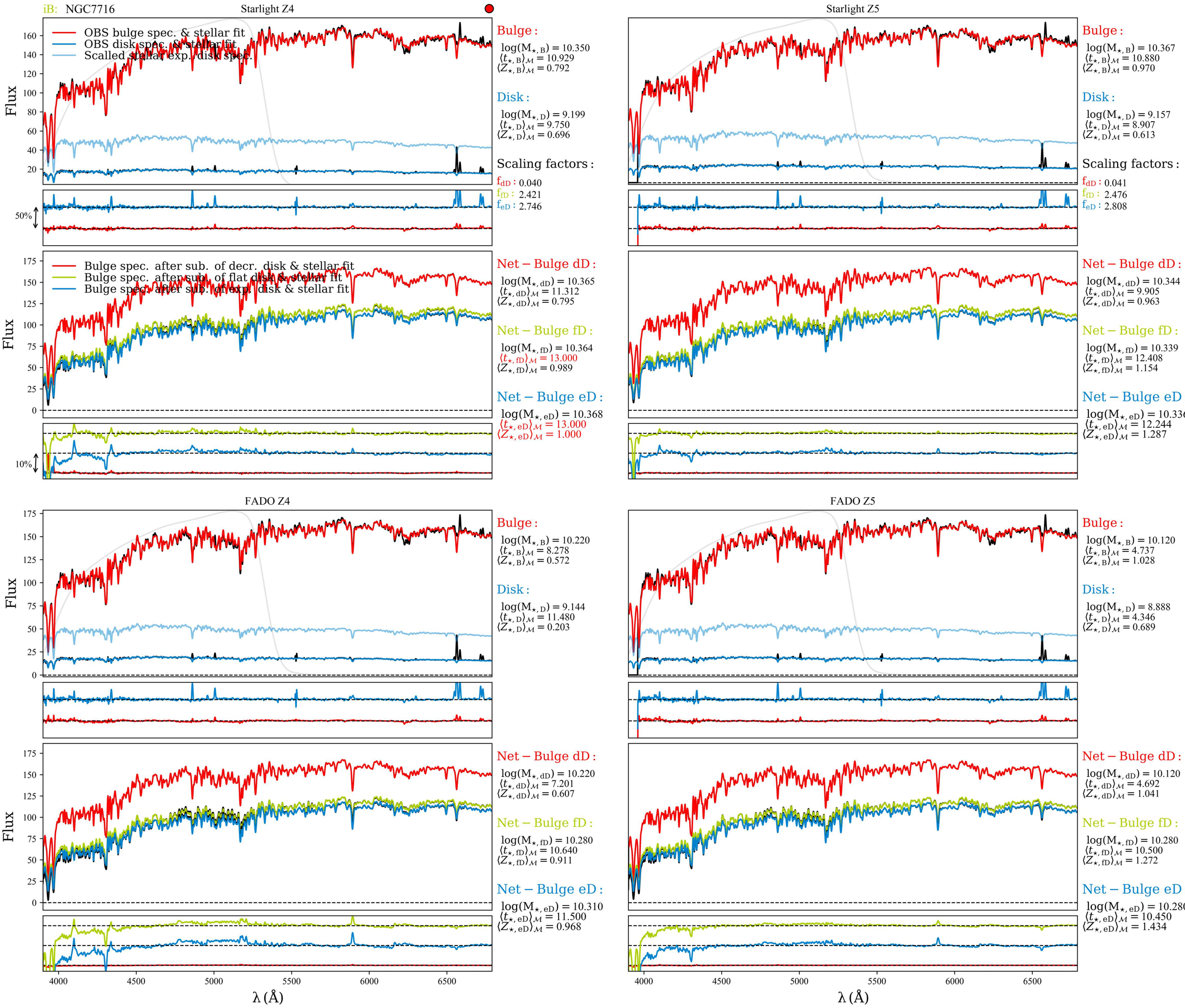
iB: NGC7716
Starlight Z4
OBS bulge spec. & stellar fit
OBS disk spec. & stellar fit
Scalled stellar exp. disk spec.
Flux
50%
Bulge :
log(M⋆, B) = 10.350
⟨t⋆, B⟩M = 10.929
⟨Z⋆, B⟩M = 0.792
Disk :
log(M⋆, D) = 9.199
⟨t⋆, D⟩M = 9.750
⟨Z⋆, D⟩M = 0.696
Scaling factors :
fdD : 0.040
ffD : 2.421
feD : 2.746
Bulge spec. after sub. of decr. disk & stellar fit
Bulge spec. after sub. of flat disk & stellar fit
Bulge spec. after sub. of exp. disk & stellar fit
10%
Net − Bulge dD :
log(M⋆, dD) = 10.365
⟨t⋆, dD⟩M = 11.312
⟨Z⋆, dD⟩M = 0.795
Net − Bulge fD :
log(M⋆, fD) = 10.364
⟨t⋆, fD⟩M = 13.000
⟨Z⋆, fD⟩M = 0.989
Net − Bulge eD :
log(M⋆, eD) = 10.368
⟨t⋆, eD⟩M = 13.000
⟨Z⋆, eD⟩M = 1.000
Starlight Z5
Bulge :
log(M⋆, B) = 10.367
⟨t⋆, B⟩M = 10.880
⟨Z⋆, B⟩M = 0.970
Disk :
log(M⋆, D) = 9.157
⟨t⋆, D⟩M = 8.907
⟨Z⋆, D⟩M = 0.613
Scaling factors :
fdD : 0.041
ffD : 2.476
feD : 2.808
Net − Bulge dD :
log(M⋆, dD) = 10.344
⟨t⋆, dD⟩M = 9.905
⟨Z⋆, dD⟩M = 0.963
Net − Bulge fD :
log(M⋆, fD) = 10.339
⟨t⋆, fD⟩M = 12.408
⟨Z⋆, fD⟩M = 1.154
Net − Bulge eD :
log(M⋆, eD) = 10.336
⟨t⋆, eD⟩M = 12.244
⟨Z⋆, eD⟩M = 1.287
FADO Z4
Bulge :
log(M⋆, B) = 10.220
⟨t⋆, B⟩M = 8.278
⟨Z⋆, B⟩M = 0.572
Disk :
log(M⋆, D) = 9.144
⟨t⋆, D⟩M = 11.480
⟨Z⋆, D⟩M = 0.203
Net − Bulge dD :
log(M⋆, dD) = 10.220
⟨t⋆, dD⟩M = 7.201
⟨Z⋆, dD⟩M = 0.607
Net − Bulge fD :
log(M⋆, fD) = 10.280
⟨t⋆, fD⟩M = 10.640
⟨Z⋆, fD⟩M = 0.911
Net − Bulge eD :
log(M⋆, eD) = 10.310
⟨t⋆, eD⟩M = 11.500
⟨Z⋆, eD⟩M = 0.968
FADO Z5
Bulge :
log(M⋆, B) = 10.120
⟨t⋆, B⟩M = 4.737
⟨Z⋆, B⟩M = 1.028
Disk :
log(M⋆, D) = 8.888
⟨t⋆, D⟩M = 4.346
⟨Z⋆, D⟩M = 0.689
Net − Bulge dD :
log(M⋆, dD) = 10.120
⟨t⋆, dD⟩M = 4.692
⟨Z⋆, dD⟩M = 1.041
Net − Bulge fD :
log(M⋆, fD) = 10.280
⟨t⋆, fD⟩M = 10.500
⟨Z⋆, fD⟩M = 1.272
Net − Bulge eD :
log(M⋆, eD) = 10.280
⟨t⋆, eD⟩M = 10.450
⟨Z⋆, eD⟩M = 1.434
λ (Å)

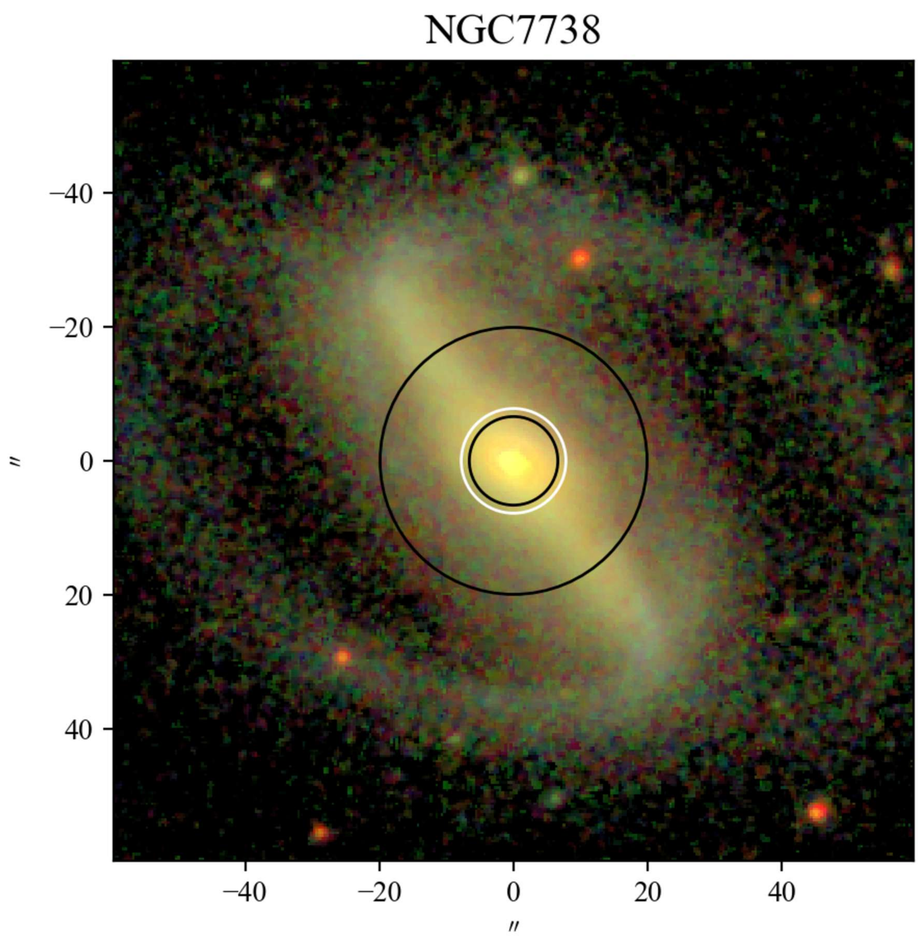
NGC7738
−40
−20
0
20
40
″
−40
−20
0
20
40
″

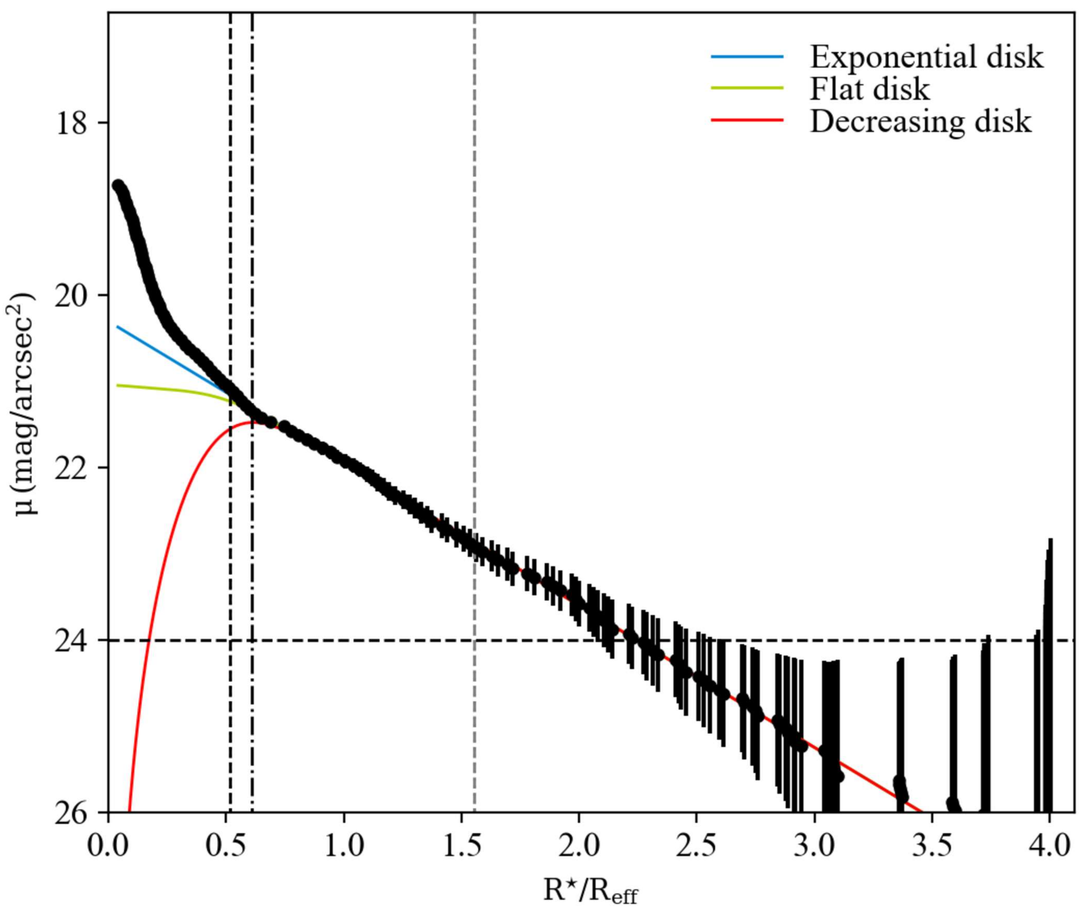
Exponential disk
Flat disk
Decreasing disk
μ (mag/arcsec²)
18
20
22
24
26
0.0
0.5
1.0
1.5
2.0
2.5
3.0
3.5
4.0
R⋆/Reff

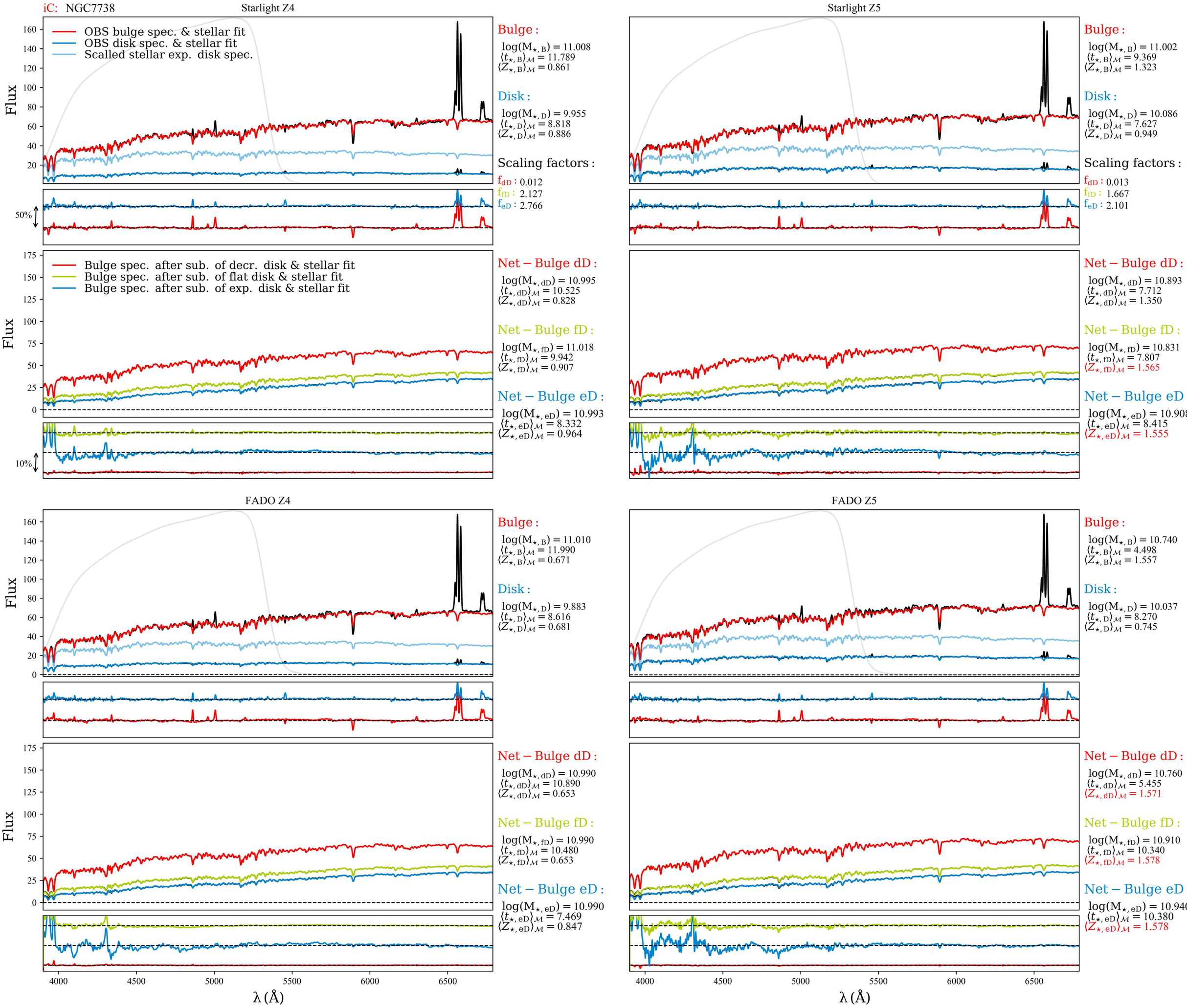
iC: NGC7738
Starlight Z4
OBS bulge spec. & stellar fit
OBS disk spec. & stellar fit
Scalled stellar exp. disk spec.
Flux
50%
Bulge :
log(M⋆, B) = 11.008
⟨t⋆, B⟩M = 11.789
⟨Z⋆, B⟩M = 0.861
Disk :
log(M⋆, D) = 9.955
⟨t⋆, D⟩M = 8.818
⟨Z⋆, D⟩M = 0.886
Scaling factors :
fdD : 0.012
ffD : 2.127
feD : 2.766
Starlight Z5
Bulge :
log(M⋆, B) = 11.002
⟨t⋆, B⟩M = 9.369
⟨Z⋆, B⟩M = 1.323
Disk :
log(M⋆, D) = 10.086
⟨t⋆, D⟩M = 7.627
⟨Z⋆, D⟩M = 0.949
Scaling factors :
fdD : 0.013
ffD : 1.667
feD : 2.101
Bulge spec. after sub. of decr. disk & stellar fit
Bulge spec. after sub. of flat disk & stellar fit
Bulge spec. after sub. of exp. disk & stellar fit
10%
Net − Bulge dD :
log(M⋆, dD) = 10.995
⟨t⋆, dD⟩M = 10.525
⟨Z⋆, dD⟩M = 0.828
Net − Bulge fD :
log(M⋆, fD) = 11.018
⟨t⋆, fD⟩M = 9.942
⟨Z⋆, fD⟩M = 0.907
Net − Bulge eD :
log(M⋆, eD) = 10.993
⟨t⋆, eD⟩M = 8.332
⟨Z⋆, eD⟩M = 0.964
Net − Bulge dD :
log(M⋆, dD) = 10.893
⟨t⋆, dD⟩M = 7.712
⟨Z⋆, dD⟩M = 1.350
Net − Bulge fD :
log(M⋆, fD) = 10.831
⟨t⋆, fD⟩M = 7.807
⟨Z⋆, fD⟩M = 1.565
Net − Bulge eD :
log(M⋆, eD) = 10.908
⟨t⋆, eD⟩M = 8.415
⟨Z⋆, eD⟩M = 1.555
FADO Z4
Bulge :
log(M⋆, B) = 11.010
⟨t⋆, B⟩M = 11.990
⟨Z⋆, B⟩M = 0.671
Disk :
log(M⋆, D) = 9.883
⟨t⋆, D⟩M = 8.616
⟨Z⋆, D⟩M = 0.681
FADO Z5
Bulge :
log(M⋆, B) = 10.740
⟨t⋆, B⟩M = 4.498
⟨Z⋆, B⟩M = 1.557
Disk :
log(M⋆, D) = 10.037
⟨t⋆, D⟩M = 8.270
⟨Z⋆, D⟩M = 0.745
Net − Bulge dD :
log(M⋆, dD) = 10.990
⟨t⋆, dD⟩M = 10.890
⟨Z⋆, dD⟩M = 0.653
Net − Bulge fD :
log(M⋆, fD) = 10.990
⟨t⋆, fD⟩M = 10.480
⟨Z⋆, fD⟩M = 0.653
Net − Bulge eD :
log(M⋆, eD) = 10.990
⟨t⋆, eD⟩M = 7.469
⟨Z⋆, eD⟩M = 0.847
Net − Bulge dD :
log(M⋆, dD) = 10.760
⟨t⋆, dD⟩M = 5.455
⟨Z⋆, dD⟩M = 1.571
Net − Bulge fD :
log(M⋆, fD) = 10.910
⟨t⋆, fD⟩M = 10.340
⟨Z⋆, fD⟩M = 1.578
Net − Bulge eD :
log(M⋆, eD) = 10.940
⟨t⋆, eD⟩M = 10.380
⟨Z⋆, eD⟩M = 1.578
λ (Å)

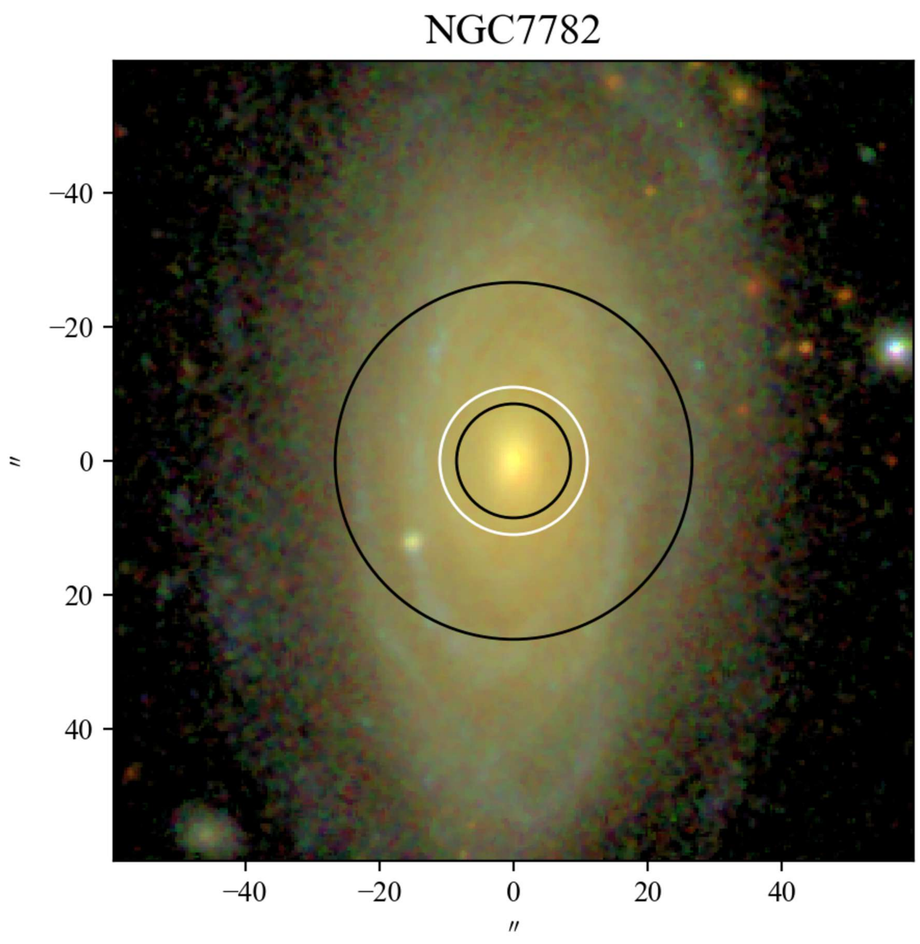
NGC7782
−40
−20
0
20
40
″
−40
−20
0
20
40
″

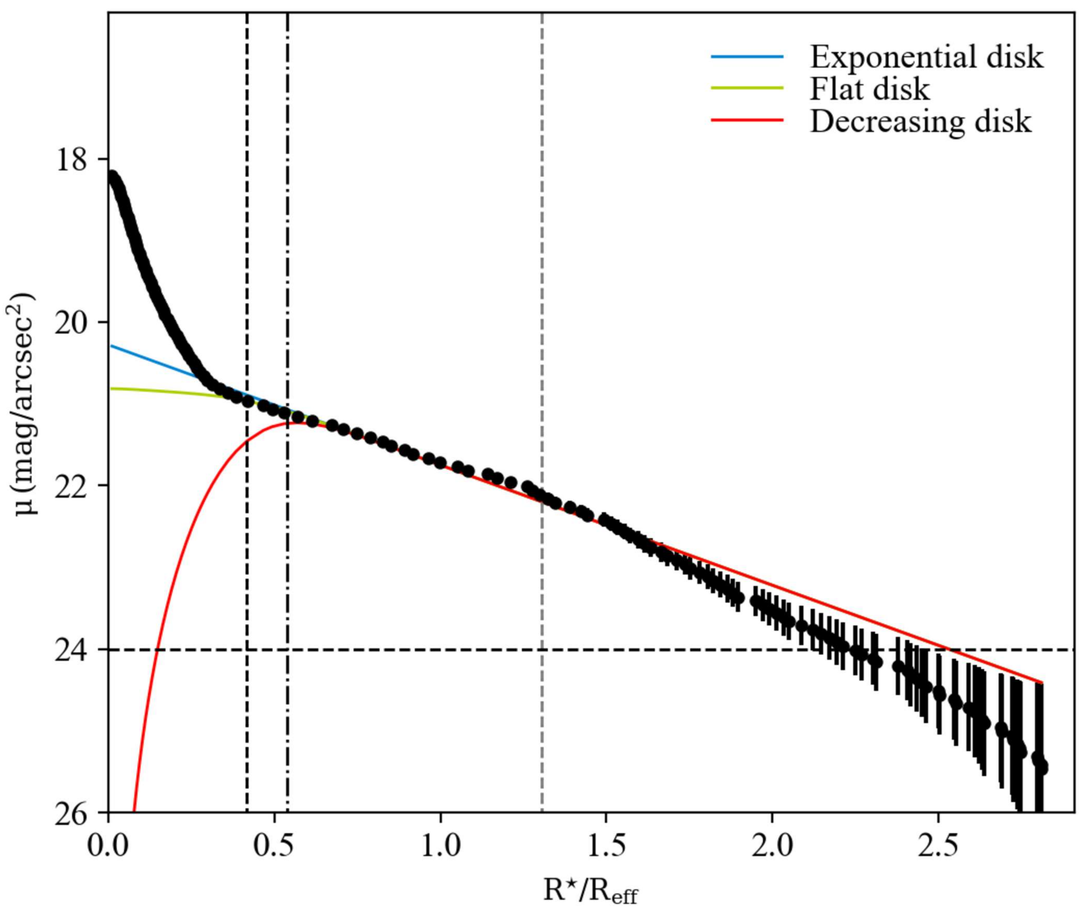
Exponential disk
Flat disk
Decreasing disk
μ (mag/arcsec²)
18
20
22
24
26
0.0
0.5
1.0
1.5
2.0
2.5
R⋆/Reff

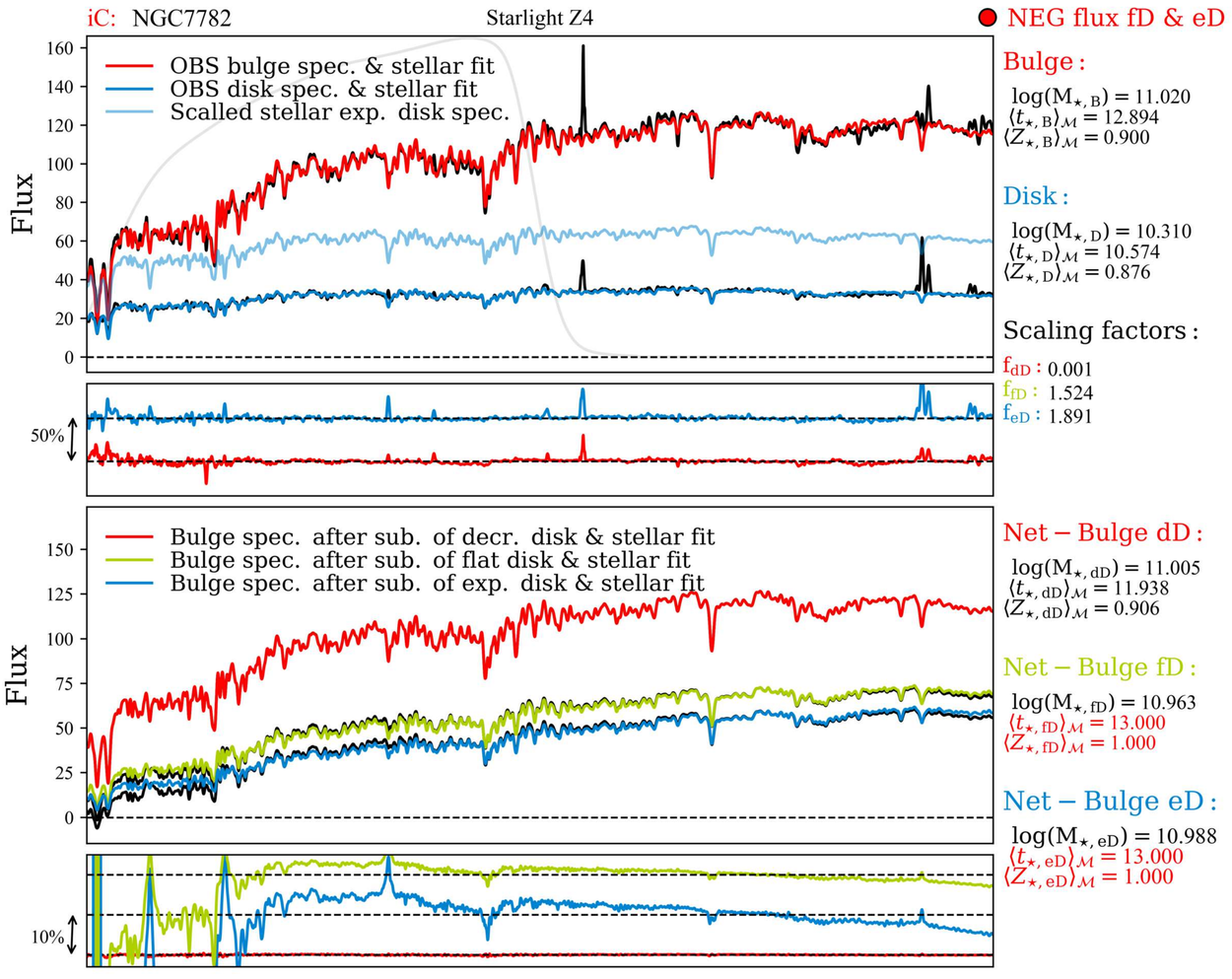
iC: NGC7782
Starlight Z4
NEG flux fD & eD
OBS bulge spec. & stellar fit
OBS disk spec. & stellar fit
Scalled stellar exp. disk spec.
Flux
Bulge :
log(M⋆, B) = 11.020
⟨t⋆, B⟩M = 12.894
⟨Z⋆, B⟩M = 0.900
Disk :
log(M⋆, D) = 10.310
⟨t⋆, D⟩M = 10.574
⟨Z⋆, D⟩M = 0.876
Scaling factors :
fdD : 0.001
ffD : 1.524
feD : 1.891
50%
Bulge spec. after sub. of decr. disk & stellar fit
Bulge spec. after sub. of flat disk & stellar fit
Bulge spec. after sub. of exp. disk & stellar fit
Net − Bulge dD :
log(M⋆, dD) = 11.005
⟨t⋆, dD⟩M = 11.938
⟨Z⋆, dD⟩M = 0.906
Net − Bulge fD :
log(M⋆, fD) = 10.963
⟨t⋆, fD⟩M = 13.000
⟨Z⋆, fD⟩M = 1.000
Net − Bulge eD :
log(M⋆, eD) = 10.988
⟨t⋆, eD⟩M = 13.000
⟨Z⋆, eD⟩M = 1.000
10%

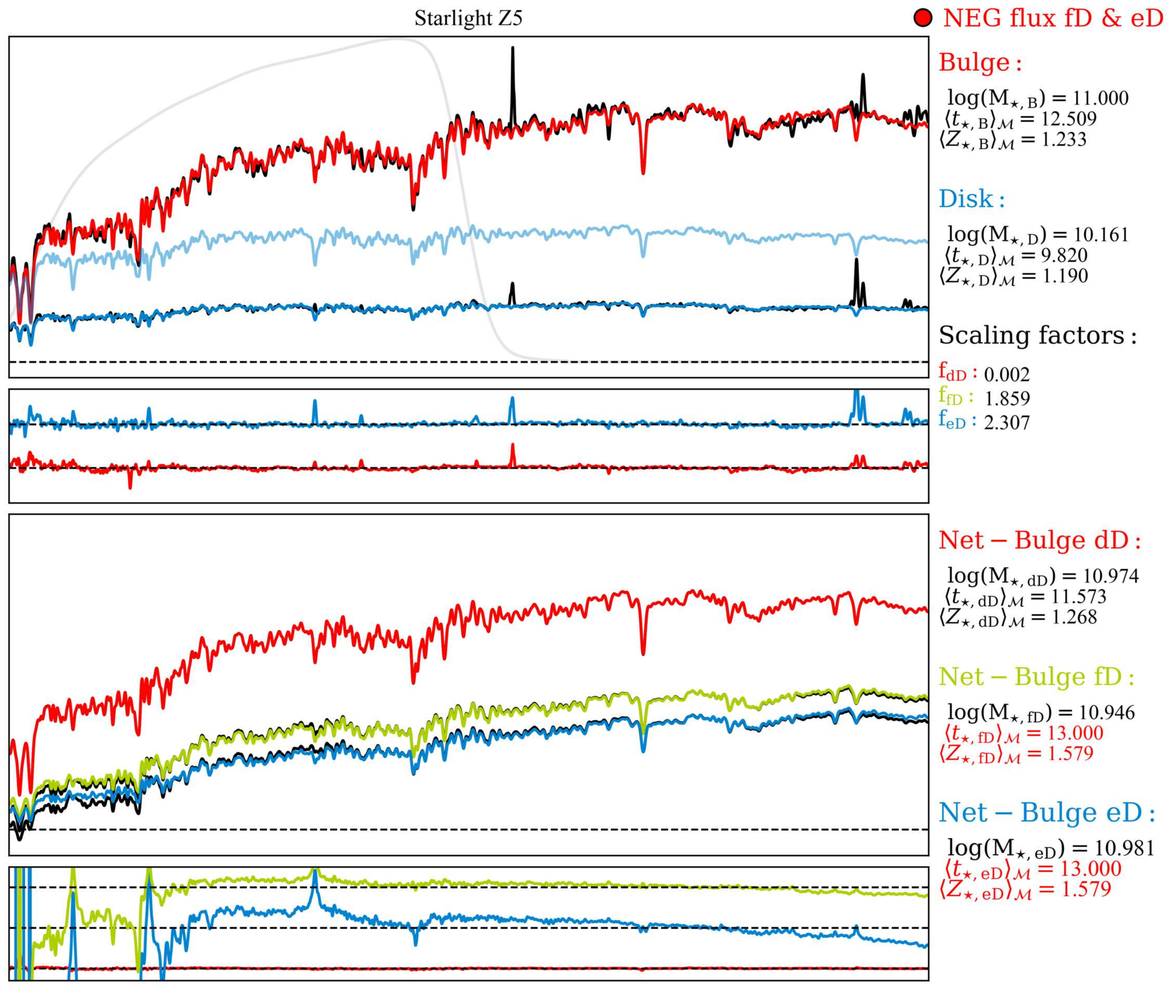
Starlight Z5
NEG flux fD & eD
Bulge :
log(M⋆, B) = 11.000
⟨t⋆, B⟩M = 12.509
⟨Z⋆, B⟩M = 1.233
Disk :
log(M⋆, D) = 10.161
⟨t⋆, D⟩M = 9.820
⟨Z⋆, D⟩M = 1.190
Scaling factors :
fdD : 0.002
ffD : 1.859
feD : 2.307
Net − Bulge dD :
log(M⋆, dD) = 10.974
⟨t⋆, dD⟩M = 11.573
⟨Z⋆, dD⟩M = 1.268
Net − Bulge fD :
log(M⋆, fD) = 10.946
⟨t⋆, fD⟩M = 13.000
⟨Z⋆, fD⟩M = 1.579
Net − Bulge eD :
log(M⋆, eD) = 10.981
⟨t⋆, eD⟩M = 13.000
⟨Z⋆, eD⟩M = 1.579

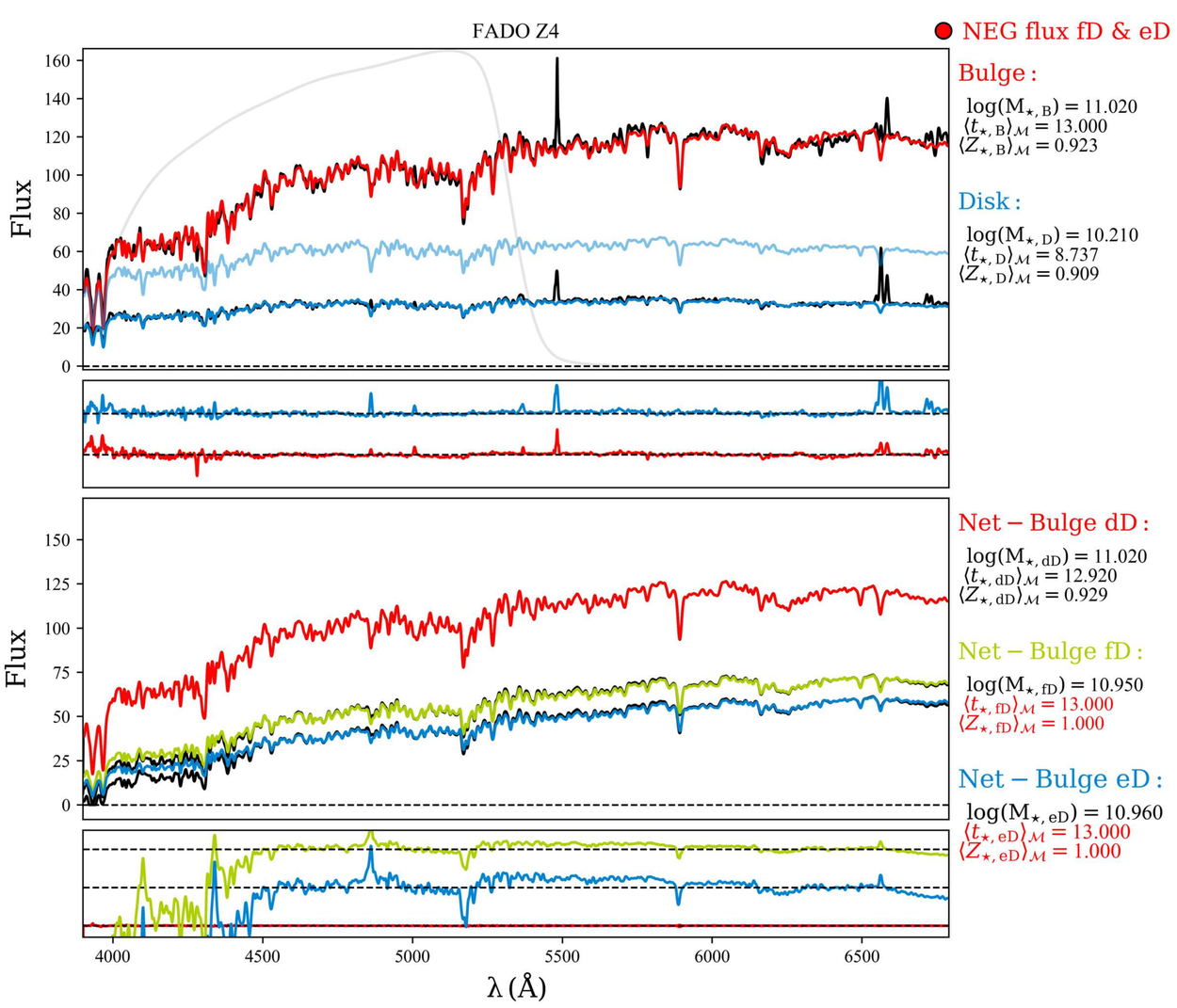
FADO Z4
NEG flux fD & eD
Flux
Bulge :
log(M⋆, B) = 11.020
⟨t⋆, B⟩M = 13.000
⟨Z⋆, B⟩M = 0.923
Disk :
log(M⋆, D) = 10.210
⟨t⋆, D⟩M = 8.737
⟨Z⋆, D⟩M = 0.909
Net − Bulge dD :
log(M⋆, dD) = 11.020
⟨t⋆, dD⟩M = 12.920
⟨Z⋆, dD⟩M = 0.929
Net − Bulge fD :
log(M⋆, fD) = 10.950
⟨t⋆, fD⟩M = 13.000
⟨Z⋆, fD⟩M = 1.000
Net − Bulge eD :
log(M⋆, eD) = 10.960
⟨t⋆, eD⟩M = 13.000
⟨Z⋆, eD⟩M = 1.000
λ (Å)

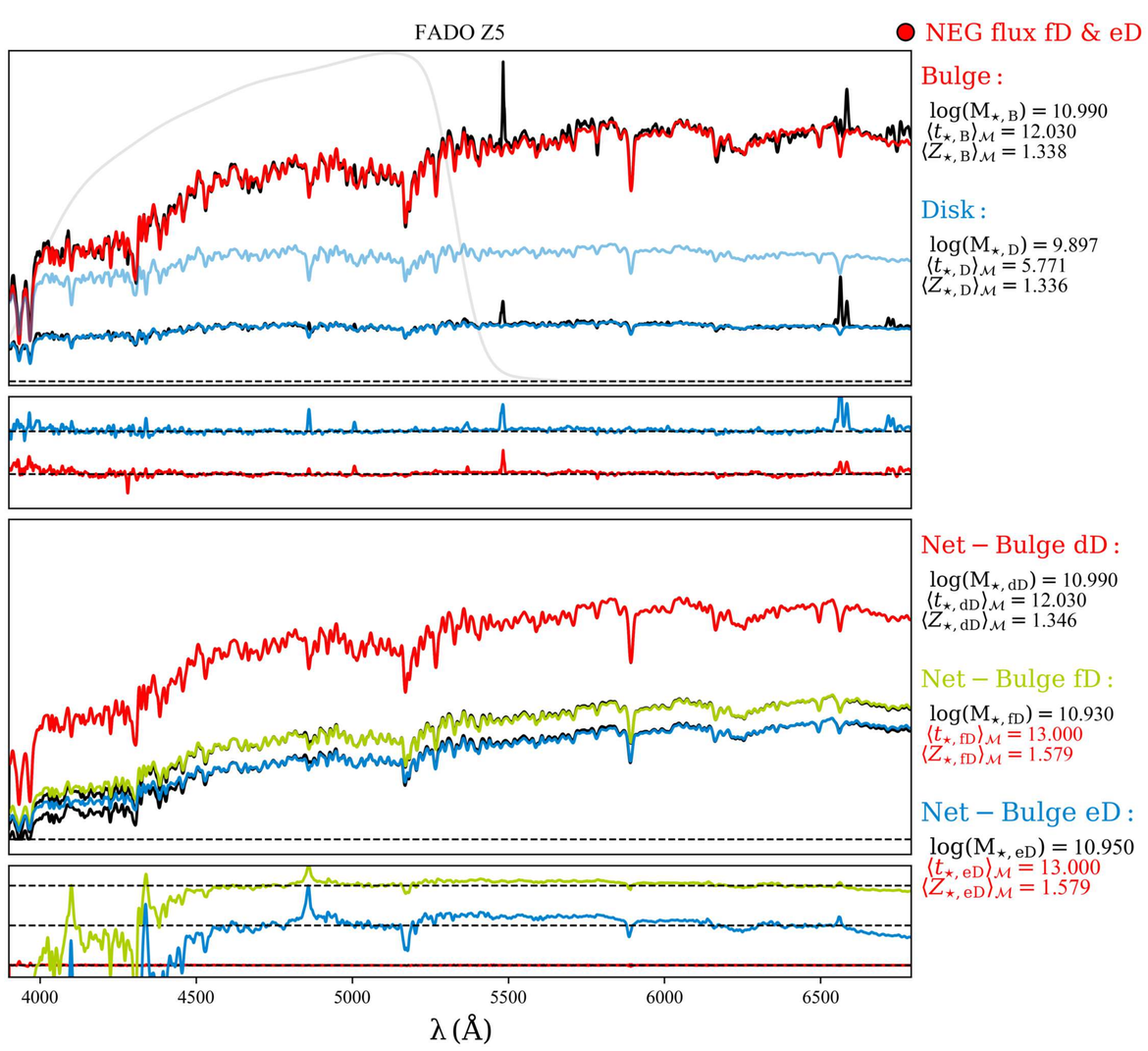
FADO Z5
NEG flux fD & eD
Bulge :
log(M⋆, B) = 10.990
⟨t⋆, B⟩M = 12.030
⟨Z⋆, B⟩M = 1.338
Disk :
log(M⋆, D) = 9.897
⟨t⋆, D⟩M = 5.771
⟨Z⋆, D⟩M = 1.336
Net − Bulge dD :
log(M⋆, dD) = 10.990
⟨t⋆, dD⟩M = 12.030
⟨Z⋆, dD⟩M = 1.346
Net − Bulge fD :
log(M⋆, fD) = 10.930
⟨t⋆, fD⟩M = 13.000
⟨Z⋆, fD⟩M = 1.579
Net − Bulge eD :
log(M⋆, eD) = 10.950
⟨t⋆, eD⟩M = 13.000
⟨Z⋆, eD⟩M = 1.579
λ (Å)

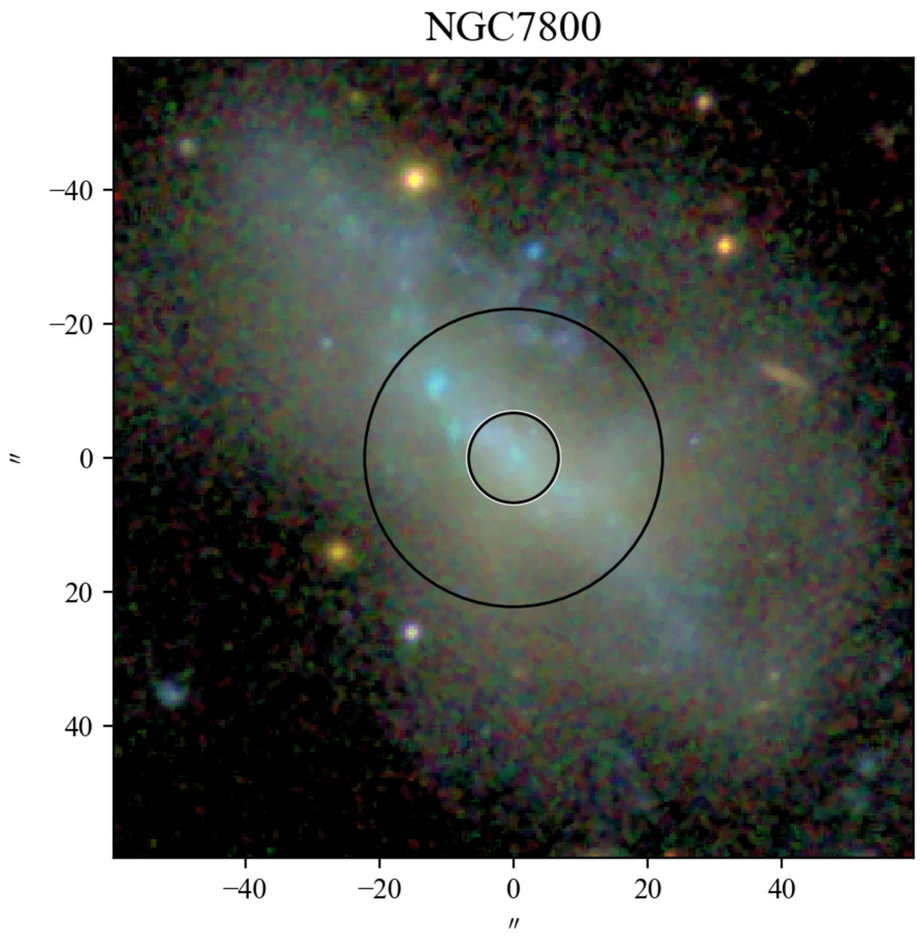
NGC7800
−40
−20
0
20
40
″
−40
−20
0
20
40
″

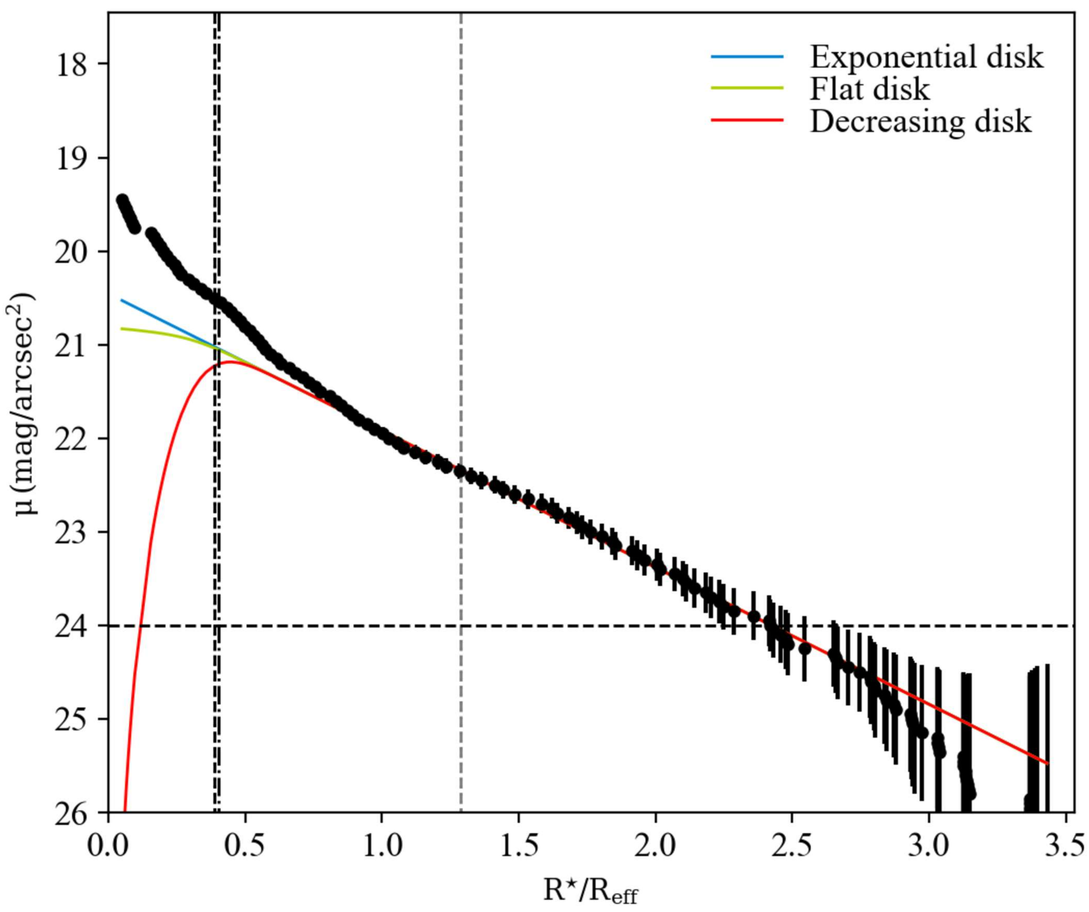
Exponential disk
Flat disk
Decreasing disk
μ (mag/arcsec²)
18
19
20
21
22
23
24
25
26
0.0
0.5
1.0
1.5
2.0
2.5
3.0
3.5
R⋆/Reff

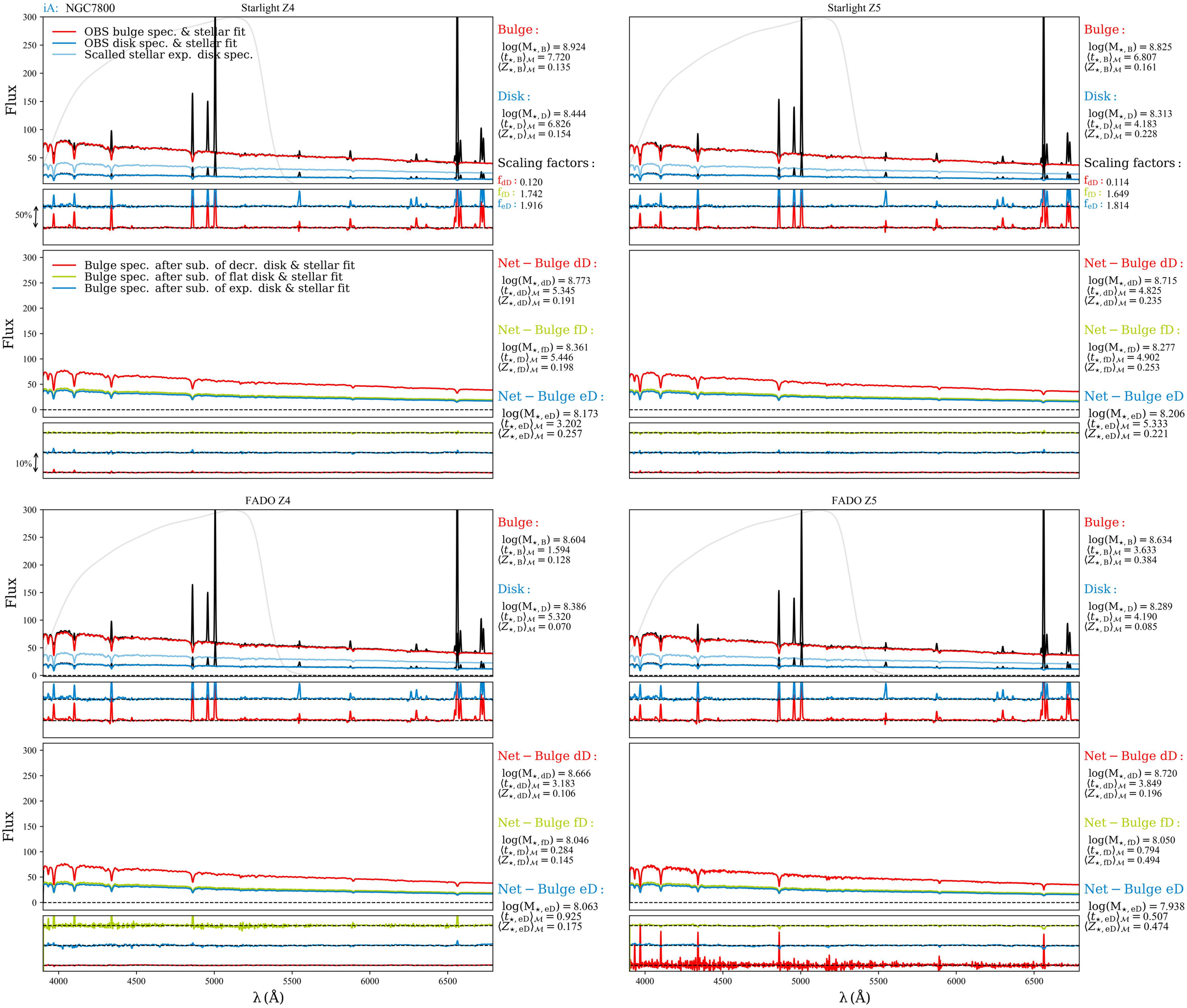
iA: NGC7800
Starlight Z4
OBS bulge spec. & stellar fit
OBS disk spec. & stellar fit
Scalled stellar exp. disk spec.
Flux
Bulge :
log(M⋆, B) = 8.924
⟨t⋆, B⟩M = 7.720
⟨Z⋆, B⟩M = 0.135
Disk :
log(M⋆, D) = 8.444
⟨t⋆, D⟩M = 6.826
⟨Z⋆, D⟩M = 0.154
Scaling factors :
fdD : 0.120
ffD : 1.742
feD : 1.916
50%
Bulge spec. after sub. of decr. disk & stellar fit
Bulge spec. after sub. of flat disk & stellar fit
Bulge spec. after sub. of exp. disk & stellar fit
Net − Bulge dD :
log(M⋆, dD) = 8.773
⟨t⋆, dD⟩M = 5.345
⟨Z⋆, dD⟩M = 0.191
Net − Bulge fD :
log(M⋆, fD) = 8.361
⟨t⋆, fD⟩M = 5.446
⟨Z⋆, fD⟩M = 0.198
Net − Bulge eD :
log(M⋆, eD) = 8.173
⟨t⋆, eD⟩M = 3.202
⟨Z⋆, eD⟩M = 0.257
10%
FADO Z4
Bulge :
log(M⋆, B) = 8.604
⟨t⋆, B⟩M = 1.594
⟨Z⋆, B⟩M = 0.128
Disk :
log(M⋆, D) = 8.386
⟨t⋆, D⟩M = 5.320
⟨Z⋆, D⟩M = 0.070
Net − Bulge dD :
log(M⋆, dD) = 8.666
⟨t⋆, dD⟩M = 3.183
⟨Z⋆, dD⟩M = 0.106
Net − Bulge fD :
log(M⋆, fD) = 8.046
⟨t⋆, fD⟩M = 0.284
⟨Z⋆, fD⟩M = 0.145
Net − Bulge eD :
log(M⋆, eD) = 8.063
⟨t⋆, eD⟩M = 0.925
⟨Z⋆, eD⟩M = 0.175
λ (Å)

Starlight Z5
Bulge :
log(M⋆, B) = 8.825
⟨t⋆, B⟩M = 6.807
⟨Z⋆, B⟩M = 0.161
Disk :
log(M⋆, D) = 8.313
⟨t⋆, D⟩M = 4.183
⟨Z⋆, D⟩M = 0.228
Scaling factors :
fdD : 0.114
ffD : 1.649
feD : 1.814
Net − Bulge dD :
log(M⋆, dD) = 8.715
⟨t⋆, dD⟩M = 4.825
⟨Z⋆, dD⟩M = 0.235
Net − Bulge fD :
log(M⋆, fD) = 8.277
⟨t⋆, fD⟩M = 4.902
⟨Z⋆, fD⟩M = 0.253
Net − Bulge eD :
log(M⋆, eD) = 8.206
⟨t⋆, eD⟩M = 5.333
⟨Z⋆, eD⟩M = 0.221
FADO Z5
Bulge :
log(M⋆, B) = 8.634
⟨t⋆, B⟩M = 3.633
⟨Z⋆, B⟩M = 0.384
Disk :
log(M⋆, D) = 8.289
⟨t⋆, D⟩M = 4.190
⟨Z⋆, D⟩M = 0.085
Net − Bulge dD :
log(M⋆, dD) = 8.720
⟨t⋆, dD⟩M = 3.849
⟨Z⋆, dD⟩M = 0.196
Net − Bulge fD :
log(M⋆, fD) = 8.050
⟨t⋆, fD⟩M = 0.794
⟨Z⋆, fD⟩M = 0.494
Net − Bulge eD :
log(M⋆, eD) = 7.938
⟨t⋆, eD⟩M = 0.507
⟨Z⋆, eD⟩M = 0.474
λ (Å)

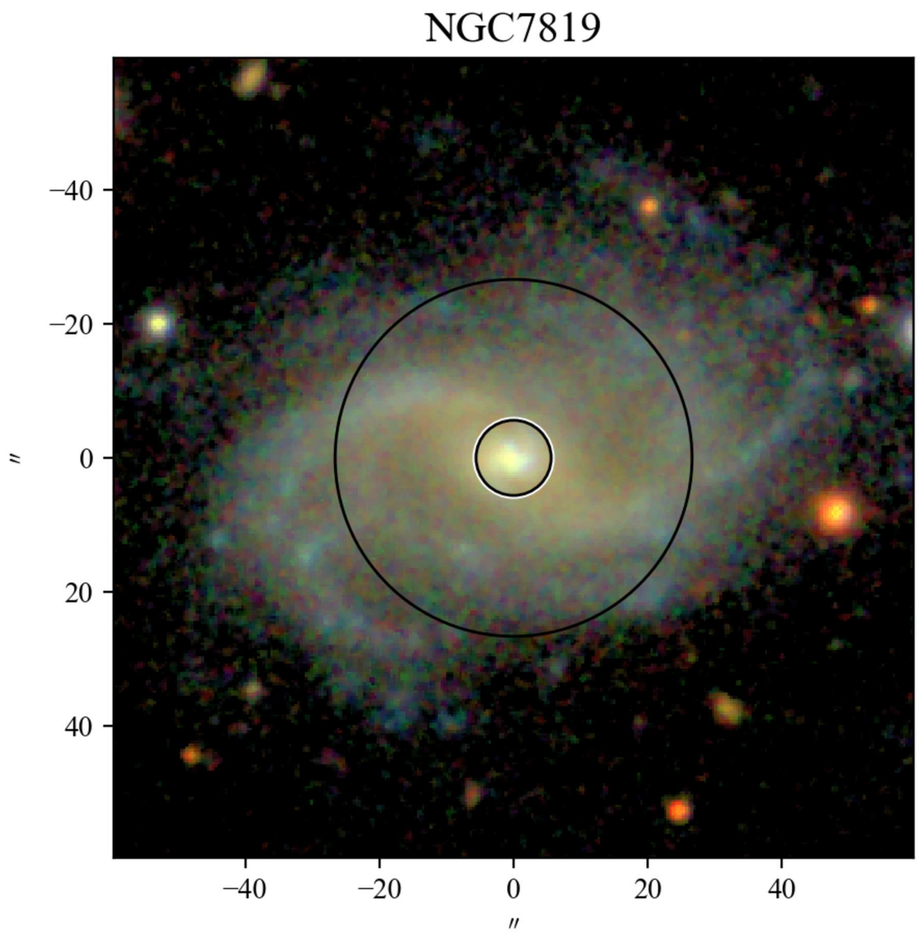
NGC7819
−40
−20
0
20
40
″
−40
−20
0
20
40
″

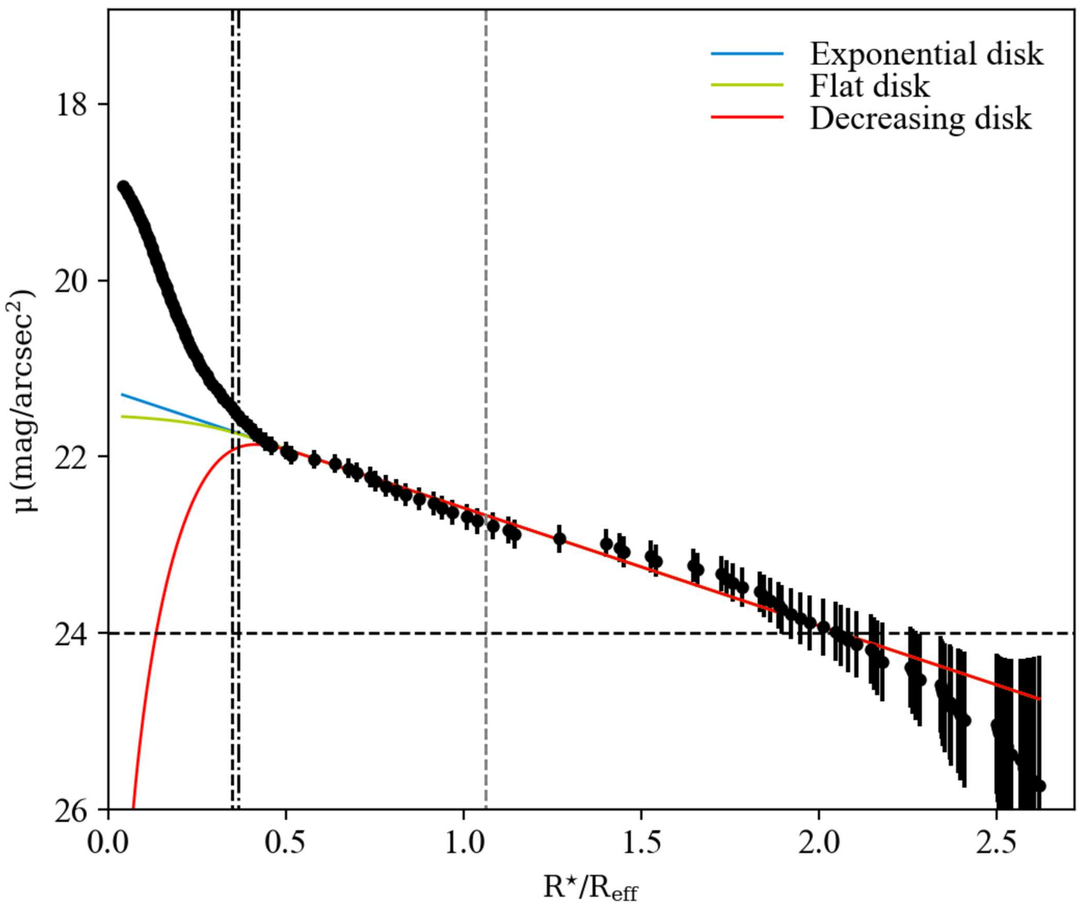
Exponential disk
Flat disk
Decreasing disk
18
20
22
24
26
μ (mag/arcsec²)
0.0
0.5
1.0
1.5
2.0
2.5
R⋆/Reff

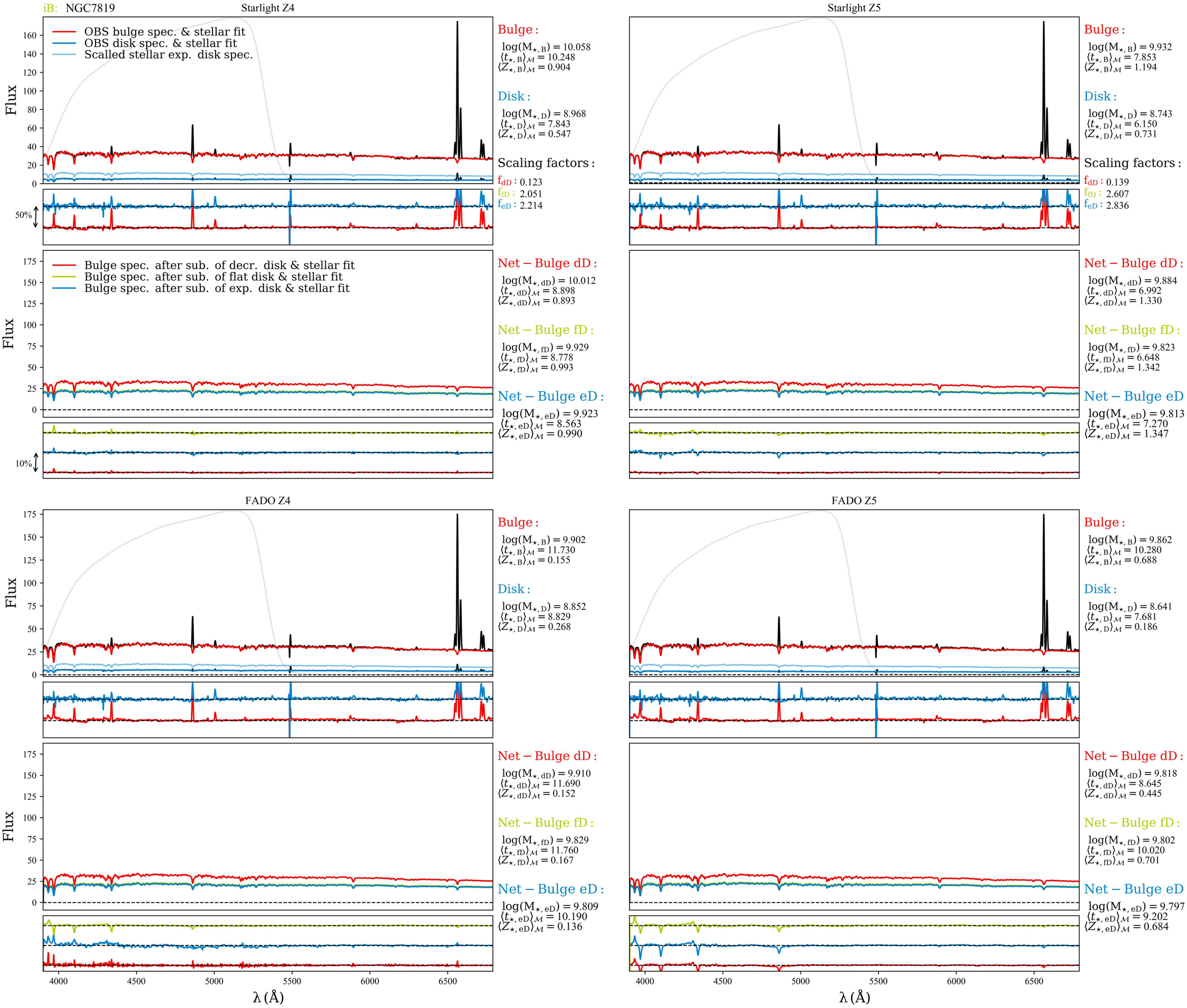
iB: NGC7819
Starlight Z4
OBS bulge spec. & stellar fit
OBS disk spec. & stellar fit
Scalled stellar exp. disk spec.
Flux
50%
Bulge :
log(M⋆, B) = 10.058
⟨t⋆, B⟩M = 10.248
⟨Z⋆, B⟩M = 0.904
Disk :
log(M⋆, D) = 8.968
⟨t⋆, D⟩M = 7.843
⟨Z⋆, D⟩M = 0.547
Scaling factors :
fdD : 0.123
ffD : 2.051
feD : 2.214
Starlight Z5
Bulge :
log(M⋆, B) = 9.932
⟨t⋆, B⟩M = 7.853
⟨Z⋆, B⟩M = 1.194
Disk :
log(M⋆, D) = 8.743
⟨t⋆, D⟩M = 6.150
⟨Z⋆, D⟩M = 0.731
Scaling factors :
fdD : 0.139
ffD : 2.607
feD : 2.836
Bulge spec. after sub. of decr. disk & stellar fit
Bulge spec. after sub. of flat disk & stellar fit
Bulge spec. after sub. of exp. disk & stellar fit
Flux
10%
Net − Bulge dD :
log(M⋆, dD) = 10.012
⟨t⋆, dD⟩M = 8.898
⟨Z⋆, dD⟩M = 0.893
Net − Bulge fD :
log(M⋆, fD) = 9.929
⟨t⋆, fD⟩M = 8.778
⟨Z⋆, fD⟩M = 0.993
Net − Bulge eD :
log(M⋆, eD) = 9.923
⟨t⋆, eD⟩M = 8.563
⟨Z⋆, eD⟩M = 0.990
Net − Bulge dD :
log(M⋆, dD) = 9.884
⟨t⋆, dD⟩M = 6.992
⟨Z⋆, dD⟩M = 1.330
Net − Bulge fD :
log(M⋆, fD) = 9.823
⟨t⋆, fD⟩M = 6.648
⟨Z⋆, fD⟩M = 1.342
Net − Bulge eD :
log(M⋆, eD) = 9.813
⟨t⋆, eD⟩M = 7.270
⟨Z⋆, eD⟩M = 1.347
FADO Z4
Bulge :
log(M⋆, B) = 9.902
⟨t⋆, B⟩M = 11.730
⟨Z⋆, B⟩M = 0.155
Disk :
log(M⋆, D) = 8.852
⟨t⋆, D⟩M = 8.829
⟨Z⋆, D⟩M = 0.268
FADO Z5
Bulge :
log(M⋆, B) = 9.862
⟨t⋆, B⟩M = 10.280
⟨Z⋆, B⟩M = 0.688
Disk :
log(M⋆, D) = 8.641
⟨t⋆, D⟩M = 7.681
⟨Z⋆, D⟩M = 0.186
Net − Bulge dD :
log(M⋆, dD) = 9.910
⟨t⋆, dD⟩M = 11.690
⟨Z⋆, dD⟩M = 0.152
Net − Bulge fD :
log(M⋆, fD) = 9.829
⟨t⋆, fD⟩M = 11.760
⟨Z⋆, fD⟩M = 0.167
Net − Bulge eD :
log(M⋆, eD) = 9.809
⟨t⋆, eD⟩M = 10.190
⟨Z⋆, eD⟩M = 0.136
Net − Bulge dD :
log(M⋆, dD) = 9.818
⟨t⋆, dD⟩M = 8.645
⟨Z⋆, dD⟩M = 0.445
Net − Bulge fD :
log(M⋆, fD) = 9.802
⟨t⋆, fD⟩M = 10.020
⟨Z⋆, fD⟩M = 0.701
Net − Bulge eD :
log(M⋆, eD) = 9.797
⟨t⋆, eD⟩M = 9.202
⟨Z⋆, eD⟩M = 0.684
λ (Å)

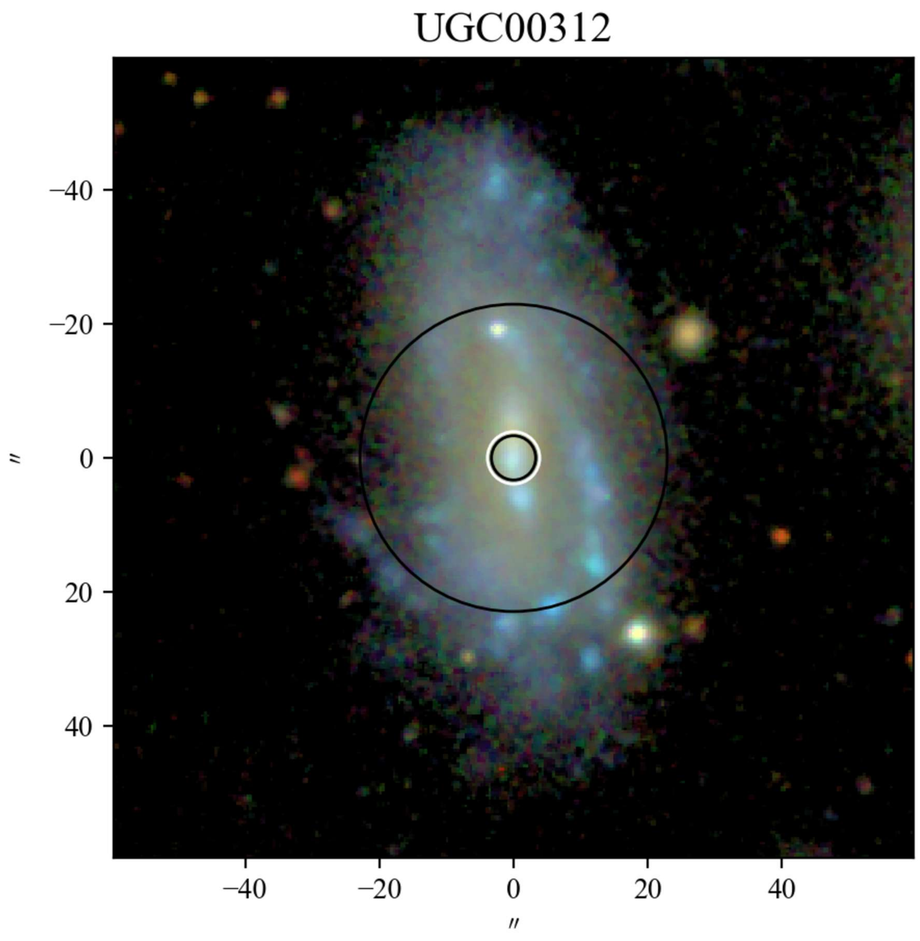
UGC00312
−40
−20
0
20
40
″
−40
−20
0
20
40
″

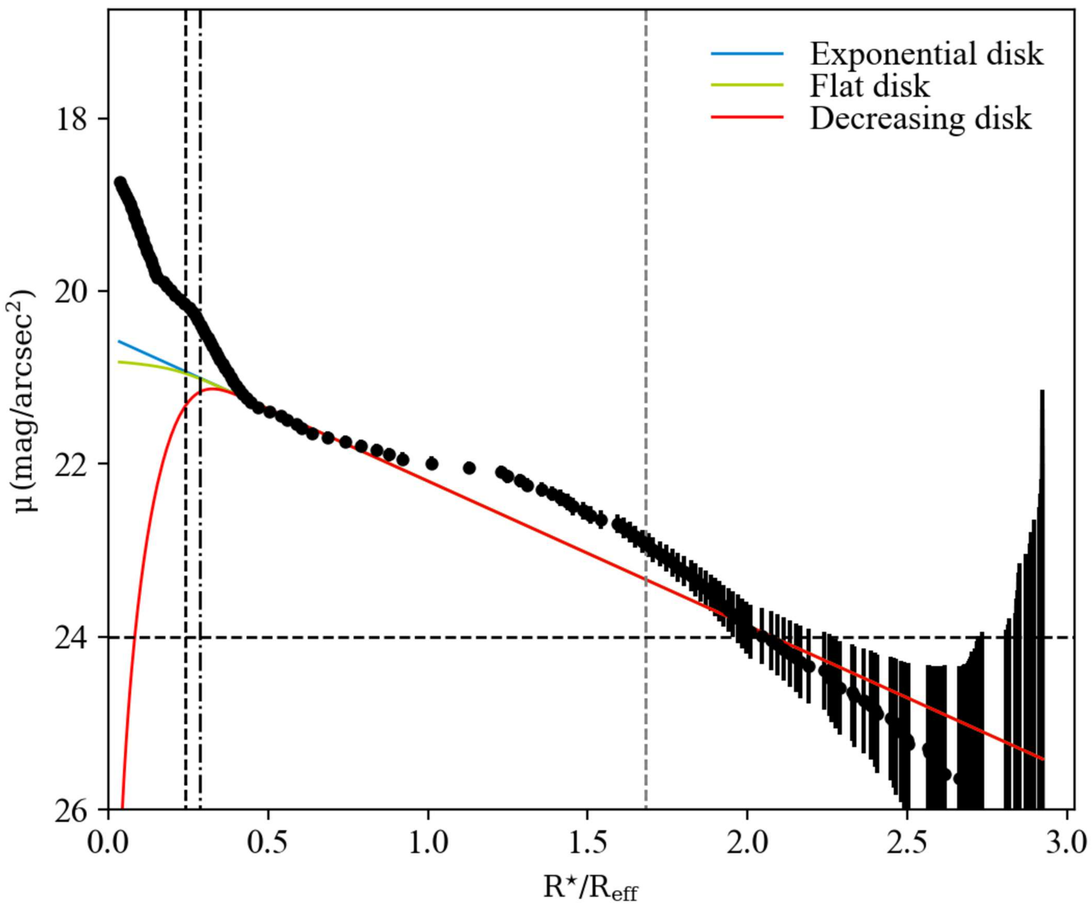
Exponential disk
Flat disk
Decreasing disk
μ (mag/arcsec²)
18
20
22
24
26
0.0
0.5
1.0
1.5
2.0
2.5
3.0
R⋆/Reff

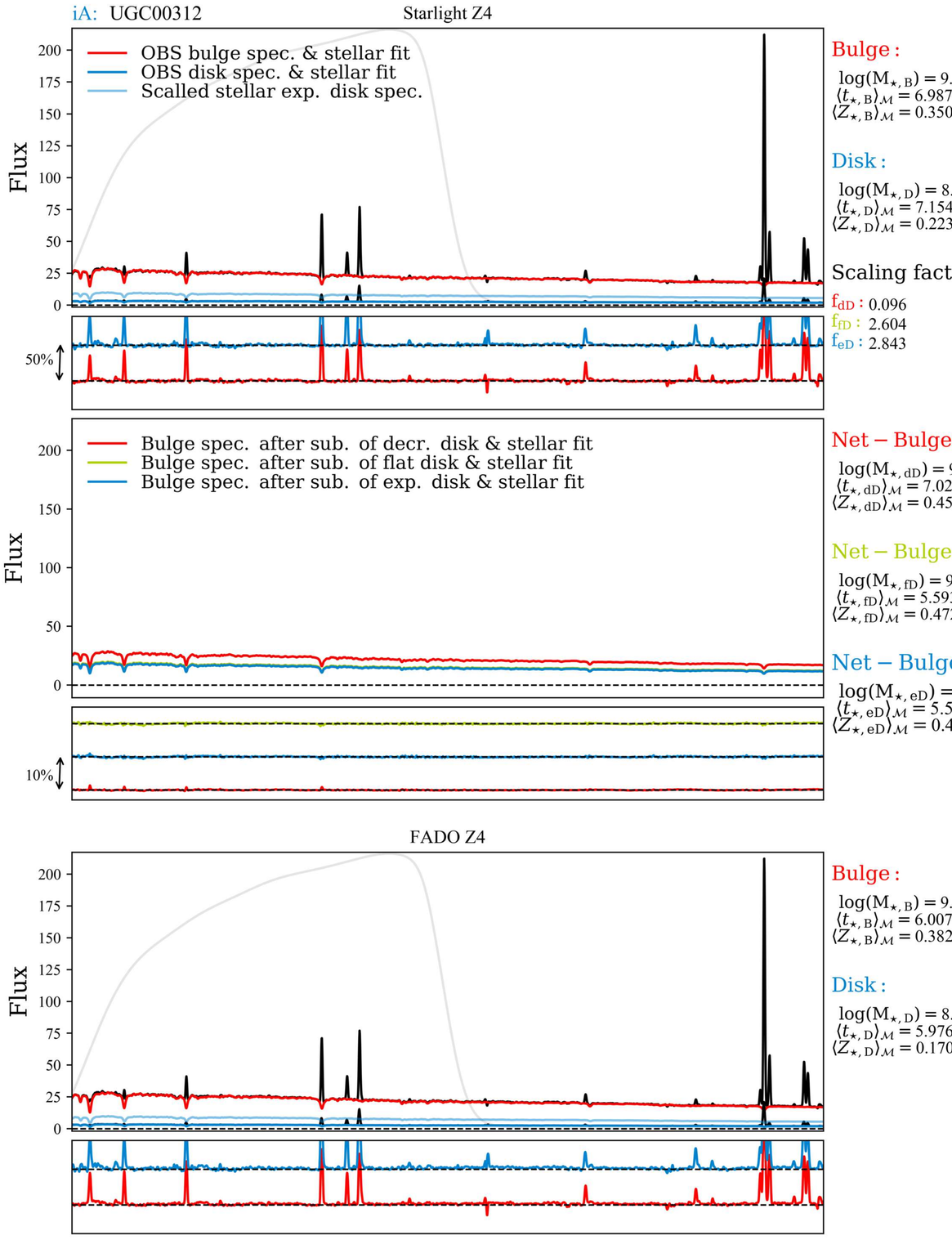
iA: UGC00312
Starlight Z4
OBS bulge spec. & stellar fit
OBS disk spec. & stellar fit
Scalled stellar exp. disk spec.
Flux
50%
Bulge :
log(M⋆, B) = 9.317
⟨t⋆, B⟩M = 6.987
⟨Z⋆, B⟩M = 0.350
Disk :
log(M⋆, D) = 8.420
⟨t⋆, D⟩M = 7.154
⟨Z⋆, D⟩M = 0.223
Scaling factors :
fdD : 0.096
ffD : 2.604
feD : 2.843
Bulge spec. after sub. of decr. disk & stellar fit
Bulge spec. after sub. of flat disk & stellar fit
Bulge spec. after sub. of exp. disk & stellar fit
10%
Net − Bulge dD :
log(M⋆, dD) = 9.336
⟨t⋆, dD⟩M = 7.027
⟨Z⋆, dD⟩M = 0.459
Net − Bulge fD :
log(M⋆, fD) = 9.073
⟨t⋆, fD⟩M = 5.593
⟨Z⋆, fD⟩M = 0.472
Net − Bulge eD :
log(M⋆, eD) = 9.073
⟨t⋆, eD⟩M = 5.551
⟨Z⋆, eD⟩M = 0.473

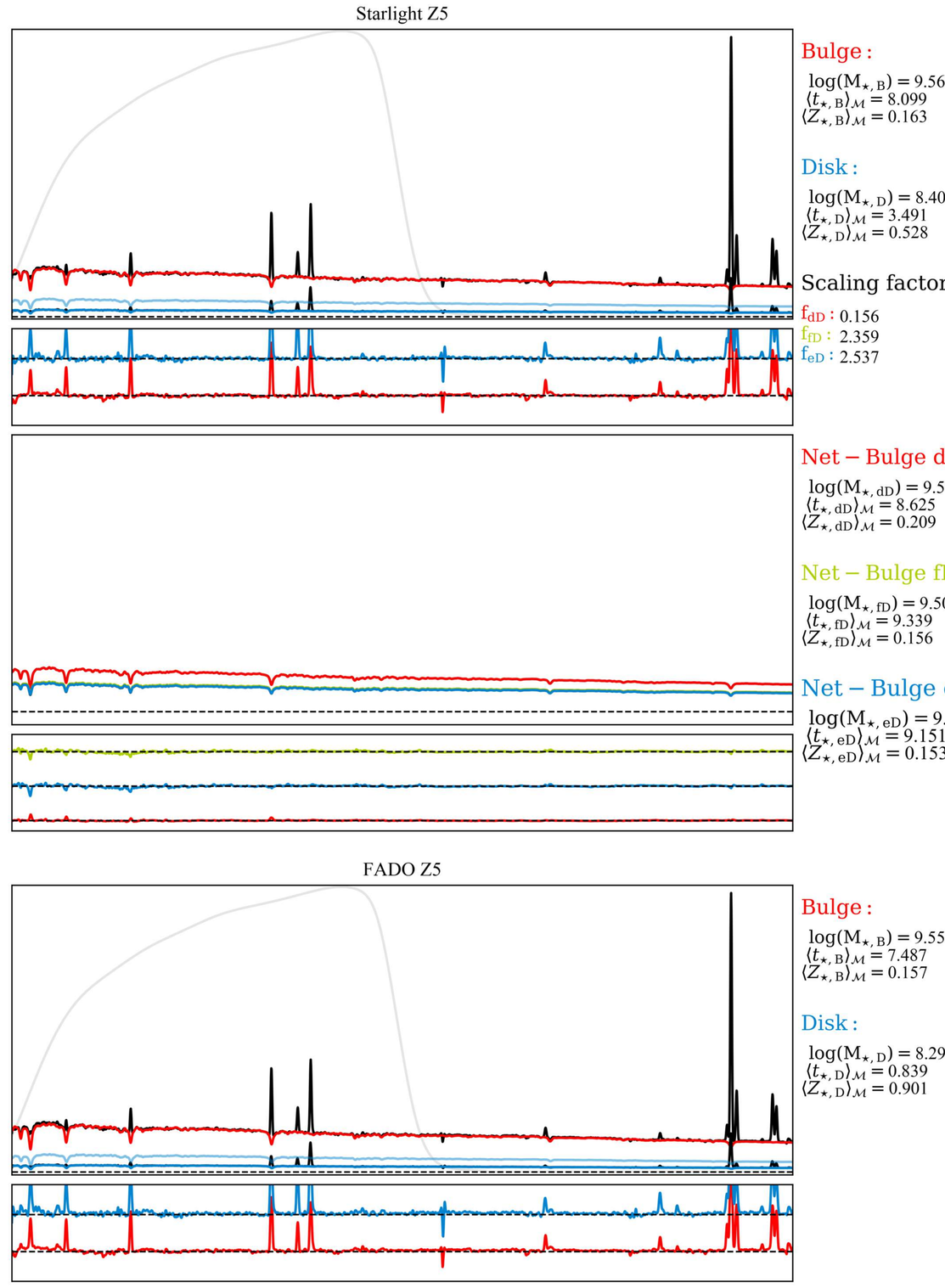
Starlight Z5
Bulge :
log(M⋆, B) = 9.560
⟨t⋆, B⟩M = 8.099
⟨Z⋆, B⟩M = 0.163
Disk :
log(M⋆, D) = 8.408
⟨t⋆, D⟩M = 3.491
⟨Z⋆, D⟩M = 0.528
Scaling factors :
fdD : 0.156
ffD : 2.359
feD : 2.537
Net − Bulge dD :
log(M⋆, dD) = 9.560
⟨t⋆, dD⟩M = 8.625
⟨Z⋆, dD⟩M = 0.209
Net − Bulge fD :
log(M⋆, fD) = 9.505
⟨t⋆, fD⟩M = 9.339
⟨Z⋆, fD⟩M = 0.156
Net − Bulge eD :
log(M⋆, eD) = 9.488
⟨t⋆, eD⟩M = 9.151
⟨Z⋆, eD⟩M = 0.153

FADO Z4
Flux
Bulge :
log(M⋆, B) = 9.422
⟨t⋆, B⟩M = 6.007
⟨Z⋆, B⟩M = 0.382
Disk :
log(M⋆, D) = 8.333
⟨t⋆, D⟩M = 5.976
⟨Z⋆, D⟩M = 0.170
Net − Bulge dD :
log(M⋆, dD) = 9.375
⟨t⋆, dD⟩M = 5.236
⟨Z⋆, dD⟩M = 0.358
Net − Bulge fD :
log(M⋆, fD) = 9.377
⟨t⋆, fD⟩M = 8.497
⟨Z⋆, fD⟩M = 0.461
Net − Bulge eD :
log(M⋆, eD) = 9.284
⟨t⋆, eD⟩M = 6.837
⟨Z⋆, eD⟩M = 0.361
λ (Å)

FADO Z5
Bulge :
log(M⋆, B) = 9.554
⟨t⋆, B⟩M = 7.487
⟨Z⋆, B⟩M = 0.157
Disk :
log(M⋆, D) = 8.298
⟨t⋆, D⟩M = 0.839
⟨Z⋆, D⟩M = 0.901
Net − Bulge dD :
log(M⋆, dD) = 9.555
⟨t⋆, dD⟩M = 9.217
⟨Z⋆, dD⟩M = 0.212
Net − Bulge fD :
log(M⋆, fD) = 9.473
⟨t⋆, fD⟩M = 9.122
⟨Z⋆, fD⟩M = 0.145
Net − Bulge eD :
log(M⋆, eD) = 9.466
⟨t⋆, eD⟩M = 8.983
⟨Z⋆, eD⟩M = 0.141
λ (Å)

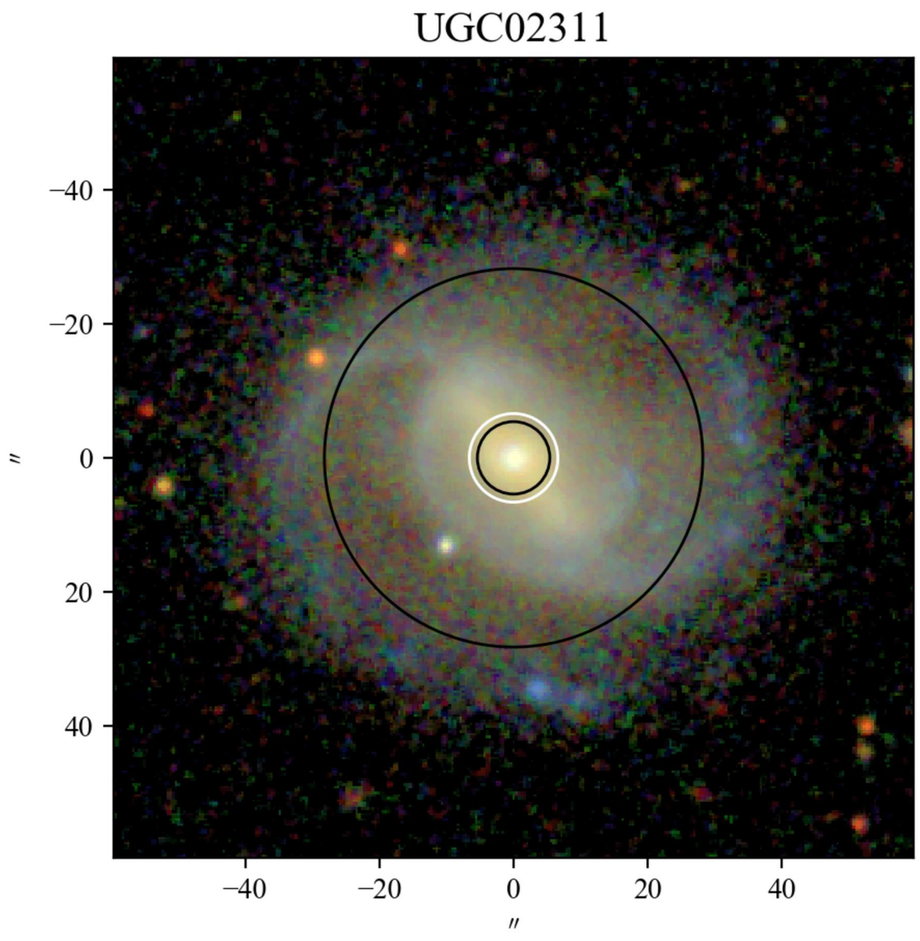
UGC02311
−40
−20
0
20
40
″
−40
−20
0
20
40
″

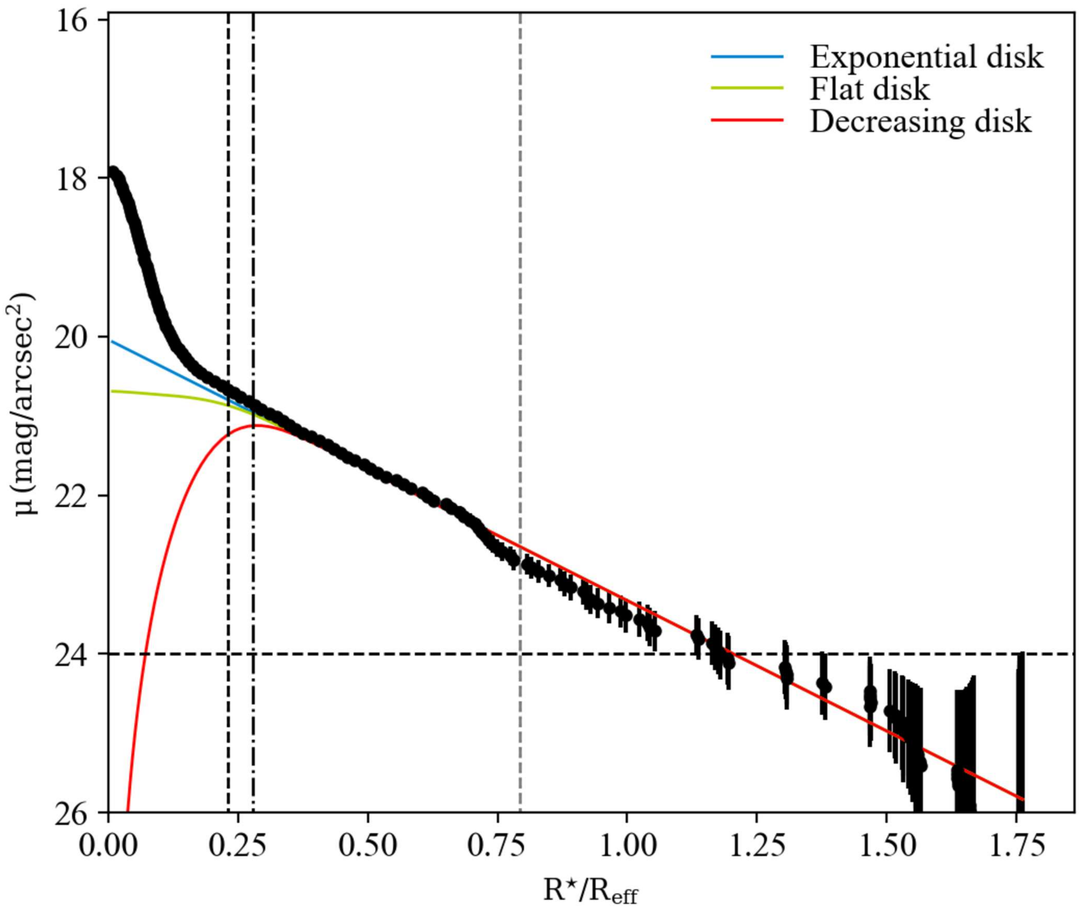
Exponential disk
Flat disk
Decreasing disk
μ (mag/arcsec²)
16
18
20
22
24
26
0.00
0.25
0.50
0.75
1.00
1.25
1.50
1.75
R⋆/Reff

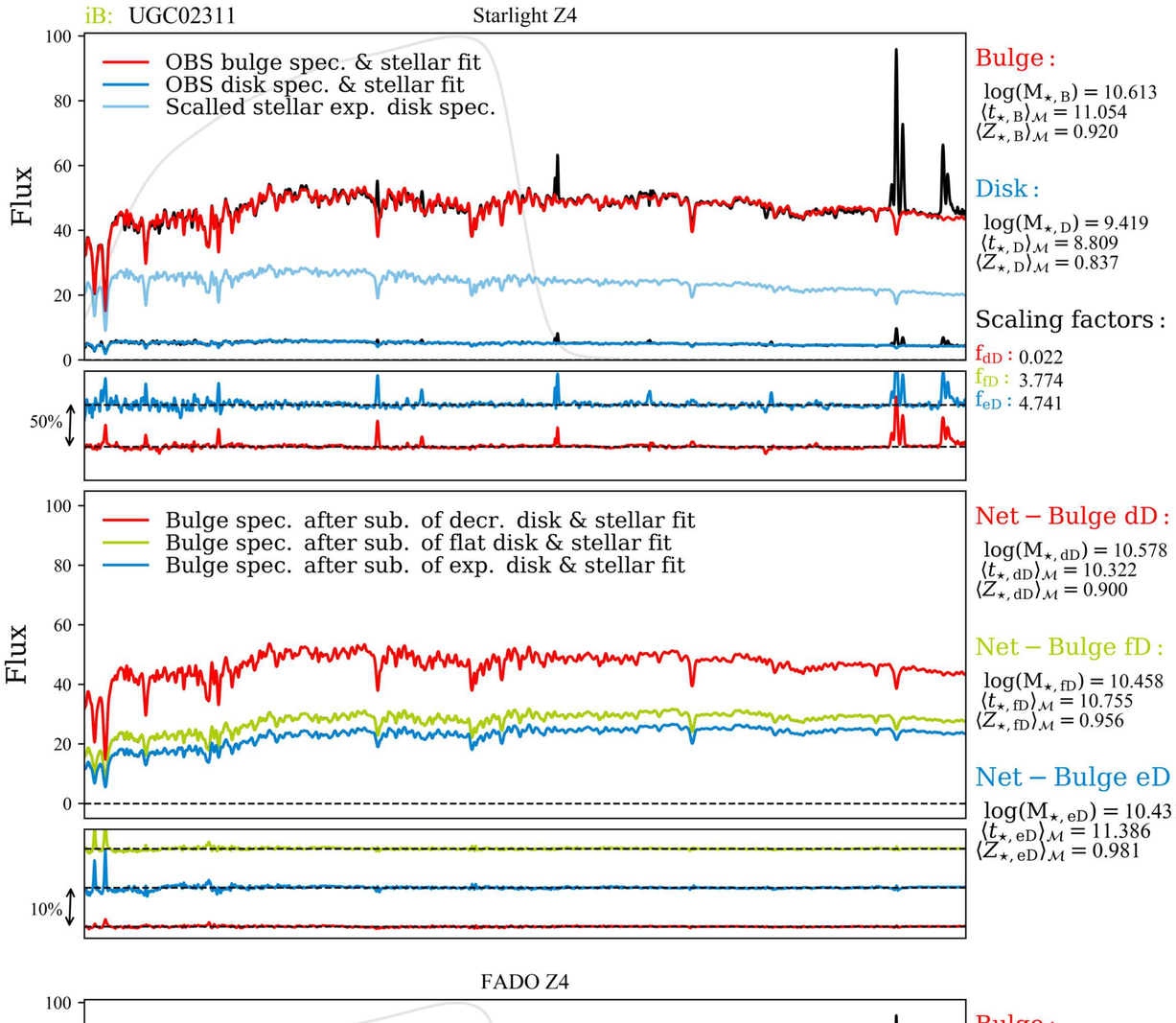
iB: UGC02311
Starlight Z4
OBS bulge spec. & stellar fit
OBS disk spec. & stellar fit
Scalled stellar exp. disk spec.
Flux
50%
Bulge :
log(M⋆, B) = 10.613
⟨t⋆, B⟩M = 11.054
⟨Z⋆, B⟩M = 0.920
Disk :
log(M⋆, D) = 9.419
⟨t⋆, D⟩M = 8.809
⟨Z⋆, D⟩M = 0.837
Scaling factors :
fdD : 0.022
ffD : 3.774
feD : 4.741
Bulge spec. after sub. of decr. disk & stellar fit
Bulge spec. after sub. of flat disk & stellar fit
Bulge spec. after sub. of exp. disk & stellar fit
10%
Net − Bulge dD :
log(M⋆, dD) = 10.578
⟨t⋆, dD⟩M = 10.322
⟨Z⋆, dD⟩M = 0.900
Net − Bulge fD :
log(M⋆, fD) = 10.458
⟨t⋆, fD⟩M = 10.755
⟨Z⋆, fD⟩M = 0.956
Net − Bulge eD :
log(M⋆, eD) = 10.431
⟨t⋆, eD⟩M = 11.386
⟨Z⋆, eD⟩M = 0.981

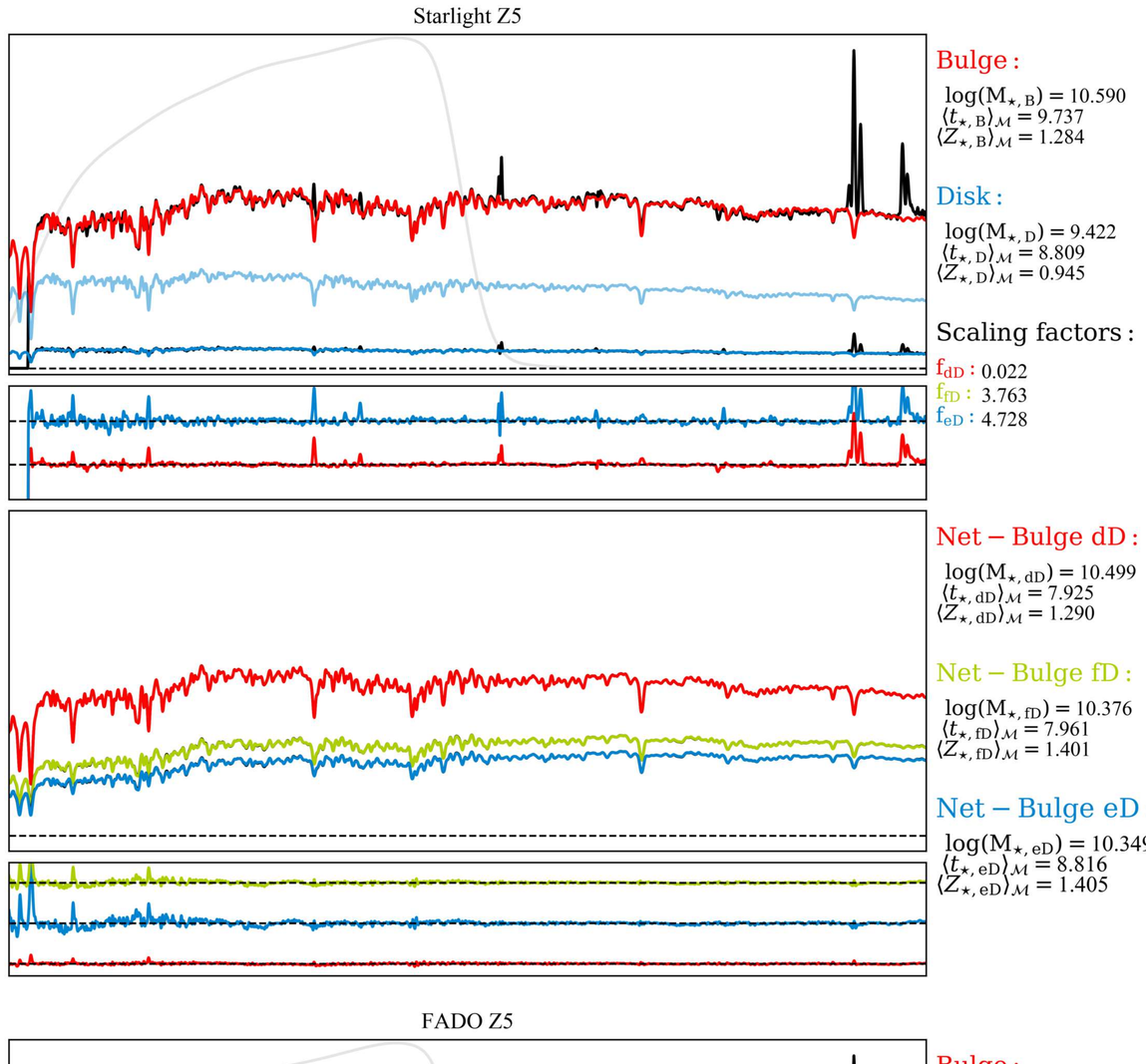
Starlight Z5
Bulge :
log(M⋆, B) = 10.590
⟨t⋆, B⟩M = 9.737
⟨Z⋆, B⟩M = 1.284
Disk :
log(M⋆, D) = 9.422
⟨t⋆, D⟩M = 8.809
⟨Z⋆, D⟩M = 0.945
Scaling factors :
fdD : 0.022
ffD : 3.763
feD : 4.728
Net − Bulge dD :
log(M⋆, dD) = 10.499
⟨t⋆, dD⟩M = 7.925
⟨Z⋆, dD⟩M = 1.290
Net − Bulge fD :
log(M⋆, fD) = 10.376
⟨t⋆, fD⟩M = 7.961
⟨Z⋆, fD⟩M = 1.401
Net − Bulge eD :
log(M⋆, eD) = 10.349
⟨t⋆, eD⟩M = 8.816
⟨Z⋆, eD⟩M = 1.405

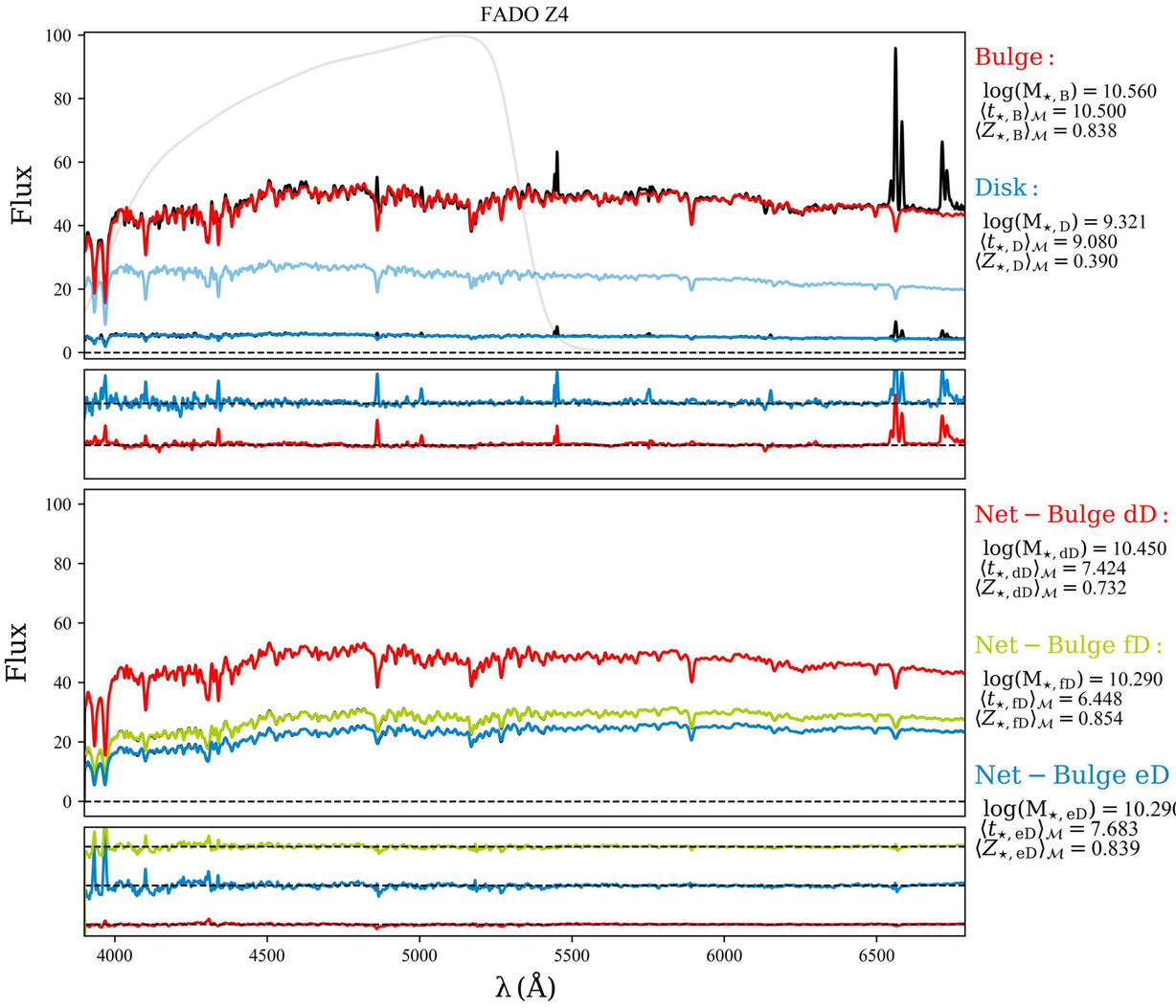
FADO Z4
Flux
Bulge :
log(M⋆, B) = 10.560
⟨t⋆, B⟩M = 10.500
⟨Z⋆, B⟩M = 0.838
Disk :
log(M⋆, D) = 9.321
⟨t⋆, D⟩M = 9.080
⟨Z⋆, D⟩M = 0.390
Net − Bulge dD :
log(M⋆, dD) = 10.450
⟨t⋆, dD⟩M = 7.424
⟨Z⋆, dD⟩M = 0.732
Net − Bulge fD :
log(M⋆, fD) = 10.290
⟨t⋆, fD⟩M = 6.448
⟨Z⋆, fD⟩M = 0.854
Net − Bulge eD :
log(M⋆, eD) = 10.290
⟨t⋆, eD⟩M = 7.683
⟨Z⋆, eD⟩M = 0.839
λ (Å)

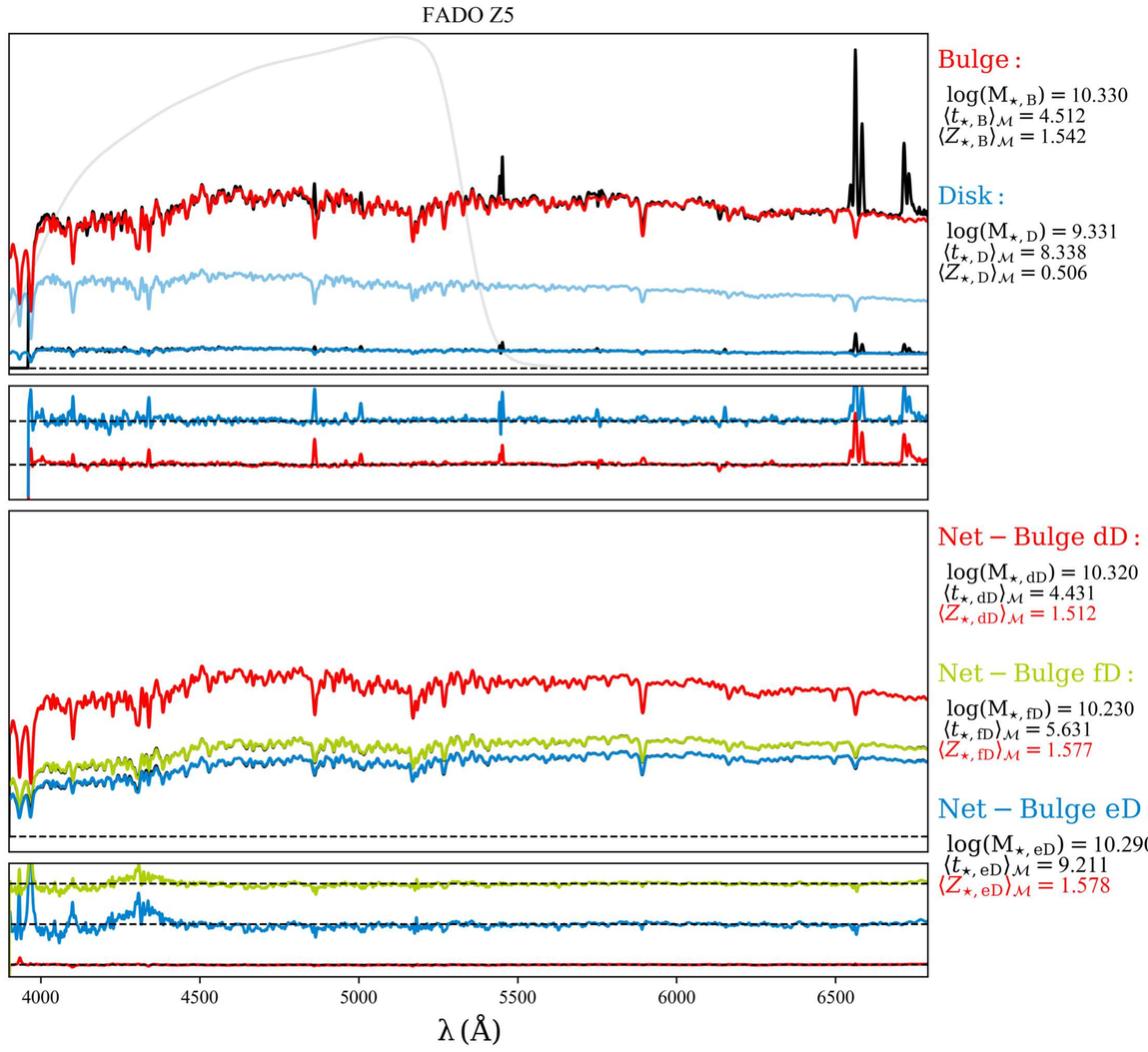
FADO Z5
Bulge :
log(M⋆, B) = 10.330
⟨t⋆, B⟩M = 4.512
⟨Z⋆, B⟩M = 1.542
Disk :
log(M⋆, D) = 9.331
⟨t⋆, D⟩M = 8.338
⟨Z⋆, D⟩M = 0.506
Net − Bulge dD :
log(M⋆, dD) = 10.320
⟨t⋆, dD⟩M = 4.431
⟨Z⋆, dD⟩M = 1.512
Net − Bulge fD :
log(M⋆, fD) = 10.230
⟨t⋆, fD⟩M = 5.631
⟨Z⋆, fD⟩M = 1.577
Net − Bulge eD :
log(M⋆, eD) = 10.290
⟨t⋆, eD⟩M = 9.211
⟨Z⋆, eD⟩M = 1.578
λ (Å)

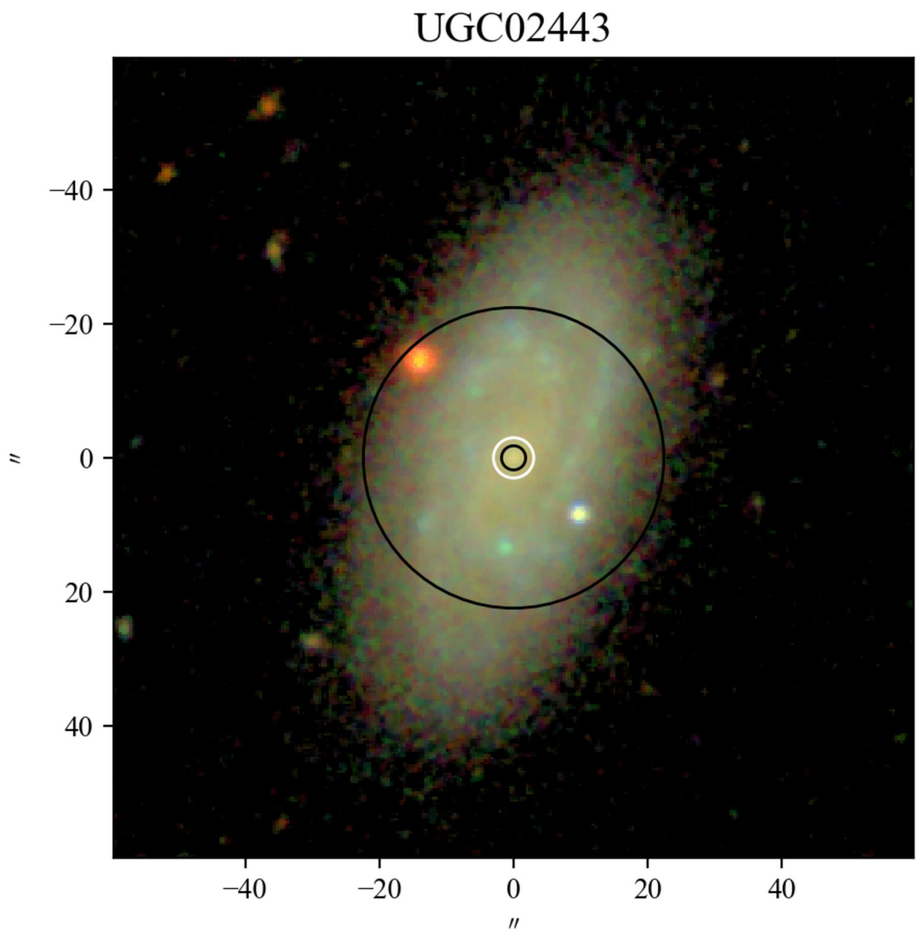
UGC02443
−40
−20
0
20
40
″
−40
−20
0
20
40
″

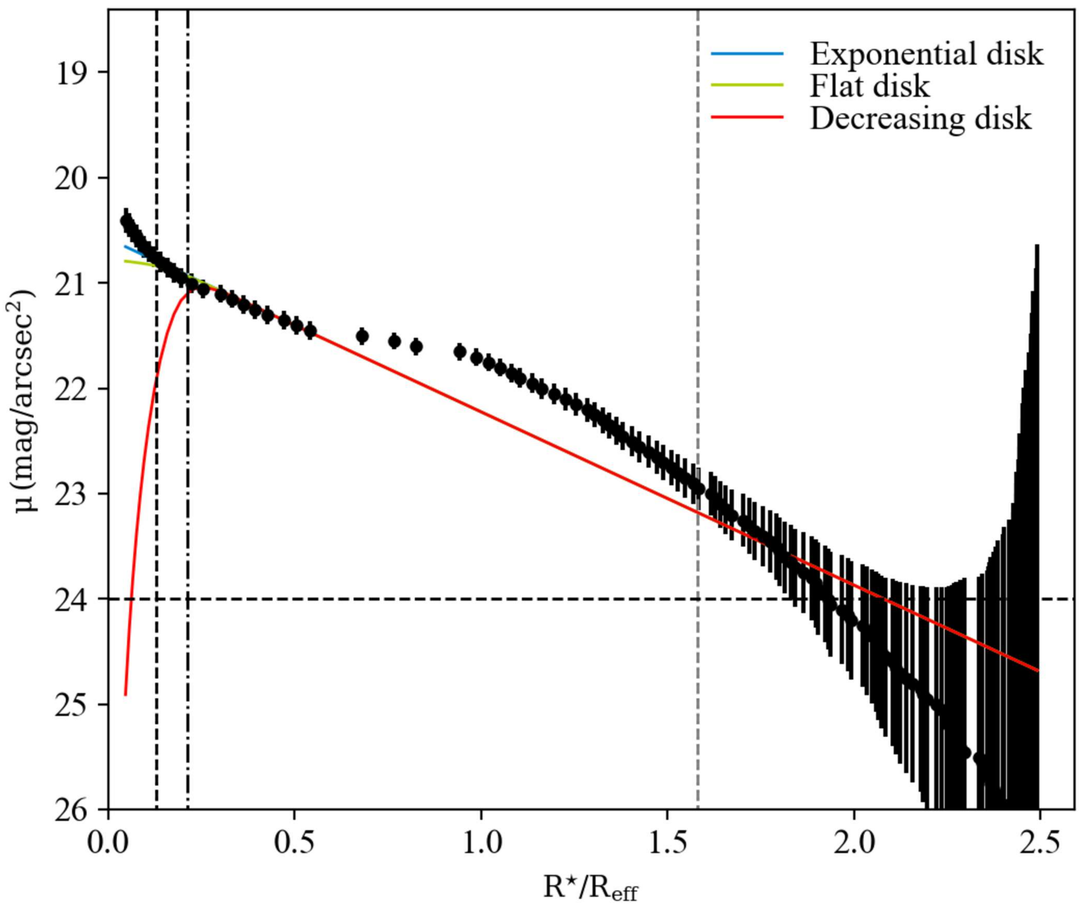
Exponential disk
Flat disk
Decreasing disk
μ (mag/arcsec²)
19
20
21
22
23
24
25
26
0.0
0.5
1.0
1.5
2.0
2.5
R⋆/Reff

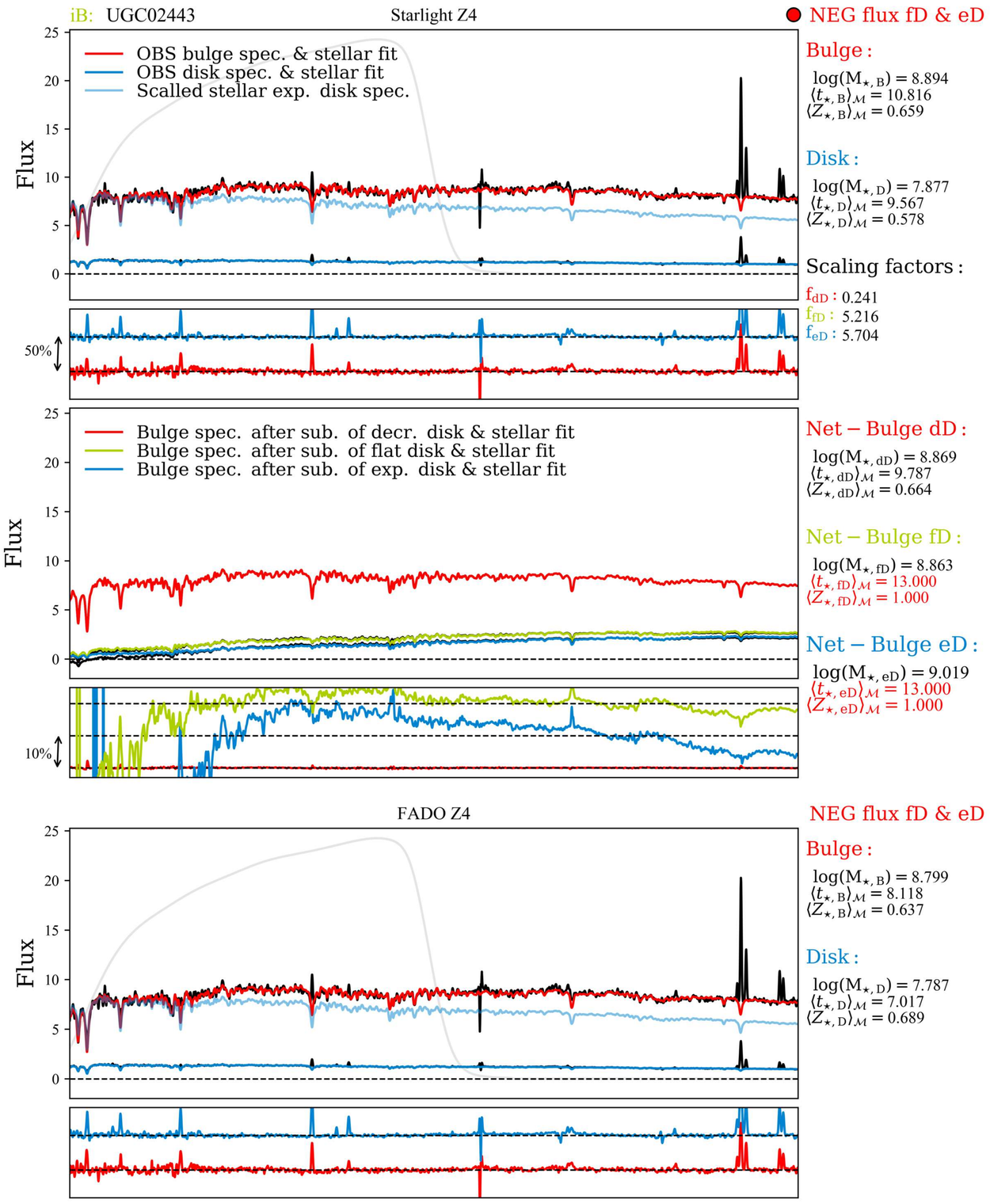
iB: UGC02443
Starlight Z4
NEG flux fD & eD
OBS bulge spec. & stellar fit
OBS disk spec. & stellar fit
Scalled stellar exp. disk spec.
Flux
50%
Bulge :
log(M⋆, B) = 8.894
⟨t⋆, B⟩M = 10.816
⟨Z⋆, B⟩M = 0.659
Disk :
log(M⋆, D) = 7.877
⟨t⋆, D⟩M = 9.567
⟨Z⋆, D⟩M = 0.578
Scaling factors :
fdD : 0.241
ffD : 5.216
feD : 5.704
Bulge spec. after sub. of decr. disk & stellar fit
Bulge spec. after sub. of flat disk & stellar fit
Bulge spec. after sub. of exp. disk & stellar fit
10%
Net − Bulge dD :
log(M⋆, dD) = 8.869
⟨t⋆, dD⟩M = 9.787
⟨Z⋆, dD⟩M = 0.664
Net − Bulge fD :
log(M⋆, fD) = 8.863
⟨t⋆, fD⟩M = 13.000
⟨Z⋆, fD⟩M = 1.000
Net − Bulge eD :
log(M⋆, eD) = 9.019
⟨t⋆, eD⟩M = 13.000
⟨Z⋆, eD⟩M = 1.000

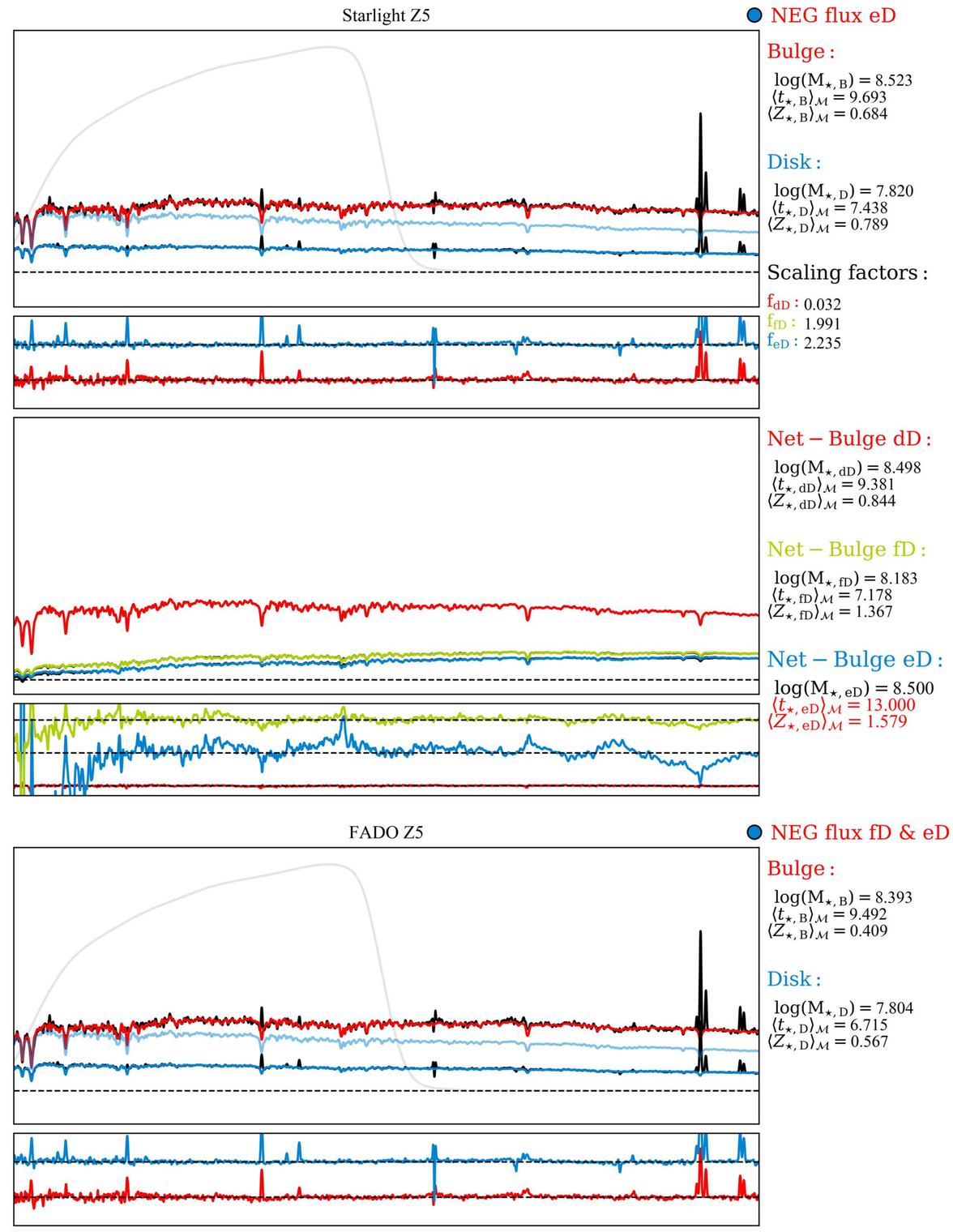
Starlight Z5
NEG flux eD
Bulge :
log(M⋆, B) = 8.523
⟨t⋆, B⟩M = 9.693
⟨Z⋆, B⟩M = 0.684
Disk :
log(M⋆, D) = 7.820
⟨t⋆, D⟩M = 7.438
⟨Z⋆, D⟩M = 0.789
Scaling factors :
fdD : 0.032
ffD : 1.991
feD : 2.235
Net − Bulge dD :
log(M⋆, dD) = 8.498
⟨t⋆, dD⟩M = 9.381
⟨Z⋆, dD⟩M = 0.844
Net − Bulge fD :
log(M⋆, fD) = 8.183
⟨t⋆, fD⟩M = 7.178
⟨Z⋆, fD⟩M = 1.367
Net − Bulge eD :
log(M⋆, eD) = 8.500
⟨t⋆, eD⟩M = 13.000
⟨Z⋆, eD⟩M = 1.579

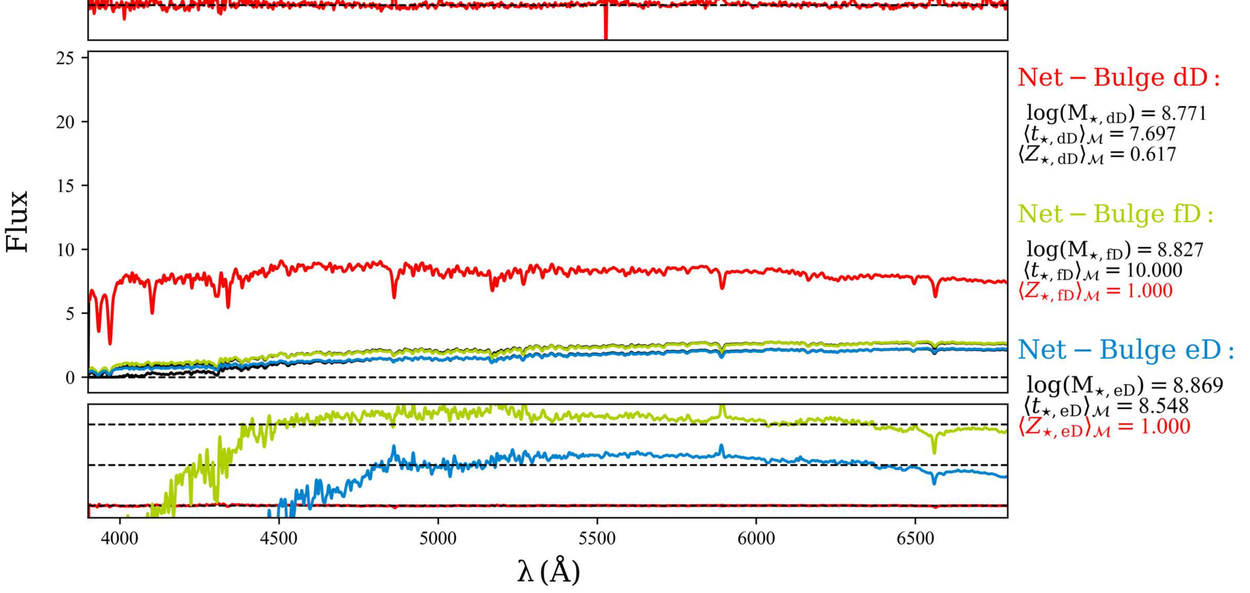
FADO Z4
NEG flux fD & eD
Flux
Bulge :
log(M⋆, B) = 8.799
⟨t⋆, B⟩M = 8.118
⟨Z⋆, B⟩M = 0.637
Disk :
log(M⋆, D) = 7.787
⟨t⋆, D⟩M = 7.017
⟨Z⋆, D⟩M = 0.689
Net − Bulge dD :
log(M⋆, dD) = 8.771
⟨t⋆, dD⟩M = 7.697
⟨Z⋆, dD⟩M = 0.617
Net − Bulge fD :
log(M⋆, fD) = 8.827
⟨t⋆, fD⟩M = 10.000
⟨Z⋆, fD⟩M = 1.000
Net − Bulge eD :
log(M⋆, eD) = 8.869
⟨t⋆, eD⟩M = 8.548
⟨Z⋆, eD⟩M = 1.000
4000
4500
5000
5500
6000
6500
λ (Å)

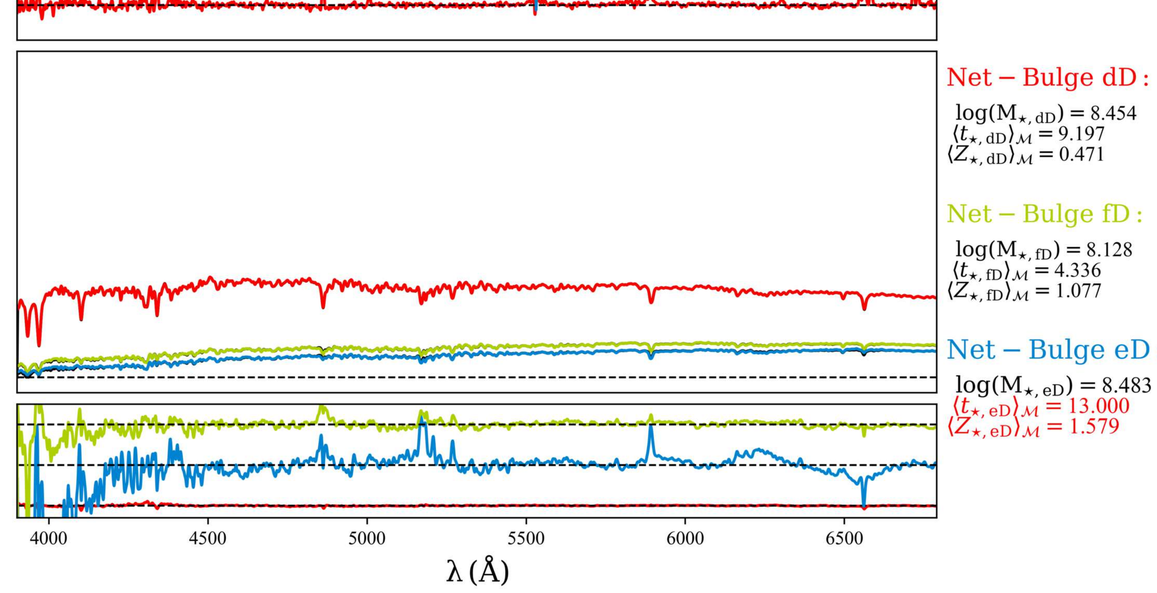
FADO Z5
NEG flux fD & eD
Bulge :
log(M⋆, B) = 8.393
⟨t⋆, B⟩M = 9.492
⟨Z⋆, B⟩M = 0.409
Disk :
log(M⋆, D) = 7.804
⟨t⋆, D⟩M = 6.715
⟨Z⋆, D⟩M = 0.567
Net − Bulge dD :
log(M⋆, dD) = 8.454
⟨t⋆, dD⟩M = 9.197
⟨Z⋆, dD⟩M = 0.471
Net − Bulge fD :
log(M⋆, fD) = 8.128
⟨t⋆, fD⟩M = 4.336
⟨Z⋆, fD⟩M = 1.077
Net − Bulge eD :
log(M⋆, eD) = 8.483
⟨t⋆, eD⟩M = 13.000
⟨Z⋆, eD⟩M = 1.579
4000
4500
5000
5500
6000
6500
λ (Å)

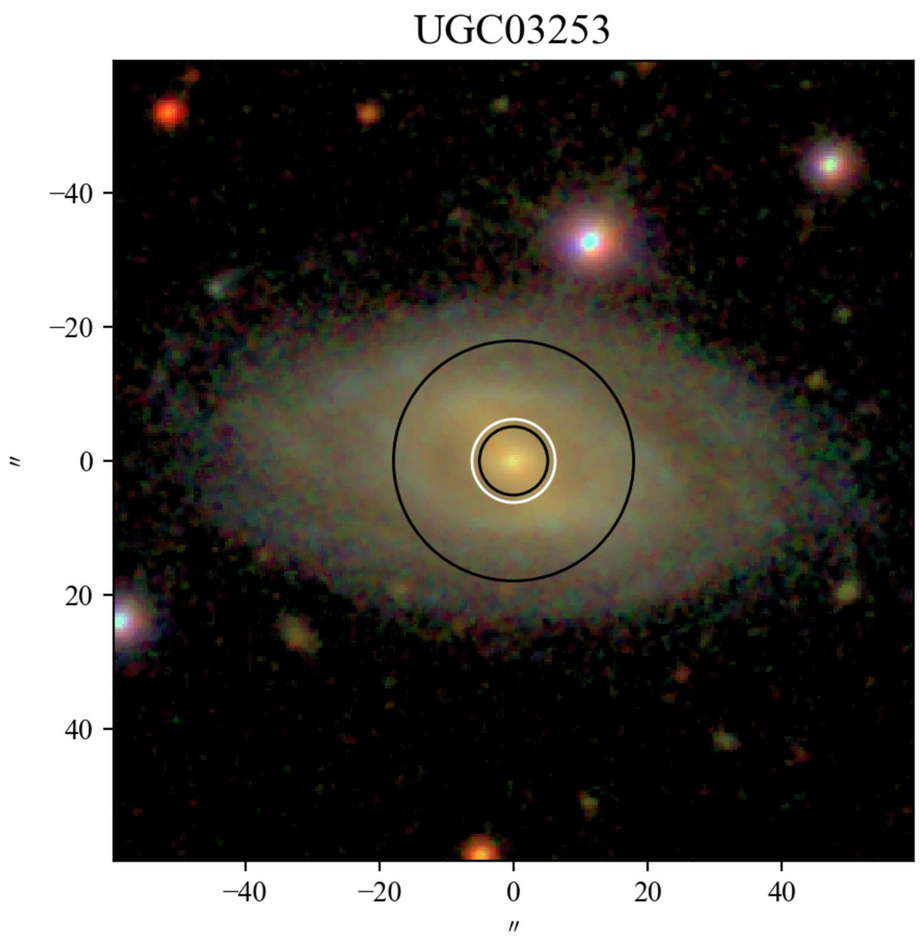
UGC03253
−40
−20
0
20
40
″
−40
−20
0
20
40
″

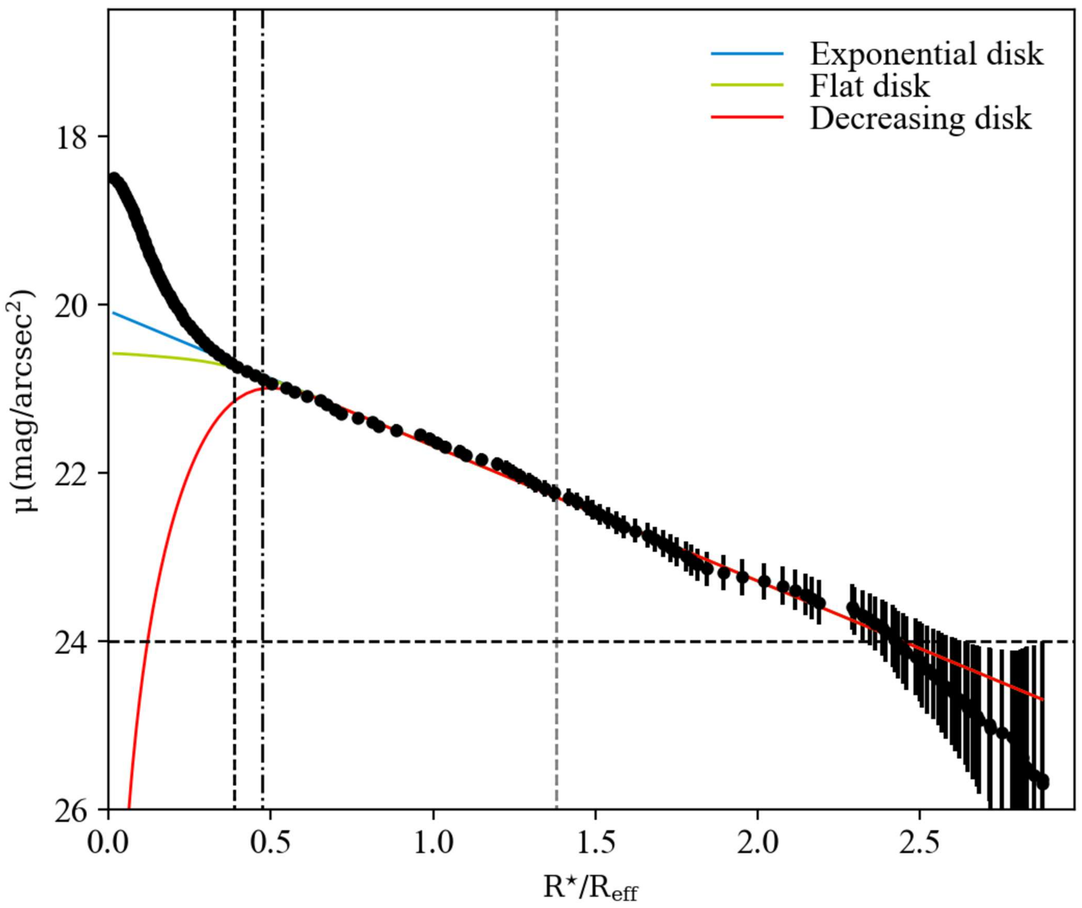
Exponential disk
Flat disk
Decreasing disk
μ (mag/arcsec²)
18
20
22
24
26
0.0
0.5
1.0
1.5
2.0
2.5
R⋆/Reff

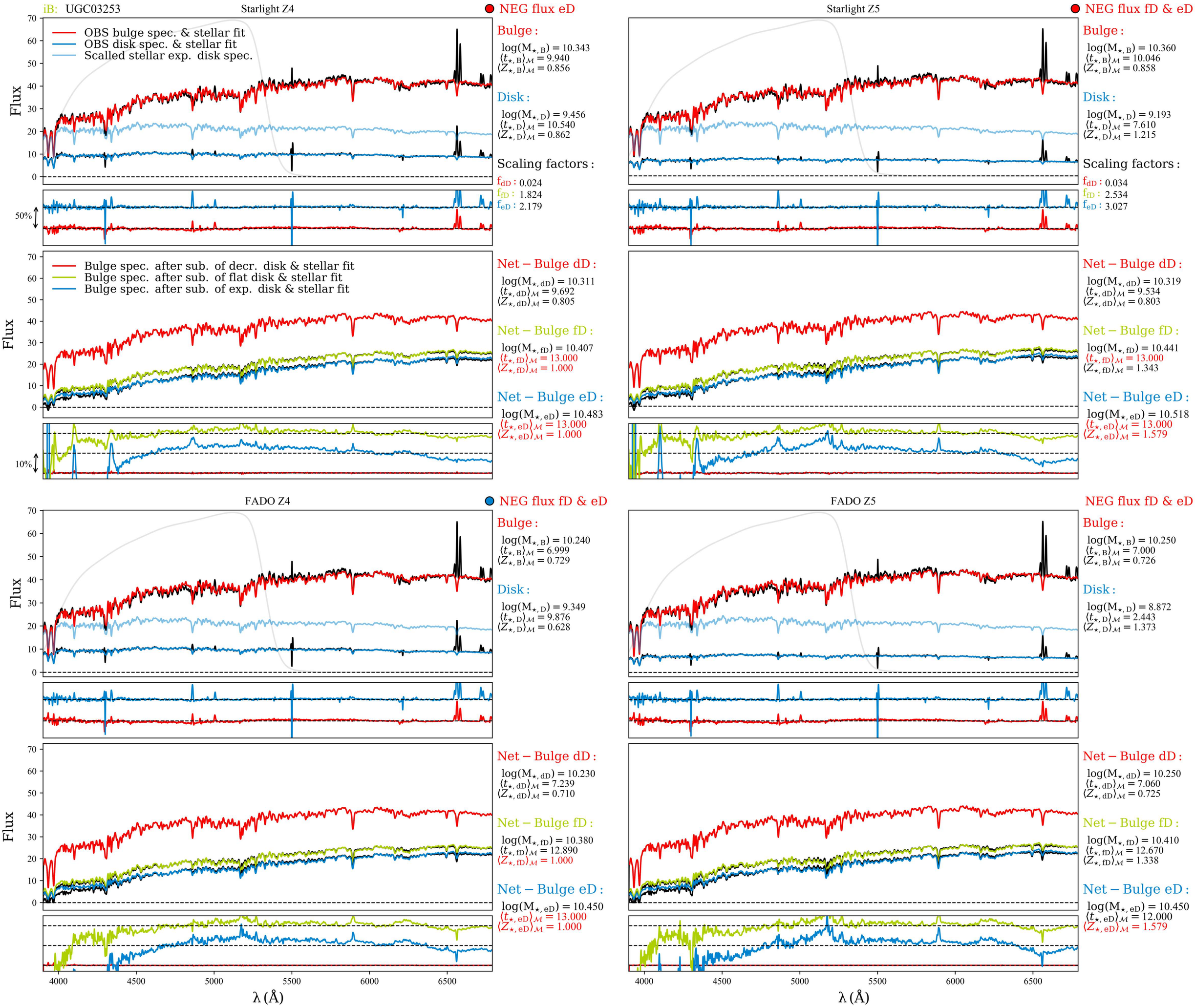
iB: UGC03253
Starlight Z4
NEG flux eD
OBS bulge spec. & stellar fit
OBS disk spec. & stellar fit
Scalled stellar exp. disk spec.
Flux
Bulge :
log(M⋆, B) = 10.343
⟨t⋆, B⟩M = 9.940
⟨Z⋆, B⟩M = 0.856
Disk :
log(M⋆, D) = 9.456
⟨t⋆, D⟩M = 10.540
⟨Z⋆, D⟩M = 0.862
Scaling factors :
fdD : 0.024
ffD : 1.824
feD : 2.179
50%
Bulge spec. after sub. of decr. disk & stellar fit
Bulge spec. after sub. of flat disk & stellar fit
Bulge spec. after sub. of exp. disk & stellar fit
Net − Bulge dD :
log(M⋆, dD) = 10.311
⟨t⋆, dD⟩M = 9.692
⟨Z⋆, dD⟩M = 0.805
Net − Bulge fD :
log(M⋆, fD) = 10.407
⟨t⋆, fD⟩M = 13.000
⟨Z⋆, fD⟩M = 1.000
Net − Bulge eD :
log(M⋆, eD) = 10.483
⟨t⋆, eD⟩M = 13.000
⟨Z⋆, eD⟩M = 1.000
10%

Starlight Z5
NEG flux fD & eD
Bulge :
log(M⋆, B) = 10.360
⟨t⋆, B⟩M = 10.046
⟨Z⋆, B⟩M = 0.858
Disk :
log(M⋆, D) = 9.193
⟨t⋆, D⟩M = 7.610
⟨Z⋆, D⟩M = 1.215
Scaling factors :
fdD : 0.034
ffD : 2.534
feD : 3.027
Net − Bulge dD :
log(M⋆, dD) = 10.319
⟨t⋆, dD⟩M = 9.534
⟨Z⋆, dD⟩M = 0.803
Net − Bulge fD :
log(M⋆, fD) = 10.441
⟨t⋆, fD⟩M = 13.000
⟨Z⋆, fD⟩M = 1.343
Net − Bulge eD :
log(M⋆, eD) = 10.518
⟨t⋆, eD⟩M = 13.000
⟨Z⋆, eD⟩M = 1.579

FADO Z4
NEG flux fD & eD
Flux
Bulge :
log(M⋆, B) = 10.240
⟨t⋆, B⟩M = 6.999
⟨Z⋆, B⟩M = 0.729
Disk :
log(M⋆, D) = 9.349
⟨t⋆, D⟩M = 9.876
⟨Z⋆, D⟩M = 0.628
Net − Bulge dD :
log(M⋆, dD) = 10.230
⟨t⋆, dD⟩M = 7.239
⟨Z⋆, dD⟩M = 0.710
Net − Bulge fD :
log(M⋆, fD) = 10.380
⟨t⋆, fD⟩M = 12.890
⟨Z⋆, fD⟩M = 1.000
Net − Bulge eD :
log(M⋆, eD) = 10.450
⟨t⋆, eD⟩M = 13.000
⟨Z⋆, eD⟩M = 1.000
4000
4500
5000
5500
6000
6500
λ (Å)

FADO Z5
NEG flux fD & eD
Bulge :
log(M⋆, B) = 10.250
⟨t⋆, B⟩M = 7.000
⟨Z⋆, B⟩M = 0.726
Disk :
log(M⋆, D) = 8.872
⟨t⋆, D⟩M = 2.443
⟨Z⋆, D⟩M = 1.373
Net − Bulge dD :
log(M⋆, dD) = 10.250
⟨t⋆, dD⟩M = 7.060
⟨Z⋆, dD⟩M = 0.725
Net − Bulge fD :
log(M⋆, fD) = 10.410
⟨t⋆, fD⟩M = 12.670
⟨Z⋆, fD⟩M = 1.338
Net − Bulge eD :
log(M⋆, eD) = 10.450
⟨t⋆, eD⟩M = 12.000
⟨Z⋆, eD⟩M = 1.579
4000
4500
5000
5500
6000
6500
λ (Å)

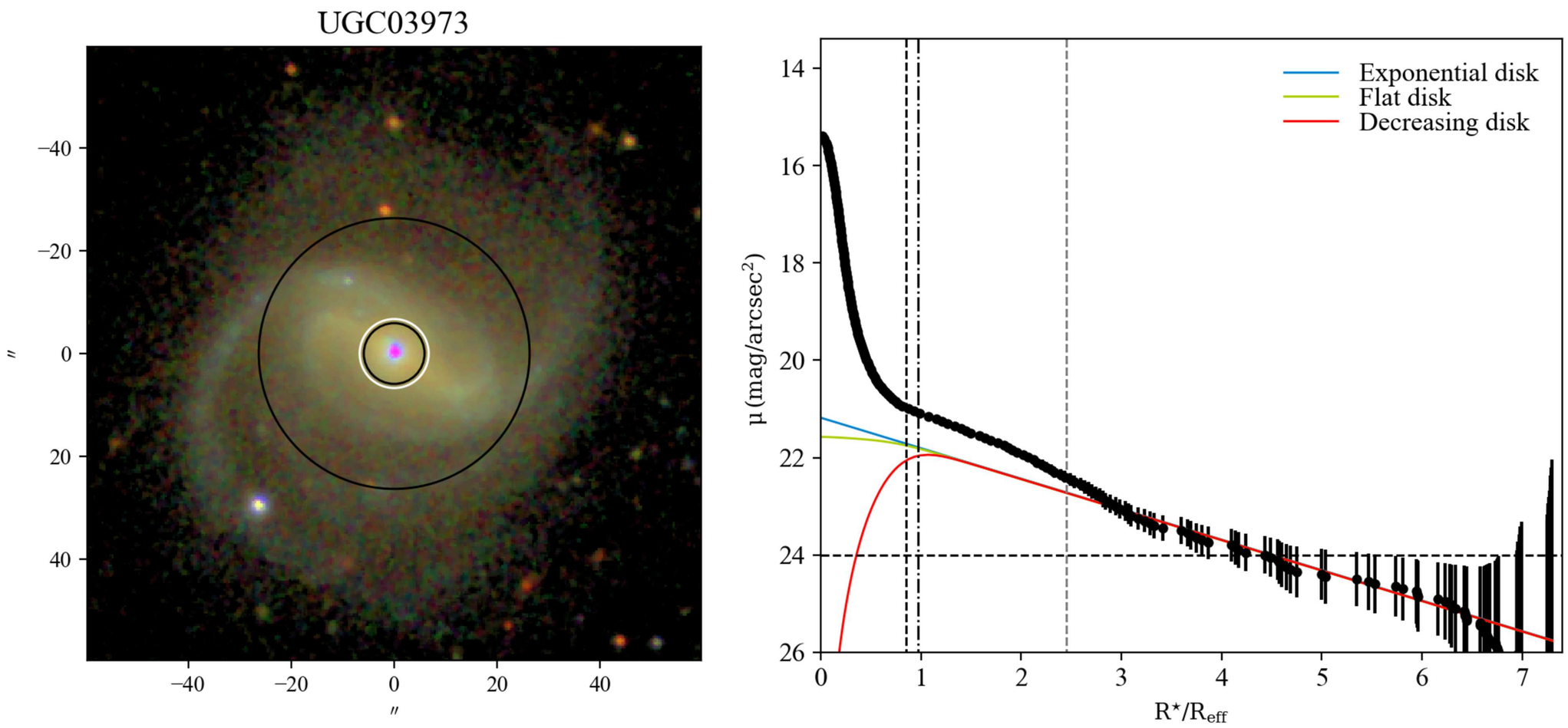
UGC03973
Exponential disk
Flat disk
Decreasing disk
μ (mag/arcsec²)
R⋆/Reff
″

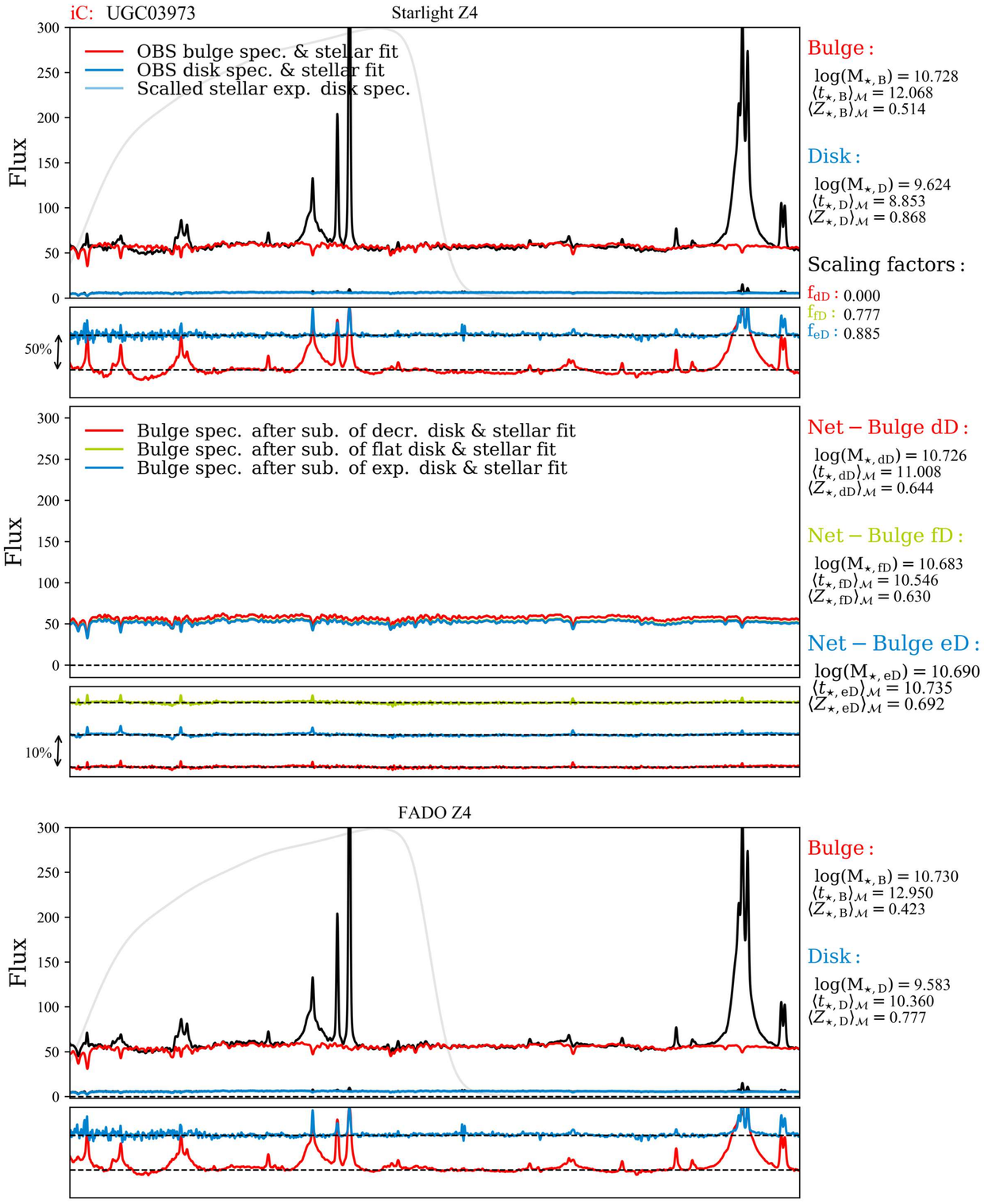
iC: UGC03973
Starlight Z4
OBS bulge spec. & stellar fit
OBS disk spec. & stellar fit
Scalled stellar exp. disk spec.
Flux
Bulge :
log(M⋆, B) = 10.728
⟨t⋆, B⟩M = 12.068
⟨Z⋆, B⟩M = 0.514
Disk :
log(M⋆, D) = 9.624
⟨t⋆, D⟩M = 8.853
⟨Z⋆, D⟩M = 0.868
Scaling factors :
fdD : 0.000
ffD : 0.777
feD : 0.885
50%
Bulge spec. after sub. of decr. disk & stellar fit
Bulge spec. after sub. of flat disk & stellar fit
Bulge spec. after sub. of exp. disk & stellar fit
Net − Bulge dD :
log(M⋆, dD) = 10.726
⟨t⋆, dD⟩M = 11.008
⟨Z⋆, dD⟩M = 0.644
Net − Bulge fD :
log(M⋆, fD) = 10.683
⟨t⋆, fD⟩M = 10.546
⟨Z⋆, fD⟩M = 0.630
Net − Bulge eD :
log(M⋆, eD) = 10.690
⟨t⋆, eD⟩M = 10.735
⟨Z⋆, eD⟩M = 0.692
10%
FADO Z4
Bulge :
log(M⋆, B) = 10.730
⟨t⋆, B⟩M = 12.950
⟨Z⋆, B⟩M = 0.423
Disk :
log(M⋆, D) = 9.583
⟨t⋆, D⟩M = 10.360
⟨Z⋆, D⟩M = 0.777
Net − Bulge dD :
log(M⋆, dD) = 10.730
⟨t⋆, dD⟩M = 12.830
⟨Z⋆, dD⟩M = 0.442
Net − Bulge fD :
log(M⋆, fD) = 10.690
⟨t⋆, fD⟩M = 11.830
⟨Z⋆, fD⟩M = 0.502
Net − Bulge eD :
log(M⋆, eD) = 10.690
⟨t⋆, eD⟩M = 11.980
⟨Z⋆, eD⟩M = 0.505
λ (Å)

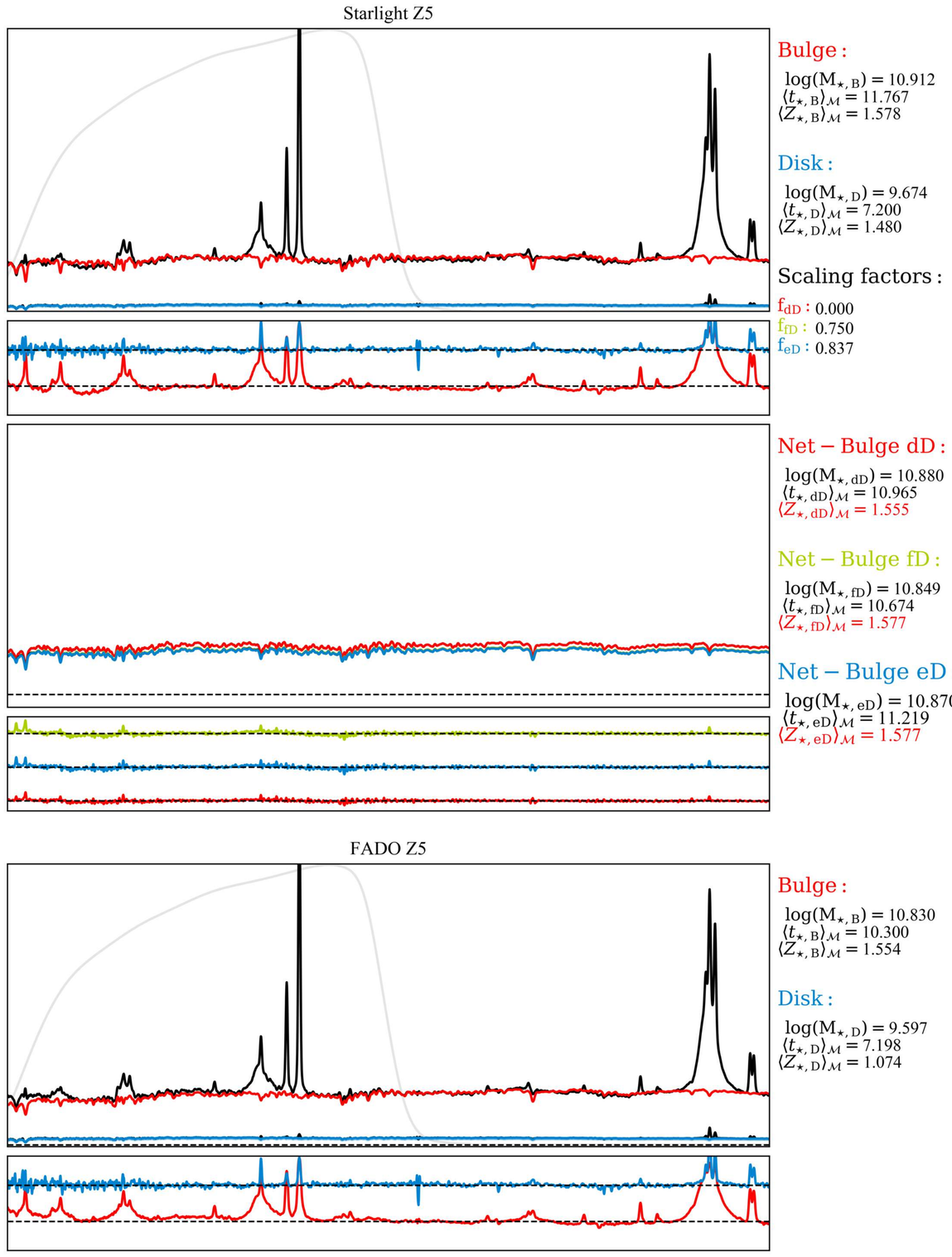
Starlight Z5
Bulge :
log(M⋆, B) = 10.912
⟨t⋆, B⟩M = 11.767
⟨Z⋆, B⟩M = 1.578
Disk :
log(M⋆, D) = 9.674
⟨t⋆, D⟩M = 7.200
⟨Z⋆, D⟩M = 1.480
Scaling factors :
fdD : 0.000
ffD : 0.750
feD : 0.837
Net − Bulge dD :
log(M⋆, dD) = 10.880
⟨t⋆, dD⟩M = 10.965
⟨Z⋆, dD⟩M = 1.555
Net − Bulge fD :
log(M⋆, fD) = 10.849
⟨t⋆, fD⟩M = 10.674
⟨Z⋆, fD⟩M = 1.577
Net − Bulge eD :
log(M⋆, eD) = 10.870
⟨t⋆, eD⟩M = 11.219
⟨Z⋆, eD⟩M = 1.577
FADO Z5
Bulge :
log(M⋆, B) = 10.830
⟨t⋆, B⟩M = 10.300
⟨Z⋆, B⟩M = 1.554
Disk :
log(M⋆, D) = 9.597
⟨t⋆, D⟩M = 7.198
⟨Z⋆, D⟩M = 1.074
Net − Bulge dD :
log(M⋆, dD) = 10.810
⟨t⋆, dD⟩M = 10.950
⟨Z⋆, dD⟩M = 1.576
Net − Bulge fD :
log(M⋆, fD) = 10.810
⟨t⋆, fD⟩M = 11.580
⟨Z⋆, fD⟩M = 1.578
Net − Bulge eD :
log(M⋆, eD) = 10.810
⟨t⋆, eD⟩M = 11.980
⟨Z⋆, eD⟩M = 1.578
λ (Å)

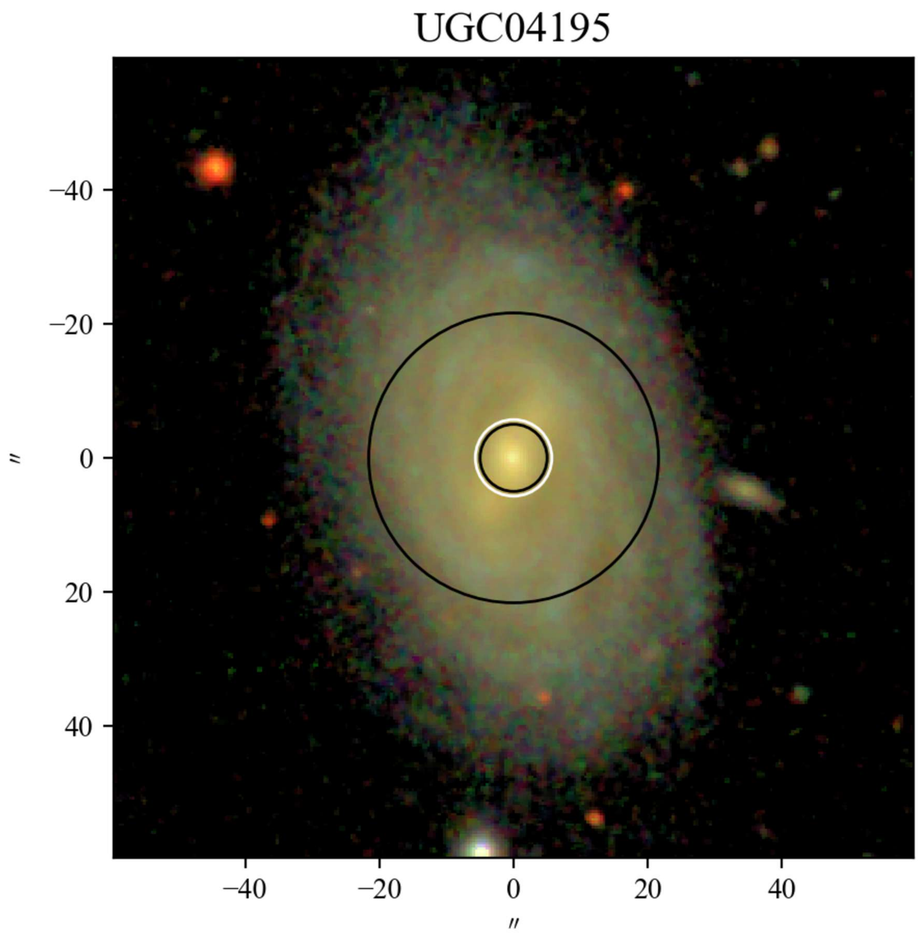
UGC04195
−40
−20
0
20
40
″
−40
−20
0
20
40
″

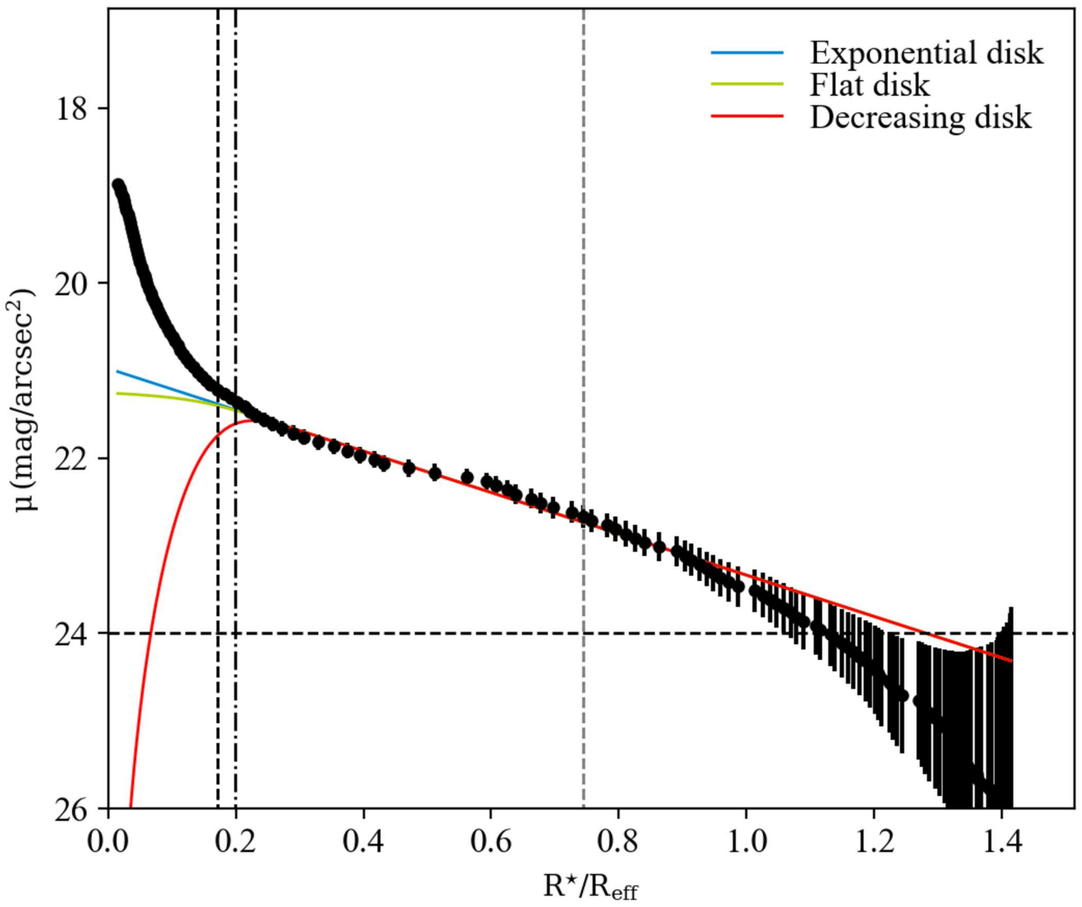
Exponential disk
Flat disk
Decreasing disk
μ (mag/arcsec²)
18
20
22
24
26
0.0
0.2
0.4
0.6
0.8
1.0
1.2
1.4
R⋆/Reff

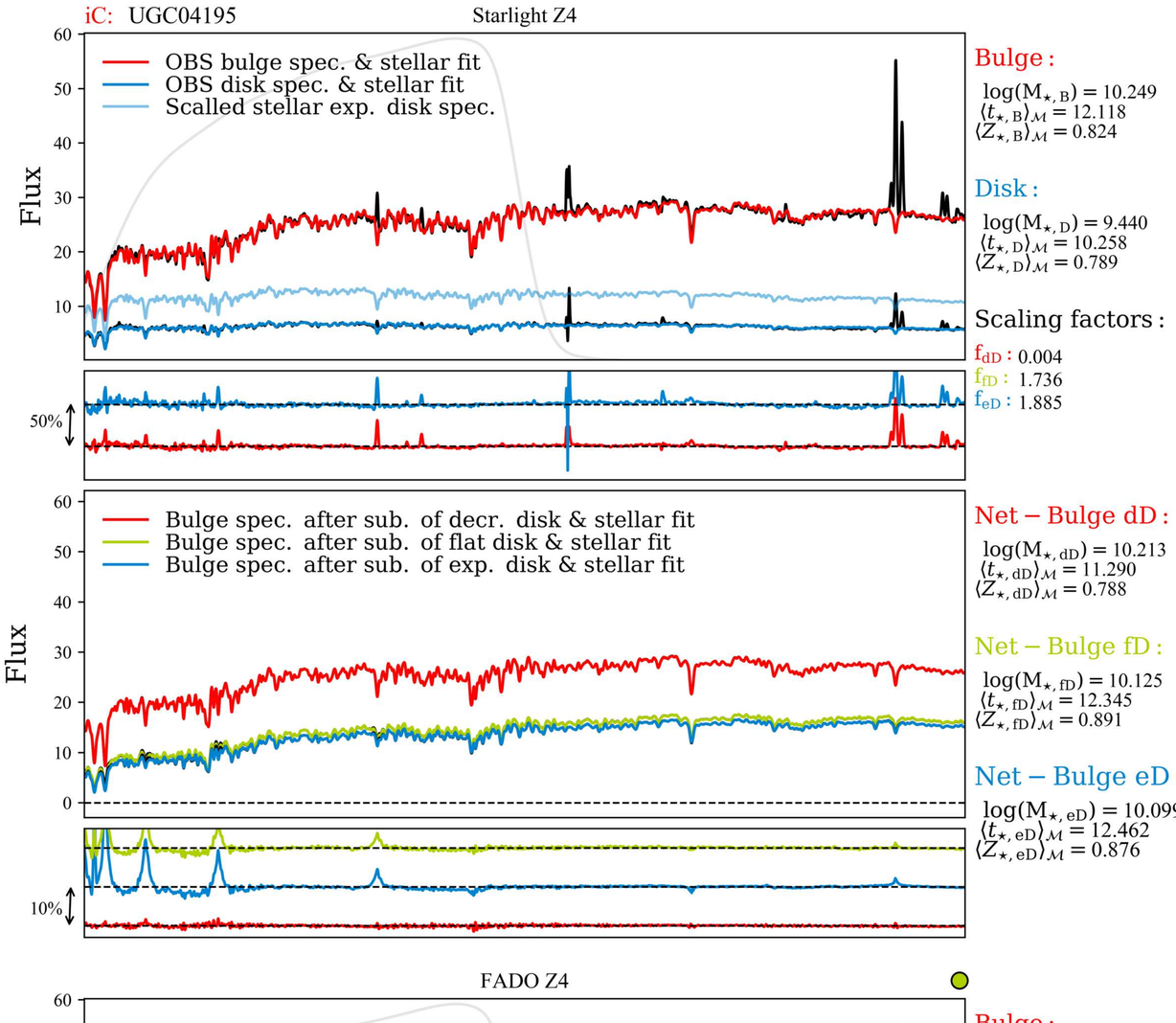
iC: UGC04195
Starlight Z4
OBS bulge spec. & stellar fit
OBS disk spec. & stellar fit
Scalled stellar exp. disk spec.
Flux
50%
Bulge :
log(M⋆, B) = 10.249
⟨t⋆, B⟩M = 12.118
⟨Z⋆, B⟩M = 0.824
Disk :
log(M⋆, D) = 9.440
⟨t⋆, D⟩M = 10.258
⟨Z⋆, D⟩M = 0.789
Scaling factors :
fdD : 0.004
ffD : 1.736
feD : 1.885
Bulge spec. after sub. of decr. disk & stellar fit
Bulge spec. after sub. of flat disk & stellar fit
Bulge spec. after sub. of exp. disk & stellar fit
10%
Net − Bulge dD :
log(M⋆, dD) = 10.213
⟨t⋆, dD⟩M = 11.290
⟨Z⋆, dD⟩M = 0.788
Net − Bulge fD :
log(M⋆, fD) = 10.125
⟨t⋆, fD⟩M = 12.345
⟨Z⋆, fD⟩M = 0.891
Net − Bulge eD :
log(M⋆, eD) = 10.099
⟨t⋆, eD⟩M = 12.462
⟨Z⋆, eD⟩M = 0.876

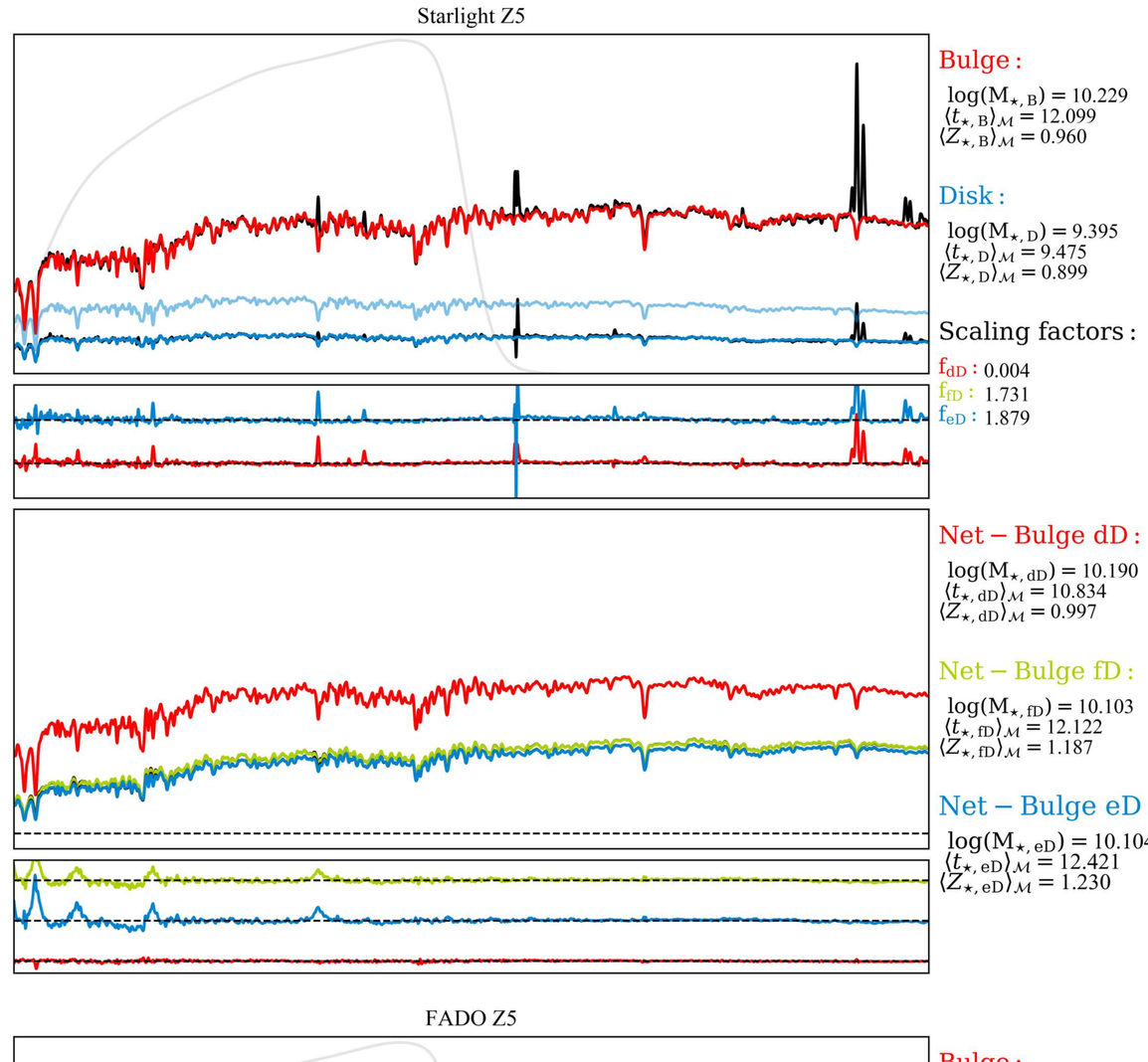
Starlight Z5
Bulge :
log(M⋆, B) = 10.229
⟨t⋆, B⟩M = 12.099
⟨Z⋆, B⟩M = 0.960
Disk :
log(M⋆, D) = 9.395
⟨t⋆, D⟩M = 9.475
⟨Z⋆, D⟩M = 0.899
Scaling factors :
fdD : 0.004
ffD : 1.731
feD : 1.879
Net − Bulge dD :
log(M⋆, dD) = 10.190
⟨t⋆, dD⟩M = 10.834
⟨Z⋆, dD⟩M = 0.997
Net − Bulge fD :
log(M⋆, fD) = 10.103
⟨t⋆, fD⟩M = 12.122
⟨Z⋆, fD⟩M = 1.187
Net − Bulge eD :
log(M⋆, eD) = 10.104
⟨t⋆, eD⟩M = 12.421
⟨Z⋆, eD⟩M = 1.230

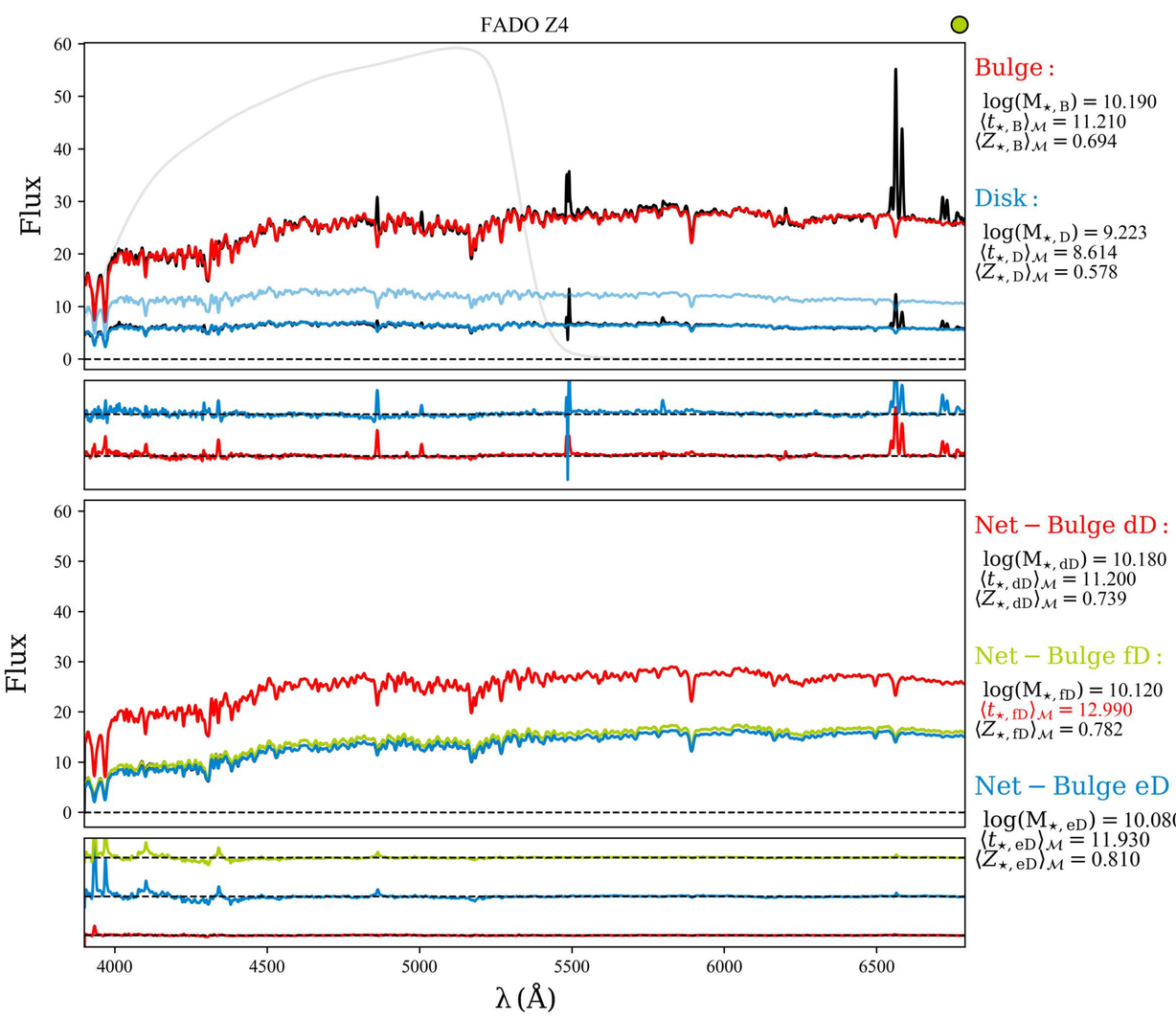
FADO Z4
Flux
Bulge :
log(M⋆, B) = 10.190
⟨t⋆, B⟩M = 11.210
⟨Z⋆, B⟩M = 0.694
Disk :
log(M⋆, D) = 9.223
⟨t⋆, D⟩M = 8.614
⟨Z⋆, D⟩M = 0.578
Net − Bulge dD :
log(M⋆, dD) = 10.180
⟨t⋆, dD⟩M = 11.200
⟨Z⋆, dD⟩M = 0.739
Net − Bulge fD :
log(M⋆, fD) = 10.120
⟨t⋆, fD⟩M = 12.990
⟨Z⋆, fD⟩M = 0.782
Net − Bulge eD :
log(M⋆, eD) = 10.080
⟨t⋆, eD⟩M = 11.930
⟨Z⋆, eD⟩M = 0.810
4000
4500
5000
5500
6000
6500
λ (Å)

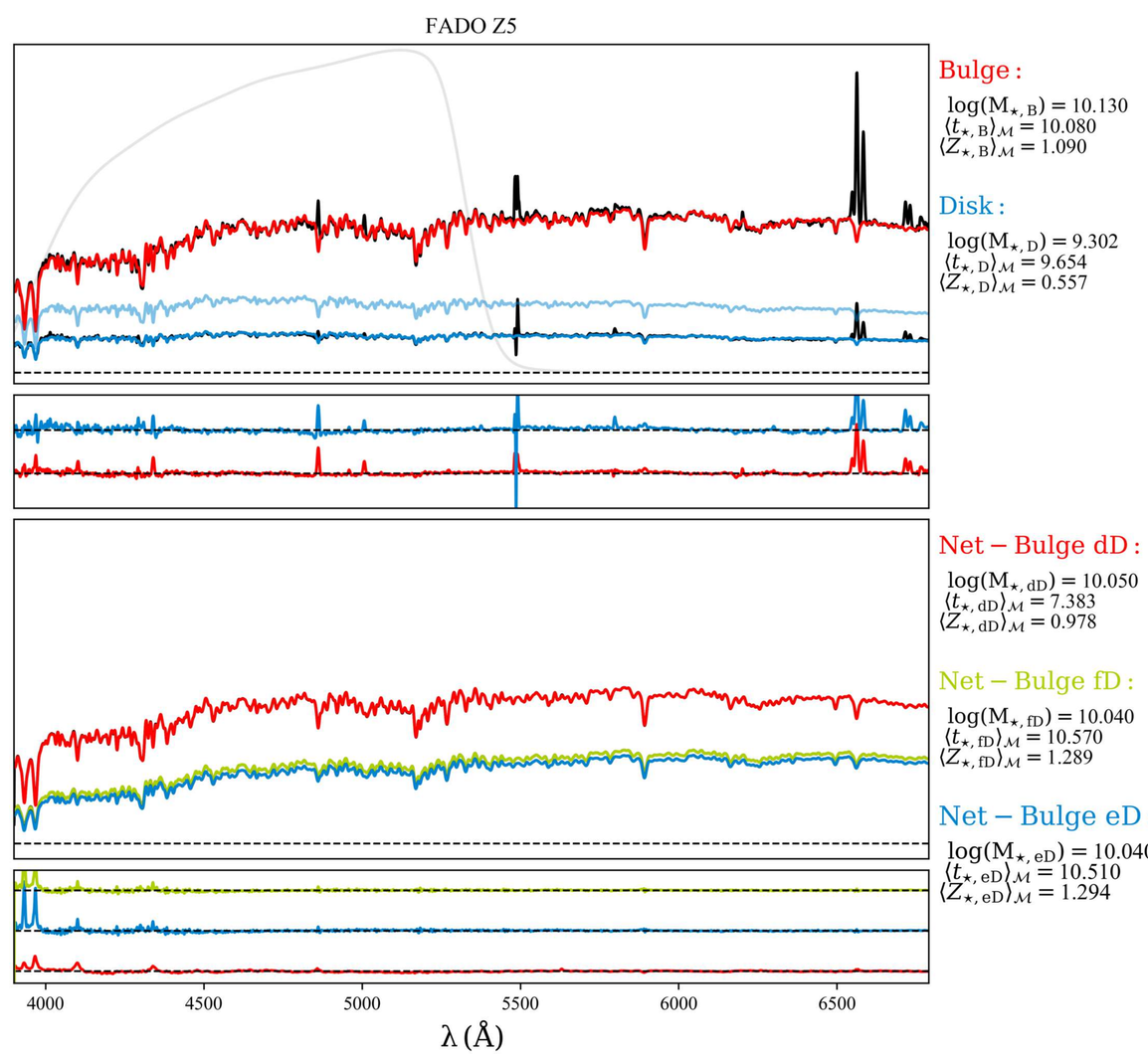
FADO Z5
Bulge :
log(M⋆, B) = 10.130
⟨t⋆, B⟩M = 10.080
⟨Z⋆, B⟩M = 1.090
Disk :
log(M⋆, D) = 9.302
⟨t⋆, D⟩M = 9.654
⟨Z⋆, D⟩M = 0.557
Net − Bulge dD :
log(M⋆, dD) = 10.050
⟨t⋆, dD⟩M = 7.383
⟨Z⋆, dD⟩M = 0.978
Net − Bulge fD :
log(M⋆, fD) = 10.040
⟨t⋆, fD⟩M = 10.570
⟨Z⋆, fD⟩M = 1.289
Net − Bulge eD :
log(M⋆, eD) = 10.040
⟨t⋆, eD⟩M = 10.510
⟨Z⋆, eD⟩M = 1.294
4000
4500
5000
5500
6000
6500
λ (Å)

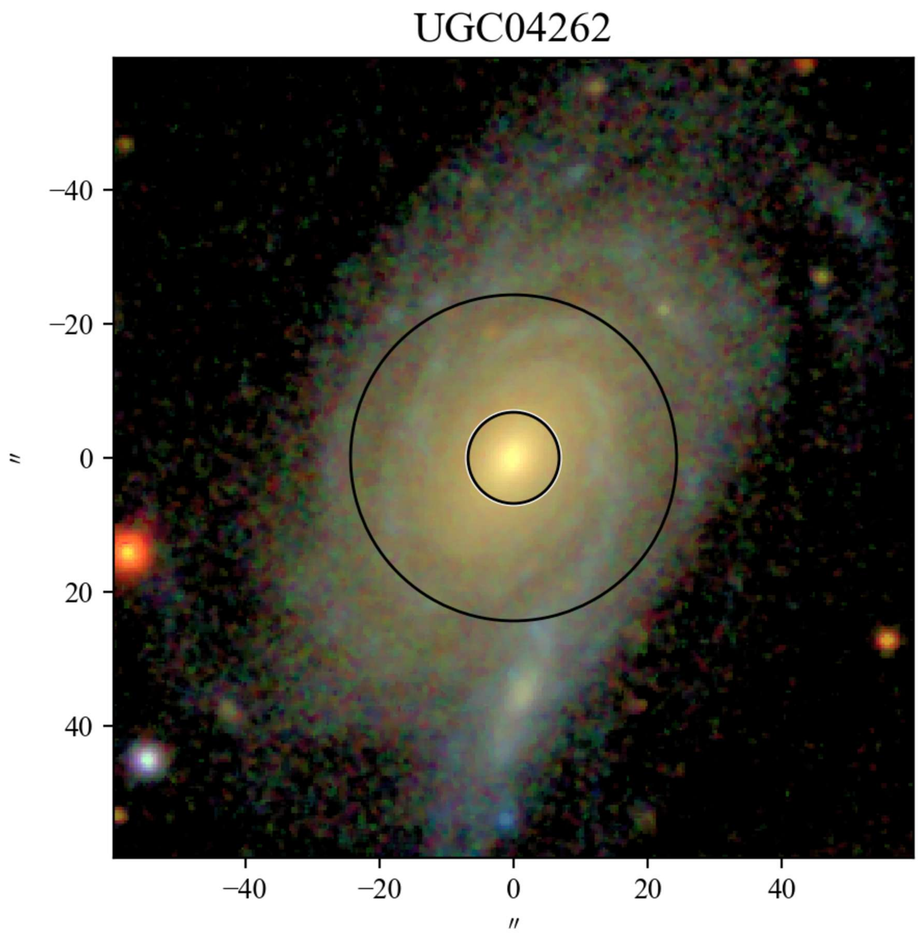
UGC04262
−40
−20
0
20
40
″
−40
−20
0
20
40
″

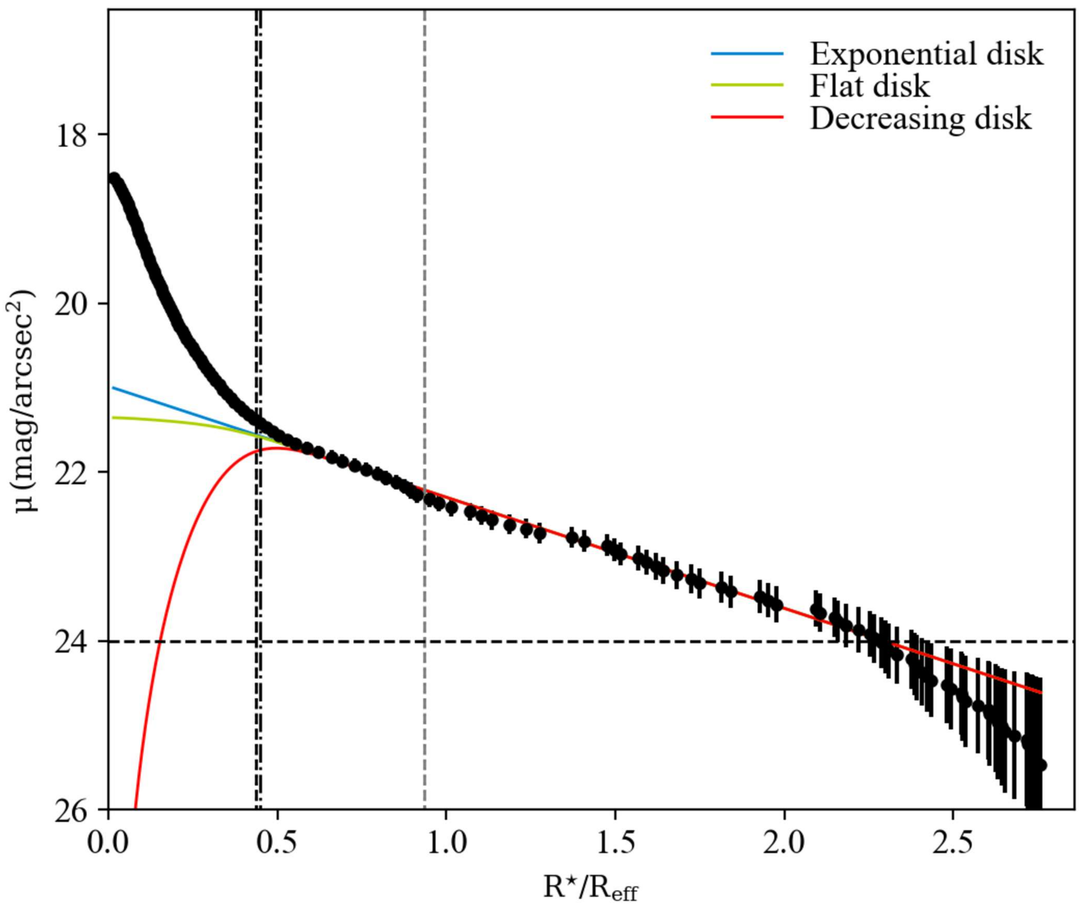
Exponential disk
Flat disk
Decreasing disk
μ (mag/arcsec²)
18
20
22
24
26
0.0
0.5
1.0
1.5
2.0
2.5
R⋆/Reff

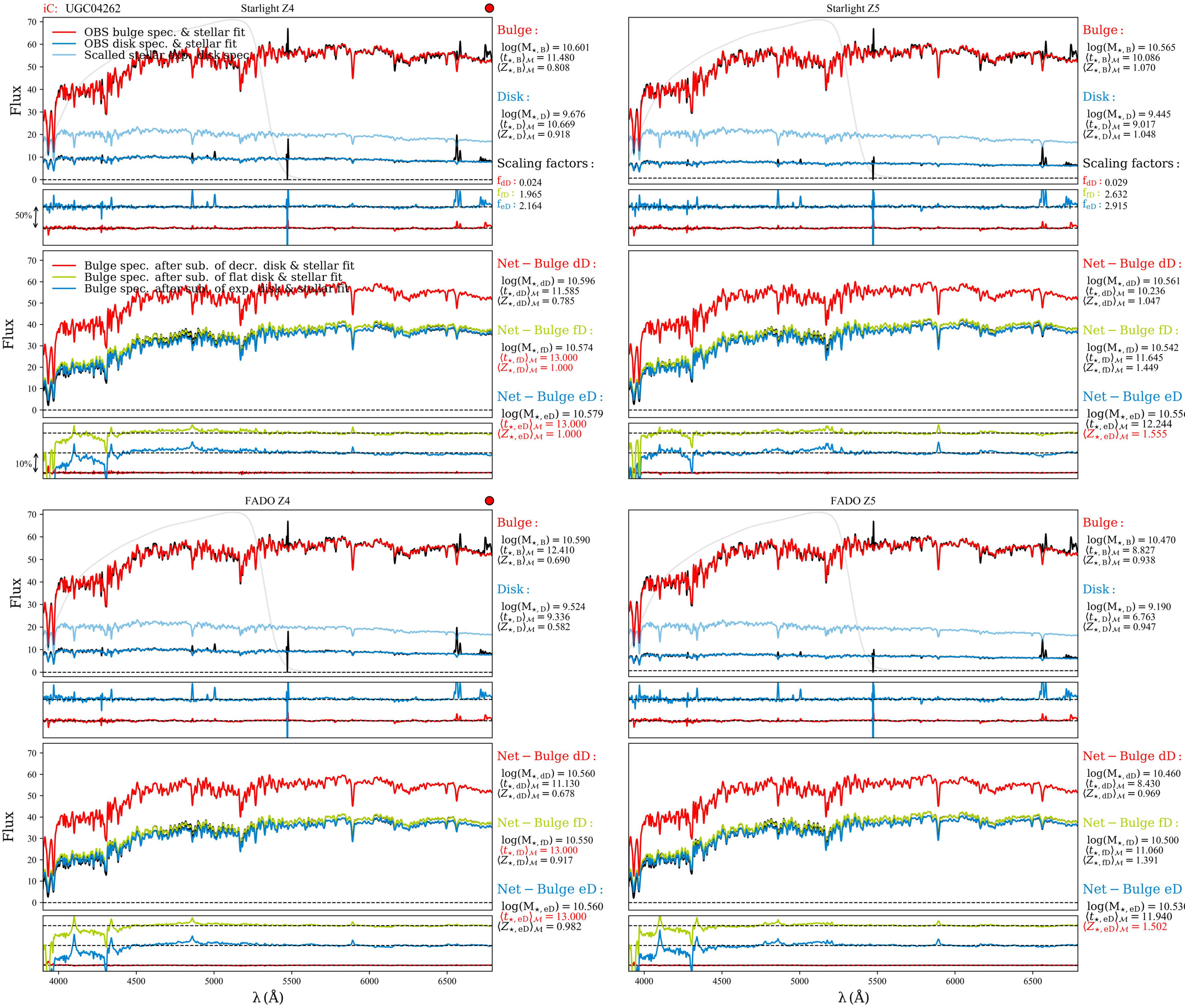
iC: UGC04262
Starlight Z4
Starlight Z5
OBS bulge spec. & stellar fit
OBS disk spec. & stellar fit
Scalled stellar exp. disk spec.
Flux
Bulge :
log(M⋆, B) = 10.601
⟨t⋆, B⟩M = 11.480
⟨Z⋆, B⟩M = 0.808
Disk :
log(M⋆, D) = 9.676
⟨t⋆, D⟩M = 10.669
⟨Z⋆, D⟩M = 0.918
Scaling factors :
fdD : 0.024
ffD : 1.965
feD : 2.164
50%
Bulge :
log(M⋆, B) = 10.565
⟨t⋆, B⟩M = 10.086
⟨Z⋆, B⟩M = 1.070
Disk :
log(M⋆, D) = 9.445
⟨t⋆, D⟩M = 9.017
⟨Z⋆, D⟩M = 1.048
Scaling factors :
fdD : 0.029
ffD : 2.632
feD : 2.915
Bulge spec. after sub. of decr. disk & stellar fit
Bulge spec. after sub. of flat disk & stellar fit
Bulge spec. after sub. of exp. disk & stellar fit
Net − Bulge dD :
log(M⋆, dD) = 10.596
⟨t⋆, dD⟩M = 11.585
⟨Z⋆, dD⟩M = 0.785
Net − Bulge fD :
log(M⋆, fD) = 10.574
⟨t⋆, fD⟩M = 13.000
⟨Z⋆, fD⟩M = 1.000
Net − Bulge eD :
log(M⋆, eD) = 10.579
⟨t⋆, eD⟩M = 13.000
⟨Z⋆, eD⟩M = 1.000
10%
Net − Bulge dD :
log(M⋆, dD) = 10.561
⟨t⋆, dD⟩M = 10.236
⟨Z⋆, dD⟩M = 1.047
Net − Bulge fD :
log(M⋆, fD) = 10.542
⟨t⋆, fD⟩M = 11.645
⟨Z⋆, fD⟩M = 1.449
Net − Bulge eD :
log(M⋆, eD) = 10.556
⟨t⋆, eD⟩M = 12.244
⟨Z⋆, eD⟩M = 1.555
FADO Z4
FADO Z5
Bulge :
log(M⋆, B) = 10.590
⟨t⋆, B⟩M = 12.410
⟨Z⋆, B⟩M = 0.690
Disk :
log(M⋆, D) = 9.524
⟨t⋆, D⟩M = 9.336
⟨Z⋆, D⟩M = 0.582
Bulge :
log(M⋆, B) = 10.470
⟨t⋆, B⟩M = 8.827
⟨Z⋆, B⟩M = 0.938
Disk :
log(M⋆, D) = 9.190
⟨t⋆, D⟩M = 6.763
⟨Z⋆, D⟩M = 0.947
Net − Bulge dD :
log(M⋆, dD) = 10.560
⟨t⋆, dD⟩M = 11.130
⟨Z⋆, dD⟩M = 0.678
Net − Bulge fD :
log(M⋆, fD) = 10.550
⟨t⋆, fD⟩M = 13.000
⟨Z⋆, fD⟩M = 0.917
Net − Bulge eD :
log(M⋆, eD) = 10.560
⟨t⋆, eD⟩M = 13.000
⟨Z⋆, eD⟩M = 0.982
Net − Bulge dD :
log(M⋆, dD) = 10.460
⟨t⋆, dD⟩M = 8.430
⟨Z⋆, dD⟩M = 0.969
Net − Bulge fD :
log(M⋆, fD) = 10.500
⟨t⋆, fD⟩M = 11.060
⟨Z⋆, fD⟩M = 1.391
Net − Bulge eD :
log(M⋆, eD) = 10.530
⟨t⋆, eD⟩M = 11.940
⟨Z⋆, eD⟩M = 1.502
λ (Å)
λ (Å)

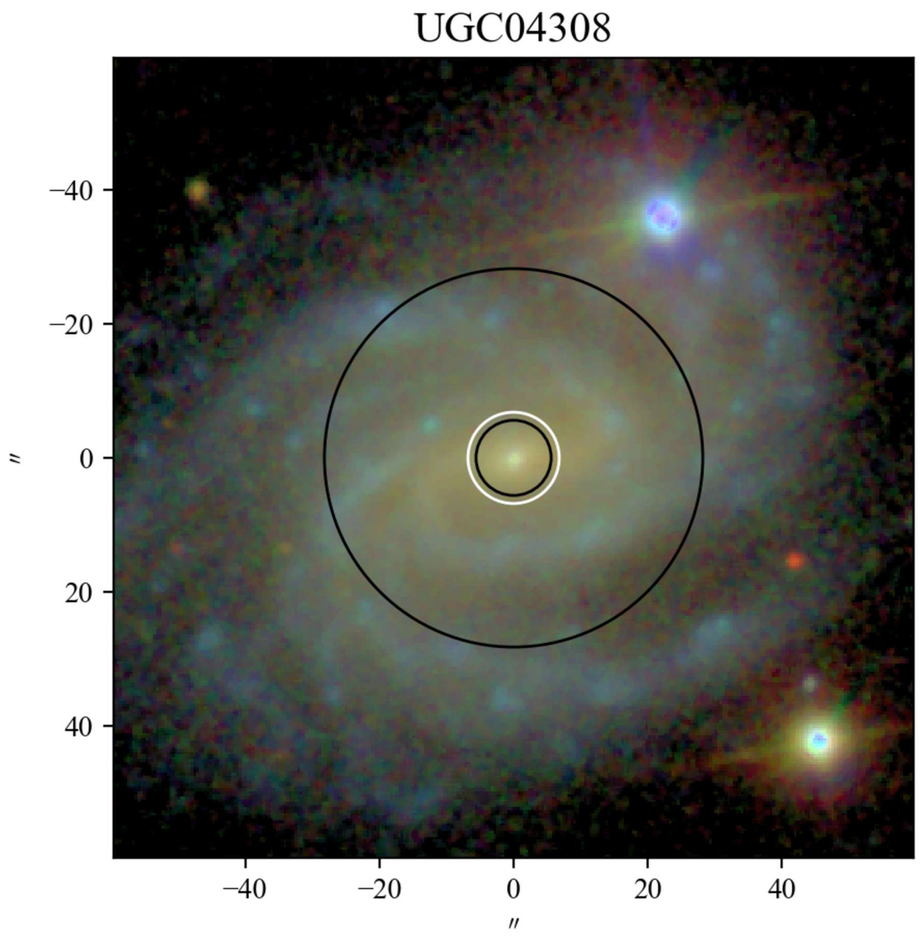
UGC04308
−40
−20
0
20
40
″
−40
−20
0
20
40
″

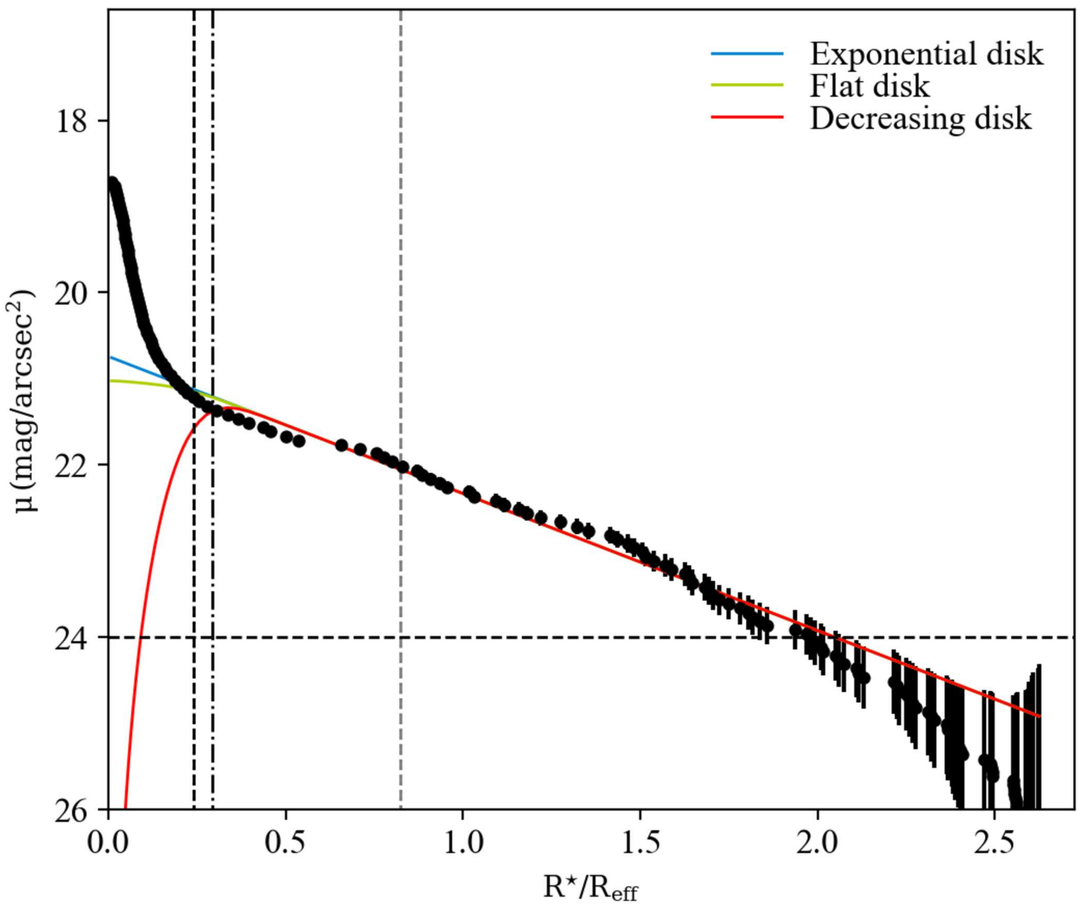
Exponential disk
Flat disk
Decreasing disk
μ (mag/arcsec²)
18
20
22
24
26
0.0
0.5
1.0
1.5
2.0
2.5
R⋆/Reff

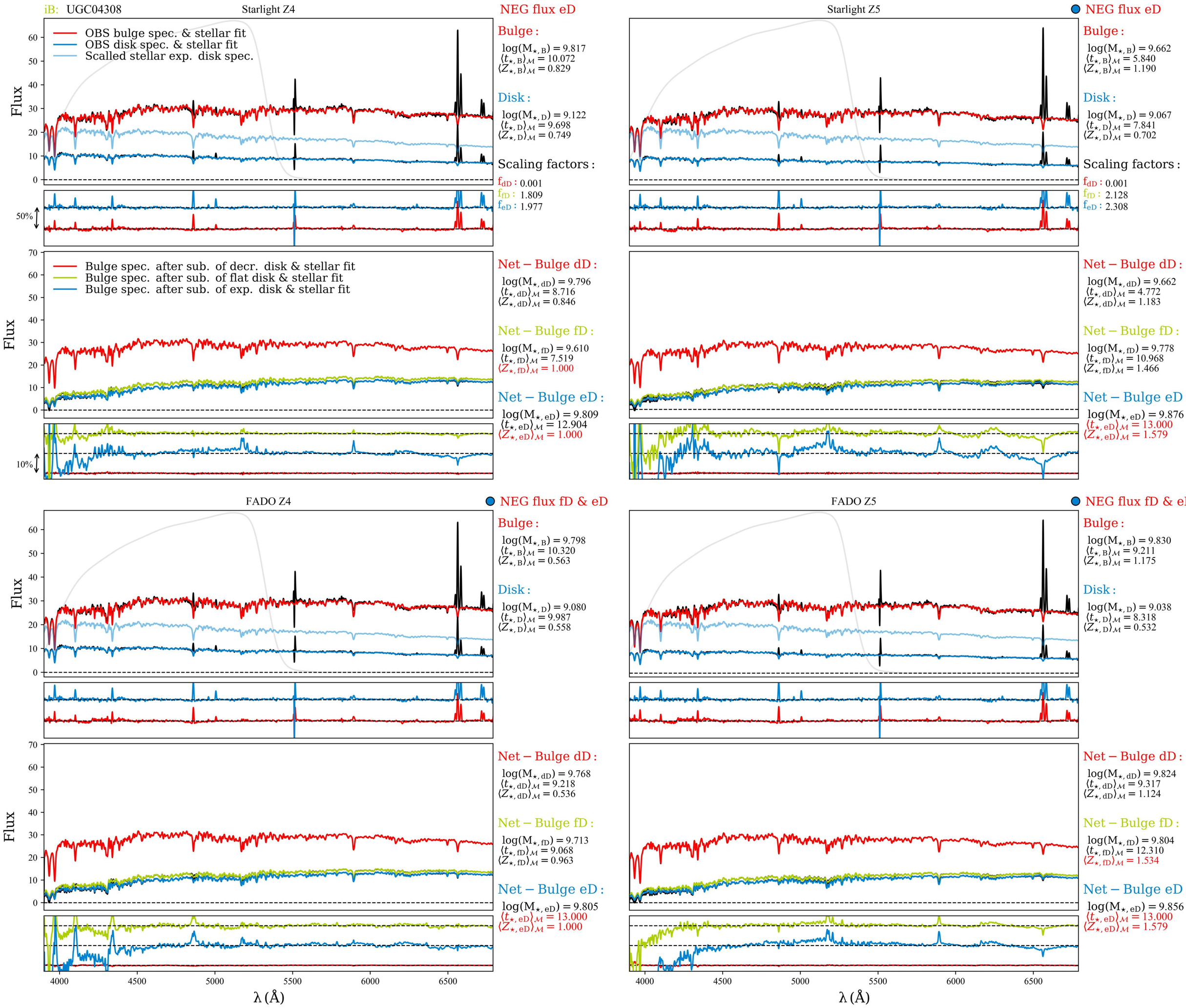
iB: UGC04308
Starlight Z4
NEG flux eD
OBS bulge spec. & stellar fit
OBS disk spec. & stellar fit
Scalled stellar exp. disk spec.
Flux
50%
Bulge :
log(M⋆, B) = 9.817
⟨t⋆, B⟩M = 10.072
⟨Z⋆, B⟩M = 0.829
Disk :
log(M⋆, D) = 9.122
⟨t⋆, D⟩M = 9.698
⟨Z⋆, D⟩M = 0.749
Scaling factors :
fdD : 0.001
ffD : 1.809
feD : 1.977
Starlight Z5
NEG flux eD
Bulge :
log(M⋆, B) = 9.662
⟨t⋆, B⟩M = 5.840
⟨Z⋆, B⟩M = 1.190
Disk :
log(M⋆, D) = 9.067
⟨t⋆, D⟩M = 7.841
⟨Z⋆, D⟩M = 0.702
Scaling factors :
fdD : 0.001
ffD : 2.128
feD : 2.308
Bulge spec. after sub. of decr. disk & stellar fit
Bulge spec. after sub. of flat disk & stellar fit
Bulge spec. after sub. of exp. disk & stellar fit
10%
Net − Bulge dD :
log(M⋆, dD) = 9.796
⟨t⋆, dD⟩M = 8.716
⟨Z⋆, dD⟩M = 0.846
Net − Bulge fD :
log(M⋆, fD) = 9.610
⟨t⋆, fD⟩M = 7.519
⟨Z⋆, fD⟩M = 1.000
Net − Bulge eD :
log(M⋆, eD) = 9.809
⟨t⋆, eD⟩M = 12.904
⟨Z⋆, eD⟩M = 1.000
Net − Bulge dD :
log(M⋆, dD) = 9.662
⟨t⋆, dD⟩M = 4.772
⟨Z⋆, dD⟩M = 1.183
Net − Bulge fD :
log(M⋆, fD) = 9.778
⟨t⋆, fD⟩M = 10.968
⟨Z⋆, fD⟩M = 1.466
Net − Bulge eD :
log(M⋆, eD) = 9.876
⟨t⋆, eD⟩M = 13.000
⟨Z⋆, eD⟩M = 1.579
FADO Z4
NEG flux fD & eD
Bulge :
log(M⋆, B) = 9.798
⟨t⋆, B⟩M = 10.320
⟨Z⋆, B⟩M = 0.563
Disk :
log(M⋆, D) = 9.080
⟨t⋆, D⟩M = 9.987
⟨Z⋆, D⟩M = 0.558
FADO Z5
NEG flux fD & eD
Bulge :
log(M⋆, B) = 9.830
⟨t⋆, B⟩M = 9.211
⟨Z⋆, B⟩M = 1.175
Disk :
log(M⋆, D) = 9.038
⟨t⋆, D⟩M = 8.318
⟨Z⋆, D⟩M = 0.532
Net − Bulge dD :
log(M⋆, dD) = 9.768
⟨t⋆, dD⟩M = 9.218
⟨Z⋆, dD⟩M = 0.536
Net − Bulge fD :
log(M⋆, fD) = 9.713
⟨t⋆, fD⟩M = 9.068
⟨Z⋆, fD⟩M = 0.963
Net − Bulge eD :
log(M⋆, eD) = 9.805
⟨t⋆, eD⟩M = 13.000
⟨Z⋆, eD⟩M = 1.000
Net − Bulge dD :
log(M⋆, dD) = 9.824
⟨t⋆, dD⟩M = 9.317
⟨Z⋆, dD⟩M = 1.124
Net − Bulge fD :
log(M⋆, fD) = 9.804
⟨t⋆, fD⟩M = 12.310
⟨Z⋆, fD⟩M = 1.534
Net − Bulge eD :
log(M⋆, eD) = 9.856
⟨t⋆, eD⟩M = 13.000
⟨Z⋆, eD⟩M = 1.579
λ (Å)

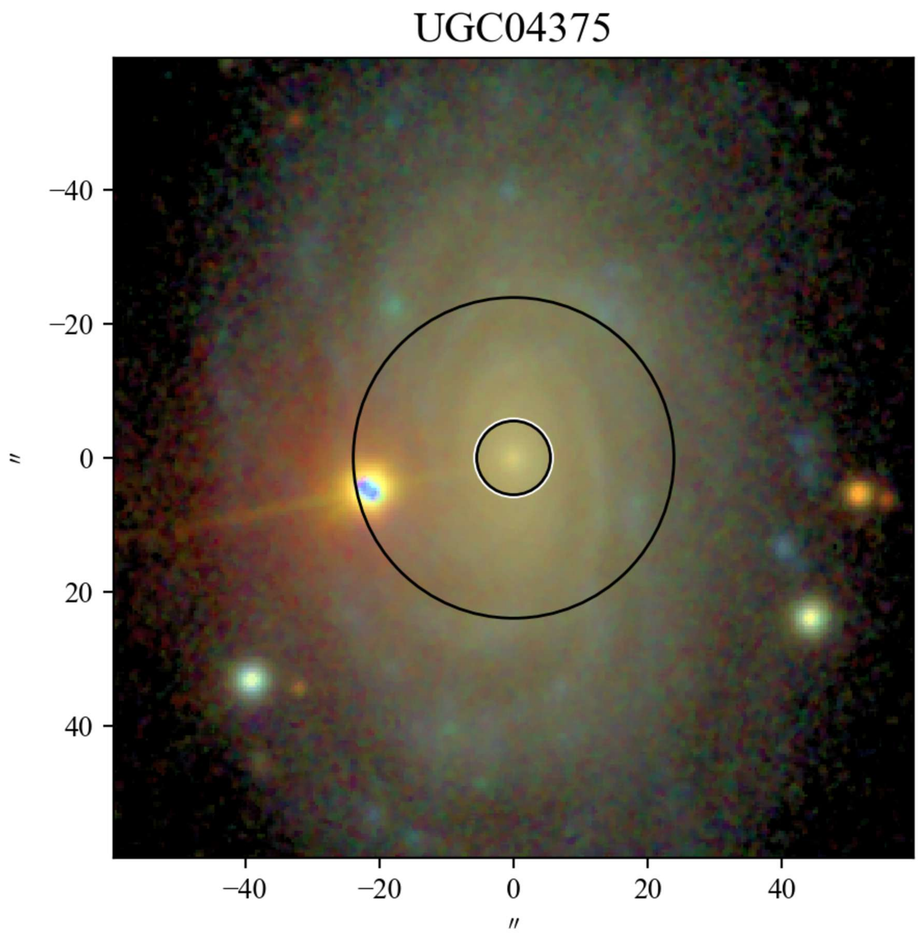
UGC04375
−40
−20
0
20
40
″
−40
−20
0
20
40
″

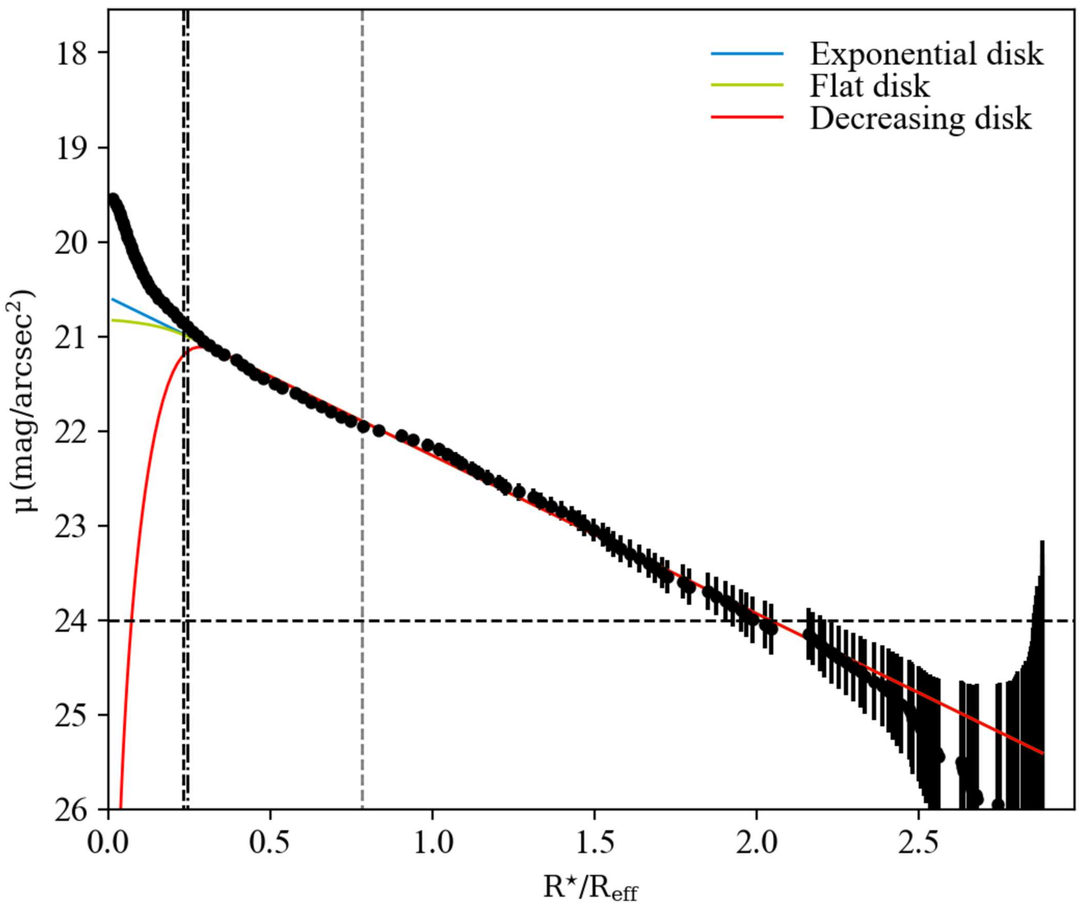
Exponential disk
Flat disk
Decreasing disk
μ (mag/arcsec²)
18
19
20
21
22
23
24
25
26
0.0
0.5
1.0
1.5
2.0
2.5
R⋆/Reff

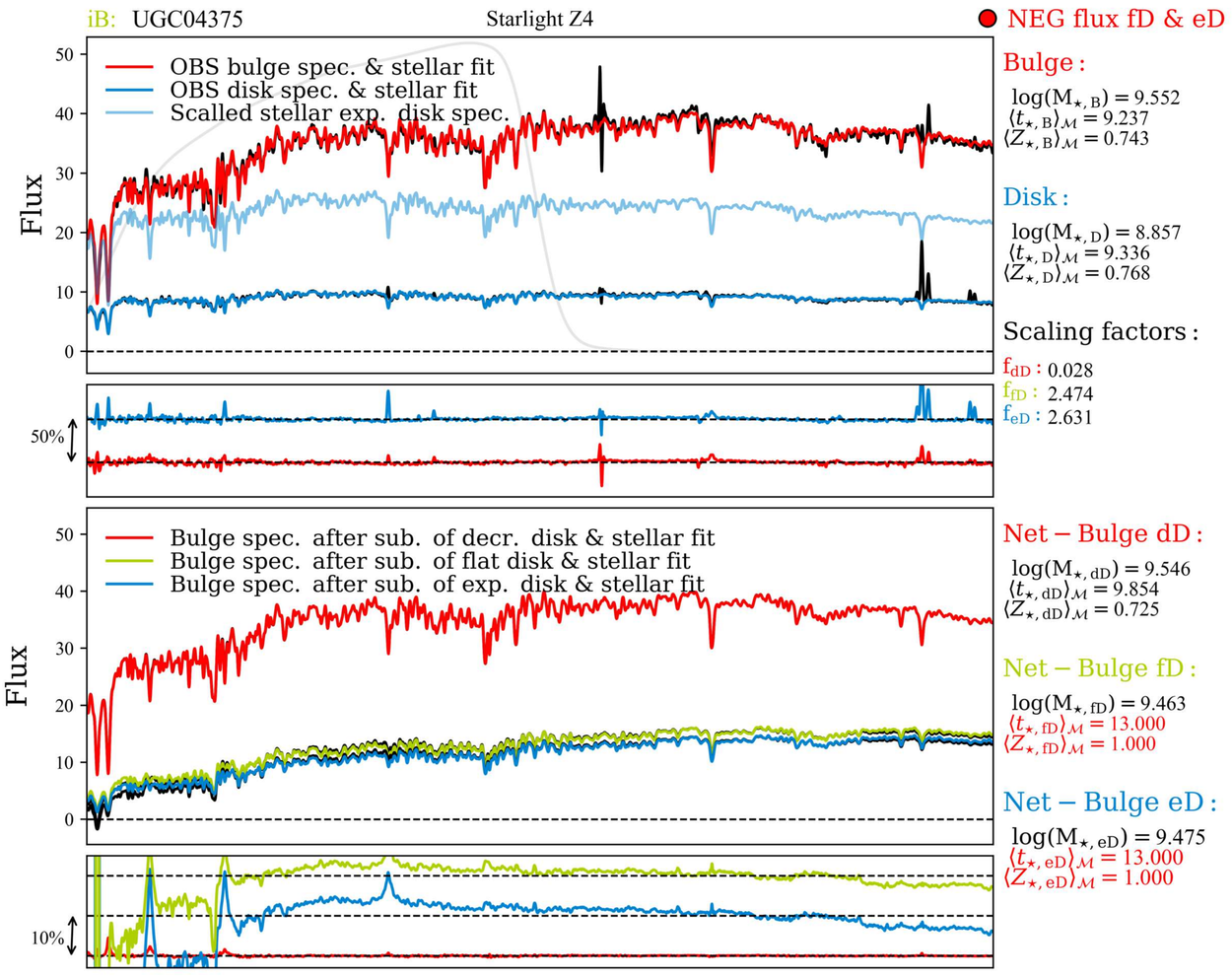
iB: UGC04375
Starlight Z4
NEG flux fD & eD
OBS bulge spec. & stellar fit
OBS disk spec. & stellar fit
Scalled stellar exp. disk spec.
Flux
50%
Bulge :
log(M⋆, B) = 9.552
⟨t⋆, B⟩M = 9.237
⟨Z⋆, B⟩M = 0.743
Disk :
log(M⋆, D) = 8.857
⟨t⋆, D⟩M = 9.336
⟨Z⋆, D⟩M = 0.768
Scaling factors :
fdD : 0.028
ffD : 2.474
feD : 2.631
Bulge spec. after sub. of decr. disk & stellar fit
Bulge spec. after sub. of flat disk & stellar fit
Bulge spec. after sub. of exp. disk & stellar fit
10%
Net − Bulge dD :
log(M⋆, dD) = 9.546
⟨t⋆, dD⟩M = 9.854
⟨Z⋆, dD⟩M = 0.725
Net − Bulge fD :
log(M⋆, fD) = 9.463
⟨t⋆, fD⟩M = 13.000
⟨Z⋆, fD⟩M = 1.000
Net − Bulge eD :
log(M⋆, eD) = 9.475
⟨t⋆, eD⟩M = 13.000
⟨Z⋆, eD⟩M = 1.000

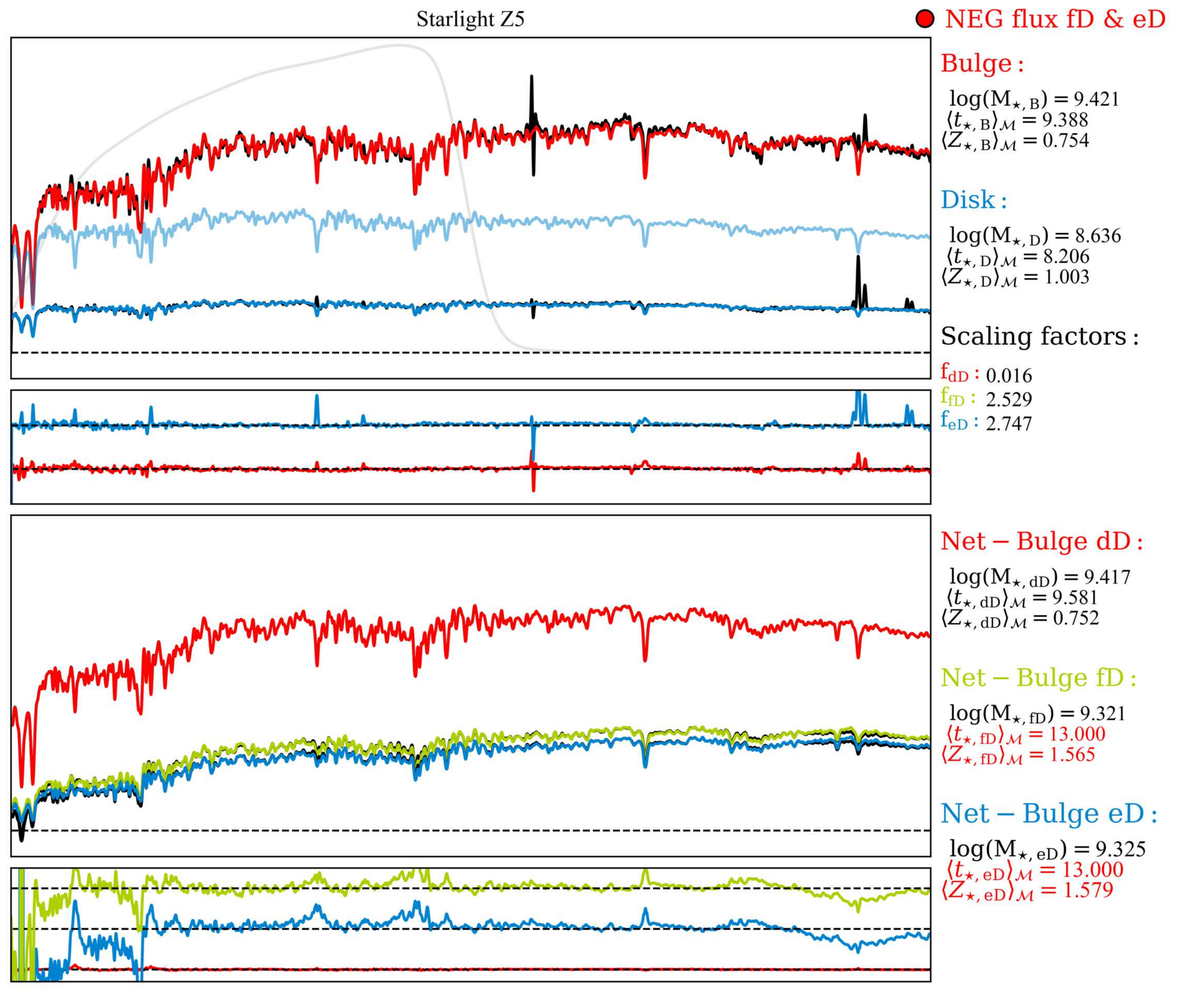
Starlight Z5
NEG flux fD & eD
Bulge :
log(M⋆, B) = 9.421
⟨t⋆, B⟩M = 9.388
⟨Z⋆, B⟩M = 0.754
Disk :
log(M⋆, D) = 8.636
⟨t⋆, D⟩M = 8.206
⟨Z⋆, D⟩M = 1.003
Scaling factors :
fdD : 0.016
ffD : 2.529
feD : 2.747
Net − Bulge dD :
log(M⋆, dD) = 9.417
⟨t⋆, dD⟩M = 9.581
⟨Z⋆, dD⟩M = 0.752
Net − Bulge fD :
log(M⋆, fD) = 9.321
⟨t⋆, fD⟩M = 13.000
⟨Z⋆, fD⟩M = 1.565
Net − Bulge eD :
log(M⋆, eD) = 9.325
⟨t⋆, eD⟩M = 13.000
⟨Z⋆, eD⟩M = 1.579

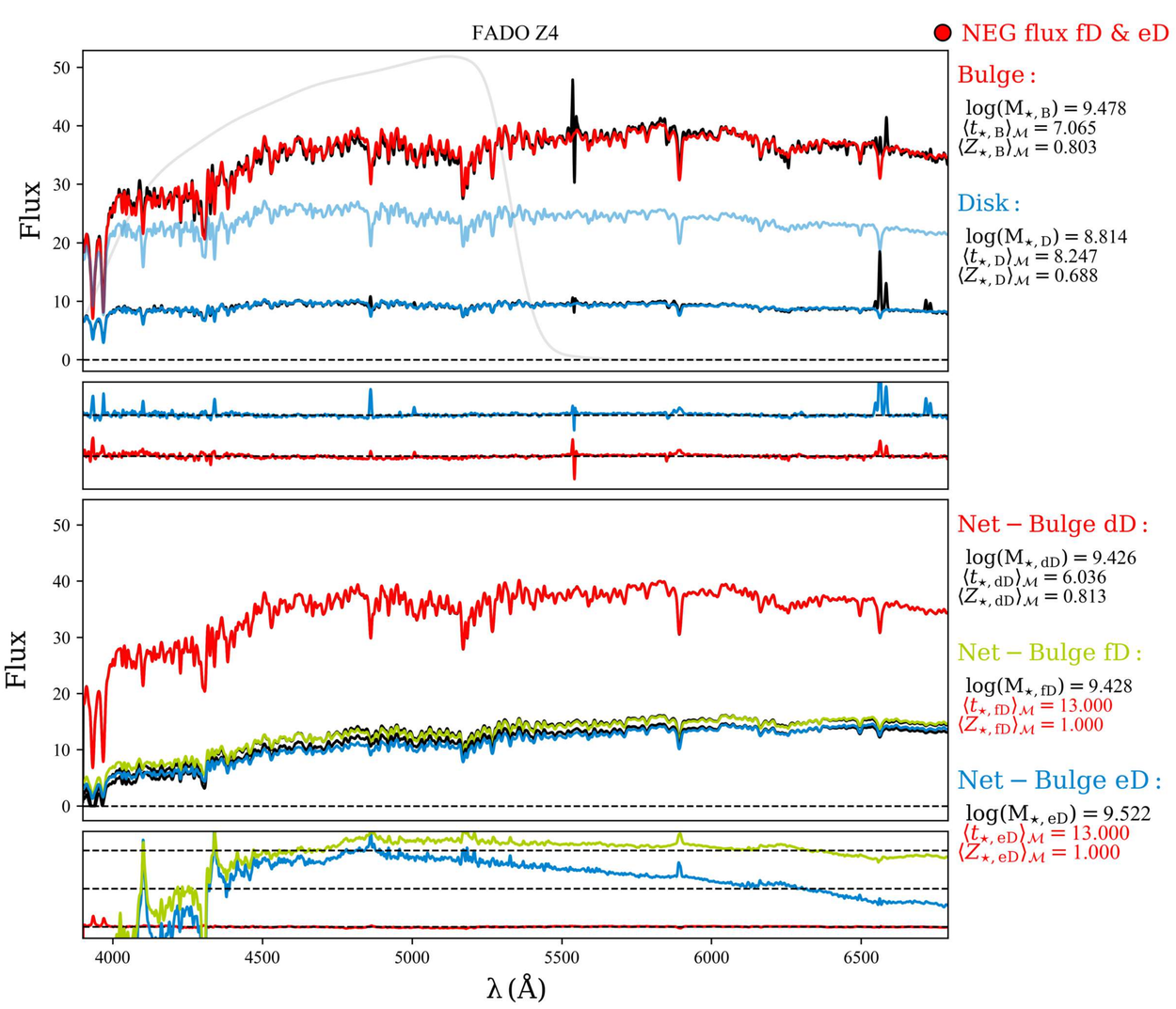
FADO Z4
NEG flux fD & eD
Flux
Bulge :
log(M⋆, B) = 9.478
⟨t⋆, B⟩M = 7.065
⟨Z⋆, B⟩M = 0.803
Disk :
log(M⋆, D) = 8.814
⟨t⋆, D⟩M = 8.247
⟨Z⋆, D⟩M = 0.688
Net − Bulge dD :
log(M⋆, dD) = 9.426
⟨t⋆, dD⟩M = 6.036
⟨Z⋆, dD⟩M = 0.813
Net − Bulge fD :
log(M⋆, fD) = 9.428
⟨t⋆, fD⟩M = 13.000
⟨Z⋆, fD⟩M = 1.000
Net − Bulge eD :
log(M⋆, eD) = 9.522
⟨t⋆, eD⟩M = 13.000
⟨Z⋆, eD⟩M = 1.000
4000
4500
5000
5500
6000
6500
λ (Å)

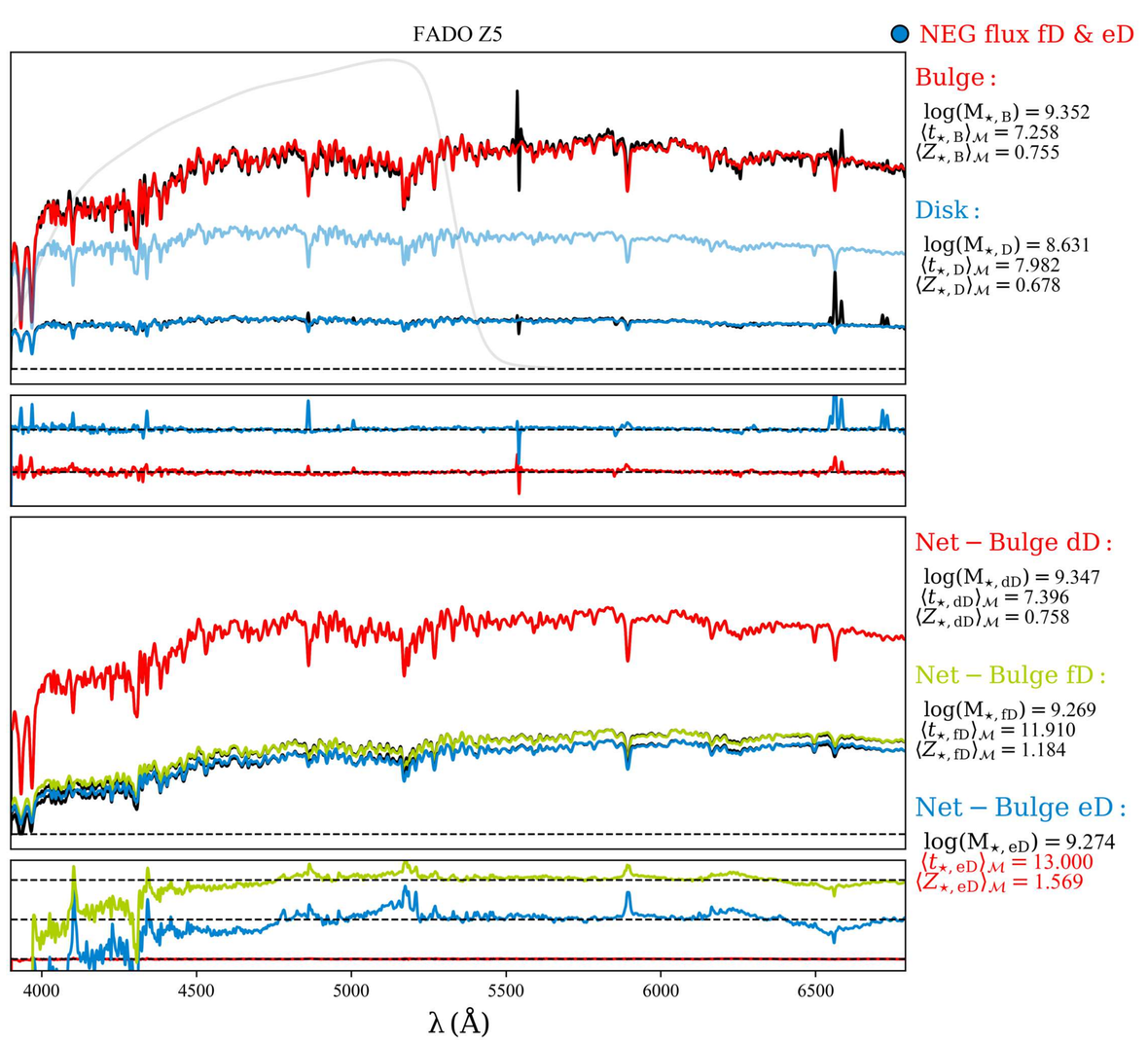
FADO Z5
NEG flux fD & eD
Bulge :
log(M⋆, B) = 9.352
⟨t⋆, B⟩M = 7.258
⟨Z⋆, B⟩M = 0.755
Disk :
log(M⋆, D) = 8.631
⟨t⋆, D⟩M = 7.982
⟨Z⋆, D⟩M = 0.678
Net − Bulge dD :
log(M⋆, dD) = 9.347
⟨t⋆, dD⟩M = 7.396
⟨Z⋆, dD⟩M = 0.758
Net − Bulge fD :
log(M⋆, fD) = 9.269
⟨t⋆, fD⟩M = 11.910
⟨Z⋆, fD⟩M = 1.184
Net − Bulge eD :
log(M⋆, eD) = 9.274
⟨t⋆, eD⟩M = 13.000
⟨Z⋆, eD⟩M = 1.569
4000
4500
5000
5500
6000
6500
λ (Å)

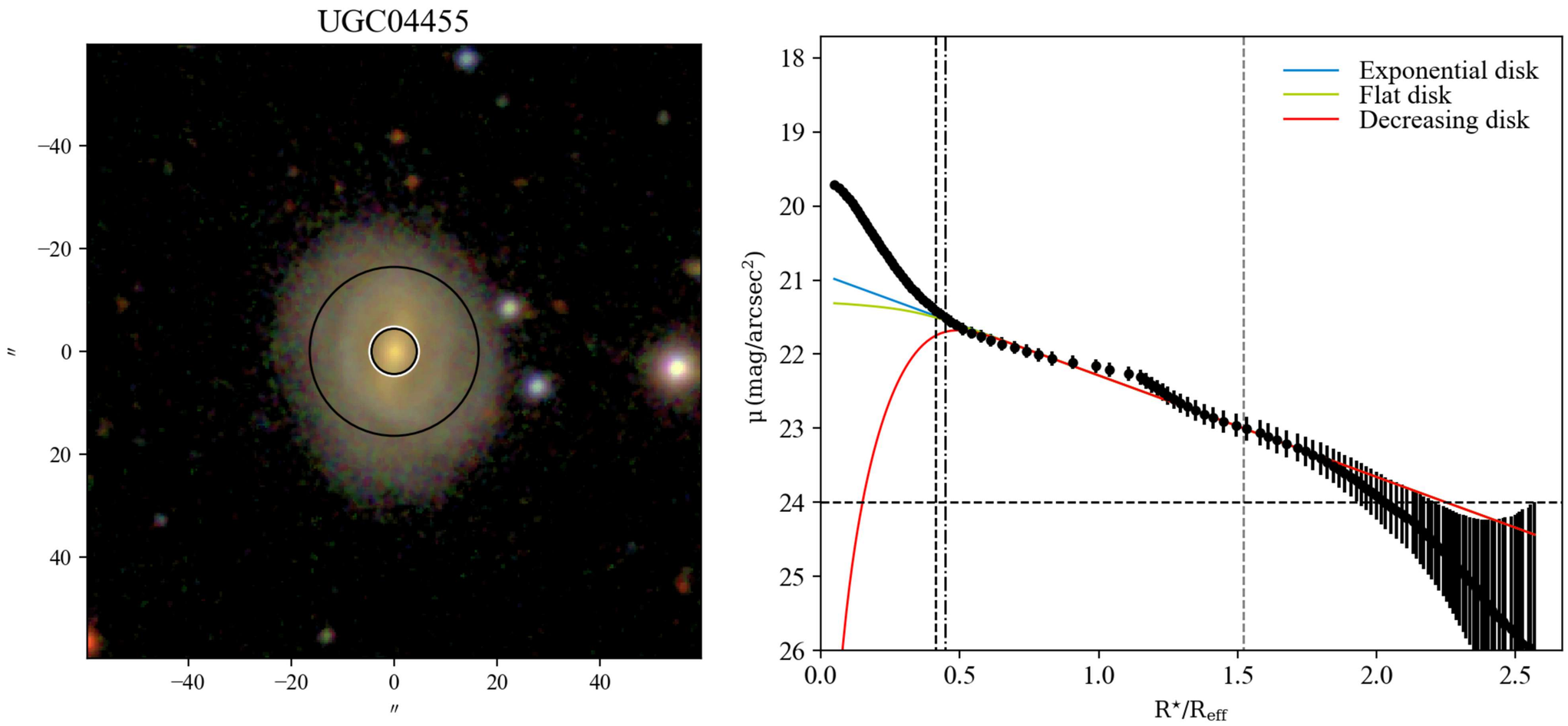
UGC04455
Exponential disk
Flat disk
Decreasing disk
μ (mag/arcsec²)
R⋆/Reff
″

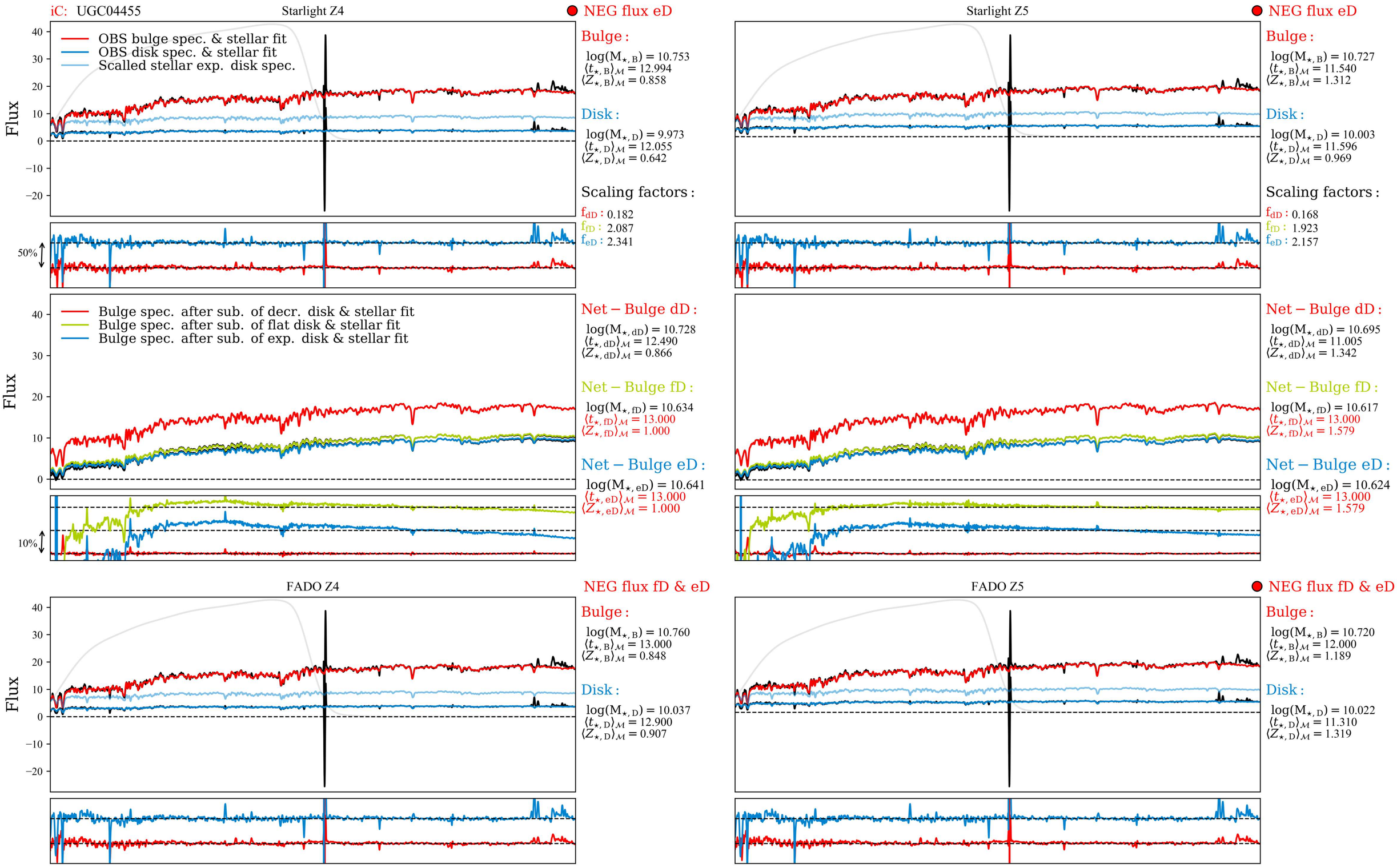
iC: UGC04455
Starlight Z4
NEG flux eD
OBS bulge spec. & stellar fit
OBS disk spec. & stellar fit
Scalled stellar exp. disk spec.
Flux
Bulge :
log(M⋆, B) = 10.753
⟨t⋆, B⟩M = 12.994
⟨Z⋆, B⟩M = 0.858
Disk :
log(M⋆, D) = 9.973
⟨t⋆, D⟩M = 12.055
⟨Z⋆, D⟩M = 0.642
Scaling factors :
fdD : 0.182
ffD : 2.087
feD : 2.341
50%
Starlight Z5
NEG flux eD
Bulge :
log(M⋆, B) = 10.727
⟨t⋆, B⟩M = 11.540
⟨Z⋆, B⟩M = 1.312
Disk :
log(M⋆, D) = 10.003
⟨t⋆, D⟩M = 11.596
⟨Z⋆, D⟩M = 0.969
Scaling factors :
fdD : 0.168
ffD : 1.923
feD : 2.157
Bulge spec. after sub. of decr. disk & stellar fit
Bulge spec. after sub. of flat disk & stellar fit
Bulge spec. after sub. of exp. disk & stellar fit
Net − Bulge dD :
log(M⋆, dD) = 10.728
⟨t⋆, dD⟩M = 12.490
⟨Z⋆, dD⟩M = 0.866
Net − Bulge fD :
log(M⋆, fD) = 10.634
⟨t⋆, fD⟩M = 13.000
⟨Z⋆, fD⟩M = 1.000
Net − Bulge eD :
log(M⋆, eD) = 10.641
⟨t⋆, eD⟩M = 13.000
⟨Z⋆, eD⟩M = 1.000
10%
Net − Bulge dD :
log(M⋆, dD) = 10.695
⟨t⋆, dD⟩M = 11.005
⟨Z⋆, dD⟩M = 1.342
Net − Bulge fD :
log(M⋆, fD) = 10.617
⟨t⋆, fD⟩M = 13.000
⟨Z⋆, fD⟩M = 1.579
Net − Bulge eD :
log(M⋆, eD) = 10.624
⟨t⋆, eD⟩M = 13.000
⟨Z⋆, eD⟩M = 1.579
FADO Z4
NEG flux fD & eD
Bulge :
log(M⋆, B) = 10.760
⟨t⋆, B⟩M = 13.000
⟨Z⋆, B⟩M = 0.848
Disk :
log(M⋆, D) = 10.037
⟨t⋆, D⟩M = 12.900
⟨Z⋆, D⟩M = 0.907
FADO Z5
NEG flux fD & eD
Bulge :
log(M⋆, B) = 10.720
⟨t⋆, B⟩M = 12.000
⟨Z⋆, B⟩M = 1.189
Disk :
log(M⋆, D) = 10.022
⟨t⋆, D⟩M = 11.310
⟨Z⋆, D⟩M = 1.319
Net − Bulge dD :
log(M⋆, dD) = 10.740
⟨t⋆, dD⟩M = 13.000
⟨Z⋆, dD⟩M = 0.853
Net − Bulge fD :
log(M⋆, fD) = 10.620
⟨t⋆, fD⟩M = 12.000
⟨Z⋆, fD⟩M = 1.000
Net − Bulge eD :
log(M⋆, eD) = 10.620
⟨t⋆, eD⟩M = 12.000
⟨Z⋆, eD⟩M = 1.000
Net − Bulge dD :
log(M⋆, dD) = 10.710
⟨t⋆, dD⟩M = 12.180
⟨Z⋆, dD⟩M = 1.237
Net − Bulge fD :
log(M⋆, fD) = 10.620
⟨t⋆, fD⟩M = 13.000
⟨Z⋆, fD⟩M = 1.579
Net − Bulge eD :
log(M⋆, eD) = 10.610
⟨t⋆, eD⟩M = 13.000
⟨Z⋆, eD⟩M = 1.579
λ (Å)

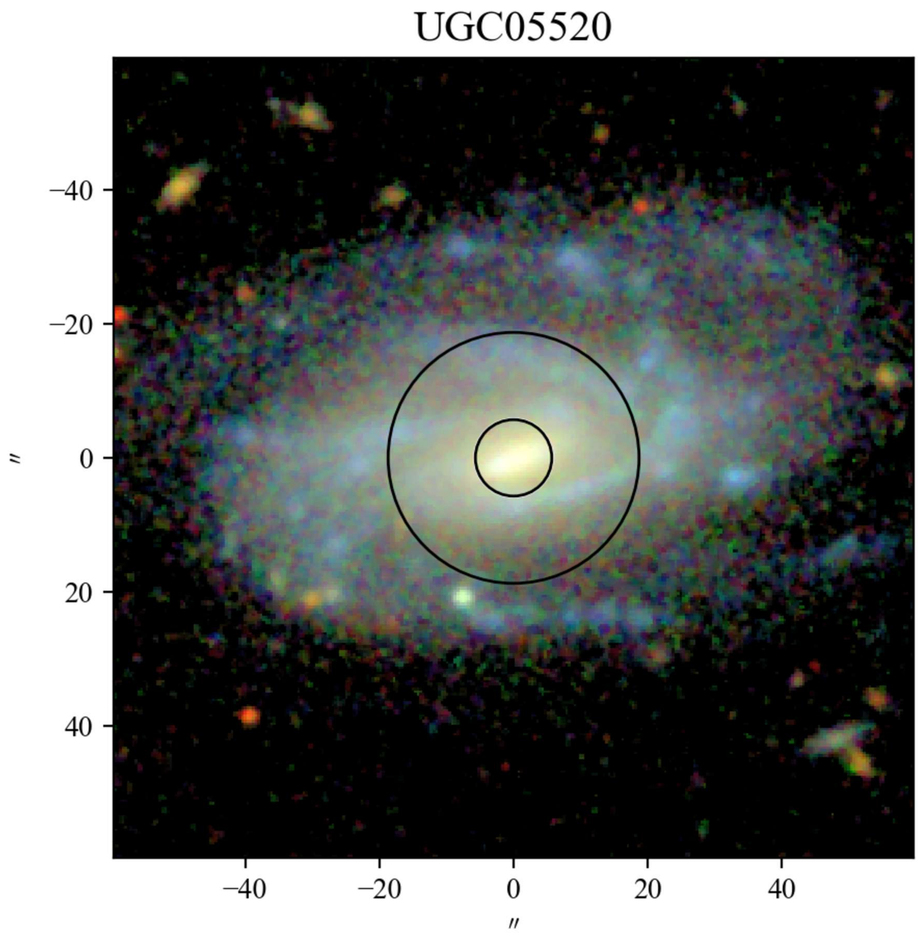
UGC05520
−40
−20
0
20
40
″
−40
−20
0
20
40
″

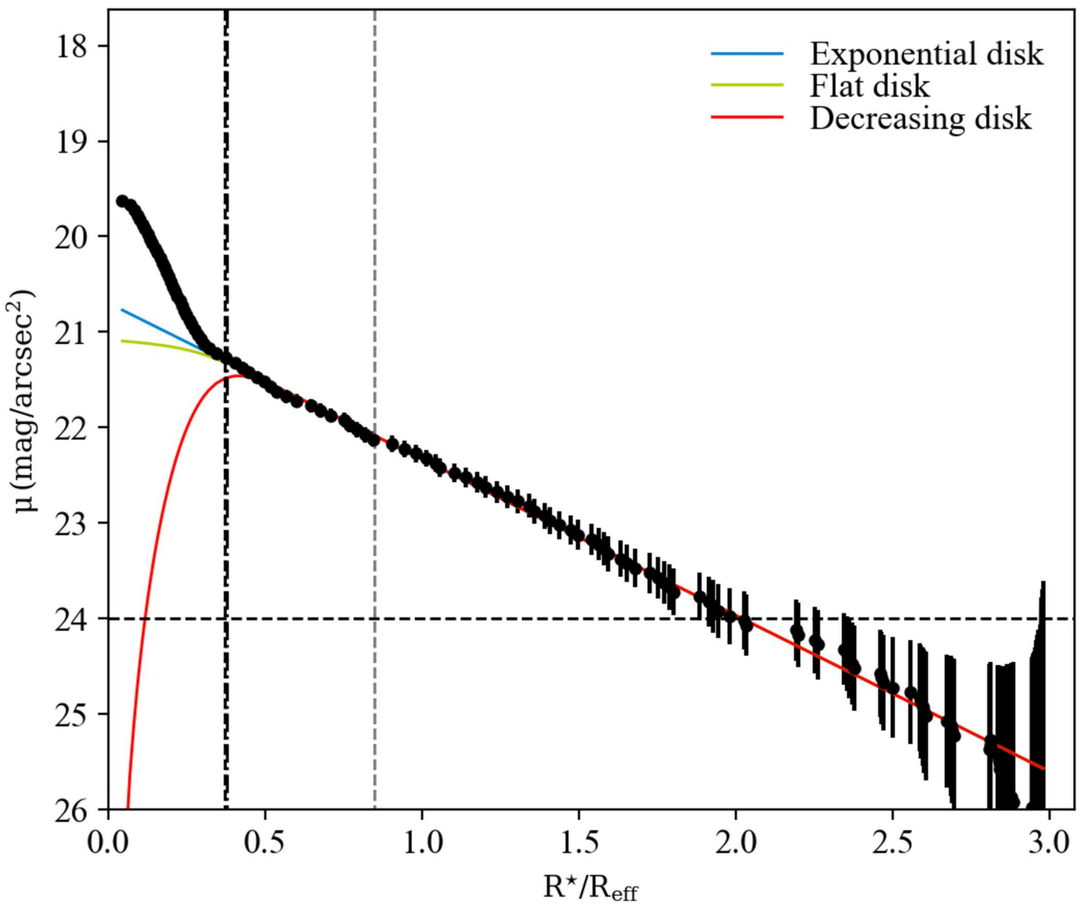
Exponential disk
Flat disk
Decreasing disk
μ (mag/arcsec²)
18
19
20
21
22
23
24
25
26
0.0
0.5
1.0
1.5
2.0
2.5
3.0
R⋆/Reff

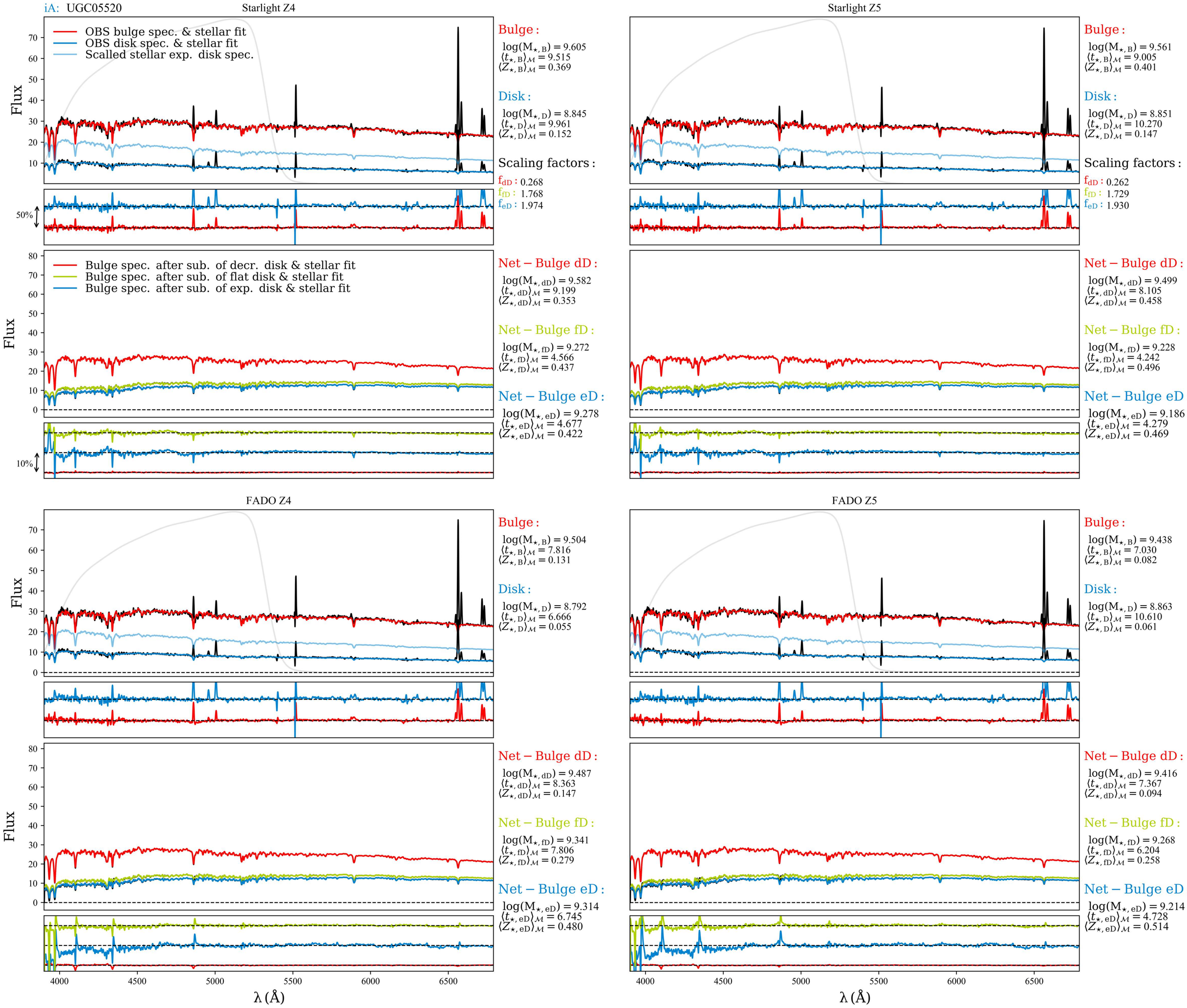
iA: UGC05520
Starlight Z4
OBS bulge spec. & stellar fit
OBS disk spec. & stellar fit
Scalled stellar exp. disk spec.
Flux
Bulge :
log(M⋆, B) = 9.605
⟨t⋆, B⟩M = 9.515
⟨Z⋆, B⟩M = 0.369
Disk :
log(M⋆, D) = 8.845
⟨t⋆, D⟩M = 9.961
⟨Z⋆, D⟩M = 0.152
Scaling factors :
fdD : 0.268
ffD : 1.768
feD : 1.974
50%
Bulge spec. after sub. of decr. disk & stellar fit
Bulge spec. after sub. of flat disk & stellar fit
Bulge spec. after sub. of exp. disk & stellar fit
Net − Bulge dD :
log(M⋆, dD) = 9.582
⟨t⋆, dD⟩M = 9.199
⟨Z⋆, dD⟩M = 0.353
Net − Bulge fD :
log(M⋆, fD) = 9.272
⟨t⋆, fD⟩M = 4.566
⟨Z⋆, fD⟩M = 0.437
Net − Bulge eD :
log(M⋆, eD) = 9.278
⟨t⋆, eD⟩M = 4.677
⟨Z⋆, eD⟩M = 0.422
10%
FADO Z4
Bulge :
log(M⋆, B) = 9.504
⟨t⋆, B⟩M = 7.816
⟨Z⋆, B⟩M = 0.131
Disk :
log(M⋆, D) = 8.792
⟨t⋆, D⟩M = 6.666
⟨Z⋆, D⟩M = 0.055
Net − Bulge dD :
log(M⋆, dD) = 9.487
⟨t⋆, dD⟩M = 8.363
⟨Z⋆, dD⟩M = 0.147
Net − Bulge fD :
log(M⋆, fD) = 9.341
⟨t⋆, fD⟩M = 7.806
⟨Z⋆, fD⟩M = 0.279
Net − Bulge eD :
log(M⋆, eD) = 9.314
⟨t⋆, eD⟩M = 6.745
⟨Z⋆, eD⟩M = 0.480
λ (Å)

Starlight Z5
Bulge :
log(M⋆, B) = 9.561
⟨t⋆, B⟩M = 9.005
⟨Z⋆, B⟩M = 0.401
Disk :
log(M⋆, D) = 8.851
⟨t⋆, D⟩M = 10.270
⟨Z⋆, D⟩M = 0.147
Scaling factors :
fdD : 0.262
ffD : 1.729
feD : 1.930
Net − Bulge dD :
log(M⋆, dD) = 9.499
⟨t⋆, dD⟩M = 8.105
⟨Z⋆, dD⟩M = 0.458
Net − Bulge fD :
log(M⋆, fD) = 9.228
⟨t⋆, fD⟩M = 4.242
⟨Z⋆, fD⟩M = 0.496
Net − Bulge eD :
log(M⋆, eD) = 9.186
⟨t⋆, eD⟩M = 4.279
⟨Z⋆, eD⟩M = 0.469
FADO Z5
Bulge :
log(M⋆, B) = 9.438
⟨t⋆, B⟩M = 7.030
⟨Z⋆, B⟩M = 0.082
Disk :
log(M⋆, D) = 8.863
⟨t⋆, D⟩M = 10.610
⟨Z⋆, D⟩M = 0.061
Net − Bulge dD :
log(M⋆, dD) = 9.416
⟨t⋆, dD⟩M = 7.367
⟨Z⋆, dD⟩M = 0.094
Net − Bulge fD :
log(M⋆, fD) = 9.268
⟨t⋆, fD⟩M = 6.204
⟨Z⋆, fD⟩M = 0.258
Net − Bulge eD :
log(M⋆, eD) = 9.214
⟨t⋆, eD⟩M = 4.728
⟨Z⋆, eD⟩M = 0.514
λ (Å)

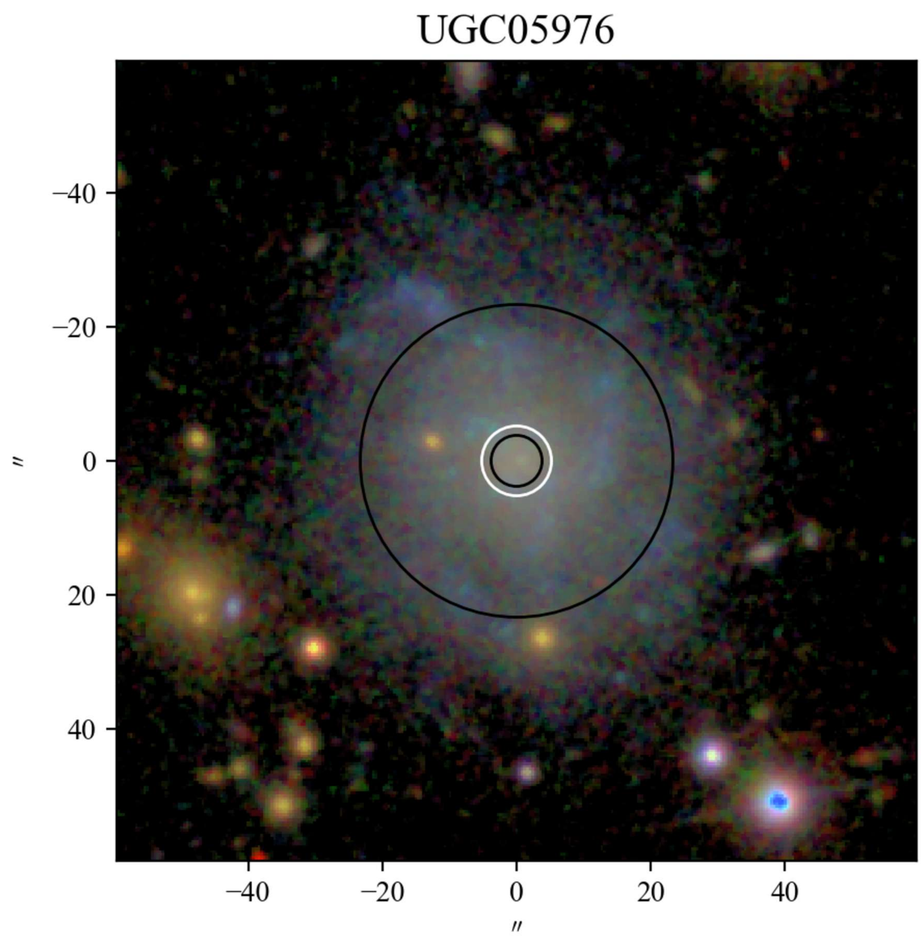
UGC05976
−40
−20
0
20
40
″
−40
−20
0
20
40
″

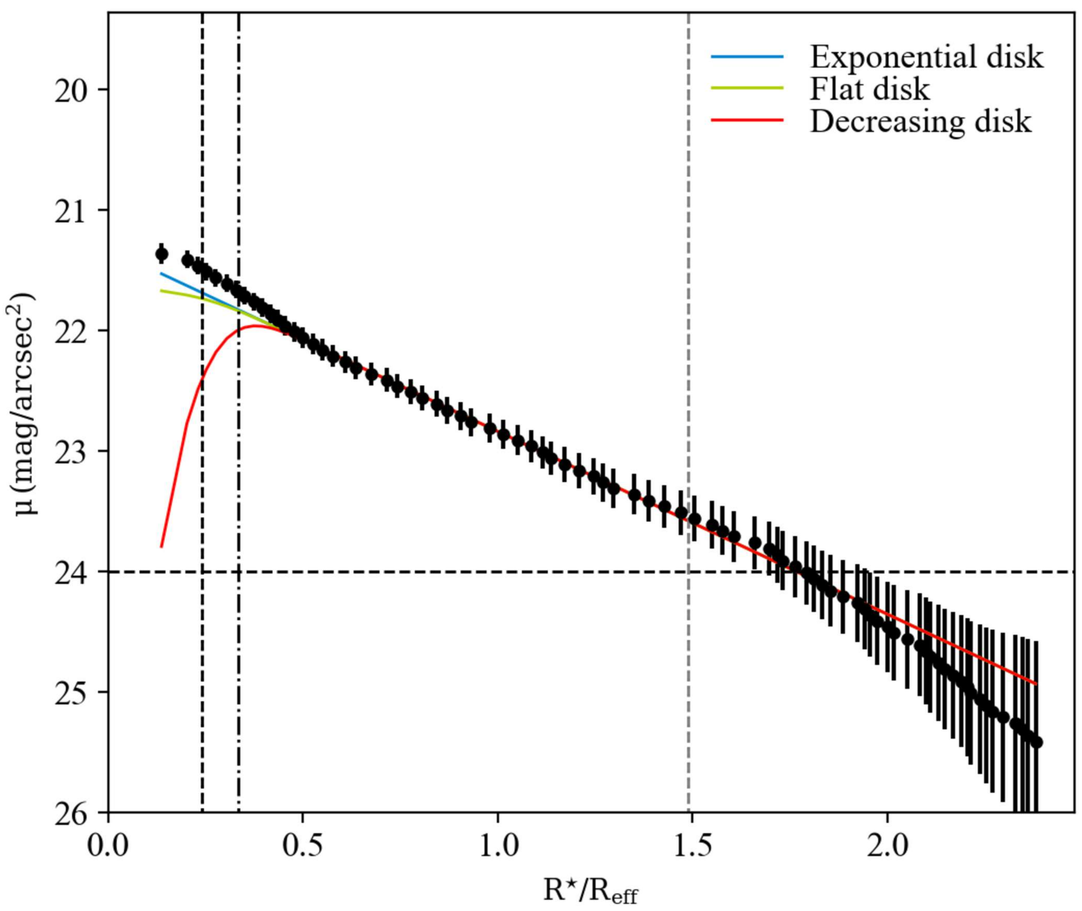
Exponential disk
Flat disk
Decreasing disk
μ (mag/arcsec²)
20
21
22
23
24
25
26
0.0
0.5
1.0
1.5
2.0
R⋆/Reff

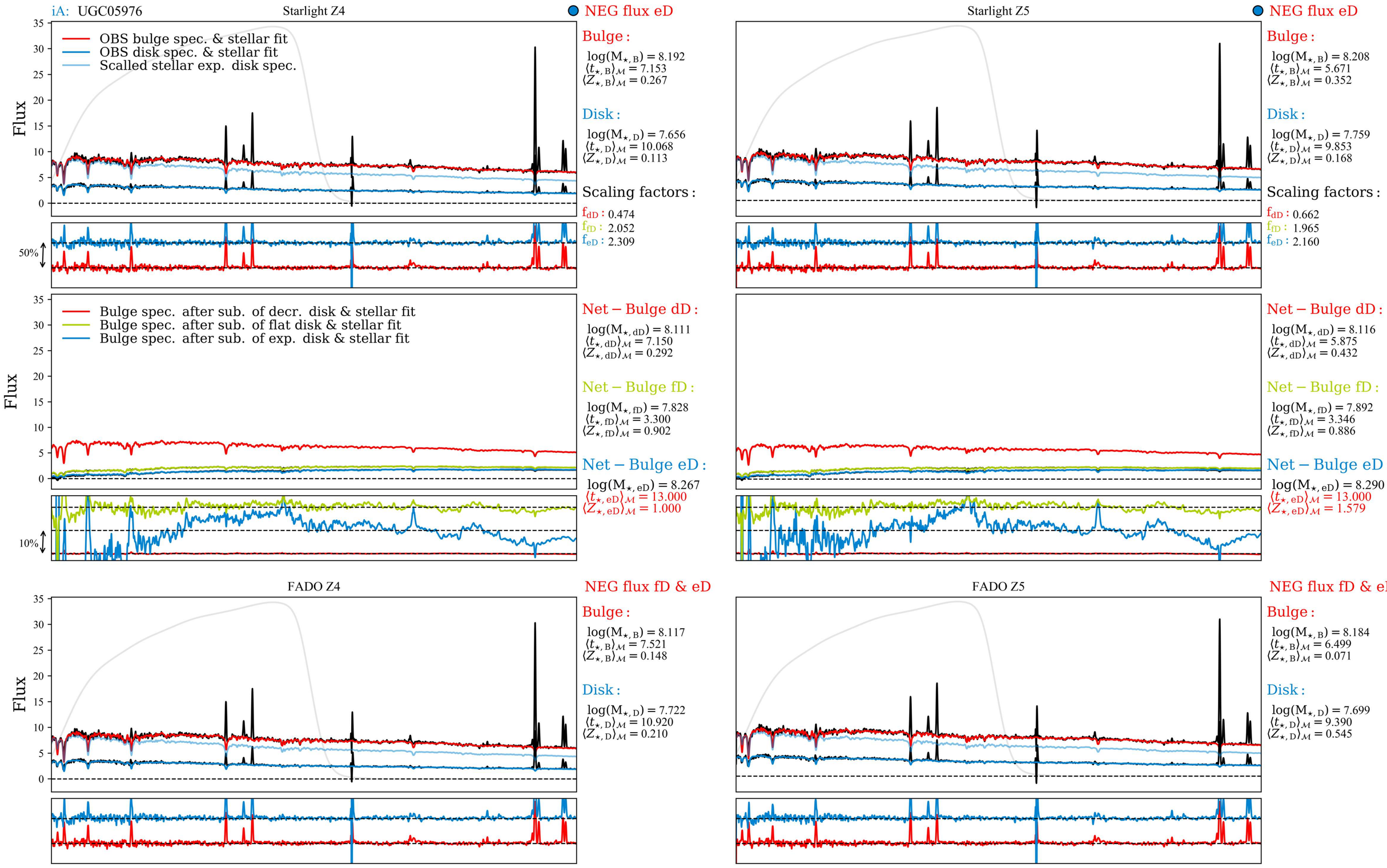
iA: UGC05976
Starlight Z4
NEG flux eD
OBS bulge spec. & stellar fit
OBS disk spec. & stellar fit
Scalled stellar exp. disk spec.
Flux
50%
Bulge :
log(M⋆, B) = 8.192
⟨t⋆, B⟩M = 7.153
⟨Z⋆, B⟩M = 0.267
Disk :
log(M⋆, D) = 7.656
⟨t⋆, D⟩M = 10.068
⟨Z⋆, D⟩M = 0.113
Scaling factors :
fdD : 0.474
ffD : 2.052
feD : 2.309
Starlight Z5
NEG flux eD
Bulge :
log(M⋆, B) = 8.208
⟨t⋆, B⟩M = 5.671
⟨Z⋆, B⟩M = 0.352
Disk :
log(M⋆, D) = 7.759
⟨t⋆, D⟩M = 9.853
⟨Z⋆, D⟩M = 0.168
Scaling factors :
fdD : 0.662
ffD : 1.965
feD : 2.160
Bulge spec. after sub. of decr. disk & stellar fit
Bulge spec. after sub. of flat disk & stellar fit
Bulge spec. after sub. of exp. disk & stellar fit
10%
Net − Bulge dD :
log(M⋆, dD) = 8.111
⟨t⋆, dD⟩M = 7.150
⟨Z⋆, dD⟩M = 0.292
Net − Bulge fD :
log(M⋆, fD) = 7.828
⟨t⋆, fD⟩M = 3.300
⟨Z⋆, fD⟩M = 0.902
Net − Bulge eD :
log(M⋆, eD) = 8.267
⟨t⋆, eD⟩M = 13.000
⟨Z⋆, eD⟩M = 1.000
Net − Bulge dD :
log(M⋆, dD) = 8.116
⟨t⋆, dD⟩M = 5.875
⟨Z⋆, dD⟩M = 0.432
Net − Bulge fD :
log(M⋆, fD) = 7.892
⟨t⋆, fD⟩M = 3.346
⟨Z⋆, fD⟩M = 0.886
Net − Bulge eD :
log(M⋆, eD) = 8.290
⟨t⋆, eD⟩M = 13.000
⟨Z⋆, eD⟩M = 1.579
FADO Z4
NEG flux fD & eD
Bulge :
log(M⋆, B) = 8.117
⟨t⋆, B⟩M = 7.521
⟨Z⋆, B⟩M = 0.148
Disk :
log(M⋆, D) = 7.722
⟨t⋆, D⟩M = 10.920
⟨Z⋆, D⟩M = 0.210
FADO Z5
NEG flux fD & eD
Bulge :
log(M⋆, B) = 8.184
⟨t⋆, B⟩M = 6.499
⟨Z⋆, B⟩M = 0.071
Disk :
log(M⋆, D) = 7.699
⟨t⋆, D⟩M = 9.390
⟨Z⋆, D⟩M = 0.545
Net − Bulge dD :
log(M⋆, dD) = 7.998
⟨t⋆, dD⟩M = 5.292
⟨Z⋆, dD⟩M = 0.177
Net − Bulge fD :
log(M⋆, fD) = 7.716
⟨t⋆, fD⟩M = 3.406
⟨Z⋆, fD⟩M = 1.000
Net − Bulge eD :
log(M⋆, eD) = 7.837
⟨t⋆, eD⟩M = 4.000
⟨Z⋆, eD⟩M = 1.000
Net − Bulge dD :
log(M⋆, dD) = 8.089
⟨t⋆, dD⟩M = 6.277
⟨Z⋆, dD⟩M = 0.053
Net − Bulge fD :
log(M⋆, fD) = 7.774
⟨t⋆, fD⟩M = 3.310
⟨Z⋆, fD⟩M = 1.000
Net − Bulge eD :
log(M⋆, eD) = 8.098
⟨t⋆, eD⟩M = 6.845
⟨Z⋆, eD⟩M = 0.706
4000
4500
5000
5500
6000
6500
λ (Å)

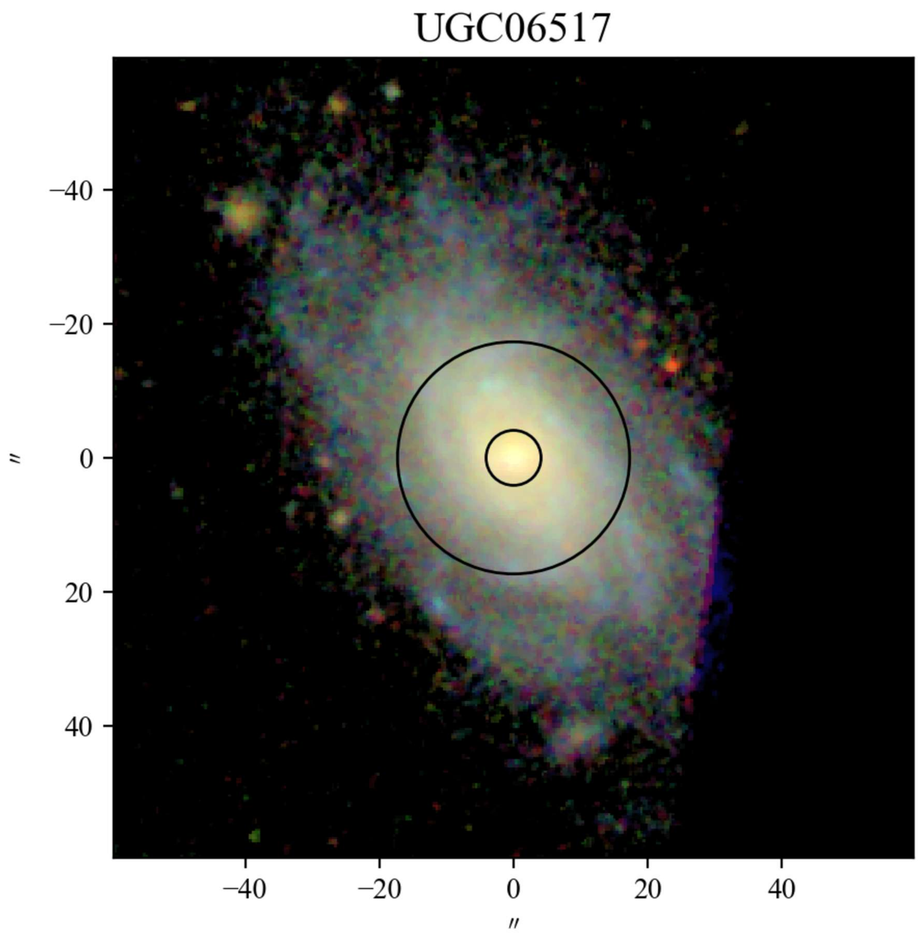
UGC06517
−40
−20
0
20
40
″
−40
−20
0
20
40
″

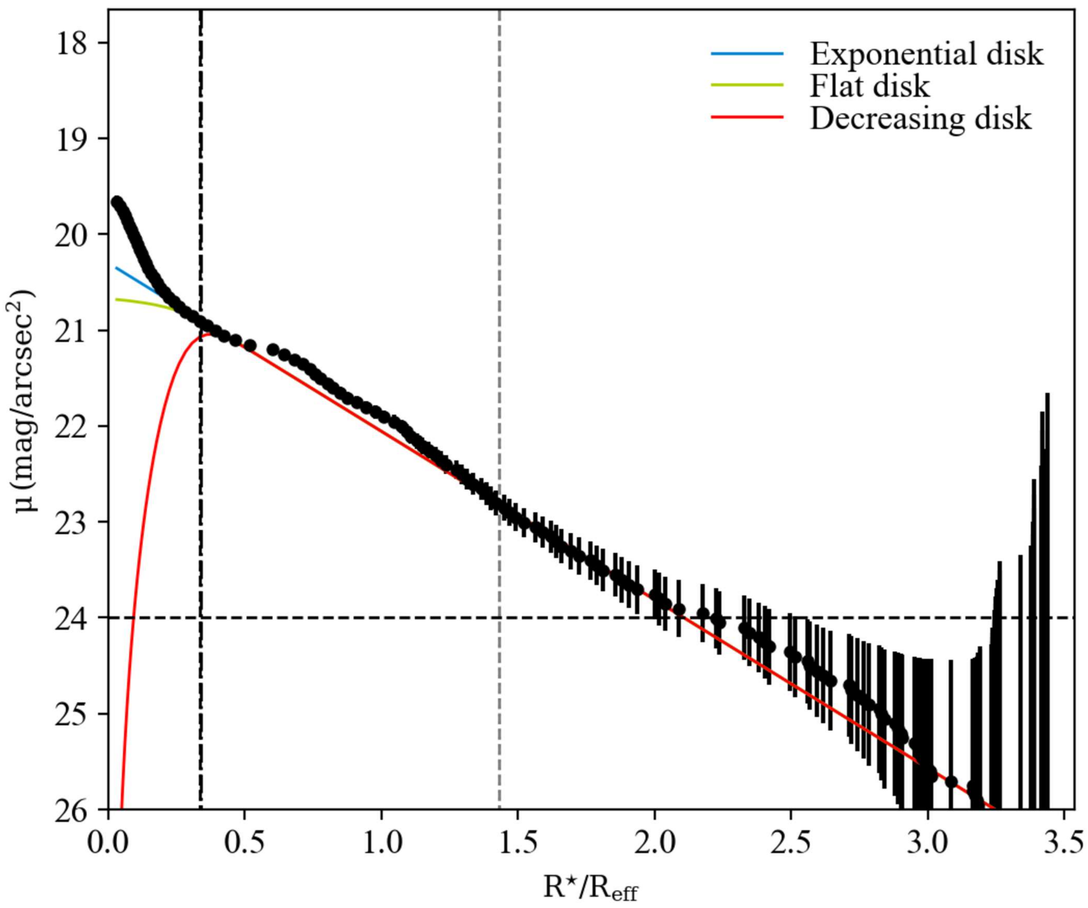
Exponential disk
Flat disk
Decreasing disk
μ (mag/arcsec²)
18
19
20
21
22
23
24
25
26
0.0
0.5
1.0
1.5
2.0
2.5
3.0
3.5
R⋆/Reff

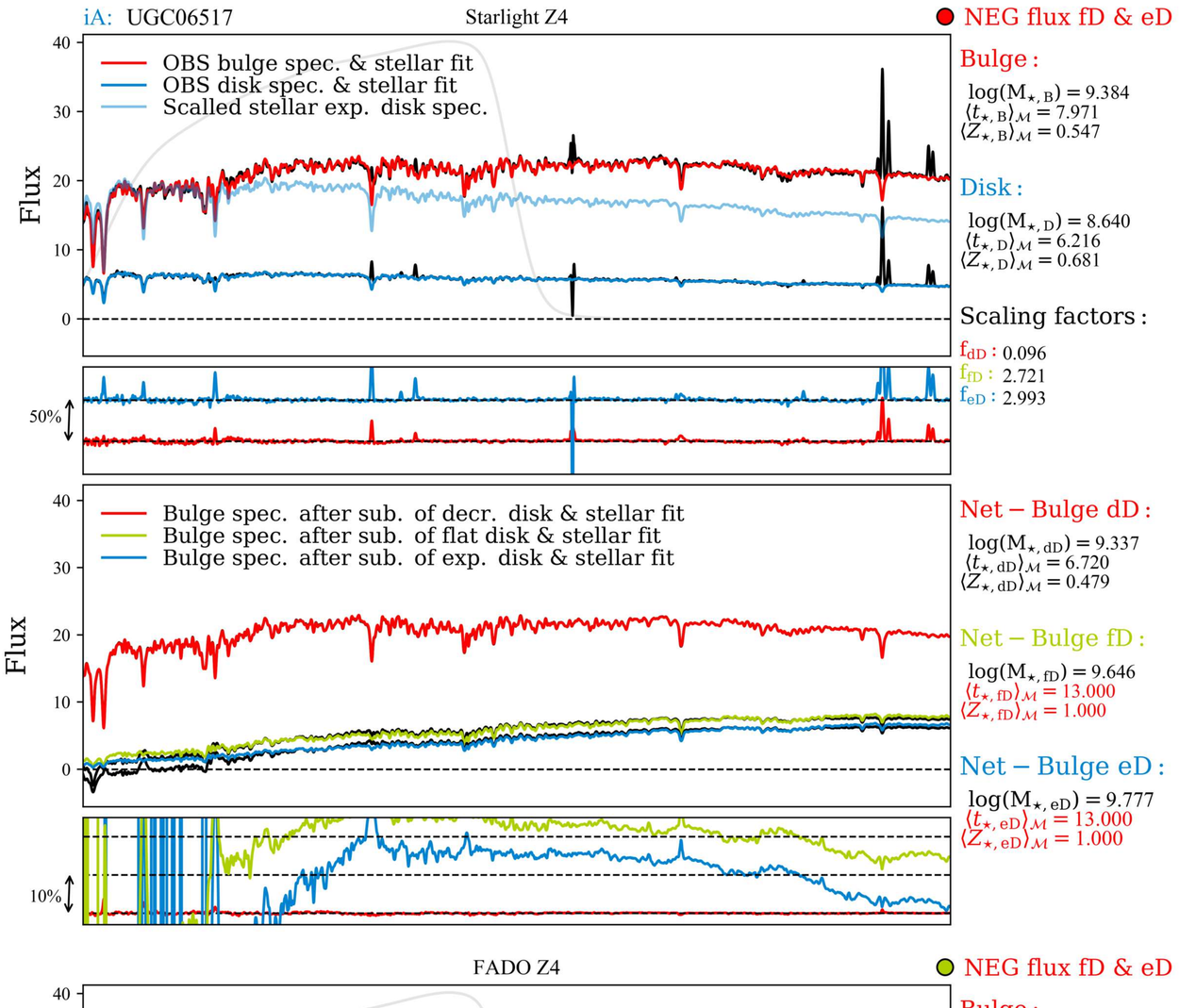
iA: UGC06517
Starlight Z4
NEG flux fD & eD
OBS bulge spec. & stellar fit
OBS disk spec. & stellar fit
Scalled stellar exp. disk spec.
Flux
50%
Bulge :
log(M⋆, B) = 9.384
⟨t⋆, B⟩M = 7.971
⟨Z⋆, B⟩M = 0.547
Disk :
log(M⋆, D) = 8.640
⟨t⋆, D⟩M = 6.216
⟨Z⋆, D⟩M = 0.681
Scaling factors :
fdD : 0.096
ffD : 2.721
feD : 2.993
Bulge spec. after sub. of decr. disk & stellar fit
Bulge spec. after sub. of flat disk & stellar fit
Bulge spec. after sub. of exp. disk & stellar fit
10%
Net − Bulge dD :
log(M⋆, dD) = 9.337
⟨t⋆, dD⟩M = 6.720
⟨Z⋆, dD⟩M = 0.479
Net − Bulge fD :
log(M⋆, fD) = 9.646
⟨t⋆, fD⟩M = 13.000
⟨Z⋆, fD⟩M = 1.000
Net − Bulge eD :
log(M⋆, eD) = 9.777
⟨t⋆, eD⟩M = 13.000
⟨Z⋆, eD⟩M = 1.000

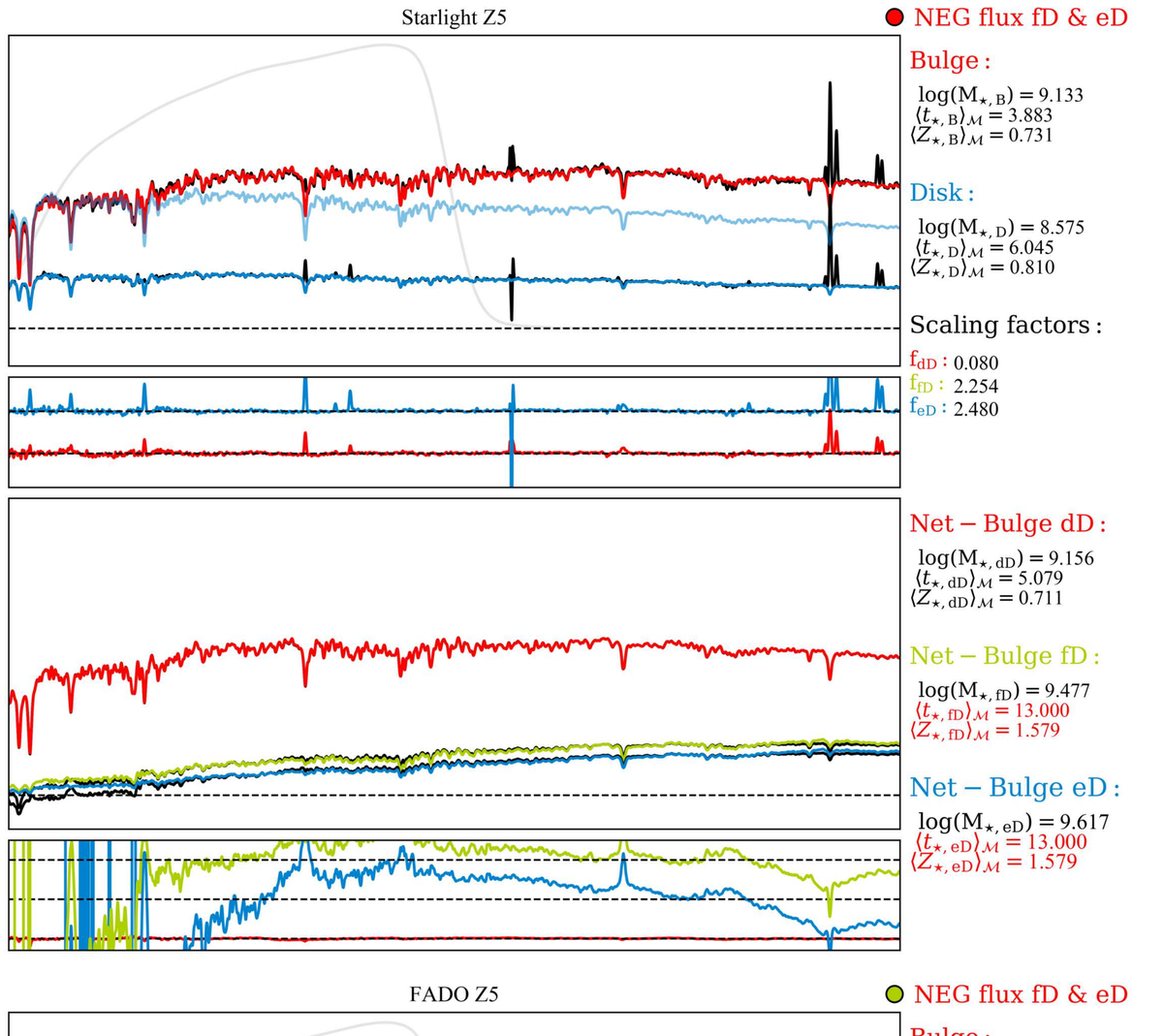
Starlight Z5
NEG flux fD & eD
Bulge :
log(M⋆, B) = 9.133
⟨t⋆, B⟩M = 3.883
⟨Z⋆, B⟩M = 0.731
Disk :
log(M⋆, D) = 8.575
⟨t⋆, D⟩M = 6.045
⟨Z⋆, D⟩M = 0.810
Scaling factors :
fdD : 0.080
ffD : 2.254
feD : 2.480
Net − Bulge dD :
log(M⋆, dD) = 9.156
⟨t⋆, dD⟩M = 5.079
⟨Z⋆, dD⟩M = 0.711
Net − Bulge fD :
log(M⋆, fD) = 9.477
⟨t⋆, fD⟩M = 13.000
⟨Z⋆, fD⟩M = 1.579
Net − Bulge eD :
log(M⋆, eD) = 9.617
⟨t⋆, eD⟩M = 13.000
⟨Z⋆, eD⟩M = 1.579

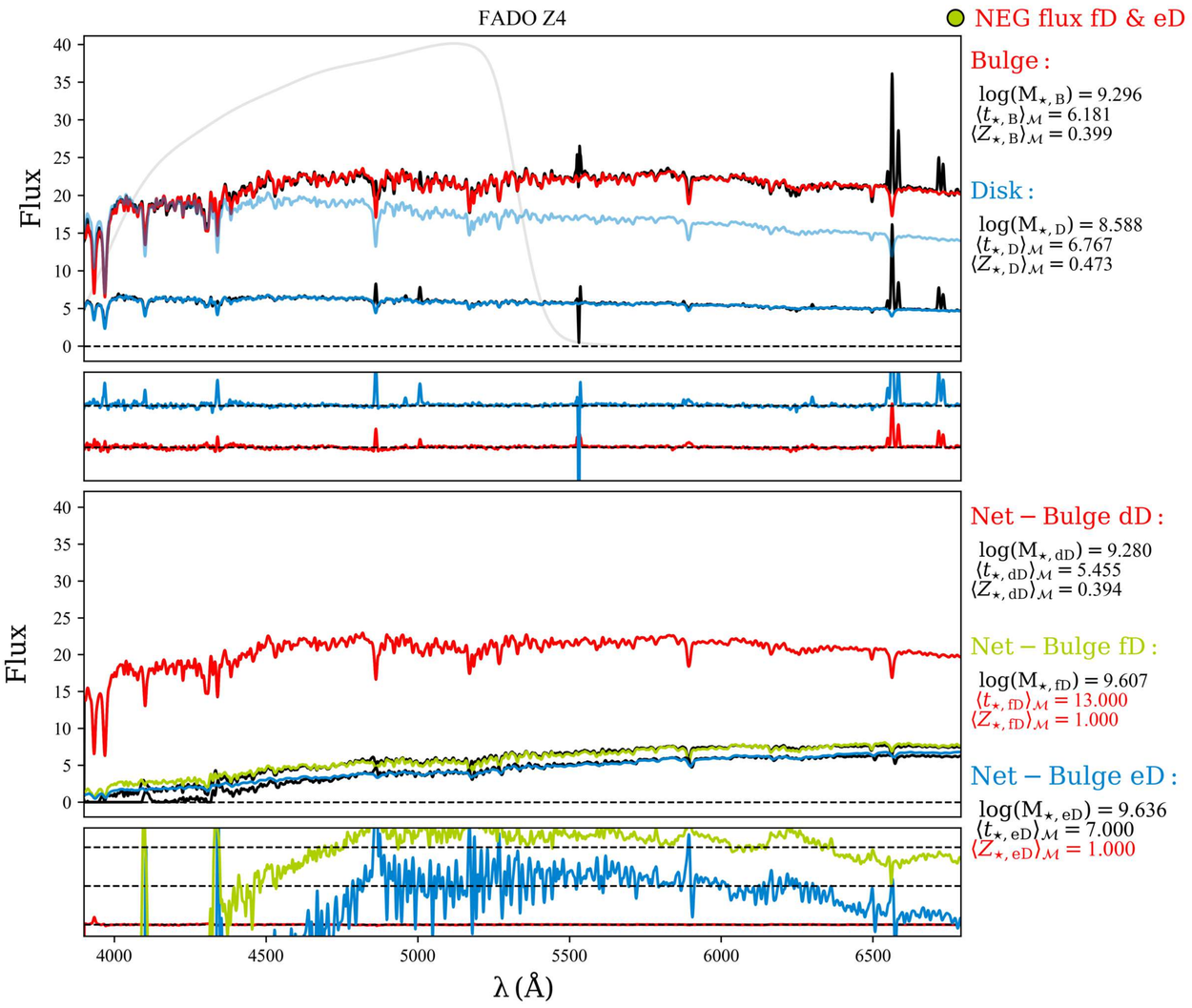
FADO Z4
NEG flux fD & eD
Flux
Bulge :
log(M⋆, B) = 9.296
⟨t⋆, B⟩M = 6.181
⟨Z⋆, B⟩M = 0.399
Disk :
log(M⋆, D) = 8.588
⟨t⋆, D⟩M = 6.767
⟨Z⋆, D⟩M = 0.473
Net − Bulge dD :
log(M⋆, dD) = 9.280
⟨t⋆, dD⟩M = 5.455
⟨Z⋆, dD⟩M = 0.394
Net − Bulge fD :
log(M⋆, fD) = 9.607
⟨t⋆, fD⟩M = 13.000
⟨Z⋆, fD⟩M = 1.000
Net − Bulge eD :
log(M⋆, eD) = 9.636
⟨t⋆, eD⟩M = 7.000
⟨Z⋆, eD⟩M = 1.000
λ (Å)

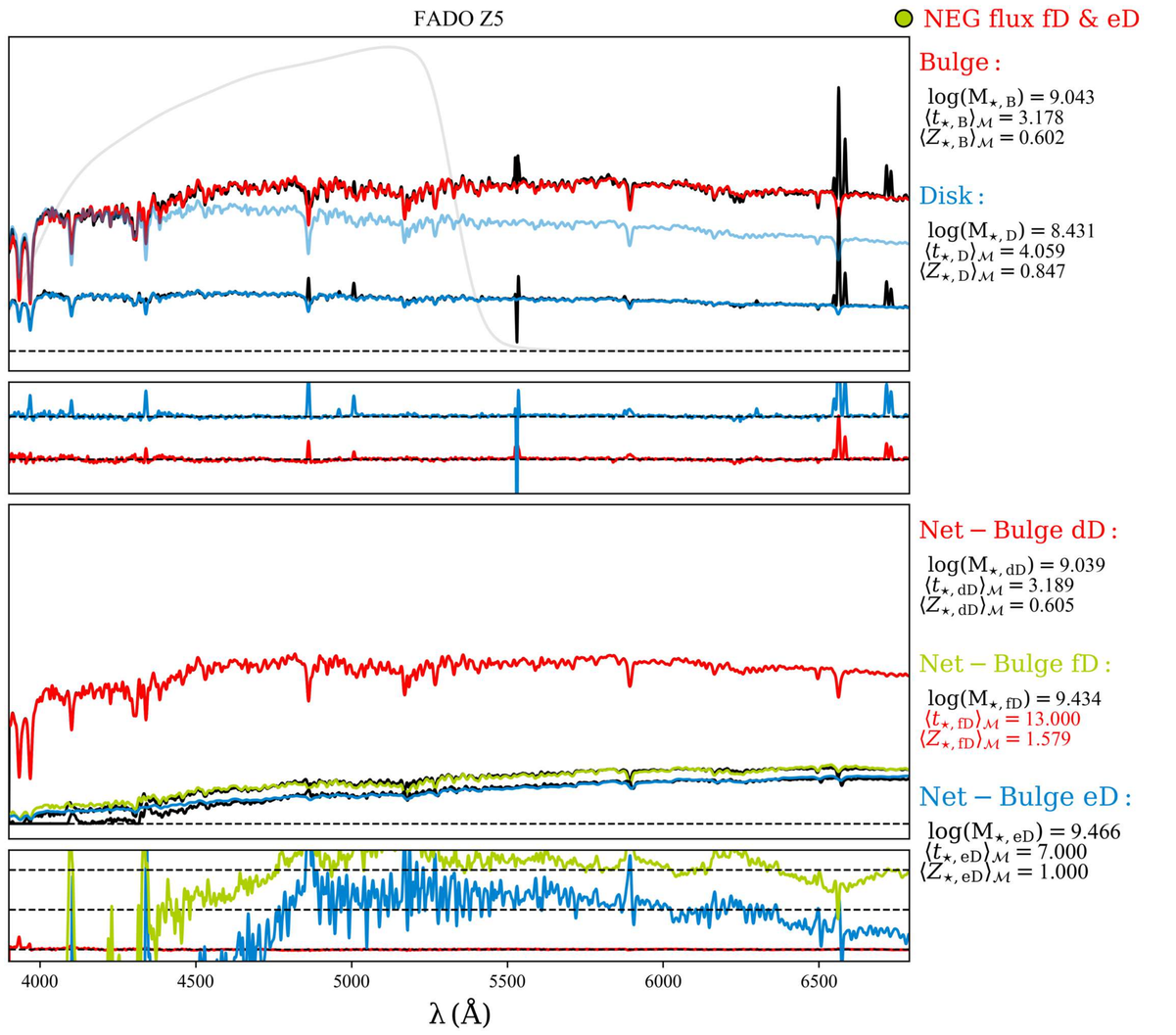
FADO Z5
NEG flux fD & eD
Bulge :
log(M⋆, B) = 9.043
⟨t⋆, B⟩M = 3.178
⟨Z⋆, B⟩M = 0.602
Disk :
log(M⋆, D) = 8.431
⟨t⋆, D⟩M = 4.059
⟨Z⋆, D⟩M = 0.847
Net − Bulge dD :
log(M⋆, dD) = 9.039
⟨t⋆, dD⟩M = 3.189
⟨Z⋆, dD⟩M = 0.605
Net − Bulge fD :
log(M⋆, fD) = 9.434
⟨t⋆, fD⟩M = 13.000
⟨Z⋆, fD⟩M = 1.579
Net − Bulge eD :
log(M⋆, eD) = 9.466
⟨t⋆, eD⟩M = 7.000
⟨Z⋆, eD⟩M = 1.000
λ (Å)

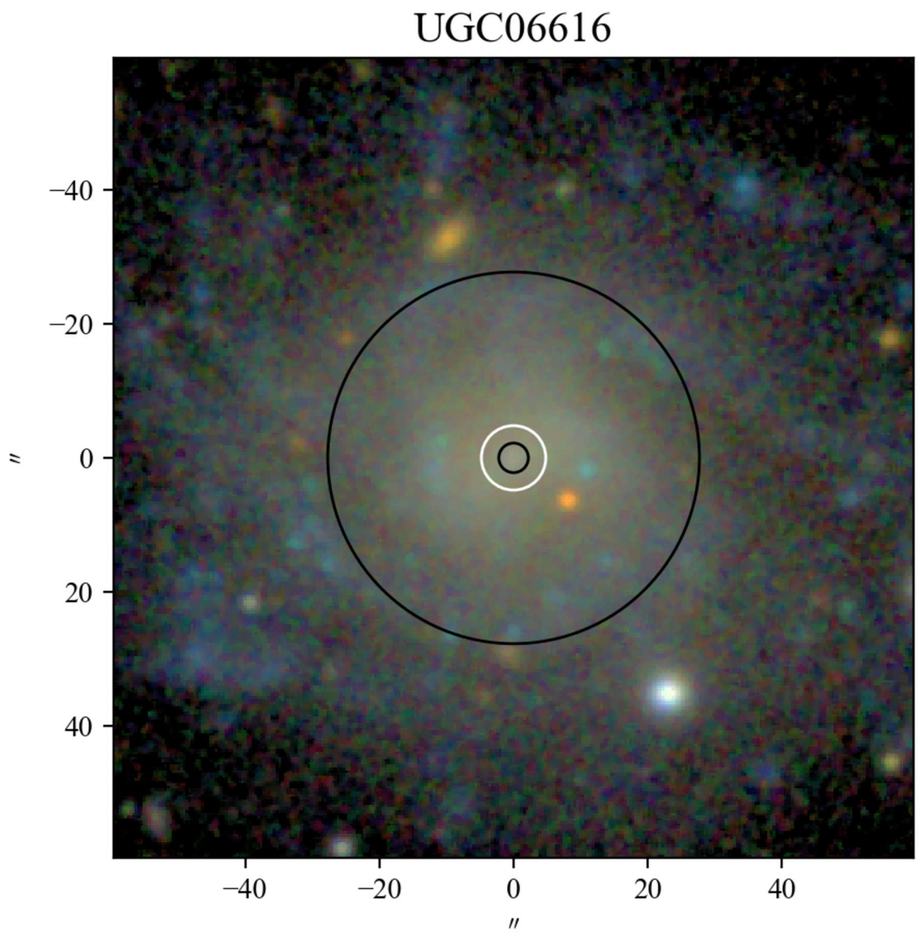
UGC06616
−40
−20
0
20
40
″
−40
−20
0
20
40
″

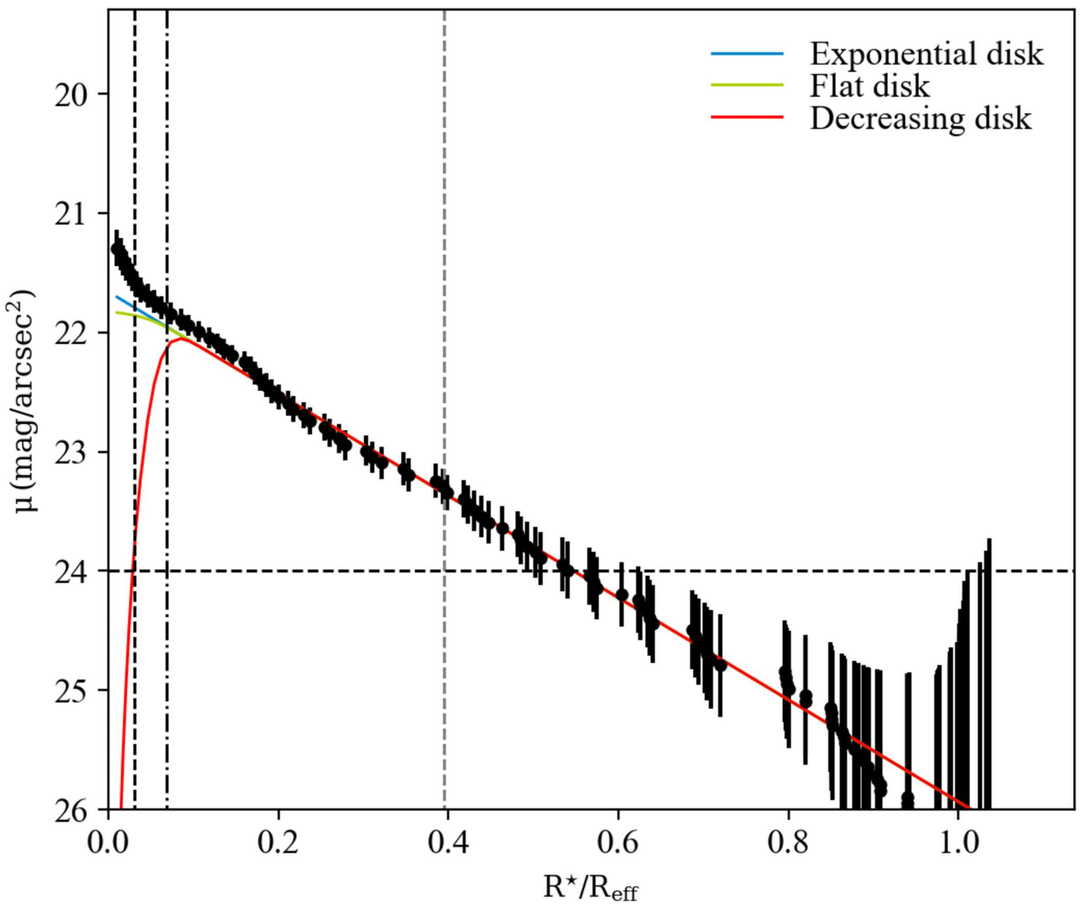
Exponential disk
Flat disk
Decreasing disk
μ (mag/arcsec²)
20
21
22
23
24
25
26
0.0
0.2
0.4
0.6
0.8
1.0
R⋆/Reff

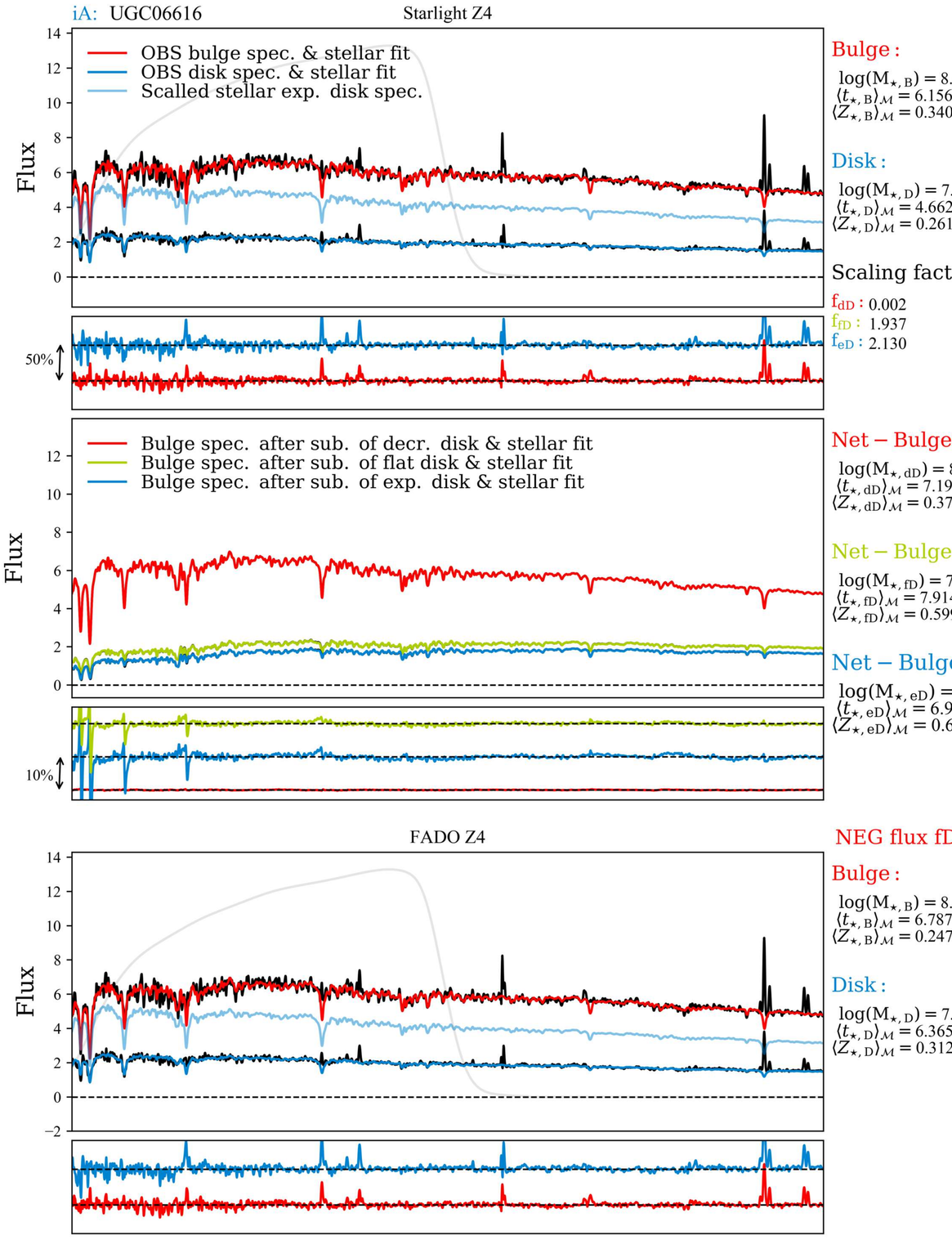
iA: UGC06616
Starlight Z4
OBS bulge spec. & stellar fit
OBS disk spec. & stellar fit
Scalled stellar exp. disk spec.
Flux
50%
Bulge :
log(M⋆, B) = 8.024
⟨t⋆, B⟩M = 6.156
⟨Z⋆, B⟩M = 0.340
Disk :
log(M⋆, D) = 7.382
⟨t⋆, D⟩M = 4.662
⟨Z⋆, D⟩M = 0.261
Scaling factors :
fdD : 0.002
ffD : 1.937
feD : 2.130
Bulge spec. after sub. of decr. disk & stellar fit
Bulge spec. after sub. of flat disk & stellar fit
Bulge spec. after sub. of exp. disk & stellar fit
10%
Net − Bulge dD :
log(M⋆, dD) = 8.034
⟨t⋆, dD⟩M = 7.198
⟨Z⋆, dD⟩M = 0.372
Net − Bulge fD :
log(M⋆, fD) = 7.793
⟨t⋆, fD⟩M = 7.914
⟨Z⋆, fD⟩M = 0.599
Net − Bulge eD :
log(M⋆, eD) = 7.744
⟨t⋆, eD⟩M = 6.952
⟨Z⋆, eD⟩M = 0.668

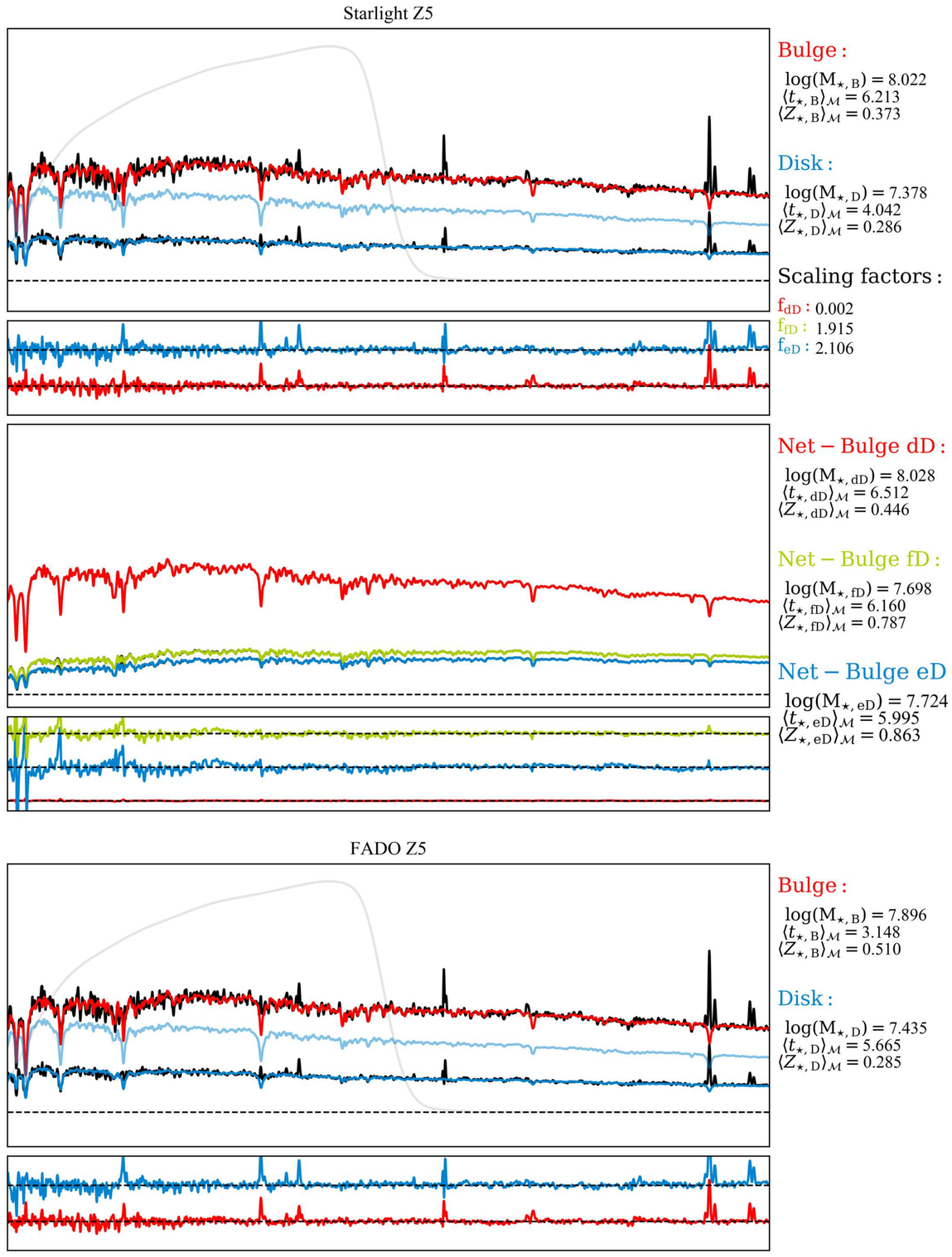
Starlight Z5
Bulge :
log(M⋆, B) = 8.022
⟨t⋆, B⟩M = 6.213
⟨Z⋆, B⟩M = 0.373
Disk :
log(M⋆, D) = 7.378
⟨t⋆, D⟩M = 4.042
⟨Z⋆, D⟩M = 0.286
Scaling factors :
fdD : 0.002
ffD : 1.915
feD : 2.106
Net − Bulge dD :
log(M⋆, dD) = 8.028
⟨t⋆, dD⟩M = 6.512
⟨Z⋆, dD⟩M = 0.446
Net − Bulge fD :
log(M⋆, fD) = 7.698
⟨t⋆, fD⟩M = 6.160
⟨Z⋆, fD⟩M = 0.787
Net − Bulge eD :
log(M⋆, eD) = 7.724
⟨t⋆, eD⟩M = 5.995
⟨Z⋆, eD⟩M = 0.863

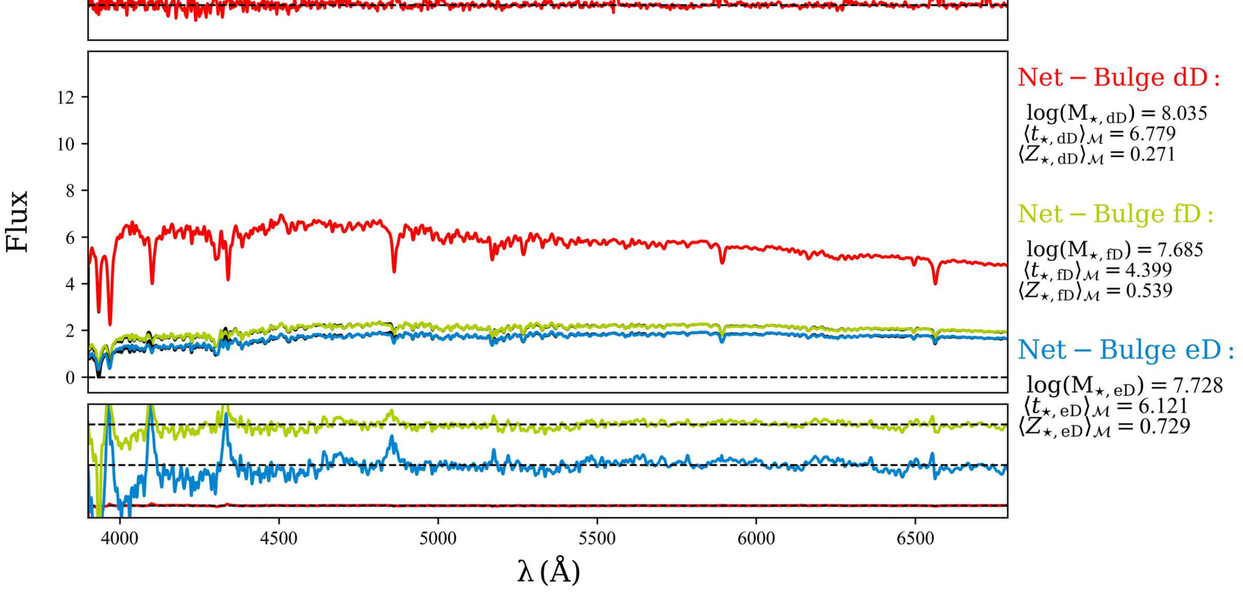
FADO Z4
NEG flux fD & eD
Flux
Bulge :
log(M⋆, B) = 8.050
⟨t⋆, B⟩M = 6.787
⟨Z⋆, B⟩M = 0.247
Disk :
log(M⋆, D) = 7.310
⟨t⋆, D⟩M = 6.365
⟨Z⋆, D⟩M = 0.312
Net − Bulge dD :
log(M⋆, dD) = 8.035
⟨t⋆, dD⟩M = 6.779
⟨Z⋆, dD⟩M = 0.271
Net − Bulge fD :
log(M⋆, fD) = 7.685
⟨t⋆, fD⟩M = 4.399
⟨Z⋆, fD⟩M = 0.539
Net − Bulge eD :
log(M⋆, eD) = 7.728
⟨t⋆, eD⟩M = 6.121
⟨Z⋆, eD⟩M = 0.729
4000
4500
5000
5500
6000
6500
λ (Å)

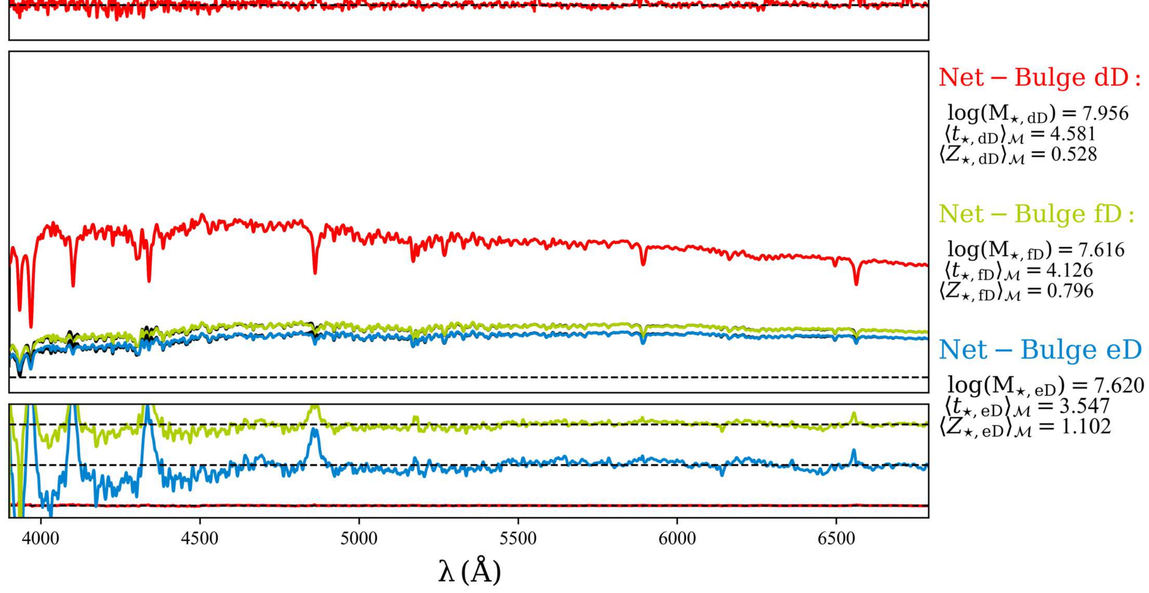
FADO Z5
Bulge :
log(M⋆, B) = 7.896
⟨t⋆, B⟩M = 3.148
⟨Z⋆, B⟩M = 0.510
Disk :
log(M⋆, D) = 7.435
⟨t⋆, D⟩M = 5.665
⟨Z⋆, D⟩M = 0.285
Net − Bulge dD :
log(M⋆, dD) = 7.956
⟨t⋆, dD⟩M = 4.581
⟨Z⋆, dD⟩M = 0.528
Net − Bulge fD :
log(M⋆, fD) = 7.616
⟨t⋆, fD⟩M = 4.126
⟨Z⋆, fD⟩M = 0.796
Net − Bulge eD :
log(M⋆, eD) = 7.620
⟨t⋆, eD⟩M = 3.547
⟨Z⋆, eD⟩M = 1.102
4000
4500
5000
5500
6000
6500
λ (Å)

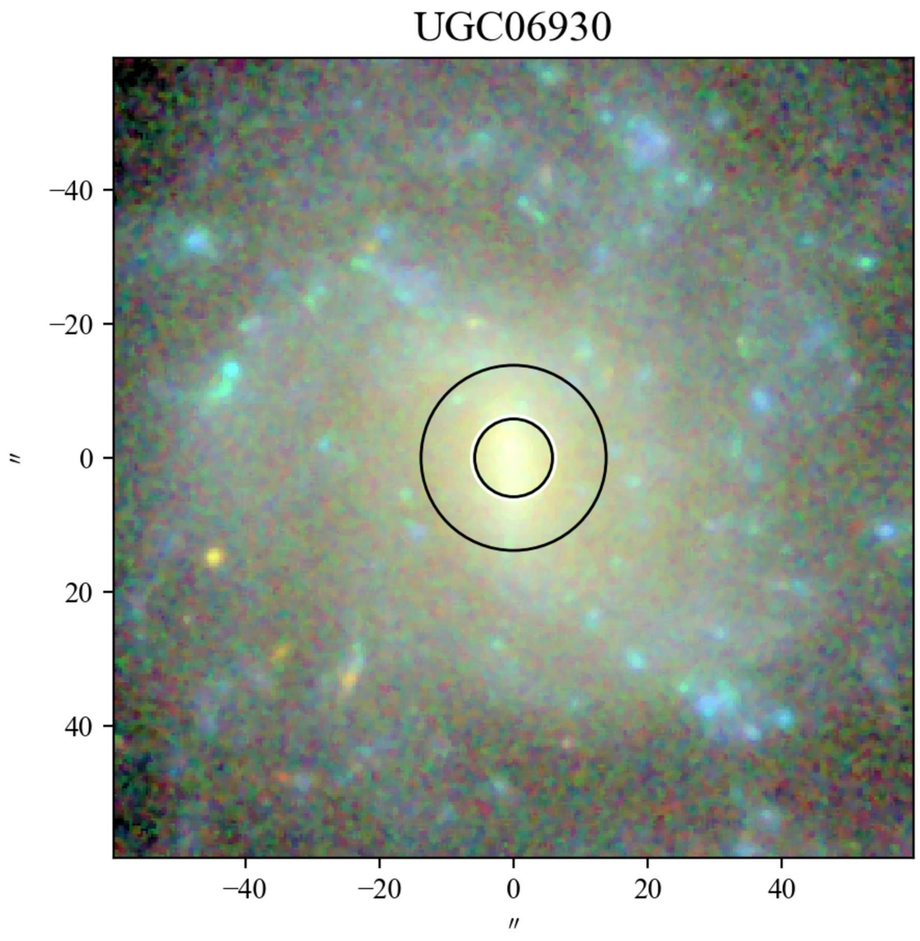
UGC06930
−40
−20
0
20
40
″
−40
−20
0
20
40
″

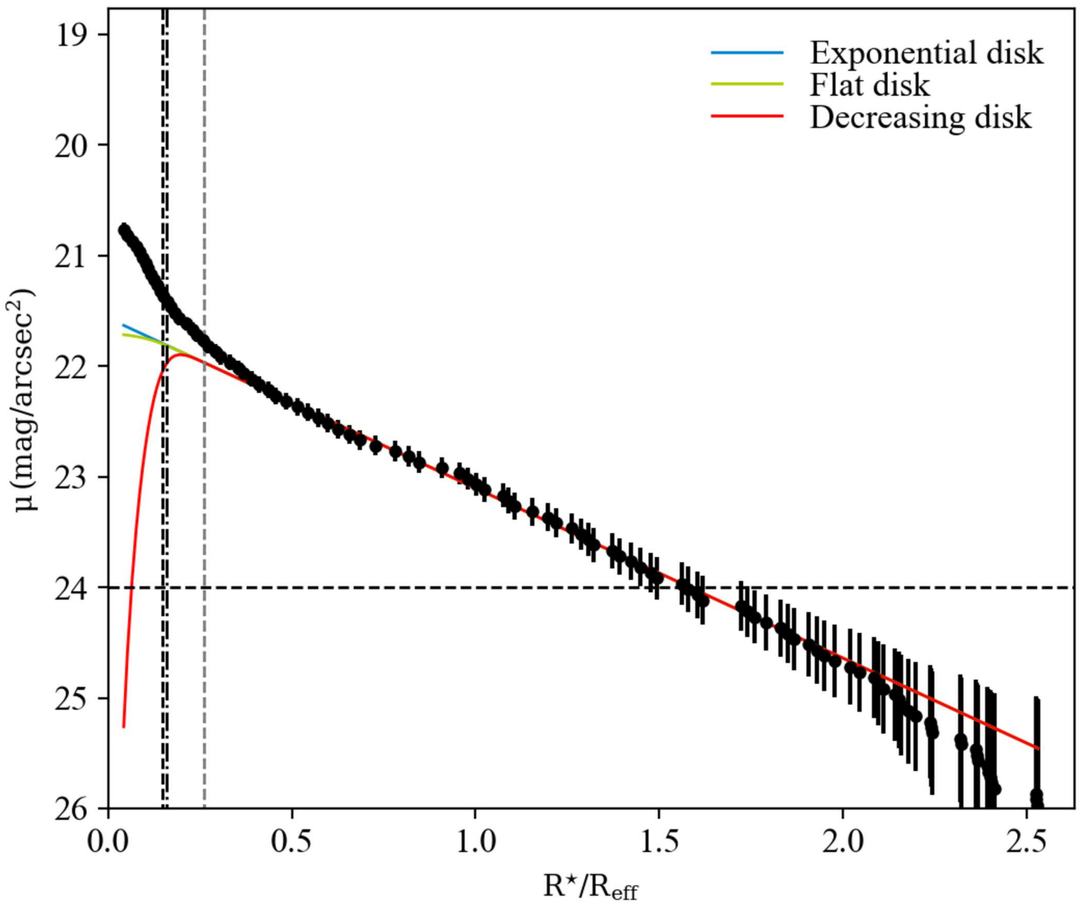
Exponential disk
Flat disk
Decreasing disk
μ (mag/arcsec²)
19
20
21
22
23
24
25
26
0.0
0.5
1.0
1.5
2.0
2.5
R⋆/Reff

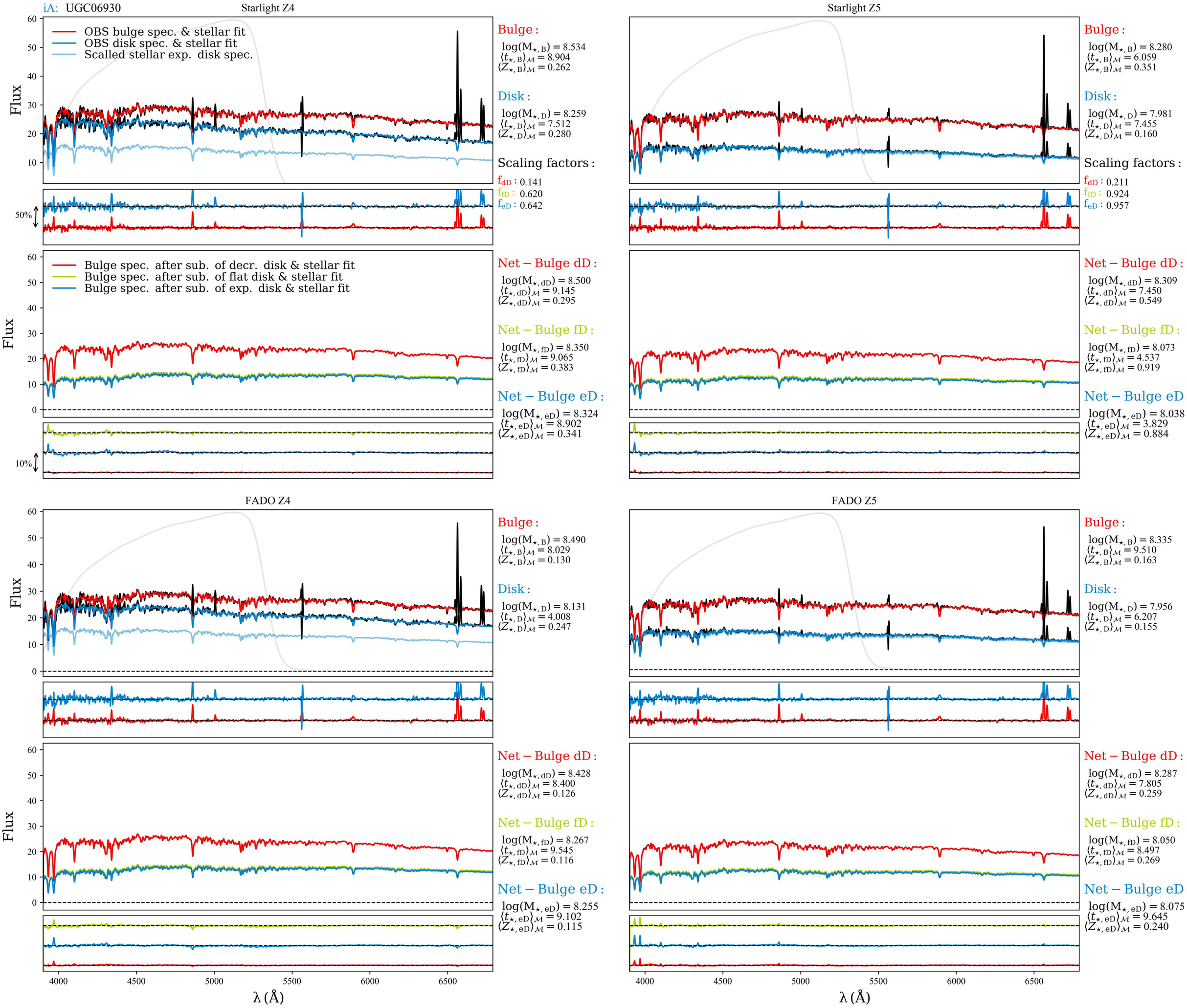
iA: UGC06930
Starlight Z4
OBS bulge spec. & stellar fit
OBS disk spec. & stellar fit
Scalled stellar exp. disk spec.
Flux
50%
Bulge :
log(M⋆, B) = 8.534
⟨t⋆, B⟩M = 8.904
⟨Z⋆, B⟩M = 0.262
Disk :
log(M⋆, D) = 8.259
⟨t⋆, D⟩M = 7.512
⟨Z⋆, D⟩M = 0.280
Scaling factors :
fdD : 0.141
ffD : 0.620
feD : 0.642
Starlight Z5
Bulge :
log(M⋆, B) = 8.280
⟨t⋆, B⟩M = 6.059
⟨Z⋆, B⟩M = 0.351
Disk :
log(M⋆, D) = 7.981
⟨t⋆, D⟩M = 7.455
⟨Z⋆, D⟩M = 0.160
Scaling factors :
fdD : 0.211
ffD : 0.924
feD : 0.957
Bulge spec. after sub. of decr. disk & stellar fit
Bulge spec. after sub. of flat disk & stellar fit
Bulge spec. after sub. of exp. disk & stellar fit
10%
Net − Bulge dD :
log(M⋆, dD) = 8.500
⟨t⋆, dD⟩M = 9.145
⟨Z⋆, dD⟩M = 0.295
Net − Bulge fD :
log(M⋆, fD) = 8.350
⟨t⋆, fD⟩M = 9.065
⟨Z⋆, fD⟩M = 0.383
Net − Bulge eD :
log(M⋆, eD) = 8.324
⟨t⋆, eD⟩M = 8.902
⟨Z⋆, eD⟩M = 0.341
Net − Bulge dD :
log(M⋆, dD) = 8.309
⟨t⋆, dD⟩M = 7.450
⟨Z⋆, dD⟩M = 0.549
Net − Bulge fD :
log(M⋆, fD) = 8.073
⟨t⋆, fD⟩M = 4.537
⟨Z⋆, fD⟩M = 0.919
Net − Bulge eD :
log(M⋆, eD) = 8.038
⟨t⋆, eD⟩M = 3.829
⟨Z⋆, eD⟩M = 0.884
FADO Z4
Bulge :
log(M⋆, B) = 8.490
⟨t⋆, B⟩M = 8.029
⟨Z⋆, B⟩M = 0.130
Disk :
log(M⋆, D) = 8.131
⟨t⋆, D⟩M = 4.008
⟨Z⋆, D⟩M = 0.247
FADO Z5
Bulge :
log(M⋆, B) = 8.335
⟨t⋆, B⟩M = 9.510
⟨Z⋆, B⟩M = 0.163
Disk :
log(M⋆, D) = 7.956
⟨t⋆, D⟩M = 6.207
⟨Z⋆, D⟩M = 0.155
Net − Bulge dD :
log(M⋆, dD) = 8.428
⟨t⋆, dD⟩M = 8.400
⟨Z⋆, dD⟩M = 0.126
Net − Bulge fD :
log(M⋆, fD) = 8.267
⟨t⋆, fD⟩M = 9.545
⟨Z⋆, fD⟩M = 0.116
Net − Bulge eD :
log(M⋆, eD) = 8.255
⟨t⋆, eD⟩M = 9.102
⟨Z⋆, eD⟩M = 0.115
Net − Bulge dD :
log(M⋆, dD) = 8.287
⟨t⋆, dD⟩M = 7.805
⟨Z⋆, dD⟩M = 0.259
Net − Bulge fD :
log(M⋆, fD) = 8.050
⟨t⋆, fD⟩M = 8.497
⟨Z⋆, fD⟩M = 0.269
Net − Bulge eD :
log(M⋆, eD) = 8.075
⟨t⋆, eD⟩M = 9.645
⟨Z⋆, eD⟩M = 0.240
4000
4500
5000
5500
6000
6500
λ (Å)

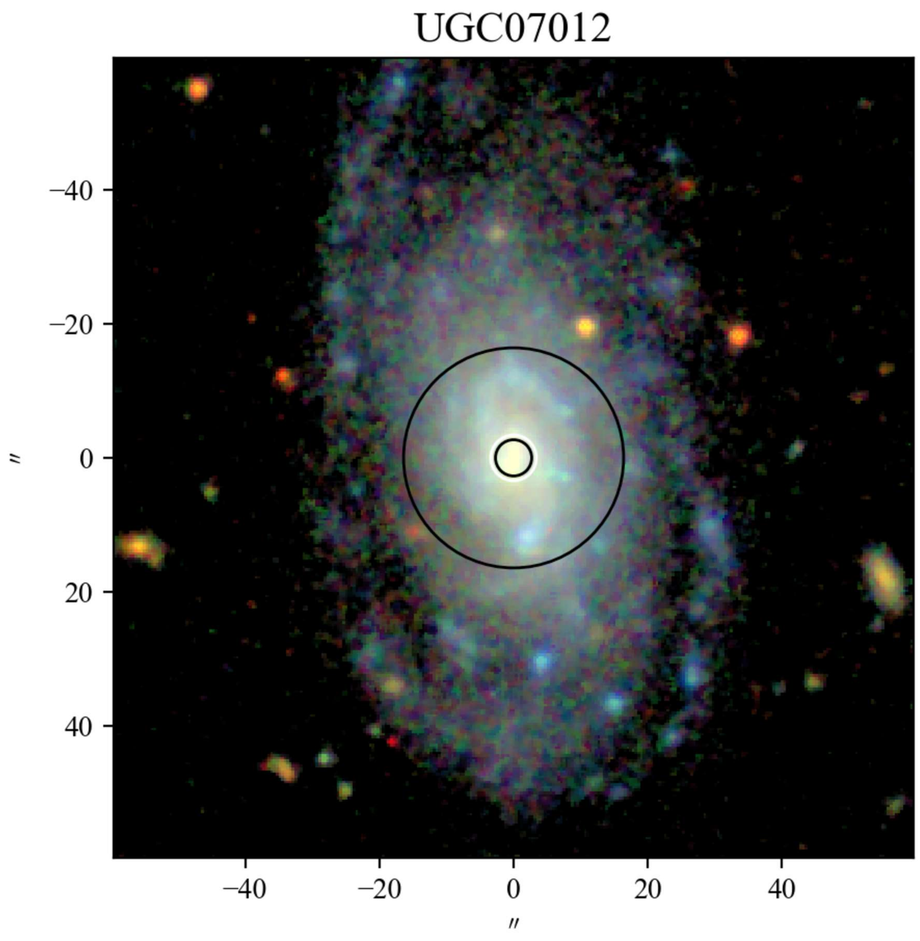
UGC07012
−40
−20
0
20
40
″
−40
−20
0
20
40
″

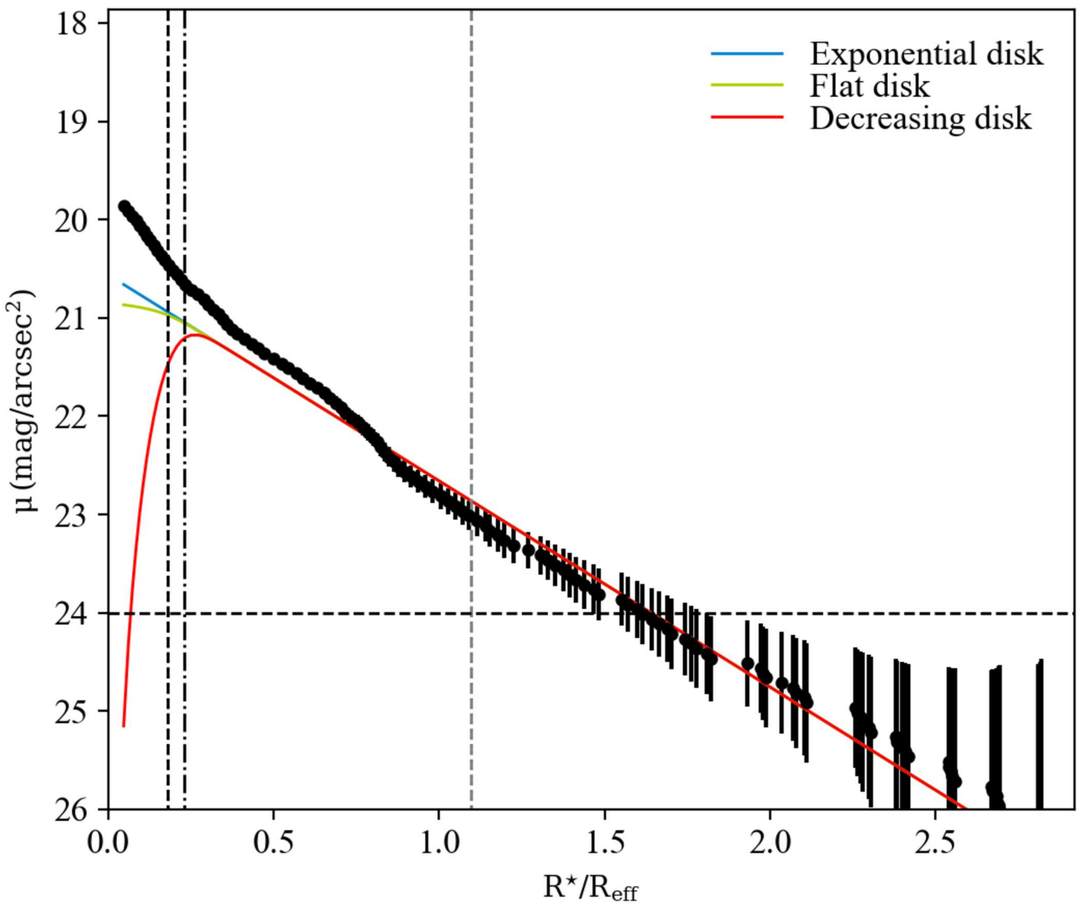
Exponential disk
Flat disk
Decreasing disk
μ (mag/arcsec²)
18
19
20
21
22
23
24
25
26
0.0
0.5
1.0
1.5
2.0
2.5
R⋆/Reff

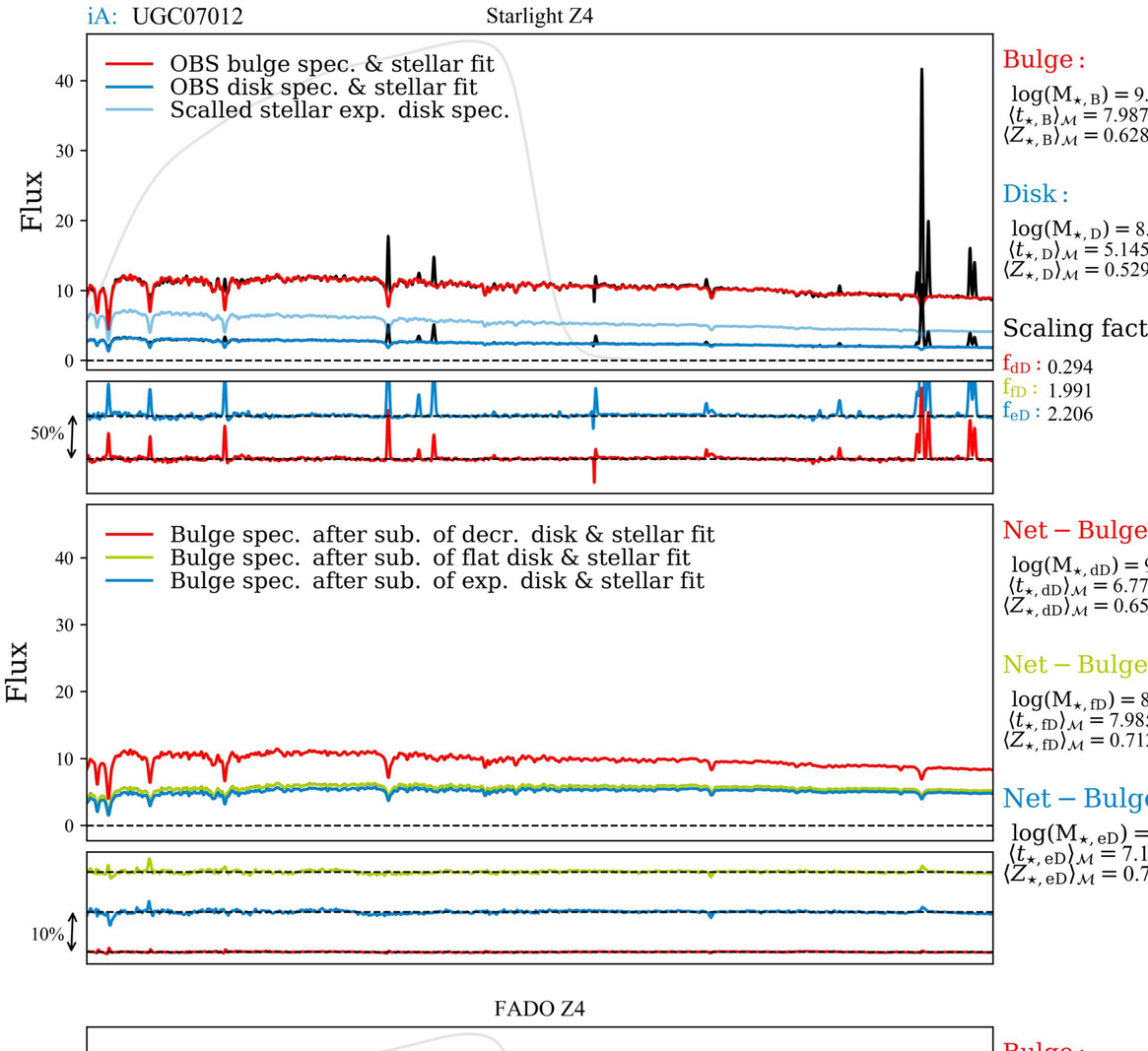
iA: UGC07012
Starlight Z4
OBS bulge spec. & stellar fit
OBS disk spec. & stellar fit
Scalled stellar exp. disk spec.
Flux
50%
Bulge :
log(M⋆, B) = 9.115
⟨t⋆, B⟩M = 7.987
⟨Z⋆, B⟩M = 0.628
Disk :
log(M⋆, D) = 8.223
⟨t⋆, D⟩M = 5.145
⟨Z⋆, D⟩M = 0.529
Scaling factors :
fdD : 0.294
ffD : 1.991
feD : 2.206
Bulge spec. after sub. of decr. disk & stellar fit
Bulge spec. after sub. of flat disk & stellar fit
Bulge spec. after sub. of exp. disk & stellar fit
10%
Net − Bulge dD :
log(M⋆, dD) = 9.080
⟨t⋆, dD⟩M = 6.773
⟨Z⋆, dD⟩M = 0.658
Net − Bulge fD :
log(M⋆, fD) = 8.990
⟨t⋆, fD⟩M = 7.985
⟨Z⋆, fD⟩M = 0.712
Net − Bulge eD :
log(M⋆, eD) = 8.969
⟨t⋆, eD⟩M = 7.132
⟨Z⋆, eD⟩M = 0.719

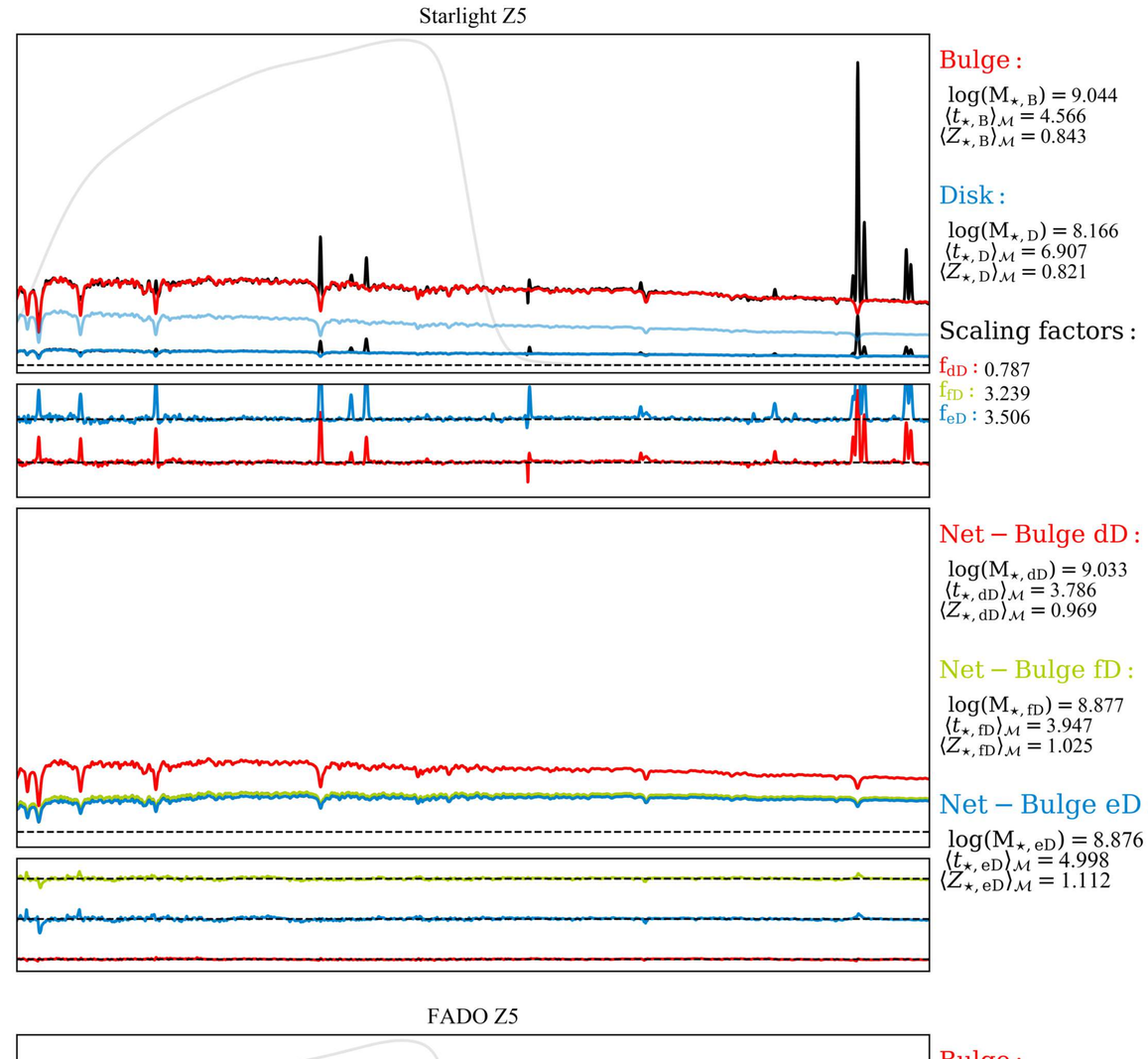
Starlight Z5
Bulge :
log(M⋆, B) = 9.044
⟨t⋆, B⟩M = 4.566
⟨Z⋆, B⟩M = 0.843
Disk :
log(M⋆, D) = 8.166
⟨t⋆, D⟩M = 6.907
⟨Z⋆, D⟩M = 0.821
Scaling factors :
fdD : 0.787
ffD : 3.239
feD : 3.506
Net − Bulge dD :
log(M⋆, dD) = 9.033
⟨t⋆, dD⟩M = 3.786
⟨Z⋆, dD⟩M = 0.969
Net − Bulge fD :
log(M⋆, fD) = 8.877
⟨t⋆, fD⟩M = 3.947
⟨Z⋆, fD⟩M = 1.025
Net − Bulge eD :
log(M⋆, eD) = 8.876
⟨t⋆, eD⟩M = 4.998
⟨Z⋆, eD⟩M = 1.112

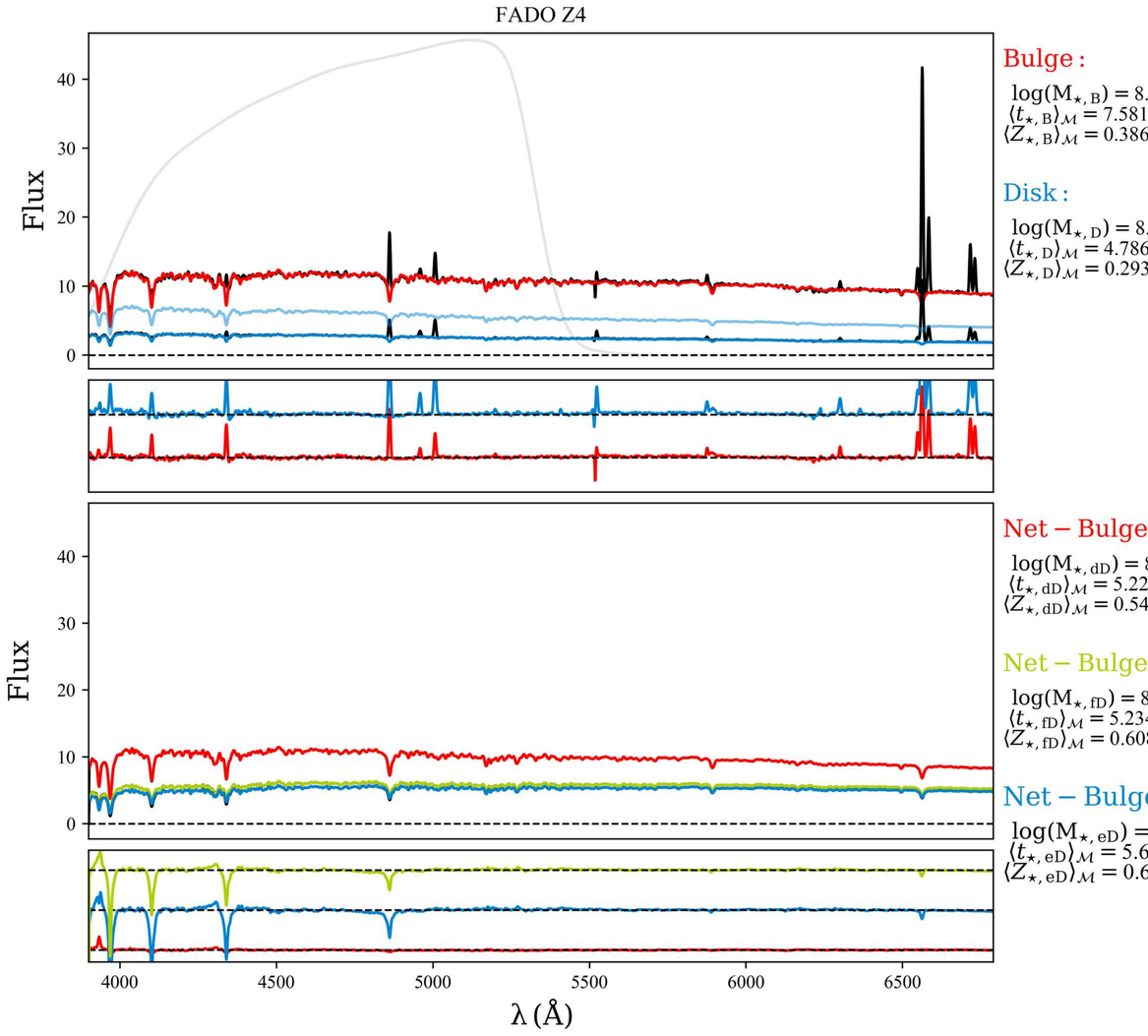
FADO Z4
Flux
Bulge :
log(M⋆, B) = 8.996
⟨t⋆, B⟩M = 7.581
⟨Z⋆, B⟩M = 0.386
Disk :
log(M⋆, D) = 8.100
⟨t⋆, D⟩M = 4.786
⟨Z⋆, D⟩M = 0.293
Net − Bulge dD :
log(M⋆, dD) = 8.989
⟨t⋆, dD⟩M = 5.221
⟨Z⋆, dD⟩M = 0.542
Net − Bulge fD :
log(M⋆, fD) = 8.854
⟨t⋆, fD⟩M = 5.234
⟨Z⋆, fD⟩M = 0.608
Net − Bulge eD :
log(M⋆, eD) = 8.850
⟨t⋆, eD⟩M = 5.642
⟨Z⋆, eD⟩M = 0.648
4000
4500
5000
5500
6000
6500
λ (Å)

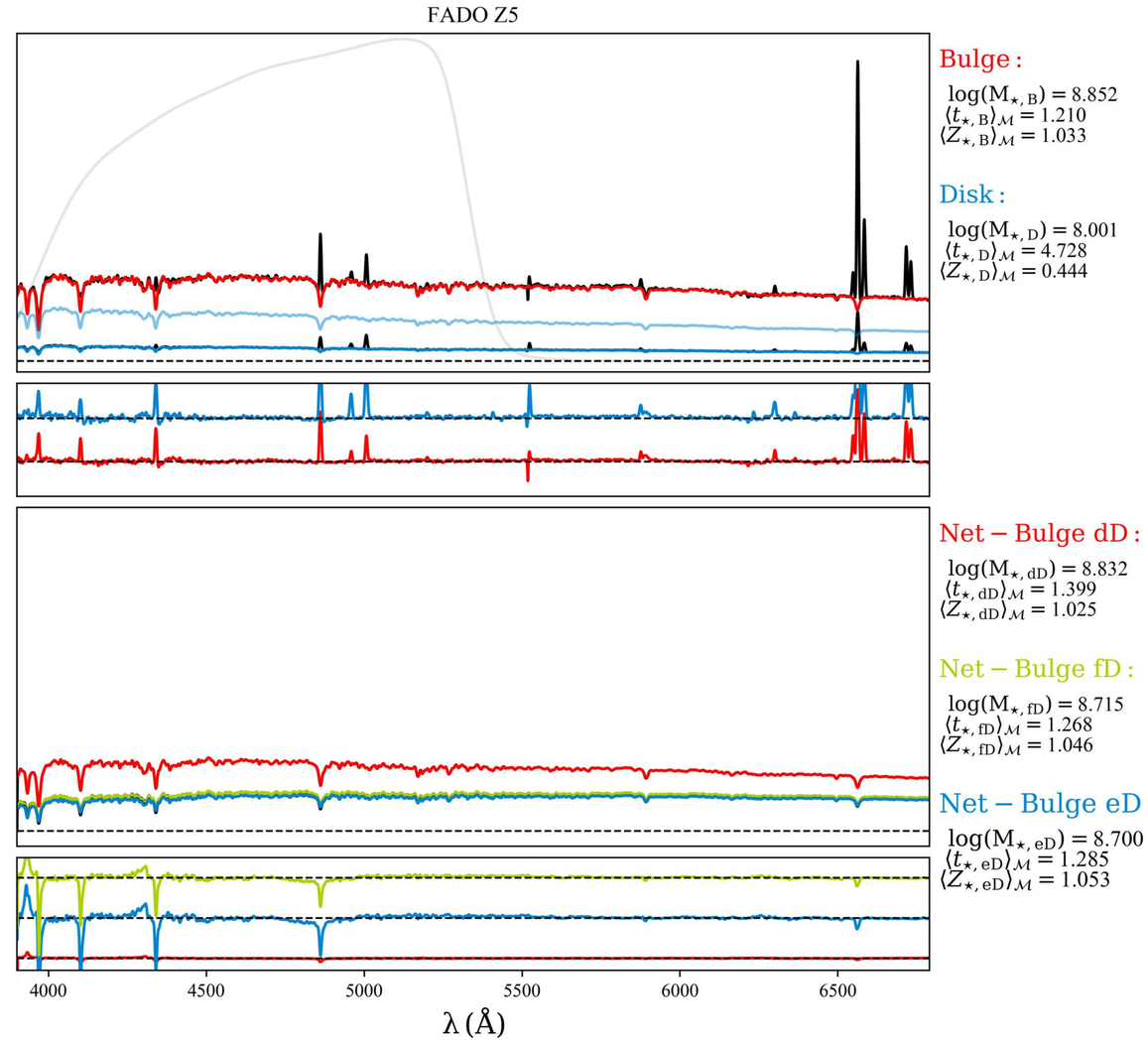
FADO Z5
Bulge :
log(M⋆, B) = 8.852
⟨t⋆, B⟩M = 1.210
⟨Z⋆, B⟩M = 1.033
Disk :
log(M⋆, D) = 8.001
⟨t⋆, D⟩M = 4.728
⟨Z⋆, D⟩M = 0.444
Net − Bulge dD :
log(M⋆, dD) = 8.832
⟨t⋆, dD⟩M = 1.399
⟨Z⋆, dD⟩M = 1.025
Net − Bulge fD :
log(M⋆, fD) = 8.715
⟨t⋆, fD⟩M = 1.268
⟨Z⋆, fD⟩M = 1.046
Net − Bulge eD :
log(M⋆, eD) = 8.700
⟨t⋆, eD⟩M = 1.285
⟨Z⋆, eD⟩M = 1.053
4000
4500
5000
5500
6000
6500
λ (Å)

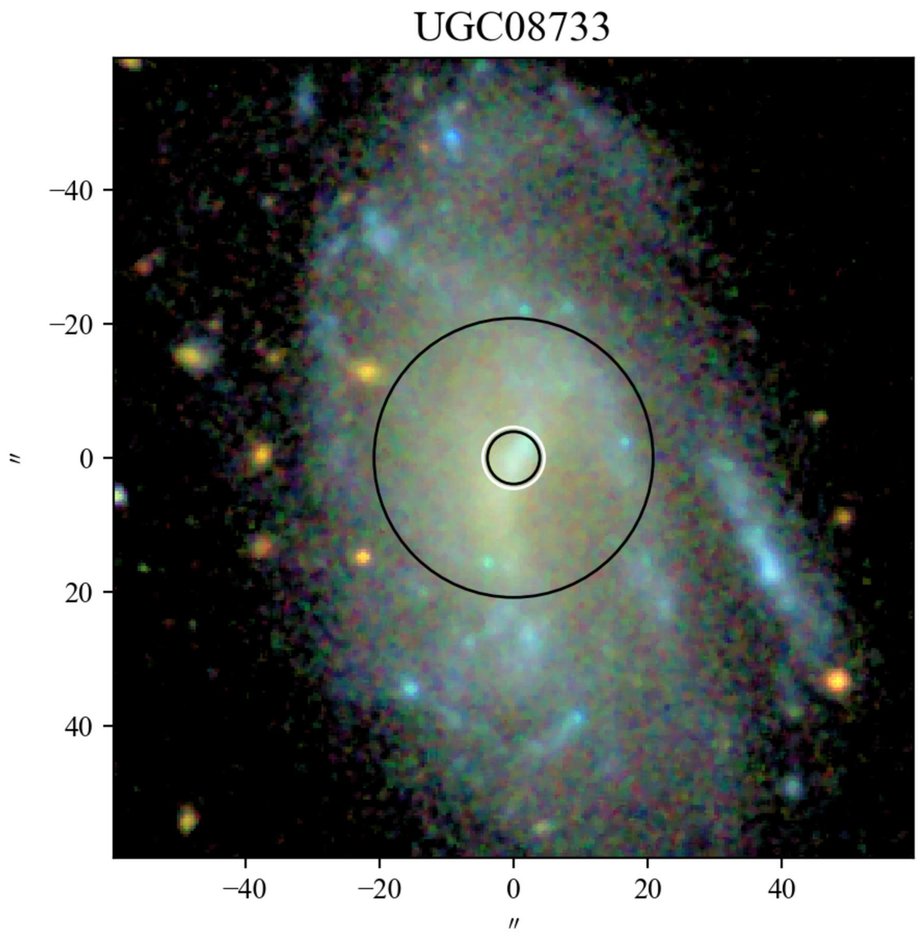
UGC08733
−40
−20
0
20
40
″
−40
−20
0
20
40
″

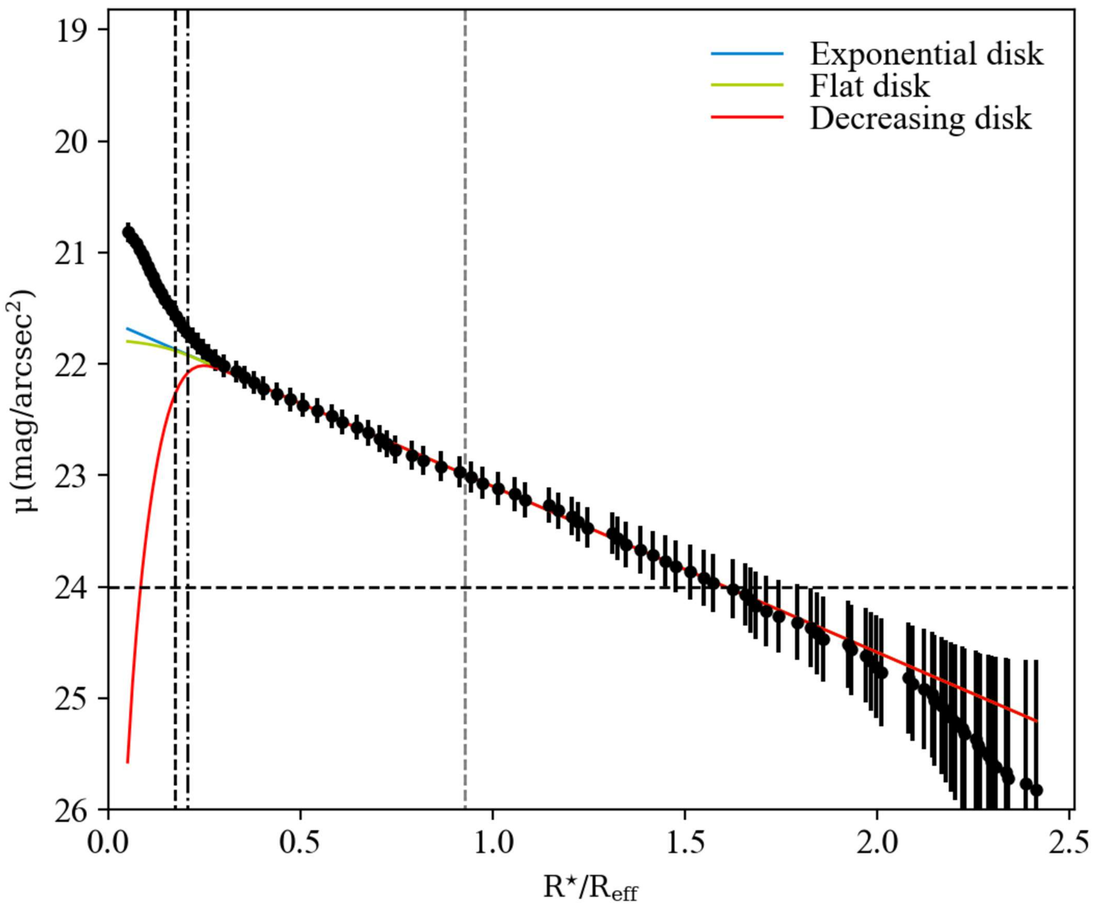
Exponential disk
Flat disk
Decreasing disk
μ (mag/arcsec²)
19
20
21
22
23
24
25
26
0.0
0.5
1.0
1.5
2.0
2.5
R⋆/Reff

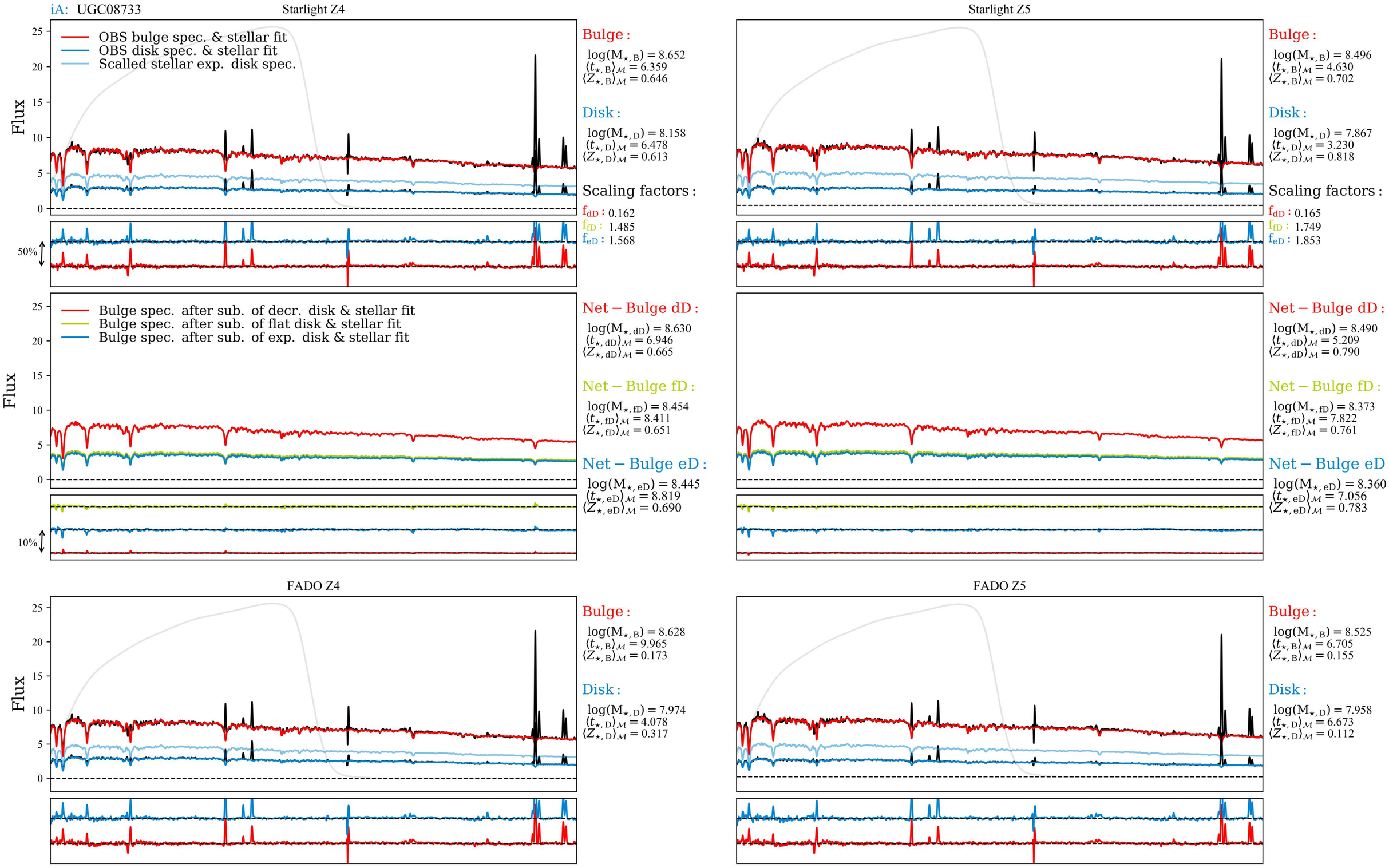
iA: UGC08733
Starlight Z4
OBS bulge spec. & stellar fit
OBS disk spec. & stellar fit
Scalled stellar exp. disk spec.
Flux
50%
Bulge :
log(M⋆, B) = 8.652
⟨t⋆, B⟩M = 6.359
⟨Z⋆, B⟩M = 0.646
Disk :
log(M⋆, D) = 8.158
⟨t⋆, D⟩M = 6.478
⟨Z⋆, D⟩M = 0.613
Scaling factors :
fdD : 0.162
ffD : 1.485
feD : 1.568
Starlight Z5
Bulge :
log(M⋆, B) = 8.496
⟨t⋆, B⟩M = 4.630
⟨Z⋆, B⟩M = 0.702
Disk :
log(M⋆, D) = 7.867
⟨t⋆, D⟩M = 3.230
⟨Z⋆, D⟩M = 0.818
Scaling factors :
fdD : 0.165
ffD : 1.749
feD : 1.853
Bulge spec. after sub. of decr. disk & stellar fit
Bulge spec. after sub. of flat disk & stellar fit
Bulge spec. after sub. of exp. disk & stellar fit
10%
Net − Bulge dD :
log(M⋆, dD) = 8.630
⟨t⋆, dD⟩M = 6.946
⟨Z⋆, dD⟩M = 0.665
Net − Bulge fD :
log(M⋆, fD) = 8.454
⟨t⋆, fD⟩M = 8.411
⟨Z⋆, fD⟩M = 0.651
Net − Bulge eD :
log(M⋆, eD) = 8.445
⟨t⋆, eD⟩M = 8.819
⟨Z⋆, eD⟩M = 0.690
Net − Bulge dD :
log(M⋆, dD) = 8.490
⟨t⋆, dD⟩M = 5.209
⟨Z⋆, dD⟩M = 0.790
Net − Bulge fD :
log(M⋆, fD) = 8.373
⟨t⋆, fD⟩M = 7.822
⟨Z⋆, fD⟩M = 0.761
Net − Bulge eD :
log(M⋆, eD) = 8.360
⟨t⋆, eD⟩M = 7.056
⟨Z⋆, eD⟩M = 0.783
FADO Z4
Bulge :
log(M⋆, B) = 8.628
⟨t⋆, B⟩M = 9.965
⟨Z⋆, B⟩M = 0.173
Disk :
log(M⋆, D) = 7.974
⟨t⋆, D⟩M = 4.078
⟨Z⋆, D⟩M = 0.317
FADO Z5
Bulge :
log(M⋆, B) = 8.525
⟨t⋆, B⟩M = 6.705
⟨Z⋆, B⟩M = 0.155
Disk :
log(M⋆, D) = 7.958
⟨t⋆, D⟩M = 6.673
⟨Z⋆, D⟩M = 0.112
Net − Bulge dD :
log(M⋆, dD) = 8.612
⟨t⋆, dD⟩M = 9.877
⟨Z⋆, dD⟩M = 0.164
Net − Bulge fD :
log(M⋆, fD) = 8.449
⟨t⋆, fD⟩M = 12.200
⟨Z⋆, fD⟩M = 0.106
Net − Bulge eD :
log(M⋆, eD) = 8.444
⟨t⋆, eD⟩M = 12.330
⟨Z⋆, eD⟩M = 0.144
Net − Bulge dD :
log(M⋆, dD) = 8.534
⟨t⋆, dD⟩M = 7.434
⟨Z⋆, dD⟩M = 0.197
Net − Bulge fD :
log(M⋆, fD) = 8.253
⟨t⋆, fD⟩M = 6.479
⟨Z⋆, fD⟩M = 0.219
Net − Bulge eD :
log(M⋆, eD) = 8.196
⟨t⋆, eD⟩M = 4.989
⟨Z⋆, eD⟩M = 0.200
4000
4500
5000
5500
6000
6500
λ (Å)

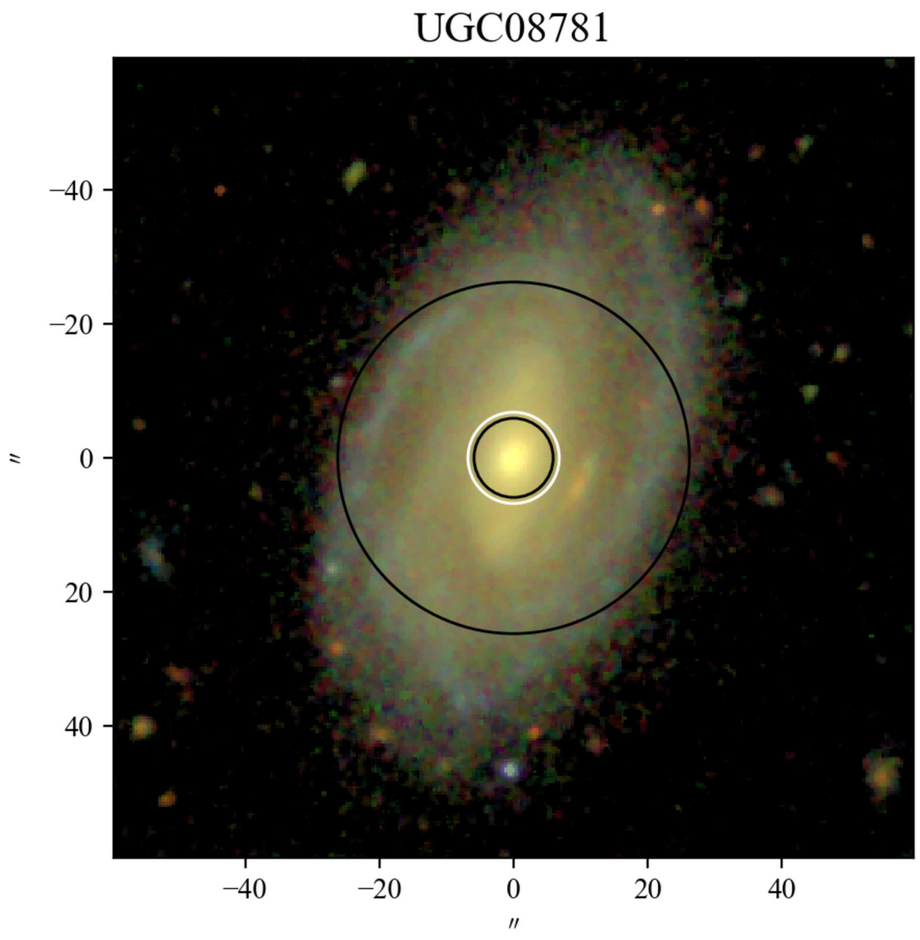
UGC08781
−40
−20
0
20
40
″
−40
−20
0
20
40
″

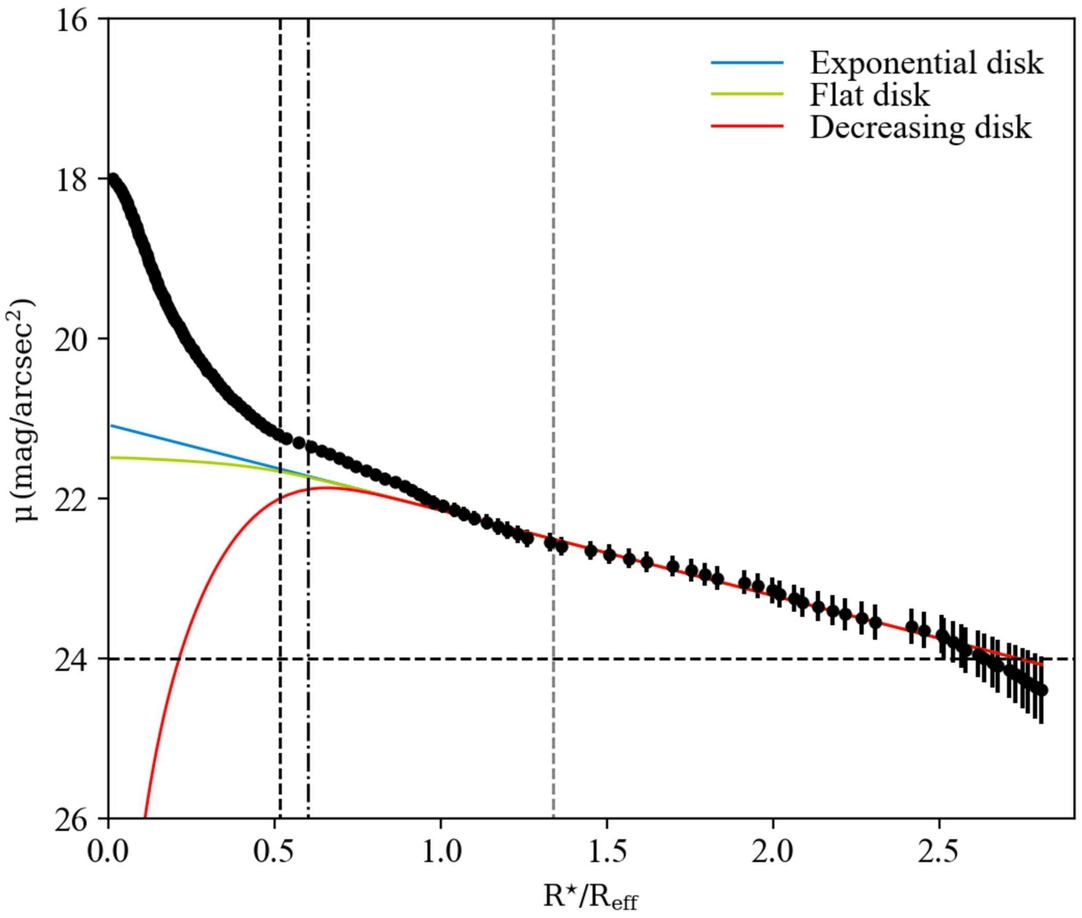
Exponential disk
Flat disk
Decreasing disk
μ (mag/arcsec²)
16
18
20
22
24
26
0.0
0.5
1.0
1.5
2.0
2.5
R*/Reff

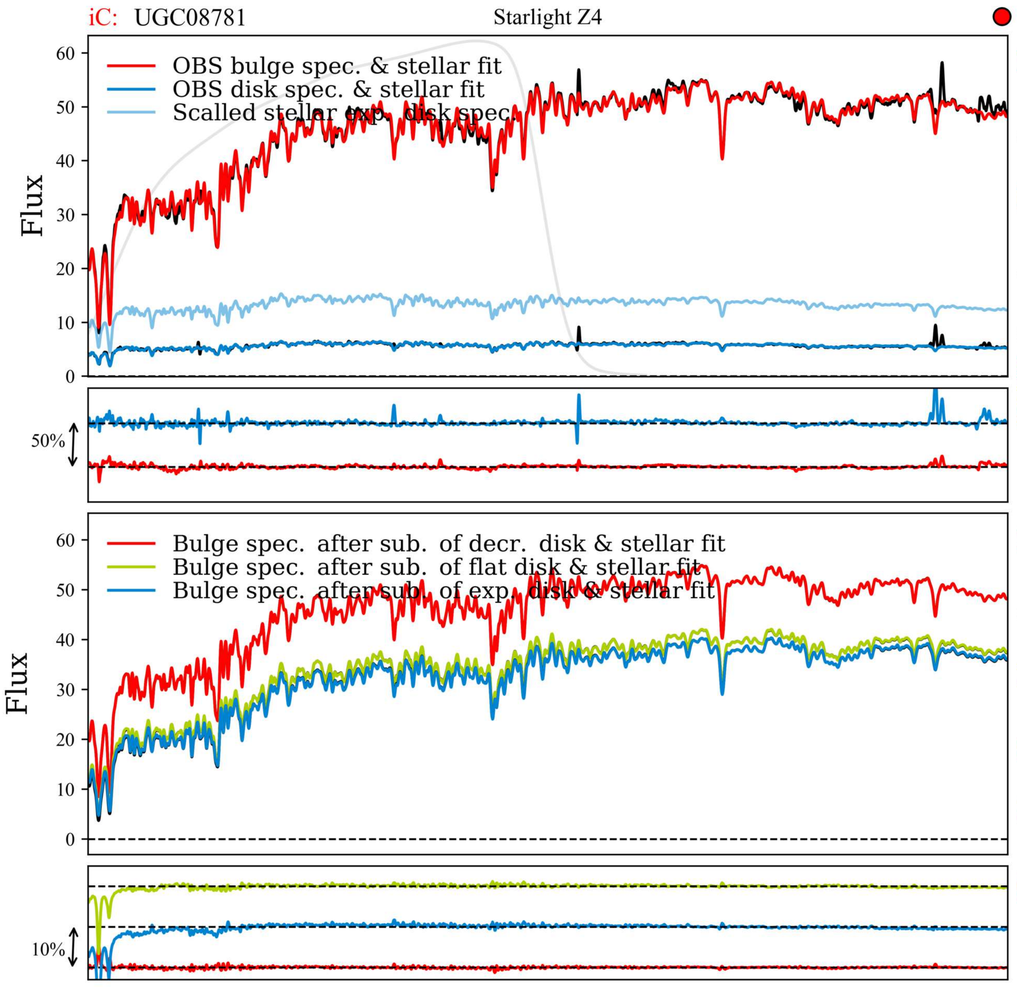
iC: UGC08781
Starlight Z4
OBS bulge spec. & stellar fit
OBS disk spec. & stellar fit
Scalled stellar exp. disk spec.
Flux
50%
Bulge spec. after sub. of decr. disk & stellar fit
Bulge spec. after sub. of flat disk & stellar fit
Bulge spec. after sub. of exp. disk & stellar fit
10%
Bulge :
log(M⋆, B) = 10.940
⟨t⋆, B⟩M = 12.787
⟨Z⋆, B⟩M = 0.953
Disk :
log(M⋆, D) = 9.796
⟨t⋆, D⟩M = 10.363
⟨Z⋆, D⟩M = 0.893
Scaling factors :
fdD : 0.003
ffD : 2.074
feD : 2.358
Net − Bulge dD :
log(M⋆, dD) = 10.925
⟨t⋆, dD⟩M = 12.270
⟨Z⋆, dD⟩M = 0.956
Net − Bulge fD :
log(M⋆, fD) = 10.878
⟨t⋆, fD⟩M = 13.000
⟨Z⋆, fD⟩M = 1.000
Net − Bulge eD :
log(M⋆, eD) = 10.875
⟨t⋆, eD⟩M = 13.000
⟨Z⋆, eD⟩M = 1.000

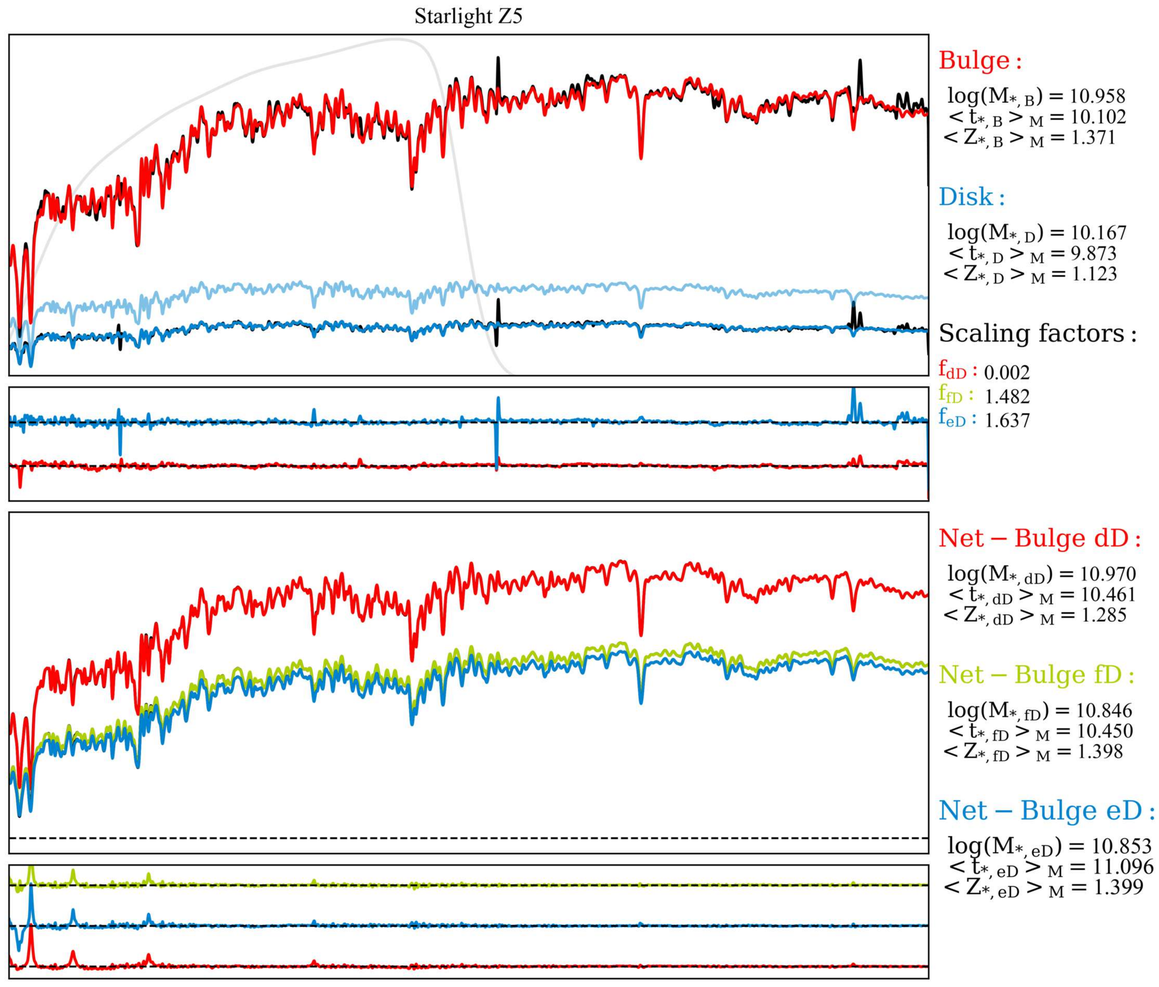
Starlight Z5
Bulge :
log(M*, B) = 10.958
< t*, B > M = 10.102
< Z*, B > M = 1.371
Disk :
log(M*, D) = 10.167
< t*, D > M = 9.873
< Z*, D > M = 1.123
Scaling factors :
fdD : 0.002
ffD : 1.482
feD : 1.637
Net − Bulge dD :
log(M*, dD) = 10.970
< t*, dD > M = 10.461
< Z*, dD > M = 1.285
Net − Bulge fD :
log(M*, fD) = 10.846
< t*, fD > M = 10.450
< Z*, fD > M = 1.398
Net − Bulge eD :
log(M*, eD) = 10.853
< t*, eD > M = 11.096
< Z*, eD > M = 1.399

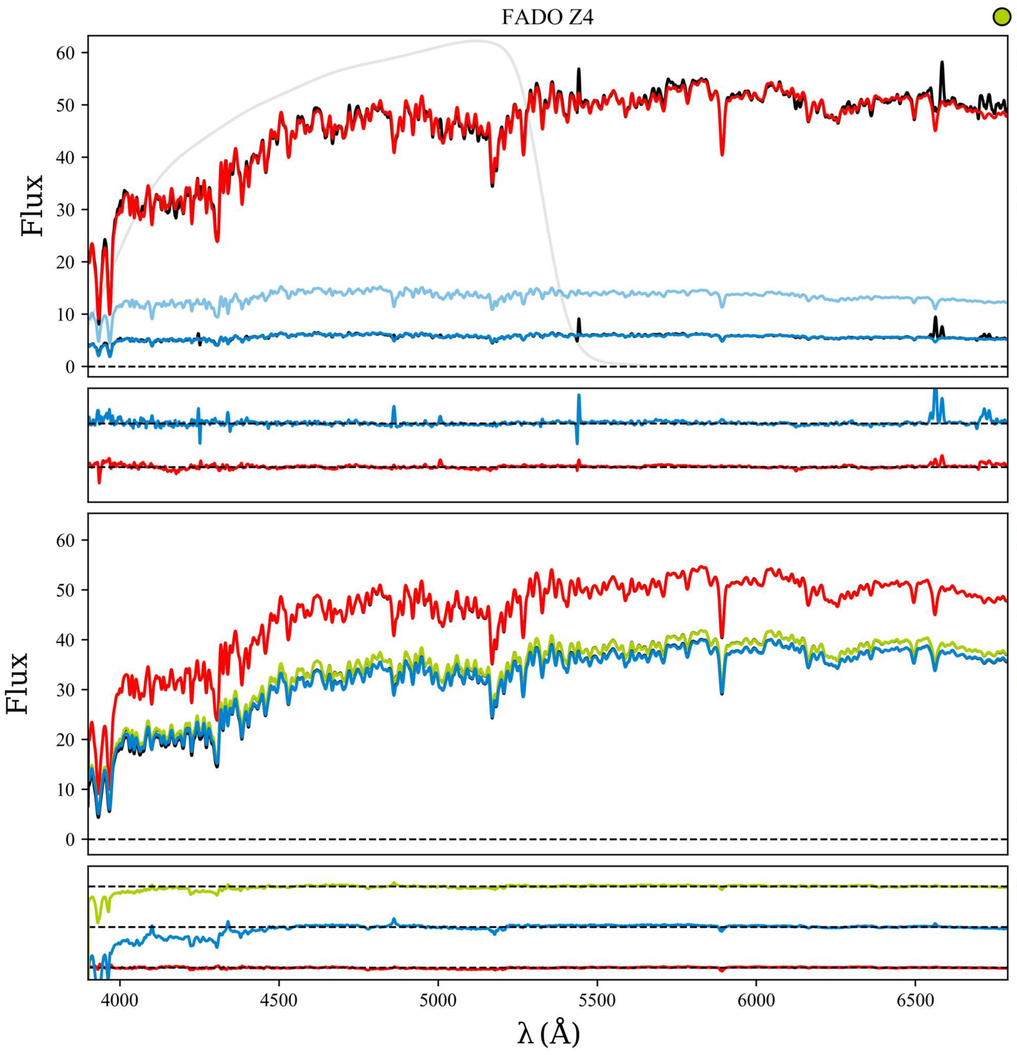
FADO Z4
Flux
Bulge :
log(M⋆, B) = 10.920
⟨t⋆, B⟩M = 13.000
⟨Z⋆, B⟩M = 0.919
Disk :
log(M⋆, D) = 9.736
⟨t⋆, D⟩M = 11.270
⟨Z⋆, D⟩M = 0.858
Net − Bulge dD :
log(M⋆, dD) = 10.910
⟨t⋆, dD⟩M = 12.540
⟨Z⋆, dD⟩M = 0.958
Net − Bulge fD :
log(M⋆, fD) = 10.860
⟨t⋆, fD⟩M = 13.000
⟨Z⋆, fD⟩M = 1.000
Net − Bulge eD :
log(M⋆, eD) = 10.850
⟨t⋆, eD⟩M = 12.000
⟨Z⋆, eD⟩M = 1.000
λ (Å)

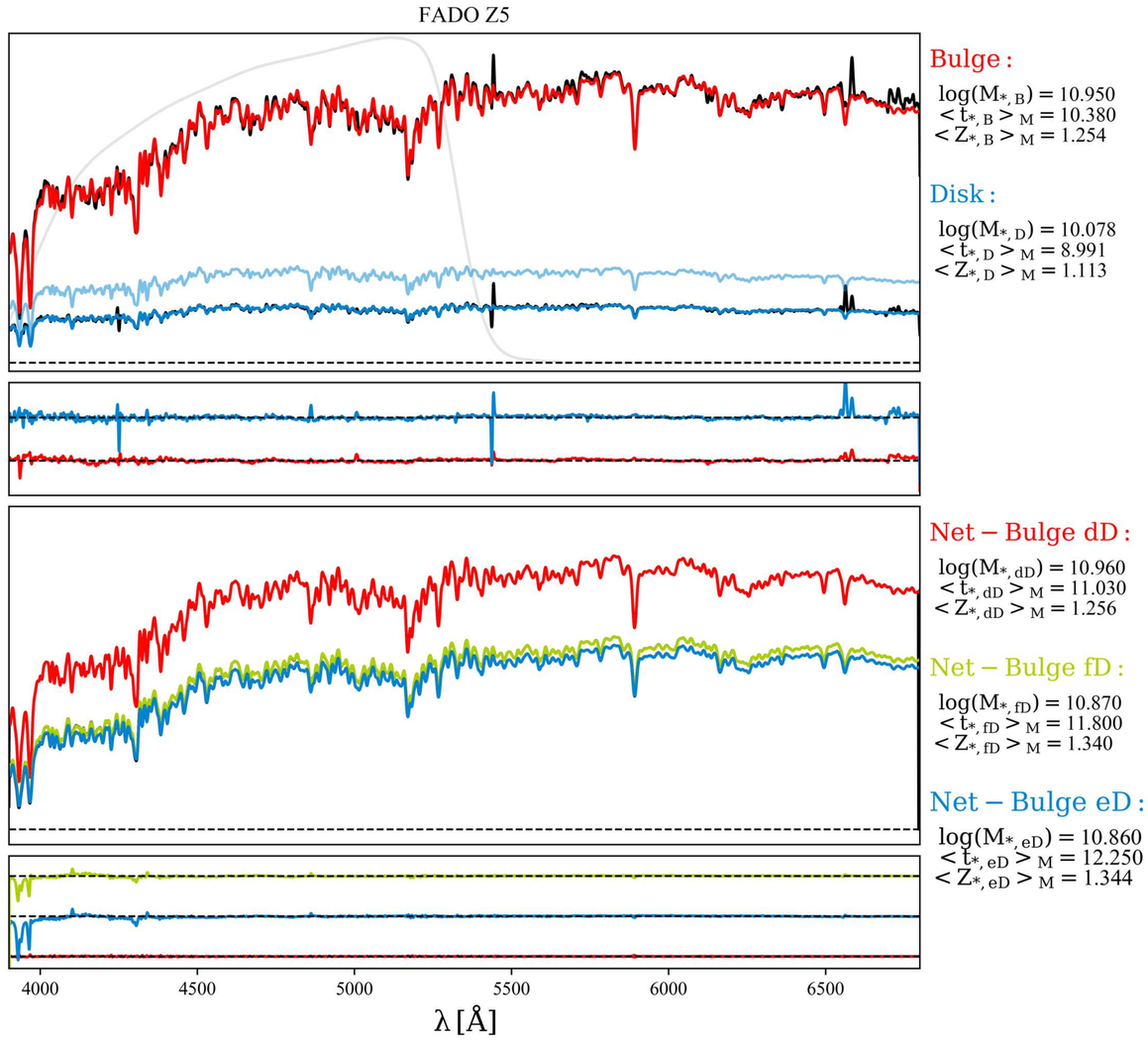
FADO Z5
Bulge :
log(M*, B) = 10.950
< t*, B > M = 10.380
< Z*, B > M = 1.254
Disk :
log(M*, D) = 10.078
< t*, D > M = 8.991
< Z*, D > M = 1.113
Net − Bulge dD :
log(M*, dD) = 10.960
< t*, dD > M = 11.030
< Z*, dD > M = 1.256
Net − Bulge fD :
log(M*, fD) = 10.870
< t*, fD > M = 11.800
< Z*, fD > M = 1.340
Net − Bulge eD :
log(M*, eD) = 10.860
< t*, eD > M = 12.250
< Z*, eD > M = 1.344
λ [Å]

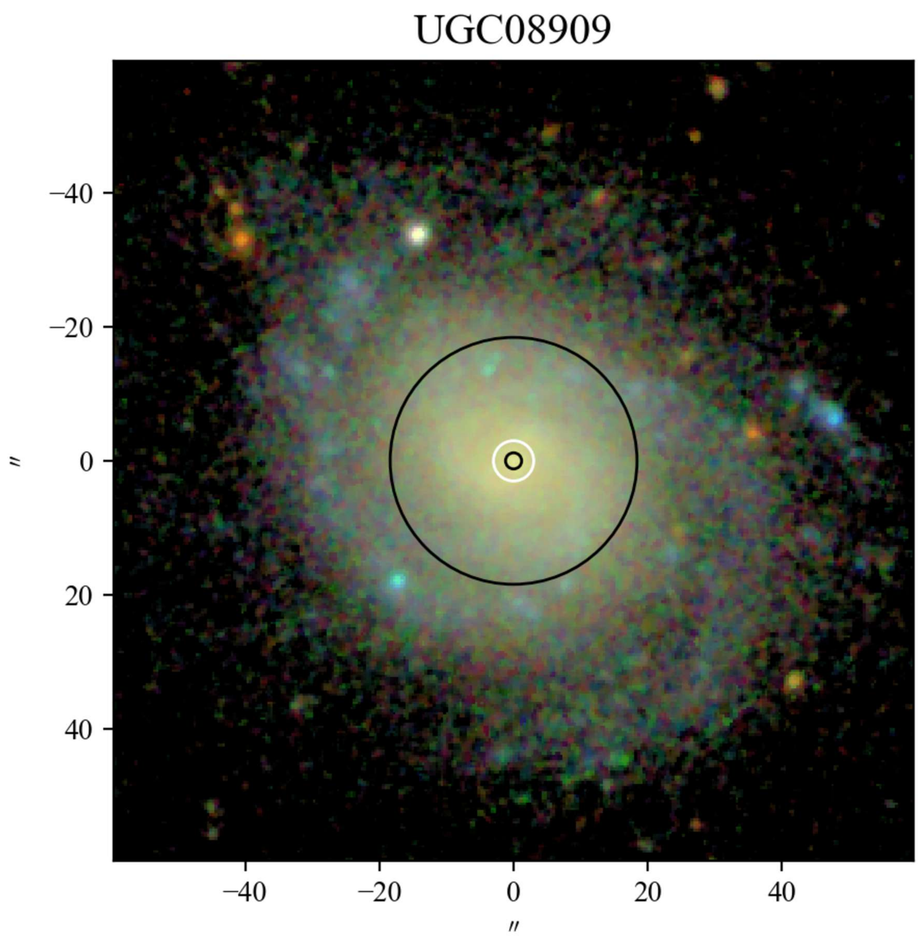
UGC08909
−40
−20
0
20
40
″
−40
−20
0
20
40
″

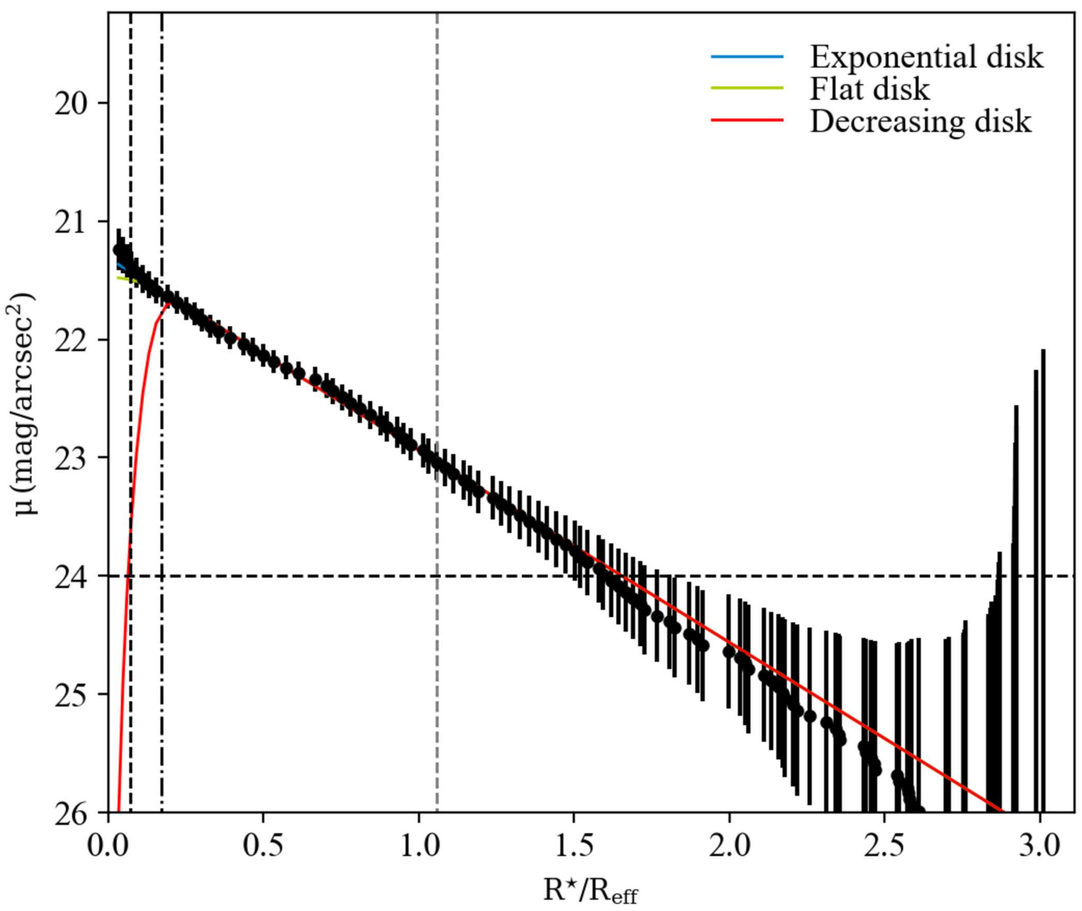
Exponential disk
Flat disk
Decreasing disk
μ (mag/arcsec²)
20
21
22
23
24
25
26
0.0
0.5
1.0
1.5
2.0
2.5
3.0
R⋆/Reff

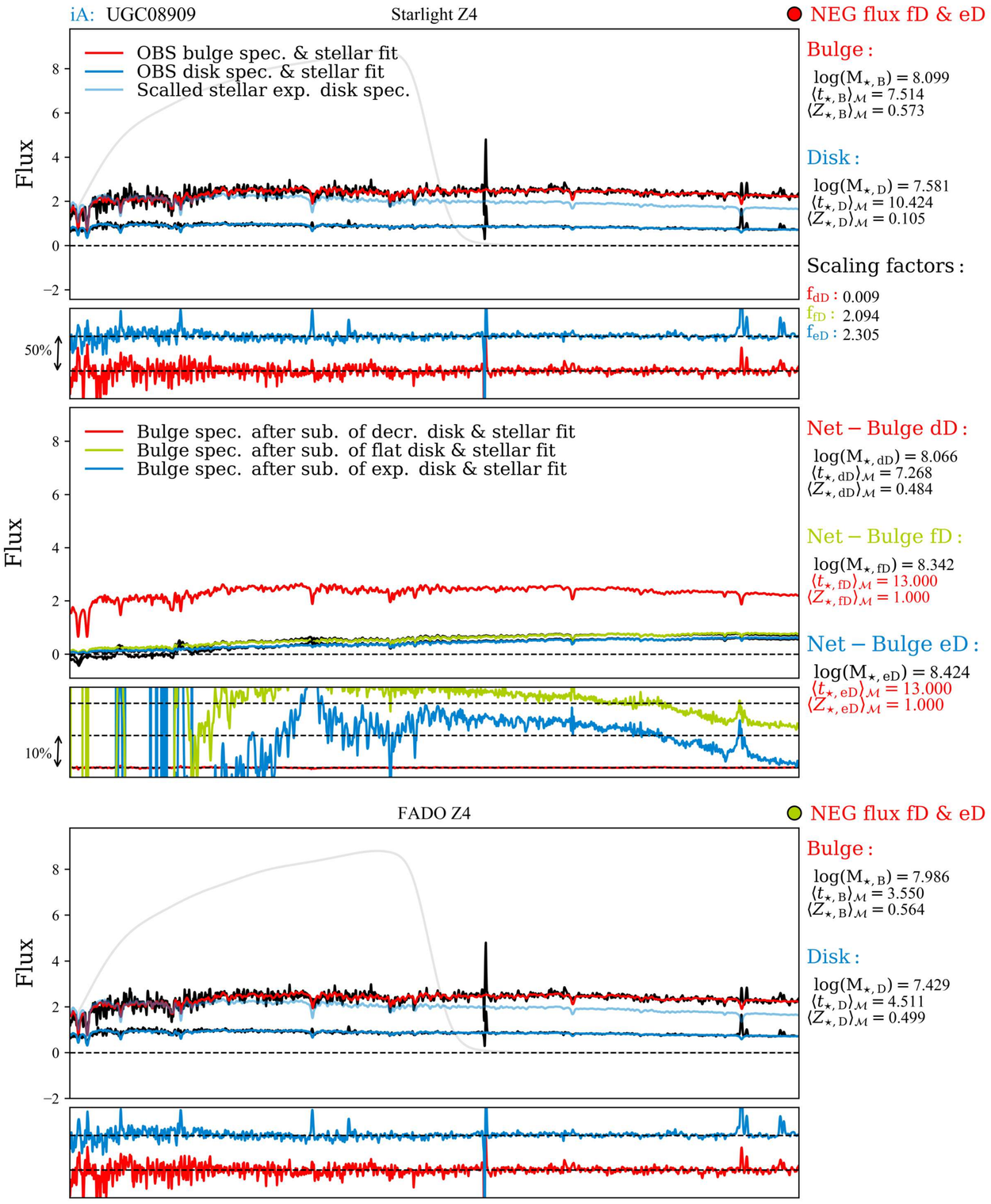
iA: UGC08909
Starlight Z4
NEG flux fD & eD
OBS bulge spec. & stellar fit
OBS disk spec. & stellar fit
Scalled stellar exp. disk spec.
Flux
50%
Bulge :
log(M⋆, B) = 8.099
⟨t⋆, B⟩M = 7.514
⟨Z⋆, B⟩M = 0.573
Disk :
log(M⋆, D) = 7.581
⟨t⋆, D⟩M = 10.424
⟨Z⋆, D⟩M = 0.105
Scaling factors :
fdD : 0.009
ffD : 2.094
feD : 2.305
Bulge spec. after sub. of decr. disk & stellar fit
Bulge spec. after sub. of flat disk & stellar fit
Bulge spec. after sub. of exp. disk & stellar fit
10%
Net − Bulge dD :
log(M⋆, dD) = 8.066
⟨t⋆, dD⟩M = 7.268
⟨Z⋆, dD⟩M = 0.484
Net − Bulge fD :
log(M⋆, fD) = 8.342
⟨t⋆, fD⟩M = 13.000
⟨Z⋆, fD⟩M = 1.000
Net − Bulge eD :
log(M⋆, eD) = 8.424
⟨t⋆, eD⟩M = 13.000
⟨Z⋆, eD⟩M = 1.000

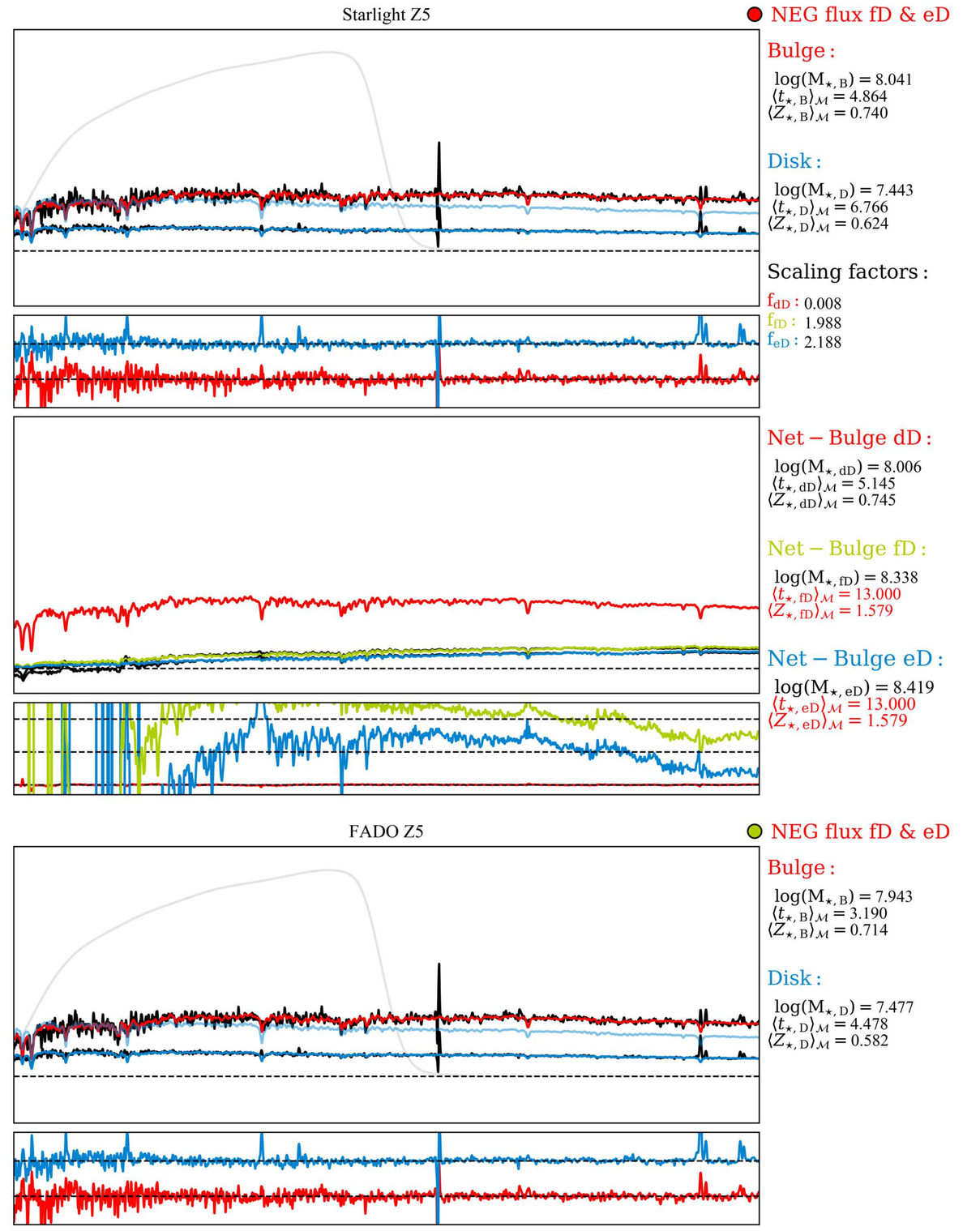
Starlight Z5
NEG flux fD & eD
Bulge :
log(M⋆, B) = 8.041
⟨t⋆, B⟩M = 4.864
⟨Z⋆, B⟩M = 0.740
Disk :
log(M⋆, D) = 7.443
⟨t⋆, D⟩M = 6.766
⟨Z⋆, D⟩M = 0.624
Scaling factors :
fdD : 0.008
ffD : 1.988
feD : 2.188
Net − Bulge dD :
log(M⋆, dD) = 8.006
⟨t⋆, dD⟩M = 5.145
⟨Z⋆, dD⟩M = 0.745
Net − Bulge fD :
log(M⋆, fD) = 8.338
⟨t⋆, fD⟩M = 13.000
⟨Z⋆, fD⟩M = 1.579
Net − Bulge eD :
log(M⋆, eD) = 8.419
⟨t⋆, eD⟩M = 13.000
⟨Z⋆, eD⟩M = 1.579

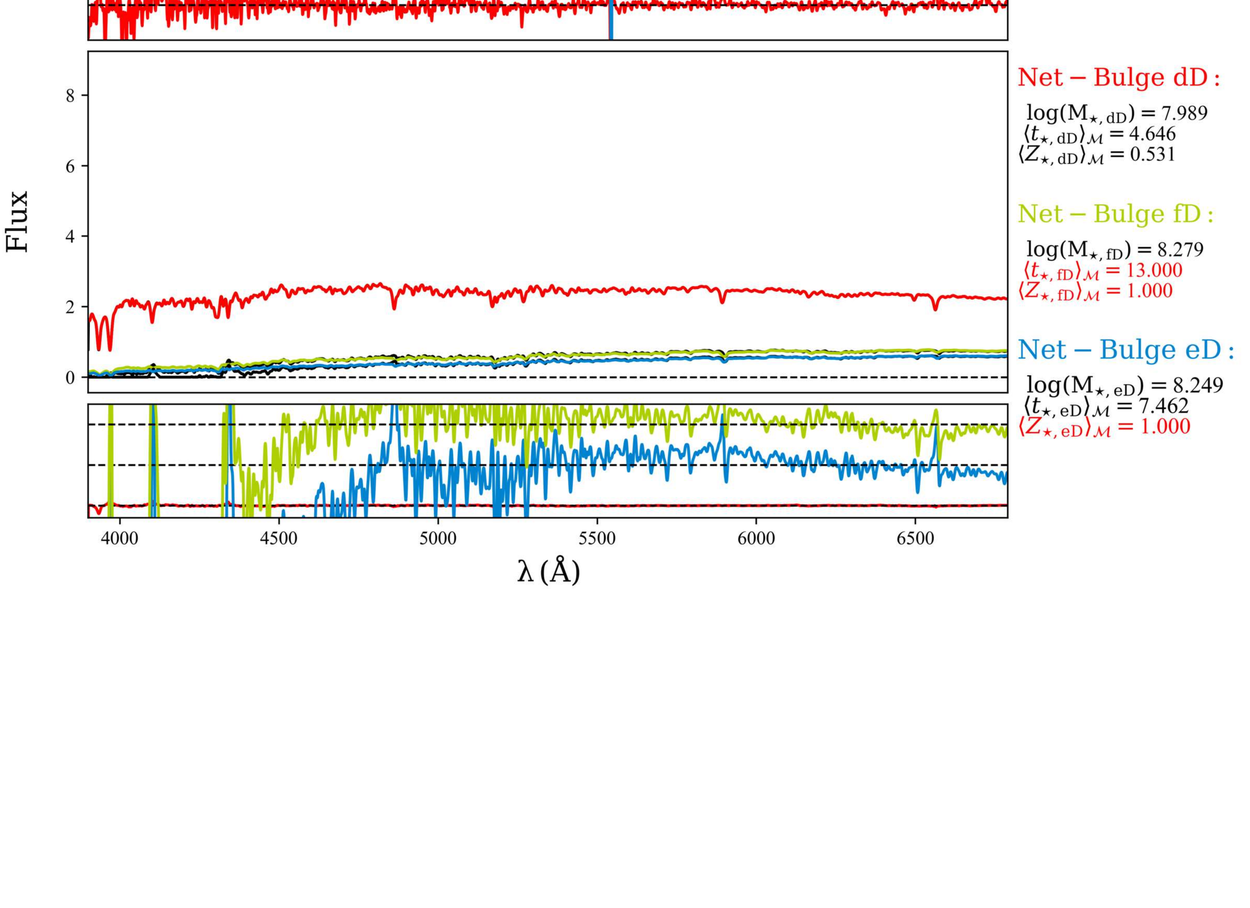
FADO Z4
NEG flux fD & eD
Flux
Bulge :
log(M⋆, B) = 7.986
⟨t⋆, B⟩M = 3.550
⟨Z⋆, B⟩M = 0.564
Disk :
log(M⋆, D) = 7.429
⟨t⋆, D⟩M = 4.511
⟨Z⋆, D⟩M = 0.499
Net − Bulge dD :
log(M⋆, dD) = 7.989
⟨t⋆, dD⟩M = 4.646
⟨Z⋆, dD⟩M = 0.531
Net − Bulge fD :
log(M⋆, fD) = 8.279
⟨t⋆, fD⟩M = 13.000
⟨Z⋆, fD⟩M = 1.000
Net − Bulge eD :
log(M⋆, eD) = 8.249
⟨t⋆, eD⟩M = 7.462
⟨Z⋆, eD⟩M = 1.000
λ (Å)

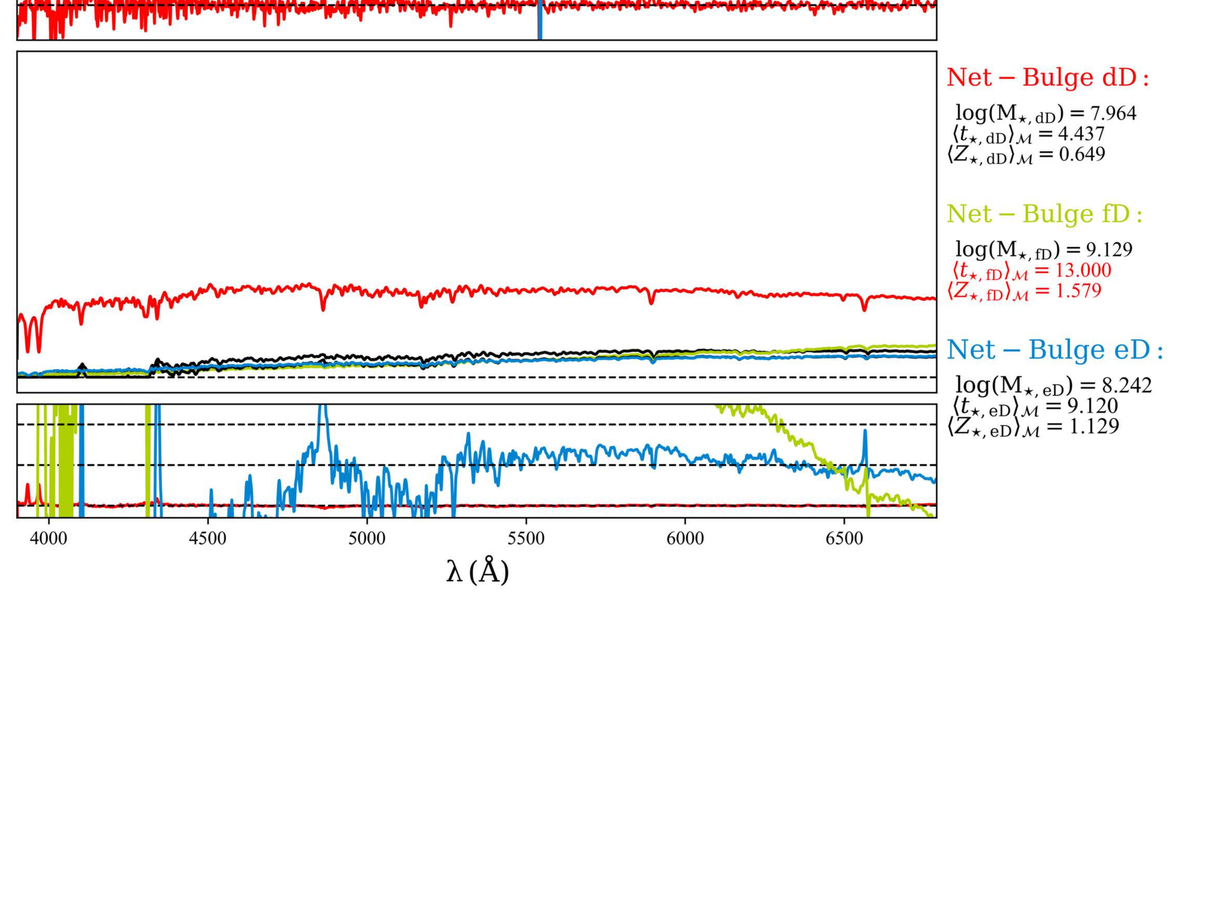
FADO Z5
NEG flux fD & eD
Bulge :
log(M⋆, B) = 7.943
⟨t⋆, B⟩M = 3.190
⟨Z⋆, B⟩M = 0.714
Disk :
log(M⋆, D) = 7.477
⟨t⋆, D⟩M = 4.478
⟨Z⋆, D⟩M = 0.582
Net − Bulge dD :
log(M⋆, dD) = 7.964
⟨t⋆, dD⟩M = 4.437
⟨Z⋆, dD⟩M = 0.649
Net − Bulge fD :
log(M⋆, fD) = 9.129
⟨t⋆, fD⟩M = 13.000
⟨Z⋆, fD⟩M = 1.579
Net − Bulge eD :
log(M⋆, eD) = 8.242
⟨t⋆, eD⟩M = 9.120
⟨Z⋆, eD⟩M = 1.129
λ (Å)

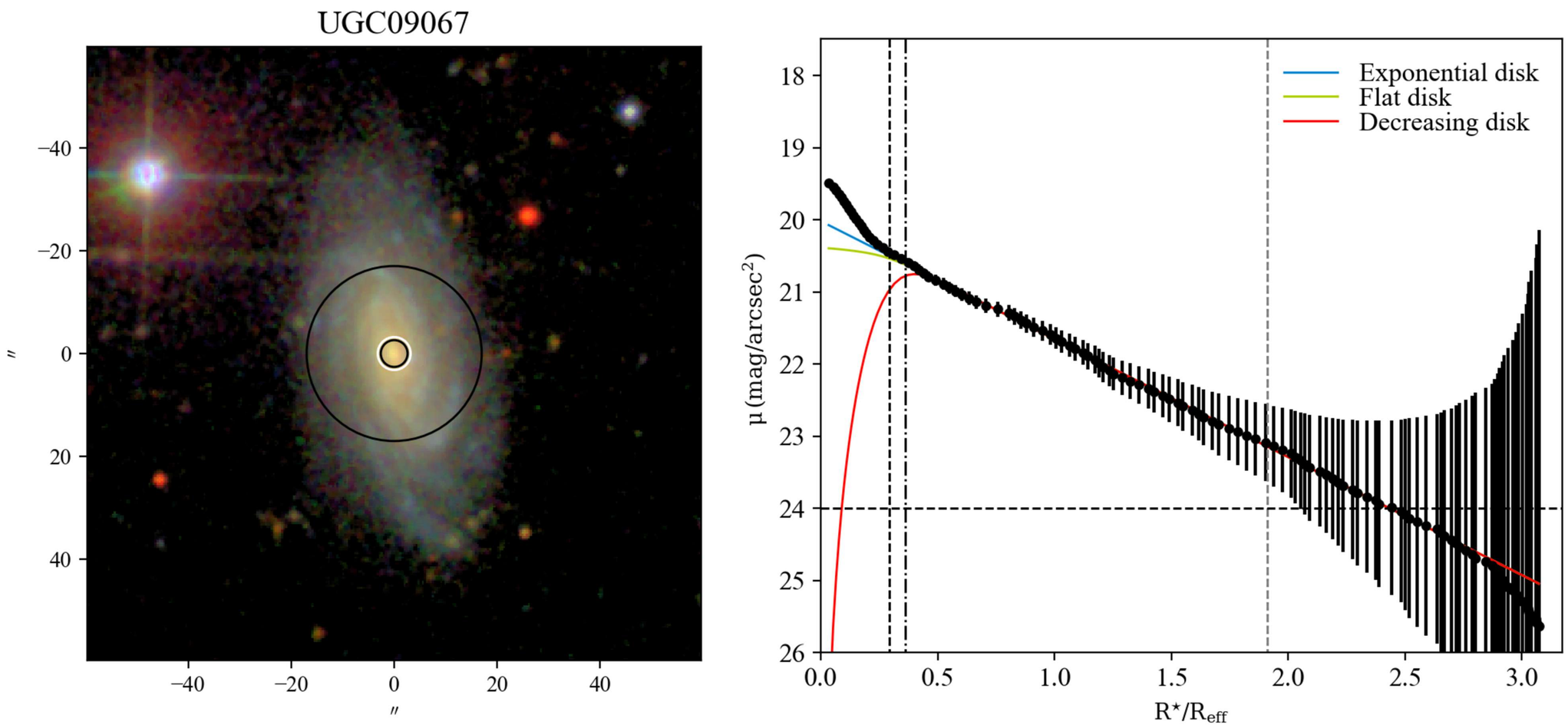
UGC09067
Exponential disk
Flat disk
Decreasing disk
μ (mag/arcsec²)
R⋆/Reff

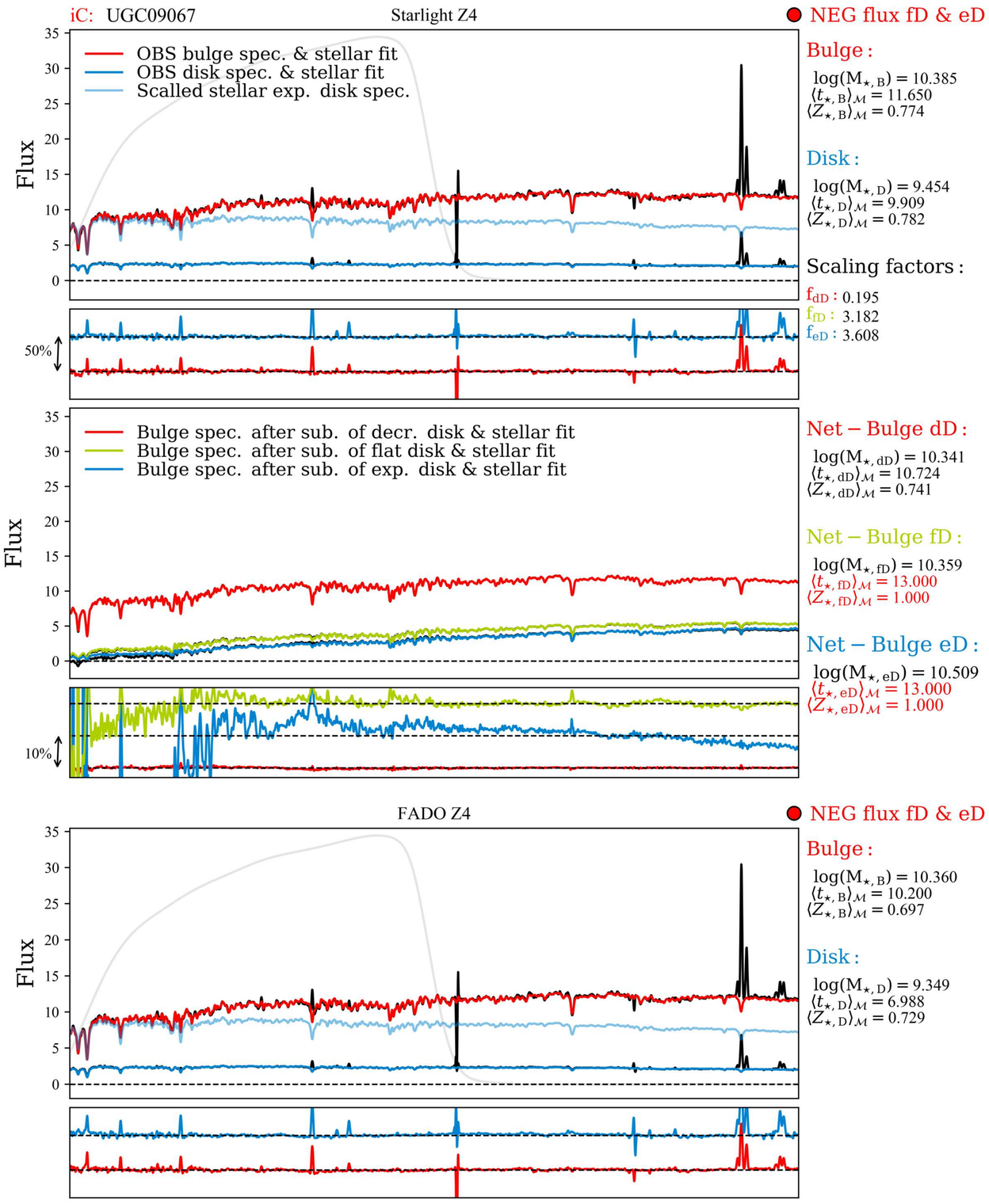
iC: UGC09067
Starlight Z4
NEG flux fD & eD
OBS bulge spec. & stellar fit
OBS disk spec. & stellar fit
Scalled stellar exp. disk spec.
Flux
Bulge :
log(M⋆, B) = 10.385
⟨t⋆, B⟩M = 11.650
⟨Z⋆, B⟩M = 0.774
Disk :
log(M⋆, D) = 9.454
⟨t⋆, B⟩M = 9.909
⟨Z⋆, B⟩M = 0.782
Scaling factors :
fdD : 0.195
ffD : 3.182
feD : 3.608
50%
Bulge spec. after sub. of decr. disk & stellar fit
Bulge spec. after sub. of flat disk & stellar fit
Bulge spec. after sub. of exp. disk & stellar fit
Net − Bulge dD :
log(M⋆, dD) = 10.341
⟨t⋆, dD⟩M = 10.724
⟨Z⋆, dD⟩M = 0.741
Net − Bulge fD :
log(M⋆, fD) = 10.359
⟨t⋆, fD⟩M = 13.000
⟨Z⋆, fD⟩M = 1.000
Net − Bulge eD :
log(M⋆, eD) = 10.509
⟨t⋆, eD⟩M = 13.000
⟨Z⋆, eD⟩M = 1.000
10%

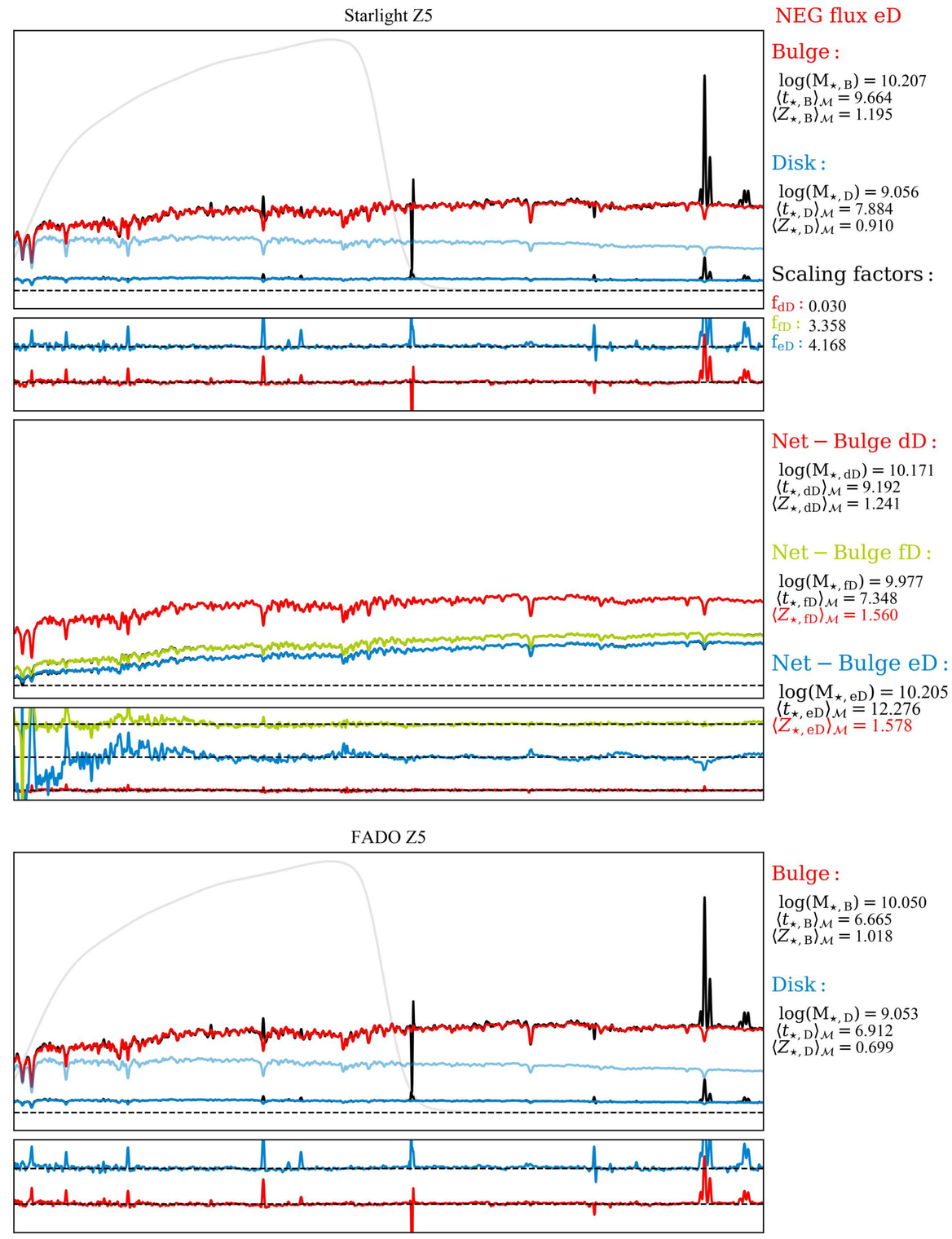
Starlight Z5
NEG flux eD
Bulge :
log(M⋆, B) = 10.207
⟨t⋆, B⟩M = 9.664
⟨Z⋆, B⟩M = 1.195
Disk :
log(M⋆, D) = 9.056
⟨t⋆, B⟩M = 7.884
⟨Z⋆, B⟩M = 0.910
Scaling factors :
fdD : 0.030
ffD : 3.358
feD : 4.168
Net − Bulge dD :
log(M⋆, dD) = 10.171
⟨t⋆, dD⟩M = 9.192
⟨Z⋆, dD⟩M = 1.241
Net − Bulge fD :
log(M⋆, fD) = 9.977
⟨t⋆, fD⟩M = 7.348
⟨Z⋆, fD⟩M = 1.560
Net − Bulge eD :
log(M⋆, eD) = 10.205
⟨t⋆, eD⟩M = 12.276
⟨Z⋆, eD⟩M = 1.578

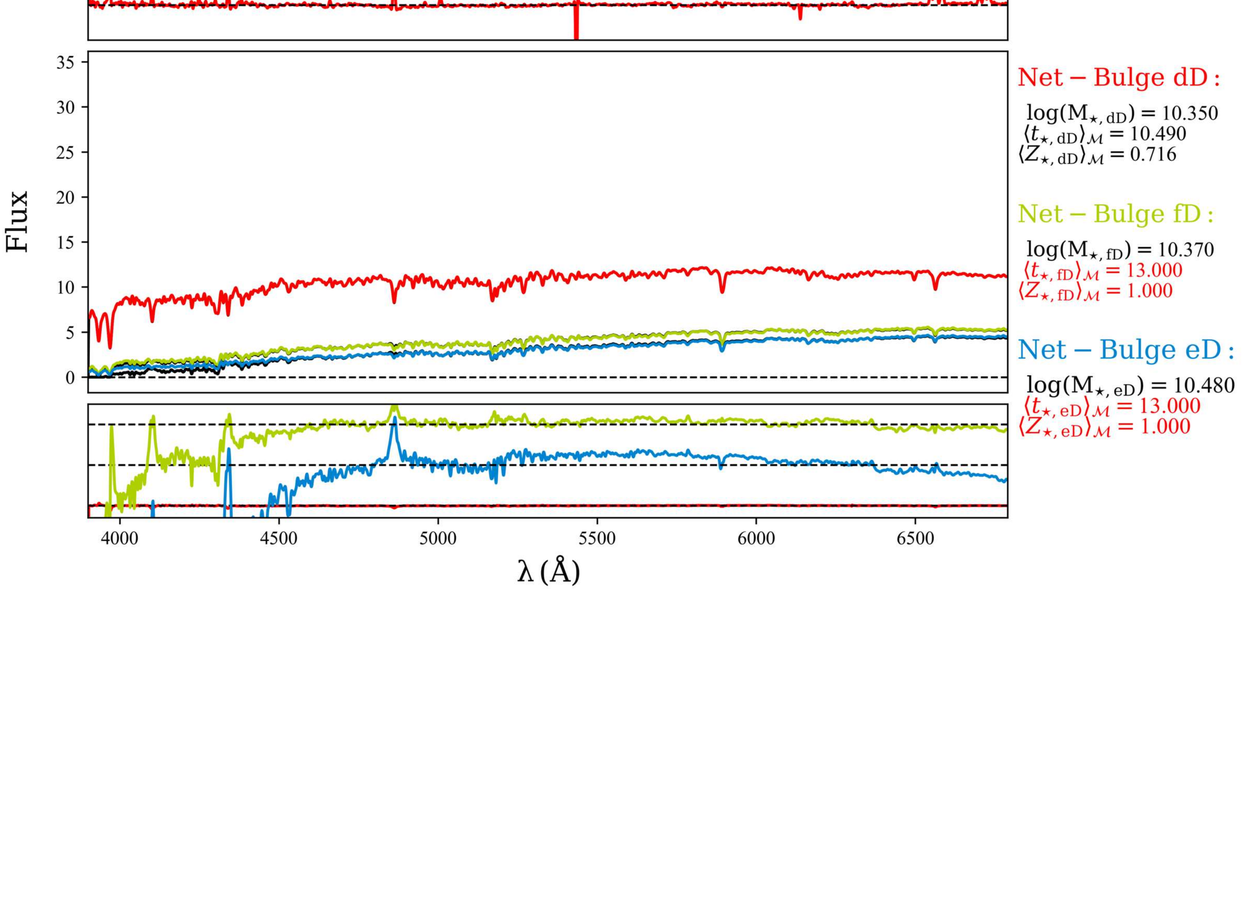
FADO Z4
NEG flux fD & eD
Flux
Bulge :
log(M⋆, B) = 10.360
⟨t⋆, B⟩M = 10.200
⟨Z⋆, B⟩M = 0.697
Disk :
log(M⋆, D) = 9.349
⟨t⋆, B⟩M = 6.988
⟨Z⋆, B⟩M = 0.729
Net − Bulge dD :
log(M⋆, dD) = 10.350
⟨t⋆, dD⟩M = 10.490
⟨Z⋆, dD⟩M = 0.716
Net − Bulge fD :
log(M⋆, fD) = 10.370
⟨t⋆, fD⟩M = 13.000
⟨Z⋆, fD⟩M = 1.000
Net − Bulge eD :
log(M⋆, eD) = 10.480
⟨t⋆, eD⟩M = 13.000
⟨Z⋆, eD⟩M = 1.000
λ (Å)

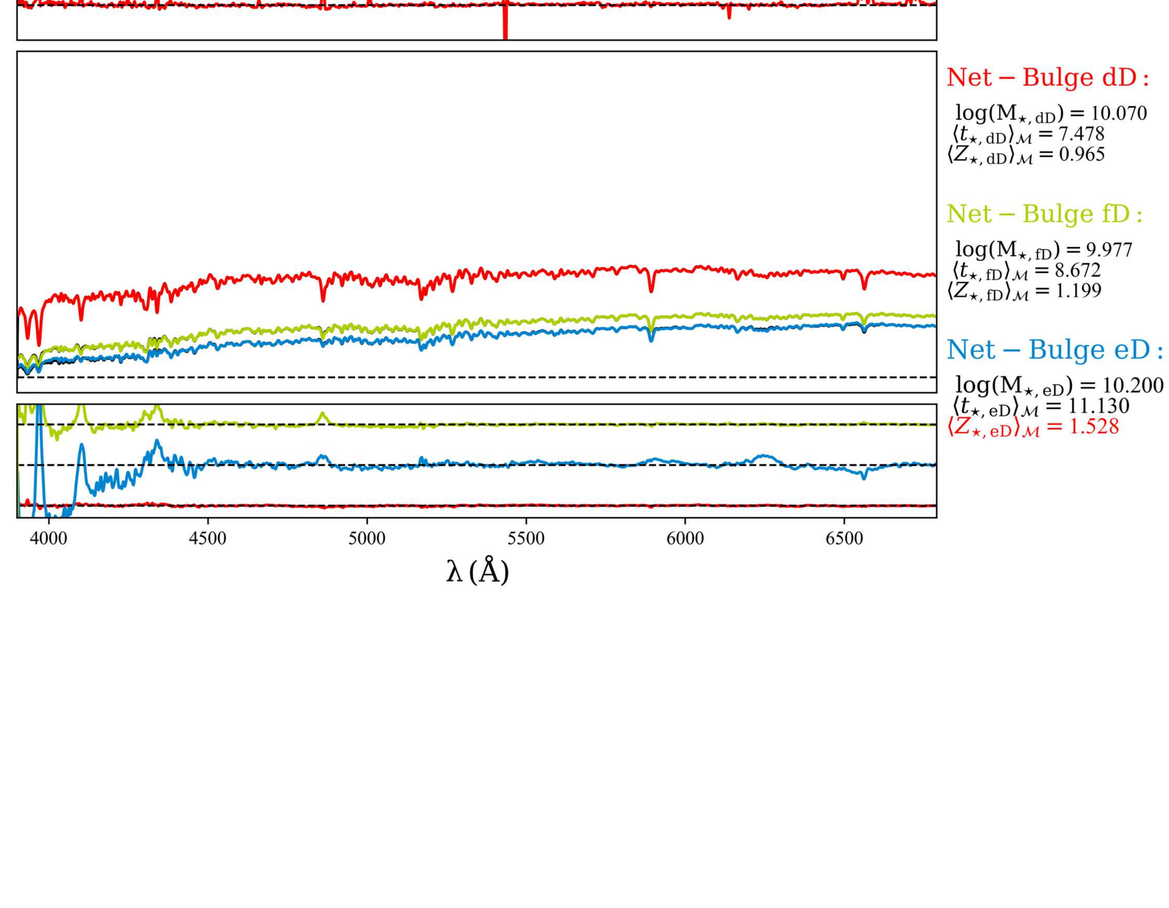
FADO Z5
Bulge :
log(M⋆, B) = 10.050
⟨t⋆, B⟩M = 6.665
⟨Z⋆, B⟩M = 1.018
Disk :
log(M⋆, D) = 9.053
⟨t⋆, B⟩M = 6.912
⟨Z⋆, B⟩M = 0.699
Net − Bulge dD :
log(M⋆, dD) = 10.070
⟨t⋆, dD⟩M = 7.478
⟨Z⋆, dD⟩M = 0.965
Net − Bulge fD :
log(M⋆, fD) = 9.977
⟨t⋆, fD⟩M = 8.672
⟨Z⋆, fD⟩M = 1.199
Net − Bulge eD :
log(M⋆, eD) = 10.200
⟨t⋆, eD⟩M = 11.130
⟨Z⋆, eD⟩M = 1.528
λ (Å)

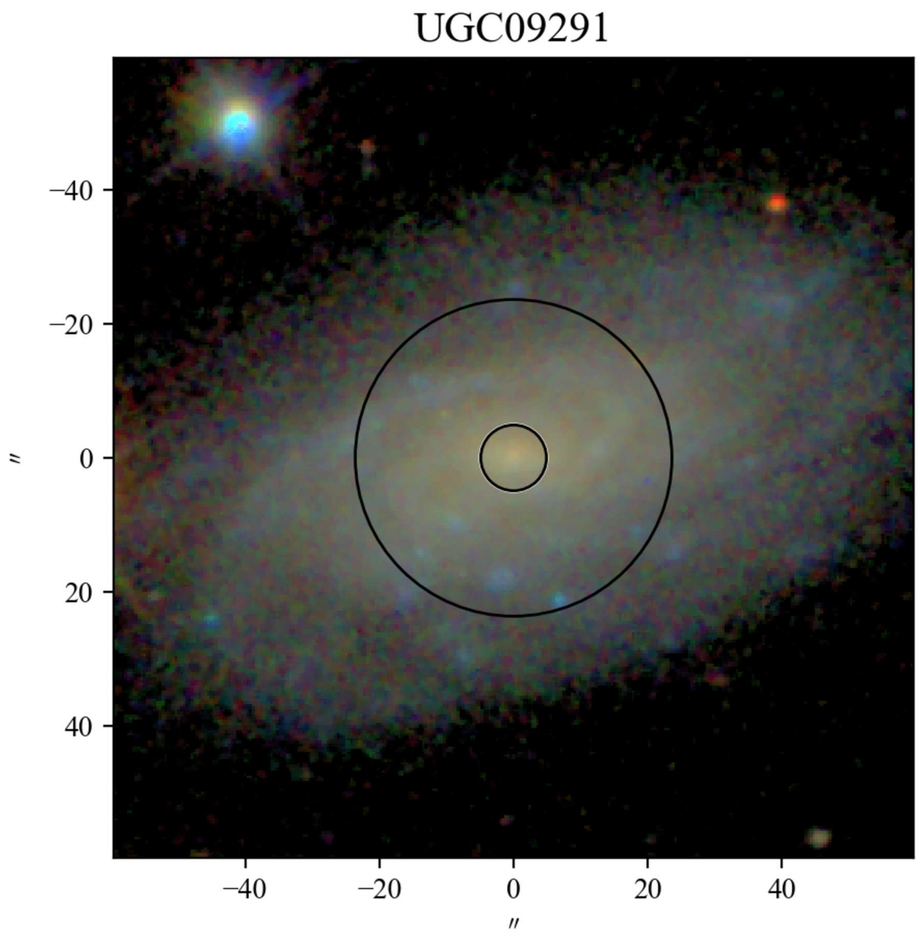
UGC09291
−40
−20
0
20
40
″
−40
−20
0
20
40
″

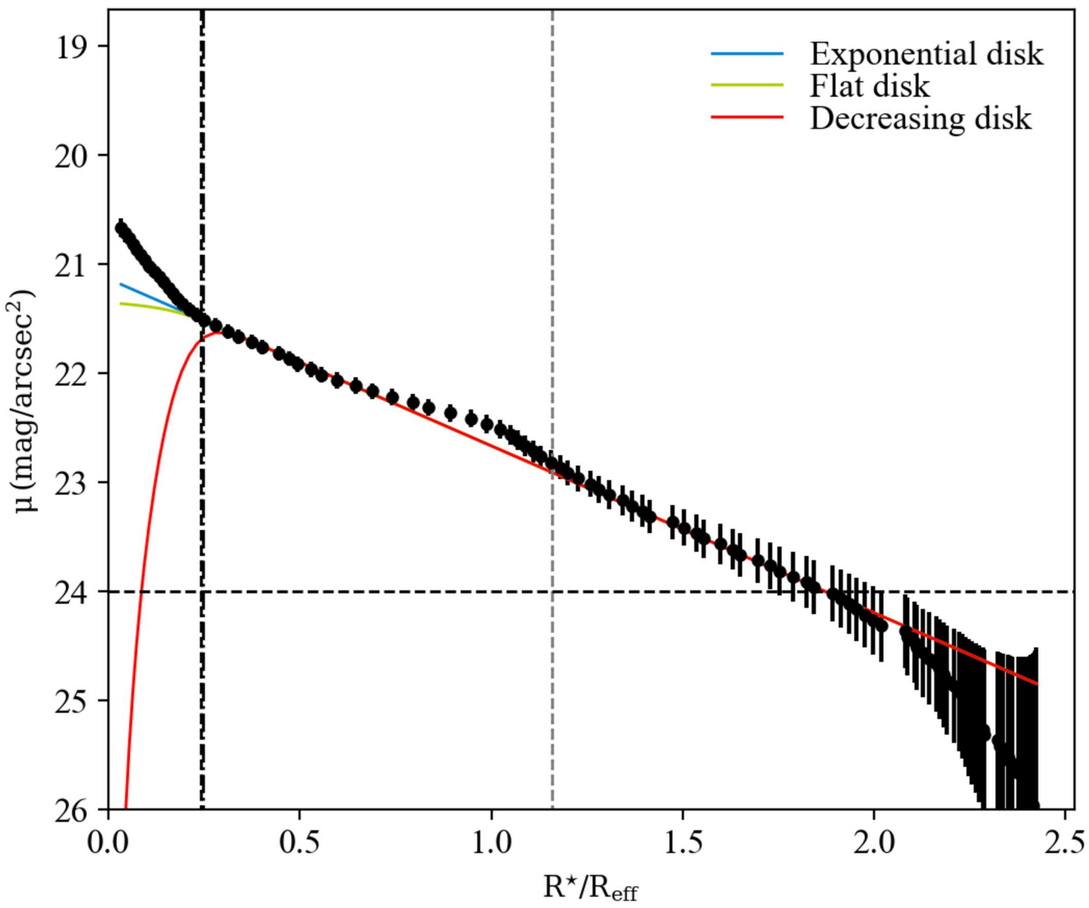
Exponential disk
Flat disk
Decreasing disk
μ (mag/arcsec²)
19
20
21
22
23
24
25
26
0.0
0.5
1.0
1.5
2.0
2.5
R⋆/Reff

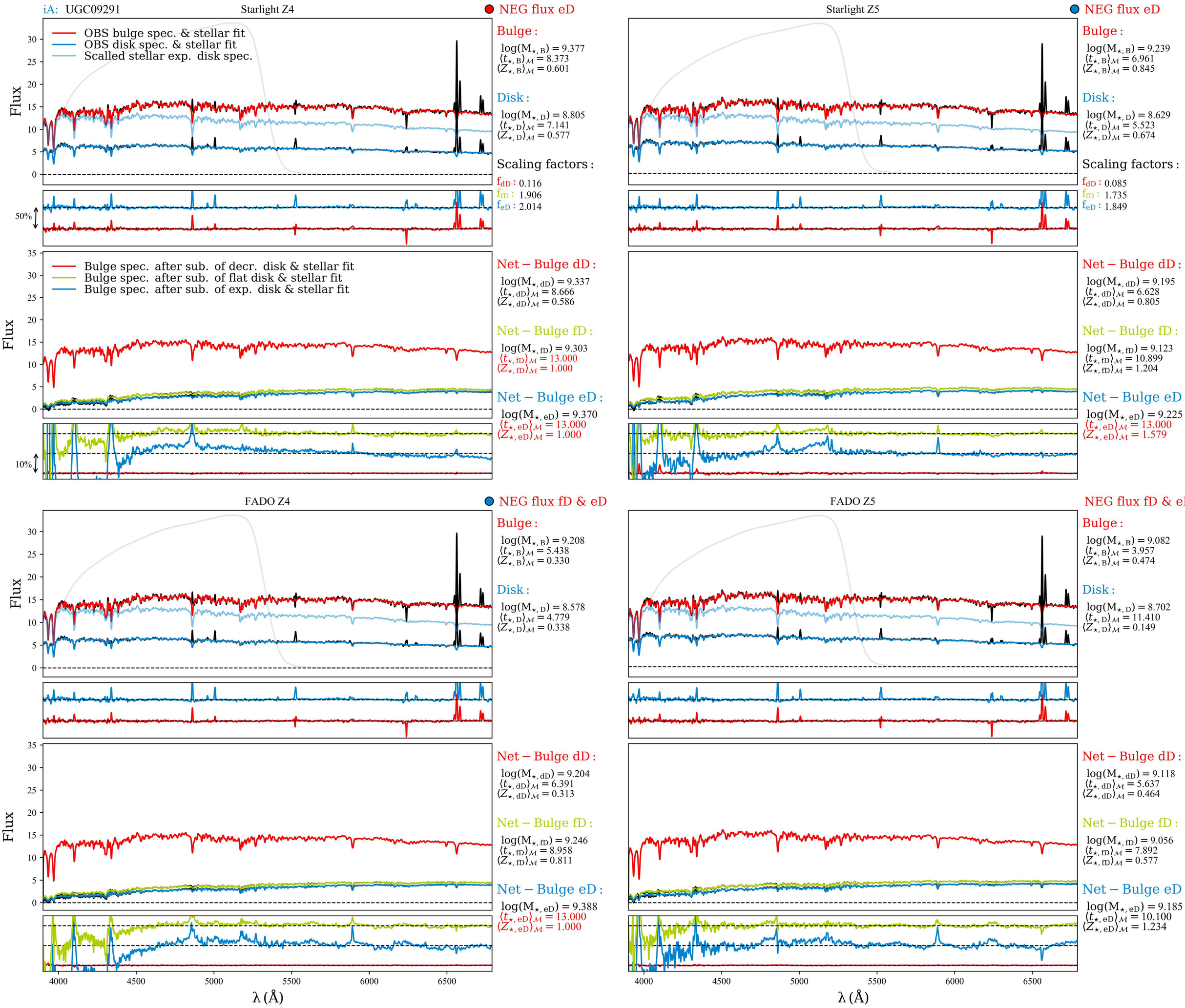
iA: UGC09291
Starlight Z4
NEG flux eD
OBS bulge spec. & stellar fit
OBS disk spec. & stellar fit
Scalled stellar exp. disk spec.
Flux
50%
Bulge :
log(M⋆, B) = 9.377
⟨t⋆, B⟩M = 8.373
⟨Z⋆, B⟩M = 0.601
Disk :
log(M⋆, D) = 8.805
⟨t⋆, D⟩M = 7.141
⟨Z⋆, D⟩M = 0.577
Scaling factors :
fdD : 0.116
ffD : 1.906
feD : 2.014
Starlight Z5
NEG flux eD
Bulge :
log(M⋆, B) = 9.239
⟨t⋆, B⟩M = 6.961
⟨Z⋆, B⟩M = 0.845
Disk :
log(M⋆, D) = 8.629
⟨t⋆, D⟩M = 5.523
⟨Z⋆, D⟩M = 0.674
Scaling factors :
fdD : 0.085
ffD : 1.735
feD : 1.849
Bulge spec. after sub. of decr. disk & stellar fit
Bulge spec. after sub. of flat disk & stellar fit
Bulge spec. after sub. of exp. disk & stellar fit
10%
Net − Bulge dD :
log(M⋆, dD) = 9.337
⟨t⋆, dD⟩M = 8.666
⟨Z⋆, dD⟩M = 0.586
Net − Bulge fD :
log(M⋆, fD) = 9.303
⟨t⋆, fD⟩M = 13.000
⟨Z⋆, fD⟩M = 1.000
Net − Bulge eD :
log(M⋆, eD) = 9.370
⟨t⋆, eD⟩M = 13.000
⟨Z⋆, eD⟩M = 1.000
Net − Bulge dD :
log(M⋆, dD) = 9.195
⟨t⋆, dD⟩M = 6.628
⟨Z⋆, dD⟩M = 0.805
Net − Bulge fD :
log(M⋆, fD) = 9.123
⟨t⋆, fD⟩M = 10.899
⟨Z⋆, fD⟩M = 1.204
Net − Bulge eD :
log(M⋆, eD) = 9.225
⟨t⋆, eD⟩M = 13.000
⟨Z⋆, eD⟩M = 1.579
FADO Z4
NEG flux fD & eD
Bulge :
log(M⋆, B) = 9.208
⟨t⋆, B⟩M = 5.438
⟨Z⋆, B⟩M = 0.330
Disk :
log(M⋆, D) = 8.578
⟨t⋆, D⟩M = 4.779
⟨Z⋆, D⟩M = 0.338
Net − Bulge dD :
log(M⋆, dD) = 9.204
⟨t⋆, dD⟩M = 6.391
⟨Z⋆, dD⟩M = 0.313
Net − Bulge fD :
log(M⋆, fD) = 9.246
⟨t⋆, fD⟩M = 8.958
⟨Z⋆, fD⟩M = 0.811
Net − Bulge eD :
log(M⋆, eD) = 9.388
⟨t⋆, eD⟩M = 13.000
⟨Z⋆, eD⟩M = 1.000
FADO Z5
NEG flux fD & eD
Bulge :
log(M⋆, B) = 9.082
⟨t⋆, B⟩M = 3.957
⟨Z⋆, B⟩M = 0.474
Disk :
log(M⋆, D) = 8.702
⟨t⋆, D⟩M = 11.410
⟨Z⋆, D⟩M = 0.149
Net − Bulge dD :
log(M⋆, dD) = 9.118
⟨t⋆, dD⟩M = 5.637
⟨Z⋆, dD⟩M = 0.464
Net − Bulge fD :
log(M⋆, fD) = 9.056
⟨t⋆, fD⟩M = 7.892
⟨Z⋆, fD⟩M = 0.577
Net − Bulge eD :
log(M⋆, eD) = 9.185
⟨t⋆, eD⟩M = 10.100
⟨Z⋆, eD⟩M = 1.234
λ (Å)

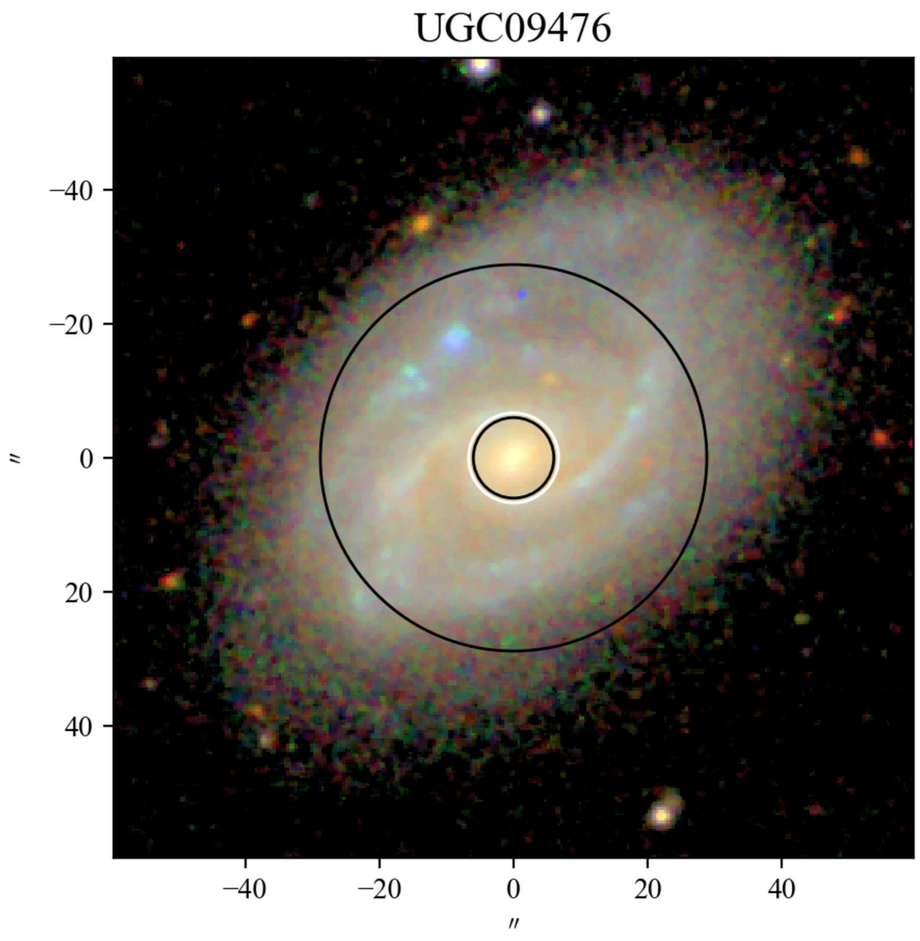
UGC09476
−40
−20
0
20
40
″

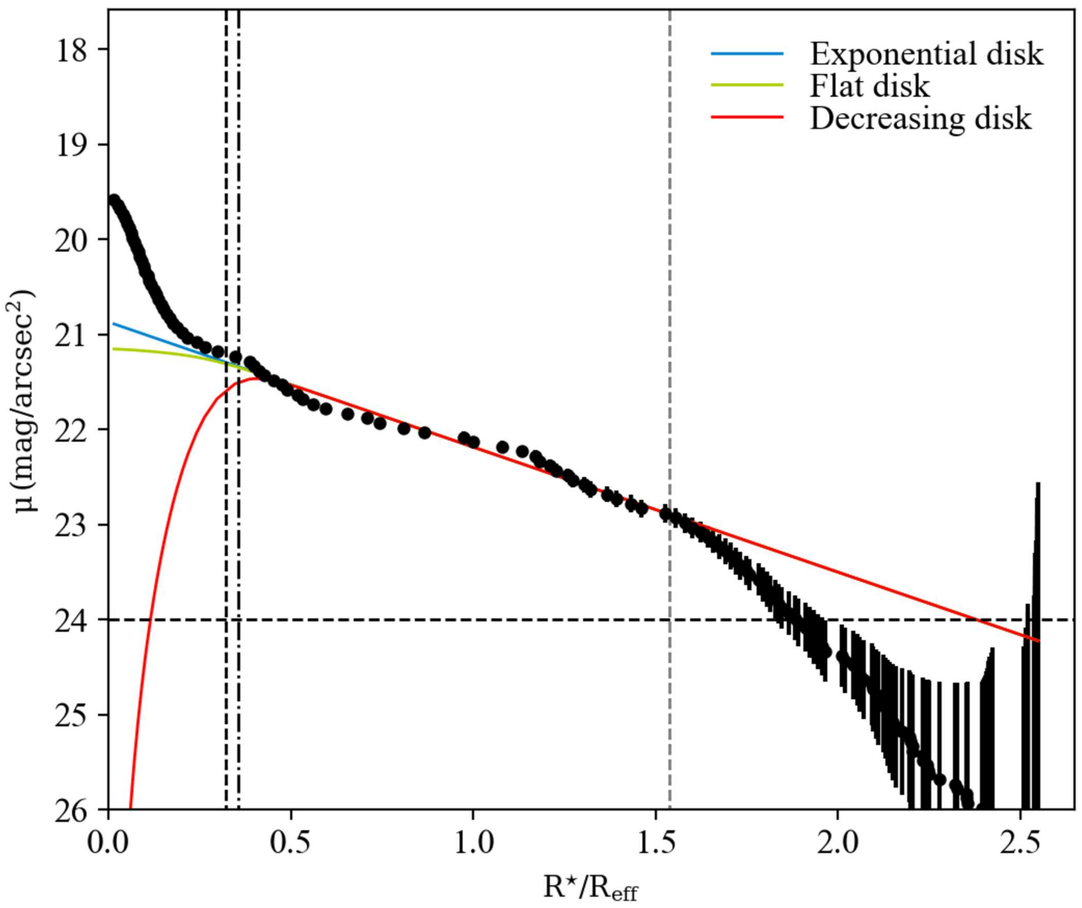
Exponential disk
Flat disk
Decreasing disk
μ (mag/arcsec²)
R⋆/Reff

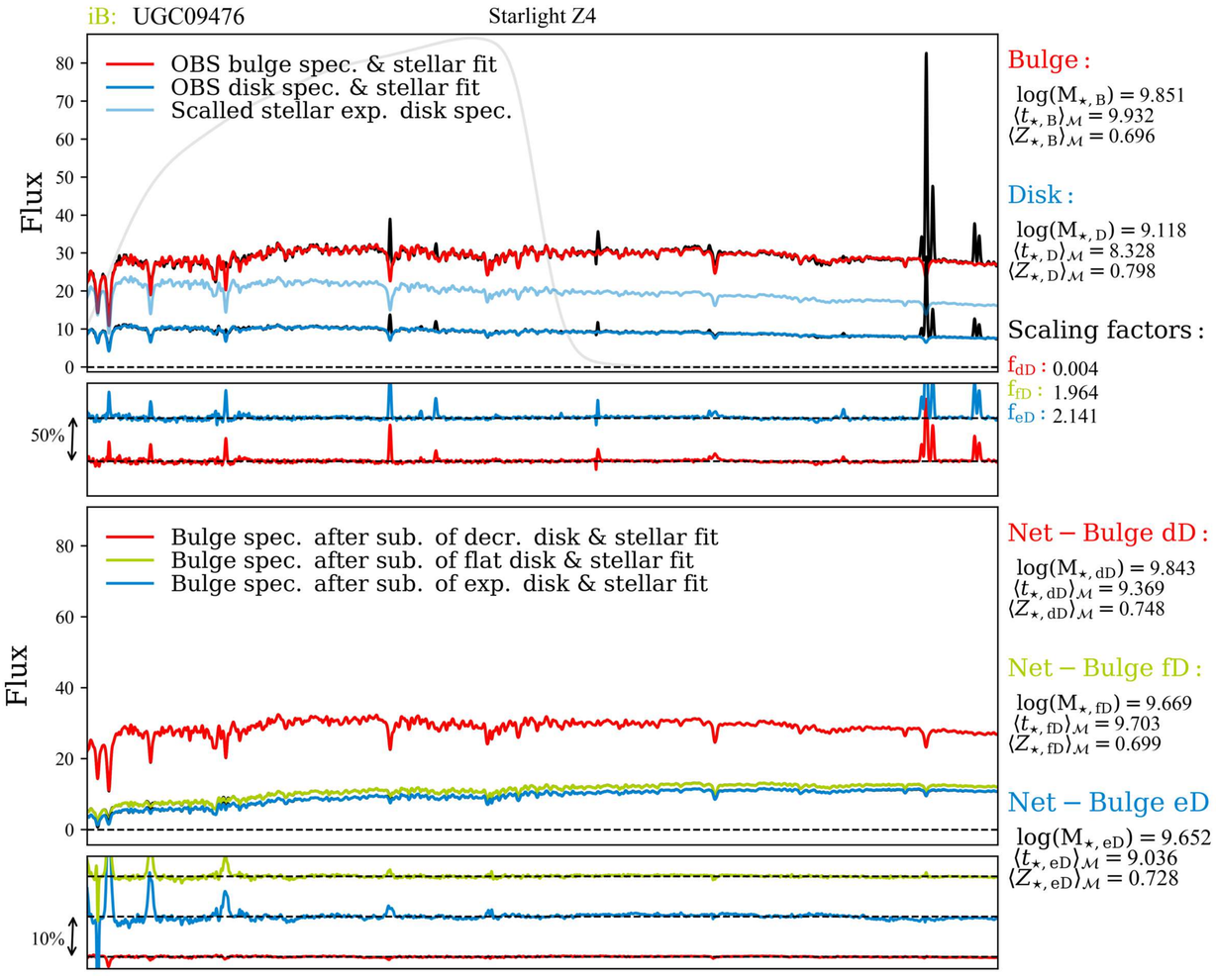
iB: UGC09476
Starlight Z4
OBS bulge spec. & stellar fit
OBS disk spec. & stellar fit
Scalled stellar exp. disk spec.
Flux
50%
Bulge :
log(M⋆, B) = 9.851
⟨t⋆, B⟩M = 9.932
⟨Z⋆, B⟩M = 0.696
Disk :
log(M⋆, D) = 9.118
⟨t⋆, D⟩M = 8.328
⟨Z⋆, D⟩M = 0.798
Scaling factors :
fdD : 0.004
ffD : 1.964
feD : 2.141

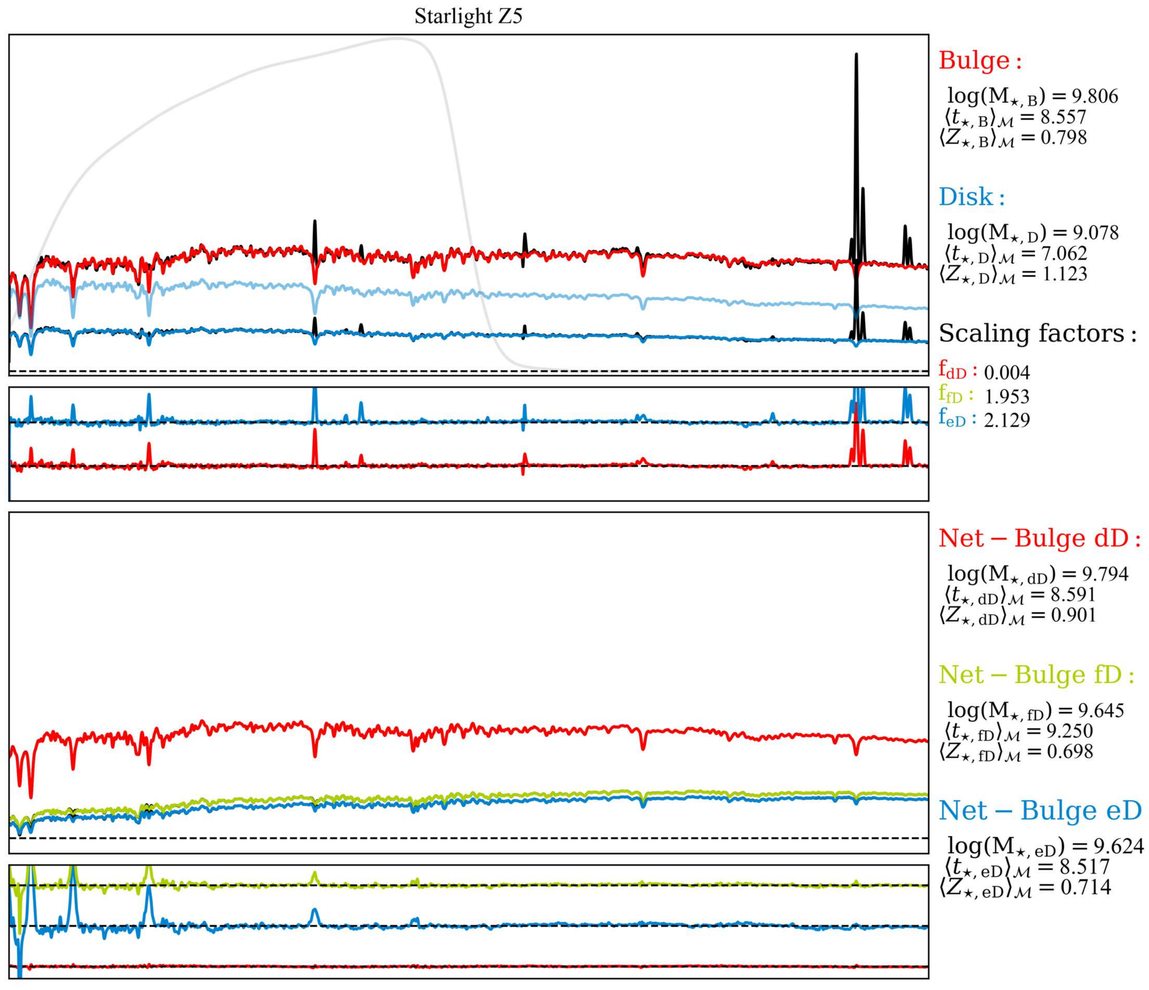
Starlight Z5
Bulge :
log(M⋆, B) = 9.806
⟨t⋆, B⟩M = 8.557
⟨Z⋆, B⟩M = 0.798
Disk :
log(M⋆, D) = 9.078
⟨t⋆, D⟩M = 7.062
⟨Z⋆, D⟩M = 1.123
Scaling factors :
fdD : 0.004
ffD : 1.953
feD : 2.129

Bulge spec. after sub. of decr. disk & stellar fit
Bulge spec. after sub. of flat disk & stellar fit
Bulge spec. after sub. of exp. disk & stellar fit
Flux
10%
Net − Bulge dD :
log(M⋆, dD) = 9.843
⟨t⋆, dD⟩M = 9.369
⟨Z⋆, dD⟩M = 0.748
Net − Bulge fD :
log(M⋆, fD) = 9.669
⟨t⋆, fD⟩M = 9.703
⟨Z⋆, fD⟩M = 0.699
Net − Bulge eD :
log(M⋆, eD) = 9.652
⟨t⋆, eD⟩M = 9.036
⟨Z⋆, eD⟩M = 0.728

Net − Bulge dD :
log(M⋆, dD) = 9.794
⟨t⋆, dD⟩M = 8.591
⟨Z⋆, dD⟩M = 0.901
Net − Bulge fD :
log(M⋆, fD) = 9.645
⟨t⋆, fD⟩M = 9.250
⟨Z⋆, fD⟩M = 0.698
Net − Bulge eD :
log(M⋆, eD) = 9.624
⟨t⋆, eD⟩M = 8.517
⟨Z⋆, eD⟩M = 0.714

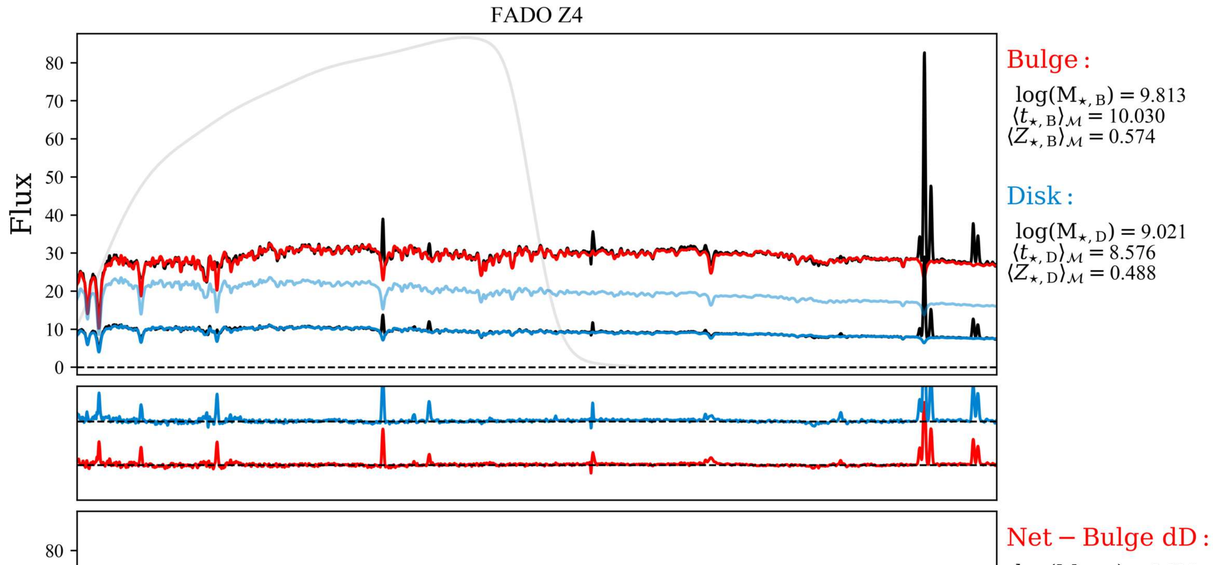
FADO Z4
Flux
Bulge :
log(M⋆, B) = 9.813
⟨t⋆, B⟩M = 10.030
⟨Z⋆, B⟩M = 0.574
Disk :
log(M⋆, D) = 9.021
⟨t⋆, D⟩M = 8.576
⟨Z⋆, D⟩M = 0.488

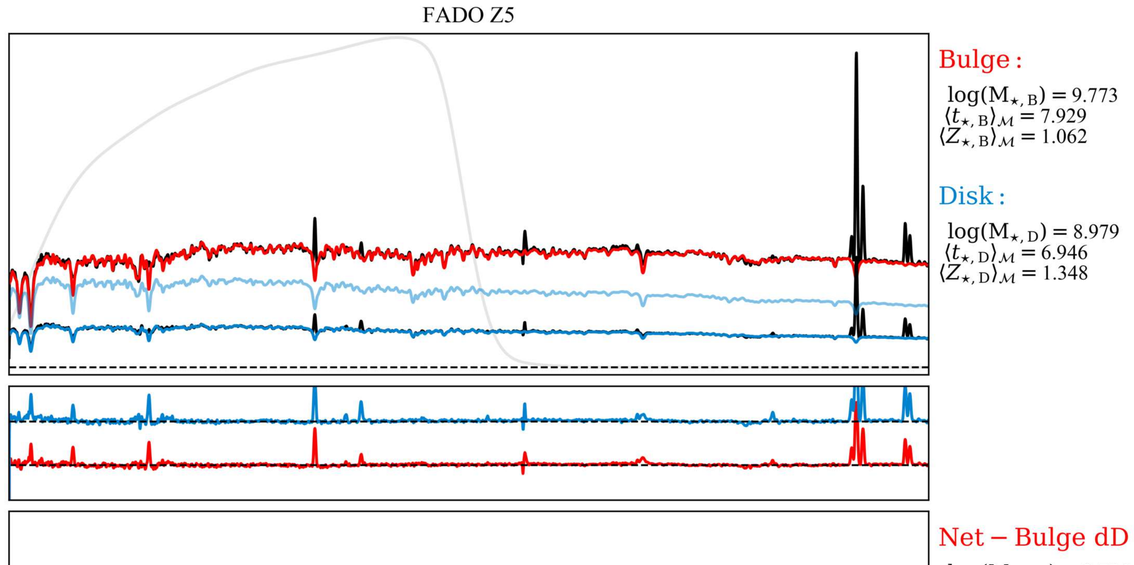
FADO Z5
Bulge :
log(M⋆, B) = 9.773
⟨t⋆, B⟩M = 7.929
⟨Z⋆, B⟩M = 1.062
Disk :
log(M⋆, D) = 8.979
⟨t⋆, D⟩M = 6.946
⟨Z⋆, D⟩M = 1.348

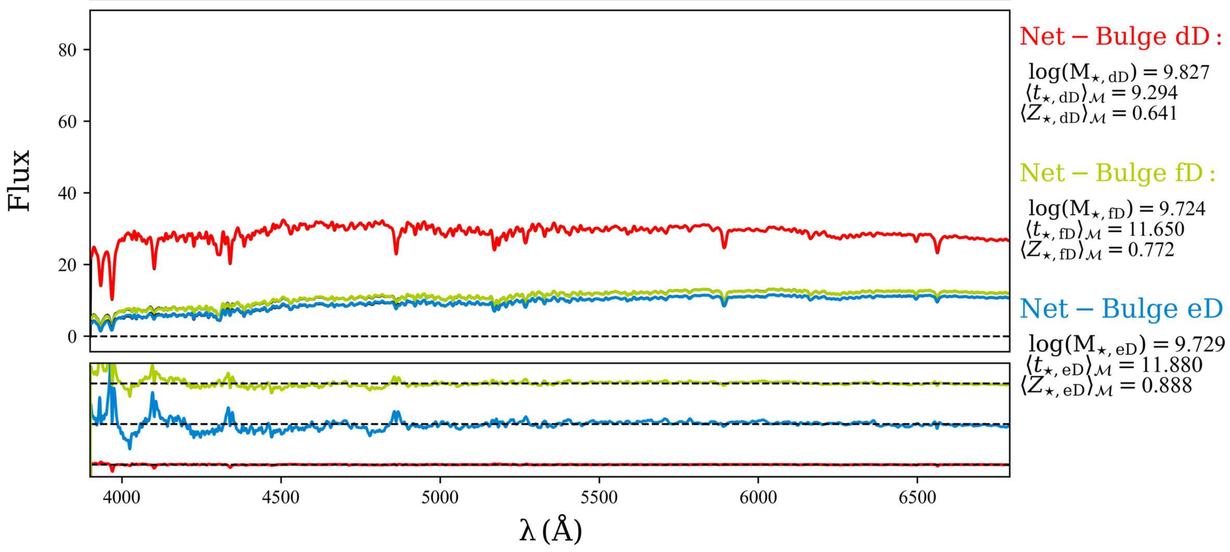
Flux
Net − Bulge dD :
log(M⋆, dD) = 9.827
⟨t⋆, dD⟩M = 9.294
⟨Z⋆, dD⟩M = 0.641
Net − Bulge fD :
log(M⋆, fD) = 9.724
⟨t⋆, fD⟩M = 11.650
⟨Z⋆, fD⟩M = 0.772
Net − Bulge eD :
log(M⋆, eD) = 9.729
⟨t⋆, eD⟩M = 11.880
⟨Z⋆, eD⟩M = 0.888
λ (Å)

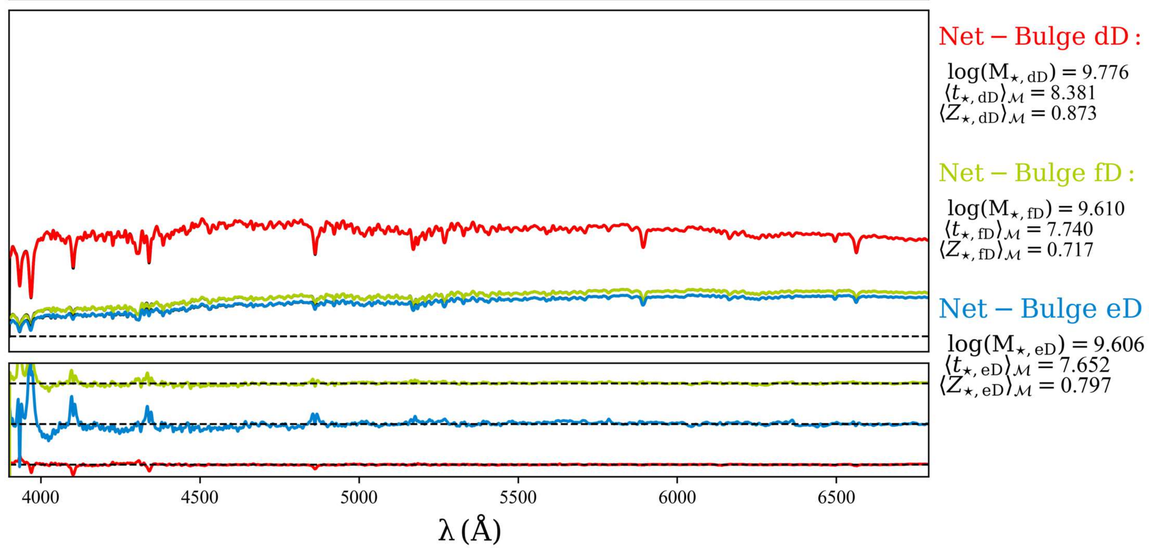
Net − Bulge dD :
log(M⋆, dD) = 9.776
⟨t⋆, dD⟩M = 8.381
⟨Z⋆, dD⟩M = 0.873
Net − Bulge fD :
log(M⋆, fD) = 9.610
⟨t⋆, fD⟩M = 7.740
⟨Z⋆, fD⟩M = 0.717
Net − Bulge eD :
log(M⋆, eD) = 9.606
⟨t⋆, eD⟩M = 7.652
⟨Z⋆, eD⟩M = 0.797
λ (Å)

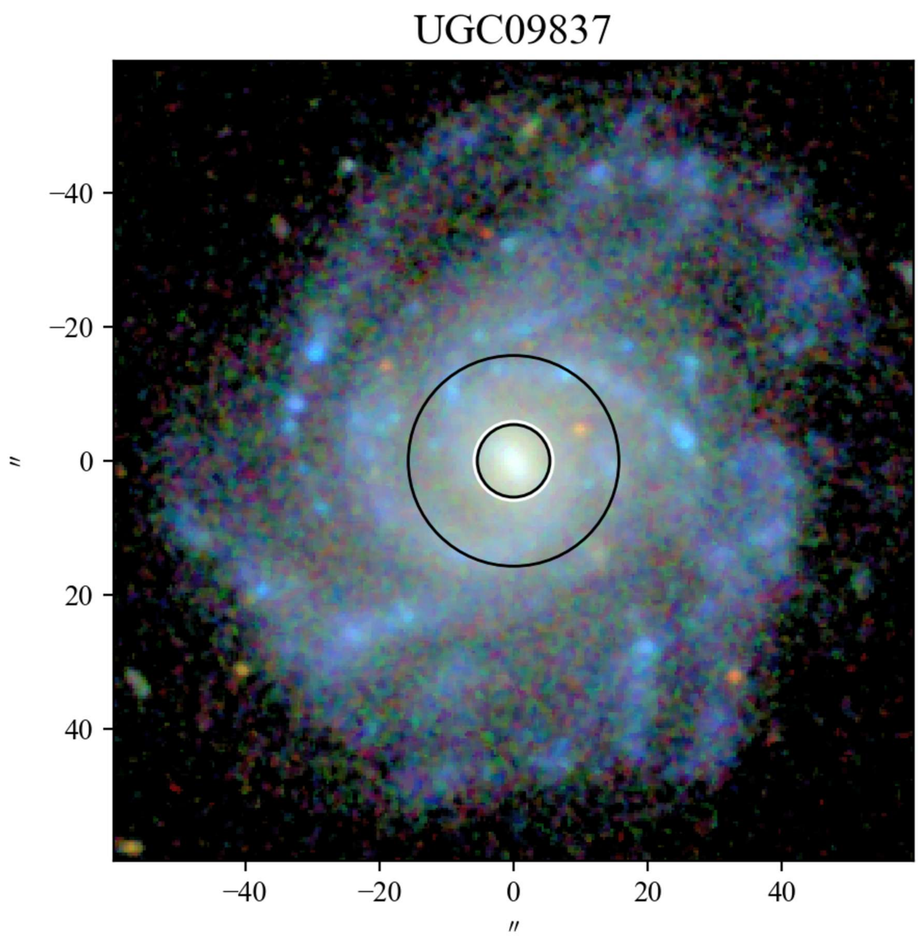
UGC09837
−40
−20
0
20
40
″
−40
−20
0
20
40
″

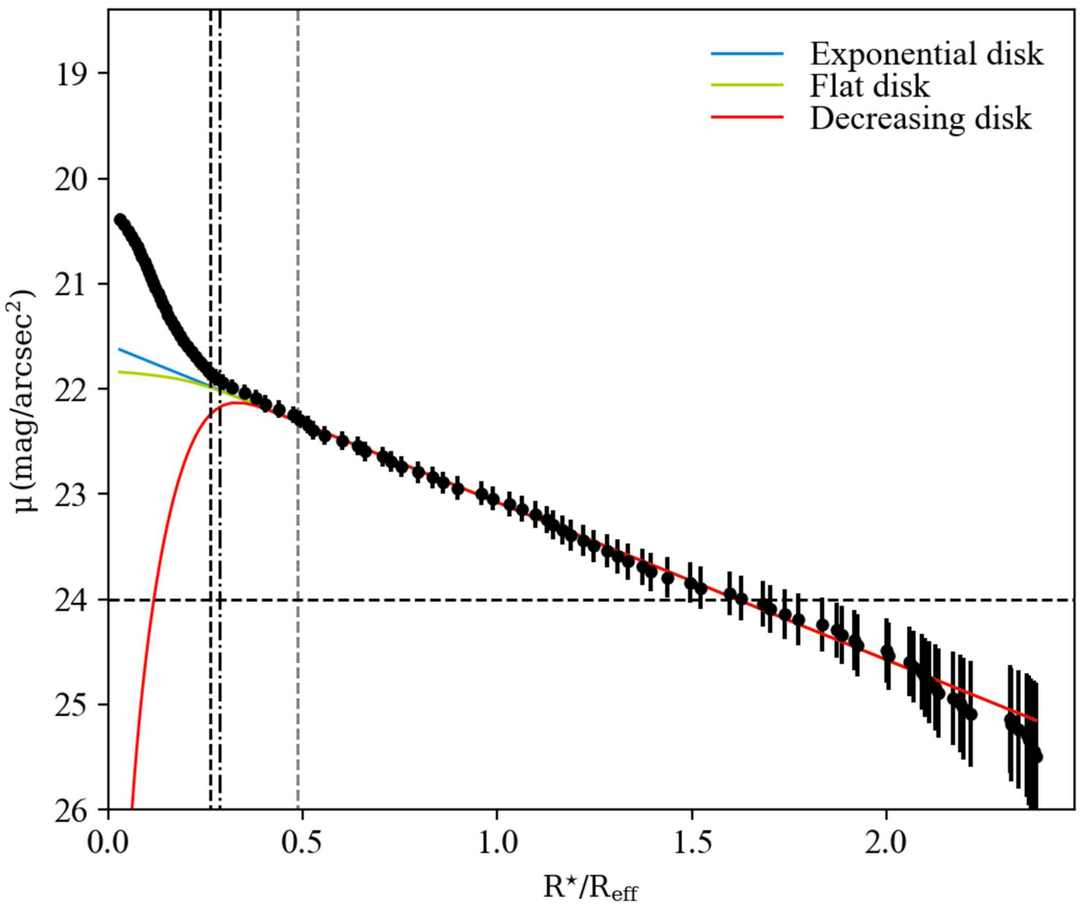
Exponential disk
Flat disk
Decreasing disk
μ (mag/arcsec²)
19
20
21
22
23
24
25
26
0.0
0.5
1.0
1.5
2.0
R⋆/Reff

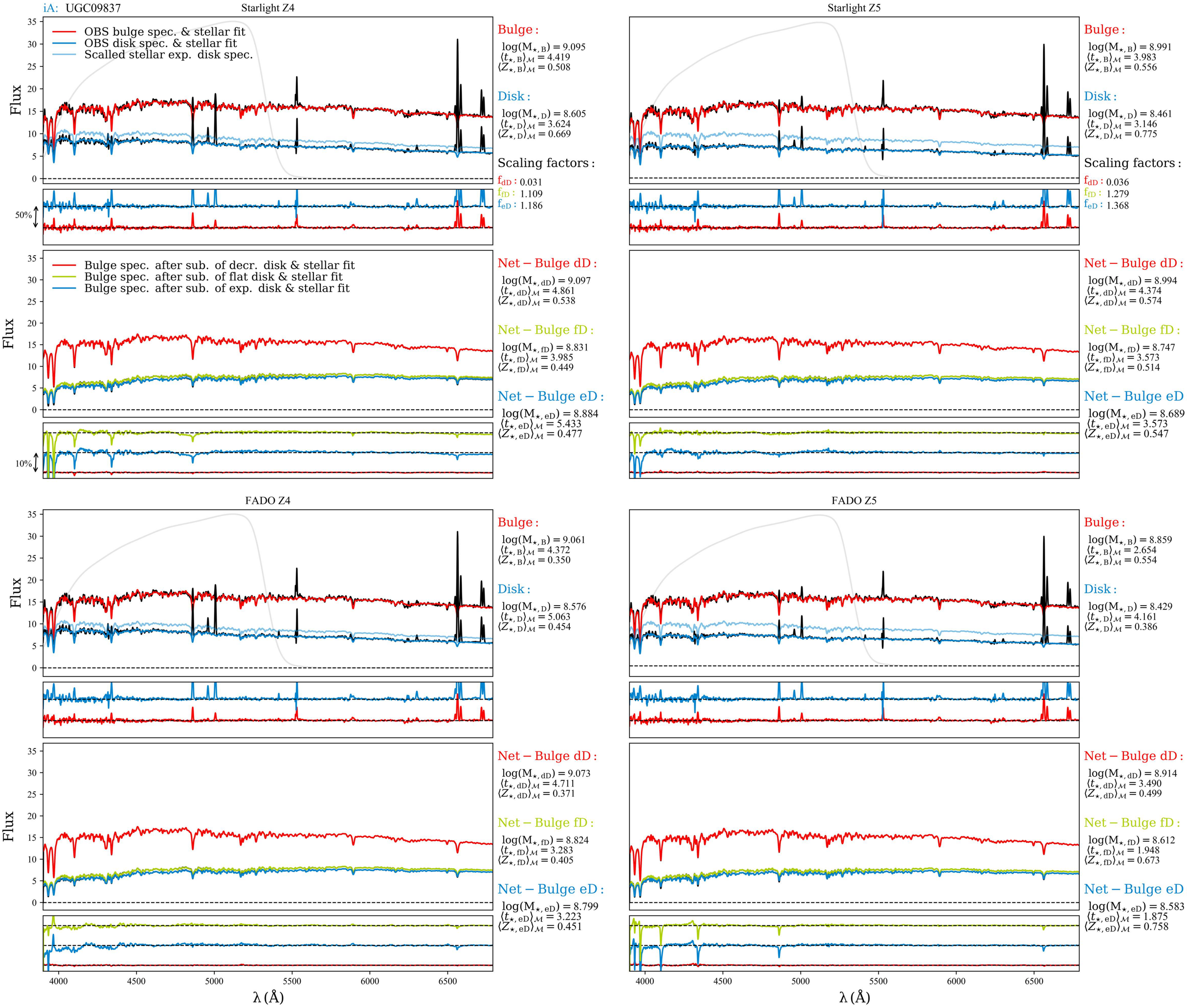
iA: UGC09837
Starlight Z4
OBS bulge spec. & stellar fit
OBS disk spec. & stellar fit
Scalled stellar exp. disk spec.
Flux
Bulge :
log(M⋆, B) = 9.095
⟨t⋆, B⟩M = 4.419
⟨Z⋆, B⟩M = 0.508
Disk :
log(M⋆, D) = 8.605
⟨t⋆, D⟩M = 3.624
⟨Z⋆, D⟩M = 0.669
Scaling factors :
fdD : 0.031
ffD : 1.109
feD : 1.186
50%
Bulge spec. after sub. of decr. disk & stellar fit
Bulge spec. after sub. of flat disk & stellar fit
Bulge spec. after sub. of exp. disk & stellar fit
Net − Bulge dD :
log(M⋆, dD) = 9.097
⟨t⋆, dD⟩M = 4.861
⟨Z⋆, dD⟩M = 0.538
Net − Bulge fD :
log(M⋆, fD) = 8.831
⟨t⋆, fD⟩M = 3.985
⟨Z⋆, fD⟩M = 0.449
Net − Bulge eD :
log(M⋆, eD) = 8.884
⟨t⋆, eD⟩M = 5.433
⟨Z⋆, eD⟩M = 0.477
10%
Starlight Z5
Bulge :
log(M⋆, B) = 8.991
⟨t⋆, B⟩M = 3.983
⟨Z⋆, B⟩M = 0.556
Disk :
log(M⋆, D) = 8.461
⟨t⋆, D⟩M = 3.146
⟨Z⋆, D⟩M = 0.775
Scaling factors :
fdD : 0.036
ffD : 1.279
feD : 1.368
Net − Bulge dD :
log(M⋆, dD) = 8.994
⟨t⋆, dD⟩M = 4.374
⟨Z⋆, dD⟩M = 0.574
Net − Bulge fD :
log(M⋆, fD) = 8.747
⟨t⋆, fD⟩M = 3.573
⟨Z⋆, fD⟩M = 0.514
Net − Bulge eD :
log(M⋆, eD) = 8.689
⟨t⋆, eD⟩M = 3.573
⟨Z⋆, eD⟩M = 0.547
FADO Z4
Bulge :
log(M⋆, B) = 9.061
⟨t⋆, B⟩M = 4.372
⟨Z⋆, B⟩M = 0.350
Disk :
log(M⋆, D) = 8.576
⟨t⋆, D⟩M = 5.063
⟨Z⋆, D⟩M = 0.454
Net − Bulge dD :
log(M⋆, dD) = 9.073
⟨t⋆, dD⟩M = 4.711
⟨Z⋆, dD⟩M = 0.371
Net − Bulge fD :
log(M⋆, fD) = 8.824
⟨t⋆, fD⟩M = 3.283
⟨Z⋆, fD⟩M = 0.405
Net − Bulge eD :
log(M⋆, eD) = 8.799
⟨t⋆, eD⟩M = 3.223
⟨Z⋆, eD⟩M = 0.451
FADO Z5
Bulge :
log(M⋆, B) = 8.859
⟨t⋆, B⟩M = 2.654
⟨Z⋆, B⟩M = 0.554
Disk :
log(M⋆, D) = 8.429
⟨t⋆, D⟩M = 4.161
⟨Z⋆, D⟩M = 0.386
Net − Bulge dD :
log(M⋆, dD) = 8.914
⟨t⋆, dD⟩M = 3.490
⟨Z⋆, dD⟩M = 0.499
Net − Bulge fD :
log(M⋆, fD) = 8.612
⟨t⋆, fD⟩M = 1.948
⟨Z⋆, fD⟩M = 0.673
Net − Bulge eD :
log(M⋆, eD) = 8.583
⟨t⋆, eD⟩M = 1.875
⟨Z⋆, eD⟩M = 0.758
4000
4500
5000
5500
6000
6500
λ (Å)

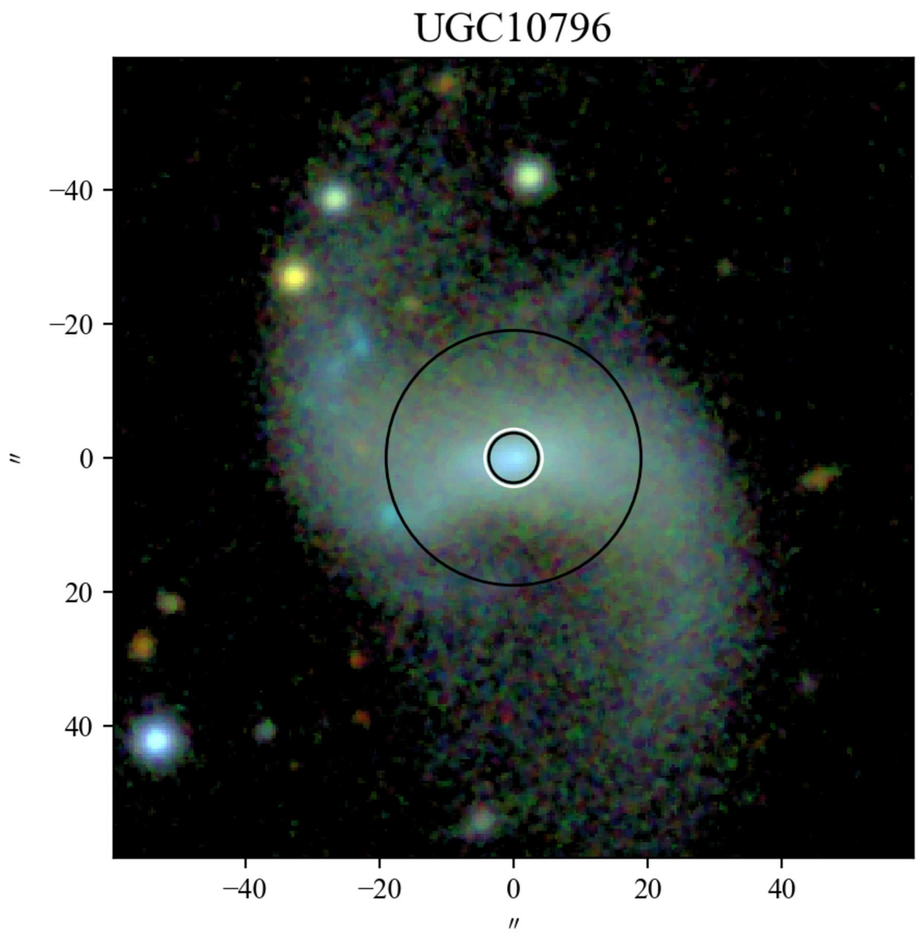
UGC10796
−40
−20
0
20
40
″
−40
−20
0
20
40
″

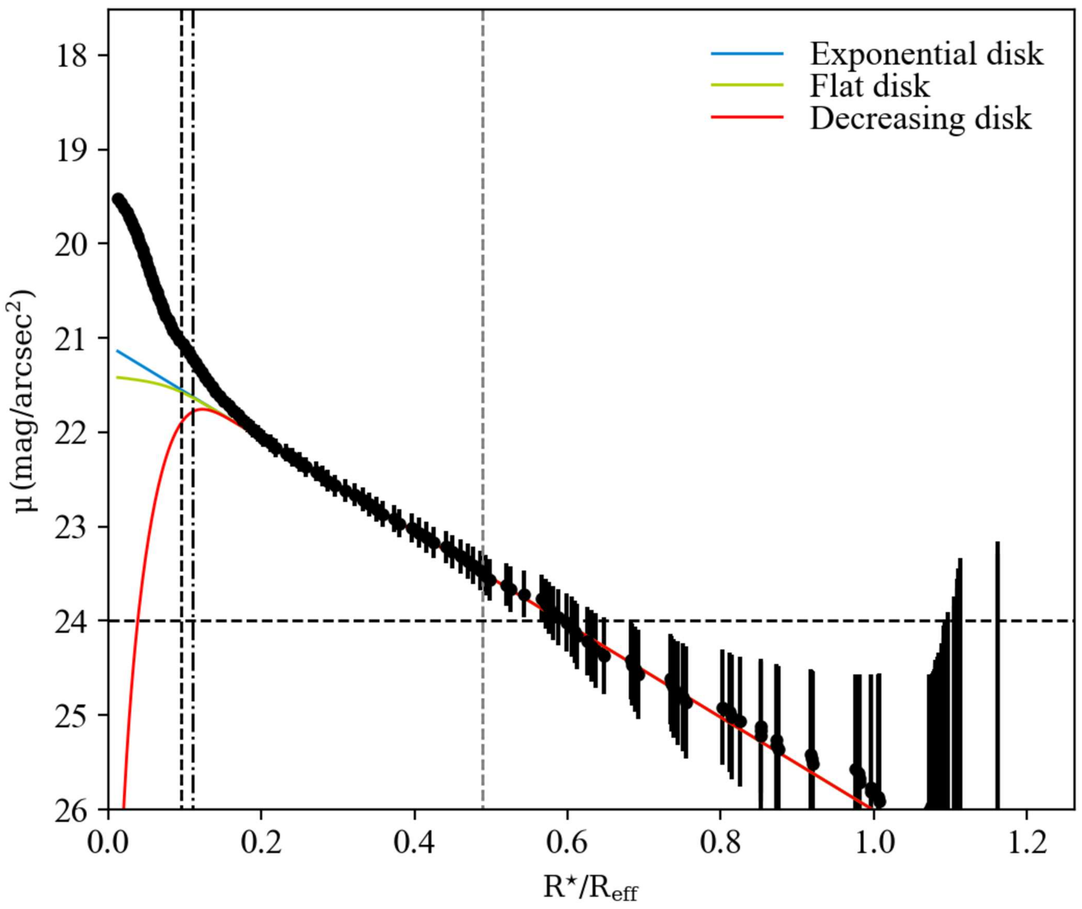
Exponential disk
Flat disk
Decreasing disk
μ (mag/arcsec²)
R⋆/Reff

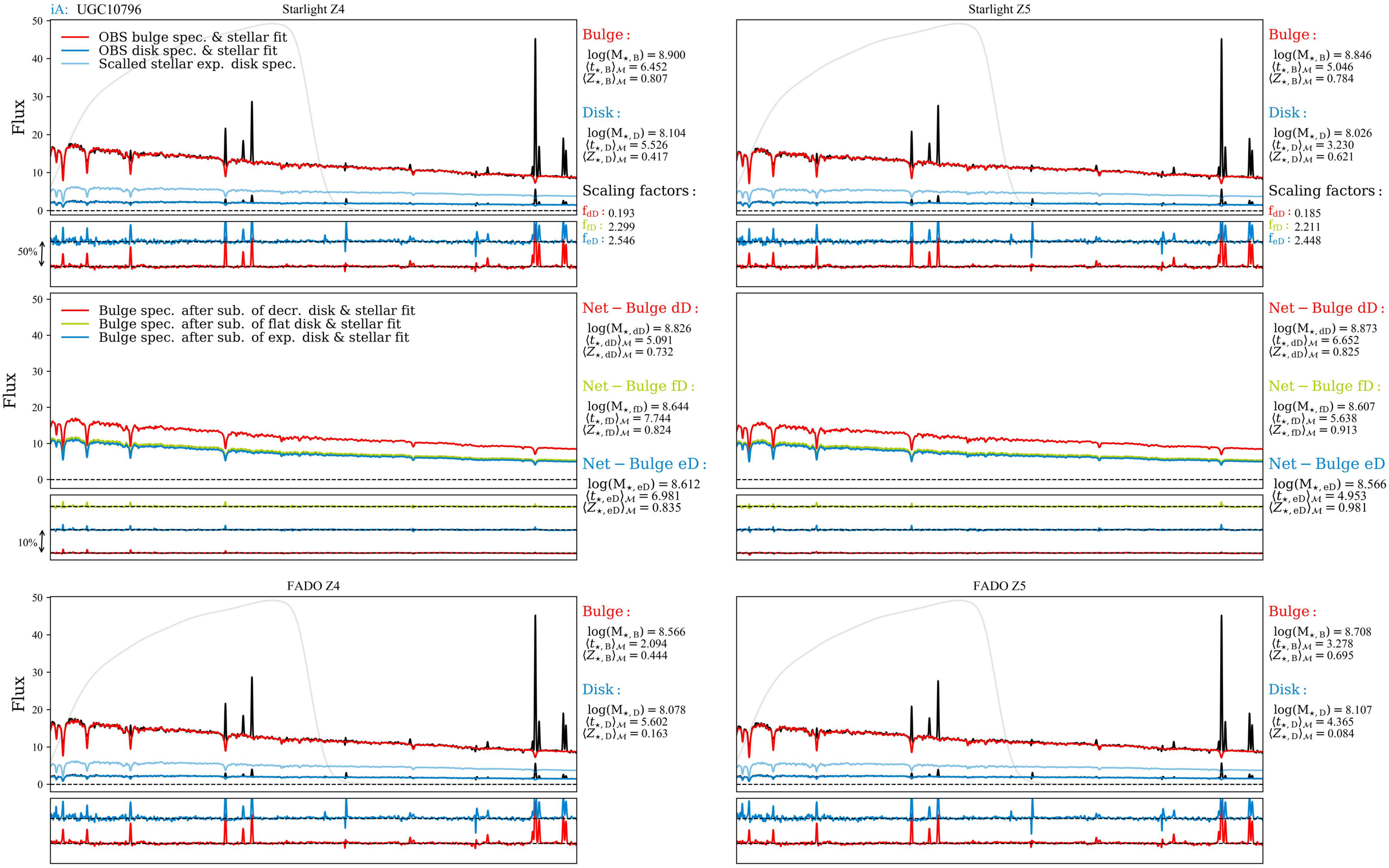
iA: UGC10796
Starlight Z4
OBS bulge spec. & stellar fit
OBS disk spec. & stellar fit
Scalled stellar exp. disk spec.
Flux
50%
Bulge :
log(M⋆, B) = 8.900
⟨t⋆, B⟩M = 6.452
⟨Z⋆, B⟩M = 0.807
Disk :
log(M⋆, D) = 8.104
⟨t⋆, D⟩M = 5.526
⟨Z⋆, D⟩M = 0.417
Scaling factors :
fdD : 0.193
ffD : 2.299
feD : 2.546
Bulge spec. after sub. of decr. disk & stellar fit
Bulge spec. after sub. of flat disk & stellar fit
Bulge spec. after sub. of exp. disk & stellar fit
10%
Net − Bulge dD :
log(M⋆, dD) = 8.826
⟨t⋆, dD⟩M = 5.091
⟨Z⋆, dD⟩M = 0.732
Net − Bulge fD :
log(M⋆, fD) = 8.644
⟨t⋆, fD⟩M = 7.744
⟨Z⋆, fD⟩M = 0.824
Net − Bulge eD :
log(M⋆, eD) = 8.612
⟨t⋆, eD⟩M = 6.981
⟨Z⋆, eD⟩M = 0.835

Starlight Z5
Bulge :
log(M⋆, B) = 8.846
⟨t⋆, B⟩M = 5.046
⟨Z⋆, B⟩M = 0.784
Disk :
log(M⋆, D) = 8.026
⟨t⋆, D⟩M = 3.230
⟨Z⋆, D⟩M = 0.621
Scaling factors :
fdD : 0.185
ffD : 2.211
feD : 2.448
Net − Bulge dD :
log(M⋆, dD) = 8.873
⟨t⋆, dD⟩M = 6.652
⟨Z⋆, dD⟩M = 0.825
Net − Bulge fD :
log(M⋆, fD) = 8.607
⟨t⋆, fD⟩M = 5.638
⟨Z⋆, fD⟩M = 0.913
Net − Bulge eD :
log(M⋆, eD) = 8.566
⟨t⋆, eD⟩M = 4.953
⟨Z⋆, eD⟩M = 0.981

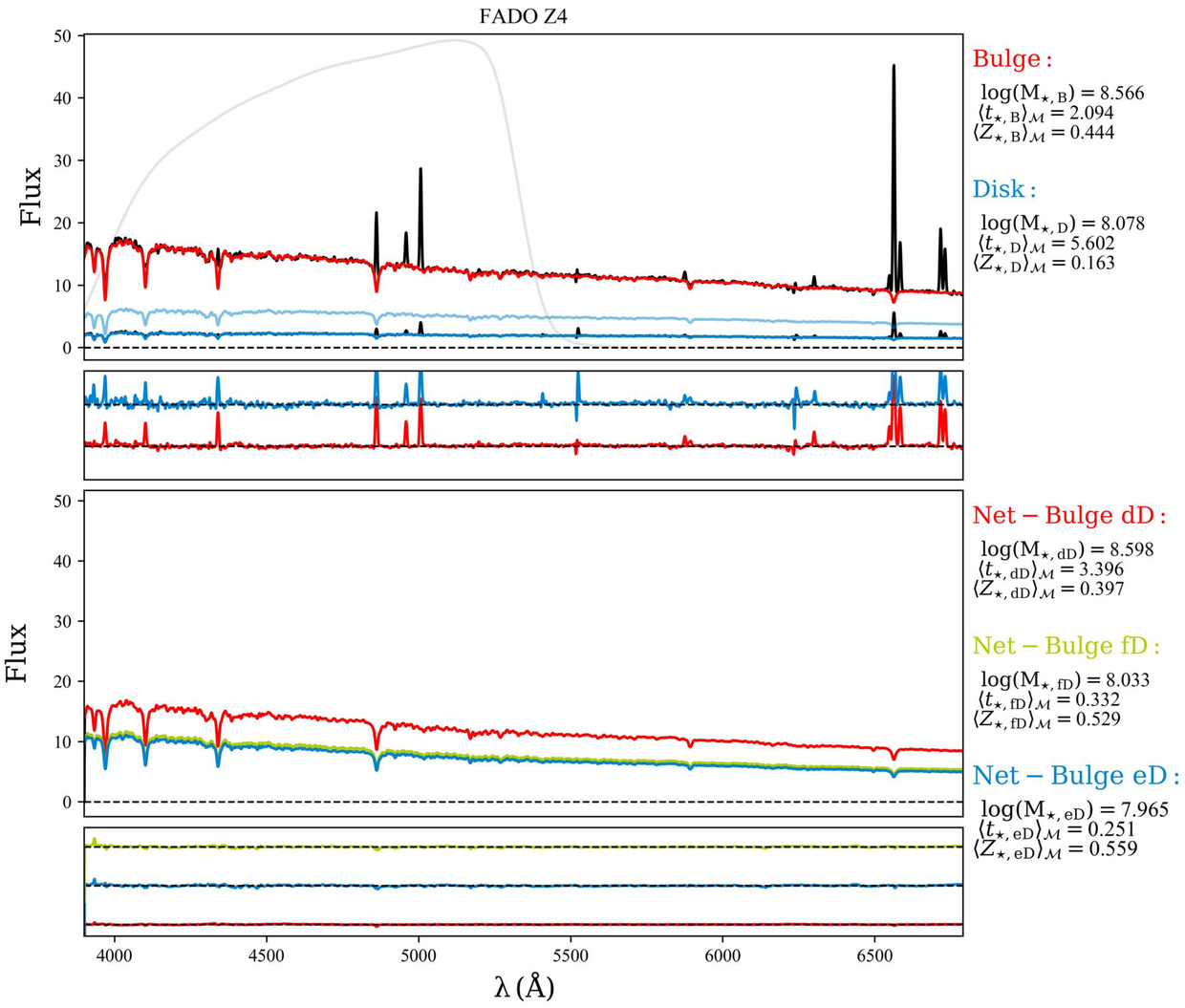
FADO Z4
Flux
Bulge :
log(M⋆, B) = 8.566
⟨t⋆, B⟩M = 2.094
⟨Z⋆, B⟩M = 0.444
Disk :
log(M⋆, D) = 8.078
⟨t⋆, D⟩M = 5.602
⟨Z⋆, D⟩M = 0.163
Net − Bulge dD :
log(M⋆, dD) = 8.598
⟨t⋆, dD⟩M = 3.396
⟨Z⋆, dD⟩M = 0.397
Net − Bulge fD :
log(M⋆, fD) = 8.033
⟨t⋆, fD⟩M = 0.332
⟨Z⋆, fD⟩M = 0.529
Net − Bulge eD :
log(M⋆, eD) = 7.965
⟨t⋆, eD⟩M = 0.251
⟨Z⋆, eD⟩M = 0.559
λ (Å)

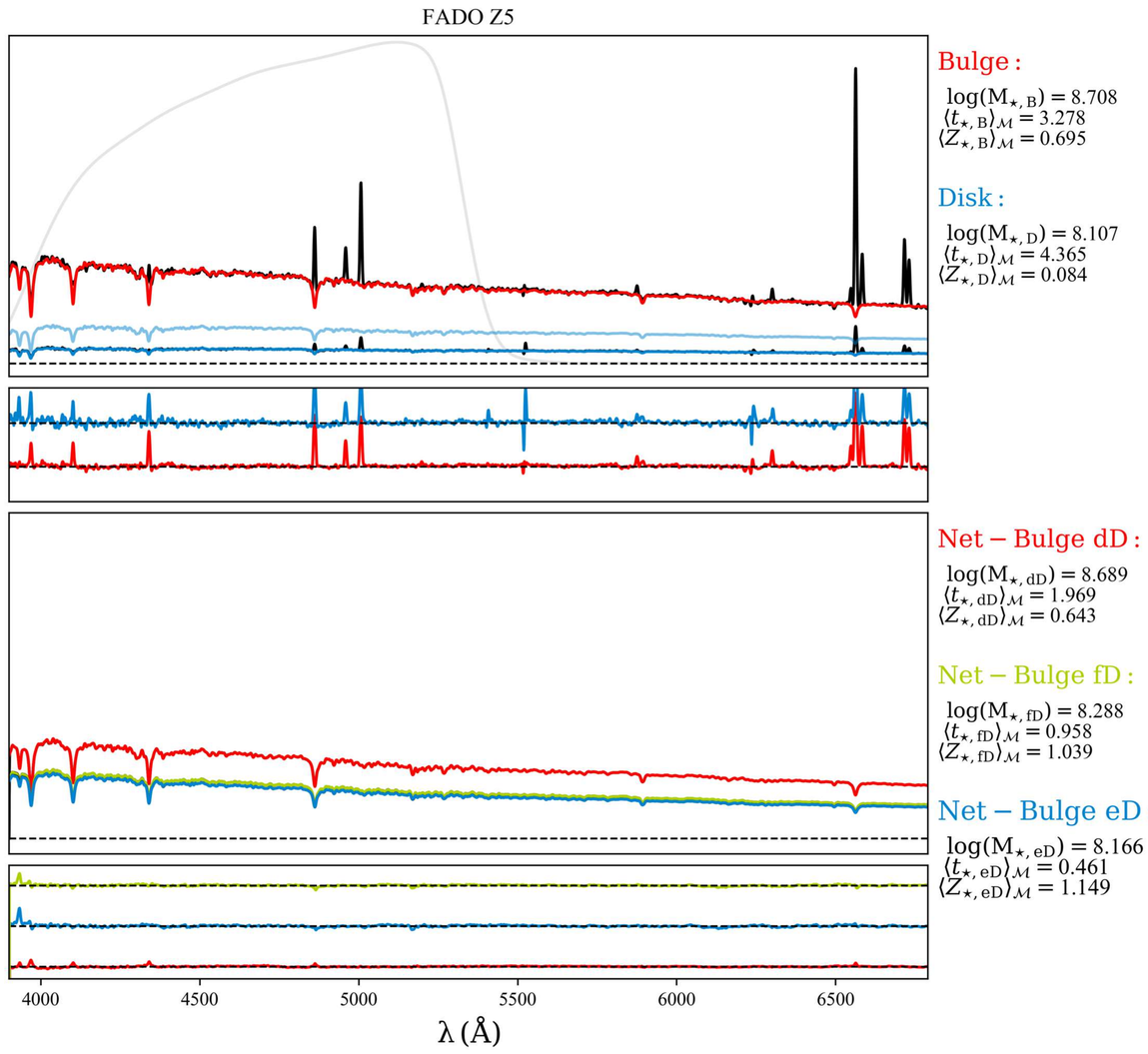
FADO Z5
Bulge :
log(M⋆, B) = 8.708
⟨t⋆, B⟩M = 3.278
⟨Z⋆, B⟩M = 0.695
Disk :
log(M⋆, D) = 8.107
⟨t⋆, D⟩M = 4.365
⟨Z⋆, D⟩M = 0.084
Net − Bulge dD :
log(M⋆, dD) = 8.689
⟨t⋆, dD⟩M = 1.969
⟨Z⋆, dD⟩M = 0.643
Net − Bulge fD :
log(M⋆, fD) = 8.288
⟨t⋆, fD⟩M = 0.958
⟨Z⋆, fD⟩M = 1.039
Net − Bulge eD :
log(M⋆, eD) = 8.166
⟨t⋆, eD⟩M = 0.461
⟨Z⋆, eD⟩M = 1.149
λ (Å)

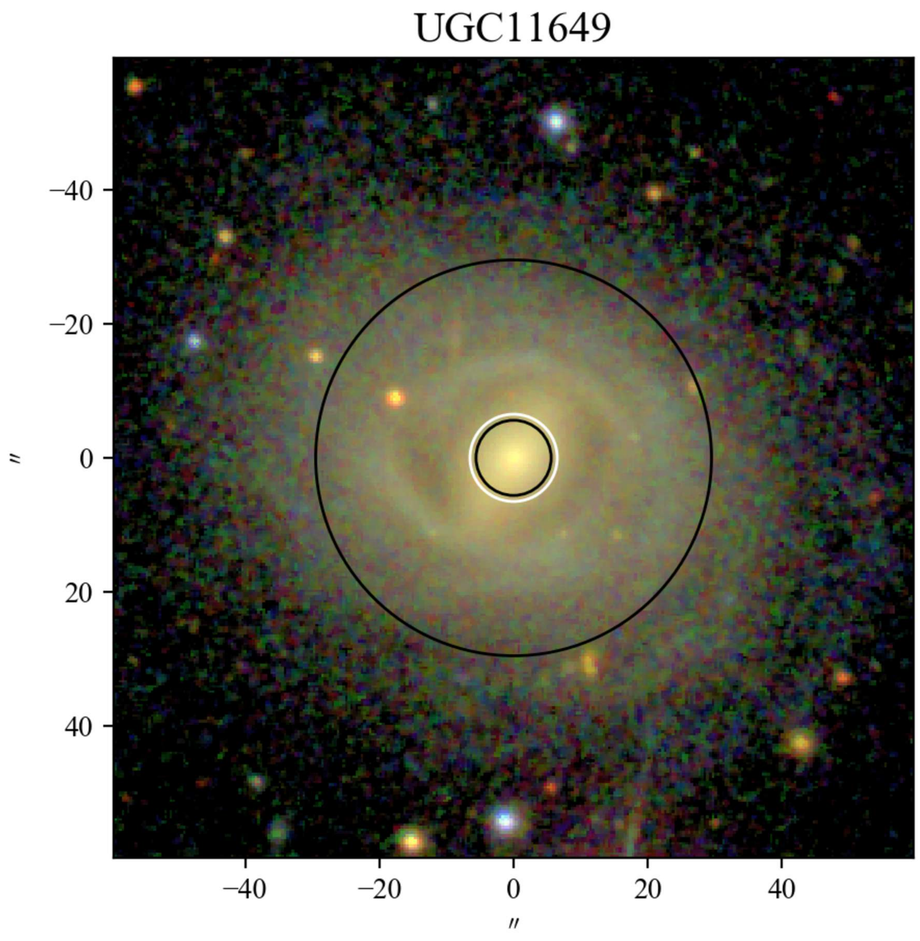
UGC11649
−40
−20
0
20
40
″
−40
−20
0
20
40
″

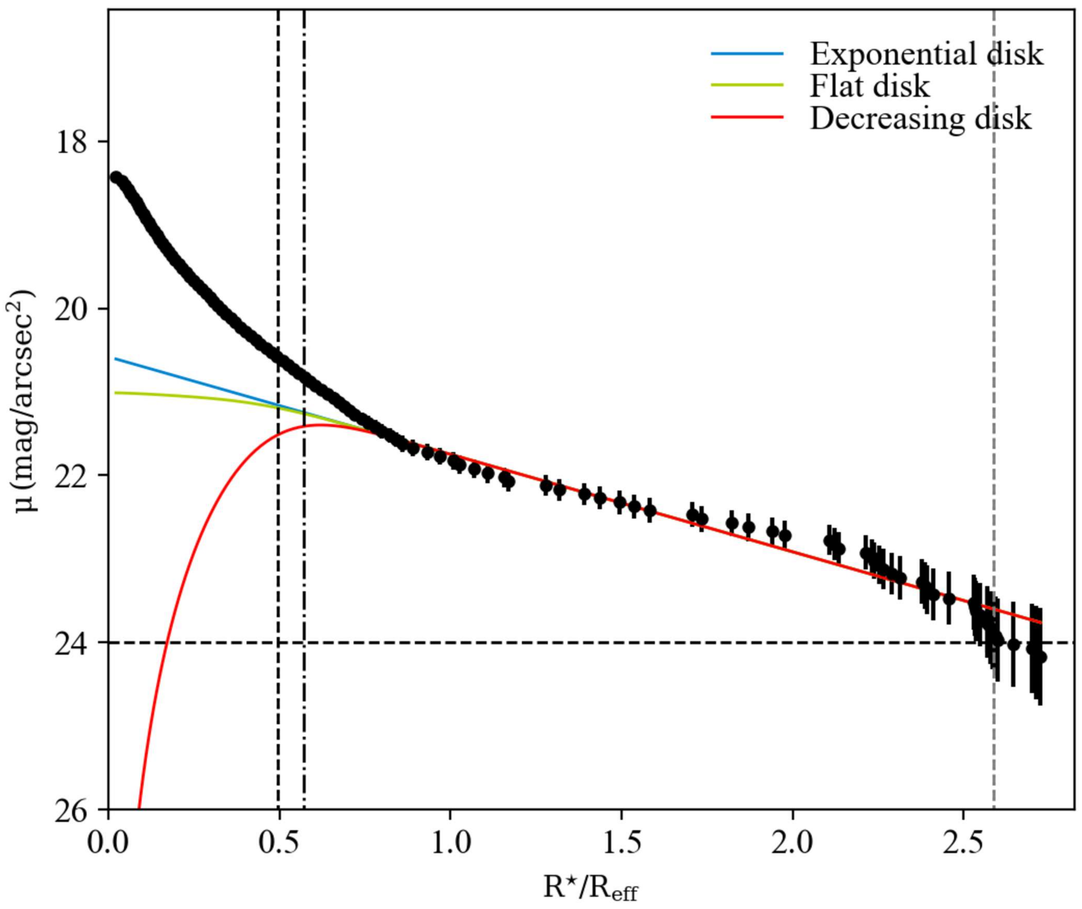
Exponential disk
Flat disk
Decreasing disk
μ (mag/arcsec²)
18
20
22
24
26
0.0
0.5
1.0
1.5
2.0
2.5
R⋆/Reff

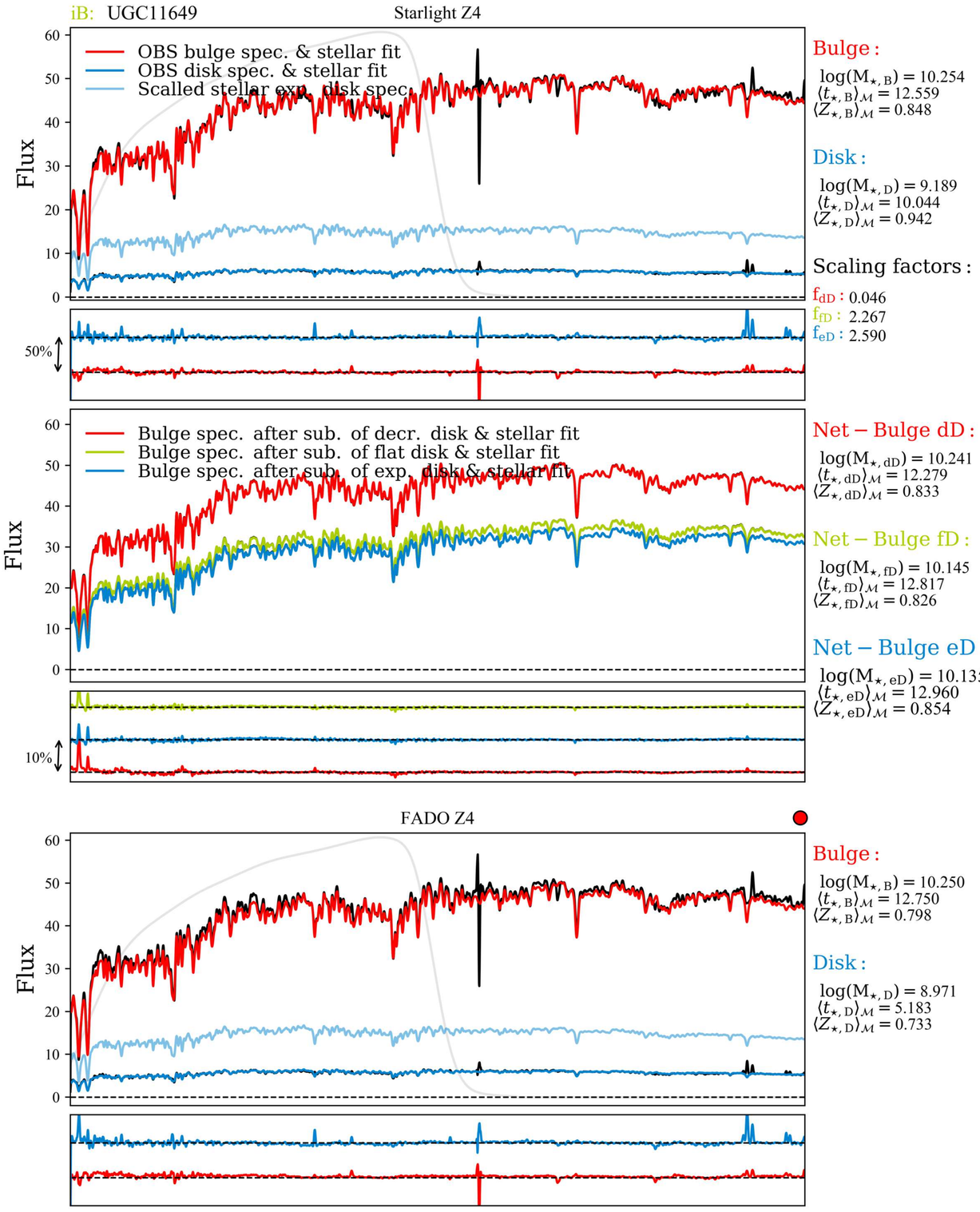
iB: UGC11649
Starlight Z4
OBS bulge spec. & stellar fit
OBS disk spec. & stellar fit
Scalled stellar exp. disk spec.
Flux
50%
Bulge :
log(M⋆, B) = 10.254
⟨t⋆, B⟩M = 12.559
⟨Z⋆, B⟩M = 0.848
Disk :
log(M⋆, D) = 9.189
⟨t⋆, D⟩M = 10.044
⟨Z⋆, D⟩M = 0.942
Scaling factors :
fdD : 0.046
ffD : 2.267
feD : 2.590
Bulge spec. after sub. of decr. disk & stellar fit
Bulge spec. after sub. of flat disk & stellar fit
Bulge spec. after sub. of exp. disk & stellar fit
10%
Net − Bulge dD :
log(M⋆, dD) = 10.241
⟨t⋆, dD⟩M = 12.279
⟨Z⋆, dD⟩M = 0.833
Net − Bulge fD :
log(M⋆, fD) = 10.145
⟨t⋆, fD⟩M = 12.817
⟨Z⋆, fD⟩M = 0.826
Net − Bulge eD :
log(M⋆, eD) = 10.135
⟨t⋆, eD⟩M = 12.960
⟨Z⋆, eD⟩M = 0.854

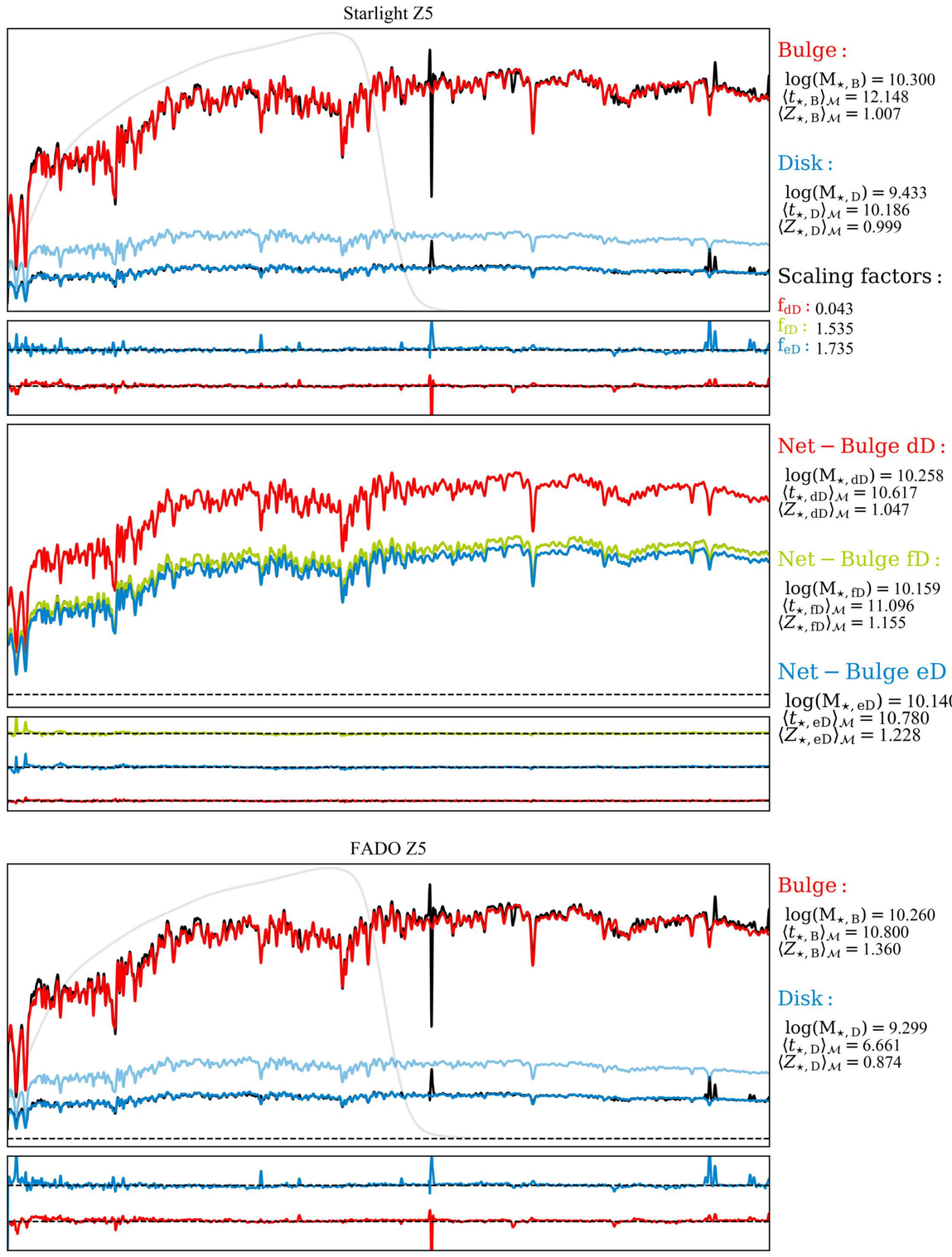
Starlight Z5
Bulge :
log(M⋆, B) = 10.300
⟨t⋆, B⟩M = 12.148
⟨Z⋆, B⟩M = 1.007
Disk :
log(M⋆, D) = 9.433
⟨t⋆, D⟩M = 10.186
⟨Z⋆, D⟩M = 0.999
Scaling factors :
fdD : 0.043
ffD : 1.535
feD : 1.735
Net − Bulge dD :
log(M⋆, dD) = 10.258
⟨t⋆, dD⟩M = 10.617
⟨Z⋆, dD⟩M = 1.047
Net − Bulge fD :
log(M⋆, fD) = 10.159
⟨t⋆, fD⟩M = 11.096
⟨Z⋆, fD⟩M = 1.155
Net − Bulge eD :
log(M⋆, eD) = 10.140
⟨t⋆, eD⟩M = 10.780
⟨Z⋆, eD⟩M = 1.228

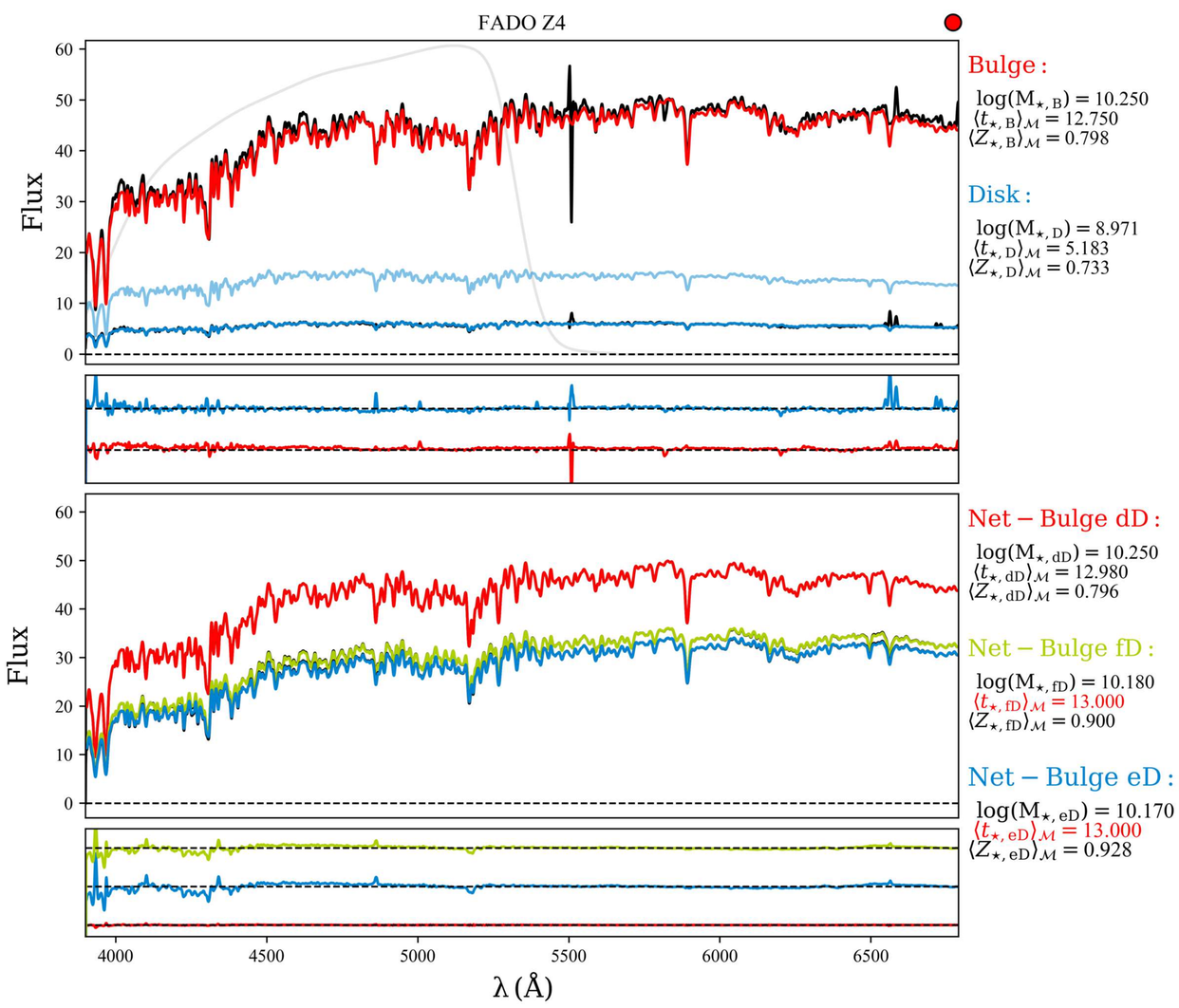
FADO Z4
Flux
Bulge :
log(M⋆, B) = 10.250
⟨t⋆, B⟩M = 12.750
⟨Z⋆, B⟩M = 0.798
Disk :
log(M⋆, D) = 8.971
⟨t⋆, D⟩M = 5.183
⟨Z⋆, D⟩M = 0.733
Net − Bulge dD :
log(M⋆, dD) = 10.250
⟨t⋆, dD⟩M = 12.980
⟨Z⋆, dD⟩M = 0.796
Net − Bulge fD :
log(M⋆, fD) = 10.180
⟨t⋆, fD⟩M = 13.000
⟨Z⋆, fD⟩M = 0.900
Net − Bulge eD :
log(M⋆, eD) = 10.170
⟨t⋆, eD⟩M = 13.000
⟨Z⋆, eD⟩M = 0.928
4000
4500
5000
5500
6000
6500
λ (Å)

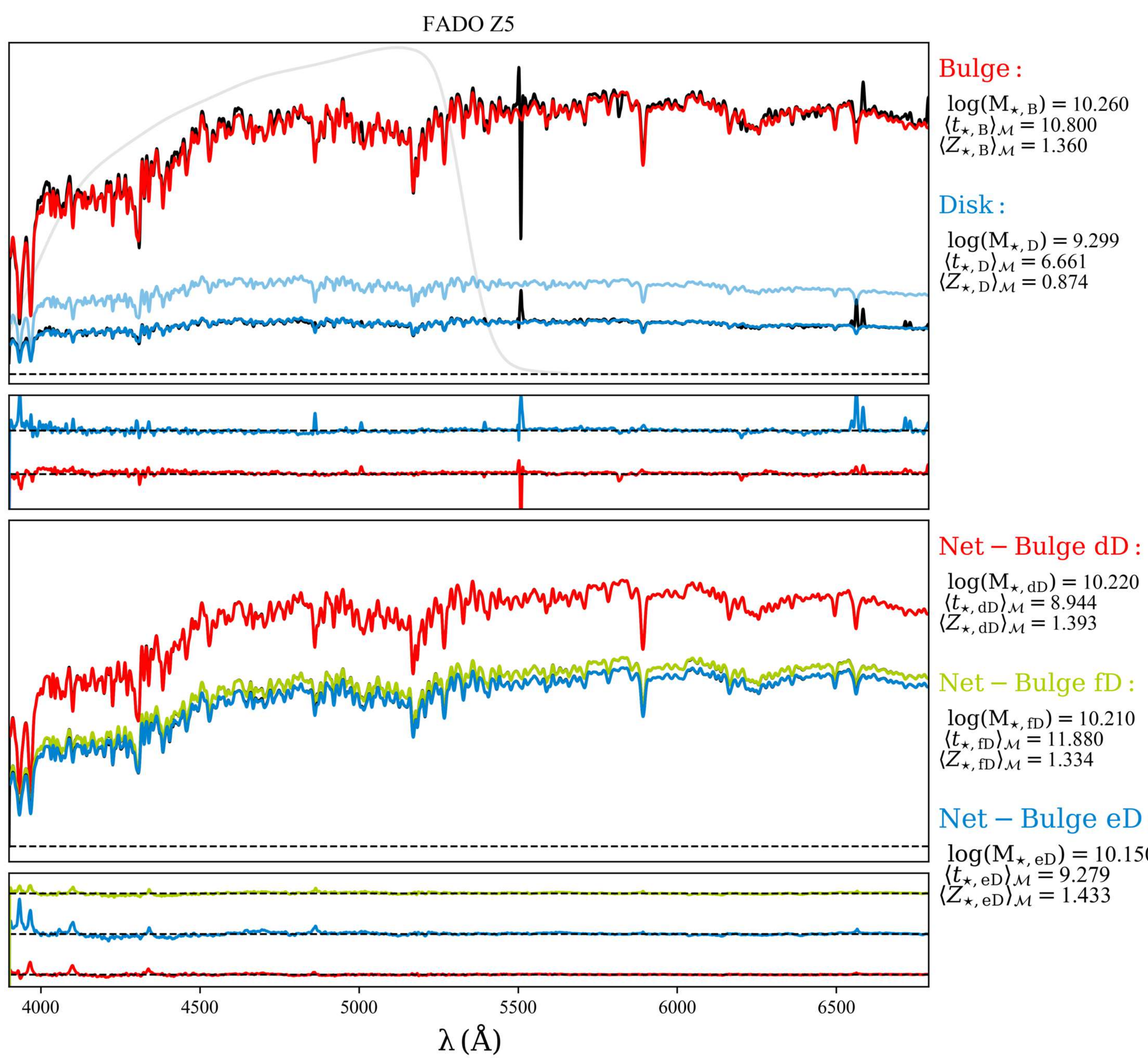
FADO Z5
Bulge :
log(M⋆, B) = 10.260
⟨t⋆, B⟩M = 10.800
⟨Z⋆, B⟩M = 1.360
Disk :
log(M⋆, D) = 9.299
⟨t⋆, D⟩M = 6.661
⟨Z⋆, D⟩M = 0.874
Net − Bulge dD :
log(M⋆, dD) = 10.220
⟨t⋆, dD⟩M = 8.944
⟨Z⋆, dD⟩M = 1.393
Net − Bulge fD :
log(M⋆, fD) = 10.210
⟨t⋆, fD⟩M = 11.880
⟨Z⋆, fD⟩M = 1.334
Net − Bulge eD :
log(M⋆, eD) = 10.150
⟨t⋆, eD⟩M = 9.279
⟨Z⋆, eD⟩M = 1.433
4000
4500
5000
5500
6000
6500
λ (Å)

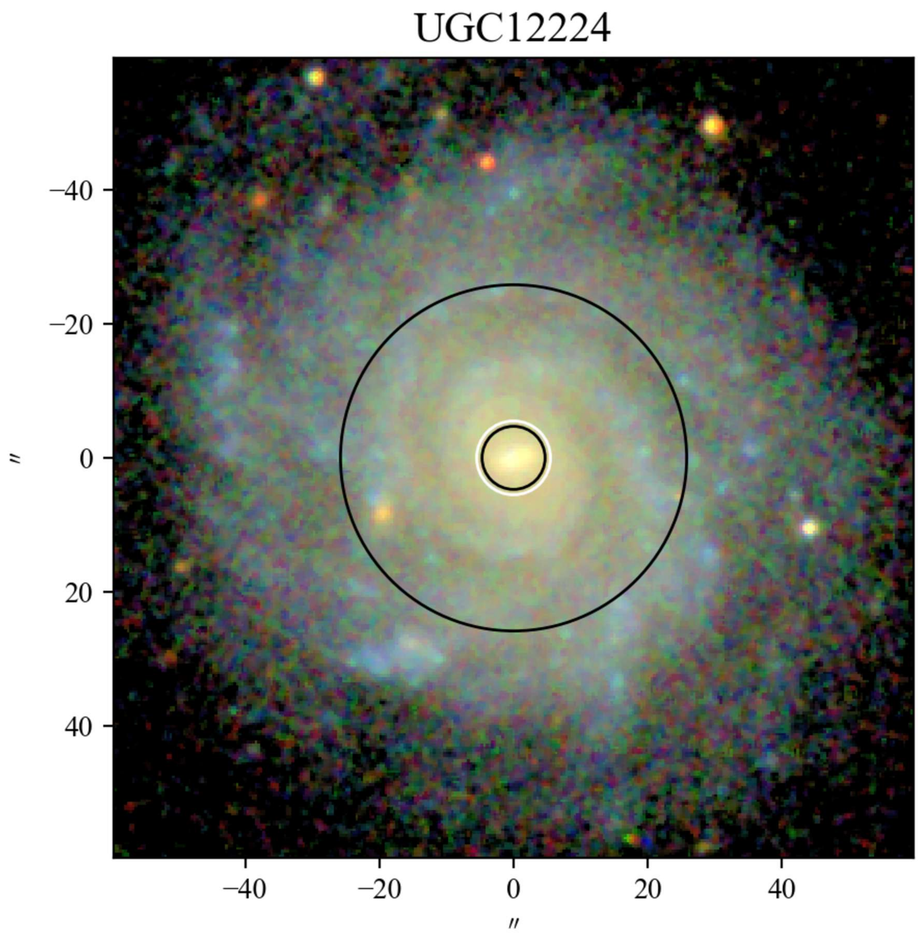
UGC12224
−40
−20
0
20
40
″
−40
−20
0
20
40
″

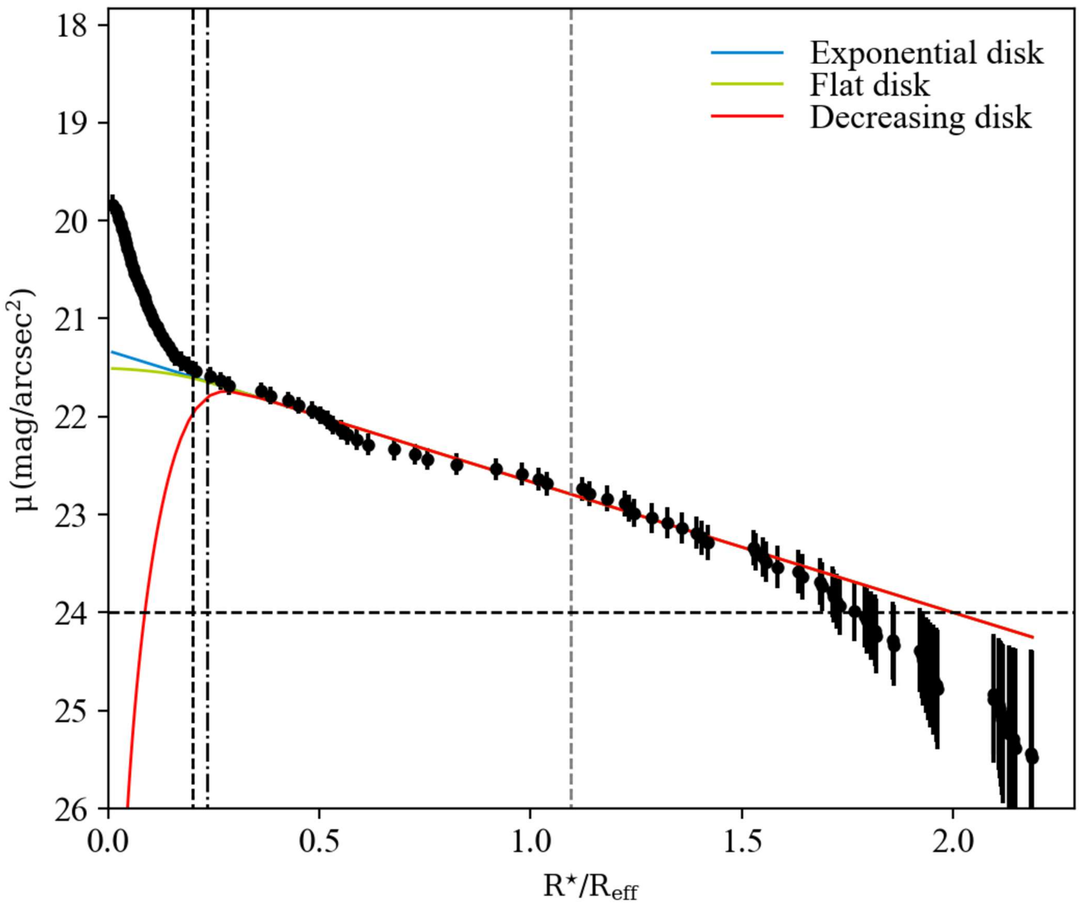
Exponential disk
Flat disk
Decreasing disk
μ (mag/arcsec²)
18
19
20
21
22
23
24
25
26
0.0
0.5
1.0
1.5
2.0
R⋆/Reff

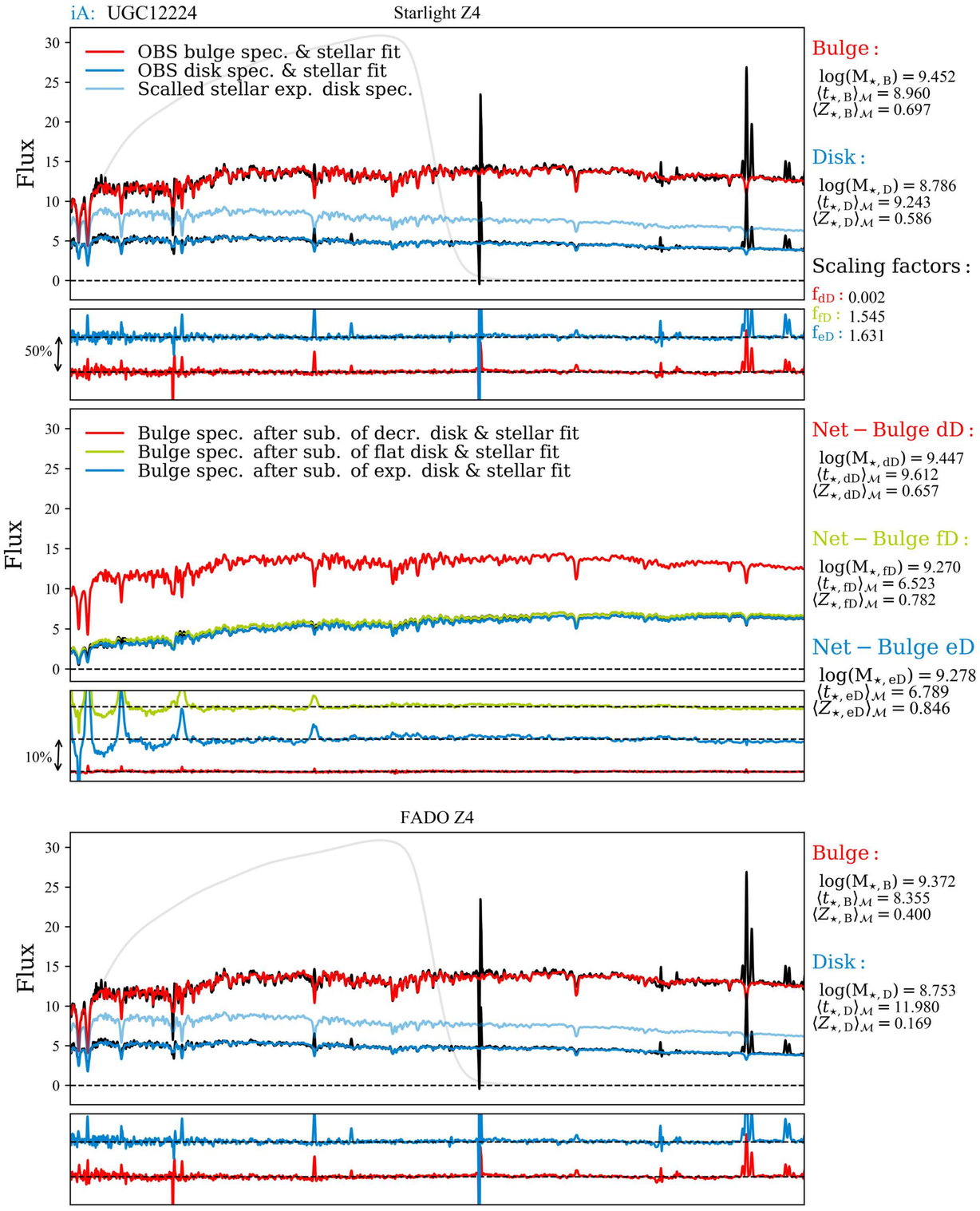
iA: UGC12224
Starlight Z4
OBS bulge spec. & stellar fit
OBS disk spec. & stellar fit
Scalled stellar exp. disk spec.
Flux
50%
Bulge :
log(M⋆, B) = 9.452
⟨t⋆, B⟩M = 8.960
⟨Z⋆, B⟩M = 0.697
Disk :
log(M⋆, D) = 8.786
⟨t⋆, D⟩M = 9.243
⟨Z⋆, D⟩M = 0.586
Scaling factors :
fdD : 0.002
ffD : 1.545
feD : 1.631
Bulge spec. after sub. of decr. disk & stellar fit
Bulge spec. after sub. of flat disk & stellar fit
Bulge spec. after sub. of exp. disk & stellar fit
10%
Net − Bulge dD :
log(M⋆, dD) = 9.447
⟨t⋆, dD⟩M = 9.612
⟨Z⋆, dD⟩M = 0.657
Net − Bulge fD :
log(M⋆, fD) = 9.270
⟨t⋆, fD⟩M = 6.523
⟨Z⋆, fD⟩M = 0.782
Net − Bulge eD :
log(M⋆, eD) = 9.278
⟨t⋆, eD⟩M = 6.789
⟨Z⋆, eD⟩M = 0.846

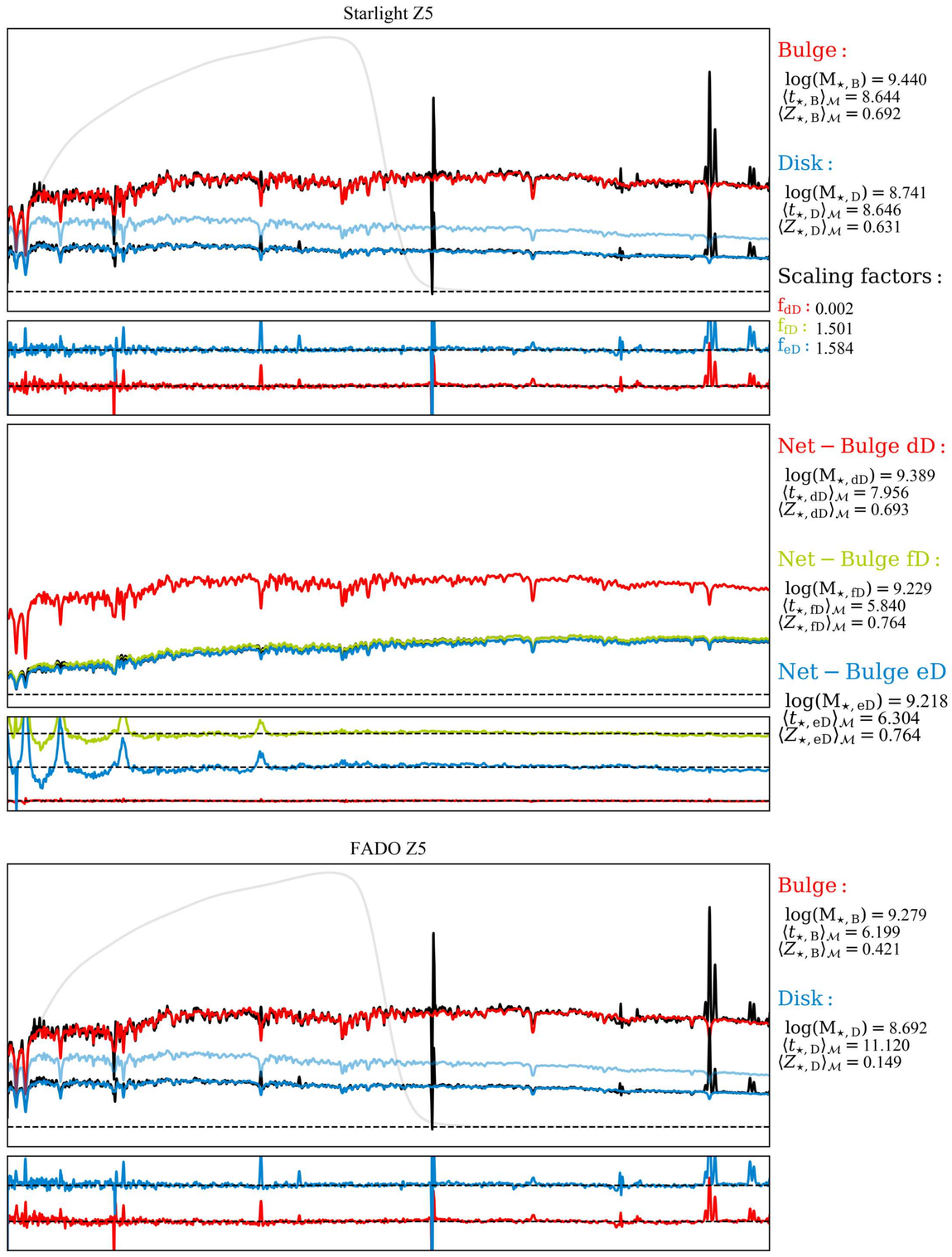
Starlight Z5
Bulge :
log(M⋆, B) = 9.440
⟨t⋆, B⟩M = 8.644
⟨Z⋆, B⟩M = 0.692
Disk :
log(M⋆, D) = 8.741
⟨t⋆, D⟩M = 8.646
⟨Z⋆, D⟩M = 0.631
Scaling factors :
fdD : 0.002
ffD : 1.501
feD : 1.584
Net − Bulge dD :
log(M⋆, dD) = 9.389
⟨t⋆, dD⟩M = 7.956
⟨Z⋆, dD⟩M = 0.693
Net − Bulge fD :
log(M⋆, fD) = 9.229
⟨t⋆, fD⟩M = 5.840
⟨Z⋆, fD⟩M = 0.764
Net − Bulge eD :
log(M⋆, eD) = 9.218
⟨t⋆, eD⟩M = 6.304
⟨Z⋆, eD⟩M = 0.764

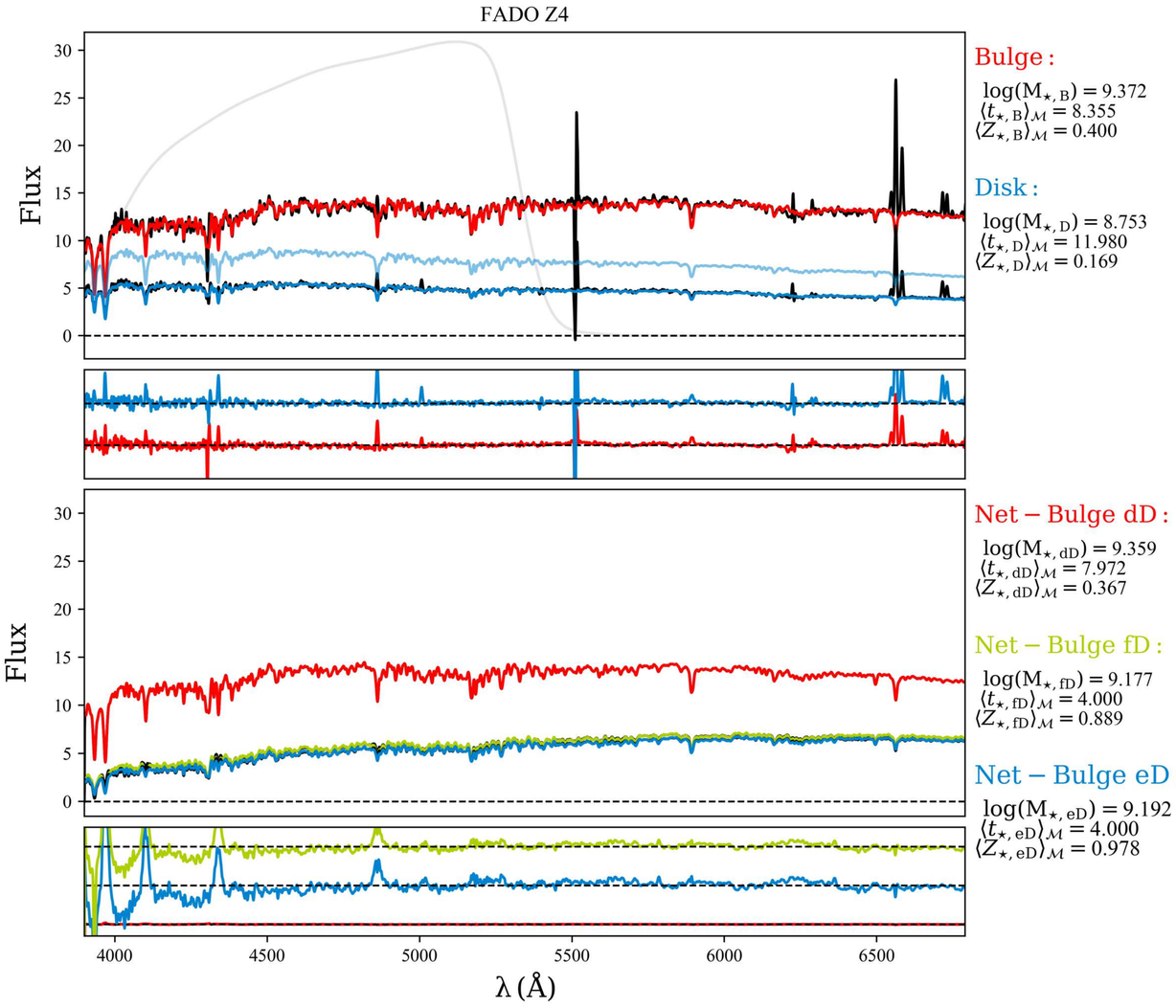
FADO Z4
Flux
Bulge :
log(M⋆, B) = 9.372
⟨t⋆, B⟩M = 8.355
⟨Z⋆, B⟩M = 0.400
Disk :
log(M⋆, D) = 8.753
⟨t⋆, D⟩M = 11.980
⟨Z⋆, D⟩M = 0.169
Net − Bulge dD :
log(M⋆, dD) = 9.359
⟨t⋆, dD⟩M = 7.972
⟨Z⋆, dD⟩M = 0.367
Net − Bulge fD :
log(M⋆, fD) = 9.177
⟨t⋆, fD⟩M = 4.000
⟨Z⋆, fD⟩M = 0.889
Net − Bulge eD :
log(M⋆, eD) = 9.192
⟨t⋆, eD⟩M = 4.000
⟨Z⋆, eD⟩M = 0.978
4000
4500
5000
5500
6000
6500
λ (Å)

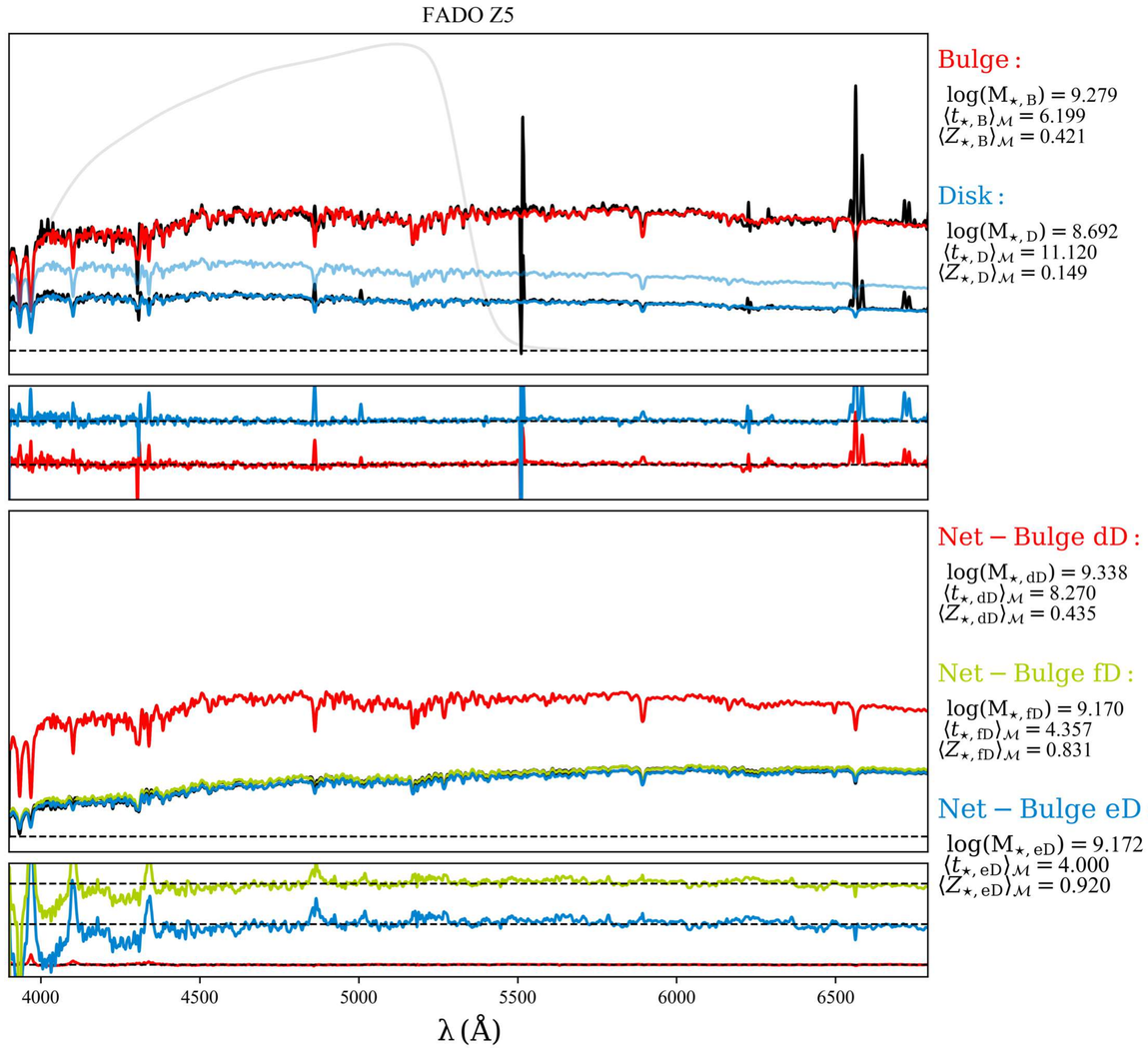
FADO Z5
Bulge :
log(M⋆, B) = 9.279
⟨t⋆, B⟩M = 6.199
⟨Z⋆, B⟩M = 0.421
Disk :
log(M⋆, D) = 8.692
⟨t⋆, D⟩M = 11.120
⟨Z⋆, D⟩M = 0.149
Net − Bulge dD :
log(M⋆, dD) = 9.338
⟨t⋆, dD⟩M = 8.270
⟨Z⋆, dD⟩M = 0.435
Net − Bulge fD :
log(M⋆, fD) = 9.170
⟨t⋆, fD⟩M = 4.357
⟨Z⋆, fD⟩M = 0.831
Net − Bulge eD :
log(M⋆, eD) = 9.172
⟨t⋆, eD⟩M = 4.000
⟨Z⋆, eD⟩M = 0.920
4000
4500
5000
5500
6000
6500
λ (Å)

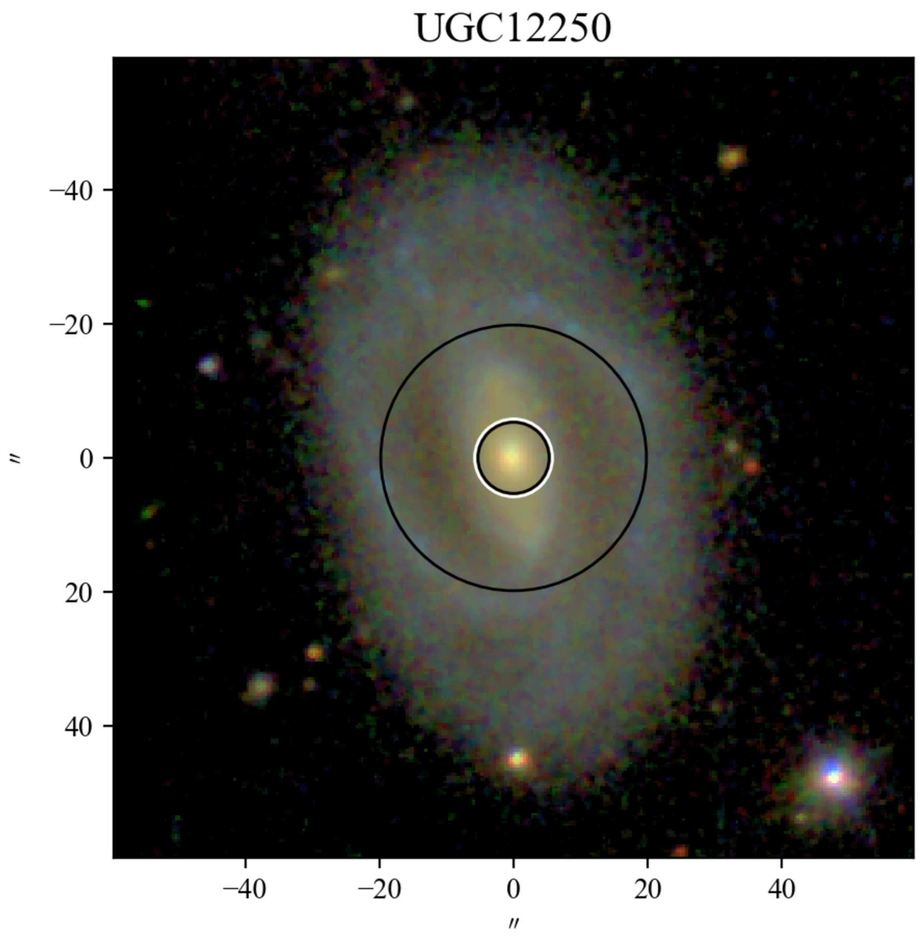
UGC12250
−40
−20
0
20
40
″
−40
−20
0
20
40
″

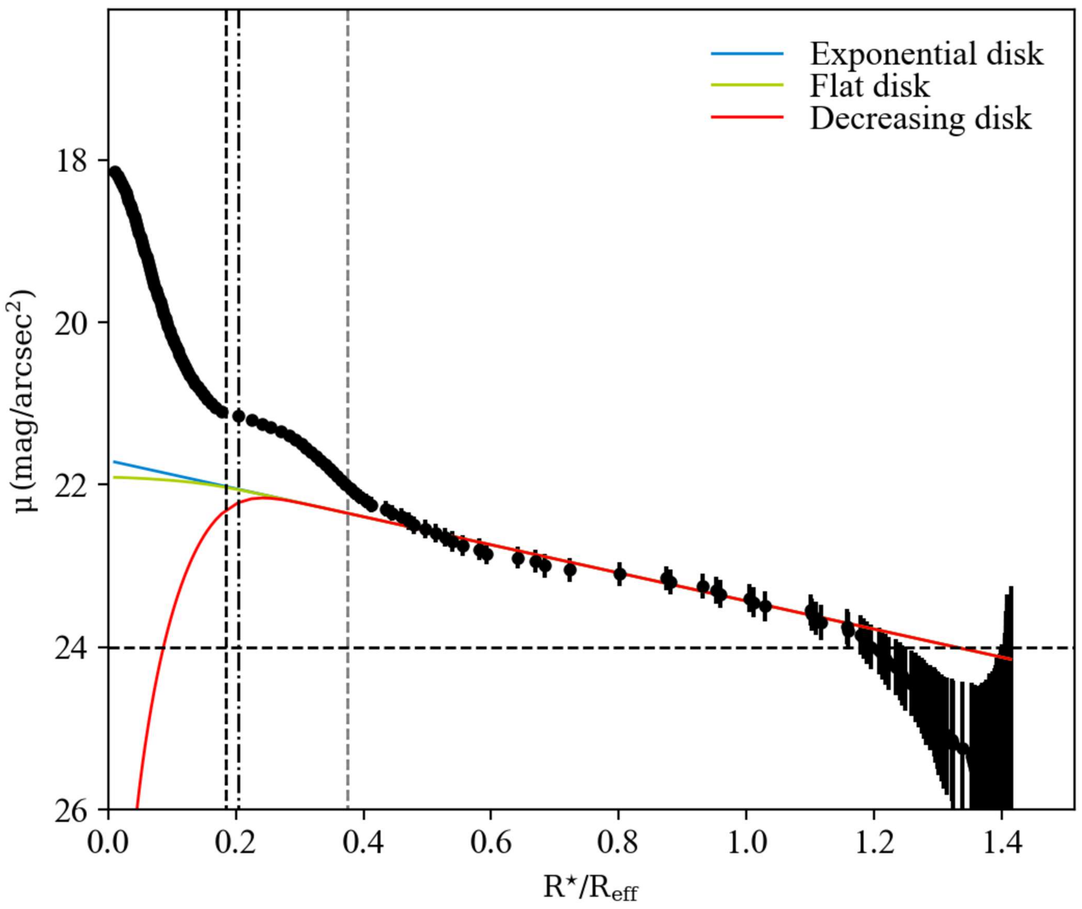
Exponential disk
Flat disk
Decreasing disk
μ (mag/arcsec²)
18
20
22
24
26
0.0
0.2
0.4
0.6
0.8
1.0
1.2
1.4
R⋆/Reff

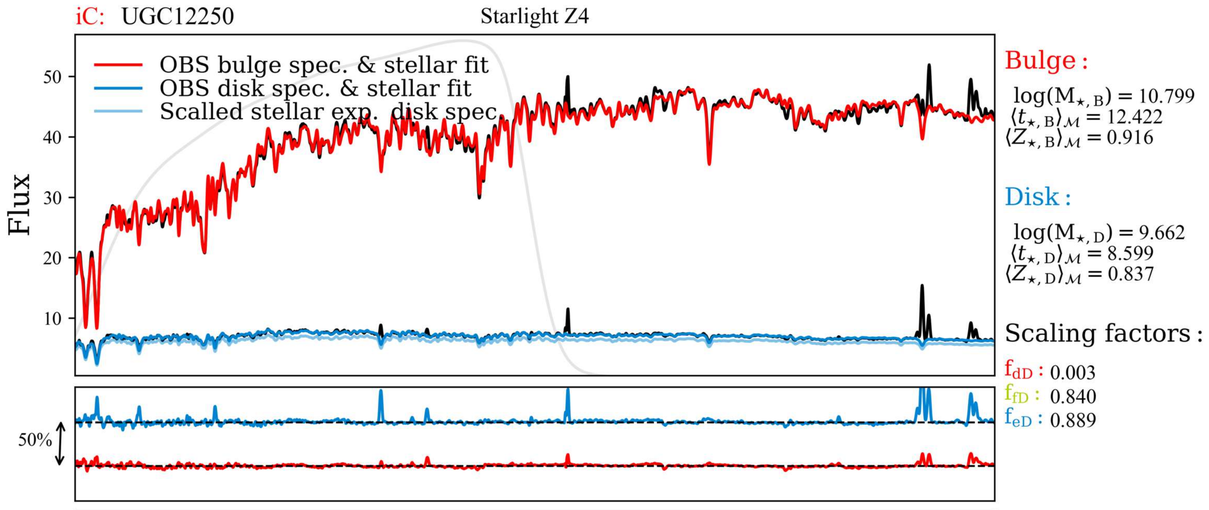
iC: UGC12250
Starlight Z4
OBS bulge spec. & stellar fit
OBS disk spec. & stellar fit
Scalled stellar exp. disk spec.
Flux
50%
Bulge :
log(M⋆, B) = 10.799
⟨t⋆, B⟩M = 12.422
⟨Z⋆, B⟩M = 0.916
Disk :
log(M⋆, D) = 9.662
⟨t⋆, D⟩M = 8.599
⟨Z⋆, D⟩M = 0.837
Scaling factors :
fdD : 0.003
ffD : 0.840
feD : 0.889

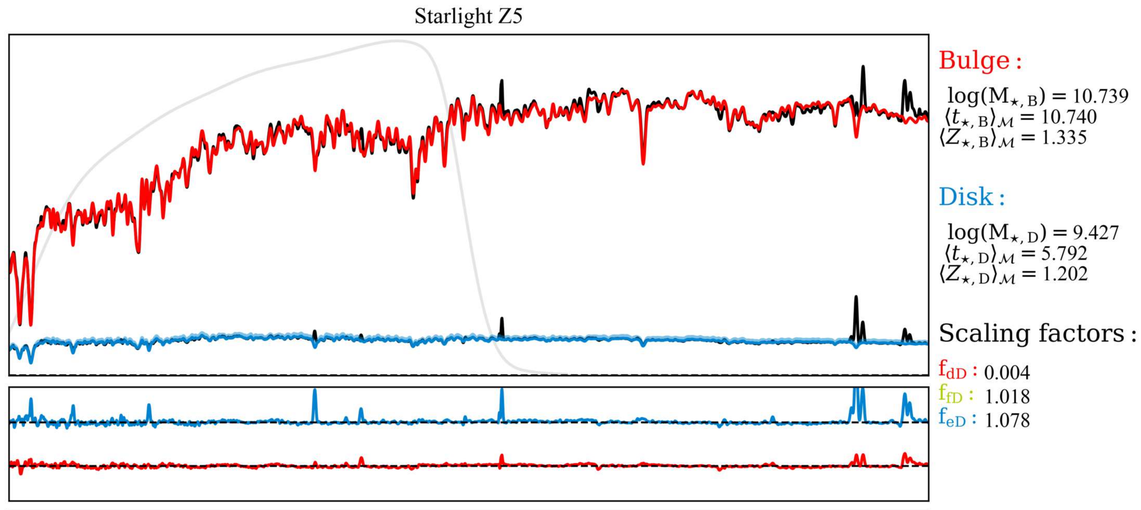
Starlight Z5
Bulge :
log(M⋆, B) = 10.739
⟨t⋆, B⟩M = 10.740
⟨Z⋆, B⟩M = 1.335
Disk :
log(M⋆, D) = 9.427
⟨t⋆, D⟩M = 5.792
⟨Z⋆, D⟩M = 1.202
Scaling factors :
fdD : 0.004
ffD : 1.018
feD : 1.078

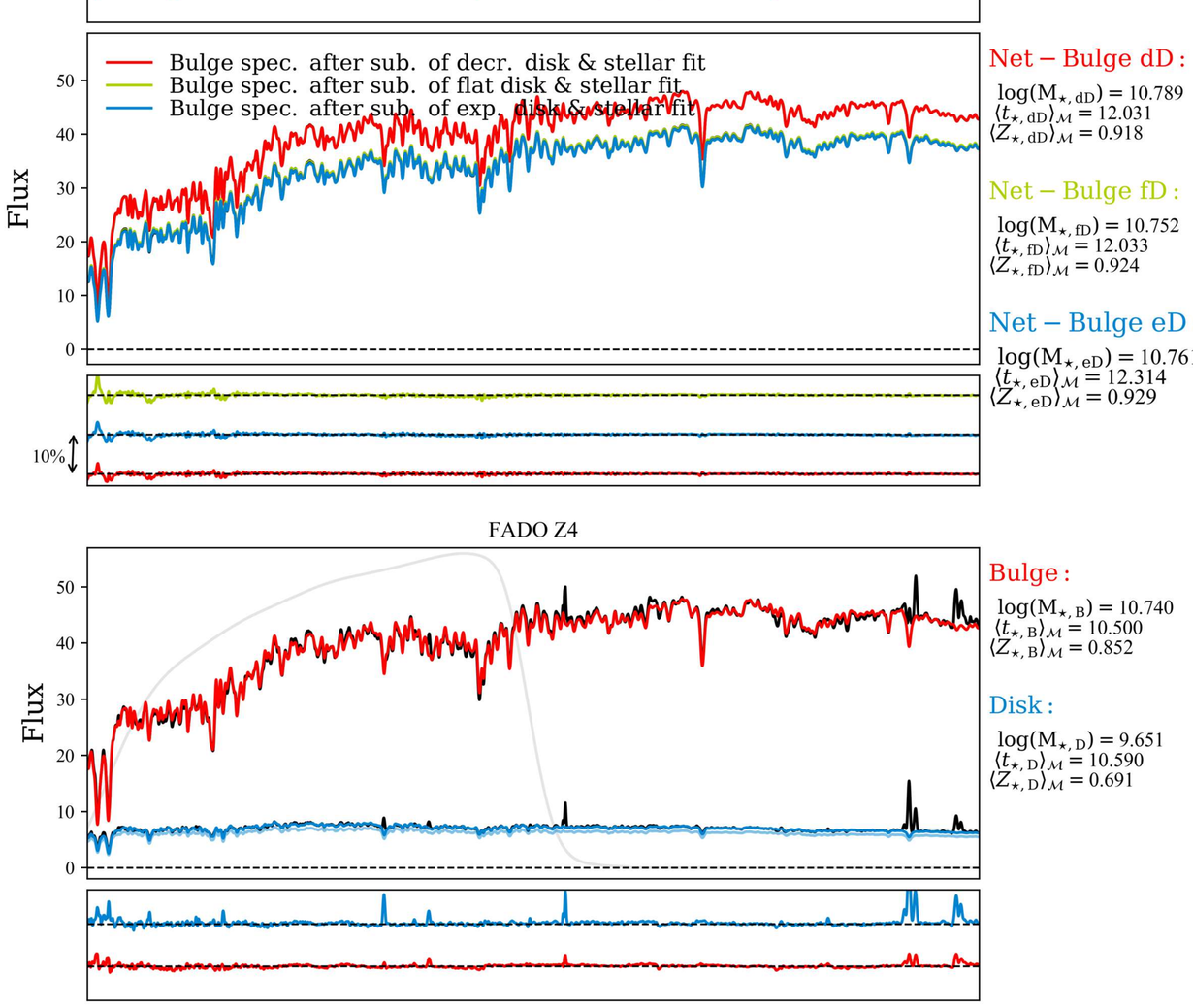
Bulge spec. after sub. of decr. disk & stellar fit
Bulge spec. after sub. of flat disk & stellar fit
Bulge spec. after sub. of exp. disk & stellar fit
Flux
10%
Net − Bulge dD :
log(M⋆, dD) = 10.789
⟨t⋆, dD⟩M = 12.031
⟨Z⋆, dD⟩M = 0.918
Net − Bulge fD :
log(M⋆, fD) = 10.752
⟨t⋆, fD⟩M = 12.033
⟨Z⋆, fD⟩M = 0.924
Net − Bulge eD :
log(M⋆, eD) = 10.761
⟨t⋆, eD⟩M = 12.314
⟨Z⋆, eD⟩M = 0.929

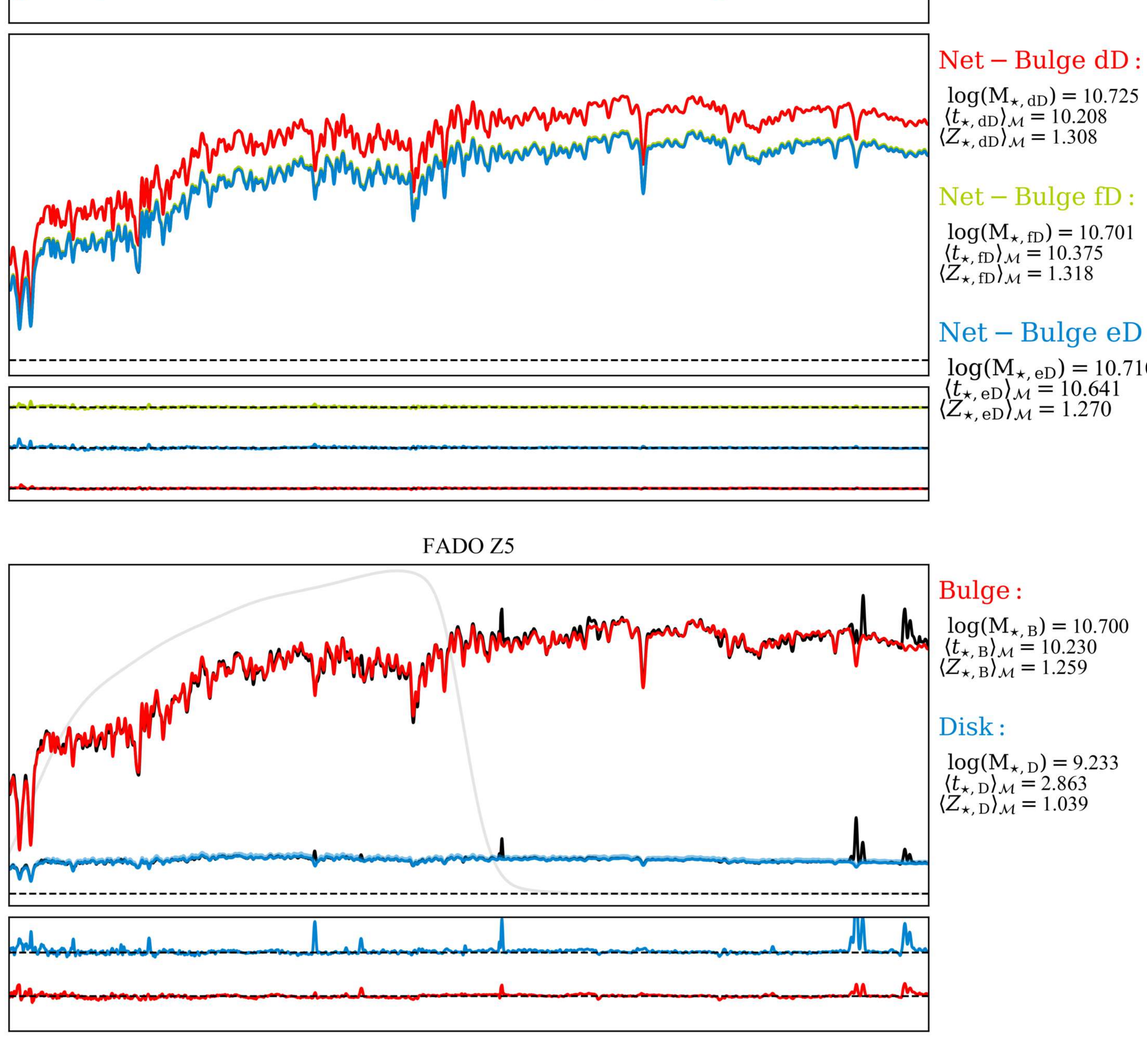
Net − Bulge dD :
log(M⋆, dD) = 10.725
⟨t⋆, dD⟩M = 10.208
⟨Z⋆, dD⟩M = 1.308
Net − Bulge fD :
log(M⋆, fD) = 10.701
⟨t⋆, fD⟩M = 10.375
⟨Z⋆, fD⟩M = 1.318
Net − Bulge eD :
log(M⋆, eD) = 10.710
⟨t⋆, eD⟩M = 10.641
⟨Z⋆, eD⟩M = 1.270

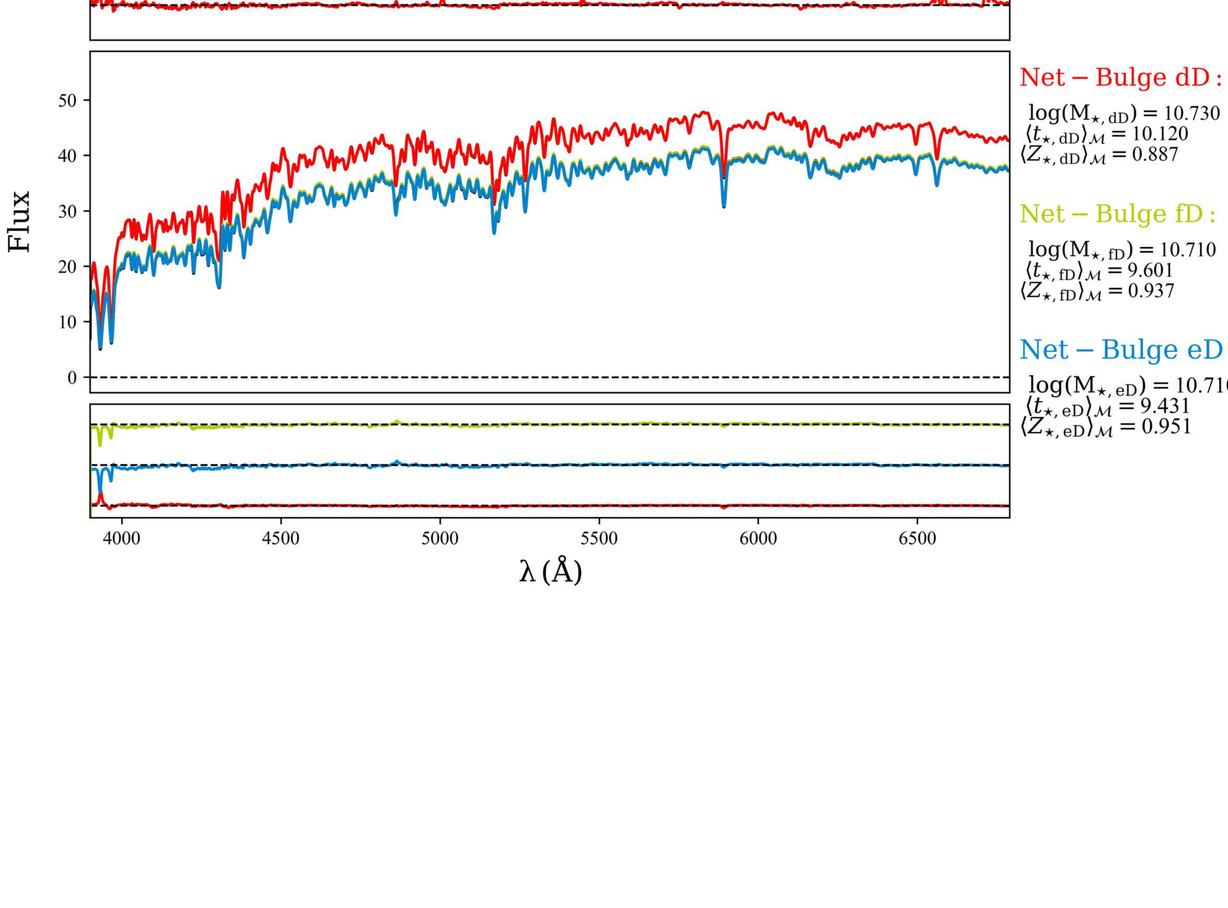
FADO Z4
Flux
Bulge :
log(M⋆, B) = 10.740
⟨t⋆, B⟩M = 10.500
⟨Z⋆, B⟩M = 0.852
Disk :
log(M⋆, D) = 9.651
⟨t⋆, D⟩M = 10.590
⟨Z⋆, D⟩M = 0.691

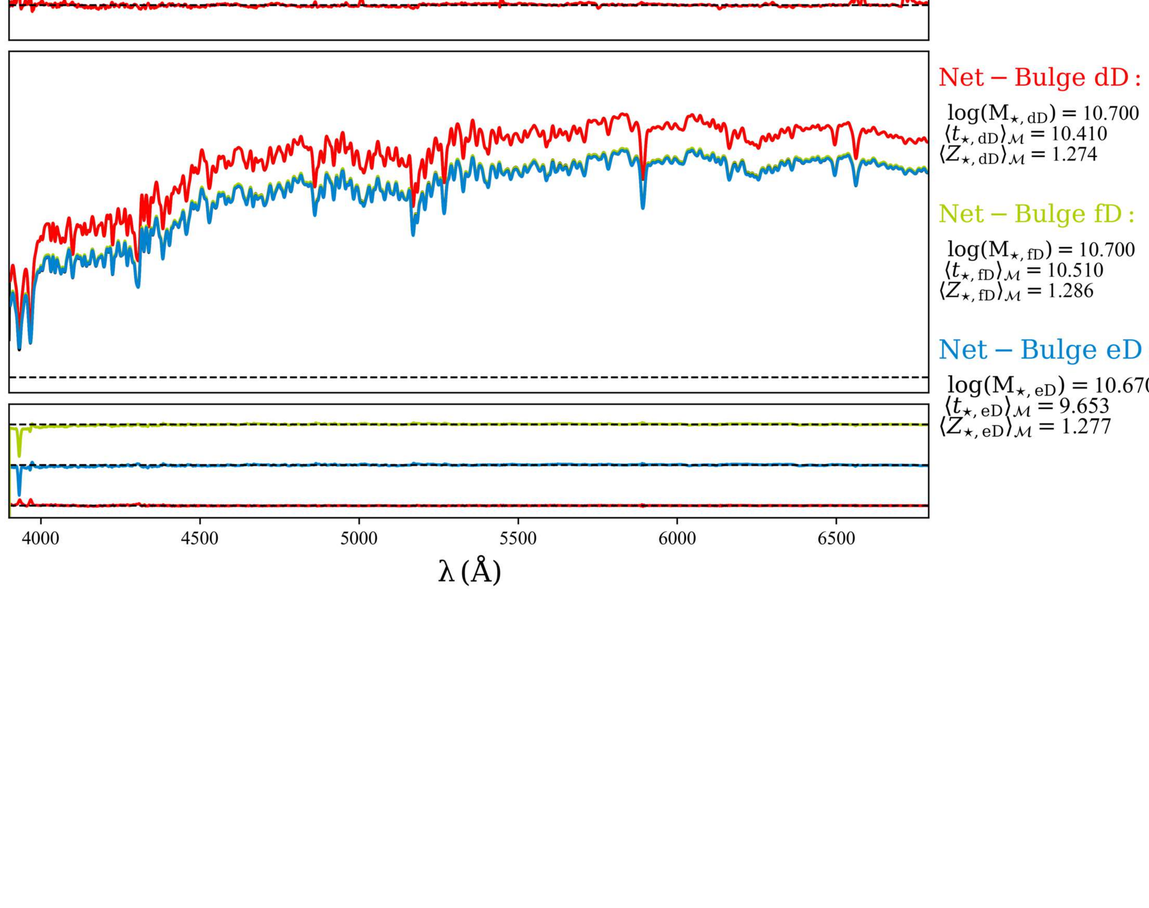
FADO Z5
Bulge :
log(M⋆, B) = 10.700
⟨t⋆, B⟩M = 10.230
⟨Z⋆, B⟩M = 1.259
Disk :
log(M⋆, D) = 9.233
⟨t⋆, D⟩M = 2.863
⟨Z⋆, D⟩M = 1.039

Flux
Net − Bulge dD :
log(M⋆, dD) = 10.730
⟨t⋆, dD⟩M = 10.120
⟨Z⋆, dD⟩M = 0.887
Net − Bulge fD :
log(M⋆, fD) = 10.710
⟨t⋆, fD⟩M = 9.601
⟨Z⋆, fD⟩M = 0.937
Net − Bulge eD :
log(M⋆, eD) = 10.710
⟨t⋆, eD⟩M = 9.431
⟨Z⋆, eD⟩M = 0.951
λ (Å)

Net − Bulge dD :
log(M⋆, dD) = 10.700
⟨t⋆, dD⟩M = 10.410
⟨Z⋆, dD⟩M = 1.274
Net − Bulge fD :
log(M⋆, fD) = 10.700
⟨t⋆, fD⟩M = 10.510
⟨Z⋆, fD⟩M = 1.286
Net − Bulge eD :
log(M⋆, eD) = 10.670
⟨t⋆, eD⟩M = 9.653
⟨Z⋆, eD⟩M = 1.277
λ (Å)

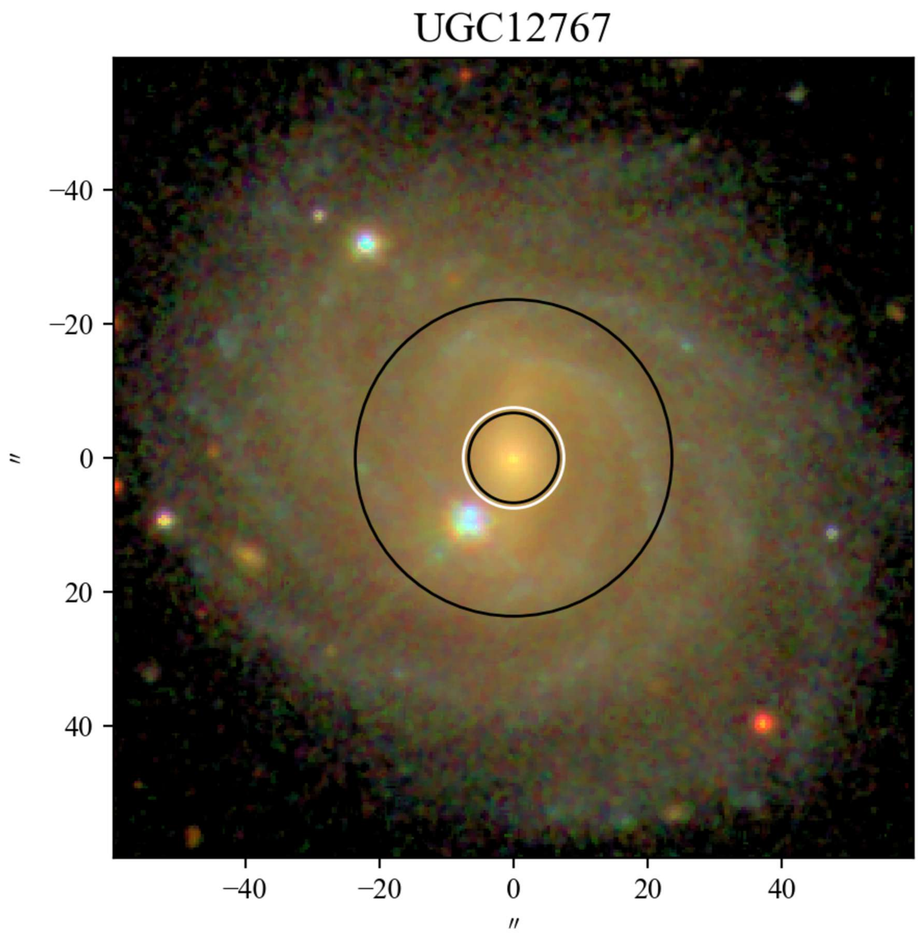
UGC12767
−40
−20
0
20
40
″
−40
−20
0
20
40
″

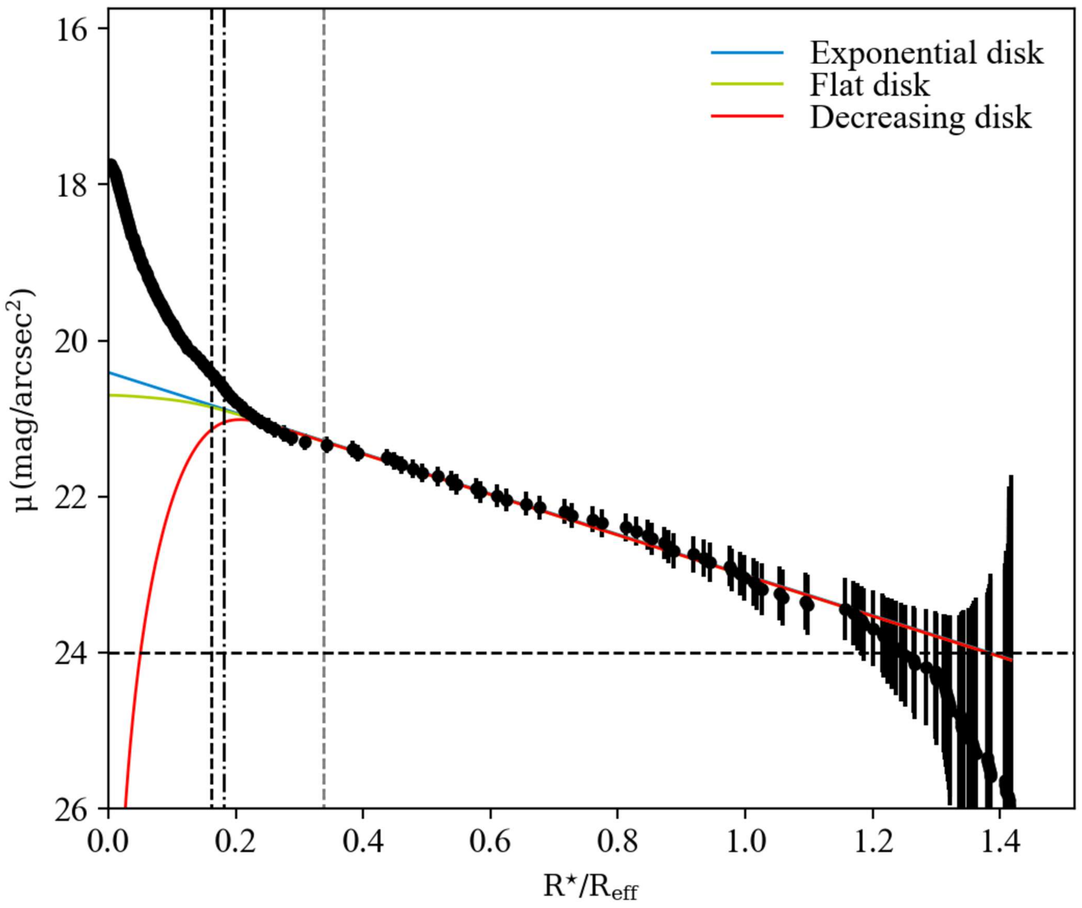
Exponential disk
Flat disk
Decreasing disk
μ (mag/arcsec²)
16
18
20
22
24
26
0.0
0.2
0.4
0.6
0.8
1.0
1.2
1.4
R⋆/Reff

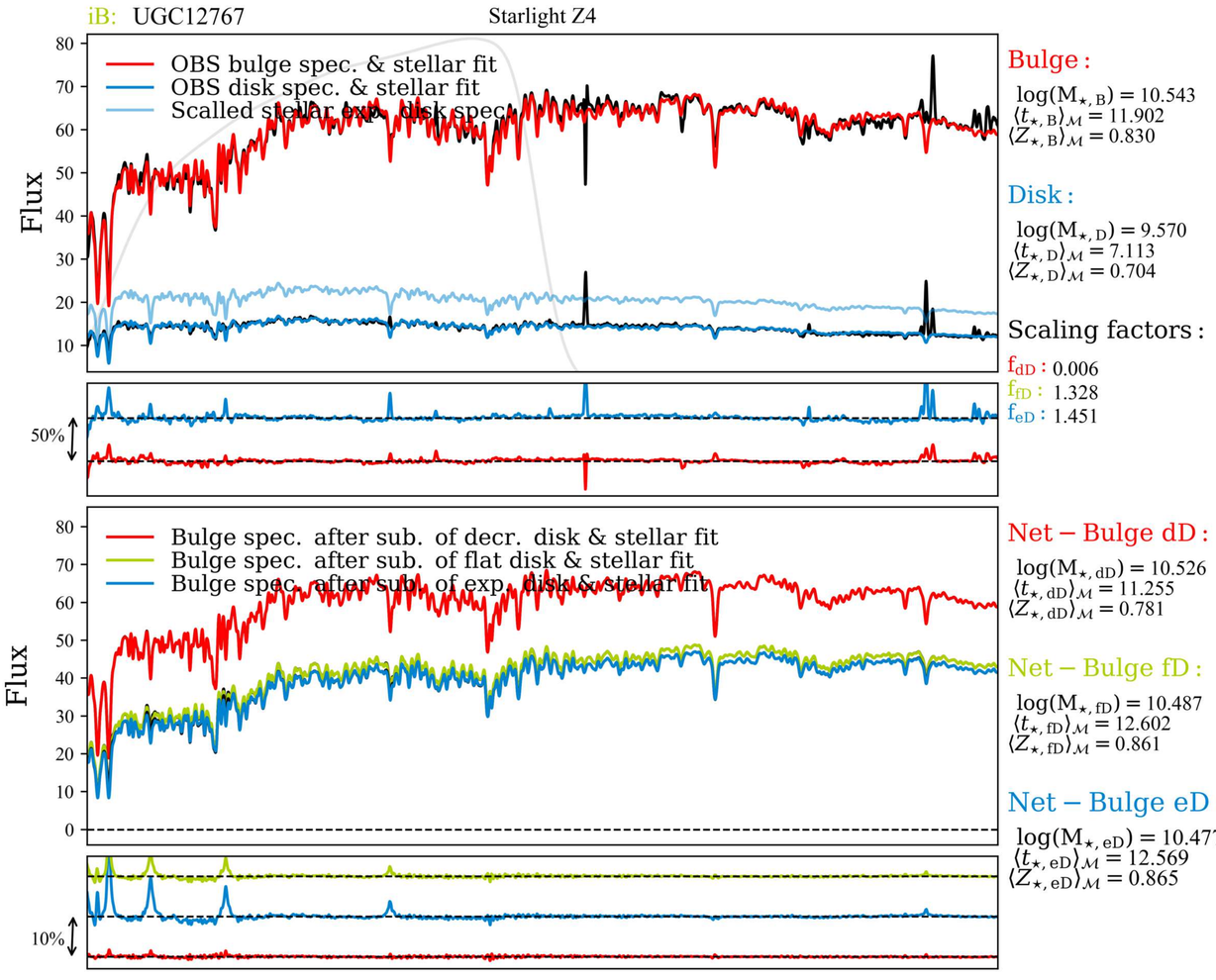
iB: UGC12767
Starlight Z4
OBS bulge spec. & stellar fit
OBS disk spec. & stellar fit
Scalled stellar exp. disk spec.
Flux
50%
Bulge :
log(M⋆, B) = 10.543
⟨t⋆, B⟩M = 11.902
⟨Z⋆, B⟩M = 0.830
Disk :
log(M⋆, D) = 9.570
⟨t⋆, D⟩M = 7.113
⟨Z⋆, D⟩M = 0.704
Scaling factors :
fdD : 0.006
ffD : 1.328
feD : 1.451
Bulge spec. after sub. of decr. disk & stellar fit
Bulge spec. after sub. of flat disk & stellar fit
Bulge spec. after sub. of exp. disk & stellar fit
10%
Net − Bulge dD :
log(M⋆, dD) = 10.526
⟨t⋆, dD⟩M = 11.255
⟨Z⋆, dD⟩M = 0.781
Net − Bulge fD :
log(M⋆, fD) = 10.487
⟨t⋆, fD⟩M = 12.602
⟨Z⋆, fD⟩M = 0.861
Net − Bulge eD :
log(M⋆, eD) = 10.477
⟨t⋆, eD⟩M = 12.569
⟨Z⋆, eD⟩M = 0.865

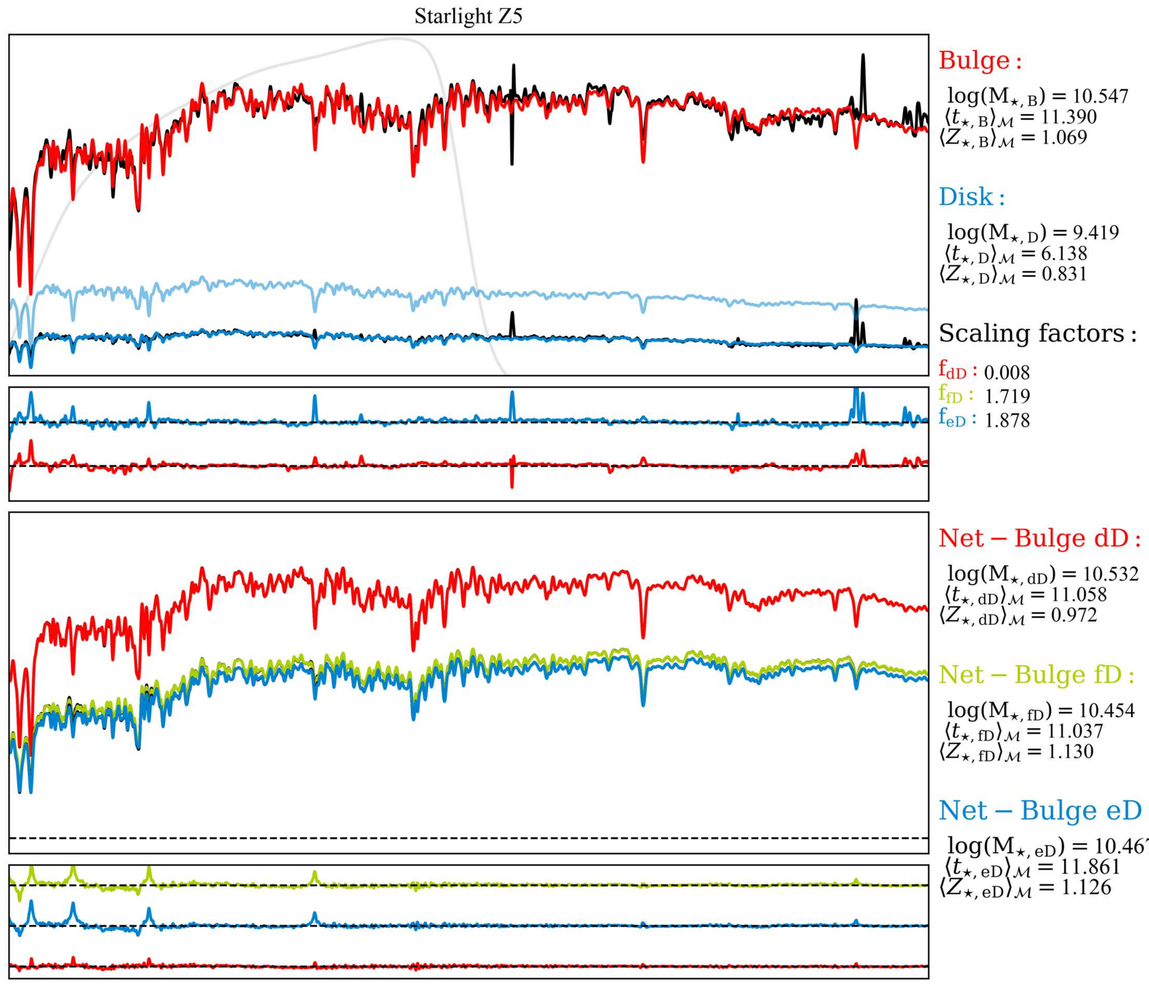
Starlight Z5
Bulge :
log(M⋆, B) = 10.547
⟨t⋆, B⟩M = 11.390
⟨Z⋆, B⟩M = 1.069
Disk :
log(M⋆, D) = 9.419
⟨t⋆, D⟩M = 6.138
⟨Z⋆, D⟩M = 0.831
Scaling factors :
fdD : 0.008
ffD : 1.719
feD : 1.878
Net − Bulge dD :
log(M⋆, dD) = 10.532
⟨t⋆, dD⟩M = 11.058
⟨Z⋆, dD⟩M = 0.972
Net − Bulge fD :
log(M⋆, fD) = 10.454
⟨t⋆, fD⟩M = 11.037
⟨Z⋆, fD⟩M = 1.130
Net − Bulge eD :
log(M⋆, eD) = 10.467
⟨t⋆, eD⟩M = 11.861
⟨Z⋆, eD⟩M = 1.126

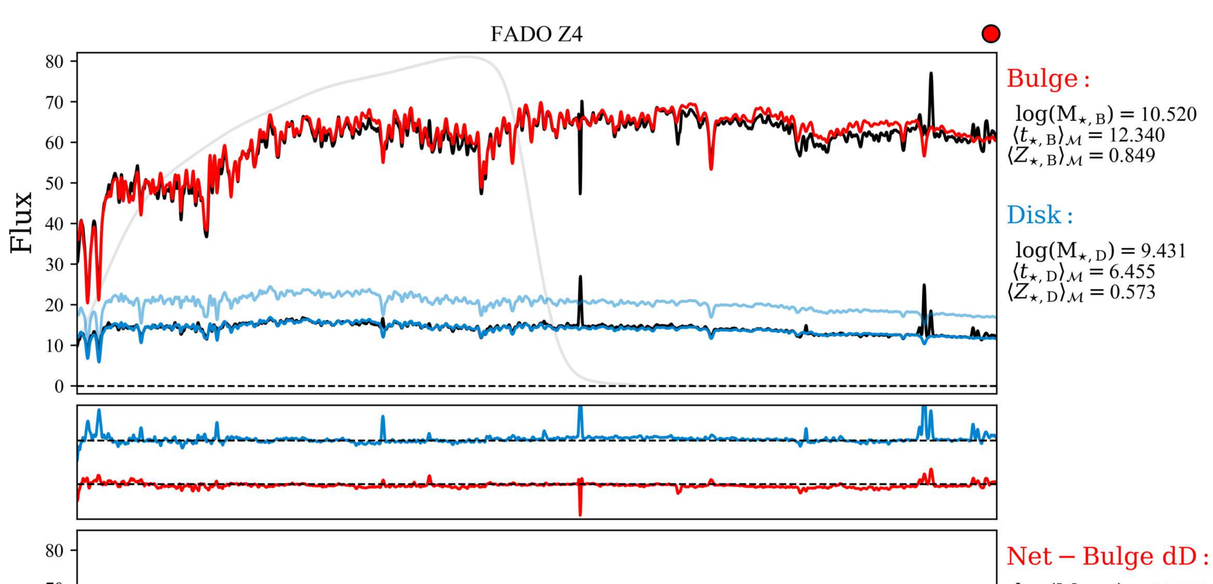
FADO Z4
Flux
Bulge :
log(M⋆, B) = 10.520
⟨t⋆, B⟩M = 12.340
⟨Z⋆, B⟩M = 0.849
Disk :
log(M⋆, D) = 9.431
⟨t⋆, D⟩M = 6.455
⟨Z⋆, D⟩M = 0.573
Net − Bulge dD :
log(M⋆, dD) = 10.530
⟨t⋆, dD⟩M = 12.500
⟨Z⋆, dD⟩M = 0.814
Net − Bulge fD :
log(M⋆, fD) = 10.480
⟨t⋆, fD⟩M = 13.000
⟨Z⋆, fD⟩M = 0.897
Net − Bulge eD :
log(M⋆, eD) = 10.480
⟨t⋆, eD⟩M = 13.000
⟨Z⋆, eD⟩M = 0.915
λ (Å)

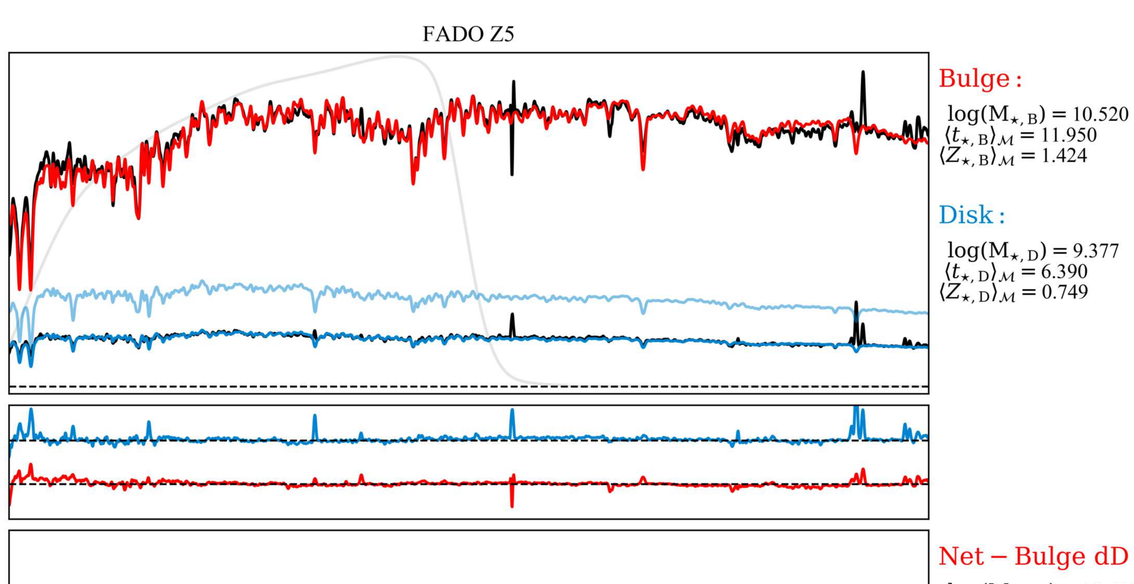
FADO Z5
Bulge :
log(M⋆, B) = 10.520
⟨t⋆, B⟩M = 11.950
⟨Z⋆, B⟩M = 1.424
Disk :
log(M⋆, D) = 9.377
⟨t⋆, D⟩M = 6.390
⟨Z⋆, D⟩M = 0.749
Net − Bulge dD :
log(M⋆, dD) = 10.490
⟨t⋆, dD⟩M = 10.480
⟨Z⋆, dD⟩M = 1.302
Net − Bulge fD :
log(M⋆, fD) = 10.470
⟨t⋆, fD⟩M = 12.980
⟨Z⋆, fD⟩M = 1.430
Net − Bulge eD :
log(M⋆, eD) = 10.420
⟨t⋆, eD⟩M = 11.010
⟨Z⋆, eD⟩M = 1.495
λ (Å)

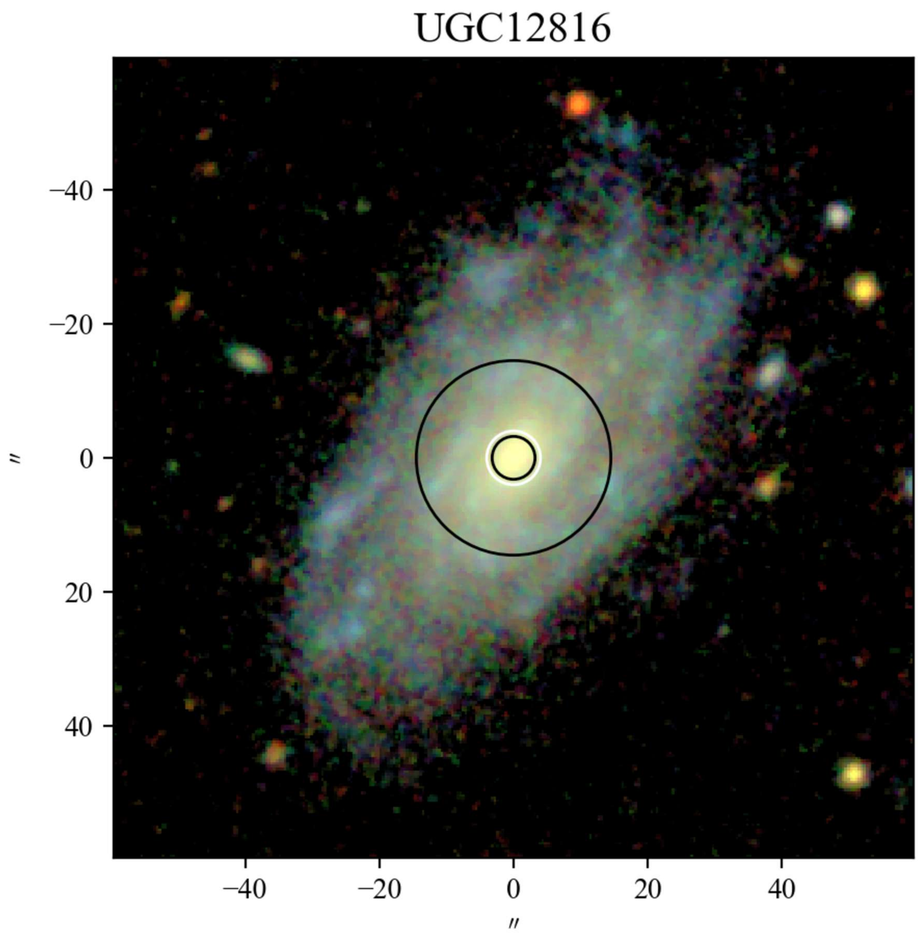
UGC12816
−40
−20
0
20
40
″
−40
−20
0
20
40
″

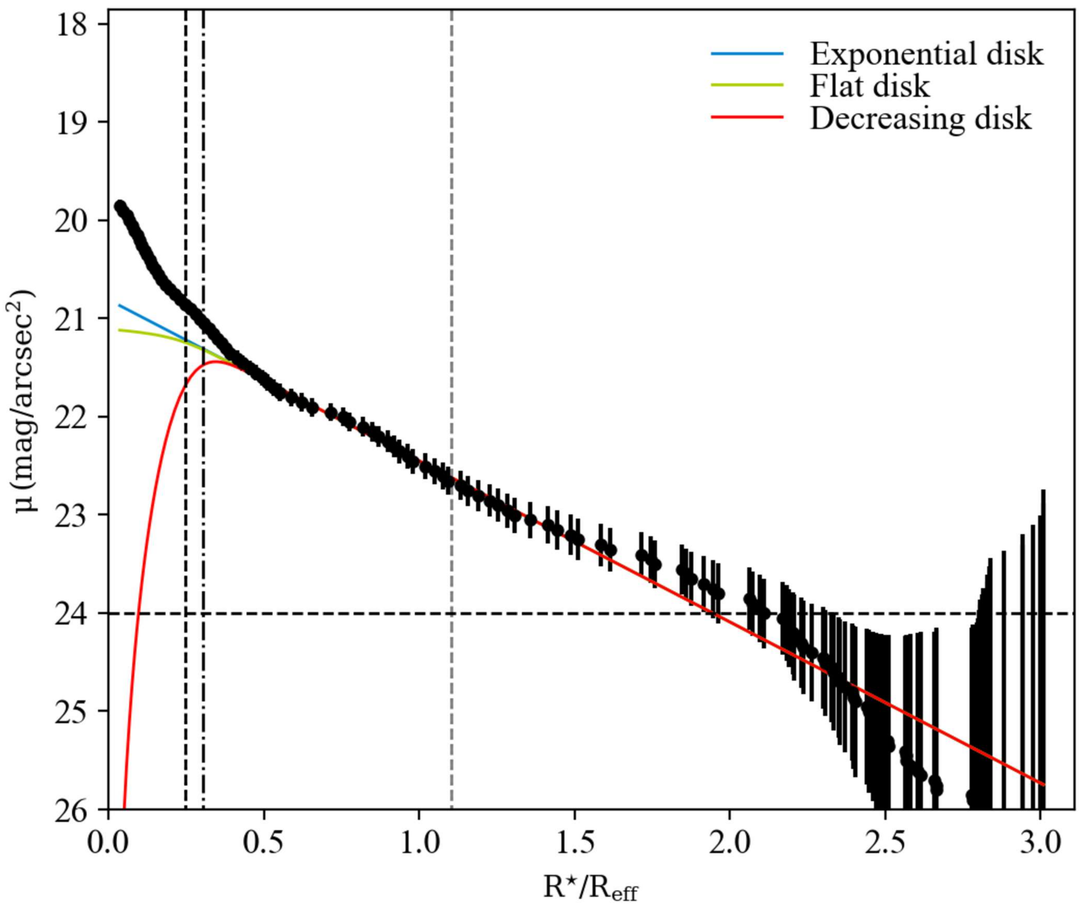
Exponential disk
Flat disk
Decreasing disk
μ (mag/arcsec²)
18
19
20
21
22
23
24
25
26
0.0
0.5
1.0
1.5
2.0
2.5
3.0
R⋆/Reff

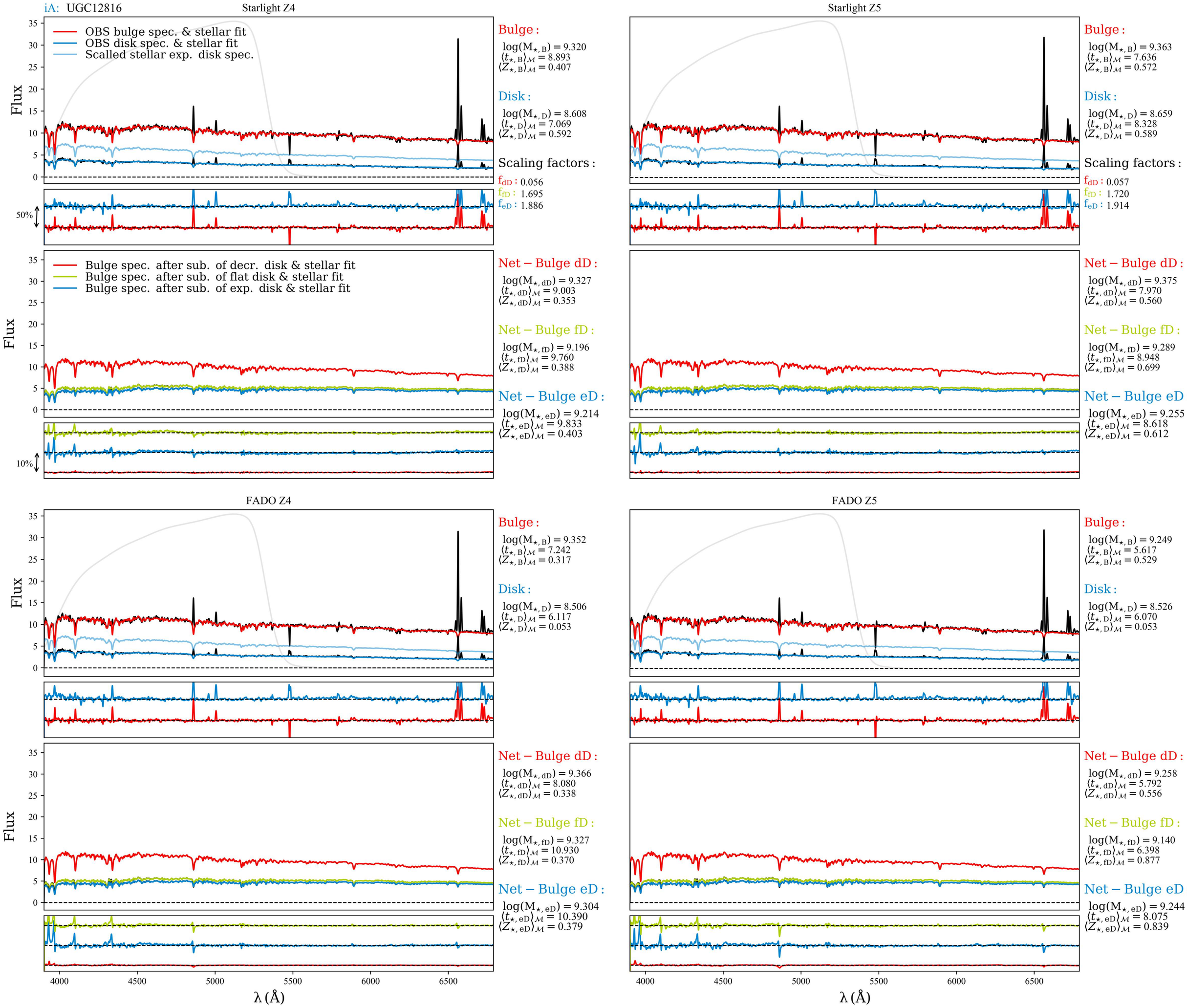
iA: UGC12816
Starlight Z4
OBS bulge spec. & stellar fit
OBS disk spec. & stellar fit
Scalled stellar exp. disk spec.
Flux
Bulge :
log(M⋆, B) = 9.320
⟨t⋆, B⟩M = 8.893
⟨Z⋆, B⟩M = 0.407
Disk :
log(M⋆, D) = 8.608
⟨t⋆, D⟩M = 7.069
⟨Z⋆, D⟩M = 0.592
Scaling factors :
fdD : 0.056
ffD : 1.695
feD : 1.886
50%
Bulge spec. after sub. of decr. disk & stellar fit
Bulge spec. after sub. of flat disk & stellar fit
Bulge spec. after sub. of exp. disk & stellar fit
Net − Bulge dD :
log(M⋆, dD) = 9.327
⟨t⋆, dD⟩M = 9.003
⟨Z⋆, dD⟩M = 0.353
Net − Bulge fD :
log(M⋆, fD) = 9.196
⟨t⋆, fD⟩M = 9.760
⟨Z⋆, fD⟩M = 0.388
Net − Bulge eD :
log(M⋆, eD) = 9.214
⟨t⋆, eD⟩M = 9.833
⟨Z⋆, eD⟩M = 0.403
10%
FADO Z4
Bulge :
log(M⋆, B) = 9.352
⟨t⋆, B⟩M = 7.242
⟨Z⋆, B⟩M = 0.317
Disk :
log(M⋆, D) = 8.506
⟨t⋆, D⟩M = 6.117
⟨Z⋆, D⟩M = 0.053
Net − Bulge dD :
log(M⋆, dD) = 9.366
⟨t⋆, dD⟩M = 8.080
⟨Z⋆, dD⟩M = 0.338
Net − Bulge fD :
log(M⋆, fD) = 9.327
⟨t⋆, fD⟩M = 10.930
⟨Z⋆, fD⟩M = 0.370
Net − Bulge eD :
log(M⋆, eD) = 9.304
⟨t⋆, eD⟩M = 10.390
⟨Z⋆, eD⟩M = 0.379
λ (Å)

Starlight Z5
Bulge :
log(M⋆, B) = 9.363
⟨t⋆, B⟩M = 7.636
⟨Z⋆, B⟩M = 0.572
Disk :
log(M⋆, D) = 8.659
⟨t⋆, D⟩M = 8.328
⟨Z⋆, D⟩M = 0.589
Scaling factors :
fdD : 0.057
ffD : 1.720
feD : 1.914
Net − Bulge dD :
log(M⋆, dD) = 9.375
⟨t⋆, dD⟩M = 7.970
⟨Z⋆, dD⟩M = 0.560
Net − Bulge fD :
log(M⋆, fD) = 9.289
⟨t⋆, fD⟩M = 8.948
⟨Z⋆, fD⟩M = 0.699
Net − Bulge eD :
log(M⋆, eD) = 9.255
⟨t⋆, eD⟩M = 8.618
⟨Z⋆, eD⟩M = 0.612
FADO Z5
Bulge :
log(M⋆, B) = 9.249
⟨t⋆, B⟩M = 5.617
⟨Z⋆, B⟩M = 0.529
Disk :
log(M⋆, D) = 8.526
⟨t⋆, D⟩M = 6.070
⟨Z⋆, D⟩M = 0.053
Net − Bulge dD :
log(M⋆, dD) = 9.258
⟨t⋆, dD⟩M = 5.792
⟨Z⋆, dD⟩M = 0.556
Net − Bulge fD :
log(M⋆, fD) = 9.140
⟨t⋆, fD⟩M = 6.398
⟨Z⋆, fD⟩M = 0.877
Net − Bulge eD :
log(M⋆, eD) = 9.244
⟨t⋆, eD⟩M = 8.075
⟨Z⋆, eD⟩M = 0.839
λ (Å)

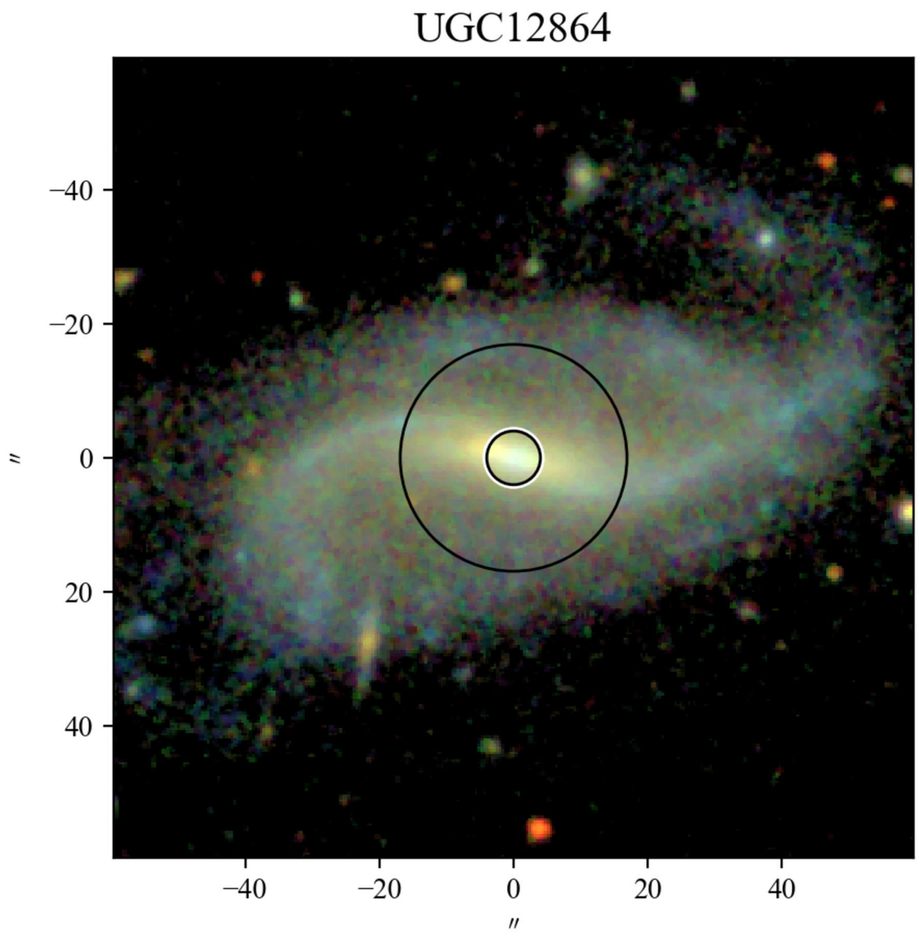
UGC12864
−40
−20
0
20
40
″
−40
−20
0
20
40
″

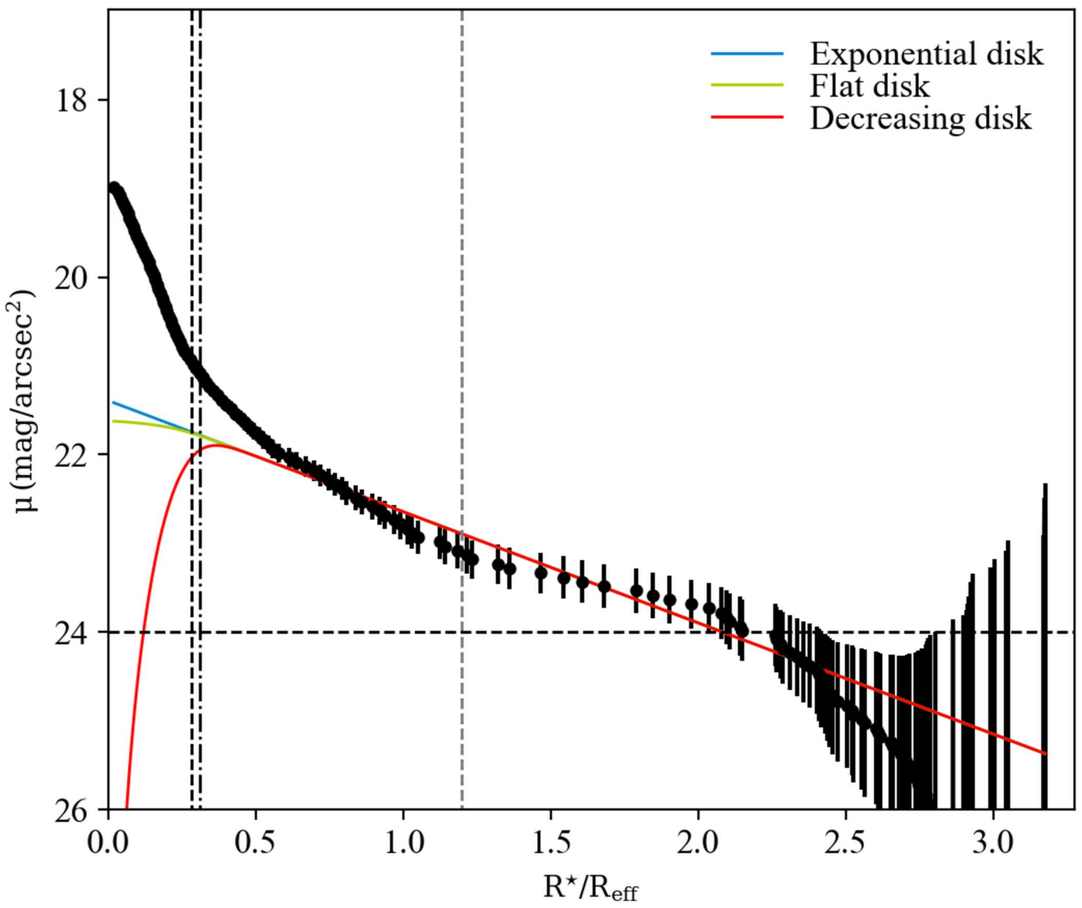
Exponential disk
Flat disk
Decreasing disk
μ (mag/arcsec²)
18
20
22
24
26
0.0
0.5
1.0
1.5
2.0
2.5
3.0
R⋆/Reff

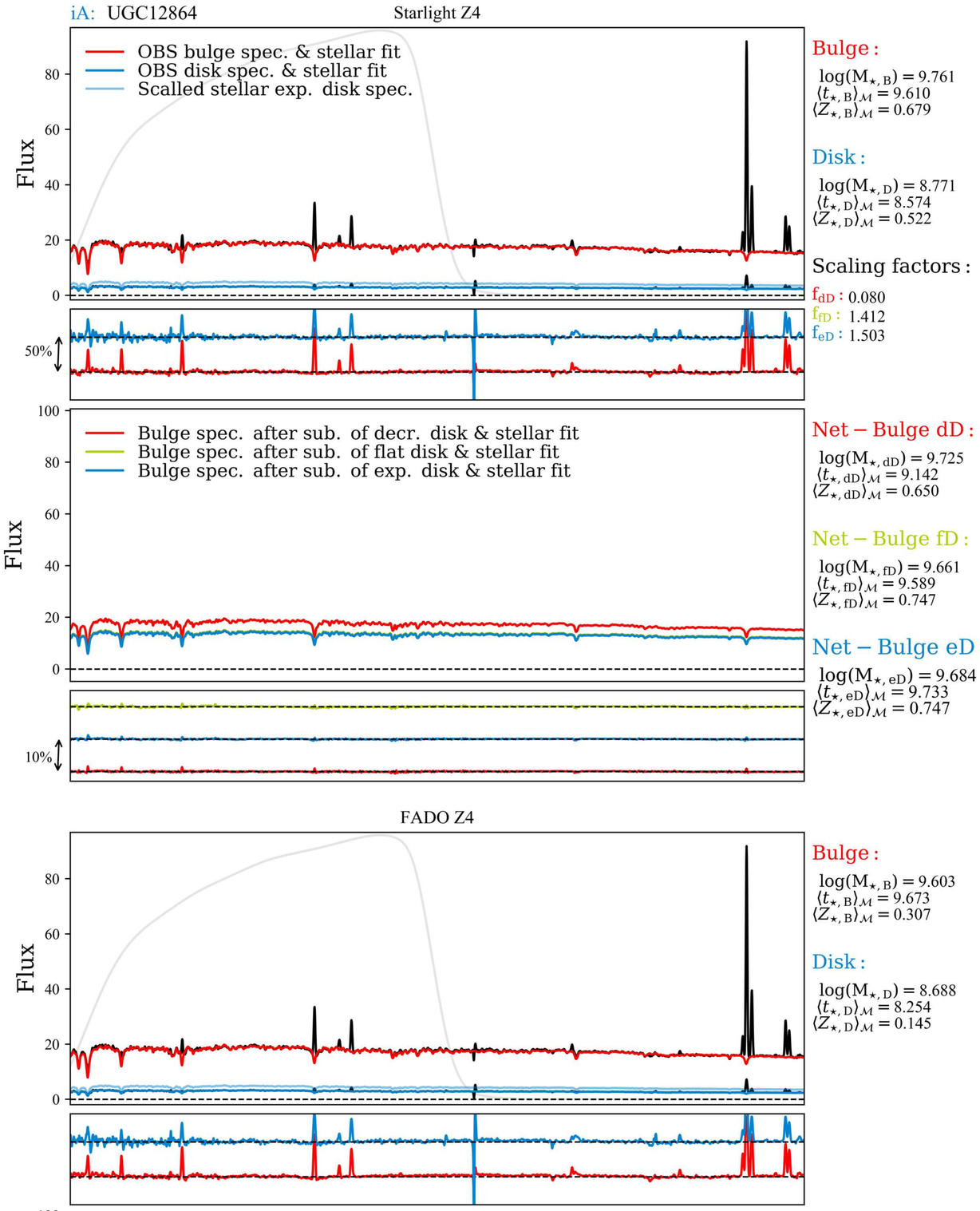
iA: UGC12864
Starlight Z4
OBS bulge spec. & stellar fit
OBS disk spec. & stellar fit
Scalled stellar exp. disk spec.
Flux
50%
Bulge :
log(M⋆, B) = 9.761
⟨t⋆, B⟩M = 9.610
⟨Z⋆, B⟩M = 0.679
Disk :
log(M⋆, D) = 8.771
⟨t⋆, D⟩M = 8.574
⟨Z⋆, D⟩M = 0.522
Scaling factors :
fdD : 0.080
ffD : 1.412
feD : 1.503
Bulge spec. after sub. of decr. disk & stellar fit
Bulge spec. after sub. of flat disk & stellar fit
Bulge spec. after sub. of exp. disk & stellar fit
10%
Net − Bulge dD :
log(M⋆, dD) = 9.725
⟨t⋆, dD⟩M = 9.142
⟨Z⋆, dD⟩M = 0.650
Net − Bulge fD :
log(M⋆, fD) = 9.661
⟨t⋆, fD⟩M = 9.589
⟨Z⋆, fD⟩M = 0.747
Net − Bulge eD :
log(M⋆, eD) = 9.684
⟨t⋆, eD⟩M = 9.733
⟨Z⋆, eD⟩M = 0.747

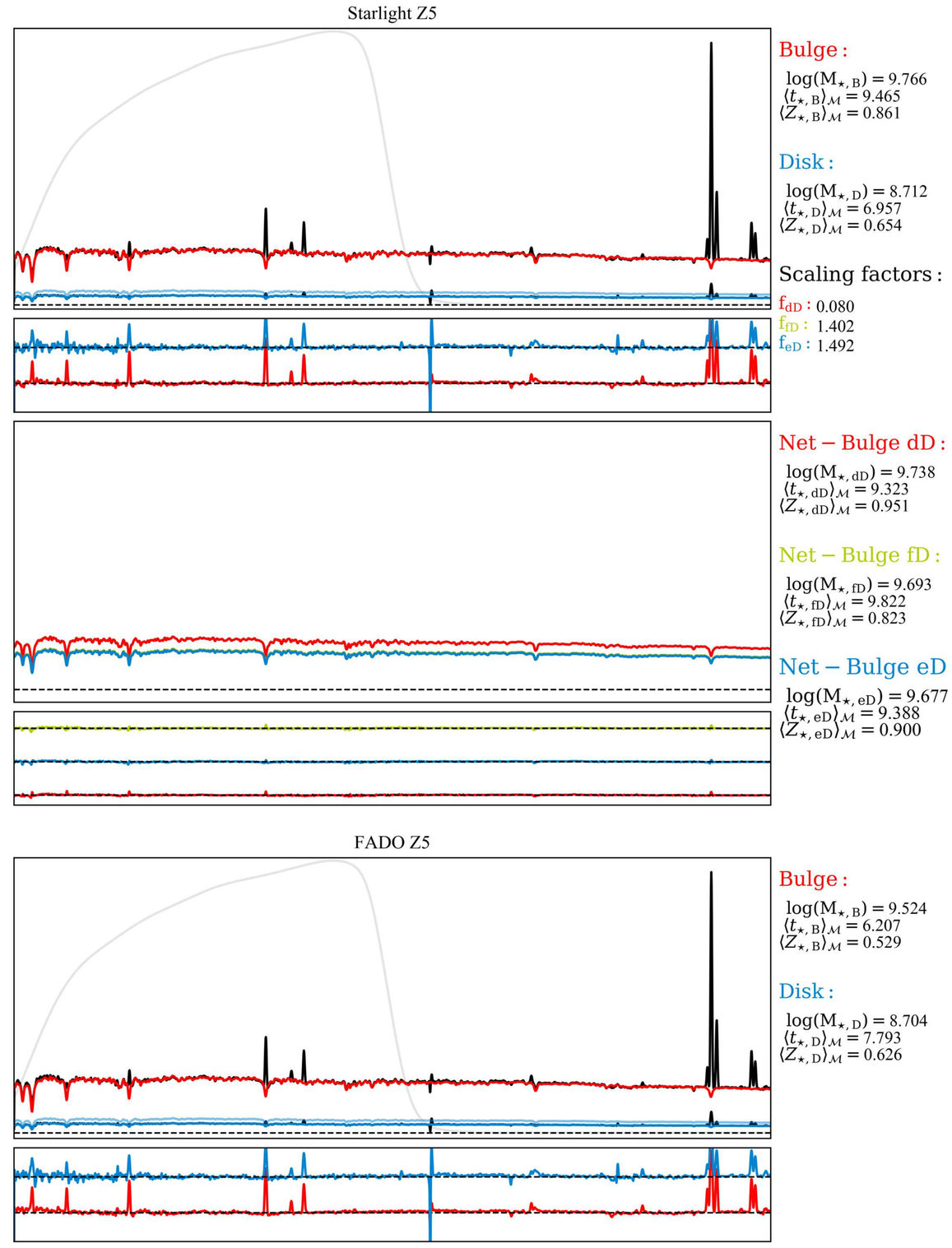
Starlight Z5
Bulge :
log(M⋆, B) = 9.766
⟨t⋆, B⟩M = 9.465
⟨Z⋆, B⟩M = 0.861
Disk :
log(M⋆, D) = 8.712
⟨t⋆, D⟩M = 6.957
⟨Z⋆, D⟩M = 0.654
Scaling factors :
fdD : 0.080
ffD : 1.402
feD : 1.492
Net − Bulge dD :
log(M⋆, dD) = 9.738
⟨t⋆, dD⟩M = 9.323
⟨Z⋆, dD⟩M = 0.951
Net − Bulge fD :
log(M⋆, fD) = 9.693
⟨t⋆, fD⟩M = 9.822
⟨Z⋆, fD⟩M = 0.823
Net − Bulge eD :
log(M⋆, eD) = 9.677
⟨t⋆, eD⟩M = 9.388
⟨Z⋆, eD⟩M = 0.900

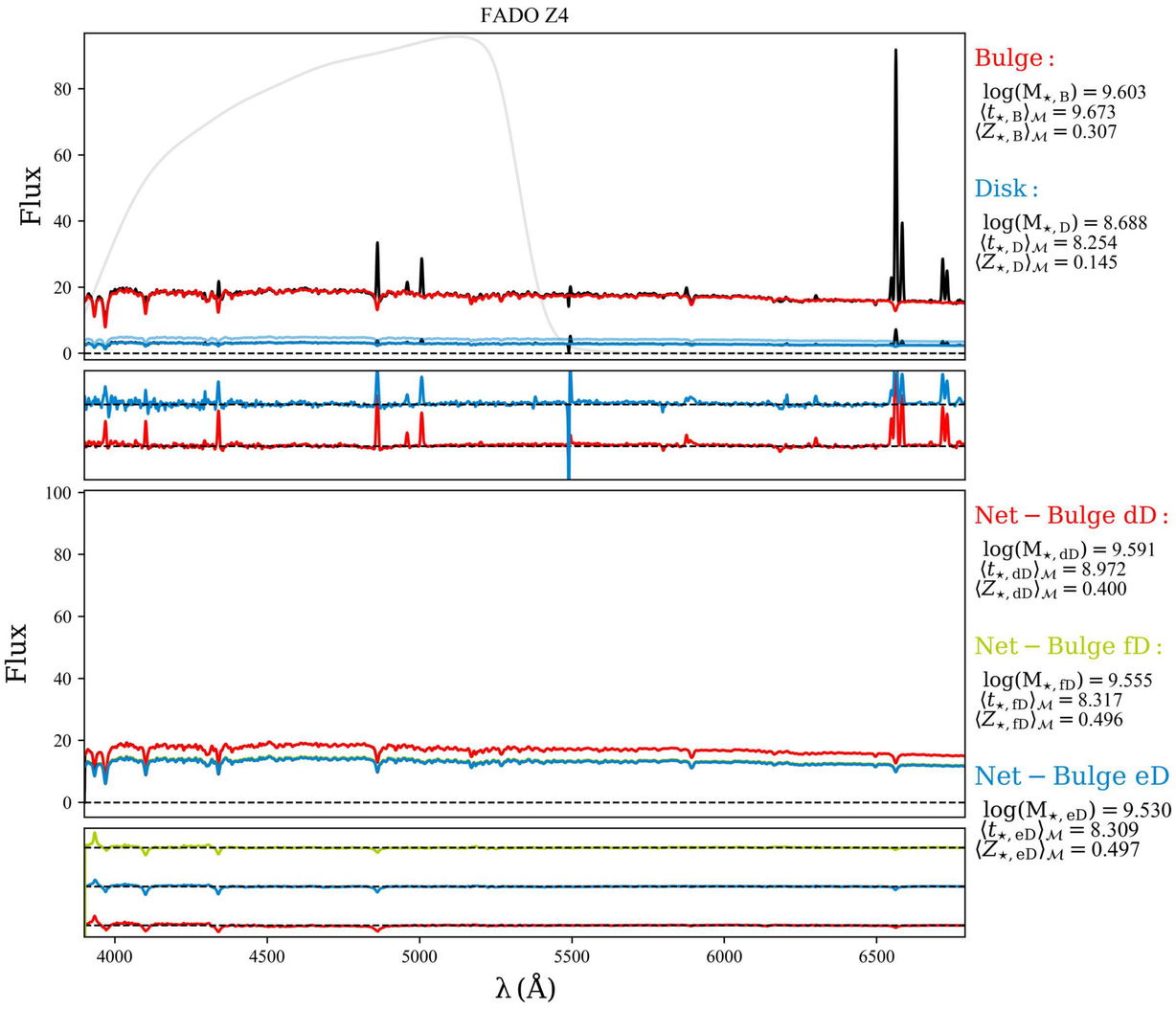
FADO Z4
Flux
Bulge :
log(M⋆, B) = 9.603
⟨t⋆, B⟩M = 9.673
⟨Z⋆, B⟩M = 0.307
Disk :
log(M⋆, D) = 8.688
⟨t⋆, D⟩M = 8.254
⟨Z⋆, D⟩M = 0.145
Net − Bulge dD :
log(M⋆, dD) = 9.591
⟨t⋆, dD⟩M = 8.972
⟨Z⋆, dD⟩M = 0.400
Net − Bulge fD :
log(M⋆, fD) = 9.555
⟨t⋆, fD⟩M = 8.317
⟨Z⋆, fD⟩M = 0.496
Net − Bulge eD :
log(M⋆, eD) = 9.530
⟨t⋆, eD⟩M = 8.309
⟨Z⋆, eD⟩M = 0.497
λ (Å)

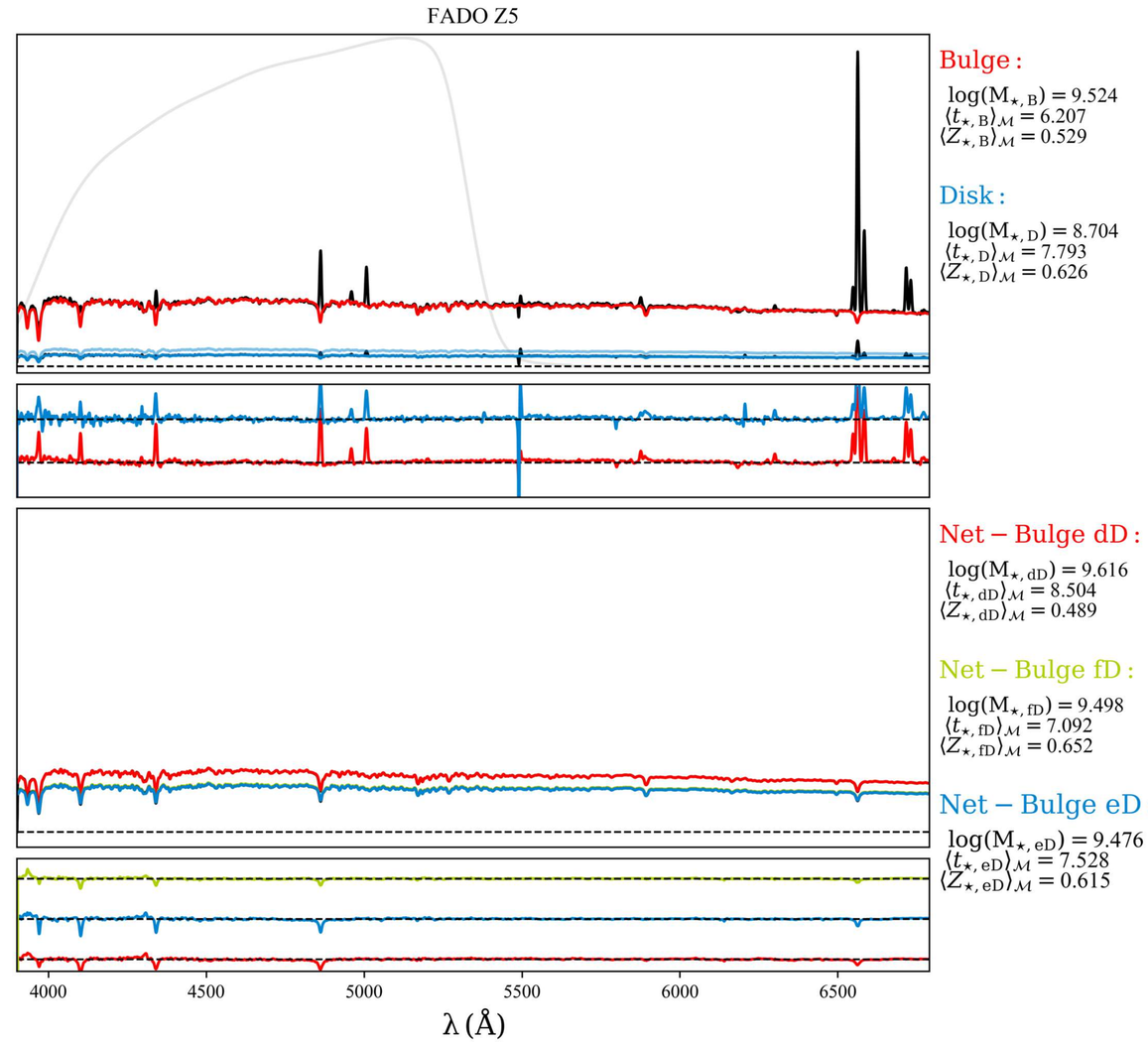
FADO Z5
Bulge :
log(M⋆, B) = 9.524
⟨t⋆, B⟩M = 6.207
⟨Z⋆, B⟩M = 0.529
Disk :
log(M⋆, D) = 8.704
⟨t⋆, D⟩M = 7.793
⟨Z⋆, D⟩M = 0.626
Net − Bulge dD :
log(M⋆, dD) = 9.616
⟨t⋆, dD⟩M = 8.504
⟨Z⋆, dD⟩M = 0.489
Net − Bulge fD :
log(M⋆, fD) = 9.498
⟨t⋆, fD⟩M = 7.092
⟨Z⋆, fD⟩M = 0.652
Net − Bulge eD :
log(M⋆, eD) = 9.476
⟨t⋆, eD⟩M = 7.528
⟨Z⋆, eD⟩M = 0.615
λ (Å)

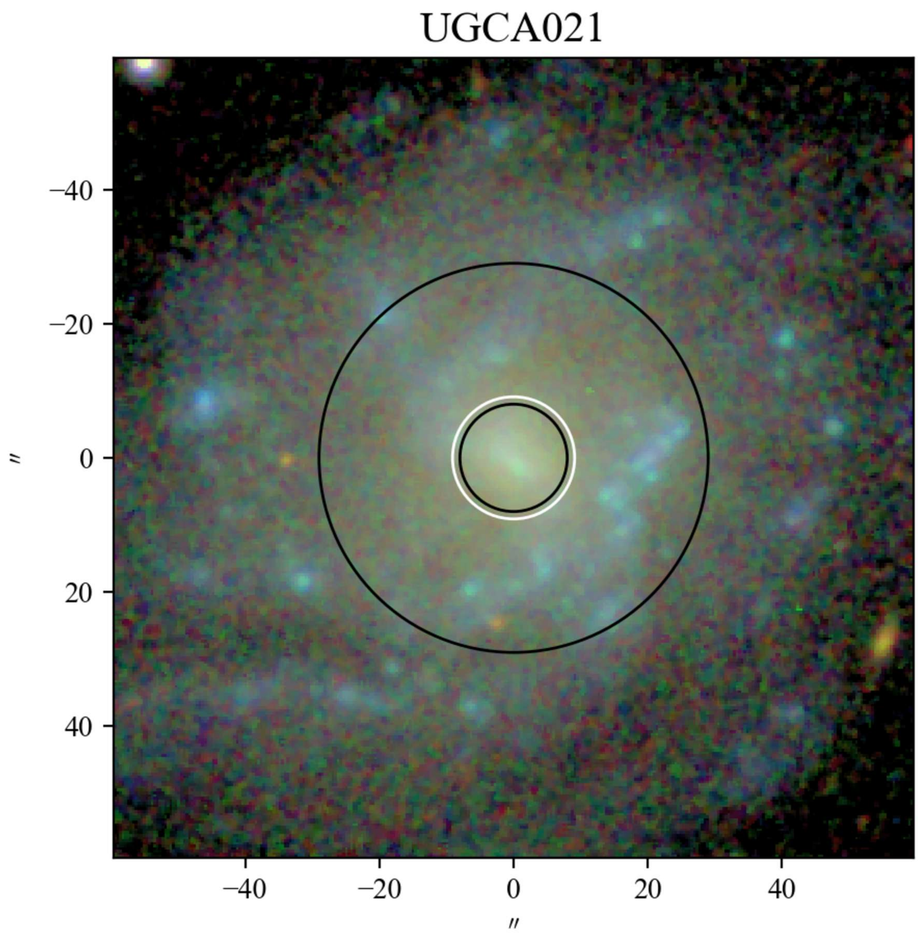
UGCA021
−40
−20
0
20
40
″
−40
−20
0
20
40
″

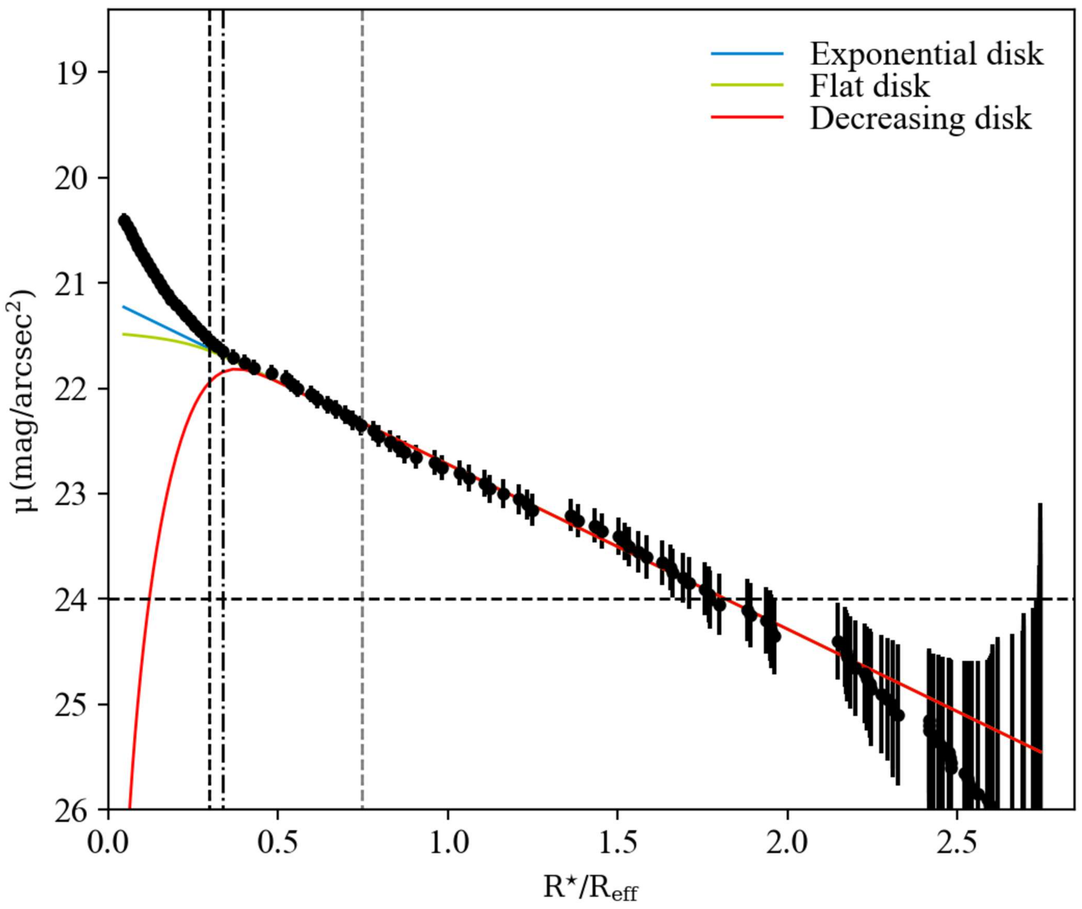
Exponential disk
Flat disk
Decreasing disk
μ (mag/arcsec²)
19
20
21
22
23
24
25
26
0.0
0.5
1.0
1.5
2.0
2.5
R⋆/Reff

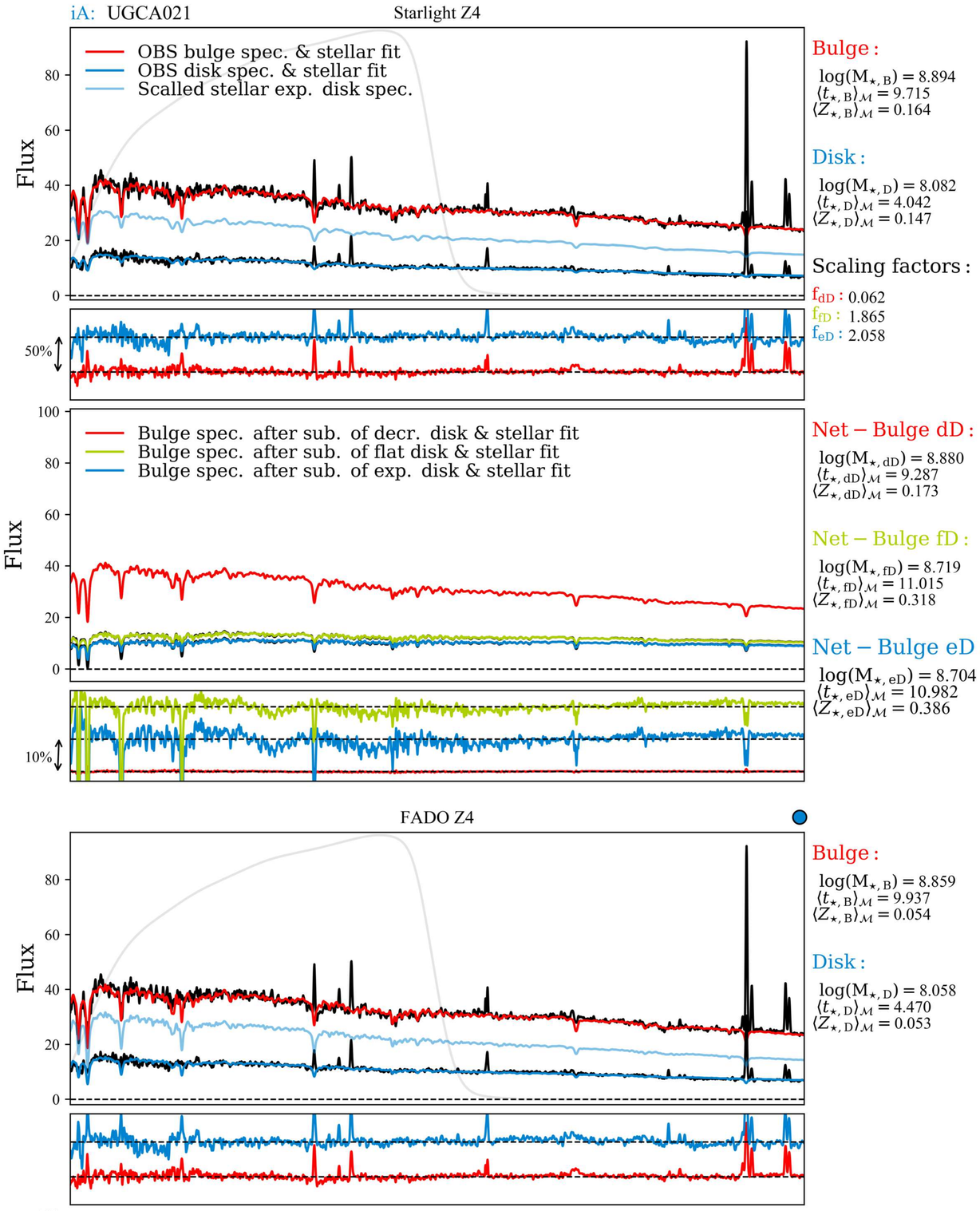
iA: UGCA021
Starlight Z4
OBS bulge spec. & stellar fit
OBS disk spec. & stellar fit
Scalled stellar exp. disk spec.
Flux
50%
Bulge :
log(M⋆, B) = 8.894
⟨t⋆, B⟩M = 9.715
⟨Z⋆, B⟩M = 0.164
Disk :
log(M⋆, D) = 8.082
⟨t⋆, D⟩M = 4.042
⟨Z⋆, D⟩M = 0.147
Scaling factors :
fdD : 0.062
ffD : 1.865
feD : 2.058
Bulge spec. after sub. of decr. disk & stellar fit
Bulge spec. after sub. of flat disk & stellar fit
Bulge spec. after sub. of exp. disk & stellar fit
10%
Net − Bulge dD :
log(M⋆, dD) = 8.880
⟨t⋆, dD⟩M = 9.287
⟨Z⋆, dD⟩M = 0.173
Net − Bulge fD :
log(M⋆, fD) = 8.719
⟨t⋆, fD⟩M = 11.015
⟨Z⋆, fD⟩M = 0.318
Net − Bulge eD :
log(M⋆, eD) = 8.704
⟨t⋆, eD⟩M = 10.982
⟨Z⋆, eD⟩M = 0.386

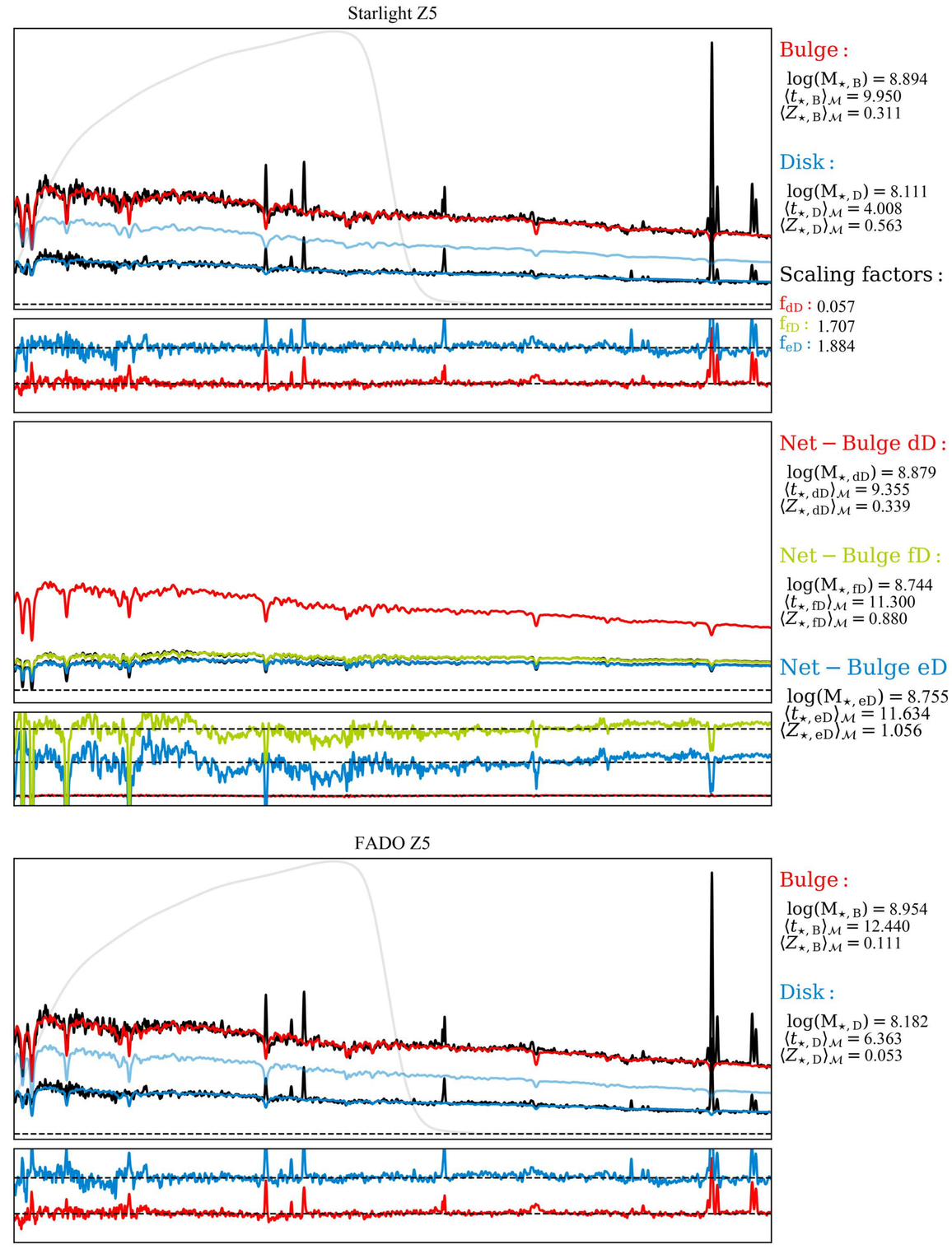
Starlight Z5
Bulge :
log(M⋆, B) = 8.894
⟨t⋆, B⟩M = 9.950
⟨Z⋆, B⟩M = 0.311
Disk :
log(M⋆, D) = 8.111
⟨t⋆, D⟩M = 4.008
⟨Z⋆, D⟩M = 0.563
Scaling factors :
fdD : 0.057
ffD : 1.707
feD : 1.884
Net − Bulge dD :
log(M⋆, dD) = 8.879
⟨t⋆, dD⟩M = 9.355
⟨Z⋆, dD⟩M = 0.339
Net − Bulge fD :
log(M⋆, fD) = 8.744
⟨t⋆, fD⟩M = 11.300
⟨Z⋆, fD⟩M = 0.880
Net − Bulge eD :
log(M⋆, eD) = 8.755
⟨t⋆, eD⟩M = 11.634
⟨Z⋆, eD⟩M = 1.056

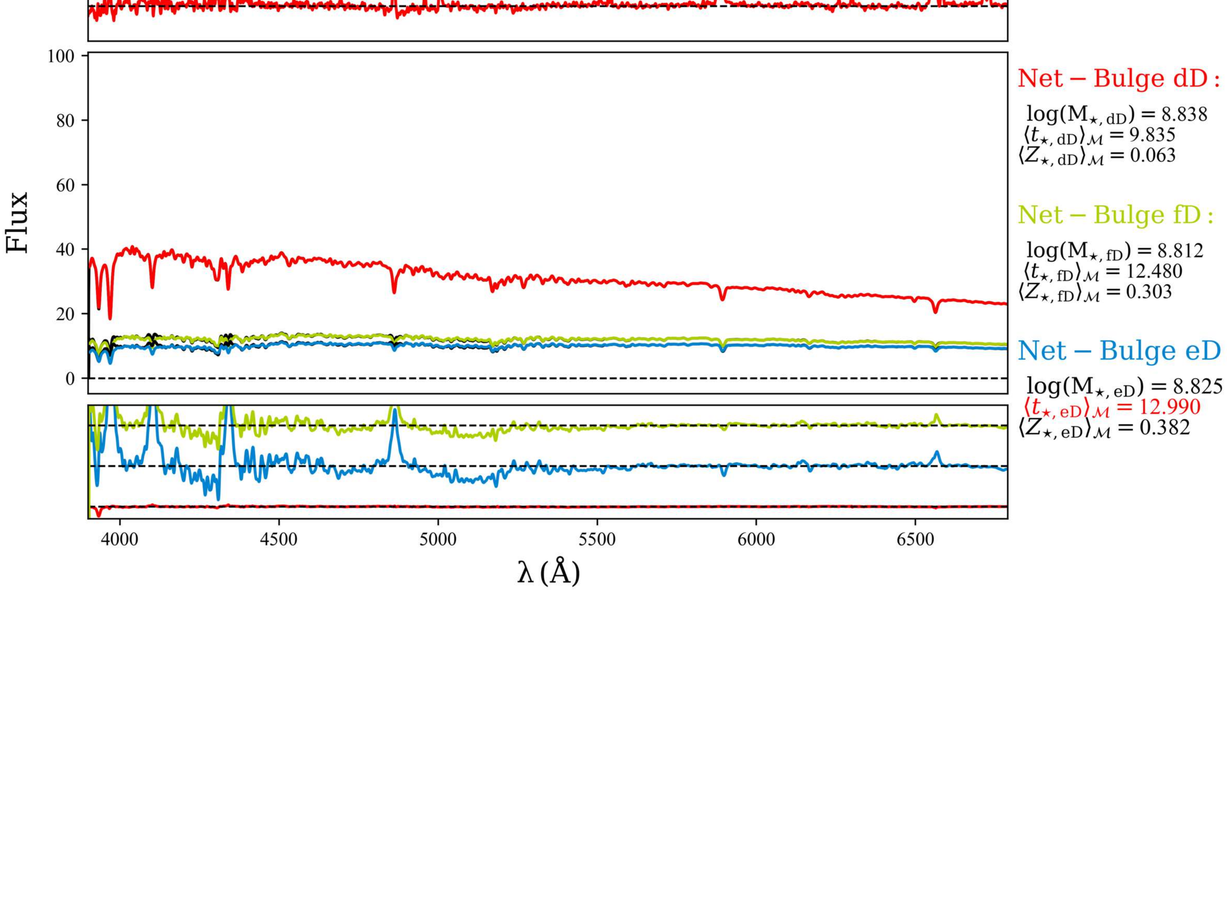
FADO Z4
Flux
Bulge :
log(M⋆, B) = 8.859
⟨t⋆, B⟩M = 9.937
⟨Z⋆, B⟩M = 0.054
Disk :
log(M⋆, D) = 8.058
⟨t⋆, D⟩M = 4.470
⟨Z⋆, D⟩M = 0.053
Net − Bulge dD :
log(M⋆, dD) = 8.838
⟨t⋆, dD⟩M = 9.835
⟨Z⋆, dD⟩M = 0.063
Net − Bulge fD :
log(M⋆, fD) = 8.812
⟨t⋆, fD⟩M = 12.480
⟨Z⋆, fD⟩M = 0.303
Net − Bulge eD :
log(M⋆, eD) = 8.825
⟨t⋆, eD⟩M = 12.990
⟨Z⋆, eD⟩M = 0.382
λ (Å)

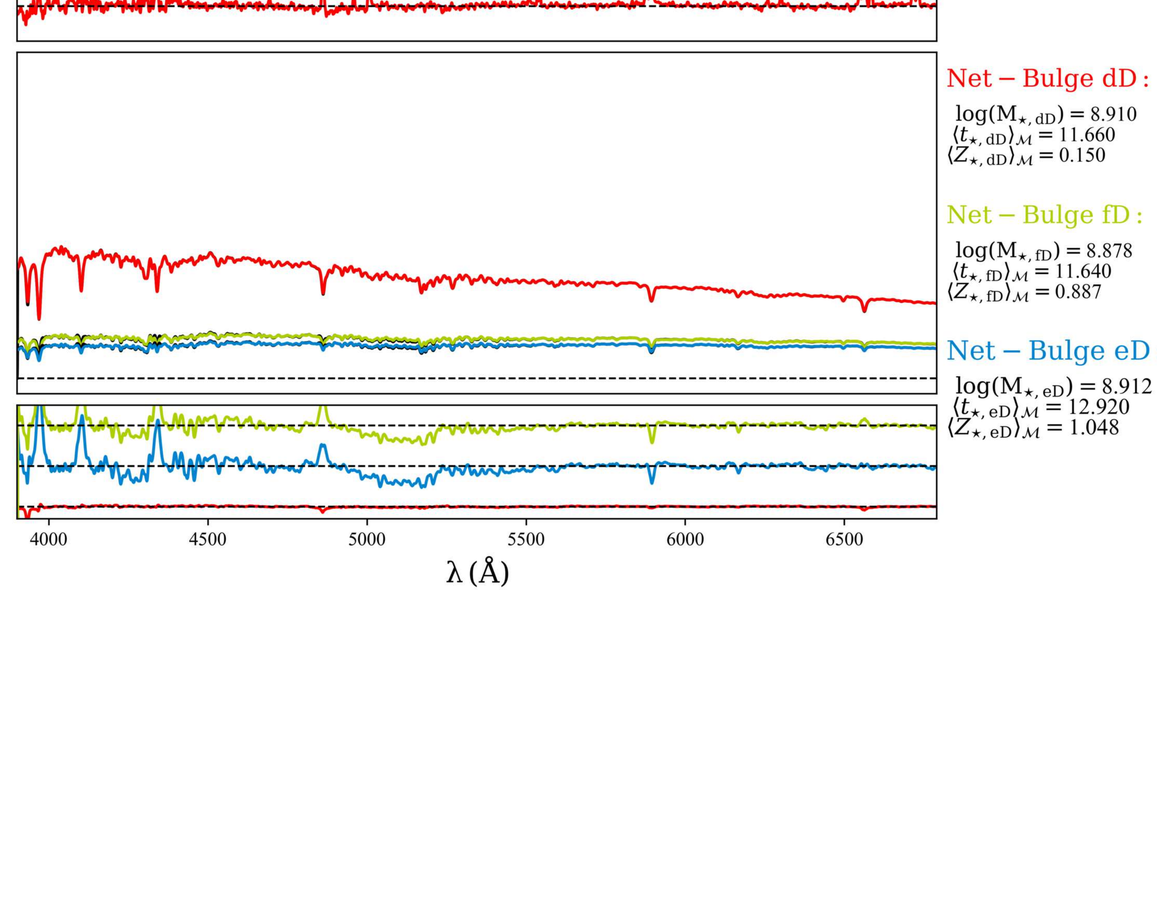
FADO Z5
Bulge :
log(M⋆, B) = 8.954
⟨t⋆, B⟩M = 12.440
⟨Z⋆, B⟩M = 0.111
Disk :
log(M⋆, D) = 8.182
⟨t⋆, D⟩M = 6.363
⟨Z⋆, D⟩M = 0.053
Net − Bulge dD :
log(M⋆, dD) = 8.910
⟨t⋆, dD⟩M = 11.660
⟨Z⋆, dD⟩M = 0.150
Net − Bulge fD :
log(M⋆, fD) = 8.878
⟨t⋆, fD⟩M = 11.640
⟨Z⋆, fD⟩M = 0.887
Net − Bulge eD :
log(M⋆, eD) = 8.912
⟨t⋆, eD⟩M = 12.920
⟨Z⋆, eD⟩M = 1.048
λ (Å)



The nature and formation history of bulges in spiral galaxies

Iris Breda

Programa Doutoral em Astronomia

Faculdade de Ciências da Universidade do Porto

2019

Orientador

Polychronis Papaderos

Investigador Coordenador, Instituto de Astrofísica e Ciências do Espaço

Coorientador

Jean Michel Gomes

Investigador, Instituto de Astrofísica e Ciências do Espaço

PhD

U.PORTO

FACULDADE DE CIÊNCIAS
UNIVERSIDADE DO PORTO

PD+F FCT PhD PROGRAMMES

The nature and formation history of bulges in spiral galaxies

Iris Breda

Advisors:
Polychronis Papaderos
Jean Michel Gomes

Thesis submitted to Faculdade de Ciências da Universidade do Porto in conformity with the requirements for the degree of Doctor of Philosophy

Departamento de Física e Astronomia da
Faculdade de Ciências da Universidade do Porto

January 2019

To my father, the one that inspired my first love,
the Universe and its mysteries.

Acknowledgements

I acknowledge Fundação para a Ciência e a Tecnologia (FCT) and POPH/FSE (EC) which supported this project by the PhD::SPACE fellowship PD/BD/52707/2014 and by the fellowship CAUP-07/2014-BI in the context of the FCT project PTDC/FIS-AST/3214/2012 & FCOMP-01-0124-FEDER-029170.

I would like to express my sincere gratitude to my main advisor PD Polychronis Papaderos. More than a mere advisor, you were a mentor, always holding my hands through all these years, instilling in me the wisdom, patience, perseverance and courage to continue, not only in my journey into science but into life. Your brilliant mind along with your kind heart made you one of the most extraordinary human beings I had the pleasure to meet. Your unconditional support and encouragement allowed me to grow as a scientist, inspiring me and enlightening every step of this long odyssey. You'll forever be part of my family.

Besides my main advisor, I would also like to thank my co-advisor Dr. Jean Michel Gomes for his insightful comments and all the shared knowledge that made me grow as an independent astronomer.

I thank my father, Luis Breda, to whom I dedicate this dissertation. Our early conversations about physics awakened the aspiration of being a scientist and an astronomer was born within me the moment you showed me the Hubble Wide Field Camera pictures. For this and for all the discussions during the period of this Ph.D that have immeasurably enriched my research, I express my deepest gratitude.

I express my heart-felt gratitude to my lovely boyfriend, Stergios Amarantidis, that besides contributing to my development as a scientist with stimulating debates, has been with me through all the ups and downs, with his infinite patience, friendship and love. Without you my life would be incomplete.

Last but not the least, I would like to thank my family: mother, brother, grandparents, uncles and aunts, friends and godchilds, the backbone of my life. Although you didn't directly contribute to this dissertation in scientific terms, you inspire my heart and soul everyday, coloring my life, supporting me in every fall and helping me to stand up, stronger. Thank you for granting me with your unconditional love.

Abstract

A fundamental subject in extragalactic astronomy concerns the formation and evolution of bulges in late-type galaxies, including their build-up processes and chronology. The current paradigm recognizes two distinct formation routes, one leading to the genesis of a classical bulge (CB) through monolithic collapse prior to disks, and the other to a pseudo-bulge (PB) gradually emerging from the disk in the course of secular galactic evolution, invariably giving rise to a segregation of bulges in two categories, echoing their opposite assembly mechanisms. However, despite numerous studies in the field, a recipe that demonstrates a clear separation of bulges and their main properties still remains elusive. This fact, coupled with further uncertainties regarding the structural analysis of bulges (emerging from surface brightness decomposition techniques) and aperture and spectral modeling biases, has been the main motivation behind this PhD project.

Here we present a systematic investigation of bulges and their parent disks for a representative sample of the local, secular evolving LTG population. The sample is composed of 135 nearly face-on, non-interacting spiral galaxies, carefully selected from the CALIFA Survey, covering a range in total stellar mass in the range $10^{8.3-11.3}$ $M_{\odot}$. The main research revolves around a combination of three techniques, namely surface photometry, spatially resolved spectral modeling and the post-processing with RemoveYoung ($\mathcal{RY}$), a code that allows suppression of the contribution of stellar populations younger than an adjustable age cutoff. In addition, a new algorithm was developed allowing the robust estimation of the Sérsic model parameters (iFIT), two population spectral synthesis codes were tested and compared (Starlight & FADO) under consideration of spatial resolution effects and, finally, it was performed a thorough investigation of the validity of the standard assumption for the inwards extrapolation of the exponential disk profile beneath the bulge.

Our main results clearly reveal a *continuity* in the main properties of bulges and their host galaxy and parent disk arguing against the bimodality expected from the two formation route scenario. Instead, they suggest that bulge and disk evolve alongside. The findings are consistent with an interwoven yet asynchronous growth of the bulge, where it assembles out of the disk within a timescale which is inversely related to the total galaxy mass.

Resumo

Um tema fundamental em astronomia extragaláctica diz respeito à formação e evolução de bojos em galáxias espirais. O paradigma actual reconhece duas vias de formação distintas, uma que conduz à génese de um bojo clássica (CB) através de colapso monolítico de gás antes da formação do disco, e a outra a um pseudo-bojo (PB) que emerge gradualmente a partir do disco, no decurso da evolução galáctica secular. Espera-se portanto uma bimodalidade nas propriedades físicas de bojos, ressoando os dois mecanismos distintos de formação. No entanto, apesar dos numerosos estudos na área, permanece indefinida uma metodologia que demonstre uma clara separação de bojos e as suas principais propriedades. Este facto, juntamente com ambiguidades relacionadas com a análise estrutural de bojos, técnicas de decomposição de imagens e enviesamentos decorrentes da abertura e modelagem espectral, foram as principais motivações para uma exploração mais aprofundada das propriedades físicas e evolutivas de bojos, no contexto desta tese de Doutoramento.

Aqui apresentamos uma investigação sistemática de bojos e seus discos utilizando uma amostra representativa da população local de galáxias espirais. A amostra é composta por 135 galáxias pertencentes ao CALIFA Survey, com inclinações inferiores a 40° e sem sinais de interações recentes, com massas estelares totais de $10^{8,3-11,3}$ $M_{\odot}$. A investigação aqui realizada combina primeira vez três técnicas, nomeadamente fotometria de superfície, modelagem espectral espacialmente resolvida e o pós-processamento com RemoveYoung ($\mathcal{RY}$), um código que permite a supressão da contribuição de populações estelares com idade inferior a um número ajustável. Adicionalmente, foi desenvolvido um novo algoritmo (iFIT) com o objetivo de determinar de forma robusta os parâmetros do modelo Sérsic e foram testados dois códigos de síntese espectral (Starlight & FADO) considerando efeitos de resolução espacial. Finalmente, este projeto inclui uma investigação da validade da suposição de que o disco preserva seu perfil exponencial dentro do

bojo.

Os resultados principais revelam uma clara *continuidade* nas propriedades físicas de bojos e suas galáxias hospedeiras, argumentando contra a bimodalidade implícita no cenário standard de formação de bojos e sugerindo que bojo e disco evoluem lado a lado. Os resultados obtidos são consistentes com o crescimento mútuo ainda que assíncrono de ambos, onde o bojo é formado a partir do disco, numa escala de tempo que está inversamente relacionada com a massa total da galáxia.

Contents

1 Introduction **1**

1.1 Alternative hypotheses for the formation of bulges . . . 3

1.1.1 PBs as rejuvenated CBs . . . 3

1.1.2 The build-up of PBs through inward migration and coalescence of star-forming clumps from the disk . . . 4

1.2 Limitations in previous studies and motivation for this work . . . 6

1.2.1 Aperture biases . . . 6

1.2.2 Spectral modeling biases . . . 8

1.2.3 Uncertainties in structural analyses of bulges . . . 11

1.3 Thesis outline . . . 16

2 Data set and methodology **19**

2.1 Sample selection . . . 19

2.2 Photometric and structural analysis of the galaxy sample . . . 21

2.2.1 Post-processing of the SDSS photometric data . . . 21

2.3 Development and aplication of iFIT . . . 22

2.3.1 Technicalities . . . 23

2.3.2 iFIT's accuracy assessment . . . 31

2.3.3 Determination of the bulge radius . . . 35

2.3.4 Computation of color maps and profiles . . . 38

2.4 Analysis of integral field spectroscopy data for the galaxy sample . . . 40

2.4.1 Spatial resolved spectral modeling of CALIFA IFS data with STARLIGHT 41

2.4.2 Derivation of gas-phase metallicities . . . 45

2.4.3 Post-processing of the spectral synthesis output with REMOVEYOUNG . . 46

2.4.4 Classification of LTG bulges according to their spectroscopic activity . . 49

2.4.5 Spectral fitting with FADO & subsequent comparison with STARLIGHT . 51
2.4.6 Spectroscopic subtraction of the underlying disk from the bulge 53

3 Physical and evolutionary properties of LTG bulges 61

3.1 Structural analysis of the sample 61
3.2 Optical colors of LTG bulges 65
3.3 Properties of LTG bulges as obtained by SRSF 71
3.3.1 Physical and evolutionary properties of LTG bulges vs. $<\delta\mu_{9G}>$ 71
3.3.2 An empirical assessment of disk contamination and PSF convolution effects on the obtained trends 81
3.3.3 Gas excitation mechanisms vs. bulge $<\delta\mu_{9G}>$ 83
3.3.4 Bulge-to-disk age, metallicity and EW(Hα) contrast 83
3.3.5 Stellar age gradients in LTG bulges 86
3.4 A comparative study between STARLIGHT & FADO 89
3.4.1 Average determinations for LTG bulges 90
3.4.2 Mass- & luminosity-weighted age gradients 95
3.5 Spectroscopic subtraction of the disk 95
3.5.1 Negative net-bulge spectra 96
3.5.2 Mass-weighted age and metallicity determinations for the net-bulge spectra 99

4 Discussion 105

4.1 The continuous rise of bulges out of galactic disks 105
4.1.1 Accelerated bulge growth in proportion to galaxy mass 110
4.1.2 Accretion-powered nuclear activity along the bulge sequence 112
4.1.3 Radial age gradients in galaxy bulges and their evolutionary implications 114
4.2 IFS data and the effects of spatial resolution 115
4.3 Extrapolating the disk component within the bulge 117
4.4 Final remarks 118
4.5 Future work 121

Bibliography

A Detailed information on the LTG sample

B Outcome from the disk subtraction procedure for the LTG sample

List of Tables

3.1 Photometric properties of the sample as obtained by application of iFIT to SDSS DR7 data in the r band 64
3.2 Overview of the fits obtained for quantities inferred from analysis of the LTG sample with the Z4 and Z5 SSP library 75
3.3 Photometric, evolutionary and physical quantities for the galaxy sample under study 76

List of Figures

1.1 Exemplification of overestimation of bulge photometric characteristics by not taking into account the bar emission. 13

2.1 Histogram of the total absolute magnitude and morphologic classification of the sample 20
2.2 Histogram of the bulge's radial extent of the sample 20
2.3 Fit to the SBP of MCG +01-10-019 24
2.4 Example of a SL $\mu(\mathrm{R}^{\star})$ profile and respective flux distribution 26
2.5 iFIT pseudo-code illustrating the principal steps 30
2.6 iFIT η error by testing using unconvolved synthetic data 31
2.7 iFIT η error by testing using convolved synthetic data 32
2.8 BCD Henize 2-10 true color image and respective iFIT fits 35
2.9 True color image of I Zw 18 and respective fit with iFIT . Bottom panel displays the best-fitting Sérsic index η vs. limiting surface brightness as obtained by Papaderos & Östlin (2012) and iFIT 36
2.10 Decomposition of the SBP of NGC 0180 37
2.11 Color maps profiles of NGC1093 40
2.12 Radial profiles of various physical quantities for NGC 0760 44
2.13 Radial profiles of mass- and light-weighted age as obtained by spaxel-by-spaxel analysis with STARLIGHT Z4 & Z5 for MCG +09-22-053 45
2.14 Gas-phase metallicity maps of NGC 5480 46
2.15 Synthetic SBPs obtained with RY for three galaxy examples 48
2.16 $<\delta\mu_{9\mathrm{G}}>$ (r mag) vs. mass-weighted stellar age $\langle t_{\star,\mathrm{B}}\rangle_{\mathcal{M}}$ (Gyr) for the bulge component for lib. Z4 (left panel) & lib. Z5 (right panel) 49
2.17 Comparison of BPT determinations with different methods 52

2.18 SDSS true-color image and SDSS r-band SBP illustrating the three disk configurations assumed for LTG NGC 0036 54
2.19 Illustration of the CALIFA IFS data (spaxel-by-spaxel map) of LTG NGC 0036 . 57
2.20 Spectral fit with STARLIGHT & FADO (Z4 & Z5) of the net spectrum of the bulge after subtraction of the disk for MCG +09-22-053 59

3.1 Comparison between total and bulge's Sérsic η and galaxy's and bulge's radial extent and stellar masses 65
3.2 Comparison between total and bulge's Sérsic η and bulge's $\langle t_{\star,\mathrm{B}}\rangle_{\mathcal{M}}$, $\langle Z_{\star,\mathrm{B}}\rangle_{\mathcal{M}}$ and $\log(\Sigma_{\star,\mathrm{B}})$ 66
3.3 Comparison between bulge and disk colors 67
3.4 Absolute magnitude and logarithm of the stellar surface density vs. mean values of the colors of bulges 68
3.5 Mass-weighted mean age and metallicity (as obtained for both the Z4 and Z5 libraries) of the bulge vs. mean colors of the bulges 69
3.6 Logarithm of the total stellar mass $\log(\mathcal{M}_{\star,\mathrm{T}})$ vs. bulge's color gradient 70
3.7 Physical and evolutionary properties of LTG bulges as obtained by the spatially resolved analysis using STARLIGHT with the SSP library Z4 72
3.8 Physical and evolutionary properties of LTG bulges as obtained by the spatially resolved analysis using with the SSP lib. Z5 73
3.9 Comparison of the mean mass-weighted stellar age $\langle t_{\star,\mathrm{B}}\rangle_{\mathcal{M}}$ (Gyr) and metallicity $\langle Z_{\star,\mathrm{B}}\rangle_{\mathcal{M}}$ ($\mathrm{Z}_{\odot}$) within $\mathrm{R_B}$ with the values obtained within a radius of 3.3″ for the LTG bulges in our sample. 82
3.10 Histogram distributions of the bulge isophotal radius $\mathrm{R_B}$ of the LTGs in our sample, and its normalized values to $\mathrm{R_{eff}}$ and the radius enclosing 80% of its total bulge luminosity. 82
3.11 Bulge vs. disk mass-weighted age and metallicity contrast 84
3.12 Bulge and disk EW(Hα) contrast 86
3.13 Mass- and luminosity-weighted age gradients of the bulge as obtained by the **SbS** analysis 87
3.14 Mass- and luminosity-weighted age gradients within $\mathrm{R_{80}}$, as obtained by the **SbS** analysis 89

3.15 Stellar mass, mass-weighted age and metallicity determinations for STARLIGHT for **SbS**, **18Z-15t**, **18Z** & **Rb** adopting lib. Z4 91
3.16 Stellar mass, mass-weighted age and metallicity determinations for models with FADO for **18Z-15t**, **18Z** and **Rb**, adopting the SSP library Z4 92
3.17 Stellar mass, mass-weighted age and metallicity determinations for STARLIGHT and FADO for **18Z-15t**, **18Z** & **Rb** adopting library Z4 93
3.18 Stellar mass, mass-weighted age and metallicity determinations for STARLIGHT and FADO for **18Z-15t**, **18Z** & **Rb** adopting lib. Z5 94
3.19 Mass- and luminosity-weighted age gradients of the bulge as obtained by the **18Z-15t** analysis 96
3.20 Fraction of net bulge spectra with negative flux after disk subtraction for each $<\delta\mu_{9G}>$ interval 98
3.21 Mass-weighted age as obtained by the disk subtraction code using as reference the surface photometry of the SDSS g band 99
3.22 Mass-weighted metallicity as obtained by the disk subtraction code using constraints from surface photometry in the SDSS g-band to scale the disk emission . 100
3.23 Fraction of net-bulge spectra whose age determinations have reached the allowed maximum for each of the three $<\delta\mu_{9G}>$ intervals 103
3.24 Fraction of net-bulge spectra which metallicity determinations have reached the allowed maximum per $<\delta\mu_{9G}>$ interval 104

4.1 Schematic illustration of the scenario envisaged here 109

Glossary

Acronyms

AGB	Asymptotic Giant Branch
AGN	Active Galactic Nucleus
AMD	Age Metallicity Degeneracy
B/T	Bulge-to-Total ratio
BCD	Blue Compact Dwarf
BPT	Baldwin, Phillips & Terlevich diagram
CALIFA	Calar Alto Legacy Integral Field Area survey
CANDELS	Cosmic Assembly Near-infrared Deep Extragalactic Legacy Survey
CB	Classical Bulge
CEH	Chemical Enrichment History
CMD	Color-Magnitude Diagram
CMZ	Central Molecular Zone
CPU	Central Processing Unit
DM	Dark Matter
DR	Data Release
ESS	Evolutionary Spectral Synthesis
ETG	Early Type Galaxy

EW	Equivalent Width
FWHM	Full Width at Half Maximum
HST	Hubble Space Telescope
IFS	Integral Field Spectroscopy
IMF	stellar Initial Mass Function
IR	Infra-Red
KMOS	K-band Multi Object Spectrograph
LINER	Low-Ionization Nuclear Emission-line Region
LSST	Large Synoptic Survey Telescope
LTG	Late Type Galaxy
LyC	Lyman Continuum
M/L	Mass-to-Light ratio
MOONS	Multi-Object Optical and Near-infrared Spectrograph
MUSE	Multi Unit Spectroscopic Explorer
MW	Milky Way
NED	NASA/IPAC Extragalactic Database
NIR	Near Infra-Red
PB	Pseudo Bulge
PMAS	Potsdam Multi-Aperture Spectrometer
PSF	Point Spread Function
PSS	Population Spectral Synthesis
PV	Population Vector
RGB	Red Green Blue
$\mathcal{RY}$	RemoveYoung

S/N	Signal-to-Noise ratio	
SBP	Surface Brightness Profile	
SDSS	Sloan Digital Sky Survey	
SED	Spectral Energy Distribution	
SF	Star Formation	
SFH	Star Formation History	
SFR	Star Formation Rate	
sSFR	specific Star Formation Rate (SFR divided by stellar mass)	
SL	Sérsic Law	
SMBH	Super Massive Black Hole	
SSP	Simple Stellar Population	
UV	Ultraviolet	
VLT	Very Large Telescope	
WLR	Weighted Linear Regression	
hWLR	half-Weighted Linear Regression	

Physical Constants

Å	Ångström	10^{-10} m
pc	Parsec	$\sim 3.08 \cdot 10^{16}$ m
$M_\odot$	Solar mass	$2 \cdot 10^{30}$ kg
$Z_\odot$	Solar metallicity	0.019

Symbols

$''$	Arcsecond	
z	Redshift	
$\mathcal{M}_\bullet$	Mass of SMBH	$M_\odot$

V_{rot}	Stellar rotational velocity	km/s
$\sigma_\star$	Stellar velocity dispersion	km/s
M_r	Absolute magnitude in the SDSS r-band	mag
μ	Surface brightness	mag/$\square''$
σ_μ	Surface brightness error	mag/$\square''$
$\langle\mu\rangle$	Mean surface brightness	mag/$\square''$
$\mu_{\rm lim}$	Limiting surface brightness	mag/$\square''$
α	Disk's scale-length (radial distance for which the stellar density decreases by a factor of e)	
$R_{\rm eff}$	Effective radius (the radius that encompasses 50% of the total SBP light)	
$\mu_{\rm eff}$	Surface brightness at the effective radius	mag/$\square''$
b_η	Parameter of the SL equation that ensures that the effective radius encloses 50% of the total luminosity of the SBP when integrated to infinity	
η	Sérsic index/exponent	
$\eta_{\rm T}$	Sérsic index for a single fit to the total galaxy	
$\eta_{\rm B}$	Sérsic index of the bulge	
isan	Irregular isophotal annuli	
$R_{\rm max}$	Maximum observed radius	
$R_{3.3}$	Radius which encompasses the central $3.3''$	
$R_{\rm B}$	Bulge radius obtained by integrating the bulge SBP until a surface brightness limit of 24 mag/$\square''$	
R_{80}	Radius which encompasses 80% of the total light of the bulge	
$R_{\rm D}$	The radial extent between $R_{\rm B}$ and the radius of the 14th isan	
$R_{\rm C}$	Conservative radial extent of the bulge in the context of the disk subtraction	
$(g-r)_{\rm B}$	mean $(g-r)$ color within $R_{\rm B}$	mag

$(r-i)_{\rm B}$	mean $(r-i)$ color within $\rm R_B$	mag
$(g-i)_{\rm B}$	mean $(g-i)$ color within $\rm R_B$	mag
$(g-r)_{\rm D}$	mean $(g-r)$ color within $\rm R_D$	mag
$(r-i)_{\rm D}$	mean $(r-i)$ color within $\rm R_D$	mag
$(g-i)_{\rm D}$	mean $(g-i)$ color within $\rm R_D$	mag
$\nabla(g-r)_{\rm B}$	$(g-r)$ color gradient within $\rm R_B$	mag
$\nabla(r-i)_{\rm B}$	$(r-i)$ color gradient within $\rm R_B$	mag
$\nabla(g-i)_{\rm B}$	$(g-i)$ color gradient within $\rm R_B$	mag
Z4	Library composed by 152 SSPs with ages between 1 Myr and 13 Gyr and stellar metallicities between 0.05 and 1.0 $Z_{\odot}$	
Z5	Library composed by 190 SSPs with ages between 1 Myr and 13 Gyr and stellar metallicities between 0.05 and 1.5 $Z_{\odot}$	
$t_{\rm cut}$	User defined age cut in the context of $\mathcal{RY}$	
$<\delta\mu_{\rm 9G}>$	The arithmetic average of the difference between the light contribution of all stellar populations and stellar populations older than 9 Gyr within $\rm R_B$ mag	
iA	Galaxies displaying $<\delta\mu_{\rm 9G}> \lesssim$ -1.5 mag	
iB	Galaxies displaying -1.5 $\lesssim <\delta\mu_{\rm 9G}> \lesssim$ -0.5 mag	
iC	Galaxies displaying -0.5 $\lesssim <\delta\mu_{\rm 9G}> \lesssim$ 0 mag	
$\mathcal{M}_{\star}$	Stellar mass	$\rm M_{\odot}$
$\mathcal{M}_{\star,\rm T}$	Total stellar mass	$\rm M_{\odot}$
$\mathcal{M}_{\star,\rm B}$	Bulge stellar mass (stellar mass within $\rm R_B$)	$\rm M_{\odot}$
$\log(\mathcal{M}_{\star,\rm T})$	Logarithm of the total stellar mass	$\rm M_{\odot}$
$\log(\mathcal{M}_{\star,\rm B})$	Logarithm of the bulge stellar mass	$\rm M_{\odot}$
$\Sigma_{\star}$	Stellar mass surface density	$\rm M_{\odot}/kpc^2$
$\Sigma_{\star,\rm B}$	Stellar mass surface density of the bulge	$\rm M_{\odot}/kpc^2$

$\log(\Sigma_{\star,\mathrm{B}})$	Logarithm of the stellar surface density of the bulge	
$t_\star$	Stellar age	Gyr
$t_{\star\mathcal{M}}$	Mass-weighted stellar age	Gyr
$t_{\star\mathcal{L}}$	Luminosity-weighted stellar age	Gyr
$\langle t_\star \rangle_{\mathcal{M}}$	Mean mass-weighted stellar age	Gyr
$\langle t_\star \rangle_{\mathcal{L}}$	Mean luminosity-weighted stellar age	Gyr
$\langle t_{\star,\mathrm{B}} \rangle_{\mathcal{M}}$	Mean mass-weighted stellar age within the bulge	Gyr
$\langle t_{\star,\mathrm{B}} \rangle_{\mathcal{L}}$	Mean luminosity-weighted stellar age within the bulge	Gyr
$\langle t_{\star,\mathrm{D}} \rangle_{\mathcal{M}}$	Mean mass-weighted stellar age within the disk	Gyr
δt_{BD}	Bulge-to-disk age contrast	
$\nabla(\mathrm{t}_{\star,\mathrm{B}})_{\mathcal{M}}$	Mass-weighted stellar age gradient within $\mathrm{R_B}$	Gyr
$\nabla(\mathrm{t}_{\star,\mathrm{B}})_{\mathcal{L}}$	Luminosity-weighted stellar age gradient within $\mathrm{R_B}$	Gyr
$\nabla(\mathrm{t}_{\star,80})_{\mathcal{M}}$	Mass-weighted stellar age gradient within $\mathrm{R_{80}}$	Gyr
$\nabla(\mathrm{t}_{\star,80})_{\mathcal{L}}$	Luminosity-weighted stellar age gradient within $\mathrm{R_{80}}$	Gyr
$Z_\star$	Stellar metallicity	$\mathrm{Z}_\odot$
$Z_{\star\mathcal{M}}$	Mass-weighted stellar metallicity	$\mathrm{Z}_\odot$
$Z_{\star\mathcal{L}}$	Luminosity-weighted stellar metallicity	$\mathrm{Z}_\odot$
$\langle Z_\star \rangle_{\mathcal{M}}$	Mean mass-weighted stellar metallicity	$\mathrm{Z}_\odot$
$\langle Z_\star \rangle_{\mathcal{L}}$	Mean luminosity-weighted stellar metallicity	$\mathrm{Z}_\odot$
$\langle Z_{\star,\mathrm{B}} \rangle_{\mathcal{M}}$	Mean mass-weighted stellar metallicity within the bulge	$\mathrm{Z}_\odot$
$\langle Z_{\star,\mathrm{B}} \rangle_{\mathcal{L}}$	Mean luminosity-weighted stellar metallicity within the bulge	$\mathrm{Z}_\odot$
$\langle Z_{\star,\mathrm{D}} \rangle_{\mathcal{M}}$	Mean mass-weighted stellar metallicity within the disk	$\mathrm{Z}_\odot$
δZ_{BD}	Bulge-to-disk metallicity contrast	
Z_g	Gas-phase metallicity	12+log(O/H)

SbS	Spaxel-by-spaxel analysis performed exclusively with STARLIGHT
18Z	Analysis performed to binned spectra within each of the 18 **isan** by means of STARLIGHT and FADO
18Z-15t	Repetition of the processing of each of the **18Z** spectra 15 times, in each time adopting different seed numbers using both STARLIGHT and FADO
Rb	Analysis performed to the summed up spectra within R_B by means of STARLIGHT and FADO
n_{pB}	Number of spaxels within the bulge
$T_{SDSS}(\lambda)$	SDSS r- or g-band transmission curve
f_D	Percentage of light within the bulge component that resides in the disk
$F_C(\lambda)$	Bulge spectra created by summing the spaxels that lay within R_C
$\hat{F}^{\star}_D(\lambda)$	Emission-line free spectra of the disk component
$F_B(\lambda)$	Net spectra of the bulge created by subtraction of the scaled emission-line free spectra of the disk
expD	Assumption of the standard exponential disk within R_B in the context of the disk subtraction analysis
flatD	Assumption of an inwardly flattening disk within R_B in the context of the disk subtraction analysis
decrD	Assumption of a central intensity depression within R_B in the context of the disk subtraction analysis

Chapter 1

Introduction

The formation history of bulges in late-type galaxies (LTGs) remains an unresolved fundamental question in extragalactic astronomy, being a crucial element towards our understanding of galaxy evolution.

Conventionally, bulges were thought to invariably form early-on via violent quasi-monolithic gas collapse (Larson, 1974) or galaxy mergers (Aguerri et al., 2001; Bender, Burstein & Faber, 1992; Keselman & Nusser, 2012) triggering vigorous nuclear starbursts (Okamoto, 2012), followed by a gradual build-up of the disk around them. Thanks to a substantial improvement of observing facilities over the past three decades, our understanding on the nature of these triaxial stellar entities in the centers of galactic disks underwent a significant revision – bulges are now subdivided into two categories: classical bulges (CBs) and pseudo-bulges (PBs). The former are in many respect reminiscent of *old and dead* elliptical/early-type galaxies (ETGs), displaying a spheroidal shape with inwardly steeply increasing surface brightness profiles (SBPs) being well approximated by the Sérsic (1963) fitting law with a high (≥ 2) exponent η, stellar kinematics dominated by velocity dispersion ($\sigma_\star$), and lacking traces of ongoing star-formation (SF). In addition, they obey the Kormendy (1977) scaling relations for normal ETGs (Fisher & Drory, 2010) and host a super-massive black hole (SMBH) with a mass ($\mathcal{M}_\bullet$) tightly correlated with their stellar mass ($\mathcal{M}_{\star,\mathrm{B}}$), $\sigma_\star$ and optical and near-infrared luminosity (Ferrarese & Merritt, 2000; Ho, 2008; Kormendy & Ho, 2013). According to our current understanding, these entities have fully assembled early-on prior to disks (e.g., Larson, 1974).

On the contrary, PBs share several properties with their surrounding disks. They usually show ongoing SF, flatter shapes with nearly exponential SBPs ($\eta \leq 2$; e.g., Drory & Fisher, 2007;

Fisher & Drory, 2010) and a significant degree of rotational support (see Kormendy & Kennicutt, 2004, for a review). Although they do not follow the $\mathcal{M}_\bullet - \sigma_\star$ correlation for CBs, there are studies suggesting that they also contain a SMBH (Kormendy & Ho, 2013; Kormendy, Bender & Cornell, 2011), sometimes unveiling itself as an active galactic nucleus (AGN; e.g., Kotilainen et al., 2016; see Kormendy & Ho, 2013, for a review). Contrary to their CB counterparts, our current understanding is that these stellar entities form gradually out of disks in the course of secular galactic evolution through continuous gas inflow feeding central SF and consequently the emergence of a central bulge-like luminosity excess at their centers (e.g., Carollo et al., 2001; Courteau, de Jong & Broeils, 1996; Kormendy & Kennicutt, 2004). Other scenarios being proposed as further contributors to PB growth along the Gyr-long secular evolution of LTGs include bar-driven gas inflow (e.g., Springel & Hernquist, 2005), minor mergers with low-mass satellites or a purely dynamical re-arrangement of the disk (Bird, Kazantzidis & Weinberg, 2012; Grand et al., 2014; Guedes et al., 2013; Halle et al., 2015; Roškar et al., 2012; Scannapieco et al., 2010).

These two distinct bulge formation routes – the first leading to CB formation *prior to* disks and the second one to PB formation *out of* disks – evidently translate into diametrically different expectations on the spectrophotometric characteristics of CBs and PBs, and their age contrast to the disk. However, despite numerous studies over the past decades, this predicted age bimodality in LTG bulges could not be observationally established, preventing an objective, physically motivated separation between CBs and PBs. In fact, the available observational data show a considerable scatter or even a smooth transition in the properties of LTG bulges across their luminosity and mass range. Already two decades ago, Wyse et al. (1997), reviewing this subject, reports that bulges show a considerable heterogeneity, with merely higher luminosity ones (CBs) having a closer affinity with ellipticals and lower luminosity bulges (PBs) with disks. Furthermore, the lack of observational evidence of "naked bulges" at high-redshift (high-z) and gradual build-up of the disk throughout z raises some doubts on the validity of the monolithic collapse scenario for CBs (e.g., van Dokkum et al., 2013).

The main goal of this PhD project is to shed further light into the formation history of LTG bulges, in particular to assess whether PBs and CBs are evolutionary distinct or rather the opposite ends of a continuous sequence with respect to age and mass. To this end, spatially resolved spectral modeling and surface photometry techniques were applied to a representative sample of local LTGs from the CALIFA survey (Sánchez et al., 2016) in order to explore their

star formation history (SFH) and structural properties.

1.1 Alternative hypotheses for the formation of bulges

The secular formation scenario for PBs involves primarily in situ SF in the centers of galactic disks. However, a number of alternative scenarios or supplementary mechanisms promoting the PB growth have been proposed, the two most popular of those interpreting PBs as rejuvenated CBs or envisaging inwards migration and coalescence of star-forming clumps from the disk as the main driver of PB growth.

1.1.1 PBs as rejuvenated CBs

In the context of the monolithic bulge formation scenario, there is obviously no other option than to interpret PBs as ancient CBs being recently rejuvenated through in situ SF (e.g., Johnston et al., 2012, 2014; Morelli et al., 2012, 2016; Thomas & Davies , 2006). For example, Thomas & Davies (2006) comes to this conclusion by reproducing a subset of Lick indices (Gorgas, 1993; Worthey et al., 1994) (Hβ, H$\gamma_{\rm A}$, H$\delta_{\rm A}$, [MgFe]$'$, and <Fe>) for local bulges with a two-component evolutionary spectral synthesis (ESS) model that invokes a 15 Gyr old stellar component, which 1-2 Gyr ago underwent a SF episode producing up to 10-30% of its $\mathcal{M}_{\star,\rm B}$.

An interesting alternative CB "rejuvenation mechanism" is the one proposed by Saha (2015) & Saha et al. (2016): by means of high-resolution N-body simulation, starting with a non-rotating CB surrounded by an exponential disk and embedded in a dark matter (DM) halo, these studies indicate that bars (which in these simulations emerge naturally from the disk) will transfer angular momentum to both low and high mass CBs. This effect will result in a composite bulge, that, depending on the predominance of the original CB, might not show any characteristic of the classical component. This hypothesis should be relatively easy to observationally test. For instance, by selecting a sample of both barred and non-barred LTGs, with an inclination being low enough for visual identification of the bar component, if present, yet sufficiently high to allow for measuring of the rotational velocity ($\rm V_{\mathit{rot}}$), one could determine the bulge's $\rm V_{\mathit{rot}}/\sigma_\star$ distribution in the axis perpendicular to the disk. If this phenomenon is indeed occurring in LTGs, it should be reflected by an increase of $\rm V_{\mathit{rot}}$ in bulges of barred galaxies in contrast with their non-barred counterparts, i.e., for the same stellar mass, barred LTGs should display higher $\rm V_{\mathit{rot}}/\sigma_\star$ when compared to non-barred LTGs.

1.1.2 The build-up of PBs through inward migration and coalescence of star-forming clumps from the disk

Between the *quick* (monolithic) and *slow* (secular) bulge formation scenarios there are intermediate models conceptualizing the dominant phase of CB formation occurring in a prolonged episode of $\sim$ 1-2 Gyr through inward migration and coalescence of massive ($> 10^{8-9}$ $M_{\odot}$) star-forming clumps that continuously form in the disk out of gas instabilities (Bournaud et al., 2007; Carollo et al., 2007; Elmegreen et al., 2008; Mandelker et al., 2014, 2017; Noguchi, 1999). This hypothesis is observationally supported by the clumpiness of high-z proto-disks and the estimated stellar mass ($\mathcal{M}_{\star}$) of their star-forming clumps (Förster Schreiber et al., 2011; Wuyts et al., 2012). It should be noted though that $\mathcal{M}_{\star}$ estimates of clumps in high-z disks can be uncertain: as pointed out by Dessauges-Zavadsky et al. (2017), limited spatial resolution for these high-z galaxies can lead to an artificial increase in the estimated masses of star-forming clumps. The process of bulge buildup through inward migration of star-forming clumps from the disk could be supported by inflow of intra-clump gas (e.g., Hopkins et al., 2012; Zolotov et al., 2015), feeding in situ SF, possibly together with stellar migration, minor mergers with dwarf satellites and other dynamical effects (e.g., Bird, Kazantzidis & Weinberg, 2012; Grand et al., 2014; Guedes et al., 2013; Halle et al., 2015; Roškar et al., 2012) promoting a gradual bulge growth in the following Gyr of galactic evolution. This set of prolonged bulge formation scenarios appears compatible with a broad range of stellar ages in present-day LTG bulges, depending on the timescale and the relative contribution of the different processes.

The latter set of scenarios is consistent with a correlated evolution of bulge and disk. Indeed, this has been proposed in several studies, in particular on the basis of photometric data from local LTGs (e.g., Gadotti & dos Anjos, 2001; Gadotti, 2009). For instance, Peletier & Balcells (1996) find that "color variations from galaxy to galaxy are much larger than color differences between disk and bulge in each galaxy", following that "the underlying old population of disks and bulges is much more similar" than previously thought. Further support for an interwoven evolution of bulge and disk comes from the modest color contrast between bulge and disk (0.3 $g-i$ mag) that was reported by Fernández Lorenzo et al. (2014) for a sample of isolated galaxies (see also, e.g., Courteau, de Jong & Broeils, 1996; Gadotti & dos Anjos, 2001). Likewise, the photometric study by Carollo et al. (2007) shows that the colors of bulges are correlated with those of their host disks. These authors interpret this observational insight as evidence that

in early phases of LTG evolution, the bulge formation has been largely driven by *continuing* rejuvenation, in some cases, most of the bulge's stellar mass was assembled after the disk build up. Furthermore, they argue that the scaling relations between bulge stellar age and bulge (and galaxy) mass suggest similar formation processes for both disk and bulge, proposing that LTG bulges invariably result from an internal evolution of their parent disks.

An additional insight for the bulge formation might come from our own Milky Way (MW). By means of N-body & smooth particle hydrodynamics simulations of its bulge, Ness et al. (2014) show that the presence of young stars predominantly near the Galactic plane (An et al., 2011; Morris & Serabyn, 1996) is expected for a bulge that has formed from the disk via dynamical instabilities, whereas it cannot be explained on the basis of monolithic collapse.

Interestingly, Hubble Space Telescope (HST) imaging studies of galaxies similar to the MW at higher z strengthen the picture of a joint evolution of bulges with their surrounding disks: van Dokkum et al. (2013), by applying the abundance matching technique to MW-progenitor candidates out to $z = 2.5$ point out that there is an absence of high-density "naked bulges" at $z \sim 2$, around which disks subsequently assemble (see also Patel et al., 2013). Additionally these authors show that MW-like LTGs have built $\sim$90% of their present $\mathcal{M}_\star$ since $z = 2.5$ with most of the SF occurring before $z = 1$. Another insight from this study regards the pace at which the bulge buildup has occurred: at $1 < z < 2.5$, the mass in the central 2 kpc of MW progenitors increases by a factor of $3.2^{+0.8}_{-0.7}$, ruling out models in which bulges were fully assembled first and disks gradually formed around them.

An important question in this context is, how bulge and disk grew relative to each other since this early cosmic epoch. Using HST photometry of 1495 massive galaxies in the CANDELS field Margalef-Bentabol et al. (2016) find that the two-component (bulge & disk) systems in the redshift interval of $1.5 < z < 3$ practically maintain their bulge size whereas their disks grow by a factor of approximately 3. Another study based on bulge and disk decomposition of LTGs suggests that the $\mathcal{M}_\star$ ratio between bulge and disk remains nearly constant over the latter redshift interval (Margalef-Bentabol et al., 2017). In view of the fact that the disk shows a higher star formation rate (SFR) than the bulge, these authors draw the conclusion that about one half of the stellar mass formed in the disk must have migrated into the bulge, promoting its gradual growth. However, primarily due to the limited resolution of high-z observations,

the evolution of the bulge-to-disk mass ratio across z remains a subject of controversy. For example, opposing the previous findings, Tacchella et al. (2018) point out that galaxies with $\mathcal{M}_\star \leq 10^{11}$ $M_\odot$ have since $z \sim 2$ on average doubled their stellar mass *throughout* their radial extent.

1.2 Limitations in previous studies on bulges and motivation behind this work

Although several recent lines of evidence support an interlacing evolution of bulge and the surrounding disk, our understanding of how this process has shaped the heterogeneity of present-day bulges is far from complete. In fact, despite intensive studies on the subject over the past three decades and a vivid controversy regarding the nature of bulges, we are still lacking robust, physically motivated discriminators between PBs and CBs. This might be the result of both an intrinsic overlap or genuine continuity in the physical and evolutionary properties (e.g., $\mathcal{M}_\star$ and the mean stellar age of bulges $\langle t_{\star,\mathrm{B}} \rangle$) or methodological limitations in previous analyses that have hidden these discriminators. Conceivable methodological biases are linked to aperture effects, shortcomings in the structural analysis of bulges and degeneracies in spectral modeling techniques. It should be born in mind that previous work on bulges has been mainly based on photometry and surface photometry, and whenever spectroscopic data were available, mostly are single fiber or longslit data which capture substantially different areas of bulges, depending on their intrinsic linear extent and the distance to the galaxy. Therefore, an observational limitation that might have affected or even compromised previous work is linked to aperture biases, most of the available spectroscopic data (single fiber and long-slit) are subjected to. Another possible source of uncertainty in discriminating between CBs and PBs might be connected with the image decomposition method used to separate the bulge from the disk and determine the bulge Sérsic exponent.

1.2.1 Aperture biases

A large body of our knowledge on bulges has been gathered in the last decade through $3''$ single-fiber Sloan Digital Sky Survey (York et al., 2000) data or longslit spectra. Spectral modeling studies using these data show that bulge age and metallicity increase with increasing total stellar mass ($\mathcal{M}_{\star,\mathrm{T}}$), with CBs (PBs) generally populating the high (low) range of

a broad LTG mass sequence (e.g., Ribeiro et al., 2016; Zhao, 2012). These trends, although showing a substantial scatter, are reported from several spectral fitting studies of large galaxy samples from SDSS, and include a positive correlation between $\mathcal{M}_{\star,\mathrm{T}}$, gas-phase and stellar metallicity (Z_{g} and $Z_{\star}$, respectively) and light- and mass-weighted stellar age ($t_{\star\mathcal{L}}$ and $t_{\star\mathcal{M}}$, respectively) (e.g., Kauffmann et al., 2013; Tremonti et al., 2004). These results are considered to be consistent with the galaxy *downsizing* hypothesis, reflected in, e.g., an anti-correlation between $\mathcal{M}_{\star,\mathrm{T}}$ with specific star formation rate (sSFR) and $t_{\star\mathcal{L}}$ for local galaxies (e.g., Asari et al., 2007; Brinchmann et al., 2004; Gallazzi et al., 2005; Heavens et al., 2004; Noeske et al., 2007), implying that massive galaxies have experienced the dominant phase of their assembly early on, whereas lower-mass systems build up their stellar mass over longer timescales. Indeed, Gallazzi et al. (2005) finds a sequence of increasing $\mathcal{M}_{\star,\mathrm{T}}$ and $t_{\star\mathcal{L}}$ with increasing light-weighted stellar metallicity ($Z_{\star\mathcal{L}}$) and 4000 Å break strength, showing that low-mass galaxies are usually younger and less metal-enriched, contrary to massive ones, with a transition between these two regimes occurring at $3 \cdot 10^9 < \mathcal{M}_{\star,\mathrm{T}}\ (\mathrm{M}_{\odot}) < 3 \cdot 10^{10}$.

There have been various attempts to account for aperture biases (e.g., Brinchmann et al., 2004; Hopkins et al., 2003; Kauffmann et al., 2003; Tremonti et al., 2004) but they all rely by necessity on simplifying assumptions on the variation of physical and evolutionary properties of galaxies with galactocentric radius. For the local Universe (or more extended galaxies), the evolutionary characteristics obtained from spectral modeling of single-fiber data are representative for the entire bulge only if it lacks significant age and metallicity gradients (i.e. its stellar component is relatively homogeneous in terms of age and metallicity). As for more distant objects (or intrinsically less extended) these observations are systematically biased towards younger stellar populations, since the spectroscopic aperture encompasses the surrounding star-forming disk. Given that the $3''$ fiber of SDSS for local LTGs captures a small fraction of the bulge, whereas it might capture the surrounding disk for more distant ones, aperture biases are inevitable. This can dilute potentially significant trends and observational discriminators between PBs and CBs. Another aspect, first addressed in Gomes et al. (2016b) for the case of early-type galaxies (ETGs) and being readily applicable to LTGs, is that, in an inside-out SF quenching scenario, the upper-right *wing* of SDSS determinations on the BPT diagram (Baldwin, Phillips & Terlevich, 1981) can naturally be accounted solely by aperture effects on SDSS data. This, in turn, suggests that the spectroscopic classification of large galaxy data sets into SF, low ionization nuclear emission regions (LINERs) and Seyfert, can be strongly affected by aperture

effects. Further studies conducted by the CALIFA consortium (e.g., Iglésias-Páramo et al., 2013) underscore and quantify the importance of aperture effects in quantities, such as SFR, and Hα equivalent width (EW).

Integral field spectroscopy (IFS), capturing the entire galaxy, offers therefore the only efficient means for overcoming these aperture biases, allowing for the proper separation and spectroscopic analysis of bulge and disk emission.

1.2.2 Spectral modeling biases

Adding to observational biases linked to aperture effects, a fact that in some cases significantly obstructs the comparison of results obtained by different groups is that different recipes are used to pre-process (spatially bin) and fit spectra of bulges. This and the fact that in some cases different definitions of physical parameters are adopted by different groups (e.g., stellar age computed as the logarithm of the arithmetic average of contributions of individual simple stellar populations (SSPs) in terms of luminosity or mass, or as the average of their respective logarithmic contributions) prevents a direct comparison of results from the literature.

In order to place constraints on the SFH one can adopt several techniques that vary greatly in their concept, physical assumptions and mathematical foundation (see Gomes & Papaderos, 2017, for a recent review). A popular yet simple approach is based on (luminosity-weighted) Lick indices in which the EWs of several prominent stellar spectral absorption lines are measured and compared with predictions from evolutionary synthesis models (examples of such studies in the context of bulge evolution include Bruzual & Charlot, 2003; Schiavon et al., 2007; Thomas & Davies , 2006; Thomas et al., 2003). It should be born in mind, however, that the Lick system was conceived and calibrated for the study of instantaneously formed stellar populations (e.g., globular clusters and ETGs). Whether or not this method is also applicable in its original form to age-dating studies of systems with an extended SFH (e.g., bulges with a prolonged or even ongoing SF) is an open question that needs to be examined (cf. the cautionary remarks in this respect by, e.g., Concas et al., 2017; Serra & Trager, 2007; Yoachim & Dalcanton, 2008). Furthermore, the superposition of the featureless continuum from an AGN (Cardoso et al., 2017), or absorption-line infilling by nebular emission excited by ongoing SF and the diffuse ionizing field from the old ($\geq$ 100 Myr) post-asymptotic giant branch (AGB) stellar component (e.g. Binette et al., 1994; Gomes & Papaderos, 2017; Gomes et al., 2016a) is another issue that needs to

be dealt with for a meaningful application of Lick indices to age-dating studies of galactic bulges.

Another approach to explore the SFH of galaxies employs parametric or non-parametric ESS models (see Gomes & Papaderos, 2017, for recent review). It is important to note that by construction, ESS models have to assume a SFH and chemical enrichment history (CEH) on the basis of which the time evolution of the synthetic spectral energy distribution (SED) of a galaxy is computed. Comparison between synthetic (produced by this kind of models) and observed SEDs allows to place constraints on the formation history of galaxies. Examples of this technique applied to bulges are Ganda et al. (2007); Kauffmann et al. (2003); MacArthur et al. (2004). A limitation from this approach is that it is strongly linked to the prior assumptions made on the SFH and CEH, which obviously cannot capture the full complexity of galaxy evolutionary processes and which could substantially influence the result in the case of an unrealistic prior. For instance, the assumption of a continuous SFR in modeling the SED of a starburst galaxy would obviously flaw estimates of age and stellar mass. On the other hand, the ESS approach has been significantly refined in the past two decades, with recent codes being capable of searching for the best-fitting combination of SFH and CEH among a dense grid of pre-computed SEDs, each corresponding to a different (parametric or non-parametric) SFH (e.g., Acquaviva et al., 2011; Chevallard & Charlot, 2016; Pacifici et al., 2012). Quite importantly, as shown by Guseva et al. (2001), inclusion of nebular emission in synthetic SEDs, as well as of prescriptions ensuring consistency between the SFH and the observed Balmer line luminosities and EWs is critically important for lifting the well-known age-metallicity-attenuation degeneracy in purely stellar models for SF galaxies (e.g., Pelat, 1997, 1998).

As for population spectral synthesis (PSS) models (being per se non-parametric), their goal is to decompose a galaxy spectrum in its elementary building blocks (i.e. SSPs, each corresponding to a given age and metallicity). In principle, this method is the one that can provide the most unbiased and realistic estimates on galaxy SFHs, especially when applied to the entire UV-through-NIR spectral range. There are several publicly available PSS codes, including MOPED (Heavens et al., 2000), Starlight (Cid Fernandes et al., 2005), SEDFIT (Walcher et al., 2006), VESPA (Tojeiro et al., 2007), and more recently FADO (Gomes & Papaderos, 2017, 2018). The codes STECKMAP (Ocvirk et al., 2006b) and ULySS (Koleva et al., 2009) may be considered as partial realizations of the PSS principle, since the best-fitting SFH they provide is not truly unconstrained but subject to a SFH regularization prescription. The only PSS code currently

available that simultaneously accounts for stellar and nebular emission is FADO. As pointed out in Gomes & Papaderos (2017), a unique feature of this code is its capability to infer the SFH that self-consistently accounts for the observer Balmer line luminosities and hydrogen Balmer-line EWs in a galaxy. This strongly reduces the notorious age-metallicity-extinction degeneracy plaguing conventional (i.e. purely stellar) PSS codes (see Cardoso, Gomes & Papaderos, 2018, for comparative tests between FADO and the purely stellar PSS code STARLIGHT). Notwithstanding the advances made, it should be stressed that FADO is an evolving project, with future releases of it intended to the modeling of composite stellar and AGN spectra, as well as accounting for Lyman continuum (LyC) photon escape. As discussed above, the presence of an AGN power law continuum might significantly affect the estimation of the best-fitting SFH (Cardoso et al., 2017), in some cases leading to substantial overestimation of stellar masses and ages (Cardoso et al., 2016). Additionally, a standard assumption made in the current (v.1b) version of FADO is that the entire LyC radiation produced by stellar populations is locally reprocessed into nebular emission (i.e., the LyC escape fraction is zero). In view of an increasing observational evidence for a non-negligible LyC photon escape fraction in star-forming galaxies, both on sub-galactic and galactic scales (Izotov et al., 2018; Leitet et al., 2013; Leitherer et al., 2016; Weilbacher et al., 2018) and ETGs (Gomes et al., 2016a; Papaderos et al., 2013) in the local Universe and out to high-z (e.g., Fletcher et al., 2018; Vanzella et al., 2018), a determination of the LyC escape fraction from spectral fitting belongs to the next main goals of the FADO development project.

It also should be pointed out that divergence in the obtained results by different PSS codes might also stem from different constructions of the SSP library used (Bruzual & Charlot, 2003; Sánchez-Blázquez et al., 2006; Vazdekis et al., 2010), as well as from the adopted intrinsic extinction law (e.g., Calzetti et al., 2000; Cardelli et al., 1989). Obviously, uncertainties in the modeling of the stellar (and nebular) continuum propagate to diagnostic emission-line ratios after, e.g., BPT, that are used to constrain the dominant gas excitation mechanisms in a galaxy (see Petropoulou et al., 2011, for a discussion on spectroscopic classification biases arising from imperfect correction for the underlying stellar absorption). Likewise, a precise modeling and subtraction of the stellar continuum is essential for the extraction and analysis of faint nebular emission in galaxies and the determination of SFRs based on their Hα luminosity.

1.2.3 Uncertainties in structural analyses of bulges

The common practice is to classify bulges on the basis of their Sérsic index (η), which is postulated to be < 2 for PBs and > 2 for CBs (see, e.g., Kormendy & Kennicutt, 2004, for a review). This classification scheme is, however, purely empirical, being based on subjective considerations, and lacks a physical foundation (e.g., Gadotti, 2012). For example, studies like Fisher & Drory (2010, cf. their Fig. 7) find that across all bulge's mass range there is a substantial overlap between CBs and PBs, depending on whether they are selected relatively to their mid-infrared colors or η. Similarly, in some cases the photometric classification as PB solely relies on the absence of correlations that are known to apply to CBs. For instance, Fisher & Drory (2010) show that, unlike CBs, the exponent η of PBs does not correlate with other bulge structural properties, like half-light radius of the bulge, average surface brightness within the half-light radius, and magnitude of the bulge at 3.6 μm. These results are consistent with the study by Gadotti (2009) that concludes that for CBs there is a significant correlation between η and bulge-to-total (B/T) ratio, whereas this is not valid for PBs that populate the same locus as disks on the fundamental plane of galaxies. These authors propose that an improved recipe to classify bulges as compared to η might be based on deviations from the Kormendy (1977) relation. Another interesting result that this study has shown was that CBs are offset from ETGs in the mass-size relation, suggesting that the former are not simply dwarf ETGs embedded within disks. In the context of the two formation scenarios for bulges, a robust parameter or set of parameters that can accurately separate bulges into CBs and PBs is of high importance. For this reason, this subject continues to attract considerable interest, as apparent from the scheme recently proposed by Neumann et al. (2017) that uses a combination of η, light concentration index $C_{20,50}$, the Kormendy (1977) relation and the inner slope of the radial $\sigma_\star$ profile.

However, in all above approaches an inherent problem is linked to the extraction and fitting of the bulge component via 1D/2D surface photometry and profile decomposition techniques. A robust analysis of the different components of LTGs requires an accurate and reproducible extraction of the bulge emission and fitting of its radial intensity profile with a Sérsic model. Given the morphological complexity of LTGs and inherent uncertainties in non-linear profile decomposition and fitting codes, this task deserves special attention.

Degeneracy between η and R_{eff}

The Sérsic fitting law (SL – also referred to as generalized de Vaucouleurs law, de Vaucouleurs 1948) is a widely used functional form in structural studies of galaxies. Following its initial application by Sérsic (1963, 1968), it has been reintroduced in extragalactic research by Caon, Capaccioli & D'Onofrio (1993), who have applied it to SBPs of ETGs, and has since then been extensively used in numerous structural investigations of galaxies across their entire mass and morphology sequence (see reviews of the subject by Davies et al., 1988; Graham, 2013). Its simple, three-parameter functional form, describing the SBP $\mu(R^\star)$ of a galaxy as

$$\mu(R^\star) = \mu_0 + \frac{2.5}{\ln(10)} (R^\star/\alpha)^{1/\eta}, \tag{1.1}$$

with μ_0 and α denoting, respectively, the central surface brightness (mag/$\square''$) and an angular pseudo-scale length ($''$), and the Sérsic shape parameter η regulating the profile curvature, offers a versatile mean for approximating a wide variety of SBPs, from roughly exponential galactic disks ($\eta = 1$) to the centrally steeply increasing profiles of massive ETGs ($\eta = 4$, in the case of the de Vaucouleurs (1948) law). Another popular formulation of the SL involves the effective radius (R_{eff}, the radius that encompasses 50% of the total SBP light) and the mean surface brightness (μ_{eff}) therein, with η being coupled to these parameters through an appropriate normalization factor (cf. Eq. 2.1 and, e.g., Caon, Capaccioli & D'Onofrio, 1993; Trujillo, Graham & Caon, 2001, for details). Since the seminal work by Caon, Capaccioli & D'Onofrio (1993), SL has attracted a great deal of interest, with several studies exploring its mathematical foundation (Graham & Colless, 1997; Graham & Driver, 2005; Graham et al., 2005; Trujillo, Graham & Caon, 2001), and the intrinsic luminosity density distribution it corresponds to (Baes & Gentile, 2011; Baes & Van Hese, 2011; Chakrabarty & Jackson, 2009; Ciotti, 1991; Papaderos et al., 1996a), as well as its stellar-dynamical origin and the meaning of η in the evolutionary context of galaxies (Cen, 2014; Marquez et al., 2000).

Given the importance that is ascribed to η, specially but not exclusively for bulge classification purposes, its robust determination is essential in several fields of extragalactic research. An issue, however, that could affect Sérsic modeling studies with state-of-the-art 1D/2D SBP decomposition techniques is a severe degeneracy between the best-fitting R_{eff} and the exponent η of a Sérsic fit (Breda, 2014; Fisher & Drory, 2010; Noeske et al., 2003; Trujillo, Graham & Caon, 2001). This is especially true when a SBP deviates from the perfect Sérsic functional

form, consequently the model parameters inferred through standard χ^2 minimization between model and individual SBP data points depend on the surface brightness range considered and errors associated with individual points.

Methodology of LTG decomposition into a bulge, bar and disk

A first issue to be considered in LTG decomposition studies is the possible inclusion of a bar component, whenever meaningful. Its omission, as is common practice in most structural studies of LTGs, may lead to an artificial overestimation of the bulge luminosity and Sérsic η (cf. Breda, 2014; Méndez-Abreu et al., 2008), as demonstrated in Fig. 1.1.

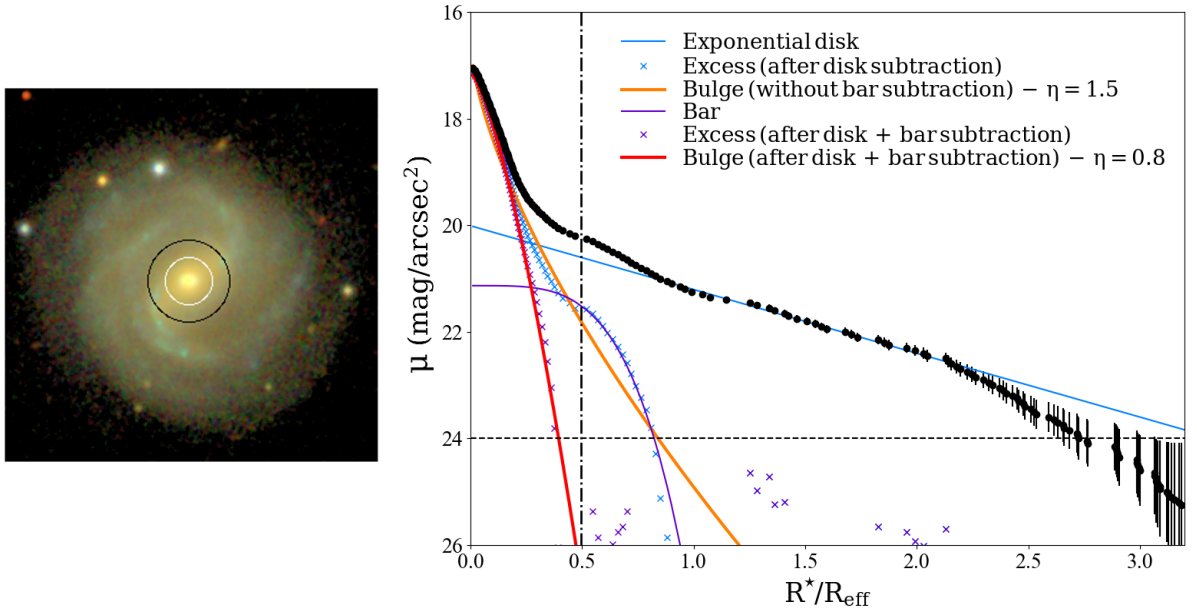

Figure 1.1: Left-hand side: true color image of the LTG NGC 0776 with the radial extent of the bulge (after subtraction of exponential disk and bar contributions) overplotted in white (**Ba**). Overplottled in black is the bulge diameter, as obtained by neglecting the bar component in the fit (**Bb**). Right-hand side: Illustrative example of the performed 1D decomposition of the SDSS r-band SBP of the LTG NGC 0776 into exponential disk (blue), bar (purple) and bulge (red, **Ba**) vs. exponential disk and bulge (orange, **Bb**) without fitting and extracting the bar luminosity contribution prior to fitting the bulge. Both **Ba** & **Bb** bulge configurations are approximated by a Sérsic model, whose η is determined to be 0.8 and 1.5, respectively. This example demonstrates how important it can be to take the bar component (if present) into account when attempting to extract the bulge emission from SBPs.

A second, and possibly more important issue that could strongly influence the Sérsic fit to a bulge, is linked to the photometric modeling of the disk. While galactic disks were initially thought to universally follow an exponential (type I) intensity profile (de Vaucouleurs, 1959), subsequent work has revealed the presence of down/up-bending SBPs (type II and type III,

respectively, Freeman, 1970), calling for a closer investigation of the disk formation process and an accurate modeling of possible divergences from the exponentiality. For instance, a recent IFS study by (Ruiz-Lara et al., 2017) attributes deviations from an exponential slope to radial stellar migration, proposing it to be more efficient in type III disks as compared to type II ones. This study reinforces this scenario by means of modeling of MW-mass disks in cosmological simulations. Another question regards the observational evidence for disks with vast extents (8 to 10 scale-lengths), much larger than those predicted from pure collapse models (see Debattista et al., 2017, for a review).

Another important question that so far has not been adequately addressed is whether exponential slope of the disk is valid all the way to the LTG center, i.e. beneath the bulge. SBPs of bulgeless [1] galaxies show a pure exponential distribution (for e.g., Sachdeva & Saha, 2016), but what will be the behavior of the disk if the galaxy hosts a *bona fide* bulge? Considering that the presence of a much brighter and denser stellar component hides the true nature of the disk in the inner region of the galaxy, it's central light distribution is unknown. To overcome this dilemma while performing structural analysis using surface photometry techniques the standard procedure is to extrapolate the exponential disk up to the galactic center, hence conserving its exponential nature.

The implications of this simplifying assumption are manyfold and fundamental: this fitting approach implies that bulge and disk co-exist without significant dynamical interaction and mass exchange (e.g., stellar migration, kinematical heating) over several Gyr of galactic evolution, which appears to be in contrast with conclusions from previous studies that advocate a joint evolution of these structures. Another implicit assumption encapsulated within the generally adopted exponentiality of the disk to the LTG center is the absence of significant stellar age or metallicity gradients within the bulge radius, as well as that the sSFR is nearly invariant throughout the disk. Recently, IFS observations allowed a spatially resolved exploration of stellar populations of galaxies across a significant part of their radial extent (up to 1.5 to 2 R_{eff}). There are many studies demonstrating that some LTGs present age and metallicity gradients across the disk radial extent (see for e.g., Goddard et al., 2017; González-Delgado et al., 2015) which can possibly compromise the supra-cited premise.

[1] In this work, *bulgeless galaxies* denotes pure disk galaxies without evidence for a central luminosity excess.

Another indication that might jeopardize the common assumption of the conservation of the disk's exponentiality to the galactic center are the results obtained by some authors while trying to model the rotation velocity profile or the stellar surface density of the disk component by means of semi-analytic models (Kuijken & Dubinski, 1995), N-body simulations (Widrow & Dubinski, 2005) or, more recently, hydrodynamical simulations (Obreja et al., 2013). These authors show that in the presence of a bulge (whose stars are characterized by significantly high $\sigma_\star$) the orbits of disk stars (mostly supported by V_{rot}) are gradually kinematically heated by cumulative weak interactions with the bulge. According to these results, interaction between both collisionless stellar populations over billions of years will eventually lead to a scarcity (or even depletion) of rotational-velocity supported stars in the galactic center, resulting in a flattening or even a sharp decrease of the disk's particle density, as shown in Fig. 2 of Obreja et al. (2013). From the observational point of view, the need for a central flattening of exponential profiles in many dwarf galaxies was established through surface photometry of early-type and late-type systems (Binggeli & Cameron, 1993; Noeske et al., 2003; Papaderos et al., 1996a). If this is indeed the case, important implications might be expected for structural studies of LTGs: a first step in the standard decomposition procedure for such galaxies involves the determination and subtraction of the disk contribution by approximating its SBP by a an exponential function. The residual central luminosity excess is attributed to the bulge and fitted with a Sérsic model, the best-fitting parameters of which (η, $R_{\rm eff}$, radial extent, total magnitude) are used for bulge classification into CBs and PBs. A possible overestimation of the disk luminosity inside the bulge radius, as implied by the aforementioned studies, would obviously impact determinations of the structural properties for the bulge, which might offer an explanation for the relatively weak correlation between η and bulge magnitude (see for e.g., Head et al., 2014; Mosenkov et al., 2014). In this regard, it is worth bearing in mind that, in disk-dominated LTGs, the assumed (inwardly extrapolated) disk emission can provide up to $\sim 80\%$ of the light inside the bulge radius. Therefore, overestimating the true luminosity fraction by the disk could lead to the erroneous classification of a high-luminosity, high-η CB as a PB. If, for instance, this bulge hosts an AGN one will conclude that some PBs display AGN activity in their cores whereas in fact this bulge is not a PB but a CB. This hypothetic scenario serves only as an example of how the adopted assumptions and methods might dictate the obtained results.

1.3 Thesis outline

With the goal of shedding further light into the formation routes and evolutionary pathways of LTGs, with special focus on their bulge component, it was considered necessary to develop and apply a methodology that combines multi-band surface photometry of SDSS data with spatially resolved spectral modeling of IFS data, thereby going significantly beyond previous studies in this field. As detailed in Sect. 1.2, several considerations, such as the lack of physically motivated observational discriminators between PBs and CBs, propagating into uncertainties in bulge classification, besides conceptual uncertainties in standard galaxy decomposition techniques and spectroscopic aperture biases, have posed a significant obstacle in developing a coherent evolutionary picture for bulges.

The methodology adopted in this study is in many respects novel and was developed with the goal of overcoming the aforementioned limitations of previous studies. For instance, the sample selection strategy adopted here does not rely on any a priori assumption on the photometric structure of PBs and CBs (e.g., their η) that could immediately introduce a bias. Instead, the entire sample of LTGs in the CALIFA survey was analyzed in a homogeneous manner, with the only pre-selection criterion being a low inclination and the absence of tidal distortions. Quite importantly, the studied sample (135 galaxies) covers the entire mass range of LTGs and their bulges (over 3 dex in log of the stellar mass; cf. Sect. 2.1 for details), from virtually bulgeless low-mass galaxies all the way to massive LTGs hosting prominent bulges. This way we ensure an unbiased investigation of the physical and evolutionary characteristics of bulges with the goal of examining possible objective discriminators between PBs and CBs.

A second novel element of this project is the development of a new algorithm that allows us to derive the Sérsic model parameters for the bulge component in a robust and consistent way. This code (iFIT, Breda et al. 2019) was constructed bearing in mind the mitigation of the aforementioned degeneracy between η and $R_{\rm eff}$, and allowed for an accurate determination of the isophotal radius of the bulge component, which was fundamental to the subsequent spatially resolved spectral modeling of its stellar populations, and the exploration of the connection between Sérsic η and the physical and evolutionary properties of LTG bulges (see Sect. 3.1). A detailed explanation of the algorithm in Sect. 2.3 is supplemented by a quantitative assessment of the accuracy of the code (Sect. 2.3.2). Furthermore, the precise determination of the bulge ra-

dius with iFIT has permitted to **1.** infer bulge colors and color gradients (cf. Sects. 2.3.4 & 3.2 for a description of our photometric analysis technique and the main results obtained, respectively) and **2.** perform an uniform spectroscopic analysis capturing virtually the whole bulge emission. This way this study could overcome aperture biases and take full advantage of the power of integral field spectroscopy. A description of the adopted spectral modeling methodology and the post-processing and analysis of the obtained results can be found in Sects. 2.4 & 3.3.

A third innovative element of this research project revolves around RemoveYoung ($\mathcal{RY}$, Gomes & Papaderos, 2016), a post-processing tool that permits to strip the galaxy's light and mass contributions of its young stellar populations, after spatially resolved spectral fitting (see Sect. 2.4.3 for a detailed explanation), allowing to trace the light and mass contributions of the different stellar populations that compose the galaxy. The analysis of the synthetic images and SBPs of successively old stellar populations back to an age of 9 Gyr has provided new key insights into the structural build-up of LTGs and led to the discovery of a powerful new discriminator of the bulge's evolutionary status ($<\delta\mu_{9\mathrm{G}}>$). The tight correlation between this distance- and nominally extinction-independent quantity with evolutionary and physical characteristics of bulges, such as stellar age and mean stellar surface density, underscores its significant potential for advancing our understanding of bulge formation and evolution.

Finally, this project examines for the first time the validity of inwards extrapolation of the exponential disk profile to the LTG center (i.e. within the bulge radius) using a combined photometric and spectral modeling approach. A detailed description of the code developed in the context of this particular task is provided in Sect. 2.4.6, and the results obtained for our sample on the intensity profile of the disk beneath the bulge are summarized in Sect. 3.5.

Chapter 2

Data set and methodology

2.1 Sample selection

The analyzed galaxy sample was selected from the 3rd Data Release of the CALIFA IFS survey (667 galaxies; Sánchez et al., 2016, see http://califa.caha.es). In pursuance of obtaining a representative sample of the local LTG population, bearing in mind an accurate decomposition of bulge and disk, SDSS images of the entire set of the observed CALIFA galaxies (667 objects) were visually inspected. All the late-type, face-on or nearly face-on galaxies were selected, excluding the ones which inclination is higher than 40° in order to minimize internal obscuration effects and disk contamination. Systems with morphological distortions (e.g., polar ring galaxy candidates) and signs of a recent or ongoing interaction were also excluded considering that our main goal is to study secular evolution of LTGs. This is also the case for galaxies strongly overlapping with bright foreground Galactic stars or extended background sources. The final sample comprises 135 non-interacting, nearly face-on, local ($\leq$ 130 Mpc) LTGs.

Spanning a range between -17.8 and -22.6 mag in SDSS r absolute magnitude (M_r, Fig. 2.1), as determined from integration of SBPs to an extinction-corrected surface brightness level of 24 mag/$\square''$, and covering nearly all late-type morphological types[1], the sample is fully representative of the (secular evolving) local LTG population. Regarding the bulge component, the sample encompasses bulges with $-20.6 \lesssim M_r$ (mag) $\lesssim -14.6$, implying a factor of ~ 250 in optical luminosity and 3 dex in $\log(\mathcal{M}_\star)$ ($10^{8.3-11.3}$ $M_\odot$) and all types of spectroscopic activity (according to the BPT diagram) permitting to investigate the relation between the incidence of AGN activity manifesting itself as Seyfert or eventually LINER characteristics with other

[1]Information collected at NASA/IPAC Extragalactic Database (NED).

physical properties of the bulge. With regard to the radial extent of the bulge (see Sect. 2.3.3 for acquaintance on the determination of the bulge radius and histogram in Fig. 2.2) the sample is diverse, encompassing bulges from ~ 0.5 to ~ 4 kpc.

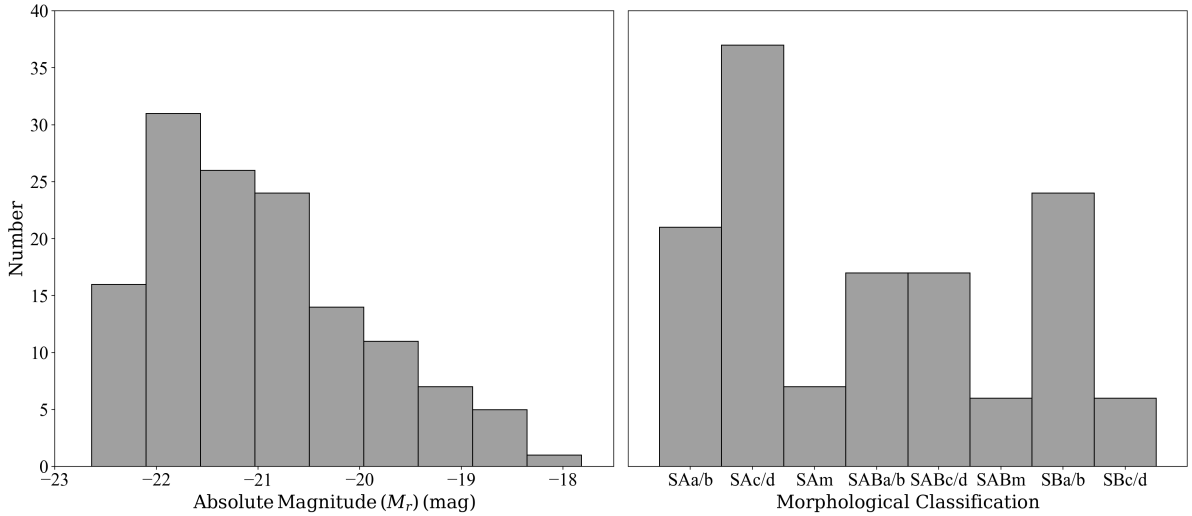

Figure 2.1: Left-hand side: distribution of extinction-corrected total absolute magnitudes in the SDSS r for the analyzed sample of 135 LTGs. Right-hand side: morphological type according to the Hubble-de Vaucouleurs classification scheme (de Vaucouleurs, 1959).

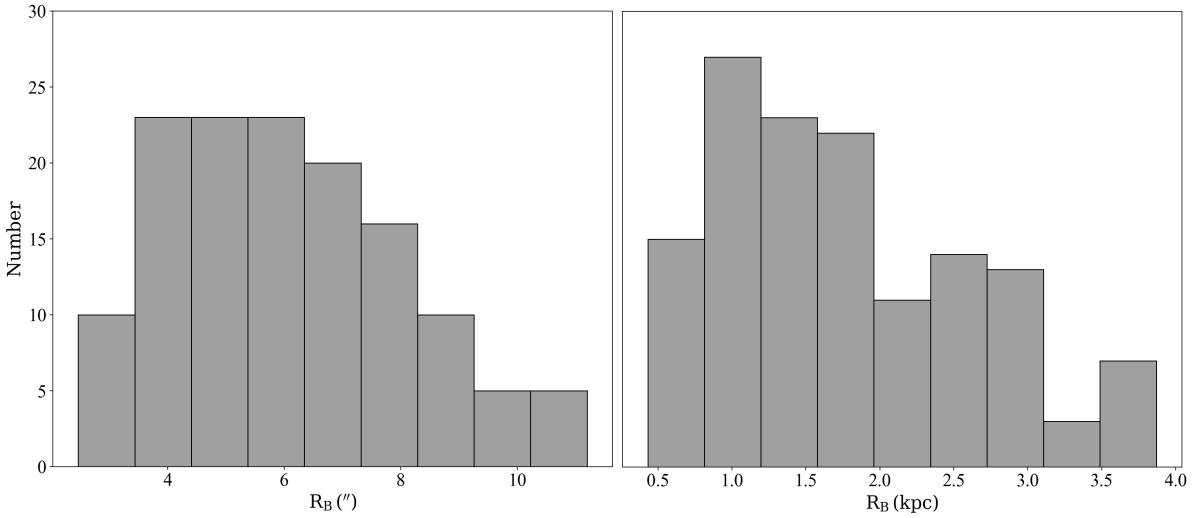

Figure 2.2: Left-hand side: distribution of the bulge's radial extent in the SDSS r band for the analyzed sample of 135 LTGs in ″. Right-hand side: distribution of the bulge's radial extent for the same galaxies but in units of kpc.

2.2 Photometric and structural analysis of the galaxy sample

This study is based on a combination of several techniques. First, we use SDSS DR7 photometric data in order to perform a detailed structural analysis and primarily to obtain a uniformly defined and largely model-independent isophotal radius for the bulge, within which subsequently all physical and evolutionary quantities derived from spectral synthesis were analyzed. This procedure ensures a homogeneous extraction and spectral fitting of nearly the total bulge emission.

2.2.1 Post-processing of the SDSS photometric data

Photometric data from SDSS DR7 (Abazajian, et al., 2009) are provided to the public in a pre-reduced form. Still, there are a few steps that must be conducted in order to improve the quality of the photometric reduction, which is essential for a precise structural and color analysis of SDSS galaxies. For that purpose, an existing in-house suite of routines (P. Papaderos, priv. comm.) was upgraded to permit simultaneous reduction of SDSS images of a galaxy in three bands, incorporating the following steps:

i. Rotation of the images to their astronomical orientation (rotate the images according to their "SDSS Photometry Position Angle");

ii. Co-registration of the images in the three bands (g, r & i) using Galactic foreground stars: even a minor error in the co-registration procedure leads to spatially extended artifacts at the level of 0.1-0.5 mag in color maps, which can obviously bias conclusions regarding stellar age and intrinsic extinction;

iii. Equalization of the point spread function (PSF) through Gaussian smoothing of better-resolved images to the lowest-resolution image available for each galaxy: as before, an imperfect PSF equalization propagates into color artifacts around compact sources. For instance, while computation of color maps, due to the non-negligible difference of the PSF of each filter (e.g., PSF *wings* of red bands are more extended than the PSF of blue bands), without PSF equalization a false red halo would be produced, which could be erroneously interpreted as an old stellar population. If the difference between the seeing in the two bands is substantial, one can produce false features that might account up to 0.5 mag. To tackle this problem, the code applied determines the full width at half

maximum (FWHM) of a Gaussian PSF model to several non-saturated field stars in three bands, and incorporates an iterative smoothing procedure to match PSFs to a precision of typically better than $0.1''$ in the final FWHM;

iv. Improved sky background subtraction through higher-order fitting of the adjacent sky: an accurate sky background subtraction (at a level better than 3% of the photon noise) is very important for a reliable surface photometry analysis. Specifically, an under/over-subtraction of the sky level leads to a flattening/truncation of SBPs, hence to a false determination of photometric quantities;

v. Removal of bright Galactic foreground stars: these sources will contaminate the images, perturbing the surface photometry analysis and radial color profiles.

vi. Determination of SDSS calibration constants after correction for foreground Galactic extinction.

The output of this routine consists of two data-cubes with three layers each (one for each band). The first data-cube, which contains the data completely reduced, was issued in all aspects of the subsequent photometric studies (e.g., surface photometry, computation of color maps and profiles). The purpose of the second data-cube is to produce true-color images where the aforementioned steps iii. and iv. are skipped. The true-color images were created by means of an own ESO-MIDAS routine that was based on the algorithm by Lupton et al. (2004) that combines Red-Green-Blue (RGB) images, ensuring that colors in the standard astronomical system (e.g., Vega, Bohlin & Gilliland, 2004) are uniquely mapped on the RGB image channel color space.

2.3 Development and aplication of a conceptually novel code (iFIT) for the robust determination of Sérsic model parameters

One important prerequisite for the execution of this project is the correct identification of the bulge radial extent (R_B). When performing the photometric decomposition of the sample we detected several problems. We tested three different tools: the available 1D surface photometry pipeline of the team, GALFIT (Peng et al., 2010) and IMFIT (Erwin, 2015). After a thorough investigation of the results produced by the available tools, by assuming different initial parameters or, for the first case, choosing different limits for the fit of the disk, we found that all

of them are very sensitive to variations in the fitting setup, making them unreliable. The high uncertainties obtained drove us to conclude that the algorithms that estimate the Sérsic parameters are heavily affected by the η-R_{eff} degeneracy (see Sect. 1.2.3). Additionally, we noticed that the 2D tools, besides being very sensitive to data-reduction aspects like sky subtraction or variables like sky noise estimation (GALFIT), modeling and subtraction of the underlying disk (e.g., Noeske et al., 2003; Papaderos et al., 1996a), and eventually the bar (Breda, 2014; Méndez-Abreu et al., 2008), produce substantial residuals in most cases, specially at the central part of the galaxy, indicating that the obtained solution is not reliable. Furthermore, we noticed that in many cases one obtains as best fit a very high Sérsic η ($5 < \eta < 10$). Such a high η would imply an unreasonable decrease in light in a very short radial range: for example, for a Sérsic model with $\eta = 10$ & $R_{eff} = 5''$ the expected decrease in light from $R^{\star} = 0$ to $R^{\star} = 0.1''$ is of 99.9998% which is virtually 100%; for the same η assuming an $R_{eff} = 50''$ the expected decrease in light for the same radius is of 99.9974%. Besides the enormous predicted stellar surface density ($\Sigma_{\star}$) in the very core of these galaxies, the extremely abrupt decrease in such short radial extent (even for high-z galaxies where $0.1''$ might imply 0.5-0.8 kpc) made us question the validity of these solutions.

These problems motivated the development of a new algorithm (iFIT) that was constructed with the main aim of breaking or at least alleviate the degeneracy between two of the three parameters of the Sérsic model (see Sect. 2.3.1 for the detailed description of the algorithm). Figure 2.3 demonstrates the case of MCG +01-10-019, a spiral galaxy situated at ~ 69.9 Mpc, where it is clear the difference between the obtained solutions for GALFIT and iFIT: although the difference in the fit is not very significant (with exception of the central region where the residuals of GALFIT indicate a difference of about 0.5 mag) the obtained Sérsic parameters differ greatly. The high disparity in the obtained parameters jointly with the similar fits is a clear example of the profound implications of the aforementioned degeneracy. For instance, a standard automated algorithm of galaxy classification based on the Sérsic index would wrongly categorize this galaxy as an ETG on the basis of its high-η.

2.3.1 Technicalities

As refereed in Sect. 1.2.3 the SBP given by the SL in mag/$\square''$ can also be expressed by the following equation:

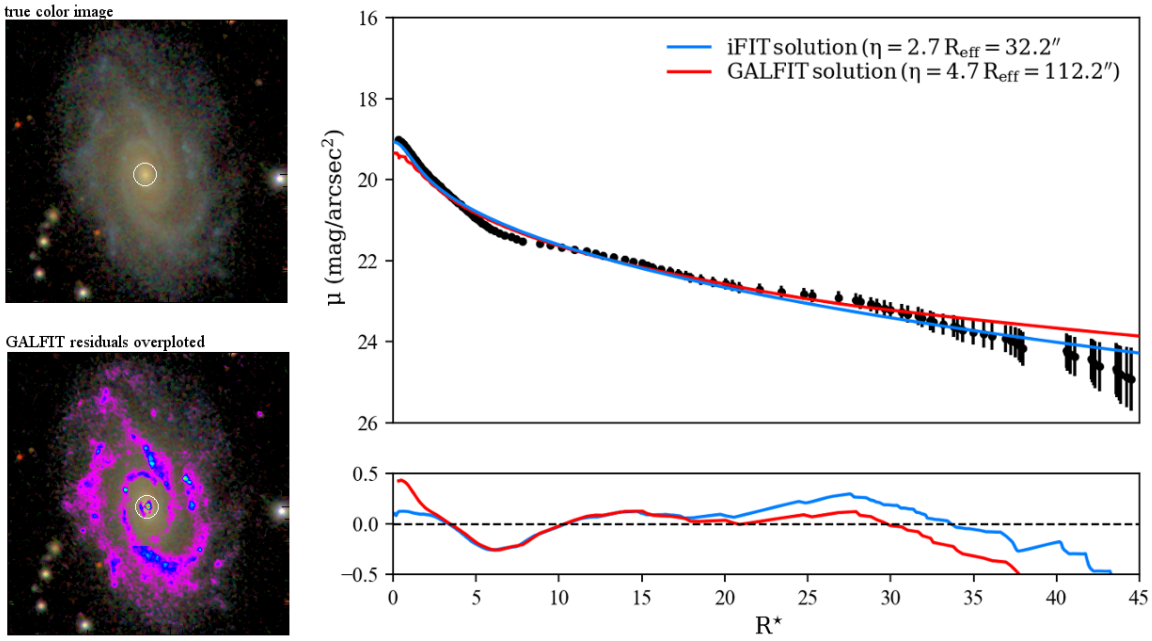

Figure 2.3: Left-hand side: true color image of the galaxy MCG +01-10-019 (top) and GALFIT residuals overplotted to the same true color image (bottom) – the white circle depicts the isophotal diameter of the bulge, as determined by applying iFIT. It is clear that the center of the galaxy is not properly fitted by GALFIT due to the large residuals. Right-hand side: fits of the total SBP with both iFIT and GALFIT of the SDSS r-band SBP of the LTG MCG +01-10-019 and respective residuals.

$$\mu(\mathrm{R}^\star) = \mu_{\mathrm{eff}} + \frac{2.5 b_\eta}{\ln(10)} \left[\left(\frac{\mathrm{R}^\star}{\mathrm{R}_{\mathrm{eff}}} \right)^{1/\eta} - 1 \right], \tag{2.1}$$

where, $\mathrm{R}_{\mathrm{eff}}$ is defined as the photometric radius that encloses 50% of the total luminosity of a SBP, μ_{eff} is the surface brightness at $\mathrm{R}_{\mathrm{eff}}$ and b_η is given by $\Gamma(2\eta) = 2\gamma(2\eta, b_\eta)$ with Γ and γ being the incomplete and complete gamma functions, respectively (Ciotti, 1991) (the b_η parameter ensures that the radius $\mathrm{R}_{\mathrm{eff}}$ encloses 50% of the total (out to $\mathrm{R}^\star = \infty$) luminosity of the SBP). At variance to the approximation $b_\eta = 1.9992\eta - 0.3271$ proposed by Graham et al. (2005) in the range of $0.5 \leq \eta \leq 10$, the exact value of b_η was computed with a Fortran code. This approach was taken due to the fact that the η of some pseudo-bulges or the underlying host of dwarf galaxies (Noeske et al., 2003) is best-fitted with a $\eta < 0.5$, i.e., off the range where the approximation by Graham et al. (2005) applies (in this range that approximation is inaccurate by $\sim 3\%$ to $\sim 700\%$).

Below, we summarize the main actions performed by the developed algorithm (see Fig. 2.5 for

pseudo-code of iFIT):

1. Preparatory steps & Integration: iFIT starts by converting the input surface brightness (μ, mag/$\square''$) data into a radial intensity distribution I(R) (counts/$\square''$) which is subsequently integrated out to the maximum observed radius R_{max}:

$$L(R_{max}) = 2\pi \int_0^{R_{max}} I(R^\star) \cdot R^\star \cdot dR \tag{2.2}$$

where $I(R) = 10^{(\mu(R)-C)/-2.5}$ and C stands for calibration constant or zero-point mag. Before integration, spline interpolation is performed by means of TSPACK, a curve-fitting package based on exponential tension splines with automatic selection of tension factors (Renka, 2009), publicly available for several programming languages. Due to the drastic steepness of high Sérsic η profiles, traditional spline interpolation techniques fail to accurately reproduce the curve resulting in major errors in flux integration (if surface brightness error – σ_μ – is provided, iFIT also interpolates the σ_μ distribution).

2. Estimation of flux-enclosing parameters: The latter permits estimation of radii enclosing an increasing fraction of $L(R_{max})$ (20, 40, 50, 60, 80 and 90%, yielding the set of parameters R_{20}, R_{40}, R_{50}, R_{60}, R_{80} and R_{90}, respectively, along with the corresponding average surface brightness levels ($\langle\mu_{20}\rangle$, $\langle\mu_{40}\rangle$, $\langle\mu_{50}\rangle$, $\langle\mu_{60}\rangle$, $\langle\mu_{80}\rangle$ and $\langle\mu_{90}\rangle$) within these flux-enclosing radii. Average surface brightness for each of the $L(R_{max})$ fractions (i) is computed by means of the following equation:

$$\langle\mu_i\rangle = -2.5\log_{10}\left(\frac{i \cdot L(R_{max})}{\pi R_i^2}\right) + C. \tag{2.3}$$

Contrasting traditional χ^2 minimization techniques iFIT determines the solution by evaluating the difference (model vs. observed) for these flux-enclosing parameters, this way preventing the few innermost points (although they show the highest intensity and $\mu(R^\star)$ they encompass a rather low fraction of $L(R_{max})$ – see Fig. 2.4) to drive the solution. Additionally, this approach secures a more robust fitting considering that deviant points do not impact the solution, since they generally have a minor effect on $L(R_{max})$.

3. Determination of R_{eff} & μ_{eff}: One of the advantages of the presented algorithm is that in early stages of the convergence procedure it fixes 2 (R_{eff} & μ_{eff}) of the three free parameters

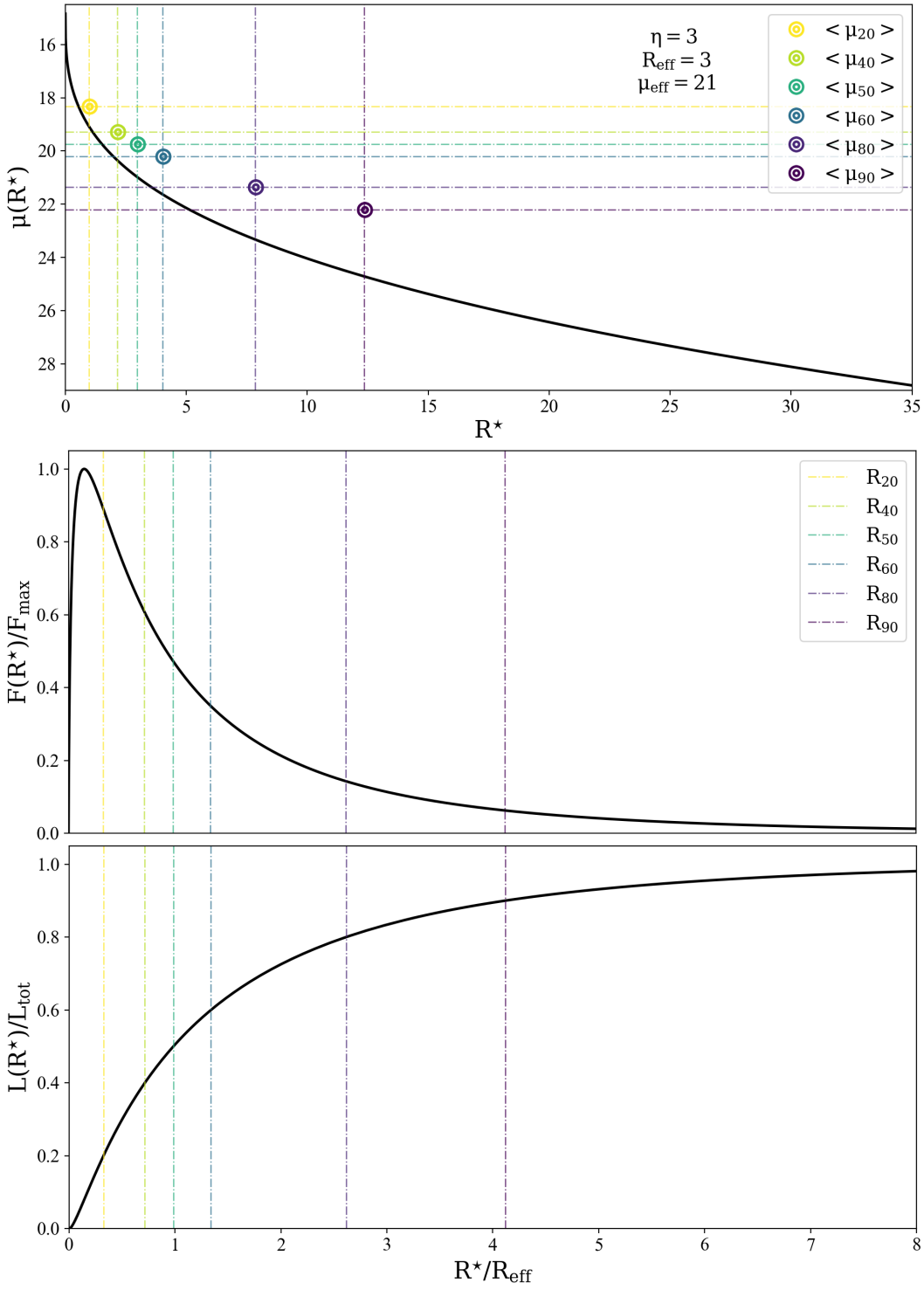

Figure 2.4: Top panel: example of a SL $\mu(R^\star)$ profile. Middle panel: respective flux distribution normalized to the maximum flux ($F(R^\star)/F_{max}$). Bottom panel: respective normalized luminosity ($L(R^\star)/L_{tot}$). It is evident that although the innermost points are the ones that enclose the highest intensity, when it comes to flux or luminosity these become nearly irrelevant. Vertical lines and markers correspond to the radial- and μ-flux enclosing parameters, respectively.

of eq. 2.1 alleviating the degeneracy between R_{eff} and η. This is done by taking advantage of SL linear nature by considering $y = \mu(R^{\star})$ and $x = R^{1/\eta}$. Assuming a range of possible η from 0.3 to 8.0, iFIT performs linear regressions ($y = mx + b$) between observed $\mu(R^{\star})$ and $R^{1/\eta}$ determining slope (m) and y-intercept (b). Having these parameters, R_{eff} & μ_{eff} are computed by means of:

$$R_{eff} = \frac{b_{\eta}^{\eta}}{(m \cdot \ln(10)/2.5)^{\eta}} \; ; \; \mu_{eff} = b + \frac{2.5 b_{\eta}}{\ln(10)} \tag{2.4}$$

By default, iFIT estimates the above mentioned parameters by performing a linear regression. However, if σ_{μ} is provided and if the final fit does not fulfill the convergence criterion ($\xi < 0.7$, cf. eq. 2.5) the algorithm repeats this step by performing weighted (WLR) or half-weighted (hWLR) linear regression (where for WLR the weight in each observed point is given by $w(i) = 1/\sigma_{\mu}(i)$ and for hWLR is equal to $w(i) = 1/\sqrt{\sigma_{\mu}(i)}$). We decided to implement these two extra methods for the derivation of R_{eff} & μ_{eff} purely based on empirical considerations: we noticed that for some galaxies, WLR would produce better results when compared to non-weighted linear regression and for some other galaxies the optimal would be to apply hWLR. For this reason we advise the user to supply σ_{μ} for the observation as the 3rd column in the input ASCII file (Breda et al., 2019).

If the observation is convolved, to ensure the PSF affected $\mu(R^{\star})$ will not impact the determination of R_{eff} & μ_{eff}, the linear regression will only occur for observational points where $R^{\star} > 3$ times the FWHM. When the FWHM of the PSF is considerable (for instance when FWHM/R_{eff} $>$ 1-2) and the observational data too shallow (when the SBP includes less than 90% of the total luminosity[2]) iFIT might not be able to retrieve the correct R_{eff} & μ_{eff} as so η (see Fig. 2.7 for acquaintance of iFIT limitations). This deficiency cannot be perceived as an exclusive iFIT limitation since all surface photometry codes will fail under these conditions.

4*a*. Estimating the Sérsic η for non-seeing convolved profiles: This step constitutes a fundamental and novel aspect of the concept presented here: its goal is to estimate η from the best match between the six aforementioned flux-enclosing radii and corresponding average μ's with the theoretically expected values for the best-fitting η. Basing the solution on flux-enclosing robust quantities is a distinctive advantage as compared to standard χ^2 mini-

[2]It is important to clarify that an SBP truncated at 90% of its total luminosity is very shallow (see top panel of Fig. 2.4 where R_{90} corresponds to a $\mu_{lim} = 24$ mag/$\square''$).

mization to individual SBP points: specifically, convergence is achieved through comparison of the theoretical R_i and μ_i for SL with η varying $0.3 \leq \eta \leq 8.0$ with the observed values. This set of multiple constraints yields a robust and unique solution for η, eliminating the risk of being trapped in local minima, as may occur with standard non-linear fitting algorithms whose best-fitting solution might depend on initial guesses and selection/weights of individual data points. Replacing them by robust (flux-enclosing) parameters leads to robust solutions. In this case the convergence criterion (ξ) is given by:

$$\begin{aligned} \Delta R_i &= (R_i^{\rm obs} - R_i^{\rm mod})^2 / R_i^{\rm mod} \\ \Delta\langle\mu_i\rangle &= (\langle\mu_i^{\rm obs}\rangle - \langle\mu_i^{\rm mod}\rangle)^2 / (1/\langle\mu_i^{\rm mod}\rangle) \\ \xi &= \sqrt{\sum \Delta R_i + \sum\langle\Delta\mu_i\rangle} \end{aligned} \tag{2.5}$$

where i stands for 20, 40, 50, 60, 80 & 90 percentages.

The η that produces the closest values between the theoretical and observed quantities (the absolute minimum ξ) is assumed to be the one that will correctly model the data.

4*b*. Estimating the Sérsic parameters for seeing convolved profiles: The code allows to recover the SL parameters from a SBP that is convolved by a Gaussian or Moffat (Moffat, 1969), the latter being described as

$$\begin{aligned} F_{\rm M}(R^\star) &= \left[1 + \left(R^\star \alpha_{\rm M}\right)^2\right]^{-\beta_{\rm M}} \\ \alpha_{\rm M} &= {\rm FWHM}(2\sqrt{2^{1/\beta_{\rm M}} - 1}) \end{aligned} \tag{2.6}$$

Additionally, iFIT allows for correction for user supplied PSF: if the user supplies a PSF, iFIT will determine the best fit parameters ($\alpha_{\rm M}$ & $\beta_{\rm M}$) for the Moffat equation by means of MINPACK (Moré et al., 1984), a publicly available set of subroutines that solves nonlinear least-squares problems using a modified version of the Levenberg-Marquardt algorithm. If, on the other hand, the user does not possess the model for the observed PSF, one might choose between a Moffat or Gaussian and render the FWHM ($''$) ($\beta_{\rm M}$ is assumed to be 4.765, Trujillo et al. 2001, in the Moffat case and ∞ for Gaussian).

Similar to the treatment of non-convolved SBPs, after having the parameters of the PSF, iFIT constructs a set of SBPs by varying η and subsequently convolving each one with the PSF. The procedure to find the correct η is the same as the one described in point **4***a* with the difference being that the synthetic SBPs whose characteristic flux-enclosing radii and mean surface brightness therein (see above) being used to constrain the best-fitting model are now PSF convolved. Another difference lies in eq. 2.5 – in the case of convolved data we implemented an extra term to facilitate quick convergence: as shown in Fig. 2.4, although the innermost points account for an almost negligible fraction of the total luminosity of a SL profile, they dominate in $\mu(\mathrm{R}^{\star})$. In practical terms this implies that especially at the high η range, the flux enclosed at R_{20} and at R_{40} are similar for different η. By introducing this single term, where it is compared the surface brightness at the first observed point ($\mu(\mathrm{R}_1)^{\mathrm{obs}}$) with the same for the model at the same radius ($\mu(\mathrm{R}_1)^{\mathrm{mod}}$), the algorithm is better stabilized avoiding convergence to an incorrect solution.

$$\begin{aligned} \Delta\mu(\mathrm{R}_1) &= (\mu(\mathrm{R}_1)^{\mathrm{obs}} - \mu(\mathrm{R}_1)^{\mathrm{mod}})^2/(1/\mu(\mathrm{R}_1)^{\mathrm{mod}}) \\ \xi &= \sqrt{\Delta\mu(\mathrm{R}_1) + \sum \Delta\mathrm{R}_i + \sum \Delta\langle\mu_i\rangle} \end{aligned} \tag{2.7}$$

The simple and novel concept of iFIT allows for a robust and quick estimation of the parameters of SL equation without the need of initial guesses or the computational expensive task of creating 2D images[3]. Due to its unique features, iFIT is best suited for the study of irregular galaxies (e.g., core-depleted ETGs, down-bending type II disks hosting a bulge, compact starburst galaxies surrounded by an extended nebular halo, BCDs and green peas) where significant deviations from the perfect SL 1D model are expected, therefore offering interesting prospects to be used in an automatic manner (e.g., without the need for an initial guess to SL model parameters, like in GALFIT/IMFIT, or a prior *training* on local galaxies, like in the case of convolutional neural networks, e.g., Huertas-Company et al., 2015, among others) to large galaxy samples (e.g., Euclid, Amiaux et al. 2012, the Large Synoptic Survey Telescope (LSST), Ivezić et al. 2008).

[3]We note that the 1D profile that iFIT requires can be computed by any 1D or 2D code. In the case of this study 1D profiles were computed by means of FIT/ELL3, a routine from ESO-MIDAS.

iFIT: pseudo-code illustrating the principal steps.

```
1  BEGIN PROGRAM
2  // Preparation of data to fit the SBP
3  Convert μ to intensities in arbitrary units;
4  TSPACK spline interpolation for intensity profiles (and their errors, if
     available);
5  Integrate fluxes
6  Compute R_i^obs & ⟨μ_i^obs⟩ for i = 20, 40, 50, 60, 80 & 90%
7  // Moffat, Gaussian or user-defined function
8  if PSF correction is activated then
9  |  Ignore first points within a radius of ~ 3×FWHM;
10 else
11 |  Use all profile data points;
12 end
13 // Linear regression of data to find R_eff & μ_eff
14 for η = 0.3 to 8 do
15 |  Linear regression to find R_eff & μ_eff;
16 end
17 // Fixing R_eff & μ_eff fit the SBP by comparing to observables
18 for η = 0.3 to 8 do
19 |  if PSF correction is activated then
20 |  |  Δμ(R_1) = (μ(R_1)^obs − μ(R_1)^mod)^2/(1/μ(R_1)^mod);
21 |  end
22 |  foreach i = 20, 40, 50, 60, 80 & 90% do
23 |  |  ΔR_i = (R_i^obs − R_i^mod)^2/R_i^mod;
24 |  |  Δ⟨μ_i⟩ = (⟨μ_i^obs⟩ − ⟨μ_i^mod⟩)^2/(1/⟨μ_i^mod⟩);
25 |  end
26 |  if PSF correction is activated then
27 |  |  ξ_η = √(Δμ(R_1) + ∑ ΔR_i + ∑ Δ⟨μ_i⟩);
28 |  else
29 |  |  ξ_η = √(∑ ΔR_i + ∑ Δ⟨μ_i⟩);
30 |  end
31 |  // Find best η and store mininum ξ
32 |  if ξ_η < ξ_min then
33 |  |  η_best = η;
34 |  |  ξ_min = ξ_η;
35 |  end
36 end
37 // iFIT Quality check
38 case ξ_min > 0.7 & error is available & First Run do
39 |  Repeat steps 8 to 29, but perform HWLR;
40 case ξ_min > 0.7 & error isavailable & Second Run do
41 |  Repeat steps 8 to 29, but perform WLR;
42 end
43 Retrieve output quantities and produce graph.
44 END PROGRAM
```

Figure 2.5: iFIT pseudo-code illustrating the principal steps

2.3.2 iFIT's accuracy assessment

In order to assess the ability of the code to recover the Sérsic model parameters we created an extended grid of synthetic profiles covering the relevant range $0.3 \leq \eta \leq 4.2$ and $1 \leq R_{eff} \leq 20$ in steps of 0.1 and $1''$, respectively. A second grid of synthetic profiles was created by convolving the above SBP set with Moffat PSF models with FWHM in the range between $0.5 \leq$ FWHM $('') \leq 2$ in steps of 0.5. Furthermore, these mock SBPs were truncated at the radius enclosing 90, 95 and 99% of the total luminosity in order to simulate different limiting $\mu(R_{max})$. The results are discussed in the following sections.

Testing iFIT with unconvolved synthetic data

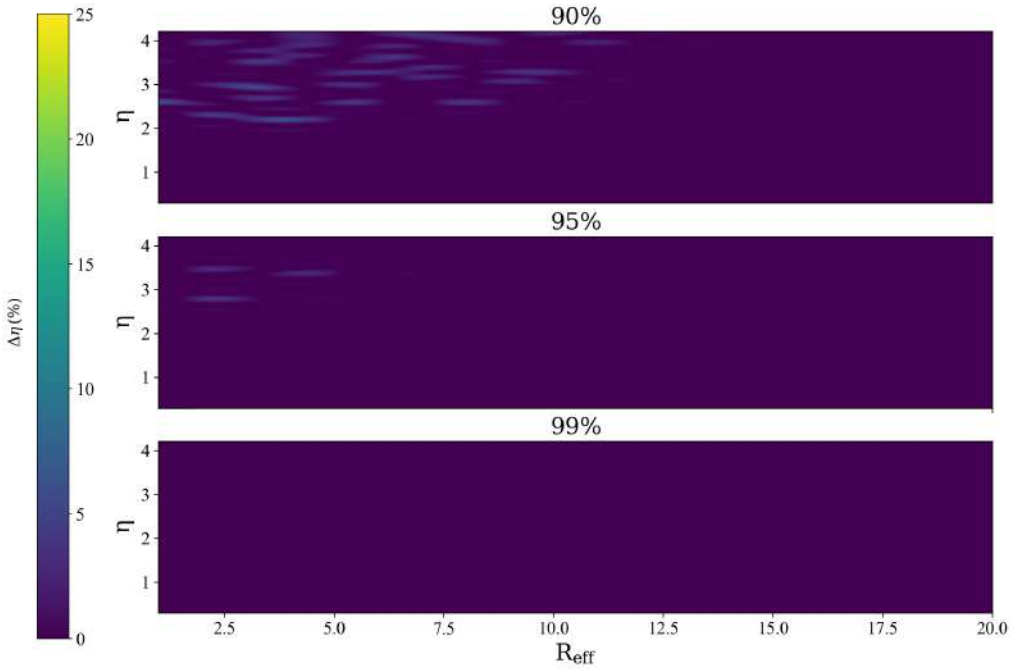

Figure 2.6: Percentual deviation between estimated and input η ($\Delta\eta$) as a function of η and effective radius R_{eff} ($''$) for the case of unconvolved Sérsic profiles encompassing 90% of the total luminosity (upper panel) 95% (middle panel) and 99% (lower panel). The left-hand vertical color bar corresponds to an absolute relative deviation between input and output Sérsic exponent $\Delta\eta = |\eta_{in} - \eta_{out}|/\eta_{in}$ between 0 and 25%.

Figure 2.6 illustrates the deviation between input and output η for the studied range in η and R_{eff}. We consider three cases, non-PSF-convolved Sérsic SBPs enclosing 90%, 95% and 99% of the total SBP luminosity. The bottom panel of the same Fig. demonstrates that, for perfect unconvolved Sérsic profiles containing 99% of the total SBP luminosity, the code recovers η over the entire considered parameter range with 0 absolute error. Absolute error of the order

of 0.1 is achieved for simulated shallow (90% & 95% of the total luminosity) SBPs.

Testing iFIT with convolved synthetic data

Obviously, the situation is far more challenging in the case of seeing-degraded Sérsic SBPs, where the ability of each code to retrieve the original η obviously depends on the degree of SBP degradation.

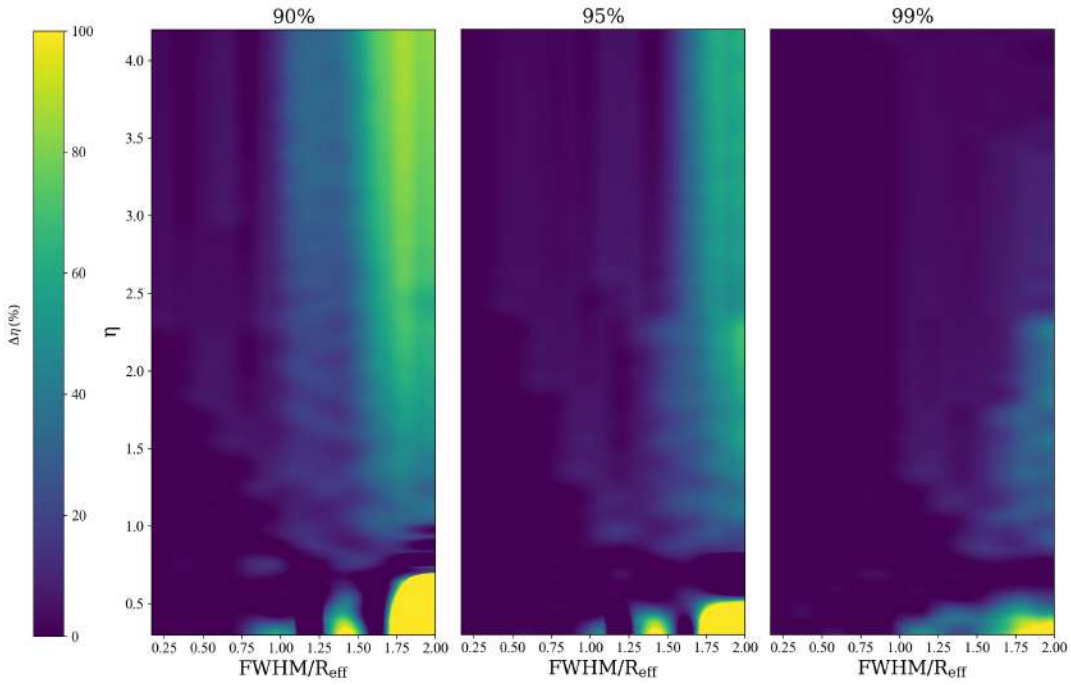

Figure 2.7: Percentual deviation between estimated and input η ($\Delta\eta$) as a function of η and FWHM/R_{eff} for the case of Sérsic SBPs reaching 90 (left pannel), 95 (middle panel) and 99% (right pannel) of the total luminosity after convolution with a Moffat PSF with $0.5 \leq$ FWHM ≤ 2 ($''$).

Figure 2.7 shows the results for synthetic SBPs covering the range $0.3 \leq \eta \leq 4.2$, $1 \leq R_{eff} \leq 3$ ($''$) and $1 \leq$ FWHM ≤ 2 ($''$) although we performed tests over all the R_{eff} parameter range between $1''$ and $20''$ (in range $3 \leq R_{eff} \leq 20$ ($''$), $1 \leq$ FWHM ≤ 3 ($''$), iFIT recovers η with a maximum absolute error of 0 (99%), 0.1 (95%) and 0.2 (90%)). Moreover it is depicted that even for SBPs that contain 99% of the total luminosity (right panel) there is a region in the parameter space where iFIT fails to recover the correct η (and consequently also R_{eff} & μ_{eff}), specially but not exclusively for very low η profiles. This happens for the region where FWHM/$R_{eff} >$ 1 showing that in order for iFIT to properly converge, the FWHM of the PSF must be lower than R_{eff}. In fact, a FWHM/$R_{eff} > 1$ is an extreme case of PSF degradation where SBPs become almost useless for fitting. This limit implies that for a pure disk, the FWHM is equal

to 1.7 exponential scale lengths, i.e., a major portion of the galactic disk is strongly affected by PSF convolution. In the even more extreme case of both strongly PSF-degraded and shallow SBPs, specifically when R_{max} is of the order of 3×FWHM, iFIT is unsurprisingly unable to correctly estimate R_{eff} & μ_{eff}, therefore also η (see Sect. 2.3.1, point **3.**). It is worth stressing that the simulated situation corresponds to studies of high-z galaxies whose SBP analyses are restricted to relatively bright rest-frame μ due to cosmological dimming, observed with, for instance, shallow SDSS data (FWHM $\sim 1.3''$) for compact higher-z galaxies. If however the same high-z galaxies are observed with HST (whose maximum FWHM $\sim 0.18''$) iFIT is able to properly recover the η within an absolute error lower than 0.1.

Testing iFIT on ETGs

iFIT was tested using 122 local ETGs observed by the Sloan Digital Sky Survey (SDSS, r-band photometry). The images were sky-subtracted, rotated to the astronomical orientation, corrected for Galactic extinction (the extinction in the SDSS bandpasses were adopted from NED and are based on the prescriptions by Schlafly & Finkbeiner, 2011) and, whenever necessary, corrected for foreground Galactic stars by substituting the projected area of contaminant MW stars by the mean intensity of the adjacent continuum. Finally, the frames were trimmed and the SBPs extracted from the 2D model computed by the function FIT/ELL3 (based on an algorithm by Bender & Möllenhoff, 1987) within the package SURFPHOT of the software ESO-MIDAS (the resulting errors are computed following Papaderos et al., 1996a). For each galaxy we used three different PSFs (three non-saturated stars extracted from the same frame as the galaxy). Although some PSFs fit with more accuracy than others the observed SBP in visual terms, it is not a main factor for the correct determination of the SL parameters, validating once again the robustness of the algorithm. Additionally, the analysis was repeated for 24 random galaxies of the sample without pre-reducing the images (they were not background subtracted, corrected for the presence of external light sources nor trimmed). By re-running iFIT on the supplementary SBPs we found that the algorithm does not depend greatly on the sky contribution (average difference of $\eta = 0.10$, $\sigma = 0.11$ & $R_{eff} = 1.60''$, $\sigma = 1.62''$).

Application of iFIT to irregular starburst galaxies

Irregular star-forming galaxies are omnipresent in the faraway Universe. Their structural analysis with standard tools poses a significant challenge given their clumpiness and asymmetry,

the absence of a geometrical center, and restricted limiting surface brightness ($\mu_{\rm lim}$) due to cosmological dimming. A robust determination of the best-fitting equivalent SL model is a crucial requirement for an automated characterization of this large galaxy population with future observing facilities, such as Euclid and LSST. Since, from the morphological and structural point of view, BCDs can be considered the best local analogs of unevolved galaxies at high-z, it is worth testing applications of iFIT to local BCDs falling into the four morphological types (iE, nE, iI/iI,C and i0) of the classification scheme by Loose & Thuan (1986a).

As an illustrative example, we show in Fig. 2.8 the SL model obtained with iFIT for the iE-BCD Henize 2-10, based on imaging data taken with the Danish 1.54m telescope at La Silla (see Papaderos & Fricke, 1998, for details). It can be seen that, iFIT yields for both B- and R-band data similar Sérsic model parameters, almost independently of the adopted $\mu_{\rm lim}$. The stability of the best-fitting SL solution with iFIT is to be contrasted with studies of BCDs with GALFIT, which, as pointed out by Amorín et al. (2007), show a strong dependence on the surface brightness interval considered. The robustness of SL model parameters with iFIT across optical passbands was further confirmed through fitting of g-, r- and i-band SDSS data for the sample of 122 ETGs. This has shown that the η exponent obtained for each galaxy in the three passbands displays a variation of typically less than 10%, which can be attributed to the distinctive concept of iFIT, in which the SL solution is constrained by flux-enclosing radii and their μ's rather than individual SBP data points. This is a significant advantage comparing with GALFIT – for the sample of 17 massive galaxies from dos Reis et al. 2019 (in prep.), GALFIT yields an average difference $|\eta_H - \eta_I|/\eta_H$ of ~ 0.38 whereas for the same sample iFIT returns 0.22. This issue is known and being addressed by different teams (e.g., the MegaMorph extension of GALFIT, Häußler et al., 2013) by forcing the η to smoothly vary across passband within a narrow, empirically estimated interval.

Another case is represented by I Zw 18, an extremely metal-poor BCD that is immersed within an extended nebular halo that contributes $\sim 1/3$ of its total R-band luminosity (Papaderos et al., 2002). As shown in Papaderos & Östlin (2012), the profile of this galaxy (SBP1) reflects the superposition of two nearly exponential components differing in their pseudo-scale length α and central surface brightness μ_0, namely the steep inner component that is primarily due to stellar emission and dominates down to ~ 24.5 mag/$\Box''$, and the surrounding shallower nebular envelope. The best-fitting η for the combined SBP depends on the limiting surface brightness of

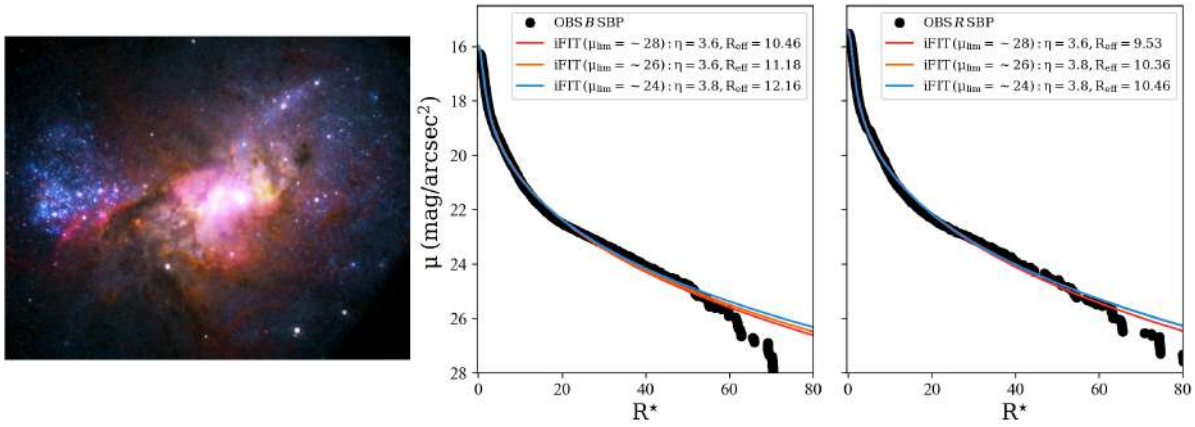

Figure 2.8: Left-hand side: BCD Henize 2-10 observed by Hubble (true-color image), Chandra (purple) and Very Large Array (yellow). Middle and right-hand side: fits with iFIT to the B (center) and R (right-hand side) bands. It can be seen that the Sérsic model parameters inferred in both bands are mutually consistent and show little dependence on the adopted $\mu_{\rm lim}$.

the data, being ~ 1.2 at a $\mu_{\rm lim} \leq 24.5$ and reaching a $\eta \sim 2$ for a $\mu_{\rm lim} \simeq 29$ (dashed gray curve in Fig. 2.9). Would the nebular envelope show a shallower profile at equal total luminosity (for instance, an α larger by a factor 2 and a μ_0 dimmer by 1.5 mag), then the best-fitting η for the resulting combined profile (SBP2) would increase to 2.5 for a $\mu_{\rm lim} = 26$ and reach a value of ~ 5 for a $\mu_{\rm lim} > 28$ (dashed-dotted gray curve in Fig. 2.9). In the latter case a marginally resolved distant morphological analog of I Zw 18 (e.g., a high-sSFR compact galaxy or quasar) could readily be misclassified as an ETG on the basis of SL fitting.

Repeated modeling of SBP1&2 with iFIT (Fig. 2.9) reveals a far weaker dependence of the SL solution on $\mu_{\rm lim}$: even for a $\mu_{\rm lim} \simeq 29$, the inferred η reaches maximal values of ~ 1.7 and ~ 2.5 for SBP1 and SBP2, respectively, faithfully reflecting the fact that $\sim 2/3$ of the total luminosity of the BCD originates from the steeper stellar emission-dominated inner exponential component.

2.3.3 Determination of the bulge radius

Considering that we do not attempt to categorize bulges into CB or PB, due to the high uncertainties associated with both the available recipes and the nature of these stellar entities (see Sect. 1.2.3), the relevant physical property that we want to estimate from the surface photometry is the bulge's radial extent. Using iFIT, this property was first determined at an extinction-corrected surface brightness level $\mu_{\rm lim}$ of 24 mag/$\Box''$ by fitting a Sérsic model to the

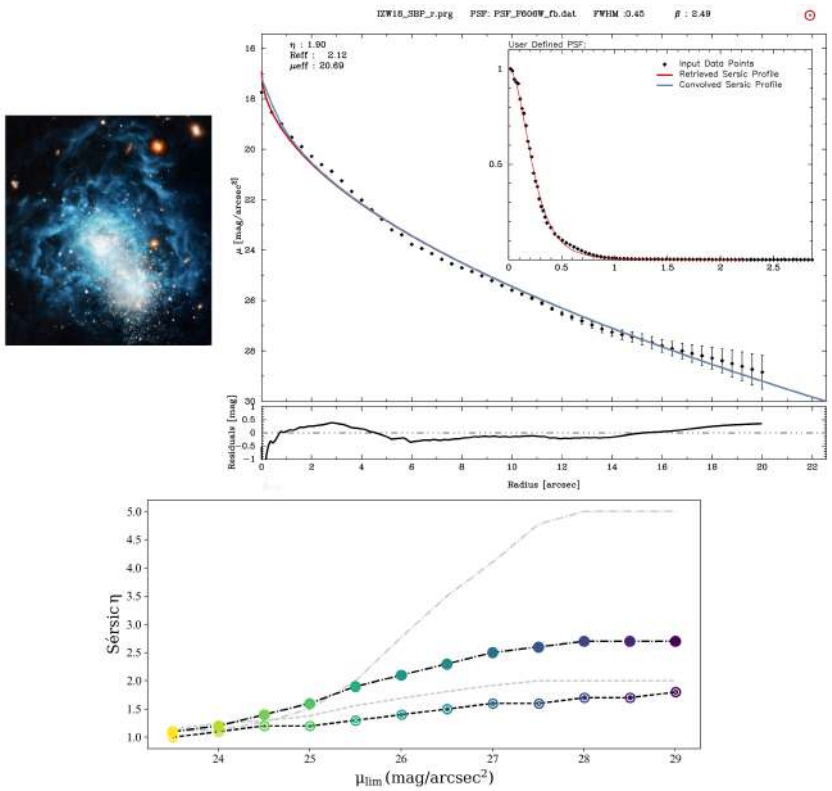

Figure 2.9: True color image of I Zw 18 obtained with HST (top panel, left-hand side) and fit with iFIT to the observed R-band stellar+nebular profile (SBP1) of I Zw 18 (blue) (top panel, right-hand side). In the bottom panel it is shown the best-fitting Sérsic index η vs. limiting surface brightness $\mu_{\rm lim}$ obtained by Papaderos & Östlin (2012) for SBP1 and SBP2 using standard χ^2 minimization (dashed and dashed-dotted curve, respectively). Open and filled circles show the result obtained with iFIT by modeling SBP1 and SBP2, respectively.

interactively selected central luminosity excess above the disk of SDSS r SBPs. Furthermore, we carried out the complete image decomposition. This step is integrated in a code that was developed in the ESO-MIDAS script language and which permits image decomposition into bulge and disk, and whenever meaningful an additional bar component. For approximately one third of the LTG sample, the results from our image decomposition tool with iFIT were compared with those from IMFIT and GALFIT, in order to estimate the dependence of R_B on different codes and profile fitting schemes. We found that performing full decomposition diminishes the bulge radius by 8% on average leading to no significant differences ($\leq$ 10%) in the quantities inferred from spectral modeling when compared to those inferred within the R_B from single Sérsic fits.

Figure 2.10 illustrates the minor difference between the isophotal radius of the bulge as obtained from a single Sérsic model and obtained by performing full bulge-bar-disk decomposition. It also

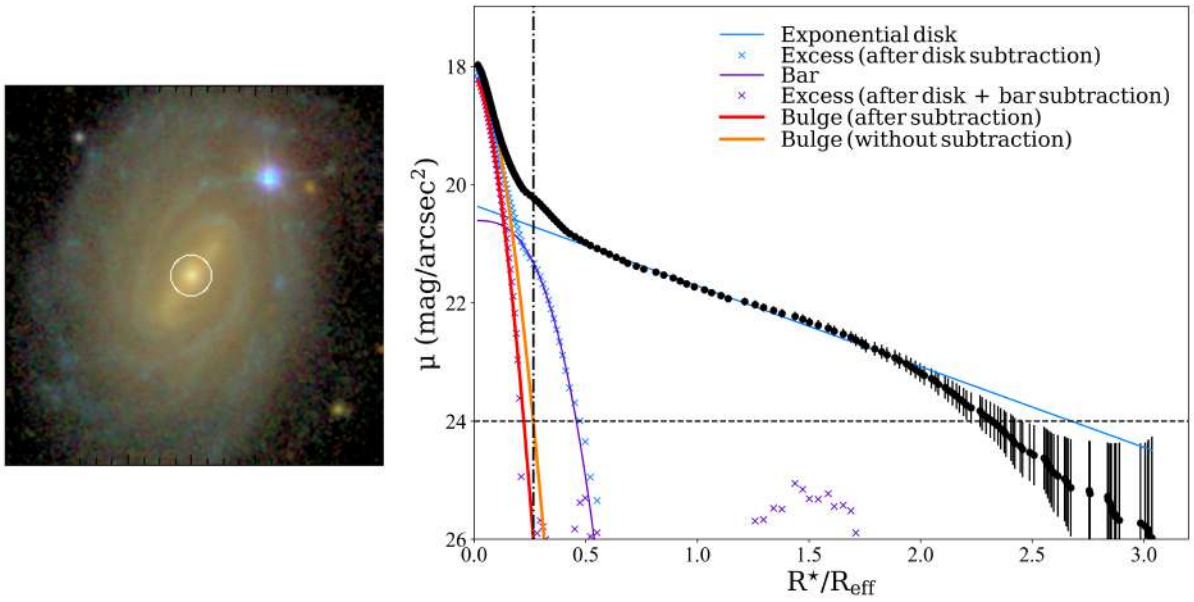

Figure 2.10: Left-hand side: true color image of the LTG NGC 0180 with the bulge diameter overplotted in white. Right-hand side: illustrative example of the performed 1D decomposition (using iFIT to model the bulge component) of the SDSS r-band SBP of the galaxy into bulge, bar and disk (red, magenta and blue, respectively). The bulge and bar are approximated by a Sérsic model, and disk by a pure exponential fitted to intermediate radii ($0.8 \leq \mathrm{R}^{\star}/\mathrm{R}_{\mathrm{eff}} \leq 1.8$, where $\mathrm{R}_{\mathrm{eff}}$ denotes the radius enclosing 50% of the total galaxy luminosity). The thick-orange curve shows a single Sérsic fit to the central luminosity excess owing to the bulge. It can be seen that its isophotal radius R_{B} at $\mu = 24$ mag/$\square''$ (dashed-dotted vertical line) determined from a single-Sérsic model closely matches the one read off the figure for the case of full bulge-bar-disk decomposition.

emphasizes that automated fitting of a pure exponential to the down-bending (type II) profile of the disk would overestimate its central surface brightness and underestimate its scale length α, leading to an underestimation of the excess emission from the bulge, and a false determination of its total magnitude, isophotal radius and Sérsic parameters. For this particular case the correct approach would be, either to model the disk with a modified exponential distribution (for example, the fitting function proposed in Papaderos et al., 1996a), or to interactively select and fit the inner exponential part of the disk ($0.8 \leq \mathrm{R}^{\star}/\mathrm{R}_{\mathrm{eff}} \leq 1.8$), as we adopted (light-blue line in Fig. 2.10). It is also apparent from the SDSS true color image and SBP that this galaxy hosts a bar component (weak bump at $20 \leq \mu$ (r mag/$\square''$) ≤ 21). Neglecting the bar 1D/2D decomposition could systematically affect the Sérsic fits to the excess emission above the disk (open blue crosses), which encompasses the more extended lower-surface brightness outskirts from the bar, leading to overestimation of η and possibly move a PB into the region that defines CBs. This might be one of the reasons for the observed scatter in any relation between η and other galaxy parameters (for example, bulge $\sigma_{\star}$, M_r, or mean surface brightness). Additionally

and more importantly, it is unclear whether the exponential disk conserves its pure exponential nature to the center of the galaxy (see Sects. 1.2.3 & 2.4.6).

Given the negligible differences when adopting the different methods, to ensure that the evolutionary and spectroscopic properties of bulges are obtained within a radius based on a uniform, clear-cut definition, we decided to adopt the simpler approach of determining R_B from fitting a single Sérsic model to the central luminosity excess upon visual inspection of the morphology and $(g-i)$ color maps of our LTG sample, eliminating the need for strong prior assumptions on the photometric structure of LTGs that might dictate the results and subsequent conclusions. By visually inspecting the true color images overplotted with a circle that represents the estimated R_B we concluded that this method provides accurate results.

2.3.4 Computation of color maps and profiles

The color of galaxies is one of the most simple ways to discern the evolutionary stage of the galaxy or galactic stellar component. It is well known that galaxy colors correlate with luminosity (which, in certain bands, is a proxy to stellar mass), galaxy type, morphology and environment (e.g., Blanton et al., 2003; Conselice, 2006; Strateva et al., 2001): on the color-magnitude diagram (Bell et al., 2004), early-type spheroidal galaxies that are usually found in high-density regions commonly belong to the *red sequence*, whereas late-type disk galaxies, mainly residing in low density environments, populate the *blue cloud* (e.g., Holmberg, 1958; Roberts & Haynes, 1994). This correlation reflects the fact that broadband colors are tightly coupled with the age (consequently, also the effective temperature) of the stellar population that dominates the UV-NIR SED of a galaxy. The observed optical colors of a galaxy are related to a combination of processes which include the galaxy's SFH (galaxy colors are strongly affected by the colors of the youngest stellar populations, hence by the SFH, de Jong 1996a) stellar initial mass function (IMF – it has a direct effect on the colors of SF galaxies (Conroy, Gunn & White, 2009) which in turn will affect its SFHs) chemical evolution and/or dust reddening and extinction (the presence of dust introduces a systematic bias translated into reddening and extinction from the ultraviolet (UV) to infra-red (IR), Draine 2003) which hampers their straight forward interpretation. Additionally, age and metallicity effects might produce very similar colors due to the age-metallicity degeneracy (AMD) (two unresolved galaxy's spectra, one composed of stellar populations three times older but half metallicity of the other, are practically indistinguishable, Worthey et al. 1994). Due to all the uncertainties associated with

the modeling of the intrinsic extinction in disk galaxies (e.g., should we consider the intrinsic extinction determined for the stellar or for the ionized gas component? How do these two differ from one another?) and the cumulative observational evidence strongly suggesting that dust extinction cannot be the driver of the measured colors and color gradients (de Jong, 1996b,c; Lian, Blanton & Kong, 2017), we decided to not correct for intrinsic extinction due to dust, but only for Galactic foreground extinction.

Although it is not clear how to disentangle between age and metallicity in the color-color or color-magnitude diagrams (O'Connell 1996 shows that by using only a few broad band colors it is not possible to break the AMD), it is well established that galaxy colors can be used as a tracer of the galaxy evolutionary stage. For this reason we considered meaningful to estimate bulge and disk colors and bulge color gradients using the available photometric SDSS data. After a complete pre-reduction of the photometric data, $(g-r)$, $(g-i)$ & $(r-i)$ color maps were computed by means of (for example for the 1st case):

$$(g-r) = -2.5\log_{10}(g/r) + (CC_g - CC_r) + (Ge_r - Ge_g), \tag{2.8}$$

where CC_g & CC_r are the calibration constants for each filter previously computed and Ge_g & Ge_r is the foreground Galactic extinction in each band.

Colors for the bulge component were computed using two different methods: $1^{\rm st}$ by performing statistics directly in the color maps (top panel of Fig. 2.11 shows an example of produced $(g-r)$, $(g-i)$ & $(r-i)$ color maps) and $2^{\rm nd}$ by subtraction of the respective SBPs of each filter (example illustrated by lower-panel of Fig. 2.11). The differences between methods are not significant lying below 0.1 mag. Furthermore, bulge and disk color gradients were computed by fitting a linear relation within the bulge/disk radial extent (for the results to be comparable with the ones obtained by analysis of the retrieved SFHs from IFS data, the linear relation was fitted using the same radial limits used for the computation of age gradients; see Sect. 2.4.1). Obtained results and subsequent discussion can be found in Sect. 3.2.

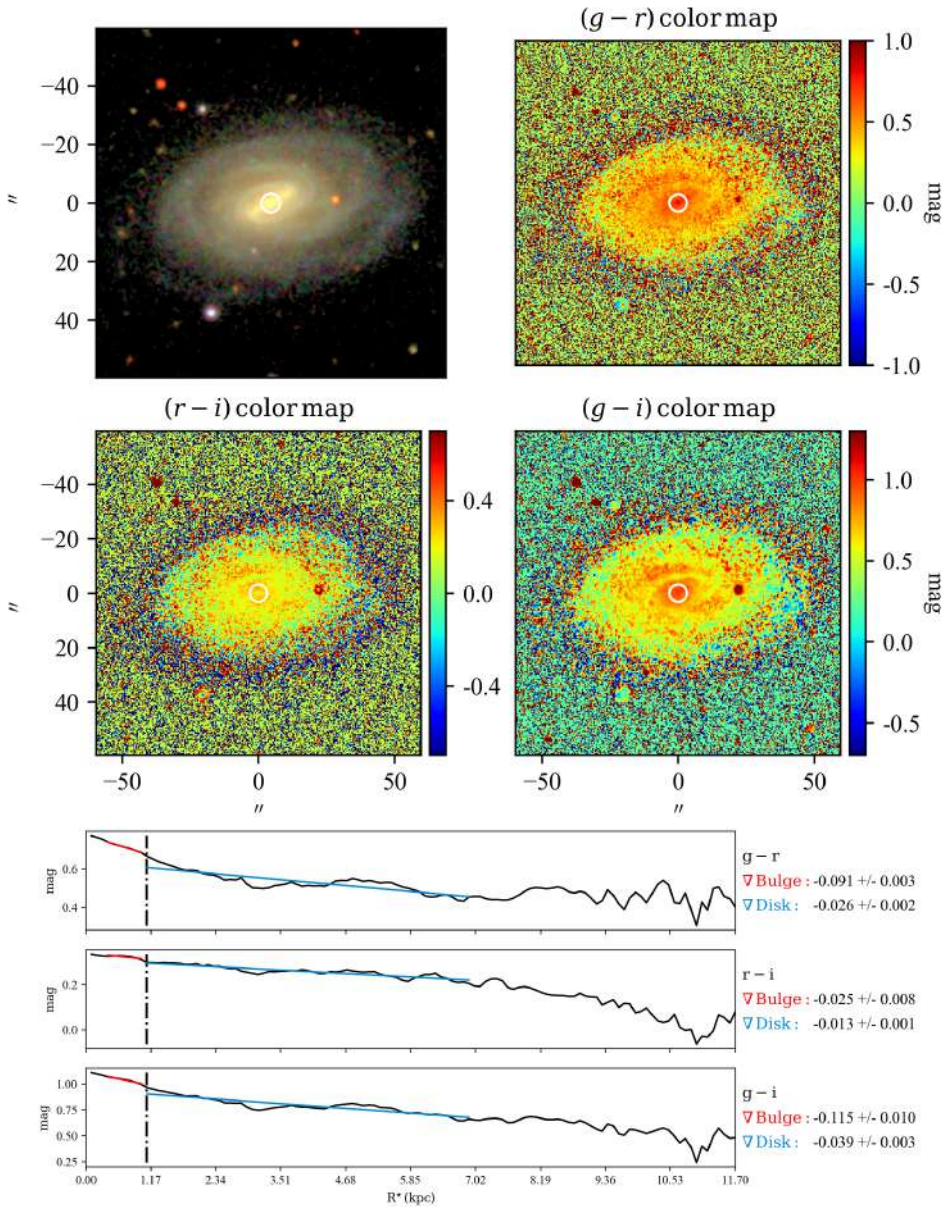

Figure 2.11: Top-panel: true-color image of NGC1093 (top-left), PSF-equalized $(g-r)$ color map (top-right), PSF-equalized $(r-i)$ color map (bottom-left) and PSF-equalized $(g-i)$ color map (bottom-right). The bulge's radial extent is depicted in the images by the overplotted white circle. Bottom-panel: respective radial color profiles.

2.4 Analysis of integral field spectroscopy data for the galaxy sample

As mentioned before, this combined structural (photometric) and IFS spectral modeling study is a key advantage. Besides the structural analysis performed mainly on SDSS r-band images, we carried out spatially resolved spectral modeling of the CALIFA V500 data using STARLIGHT

(Cid Fernandes et al., 2005). Additionally we performed for the first time the spaxel-by-spaxel post-processing of the spectral synthesis output with the code RemoveYoung ($\mathcal{RY}$; Gomes & Papaderos, 2016) aiming for a quantitative study of the contribution of stellar populations older than 9 Gyr ($\sim 2/3$ of the age of the Universe) to the optical surface brightness and $\Sigma_\star$ of both bulge and disk. Additional quantities like spatially resolved gas-phase metallicity were estimated using several recipes based on the strong line methods.

Moreover, the analysis was extended to include a comparison with the new PSS code FADO (Gomes & Papaderos, 2017). Due to the substantial investment in CPU time needed for spaxel-by-spaxel spectral fitting, it was necessary to fit binned spectra within irregular isophotal annuli (**isan**), which were defined by using an IFS-implementation of the **isan** surface photometry technique by Papaderos et al. (2002).

Finally, motivated by uncertainties described in Sect. 1.2.3, we developed a tool that permits to spectroscopically subtract the disk contribution from the central emission of the galaxy, this way obtaining the net-bulge spectra. This complex procedure permits to examine the legitimacy of the universal assumption of conservation of the exponential nature of the disk within the bulge extent and explore the validity of different disk configurations.

2.4.1 Spatial resolved spectral modeling of CALIFA IFS data with Starlight

Spectral modeling of low resolution ($\lambda/\Delta\lambda \sim 6.5$ at ~ 5000 Å) CALIFA IFS data taken with the Potsdam Multi-Aperture Spectrometer (PMAS; Roth et al., 2005) in its PPaK mode (Kelz et al., 2006; Verheijen et al., 2004) with the V500 grating, and reduced as described in García-Benito et al. (2015, and references therein) was carried out with our pipeline Porto3D (Gomes et al., 2016a; Papaderos et al., 2013, for details). Spectral fits were computed with the PSS code Starlight (Cid Fernandes et al., 2005) in the spectral range between 3900 and 6800 Å using a library of 152 SSPs spectra and an additional one of 190 SSPs. The first library (hereafter Z4) comprises SSPs from Bruzual & Charlot (2003) for 38 ages between 1 Myr and 13 Gyr for four stellar metallicities (0.05, 0.2, 0.4 and 1.0 $Z_\odot$), referring to a Salpeter IMF (Salpeter, 1955) and Padova 2000 tracks (Girardi et al., 2000). The second library (hereafter Z5) is identical to Z4 in terms of age coverage except for being supplemented by SSPs with a metallicity of 1.5 $Z_\odot$. The modeling was repeated for a subset of the data using combined V500 and V1200

(COMB)[4] CALIFA data covering the spectral range between 3700 and 7300 Å aiming to assess the dependence of the results on the considered spectral range. We found that the obtained differences (> 0.2 dex in $\mathcal{M}_\star$) are within the typical uncertainties expected from PSS modeling with STARLIGHT (Cid Fernandes et al., 2014). Although the galaxy sample was completely processed with both SSP libraries and throughout the document it is presented the results obtained with both, we decided to adopt as main results the determinations based on the Z4 SSP library. Even though this choice might entail a potential saturation of $Z_\star$ at $Z_\odot$, it may be expected that, in the presence of the AMD, a narrowing-down of the SSP metallicity space has the advantage of tighter estimates on $t_\star$, in which, in this study, we give more emphasis to as compared to the stellar metallicity. Additionally, it might be conjectured that the occupancy of the full available metallicity space in Z5 fits might be partly driven by the mathematical foundation of state-of-the-art PSS codes, thus in itself no effective evidence for a significantly over-solar mass-weighted stellar metallicity. For example, whereas the light-weighted metallicity ($Z_{\star\mathcal{L}}$) reflects the young and probably more metal-enriched stellar component (in agreement with super-solar determinations for massive galaxy spheroids from, for example, luminosity-weighted Lick indices), the mass-weighted ($Z_{\star\mathcal{M}}$) predominantly reflects the older, high mass-to-light ratio stellar component that had less time for its chemical self-enrichment. Therefore, an inequality between these two quantities, where $Z_{\star\mathcal{M}} \leq Z_{\star\mathcal{L}}$ appears plausible from the evolutionary point of view. More generally, it is noteworthy that the AMD and other potential sources of degeneracy (e.g., between $Z_\star$ and $\sigma_\star$, cf. Koleva et al., 2008) within the complexity of non-linearly coupled parameters in current PSS models, have not been fully addressed so far, making admissible to adopt a conservative limitation of the $Z_\star$. Moreover, due to a possible contribution by the disk to the integral SED within R_B, we give preference to mass-weighted quantities determinations which are dominated by the old stellar component, being robust against young (< 0.1 Gyr) stellar populations that typically dominate the light despite their very low $\mathcal{M}_\star$ fraction. Additionally, if the bulge is indeed a composition of bulge plus the contribution of an exponential disk, by adopting mass-weighted determinations it is expected to mitigate the effect of the disk, which is characterized by a higher fraction of young stellar populations.

Several quantities of interest, including the present-day and ever formed $\mathcal{M}_\star$ ($M_\odot$), mass-weighted stellar age ($t_{\star\mathcal{M}}$, Gyr) and metallicity ($Z_{\star\mathcal{M}}$, $Z_\odot$), and their luminosity-weighted values ($t_{\star\mathcal{L}}$ and $Z_{\star\mathcal{L}}$), stellar mass surface density ($\Sigma_\star$ in units of $M_\odot/\mathrm{kpc}^2$), the time when

[4]We note that CALIFA DR3 provides COMB data for 97 out of 135 galaxies from our sample

50% of the present-day $\mathcal{M}_\star$ was in place, the light and mass-fraction of stellar populations younger than 0.1, 1 and 5 Gyr, as well as emission-line fluxes and respective EWs, and stellar and ionized-gas velocity maps (see Gomes et al., 2016a, for details) are computed by Porto3D. The spatially resolved maps of the aforementioned quantities produced by Porto3D were in turn converted into radial profiles using an adaptation of **isan** surface photometry technique by Papaderos et al. (2002). This method (e.g., Gomes et al., 2016a; Kehrig et al., 2012; Papaderos et al., 2013) allows to compute statistics within logarithmically equidistant isophotal zones defined from a reference image (in this case, the emission-line-free pseudo-continuum between 6390 and 6490 Å). Using this technique, the galaxies were segmented into 18 isophotal zones. The algorithm permits to trace the galaxy morphology at all surface brightness levels, without the need for prior assumptions on galaxy structure usually made in 1D/2D surface photometry techniques (common assumptions such as approximation of a galaxy as due to the superposition of axis-symmetric components, or profile derivation within elliptical annuli with constant ellipticity and position angle), this way correctly determining the galaxy's SBPs even for irregular galaxies (see also, e.g., Noeske et al., 2003).

To ensure that average values within R_B are not biased towards a group of data points that might be eventually more densely spaced in radius, **isan** determinations were cubic-spline-interpolated to a finer radius step. Figure 2.12 presents normalized radial profiles of some quantities of interest as an example. It is shown, from top to bottom, the radial distribution of the enclosed present-day stellar mass $\mathcal{M}_\star$, the logarithm of the stellar surface density ($\log(\Sigma_{\star,B})$), mass- and light-weighted stellar age ($t_{\star\mathcal{M}}$ and $t_{\star\mathcal{L}}$, respectively) in Gyr, mass- and light-weighted stellar metallicity ($Z_{\star\mathcal{M}}$ and $Z_{\star\mathcal{M}}$, respectively) in $Z_\odot$. The grey dots mark the average value within each **isan** and the black solid line the respective spline-interpolation.

Arithmetic average values for all the quantities of interest within R_B and R_D (R_D is defined to be the radial extent between R_B and the radius of the 14th **isan**[5] which, throughout the sample has an average value of $\mu = 23.6$ mag/$\square''$) were computed from the splined interpolated radial profiles and additionally by performing statistics directly on 2D maps within the isophote corresponding to R_B (the two methods produce very similar results with an overall difference lower than 10%). The present stellar mass of the bulge ($\mathcal{M}_{\star,B}$) was computed by

[5]We decided to exclude the last 4 zones from the analysis due to the decreasing μ, and consequently decreasing signal-to-noise ratio (S/N), of the outermost spaxels.

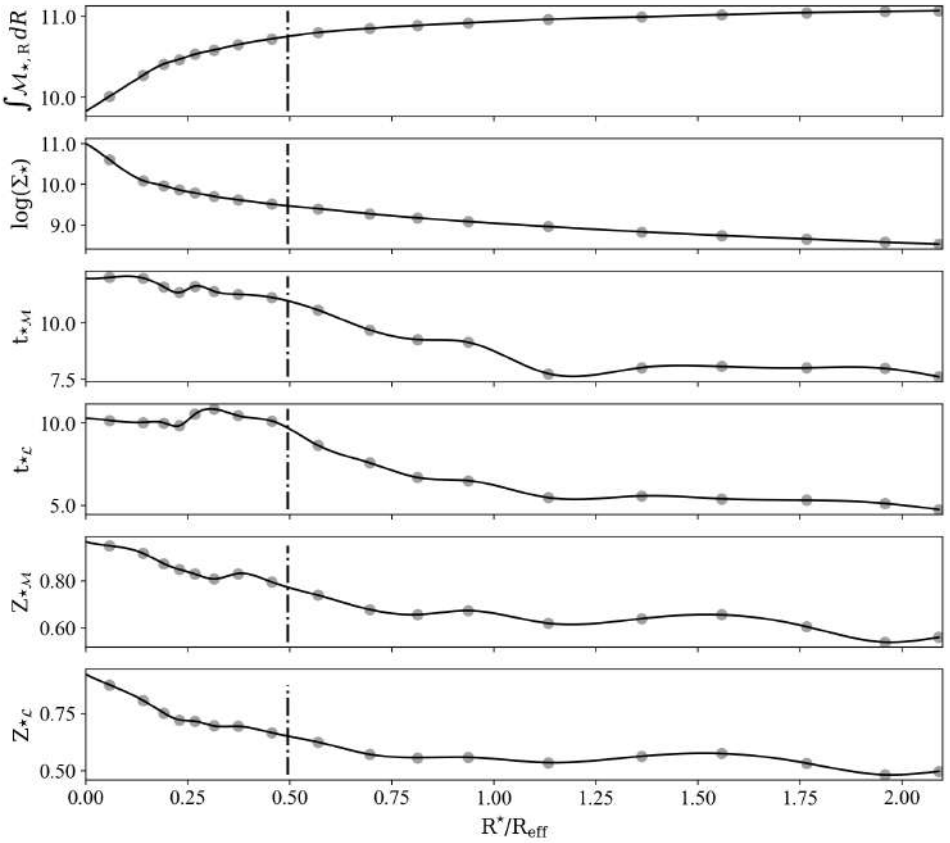

Figure 2.12: Radial profiles for various quantities obtained for NGC 0776 with the **isan** technique and auxiliary codes for spline interpolation and statistical analysis. From top to bottom the panels show: i) the enclosed present-day stellar mass $\mathcal{M}_\star$, ii) a logarithmic representation of the stellar surface density $\Sigma_\star$ in $M_\odot/kpc^2$, iii&iv) the mass- and light-weighted stellar age in Gyr, v&iv) the mass- and light-weighted stellar metallicity in $Z_\odot$. All are functions of the photometric radius $R^\star$ normalized to the effective radius R_{eff}. The bulge radius R_B is depicted by the vertical dashed line.

integrating $\mathcal{M}_\star$ profiles out to R_B. In order to complement the insights obtained with regard to the mean age and metallicity of both bulge and disk, we performed an additional analysis of age and metallicity gradients within R_B and R_D, shedding extra light on how age and metallicity change within the different stellar components. For this purpose, linear relations in the radial profiles of both mass- and light-weighted age and metallicity are fitted for $R^\star \leq R_B$ and $R_B < R^\star < R_D$ as partially illustrated in Fig. 2.13.

Subsequently, the obtained age and metallicity gradients within the bulge were multiplied by R_B (kpc) obtaining the gradients normalized by the bulge radial extent. Section 3.3.5 is dedicated to the presentation and discussion of the obtained results.

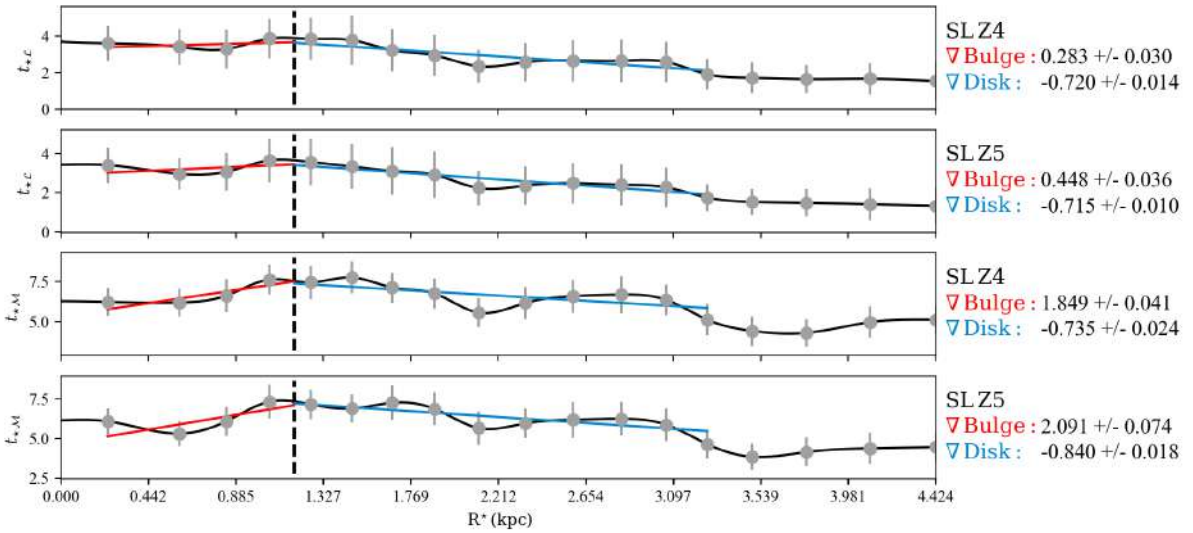

Figure 2.13: Example of radial profiles of mass- and light-weighted ages as obtained by the spaxel-by-spaxel analysis with Starlight for both libraries Z4 & Z5 for the galaxy MCG +09-22-053. The right-hand side of the diagrams is labeled with the slopes of the linear fits for each profile for both bulge and disk (Gyr/kpc).

2.4.2 Derivation of gas-phase metallicities

Using spectroscopic data, 2D gas-phase metallicity (Z_g) maps were determined with a variety of methods. Since for most of the CALIFA galaxies the [OIII]4363 Å emission line has a very low S/N it is not possible to accurately determine Z_g using the direct T_e method (Osterbrock, 1989). For this reason, various widely used semi-empirical methods were applied: strong line methods (Marino et al., 2013; Pettini & Pagel, 2004) as well as the method devised by Pérez-Montero (2014) which estimates the oxygen abundance (commonly used indicator of the gas-phase metallicity) from a set of optical emission-line intensities consistent with the direct method. To achieve this goal, a code was developed for the spaxel-by-spaxel computation of Z_g with the Pettini & Pagel (2004) calibration and an IFS adaptation of the Python program from Pérez-Montero (2014). It should be noted that all the above calibrations were established for classical HII regions, i.e. their validity for the intra-HII region diffuse ionized gas component is uncertain.

Figure 2.14 shows the gas-phase metallicity distribution of the galaxy NGC 5480 computed with four different methods: Pettini & Pagel (2004), methods N2 and O3N2, Marino et al. (2013) and Pérez-Montero (2014), respectively. As apparent from this Fig. the results can vary substantially from method to method. Some extreme values (like 9.71 for the (Pettini & Pagel, 2004), N2 calibration, which is $\sim$ 1 dex above solar metallicity) can be found in the periphery

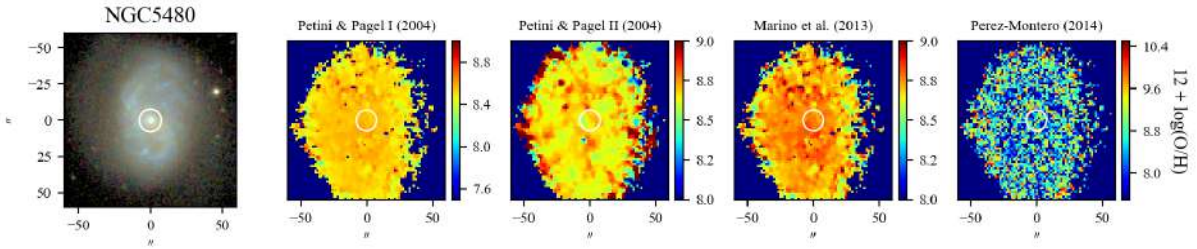

Figure 2.14: Example of the oxygen abundance distribution 12+log(O/H) obtained from four empirical methods for the galaxy NGC 5480 (true-color image at the left-side panel). The following panels show determinations after Pettini & Pagel (2004), methods N2 and O3N2, respectively, Marino et al. (2013) and Pérez-Montero (2014).

of the galaxy where the S/N might be insufficient to robustly estimate Z_g. For this reason, and for the observed significant changes on the slope of obtained correlations between Z_g and, for instance, total stellar mass or mass-weighted stellar metallicity, we concluded that the tested methods are not reliable enough to obtain unambiguous information on Z_g and as consequence they were put aside in the forthcoming analysis.

2.4.3 Post-processing of the spectral synthesis output with REMOVEYOUNG

REMOVEYOUNG ($\mathcal{RY}$; Gomes & Papaderos, 2016) is a tool that permits to spectroscopically subtract the light and mass contributions of stellar populations older than a user defined age (hereafter $t_{\rm cut}$). It works by analyzing the population vector (PV; i.e., the best-fitting combination of the fractional contributions of individual SSPs) obtained after modeling a spectrum with a PSS code (e.g., STARLIGHT, FADO), computing the synthetic spectrum, magnitudes in different filters (e.g., SDSS u, g, r, i, z) and the stellar mass of the older stellar component. By applying $\mathcal{RY}$ to the spatially resolved spectral synthesis output from PORTO3D for eight $t_{\rm cut}$ values (0.03, 0.1, 0.3, 1, 3, 5, 7 and 9 Gyr) we produced synthetic images of the underlying older stellar background in various photometric bands ($\mathcal{RY}$ convolves the residual SED with the filter transmission functions) and maps of the stellar mass for the different aforementioned $t_{\rm cut}$ values. In turn, by applying the **isan** method as described in the previous Sect., we constructed 1D radial profiles tracing the light and mass contributions of the different stellar populations that compose the galaxy. Figure 2.15 illustrates the application of $\mathcal{RY}$ on three LTGs from our sample. The synthetic r band SBPs for the eight adopted age cutoffs are shown color coded. SBPs labeled "r SDSS" were obtained for a $t_{\rm cut} = 0$ Gyr, that is, through convolution of the *observed* IFS data cubes with the SDSS r band transmission curve. For comparison, we overlay the r band SBPs obtained from SDSS images (light-gray curves labeled "OBS r SDSS"),

which due to their better resolution (FWHM $\sim 1.3''$ as compared to $\sim 2.6''$ for CALIFA IFS data) trace better the central luminosity peak of the bulge. The output from $\mathcal{RY}$ allowed us to compute the difference $\mu_{0\,\mathrm{Gyr}} - \mu_{9\,\mathrm{Gyr}}$ where $\mu_{0\,\mathrm{Gyr}}$ and $\mu_{9\,\mathrm{Gyr}}$ correspond to the synthetic r-band SBP of each LTG for a t_{cut} of 0 and 9 Gyr, respectively. The arithmetic average of this quantity within $\mathrm{R_B}$ is referred to in the following as $<\delta\mu_{9\mathrm{G}}>$ (mag).

Figure 2.15 displays three characteristic snapshots in a sequence of increasing total $\mathcal{M}_\star$ and bulge $<\delta\mu_{9\mathrm{G}}>$. It illustrates that although the three LTGs display a considerable (> 1.5 mag) surface brightness dimming with increasing t_{cut} in the disk ($\mathrm{R}^\star \geq \mathrm{R_B}$), indicating its progressive build-up in the last 9 Gyr, the bulge's $<\delta\mu_{9\mathrm{G}}>$ spans a broad range between ~ 0 and $\sim$ -4 mag ($<\delta\mu_{9\mathrm{G}}>= 0$ mag corresponds to the case where stellar populations with age ≥ 9 Gyr entirely dominate the r-band surface brightness within $\mathrm{R_B}$, whereas a $<\delta\mu_{9\mathrm{G}}>$ of -4 mag translates into a contribution of $\sim 3\%$ by this old stellar component).

The sample was then subdivided into intervals according to their $<\delta\mu_{9\mathrm{G}}>$ (see. left panel of Fig. 2.16) – interval **iA** (34 galaxies): $<\delta\mu_{9\mathrm{G}}> \leq$ -1.5 mag; these are almost bulgeless LTGs (e.g., IC 0776), with a practically uniform dimming in μ with increasing t_{cut} throughout the galaxy's radial extent, which is consistent with a nearly homologous growth of $\Sigma_\star$ – interval **iB** (58 galaxies): -1.5 $< <\delta\mu_{9\mathrm{G}}> <$ -0.5; intermediate galaxies (e.g., NGC 0001) that display a significant contribution from stars younger than 9 Gyr to the bulge luminosity but not as considerable as in **iA** galaxies – interval **iC** (43 galaxies): $<\delta\mu_{9\mathrm{G}}> \geq$ -0.5 mag; LTGs whose bulge is mainly constituted by old stellar populations with no significant SF occurring over the past 9 Gyr. This color scheme and classification will be used throughout the document referring always to the spatially resolved results obtained by using Starlight with the SSP library Z4 unless mentioned otherwise.

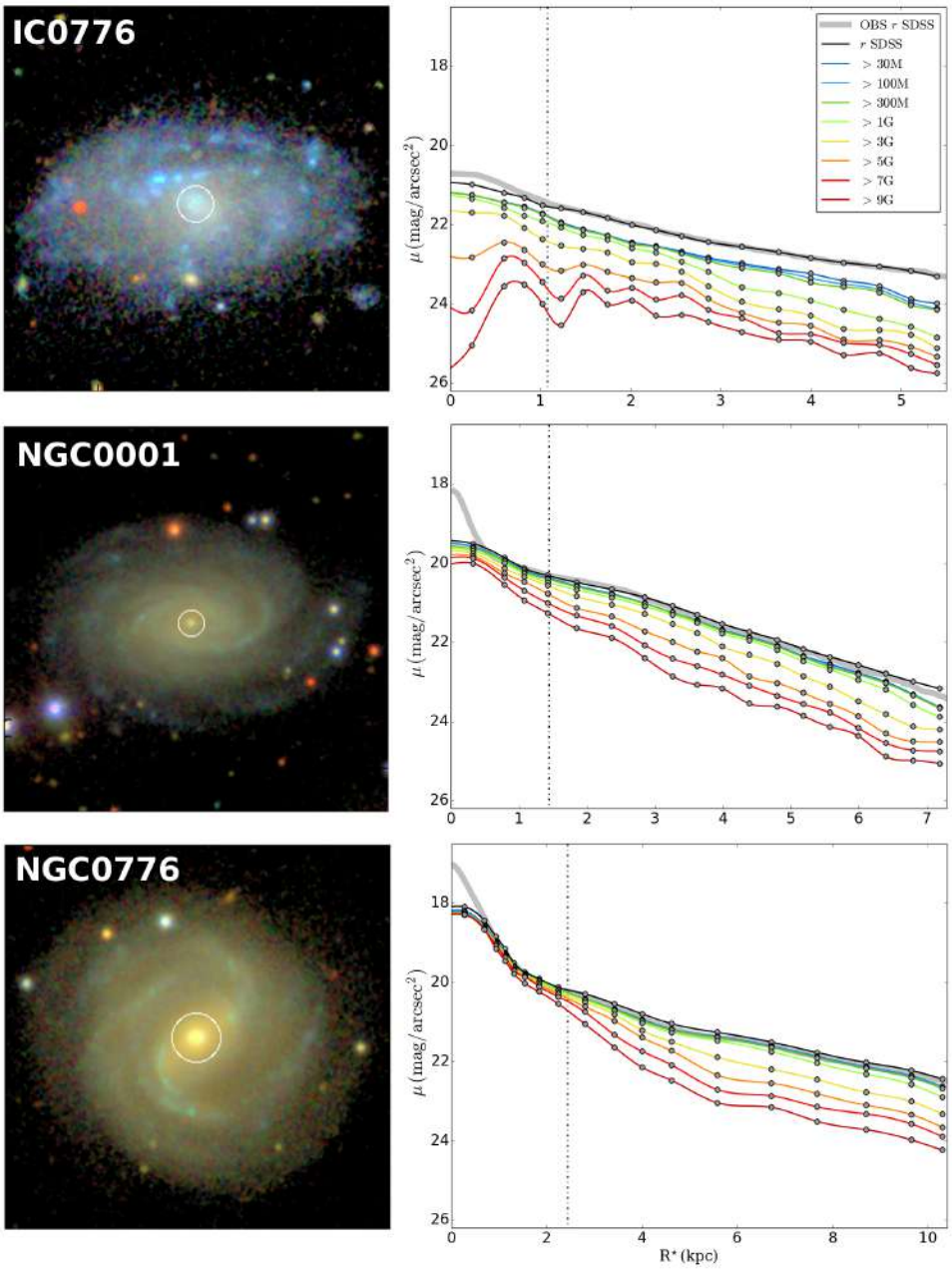

Figure 2.15: SDSS true-color images and SBPs (left- and right-side panel, respectively) for three LTGs illustrating the prominence of the bulge relatively to the disk: IC 0776 ($\log(\mathcal{M}_{\star,\mathrm{T}}) = 9.58$; interval **iA**), NGC 0001 ($\log(\mathcal{M}_{\star,\mathrm{T}}) = 10.99$; interval **iB**) and NGC 0776 ($\log(\mathcal{M}_{\star,\mathrm{T}}) = 11.09$; interval **iC**). Synthetic SBPs computed through convolution of the observed IFS data with the SDSS r-band filter transmission curve are shown in black, and those after removal with $\mathcal{RY}$ of stellar populations younger than 0.03, 0.1, 0.3, 1, 3, 5, 7 and 9 Gyr with the color coding in the upper-right panel. Thick-gray curves depict r-band SBPs computed from SDSS images and used for fitting a Sérsic model to infer the bulge radius $\mathrm{R_B}$ (dashed vertical lines). The circles overlaid with SDSS images depict the bulge diameter.

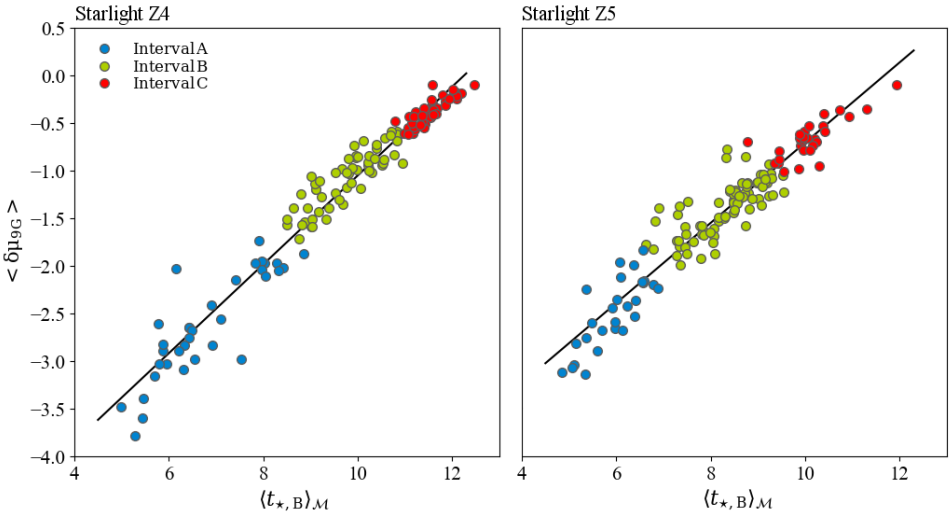

Figure 2.16: $<\delta\mu_{9G}>$ (r mag) vs. mass-weighted stellar age $\langle t_{\star,B}\rangle_{\mathcal{M}}$ (Gyr) for the bulge component of our sample LTGs obtained by spaxel-by-spaxel analysis with Starlight adopting lib. Z4 (left panel) & lib. Z5 (right panel). The solid line shows a linear fit to the data.

We verified that this quantity, first introduced by this study, tightly correlates with all the bulge's fundamental properties, offering a simple, distance- and formally extinction-independent proxy to the evolutionary and physical properties of LTG bulges.

2.4.4 Classification of LTG bulges according to their spectroscopic activity

Luminosity-weighted emission-line ratios within R_B, therefore free from aperture biases, were estimated across a relevant range in bulge $\mathcal{M}_\star$ and $\Sigma_\star$ by using a combination of methods. First, emission-line maps were determined by Porto3D by spaxel-by-spaxel subtraction of the best-fitting stellar model. From these maps we determined the fluxes and EW of the four emission lines ([OIII]5007, Hβ, [NII]6584 and Hα) used for spectroscopic classification in the optical BPT diagram.

In areas with weak nebular emission, hydrogen Balmer lines embedded within broader stellar absorption profiles might be strongly underestimated when measured with standard line fitting techniques. For this reason, an accurate continuum subtraction is mandatory for a correct spectroscopic classification. As pointed out in Petropoulou et al. (2011), weak nebular emission spaxels might have its [OIII]/Hβ ratio artificially increased, moving it upward on BPT diagrams leading to their erroneous classification as Seyfert. The BPT ratios estimated for the bulge component of our LTG sample were determined by means of three different methods: **a**) the first one simulates SDSS measurements within a 3″ aperture centered on the maximum of

the emission-line-free pseudo-continuum maps (this aperture diameter yields a good match to the angular resolution of CALIFA data being generally much smaller than R_B (see Sect. 3.3.2), and it minimizes the possible dilution of potential spectroscopic signatures from an AGN); **b**) the second method where BPT ratios were determined by averaging cubic-spline-interpolated [OIII]/Hβ and [NII]/Hα ratios within R_B; **c**) the third method where BPT ratios were determined from the integrated [OIII]5007, Hβ, [NII]6584 and Hα line fluxes within R_B.

Determinations with method **a** are more sensitive to a central AGN as compared to the area-weighted BPT ratios from method **b** which are only weakly dependent on the luminosity contribution from a bright central point source. If present and even dominating the total nebular luminosity within the bulge, the $\log$ [OIII]/Hβ and $\log$ [NII]/Hα profiles would be affected only locally (out to $R^\star \sim$ FWHM), thereby having little influence on their mean value within R_B. On the other hand, method **c** grants purely luminosity-weighted BPT ratios within R_B and simulates the (idealized) situation where the SDSS fiber precisely matches the isophotal bulge diameter of a LTG. Differences between the three methods were found to be generally small ($\leq$ 0.3 dex) therefore not altering the spectroscopic classification of the analyzed bulges, specially for sources classified as SF. However, as visualized in the upper-right part of Fig. 2.17, there is a tendency for method **b** (large circles) to shift determinations within a 3″ aperture (method **a**, small circles) from the locus of LINERs (Heckman, 1980) and Seyferts into Composites. This trend, which can be attributed to dilution of central AGN/LINER emission by circumnuclear SF, is compatible with the hypothesis formulated by Gomes et al. (2016b) where it is proposed that the upper-right *wing* delineated by SDSS galaxies on the BPT diagram is partly due to aperture effects and consistent with an inside-out galaxy formation (or SF quenching) scenario.

In this context, it is interesting to note that using CALIFA IFS data, Iglésias-Páramo et al. (2016) found that integrated [OIII]/Hβ and [NII]/Hα ratios for local LTGs can differ from single-fiber SDSS determinations by up to $\sim$ 0.3 dex. It is worth pointing out that, whereas Seyfert or Composite BPT ratios imply that an AGN dominates or substantially contributes to the gas excitation, the nature of accretion-powered nuclear activity in bulges classified as LINERs is not that clear. Traditionally, LINER emission-line ratios in massive, high-$\Sigma_\star$ spheroids (early-type galaxies and bulges) were thought to come from the diffuse floor of photoionization powered by the hard radiation field from hot evolved ($\geq 10^8$ yr) post-AGB stars (e.g., Binette et al., 1994; Cid Fernandes et al., 2010, 2011; Macchetto et al., 1996; Sarzi et al., 2010; Stasińska et al.,

2008; Trinchieri & di Serego Alighieri, 1991; Yan & Blanton, 2012). Nevertheless, given that the maximum, nearly metallicity-independent EW(Hα)$_{\rm obs}$ predicted by zero-dimensional ESS models for an old, instantaneously formed stellar population (assuming case B recombination, e.g., Cid Fernandes et al., 2011; Gomes et al., 2016a) is $\sim$ 3 Å, the post-AGB photoionization hypothesis is valid only as long as the observed EW(Hα) does not exceed this threshold. As pointed out in Papaderos et al. (2013), whereas an EW(Hα)$_{\rm obs} \leq$ 3 Å is a necessary condition for the post-AGB photoionization hypothesis to be a valid explanation, it is in itself no effective evidence against an AGN [6].

There are alternative scenarios for the source of LINER emission such as fast shocks (e.g., Allen et al., 2008; Dopita & Sutherland, 1995) and gas excitation by a radiatively inefficient low-luminosity AGN (e.g., Ho, 1999). Papaderos et al. (2013) argue that many ETGs which show LINER emission might hold an energetic AGN, although concealed due the high LyC photon escape fraction (for $\sim$ 60% of the systems they analyzed can exceed 0.9), implying that most of the ionizing radiation produced by an AGN escapes without being locally reprocessed into nebular emission. If this hypothesis is valid for ETGs it is also conceivable for massive LTG bulges hosting an AGN, consequently, we do not exclude the possibility of LTG bulges that fall within the LINER locus of BPT diagrams to host significant accretion-powered nuclear activity.

2.4.5 Spectral fitting with FADO & subsequent comparison with Starlight

FADO (Gomes & Papaderos, 2017) is a conceptually novel PSS code that allows to decipher the SFH of a galaxy from its spectrum. This tool is currently unique among PSS codes by the fact that it includes the nebular component in the best-fitting SED and ensures consistency between observed and predicted hydrogen Balmer line luminosities and EWs. The code also computes several primary and secondary products of the spectral modeling, such as stellar mass, and the mass- and light-weighted mean stellar age and metallicity. The self-consistency concept of FADO, as well as its mathematical foundation (genetic differential evolution opti-

[6] Considering that, in a triaxial geometry, the stellar background along the line of sight will dilute the intrinsic (nuclear) EW(Hα)$_{\rm nuc}$ implying EW(Hα)$_{\rm nuc} \geq$ EW(Hα)$_{\rm obs}$, with equality between these quantities representing a special case. As observed in many star-forming galaxies, the spatial anti-correlation between emission-line EWs and $\Sigma_\star$ demonstrates this effect (Papaderos et al., 2002), being noteworthy that interpreting projected observables and byproducts thereof (e.g., colors, EWs, Lick indices and ages, SFHs, metallicity enrichment histories, respectively) on basis of predictions from standard 0D evolutionary synthesis models is not a simple exercise.

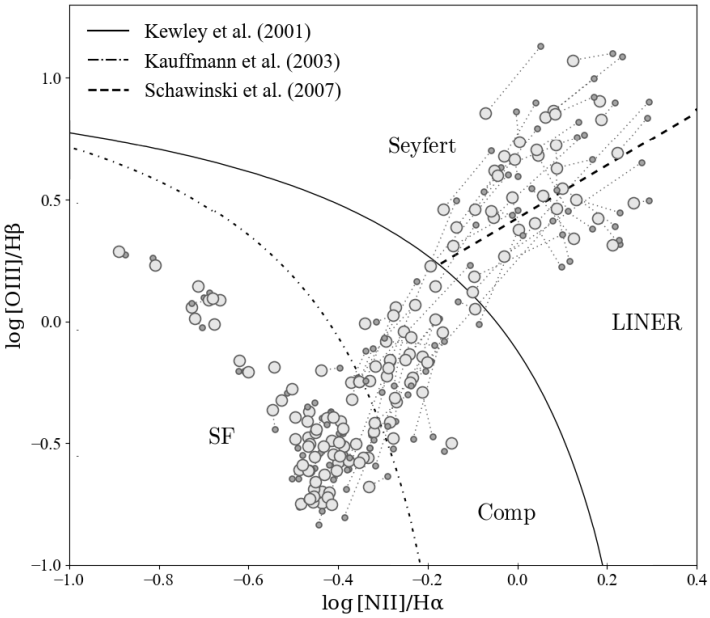

Figure 2.17: Comparison of diagnostic emission-line ratios after Baldwin, Phillips & Terlevich (1981), as obtained within a 3″ aperture (small circles; method **a**), connected by dotted lines with determinations from method **b** (mean ratios within R_B from radial [OIII]/Hβ and [NII]/Hα profiles; big circles). Data based on method **c** (luminosity-weighted determinations using integral [OIII]5007, Hβ, [NII]6584 and Hα line fluxes within R_B) and error bars are omitted for the sake of better visibility. The loci of Seyfert, LINERs and Composites, and that corresponding to photoionization by SF are demarcated following Kauffmann et al. (2003b, dashed-dotted curve), Kewley et al. (2001, solid curve) and Schawinski et al. (2007, dashed line).

mization) result in a robust characterization of the galaxy SFH (cf., e.g. Cardoso, Gomes & Papaderos, 2018). A series of empirical tests shows that FADO can fit spectra and retrieve SFHs adequately well if their S/N in the blue spectral range is typically greater than ~ 8 and the Hα and Hβ are detectable at a level of 5-6 Å.

Whereas the modeling of the whole LTG sample with the current, further refined version of FADO (version v.1b, October 2018) is intended and a valuable supplement to the previously described analysis, we opted for carrying out the CPU time consuming spaxel-by-spaxel (**SbS**) fitting with FADO after completion of the study by Pappalardo et al. (in prep.), which, among other issues, will address in further detail the precision to which FADO can recover evolutionary and physical properties of galaxies as a function of the S/N ratio.

Nevertheless, to facilitate a comparison of the SFHs from these two PSS codes, it was deemed meaningful to fit binned spectra (**18Z**) within **isan** using both FADO and STARLIGHT. Prior

to coaddition, individual-spaxel spectra within each **isan** were corrected for intrinsic stellar motions. For each galaxy, a total of 18 **isan**-spectra were extracted and fitted with both PSS codes using two different SSP libraries (Z4 and Z5) previously defined in the spectral range between 3900 and 6800 Å. Subsequently we created radial profiles of several quantities of interest for the whole sample (see Fig. 2.12) that were compared with the ones created by spaxel-by-spaxel analysis. Additionally, we computed the arithmetic average of these quantities within R_B and R_D.

Furthermore, each of the **isan** within the bulge radius was repeatedly processed, totaling 15 times (**18Z-15t**), in order to obtain improved empirical estimates of the standard deviation values for the determined physical quantities. This analysis was performed using Starlight and FADO (v.1a) with the SSP libraries Z4 & Z5, adopting the same set of parameters as for the spaxel-by-spaxel analysis (identical spectral and normalization ranges) with exception of the seed number in the fitting procedure which gives the initial guesses in the parameter space. After repeatedly processing the same spectrum, the adopted values for each of the determined bulge properties was computed by the arithmetic average of all the 15 determinations.

In order to complement this analysis and gain more insight on the effects of spatial resolution on the results obtained by means of spectral synthesis codes, a supplementary test was executed: **isan** spectra (previously corrected for intrinsic stellar motions) that are within the bulge's radial extent were summed, this way obtaining the integral spectrum for the bulge (**Rb**) for each LTG. These spectra were processed with Starlight and FADO in the same manner as described above. A detailed analysis and comparison summarizing the results obtained by adopting the aforementioned methodology can be found in Sect. 3.4.

2.4.6 Spectroscopic subtraction of the underlying disk from the bulge

As an attempt to investigate the disk's radial distribution within R_B and evaluate the standard hypothesis of extrapolation of its exponential nature, part of this project was dedicated to the development of a tool that allows to estimate the net SED of the bulge after removal of the disk contribution.

Surface photometry was carried out on SDSS r- and g-band images with the goal of evaluating possible light distributions for the disk component. For each galaxy we tested three disk

configurations with respect to the disk nature within R_B as shown in Fig. 2.18: the standard assumption of the conservation of the disk exponential structure, an inwardly flattening disk's contribution and finally, a centrally depressed disk profile, so that at the galactic center its contribution is virtually zero. The key goal of this exercise is to determine the percentage of light within the bulge component that resides in the disk (f_D), for these three disk configurations. In parallel, we conducted the spectral analysis: after having clear-cut definition of the boundaries for bulge (R_B) and disk (R_D), individual spaxels were integrated into one normalized spectrum for the respective stellar components. For each galaxy, bulge and disk spectra were modeled by both STARLIGHT & FADO using the two sets of SSPs spectra libraries (Z4 & Z5). Disk spectral fits were scaled according to previous determined f_D (after correction from the SDSS r- or g-band transmission curve) and subsequently subtracted from the bulge spectral fits, this way theoretically obtaining the net bulge spectrum, free from any disk contribution. Finally, the obtained spectra of the net bulge were re-fitted. The resulting spectral fits were analyzed in order to determine whether the three different assumptions for the adopted disk configurations produce physically meaningful outcome.

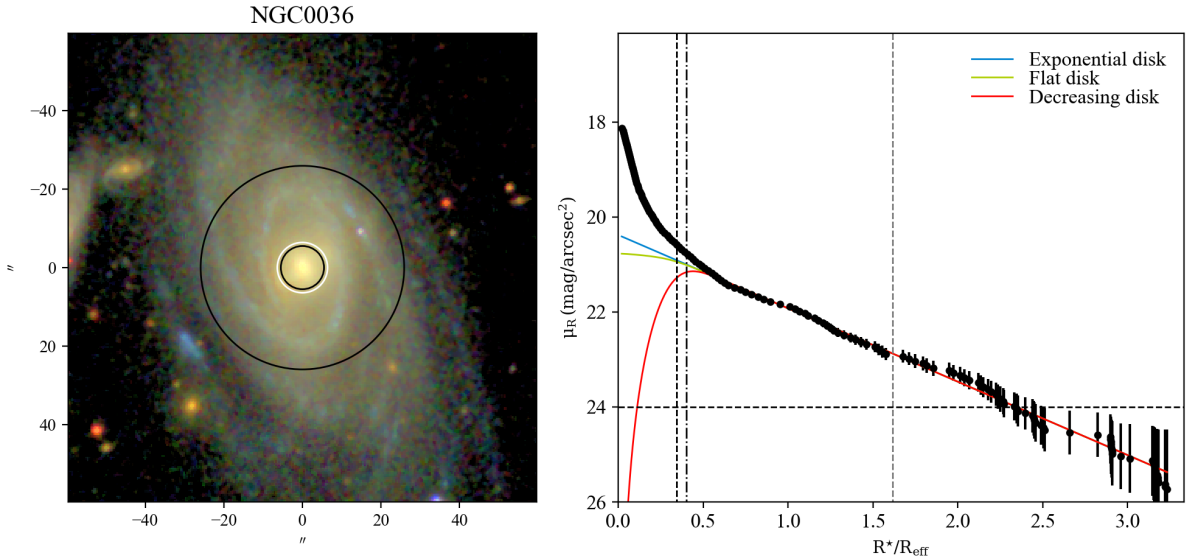

Figure 2.18: Left-hand side: SDSS true-color image of LTG NGC 0036. The white circle overlaid in the SDSS image depicts the bulge diameter (with radius R_B) and the black circle illustrates the bulge radius that was actually considered for this study (with radius R_C, defined at Sect. 2.4.6). Additionally it is overlaid a circle which radius is equivalent to the limit for the disk (with radius R_D, big black circle)[7]. Right-hand side: SDSS g-band SBP illustrating the three disk configurations assumed (black points – observed SBP; blue solid line – standard exponential disk (**expD**); green solid line – inwardly flattening disk (**flatD**); red solid line – centrally depressed disk (**decrD**)). Dashed-dotted vertical line denotes the isophotal radius R_B at $\mu = 24$ mag/$\square''$ and dashed vertical line indicates the bulge radius that was considered for the analysis (R_C). Grey dashed vertical line denotes the limit of the disk (R_D) considered in this study. The galactocentric distance (x axis) is normalized to R_{eff}.

Photometric decomposition assuming three distinct disk configurations

Under the simplified assumption that LTGs are the sum of a disk plus a bulge (and bar when meaningful), structural analysis permits to decompose these complex galactic systems into their main stellar components. Such an exercise is certainly valuable since it allows to estimate important structural parameters for each of the considered stellar components like radial extents, magnitudes and other model- dependent or independent parameters.

As explained in Sect. 2.3.3, as a first approach, the sample was decomposed into bulge (by fitting a Sérsic model to the central luminosity excess of SDSS r & g SBPs), a disk (by fitting the standard exponential model – Sérsic model with $\eta = 1$ fitted at intermediate radii) and a bar when there is a clear sign of the presence of an extra stellar component (by fitting a Sérsic model with $\eta < 1$) which allowed to estimate, among other quantities of interest, the scale-length of the exponential disk. The exponential disk equation in intensity units is given by:

$$\mathrm{I_{exp}(R^\star) = I_0 \cdot e^{R^\star/\alpha}}, \tag{2.9}$$

where $\mathrm{I_0}$ is the intensity at the galactic center and α is the scale-length.

The following procedure was to modify the standard exponential disk distribution in such manner that its contribution decreases within $\mathrm{R_B}$. To this end we used the set of equations 1 & 2 from Papaderos et al. (1996a):

$$\begin{aligned} \mathrm{I(R^\star)} &= \mathrm{I_{exp}[1 - \epsilon_1 e^{P_3(R^\star)}]} \\ \mathrm{P_3(R^\star)} &= \mathrm{(R^\star \epsilon_2 \alpha)^3 + (R^\star (1-\epsilon_1)\alpha\epsilon_1)} \end{aligned} \tag{2.10}$$

The core radius $\mathrm{R_{core}} = \epsilon_2\alpha$ was in every case assumed to be equal to $\mathrm{R_B}$ so that $\mathrm{I/I_{exp}}$ starts diverging from 1 (decreasing the disk contribution) at $\mathrm{R_B}$. As for the central intensity depression $\epsilon_1 = \Delta\mathrm{I/I_0}$ we tested two distinctive cases: an intermediate case between exponential and absence of flux characterized by a flattening of the disk contribution within $\mathrm{R_B}$ (adopted $\epsilon_1 = \epsilon_2/1.5$) and a systematically decreasing disk (adopted $\epsilon_1 = 1$) as it can be seen from

[7]The circle depicting $\mathrm{R_D}$ does not precisely correspond to the area analyzed by the spatially-resolved analysis, given that for this purpose we used the area covered by the **isan**s belonging to the disk. The circle's radius is equivalent to the same of a circumference with the area occupied by the sum of the spaxels that belong to the disk's **isan**s.

Fig. 2.18.

Construction of bulge and disk spectra

To conduct this analysis we required to integrate IFS CALIFA data in order to construct two spectra per galaxy: a summed up spectrum of the bulge and an average spectrum of the disk, normalized to 1 spaxel. Figure 2.19 illustrates the spaxels that were used to construct the two spectra for the case of NGC 0036: the total spectrum in the bulge region (i.e., bulge plus possible disk contribution – $F_{\rm C}(\lambda)$) was created by summing up the spaxels residing within the contour in the left panel whereas the normalized disk spectrum ($\hat{F}_{\rm D}(\lambda)$) was constructed by summing up the spaxels that occupy the locus between the two contours in the right panel, subsequently dividing by the considered number of spaxels. The spaxel selection was performed by taking advantage of previously computed isophotal zones. Having the sample galaxies already segmented into 18 zones and the information on the radial extent of the bulge, the next step was to determine the zones that lie within the bulge and the ones within the disk, as pictured in Fig. 2.19. Here we defined a more conservative radial extent of the bulge ($R_{\rm C}$, see black circle overlaid with SDSS true color image at the left panel and dashed vertical line at the right panel of Fig. 2.18) which is the galactocentric radius of the last zone that lies within $R_{\rm B}$, as given by the structural analysis.

Spectral modeling of the disk average spectra was carried out using the two available PSS codes (STARLIGHT & FADO) in the spectral range between 3900 and 6800 Å using the two sets of libraries. Spectral fitting of the average spectra of the disk permits to compute emission-line free spectra ($\hat{F}^{\star}_{\rm D}(\lambda)$), composed exclusively by the stellar component of the disk so that in the following step where the disk spectra are subtracted from $F_{\rm C}(\lambda)$ there is no risk of over-subtraction of emission-lines producing artificially increased absorption features in the net spectra of the bulge ($F_{\rm B}(\lambda)$).

Scaling of $\hat{F}^{\star}_{\rm D}(\lambda)$:

The aforementioned procedure describes how we defined the three disk configurations that are going to be tested. The next step is to estimate how much light within $R_{\rm C}$ belongs to the disk component and accordingly how much it is needed to scale $\hat{F}^{\star}_{\rm D}(\lambda)$ for the two approaches to be consistent. By integrating the observed SBP emission and the three disk light distributions

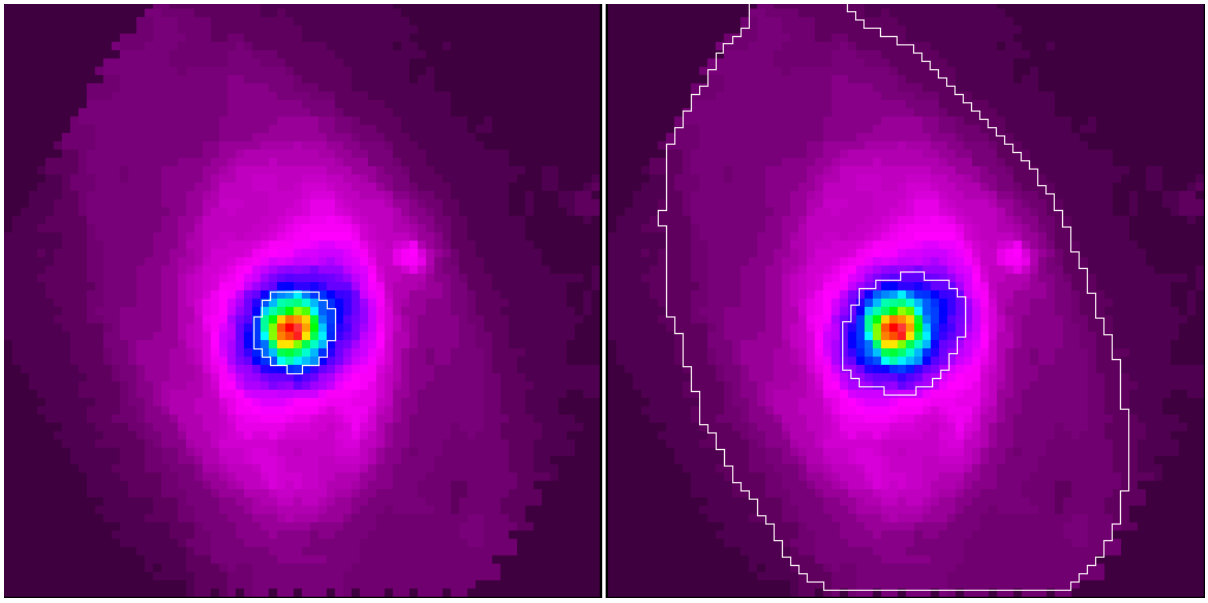

Figure 2.19: Illustration of the CALIFA IFS data (spaxel-by-spaxel map) of LTG NGC 0036: it is shown the emission-line-free pseudo-continuum between 6390 and 6490 Å. Within the contour at the left-hand side are shown the spaxels that were integrated in pursuance of obtaining a single bulge spectrum. As for the average disk spectrum it was obtained by integrating the spaxels that lay between the two contours in the right-hand side and subsequent division by the considered number of spaxels.

from the galactic center until $\mathrm{R_C}$ it is computed f_D, the light fraction within the bulge residing in the disk under each of the assumptions. At this point, the only missing element to obtain the final scaling factor (f_S) is to correct for the SDSS r- or g-band transmission curve ($T_{\mathrm{SDSS}}(\lambda)$). The corrective factor (f_C) was obtained by multiplying $\hat{F}^{\star}_{\mathrm{D}}(\lambda)$ (after multiplying by the number of spaxels within the bulge (n_{pB}) given that $\hat{F}^{\star}_{\mathrm{D}}(\lambda)$ is normalized to 1 spaxel) and $F_{\mathrm{C}}(\lambda)$ by $T_{\mathrm{SDSS}}(\lambda)$ in the considered λ range, integrating the flux of each spectra and dividing one by the other.

Summarizing, to compute the final scaling factor for each of the three disk configurations:

$$
\begin{aligned}
f_D &= \frac{\int_0^{\mathrm{R_C}} \mathrm{R}^{\star} 10^{(\mu_D(\mathrm{R}^{\star})-25)/-2.5} d\mathrm{R}^{\star}}{\int_0^{\mathrm{R_C}} \mathrm{R}^{\star} 10^{(\mu(\mathrm{R}^{\star})-25)/-2.5} d\mathrm{R}^{\star}} \\
f_C &= \frac{n_{\mathrm{pB}} \int_{\lambda_{\mathrm{min}}}^{\lambda_{\mathrm{max}}} \hat{F}^{\star}_D(\lambda) T_{\mathrm{SDSSr}}(\lambda) d\lambda}{\int_{\lambda_{\mathrm{min}}}^{\lambda_{\mathrm{max}}} F_C(\lambda) T_{\mathrm{SDSSr}}(\lambda) d\lambda} \\
f_S &= f_D / f_C
\end{aligned}
\tag{2.11}
$$

where $\mu(R^{\star})$ is the surface brightness distribution of the observed SDSS r-band SBP and $\mu_D(R^{\star})$ is the surface brightness distribution of the assumed disk component.

The individual bulge net spectra for each of the three different disk configurations were computed by subtracting the scaled disk spectra to $F_{\rm C}(\lambda)$:

$$F_B(\lambda) = F_C(\lambda) - n_{\rm pB} \cdot f_S \cdot \hat{F}^{\star}_D(\lambda) \tag{2.12}$$

Finally, the three $F_B(\lambda)$ (one for each disk configurations) for each galaxy were re-fitted with STARLIGHT & FADO, for both libraries Z4 & Z5.

Summarizing, the developed suite of codes in Fortran, ESO-MIDAS and Python:

i. computes the integrated observed spectrum of the bulge (OBS bulge) and the average spectrum of the disk (OBS disk);

ii. by integrating the observed SBPs and those assumed for the disk, computes the scaling factors for the disk SED within $\rm R_C$ under consideration of the SDSS g- or r-band filter transmission curves;

iii. extracts and models with STARLIGHT & FADO the OBS bulge & OBS disk, and determines the respective best-fitting stellar SED;

iv. scales and subtracts the latter from OBS bulge and re-fit (four times; i.e. with STARLIGHT & FADO for both the Z4 and Z5 SSP libraries) of the net spectrum of the bulge for the three different functional forms of the disk within $\rm R_B$;

Figure 2.20 shows the results obtained for LTG MCG +09-22-053 and it can be seen that, according to the outcome by STARLIGHT, extrapolation of a pure exponential profile for the disk to the center yields a negative flux for $\lambda \leq 4000$ Å, which in turn implies that the disk profile has to flatten or show a central depression within $\rm R_B$. As for FADO, even the flattened disk distribution produces unphysical results since the obtained spectra also yields negative flux for $\lambda \leq 4000$ Å. This central deviation from the exponential law, if proven for a significant fraction of LTG disks, will obviously have far-reaching implications on our understanding of the photometric structure and assembly history of LTGs. The complete set of results obtained from application of this tool to the whole sample can be found in Sect. 3.5.

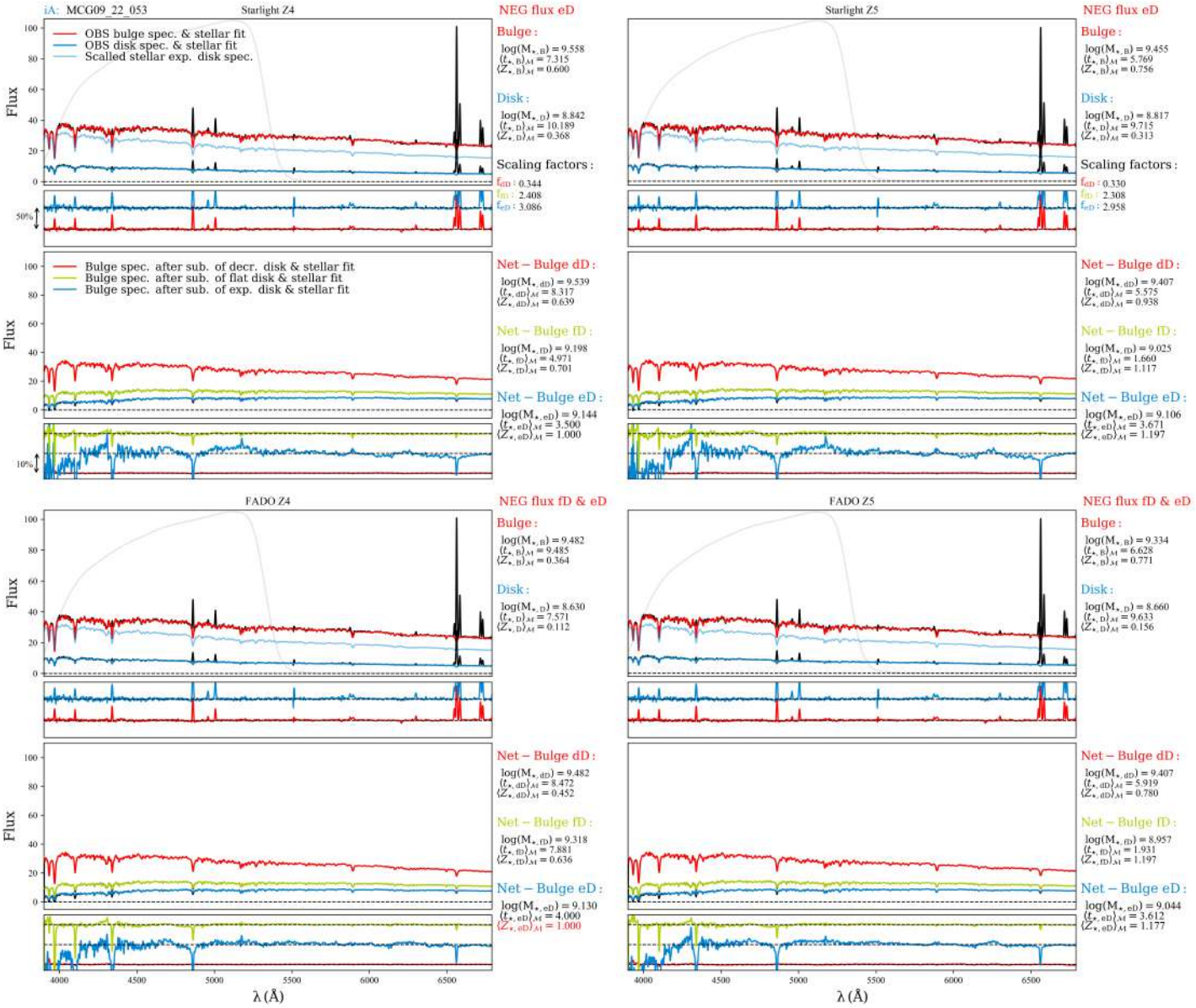

Figure 2.20: The resulting spectra and respective fits for LTG MCG +09-22-053 – in the top panel it is shown the spectrum of bulge (red), disk (blue) and scaled disk (light-blue) according to the exponential disk distribution (additionally it can be seen the overplotted SDSS g-band transmission curve in soft grey); in the bottom panel it is shown the resulting net spectra of the bulge after subtraction of the three different models for the disk and the respective residuals. Labels on the r.h.s of the panel list the stellar mass $\log(\mathcal{M}_\star)$, and mass-weighted mean age and metallicity ($\langle t_{\star,\mathrm{B}}\rangle_{\mathcal{M}}$ and $\langle Z_{\star,\mathrm{B}}\rangle_{\mathcal{M}}$, respectively for each of the fits), as obtained with Starlight - Z4 at top left, Starlight - Z5 at top right, FADO - Z4 at bottom left, FADO - Z5 at bottom right.

Chapter 3

Physical and evolutionary properties of LTG bulges

In this Chapter we provide an overview of the main results obtained through the combined structural and spectral synthesis analysis of LTG bulges in the framework of this project.

3.1 Structural analysis of the sample

As detailed in Sect. 2.3.3, iFIT was used for the structural characterization of the LTG sample. Table 3.1 lists some quantities of interest obtained by a) fitting a Sérsic model to the whole galaxy SBP in the SDSS r-band, and b) by performing a full decomposition by fitting a Sérsic model to the residual emission of the bulge that was inferred from subtraction from each SBP of a model to the disk, and whenever necessary also of a bar. We note that, in either case, fits were computed by taking into account PSF convolution effects.

Name	$M_{r\,\mathrm{T}}$ (mag)	$\mathrm{R_T}$ (kpc)	η_T	$\mathrm{R_{eff\,T}}$ (kpc)	$M_{r\,\mathrm{B}}$ (mag)	$\mathrm{R_B}$ (kpc)	η_B	$\mathrm{R_{eff\,B}}$ (kpc)	B/T
CGCG163_062	-19.64	6.46	1.00	3.23	-17.29	1.37	0.40	0.61	0.12
IC0159	-20.15	7.31	1.70	3.21	-17.17	0.87	0.30	0.39	0.06
IC0208	-20.24	8.92	2.20	4.32	-17.35	1.22	0.40	0.53	0.07
IC0776	-19.09	6.58	1.40	3.51	-16.33	1.07	0.30	0.54	0.08
IC1256	-21.14	10.96	*	4.41	-18.06	1.44	0.70	0.47	0.06
IC1528	-20.84	9.83	1.40	3.71	-17.55	1.01	0.40	0.41	0.05
IC1683	-20.95	9.42	2.20	2.96	-19.24	1.91	0.80	0.53	0.21
IC2604	-18.53	3.89	1.00	1.81	-15.15	0.46	0.30	0.23	0.04
IC3918	-20.05	6.22	1.00	2.50	-17.84	1.17	0.30	0.53	0.13
IC4566	-21.78	14.48	2.60	5.46	-19.95	2.97	0.80	0.86	0.19
MCG01_10_019	-20.89	12.68	2.70	5.95	-18.19	1.63	0.50	0.63	0.08
MCG09_22_053	-19.71	5.72	1.30	1.80	-17.87	1.18	0.50	0.44	0.18

NGC0001	-21.52	11.57	2.80	2.92	-19.99	1.92	0.60	0.58	0.24
NGC0036	-22.13	17.67	3.00	6.02	-19.84	2.52	0.80	0.70	0.12
NGC0160	-22.00	16.16	3.70	5.37	-20.41	3.14	0.80	0.87	0.23
NGC0165	-21.40	16.14	*	5.96	-19.17	2.00	0.50	0.73	0.13
NGC0171	-21.70	14.22	2.90	5.45	-19.33	1.98	0.60	0.65	0.11
NGC0180	-22.18	18.99	3.30	8.18	-19.48	2.17	0.60	0.71	0.08
NGC0214	-22.07	14.08	1.90	4.55	-19.58	1.88	0.50	0.65	0.10
NGC0234	-21.95	16.51	*	5.74	-19.39	2.33	0.70	0.73	0.09
NGC0237	-20.93	9.14	1.40	2.90	-18.41	1.22	0.40	0.48	0.10
NGC0257	-22.02	14.46	3.20	5.66	-19.89	2.66	0.80	0.75	0.14
NGC0309	-22.51	22.80	3.30	10.46	-19.66	2.78	0.80	0.83	0.07
NGC0447	-22.18	24.37	3.80	6.48	-20.57	3.81	1.00	0.96	0.23
NGC0477	-21.53	14.42	2.40	6.46	-18.77	1.89	0.50	0.71	0.08
NGC0496	-21.34	12.94	1.90	5.64	-18.01	1.48	0.50	0.57	0.05
NGC0768	-21.48	12.01	2.70	4.77	-19.05	1.90	0.70	0.59	0.11
NGC0776	-21.82	14.69	3.80	4.93	-19.97	2.44	0.80	0.66	0.18
NGC0873	-21.48	9.86	*	3.57	-18.43	1.10	0.60	0.34	0.06
NGC0941	-19.25	5.69	*	2.26	-15.37	0.47	0.70	0.16	0.03
NGC0976	-22.07	12.00	2.10	2.93	-20.43	2.49	0.80	0.64	0.22
NGC0991	-19.55	6.56	1.50	3.15	-15.99	0.70	0.40	0.31	0.04
NGC1070	-22.25	16.31	2.50	4.60	-20.13	2.55	0.80	0.69	0.14
NGC1093	-21.42	11.68	2.00	3.43	-18.67	1.10	0.40	0.41	0.08
NGC1094	-21.92	13.99	2.10	3.73	-20.17	2.77	0.80	0.76	0.20
NGC1590	-21.10	6.23	*	1.89	-18.48	0.87	0.40	0.32	0.09
NGC1645	-21.71	13.01	2.60	3.29	-20.07	1.92	0.50	0.63	0.22
NGC1659	-21.59	11.35	2.70	3.94	-19.11	1.38	0.60	0.42	0.10
NGC1667	-22.43	13.66	1.80	4.13	-20.40	2.63	0.70	0.75	0.15
NGC2253	-21.47	9.76	2.90	3.53	-18.99	1.25	0.60	0.38	0.10
NGC2347	-21.93	12.74	2.10	3.57	-19.67	1.72	0.60	0.52	0.12
NGC2486	-21.14	10.95	4.60	3.86	-19.49	1.87	0.80	0.50	0.22
NGC2487	-21.86	17.34	5.20	6.55	-19.55	2.68	1.20	0.64	0.12
NGC2530	-21.06	12.56	2.80	5.29	-18.21	1.51	0.60	0.53	0.07
NGC2540	-21.50	13.03	*	5.31	-18.70	1.72	0.60	0.58	0.08
NGC2543	-20.80	8.88	3.80	3.41	-18.58	1.50	0.90	0.40	0.13
NGC2558	-21.74	14.42	3.50	4.74	-20.02	2.15	0.70	0.61	0.21
NGC2595	-21.83	19.09	*	7.75	-19.64	2.35	0.60	0.77	0.13
NGC2604	-19.99	7.97	2.30	3.57	-16.31	0.59	0.60	0.20	0.03
NGC2730	-20.72	10.76	2.10	5.28	-17.17	1.04	0.40	0.44	0.04
NGC2780	-19.21	4.18	*	1.94	-15.75	0.49	0.30	0.23	0.04
NGC2805	-20.10	11.00	2.30	4.64	-16.25	0.69	0.50	0.27	0.03
NGC2906	-20.73	6.83	*	2.41	-18.36	1.11	0.70	0.32	0.11
NGC2916	-21.95	14.04	3.50	5.42	-19.73	2.86	1.00	0.75	0.13
NGC3057	-18.94	5.48	1.10	2.79	-16.32	0.96	0.30	0.48	0.09
NGC3381	-19.90	6.81	1.70	2.70	-16.95	0.72	0.40	0.29	0.07
NGC3614	-20.89	12.40	1.90	5.85	-17.62	1.41	0.60	0.52	0.05
NGC3687	-20.83	9.44	2.80	3.32	-19.09	2.13	1.00	0.56	0.20
NGC3811	-21.16	10.19	3.10	3.76	-19.25	2.08	1.00	0.52	0.17

NGC3913	-18.52	4.08	1.90	1.75	-16.38	0.75	0.50	0.30	0.14
NGC4047	-21.69	11.37	1.50	3.62	-19.62	2.28	0.60	0.74	0.15
NGC4185	-21.71	15.79	2.40	7.19	-18.70	2.04	0.60	0.73	0.06
NGC4210	-20.85	9.22	2.70	4.03	-18.18	1.41	0.60	0.48	0.09
NGC4711	-20.92	8.86	*	3.77	-17.86	1.25	0.50	0.47	0.06
NGC4961	-20.01	6.70	1.30	2.22	-16.66	0.60	0.30	0.27	0.05
NGC5000	-21.51	14.48	2.50	5.57	-19.00	2.18	0.80	0.66	0.10
NGC5016	-20.92	9.37	1.40	3.28	-17.67	0.96	0.40	0.38	0.05
NGC5056	-21.66	14.35	1.60	5.02	-18.98	1.74	0.40	0.69	0.08
NGC5157	-22.24	19.03	2.10	7.28	-20.40	3.84	0.60	1.31	0.18
NGC5205	-19.96	6.32	2.10	2.29	-18.00	1.30	0.70	0.41	0.16
NGC5320	-20.92	10.76	1.70	4.22	-17.96	1.34	0.50	0.51	0.07
NGC5378	-21.08	13.40	3.90	4.47	-19.35	2.69	1.20	0.67	0.20
NGC5406	-22.36	18.01	2.90	6.47	-20.43	3.61	1.00	0.91	0.17
NGC5480	-20.55	7.68	*	3.00	-18.09	1.23	0.80	0.35	0.10
NGC5519	-21.73	15.42	2.10	5.44	-19.57	2.64	0.60	0.91	0.14
NGC5622	-20.59	8.44	1.40	3.46	-17.94	1.29	0.40	0.53	0.09
NGC5633	-20.79	6.87	1.00	2.20	-18.18	1.10	0.40	0.43	0.09
NGC5656	-21.43	9.58	*	2.98	-19.31	1.86	0.90	0.47	0.14
NGC5665	-20.97	8.75	1.80	3.14	-17.92	1.05	0.60	0.35	0.06
NGC5720	-22.06	17.87	3.20	6.97	-20.16	3.09	0.70	0.95	0.17
NGC5732	-20.30	7.88	1.60	3.07	-17.73	1.17	0.40	0.48	0.09
NGC5735	-21.23	13.02	2.10	5.65	-18.58	2.06	0.70	0.71	0.09
NGC5772	-21.99	15.42	3.30	4.85	-20.45	3.62	1.20	0.81	0.24
NGC5829	-21.48	16.18	2.30	7.39	-18.28	1.68	0.50	0.65	0.05
NGC5888	-22.64	19.41	2.30	7.66	-20.45	3.59	0.60	1.20	0.13
NGC5947	-21.48	13.66	4.10	5.02	-19.71	2.55	0.80	0.73	0.20
NGC5950	-19.91	6.64	1.30	2.81	-17.40	1.00	0.30	0.46	0.10
NGC5957	-20.52	7.71	3.90	3.31	-18.24	1.48	0.90	0.42	0.12
NGC6004	-21.73	14.49	4.20	6.45	-19.12	2.56	1.10	0.69	0.09
NGC6032	-21.17	12.01	3.00	4.77	-18.57	1.71	0.80	0.51	0.09
NGC6063	-20.42	7.90	*	3.66	-16.61	0.76	0.40	0.32	0.03
NGC6154	-21.97	17.55	3.10	6.59	-20.14	3.47	0.90	0.97	0.18
NGC6155	-20.63	7.38	*	2.76	-17.57	0.98	0.50	0.36	0.06
NGC6301	-22.52	23.30	2.60	10.74	-19.03	2.74	0.70	0.96	0.04
NGC6941	-22.22	19.15	4.30	7.15	-20.12	2.97	0.80	0.84	0.14
NGC7321	-22.36	17.62	2.20	5.93	-20.14	3.07	0.70	0.94	0.13
NGC7489	-22.24	17.15	*	5.97	-18.98	1.75	0.50	0.63	0.05
NGC7653	-21.50	11.66	3.40	3.44	-19.95	2.68	1.00	0.66	0.24
NGC7691	-21.16	15.70	1.90	6.25	-17.35	1.10	0.40	0.46	0.03
NGC7716	-20.83	8.25	3.40	2.44	-19.24	1.44	0.80	0.37	0.23
NGC7738	-21.89	14.07	2.30	4.52	-20.29	3.47	0.90	0.94	0.23
NGC7782	-22.43	17.78	3.50	6.48	-20.45	3.87	1.00	1.00	0.16
NGC7800	-19.39	5.61	1.50	2.14	-16.95	0.83	0.30	0.38	0.11
NGC7819	-20.92	11.82	3.40	5.05	-18.94	1.91	0.60	0.65	0.16
UGC00312	-20.42	7.01	*	3.24	-18.05	1.10	0.40	0.41	0.11
UGC02311	-21.98	16.22	2.40	4.86	-20.14	3.01	0.80	0.85	0.18

UGC02443	-19.39	4.90	0.90	2.28	-15.49	0.48	0.30	0.23	0.03
UGC03253	-21.06	9.52	2.40	3.44	-18.99	1.77	0.70	0.54	0.15
UGC03973	-22.05	18.28	2.60	5.43	-20.37	3.02	0.70	0.89	0.21
UGC04195	-21.17	11.41	3.70	4.99	-18.76	1.94	0.80	0.59	0.11
UGC04262	-21.68	14.99	3.20	5.52	-19.83	2.75	0.70	0.85	0.18
UGC04308	-21.16	12.47	*	5.44	-18.24	1.73	0.80	0.55	0.07
UGC04375	-20.33	9.33	1.80	3.37	-17.08	0.90	0.50	0.34	0.05
UGC04455	-21.75	14.72	1.90	6.20	-19.81	3.05	0.50	1.14	0.17
UGC05520	-20.17	8.98	1.80	3.42	-18.00	1.40	0.40	0.58	0.13
UGC05976	-17.82	3.26	1.00	1.65	-15.11	0.57	0.30	0.29	0.08
UGC06517	-19.55	5.45	*	2.12	-16.76	0.82	0.50	0.31	0.08
UGC06616	-18.56	4.74	1.20	2.69	-14.75	0.52	0.30	0.26	0.03
UGC06930	-18.78	5.22	1.50	2.70	-15.14	0.47	0.30	0.23	0.03
UGC07012	-19.72	6.19	1.50	2.39	-17.01	0.82	0.30	0.37	0.08
UGC08733	-19.42	7.72	1.50	3.74	-16.26	0.89	0.30	0.43	0.05
UGC08781	-22.23	17.85	3.80	5.94	-20.59	3.75	0.90	0.99	0.22
UGC08909	-18.64	5.52	1.10	2.28	-14.63	0.43	0.30	0.21	0.03
UGC09067	-21.71	14.00	1.40	4.91	-18.99	1.81	0.40	0.73	0.08
UGC09291	-20.38	9.89	1.40	4.55	-17.02	1.16	0.40	0.51	0.05
UGC09476	-20.80	9.74	2.10	4.61	-18.05	1.69	0.60	0.63	0.08
UGC09837	-19.55	8.41	2.00	3.72	-16.99	1.23	0.50	0.51	0.09
UGC10796	-19.44	7.02	2.10	2.98	-17.04	0.99	0.40	0.42	0.11
UGC11649	-20.94	8.56	2.90	3.10	-19.07	1.75	0.70	0.52	0.18
UGC12224	-20.59	10.31	2.50	5.20	-17.33	1.29	0.60	0.49	0.05
UGC12250	-22.00	17.54	4.10	6.02	-20.26	2.80	0.70	0.82	0.20
UGC12767	-22.44	18.62	3.20	7.26	-20.05	2.57	0.80	0.70	0.11
UGC12816	-20.46	9.82	2.00	4.04	-17.90	1.39	0.40	0.58	0.09
UGC12864	-20.46	10.19	2.60	3.97	-18.33	1.35	0.40	0.54	0.14
UGCA021	-19.53	7.05	1.60	3.44	-16.85	1.16	0.40	0.52	0.09

Table 3.1: Photometric properties of the LTG sample, as obtained by applying iFIT to SDSS DR7 r-band data after full reduction of the latter (cf. Sect. 2.2). The table lists, from the left to the right: the name of the galaxy, total absolute magnitude, radial extent of the galaxy in kpc, obtained at an extinction-corrected surface brightness level 24 mag/$\Box''$, exponent η obtained by fitting a Sérsic model to the total SBP, $R_{\rm eff}$ of the galaxy in kpc, bulge absolute magnitude, radial extent of the bulge in kpc, η obtained by fitting a Sérsic model to the bulge (i.e. the residual emission after subtraction of the exponential disk and, whenever meaningful, also of a bar, $R_{\rm eff}$ of the bulge in kpc and the bulge-to-total (B/T) ratio. The * symbol marks cases where convergence to a reliable solution for the Sersic model could not be achieved.

A comparison of the obtained Sersic index of the bulge and the total SBP ($\eta_{\rm B}$ and $\eta_{\rm T}$, respectively) with other physical properties like $\langle t_{\star,{\rm B}}\rangle_{\mathcal{M}}$ or $\langle Z_{\star,{\rm B}}\rangle_{\mathcal{M}}$ reveals a weak (if any at all) correlation. This is also the case when η is compared with the isophotal radial extent of LTGs and their bulge component, as apparent from Figs. 3.2 & 3.1. As a cautionary note, one must be prudent when interpreting the results obtained for $\eta_{\rm B}$ since the beta-version of iFIT used for this study has not reached its maximum potential in profile decomposition and the precision of the η_B values listed above is on the order of 10%. However, the exercise was repeated for $\sim 1/3$

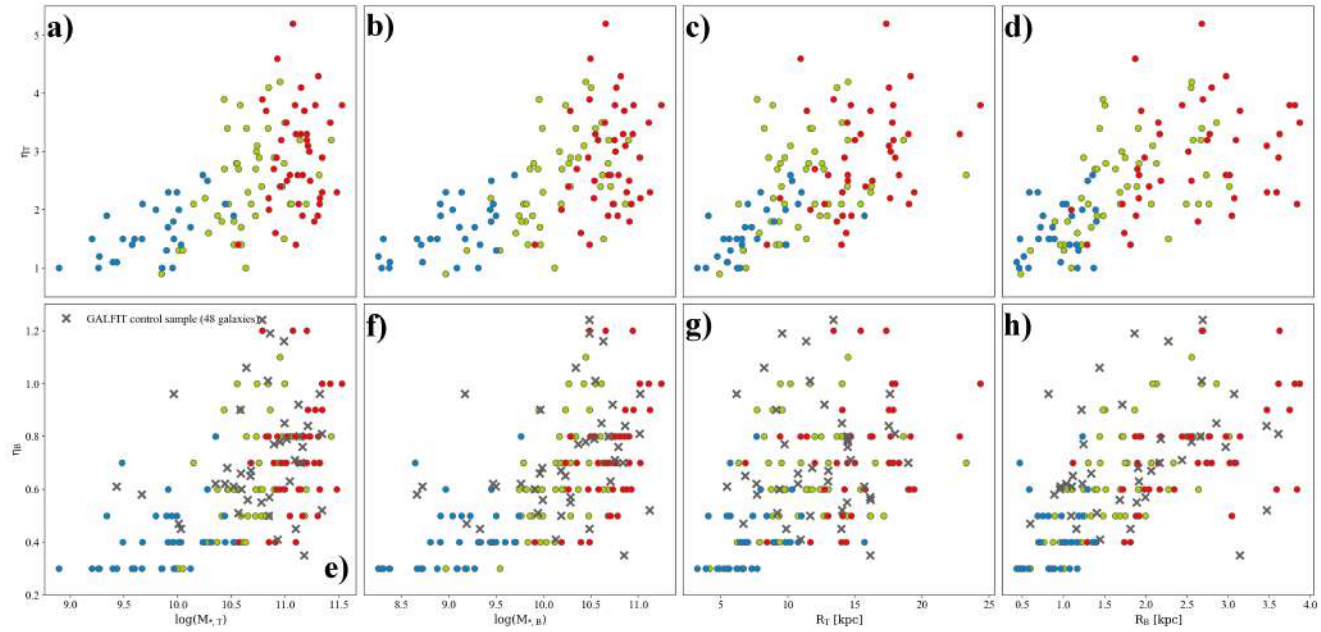

Figure 3.1: **a**) Logarithm of the total stellar mass $\log(M_{\star,T})$ ($M_{\odot}$) vs. η_T; **b**) Logarithm of the bulge's stellar mass $\log(M_{\star,B})$ ($M_{\odot}$) vs. η_T; **c**) Radial extent of the galaxy R_T (kpc) vs. η_T; **d**) Radial extent of the bulge R_B (kpc) vs. η_T; **e**) $\log(M_{\star,T})$ vs. bulge's Sérsic η (η_B); **f**) $\log(M_{\star,B})$ vs. η_B; **g**) R_T vs. η_B; **h**) R_B vs. η_B. Crosses show the results obtained by GALFIT for a reduced sample of 48 galaxies.

(48/135) of the sample with both GALFIT and IMFIT and the lack of significant correlations was confirmed. These results suggest that the much-debated ambiguity in bulge classification via η is not mainly due to fitting uncertainties but primarily reflects a lack of a strong coupling between η and the physical and evolutionary properties of bulges, or a LTG as a whole. For instance, as apparent from Figs. 3.2 & 3.1, at a $\eta_T \simeq 2$, LTG bulges span a range of 5 Gyr in their age and 1.5 dex in mass. Important is also to remark that the decomposition made does not reveal any bulge with $\eta_B > 1.5$, which contrasts previous work with, e.g. GALFIT and the notion that a $\eta_B \simeq 2$ is a useful discriminator between PBs and CBs.

3.2 Optical colors of LTG bulges

Due to the fact that, as stellar populations grow older their colors evolve from blue to red, even-though the biases mentioned in Sect. 2.3.4, optical colors are widely used to age-date galaxies and their structural components.

In order to complement the insights obtained by the spatially resolved analysis of the CALIFA data cubes we perform in this section a determination and comparative analysis of the colors

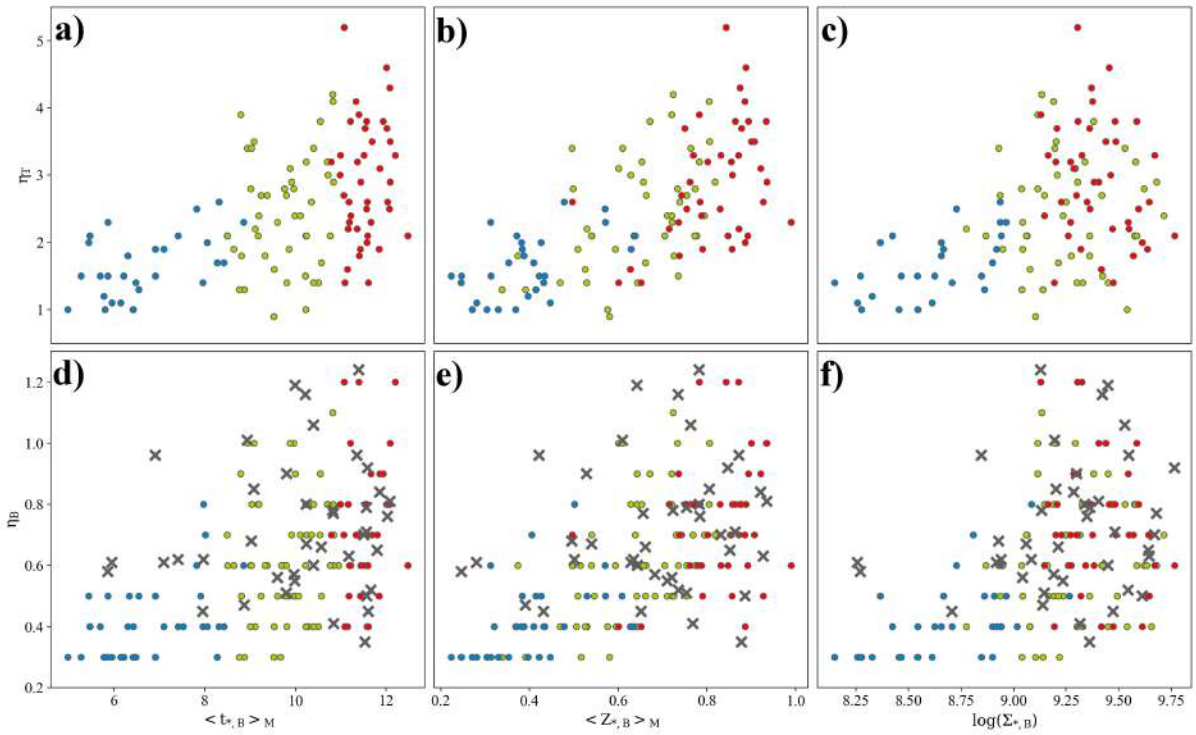

Figure 3.2: **a**) Mass-weighted stellar age $\langle t_{\star,\mathrm{B}}\rangle_{\mathcal{M}}$ (Gyr) of the bulge component vs. Sérsic η (η_{T}) of the total SBP; **b**) Mass-weighted stellar metallicity $\langle Z_{\star,\mathrm{B}}\rangle_{\mathcal{M}}$ ($\mathrm{Z}_{\odot}$) of the bulge component vs. η_{T}; **c**) Logarithm of the bulge stellar surface density $\log(\Sigma_{\star,\mathrm{B}})$ ($\mathrm{M}_{\odot}/\mathrm{kpc}^2$) vs. η_{B}; **d**) $\langle t_{\star,\mathrm{B}}\rangle_{\mathcal{M}}$ vs. Sérsic η (η_{B}) of the bulge; **e**) $\langle Z_{\star,\mathrm{B}}\rangle_{\mathcal{M}}$ vs. η_{B}; **f**) $\log(\Sigma_{\star,\mathrm{B}})$ vs. η_{B}. Crosses show the results obtained by GALFIT for a reduced sample of 48 galaxies.

of the bulge and the disk in our LTG sample.

The left-hand side of Fig. 3.3 displays the total stellar mass of the galaxy, $\log(\mathcal{M}_{\star,\mathrm{T}})$, versus the mean color of the bulge (big circles) and that of the disk (small circles). To ease the visualization of the obtained results, in the right-hand side of the same figure, a set of panels was added displaying $\log(\mathcal{M}_{\star,\mathrm{T}})$ versus the difference between bulge and disk colors. A review of the results shows a correlation with mass with regard to all three measured colors: high mass galaxies tend to consist of both redder bulges and disks as compared to lower mass galaxies, whose bulge and disk component appears on the statistical average almost indistinguishable from one another with respect to their optical color (for example, MacArthur et al., 2008, reach a similar conclusion from a photometric study of 137 spiral galaxies within the redshift range $0.1 < z < 1.2$). Another interesting feature is that the difference between bulge and disk colors tends to be higher for higher mass galaxies. These results are compatible with the ones obtained from a spatially resolved analysis of CALIFA IFS data that indicates that the contrast

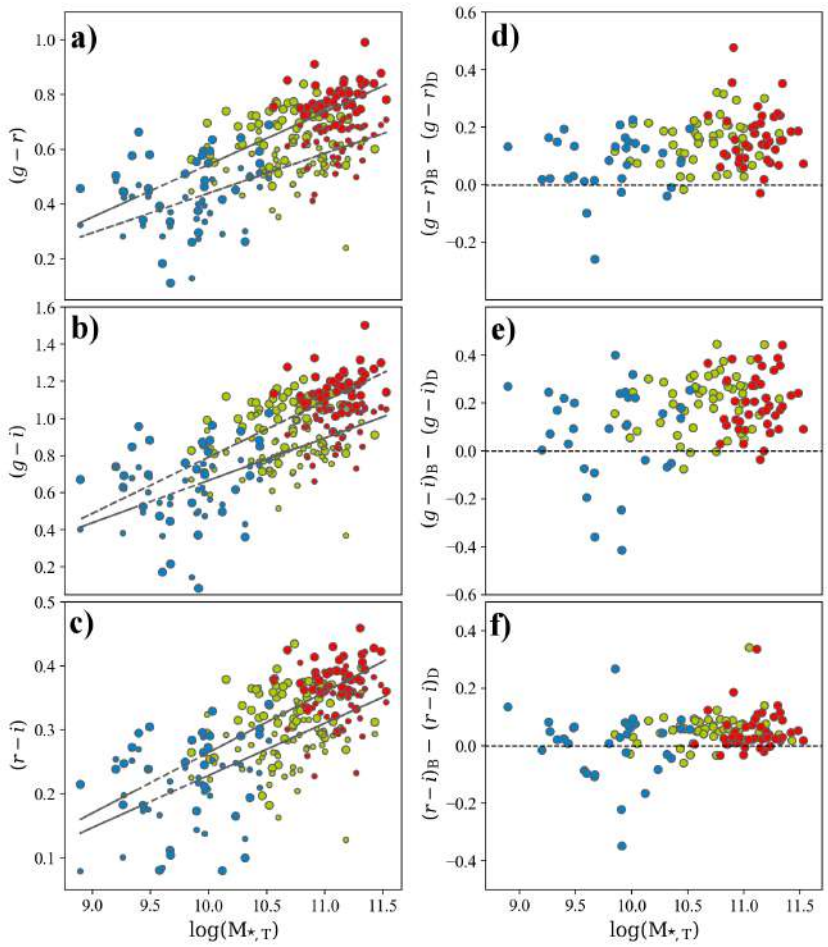

Figure 3.3: **a**) Logarithm of the total stellar mass $\log(\mathcal{M}_{\star,\mathrm{T}})$ vs. mean bulge $(g-r)$ (big circles) and disk $(g-r)$ (small circles) colors; **b**) $\log(\mathcal{M}_{\star,\mathrm{T}})$ vs. $g-i$ color for the bulge and disk ($(g-i)_{\mathrm{B}}$ and $(g-i)_{\mathrm{D}}$, respectively); **c**) $\log(\mathcal{M}_{\star,\mathrm{T}})$ vs. $r-i$ color for the bulge and disk ($(r-i)_{\mathrm{B}}$ & $(r-i)_{\mathrm{D}}$, respectively); **d**) $\log(\mathcal{M}_{\star,\mathrm{T}})$ vs. difference between bulge and disk $g-r$ color $(g-r)_{\mathrm{B}}$–$(g-r)_{\mathrm{D}}$; **e**) $\log(\mathcal{M}_{\star,\mathrm{T}})$ vs. difference between $(g-i)_{\mathrm{B}}$ and $(g-i)_{\mathrm{D}}$; **f**) $\log(\mathcal{M}_{\star,\mathrm{T}})$ vs. difference between $(r-i)_{\mathrm{B}}$ and $(r-i)_{\mathrm{D}}$. Markers are color-coded according to the classification scheme proposed in the left-hand side of Fig. 2.16.

in mass-weighted age and metallicity between bulge and disk increases with LTG mass (see Sect. 3.3.1). It is interesting to note that independently of the mass range, bulges have similar colors with their host disks suggesting a common evolution (for e.g., Balcells & Peletier, 1994; Peletier & Balcells, 1996, document the same results and arrive at the same conclusion).

When comparing average colors within each $<\delta\mu_{9\mathrm{G}}>$ interval we find that low-mass galaxies have a much higher spread than higher mass galaxies. Mean color values and their dispersion for the three $<\delta\mu_{9\mathrm{G}}>$ intervals are as follows: **iA**: $(g-r)_{\mathrm{B}} = 0.466$, $\sigma = 0.138$, $(g-i)_{\mathrm{B}} = 0.666$, $\sigma = 0.236$, $(r-i)_{\mathrm{B}} = 0.202$, $\sigma = 0.108$; **iB**: $(g-r)_{\mathrm{B}} = 0.682$, $\sigma = 0.086$, $(g-i)_{\mathrm{B}} = 1.012$, σ

$= 0.129$, $(r-i)_{\rm B} = 0.331$, $\sigma = 0.048$; **iC**: $(g-r)_{\rm B} = 0.779$, $\sigma = 0.102$, $(g-i)_{\rm B} = 1.161$, $\sigma = 0.142$, $(r-i)_{\rm B} = 0.391$, $\sigma = 0.051$. These results are compatible with previous works, as for e.g., Bower et al. (1998) which state that colors of younger stellar populations show a stronger dependence on age than those of old stellar populations, which offers an explanation for the significant color dispersion observed at the low-mass end of the color-magnitude diagram in Fig. 3.4.

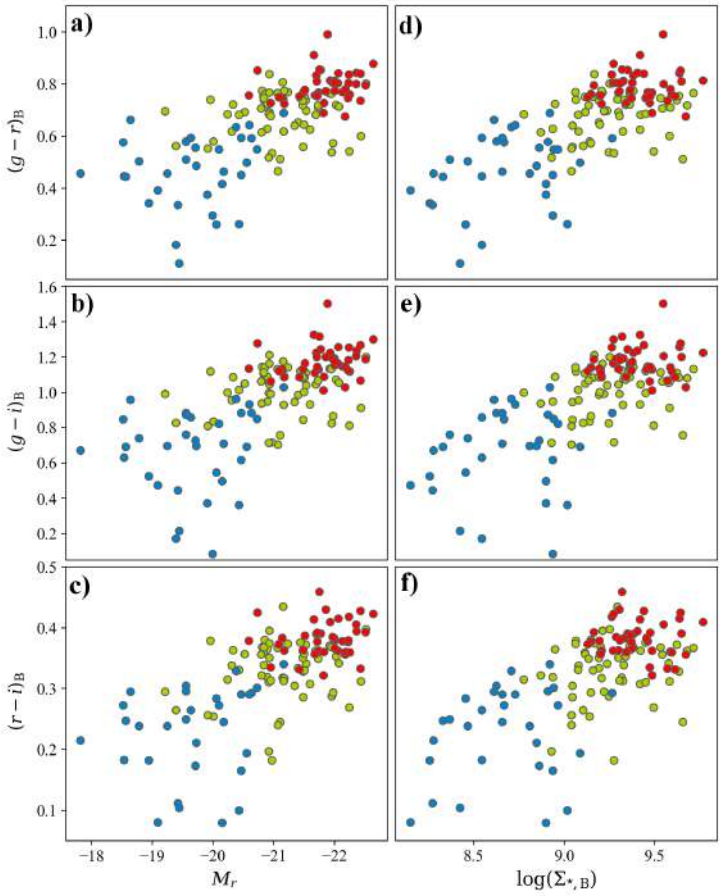

Figure 3.4: **a**) Absolute magnitude M_r vs. mean bulge color $(g-r)_{\rm B}$; **b**) M_r vs. $(g-i)_{\rm B}$; **c**) M_r vs. $(r-i)_{\rm B}$; **d**) Logarithm of the bulge stellar surface density $\log(\Sigma_{\star,{\rm B}})$ ($M_\odot$/kpc^2) vs. $(g-r)_{\rm B}$; **e**) $\log(\Sigma_{\star,{\rm B}})$ vs. $(g-i)_{\rm B}$; **f**) $\log(\Sigma_{\star,{\rm B}})$ vs. $(r-i)_{\rm B}$.

Not surprisingly, when comparing the bulge colors with the galaxy absolute magnitude (left-hand side of Fig. 3.4) there is again a clear color trend similar to that in Fig. 3.3, since luminosity is a proxy to stellar mass. Furthermore, when considering the bulge's colors versus the logarithm of the bulge stellar surface density $\log(\Sigma_{\star,{\rm B}})$ ($M_\odot$/kpc^2) (right-hand side of Fig. 3.4) a trend is also visible for more dense bulges which tend to show redder colors and vice versa.

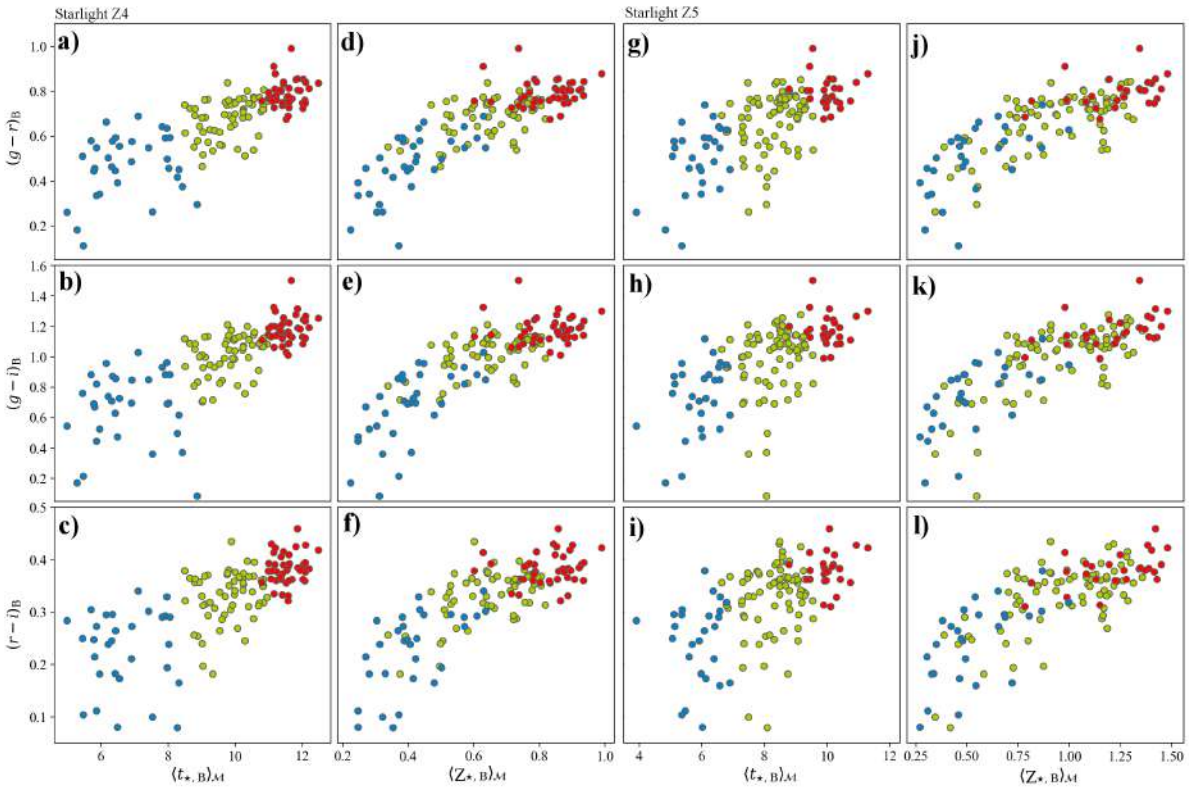

Figure 3.5: **a**) Mean bulge mass-weighted stellar age $\langle t_{\star,\mathrm{B}}\rangle_{\mathcal{M}}$ (Gyr) as obtained with the Z4 SSP library vs. mean bulge color $(g-r)_{\mathrm{B}}$; **b**) $\langle t_{\star,\mathrm{B}}\rangle_{\mathcal{M}}$ as obtained for the Z4 library vs. $(g-i)_{\mathrm{B}}$; **c**) $\langle t_{\star,\mathrm{B}}\rangle_{\mathcal{M}}$ as obtained for the Z4 library vs. $(r-i)_{\mathrm{B}}$; **d**) Mean bulge mass-weighted stellar metallicity $\langle Z_{\star,\mathrm{B}}\rangle_{\mathcal{M}}$ ($\mathrm{Z}_{\odot}$) as obtained for the Z4 SSP library vs. $(g-i)_{\mathrm{B}}$; **e**) $\langle Z_{\star,\mathrm{B}}\rangle_{\mathcal{M}}$ as obtained for Z4 vs. $(r-i)_{\mathrm{B}}$; **f**) $\langle Z_{\star,\mathrm{B}}\rangle_{\mathcal{M}}$ as obtained for Z4 vs. $(g-r)_{\mathrm{B}}$. Panels **g**) to **l**) present the same quantities as panels **a**-**f**, but for $\langle t_{\star,\mathrm{B}}\rangle_{\mathcal{M}}$ & $\langle Z_{\star,\mathrm{B}}\rangle_{\mathcal{M}}$ determinations obtained from spectral fitting with the Z5 SSP library. The color coding is identical to that used in the right-hand side of Fig. 2.16.

In Fig. 3.5 we plot bulge average colors vs. mass-weighted mean age ($\langle t_{\star,\mathrm{B}}\rangle_{\mathcal{M}}$, left-hand side) and metallicity ($\langle Z_{\star,\mathrm{B}}\rangle_{\mathcal{M}}$, right-hand side) within $\mathrm{R_B}$ obtained from spectral synthesis models with Starlight and the Z4 and Z5 SSP libraries. Since there is a strong correlation between total stellar mass and $\langle t_{\star,\mathrm{B}}\rangle_{\mathcal{M}}$ & $\langle Z_{\star,\mathrm{B}}\rangle_{\mathcal{M}}$ (see Sect. 3.3.1), the documented trends are to be expected: bulge's colors correlate with both $\langle t_{\star,\mathrm{B}}\rangle_{\mathcal{M}}$ & $\langle Z_{\star,\mathrm{B}}\rangle_{\mathcal{M}}$ although the observed $\langle t_{\star,\mathrm{B}}\rangle_{\mathcal{M}}$ correlation is tighter for Z4-SSP results. This is probably due to the increase in the SSP metallicity space which might aggravate the AMD (at the expense of precision in estimating ages) as discussed in detail in Sect. 2.4.1. Panels from **d** to **f** compare colors with $\langle Z_{\star,\mathrm{B}}\rangle_{\mathcal{M}}$: it appears that the obtained correlation is non-linear, or that it exhibits a plateau for the higher metallicity regime. By inspection of the panels from **j** to **l**, where stellar metallicities were obtained by a spatially resolved analysis with Starlight with the Z5 library (covering metallicities of up

to 1.5 $Z_{\odot}$), we verify that the plateau is still present which might suggest that bulges with $\langle Z_{\star,\mathrm{B}} \rangle_{\mathcal{M}} > 0.8$ $Z_{\odot}$ display the same color-metallicity trend, becoming indistinguishable from highly enriched bulges.

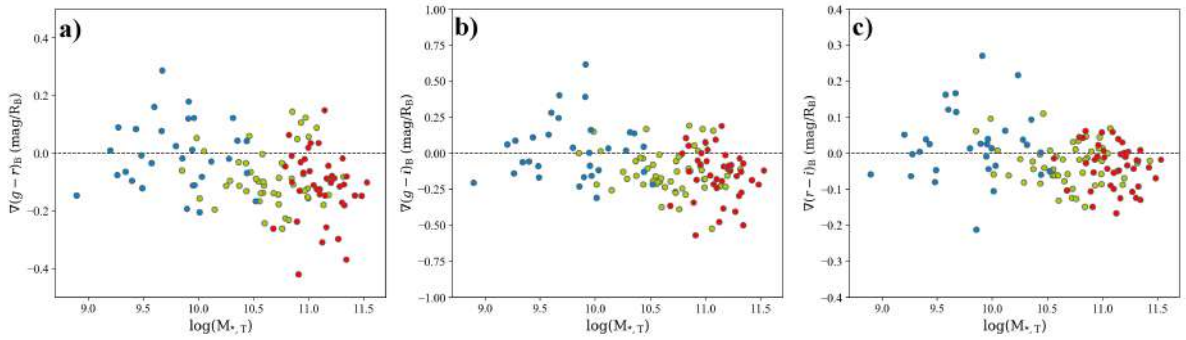

Figure 3.6: **a**) Logarithm of the total stellar mass $\log(\mathcal{M}_{\star,\mathrm{T}})$ vs. bulge color gradient within $\mathrm{R_B}$, $\nabla(g-r)_{\mathrm{B}}$; **b**) $\log(\mathcal{M}_{\star,\mathrm{T}})$ vs. $\nabla(g-i)_{\mathrm{B}}$; **c**) $\log(\mathcal{M}_{\star,\mathrm{T}})$ vs. $\nabla(r-i)_{\mathrm{B}}$.

Figure 3.6 displays the logarithm of the total stellar mass $\log(\mathcal{M}_{\star,\mathrm{T}})$ versus the color gradient within $\mathrm{R_B}$. The obtained results are in agreement with previous studies: by exploring the surface photometry in various bands of a sample of 45 early-type spiral galaxies, Balcells & Peletier (1993) find a correlation between bulge absolute magnitude and color gradient: bulges with low absolute magnitude tend to present positive color gradients whereas the opposite is valid for intrinsically luminous bulges. They add that the observed correlation cannot be explained by dust effects. In a later work (Balcells & Peletier, 1994), where only galaxies unaffected by dust were analyzed (18 out of 45), these authors claim that the observed correlation is only valid for bulges which absolute magnitude in the R band $<$ -20, since for bulges with absolute magnitude $>$ -20 the color gradients are strongly negative and do not correlate with bulge's luminosity. The favored interpretation was that this distinct behavior is a reflection of different formation routes, and since dissipative collapse models predict that abundance gradients increase with luminosity, it is suggested that the observed correlation for massive bulges is a manifestation of its dissipative origin.

Interestingly, the observed trend is consistent with the one obtained for mass-weighted age gradients within $\mathrm{R_B}$ (Sect. 3.3.5). In any case we document a segregation in two nodes as expected from two distinct formation processes. On the contrary, both cases show a continuous sequence with increasing total stellar mass with more massive galaxies tending to present negative color/age gradients and vice versa.

3.3 Properties of LTG bulges as obtained by a spatially resolved spectral fitting analysis

This section is dedicated to a discussion of the main results obtained from the spatially resolved spectral fitting analysis of the LTG bulges in our sample. First, we will discuss the relation between $<\delta\mu_{9G}>$ and the evolutionary and physical characteristics of LTG bulges and lay emphasis on the tight correlation between this quantity and others implying that $<\delta\mu_{9G}>$ can be a powerful discriminator of the bulge (and galaxy) evolutionary status. Moreover, we investigate the relation between bulge and disk age and metallicity as a function of LTG mass, as well as the dominant gas excitation mechanisms along the bulge mass and age sequence. Finally, we examine mass and light-weighted age gradients within the bulge radial extent.

3.3.1 Physical and evolutionary properties of LTG bulges vs. $<\delta\mu_{9G}>$

Figure 3.7 (adopted from Breda & Papaderos, 2018) illustrates how physical and evolutionary properties of LTG bulges vary across the three $<\delta\mu_{9G}>$ intervals defined in Sect. 2.4.3.

Panel **a** of Fig. 3.7 displays a nearly linear relation between $<\delta\mu_{9G}>$ and the mass-weighted stellar age $\langle t_{\star,B}\rangle_{\mathcal{M}}$ within the bulge. The transition from interval **iA** (blue dots) to interval **iB** (green dots) corresponds to a $\langle t_{\star,B}\rangle_{\mathcal{M}} \sim 9$ Gyr, and the one from interval **iB** to interval **iC** to a $\langle t_{\star,B}\rangle_{\mathcal{M}} \geq 11$ Gyr. The bulges of the sample have a broad span in mean age ranging from ~ 2 to 13.5 Gyr (cf. e.g., Moorthy & Holtzman, 2006; Peletier et al., 2007) and metallicities from ~ 0.2 to 1 $Z_{\odot}$. This panel reveals a tight trend between age and $<\delta\mu_{9G}>$ that can be approximated by the relation $\langle t_{\star,B}\rangle_{\mathcal{M}}$ (Gyr) = (12.14 ± 0.06) + (2.05 ± 0.04) · $<\delta\mu_{9G}>$ (solid line). We note that all linear fits were computed through χ^2 minimization for both quantities considered, given that none of them is strictly independent. The correlation between the age of LTG bulges (Gyr) and the logarithm of their stellar mass ($M_{\odot}$) is presented in panel **b** and can be approximated by the relation $\langle t_{\star,B}\rangle_{\mathcal{M}}$ = (2.30 ± 0.11) · log($\mathcal{M}_{\star,B}$) - (13.44 ± 1.13), implying that old ($\geq$ 11 Gyr) bulges in the $<\delta\mu_{9G}>$ interval **iC** (mean age of 10.7 ± 0.4 Gyr) are by ~ 2 orders of magnitude more massive than bulges falling in the $<\delta\mu_{9G}>$ interval **iA** (mean age of 6.82 ± 1.06 Gyr), with bulges in the interval **iB** having an average age of 9.80 ± 0.7 Gyr. Another interesting insight comes from panel **c** that shows that more massive bulges are hosted by more massive (and luminous) LTGs. A linear relation of the form log($\mathcal{M}_{\star,B}$) = (1.22 ± 0.02) log($\mathcal{M}_{\star,T}$) – (2.87 ± 0.25) is obtained, or, equivalently, $\mathcal{M}_{\star,B}/\mathcal{M}_{\star,T}$ = (0.13 ±

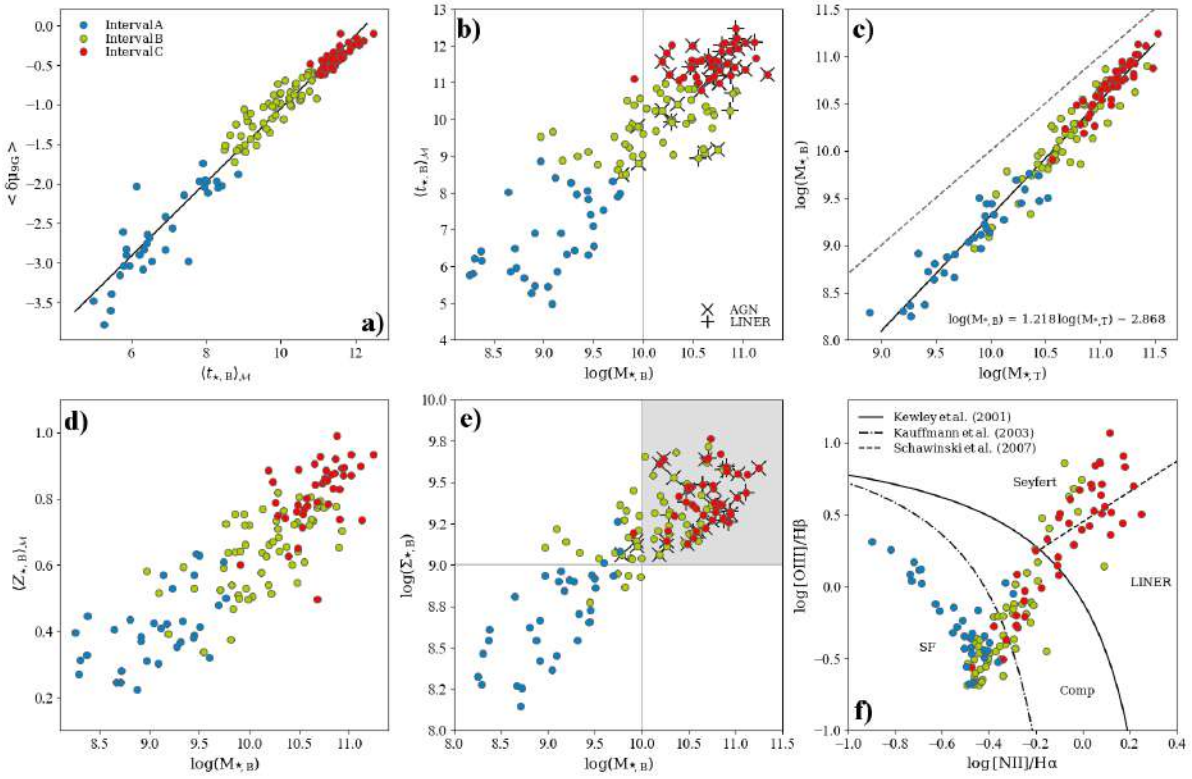

Figure 3.7: **a**) $<\delta\mu_{9G}>$ (r mag) vs. mass-weighted stellar age $\langle t_{\star,B}\rangle_{\mathcal{M}}$ (Gyr) for the bulge component of our sample LTGs. The solid line shows a linear fit to the data. **b**) Logarithm of the stellar mass $\mathcal{M}_{\star,B}$ ($M_\odot$) in the bulge vs. mass-weighted stellar age $\langle t_{\star,B}\rangle_{\mathcal{M}}$ (Gyr). Galaxies spectroscopically classified as Seyfert and LINER are marked. **c**) Logarithm of the total stellar mass $\log(\mathcal{M}_{\star,T})$ vs. $\log(\mathcal{M}_{\star,B})$. The solid and dashed lines show, respectively, a linear fit to the data and equality between both quantities. **d**) Logarithm of $\mathcal{M}_{\star,B}$ vs. mass-weighted stellar metallicity $\langle Z_{\star,B}\rangle_{\mathcal{M}}$ ($Z_\odot$). **e**) Logarithm of $\mathcal{M}_{\star,B}$ vs. logarithm of the mean stellar surface density $\Sigma_{\star,B}$ ($M_\odot$/kpc^2) in the bulge. The gray-shaded quadrant at $\log(\mathcal{M}_\star) \geq 10$ and $\log(\Sigma_{\star,B}) \geq 9$ delineates the parameter space containing 93% of all Seyfert and LINER galaxies in our sample. **f**) Spectroscopic classification after BPT within simulated 3″ SDSS fibers (method **a** in Sect. 2.4.4; cf. Fig. 2.17). These results are based on the spatially resolved analysis obtained with STARLIGHT, SSP library Z4.

0.02) · $\log(\mathcal{M}_{\star,T})$ – (1.12 ± 0.17).

The tight linear relation obtained (solid line) implies that bulges in the $<\delta\mu_{9G}>$ interval **iC** contain on average ∼ 40% of the total stellar mass whereas **iA** bulges enclose approximately half of it. Panels **d**&**e** illustrate that massive, old bulges (**iC**) are the ones exhibiting more metal enriched stellar populations and the highest $\Sigma_{\star,B}$, which in all cases exceeds 10^9 $M_\odot$/kpc^2 and reaches up to $\sim 6 \cdot 10^9$ $M_\odot$/kpc^2. The bulge stellar surface density scales as $\log(\Sigma_{\star,B}) = (4.96 \pm 0.23) + (0.42 \pm 0.02) \cdot \log(\mathcal{M}_{\star,B})$ and $\log(\Sigma_{\star,B}) = (7.63 \pm 0.09) + (0.16 \pm 0.01) \cdot \langle t_{\star,B}\rangle_{\mathcal{M}}$. Combining the evidence from panels **a**, **b** and **e**, a trend is expected between $<\delta\mu_{9G}>$ and bulge mass that can be approximated by the relation $\log(\mathcal{M}_{\star,B}) = (10.87 \pm 0.06) + (0.67 \pm$

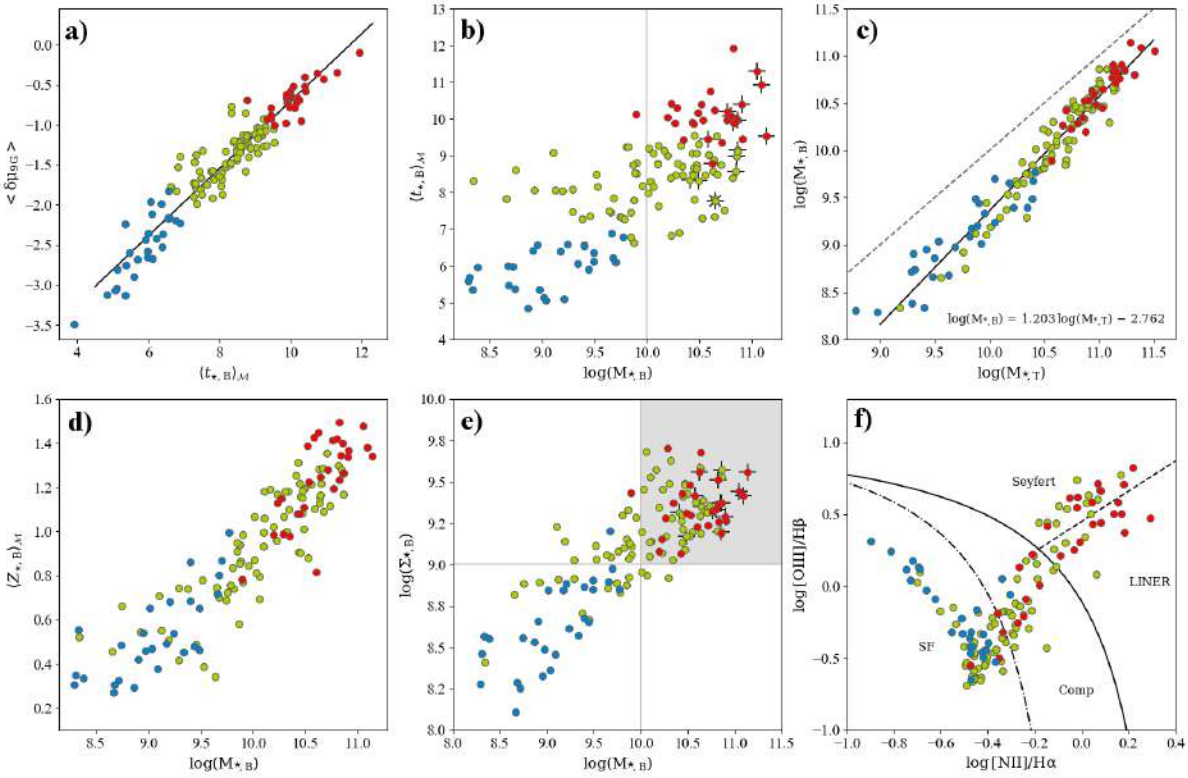

Figure 3.8: **a**) $<\delta\mu_{9G}>$ (r mag) vs. mass-weighted stellar age $\langle t_{\star,B}\rangle_{\mathcal{M}}$ (Gyr) for the bulge component, with the solid line showing a linear fit to the data. **b**) Logarithm of the stellar mass $\log(\mathcal{M}_{\star,B})$ ($M_\odot$) in the bulge vs. mass-weighted stellar age $\langle t_{\star,B}\rangle_{\mathcal{M}}$ (Gyr). Galaxies spectroscopically classified as Seyfert and LINER (cf. panel **f**) are marked. **c**) Logarithm of the total stellar mass $\log(\mathcal{M}_{\star,T})$ vs. $\log(\mathcal{M}_{\star,B})$. The solid and dashed lines show, respectively, a linear fit to the data and equality between both quantities. **d**) Logarithm of $\mathcal{M}_{\star,B}$ vs. mass-weighted stellar metallicity $\langle Z_{\star,B}\rangle_{\mathcal{M}}$ ($Z_\odot$). **e**) Logarithm of $\mathcal{M}_{\star,B}$ vs. logarithm of the mean stellar surface density $\Sigma_{\star,B}$ ($M_\odot$/kpc^2) in the bulge. **f**) Spectroscopic classification after BPT line ratios within simulated 3″ SDSS fibers (cf. Sect. 2.4.4). These results are based on the spatially resolved analysis obtained with Starlight with the SSP library Z5.

0.04) · $<\delta\mu_{9G}>$ and $\log(\Sigma_{\star,B}) = (9.56 \pm 0.03) + (0.32 \pm 0.02) \cdot <\delta\mu_{9G}>$. The resulting linear fits yield tight correlations, suggesting that $<\delta\mu_{9G}>$ offers a useful semi-empirical proxy to the evolutionary and physical properties of LTG bulges. Moreover, within the considered range of stellar metallicities ($Z_\odot$/20 to $Z_\odot$), linear fits to $\langle Z_{\star,B}\rangle_{\mathcal{M}}$ (panel **d**) yield the relations $\langle Z_{\star,B}\rangle_{\mathcal{M}}$ ($Z_\odot$) = $(0.23 \pm 0.01) \cdot \log(\mathcal{M}_{\star,B})$ – (1.60 ± 0.11) and $\langle Z_{\star,B}\rangle_{\mathcal{M}}$ ($Z_\odot$) = $(0.28 \pm 0.02) \cdot \log(\mathcal{M}_{\star,T})$ – (2.37 ± 0.15). We note that these results are qualitatively consistent with reports from other studies, for example Thomas & Davies (2006), that by means of Lick index indicates that less massive bulges display the lowest light-weighted ages and late enrichment in iron from SNe Ia, contrary to high mass bulges.

Comparison of Fig. 3.7 with Fig. 3.8 shows that the AMD is reflected in an increase of the

metallicity and decrease in the age of high-$\mathcal{M}_\star$ bulges. However the effect on $<\delta\mu_{9\mathrm{G}}>$ by performing spectral modeling with the Z5 SSP library is relatively small ($\pm$ 0.5 mag) (also for $\mathcal{M}_\star$ which displays $\leq$ 0.2-0.3 dex difference between Z4 & Z5 results) and there are no significant differences in the trends between $<\delta\mu_{9\mathrm{G}}>$ and physical and evolutionary quantities of LTG bulges. The key insight obtained from this analysis is that all main physical properties of bulges comprising a representative sample of local LTGs are distributed linearly showing a continuity instead of a segregation in two nodes (a bimodality), as should be the expected result from two distinct formation routes.

Table 3.2 provides a synopsis of relations inferred from regression analysis for quantities obtained from spectral modeling with the Z4 and Z5 SSP libraries (panels **a**-**e** in Figs. 3.7 & 3.8, respectively). The upper block lists relations computed by minimizing χ^2 with regard to both quantities considered, whereas the lower block refers to fits where χ^2 minimization was done only with regard to the quantity listed in the right-hand side of each equation. Table 3.3 presents photometric, evolutionary and physical quantities for the galaxy sample as obtained by the spatially resolved analysis with STARLIGHT adopting SSP library Z4.

Z4 SSP Library	Z5 SSP Library
$\langle t_{\star,\mathrm{B}}\rangle_{\mathcal{M}} = (2.05\pm0.04) \cdot <\delta\mu_{9\mathrm{G}}> + (12.14\pm0.06)$	$\langle t_{\star,\mathrm{B}}\rangle_{\mathcal{M}} = (2.26\pm0.07) \cdot <\delta\mu_{9\mathrm{G}}> + (11.52\pm0.11)$
$\langle t_{\star,\mathrm{B}}\rangle_{\mathcal{M}} = (2.30\pm0.11) \cdot \log(\mathcal{M}_{\star,\mathrm{B}})$ - (13.44 ± 1.13)	$\langle t_{\star,\mathrm{B}}\rangle_{\mathcal{M}} = (1.69\pm0.12) \cdot \log(\mathcal{M}_{\star,\mathrm{B}})$ - (8.71 ± 1.23)
$\log(\Sigma_{\star,\mathrm{B}}) = (0.42\pm0.02) \cdot \log(\mathcal{M}_{\star,\mathrm{B}}) + (4.96\pm0.23)$	$\log(\Sigma_{\star,\mathrm{B}}) = (0.39\pm0.02) \cdot \log(\mathcal{M}_{\star,\mathrm{B}}) + (5.20\pm0.24)$
$\log(\Sigma_{\star,\mathrm{B}}) = (0.16\pm0.01) \cdot \langle t_{\star,\mathrm{B}}\rangle_{\mathcal{M}} + (7.63\pm0.09)$	$\log(\Sigma_{\star,\mathrm{B}}) = (0.16\pm0.01) \cdot \langle t_{\star,\mathrm{B}}\rangle_{\mathcal{M}} + (7.76\pm0.10)$
$\log(\Sigma_{\star,\mathrm{B}}) = (0.32\pm0.02) \cdot <\delta\mu_{9\mathrm{G}}> + (9.56\pm0.03)$	$\log(\Sigma_{\star,\mathrm{B}}) = (0.39\pm0.03) \cdot <\delta\mu_{9\mathrm{G}}> + (9.69\pm0.05)$
$\langle Z_{\star,\mathrm{B}}\rangle_{\mathcal{M}} = (0.23\pm0.01) \cdot \log(\mathcal{M}_{\star,\mathrm{B}})$ - (1.60 ± 0.11)	$\langle Z_{\star,\mathrm{B}}\rangle_{\mathcal{M}} = (0.42\pm0.02) \cdot \log(\mathcal{M}_{\star,\mathrm{B}})$ - (3.26 ± 0.17)
$\langle Z_{\star,\mathrm{B}}\rangle_{\mathcal{M}} = (0.28\pm0.01) \cdot \log(\mathcal{M}_{\star,\mathrm{T}})$ - (2.30 ± 0.15)	$\langle Z_{\star,\mathrm{B}}\rangle_{\mathcal{M}} = (0.51\pm0.02) \cdot \log(\mathcal{M}_{\star,\mathrm{T}})$ - (4.48 ± 0.23)
$\langle t_{\star,\mathrm{D}}\rangle_{\mathcal{M}} = (1.88\pm0.12) \cdot \log(\mathcal{M}_{\star,\mathrm{T}})$ - (11.85 ± 1.32)	$\langle t_{\star,\mathrm{D}}\rangle_{\mathcal{M}} = (1.42\pm0.12) \cdot \log(\mathcal{M}_{\star,\mathrm{T}})$ - (7.86 ± 1.25)
$\langle Z_{\star,\mathrm{D}}\rangle_{\mathcal{M}} = (0.20\pm0.02) \cdot \log(\mathcal{M}_{\star,\mathrm{T}})$ - (1.55 ± 0.16)	$\langle Z_{\star,\mathrm{D}}\rangle_{\mathcal{M}} = (0.29\pm0.02) \cdot \log(\mathcal{M}_{\star,\mathrm{T}})$ - (2.31 ± 0.20)
$\log(\mathcal{M}_{\star,\mathrm{B}}) = (0.67\pm0.04) \cdot <\delta\mu_{9\mathrm{G}}> + (10.87\pm0.06)$	$\log(\mathcal{M}_{\star,\mathrm{B}}) = (0.86\pm0.06) \cdot <\delta\mu_{9\mathrm{G}}> + (11.26\pm0.09)$
$\log(\mathcal{M}_{\star,\mathrm{B}}) = (1.22\pm0.02) \cdot \log(\mathcal{M}_{\star,\mathrm{T}})$ - (2.87 ± 0.25)	$\log(\mathcal{M}_{\star,\mathrm{B}}) = (1.20\pm0.03) \cdot \log(\mathcal{M}_{\star,\mathrm{T}})$ - (2.67 ± 0.27)
$\mathcal{M}_{\star,\mathrm{B}}/\mathcal{M}_{\star,\mathrm{T}} = (0.13\pm0.02) \cdot \log(\mathcal{M}_{\star,\mathrm{T}})$ - (1.12 ± 0.17)	$\mathcal{M}_{\star,\mathrm{B}}/\mathcal{M}_{\star,\mathrm{T}} = (0.13\pm0.02)\cdot \log(\mathcal{M}_{\star,\mathrm{T}})$ - (1.09 ± 0.18)
$\langle t_{\star,\mathrm{B}}\rangle_{\mathcal{M}} = (1.21\pm0.06) \cdot \langle t_{\star,\mathrm{D}}\rangle_{\mathcal{M}}$ - (0.18 ± 0.49)	$\langle t_{\star,\mathrm{B}}\rangle_{\mathcal{M}} = (1.07\pm0.08) \cdot \langle t_{\star,\mathrm{D}}\rangle_{\mathcal{M}} + (0.64\pm0.55)$
$\langle Z_{\star,\mathrm{B}}\rangle_{\mathcal{M}} = (1.09\pm0.05) \cdot \langle Z_{\star,\mathrm{D}}\rangle_{\mathcal{M}} + (0.05\pm0.03)$	$\langle Z_{\star,\mathrm{B}}\rangle_{\mathcal{M}} = (1.42\pm0.06) \cdot \langle Z_{\star,\mathrm{D}}\rangle_{\mathcal{M}}$ - (0.17 ± 0.04)
$\delta t_{\mathrm{BD}} = (1.00\pm0.12) \cdot \log(\mathcal{M}_{\star,\mathrm{T}})$ - (9.07 ± 1.28)	$\delta t_{\mathrm{BD}} = (0.74\pm0.14) \cdot \log(\mathcal{M}_{\star,\mathrm{T}})$ - (6.65 ± 1.45)
$\delta Z_{\mathrm{BD}} = (0.08\pm0.01) \cdot \log(\mathcal{M}_{\star,\mathrm{T}})$ - (0.75 ± 0.12)	$\delta Z_{\mathrm{BD}} = (0.22\pm0.02) \cdot \log(\mathcal{M}_{\star,\mathrm{T}})$ - (2.18 ± 0.16)
$\langle t_{\star,\mathrm{B}}\rangle_{\mathcal{M}} = (2.13\pm0.04) \cdot <\delta\mu_{9\mathrm{G}}> + (12.23\pm0.23)$	$\langle t_{\star,\mathrm{B}}\rangle_{\mathcal{M}} = (2.49\pm0.07) \cdot <\delta\mu_{9\mathrm{G}}> + (11.86\pm0.37)$
$\langle t_{\star,\mathrm{B}}\rangle_{\mathcal{M}} = (2.93\pm0.15) \cdot \log(\mathcal{M}_{\star,\mathrm{B}})$ - (19.81 ± 1.06)	$\langle t_{\star,\mathrm{B}}\rangle_{\mathcal{M}} = (2.66\pm0.20) \cdot \log(\mathcal{M}_{\star,\mathrm{B}})$ - (18.39 ± 1.45)
$\log(\Sigma_{\star,\mathrm{B}}) = (0.44\pm0.03) \cdot \log(\mathcal{M}_{\star,\mathrm{B}}) + (4.70\pm0.30)$	$\log(\Sigma_{\star,\mathrm{B}}) = (0.42\pm0.03) \cdot \log(\mathcal{M}_{\star,\mathrm{B}}) + (4.93\pm0.31)$
$\log(\Sigma_{\star,\mathrm{B}}) = (0.16\pm0.01) \cdot \langle t_{\star,\mathrm{B}}\rangle_{\mathcal{M}} + (7.62\pm0.10)$	$\log(\Sigma_{\star,\mathrm{B}}) = (0.17\pm0.01) \cdot \langle t_{\star,\mathrm{B}}\rangle_{\mathcal{M}} + (7.74\pm0.12)$
$\log(\Sigma_{\star,\mathrm{B}}) = (0.34\pm0.02) \cdot <\delta\mu_{9\mathrm{G}}> + (9.58\pm0.07)$	$\log(\Sigma_{\star,\mathrm{B}}) = (0.43\pm0.03) \cdot <\delta\mu_{9\mathrm{G}}> + (9.75\pm0.14)$
$\langle Z_{\star,\mathrm{B}}\rangle_{\mathcal{M}} = (0.24\pm0.01) \cdot \log(\mathcal{M}_{\star,\mathrm{B}})$ - (1.64 ± 0.11)	$\langle Z_{\star,\mathrm{B}}\rangle_{\mathcal{M}} = (0.43\pm0.02) \cdot \log(\mathcal{M}_{\star,\mathrm{B}})$ - (3.40 ± 0.15)
$\langle Z_{\star,\mathrm{B}}\rangle_{\mathcal{M}} = (0.28\pm0.02) \cdot \log(\mathcal{M}_{\star,\mathrm{T}})$ - (2.37 ± 0.15)	$\langle Z_{\star,\mathrm{B}}\rangle_{\mathcal{M}} = (0.54\pm0.02) \cdot \log(\mathcal{M}_{\star,\mathrm{T}})$ - (4.76 ± 0.20)
$\langle t_{\star,\mathrm{D}}\rangle_{\mathcal{M}} = (2.80\pm0.19) \cdot \log(\mathcal{M}_{\star,\mathrm{T}})$ - (21.56 ± 1.48)	$\langle t_{\star,\mathrm{D}}\rangle_{\mathcal{M}} = (2.44\pm0.21) \cdot \log(\mathcal{M}_{\star,\mathrm{T}})$ - (18.64 ± 1.65)
$\langle Z_{\star,\mathrm{D}}\rangle_{\mathcal{M}} = (0.21\pm0.02) \cdot \log(\mathcal{M}_{\star,\mathrm{T}})$ - (1.61 ± 0.16)	$\langle Z_{\star,\mathrm{D}}\rangle_{\mathcal{M}} = (0.31\pm0.02) \cdot \log(\mathcal{M}_{\star,\mathrm{T}})$ - (2.45 ± 0.20)
$\log(\mathcal{M}_{\star,\mathrm{B}}) = (0.76\pm0.04) \cdot <\delta\mu_{9\mathrm{G}}> + (10.98\pm0.30)$	$\log(\mathcal{M}_{\star,\mathrm{B}}) = (1.11\pm0.08) \cdot <\delta\mu_{9\mathrm{G}}> + (11.63\pm0.57)$
$\log(\mathcal{M}_{\star,\mathrm{B}}) = (1.26\pm0.02) \cdot \log(\mathcal{M}_{\star,\mathrm{T}})$ - (3.27 ± 0.23)	$\log(\mathcal{M}_{\star,\mathrm{B}}) = (1.25\pm0.03) \cdot \log(\mathcal{M}_{\star,\mathrm{T}})$ - (3.12 ± 0.24)
$\mathcal{M}_{\star,\mathrm{B}}/\mathcal{M}_{\star,\mathrm{T}} = (0.14\pm0.02) \cdot \log(\mathcal{M}_{\star,\mathrm{T}})$ - (1.17 ± 0.17)	$\mathcal{M}_{\star,\mathrm{B}}/\mathcal{M}_{\star,\mathrm{T}} = (0.14\pm0.02) \cdot \log(\mathcal{M}_{\star,\mathrm{T}})$ - (1.15 ± 0.19)
$\langle t_{\star,\mathrm{B}}\rangle_{\mathcal{M}} = (1.46\pm0.07) \cdot \langle t_{\star,\mathrm{D}}\rangle_{\mathcal{M}}$ - (2.23 ± 0.54)	$\langle t_{\star,\mathrm{B}}\rangle_{\mathcal{M}} = (1.52\pm0.12) \cdot \langle t_{\star,\mathrm{D}}\rangle_{\mathcal{M}}$ - (2.56 ± 0.70)
$\langle Z_{\star,\mathrm{B}}\rangle_{\mathcal{M}} = (1.26\pm0.06) \cdot \langle Z_{\star,\mathrm{D}}\rangle_{\mathcal{M}}$ - (0.04 ± 0.03)	$\langle Z_{\star,\mathrm{B}}\rangle_{\mathcal{M}} = (1.63\pm0.07) \cdot \langle Z_{\star,\mathrm{D}}\rangle_{\mathcal{M}}$ - (0.33 ± 0.04)
$\delta t_{\mathrm{BD}} = (2.35\pm0.31) \cdot \log(\mathcal{M}_{\star,\mathrm{T}})$ - (23.42 ± 2.68)	$\delta t_{\mathrm{BD}} = (3.11\pm0.64) \cdot \log(\mathcal{M}_{\star,\mathrm{T}})$ - (31.57 ± 6.00)
$\delta Z_{\mathrm{BD}} = (0.08\pm0.01) \cdot \log(\mathcal{M}_{\star,\mathrm{T}})$ - (0.76 ± 0.12)	$\delta Z_{\mathrm{BD}} = (0.23\pm0.01) \cdot \log(\mathcal{M}_{\star,\mathrm{T}})$ - (2.25 ± 0.16)

Table 3.2: Overview of the fits obtained for quantities inferred from analysis of the LTG sample with the Z4 and Z5 SSP library. The $<\delta\mu_{9\mathrm{G}}>$ is expressed in SDSS r mag, $\langle t_{\star,\mathrm{B}}\rangle_{\mathcal{M}}$ and $\langle t_{\star,\mathrm{D}}\rangle_{\mathcal{M}}$ in Gyr, $\mathcal{M}_{\star,\mathrm{B}}$ and $\mathcal{M}_{\star,\mathrm{T}}$ in $\mathrm{M}_{\odot}$, $\Sigma_{\star,\mathrm{B}}$ in 10^9 $\mathrm{M}_{\odot}/\mathrm{kpc}^2$ and $\langle Z_{\star,\mathrm{B}}\rangle_{\mathcal{M}}$ in $\mathrm{Z}_{\odot}$.

Table 3.3: Photometric, evolutionary and physical quantities for the galaxy sample under study. **Col. 1:** name of the galaxy, **Col. 2:** adopted distance in Mpc, **Col. 3:** isophotal radius of the bulge (R_B) in kpc, **Col. 4:** logarithm of the total stellar mass ($\mathcal{M}_{\star,T}$ in $M_\odot$), **Col. 5:** logarithm of the present-day stellar mass ($\mathcal{M}_{\star,B}$ in $M_\odot$) within R_B, **Cols. 6&7:** mean mass-weighted stellar age of the bulge ($\langle t_{\star,B}\rangle_{\mathcal{M}}$ in Gyr) and its dispersion ($\sigma\ \langle t_{\star,B}\rangle_{\mathcal{M}}$), **Cols. 8&9:** mean mass-weighted stellar age of the disk ($\langle t_{\star,D}\rangle_{\mathcal{M}}$ in Gyr) and its dispersion ($\sigma\ \langle t_{\star,D}\rangle_{\mathcal{M}}$), **Cols. 10&11:** mean mass-weighted stellar metallicity of the bulge ($\langle Z_{\star,B}\rangle_{\mathcal{M}}$ in $Z_\odot$) and its dispersion ($\sigma\ \langle Z_{\star,B}\rangle_{\mathcal{M}}$), **Cols. 12&13:** mean mass-weighted stellar metallicity of the disk ($\langle Z_{\star,D}\rangle_{\mathcal{M}}$ in $Z_\odot$) and its dispersion ($\sigma\ \langle Z_{\star,B}\rangle_{\mathcal{M}}$), **Col. 14:** logarithm of the mean stellar mass surface density in the bulge ($\Sigma_{\star,B}$ in $M_\odot/kpc^2$) and **Col. 15:** mean $<\delta\mu_{9G}>$ (r mag) within R_B. Quantities listed in cols. 4–15 were obtained from spectral modeling with STARLIGHT of CALIFA V500 data with the Z4 SSP library and refer to the present-day $\mathcal{M}_\star$.

Name	Distance (Mpc) (2)	R_B (kpc) (3)	$\log(\mathcal{M}_{\star,T})$ ($M_\odot$) (4)	$\log(\mathcal{M}_{\star,B})$ ($M_\odot$) (5)	$\langle t_{\star,B}\rangle_{\mathcal{M}}$ (Gyr) (6)	$\sigma\ \langle t_{\star,B}\rangle_{\mathcal{M}}$ (Gyr) (7)	$\langle t_{\star,D}\rangle_{\mathcal{M}}$ (Gyr) (8)	$\sigma\ \langle t_{\star,D}\rangle_{\mathcal{M}}$ (Gyr) (9)	$\langle Z_{\star,B}\rangle_{\mathcal{M}}$ ($Z_\odot$) (10)	$\sigma\ \langle Z_{\star,B}\rangle_{\mathcal{M}}$ ($Z_\odot$) (11)	$\langle Z_{\star,D}\rangle_{\mathcal{M}}$ ($Z_\odot$) (12)	$\sigma\ \langle Z_{\star,D}\rangle_{\mathcal{M}}$ ($Z_\odot$) (13)	$\log(\Sigma_{\star,B})$ ($M_\odot/kpc^2$) (14)	$<\delta\mu_{9G}>$ (mag) (15)
CGCG163_062	68.1	1.37	9.95	9.31	6.43	0.89	4.80	0.76	0.37	0.22	0.34	0.22	8.54	-2.64
IC0159	52.0	0.87	10.12	9.27	8.28	1.14	6.67	1.19	0.35	0.16	0.38	0.19	8.90	-1.97
IC0208	46.6	1.22	10.25	9.44	9.11	0.99	7.68	1.01	0.53	0.24	0.62	0.31	8.77	-1.20
IC0776	40.2	1.07	9.58	8.71	6.49	1.02	7.41	1.12	0.25	0.10	0.30	0.16	8.15	-2.67
IC1256	72.1	1.44	10.93	10.13	10.85	0.67	8.67	1.03	0.77	0.32	0.68	0.31	9.32	-0.63
IC1528	51.6	1.01	10.52	9.83	10.51	0.71	6.95	0.98	0.47	0.18	0.44	0.22	9.33	-0.94
IC1683	65.4	1.91	10.85	10.53	11.16	0.73	8.28	0.99	0.71	0.32	0.72	0.36	9.47	-0.60
IC2604	28.9	0.46	9.26	8.37	6.42	0.97	6.81	0.99	0.33	0.15	0.38	0.27	8.54	-2.75
IC3918	97.7	1.17	9.85	9.09	4.99	1.27	6.13	1.11	0.30	0.14	0.36	0.22	8.45	-3.48
IC4566	86.3	2.97	11.16	10.79	12.03	0.50	9.81	0.82	0.78	0.47	0.72	0.38	9.35	-0.20
MCG01_10_019	69.9	1.63	10.43	9.86	9.24	0.89	8.78	0.92	0.75	0.33	0.67	0.33	8.94	-1.27
MCG09_22_053	55.0	1.18	9.89	9.50	6.55	0.94	6.56	1.00	0.41	0.15	0.34	0.16	8.86	-2.98
NGC0001	61.6	1.92	10.99	10.68	9.76	0.97	8.12	0.98	0.77	0.30	0.59	0.27	9.62	-1.18
NGC0036	81.0	2.52	11.22	10.76	10.99	0.93	9.11	0.91	0.86	0.50	0.72	0.36	9.46	-0.61
NGC0160	70.5	3.14	11.18	10.85	11.54	0.63	8.86	0.80	0.88	0.57	0.85	0.57	9.36	-0.44
NGC0165	78.9	2.00	10.85	10.29	9.97	0.76	9.01	0.98	0.68	0.34	0.58	0.27	9.19	-0.86
NGC0171	52.8	1.98	10.92	10.47	11.44	0.76	9.00	0.90	0.76	0.51	0.65	0.34	9.38	-0.40
NGC0180	70.6	2.17	11.14	10.84	11.51	0.63	10.39	0.84	0.83	0.49	0.82	0.39	9.67	-0.44
NGC0214	61.0	1.88	11.16	10.68	11.43	0.65	9.21	0.85	0.79	0.40	0.64	0.39	9.64	-0.51
NGC0234	59.7	2.33	11.00	10.48	10.54	0.89	8.67	1.04	0.73	0.32	0.62	0.27	9.25	-0.92
NGC0237	55.9	1.22	10.58	9.97	9.81	0.99	7.92	1.01	0.53	0.23	0.41	0.19	9.30	-1.03
NGC0257	70.4	2.66	11.13	10.69	10.24	0.87	8.36	0.88	0.78	0.33	0.60	0.34	9.34	-0.98

NGC0309	75.8	2.78	11.1	10.55	10.99	0.72	9.29	0.95	0.77	0.48	0.68	0.30	9.16	-0.61
NGC0447	75.1	3.81	11.53	11.24	11.21	0.62	9.14	1.00	0.93	0.60	0.80	0.43	9.59	-0.57
NGC0477	79.1	1.89	10.78	10.29	9.99	0.83	8.52	0.95	0.71	0.33	0.57	0.23	9.24	-0.99
NGC0496	80.5	1.48	10.72	9.88	9.86	0.73	8.42	0.97	0.51	0.19	0.42	0.19	9.04	-1.13
NGC0768	93.3	1.90	10.89	10.35	11.07	0.64	8.14	0.98	0.74	0.34	0.48	0.21	9.30	-0.55
NGC0776	65.5	2.44	11.09	10.76	11.57	0.58	9.29	0.94	0.86	0.44	0.67	0.31	9.48	-0.30
NGC0873	53.2	1.10	10.76	10.22	10.95	0.76	8.35	1.11	0.51	0.23	0.47	0.23	9.63	-0.92
NGC0941	21.3	0.47	9.48	8.64	8.02	0.97	6.48	1.08	0.41	0.15	0.36	0.19	8.81	-1.97
NGC0976	57.0	2.49	11.05	10.86	10.23	0.73	7.91	0.78	0.78	0.44	0.62	0.42	9.58	-0.94
NGC0991	20.2	0.70	9.49	8.81	5.69	0.94	6.23	1.07	0.43	0.19	0.39	0.19	8.62	-3.16
NGC1070	54.0	2.55	11.23	10.91	12.07	0.48	10.82	0.70	0.83	0.48	0.76	0.39	9.59	-0.18
NGC1093	70.8	1.10	10.85	10.19	11.58	0.57	9.46	0.93	0.89	0.49	0.69	0.29	9.61	-0.29
NGC1094	85.8	2.77	11.06	10.74	9.18	0.84	9.01	0.87	0.77	0.37	0.53	0.30	9.36	-1.43
NGC1590	52.2	0.87	10.6	10.03	10.29	0.94	7.57	0.89	0.51	0.21	0.39	0.22	9.65	-1.02
NGC1645	65.9	1.92	11.04	10.71	11.18	0.93	9.52	0.73	0.93	0.71	0.71	0.41	9.65	-0.54
NGC1659	61.7	1.38	10.73	10.2	9.38	0.95	8.03	1.04	0.66	0.38	0.55	0.34	9.42	-1.39
NGC1667	61.2	2.63	11.27	10.91	11.4	0.70	9.61	0.84	0.74	0.37	0.54	0.27	9.57	-0.55
NGC2253	51.3	1.25	10.9	10.37	10.84	0.79	9.35	0.95	0.66	0.25	0.52	0.20	9.68	-0.58
NGC2347	63.0	1.72	11.12	10.73	11.59	0.64	10.13	0.88	0.85	0.43	0.59	0.25	9.77	-0.36
NGC2486	66.3	1.87	10.93	10.5	12.00	0.45	10.28	0.67	0.89	0.69	0.77	0.45	9.45	-0.23
NGC2487	68.9	2.68	11.07	10.66	11.07	0.76	9.47	0.90	0.84	0.45	0.67	0.32	9.3	-0.62
NGC2530	71.7	1.51	10.55	9.90	9.01	1.01	6.91	1.05	0.5	0.22	0.36	0.17	9.04	-1.58
NGC2540	89.0	1.72	10.79	10.13	9.69	0.85	7.77	1.00	0.64	0.31	0.48	0.24	9.16	-1.35
NGC2543	37.4	1.5	10.58	10.23	10.55	0.71	8.35	0.97	0.67	0.36	0.53	0.25	9.38	-0.88
NGC2558	71.6	2.15	11.01	10.65	11.69	0.62	9.51	0.79	0.91	0.62	0.81	0.49	9.48	-0.34
NGC2595	62.7	2.35	11.00	10.58	11.6	0.56	9.50	0.87	0.78	0.41	0.66	0.31	9.34	-0.36
NGC2604	32.3	0.59	9.91	8.97	8.86	0.86	6.49	0.98	0.31	0.17	0.34	0.21	8.94	-1.87
NGC2730	56.7	1.04	10.44	9.47	7.42	0.98	6.87	0.98	0.63	0.19	0.43	0.20	8.94	-2.14
NGC2780	31.8	0.49	9.98	9.09	9.67	0.88	7.84	0.98	0.52	0.18	0.53	0.26	9.22	-0.98
NGC2805	28.7	0.69	9.99	9.13	5.87	0.93	6.96	0.97	0.57	0.21	0.46	0.25	8.96	-2.90
NGC2906	33.5	1.11	10.68	10.23	11.80	0.51	9.66	0.92	0.85	0.43	0.60	0.27	9.64	-0.20
NGC2916	56.0	2.86	11.00	10.61	9.09	0.98	8.84	0.97	0.81	0.45	0.52	0.25	9.20	-1.14
NGC3057	25.9	0.96	9.43	8.72	5.96	0.93	6.41	1.07	0.28	0.11	0.32	0.16	8.26	-3.03

NGC3381	28.8	0.72	9.91	9.11	8.42	0.98	6.95	1.14	0.41	0.17	0.40	0.17	8.90	-2.02
NGC3614	38.4	1.41	10.37	9.74	8.64	1.16	7.87	1.07	0.59	0.23	0.51	0.22	8.95	-1.39
NGC3687	41.1	2.13	10.55	10.27	9.96	1.10	8.74	0.97	0.73	0.34	0.59	0.25	9.11	-0.84
NGC3811	49.0	2.08	10.74	10.43	9.88	1.06	7.70	1.07	0.60	0.25	0.49	0.22	9.29	-0.97
NGC3913	19.2	0.75	9.34	8.91	6.91	0.98	6.81	1.03	0.38	0.16	0.39	0.20	8.67	-2.83
NGC4047	53.3	2.28	10.99	10.63	10.22	0.88	9.39	0.96	0.73	0.29	0.55	0.21	9.42	-0.91
NGC4185	61.0	2.04	10.95	10.26	11.22	0.64	10.43	0.79	0.79	0.40	0.80	0.40	9.15	-0.38
NGC4210	43.2	1.41	10.57	9.94	9.80	0.95	8.8	1.02	0.75	0.33	0.61	0.23	9.15	-0.88
NGC4711	63.3	1.25	10.82	9.86	9.77	0.98	7.93	0.94	0.64	0.25	0.46	0.22	9.17	-1.02
NGC4961	42.5	0.60	10.01	9.19	8.87	1.02	7.13	1.06	0.39	0.14	0.29	0.14	9.14	-1.54
NGC5000	84.9	2.18	11.02	10.54	11.57	0.52	9.87	0.84	0.75	0.44	0.64	0.32	9.36	-0.25
NGC5016	43.5	0.96	10.59	9.91	10.4	0.76	8.73	0.89	0.64	0.28	0.53	0.28	9.45	-0.77
NGC5056	84.6	1.74	10.91	10.4	11.14	0.66	8.18	0.98	0.63	0.29	0.48	0.20	9.42	-0.50
NGC5157	108.0	3.84	11.32	10.93	12.48	0.47	9.72	0.86	0.89	0.69	0.78	0.40	9.26	-0.1
NGC5205	30.9	1.30	10.15	9.79	8.49	1.12	7.44	0.94	0.64	0.30	0.44	0.23	9.06	-1.57
NGC5320	43.6	1.34	10.59	9.96	10.57	0.84	8.85	1.00	0.66	0.27	0.51	0.21	9.21	-0.66
NGC5378	49.6	2.69	10.79	10.49	11.40	0.71	9.98	0.76	0.78	0.46	0.73	0.42	9.13	-0.34
NGC5406	79.0	3.61	11.34	11.02	12.09	0.50	9.94	0.80	0.93	0.61	0.73	0.35	9.4	-0.24
NGC5480	32.9	1.23	10.35	9.76	7.97	0.94	7.94	1.06	0.50	0.23	0.44	0.22	9.09	-1.95
NGC5519	111.3	2.64	11.20	10.93	10.76	0.56	8.32	0.98	0.70	0.33	0.65	0.28	9.59	-0.83
NGC5622	60.2	1.29	10.56	9.91	11.09	0.69	8.96	0.99	0.6	0.27	0.52	0.21	9.19	-0.43
NGC5633	39.6	1.10	10.63	10.12	10.23	0.86	8.61	1.00	0.58	0.22	0.39	0.18	9.54	-1.00
NGC5656	51.4	1.86	10.86	10.49	9.99	0.95	8.40	0.95	0.64	0.23	0.41	0.17	9.45	-0.85
NGC5665	37.3	1.05	10.52	9.81	9.33	0.91	7.89	1.14	0.37	0.15	0.43	0.19	9.27	-1.51
NGC5720	113.0	3.09	11.20	10.75	11.36	1.05	8.78	0.97	0.85	0.55	0.68	0.31	9.27	-0.49
NGC5732	59.3	1.17	10.29	9.71	9.54	0.88	7.36	0.94	0.53	0.18	0.33	0.15	9.08	-1.23
NGC5735	59.6	2.06	10.68	10.19	10.24	0.90	7.60	1.04	0.54	0.25	0.50	0.24	9.06	-0.84
NGC5772	74.8	3.62	11.2	10.94	12.2	0.46	10.13	0.79	0.87	0.59	0.70	0.35	9.33	-0.19
NGC5829	85.8	1.68	10.65	9.99	9.6	1.00	7.68	1.04	0.72	0.33	0.52	0.27	9.04	-1.3
NGC5888	126.7	3.59	11.48	10.88	11.19	0.92	8.49	1.00	0.99	0.32	0.88	0.31	9.27	-0.44
NGC5947	88.0	2.55	10.85	10.5	10.83	0.99	8.04	1.05	0.80	0.38	0.63	0.24	9.19	-0.62
NGC5950	43.3	1.00	10.05	9.54	8.77	0.84	7.85	1.06	0.34	0.13	0.42	0.29	9.04	-1.72
NGC5957	32.0	1.48	10.43	9.95	8.80	1.19	8.78	0.92	0.72	0.37	0.75	0.38	9.11	-1.24

NGC6004	60.8	2.56	10.95	10.45	10.82	0.71	8.61	0.93	0.72	0.34	0.59	0.26	9.13	-0.69
NGC6032	67.0	1.71	10.73	10.17	10.72	0.87	8.90	0.90	0.63	0.35	0.67	0.42	9.21	-0.59
NGC6063	46.7	0.76	10.36	9.34	9.01	1.02	7.58	1.03	0.60	0.20	0.50	0.22	9.08	-1.05
NGC6154	88.7	3.47	11.21	10.86	11.86	0.60	9.61	0.93	0.92	0.68	0.80	0.40	9.29	-0.28
NGC6155	40.3	0.98	10.44	9.74	7.91	1.04	6.29	1.01	0.61	0.19	0.44	0.20	9.26	-1.74
NGC6301	120.3	2.74	11.32	10.62	10.36	0.66	8.63	0.89	0.74	0.42	0.63	0.34	9.25	-0.88
NGC6941	88.6	2.97	11.31	10.81	12.08	0.57	9.89	0.79	0.87	0.62	0.73	0.43	9.37	-0.2
NGC7321	97.9	3.07	11.32	11.02	11.36	0.68	8.62	0.96	0.87	0.47	0.61	0.27	9.55	-0.42
NGC7489	85.1	1.75	11.18	10.48	10.07	0.80	8.03	0.88	0.55	0.25	0.44	0.23	9.49	-1.19
NGC7653	58.3	2.68	10.84	10.55	8.94	0.91	7.27	0.98	0.61	0.24	0.47	0.21	9.20	-1.39
NGC7691	55.2	1.10	10.52	9.50	7.10	0.87	7.32	0.71	0.63	0.32	0.67	0.49	8.92	-2.56
NGC7716	35.6	1.44	10.64	10.34	10.40	1.08	9.17	0.92	0.76	0.36	0.50	0.22	9.53	-0.73
NGC7738	91.4	3.47	11.34	11.12	11.66	0.60	9.46	0.81	0.74	0.45	0.78	0.43	9.55	-0.40
NGC7782	72.6	3.87	11.42	11.11	12.09	0.32	10.26	0.70	0.90	0.74	0.66	0.38	9.44	-0.21
NGC7800	24.7	0.83	9.60	8.88	5.28	1.15	4.79	1.05	0.22	0.10	0.24	0.13	8.54	-3.78
NGC7819	67.2	1.91	10.46	9.99	9.03	0.93	6.94	1.02	0.50	0.22	0.46	0.20	8.93	-1.5
UGC00312	58.5	1.10	10.31	9.60	7.53	0.96	6.17	1.04	0.32	0.14	0.28	0.15	9.02	-2.98
UGC02311	94.5	3.01	10.97	10.60	9.19	0.85	7.80	0.95	0.72	0.42	0.56	0.29	9.15	-1.11
UGC02443	33.2	0.48	9.85	8.97	9.53	1.08	7.55	0.94	0.58	0.24	0.42	0.21	9.10	-1.02
UGC03253	59.5	1.77	10.96	10.71	10.11	0.79	9.12	0.91	0.79	0.49	0.61	0.27	9.71	-0.69
UGC03973	93.1	3.02	11.11	10.68	11.59	0.51	10.33	0.71	0.50	0.33	0.50	0.27	9.23	-0.1
UGC04195	69.8	1.94	10.82	10.28	12.02	0.44	9.81	0.87	0.75	0.46	0.72	0.36	9.21	-0.15
UGC04262	80.8	2.75	10.96	10.58	10.79	0.84	10.29	0.81	0.80	0.44	0.70	0.35	9.20	-0.48
UGC04308	52.1	1.73	11.07	10.3	9.04	0.90	8.05	1.03	0.64	0.32	0.54	0.25	9.32	-1.59
UGC04375	31.7	0.90	10.41	9.76	8.81	0.82	8.11	0.90	0.73	0.37	0.63	0.30	9.36	-1.57
UGC04455	130.0	3.05	11.3	10.78	11.85	0.43	8.21	0.64	0.86	0.68	0.62	0.42	9.32	-0.32
UGC05520	50.1	1.40	9.96	9.44	6.31	0.89	7.18	0.99	0.39	0.15	0.28	0.15	8.66	-3.08
UGC05976	22.6	0.57	8.89	8.29	5.80	0.91	6.55	1.03	0.27	0.12	0.35	0.23	8.28	-3.03
UGC06517	40.9	0.82	9.94	9.23	6.34	1.10	6.78	0.98	0.53	0.19	0.41	0.17	8.91	-2.83
UGC06616	22.2	0.52	9.27	8.25	5.78	1.01	6.22	0.97	0.40	0.17	0.41	0.27	8.33	-2.61
UGC06930	15.5	0.47	9.2	8.31	6.21	1.02	6.66	1.02	0.31	0.12	0.32	0.14	8.46	-2.9
UGC07012	49.4	0.82	9.97	9.17	6.91	1.07	6.36	1.06	0.42	0.14	0.31	0.15	8.85	-2.41
UGC08733	39.7	0.89	9.67	8.67	5.87	1.11	5.14	0.97	0.25	0.12	0.32	0.17	8.27	-2.82

UGC08781	113.0	3.75	11.28	10.95	11.93	0.60	10.08	0.86	0.89	0.59	0.74	0.36	9.31	-0.24
UGC08909	29.8	0.43	9.40	8.38	6.15	1.34	5.35	0.86	0.45	0.22	0.40	0.26	8.61	-2.03
UGC09067	116.0	1.81	11.1	10.49	11.61	0.51	8.85	0.86	0.65	0.29	0.50	0.25	9.47	-0.41
UGC09291	47.6	1.16	10.03	9.33	7.96	1.00	6.97	1.05	0.43	0.17	0.40	0.18	8.71	-2.04
UGC09476	52.3	1.69	10.47	9.82	8.50	1.00	7.30	1.09	0.54	0.18	0.51	0.21	8.87	-1.51
UGC09837	43.2	1.23	9.80	9.04	5.45	0.81	5.57	0.89	0.43	0.17	0.32	0.14	8.37	-3.6
UGC10796	48.0	0.99	9.67	8.91	5.47	1.11	4.54	0.95	0.37	0.13	0.31	0.17	8.42	-3.39
UGC11649	55.3	1.75	10.76	10.29	9.92	0.95	6.81	0.98	0.82	0.37	0.96	0.37	9.3	-0.74
UGC12224	48.7	1.29	10.28	9.45	7.82	1.03	7.47	1.04	0.57	0.23	0.48	0.22	8.73	-1.97
UGC12250	98.9	2.80	11.15	10.77	11.33	0.73	9.57	0.82	0.89	0.55	0.66	0.33	9.38	-0.52
UGC12767	71.2	2.57	11.43	10.9	10.70	0.70	8.36	0.93	0.65	0.34	0.53	0.26	9.58	-0.63
UGC12816	71.9	1.39	10.01	9.44	8.05	1.01	5.75	1.04	0.38	0.16	0.31	0.15	8.66	-2.11
UGC12864	63.6	1.35	10.23	9.70	8.32	1.01	6.08	1.03	0.48	0.19	0.40	0.17	8.94	-2.05
UGCA021	26.4	1.16	9.39	8.88	7.33	1.07	4.18	0.83	0.32	0.16	0.32	0.23	8.26	-2.28

3.3.2 An empirical assessment of disk contamination and PSF convolution effects on the obtained trends

In order to minimize the contribution of the host disk to quantities derived within the bulge radius, stellar ages and metallicities computed in this study are weighted by $\mathcal{M}_{\star}$, this way reducing their sensitivity to the luminosity contribution by the star-forming disk. Even so, it is important to check whether the latter has a significant influence on $\langle t_{\star,\mathrm{B}}\rangle_{\mathcal{M}}$ and $\langle Z_{\star,\mathrm{B}}\rangle_{\mathcal{M}}$ determinations within the bulge radius $\mathrm{R_B}$.

In view of the fact that the B/T mass ratio increases by a factor of ~ 2 across the considered range in $\mathcal{M}_{\star,\mathrm{T}}$, it is possible that the degree of disk contamination scales inversely with $\mathcal{M}_{\star,\mathrm{T}}$, therefore specially affecting low-B/T (i.e., low-$<\delta\mu_{9\mathrm{G}}>$, **iA**) galaxies and leading to an artificial steepening of the $\log(\mathcal{M}_{\star,\mathrm{B}})$ vs. $\langle t_{\star,\mathrm{B}}\rangle_{\mathcal{M}}$ relation in Figs. 3.7 & 3.8, panel **b**. For this reason, we performed a series of extra tests in order to study and quantify the dependence of $\langle t_{\star,\mathrm{B}}\rangle_{\mathcal{M}}$ and $\langle Z_{\star,\mathrm{B}}\rangle_{\mathcal{M}}$ on the considered isophotal aperture. This analysis was repeated taking into consideration only the three innermost **isan** and the spaxels that lie within $\mathrm{R}^{\star} < 3.3''$ (hereafter $\mathrm{R_{3.3}}$), where the disk contamination should be minimal. Given that the typical FWHM of CALIFA DR3 data is $\simeq 2.6''$, $\mathrm{R_{3.3}}$ encompasses the total emission of a point-like source (e.g., a compact bulge).

Figure 3.9 reveals that mass-weighted age and metallicity determinations within $\mathrm{R_{3.3}}$ do not significantly differ from those within $\mathrm{R_B}$, suggesting that the trends reported in Figs. 3.7, 3.8 & 3.11 are not affected by a possible light contamination of the bulge by the surrounding star-forming disk.

The good agreement between $\langle t_{\star,\mathrm{B}}\rangle_{\mathcal{M}}$ and $\langle Z_{\star,\mathrm{B}}\rangle_{\mathcal{M}}$ determinations within $\mathrm{R_{3.3}}$ and $\mathrm{R_B}$ is most probably not due to PSF smearing effects. Actually, Fig. 3.10 shows that for the majority ($\sim$ 95%) of the LTGs the bulge radius is by a factor $\sim$ 2-4.6 larger than the FWHM of CALIFA IFS data (vertical dashed line in panel a of Fig. 3.10) and that $\mathrm{R_B}$ is typically $\sim$ 2-3 times larger than the effective radius $\mathrm{R_{eff}}$ and contains in all cases at least 80% of the total emission of the bulge (cf. panels **b**&**c**).

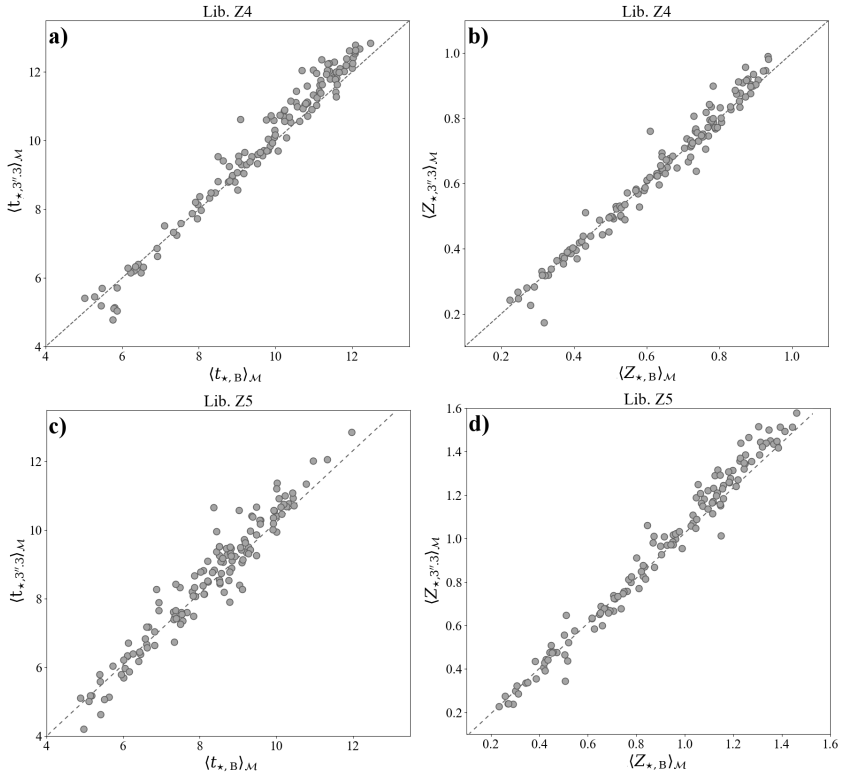

Figure 3.9: Comparison of the mean mass-weighted stellar age $\langle t_{\star,\mathrm{B}}\rangle_{\mathcal{M}}$ (Gyr) and metallicity $\langle Z_{\star,\mathrm{B}}\rangle_{\mathcal{M}}$ ($\mathrm{Z}_{\odot}$) within $\mathrm{R_B}$ with the values obtained within a radius of $3.3''$ for the LTG bulges in our sample ($\langle t_{\star,3.3}\rangle_{\mathcal{M}}$ and $\langle Z_{\star,3.3}\rangle_{\mathcal{M}}$, respectively). Dashed diagonal lines indicate equality between both plotted quantities for spectral models based on the Z4 and Z5 SSP library (upper and lower panels, respectively). It can be seen that the scatter of points relative to the equality lines is relatively small (standard deviation in age and metallicity of, respectively, 0.56 Gyr and 0.33 dex for spectral fits with the Z4 SSP library and 0.63 Gyr and 0.60 dex for those based on the Z5 SSP library) and do not show a significant dependence on age and metallicity.

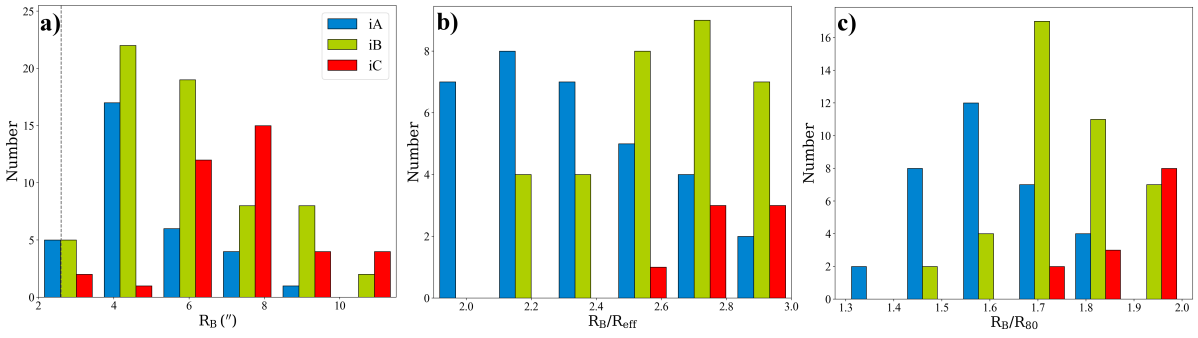

Figure 3.10: Histogram distributions of the bulge isophotal radius $\mathrm{R_B}$ ($''$) of the LTGs in our sample (panel **a**), and its normalized values to $\mathrm{R_{eff}}$ and the radius enclosing 80% of its total bulge luminosity (panels (panel **b** and **c**, respectively). The dashed vertical line in panel **a** marks the FWHM of CALIFA DR3 data ($2.6''$). The color coding is identical to that in Fig. 3.7 and is meant to illustrate the variation of the extent of bulges falling into the three tentatively defined $<\delta\mu_{9\mathrm{G}}>$ intervals.

3.3.3 Gas excitation mechanisms vs. bulge $<\delta\mu_{9G}>$

In panel **f** of Figs. 3.7 & 3.8 we examine the importance of various gas excitation mechanisms across the three $<\delta\mu_{9G}>$ intervals. This study is based on BPT diagnostics within simulated 3″ SDSS apertures (method **a** in Sect. 2.4.4). The central insight from this figure is that accretion-powered nuclear activity (reflected in Seyfert- and eventually also LINER-specific BPT line ratios) does not manifest itself uniformly along the bulge $<\delta\mu_{9G}>$ vs. $\mathcal{M}_{\star,B}$ – $\Sigma_{\star,B}$ – $\langle t_{\star,B}\rangle_{\mathcal{M}}$ sequence, but it is confined to the $<\delta\mu_{9G}>$ interval **iB-iC**, whereas gas excitation in **iA** bulges is almost invariably powered by SF activity.

Although these results are consistent with the previously reported rarity of Seyfert activity in low-luminosity bulges that are commonly classified as PBs (Kormendy & Ho, 2013, for a review), an insight from this panel pertains to the association between physical and evolutionary properties of bulges with their activity: lower $\mathcal{M}_{\star,B}$ and $\Sigma_{\star,B}$, **iA** bulges fall systematically in the SF region of the diagram whereas higher-mass ($\geq 10^{10}$ $M_\odot$), higher-$\Sigma_{\star,B}$ ($\geq 10^9$ $M_\odot$/kpc^2) **iC** bulges show in their majority Seyfert- and LINER-typical BPT ratios. Quantitatively, $\sim$ 93% (38/41) of the bulges classified as Seyfert and LINER are located within the gray-shaded quadrant in panel **e** that encompasses the area ($\log(\mathcal{M}_{\star,B})$; $\log(\Sigma_{\star,B})$) $\geq$ (10;9). Out of the 76 LTG bulges that fall in this locus of the diagram, 16 are classified as Composite, presenting gas excitation by a mixture of accretion-powered and SF activity.

As already mentioned in Sect. 2.4.4, the proportion among different spectroscopic classes does not severely change for area-weighted determinations within R_B. Within the gray-shaded quadrant, these yield a proportion 23:11:22:20 between Seyfert, LINER, Composite and SF. This adds further support to the conjecture that accretion-powered nuclear activity is mainly associated with old, high-$\mathcal{M}_{\star,B}$ and high-$\Sigma_{\star,B}$ bulges in the upper range of the $<\delta\mu_{9G}>$ sequence.

3.3.4 Bulge-to-disk age, metallicity and EW(Hα) contrast

An additional observational insight into LTG bulge assembly history comes from comparison of the evolutionary properties of bulges relative to those of their host disks. It is noteworthy that, according to both modeling results with the Z4 and Z5 SSP library, all bulges in our sample contain a non-negligible mass fraction m_9 (%) of stars older than 9 Gyr, with average values of 21 $\pm$ 0.10 (28 $\pm$ 0.08 for Z5), 59 $\pm$ 0.15 (52 $\pm$ 0.09) and 85 $\pm$ 0.07 (75 $\pm$ 0.07) in the $<\delta\mu_{9G}>$

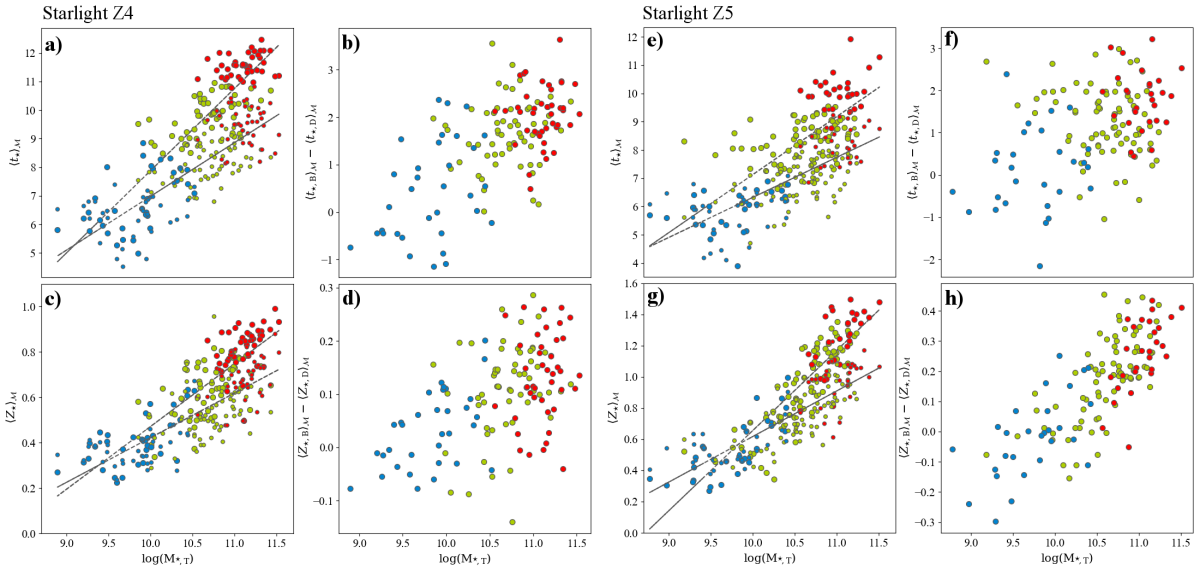

Figure 3.11: **a**) Logarithm of the total stellar mass $\mathcal{M}_{\star,\mathrm{T}}$ ($\mathrm{M}_\odot$) vs. mass-weighted stellar age $\langle t_\star \rangle_\mathcal{M}$ (Gyr) of the bulge and disk component (large and small dots, respectively). Linear fits to the data for the bulge and the disk are shown with solid lines. **b**) $\log(\mathcal{M}_{\star,\mathrm{T}})$ vs. mass-weighted stellar metallicity ($\mathrm{Z}_\odot$) for the bulge and the disk. The layout is identical to that in panel a. **c**) $\log(\mathcal{M}_{\star,\mathrm{T}})$ vs. age contrast δt_{BD} ($\langle t_{\star,\mathrm{B}} \rangle_\mathcal{M} - \langle t_{\star,\mathrm{D}} \rangle_\mathcal{M}$) (Gyr) between bulge and disk. **d**) $\log(\mathcal{M}_{\star,\mathrm{T}})$ vs. metallicity contrast δZ_{BD} ($\langle Z_{\star,\mathrm{B}} \rangle_\mathcal{M} - \langle Z_{\star,\mathrm{D}} \rangle_\mathcal{M}$) in $\mathrm{Z}_\odot$ between bulge and disk. Panels **e** through **h** display the same quantities as panels **a** to **d** as obtained from spectral models with the Z5 SSP library. Color coded as proposed in Fig. 2.16.

intervals **iA**, **iB** and **iC**, respectively. The respective m_9 determinations for the disk (24 ± 0.09, 48 ± 0.08 and 49 ± 0.11, for Z4) suggest that the oldest bulges are hosted by the oldest disks, and vice versa, which is further supported by the determinations obtained by lib. Z5 (27 ± 0.15, 49 ± 0.08 and 59 ± 0.09).

Similar to the trends documented for the bulge, the age and metallicity of the disk follow a trend with total stellar mass $\mathcal{M}_{\star,\mathrm{T}}$ ($\mathrm{M}_\odot$), as $\langle t_{\star,\mathrm{D}} \rangle_\mathcal{M} = (1.88 \pm 0.12) \cdot \log(\mathcal{M}_{\star,\mathrm{T}}) - (11.85 \pm 1.32)$ and $\langle Z_{\star,\mathrm{D}} \rangle_\mathcal{M}$ ($\mathrm{Z}_\odot$) $= (0.20 \pm 0.02) \cdot \log(\mathcal{M}_{\star,\mathrm{T}}) - (1.55 \pm 0.16)$.

Panels **a**&**b** (and **e**&**f** for Z5 models) of Fig. 3.11, that show the mass-weighted age and metallicity of the bulge and disk (large and small dots, respectively) as a function of total stellar mass $\mathcal{M}_{\star,\mathrm{T}}$, suggest a connection between the evolutionary properties of the disk and the bulge. Linear fits to the data (solid lines) demonstrate that LTG disks follow similar (yet not as tight) trends with $\mathcal{M}_{\star,\mathrm{T}}$ as bulges, being consistent with a synchronized evolution of the age and metallicity of the disk ($\langle t_{\star,\mathrm{D}} \rangle_\mathcal{M}$ and $\langle Z_{\star,\mathrm{D}} \rangle_\mathcal{M}$, respectively) with $\langle t_{\star,\mathrm{B}} \rangle_\mathcal{M}$ and $\langle Z_{\star,\mathrm{B}} \rangle_\mathcal{M}$. Our data yield the relations $\langle t_{\star,\mathrm{B}} \rangle_\mathcal{M} = (1.21 \pm 0.06) \cdot \langle t_{\star,\mathrm{D}} \rangle_\mathcal{M} - (0.18 \pm 0.49)$ and $\langle Z_{\star,\mathrm{B}} \rangle_\mathcal{M} = (1.09$

$\pm$ 0.05) $\cdot$ $\langle Z_{\star,\mathrm{D}}\rangle_{\mathcal{M}}$ – (0.05 $\pm$ 0.03).

As evident from panel **c** (and **f**) roughly all bulges of our sample are older than the disk except for low-mass LTGs whose bulge and disk are barely indistinguishable from one another regarding their mean age and metallicity. An interesting feature is the increase of the the bulge-to-disk age contrast δt_{BD} ($\langle t_{\star,\mathrm{B}}\rangle_{\mathcal{M}}$ – $\langle t_{\star,\mathrm{D}}\rangle_{\mathcal{M}}$) with $\mathcal{M}_{\star,\mathrm{T}}$, following the relation δt_{BD} (Gyr) = (1.00 $\pm$ 0.12) $\cdot$ log($\mathcal{M}_{\star,\mathrm{T}}$) – (9.07 $\pm$ 1.28). Panel **d** shows a similar, though weaker, trend for the bulge-to-disk metallicity contrast δZ_{BD} ($\langle Z_{\star,\mathrm{B}}\rangle_{\mathcal{M}}$ – $\langle Z_{\star,\mathrm{D}}\rangle_{\mathcal{M}}$), which scales with galaxy mass as δZ_{BD} ($\mathrm{Z}_{\odot}$) = (0.08 $\pm$ 0.01) $\cdot$ log($\mathcal{M}_{\star,\mathrm{T}}$) – (0.75 $\pm$ 0.12). The mean δt_{BD} in the $<\delta\mu_{9\mathrm{G}}>$ intervals **iA**, **iB** and **iC** was determined to be 0.50 $\pm$ 1.1, 1.65 $\pm$ 0.7 and 2.07 $\pm$ 0.6 Gyr for models with the Z4 SSP library, and 0.10 $\pm$ 1.0, 1.26 $\pm$ 0.8 and 1.79 $\pm$ 0.7 Gyr for models with the Z5 SSP library. It can be seen that the age contrast in **iC** bulges shows a large spread between $\sim$ 0.5 and $\sim$ 3.6 Gyr and $\sim$ 40% of the bulges within interval **iA** it is slightly negative ($\sim$ -1 Gyr) suggesting a rise of SF activity in the bulge over the recent few Gyrs. As expected from the evidence of Fig. 3.7, δt_{BD} and δZ_{BD} also show a positive correlation with $<\delta\mu_{9\mathrm{G}}>$.

The obtained results and conclusions are in qualitative agreement with those by Sánchez-Blázquez et al. (2014) that by spaxel-by-spaxel spectral modeling of 62 nearly face-on spiral galaxies from CALIFA find that bulges show, on average, higher luminosity-weighted ages and metallicities than disks. Likewise, this study shows that the metallicities of bulge and disk are correlated (see also, e.g., Moorthy & Holtzman, 2006), in agreement with the evidence from panel **b** of Fig. 3.11, although they do not find any significant correlation between the age of the two components (see also, Sánchez-Blázquez, 2016). Sánchez-Blázquez et al. (2014) also show that the slope of the relation between central velocity dispersion and luminosity-weighted age and metallicity is similar, both for the central parts of bulges and at a galactocentric radius equivalent to $\sim$ 2.4 exponential disk scale lengths.

Figure 3.12 illustrates the variation of the logarithm of the mean EW(Hα), a proxy to the level of ongoing SF, with total stellar mass for both bulge and disk components. From inspection of this figure it is apparent that a) disks present generally higher values of mean EW(Hα), indicating a higher level of ongoing SF than bulges, with the exception of **iA** galaxies where the mean EW(Hα) is similar in the bulge and disk; b) for both stellar components, the higher the total stellar mass of a galaxy the lower the mean EW(Hα), with the notable trend of a

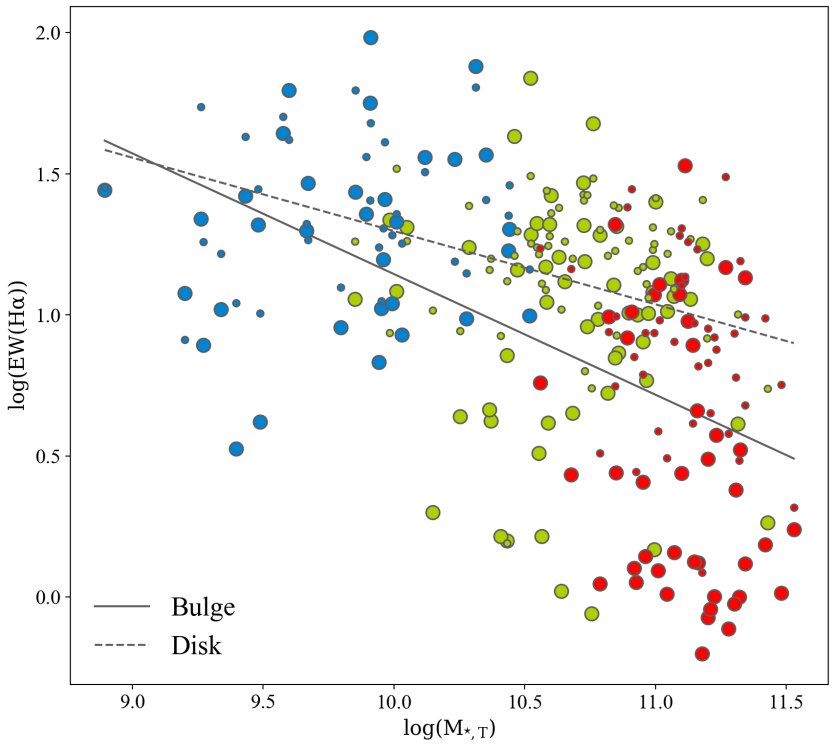

Figure 3.12: Logarithm of the total stellar mass $\mathcal{M}_{\star,\mathrm{T}}$ ($\mathrm{M}_{\odot}$) vs. logarithm of the mean EW(Hα) (Å) for the bulge (big circles) and disk (small circles). Linear fits to the data are shown with solid and dashed lines, respectively. The color coding is identical to that in the left panel of Fig. 2.16.

steeper decrease of the mean EW(Hα) in bulges than in disks. This result indicates that low-mass LTGs tend to be producing stars in their centers (along with their disks), whereas in higher-mass LTGs SF is mostly quenched in the bulge yet maintained in the disk.

3.3.5 Stellar age gradients in LTG bulges

Figure 3.13 shows the variation with total stellar mass of the normalized mass- (upper panels) and luminosity-weighted (lower panels) age gradients measured within $\mathrm{R_B}$ for the LTG sample obtained by the spaxel-by-spaxel analysis with STARLIGHT and adopting both Z4 and Z5 SSP libraries (left-hand side and right-hand side panels, respectively). Besides determinations for individual bulges, it additionally displays with the star symbol the arithmetic average within each $<\delta\mu_{9\mathrm{G}}>$ interval ($\nabla(\mathrm{t}_{\star,\mathrm{B}})_{\mathcal{M}}$ – lib. Z4 **iA**: 0.209, **iB**: -1.536, **iC**: -2.044; lib. Z5 **iA**: 0.781, **iB**: -1.621, **iC**: -1.875; $\nabla(\mathrm{t}_{\star,\mathrm{B}})_{\mathcal{L}}$ – lib. Z4 **iA**: 0.372, **iB**: -1.330, **iC**: -2.343; lib. Z5 **iA**: 0.456, **iB**: -1.159, **iC**: -1.796) and a linear fit to the data plotted in each panel.

In all cases, our results point to a decrease in the age gradient towards higher total stellar masses:

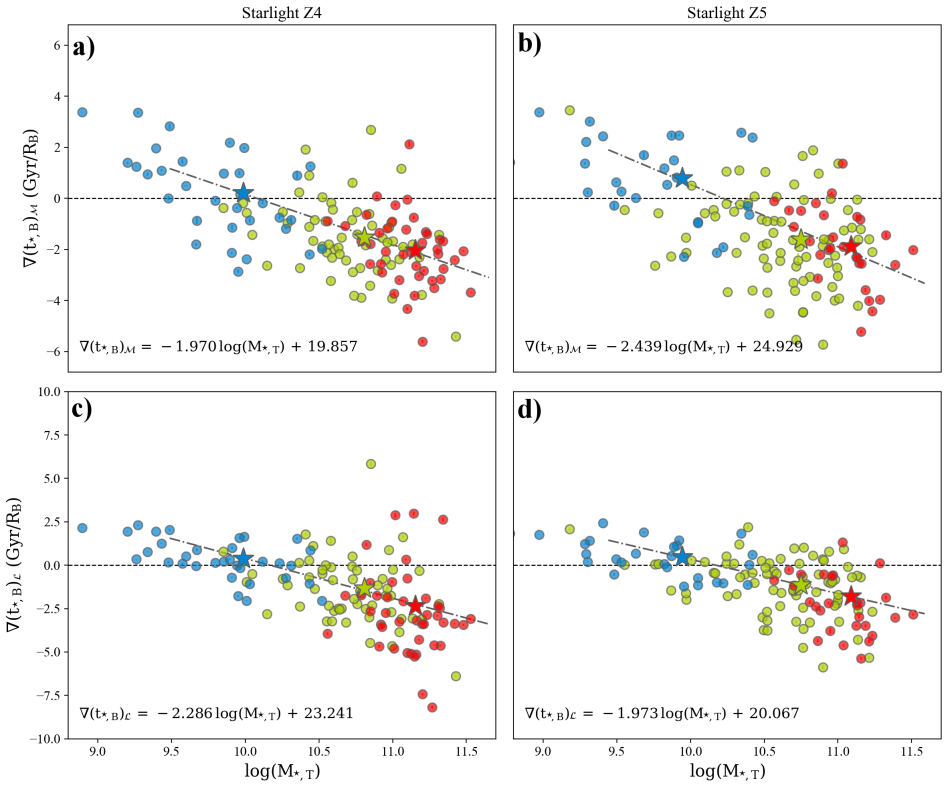

Figure 3.13: **a**) Logarithm of the total stellar mass $\mathcal{M}_{\star,T}$ ($M_\odot$) vs. gradient $\nabla(t_{\star,B})_{\mathcal{M}}$ (Gyr/R_B) of mass-weighted stellar age, normalized to bulge radius R_B, as obtained through spaxel-by-spaxel modeling with Starlight and the SSP library Z4. **b**) $\log(\mathcal{M}_{\star,T})$ vs. $\nabla(t_{\star,B})_{\mathcal{M}})$, inferred as above with the SSP library Z5. **c&d**) $\log(\mathcal{M}_{\star,T})$ vs. luminosity-weighted stellar age gradient $\nabla(t_{\star,B})_{\mathcal{L}})$ normalized to R_B, obtained, respectively, from spectral models with Starlight and the Z4 and Z5 SSP library. The color coding follows that in Fig. 2.16. Stars represent the arithmetic average of each quantity within the respective $<\delta\mu_{9G}>$ interval, and lines show linear fits to the plotted quantities.

low mass **iA** galaxies tend to display positive age gradients ($\nabla(t_{\star,B})_{\mathcal{M}}$), whereas the opposite is the case for higher-mass **iC** galaxies, with intermediate-mass **iB** galaxies showing intermediate $\nabla(t_{,B})_{\mathcal{M}}$ values. This evidence, together with the fact that **iA** galaxies show the highest mean EW(Hα) values in their bulges, contrary to **iC** systems (see Fig. 3.12), suggests a high degree of SF confinement to their centers, which is consistent with their positive age gradients. It is conceivable that these lower-mass LTGs, due to their shallower potential well have experienced a *delayed maturation* (i.e. build-up of their bulge component) as compared to high-mass LTGs, in agreement with their comparatively young age. Supportive evidence for this scenario comes from the fact that **iA** galaxies still retain considerable amounts of neutral gas: this is apparent from a preliminary analysis of gas mass determinations for 86 galaxies of our sample from Zaritsky et al. (2014), showing that the specific gas mass (HI-to-stellar mass ratio) is higher for **iA** galaxies when compared to **iB** and **iC**. On the opposite side of the mass sequence, **iC** galaxies

exhibit older stellar populations in their very center as compared to their periphery. Indeed, Fig. 3.12 demonstrates the lack of significant ongoing SF in these bulges, in agreement with the evidence gained from the analysis with $\mathcal{RY}$, showing that most of them are entirely composed of stars older than 9 Gyr. This insight, along with the occurrence of accretion-powered nuclear activity in these high-mass bulges (expected from the robustly established correlation between SMBH and bulge stellar mass (cf. Sect. 1 and further supported by the analysis of BPT ratios in Sect. 3.3.3) hints at a scenario in which bulges experienced inside-out SF quenching several Gyr ago. Quite interestingly, the slope of normalized age gradients suggests that the inside-out quenching process did not occur abruptly but on a Gyr-timescale, as already suggested by the age span ($\sim$ 2 Gyr) covered by the gray-shaded quadrant in Fig. 3.7**e**. Whereas the details of this inside-out SF quenching are difficult to be firmly constrained from the present data, it appears unlikely that a single episode has been responsible for the cessation of SF within R_B. A more plausible hypothesis is that this process has been driven by a prolonged injection of energy and momentum by an AGN and a series of minor SF episodes. In a simplified picture of an outwardly propagating *SF quenching wave* of constant radial velocity (V_r), the age gradients inferred for **iC** bulges in this study translate to a $V_r \simeq 1$ km/s. As for **iB** galaxies, their very shallow age gradients might witness a balance between SF activity and quenching along the pathway of slow transition to the **iC** evolutionary stage.

As for age gradients in the disk and metallicity gradients regarding both bulge and disk it was found a lack of correlation with total stellar mass or with bulge/disk stellar mass.

To ascertain that the inversion of age gradients from low-mass **iA** bulges to high-mass **iC** bulges does not result from increasing light contamination from the disk at the bulge's periphery, $\nabla(t_{\star,B})_{\mathcal{M}}$ values were re-computed within the radius R_{80} that encompasses 80% of the total emission of a bulge and contains a nearly negligible light fraction owing to the disk ($\nabla(t_{\star,80})_{\mathcal{M}}$). As apparent from Fig. 3.14, all trends from Fig. 3.13 are preserved, which adds support to the conclusion that the observed dependence of $\nabla(t_{\star,B})_{\mathcal{M}}$ on LTG mass reflects an evolutionary transition from star-forming to SF quenched bulges and is not driven by light contamination from the disk.

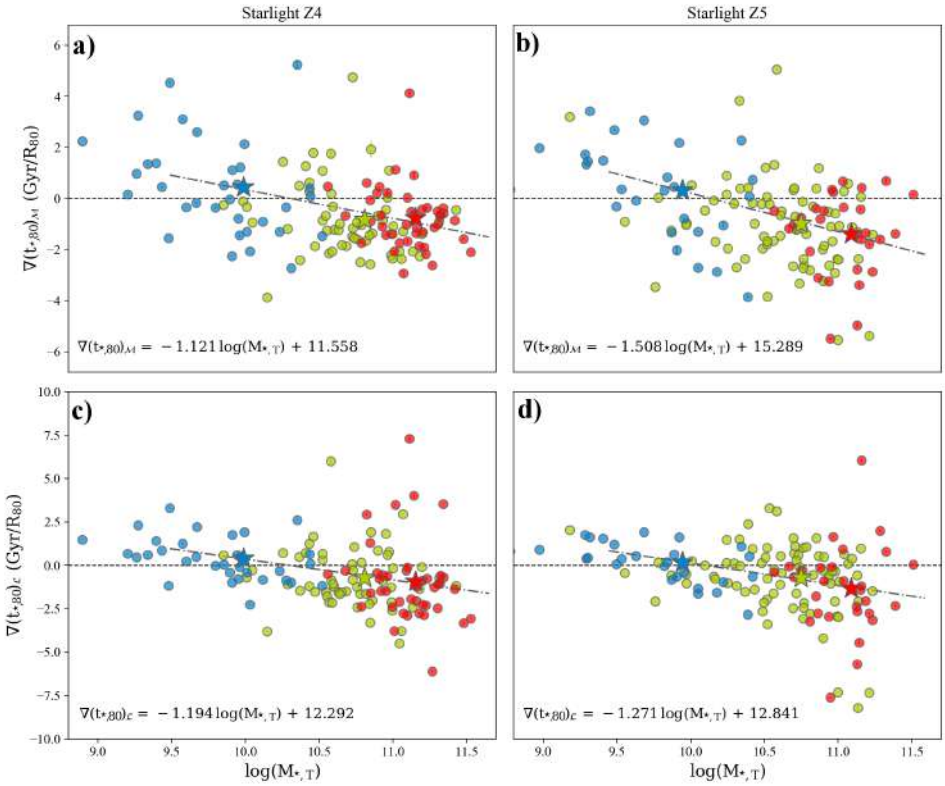

Figure 3.14: **a**) Logarithm of the total stellar mass $\mathcal{M}_{\star,\mathrm{T}}$ ($\mathrm{M}_{\odot}$) vs. normalized mass-weighted stellar age gradient $\nabla(\mathrm{t}_{\star,80})_{\mathcal{M}}$ ($\mathrm{Gyr/R}_{80}$), as obtained from spaxel-by-spaxel modeling with STARLIGHT fits and the Z4 SSP library. **b**) same as in panel a, for spectral fits with the Z5 SSP library. **c&d**) $\log(\mathcal{M}_{\star,\mathrm{T}})$ vs. normalized bulge luminosity-weighted stellar age gradient $\nabla(\mathrm{t}_{\star,80})_{\mathcal{L}}$ ($\mathrm{Gyr/R}_{80}$), obtained from spectral fits with STARLIGHT and the Z4 and Z5 SSP library, respectively. The color coding follows that in Fig. 2.16. Stars mark the arithmetic average of each quantity within each of the three $<\delta\mu_{9\mathrm{G}}>$ intervals and the overplotted lines show linear fits to the data.

3.4 A comparative study between STARLIGHT & FADO

An important component of this work is a careful examination and comparison of the results obtained from spectral modeling with the codes STARLIGHT and FADO. As detailed in Sect. 2.4.5, for this analysis to be possible within the time frame of this PhD project, it was deemed necessary to apply FADO to binned spectra within irregular annuli (**isan**), after correction of spectra in individual spaxels for intrinsic stellar motions. Furthermore, the summed up spectra within **isan** were repeatedly modeled (both with libraries Z4 and Z5) for 15 times with the identical fitting setup yet different seed numbers (see Sect. 2.4.5 for detailed explanation) in order to obtain a further estimate of formal uncertainties (internally computed only in the case of FADO). Additionally, this investigation was complemented by fits to the summed up spectrum of **isan**'s subtended within the $\mathrm{R_B}$ radius of each LTG. In the following discussion we denote with **SbS**

results based on the spaxel-by-spaxel analysis (solely performed with STARLIGHT, with the complete results obtained therefrom presented in Sect. 3.3), with **18Z-15t** results from analysis performed by repeatedly processing the **isan** spectra adopting different initial seed numbers, **18Z** for the model output from fitting one time **isan** spectra, and, finally, **Rb** for results from processing the sum of all the **isan** within R_B.

3.4.1 Average determinations for LTG bulges

STARLIGHT

Figure 3.15 summarizes the results obtained by STARLIGHT with the library Z4, illustrating how the decrease in spatial resolution affects some of the inferred properties for bulges and associated trends. Furthermore, the comparison between panels **c**, **h** & **m** with panels **d**, **i** & **n**, respectively, shows the effect that different initial guess values (seed numbers) have on the determined properties.

As apparent from Fig. 3.15, although the scatter increases towards lower spatial resolution, the main trends for mass-weighted age and metallicity revealed by the **SbS** analysis are conserved, safeguarding the conclusion that low-mass bulges tend to be younger and chemically less enriched, and vice versa. Furthermore, previously reported trends with stellar mass remain valid, strengthening our conclusion that LTG bulges show an overall continuity in their physical and evolutionary properties instead of the dichotomy implied by the PB–CB formation hypothesis (see Sect. 1). It also can be seen that the higher the spatial resolution the tighter are the obtained trends, specially in the low mass regime (**iA** galaxies). The former result is expected mainly due to the fact that these bulges are star forming. Consequently they exhibit significant nebular emission (both continuum and emission lines) that can conceal stellar absorption features and obstruct the correct determination of stellar population properties. Moreover, since HII regions are generally localized, their light-weighted sum with emission from non-SF spaxels in the intra-HII region component is expected to result in a higher continuum contribution, on average, which will alter the best-fitting spectral modeling result. Another insight from Fig. 3.15 concerns the effect of a variation in the initial parameter guess (seed number) in improving the statistical significance of the determined physical properties. By comparing panels **b**, **f** & **j** with **c**, **g** & **k**, respectively, it is evident that this CPU time-consuming approach leads to an improvement in average determinations with STARLIGHT. This is particularly true for

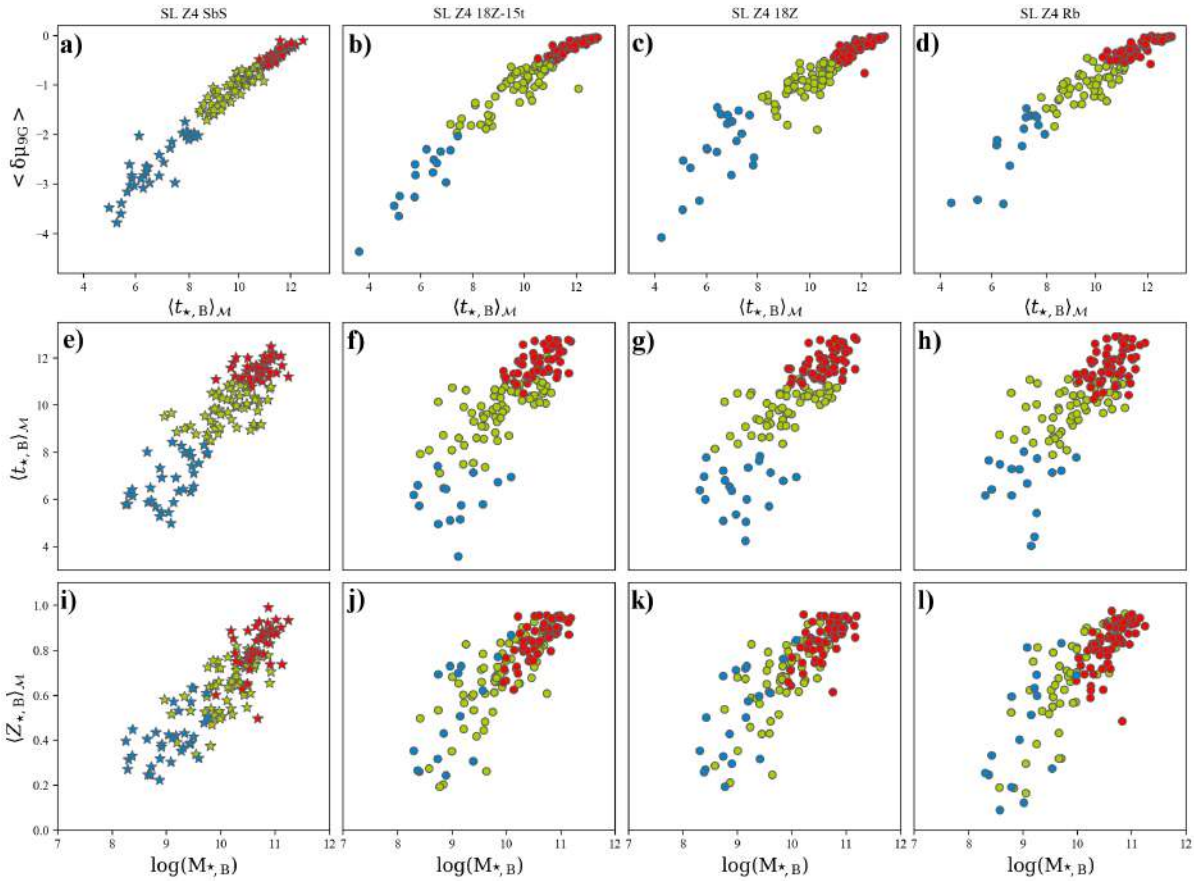

Figure 3.15: **a-d**): mass-weighed stellar age $\langle t_{\star,\mathrm{B}}\rangle_{\mathcal{M}}$ (Gyr) vs. $<\delta\mu_{9\mathrm{G}}>$ (r mag) for the bulge. **e-h**): logarithm of the bulge's stellar mass $\mathcal{M}_{\star,\mathrm{B}}$ ($\mathrm{M}_{\odot}$) vs. $\langle t_{\star,\mathrm{B}}\rangle_{\mathcal{M}}$ (Gyr). **i-l**): logarithm of $\mathcal{M}_{\star,\mathrm{B}}$ ($\mathrm{M}_{\odot}$) vs. mass-weighted stellar metallicity $\langle Z_{\star,\mathrm{B}}\rangle_{\mathcal{M}}$ ($\mathrm{Z}_{\odot}$) for the bulge. The different panels display the determinations obtained with STARLIGHT and the SSP library Z4 for the case of **SbS** (**b,f,g**), **18Z-15t** (**c,g,k**) and **18Z** (**d,h,l**). Stars display **SbS** determinations and circles the remaining. Panels displayed in the second and third rows are color coded according to the division after $<\delta\mu_{9\mathrm{G}}>$ made in the first row.

$<\delta\mu_{9\mathrm{G}}>$ determinations that in this way are better separable into intervals (the color code presented in panels **f** & **j** accounts for the partition performed in panel **b** – it is important to note the scarcity of **iA** galaxies ($<\delta\mu_{9\mathrm{G}}>$ < -2 mag) implying that less bulges where determined to display a mean age $\lesssim$ 8 Gyr. Although the color scatter in panels **f** & **j** is higher than the same in panels **e** & **i**, globally still confirms the obtained conclusions given in Sect. 3.3.1 regarding the distribution of mass-weighted age and metallicity with bulge's stellar mass.

FADO

An analogous comparison to Fig. 3.15 (except for the **SbS** analysis) was also performed with FADO. The results are summarized in Fig. 3.16.

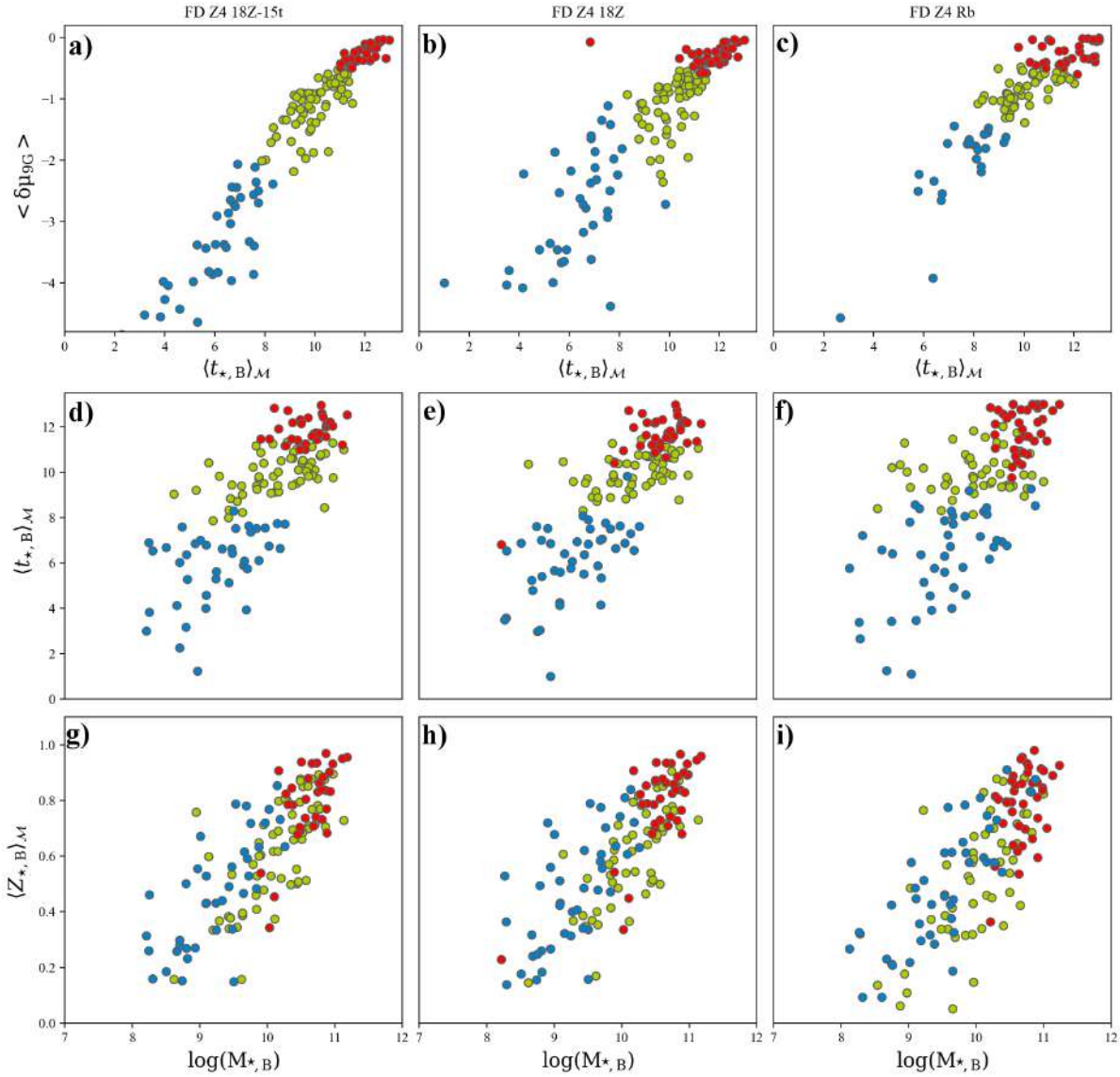

Figure 3.16: **a-c**): mass-weighed stellar age $\langle t_{\star,\mathrm{B}}\rangle_{\mathcal{M}}$ (Gyr) vs. $<\delta\mu_{9\mathrm{G}}>$ (r mag) for the bulge. **d-f**): logarithm of the bulge stellar mass $\mathcal{M}_{\star,\mathrm{B}}$ ($\mathrm{M}_\odot$) vs. $\langle t_{\star,\mathrm{B}}\rangle_{\mathcal{M}}$ (Gyr). **g-i**): logarithm of $\mathcal{M}_{\star,\mathrm{B}}$ ($\mathrm{M}_\odot$) vs. mass-weighted stellar metallicity of the bulge ($\langle Z_{\star,\mathrm{B}}\rangle_{\mathcal{M}}$ in $\mathrm{Z}_\odot$). The different panels display the determinations obtained through **18Z-15t** (panels **a,d,g**), **18Z** (panels **b,e,h**) and **Rb** (panels **c,f,i**). Diagrams in the second and third row are color coded according to the division performed in the first row.

From inspection of Fig. 3.16 it is apparent that all conclusions drawn from Fig. 3.15 remain valid for FADO determinations. It is interesting to note that determinations with FADO in the case of **18Z-15t** are reliable enough to once more separate the results into $<\delta\mu_{9\mathrm{G}}>$ intervals

(the color code presented in panels **d** and **g** regard the separation presented in panel **a**, this way showing that FADO confirms the results obtained with STARLIGHT) although there is a significant increase of the spread, in particular for $\langle Z_{\star,\mathrm{B}}\rangle_{\mathcal{M}}$ determinations of **iA** LTGs.

Figure 3.17 permits visualization and comparison of the obtained determinations for the two spectral synthesis codes:

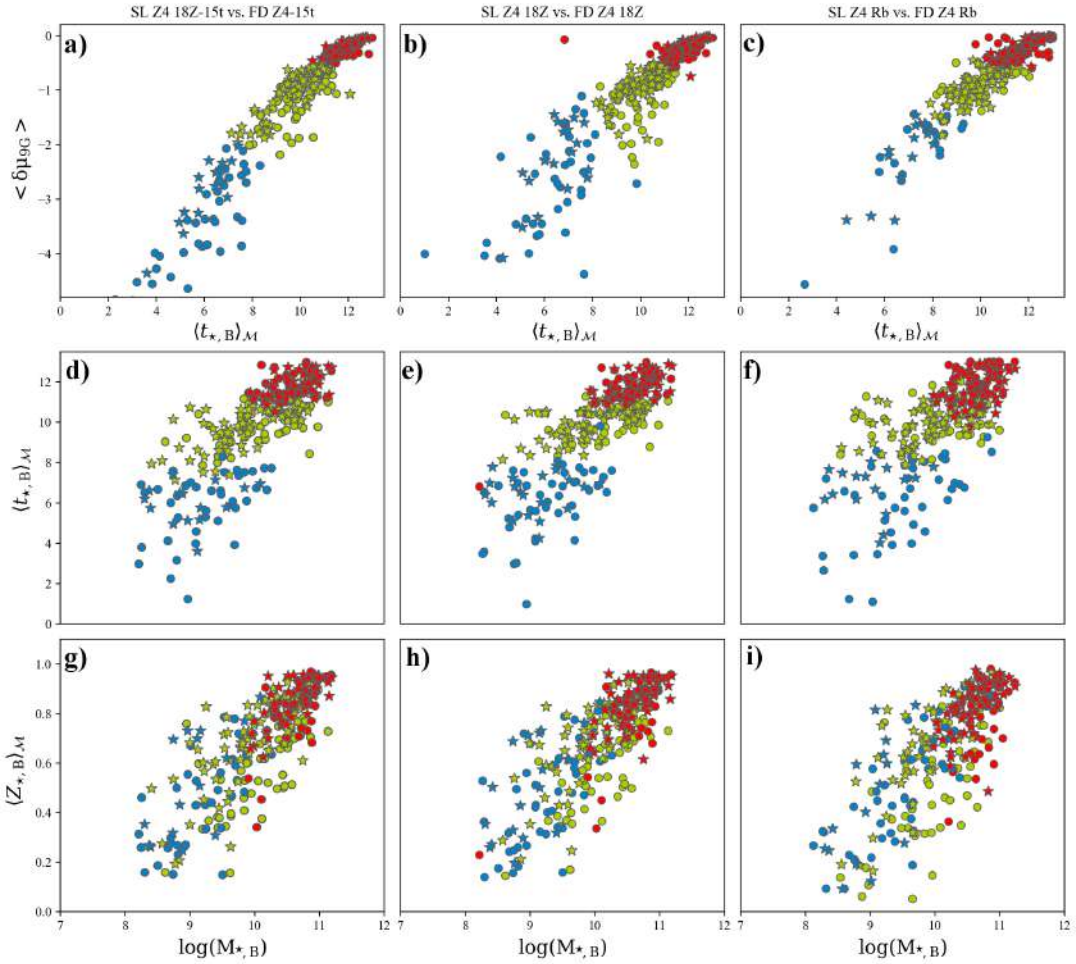

Figure 3.17: **a-c**): bulge mass-weighed stellar age $\langle t_{\star,\mathrm{B}}\rangle_{\mathcal{M}}$ (Gyr) vs. $<\delta\mu_{9\mathrm{G}}>$ (r mag). The different panels display the determinations obtained by **a**/**d**/**g** – **18Z-15t**, **b**/**e**/**h** – **18Z** & **c**/**f**/**j** – **Rb**. Panels **a**, **d** & **g** are color coded according to the $<\delta\mu_{9\mathrm{G}}>$ division illustrated in panel **a** & panels **b**, **e** and **h** according to **b**. STARLIGHT determinations are displayed by stars and FADO by circles. **d-f**): logarithm of the bulge's stellar mass $\mathcal{M}_{\star,\mathrm{B}}$ ($\mathrm{M}_{\odot}$) vs. $\langle t_{\star,\mathrm{B}}\rangle_{\mathcal{M}}$ (Gyr). **g-j**): $\mathcal{M}_{\star,\mathrm{B}}$ ($\mathrm{M}_{\odot}$) vs. mass-weighted stellar metallicity of the bulge ($\langle Z_{\star,\mathrm{B}}\rangle_{\mathcal{M}}$ in $\mathrm{Z}_{\odot}$).

It is apparent from Fig. 3.17 that the overall trends obtained with STARLIGHT and FADO are in mutual agreement, although the scatter in determinations with FADO is slightly larger. Another visible difference is that in the low-mass regime FADO tends to yield lower mass-weighted

ages than STARLIGHT, and it is also for this mass range where differences in age and metallicity from the two codes are more evident (as compared to the medium-to-high mass regime, where differences between STARLIGHT and FADO are not so significant). This was also expected since, as shown in Fig. 3.12, low-mass galaxies exhibit moderate-to-high EW(Hα) (indicating ongoing SF) in their centers. Since FADO is the only currently available self-consistent PSS code that takes nebular emission into account and seeks consistency between observed and predicted nebular characteristics (unlike STARLIGHT that considers stellar emission only), a plausible expectation is that differences between determinations from the two codes are more pronounced in the presence of significant nebular emission, whereas in the case of gas-depleted or old regions determinations from both codes are similar (Cardoso, Gomes & Papaderos, 2018).

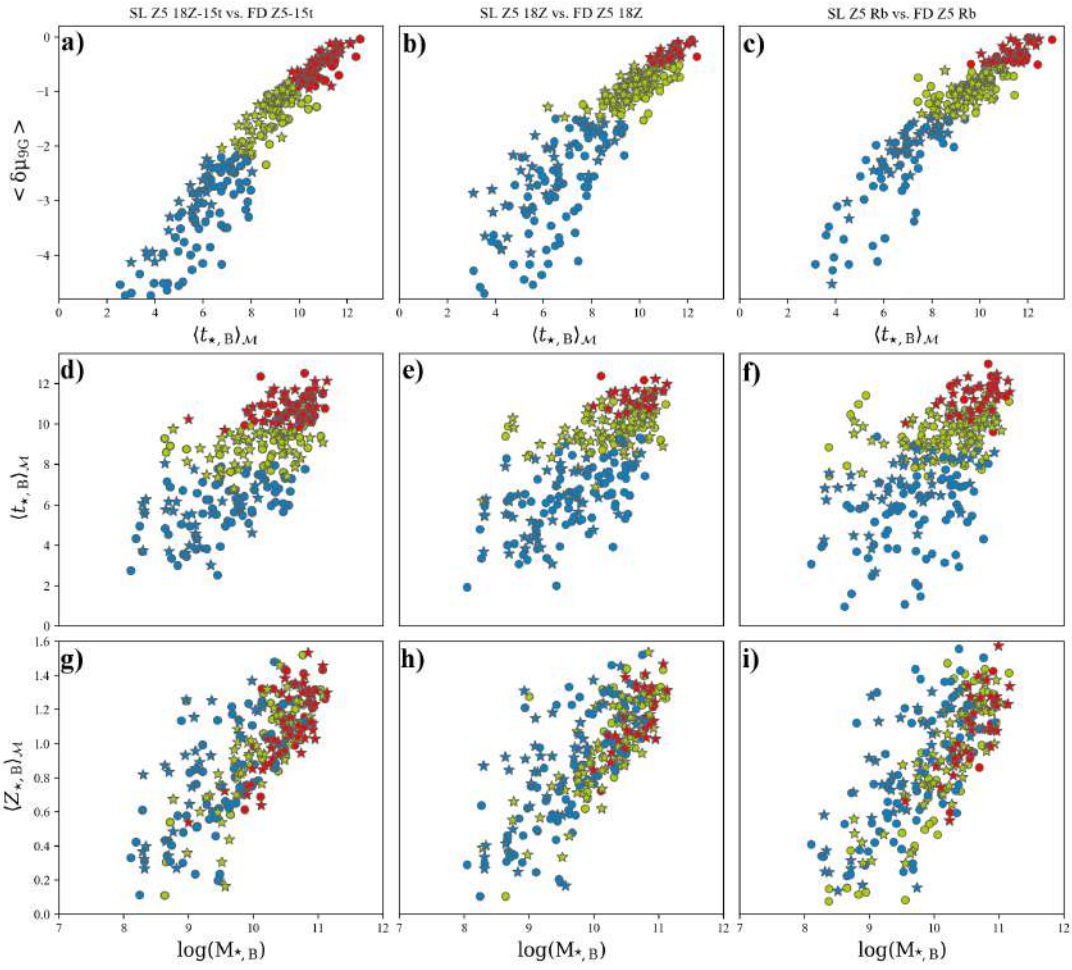

Figure 3.18: Comparison of results from STARLIGHT and FADO for **18Z-15t**, **18Z** & **Rb** adopting the SSP library Z5. The layout is identical to that in Fig. 3.17.

As for the relations obtained with both PSS codes adopting the SSP library Z5 (Fig. 3.18) they are in agreement with those based on modeling with the Z4 SSP library (Fig. 3.17). It is noteworthy that FADO yields a higher number of **iA** galaxies ($<\delta\mu_{9G}>$ < -2 mag) as compared to STARLIGHT (Z4 & Z5) and FADO (Z4), suggesting that FADO in conjunction with the Z5 SSP library estimates lower ages for the bulge of some of our sample galaxies. This is unlikely to result from the AMD, given the self-consistency concept of FADO that alleviates this issue (cf. quantitative analysis in Cardoso, Gomes & Papaderos 2018). A comparison between both figures reveals that the trends obtained by determinations based on the SSP library Z4 are less scattered than those using the Z5 library, as previously reported for STARLIGHT, **SbS** (see Sect. 3.3.1).

3.4.2 Mass- & luminosity-weighted age gradients

In view of the good agreement between the mean age values obtained by the **SbS** analysis and the **18Z-15t** (see Figs. 3.7, 3.8, 3.17 & 3.18), we repeated the analysis of age gradients within the bulge component using **18Z-15t** for both PSS codes and the Z4 and Z5 SSP library. A summary of the results is presented in Fig. 3.19.

From inspection of Fig. 3.19 and comparison with Fig. 3.13 it is obvious that the scatter significantly increases from **SbS** analysis to **18Z-15t**, with determinations from FADO displaying even higher scatter. The considerable increase of dispersion in the trend between age gradients derived from STARLIGHT, **SbS** and STARLIGHT, **18Z-15t** with total stellar mass indicates the importance of spatially resolved spectroscopy to reveal correlations between such sensitive determinations as age gradients. As for the results obtained with FADO, although the linear relations fitted to the average within each $<\delta\mu_{9G}>$ interval are conserved, the significant dispersion in results from modeling summed-up spectra calls for a spaxel-by-spaxel fitting to draw firm conclusions on the precise slope of radial age gradients as a function of bulge mass.

3.5 Spectroscopic subtraction of the disk and first insights into the validity of its exponential intensity profile inside the bulge radius

The code presented in Sect. 2.4.6 for the spectroscopic subtraction of the disk emission within R_C (mean $R_C \sim 0.87 \cdot R_B$; $\sigma = 0.13$ for the LTG sample, lib. Z4) was applied to the entire

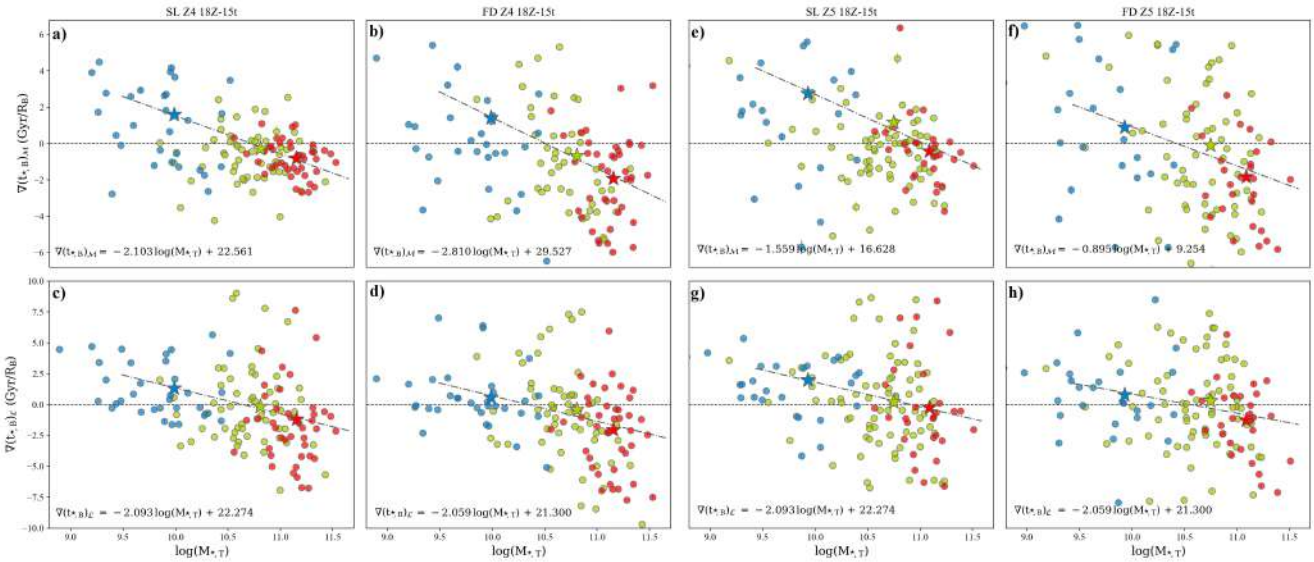

Figure 3.19: **a**) Logarithm of the total stellar mass $\mathcal{M}_{\star,\mathrm{T}}$ ($\mathrm{M}_{\odot}$) vs. normalized mass-weighted stellar age gradient $\nabla(\mathrm{t}_{\star,\mathrm{B}})_{\mathcal{M}}$ ($\mathrm{Gyr/R_B}$), as obtained by the **18Z-15t** analysis using STARLIGHT for library Z4. **b**) $\log(\mathcal{M}_{\star,\mathrm{T}})$ vs. $\nabla(\mathrm{t}_{\star,\mathrm{B}})_{\mathcal{M}}$ (Gyr), as obtained by the **18Z-15t** analysis using FADO and library Z4. **c**) As panel a, for the normalized luminosity-weighted stellar age gradient $\nabla(\mathrm{t}_{\star,\mathrm{B}})_{\mathcal{L}}$ ($\mathrm{Gyr/R_B}$). **d**) As panel b, for $\nabla(\mathrm{t}_{\star,\mathrm{B}})_{\mathcal{L}}$ ($\mathrm{Gyr/R_B}$). **e-h**) As in panels **a-b**) but using the SSP library Z5. The color coding follows that in Fig. 2.16 (left panel for lib. Z4 and right panel for lib. Z5), to ease comparison with Fig. 3.13. Stars represent the arithmetic average of each quantity within the respective $<\delta\mu_{9\mathrm{G}}>$ intervals, and dashed lines show linear fits to the data.

sample using photometric constraints in both r- and g-band to scale the normalized spectrum for the disk. Since the results for both passbands are in agreement (within $\lesssim 15\%$) it was decided to present here only the results obtained from photometric decomposition g-band SBPs. This is because the g-band transmission curve covers a significant part of the blue spectral range ($\sim$ 3830 - 5480 Å), therefore better tracing the emission of a star-forming disk.

3.5.1 Negative net-bulge spectra

The first and possibly most decisive test of the validity of the exponential fitting function for the disk within $\mathrm{R_C}$ is to examine the physical significance of the residual net spectrum of the bulge after subtracting the estimated contribution from the underlying disk. Since the latter relies on the standard assumption that the disk exponential slope is preserved all the way to the center, a possible negative flux of the net spectrum of the bulge must yield a strong indication against the validity of the background assumption of the disk exponentiality. Whereas this *reductio ad absurdum* approach does not permit to directly constrain the intensity of the disk beneath the bulge, it allows to confirm or exclude a range of functional forms for the disk profile.

The central outcome from the performed analysis is that, correction of the summed-up spectrum within R_C for the underlying disk with the assumption of a pure exponential disk (**expD**) or an inwardly flattening disk (**flatD**) leads in many cases to negative flux values in the blue range of the net bulge spectrum. This incidence never occurred when a central intensity depression was assumed for the disk (**decrD**).

The histogram distribution in Fig. 3.20 illustrates the number of unphysical (i.e. partly negative) net spectra for the bulge produced by subtracting from the integrated spectrum within R_C (see Sect. 2.4.6) the estimated spectrum of the underlying disk under the assumption of the latter following an **expD** and and **flatD** profile. It can be seen that there is no significant preference for any $<\delta\mu_{9G}>$ interval (i.e. bulge classification in **iA**, **iB** and **iC**), and that a significant fraction (up to 40%) of bulges do not contain enough emission in their blue spectral range to accommodate the inwardly extrapolated disk emission. This suggests that, for galaxies with a net bulge spectrum classified as unphysical, the emission from the disk within R_C cannot conserve its exponential (or even flat) slope as invariably assumed in surface photometry studies. Quite importantly, the analysis shows that the disk emission within R_C is much lower than commonly assumed or shows a redder spectral slope than for $R^\star > R_C$.

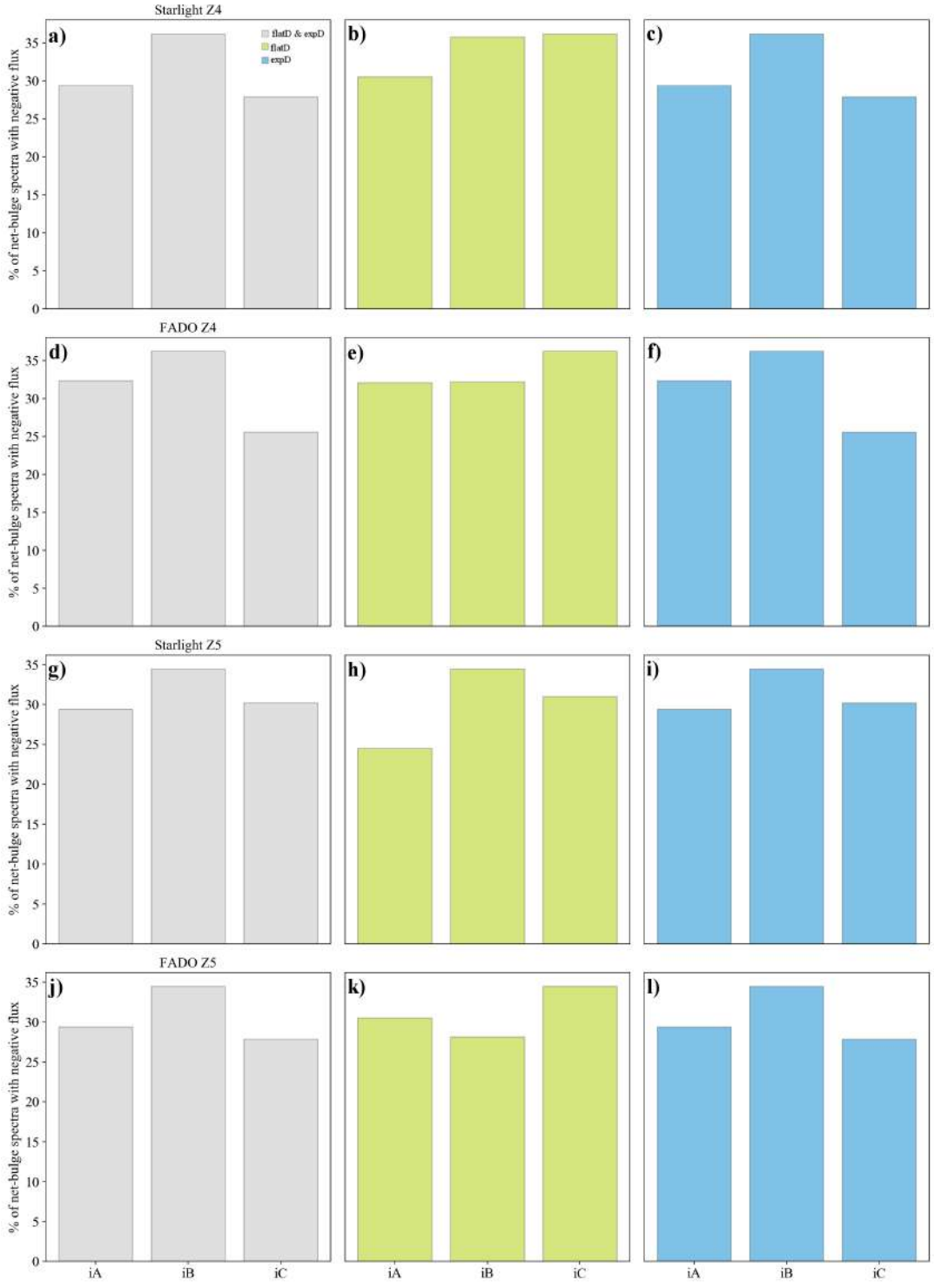

Figure 3.20: **a**) Histogram of the fraction of spectra with negative flux after disk subtraction in the three $<\delta\mu_{9G}>$ intervals for the three disk configurations considered. The results refer to spectral modeling with STARLIGHT and the SSP library Z4. **b**) like panel **a**, however for disk subtraction assuming a **flatD** model. **c**) like panel **a**, however for disk subtraction assuming a **expD** model. **d-f**) repetition of **a** to **c** based using FADO with the Z4 SSP libary. **e-h**) as **a** to **c** but using STARLIGHT with the Z5 SSP library. **i-l**) as **a** to **c** but using FADO with the Z5 SSP library.

3.5.2 Mass-weighted age and metallicity determinations for the net-bulge spectra

The next step performed with the disk subtraction tool was to re-fit with both STARLIGHT and FADO the obtained net spectra for the bulge for each of the three assumed disk configurations using both available SSP libraries.

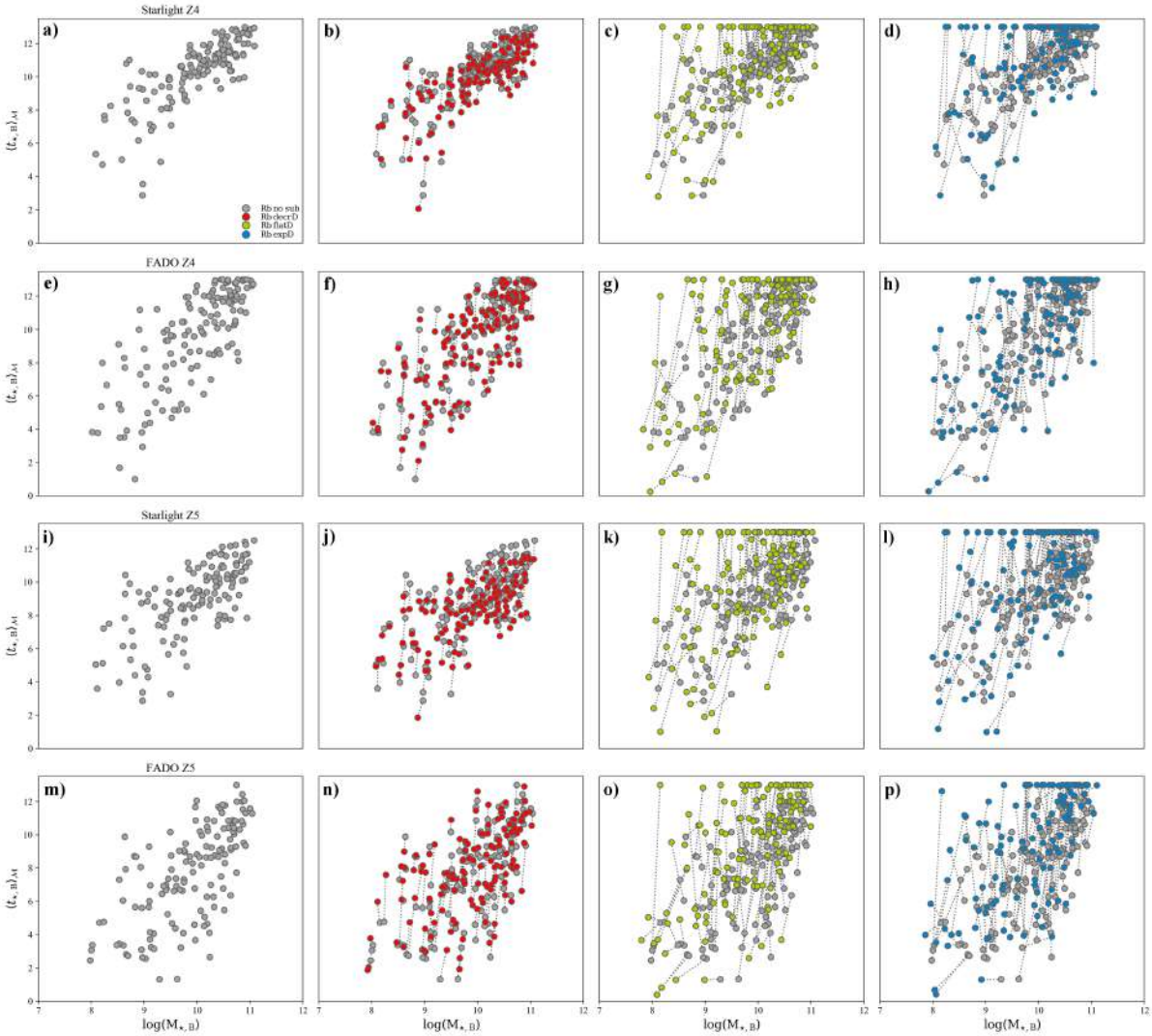

Figure 3.21: **a**) Logarithm of the bulge stellar mass $\mathcal{M}_{\star,\mathrm{B}}$ ($\mathrm{M}_\odot$) vs. mass-weighted stellar age $\langle t_\star \rangle_\mathcal{M}$ (Gyr), as obtained by the **Rb** analysis using STARLIGHT with the Z4 SSP library. **b**) $\log(\mathcal{M}_{\star,\mathrm{B}})$ vs. $\langle t_\star \rangle_\mathcal{M}$, after subtraction of a centrally depressed disk (**decrD**). **c**) $\log(\mathcal{M}_{\star,\mathrm{B}})$ vs. $\langle t_\star \rangle_\mathcal{M}$, after subtraction of an inwardly flattening disk (**flatD**). **d**) $\log(\mathcal{M}_{\star,\mathrm{B}})$ vs. $\langle t_\star \rangle_\mathcal{M}$, after subtraction of the standard exponential disk (**expD**). **e-h**) as panels **a** to **d** for models with FADO and the SSP library Z4. **i-l**) as panels **a** to **d** for models with STARLIGHT and the Z5 SSP library. **m-p**) as panels **a** to **d** for models with FADO with the Z5 SSP library. In all panels, determinations refer to average values within $\mathrm{R_B}$. Dashed lines connect the two obtained values to ease visual check of the shift implied by subtraction of the disk.

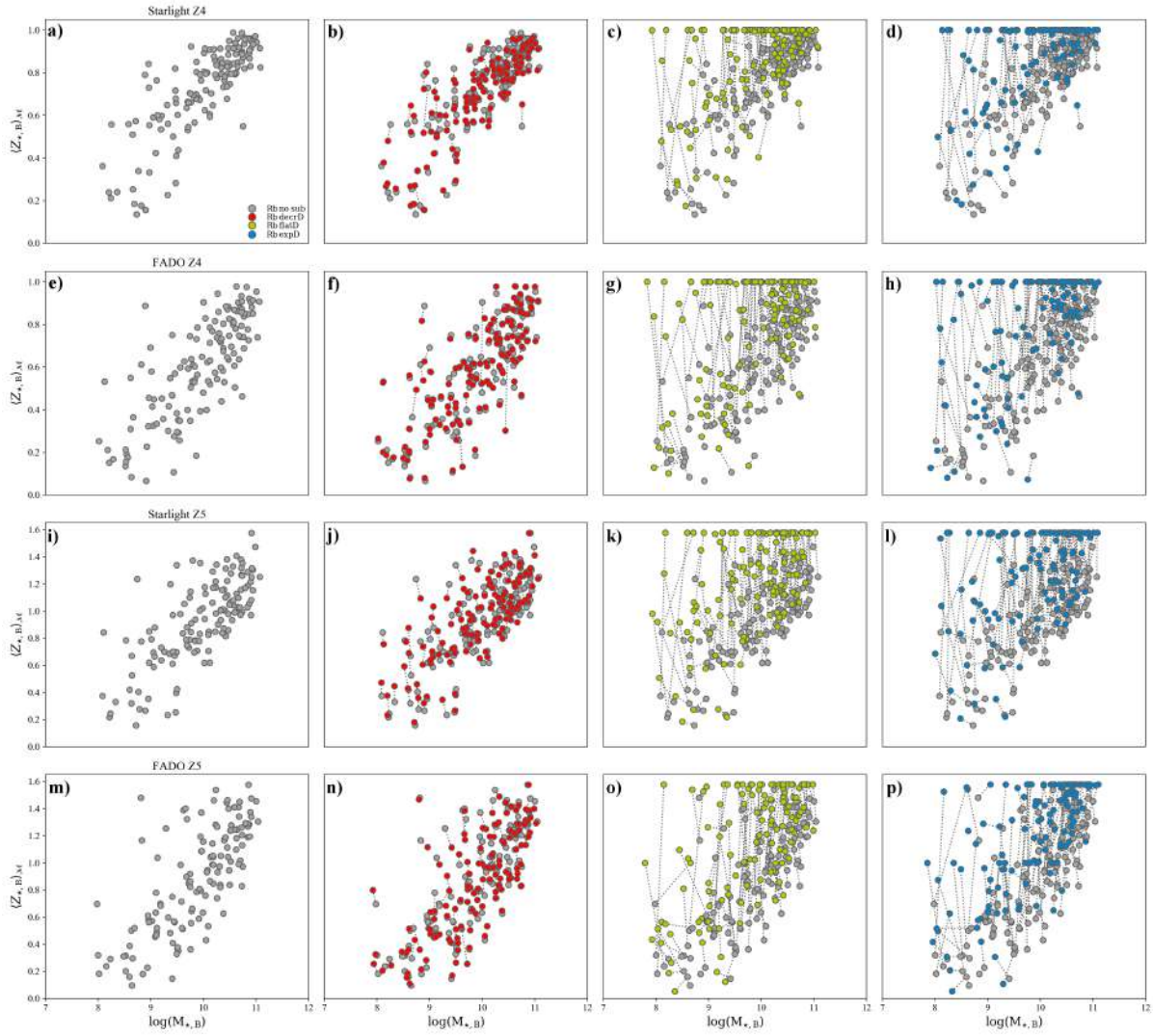

Figure 3.22: Same layout as in Fig. 3.21 but for mass-weighted metallicity determinations instead of mass-weighted age.

Figure 3.21 displays the obtained mass-weighted age determinations for each of the tested cases, whereas Fig. 3.22 displays the obtained mass-weighted metallicity determinations. Inspection of both figures reveals that:

i. mass-weighted age and metallicity determinations are not significantly affected after subtraction of a centrally depressed disk;

ii. without exception, the values of the displayed values within **Rb** increase as compared to those prior to disk subtraction;

iii. the stellar mass determinations are also affected by the disk subtraction and in some cases quite significantly. Counter-intuitively, stellar mass determinations increase for the

net-bulge spectra. This is also an unphysical result, since the resulting spectra, after subtraction of a possible disk component, cannot comprise more stellar mass than the spectra that incorporate the light from both components. This result can be explained by the fact that the PSS codes compensate for the severe (and probably unreasonable) loss of flux in the blue spectral range by assuming that the abnormally red resulting net-spectra for the bulge are composed of very old, high M/L SSPs, which artificially increases the estimated total stellar mass;

iv. the higher the assumed disk contribution inside **Rb** (from **decrD** to **flatD** to **expD**), the higher is the fraction of LTGs for which the determined age and/or metallicity converges to the maximum allowed value by the adopted SSP library. The fraction of LTGs for which the determined mass-weighted age and/or metallicity reaches the maximum allowed by the construction of SSP libraries increases from **flatD** to **expD** model configurations.

Figures 3.23 & 3.24 show for each $<\delta\mu_{9G}>$ interval the fraction of net-bulge spectra whose determined mass-weighted age and metallicity has reached the maximum allowed value by the SSP library. Such *failed* fits obviously yield indirect constraints on the validity of the assumed model for the intensity profile of the disk within the bulge radius. Inspection of these results demonstrates that independently of the used PSS code or adopted SSP library, a higher fraction of bulges in the $<\delta\mu_{9G}>$ interval **iC** tend to reach maximum values of age and metallicity, followed by **iB** bulges and finally by **iA** bulges, which display the lowest fractions. This insight can be interpreted in terms of: considering that **iC** & **iB** bulges (by this order) are intrinsically the oldest and most metal-rich in the sample, it is to be expected that, mostly for these bulges, subtraction of the rather blue spectrum of the disk will lead to a strong deficit of flux in the blue spectral range, thereby forcing PSS codes to reach maximum age and metallicity determinations.

Although this project has produced interesting results, placing us one step further in answering the fundamental question of whether the disk preserve its intensity slope, or even exists, inside the bulge radius, this exercise alone is not sufficient for definitively settling this issue. Nevertheless, this investigation has placed important constraints on the possible light distribution by the disk within R_B: for a substantial part of the sampled LTGs, independently of their $<\delta\mu_{9G}>$ classification, the assumption of inward extrapolation of the exponential intensity profile of the disk yields unphysical results. This suggests that the true intensity profile of the disk inside R_B shows a flattening or central depression, as theoretically proposed in Kuijken & Dubinski (1995); Obreja et al. (2013); Widrow & Dubinski (2005). If, on the other hand, the disk contribution within R_B indeed follows an exponential profile, these results indicate that, for a significant fraction of the analyzed galaxies, the disk distribution for $R^\star < R_B$ should be much redder than the host disk, resembling more the bulge than the disk.

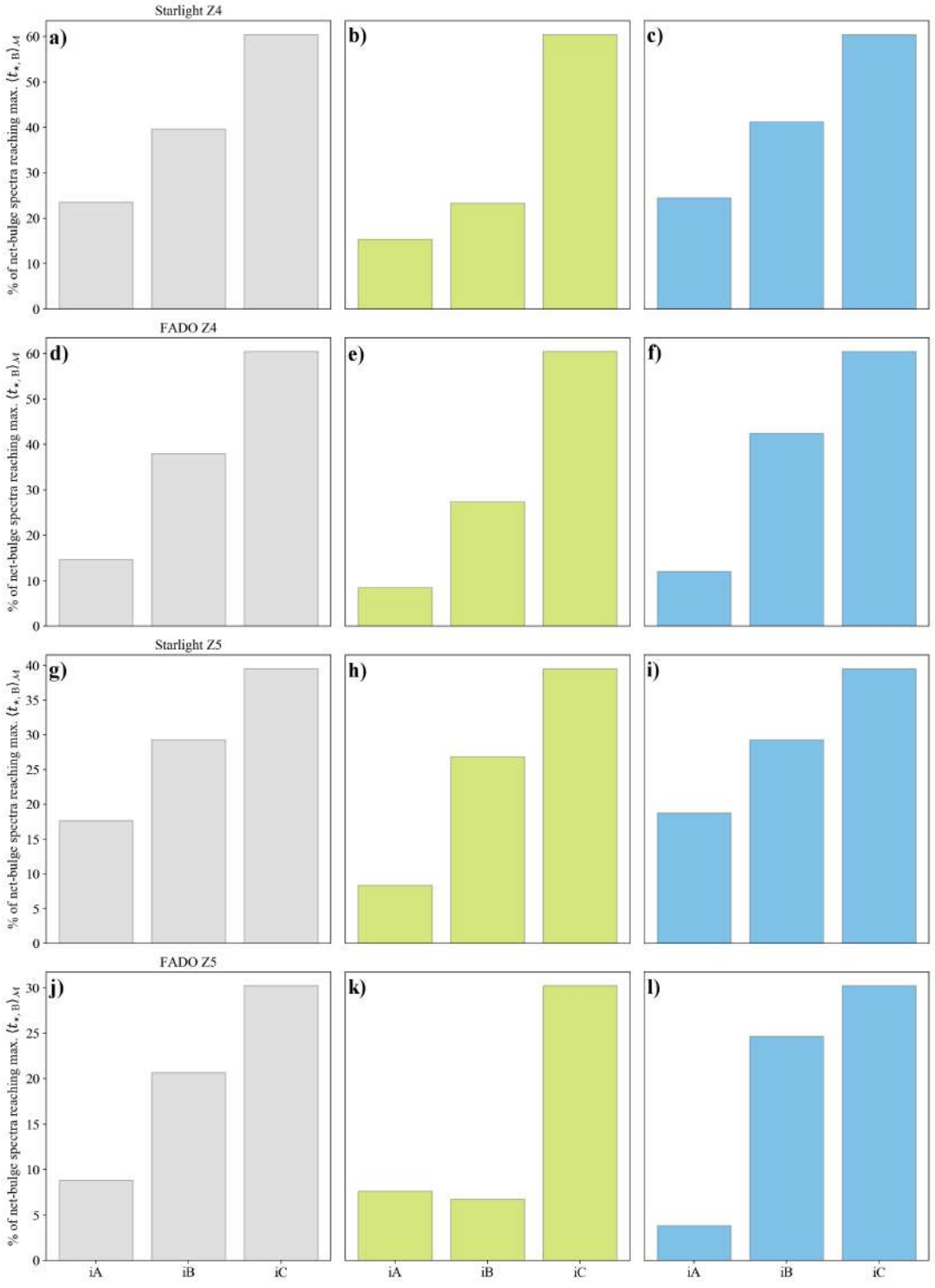

Figure 3.23: **a**) Histogram of the fraction of spectra in each of the three $<\delta\mu_{9G}>$ intervals whose age determinations have reached the allowed maximum for all disk configurations. This figure refers to results with STARLIGHT and the SSP library Z4. **b**) Histogram of the fraction of net-bulge spectra whose estimated age has reached the allowed maximum in the case of the **flatD** disk configuration and spectral modeling with STARLIGHT and the SSP library Z4. **c**) Histogram of the fraction of net-bulge spectra with maximum age for the **expD** disk configuration and spectral modeling with STARLIGHT and the SSP library Z4. **d**) to **f**) – repetition of **a** to **c** but using FADO and the SSP library Z4. **e**) to **h**) – repetition of **a** to **c** but using STARLIGHT and library Z5. **i**) to **l**) – repetition of **a** to **c** but using FADO and the SSP library Z5.

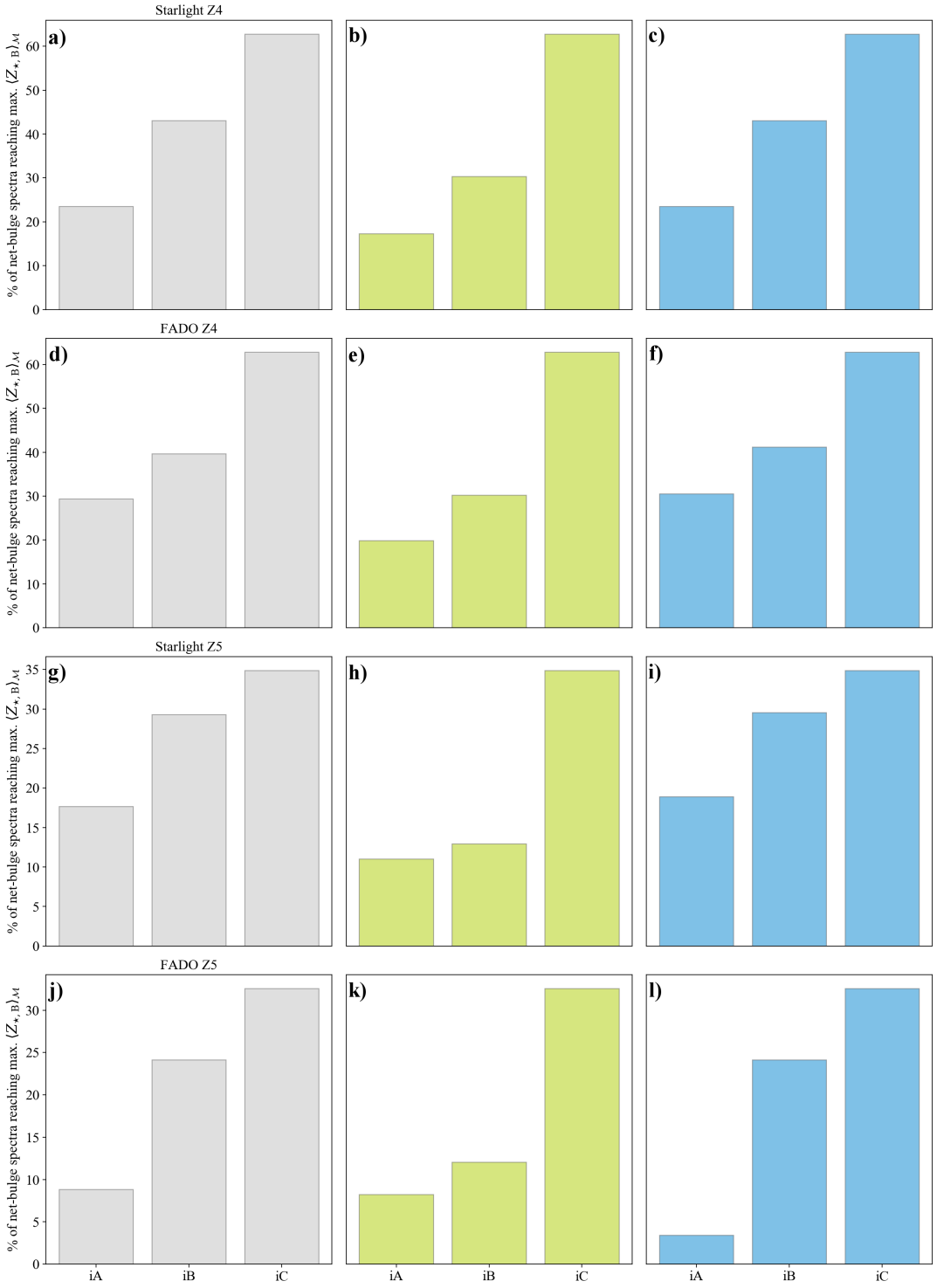

Figure 3.24: Same layout as in Fig. 3.21 but for the mass-weighted metallicity determinations instead of mass-weighted age.

Chapter 4

Discussion

4.1 The continuous rise of bulges out of galactic disks

A fundamental insight from this study is that, after an accurate decomposition of the structural components of our sample LTGs by means of iFIT a code developed in the framework of this PhD project with the goal of robust determination of Sérsic model parameters, LTG bulges across ~ 3 dex in $\log(\mathcal{M}_\star)$ and > 1 dex in $\log(\Sigma_\star)$ form a *continuous* sequence with regard to their $<\delta\mu_{9G}>$, B/T, $\langle t_{\star,B}\rangle_{\mathcal{M}}$, $\langle Z_{\star,B}\rangle_{\mathcal{M}}$, $\Sigma_\star$ and colors (see Figs. 3.4, 3.7 & 3.8). This result was not only obtained on the basis of a single analysis methodology, but it was confirmed by repeating the modeling of CALIFA IFS data within irregular annuli with two conceptually distinct PSS codes each applied with two different SSP libraries (Z4 & Z5). Additionally, an analysis of the retrieved SFHs has shown that the evolutionary properties of bulges and their host disks are correlated (see Figs. 3.3, 3.11 & 3.12). These findings strongly argue against the age bimodality expected from the standard scenario of two bulge assembly routes, one leading to CBs via monolithic collapse and the other one to PBs via quasi-continuous SF in the centers of secularly evolving disks. If this scenario was valid, one would expect a segregation of bulges into two evolutionary distinct branches that would echo these two different formation routes. Likewise, our results are hardly compatible with the rejuvenation scenario proposed by some authors: First, it can be argued that, if the SF episode that led to the rejuvenation of CBs was relatively brief (e.g., a starburst with a *burst parameter b* of 0.1-0.3, occurring 1-2 Gyr ago, as proposed by Thomas & Davies , 2006), a large fraction of LTGs at $0.08 < z < 0.16$ would be similar with regard to their integrated SEDs to extreme starburst galaxies, such as green peas (GPs; e.g., Amorín et al., 2012; Cardamone et al., 2009, among others) and luminous blue compact galaxies (BCGs; e.g. Bergvall & Östlin, 2002; Guzmán et al., 1998; Papaderos et

al., 1996a). More specifically, the high SFRs implied by the rejuvenation scenario proposed by Thomas & Davies (2006) translate to a high ($> 10^3$ Å) EW(Hα) and a nebular (line and continuum) contribution that exceeds 50% of the integral optical and near-infrared emission (e.g., Krüger et al., 1995). However, both our spectral modeling analysis and a review of the existing literature yield no support to the hypothesis that such extreme starbursts were ignited in the centers of fully developed LTG disks some 1-2 Gyr ago, transforming old CBs into present-day PBs. Furthermore, if the rejuvenation scenario was invariably valid, one would statistically expect indications of a recent phase of strongly elevated sSFR in the SFHs of some of the most massive bulges (equivalent to CBs) in our sample, in disagreement with our spectral modeling analysis. Finally, if PBs were disguised CBs due to recent in-situ SF, one would expect them to follow the $M_\bullet - \sigma_\star$ correlation observed for CBs, which is incompatible with the available observational evidence (e.g., Kormendy & Ho, 2013; Kormendy, Bender & Cornell, 2011).

The entire evidence gathered during this project coherently suggests that, throughout the LTG mass sequence, bulges and disks evolve alongside through a combination of processes that lead to a continuum of physical and evolutionary properties. These are reflected in the increase of $<\delta\mu_{9\mathrm{G}}>$ with increasing LTG mass and exemplified by the three $<\delta\mu_{9\mathrm{G}}>$ intervals (**iA**–**iC**) in Fig. 2.15. For high-mass ($\log(\mathcal{M}_{\star,\mathrm{B}}) > 10$) bulges (interval **iC**) that are hosted by higher-mass LTGs, SF has ceased earlier than 9 Gyr ago, whereas for intermediate-mass ones (**iB**) it was extended to later cosmic epochs, with the least massive bulges (**iA**) displaying ongoing SF and being composed by $\sim 80\%$ of stars younger than 9 Gyr. Furthermore, comparison of the m_9 ratio in the bulge and disk, and examination of Fig. 3.11**a** & **c** demonstrate that older disks host older bulges with both displaying a similar (within ~ 0.2 dex) metallicity (panel **d**). This fact points to an interwoven bulge–disk evolution as previously suggested by some photometric or spectroscopic studies in the local Universe and at higher redshift (e.g., Carollo et al., 2007; Lang et al., 2014; Margalef-Bentabol et al., 2017; Papovich et al., 2015; Sánchez-Blázquez et al., 2014; Sánchez-Blázquez, 2016; Tacchella et al., 2018; van Dokkum et al., 2013, see also Sect. 1).

The results obtained in this study are consistent with a scenario where the development and growth of the bulge component in LTGs is driven by a superposition of quick-early and slow-secular processes, the relative importance of which increases with increasing galaxy mass. By assuming that the gas cloud from which a LTG forms has an angular momentum, a rotating disk is the first structure to be formed (according to observations of galaxies at high-z, the

disk exhibits at this stage a clumpy and irregular morphology). For high-mass systems (the precursors of local **iC** galaxies), which possess a deep gravitational pool promoting central gas inflow and intense in situ SF (and eventually also the genesis of a SMBH seed), it is plausible to assume that the formation of a massive nuclear cluster or a low-mass proto-bulge will be early and quick. In addition, inward migration and coalescence of massive ($> 10^{8-9}$ $M_{\odot}$) SF clumps forming continuously out of violent disk instabilities (e.g., Bournaud et al., 2007; Mandelker et al., 2014, 2017) and inflow of inter-clump gas (e.g., Hopkins et al., 2012; Zolotov et al., 2015) will support the buildup of the bulge during its dominant formation phase and beyond. Bournaud et al. (2007) uses a particle-mesh sticky-particle code to model the evolution of a $7 \cdot 10^{10} M_{\odot}$ Jeans-unstable gas-rich galactic flat-density disk. Even though the model does not incorporate SNe feedback, their results suggest that the bulge naturally emerge from the disk, and that on a timescale of 0.5–0.7 Gyr several high-mass ($\geq 2 \cdot 10^{8} M_{\odot}$) clumps migrate to the center accounting on average for $\sim$ 70% of the final bulge stellar mass. Later on, but still in early stages of galaxy formation (no later than $\sim$ 3 to 4 Gyr, according to the results obtained with $\mathcal{RY}$ that indicate a lack of in situ SF in the past 9 Gyr in the very center of these galaxies) it is reasonable to assume that SF activity and the associated SNe feedback yields to depletion, heating and expulsion of the gas. This, together with negative AGN feedback, is expected to initiate a gradual SF quenching, as apparent from the red colors and old ages of massive bulges in Figs. 3.3, 3.7 & 3.8. However, Fig. 3.3.5 suggests that the timescale for SF quenching over the total bulge extent is rather long, reaching up to $\sim$4 Gyr. This quenching timescale is consistent with a prolonged inside-out low-level SF activity or a series of weak SF episodes, or energy injection by an AGN, rather than one single major SF episode that gave rise to a sudden removal of the gas.

As for low-mass systems (the progenitors of local **iA** galaxies), due to their modest gravitational well, the pace of their bulge formation and general evolution is likely substantially slower as compared to their higher mass counterparts. The slow secular evolution of LTGs in the low-mass end, dictated by their shallower gravitational potential is presumably the reason why still today bulges in these LTGs are in the process of building up, as reflected in their blue colors (Fig. 3.3), low mass-weighted ages (Figs. 3.7 & 3.8) and positive age and color gradients (Figs. 3.6 & 3.3.5). Regarding LTGs with an **iB** bulge, their intermediate initial mass favors a delayed evolution as compared to their more massive analogs (**iC**) but not so passive as **iA** galaxies. In terms of standard SFH parametrizations, the superposition of these processes might

be empirically approximated by *delayed* exponentially declining SFR models (e.g., Cardoso et al., 2017) with an e-folding timescale and a delay of the SFR peak scaling inversely to the present-day $\mathcal{M}_{\star,\mathrm{T}}$.

The qualitative agreement of our results with those from other authors, who have documented an evolutionary pace that is dependent on the initial baryonic mass of a galaxy (e.g., Heavens et al., 2004; van Dokkum et al., 2013), does not necessarily rule out that the current evolutionary status of a LTG reflects a short/prolonged phase of mass accumulation through accretion of gas from the Cosmic Web: galaxies classified as **iA** might have gathered their baryonic mass onto their shallow gravitational pools over a longer time scale, that would be consistent with their observed delayed development.

It is clear that, in order to develop a detailed picture of the proposed scenario it is necessary to gain a deeper understanding of timescales and drivers of bulge growth including the possible regulatory role of AGN- and SF-driven feedback. To achieve this goal one needs improved observational constraints (for instance, on the mass function of SF clumps in high-z proto-disks; cf. e.g., Cava et al., 2018; Tamburello et al., 2017) and a better understanding of stellar-dynamical processes, such as stellar migration and its observational imprints (e.g., Roškar et al., 2012; Ruiz-Lara et al., 2016; Sánchez-Blázquez et al., 2009), the dissolution and regeneration of stellar bars (e.g., Berentzen et al., 2004), and, more generally, of all intrinsic and environmental parameters that shape the dynamical coupling of stars, gas and dark matter (DM) in an evolving galaxy ecosystem. For instance, a process that might contribute to the steepening of the density profile of a bulge, possibly promoting nuclear starburst activity (Loose et al., 1982), is the adiabatic contraction of the stellar component in response to gas inflow. Papaderos et al. (1996b) proposed this effect as a justification for the steeper stellar density profile of the underlying host of starbursting dwarfs when compared to the same of quiescent dwarf irregulars. This process could occur if accreted gas from the disk or from the cosmic web (e.g., Dekel & Burkert, 2014; Dekel et al., 2009) yields a significant ($\geq 30\%$) fraction of the dynamical mass in the central parts of proto-LTGs, which might be the case if baryons dominate in those radii (see Genzel et al., 2017, for recent observational evidence for baryon dominated disks ~ 10 Gyr ago), or the DM halo has an extended core of nearly constant density (i.e., a Burkert 1995 profile, see also Salucci & Burkert, 2000).

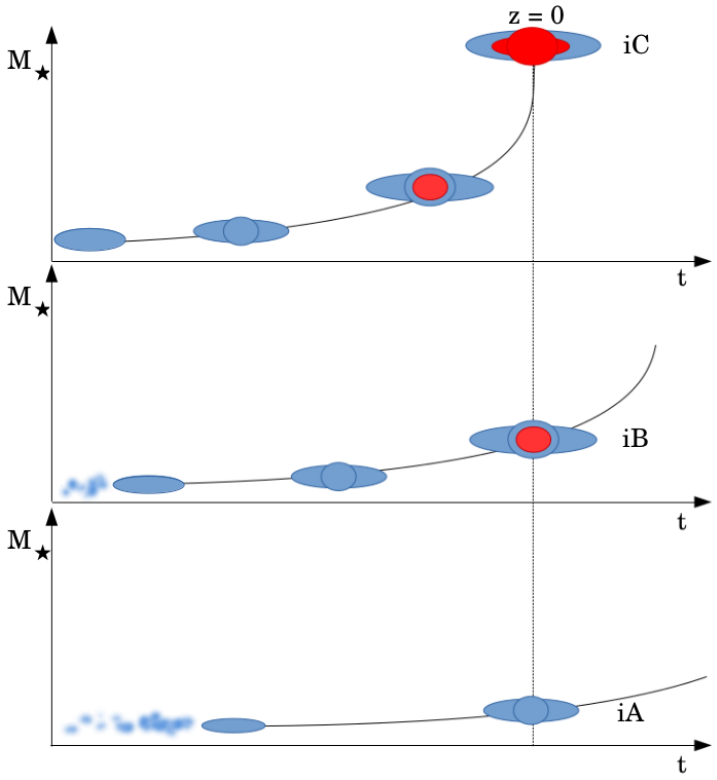

Figure 4.1: Schematic illustration of the proposed scenario for formation and evolution of bulges: the three LTGs in Fig. 2.15 may be regarded as morphological snapshots in a sequence of increasing bulge stellar mass $\mathcal{M}_{\star,\mathrm{B}}$, age $\langle t_{\star,\mathrm{B}}\rangle_{\mathcal{M}}$, surface density $\Sigma_{\star,\mathrm{B}}$ and $<\delta\mu_{9\mathrm{G}}>$. The progenitors of high-mass LTGs (e.g., NGC 0776, i.e., systems in the $<\delta\mu_{9\mathrm{G}}>$ interval **iC**; $\geq$ -0.5 mag) form in more massive halos and experience the dominant phase of their bulge assembly earlier than 9 Gyr ago. Conversely, the precursors of low-$<\delta\mu_{9\mathrm{G}}>$ ($\leq$ -1.5 mag; i.e., **iA**) LTGs, such as IC 0776, assemble at a calm pace within lower-mass halos and undergo an overall retarded structural and chemical evolution toward intermediate-$<\delta\mu_{9\mathrm{G}}>$ LTGs (**iB**), such as NGC 0001. Once the bulge has grown to (log $\mathcal{M}_{\star,\mathrm{B}}$; log $\Sigma_{\star,\mathrm{B}}$) $\geq$ (10;9), AGN-driven feedback initiates a gradual cessation of SF (depicted in red).

It is noteworthy that by selecting 15 galaxies of our sample with total stellar mass $5.08 \cdot 10^{10} < \mathcal{M}_{\star} < 7.08 \cdot 10^{10}$ (i.e. in the range of MW's total stellar mass of $\sim 6.08 \cdot 10^{10}$, Licquia & Newman 2015) we find as average values a B/T of $\sim$ 30% in stellar mass, a $\mathrm{R_B}$ of $\sim$ 1.8 kpc, a mass-weighted stellar age of 10.4 Gyr and a mass fraction of 18% for stars younger than 7 Gyr. These mean values are compatible with those given for the MW in the review by Barbuy, Chiappini & Gerhard (2018, B/T $\sim$ 25%, $\mathrm{R_B} \sim$ 2 kpc, an average stellar age of $\sim$ 10 Gyr and a fraction by mass of $\sim$ 15% for stellar populations younger than 8 Gyr in the bulge). Additionally, 11 of these 15 galaxies are classified as **iB** and 6 of their bulges fall in the SF locus on the BPT diagram. The agreement between the physical properties measured in these mass-selected LTGs and the MW yields indirect support to our main conclusion that the initial mass of a LTG regulates the timescale of its bulge formation and the B/T ratio.

4.1.1 Accelerated bulge growth in proportion to galaxy mass

Figures 3.7**c** & 3.8**c** demonstrate that the B/T mass fraction increases with LTG mass: low-mass **iA** bulges contain on average 20% of the total mass of a LTG, whereas this percentage rises to 40% in high-mass LTGs hosting an **iC** bulge, with intermediate-mass LTGs typically containing **iB** bulges that comprise, on average, 30% of their mass. Additionally, Figs. 3.7**e** & 3.8**e** show an increase of $\Sigma_\star$ with $\mathcal{M}_{\star,\mathrm{B}}$. This combined evidence hints at a non-homologous growth of radial $\Sigma_\star$, $\mathcal{M}_{\star,\mathrm{B}}$ and μ profiles in LTGs with increasing total stellar mass. The increase of the stellar mass fraction of the bulge with increasing $\mathcal{M}_{\star,\mathrm{T}}$ reinforces the proposed scenario of an accelerated build-up of the bulge in proportion to $\Sigma_\star$. This can be understood as the result of efficient gas inflow and star formation in the deep gravitational pool of more massive LTGs, leading then to quick chemical self-enrichment and in turn a high gas cooling efficiency (cf., e.g., Böhringer & Hensler, 1989) that further promotes in situ SF and the growth of $\mathcal{M}_{\star,\mathrm{B}}$ on a timescale being inversely related to the LTG mass. This process may continue until the bulge reaches a characteristic value ($\log(\mathcal{M}_{\star,\mathrm{B}})$; $\log(\Sigma_{\star,\mathrm{B}}) \geq (10;9)$) above which accretion-powered nuclear activity becomes significant (cf. Sec. 4.1.2) and gas heating and depletion gradually lead to SF quenching. In this context, bulge growth in the center of galactic disks might be seen as a manifestation of (sub)galactic downsizing, where the buildup timescale scales inversely with the mass and initial density of the baryonic condensation out of which galaxies form, which is in qualitative agreement with the *staged galaxy formation scenario* by Noeske et al. (2007).

Besides the trends documented in Figs. 3.7 & 3.8, panels **a** to **c**, showing an increase of $<\delta\mu_{9\mathrm{G}}>$ and $\langle t_{\star,\mathrm{B}}\rangle_{\mathcal{M}}$ with increasing $\mathcal{M}_{\star,\mathrm{B}}$ and $\mathcal{M}_{\star,\mathrm{T}}$, lent supplementary support to the hypothesis of an accelerated bulge growth in proportion to the LTG mass, as also apparent from Fig. 3.11**c**. The latter displays the bulge-to-disk age contrast (δt_{BD}) as a function of $\mathcal{M}_{\star,\mathrm{T}}$: if bulges where formed purely through monolithic collapse prior to and thus independently from disks, then one would expect a roughly constant (> 0) δt_{BD} across the entire LTG mass range. Conversely, if bulges were assembling strictly in lockstep with secularly evolving disks, having thus the same SFH and being merely rearranged disk material, then their δt_{BD} would also be independent on $\mathcal{M}_{\star,\mathrm{T}}$. Neither of these two cases is documented by our analysis, which revels an increasing bulge-to-disk age contrast with increasing $\mathcal{M}_{\star,\mathrm{T}}$. This implies that high-mass bulges, residing at the centers of higher-mass disks, have assembled earlier and quicker than low-mass bulges. We remark that it is improbable that the relation between δt_{BD} and $\mathcal{M}_{\star,\mathrm{T}}$ (or, similarly, $<\delta\mu_{9\mathrm{G}}>$)

for high-mass LTGs is due to a premature interruption of SF. If this was the case, we would expect a diminishing in $\delta t_{\rm BD}$, contrary to the evidence of Fig. 3.11**c**.

Another insight from Fig. 3.11 is the lack of a bimodality or discontinuity in the bulge vs. disk age and metallicity contrast over $\sim$ 2.5 dex in $\mathcal{M}_{\star,\rm T}$. This again suggests an interwoven yet asynchronous build-up of the two stellar components, where, apparently bulges are assembled from disks on a timescale that scales inversely with $\mathcal{M}_{\star,\rm T}$. Hereupon, the results from this study are incompatible with both a pure monolithic formation scenario and a secular origin for LTG bulges, pointing instead to galactic downsizing phenomenon of an accelerated bulge build-up in the center of massive proto-disks, and vice versa. This interpretation is consistent with a non-homologous radial growth of $\Sigma_\star$ and the observed trend between $\mathcal{M}_{\star,\rm B}/\mathcal{M}_{\star,\rm T}$ ratio and $\mathcal{M}_{\star,\rm T}$ (Figs. 3.7**c** & 3.8**c**), as well as with a trend for an increasing Sérsic index η with $\mathcal{M}_{\star,\rm T}$ (or M_r) for present-day LTGs.

Figure 2.15 displays three LTGs that may be seen as morphological snapshots in a chronological sequence of increasing $\mathcal{M}_{\star,\rm B}$, $\Sigma_{\star,\rm B}$ and $<\delta\mu_{\rm 9G}>$. The continuity that is here documented for bulge physical properties and for their difference ($\delta t_{\rm BD}$ and $\delta Z_{\rm BD}$) to their host disks disfavors segregation into evolutionary distinct classes, despite the tentative subdivision of LTG bulges into three intervals (**iA**–**iC**) that was performed here only for illustration purposes.

Summarizing, the combined results from this project can be explained by a simple scenario where high-mass bulges ($<\delta\mu_{\rm 9G}>$ interval **iC**) correspond to the endpoint of an evolutionary pathway across an increasing $<\delta\mu_{\rm 9G}>$ (**iA** $\rightarrow$ **iB** $\rightarrow$ **iC**) whose timescale scales inversely with the baryonic mass of a LTG. The initial mass of a LTG might in turn depend on its environmental properties, since gas accretion from the cosmic web is more efficient in high-density environments (e.g., Dekel et al., 2009), promoting accelerated growth of galaxies and their structural components. By contrast, LTGs forming within lower-mass halos that usually reside in less *privileged* regions of the cosmic network (filaments and the extreme field) are likely to experience a delayed build-up due to a lower efficiency of gas accretion onto their shallow gravitational well. The slower build-up of these present-day **iA** LTGs (i.e. their lower *metabolism*, as quantified by their time-averaged sSFR) is reflected in their lower age, metallicity, stellar surface density and $\mathcal{M}_{\star,\rm B}/\mathcal{M}_{\star,\rm T}$ ratio. Despite their lower mass-weighted ages, these systems are not truly young since our spectral modeling analysis implies that their bulges contain a minor fraction ($\sim$ 20%)

of stars older than 9 Gyr (cf. Sect. 3.3.4). This old stellar component might have originated from low-level SF occurring early on and minor mergers with, e.g., dwarf spheroidals formed prior to the epoch of reionization (e.g., Grebel & Gallagher, 2004).

These considerations are in qualitative agreement with conclusions obtained from abundance matching studies of higher-z galaxies (e.g., Papovich et al., 2015; Patel et al., 2013; van Dokkum et al., 2013). For instance, Papovich et al. (2015) studied how the progenitors of present-day LTGs with the stellar mass of the MW and M31 ($5 \cdot 10^{10}$ $M_\odot$ and 10^{11} $M_\odot$, respectively) may have developed and grown from $z = 3$ to 0.5. Their findings suggest that both LTGs commenced their evolution as star-forming disks that passed an IR-luminous phase and subsequently evolved to the redder and more quiescent galaxies of today. These authors add that "the progenitors of MW-mass galaxies reached each evolutionary stage at later times (lower redshifts) and with stellar masses that are a factor of two to three lower than the progenitors of the M31-mass galaxies.". Additionally, these studies report an increase of Sérsic η with z, whereby higher-mass galaxies reach a higher η earlier than lower-mass galaxies, being in agreement with the proposed scenario of sub-galactic downsizing.

4.1.2 Accretion-powered nuclear activity along the bulge sequence

In the last decades, accretion-powered nuclear activity in galactic bulges has motivated numerous studies (see Kormendy & Ho, 2013, for a recent review). A central insight that has emerged on this subject is the scarcity of Seyfert activity in bulges classified as PB, although there is kinematical evidence for them containing a SMBH. This is commonly attributed to an inefficient (sub-Eddington) and sporadic matter accretion (e.g., Kormendy, Bender & Cornell, 2011). Another explanation involves the premature termination of SMBH growth, possibly due to the dissolution of short inner bars (Du et al., 2017). Indeed, Figs. 3.7 & 3.8, panel **f**, are in concordance with previous findings: $\sim 94\%$ (31 of the 33) low-mass **iA** bulges are spectroscopically classified as SF according to BPT emission-line diagnostics, with the remaining two falling in the locus of Composites. Assuming that the mean $M_\bullet/\mathcal{M}_{\star,\mathrm{T}}$ ratio of $\sim 10^{-3}$ for galaxies with $\log(\mathcal{M}_{\star,\mathrm{T}}) \geq 10$ (Kormendy & Ho, 2013) applies to lower-mass bulges and a radiative efficiency of 0.1, the predicted $M_\bullet$ of $\sim 10^{6-7}$ $M_\odot$ for **iA** bulges would translate to maximum Eddington rates of 0.02-0.2 $M_\odot$/yr. If so, even after convolution by the PSF of CALIFA IFS data, and taking into consideration that the surface brightness of these bulges is by 2-3 SDSS r mag fainter than that of high-mass (**iC**) bulges, it should be expected that weak AGN would

be detectable, if the central black hole would be fed by nearly constant matter accretion. Furthermore, the fact that these bulges sustain significant star formation (reflected in an average EW(Hα) = 26.3 Å) implies the presence of a reservoir of cold dense gas, indicating that the lack of Seyfert line emission is not due to a high LyC photon escape fraction (in contrast to many massive ETGs, Gomes et al. 2016a; Papaderos et al. 2013). Dilution of AGN-specific line ratios by HII regions is also improbable given that our analysis of emission-line diagnostics was repeated within small (3″) apertures that exclude circumnuclear SF regions (see Fig. 2.17 in Sect. 2.4.4). Likewise, obscuration of a putative AGN by dust does not offer an explanation for the scarcity of Seyfert activity in these fainter bulges, given their nearly face-on geometry and moderate-to-low intrinsic extinction ($A_V \leq 0.24 \pm 0.12$ mag). The evidence panel **f** from Figs. 3.7 & 3.8 is in agreement with inefficient or sporadic gas accretion onto an intermediate-$M_\bullet$ SMBH, as previously suggested by other studies, or might be due to the asynchronous growth of SMBHs relative to their galaxy hosts with the $M_\bullet/\mathcal{M}_{\star,\mathrm{B}}$ ratio, or the Eddington ratio and the SMBH spin parameter being non-linearly coupled to $\mathcal{M}_{\star,\mathrm{T}}$. Regarding moderate-to-massive bulges (**iB** and **iC**), the gray-shaded quadrant in Figs. 3.7**e**, includes 93% (38/41) of all Seyfert and LINER in our sample, suggesting that the deeper gravitational potential of bulges in the range $\log(\mathcal{M}_{\star,\mathrm{B}};\Sigma_{\star,\mathrm{B}})\geq(10;9)$ is related to efficient SMBH nourishment.

Another subject of intense examination and debate is the regulatory role of AGN on SF quenching in high-mass bulges both in local Universe and at intermediate z (e.g., Cattaneo et al., 2009; Harrison, 2017; Kormendy & Ho, 2013, and references therein). By carrying out bulge-to-disk decomposition in 6764 galaxies with $\mathcal{M}_{\star,\mathrm{T}} > 10^{10}$ M$_\odot$ at $0.5 < z < 2.5$, Lang et al. (2014) find that bulges and SMBHs assemble their mass in tandem by means of mergers and/or disk instabilities, and AGN-feedback is a major driver of SF quenching. Similarly, Tacchella et al. (2018) hypothesize that mechanisms associated with SF quenching must be internal to the galaxies and intimately related to bulge growth. These authors conclude that for bulges with $\mathcal{M}_{\star,\mathrm{T}} > 10^{11}$ M$_\odot$, the quenching of SF occurs gradually in an inside-out manner. This is consistent with our results shown in Fig. 3.7**e** where 16 out of 76 LTGs fall in the gray-shaded and are classified as Composites, indicating a co-existence of SF with AGN-driven feedback over a time span of at least 2 Gyr (cf. panel **b** with panel **f**). This points against a sudden SF quenching by accretion-powered nuclear activity (Fig. 3.13), adding further support to the aforementioned proposition.

4.1.3 Radial age gradients in galaxy bulges and their evolutionary implications

Inspection of Fig. 3.13 reveals once again a continuity in the properties of LTG bulges, this time with respect to the radial variation of stellar age out to the bulge periphery, as defined at the isophotal radius R_B. This diagram documents a trend between stellar age gradient and $\mathcal{M}_{\star,T}$, with low-mass LTGs exhibiting positive mass- and luminosity-weighted age gradients in their bulges whereas the opposite tendency is apparent for high-mass LTGs. This trend remains valid (cf. Fig. 3.14) when age gradients are computed within the radius R_{80} that encompasses 80% of the bulge's r-band luminosity, which reassures that the obtained trends are not artificially arising due to an increasing light contamination from the disk in the bulge periphery. It is interesting to note that analysis of color gradients using SDSS data yields the same trend (cf. Fig. 3.6, in agreement with previous work, e.g., Balcells & Peletier 1993).

Positive age gradients reflect an increase in SF activity at the center of the bulge as compared to its periphery (or R_{80}). Indeed, by examining the EW(Hα) profiles (provided in the electronic appendix for the whole LTG sample) it becomes evident that the lower the LTG mass is, the higher is the EW(Hα), thus, the sSFR at the center of its bulge. This observational insight is in agreement with the proposed scenario where the three intervals in $<\delta\mu_{9G}>$ are considered as chronological snapshots in a common evolutionary sequence for LTG bulges: in an early cosmic epoch, massive LTG progenitors, initially resembling nearly bulgeless disks (i.e. qualitatively similar to present-day **iA** bulges), were able to rapidly form a massive **iC** bulge. This picture is consistent with the results from Welikala & Kneib (2012) who measure color gradients in 3248 galaxies out to $z \sim 3$ in the GOODS-South field. These authors report that "the star formation rate in galaxies increases towards $z \sim 3$ (galaxies becoming bluer), it is the central regions of galaxies where this increase is most marked, possibly due to increased gas densities in the central regions".

Another insight from Fig. 3.13 is that high-mass bulges show negative age gradients suggesting a bulge formation timescale of up to 4 Gyr/R_B. A possible interpretation for this is that these bulges have formed and/or quenched their SF in an inside-out manner over a time scale of up to ~ 4 Gyr. As discussed in Sect. 3.3.5 and above in greater detail, a relatively slow inside-out SF quenching could be due to the release of energy and momentum by an AGN or a series of

minor SF episodes eventually leading to the expulsion and depletion of cold gas within R_B.

4.2 The importance of spatially resolved IFS data for advancing our understanding on bulge formation and evolution

The tight trends emerging from this study are presumably due to the consistent application of an advanced analysis methodology on a representative set of high-quality IFS data for local LTGs. An important advantage of the conducted study is that it is free of aperture biases, given that both average and spatially resolved properties of LTG bulges refer to a clear-cut isophotal definition of the bulge radius that has been uniformly applied to the whole sample in the framework of a profile fitting analysis of SDSS data. Of special relevance is also that the SFH of stellar populations in the sample LTGs has been analyzed with two different state-of-the-art PSS codes (Sect. 3.4), one taking self-consistently into account nebular and stellar emission (FADO) while the other (STARLIGHT) fitting spectra purely in terms of stellar templates. Additionally, this study explores how spatial resolution (specifically, determinations for single spaxels, as opposed to those for larger segments of binned spaxels) affects the estimated SFH and secondary products from spectral modeling, such as $\mathcal{M}_\star$, $t_{\star,\mathcal{M}}$ and $Z_{\star,\mathcal{M}}$. This task is specially relevant in view of the high angular resolution permitted by modern IFS units attached to 10m-class telescopes, such as the Multi Unit Spectroscopic Explorer (MUSE) at the Very Large Telescope (VLT). In this regard, we carry out a comparative analysis of the results obtained with STARLIGHT for $<\delta\mu_{9G}>$, $\log(\mathcal{M}_{\star,T})$, $\langle t_{\star,B}\rangle_{\mathcal{M}}$ and $\langle Z_{\star,B}\rangle_{\mathcal{M}}$ by averaging determinations within single spaxels and from fitting integrated spectra within **isan**. Additionally, given that a spaxel-by-spaxel analysis of the LTG sample with FADO has not been feasible (due to a high CPU-time expense and the fact that its upgraded version v.1b became available only in October 2018), we compare modeling results from STARLIGHT and FADO only within **isan**. This series of comparisons is presented in Fig. 3.15:

i. Results from panels **a**, **e** & **i** are based on spaxel-by-spaxel modeling (i.e. at the highest resolution that the available IFS data yield) and display the tightest trends and a better separation of $<\delta\mu_{9G}>$ intervals in their physical properties.

ii. Panels **b**, **f** & **j** exhibit the results from STARLIGHT by fitting the summed up spectrum of all spaxels that lie in the same **isan**. Additionally, each of the combined spectra were fed to STARLIGHT 15 times, each time changing the seed random number that controls the

initial guess in the parameters space for each fit. The number of **isan** spectra that were used for the analysis of each LTG bulge depends on the bulge angular extent that varies between ~ 2.5 and $\sim 11.2''$.

iii. Panels **c**, **j** & **k** are similar to panels **b**, **f** & **j** with the exception being that they were fed to STARLIGHT only once. Comparison of these panels with panels **b**, **f** & **j** shows how the seed number influences the spectral modeling results. Although in terms of $\log(\mathcal{M}_{\star,\mathrm{T}})$, $\langle t_{\star,\mathrm{B}}\rangle_{\mathcal{M}}$ and $\langle Z_{\star,\mathrm{B}}\rangle_{\mathcal{M}}$ the differences are rather small, this is not the case for $<\delta\mu_{9\mathrm{G}}>$, and consequently for the subdivision of the sample into the bulge classes **iA**, **iB** and **iC**.

iv. Panels **d**, **h** & **l** were obtained by summing all the zones that lay within $\mathrm{R_B}$ and subsequently feeding them to STARLIGHT. While the other methods analyze spectra within several radial zones of a LTG, this method considers only the integrated spectrum of each LTG within $\mathrm{R_B}$.

v. A notable trend from comparison of panels **a** to **i** with panels **b** to **j** is, respectively, the decrease of the goodness of models and the increase of the spread within $<\delta\mu_{9\mathrm{G}}>$ intervals. These variations are more evident for lower mass galaxies which usually contain a higher percentage of spaxels with strong SF and they can be attributed to the fact that co-addition of luminous SF-dominated spaxels with fainter spaxels from non-SF regions leads the former set of spaxels to dominate the fitting solution to the combined luminosity-weighted integrated spectrum. For instance, it is evident that the correlation between $\langle t_{\star,\mathrm{B}}\rangle_{\mathcal{M}}$ and $\log(\mathcal{M}_{\star,\mathrm{T}})$ (panels **e**, **f**, **g** & **h**), notably strong from the **SbS** analysis, has now much higher dispersion (the coefficient of determination R^2 decreased from 0.76 (**SbS**) to 0.65 (**18Z-15t**), 0.64 (**18Z**) & 0.61 (**Rb**)).

vi. Regarding $\langle Z_{\star,\mathrm{B}}\rangle_{\mathcal{M}}$ estimations, whereas panel **i** shows a satisfactory separation into $<\delta\mu_{9\mathrm{G}}>$ intervals, it is not the case for the estimates obtained with the other methods. For instance, the maximum value obtained for $\langle Z_{\star,\mathrm{B}}\rangle_{\mathcal{M}}$ within **iA** is 0.40 $\mathrm{Z_\odot}$ (**SbS**), 0.52 (**18Z-15t**) 0.51 (**18Z**) and 0.45 (**Rb**). As for the minimum & maximum $\langle Z_{\star,\mathrm{B}}\rangle_{\mathcal{M}}$ within **iB**, respectively: 0.33 & 0.81 (**SbS**), 0.19 & 0.92 (**18Z-15t**), 0.21 & 0.93 (**18Z**) & 0.16 & 0.96 (**Rb**). Regarding the minimum $\langle Z_{\star,\mathrm{B}}\rangle_{\mathcal{M}}$ within **iC** we measure 0.50 (**SbS**), 0.62 (**18Z-15t**), 0.61 (**18Z**) & 0.48 (**Rb**). From these numbers it is clear the increasing mixture within each $<\delta\mu_{9\mathrm{G}}>$ interval.

Despite the fact that there is a significant increase of the dispersion in the documented trends

from **SbS** to **isan** determinations, showing that a clear separation into $<\delta\mu_{9G}>$ intervals is only possible to obtain with **SbS** analysis, the observed continuity is still fairly visible. This is probably related to the fact that, although spaxel binning within **isan** entails a substantial decrease in spatial resolution, we use exclusively spectra that lay within R_B. This approach is still superior to studies with a fixed aperture where the fiber might capture only a small part of the bulge or encompass part of the disk, depending to the distance of the LTG and the radial extent of its bulge. Additionally, by examining Fig. 3.19, one can verify that the dispersion in the correlation between $\log(\mathcal{M}_{\star,T})$ and $\nabla(t_{*,B})_M$ & $\nabla(t_{*,B})_L$ significantly increases to a point where conclusions become uncertain, indicating that the **SbS** approach is preferable for the determination of stellar age gradients.

The fact that a better spatial resolution (i.e. the **SbS**-based analysis) supports a more accurate analysis of the evolutionary properties of stellar populations in bulges calls for an extension of this project with the determination of $<\delta\mu_{9G}>$ for high-quality MUSE data for a representative sample of local LTGs.

4.3 A critical examination of the standard assumption that the disk preserves its exponential profile within R_B

The last part of this project is dedicated to the exploration of the disk's radial distribution within R_B. For this purpose we developed a routine that permits to determine the net SED of the bulge after spectroscopic subtraction of the expected contribution from the underlying disk (see Sect. 2.4.6 for detailed explanation). Although quite rudimentary at this stage, this technique allowed to draw some important conclusions on the validity of the standard assumption that the disk preserves its exponential slope all the way to the LTG center:

i. Figure 3.20 shows that, independently of the $<\delta\mu_{9G}>$ interval considered, hence the galaxy total mass, up to 35% of the SEDs obtained for the bulge after subtraction of an exponential (or inwardly flattening) model for the disk yield negative flux in the blue spectral range. This implies that in a significant fraction of LTGs the disk component must show a central flat core or intensity depression inside R_B.

ii. Further support against the standard assumption of the exponentiality of the disk within R_B comes from the fact that spectral modeling obtained in that case for the net SED

of the bulge leads to dubious results. Specifically, we find that $\sim 30\%$ ($\sim 33\%$) of the disk-subtracted bulges reach the maximum allowed age (metallicity), and for $\sim 30\%$ the stellar mass is higher than that estimated prior to disk subtraction.

iii. By assuming a flat intensity profile for the disk within R_B, spectral modeling of $\sim 20\%$ ($\sim 22\%$) of the net SED of bulges in our sample yields the maximum allowed age (metallicity), and for $\sim 20\%$ of all cases the stellar mass exceeds that estimated within R_B prior to disk subtraction.

The above lines of evidence suggest that the disk component in a significant fraction of LTGs shows a central intensity depression inside R_B. This conclusion, if corroborated through further studies, will necessitate a fundamental revision in image decomposition techniques and have far-reaching implications on our understanding of the structural build-up of LTGs.

4.4 Final remarks

This project was carried out with the purpose of a systematic investigation of the physical and evolutionary properties of bulges in LTGs, whereby special attention was placed on the mitigation of limitations in previous studies, most importantly of aperture effects. One decisive advantage of this study compared to previous ones is the combined use of good quality IFS data and surface photometric techniques that has allowed to extract virtually the total emission of the bulge, minimizing contamination by the surrounding disk. Moreover, utilizing a new algorithm (iFIT), that was developed in the context of this study it has been possible to overcome the degeneracy between two of the three free parameters from the Sérsic fitting law and accurately determine the isophotal radius of the bulge. Additionally, as shown in Sect. 3.4, spectral modeling IFS data both spaxel-by-spaxel and within isophotal annuli has permitted to robustly establish trends between physical and evolutionary properties of LTG bulges, and advance our understanding on their connection with their parent disks.

An important feature of the approach taken here is the omission of a pre-classification of LTG bulges into CBs and PBs on the basis of their SL index η. This is because such an empirical prior subdivision into PBs and CBs would have to rely on subjective cutoff in η, and it would therefore immediately introduce a bias in our analysis. Our study considers instead the entire set of available IFS data for LTGs in the CALIFA survey with the only pre-selection criterion

used being their nearly face-on geometry and undisturbed morphology. Additionally, no attempt was made to estimate the photometric properties of the bulge (for instance, magnitudes, radial extent, η) through image decomposition into the bulge and an exponential disk, as is the case of previous studies. This is mainly because, as shown in Sect. 3.5, the common assumption of a perfect exponential disk all the way to the LTG center is invalid for a large fraction of LTGs.

Quite importantly, our sample covers the entire mass range of LTGs and their bulges, providing a representative base for the exploration of bulge properties in local galaxies. By combining, for the first time, three powerful techniques (surface photometry of SDSS data, spectral modeling of IFS data and post-processing of the spectral synthesis output with the code $\mathcal{RY}$) on such representative sample, we were able to significantly advance in this topic, shedding new light in the formation and evolution of bulges:

i. We devised an effective bulge classification diagnostic ($<\delta\mu_{9\mathrm{G}}>$), a distance- and nominally extinction-independent quantity that proved to be much more reliable and physically meaningful than the SL index η (see Sect. 3.1). Unlike η, this quantity follows tight correlations with the several other physical properties of bulges (e.g., present-day stellar mass $\mathcal{M}_{\star,\mathrm{B}}$, stellar surface density $\Sigma_{\star,\mathrm{B}}$, mass-weighted age $\langle t_{\star,\mathrm{B}}\rangle_{\mathcal{M}}$ and metallicity $\langle Z_{\star,\mathrm{B}}\rangle_{\mathcal{M}}$), offering a new powerful means for the characterization of bulges.

ii. We found a *continuity* in the distribution of the bulge's physical properties: B/T, $\mathcal{M}_{\star,\mathrm{B}}$, $\langle t_{\star,\mathrm{B}}\rangle_{\mathcal{M}}$ and $\langle Z_{\star,\mathrm{B}}\rangle_{\mathcal{M}}$ all scale linearly with $\log(\mathcal{M}_{\star,\mathrm{T}})$, with the highest-mass LTGs hosting the oldest, most massive and dense and least chemically enriched bulges, and vice versa. This continuity is reinforced by being consistently documented both with STARLIGHT and FADO, and adopting two different SSP libraries in modeling of binned spectra.

iii. Based on $<\delta\mu_{9\mathrm{G}}>$ we tentatively subdivide LTG bulges in three characteristic intervals: low-mass ($\log(\mathcal{M}_{\star,\mathrm{B}}) \leq 9.7$) bulges with a $<\delta\mu_{9\mathrm{G}}> \leq$ -1.5 mag (interval **iA**) are hosted by low-mass ($\log(\mathcal{M}_{\star,\mathrm{T}}) \leq 10.5$) disk-dominated LTGs, are comparatively young ($\langle t_{\star,\mathrm{B}}\rangle_{\mathcal{M}} \simeq 6.8$ Gyr) and show ongoing SF with an average EW(Hα) $\simeq$ 25 Å. High-mass bulges ($<\delta\mu_{9\mathrm{G}}> \geq$ -0.5 mag; interval **iC**) reside in high-mass ($\log(\mathcal{M}_{\star}) \geq 11$) LTGs, have a mean age of $\simeq$ 11.5 Gyr and are characterized by a high stellar mass surface density ($\Sigma_{\star,\mathrm{B}} \geq 10^9$ $\mathrm{M}_{\odot}/\mathrm{kpc}^2$) and weak nebular emission ($\langle\mathrm{EW(H}\alpha)\rangle \simeq 5$ Å. As for bulges in the intermediate range of $<\delta\mu_{9\mathrm{G}}>$ (interval **iB**), they also display intermediate values in $\mathcal{M}_{\star,\mathrm{B}}$, $\Sigma_{\star,\mathrm{B}}$, $\langle t_{\star,\mathrm{B}}\rangle_{\mathcal{M}}$, $\langle Z_{\star,\mathrm{D}}\rangle_{\mathcal{M}}$, absolute r-band magnitude and EW(Hα).

vi. By extending this project with a comparative analysis of the bulge and the disk, we found that these two components evolve alongside. However, the bulge-to-disk age and metallicity contrast increases with $\mathcal{M}_{\star,\mathrm{T}}$ and $<\delta\mu_{9\mathrm{G}}>$: whereas the bulge and the disk are of similar age and metallicity in low-mass LTGs, high-mass bulges are, on average, by $\sim$ 2 Gyr older and by 0.9 dex more metal-rich than their parent disks.

v. An analysis of BPT diagnostics indicates that in lower-mass bulges, SF is the dominant gas excitation mechanism whereas accretion-powered nuclear activity is practically confined to higher-mass ($\geq 10^{10}$ $\mathrm{M}_{\odot}$), higher-$\Sigma_{\star,\mathrm{B}}$ ($\geq 10^{9}$ $\mathrm{M}_{\odot}\mathrm{kpc}^{2}$) bulges.

vi. An exploration of radial age gradients in bulges reveals once more a relation with $\mathcal{M}_{\star,\mathrm{T}}$: in the low-mass regime, mass- and luminosity-weighted age gradients are generally positive, which indicates an increase of SF activity in the very center of these bulges. To the contrary, for high-mass LTGs, our analysis documents negative age gradients reflecting a decreasing stellar age from the center to the periphery of the bulge. Quantitatively, negative age gradients in the high-mass LTG regime might reach 4 $\mathrm{Gyr}/\mathrm{R}_{\mathrm{B}}$, which is consistent with a prolonged phase of inside-out formation and/or SF quenching.

The essential insight from this analysis is that LTG bulges across $\sim$ 3 dex in $\log(\mathcal{M}_{\star})$ and $>$ 1 dex in $\log(\Sigma_{\star})$ form a *continuous* sequence with regard to $<\delta\mu_{9\mathrm{G}}>$, $\langle t_{\star,\mathrm{B}}\rangle_{\mathcal{M}}$ and $\langle Z_{\star,\mathrm{B}}\rangle_{\mathcal{M}}$, strongly challenging the standard picture of bulge formation, which implies distinct assembly routes for old, quasi-monolithically formed CBs and comparatively young secularly forming PBs. The combined lines of evidence emerging from this project support the view that bulges and disks in LTGs evolve alongside, whereby bulge growth is driven by a superposition of quick-early and slow-secular processes, the relative importance of which is increasing with increasing galaxy mass. This formation process leads to a continuum of evolutionary properties that is reflected in the tight correlation between $<\delta\mu_{9\mathrm{G}}>$ and LTG mass $\mathcal{M}_{\star,\mathrm{T}}$.

Additionally, the trend for an increasing $\mathcal{M}_{\star,\mathrm{B}}/\mathcal{M}_{\star,\mathrm{T}}$ ratio and bulge-to-disk age contrast with increasing $\mathcal{M}_{\star,\mathrm{T}}$ (or, equivalently, $<\delta\mu_{9\mathrm{G}}>$), and the absence of a bimodality or even discontinuity in this relation over three dex in bulge mass, lend support to the interpretation of an interwoven yet asynchronous growth of bulge and disk, with the former assembling out of the latter on a timescale that is inversely related to $\mathcal{M}_{\star,\mathrm{T}}$. This process is expected to lead to a non-homologous radial growth of $\Sigma_{\star}$ in LTGs and a trend for an increasing Sérsic index η with increasing $\mathcal{M}_{\star,\mathrm{T}}$.

4.5 Future work

The build-up history of bulges in late-type galaxies is a fundamental subject in extragalactic research and intimately linked to the genesis and growth of galaxies and their SMBHs. Therefore a comprehensive exploration of this phenomenon both in local and higher-z galaxies is of paramount importance. With high-quality IFS data taken with 10m-class telescopes (e.g., MUSE@VLT spectrograph), advanced consistency-ensuring PSS codes like FADO and continuously refined numerical simulations, a comprehensive understanding of bulge evolution across cosmic time is now at reach.

The analysis of local LTGs in this PhD project yields testable predictions on the structural build-up of bulges across cosmic time and calls for an observational investigation of the proposed bulge evolutionary scenario back to ∼9 Gyr ago ($z \sim 1.3$). If correct, one would expect precursors of present-day iC bulges in massive LTGs to have almost assembled their stellar mass and eventually still show significant SF activity or post-starburst spectra with prominent stellar Balmer absorption features, whereas less massive LTGs ($\log(\mathcal{M}_{\star,\mathrm{T}}) < 10$) to host a weak, if any at all, bulge component. An interesting and quite revealing exercise would be to use, for instance, archival data from the K-band Multi Object Spectrograph (KMOS) at VLT to study the bulge and disk in nearly face-on LTGs at $1 < z < 2$, while supplementing the sample for lower-z bins with archival data with MUSE@VLT. Some of the questions to be investigated with FADO within different bins in galaxy mass concern the evolutionary and physical properties of the bulge and disk, and the B/T ratio. A kinematical study of stars and ionized gas for an additional sample of higher-inclination LTGs at those redshifts would supplement this project with information on the connection between LTG angular momentum and bulge characteristics (e.g., $\Sigma_\star$, $\mathrm{V}_{rot}/\sigma_\star$). Additionally, a spatially resolved kinematical analysis would allow us to investigate $\mathrm{V}_{rot}/\sigma_\star$ radial profiles, which might give further insights on the validity of the inward exponentiallity of galactic disks.

Another component of future studies could center on MOONS@VLT. Although single-aperture spectroscopy is affected by the disk, a careful selection of a LTG sample using supplementary photometric data will certainly yield a significant number of galaxies where the MOONS fiber matches the bulge component. This sample, analyzed with FADO, will then provide a statistically significant probe for studying the evolutionary properties of bulges at intermediate

redshifts.

Finally, it is planned to further develop iFIT so that it becomes a complete 1D surface photometry decomposition tool. The planned concept includes the incorporation of the **isan** technique for the extraction of the SBPs and will allow both for an interactive and automatic definition of the disk, and its possible deviations from the exponentiality within the bulge radius. We anticipate that iFIT (v.2) will be of great interest to the community given that it will facilitate fast and robust structural decomposition and it may have significant potential for applications to imaging data from the Euclid mission and LSST.

Bibliography

Abazajian K. N., et al., 2009, ApJS, 182, 543

Acquaviva, V., Guaita, L., Gawiser, E., & Padilla, N. 2011, Bulletin of the American Astronomical Society, 43, 407.04

Aguerri, J. A. L., Balcells, M. & Peletier, R. F. 2001, A&A, 367, 428

Allen, M. G., Groves, B. A., Dopita, M. A., Sutherland, R. S., & Kewley, L. J. 2008, ApJS, 178, 20

Amiaux J., et al., 2012, Space Telescopes and Instrumentation 2012: Optical, Infrared, and Millimeter Wave, 84420Z, SPIE.8442

Amorín, R. et al. 2007, A&A 467, 541

Amorín, R., Pérez-Montero, E., Vílchez, J. M., Papaderos, P. 2012, ApJ, 749, 185A

An, D., Ramírez, S. V., Sellgren, K., Arendt, R. G. A., Boogert, A. C., Robitaille, T. P., Schultheis, M., Cotera, A. S., Smith, H. A., Stolovy, S. R. 2011, ApJ, 736, 133

Asari, N. V., Cid Fernandes, R., Stasińska, G., et al. 2007, MNRAS, 381, 263

Baes, M. & Gentile, G. 2011, A&A, 525, A136

Baes, M. & Van Hese, W. 2011, A&A, 534, A69

Balcells, M., & Peletier, R. F. 1993, Galactic Bulges, 153, 409

Balcells, M., & Peletier, R. F. 1994, AJ, 107, 135

Baldwin, J. A., Phillips, M. M. & Terlevich, R. 1981, PASP, 93, 5 (BPT)

Barbuy B., Chiappini C., Gerhard O., 2018, ARAA, 56, 223

Bell, E. F., et al. 2004, ApJ, 608, 752

Bender, R. & Möellenhoff, C. 1987, A&A, 177, 71

Bender, R., Burstein, D. & Faber, S. M. 1992, ApJ, 399, 462

Berentzen, I., Athanassoula, E., Heller, C. H. & Fricke, K. J. 2004, MNRAS, 347, 220

Bergvall, N. & Östlin, G. 2002, A&A, 390, 891

Bigiel F., Blitz L., 2012, ApJ, 756, 183

Binette, L., Magris, C. G., Stasińska, G., & Bruzual, A. G. 1994, A&A, 292, 13

Binggeli, B., Cameron, L.M. 1993, A&AS 98, 297

Bird, J. C., Kazantzidis, S. & Weinberg, D. H. 2012, MNRAS, 420, 913

Blanton, M. R. et al. 2003b, ApJ, 594, 186

Bohlin, R. C. & Gilliland, R. L. 2004, AJ, 127, 3508

Böhringer, H. & Hensler, G. 1989, A&A, 215, 147

Bournaud, F., Elmegreen, B. G., Elmegreen, D. M. 2007, ApJ, 670, 237

Bower, R. G., Kodama, T., & Terlevich, A. 1998, MNRAS, 299, 1193

Breda, I. 2014, MSc Thesis, University of Porto

Breda, I. & Papaderos, P. 2018, A&A, 614, 48

Breda, I., Papaderos, P., Gomes, J.M., Amarantidis, S. 2019, A&A, submitted

Brinchmann, J., Charlot, S., White, S. D. M., et al. 2004, MNRAS, 351, 1151

Bruzual, G. & Charlot, S. 2003, MNRAS, 344, 1000

Calzetti, D., Armus, L., Bohlin, R.C., Kinney, A.L., Koornneef J., Storchi-Bergmann T. 2000, ApJ, 533, 682

Caon, N., Capaccioli, M. & D'Onofrio, M. 1993, MNRAS, 265, 1013

Cardamone, C., Schawinski, K., Sarzi, M. et al. 2009, MNRAS, 399, 1191

Cardelli, J. A., Clayton, G. C., & Mathis, J. S. 1989, ApJ, 345, 245

Cardoso, L. S. M., Gomes, J.-M., & Papaderos, P. 2016, A&A, 594, L2

Cardoso, L., Gomes, J. M. & Papaderos, P. 2017, A&A, 604A, 99C

Cardoso, L., Gomes, J.M. & Papaderos, P. 2018, A&A, in press

Carollo, C. M., Stiavelli, M., de Zeeuw, P. T., Seigar, M. & Dejonghe, H. 2001, ApJ, 546, 216

Carollo, C.M., Scarlata, C., Stiavelli, M., Wyse, R. F. G., Mayer, L. 2007, ApJ, 658, 960

Cattaneo, A., Faber, S. M., Binney, J., Dekel, A., Kormendy, J., et al. 2009, Nature, 460, 213

Cava, A., Schaerer, D., Richard, J., et al. 2017, Nature Astronomy, 2, 76

Cen, R. 2014, ApJ, 790, L24

Chakrabarty, D. & Jackson, B. 2009, A&A, 498, 615

Chevallard, J., & Charlot, S. 2016, MNRAS, 462, 1415

Cid Fernandes, R., Mateus, A., Sodré, L., Stasińska, G., Gomes, J. M. 2005, MNRAS, 358, 363

Cid Fernandes, R. González Delgado, R. García Benito, R., et al. 2014, A&A, 561, A130

Cid Fernandes, R., Stasinka, G., Schlickmann, M. S., et al. 2010, MNRAS, 403, 1036

Cid Fernandes, R., Stasińska, G., Mateus, A., et al. 2011, MNRAS, 413, 1687

Ciotti, L. 1991, A&A, 249, 99

Concas, A., Pozzetti, L., Moresco, M., & Cimatti, A. 2017, MNRAS, 468, 1747

Conroy, C., Gunn, J. E., & White, M. 2009, ApJ, 699, 486

Conselice C. J. 2006, ApJ, 638, 686

Courteau, S., de Jong, R. S. & Broeils, A. H. 1996, ApJ, 457, L73

Davies, J.I., Phillipps, S., Cawson, M.G.M. et al. 1988, MNRAS, 232, 239

de Jong, R. S. 1996, A&A, 313, 377

de Jong, R. S. 1996, Spiral Galaxies in the Near-IR, 43

de Jong, R. S. 1996, A&A, 313, 45

de Vaucouleurs, G. 1948, Ann. Astrophys., 11, 247

de Vaucouleurs, G. 1959, ApJ, 130, 728

de Vaucouleurs, G. 1959, Handbuch der Physik, 53, 275

Debattista, V. P., Roškar, R., Loebman, S. R. 2017, vol. 434. Springer, Cham

Dekel, A. & Burkert, A. 2014, MNRAS, 438, 1870

Dekel, A., Birnboim, Y., Engel, G., Freundlich, J., et al. 2009, Nature, 457, 451

Dessauges-Zavadsky, M., Schaerer, D., Cava, A., Mayer, L., & Tamburello, V. 2017, ApJ, 836, L22

Dopita, M. A. & Sutherland, R. S. 1995, ApJ, 455, 468

dos Reis, S. et al. 2019, in prep.

Draine B. T. 2003, ARA&A, 41, 241

Drory, N. & Fisher, D. 2007, ApJ, 664, 640

Du, M., Debattista, V. P., Shen, J., et al. 2017, ApJ, 844L, 15D

Elmegreen, B. G., Bournaud F., Elmegreen D. M. 2008, ApJ, 688, 67

Erwin, P. 2015, ApJ, 799, 226

Fernandez Lorenzo, M., Sulentic, J., Verdes-Montenegro, L., et al. 2014, ApJL, 788, L39

Ferrarese, L., & Merritt, D. 2000, ApJL, 539, L9

Fisher, D. & Drory, N. 2010, ApJ, 716, 942

Fletcher, T. J., Robertson, B. E., Nakajima, K., et al. 2018, arXiv:1806.01741

Freeman, K. C. 1970, ApJ, 160, 811

Förster Schreiber, N., Shapley, A. E., Genzel, R., et al. 2011, ApJ, 739, 45

Gadotti, D. A. & dos Anjos, S. 2001, AJ, 122, 1298

Gadotti, D. A. 2009, MNRAS, 393, 1531

Gadotti, D. A. 2012, in *notes to the PhD School of Astrophysics "F. Lucchin"*, Erice, Italy, September 2011; G. Bono, M., Zoccali (eds.), arXiv1208.2295G

Gallazzi A., Charlot S., Brinchmann J., White, S. D. M., Tremonti, C. A. 2005, MNRAS, 362, 41

Ganda K., Peletier R. F., McDermid R. M., Falcón-Barroso J., de Zeeuw P. T., Bacon R., Cappellari M., Davies R. L., Emsellem E., Krajnovic D., Kuntschner H., Sarzi M., van de Ven G., 2007, MNRAS, 380, 506

Carcía-Benito, R., Zibetti, S., Sánchez, S. F., et al. 2015, A&A, 576. A135

Genzel, R., Förster Schreiber, N., Übler, H., et al. 2017, Nature, 543, 397

Girardi, L., Bressan, A., Bertelli, G., Chiosi, C. 2000, A&AS, 141, 371

Goddard, D., Thomas, D., Maraston, C., et al 2017, MNRAS, 466, 4, 4731

Gomes, J. M. & Papaderos, P. 2016, A&A, 594, A49

Gomes, J.M., Papaderos, P. 2017, A&A 603, A63

Gomes, J.M., Papaderos, P. 2017, A&A 618, 3

Gomes, J. M., Papaderos, P., Kehrig, C., et al. 2016, A&A, 588, 68

Gomes, J. M., Papaderos, P., et al. 2016, A&A, 586A, 22G

González Delgado, R., García-Benito, R., Peréz, E., et al. 2015, A&A, 581, A103

Gorgas, J. et al. 1993, ApJS, 86, 153

Graham, A. & Colless, M. 1997, MNRAS, 287, 221

Graham, A. & Driver, S. 2005, PASA, 22, 118

Graham, A., Driver, S., Petrosian, V. et al. 2005, AJ, 130, 1535

Graham, A. W. 2013, Planets, Stars and Stellar Systems. Volume 6: Extragalactic Astronomy and Cosmology, 6, 91

Grand, R. J. J., Daisuke, K. & Cropper, M. 2014, MNRAS 439, 623

Grebel, E. K. & Gallagher, J. S. 2004, ApJ, 610, L89

Guedes, J., Mayer, L., Carollo, M. & Madau, P. 2013, ApJ, 772, 36

Guseva, N.G., Izotov, Y.I., Papaderos, P., et al. 2001, A&A, 378, 756

Guzmán, R., Jangren, A., Koo, D.C., Bershady, M. A., Simard, L. 1998, ApJ, 495, L13

Halle, A., Di Matteo, P., Haywood. M., Combes, F. 2015, A&A, 578, A58

Häußler, B. et al. 2013, MNRAS, 430, 330

Harrison, C. 2017, Nature Astronomy, 1E, 165H

Head, J. T. C. G., Lucey, J. R., Hudson, M. J., & Smith, R. J. 2014, MNRAS, 440, 1690

Heavens A. F., Jimenez R., Lahav O., 2000, MNRAS, 317, 965

Heavens, A., Panter, B., Jimenez, R. & Dunlop, J. 2004, Nature, 428, 625

Heckmann, T. M. 1980, A&A, 87, 152

Ho, L. C. 1999, Adv. Space Res., 23, 813

Ho, L. C. 2008, ARA&A, 46, 475

Holmberg, E. 1958, Meddelanden Lunds Astron. Obser. Ser. II, 136, 1

Hopkins, A. M., Miller, C. J., Nichol, R. C., et al., 2003, ApJ, 599, 971

Hopkins, P. F., Kereš, D., Murray, N., Quataert, E., & Hernquist, L. 2012, MNRAS, 427, 968

Huertas-Company, M., Gravet, R., Cabrera-Vives, G. et al. 2015, ApJS, 221, 8

Iglésias-Páramo, J., Vílchez, J. M., Galbany, L., et al. 2013, A&A 553, L7

Iglésias-Páramo, J., Vílchez, J. M., Rosales-Ortega, F. F., et al. 2016 ApJ, 826, 71

Ivezić Ž., et al., 2008, arXiv e-prints, arXiv:0805.2366

Izotov, Y. I., Schaerer, D., Worseck, G., et al. 2018, MNRAS, 474, 4514

Johnston, E. J., Aragón-Salamanca, A., Merrifield, M. R., Bedregal, A. G. 2012, MNRAS, 422, 2590

Johnston, E. J., Aragón-Salamanca, A., Merrifield, M. R. 2014, MNRAS, 441, 333

Kauffmann, J., Pillai, T., Zhang, Q., et al. 2017, A&A, 603, A90

Kauffmann, G., Heckman, T. M., Tremonti, C., et al. 2003, MNRAS, 346, 1055

Kauffmann, G., Heckman, T. M., Tremonti, C., et al. 2003, MNRAS, 346, 1055

Kauffmann, G., Heckman, T. M., White, S. D. M., et al. 2013, MNRAS, 341, 54

Kehrig, C., Monreal-Ibero, A. & Papaderos, P., et al. 2012, A&A, 540, 11

Kelz, A., Verheijen, M. A. W., Roth, M. M., et al. 2006, PASP, 118, 129

Keselman, J. A., Nusser, A. 2012, MNRAS, 424, 1232

Kewley, L. J., Dopita, M. A., Sutherland, R. S., Heisler, C. A., Trevena, J. 2001, ApJ, 556, 121

Koleva, M., Prugniel, P., Ocvirk, P., et al. 2008, MNRAS, 385, 1998

Koleva M., Prugniel P., Bouchard A., Wu Y., 2009, A&A, 501, 1269

Kormendy, J. & Ho, L. C. 2013, ARA&A, 51, 511

Kormendy, J. & Kennicutt Jr, R. 2004, ARA&A, 42, 603

Kormendy, J., Bender, R. & Cornell, M. 2011, Nature, 469, 374

Kormendy, J. 1977, ApJ, 217, 406

Kotilainen, J. K., León-Tavares, J., Olguín-Iglesias, A., et al. 2016, ApJ, 832, 157

Krüger et al. 1995, A&A, 303, 41

Kuijken, K. Dubinski, J. 1995, MNRAS, 277, 1341

Lang P., Wuyts, S., Somerville, R. S., et al. 2014, ApJ, 788, 11

Larson, R. 1974, MNRAS, 166, 585

Leitet, E., Bergvall, N., Hayes, M., Linné, S., & Zackrisson, E. 2013, A&A, 553, A106

Leitherer, C., Hernandez, S., Lee, J. C., & Oey, M. S. 2016, ApJ, 823, 64

Lian J., Yan R., Blanton M. & Kong X., 2017, MNRAS, 472, 4679

Licquia T. C., Newman J. A., 2015, ApJ, 806, 96

Loose, H.-H., & Thuan, T.X. 1986a, in Star Forming Dwarf Galaxies and Related Objects, ed. D. Kunth, T. X. Thuan & J. T. T.Van (Editions Frontières), 73 (LT86)

Loose, H. H., Krügel, E. & Tutukov, A. 1982, A&A 105, 342

Lupton, R., Blanton, M. R., Fekete, G., et al. 2004, PASP, 116, 133

MacArthur L. A., Courteau S., Bell E., Holtzman J. A., 2004, ApJS, 152, 175

MacArthur, L. A., Ellis, R. S., Treu, T., et al. 2008, ApJ, 680, 70

Macchetto, F., Pastoriza, M., Caon, N., et al. 1996, A&AS, 120, 463

Madau, P., & Dickinson, M. 2014, ARA&A, 52, 415

Mandelker, N., Dekel, A., Ceverino, D., et al. 2014, MNRAS 443, 3675

Mandelker, N., Dekel, A, Ceverino, D., et al. 2017, MNRAS, 464, 635

Margalef-Bentabol, B., Conselice, C., Mortlock, A., et al. 2016, MNRAS, 461, 2728

Margalef-Bentabol, B., Conselice, C., Mortlock, A., et al. 2017, MNRAS, 473, 5370

Marino, R., Rosales-Ortega, F. & Sánchez, S. et al. 2013, A&A, 559, A114

Márquez, I. et al. 2000, A&A, 353, 873

Méndez-Abreu, J., Aguerri, J. A. L., Corsini, E. M. & Simonneau, E. 2008, A&A, 478, 353

Moffat, A.F.J. 1969, A&A, 3, 455

Moorthy, B. K. & Holtzman, J. A. 2006, MNRAS, 371, 583

Moré, J. J., Sorensen, D. C., Hillstrom, K. E., & Garbow, B. S. 1984, The MINPACK Project, Sources and Development of Mathematical Software, pages 88-111

Morelli, L., Corsini, E. M., Pizzella, A., et al. 2012, MNRAS, 423, 962

Morelli, L., Parmiggiani, M., Corsini, E. M., et al. 2016, MNRAS, 463, 4396

Morris, M., & Serabyn, E. 1996, ARA&A, 34, 645

Mosenkov, A. V., Sotnikova, N. Y., & Reshetnikov, V. P. 2014, MNRAS, 441, 1066

Ness, M., Debattista, V. P., Bensby, T., Feltzing, S., Roškar, R., Cole, D. R., Johnson, J. A., Freeman, K. 2014, ApJ, 787, L19

Neumann, J., Wisotzki, L., Cloudhury, O. S., Gadotti, D. A., Walcher, C. J., et al. 2017, A&A, 604, 30

Noeske, K. G., Papaderos, P., Cairós, L. M. & Fricke, K. J. 2003, A&A, 410, 481

Noeske, K. G., Faber, S. M., Weiner, B. J., et al. 2007, ApJL, 660, 47

Noguchi, M. 1999, ApJ, 514, 77

O'Connell, R. W. 1996, From Stars to Galaxies: the Impact of Stellar Physics on Galaxy Evolution, 98, 3

Obreja, A., Domínguez-Tenreiro, R., Brook, C., Martínez-Serrano, F.J., Doménech-Moral, M., et al. 2013, ApJ, 763, 26

Ocvirk P., Pichon C., Lançon A., Thiébaut E., 2006b, MNRAS, 365, 46

Okamoto, T. 2013, MNRAS, 428, 718

Osterbrock, D. E. 1989, Astrophysics of Gaseous Nebulae and Active Galactic Nuclei (Mill Valley, CA: University Science Books)

Pacifici, C., Charlot, S., Blaizot, J., & Brinchmann, J. 2012, MNRAS, 421, 2002

Papaderos, P. & Östlin, G. 2012, A&A, 537, A126

Papaderos, P. & Fricke, K.J. 1998, *X-rays from Blue Compact Dwarf Galaxies*, in Highlights in X-ray astronomy : international symposium in honor of Joachim Trümper's 65th birthday, June 17-19, 1998, Garching, Germany, Symposium proceedings / edited by Bernd Aschenbach & Michael J. Freyberg. Garching : Max-Planck-Institut für extraterrestrische Physik, 1999. (MPE report, No. 272, ISSN 0178-0719), p.193 (arXiv:astro-ph/9810101)

Papaderos, P., Loose, H. H., Thuan, T. X., & Fricke, K. J. 1996a, A&AS, 120 207

Papaderos, P., Loose, H. H., Fricke, K. J., Thuan, T. X. 1996b, A&A 314, 59

Papaderos, P., Izotov, Y. I., Thuan, T. X., et al. 2002, A&A, 393, 461

Papaderos, P., Gomes, J. & Vílchez, J., et al. 2013, A&A, 555, L1

Papovich, C., Labbé, I., Quadri, R., et al. 2015, ApJ, 803, 26

Patel, S. G., van Dokkum, P. G., Franx, M., et al. 2013, ApJ, 766, 15

Pelat, D. 1997, MNRAS, 284, 365

Pelat, D. 1998, MNRAS, 299, 877

Peletier, R. F., & Balcells, M. 1996, AJ, 111, 2238

Peletier, R. F., Falcón-Barroso, J., Bacon R., et al. 2007, MNRAS, 379, 445

Peng, C. Y., Ho., L. C., Impey, C. D. & Rix, H. W. 2010, AJ, 139, 2097

Pérez-Montero, E. 2014, MNRAS, 441, 2663S

Petropoulou, V., Vílchez, J., Iglésias-Páramo, J., Papaderos, P., Magrini, L., Cedrés, B., Reverte, D. 2011, ApJ, 734, 32

Pettini, M., & Pagel, B. E. J. 2004, MNRAS, 348, L59

Renka, R. J. 2009, ACM Trans. Math. Softw., Vol. 36 Issue 1, Article No. 7

Ribeiro, B., Lobo, C., Antón, S., Gomes, J. M., Papaderos, P. 2016, MNRAS, 456, 3899

Roškar, R., Debattista, V. P., Quinn, T. R., Wadsley J. 2012, MNRAS, 426, 2089

Roberts, M. S. & Haynes, M. P. 1994, ARA&A, 32, 115

Roth, M. M., Kelz, A., Fechner, T., et al. 2005, PASP, 117, 620

Ruiz-Lara, T., Pérez, I., Florido, E., et al. 2016, MNRAS, 456, L35

Ruiz-Lara, T., Few, C. G., Florido, E., et al. 2017, A&A, 608, A126

Sachdeva, S. & Saha, K. 2016, ApJL, 820, 4

Saha, K., Gerhard, O., & Martinez-Valpuesta, I. 2016, A&A, 588, A42

Saha, K. 2015, ApJL, 806, L29

Salpeter, E. E. 1955, ApJ, 121, 161

Salucci, P. & Burkert, A. 2000, ApJ, 537, L9

Sánchez, S. F., García-Benito, R., Zibetti, S., et al. 2016, A&A 594, 36

Sánchez-Blázquez P., Peletier R. F., Jiménez-Vicente J., Cardiel N., Cenarro A. J., Falcón-Barroso J., Gorgas J., Selam S., Vazdekis A., 2006b, MNRAS, 371, 703

Sánchez-Blázquez, P., Courty, S., Gibson, B. K. & Brook, C. B. 2009, MNRAS, 398, 591

Sánchez-Blázquez, P., Rosales-Ortega, F. F., Méndez-Abreu J., et al. 2014, A&A, 570, A6

Sánchez-Blázquez, P. 2016, in *Galactic Bulges*, Astrophysics and Space Science Library, Springer, Volume 418, p. 127

Sarzi, M., Shields, J. C., Schawinski, K., et al. 2010, MNRAS, 402, 2187

Scannapieco, C., Gadotti, D. A., Jonsson, P., White, S. D. M. 2010, MNRAS, 407, 41

Schawinski, K., Thomas, D., Sarzi, M., et al. 2007, MNRAS, 382, 1415

Schiavon R. P., 2007, ApJS, 171, 146

Schlafly, E. & Finkbeiner, D. 2011, ApJ, 737, 103

Serra, P. & Trager, S. C., 2007, MNRAS, 374, 769

Sérsic, J. L. 1963, Boletin de la Asociacion Argentina de Astronomia, vol.6, p.41

Sérsic, J.-L. 1968, Atlas de galaxias australes. Observatorio Astronomico, Cordoba

Springel V. & Hernquist L. 2005, ApJ, 622, L9

Stasińska, G., Vale Asari, N., Cid Fernandes, R., et al. 2008, MNRAS, 391, L29

Strateva I., et al. 2001, AJ, 122, 1861

Tacchella S., et al., 2018, ApJ, 859, 56

Tamburello, V., et al. 2017, MNRAS, 468, 4792

Thomas, D. & Davies, R. 2006, MNRAS, 366, 510

Thomas D., Maraston C., Bender R., 2003, MNRAS, 339, 897

Tissera, P. B., Machado, R. E. G., Sánchez-Blazquez, P., et al. 2016, A&A, 592, 93

Tojeiro R., Heavens A. F., Jimenez R., Panter B., 2007, MNRAS, 381, 1252

Tremonti, C. A., et al. 2004, ApJ, 613, 898

Trinchieri, G. & di Serego Alighieri, S. 1991, AJ, 101, 1647

Trujillo, I., Aguerri, J. A. L., Cepa, J., & Gutiérrez, C. M. 2001, MNRAS, 328, 977

Trujillo, I., Graham, A.W. & Caon, N. 2001, MNRAS, 326, 869

van Dokkum, P. G., Leja, J., Nelson, E. J., et al. 2013, ApJL, 771, 354

Vanzella, E., Nonino, M., Cupani, G., et al. 2018, MNRAS, 476, L15

Vazdekis A., Sánchez-Blázquez P., Falcón-Barroso J., Cenarro A. J., Beasley M. A., Cardiel N., Gorgas J., Peletier R. F., 2010, MNRAS, 404, 1639

Verheijen, M., Bershady, M., Andersen, D., et al. 2004, Astronomische Nachrichten, 325, 151

Walcher C. J., Böker T., Charlot S., Ho L. C., Rix H.-W., Rossa J., Shields J. C., van der Marel R. P., 2006, ApJ, 649, 692

Weilbacher, P. M., Monreal-Ibero, A., Verhamme, A., et al. 2018, A&A, 611, A95

Welikala, N., & Kneib, J.-P. 2012, arXiv:1202.0494

Widrow, L.M., & Dubinski, J. 2005, ApJ, 631, 838

Worthey. G., Faber, S. M., Gonzalez J. J., Burstein, D. 1994, ApJS, 94, 687

Wuyts, S., Förster Schreiber, N., Genzel, R., et al. 2012, ApJ, 753, 114

Wyse, R. F. G., Gilmore, G., & Franx, M., 1997, ARA&A, 35, 637

Yan, R. & Blanton, M. R. 2012, ApJ, 747, 61

Yoachim, P., & Dalcanton, J. J. 2008, ApJ, 682, 1004

York D. G. et al., 2000, AJ, 120, 1579

Zaritsky, D., Courtois, H., Mũnoz-Mateos, J.-C., et al. 2014, AJ, 147, 134

Zhao, Y. 2012, Ap&SS, 337, 719

Zolotov, A., Dekel, A., Mandelker, N., et al. 2015, MNRAS, 450, 2327

Appendix A

Detailed information on the LTG sample

The following appendix presents, from top to bottom and from left to right:

i. A true-color image of each galaxy and $(g-r)$, $(r-i)$ and $(g-i)$) color maps with the white circle representing the diameter of the bulge component, as inferred with iFIT. The respective radial color profiles, labeled with the color gradient (mag/kpc) determined within the bulge and disk component, are displayed in the right-hand side.

ii. SDSS r-band SBP with a) the Sérsic model obtained with iFIT by fitting the central luminosity excess (orange curve) and b) the result from decomposition into bulge and disk (red curve and blue line, respectively).

iii. SBPs obtained by applying $\mathcal{RY}$ to the spectral synthesis output from Porto3D for CALIFA V500 data (with the SSP library Z4) for nine $t_{\rm cut}$ values (30M, 100M, 300M, 1G, 3G, 5G, 7G and 9G yr). The profiles display the surface brightness distribution of stellar populations with age $\geq t_{\rm cut}$.

iv. Spatially resolved maps of several quantities of interest (stellar continuum, present-day stellar mass ($\mathcal{M}_{\star,\rm P}$), luminosity-weighted stellar metallicity ($Z_{\star,\mathcal{L}}$), mass-weighted stellar metallicity ($Z_{\star,\mathcal{M}}$), luminosity-weighted stellar age ($t_{\star,\mathcal{L}}$), mass-weighted stellar age ($t_{\star,\mathcal{M}}$), Hα flux and EW(Hα)), as obtained by processing the CALIFA V500 data with Porto3D (with the SSP library Z4). The bulge diameter is depicted with the circle in white color. The radial profiles of these quantities as obtained with Porto3D for both the Z4 and Z5 SSP library are shown in the right-hand side together with their respective gradients within the bulge and disk component.

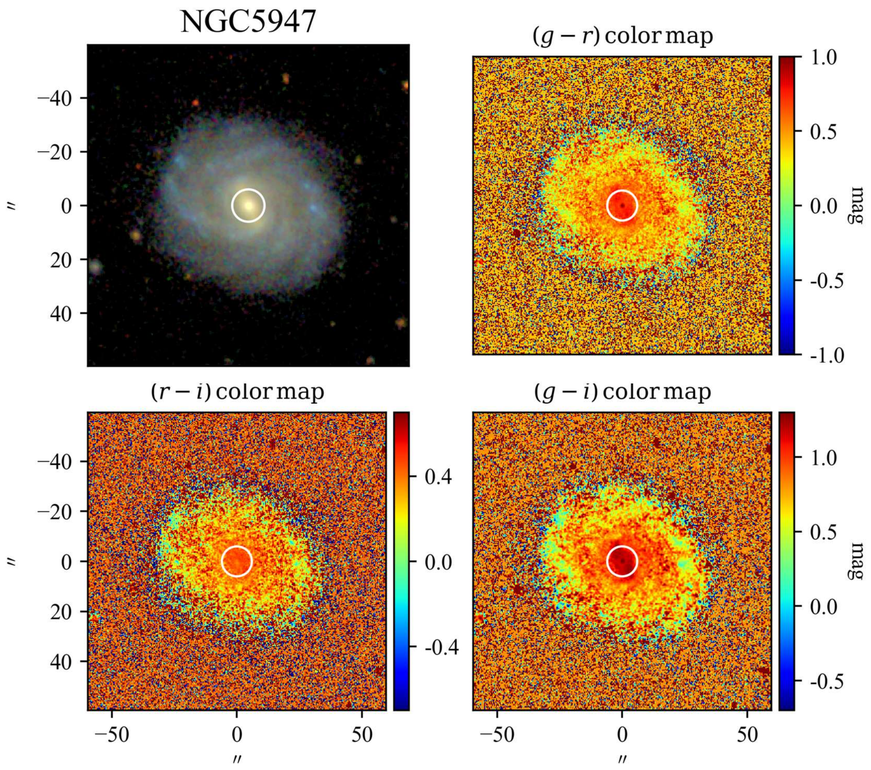

SBP decomposition of SDSS r band

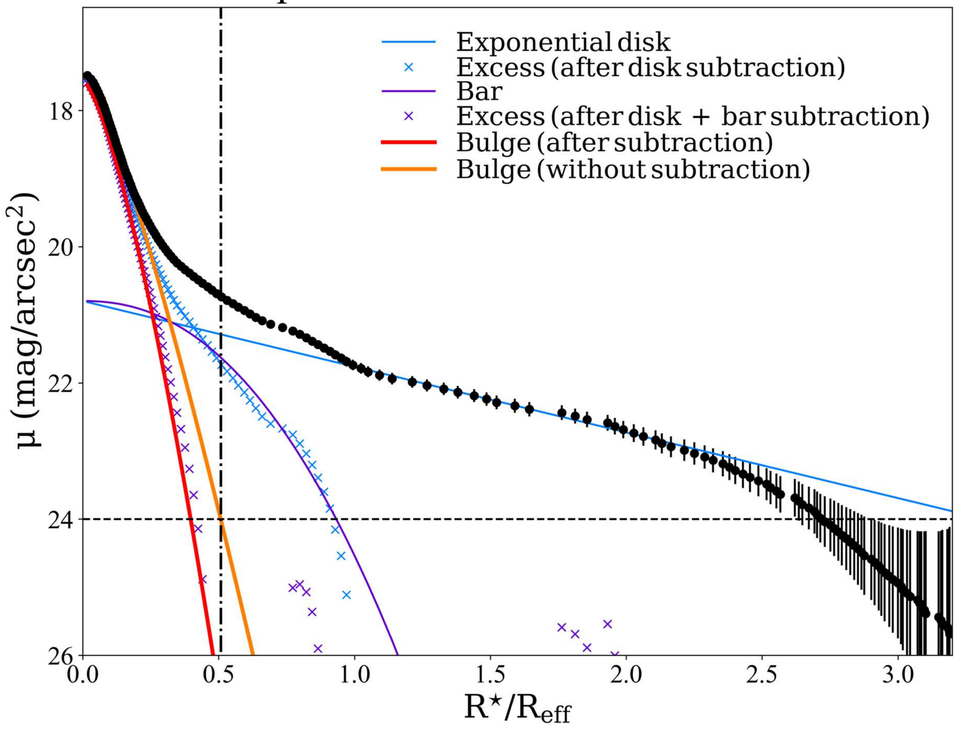

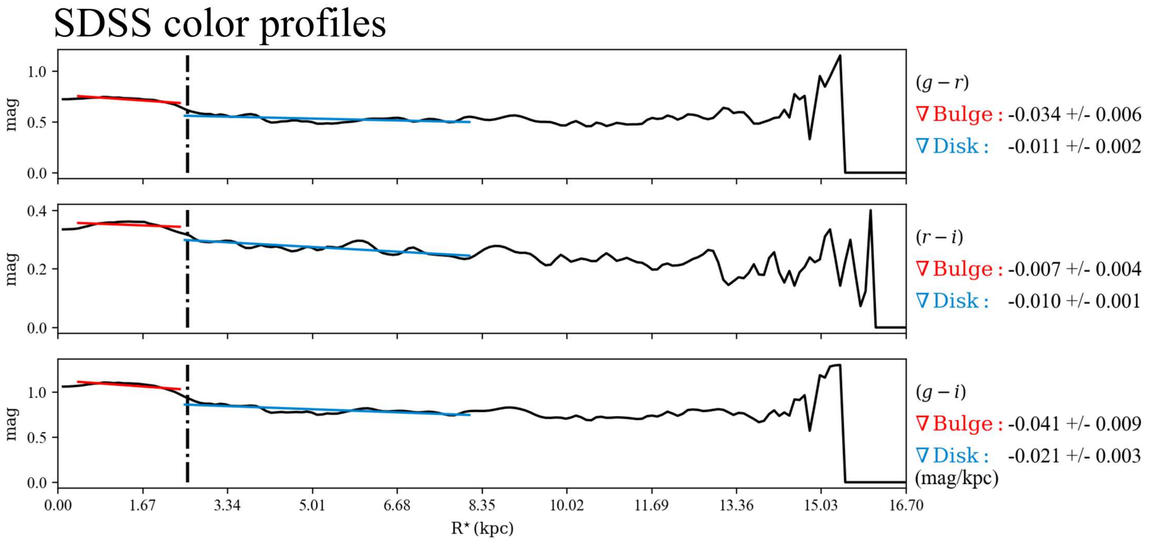

$\mathcal{RY}$ SBPs

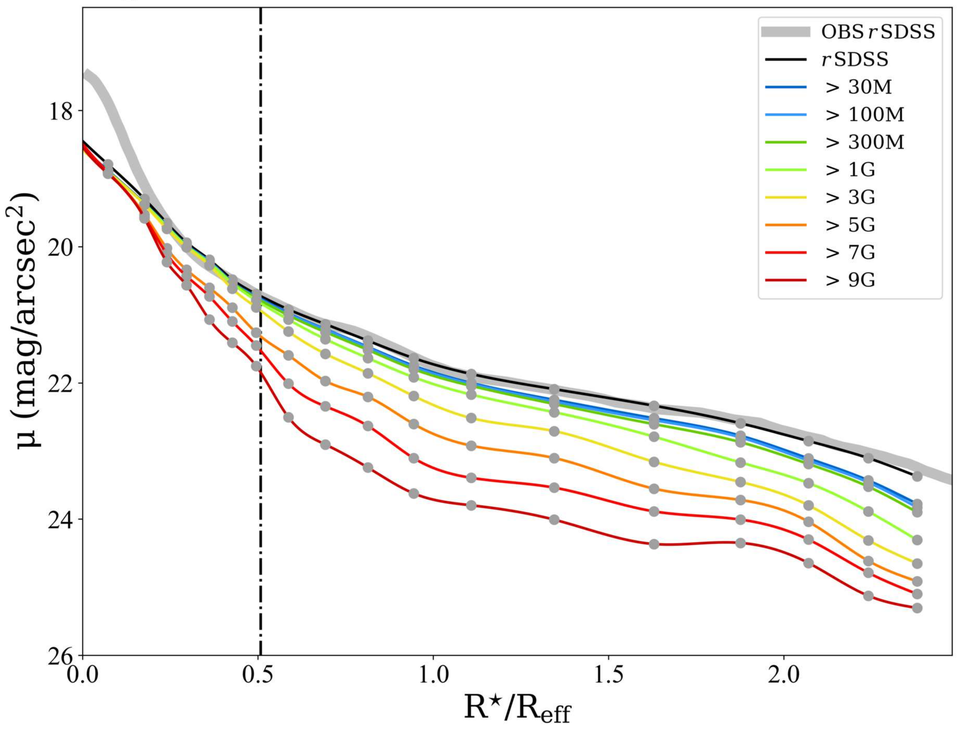

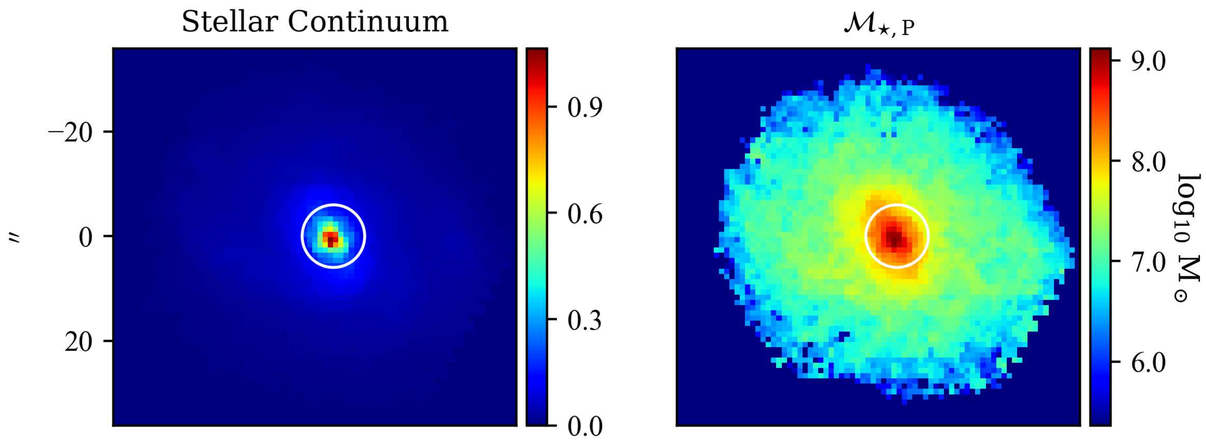

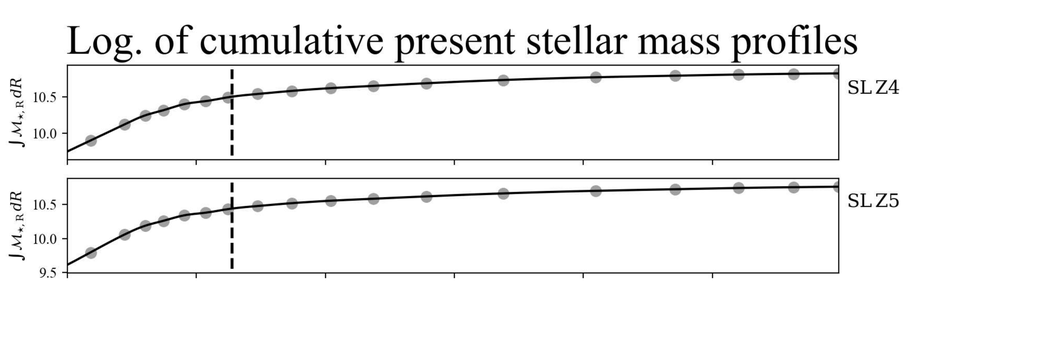

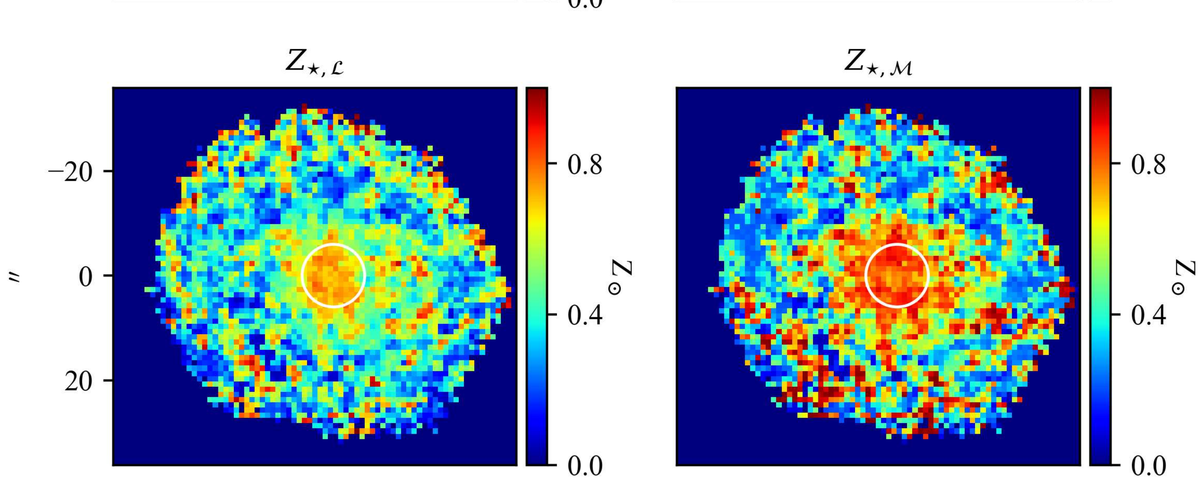

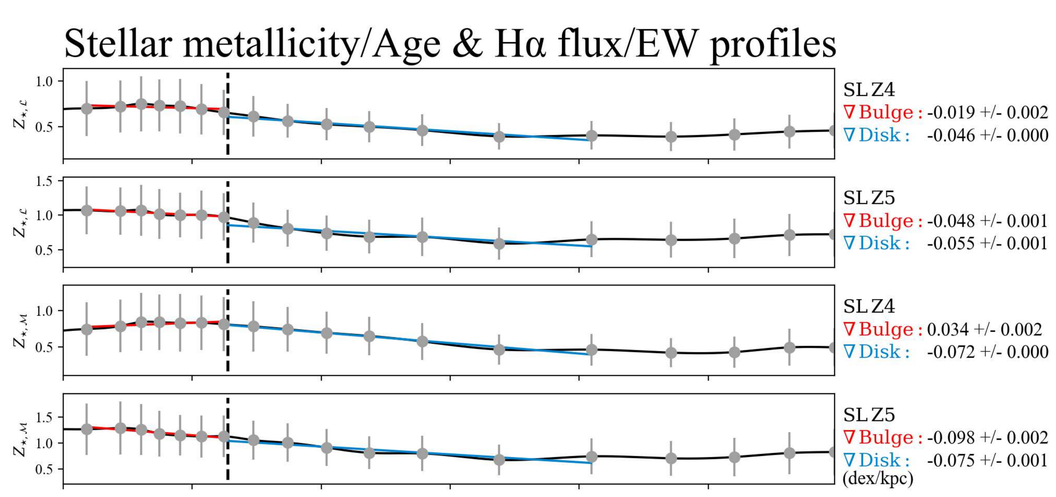

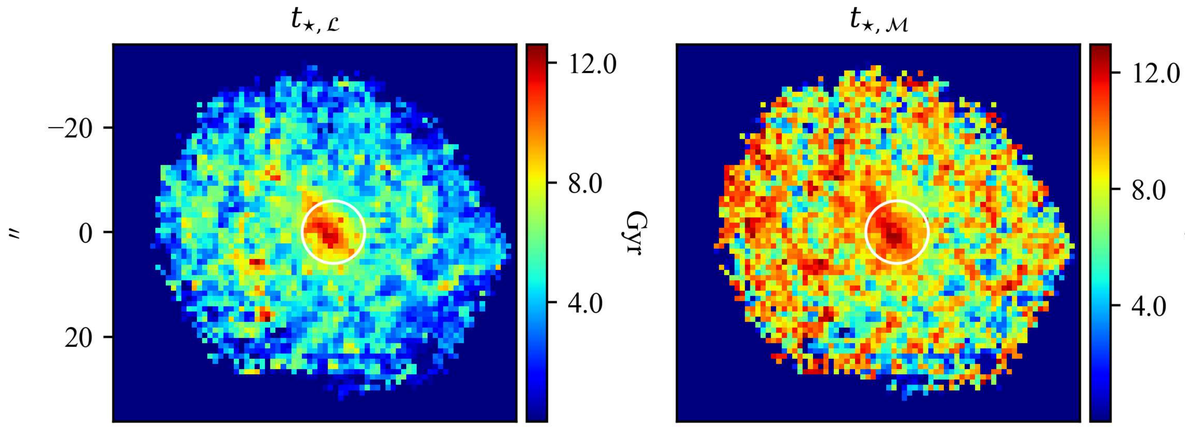

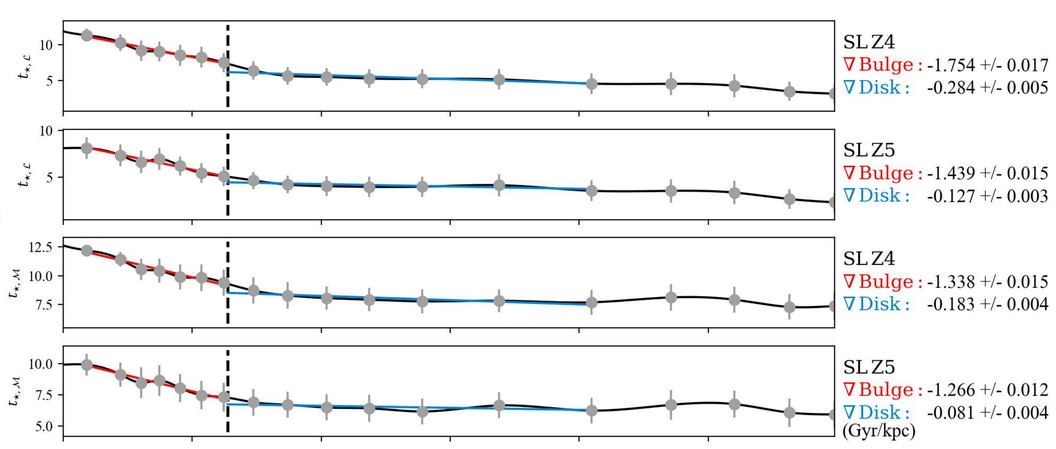

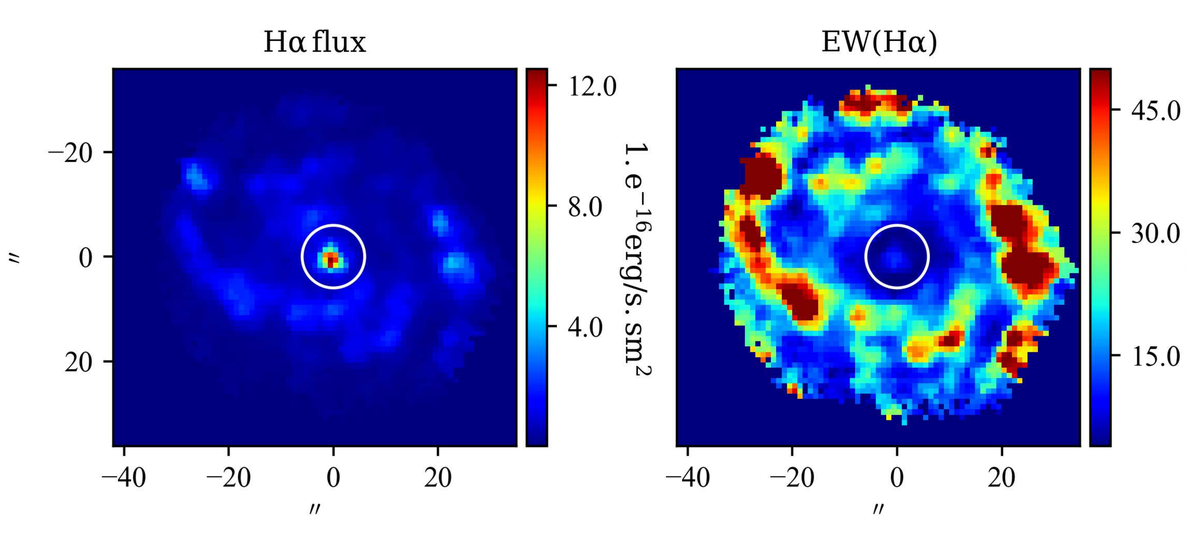

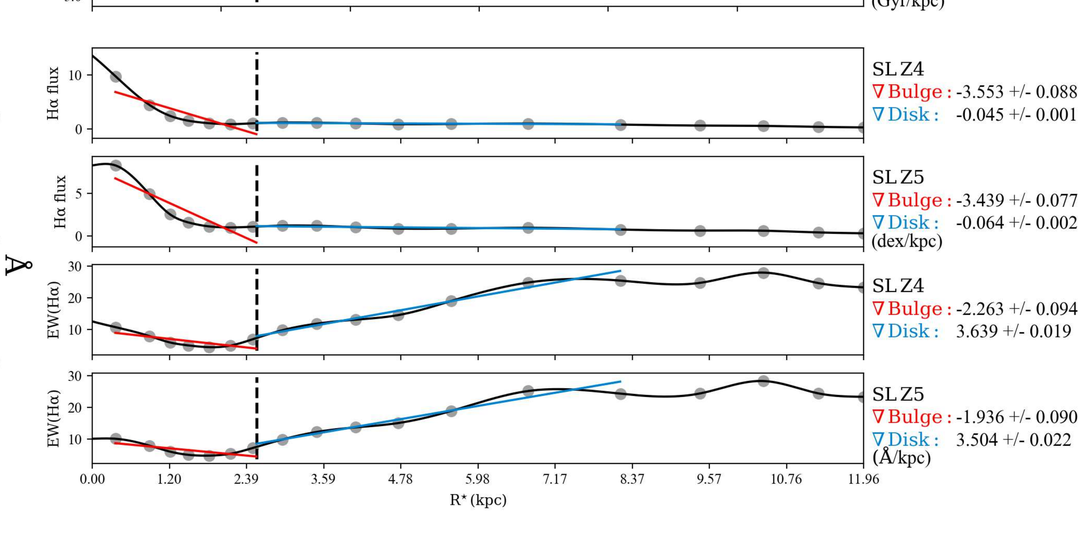

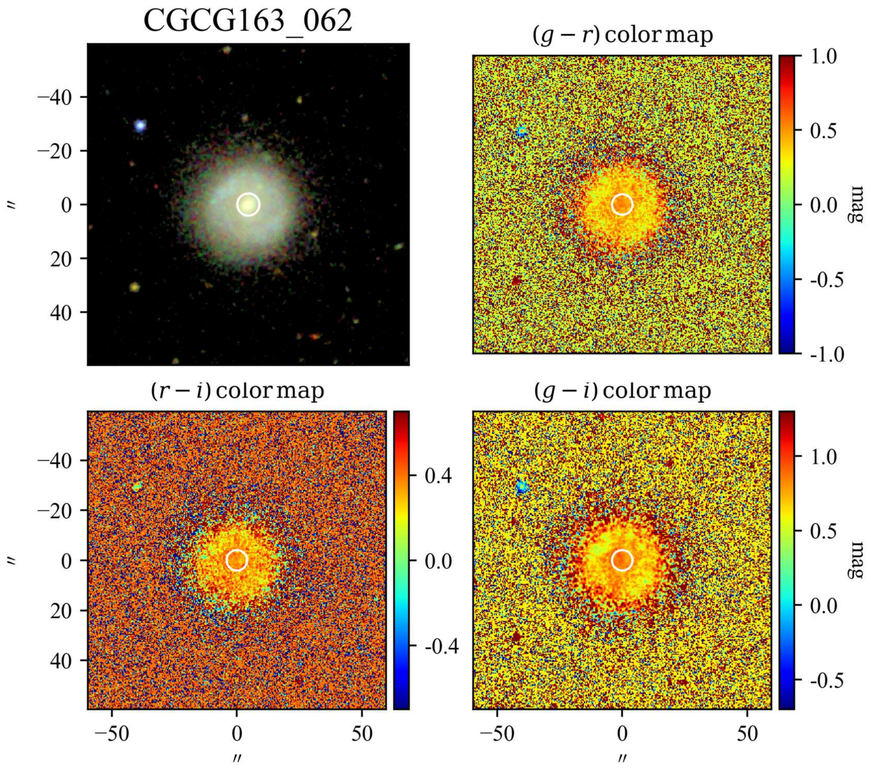
CGCG163_062
$(g-r)$ color map
$(r-i)$ color map
$(g-i)$ color map
mag
″

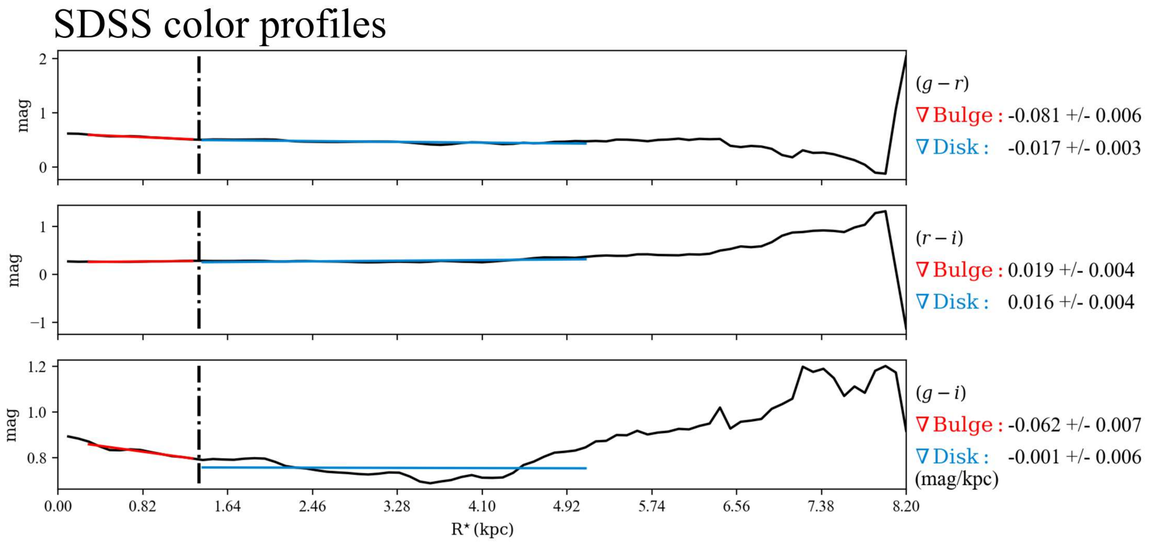
SDSS color profiles
$(g-r)$
∇ Bulge : -0.081 +/- 0.006
∇ Disk : -0.017 +/- 0.003
$(r-i)$
∇ Bulge : 0.019 +/- 0.004
∇ Disk : 0.016 +/- 0.004
$(g-i)$
∇ Bulge : -0.062 +/- 0.007
∇ Disk : -0.001 +/- 0.006
(mag/kpc)
mag
R* (kpc)

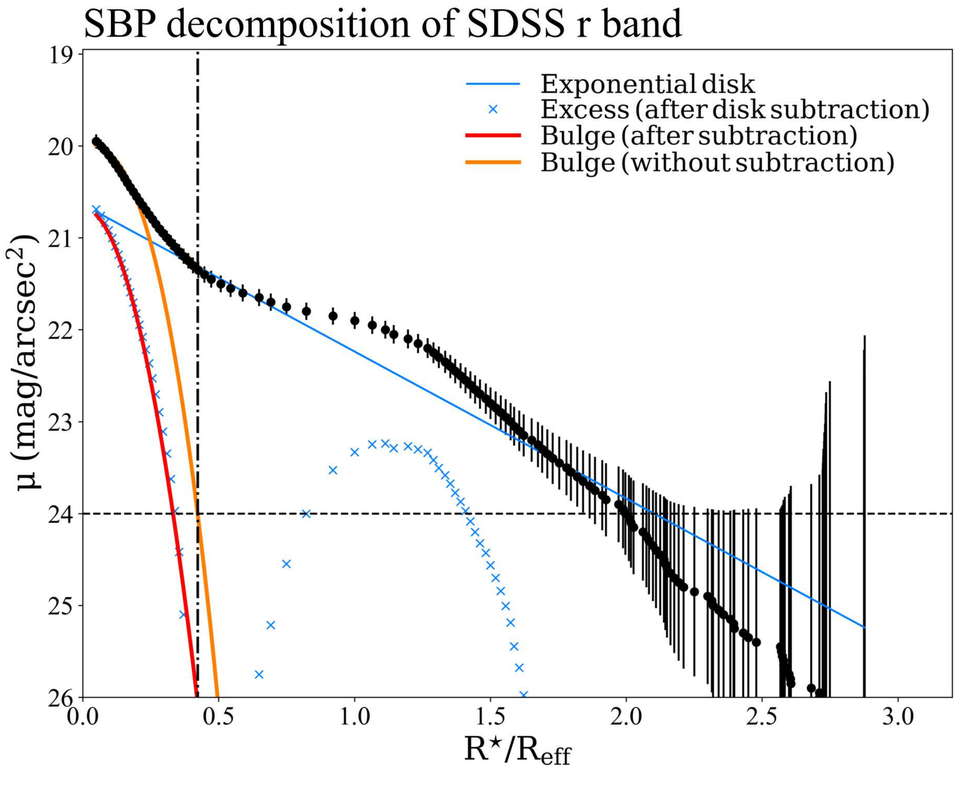
SBP decomposition of SDSS r band
Exponential disk
Excess (after disk subtraction)
Bulge (after subtraction)
Bulge (without subtraction)
μ (mag/arcsec²)
R*/Reff

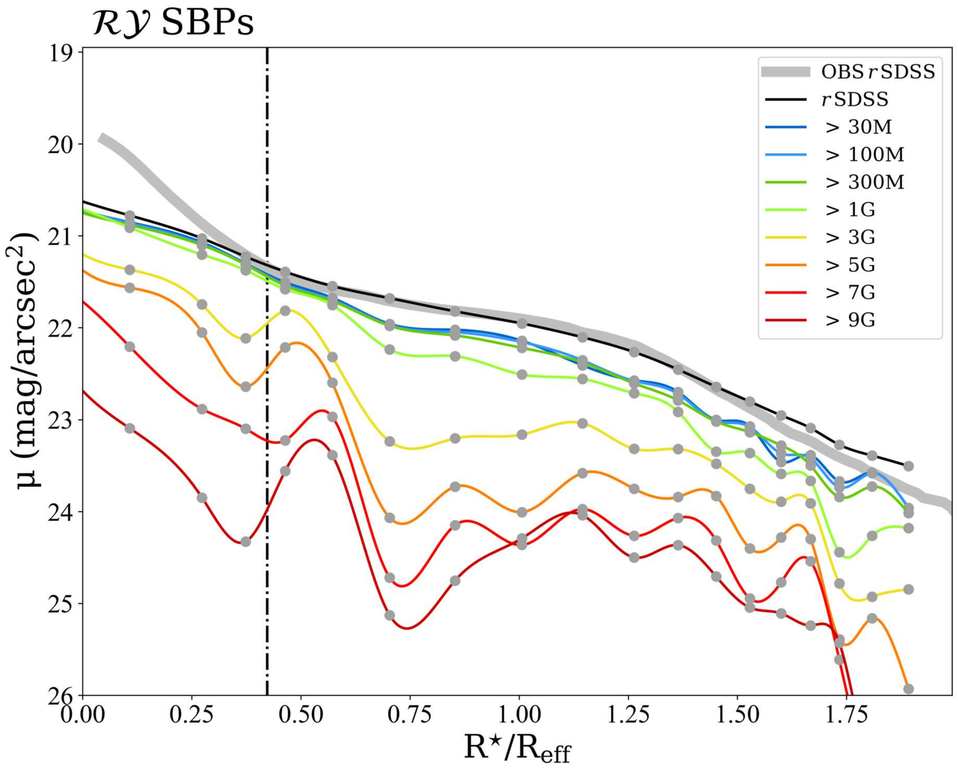
$\mathcal{RV}$ SBPs
OBS rSDSS
rSDSS
> 30M
> 100M
> 300M
> 1G
> 3G
> 5G
> 7G
> 9G
μ (mag/arcsec²)
R*/Reff

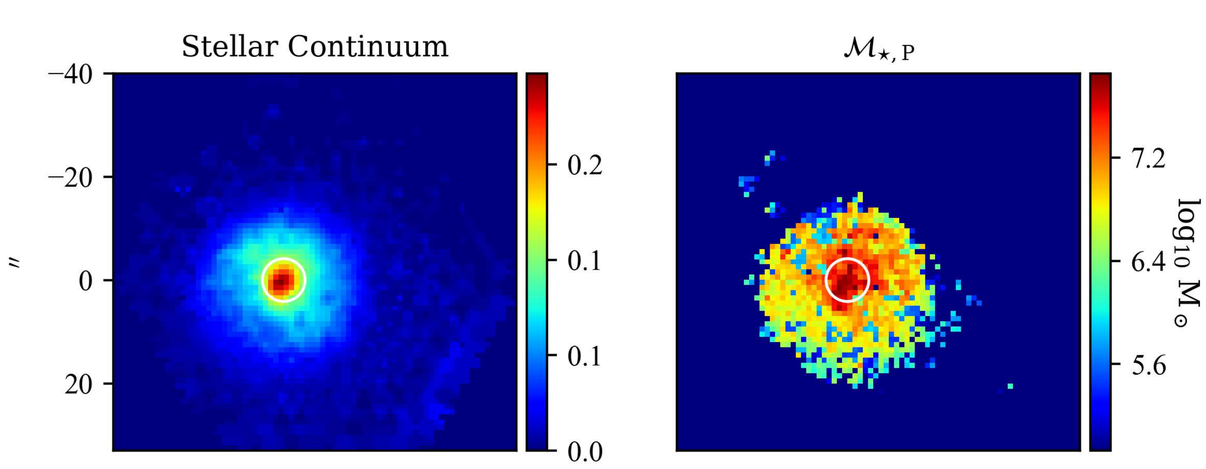
Stellar Continuum
$\mathcal{M}_{\star,\mathrm{P}}$
log10 M⊙

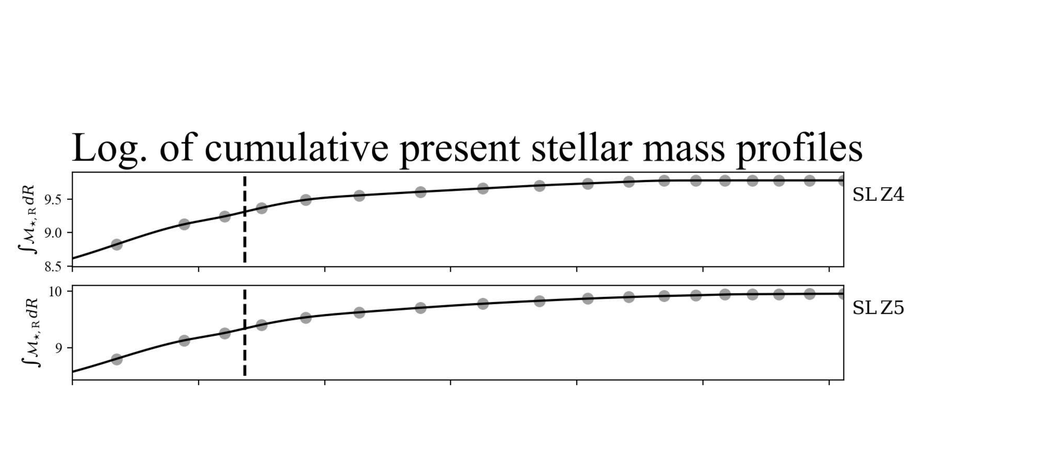
Log. of cumulative present stellar mass profiles
SL Z4
SL Z5

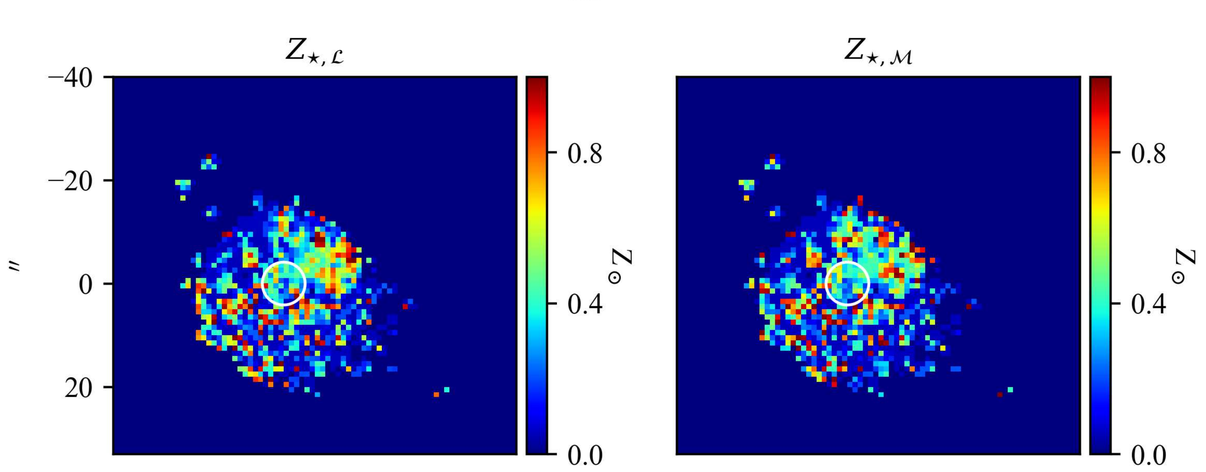
$Z_{\star,\mathcal{L}}$
$Z_{\star,\mathcal{M}}$
Z⊙

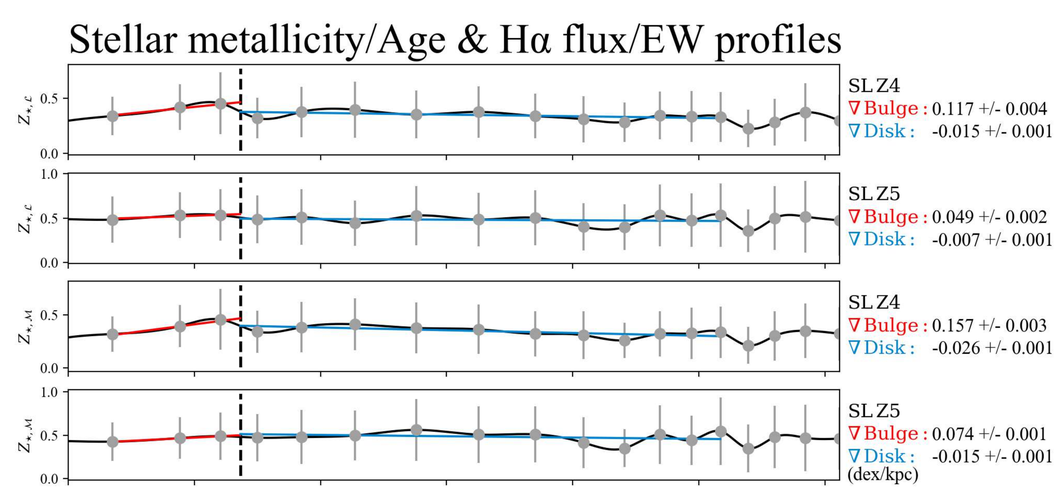
Stellar metallicity/Age & Hα flux/EW profiles
SL Z4
∇ Bulge : 0.117 +/- 0.004
∇ Disk : -0.015 +/- 0.001
SL Z5
∇ Bulge : 0.049 +/- 0.002
∇ Disk : -0.007 +/- 0.001
SL Z4
∇ Bulge : 0.157 +/- 0.003
∇ Disk : -0.026 +/- 0.001
SL Z5
∇ Bulge : 0.074 +/- 0.001
∇ Disk : -0.015 +/- 0.001
(dex/kpc)

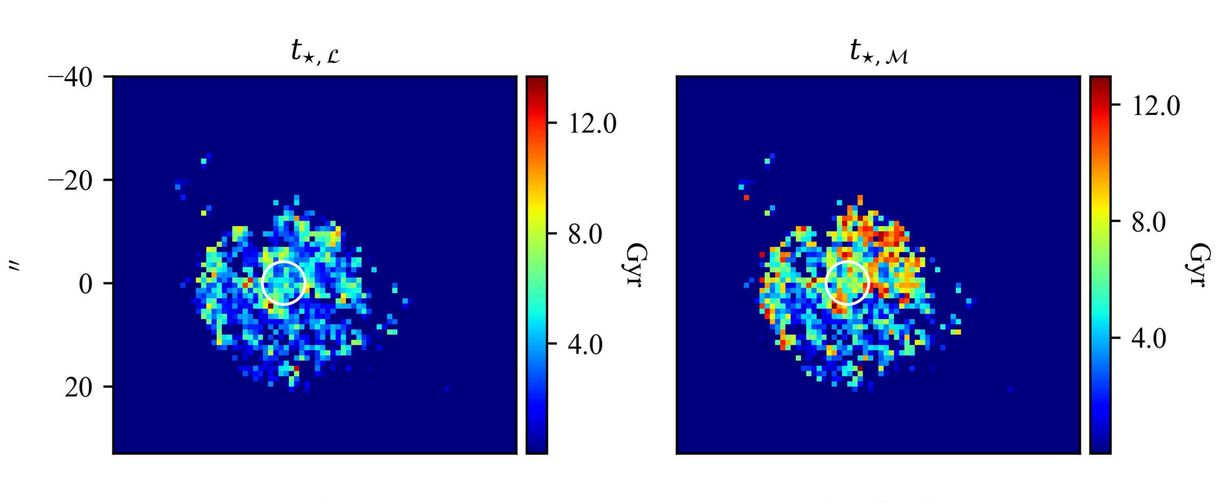
$t_{\star,\mathcal{L}}$
$t_{\star,\mathcal{M}}$
Gyr

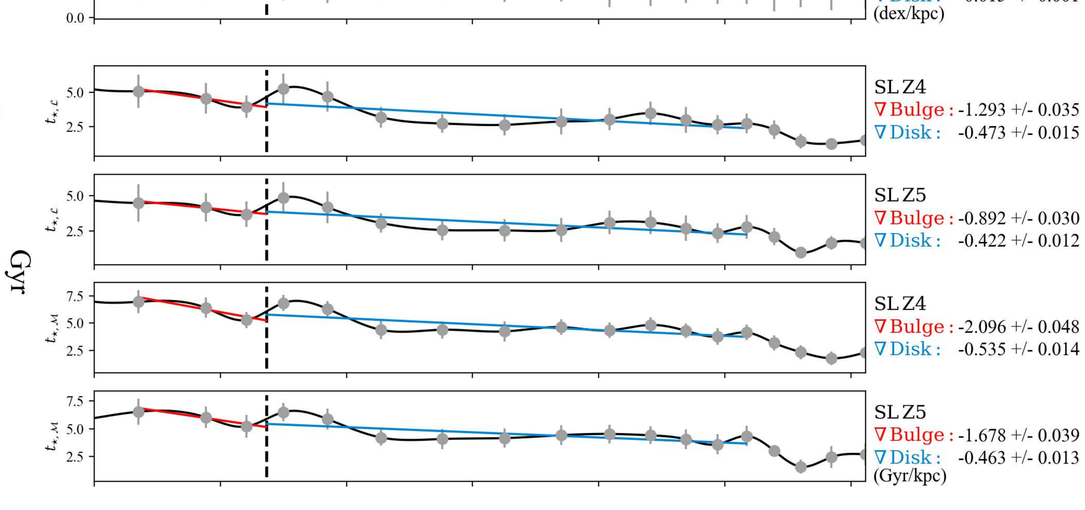
SL Z4
∇ Bulge : -1.293 +/- 0.035
∇ Disk : -0.473 +/- 0.015
SL Z5
∇ Bulge : -0.892 +/- 0.030
∇ Disk : -0.422 +/- 0.012
SL Z4
∇ Bulge : -2.096 +/- 0.048
∇ Disk : -0.535 +/- 0.014
SL Z5
∇ Bulge : -1.678 +/- 0.039
∇ Disk : -0.463 +/- 0.013
(Gyr/kpc)

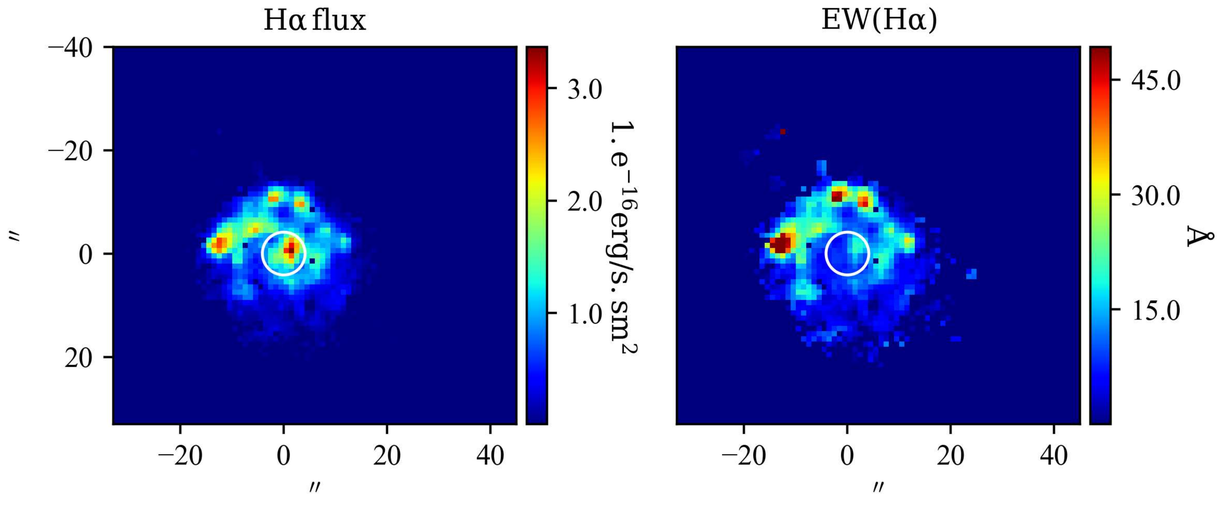
Hα flux
EW(Hα)
1. e⁻¹⁶erg/s. sm²
Å

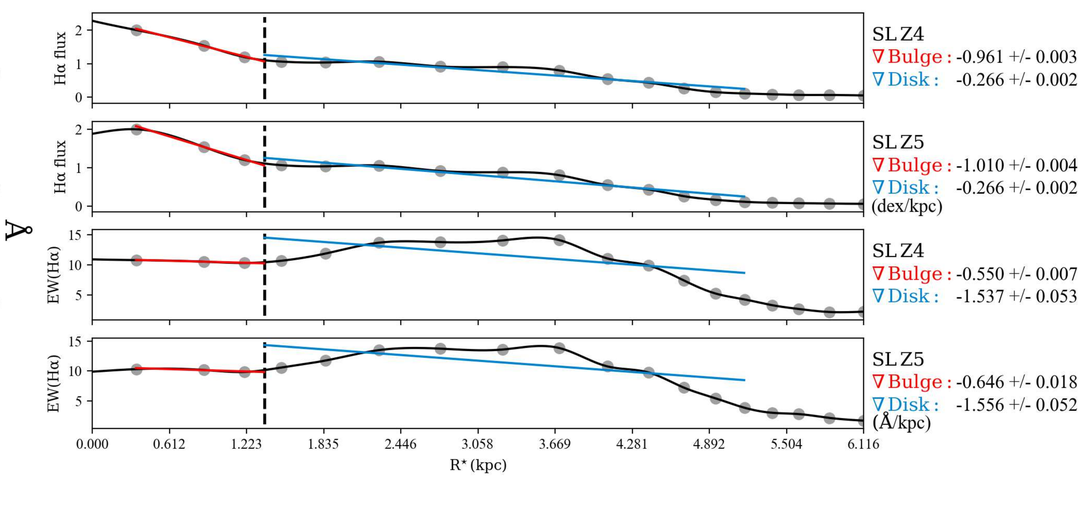
SL Z4
∇ Bulge : -0.961 +/- 0.003
∇ Disk : -0.266 +/- 0.002
SL Z5
∇ Bulge : -1.010 +/- 0.004
∇ Disk : -0.266 +/- 0.002
(dex/kpc)
SL Z4
∇ Bulge : -0.550 +/- 0.007
∇ Disk : -1.537 +/- 0.053
SL Z5
∇ Bulge : -0.646 +/- 0.018
∇ Disk : -1.556 +/- 0.052
(Å/kpc)
R* (kpc)

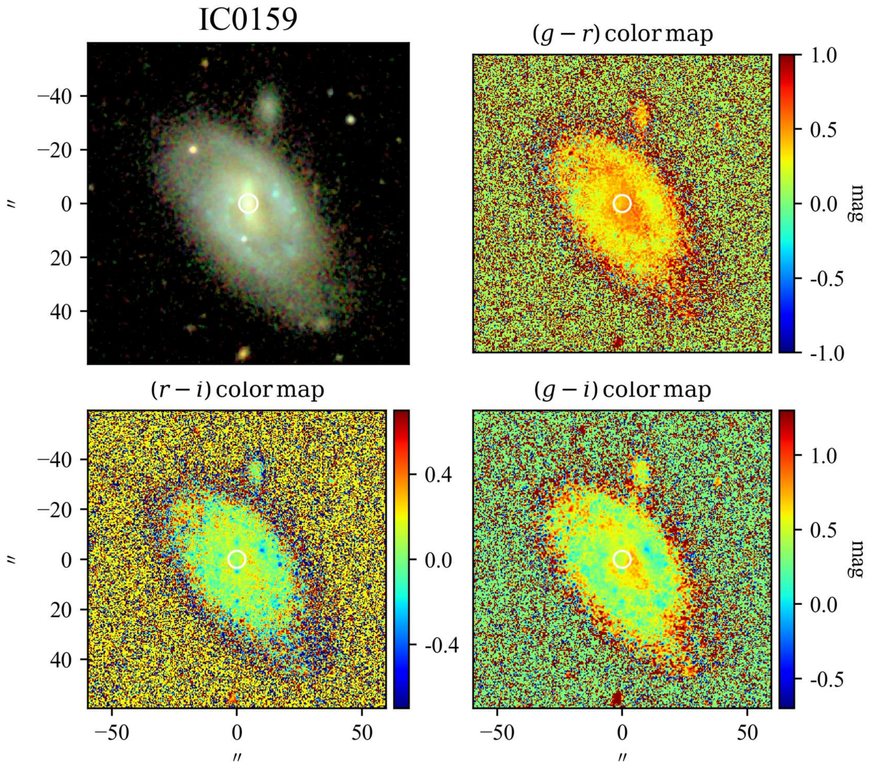

SBP decomposition of SDSS r band

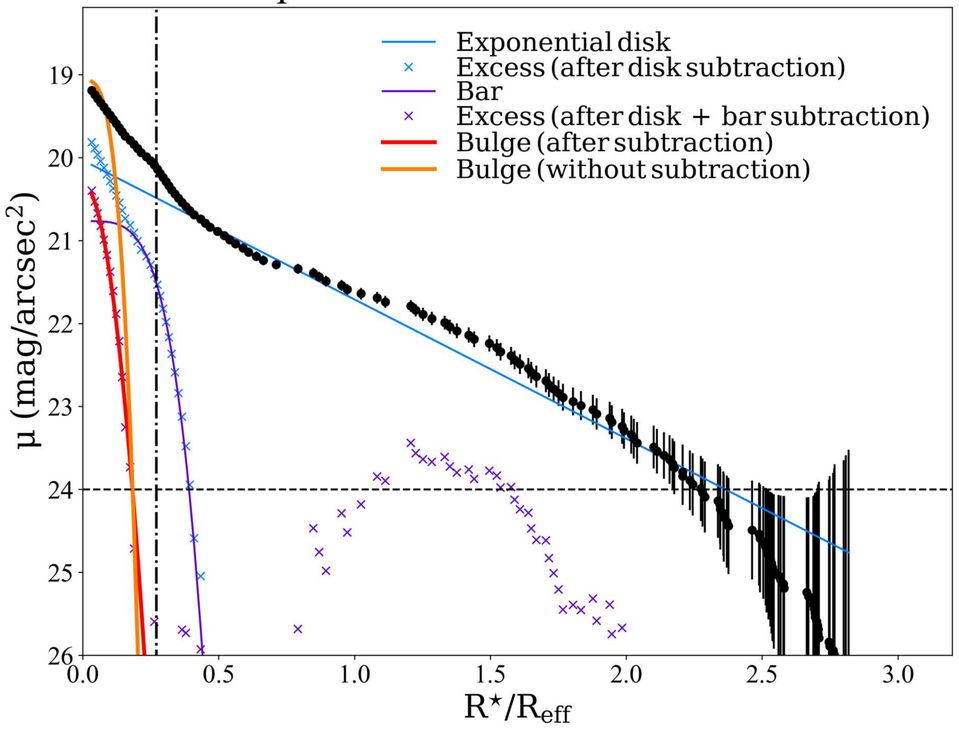

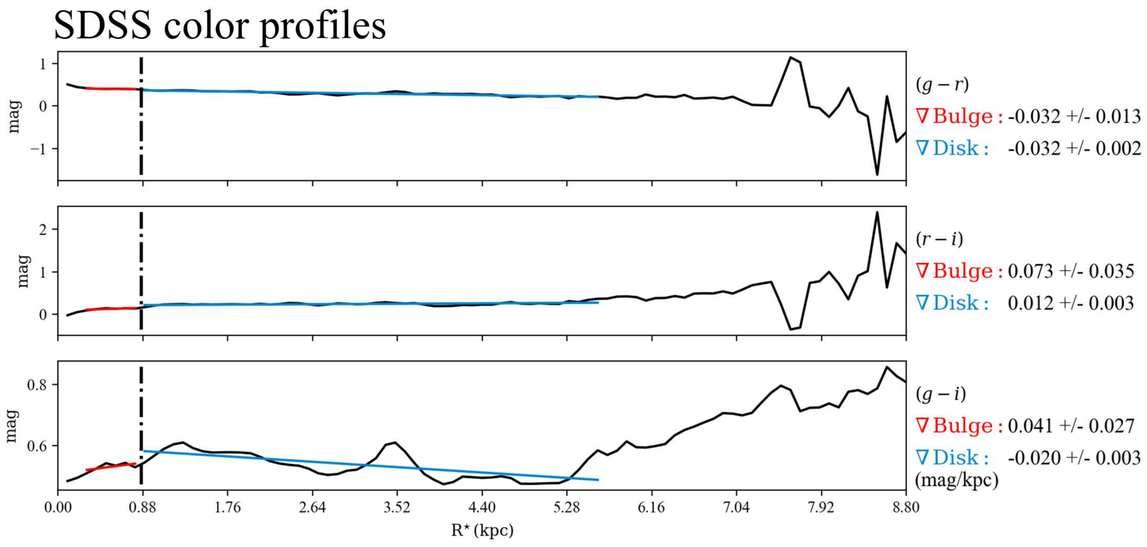

$\mathcal{RY}$ SBPs

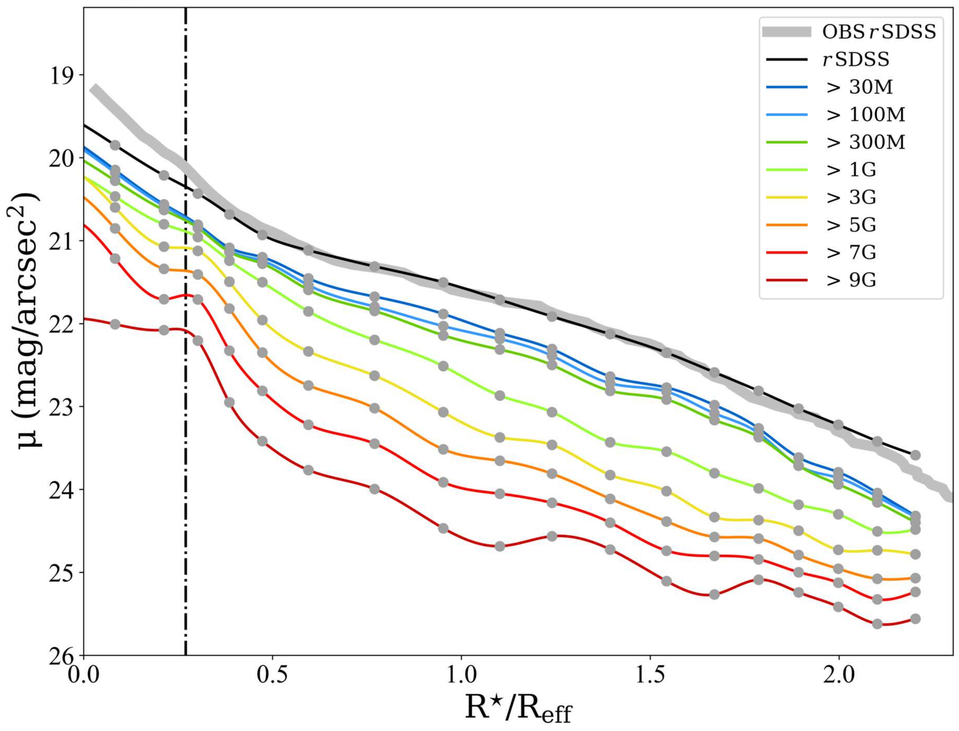

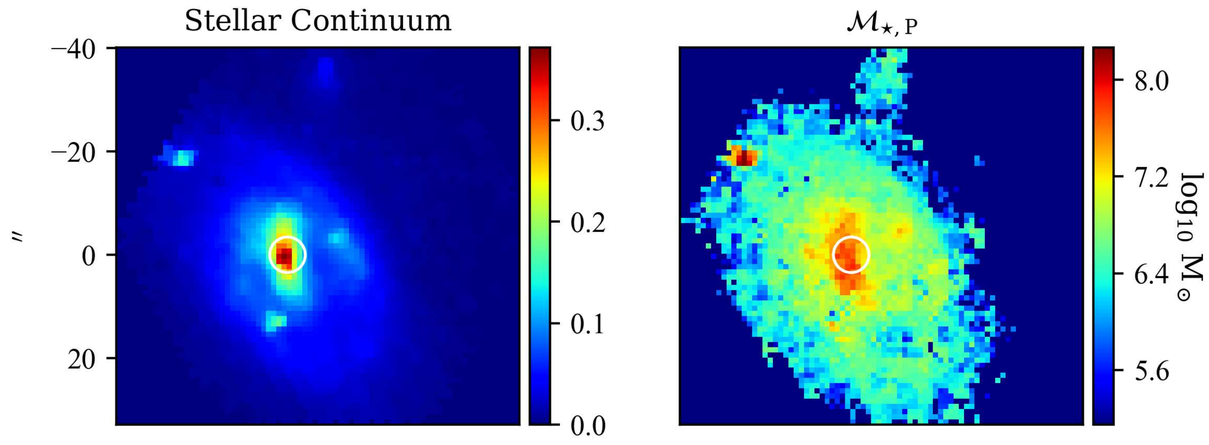

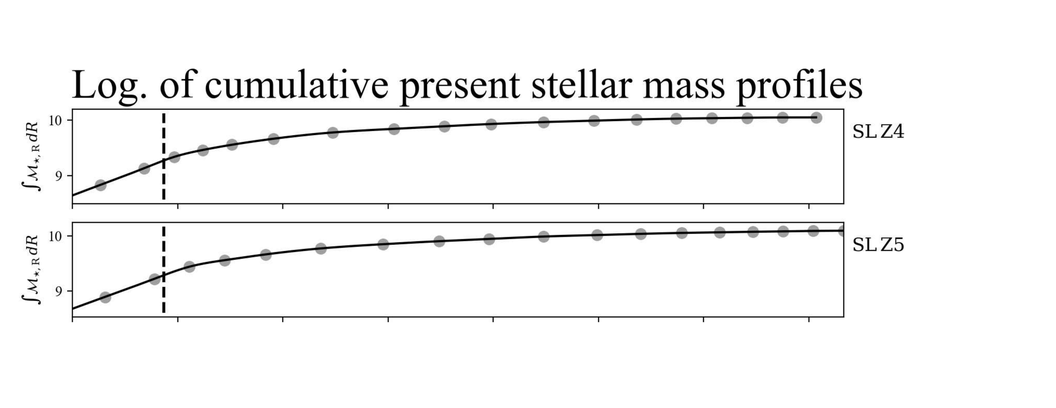

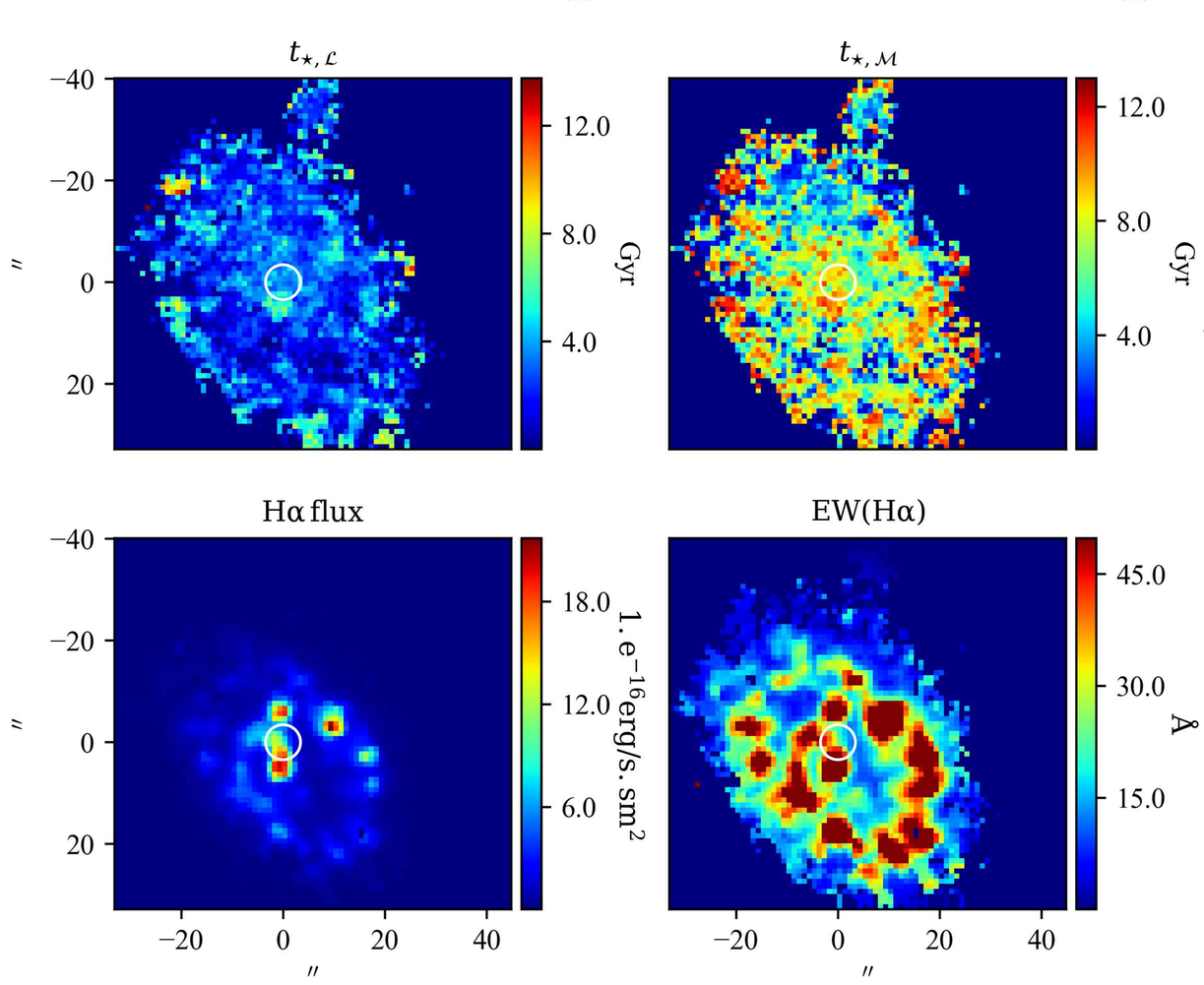

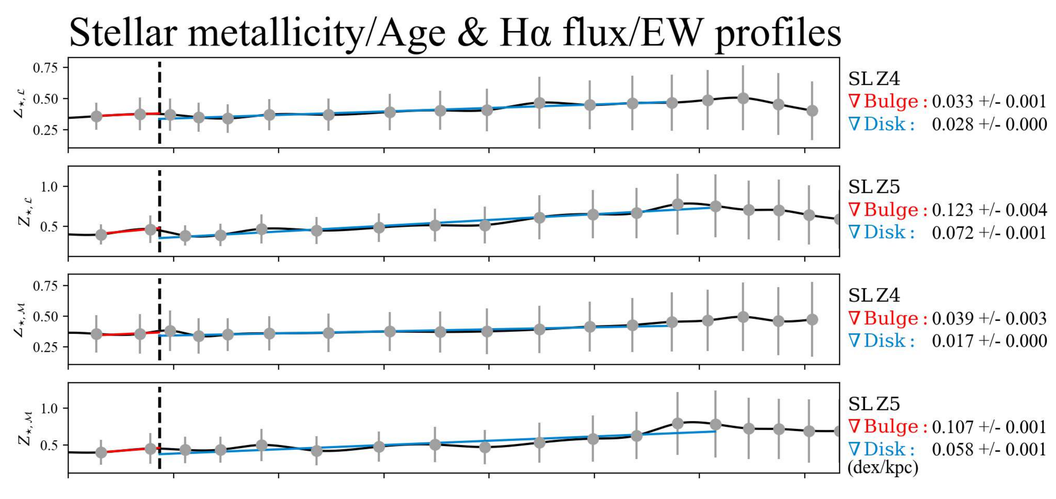

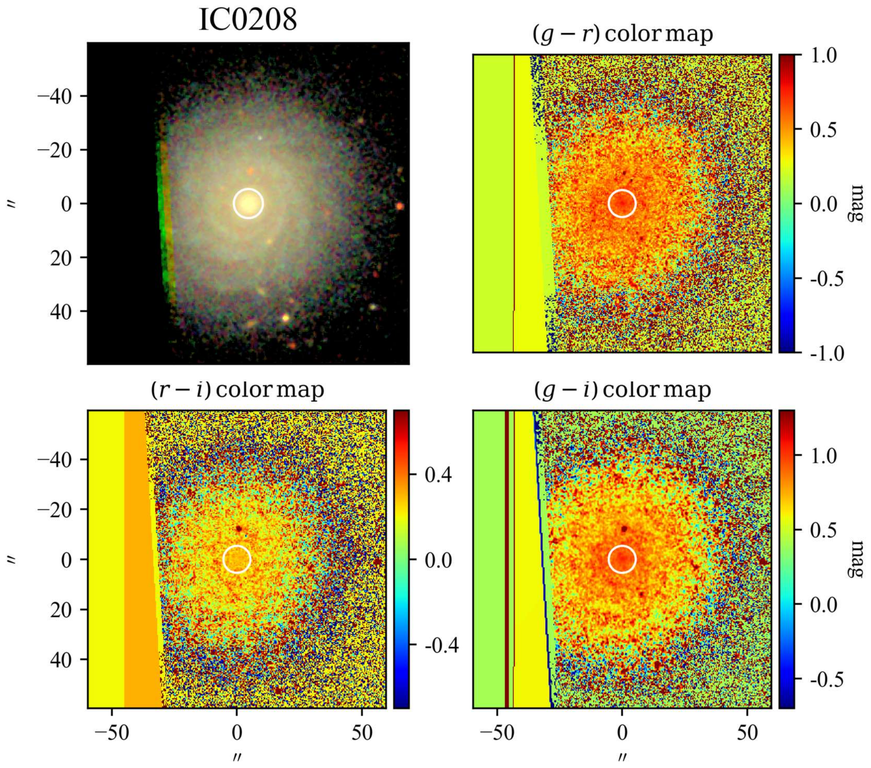

SBP decomposition of SDSS r band

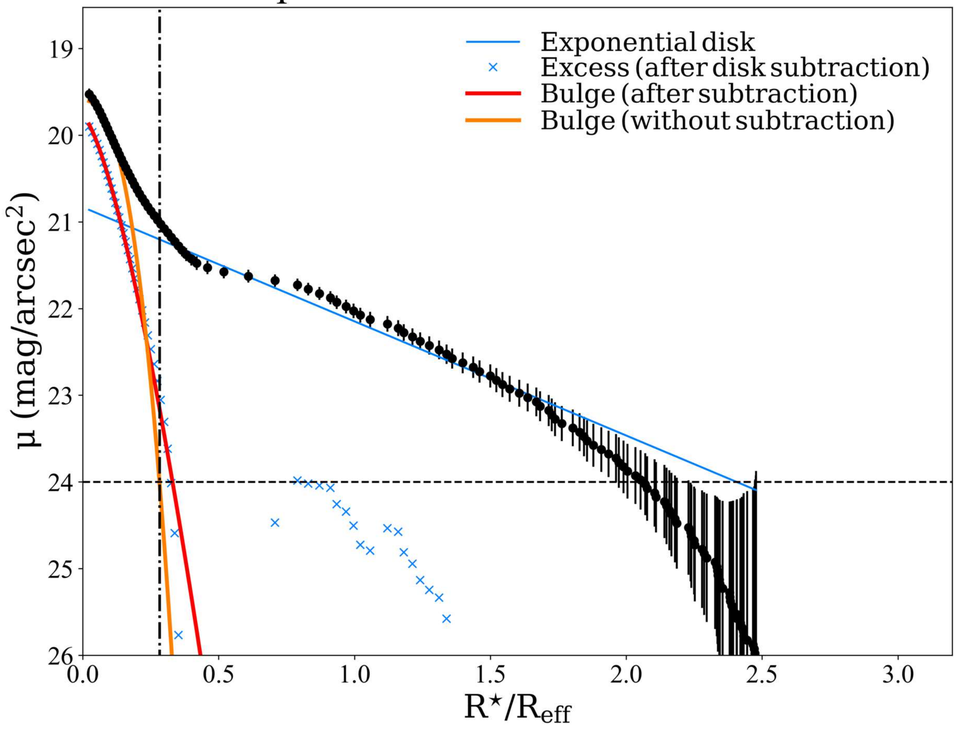

SDSS color profiles

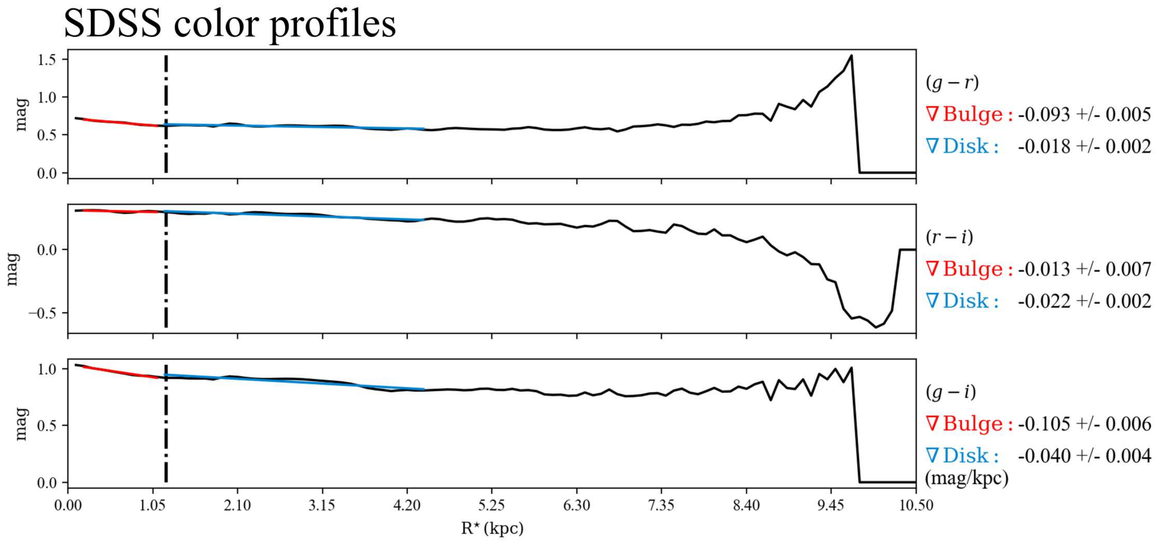

$\mathcal{RV}$ SBPs

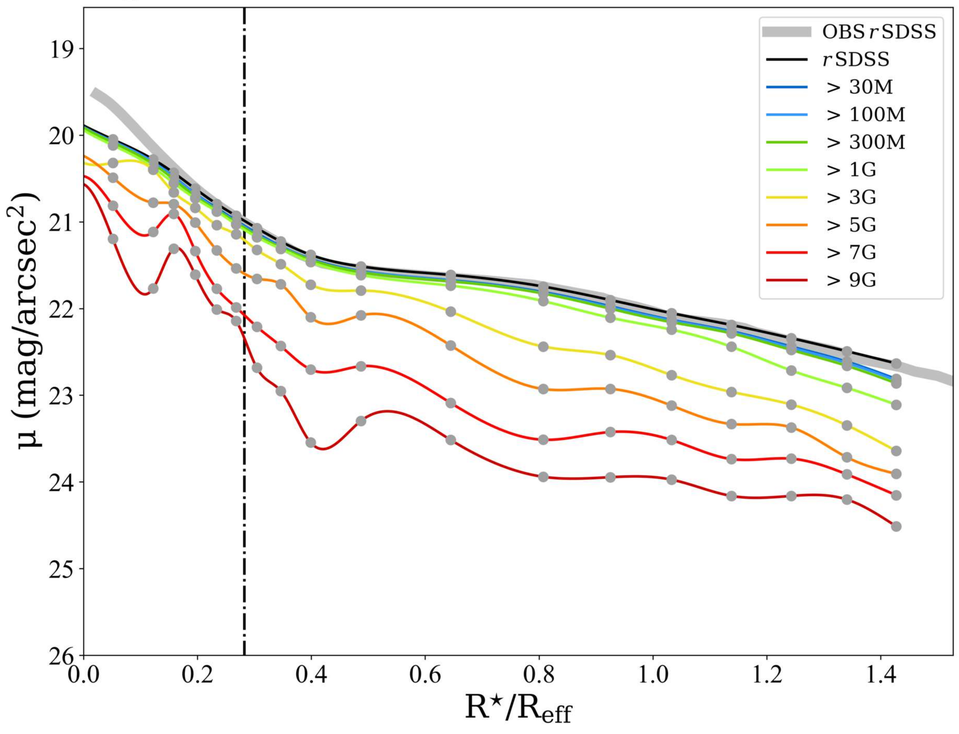

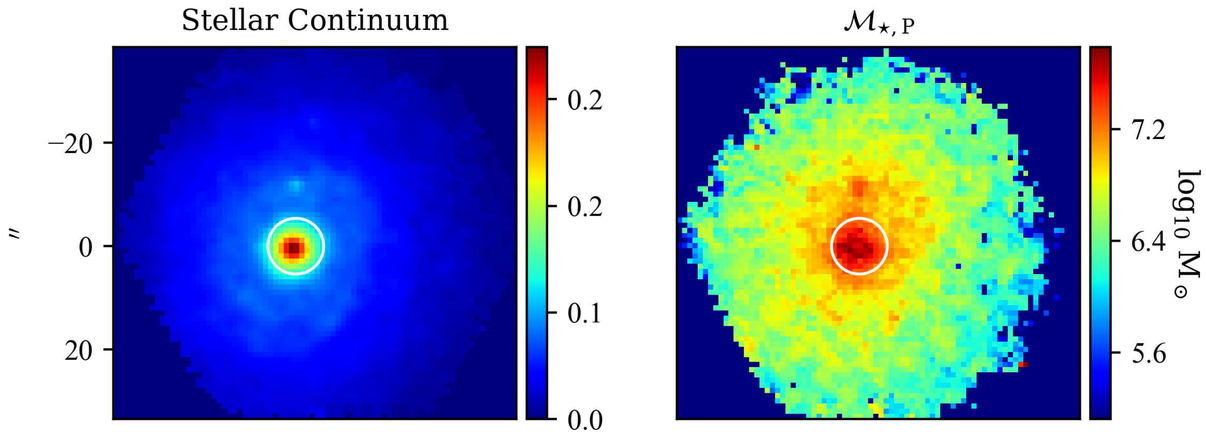

Log. of cumulative present stellar mass profiles

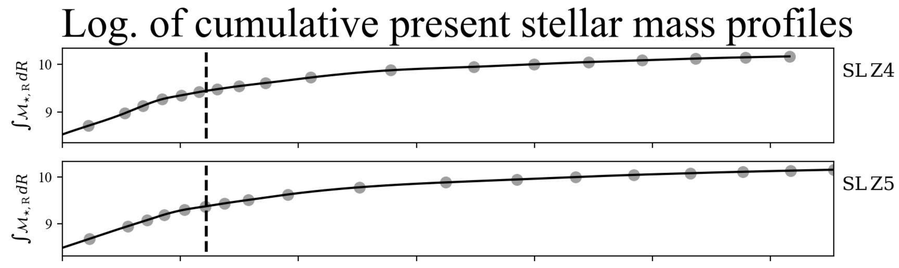

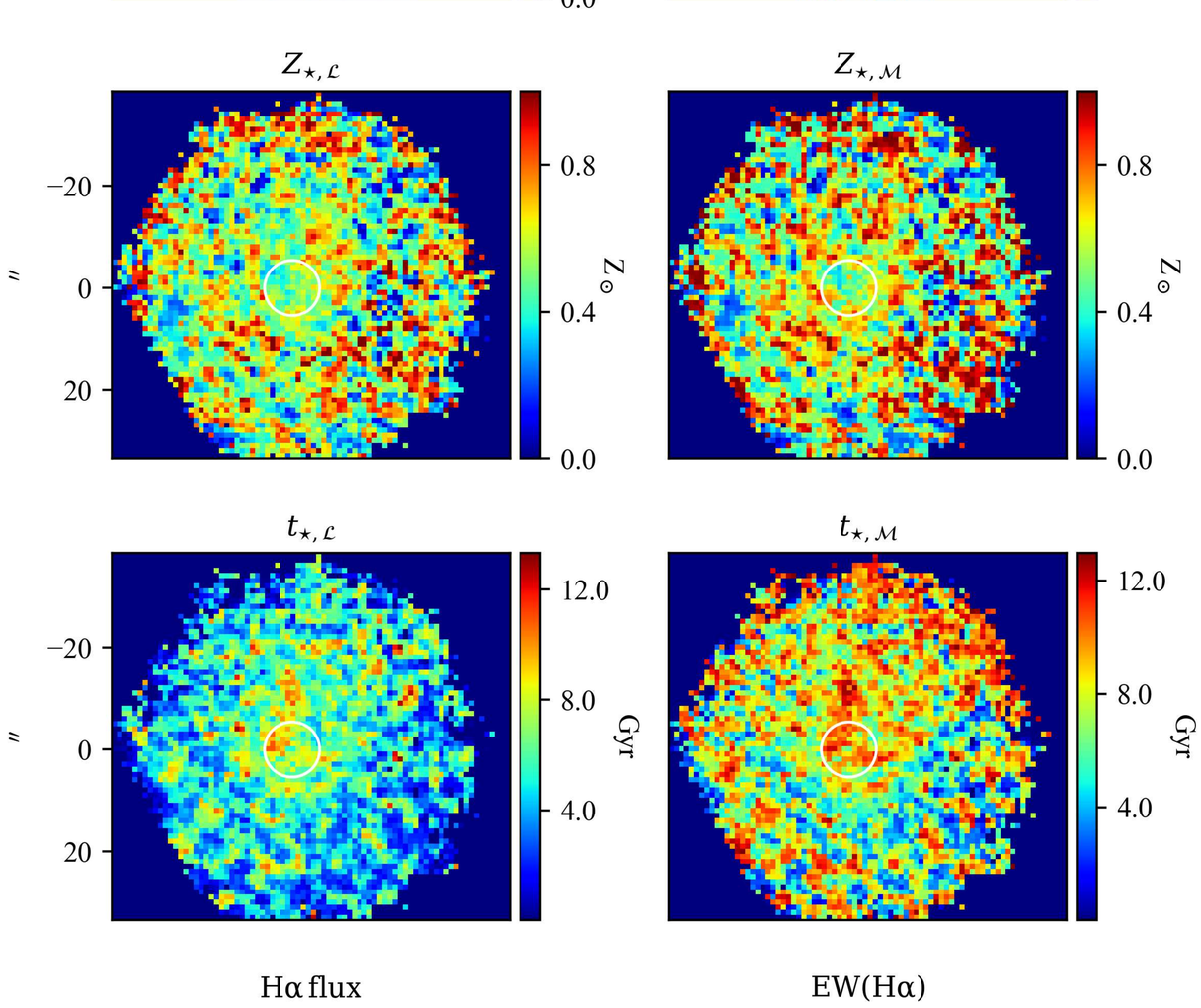

Stellar metallicity/Age & Hα flux/EW profiles

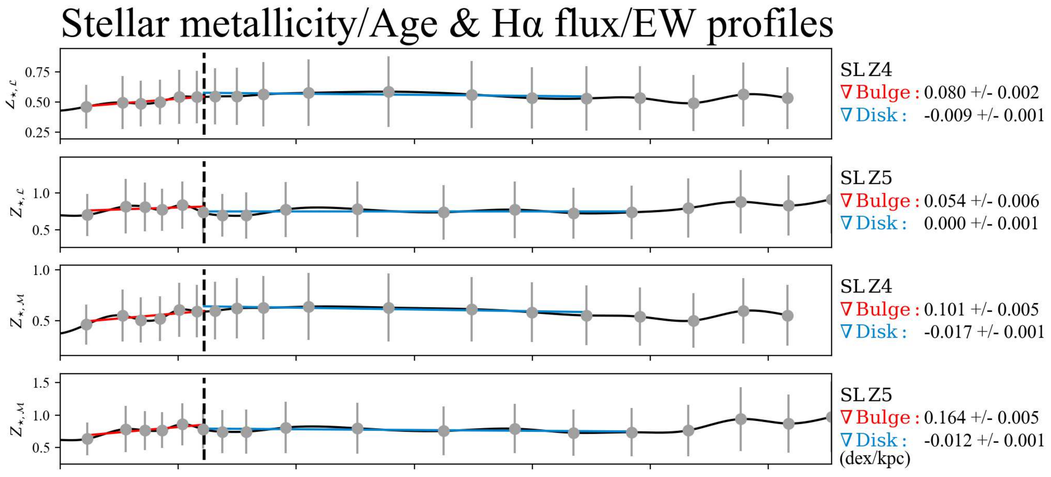

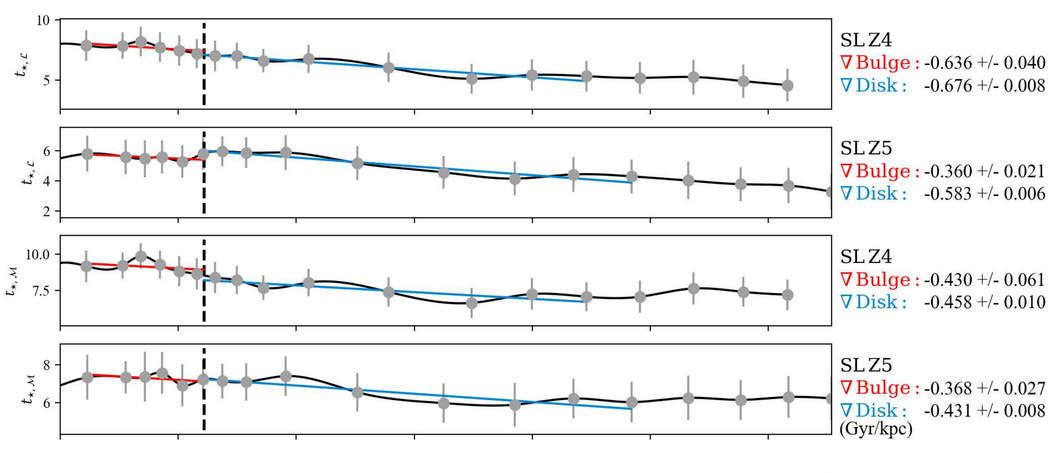

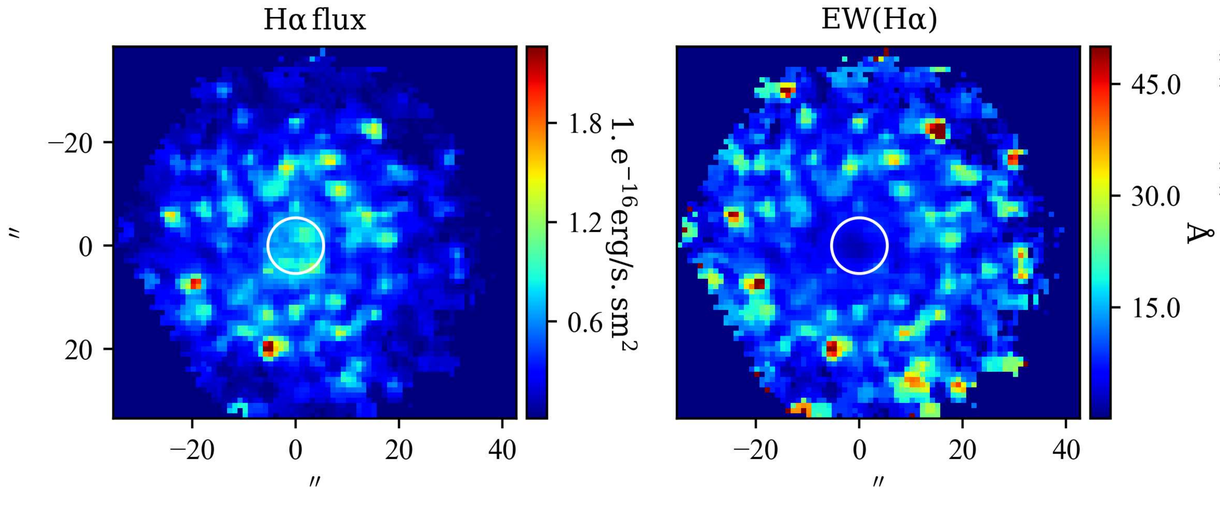

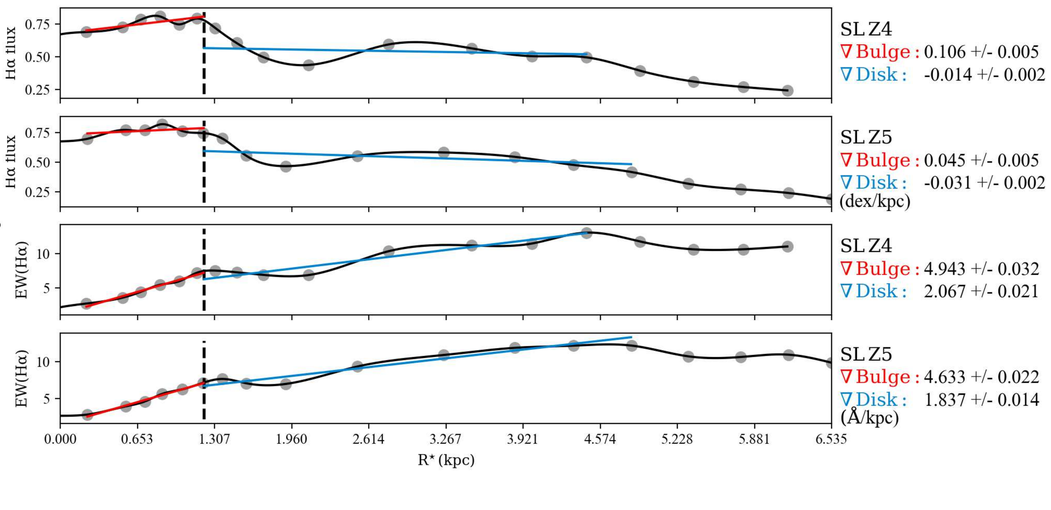

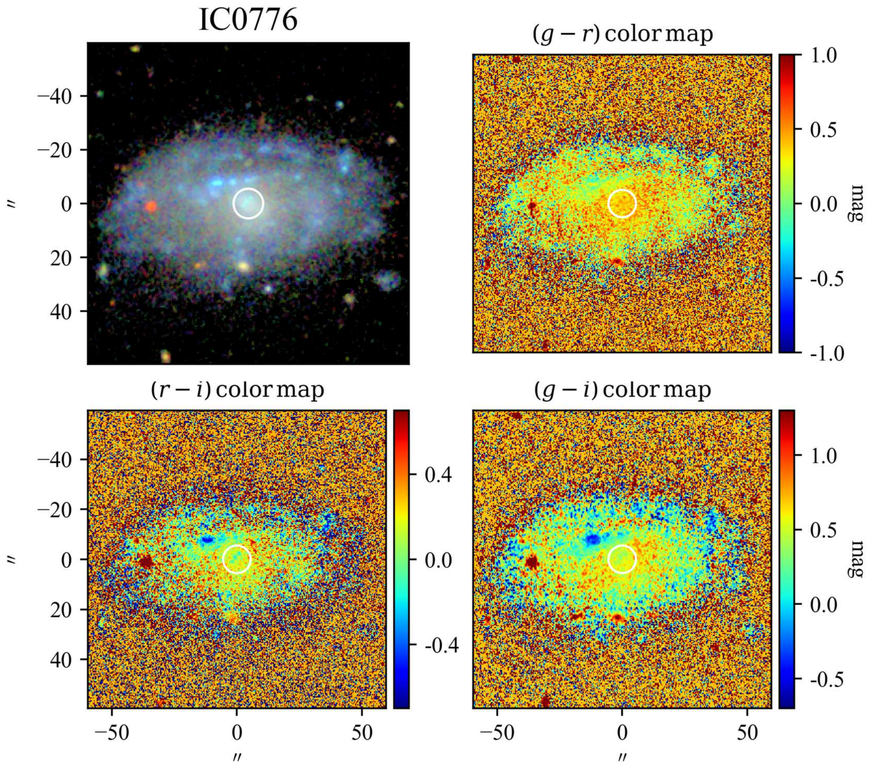

SBP decomposition of SDSS r band

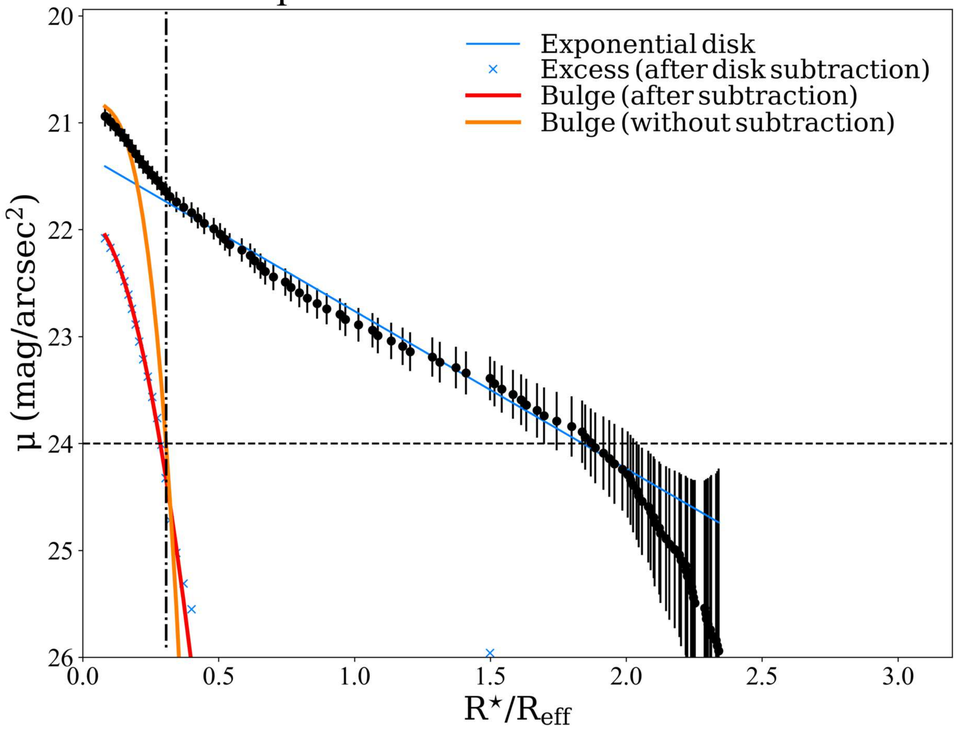

SDSS color profiles

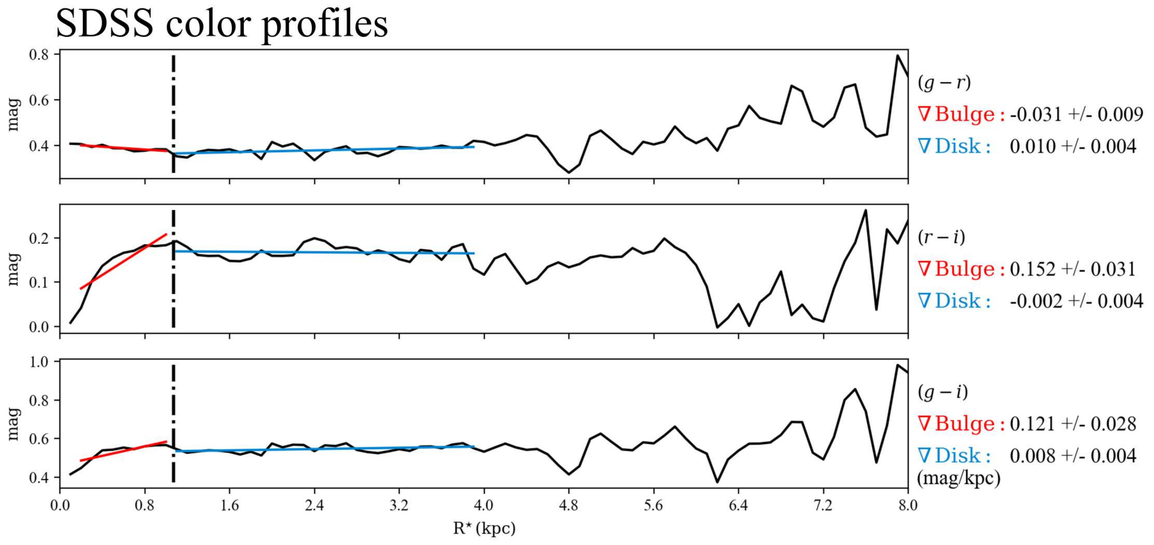

$\mathcal{RY}$ SBPs

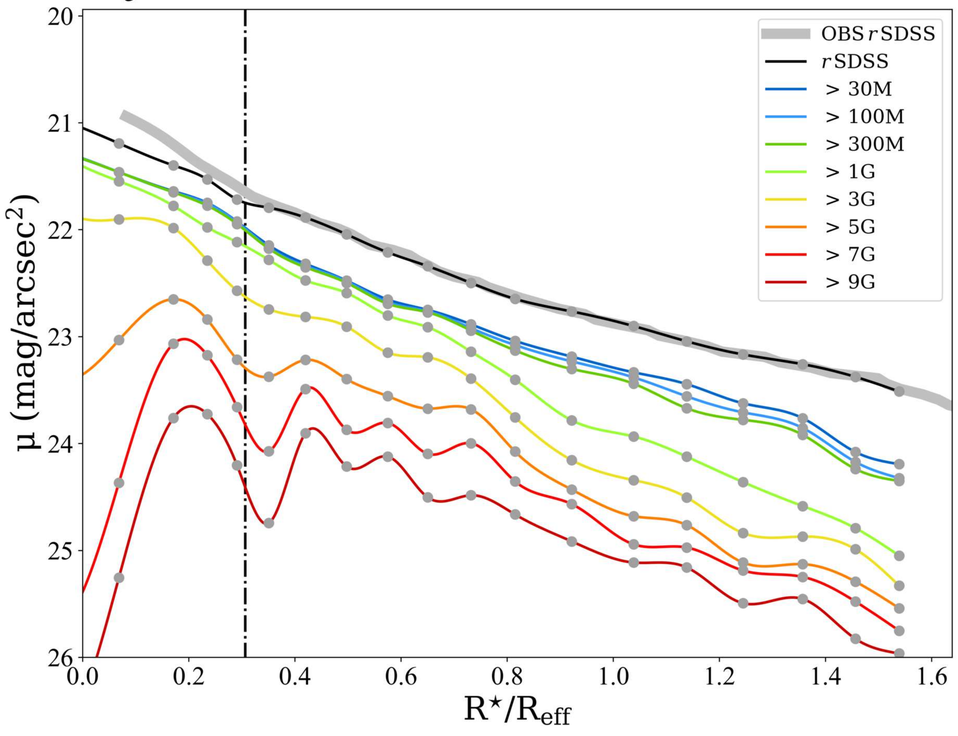

Stellar Continuum

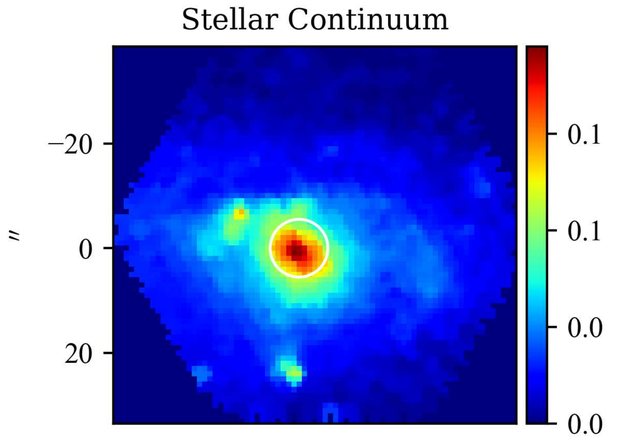

$\mathcal{M}_{\star,\mathrm{P}}$

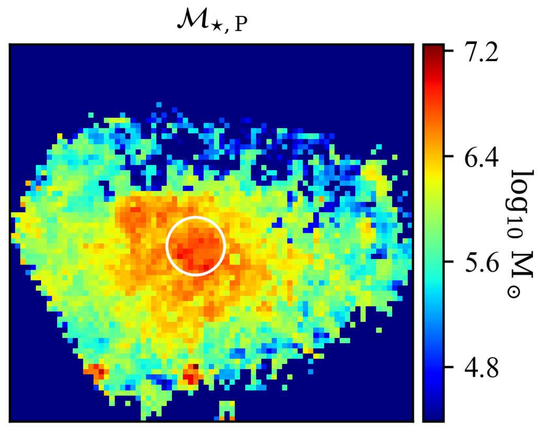

Log. of cumulative present stellar mass profiles

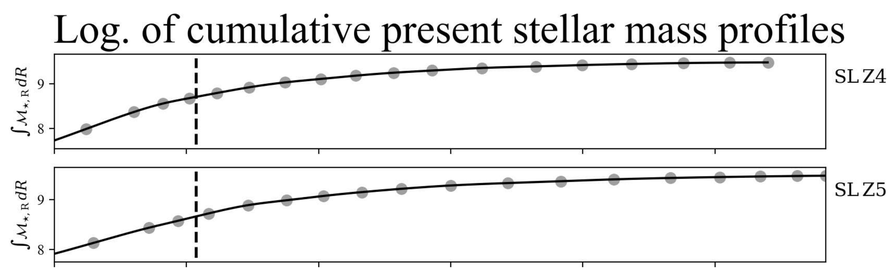

$Z_{\star,\mathcal{L}}$

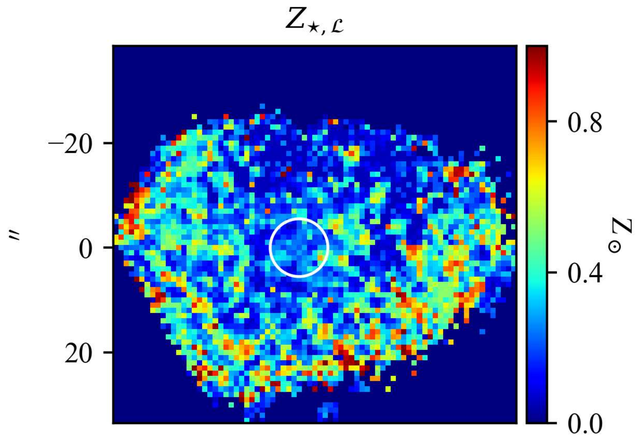

$Z_{\star,\mathcal{M}}$

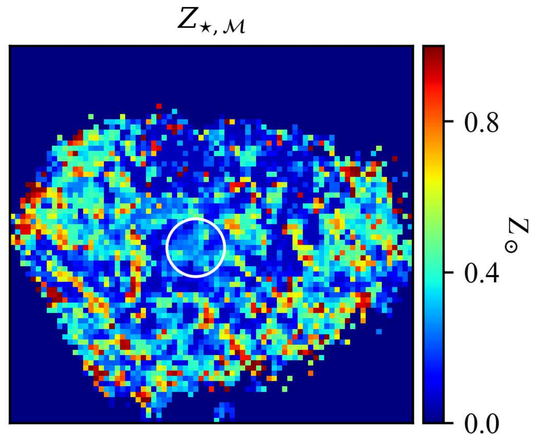

Stellar metallicity/Age & Hα flux/EW profiles

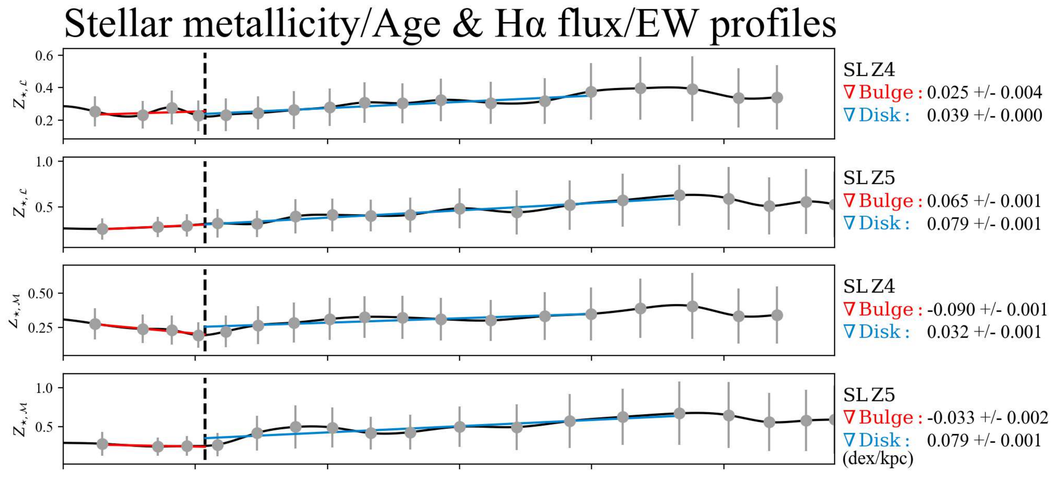

$t_{\star,\mathcal{L}}$

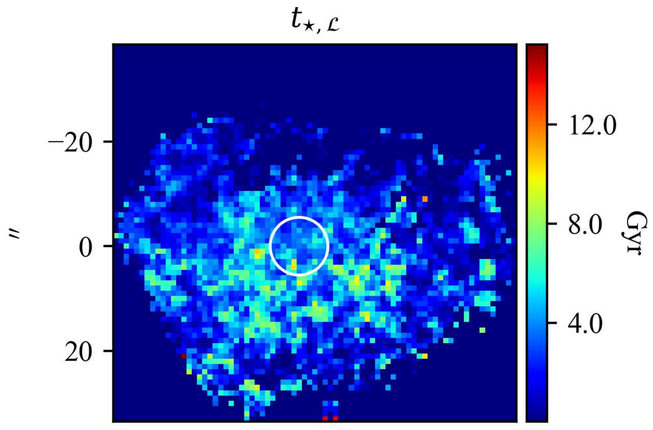

$t_{\star,\mathcal{M}}$

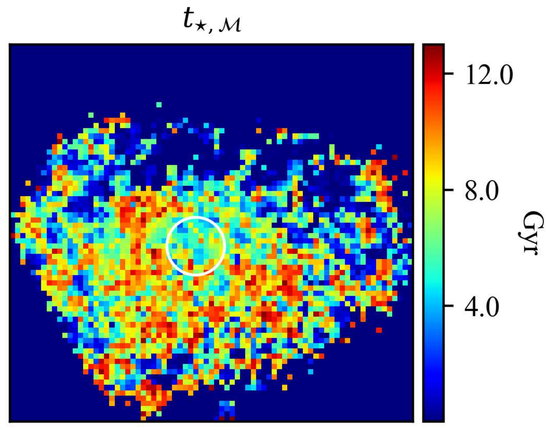

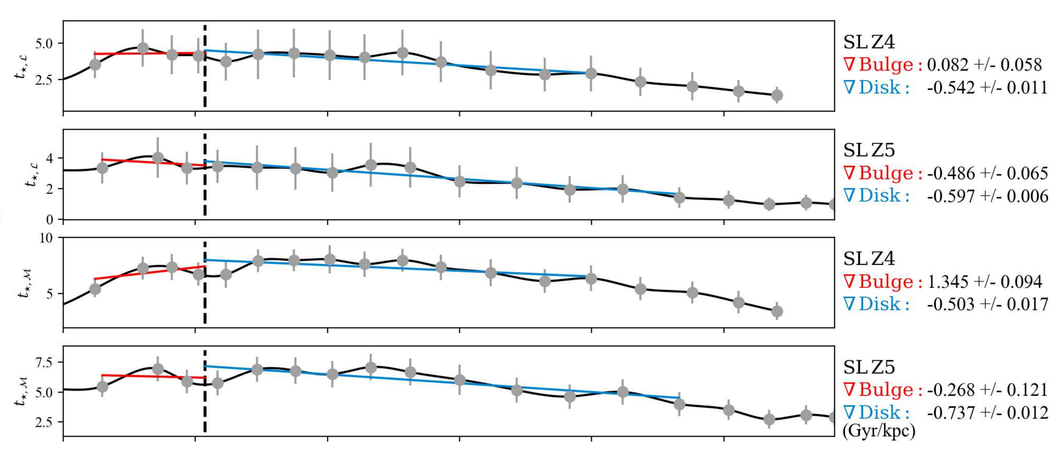

Hα flux

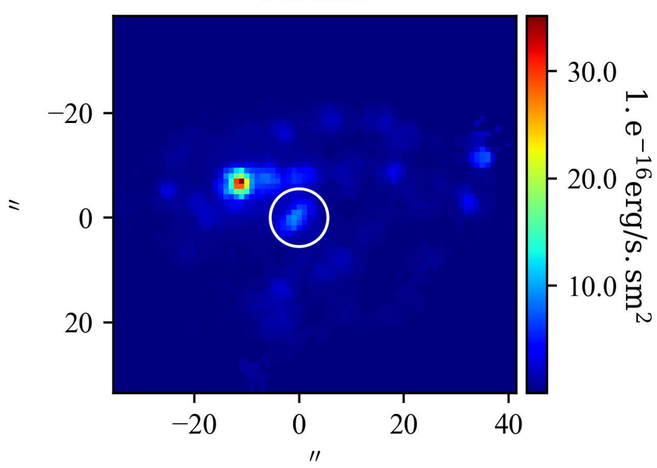

EW(Hα)

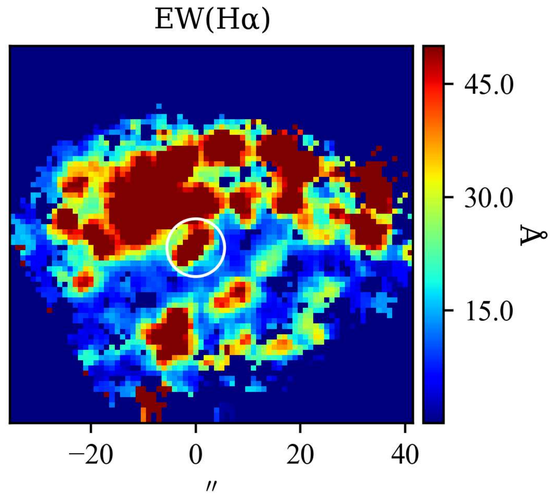

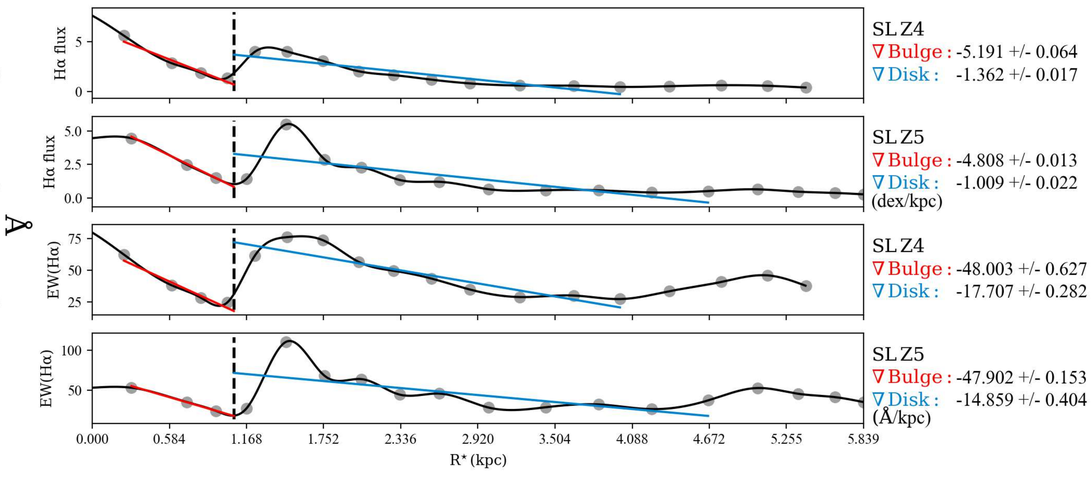

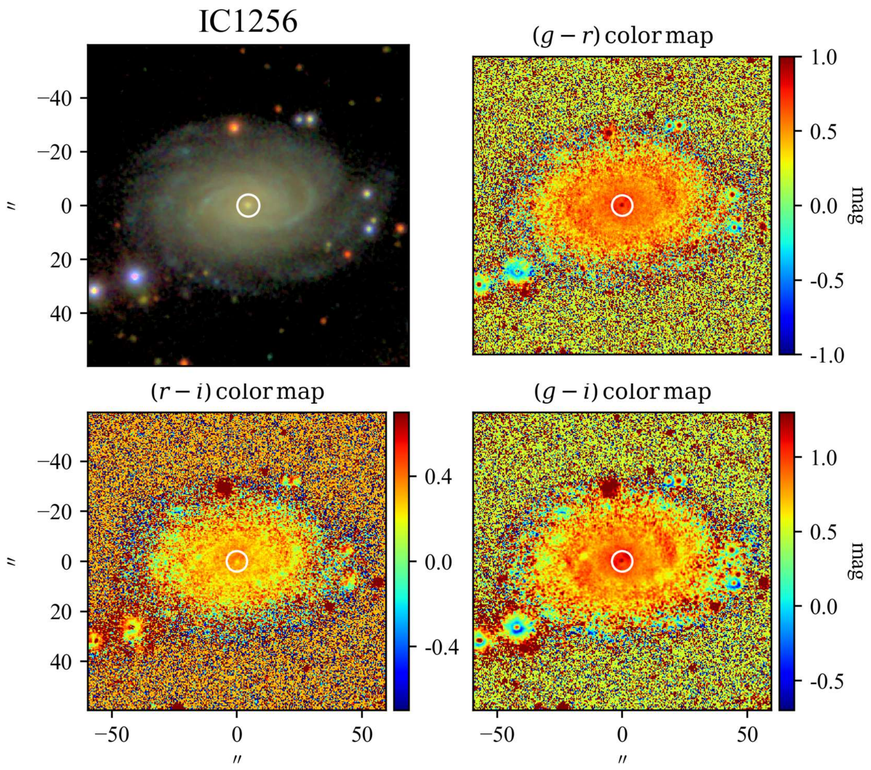

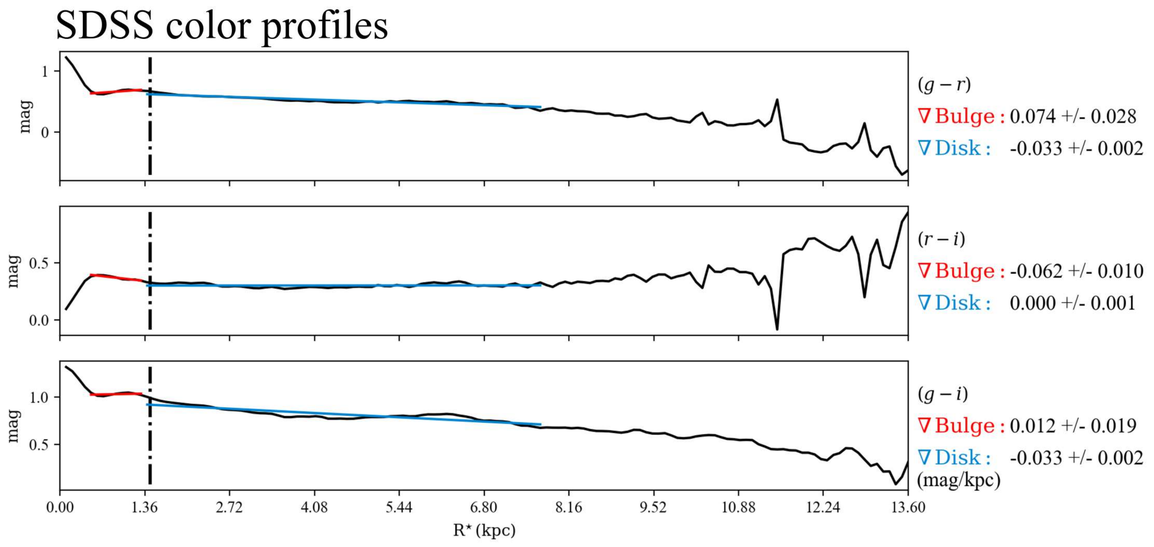

SBP decomposition of SDSS r band

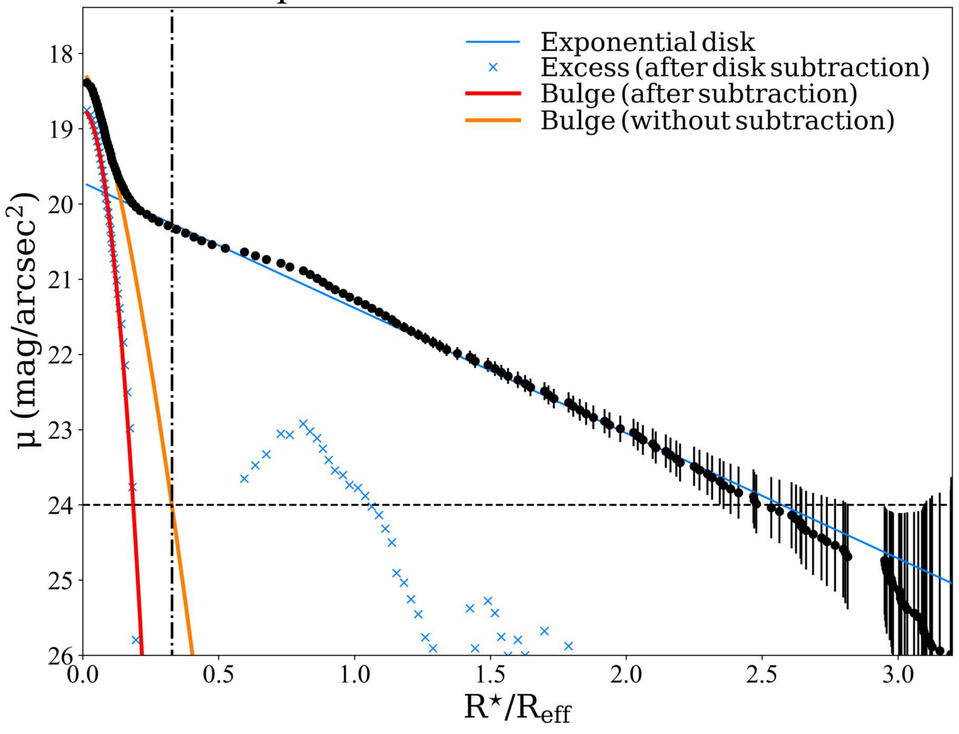

$\mathcal{RV}$ SBPs

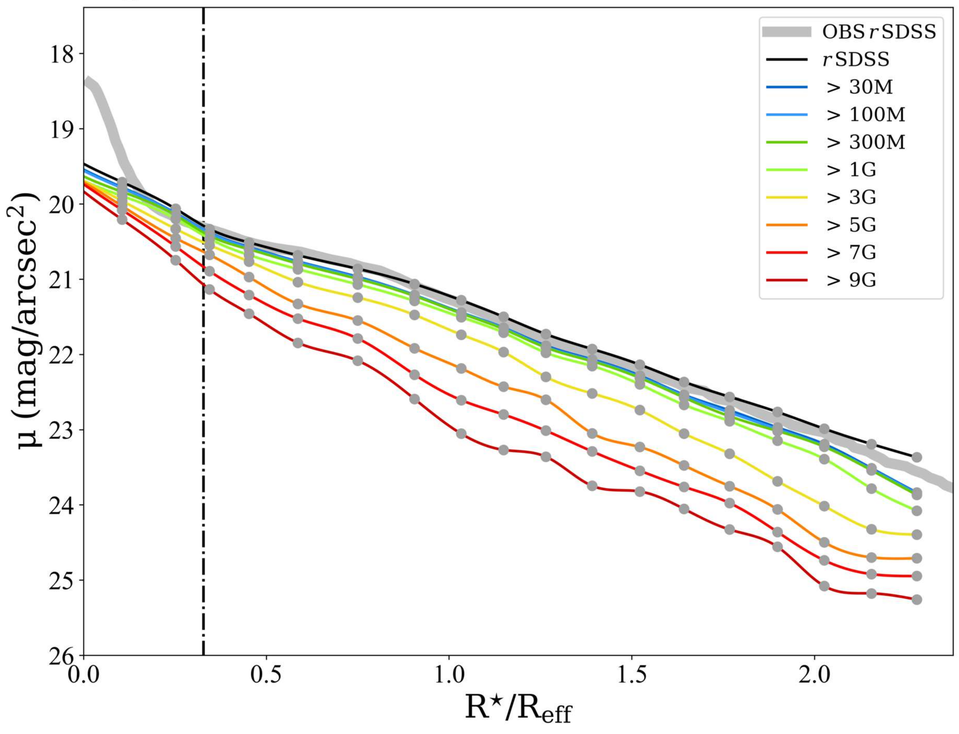

Stellar Continuum

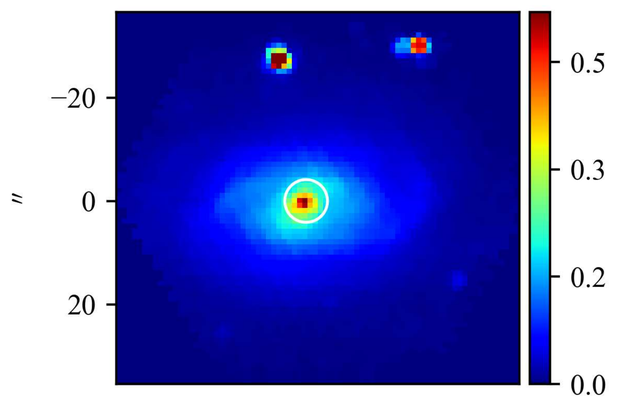

$\mathcal{M}_{\star,\mathrm{P}}$

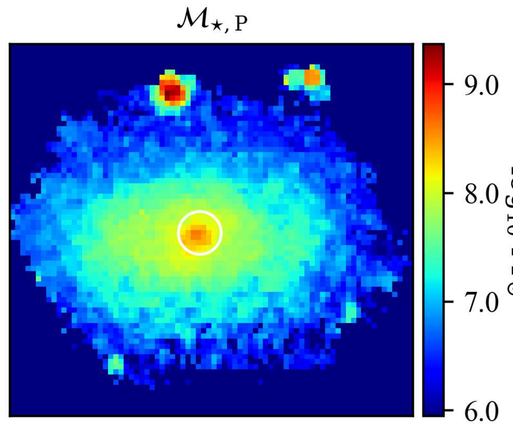

Log. of cumulative present stellar mass profiles

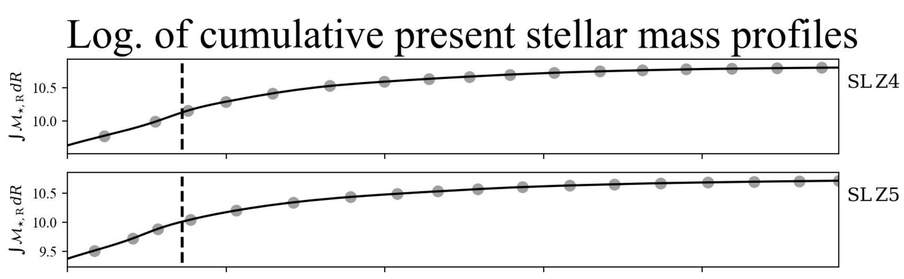

$Z_{\star,\mathcal{L}}$

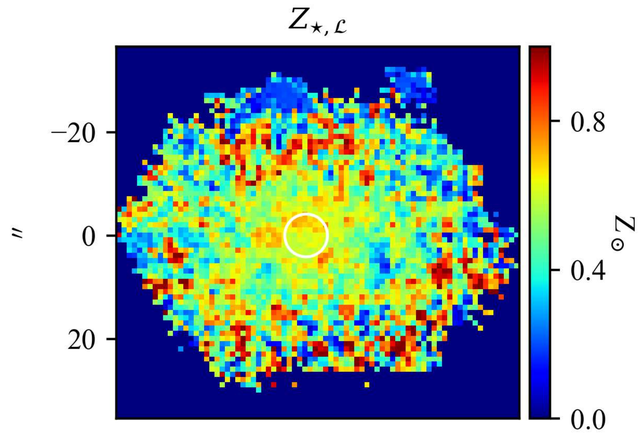

$Z_{\star,\mathcal{M}}$

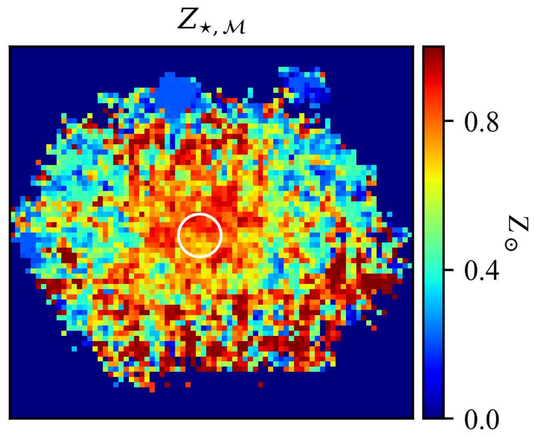

Stellar metallicity/Age & Hα flux/EW profiles

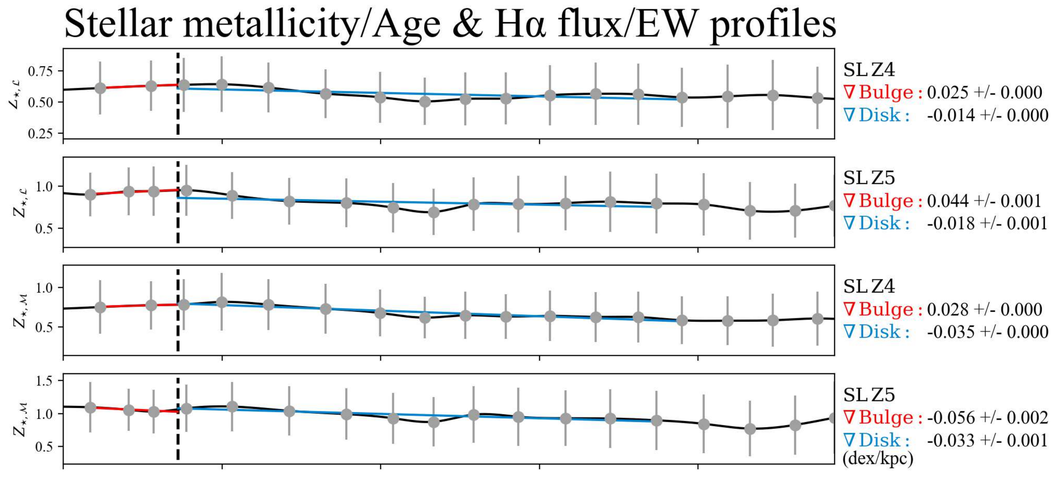

$t_{\star,\mathcal{L}}$

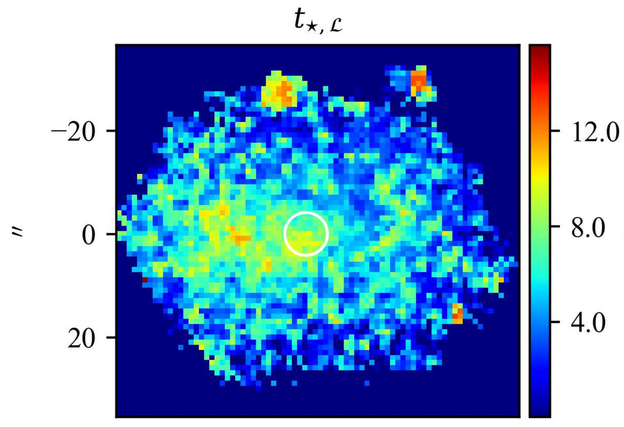

$t_{\star,\mathcal{M}}$

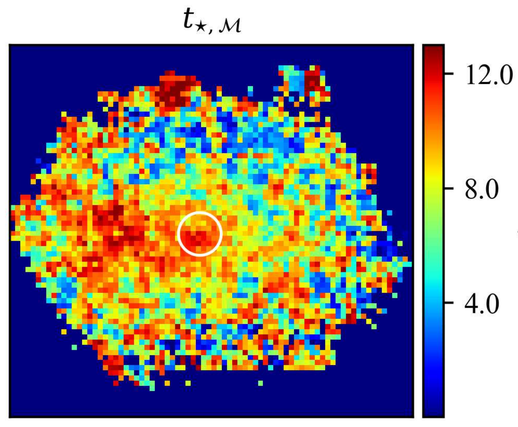

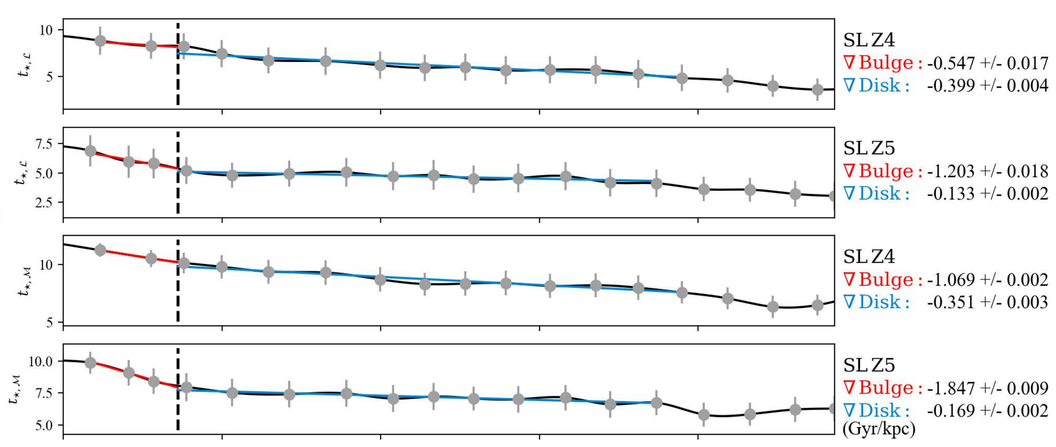

Hα flux

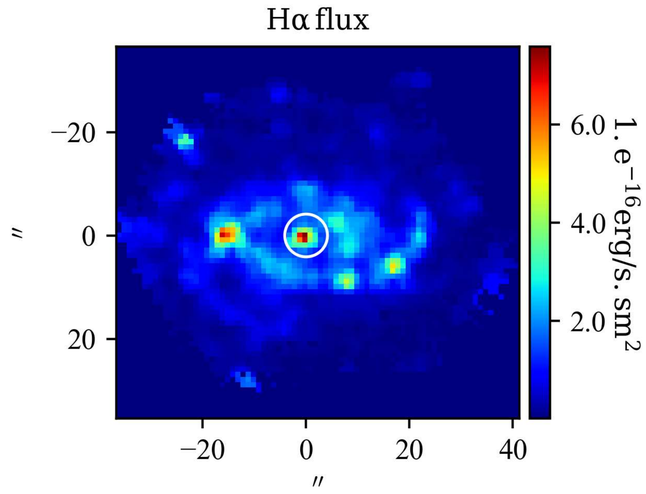

EW(Hα)

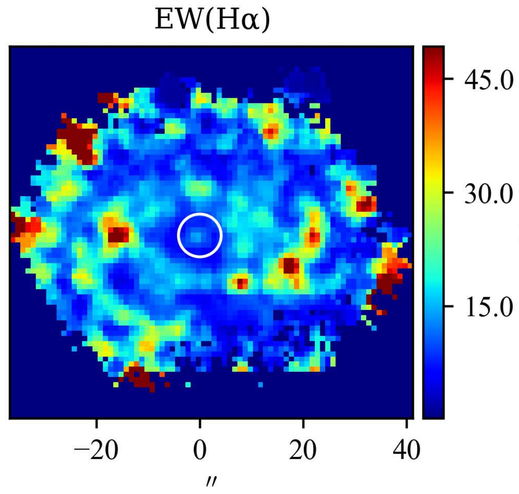

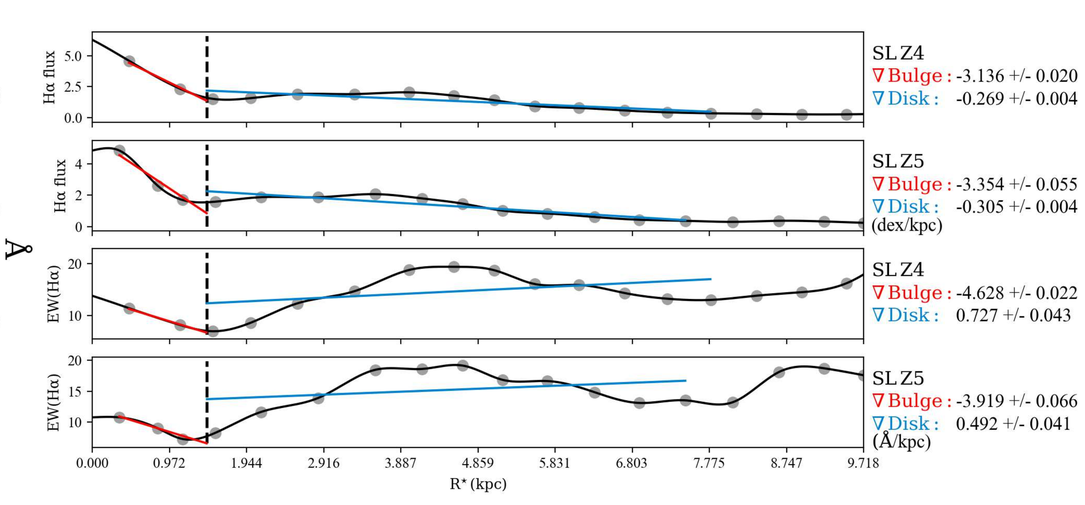

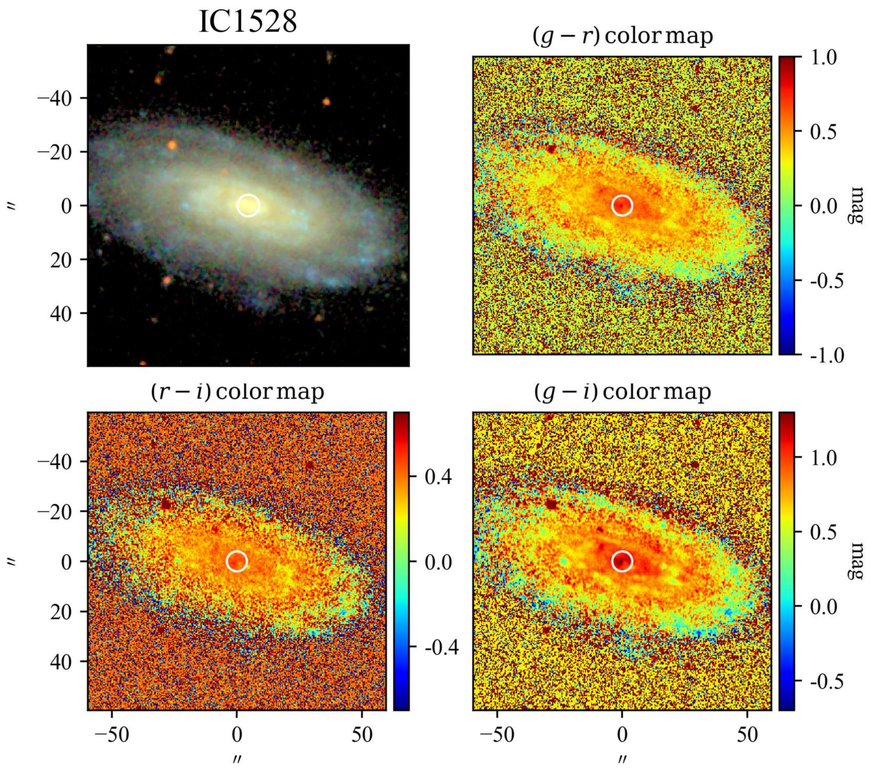

SBP decomposition of SDSS r band

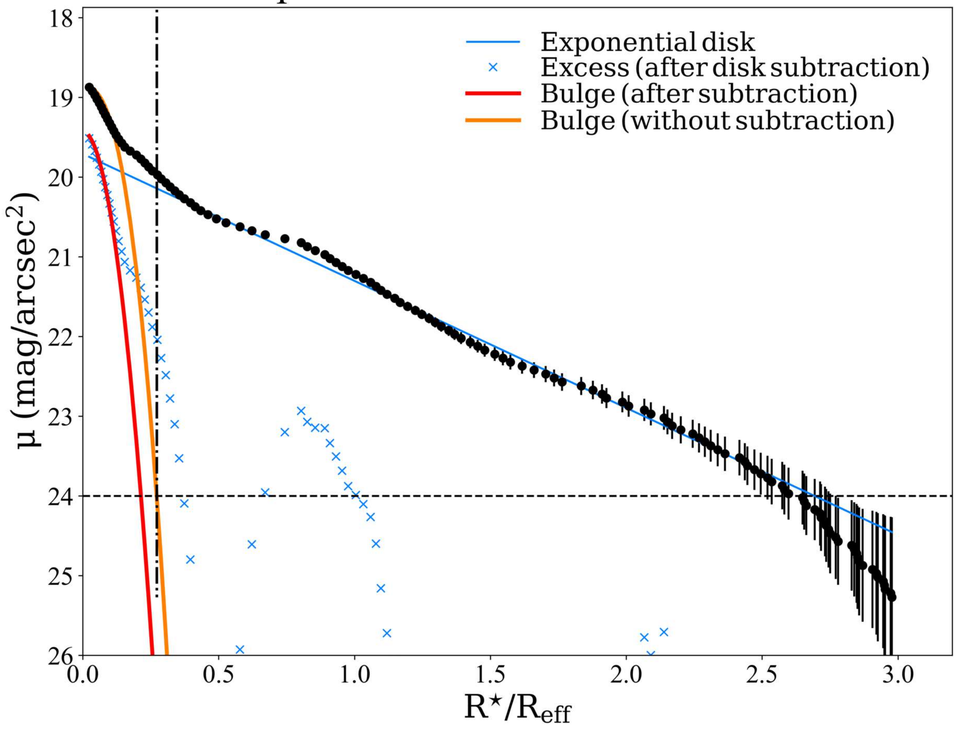

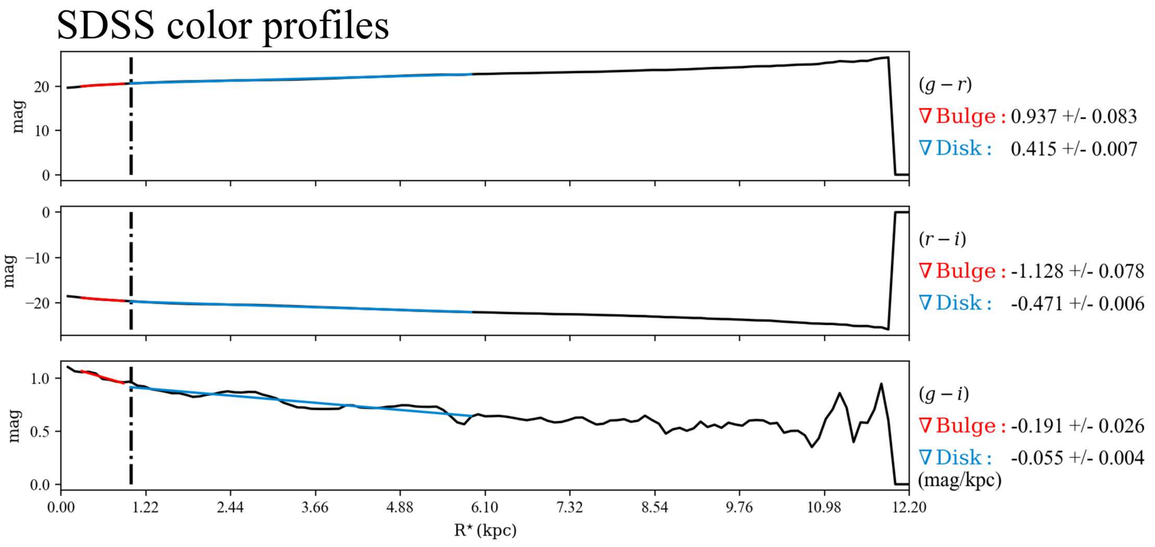

$\mathcal{RY}$ SBPs

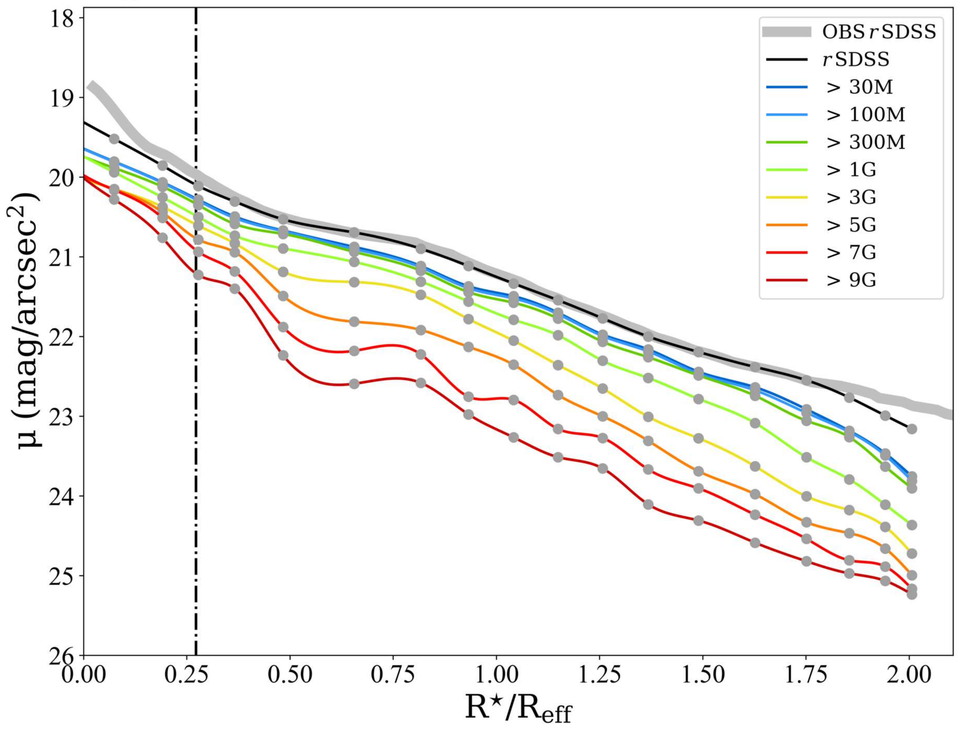

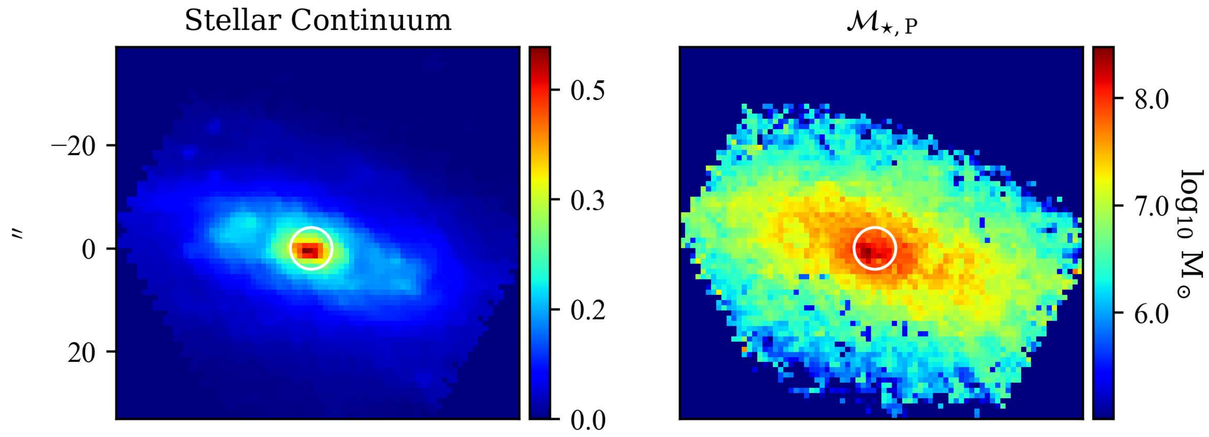

Log. of cumulative present stellar mass profiles

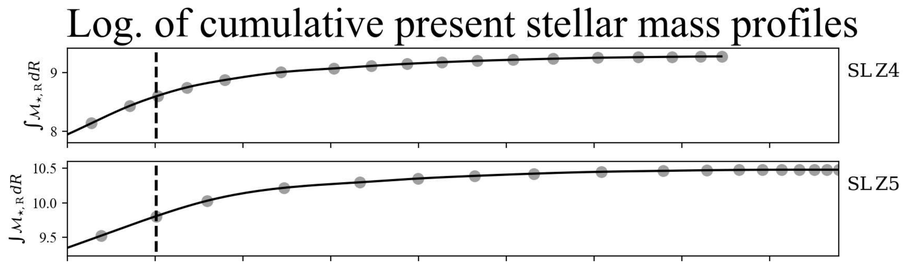

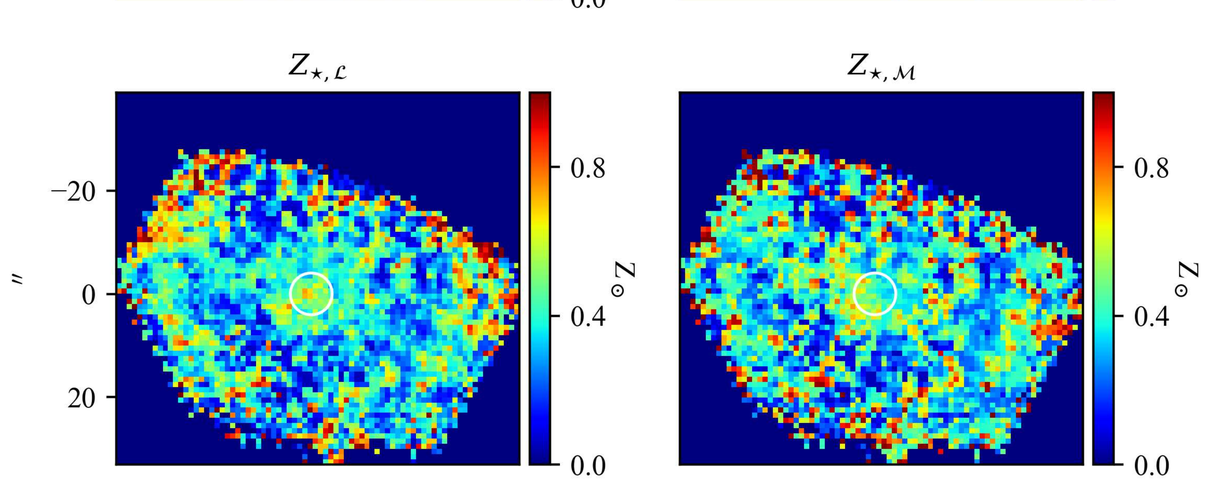

Stellar metallicity/Age & Hα flux/EW profiles

